

Structure of oligourethanes: 6. Fine structure of melt crystallized oligourethanes

Masanobu Nagura and H. Ishikawa.

Faculty of Textile and Technology, Shinshu University, Ueda, Nagano Prefecture, Japan

and Hiroyuki Tagawa and Eiichi Wada

Department of Engineering Chemistry, College of Science and Technology, Nihon University, Tokyo, Japan

(Received 13 June 1975)

The structure and the structure change of the melt crystallized oligourethanes, $\text{CH}_3\text{CO}-\text{-(CH}_2)_5\text{NHCO-}_n\text{OCH}_3$, having strictly homogeneous molecular weight, were studied. The crystal system of every melt crystallized oligourethane was similar to that of the single crystal of $n = 2$. In the case of $n = 2$, crystalline rearrangement by annealing does not occur, although the number of hydrogen bonds increases. On the other hand, rearrangement occurs for $n = 3$ and higher oligomers. It was considered that the rearrangement for $n = 3$ was the transformation from the spherulite to the plate-like crystal, whilst for those of $n = 5$ and 8 the growth of the new spherulitic type of crystal by secondary crystallization occurs. For $n = 10$ and the polymer crystal the thickening was accompanied by an increase of ordered regions.

INTRODUCTION

The synthesis and the fine structure of oligourethanes have been previously studied by Kern¹ and Zahn². The structure and the physical properties of solid state of oligomer, however, have not been investigated in detail.

In previous papers^{3,4}, the dependence of the degree of polymerization on the crystal structure of the solution grown crystal of oligourethane was elucidated. In this paper, the structure and the structure change of the melt crystallized oligomer have been studied.

EXPERIMENTAL

Acetoxy-oligopentamethyleneurethane, $\text{CH}_3\text{CO}-\text{-(CH}_2)_5\text{NHCO-}_n\text{OCH}_3$ with $n = 2$ to 10, synthesized by a stepwise addition polymerization method⁵ and having strictly homogeneous molecular weights and the polymer having $\bar{M}_n 5.3 \times 10^4$, were used as samples.

The melt crystallized samples were prepared as shown in Table 1.

The thermal properties were determined by differential scanning calorimetry (d.s.c.) and differential thermal analysis (d.t.a.).

Infra-red spectra was measured by the KBr and Nujol method.

Wide angle X-ray scattering (WAXS) was measured with a diffractometer at room temperature.

Small angle X-ray scattering (SAXS) was measured with a Kratky type U-slit camera using $\text{CuK}\alpha$ radiation and a scintillation counter with pulse height analyser.

Density was measured by the floatation method using a mixture of n-heptane and carbon tetrachloride.

The dependence of the specific volume on temperature was measured by dilatometry.

RESULTS

Infra-red spectra of unannealed and annealed samples are shown in Figure 1. The intensity of the absorption band of $3400-3500 \text{ cm}^{-1}$, which is due to the free hydrogen bonds, was reduced by annealing for every sample.

Figure 2 shows WAXS patterns of the unannealed and annealed samples. In the case of $n = 2$ to 8, the intensity of two strong diffraction peaks of the annealed sample does not change. On the other hand, for $n = 10$ and the polymer the diffraction peak shifts into the wide angle side on annealing, namely the same angle as that obtained with oligomers of $n = 8$ and lower. This means that the crystal system of every melt crystallized sample is similar to that of $n = 2$.

Densities of the before and after annealing are shown in Table 2.

Figure 3 shows d.s.c. thermograms. Those of $n = 2, 10$ and the polymer show only a simple endothermic peak,

Table 1 Preparation condition of sample

Degree of polymerization, n	Crystallization conditions		Annealing conditions	
	Temperature ($^{\circ}\text{C}$)	Time (h)	Temperature ($^{\circ}\text{C}$)	Time (h)
2	0	1	50	2
3	0	1	80	5
5	0	1	105	2
8	0	1	120	2
10	0	1	120	2
	125	1		
		3		
Polymer	0	1	120	2
	125	1		
		3		

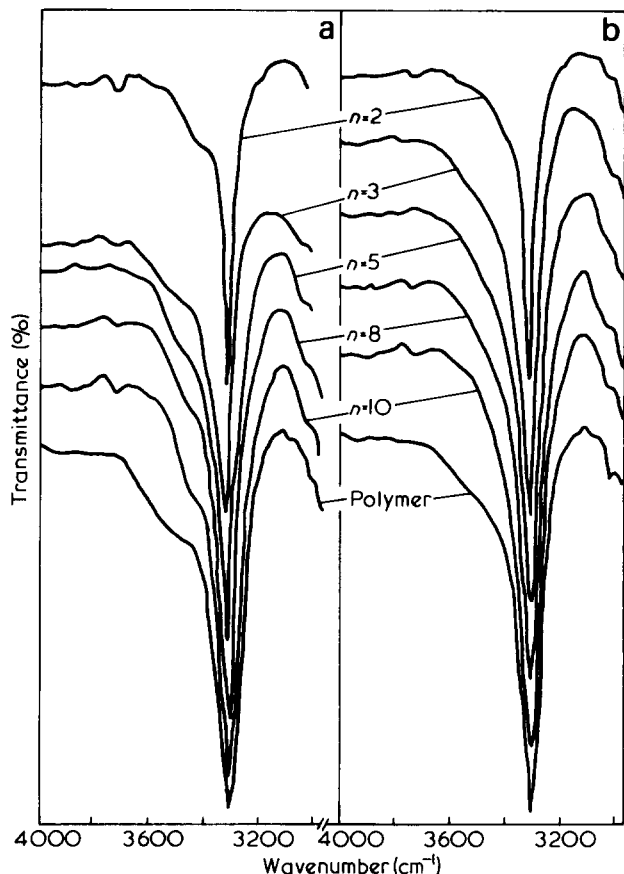


Figure 1 Infra-red spectra of (a) unannealed and (b) annealed samples

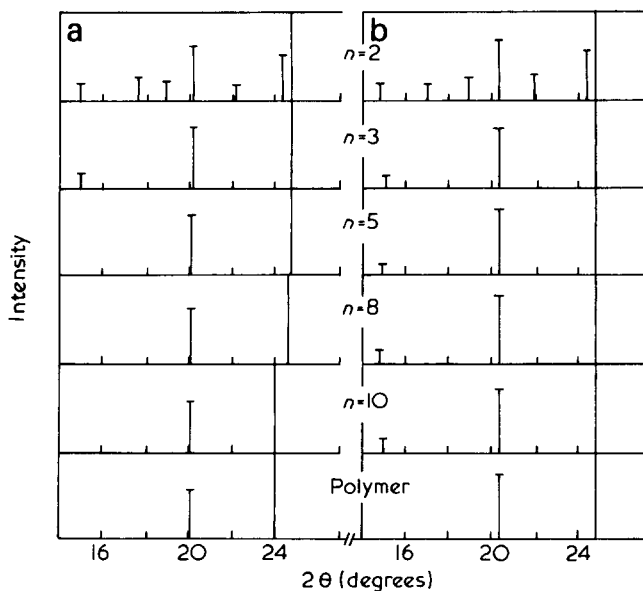


Figure 2 WAXS patterns of (a) unannealed and (b) annealed samples

that of $n = 3$ shows two endothermic peaks and one exothermic peak. Exothermic and endothermic peaks appear for $n = 5$ and 8. By annealing a simple endothermic peak appears in every sample.

Plots of the specific volume against temperature are shown in Figure 4.

The long periods calculated from the results of SAXS pattern by Bragg's law is shown in Figure 5.

DISCUSSION

The process of heating in the d.s.c. measurement corresponds to the annealing and the d.s.c. thermogram of $n = 2$ shows only a simple endothermic peak. The infra-red spectra shows an increase in the number of hydrogen bonds in the sample. Therefore, it is considered that the rearrangement of the whole crystal solid by annealing does not occur, although the number of hydrogen bonds increases.

The d.s.c. thermogram of $n = 3$ shows exothermic and endothermic peaks and by annealing for 5 h at 80°C , the thermogram shows only an endothermic peak on the higher temperature side as shown in Figure 3.

As seen in Figure 5 specific volume increases and decreases abruptly at temperatures close to those of the endothermic and exothermic peaks, respectively. The above results show that the rearrangement of crystallites occurs in the $n = 3$ sample.

To study the rearrangement of the $n = 3$ sample the influence of heating rate on the d.t.a. thermogram and dilatometry was measured. Figure 6 shows the dependence of the endothermic peak temperature on the heating rate. At heating rates higher than $5^\circ\text{C}/\text{min}$ one endothermic peak on the higher temperature side disappears and the other on

Table 2 Degree of polymerization and density

Degree of polymerization, n	Density (g/cm^3)	
	Unannealed sample	Annealed sample
2	1.229	1.231
3	1.231	1.248
5	1.230	1.249
8	1.227	1.250
10	1.225	1.240
Polymer	1.227	1.235

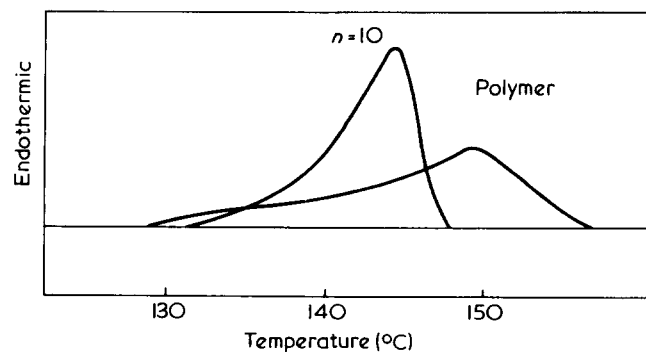
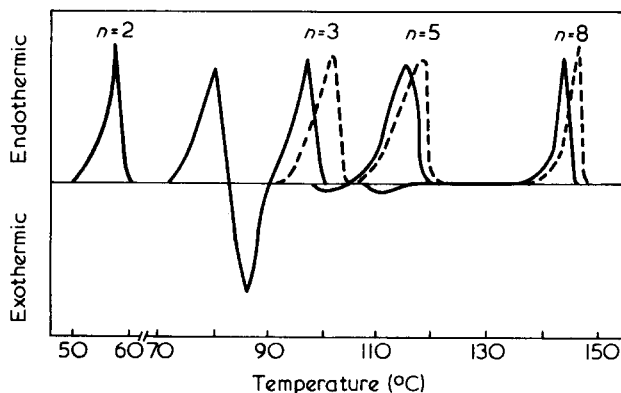


Figure 3 D.s.c. thermograms of unannealed (—) and annealed (---) samples

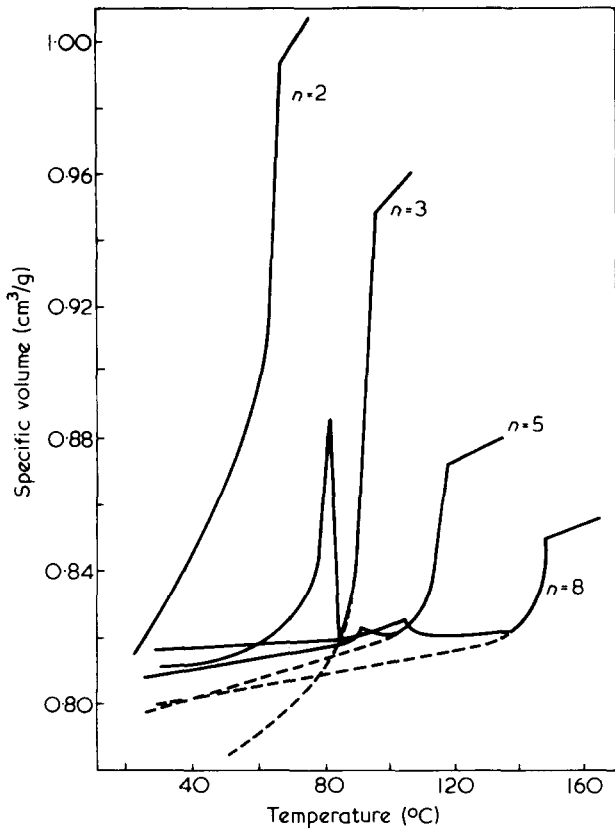


Figure 4 Plots of the specific volume against temperature of unannealed (—) and annealed (---) samples

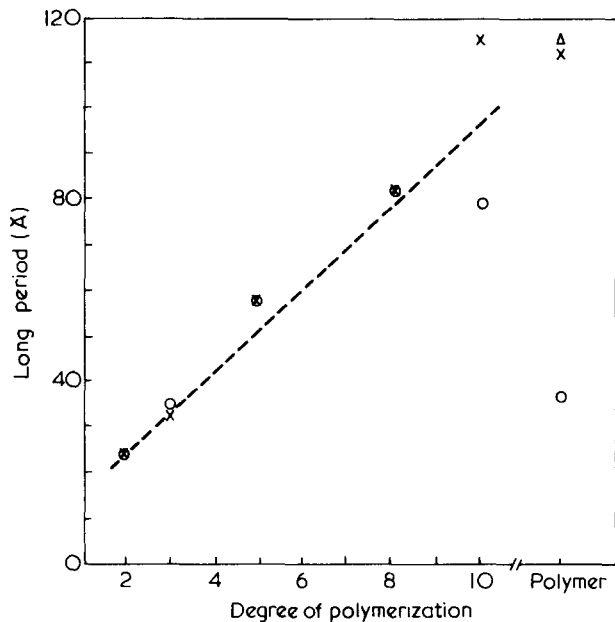


Figure 5 Degree of polymerization dependence of long period; ○, unannealed sample; X, annealed sample; △, isothermal crystallized at 125°C for 3 h; ---, calculated spacing (OKO)

the lower temperature side remains. At very low heating rates, which corresponds to annealing, only one peak appears on the higher temperature side. As shown in Figure 2, the annealed and unannealed samples show almost same WAXS pattern. These results suggest that the metastable crystalline structure at lower temperatures transforms to the stable one at higher temperatures which have the same value of the long period with the metastable one and the same crystal system.

To elucidate the nature of the metastable and stable crystals, the volume contraction was observed by dilatometry, and the volume contraction versus time curves were analysed by using the Avrami equation⁷:

$$\ln \frac{h_0 - h_\infty}{h_t - h_\infty} = kt^n$$

where h_0 is the initial height of mercury in the dilatometry, h_∞ is the final height, h_t is the height at time t and k and n are constant. In the case of the volume contraction for isothermal crystallization at 65°C, the slope of the Avrami plot was 3.2 (Figure 7). This value indicates the formation of spherulitic type of crystal. On the other hand, the spherulitic type of crystal packed in the dilatometer, at 85°, 88° and 92°C, corresponding to the exothermic peak

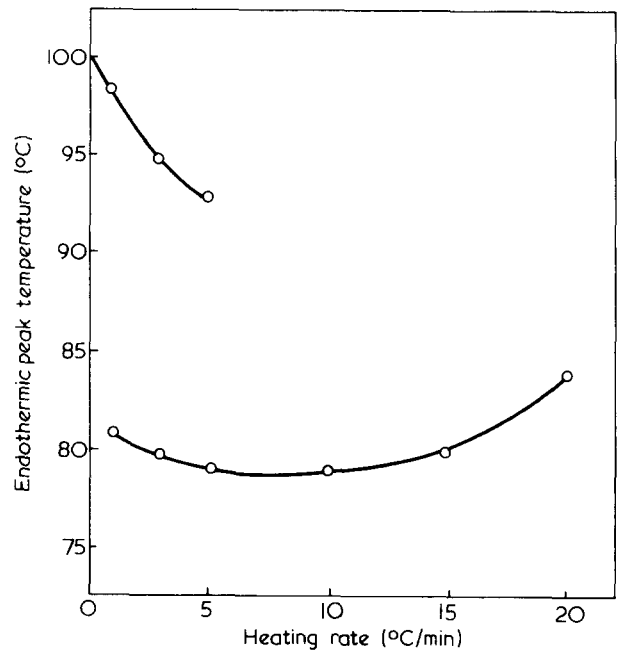


Figure 6 Dependence of the endothermic peak temperature of d.t.a. thermogram on the heating rate

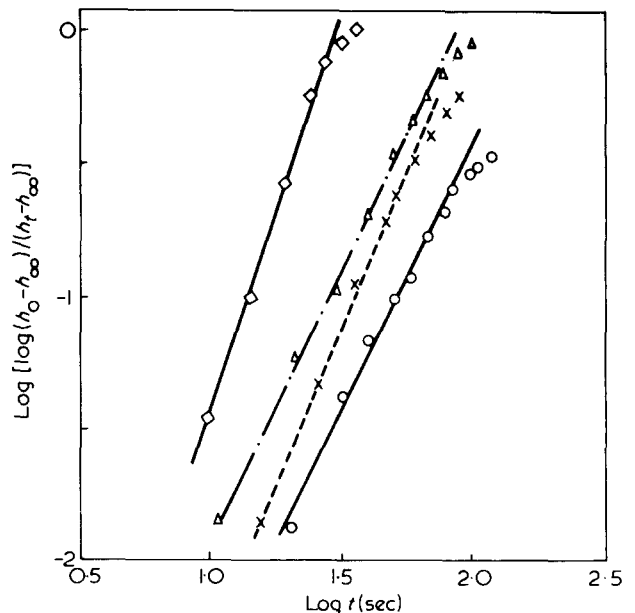


Figure 7 Avrami plots for $n = 3$. ◇, 65°; △, 85°; X, 88°; ○, 92°C

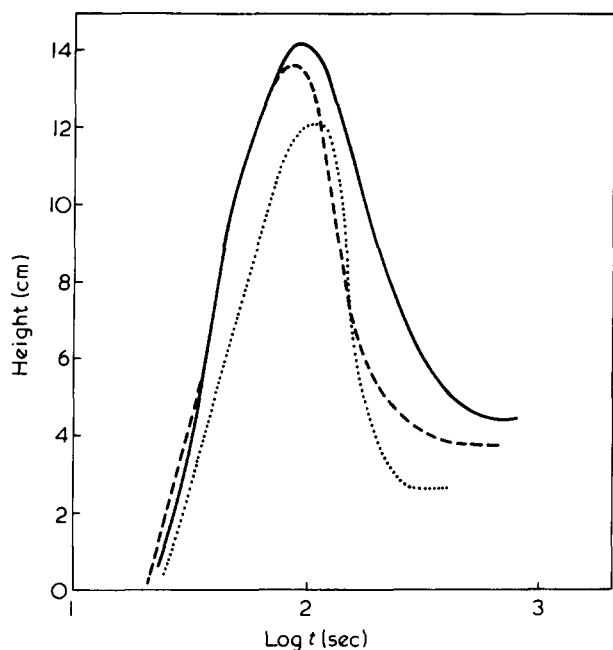


Figure 8 Plots of height of mercury of dilatometer against log t . —, 92°; ---, 88°; ·····, 85°C

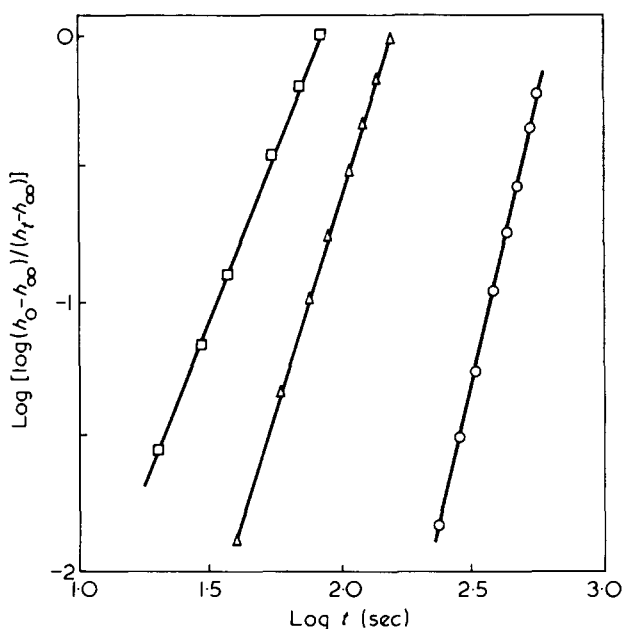


Figure 9 Avrami plots for $n = 5$. □, 100°; △, 105°; ○, 110°C

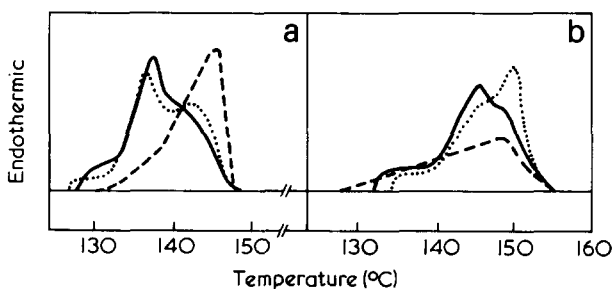


Figure 10 Dependence of d.s.c. thermograms of (a) $n = 10$ and (b) polymer on crystallization time: —, unannealed sample; ---, 1 h; ·····, 3 h

temperature in the d.s.c. thermograms, expands and then contracts as shown in Figure 8. This volume contraction versus time curve was also analysed by using the Avrami equation. The slope of this Avrami plot was 2.0 and this value may mean that the growth of new crystal is two dimensional, or plate-like crystal. These results suggest that the rearrangement from the metastable to the stable crystal is the transformation from the spherulite to the plate-like crystal.

It is clear that the specific volume either increases or decreases at temperatures close to those of the endothermic and exothermic peaks, respectively. Each annealed sample shows a simple fusion curve (Figures 3 and 4) and thus the rearrangement also occurs in these samples.

When the temperature was kept at the maximum point of the plot of specific volume and temperature curve, the slope of the Avrami plot calculated from the volume contraction was about 3.5 as shown in Figure 9. It is thus reasonable to consider that the new spherulitic type of crystal grows from the amorphous parts by secondary crystallization in the samples of $n = 5$ and 8.

As shown in Figure 5, the long periods of $n = 10$ and polymer increase by annealing. The calculated spacing⁴ ($0k0$) assuming that the unit cell expands along \vec{b}_s of sub-cell axis, the length of repeating unit, $-\text{O}(\text{CH}_2)_5\text{NHCO}-$, having that of the planar zigzag configuration is also shown in Figure 5. The Figure shows the thickening phenomena of the crystal of $n = 10$ and polymer by annealing. Furthermore, the $2\theta = 24.8^\circ$ diffraction peak, which corresponds to the lattice plane composed of the molecular sheet connected side by side, shows a decrease of this lattice distance on annealing. Therefore, in the unannealed sample the disordered region changes into the ordered region, or the intermolecular sheet distance decreases. Consequently, density increases as shown in Table 2.

In addition to the endothermic peak for quenched sample a new endothermic peak on the lower temperature side appears in the d.s.c. thermogram for isothermal crystallization at 125°C (Figure 10). The area of the new peak increases with increasing crystallization time and both the long period of the $n = 10$ and polymer increase as shown in Figure 5. Therefore, it is considered that the crystal is thickened gradually during the long period of isothermal crystallization. The decrease of the endothermic peak temperature in the d.s.c. thermogram may be explained if the entropy difference between the solid state of crystal and the melt increases with increasing time.

ACKNOWLEDGEMENTS

The authors express their grateful thanks to Dr Y. Iwakura of University of Tokyo and Dr K. Iwata of Central Institute of Teijin Co. Ltd for donating the sample.

REFERENCES

- 1 Kern, W., Davidovits, J., Rauterkus, K. I. and Schmidt, G. F. *Makromol. Chem.* 1961, **43**, 106
- 2 Zahn, H. and Pieper, W. *Kolloid-Z.* 1962, **180**, 97
- 3 Nagura, M., Tagawa, H. and Wada, E. *Makromol. Chem.* 1973, **165**, 325
- 4 Nagura, M., Tagawa, H. and Wada, E. *ibid.* 1973, **168**, 251
- 5 Iwakura, Y., Hayashi, K. and Iwata, K. *ibid.* 1965, **89**, 214
- 6 Tagawa, H., Wada, E. and Sakurai, T. *ibid.* 1972, **154**, 215
- 7 Mandelkern, L. 'Crystallization of Polymers', McGraw-Hill, New York, 1964.

Reaction field in anisotropic dielectrics

K. H. Lau and K. Young

Department of Physics, The Chinese University of Hong Kong, Shatin, N.T., Hong Kong
(Received 3 June 1975)

Drawn polymers are often characterized by dielectric anisotropy. This is determined by the anisotropy in the molecular polarizability, averaged over the distribution of polymer chains. Since each dipole in the dielectric is situated in a macroscopically anisotropic medium, corrections arise from the anisotropic cavity field and reaction field. The necessary reaction field correction is explicitly evaluated for an axially symmetric dielectric with negligible electronic polarizability and is found not to exceed 2–3%. This shows that the *ad hoc* anisotropic generalization of Onsager's equation used in the literature need only be corrected for the cavity field effect in the manner recently discussed.

INTRODUCTION

A useful tool for determining the orientation function in a drawn polymer is the measurement of dielectric anisotropy. From the measured permittivity tensor ϵ_{ij} , one first obtains the molecular polarizability $\overline{\alpha_{ij}}$, where $\overline{\quad}$ denotes an average over the polymer chain distribution. Comparison with the polarizability α_{ij} of a single molecule yields the orientation function. Our purpose here is to examine in some detail the relation between ϵ_{ij} and $\overline{\alpha_{ij}}$; this relation for the isotropic case is the Onsager equation¹. Previous analyses of anisotropic data^{2–4} have not used a proper anisotropic generalization of the Onsager equation. This is particularly worrying because (a) it is the anisotropy, rather than the average value, which is of main interest in polymer physics, and (b) the likely size of the error involved has not hitherto been estimated.

We give a systematic formulation of dielectric theory in the anisotropic case and show that two effects need be taken into account: (a) the cavity field effect recently discussed⁵; and (b) the reaction field. The latter is the main concern of this paper, and the necessary correction is evaluated for an axially symmetric dielectric with negligible electronic polarizability. Our main result is that the reaction field correction turns out to be very small. It is fortunate, but not *a priori* obvious, that this should be so.

The rest of the paper is organized as follows. In the next section, we consider the response of an isolated molecule to an external field and define the polarizability α_{ij} . Next the response of a molecule in a medium is considered and a general expression is found for the permittivity ϵ_{ij} . In both cases, the example of an axially symmetric material with negligible electronic polarizability serves to illustrate the main ideas. Finally, the reaction field is studied for this special case and the correction is estimated.

MODEL FOR AN ISOLATED MOLECULE

General formulation

The molecular dipole will be assumed to be made of two parts: a rigid permanent dipole of magnitude μ_0 and a bound electron of charge $-e$:

$$\vec{\mu} = \mu_0 \vec{a} - e\vec{x} \quad (1)$$

Here \vec{a} is a unit vector specifying the direction of the permanent dipole and \vec{x} is the position of the electron. The generalization to several electrons is straightforward. The thermal average of the dipole moment is:

$$\langle \mu_i \rangle = \frac{\int \mu_i \exp(-\beta U) d^3x d\Omega}{\int \exp(-\beta U) d^3x d\Omega} \quad (2)$$

Here Ω denotes the orientation of the unit vector \vec{a} , $\beta = (kT)^{-1}$ and U is the energy of the dipole. For an isolated molecule, U is taken to be of the form:

$$U = \Delta(\vec{a}) + \frac{1}{2} x_i k_{ij} x_j - \vec{\mu} \cdot \vec{E} = U_0 - \vec{\mu} \cdot \vec{E} \quad (3)$$

Here $\Delta(\vec{a})$ is the orientation energy of the permanent dipole, the symmetric matrix k_{ij} represents an anisotropic 'spring' binding the electron and \vec{E} is an external electric field. To first order in \vec{E} , equation (2) may be written as:

$$\langle \mu_i \rangle = \alpha_{ij} E_j \quad (4)$$

where the polarization tensor α_{ij} is:

$$\alpha_{ij} = \beta \frac{\int \mu_i \mu_j \exp(-\beta U_0) d^3x d\Omega}{\int \exp(-\beta U_0) d^3x d\Omega} \quad (5)$$

A special case

We shall focus attention on a special case of equation (5) in order to bring out the essential physics. First, we assume the electronic contribution can be ignored, so that equation (5) reduces to:

$$\alpha_{ij} = \beta \mu_0^2 \frac{\int a_i a_j \exp(-\beta \Delta) d\Omega}{\int \exp(-\beta \Delta) d\Omega} \quad (6)$$

Define

$$Q(\Omega) = \exp(-\beta \Delta) \quad (7)$$

which is just the Boltzmann distribution function for the permanent dipole. Further assume that $Q(\Omega)$ is axially symmetric about the chain axis (of the monomer molecule). If

the angle between the chain and the dipole \vec{a} is denoted by γ , $Q(\Omega)$ may be written as:

$$Q(\Omega) = \frac{1}{4\pi} \sum_l Q_l P_l(\cos \gamma) \quad (8)$$

Putting these into equation (6) gives:

$$\alpha_{ij} = \frac{\beta\mu_0^2}{4\pi Q_0} \sum_l Q_l \int a_i a_j P_l(\cos \gamma) d\Omega \quad (9)$$

In a frame where the z-axis coincides with the chain, α_{ij} takes the diagonal form:

$$\alpha_{ij} = \alpha(\delta_{ij} + \nu\eta_{ij}) \quad (10)$$

where η_{ij} is the matrix (matrices will be denoted by $\hat{\eta}$)

$$\hat{\eta} = \begin{pmatrix} 1 & & \\ & 1 & \\ & & -2 \end{pmatrix} \quad (11)$$

Thus $\alpha = \text{tr } \alpha_{ij}/3$ is the average value (over the principal directions) of the polarizability and ν is a measure of the anisotropy. Taking the trace of equation (9) and noting that $a^2 = 1$, we get:

$$\alpha = \beta\mu_0^2/3 \quad (12)$$

which is the classical result of Langevin and Debye⁶, here found to be unmodified so long as we talk about the average. For the anisotropy we obtain:

$$\nu = -\frac{1}{5} \frac{Q_2}{Q_0} \quad (13)$$

It is to be noticed that α_{ij} is insensitive to Q_l with $l > 2$; therefore measurement of the polarizability will yield no information on the higher Q_l . This comes as no surprise since α_{ij} is a rank two tensor and therefore involves only $l = 0$ and 2.

Averaging over the chain distribution

Let us now transform to a frame suitable for macroscopic discussion: we take the z-axis to be the draw direction (rather than the chain direction). In this frame, let the direction of the dipole be Ω and that of the chain be Ω' , with the angle between them being γ . Then equation (8) becomes, by the addition theorem for spherical harmonics*.

$$Q(\Omega) = \sum_{lm} \frac{Q_l}{2l+1} Y_{lm}^*(\Omega') Y_{lm}(\Omega) \quad (14)$$

We are interested not so much in $Q(\Omega)$ as in its average value $\bar{Q}(\Omega)$ over the chain distribution. Let the chains be distributed according to $f(\Omega')$; this is, of course, the orientation function one wants to study. Let $f(\Omega')$ be axially symmetric about the draw direction:

$$\begin{aligned} f(\Omega') &= \frac{1}{4\pi} \sum_l f_l P_l(\cos \theta') \\ &= \frac{1}{(4\pi)^{1/2}} \sum_l \frac{1}{(2l+1)^{1/2}} f_l Y_{l0}(\Omega') \end{aligned} \quad (15)$$

Here θ' is the polar angle between the chain and the draw direction. The distribution (15) is normalized to unity if $f_0 = 1$. With these definitions in hand, $\bar{Q}(\Omega)$ can be evaluated:

$$\begin{aligned} \bar{Q}(\Omega) &\equiv \int Q(\Omega) f(\Omega') d\Omega' \\ &= \frac{1}{4\pi} \sum_l \frac{1}{2l+1} Q_l f_l P_l(\cos \theta) \end{aligned} \quad (16)$$

where we have used equations (14) and (15) and the orthogonality of the spherical harmonics.

Comparing with equation (8), we see that Q_l has been replaced by $Q_l f_l/(2l+1)$. Thus if we parametrize the average polarizability as:

$$\bar{\alpha}_{ij} = \bar{\alpha}(\delta_{ij} + \bar{\nu}\eta_{ij}) \quad (17)$$

then $\bar{\alpha} = \alpha$, which is physically obvious. The average anisotropy $\bar{\nu}$ can evidently be obtained from equation (13) with the replacement $Q_l \rightarrow Q_l f_l/(2l+1)$:

$$\bar{\nu} = -\frac{1}{5} \frac{Q_2 f_2/5}{Q_0 f_0} = -\frac{1}{25} \frac{Q_2 f_2}{Q_0 f_0} \quad (18)$$

Again $l > 2$ is not involved. The proportionality to f_2 is physically reasonable: it expresses the fact that no matter how anisotropic each molecule is, there will be no average anisotropy $\bar{\nu}$ if the molecules are randomly oriented.

THE MOLECULE IN A DIELECTRIC MEDIUM

General formulation

We next consider a substance with N such molecules or monomers per unit volume. Our treatment will draw on the method of Fröhlich⁷. In contrast to the case of the isolated molecule, it will be necessary to consider interaction between molecules. We consider a sphere of radius R containing one molecule; this molecule will be treated microscopically while the rest of the medium will be treated macroscopically as a dielectric with permittivity ϵ_{ij} . An alternate but equivalent method is to consider a larger sphere containing many molecules but to neglect the short range interaction between these molecules. Thus we are not concerned here with Kirkwood's generalization⁸ of the Onsager equation to include short range effects.

Now the energy of the molecule in question will still have the intrinsic pieces $\Delta(a) + \frac{1}{2} x_i k_{ij} x_j$ of molecular origin. In addition, there will be the energy used to set up the dipole:

$$-\int_0^{\vec{\mu}} \vec{F} \cdot d\vec{\mu} \quad (19)$$

where \vec{F} is the electric field at the origin, other than that due to the dipole itself, i.e. \vec{F} is defined by:

$$\phi(r) = \frac{\vec{\mu} \cdot \vec{r}}{r^3} - \vec{F} \cdot \vec{r} + O(r^2) \quad (20)$$

as $r \rightarrow 0$, where ϕ is the electrostatic potential. The linearity of the dielectric can be used to write \vec{F} as the sum of two

* We shall not explicitly indicate the Ω dependence of Q .

terms respectively proportional to the external field \vec{E} and to μ :

$$F_i = X_{ij}E_j + Y_{ij}\mu_j \quad (21)$$

The first term, known as the cavity field, is the field at the origin when the external field is E and the cavity contains no dipoles:

$$\begin{aligned} \phi(r) &\rightarrow -\vec{E} \cdot \vec{r} & r \rightarrow \infty \\ \phi(r) &\rightarrow -(X_{ij}E_j)r_i + O(r^2) & r \rightarrow 0 \end{aligned} \quad (22)$$

The second term, known as the reaction field, is the field at the origin when there is no external field, but with a dipole μ in the cavity:

$$\begin{aligned} \phi(r) &\rightarrow 0 & r \rightarrow \infty \\ \phi(r) &\rightarrow \frac{\mu \cdot \vec{r}}{r^3} - (Y_{ij}\mu_j)r_i + O(r^2) & r \rightarrow 0 \end{aligned} \quad (23)$$

The symmetric matrices X_{ij} and Y_{ij} are completely defined by equations (22) and (23) and will be functions of the macroscopic permittivity ϵ_{ij} . For reference, we quote the well-known isotropic result:

$$X_{ij} = \frac{3\epsilon}{2\epsilon + 1} \delta_{ij} \quad (24)$$

$$Y_{ij} = \frac{2}{R^3} \frac{\epsilon - 1}{2\epsilon + 1} \delta_{ij} = \frac{8\pi}{3} N \frac{\epsilon - 1}{2\epsilon + 1} \delta_{ij} \quad (25)$$

where in equation (25) we have made the usual assumption $(4\pi/3)R^3N = 1$. We are of course concerned here with the anisotropic case. The form of X_{ij} for this more complicated situation has recently been found and its effect discussed⁵. The rest of the paper will concentrate on the effect of Y_{ij} .

If we now substitute equation (21) into equation (19), we get:

$$-\int_0^{\vec{\mu}} \vec{F} \cdot d\vec{\mu} = -\mu_i X_{ij} E_j - \frac{1}{2} \mu_i Y_{ij} \mu_j \quad (26)$$

so that the total configuration energy is now:

$$\begin{aligned} U &= \Delta(\vec{a}) + \frac{1}{2} x_i k_{ij} x_j - \frac{1}{2} \mu_i Y_{ij} \mu_j - \mu_i X_{ij} E_j \\ &= U_1 - \mu_i X_{ij} E_j \end{aligned} \quad (27)$$

This can now be inserted into equation (2), which is valid in general, to yield the following result to first order in \vec{E} :

$$\langle \mu_i \rangle = \beta \frac{\int \mu_i \mu_j \exp(-\beta U_1) d^3 x d\Omega}{\int \exp(-\beta U_1) d^3 x d\Omega} X_{jk} E_k \quad (28)$$

Recall that the permittivity tensor ϵ_{ij} is defined by:

$$4\pi N \langle \mu_i \rangle = (\epsilon_{ik} - \delta_{ik}) E_k \quad (29)$$

so that comparison with equation (28) gives:

$$\epsilon_{ik} - \delta_{ik} = 4\pi N Z_{ij} X_{jk} \quad (30)$$

or in matrix notation:

$$\hat{\epsilon} - \hat{1} = 4\pi N \hat{Z} \hat{X} \quad (31)$$

where:

$$Z_{ij} = \beta \frac{\int \mu_i \mu_j \exp(-\beta U_1) d^3 x d\Omega}{\int \exp(-\beta U_1) d^3 x d\Omega} \quad (32)$$

Comparison with equation (5) shows that Z_{ij} differs from α_{ij} by the replacement $U_0 \rightarrow U_1$. Physically this just means that the presence of the dielectric modifies the configuration energy, and hence the response to an external field. It is precisely the difference between \hat{Z} and $\hat{\alpha}$ that concerns us here.

It will in fact be instructive for the reader to evaluate equation (32) for the isotropic case (where $\Delta = \text{constant}$; \hat{X} , \hat{Y} are given by equations (24) and (25) and $k_{ij} = k\delta_{ij}$) and thus show that equation (31) reduces to the usual form of the Onsager equation. Indeed such a derivation of the Onsager equation avoids the introduction of various ambiguous concepts such as the 'effective dipole'.

Special case

Again, to simplify matters, we ignore the electronic contribution, then equation (32) becomes:

$$Z_{ij} = \beta \mu_0^2 \frac{\int a_i a_j \exp(-\beta \Delta) \exp(\frac{1}{2} \beta \mu_0^2 a_i Y_{ij} a_j) d\Omega}{\int \exp(-\beta \Delta) \exp(\frac{1}{2} \beta \mu_0^2 a_i Y_{ij} a_j) d\Omega} \quad (33)$$

Note that in the isotropic case $a_i Y_{ij} a_j \propto a^2 = 1$ is independent of Ω and hence can be dropped. Thus the reaction field has no effect in the isotropic limit when the electronic contribution is ignored; it is a specifically anisotropic effect. This is in fact physically obvious: in the isotropic case, the reaction field \vec{E}_R is necessarily in the same direction as the rigid dipole, therefore the torque tending to orient the dipole: $\tau = \mu \times \vec{E}_R$ vanishes. When the medium is anisotropic and $Y_{ij} \neq Y\delta_{ij}$, \vec{E}_R is no longer parallel to μ , so there is a non-zero torque.

The matrix Y_{ij} is of course a function of ϵ_{ij} . We consider a case where ϵ_{ij} is symmetric about the z-axis:

$$\hat{\epsilon} - \hat{1} = (\epsilon - 1) [\hat{1} + u\hat{\eta}] \quad (34)$$

with $\hat{\eta}$ defined as in equation (11). Here:

$$\epsilon = \text{tr} \hat{\epsilon} / 3 \quad (35)$$

is the average value (over the principal directions) of the permittivity, while:

$$u = \frac{\epsilon_{xx} + \epsilon_{yy} - 2\epsilon_{zz}}{6(\epsilon - 1)} \quad (36)$$

is a measure of dielectric anisotropy*. We have calculated

* The parameter u here corresponds to u in ref 5.

Y_{ij} in terms of ϵ and u , using a method similar to that in ref 5, with the result:

$$Y_{ij} = \frac{2}{R^3} \frac{\epsilon - 1}{2\epsilon + 1} \left\{ \delta_{ij} + u \frac{3}{10} \frac{1}{2\epsilon + 1} \eta_{ij} + O(u^2) \right\} \quad (37)$$

It is anticipated that the $O(u^2)$ contribution will be negligible; this is the case with X_{ij} , which we have previously calculated to $O(u^2)$ ⁵.

Insert equation (37) in equation (33) and note that the δ_{ij} piece in Y_{ij} affects only the overall normalization and may be dropped. Thus:

$$Z_{ij} = \beta\mu_0^2 \frac{\int a_i a_j \bar{Q}(\Omega) \exp(Au a_i \eta_{ij} a_j) d\Omega}{\int \bar{Q}(\Omega) \exp(Au a_i \eta_{ij} a_j) d\Omega} \quad (38)$$

where we have made the replacement, $\exp(-\beta\Delta) = Q \rightarrow \bar{Q}$, as discussed earlier and where A stands for:

$$A = \frac{3}{10} \frac{\beta\mu_0^2}{R^3} \frac{\epsilon - 1}{(2\epsilon + 1)^2} \quad (39)$$

Since the calculation will be carried only to first order in the anisotropy u , we only need A to zero order in u , i.e. for the isotropic case. In that case, equation (30) is:

$$\epsilon - 1 = 4\pi N \frac{\beta\mu_0^2}{3} \frac{3\epsilon}{2\epsilon + 1} \quad (40)$$

so that comparing equations (39) and (40) gives:

$$A = \frac{1}{10} \frac{(\epsilon - 1)^2}{\epsilon(2\epsilon + 1)} \quad (41)$$

Note that A does not exceed 0.05.

Let us parameterize Z_{ij} as:

$$\hat{Z} = \alpha(\hat{1} + w\hat{\eta}) \quad (42)$$

then solving for w from equation (38) gives:

$$w = - \frac{\int P_2(Z) \bar{Q}(Z) \exp(-2AuP_2(Z)) dZ}{\int \bar{Q}(Z) \exp(-2AuP_2(Z)) dZ} \quad (43)$$

where we have used:

$$a_i \eta_{ij} a_j = -2P_2(\cos \theta) = -2P_2(Z) \quad (44)$$

For reference note that the usual treatment in the literature^{2,3} ignores the anisotropy in the reaction field and corresponds to putting $A = 0$. Provided that neither the reaction field correction (owing to $A \neq 0$) nor the cavity field correction (owing to $\bar{X} \neq X\bar{1}$) is too large, the two corrections may be independently applied. The cavity field correction has already been discussed⁵, so in this paper we take \bar{X} to be isotropic as in equation (24) and concentrate on the reaction field. Thus comparing anisotropies in equation (31), we find $u = w$. Hence equation (43) now reads:

$$u = - \frac{\int P_2(Z) \bar{Q}(Z) \exp(-2AuP_2(Z)) dZ}{\int \bar{Q}(Z) \exp(-2AuP_2(Z)) dZ} \quad (45)$$

Thus we have derived an implicit equation relating u to

molecular parameters embodied in $\bar{Q}(Z)$. It remains to investigate how a non-zero A affects equation (45).

The reaction field correction

We expand the exponential in equation (45) and also insert equation (16) to get:

$$u = - \frac{\sum_n \sum_l \frac{Q_l f_l}{2l+1} \frac{(-2Au)^n}{n!} \int P_2(Z)^{n+1} P_l(Z) dZ}{\sum_n \sum_l \frac{Q_l f_l}{2l+1} \frac{(-2Au)^n}{n!} \int P_2(Z)^n P_l(Z) dZ} \quad (46)$$

Since $A < 0.05$ and $|u| < 1$, we terminate the series at $n = 1$:

$$u = - \frac{N_0 - 2AuN_1}{D_0 - 2AuD_1} \quad (47)$$

where:

$$N_0 = \sum_l \frac{Q_l f_l}{2l+1} \int P_2(Z) P_l(Z) dZ = \frac{2}{25} Q_2 f_2$$

$$N_1 = \sum_l \frac{Q_l f_l}{2l+1} \int P_2(Z)^2 P_l(Z) dZ$$

$$= \frac{2}{5} Q_0 f_0 + \frac{4}{175} Q_2 f_2 + \frac{4}{315} Q_4 f_4$$

$$D_0 = \sum_l \frac{Q_l f_l}{2l+1} \int P_l(Z) dZ = 2Q_0 f_0$$

$$D_1 = \sum_l \frac{Q_l f_l}{2l+1} \int P_2(Z) P_l(Z) dZ = \frac{2}{25} Q_2 f_2 \quad (48)$$

Notice that since

$$\int P_2(Z)^n P_l(Z) dZ = 0 \quad (49)$$

for $l > n$, by terminating the sum over n we automatically terminate the sum over l as well.

We are now in a position to look at the properties of equation (47). Recall that the molecular polarizability determines $Q_2 f_2$ by means of equation (17), but does not determine $Q_4 f_4$, which appears in N_1 . This is an interesting breakdown of classical dielectric theory, where 'normally' molecular polarizability determines the permittivity. In practice, however, this will not be an important effect, since the coefficient of $Q_4 f_4$ is small. So in the rest of the discussion, we shall set $Q_4 f_4$ to zero. This will be discussed in the Appendix.

Ignoring $Q_4 f_4$, and relating $Q_2 f_2$ to \bar{v} by equation (18), equation (47) can be written as:

$$u = \frac{\bar{v} + Au \left(\frac{2}{5} - \frac{4}{7} \frac{\bar{v}}{v} \right)}{1 + 2Au\bar{v}} \quad (50)$$

Solving for \bar{v} :

$$\bar{v} = u \left[1 + A \left(2u^2 + \frac{4}{7}u - \frac{2}{5} \right) \right] \quad (51)$$

where $O(A^2)$ terms have not been kept. In practice, one measures the anisotropy $u = [\epsilon_{xx} + \epsilon_{yy} - 2\epsilon_{zz}]/[6(\epsilon - 1)]$ and determines \bar{v} from it, so equation (51) is the experimentally useful equation. (The determination of the orientation function from \bar{v} is standard and will not be discussed here; see for example ref 5.) The square bracket in equation (51) is the correction factor to be applied to the naive result $\bar{v} = u$ often used in the literature; the correction is of course proportional to A . In view of the bound $A < 0.05$, the correction never amounts to more than 2–3% and is totally negligible at the present level of experimental accuracy.

Thus the only significant correction, of up to 10%, comes from the cavity field effect⁵.

CONCLUSION

Our main result is that the reaction field correction is small; if a correction is nevertheless desired, equation (51) may be applied. It is well to recall the limitations of the present calculation. First, we restricted our attention to axially symmetric systems. This is the most common situation in polymer physics, and in any case it is inconceivable that the qualitative conclusion of this paper will be altered if one removes this restriction. Secondly, electronic polarizability has been ignored. Thus we expect our result to be applicable in detail only if $|\hat{\epsilon}_0| \gg |\hat{\epsilon}_\infty|$ (where the subscript denotes the frequency) or if we consider the dispersion $\Delta\hat{\epsilon} = \hat{\epsilon}_0 - \hat{\epsilon}_\infty$, which should be due to the permanent dipoles alone. Whether the reaction field has any appreciable effect on the birefringence (i.e. the anisotropy in $\hat{\epsilon}_\infty$) is a separate question to be looked at.

REFERENCES

- 1 Onsager, L. *J. Am. Chem. Soc.* 1936, **58**, 1486
- 2 Bares, J. *Kolloid-Z.* 1969, **239**, 552

- 3 Kakutani, H. *J. Polym. Sci. (A-2)* 1970, **8**, 1177
- 4 Phillips, P. J., Kleinheins, G. and Stein, R. S. *J. Polym. Sci. (A-2)* 1972, **10**, 1593
- 5 Lau, K. H. and Young, K. *Polymer* 1975, **16**, 477
- 6 Langevin, P. *J. Phys.* 1905, **4**, 678;
Debye, P. *Phys. Z.* 1912, **13**, 97
- 7 Fröhlich, H. 'Theory of Dielectrics', Oxford Univ. Press, London, 1949
- 8 Kirkwood, J. G. *J. Chem. Phys.* 1939, **7**, 911

Note added in proof

Similar problems have been considered in the context of liquid crystals by Bordewijk (*Physica* 1974, **75**, 146). We thank Dr Bordewijk for bringing this work to our attention.

APPENDIX

Here we wish to justify the neglect of Q_4f_4 , which, we stress again, cannot be calculated from the polarizability. If we keep the Q_4f_4 term in equation (48), (51) acquires an extra term:

$$\bar{v} = u \left[1 + A \left(2u^2 + \frac{4}{7}u - \frac{2}{5} + \xi \right) \right] \quad (51')$$

where $\xi = 4/315 (Q_4f_4/Q_0f_0)$. By the positive of f , we can deduce

$$|f_4| = \frac{9}{2} \left| \int f(Z)P_4(Z)dZ \right| \leq \frac{9}{2} \int f(Z)dZ = \frac{9}{2} f_0$$

since $|P_4(Z)| \leq 1$. A similar bound applies to Q_4 , hence

$$|\xi| \leq \frac{4}{315} \left(\frac{9}{2} \right)^2 = \frac{9}{35}$$

Therefore the inclusion of ξ does not alter the fact that the correction will be quite small, on account of $A < 0.05$.

Comparative study of crystallization rates by d.s.c. and depolarization microscopy

C. F. Pratt and S. Y. Hobbs

General Electric Research and Development Center, P.O. Box 8, Schenectady, NY 12301, USA

(Received 17 June 1975; revised 20 September 1975)

Markedly slower crystallization half times for poly(butylene terephthalate) and poly(ethylene terephthalate) are found by d.s.c. than by depolarization microscopy although similar values are obtained for isotactic polypropylene. In both the microscopic and calorimetric experiments an Avrami analysis of data on each polymer gives $n \sim 3$ (predetermined nucleation, spherulitic growth), over the range of crystallization temperatures investigated. Possible reasons for the observed discrepancies are discussed.

INTRODUCTION

Measurements of isothermal crystallization rates by the depolarization of light in the hot stage microscope have been reported by several authors¹⁻⁵. In this method the light transmission through crossed polarizers, is monitored as a function of time with a photocell and chart recorder. Crystallization half-times can be interpolated directly from the I versus t profiles or, as suggested by Magill^{1,2}, from normalized light transmission/time plots of the form $(I_c - I_t)/(I_c - I_0)$ vs. $\log t$ where I_0 and I_c are initial and final intensities and I_t the intensity at time t . Rate constants can be calculated from the Avrami equation:

$$\theta = e^{-kt^n} \quad (1)$$

where θ is the fraction of untransformed material, k is a constant and n an integer depending on the type of nucleation and growth⁶⁻⁷. With $\theta = (I_c - I_t)/(I_c - I_0)$, n can be obtained directly from $\ln(-\ln\theta)$ vs. $\ln t$ plots.

In spite of the widespread use of this technique it is not obvious that the depolarized light/time traces should provide a correct measure of polymer crystallization rates or should give the proper Avrami exponent. Binsbergen has shown, for example, that only when it is assumed that the birefringent entities in the crystallizing aggregates increase in number and length with time, (probably a reasonable model for spherulite development), is there a linear relationship between the birefringence and volume of crystalline material⁸. Other analytical techniques may show a similar sensitivity to the details of the crystallization process. Godovsky has recently indicated that for some polymers calorimetry may give $n = 2$ while dilatometry gives $n = 3$ ⁹. In explanation he suggests that the first technique is more sensitive to the development of two-dimensional lamellae while the second reflects the formation of three-dimensional spherulites. Gilbert and Hybart have noted a similar but smaller difference in d.t.a. and dilatometric measurements of aliphatic polyester crystallization rates¹⁵. In general, however, when different analyses give similar Avrami exponents on a given system other kinetic parameters such as the crystallization half-times are found to be comparable.

Some recent studies of the crystallization kinetics of isotactic polypropylene, poly(butylene terephthalate) (PBT), and poly(ethylene terephthalate) (PET) by differen-

tial scanning calorimetry (d.s.c.) and depolarization microscopy, have been reported. Our calorimetric data on PBT are in quantitative agreement with those recently presented by Shultz and Stang¹⁰. The comparative results are noteworthy in that the two polyesters appear to exhibit similar Avrami kinetics but quite different crystallization half-times when examined by the two techniques. In contrast, similar $t_{1/2}$ values are obtained for polypropylene by the two methods.

EXPERIMENTAL

PBT samples were obtained from the GE Plastics Division (Pittsfield, Mass.) (Valox® 310 resin, $[\eta]$ at 25°C in hexafluoroisopropanol (HFIP) = 1.32 dl/g), PET from Cellomer Associates ($[\eta]_{\text{HFIP}}^{25^\circ\text{C}} = 0.67$ dl/g), and polypropylene from the GE Capacitor Department in Hudson Falls (Rexene PP41E3 resin). All calorimetry was carried out in a DSC-2 calorimeter and all microscopy in a Zeiss polarizing microscope equipped with a Mettler FP-2 hot stage. Light transmission between crossed polarizers was monitored as a function of time using a beam splitter and photocell whose output was channeled into a Hewlett-Packard $x-y$ recorder. Both instruments were calibrated over the temperature range 30°–300°C using the following standards: naphthalene, (80.24°C ± 0.05°C); adipic acid, (151.46°C ± 0.05°C); 2-chloroanthraquinone, (208.95°C ± 0.05°C); anthraquinone, (284.23°C ± 0.05°C). Equilibrium temperatures were determined by scanning the standards at increasingly slower rates and extrapolating to zero cooling rate. In the hot stage these values were checked using a copper-constantan thermocouple sandwiched between 9 mil glass cover slips. The values agreed within ±0.2°C.

All samples were melted for 2 min prior to crystallization; polypropylene at 210°C, PBT at 250°C, and PET at 290°C. No changes in the measured crystallization rates were observed on increasing the melting temperature or time and it is assumed that in all cases crystallization proceeded from the equilibrium melt. In both the calorimeter and the hot stage the samples were first cooled to an intermediate temperature* sufficiently high that no measurable crystallization took place, equilibrated for 1 min, and then dropped

* For polypropylene 140°C, PBT 210°C, and PET 240°C.

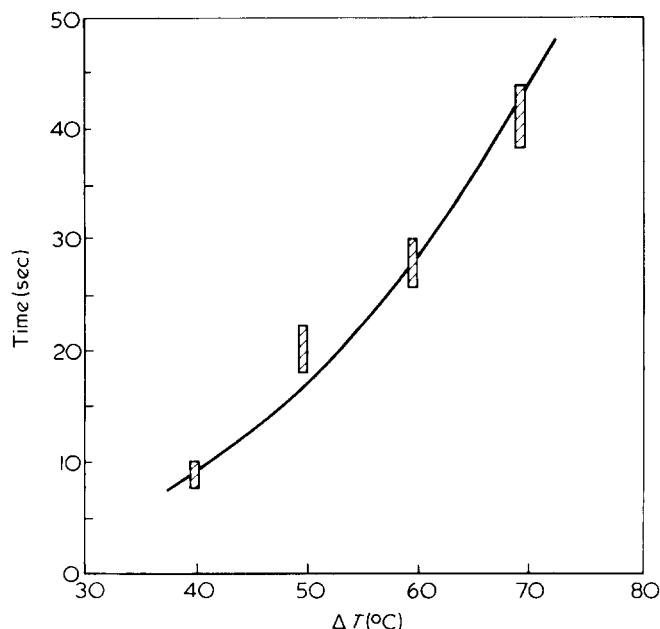


Figure 1 Time for sample to reach thermal equilibrium as a function of supercooling, ΔT

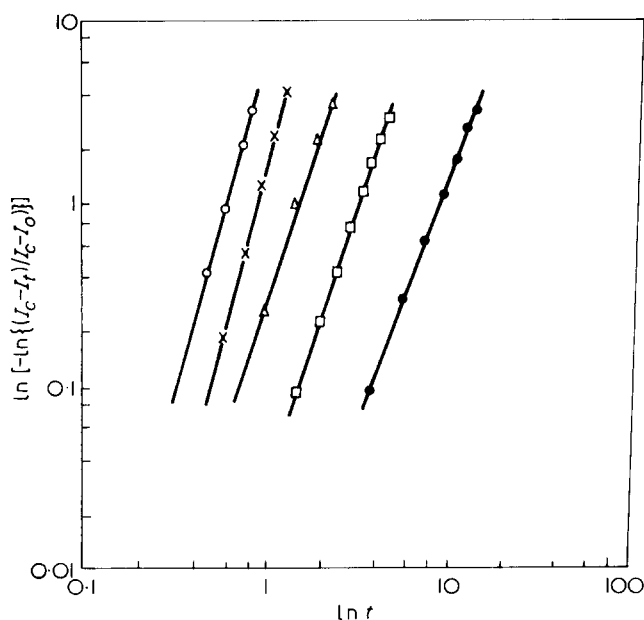


Figure 2 Avrami plot of d.s.c. data for polypropylene. \circ , $T_c = 110^\circ\text{C}$, $n = 3.0$; \times , $T_c = 115^\circ\text{C}$, $n = 3.1$; \triangle , $T_c = 120^\circ\text{C}$, $n = 2.9$; \square , $T_c = 125^\circ\text{C}$, $n = 2.9$; \bullet , $T_c = 130^\circ\text{C}$, $n = 2.7$

to the crystallization temperature. This procedure allowed any thermal stresses to be relieved and permitted more rapid equilibration at T_c . Indicator lights on the two pieces of apparatus were found to give an accurate measure of temperature stabilization. Other investigators employing the depolarization technique have used two furnaces, one at T_m and one at T_c and transferred the sample into the low temperature furnace to initiate crystallization. Our experiments with imbedded thermocouples have indicated that a fairly large but variable time may be required to reach thermal equilibrium using this technique (see Figure 1), giving rise to appreciable uncertainty in the determination of t_0 . By dropping the entire stage temperature with a cool nitrogen jet, t_0 could be accurately fixed although the maximum measurable crystallization rate was somewhat reduced.

The calorimetric data were reduced by setting $\theta = \Delta H_c^t / \Delta H_c^0$ where ΔH_c^t is the integral heat of crystallization at time

t and ΔH_c^0 the total measured heat of crystallization. The depolarization data were reduced as described by Magill. In both cases (see Figures 3 and 5) the times in the $\ln(-\ln\theta)$ vs. $\ln t$ plots include induction times. Slopes were determined graphically over the range $\theta = 0.2-0.8$ to avoid difficulties associated with unusual birefringence variations during the

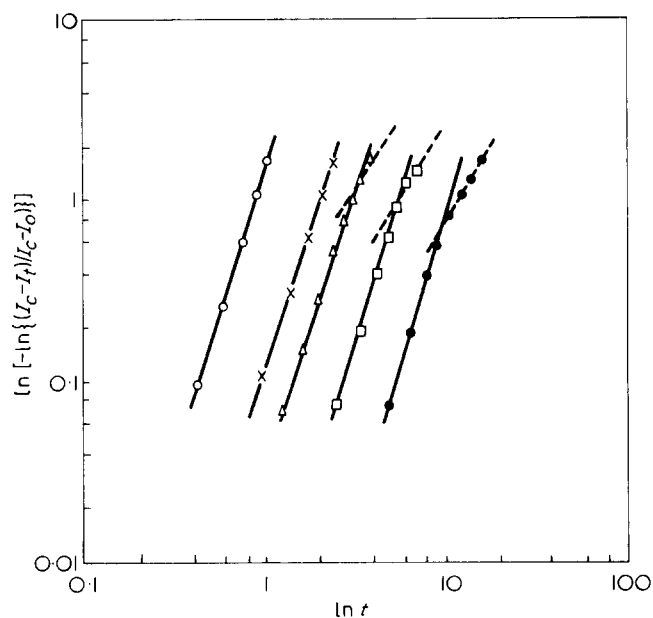


Figure 3 Avrami plot of depolarization data for polypropylene. Note shift in exponent from 3 to 2 as spherulite diameters approach film thickness at higher T_c values. \circ , $T_c = 120^\circ\text{C}$, $n = 3.0$; \times , $T_c = 123^\circ\text{C}$, $n = 2.9$; \triangle , $T_c = 125^\circ\text{C}$, $n = 2.9$; \square , $T_c = 127^\circ\text{C}$, $n = 2.9$; \bullet , $T_c = 130^\circ\text{C}$, $n = 3.0$

Table 1 Avrami exponents obtained from d.s.c. and depolarization data

Polymer	Technique	Crystallization temperature ($^\circ\text{C}$)	Avrami exponent n		
polypropylene	D.s.c.	110	3.0		
		115	3.1		
		120	2.9		
		125	2.9		
		130	2.7		
	depolarized light	120	3.0		
		123	2.9		
		125	2.9		
		127	2.9		
		130	3.0		
poly(butylene terephthalate)	D.s.c.	200	2.7		
		205	2.9		
		210	2.8		
	depolarized light	200	2.9		
		203	3.0		
		205	3.0		
		207	3.0		
		210	3.1		
		poly(ethylene terephthalate)	D.s.c.	200	3.1
				205	3.2
210	3.0				
215	3.1				
220	3.2				
225	3.1				
depolarized light	210	2.9			
	215	3.0			
	220	3.1			
	225	3.5			

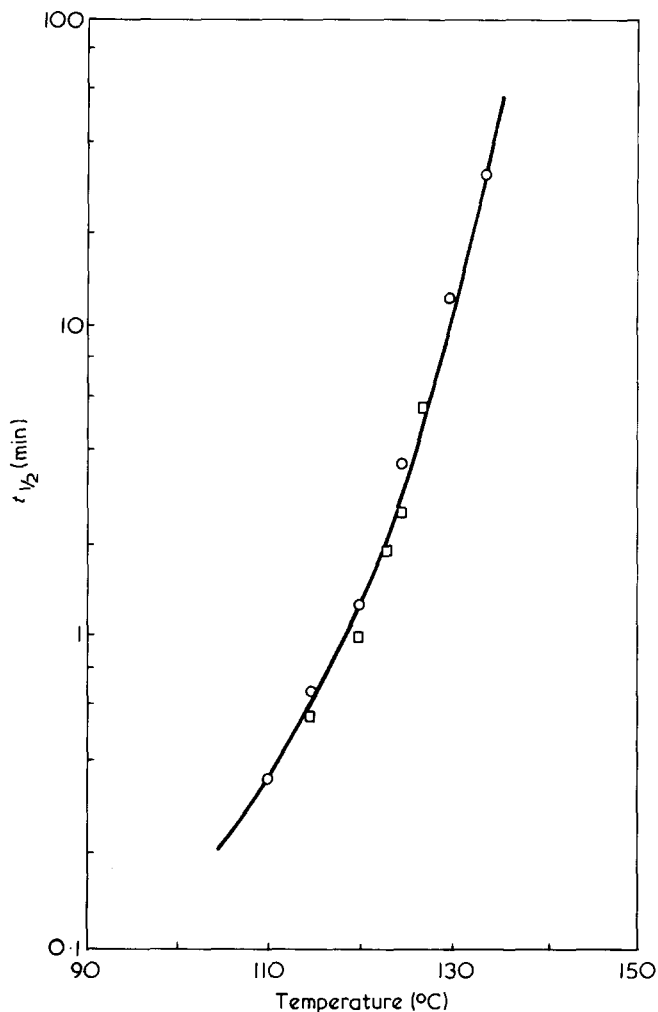


Figure 4 Crystallization half times for polypropylene. \circ , D.s.c.; \square , hot stage

early, non-spherulitic stage of crystallization and truncation effects near the end of crystallization. Independent linear regression analyses of the data gave slopes within ± 0.05 of the graphical values.

RESULTS

Avrami plots obtained by d.s.c. and depolarization microscopy for polypropylene are shown in Figures 2 and 3 and the crystallization temperatures and the corresponding n values for each polymer are listed in Table 1. In the polypropylene samples crystallized in the hot stage above 127°C the diameters of the growing spherulites become comparable to the film thickness and two-dimensional growth ensues. This change is reflected as a shift from 3 to 2 in the slopes of the Avrami plots as shown in Figure 3. In all other cases the slopes of the isotherms remain approximately equal to 3.

The crystallization half times for the three polymers are presented in Figures 4–6. In the case of polypropylene the agreement is excellent between the two techniques over the range of crystallization temperatures investigated, whereas there is considerable disparity in the case of PBT and PET. (The log scale on the ordinate minimizes the displacement in the curves which is approximately a factor of 2.) Crystallization half times for PBT samples with different thermal and processing histories as measured by the two techniques are shown in Figure 6. (The key 450/70, etc. indicates the

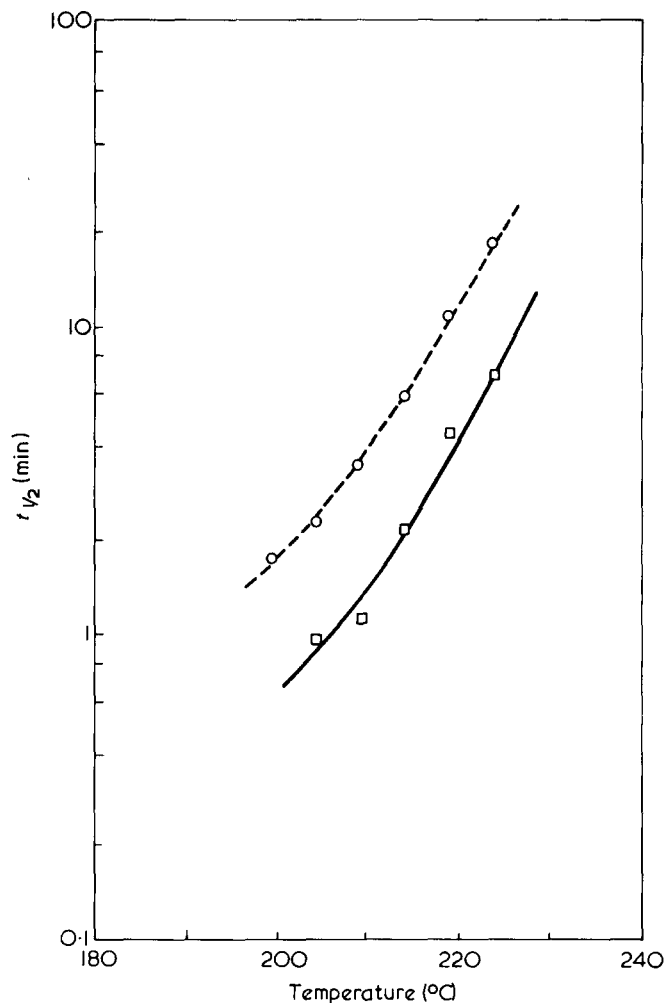


Figure 5 Crystallization half times for poly(ethylene terephthalate). -----, D.s.c.; ———, hot stage

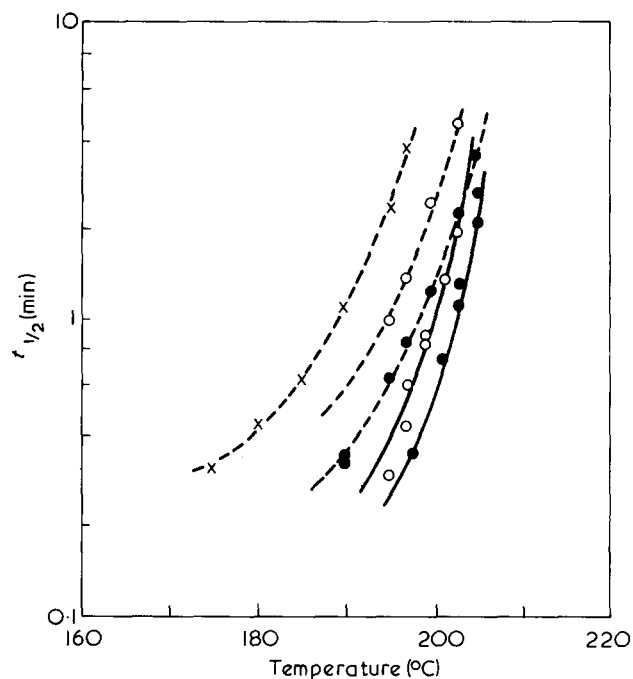


Figure 6 Crystallization half times for poly(butylene terephthalate). X, Valox 310; \circ , Valox 310, moulding 450/70; \bullet , Valox 310, moulding 450/250. Note relatively large sample to sample variation in both techniques. -----, D.s.c.; ———, hot stage

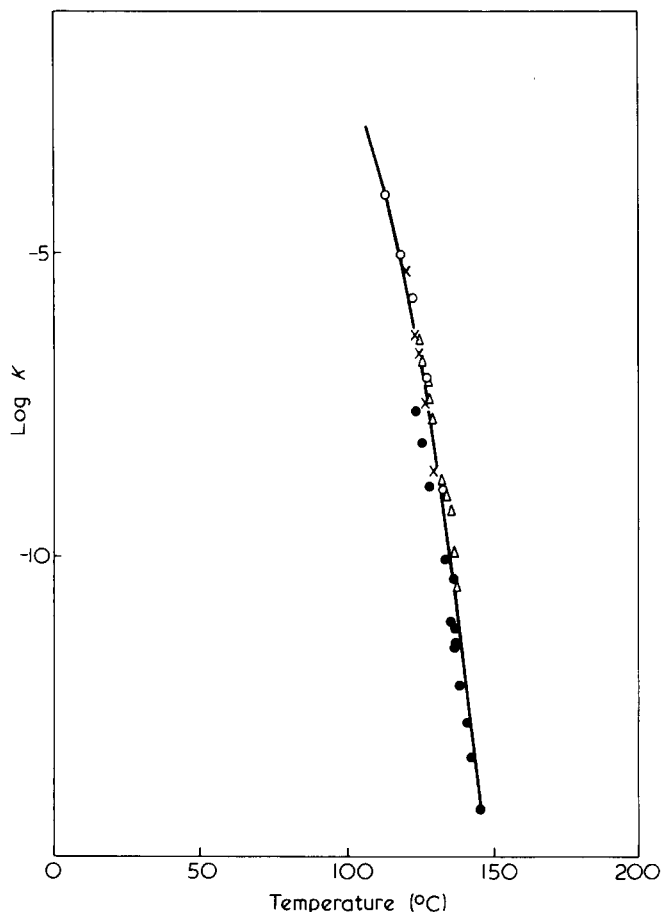


Figure 7 Comparison of Avrami k values obtained by different techniques on several polypropylene samples. Δ , Magill²; \bullet , Marker *et al.*¹¹; O.d.s.c.; X, depolarization

melt and mould temperatures respectively in °F.) Again the $t_{1/2}$ values obtained from the depolarization experiments are approximately half of those measured by d.s.c. although the data appear to show some convergence at higher crystallization temperatures. In all cases the measured Avrami n values ranged from 2.8–3.0. It is noteworthy that there is a considerable increase in the crystallization rate of PBT resin which has been injection moulded although very little change in the viscosity average molecular weight is observed. Very likely the nucleation density is increased in these samples.

A comparison of our data with those obtained by dilatometry on Profax 6513E¹¹ polypropylene and by depolarization microscopy on Shell Carbona White polypropylene² is presented in Figure 7. The respective values for $t_{1/2}$ are conveniently replaced with the respective values for Avrami's k since $n = 3$ in all cases. The three sets of data show surprisingly good agreement for independent measurements on three different polymer samples using three analytical techniques.

DISCUSSION

At the present time we cannot offer a totally satisfactory explanation for the differences in the $t_{1/2}$ vs. T plots obtained for PBT and PET by calorimetric and depolarized light techniques. Repeated measurements showed that the differences are real and reproducible. Although it appears that the curves can be nearly superimposed by a shift along the temperature axis, repeated calibration of both instru-

ments with melting standards indicate that there is less than 0.5°C temperature error in the data points. Similarly there is no evidence that the differences can be attributed to differences in sample configuration or to heterogeneous nucleation on the glass cover slips. The observed spread in $t_{1/2}$ values was maintained when microtomed films of identical thickness were used in the hot stage and calorimeter. Similar half times were measured for unfilled- and glass-filled polyester resins in the calorimeter and no preferential nucleation could be observed on the glass cover slips in the optical microscope.

It has been suggested that the value of I_c obtained from the depolarized light intensity curves may be too low because of improper correction for scattering. This argument finds some support as there are other reports of anomalous maxima in some intensity time traces which may be attributed to competing depolarization and scattering effects. These peaks occur most commonly in samples which are excessively thick or which crystallize extremely rapidly. It is not considered that such effects lead to major errors in the present analyses. Data points were collected only from sigmoidal curves showing no decrease in intensity after reaching maximum height. The half-times normally fell in the steepest section of the traces requiring an unacceptably large 'error' in I_c to displace $t_{1/2}$ to the values obtained by calorimetry. Furthermore, it is unlikely that such competing effects could combine to give 'correct' integral Avrami exponents. Another common reported problem in these experiments is in the selection of τ , the induction time, as the slopes of the $\ln(-\ln\theta)$ vs. $\ln t$ plots are very sensitive to the value of τ . However, we would expect such errors to show up as fluctuations in the Avrami n well before deviations in $t_{1/2}$ are observed. Such variations were not observed. Furthermore inbedded thermocouples indicate that t_0 , the time at which equilibrium temperature is obtained, is accurate 3% or better even in the most rapidly crystallized samples.

Stein has found upon annealing quenched samples of PBT that considerable non-birefringent crystallization may occur which is detectable by low angle light scattering and density measurements but which is not detectable in the optical microscope¹². It is possible that the rate of primary spherulitic development is given accurately by the depolarization measurements while the calorimetric data more accurately reflects the overall rate of crystallization. The latter may include contributions from numerous small crystals which mirror the development of more well developed spherulites but do not contribute appreciably to increases in birefringence. In support of this argument we note that significant heat output is observed in the calorimeter, before the first signs of birefringence develop in the hot stage, especially at higher temperatures. It is also likely that secondary growth processes which proceed at a much lower rate than spherulite development make substantial contributions to the heat of crystallization but only small contributions to increased birefringence. This explanation is undoubtedly oversimplified in that several theoretical treatments have indicated that substantial secondary crystallization should introduce a large fractional component to the Avrami exponents^{13,14}. This result is partly attributable to the fact that such growth is proportional to the time a given volume element has resided in a growing spherulite. We hope that more extensive light scattering experiments, in which contributions from primary spherulite growth are separated from other types of crystallization, will help to explain the observed discrepancy in half-times.

REFERENCES

- 1 Magill, J. H. *Polymer* 1961, 2, 221
- 2 Magill, J. H. *Polymer* 1962, 3, 35
- 3 Hock, C. W. and Arbogast, J. F. *Anal. Chem.* 1961, 33, 462
- 4 Jackson, J. B. and Longman, G. W. *Polymer* 1969, 10, 873
- 5 Binsbergen, F. L. and deLange, B. G. M. *Polymer* 1970, 11, 309
- 6 Avrami, M. J. *J. Chem. Phys.* 1939, 7, 1103
- 7 Morgan, L. B. *J. Appl. Chem.* 1954, 4, 160
- 8 Binsbergen, F. L. *J. Macromol. Sci. (B)* 1970, 4, 837
- 9 Godovsky, Yu. K. and Slonimsky, G. L. *J. Polym. Sci.* 1974, 12, 1053
- 10 Shultz, A. R. and Stang, L. D. *General Electric Analyt. Symp., Cleveland*, 1974
- 11 Marker, L., Hay, P. M., Tilley, G. P., Early, R. M. and Sweeting, O. J. *J. Polym. Sci.* 1959, 38, 33
- 12 Misra, A. and Stein, R. S. *Internal Reports to the General Electric Company*, December, 1973; May, 1974
- 13 Hillier, I. H. *J. Polym. Sci. (A)* 1965, 3, 3067
- 14 Price, F. P. *J. Polym. Sci. (A)* 1965, 3, 3079
- 15 Gilbert, M. and Hybart, F. J. *Polymer* 1974, 15, 407

A rapid technique for the qualitative analysis of polymers and additives using stop-and-go g.p.c. and i.r.*

Francis M. Mirabella Jr[§] and Edward M. Barrall II[†]

Institute of Materials Science and Department of Chemistry University of Connecticut, Storrs, Connecticut 06268, USA

and Julian F. Johnson[‡]

IBM Research Laboratory, San Jose, California 95193, USA

(Received 23 May 1975)

The use of gel permeation chromatography operated in a stop-and-go mode combined with an infra-red spectrometer detector permits rapid qualitative and quantitative analysis of additives in polymers. Additionally, the chemical composition of the polymer and its molecular weight and molecular weight distribution may be determined. The method does not require any preliminary separation steps.

INTRODUCTION

Polymers are often modified with various additives to improve their usefulness. Plasticizers, such as phthalate esters, phosphate esters, fatty acid esters and sulphonamides, are added to improve processability and flexibility of the compounded polymer. Antioxidants, such as phenols, aromatic amines, and condensation products of amines and aminophenols with aldehydes, ketones and thio compounds, are added to prevent or inhibit the oxidation of the polymer. Other additives include colorants, flame retardants and stabilizers. The analysis of polymeric materials routinely includes the qualitative and quantitative analysis for these additives.

The additives present in polymeric materials have been determined in various ways. One of the most common techniques is extraction followed by infra-red spectroscopic analysis¹. The extraction techniques, generally, involve the preparation of a thin film of the sample, e.g. by slicing in the microtome. The films are then extracted in a Soxhlet, Kumagawa or similar apparatus with a solvent that leaches out the monomeric additives present without dissolving, essentially, any of the polymeric material. The polymer and additives, thus separated, can then be analysed separately. Extractions are generally continued for 8–10 h and drying of the polymeric films is done overnight¹. Thus this method is not rapid. A more rapid technique involves the dissolution of the entire sample in a suitable solvent followed by the ultra-violet spectroscopic (u.v.) analysis of the solution². The u.v. spectrum is usually scanned from 200–400 nm and the additive identified and then quantified by direct calibration with the use of standard curves. The solvent and polymer must not absorb u.v. radiation in the region where the additive absorbs. This is a rapid

method but has the disadvantage that the identification of the additive is not readily determined from a u.v. spectrum alone. This would be further complicated if the polymer were unknown. Thus, the method is usually used with known polymers when only one of several additives are suspected as present. A similar u.v. technique has been described by Luongo³, using thin compression moulded films of the polymer. It is subjected to the difficulties mentioned for the solution technique, except there is no solvent which can interfere.

This paper describes a rapid technique for the determination of the chemical composition of the polymeric portion of the sample and the identification of the additives present. The technique can be extended to allow the molecular weight (*MW*) averages and molecular weight distribution (*MWD*) of the polymeric portion of the sample to be determined and to permit the quantification of the additives present, also. This method involves the dissolution of the entire sample in a suitable solvent, followed by the separation of the components on a gel permeation chromatograph. Then using the stop-and-go g.p.c./i.r. method, previously described⁴, the infrared (i.r.) spectrum of each component is scanned while the g.p.c. flow is stopped. This allows for the identification of the polymeric and additive portions of the sample.

EXPERIMENTAL

The experimental apparatus has been described in detail, previously⁴. It consisted of a simple gel permeation chromatograph with a 4.0 cm³ injection loop, stainless steel, 6.35 mm (0.25 in), 1 m columns, packed with Bioglas (Richmond, Cal. USA) glass beads and a Perkin-Elmer 21 infrared spectrometer as a detector. The i.r. detector was fitted with a refracting beam condenser, a 3 mm pathlength, 50 μ l flow-through cell and a 3 mm pathlength, adjustable reference cell.

Two columns sets were employed. Column set 1 consisted of three, 1 m, 6.35 mm (0.25 in) columns packed with 1000, 200 and 200 Å nominal exclusion limit glass beads respectively. Column set 2 consisted of five, 1 m, 6.35 mm

* Part XXXVIII of a series on Column Fractionation of Polymers.

[§] To whom enquiries should be addressed, c/o ARCO/Polymers, Inc., Monroeville, Pa 15146, USA,

[†] On leave from IBM Research Laboratory, San Jose, California, USA.

[‡] On leave from University of Connecticut, Storrs, Connecticut, USA.

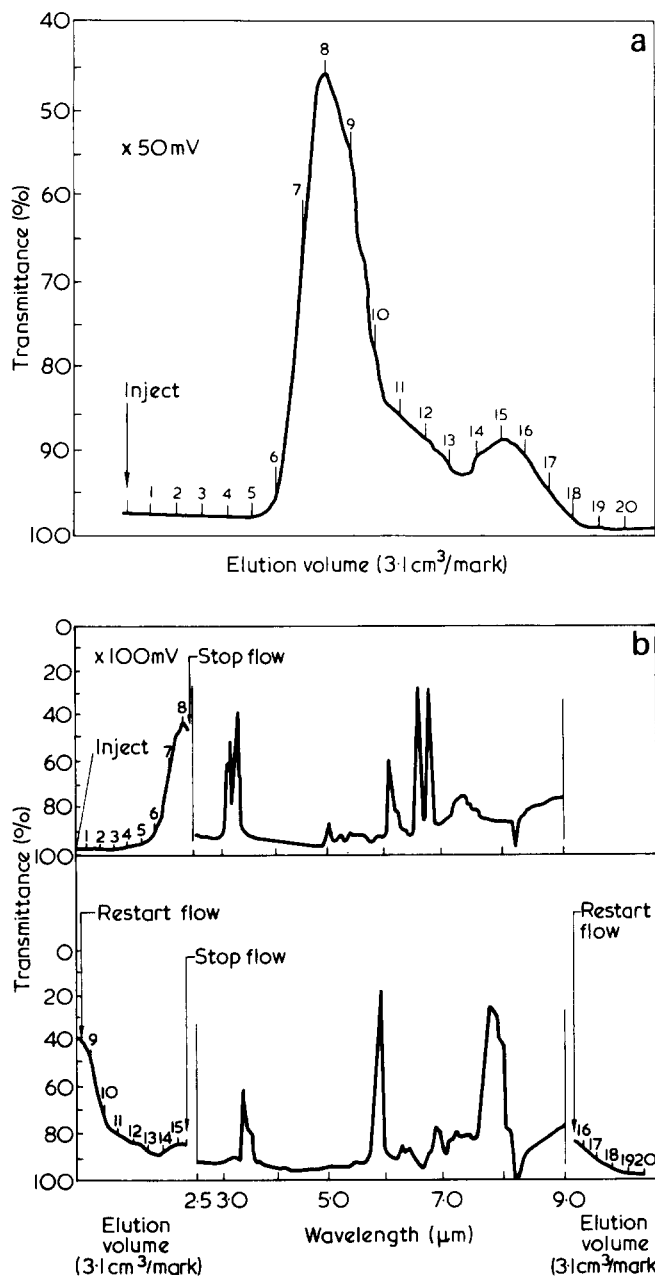


Figure 1 (a) G.p.c. of sample 1 (polystyrene and dibutyl phthalate) on column set 1; see text for details. (b) Stop-and-go g.p.c. of sample 1 on column set 1, showing the i.r. spectra of the polymeric portion and additive portion of the sample

(0.25 in) columns, packed with 1250, 370, 2000 and 1000 glass beads, respectively. Particle sizes of the glass beads used ranged from 50 to 400 mesh.

Column set 1 was used to demonstrate rapid qualitative analysis. Column set 2 was used to demonstrate the feasibility of higher resolution quantitative analysis.

Chromatograms and i.r. spectra were both recorded on a Varian A-25 recorder. Wavelength calibration of the i.r. spectra was performed manually, using the wavelength counter of the spectrometer as a reference.

The following polymer formulations were prepared to demonstrate the method of analysis. All formulations were made using a broad *MWD* polystyrene. Sample 1 contained 7.2% w/w dibutyl phthalate in polystyrene. Sample 2 contained 3.2% w/w didecyl phthalate in polystyrene. Sample 3 contained 1.0% w/w BHT, (2,6-di-*t*-butyl-4-methyl phenol), in polystyrene. Each sample was dissolved at a

concentration of 15 mg/cm³ (based on polymer) in tetrachloroethylene (Fisher Scientific Co., technical grade) which was freshly distilled prior to use. This same solvent was used as the g.p.c. solvent.

The solutions were syringed up through a Millipore filter to remove any insoluble materials. They were chromatographed at a flow rate of 0.8 ml/min and at room temperature. Since 4.0 ml of each solution were injected, the sample load was 60 mg of polymer.

RESULTS AND DISCUSSION

Figures 1a and 1b show, respectively, the g.p.c. of sample 1 (15 mg/cm³ in tetrachloroethylene of polystyrene containing 7.2% w/w dibutyl phthalate) and the stop-and-go g.p.c. of sample 1, showing the i.r. spectra of the polymeric portion and the additive portion of the sample. The g.p.c. were run on column set 1, as described above. The spectra were scanned from 2.50 μm (4000 cm⁻¹) to 9.00 μm (1111 cm⁻¹) since a continuous 'window' was obtained within these limits for tetrachloroethylene solvent. Figures 2a and 2b show standard spectra of polystyrene and dibutyl phthalate in tetrachloroethylene, respectively. Comparison of Figures 2a and 2b with Figure 1b indicates how this method permits the qualitative identification of both polymer and additive. Total analysis time was 1½ h for running one chromatogram and two i.r. spectra.

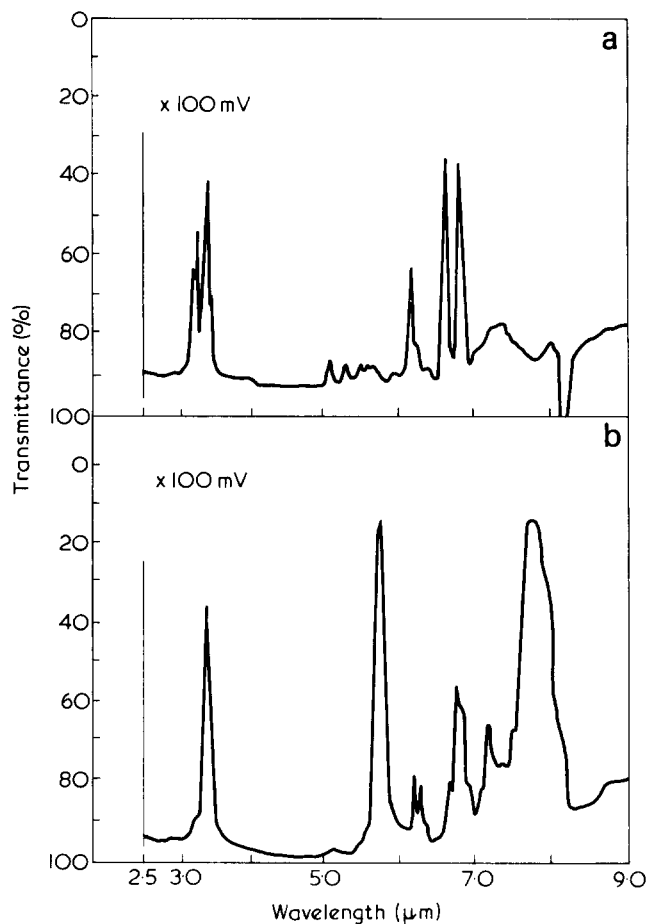


Figure 2 (a) I.r. spectrum of polystyrene, 1 mg/cm³ in tetrachloroethylene, 3 mm pathlength solution versus 3 mm pathlength tetrachloroethylene reference. (b) I.r. spectrum of dibutyl phthalate, 1 mg/cm³ in tetrachloroethylene, 3 mm pathlength solution versus 3 mm pathlength tetrachloroethylene reference

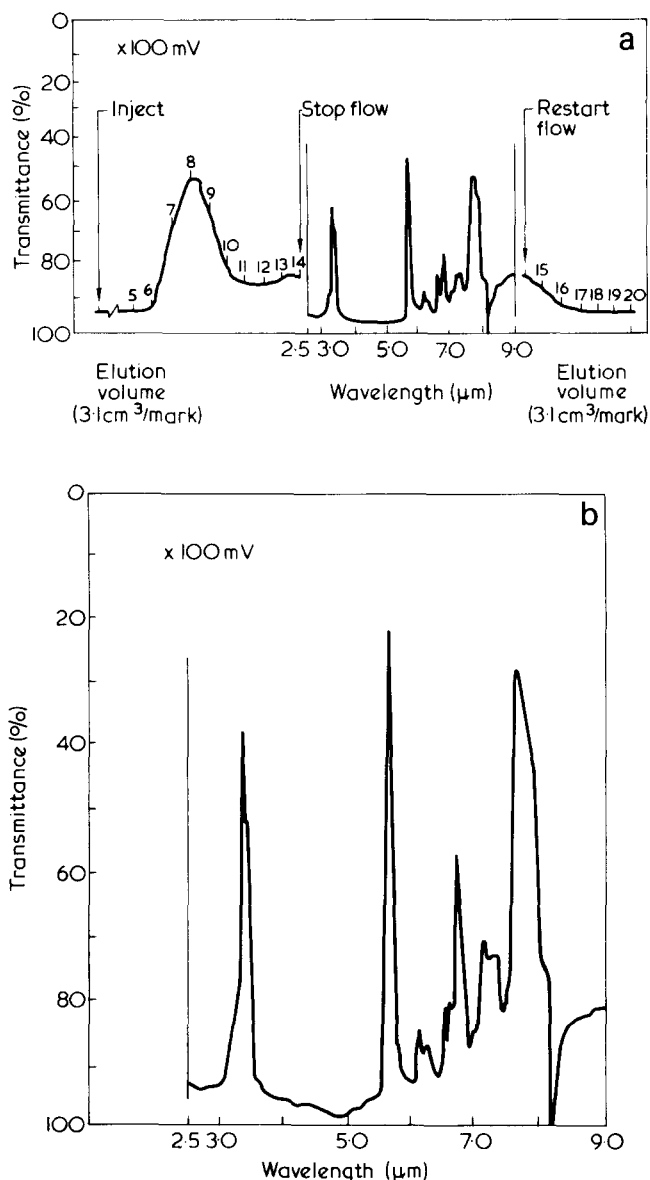


Figure 3 (a) Stop-and-go g.p.c. of sample 2 (polystyrene and didecyl phthalate) on column set 1, showing the i.r. spectrum of the additive peak; see text for details. (b) I.r. spectrum of didecyl phthalate, 1 mg/cm^3 in tetrachloroethylene, 3 mm pathlength solution versus 3 mm pathlength tetrachloroethylene reference

Analogous rapid analyses for samples 2 and 3 are shown in *Figures 3* and *4*, respectively. The i.r. scan of the polymer peak is not shown. *Figures 3a* and *3b* show the stop-and-go g.p.c. of sample 2 (15 mg/cm^3 in tetrachloroethylene of polystyrene containing 3.2% w/w didecyl phthalate) with the i.r. spectrum of the additive peak and a standard spectrum of didecyl phthalate in tetrachloroethylene, respectively. *Figures 4a* and *4b* show the stop-and-go g.p.c. of sample 3 (15 mg/cm^3 in tetrachloroethylene of polystyrene containing 1.0% w/w BHT) with the i.r. spectrum of the additive peak and a standard spectrum of BHT in tetrachloroethylene, respectively.

Comparison of the standard spectrum in each of *Figures 3b* and *4b* to the spectrum obtained for the additive peak in each case, again shows the application of this technique to qualitative analysis. The additional peaks observed in the i.r. spectrum of the additive peak in *Figure 4a* are due to polystyrene which was not resolved on the g.p.c. columns. However, the additive can be identified as BHT from the

other peaks, not interfered with by the residual polystyrene, especially the hydroxyl absorption at $\sim 2.70 \mu\text{m}$ (3700 cm^{-1}).

Polymer formulations which contain more than one polymer and/or additive could be analysed by this method with somewhat more difficulty in interpreting the i.r. spectra.

The method can be extended to the quantitative analysis of both polymeric and additive portions of the sample. This was demonstrated for sample 1 using column set 2, as described in the experimental sections. *Figure 5* shows a stop-and-go g.p.c. of sample 1, showing the i.r. spectrum of the additive peak. Under these higher resolution conditions the polymer peak was well resolved from the additive peak. Thus the *MW* averages and *MWD* of the polymeric portion of the sample could be determined in the usual way. The concentration of the additive could be determined by direct calibration with standard solutions of the additive chromatographed on the same system in order to obtain a

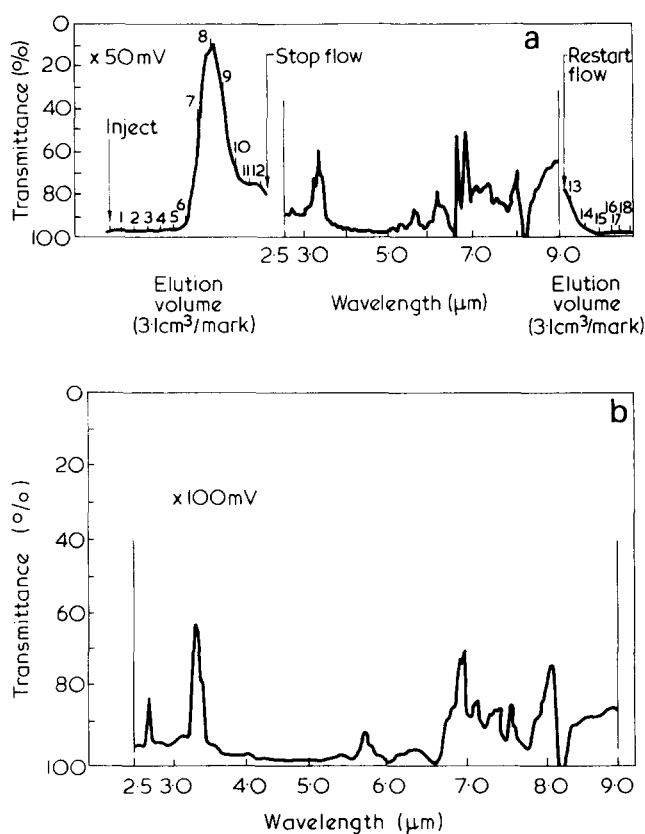


Figure 4 (a) Stop-and-go g.p.c. of sample 3 (polystyrene and BHT) on column set 1 showing the i.r. spectrum of the additive peak; see text for details. (b) I.r. spectrum of BHT, 0.4 mg/cm^3 in tetrachloroethylene, 3 mm pathlength solution versus 3 mm pathlength tetrachloroethylene reference

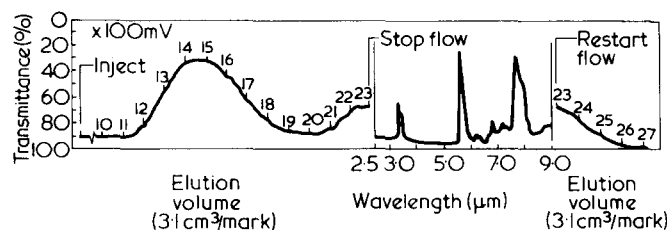


Figure 5 Stop-and-go g.p.c. of sample 1 on column set 2, showing the i.r. spectrum of the additive peak

calibration curve. Analysis time for a sample was 2 h per g.p.c. run at the higher resolution conditions.

ACKNOWLEDGEMENT

A portion of this work was supported by the National Science Foundation through Grant No. MPS 75-01915.

REFERENCES

- 1 Henniker, C. J., 'Infrared Spectrometry of Industrial Polymers', Academic Press, New York, 1967, pp38-41
- 2 Harple, W. personal communication
- 3 Luongo, J. P. *Appl. Spectros.* 1965, 19 (4), 117
- 4 Mirabella, Jr, F. M., Barrall, II, E. M. and Johnson, J. F. *J. Appl. Polym. Sci.* 1975, 19, 2131

Relationship of temperature to composition of copolymers of α -methylstyrene and maleic anhydride

Raymond B. Seymour and David P. Garner

Department of Chemistry, University of Houston, Houston, Texas 77004, USA

(Received 19 August 1975; revised 16 September 1975)

Alternating copolymers of α -methylstyrene and maleic anhydride were prepared in good yields in a decalin solution at temperatures below 80°C. Random copolymers with large percentages of α -methylstyrene were obtained in good yields at higher temperatures. These results were in accord with the charge transfer complex which was characterized by n.m.r. and u.v. spectrophotometry and shown to exist below 80°C. The copolymers were characterized by pyrolysis/gas chromatography and differential scanning calorimetry. The glass transition temperature of poly(α -methylstyrene) and the random copolymer of this monomer and maleic anhydride were approximately 450 and 458 K respectively.

INTRODUCTION

Polymers of α -methylstyrene¹ and maleic anhydride² as well as alternating copolymers of these two monomers³ have been described. Likewise, the alternating copolymer of styrene and maleic anhydride was one of the first recognizable copolymers⁴. Both block copolymers and random copolymers of this system have also been described^{5,6}.

The formation of block copolymers is the result of the addition of excess styrene monomer to styrene-maleic anhydride macroradicals⁷. The formation of random copolymers has been attributed to the decomposition of the charge transfer complex at elevated temperatures⁸. It is assumed that this complex is formed when the electron-poor maleic anhydride accepts a charge from the electron-rich styrene⁹. Absorbance bands attributable to this complex and not characteristic of either monomer species have been observed in the u.v. spectra of a solution of these monomers¹⁰. The presence of this complex has also been demonstrated by n.m.r. techniques¹¹.

EXPERIMENTAL

Copolymers of α -methylstyrene and maleic anhydride were prepared from freshly distilled α -methylstyrene and maleic anhydride, which had been crystallized from benzene. Mixtures of these monomers as a 10% w/w solution in purified decalin were polymerized in oxygen-free sealed containers at specified temperatures. Azobisisobutyronitrile (AIBN) was used as the initiator.

The decalin was washed with concentrated sulphuric acid, washed with water, dried over sodium and freshly distilled. Yields of better than 90% w/w of alternating copolymers were obtained in the presence of 2.5% w/w AIBN. However, it was necessary to increase this concentration to 10% w/w in order to obtain comparable yields of random copolymers at higher temperatures.

U.v. absorbance data were obtained from 0.001 M solutions of the monomeric mixtures in decalin using a Carey Model 14 spectrophotometer. N.m.r. data were obtained from solvent free α -methylstyrene, 10% w/w solution of maleic anhydride in carbon tetrachloride, and 10% w/w

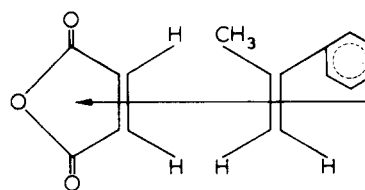
solution of the maleic anhydride/ α -methylstyrene complex in carbon tetrachloride using a Varian T-60 spectrophotometer. The d.s.c. data were obtained on a Perkin-Elmer Differential Scanning Calorimeter 1B.

Pyrolysis/g.c. data were obtained from small samples of copolymers which were thermally decomposed by a current of 8 A for 6 sec in a Varian Aerograph A-25 pyrolysis unit. Helium at a flow rate of 60ml/min was used as the carrier gas for the decomposition products in a Varian Aerograph A 100 C Gas Chromatograph.

RESULTS

Charge transfer complex of α -methylstyrene and maleic anhydride

Since α -methylstyrene is a better electron donor than styrene, it forms a stronger charge transfer complex with maleic anhydride as shown below:



As shown in *Figure 3*, the n.m.r. absorbance for maleic anhydride has shifted from 7.1 δ (*Figure 1*) to 5.9 δ in the mixture of this monomer and α -methylstyrene. The n.m.r. absorbance for the latter is shown in *Figure 2*.

Effect of temperature on the charge transfer complex

Since the effect of temperature on the charge transfer complex is not readily determined by n.m.r. techniques, u.v. spectrophotometry was used to investigate this effect. The change in the absorbance band at 291 nm in the u.v. spectrum was followed with the change in temperature. As shown in *Figure 4*, the intensity of this absorbance decreased as the temperature was increased. Extrapolation of these

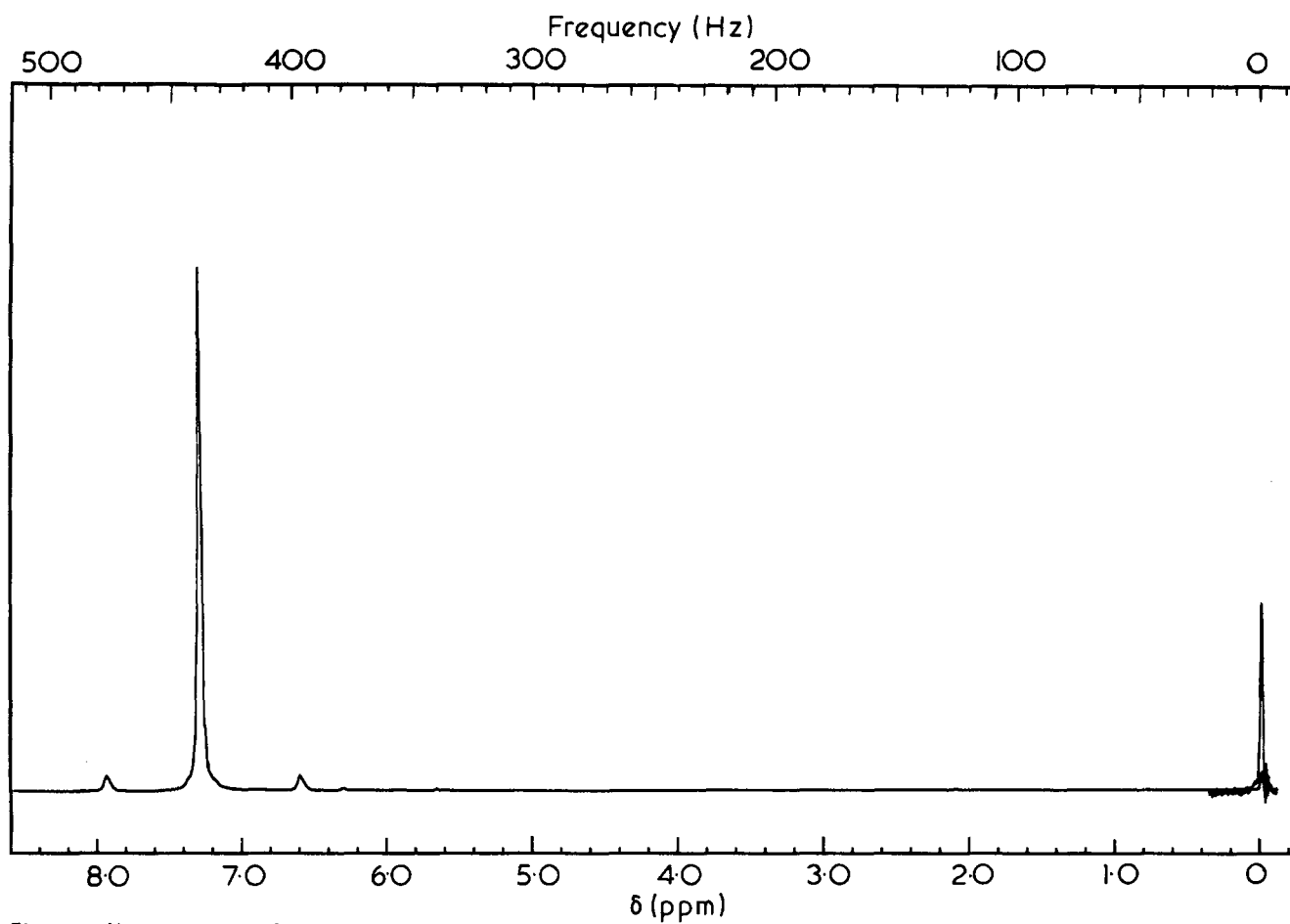


Figure 1 N.m.r. spectrum of maleic anhydride

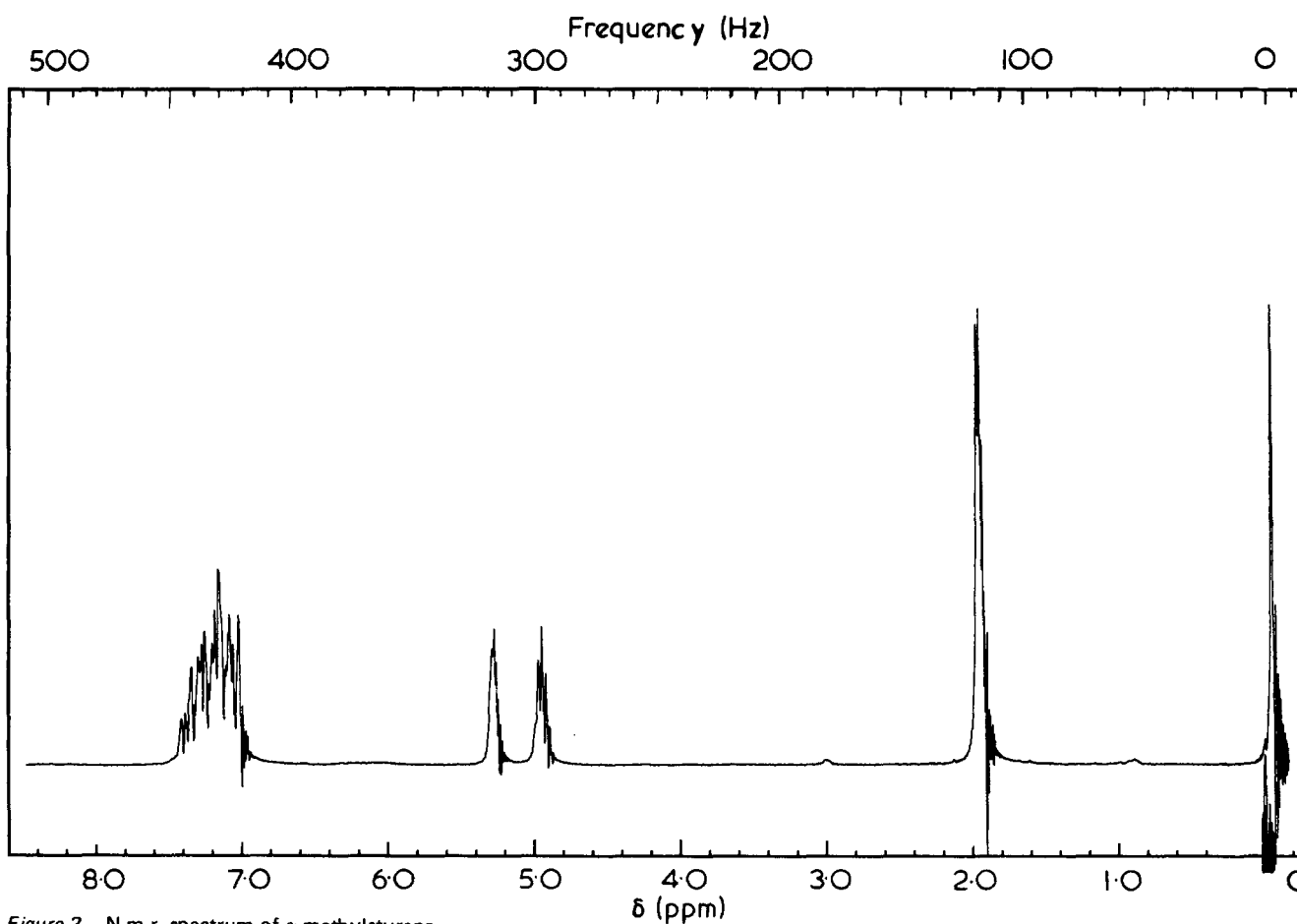


Figure 2 N.m.r. spectrum of α -methylstyrene

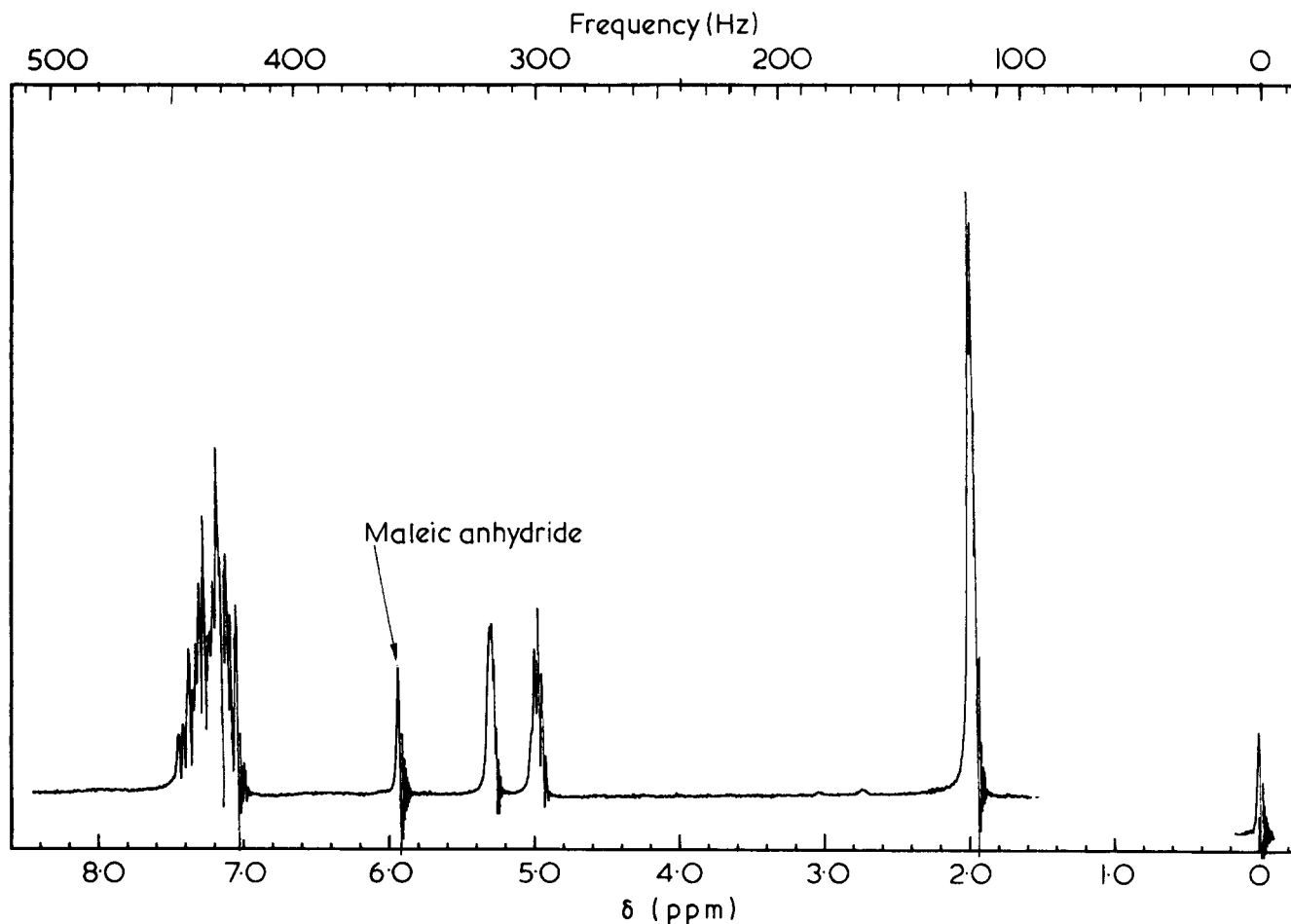


Figure 3 N.m.r. spectrum of an equimolar mixture of maleic anhydride and α -methylstyrene

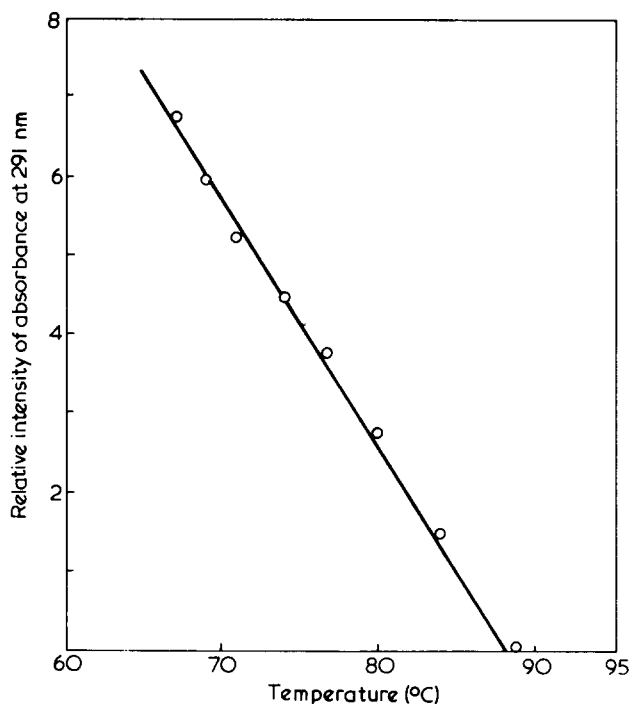


Figure 4 Effect of temperature on absorbance of α -methylstyrene-maleic anhydride charge transfer complex at 291 nm

data showed zero absorbance at temperatures above 85°C. Since the formation of an alternating copolymer is dependent on the presence of a charge transfer complex, the composition of the copolymer is independent of compositions at temperatures below 85°C.

Copolymers of α -methylstyrene and maleic anhydride

As shown in Table 1, good yields of decalin insoluble alternating copolymers were obtained when 10% solution of equimolar ratios of α -methylstyrene and maleic anhydride in decalin were heated at temperatures below 80°C for 72 h in the presence of 2.5% AIBN. These compositions were determined by pyrolysis/gas chromatography. Typical pyrograms are shown in Figure 5.

As shown in Table 2, the composition of the copolymer was independent of the monomer ratio in the feed at temperatures below 80°C. However, random copolymers with large proportions of α -methylstyrene were obtained at 100°C

CHARACTERIZATION OF COPOLYMERS

The d.s.c. thermograms, shown in Figure 6, indicate that the copolymers prepared at 100°C were random copolymers while those prepared at temperatures less than 80°C (B) were alternating copolymers. Scan A for poly(α -methylstyrene) shows a glass transition temperature of approximately 450 K, which corresponds well with the previously obtained range of 446–453 K¹².

Table 1 Effect of temperature (60°–80°C) on composition of copolymers of α -methylstyrene (α -MS) and maleic anhydride (MA)

Temperature (°C)	Feed ratio (α -MS/MA)	Polymer composition (α -MS/MA)
60	1:1	1:1
70	1:1	1:1
80	1:1	1.1:1



Figure 5 Typical g.c. pyrograms of copolymers of α -methylstyrene and maleic anhydride. A, 1:1 ratio; B, 20:1 ratio of monomers

Table 2 Effect of temperature (60°–100°C) on composition of copolymers of α -methylstyrene (α -MS) and maleic anhydride (MA)

Temperature (°C)	Feed ratio (α -MS/MA)	Polymer composition (α -MS/MA)
60	5:1	1:1
70	5:1	1:1
80	5:1	1:1
100	10:3	7:2
100	50:3	20:1

No transition at $\sim 450\text{K}$ was observed for the alternating copolymer (B), which melted at about 480K . Scan C for the copolymer produced at 100°C resembles scan A. However, since α -methylstyrene does not form a homopolymer at temperatures above 61°C , and g.c. pyrograms showed the presence of two monomers in a 7:2 ratio, this scan is for a random copolymer.

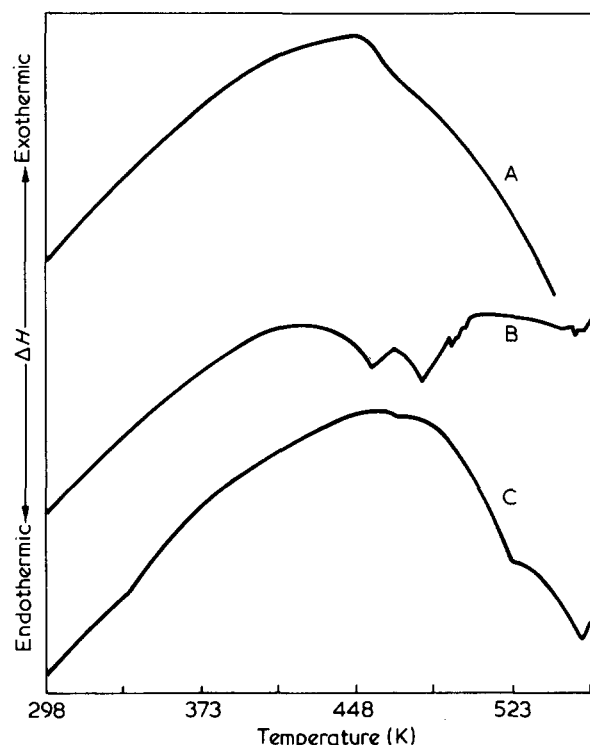


Figure 6 D.s.c. thermograms of α -methylstyrene-maleic anhydride copolymers. A, poly(α -methylstyrene) $T_g = 450\text{K}$; B, alternating copolymer prepared at 70°C ; C, random copolymer (7:2) prepared at 100°C

REFERENCES

- 1 Kilroe, J. G. and Weale, K. E. *J. Chem. Soc.* 1960, p3849
- 2 Lang, J. L., Pavelich, W. A. and Clarey, H. D. *J. Polym. Sci. (A)* 1963, 1, 1123
- 3 Oshima, K. *Kogyo Kagaku Zasshi* 1964, 67, 2159
- 4 Wagner-Jauregg, T. *Ber Dtsch Chem. Ges.* 1930, 63, 3213
- 5 Seymour, R. B., Tsang, H. S., Jones, E. E., Kincaid, P. D. and Patel, A. K. *Adv. Chem. Ser.* 1971, 99, 418
- 6 Muskat, I. E. U.S. Pat. 3 388 106 (1.6.68)
- 7 Seymour, R. B., Kincaid, P. D. and Owen, D. R. *J. Paint Technol.*, 1973, 45, 33
- 8 Seymour, R. B. and Garner, D. P. *J. Paint Technol.* in press
- 9 Bartlett, P. D. and Nazaki, K. *J. Chem. Soc.* 1946, 68, 1495
- 10 Andrews, L. J. and Keefer, R. M. *J. Chem. Soc.* 1953, 75, 3776
- 11 Tsuchida, E., Tomono, T. and Sono, H. *J. Macromol. Sci. (A)* 1972, 6, 151, 295
- 12 Cowie, J. M. G. and Toporowski, P. M. *J. Macromol. Sci. (B)* 1969, 3, 81

A study of molecular orientation in drawn and shrunk poly(ethylene terephthalate) by means of birefringence, polarized fluorescence and X-ray diffraction measurements

J. H. Nobbs, D. I. Bower and I. M. Ward

Department of Physics, University of Leeds, Leeds LS2 9JT, UK

(Received 21 July 1975)

Amorphous tapes of poly(ethylene terephthalate) (PET) containing the fluorescent additive 4,4'-(dibenzoxazoly) stilbene, prepared by a method previously described, were drawn around a 'pin' at 80°C to draw ratios, λ , of 2.0, 2.5, 3.4, 3.5 and 4.2. Values of $\langle P_2(\cos\theta) \rangle$ were determined for samples from the tapes, either as-drawn or shrunk and crystallized in air under various conditions. $P_2(\cos\theta)$ is the second order Legendre polynomial, θ is the angle between a chain axis and the draw direction and the angle brackets denote an average value. Measurements of refractive index and of the intensity of X-ray scattering were used to derive $\langle P_2(\cos\theta) \rangle_{\text{opt}}$ and $\langle P_2(\cos\theta) \rangle_c$ which refer, respectively, to the whole polymer and to the crystalline regions only. By making certain assumptions, values of $\langle P_2(\cos\theta) \rangle_a$ for the amorphous regions only, were derived from measurements of the intensity of polarized fluorescence. The expected relationship between the three measures of orientation and the degree of crystallinity was verified, which justified the assumptions made in deriving $\langle P_2(\cos\theta) \rangle_a$. The PET samples appeared to behave as a rubber with 5.6 freely-jointed links between crosslink points when drawn and shrunk at 80°C for $\lambda < 2.5$. For higher λ , although the shrinkage was dramatically reduced, it was always associated with considerable disorientation of the amorphous regions, which suggests that this is the primary mechanism of shrinkage.

INTRODUCTION

In a previous paper¹ we have presented the theory of the polarized fluorescence method for studying molecular orientation in polymers, together with quantitative results for a series of uniaxially drawn amorphous tapes of poly(ethylene terephthalate) (PET), in which molecules of the fluorescent compound 4,4'-(dibenzoxazoly) stilbene were dispersed. This previous investigation was deliberately concerned with oriented polymers of low crystallinity, so that the effects of crystallization were minimized. By comparing the fluorescence results with measurements of optical birefringence it was shown that, although the fluorescent molecules were more highly oriented than the polymer segments, the two distributions of orientations maintained a constant relationship.

The most useful application of polarized fluorescence is, however, to study the distribution of orientations within the amorphous regions of a semi-crystalline polymer, if, as is believed, the large fluorescent probe molecules are too bulky to be accommodated in the crystal lattice of the polymer. In the present paper, we describe a study of similar PET tapes which were first drawn and then shrunk under various conditions, some of which induced crystallinity. The results confirm that the fluorescent probes are indeed located in the amorphous regions of the polymer and provide valuable information about the shrinkage and crystallization processes. In this investigation, fluorescence measurements, have been combined with X-ray diffraction and optical measurements which provide direct measures of the orientation of the crystalline regions and of the overall molecular orientation, respectively.

ORIENTATION AVERAGES

For transversely isotropic samples we define an orientation average $\langle P_2(\xi) \rangle$, the mean value of $P_2(\xi)$, where ξ is the cosine of the angle θ between the axis of a structural unit in the polymer and the draw direction and $P_2(\xi) = \frac{1}{2}(3\xi^2 - 1)$ is a second order Legendre polynomial.

The optical orientation averages, which are determined from measurements of refractive index and which we call $\langle P_2(\xi) \rangle_{\text{opt}}$, relate to the overall chain axis orientation to a good approximation. This has been confirmed directly by infra-red² and Raman³ spectroscopic studies, where it has been shown that there is an excellent correlation between the optical orientation averages and those obtained from intensity measurements on infra-red or Raman lines assigned to specific benzene ring vibrational modes.

It will be assumed that the semi-crystalline polymer can be regarded as a two-phase system consisting of a mixture of crystalline and amorphous phases. Although it has to be borne in mind that the state of order required to produce X-ray diffraction is not necessarily the same as that required to exclude a fluorescent molecule it will be assumed, as a first step, that it is the same. In the previous paper¹ a set of equations was developed which enables the determination, from suitable measurements of fluorescent intensities, of $\langle \cos^2\theta_M \rangle$ and $\langle \cos^4\theta_M \rangle$, the average values of $\cos^2\theta_M$ and $\cos^4\theta_M$, where θ_M is the angle between a unique axis M in a typical molecule of the fluorescent additive and the symmetry axis of the sample. As explained later, $\langle P_2(\xi_M) \rangle = \frac{1}{2}(3\langle \cos^2\theta_M \rangle - 1)$ can be used to estimate the value of $\langle P_2(\xi) \rangle_a$, where the subscript a signifies that the average extends only over the polymer chains in the amorphous

regions. A similar average, $\langle P_2(\xi) \rangle_c$, for the crystalline regions can be obtained from X-ray diffraction measurements, in a manner to be described.

If the assumptions made are correct the three orientation averages $\langle P_2(\xi) \rangle_{\text{opt}}$, $\langle P_2(\xi) \rangle_a$ and $\langle P_2(\xi) \rangle_c$ should be related by:

$$\langle P_2(\xi) \rangle_{\text{opt}} = f_c \langle P_2(\xi) \rangle_c + (1 - f_c) \langle P_2(\xi) \rangle_a \quad (1)$$

where f_c is the fraction of polymer in the crystalline phase. The accuracy with which the experimental values satisfy this equation is a measure of the adequacy of the underlying assumptions and of the accuracy of the three measures of orientation.

EXPERIMENTAL

Specimen preparation

Amorphous tapes of PET, approximately 1.5×10^{-3} m by 1.0×10^{-4} m in cross-section and containing the photo-stable compound 4,4'-(dibenzoxazoly) stilbene as the fluorescent additive, were prepared by the method described in the previous paper¹. Tapes containing the compound at a concentration of 50 or 200 ppm by wt, were subsequently oriented by drawing around a smooth stationary 'pin' to produce a series of tapes with draw ratios 2.0, 2.5, 3.4, 3.5 and 4.2. The 'pin' was heated to a temperature of $80 \pm 1^\circ\text{C}$ and was located between feed and wind-up rollers rotating at different rates.

In the first set of experiments, tapes with an initial draw ratio, λ , of 2.0 were shrunk in a controlled way at a temperature of 80°C to a series of final effective draw ratios in the range 2.0 to 1.0 by passing them through a hot-air oven held at 80°C and located between the feed and wind up rollers of the frame originally used to draw them. The oven was constructed from sections of expanded polyurethane foam and consisted of two regions. The tape was first led through a slit into a region fed with hot air at 80°C and then passed through a slot to a second region fed with air at 10°C . The air flow rate through both regions was 200 ft³/h. The temperature in the hot region was monitored by a thermocouple and was found to be within 1° of 80°C throughout the hot region. Each part of the tape took approximately 30 sec to travel through the hot region and a similar time to travel through the cold region.

For the second group of experiments, drawn tapes were placed in a conventional air oven and allowed to shrink free from constraints. The tapes were in the oven for various lengths of time within the range 5–1000 min, for a series of temperatures from 70° to 180°C .

Refractive index measurements

The refractive indices of the samples for light polarized with the electric vector parallel to the draw direction, n_z , or normal to this direction but parallel to the plane of the tape, n_x , were measured using an image-splitting interference microscope (Zeiss Zena Interphako) with accurately calibrated immersion liquids. All measurements were made at 551 nm. The results are shown in Tables 1–6.

$\langle P_2(\xi) \rangle_{\text{opt}}$ can be most simply obtained from the refractive index data using the relationship⁴:

$$\frac{\Delta\alpha}{3\alpha_0} \langle P_2(\xi) \rangle_{\text{opt}} = \frac{\phi_z^e - \phi_x^e}{\phi_z^e + 2\phi_x^e} \quad (2)$$

where $\phi_i^e = (n_i^2 - 1)/(n_i^2 + 2)$, $\Delta\alpha$ is the difference between the electronic polarizabilities of a polymer repeat unit parallel and perpendicular to the chain axis, and α_0 is the isotropic polarizability.

In the present work $\Delta\alpha/\alpha_0$ was estimated from measurements on a series of drawn amorphous samples. A plot of $(\phi_z^e - \phi_x^e)/(\phi_z^e + 2\phi_x^e)$ against $\langle P_2(\xi_M) \rangle$, measured by polarized fluorescence, was extrapolated to the point where $\langle P_2(\xi_M) \rangle = 1$. The corresponding value of $(\phi_z^e - \phi_x^e)/(\phi_z^e + 2\phi_x^e)$, 0.106 ± 0.005 , was taken as $\Delta\alpha/(3\alpha_0)$. The assumption here is that the axes of the fluorescent molecules are fully aligned only when the polymer segments are fully aligned. It is further assumed that the value of $\Delta\alpha/(3\alpha_0)$ is the same for polymer segments in the crystalline and amorphous phases.

As in previous studies^{1,2}, the assumption of transverse isotropy was checked by calculating the refractive index of isotropic amorphous PET, n_d^0 , from n_z and n_x using the relationship:

$$\frac{n_d^{02} - 1}{n_d^{02} + 2} = \frac{\rho_d^0}{3\rho} \left[\frac{n_z^2 - 1}{n_z^2 + 2} + \frac{2(n_x^2 - 1)}{n_x^2 + 2} \right] \quad (3)$$

where ρ is the density of the sample and ρ_d^0 is the density of an isotropic amorphous sample. The values of n_d^0 obtained are shown in Tables 1–6 and are essentially constant.

Fluorescence measurements

The fluorescence experiment consists of measuring the intensity and polarization of light emitted by the sample when the fluorescence is excited by linearly polarized light. The same theory, apparatus and method of analysis of the intensity measurements were used in this study as are described in a previous paper¹ and reference should be made there for further details.

In the previous investigation it was concluded that there was a unique relationship between the birefringence of the sample and $\langle \cos^2\theta_M \rangle$ for PET samples of low crystallinity containing the same fluorescent additive as used in the present work. In Figure 1, $\langle P_2(\xi_M) \rangle$ is plotted against $\langle P_2(\xi) \rangle_{\text{opt}}$. Note that $\langle P_2(\xi_M) \rangle$ and $\langle P_2(\xi) \rangle_{\text{opt}}$ take the value unity simultaneously as a result of the method used to derive $\langle P_2(\xi) \rangle_{\text{opt}}$. In this paper it will be assumed that the relationship between the distribution of orientations of the fluorescent molecules and the polymer chains in the amorphous regions of semi-crystalline PET is the same as that in completely amorphous PET. This assumption will be adopted as a working hypothesis, to be justified by detailed comparison of measurements of orientation obtained from optical, fluorescence and X-ray diffraction measurements. With this assumption Figure 1 can be used to obtain a value of $\langle P_2(\xi) \rangle_o$ from the measured value of $\langle P_2(\xi_M) \rangle$. For example, a value of $\langle P_2(\xi_M) \rangle$ of 0.25 corresponds to a value of 0.119 for $\langle P_2(\xi) \rangle_o$.

X-ray diffraction measurements

The distribution of orientations of a particular crystal-plane normal for the crystallites in a semi-crystalline polymer can be determined from X-ray diffraction measurements⁵. Figure 2 illustrates schematically the experimental arrangement used, in which the X-ray source, S, the detector, D, and the centre of the sample, O, all lie in the same horizontal plane. \angle TOD formed by the transmitted beam, OT, and the line OD from the centre of the sample to the detector we call 2β . The angle between the bisector of

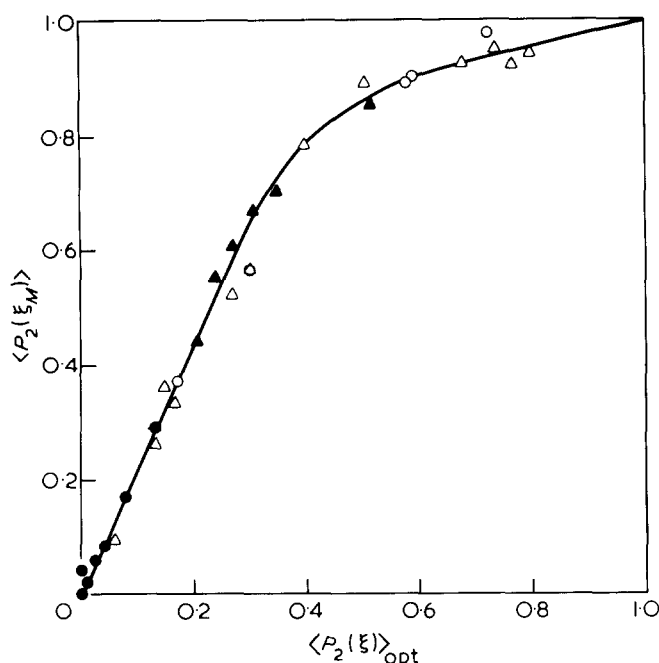


Figure 1 $\langle P_2(\xi_M) \rangle$ compared with $\langle P_2(\xi) \rangle_{opt}$ for samples of low crystallinity. Δ , Samples from previous work¹ drawn at 80°C to various draw ratios; \blacktriangle , samples from previous work¹ drawn to draw ratio 2.66 at various temperatures between 65 and 90°C; \circ , samples from present work drawn at 80°C to various draw ratios; \bullet , samples from present work drawn and shrunk at 80°C

\angle SOD and the draw direction of the sample, Oz, is called χ . Oz lies in the horizontal plane.

To determine the distribution of orientations of a particular plane normal, the value of 2β is fixed so that the detector is at the peak of the diffraction profile for that plane. The intensity of the diffracted beam, $I(\chi)$, is measured as χ is varied by rotating the sample about a vertical axis. $I_0(\chi)$ is derived from the measured intensity $I(\chi)$ by subtracting the background intensity (noise and amorphous scattering) and correcting for any variation with χ of the volume of sample illuminated with X-rays or of the absorption by the sample due to changes in its orientation with respect to the incident and diffracted beams.

This procedure involves the assumption that the peak intensity, $I_0(\chi)$, is directly proportional to the amount of crystalline material having the particular plane normal in the direction χ . This is justified if the peak intensity is proportional to the total intensity integrated over a range of values of 2β around the peak.

The orientation averages are calculated from the observed intensity function by means of the equation:

$$\langle P_n(\cos\chi) \rangle = \frac{\int_0^\pi I_0(\chi) P_n(\cos\chi) \sin\chi d\chi}{\int_0^\pi I_0(\chi) \sin\chi d\chi} \quad (4)$$

The unit cell of PET is triclinic with the direction of the molecular chain axis parallel to the crystallographic c -axis. Unfortunately there are no planes whose normals are parallel to the c -axis and which strongly diffract the X-ray beam. The diffraction from the $(\bar{1}05)$ plane was therefore used and the results were corrected to allow for the angle

$\delta (= 9^\circ 46')$ between the $(\bar{1}05)$ plane normal and the c -axis.

We require to obtain the orientation averages $\langle P_2(\xi) \rangle_c$ and $\langle P_4(\xi) \rangle_c$ which characterize the orientation of the crystallographic c -axes in the specimens. If we assume that there is no preferential alignment of the a and b crystallographic axes about the c -axis, the Legendre addition theorem gives:

$$\langle P_2(\cos\chi) \rangle = \langle P_2(\xi) \rangle_c \langle P_2(\cos\delta) \rangle \quad (5)$$

$$\langle P_4(\cos\chi) \rangle = \langle P_4(\xi) \rangle_c \langle P_4(\cos\delta) \rangle \quad (6)$$

X-ray samples were prepared from the tapes by first cutting across each tape at right angles to the initial draw direction and then glueing the two halves together to form a tape twice as thick. This composite tape was then cut in two and the halves glued together to form a four-layer tape. This process was repeated until a stack of tape 32 layers high was formed. The stack was then trimmed to form a 3 mm long rod with a square cross-section of side 1.5 mm in such a way that the initial draw direction was parallel to one of these short sides. A poly(vinyl alcohol) adhesive was used since it was found to give a strong bond, produced very little background scatter and no discrete X-ray diffraction peaks. Microscopic examination of samples produced in this way showed that the draw directions of the tapes within the stack were parallel to each other to within one degree.

The sample was mounted on the goniometer stage of a Siemens K4 recording X-ray diffractometer and aligned so that the centre of the sample was at the centre of rotation of the diffractometer stage and the draw direction of the sample was in the horizontal plane (see Figure 2.) The $\text{CuK}\alpha$ radiation passed through a nickel filter and a slit system so that an X-ray beam that almost fully illuminated the sample yet diverged less than $15'$ from parallel was formed. The effective solid angle sampled by the diffractometer was ellipsoidal in shape. It was estimated from the diffractometer dimensions that the detector sampled plane normals within approximately $\pm 1/2^\circ$ of χ in the horizontal plane and $\pm 1 1/2^\circ$ in the vertical plane. This was not corrected for, since the ranges of angles involved are far smaller than the smallest half-width of the intensity *versus* χ plots. The corrected values of $\langle P_n(\xi) \rangle_c$ would be slightly greater than the uncorrected values. The diffracted beam was detected by a scintillation counter and the signal passed through a pulse-height selector to eliminate background pulses before being recorded by a chart recorder.

Daubeny *et al.*⁶ have given the lattice parameters of the PET crystal as $A = 4.56\text{\AA}$, $b = 5.94\text{\AA}$, $c = 10.75\text{\AA}$, $\alpha = 98^\circ 30'$, $\beta = 118^\circ$ and $\gamma = 112^\circ$. These values, together with a value of 1.5416\AA for the wavelength of the radiation, give

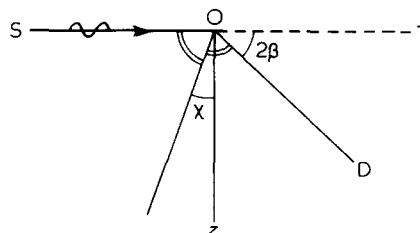


Figure 2 Schematic diagram of arrangements for X-ray diffraction measurements. S, source; D, detector; O, centre of sample; Oz draw direction in sample

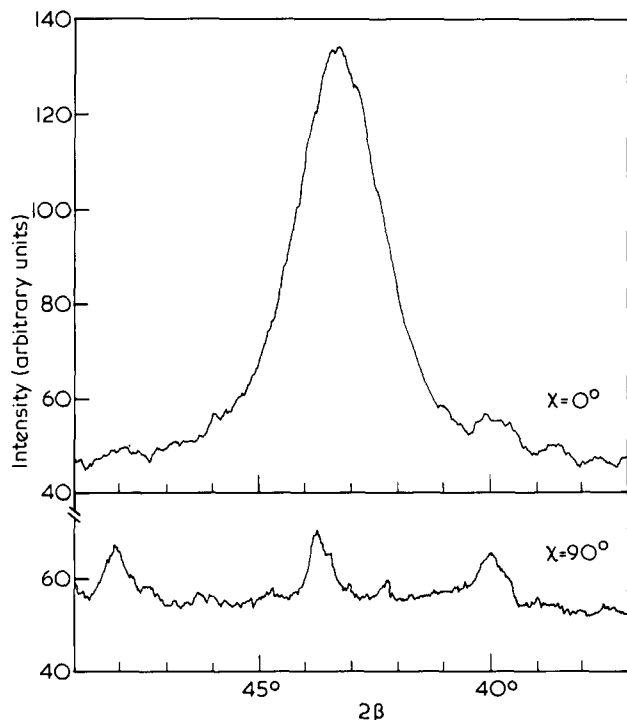


Figure 3 Diffracted X-ray intensity as a function of 2β in the region of the $(\bar{1}05)$ plane diffraction for sample 3f

$2\beta = 42.8^\circ$ for the $(\bar{1}05)$ plane diffraction. For our samples 2β was found to lie between 42.9 and 43.6° .

When the diffraction peak was recorded the detector was rotated at twice the rate of rotation of the sample, in the usual way, so that the same set of crystal planes was potentially able to give rise to Bragg 'reflection'. The intensities observed for the angular range $2\beta = 37^\circ$ to 49° for $\chi = 0^\circ$ and $\chi = 90^\circ$ are shown in Figure 3 for sample 3f. The amorphous background intensity was determined for each sample from the distribution of diffracted intensity as a function of 2β for $\chi = 90^\circ$ by drawing a straight line through it in the regions well away from the diffraction peak. The height of this line at the diffraction peak was taken as the background intensity and the ratio of this height to that at $2\beta = 37.5^\circ$ was called C . The background intensity at the diffraction peak for any other value of χ was found by multiplying the observed background at $2\beta = 37.5^\circ$ by C . Figure 4 shows the observed intensities as a function of χ for $2\beta = 43.3^\circ$ and 37.5° for sample 3f. For this sample $C = 1.11$.

The values of $\langle P_n(\xi) \rangle_c$ were obtained from equations (4), (5) and (6) by performing the integration by Simpson's method. A total of 27 points was used in the range 0° to 90° ; the range 0° to 20° was divided into 10 intervals, 20° to 60° into 10 intervals and 60° to 90° into 6 intervals. The corresponding range from 0° to -90° was similarly divided.

In order to determine whether the peak intensity $I_0(\chi)$ was proportional to the intensity integrated over a range of values of 2β around the peak, the diffraction peak from sample 3f was recorded for several values of χ . For each peak the corrected intensity $I_0(\chi)$ was integrated from $2\beta = 41.5$ to $2\beta = 45.5^\circ$ and the integral was plotted against the corrected intensity of the diffraction peak. A least squares fitted straight line gave a correlation factor of 0.995, confirming the proportionality.

No correction was made for the change with χ of the effective volume or absorption of the sample. The rod-shaped samples were almost completely illuminated with

radiation and the correction was expected to be small. The background-corrected intensity from a highly crystalline sample with randomly oriented crystallites was found to be independent of χ , which further justifies the neglect of the correction.

Determination of crystallinity

A comparison of X-ray, infra-red and density measurements of crystallinity by Farrow and Ward⁷ showed poor agreement between the crystallinity as measured by density and the crystallinity measured by X-rays for drawn yarns of PET. They concluded that for drawn oriented yarns it is not permissible to regard the non-crystalline material as having a constant density and suggested that the density of these regions increases as the orientation of the chains increases. We have made an estimate, using a simple model (see Appendix), of the way in which the density, ρ_a , of the amorphous material should vary with orientation of the amorphous regions, and the curve in Figure 5 shows the estimated variation. f_c , the fraction of polymer in the crystalline regions, is given by $f_c = f_v \rho_c / \rho$, where f_v is the volume fraction that is crystalline and ρ_c is the density of

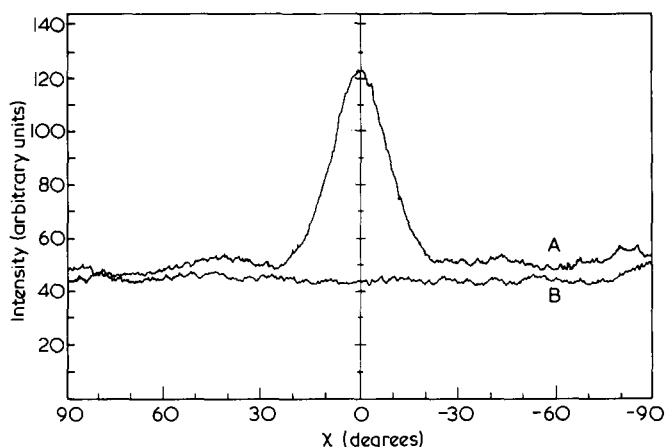


Figure 4 Diffracted X-ray intensity as a function of the orientation of the draw direction for sample 3f. A, $2\beta = 43.3^\circ$; B, $2\beta = 37.5^\circ$

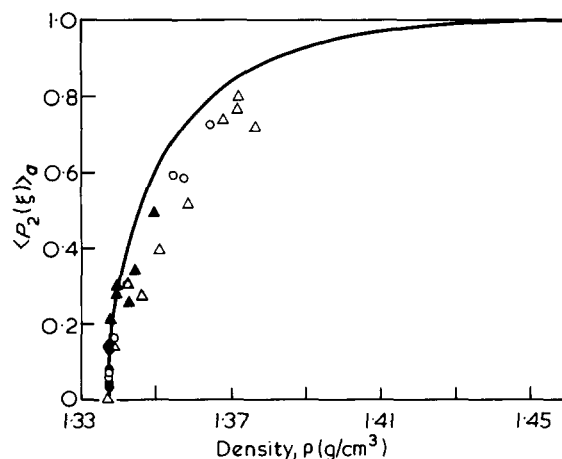


Figure 5 The curve shows the estimated relationship between density and $\langle P_2(\xi) \rangle_a$ for amorphous PET. The points show the relationship for samples of low crystallinity. Δ , Samples from previous work¹ drawn at 80°C to various draw ratios; \blacktriangle , samples from previous work¹ drawn to draw ratio 2.66 at various temperatures between 65 and 90°C ; \circ , samples from present work drawn at 80°C to various draw ratios; \bullet , samples from present work drawn and shrunk at 80°C

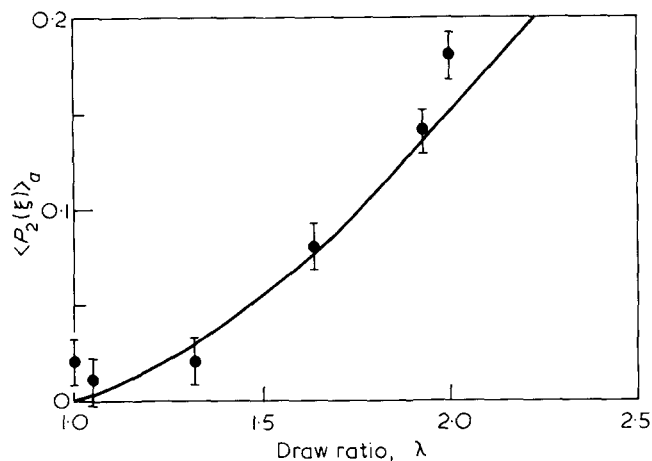


Figure 6 $\langle P_2(\xi) \rangle_a$ plotted against final effective draw ratio for samples drawn at 80°C to draw ratio 2.0 and then shrunk at 80°C to controlled final effective draw ratios. The curve represents a smooth line through points (not shown) for all samples from the previous¹ and present work which were drawn at 80°C but not subsequently shrunk

the crystalline fraction. Now

$$f_v = (\rho - \rho_a)/(\rho_c - \rho_a)$$

Hence, using the known crystalline and estimated amorphous densities, f_c may be obtained from:

$$f_c = (\rho_c/\rho)(\rho - \rho_a)/(\rho_c - \rho_a) \quad (7)$$

This method of obtaining the crystallinity involves assuming that there is a unique relationship between the density of the amorphous regions and their orientation, which may not be quite correct. We have, however, only used the calculated crystallinities in verifying equation (1) for samples for which either the crystallinity or the amorphous orientation was low and any errors in the estimated crystallinity values should be small for such samples.

RESULTS

Tables 1–6 contain the complete list of results for all the samples, including details of the mechanical and heat treatment and the sample density, crystallinity, refractive index, $\langle P_2(\xi) \rangle_{\text{opt}}$, $\langle P_2(\xi) \rangle_a$ and $\langle P_2(\xi) \rangle_c$. The calculated values of the isotropic refractive index, n_a^0 , are also shown. The values of n_a^0 were the same within experimental error for all samples, which confirmed that the samples were uniaxial and that the assumptions used in deriving equation (2) were probably justified. Several samples were also checked by means of wide-angle X-ray photographs, which confirmed that the crystallite distribution was uniaxial for these samples.

For sample 4e, $\langle P_2(\xi) \rangle_c$ was determined for three different X-ray specimens made from different parts of the same tape and the results were the same to within 0.012. Samples 3u and 3i underwent the same mechanical and heat treatments but contained 200 ppm and 50 ppm by wt of the fluorescent molecules respectively; the results were the same to within experimental error. The concentration used was 200 ppm for all samples except 3a–3g and 3i, for which it was 50 ppm.

For seventeen out of the twenty-six samples 3a to 3u and 4a to 4e the values of the three averages $\langle P_2(\xi) \rangle_{\text{opt}}$, $\langle P_2(\xi) \rangle_a$ and $\langle P_2(\xi) \rangle_c$ were determined. These values do not generally satisfy equation (1). If we temporarily denote the experimental values by a superscript m , then in general,

$$\langle P_2(\xi) \rangle_{\text{opt}}^m \neq f_c^m \langle P_2(\xi) \rangle_c^m + (1 - f_c^m) \langle P_2(\xi) \rangle_a^m$$

There is no simple way of deciding which of the measured quantities are in error and lead to the inequality. We can, however, calculate a set of values $\langle P_2(\xi) \rangle_a$, $\langle P_2(\xi) \rangle_c$, $\langle P_2(\xi) \rangle_{\text{opt}}$ and f_c which satisfy equation (1) exactly and at the same time minimize the sum

$$S = (E_a/D_a)^2 + (E_c/D_c)^2 + (E_t/D_t)^2 + (E'_c/D'_c)^2 \quad (8)$$

where the E 's are defined as:

$$E_a = \langle P_2(\xi) \rangle_a - \langle P_2(\xi) \rangle_a^m$$

$$E_c = \langle P_2(\xi) \rangle_c - \langle P_2(\xi) \rangle_c^m$$

$$E_t = \langle P_2(\xi) \rangle_{\text{opt}} - \langle P_2(\xi) \rangle_{\text{opt}}^m$$

$$E'_c = f_c - f_c^m$$

and the D 's are estimates of the standard deviation of the corresponding measured values. The degree of agreement between this calculated set of values and the corresponding experimental ones may be taken as a measure of the reasonableness of the assumptions made in deriving the experimental values.

In this investigation the values of $\langle P_2(\xi) \rangle_a^m$, $\langle P_2(\xi) \rangle_c^m$, $\langle P_2(\xi) \rangle_{\text{opt}}^m$ and f_c^m were calculated as described above and the standard deviation of all these values was arbitrarily assumed to be the same. The sum S in equation (8) was minimized by computer and the corresponding best fit values of $\langle P_2(\xi) \rangle_{\text{opt}}$, $\langle P_2(\xi) \rangle_a$, $\langle P_2(\xi) \rangle_c$ and f_c were derived and they are shown below the corresponding measured values in Tables 1, 4, 5 and 6.

DISCUSSION

Rubber-like behaviour for low initial draw ratio

Figure 6 is a plot of $\langle P_2(\xi) \rangle_a$ against the final draw ratio for essentially non-crystalline samples ($f_c < 0.03$). The curve is derived from the results given in Tables 2 and 6 of our previous paper¹ for samples which were simply drawn at 80°C. The values of $\langle \cos^2 \theta_M \rangle$ in these Tables have been converted to $\langle P_2(\xi_M) \rangle$ and then to $\langle P_2(\xi) \rangle_a$ by means of the curve in Figure 1. The curve in Figure 6 is a smooth curve drawn through these values and the points shown are the results for samples 1a to 1g (Tables 1 and 2), which lie on the curve within experimental error. These samples were drawn at 80°C to a draw ratio of 2.0 and subsequently shrunk to various predetermined final effective draw ratios. The reversibility of the deformation and the dependence of the distribution of orientations only on the final effective draw ratio suggests that the PET tape is behaving as a rubber for uniaxial deformations at 80°C up to at least a draw ratio of 2.0.

Using the inverse Langevin approximation to the rubber model, Roe and Krigbaum⁸ have derived the following

Table 1 As-drawn samples

Sample	Draw ratio, λ	Density, ρ	Refractive index			Crystal- linity, f_c	$\langle P_2(\xi) \rangle_{opt}$	$\langle P_2(\xi) \rangle_a$	$\langle P_2(\xi) \rangle_c$	
			n_z	n_x	n_a^0					
1a	2.0	1.3388	1.611	1.571	1.583	0.01	0.17	0.18		
2a	2.5	1.3418	1.630	1.561	1.582	0.03	0.30	0.27		
3a	3.4 ₄	1.3541	1.685	1.545	1.582	0.06	0.59	0.58	0.54	meas.
3j	3.5	1.3574	1.682	1.545	1.579	0.06	0.58	0.59	0.54	fit
						0.11	0.58	0.55	0.57	meas.
4a	4.2	1.3648	1.713	1.540	1.580	0.11	0.56	0.56	0.57	fit
						0.06	0.72	0.74	0.72	meas.
						0.07	0.73	0.73	0.72	fit

Table 2 Samples initially drawn to $\lambda = 2.0$ and shrunk at 80°C for 30 sec to controlled final length

Sample	Final draw ratio, λ	Density, ρ	Refractive index			Crystal- linity, f_c	$\langle P_2(\xi) \rangle_{opt}$	$\langle P_2(\xi) \rangle_a$
			n_z	n_x	n_a^0			
1b	1.93	1.3382	1.605	1.575	1.585	0.00	0.13	0.14
1c	1.64	1.3377	1.595	1.577	1.583	0.00	0.08	0.08
1d	1.43	1.3375	1.588	1.578	1.582	0.00	0.04	0.04
1e	1.32	1.3370	1.585	1.580	1.582	0.00	0.02	0.03
1f	1.05	1.3373	1.582	1.582	1.582	0.00	0.00	0.01
1g	1.00	1.3372	1.582	1.581	1.582	0.00	0.00	0.02

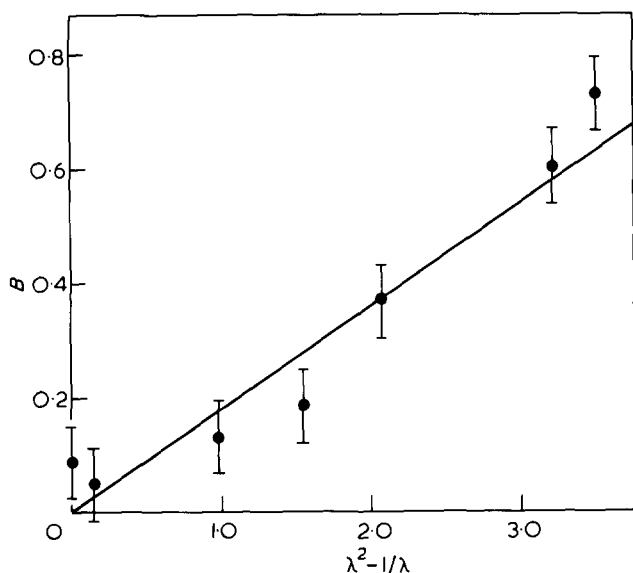


Figure 7 B plotted against $\lambda^2 - 1/\lambda$ for samples drawn and shrunk at 80°C . Linear region for rubber model

relationship between $\langle P_2(\xi) \rangle$ and draw ratio:

$$\langle P_2(\xi) \rangle = \frac{1}{5N} \left(\lambda^2 - \frac{1}{\lambda} \right) + \frac{36}{875N^2} \left(\lambda^4 + \frac{\lambda}{3} - \frac{4}{3\lambda^2} \right) + \frac{108}{6125N^3} \left(\lambda^6 + \frac{3\lambda^3}{5} - \frac{8}{5\lambda^3} \right) + \dots \quad (10)$$

where N is the number of freely jointed links between crosslink points. This equation can be simplified by setting:

$$B = (1/N) \left(\lambda^2 - \frac{1}{\lambda} \right) \quad (11)$$

to obtain the following approximation to equation (10):

$$\langle P_2(\xi) \rangle = \frac{1}{5} B + \frac{36}{875} B^2 + \frac{108}{6125} B^3 + \dots \quad (12)$$

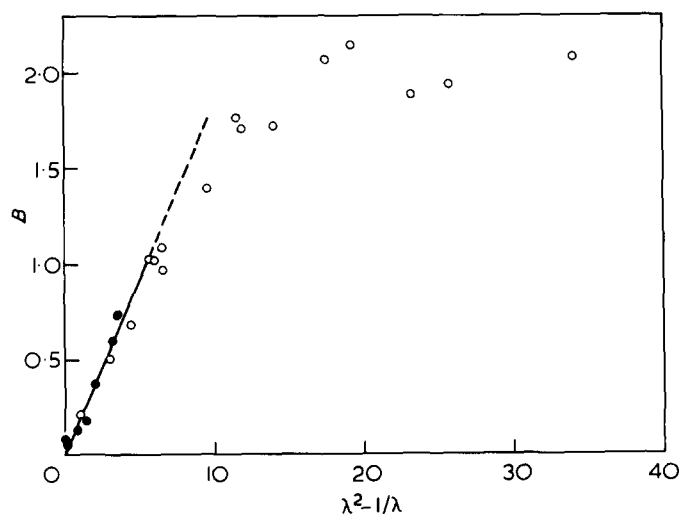


Figure 8 B plotted against $\lambda^2 - 1/\lambda$ for samples drawn at 80°C . \circ , Samples drawn but not shrunk, present and previous work¹; \bullet , samples drawn to draw ratio 2.0 and shrunk at 80°C

Equation (12) gives $\langle P_2(\xi) \rangle$ within 1% of the value given by equation (10) for $\lambda < 3$ and $N = 6$, which is close to the value of N found in the present work.

By plotting a graph of $\langle P_2(\xi) \rangle$ against B , a value of B can be read off for each experimental value of $\langle P_2(\xi) \rangle_a$. The rubber model predicts that a plot of B against $(\lambda^2 - 1/\lambda)$ should be a straight line of gradient $1/N$. Figure 7 is a plot of B against $(\lambda^2 - 1/\lambda)$ for samples 1a to 1g. The plot is a straight line of slope $1/5.6$, which corresponds to a rubber network with 5.6 freely jointed links between crosslink points. Figure 8 is a plot of B against $(\lambda^2 - 1/\lambda)$ for all samples from the present and previous¹ work that were drawn at 80°C and were subsequently not shrunk or were shrunk at 80°C . Initially the plot is linear, with a gradient of $1/5.6$. However, for values of $(\lambda^2 - 1/\lambda)$ greater than 6, the results deviate from the straight line. This value of $(\lambda^2 - 1/\lambda)$ corresponds to a draw ratio of 2.53, which is in the region of maximum extension for a rubber network with $N = 5.6$, since the maximum draw ratio of a rubber network with N freely jointed links between crosslink points

Table 3 Samples initially drawn to $\lambda = 2.0$ or $\lambda = 2.5$ and shrunk freely for 10 min

Sample	Draw ratio, λ	Shrinkage temp. ($^{\circ}\text{C}$)	Final draw ratio, λ	Density, ρ	Refractive index			Crystallinity, f_c	$\langle P_2(\xi) \rangle_{\text{opt}}$	$\langle P_2(\xi) \rangle_a$
					n_z	n_x	n_a^0			
1h	2.0	80	1.00	1.3370	1.583	1.582	1.583	0.00	0.00	0.00
1i	2.0	120	1.07	1.3690	1.597	1.594	1.578	0.30	0.01	0.05
1j	2.0	150	1.00	1.3798		Sample opaque		0.40		
1k	2.0	180	1.00	1.3855		Sample opaque		0.45		
2b	2.5	80	1.04	1.3370	1.583	1.583	1.583	0.00	0.01	0.00
2c	2.5	120	1.10	1.3707	1.606	1.585	1.575	0.31	0.08	0.02
2d	2.5	150	1.10	1.3787		Sample opaque		0.39		
2e	2.5	180	1.10	1.3855		Sample opaque		0.45		

Table 4 Samples initially drawn to $\lambda = 3.4_4$ and shrunk freely for 10 min

Sample	Shrinkage temp. ($^{\circ}\text{C}$)	Shrinkage (%)	Density, ρ	Refractive index			Crystallinity, f_c	$\langle P_2(\xi) \rangle_{\text{opt}}$	$\langle P_2(\xi) \rangle_a$	$\langle P_2(\xi) \rangle_c$	
				n_z	n_x	n_a^0					
3b	70	2.9	1.3557	1.656	1.556	1.579	0.13	0.43	0.41	0.58	meas.
3c	80	9.6	1.3593	1.652	1.561	1.579	0.13	0.43	0.41	0.58	fit
							0.18	0.39	0.37	0.66	meas.
3d	90	14.0	1.3626	1.655	1.563	1.580	0.17	0.40	0.35	0.66	fit
							0.22	0.39	0.27	0.73	meas.
3e	100	14.8	1.3691	1.677	1.558	1.580	0.23	0.38	0.28	0.73	fit
							0.28	0.50	0.30	0.76	meas.
3f	110	17.7	1.3718	1.676	1.561	1.580	0.30	0.46	0.32	0.78	fit
							0.31	0.48	0.24	0.83	meas.
3g	120	16.6	1.3761	1.686	1.559	1.580	0.33	0.45	0.26	0.84	fit
							0.36	0.53	0.20	0.73	meas.
3h	150	20.8	1.3841	1.688	1.561	1.577	0.40	0.45	0.24	0.76	fit
							0.43	0.53	0.19	0.76	meas.
3i	180	18.3	1.3907	1.704	1.560	1.580	0.46	0.47	0.21	0.78	fit
							0.49	0.59	0.19	0.76	meas.
							0.53	0.52	0.22	0.80	fit

is approximately equal to $(N)^{1/2}$. The value of 5.6 compares well with the value of 5.3 deduced by suitably averaging values previously reported from stress-optical data⁹ on higher and lower molecular weight polymer and with the value 4.8 previously obtained by means of infra-red measurements². If the previous data are re-evaluated using equations (11) and (12) above, values of 6.2 and 5.7 are obtained from the stress-optical and infra-red measurements, respectively.

The density measurements showed that samples 1a to 1h had very low crystallinity. When freely shrunk in an air oven at higher temperatures, specimens 1i to 1k (Table 3) returned to their original length. The final crystallinities were, however, no longer low. Sample 1k was shrunk at the highest temperature and had a crystallinity of 0.45 after ten minutes in the air oven held at 180 $^{\circ}\text{C}$.

The tapes 2b to 2c (Table 3) were drawn to an initial draw ratio of 2.5, which is very close to the maximum rubber-like extension ratio of 2.4 calculated on the basis of 5.6 freely jointed links between crosslink points. These tapes shrank back to very nearly their original length when placed in the hot air oven for 10 min, and generally behaved in a similar way to the tapes with an initial draw ratio of 2.0.

Shrinkage of samples with higher initial draw ratio

The third series of tapes, 3a to 3u were drawn to an initial draw ratio of 3.4₄ (3a to 3i) or 3.5 (3j to 3u). This was well beyond the extension limit of the equivalent rub-

ber network. These tapes were studied in greater detail and refractive index, density, polarized fluorescence and X-ray diffraction measurements were made.

Samples 3b to 3i (Table 4) were freely shrunk in an oven for 10 min at 8 different temperatures in the range 70 $^{\circ}$ to 180 $^{\circ}\text{C}$. The as-drawn sample, sample 3a, had a crystallinity of 0.06, and consequently the crystalline orientation $\langle P_2(\xi) \rangle_c$ had a large uncertainty arising from the low diffracted X-ray intensity for this sample. The percentage shrinkage, the crystallinity, $\langle P_2(\xi) \rangle_{\text{opt}}$, $\langle P_2(\xi) \rangle_a$ and $\langle P_2(\xi) \rangle_c$ are plotted against oven temperature in Figure 9. As the temperature of the oven was increased, the amount by which the samples shrank increased. This was accompanied by a decreasing amorphous orientation and increasing crystallinity and crystalline orientation. The overall average orientation initially decreased in step with the amorphous orientation, then increased as the fraction of the more highly oriented crystalline material increased.

Samples 3k to 3o (Table 5) were all freely shrunk at 80 $^{\circ}\text{C}$ for various times in the range 5 to 1000 min. The results are plotted against time in Figure 10. The shrinkage initially increases with the length of time the sample spends in the oven until a plateau is reached after 20 min oven time. Each sample which spent longer than 20 min in the oven had a similar value of crystallinity, shrinkage, $\langle P_2(\xi) \rangle_{\text{opt}}$, $\langle P_2(\xi) \rangle_a$ and $\langle P_2(\xi) \rangle_c$. Results for samples 3p to 3t (Table 5) are shown in Figure 11. They were freely shrunk at 120 $^{\circ}\text{C}$ in the oven for the same range of times as samples 3k to 3o and they behaved in a similar way to that

set except that the plateau was reached more quickly, after about 8 min, and the final shrinkage was greater than for the corresponding sample shrunk at 80°C.

The final series of samples had an initial draw ratio of 4.2. The four samples 4b to 4e were freely shrunk for 10 min in the air oven at temperatures in the range 80° to 180°C. The behaviour of this series was similar to that of the corresponding series drawn to an initial draw ratio of 3.44.

The behaviour of the two series of tapes initially drawn to draw ratios of 3.44 (or 3.5) and 4.2 were very different from those initially drawn to draw ratios of 2.0 and 2.5. At 80°C the latter two series shrank back to their original length, whereas the former two series shrank by less than 25% at this temperature. The significant fall in shrinkage is attributed to the increased crystallinity of the more highly drawn tapes, even though the level of crystallinity is still very low (<10%).

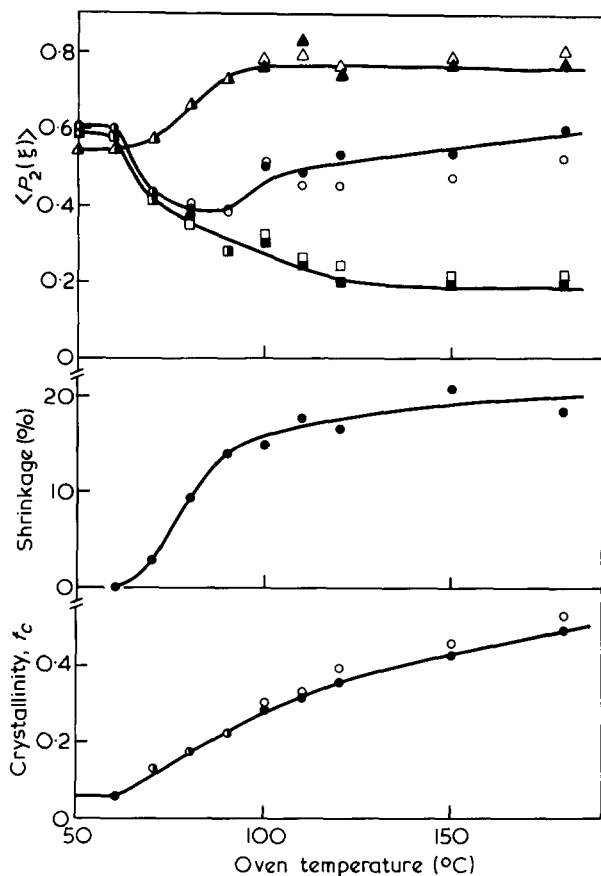


Figure 9 $\langle P_2(\xi) \rangle_c$ (Δ , \blacktriangle), $\langle P_2(\xi) \rangle_{opt}$ (\circ , \bullet), $\langle P_2(\xi) \rangle_a$ (\square , \blacksquare), f_c and shrinkage plotted against oven temperature for samples 3a–3i, which were initially drawn to $\lambda = 3.44$ at 80°C and subsequently shrunk freely for 10 min in an air oven. Solid points denote experimental data; open points denote best fit to equation (1)

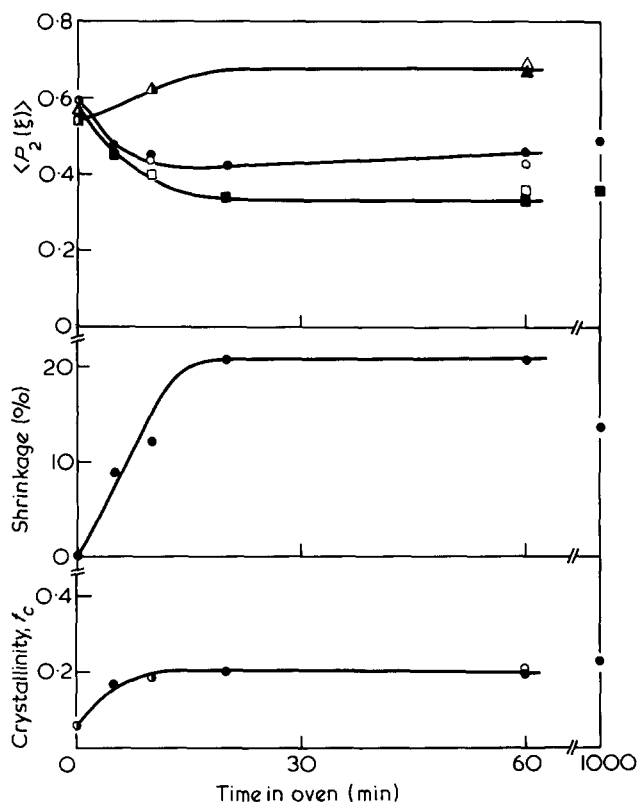


Figure 10 $\langle P_2(\xi) \rangle_c$ (Δ , \blacktriangle), $\langle P_2(\xi) \rangle_{opt}$ (\circ , \bullet), $\langle P_2(\xi) \rangle_a$ (\square , \blacksquare), f_c and shrinkage plotted against time in oven for samples 3k to 3o which were initially drawn to $\lambda = 3.5$ and subsequently shrunk freely in an air oven at 80°C for various times. Solid points denote experimental data; open points denote best fit to equation (1)

Table 5 Samples initially drawn to $\lambda = 3.5$ and shrunk freely at 80°C, 120°C or 180°C

Sample	Shrinkage temp. (°C)	Shrinkage time (min)	Shrinkage (%)	Density, ρ	Refractive index			Crystallinity, f_c	$\langle P_2(\xi) \rangle_{opt}$	$\langle P_2(\xi) \rangle_a$	$\langle P_2(\xi) \rangle_c$	
					n_z	n_x	n_a^0					
3k	80	5	8.7	1.3605	1.667	1.555	1.579	0.17	0.47	0.45		
3l	80	10	12.2	1.3605	1.663	1.557	1.580	0.18	0.45	0.39	0.62	meas.
								0.18	0.44	0.40	0.62	fit
3m	80	20	20.7	1.3614	1.658	1.560	1.579	0.20	0.42	0.34		
3n	80	60	20.6	1.3608	1.660	1.561	1.581	0.20	0.46	0.33	0.67	meas.
								0.21	0.43	0.36	0.69	fit
3o	80	1000	13.6	1.3649	1.675	1.557	1.581	0.23	0.49	0.36		
3p	120	5	20.1	1.3750	1.676	1.562	1.579	0.35	0.48	0.19		
3q	120	10	27.2	1.3752	1.675	1.562	1.579	0.35	0.47	0.16	0.63	meas.
								0.39	0.39	0.21	0.66	fit
3r	120	20	24.1	1.3777	1.678	1.563	1.579	0.37	0.48	0.15		
3s	120	60	24.1	1.3782	1.678	1.563	1.580	0.38	0.48	0.14	0.75	meas.
								0.41	0.42	0.17	0.77	fit
3t	120	1000	27.7	1.3807	1.687	1.562	1.579	0.40	0.52	0.16		
3u	180	10	18.7	1.3928	1.706	1.562	1.579	0.51	0.21	0.58	0.78	meas.
								0.53	0.23	0.54	0.81	fit

Table 6 Samples initially drawn to $\lambda = 4.2$ and shrunk freely for 10 min

Sample	Shrinkage temp. (°C)	Shrinkage (%)	Density, ρ	Refractive index			Crystallinity, f_c	$\langle P_2(\xi) \rangle_{\text{opt}}$	$\langle P_2(\xi) \rangle_a$	$\langle P_2(\xi) \rangle_c$	
				n_z	n_x	n_a^0					
4b	80	5.7	1.3673	1.705	1.544	1.580	0.13	0.67	0.70		
4c	120	15.4	1.3778	1.702	1.553	1.579	0.34	0.62	0.44		
4d	150	21.4	1.3855	1.708	1.558	1.581	0.42	0.61	0.38		
4e	180	25.0	1.3933	1.713	1.560	1.579	0.50	0.62	0.36	0.78	
							0.51	0.59	0.37	0.80	meas. fit

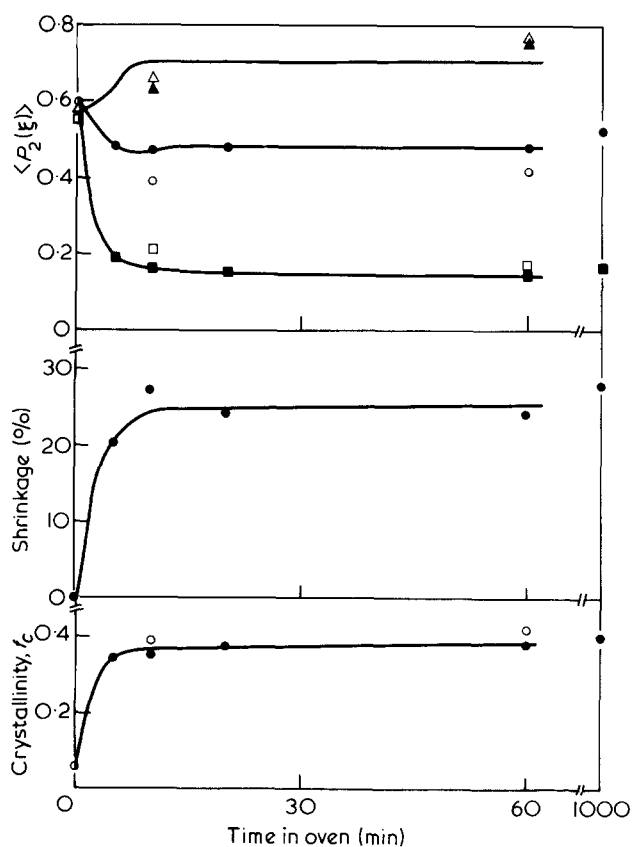


Figure 11 $\langle P_2(\xi) \rangle_c$ (Δ , \blacktriangle), $\langle P_2(\xi) \rangle_{\text{opt}}$ (\circ , \bullet), $\langle P_2(\xi) \rangle_a$ (\square , \blacksquare), f_c and shrinkage plotted against time in oven for samples 3p to 3t, which were initially drawn to $\lambda = 3.5$ and subsequently shrunk freely in an air oven at 120°C for various times. Solid points denote experimental data; open points denote best fit to equation (1)

Intercomparison of shrinkage with amorphous, crystalline and overall orientation

For seventeen out of the twenty-six samples 3a to 3u and 4a to 4e the value of $\langle P_2(\xi) \rangle_c$ was measured, enabling a second set of values of $\langle P_2(\xi) \rangle_a$, $\langle P_2(\xi) \rangle_c$, $\langle P_2(\xi) \rangle_{\text{opt}}$ and f_c to be calculated for a best fit to equation (1). These best fit values are displayed below the corresponding measured values in Tables 1, 4, 5 and 6 and are plotted as open points in Figures 9, 10 and 11.

Comparison of the experimental and best fit results throughout the series reveals a systematic error. This can be interpreted as a systematic error in one or a number of the experimental results and such an error is not surprising considering the number of assumptions involved in deriving each of the four quantities from the data. Taking this into account, the agreement between the experimental and best fit values is reasonable. This result supports the hypothesis that the fluorescent molecules are excluded from the crystalline regions and that the relationship between the distribution of orientations of the fluorescent molecules and

that of the polymer chains in the amorphous regions of the crystalline polymer is the same as in the completely amorphous polymer. We are therefore justified in interpreting $\langle P_2(\xi) \rangle_a$, determined from measurements of the fluorescence intensities in the way described, as the value of $\langle P_2(\xi) \rangle$ for the amorphous regions of the polymer.

Figures 9, 10 and 11 show both the shrinkage and the crystallinity of the samples. The results in Figure 9 for samples originally drawn to draw ratio 3.4 are the most revealing because they show a separation between the shrinkage and crystallization processes. For this series of samples the shrinkage increases very markedly, from zero to 15%, as the temperature of the oven rises from 60° to 90°C and then increases less rapidly with temperature. The crystallinity, on the other hand, shows a more gradual increase over the whole range of oven temperatures from 60° to 180°C. It is notable that $\langle P_2(\xi) \rangle_{\text{opt}}$ shows a clear minimum for oven temperatures near 80°C. We can conclude from this that shrinkage is associated with a decrease in overall molecular orientation, whilst for these samples crystallization produces an increase in molecular orientation and that this is the major effect above 100°C. These results and those for the samples of lower draw ratio shrunk at 80°C, which do not crystallize, show that there can be no doubt that at the lower temperatures shrinkage is primarily due to the disorientation of the amorphous regions, as was concluded from a much earlier study of the dichroism of dyestuffs incorporated in PET¹⁰. It has been proposed¹¹⁻¹³, notably by Statton *et al.*¹³, that shrinkage should be attributed primarily to the refolding of chains which have been pulled out in the drawing process. The present results for shrinkage at 80°C, however, support the dichroism studies^{10,14} and the view of Wilson¹⁵ that the shrinkage of PET is essentially associated with the disorientation of the amorphous regions and that crystallization occurs at a later stage. The observed rise in orientation of the crystalline regions can be explained either by Wilson's suggestion that the molecules in the amorphous regions preferentially crystallize onto pre-existing more highly oriented crystallites or by the assumption that shrinkage forces in the amorphous regions cause re-orientation of the crystallites. Both of these processes may occur.

At higher temperatures the separation between the shrinkage and crystallization processes is not so clear cut. Figure 11 indeed suggests that the rates of these processes are roughly comparable at 120°C, although our results cannot rule out a very fast component of shrinkage taking place in times of the order of a few minutes, or even less, as found by Wilson. Although it may well be that the driving force for shrinkage is still molecular disorientation rather than chain folding, these two processes seem to be occurring simultaneously in the samples for which the results are shown in Figures 10 and 11.

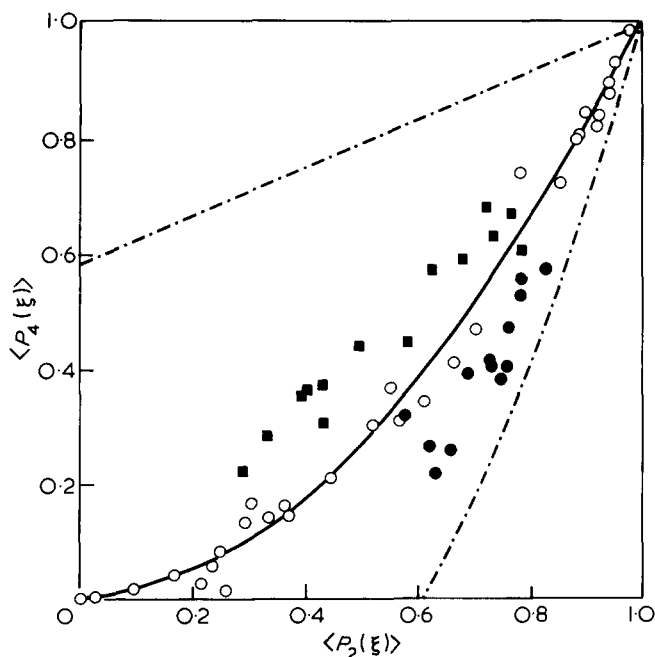


Figure 12 $\langle P_4(\xi) \rangle$ plotted against $\langle P_2(\xi) \rangle$. \circ , $\langle P_4(\xi_M) \rangle$ plotted against $\langle P_2(\xi_M) \rangle$ for all the samples of low crystallinity from the present and previous¹ work, including those drawn to draw ratio 2.0 and shrunk at 80°C; \bullet , X-ray data for $\langle P_4(\xi)_c \rangle$ against $\langle P_2(\xi)_c \rangle$; \blacksquare , fluorescence data for $\langle P_4(\xi_M) \rangle$ against $\langle P_2(\xi_M) \rangle$ for the shrunk samples 3b to 3i and 3l, 3n, 3q, 3s, 3u and 4e. —, —, —, mathematical upper and lower bounds on the value of $\langle P_4(\xi) \rangle$ for any value of $\langle P_2(\xi) \rangle$; —, relationship predicted by the pseudo-affine deformation scheme¹⁶.

Fourth-order orientation averages

The fluorescence method can provide¹ values of $\langle P_4(\xi_M) \rangle = 1/8(35\langle \cos^4\theta_M \rangle - 30\langle \cos^2\theta_M \rangle + 3)$ as well as values of $\langle P_2(\xi_M) \rangle$, and the X-ray method can give similar and higher-order orientation averages for the crystallites, as already explained.

Figure 12 shows, as open circles, the values of $\langle P_4(\xi_M) \rangle$ plotted against the corresponding values of $\langle P_2(\xi_M) \rangle$ for all the samples of low crystallinity from the present and previous¹ work, including those drawn to draw ratio 2.0 and shrunk at 80°C. The continuous line, which they lie close to, is the relationship between $\langle P_4(\xi) \rangle$ and $\langle P_2(\xi) \rangle$ predicted according to the pseudo-affine deformation scheme¹⁶ for the preferential orientation of a set of unique axes. As previously suggested¹, the agreement between the points and this line may be fortuitous. Also shown in Figure 12 are values of $\langle P_4(\xi_M) \rangle$ plotted against $\langle P_2(\xi_M) \rangle$ and $\langle P_4(\xi)_c \rangle$ plotted against $\langle P_2(\xi)_c \rangle$ for all the shrunk samples for which X-ray measurements were made. The upper broken curve is the theoretical upper limit on $\langle P_4(\xi) \rangle$, which corresponds to $\langle \cos^4\theta \rangle = \langle \cos^2\theta \rangle$ and thus to a distribution in which the unique axes lie parallel or perpendicular to the draw direction. The lower broken curve corresponds to the lower theoretical limit, where $\langle \cos^4\theta \rangle = (\langle \cos^2\theta \rangle)^2$ and the unique axes lie on a cone around the draw direction with semi-angle θ .

The fluorescence points lie in general between the upper limit and the pseudo-affine curve and the X-ray points between this curve and the lower limit. The first of these results suggests that it may not be quite correct to deduce $\langle P_2(\xi)_a \rangle$ for the amorphous regions in the semi-crystalline polymer from the curve in Figure 1, which refers to non-crystalline samples, since the natures of the distributions of orientations of the fluorescent molecules for the two kinds

of samples appear to be different. Since, however, the points for the semi-crystalline sample do not lie far from the pseudo-affine curve the approximation may be reasonably good.

The fact that the fluorescence and X-ray points for the shrunk samples lie on opposite sides of the curve on which the original drawn samples lie suggests the possibility that points representing the overall distribution of molecular orientations after shrinkage might also lie on this curve. To test this hypothesis it is first necessary to deduce values of $\langle P_4(\xi)_a \rangle$. This may be done by making two assumptions. The first is that $\langle P_4(\xi)_a \rangle$ is related uniquely to $\langle P_4(\xi_M) \rangle$, which is similar to the assumption made in deriving $\langle P_2(\xi)_a \rangle$. The second is that $\langle P_4(\xi)_a \rangle$ may be deduced approximately for totally amorphous samples from the value $\langle P_2(\xi)_a \rangle = \langle P_2(\xi) \rangle_{\text{opt}}$ by taking the corresponding value on the pseudo-affine curve. We do not imply here that the mechanism of orientation is in fact that of the 'floating rod' model to which the pseudo-affine curve applies exactly; on the contrary, we have already shown that for low orientation the rubber model is appropriate. It is only necessary for the present purpose to note that the two models do not differ greatly in their prediction of the relationship between $\langle P_4(\xi) \rangle$ and $\langle P_2(\xi) \rangle$. It thus seems very likely that the use of the pseudo-affine curve, which is well-defined for all degrees of orientation (in contrast to the curve for the rubber model, which applies only for low orientation) will lead to values of $\langle P_4(\xi)_a \rangle$ for amorphous samples which are correct to a good approximation.

Once $\langle P_4(\xi)_a \rangle$, $\langle P_4(\xi)_c \rangle$ and f_c are known, a value of $\langle P_4(\xi)_0 \rangle$ for the overall distribution of molecular orientations may be derived using a similar equation to (1). In Figure 13, $\langle P_4(\xi)_0 \rangle$ is plotted against $\langle P_2(\xi) \rangle_{\text{opt}}$ (which also refers to the overall distribution of orientations), $\langle P_4(\xi)_c \rangle$ is plotted against $\langle P_2(\xi)_c \rangle$ and $\langle P_4(\xi)_a \rangle$ is plotted against $\langle P_2(\xi)_a \rangle$ for samples 3a–3i. Despite the scatter of the points, the values of $\langle P_4(\xi) \rangle$ and $\langle P_2(\xi) \rangle$ for the overall distribution are indeed seen to lie closer to the pseudo-affine

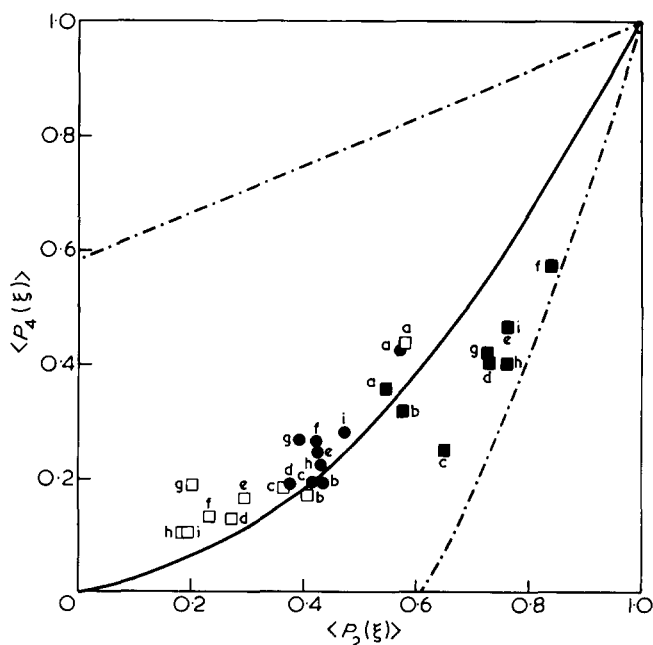


Figure 13 $\langle P_4(\xi) \rangle$ plotted against $\langle P_2(\xi) \rangle$ for samples 3a to 3i. \blacksquare , X-ray data for $\langle P_4(\xi)_c \rangle$ against $\langle P_2(\xi)_c \rangle$; \square , $\langle P_4(\xi)_a \rangle$ against $\langle P_2(\xi)_a \rangle$; \bullet , denotes $\langle P_4(\xi)_0 \rangle$ against $\langle P_2(\xi) \rangle_{\text{opt}}$ (which both refer to the overall distribution of orientations). —, —, —, and — as in Figure 12

curve than the corresponding values for either the amorphous or crystalline regions. This is consistent with the view that shrinkage takes place before crystallization so that the overall orientation is reduced by the polymer re-tracing the orientation states through which it passed during drawing, prior to subsequent crystallization.

Although much further work is required in order to deduce the precise nature of the changes in molecular orientation which take place during shrinkage, the present results illustrate clearly the importance of developing methods such as the fluorescence method which can give more information about amorphous orientation than $\langle P_2(\xi) \rangle$, which is the only information deducible from, for instance, birefringence or dichroism, whether optical or infra-red.

CONCLUSIONS

The results of the present work show that for the fluorescent-molecule-polymer system used in the experimental work, the fluorescent molecules are excluded from the crystalline regions in the semi-crystalline polymer and confirm that the unique relationship between the distribution of orientations of the fluorescent molecules and that of the chain axes, reported previously, still applies to a good approximation in the amorphous regions of the semi-crystalline polymer. We conclude that the fluorescence method is capable of characterizing quantitatively the distribution of chain orientations in the non-crystalline regions of semi-crystalline polymers.

The samples of PET studied appear to behave as a rubber with 5.6 freely joined links between crosslink points when uniaxially drawn and shrunk at 80°C, provided the draw ratio is less than 2.5. At higher draw ratios strain-induced crystallization occurs and the shrinkage is significantly reduced.

In all cases it can be concluded that shrinkage is associated with the disorientation of the amorphous regions. The results suggest that further crystallization takes place independently of the disorientation process.

ACKNOWLEDGEMENTS

This research was undertaken with financial support from the Science Research Council, and J. H. N. also held an SRC CAPS studentship sponsored by ICI Ltd, Fibres Division. We wish to thank Dr H. Brody and Dr M. P. W. Wilson at ICI Ltd, and Dr D. Patterson, Department of Colour Chemistry, University of Leeds, for helpful discussions.

REFERENCES

- 1 Nobbs, J. H., Bower, D. I., Ward, I. M. and Patterson, D. *Polymer* 1974, **15**, 287
- 2 Cunningham, A., Ward, I. M., Willis, H. A. and Zichy, V. *Polymer* 1974, **15**, 749
- 3 Purvis, J., Bower, D. I. and Ward, I. M. *Polymer* 1973, **14**, 398
- 4 Cunningham, A., Davies, G. R. and Ward, I. M. *Polymer* 1974, **15**, 743
- 5 Krigbaum, W. R. and Roe, R-J. *J. Polym. Sci. (A)* 1964, **2**, 4391
- 6 Daubeny, R. DeP., Bunn, C. W. and Brown, C. J. *Proc. R. Soc. (A)* 1954, **226**, 531
- 7 Farrow, G. and Ward, I. M. *Polymer* 1960, **1**, 330
- 8 Roe, R-J. and Krigbaum, W. R. *J. Appl. Phys.* 1964, **35**, 2215
- 9 Pinnock, P. R. and Ward, I. M. *Trans. Faraday Soc.* 1966, **62**, 1308

- 10 Patterson, D. and Ward, I. M. *Trans. Faraday Soc.* 1957, **53**, 1516
- 11 Dumbleton, J. H. *J. Polym. Sci. (A-2)* 1969, **7**, 667
- 12 Dumbleton, J. H. *Polymer* 1969, **10**, 539
- 13 Statton, W. O., Koenig, J. L. and Hannon, M. *J. Appl. Phys.* 1970, **41**, 4290
- 14 Okajima, S., Nakayama, K., Kayama, K. and Kato, Y. *J. Appl. Polym. Sci.* 1970, **14**, 1069
- 15 Wilson, M. P. W. *Polymer* 1974, **15**, 277
- 16 'Structure and Properties of Oriented Polymers'. (Ed. Ward, I. M.), Applied Science, London 1975, Ch. 1

APPENDIX

The following simple ideas have been used to estimate the dependence of the density of the amorphous regions on the value of $\langle P_2(\xi) \rangle_a$.

A unit volume of amorphous polymer is imagined to be divided into two parts, V_c and ΔV . Thus

$$1 = V_c + \Delta V \quad (\text{A1})$$

V_c is defined as the volume of the same mass of material if it were fully crystalline. It follows that ΔV is the volume of the sample that is orientation dependent. In *Figure 14*, the two unit vectors S_1 and S_2 represent two adjacent polymer chains. We assume that the shaded area, A , is proportional to the volume that is reduced to zero when S_1 is completely aligned with S_2 . If G is the angle between S_1 and S_2 the area A is equal to $\frac{1}{2} \sin G$. It follows that

$$\Delta V = k \langle \sin G \rangle \rho_a / \rho_a^0 \quad (\text{A2})$$

where k is a constant of proportionality and $\langle \sin G \rangle$ is the average value of $\sin G$ for the amorphous sample.

From equation (A1) we obtain:

$$\Delta V = 1 - \rho_a / \rho_c \quad (\text{A3})$$

and if R is defined by:

$$R = \langle \sin G \rangle / \langle \sin G \rangle_0 \quad (\text{A4})$$

where $\langle \sin G \rangle_0$ refers to an isotropic amorphous sample, it can be shown from equations (A2) and (A3) that

$$\rho_a = \rho_a^0 \rho_c / [\rho_a^0 + R(\rho_c - \rho_a^0)] \quad (\text{A5})$$

If we assume that there is no correlation between the position and orientation of a chain it follows from the Legendre addition theorem that for a sample with a uni-

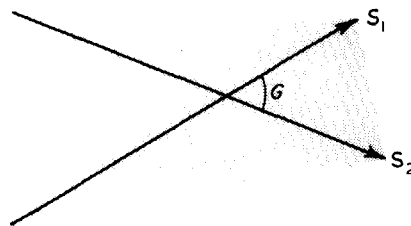


Figure 14 The unit vectors S_1 and S_2 represent two adjacent chains in the amorphous regions of a polymer. The shaded area is assumed to be proportional to the volume that is reduced to zero when S_1 is completely aligned with S_2

axial distribution of chain orientations,

$$\langle P_2(\cos G) \rangle = [\langle P_2(\xi) \rangle]^2 \quad (\text{A6})$$

It is not possible to obtain an exact expression for $\langle \sin G \rangle$ in terms of $\langle P_2(\cos G) \rangle$ and we have therefore used the approximation

$$\langle \sin G \rangle = |1 - \langle \cos^2 G \rangle|^{1/2} = \left| \left\{ \frac{2}{3} [1 - \langle P_2(\cos G) \rangle] \right\}^{1/2} \right| \quad (\text{A7})$$

which gives in fact the maximum value for $\langle \sin G \rangle$ for a given $\langle P_2(\cos G) \rangle$, since by Schwartz's inequality $\langle \sin^2 G \rangle$ is greater than or equal to $(\langle \sin G \rangle)^2$. The same approxima-

tion was used for $\langle \sin G \rangle_0$ in an attempt to reduce the error in R .

For PET appropriate values are $\rho_d^0 = 1.3375$ and $\rho_c = 1.445$. Thus equation (A5) becomes:

$$\rho_a = 1.9327 / (1.3375 + 0.1075R) \quad (\text{A8})$$

The curve in *Figure 5* corresponds to this equation. The points shown are for all the samples, from this and the previous work¹, which were drawn at 80°C and which are believed to be of low crystallinity. The general relationship between the points and the curve suggests that, despite the simplicity of the ideas and approximations used to derive it, the curve may be sufficiently good to be used for deriving values of f_c for oriented samples.

Trajectory of polyethylene chains in single crystals by low angle neutron scattering

D. M. Sadler and A. Keller

H. H. Wills Physics Laboratory, University of Bristol, Bristol BS8 1TL, UK

(Received 9 May 1975; revised 1 September 1975)

Measurements of coherent neutron diffraction of oriented single crystals of blends of hydrogenous and deuterated polyethylene have been undertaken in order to study the mutual arrangements of the crystalline 'stems' of the same molecule. In the appropriate range of diffraction angle, the scatter is fully consistent with thin lamellae, the planes of which contain the stems. The thickness of these lamellae agrees with that expected for neighbouring stems of one molecule being restricted to the same (110) plane. The density of deuterium atoms in the lamellae is consistent with largely adjacent re-entrant folding; for crystals grown at low supercooling there is a possibility of some segregation according to isotope. Outside the above range of diffraction angle, effects are observed which are attributable to the finite lateral dimensions of the proposed lamellae. At the smallest angles of measurement an artifactual signal attributable to voids can be observed, which can be avoided by suitable sample treatment.

INTRODUCTION

In the period following the discovery of chain folding in crystallizable polymers, there has been a continuing effort to define the degree and nature of crystal disorder and, in addition, how the chains thread through the crystalline lamellae. Two newly applied techniques promise to provide some evidence on the second of these two related matters: both infra-red (i.r.) and low angle neutron diffraction are sensitive to the 'trajectory' of an isotopically labelled chain in its unlabelled matrix. I.r. results¹ suggest that in single crystals composed of blends of polyethylene (PE) and deuterio-polyethylene (DPE), nearest neighbour chains along the $\langle 110 \rangle$ direction are of the same isotopic composition. This indicates adjacent re-entrant folding, leading to one molecule forming a slab along the growth face. This was the chain trajectory proposed when chain folding was first discovered. *Figure 1* shows a chain folded in this manner, with crystal 'stems' (i.e. those parts of the chain passing through the crystals) adjacent to one another. Other modes of folding will result in the stems of the same molecule being arranged differently, and in the case of labelled chains the coherent neutron scattering will depend on the resulting spacial arrangement of these stems. *Figure 2* illustrates several possibilities; the position of each stem in the plane of the crystal being indicated. It should be emphasized that the degree and nature of the disorder in the crystal is not directly in question here, since the scattering will only be affected to a minor extent by the chain sequence in any disordered regions (e.g. in the fold surface).

Preliminary results² on bulk crystallized material, in conjunction with a study on molten PE, concern very small angles of diffraction (equivalent Bragg spacings in the region of 500 Å). These results lead to molecular weights and radii of gyration of the deuterated particles consisting of molecules or groups of molecules in the PE matrix. The present results concern crystals grown from solution; the angles of diffraction correspond to equivalent Bragg spacings of 200–15 Å, in which case the intensities of diffraction depend on the variations of scattering density according to the stem arrangements as outlined above.

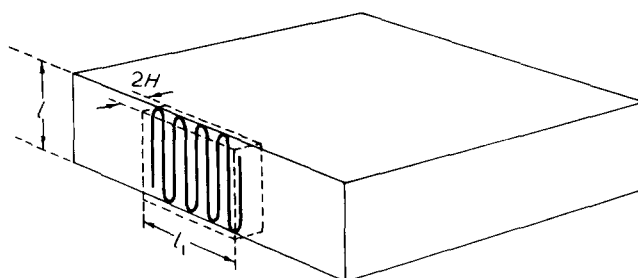


Figure 1 Diagrammatic representation of a polyethylene crystal, showing how adjacent re-entrant folding leads to lamellar diffracting objects

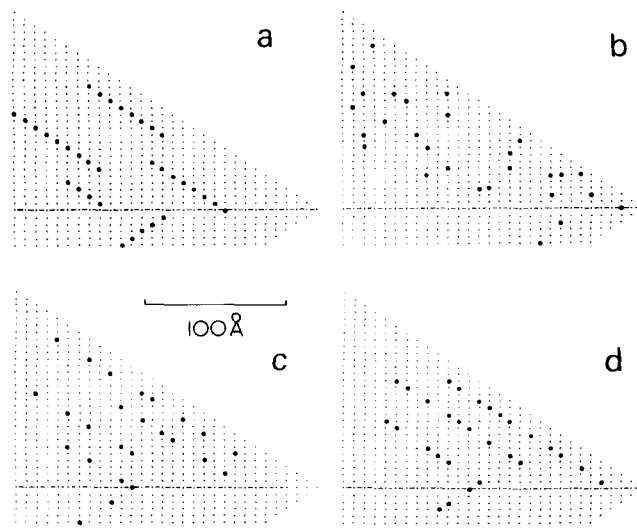


Figure 2 Representation of the positions of intersections of stems (i.e. chain sequences passing through the crystalline region) and a (001) plane. The small points represent PE chains, the large points DPE. The examples of chain trajectory are: (a) adjacently re-entrant folding; (b) randomly re-entrant folding; (c) and (d) other forms of folding restricted to (110) planes; (c) large gaps between stems; (d) small gaps. The broken line indicates a fold sector boundary

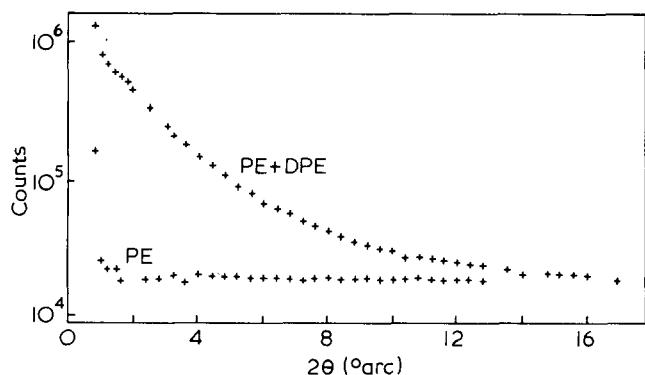


Figure 3 Example of data used for the analysis. In general only at larger values of 2θ were the total counts as high as shown on the ordinate: for smaller angles the values plotted were calculated using shorter times of counting. These data were interpolated and analysed as explained in the text to give Figures 4 and 6. Some measurements were taken at even higher 2θ than shown, and were fully consistent with the way in which the two spectra, PE and PE with DPE, were subtracted to give a measure of coherent scattering from the DPE component. Results from the diffractometer at Harwell⁴.

The results presented here have been analysed with a view to testing whether the diffraction could be from lamellar structures (e.g. as in Figure 1). It remains to be tested how much of the labelled stems are in lamellae only one molecule in thickness, and in addition to investigate to what extent alternative structures can be excluded.

EXPERIMENTAL

DPE from Merck Sharpe and Dohme was specified as being of 99% isotopic purity; the PE used was Rigidex 9. The DPE was dissolved by boiling in xylene together with PE; the mixing in solution was continued for at least 1 h. Total concentration of polymer was 0.04% w/v, the weight fraction of DPE in the polymer being 0.13. The solution was poured into thin-walled tubes held at 70° or 85°C. For the crystallization temperature $T_x = 85^\circ\text{C}$ a seeding procedure was employed³ in order to produce a uniform crystal size. The crystal suspension was filtered (at 85°C in the case of that crystallization temperature) so that the final filtrate consisted of a concentrated sludge on filter paper. This was dried so as to produce flat mats about 0.1 mm thick. For $T_x = 70^\circ\text{C}$ the dry mat was pressed at 60°C so as to produce a translucent material. For $T_x = 85^\circ\text{C}$ one of the samples remained white in colour. The isotopic composition of the samples was monitored by i.r. The sample sheets were cut and mounted in aluminium holders, usually with the mat planes (hence the crystal layers) parallel to the plane of the holder. In these cases an area of 7×20 mm was uniformly filled with a weighed amount of polymer (~130 mg). In two instances, mentioned in the text, the mats were cut into strips and mounted with the mat normals in the plane of the holder. Two small angle scattering instruments were used: at Harwell⁴ where the normal to the holder was held at an angle of θ to the incident beam (where 2θ is the angle at which the scattering is being measured) and at the high flux reactor of the Institut Max von Lane–Paul Langevin at Grenoble⁵ where the normal to the holder was parallel to the incident beam. The aperture defining the beam at the sample was slightly larger than the area defined by the sample. Orientations of the crystal layers and the crystal lattice within the mats were monitored by low- and wide-angle X-ray diffraction, respectively. The layer normals are concentrated within about 30° to

the normal to the mats. The 110 arcs were equatorial (most intense along a direction parallel to the plane of the mats). The long spacing l was 107 Å for $T_x = 70^\circ\text{C}$ and 132 Å for $T_x = 85^\circ\text{C}$.

RESULTS

Figure 3 shows the variation of neutron count rate as a function of 2θ , for a mat of PE and of a blend of 0.13 DPE and 0.87 PE using the scanning diffractometer⁴. The former show scatter which is almost independent of 2θ , which corresponds to the high H content and high incoherent scatter. The latter shows an additional intense scatter attributable to the DPE component. The latter contribution was separated by taking the difference between the signal from the blend, and the signal from PE which is rescaled slightly so that it corresponds to the same total incoherent cross-section as in the blend. To enable this to be done accurately, the PE scatter was measured for several sample thicknesses. A (small) desmearing correction⁶ was applied to the difference curve to allow for the finite size of the sample and of the counter aperture. The resultant measure of diffracted intensity I decreases sharply with 2θ ; the results are conveniently expressed as a plot of $I s^2 \cos \theta$ versus s , where

$$s = 2 \sin \theta / \lambda \quad (\lambda, \text{neutron wavelength})$$

Such a plot is shown in Figure 4.

Figure 5 shows results on mats mounted edgewise ($T_x = 85^\circ\text{C}$) using the high flux reactor device. The total scatter from the blend is shown since these samples do not have a uniform thickness, so that background subtraction cannot be accurate. Figure 5a corresponds to a mat as dried, i.e. white in colour and containing large numbers of voids. The scatter in a direction parallel to the mat normals (broken line) is much higher than that at right angles to the normals (solid line). This is not consistent with scatter from PE–DPE contrast from any of the models of the type shown in Figure 2 (see below). Figure 5b shows the corresponding results for mats which have been pressed at 60°C so as to remove most of the voids; a translucent sample then results. The anomalous signal in a direction parallel to the mat normals has been removed. We tentatively

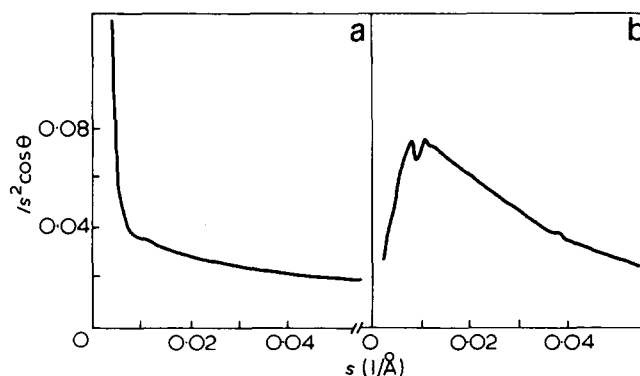


Figure 4 Plot of the data as $I s^2 \cos \theta$ versus s after background subtraction, desmearing, and corrections for attenuation and preferred orientations (see text). The units of I are arbitrary, being expressed as $I_{\text{diff}}/I_{\text{D}}$ where I_{diff} is the count rate difference from Figure 3. I_{D} is the sum of the coherent diffraction intensities for the same number of labelled individual atoms as in the PE and DPE blend, calculated on the basis of the vanadium calibration. (a) $T_x = 85^\circ\text{C}$, mat unpressed; (b) $T_x = 70^\circ\text{C}$, mat pressed. For the effect of pressing see also Figure 5

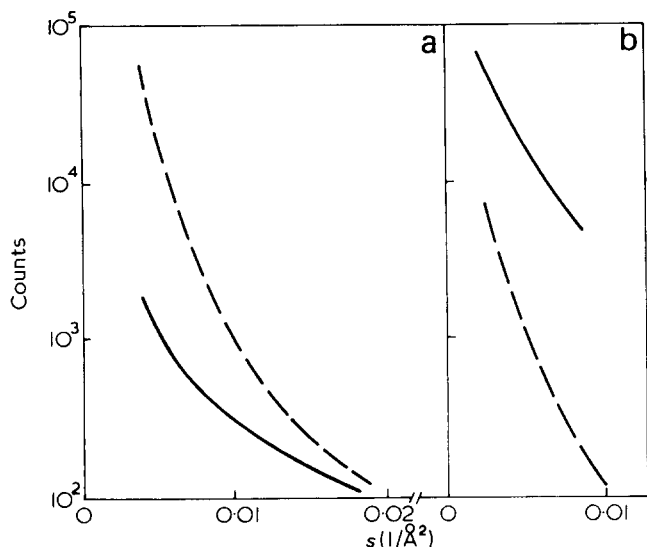


Figure 5 Dependence of uncorrected scattered intensity (in counts per cell of the multidetector array) on orientation of the mats. —, direction in the plane of the mats; ----, direction parallel to the mat normals. $T_x = 85^\circ\text{C}$; (a) mat as dried, containing many voids; (b) after pressing at 60°C to minimize voids. The intensity scale of (a) relative to (b) is arbitrary. Results from the high flux reactor, Grenoble⁵

attribute the anomalous signal to multiple total internal reflection at interfaces between voids and stacks of crystals.

General considerations

The small angle scatter from the DPE component of PE-DPE blends is clearly significant (the intensity is quantified in the discussion below). If the DPE was segregated into blocks much larger than 200 \AA , most of the diffraction would not be included within the measured range, and would be at very small angles and at wide angle peaks. Much of the DPE must be dispersed in particles of a size of the order of magnitude of 100 \AA .

The reader is referred to Guinier and Fournet⁷ for the detailed interpretation of low angle intensity measurements. For the present purposes it is convenient to quote some formulae in the form below, which are relevant to samples where the scattering particles take up a range of orientations.

Rods of radius R_0 and length L . For $s \gg 1/L$ diffraction occurs only for s perpendicular to the direction of the rod; the intensity is then given by:

$$I = (N\sigma n_L / 2s \cos \theta) \exp - (2s^2 \pi^2 R^2) \quad (1)$$

where N is the number of scattering centres defined as the number of deuterium atoms, σ is the corresponding coherent cross-section, n_L is the number of centres per unit length, and the exponential factor applies for $s \ll 1/R_0$. R is analogous to the usual radius of gyration: $R \equiv r^2$ where r is the distance of each centre from the centre line of the rod.

Lamellae of thickness $2H$ and width W . For $s \gg 1/W$ diffraction only occurs for s parallel to the lamellar normals, and the intensity is given by:

$$I = (N\sigma n_A / 2\pi s^2 \cos \theta) \exp - (4\pi^2 D^2 s^2) \quad (2)$$

where n_A is the number of centres per unit area, and the exponential factor applies for $s \ll 1/2H$. $D \equiv z^2$ where z is the distance of a scattering centre from the central plane of the lamella. In these equations the additional $\cos \theta$ term arises in order to avoid the restriction to small values of 2θ ⁷.

For both particle shapes a preferred particle orientation will result in scattered intensities which are higher in a direction either perpendicular to the rod direction or parallel to the lamellar normals.

The validity of these two equations depends not only on whether rods or lamellae are suitable structural models (see Figures 2b and 2a respectively). In addition the range of s must be examined. The maximum value of s measured was 0.07 \AA^{-1} , so that both conditions $s \ll 1/R_0$ and $s \ll 1/2H$ (see above) are likely to be satisfied. The length of a stem (approximately equal to the fold length l) is, however, within the experimental range of $1/s$. Equations (1) or (2) can therefore only be valid as asymptotes. To predict the variation of I with s for values of $s \lesssim 1/l$, numerical calculations would be necessary. These would need to allow for the distribution of orientations and the dimensions l and l_1 (see Figure 1). Qualitatively, it may be said that I may be both above or below the asymptotic value for $s \approx 1/l$ (Fig. 8⁷). For $s \ll 1/l$ will be below the asymptotic value.

It must be considered whether interference caused by the phase relationship between the scattering from neighbouring rods or lamellae should be significant for the prediction of I . For non-overlapping spheres spaced at random it has been calculated⁷ that the importance of interference effects, depends on the concentration and the relative value of $1/s$ compared with the average sphere separation. For a DPE concentration of 0.13, the average spacing between stems arranged randomly within the crystal would be of the order of 11 \AA , and between rows of stems (i.e. lamellae) about 30 \AA . These estimates are made from simple geometry based on the cross-sectional area per stem of 18 \AA^2 . Based on these figures, estimates of interference effects which are analogous to previous calculations⁷ suggest that for lamellae (equation (2)) they should be small, for s more than about 0.03 \AA^{-1} , but that for rods should be quite significant for all s measured.

Finally, in order to be able to deduce values of n_L or n_A from the equations, it is necessary for all the DPE to be dispersed within the crystals. Some partial segregation would of course lead to low measured values.

DISCUSSION

It is immediately apparent that equation (1) (using $R \approx 2\text{ \AA}$ i.e. for a single chain) bears no relation to the experimental results (Figure 4) since $I s^2$ decreases and not increases as a function of s . It must be borne in mind, however, that interference between different stems (see above) has not been considered, so that equation (1) cannot be expected to predict accurately the scatter from structures such as shown in Figure 2b. Equation (2) predicts a decrease of $I s^2$ for larger values of s ; to test this equation further $I s^2 \cos \theta$ is plotted on a log scale against s^2 (Figure 6). The predicted variation for infinitely wide sheets [corresponding to (110) pleated sheets: $D = 1.57\text{ \AA}$; $n_A = 0.35\text{ \AA}^{-2}$] is also shown. The absolute calibration of I was estimated from a measure of the (incoherent) scatter from a vanadium sheet; very similar results are obtained by using the incoherent scatter from PE. Corrections were also made for beam attenuation (a factor of 2) and for preferred orientation (a factor of 0.45 for $T_x = 70^\circ\text{C}$ and 0.66 for $T_x = 85^\circ\text{C}$).

It can be seen that the experimental curves as plotted in Figure 6 are linear for large s , hence the results are consistent with sheet structures. In addition, the linear portions of the experimental curves are approximately parallel to the predicted one. Hence the thickness of the sheets (as specified by D) is that predicted on the basis of the

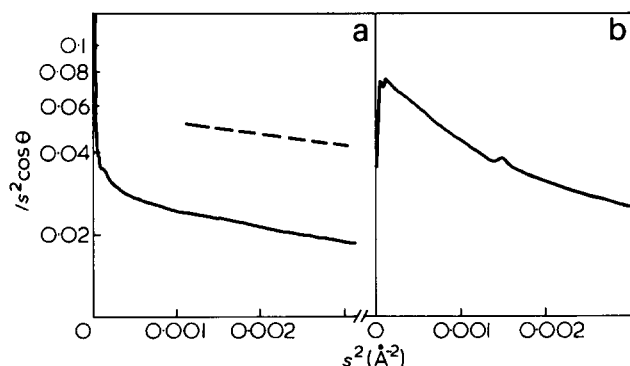


Figure 6 The data of Figure 4 replotted as $Is^2 \cos \theta$ on a logarithmic scale versus s^2 . (a) $T_x = 85^\circ\text{C}$ (b) $T_x = 70^\circ\text{C}$. ----- predicted for (110) adjacent re-entrant folding for 100% of DPE in the form of stems. No account is made for finite width of sheet, or intersheet interference (see text)

Table 1

Single crystals	$D(\text{\AA})$	$n_A(1/\text{\AA}^2)$
Calculated	1.57	0.35
$T_x = 70^\circ\text{C}$	2.2	0.29
$T_x = 85^\circ\text{C}$	1.9	0.18

The calculated values of n_A assume that all the deuterium in the blend is in the form of rows of stems of the same length. The folding has been assumed to be on (110) planes for this calculation. Other directions of folding [e.g. on the (100) plane] would give slightly different values. The measured results are obtained from the experimental curves in Figure 6, as discussed in the text

stems of a DPE molecule being restricted to the same (110) plane. Of such structures (Figures 1, 2a, 2c, and 2d) only those where the interstem spacing within the sheets is not too high, i.e. with few gaps of more than two stems in the folded sequence will still scatter as sheets in the observed range of s .

Table 1 shows predicted values for D and n_A for adjacent re-entrant folding, together with values derived from the linear portions of the experimental curves. (For $T_x = 70^\circ\text{C}$ there is an uncertainty introduced by the slight concavity of the measured curve; the tabulated D and n_A values refer to the slope at the highest values of s^2 , for which, unfortunately, the experimental uncertainties in I are greatest.) As discussed above, the dimension D (related to the slopes in Figure 6) agrees well with those predicted. For $T_x = 70^\circ\text{C}$, there is also good agreement for n_A , when it is borne in mind that any measured value of n_A should be about 20% lower than that shown for (110) folding in the Table, because of exclusion of DPE chains into a superficial amorphous layer, and because of variations in stem length⁸⁻¹⁰.

For $T_x = 85^\circ\text{C}$, the measured value of n_A is rather low on this basis. There are a number of reasons why this should be so, for example gaps in the rows of stems (Figure 2d). We suggest that a likely hypothesis for this discrepancy is partial segregation according to isotope or molecular weight at $T_x = 85^\circ\text{C}$. This is not unreasonable since $T_x = 85^\circ\text{C}$ represents a lower supercooling than $T_x = 70^\circ\text{C}$, and hence sensitivity to slight thermodynamic differences. This interpretation is consistent with measurements of overall PE/DPE contents¹¹. If there is partial segregation, no information is available as to the folding within the aggregates. A second explanation which cannot be excluded is less efficient dispersal in xylene prior to crystallization for this sample.

It remains to consider qualitatively the intensities at

low s when neither equations (1) nor (2) are likely to be valid. For $T_x = 85^\circ\text{C}$, the sample used for the data in Figures 4a and 6a had not been pressed. In addition its degree of orientation was such that a few lamellae were edge-on to the beam. Thus an artifactual signal from voids is to be expected (see above); the sharp increase of Is^2 with decreasing s at small s is therefore attributed to voids. By comparison, for $T_x = 70^\circ\text{C}$, for which the mats had been pressed, Figures 4b and 6b show a decrease in Is^2 at small s . The value of s at which the decrease commences (0.01\AA^{-1}) is fully consistent with the sheets containing the stems only being 100\AA wide⁷.

At $s \approx 0.02 \text{\AA}^{-1}$ there is, especially for $T_x = 70^\circ\text{C}$, still an increase of Is^2 above the asymptotic line (Figure 6). Some such departure could be expected for $1/s$ slightly smaller than l or l_1 (see above). Another, perhaps more likely, possibility is intersheet interference.

Experiments are continuing, employing both instruments, in order to test the generality of these results and to investigate to what extent alternative structural models can be eliminated.

CONCLUSIONS

The intensity of coherent neutron scattering from a blend of DPE in PE agrees with that expected for lamellae (equation (2) for $0.03 < s < 0.07 \text{\AA}^{-1}$). Table 1 shows, furthermore, that these lamellae have a thickness as predicted for rows of stems along (110) planes. The density of deuterium atoms in the lamellae is consistent with predominantly adjacent re-entrant folding along (110) in the case of crystals grown at high supercooling. At low supercooling there is a possibility of partial segregation of the deuterated chains in the hydrogenous matrix.

It seems that at low angles of diffraction there can be an artifactual signal originating from voids.

ACKNOWLEDGEMENTS

Thanks are due to Dr D. L. Worcester whose generous assistance made these experiments possible. Among those with whom we have had valuable discussions, we would like to thank in particular M. V. Luzzati, Professor G. Allen and Dr J. S. Higgins. Thanks are due to Dr C. G. Vonk for a listing of his deconvolution program. The work is supported by the Science Research Council.

REFERENCES

- 1 Bank, M. I. and Krimm, S. *J. Polym. Sci. (A-2)* 1969, 7, 1785
- 2 Schelten, J., Wignall, G. D. and Ballard, D. G. H. *Polymer* 1974, 15, 682
- 3 Blundell, D. J., Keller, A. and Kovacs, A. J. *J. Polym. Sci. (B)* 1966, 4, 481
- 4 Haywood, B. C. G. and Worcester, D. L. *J. Phys. (E)* 1973, 6, 568
- 5 Schmatz, W., Springer, T., Schelten, J. and Ibel, K. *J. Appl. Crystallog.* 1974, 7, 96
- 6 Vonk, C. G. *J. Appl. Crystallog.* 1971, 4, 340
- 7 Guinier, A. and Fournet, G. 'Small Angle Scattering of X-rays', Chapman and Hall, London, 1955
- 8 Sadler, D. M. and Keller, A. *Kolloid-Z. Z. Polym.* 1970, 242, 1081
- 9 Keller, A., Martuscelli, E., Priest, D. J. and Udagawa, Y. *J. Polym. Sci. (A-2)* 1971, 9, 1807
- 10 Hoffman, J. D., Lauritzen, J. I., Passaglia, E., Ross, C. S., Frohman, L. J. and Weeks, I. J. *Kolloid-Z. Z. Polym.* 1969, 231, 564
- 11 Stehling, F. C., Ergos, E. and Mandelkern, L. *Macromolecules* 1971, 4, 672

Pulsed n.m.r. of a SBS 'macroscopic single crystal'

G. E. Wardell

Physical Laboratory, University of Dublin, Trinity College, Dublin 2, Eire

and D. C. Douglass and V. J. McBrierty

Bell Laboratories, Murray Hill, New Jersey 07974, USA

(Received 2 September 1975)

Pulsed n.m.r. T_1 , T_2 and $T_{1\rho}$ results are reported for a macroscopic single crystal of styrene-butadiene-styrene copolymer, recorded as a function of the angle between the extrusion axis of the sample and the magnetic field direction. The data confirm the absence of molecular orientation in either component of the copolymer. T_1 and $T_{1\rho}$ results indicate a coupling via spin diffusion, between the polystyrene and polybutadiene regions. These spin diffusion effects are analysed in terms of a simple model, presented earlier, which demonstrates a stronger spin diffusion coupling in the rotating frame than in the laboratory frame.

INTRODUCTION

Styrene-butadiene-styrene (SBS) is a three block copolymer which may be extruded into a material of unique morphological character, in which the dispersed polystyrene (PS) component is in the form of cylinders, parallel to the extrusion axis, and arranged in a hexagonal array within a continuous polybutadiene (PB) matrix¹⁻³. This form of the copolymer is referred to as a macroscopic 'single crystal'¹. Although such systems are anisotropic in their optical and mechanical properties⁴ experimental observations so far indicate a random molecular orientation in both the PS and PB components⁵.

EXPERIMENTAL

In the work reported here, T_1 , T_2 and $T_{1\rho}$ relaxation times have been recorded over a wide temperature range for a SBS single crystal of the type described above. The sample, kindly provided by Professor A. Keller of the University of Bristol, was in the form of an extruded plug made from the copolymer Kraton 102 (Shell). The molecular weights of the PS and PB components were 10^4 and 5.5×10^4 , respectively⁶. The sample was annealed at $\pm 150^\circ\text{C}$ for 16 h in order to enhance the features of the macrolattice³. Measurements were carried out for orientation angles $\gamma = 0^\circ$, 54° and 90° between the extrusion direction (cylinder axis) and the direction of the applied magnetic field.

Data were recorded on a Bruker B-KR301 spectrometer operating at a resonant frequency of 20 MHz with a recovery time of about 9 μsec . A 90° pulse was of 2.5 μsec duration. The Bruker temperature control facility provided sample temperatures to an accuracy of $\pm 1^\circ\text{C}$. Rotating frame data were recorded at a r.f. field, H_1 , of 10 G. The details of data acquisition and analysis have been described previously^{7,8}.

RESULTS AND DISCUSSION

The single crystal results are presented in Figures 1 to 3 along with data on homopolymers of comparable molecular weights. Connor's rotating frame data ($H_1 = 10$ G) for PS,

of molecular weight 1.08×10^6 , have been used for comparison⁹.

It is immediately apparent from the data that there is no T_1 , T_2 or $T_{1\rho}$ dependence on the orientation angle γ . This result implies that there is no measurable molecular orientation, in a n.m.r. sense, in either region of the polymer, which is in agreement with earlier conclusions from infra-red measurements⁵.

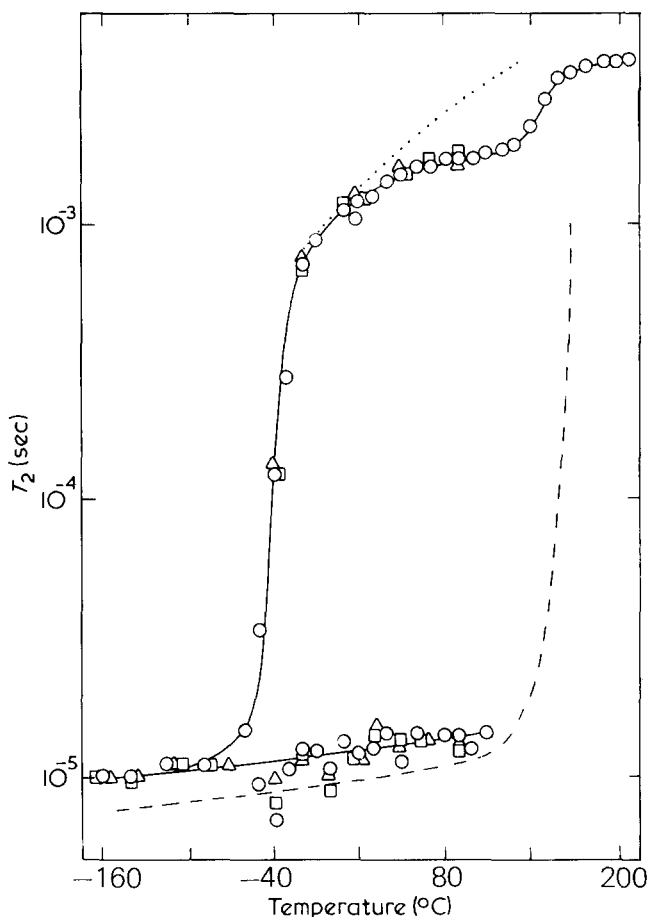


Figure 1 T_2 data for a SBS single crystal: \circ , $\gamma = 0^\circ$; \triangle , $\gamma = 54^\circ$; \square , $\gamma = 90^\circ$; -----, data for PS homopolymer; data for PB homopolymer

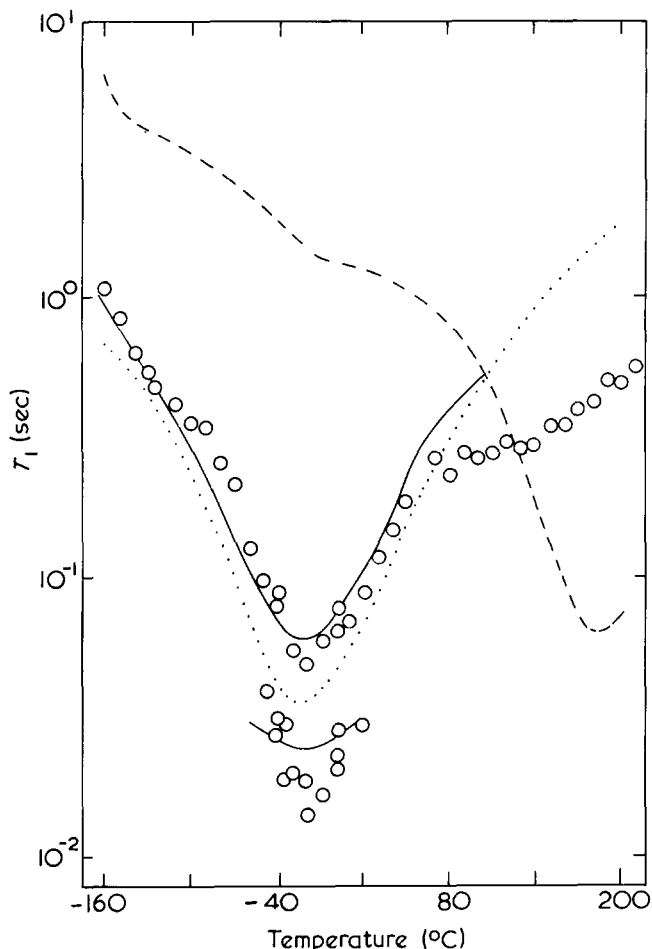


Figure 2 T_1 data for a SBS single crystal: -----, data for PS homopolymer;, data for PB homopolymer. ———, values predicted by the spin diffusion model (see text). Data points for orientations $\gamma = 54^\circ$ and 90° which are essentially the same as for $\gamma = 0^\circ$ have been omitted for clarity

The T_1 and T_2 results for the single crystal are similar to those for the comparable unextruded material⁸, at least up to 150°C , which is the upper limit of the earlier work. From this, it would appear that the molecular motions in this temperature region are insensitive to the *shape* of the PS domains in the copolymer. There are a number of additional features in the more comprehensive single crystal data, not included in the detailed treatment presented earlier, which require explanation.

The minimum in the short $T_{1\rho}$ component at -50°C is the $T_{1\rho}$ analogue for the T_1 minimum at -20°C and the sharp transition in the long T_2 component in the region of -40°C ; they are all manifestations of the PB first order transition⁸. The high temperature T_2 transition from 2 msec at $+140^\circ\text{C}$ to 3.6 msec at $+180^\circ\text{C}$ is associated with the PS glass transition. Furthermore, the constraints on the motion of the PB chains which are in force below the glass transition temperature T_g are removed⁸. This may be deduced from the magnitude of the plateau, which is greater than would be expected from the onset of the glass transition in PS, alone. There are indications of a correspondingly high temperature minimum in the short $T_{1\rho}$ component, although the exact location of the minimum is not possible. A short $T_{1\rho}$ component was just detectable in the temperature range -20°C to $+150^\circ\text{C}$ but the intensity was too small to permit a reasonable quantitative assessment of its magnitude. Above $+150^\circ\text{C}$ the intensity was of the order of 25%.

The variation in the component intensities indicates that it is most probable that there is coupling, via spin diffusion, between the PS and PB regions at these temperatures. A consequence of this would be a recorded $T_{1\rho}$ minimum for the glass transition process in PS which is greater in magnitude than the predicted value of 60 μsec in the absence of spin diffusion¹⁰.

The T_1 and $T_{1\rho}$ data indicate that spin diffusion is operative between the PS and PB components in the region of the minima associated with the first order transition in PB. This effect has been treated in detail in an earlier paper⁸, on the basis of a simple spin diffusion model in which a uniform spin temperature is assumed in each region of the copolymer and, in addition, the geometry of the interface is neglected. The strength of the coupling between the two regions is controlled by the parameter K , the only variable of the model. The solid lines in Figures 2 and 3 indicate the computed magnitudes of the T_1 and $T_{1\rho}$ components, respectively, which are seen to be in good agreement with the experimental results. The intensities of the long components in each case, which are also spin diffusion controlled, compare favourably with the measured values (see Figures 4 and 5). In order to achieve this fit, however, different values had to be assigned to the coupling parameter K for the T_1 and $T_{1\rho}$ data, respectively; for the T_1 data $K = 4.4$ as compared with the value of $K = 20$ for the $T_{1\rho}$ results.

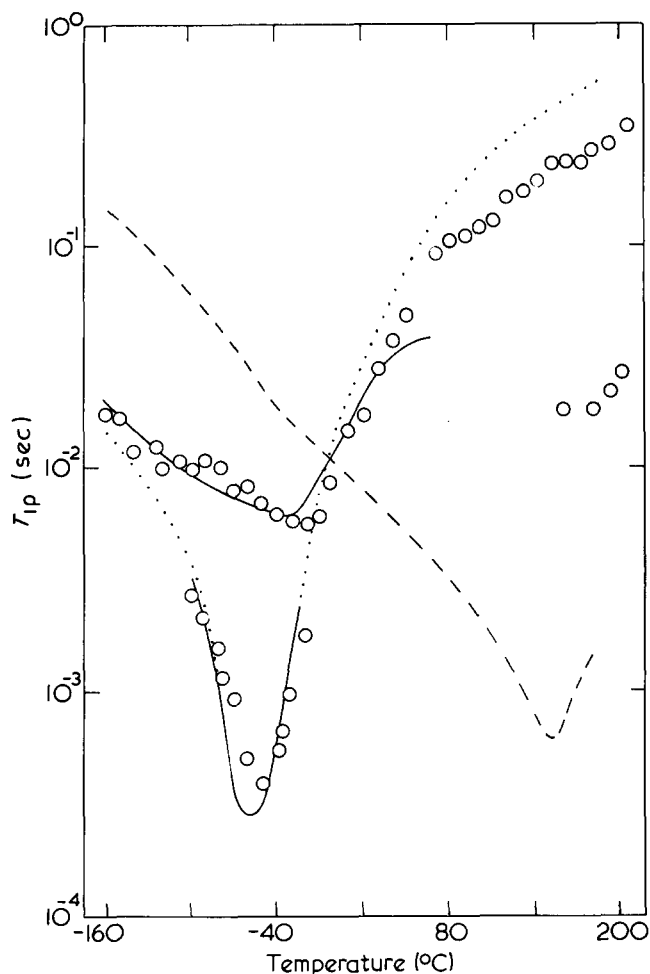


Figure 3 $T_{1\rho}$ data for a SBS single crystal: -----, data for PS homopolymer, (due to Connor⁹);, data for PB homopolymer. ———, Values predicted by the spin diffusion model (see text). Data points for orientations $\gamma = 54^\circ$ and 90° which are essentially the same as for $\gamma = 0^\circ$ have been omitted for clarity

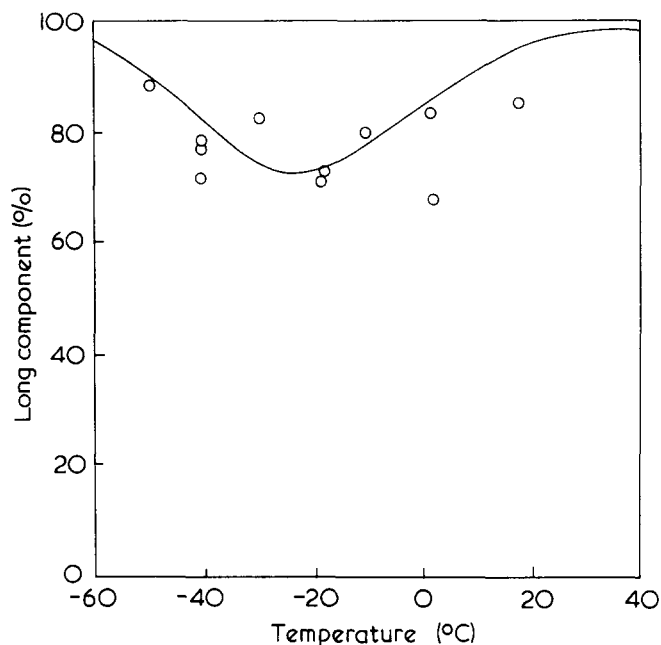


Figure 4 Intensity of the T_1 long component as a function of temperature. —, theoretical predictions from the spin diffusion model (see text)

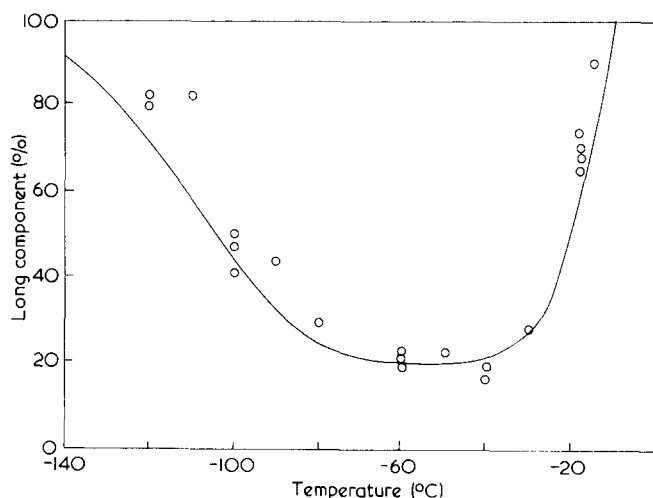


Figure 5 Intensity of the $T_{1\rho}$ long component as a function of temperature. —, theoretical predictions from the spin diffusion model (see text)

While this variation may derive from inadequacies of the model, there is also longstanding recognition that the spin diffusion coefficient can depend upon field strength for applied fields comparable to the dipolar fields¹¹⁻¹³. Since the coupling parameter is proportional to the spin diffusion coefficient, D this result implies an increased D in the rotating frame. Measurement of relaxation in normal alkanes indicates that D does indeed increase with decreasing field in the resonant rotating frame¹². This result is consistent with the intuitive notion that additional paths for spin exchange become energetically possible when the Zeeman and dipolar energies are comparable. However, no data on calculations directly applicable to comparison of spin diffusion in the rotating and laboratory frames seem to exist.

ACKNOWLEDGEMENTS

Mr S. Doherty provided valuable assistance throughout the course of the work. The research was supported in part by a grant from the National Science Council of Ireland.

REFERENCES

- 1 Keller, A., Pedemonte, E. and Willmouth, F. M. *Nature* 1970, **225**, 538
- 2 Keller, A., Pedemonte, E. and Willmouth, F. M. *Kolloid-Z.* 1970, **238**, 385
- 3 Dlugosz, J., Keller, A. and Pedemonte, E. *Kolloid-Z.* 1970, **242**, 1125
- 4 Folkes, M. J. and Keller, A. *Polymer* 1971, **12**, 222
- 5 Folkes, M. J., Keller, A. and Scalisi, F. P. *Polymer* 1971, **12**, 793
- 6 Biarchi, U., Pedemonte, E. and Turturro, A. *Polymer* 1970, **11**, 268
- 7 Wardell, G. E. and McBrierty, V. J. *Proc. R. Ir. Acad. (A)* 1973, **73**, 63
- 8 Wardell, G. E., McBrierty, V. J. and Douglass, D. C. *Am. J. Appl. Phys.* 1974, **45**, 3441
- 9 Connor, T. M. *J. Polym. Sci. (A-2)* 1970, **8**, 191
- 10 Douglass, D. C. and McBrierty, V. J. *J. Chem. Phys.* 1971, **54**, 4085
- 11 Solomon, I. and Ezratty, J. *Phys. Rev.* 1962, **127**, 78
- 12 Douglass, D. C. and Jones, G. P. *J. Chem. Phys.* 1966, **45**, 956
- 13 Redfield, A. G. and Yu, W. N. *Phys. Rev.* 1968, **169**, 443

Structural order in heat treated vinyl chloride polymers

A. Gray* and M. Gilbert

Institute of Polymer Technology, University of Technology, Loughborough, Leicestershire LE11 3TU, UK
(Received 3 June 1975; revised 16 July 1975)

Three vinyl chloride polymers were annealed at temperatures in the range 40–160°C for times varying from 0.5 to 5 h. Structural changes occurring in the polymers were examined by density measurement, differential thermal analysis and X-ray diffraction. It was shown that the three polymers varied in their original crystallinity. Attempts to totally remove this crystallinity, were unsuccessful; further crystallinity could be introduced by annealing above T_g . Changes induced by annealing below T_g were not due to crystallization. Methods used to measure crystallinity in poly(vinyl chloride) (PVC) were assessed.

INTRODUCTION

Several workers^{1–6} have investigated the morphological changes which can be induced by suitable heat treatment of poly(vinyl chloride) (PVC). Methods used for such investigations have included density measurements^{1–4}, X-ray diffraction⁴, infra-red spectroscopy⁵ and differential scanning calorimetry (d.s.c.)^{2–6}. Changes in various mechanical properties have also been reported^{1–3,7}. Phillips *et al.*¹ have attributed property changes caused by heat treatment near and above the glass transition temperature T_g to changes in free volume. Foltz and McKinney have interpreted their d.s.c. results in a similar manner. Again, most of their samples were given heat treatments at temperatures below T_g . Rybníkář⁴ and Witenhafer⁵ have heat treated at higher temperatures (up to 180°C in the latter case) and have attributed observed changes to crystallization. Rybníkář and Juijn *et al.*^{3,8} distinguish primary and secondary crystallization processes, the latter workers discussing the thermal analysis of PVC polymers in some detail. Illers² also used this technique extensively, and compared structural changes occurring under various conditions. He suggested that heat treatment above T_g caused crystallization, while heat treatment below T_g caused decrease in free volume. Crystallinity changes were shown to have a greater effect on density, solvent sorption and shear modulus than free volume changes.

The present work was carried out as part of a project investigating the relationships between thermal history, crystallinity and properties for PVC polymers containing different types and levels of additives in an attempt to find the effect of structural changes occurring in PVC during processing. Initially the effects of time and temperature of annealing on the crystallinity of three PVC polymers have been examined. The polymers selected are a commercial suspension PVC homopolymer, a copolymer in which crystallization would be expected to be hindered, and a polymer prepared at –30°C which has increased syndiotacticity, hence increased crystallinity⁹.

* Present address: BP Chemicals International Ltd, Sully, Penarth, Glamorgan, UK.

EXPERIMENTAL

Materials

Details of polymers used are given in *Table 1a*. Molecular weights were obtained by gel permeation chromatography (g.p.c.), at 25°C using tetrahydrofuran as solvent. The copolymer and PVC 2 homopolymer could be dissolved at room temperature. While the low temperature PVC apparently dissolved under these conditions, two peaks were observed in the g.p.c. trace. The high molecular weight peak was attributed to incomplete solution of PVC mole-

Table 1a Polymers examined

Polymer	Details	\bar{M}_n	\bar{M}_w	Diad concentration (%)		T_g (°C)
				Syndio-tactic	Iso-tactic	
PVC 2	BP suspension polymer supplied by RAPRA PSCC	23 300	59 200	58	42	82
Breon AS 60/41	BP suspension copolymer containing 15% vinyl acetate	34 800	77 020	49.5	50.5	75
–30°C polymerized	Montecatini Edison homopolymer	43 600	88 800	66.5	33.5	91

Table 1b Conditions of sample preparation

Polymer	Milling temperature (°C)	Moulding temperature (°C)	Moulding time (min)	Pre-treatment temperature (°C)
PVC 2	160	180	3	200
PVC/PVAC copolymer	140	140	3	175
low temp. polymerized PVC	170	200	3	220

cules. After heating the polymer at 90°C for 5 days in a sealed tube the size of this peak became insignificant and the resulting trace was used to obtain the molecular weights quoted for this polymer.

To obtain a measure of syndiotacticity, the diad concentrations shown were calculated from spin decoupled ¹³C n.m.r. spectra using the method described by Carman *et al.*¹⁰. The figure for the copolymer is an approximate one since some peak overlap occurred; however, it suggests that the copolymer is virtually atactic.

Glass transition temperatures were obtained by thermo-mechanical analysis as described below.

Sample preparation

Four parts per hundred (w/w) of dibasic lead stearate were added to each polymer as stabilizer and lubricant. Each compound was dry blended, milled, then compression moulded to form sheets 0.5 mm thick. Details of milling and moulding conditions are shown in columns 2–4 of *Table 1b*. The moulded samples were cooled under pressure to room temperature.

Temperatures were selected to be high enough to achieve fusion of PVC particles. Scanning electron micrographs obtained by Pezzin *et al.*⁷ for PVC polymers milled at various temperatures suggest that temperatures used should give adequate fusion. An acetone immersion test indicated that samples were homogeneous. If fusion is inadequate, individual PVC particles are observed and fragmentation of the sample occurs on swelling in acetone.

Heat treatment

In an attempt to destroy existing crystallinity, and to ensure a uniform thermal history, all samples were subjected to a 3 min pre-treatment under nitrogen, prior to crystallization. Pre-treatment temperatures are shown in column 5 of *Table 1b*. These temperatures were the highest that could be used without degradation occurring. Samples were quenched in an ice/water mixture, then immediately subjected to annealing or stored at about –50°C until the annealing treatment was carried out. Density and d.t.a. measurements on the stored samples indicated that no detectable changes occurred during this period.

Subsequently samples of all three polymers wrapped in aluminium foil were packed in a glass tube which was suspended in a thermostated bath controlled to ±0.15°C. Annealing treatments (under nitrogen) varied from 0.5 to 5.0 h at temperatures of 40°–160°C. Some samples were stored at room temperature for longer periods of time.

Differential thermal analysis (d.t.a.)

Thermograms were recorded using a Du Pont 900 Thermal Analyser fitted with a d.s.c. cell. Samples of 10 ± 1 mg were heated at 30°C/min from –40°C. In order to convert peak areas into energy units the instrument was calibrated using indium (melting temperature 157°C, heat of fusion 28.4 J/g). The reproducibility of the method was estimated by obtaining results for ten similar samples. The standard deviation on the mean was found to be 5%.

Glass transition temperatures of the quenched polymers were measured using the thermal analyser fitted with a thermomechanical analyser (t.m.a.) attachment. The penetration probe used was loaded with a weight of 10 g and the t.m.a. trace was recorded from –50°C, using a heating rate of 5°C/min. The temperature at which the probe first star-

ted to penetrate into the polymer was taken to be the glass transition temperature, T_g .

Density measurement

Sample densities were measured at 23°C using a Davenport density gradient column filled with an aqueous solution of calcium nitrate. Each measurement was made by averaging results from four samples. In order to find the density of the PVC in the samples, measured values were corrected to allow for the 4 pph of dibasic lead stearate (density 2000 kg/m³) present.

Crystallinity X_d of the PVC was calculated from the equation

$$X_d = \frac{\rho_c}{\rho} \frac{\rho - \rho_a}{\rho_c - \rho_a} \times 100\%$$

where ρ_c is density of totally crystalline polymer = 1530 kg/m³¹¹, ρ_a is density of totally amorphous polymer = 1373 kg/m³¹², and ρ is the density of the PVC in the samples. Although values of X_d have been calculated for polymers annealed at 40°C (*Table 5*) it is considered that the true crystallinities of these polymers are equal to the crystallinities of quenched samples (see Discussion).

X-ray diffraction

X-ray diffractometer traces were obtained from compression moulded sheets of the polymers using Ni filtered CuK α radiation (40 kV, 20 mA). Order factors were calculated as described by Rayner and Small¹³. To obtain diffractometer traces for amorphous PVC, templates were prepared from the graphs in ref. 12 using a horizontal scale corresponding to that of the experimental traces. Each trace was then analysed by fitting the appropriate template which touched the experimental curve as shown in *Figure 5b*.

$$\text{Then, order factor} = \frac{A_x}{A_x + A_a} \times 100\%$$

No corrections were made for the variation of scattering intensity with θ .

RESULTS

Differential thermal analysis

A typical series of thermograms for the commercial homopolymer (PVC 2), annealed for 5 h is shown in *Figure 1*. The thermogram of a quenched sample (i.e. one heated at 200°C for 3 min and quenched in ice–water) is shown in *Figure 1(A)*, and is similar to that reported by Illers² for samples subjected to similar treatments. A baseline shift due to the glass transition at about 84°C is followed by an exotherm peaking at approximately 107°C which has been attributed to crystallization². A broad melting endotherm is observed in the 120°–200°C range. For a quenched sample of the low temperature polymerized PVC the trace is similar but the exothermic peak is smaller and the melting endotherm extends to 220°C. In both cases the three transitions merge into one another.

It can be noted that owing to the relatively high heating rates used for these measurements, the glass transition temperatures are higher than those obtained from the t.m.a. experiments.

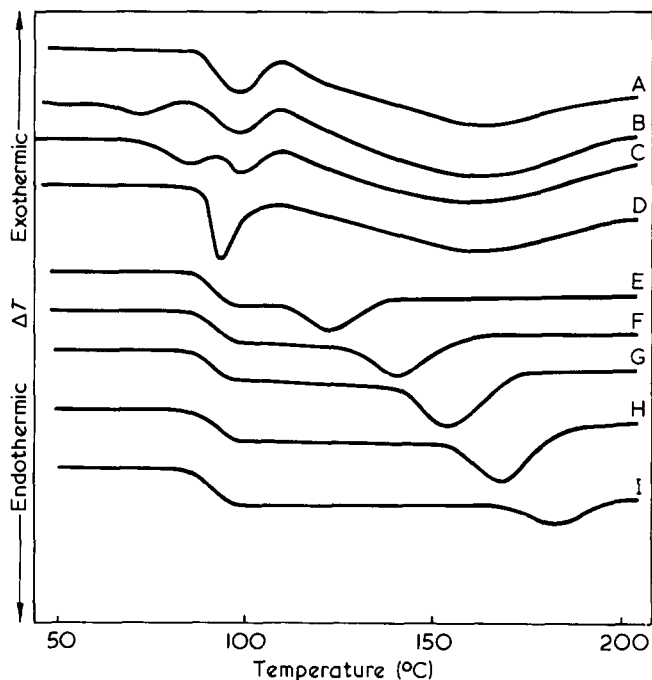


Figure 1 Thermograms for PVC 2: A, quenched, and annealed for 5 h at B, 40°; C, 55°; D, 70°; E, 100°; F, 115°; G, 130°; H, 145°; I, 160°C

Table 2 Effect of annealing on d.t.a. peak temperature (°C) for PVC-2

Annealing time (h)	Annealing temperature (°C)							
	40	55	70	100	115	130	145	160
0.5	—	—	—	121	134	148	162	176
1.0	—	—	—	121	135	148	163	177
1.5	—	—	—	122	137	150	164	179
3.0	—	—	—	123	138	151	164	180
5.0	72	83	94	125	139	152	166	180

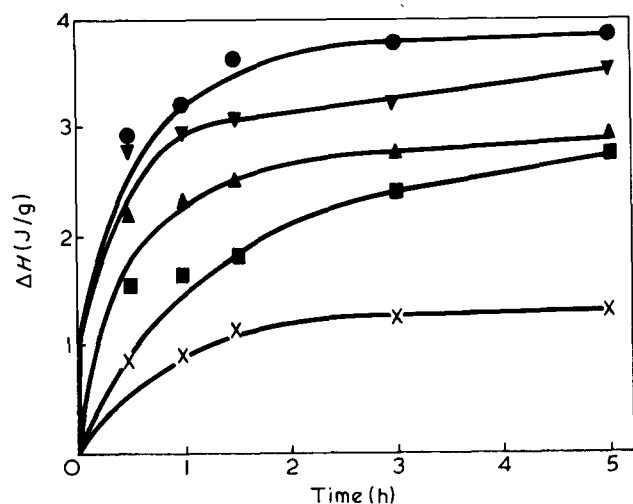


Figure 2 Enthalpy changes of low temperature polymerized PVC as a function of annealing time. Annealing temperatures: X, 100°, ■, 115°; ▲, 130°; ●, 145°; ▼, 160°C

Sharper endotherms are observed in thermograms of the annealed polymers, the peak temperature occurring at approximately 20°C above the annealing temperature in each case. Peak temperatures for PVC 2 are listed in Table 2. It is apparent that the peak temperature is also influenced

to some extent by annealing time. Results for the low temperature polymerized PVC were very similar, peak temperatures being 1°–2°C lower at the lower annealing temperatures, and 1°–2°C higher at the higher annealing temperatures.

For samples annealed at 100°C and above (i.e. above the glass transition temperature) the main features of the thermograms are the baseline shift due to the glass transition and the endotherm described above. No exothermic peak is observed. For samples annealed in the 40°–70°C region or stored at room temperature, the exothermic peak present in the quenched samples is still present [e.g. Figure 1(B)]. For the samples annealed at 55°C and 70°C the endothermic peak and glass transition occur very close together so that it is difficult to make any accurate measurements of area or temperature [Figure 1(C and D)]. In these cases peak areas were estimated by superimposing d.t.a. traces for quenched samples on those for the annealed samples.

Endotherms increase in area as annealing time is increased. In Figure 2 enthalpy changes are plotted as a function of time for the low temperature polymerized PVC. The corresponding plot for PVC 2 is similar except that the highest enthalpy changes are observed after heat treatment at 130°C.

The relationship between enthalpy change and temperature is shown in Figure 3 for PVC 2, and in Figure 4 for the low temperature polymerized PVC. Results for samples

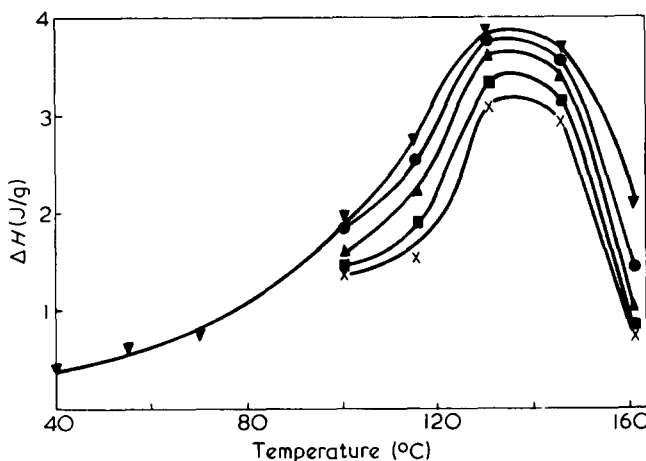


Figure 3 Enthalpy changes of PVC 2 as a function of annealing temperature. Annealing times: X, 0.5; ■, 1.0; ▲, 1.5; ●, 3.0; ▼, 5.0 h

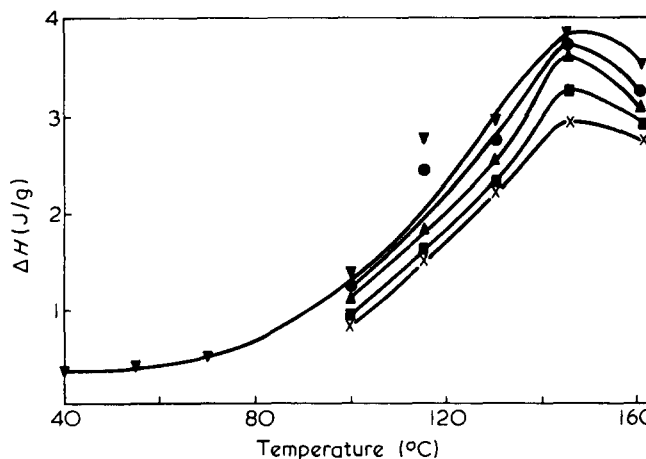


Figure 4 Enthalpy changes of low temperature polymerized PVC as a function of annealing temperature. Annealing times: X, 0.5, ■, 1.0; ▲, 1.5; ●, 3.0; ▼, 5.0 h

Table 3 Enthalpy changes and d.t.a. peak temperatures for quenched samples stored at room temperature

Polymer	Storage time (days)	ΔH (J/g)	Peak temperature ($^{\circ}\text{C}$)
PVC 2	81	0.766	69
low temperature 77 polymerized PVC		0.576	69

Table 4 Enthalpy changes and d.t.a. peak temperatures for PVC/PVAC copolymer annealed for 5 h at temperatures shown

Annealing temperature ($^{\circ}\text{C}$)	ΔH (J/g)	Peak temperature ($^{\circ}\text{C}$)
110	1.104	126
115	1.021	142
130	1.058	152

Table 5 Effect of annealing on crystallinity X_d (%) for PVC homopolymers

Annealing time (h)	Polymer	Annealing temperature ($^{\circ}\text{C}$)					
		100	115	130	145	160	40
0.5	PVC 2	16.88	17.16	17.02	14.79	13.88	(12.48)
1.0	PVC 2	17.58	16.95	17.16	15.07	13.88	
1.5	PVC 2	17.72	17.65	17.37	15.15	13.67	
3.0	PVC 2	17.79	17.63	17.23	15.35	13.74	(12.90)
5.0	PVC 2	18.07	17.51	17.37	15.70	13.54	(13.11)
0.5	low temp. polymerized PVC	19.80	20.63	21.25	21.11	19.80	(16.88)
1.0	low temp. polymerized PVC	19.94	20.84	20.84	21.04	20.08	
1.5	low temp. polymerized PVC	20.22	21.05	21.18	21.60	20.02	
3.0	low temp. polymerized PVC	20.63	21.18	21.32	21.25	18.90	(17.23)
5.0	low temp. polymerized PVC	20.84	21.25	21.11	21.39	20.35	(17.37)

stored at room temperature for longer periods of time are shown in *Table 3*.

Although endotherms were observed in thermograms of the PVC/PVAC copolymer after annealing, these were very much smaller than those observed for the other two polymers. It was not possible to anneal above 130°C as at higher temperatures acetic acid is released from the vinyl acetate units present. This volatilizes, causing voids in the sample. Results obtained for the copolymer annealed for 5 h at temperatures shown are listed in *Table 4*; again, peak temperatures are similar to those observed for the other two polymers.

Density results

The calculated crystallinities (X_d) for the two polymers are shown in *Table 5*. The time and temperature dependence of the density changes is similar to that of the enthalpy changes although the densities of samples annealed at 160°C are lower than would be expected from the observed enthalpy changes. Also, density results for PVC 2 showed a considerable scatter although four measurements were averaged to obtain each result. The lower reliability of the density measurements is thought to be partly due to the very small density changes being measured. A minor amount of degradation could have a significant effect on density measurements, but less effect on the order measured by thermal analysis. Since the density measurements for the low temperature polymerized PVC showed less scatter than those for PVC 2, the former polymer appears more thermally stable under the conditions used.

X-ray diffraction

Order factors calculated by the method described are shown in *Table 6*. As expected, the low temperature poly-

Table 6 Effect of annealing on order factor for vinyl chloride polymers

Annealing temperature ($^{\circ}\text{C}$)	PVC 2 annealed 0.5 h	PVC 2 annealed 5 h	low temp PVC annealed 0.5 h	low temp PVC annealed 5 h	PVAC annealed 5 h
40	8.5	8.4	20.7	19.5	
55	9.3	9.8	23.7	15.0	
70	7.8	7.8	19.6	21.2	
100	15.0	14.4	23.2	25.2	
115	16.8	11.9	23.7	24.6	2.0
130	14.4	14.6	26.9	20.8	
145	14.1	14.3	23.7	24.0	
160	11.6	11.9	27.5	23.1	

merized PVC is the most crystalline of the three polymers, while the copolymer is the least crystalline. For PVC 2 the order factor for a quenched sample (i.e. before annealing) was found to be 8.7. Heat treatment in the 40° – 70°C range did not appear to alter crystallinity significantly, while heat treatment above 70°C increased crystallinity by a factor of approximately 1.6. Diffractometer traces for samples of PVC 2 annealed for 5 h at 100°C and 40°C are shown in *Figure 5(B and C)*. No significant differences in order factor were observed when annealing time was increased from 0.5 to 5 h, nor at different temperatures in the 100° – 160°C range. For a quenched sample of the low temperature polymerized PVC the order factor was 20.1. Annealing at 100°C and above increased the figure by a factor of approximately 1.2, but results were rather erratic particularly after annealing for 5 h. A diffractometer trace for this polymer annealed for 5 h at 100°C is shown in *Figure 5(A)*. Diffraction maxima assignments are those reported by Garbuglio *et al.*¹⁴

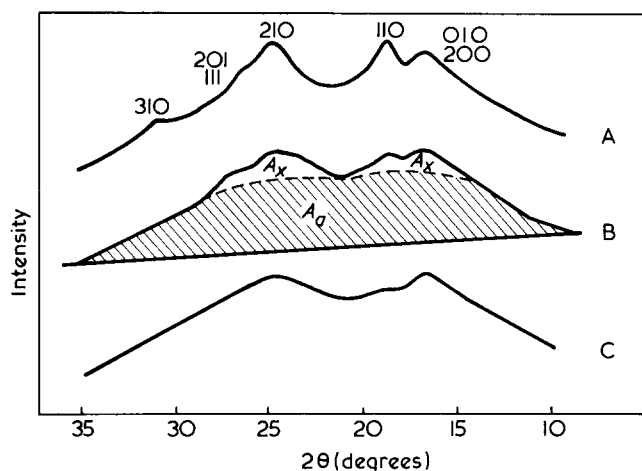


Figure 5 X-ray diffraction patterns for polymers annealed 5 h: (A) low temperature polymerized PVC at 100°C; (B) PVC2 at 100°C; (C) PVC 2 at 40°C

DISCUSSION

Effect of pre-treatment and quenching

A pre-treatment and quenching procedure was used prior to annealing in an attempt to destroy existing order in the polymers. However, it is apparent from subsequent investigations either that this did not occur or that crystallinity was re-introduced on cooling. Corrected densities for quenched samples of PVC 2 and low temperature polymerized PVC were 1389 kg/m³ and 1396 kg/m³, corresponding to calculated crystallinities of 11.35 and 16.26% respectively. X-ray measurements confirmed this conclusion, order factors of 8.7 and 20.1% being obtained in the two cases. Both methods show that the crystallinity remaining in the low temperature PVC is greater.

D.t.a. traces of the quenched polymers can also be explained by this residual crystallinity. The exotherm observed in heating quenched samples is considered to be due to rapid crystallization which occurs when the polymers are heated above T_g ². Approximate areas were obtained for this exotherm and the broad melting endotherm. It was shown that the exotherm was equivalent to 40% of the endotherm for PVC 2 and 15% for the low temperature polymerized PVC.

The smaller value obtained in the latter case is consistent with the relatively high level of crystallinity already present in this material, which limits the amount of material available for further rapid crystallization on heating. The broad melting endotherm observed for both polymers will be due to melting of crystallites introduced during heating, together with those which remain in the sample after pre-treatment and quenching. It would seem likely that residual crystallites will melt at the higher end of the melting range. This range extends to higher temperatures for the low temperature polymerized PVC than for PVC 2.

Effect of annealing below T_g

As reported previously, annealing, or storage below T_g was found to increase the density of samples and also give rise to additional endothermic peaks below or at T_g in the d.t.a. traces. The conditions under which such peaks are obtained have been discussed in considerable detail². Both

sample density and endothermic peak area increase with time and temperature of annealing. Crystallization would not be expected to occur below T_g and this was confirmed by X-ray measurements, no significant changes in order factor being observed for the samples annealed below T_g . Thus the densifying process which occurs does not give rise to three-dimensional order and has been attributed to change in free volume^{1,2,6}. It is of interest that larger enthalpy changes and density increases are observed for PVC 2 than for the low temperature polymerized PVC during annealing or storage below T_g . It seems reasonable to assume that free volume changes occur in amorphous regions, so are observed to a lesser degree in the higher crystallinity polymer.

Effect of annealing above T_g

X-ray results showed that annealing PVC 2 and the low temperature polymerized PVC above T_g caused an increase in crystallinity as shown by order factor (Table 6 and Figure 5). A small amount of crystallinity was present in the copolymer after annealing for 5 h. This was confirmed by d.t.a. results (Table 4).

The accuracy of the X-ray results is at present insufficient to investigate time and temperature dependence of crystallinity in detail, owing to the problem of resolving crystalline and amorphous areas, although the 210 diffraction maximum appeared to increase in height with time of annealing, particularly for the low temperature polymerized PVC. Additional information can be obtained from density measurements and d.t.a. The endotherms observed in d.t.a. traces of annealed samples are considered to be due to the formation of crystallites which melt about 20°C above the annealing temperature. Enthalpy changes corresponding to the fusion of these crystallites are found to pass through a maximum with respect to temperature (Figures 3 and 4) suggesting that crystallization rate passes through a maximum between T_g and the melting temperature T_m in a manner typical of most crystallizing polymers. Density measurements for the low temperature polymerized PVC show a similar trend, but the scattered points observed for PVC 2 did raise the question of degradation, particularly for the samples annealed at 145°C and above for longer periods of time. No voids were detectable by visual or microscopic examination of any of the samples. PVC 2 samples were yellow in colour suggesting that very little degradation had occurred, although low temperature polymerized PVC samples were reddish-brown. As points in Figures 3 and 4 are on reasonably smooth curves it is felt that results are not significantly affected by degradation.

The higher temperature maximum observed for the low temperature polymerized PVC is not unexpected since T_g is higher for this polymer, and T_m is expected to be higher owing to the higher proportion of syndiotacticity. The maximum increase in crystallinity is similar for the two polymers.

Enthalpy changes and density measurements demonstrate an increase of crystallinity with annealing time (e.g. Figure 2). Results show that the increase in crystallinity on annealing occurs fairly rapidly. Even at 100°C half the crystallization has occurred within less than 0.5 h. Further investigation of much shorter annealing times is necessary since it appears that changes will occur in the PVC structure during processing. The exotherm obtained in d.t.a. traces of quenched samples also indicates the rapidity of the crystallization process.

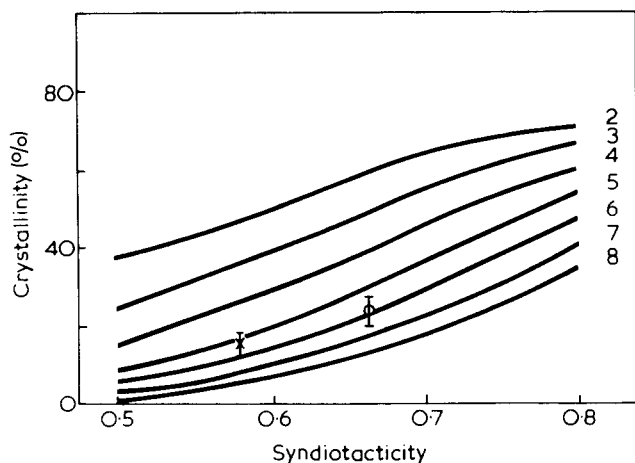


Figure 6 Calculated crystallinity as a function of syndiotacticity for values of ξ_{\min} from 2 to 8. Experimentally determined range of crystallinity from density measurements and X-ray order factors for PVC 2 (X) and low temperature polymerized PVC (O)

Comparison of ordering processes above and below T_g

Density measurements and differential thermal analysis do not show conclusively that different processes are occurring when vinyl chloride polymers are annealed above and below T_g . However, X-ray diffraction shows that crystallization is occurring above T_g while annealing below T_g produces no additional three-dimensional order.

Solvent sorption measurements, reported elsewhere¹⁵, also serve to distinguish between annealing above and below T_g for PVC 2, but show no structural differences for the PVC/PVAC copolymer after quenching, annealing below T_g or annealing above T_g .

Relationship between % crystallinity and syndiotacticity

It is of interest to compare maximum crystallinities obtained for the polymers with the amount of crystallizable material available. Using the relationship of Fordham¹⁶, it is possible to calculate the fraction of the total polymer in syndiotactic sequences from the tacticity.

$$F_{\text{SYNDIO}}^N = N(1 - \alpha)^2 \alpha^N$$

where N is the number of repeat units in a syndiotactic sequence, α is the degree of syndiotacticity.

If PVC is considered as a copolymer in which only the syndiotactic portion is crystallizable Flory's theory of crystallization of copolymers¹⁷ can be applied. This states that on thermodynamic grounds, the crystallites should have a minimum length. Then the parts of the polymer chain which contribute to the crystallite should also have a minimum sequence length, ξ_{\min} .

Using the distribution of syndiotactic sequences obtained from Fordham's relationship it is possible to calculate the degree of crystallinity obtainable, with ξ_{\min} as a variable, by the summation of F_{SYNDIO}^N for $N = 1-20$ (larger N values are neglected as their contribution to the degree of crystallinity becomes very small).

In Figure 6 the calculated crystallinity is plotted against syndiotacticity. Experimental values of crystallinity obtained by the density method, and X-ray order factor are plotted on this graph. These values are consistent with a minimum number of sequences necessary for crystallization of 5-6,

in agreement with Lebedev *et al.*¹⁸ and Talamini and Vidotto¹⁹. However, Kockott²⁰ found a value of 12 for ξ_{\min} , which, according to Lebedev *et al.* is due to the former's low estimation of the degree of crystallinity, for example, a value of zero is quoted for a commercial PVC.

Juijn *et al.*⁸, using values of $\alpha = 0.55$ and $\xi_{\min} = 12$ for commercial PVC obtained a low crystallinity figure of 0.45%. They explained this result by showing how the isotactic portion of the chain could also be incorporated into the crystal lattice. The value of 12 for ξ_{\min} was used as it was 'in agreement with values for other polymers'. However, other evidence suggests that crystallites in PVC are likely to be smaller than those in other crystalline polymers, so that a lower value of ξ_{\min} does not seem unreasonable. The broad d.t.a. melting endotherm indicates that a wide range of crystallite size and/or perfection exists. X-ray diffraction peaks are also broad and ill-defined, and an estimation of crystallite size from diffraction peak width gives a mean value of only about 5.0 nm.

Measurement of crystallinity in PVC

Owing to the low levels of crystallinity in PVC all methods of measurement provide problems.

Thermal analysis is a sensitive method which permits accurate measurement of crystallinity developed in PVC under carefully controlled conditions, so it is a particularly good technique for following small changes in crystallinity. However, it cannot be used to measure total crystallinity in polymers which have not been subjected to a special treatment, since the broad, shallow endotherm produced in these cases cannot be measured accurately.

Density measurements provide some information, but density changes can result from various causes, so the method is unselective. Its accuracy is limited for following the very small changes caused by special treatment of the polymers, and it appears susceptible to minor amounts of degradation.

X-ray diffraction is the only technique used which shows conclusively whether or not crystallinity is present. However, the technique used in this work was not sufficiently accurate to follow changes with time or temperature. There is some scope for improvement here, for example, the step scanning and data averaging techniques discussed by Brunner²¹.

In many respects techniques used are complementary and it is of value to use more than one technique to solve a particular problem.

ACKNOWLEDGEMENTS

We are grateful to the Science Research Council for the award of a Research Studentship to A.G.

Thanks are also due to Mr M. Cudby of ICI Plastics Division who made n.m.r. measurements on the polymers and Mr J. Maisey of the Polymer Supply and Characterization Centre, Rubber and Plastics Research Association for molecular weight determinations.

REFERENCES

- Phillips, R., Cox, R. L. and Heiberger, C. A. *26th SPE ANTEC Meeting New York*, 1968
- Illers, K. H. *Makromol. Chem.* 1969, 127, 1

Structural order in heat treated vinyl chloride polymers: A. Gray and M. Gilbert

- 3 Juijn, J. A., Gisolf, J. H. and de Jong, W. A. *Kolloid-Z. Z. Polym.* 1969, **235**, 1157
- 4 Rybníkář, F. *Makromol. Chem.* 1971, **140**, 91
- 5 Witenhafer, D. E. *J. Macromol. Sci. (B)* 1970, **4**, 915
- 6 Foltz, C. R. and KcKinney, P. V. *J. Appl. Polym. Sci.* 1969, **13**, 2235
- 7 Pezzin, G., Ajroldi, G., Casiraghi, T. and Garbuglio, C. *J. Appl. Polym. Sci.* 1972, **16**, 1839
- 8 Juijn, J. A., Gisolf, J. H. and de Jong, W. A. *Kolloid-Z. Z. Polym.* 1973, **251**, 456
- 9 Pezzin, G. *Plast. Polym.* 1969, **37**, 275
- 10 Carman, C. J., Tarpley, A. R. and Goldstein, J. H. *Macromolecules* 1971, **4**, 445
- 11 Wilkes, C. E., Folt, V. L. and Krimm, S. *Macromolecules* 1973, **6**, 235
- 12 Glazkovskii, Y. V., Zav'yalov, A. N., Bakardzhiyev, N. M. and Novak, I. I. *Polym. Sci. USSR* 1970, **12**, 3061
- 13 Rayner, L. S. and Small, P. A. Br. Pat. 847 676
- 14 Garbuglio, C., Rodella, A., Borsini, G. C. and Gallinella, E. *Chim. Ind. (Milan)* 1964, **46**, 166
- 15 Gray, A. and Gilbert, M. *Polymer* 1975, **16**, 387
- 16 Fordham, J. W. L. *J. Polym. Sci.* 1959, **39**, 321
- 17 Flory, P. J. *Trans. Faraday Soc.* 1955, **51**, 848
- 18 Lebedev, V. P., Tsvankin, D. Ya. and Glazkovskii, Ya. V. *Polym. Sci. USSR* 1972, **14**, 123
- 19 Talamini, G. and Vidotto, G. *Makromol. Chem.* 1967, **100**, 48
- 20 Kockott, D. *Kolloid-Z. Z. Polym.* 1964, **198**, 17
- 21 Brunner, A. J. *J. Polym. Sci. (Polym. Lett. Edn)* 1972, **10**, 379

Effect of molecular weight on the thermal properties of polycarbonates

G. A. Adam, J. N. Hay, I. W. Parsons and R. N. Haward

Department of Chemistry, University of Birmingham, PO Box 363, Birmingham B15 2TT, UK
(Received 26 August 1975)

The relationships between the molecular weight and several thermal properties of 2,2-bis(4-hydroxyphenyl)propane polycarbonate are reported. It is shown that the amount of thermal degradation, measured thermogravimetrically, increases with decrease in molecular weight and is affected by the nature of the end groups present. The heat of fusion at the crystalline melting point has been measured by differential scanning calorimetry and correlated with density and X-ray diffraction estimates of total crystallinity. The heats of melting obtained were 30.4 cal/g and 32.9 cal/g respectively. The effect of molecular weight on specific heat, annealing peaks and glass transition temperature are also reported.

INTRODUCTION

During an earlier programme of research we synthesized a number of polycarbonates from 2,2-bis(4-hydroxyphenyl)propane and compared their properties with commercial materials and with new synthetic copolymers¹. The copolymers made under varying experimental conditions had different molecular weights and it was necessary (for comparison purposes) to make polymers with similar molecular weights. In the course of this programme we observed a number of previously unreported correlations between molecular weight and physical properties.

In this paper results are presented which illustrate both the effects of molecular weight on thermal properties and also the quite significant differences which exist between currently marketed commercial materials and those which may be synthesized by conventional methods^(2,3). Among the subjects studied were: the formation of volatiles by heating at high temperatures, the glass transition temperatures, specific heats, heats of crystallization and annealing peaks as measured by differential scanning calorimetry (d.s.c.). Details of the methods used are given in the experimental section.

EXPERIMENTAL

Polymer preparation

Experimental samples of poly[2,2-propane-bis(4-phenyl carbonate)] used in this study was either prepared by interfacial polycondensation or in a homogeneous (pyridine/methylene chloride) system¹⁻³. Where polymers of different molecular weight were synthesized this was generally achieved by varying the reactant molar ratio but in some cases *p*-cresol was used as a chain terminating reagent. Other samples were obtained from commercial sources.

The polymers used are listed in Table 1.

Acetylation

Polycarbonates, whose molecular weights had been controlled by varying the reactants' ratio, were treated with excess of acetyl chloride in the presence of pyridine and methylene chloride. The latter was used as a solvent for the polymer.

Thermal analyses

Thermogravimetric analysis was carried out on a Perkin-Elmer thermobalance TGS-1 using nitrogen as the carrier gas, and d.s.c. on the Perkin-Elmer DSC.2. Zone refined stearic acid and purified metals (indium, tin, zinc and lead) were used as thermal standards. Heating rate and sample size effects were apparent in measuring T_g but extrapolation to zero weight at constant rate and to zero heating rate at constant weight gave similar values for T_g (± 0.5 K). In specific heat measurements a sample weight of 30 mg was used over a temperature range 350–470 K.

Table 1 Polymer characterization

A. Experimental polymers

Sample No.	$\bar{M}_v \times 10^{-3}$	$\bar{M}_n \times 10^{-3}$
1 (P)	2.5	—
2	6.0	2.45
3 (P)	6.3	2.40
4	12.5	4.87
5	16.0	6.00
6 (P)	25.7	10.3
7	25.5	12.5
8	40.0	16.7
9	56.9	22.7
10	62.2	25.9
11 (P)	70.0	30
12	76	32
13	80	33

B. Commercial*

Commercial grade	Source	$\bar{M}_v \times 10^{-3}$	$\bar{M}_n \times 10^{-3}$
M39	Mobay (Merlon)	25.5	12.0
M40	Mobay (Merlon)	31.0	14.5
M50	Mobay (Merlon)	35.0	16.5
M60	Mobay (Merlon)	41.5	19.5
5730 ^a	Bayer (Makrolon)	71.0	37.0
5705	Bayer (Makrolon)	78.0	34.0
Makrofol-E	Bayer (Makrolon)	20.8	—

P = Molecular weight was controlled by using *p*-cresol

* Data as supplied by the manufacturers except ^a

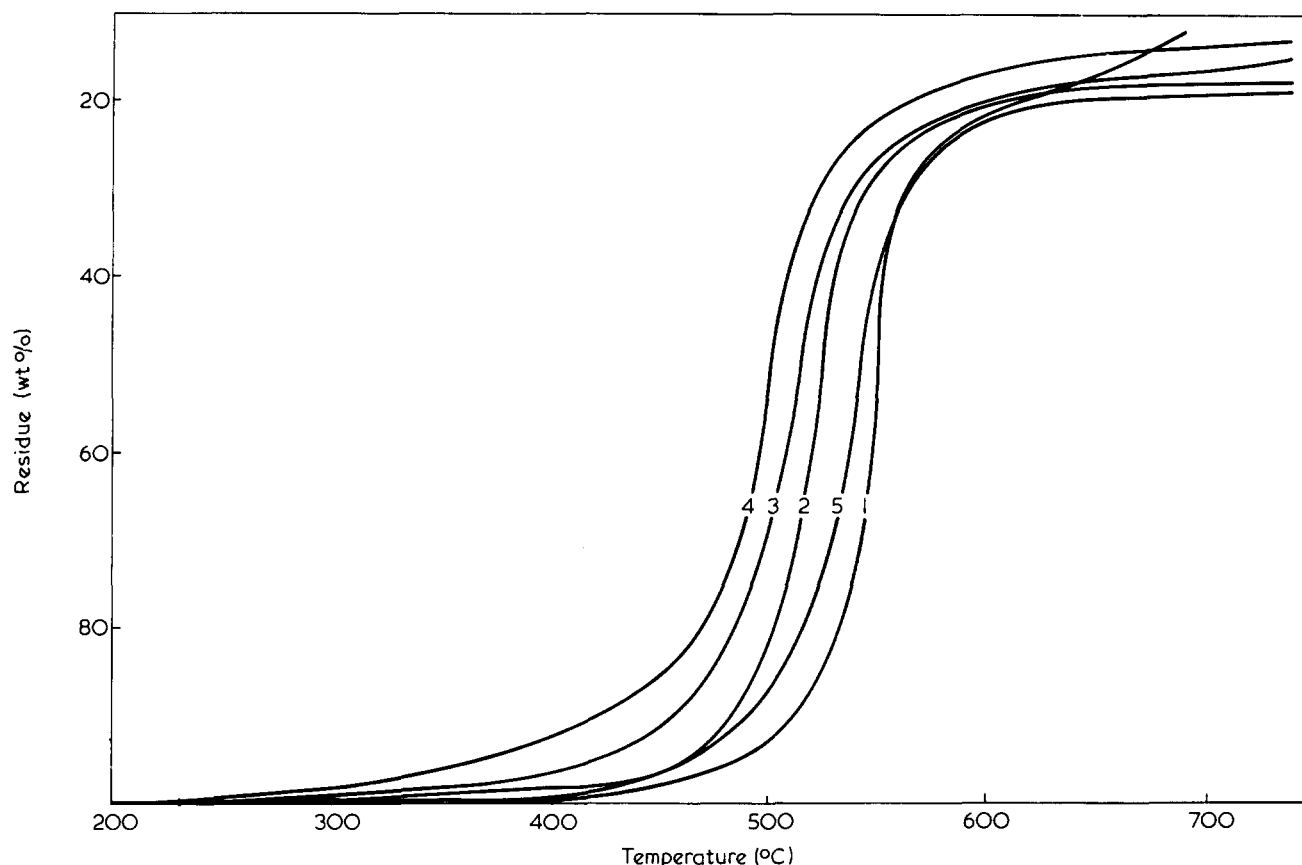


Figure 1 Weight loss by thermal decomposition of different polycarbonates heated at increasing temperatures: 1, commercial material, $\bar{M}_v = 71\ 000$; 2, experimental polycarbonate, $\bar{M}_v = 80\ 000$; 3, experimental polycarbonate, $\bar{M}_v = 16\ 000$; 4, experimental polycarbonate, $\bar{M}_v = 6000$; 5, acetylated polymer, $\bar{M}_v = 62\ 200$. Rate of heating $20^\circ\text{C}/\text{min}$

Molecular weights

Viscosity-average molecular weights (\bar{M}_v) were determined from the limiting viscosity number $[\eta]$ in methylene dichloride solution using the relationship⁴:

$$[\eta] = 1.11 \times 10^{-2} \bar{M}_v^{0.82}$$

The number-average molecular weights (\bar{M}_n) up to 3×10^4 , were measured in chloroform solutions at 32°C with a Hitachi Perkin-Elmer Vapour Pressure Osmometer, model 115. Values above this were estimated from \bar{M}_v (Table 1) using a dispersity (\bar{M}_v/\bar{M}_n) of 2.4 which was checked by gel permeation chromatography for certain of the samples.

Crystallization

Polycarbonates were crystallized by: hot precipitation from 1,2-dichloroethane solutions, treatment with acetone, and melt crystallization in sealed tubes under vacuum at 195°C for 8 and 21 days.

I.r. measurements

Measurements were made on methylene chloride solutions ($40\ \text{g}/\text{dm}^3$) in KBr solution cells of path length 0.3–1.0 cm. Methylene chloride was dried with silica gel immediately before use, and has a limited window region for $3600\text{--}3400\ \text{cm}^{-1}$.

Density measurements

These were carried out on cast films by flotation on aqueous NaNO_3 solutions.

X-ray diffractometer

A Picker Powder Diffractometer was used to measure the degree of crystallinity of finely powdered or film samples. The instrument was used with $\text{CuK}\alpha$ radiation for 2θ values of 4° to 40° at $2^\circ/\text{min}$. The instrument was standardized with α -quartz as a test sample.

RESULTS AND DISCUSSION

Thermogravimetric measurements

This technique measures the weight loss of a polymer sample. The measurement may be carried out either by keeping the polymer at a constant temperature and observing the weight loss, or by raising the temperature at a steady rate until the polymer is substantially decomposed (see Figure 1). These and other similar results showed that the commercial polycarbonates had a better thermal stability than our experimental material and that there was a strong effect of molecular weight which was not just an initial effect but persisted through the main part of the decomposition process. These two factors were investigated separately and for this purpose the constant temperature procedure which gave a linear first order curve suitable for characterizing thermal stability was used.

The results showing the effect of molecular weight on the initial isothermal weight loss at 410°C are given in Figures 2a and 2b. The measurements confirm the observations illustrated in Figure 1 and show that the commercial polymers are significantly superior to the experimental material. With both types of material the amount of decomposition is much greater with low molecular weight

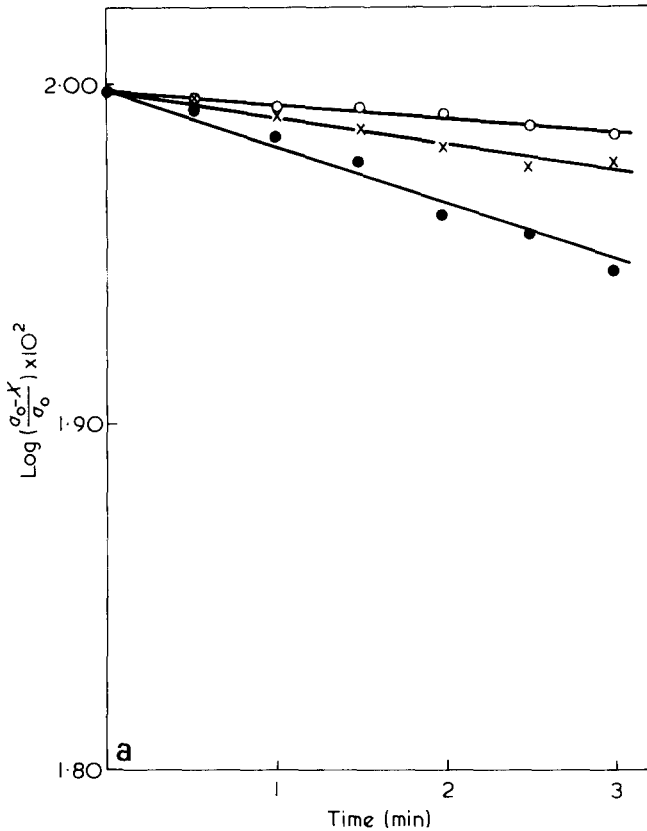


Figure 2a Effect of molecular weight on the thermal decomposition of commercial polycarbonates: \circ , $\bar{M}_v = 78\,000$; \times , $\bar{M}_v = 71\,000$; \bullet , $\bar{M}_v = 25\,500$; where a_0 is the initial weight and X is the weight loss

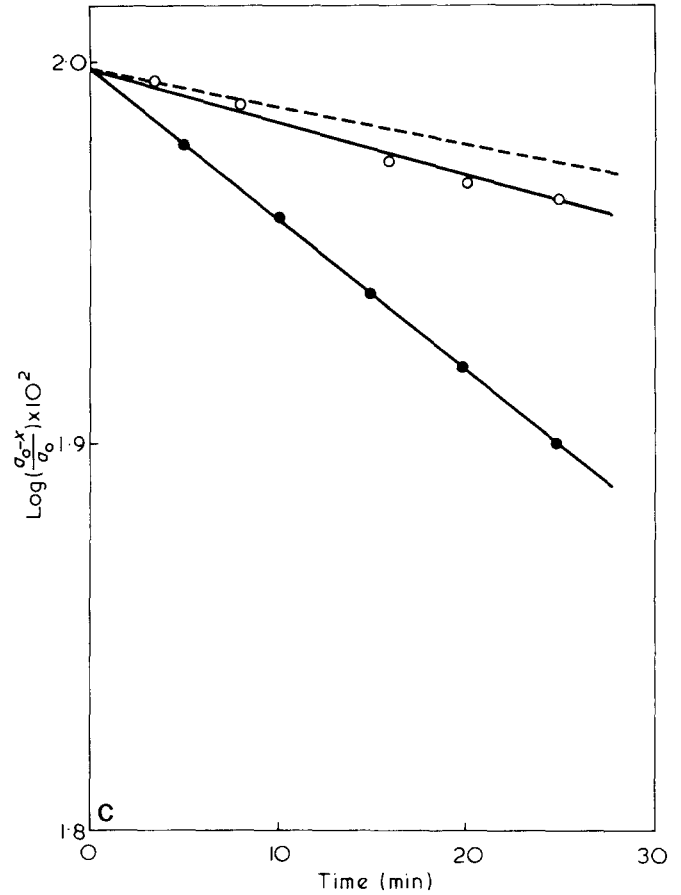


Figure 2c Isothermal decomposition curves. \bullet , experimental polycarbonate ($\bar{M}_v = 62\,000$); \circ , acetylated polymer; ----, commercial material, this line was interpolated for \bar{M}_v of 62 200 from Figure 2a

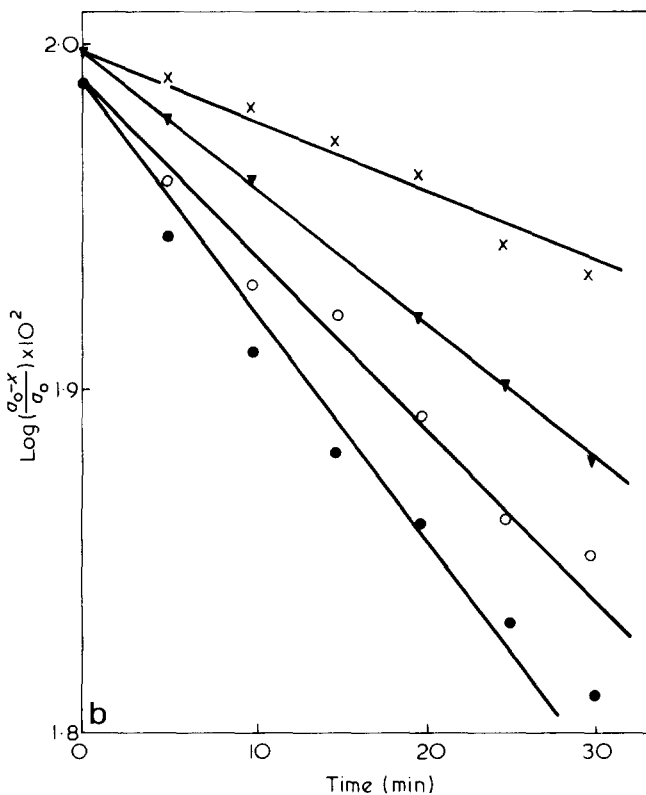
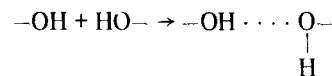


Figure 2b Effect of molecular weight on the thermal decomposition of experimental polycarbonates: \times , $\bar{M}_v = 80\,000$; ∇ , $\bar{M}_v = 62\,200$; \circ , $\bar{M}_v = 16\,000$; \bullet , $\bar{M}_v = 6\,000$

samples. Polymers terminated by *p*-cresol were not used in these studies.

Nature of the degradation process

Previous work has indicated that the degradation of polycarbonate involves the reaction of end groups^{5,6} (either phenyl or hydroxyl) and this seems to be at least superficially confirmed by our measurements. Also a study of the patent literature⁷ suggested that esterification of the hydroxyl end groups might have a useful stabilizing effect. One of the experimental polymers was therefore acetylated, and so removed $70 \pm 10\%$ of the hydroxyl groups (estimated by i.r. spectroscopy). As shown in Figure 2c the resulting polymer showed a marked increase in thermogravimetric stability although it did not quite reach the level interpolated for a commercial polymer of the same molecular weight. This result points strongly to a catalytic effect on the decomposition process. Indeed, i.r. analysis of the polymers indicated that free and associated hydroxyl groups were present, and that the concentration of free hydroxyl groups measured in methylene chloride solution varied inversely with the square root of the degree of polymerization (Figures 3a, and 3b). This dependence is consistent with association of end groups, as observed previously with polyethylene oxide in benzene⁸, i.e.



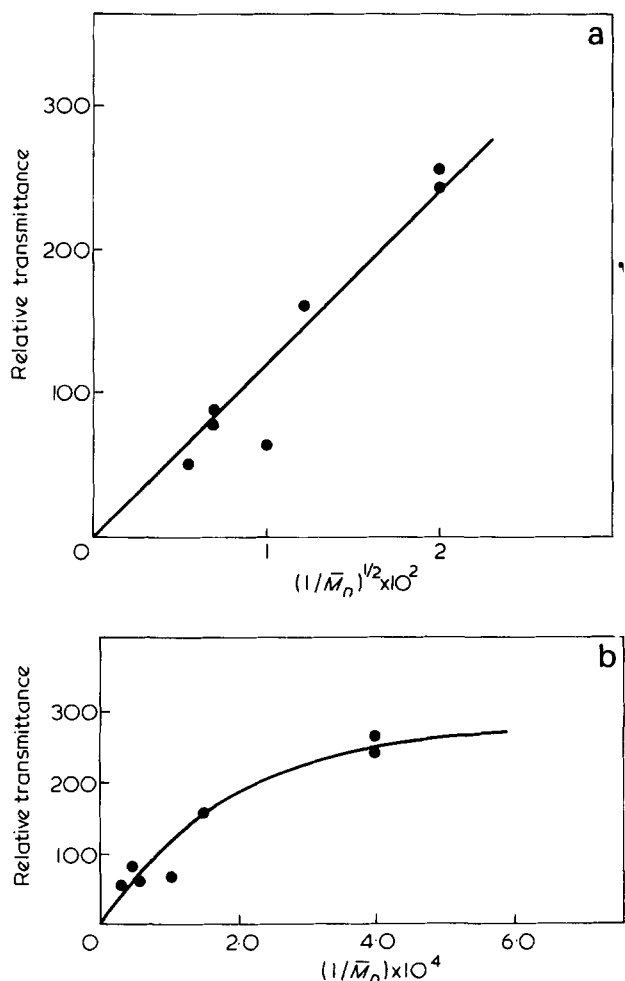


Figure 3 Effect of molecular weight on the i.r. hydroxyl absorption peak (3500 cm^{-1})

Acetylated polymers contained a reduced concentration of hydroxyl groups (reduced by 60–80% as determined from Figure 3b). On the other hand, commercial materials contained an apparently high level of hydroxyl groups which we ascribed to the presence of additives. This is also suggested by the work of Bartosiwiz and Booth⁹ who observed a decrease in polymer stability on purification. Thus the major processes of degradation are different in the two types of polymer and this is further supported by a study of weight loss at increasing temperature as shown in Figure 1. From the instantaneous slopes of these curves at different temperatures it is possible to calculate the energy of activation of the decomposition process over the initial 10% weight loss. The results obtained, which are included in Table 2, show a very significant difference between the commercial and the laboratory materials, which presumably corresponds to the absence of terminal hydroxy groups in the commercial polymers.

It should, however, be appreciated that in this type of measurement an inverse dependence on molecular weights does not itself indicate end group catalysis, since the small molecules which are volatilized in the early stages of decomposition are most likely to be formed from the ends of the polymer molecules and this would therefore give a molecular weight effect even if the degradation process was one of random molecular fracture.

Thermal studies of the glass transition

The glass transition temperature (T_g) may be readily estimated by d.s.c.^{10,11} making use of the marked change in the specific heat which occurs at the glass transition. However, the results directly obtained are dependent both on the rate of heating used (as also occurs with other methods of measurement) and on the sample size. Consistent values of T_g were obtained either by linear extrapolation to zero weight or to zero heating rate (heating rate of 2.5–80 K/min). The results (see Figure 4) followed the conventional type of relationship between T_g and M_n^{-1} ^{12,13} so that:

$$T_g = T_g^\infty - AM_n^{-1}$$

where $T_g = 432 \text{ K}$ and $A = 1.45 \times 10^5 \text{ mol K}$. In this case, it was also found that both commercial and synthetic polymers gave similar results for $T_g: M_n$, (Figure 4).

Another feature which was observed by d.s.c. studies of T_g was the occurrence of annealing peaks^{14–16}. If the polymer is heated at a temperature below T_g , say between T_g and $(T_g - 60) \text{ K}$, a change takes place which leads to an endothermic peak on later heating through T_g . The precise nature of this process is not fully understood but it is probably connected with volume relaxation which has been shown to occur under the same conditions¹⁷, and it may be associated with the formation of nodules reported to be observable under the electron microscope¹⁸. The process is unlikely to be one of nucleation and growth of a new phase since it could be fitted with an Avrami equation:

$$1 - X_t = e^{-Kt^n}$$

Table 2 Activation energies from thermal decomposition curves

Sample	Activation energy (kJ/mol)
Commercial 5705	125 ± 25
Commercial 5730	125 ± 25
Commercial M39	125 ± 25
Experimental polymer 2	65 ± 10
Experimental polymer 5	65 ± 10
Experimental polymer 10	75 ± 15
Experimental polymer 13	80 ± 10
Acetylated polymer	140 ± 30

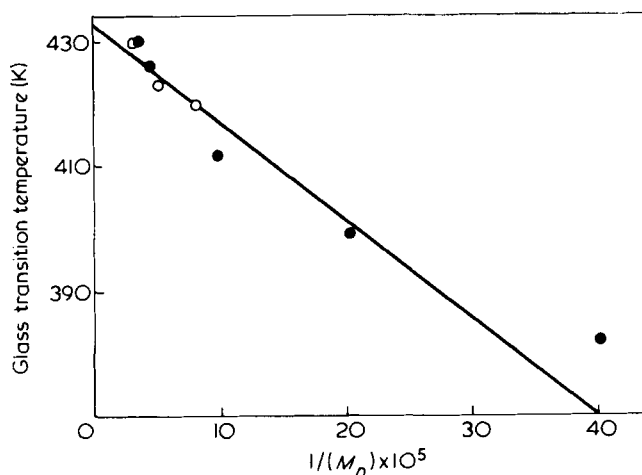


Figure 4 Effect of molecular weight on the glass-transition temperature of polycarbonate: ○, commercial materials; ●, experimental polycarbonates

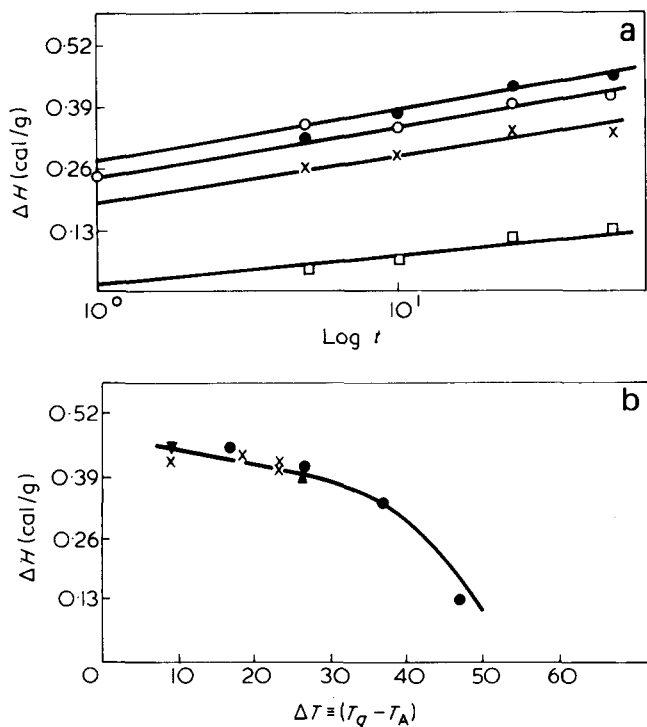


Figure 5 The endothermic peak measured by differential scanning calorimetry: (a) the effect of annealing time and temperature on the endothermic heat absorption at the glass transition temperature: \square , 110° ; \times , 120° ; \circ , 130° ; \bullet , 140°C . (b) the endothermic d.s.c. peaks measured after 48 h, related to the difference between the annealing temperature T_A and the relevant glass transition temperature: \times , experimental polycarbonates of different molecular weights; \blacktriangle , commercial materials of different molecular weights; \bullet , experimental polycarbonate $\bar{M}_v = 80\,000$ at different annealing temperatures

relating X_t , the extent of development of the new phase, to time t with an n value of 1.0, and with a rate constant K which was dependent on temperature rather than on the under-cooling from the glass transition temperature ΔT . The enthalpic change Q_E increased logarithmically with the annealing time (Figure 5a) and was consistent with a relaxation to the equilibrium glassy state for which at constant temperatures:

$$Q_{E,T_A} - Q_{t,T_A} = A \ln t + A \ln k$$

where A is a constant, k a first order rate constant, Q_{t,T_A} the enthalpy change at time t and annealing temperature T_A , and Q_{E,T_A} the maximum change in energy associated with the transition. This relation is similar to that used by Petrie¹⁹ for polystyrene, though we attach no theoretical significance to the observation of a linear relation over the range studied. However, one would expect Q_E to be equivalent to the specific heat change between liquid and glass multiplied by the temperature interval, i.e.:

$$Q_{E,T_A} = \Delta C_p (T_g - T_A)$$

where $\Delta C_p = C_{p,L} - C_{p,g}$, i.e. the difference in C_p above and below T_g . Times required for relaxation of the enthalpy to the equilibrium glassy state were very long, and annealing was not continued above 100 h. The measured enthalpy changes (0.5 cal/g) were less than Q_{E,T_A} (0.80–2.00 cal/g), and depended on the annealing temperatures. Annealing at 130°C for 48 h established that the enthalpic changes of different molecular weight samples exhibited a similar

dependence on temperature of under cooling (ΔT) (see Figure 5b and Figure 6). It would appear that the enthalpic effects on annealing polycarbonate below the glass transition temperature are sensitive to the degree of undercooling, and perhaps to the free volume of the system. Further studies are required to establish the structure, formation mechanism, size and number of the nodules reported¹⁷ on annealing to see if there is any correlation of these with the enthalpic effect.

Heat of fusion and melting of polycarbonates

Polycarbonate crystallizes only slowly in bulk and samples generally do not have crystallinities in excess of 40%. The heat of fusion was determined by d.s.c. using samples crystallized in different ways, i.e. isothermally in bulk, by precipitation from hot dichloroethane solution and by treatment with acetone. The degree of crystallinity was determined in two ways, by density and by X-ray diffraction.

Density method

For a two phase system, amorphous density ρ_A and crystalline density ρ_C the degree of crystallinity of a sample of density ρ is given by:

$$X_c = \frac{(\rho - \rho_A)}{(\rho_C - \rho_A)}$$

The crystalline density was calculated as $1.30(7) \text{ g/cm}^3$ from the X-ray structure²⁰. However, the probable error in ρ_C obtained in this way (up to 2%) was highly significant in deriving ρ_C and consequently in determining the heat of fusion. The density of the amorphous polymer was not sensibly affected by the rate of cooling but varied from one sample to another. We measured the value of 1.188 for the commercial polymer (\bar{M}_n 19 500) used and 1.204 for the hydroxyl terminated (experimental) material (\bar{M}_n 33 000).

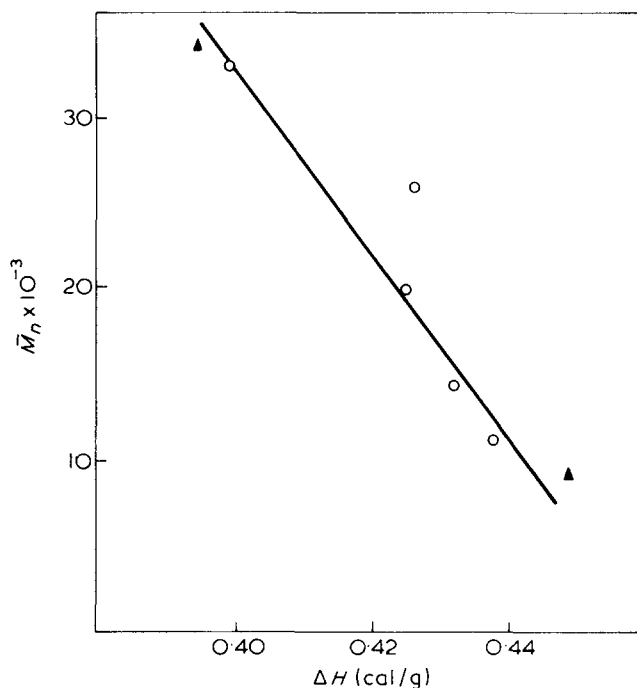


Figure 6 Effect of molecular weight on the endothermic d.s.c. peak: \circ , experimental polycarbonates; \blacktriangle , commercial materials

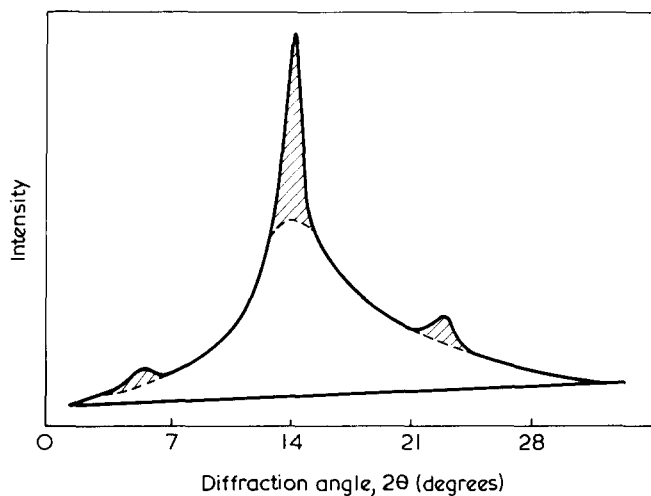


Figure 7 X-ray diffraction peaks for a partly crystalline polycarbonate. The % crystallinity is obtained from the relative area of the shaded portions

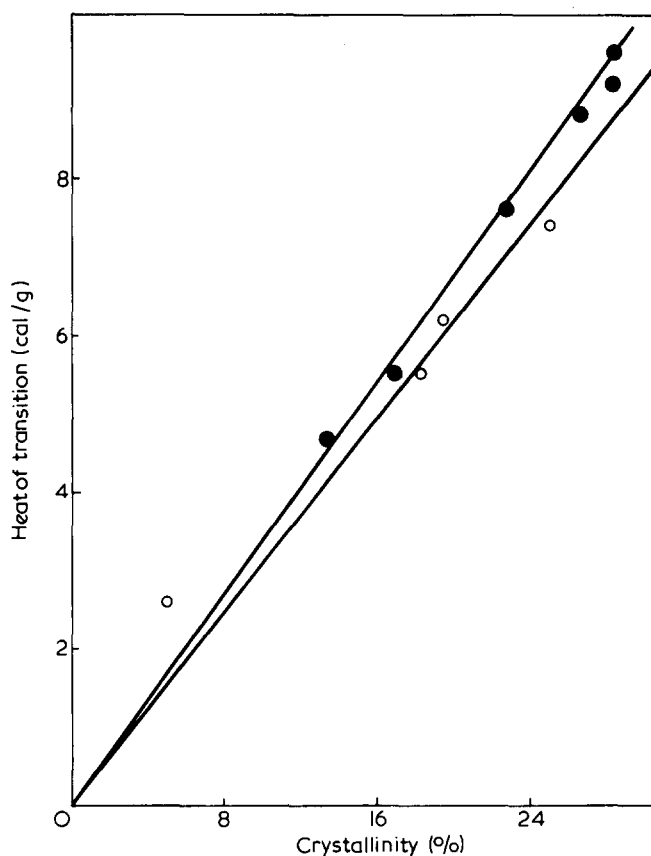


Figure 8 Heat of fusion of polycarbonates with different levels of crystallinity. ○, % crystallinity from density measurements ($\Delta H_f = 30.4 \text{ cal/g} \pm 20\%$); ●, % crystallinity from X-ray diffractometry ($\Delta H_f = 32.9 \text{ cal/g} \pm 4\%$)

X-ray diffraction

Partly crystalline polymers were characterized on an X-ray powder diffractometer, in which scattered intensities were plotted as a function of the Bragg angle 2θ . The amorphous and crystalline contents were measured directly from the areas under the curves shown in Figure 7. With this method it was possible to use polymers prepared by hot precipitation, which had a slightly higher crystallinity than could be reached by isothermal bulk crystallization ($\sim 30\%$ compared with $\sim 25\%$) and this was an advantage

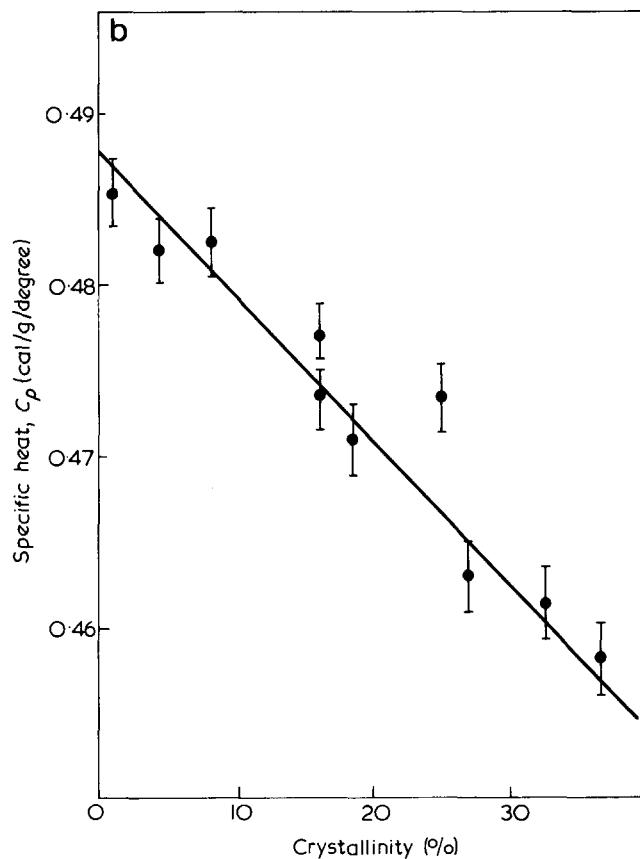
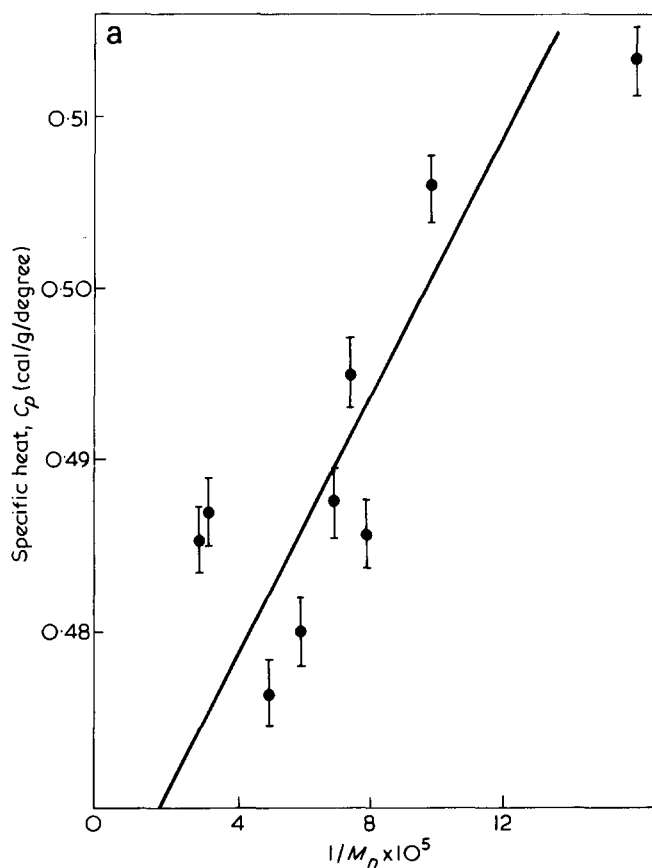


Figure 9 The specific heats of polycarbonates. (a) the effect of molecular weight on the specific heat of amorphous polycarbonate; (b) the effect of crystallinity on the specific heat of polycarbonates. Crystallinity determined from d.s.c. measurements using a heat of fusion of 32 cal/g

Table 3 Specific heat of polycarbonate

Temperature (K)	Specific heat (cal/g)	
	Crystalline	Amorphous
350	0.243	0.327
355	0.247	0.331
360	0.251	0.335
365	0.251	0.338
370	0.258	0.342
375	0.261	0.345
380	0.265	0.349
385	0.268	0.352
390	0.272	0.356
395	0.275	0.359
400	0.279	0.363
405	0.282	0.366
410	0.286	0.370
415	0.289	0.373
420	0.293	0.377
	Glass-transition region	
	(cal/g)	(cal/g)
435	0.345	0.429
440	0.350	0.434
445	0.354	0.438
450	0.359	0.443
455	0.364	0.448
460	0.368	0.452
465	0.373	0.457
470	0.378	0.462

of the X-ray method. As is clear from *Figure 7* the limitation of the method lies in the estimation of peak areas from the X-ray diffraction curves.

Measured heats of fusion

The results of the two sets of measurements are given in *Figure 8* where the measured heat of fusion is plotted against the estimated crystallinity. From the slopes of the curves, the heat of fusion for the 100% crystalline material may be estimated. The value obtained from the density method (30.4 cal/g) agrees with that given by Wineman^{21,22}. The value obtained by X-ray diffraction is higher (32.9 cal/g), but in view of the problems concerning the precise determination of crystal density it could well be correct in spite of the disagreement with Wineman's work.

Both values are inconsistent with the value of 13.4 cal/g given by Conix and Jeurissen²³ determined by melting point depression. Analysis of the molecular weight dependence of the melting point of the selected samples gave a very similar low value of the heat of fusion. This would seem to indicate that the assumption of equilibrium in the melting studies cannot be valid. Therefore it is concluded that the two higher figures reported above are a better estimate of the true heat of fusion.

Heat capacity

The specific heats were also measured by extrapolation to zero heating rate and the results obtained varied with the particular material used. Two parameters proved to affect the specific heat significantly, viz, crystallinity and molecular weight.

Samples of amorphous polymer quenched to room temperature showed no endotherm in the melting range so that specific heats could be directly measured and so related to \bar{M}_n as shown in *Figure 9a*. The results may be represented by:

$$C_p(\text{amorphous}) = C_p^\infty + \frac{360}{\bar{M}_n} \text{ cal/g [where } \bar{M}_n = 2.5 \times 10^3 \text{ to } 3.3 \times 10^4]$$

Differences in specific heats for materials of different crystallinities (corrected for differences in molecular weight) are shown in *Figure 9b* from which it may be inferred that

$$C_p(\text{crystalline}) - C_p(\text{amorphous}) = 0.084 \text{ cal/g at } 180^\circ\text{C}$$

The specific heats for crystalline and amorphous polymers are listed in *Table 3* as a function of temperature from which

$$C_p(\text{crystalline}) = 0.243 + (T - 350) \times 9.0 \times 10^{-4} \text{ cal/g}$$

$$C_p(\text{amorphous glass}) = 0.327 + (T - 350) \times 8.0 \times 10^{-4} \text{ cal/g}$$

The change in heat capacity between amorphous glass and liquid at the glass transition temperature was 0.040 cal/g which for our range of annealing temperatures corresponded with $Q_{E,TA}$ values of 0.80–2.00 cal/g.

ACKNOWLEDGEMENTS

We wish to thank Dr J. I. Langford for assistance in carrying out our X-ray diffraction measurements, Dr F. W. Peaker for the g.p.c. measurements and Dr J. K. Brown for i.r. analysis. G.A.A. is indebted to the Iraqi Ministry of Higher Education for financial support.

REFERENCES

- 1 Adam, G. A., Haward, R. N. and Parsons, I. W. *Polymer* 1975, **16**, 433
- 2 Sorenson, W. R. and Campbell, T. W. 'Preparative Methods in Polymer Chemistry', Wiley, New York, 1968
- 3 Schnell, H. 'Chemistry and Physics of Polycarbonates', Interscience, New York, 1964
- 4 Schulz, G. V. and Horbach, A. *Makromol. Chem.* 1959, **29**, 93
- 5 Davis, A. and Golden, J. H. *J. Gas Chromatogr.* 1967, **81**
- 6 Davis, A. and Golden, J. H. *J. Macromol. Sci. (C)* 1969, **3**, 49
- 7 U.S. Pat. 3 475 373 (1969)
- 8 Affifi, A. M. and Hay, J. N. *Eur. Polym. J.* 1972, **8**, 289
- 9 Bartosiwiz, R. L. and Booth, C. *Eur. Polym. J.* 1974, **10**, 791
- 10 O'Neill, M. J. and Fyans, R. L. *The Eastern Analytical Symposium, New York, 1971*
- 11 Lambert, A. *Polymer* 1969, **10**, 39
- 12 Flory, P. J. *J. Appl. Phys.* 1950, **21**, 581; *J. Polym. Sci.* 1954, **14**, 315
- 13 Beevers, R. B. and White, E. F. T. *Trans. Faraday Soc.* 1960, **56**, 1928
- 14 Illers, K. H. *Makromol. Chem.* 1969, **127**, 1
- 15 Ali, M. S. and Sheldon, R. P. *J. Appl. Polym. Sci.* 1970, **14**, 2619
- 16 Haward, R. N. 'Molecular Behaviour and the Development of Polymeric Materials', (Eds A. Ledwith and A. M. North), Chapman and Hall, London, 1975, p 434
- 17 Rehage, G. 'The Physics of Glassy Polymers', (Ed. R. N. Haward), Appl. Science, London, 1974, Ch I
- 18 Siegman, A. G. and Gell, P. H. *J. Macromol. Sci. (B)* 1970, **4**, 239
- 19 Petrie, S. E. B. *J. Polym. Sci. (A-2)* 1972, **1255**
- 20 Preistzschk, A. *Kolloid-Z.* 1958, **8**, 156
- 21 Wineman, P. see Kambour, R. P., Karasz, F. E. and Deane, J. H. *J. Polym. Sci. (A-2)* 1966, **4**, 327
- 22 Wineman, P. see O'Reilly, J. M., Kavasz, F. E. and Bair, H. E. *J. Polym. Sci. (C)* 1964, **6**, 109
- 23 Conix, A. and Jeurissen, L. *ASC Symp. No. 147, Philadelphia, 1964*

Effect of phosphine ligand on the activity of palladium/ π -catalysts

Fereidun Hojabri

Department of Chemistry, Arya-Mehr University of Technology, PO Box 3406, Tehran, Iran
(Received 8 May 1975)

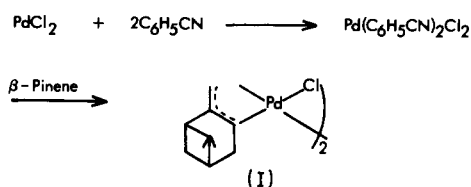
Homogeneous palladium/ π -catalysts for olefin polymerization were converted to supported catalysts with styrene-divinylbenzene copolymer as supporting matrix. Phosphine ligand was used for linkage of palladium to the support. The effect of phosphine ligand on the catalytic activity for the polymerization of olefins was studied. A reaction mechanism on the basis of preferred maximum coordination number of Pd(II) is proposed and discussed to explain the reduced activity of phosphinated palladium complexes for olefin polymerization.

INTRODUCTION

Homogeneous catalysts have several advantages over heterogeneous catalysts: (a) they have better defined active sites; (b) usually all of their metal atoms are available to the reactant as catalyst; and (c) they have better mass and heat characteristics. But especially the problem of separation of a homogeneous catalyst from the solution in which it has served as a catalyst has been the major hindrance to the greater employment of homogeneous catalysts in commercial processes. To remove this disadvantage the homogeneous catalysts can be linked to a variety of support materials^{1,2}. Polystyrene-divinylbenzene copolymers have recently been used to chemically bond Rh and Ti to prepare hydrogenation catalysts with interesting selectivity and stability^{3,4}. Phosphine ligand is usually used to link metals to the supports. The same method was applied to this work to bond palladium/ π -allylic complexes to polymer support. The effect of phosphine ligand on the activity of palladium/ π -complex for olefin polymerization is described here.

ATTACHMENT OF PALLADIUM TO POLYMER SUPPORT

The homogeneous palladium catalyst (I) used in these experiments was a palladium/ π -allylic complex⁵. The catalyst was prepared from palladium chloride and β -pinene according to the following scheme:

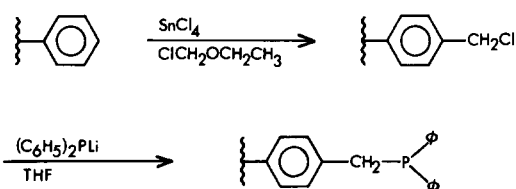


The supporting matrix was a styrene-divinylbenzene copolymer with a divinylbenzene content of 2% and bead size ranging from 200 to 600 mesh.

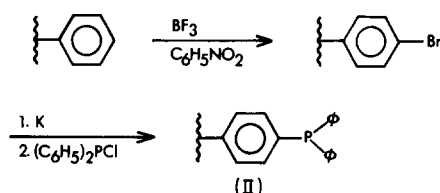
The crosslinking with divinylbenzene gives the copolymer a pore-containing structure and increases the ability of substrate to penetrate into the inner parts of the beads.

Since the π -allylic complex of palladium is a bridged compound⁵ and triphenyl phosphine is a well-known bridge-

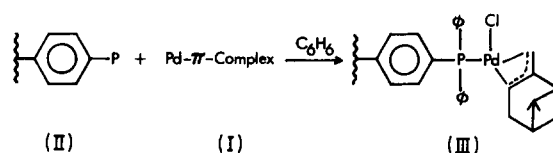
splitting agent⁶, it was decided to functionalize the polymer with a similar ligand. For the attachment of this ligand, usually, the polymer is first chloromethylated⁷ and then treated with lithiodiphenylphosphide³:



But owing to reported cancer causing properties of chloromethyl ethyl ether, phosphination of the polymer support was carried out through another method:



Phosphinated polymer beads (II) were then equilibrated with an excess of palladium/ π -allylic complex (I) for 20 days.



The polymer-attached palladium complex (3) was deep red in benzene. The catalyst was washed several times with benzene and dried.

CATALYTIC ACTIVITY OF THE SUPPORTED PALLADIUM COMPOUND

To compare the catalytic activity of the supported palladium catalyst with the activity of the homogeneous palladium one, both catalysts were used in polymerization of bicyclohepta-(2, 5)-diene under the same reaction condi-

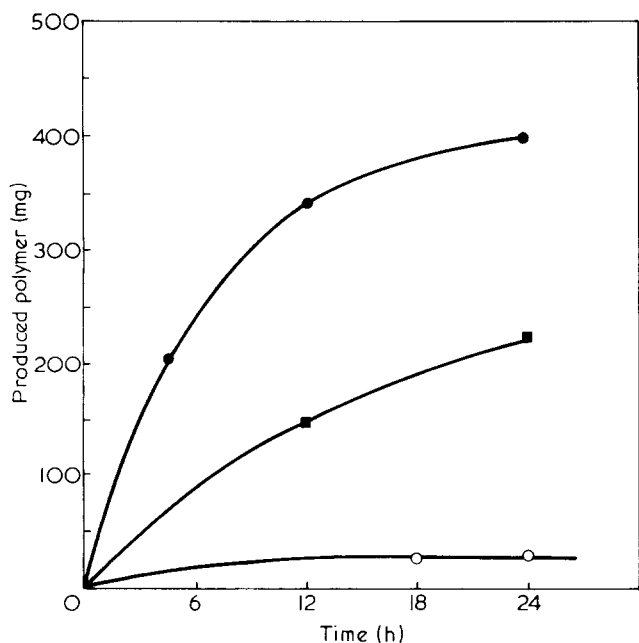


Figure 1 Polymerization of bicyclohepta-(2,5)-diene at 80°C. ●, Homogeneous Pd catalyst; ■, supported Pd catalyst; ○, supported Pd catalyst refluxed with benzene

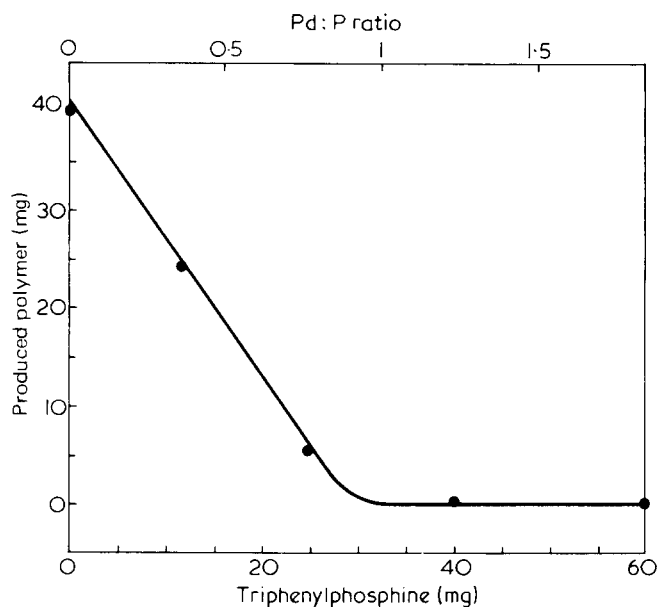


Figure 2 Effect of triphenylphosphine on polymerization of bicyclohepta-(2,5)-diene at 80°C with palladium/ π -allylic complex (30 mg)

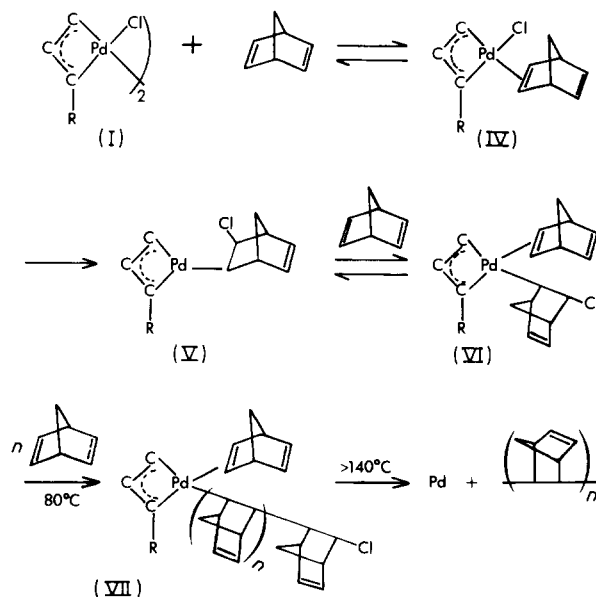
tions. It was found that the polymerization with the supported catalyst, although slower than with the homogeneous catalyst, was still a fast reaction. But when the supported palladium catalyst was refluxed with benzene for 30 min, prior to its application in polymerization reaction, the catalytic activity was reduced to almost zero. Figure 1 shows the results of polymerization at 80°C, using the same amounts of homogeneous and supported catalyst in respect to palladium content. Apparently residues of uncoordinated palladium/ π -complex were responsible for the remaining catalytic activity. These residues were firmly adsorbed by the polymer support and could be removed only after long treatment with benzene solvent. To determine whether the decline in catalytic activity of the supported palladium was due to coordination of the palladium/

π -complex with phosphine ligand or due to other factors, the homogeneous palladium/ π -complex with different amounts of triphenylphosphine was used in polymerization. As it can be seen from Figure 2, polymerization of bicyclohepta-(2,5)-diene was decreased with increasing amounts of added triphenylphosphine. The activity of the catalyst mixture diminished totally when the ratio Pd:P reached 1:1. Addition of more triphenylphosphine did not change the activity of the catalyst system.

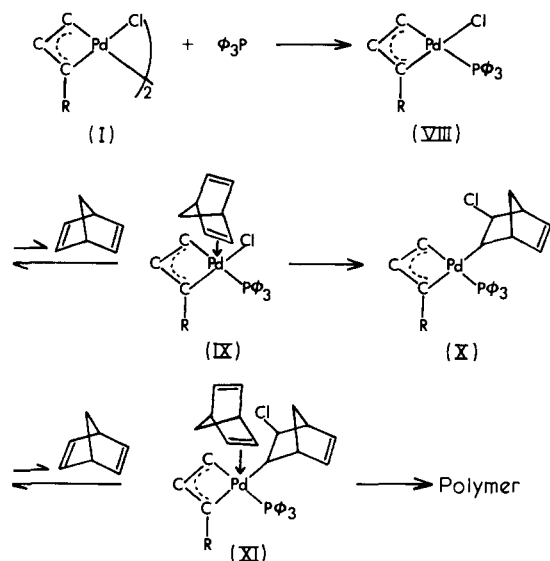
Olefin polymerization by transition metal complexes normally occurs by a π -olefin mechanism, involving an intermediate metal-carbene complex. Such an intermediate might be involved in addition of olefins to palladium/ π -allylic complexes, by olefins acting as bridge-splitting agents (Scheme 1). Rearrangement of π -complex (IV) to (V) and further addition of olefin to these intermediates with vacant coordination site leads to polymerization.

This mechanism is consistent with the experimental results. Palladium remained attached to the produced polymer and it was not possible to separate the applied homogeneous palladium/ π -complexes from the product by solvent extraction. Furthermore, if the polymerization was stopped in the early stages of the reaction, the produced polymer was active and could be used to polymerize more bicyclohepta-(2,5)-diene. The yellow colour of the polymer was another indication that the π -allylic system of the palladium complex was present as part of the produced polymer. More than 90% of palladium present in the original catalyst was also found in the polymer. Dissociation of (VII) and participation of palladium metal occurs at temperatures higher than 140°C.

The mechanism shown in Scheme II best explains the observation on the effect of triphenylphosphine addition. Palladium is in π -allylic complexes, $[\text{PdCl}(\text{allyl})]_2$ in the Pd(II) state and, therefore, has a 8d electronic structure. The maximum coordination number for a 8d configuration is 5 but the tendency for five coordination depends on the ligand and the metal. Palladium, as opposed to Ni or Rh, has little tendency to accept the coordination number 5. Only a few palladium complexes with 5-coordinate structure have so far been determined⁸. Triphenylphosphine adduct (VIII), which is formed by addition of $(\text{C}_6\text{H}_5)_3\text{P}$ to palladium/ π -allylic complex (I), has also the preferred 8d



Scheme 1



Scheme II

structure. However, to add olefin, the complex (VIII) must change to the intermediate (IX) with the coordination number 5. Rearrangement of (IX) to (X) and further addition

of olefin (XI) could lead to final polymerization of bicyclohepta-(2, 5)-diene. Apparently owing to the higher energy of five coordinate structure, the intermediates (IX) and (XI) are not formed and the polymerization does not take place.

The lack of polymerization activity of the supported palladium catalyst may be explained in the same way by a reaction mechanism involving the phosphine ligand as linkage to the support.

REFERENCES

- 1 Haag, W. O. and Whitehurst, D. D. Belg. Pat. 721 686 (1969)
- 2 British Petroleum Co. Ltd, US Pat. 3 726 809 (1972)
- 3 Grubbs, R. H. and Kroll, L. C. *J. Am. Chem. Soc.* 1971, **93**, 3062
- 4 Grubbs, R. H., Gibbons, C., Kroll, L. C., Bond, W. D. and Brubaker, C. H. *J. Am. Chem. Soc.* 1973, **95**, 2373
- 5 Hojabri, F. *J. Appl. Chem. Biotechnol.* 1973, **23**, 205
- 6 Powell, J. and Shaw, B. L. *J. Chem. Soc. (A)* 1967, p 1839
- 7 Pepper, K. W., Paisley, H. M. and Young, M. A. *J. Chem. Soc. (A)* 1953, p 4097
- 8 Churchill, M. R. and O'Brien, T. A. *J. Chem. Soc. (A)* 1970, p 206

Thermal oxidation of poly(1-pentene): 1. Identification of products and mechanisms*

S. M. Gabbay and S. S. Stivala

Department of Chemistry and Chemical Engineering, Stevens Institute of Technology, Hoboken, New Jersey 07030, USA

(Received 18 August 1975)

Isotactic poly(1-pentene) was degraded in the presence of pure oxygen at 115°C. The functional groups present in the non-volatile products were identified using infra-red spectroscopy. The volatile products formed were identified by means of a relatively new technique which combines thermal and mass chromatography. In this study, fourteen volatile products were detected and identified and their relative abundance estimated. The results obtained could readily be reproduced. Various oxidation mechanisms for these products are postulated.

INTRODUCTION

Earlier studies¹⁻⁵ have indicated that isotactic poly(1-pentene) (IPP-1) may crystallize into two modifications: modification 1, having a melting temperature at 130°C, and modification 2, having a melting temperature at 80°C. These melting temperatures are regularly affected by molecular weight but exceptionally dependent on crystallization temperature⁶. Both polymorphous modifications have distinct X-ray crystal structures⁷, (e.g. the chain conformations are 3₁ and 4₁ helix for modification 1 and 2, respectively), and characteristic infra-red spectra, as reported elsewhere⁸.

Since the study of the kinetics and mechanism of thermal oxidative degradation provides a basis from which the most diverse technological phenomena can be controlled, several investigations have been carried out on the mechanism and kinetics of polyolefins, e.g. polyethylene, polypropylene, and poly(1-butene), autoxidation, both in the presence and absence of additives using different methods^{9,10}. However, relatively very little work was reported on the nature and the mechanisms of formation of volatile products (*VP*) evolved during the thermal oxidation of polyolefins^{11,12}.

Recently, a relatively new technique (thermal and mass chromatography) was used to identify the *VP* evolved during the thermal degradation of polyethylene¹³ and polystyrene¹⁴. A modification of this technique was adopted for the detection and identification of *VP* resulting from thermal oxidation of polymers¹⁵. Additionally, a procedure combining thermal chromatography with mass spectrometry was described in an earlier paper for the identification of volatile oxidation products of poly(4-methyl-1-pentene)¹⁶.

The purpose of this paper is to examine the non-volatile products (*NVP*) and the volatile products formed from the oxidation (115°C, 100% O₂) of modification 1 of IPP-1, using the methods of i.r. spectroscopy and thermal/mass chromatography (t.m.c.) respectively.

* Presented at the IUPAC International Symposium on Macromolecules and the Third Aharon Katzir-Katchalsky Conference, Jerusalem, July 1975.

EXPERIMENTAL

Starting material

The IPP-1 sample used in this study was an unstabilized pure polymer obtained through the courtesy of Dr Gianotti from Montedison, Italy. Its intrinsic viscosity in tetralin at 135°C was 4.7 dl/g. Upon ignition, the sample gave an ash content of 0.01% by wt. A crystalline melting point of 78°C was determined by a Perkin-Elmer Differential Scanning Calorimeter (d.s.c.) using a programmed heating rate of 10°C/min. IPP-1 studied in this work was modification 1.

Apparatus

A Perkin-Elmer spectrophotometer, Model 21, equipped with a sodium chloride prism was used to record the i.r. spectra of oxidized IPP-1 in order to identify the functional groups formed in the *NVP*.

A thermal chromatograph (MP-3) coupled in series with a mass chromatograph (MC-2) (Chromalytics, Division of Spex Industries) were used to identify the *VP* evolved during the thermal oxidation of IPP-1.

Procedure

Clear and uniform films of ~2 to 2.5 mil thickness of modification 2 were prepared when IPP-1 sample was compression moulded in vacuum¹⁷ at 140°C and cooled to room temperature over a 20 min period. These films were converted to modification 1 by refluxing them in absolute ethanol¹⁸ overnight and subsequently dried in a vacuum oven at 50°C for 12 h (thickness not appreciably affected). These films were oxidized at 115°C under 100% oxygen for 75 min in the MP-3. The volatile oxidation products evolved were rapidly swept from the sample chamber for gas chromatographic separation and identification by retention times, mass chromatography (using MC-2 in order to determine the molecular weight of the major *VP*), and peak enhancement. Detailed experimental conditions were described earlier¹⁵. Weight loss of modification 1, owing to formation of *VP*, was 1% at 115°C. Several repeat runs indicated excellent reproducibility.

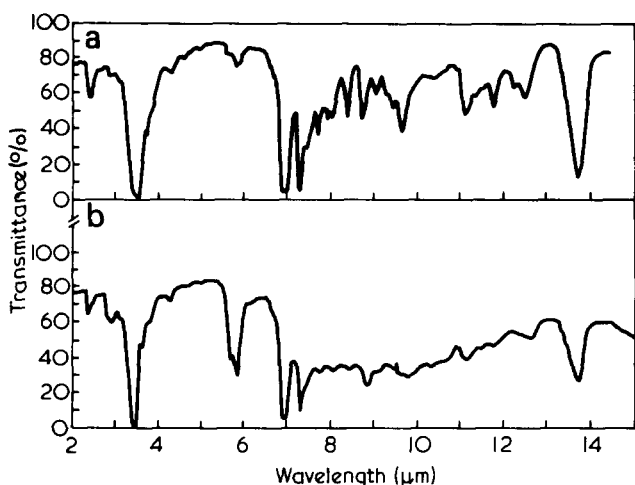


Figure 1 I.r. spectra of IPP-1 (modification 1) at (a) initial and (b) final stages of oxidation at 115°C

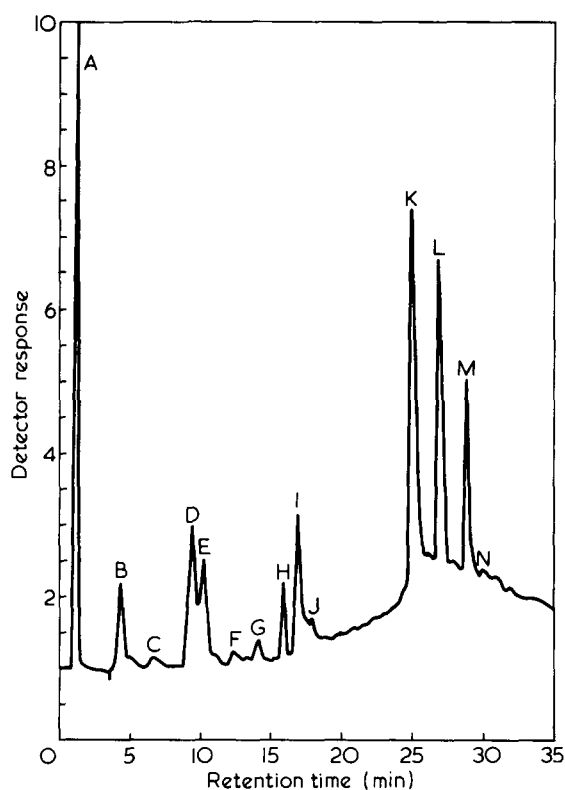


Figure 2 Chromatogram of volatile oxidative degradation products of IPP-1 obtained at 115°C¹⁵. A, CO₂; B, acrolein; C, acetaldehyde; D, propionaldehyde; E, acetone; F, methanol; G, ethanol; H, butyraldehyde; I, water; J, propanol; K, acetic acid; L, propionic acid; M, butyric acid; N, oxalic acid

By means of i.r. spectra, it was ascertained that the oxidized film of IPP-1 was that of modification 1 (see Figure 1) and the *NVP* formation was assessed in terms of hydroxyl, carbonyl, and vinyl groups as described earlier¹⁶.

RESULTS AND DISCUSSION

Figure 1 represents i.r. spectra of modification 1 of IPP-1 at an initial and final stage of oxidation at 115°C. It can be seen that a strong band appeared at 2.85 μm due to the presence of hydroxyl groups. A triplet formation in the carbonyl stretching region (5.70–5.85 μm) indicated the

presence of such functional groups as aldehyde, ketone, ester, and carboxylic acid¹⁹ and a band ingrowth at 11.35 μm indicated the formation of substituted vinylidene bonds²⁰. A representative gas chromatogram of modification 1 oxidized for 75 min is shown in Figure 2. The relative abundance, h_p/h_{CO_2} , of the fourteen volatiles was calculated from the peak heights, h , of an oxidation product, p , to that of CO₂ (the first product appearing in the chromatogram and the most abundant). Values of h_p/h_{CO_2} ratios and their relative percentages are given in Table 1 in an order of decreasing abundance of the *VP* relative to CO₂. The molecular weights of five major *VP* are also given in Table 1. As noted, the molecular weights of some of the *VP* could not be determined owing to their low concentrations. The assessment of the precision and accuracy of the MC-2 over a wide range of molecular weights was previously reported²¹.

Since it has been established that peroxides or hydroperoxides^{22–25} are predominantly formed at the early stages of oxidation, the decomposition of unstable peroxides will give rise to a whole series of secondary compounds, generally containing carbonyl and hydroxyl groups. Based on this observation, various mechanisms for the formation of polar volatile products resulting from the thermal oxidation of poly(4-methyl-1-pentene) were postulated in an earlier publication¹⁶. In a similar manner it is possible to account for the formation of the volatiles of IPP-1 in this work.

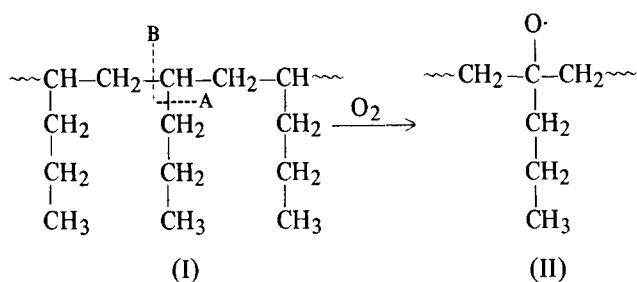
In the case of IPP-1, fourteen *VP* were detected (115°C under 100% oxygen for 75 min) whereas in isotactic poly(4-methyl-1-pentene) (IPMP) seventeen *VP* were detected (145°C under 100% oxygen for 10 min). Propionic acid, propionaldehyde, butyraldehyde, butyric acid, and n-propanol were detected in IPP-1 but not in IPMP. The remaining nine *VP* shown in Table 1 were also detected in IPMP and their mechanism of formation was postulated¹⁶. The mechanism of formation of the above five volatile products of IPP-1 is postulated below, including only those *VP* also evolved from IPMP but whose mechanism may differ by virtue of the composition of IPP-1.

The poly(1-pentene) molecule possesses tertiary hydrogens on the main chain. These hydrogens should be more readily abstracted by free radicals and oxygen than the neighbouring secondary hydrogens. Nevertheless, it should be noted that secondary hydrogens would also be expected to participate in reactions along with tertiary hydrogens albeit to a lesser extent.

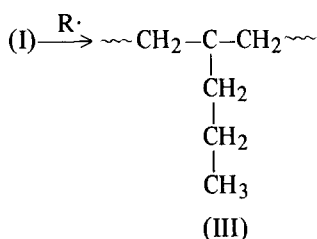
Table 1 Relative abundance, h_p/h_{CO_2} , of volatile oxidation products of IPP-1 at 115°C¹⁵

Volatiles	h_p/h_{CO_2}	Relative abundance (%)	Calculated MW	Actual MW
Carbon dioxide	1.00	65.3	—	—
Acetic acid	0.125	8.1	61.53	60
Propionic acid	0.116	7.6	74.50	74
Water	0.061	4.0	—	—
Propionaldehyde	0.055	3.6	58.58	58
Acetone	0.041	2.7	59.5	58
Butyric acid	0.036	2.3	91.83	88
Butyraldehyde	0.033	2.2	—	—
Acrolein	0.033	2.2	—	—
Ethanol	0.011	0.7	—	—
Methanol	0.008	0.5	—	—
n-Propanol	0.005	0.3	—	—
Acetaldehyde	0.005	0.3	—	—
Oxalic acid	0.003	0.3	—	—

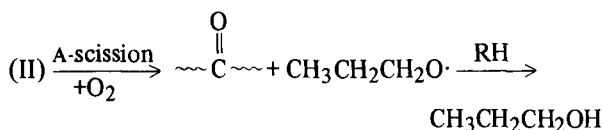
Thus:



or

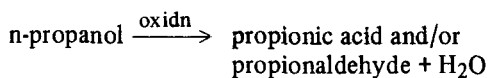


In these reactions, the IPP-1 moieties II and III are considered to form according to the equations reported earlier¹⁶. The broken lines on structure I indicate bonds which may undergo scission, and also apply to structures II and III.

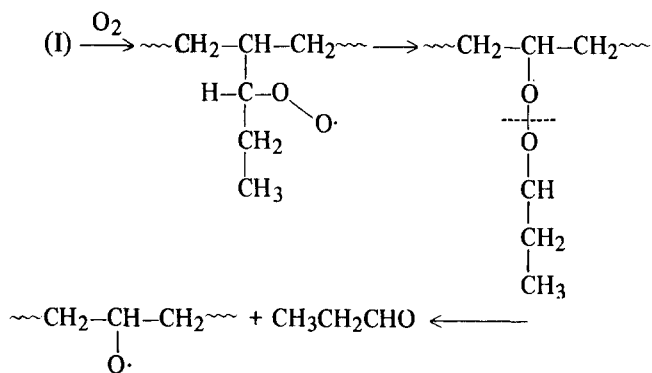


where RH is the polyolefin chain I

The resulting non-volatile fragment could be ketone which, indeed, was detected by i.r. in the IPP-1 residue following oxidation (see Figure 1). The resulting n-propanol has been identified (Table 1) and may undergo further reaction:



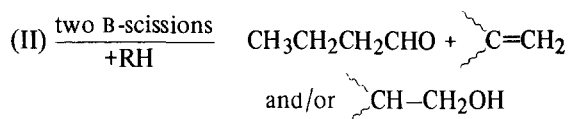
Propionaldehyde may also be derived in the following manner, which involves secondary side chain hydrogen and an isomerization²⁶:



The resulting propionaldehyde can undergo oxidation to the corresponding acid (a major product) while the re-

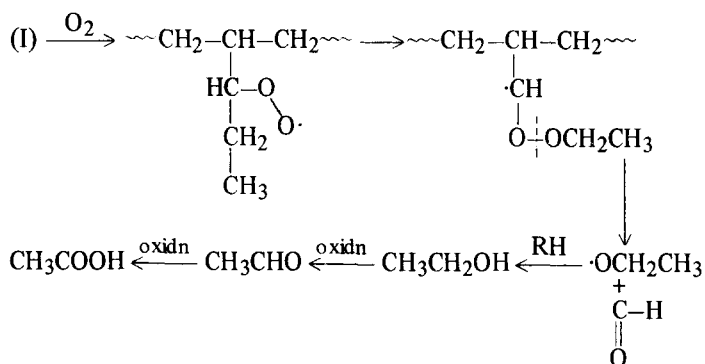
sulting alkoxide may either liberate H⁺ to form a ketone or may abstract a hydrogen to form the corresponding alcohol (hydroxyl groups have been detected by i.r., see Figure 1).

If two B-scissions are assumed, one of the VP identified, butyraldehyde, may form, thus:

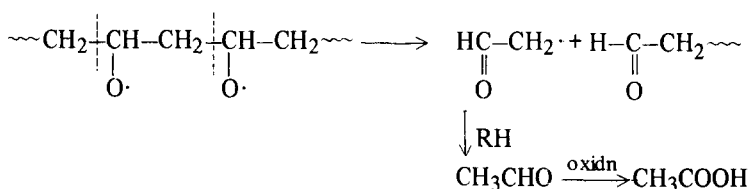


The resulting butyraldehyde may undergo oxidation to yield the corresponding acid, butyric acid (one of the VP identified).

A major product, acetic acid, may be obtained from the oxidation of the corresponding aldehyde (acetaldehyde) which is depicted:



It has been reported in the thermal oxidation of polypropylene²⁷ that acetic acid was an abundant VP formed from further oxidation of an acetyl radical produced by successive scissions as shown:



ACKNOWLEDGEMENTS

The authors wish to express their gratitude to Dr Gianotti from Montedison Company, Italy for the polymer sample.

REFERENCES

- Natta, G. and Corradini, P. *Makromol. Chem.* 1955, **16**, 213
- Natta, G. and Corradini, P. *Chim. Ind. (Milan)* 1955, **37**, 888
- Danusso, F. and Gianotti, G. *Makromol. Chem.* 1963, **61**, 164
- Campbell, W. and Haven, A. C. *J. Appl. Polym. Sci.* 1959, **1**, 73
- Danusso, F. *Polymer* 1962, **3**, 439
- Danusso, F. and Gianotti, G. *Makromol. Chem.* 1964, **80**, 1
- Turner-Jones, A. and Aizlewood, J. M. *J. Polym. Sci. (B)* 1963, **1**, 471
- Gabbay, S. M. and Stivala, S. S. to be published
- Reich, L. and Stivala, S. S. 'Autoxidation of Hydrocarbons and Polyolefins', Marcel Dekker, New York, 1969

- 10 Reich, L. and Stivala, S. S. 'Elements of Polymer Degradation', McGraw-Hill, New York, 1971
- 11 Bevilacqua, E. M., English, E. S. and Gall, J. S. *J. Appl. Polym. Sci.* 1964, 8, 1961
- 12 Neiman, M. B. *Usp. Khim.* 1964, 33, 28
- 13 Kiran, E. and Gilham, J. K. *J. Macromol. Sci (A)* 1974, 8, 211
- 14 Gilham, J. K. personal communication
- 15 Gabbay, S. M., Stivala, S. S. and Reed, P. R. *Analyt. Chim. Acta* in press
- 16 Gabbay, S. M., Stivala, S. S. and Reich, L. *J. Appl. Polym. Sci.* in press
- 17 Rogers, C. E., Vroom, W. I. and Westover, R. F. *Mod. Plast.* 1968, No. 9, p 200
- 18 Natta, G., Danusso, F. and Gianotti, G. *Ital. Pat. Appl.* 32, 222 (1963)
- 19 Adams, J. H. *J. Polym. Sci. (A-1)* 1970, 8, 1077
- 20 Zitomer, F. and DiEdwardo, A. H. *J. Macromol. Sci. (A)* 1974, 8, 119
- 21 Lanser, A. C., Ernst, J. D., Kwolek, W. F. and Dutton, H. J. *Analyt. Chem.* 1973, 45, 14, 2344
- 22 Hawkins, E. G. E. 'Organic Peroxides', Van Nostrand, New Jersey, 1961
- 23 Karyakini, A. V., Niltin, V. A. and Ivanov, K. I. *Zh. Khim. Prom.* 1953, 27, 1856
- 24 Swern, D., Coleman, J. E., Knight, H. B., Ricciniti, C., Willits, C. O. and Eddy, C. R. *J. Am. Chem. Soc.* 1953, 75, 3135
- 25 Dasgupta, S., Pande, J. B. and Ramakrishnan, C. S. *J. Polym. Sci.* 1955, 17, 84
- 26 Shtern, V. Y. 'The Gas-Phase Oxidation of Hydrocarbons', MacMillan, New York, 1964
- 27 Bevilacqua, E. M., English, E. S., Gall, J. S. and Norling, P. *J. Appl. Polym. Sci.* 1964, 8, 1029

Model polyurethane networks

G. Allen*, P. L. Egerton and D. J. Walsh

Department of Chemistry, University of Manchester, Manchester M13 9PL, UK

(Received 12 March 1975)

Polyurethane model networks have been prepared in various solvents at different polymer concentrations, in such a way that the topology of the networks could be controlled. The effects of the network defects, i.e. unreacted functionalities, closed loops and entanglements, on the theoretical value of the modulus has been estimated and these theoretical values have been compared with the experimentally determined values of the modulus. The results imply that the front factor A in the equation for the free energy of deformation of the network tends to half rather than unity. In dry networks the effect of physical entanglements on the modulus of the network appears to be comparable in magnitude to that of chemical crosslinking.

INTRODUCTION

The various theories of rubber elasticity lead to a general expression for the free energy of deformation of a network of the form:

$$\Delta F_{eL} = A \left(\frac{\nu}{2} \right) kT(\lambda_x^2 + \lambda_y^2 + \lambda_z^2 - 3) - B\nu kT \ln \lambda_x \lambda_y \lambda_z \quad (1)$$

where ν = no. of elastically effective chains, k = the Boltzmann constant, T = absolute temperature, $\lambda_x, \lambda_y, \lambda_z$ = deformation ratios in the $x, y,$ and z directions and A and B are constants.

The values of A, B differ in the various theories of rubber elasticity. The theories of Flory and Wall¹⁻⁴ sum over all the chains in the network before and after deformation and give a form of equation (1) with $A = 1, B = \frac{1}{2}$. James and Guth⁵⁻⁸ sum over all the crosslink positions and consider the effects of a gradual rather than an instantaneous crosslinking of chains, resulting in $A = \frac{1}{2}, B = 0$. Edwards⁹ considers the network to be an infinitely long polymer molecule, where the entropy of the system is limited by crosslinks which are put in as delta functions. The crosslinks are considered to be random and free to slide along the chains, and then frozen in position. The result obtained here is that $A = \frac{1}{2}, B = 0$. This is in agreement with that obtained by James and Guth although in this latter case no particular crosslinking process is assumed.

The shear modulus, G , of the network is:

$$G = \frac{3}{2} AnkT = AvkT \quad (2)$$

for a network with trifunctional crosslinks where n is the number of crosslinks per unit volume. Thus, if we measure the modulus of a network containing a known number of elastically effective chains it is, in principle, possible to determine the value of A . The value of B can only be determined for network deformations accompanied by changes in volume.

Previous papers^{10,11} have described a procedure for pre-

paring polystyrene networks containing a known number of elastically effective chains at various concentrations in inert solvents. An estimation was made of the commonly considered network defects: (i) unreacted functionalities and free chain ends; (ii) closed loops; (iii) entanglements. The results obtained^{10,11} were consistent with the value of $A = \frac{1}{2}$.

In this paper, simple polyurethane networks have been prepared from propylene oxide polyols which have narrow molecular weight distributions. Thus the crosslinks are distributed more regularly than in the polystyrene gels^{10,11}. Elastic moduli have been measured for gels of different concentrations and crosslink density and the results have been interpreted in a similar manner to that used previously. In general the results support the previous analysis^{10,11}.

EXPERIMENTAL

Preparation of networks

Simple polyurethane networks were prepared by the reaction of long chain poly(propylene oxide) polyols with 4,4'-diphenylmethane diisocyanate (MDI) an aromatic diisocyanate. Two types of polyol were used, one trifunctional (T56) and the other bifunctional (B56); each had an equivalent weight per hydroxyl group of about 1000 and the poly(propylene oxide) chains were terminated by a secondary alcohol group. Both polyols were kindly supplied by ICI Ltd Organics Division.

Prior to use, both T56 and B56 were filtered using a G3 sintered glass filter. The polyols were then dried by passing nitrogen through at reduced pressure and heating for about 1 h at 100–110°C. Once dried, the polyols were stored in an evacuated vessel until required. Polyols used in gel preparation were stored under these conditions for no longer than one week.

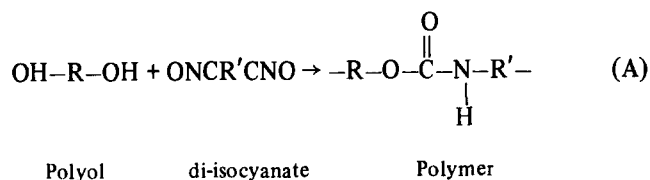
MDI was distilled under reduced pressure prior to use. Using a rotary vacuum pump to obtain reduced pressure, the MDI normally distilled in the range 180–188°C depending on precise value of the pressure. The melting point of the MDI was determined to be 42°C. MDI was used on the same day as it had been distilled thus minimising any deterioration of the MDI which would result in inefficient crosslinking.

* Present address: Department of Chemical Engineering and Chemical Technology, Imperial College, London SW7, UK.

Generally, the solvent used in the gel preparation was dibutyl phthalate (DBP). Prior to use it was dried over calcium hydride for at least one week. Immediately before use it was passed through a G3 sintered glass filter. Other solvents used were diethyl phthalate (DEP), dimethyl phthalate (DMP), diheptyl phthalate (DHP), dinonyl phthalate (DNP), tetralin and diglyme. All were dried and filtered in a way similar to that previously described. It was found necessary to distil the tetralin and diglyme before use to remove peroxides; the presence of peroxides resulted in yellow gels, and reduced modulus.

The method of preparation was simple, all the components being mixed in a 250 ml flask. The amount of MDI used was a few per cent less than that required stoichiometrically. Solid MDI ground to a powder was first weighed accurately into the flask, and then the polyol and solvent were added. The mixture was then heated to about 40°C to dissolve the MDI and the flask was then cooled to room temperature. The mixture was then degassed for a few minutes in order to remove dissolved air. Catalyst was then added. The amount of catalyst added depended on the concentration of polymer in the mixture. Generally one small drop was added to the 100% polymer mixtures and more was added to the less concentrated mixtures; typically about 10 drops of catalyst were added to the 15% polymer mixtures. The catalyst generally used was dibutyltin dilaurate (DBTDL) although different catalysts were also used [triethylene diamine (DABCO) and stannous octoate (SnOc)]. After addition of the catalyst the contents of the flask were mixed under vacuum for about 1 min to ensure uniformity of the components and then poured into a mould, which was then placed into a desiccator containing dried silica gel. This prevented any atmospheric water vapour effecting the mixture during gelation. The mould was typically a 3.5 in diameter crystallizing dish. Gelation took place in a period of 1–5 h at room temperature depending on the initial polymer concentration.

Under these conditions any side reactions were kept to a minimum; rate constants of allophanate reactions (i.e. reaction between urethane and isocyanate groups) are much less than the rate constant for the normal urethane forming reaction. We can also assume that the effect of water can be ignored since all reagents were carefully dried. We assume that the main reaction in the formation of the network is:



This is supported by studies on the structure of similar polyurethane elastomers by n.m.r. spectra¹⁷. Sumi *et al.* found that for a polymer made from poly(propylene glycol) and MDI at 85°C for 3 h, only a single NH peak was observed in the n.m.r. spectra, indicating the presence of simple urethane links only in the polymer. Much of the previous work on polyurethanes has been carried out on materials synthesized under conditions where complex crosslinking reactions occur¹⁸ including allophanate and biuret reactions. The results described here should be simpler to interpret since we can assume that reaction (A) is the only one occurring to any appreciable extent.

Networks were prepared at different solvent concentrations (DBP) and at 3 different ratios of T56: B56. These

were 100% T56, 75% T56, 60% T56 by wt. Thus polymer concentration and crosslink density were varied.

Reaction efficiency

The method used in previous work^{10,11} was used to estimate reaction efficiency. The number of unreacted isocyanate groups remaining in the gel was measured using a ¹⁴C labelling technique. After the gel had been used, and mechanically tested, a sample of ~10 g was broken into small pieces and placed in a stoppered vessel. ¹⁴C-methanol (~1 ml of a suitable activity) was added with about 100 ml of tetrahydrofuran to label the residual isocyanate in the gel. The mixture was left to stand for a week to ensure complete reaction. The remaining unreacted ¹⁴C-methanol was then extracted from the gel by standing in excess of solvent. The solvent was changed daily; heptane and methanol were used alternately. After about 10 series of washings a constant value was obtained. Then the gel was dried, swollen in methanol and redried. The activity of the samples was then measured on a Packard Model 3320 liquid scintillation counter, and compared with a dilute solution of the original ¹⁴C-methanol, and a blank. The scintillation 'cocktail' used consisted of 0.30% diphenyl oxazole and 0.03% bis(5 phenyloxazole-2-yl)benzene in xylene.

Modulus measurement

Modulus measurements were determined in the same manner as described in previous papers^{10,11}. This method is based on the indentation of the gel surface with a solid sphere. A modified dial gauge was used to measure the indentations produced by different loads. The equation used to relate modulus (*G*) to applied force (*P*) sphere radius (*r*), and indentation (*d*), is given by Waters¹³:

$$G = \frac{3P}{16d^3/2R^{1/2}} \quad (3)$$

This method was used to compare the moduli of all gels produced. Two sizes of spheres were used on each gel. If the results obtained from both measurements were not consistent, the measurements were repeated until reproducible modulus values were obtained.

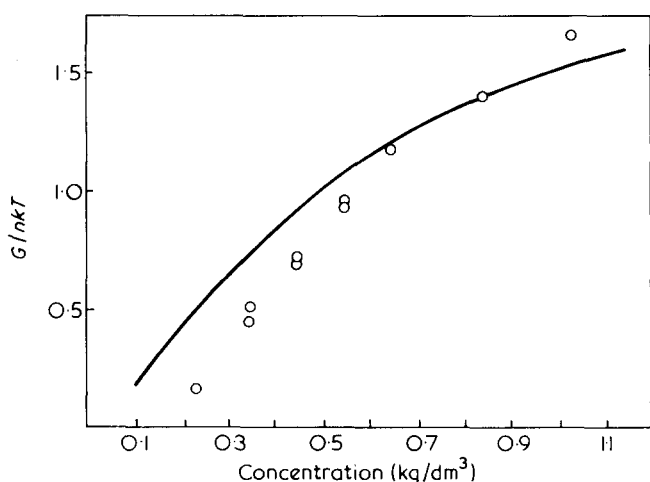
In order to test the reliability of the previous method of modulus measurement further tests were carried out on some of the harder samples produced. In these measurements samples were subject to compressive or extensive forces.

For the simple compression tests a mould was made of PTFE of internal height 4 cm and diameter 2 cm. The mould was filled with the reaction mixture. On completion of the reaction the sample was removed by removing the end caps from the mould and pushing the sample through the mould. The sample was then placed on a comparator bench with a flat glass plate placed over it. Loads were then applied on the load platform above the dial gauge and indentations measured on the gauge.

Sheets of polyurethane were prepared for samples to be used in the extension tests. Two glass sheets were cleaned and, using PTFE and silicon sprays, a thin coating of PTFE was applied followed by a thin coating of silicon grease. These coatings aided removal of the sample. A rubber gasket was cut and the plates and gasket held in position with clamps. The reactants were then paired into the slit at the top of the mould and allowed to set. The sample was removed and suitable strips cut for use on a type E, Houns-

Table 1 Agreement between various methods of modulus measurement

Sample	Method of measurement	Modulus $\times 10^{-4}$ (N/m ²)
A	Extension of strip	84
	Indentation of sphere	96
B	Extension of strip	100
	Indentation with sphere	110
C	Compression of block	73
	Indentation with sphere	76
D	Compression of block	22
	Indentation with sphere	26
E	Indentation with sphere	32.0
	Compression of block	27.6
	Extension of strip	28.2
F	Indentation with sphere	17.1
	Compression of block	15.3
	Extension of strip	13.0

Figure 1 Plot of G/nkT versus concentration for 100% T56 networks

field Tensometer. Using this machine the stress applied to the sample was measured automatically by strain gauges and the data were fed to a chart recorder. The extension was measured at various applied stresses by measuring the distance between fiducial marks on the sample using a cathetometer.

Sample dimensions were measured using callipers, and deformations in extension and compression were generally less than 10%. Equation (4) describes the behaviour of the samples approximately under these conditions.

$$f = \frac{E}{3} (\alpha - \alpha^{-2}) \quad (4)$$

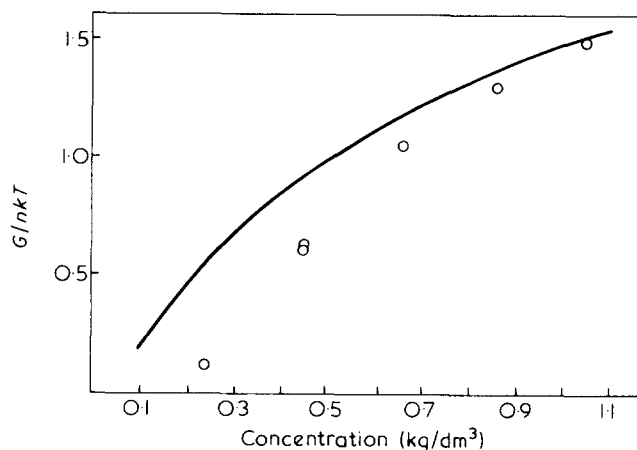
where f is the force applied to the sample per unit unstrained cross-section of the sample, E is Young's modulus and α is the extension ratio. Thus a value of E can be obtained if f is plotted against $(\alpha - \alpha^{-2})$. Assuming Poisson's ratio is $\frac{1}{2}$ we can use the relationship, $E = 3G$, and so determine G , the shear modulus of the material. Table 1 shows the agreement obtained in the various samples tested by more than one method. The agreement between the various methods shows that the modulus values obtained by the indentation method are reasonable when compared with other methods of estimating shear modulus.

CALCULATION AND RESULTS

It is necessary to determine the number of chemical crosslinks in the network. In the calculation it has been assumed that the number of T56 units totally incorporated into the network gave the number of crosslinks in the network. Unless all three 'arms' of the T56 molecule are reacted no crosslink is incorporated in the network. This implies that, if we ignore closed loops and entanglements, no continuous network is formed until the reaction is 66.7% complete in the case of T56 networks, 75% complete for 75% T56, 25% B56 networks and 80% complete for 60% T56/40% B56 networks, assuming we have initially equimolar amounts of isocyanate and hydroxyl groups.

On this basis the number of crosslinks in the network (n) has been estimated. Allowance must be made for the fact that exactly equimolar amounts of isocyanate and hydroxyl groups were not used and for the fact that the reaction was never 100% efficient. The number of T56 molecules totally incorporated into the network gives the number of crosslinks in the network. In 100% T56 networks, 3 isocyanate-polyol reactions are required for each T56 molecule to be incorporated completely into the network. In networks of 75% T56 by wt, 2 T56 molecules exist for each B56 molecule. Thus, on average, 4 isocyanate-polyol reactions are required to incorporate each T56 molecule into the network. In networks of 60% T56 by wt, where 1 B56 molecule is present for each T56 molecule, 5 isocyanate-polyol reactions are required to incorporate each T56 molecule into the network. Thus, an $x\%$ inefficiency of reaction reduces the value of n by $3x\%$: for T56 networks, $4x\%$ for 75% networks, and $5x\%$ for 60% networks. Thus n is a sensitive function of the inefficiency of reaction, and the proportions of initial reactants. It can be seen from the table of results that in this experiment the efficiency of reaction is generally close to 100%. This is in agreement with results of Conway *et al.*¹⁹ where a similar value of the efficiency of reaction was found by nitrogen analysis of the urethane network formed by reaction of poly(propylene oxide) with²⁴ toluene di-isocyanate. Using equation (2) an estimate of the modulus excluding effects of defects can be obtained. In the graphs (Figures 1-3) values of G/nkT are shown, where G is the experimental modulus, and $0.75 nkT$ is the theoretical modulus assuming $A = \frac{1}{2}$ and that no closed loops or entanglements are present.

A series of measurements was made at $\sim 50\%$ polymer concentration in a wide range of solvents. These results are shown in Table 2. They suggested that the modulus of the

Figure 2 Plot of G/nkT versus concentration for 75% T56/25% B56 networks

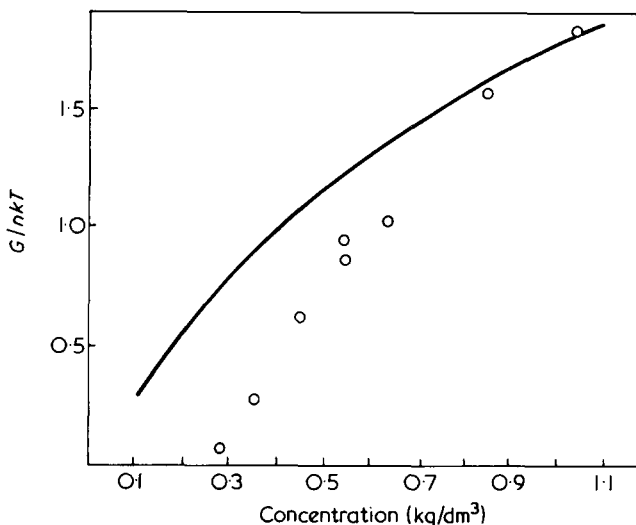


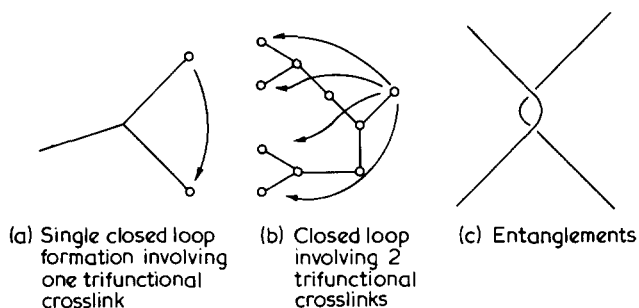
Figure 3 Plot of G/nkT versus concentration for 60% T56/40% B56 networks

gel was independent of the solvent used. Some variation in the value of G/nkT was observed but this was no more than the variation normally observed for any one solvent. The effect of different catalysts was also negligible. Thus we can assume that the results obtained for the system using DBP as solvent and DBDTL as catalyst are not peculiar to this particular system.

Interpretation

If there are no defects in the network we would expect that $G/nkT = 0.75$ for all the series of results. We assume the variation from this result can be explained in terms of network defects. Closed loops result in a loss of elastically effective chain from the network; entanglements result in an increase of effective crosslinks.

Closed loops.



Using the analysis shown in the Appendix, similar to that used previously by Kuhn¹⁴, and Jacobson and Stockmayer¹⁵ we obtain:

$$G/nkT = \frac{3}{2} A \left(1 - \frac{3}{1 + 30C} \right) \left(1 - \frac{3}{1 + 44C} \right) \quad (5)$$

where C = concentration of polymers, and where single closed loops and closed loops involving 2 chains are considered.

For gels with both T56 and B56 present a similar analysis leads equation (A1), to:

$$G/nkT = \frac{3}{2} A \left(1 - \frac{3}{1 + 30C} \right) \left(1 - \frac{3}{1 + K'C} \right) \quad (6)$$

where K' is a constant which can be calculated from the actual ratio of B56 and T56 used. For simplicity, we neglect the effect of larger closed loops which might also be expected to reduce the modulus. Some of the larger loops may also tend to be elastically effective and contribute to the modulus.

Entanglements. Previous results on polystyrene gels^{10,11} have suggested that the effect of entanglements is proportional to C^2 as predicted by Edwards¹⁶. Thus for T56/B56 gels the total variation in G/nkT is described by:

$$\frac{G}{nkT} = \frac{3}{2} A \left(1 - \frac{3}{1 + 30C} \right) \left(1 - \frac{3}{1 + K'C} \right) + 2AR \left(\frac{C}{nkT} \right) C \quad (7)$$

In Figures 1–3 the plots of G/nkT according to equation (7) have been drawn using values of $R = 6 \times 10^5$, 4×10^5 , 3.75×10^5 , where R has been adjusted to give the best fit with experimental results in the high concentration region. These values of R are of the same order as the value of $R = 1 \times 10^5$ determined in the studies of polystyrene gels¹⁰. We might expect that R would be greater for poly(propylene oxide) chains than for polystyrene chains owing to the greater configurational flexibility of the former. The use of different values of R in the three cases might support the view that the effect of entanglements is greater in gels where crosslink density is greater, i.e. the number of entanglement is not only a function of C^2 but also of crosslink density.

A series of measurements have also been obtained of modulus of bulk polymers of varying T56/B56 ratios. Extrapolation of the modulus values to zero T56 concentration allows an estimate to be made of the effect of entanglements in this system at zero chemical crosslink density. The value of R obtained from these results is similar to the value of R used here, for gels with B56 present, i.e. 2×10^5 (Figure 4).

Errors in the experimental value of G/nkT should be small. Values of G/nkT obtained for different gels in similar conditions were within 10% of each other as shown by results in Table 3. This uncertainty arises chiefly from the

Table 2 Effect of solvent and catalyst

No.	Concentration polymer, C (kg/dm ³)	Solvent	Catalyst	Experimental modulus, $G_{\text{exp}} \times 10^{-4}$ (N/m ²)	Theoretical modulus, $nkT \times 10^{-4}$ (N/m ²)	G/nkT
29	0.55	DMP	DBTDL	33.6	36.9	0.93
30	0.55	DEP	DBTDL	32.0	36.4	0.90
31	0.55	DHP	DBTDL	33.4	35.7	1.00
32	0.55	DNP	DBTDL	33.0	33.5	0.94
33	0.56	DBP	DBTDL	38.9	35.3	1.10
34	0.56	DBP	DABCO	33.5	31.7	1.06
35	0.56	DBP	SnOc	32.5	32.0	1.03
36	0.73	DBP	DBTDL	63.5	48.3	1.34
37	0.73	Tetralin	DBTDL	63.5	46.8	1.36
38	0.73	Diglyme	DBTDL	58.0	47.3	1.24

DMP = dimethyl phthalate; DEP = diethyl phthalate; DBP = dibutyl phthalate; DHP = diheptyl phthalate; DNP = dinonyl phthalate; DBTDL = dibutyltin dilaurate; DABCO = triethylene diamine; SnOc = stannous octoate

Table 3 Results

Sample No.	Polymer (%)	Polymer conc. C (kg/dm ³)	Experimental modulus $\times 10^{-4}$ (N/m ²)	$nkT \times 10^{-4}$ (N/m ²)	$G/nkT \times 10^6$	C/nkT
1	100	1.045	106.5	64.94	1.60	1.64
2	81.77	0.849	74.0	53.72	1.58	1.38
3	62.60	0.649	48.8	41.75	1.55	1.17
4	52.89	0.548	33.0	34.91	1.56	0.945
5	42.53	0.445	19.5	27.8	1.60	0.701
6	43.06	0.448	18.5	27.3	1.64	0.678
7	33.16	0.344	8.55	19.63	1.75	0.436
8	33.46	0.348	9.7	19.78	1.75	0.492
9	21.94	0.228	2.149	14.45	1.57	0.149
10	52.90	0.55	32.0	34.80	1.58	0.920
11	100	1.05	75.0	49.56	2.12	1.51
12	81.38	0.86	53.0	40.52	2.11	1.31
13	62.90	0.66	32.0	30.59	2.16	1.05
14	42.98	0.45	12.9	20.72	2.18	0.62
15	42.60	0.45	13.8	21.34	2.09	0.65
16	22.27	0.24	1.10	10.42	2.24	0.11
17	100	1.05	71	34.03	2.67	1.819
18	82	0.86	48.7	31.02	2.76	1.570
19	62	0.64	23.8	23.49	2.74	1.013
20	53	0.55	18.9	20.15	2.72	0.938
21	44	0.45	7.8	12.58	3.59	0.620
22	35	0.36	3.5	13.43	2.70	0.261
23	26	0.28	0.36	5.73	4.80	0.063
24	53	0.55	17.0	20.0	27.6	0.85

Samples 1–10: 100% T56 gels

Samples 11–16: 75% T56 gels

Samples 17–24: 60% T56 gels

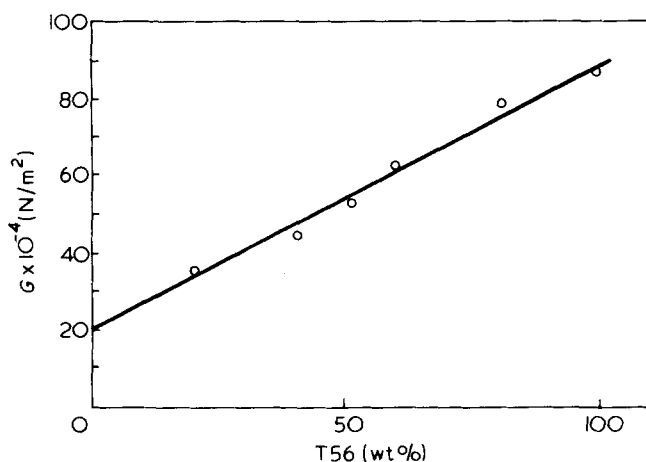


Figure 4 Modulus of 100% polymer networks of various T56: B56 ratios

modulus measurements which have random errors of about 1.5%.

The curves plotted in Figures 1–3 have been calculated using equation (7). Other theoretical curves have been plotted assuming $A = 1$, and assuming that no entanglements exist in the networks. Of all the curves plotted those predicted by equation (7) give the best agreement with experimental results. Thus our results support the view that the front factor, A , in equation (1) is $\frac{1}{2}$ and that the effect of entanglements is proportional to C^2 .

We see that at lower concentrations theoretical curves predict a higher value of modulus than that experimentally determined. This effect becomes more noticeable as the proportion of B56 in the polymer increases. We might ex-

pect that in the region of low concentration of polymer, where the effect of closed loop formation is greatest, our simple analysis of the fraction of closed loops would underestimate the total number of chains lost in closed loop formation since we consider only two possible types of loop. Hence this could explain our observations at low concentration. Future experiments hope to document this effect more thoroughly.

CONCLUSION

Generally there is a fair agreement between experiment and theory as shown in Figures 1–3. This suggests that the estimate of the network defects, i.e. closed loops and entanglements, in the gels are of the correct order of magnitude. The theoretical curves are plotted with a value of $A = \frac{1}{2}$, supporting the use of this value in theoretical equations. It would be difficult to interpret the results using $A = 1$ in equations (6) and (7). The results of these experiments in poly(propylene oxide) networks, thus support the theoretical conclusions reached in previous work on polystyrene networks^{10,11}. The present results, however, were obtained over a wider range of polymer concentration than was possible for the polystyrene gels used previously. In particular it was possible to study dry rubbers.

REFERENCES

- 1 Flory, P. J. 'Principles of Polymer Chemistry', Cornell University Press, Ithaca, 1953
- 2 Flory, P. J. *J. Chem. Phys.* 1950, 18, 108, 112
- 3 Wall, F. T. and Flory, P. J. *J. Chem. Phys.* 1951, 19, 1435
- 4 Wall, F. T. *J. Chem. Phys.* 1953, 11, 527
- 5 James, H. M. and Guth, E. *J. Chem. Phys.* 1947, 15, 669
- 6 James, H. M. *J. Chem. Phys.* 1947, 15, 651

- 7 James, H. M. and Guth, E. *J. Chem. Phys.* 1953, **21**, 1039
- 8 Guth, E. *J. Polym. Sci. (C)* 1966, **12**, 89
- 9 Edwards, S. F. and Freed, E. K. *J. Phys. (C: Solid St. Phys.)* 1970, **3**, 739, 750, 760
- 10 Walsh, D. J., Allen, G. and Ballard, G. *Polymer*, 1974, **15**, 366
- 11 Allen, G., Holmes, P. and Walsh, D. J. *Discuss Faraday Soc.* 1974
- 12 Saunders, J. M. and Frisch, K. C. 'Polyurethane chemistry', Interscience, New York
- 13 Waters, N. E. *Br. J. Appl. Phys.* 1965, **16**, 557
- 14 Kuhn, W. *Kolloid-Z.* 1934, **68**, 2
- 15 Jacobson, W. and Stockmayer, W. H. *J. Chem. Phys.* 1950, **18**, 160
- 16 Edwards, S. F. *3rd Int. Conf. Non-Cryst. Solids*
- 17 Sumi, M. et al. *Makromol. Chem.* 1964, **78**, 146
- 18 Saunders, J. M. *Rubber Chem. Technol.* 1960, **33**, 1259
- 19 Conway, B. E. et al. *J. Polym. Sci.* 1960, **46**, 129
- 20 Allen, G., Booth, C. and Price, C. *Polymer* 1967, **8**, 397

APPENDIX

Estimation of the effects of closed loops in polyurethane gels

If we neglect the effect of closed loops:

$$G = \frac{3}{2} AnkT \tag{A1}$$

$$\frac{G}{nkT} = \frac{3}{2} A \tag{A2}$$

Suppose that x is the fraction of wasted crosslinks, in closed loops, then x is also the fraction of -OH groups wasted in closed loops. At least 2/3 of the -OH groups on the trifunctional polyol must be incorporated into the network for a truly infinite network to be formed. If n' is the total number of -OH groups:

$$G = 0.75(n'kT) \left(1 - \frac{2}{3} - x\right) \tag{A3}$$

$$\frac{G}{n'kT} = 0.75 \left(\frac{1}{3} - x\right) \tag{A4}$$

As $n' = 3n$, for a network of T56 molecules:

$$\frac{G}{nkT} = 0.75(1 - 3x) \tag{A5}$$

Thus if we can calculate x , the fraction of wasted crosslinks, we can estimate the effect of closed loops on the modulus.

We assume a Gaussian distribution of ends:

$$W(x, y, z) = \left(\frac{B}{\pi^{1/2}}\right)^3 e^{-B^2(x^2+y^2+z^2)} dx dy dz \tag{A6}$$

Where $W(x, y, z)$ is the probability of one end of the molecule lying in the volume $dx dy dz$ if the other end is at the origin, and $B = (3/2nl^2)^{1/2}$ where $(nl^2)^{1/2}$ is the root mean square end-to-end distance. If the two chain ends are in the same unit volume $dx dy dz$:

$$W(dv) = \left(\frac{3}{2nl^2\pi}\right)^{3/2} \tag{A7}$$

We assume that the reaction probability is proportional to the concentration of groups in its vicinity.

Single closed loops

For a trifunctional polyol there are two possibilities of closed loop formation. Thus:

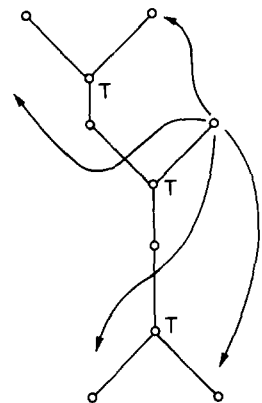
$$W(dv)_{loop} = 2 \left(\frac{3}{2(99)2.14\pi 5.5}\right)^{3/2} \tag{A8}$$

where we have 99 bonds between crosslinks and the average value of l^2 for the chain is 2.14 \AA^2 , and 5.5 is the characteristic ratio for poly(propylene oxide)²⁰.

Closed loop involving 2 trifunctional chains

There are 4 possibilities of closed loop formation:

$$W(dv)_{loop} = 4 \left(\frac{3}{4(99)2.14\pi 5.5}\right)^{3/2} \tag{A9}$$



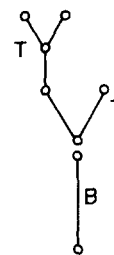
$$W(dv)_{loop} = 11.8 \times 10^{-6}$$

We only consider the effects of these two types of loops. Larger loops will become more elastically effective. The choice of two types of loops only is however an approximation.

Effect of closed loops in T56/B56 mixtures

For the case of single closed loops, we need only consider closed loops involving T56 units. The presence or absence of B56 in the gel will not affect the number of crosslinks, and hence the modulus. Thus the first effects of single closed loops will be in equation (A8). However, the value of $W(dv)_{loop}$ for closed loops involving two chains will depend on the ratios of B56 to T56 in the network.

Thus, for a polyol mixture 75% T56 by wt, two T56 molecules exist for each B56 molecule, as shown in the diagram:



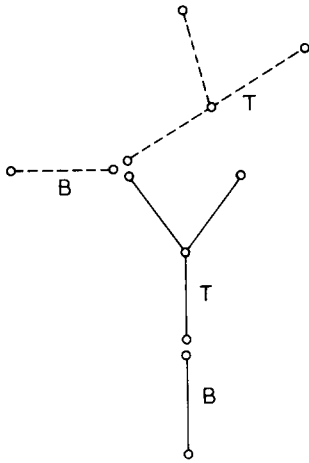
Thus in this case:

$$W(dv)_{loop} = 3 \left(\frac{3}{4(99)2.14\pi 5.5}\right) \tag{A10}$$

In a polyol mixture 60% T56 by wt, two T56 molecules exist for two B56 molecules in the mixture. Thus, one T56 molecule has an equal probability of being adjacent to two B56 molecules or one T56 and one B56 molecule.

This gives:

$$W(dv)_{loop} = 2.5 \left(\frac{3}{4(99)2.14\pi 5.5}\right) \tag{A11}$$



Intermolecular chains

Here we must consider the density of end groups per Å, this will again be proportional to the reaction probability:

$$W(d\nu)_{\text{loop}} = \frac{C \times N_0 \times 10^{-24}}{1000} \quad (\text{A12})$$

where C = concentration of polymer in kg/dm^3 ; N_0 = Avogadro's number; 1000 = equivalent weight of T56, B56; $W(d\nu)_{\text{cross}} = 5.3C \times 10^{-4}$.

Effect of modulus

Fraction of closed loops (f) is given by:

$$\begin{aligned} f &= \frac{W(d\nu)_{\text{loop}}}{W(d\nu)_{\text{loop}} + W(d\nu)_{\text{cross}}} \\ &= \frac{1}{1 + 30C} \quad \text{for single loops} \\ &= \frac{1}{1 + 44C} \quad \text{for loops involving 2 chains in 100\% T56} \\ &= \frac{1}{1 + 60C} \quad \text{for loops involving 2 chains in 75\% T56} \\ &= \frac{1}{1 + 72C} \quad \text{for loops involving 2 chains in 60\% T56} \end{aligned} \quad (\text{A13})$$

Substituting these values of f into equation (A5) we obtain the effect of closed loops on the modulus, given by:

$$\frac{G}{nkT} = \frac{3}{2} A \left(1 - \frac{3}{1 + 30C} \right) \left(1 - \frac{3}{1 + K'C} \right) \quad (\text{A14})$$

For T56, B56 networks K' varies as shown in equation (A13).

In equation (A14) the reduction in n due to single and double closed loops formed simultaneously is obtained by multiplying the two separate terms calculated for single and closed loops respectively.

Correlation between physical-mechanical properties and morphological features of cruciform styrene – butadiene block copolymers

Enrico Pedemonte and Giovanni Dondero

Istituto di Chimica Industriale, Università di Genova, 16132 Genova, Italy

and Francesco de Candia and Gennaro Romano

Laboratorio di Ricerche su Tecnologia dei Polimeri e Reologia, CNR, 80072 Arco Felice (Napoli), Italy

(Received 10 June 1975; revised 11 July 1975)

The structural and morphological characterization of a cruciform styrene–butadiene block copolymer of the $(SB)_4Si$ type is reported together with the stress–strain properties of films prepared by compression moulding. The influence of the compression on the morphology (and therefore on the mechanical properties) are considered in detail because the structure of the specimen becomes particularly simple; it consists of polystyrene cylinders arranged perpendicularly to the compression plane. The rods lead to a semi-continuous polystyrene phase, so that the film exhibits the Mullins and hardening effects already observed for linear three block copolymers. Explanations for these phenomena are given, supported by optical observations and by electron microscopical views of sections cut after deformation.

INTRODUCTION

It is well known that ABA type three block copolymers of styrene (monomer A) with butadiene or isoprene (monomer B) give rise to the unusual ‘thermoplastic elastomers’; these can be easily moulded at temperatures higher than 120°C while at room temperature they behave as vulcanized rubbers even though the polymer molecules are perfectly linear and have no chemical crosslinks. These properties are ascribed to the fact that the polystyrene ends aggregate into domains owing to thermodynamic incompatibility of the A and B blocks; at room temperature the domains are glassy and set as rigid network junctions^{1–10}.

Morphology and physical properties of these materials have been widely studied and comprehensively reviewed^{11,12}. The correlation between them is now made sufficiently clear^{12–16}.

In this paper is discussed the relationship between structural characteristics, morphology and mechanical properties of films obtained by compression moulding of a copolymer whose macromolecules are characterized by four polystyrene–polybutadiene blocks coupled to a tetra-functional silicon group: it is a member of a new set of materials having the general formula $(AB)_nX$ which have been recently prepared^{17,18} and studied with regard to the effect of chain geometry on domain morphology¹⁹.

EXPERIMENTAL

Material and molecular characterization

The material used in our experiments has been a laboratory preparation supplied by Anic Company and labelled Europrene T–162. It is a styrene (S)–butadiene (B) block copolymer of the $(SB)_4Si$ type and several of its molecular

and physical characteristics are summarized in *Table 1*.

The techniques employed to obtain the reported data have been extensively described in a previous paper²⁰. The molecular weights have been measured by light scattering and by osmometry in the Anic Laboratories at S. Donato Milanese (Italy). The polystyrene content has been averaged between the values obtained by u.v. analysis at 262 nm^{21,22} (47.5%), and at 269.5 nm (49.5%) and by refractive index increment²³ (49.6%). Infra-red spectroscopy was used to measure the configurational composition of the elastic fraction²⁴ while the length of the elastic chains was obtained by swelling^{25,26}.

The data clearly show that this copolymer has a rather high molecular weight and about the same contents of polystyrene and polybutadiene; hence the lengths of the blocks are similar and owing to the star-structure of the macromolecule, rather short. Only few entanglements are present in the rubber phase, which is mainly in the *cis*–1,4 configuration.

Table 1 Molecular and physical characteristics of the Europrene T-162

Weight-average molecular weight, \bar{M}_w	1.48×10^5
Number-average molecular weight, \bar{M}_n	0.98×10^5
\bar{M}_w/\bar{M}_n	1.51
Polystyrene (% by wt)	49
Molecular weight of each polystyrene terminal block	1.8×10^4
Molecular weight of each polybutadiene block	1.9×10^4
Configurational composition of the elastic phase:	
<i>trans</i> -1,4-polybutadiene (%)	36
<i>cis</i> -1,4-polybutadiene (%)	56
1,2-polybutadiene	8
M_c , (molecular weight of the elastically efficient chain)	1.75×10^4

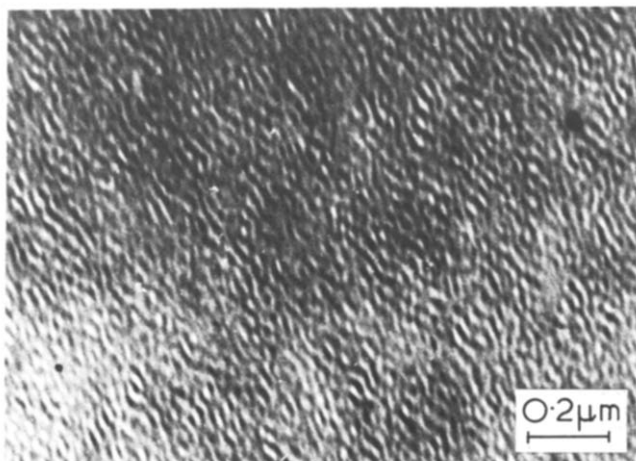


Figure 1 Electron micrograph of an ultra-thin section of Europrene T 162 original copolymer

Compression moulded films preparation and stress-strain measurements

Films of the material were obtained by die casting at 120° – 130° C and under slight pressure (2 – 3 kg/cm²).

Stress-strain measurements were carried out using a tensile tester of the Toyo Measuring Instruments Ltd. The deformation rate was 10 mm/min. The sample length was 2 cm in all the experiments; this gives a strain rate of 0.5 min⁻¹. The stress-strain plots were detected at room temperature (20° C).

The effects of the mechanical history on the sample properties were investigated by resting for 30 min at zero load between two successive deformation cycles.

Morphology

For the morphological analysis by electron microscopy, ultra-thin sections were cut at low temperature²⁷. The

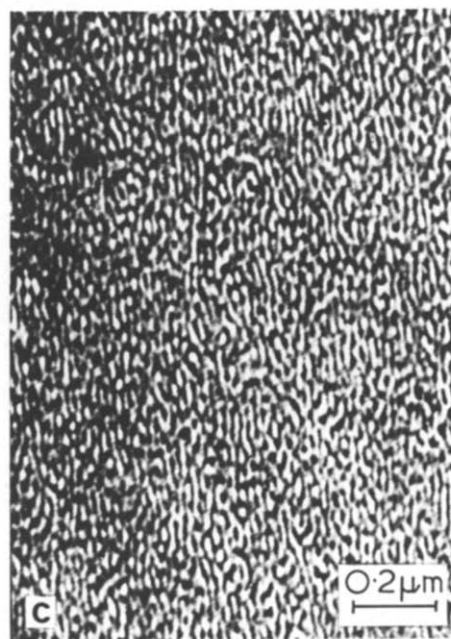
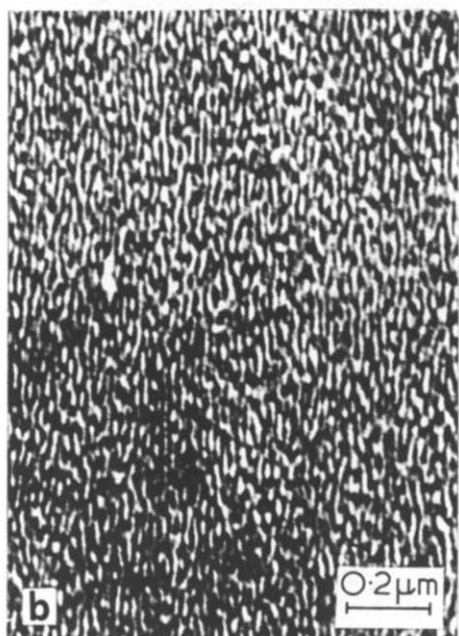
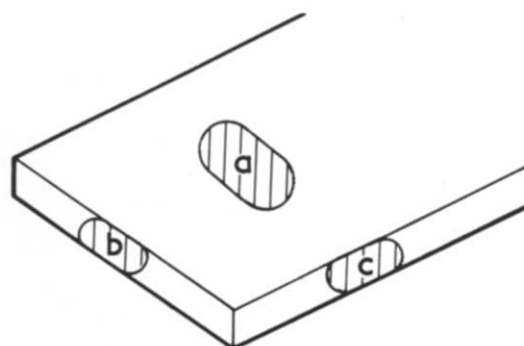


Figure 2 Electron micrograph of ultra-thin sections of compression moulded Europrene T 162 film. Section (a) corresponds to the surface parallel to the compression plane; sections (b) and (c) have been cut along the compression direction and their orientations differ 90°

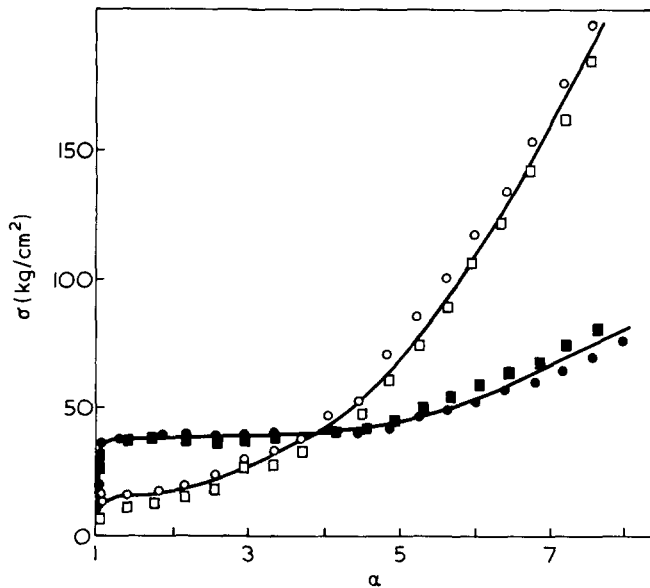


Figure 3 Stress-strain isotherms of the compression moulded Europrene T 162 films, detected at room temperature. ■, Sample A, first run; □, sample A, second run after 30 min of relaxation at zero load; ●, sample B, first run; ○, sample B, second run (same conditions)

rubbery phase of the specimen was contrasted by exposing the sections to the vapours of an aqueous OsO_4 solution²⁸ at room temperature for several minutes; so that in the electron micrographs the butadiene phase will appear dark and the styrene bright.

The copolymer was studied both as supplied by the manufacturer and as a compression moulded film. In the latter case the effect of the deformation on the morphology has also been investigated.

RESULTS

Figures 1 and 2 show the morphologies of the original material and of the compression moulded film. In the first case morphology is characterized by short rods of polystyrene oriented along a well defined direction, probably as the consequence of an uncontrolled mechanical treatment which follows the polymerization process. In the latter case we can reach some conclusions on the structure of the specimen provided. We were able to look at three sections, cut perpendicularly to each other and corresponding to the planes indicated in Figure 2; it appears that compression arranges the rods almost perpendicularly to the compression plane.

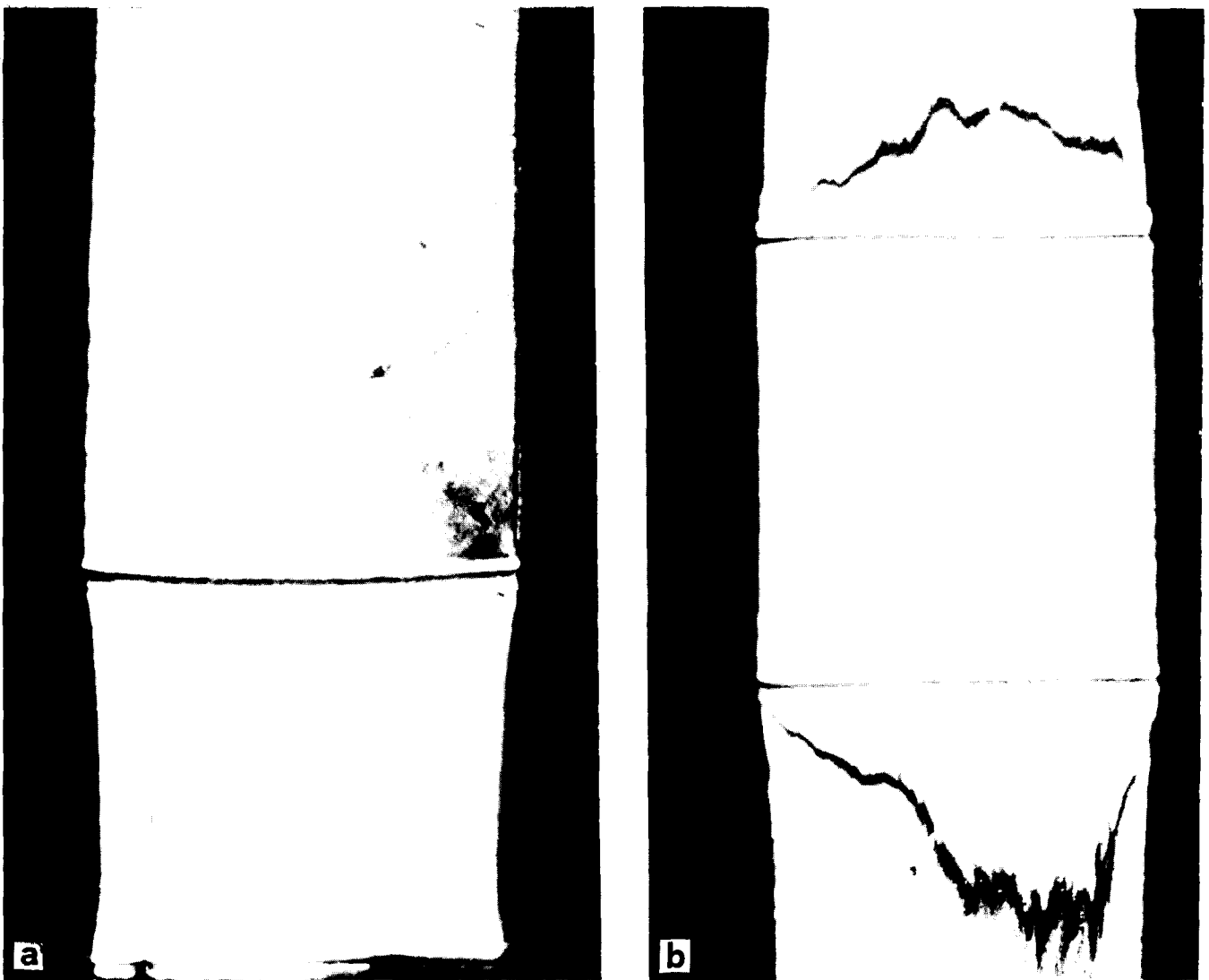


Figure 4 (a) Neck present in a sample deformed at $\alpha = 1.5$. (b) Double neck present in a sample deformed at $\alpha = 4$. The photographs were detected in polarized light, at crossed Nicols

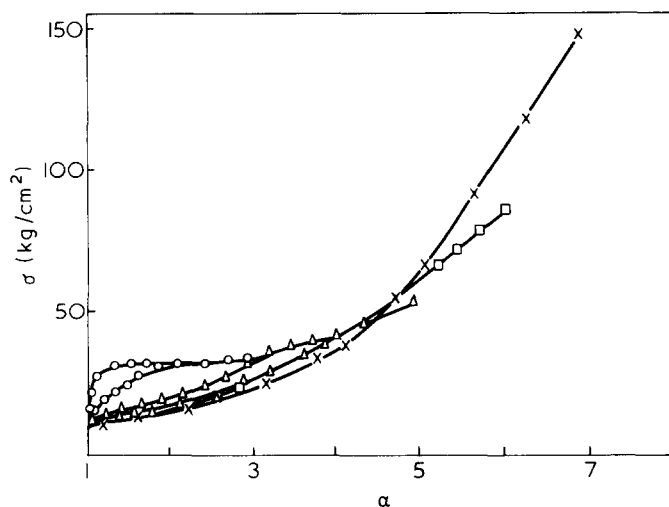


Figure 5 Mullins effect as observed in a sample deformed increasing step by step the maximum strain value

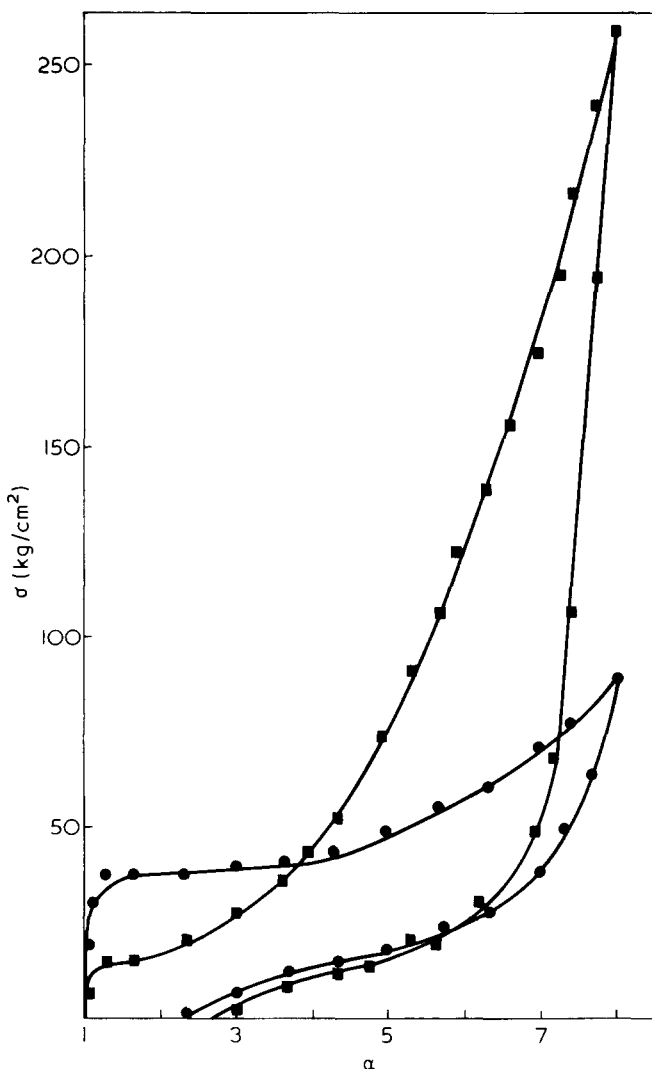


Figure 6 Hysteresis loops detected on a compression moulded film. ●, first run; ■, second run (same conditions of Figure 3)

Figure 3 shows the stress-strain isotherms obtained using compression moulded films. Plots, detected on two different samples, show the effects on the mechanical behaviour when two successive deformation runs are performed, allowing 30 min relaxation at zero load between the first and the second cycle. There is clearly a strong influence of the previous mechanical treatment.

Macroscopic observations give evidence that in the first deformation run the strain increases by neck propagation, while necks are absent in the second run. In Figure 4a the neck which is present in a sample deformed at $\alpha = 1.5$ and in Figure 4b a double neck is present in a sample deformed at $\alpha = 4$. These pictures were obtained with crossed Nicols using light polarized at 45° with respect to the deformation axis.

The effect shown in Figure 3 is stressed in Figure 5, where the mechanical behaviour is studied as function of the previous mechanical history of the specimen, increasing step by step the maximum strain value between two successive deformations. Data of Figure 5 indicate the presence of the well known Mullins effect^{29,30}.

Figure 6 shows the hysteresis loops detected in two successive cycles, observing the same conditions of Figure 3, i.e. 30 min relaxation at zero load between the first and the second cycle.

Figures 7 and 8 show the morphologies of compression moulded films after stretching, at deformation ratios of $\alpha = 3$ and $\alpha = 6$ respectively; the sections have always been cut along the stretching direction.

DISCUSSION

It is evident from Figures 7 and 8 that the deformation of the specimen produces the orientation of the polystyrene rods in the stretching direction. These rods are oriented normally to this direction in the compressed film (Figure 2). Some differences may be observed between Figures 7 and 8, which correspond to different degrees of deformation; in particular the continuity of the polystyrene phase is more pronounced at $\alpha = 3$ than at $\alpha = 6$, where the polystyrene rods are shorter owing to the rods breaking under the strain¹⁵.

On the basis of these morphological features the mechanical behaviour as reported in the previous section can be analysed.

The most important phenomenon observed is the macroscopic deformation mechanism of the sample, i.e. the neck propagation. The presence of a neck is generally due to structural changes induced by the stretching; in the present case the structural change involves orientation of the polystyrene rods. As stated previously, before stretching the rods are perpendicular to the compression plane of the film (and therefore to the strain direction) but they become parallel to it after stretching. The neck formation would

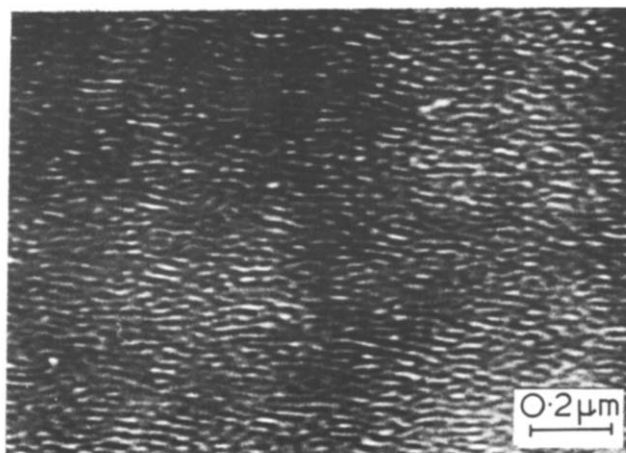


Figure 7 Electron micrograph of ultra-thin section of compression moulded Europrene T 162 film after stretching at $\alpha = 3$. Section cut perpendicular to the compression plane and along the stretching direction

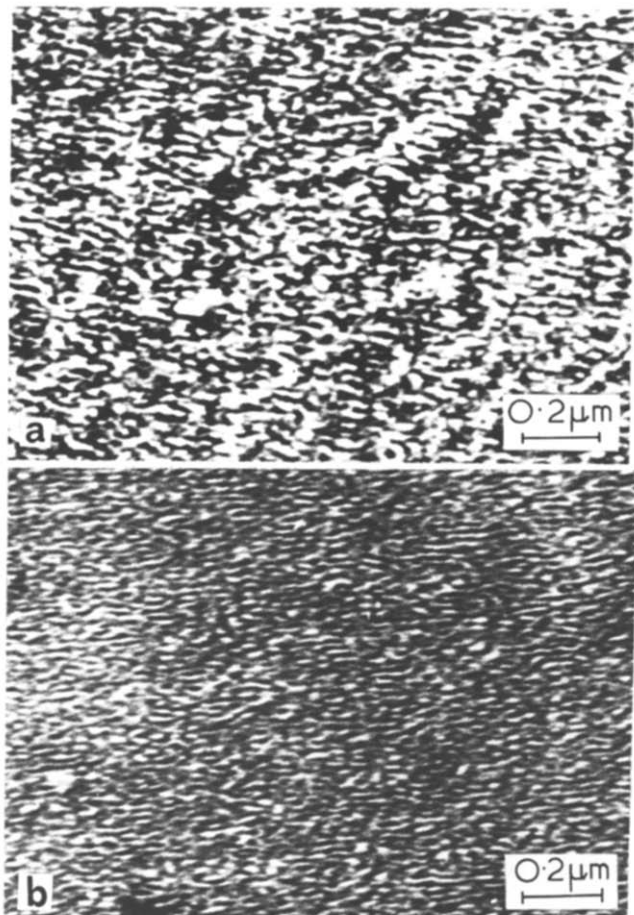


Figure 8 Electron micrograph of ultra-thin sections of compression moulded Europrene T 162 film after stretching at $\alpha = 6$. Section (a) corresponds to the surface of the compression plane; section (b) is perpendicular to it; both have been cut along the stretching direction

correspond to this mechanism. This mechanism is irreversible and necks are present only in the first deformation run; they are not observed in the second one.

The presence of necks gives rise to a plastic deformation which, as far as the mechanical behaviour is concerned, corresponds to the yield region observed in the first stress-strain run of Figure 3. This yield region covers the strain range 1.05–4.5.

The orientation mechanism and rod breaking observed in Figure 8 also explain the stress softening of the second deformation run for the lower values of the strain, generally up to $\alpha = 4$. This phenomenon, clearly shown in Figure 5 where the strain is increased step by step, is due to the irreversibility of the two effects. The mechanical work necessary to orientate and to break some of the rods, is not necessary in the second run and therefore the same values of the strain can be reached with a lower force.

In a previous paper¹⁵ we have shown that when the polystyrene rods are well oriented along the stretching direction, the Mullins effect is due to the breaking of the cylinders. If the rod's axis does not correspond to the stretching direction, it seems reasonable that the organization of the structure needs additional mechanical work which gives its contribution to the irreversible stress-softening effect.

One must seek a different explanation for the stress hardening observed in the second run for the higher values of the strain. As suggested in a previous paper¹⁶, this phenomenon can be due to a kinetic mechanism. The presence of hard polystyrene rods, which behave as fillers, reduces sensitively the conformational freedom of the elastomeric polybuta-

diene chains. The orientation of these chains, owing to the first deformation cycle, is partly irreversible in the time scale of the experiment and therefore, in the second run, we stretch chains that are still stretched, even if partly. Work is in progress to give a more direct evidence of the suggested mechanism.

One may conclude with some considerations about Figure 6. Graphical integration of the two hysteresis loops gives for the first run $\Delta F = 5.26 \text{ cal/cm}^3$ and for the second run $\Delta F = 9.88 \text{ cal/cm}^3$, where ΔF is the free energy dissipated in the hysteresis cycle. The ratio $\Delta F/\Delta F_{\text{tot}}$, where ΔF_{tot} is the energy given to the system on increasing the strain, is the relative amount of dissipated energy; calculation gives 0.58 and 0.64 for the first and second runs, respectively. These results indicate that the absolute value of the dissipated energy is very different in the two runs while the relative values are rather similar. On the basis of the proposed mechanisms, i.e. in the first run a dissipation due mainly to the rods orientation and breaking and in the second one a dissipation due mainly to the low chain mobility, the latter results are surprising. Work is in progress to obtain more experimental data in this field, particularly for specimens whose deformation does not involve any orientation of rods but only breaking.

REFERENCES

- 1 Bianchi, U., Pedemonte, E. and Turturro, A. *Polymer* 1970, **11**, 268
- 2 Leary, D. F. and Williams, M. C. *J. Polym. Sci. (B)* 1970, **8**, 335
- 3 Leary, D. F. and Williams, M. C. *J. Polym. Sci. (Polym. Phys. Edn)* 1973, **11**, 345
- 4 Lo Flair, R. T. *Pure Appl. Chem.* 1971, **8**, 195
- 5 Meier, D. J. *J. Polym. Sci. (C)* 1969, **26**, 81
- 6 Meier, D. J. *Polym. Prepr.* 1970, **11**, 400
- 7 Kromer, H., Hoffmann, M. and Kampf, G. *Ber. Bunsenges, Phys. Chem.* 1970, **74**, 859
- 8 Soen, T., Inoue, T., Miyoshi, K. and Kawai, H. *J. Polym. Sci. (A-2)* 1972, **10**, 1757
- 9 Krause, S. *J. Polym. Sci. (A-2)* 1969, **7**, 249
- 10 Krause, S. *Macromolecules* 1970, **3**, 84
- 11 Folkes, M. J. and Keller, A. 'The Physics of Glassy Polymers', (Ed. R. N. Haward), Applied Science, London, 1973, p 548
- 12 Estes, G. M., Cooper, S. L. and Tobolsky, A. V. *J. Macromol. Sci. (C)* 1970, **4**, 313
- 13 Inoue, T., Moritani, M., Hashimoto, T. and Kawai, H. *Macromolecules* 1971, **4**, 500
- 14 Turturro, A., Bianchi, U., Pedemonte, E. and Ravetta, P. *Chim. Ind. (Milan)* 1972, **54**, 782
- 15 Pedemonte, E., Turturro, A. and Dondero, G. *Br. Polym. J.* 1974, **6**, 277
- 16 Pedemonte, E., Dondero, G., Alfonso, G. C. and De Candia, F. *Polymer* 1975, **16**, 531
- 17 Price, C., Watson, A. and Chow, M. T. *Polymer* 1972, **13**, 333
- 18 Price, C. and Woods, D. *Polymer* in press
- 19 Price, C., Lally, T. P., Watson, A. G., Woods, D. and Chow, M. T. *Br. Polym. J.* 1972, **4**, 413
- 20 Conio, O., Orlandini, D. and Pedemonte, E. *Rass. Chim. (Rome)* in press
- 21 Cunningham, R. E. and Treiber, M. R. *J. Appl. Polym. Sci.* 1968, **12**, 23
- 22 Uchida, T., Soen, T., Inoue, T. and Kawai, H. *J. Polym. Sci. (A-2)* 1972, **10**, 101
- 23 Huglin, M. B. *J. Appl. Polym. Sci.* 1965, **9**, 4003
- 24 Silas, S., Vates, J. and Thornton, V. *Analyt. Chem.* 1959, **31**, 529
- 25 Flory, P. J. and Rehner, J. *J. Chem. Phys.* 1943, **18**, 108
- 26 Bishop, E. T. and Davison, S. *J. Polym. Sci. (C)* 1969, **26**, 59
- 27 Dondero, G., Olivero, L., Devetta, P., Cartasegna, S. and Pedemonte, E. *Nuova Chimica (Milan)* 1972, (10), 48
- 28 Kato, K. *Polym. Eng. Sci.* 1967, **7**, 38
- 29 Mullins, L. and Tohin, N. R. *Proc. 3rd Rubber Technol. Conf. London* 1954
- 30 Bueche, F. *J. Appl. Polym. Sci.* 1960, **4**, 107

Creep behaviour of annealed UPVC and PMMA

D. C. Wright

Rubber and Plastics Research Association, Shawbury, Shrewsbury SY4 4NR, UK
(Received 26 March 1975)

The 20°C creep compliance of UPVC is temporarily increased by prior annealing at temperatures above ~45°C and below T_g . This effect increases with decreasing annealing time. Similar behaviour is observed with PMMA which suggests that this may be a general phenomenon shared by polymers in the 'glassy amorphous state'. The temporary, and therefore unstable nature of the annealed state is inappropriate for a test specimen, particularly for tests of long duration. It is suggested that volume relaxation in UPVC below 45°C proceeds by short range separation into regions of molecular order and disorder. This state is rapidly disrupted at temperatures above 45°C.

INTRODUCTION

Thermal conditioning prior to property evaluation is a favoured method of minimizing batch-to-batch variability. A relatively severe and recent thermal conditioning treatment supposedly erases the influence of the (often unknown) previous thermal history. This provides an easily accessible materials reference state which, however, is almost certainly arbitrary. The reference state in addition may be only a transient one and therefore not stable over the period of test. An arbitrary unstable reference state is particularly inappropriate for creep testing, where long test durations are common and creep data are often intended for use in design calculations.

According to classical concepts of the glassy amorphous state, a polymer at any temperature below its glass transition temperature (T_g) undergoes volume relaxation (densification). The rate of this relaxation at temperatures far below T_g is so small that for normal periods of observation the state is apparently stable. At temperatures approaching T_g , the rate of volume relaxation will be increased, resulting in a detectable change in the density and properties of the polymer.

Retting¹ investigated the effect on the tensile modulus of UPVC after annealing for various periods at a temperature of ($T_g - 17$)°C. The modulus (25°C) at low strain rates increased substantially with annealing time. At high strain rates the modulus was not significantly affected. Foltz and McKinney² employed a similar heat treatment on UPVC and attributed the observed increase in the pre-glass transition endotherm to an increase in crystallinity. Illers³ attributed a similar effect to a decrease in free volume. These observations are compatible with classical expectations. Volume relaxation involves an increase in molecular order; this decreases molecular mobility and therefore increases the long term (low strain rate) modulus. The high strain rate modulus is not primarily dependent on molecular mobility and is therefore not sensitive to annealing.

Turner⁴ investigated the effect of pre-conditioning period at 60°C on the creep response of UPVC at 60°C. It was reported that the time dependent creep compliance decreased with increasing pre-conditioning period. Therefore in this respect the response is apparently classical and

indicative of volume relaxation in the direction of equilibrium.

The procedure adopted here involves room temperature creep testing after annealing periods at various temperatures. Although annealing as compared with pre-conditioning introduces an additional interaction (the cooling cycle) it does offer a distinct advantage. The effect of thermal treatment can only be ascertained unambiguously by comparison with the state or response of the untreated material. The creep behaviour with no annealing presents no problem, but the zero pre-conditioning state is unattainable.

EXPERIMENTAL

The following sequence was adopted:

- (1) Calendered sheets of UPVC (Cobex 018 grade supplied by BXL Ltd) were stored for 2 years at 20°C.
- (2) Creep specimens of nominal dimensions 3 × 5 × 140 mm were prepared.
- (3) Creep specimens were stored in ovens at either 60° ± 1°, 50° ± 1°C, or 40° ± 1°C.
- (4) After a specified annealing period covering a range between 1 and 2000 h, specimens were removed and cooled (to 20°C) under controlled forced air convection for 30 min.
- (5) The cross-sectional areas of the cooled specimens were measured and the specimens prepared for tensile creep testing.
- (6) 1 h, 24 h, or 336 h after the removal of the specimen from its oven (termed the delay time) a tensile stress of 25 MN/m² was applied and the creep strain recorded for 10⁴ sec.

A similar sequence but with only one annealing temperature of 60°C, and one delay time of 1 h was applied to PMMA (cast Perspex, ICI Ltd).

The tensile creep machines used in the study have been described previously⁵. A Moiré fringe extensometer, employing crossed diffraction gratings with a ruling pitch of 4 μm provides the means of automatic strain detection. The Moiré fringe image illuminates an assembly of 4 silicon photodiodes. The photodiode signal is amplified and shaped to provide 2 or 4 counter compatible pulses for each 4 μm extension or contraction of the 66.67 mm gauge length.

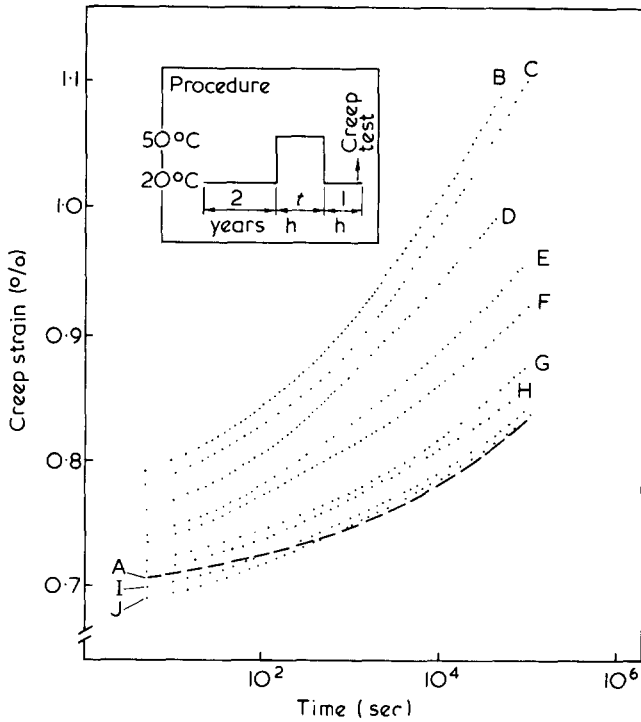


Figure 1 Tensile creep characteristics for UPVC at 20°C and 25MN/m². The parameter is the annealing time in hours. The delay time between cooling and testing is 1 h. Hours (t) stored at 50°C prior to room temperature creep test: A, t = 0; B, t = 1; C, t = 2; D, t = 6; E, t = 14; F, t = 24; G, t = 96; H, t = 600; I, t = 1900; J, t = 2400

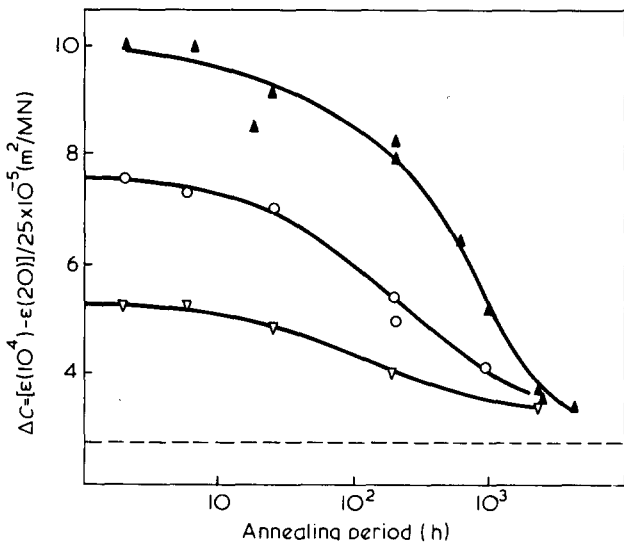


Figure 2 Time dependent tensile creep compliance ΔC of UPVC at 20°C vs. annealing time at 60°C. Delay time between annealing and testing: ▲, 1; ○, 24; ▽, 336 h. -----, no annealing

Thus strain increments of 0.0015% can be totalized on a bi-directional counter and/or used to trigger a digital event recorder which essentially records the time coordinate for each positive or negative strain increment for the duration of the creep test.

RESULTS

The family of creep curves shown in Figure 1 are for UPVC with various annealing periods at 50°C with a 1 h delay before testing. The creep characteristic with no thermal treatment is identified by the broken line. Similar data were

generated after longer delay times and at different annealing temperatures. The initial creep response tended to be rather erratic for these annealing treatments, but the time dependent response defined as ΔC , shown in Figure 2, 3, 4 and 5, proved to be smoothly related to annealing and delay time. The time dependent compliance ΔC is defined here:

$$\Delta C = [\epsilon(10^4) - \epsilon(20)] / \sigma$$

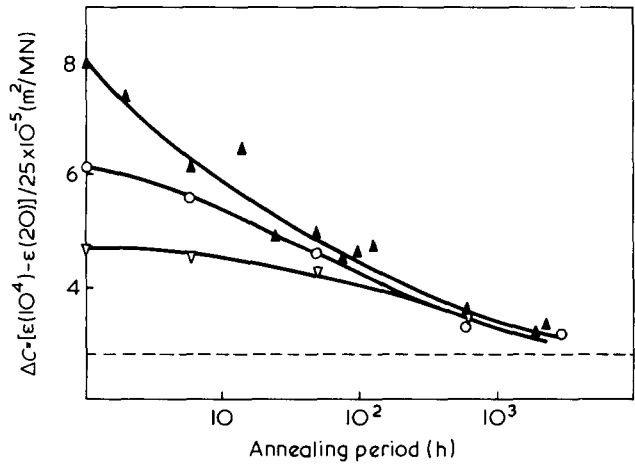


Figure 3 Time dependent tensile creep compliance ΔC of UPVC at 20°C vs. annealing time at 50°C. Delay time between annealing and testing: ▲, 1; ○, 24; ▽, 336 h. -----, No annealing

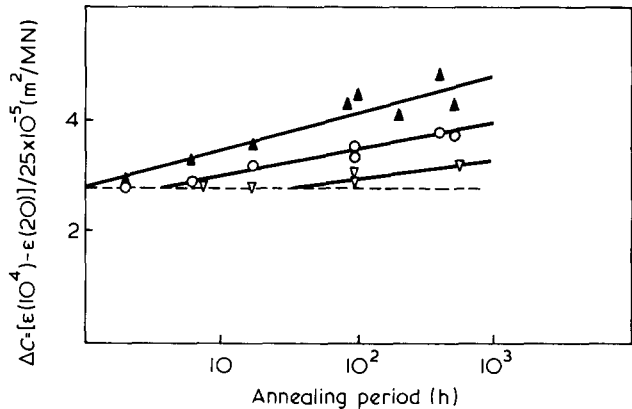


Figure 4 Time dependent tensile creep compliance ΔC of UPVC at 20°C vs. annealing time at 40°C. Delay time between annealing and testing: ▲, 1; ○, 24; ▽, 336 h. -----, No annealing

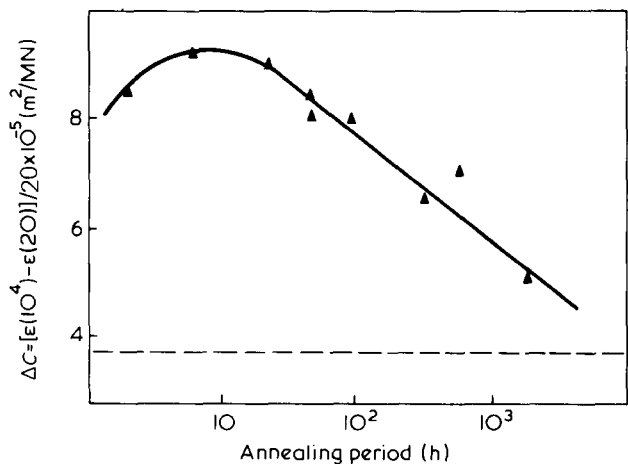


Figure 5 Time dependent tensile creep compliance ΔC of cast PMMA at 20°C vs. annealing time at 60°C. Delay time between annealing and testing is 1 h. -----, No annealing

where $\epsilon(20)$ and $\epsilon(10^4)$ are the strains recorded 20 sec and 10^4 sec after a stress application of $\sigma = 25 \text{ MN/m}^2$ (UPVC), and $\sigma = 20 \text{ MN/m}^2$ (PMMA). The ΔC versus annealing time format is convenient in that it enables the gross effects of annealing time, delay time, and annealing temperature to be conveniently compared. It is these gross effects rather than detailed changes in the shape of the creep characteristic that are the subject of the discussion.

DISCUSSION

The following features are observed in *Figures 2, 3 and 4*.

- (a) UPVC specimens which have been annealed at 50° and 60°C show a decreased resistance to creep deformation (increase in ΔC compared with unannealed specimens). This effect is enhanced for short annealing and delay periods.
- (b) UPVC specimens which have been annealed for very long periods at 50° or 60°C exhibit similar creep behaviour to those with no heat treatment.
- (c) The severe effect of short annealing periods observed at annealing temperatures of 50° and 60° are not observed after annealing at a temperature of 40°C .
- (d) The effect of increasing the delay time between annealing and testing is to generally reduce the effects of annealing. The material state after short annealing periods is particularly unstable.

The observed increase of the time-dependent compliance after annealing is the reverse of that anticipated for a classical glassy amorphous polymer. *Figure 5* shows that this anomalous behaviour is not peculiar to PVC but also occurs with PMMA. This conclusion is derived from comparison with the non-annealed reference state response. If this response was not known then the data in *Figure 2 and 3* would appear to be classical, i.e. a decrease in compliance with increasing annealing time. This is qualitatively similar to the trend observed by Turner⁴ and discussed in the introduction.

It would be logical in the absence of any other evidence to seek an explanation for this anomalous behaviour by reference to observed morphological differences between UPVC and that of a classical glassy amorphous polymer. Morphological studies have revealed direct evidence of ordered regions in UPVC⁶⁻⁸. These regions might be regarded as small crystallites or regions of molecular orientation with a characteristic cohesive energy and a specific melt temperature, or simply as regions of zero configurational entropy which are stable below a particular temperature. Clearly, both aspects describe the same phenomenon but at this stage it is considered preferable to treat each one separately.

Iobst⁹ has estimated that the smallest stable unit of molecular order in plasticized PVC would be disrupted at temperatures above 50°C . Larger ordered units have a higher melt temperature but their formation is less probable. Stafford¹⁰ has used the argument that the disruption of 'crystallites' is responsible for the phenomenon of 'reversible stiffening in plasticized PVC'. The compliance of plasticized PVC increases dramatically after annealing but slowly returns to its original stiffness with time after annealing. In this respect the response to annealing is similar to that reported here, but Stafford did not observe the transition in short period annealing effects at 45°C . This transition being close to the minimum 'crystal melt' temperature as calculated by Iobst adds considerably to the case for a thermal disruption model. The effect of thermal

history on the creep response of UPVC could be explained by the following sequence:

- (1) Over extended periods (2 years in this case) at 20°C , small crystallites are formed which are stable at this temperature. The low (or zero) free volume within the crystallite structure is responsible for deformation processes with very long retardation times. Hence the presence of crystallites might be considered as delaying the strain response and decreasing the creep compliance after long creep times.
- (2) After short periods of annealing at 50° or 60°C , the crystallites suffer rapid thermal disruption leading to an increase in creep compliance particularly after long periods under load.
- (3) After long periods of annealing above 45°C , the free volume is slowly reduced by the classical process of volume relaxation. As this proceeds the creep compliance will slowly decrease.
- (4) With increasing delay time after annealing, crystallites are slowly reformed with an attendant decrease in compliance.

The second approach is to consider the entropy of the system. Gibbs and Di Marzio¹¹ have proposed that even though the observed T_g is a kinetic phenomenon, there is an underlying thermodynamic transition at a lower temperature T_2 . If the polymer is cooled infinitely slowly, then at T_2 the configurational entropy of the specimen as a whole, would be zero. Adam and Gibbs¹² calculated that a universal expression for T_2 could be:

$$T_2 = (T_g - 53)^\circ\text{C}$$

According to Adam *et al.* the activation volume in the Eyring¹³ viscosity equation is identified as the minimum cooperatively rearranging region. The transition probability, the mobility, and hence the relaxation or creep rate increases as this minimum activation volume decreases. Clearly this cooperative entity must contain free volume for internal rearrangement, or more precisely a unit value of quantized free volume (hole) must be present. The volume of the cooperative entity, and hence the rate of relaxation and creep, might therefore depend significantly on the distribution of free volume or on the size of the quantized unit of free volume. At temperatures below T_2 , close packing is energetically favourable because the equilibrium configurational entropy is zero. This cannot be achieved on a macroscopic scale within a finite time as this involves large diffusion distances and a high degree of molecular cooperation.

It is proposed here, however, that explosion of free volume could be achieved within a finite time at the short range level. The result of such a process would be small regions of aligned molecular segments (crystallites) with zero configurational entropy, bounded by a region with a high free volume content. Pictorially, this is similar to the fringed micellar grain model of the 'glassy' state adopted by Yeh¹⁴. Therefore it could be envisaged that after a finite period of storage at 20°C the quantized unit of free volume would increase in size with a resultant increase in the minimum volume of molecular cooperation and a decrease in creep compliance. On raising the temperature above T_2 the ordered regions are rapidly disrupted with a resultant decrease in the volume of the cooperative entity and increase in compliance.

Both the energy and entropy approach combine strongly to support the hypothesis that the volume relaxation process below $\sim 45^\circ\text{C}$ is quite different from that operating

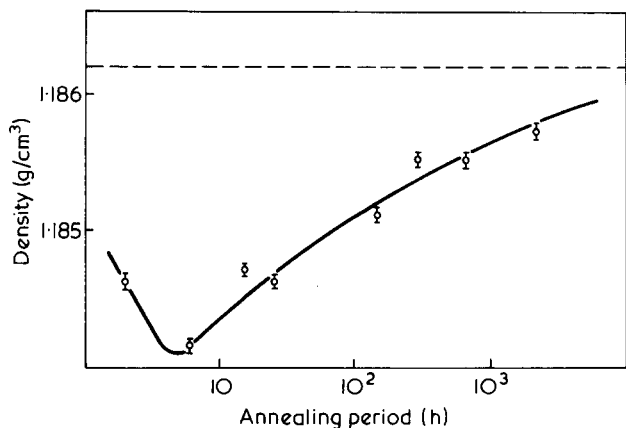


Figure 6 Density of cast PMMA after a range of annealing periods at 60°C. -----, Density with no annealing

above this temperature. Above 45°C, volume relaxation proceeds classically by a uniform diffusion of free volume. Below ~45°C (T_2) the uniform diffusion process is no longer energetically favourable and is replaced by a short range process which results in the formation of 'small islands' of order in a matrix of disorder. The short range ordered regions are disrupted rapidly on annealing above 45°C and it is proposed that this is responsible for the anomalous creep behaviour reported here for UPVC.

The existence of two different volume relaxation processes could also explain why in some cases (e.g. Retting¹) apparently classical effects are observed after annealing. The period at room temperature prior to annealing determines whether sufficient localized volume relaxation has accumulated to give a non-classical response. Thus a recently processed polymer may be expected to react differently to annealing than one stored below T_2 for a long period prior to annealing.

It is not necessary to predict that on annealing above T_2 the disruption of ordered regions will result in a net decrease in density. The redistribution of free volume can be sufficient to qualitatively account for the effects observed. However, the model would predict a density decrease with further annealing owing to normal volume relaxation. An attempt was made to detect the change in density of UPVC after various annealing treatments but, with the resolution available, this could not be achieved. Density measurements on cast PMMA using a density column gradient of ~0.0005 (g/cm)/cm did, however, reveal a significant decrease in density after annealing for short periods at 60°C, followed by an increase in density with increasing annealing period. These density data are shown in Figure 6. Similar density

changes have been observed by Golden *et al.*¹⁵ for annealed polycarbonate.

CONCLUSION

The materials reference state generated by annealing PVC above ~45°C is not stable at room temperature. The instability is liable to distort the creep characteristics and thereby render this method of specimen conditioning counter-productive. The effect is particularly severe after short (practical) annealing periods.

The effect of annealing UPVC between ~45°C and T_g is to decrease the time dependent creep modulus of the polymer. This phenomenon was also apparent with PMMA at an annealing temperature of 60°C. In the case of PMMA the reduction of creep modulus coincided with a significant decrease in density. The transition temperature, $T_2 = 45^\circ\text{C}$, for UPVC could be associated with either the 'melt' temperature of small crystallites or the equilibrium temperature for zero configurational entropy. It follows from both concepts that the processes of volume relaxation that operate above and below this transition (T_2) are quite different, it is suggested that below T_2 the predominant process is that of local diffusion of free volume to give small but definite regions of molecular order and disorder. Above T_2 the ordered regions are no longer stable and after disruption, volume relaxation proceeds by the operation of a more diffuse or homogeneous contraction of free volume.

REFERENCES

- 1 Retting, W. *Angew. Makromol. Chem.* 1969, 8, 87
- 2 Foltz, C. R. and Mckinney, P. V. *J. Appl. Polym. Sci.* 1969, 13, 2235
- 3 Illers, K. H. *Makromol. Chem.* 1969, 127, 1
- 4 Turner, S. *Br. Plast.* 1964, 37, 682
- 5 Wright, D. C. *RAPRA Bull.* 25, 1971, p 133
- 6 Natta, G. and Corradini, P. *J. Polym. Sci.* 1956, 20, 251
- 7 Koenig, J. L. and Druedow, D. *J. Polym. Sci. (A-2)* 1969, 7, 1075
- 8 Witenbafer, D. E. *J. Macromol. Sci. (B)* 1970, 4, 915
- 9 Iobst, S. A. *Thesis Lehigh University* (1970)
- 10 Stafford, T. G. *Thesis Bradford University* (1973)
- 11 Di Marzio, E. A. and Gibbs, J. H. *J. Polym. Sci. (A)* 1963, 1, 1417
- 12 Adam, G. and Gibbs, J. H. *J. Chem. Phys.* 1965, 43, 139
- 13 Eyring, H. *J. Chem. Phys.* 1936, 4, 283
- 14 Yeh, G. S. Y. *J. Macromol. Sci. (B)* 1972, 6, 465
- 15 Golden, J. H., Hammant, B. L. and Hazell, E. A. *J. Appl. Polym. Sci.* 1967, 11, 1571

Drag reduction effectiveness of macromolecules

B. Hlavacek, L. A. Rollin and H. P. Schreiber*

Department of Chemical Engineering, Ecole Polytechnique, Montreal, P.Q., Canada

(Received 20 July 1975)

A working hypothesis has been developed to account for observed drag reduction properties of dilute polymer solutions. Drag reduction effectiveness of polymer solutes is attributed to their ability to form a deformable network structure which inhibits the formation of microvortices in the solvent and retards their ability to migrate through the fluid, coalesce, and result in fully developed turbulence centres. The size of microvortex precursors is tentatively set in the range of 100 Å, and it is assumed that the damping (drag reduction) effect of macromolecules is due to strong association between solvent molecules and polymer chains, immobilizing many of these active precursors. The hypothesis indicates that drag reduction effectiveness of polymers should depend strongly on polymer/solvent interactions in addition to the recognized variables of molecular weight, concentration and geometry of the flow system. The hypothesis accounts for a number of published anomalous observations and leads to new predictions of drag reduction variations with polymer molecular weight distribution, and temperature. These and related predictions are the focal points of new experimental research studies of the drag reduction phenomenon.

INTRODUCTION

The wide range of potential applications for drag reduction (*DR*) effects of dilute polymer solutions, coupled with the challenge of accounting for *DR* phenomena, have led to numerous studies of the subject. In some¹⁻¹² (only a few of the more recent articles have been noted), successful correlations have been developed for the drag reduction effectiveness (*DRE*) of many polymers over a wide range of shear gradients. However, as noted in recent papers¹³⁻¹⁵, a comprehensive understanding of *DR* mechanisms remains obscure. A pattern is emerging, nevertheless, that accentuates the importance of molecular properties of the drag reducing agent in accounting for *DR* effects. The conceptual basis for our work lies in the molecular characteristics of the *DR* agent and in those characteristics of the solvent which respond to them. In this initial article a working hypothesis which accounts for some apparent conflicts in published studies of *DR* is presented. Important also are experimental consequences which follow from the conceptual approach; tests of these form the goals for our ongoing research, and may motivate a wider research response elsewhere.

Two fundamental prerequisites for the *DR* effect can be postulated:

- (1) The phenomenon reflects an inherent property of the matrix fluid (solvent) to form a microstructure of turbulent eddies under critical gradient conditions.
- (2) *DR* follows from an intervention on the part of macromolecules. Logically, their *DRE* should reflect the influence of those variables which control the size, shape and mobility of the macromolecule under the conditions of observed drag reduction.

In evaluating earlier rationalizations of *DR*, as well as in laying a foundation for the present approach, it is con-

venient to consider turbulence suppression in terms of three kinetic stages:

(a) disturbance initiation. This stage postulates the activation of microeddies from pre-existing microcentres of discontinuity in the solvent.

(b) growth (propagation) stage. In the second stage, one may postulate the growth and diffusion of eddies through the continuum. Growth and mutual interaction of disturbances leads to:

(c) disturbance decay (termination). The decay rate will be a function of energy dissipation as well as of recombination or partial coalescence of eddies. Thus, it does not necessarily follow that the initiation and decay rates must be numerically equal.

A more complete theoretical argument of these concepts is to be published separately¹⁶.

The kinetics of each of the three stages should depend upon the inherent properties of the continuum fluid, on the modifying influence of a macromolecular solute and on the geometry of the flow system. Clearly, stage (a) and, in part, stage (b) are concerned with events of 'incipient disturbance' on a dimensional level much smaller than the events of optically observable macrodisturbance [stages (b) and (c)]. In general, published accounts of *DR* are concerned with the role of polymers as agents for the suppression of macrodisturbances in the late stages of their kinetic development. Thus, Astarita^{7,8} and Fabula⁵ are concerned with the dynamic and relaxation properties of polymers, hence focusing on stages (b) and (c). Others, notably Seyer and Metzner⁹ stress the effect of increased elongational viscosity in polymer solutions and so are concerned with the decay rate of stage (c). Recently, Lacey¹⁴, also focusing on stage (c), has suggested that an eddy-damping effect arises from the migration of macromolecules and thread-like particles to regions of flow disturbance. The approach of Virk and coworkers⁴, to which our concepts relate, introduces specific dimensions in considering the influence of macromolecules on fully developed disturbances, with diameters exceeding 10⁻³ cm. The expectations of Virk's effective

* To whom enquiries should be addressed.

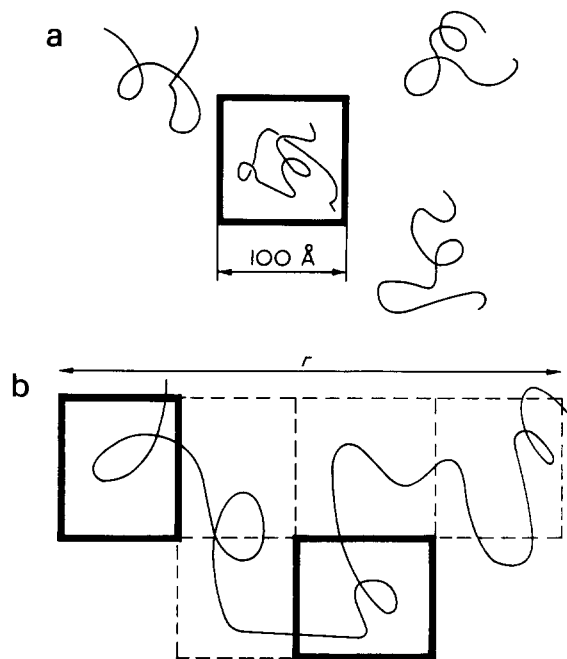


Figure 1 Schematic representation of function in drag reducing polymers. (a) $\langle r_g \rangle \approx d$ microdomains (turbulence precursors); (b) $\langle r_g \rangle \gg d$ microdomains (turbulence precursors)

slip correlations are not universally substantiated. Thus, Peyser and Little¹² reported apparent contradictions to Virk's theory, in that the *DRE* of polystyrene increased with the viscosity of the solvent. It is our opinion that a shortcoming in the Virk approach lies in its attempt to account for the behaviour of fully developed disturbances [in stages (b) and (c)], which are dimensionally inconsistent (much larger) with the average dimensions of the drag reducing macromolecule.

In order to overcome this problem, it would be necessary to consider the properties of macromolecular aggregates or entanglement domains with overall dimensions equal to or greater than the 10^{-3} cm range proposed for the linear dimensions of turbulent eddies⁴. Astarita's treatment^{7,8} of characteristic (bulk) relaxation times can be seen as a step in this direction. The aggregation and entanglement tendencies of polymers in solution are principally dependent on molecular size, flexibility and deformability, under the conditions of relevant stress gradients. These properties will be strongly influenced by the thermodynamics of polymer/solvent interaction, and progress towards the further evolution of *DR* mechanism therefore should be possible from detailed consideration along these lines. Our approach involves the question of molecular structure, and thus resembles the statements of Little and coworkers^{12,13}, of Balakrishnan and Gordon¹⁵ and Kiran¹⁷. An important feature of our approach, however, is its focus on the role of macromolecule as an inhibitor for the initiation stage (a) of micro-disturbance formation.

MOLECULAR MODEL FOR *DR*

To account for the *DRE* of macromolecular solutes, we note that: (1) the concentration of macromolecules needed for *DR* must exceed a minimum¹¹, below which no significant *DR* is noted in any given system; and (2) the molecular size of the solute is important and appreciable *DR* is observed only when the molecular weight exceeds a 'benchmark' parameter, such as the entanglement weight M_c ^{11,18}.

The points suggest that the macromolecule reports on events occurring on a size level comparable with those of the indicating species. In combination, the criteria re-iterate that *DR* is evident only when there is dimensional consistency between turbulence precursors in the solvent and the effective size of the polymer. This size should be related to a critical effective radius of gyration of the macromolecule, $\langle r_g \rangle$. Through changes in polymer molecular weight, concentration and solvent-solute interaction, the right order of $\langle r_g \rangle$ must be attained for any fluid-flow geometry situation, in order for the polymer to act as an effective *DR* agent.

The basis of our argument is represented schematically in Figure 1. The solvent is thought to contain microdisturbances or turbulence precursors, and the macromolecule becomes an effective suppressor only when it is capable of linking, or 'penetrating' two or more of these, thus hindering their free movement and growth. The above criteria for *DR* strongly relate *DR* effectiveness with events which will tend to increase the apparent 'size' of the polymer. Chain entanglement is one such event¹⁸. An important additional effect will be the tendency for multilayers of solvent to form a jacket about the polymer chain, an interfacial effect discussed by Jellinek¹⁹ for polymer/water systems. These stipulations of our model suggest that turbulence precursors will have linear dimensions in the 100 Å range.

Expectedly, *DRE* should increase as $\langle r \rangle$ increases beyond $\langle r_g \rangle$ i.e. as the macromolecule becomes capable of hindering the motion of an increasing mass of discontinuity elements. A limit to the rise in *DRE* is clearly necessary however; at $\langle r \rangle$ much greater than $\langle r_g \rangle$, the energy requirement for transport of the macromolecules through the fluid matrix rises sharply, and significant increases in the friction coefficient of larger units will tend to reduce the relative *DRE* of the macromolecular additive.

Further clarification of the role played by macromolecules in *DR* follows from a consideration of the mechanisms for 'activating' turbulence microdomains. A detailed analysis of the process will be given in a separate publication¹⁶. Here a simple model is adopted which assigns Brownian translation motion to any microdomain:

$$1/2(m\bar{u}^2) = 3/2(kT) \quad (1)$$

Assuming the linear dimension of the domain to be 100 Å and the liquid density $\rho = 1.00$ then:

$$m = \rho D^3 = 10^{-18} \text{g}$$

At 300 K, $(\bar{u}^2)^{1/2} = 3$ m/sec; in a much larger domain, say 1000 Å, $(\bar{u}^2)^{1/2} \approx 0.11$ m/sec. These average values of the Brownian velocity are comparable with the characteristic velocity, ν_0 , of boundary layers in pipe flow as given by^{4,5}:

$$\nu_0 = \left(\frac{\tau\omega}{\rho} \right)^{1/2} \quad (2)$$

According to Levich²⁰, this velocity pertaining to a boundary layer of thickness δ_0 is also characteristic of annihilation of micro-eddies in the continuum fluid.

These concepts are expressed schematically in Figure 2. Here the boundary layer, δ_0 , contains a typical domain, A, populated by N independent hydrodynamic units. Choosing Cartesian coordinates for this system, a Gaussian velocity distribution can be assigned thereto. A similar domain

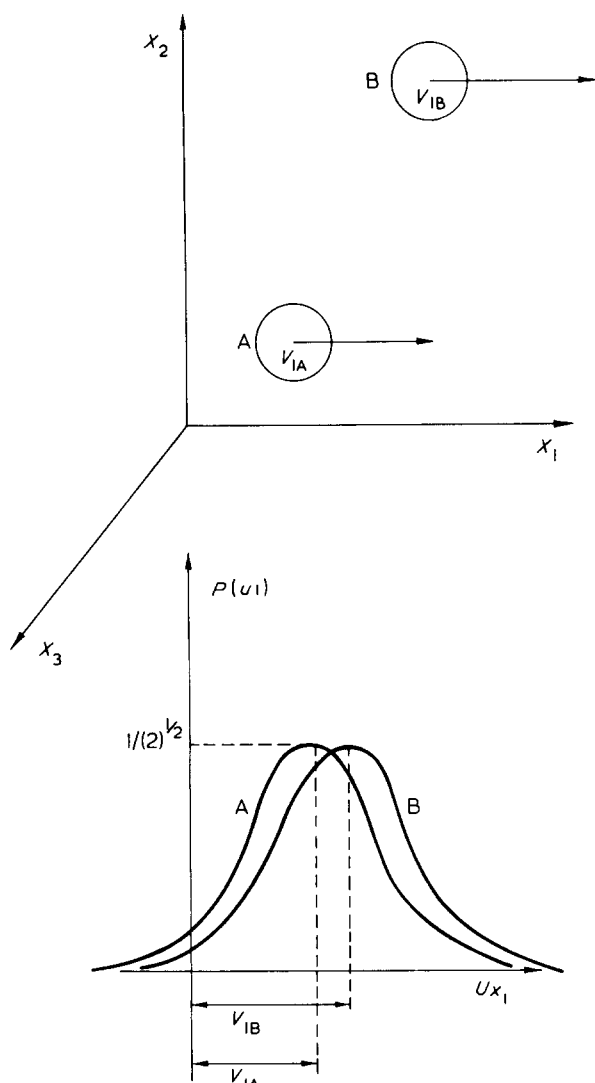


Figure 2 Schematic representation of velocity distribution in Brownian motion of domains in laminar boundary layer (A) and main stream (B)

B located outside the boundary layer will have velocity distributions related to those in A but shifted, as shown, by a component dimensionally equal to v_0 . The situation is tantamount to the existence of a local entropy gradient ΔS , and a restoring force related to the gradient via:

$$F \propto \Delta S / \delta_0 \quad (3)$$

The magnitude of ΔS will depend on the total number of independent hydrodynamic units involved, as well as on v_0 .^{*} In this context, the role of the macromolecule as drag reducer, rests in its ability to reduce ΔS by reducing the number of independently moving hydrodynamic units. Accordingly, *DRE* will be proportional to D^3 , but in addition, a positive contribution to *DRE* should arise from an increase in δ_0 owing to the presence of polymer. The penetration of microdomains by the macromolecule, its dimensions increased through chain entanglements, and/or the reduction in the degree of translational freedom of microdomains located in a solvent jacket strongly associated with

* We note that with increasing D , both $(\bar{u}^2)^{1/2}$ (equation 1) and v_0 will decrease, the latter variation leading to the empirical statement⁶ $v_0 \propto 1/D$. Thus, the magnitude ΔS will depend most heavily on D , i.e. on the total number of independent hydrodynamic units involved.

the polymer chain¹⁹, are proposed as the major stabilizing effects of the solute. Both routes to a reduction of the local entropy effect must depend on molecular size and on the architecture of the polymer/solvent interface; hence an interdependence is expected between *DRE* and parameters descriptive of thermodynamic interactions in polymer solutions²¹.

Initial tests of the model

The need for the macromolecule to conform in such a way as to immobilize a substantial number of turbulence precursors, indicates a molecular flexibility arising from favourable thermodynamic interactions, and from a molecular weight greater than the critical weight for chain entanglement¹⁸. A rough correlation between *DRE* and M/M_c should be expected and has in fact been reported by several authors. The intrinsic viscosity, $[\eta]$, being a convenient measure of the quality of solvent/solute interaction for a given macromolecule, should also be an acceptable, though approximate normalizing parameter for *DRE*. Thus, we could expect the effective linear dimension of the turbulence-suppressing agent as given by a parameter involving both $[\eta]$ and M/M_c to be particularly useful in accounting for the *DR* performance of a wide range of polymers.

The recent data reported by Liaw *et al.*¹¹ provide a suitable test of this point. These authors tabulate M/M_c , $[\eta]$ and the Mark-Houwink exponent a , for a number of equally effective *DR* systems, and note a qualitative link between *DRE* and $[\eta]$. Expressing the effective dimension of the macromolecule by:

$$\langle r_e \rangle = f[\eta] / (M/M_c)^a \quad (4)$$

it is found that this new parameter correlates with *DRE* more satisfactorily than either $[\eta]$ or M/M_c alone, ($\langle r_e \rangle$ may be thought of as an index of microdomain immobilization on the subchain level). The relevant data are given in Table 1. With one exception the $\langle r_e \rangle$ values are reasonably invariant – a noteworthy fact when considering an inherent error of some 20% in M_c evaluations¹⁸. The exception is ethyl cellulose; the molecular flexibility here may be much more restricted because of the internal bonding capacity of the polymer. The point emphasizes the fact that a given value of $[\eta]$ is not necessarily synonymous with a specific molecular flexibility, i.e. with an equivalent capacity of the macromolecule to immobilize precursor centres by the mechanisms elaborated above. A similar point has been made recently by Frommer and coworkers²².

Some additional progress can be made in rationalizing the *DRE* of macromolecules. If our mechanistic approach is valid, then the following simple considerations should apply. Let (C_s/M) be the number of macromolecules per unit volume, and V_m be the volume of one macromolecule. In the light of our assumptions at any M , the product $(C_s/M) \times V_m$ represents the number of *DR* units necessary to just fill the continuum fluid space. This, however, does not evaluate the efficiency with which the turbulence precursors resident within that space will be immobilized. We therefore introduce the parameter ξ to be proportional to the effective number of turbulence precursors immobilized within V_m . Inherently ξ must be a function again of molecular mass (M) and also of solvent/solute thermodynamic interaction parameters, such as the free energy of mixing value χ_{12} , or the contact energy value X_{12} , drawn from con-

Table 1 Values of $[\eta]/(M/M_c)^a$ for various drag reduction systems. All source data taken from ref 11

Polymer	Code	M	M/M_c	$[\eta]$ (dl/g)	a	$[\eta]/(M/M_c)^a$
Polydimethyl-siloxane	SR 130	1.1×10^7	380	8.0	0.62	0.201
	SR 54	5.6×10^6	193	5.3	0.62	0.203
	SE	3.0×10^5	10	0.83	0.62	0.199
Poly(ethylene oxide)	PEO-Coag	2.8×10^6	458	13.2	0.82	0.087
	WSR-301	2.3×10^6	383	11.4	0.82	0.087
	WSR-205	7.8×10^5	133	4.95	0.82	0.090
	WSR-35	4.0×10^5	67	2.95	0.82	0.094
	WSRN-10	7.8×10^4	13	0.8	0.82	0.098
<i>cis</i> -Polybutadiene	PBD	3.5×10^5	60	3.6	0.725	0.185
<i>cis</i> -Polyisoprene	PIP-280	2.7×10^6	191	8.5	0.728	0.186
	PIP-70	7.1×10^5	50	4.0	0.728	0.232
Ethyl cellulose	ECN	10^5	5	3.1	0.81	0.842

temporary polymer solution theories^{23,24}. This argument indicates that:

$$(C_s/M) \times V_m \cdot \xi = \text{constant} \quad (5)$$

If we assume, for simplicity, that the molecular weight effect predominates, then $\xi \propto M$, and

$$C_s \times V_m = \text{constant} \quad (6)$$

whence $C_s \times D^3 = C_s^{1/3} D = \text{constant} \quad (7)$

Re-introducing the interaction concept, we follow the frequent procedure of using $[\eta]$ as a more convenient measure of solvent/solute interactions. As a first approximation then, $D \propto [\eta]^\kappa$, and at $\kappa = 1.0$,

$$C_s^{1/3} [\eta] = \text{constant} \quad (8)$$

A major problem resides in the fact that $[\eta]$ is defined in the limit $\dot{\gamma} \rightarrow 0$, whilst DR occurs at high rates of shear. Following Subirana²⁵, we note that at high shear rates the $[\eta]$ of all macromolecules corresponds to that of a θ condition, whence a preferred statement is

$$C_s^{1/3} [\eta]_\theta = \text{constant} \quad (9)$$

This development can be tested approximately, again using the data of ref 11. A set of $C_s^{1/3} [\eta]$ values has been calculated from that source, and entered in Table 2. The evidence is strongly in favour of the present argument, for with variations in C_s over a range of 3 decades, the variation in $C_s^{1/3} [\eta]$ is reduced to a fairly narrow range centred on a value of about 1.5. The scatter is random, apparently independent of molecular weight or intrinsic viscosity, and could well reflect the error introduced in using $[\eta]$ instead of the theoretically preferred $[\eta]_\theta$.

A final reminder is made, however, that ideal correlations involving DRE, should include a specific representation of ξ ; we re-iterate that this will be functionally dependent on the free energy of mixing for the polymer/solvent pair, ΔG_M , and consequently on the independent variables of ΔG_M , such as the temperature and concentration.

DISCUSSION

(1) Our molecular approach to DR events bears some similarities to previously reported theories of fluid instability,

in particular the extensive field analysis of fluids due to Denn and Porteous²⁶. These authors concluded that flow instabilities in liquids bear a close similarity to field instabilities in supersonic flow of gases. Our approach is closely analogous, but $(\bar{u}^2)^{1/2}$ of the large flow units in our systems is much less than that in air flow²⁶, hence our flow units can be affected significantly by the velocities v_0 of the relevant boundary layers.

Analogy is also noted to the empirical relationship of Virk⁶

$$K^* \times D = \text{constant} \quad (12)$$

where K^* is the wavenumber and D the particle diameter of vortices. According to Hinze²⁷, K^* is related to the size of energy-dissipating eddies. Thus:

$$K^* \times D \sim \frac{D}{\delta} = \text{constant} \quad (12')$$

and $\frac{D^3}{\delta^3} = \frac{V_m}{\delta^3} = \text{constant} \quad (12'')$

Table 2 Values of $(C_s)^{1/3} [\eta]$ for drag reduction systems reported in ref 11

Polymer code*	C_s (wt %)	$(C_s)^{1/3} [\eta]$
SR 130	~0.001	0.8
SR 54	~0.003	0.76
SE 30	0.7-1.5	0.78-1.00
PEO-Coag	0.001-0.003	1.35-1.93
WSR-310	<0.003	<1.83
WSR-205	0.008-0.02	0.9-1.22
WSR-35	0.02-0.05	0.68-0.92
WSRN-10	≥0.4	≥0.58
Hydrin	<0.1	<1.44
PIP 60	~0.2	1.46
CIS PBD	>0.2	>2.1
CIS PIP-280	0.008-0.02	1.68-2.28
CIS PIP-70	0.15-0.30	2.12-2.68
PIB L 200	0.1-0.4	1.95-3.08
PIB L 200	0.05-0.20	2.42-3.78
PIB L 80	0.1-0.3	1.63-2.34
PIB L 80	>0.9	>0.79
ECN	>0.25	>1.57
PMME	>0.9	>1.64
Polystyrene	>0.94	>0.98

* Codes are fully described in ref 11 from which they are reproduced

This leads to the consistent suggestion that the lower limit of observable turbulence is associated with a constant number of hydrodynamically independent units, regardless of the chemical nature of either solvent or solute.

(2) In a future publication, we will account more formally for the response of *DRE* to independent variables such as *T*, concentration and polymer molecular weight, through analysis of correlation equations derived from the foregoing arguments. Some qualitative experimental expectations are noted at this time, however. We regard these as useful starting points for newer research goals in the *DR* area. (a) The general correlation of molecular weight and *DRE* has been noted frequently, but little concern appears to have been given to the question of which moment of the distribution of a polymer is important. The high molecular weight end of the distribution spectrum will weigh most heavily in immobilizing turbulence centres. Thus, it is suggested that in polydisperse systems, *DRE* will correlate more strongly with *z*-average and weight-average values than with *M_p*, or number-average values of the molecular weight. Further, in the present work, the envisaged role of *DR* agents suggests that a minimum effective number of chain segments must be available before an average molecular unit of the material can produce measurable *DR* results. The existence of a material constant based on a function of the type $F(C_g/M_z)$ is therefore proposed for constant thermodynamic conditions of polymer/solvent interaction. (b) The influence of polymer/solvent interactions on *DRE* is held to be important. The tacit assumption is often made that the intrinsic viscosity can be used as a convenient index of polymer/solvent interactions. As already noted, we regard this choice as too limiting. Among the reasons for this is the fact that $[\eta]$ relates to macromolecular dimensions at vanishing concentration and very low shear rates. In contrast, *DR* occurs at finite concentrations and at very high rates of shear. Although the former problem is likely of little importance, a change to other parameters of interaction, such as the χ or *X* value already referred to earlier should increase the precision of correlations. The difference in shear levels however, would seem to be of great importance²⁵, and it is proposed that more accurate predictions of *DRE* will follow from the inclusion of an index of the shear dependence of solution viscosity in the molecular descriptors of the *DR* agents, or as suggested in equation (9), from the use of experimentally evaluated $[\eta]_\theta$ results. (c) The temperature dependence of *DRE* should reflect the unique temperature dependence patterns of polymer/solvent interaction parameters^{23,24}. In particular, we cite the existence in polymer solutions of both a low and high temperature solubility limit. From these considerations it follows that: a given polymer/solvent system must have an optimum temperature for *DRE*; both positive and negative variations of *DRE* with temperature should exist, depending on which side of the optimum temperature observations are being made.

CONCLUSIONS

We conclude that turbulent eddies in fluids arise from three dynamic processes. Incipient turbulence is associated with microvortex precursors having dimensions in the range of 100 Å, while fully developed turbulence domains are associated with linear dimensions of the order of 10⁻³ cm. *DR* effects of macromolecules are associated with their ability

to form penetrated domains which damp and stabilize the discontinuities of the solvent at the incipient formation stage. By a principle of dimensional consistency this calls for entanglement or penetration domains with linear dimensions of at least 100 Å. It follows that *DRE* will depend on those variables of the system which influence the effective linear dimensions of the macromolecule as well as on the variables which determine the size of microdisturbances in the solvent and the shear gradient at which these first occur.

NOMENCLATURE

C_s	= critical concentration of macromolecules
D	= diameter of volume defined by macromolecule
M, M_c	= molecular weight, and critical weight for chain entanglement of macromolecule
ΔS	= local entropy gradient
m	= mass of turbulence domain
F	= restoring force to entropy gradient
ν_0	= characteristic velocity of boundary layers in tube flow
V_m	= internal volume of macromolecule
$\langle r \rangle$	= gyration radius of macromolecule
u	= mean Brownian translational velocity
$[\eta]$	= inherent viscosity of polymer
$\tau\omega$	= wall stress
$\dot{\gamma}$	= shear rate
δ_0	= thickness of boundary layer
ρ	= density of continuum fluids
K^*	= wavenumber
ξ	= number of turbulence precursors immobilized by macromolecule
χ_{12}	= free energy of mixing
X_{12}	= contact energy

} for solvent/solute pair

ACKNOWLEDGEMENTS

We thank Drs J. P. Carreau and J. M. Sangster for fruitful discussions. We acknowledge with gratitude financial support from a Regional Development Grant, National Research Council of Canada and from the Defence Research Board of Canada.

REFERENCES

- Hershey, H. C. and Zakin, J. L. *Chem. Eng. Sci.* 1967, **22**, 1847
- Dodge, D. W. and Metzner, A. B. *AIChE J.* 1959, **5**, 189
- Savins, J. G. *J. Inst. Pet.* 1961, **47**, 329
- Virk, P. S., Merrill, E. W., Mickley, H. S. and Smith, K. A. *J. Fluid Mech.* 1967, **30**, 305
- Fabula, A. C., Lumley, J. L. and Taylor, W. D. 'Modern Developments in the Mechanics of Continua', (Ed. S. Eskinazi), Academic Press, New York and London, 1966
- Virk, P. S., Merrill, E. W., Mickley, H. S. and Smith, K. A. 'Modern Developments in the Mechanics of Continua', (Ed. S. Eskinazi), Academic Press, New York and London, 1966
- Astarita, G. *Ind. Eng. Chem. (Fundamentals)* 1965, **4**, 355
- Astarita, G., Greco, G. and Nicodemo, L. *AIChE J.* 1969, **15**, 4
- Sayer, F. A. and Metzner, A. B. *Can. J. Chem. Eng.* 1967, **45**, 121

Drag reduction effectiveness of macromolecules: B. Hlavacek et al.

- 10 Patterson, G. K., *et al. Ind. Eng. Chem.* 1969, **61**, 23
- 11 Liaw Gin-Chain, Zakin, J. L. and Patterson, G. K. *AIChE J.* 1971, **17**, 391
- 12 Peyser, P. and Little, R. C. *J. Appl. Polym. Sci.* 1971, **15**, 2623
- 13 Ting, R. Y. and Little, R. C. *J. Appl. Polym. Sci.* 1973, **17**, 3345
- 14 Lacey, P. M. C. *Chem. Eng. Sci.* 1974, **29**, 1495
- 15 Balakrishnan, C. and Gordon, R. J. 'Influence of Molecular Conformation and Intermolecular Interactions on Turbulent Drag Reduction', *44th Meeting, American Society of Rheology, Montreal, Canada* 1973
- 16 Hlavacek, B, and Sangster, J. M. to be published
- 17 Kiran, E. *Nature (Phys. Sci.)*. 1972, **238**, 29
- 18 Porter, R. S. and Johnson, J. F. *Chem. Rev.* 1966, **66**, 1
- 19 'Water Structure at the Water-Polymer Interface', (Ed. H. H. G. Jellinek), Plenum Press, New York, 1972
- 20 Levich, V. G. 'Physicochemical Hydrodynamics', Prentice-Hall, Englewood Cliffs, N. J., 1962
- 21 Morawetz, H. 'Macromolecules in Solution', Interscience, New York, 1965
- 22 Frommer, M. A., Feder-Lavy, A. and Kraus, M. A. *J. Colloid Interface Sci.* 1974, **48**, 165
- 23 Orwoll, R. A. and Flory, P. J. *J. Am. Chem. Soc.* 1967, **89**, 6814
- 24 Patterson, D. *Macromolecules* 1969, **2**, 672
- 25 Subirana, J. A. *J. Chem. Phys.* 1964, **41**, 3852
- 26 Denn, M. M. and Porteous, K. C., *Chem. Eng. J.* 1971, **2**, 280
- 27 Hinze, J. O. 'Turbulence', McGraw-Hill, New York, 1959

Time effects on the thermochemical behaviour of natural rubber

L. Araimo, F. de Candia and V. Vittoria

Laboratorio di Ricerche su Tecnologia dei Polimeri e Reologia, CNR, 80072 Arco Felice (Napoli) Italy
(Received 30 June 1975; revised 30 July 1975)

Some preliminary results, obtained by studying the time effects on the thermomechanical behaviour of a natural rubber network, are reported. Experimental data indicate some thermodynamic features of the relaxation phenomenon under stress. The observed effects are discussed.

INTRODUCTION

At constant pressure and temperature the thermomechanical analysis of the deformation process of a rubberlike material can be carried out using the following state equation¹:

$$\Delta F = \Delta W + \Delta Q - T\Delta S \quad (1)$$

where ΔF is the change in free energy, ΔW is the elastic work and is given by the integral

$$\int_1^\alpha \tau d\alpha$$

where τ is the force on the unit of undeformed cross-sectional area and α is the strain ratio, ΔQ is the heat change and $T\Delta S$ is the entropic term. In equilibrium conditions $\Delta Q = T\Delta S$ and:

$$\Delta F = \int_1^\alpha \tau d\alpha \quad (1a)$$

while in non-equilibrium conditions, taking into account that:

$$T\Delta S = \Delta Q + T\Delta S_{\text{irr}} \quad (2)$$

where ΔS_{irr} is related to the irreversibility of the process, then:

$$\Delta F = \int_1^\alpha \tau d\alpha - T\Delta S_{\text{irr}} \quad (3)$$

and

$$\Delta H = \int_1^\alpha \tau d\alpha + \Delta Q \quad (3a)$$

All the thermodynamic terms of equations (1)–(3) refer to the volume unit.

Therefore, a direct graphical integration of the experimental τ vs. α plots gives the experimental numerical value of ΔW , while, ΔQ can be given by a direct microcalorimetric measurement. In the present paper, using this kind of analysis, time effects on the thermomechanical behaviour of a vulcanized rubber sample have been investigated. In

particular, the thermodynamic functions ΔQ , ΔW , ΔH for increasing and decreasing strain, have been calculated from experimental data, in order to obtain information about the relaxation phenomena at thermodynamic level, for short and long times of relaxation. Moreover, at a qualitative level, information about the entropic term $T\Delta S$ can be obtained.

It is of interest to see if, from the thermomechanical data, it is possible to obtain evidence of chain–chain interactions or aggregation, induced by strain, and some information on the degree of irreversibility of such effects eventually present. This study is related to well known problems of rubber elasticity, where the experimental deviations from the Gaussian theory², suggest connections with intermolecular phenomena such as chain–chain interactions or aggregations^{3–5}.

EXPERIMENTAL

A sample of vulcanized natural rubber was prepared using dicumyl peroxide as initiator; vulcanization was carried out at 145°C for 45 min.

The apparatus used to analyse the thermomechanical behaviour of the sample consists of a Calvet microcalorimeter equipped with a cell previously described³. The microscrew of the deformation cell is connected with a strain gauge that gives the value of the tensile stress. The sample is clamped in part of the cell inside the microcalorimeter which gives the measure of the heat exchanged during the deformation. The use of the microcalorimeter, in this kind of measurement, is based on the Tian equation³. As explained before³, in the present experiment the heat exchanged during the deformation is proportional to the area under the recorded line, and can be easily calculated when the calibration constant is known. A calibration plot (recorded area vs. energy) was obtained using a calibration cell based on the Joule effect. The work temperature was 40°C. The time interval between stretching and relaxing was 20 min. A general view of the apparatus is given in *Figure 1*.

RESULTS

The sample was deformed step by step, relaxing to zero load before stretching to the next strain value. The time interval between stretching and relaxing, and again stretching to the next α value was always 20 min. In this way, for each deformation value, the stress, immediately after stretching and

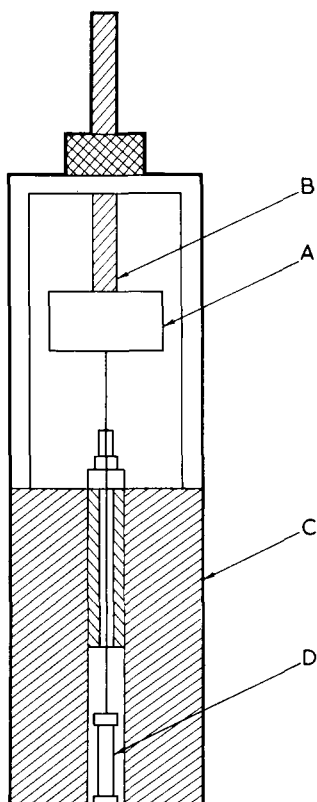


Figure 1 Schematic illustration of the apparatus used in the thermomechanical measurements: A, force transducer; B, deformation microscrew; C, calorimeter cell; D, sample

Table 1 Experimental data of ΔW and ΔQ

α	$\Delta W \uparrow$ $\times 10^{-2}$ (J/cm ³)	$\Delta W \downarrow$ $\times 10^{-2}$ (J/cm ³)	α	$\Delta Q \uparrow$ $\times 10^{-2}$ (J/cm ³)	$\Delta Q \downarrow$ $\times 10^{-2}$ (J/cm ³)
1.200	1.4	1.5	1.659	7.52	4.46
1.500	9.3	8.8	1.989	20.46	13.72
2.100	39.6	36.6	2.319	36.69	30.09
2.400	59.1	55.0	2.648	60.08	50.11
2.700	81.3	75.7			

The arrows indicate increasing (\uparrow) and decreasing (\downarrow) strain

before relaxing the sample, has been detected. Therefore, the calorimeter gives two signals, the first on stretching and the second on relaxing. Using these experimental data, (see Table 1), the curves ΔW vs. α and ΔQ vs. α for increasing and decreasing strain were obtained. Using equation (3a), we have calculated the plot ΔH vs. α for increasing and decreasing strain. Results are reported in Figure 2. Repeating the complete deformation cycle, after a few hours and after two days, the data of Figure 2 are reproducible in the range of experimental errors.

DISCUSSION

In order to give an interpretation of the results obtained, the significance of the measurements as carried out must first be discussed. The difference observed in the thermodynamic functions, between increasing and decreasing strain, takes into account the effects, at thermodynamic

level, of the relaxation phenomenon, occurring when the sample is stretched. Therefore, the comparative analysis of the data of Table 1 and of Figure 2, giving a thermodynamic picture of the mechanical relaxation, provides evidence concerning the relaxation mechanism.

The effect of the relaxation, as is well known, is a dissipation of mechanical energy; this is clearly shown in Table 1, where all the values detected decreasing the strain are smaller than those during increase. From Table 1 it appears that thermal energy also, is dissipated in the deformation process.

Reporting these main results in terms of the cyclic integrals of the two functions ΔW and ΔQ related to cyclic deformation, the data of Table 1 give: $|\oint \Delta Q d\alpha| > |\oint \Delta W d\alpha|$.

The last result indicates that in the overall process, the dissipation of thermal energy is more pronounced and, this gives, as is clear from Figure 2: $\oint \Delta H d\alpha < 0$. As ΔH is a state function this datum is evidence of the irreversibility of the process in the time scale of the experiment.

Moreover, it can be suggested that the negative value of the cyclic integral of the enthalpic term could be related to ordering phenomena. Ordering phenomena, such as the formation or orientation of bundles, or simple chain orientation with interchain aggregation, are consistent with the behaviour observed for the enthalpic term. The suggestion that the relaxation can take place with such a mechanism is supported by results obtained by analysing the infra-red dichroism of stretched natural rubber networks⁶, where it is evident that orientation phenomena take place during the relaxation process. On the other hand, the possibility that aggregation phenomena can occur during the stretching seems to be supported by experimental data obtained analysing the crystallization behaviour of stretched natural rubber^{7,8}. This does not exclude the occurrence of other kind of relaxation mechanisms, e.g. entanglements, or free chains or chain ends slipping.

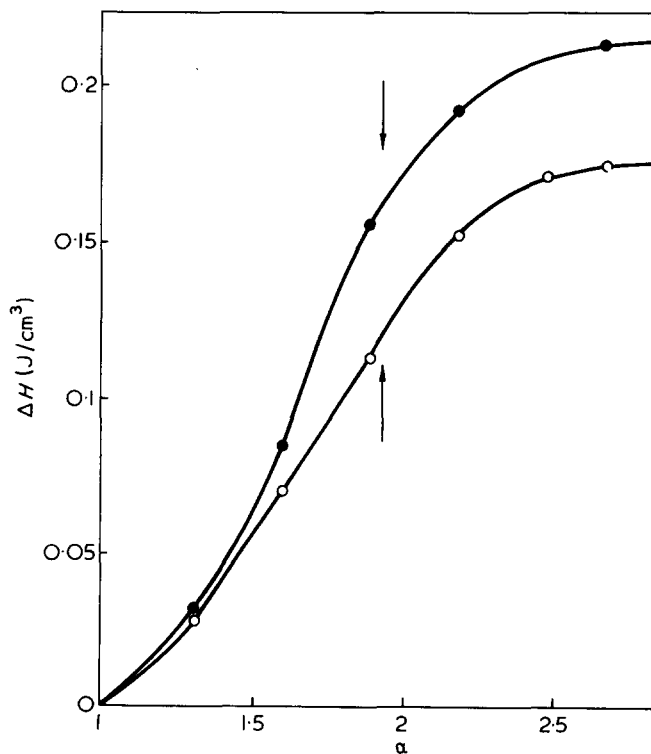


Figure 2 Enthalpic term as a function of the deformation ratio: ○, increasing the strain; ●, decreasing the strain

Some comment can be made about the entropic term. From equation (2) where $T\Delta S_{irr}$ is always larger than zero, it follows that, even if the entropic term cannot be calculated quantitatively, this term is qualitatively related to the heat term. Thus *Table 1* shows that the difference in entropy between the strained and unstrained state is greater on stretching than on relaxing.

This observation is valid in the hypothesis that ΔS_{irr} on stretching and ΔS_{irr} on relaxing are not drastically different, can be in agreement with the occurrence of ordering phenomena such as chain orientation and aggregation which are irreversible in the time scale of the experiment. Ordering phenomena also seem to be suggested by the residual creep after the relaxing.

In addition, the evidence regarding the reversibility of the data of *Table 1* and *Figure 2* on repeating the deformation cycle after a few hours and a few days, indicate that the phenomena responsible for the observed effects that take place during relaxation under stress, are reversible after a moderate time of relaxation at zero load. In conclusion, at this stage, we cannot prove without doubt, from the time effects on the thermomechanical behaviour the existence of ordering phenomena. However, we have no results that disagree with this hypothesis, which is so important for the understanding of the mechanical behaviour

of the rubber-like materials. On the other hand, the hypothesis seems to be directly supported by other kinds of experimental observations⁶⁻⁸

ACKNOWLEDGEMENT

We wish to thank Mr G. Permicola for the technical assistance in the realization of the apparatus of *Figure 1*.

REFERENCES

- 1 Treolar, L. R. G. 'The Physics of Rubber Elasticity', Oxford, 1958
- 2 Flory, P. J. *J. Am. Chem. Soc.* 1956, **78**, 5222
- 3 Price, C., Evans, K. A. and de Candia, F. *Polymer* 1973, **14**, 338
- 4 Dusek, K. and Prins, W. *Adv. Polym. Sci.* 1969, **6**, 1
- 5 de Candia, F. and Vittoria, V. *J. Appl. Polym. Sci.* 1973, **17**, 3243
- 6 Gotoh, R., Takenaka, T. and Hayama, N. *Kolloid-Z. Z. Polym.* 1966, **205**, 18
- 7 Mitchell, J. C. and Meier, D. J. *J. Polym. Sci. (A-2)* 1968, **6**, 1689
- 8 Jee, E., Luch, D. and Yeh, G. S. Y. *J. Polym. Sci. (A-2)* 1973, **11**, 467

A new approach in permeation chromatography calibration

Paweł Szewczyk

Polish Academy of Sciences, Institute of Polymer Chemistry 41-800 Zabrze, Poland
(Received 22 May 1975)

The first step in the determination of molecular weight distribution (*MWD*) of polymers using the gel permeation chromatography (g.p.c.) technique is to calibrate a given set of columns with a series of reference solutes. True molecular weight averages may be calculated from a g.p.c. chromatogram when a complete form of the calibration curve is known and corrections for imperfect resolution are made¹.

A large variety of calibration methods have been proposed²⁻⁶, involving narrow or broad *MWD* standards or using the hydrodynamic volume concept. Among the existing calibration procedures incorporating both of the above mentioned conditions, only the effective linear calibration method proposed by Balke *et al.*⁷ is relatively simple and has potential general utility. However, the linearity of this effective calibration becomes questionable when the calibration line is to be extrapolated to interstitial volume on one end and elution volume for monomers on the other.

In this paper a new concept in the effective g.p.c. calibration approach is presented. It is assumed that for a given type of polymer and fixed experimental conditions the molecular weight calibration curve in the elution volume range of practical importance may be accurately represented by a polynomial of degree n , i.e.:

$$\log M = a_0 + a_1 V + a_2 V^2 + \dots + a_n V^n = f(V) \quad (1)$$

where M , V , a_0 , a_1 , ..., a_n are the molecular weight of a hypothetically monodisperse fraction, the peak elution volume and polynomial coefficients, respectively. If equation (1) holds for monodisperse fractions, the coefficients a_0 , a_1 , ..., a_n are evaluated from an identical equation (2) by means of the least squares method⁸:

$$\log \bar{M}_r = a_0 + a_1 \bar{V}_p + a_2 \bar{V}_p^2 + \dots + a_n \bar{V}_p^n = f(\bar{V}_p) \quad (2)$$

in which \bar{M}_r denotes any type of polymer average molecular weight (e.g. number-, viscosity-, weight-average molecular weight, etc.) and \bar{V}_p represents a suitably averaged value of its elution volume. From the definition of the reciprocal function the following relation for \bar{V}_p is obtained from equation (2):

$$\bar{V}_p = f^{-1}(\log \bar{M}_r) = b_0 + b_1 (\log \bar{M}_r) + \dots + b_n (\log \bar{M}_r)^n \quad (3)$$

where b_0 , b_1 , ..., b_n are coefficients of the reciprocal polynomial.

Equations (2) and (3) are the basis of the proposed calibration procedure. In order to calculate $(n + 1)$ values of the a_i and b_i ($i = 0, 1, 2, \dots, n$), polynomial coefficients at

least $(n + 2)$ values of average molecular weights \bar{M}_r , and the chromatograms of samples of which the \bar{M}_r are measured, have to be known.

Starting values of the a_i and b_i coefficients are evaluated from the $\log \bar{M}_r$ versus V_{peak} , and V_{peak} versus $\log \bar{M}_r$ relations using the known $(n + 2)$ values of average molecular weights \bar{M}_r and peak elution volumes V_{peak} of samples chosen as standards for the polymer investigated. Values of the average elution volumes \bar{V}_p are then calculated for each of the standards. If the number-average molecular weight \bar{M}_n of a standard is known, $\bar{V}_p \equiv \bar{V}_1$, is calculated according to a formula derived from equations (3) and (2) and the definition of \bar{M}_n :

$$\begin{aligned} \bar{V}_1 &= f^{-1}(\log \bar{M}_n) = f^{-1} \left[\log \left(\sum_i w_i M_i^{-1} \right) - 1 \right] \\ &= f^{-1} \left[-\log \left(\sum_i w_i 10^{-f(V_i)} \right) \right] \end{aligned} \quad (4)$$

In the case when viscosity-average \bar{M}_v or weight-average \bar{M}_w molecular weights of the chosen standards are known, equations from which the corresponding \bar{V}_2 or \bar{V}_3 average elution volumes may be evaluated are as follows:

$$\bar{V}_2 = f^{-1}(\log \bar{M}_v) = f^{-1} \left[\alpha^{-1} \log \left(\sum_i w_i 10^{\alpha f(V_i)} \right) \right] \quad (5)$$

$$\bar{V}_3 = f^{-1}(\log \bar{M}_w) = f^{-1} \left[\log \left(\sum_i w_i 10^{f(V_i)} \right) \right] \quad (6)$$

In equations (4)–(6) f and f^{-1} denote the polynomials defined in equations (2) and (3), w_i are the established from the chromatogram weight fractions of polymer with molecular weight M_i and α is the corresponding Mark–Houwink equation exponent.

In this way $(n + 2)$ values of average elution volumes \bar{V}_p are obtained and the least squares evaluation of the a_i and b_i coefficients repeated. An iteration procedure is then performed on the successive a_i and b_i coefficients until a minimum value of the average percentage accuracy of the calculated from the corresponding chromatograms average molecular weights $\bar{M}_r(\text{calc.})$ using the latest calibration polynomial is obtained, i.e.:

$$1/(n + 2) \sum_{i=1}^{n=2} 100(\bar{M}_r^i - \bar{M}_r^i(\text{calc.}))/\bar{M}_r^i \quad (7)$$

In analogy to the ultracentrifugation method of establishing the sedimentation coefficient—molecular weight relation, using averaged values of sedimentation coefficients^{9,10}, the concept of averaging the experimental g.p.c. elution volumes was used in the above presented calibration procedure. Peak elution volumes almost exclusively applied in calibrating the g.p.c. columns are known not to correspond to any of the experimentally measurable average molecular weights¹¹. This may lead to serious errors in the case of generally encountered polydisperse polymer samples. In the presented method polymer samples of any polydispersity may be used as standards, yet their molecular weights should cover as broad a molecular weight range as possible.

This new calibration method is presently being tested to establish whether it does in fact correct for the g.p.c. instrumental spreading, and how its accuracy is influenced by experimental errors in average molecular weights and polydispersity of standards.

REFERENCES

- 1 Bly, D. D. 'Physical Methods of Macromolecular Chemistry', (Ed. B. Carroll), Dekker, New York, 1971, Vol 2
- 2 Cantow, M. J. R., Porter, R. S. and Johnson, J. F. *J. Polym. Sci. (A-1)* 1967, **5**, 1391
- 3 Frank, F. C., Ward, I. M. and Williams, T. *J. Polym. Sci. (B)* 1968, **6**, 1357
- 4 Purdon, Jr. J. R. and Mate, R. D. *J. Polym. Sci. (A-1)* 1968, **6**, 243
- 5 Benoit, H., Grubisic, Z., Rempp, P., Dekcer, D. and Zilliox, J. G. *J. Chim. Phys.* 1966, **63**, 1507
- 6 Dawkins, J. V. *J. Macromol. Sci. (B)* 1968, **2**, 623
- 7 Balke, S. T., Hamielec, A. E., Le Clair, B. P. and Pearce, S. L. *Ind. Eng. Chem. (Prod. Res. Dev.)* 1969, **8**, 54
- 8 Brandt, S. 'Statistical and Computational Methods in Data Analysis', North-Holland, Amsterdam, 1970, Ch. 9
- 9 McCormick, H. W. *J. Polym. Sci.* 1959, **36**, 341
- 10 Szweczyk, P. and Kalfus, M. *J. Macromol. Sci. (A)* 1973, **7**, 737
- 11 Elias, H.-G., Bareiss, R. and Watterson, J. G. *Adv. Polym. Sci.* 1973, **11**, 111

Spin-labelling of hydroxyl groups in polysaccharides

Michael C. Cafe, Norman G. Pryce and Ian D. Robb

Unilever Research Laboratory, Port Sunlight, Wirral, Merseyside L62 4XN, UK

(Received 21 August 1975; revised 29 September 1975)

INTRODUCTION

Spin labelled polymers have been used to study both the solution properties of polymers^{1,2} and their behaviour when adsorbed at the solid/liquid interface^{3,4}. Various methods for labelling polymers have been used, though one of the more difficult problems has been the labelling of hydroxyl groups on polymers such as polysaccharides that are soluble only in water or other hydroxylic solvents. Serine-OH groups on proteins have been labelled⁵, though the toxicity of the label requires great caution with the experiment. Labelling hydroxyl groups in proteins or polysaccharides by other methods such as using water soluble carbodiimides⁶, Woodward's reagent K⁷ or cyanuric chloride⁸ has been briefly reviewed^{9,10}. These methods however can sometimes lead to crosslinking.

The method of spin-labelling polysaccharides outlined in this note involves modifying the hydroxyl group with cyanogen bromide. This method has been used to attach proteins and polypeptides to cellulose or Sephadex gels¹¹⁻¹³. Although the pH in this work was 11, the reaction can be carried out in more moderately alkaline conditions (9.5-10). At pH 11, degradation of the polymer which occasionally occurs in acid conditions is avoided and a high efficiency of labelling can be achieved. Provided the polymer is completely dissolved, labels will be attached to OH groups and be randomly distributed along the chain. The polysaccharide to be labelled was sodium carboxymethylcellulose (SCMC) and the spin-label was 4-amino-2,2,6,6-tetramethylpiperidine-*N*-oxyl (I), (as supplied by Aldrich Chem. Co. Ltd).

EXPERIMENTAL AND RESULTS

A 2% solution of the SCMC (F4 grade from British Celanese Products, degree of substitution, 0.6) was filtered through a No. 4 sintered glass filter and then dialysed against distilled water for 2 weeks. Its molecular weight determined by viscosity¹⁴ in 0.1 M NaCl was 32 500. Purified SCMC (2 g) was dissolved in 40 ml H₂O and the pH adjusted to 11 with 1.0 M NaOH. Cyanogen bromide, (0.1 g, supplied by BDH) in 2 ml H₂O, was added and the mixture stirred for 4 h at room temperature, while keeping the pH constant at 11, using an automatic titrator. Spin label (I) (0.1 g) was added and the solution left a further 18 h at room temperature and at pH 11. The SCMC solution was then dialysed against distilled water until no further spin label (I) could be detected in the external solution by e.p.r. methods and then freeze-dried. Spectra were recorded on a Varian E-4 X-band spectrometer.

The molecular weight of the labelled SCMC¹¹, again determined by viscosity in 0.1 M NaCl was 34 000, indicating a minimum degree of crosslinking. The ¹H and ¹³C spectra measured on a Bruker WH90, showed no difference in the linewidths or chemical shifts of the labelled or unlabelled samples, again indicating that no significant crosslinking had taken place. Solutions of the labelled polymer were optically clear. The e.p.r. intensity of a 2% solution of the labelled polymer was compared with that of a known concentration of spin label (I). From this comparison it was calculated that there was 1 label per 24 glucose units. The spectrum from the labelled polymer is shown in *Figure 1*.

In analogy to the ultracentrifugation method of establishing the sedimentation coefficient—molecular weight relation, using averaged values of sedimentation coefficients^{9,10}, the concept of averaging the experimental g.p.c. elution volumes was used in the above presented calibration procedure. Peak elution volumes almost exclusively applied in calibrating the g.p.c. columns are known not to correspond to any of the experimentally measurable average molecular weights¹¹. This may lead to serious errors in the case of generally encountered polydisperse polymer samples. In the presented method polymer samples of any polydispersity may be used as standards, yet their molecular weights should cover as broad a molecular weight range as possible.

This new calibration method is presently being tested to establish whether it does in fact correct for the g.p.c. instrumental spreading, and how its accuracy is influenced by experimental errors in average molecular weights and polydispersity of standards.

REFERENCES

- 1 Bly, D. D. 'Physical Methods of Macromolecular Chemistry', (Ed. B. Carroll), Dekker, New York, 1971, Vol 2
- 2 Cantow, M. J. R., Porter, R. S. and Johnson, J. F. *J. Polym. Sci. (A-1)* 1967, **5**, 1391
- 3 Frank, F. C., Ward, I. M. and Williams, T. *J. Polym. Sci. (B)* 1968, **6**, 1357
- 4 Purdon, Jr. J. R. and Mate, R. D. *J. Polym. Sci. (A-1)* 1968, **6**, 243
- 5 Benoit, H., Grubisic, Z., Rempp, P., Dekcer, D. and Zilliox, J. G. *J. Chim. Phys.* 1966, **63**, 1507
- 6 Dawkins, J. V. *J. Macromol. Sci. (B)* 1968, **2**, 623
- 7 Balke, S. T., Hamielec, A. E., Le Clair, B. P. and Pearce, S. L. *Ind. Eng. Chem. (Prod. Res. Dev.)* 1969, **8**, 54
- 8 Brandt, S. 'Statistical and Computational Methods in Data Analysis', North-Holland, Amsterdam, 1970, Ch. 9
- 9 McCormick, H. W. *J. Polym. Sci.* 1959, **36**, 341
- 10 Szweczyk, P. and Kalfus, M. *J. Macromol. Sci. (A)* 1973, **7**, 737
- 11 Elias, H.-G., Bareiss, R. and Watterson, J. G. *Adv. Polym. Sci.* 1973, **11**, 111

Spin-labelling of hydroxyl groups in polysaccharides

Michael C. Cafe, Norman G. Pryce and Ian D. Robb

Unilever Research Laboratory, Port Sunlight, Wirral, Merseyside L62 4XN, UK

(Received 21 August 1975; revised 29 September 1975)

INTRODUCTION

Spin labelled polymers have been used to study both the solution properties of polymers^{1,2} and their behaviour when adsorbed at the solid/liquid interface^{3,4}. Various methods for labelling polymers have been used, though one of the more difficult problems has been the labelling of hydroxyl groups on polymers such as polysaccharides that are soluble only in water or other hydroxylic solvents. Serine-OH groups on proteins have been labelled⁵, though the toxicity of the label requires great caution with the experiment. Labelling hydroxyl groups in proteins or polysaccharides by other methods such as using water soluble carbodiimides⁶, Woodward's reagent K⁷ or cyanuric chloride⁸ has been briefly reviewed^{9,10}. These methods however can sometimes lead to crosslinking.

The method of spin-labelling polysaccharides outlined in this note involves modifying the hydroxyl group with cyanogen bromide. This method has been used to attach proteins and polypeptides to cellulose or Sephadex gels¹¹⁻¹³. Although the pH in this work was 11, the reaction can be carried out in more moderately alkaline conditions (9.5-10). At pH 11, degradation of the polymer which occasionally occurs in acid conditions is avoided and a high efficiency of labelling can be achieved. Provided the polymer is completely dissolved, labels will be attached to OH groups and be randomly distributed along the chain. The polysaccharide to be labelled was sodium carboxymethylcellulose (SCMC) and the spin-label was 4-amino-2,2,6,6-tetramethylpiperidine-*N*-oxyl (I), (as supplied by Aldrich Chem. Co. Ltd).

EXPERIMENTAL AND RESULTS

A 2% solution of the SCMC (F4 grade from British Celanese Products, degree of substitution, 0.6) was filtered through a No. 4 sintered glass filter and then dialysed against distilled water for 2 weeks. Its molecular weight determined by viscosity¹⁴ in 0.1 M NaCl was 32 500. Purified SCMC (2 g) was dissolved in 40 ml H₂O and the pH adjusted to 11 with 1.0 M NaOH. Cyanogen bromide, (0.1 g, supplied by BDH) in 2 ml H₂O, was added and the mixture stirred for 4 h at room temperature, while keeping the pH constant at 11, using an automatic titrator. Spin label (I) (0.1 g) was added and the solution left a further 18 h at room temperature and at pH 11. The SCMC solution was then dialysed against distilled water until no further spin label (I) could be detected in the external solution by e.p.r. methods and then freeze-dried. Spectra were recorded on a Varian E-4 X-band spectrometer.

The molecular weight of the labelled SCMC¹¹, again determined by viscosity in 0.1 M NaCl was 34 000, indicating a minimum degree of crosslinking. The ¹H and ¹³C spectra measured on a Bruker WH90, showed no difference in the linewidths or chemical shifts of the labelled or unlabelled samples, again indicating that no significant crosslinking had taken place. Solutions of the labelled polymer were optically clear. The e.p.r. intensity of a 2% solution of the labelled polymer was compared with that of a known concentration of spin label (I). From this comparison it was calculated that there was 1 label per 24 glucose units. The spectrum from the labelled polymer is shown in *Figure 1*.



Figure 1 Spectrum of 3% polymer solution, pH 7

The correlation time was calculated to be about 5×10^{-10} sec, indicating slower tumbling of the label on the polymer, than when free in solution.

Thus it is possible to spin-label polysaccharides under alkaline conditions, causing a minimal change in the solubility, crosslinking or degradation.

REFERENCES

- 1 Bullock, A. T., Cameron, G. G. and Elsom, J. M. *Polymer* 1974, **15**, 74 and refs therein
- 2 Törmälä, P. and Tulikoura, J. *Polymer* 1974, **15**, 248
- 3 Fox, K. K., Robb, I. D. and Smith, R. *JCS. Faraday Trans. I* 1974, **70**, 1186
- 4 Robb, I. D. and Smith, R. *Eur. Polym. J.* 1974, **10**, 1005
- 5 Morrisett, J. D., Broomfield, C. A. and Hacklay, B. E. *J. Biol. Chem.* 1969, **244**, 5758
- 6 Hoare, D. G. and Koshland, D. E. Jr. *J. Biol. Chem.* 1967, **242**, 2447
- 7 Patel, R., Lopiekes, D. V., Brown, S. P. and Price, S. *Biopolymers* 1967, **5**, 577
- 8 Kay, G. and Lilly, M. D. *Biochem. Biophys. Acta* 1970, **198**, 276
- 9 Silman, I. H. and Katchalski, E. *Annu. Rev. Biochem.* 1966, **35**, 873
- 10 Weliky, N. and Weetall, H. H. *Immunochemistry* 1965, **2**, 293
- 11 Axén, R., Porath, J. and Ernback, S. *Nature* 1967, **214**, 1302
- 12 Axén, R. and Ernback, S. *Eur. J. Biochem.* 1971, **18**, 351
- 13 Porath, J., Axen, R. and Ernback, S. *Nature* 1967, **215**, 1491
- 14 Sitaramaiah, G. and Goring, D. A. I. *J. Polym. Sci.* 1962, **58**, 1107

ERRATA

'Small angle neutron and X-ray scattering by poly(methyl methacrylate) chains' by D. Y. Yoon and P. J. Flory, *Polymer* 1975, **16**, 645-648

Page 646, right-hand column, equations (8), (9) and (10) should read:

$$U' = \begin{bmatrix} 1 & 1 \\ 1 & 0 \end{bmatrix} \quad (8)$$

$$U''_m = \begin{bmatrix} 1 & \alpha \\ \alpha & \alpha^2/\beta \end{bmatrix} \quad (9)$$

$$U''_r = \begin{bmatrix} \beta & \alpha \\ \alpha & \alpha^2/\beta \end{bmatrix} \quad (10)$$

We apologize for these errors.



Figure 1 Spectrum of 3% polymer solution, pH 7

The correlation time was calculated to be about 5×10^{-10} sec, indicating slower tumbling of the label on the polymer, than when free in solution.

Thus it is possible to spin-label polysaccharides under alkaline conditions, causing a minimal change in the solubility, crosslinking or degradation.

REFERENCES

- 1 Bullock, A. T., Cameron, G. G. and Elsom, J. M. *Polymer* 1974, **15**, 74 and refs therein
- 2 Törmälä, P. and Tulikoura, J. *Polymer* 1974, **15**, 248
- 3 Fox, K. K., Robb, I. D. and Smith, R. *JCS. Faraday Trans. I* 1974, **70**, 1186
- 4 Robb, I. D. and Smith, R. *Eur. Polym. J.* 1974, **10**, 1005
- 5 Morrisett, J. D., Broomfield, C. A. and Hacklay, B. E. *J. Biol. Chem.* 1969, **244**, 5758
- 6 Hoare, D. G. and Koshland, D. E. Jr. *J. Biol. Chem.* 1967, **242**, 2447
- 7 Patel, R., Lopiekes, D. V., Brown, S. P. and Price, S. *Biopolymers* 1967, **5**, 577
- 8 Kay, G. and Lilly, M. D. *Biochem. Biophys. Acta* 1970, **198**, 276
- 9 Silman, I. H. and Katchalski, E. *Annu. Rev. Biochem.* 1966, **35**, 873
- 10 Weliky, N. and Weetall, H. H. *Immunochemistry* 1965, **2**, 293
- 11 Axén, R., Porath, J. and Ernback, S. *Nature* 1967, **214**, 1302
- 12 Axén, R. and Ernback, S. *Eur. J. Biochem.* 1971, **18**, 351
- 13 Porath, J., Axen, R. and Ernback, S. *Nature* 1967, **215**, 1491
- 14 Sitaramaiah, G. and Goring, D. A. I. *J. Polym. Sci.* 1962, **58**, 1107

ERRATA

'Small angle neutron and X-ray scattering by poly(methyl methacrylate) chains' by D. Y. Yoon and P. J. Flory, *Polymer* 1975, **16**, 645-648

Page 646, right-hand column, equations (8), (9) and (10) should read:

$$U' = \begin{bmatrix} 1 & 1 \\ 1 & 0 \end{bmatrix} \quad (8)$$

$$U''_m = \begin{bmatrix} 1 & \alpha \\ \alpha & \alpha^2/\beta \end{bmatrix} \quad (9)$$

$$U''_r = \begin{bmatrix} \beta & \alpha \\ \alpha & \alpha^2/\beta \end{bmatrix} \quad (10)$$

We apologize for these errors.

Letters

Small-angle X-ray scattering from ultrathin films of cellulose acetate

Thin films (300–4000 Å) of cellulose acetate can be used to make composite reverse osmosis membranes¹. Since the mechanism of reverse osmosis separation is not fully understood, the structure of these films is of interest. Schultz and Asunmaa² obtained electron micrographs of shadowed films of cellulose acetate which they interpreted as showing an irregular close-packed array of roughly spherical particles, about 188 Å in diameter.

In the present study, thin films of cellulose 2.5 acetate (Eastman Kodak E-398-3) were made from a 2% w/w solution in acetone by the Carnell–Cassidy^{3,4} method. Assuming a film density of 1.3 g/cm³, the film thickness (determined by weighing) was 1900 ± 100 Å. The true film density may be considerably less than 1.3 g/cm³ in view of the structural model discussed below. A stack of the films (not heat-treated) was examined using a Kratky camera and a version of the Franks camera with the X-ray beam (CuKα) perpendicular to the plane of the films. A range of s down to $s = 0.0012 \text{ \AA}^{-1}$ was studied with the Franks camera (photographic detection) and down to $s = 0.00044 \text{ \AA}^{-1}$ with the Kratky (counter detection) where $s = 2 \sin \theta / \lambda$. Kratky data were desmeared by the method of Glatter⁵.

From $s = 0.00044$ to 0.025 \AA^{-1} the scattered intensity decreases monotonically apart from two 'shoulders' at $s = 0.0043$ and 0.0084 \AA^{-1} (Figure 1). If the films consist of a paracrystalline array of particles then the shoulder at $s = 0.0084 \text{ \AA}^{-1}$ could be due to the structure factor of individual particles. The first subsidiary maximum in the structure factor of a sphere radius R , occurs at $sR = 0.92$, and the (110) reflection of spheres in an hexagonal close packed (h.c.p.) lattice occurs at $sR = 1.00$. Spherical particles would then have a radius of 110–120 Å. The $s = 0.0043 \text{ \AA}^{-1}$ reflection is probably due to interparticle interference. The (002) reflection for an infinite h.c.p. lattice of spheres occurs at $sR = 0.613$. However, the structure factor of a sphere is changing rapidly at this value of sR and if a crystalite contained only 3 lattice repeats in the z direction then the (002) peak would be displaced⁷ to about $sR = 0.571$, i.e. to $s = 0.0050 \text{ \AA}^{-1}$ for $R = 115 \text{ \AA}$. The shoulder at $s =$

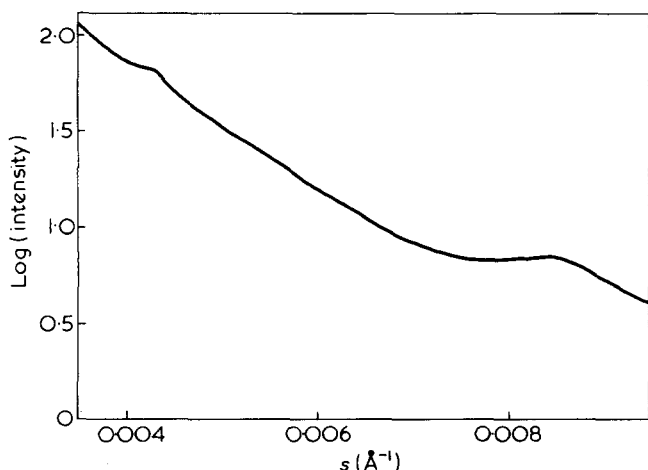


Figure 1 Scattering from cellulose acetate films. Desmeared Kratky camera data (small angle region)

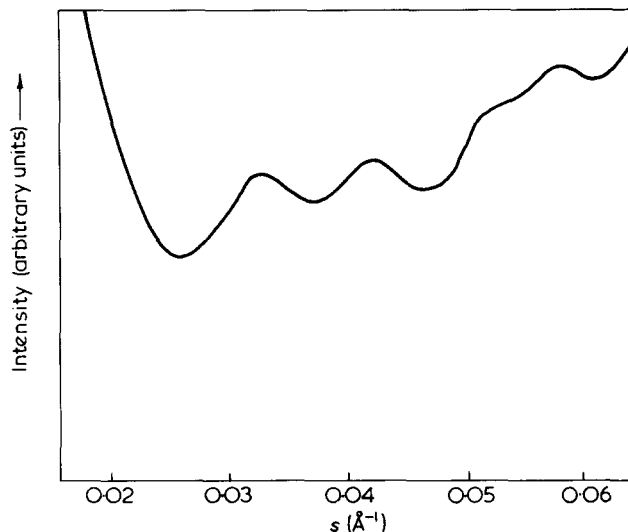


Figure 2 Scattering from cellulose acetate films. Desmeared Kratky camera data (higher angle region)

0.0043 \AA^{-1} thus seems consistent with rather irregular packing, with some gaps between the spheres.

The above results are in reasonable agreement with those of Schultz and Asunmaa². Contrary to the assertion of Kesting⁸, the results confirm that the postulated paracrystalline structure of these films can be detected by X-ray scattering.

The minimum scattered intensity occurs at $s = 0.0256 \text{ \AA}^{-1}$. At higher angles there are several broad subsidiary maxima, notably at $s = 0.0324$ and 0.0422 \AA^{-1} (Figure 2). A very small percentage of material present in the CTA II crystal structure⁹ would produce a (100) reflection at $s = 0.0408 \text{ \AA}^{-1}$ which might account for the latter peak, but not for the former. Alternatively, if the $s = 0.0422 \text{ \AA}^{-1}$ peak were due to the first subsidiary maximum in the structure factor of a sphere, then this would correspond to a sphere radius of 21.9 Å and (assuming a density of 1.3 g/cm³) a mass of about 34 000 amu. The stated mean molecular weight of the polymer is 27 000 amu which suggests that the 115 Å radius particles are made up of globular sub-units, each consisting of one molecule. If the 21.9 Å subunits were close packed on an f.c.c. lattice they would give (200) type reflections at $s = 0.0323 \text{ \AA}^{-1}$ in good agreement with the observed peak at $s = 0.0324$. No (111) reflection was observed. However, if the paracrystalline regions were small then the (111) reflection would be displaced to smaller angles in the same way as the (002) reflection of the h.c.p. lattice of 115 Å particles. The peak would then be inseparable from the start of the small angle scattering.

SAXS studies of these cellulose acetate films are continuing.

Acknowledgements

Kratky-camera data were obtained at the Institute for Physical Chemistry, University of Graz. Thanks are due to Professor I. Pilz and the staff of the Institute for kindly providing facilities.

Philip H. Stothart

The National Institute for Research in Dairying,
Shinfield, Reading, RG2 9AT, UK
(Received 27 October 1975)

References

- Riley, R. L., Lonsdale, H. K., Lyons, C. R. and Merten, U. *J. Appl. Polym. Sci.* 1967, 11, 2143
- Schultz, R. D. and Asunmaa, S. K. *Recent Progr. Surface Sci.* 1970, 3, 294
- Carnell, P. H. and Cassidy, H. G. *J. Polym. Sci.* 1961, 55, 233
- Carnell, P. H. *J. Appl. Polym. Sci.* 1965, 9, 1863
- Glatter, O. *Acta. Phys. Austriaca* 1972, 36, 307
- Guinier, A., Fournet, G., Walker, C. B. and Yudowitch, K. L. 'Small-angle scattering of X-rays', Chapman and Hall, London, (Wiley, New York), 1955, pp 54-57
- James, R. W. 'The Optical Principles of the Diffraction of X-rays', Bell, London, 1962, Ch X
- Kesting, R. E. 'Synthetic Polymeric Membranes', McGraw-Hill, New York, 1971, p 68
- Dulmage, W. J. *J. Polym. Sci.* 1957, 26, 277

New thermal initiators of free-radical polymerization and block copolymerization

Much information is available about the initiation of free-radical polymerization by organo-transition metal complexes in the presence of reactive organic halides^{1,2}. We now report two types of thermally initiating systems based on transition metal carbonyls which either contain no abstractable halide atoms or are free from halides.

Systems containing transition metal carbonyls (I)

In addition to a transition metal carbonyl, notably manganese or rhenium carbonyl ($Mn_2(CO)_{10}$, $Re_2(CO)_{10}$, respectively), these systems contain a low concentration of an additive such as tetrafluoroethylene or other ethylenic derivative carrying electron-withdrawing groups or an acetylenic derivative. *Figure 1* illustrates the characteristics of initiators of this type based on $Mn_2(CO)_{10}$ and $Re_2(CO)_{10}$. Rates of polymerization of methyl methacrylate at 100°C, ω , are shown as a function of the concentration of additive, either tetrafluoroethylene or acetylene dicarboxylic acid dimethyl ester (ADCADME). The curves are highly reminiscent of the 'halide' curves in initiating systems containing reactive halides, showing a plateau value at high additive concentrations^{1,2}. For comparison, the dependence of ω on $[CCl_4]$ for initiation by $Mn_2(CO)_{10}/CCl_4$ at 100°C is also illustrated in *Figure 1*; evidently C_2F_4 and ADCADME

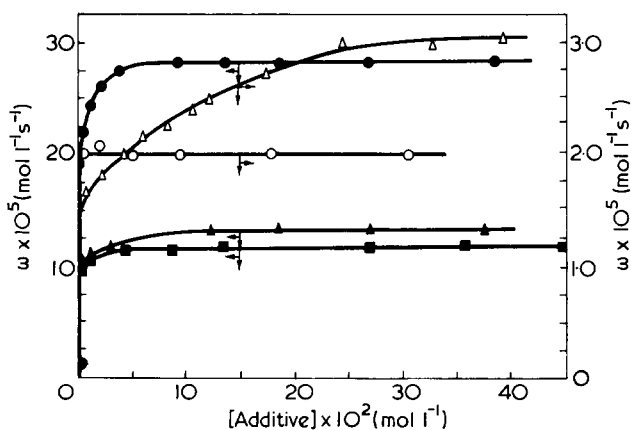


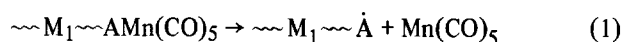
Figure 1 Thermal initiation by systems of type I. Methyl methacrylate (bulk), 100°C. ■, $Mn_2(CO)_{10}$ (4.77×10^{-4} mol/l) + ADCADME; ▲, $Mn_2(CO)_{10}$ (4.77×10^{-4} mol/l) + C_2F_4 ; ●, $Mn_2(CO)_{10}$ (4.77×10^{-4} mol/l) + CCl_4 ; ○, $Re_2(CO)_{10}$ (5.48×10^{-4} mol/l) + ADCADME; △, $Re_2(CO)_{10}$ (5.48×10^{-4} mol/l) + C_2F_4 . The concentrations of C_2F_4 given are nominal values only, being calculated on the assumption that all the gas is dissolved in the methyl methacrylate. When [additive] = 0, $\omega = 1.02 \times 10^{-5}$ mol $l^{-1} s^{-1}$

are less effective than CCl_4 in producing high rates of initiation in association with $Mn_2(CO)_{10}$.

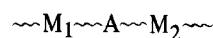
Under suitable conditions, polymers prepared with the new initiators show absorption in the infra-red near 2000 cm^{-1} similar to that of $(CO)_5MnA-$ or $(CO)_5ReA-$ end-groups³⁻⁵, where A represents a ligand derived from the additive, e.g. $-CF_2CF_2-$ or $-C(COOMe)=C(COOMe)-$. Thus the primary radicals probably have structures such as $(CO)_5MnCF_2\dot{C}F_2$ or $(CO)_5MnC(COOMe)=\dot{C}(COOMe)$, which may conveniently be abbreviated to $(CO)_5Mn\dot{A}$, although more complex variants cannot be excluded. The final polymers contain covalently bound atoms of manganese or rhenium.

Macromolecular initiators: block copolymerization (II)

In earlier papers³⁻⁷ we have shown that some transition metal carbonyls, particularly $Mn_2(CO)_{10}$, $Re(CO)_{10}$, in the presence of an additive of the types described above can photoinitiate the polymerization of common vinyl monomers at ambient temperatures. The resulting polymers have end-groups of structure $(CO)_5MnA-$ or $(CO)_5ReA-$. In the examples described below the additives were C_2F_4 and $MeOOC\equiv CCOOMe$, so that the corresponding end-groups [from $Mn_2(CO)_{10}$] were $(CO)_5MnCF_2CF_2-$ and $(CO)_5MnC(COOMe)=C(COOMe)-$, respectively. These polymers are active thermal initiators at higher temperatures (e.g. 100°C); we believe that initiation results from a homolytic process of the type:



in which $\sim M_1 \sim$ represents a polymer chain derived from monomer M_1 . The polymeric product obtained from a monomer M_2 is, therefore, in the simplest case, (when termination in M_2 is 100% disproportionation) a block copolymer:



When an additive of the type described is present the species $Mn(CO)_5$ also initiates, giving rise to primary radicals such as $(CO)_5Mn\dot{A}$; the rate of polymerization is therefore increased.

Preparative details and molecular weights of typical macroinitiators are given in *Table 1*. The experimental arrangements have been described in earlier papers^{3,5-7}.

Figure 2 presents conversion-time data for the polymerization of methyl methacrylate at 100°C in the presence of the macroinitiators 1 and 2 (*Table 1*). Some corresponding data for the rhenium macroinitiators are given in *Table 2*. These experiments also show that the presence

Table 1 Preparation of macroinitiators at 25°C

No.	M_1 , concentration	Solvent	Total volume (ml)	Additive (~0.2 mol/l)	$M_n \times 10^{-5}$
[$Mn_2(CO)_{10}$] = 8.54×10^{-4} mol/l; $\lambda = 435.8$ nm:					
1	MMA, bulk	none	60	ADCADME	2.12
2	MMA, bulk	none	60	C_2F_4	1.83
3	C_2F_4 , 2.6 mol/l	acetic acid	~2	—	—
[$Re_2(CO)_{10}$] = 8.60×10^{-4} mol/l; $\lambda = 365$ nm:					
4	MMA, bulk	none	5	ADCADME	1.88
5	MMA, bulk	none	5	C_2F_4	1.88

References

- Riley, R. L., Lonsdale, H. K., Lyons, C. R. and Merten, U. *J. Appl. Polym. Sci.* 1967, 11, 2143
- Schultz, R. D. and Asunmaa, S. K. *Recent Progr. Surface Sci.* 1970, 3, 294
- Carnell, P. H. and Cassidy, H. G. *J. Polym. Sci.* 1961, 55, 233
- Carnell, P. H. *J. Appl. Polym. Sci.* 1965, 9, 1863
- Glatter, O. *Acta. Phys. Austriaca* 1972, 36, 307
- Guinier, A., Fournet, G., Walker, C. B. and Yudowitch, K. L. 'Small-angle scattering of X-rays', Chapman and Hall, London, (Wiley, New York), 1955, pp 54-57
- James, R. W. 'The Optical Principles of the Diffraction of X-rays', Bell, London, 1962, Ch X
- Kesting, R. E. 'Synthetic Polymeric Membranes', McGraw-Hill, New York, 1971, p 68
- Dulmage, W. J. *J. Polym. Sci.* 1957, 26, 277

New thermal initiators of free-radical polymerization and block copolymerization

Much information is available about the initiation of free-radical polymerization by organo-transition metal complexes in the presence of reactive organic halides^{1,2}. We now report two types of thermally initiating systems based on transition metal carbonyls which either contain no abstractable halide atoms or are free from halides.

Systems containing transition metal carbonyls (I)

In addition to a transition metal carbonyl, notably manganese or rhenium carbonyl ($Mn_2(CO)_{10}$, $Re_2(CO)_{10}$, respectively), these systems contain a low concentration of an additive such as tetrafluoroethylene or other ethylenic derivative carrying electron-withdrawing groups or an acetylenic derivative. *Figure 1* illustrates the characteristics of initiators of this type based on $Mn_2(CO)_{10}$ and $Re_2(CO)_{10}$. Rates of polymerization of methyl methacrylate at 100°C, ω , are shown as a function of the concentration of additive, either tetrafluoroethylene or acetylene dicarboxylic acid dimethyl ester (ADCADME). The curves are highly reminiscent of the 'halide' curves in initiating systems containing reactive halides, showing a plateau value at high additive concentrations^{1,2}. For comparison, the dependence of ω on $[CCl_4]$ for initiation by $Mn_2(CO)_{10}/CCl_4$ at 100°C is also illustrated in *Figure 1*; evidently C_2F_4 and ADCADME

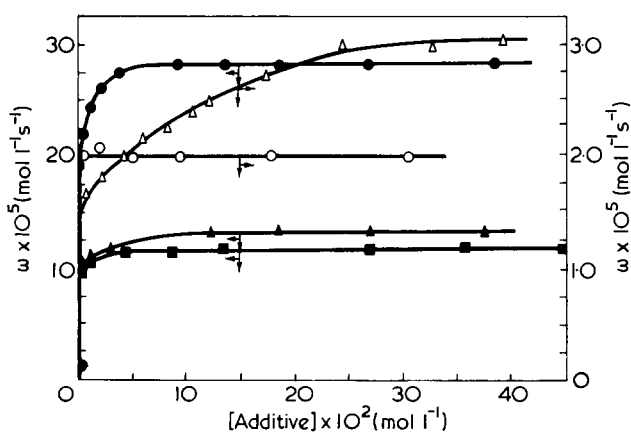


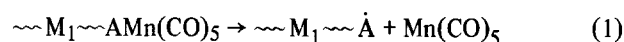
Figure 1 Thermal initiation by systems of type I. Methyl methacrylate (bulk), 100°C. ■, $Mn_2(CO)_{10}$ (4.77×10^{-4} mol/l) + ADCADME; ▲, $Mn_2(CO)_{10}$ (4.77×10^{-4} mol/l) + C_2F_4 ; ●, $Mn_2(CO)_{10}$ (4.77×10^{-4} mol/l) + CCl_4 ; ○, $Re_2(CO)_{10}$ (5.48×10^{-4} mol/l) + ADCADME; △, $Re_2(CO)_{10}$ (5.48×10^{-4} mol/l) + C_2F_4 . The concentrations of C_2F_4 given are nominal values only, being calculated on the assumption that all the gas is dissolved in the methyl methacrylate. When [additive] = 0, $\omega = 1.02 \times 10^{-5}$ mol $l^{-1} s^{-1}$

are less effective than CCl_4 in producing high rates of initiation in association with $Mn_2(CO)_{10}$.

Under suitable conditions, polymers prepared with the new initiators show absorption in the infra-red near 2000 cm^{-1} similar to that of $(CO)_5MnA-$ or $(CO)_5ReA-$ end-groups³⁻⁵, where A represents a ligand derived from the additive, e.g. $-CF_2CF_2-$ or $-C(COOMe)=C(COOMe)-$. Thus the primary radicals probably have structures such as $(CO)_5MnCF_2\dot{C}F_2$ or $(CO)_5MnC(COOMe)=\dot{C}(COOMe)$, which may conveniently be abbreviated to $(CO)_5Mn\dot{A}$, although more complex variants cannot be excluded. The final polymers contain covalently bound atoms of manganese or rhenium.

Macromolecular initiators: block copolymerization (II)

In earlier papers³⁻⁷ we have shown that some transition metal carbonyls, particularly $Mn_2(CO)_{10}$, $Re(CO)_{10}$, in the presence of an additive of the types described above can photoinitiate the polymerization of common vinyl monomers at ambient temperatures. The resulting polymers have end-groups of structure $(CO)_5MnA-$ or $(CO)_5ReA-$. In the examples described below the additives were C_2F_4 and $MeOOC\equiv CCOOMe$, so that the corresponding end-groups [from $Mn_2(CO)_{10}$] were $(CO)_5MnCF_2CF_2-$ and $(CO)_5MnC(COOMe)=C(COOMe)-$, respectively. These polymers are active thermal initiators at higher temperatures (e.g. 100°C); we believe that initiation results from a homolytic process of the type:



in which $\sim M_1 \sim$ represents a polymer chain derived from monomer M_1 . The polymeric product obtained from a monomer M_2 is, therefore, in the simplest case, (when termination in M_2 is 100% disproportionation) a block copolymer:



When an additive of the type described is present the species $Mn(CO)_5$ also initiates, giving rise to primary radicals such as $(CO)_5Mn\dot{A}$; the rate of polymerization is therefore increased.

Preparative details and molecular weights of typical macroinitiators are given in *Table 1*. The experimental arrangements have been described in earlier papers^{3,5-7}.

Figure 2 presents conversion-time data for the polymerization of methyl methacrylate at 100°C in the presence of the macroinitiators 1 and 2 (*Table 1*). Some corresponding data for the rhenium macroinitiators are given in *Table 2*. These experiments also show that the presence

Table 1 Preparation of macroinitiators at 25°C

No.	M_1 , concentration	Solvent	Total volume (ml)	Additive (~0.2 mol/l)	$M_n \times 10^{-5}$
[$Mn_2(CO)_{10}$] = 8.54×10^{-4} mol/l; $\lambda = 435.8$ nm:					
1	MMA, bulk	none	60	ADCADME	2.12
2	MMA, bulk	none	60	C_2F_4	1.83
3	C_2F_4 , 2.6 mol/l	acetic acid	~2	—	—
[$Re_2(CO)_{10}$] = 8.60×10^{-4} mol/l; $\lambda = 365$ nm:					
4	MMA, bulk	none	5	ADCADME	1.88
5	MMA, bulk	none	5	C_2F_4	1.88

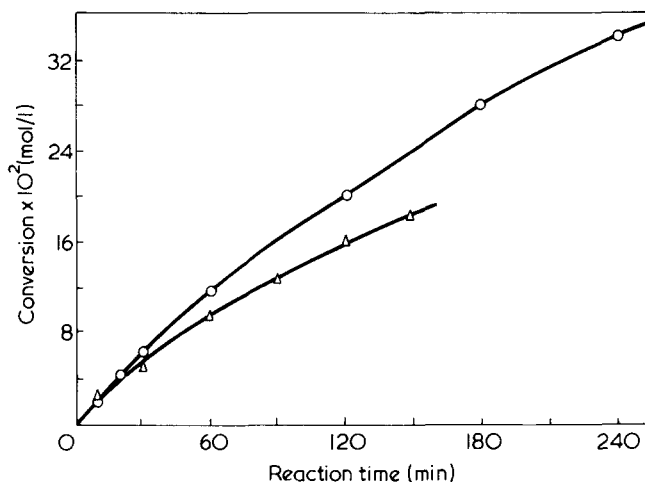


Figure 2 Thermal initiation by systems of type II. Methyl methacrylate (bulk), 100°C. No additive. Δ , Macroinitiator No. 1 (Table 1): 1.0 g/l; \circ , macroinitiator No. 2 (Table 1): 1.0 g/l

Table 2 Initiation by rhenium macroinitiators

No. of macro-initiator (Table 1)	Additive, weight (mg)	Weights of final polymers (mg)	
		30 min	60 min
4	—	54	74
4	ADCADME, 151	72	127
4	C ₂ F ₄ , 153	69	—
5	—	46	62
5	ADCADME, 151	66	117
5	C ₂ F ₄ , 153	65	—

In each experiment 10 mg macroinitiator in 10 ml methyl methacrylate were used and the mixture was heated at 100°C

of the additive increases the rate of polymerization, as already mentioned. The dependence of the rate of polymerization initiated by polymers 1 and 2 (Table 1) on the concentration of ADCADME is presented in Figure 3. The results with polymer 2, showing a plateau value with increasing [ADCADME], are as would be expected, but polymer 1 behaves in a more complicated fashion which at present is being studied in detail.

Block copolymer formation has been demonstrated in the polymerization of acrylonitrile (AN) initiated by the polymers 1 and 2 (Table 1) and in the polymerization of methyl methacrylate (MMA) initiated by polymer 3 (Table 1). Details are given in Table 3. In three cases the products were separated into fractions soluble and insoluble in chloroform as indicated in Table 3. Infra-red spectra of the polymeric products from macroinitiators 1 and 2 (Table 3) showed that in the chloroform-insoluble fractions both AN and MMA units were present, while in the chloroform-soluble portions no AN could be detected. The latter fractions therefore contained mainly the unreacted macroinitiator together perhaps with reacted material with very short AN chains. Both fractions of the polymer from experiment 3 (Table 3) contained tetrafluoroethylene and methyl meth-

Table 3 Block copolymerization at 100°C

Macro-initiator	Weight (mg)	Additive, M ₂ , weight (mg)	M ₂ , volume (ml)	Reaction time (min)	Product	
					CHCl ₃ soluble/ (mg)	CHCl ₃ insoluble (mg)
1	50	—	AN, 5	60	42	150
2	50	—	AN, 5	60	44	141
3	30	ADCAD- ME, 151	MMA, 10	60	90	63
3	30	—	MMA, 10	60	133	—
3	10	ADCAD- ME, 151	MMA, 10	30	64	—
3	10	—	MMA, 10	30	50	—

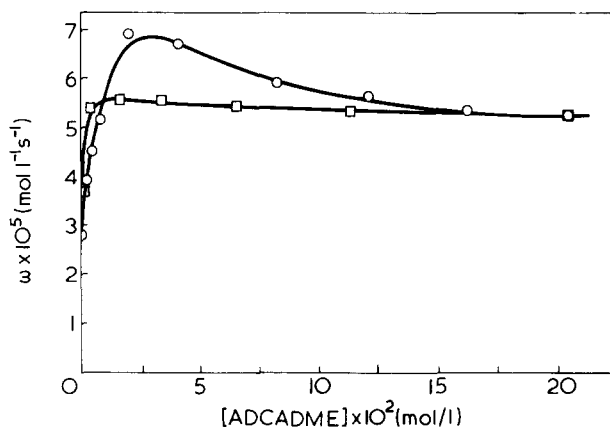


Figure 3 Thermal initiation by systems of type II in presence of ADCADME. \circ , Macroinitiator No. 1 (Table 1): 1.0 g/l; \square , macroinitiator No. 2 (Table 1): 1.0 g/l

acrylate units, but the former predominated in the insoluble fractions.

It seems clear that these macroinitiators are of considerable potential value in the synthesis of block copolymers.

C. H. Bamford and S. U. Mullik

Department of Inorganic, Physical and Industrial Chemistry,
University of Liverpool,
PO Box 147,
Liverpool L69 3BX, UK
(Received 17 October 1975)

References

- Bamford, C. H. in 'Reactivity, Mechanism and Structure in Polymer Chemistry', (Ed. A. D. Jenkins and A. Ledwith), Wiley, London and New York, 1974, Ch 3
- Bamford, C. H. *Pure Appl. Chem.* 1973, **34**, 173
- Bamford, C. H. and Mullik, S. U. *JCS Faraday Trans. I* 1975, **71**, 625
- Aliwi, S. M., Bamford, C. H. and Mullik, S. U. *IUPAC Symp. Macromolecules, Madrid*, 1974; *J. Polym. Sci. (C)* in press
- Bamford, C. H. and Mullik, S. U. *JCS Faraday Trans. I* in press
- Bamford, C. H. and Mullik, S. U. *JCS Faraday Trans. I* 1973, **69**, 1127
- Bamford, C. H. and Mullik, S. U. *Polymer* 1973, **14**, 38

Book Reviews

Peptides, polypeptides and proteins

Edited by E. R. Blout, F. A. Bovey, M. Goodman and N. Lotan

John Wiley, New York, 1975. 656 pp. £12.25

This volume contains forty-six papers given at a symposium held in Israel in May 1974. They are grouped under six main headings: Conformational calculations, Polypeptide and protein conformations, Cyclic and linear oligopeptides, Optical spectroscopy, Intermolecular interactions and Biological properties. While these papers might have been published in the usual journals, together they give a spectrum of current experimental and theoretical work for research workers in these areas. The discussions that followed the papers are not reported, but the authors had the opportunity to revise their papers following the meeting, and the substantial revision and editing of the preprint versions (which weighed 5 kilos!) is evident and beneficial.

While it may be, as Traub suggests, that the usefulness of X-ray studies of poly(amino acids) as models in relation to proteins has now largely been exhausted, undoubtedly the relative simplicity of these polymers is still of great value in providing a sound experimental and theoretical basis for n.m.r., optical and conformational studies of proteins, as is shown by many papers. Similarly, work on the cyclic peptides, which are of considerable intrinsic interest, may be relevant to the turns in protein structures. Undoubtedly the hope of predicting (successfully) the full conformation of a protein is a strong motivating factor here, but a spin-off from this extensive work is a better understanding of polymeric systems in general, and workers in other fields could find this book stimulating.

The accounts of the use of linear and branched chain polypeptides as synthetic antigens to study the immune response will be of particular interest to biologists.

Many will find the volume a valuable compilation at a not unrealistic price, and all concerned are to be congratulated on its speedy publication.

B. R. Malcolm

Progress in polymer science, Japan, Volume 7

Edited by T. Otsu and M. Takayanagi

Kodansha, Tokyo and John Wiley, New York, 1974, 380 pp. £14.50

Much Japanese work in polymer science is published in English, but there is still a large amount which is published in Japanese and hence not readily available internationally. This series is aimed at publicising fundamental studies currently in hand in Japanese laboratories by an annual selection of areas of work of topical interest and importance.

The present volume is divided between the synthesis of polymers and selected aspects of the study of physical properties.

Three articles on synthetic chemistry deal with photoresponsive polymers, polymers containing nucleic acid bases and their derivatives, and the polymerization of diallyl dicarboxylates. Current interest in photoresponsive polymers deal with all aspects of properties influenced by light such as colour, conduction, fluorescence and redox catalysis. The incorporation of nucleic acid bases in a variety of synthetic backbones is of obvious biochemical and biological interest and the article includes some comments on possible uses for these special molecules. The polymerization of diallyl dicarboxylates leads ultimately to the formation of extensive gel structures and in addition to further studies of the kinetics of reaction, attention has been given to gelation and copolymerization mechanisms together with the compilation of much quantitative information.

The structural articles are three in number and deal with solid state polymerization products, properties of crystalline polymers under high pressure and the structure of polypeptides and protein molecules. In the solid state work a variety of mechanisms is described and the morphology of the polymer studied in relation to the structure of the monomer in the solid state. The effect of pressure on polymers has also been extensively reviewed and includes instrumentation to measure a variety of properties including transitions and mechanical relaxation. Several vinyl and condensation polymers have been examined in this respect. The structure of the polypeptides section includes studies of model compounds for polypeptide chains and of vibrational spectra for poly(α -amino acids).

All the articles are well documented and provided with much quantitative information. For those interested in these fields this work must be a valuable review and even for those with more general interests, the clear presentation is conducive to browsing. The price is not low but the book represents good value by present day standards.

J. C. Robb

Conference Announcement

IVth European Symposium on Polymer Spectroscopy

Strasbourg, France, 22–24 March 1976

This conference is organized on behalf of the European Physical Society (Section of Macromolecular Physics of the Condensed Matter Division), the European Group on Polymer Spectroscopy, the French Physical Society and the French Polymer Group and will take place at Louis Pasteur University in Strasbourg from 22 to 24 March 1976. There will be five scientific sessions, each introduced by an invited lecture and followed by short contributed communications in the following fields: infra-red and Raman spectroscopy, inelastic neutron scattering, n.m.r., e.p.r., e.s.c.a., optical spectroscopy and fluorescence. The number of participants will be limited to 120. The second circular and registration form are now available from Professor G. Weill, Symposium Européen de Spectroscopie des Polymères, Centre de Recherches sur les Macromolécules, CNRS, 6 Rue Boussingault, 67083 Strasbourg, France and to whom completed registration forms should be sent by 31 January 1976.

Conference Announcement

Second Symposium on Poly(vinyl chloride)

Lyon, France, 5–9 July 1976

Following the first symposium held in Prague in 1970, a second symposium on poly(vinyl chloride), sponsored by IUPAC, CNRS and GRP will be organized in Lyon from 5 to 9 July 1976. It will cover eight topics: polymerization, chemical modifications, characterization, rheology, processing, properties, degradation and stabilization, and combustion and toxicity. Each topic will include a main lecture, short communications and a panel discussion. Further information may be obtained from the Symposium Secretary: Dr A. Michel, LA 199—CNRS, 39 Bd du 11 novembre 1918, 69626 Villeurbanne, France.

Crystallization of dilute polyethylene solutions: influence of molecular weight

E. Riande and J. M. G. Fatou

Sección de Fisicoquímica y Física de polímeros, Instituto de Plásticos y Caucho, Juan de la Cierva 3, Madrid-6, Spain

(Received 30 June 1975)

The crystallization kinetics of linear polyethylene over the molecular weight range 14 000–1 200 000 was studied in dilute solutions of α -chloronaphthalene by dilatometric techniques. The experimental results could be quantitatively described by the Avrami and Göler–Sachs theories for a significant part of the transformation. The influence of molecular weight on the time necessary for 10% of crystallinity to develop was also analysed and the obtained curves follow the same pattern as in the bulk. The temperature coefficient of crystallization was studied by using the two-dimensional nucleation theory and it was found that the basic interfacial free energy is about four times lower than the value reported previously for the pure polymer.

INTRODUCTION

The nucleation process plays an important role in the crystallization of polymers. Nucleation theories for finite molecular weight were developed in the past¹ and significant departures from monomer theory have been observed in the molecular weight range of interest. Accordingly, the crystallization kinetics of polymers strongly depends on the crystallization temperature, molecular weight and diluent concentration. Earlier work² has re-investigated the nucleation theory for fractionated polymer diluent systems (polyethylene in α -chloronaphthalene) over a composition range extending from pure polymer to 0.30 polymer fraction solutions and we have shown that the crystallization process in polymer/diluent mixtures is governed by the nucleation of the system and that the phase transformation is described by a function of the free energy required for nucleation. In the present paper this analysis is extended to very dilute solutions ($v_2 = 0.0030$) in the system polyethylene/ α -chloronaphthalene over a wide range of molecular weights.

EXPERIMENTAL

Materials

The linear polyethylene fractions were obtained from unfractionated Marlex 50 using the column fractionation technique that has been described elsewhere³. The solvent/non-solvent system used was tetralin/*n*-butyl glycol. The polyethylene fractionation was carried out at 128.0°C under a nitrogen atmosphere to prevent oxidation. The highest molecular fraction used in this work was obtained from a NBS linear high molecular weight polyethylene sample using a liquid–liquid phase separation technique which has been described previously⁴.

The α -chloronaphthalene (Fluka, AG) used in this work was of high purity.

Viscosity measurements

The determination of the intrinsic viscosities of the polyethylene fractions has been described elsewhere³. Viscosity-average molecular weights, M_η , were obtained from the rela-

tion given by Chiang⁵ for decalin at 135°C. The viscosity-average molecular weights for polyethylene fractions studied in this work were: 14 000; 20 000; 47 000; 190 000 and 1 200 000.

Crystallization

The sample and solvent were introduced into the bulb of the dilatometer and the sample was dissolved under a nitrogen atmosphere. Then the dilatometer was sealed. Filling the dilatometer with mercury was carried out according to the procedure described by Mandelkern *et al.*⁶. The crystallization was conducted in a silicone oil thermostat bath and the column of the mercury in the dilatometer was recorded as a function of time and could be measured to within ± 0.1 mm. The total change in the mercury height to completion of the crystallization was about 4 cm. Prior to the initiation of the crystallization the polymer sample in the dilatometer was dissolved by heating and the dilatometer was quickly transferred to a thermostat at a pre-assigned temperature. Thermal equilibrium was reached in about 10 min.

RESULTS AND DISCUSSION

At very high dilutions, comparative large undercoolings are necessary to obtain kinetic data in a reasonable time period. The data could be obtained in the temperature range from 96° to 102°C. The total crystallization time involved in the results reported here range from 1400 minutes to 10 000 min depending on the crystallization temperature. The lower crystallization temperature used in these experiments was that one with which a slight transformation (0.4%) was obtained in about 40 min.

It was found that the crystallization rates depend on the thermal history of the solution. Reproducible isotherms were obtained for low molecular weights when the dilatometer was kept in a bath for 60 min at a temperature of 150.0°C. As the molecular weight increases longer times and higher solution temperatures were necessary to achieve complete solubility. With the two higher molecular weight fractions, reproducible isotherms were obtained once the

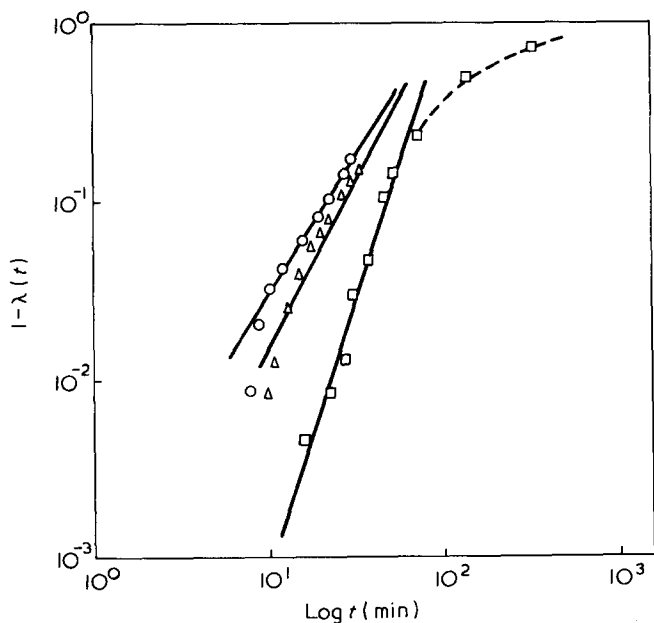


Figure 1 Plot of degree of crystallinity as function of log t for fraction $M = 190\,000$. Solution temperatures: \circ , 180° ; Δ , 190° ; \square , 210°C

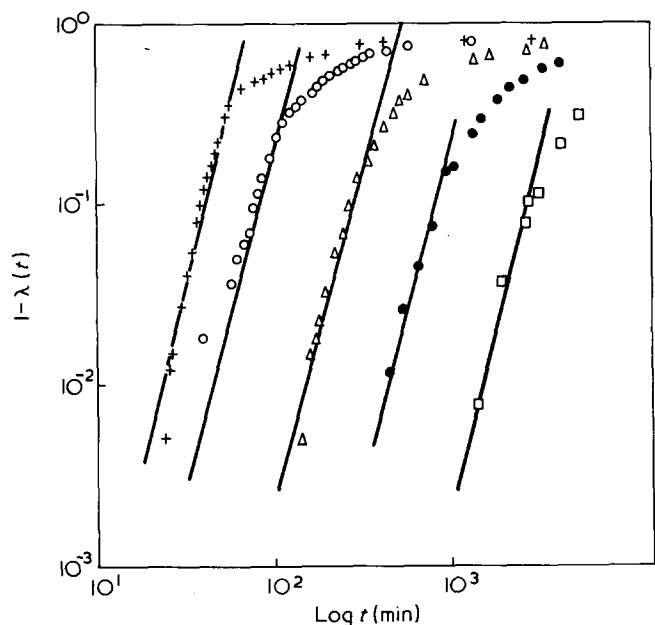


Figure 2 Double logarithmic plot of degree of crystallinity against t at different crystallization temperatures, for fraction $M_\eta = 14\,000$. $+$, 98° ; \circ , 98.9° ; Δ , 100.1° ; \bullet , 100.9° ; \square , 101.9°C

dilatometers were kept in a bath at 220°C for 12 h as is shown in Figure 1.

The prior thermal history strongly influences the crystallization kinetics. As an example, the first stages of the crystallization isotherms as a function of the thermal history will be analysed for the molecular weight fraction of 190 000. The experiments were carried out one after another in which the sample was crystallized at 99.0°C . As indicated in Figure 1 the crystallization rates are higher the lower the solution temperatures and the induction time increases as long as the solution temperature increases. It would appear that a very high solution temperature is necessary to get the polymer chains completely at random in solution and completely homogenized solutions. The same behaviour concerning the irreproducibility of the isotherms

was found by Ergoz *et al.*⁷ with undilute high molecular weight fractions ($\bar{M}_\eta = 1.2 \times 10^6$). However, these authors reported that if the sample was never cooled below the crystallization temperature, then on the third and subsequent melting and crystallization the results were reproducible.

Kinetic analysis

The kinetic data were analysed using the G6ler-Sachs or free growth approximation⁸. Accordingly, for the initial portion of the transformation it is found that:

$$1 - \lambda(t) = (k_3 t)^4 / 4$$

$$1 - \lambda(t) = (k_2 t)^3 / 6 \tag{1}$$

$$1 - \lambda(t) = (k_1 t)^2 / 2$$

depending on the respective growth geometries, i.e. the exponent in equation (1) defines, respectively, three, two or one-dimensional growth. The experimental results, concerning the complete molecular weight range studied, are plotted in Figures 2-6 according to equation (1). For a given molecular weight fraction a linear relation is obtained for a significant part of the total transformation and the slope of these portions is found to be independent of crystallization temperature. However, the slope of the linear portion of the double logarithmic plot $1 - \lambda(t)$ vs. t , is dependent on molecular weight. For the two lowest molecular weights analysed here, the slope is four. As the molecular weight increases up to and including $M = 1.2 \times 10^6$, the slope is three. Similar results were obtained in previous work⁷ for undiluted fractionated polyethylene covering the same molecular weight range. The slopes have the exact integral value and the close adherence of these straight lines to the experimental data is quite clear.

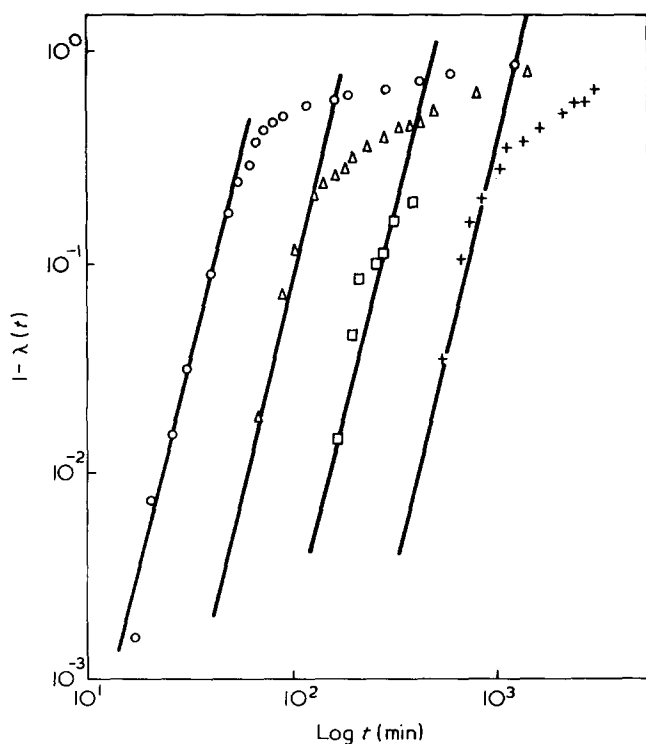


Figure 3 Double logarithmic plot of degree of crystallinity against t at different crystallization temperatures for fraction $M_\eta = 20\,000$. \circ , 98° ; Δ , 99° ; \square , 99.9° ; $+$, 100.9°C

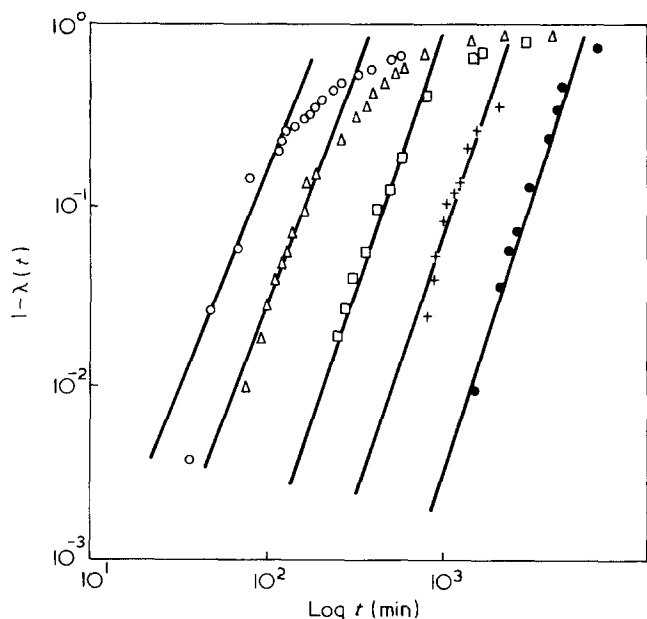


Figure 4 Double logarithmic plot of degree of crystallinity against t at different crystallization temperatures for fraction $M_n = 47\,000$. \circ , 98.25° ; \triangle , 99.2° ; \square , 100.1° ; $+$, 100.9° ; \bullet , 101.8° C

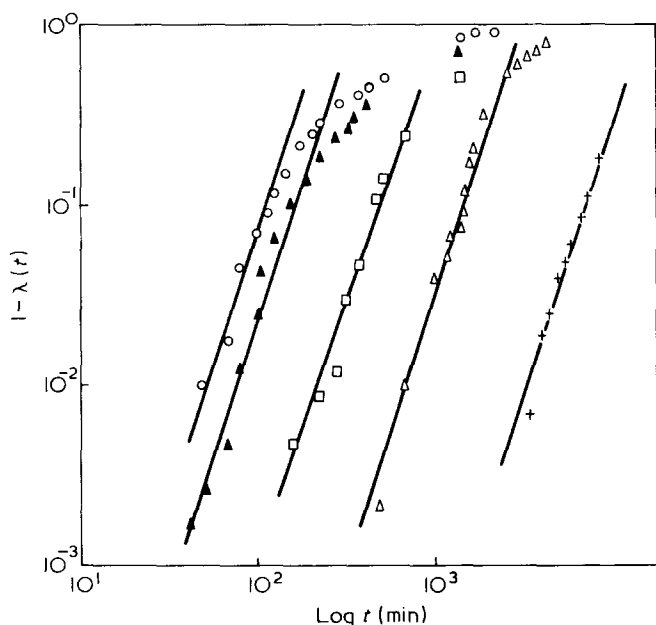


Figure 5 Double logarithmic plot of degree of crystallinity against t at different crystallization temperatures for fraction $M_n = 190\,000$. \circ , 98.1° ; \blacktriangle , 98.9° ; \square , 100° ; \triangle , 100.9° ; $+$, 102° C

The fact that integral values of 3 for the slope are obtained is very important. As will be seen below, the magnitude of the slope corresponds to the exponent in the Avrami equation.

As occurs with the crystallization in bulk, after deviations from linearity develop, the experimental results for each temperature and for a given molecular weight form a common straight line of very small slope.

The G6ler-Sachs approximation assumes a free growth over the complete range of the transformation, i.e. it neglects the impingement. On the contrary, the Avrami equation takes into account the mutual impingement of growing centres upon each other. The assumption is made that upon impingement, further crystal growth ceases. The Avrami equation⁹ can be written as:

$$\ln(1 - X) = kt^n \quad (2)$$

It is very easy to show that equation (2) reduces to equation (1) for small extents of the transformation.

The agreement of the experimental data with the Avrami theory is about the same as with the G6ler-Sachs theory so that deviation from either of the theories occurs at about the same level of crystallinity. Then, the introduction of impingement does not improve the agreement between theory and experiment for crystallization of long chains from solutions. This conclusion is analogous to that obtained in the crystallization of long chains in bulk.⁷

Therefore in the first stages of the transformation the curves $1 - \lambda(t)$ vs. $\log t$ show, for a given molecular weight, good agreement with the theoretical equations and the superposition principle holds. However, in the final stages, deviations occur so that the same time-temperature reduce variable is no longer maintained throughout the transformation. In the analysis of the crystallization kinetics of fractionated polyethylene carried out by Ergoz *et al.*⁷, it is shown that for a given molecular weight and below a critical undercooling the superposition principle holds over the complete extent of the transformation. Deviations occur at lower undercoolings. Our data were obtained at relatively low undercoolings and we do not have sufficient experimental evidence to reach any reliable conclusion relative to this point.

It should be stressed that our data seem to indicate that in comparison with the crystallization in bulk higher crystallinity levels are obtained in solution.

Crystallinity slightly depends on molecular weight and reaches an asymptotic value for infinite time, independent of crystallization temperature. In the lower molecular weight range, from 14 000 to 190 000, the total crystallinity after two decades in the time scale, varies from 90 to 85%. The highest molecular weight develops 75% crystallinity, relatively higher than the crystallinity levels obtained for this fraction crystallized from the bulk, which corresponds to 40%.⁷

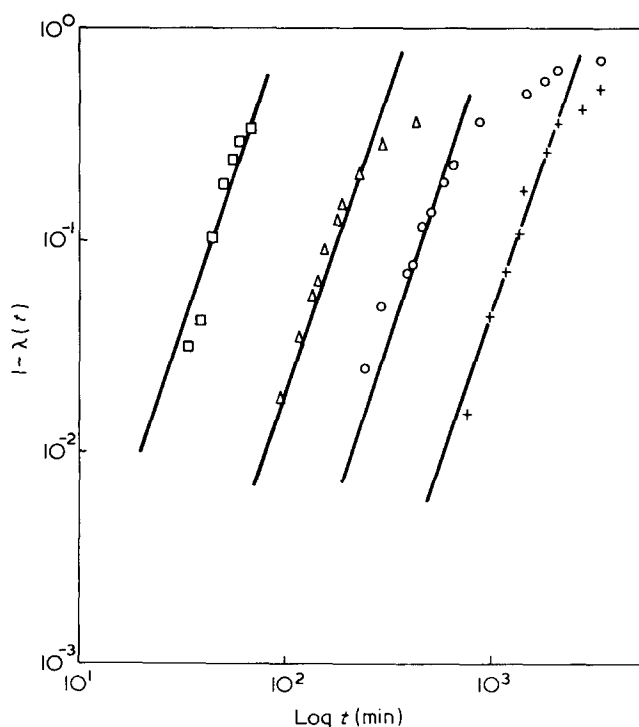


Figure 6 Double logarithmic plot of degree of crystallinity against t at different crystallization temperatures for fraction $M_n = 1.2 \times 10^6$. \square , 96.4° ; \triangle , 98.4° ; \circ , 99.4° ; $+$, 100.4° C

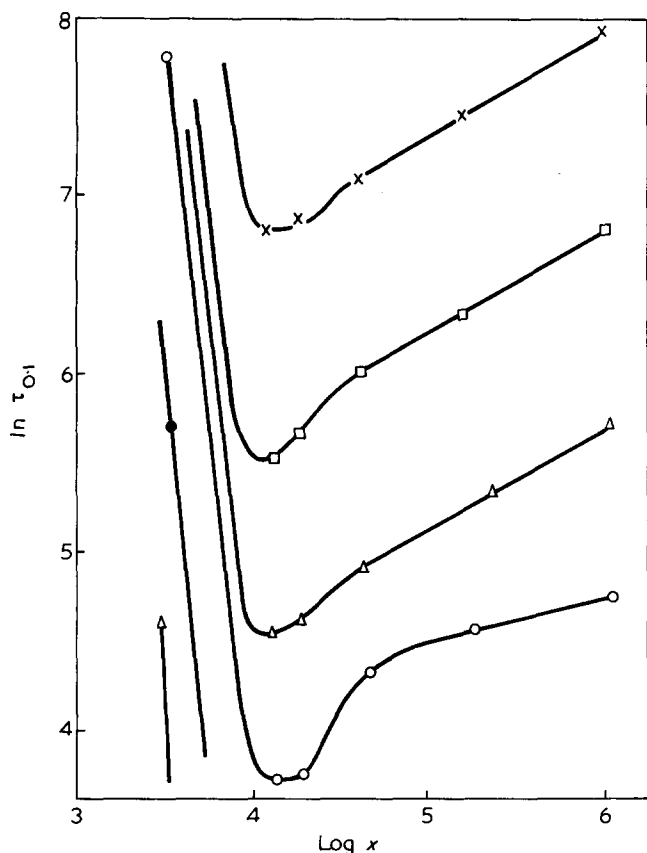


Figure 7 Double logarithmic plot of $\tau_{0.1}$ against molecular weight for different crystallization temperatures. \blacktriangle , 368.2; \bullet , 369.2; \circ , 371.2; \triangle , 372.2; \square , 373.2; \times , 374.2K

These results indicate that in comparison with the crystallization in bulk, higher crystallinity levels are obtained in solution with the higher molecular weight and about the same in the lowest molecular weight range.

Finally, it is of interest to investigate the influence of molecular weight on the time scale of the crystallization process. The time required for 10% of the absolute amount of crystallinity to develop as a function of the molecular weight is plotted in Figure 7. The obtained curves follow the same pattern as in the bulk. Thus, the crystallization time decreases as the molecular weight increases, reaching a minimum within the molecular weight interval 10 000–20 000. For molecular weights higher than 20 000 the crystallization times increase as the molecular weight increases. Again the polyethylene in solution behaves as the polymer in bulk as far as the relation crystallization time–molecular weight, is concerned. This is a very important conclusion.

Temperature coefficient of the crystallization

In order to analyse the temperature coefficient of the crystallization, it is important to consider the nucleation act. The crystallization process is governed by the nucleation of the system, and the phase transformation is described by the free energy required to form a stable critical nucleus^{10,11}. Nucleation theory has been developed for finite molecular weights in diluent–polymer systems² and the importance of molecular weight and concentration in analysing the temperature coefficient in high and moderate concentrations has been shown.

The free energy change involved in forming a cylindrically arranged crystalline array of ξ units long and ρ sequen-

ces in cross-section for a diluted system containing N polymer molecules each comprised of x repeating units in which the volume fraction of diluent is v_2 , is given by^{2,12,13}:

$$\Delta F_d = 2\pi^{1/2}\rho^{1/2}\sigma_u\xi - 2\rho\sigma_e\ln v_2 - \xi\rho\Delta f'_u + \xi\rho\frac{RT}{x}v_2 - \rho RT \ln \frac{x - \xi + 1}{x} \quad (3)$$

where σ_u is the lateral interfacial free energy, σ_e is the excess interfacial free energy per repeating unit as it emerges from the crystal face normal to the chain direction. The first two terms in equation (3) represent the positive contribution to the total free energy of interfaces present. The third term of equation (3) represents the depressed energy of fusion for the $\xi\rho$ units involved in the transformation and is given by:

$$\Delta f'_u = \Delta f_u - RT \left\{ \frac{V_u}{V_l} (1 - v_2) - \mu(1 - v_2)^2 \right\} \quad (4)$$

where Δf_u is the energy of fusion per repeating unit for a chain of infinite molecular weight, V_u is the volume per repeating unit of the polymer and V_l is the molar volume of the diluent, μ is a parameter depending of the interaction polymer–diluent.

The last two terms result from the finite length of the chains. The first of these terms expresses the entropy gain which results from the increased volume available to the ends of the molecule after melting. The last term represents the entropy gain that arises from the number of different ways a sequence of ξ units can be located in a chain x units long with the terminal unit being excluded from the sequence in question. The surface described by equation (3) contains a saddle point and the coordinates of this point prescribe the dimensions of a nucleus of critical size. These dimensions are given by the relations²:

$$\rho^{1/2} = \frac{2\pi^{1/2}\sigma_u}{\Delta f'_u - (RT/x)v_2 - RT/(x - \xi + 1)} \quad (5)$$

$$\frac{\xi}{2} \left(\Delta f'_u - \frac{RT}{x}v_2 + \frac{RT}{x - \xi + 1} \right) = 2\sigma_e - RT \ln v_2 - RT \ln \frac{x - \xi + 1}{x}$$

Accordingly, the free energy change, ΔF^* , involved in forming the critical nucleus is given by²:

$$\Delta F^* = \pi^{1/2}\xi\rho^{1/2}\sigma_u \quad (6)$$

If a two-dimensional nucleation is assumed and we use the concepts and notation of the previous analysis, the change in free energy that accompanies the formation of a monomolecular nucleus, ξ units long and ρ sequences breadth is given by²:

$$\Delta F^* = 2\sigma_u\xi \quad (7)$$

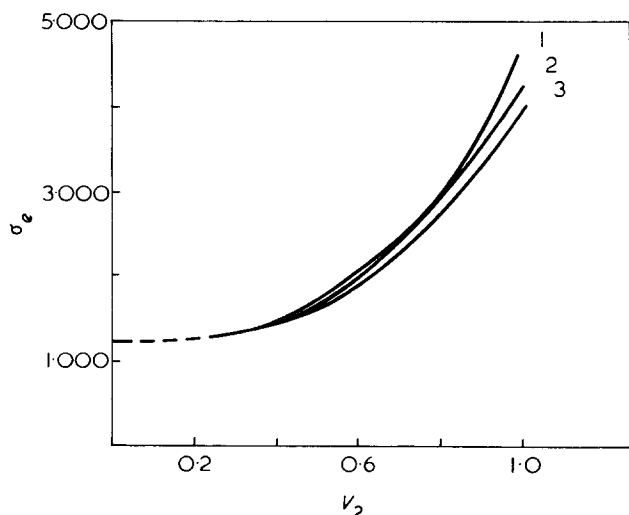


Figure 8 Plot of σ_e against volume fraction v_2^2 . 1, $M = 250\,000$; 2, $M = 10\,000$; 3, $M = 4\,000$

where ξ is expressed by the transcendent equation:

$$\xi = \frac{2\sigma_e - RT \ln \left(\frac{x - \xi + 1}{x} \right) - RT \ln v_2}{\Delta f_u' - \frac{RT}{x} v_2} \quad (8)$$

These theories rest heavily on the Flory-Huggins theory which, as is well known, only holds for high and moderate concentrations in which the excluded volume effects are not important. Basically, in dilute solutions, the free energy of mixing departs drastically from that predicted by the Flory-Huggins theory because of the lack of homogeneity in the solution. Therefore, from a rigorous point of view, the nucleation theories described above are only applicable to concentrated solutions and to those dilute solutions in which the excluded volume effects are negligible.

With these reservations in mind we will apply the nucleation theories to analyse the coefficient temperature of the kinetic data. Owing to the fact that n equals three, we have used two-dimensional theory. The results and conclusions do not depend on this assumption. Consequently, no unique conclusions can be made with regard to the molecular nature of the nucleus because the experimental data fit the form for either of the two major types of nucleation.

In order to analyse the temperature coefficient of the crystallization process it is convenient to take $\tau_{0.1}$ the time required for 10% of the transformation to occur, as a measure of the rate constant. Then the data can be analysed by the equation:

$$\ln \tau_{0.1}^{-1} = \ln(\tau_{0.1})_0 - \frac{\Delta F^*}{RT} \quad (9)$$

By introducing equation (7) into equation (9) one obtains:

$$\ln \tau_{0.1}^{-1} = \ln(\tau_{0.1})_0 - \sigma_u \frac{\xi}{T} \quad (10)$$

It is quite clear from equation (10) that by plotting $\ln \tau_{0.1}^{-1}$ against ξ/T a straight line should be obtained whose slope should be the interfacial lateral free energy.

It is clear that this analysis does not involve the independent establishment of values for T_s , the equilibrium melting temperature (or dissolution temperature) of the dilute solution as has been done previously⁶. However, in order to proceed with the present treatment the basic interfacial free energy σ_e needs to be specified.

Recent work² has established that for undiluted polyethylene σ_e ranges from 4600 cal/mol to 4000 cal/mol for the molecular weight range 4000–250 000 if σ_u has a constant value of 25 cal/mol. Furthermore, it has been stated that in the system polyethylene/ α -chloronaphthalene for high and moderate concentrations, σ_e decreases sharply with dilution at very high concentrations and slowly at moderate concentrations if σ_u remains constant.

For very dilute systems, a lower value of σ_e of about 1000 cal/mol can be extrapolated although this extrapolation is very risky since the lowest experimental concentration corresponds to $v_2 = 0.30$ (Figure 8).

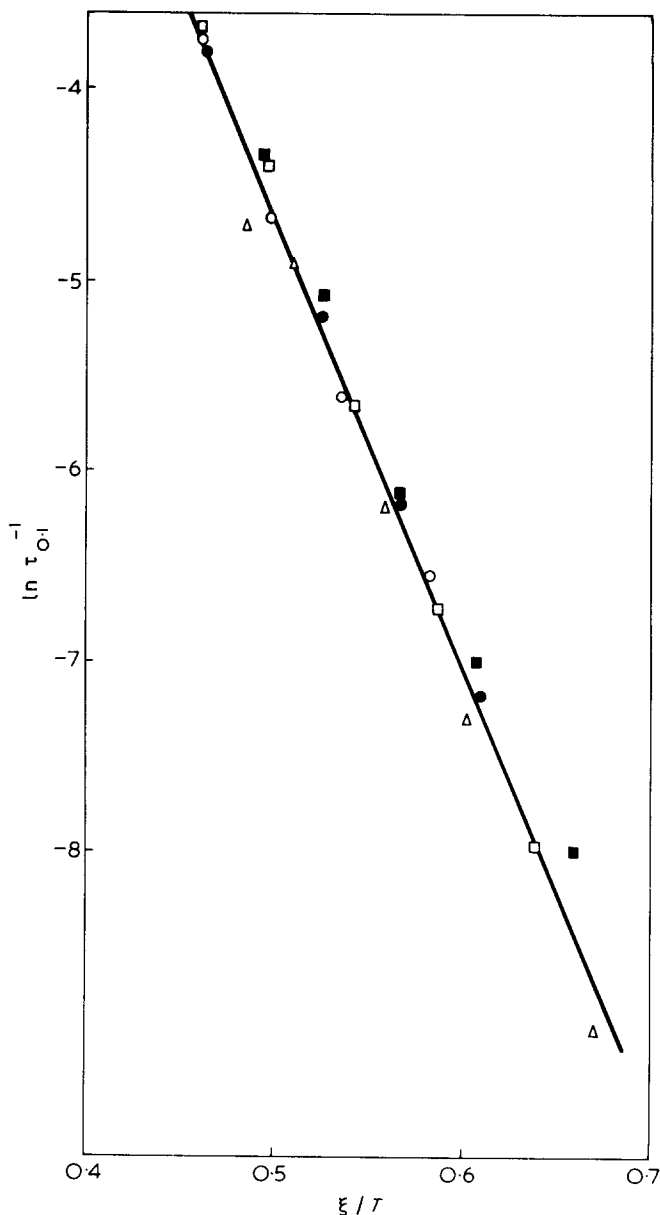


Figure 9 Plot of $\ln \tau_{0.1}^{-1}$ against ξ/T for various molecular weights. $\sigma_e = 1000$ cal/mol for 14 000 and 20 000 molecular weight fractions; $\sigma_e = 1.200$ cal/mol for 47 000 and 190 000; $\sigma_e = 1.400$ cal/mol M : \square , 14 000; \circ , 20 000; \blacksquare , 47 000; \triangle , 190 000; \bullet , 1 200 000

Taking into account these earlier findings the temperature coefficient of our data has been analysed by equation (9). By plotting $\ln \tau_0^{-1}$ against ξ/T a set of non-parallel straight lines is obtained if a unique value of σ_e is considered for all molecular weights. This result means that σ_u changes with molecular weight, a conclusion which is very difficult to accept.

Assuming that σ_u does not change with dilution a unique straight line is obtained independent of molecular weight and parallel to that of undiluted polymer if the basic interfacial free energy is allowed to change slightly from 1000 cal/mol ($M = 14\,000$) to 1400 cal/mol ($M = 1.2 \times 10^6$) as can be seen in Figure 9.

The conclusion is very important. The values of σ_e are, in this concentration range, slightly dependent on molecular weight in the range analysed in this work and about four times lower than the values reported earlier for pure polymer.²

The theory presents limitations when it is applied to very dilute solutions, because the tacit assumption of a uniform distribution of polymer segments through the amorphous regions is made. The inaccuracy should become serious at the lowest chain length. However, in spite of the limitation of equations (4) and (7), the general conclusion

stated above may be reached if small excluded volume effects are present in this system. Further investigation is in progress using other polymer-diluent systems to assess the reliability of this approach.

REFERENCES

- 1 Mandelkern, L., Fatou, J. G. and Howard, C. *J. Phys. Chem.* 1965, **69**, 956
- 2 Fatou, J. G., Riande, E. and Valdecasas, R. G. *J. Polym. Sci.* 1975, **13**, 2103
- 3 Fatou, J. G. and Mandelkern, L. *J. Phys. Chem.* 1965, **69**, 71
- 4 Ikamoto, H. and Sekikawa, K. *J. Polym. Sci.* 1961, **55**, 597
- 5 Chiang, R. *J. Polym. Sci.* 1959, **36**, 91
- 6 Devoy, C., Mandelkern, L. and Bourland, L. *J. Polym. Sci. (A-2)* 1970, **8**, 869
- 7 Ergoz, E., Fatou, J. G. and Mandelkern, L. *Macromolecules* 1972, **5**, 147
- 8 Göler, V., Sachs, F. and Sachs, G. *Z. Phys.* 1932, **77**, 281
- 9 Avrami, M. *J. Chem. Phys.* 1939, **7**, 1103
- 10 Devoy, C. and Mandelkern, L. *J. Polym. Sci. (A-2)* 1969, **7**, 1883
- 11 Jackson, J. F. and Mandelkern, L. *Macromolecules* 1968, **1**, 546
- 12 Flory, P. J. *J. Chem. Phys.* 1949, **17**, 223
- 13 Mandelkern, L. *J. Appl. Phys.* 1955, **26**, 443

Melting of ethylene oxide – propylene oxide type P(EP)_n block copolymers

P. C. Ashman and C. Booth

Department of Chemistry, University of Manchester, Manchester M13 9PL, UK
(Received 30 May 1975)

Multiblock copolymers of poly(ethylene oxide) and poly(propylene oxide), type P(EP)_n, have been prepared by condensation of hydroxy- and chlorocarboxy-ended polymers. Small-angle X-ray scattering and dilatometry have been used to determine lamella spacings and melting points of the copolymers. The melting points of the multiblock copolymers can be predicted from the melting points of corresponding triblock (PEP) copolymers.

INTRODUCTION

It is possible to avoid undue complexity in the molecular interpretation of the thermodynamic properties of crystallizable block copolymers provided that the polymeric components are compatible in the melt and that only one component is crystallizable. These criteria are fulfilled by poly(ethylene oxide)–poly(propylene oxide) block copolymers with fairly short block lengths. We have reported elsewhere the melting behaviour of model block copolymers of type PE¹, PEP^{2,3} and EPE⁴. Here we present results for multiblock copolymers of type P(EP)_n where $n = 1-7$.

EXPERIMENTAL AND RESULTS

Preparation

P(EP)_n block copolymers were prepared by the condensation of α , ω -hydroxy-poly(ethylene oxide) with α , ω -chlorocarboxy-poly(propylene oxide) for $n > 1$ or with α -methoxy, ω -chlorocarboxy-poly(propylene oxide) for $n = 1$. Reagents and solvents were purified as described earlier¹.

Samples of α , ω -hydroxy-poly(ethylene oxide) were prepared using potassium hydroxide as catalyst and ethylene glycol as initiator as described previously³ (samples 48 and 75) or were commercial samples (Hoechst Chemicals Ltd, samples 45 and 136). Samples of α , ω -hydroxy-poly(propylene oxide) were similarly prepared, but with 1,2-propanediol (dried over anhydrous sodium sulphate and distilled, 104°C and 32 mmHg, before use) as initiator.

Samples of α -methoxy, ω -hydroxy-poly(propylene oxide) were prepared using a sodium methanol mixture as catalyst/initiator. The polymerizations were carried out in dry evacuated sealed ampoules kept in the dark at room temperature for 3 months. Polymers were neutralized with a solution of dilute hydrochloric acid in methanol (50% v/v). Water and methanol were removed by rotary evaporation, and sodium chloride by centrifugation (15 000 \times g for 1 h). In a typical experiment sodium (0.29 g), methanol (1.65 g) and propylene oxide (10.30 g) gave polymer with $\bar{M}_n = 220$ (calculated 200).

The hydroxy-ended poly(propylene oxide) samples were reacted with phosgene (ICI Ltd) to form the chloroformate intermediates. The polymer was dried by evacuation (<1 N/m², 50°C, 1 h) and dissolved (10 g) in dry benzene

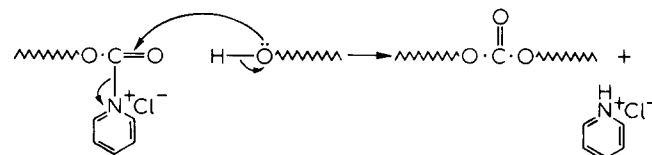
(75 cm³). Phosgene was bubbled slowly through the stirred solution at 20°C for 1 h. Thereafter dry nitrogen was bubbled slowly through the solution to remove excess phosgene. Benzene and remaining traces of phosgene were removed by distillation under reduced pressure, and finally by evacuation (<1 N/m², 24 h). The polymers were stored under dry nitrogen in order to avoid hydrolysis. The infra-red spectra of the polymers prepared in this way were consistent with complete conversion of hydroxy- to chlorocarboxy-end groups⁵. Gel permeation chromatography served to show that the molecular weight distributions (*MWD*) of the polymers were unchanged during the phosgenation.

The α , ω -hydroxy-poly(ethylene oxide) was dried by evacuation (<1 N/m², 2 h, $T > T_m$) and dissolved (5 g) in pyridine* (20 cm³, dried over and distilled from calcium hydride). To this solution blanketed with dry nitrogen and stirred at 60°C under reflux, was added, using a syringe, a solution of the chlorocarboxy-ended poly(propylene oxide) in dry benzene (10 cm³). Preliminary experiments (*Table 1*)

Table 1 Effect of mole ratio on the degree of condensation (n) in the formation of 12(136–12)_n copolymers

Mole ratio (P:E)	Degree of condensation
0.86	1.3
1.00	2.1
1.08	2.9
1.19	3.7
1.34	5.9
1.42	4.0
1.83	3.2

* In preliminary experiments we found that a chlorocarboxy-group reacts more readily with a hydroxy-group in solution in pyridine than with an alkoxy-group in the melt. This is attributable to the formation of a complex which is particularly susceptible to nucleophilic attack by an alcohol:



This reaction is favoured by primary hydroxy-groups, such as the end groups of poly(ethylene oxide), rather than by secondary hydroxy-groups, such as the end groups of poly(propylene oxide)⁶.

Table 2 Characteristics of homopolymers

Sample	M_n				\bar{M}_w/\bar{M}_n (g.p.c.)
	(v.p.o.)	(e.g.a.)	(g.p.c.)	(predicted) ^a	
α, ω -hydroxy-poly(ethylene oxide) ^b :					
45	2030	1910	2040	—	1.05
48	1900	2100	2000	2100	1.10
75	3400	—	3000	3300	1.08
136	6100	6040	6010	—	1.23
α, ω -hydroxy-poly(propylene oxide):					
5	280	275	—	—	—
7	430	375	—	—	—
9	550	500	—	—	—
12	700	710	—	—	—
α -methoxy, ω -hydroxy-poly(propylene oxide):					
4	—	220	—	200	—
6	—	330	—	330	—

^a Predicted from preparative conditions

^b Data mainly from Refs 1, 2 and 10

served to define a mole ratio (P:E) of 1.3:1 as optimum for obtaining a high degree of condensation when using α, ω -chlorocarboxy-poly(propylene oxide) in the preparation of multiblock copolymers. A mole ratio of 4:1 was used for α -methoxy, ω -hydroxy-poly(propylene oxide) in the preparation of triblock copolymers. Reaction was complete in 15 min (prolonged heating at 60°C led to chain scission, detectable by gel permeation chromatography). Termination of P(EP)_n chains by poly(propylene oxide) blocks was ensured at this stage by the addition of further α, ω -chlorocarboxy-poly(propylene oxide) to bring the overall mole ratio to 1.6:1.

The condensation was terminated by adding methanol (10 cm³). Pyridine and methanol were removed by rotary evaporation followed by evacuation of the melt (<1 N/m², 50°C, 24 h). Pyridinium hydrochloride was removed by dissolving the dry polymer in dry benzene and centrifuging the mixture (15 000 × g for 15 min). The copolymer was separated from poly(propylene oxide) homopolymer by adding excess iso-octane to the benzene solution at 0°C, followed by repeated washing with iso-octane at room temperature.

Notation

We refer to samples by their number-average block lengths (expressed in monomer units) and their degree of condensation as established by their preparation and subsequent characterization. For example, sample 5(45–5)₇ denotes an alternating block copolymer composed of 8 poly(propylene oxide) blocks of length 5 units and 7 poly(ethylene oxide) blocks of length 45 chain units.

Characterization

Vapour pressure osmometry (v.p.o.) (Mechrolab, benzene at 25°C) and end group analysis (e.g.a.) (phthaloylation of hydroxy-groups^{7–9}) were used to characterize the homopolymers, as indicated in Table 2. Gel permeation chromatography (g.p.c.) was used to determine *MWD* of the poly(ethylene oxide) homopolymers; details are given elsewhere^{3,10}. Results are listed in Table 2.

G.p.c. was used to check that the PEP copolymers were free from polymeric impurities. Five Styragel columns (Waters Associates) with nominal pore sizes in the range 150

to 1500 nm were used with tetrahydrofuran solvent (25°C, flow rate 1 cm³/min). Chromatograms showed a complete absence of multiblock copolymer or excess homopolymer. (Chromatograms of the poly(propylene oxide) homopolymers under the same conditions were resolved into individual oligomers). In addition proton magnetic resonance spectroscopy¹¹ (p.m.r.) was used to check that the composition of the PEP copolymers was as expected; the results are given in Table 3.

G.p.c. was also used to check the degree of condensation of the multiblock copolymers, and to investigate their *MWD*. Four Styragel columns with nominal pore sizes in the range 70 to 5 × 10⁵ nm were used with *N,N*-dimethylacetamide as solvent (80°C, flow rate 1 cm³/min). Calibration was by fractions of poly(ethylene oxide) and poly(propylene oxide), which gave coincident plots. The results are summarized in Table 4. Number-average values of *n* were in the range 2 to 7; weight- to number-average molecular weight ratios were generally greater than 2. For a condensation, the distribution should be most probable with $\bar{M}_w/\bar{M}_n = (2n + 1)/(n + 1)$ varying from 1.7 (*n* = 2) to 1.9 (*n* = 7)¹². The generally higher values of \bar{M}_w/\bar{M}_n observed are attributable in part to instrumental spreading and in part to adventitious termination by hydrolysis during the condensation.

Dilatometry and X-ray scattering

The methods used to determine melting points by dilatometry and lamella spacings by small-angle X-ray scattering have been described earlier¹.

All polymers were crystallized as completely as possible. The degree of crystallinity attained with the multiblock copolymers was lower than that attained with triblock (PEP) copolymers, e.g. the dilatometric contractions observed for the multiblock samples were only about 60% of those observed for comparable PEP copolymers. A similar effect has been noted with segmented poly(ethylene oxide) samples¹³.

Melting points are listed in Table 5. Multiple melting points were observed only for the P(45–P)_n type copoly-

Table 3 Compositions of PEP copolymers

Sample	Weight fraction of poly(ethylene oxide)	
	p.m.r.	Predicted
4–45–4	0.80	0.82
6–45–6	0.77	0.76
4–48–4	0.82	0.84
6–48–6	0.80	0.79
4–75–4	0.88	0.89
6–75–6	0.82	0.84

Table 4 Molecular characteristics of P(EP)_n copolymers

Sample	\bar{M}_n	\bar{n}	\bar{M}_w/\bar{M}_n
5(45–5) ₇	15 400	6.7	2.5
7(45–7) ₂	4 400	1.7	1.5
9(45–9) ₅	13 200	5.1	2.1
12(45–12) ₅	14 400	5.1	2.5
5(75–5) ₄	13 200	3.6	2.2
9(75–9) ₅	19 000	4.8	2.3
5(136–5) ₄	23 000	3.6	2.2
7(136–7) ₃	19 500	3.0	2.3
9(136–9) ₄	24 100	3.6	2.3
12(136–12) ₆	39 500	5.8	2.2

Table 5 Melting points (T_m) and lamella spacings (l) of P(EP) $_n$ copolymers

Sample	T_c (°C)	T_m (°C)	l (nm)
4-45-4	25	38.5	—
	30	39.2	—
6-45-6	25	37.4	—
	30	37.6	—
5(45-5) $_7$	20	40.9	—
	25	41.1	13.0
	28	41.0	—
7(45-7) $_2$	20	38.9(37.3)	12.3
	25	38.8	—
	28	38.7	13.1
9(45-9) $_5$	20	39.6(37.0)	—
	25	39.7(38.0)	12.7
	28	39.9(38.9)	—
12(45-12) $_5$	20	37.0	12.7
	25	37.6(35.7)	14.7
	28	37.6(36.0)	16.6
4-48-4	25	—	11.1
6-48-6	30	—	11.3
4-75-4	30	47.7	—
	35	48.5	12.3
6-75-6	30	46.0	—
	35	46.3	12.8
5-(75-5) $_4$	25	47.4	—
	30	47.4	13.3
	35	48.2	—
9(75-9) $_5$	40	49.3	16.3
	25	46.0	—
	30	46.1	14.2
5(136-5) $_4$	35	46.6	—
	40	47.6	15.5
	30	53.7	17.3
7(136-7) $_3$	35	54.4	—
	40	55.0	18.0
	45	56.0	—
9(136-9) $_4$	28	53.0	—
	35	53.4	16.1
	40	53.8	—
12(136-12) $_6$	30	53.0	16.7
	35	53.5	—
	40	54.0	16.8
	45	54.8	—
	28	52.6	—
	35	52.6	17.3
	40	53.7	—

mers, as indicated in Table 5 (lower melting points in parentheses). Melting ranges were similar for both tri- and multi-block copolymers, and were from 3 to 4 K. The melting points were more dependent on crystallization temperature T_c than hitherto observed¹⁻⁴ with poly(ethylene oxide)/poly(propylene oxide) block copolymers, especially those of the multiblock copolymers.

The small-angle X-ray scattering patterns of the PEP copolymers were similar to those observed for homopolymers^{10,14} and copolymers¹⁻³ and consisted of several sharp peaks. By contrast the peaks derived from the multiblock copolymers were broad. Sharp peaks could be obtained for samples annealed for several days at temperatures 5 K below T_m . The annealing did not change the peak position. Lamella spacings¹ obtained from small-angle X-ray measurements are listed in Table 5. Comparison of the results of Table 5 with those obtained earlier for ether linked PEP block copolymers (e.g. sample 5-48-5 crystallized at 29°C had² $l = 10.9$ nm, 3-75-3 crystallized at 37°C had³ $l = 12.6$ nm) is sufficient to identify the PEP polycrystals as predominantly once-folded chain type. Similar comparison of the lamella spacings of the multiblock copolymers is complicated by their relatively low degree of crystallinity

(with the possibility that the amorphous material is located in the amorphous lamellae of the polycrystal). With this in mind we identify the 45 and 75 series of multiblock copolymers as forming predominantly once-folded chain polycrystals, and the 136 series as forming predominantly twice-folded chain polycrystals. We assign the lower melting points observed for samples 7(45-7) $_2$, 9(45-9) $_5$ and 12(45-12) $_5$ to predominantly twice-folded chain polycrystals.

DISCUSSION

Compared to the melting points of poly(ethylene oxide) homopolymers of corresponding (block) length, the melting points of the copolymers are substantially reduced, e.g. compare the results of Table 5 with^{10,15} $T_m = 53.8^\circ\text{C}$ for poly(ethylene oxide) 2000 ($\bar{x}_n = 45$); $T_m = 60.2^\circ\text{C}$ for poly(ethylene oxide) 3300 ($\bar{x}_n = 75$); and $T_m = 64.1^\circ\text{C}$ for poly(ethylene oxide) 6000 ($\bar{x}_n = 136$). The melting point depression is due in part to chain folding in the crystalline lamellae [compare $T_m = 60.1^\circ\text{C}$ for once-folded chain poly(ethylene oxide) 6000] and in part to the inclusion of the poly(propylene oxide) blocks in the amorphous lamellae of the polycrystal^{1,2}.

We have shown elsewhere^{1,2} that successful quantitative interpretation of the melting of homopolymers and block polymers is possible only when information is available concerning the polycrystalline structure. In terms of the stacked lamella model we have used^{1,2}, this information is the thickness of the crystalline and amorphous lamellae. Nevertheless it is possible to qualitatively interpret the results of Table 5 in the light of the Flory-Vrij¹⁶ model of melting of short polymer chains, the use of which is justified elsewhere¹. Here it is sufficient to consider the simplified case of an alternating block copolymer, P(EP) $_n$, having monodisperse E- and P-blocks. The feature of this model is that the E block ends are paired at the surface of the crystalline lamella. We envisage two extreme cases.

Long P blocks. The E blocks are haphazardly placed in the crystalline lamellae (Figure 1a). Assuming random placement of the E blocks in the lamellae, the free energy of fusion per chain (ΔG) is given by^{1,16,17}:

$$\Delta G = n(x\Delta g - 4\sigma_e - RT\ln x + RT\ln\phi_e) \quad (1)$$

where n is the number of E blocks (length x) in the copolymer chain, ΔG is the free energy of fusion per chain unit of perfectly crystalline poly(ethylene oxide), σ_e is the free

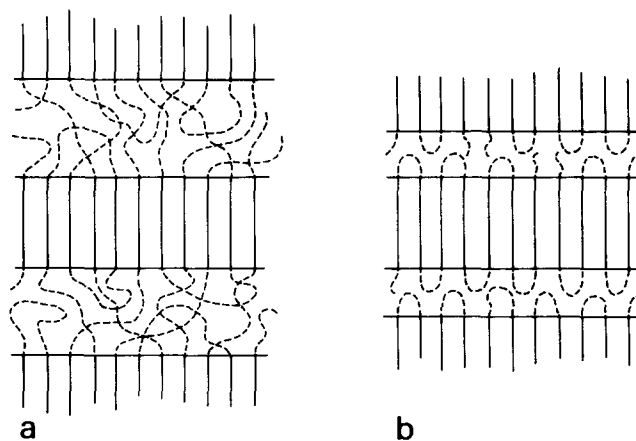


Figure 1 Model polycrystals of P(EP) $_n$ block copolymers: (a) long P blocks; (b) short P blocks

Table 6 Calculated melting points (equation 4) of 5(45-5)_n copolymers

<i>n</i>	ϕ_e	<i>z</i>	T_m^0 (°C)
1	0.752	45	36.5
2	0.802	96	40.4
3	0.821	146	42.0
5	0.836	247	43.4
10	0.847	501	44.6
∞	0.858	∞	46.2

Table 7 Comparison of experimental and predicted melting point differences

Sample	Experimental		Predicted ΔT	
	T_m (°C, approx.)	ΔT	a	b
5-45-5	38	3	0	7.6
5(45-5) ₇	41			
5-75-5	47	1	0	4.5
5(75-5) ₄	48			

energy of formation from the melt of the crystal/amorphous interface and the amorphous lamella, and ϕ_e is the segment fractions of E in the copolymer melt (one segment has the volume of one poly(ethylene oxide) unit). The term $RT\ln\phi_e$ arises from the necessity that the first segment of a chosen sequence (which must be paired at the interface) is a poly(ethylene oxide) unit; the term $RT\ln x$ from the necessity that the sequence is *x* E units long. The factor 4 in the interfacial free energy term is introduced because our data pertain to once-folded chain polycrystals in which the E block occupies 4 interfacial sites. This equation is identical to that for *n* independent PEP copolymers and leads directly to the melting point expression*:

$$T_m = T_m^0 [1 - 4\sigma_e/x\Delta h] / [1 - (RT_m^0/x\Delta h)\ln(\phi_e/x)] \quad (2)$$

where T_m^0 and Δh are, respectively, the melting point and the enthalpy of fusion per chain unit of perfectly crystalline poly(ethylene oxide). The melting point T_m is independent of *n*.

Short P blocks. The -EPEPEPE- chain forms a regularly folded lamella (Figure 1b) in which the E blocks are sequentially placed and in which the inner P blocks form identical folds. In this case proper location of the end unit of the -EPEPEPE- chain uniquely locates the rest. For this restrictive case the free energy of fusion per chain, in a once-folded chain polycrystal is:

$$\Delta G = nx\Delta g + 4n\sigma_e' - RT\ln z + RT\ln\phi_e \quad (3)$$

where σ_e' is the free energy of formation from the melt of the interface and *z* is the chain length in segments of the -EPEPEPE- chain (i.e. the chain length excluding the two end P blocks). This equation leads to the melting point expression:

$$T_m = T_m^0 [1 - (4\sigma_e'/x\Delta h)] / [1 - (RT_m^0/nx\Delta h)\ln(\phi_e/z)] \quad (4)$$

The melting point T_m depends upon *n*.

* We use the condition $\Delta G = 0$ when $T = T_m$ and the relationship $\Delta g = \Delta h [1 - (T_m/T_m^0)]$

Values of T_m calculated from equation (4) for a typical copolymer series, 5(45-5)_n are listed in Table 6. We use $T_m^0 = 349^{18-20}$ and $\Delta h = 8.4$ kJ/mol²¹ and choose σ_e' to be 8.0 kJ/mol in order to bring the calculated melting points into approximate agreement with those observed. Parameters ϕ_e and *z* are calculated assuming that the specific volumes of supercooled poly(ethylene oxide) and poly(propylene oxide) melts at 40°C are, respectively, 0.901 cm³/g and 1.012 cm³/g¹.

A comparison of the experimental and the predicted variation of T_m with *n* is made in Table 7. Experimental results fall between those predicted from the extreme models. This is in keeping with our finding a low degree of crystallinity in the multiblock copolymers; presumably, although the P blocks are short in our systems, a random structure of type (a) (Figure 1) is approached by the incorporation of E blocks in the amorphous layer.

The fact that the experimental values of ΔT in Table 7 are fairly small means that the melting point of a copolymer with alternating blocks of crystallizable (E) and non-crystallizable (P) polymers can be predicted with success, say to within a degree, from the melting point of the corresponding triblock (PEP) copolymer.

ACKNOWLEDGEMENTS

We thank Dr R. Mobbs for practical assistance in the preparation of the copolymers and Messrs D. J. Roy and D. Rowlinson for help with their characterization. P.C.A. acknowledges receipt of a Science Research Council Student ship.

REFERENCES

- Ashman, P. C. and Booth, C. *Polymer* 1975, **16**, 889
- Ashman, P. C., Booth, C., Cooper, D. R. and Price, C. *Polymer* 1975, **16**, 897
- Booth, C. and Pickles, C. J. *J. Polym. Sci. (A-2)* 1973, **11**, 249
- Booth, C. and Dodgson, D. V. *J. Polym. Sci. (A-2)* 1973, **11**, 265
- Gallin, J. C., Rempp, P. and Parrod, J. *C.R. Acad. Sci.* 1965, **260**, 5558
- Case, L. C. and Rent, N. H. *J. Polym. Sci. (B)* 1964, **2**, 417
- Price, C. C. and St. Pierre, L. E. *J. Am. Chem. Soc.* 1956, **78**, 3432
- Havlik, A. J., Moacanin, J. and Otterness, I. *J. Polym. Sci. (A)* 1963, **1**, 2213
- Blanchard, L. P. and Baijal, M. D. *J. Polym. Sci. (B)* 1966, **4**, 837
- Beech, D. R., Booth, C., Dodgson, D. V., Sharpe, R. R. and Waring, J. R. S. *Polymer* 1972, **13**, 73
- Mathias, A. and Mellor, R. *Analyt. Chem.* 1966, **38**, 472
- Peebles, L. H. 'Molecular Weight Distributions in Polymers', Interscience, New York, 1971
- Gallin, J.-C., Spegt, P., Suzuki, S. and Skoulios, A. E. *Makromol. Chem.* 1974, **175**, 991
- Arlie, J. P., Spegt, P. and Skoulios, A. E. *Makromol. Chem.* 1966, **99**, 160
- Beech, D. R., Booth, C., Pickles, C. J., Sharpe, R. R. and Waring, J. R. S. *Polymer* 1972, **13**, 246
- Flory, P. J. and Vrij, A. *J. Am. Chem. Soc.* 1963, **85**, 3548
- Flory, P. J. *J. Chem. Phys.* 1949, **17**, 273
- Beech, D. R. and Booth, C. *J. Polym. Sci. (B)* 1970, **8**, 731
- Afifi-Effat, A. M. and Hay, J. N. *J. Chem. Soc. Faraday Trans. II* 1972, **68**, 656
- Rijke, A. M. and McCoy, S. *J. Polym. Sci. (A-2)* 1972, **10**, 1845
- Devoy, C. J. *PhD Thesis* Manchester University (1966)

Effect of chain structure on the melting of low molecular weight poly(ethylene oxide)

J. O. G. Maclaine, P. C. Ashman and C. Booth

Department of Chemistry, University of Manchester, Manchester, M13 9PL, UK

(Received 30 May 1975)

Linked poly(ethylene oxide) samples have been prepared by the condensation of α -methoxy- ω -chlorocarboxy-poly(ethylene oxide) with alcohols of various functionalities. Melting points (by dilatometry) and lamella spacings (by small-angle X-ray scattering) have been determined. The linked polymers have higher melting points than their unlinked precursors. The increased melting point is interpreted in the light of the model of Flory and Vrij.

INTRODUCTION

Investigations have been made of the crystalline structure¹⁻⁵ and the melting⁴⁻⁶ of linear low molecular weight α , ω -hydroxy-poly(ethylene oxide), of poly(ethylene oxide) samples with other end groups^{7,8} or with segmented structure⁹, and of block copolymers of poly(ethylene oxide) with poly(propylene oxide)¹⁰⁻¹⁴, polystyrene^{15,16} or poly(ϵ -caprolactam)¹⁷. In the absence of effects attributable to incompatibility in the melt^{15,16} or crystallization of the copolymerized component¹⁷ the experimental results can be broadly interpreted in terms of a polycrystalline structure of alternating crystalline and amorphous lamellae^{12,13}. In this paper we report an extension of the range of investigations to include branched poly(ethylene oxide) samples.

EXPERIMENTAL AND RESULTS

Preparation

Poly(ethylene oxide) samples were prepared by the condensation of α -methoxy- ω -chlorocarboxy-poly(ethylene oxide) with alcohols of various functionalities.

Samples of α -methoxy- ω -hydroxy-poly(ethylene oxide) were prepared by use of a sodium methoxide/methanol mixture as catalyst/initiator. These polymers were reacted with phosgene to form the α -methoxy- ω -chlorocarboxy-polymer intermediates for the condensation. The preparative methods have been described elsewhere¹⁴.

The chloroformate intermediates were reacted with either methanol (distilled from magnesium activated by iodine), ethylene glycol (distilled from calcium sulphate), glycerol (dried under high vacuum for 4 days at 40°C), or penta-erythritol (Hopkins and Williams Ltd, m.p. 260.5°C, used as received). The liquid alcohols were stored over type 4A molecular sieves and were degassed before use. Reactions were carried out in pyridine which had been distilled from calcium hydride. The α -methoxy- ω -chlorocarboxy-poly(ethylene oxide) was melted at 60°C under vacuum (<1 N/m², 2 h). The system was then blanketed with dry nitrogen and a solution of the appropriate alcohol in pyridine (~0.1 g/cm³ in sufficient quantity to ensure a 20% molar excess of chlorocarboxy- over hydroxy-groups in the linking reactions and *vice versa* in the reaction with methanol) was added using a syringe. The mixture was held under reflux at 60°C for 1 h. The condensation was terminated by atmospheric moisture. Volatiles were removed by rotary evacuation. Pyridinium hydrochloride was re-

moved by dissolving the dry polymer in dry benzene and centrifuging the mixture (15 000 \times g for 15 min). The polymer was recovered by freeze-drying.

Nomenclature

Starting from α -methoxy- ω -hydroxy-poly(ethylene oxide) samples of molecular weight $\bar{M}_n = 1600$ or 2700 we prepared two series of polymers. We refer to these by their chain lengths (36 or 61 chain units respectively); by their end groups (M = methoxy-, H = hydroxy-, C = carboxy-methoxy-); by the alcohol used in the condensation (O = hydroxy-ended polymer, E = ethylene glycol, G = glycerol and P = penta-erythritol); and by the number of poly(ethylene oxide) blocks. This is illustrated, for the 36 series, in Table 1.

Fractionation

The preparative conditions for the α -methoxy- ω -hydroxy-poly(ethylene oxide) samples lead to the formation of a small proportion of α , ω -hydroxy-poly(ethylene oxide) initiated by adventitious water. This polymer will form α , ω -chlorocarboxy-poly(ethylene oxide) at the second stage of the preparation and so may undergo chain extension by reactions with the polyfunctional alcohols. Moreover, because of the excess of chloroformate in the reaction mixture, condensation with a polyfunctional alcohol gives both linked and unlinked polymers. Consequently the molecular weight distributions of the linked polymers may be wide. Accordingly the polymers were all fractionated before use. Fractionation was from a dilute solution of toluene (<5 g/dm³) by addition of isoctane in the manner described elsewhere¹⁸. Generally 3 or 4 fractionations were needed to reduce the width of the molecular weight distribution to an acceptable figure (see Table 2).

Characterization

Vapour pressure osmometry (v.p.o.) (Mechrolab Model 301A, benzene at 25°C), end group analysis (e.g.a.) (phthaloylation of hydroxy end-groups^{19,20}), dilute solution viscometry (d.s.v.) (tetrahydrofuran at 25°C) and gel permeation chromatography (g.p.c.) (tetrahydrofuran at 25°C) were used to characterize the polymers with respect to molecular weight. Results are given in Table 2. Infra-red spectroscopy and reaction with phthalic anhydride served to demonstrate an absence of hydroxy end-groups in all samples but MH36 and MH61.

Table 1 The 36 series of polymers

Name	Structure
MH36	$\text{CH}_3(\text{O}.\text{CH}_2\text{CH}_2)_{36}\text{OH}$
MC36	$\text{CH}_3(\text{O}.\text{CH}_2\text{CH}_2)_{36}\text{O}.\text{CO}.\text{O}.\text{CH}_3$
(M36) ₂ O	$\text{CH}_3(\text{O}.\text{CH}_2\text{CH}_2)_{36}\text{O}.\text{CO}.\text{O}(\text{CH}_2\text{CH}_2\text{O})_{36}\text{CH}_3$
(M36) ₂ E	$\text{CH}_3(\text{O}.\text{CH}_2\text{CH}_2)_{36}\text{O}.\text{CO}.\text{O}.\text{CH}_2\text{CH}_2\text{O}.\text{CO}.\text{O}(\text{CH}_2\text{CH}_2\text{O})_{36}\text{CH}_3$
(M36) ₃ G	$\text{CH}_3(\text{O}.\text{CH}_2\text{CH}_2)_{36}\text{O}.\text{CO}.\text{O}.\text{CH}_2$
(M36) ₄ P	$\text{CH}_3(\text{O}.\text{CH}_2\text{CH}_2)_{36}\text{O}.\text{CO}.\text{O}.\text{CH}$
	$\text{CH}_3(\text{O}.\text{CH}_2\text{CH}_2)_{36}\text{O}.\text{CO}.\text{O}.\text{CH}_2$
	$\text{CH}_3(\text{O}.\text{CH}_2\text{CH}_2)_{36}\text{O}.\text{CO}.\text{O}.\text{CH}_2$ $\text{CH}_2\text{O}.\text{CO}.\text{O}(\text{CH}_2\text{CH}_2\text{O})_{36}\text{CH}_3$
	$\text{CH}_3(\text{O}.\text{CH}_2\text{CH}_2)_{36}\text{O}.\text{CO}.\text{O}.\text{CH}_2$ $\text{CH}_2\text{O}.\text{CO}.\text{O}(\text{CH}_2\text{CH}_2\text{O})_{36}\text{CH}_3$

Table 2 Characteristics of the poly(ethylene oxide) fractions

Sample	\bar{M}_n			\bar{M}_w/\bar{M}_n	[η] (cm ³ /g)	\bar{M}_n (predicted)
	v.p.o.	e.g.a.	g.p.c.			
MH36	1500	1400	1600	1.05	6.2	—
MC36	1600	—	1600	1.05	5.9	—
(M36) ₂ O	2900	—	3000	1.05	9.3	3200
(M36) ₂ E	3600	—	3300	1.08	9.7	3300
(M36) ₃ G	4600	—	5000	1.07	10.0	4900
(M36) ₄ P	5900	—	6800	1.16	13.6	6600
MH61	2800	2500	2700	1.05	7.9	—
MC61	2700	—	2700	1.05	7.5	—
(M61) ₂ E	—	—	4700	1.13	14.0	5400
(M61) ₃ G	—	—	8800	1.12	15.5	8300

Table 3 Lamella spacings (nm) for poly(ethylene oxide) fractions

Sample	T_c (°C)			
	30.5	39	43	48
MH36	10.6	10.7	—	—
MC36	10.6	—	—	—
(M36) ₂ O	—	10.7	—	—
(M36) ₂ E	11.3	11.7	—	—
(M36) ₃ G	—	12.4	12.7	—
(M36) ₄ P	—	12.8	—	—
MH61	—	15.5	16.0	—
MC61	—	—	16.0	—
(M61) ₂ E	—	—	17.5	18.3
(M61) ₃ G	—	—	17.9	18.8

D.s.v. was carried out with modified Desreux–Bischoff viscometers. Kinetic energy and shear corrections were negligible. A density correction was applied²¹.

G.p.c. was carried out with 5 Styragel columns of nominal pore sizes in the range 15 to 1500 nm. Calibration was with narrow fractions of known molecular weight⁴; the calibration curve was adjusted to reproduce the values of \bar{M}_n for the calibrants. Values of \bar{M}_n for the branched samples were based upon a 'universal' calibration²² i.e. a plot of $\log_{10}[\eta]M$ against elution volume. Corrections for instrumental spreading were not made.

Values for \bar{M}_n obtained by end group analysis are low compared with those obtained by the other methods; this is as expected if the samples (MH36 and MH61) contain a fraction of α , ω -hydroxy-poly(ethylene oxide).

Values of \bar{M}_n , based on those established for samples MH36 (1600) and MH61 (2700) taking into account the structure of the polymers, are listed in the last column of Table 2. The agreement between the predicted and the experimental values is satisfactory.

Small-angle X-ray scattering

The methods used for small-angle X-ray scattering have been described earlier¹². The scattering patterns were similar to those observed for other poly(ethylene oxide) homopolymers^{1,4} and copolymers¹². Lamella spacings were calculated directly from Bragg's Law, slit smearing effects being unimportant.

Lamella spacings are listed in Table 3. Polymers were crystallized at several temperatures (T_c); scattering was at

20°C. The chain length of poly(ethylene oxide) homopolymer of length 36 chain units is 10.1 nm and that of length 61 chain units is 17.1 nm. (Calculated assuming 0.28 nm per chain unit, in keeping with a repeat distance of 1.95 nm for the 7–2 helix of crystalline poly(ethylene oxide)²³. The spacings indicate that the polymers form predominantly extended chain lamellae, as is found for other poly(ethylene oxide) homopolymers of comparable chain (block) length^{1,4,5}. The increase in lamella spacing with degree of branching is possibly due to rejection of the shorter branches from the crystalline lamellae; the temperature dependence of lamella spacing is also consistent with a fractionation mechanism of this kind.

Dilatometry

The methods used for dilatometry have been described elsewhere^{12,24}. Contractions on crystallization (Δv , cm³/g) are listed in Table 4. These may be compared (see Table 4) with those for the process*:

melt → perfect crystal

The volume contractions must be considered in conjunction with the melting temperatures of the samples (Table 5) since, due to fractionation during the crystallization process^{1,26}, Δv can vary considerably with undercooling. The

* We use the following specific volumes to calculate Δv for the perfect crystallization^{2,23,25}:
Melt $v = 0.891$ cm³/g at 25°C $\alpha = 0.00069$ cm³/g K
Crystal $v = 0.813$ cm³/g at 25°C $\alpha = 0.00015$ cm³/g K.

Table 4 Contraction on crystallization ($10^2 \times \text{cm}^3/\text{g}$) for poly(ethylene oxide) fractions

Sample	T_c (°C)		
	36.1	40.0	43.2
MH36	6.1	5.5	—
MC36	—	5.6	—
(M36) ₂ O	—	6.4	—
(M36) ₂ E	6.5	5.5	—
(M36) ₃ G	—	5.5	—
(M36) ₄ P	4.8	4.7	—
MH61	—	7.3	5.1
(M61) ₂ E	—	5.7	6.3
(M61) ₃ G	—	6.1	6.5
Perfect crystallization	8.4	8.6	8.8

evidence we have is that Δv is not greatly affected by branching (with the possible exception of sample (M36)₄P).

Melting points (Table 5) are defined by the point of disappearance of the last trace of crystallinity¹². Within the temperature range $T_m \pm 5$ K we found only one melting point in any fraction; this is in keeping with other results on poly(ethylene oxide) homopolymers of molecular length⁶⁻⁸ less than 70 chain units. Melting points of the branched samples are slightly dependent on T_c ; those of the linear samples are independent of T_c .

DISCUSSION

Replacement of the hydroxy-end groups of samples MH36 and MH61 by methoxycarbonyl-end groups in samples MC36 and MC61 changes the melting point very little (<0.5 K, see Table 5). This is in keeping with a recent²⁷ comparison of hydroxy- and methoxy-ended poly(ethylene oxide) fractions which revealed a similarly small divergence in melting behaviour. We take these results to mean that the contribution of the free energy of mixing of end- and chain-groups to the free energy of formation from the melt of the amorphous lamellae of the polycrystal is small¹². Consequently we are able, in these systems, to ascribe changes in melting point between single and linked chains mainly to changes in structure. We note that this is not so for poly(ethylene oxide) linked with 2,4-toluene di-isocyanate⁹ because the introduction of aryl groups is known to depress the melting point of low molecular weight poly(ethylene oxide)⁷. (In fact melting point depressions were found by Galin *et al*⁹ for the 2,4-toluene di-isocyanate linked polymers.)

Effect of chain structure on melting

For simplicity we consider firstly the melting of polymers composed of p branches each of equal length (x chain units) which form crystalline lamellae of thickness x chain units. The case of single chains ($p = 1$) has been treated by Flory and Vrij²⁸ who write the free energy of fusion per chain:

$$\Delta G = x\Delta g - 2\sigma_0 - RT\ln x \quad (1)$$

where Δg is the free energy of fusion per chain unit of perfectly crystalline poly(ethylene oxide) and σ_0 is the free energy of formation from the melt of the crystal/melt interface (i.e. the layer of end groups). This equation leads to the melting point expression*:

* We use the condition $\Delta G = 0$ when $T = T_m$ and the relationship $\Delta g = \Delta h[1 - (T_m/T_m^0)]$.

$$T_m = T_m^0 [1 - (2\sigma_0/x\Delta h)] / [1 + (RT_m^0/x\Delta h)\ln x] \quad (2)$$

where T_m^0 and Δh are, respectively, the melting point and the enthalpy of fusion per chain unit of perfectly crystalline poly(ethylene oxide).

For the case $p \geq 1$, the free energy of fusion per chain can be written:

$$\Delta G = px\Delta g - 2p\sigma_0 - RT\ln z \quad (3)$$

where z is the total chain length. In formulating the term $RT\ln z$ we note that all p branches of length x enter the crystal and so the pairing of a chain end, in a crystal of thickness x units, is sufficient to ensure that all other ends are paired. The melting point expression corresponding to equation (3) is:

$$T_m = T_m^0 [1 - (2\sigma_0/x\Delta h)] / [1 + (RT_m^0/px\Delta h)\ln z] \quad (4)$$

The Flory-Vrij model can be extended²⁸ to take account of a crystalline lamella of thickness $l_c < x$, i.e. the case of partial melting²⁸. The free energy of fusion per chain can be written:

$$\Delta G = pl_c\Delta g - 2p\sigma_e - RT\ln z + pRT\ln(x - l_c + 1) \quad (5)$$

where σ_e is the free energy of formation from the melt of the crystal/amorphous interface and the amorphous layer of uncrystallized chain ends. The term $RT\ln(x - l_c + 1)$ originates in the additional combinatorial entropy of the partly melted crystal. We assume here an identical contribution of $RT\ln(x - l_c + 1)$ from each branch. (This is for an idealized model in which the constraints of one branch on another are ignored.) The melting point expression corresponding to equation (5) is:

$$T_m = T_m^0 [1 - (2\sigma_e/l_c\Delta h)] / [1 - (RT_m^0/pl_c\Delta h)\ln I] \quad (6)$$

where:

$$I = (x - l_c + 1)^p/z \quad (7)$$

We have shown elsewhere^{6,12} how these equations can be recast to take account of polydispersity of chain length, provided that simple assumptions are made concerning the nature of chain folding of the longer chains in the distributions. In fact we can demonstrate the important effects of chain structure without recourse to more complex equations than those above.

Table 5 Melting points (°C) of poly(ethylene oxide) fractions

Sample	T_c (°C)							
	30.5	33.3	34.8	35.1	36.1	40.0	43.2	48.0
MH36	49.5	49.5	49.5	—	—	—	—	—
MC36	49.1	49.1	49.1	—	49.1	—	—	—
(M36) ₂ O	53.4	53.5	—	—	53.5	53.7	—	—
(M36) ₂ E	53.1	53.1	—	53.0	—	53.2	—	—
(M36) ₃ G	52.3	—	52.5	—	52.6	52.5	—	—
(M36) ₄ P	51.9	—	52.1	—	52.2	52.4	—	—
MH61	—	—	—	—	57.6	57.4	57.4	57.6
MC61	—	—	—	—	56.8	56.9	56.9	—
(M61) ₂ E	—	—	—	—	58.3	58.3	58.7	59.3
(M61) ₃ G	—	—	—	—	58.4	58.4	58.8	59.5

Table 6 Calculated melting points (T_m) and interfacial free energies (σ_e)

Sample	Observed T_m (°C)	Calculated		
		Equation (4) T_m (°C) ^a	Equation (6)	
			T_m (°C) ^a	σ_e (kJ/mol)
MC36	49.1	49.0	49.1	6.6
(M36) ₂ E	53.1	53.4	55.5	7.3
(M36) ₃ G	52.5	55.0	58.2	8.3
(M36) ₄ P	52.1	56.2	59.6	8.8
MC61	56.9	56.9	56.8	8.2
(M61) ₂ E	58.4	60.1	61.4	9.7
(M61) ₃ G	58.5	61.3	63.2	10.6

^a Calculated assuming that for the 36 series of copolymers $\sigma_0 = 6.8$ kJ/mol and $\sigma_e = 6.6$ kJ/mol, and that for the 61 series $\sigma_0 = \sigma_e = 8.2$ kJ/mol

Comparison of theory and experiment

Values of T_m calculated according to equations (4) and (6) are listed in Table 6. We use $T_m = 349K^{29-31}$ and $\Delta h = 8.4$ kJ/mol³². The lamella thickness l_c is assumed to be $0.7x$, in keeping with the values of l_c found¹² for extended chain polycrystals. The values of σ_0 and σ_e (indicated in Table 6) were chosen so as to bring measured and calculated melting points into agreement for the single chains MC36 and MC61.

At constant end interfacial free energy the theoretical prediction is that T_m is increased as p is increased. The predicted increase varies somewhat with the model used. However the end-paired model is for chains with zero combinatorial entropy in the polycrystal so that we might expect to observe increases in T_m at least as large as those predicted by equation (4). In fact we do not observe a constant increase in T_m with p ; moreover the observed increases in T_m are markedly lower than those predicted. We interpret this to mean that the interfacial free energy is increased as p is increased.

For the more realistic partly melted model, represented by equation (6), we have determined the values of σ_e required to bring theory and experiment into agreement. These values are listed in Table 6. An increase in σ_e of up to 2.5 kJ/mol is sufficient to explain the observed melting points. Such an increase in σ_e would be consistent^{12,13} with conformational distortions of the poly(ethylene oxide) chains in the amorphous layer (as a consequence of accommodating linking points in the amorphous layer whilst maintaining a high extent of crystallinity), or with an increase in thickness of the amorphous lamellae (as might be the case with sample (M36)₄P, see Table 4).

ACKNOWLEDGEMENTS

We thank Dr R. Mobbs for help with the preparation of the linked polymers and Messrs D. J. Roy and D. Rowlinson for assistance with their characterization. P.C.A. and J.Q.G.M. acknowledge receipt of Science Research Council Studentships.

REFERENCES

- 1 Arlie, J. P., Spegt, P. A. and Skoulios, A. E. *Makromol. Chem.* 1966, **99**, 160
- 2 Arlie, J. P., Spegt, P. A. and Skoulios, A. E. *Makromol. Chem.* 1967, **104**, 212
- 3 Spegt, P. A. *Makromol. Chem.* 1970, **140**, 167
- 4 Beech, D. R., Booth, C., Dodgson, D. V., Sharpe, R. R. and Waring, J. R. S. *Polymer* 1972, **13**, 73
- 5 Beech, D. R., Booth, C., Pickles, C. J., Sharpe, R. R. and Waring, J. R. S. *Polymer* 1972, **13**, 246
- 6 Ashman, P. C., and Booth, C. *Polymer* 1972, **13**, 459
- 7 Booth, C., Bruce, J. M. and Buggy, M. *Polymer* 1972, **13**, 475
- 8 Ashman, P. C. and Booth, C. *Polymer* 1973, **14**, 300
- 9 Galin, J.-C., Spegt, P. A., Suzuki, S. and Skoulios, A. E. *Makromol. Chem.* 1974, **175**, 991
- 10 Booth, C. and Pickles, C. J. *J. Polym. Sci. (A-2)* 1973, **11**, 249
- 11 Booth, C. and Dodgson, D. V. *J. Polym. Sci. (A-2)* 1973, **11**, 265
- 12 Ashman, P. C. and Booth, C. *Polymer* 1975, **16**, 889
- 13 Ashman, P. C., Booth, C., Cooper, D. R. and Price, C. *Polymer* 1975, **16**, 897
- 14 Ashman, P. C. and Booth, C. *Polymer* 1976, **17**, 105
- 15 Skoulios, A. E., Tsouladze, G. and Fanta, E. *J. Polym. Sci. (C)* 1964, **4**, 507
- 16 Short, J. M. and Crystal, R. G. *Appl. Polym. Symp.* 1971, **16**, 137
- 17 Perret, R. and Skoulios, A. E. *Makromol. Chem.* 1972, **162**, 147, 163
- 18 Booth, C. and Price, C. *Polymer* 1966, **7**, 85
- 19 Price, C. C. and St. Pierre, L. E. *J. Am. Chem. Soc.* 1956, **78**, 3432
- 20 Havlik, A. J., Moacanin, J. and Otterness, I. *J. Polym. Sci. (A)* 1963, **1**, 2213
- 21 Beech, D. R. and Booth, C. *J. Polym. Sci. (A-2)* 1969, **7**, 575
- 22 Grubisic, Z., Rempp, P. and Benoit, H. *J. Polym. Sci. (B)* 1967, **5**, 753
- 23 Price, F. P. and Kilb, R. W. *J. Polym. Sci.* 1962, **57**, 395
- 24 Maclaine, J. Q. G. and Booth, C. *Polymer* 1975, **16**, 680
- 25 Simon, F. T. and Rutherford, J. H. *J. Appl. Phys.* 1964, **35**, 82
- 26 Beech, D. R., Booth, C., Dodgson, D. V. and Hillier, I. H. *J. Polym. Sci. (A-2)* 1972, **10**, 1555
- 27 Cooper, D. R., Timson, M. J. and Booth, C. to be published
- 28 Flory, P. J. and Vrij, A. *J. Am. Chem. Soc.* 1963, **85**, 3548
- 29 Beech, D. R. and Booth, C. *J. Polym. Sci. (B)* 1970, **8**, 731
- 30 Afifi-Effat, A. M. and Hay, J. N. *JCS Faraday Trans. II* 1972, **68**, 656
- 31 Rijke, A. M. and McCoy, S. *J. Polym. Sci. (A-2)* 1972, **10**, 1845
- 32 Devoy, C. J. *PhD Thesis* Manchester University (1966)

Sequence distribution of *cis*-1,4- and *trans*-1,4-units in polyisoprenes

Yasuyuki Tanaka and Hisaya Sato

Department of Textiles and Polymer Science, Faculty of Technology, Tokyo University of Agriculture and Technology, Tokyo, Japan

(Received 9 June 1975)

The ^{13}C n.m.r. spectra of chicle polyisoprene and *cis*-*trans* isomerized 1,4-polyisoprenes were studied. The splittings of signals were observed in the C_1 , C_2 , and C_4 carbon signals of the isomerized polyisoprenes. The newly appearing signals were assigned to the carbon atoms in *cis*-*trans* linkages. The fractions of the diad sequences (*trans*-*trans*, *trans*-*cis*, *cis*-*trans*, and *cis*-*cis*) were determined by using the four signals of C_1 carbon. It was found that the *cis*-1,4- and *trans*-1,4-units were randomly distributed in the isomerized polyisoprenes and it was confirmed that the chicle polyisoprene was a mixture of *cis*-1,4- and *trans*-1,4-polyisoprenes.

INTRODUCTION

Recently ^{13}C n.m.r. spectroscopy has been successfully applied to investigate the sequence distribution of 1,2- and 1,4-units or *cis*-1,4- and *trans*-1,4-units in polybutadienes¹⁻⁴. As for polyisoprenes, however, few investigations have been made on the sequence distribution of isomeric structures using this technique, although Duch and Grant have assigned the ^{13}C n.m.r. signals of *cis*-1,4- and *trans*-1,4-homopolyisoprenes⁵.

In previous work we have found new signals attributed to *cis*-*trans* linkages in the ^{13}C n.m.r. spectra of *cis*-*trans* isomerized polyisoprenes and assigned the signals using diad sequences of *cis*-1,4- and *trans*-1,4-units⁶. We have also studied the ^{13}C n.m.r. spectra of hydrogenated polyisoprenes containing various amounts of 1,4- and 3,4-units and the sequence distribution of 1,4- and 3,4-units were discussed for *n*-BuLi catalysed polyisoprenes⁷. In this work we have investigated the sequence distribution of chicle polyisoprene and *cis*-*trans* isomerized 1,4-polyisoprenes containing various ratios of *cis*-1,4- and *trans*-1,4-units.

EXPERIMENTAL

Materials

Chicle polyisoprene was obtained by the extraction of crude chicle with benzene after removing the acetone-soluble compounds. This polyisoprene was purified by repeated reprecipitation from a benzene solution into acetone. The purified chicle polyisoprene consisted of exclusively 1,4-polyisoprene, which was confirmed by ^1H n.m.r. and infra-red spectroscopies.

Gutta percha (*trans*-1,4-: 100%) and synthetic *cis*-1,4-polyisoprene (*cis*-1,4-: 97.1%, *trans*-1,4-: 1.9%, 3,4-: 1.0%) were used for the starting polymer of *cis*-*trans* isomerization without further purification. The benzene solution of the polymer (2 or 3 % w/v) was irradiated with a high pressure mercury lamp in the presence of thiobenzoic acid (1-8% w/w of the polymer) stirring with a magnetic stirrer at 20°C under nitrogen atmosphere. The isomerized polymer was purified by repeated reprecipitation

from a benzene solution into acetone. The ratio of *cis*-1,4- and *trans*-1,4-units of the polymer was determined by ^1H n.m.r. spectroscopy.

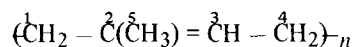
Measurement

The ^{13}C n.m.r. spectra were obtained at 25.1 or 15.0 MHz using respectively a JEOL JNM-PS 100 or a Varian CFT-20 spectrometer equipped with a Fourier transfer accessory. Measurements were made at room temperature or 60°C in CDCl_3 (about 25% w/v). Chemical shifts were referred to tetramethylsilane added as an internal standard. All the spectra were proton noise decoupled and obtained with multiple scans at a pulse repetition time of 2.0 or 2.2 sec.

RESULT AND DISCUSSION

Assignments of ^{13}C n.m.r. signals

The ^{13}C n.m.r. spectrum of chicle polyisoprene was identical to that of a mixture of *cis*-1,4- and *trans*-1,4-polyisoprenes showing five signals due to *cis* polymer at 134.85, 124.65, 32.25, 26.36, and 23.25 ppm and also five signals due to *trans* polymer at 134.38, 123.87, 39.67, 26.67, and 15.87 ppm (Figure 1). These signals were assigned to the C_2 , C_3 , C_1 , C_4 , and C_5 carbons in the order of increasing magnetic field for both *cis*-1,4- and *trans*-1,4-polymers⁵. The symbols of carbon atoms are denoted as follows:



The observation that chicle contains both *cis*-1,4- and *trans*-1,4-polyisoprenes is in accord with the finding obtained by Schlesinger and Leeper using fractionation⁸.

Polyisoprenes containing various ratios of *cis*-1,4- and *trans*-1,4-units were obtained by *cis*-*trans* isomerization of 1,4-polyisoprenes. Figure 2 shows the differences between the ^{13}C n.m.r. spectra of chicle and isomerized polyisoprenes. In the spectra of isomerized polyisoprenes signals due to C_1 carbon split into two peaks for both *cis* and *trans* resonances. Similar splittings were observed in

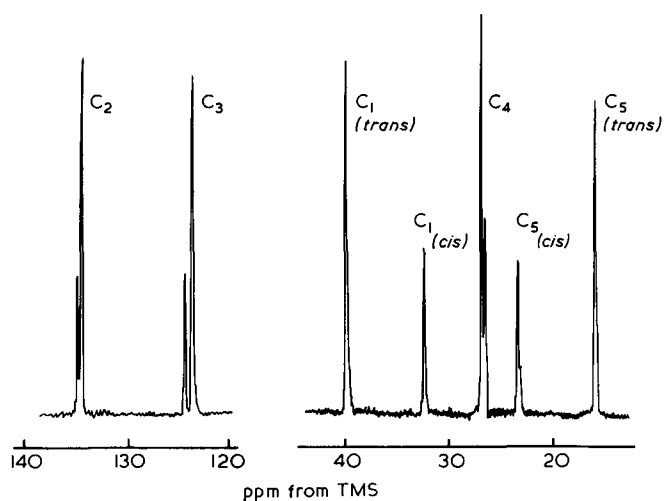


Figure 1 ^{13}C n.m.r. spectrum of chicle polyisoprene (25.1 MHz)

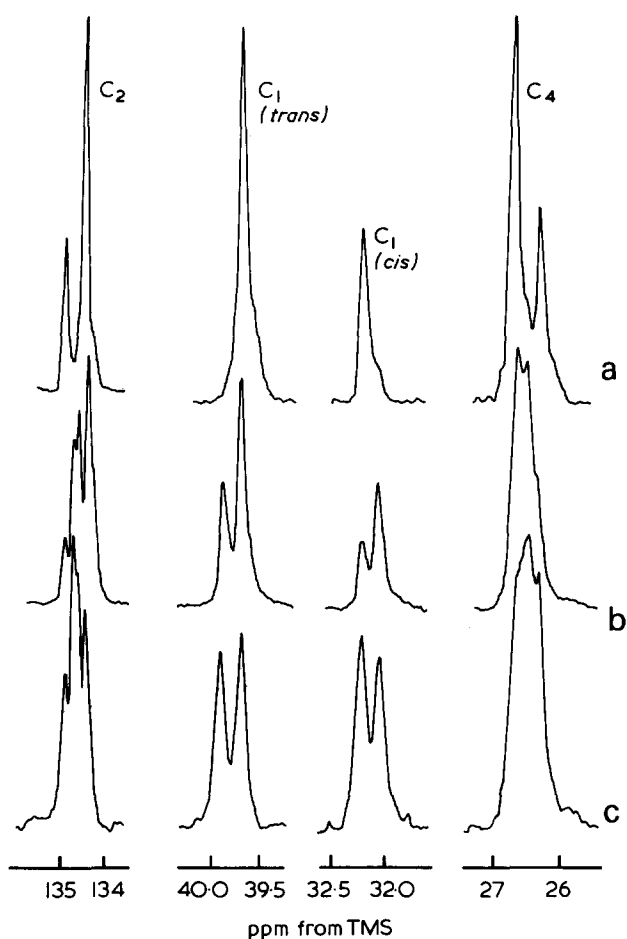


Figure 2 ^{13}C n.m.r. spectra of 1,4-polyisoprenes (25.1 MHz). (a) Chicle polyisoprene; (b) isomerized gutta percha (*trans*-1,4-: 64%); (c) isomerized *cis*-1,4-polyisoprene (*trans*-1,4-: 50%)

the signals due to C_2 and C_4 carbons of isomerized polymers, though new signals appeared between the original *cis* and *trans* peaks and overlapped with one another. These new signals were not observed for chicle polyisoprene, gutta percha, and synthetic *cis*-1,4-polyisoprene.

The structures of the isomerized polyisoprenes were also investigated by X-ray diffraction. The crystallinity of gutta percha drastically decreased by the isomerization as shown in Figure 3. On the other hand, the isomerized *cis*-1,4-polyisoprene displayed no peaks due to the crystallinity of long sequences of *trans*-1,4-unit, even though it had

more than 50% of *trans*-1,4-unit (Figure 3c). This finding shows that the long sequences of the *trans*-1,4-unit disappeared by the isomerization of the *trans* polymer and was not produced by the isomerization of the *cis* polymer. Hence, it is concluded that *cis*-*trans* linkages were produced by the isomerization of both *cis* and *trans* polymers. It was confirmed that side reactions such as main chain scission reaction and cyclization were negligible in the course of *cis*-*trans* isomerization as discussed later. Consequently, the newly appearing signals were attributed to the carbon atoms in the *cis*-*trans* or *trans*-*cis* linkages. The signals due to C_1 , C_2 , and C_4 carbon atoms were assigned to the carbon atoms in diad sequences of *cis*-1,4- and *trans*-1,4-units as shown in Table 1.

Sequence distribution of *cis*-1,4 and *trans*-1,4 units

The fractions of diad sequences of *cis*-1,4- and *trans*-1,4-units, i.e., *trans*-*cis*, *trans*-*trans*, *cis*-*cis*, and *cis*-*trans* were determined from the relative intensities of the four signals of C_1 carbon atom. These diad fractions are plotted against the fraction of *trans*-1,4-unit for the isomerized polyisoprenes as shown in Figure 4. The observed values of

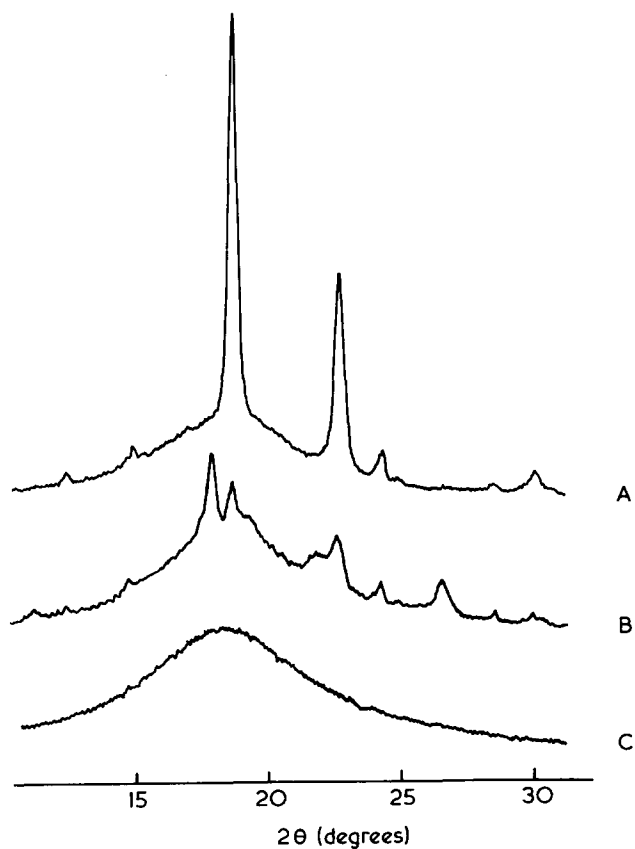


Figure 3 X-ray diffraction patterns of 1,4-polyisoprenes. A, gutta percha; B, isomerized gutta percha (*trans*-1,4-: 87%); C, isomerized *cis*-1,4 polyisoprene (*trans*-1,4-: 50%)

Table 1 Assignment of ^{13}C n.m.r. signals

Carbon	Chemical shift (ppm from TMS)			
	<i>trans</i> - <i>trans</i>	<i>trans</i> - <i>cis</i>	<i>cis</i> - <i>trans</i>	<i>cis</i> - <i>cis</i>
C_1	39.67	39.91	32.01	32.25
C_2	134.38	134.55	134.68	134.85
C_4	26.69	~26.55	~26.45	26.36

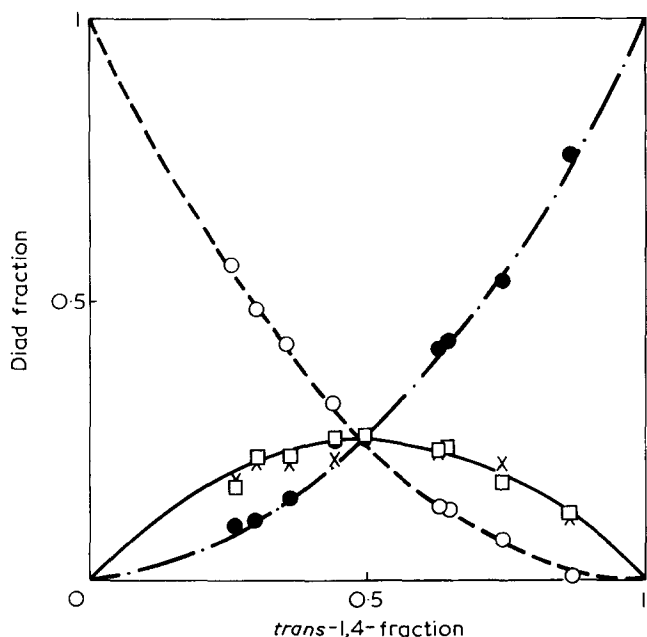


Figure 4 Diad sequence fraction of *cis*-1,4- and *trans*-1,4-units. Points show experimental points, and curves the theoretical dependence assuming Bernoullian distribution; \circ , *cis*-*cis*; \square , *cis*-*trans*; \times , *trans*-*cis*; \bullet , *trans*-*trans* fraction

each diad sequence lay on the theoretical curves assumed for a random distribution of *cis*-1,4- and *trans*-1,4-units. Therefore it is concluded that the *cis*-*trans* isomerization proceeded randomly regardless of the ultraviolet irradiation time, the concentration of thiobenzoic acid, and the microstructure of the starting polymer. It is noteworthy that the fractions of *cis*-*trans* and *trans*-*cis* linkages were almost equal for all polymers, which indicates the validity of the signal assignments. The fractions of *trans*-1,4-unit determined from relative intensities between C_1 -*cis* and C_1 -*trans* signals were in good agreement with those obtained by ^1H n.m.r. spectroscopy. This indicates that the differences of the nuclear Overhauser enhancement factor and the effect of spin-lattice relaxation time among these C_1 carbon atoms were negligible in these measurements. However, the fractions of *trans*-1,4-unit determined from the signals of C_5 carbon atom were lower than those obtained by ^1H n.m.r. spectroscopy up to 8%.

The chicle polyisoprene did not exhibit definite signals characteristic of the *cis*-*trans* or *trans*-*cis* linkages, which indicates that this polymer is a mixture of *cis*-1,4- and *trans*-1,4-polyisoprenes or a block copolymer consisting of long sequences of *cis*-1,4- and *trans*-1,4-units. The fractionation of the chicle polyisoprene was carried out according to the method of Schlesinger and Leeper⁸. The polymer was separated into a pure *trans*-1,4-polymer and *cis*-1,4-polymer containing 10% of *trans*-1,4-unit. Characteristic signals due to *cis*-*trans* linkages were not observed in either fraction. Therefore it is confirmed that the chicle polyisoprene is a mixture of *cis*-1,4- and *trans*-1,4-homopolymers, although a pure *cis* polymer was not obtained by the fractionation.

cis-*trans* Isomerization by ultra-violet irradiation

The *trans*-1,4-fractions of the isomerized polymers were plotted as a function of ultra-violet irradiation time in Figure 4. The isomerization proceeded as the irradiation

time increased and the isomerization rate increased with the concentration of thiobenzoic acid. Both *cis* and *trans* polymers were isomerized to a common equilibrium structure containing 50 to 65% of *trans*-1,4-unit. This equilibrium composition is almost in agreement with one obtained by Cunneen *et al.*⁹.

Golub *et al.* reported that 3,4-, 1,2-, and cyclic-units were produced resulting from the side reactions of *cis*-*trans* isomerization of 1,4-polyisoprenes by the u.v. irradiation in the absence of sensitizer¹⁰. The microstructure of the isomerized polymers was examined according to the method of Golub *et al.* using ^1H n.m.r. and i.r. spectroscopies. Under the present experimental conditions the isomerized polymers contained 3,4-, 1,2- and cyclic-units less than 3, 1, and 1%, respectively. This result indicates that thiobenzoic acid accelerated exclusively *cis*-*trans* isomerization. In the course of *cis*-*trans* isomerization process only a slight amount of side reactions was also confirmed by the analysis of hydrogenated polyisoprenes⁷. Only four signals corresponding to four types of carbon atoms linked by head-to-tail 1,4 structure were observed in the ^{13}C n.m.r. spectra of hydrogenated polyisoprenes prepared by the hydrogenation of isomerized polymers using *p*-toluenesulphonylhydrazide.

^{13}C n.m.r. spectra of polyisoprenes containing only *cis*-1,4- and *trans*-1,4-units were rather simple. The sequence distributions of these units were determined for chicle polyisoprene and *cis*-*trans* isomerized 1,4-polyisoprenes. It was found that *cis*-1,4- and *trans*-1,4-units were distributed randomly along the *cis*-*trans* isomerized polyisoprenes. A similar random distribution of *cis*-1,4- and *trans*-1,4-units was also observed for *cis*-*trans* isomerized polybutadienes³. The sequence distribution of 3,4- and 1,4-units were also determined by ^{13}C n.m.r. measurement of hydrogenated polyisoprenes as described in a previous paper⁷. On the other hand, polyisoprenes containing *cis*-1,4-, *trans*-1,4 and 3,4-units exhibited quite complicated ^{13}C n.m.r. signals due to various types of carbon atoms in different sequences. These complicated resonances can be analysed by referring to the results obtained

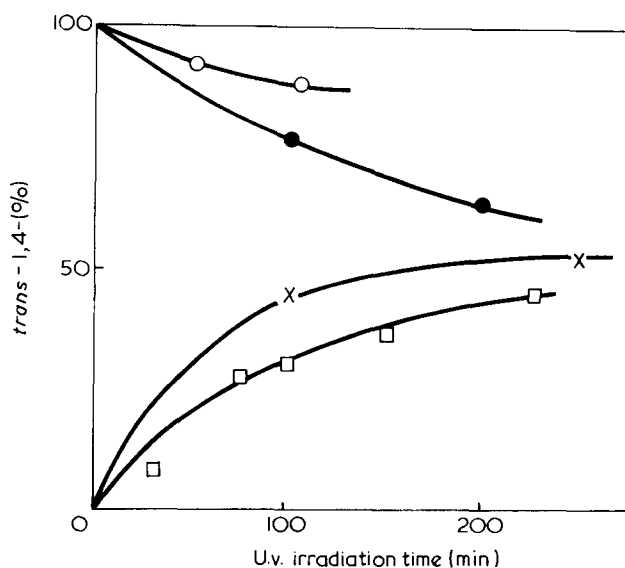


Figure 5 Isomerization of 1,4-polyisoprenes. \square Thiobenzoic acid; \circ , 1; \times , 3; \bullet , 8% w/w polymer

hitherto and the sequence distribution of *cis*-1, 4-, *trans*-1, 4 and 3, 4-units will be discussed in a subsequent paper.

ACKNOWLEDGEMENTS

The authors are very grateful to Mr Ichiro Nagoya of Asahi Chemical Industry Co. and Mr Kiyoshi Aoki of Nippon Electric Varian Co. for the measurement of ^{13}C n.m.r. spectra.

REFERENCES

- 1 Elgert, K. F., Stützel, B., Frenzel, P., Cantow, H. J. and Streck, R. *Makromol. Chem.* 1973, **170**, 257
- 2 Conti, F., Segre, A., Pini, P. and Porri, L. *Polymer* 1974, **15**, 5
- 3 Tanaka, Y., Sato, H., Ogawa, M., Hatada, K. and Terawaki, Y. *J. Polym. Sci. (B)*, 1974, **12**, 369
- 4 Furukawa, J., Kobayashi, E. and Kawagoe, T. *Polym. J.* 1973, **5**, 231
- 5 Duch, M. W. and Grant, D. M. *Macromolecules* 1970, **3**, 165
- 6 Tanaka, Y., Sato, H. and Seimiya, T. *Polym. J.* 1975, **7**, 264
- 7 Tanaka, Y., Sato, H. and Ogura, A. *J. Polym. Sci. (A-1)* in press
- 8 Schlesinger, W. and Leeper, H. M. *Ind. Eng. Chem.* 1951, **43**, 398
- 9 Cunneen, J. I., Higgins, G. M. C. and Watson, W. F. *J. Polym. Sci.* 1957, **11**, 1
- 10 Golub, M. A. and Stephens, C. L. *J. Polym. Sci. (A-1)* 1968, **6**, 763

Diimide reduction of *cis*-1,4-polyisoprene with *p*-toluenesulphonylhydrazide

Tran Dai Nang*, Yasuo Katabe and Yuji Minoura

Department of Chemistry, Research Institute for Atomic Energy, Osaka City University, Sugimoto-cho, Sumiyoshi-ku, Osaka, Japan

(Received 29 August 1975)

The hydrogenation of *cis*-1,4-polyisoprene with diimide generated *in situ* from *p*-toluenesulphonylhydrazide (TSH), was investigated under various conditions. In aromatic solvents at 100–140°C, the rate of hydrogenation was increased with increase in concentration of polyisoprene and of TSH. Part of the polymer was depolymerized and cyclized during the reaction. Increasing the hydrogenation tended to decrease the rate of sulphur vulcanization, of the compounded rubber and the physical properties of vulcanizates were poor. The reaction of polyisoprene rubber with TSH, was also carried out in a solid state at 140°C for 20–60 min. It was found that by using a large amount of TSH hydrogenation and cyclization of rubber occurred. The quantity of TSH used as a blowing agent, for rubber in the manufacture of sponge rubber, i.e. 5–10 phr, did not cause hydrogenation.

INTRODUCTION

The hydrogenation of unsaturated polymers, especially polydienes, has been studied for many years, in order to derive polymers exhibiting substantially altered physical properties and generally improved resistance to oxidative and thermal degradation.

Previously, hydrogenation techniques usually required the use of highly reactive chemicals or heterogeneous catalysts, which generally resulted in appreciable degradation to the polymer chain.

Recently, the transitory species diimide, $N_2H_2^{1,2}$, has been extensively studied as a general hydrogenation reagent for low molecular weight olefins^{3,4}. The use of diimide with polymeric substrates was first reported by Okawara and coworkers⁵, who employed it to remove residual unsaturation from polyvinylchloride.

Lenz *et al.*^{6,7} and Harwood *et al.*⁸ have investigated the hydrogenation of polydienes (i.e. *cis*- and *trans*-1,4-polybutadiene, *cis*-1,4-polyisoprene, random and block SBR, poly(2,3-dimethylbutadiene), polycyclohexadiene, etc.) with diimide generated *in situ* from *p*-toluenesulphonylhydrazide.

In the present work, the reduction of *cis*-1,4-polyisoprene with diimide, has been studied in order to clarify the effect of reaction conditions on the hydrogenation and of polymer composition on the physical properties of the product.

EXPERIMENT

Commercial *cis*-1,4-polyisoprene (Natsyn 2200) as provided by the Goodyear Tyre and Rubber Company, and of composition 96.9% *cis* and 3.1% 3,4-bond content, was purified by dissolving it in benzene, followed by filtration and precipitation in methanol. The precipitated polymer was washed with alcohol and dried at room temperature *in vacuo*. Commercial *p*-toluenesulphonylhydrazide (TSH) was purified by recrystallization from ethanol and dried *in vacuo*. (TSH has decomposition point 107°C). Solvents used were purified by distillation.

* Present address: Chemical Engineering School, National Technical Institute, Saigon, South Vietnam.

Reduction

Polymer samples (10 g) and 500 ml of solvent (xylene, dichlorobenzene, pyridine etc.) were heated under nitrogen with stirring until the polymer dissolved. The solution was kept at a suitable temperature (100°–135°C) and the *p*-toluenesulphonylhydrazide (TSH) was added. Aliquots of 30 ml were removed from the reaction mixture at suitable times and the polymers were isolated by precipitation from methanol. After washing with methanol, water and more methanol, the hydrogenated polymers were purified by reprecipitation from benzene solution by methanol and dried at room temperature *in vacuo* to constant weight.

Physical measurements and analysis

Polymer characterizations were carried out by elemental analysis, infra-red spectroscopy, the determination of the unsaturation of rubber by Wij's method⁹ and n.m.r. spectroscopy.

Infra-red analyses were carried out using a Jasco IR type spectrometer of Japan Spectroscopic Co. Ltd. Films suitable for infra-red measurements were prepared on a NaCl plate by casting from the benzene solution. N.m.r. measurements were carried out using Hitachi–Perkin Elmer Corp. R-2018 instrument at 60 MHz.

The intrinsic viscosities of polyisoprene and the reaction products, were measured by means of Ubbelohde viscometer in toluene at 30°C. The molecular weights of polyisoprene were calculated using the equation, $[\eta] = 5 \times 10^{-4} M^{0.67}$.

Physical properties of vulcanizates

The hydrogenated rubbers that had been kept in methanol, plus 0.2% phenyl β -naphthylamine, were washed with methanol then dried *in vacuo*. The original rubber, was dissolved in xylene, precipitated in methanol, and treated as above.

All the rubbers were compounded with curing agents, according to the following method; rubber (10 g), zinc stearate (0.2 g), zinc oxide (0.6 g), zinc dimethyl dithiocarbamate (0.06 g) and sulphur (0.2 g). The rubber and ingredients were compounded on a Micro 'RAPRA–Shawbury' mill at a temperature of 40°C for about 15 min.

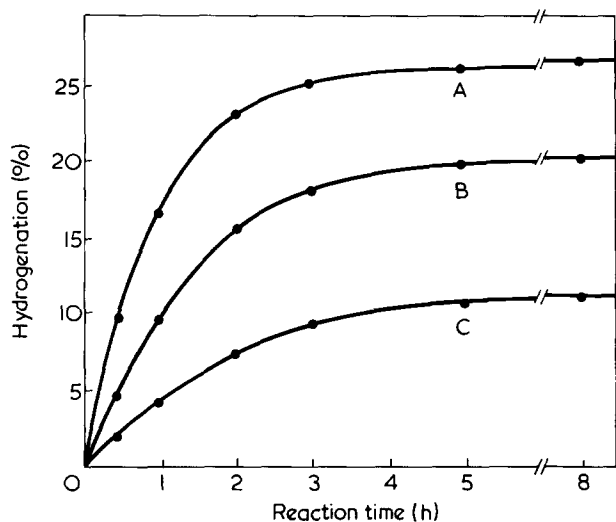


Figure 1 Effect of TSH on hydrogenation of polyisoprene (Natsyn) at 100°C. Concentration of polyisoprene: 0.29 mol/l, i.e. polyisoprene (10 g)/xylene (400 ml) + pyridine (100 ml). Concentration of TSH (mol/l); A, 0.88, B, 0.59; C, 0.29

Using the 'Wallace Shawbury MK V', curometer a cure chart of each compound was recorded at 130°C. The vulcanization of each sample was carried out at 130°C and for T_{90} min.

The physical properties of vulcanizates i.e. tensile strength, modulus, elongation and hardness, were measured according to the JIS K 6301 method. The heat ageing test was carried out simultaneously for each sample at 70°C for 24 h.

RESULTS AND DISCUSSION

Determination of suitable conditions

The diimide reductions of polyisoprene were carried out in various solvents. In *o*-dichlorobenzene, the reaction system turned brown after about 3 h and black after 5 h at 135°C, whilst, in xylene, the reaction mixture turned brown and then black at 135°C after about 5 h, owing to decomposition of the polymer. *p*-Toluenesulphonic acid produced from TSH, was partly converted to *p*-toluenesulphonic acid which caused the cyclization of polyisoprene and the acceleration of the thermal decomposition of the polymer. The effect of the *p*-toluenesulphonic acid was prevented by use of a basic solvent, i.e. pyridine. The diimide reduction carried out at 125°C in the mixed solvent, (i.e. xylene/pyridine = 4:1), gave a dark brown product after 8 h but at a lower temperature, (100°C), the decomposition was avoided and a clear product was produced.

Effect of concentration of TSH

At constant concentration of polyisoprene (10 g/500 ml), the rate of hydrogenation increased at a rate directly proportional to concentration of TSH (Figure 1).

Table 1 Effect of concentration of *p*-toluenesulphonylhydrazide on degree of hydrogenation. Natsyn (10 g); solvent [xylene (400 ml), pyridine (100 ml)] at 100°C for 8 h

Natsyn/TSH (mol ratio)	C (%)	H (%)	$[\eta]$	$M_w \times 10^{-3}$	Hydrogenation (%)
1:0	87.72 (88.23)	12.35 11.77 calc. for C_5H_8	2.38	308	0
1:1	85.91	12.82	1.14	103	11.7
1:2	85.90	13.64	1.19	110	20.2
1:3	86.01	14.04	1.18	109	26.5

The partly hydrogenated *cis*-polyisoprene and natural rubber were soluble in aromatic and chlorinated hydrocarbon solvents at room temperature and were analysed for residual unsaturation by i.r. and n.m.r. spectroscopy.

The n.m.r. spectrum of the original polyisoprene compared with that of the partly hydrogenated sample, show that the resonance of $-C=CH-$ units (5.1 ppm) is decreased and the resonance at 1.3–1.2 and 0.9–0.8 ppm due to hydrogenated isoprene units appeared in the spectrum.

The results of elemental analysis of products (Table 1), show H% clearly increased and C% decreased compared with the original polyisoprene. The results were not satisfactory for the calculation of degree of hydrogenation, and this was determined by Wij's method.

Intrinsic viscosity measurements (Table 1) show that polyisoprene degrades under the reaction conditions required to generate diimide. The i.r. spectrum of the hydrogenated *cis*-polyisoprene (Figure 2) showed a decrease in percentage absorption of the C=C peaks at 570, 835 and 1665 cm^{-1} proving that the hydrogenation had occurred. The slight shifts of the CH_3 deformation vibration at 1450 cm^{-1} of the hydrogenated polymer, also showed the occurrence of cyclization¹⁰.

Effect of concentration of polyisoprene

The diimide reductions of polyisoprene, carried out at 100°C for varying concentrations of rubber and at constant concentration of TSH, are shown in Figure 3. The degrees of hydrogenation and the rate of hydrogenation increased with increase in the concentration of rubber, and in each case reached a saturation value at almost the same reaction time. Therefore, the rate of hydrogenation of polyisoprene by diimide obeys the equation:

$$\text{rate of hydrogenation} = K [\text{polymer}] [\text{TSH}]$$

where K is the rate constant.

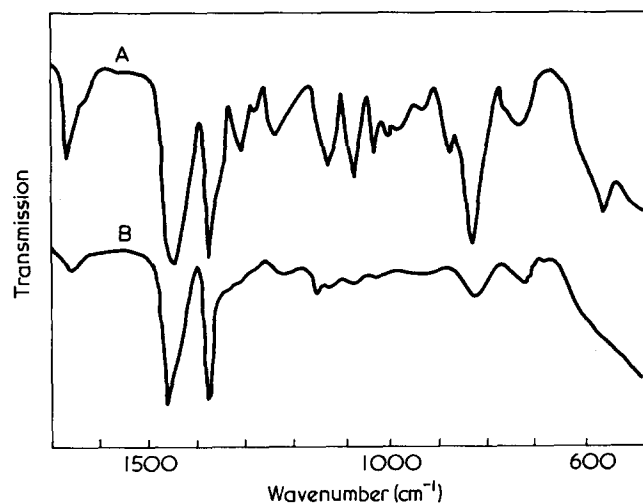


Figure 2 Infra-red spectrum of *cis*-1,4-polyisoprene (A) and hydrogenated *cis*-1,4-polyisoprene (26.5%) (B)

Effect of solvents

General reaction conditions of constant polyisoprene concentration (0.441 mol/l), TSH concentration (0.882 mol/l) and reaction temperature (100°C–102°C), were applied to four reactions using different solvent mixtures of 100:0, 80:20, 40:60 and 0:100 v/v of *m*-xylene and pyridine.

Iodine titrations on the samples taken at determined reaction times, were used to measure the degree of hydrogenation. The results (Figure 4) show that the rate of hydrogenation was decreased with increasing amounts of pyridine in the reaction solvent.

The infra-red spectra of reaction products showed that the hydrogenation occurred with all the samples and that the degree of hydrogenation decreased continuously from *m*-xylene to pyridine.

The shifts of the peak at 1450 cm⁻¹ were observed in *m*-xylene, and in *m*-xylene and pyridine mixtures, but not in pure pyridine, showing that the cyclization could be avoided in the pyridine solution. These results were summarized in Table 2.

Physical properties of hydrogenated rubber

All the hydrogenated rubbers obtained as described above, were compounded to observe their vulcanizing characteristics and to measure the physical properties of vulcanizates. *T*₉₀ was chosen as the cure time for each compound. After curing, the physical properties (Table 3) were measured on dumb bell specimens of the vulcanizates.

In general, the physical properties of vulcanizates from the hydrogenated rubbers were poor, owing to the depolymerization during the hydrogenation reaction. It was found that increase of the hydrogenation tended to decrease the rate of vulcanization.

Table 2 Effect of *m*-xylene/pyridine mixture on hydrogenation reaction at 100°C. Natsyn 15 g (0.441 mol/l); TSH 82.2 g (0.882 mol/l), mole ratio = ½; solvent 500 ml

Xylene/ pyridine (vol %)	Hydrogenation after 8 h (%)	Hydrogenation rate $R_H \times 10^6$ (mol/l/sec)	Cyclic units
100:0	62.0	49.0	++
80:20	34.0	40.3	+
40:60	23.3	26.1	+
0:100	16.1	21.1	-

Table 3 Physical properties of hydrogenated polyisoprene vulcanizates

Hydrogenation (%)	Appearance of polymer	<i>T</i> ₁₀ * (scorch time)	<i>T</i> ₉₀ * (opt. cure time)	Tensile strength† (kg/cm ²)	<i>M</i> ₁₀₀ † (kg/cm ²)	Elongation† (g)	Hardness**†
0 Natsyn	clear and soft	4.4	11.5	93.2 (83.0)	4.1 (4.3)	952 (902)	28 (28)
11.7	light brown	1.5	4.5	14.7 (12.1)	7.4 (7.5)	300 (250)	40 (36)
20.2	a little tacky	2.6	10.0	11.4 (11.2)	6.9 (7.4)	183 (150)	43 (40)
23.3	light brown soft	3.0	11.0	12.0 (11.4)	9.1 (8.2)	166 (150)	43 (40)
26.5	brown	8.0	27.5	13.6 (13.3)	7.9 (8.0)	283 (308)	43 (41)
33.3	a little hard	9.0	30.0	14.2 (10.9)	8.6 (6.4)	258 (225)	39 (37)
	brown						
	a little hard						

* Wallace Shawbury MK V curometer ** ASKER Hardness Tester-type JA A-degrees † Values in parenthesis are for ageing test at 70°C for 24

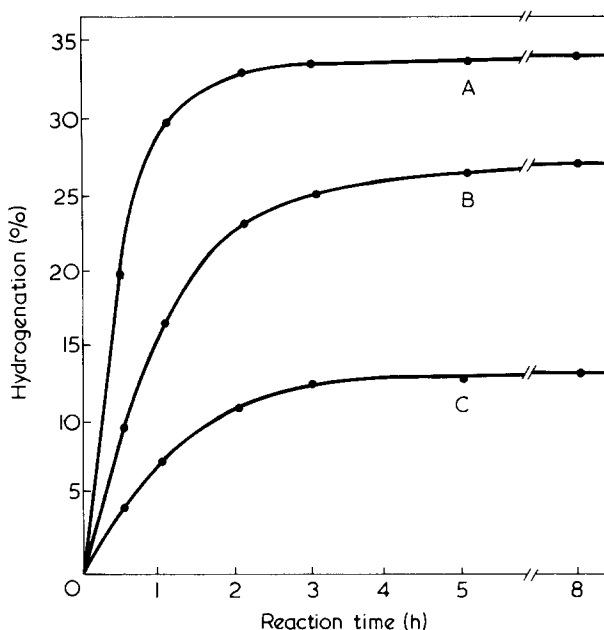


Figure 3 Effect of concentration of polyisoprene on hydrogenation at 100°C. Concentration of TSH: 0.88 mol/l; concentration of polyisoprene (mol/l): A, 0.59; B, 0.44; C, 0.29

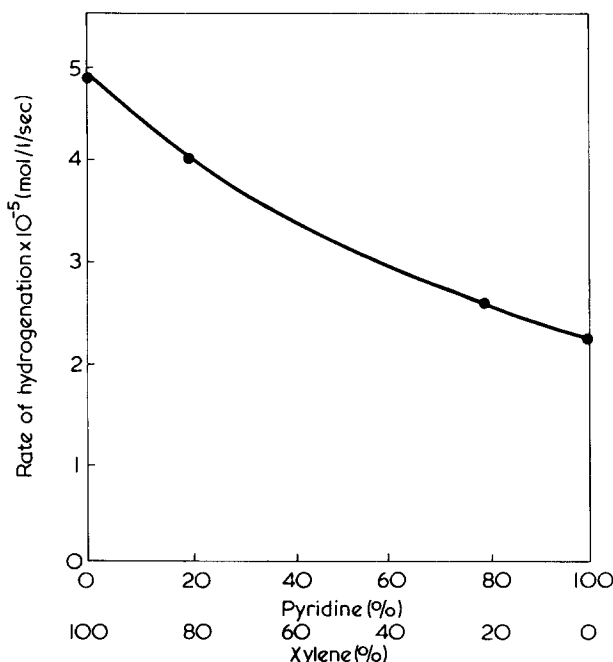


Figure 4 Effect of solvent on hydrogenation rate of polyisoprene at 100°C. Concentration of polyisoprene, 0.44 mol/l; concentration of TSH, 0.88 mol/l

Solid reaction of TSH with polyisoprene

p-Toluenesulphonylhydrazide (TSH) is usually used as a blowing agent in the rubber sponge industry. The reaction of TSH with rubber was carried out in a solid state by mixing various amounts of TSH and rubber, on rolls heated to 140°C for 20 and 60 min. After heating, the rubber was dissolved in benzene and the unreacted TSH was removed by filtration. The filtrate was concentrated, poured in methanol, and the rubber was recovered as a precipitate. The degree of hydrogenation was measured by n.m.r., and the results are shown in Table 4.

The results of n.m.r. and i.r., show that, the use of large amounts of TSH led to the hydrogenation and cyclization of rubber. The amount of TSH used for rubber in the actual

sponge manufacture is generally up to 5–10 phr, and under these conditions the hydrogenation of rubber would be negligible.

ACKNOWLEDGEMENTS

The authors thank Dr K. Yamaguchi and Mr H. Ishikawa of the Industrial Research Institute of Hyogo Prefecture for their collaboration in the measurements of n.m.r. and physical properties of vulcanizates.

REFERENCES

- 1 Dows, D. A., Pimental, G. C. and Whittle, E. *J. Chem. Phys.* 1955, **23**, 1606
- 2 Foner, S. F. and Hudson, R. C. *J. Chem. Phys.* 1958, **28**, 719
- 3 Huning, S., Muller, H. and Thier, W. *Angew. Chem.* 1965, **77**, 368
- 4 Miller, C. E. *J. Chem. Educ.* 1965, **42**, 254
- 5 Nakagawa, T. and Okawara, M. *J. Polym. Sci. (A-1)* 1968, **6**, 1795
- 6 Mango, L. A. and Lenz, R. W. *Makromol. Chem.* 1973, **163**, 13
- 7 Sanui, K., MacKnight, W. J. and Lenz, R. W. *J. Polym. Sci. (B)* 1973, **11**, 427
- 8 Harwood, H. J., Rusell, D. B., Verthe, J. A. and Zymonas, J. *Makromol. Chem.* 1973, **163**, 1
- 9 Kemp, A. R. and Mueller, G. S. *Ind. Eng. Chem. (Analyt. Edn.)* 1934, **6**, 52
- 10 Kossler, I. and Vodekna, J. *Analyt. Chem.* 1968, **40**, 825

Table 4 Hydrogenation reaction of polyisoprene with TSH in solid state at 140°C

Poly-isoprene (I.R.) (g)	TSH (g)	TSH/IR (mol ratio)	Reaction time (min)	Degree of hydrogenation (g)
100	0	0	60	0
100	10	0.037	20	—
			60	0.2
100	50	0.182	20	1.1
			60	1.9
100	140	0.511	20	7.1
			60	11.7

Infra-red study of poly(1-pentene) and poly(4-methyl-1-pentene)*

S. M. Gabbay and S. S. Stivala

Department of Chemistry and Chemical Engineering, Stevens Institute of Technology, Hoboken, New Jersey 07030, USA

(Received 14 April 1975; revised 13 October 1975)

The infra-red (i.r.) spectra of the two polymorphous forms (modification 1 and 2) of isotactic poly(1-pentene) are reported. Several absorption bands characteristic of the two modifications have been detected and attributed to the helical conformation of the polymer chains. The differences between the two modifications are reproducible, thus enabling their identification from i.r. spectroscopy. The infra-red spectra of isotactic poly(4-methyl-1-pentene) is also reported, and compared with that of the atactic polymer. General assignment of absorption bands is presented.

INTRODUCTION

The i.r. spectra of several hydrocarbons and polymers have been studied extensively. Much of this work has been concerned with establishing and determining the origin of characteristic group frequencies. These data have been summarized and critically reviewed by several investigators¹⁻⁵.

In previous publications on the i.r. spectra of polyolefins, e.g. polyethylene⁶⁻⁷, isotactic polypropylene (IPP)⁸⁻¹², syndiotactic polypropylene^{13,14}, and isotactic poly(1-butene) (IPB)¹⁵⁻¹⁹, assignments for the principal vibrations were reported. The correlations of the i.r. spectra with crystallinity and stereoregularity of IPB, were studied by Nishioka and Yanagisawa²⁰. Their studies showed that certain absorption bands are related to the crystallinity, while others were not assigned because of the complexity of the molecule. In the case of isotactic and atactic polypropylene, Luongo²¹ obtained an analytical curve for determining atactic or isotactic content in a polypropylene sample from i.r.

The present investigation considers a general assignment of the i.r. absorption bands of isotactic poly(1-pentene) (IPP-1), isotactic poly(4-methyl-1-pentene) (IPMP), and atactic poly(4-methyl-1-pentene) (APMP), including the correlation of certain bands to crystallinity and tacticity, which depend upon the thermal history and stereoregularity of the samples.

EXPERIMENTAL

The samples selected for this study were: (a) a highly isotactic poly(1-pentene) obtained from Montedison Company, Italy through the courtesy of Dr G. Gianotti; (b) a highly isotactic poly(4-methyl-1-pentene) obtained from Imperial Chemical Industries Ltd, England; (c) atactic poly(4-methyl-1-pentene), extracted from a commercial sample from Poly-science, and (d) mixtures of 100/0, 75/25, 50/50, 25/75, 0/100, by wt of IPMP/APMP, prepared by dissolution in cyclohexane at 60°C with subsequent recovery by freeze-drying.

Films of modification 1 of IPP-1 were obtained by refluxing films of modification 2 in absolute ethanol overnight and subsequently dried in a vacuum oven at 50°C for 12 h²².

* From the thesis submitted by S. M. Gabbay in partial fulfillment of the requirements for the degree of Doctor of Philosophy, Stevens Institute of Technology, 1975.

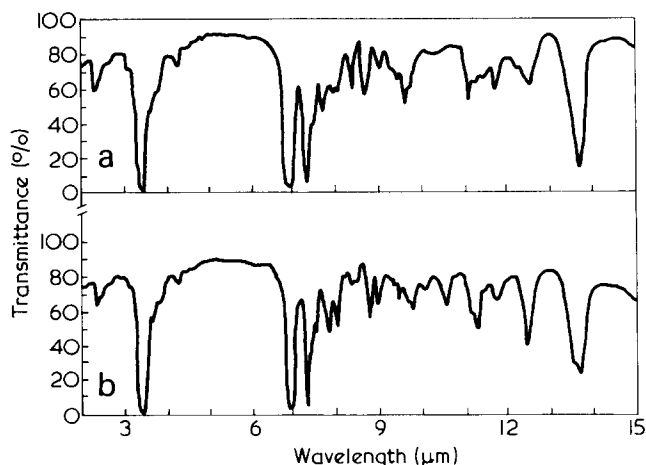


Figure 1 (a) i.r. spectrum of IPP-1 modification 1; (b) i.r. spectrum of IPP-1 modification 2

The identity of these samples (modification 1 and 2), was established by reference to their crystalline melting temperature¹⁵. Uniform and clear films of the above samples of approximately 2–2.5 mils thickness were prepared following the procedure described in an earlier publication²².

All spectra were recorded on a Perkin Elmer Model 21 infra-red spectrophotometer equipped with NaCl prism.

RESULTS AND DISCUSSION

Poly(1-pentene)

Significant differences in the characteristic i.r. spectra were detected between 7.0 to 14.0 μm of the two polymorphous forms (modification 1 and 2), in Figure 1. Of particular note in Figure 1a, the bands at 7.73, 8.40, 9.65, 11.15 μm appear to be specific to modification 1. The modification 2 spectra shown in Figure 1b does not contain these bands, but does show others, e.g. 7.37 (shoulder), 7.42 (shoulder), 7.52, 7.80, 7.85, 8.02, 9.80, 10.07, 10.60, 11.32, and 13.55 μm (shoulder), which distinguishes it from modification 1. The appearance of these characteristic bands confirms the reproducibility of the method of preparation of modification 1, and it is possible to identify which modification of IPP-1 is present from the i.r. spectra of the sample. These spectral differences reflect variation in helical chain conformation between the two modifications and not their isotacticity nor any new chemical groups. In fact, Turner-Jones and Aizlewood²³ reported that both polymorphous forms have

distinct X-ray crystal structure and the chain conformations are 3, and 4, helix for modification 1 and 2, respectively.

Grant and Ward¹⁴, used a simplified approach in assigning absorption bands in isotactic and syndiotactic polypropylene. Their work was examined in this study, in light of the applicability of their simplified approach in assigning absorption bands for the case of poly(1-pentene) and to search for a trend among polyolefins existing in two modifications. The close agreement that they obtained between the ratios of the calculated and observed number of modes of vibrations in the i.r. spectra would seem to render their method acceptable. Briefly, the number of fundamental vibrations for a repeat unit of a polymer helix, is calculated from the selection rules ($3N - 4$) where N is the number of atoms in one complete turn of the helix. These selection rules, which yields the maximum number of calculated fundamental absorption bands, were derived from a simplified model of a single polymer molecule by Liang *et al.*²⁴.

In modification 1 and 2 of IPP-1 there are three and four monomer units respectively, in one complete turn of the

helix²³. Thus, by applying the same selection rules and comparing the ratios of the calculated and observed number of modes of vibrations in the i.r. spectra, a satisfactory agreement was obtained. Additionally, by examining the i.r. spectra of the two polymorphous forms of IPB reported by Calpitt and Hughes¹⁷ and by applying the same selection rules, we also found a satisfactory agreement. These results are presented in *Table 1*. It is reasonable to presume therefore that there is a certain trend among polyolefins assuming different helical chain conformations in two polymorphous forms. Finally, by following these selection rules together with band assignments from the literature of similar polymers it was possible to make a tentative assignment of most of the absorption bands of IPP-1, listed in *Table 2*. No practical assignment of bands was given to modification 2 since they closely correspond to the bands in modification 1.

Poly(4-methyl-1-pentene)

Natta *et al.*²⁵ indicated that, the 'isotactic' synthesis ensures that the side groups in a polymer are sterically all in

Table 1 Comparison between observed and calculated ratios of i.r. bands of IPB and IPP-1

Polymer	Repeating Unit	Form	No of monomer per turn	Observed no of bands	Calculated no of bands	Observed ratio	Calculated ratio
IPB	$\begin{array}{c} -\text{CH}_2-\text{CH}- \\ \\ \text{CH}_2 \\ \\ \text{CH}_3 \end{array}$	1	3	17	104	0.77	0.74
		2	4	22	140		
IPP-1	$\begin{array}{c} -\text{CH}_2-\text{CH}- \\ \\ \text{CH}_2 \\ \\ \text{CH}_2 \\ \\ \text{CH}_3 \end{array}$	1	3	20	131	0.77	0.74
		2	4	26	176		

Table 2 Characteristics of i.r. absorption bands of poly(1-pentene)

modification 1			modification 2		
Wavelength	Relative intensity	Tentative assignment	Wavelength	Relative intensity	Tentative assignment
7.32	S	$\delta_s(\text{CH}_3)$	7.30	S	--
7.47	s	w(CH ₂)	7.37	s	conformation
7.73	M	conformation	7.42	s	
7.98	W	$\tau(\text{CH}_2)$	7.52	W	
8.09	W	w(CH)	7.80	W	
8.40	M	conformation	7.85	W	
8.75	M	$\delta_a[(\text{CH}_2)_2\text{CH}_3]$	8.02	M	conformation
9.05	M	$\rho(\text{CH}_3)$	8.23	W	
9.35	s	$\nu_s(\text{CC})$	8.35	W	conformation
9.48	W	$\tau(\text{CH}_2)$	8.45	s	
9.65	M	conformation	8.77	M	conformation
10.40	W	$\rho(\text{CH}_3)$	8.82	s	
10.92	W		9.00	M	
11.15	M	conformation	9.35	W	conformation
11.35	s	$\rho(\text{CH}_2)$	9.45	M	
11.50	W		9.65	s	
11.75	M	$\nu(\text{CC})$	9.80	M	conformation
12.25	s	$\rho(\text{CH}_2)$	10.07	W	
12.52	M	$\nu_a(\text{CC})$	10.60	M	conformation
13.70	S	$\rho[(\text{CH}_2)_2\text{CH}_3]$	11.20	s	
			11.32	M	conformation
			11.50	s	--
			11.75	M	--
			12.45	S	--
			13.55	s	conformation
			13.70	S	--

δ , bending; w, wagging; ν , stretching; τ , twisting; ρ , rocking; S, strong; M, medium; W, weak; s, shoulder. Subscripts: a, asymmetric; s, symmetric

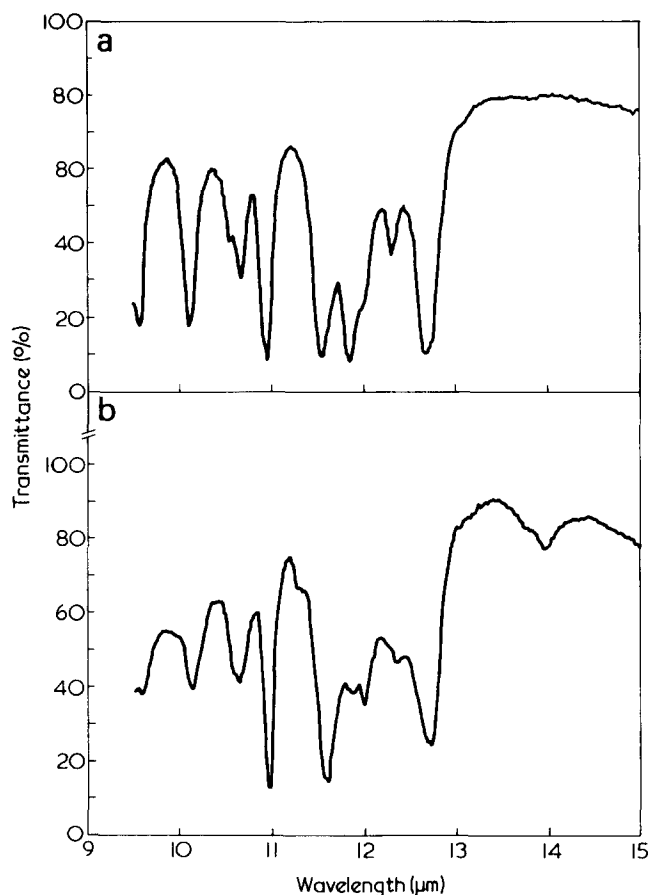


Figure 2 I.r. spectrum of poly(4-methyl-1-pentene) (a) isotactic (b) atactic

the same orientation, i.e. they are either all in a right-handed or all in a left-handed position with respect to the carbon atom in the chain. Because of this regularity of the side groups, an isotactic polymer can be obtained in crystalline

form in contrast to the so-called atactic polymer where the steric positions of the side groups are in an irregular sequence and thus is completely amorphous. Therefore, IPMP has been assumed to be fully crystalline whereas the APMP is considered to be fully amorphous. In fact, its amorphicity was established by X-ray diffraction. Significant differences in the characteristics of the i.r. spectra were noted between 10.0 to 14.50 μm of isotactic and atactic poly(4-methyl-1-pentene), in Figure 2. The wavelengths of the absorption bands with indications of their intensity and tentative assignment are listed in Table 3. As can be seen in Figure 2a, the absorption bands in the IPMP spectrum at 10.55 (shoulder), 11.85, and 12.35 μm, either are extremely weak or eliminated in the spectrum of APMP. The 10.70 μm band with a shoulder at 10.55 μm in IPMP becomes a broad band at 10.70 μm in APMP. The 11.55 μm strong band in IPMP is shifted to 11.60 μm in APMP with a shoulder at 11.30 μm. The sharp band at 12.00 μm, in APMP becomes a shoulder in IPMP and the band 13.95 μm, in APMP is completely absent in IPMP. This indicates that these bands are sensitive to tacticity, however, the 11.85 μm and 12.35 μm bands in IPMP were also found to be sensitive to crystallinity. This conclusion was based on the fact that, in the i.r. spectra of molten IPMP (recorded at 245°C under nitrogen) only these two bands disappeared completely (see Figure 3) and reappeared when the polymer was brought back to room temperature. Film samples containing 100, 75, 25, and 0% (w/w) APMP, were subjected to i.r. analysis. The 11.85 μm absorbance band gradually diminishes from the 0 to 100% atactic sample, while the 13.95 μm absorbance band gradually increases from 100 to 0% atactic sample. Since the 11.85 μm band has disappeared in the molten state (see Figure 3) of IPMP and significantly diminished in APMP at 25°C, it would thus appear that this band shows that isotactic content and crystallinity are closely related. An 11.85 μm band in the case of polypropylene was also correlated to crystallinity by Heinen²⁶.

Table 3 Characteristics of i.r. absorption bands of poly(4-methyl-1-pentene)

Wavelength	Relative intensity	Tentative assignment	Wavelength	Relative intensity	Tentative assignment
3.35	S	$\nu_a(\text{CH}_3)$	7.92	M	$\omega(\text{CH})$
3.43	S	$\nu_a(\text{CH}_2)$	8.17	W	$\omega(\text{CH})$
3.48	S	$\nu_s(\text{CH}_3)$	8.46	M	—
3.60	M	$\nu_s(\text{CH}_2)$	8.61	S	$\delta_a[\text{CH}(\text{CH}_3)_2]$
3.80	M	$\nu_s(\text{CH})$	8.67	s	$\omega(\text{CH}_3)$
6.85	S	$\delta_a(\text{CH}_3)$	8.75	s	
6.95	S	$\delta_a(\text{CH}_2)$	8.86	M	$\nu_s(\text{CC})$
7.25	S	$\delta_s[\text{CH}(\text{CH}_3)_2]$	9.14	M	$\rho(\text{CH}_3)$
7.35	S	$\delta(\text{CH})$	9.45	s	$\tau(\text{CH}_2)$
7.50	M	$\omega(\text{CH}_2)$	9.57	W	
7.73	M	$\tau(\text{CH}_2)$	10.15	M	$\rho(\text{CH}_3)$
IPMP			APMP		
10.55	s	Tacticity	—	—	—
10.70	M	$\delta(\text{CH})$	10.70	M	$\delta(\text{CH})$
10.97	S	$\rho(\text{CH}_3)$	10.97	S	$\rho(\text{CH}_3)$
11.55	S	$\rho(\text{CH}_2)$	11.30	s	Tacticity
11.85	S	Tacticity (Crystallinity)	11.60	S	—
12.00	s	—	11.85	W	—
12.35	M	Tacticity (Crystallinity)	12.00	M	Tacticity
12.70	S	$\nu_a(\text{CC})$	12.35	W	—
			12.70	S	$\nu_a(\text{CC})$
			13.95	S	Tacticity

δ , bending; ω , wagging; ν , stretching; τ , twisting; ρ , rocking; S, strong; M, medium; W, weak; s, shoulder. Subscripts: a, asymmetric; s, symmetric

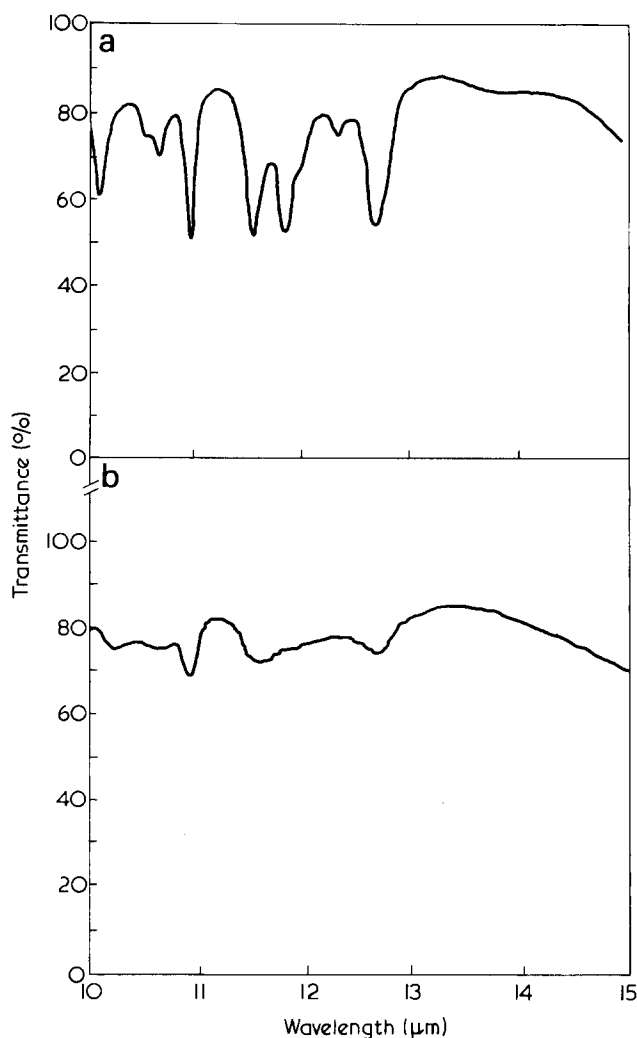


Figure 3 I.r. spectrum of IPMP (a) at 25°C (b) in molten state

REFERENCES

- 1 Bellamy, L. J. 'The Infrared Spectra of Complex Molecules', Wiley, New York, 1958
- 2 Brügel, 'Einführung in Die Ultrarotspectroskopie', Steinkopff, Darmstadt, 1954
- 3 Colthup, N. B. *J. Opt. Soc. Am.* 1950, **40**, 397
- 4 Conley, R. T. 'Infrared Spectroscopy', Allyn and Bacon, Boston, 1966
- 5 Zbinden, R. 'Infrared Spectroscopy of High Polymers', Academic Press, New York, 1964
- 6 Krimm, S., Liang, C. Y. and Sutherland, G. B. B. M. *J. Chem. Phys.* 1956, **25**, 549
- 7 Snyder, R. G. *J. Chem. Phys.* 1967, **47**, 1316
- 8 Krimm, S. *Adv. Polym. Sci.* 1960, **2**, 51
- 9 Tobin, M. C. *J. Phys. Chem.* 1960, **64**, 216
- 10 Liang, C. Y., Lytton, M. R. and Boone, C. J. *J. Polym. Sci.* 1961, **54**, 523
- 11 Miyazawa, T. and Ideguchi, Y. *Bull. Chem. Soc. Japan* 1964, **37**, 1065
- 12 Snyder, R. G. and Schatschneider, J. H. *Spectrochim. Acta*, 1964, **20**, 853
- 13 Peraldo, M. and Cambini, M. *Spectrochim. Acta* 1965, **21**, 1509
- 14 Grant, I. J. and Ward, I. M. *Polymer* 1965, **6**, 223
- 15 Natta, G. *Angew. Makromol. Chem.* 1960, **35**, 94
- 16 Yasuda and Takayanagi, M. *Progr. Polym. Sci. Japan* 1964, **7**, 245
- 17 Clampitt, B. H. and Hughes, R. H. *J. Polym. Sci. (C)* 1964, **6**, 43
- 18 Luongo, J. P. and Salovey, R. *J. Polym. Sci. (B)* 1965, **3**, 513
- 19 Ukita, M. *Bull. Chem. Soc. Japan* 1966, **39**, 742
- 20 Nishioka, T. and Yanagisawa, K. *Kobunshi Kagaku* 1962, **19**, 671
- 21 Luongo, J. P. *J. Appl. Polym. Sci.* 1960, **3**, 302
- 22 Gabbay, S. M., Stivala, S. S. and Reich, L. *Polymer* 1975, **16**, 749
- 23 Turner-Jones, A. and Aizlewood, J. M. *J. Polym. Sci. (B)* 1963, **1**, 471
- 24 Liang, C. Y., Krimm, S. and Sutherland, G. B. B. M. *J. Chem. Phys.* 1956, **25**, 543
- 25 Natta, G., Pino, P., Mazzanti, G., Corradini, P. and Giannini, U. *Atti Accad. Naz. Lincei.* 1955, **19**, 397
- 26 Heinen, W. *J. Polym. Sci.* 1959, **38**, 545

Interpretation of broad line nuclear magnetic resonance in oriented poly(ethylene terephthalate)

A. Cunningham*, A. J. Manuel and I. M. Ward

Department of Physics, University of Leeds, Leeds LS2 9JT, UK

(Received 23 July 1975; revised 15 September 1975)

Broad line nuclear magnetic resonance measurements on oriented poly(ethylene terephthalate) sheets have been reconsidered, in the light of recent infra-red data on similar materials. It is shown that the n.m.r. anisotropy is consistent with a model for the molecular orientation, in which the fraction of the polymer in the *trans* conformation is highly oriented, whereas the *gauche* fraction is sensibly isotropic.

INTRODUCTION

In a recent publication¹, polarized infra-red spectroscopy was used to study the changes in molecular orientation and conformation which occur in drawing poly(ethylene terephthalate) (PET) sheets. Detailed information was obtained, concerning both the development of overall orientation and the changes in molecular conformation in the glycol residue; the *trans/gauche* conformations. It was found that drawing decreased the proportion of *gauche* conformations at the expense of *trans*, and moreover, that the remaining *gauche* conformations remained sensibly unoriented, as overall molecular orientation increased with drawing.

In a previous publication we have attempted to use broad line nuclear magnetic resonance (n.m.r.) measurements and optical anisotropy to characterize the molecular orientation in PET². This investigation remained incomplete, however, partly because of the intrinsic difficulties in using the n.m.r. method to deal with orthorhombic symmetry, and partly because the *trans/gauche* content of the sheets was not known. In the present paper, we will now examine these earlier n.m.r. results and show that they provide excellent support for the conclusions made on the basis of the infra-red data, regarding the development of molecular orientation in drawn PET films.

NUCLEAR MAGNETIC RESONANCE

In the study of anisotropic materials by nuclear magnetic resonance (n.m.r.), the second moment $\langle \Delta H^2 \rangle$ of the absorption line, is measured for different orientations of the applied magnetic field with respect to the symmetry axes of the specimen. In PET film², we take a set of orthogonal axes with the *z* axis in the draw direction, the *x* axis in the plane of the film and the *y* axis normal to the plane of the film. The direction of the magnetic field *H*, may then be specified by the polar angle γ , between the direction of *H* and the *z* axis, and the azimuthal angle ϕ_γ between the *x* axis and the plane containing *H* and the *z* axis (Figure 1). The value of $\langle \Delta H^2 \rangle$ for a given direction of *H*, depends on a combination of a set of numbers S_{lm} (the lattice sums), characteristic of the structural units, and an orientation

distribution function for the structural units. For an anisotropic structural unit, a set of orthogonal axes *uvw* may be defined and their orientation with respect to the specimen axes (*x, y, z*) may be related through the Euler angles (ϕ, θ, ψ), as shown in Figure 1. The orientation distribution of the structural units may then be represented by a function $\rho(\phi, \theta, \psi)$, where $\rho(\phi, \theta, \psi)d\phi d\theta d\psi$ represents the volume fraction of structural units with Euler angles in the range ϕ to $\phi + d\phi, \theta$ to $\theta + d\theta$ and ψ to $\psi + d\psi$. Knowledge of the lattice sums for the structural units and the orientation functions $\rho(\phi, \theta, \psi)$ permits the calculation of $\langle \Delta H^2 \rangle$ as a function of γ and ϕ_γ . To carry out the inverse procedure and obtain information about the orientation distribution of the structural units from the measured variation of $\langle \Delta H^2 \rangle$ with γ and ϕ_γ and the calculated lattice sums, it is necessary to expand $\rho(\phi, \theta, \psi)$ in a suitable set of orthogonal functions and solve the relevant equations for the coefficients of the expansion. This can only be done for certain symmetry conditions or simplifying assumptions. These are discussed in ref. 2, where for PET films of low draw ratio (2:1 and 2.5:1) and for drawn rods, the structural units are taken as small aggregates of crystalline and amorphous material, with the chain axes (crystalline *c* axis), in both the crystalline and amorphous regions, lying along the *w* axis of Figure 1, but with no preferred orientation.

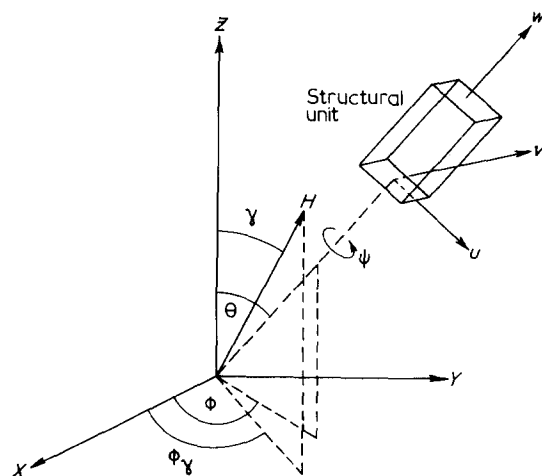


Figure 1 The relationship of the axes (*u, v, w*) of a structural unit to the symmetry axes *x, y, z* of a specimen of drawn material through the Euler angles (ϕ, θ, ψ) and the definitions of the angles γ and ϕ_γ specifying the direction of the magnetic field *H* with respect to the specimen axes

* Present address: ICI Corporate Laboratory, Runcorn, Cheshire WA7 4QE

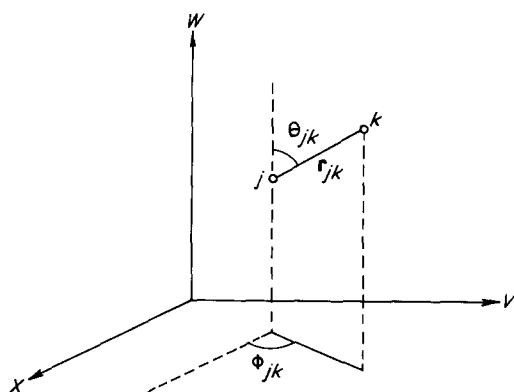


Figure 2 The vector r_{jk} and the angles θ_{jk} and ϕ_{jk} for the protons j and k of a structural unit for the calculation of the lattice sums

tation of the u and v axes about w . This means that for the low draw ratio films it is permissible to take the orientation distribution function $\rho(\phi, \theta, \psi)$ as independent of ψ , and it can be reduced to the form $\rho(\theta, \phi)$, where θ and ϕ are the polar and azimuthal angles specifying the w (crystalline) axis of the transversely isotropic aggregate, with respect to the specimen axis. This situation corresponds to case (ii) a ref. 2, for which the following equations are valid:

$$\rho(\theta, \phi) = \sum_{l=0}^{\infty} \sum_{m=0}^l 2\pi \left(\frac{4\pi}{2l+1} \right)^{1/2} \rho_{lm0} Y_{lm}^e(\theta, \phi) \quad (1)$$

$$B_{lm} = 4G \frac{4\pi a_l}{2l+1} \frac{8\pi^2}{2l+1} S_{l0} \rho_{lm0} \quad (2)$$

$$\langle \Delta H^2 \rangle = \sum_{l=0, 2, 4} \sum_{m=0}^l B_{lm} Y_{lm}^e(\gamma, \phi_\gamma) \quad (3)$$

$G = 3/2 [I(I+1)g^2\mu_n^2]$ where I is the nuclear spin quantum number, g the nuclear g factor and μ_n the nuclear magneton and $a_0 = 1/5$, $a_2 = 2/7$ and $a_4 = 18/35$. These equations correspond to equations (18)–(20) of ref. 2 but are written here with the real form of spherical harmonics. The factor of 2π appearing in equation (1) should also be present in equation (18) of ref. 2. It arises, because in going from $\rho(\theta, \phi, \psi)$ to $\rho(\theta, \phi)$, there is an effective integration over ψ . For a similar reason the right hand side of equation (15) of ref. 2 should be multiplied by $4\pi^2$. The lattice sums S_{l0} are determined from the general form S_{lm} given by:

$$S_{lm} = \frac{1}{N} \sum_{j>k} r_{jk}^{-6} Y_{lm}^e(\theta_{jk}, \phi_{jk}) \quad (4)$$

corresponding to equation (8) of ref. 2.

$$S_{l0} = \frac{1}{N} \sum_{j>k} r_{jk}^{-6} \left[\frac{2l+1}{4\pi} \right]^{1/2} P_l(\cos \theta_{jk}) \quad (5)$$

r_{jk} is the internuclear vector between protons j and k of a structural unit and θ_{jk} the angle between r_{jk} and the w axis of the structural unit. This is illustrated in Figure 2. For the case of a drawn rod having transverse isotropy, the dependence of $\langle \Delta H^2 \rangle$ on ϕ_γ vanishes and equations (1)–(3) are simplified.

The six coefficients B_{lm} for $l = 0, 2, 4$, are determined from the experimental measurements of $\langle \Delta H^2 \rangle$ for various γ and ϕ_γ , through equation (3), by a least squares fitting procedure. Values for ρ_{lm} for $l = 0, 2, 4$ may then be obtained from equation (2), using calculated values for S_{l0} . The lattice sums are intrinsic properties of the structural units and were calculated, in ref. 2, for the *trans* conformation which exists in the crystalline regions of PET. They are reproduced in Table 1. The calculations are based on the crystal structure determination of Daubeny, Bunn and Brown³. The intramolecular contributions to the lattice sums which are shown separately in Table 1, can be seen to be of major importance, and for S_{20} and S_{40} , which determine the anisotropic n.m.r. behaviour, they are dominant. It can therefore be inferred that for molecules in an amorphous environment, the lattice sums will also be dominated by the intramolecular interactions. We must in this case, however, also consider the effect of the *gauche* conformations.

It is now generally accepted that the *gauche* conformation arises from a rotation within the glycol group^{4,5}. Figure 3 shows a projection of the glycol group along the methylene C–C bond, in both the *trans* and in a hypothetical *gauche* conformation which is produced from the *trans* conformation by a rotation about the C1–C1' methylene bond; with the further assumption that the C1–O2 bond length remains constant (i.e. C1'–O2' bond length = C1–O2 bond length). The coordinates of this molecule are listed in Table 2, and the projections of the molecular positions on the xz plane are shown in Figure 4.

Although these coordinates are not expected to be very accurate numerically, it is reasonable to assume that the qualitative anisotropy of the resultant intramolecular *gauche* lattice sums, is correct. The values for these lattice sums are given in Table 1, together with the differences between the intramolecular contributions to S_{00} , S_{20} and S_{40} for the *trans* and *gauche* conformations. There is little difference between the values of S_{00} but S_{20} and S_{40} are of opposite sign for the two conformations. This difference is not dependent on the exact form of the *gauche* molecule as can be seen by comparing the contributions to S_{00} , S_{20} and S_{40} of the four protons in the glycol group in the *trans* and *gauche* conformations, which are also given in Table 1.

Table 1 Total lattice sums for *trans* and *gauche* conformations in PET and contributions from intramolecular interactions

	S_{00}	S_{20}	S_{40}
1 Total S_{l0} for transversely isotropic structural units in <i>trans</i> configuration	+0.00424	–0.00227	+0.00276
2 Intramolecular contribution to S_{l0} in <i>trans</i> configuration	+0.00303	–0.00206	+0.00315
3 Intramolecular contribution to S_{l0} in <i>gauche</i> configuration	+0.00325	+0.00202	–0.00177
4 Difference (3 – 2)	+0.00022	+0.00408	+0.00492
5 Contribution to S_{l0} for four methylene protons in <i>trans</i> configuration	+0.00260	–0.00281	+0.00262
6 Contribution to S_{l0} for four methylene protons in <i>gauche</i> configuration	+0.00274	+0.00123	–0.00226
7 Difference 6 – 5	+0.00014	+0.00404	+0.00488

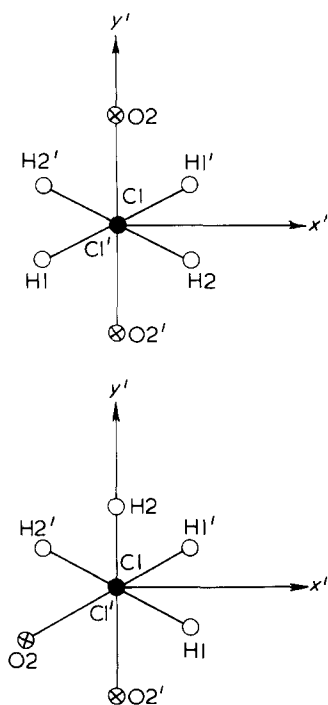


Figure 3 Projection of the glycol group in PET along the methylene C-C bond in (a) *trans* (b) *gauche* conformation

OPTICAL ANISOTROPY

The principal refractive indices n_q for an oriented sample can be related to the average molecular polarizabilities $\langle\alpha_{qq}\rangle$ by the Lorentz-Lorenz equation:

$$\frac{n_q^2 - 1}{n_q^2 + 2} = \frac{4\pi}{3} N \langle\alpha_{qq}\rangle \quad (6)$$

where, N is the number of polarizable units per unit volume. If, for a transversely isotropic structural unit, the principal polarizabilities are represented by α_{33} , along the axis of a symmetry and α_{tt} , in the transverse directions, then it has been shown² that for a transversely isotropic distribution of the structural units:

$$\begin{aligned} \langle\alpha_{11}\rangle &= \langle\sin^2\theta \cos^2\phi\rangle (\alpha_{33} - \alpha_{tt}) + \alpha_{tt} \\ \langle\alpha_{22}\rangle &= \langle\sin^2\theta \sin^2\phi\rangle (\alpha_{33} - \alpha_{tt}) + \alpha_{tt} \\ \langle\alpha_{33}\rangle &= \frac{2}{3} \langle P_2(\cos\theta)\rangle (\alpha_{33} - \alpha_{tt}) + \frac{1}{3} (\alpha_{33} + 2\alpha_{tt}) \end{aligned} \quad (7)$$

These equations correspond to equation (30) of ref. 2, reduced to the case of a transversely isotropic distribution of structural units. The α_{33} and α_{tt} are seen to depend only on the intrinsic molecular state and not on the overall orientation, and for the optical measurements have the same significance as the lattice sums in n.m.r.

The values of the principal polarizabilities, α_{11} , α_{22} and α_{33} for the *trans* and *gauche* configurations of molecules, are now calculated by the addition of bond polarizabilities as discussed in ref. 2. They yield the values shown in Table 3 from which $\alpha_{tt} = \frac{1}{2}(\alpha_{11} + \alpha_{22})$ can be calculated. The results in Table 3 show that the values of α_{33} and α_{tt} for the *trans* and *gauche* conformations, are essentially identical and hence the overall optical anisotropy cannot be sensitive to the *trans/gauche* ratio or to changes in that ratio.

It is therefore to be expected, that the optical anisotropy of PET should be primarily a function of the overall chain axis orientation. This conclusion was confirmed directly by the infra-red spectroscopic studies¹, where it was shown that there is an excellent correlation between the orientation function derived from birefringence and from absorption assigned to benzene ring mode vibrations. For these calculations of $\langle P_2(\cos\theta)\rangle^{\text{overall}}$, the procedure followed has been described in the previous publications^{1,2}. It is recognised that the calculated values for bond polarizabilities can be in error by a small amount ($\sim 2-3\%$). The value of α_{33} was therefore adjusted to a value of $2.3 \times 10^{-23} \text{ cm}^3$ to be consistent with values obtained from birefringence measurements on drawn samples of PET. No alteration was required in the values of α_{tt} , but an average value of $1.70 \times 10^{-23} \text{ cm}^3$ was assumed. These values of α_{33} and α_{tt} lead to the value of 0.105 for $\Delta\alpha/3\alpha_0$ used in ref. 1.

In contrast to the optical situation, the n.m.r. lattice sums S_{20} and S_{40} , are extremely sensitive to the conformation of the molecule, being of opposite signs for the *trans* and *gauche* cases and their contributions to the second mo-

Table 2 Atomic coordinates in *trans* and *gauche* conformations of PET molecule

Atom	$\delta(3^\circ)$ (Å)	y (Å)	x (Å)
(a) <i>trans</i> conformation coordinates			
H1	+0.284	+0.160	-1.481
H2	+0.127	+1.483	-0.292
H2'	-0.127	-1.483	+0.292
H1'	-0.284	-0.160	+1.481
H3	+3.514	-0.228	+1.546
H4	+4.974	+0.498	-2.354
H3'	+7.236	+0.228	-1.546
H4'	+5.776	-0.498	+2.354
O2	+1.770	+0.209	+0.000
O	+2.402	+0.845	-2.100
C1	+0.408	+0.435	-0.430
C1'	-0.408	-0.435	+0.430
C2	+2.707	+0.541	-0.916
C3	+4.057	+0.233	-0.395
C4	+4.345	-0.105	+0.860
C5	+5.131	+0.297	-1.300
C2'	+8.043	-0.541	+0.916
O2'	+8.980	-0.209	+0.000
O'	+8.348	-0.845	+2.100
C1''	+10.342	-0.435	+0.430
C4'	+6.405	+0.105	-0.860
C5'	+5.619	-0.297	+1.300
C3'	+6.693	-0.233	+0.395
(b) <i>gauche</i> conformation coordinates (Model)			
H1	-0.213	+0.400	-1.355
H2	+0.901	-0.953	-1.666
H1'	-1.195	-1.726	-0.607
H2'	+0.212	-2.006	+0.445
H3	+3.126	-0.228	+1.546
H4	+4.586	+0.498	-2.354
H3'	+6.848	+0.228	-1.546
H4'	+5.388	+0.498	+2.354
O2	+1.381	+0.209	+0.000
O	+2.014	+0.845	-2.100
C1	+0.408	-0.368	-0.885
C1'	-0.408	-1.239	-0.024
C2	+2.318	+0.541	-0.916
C3	+3.668	+0.233	-0.395
C4	+3.956	-0.105	+0.860
C5	+4.742	+0.297	-1.300
C2'	+7.655	-0.541	+0.916
O2'	+8.993	-0.353	+0.951
O'	+7.959	-0.845	+2.100
C1''	+9.565	-1.239	-0.024

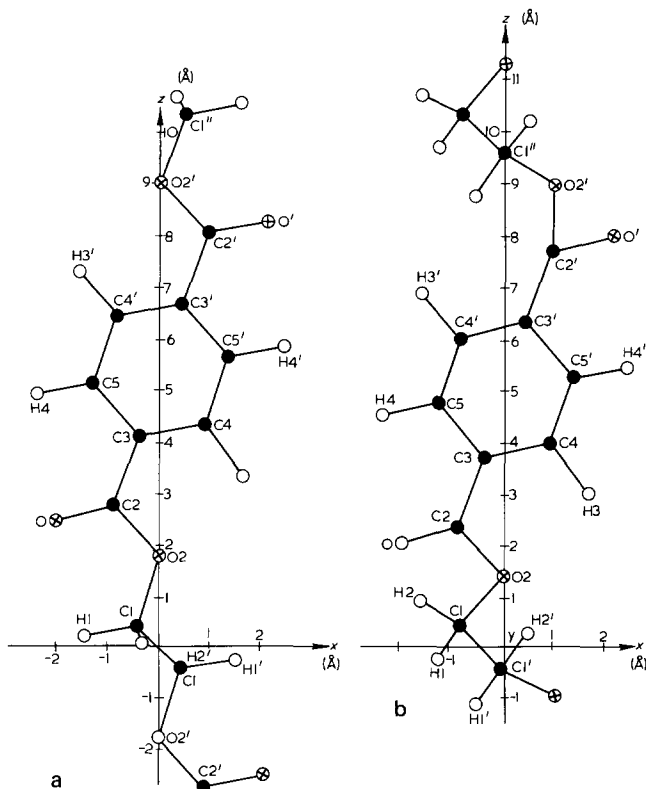


Figure 4 Projection of the atomic position of the atoms in the PET molecule on the xz plane in the (a) *trans* (b) *gauche* conformation. ●, carbon; ⊕, oxygen; ○, hydrogen. The monomer repeat distances are 10.75 Å for the *trans* and 9.97 Å for the *gauche* configuration

ment anisotropy act in opposition to each other. Because of this, although the wide line n.m.r. technique cannot on its own determine the *trans/gauche* ratio or the orientation distribution, the extreme sensitivity of S_{20} and S_{40} to the configuration can be used to examine the validity of the model for the structure of oriented PET films put forward in ref. 2.

If we consider a model comprising a fraction f of *trans* molecules with orientation characterized by coefficients ρ_{100}^t and $(1-f)$ of *gauche* molecules with orientation coefficients ρ_{100}^g , and we assume that the contributions to the overall second moment are additive we should find:

$$\rho_{100}(\text{experimental}) = f\rho_{100}^t + (1-f)\rho_{100}^g \quad (8)$$

for ρ_{200} this leads, using equation (2), to:

$$\frac{B_{20}}{a_2} = 4G \left(\frac{4\pi}{5}\right) \left(\frac{8\pi^2}{5}\right) [fS_{20}^t\rho_{200}^t + (1-f)S_{20}^g\rho_{200}^g] \quad (9)$$

where S_{20}^t and S_{20}^g are the relevant lattice sums for the *trans* and *gauche* materials.

A value of B_{20} for the proposed model² specifying f , ρ_{200}^t and ρ_{200}^g can thus be calculated and compared with the value obtained from n.m.r. measurements through equation (1).

The detailed analysis of the infra-red spectra described in ref. 1, resulted in considerable information on the molecular state of oriented PET. It was shown that to a good approximation, the *gauche* molecular distribution could be taken as isotropic over the range of molecular orientations and drawing conditions investigated.

This result will now be used to predict the overall n.m.r. response (as reflected through B_{20}) for such oriented polymers.

For isotropic *gauche* material we have $\rho_{200}^g = 0$. Equation (8) now becomes:

$$\frac{B_{20}}{a_2} (\text{proposed}) = 4G \left(\frac{4\pi}{5}\right) \left(\frac{8\pi^2}{5}\right) fS_{20}^t\rho_{200}^t \quad (10)$$

Let the average value of the coefficient of $P_2(\cos\theta)$ for the molecular orientation function of the *trans* material be $\langle P_2(\cos\theta) \rangle^t$. Then $\langle P_2(\cos\theta) \rangle^{\text{overall}} = f\langle P_2(\cos\theta) \rangle^t$

$$= f\rho_{200}^t \left(\frac{8\pi^2}{5}\right)$$

Substitution into equation (9) gives:

$$\frac{B_{20}}{a_2} (\text{proposed}) = 4G \left(\frac{4\pi}{5}\right) S_{20}^t \langle P_2(\cos\theta) \rangle^{\text{overall}} \quad (11)$$

This equation is valid for films with orthorhombic specimen symmetry, as well as for cylindrically symmetrical rod specimens. It is to be noted that equation (11) is independent of f . If therefore the model is correct, the value of B_{20} determined experimentally from n.m.r. measurements, should be a linear function of the $\langle P_2(\cos\theta) \rangle^{\text{overall}}$ values obtained from refractive index measurements.

For the other extreme situation of isotropic *trans* and oriented *gauche* material, equation (11) would require the use of S_{20}^g instead of S_{20}^t . Remembering that these values are nearly equal in magnitude and opposite in sign this equation becomes a very sensitive test of the proposed model, particularly as the infra-red investigation showed that on average at least 50% of the monomers were in their *gauche* conformation.

RESULTS AND DISCUSSION

The experimental work on the three drawn films of orthorhombic symmetry (draw ratios 2:1, 2.5:1 and 5:1) and the cylindrically symmetrical rod (draw ratio 3.25:1) is described in detail in ref. 2. The results are summarized in Table 4 together with values of $\langle P_2(\cos\theta) \rangle^{\text{overall}}$ and the equivalent isotropic refractive indices \bar{n} calculated from the experimental values of n_1 , n_2 and n_3 . The values of \bar{n} lie close to the experimentally determined refractive index of 1.583 for an isotropic sample of density $\rho = 1.338$. This reflects the insensitivity of the average principal polarizabilities of the monomer units in the transversely isotropic

Table 3 Principal polarizabilities for PET monomers and their average values in transversely isotropic structural unit

	<i>Trans</i> (calc.) (10^{-23} cm ²)	<i>Gauche</i> (calc.) (10^{-23} cm ²)	<i>Trans</i> (exp.) (10^{-23} cm ²)
α_{11}	2.12	2.12	—
α_{22}	1.22	1.26	—
α_{33}	2.22	2.16	—
α_{ff}	1.67	1.69	1.70
α_{33}	2.22	2.16	2.30

Table 4

Draw ratio	Density	n_3	n_2	n_1	\bar{n}	$\langle P_2(\cos \theta) \rangle_{\text{overall}}$	B_{20}/a_2 (exp.)	B_{00}/a_0 (exp.)
2:1	1.349	1.628	1.571	1.548	1.576	0.32	-3.57	+182.3
2.5:1	1.354	1.645	1.566	1.546	1.577	0.40	-4.76	+182.8
3.25:1	1.351	1.679	1.543	1.543	1.588	0.59	-8.48	+196.5
5:1	1.372	1.708	1.580	1.509	1.578	0.70	-7.65	+181.2

exp. isotropic refractive index $n_i = 1.583$, $\rho_i = 1.338$

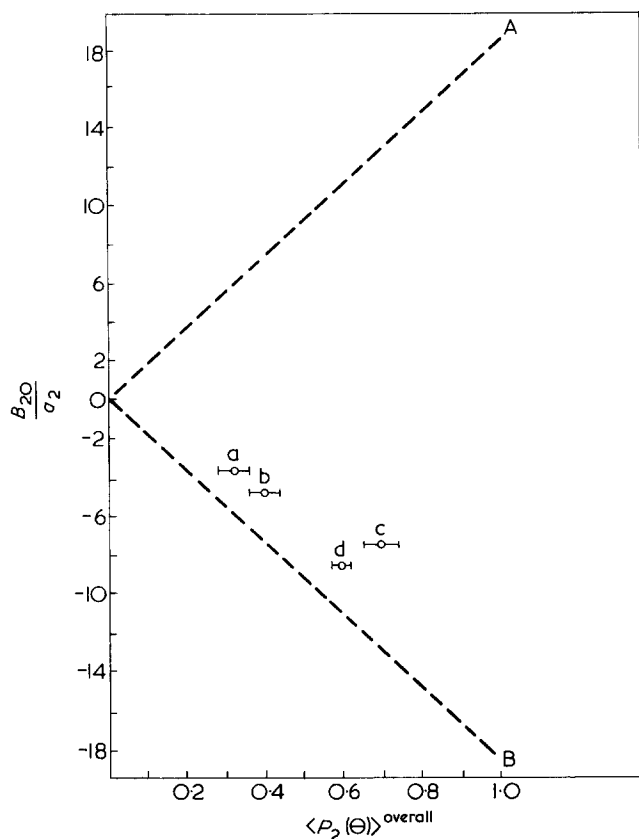


Figure 5 B_{20}/a_2 plotted against $\langle P_2(\cos \theta) \rangle_{\text{overall}}$ from Table 4 together with the theoretical boundaries (A) for wholly *gauche* oriented material. (B) for wholly *trans* oriented material. Draw ratios (a) 2:1; (b) 2.5:1; (c) 5:1 for two way drawn film; (d) 3.25:1 uniaxial drawn rod

structural unit to the conformation, as shown in Table 3. A similar situation, is shown by the experimental value of B_{00}/a_0 of Table 4 which reflects the insensitivity of S_{00} to the conformation (Table 1).

However B_{20}/a_0 in Table 4 shows a behaviour which correlates with $P_2(\cos \theta)_{\text{overall}}$. Figure 5 shows these two quantities plotted against each other, together with the boundaries between which they should lie for the two extreme cases in which the oriented material is wholly *trans* or wholly *gauche*.

The experimental results for the 2:1, 2.5:1 draw ratio film and 3.25:1 draw ratio rod do, in fact, lie close to the line predicted on the assumption of isotropic distribution of *gauche* conformer material, the oriented parts of the specimens being those with the *trans* conformation.

The point in Figure 5 for the 5:1 draw ratio film, shows less good agreement with the points for the other material. This is not surprising since as was shown in ref. 3, there is a distinct preferred orientation distribution of the molecules with respect to the plane of the film. The position of the point in Figure 5 for this specimen does suggest, however, that here also the *gauche* material is sensibly isotropic in molecular orientation distribution.

REFERENCES

- Cunningham, A., Ward, I. M., Willis, H. A. and Zichy, V. *Polymer* 1974, 15, 749
- Kashiwagi, M., Cunningham, A., Manuel, A. J. and Ward, I. M. *Polymer* 1973, 14, 111
- Daubeny, R de P., Bunn, C. W., and Brown, C. J. *Proc. R. Soc. (A)* 1954, 226, 531
- Ward, I. M. *Chem. Ind.* 1956, p. 905
- Grime, D. and Ward, I. M. *Trans. Faraday Soc.* 1958, 54, 959

Ziegler–Natta catalysis: 7. The settling period

D. R. Burfield,* I. D. McKenzie† and P. J. T. Tait

Department of Chemistry, University of Manchester Institute of Science and Technology, Manchester M60 1QD, UK

(Received 24 July 1975; revised 17 October 1975)

Factors affecting the duration of the settling period in the polymerization of 4-methylpentene-1 by the catalyst system $\text{VCl}_3/\text{AlR}_3$ in benzene have been systematically investigated. Plots of $\log_{10}(100 - \%R_p)$ versus time show that the so-called settling period can be divided into two distinct regions; an initial region which is not time dependent and a steady state region in which the formation of C_0 follows a strictly first order time dependence. The initial region is believed to arise from the removal of adsorbed AlR_2Cl species, while the steady state region can be interpreted as describing a rearrangement reaction involving the production of initiated chains.

INTRODUCTION

One of the puzzling features of many Ziegler–Natta polymerization systems, when using catalysts derived from solid transition metal halides and aluminium alkyls, is the initial period during which the rate of polymerization gradually increases to reach either a maximum or a steady state value. This so-called ‘settling period’ has been observed in a large number of systems^{1–5} and is a characteristic feature of these polymerization systems⁶. Typical kinetic curves for these systems are shown in *Figure 1* and can be seen to be divided into either three [as in (a)] or two [as in (b)] parts. Curve (a) shows a settling period I, during which the rate of polymerization increases rapidly to a maximum followed by a decay period, II, when the rate decreases gradually to reach that of the steady state, III. In the case of Curve (b) there is a gradual increase in the rate of polymerization during the settling period, I until the steady state, III is reached directly.

The duration of the settling period appears to be influenced by the majority of the variable parameters in these complex polymerization systems, e.g. monomer and alkyl concentrations, and its cause has been variously interpreted as arising from a number of factors. These factors include the breakdown of catalyst crystals to expose additional active centres², slow initiation by monomer^{4,7}, and the presence of impurities⁸. It is now generally believed, however, that its origin may be more complex.

The present study is concerned with an investigation of the settling period, as observed in the polymerization of 4-methylpentene-1 by the catalyst system $\text{VCl}_3/\text{AlR}_3$ in benzene, and forms part of a detailed study⁷ of the kinetics of Ziegler–Natta polymerization systems, by this highly pure and stable catalyst system.

EXPERIMENTAL

Materials

Details of catalysts have already been published⁷.

* Present address: Department of Chemistry, University of Malaya, Kuala Lumpur, Malaysia.

† Present address: Imperial Chemical Industries Ltd., Plastics Division Welwyn Garden City, Herts, UK

Procedure

All polymerization runs were carried out under high vacuum in specially constructed dilatometers. However, two distinct procedures were employed for the preparation of the catalyst systems.

Method A. The vanadium trichloride addition was followed by the desired amounts of benzene and then alumin-

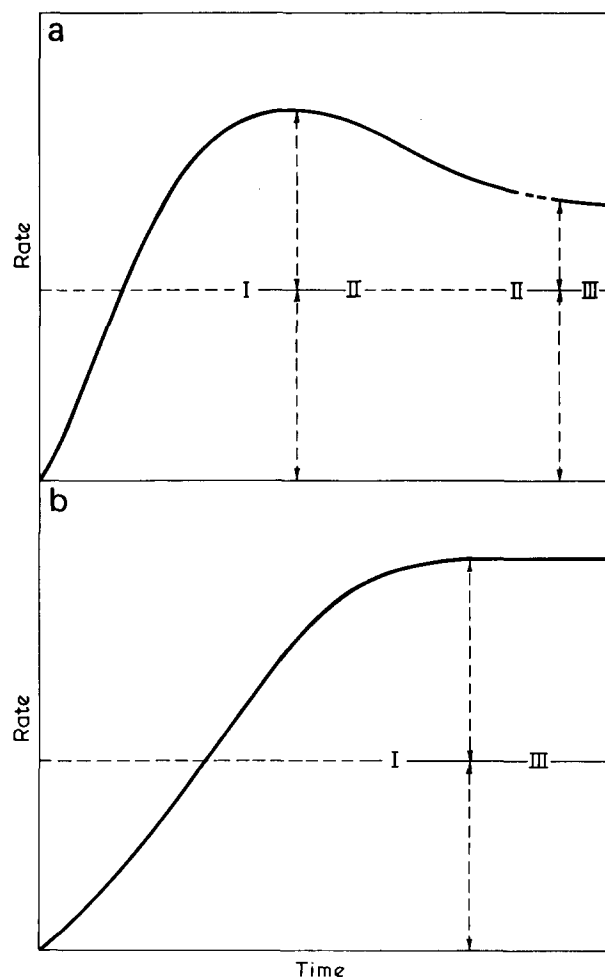


Figure 1 Plots of rate versus time (a) showing decay characteristics; (b) showing steady state characteristics

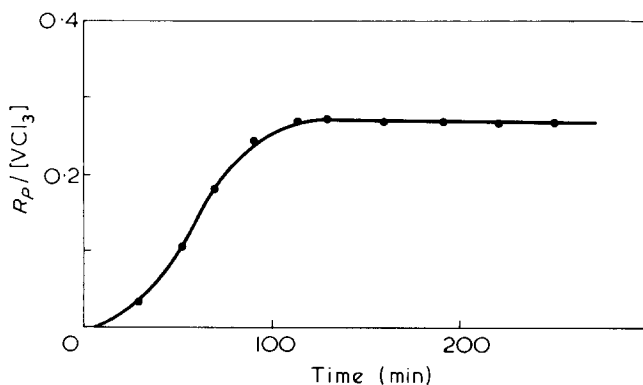


Figure 2 Plot of $R_p/[VCl_3]$ versus time. $[VCl_3] = 18.5$ mmol/l; $[Al(iBu)_3] = 37.0$ mmol/l; $[4-MP-1] = 2.0$ mol/l; solvent = benzene; temperature = $30^\circ C$

ium alkyl in benzene by means of graduated syringes. The dilatometer filler or reaction vessel was then quickly stoppered, removed from the dry box, and attached to the high vacuum system. The contents were degassed twice, and the catalyst 'aged' for 10 and 15 min respectively at $30^\circ C$, before the required amount of degassed monomer was distilled in from a graduated tube.

Method B. In this method the vanadium trichloride addition was followed by addition of the required quantities of monomer, benzene and aluminium alkyl in benzene in that order. The reaction mixture was then degassed on the vacuum line as in Method A, but without ageing.

RESULTS

All polymerization runs were characterized by an initial settling period during which the overall rate of polymerization increased. This period was followed by a much longer period of decreasing rate owing to depletion in monomer concentration. It can be shown^{5,7}, that if correction is made for the decrease in the monomer concentration, the rate of polymerization has now reached a steady value during this latter period. A typical plot of steady rate versus time is shown in Figure 2, and this rate plot is analogous to Curve (b) in Figure 1. The duration of the settling period can be determined, either by extrapolation of the steady state portion of the percentage conversion versus time plot to zero conversion and measuring the intercept on the time axis, or by extrapolation of the linear portion of the $\log(100 - \% \text{ conversion})$ versus time plot to zero conversion (Figure 3). This latter procedure is considered to be the more satisfactory, and was usually adopted in this work.

The effect of ageing of catalyst on catalyst activity and duration of settling period

The effect of ageing the catalyst is shown in Table 1. It is apparent that the steady state rate of polymerization is not greatly affected by the ageing process. However, the observed settling period is increased when the catalyst is aged. In addition it was found that the rates of polymerization were less reproducible when aged catalysts were used; in general the measured rates showed a spread of $\pm 7\%$ for Method A, but only a spread of $\pm 4\%$ for Method B. Furthermore, the duration of the settling period was very much more reproducible when Method B was used. It was found that polymerization runs carried out under identical conditions using Method A, could have settling periods that differed by twenty or more minutes.

The observation that the settling period is shorter when the catalyst is unaged suggests that in the absence of monomer, VCl_3 reacts with $Al(iBu)_3$ to form a strong complex which has to be broken up subsequently when monomer is added. It also indicates that the settling period is not due to a slow alkylation process, and is consistent with other evidence⁹ that the alkylation reaction is rapid.

Effect of concentration of components of polymerization system on duration of settling period

The effect of the monomer concentration on the duration of the settling period was investigated at 30° and $40^\circ C$, and the results are shown in Table 2. A marked decrease in the duration of the settling period with increase in monomer concentration, is observed at both temperatures.

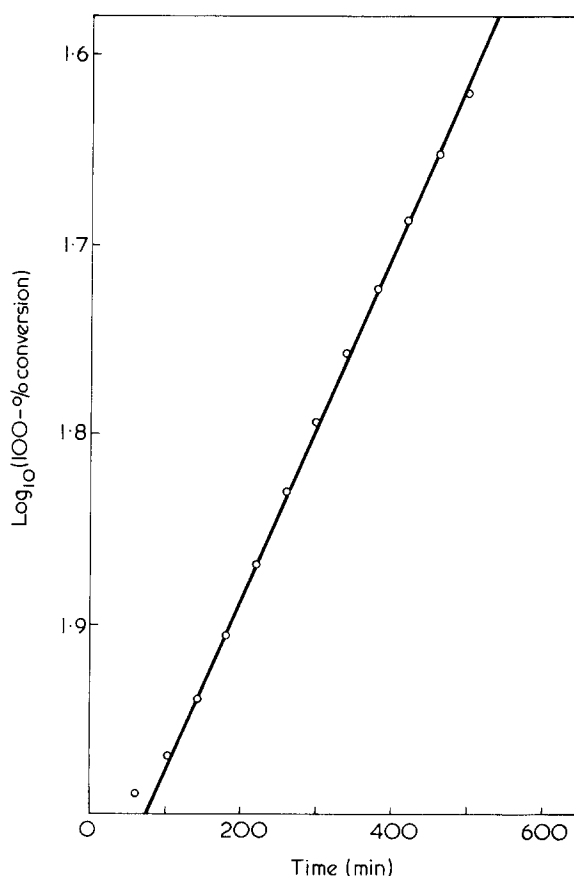


Figure 3 Plot of $\log_{10}(100 - \% \text{ conversion})$ versus time. Experimental conditions same as for Figure 2

Table 1 Effect of ageing on the duration of the settling period $[4\text{-Methylpentene-1}] = 2.00$ mol/l; $[Al(iBu)_3] : [VCl_3] = 2.0:1$; solvent benzene; temperature = $30^\circ C$

Method	$[VCl_3] \times 10^3$ (mol/l)	Rate [VCl_3]	Settling Period (min)
A	18.8	0.281	120
A	17.3	0.267	140
A	17.1	0.252	200
A	17.6	0.284	155
A	15.1	0.269	150
B	18.8	0.258	73
B	18.5	0.268	67
B	18.9	0.291	78
B	18.7	0.266	75

Table 2 Effect of monomer concentration on the duration of the settling period
 $[\text{VCl}_3] = 18.0 \text{ mmol/l}$ at 30°C , 8.8 mmol^{-1} at 40°C ; $[\text{Al}(\text{iBu})_3] : [\text{VCl}_3] = 2.0:1$; solvent = benzene; Method A

Temperature 30°C		Temperature 40°C	
[4-MP-1] (mol/l)	Duration of settling period (min)	[4-MP-1] (mol/l)	Duration of settling period (min)
0.25	350	0.50	140
0.50	260	1.00	115
1.00	248	1.50	92
1.50	200	2.00	100
2.00	150	2.50	85
3.00	155	2.50	100
4.00	140	3.00	68

Table 3 Effect of vanadium trichloride concentration on the duration of the settling period
 $[\text{4-MP-1}] = 2.00 \text{ mol/l}$; $[\text{Al}(\text{iBu})_3] : [\text{VCl}_3] = 2.0:1$; solvent = benzene; Method A

Temperature 30°C		Temperature 40°C	
$[\text{VCl}_3] \times 10^3$ (mol/l)	Duration of settling period (min)	$[\text{VCl}_3] \times 10^3$ (mol/l)	Duration of settling period (min)
10.2	208	3.9	116
15.7	235	4.8	151
17.5	150	7.4	95
21.5	143	7.5	110
22.6	190	8.7	80
48	100	11.2	82
58	53	14.7	62
110	70	18.4	35
126	40		

Table 4 Effect of vanadium trichloride concentration on the duration of the settling period at 30°C
 $[\text{4-MP-1}] = 2.00 \text{ mol/l}$; $[\text{Al}(\text{iBu})_3] = 37.0 \text{ mmol/l}$; solvent = benzene; Method B

$[\text{VCl}_3] \times 10^3$ (mol/l)	Duration of settling period (min)
3.51	80
5.44	92
8.61	92
18.2	70

Table 5 Effect of tri-isobutylaluminium concentration on the duration of the settling period
 $[\text{4-MP-1}] = 2.00 \text{ mol/l}$; $[\text{VCl}_3] = 17.6 \text{ mmol/l}$ at 30°C , 8.6 mmol/l at 40°C ; solvent = benzene; Method A

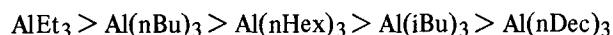
Temperature 30°C		Temperature 40°C	
[Alkyl] [VCl ₃]	Duration of settling period (min)	[Alkyl] [VCl ₃]	Duration of settling period (min)
0.5	190	0.5	115
1.0	135	1.0	104
2.0	95	2.0	100
4.0	105	4.0	104
6.0	110	4.0	89
8.0	93	8.0	100
16.0	90	16.0	93
22.0	100	24.0	86
28.0	87	32.0	68
32.0	110		

Variation in the concentration of vanadium trichloride had a complex effect on the duration of the settling period. Provided that the ratio of $[\text{Al}] : [\text{V}]$ remained constant, an increase in the concentration of vanadium trichloride caused a decrease in the length of the settling period, as is evident from *Table 3*. However, if the concentration of aluminium alkyl remained constant, i.e. when using constant $[\text{M}] : [\text{Al}]$ ratios, the initial region of increasing rate is unaffected by change in the vanadium trichloride concentration (*Table 4*).

Table 5 shows that, the concentration of the aluminium alkyl compound has little or no effect on the duration of the settling period, except at low $[\text{Al}] : [\text{V}]$ ratios where the settling period tends to be longer, especially at 30°C .

Effect of different aluminium alkyl compounds on the duration of the settling period

The durations of the settling period observed for a number of different aluminium alkyl compounds are listed in *Table 6*. It can be seen that the ability of these alkyls to reduce the settling period is in the following order:



This order is similar to that already established for overall rates of polymerization⁷, except that $\text{Al}(\text{iBu})_3$ is much lower in the above series. If the alkylation of the surface is a rapid reaction, the above order may correspond to the rate of initiation, i.e. the rate of addition of the first monomer unit to the metal-carbon bond in the newly formed transition metal alkyl. Initiation with the branched chain alkyl, $\text{Al}(\text{iBu})_3$, may be slower than that with its unbranched isomer, $\text{Al}(\text{nBu})_3$, because of steric effects.

Effect of ball-milling on the duration of the settling period

The polymerizations listed in *Table 7*, were carried out using a sample of vanadium trichloride which had been ball-milled, and whose surface area, as determined by a BET method was $5.3 \text{ m}^2/\text{g}$ as compared to a value of $2.3 \text{ m}^2/\text{g}$ for the unground vanadium trichloride.

Table 6 Effect of different alkylaluminium compounds on the duration of the settling period at 30°C
 $[\text{4-MP-1}] = 2.00 \text{ mol/l}$; $[\text{AlR}_3] : [\text{VCl}_3] = 2.0:1$; solvent = benzene; Method B

Alkylaluminium Compound	$[\text{VCl}_3] \times 10^3$ (mol/l)	Rate/ $[\text{VCl}_3]$	Settling period (min)
AlEt_3	17.6	0.247	38
$\text{Al}(\text{iBu})_3$	18.5	0.271	70
$\text{Al}(\text{nBu})_3$	18.3	0.221	45
$\text{Al}(\text{nHex})_3$	18.1	0.149	69
$\text{Al}(\text{nDec})_3$	18.6	0.107	105

Table 7 Effect of ball-milling on the duration of the settling period at 30°C
 $[\text{4-MP-1}] = 2.00 \text{ mol/l}$; $[\text{Al}(\text{iBu})_3] : [\text{VCl}_3] = 2.0:1$; solvent = benzene; Method A

$[\text{VCl}_3] \times 10^3$ (mol/l)	Duration of settling period (min)
6.0	80
8.8	73
13.7	45
15.2	45

Table 8 Effect of temperature and polymerization media on the duration of the settling period
[4-MP-1] = 2.0 mol/l; [Al(iBu)₃] : [VCl₃] = 2.0:1; Method A

Temp. (°C)	Benzene solution		n-heptane solution	
	[VCl ₃] × 10 ³ (mol/l)	Settling period (min)	[VCl ₃] × 10 ³ (mol/l)	Settling period (min)
30	18.9	85	7.9	130
30	16.8	95	16.3	70
35	—	—	11.1	130
40	18.4	35	7.9	125
40	4.8	151		
45	4.8	107		
50	5.4	67	7.5	85
60	4.8	96	4.3	110
70	4.8	73	4.7	60

* Ball-milled sample

Comparison with the values listed in Table 3 shows, that the duration of the settling period, when a ball-milled sample of vanadium trichloride is used, is considerably reduced. These results are broadly in agreement with the findings of Natta¹.

Effect of polymerization media and temperature on the duration of the settling period

In Table 8, the effect of temperature on the duration of the settling period is shown for polymerizations carried out in benzene and in n-heptane.

The polymerizations in n-heptane were carried out using a ball-milled sample of vanadium trichloride. If the results of these polymerizations at 30°C are compared with those obtained using the ball-milled catalyst in benzene at 30°C (Table 7), it is evident that the settling period is considerably longer when n-heptane is used as the polymerization media. These results may suggest that the duration of the settling period is affected by the presence of a good solvent for the polymer, or that these partially ionic reactions occur faster in the slightly more polar benzene.

DISCUSSION

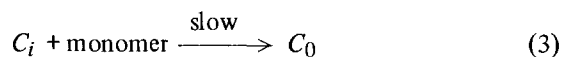
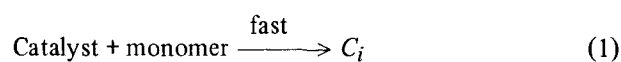
Natta² has explained the settling period by assuming that large crystals and crystal aggregates, present in these solid transition metal halides, were cleaved during the settling period by the mechanical action of the growing polymer chains, and that this process exposed more lattice defects for the formation of further numbers of active centres. Factors which increased the polymerization rate, such as high monomer concentration and temperature, were considered to shorten the settling period by increasing the rate of disruption of metal halide crystals by the growing polymer chains.

The above model does not, however, explain all the dependencies of the settling period observed for the present system, when using the particular variety of highly pure vanadium trichloride employed as the transition metal halide compound. Thus the model does not explain the reduction in the duration of the settling period observed as the catalyst concentration is increased, for although the rate is increased, the rate per unit catalyst concentration remains constant over a fairly wide range⁷. Further, the model does not explain, the variation in the settling period observed with different metal alkyls as in this work, nor the

dependence of the rate of polymerization on the initial surface area of the metal halide observed by several authors¹⁰⁻¹³

It is possible, however, to obtain additional information concerning the nature of the initial settling period by means of a detailed examination of the change in polymerization rate with time. Thus Keii¹⁴ has shown that Natta's data² on the acceleration period, are consistent with a first order rate law for the change in polymerization rate with time. A similar first order relationship is found in this work.

If it is supposed that the formation of active centres follows the general scheme:



where C_i is the number of potentially active centres on the VCl₃ surfaces, either formed by the fast interaction of catalyst components and monomer (equation 1), or already formed before monomer is added. Equations (2) and (3) thus describe slow processes which give rise to actual active centres, either in the absence (equation 2), or in the presence (equation 3) of monomer.

Now if C_0 is the total number of centres which can become active (at this stage the overall rate of polymerization will reach a maximum value and will be time independent), and if $C_{0(t)}$ is the number of active centres which have been converted from potential to actual active centres at time t , then under these circumstances the rate of formation of C_0 will be given by:

$$\frac{dC_{0(t)}}{dt} = k_i C_i \quad (4a)$$

or

$$\frac{dC_{0(t)}}{dt} = k_i \theta_M C_i \quad (4b)$$

where θ_M is the fraction of surface covered by adsorbed monomer^{7,15,16}.

In either case, if the monomer concentration is constant, the relationship will be:

$$\frac{dC_{0(t)}}{dt} = k'_i C_i \quad (5)$$

where $k'_i = k_i$ or $k_i \theta_M$ depending on the validity of the above expressions. Since $C_i = C_0 - C_{0(t)}$, integration of equation (5) gives rise to the result:

$$\ln \left(\frac{C_0}{C_0 - C_{0(t)}} \right) = k'_i t \quad (6)$$

Since it has already been established that during the steady state period the overall rate of polymerization, R_p , is given by the equation^{7,15,16}:

$$R_p = k_p \theta_M C_0 \quad (7)$$

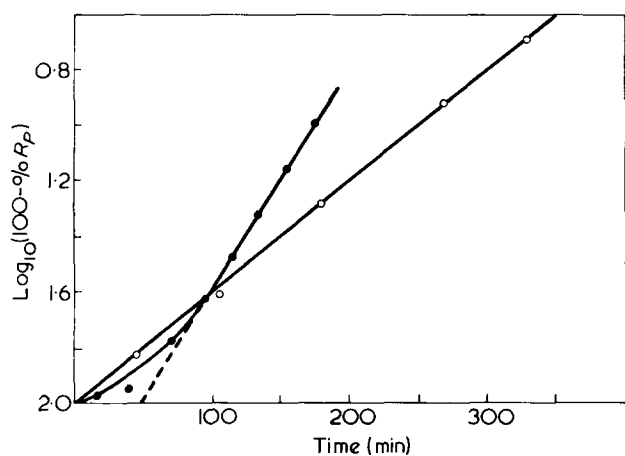


Figure 4 Plot of $\log_{10}(100 - \%R_p)$ versus time. \circ , Al(nDec)₃; \bullet , Al(iBu)₃. Experimental conditions as for Figure 2

then the overall rate of polymerization at time t , $R_{p(t)}$, corrected for decrease in monomer concentration, will be directly proportional to the number of propagating active centres at time t , $C_{0(t)}$. Thus the variation of propagating active centres with time can be followed by an examination of the polymerization rate, since at constant $k_p\theta_M$, equation (6) becomes:

$$\ln \left(\frac{R_p}{R_p - R_{p(t)}} \right) = k'_i t \quad (8)$$

which rearranges to give:

$$-\ln \left(1 - \frac{R_{p(t)}}{R_p} \right) = k'_i t \quad (9)$$

Now if this expression holds for the acceleration period, a plot of $\ln(1 - R_{p(t)}/R_p)$ versus t should be linear. In practice plots of $\log_{10}(100 - \%R_p)$, where $\%R_p = 100R_{p(t)}/R_p$, were more often made. Typical plots for the alkyls Al(iBu)₃ and Al(nDec)₃ are shown in Figure 4.

It is apparent that when the results are plotted in this way that the acceleration period can be seen to be characterized by two regions:

- (i) an initial region where the rate of formation of C_0 is increasing, followed by
- (ii) a steady region, where the formation of C_0 follows a strictly first order dependence.

That the initial region is not due to extraneous impurities, is shown by the observation that it is dependent on the nature of the aluminium alkyl. Also, since the initial region is shortest for Al(nDec)₃, the least reactive alkyl, it cannot be associated with slow alkylation. It could, however, conceivably involve the removal of some adsorbed AlR_2Cl species, the concentration of which, would be expected to be higher for the more reactive alkyls. The exceptionally long initial region in the case of Al(iBu)₃, may then reflect difficulty in the removal of Al(iBu)₂Cl because of the limited dimerisation of this sterically hindered alkyl¹⁷.

The variation of the slope of the first order plot (k'_i) with variation in polymerization component concentrations and conditions will now be discussed.

Variation of k'_i with monomer concentration

The effect of the initial monomer concentration on k'_i is shown in Table 9. It can be seen that k'_i is virtually inde-

pendent of the monomer concentration over a twelvefold range. This strongly suggests that the monomer is not involved in the slow step of active site formation; i.e. this reaction may be formulated:



This is not to say that monomer is not involved in the formation of a precursor of the active sites, e.g. in the formation of C_i . Earlier work has shown, that the concentration¹⁶ and order of addition¹⁷ of monomer does significantly affect the final C_0 value, presumably by affecting the concentration of C_i .

Interestingly, the value of the initial region is affected by the monomer concentration, being much longer at low monomer concentrations, presumably due to the slower formation of C_i . Thus the longer initial region, rather than a lower k'_i value is the reason for the observed variation of the settling period with monomer concentration.

Variation of k'_i with the nature of the aluminium alkyl

The effect of the alkyl group on k'_i is shown in Table 10. The rate of formation of C_0 is seen to be very dependent on the nature of the alkyl group. This is irreconcilable with the view that the acceleration region is due to breakdown of the catalyst particles to a limiting size. It suggests that the intermediate (C_i) is a species such as VCl_2RM whose rate of rearrangement to form C_0 is dependent on the nature of R .

Variation of k'_i with catalyst component concentration

Inspection of Tables 11 and 12 shows that k'_i is independent of the concentration of VCl_3 and Al(iBu)₃ over a five-fold range. This again fits the picture of a fairly rapid formation of a reactive intermediate, whose decomposition is not affected by the concentration of the polymerization components.

Effect of donor addition

Addition of triethylamine does not affect the value of k'_i but does considerably shorten the initial region. This is

Table 9 Effect of monomer concentration on k'_i at 30°C
[VCl₃] = 18.5 mmol/l; [Al(iBu)₃] = 37.0 mmol/l; solvent = benzene

[4-MP-1] (mol/l)	k'_i (min ⁻¹)
0.025	0.016 ± 0.004
0.50	0.016
1.00	0.024
	0.015
2.00	0.018
	0.020
3.00	0.022

Table 10 Variation of k'_i with nature of aluminium alkyl at 30°C
[4-MP-1] = 2.0 mol/l; [VCl₃] = 18.5 mmol/l; [AlR₃] = 37.0 mmol/l; solvent = benzene

Aluminium alkyl	k'_i (min ⁻¹)	Initial Region (min)
AlEt ₃	0.037	20
Al(nBu) ₃	0.023	25
Al(iBu) ₃	0.019	50
Al(nHex) ₃	0.015	11
Al(nDec) ₃	0.009	4

Table 11 Effect of vanadium trichloride concentration on k'_i at 30°C
[4-MP-1] = 2.00 mol/l; [Al(iBu)₃] = 37.0 mmol/l; solvent = benzene

[VCl ₃] × 10 ³ (mol/l)	k'_i (min ⁻¹)
18.5	0.018
	0.020
8.61	0.022
5.44	0.021
3.54	0.023

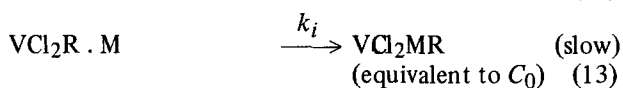
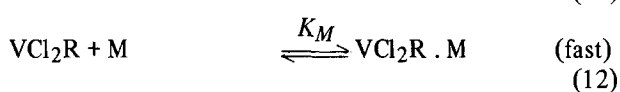
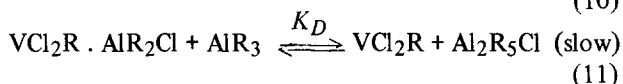
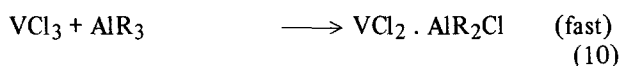
consistent with earlier proposals¹⁷ that donors primarily activate the polymerization by removal of AlR₂Cl species rather than by interaction with the active centre.

Effect of temperature

The value of k'_i is increased by increase in temperature as would be expected (Table 13). The value of the activation energy for this process is found to be about 68.6 kJ/mol (16.4 kcal/mol) for Al(iBu)₃. It should be emphasized that this is only an approximate figure since appreciable catalyst deactivation occurs at 50°C which makes derivation of an accurate k'_i value impossible.

The present study does not unfortunately shed much information on the basic chemical steps which give rise to chain initiation. It does, nevertheless, clearly establish the complexity of these processes and shows that the so-called settling period is itself composed of at least two phases, the first of which has been ascribed to the removal by complexation of adsorbed chloroalkyl, and the second of which is believed to describe a rearrangement reaction producing an initiated chain.

The catalyst forming reactions have been formulated in a previous paper⁷ as:



These equations are in qualitative agreement with the experimental findings detailed in the results section of this paper. Increase in monomer concentration should lead to an increase in the rate of initiation according to equations (12) and (13). Equations (12) and (14) would explain the complex effect of increase in vanadium trichloride concentration. The relatively slight effect of increase in tri-isobutylaluminium concentration arises because reactions (11) and (14) tend to cancel each other out.

The fact that an 'initial region' can be observed in the induction period is believed to arise because the establishment of reaction (11) is so much slower than reaction (10). In this respect the results of the analyses presented in this paper are in agreement with the catalyst forming reactions proposed in previous papers. The major difficulty lies in

identifying the nature of C_i and C_0 . It might seem reasonable to suppose that C_i is some monomer containing complex (formulated VCl₂R · M in equation 12), which rearranges by means of a slow reaction to give an entity of the type VCl₂MR, i.e. the first monomer molecule is inserted into the metal–carbon bond.

The observed dependence of k'_i on the nature of R is in keeping with such a hypothesis. However, this raises the problem as why the first monomer unit should be more difficult to insert than subsequent monomer units. Therefore, it might seem more reasonable to believe that the slow rearrangement step occurs before complexation with monomer. However, this is at variance with the observation that C_0 (and hence R_p) decreases sharply at low monomer concentrations¹⁶. There is also the possibility that reaction (2) is connected with a slow production of vacant sites owing to some surface decomposition reaction, or that it arises from some structural rearrangement on the catalyst surface. The present study does not allow an unequivocal decision to be reached on this matter.

It can nevertheless be concluded that the apparent dependence of the settling period on the monomer concentration, arises because of the slow formation of C_i , a reaction involving the monomer, together with a dependence of the 'initial region' on the monomer concentration, in spite of the fact that k'_i is independent of the monomer concentration.

One of the largest areas of uncertainty in the literature is doubtless the effect of ball-milling on the settling period. Keii⁶ has demonstrated quite thoroughly that the steady state rate is dependent, and quite likely proportional, to the initial surface area of the catalyst, i.e. that in these polymerization systems there is little change in the surface area as the polymerization proceeds. Also, it seems quite clear that when using pure vanadium trichloride catalysts of the type employed in the present study, there is little breakdown of the catalyst particles during the polymerization process. However, the situation with more complex catalysts, e.g. those based on TiCl₃·0.3AlCl₃ may be very different.

One possible reason for the reduced settling periods on ball-milling could be the production of extremely small particles, perhaps by 'chipping off' corners from the main crystal lattice of large particles. These very small species

Table 12 Effect of aluminium alkyl concentration on k'_i at 30°C
[4-MP-1] = 2.0 mol/l; [VCl₃] = 18.5 mmol/l; solvent = benzene

[Al(iBu) ₃] × 10 ³ (mol/l)	k'_i (min ⁻¹)
37.0	0.018
37.0	0.020
111	0.020
222	0.019

Table 13 Variation of k'_i with temperature
[4-MP-1] = 2.00 mol/l; [VCl₃] = 18.5 mmol/l; [Al(iBu)₃] = 37.0 mmol/l; solvent = benzene

Temperature (°C)	k'_i (min ⁻¹)
30	0.019
50	0.104

might then be solubilized by the reaction media (containing monomer), and behave somewhat akin to soluble systems, i.e. having a very high but decaying initial rate. This behaviour superimposed on the conventional polymerization would result in an apparently shortened settling period. This hypothesis is consistent with the observation that, finely ball-milled catalysts often show an initial decaying rate which can be eliminated by washing or by prolonged storage.

Finally, it is not considered that impurities play any role in the settling periods which are observed in this polymerization system. Impurities can, nevertheless, affect the duration of the settling period as has been demonstrated by Vesely¹⁰ in the case of H₂O and by McKenzie¹⁸ in the case of impurities in 4-methylpentene-1. Certainly some of the confusion found in the literature may well arise from the presence of impurities of one kind or another.

REFERENCES

- 1 Natta, G. *J. Polym. Sci.* 1959, **34**, 21
- 2 Natta, G. *Adv. Catal.* 1959, **11**, 1
- 3 Burnett, G. and Tait, P. J. T. *Polymer* 1960, **1**, 151
- 4 Novokshonova, L. A., Tovetkova, V. I. and Chirkov, N. M. *Izv. Akad. Nauk. SSSR Ser. Khim.* 1963, **7**, 1176
- 5 Tait, P. J. T. and McKenzie, I. D. 'Kinetics and Mechanisms of Polyreactions', Hungarian Academy, Vol. 2, Budapest, 1969, p 259
- 6 Keii, T. 'Kinetics of Ziegler-Natta Polymerization', Chapman & Hall, London, 1972, p 15
- 7 McKenzie, I. D., Tait, P. J. T. and Burfield, D. R. *Polymer* 1972, **13**, 307
- 8 Ehrig, R. J., Godfrey, J. J. and Krishnamurthy, G. S. 'Elastomer Stereospecific Polymerization' *Am. Chem. Soc. Symp. New Aspects of Elastomer Stereospecific Polymerization*, Chicago, 1964, p 105
- 9 Rodriguez, L. A. M., Van Looy, H. M. and Gabant, J. A. *J. Polym. Sci. (A-1)* 1966, **4**, 1905
- 10 Vesely, K., Ambroz, J., Villim, R. and Hamrik, O. *J. Polym. Sci.* 1961, **55**, 25
- 11 Keii, T. *Nature* 1964, **203**, 76
- 12 Keii, T., Suzuki, T. and Soga, K. *Asahi Glass Kogyogijitsu Shoreikai Report* 1966, **12**, 155
- 13 Kollar, L., Simon, A. and Kallo, A. *J. Polym. Sci. (A)* 1968, **6**, 937
- 14 Keii, T. 'Kinetics of Ziegler-Natta Polymerization' Chapman & Hall, London, 1972, p 18
- 15 Burfield, D. R., McKenzie, I. D., and Tait, P. J. T. *Polymer* 1972, **13**, 302
- 16 Burfield, D. R., Tait, P. J. T. and McKenzie, I. D. *Polymer* 1972, **13**, 321
- 17 Burfield, D. R. and Tait, P. J. T. *Polymer* 1974, **15**, 87
- 18 McKenzie, I. D. *Ph.D Thesis* University of Manchester (1967)

Kinetics of the thermal oxidation of poly(4-methyl-1-pentene)*

S. M. Gabbay and S. S. Stivala

Department of Chemistry and Chemical Engineering, Stevens Institute of Technology, Hoboken, New Jersey 07030, USA

(Received 30 June 1975; revised 30 September 1975)

The kinetics of the thermal oxidation of isotactic and atactic poly(4-methyl-1-pentene) were studied in the bulk phase using infra-red (i.r.) spectroscopy. The rates of formation of the non-volatile products were assessed from the i.r. bands of the carbonyl groups at different temperatures and various oxygen concentrations. Reaction temperature varied from 120° to 185°C and oxygen concentrations from 10 to 100%, by volume. A general kinetic scheme and mathematical expressions, previously reported for the thermal oxidation of polyolefins, satisfactorily explained the experimental results. Single activation energies for the major oxidation stages in the scheme, were estimated from various Arrhenius plots.

INTRODUCTION

The thermal oxidation of poly(4-methyl-1-pentene) (PMP) was first examined by Winslow and coworkers¹ using oxygen uptake methods. These investigators found that isotactic poly(4-methyl-1-pentene) (IPMP), was more susceptible to oxidation, than polyethylene and polypropylene. They attributed this observation to the presence of ordered and disordered regions of nearly identical densities at 100°C, as reported by Griffith and Ranby². Recently, the authors³ identified the main volatile products evolved during the thermal oxidation of IPMP and atactic poly(4-methyl-1-pentene) (APMP), using thermal and mass spectroscopy. In an earlier paper⁴, the kinetics of the thermal oxidation of isotactic poly(1-pentene) (IPP-1) was reported and compared to atactic and isotactic polypropylene and poly(1-butene). The purpose of this paper, is to examine the kinetics of the thermal oxidation of PMP and to compare the IPMP to the APMP under similar experimental conditions, particularly since the former has been reported to be less resistant to oxidation than the latter^{1,9}. The interesting aspect of the tertiary carbon in the pendant group of PMP, lacking in the pendant groups of polypropylene and its higher homologues, may present some differences, particularly at higher temperatures of oxidation.

EXPERIMENTAL

Starting Material

(a) The IPMP used in this study, was an unstabilized pure homopolymer obtained from Imperial Chemical Industries. Upon ignition, the sample gave an ash content of 0.004%. A number average molecular weight of 108 000 was determined from osmotic pressure in cyclohexane at 35°C using a Mechrolab automatic membrane osmometer. A crystalline melting point of 235°C was determined on a Perkin Elmer differential scanning calorimeter (d.s.c.), using a programmed heating rate of 10°C/min.

(b) The APMP sample was obtained from a double extraction with boiling ether, of a commercial poly(4-methyl-1-pentene) from Polysciences. After extraction (1% yield), the APMP was purified several times by standard precipitation procedures using cyclohexane-methanol as solvent-nonsolvent. Its amorphicity was established by X-ray diffraction (powder technique using a cylindrical camera). Upon ignition the APMP gave an ash of 0.03%, by weight. A number average molecular weight of 88 000 was obtained from osmotic pressure measurements in cyclohexane at 35°C using a Mechrolab membrane osmometer. Weight loss, due to formation of volatile products, was ~3% at 145°C and 100% oxygen.

Apparatus

(a) A Perkin Elmer Recording Spectrophotometer, Model 21, was used, to which was attached an oxidation cell similar to that previously described⁴.

(b) A Dupont Thermogravimetric Analyzer Model 950 was used to record the weight losses of IPMP films as a function of time at different temperatures above 150°C and under various oxygen concentrations. The rate of flow of O₂/N₂ mixtures was 30 cm³/min, using isothermal mode.

Procedure

Clear and uniform films of IPMP and APMP of 2–2.5 mils thickness were prepared by compression moulding and solution casting, respectively, as described elsewhere^{4–6}. The films were then placed on sodium chloride discs, which were assembled in the oxidation cell mounted onto the infra-red spectrophotometer. By means of i.r. spectra, it was ascertained that no pre-oxidation of the sample occurred, during film preparation or when the sample was heated to the desired reaction temperature, under a blanket of nitrogen, as noted by the absence of any carbonyl bands. Known mixtures of purified oxygen and nitrogen were passed into the oxidation cell at a constant rate of 30 cm³/min, after the desired reaction temperature had been reached. The concentrations of oxygen in nitrogen varied between 10 to 100%, by volume. Reaction temperatures ranged from 120° to 135°C for the APMP, and 125° to 185°C for the IPMP. Infra-red spectra of the carbonyl

* From the thesis submitted by S. M. Gabbay in partial fulfillment of the requirements for the degree of Doctor of Philosophy, Stevens Institute of Technology, 1975.

Table 1 Comparison of theoretical and observed maximum rates (ρ_m) of total carbonyl at different temperatures and oxygen concentrations for APMP

Temp. (°C)	[O ₂] (vol. %)	$K_1 \times 10^4$	K_2	K_3	ρ_m (cm ² /min)	
					Calc.	Obs.
135		17.20	48.14	50.00		
	100				0.253	0.258
	75				0.209	0.214
	50				0.166	0.172
	25				0.119	0.118
130	10	14.80	37.08	39.18	0.086	0.072
	100				0.201	0.206
	75				0.164	0.170
	50				0.126	0.130
	25				0.087	0.090
125	10	10.20	27.90	31.37	0.060	0.052
	100				0.129	0.134
	75				0.104	0.110
	50				0.078	0.082
	25				0.050	0.058
120	10	6.60	17.41	24.24	0.031	0.032
	100				0.077	0.082
	75				0.060	0.064
	50				0.043	0.048
	25				0.025	0.030
	10				0.013	0.014

K_1, K_2, K_3 defined in equations (10a), (10b) and (10c), ref. (4)

(5.50–6.00 μm) region were recorded, at various temperatures and oxygen concentrations, as a function of exposure time. The carbonyl absorbance areas for a given film, were computed in terms of the total absorbance area (cm²) and normalized to unit thickness as described earlier⁴. Diffusion control was found to be absent for the mil thickness of the films used in this study, pursuant to procedure described elsewhere^{5,6}.

RESULTS

As in the case of IPP-1⁴ and other polyolefins^{6,7}, it was observed that for IPMP and APMP, at all oxygen concentrations employed, the reaction rate increased while the induction period decreased with increasing reaction temperature. Further, as the oxygen concentration was increased, the rate of formation of total carbonyl increased while the induction time decreased, at any one given temperature. Maximum rates of formation of total carbonyl (ρ_m) were determined from plots of carbonyl absorbance area versus time, for various temperatures and oxygen concentrations. These plots were similar in nature to those described for IPP-1⁴. Values of observed ρ_m for APMP and IPMP are listed in Tables 1 and 2, respectively.

DISCUSSION

The general kinetic scheme for the thermal oxidation of polyolefins^{6,7}, including the mathematical expressions derived therefrom, were reproduced for convenience in a recent paper⁴ on IPP-1. Accordingly, all kinetic parameters and equation numbers designated in this paper, refer to those of the paper on the IPP-1. Values of $A, A',$ and k' calculated from equation (4) are shown in Tables 3 and 4. The observed maximum rates of formation of nonvolatile (NVP) carbonyl products, (ρ_m)_{obs.} for APMP, were found

to satisfactorily agree to those calculated, (ρ_m)_{calc.} (see Table 1), in the temperature range examined (120°–135°C). However, in the case of the IPMP, where the oxidation was conducted in the range of 125°–185°C, the (ρ_m)_{obs.} was found to agree within $\pm 3\%$ to the (ρ_m)_{calc.} for the oxidation conducted between 125° to 145°C (see Table 2). It should be noted that PMP contains a tertiary carbon on each pendant group, in addition to the tertiary carbons contained on the main chain. Since it was noted from the i.r. bands of the isopropyl moiety of the pendant group (7.25 μm), that there was no perceptible decrease in the maximum absorbance band, it is reasonable to assume that the oxidation occurred primarily on the main chain. Accordingly, one can assert that this pendant group, effectively behaved as if it contained no reactive site. However, the use of the derived mathematical expressions for the IPMP oxidation above 150°C, showed deviations between observed and calculated ρ_m , which increased with increasing reaction tem-

Table 2 Comparison of theoretical and observed maximum rate (ρ_m) of total carbonyl at different temperatures and oxygen concentrations for IPMP

Temp. (°C)	[O ₂] (vol. %)	$K_1 \times 10^4$	K_2	K_3	ρ_m (cm ² /min)	
					Calc.	Obs.
125		9.06	33.24	35.32		
	100				0.120	0.122
	75				0.097	0.100
	50				0.074	0.078
	25				0.050	0.053
130	10	11.6	54.85	58.62	0.034	0.028
	100				0.177	0.186
	75				0.147	0.156
	50				0.117	0.126
	25				0.084	0.078
135	10	14.2	60.91	64.78	0.057	0.036
	100				0.225	0.233
	75				0.189	0.194
	50				0.151	0.156
	25				0.110	0.092
140	10	16.0	69.91	87.10	0.076	0.048
	100				0.255	0.257
	75				0.211	0.220
	50				0.163	0.180
	25				0.106	0.106
155	10	28.8	90.59	94.44	0.057	0.050
	100				0.540	0.560
	87.5				0.501	0.520
	75				0.464	0.480
165	100	38.0	104.50	106.06	0.771	0.780
	87.5				0.722	0.730
	75				0.673	0.690
175		49.0	107.73	110.20		
	100				1.005	1.030
	87.5				0.942	0.961
	75				0.878	0.900
	50				0.748	0.780
	35				0.664	0.680
185	25	62.0	127.73	129.03	0.603	0.640
	10				0.472	0.500
	100				1.401	1.420
	87.5				1.322	1.340
	75				1.243	1.260

K_1, K_2, K_3 defined in equations (10a), (10b), and (10c), ref. (4).

Table 3 Values of A , A' and k' at different temperatures and oxygen concentrations for IPMP

Temp. (°C)	[O ₂] (vol. %)	A'	A (min ⁻¹)	k' (min ⁻¹)
125	100	0.754	0.009	0.012
	75	0.698	0.008	0.011
	50	0.610	0.008	0.013
	25	0.499	0.007	0.014
130	100	0.622	0.011	0.017
	75	0.549	0.010	0.018
	50	0.441	0.008	0.018
	25	0.266	0.007	0.020
135	100	0.631	0.019	0.030
	75	0.565	0.014	0.025
	50	0.470	0.012	0.025
	25	0.322	0.010	0.030
140	100	0.627	0.021	0.033
	75	0.569	0.020	0.035
	50	0.500	0.019	0.038
	25	0.377	0.016	0.042
145	100	0.589	0.035	0.059
	75	0.535	0.028	0.052
	50	0.466	0.023	0.049
	25	0.372	0.022	0.059
155	100	0.534	0.873	0.1634
	87.5	0.5021	0.0657	0.1308
	75	0.4654	0.0419	0.0900
165	100	0.4929	0.1151	0.2335
	87.5	0.4601	0.0936	0.2034
	75	0.4229	0.0802	0.1896
175	100	0.4875	0.1820	0.3733
	87.5	0.4551	0.1663	0.3654
	75	0.4183	0.1506	0.3600
185	100	0.4423	0.2925	0.6613
	87.5	0.4101	0.2022	0.4930
	75	0.3740	0.1619	0.4328

perature, e.g. about 25% deviation at 175°C. It should be mentioned that in prior work reported by Stivala and co-workers on the thermal oxidation of the polypropylenes⁶, poly(1-butenes)⁶, and poly(1-pentene)⁴, the weight loss following any oxidation was less than 1%. A low weight loss was also observed for APMP, and for IPMP below 150°C (3% at 145°C under 100% oxygen). This is consistent with the assumptions made by Stivala and Reich^{6,7}, that the scheme is applicable for conditions where volatile losses are low. On the other hand, in the case of IPMP oxidation conducted above 150°C, the weight loss following oxidation was as high as 16%. Therefore, it would not have been expected that one would obtain good agreement between calculated and observed ρ_m . The higher weight loss in the case of IPMP oxidized above 150°C, compared to IPMP oxidized below 150°C and the polyolefins studied earlier^{6,7}, is due to increased volatile formation resulting from attack by oxygen on the tertiary carbons of the pendant groups in IPMP. This was confirmed by the observed decrease in the maximum absorbance band of the isopropyl moiety in the pendant group with reaction time. Further, % relative abundance of volatile products, e.g. acetone, was higher at 175°C compared to oxidation at 145°C³. It is interesting to note that in isotactic polypropylene (IPP), where the pendant group contains no tertiary carbon, only a 4% weight loss was observed by the authors when this polymer was oxidized in pure oxygen at 165°C (m.p. ~171°C) for 3 h.

The question that one has to consider is whether the general kinetic scheme for the thermal oxidation of polyolefins, might not be still applicable to IPMP oxidized above 150°C. Therefore, in considering this question it was believed that the poor agreement between calculated and observed ρ_m , may have been due to the lower magnitude of maximum absorption of the carbonyl groups (assessed from the absorbance area), by virtue of the high losses of the volatile carbonyl containing products. Therefore, a correction to the observed area was deemed necessary to account for the high volatile losses. The observed carbonyl absorbance areas were corrected as follows:

$$A_c = \frac{A_m \times 100}{(100 - x)}$$

where: A_c = corrected carbonyl absorbance area; A_m = measured carbonyl absorbance area; x = percentage weight loss.

In the above correction, it was assumed that the weight of carbonyl per unit weight of solid film approximately equals the weight of carbonyl per unit weight of volatiles. The weight losses, at a given temperature and oxygen concentration as a function of time, were obtained from thermal gravimetric analysis (t.g.a.).

When the areas were corrected in this manner for all oxidations conducted at 155°, 165°, 175°, and 185°C, satisfactory agreement between observed and calculated ρ_m within an experimental error of ±4%, was obtained (see Table 2). On the basis of the satisfactory agreement between observed and calculated ρ_m , following the correction, it may appear that the general kinetic scheme also holds for the thermal oxidation of IPMP above 150°C.

Arrhenius plots of $-\ln \rho_m A / [O_2]$, $\ln K_2 / K_1 K_3$, $\ln K_3$, and $-\ln k' K_2 / K_3$ versus $1/T$, as in the previous paper⁴ on IPP-1, afforded values of energies of activation of $E_1 + E_6$, $E_1 + E_6 - E_5$, $E_8 - E_9$, and E_5 , respectively. It was noted in the case of IPMP, that each plot yielded two linear relationships of different slopes (e.g. see Figure 1), depending on the temperature range of oxidation. Hence, two values of energies of activation were obtained for any given stage (or combined stages of oxidation), see Table 5. In this context it is noteworthy to mention the work of Grieverson *et al.*⁸, who investigated the effect of temperature on the rate of oxidation of Zeigler polyethylene. They found that at temperatures between 140° and 170°C, the activation energy of the reaction was constant at 31 kcal/mol but that above 170°C, it decreased progressively until at 200°C the value was about 15 kcal/mol. Between 80° and 125°C an

Table 4 Values of A , A' and k' for different temperatures and oxygen concentrations for APMP

Temp. (°C)	[O ₂] (vol. %)	A'	A (min ⁻¹)	k' (min ⁻¹)
135	100	0.680	0.025	0.037
	75	0.615	0.019	0.031
	50	0.519	0.012	0.023
	25	0.359	0.009	0.025
130	100	0.734	0.020	0.027
	75	0.676	0.013	0.019
	50	0.585	0.008	0.014
	25	0.423	0.005	0.011
125	100	0.788	0.010	0.012
	75	0.738	0.007	0.009
	50	0.658	0.006	0.008
	25	0.505	0.004	0.007
120	100	0.860	0.009	0.010
	75	0.825	0.007	0.008
	50	0.766	0.005	0.006
	25	0.647	0.004	0.006

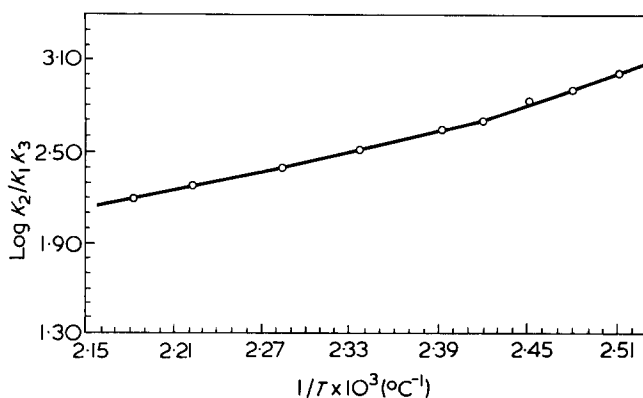
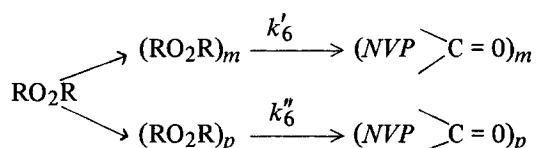


Figure 1 Arrhenius plot of $\log K_2/K_1K_3$ versus reciprocal temperature for IPMP

activation energy of 21 kcal/mol was found. They ascribed their results to phase changes and to diffusional factors. Thus, the temperature range of 140° to 170°C is above the crystalline melting point of linear polyethylene, and it was postulated that above 170°C , the rate of oxygen diffusion into the polymer could no longer keep pace with the chemical reaction rate between the oxygen and the polymer. In the case of IPMP, it is unlikely that the lower activation energies obtained above 150°C is attributed to diffusional factors, since no diffusion barrier for film thickness 2.5 mil exists. It would appear, therefore, that in the case of the thermal oxidation of IPMP above 150°C , attack on the tertiary carbons on the pendant groups should be considered. This would require a knowledge of the energy of activation of each step in the kinetic scheme, particularly that of step 6, i.e. the decomposition of RO_2R into non-volatile carbonyl products. It was possible, as described below, to estimate E_6 , from which E_1 is then obtained from the value of $E_1 + E_6$.

Thus, in the Arrhenius plot of $-\ln k'K_2/K_3$ versus $1/T$ (from which E_5 is obtained) the intercept yields $\ln Z_5$, where Z_5 is the frequency (pre-exponential) factor for step 5; from which k_5 is obtained from $k = Ze^{-E/RT}$. In this manner values of k_5 were calculated at different temperatures. In the kinetic scheme, k' represents $k_5 + k_6$ (see equation 3a) calculated from the ratio of A/A' . Values of k' , A , and A' at different temperatures are shown in Table 3. From the above, values of k_6 were obtained at the different temperatures and Arrhenius plots of $\ln k_6$ versus $1/T$ afforded E_6 for oxidations conducted above and below 150°C . E_1 was found to be constant over the temperature range of 125° to 185°C , whereas, E_6 decreased in the range above 150°C (Table 5 summarizes the estimated activation energies). It may well be that the rate constant k_6 for that step (formation of *NVP*, above 150°C becomes a complicated function of rate constants which could be represented in the following way:



where the subscripts m and p represent the main chain and pendant group, respectively. Thus:

$$k_6[\text{RO}_2\text{R}] = k'_6[\text{RO}_2\text{R}]_m + k''_6[\text{RO}_2\text{R}]_p$$

Table 5 Activation energies of APMP, IPMP, isotactic polypropylene (IPP) and atactic polypropylene (APP) for various oxidation stages

Polyolefin	Activation energies (kcal/mol)				
	$E_8 - E_9$	$E_1 + E_6 - E_5$	$E_1 + E_6$	E_5	E_6
APMP	16	17	43	27	30
IPMP, below 150°C	19	16	33	17	23
IPMP, above 150°C	4	7	28	19	18
IPP ¹¹	6	18	51	33	24
APP ¹¹	9	17	48	31	30

Below 150°C , the tertiary carbons on the main chain are the major reactive sites, thus $k_6 = k'_6$. Above 150°C , the tertiary carbons on the pendant groups become reactive. This may be due to morphological changes, where the chains become more mobile exposing the hidden tertiary carbons from the pendant group to the surface, and/or chain fold enhancement (see below). Indeed, the relative abundance of acetone formation at 175°C , was much greater than at 145°C ⁷ and this observation may account for side chain tertiary carbon oxidation. As stated earlier, the isopropyl i.r. band ($7.25 \mu\text{m}$), diminished significantly during the oxidation above 150°C whereas below 150°C no perceptible change was noted.

It would thus appear that the general kinetic scheme reported by Stivala and coworkers^{6,7} for the thermal oxidation of polyolefins, has not been violated in the case of IPMP above 150°C , where side chain oxidation occurs along with main chain attack. This is supported by a subsequent study on the kinetics of IPMP oxidation above 150°C from volatile product formation from t.g.a. data (to be published).

Examination of the energies of activation, for the various steps of the thermal oxidation of IPMP and APMP, indicate that IPMP is more susceptible to oxidation than APMP. This observation is consistent with those made by the authors reported in an earlier publication³ and by Bassett⁹. Bassett explained his observation by suggesting that in aggregated IPMP crystals, oxidation preferentially selects chain folds as reaction sites, since the strained backbone configuration would reduce the energy of activation for reaction. The suggestion was based on low angle X-ray scattering of oxidized films of IPMP. The observed lower energies of activation for the oxidation of IPMP conducted above 150°C (see Table 5) may indicate chain fold enhancement at the high temperatures. It is noteworthy to mention that, in the case of poly(1-butene), the isotactic form had a lower energy of activation than the atactic polymer for oxidation⁶, and in the case of polystyrene the isotactic form was more susceptible to oxidation than the atactic form, reported by Jellinek¹⁰.

Table 5 also contains energies of activation for the various steps of PMP in the kinetic scheme compared to IPP and APP. It is noted from these values, for example, E_5 that PMP is more susceptible to oxidation than polypropylene. This is consistent with the observation made by Winslow *et al.*¹.

ACKNOWLEDGEMENTS

The authors are most grateful to Imperial Chemical Industries, England, and to Polysciences for supplying the polymers, to Mr R. F. Westover and Bell Telephone Labora-

ories for the preparation of the preliminary compression moulded films and to Dr T. Dougherty and Dr R. Jones for useful discussions.

REFERENCES

- 1 Winslow, F. H. and Matreyek, W. Papers presented at the Washington Meeting, Division of Polymer Chemistry, ACS, (March, 1962)
- 2 Griffith, J. H. and Ranby, B. J. *J. Polym. Sci.* 1960, **44**, 369
- 3 Gabbay, S. M., Stivala, S. S. and Reich, L. *J. Appl. Polym. Sci.*, in press
- 4 Gabbay, S. M., Stivala, S. S. and Reich, L. *Polymer* 1975, **16**, 749
- 5 Gabbay, S. M. *Ph. D. Thesis*, Stevens Institute of Technology (1975)
- 6 Reich, L. and Stivala, S. S. 'Autoxidation of Hydrocarbons and Polyolefins', Marcel Dekker, New York, 1969
- 7 Reich, L. and Stivala, S. S. 'Elements of Polymer Degradation', McGraw-Hill, New York, 1971
- 8 Grieveson, B. M., Howard, R. N. and Wright, B., Ind. Chem. Soc., (London), Monograph No. 13 (1961)
- 9 Bassett, D. C. *Polymer* 1964, **5**, 457
- 10 Jellinek, H. H. G. Nat. Bur. Stand. Spec. Publ. 1972, **357**, 101
- 11 Gabbay, S. M. and Stivala, S. S. Degradation and Stabilization of Polyolefins, IUPAC 15th Prague Microsymposium on Macromolecules, (July 1975)

Swelling of bonded-rubber cylinders

L. R. G. Treloar

Department of Polymer and Fibre Science, University of Manchester Institute of Science and Technology, PO Box 88, Manchester M60 1QD, UK

(Received 18 July 1975; revised 14 August 1975)

The equations governing the equilibrium of the stresses, and the equilibrium between the stresses and the degree of swelling at any point, for a rubber cylinder bonded to a rigid cylindrical core and immersed in a swelling liquid are derived. These equations may be solved numerically, for given values of the parameters defining the system, assuming the Flory–Huggins equation for the free energy of swelling to apply. A typical example of the resultant stress and swelling distribution is included.

STATEMENT OF PROBLEM

The objective of the paper is to calculate the equilibrium degree of swelling of an infinitely long rubber cylinder containing a cylindrical metal core to which it is rigidly bonded, when immersed in a swelling liquid. This system approximates closely to the practical problem of the swelling of an ‘O-ring’, consisting of a rubber toroid bonded to a toroidal metal core, provided that the radius of the cross-section of the toroid is small compared with the radius of the axis of the ring.

The presence of the metal core, which is considered to be perfectly rigid, imposes restraints on the swelling of the rubber which give rise to a distribution of stress throughout the system. As a result, an inhomogeneous state of swelling is brought about. The problem is to determine the relations between the local stresses and the corresponding equilibrium degree of swelling at any point, and hence by integration to obtain the total amount of liquid absorbed in the final equilibrium state. The equations derived to represent this equilibrium do not yield an explicit solution in general terms, but may be solved numerically for specific values of the geometrical and physical parameters defining the system. An example of the type of solution obtained is included by way of illustration.

NATURE OF SOLUTION

Before proceeding with the detailed analysis, it may be helpful to consider in a general way the nature of the solution ultimately obtained. In this, and in the later full treatment, the following symbols will be used:

v_2	volume fraction of rubber in swollen state
l_1, l_2, l_3	principal extension ratios, referred to unstrained, unswollen state
t_1, t_2, t_3	principal (tensile) stresses
a_0	radius of cylinder in unswollen state
a	radius of cylinder in swollen state
b_0	radius of core
r_0	radial position of element in unswollen state
r	radial position of element in swollen state
ρ	density of unswollen rubber
M_c	mean molecular weight of network chains
V_0	molar volume of swelling liquid
A_{0m}	molar free energy of dilution

The geometry of the system is indicated in *Figure 1*. Since the system possesses axial symmetry, any given element of the rubber at a distance r_0 from the axis is displaced radially outwards, on swelling to a new position r , without change of its angular coordinate. Also, the presence of the inextensible core requires that there shall be no strain in the axial direction, i.e. no change in the axial coordinate. The problem is thus a two-dimensional one, and by symmetry the principal axes of the strain ellipsoid in any plane normal to the axis must be along and perpendicular to the radial direction. Denoting the circumferential, radial and axial extension ratios by l_1, l_2 , and l_3 respectively we have then $l_3 = 1$. If we consider an element of unit volume in the unswollen state, its volume in the swollen state is $1/v_2$, where v_2 is the volume fraction of rubber corresponding to the radial position r . Assuming additivity of volumes it follows that:

$$1/v_2 = l_1 l_2 l_3 = l_1 l_2 \quad (1)$$

i.e. that the state of swelling at any point is determined by the two strain parameters l_1 and l_2 .

As will be shown later, particular significance is attached to the state existing at the inner and outer boundaries. At the inner boundary ($r = b_0$), it is clear that $l_1 = 1$. Since also $l_3 = 1$, it follows that the swelling in the immediate vicinity of this boundary is associated solely with an increase in the radial dimension l_2 . This generates a lateral *compressive* stress, represented by a negative value of t_1 , together with a radial *tensile* stress, t_2 . On proceeding outwards, the restraining influence of the core diminishes, per-

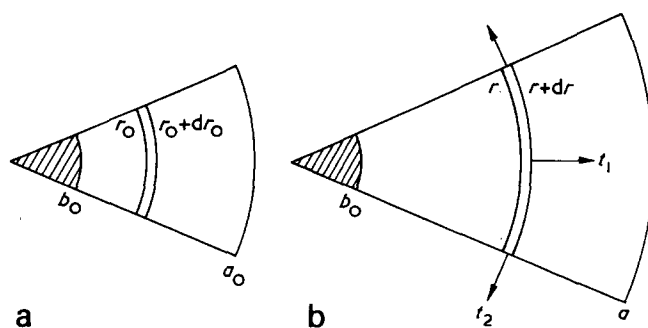


Figure 1 Strain geometry and principal stresses in cylindrical system: (a) unswollen; (b) swollen

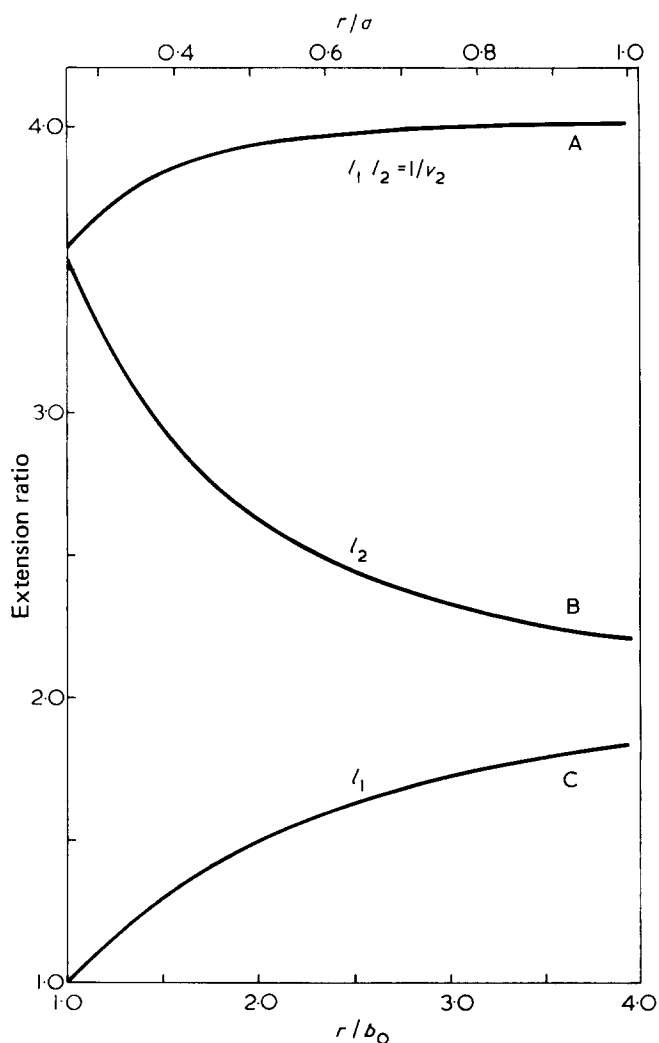


Figure 2 Typical variation of circumferential (l_1) and radial (l_2) extension ratios, and of volume swelling ratio ($1/v_2$) with radial position referred to core radius b_0 (lower scale) or to external radius b of swollen cylinder (upper scale): A, $l_1 l_2 = 1/v_2$; B, l_2 ; C, l_1

mitting an increase both in l_1 and in the degree of swelling $1/v_2$. Correspondingly, the numerical values of both t_1 and t_2 progressively diminish, until at the surface ($r = a$), the radial stress t_2 falls to zero, though t_1 (and also t_3) remain finite, (see Figures 5 and 6).

The changes in the geometrical parameters l_1 and l_2 are illustrated in Figure 2. This refers to the particular case $b_0/a_0 = 0.4601$, and is taken from the data presented in Figures 3 and 4, the scale of abscissae being converted to r/b_0 . It is seen that as r increases the two lateral strains tend to converge; at the same time the volume swelling ratio $l_1 l_2$ increases, becoming a maximum at the outer boundary ($r = a$).

DERIVATION OF EQUATIONS

The quantitative treatment of the problem involves four types of equations. These are concerned with the following considerations: (a) Compatibility of strains; (b) relations between stresses and strains; (c) equilibrium of stresses; (d) relations between swelling equilibrium and stresses. These will be dealt with in succession.

Compatibility of strains

The radial variation of l_1 and l_2 is not entirely arbitrary, but is subject to certain geometrical conditions of compat-

ibility. From Figure 1 we see that the initial radius r_0 of a circular arc is changed on swelling to the value r ; the circumferential extension ratio is therefore r/r_0 . Also, the thickness of a cylindrical shell is correspondingly changed from dr_0 to dr , giving the radial extension ratio dr/dr_0 .

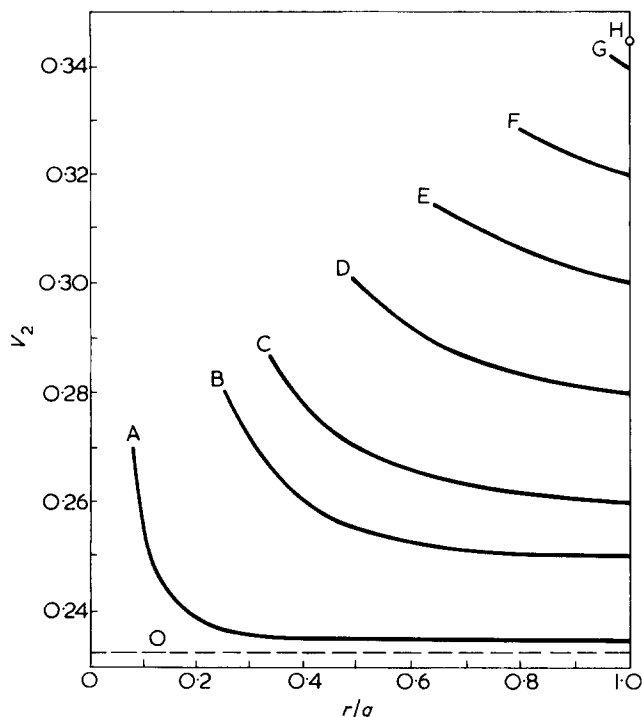


Figure 3 Radial variation of v_2 (volume fraction of rubber) for values of b_0/a_0 : A, 0.1634; B, 0.4601; C, 0.5695; D, 0.7249; E, 0.8354; F, 0.9201; G, 0.9880; H, 1.000; O, 0

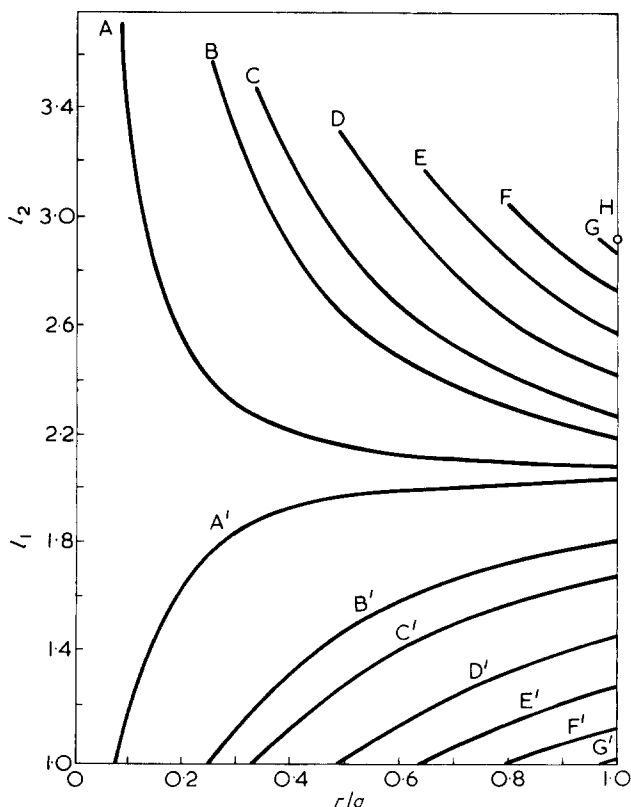


Figure 4 Radial variation of principal extension ratios l_1 and l_2 (referred to unswollen unstrained dimensions). b_0/a_0 values: A A', 0.1634; B B', 0.4601; C C', 0.5695; D D', 0.7249; E E', 0.8354; F F', 0.9201; G G', 0.9880; H, 1.0000

Remembering that $l_3 = 1$, the three principal extension ratios are therefore:

$$l_1 = \frac{r}{r_0}; \quad l_2 = \frac{dr}{dr_0}; \quad l_3 = 1 \quad (2)$$

From these equations we have:

$$l_2 = \frac{dr}{dr_0} = \frac{d(l_1 r_0)}{dr_0} = l_1 + r_0 \frac{dl_1}{dr_0}$$

whence:

$$\frac{dl_1}{dr_0} = \frac{l_2 - l_1}{r_0}$$

We thus obtain:

$$\frac{dl_1}{dr} = \frac{dl_1}{dr_0} \times \frac{dr_0}{dr} = \frac{l_2 - l_1}{r_0} \times \frac{dr_0}{dr}$$

Substituting for r_0 and dr_0/dr from equation (2) this gives:

$$\frac{dl_1}{dr} = \frac{1}{r} \left(l_1 - \frac{l_1^2}{l_2} \right) \quad (3)$$

Equation (3) implies that, if the values of the principal extension ratios at any point r are known, the rate of change of l_1 with respect to r is determined.

Relations between stresses and strains

The relations between the principal stress differences ($t_1 - t_2$), ($t_2 - t_3$), ($t_3 - t_1$) and the principal extension ratios, in a pure homogeneous deformation, are given by the Gaussian network theory of rubber elasticity in the form¹:

$$t_1 - t_2 = \frac{\rho RT}{M_c} v_2 (l_1^2 - l_2^2) \text{ etc.} \quad (4)$$

where t_1, t_2, t_3 are the respective forces per unit area, measured in the strained swollen state.

Equilibrium of stresses

It may easily be shown² that the conditions for internal equilibrium of the stresses in a cylindrical system lead to the differential equation:

$$\frac{dt_2}{dr} = \frac{t_1 - t_2}{r} \quad (5)$$

By virtue of equation (4), this may be put in the alternative form:

$$\frac{dt_2}{dr} = \frac{\rho RT}{M_c} \times \frac{l_1^2 - l_2^2}{r} \times v_2 \quad (5a)$$

Relation between swelling equilibrium and stresses

The relations between the equilibrium swelling and the principal stresses, in a pure homogeneous strain, have been

given by the author¹. For the present purpose the relevant relation is of the form:

$$t_2 = \frac{A_{0m}}{V_0} + \frac{\rho RT}{M_c} v_2 l_2^2 \quad (6)$$

in which A_{0m} is the free energy of dilution of the polymer (in the non-crosslinked state) by the swelling liquid. In the present numerical analysis this will be assumed to be given by the Flory-Huggins relation³:

$$A_{0m} = RT \left(\ln(1 - v_2) + v_2 + \chi v_2^2 \right) \quad (7)$$

where χ is an interaction parameter which is specific to the particular polymer-liquid system considered. The method of analysis is, however, not restricted to any particular form of A_{0m} .

RADIAL VARIATION OF v_2

Equations (1) to (7) provide the essential basis for the solution of the present problem. For the purpose of computation, however, it is convenient to derive a further relation expressing the radial variation of the degree of swelling, as represented by the parameter v_2 . (This avoids the necessity of having to work directly with the cumbersome equation 7.)

Putting $l_2 = 1/l_1 v_2$ in equation (6) and differentiating with respect to r , we obtain:

$$\begin{aligned} \frac{dt_2}{dr} &= \frac{1}{V_0} \frac{dA_{0m}}{dr} + \frac{\rho RT}{M_c} \times \frac{d}{dr} \left(\frac{1}{v_2 l_1^2} \right) \\ &= \frac{RT}{V_0} \left[-\frac{1}{(1-v_2)} + 1 + 2\chi v_2 \right] \frac{dv_2}{dr} \\ &\quad + \frac{\rho RT}{M_c} \left[-\left(\frac{1}{v_2^2 l_1^2} \times \frac{dv_2}{dr} \right) - \left(\frac{2}{v_2 l_1^3} \times \frac{dl_1}{dr} \right) \right] \end{aligned}$$

or

$$\begin{aligned} \frac{dt_2}{dr} &= \frac{RT}{V_0} \left\{ \left[2\chi - \frac{1}{(1-v_2)} \right] v_2 - \frac{\rho V_0}{M_c} l_2^2 \right\} \frac{dv_2}{dr} \\ &\quad - \left(\frac{\rho RT}{M_c} \times \frac{2l_2}{l_1^2} \frac{dl_1}{dr} \right) \end{aligned} \quad (8)$$

Introducing dt_2/dr from equation (5) and dl_1/dr from equation (3):

$$\begin{aligned} \frac{t_1 - t_2}{r} &= \frac{RT}{V_0} \left\{ \left[2\chi - \frac{1}{(1-v_2)} \right] v_2 - \frac{\rho V_0}{M_c} l_2^2 \right\} \frac{dv_2}{dr} \\ &\quad - \left[\frac{\rho RT}{M_c} \times \frac{2l_2}{l_1^2} r \left(l_1 - \frac{l_1^2}{l_2} \right) \right] \end{aligned}$$

or

$$\frac{dv_2}{dr} = \frac{(M_c/\rho RT) (t_1 - t_2) + 2(l_2/l_1 - 1)}{\left\{ \frac{M_c}{\rho V_0} \left[2\chi - \frac{1}{(1-v_2)} \right] v_2 - l_2^2 \right\} r} \quad (9)$$

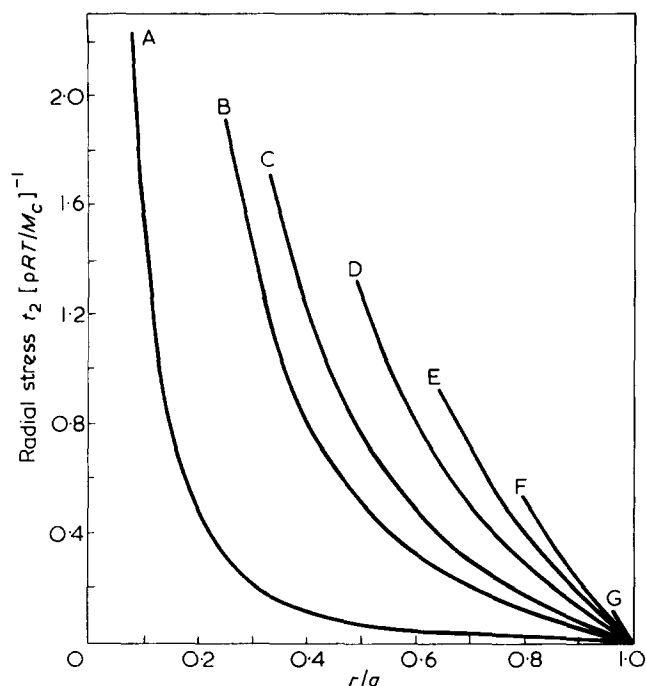


Figure 5 Variation of tensile stress (t_2) in radial direction. b_0/a_0 values: A, 0.1634; B, 0.4601; C, 0.5695; D, 0.7249; E, 0.8354; F, 0.9201; G, 0.9880

NUMERICAL ANALYSIS

Procedure

The problem cannot be solved directly, given the values of a_0 , b_0 , and the parameters defining the material properties. The boundary conditions are: (1) at $r = a$, $t_2 = 0$ and (2) at $r = b_0$, $l_1 = 1$. Neither of these gives a unique solution for the remaining variables at the respective boundary. The problem may, however, be solved indirectly by choosing an arbitrary value of one of the variables at either the inner or the outer boundary, solving for the remaining variables at this boundary, and then applying the above equations to obtain the values at a neighbouring point. The latter process is then repeated in a stepwise manner until a value of r is reached at which the required condition at the other boundary is satisfied; this then defines the second boundary.

In the present case, the calculation was started from the outer boundary, $r = a$. Assuming an arbitrary value of v_2 , and inserting the condition $t_2 = 0$, equation (6) was solved for l_2 . Knowing l_2 and v_2 , l_1 was then obtained from equation (1), following which t_1 was obtained from equation (4). The values of v_2 and t_2 at a neighbouring point ($r - \delta r$) were then obtained, using the gradients dt_2/dr and dv_2/dr as given by equations (5a) and (9) respectively; using these values the solution for l_2 and t_1 was then obtained as before. The process was repeated until the condition $l_1 = 1$ was attained; this corresponds to the inner boundary ($r = b_0$), and hence determines the value of b_0 .

Numerical values

To obtain a typical numerical solution, values of the parameters were chosen to correspond to a vulcanized natural rubber swollen with benzene, as used in a preceding study of swelling under compression⁴. These values were as follows:

$$\rho = 950 \text{ kg/m}^3; V_0 = 8.94 \times 10^{-5} \text{ m}^3/\text{mol}; \chi = 0.41.$$

Taking $M_c = 8.490 \text{ kg/mol}$ we then have $\rho V_0/M_c = 1/100$. For a temperature of 298 K this yields the value of shear modulus for the unswollen rubber $\rho RT/M_c = 0.2772 \text{ MN/m}^2$

The accuracy of the calculations depends on the interval δr between successive radial positions. Two values of this interval were used, i.e. $\delta r/r = 0.005$ and $\delta r/r = 0.001$. The resulting figures differed only slightly (i.e. in the 4th significant digit in l_1 and v_2), indicating that the smaller interval gives reasonably accurate results. For any chosen value of v_2 at the surface, there is a corresponding value of b_0 ; this, as already noted, is the value of r at which $l_1 = 1$, which was obtained by interpolation.

Figure 3 shows the radial variation of v_2 , for 7 values of b_0/a_0 , obtained in this way. The circumferential and radial strains are shown in Figure 4. Figure 5 gives the variation of the radial (tensile) stress t_2 and Figure 6 the circumferential (compressive) stress, $-t_1$, and the (compressive) stress parallel to the axis, $-t_3$. All the stresses are given relative to the shear modulus $\rho RT/M_c$.

Overall degree of swelling

The effect of the solid core on the overall swelling ratio of the rubber component is obtained from the formula:

$$Q = \frac{a^2 - b_0^2}{a_0^2 - b_0^2} \quad (10)$$

This quantity is shown in Figure 7, as a function of b_0/a_0 .

LIMITING CASES

Two limiting cases may be treated generally. These are: (a) infinitesimal thickness of rubber ($b_0/a_0 \rightarrow 1$) and (b) infinitesimal core radius ($b_0/a_0 \rightarrow 0$).

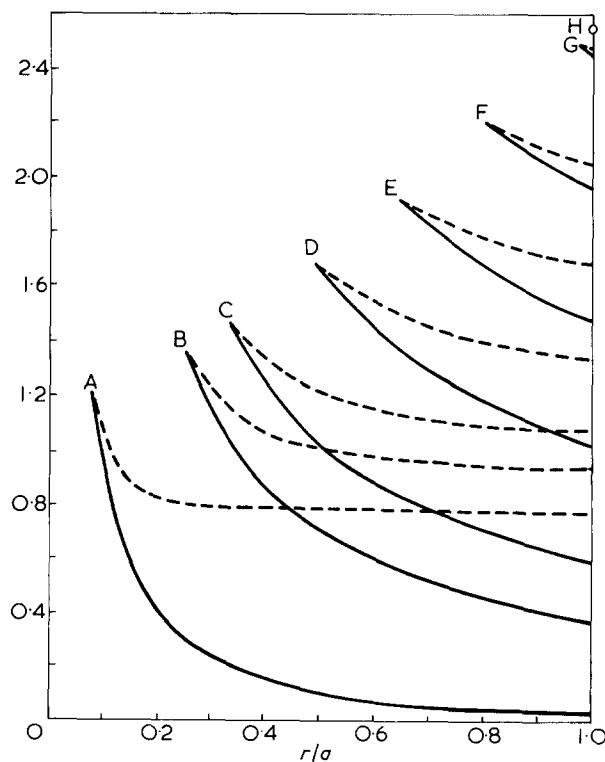


Figure 6 Radial variation of compressive stresses in circumferential direction ($-t_1$) and in axial direction ($-t_3$). —, $-t_1/(\rho RT/M_c)$; ---, $-t_3/(\rho RT/M_c)$. b_0/a_0 values: A, 0.1634; B, 0.4601; C, 0.5695; D, 0.7249; E, 0.8354; F, 0.9201; G, 0.9880; H, 1.0000

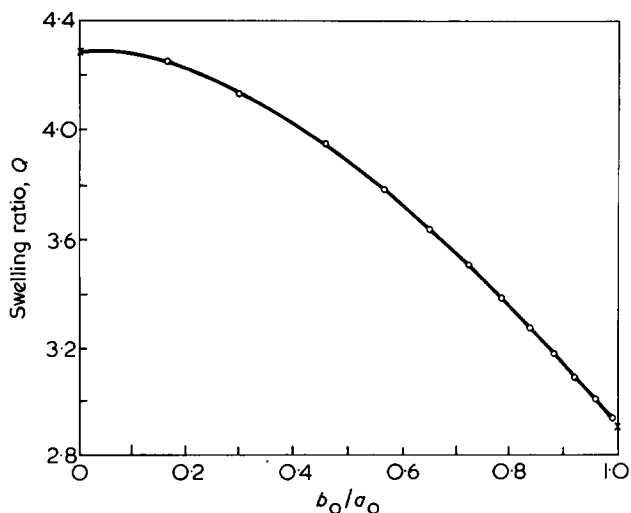


Figure 7 Dependence of overall swelling ratio Q on ratio of internal to external radii of unswollen cylinder. X, calculated from equations (10) and (11)

(a) For this case $l_1 = l_3 = 1$, $\nu_2 = 1/l_2$, $t_2 = 0$. Substituting these values in equation (6), we obtain an equation for ν_2 , namely:

$$\frac{A_0 m}{RT} + \frac{\rho V_0}{M_c} \nu_2^{-1} = 0 \tag{11}$$

The remaining variables are then obtained directly.

(b) For this case it may be assumed that the region of non-uniform strain is restricted to an infinitesimal distance from the axis. Except for this infinitesimal region the swelling and strain will be homogeneous, the effect of the core being merely to restrict the axial extension. The only stress present will be the axial compressive stress $-t_3$. Hence $l_1^2 = l_2^2 = 1/\nu_2$; $t_1 = t_2 = 0$; and equation (6) becomes:

$$\frac{A_0 m}{RT} + \frac{\rho V_0}{M_c} = 0 \tag{12}$$

The solutions for ν_2 corresponding to these two limiting cases are represented in Figure 3 by the point for $b_0/a_0 = 1$ and the horizontal line for $b_0/a_0 = 0$. Corresponding values for case (a) are shown also in Figures 4 and 6.

DISCUSSION

Origin of swelling stresses

The origin of the stresses developed on swelling, already briefly referred to earlier, can easily be understood in a qualitative way. If the core were removed, leaving a hollow cylinder of rubber, this would swell isotropically. Such a swollen cylinder would have a greater axial length, and a greater internal radius, than the core to which it was originally attached in the unswollen state. In order to fit the internal surface of the swollen cylinder to the core, it is necessary to apply forces to the boundary surfaces so as to reduce the internal radius and the axial length to their original values. Given that the outer surface is stress-free, the necessary forces are obviously: (1) a radial tensile force on the inner surface, and (2) an axial compressive force on the end surfaces. These forces correspond to the radial tensile stress t_2 and the axial compressive stress $-t_3$ derived from the above calculations. The circumferential compressive stress $-t_1$ is a result of the radial tensile stress t_2 .

ACKNOWLEDGEMENTS

The author is indebted to Dr M. D. Heaton for carrying out the necessary computational work, and to Dr W. F. Watson of the Rubber and Plastics Research Association for discussions related to the problem considered.

REFERENCES

- 1 Treloar, L. R. G. *Proc. R. Soc. (A)* 1950, **200**, 176
- 2 Rivlin, R. S. *Philos. Trans. R. Soc. (A)* 1949, **242**, 173
- 3 Flory, P. J. *J. Chem. Phys.* 1942, **10**, 51
- 4 Treloar, L. R. G. *Polymer* 1967, **8**, 433

Comparison of bound rubber and swelling in silicone rubber/silica mixes and in silicone rubber vulcanizates

David W. Southwart

Dunlop Limited, Precision Rubbers Division, Shepshed, Loughborough, Leics. LE12 9 EQ, UK

(Received 8 January 1975; revised 5 August 1975)

Unextracted polymer and liquid absorption values have been determined on unvulcanized silicone rubber/silica mixes and on unfilled silicone rubber vulcanizates, for comparison of the two different types of three-dimensional structure which must exist. In both types, the amount of rubber extracted on immersion in liquid is dependent on the expansion of the respective network but only in the former is the amount dependent on the method of extraction; this is attributed to interaction between filler and rubber continuing as a result of immersion. Even at equilibrium, the amount of unextracted polymer can be greater than that of bound rubber. In some mixes, liquid absorption is substantially constant during extraction of considerable amounts of soluble rubber. This is attributed, in the presence of filler, to a dependence of the absorption on the previously postulated interparticular rubber which, in turn, is dependent on the mean distance between filler particles. Although unextracted polymer is also dependent on that mean distance, it is proposed that this is a secondary effect of network expansion by the absorbed liquid. As some published values of bound rubber have undoubtedly been of unextracted polymer, these results help to explain published differences of opinion on the value of bound rubber for investigation of filler reinforcement phenomena.

INTRODUCTION

In previous work, the author has attempted to correlate various changes occurring in mixtures of silicone rubber and fine particle fume silica, on storage. The well known increase in bound rubber was shown to be more complex than previously realized, e.g. immersion times in excess of six months¹ were sometimes required to reach an equilibrium (constant) value; furthermore, the increase in bound rubber on storage, accompanied by a decrease in swelling, was shown not to correlate directly with processability, the latter sometimes passing through a minimum as the bound rubber continued to increase. Similarly, heat of melting was shown to pass through a minimum on storage².

Comparison of unvulcanized and vulcanized mixes was restricted to modulus measurements³. Vulcanization was found to decrease the rate, but not the extent, of increase of (low strain) Young's modulus on storage. Sometimes the maximum Young's modulus of the unvulcanized mix was greater than that of the corresponding vulcanizate.

To account for these results, the author⁴ proposed that silicone rubber and silica interact to produce two different structures in the unvulcanized state; one giving an effective three-dimensional structure but both immobilizing some of the rubber. These were described as:

(a) adsorbed rubber: polymer segments immobilized in the immediate vicinity of filler particles, whether by orientation on the filler surface or by entrapment in filler agglomerates;

(b) interparticular rubber: polymer segments joining filler particles to give effective crosslinkages, and (interlocking) polymer loops attached to filler particles.

The two terms are synonymous with the 'shell of rubber' and 'rubber bridgehead chains' respectively described by Gessler⁵. The polymer free of interaction with filler was termed matrix rubber.

In this paper further experiments are reported on the comparison of the behaviour in liquids of (unvulcanized) silicone rubber/silica mixes, with that of (pure gum) silicone rubber, lightly vulcanized with peroxide so that up to 30% of the rubber remained soluble (i.e. bound rubber ~70%). Interesting observations have been made, which help to demonstrate the differences in structure between silicone rubber conventionally crosslinked by peroxide, and silicone rubber 'effectively crosslinked' by interaction with a fine particle reinforcing filler.

MATERIALS

The silicone rubber was a commercial methyl vinyl polysiloxane obtained from Imperial Chemical Industries Limited. It was used in its original form, E302, and in its devolatilized form, E303; the latter having reduced loss during high temperature post curing of its vulcanizates, for normal commercial applications. The fine particle fume silica was Aerosil 300, produced by Degussa and supplied by Bush Beach and Segner Bayley Ltd. It has a nominal specific surface area of 300 m²/g. The peroxide was a commercial form of 2,4-dichlorobenzoyl peroxide in an equal weight of unspecified silicone oil, obtained from Novadel Limited as Perkadox PDS-50. The liquids used were generally of analar or similar high purity grades.

BOUND RUBBER

Time to equilibrium

Bound rubber is generally reported as % original rubber, remaining in a sample after immersion in a good solvent for a time considered sufficient to reach an equilibrium condition, i.e. a state where there is no further change in composition of the swollen gel during continued immersion.

Such values of bound rubber include any soluble rubber remaining in the swollen gel. A better term, which can also be used for values obtained under non-equilibrium conditions, is 'unextracted polymer'. It will generally be greater than the bound rubber, if that term is reserved for the sum of the adsorbed rubber and interparticular rubber as defined above.

In the case of a silicone rubber/fume silica mix, the rate of extraction of soluble rubber is dependent on the storage time of that mix and on the type and concentration of filler. In addition the rate and amount of extraction are affected by repeatedly replacing the solvent containing extracted rubber by fresh solvent. If the solvent contains soluble rubber there is an effect on the swelling of the gel and on the amount of soluble rubber remaining in the gel. This arises from a back pressure effect⁶ which has been confirmed by others^{7,8} and recently analysed by Blow⁹, using the concept of a partition coefficient, for the distribution of soluble rubber between the solvent present in the gel and that in which the gel is immersed. It was claimed that the bound rubber, as defined in the previous paragraph, can be calculated from values of extracted rubber, obtained from the immersion of samples of the mix in a range of silicone rubber solutions instead of in the pure solvent; it is, however, necessary to ensure equilibrium¹⁰.

Several samples (~0.4 g) of silicone rubber (E302) containing 26 parts by weight per hundred of rubber (phr) of fume silica were immersed in toluene for varying periods up to 4 years, with occasional transfer of the swollen jelly to fresh solvent. Unextracted polymer was found to be linearly related to the square root of the immersion time. Extrapolation of the line indicated that all the rubber would be extracted in approximately 20 years.

It is possible that the slow and continuing fall in the unextracted polymer value in the case of the above experimental procedure is due not to a low rate of diffusion of soluble polymer but to solubilization of bound rubber by hydrolysis, or by some other mechanism.

To study the rate of extraction of soluble rubber in the absence of filler, lightly crosslinked unfilled silicone rubber

has been used as a model system. Although variation of peroxide concentration would have provided the desired variation in liquid absorption through crosslink density effects, it would also have varied the soluble rubber concentration. To provide variation of liquid absorption, at constant soluble rubber concentration, the vulcanizate was swollen in several liquids covering a wide range of solubility parameters.

Effect of liquid composition

Silicone rubber (E303) containing 0.5 phr of peroxide was moulded for 10 min at 110°C into nominally 175 × 175 × 2.5 mm sheets. Test pieces (~0.4 g) were immersed in various liquids, then dried at room temperature to determine the unextracted polymer. Some test pieces were subjected to successive determinations, by being reswollen and extracted for longer periods until equilibrium was attained, as shown by a horizontal portion of the line obtained when unextracted polymer was plotted against the square root of immersion time. Other test pieces were immersed concurrently and continuously until equilibrium had been attained by the method of successive determinations. In all cases the liquid was replaced frequently so that final values were not subject to any significant back pressure effect. As no correction was made for residual peroxide etc. values are subject to a small error not exceeding 0.5%.

The data in *Table 1* show that, with one exception, there was a small, but probably significant, increase in unextracted polymer with increase of solubility parameter of the extracting liquid, when values were obtained by successive determinations. Similarly, with the exception of the values obtained in toluene, unextracted polymer determined by continuous immersion, also increased with increases of solubility parameter. Although the differences in values are small there appears to be no significant effect of test method, i.e. unextracted polymer is the same whether or not immersion is interrupted by drying down and reswelling. When test pieces dried after successive determinations for 5 weeks were transferred to hexane they gave values identical within likely experimental error.

Table 1 Effect of liquid composition on unextracted polymer (%) of a silicone rubber vulcanizate

Immersion time	Solubility parameter ¹⁶				
	9.7 Acetone	9.6 Methyl isobutyl ketone	9.3 THF	8.9 Toluene	7.2 Hexane
	Successive determinations				
7 h	95.2	94.8	94.9	93.9	93.0
2 days	94.4	93.9	93.8	93.6	92.4
1 week	93.9	92.9	92.3	92.6	91.3
2 weeks	93.8	92.7	92.0	92.3	91.0
3 weeks	93.8	92.8	91.7	92.3	90.7
4 weeks	93.8	92.7	91.6	92.3	90.6
5 weeks	93.8	92.7	91.6	92.3	90.6
	Continuous immersion				
7 weeks (sample 1)	94.0	93.0	91.1	92.6	90.5
(sample 2)	93.0	92.6	91.3	93.0	90.8
	Samples from successive determinations for 5 weeks transferred to hexane				
1 week	92.1	91.4	91.1	91.5	90.6
3 weeks	90.9	91.0	91.0	91.1	90.6
5 weeks	90.7	90.8	90.7	90.9	90.6
7 weeks	90.7	90.7	90.7	90.5	90.6
9 weeks	90.7	90.7	90.7	90.5	90.6

Table 2 Effect of liquid composition on unextracted polymer (%) of a silicone rubber/fume silica mix (mean of duplicate values)

Immersion time	Acetone	Methyl isobutyl ketone	THF	Toluene	Hexane
			Successive determinations		
1 day	94.0	92.9	90.5	91.0	86.0
1 week	93.6	89.1	86.9	88.2	82.2
2 weeks	93.3	87.7	85.9	86.7	80.7
3 weeks	93.0	86.7	85.4	86.0	79.8
4 weeks	92.9	86.7	84.2	85.5	79.1
5 weeks	92.9	86.6	84.1	85.4	79.1
6 weeks	92.9	86.6	84.1	85.5	79.0
7 weeks	92.9	86.7	84.0	85.4	79.0
8 weeks	92.9	86.6	84.0	85.4	79.0
			Further successive determinations after transfer to hexane		
1 day	92.1	86.7	84.1	85.4	ND
1 week	91.3	86.6	84.1	85.5	ND
2 weeks	91.1	86.7	84.0	85.5	ND
4 weeks	91.0	86.7	84.0	85.5	ND
6 weeks	91.0	86.7	84.0	85.5	ND
			Continuous immersion		
8 weeks	93.3	75.5	74.0	67.3	64.8

ND = not determined

The data in Table 2 show that, in a similar series of determinations on unvulcanized portions of silicone rubber (E303) containing 32 phr of fume silica, unextracted polymer on successive determinations was similarly, but considerably more, dependent on the liquid. On the other hand: (a) no more soluble rubber was extracted on subsequent immersion in hexane (except in the case of samples originally immersed in acetone); (b) more (sometimes considerably more) rubber was extracted by continuous immersion than by repeated immersion and drying (again with the exception of the samples immersed in acetone).

Comparison of the two sets of data reveals several differences between vulcanized (unfilled) silicone rubber and unvulcanized silicone rubber containing silica, but also some similarities. These can be summarized as follows.

(1) In both systems unextracted polymer is liquid dependent.

(2) In the case of a filled unvulcanized mix, unextracted polymer is greater when determined by successive determinations to equilibrium than by continuous immersion whereas a gum vulcanizate shows little, if any, dependence on the test method.

(3) Gum vulcanizate samples, previously extracted in the various liquids (successive drying and reswelling) undergo further extraction on immersion in hexane to give the same value as a sample not previously extracted. Filled unvulcanized samples, on the other hand, undergo no further extraction when immersed in hexane.

The dependence of unextracted polymer on the solubility parameter of the liquid, could be due to the differing solubility of the polymer in the various liquids and/or to the variation in the amount of network expansion produced by the liquids. In the case of the filled unvulcanized mix, it is particularly significant that the higher values of unextracted polymer obtained by successive determinations (rather than by continuous immersion) in the various liquids, were not reduced by subsequent immersion in the most powerful solvent, i.e. hexane, except for a small reduction when the first liquid had been acetone.

The effects of acetone and hexane were also compared at higher soluble rubber concentration by using separate

portions of silicone rubber (E303) vulcanized with only 0.2 phr of peroxide. Acetone, in which the rubber is only partly soluble, extracted only 5.5% of the polymer at equilibrium in approximately 5 days, by which time hexane has extracted 25%. The extract in hexane continued to increase and had attained 34% in 132 days. In a further sample, the 4 and 12 day acetone extracts were both found to have a molecular weight of 0.35×10^6 as determined by intrinsic viscosity in toluene after drying down, whereas the first extract after transfer to hexane for 1 day had a molecular weight of 0.48×10^6 ; (original polymer 0.64×10^6). This provides some limited evidence for a belief that the amount of polymer extracted and its molecular weight are dependent upon the degree of expansion of the network, possibly through some fractionation or molecular 'window' effect, similar to that proposed by Cooper and Smith for natural rubber¹¹.

RELATIONSHIP BETWEEN LIQUID ABSORPTION AND UNEXTRACTED POLYMER

The swelling of a 'bound rubber gel', expressed as the weight of liquid per 100 parts by weight of unextracted polymer, can be linearly related to the 'bound rubber', or more correctly to the unextracted polymer. This has been established both for unvulcanized silicone rubber containing silica, in toluene with variation of storage and immersion times and, from the data of J. W. Watson¹², for unvulcanized natural rubber containing carbon black, in benzene¹; also for unvulcanized nitrile rubber containing silica, in acetone, methyl isobutyl ketone and toluene¹³.

In the experiments reported in this paper the weight of the test piece increased rapidly on immersion and attained a near constant value within one day. Thereafter there were generally further small but comparatively insignificant weight changes over several weeks while rubber continued to be extracted. In Figure 1, the unextracted polymer values from Tables 1 and 2 for the various liquids, taking those at 3 weeks and 8 weeks (continuous immersion) respectively as representing equilibrium, are plotted against the liquid absorption, expressed as the volume of liquid

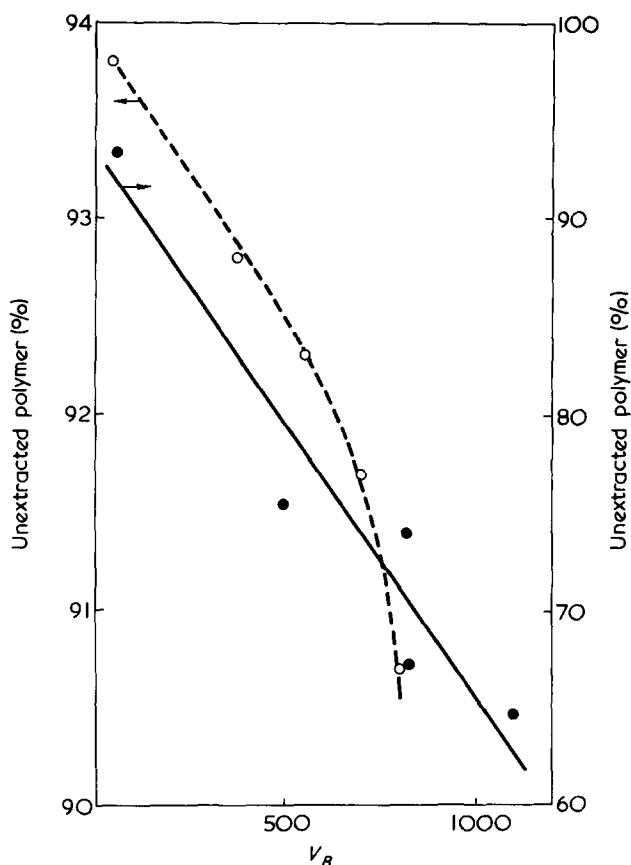


Figure 1 Relationship between unextracted polymer and volume swelling (V_B) for a silicone rubber vulcanizate (○) and an unvulcanized silicone rubber/silica mix (●)

(V_B) per 100 volumes of unextracted polymer. Both plots show the same decrease of unextracted polymer with increase of swelling.

There is an alternative way of expressing liquid absorption, i.e. as the parts by weight of liquid absorbed per 100 parts of original mix (S_M). This value is substantially independent of storage time before immersion¹⁰; it is also substantially independent of immersion time as the following experiment demonstrates.

Eight portions of five silicone rubber (E302) mixes containing various proportions (8–48 phr) of fume silica were immersed in toluene (which was renewed frequently), and removed successively during 100 days. In Figure 2, unextracted polymer versus S_M is plotted for the five mixes after the varying immersion times. The slope of the linear portions of these plots varies slightly and is a maximum for the mix with 24 phr of filler, which had substantially constant toluene absorption.

A similar series of mixes was extracted, with weekly changes of toluene, until there was no residue on drying down the replaced solvent on three successive weeks. Excluding the lowest filler concentration, there was an approximately linear relationship between the unextracted polymer and the liquid absorption expressed (in this instance to take account of varying silica content) as parts by weight of toluene (S_P) per 100 parts of E302 originally present in the mix (Figure 3).

DISCUSSION

Unextracted polymer is believed to comprise three different types: (1) bound rubber, as interparticular rubber and/or adsorbed rubber; (2) soluble rubber which cannot be

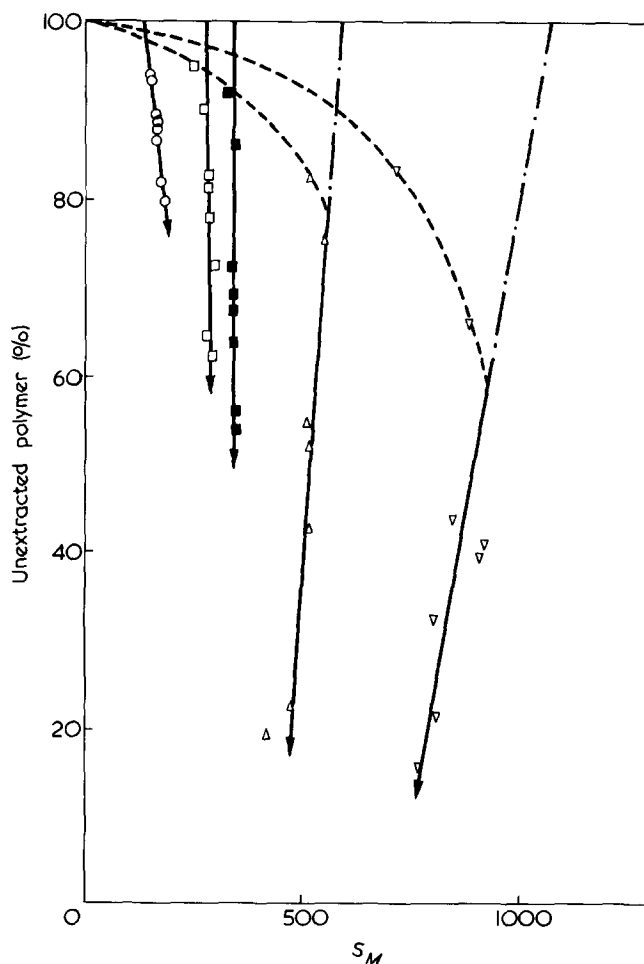


Figure 2 Relationship between unextracted polymer and liquid absorption (S_M) with increase of immersion time as arrowed; filler concentration (phr): ○, 48; □, 32; ■, 24; △, 16; ▽, 8

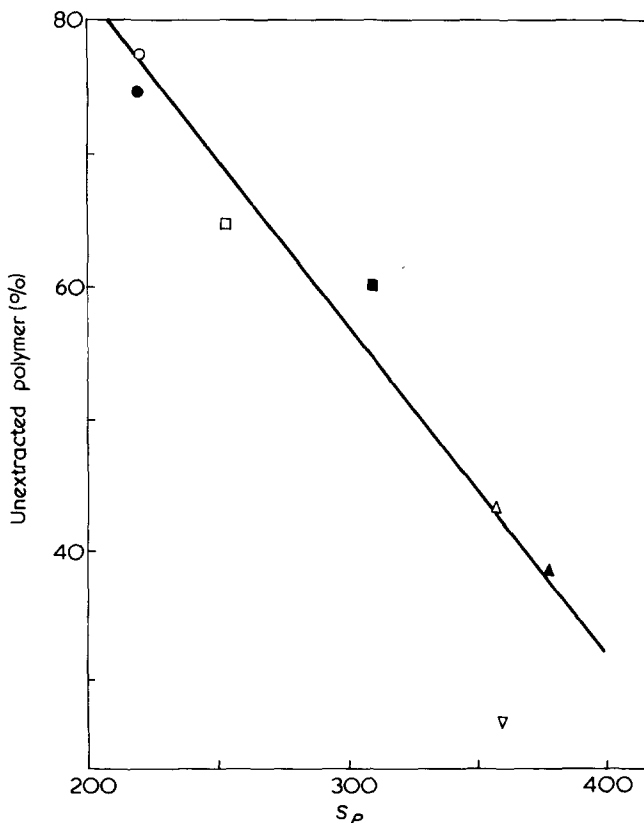


Figure 3 Relationship between unextracted polymer and liquid absorption (S_P) in silicone rubber with variation of filler concentration (phr) ○, 48; ●, 40; □, 32; ■, 24; △, 16; ▲, 12; ▽, 8

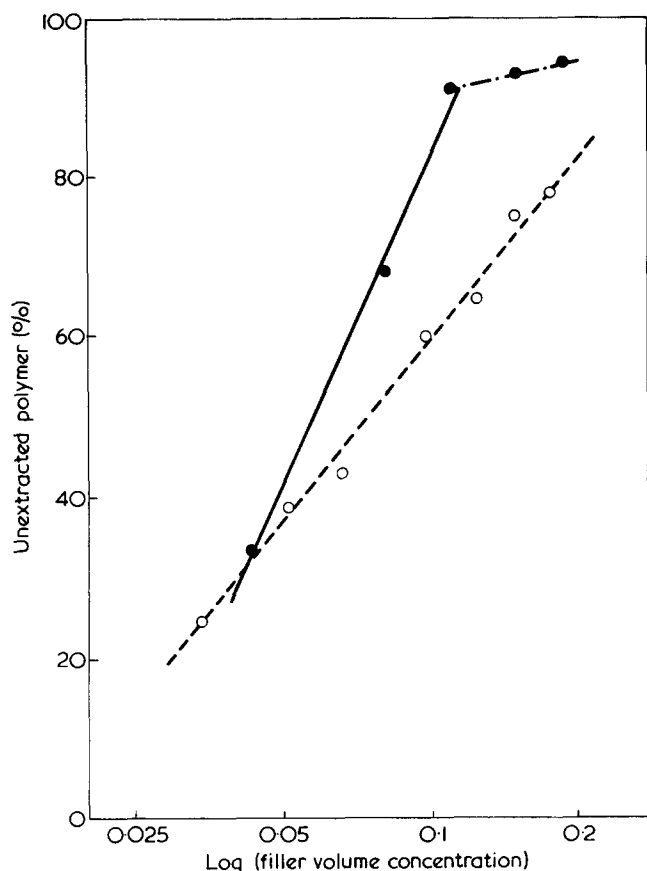


Figure 4 Relationship between unextracted polymer and log (filler volume concentration). Filler nominal specific surface area (m^2/g) \circ , 300; \bullet , 80 (data from Vondráček, personal communication, 1974)

extracted through available 'windows' in the network because of its molecular size, or for other reasons; (3) soluble rubber which will be extracted if immersion is sufficiently prolonged, with sufficiently frequent replacement of the extracting liquid by fresh solvent.

Changes may well occur during determinations of unextracted polymer because bound rubber is desorbed, or because networks have expanded under the influence of liquid pressure — the well known swelling increment. One of the most significant observations is that, equilibrium values of unextracted polymer obtained by successive determinations of unvulcanized silicone rubber containing fine particle fume silica, are higher than values obtained by continuous immersion. This is attributed to an increase in bound rubber, particularly on drying after an increase in the mobility of the reactive species in the swollen expanded network. On the other hand, vulcanized but unfilled silicone rubber, whose network structure should not be changed by the liquid, gives values of unextracted polymer which are little, if at all, affected by the method of determination.

At equilibrium the amount of soluble rubber extracted from a three-dimensional silicone rubber network is related to the amount of expansion of that network imposed by the extracting liquid; whether the network consists of rubber molecules joined by peroxide-induced linkages or by adsorption to filler particles (Figure 1). In lightly vulcanized silicone rubber it seems unlikely that the amount of soluble rubber present depends on the solvent used; the increase in the amount of soluble rubber extracted with increase in solvent absorption is therefore attributed to the increase there must be in network expansion. In unvul-

canized silicone rubber containing silica, liquid might desorb rubber adsorbed on the filler surface, thus effectively increasing the soluble rubber content. However, hexane was apparently unable to desorb the rubber bound during the successive determinations in all but acetone (Table 2). The similarity between the two curves in Figure 1 is therefore attributed to a dependence of the amount of rubber extracted on the degree of expansion of the two types of three-dimensional network.

Another significant observation is the tendency for the amount of liquid absorbed to be substantially independent of storage time and immersion time, for a given mix and liquid, even when further rubber is adsorbed (by the filler) during the determination. It is proposed that the liquid absorption is largely determined by the length of the interparticular rubber chains in a silicone rubber/silica mix, rather than by their number and thus related to the mean distance between filler particles in the unswollen mix.

It is in the effect of additional linkages that the two three-dimensional structures are believed to differ most. In a gum vulcanizate the effect is well known, and characterized by the Flory-Rehner relationship¹⁴; generally each additional crosslink reduces the mean distance between crosslinks, and thus the extent of swelling. It is postulated that in a uniform three-dimensional network in a filled unvulcanized mix, filler particles are joined by rubber chains of constant length (interparticular rubber). The addition of a further chain will reduce the degree of swelling in a liquid but this reduction will be less than that of an additional crosslink in a vulcanizate. Additional linkages introduced during drying after immersion will however tend to be of greater chain length than the original ones and thus have even less subsequent effect. In other words, if, during the determination of unextracted polymer, additional linkages form and insolubilize some previously soluble rubber, the liquid absorption will not be appreciably altered.

The data in Figure 2, obtained by continuous immersion, show that liquid absorption is dependent on filler concentration. At high filler concentrations liquid absorption increases with increase of immersion time; probably owing to the swelling increment mentioned earlier. At low filler concentrations immersion time has the opposite effect on liquid absorption, probably owing to greater absorption of liquid by the soluble rubber before its extraction. At the median filler concentration liquid absorption is remarkably constant. The deviation of the first one or two values from the straight lines drawn, particularly for the mix with the highest liquid absorption, is attributed to a normal diffusion rate effect on the liquid.

The relationship between unextracted polymer and filler concentration is considered next. Vondráček and Schätz have recently proposed¹⁵ that bound rubber is directly proportional to filler contact area, up to a limiting volume concentration of approximately 0.08 with a lower specific area fume silica. This is equivalent to direct proportionality of bound rubber to filler volume concentration, as found in an earlier stage of the present work when only four filler concentrations were used. However the data obtained from near-equilibrium conditions (Figure 3) did not fit that relationship but instead indicated that unextracted polymer is proportional to the logarithm of filler volume concentration as shown in Figure 4. Similarly the data of Vondráček and Schätz were found to agree with that relationship, up to a high unextracted polymer value.

It is interesting finally to examine the relationship between unextracted polymer and mean interparticle distance.

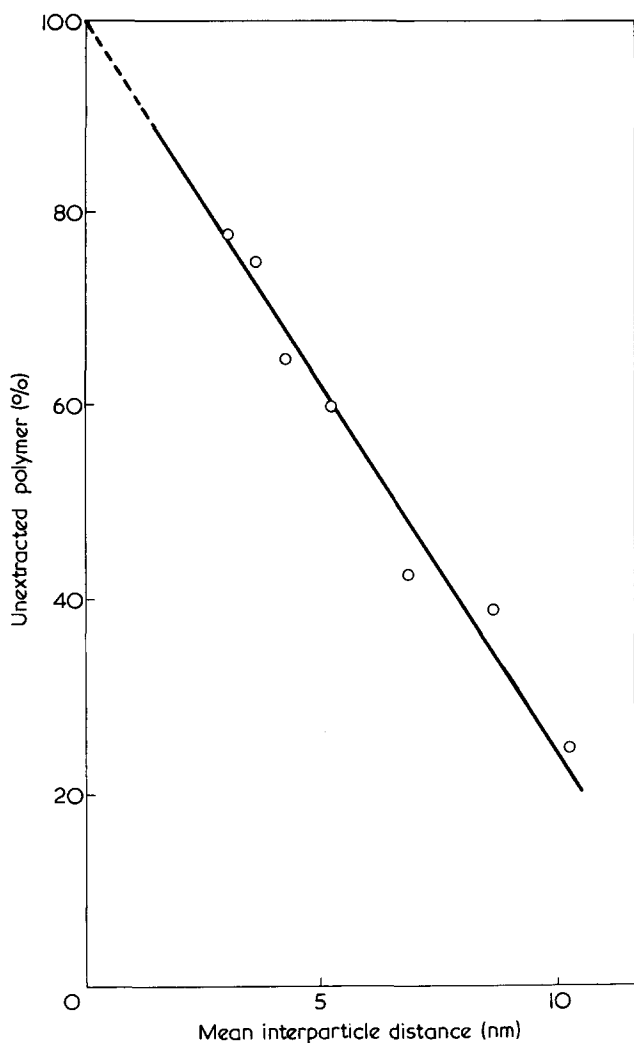


Figure 5 Relationship between unextracted polymer and the calculated mean distance between filler particles before immersion. Data from Figure 3

Again using the data from near-equilibrium conditions (Figure 3), there is found to be a linear relationship (Figure 5), with the line indicating complete insolubility when the filler particles are touching, i.e. at a volume concentration of 0.52, this is equivalent to nearly 250 phr of Aerosil 300, far in excess of practical concentrations.

CONCLUSIONS

It appears that both the liquid absorption and the unextracted polymer of a three-dimensional silicone rubber/

fume silica network, are dependent upon the mean distance between filler particles. However, the work with different liquids indicated that unextracted polymer often included unextracted, or unextractable, matrix rubber as well as true bound rubber i.e. adsorbed rubber and interparticular rubber. It is therefore concluded that liquid absorption is the primary parameter, dependent on the interparticular rubber and the mean distance between filler particles, while unextracted polymer is largely a secondary parameter, dependent on the liquid absorption.

In the mathematical model recently called for by Blow⁹, the importance of filler particle diameter was emphasized, it is now suggested that this is because of its effect upon the mean distance between the filler particles at any given loading.

ACKNOWLEDGEMENTS

This paper is based on a thesis recently accepted by Loughborough University of Technology in partial fulfilment of the requirements of the award of PhD. Further acknowledgement is made to the persons named therein, to the Directors of Dunlop Limited for permission to publish this paper and particularly to Dr C. M. Blow for his continuing interest and constructive criticism.

REFERENCES

- 1 Southwart, D. W. *M.Sc. Thesis* University of Manchester (1969)
- 2 Southwart, D. W. *Proc. Int. Rubber Conf., Brighton 1972*, paper G9
- 3 Southwart, D. W. and Hunt, T. *J. Inst. Rubber Ind.* 1970, 4, 74
- 4 Southwart, D. W. *Division of Rubber Chemistry, American Chemical Society, Cleveland 1971*, paper 70
- 5 Gessler, A. M. *Rubber Age* 1969, 101, 12, 54
- 6 Blow, C. M. and Stamberger, P. *Rec. Trav. Chim.* 1929, 48, 681
- 7 Boyer, R. F. *J. Chem. Phys.* 1945, 13, 363
- 8 Southwart, D. W. and Hunt, T. *J. Inst. Rubber Ind.*, 1968, 2, 140
- 9 Blow, C. M. *Polymer* 1973, 14, 309
- 10 Southwart, D. W. to be reported
- 11 Cooper, W. and Smith, R. K. *J. Appl. Polym. Sci.* 1962, 6, 64
- 12 Watson, J. W. *Trans. Inst. Rubber Ind.* 1956, 32, 204
- 13 Southwart, D. W. *Inst. Rubber Ind. Conf., Loughborough 1969*
- 14 Flory, P. J. 'Principles of Polymer Chemistry', Cornell University Press, Ithica, 1953, p 579
- 15 Vondráček, P. and Schätz, M. *Int. Rubber Conf. Prague 1973*
- 16 Bristow, G. M. and Watson, W. F. *Trans. Faraday Soc.* 1958, 54, 1731

Polarized far infra-red studies of hot-drawn polytetrafluoroethylene

R. G. Jones, Elisabeth A. Nicol, J. R. Birch, G. W. Chantry and J. W. Fleming
Electrical Science Division, National Physical Laboratory, Teddington, Middlesex, UK

and H. A. Willis and M. E. A. Cudby
ICI Plastics Division, Welwyn Garden City, Herts, UK
(Received 7 July 1975; revised 15 August 1975)

The three strong sharp lines in the 50 cm^{-1} region of the infra-red spectrum of polytetrafluoroethylene (PTFE) at liquid nitrogen temperature, have been shown to be strongly polarized, with the transition moments lying perpendicular to the molecular axes. This result is interpreted in terms of the lattice-mode theory and in terms of possible symmetries for the unit cell.

INTRODUCTION

Recently there has been considerable interest in the far infra-red spectrum of polytetrafluoroethylene (PTFE). The absorption bands observed, have been interpreted in terms of specific models for the dependence of the crystal structure on temperature¹. Further information may be obtained, by observing the spectra of specimens in which some degree of molecular alignment has been introduced e.g. by stretching in a tensile testing machine²⁻⁴. The polarization of the absorption bands may be predicted from the models and compared with experiment.

EXPERIMENTAL

Samples cut from a commercial sheet were stretched at 250°C in air, to a draw ratio of 2.3 at a rate of 100 mm/min and cooled slowly (3-4 h) at constant extension. Spectra were recorded between 30 and 100 cm^{-1} , both at room and liquid nitrogen temperatures using an NPL - Grubb Parsons modular Michelson interferometer, with a wire grid polarizer in the beam.

RESULTS AND DISCUSSION

The room temperature spectra showed the presence of the weak broad feature at 50 cm^{-1} and this was clearly, polarized strongly with the transition moment perpendicular to the draw direction. This result is exactly what would be expected if, as has been postulated, this band arises from the z-axis rotational lattice mode. On cooling to low temperature, the set of absorption bands in the $30-90\text{ cm}^{-1}$ region appears. This phenomenon is well known for unstretched PTFE and has been attributed to the onset of a two segment unit cell¹. Its persistence in the stretched material must mean that on stretching there is an orientation of crystallites, each of which is still able to undergo the phase transitions. A model for this would be a set of randomly oriented crystallites connected by disordered chains. On stretching, the disordered regions take the strain and pull the crystallites into alignment.

The nature of the 19°C transition in PTFE is still a matter for controversy, but the infra-red results are consistent with a model, in which rotational disorder leads essentially to there being one segment per unit cell above 19°C , i.e. a hexagonal form. Then there is a progressively closer

approach to a perfect two segment per unit cell structure (the monoclinic form) as the temperature continues to fall below the 19°C transition. This fact does not mean of course that this model is established, since i.r. studies are not the most sensitive way of establishing phase transitions, but nevertheless we will use the model to interpret our present results.

For an isolated chain molecule, there are four modes of vibration which have zero frequency for $k = 0$, these are the three translations T_x, T_y, T_z , and the rotation about the chain axis R_z . Because of the strong covalent bonding between repeat units, the two other rotations R_x and R_y take on the form of bond stretching or angle deformation modes and have finite and in fact quite high frequencies. When the chain-molecule forms part of a crystal lattice, the z-axis rotation has likewise a finite frequency, as the molecule does not have cylindrical symmetry nor is it moving in a cylindrically symmetric force field. The three translations are still of zero frequency, for one segment per unit cell, since they correspond to overall translation of the crystal. When there are two segments per unit cell, the in- and out-of phase coupling splits the z-axis rotation into a doublet and produces a finite frequency for each of the out of phase translational modes. One would then expect five lattice modes, but their spectral activity will depend on the cell symmetry. It is natural to compare results with the well known case^{5,6} of polyethylene but this has to be done with care because of the much higher symmetry (V_h) of the polyethylene unit cell. For PE* one has two i.r. active modes (T_x and T_y belonging to the irreducible representations B_{2u} and B_{3u} respectively), two Raman active modes (the split R_z in A_g and B_{1g} respectively) and an inactive mode in class A_u . For PTFE, where the current model postulates no higher than C_2 symmetry for the two segment unit cell, all five modes would be active in both i.r. and Raman scattering. In the i.r. case, the two translations T_x and T_y and both components of the split R_z would be polarized perpendicular to the draw direction and the fifth mode, now corresponding to z-axis translation, would be polarized parallel to the draw direction. In our previous assignment, we assumed that the line at 45 cm^{-1} was the analogue of the

* The point group $V_h(D_{2h})$ has an unavoidable ambiguity of axis labelling and consequently one may see one and the same vibration referred to as B_{1u} or B_{2u} ; this confusing situation is especially prevalent for the 73 cm^{-1} lattice mode.

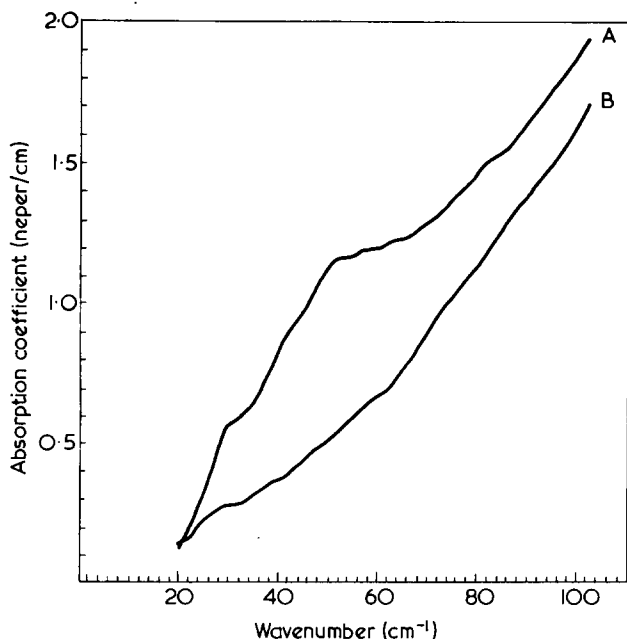


Figure 1 Polarized far infra-red spectra of a stretched sample of PTFE at room temperature. Resolution 4 cm^{-1} . A, Electric field perpendicular to draw axis; B, Electric field parallel to draw axis

B_{2u}^* (73 cm^{-1}) lattice mode of PE and that, the lines at 53.5 and 56.7 cm^{-1} were the components of the R_z doublet. This assumption is strongly confirmed by our present results. The location of the two other lattice bands is however much more problematical. In Figure 2 there will be seen weak lines at 70 , 76 and 86 cm^{-1} all of which are polarized perpendicularly and are therefore candidates for the B_{3u} mode. However, by analogy with PE, one would expect the B_{3u} (often referred to as the B_{2u} !) line to lie at higher frequency and to be much weaker than the B_{2u} (45 cm^{-1}) line; so perhaps the 70 or 76 cm^{-1} line can be identified with the B_{3u} mode. The 86 cm^{-1} line is probably at too high a frequency for consideration. There are no parallel polarized lines evident in Figure 2, so we have not yet succeeded in identifying the T_z lattice mode. Again by analogy with PE where calculations have placed the A_u mode below the B_{2u} mode, one would expect the T_z mode for PTFE to be below 45 cm^{-1} . It will however almost certainly be extremely weak, for it is only active in principle because of the slight helical distortion away from the planar zig zag. The perpendicularly polarized line at 34 cm^{-1} has previously¹ been assigned to the E_1 intersection of B_8 , and since this mode should give a perpendicularly polarized line, our present results confirm the assignment. We have as yet no clear explanation for the line at 86 cm^{-1} or for whichever of the 76 , 70 cm^{-1} pair is not the second perpendicular lattice mode. However the polarization evidence shown in Figures 1 and 2 provides further strong evidence in support of the two segment unit cell theory for the structure below 19°C .

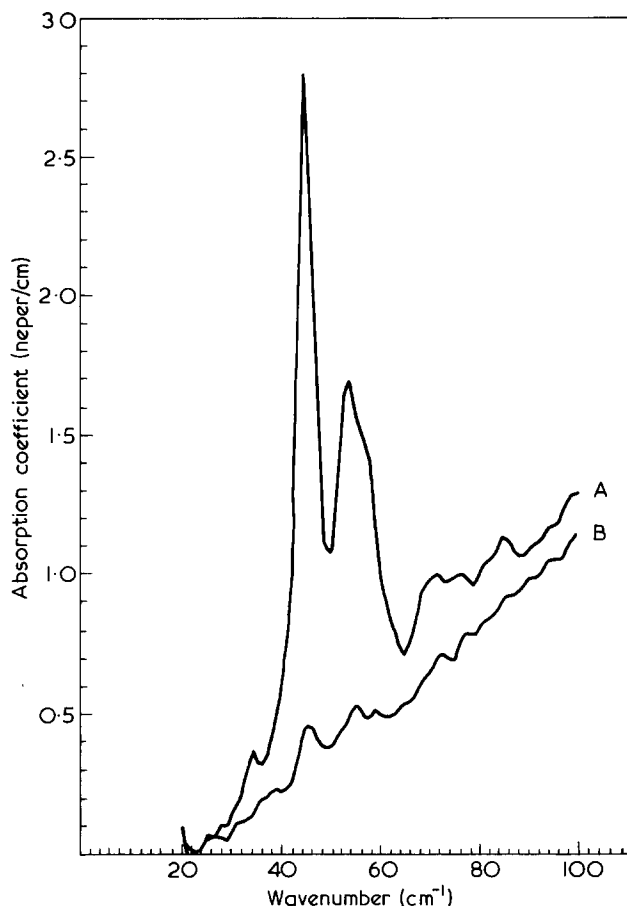


Figure 2 Polarized far infra-red spectra of a stretched sample of PTFE cooled by liquid nitrogen ($T = 110\text{ K}$). Resolution 2 cm^{-1} . A, Electric field perpendicular to draw axis; B, Electric field parallel to draw axis

ACKNOWLEDGEMENTS

We would like to thank Dr B. E. Read, Dr J. White and Dr R. J. Cook for much helpful advice and comment and Mr M. F. Markham for the use of the tensile testing apparatus.

REFERENCES

- 1 Chantry, G. W., Fleming, J. W., Nicol, E. A., Willis, H. A., Cudby, M. E. A. and Boerio, F. J. *Polymer* 1974, **15**, 69
- 2 Zbinden, R. 'Infra-red Spectroscopy of High Polymers', Academic Press, New York, 1964
- 3 Mills, N. J. in 'Polymer Science' (Ed. A. J. Jenkins), North Holland, Amsterdam, 1972
- 4 Frank, W. and Rabus, G. *Colloid Polym. Sci.* 1974, **252**, 1003
- 5 Dean, G. D. and Martin, D. H. *Chem. Phys. Lett.* 1967, **1**, 415
- 6 Fleming, J. W., Chantry, G. W., Turner, P. A., Nicol, E. A., Willis, H. A. and Cudby, M. E. A. *Chem. Phys. Lett.* 1972, **17**, 84

Non-Newtonian viscosity and non-linear flow birefringence of cellulose tricarbaniolate

J. W. M. Noordermeer, R. Daryanani and H. Janeschitz-Kriegl

Laboratory of Physical Chemistry, Delft University of Technology, Delft 8, The Netherlands
(Received 30 June 1975; revised 21 August 1975)

The shear rate dependence of the intrinsic viscosity and of the intrinsic property, which can be derived from the extinction angle, was investigated for a sample of cellulose tricarbaniolate. Its number-average molecular weight was 4.4×10^5 ; the solvents used were dioxane at 25°C and phenyl benzoate at 75°C , the latter being known to break most intramolecular hydrogen bonds. The onset of non-Newtonian viscosity was found at a reduced shear rate of about 0.1, whereas non-linear behaviour in the extinction angle was noticed already at 0.02. The obtained data were compared with the theory by Noda and Hearst¹⁰, which deals with the influence of chain stiffness on the viscoelastic properties of polymer solutions. The qualitative outcome of this theory agrees fairly well with the experimental results. However, the onset of non-linear behaviour, especially in the extinction angle, occurs at lower values of the reduced shear rate than predicted. The stress-optical law remains surprisingly valid for this stiff polymer throughout almost the whole accessible range of reduced shear rates. However, some experiments with the highly viscous solvent tri-*o*-cresyl phosphate at 30°C show appreciable deviations at reduced shear rates larger than 1.0.

INTRODUCTION

At the present time the shear rate dependence of the hydrodynamic properties of macromolecules is the subject of intensive study, both theoretical and experimental. The theory for the non-Newtonian viscosity of solutions of rigid ellipsoidal particles is satisfactorily developed¹ and is reasonably well confirmed by experiments^{2,3}. On the other hand, for solutions of flexible linear macromolecules the theoretical and experimental situations are still rather obscure. In a previous work⁴ we described the linear viscosity and flow birefringence behaviour of cellulose tricarbaniolate. We showed that the chain stiffness of this polymer depends on the temperature and the type of solvent. In etheric solvents this polymer has a stiffer conformation than in an ester or ketone.

The purpose of this paper is to report upon the non-linear behaviour of the viscosity and flow birefringence of this cellulose tricarbaniolate. Because of the great chain stiffness of cellulose derivatives, these polymers usually have too low a degree of polymerization to behave in solution as Gaussian coils⁵. This results in a hydrodynamic behaviour, which may differ appreciably from that of flexible Gaussian polymers such as polyethylene, polystyrene etc. The possibility of influencing the chain stiffness, in the case of cellulose tricarbaniolate, by a particular choice of solvent provides us with an additional parameter in the study of non-linear effects.

The general theories on the dynamics of dilute solutions of flexible macromolecules do not account for non-linear effects^{6,7}. This is due essentially to the linear character of the models underlying these theories. The results of these theories with respect to the polymer contributions to the stress tensor of a flowing solution, may be conveniently summarized as follows:

$$\Delta p \cos 2\chi' = p_{11} - p_{22} = \theta q^2 \quad (1)$$

$$\Delta p \sin 2\chi' = 2p_{12} = 2(\eta - \eta_s)q \quad (2)$$

where $\Delta p = p_{11} - p_{22}$ is the difference of the two principal stresses in the plane of flow, χ' , the orientation angle of the polymer contribution to the stress tensor in the plane of flow (defined as the smallest angle between the direction of one of the principal stresses and the direction of the flow), $p_{11} - p_{22}$, the so-called primary normal stress difference (related to the shear rate q by the primary normal stress coefficient, θ), p_{12} , the contribution of the polymer molecules to the shear stress, η the viscosity of the solution and η_s the solvent viscosity.

According to these theories θ and η should be independent of shear rate. In particular, the intrinsic viscosity $[\eta]$, defined as:

$$[\eta] = \lim_{c \rightarrow 0} \frac{p_{12}}{q\eta_s c} = [\eta]_0 \quad (3)$$

is independent of shear rate. In equation (3) c is the concentration (g/ml) and the subscript 0 indicates the value of $[\eta]$ at zero shear rate. Further:

$$\cot 2\chi' = \frac{p_{11} - p_{22}}{2p_{12}} = \frac{\theta q}{2(\eta - \eta_s)} \quad (4)$$

should be a linear function of shear rate.

Equation (4) can be presented in another form:

$$\cot 2\chi' = J_{eR} \beta_N \quad (5)$$

where J_{eR} is reduced steady-state shear compliance⁸, for which numerical values for flexible coil molecules^{6,7} and stiff rods^{9,10} were given earlier⁴. The reduced shear rate β_N is defined as¹¹:

$$\beta_N = \frac{Mq(\eta - \eta_s)}{cRT} \quad (6)$$

Table 1 Data of the solvents

Solvent	Temp. (°C)	Density (g/cm ³)	Viscosity × 10 ² (P)	$\Delta n_s \times 10^7$ at $q = 10^4$ (sec ⁻¹)
1, 4-Dioxane	25	1.0283	1.193	-----
Phenyl benzoate	75	1.0893	2.699	1.137
Tri- <i>o</i> -cresyl phosphate	30	1.1523	60.208	10.1

where M is the molecular weight of the polymer, R the gas constant and T the absolute temperature. The subscript N is used to indicate that the Newtonian 'zero shear' viscosity of the solution must be inserted*.

From an experimental point of view, however, it is well known that the ratios p_{12}/q and $(p_{11} - p_{22})/q^2$ both decrease with increasing q , in some cases even by several orders of magnitude. The first of both non-linear effects is usually referred to as the non-Newtonian viscosity.

Various attempts have been made to give a theoretical description of these non-linear phenomena. The reasons, usually quoted as responsible for non-linear effects are¹²: (i) changes in the excluded volume of the chain when the chain becomes extended at high shear rates¹³; (ii) an anisotropy of the hydrodynamic interaction at high shear rates^{14,15} (this is not accounted for in most molecular theories because of the necessity to preaverage the hydrodynamic interaction in order to facilitate further calculations); (iii) deviations from a perfect flexibility of the chain due to constraints imposed on the mobility of chain elements by fixed bond lengths and bond angles^{10,16}.

For the comparison with experimental results we have chosen the theory by Noda and Hearst¹⁰, as this theory seems to predict the most pronounced deviations from linearity. Moreover, it uses the parameters which were determined earlier⁴.

From a fundamental point of view it should be noted that, insofar as the mentioned theories make use of modifications of the linearized diffusion equation, this diffusion equation itself only holds for small deviations from equilibrium¹⁷. From such a linearized diffusion equation only a linear viscoelastic behaviour may be derived, in principle. Applying this equation to large deviations from equilibrium, where non-linearity appears, would seem to be incompatible with the linearization procedures needed to obtain the diffusion equation itself¹⁸. It should be mentioned as well that this doubt also holds for the basis of the theories described in refs. 1 and 24.

In terms of the stress-optical law¹⁹ there exists a direct relation between the contributions of coiled macromolecules to the stress tensor and the the flow birefringence of a streaming solution. According to this law:

$$\chi' = \chi \quad (7)$$

and

$$\Delta n \sin 2\chi = 2Cq(\eta - \eta_s) \quad (8)$$

where χ is the extinction angle, Δn the birefringence, both measured at shear rate q , and C is the so called stress-optical coefficient. The validity of the stress-optical law

* In principle, one can interpret the quantity β (without subscript N) also as a reduced shear stress. In that case, however, one has to insert the non-Newtonian viscosity of the solution, as measured at shear rate q .

is not necessarily linked to all peculiarities of the linear theories describing the hydrodynamic properties of polymers. Therefore, the non-linearity in η can tentatively be taken into account in equation (8) by inserting the non-Newtonian solution viscosity η , as measured at the finite shear rate q at which also the birefringence is measured.

Theoretically the constancy of the stress-optical coefficient can be made acceptable for polymers with Gaussian distributions of their end-to-end distances¹⁹⁻²³. For rigid ellipsoidal particles the stress-optical coefficient was predicted to decrease in value with increasing shear rate²⁴. For non-Gaussian polymers, like the cellulose tricarbanilate sample under investigation in this paper, an intermediate behaviour may be found.

EXPERIMENTAL

For the present investigation a sample of cellulose tricarbanilate (CCIV) was used. Its number-average molecular weight (M_n) was 4.4×10^5 and its polydispersity index (M_w/M_n) was about 1.5.

As solvents 1, 4-dioxane, phenyl benzoate and tri-*o*-cresyl phosphate were used. Dioxane (UCB) was dried over $MgSO_4$ and distilled afterwards. Phenyl benzoate (Fluka AG) was recrystallized from ethanol and thoroughly dried in vacuum. Tri-*o*-cresyl phosphate (K & K Laboratories) was dried over $MgSO_4$ and distilled under vacuum. Colourless products were obtained.

Solutions in dioxane were prepared by weighing dried cellulose tricarbanilate and freshly prepared solvent. In dioxane the polymer dissolved within one day at room temperature. The solutions in phenyl benzoate and in tri-*o*-cresyl phosphate were prepared by gently shaking at 75°C over several hours in a nitrogen atmosphere.

Table 1 contains data of the pure solvents for the temperatures at which measurements were carried out. The pure solvents phenyl benzoate and tri-*o*-cresyl phosphate show a measurable flow birefringence by themselves. It means that flow birefringence measurements, made in these solvents, have to be corrected for the solvent contribution Δn_s to the total birefringence Δn of the solution. Appropriate correction formulae were given by Sadron²⁵. Values of Δn_s are given as measured at a shear rate $q = 10^4$ sec⁻¹. Since, for low molecular weight fluids the dependence of Δn_s on shear rate is always linear, Table 1 contains all the information needed for these corrections.

Newtonian viscosities at low shear rates were measured with the aid of ordinary Ubbelohde viscometers. Shear rate dependent viscosities at higher rates of shear were measured with the aid of a special capillary viscometer at the Central Laboratory TNO, Delft, described by Daum and Janeschitz-Kriegl²⁶. The flow birefringence measurements were carried out in the equipment previously described by Janeschitz-Kriegl and Nauta²⁷.

RESULTS

Figure 1 gives an example for the non-Newtonian viscosity of cellulose tricarbanilate solutions. In this Figure the contributions of the solute to the viscosity are represented for solutions in dioxane at 25°C. The concentrations of the solutions range from 0.3×10^{-2} to 0.8×10^{-2} g/ml. In this Figure also a number of measurements is given, carried out with Ubbelohde viscometers. The shear rates in the

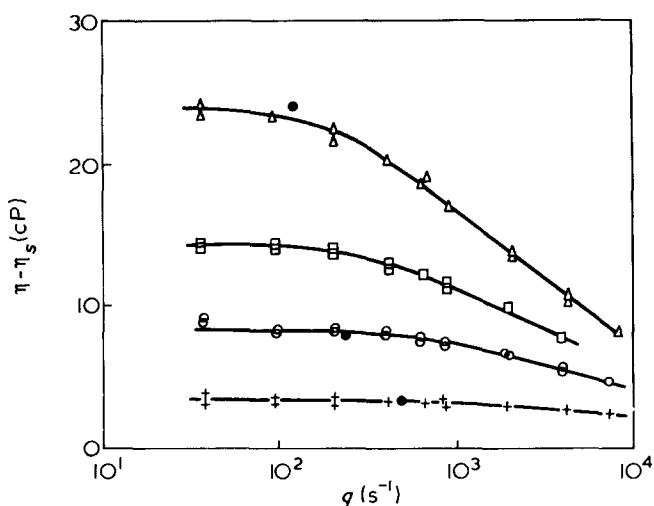


Figure 1 Shear rate dependence of the solute contribution to the viscosity for solutions of cellulose tricarbaniolate in dioxane at 25°C. Concentrations: +, 0.3×10^{-2} ; ○, 0.5×10^{-2} ; □, 0.65×10^{-2} ; △, 0.8×10^{-2} g/ml. ●, Ubbelohde measurements

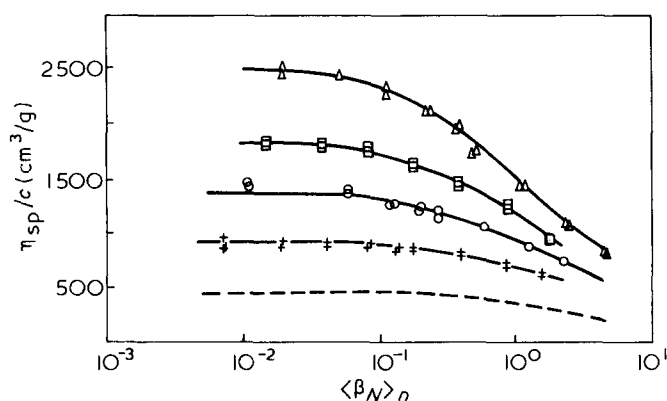


Figure 2 Data of Figure 1, replotted as the reduced viscosity η_{sp}/c against the reduced shear rate $\langle\beta_N\rangle_n$. Symbols as in Figure 1. ---, curve extrapolated to zero concentration

Ubbelohde viscometers were estimated from the dimensions of the apparatus. All viscosities measured with these Ubbelohde viscometers are in fair agreement with the Newtonian viscosities at low shear rates.

Figures 2 and 3 show the reduced viscosities of cellulose tricarbaniolate in dioxane at 25°C and in phenyl benzoate at 75°C as functions of the reduced shear rate $\langle\beta_N\rangle_n$. In the latter quantity $\langle \rangle_n$ signifies that the number-average molecular weight $\langle M \rangle_n$ is inserted in equation (6) for β_N .

From both Figures it is evident that the decrease of the reduced viscosity with increasing $\langle\beta_N\rangle_n$ is more pronounced for higher concentrations. An extrapolation of the reduced viscosities to zero concentration can be made with a reasonable accuracy. There are discussions^{28,29} on whether the extrapolations should be carried out at constant shear rate or at constant shear stress. Considering that in almost all theoretical works non-linear effects are basically expressed in terms of the reduced shear rate β_N , we chose to make the extrapolations at constant $\langle\beta_N\rangle_n$. The results, the intrinsic viscosities as functions of $\langle\beta_N\rangle_n$, are given by broken lines.

If one plots the reduced viscosity against reduced 'shear stress' $\langle\beta_n\rangle$, where the latter quantity is defined in exactly the same manner as $\langle\beta_N\rangle_n$, equation (6), except that the non-Newtonian solution viscosity is inserted, one obtains more pronounced non-Newtonian effects. All curves in Figures 2 and 3 converge in a stronger way. In extrapolat-

ing at constant $\langle\beta_n\rangle$ the Huggins constant approaches zero with increasing $\langle\beta_n\rangle$, so that the reduced viscosity seems to become more and more independent of concentration. This agrees with the observations of Munk and Peterlin³⁰ on solutions of polystyrene in Aroclor 1248.

In both solvents the non-Newtonian effects become perceptible at $\langle\beta_N\rangle_n$ values of about 10^{-1} . Further, in none of the solvents sufficiently large values of $\langle\beta_N\rangle_n$ are attained to reach a new constant value of the intrinsic viscosity (second Newtonian region).

Figures 4 and 5 show the non-linear behaviour of the extinction angle for cellulose tricarbaniolate in both solvents. Data are plotted as $\cot 2\chi/\langle\beta_N\rangle_n$ against $\langle\beta_N\rangle_n$. While according to linear theories $\cot 2\chi/\beta_N$ should be independent of β_N (equations (4) and (7)), a strong decrease is observed with increasing $\langle\beta_N\rangle_n$. A linear region is hardly found. For the solutions in dioxane the value of $\cot 2\chi/\langle\beta_N\rangle_n$ seems to level off at $\langle\beta_N\rangle_n$ values around 2×10^{-2} . The larger scatter which is observed at the lowest $\langle\beta_N\rangle_n$ values is caused by the relative inaccuracy in measuring extinction angles close to 45°. For the solutions in phenyl benzoate the measurements could not be extended to low enough shear rates to approach the linear region.

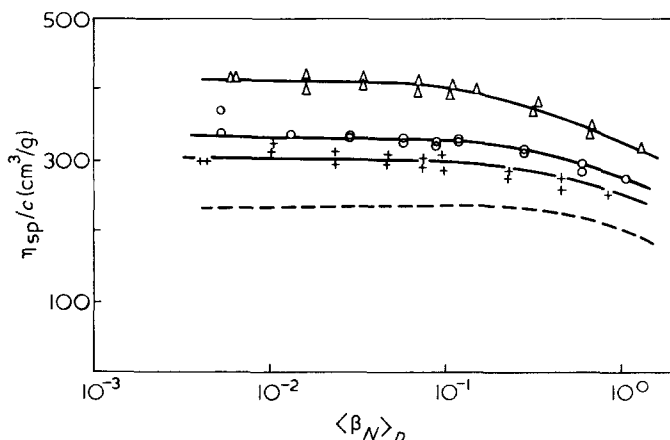


Figure 3 Shear rate dependence of the reduced viscosity for solutions of cellulose tricarbaniolate in phenyl benzoate at 75°C. Symbols as in Figure 1. ---, curve extrapolated to zero concentration

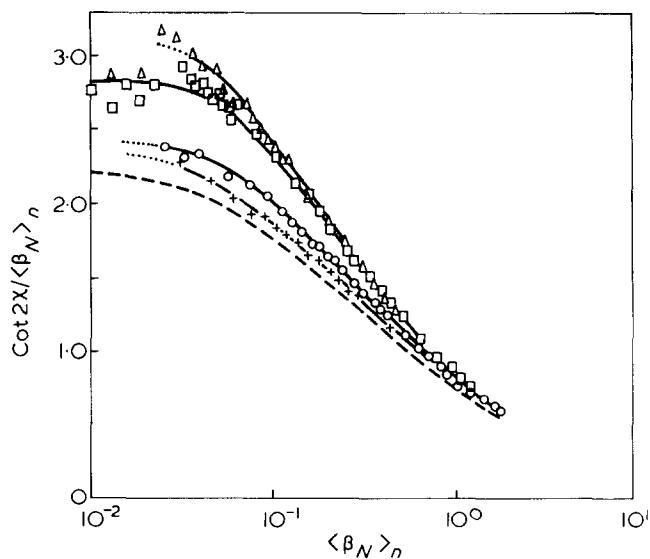


Figure 4 Shear rate dependence of the extinction angle for solutions of cellulose tricarbaniolate in dioxane at 25°C. Data plotted as $\cot 2\chi/\langle\beta_N\rangle_n$ against $\langle\beta_N\rangle_n$. Symbols as in Figure 1. ---, curve extrapolated to zero concentration

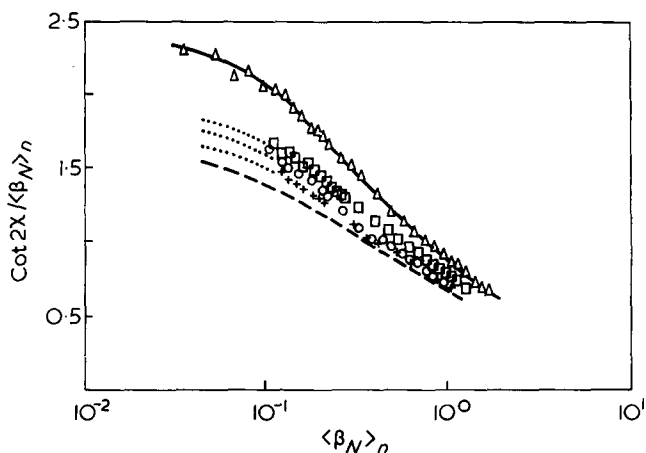


Figure 5 Shear rate dependence of the extinction angle for solutions of cellulose tricarbanilate in phenyl benzoate at 75°C. Data plotted as $\cot 2\chi/(\beta_N)_n$ against $(\beta_N)_n$. Symbols as in Figure 1. —, curve extrapolated to zero concentration

In view of the observable concentration dependence of $\cot 2\chi/(\beta_N)_n$ an extrapolation to infinite dilution was carried out, again at constant $(\beta_N)_n$. The resulting curves are given by broken lines. As to the kind of solvent no influence on the general shape of the curves can be observed, except that the curve for cellulose tricarbanilate in phenyl benzoate is lying slightly lower than the one for cellulose tricarbanilate in dioxane.

As a last type of non-linear behaviour deviations from the stress-optical law may be considered. In Figure 6 data are shown, chosen out of a variety of experimental data gathered on this subject. The given results were obtained on solutions of cellulose tricarbanilate in dioxane at 25°C (0.8×10^{-2} g/ml), in phenyl benzoate at 75°C (0.8×10^{-2} g/ml) and in the highly viscous solvent tri-*o*-cresyl phosphate at 30°C (0.564×10^{-2} g/ml). All values of the stress-optical coefficient were calculated according to equation (8), using the non-Newtonian solution viscosities. In all three solvents the stress-optical coefficient appears to be nearly independent of shear rate up to a $(\beta_N)_n$ value of about 1.0. Only the viscosity of the solution in tri-*o*-cresyl phosphate was high enough to enable measurements at sufficiently high reduced shear rates, where a significant decrease of the value of the stress-optical coefficient could be observed.

DISCUSSION

The experimental results show the occurrence of strong non-linear effects for cellulose tricarbanilate. The viscosity shows the first deviations from linear behaviour at $(\beta_N)_n$ values of about 10^{-1} . The ratio of $\cot 2\chi$ to $(\beta_N)_n$ shows a non-linear behaviour even at lower values of $(\beta_N)_n$.

A number of polystyrene samples of narrow *MWD* investigated by Janeschitz-Kriegl³¹, showed a linear relationship between $\cot 2\chi$ and $(\beta_N)_n$ up to $\beta_N = 0.5$. Also Munk and Peterlin³⁰ found similar results for polystyrene in Aroclor 1248, both on the intrinsic viscosity and on the ratio of $\cot 2\chi$ to $(\beta_N)_n$. It means that for this cellulose tricarbanilate the onset of non-linear behaviour is shifted to lower values of $(\beta_N)_n$.

It is of interest to compare the present data with the results of the theory of Noda and Hearst¹⁰. For that purpose, in Figure 7 the intrinsic viscosity of cellulose tricarbanilate in both solvents, as obtained from Figures 2 and 3, is replotted

as $[\eta]_{rel} \equiv [\eta]/[\eta]_0$ against $(\beta_N)_n$. The curves according to Noda and Hearst correspond to chains with various degrees of chain stiffness and a dominant hydrodynamic interaction. The numbers λL at the curves are the measures of chain stiffness; they correspond to the ratio of the contour length L of the chain to the length of a statistical random link l/λ . With increasing chain stiffness (smaller λL) the Noda and Hearst theory predicts that the onset of non-Newtonian viscosity shifts along the logarithmic $(\beta_N)_n$ scale to lower values of $(\beta_N)_n$. From the investigation⁴, values of λL can be derived for our sample of cellulose tricarbanilate in the solvents under consideration: $\lambda L = 17$ in dioxane at 25°C and $\lambda L = 28$ in phenyl benzoate at 75°C. The difference between these two values of λL seems to show up correctly in Figure 7. However, this difference is perhaps too small for a discrimination of the points where the solutions start to show non-Newtonian behaviour. Values of λL which apply to flexible polystyrene samples, as those investigated by Janeschitz-Kriegl, Munk and Peterlin, are at least an order of magnitude larger than those for cellulose tricarbanilate. The much greater chain stiffness of the latter may explain the shift of the onset of non-Newtonian effects to lower values of $(\beta_N)_n$. However, according to observa-

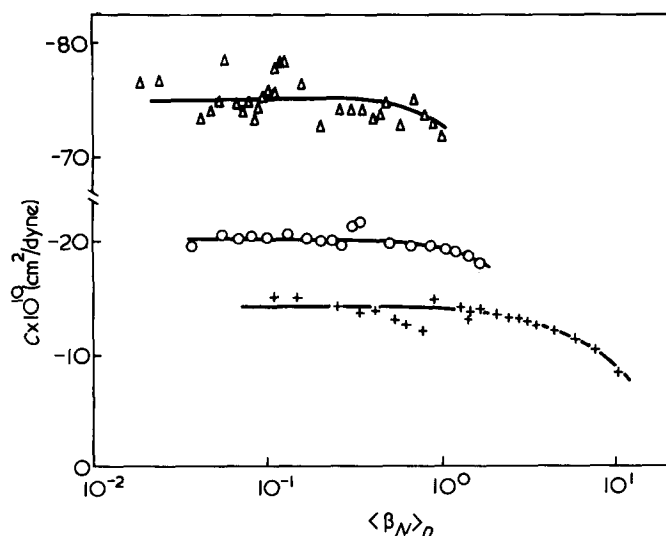


Figure 6 Stress-optical coefficient C against $(\beta_N)_n$ for a series of solutions of cellulose tricarbanilate in various solvents. Δ , 0.8×10^{-2} g/ml in dioxane at 25°C; \circ , 0.8×10^{-2} g/ml in phenyl benzoate at 75°C; +, 0.564×10^{-2} g/ml in tri-*o*-cresyl phosphate at 30°C

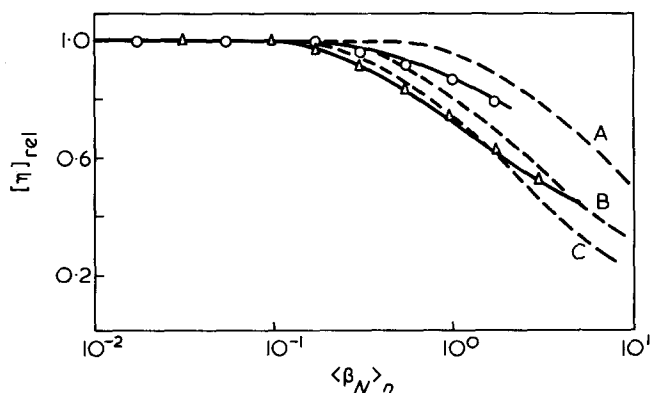


Figure 7 Plot of the relative intrinsic viscosity $[\eta]_{rel}$ against $(\beta_N)_n$ for cellulose tricarbanilate in Δ , dioxane at 25°C and \circ , phenyl benzoate at 75°C. —, theoretical lines according to Noda and Hearst. Parameters λL : A, 10; B, 1; C, 0.001

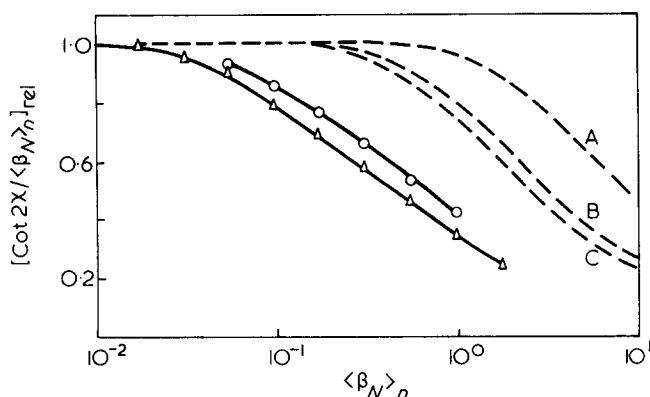


Figure 8 Plot of $[\cot 2\chi / \langle \beta_N \rangle_n]_{\text{rel}}$ against $\langle \beta_N \rangle_n$ for cellulose tricarbaniolate in \triangle , dioxane at 25°C and \circ , phenyl benzoate at 75°C. —, theoretical lines according to Noda and Hearst. Parameters λL : A, 10; B, 1; C, 0.001

tions on other polymers²⁹ the different slopes between the curves for dioxane and phenyl benzoate should be attributed to differences in solvent power. This implies that dioxane should be considered as a better solvent for cellulose tricarbaniolate than phenyl benzoate. This is noticeable, since phenyl benzoate breaks intramolecular hydrogen bonds⁴ in contrast to dioxane. The explanation may lie in the fact that cellulose tricarbaniolate has a hybrid nature with respect to solvents³⁶.

The theory predicts the total non-Newtonian behaviour of a polymer solution, i.e. the change from constant $[\eta]_0$ to a new constant $[\eta]_\infty$, to occur within about 3 decades of $\langle \beta_N \rangle_n$. This is found experimentally for solutions of monodisperse polymer samples^{3,32}. For the investigated sample of cellulose tricarbaniolate, the non-Newtonian viscosity range covers a broader region of shear rates: the whole transition seems to comprise at least 4 decades in $\langle \beta_N \rangle_n$. This broadening of the transition range is a well known polydispersity effect. The fact that the first deviations from Newtonian behaviour are observed at $\langle \beta_N \rangle_n$ values which are slightly smaller than those predicted by theory may therefore be due to the polydispersity of our sample.

The influence of the polydispersity on the behaviour of the extinction angle is appreciably more pronounced. Within the linear region (where $\cot 2\chi / \langle \beta_N \rangle_n$ is still independent of $\langle \beta_N \rangle_n$) the polydispersity raises $\cot 2\chi / \langle \beta_N \rangle_n$ to a value far outside the theoretical range for $J_e R$ ³³. Within the linear region the effect of polydispersity on the extinction angle can be calculated, if detailed information on the molecular weight distribution of the polymer and the molecular weight dependence of the intrinsic viscosity is available³⁴ and this was done previously⁴. Concerning the influence of polydispersity outside the linear region no detailed theoretical predictions are available yet.

Noda and Hearst have calculated the shear rate dependence of $[\cot 2\chi / \langle \beta_N \rangle_n]$ for monodisperse polymers with various degrees of chain stiffness. The large influence of polydispersity prohibits a quantitative comparison of the experimental data with their theory. On the other hand, a qualitative comparison can be tried by plotting $[\cot 2\chi / \langle \beta_N \rangle_n]_{\text{rel}} = [\cot 2\chi / \langle \beta_N \rangle_n] / [\cot 2\chi / \langle \beta_N \rangle_n]_0$ against $\langle \beta_N \rangle_n$. The subscript 0 refers to an extrapolation to zero shear rate. The infinite dilution curves in Figures 4 and 5 are replotted in this form in Figure 8. For the data obtained on cellulose tricarbaniolate in phenyl benzoate some arbitrariness is involved, because the value of $[\cot 2\chi / \langle \beta_N \rangle_n]_0$ had to be guessed. Besides these curves of experimental origin

Figure 8 also contains a theoretical curves for dominant hydrodynamic interaction and the same degrees of chain stiffness as in Figure 7. The shapes of the theoretical and experimental curves agree remarkably well. Furthermore, no difference in slope can be observed between the two experimental curves. This seems to indicate that polydispersity and solvent power do not influence the shape of the shear rate dependence of $[\cot 2\chi / \langle \beta_N \rangle_n]_{\text{rel}}$ to a large extent. However, the actual position of the experimental curves is shifted with respect to the theoretical curves by about one decade to lower values of $\langle \beta_N \rangle_n$.

The flexible polystyrene samples, mentioned before, start to behave non-linearly at $\langle \beta_N \rangle_n$ values of about 0.5, which is still small compared to what the Noda–Hearst theory predicts for the appropriate values of λL . It indicates that the Noda–Hearst theory underestimates the effect of non-linearity in the ratio $[\cot 2\chi / \langle \beta_N \rangle_n]$. Unfortunately, the other non-linear theories mentioned in the introduction, underestimate the non-linear effects even more.

As pointed out in Fig.8 of our previous paper⁴, the molecular weight of the sample under investigation is sufficiently high, so that any influences of polydispersity on the values of the stress–optical coefficient in Figure 6 can be neglected. By comparing the results in Figure 6 with those on the viscosity and the extinction angle, one observes quite clearly that the stress–optical law remains valid until far in the non-linear range of the former two. In this region cellulose tricarbaniolate still shows the same behaviour as Gaussian polymers, although the number of random links in dioxane, for example, amounts to only 17. At $\langle \beta_N \rangle_n$ values above 1.0, however, appreciable deviations from the stress–optical law are observed. For very flexible polymers many examples are known of a validity up to much higher values of $\langle \beta_N \rangle_n$ ^{30,33,35}. Therefore, the conclusion must be drawn that, although the stress–optical law still holds in a limited range of shear rates, it loses much of its general validity in the case of non-Gaussian polymers.

ACKNOWLEDGEMENTS

The authors wish to express their thanks to U. Daum at the Central Laboratory TNO, Delft, for giving the opportunity to measure non-Newtonian viscosities and to Professor W. Burchard, University of Freiburg, for many valuable discussions.

REFERENCES

- Scheraga, H. A. *J. Chem. Phys.* 1955, **23**, 1526
- Wada, E. *J. Sci. Instrum.* 1953, **47**, 168
- Yang, J. T. *J. Am. Chem. Soc.* 1958, **81**, 1783; 1959, **82**, 3901
- Noordermeer, J. W. M., Daryanani, R. and Janeschitz-Kriegl H. *Polymer* 1975, **16**, 359
- Flory, P., Spurr, O. K. and Carpenter, D. K. *J. Polym. Sci.* 1958, **27**, 231
- Rouse, P. E. *J. Chem. Phys.* 1953, **21**, 1272
- Zimm, B. H. *J. Chem. Phys.* 1956, **24**, 269
- Tschoegl, N. W. *J. Chem. Phys.* 1966, **44**, 4615
- Kotaka, T. *J. Chem. Phys.* 1959, **30**, 1566
- Noda, I. and Hearst, J. E. *J. Chem. Phys.* 1971, **54**, 2342
- Peterlin, A. *J. Chem. Phys.* 1963, **39**, 224
- Yamakawa, H. in 'Modern Theory of Polymer Solutions', Harper and Row, New York, 1971
- Fixman, M. *J. Chem. Phys.* 1966, **45**, 793
- Peterlin, A. and Copic, M. *J. Appl. Phys.* 1956, **27**, 434
- Copic, M. *J. Chim. Phys.* 1956, **53**, 440

Viscosity and flow birefringence of cellulose tricarbanilate: J. W. M. Noordermeer et al.

- 16 Reinhold, C. and Peterlin, A. *J. Chem. Phys.* 1966, **44**, 4333
17 Kirkwood, J. G. *J. Polym. Sci.* 1954, **12**, 1
18 Merk, H. J. *Rep. WTHD 46* Delft University of Technology, May 1973
19 Lodge, A. S. *Nature* 1955, **176**, 838; *Trans. Faraday Soc.* 1956, **52**, 127
20 Tsvetkov, V. N. in 'Newer Methods of Polymer Characterization', (Ed. B. Ke), Interscience, New York, 1964, p 563
21 Janeschitz-Kriegl, H. *Makromol. Chem.* 1959, **33**, 55; 1960, **40**, 140
22 Copic, M. *J. Chem. Phys.* 1957, **26**, 1382
23 Kuhn, W. and Gr \ddot{u} n, F. *Kolloid-Z.* 1942, **101**, 248
24 Scheraga, H. A., Edsall, J. T., and Gadd, J. O. *J. Chem. Phys.* 1951, **19**, 1101
25 Sadron, C. *J. Phys. Radium* 1938, **9**, 381
26 Daum, U. and Janeschitz-Kriegl, H. *Rheol. Acta* 1968, **7**, 349
27 Janeschitz-Kriegl, H. and Nauta, R. *J. Sci. Instrum.* 1965, **42**, 880
28 Kotaka, T., Suzuki, H. and Inagaki, H. *J. Chem. Phys.* 1966, **45**, 2770
29 Suzuki, H., Kotaka, T. and Inagaki, H. *J. Chem. Phys.* 1969, **51**, 1279
30 Munk, P. and Peterlin, A. *Rheol. Acta* 1970, **9**, 288, 294
31 Janeschitz-Kriegl, H. *Rheol. Acta* 1966, **5**, 78
32 Philippoff, W. 'Viscosit \ddot{a} t der Kolloide', Steinkopff, Dresden und Leipzig, 1942
33 Janeschitz-Kriegl, H. *Adv. Poly. Sci.* 1969, **6**, 170
34 Daum, U. *J. Polym. Sci. (A2)* 1968, **6**, 141
35 Philippoff, W. *Nature* 1956, **178**, 811; *J. Appl. Phys.* 1956, **27**, 984; *J. Poly. Sci. (C)* 1964, **5**, 1
36 Burchard, W. *Z. Phys. Chem.* 1964, **42**, 293; *Makromol. Chem.* 1965, **88**, 11

Influence of the molecular weight of poly(methyl methacrylate) on fracture surface energy in notched tension

R. P. Kusy and D. T. Turner

Dental Research Center, School of Dentistry, University of North Carolina at Chapel Hill, NC 27514, USA

(Received 11 August 1975)

Specimens of poly(methyl methacrylate) (PMMA) were prepared by the radiolysis of a polymer from an initial viscosity average molecular weight of $\bar{M}_v = 1.1 \times 10^6$ down to 1.5×10^4 . Corresponding values of fracture surface energy, ranging from 3.5×10^5 erg/cm² to 4.5×10^2 erg/cm², were calculated from tensile data using Griffith's equation. A theoretical dependence of fracture energy on molecular weight was derived on the assumption that only molecules exceeding a critical molecular weight can contribute to the work of plastic deformation. Comparison with experimental data indicates this molecular weight to be about 1×10^5 . Limitations of the theoretical treatment are discussed.

INTRODUCTION

The concepts of fracture surface energy (γ) and inherent flaw size have become more important as an understanding of their associated fracture mechanisms (e.g. crazing) has led to better materials. Starting with Griffith¹, investigators have tested many materials by different techniques, to compare experimental results with theory²⁻¹⁰. Today however, little experimental data exists describing the effect which molecular weight has on the fracture surface energy of glassy polymers (see Figure 1).

Berry¹¹, measured the fracture energy of PMMA for M in the range $(0.9-60) \times 10^5$. By an equation of the form $\gamma = A - BM^{-1}$, where A and B are arbitrary constants, he considered that γ should equal zero for $M = 2.5 \times 10^4$. He qualified this conclusion 'in view of the uncertain validity of that extrapolation', stating further that 'it would clearly be desirable to determine directly the fracture surface energy and other ultimate properties of samples with molecular weights extending down to the critical value'. In 1974, Kusy and Turner¹² carried out preliminary work in this direction, by the controlled radiation degradation of high molecular weight PMMA. While their results agreed with Berry's general statement that γ 'should become zero for a polymer of molecular weight 25 000', the functional dependence in the region of decreasing γ was not linear, but rather concave upward (see Figure 2 of ref 12). This trend was similar to data found, between the flexural strength and the reciprocal of number average molecular weight for PMMA at -196°C and ambient temperature, respectively^{13,14}. Moreover, work by Robertson¹⁵ on narrow molecular weight fractions of polystyrene, yielded a concave upward relationship for the molecular weight range below 10^5 . He also stated that, 'one deduces from this that the fracture energy vs. log (molecular weight) over the entire molecular weight range should be S-shaped with the maximum slope occurring around 10^5 '.

In general, information of this nature is hard to obtain because of inherent difficulties in preparing specimens of brittle, low molecular weight polymers. However, PMMA is an exception in that its molecular weight can be decreased in a controlled manner by exposure of specimens, conveniently machined at high molecular weight, to high

energy radiation. The objective of the present paper, is to make use of this property to document the dependence of fracture energy over a wide range of molecular weight.

EXPERIMENTAL

Material preparation

An unplasticized PMMA homopolymer, Plexiglas G (Rohm and Haas Co.), was cut at random into two sets of specimens: A, $12.7 \times 2.5 \times 0.32$ cm; B, $12.7 \times 3.2 \times 0.32$ cm. Slots were cut in the A specimens with a 0.015 cm thick circular saw, from 0.025 to 0.25 cm in depth, either before or after irradiation. Cracks were made in unirradiated B specimens using a method similar to that described by Berry¹⁶, in which a wedge was driven into a slot 0.7 cm deep. Subsequently, 0.7 cm was milled off to reduce the B specimens to the same dimensions as the A specimens. Residual stresses were relieved by heat treating at one of three equivalent time-temperature schemes: 5 h at 90°C , $10\frac{1}{2}$ h at 80°C , or 24 h at 70°C . A few specimens were not annealed for purposes of comparison.

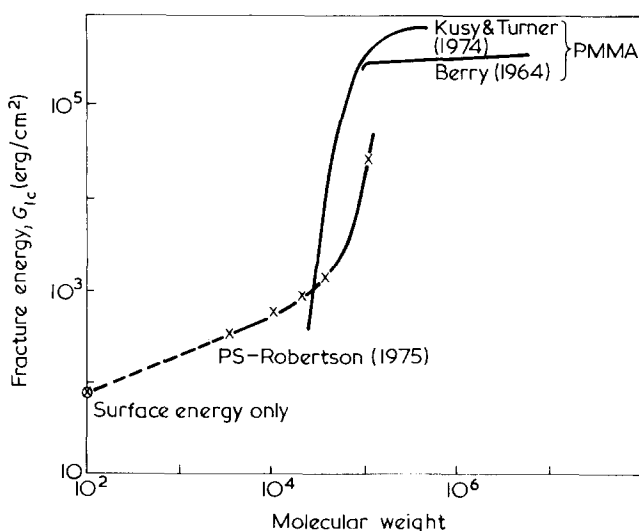


Figure 1 Influence of molecular weight of glassy polymers on fracture energy (from ref 15)

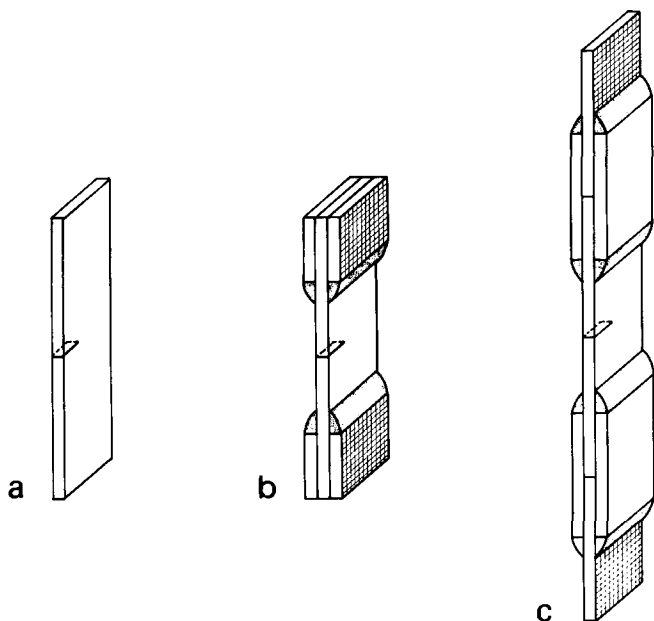


Figure 2 Preparation of notched tensile bars: (a), machined and notched; (b), with PMMA flats bonded for direct gripping; (c), with PMMA lap joints bonded for indirect gripping. Hatched regions represent gripping areas while shaded zones are epoxy fillets

Irradiation

Specimens were exposed in air at an ambient temperature of 30°–40°C to gamma rays from either a ^{137}Cs or ^{60}Co source. Nominal dose rates were 0.90 and 2.1 Mrad/h, respectively. Irradiation resulted in the formation of gaseous products, which were removed by degassing over periods ranging up to six months. Degassing was considered to be complete when gas bubbles no longer formed when specimens were heated above the glass transition temperature, i.e. above 105°C¹⁷. As reported by Charlesby¹⁸, heating immediately after irradiation resulted in such extensive outgassing, that an expanded foam was formed. In order to evaluate any influence owing to trapped gas, some specimens were tested without degassing, shortly after irradiation.

Testing procedures

The flexural modulus, E , was calculated from the deflection, δ , produced by a force, P , in a three point bending test using equation (1), in which l , b , and d are the length, width, and thickness of the unnotched specimen, respectively¹⁹:

$$E = \frac{Pl^3}{4bd^3\delta} \quad (1)$$

The engineering stress at fracture, σ_f , was determined in tension using an Instron machine at a crosshead separation of 0.1 cm/min. Specimens given high doses were extremely brittle so that lap joints were bonded to the grip areas to prevent premature fracture (Figure 2).

Limiting viscosity numbers $[\eta]$ were determined in benzene at 25°C. Viscosity molecular weights, \bar{M}_v , were calculated from the Mark–Houwink equation (2) in which $K = 5.5 \times 10^{-5}$ dl/g and $\alpha = 0.76$ ²⁰:

$$[\eta] = K\bar{M}_v^\alpha \quad (2)$$

RESULTS AND DISCUSSION

Controlled degradation by radiolysis

The PMMA made as commercially cast sheets, is a linear polymer with a Schulz-type molecular weight distribution (equation 3):

$$W(r) = \left(\frac{k}{\bar{x}_n}\right)^{k+1} \left(\frac{r^k}{k!}\right) \exp\left(\frac{-kr}{\bar{x}_n}\right); 1 \leq k \leq 2 \quad (3)$$

in which $W(r)$ is the weight fraction of r -mers and \bar{x}_n is the number average degree of polymerization²¹. On exposure to high energy radiation, PMMA molecules are fractured at random at a rate of 1.7 fractures per 100 eV of absorbed energy, i.e. $G(\text{fractures}) \equiv G(F) \approx 1.7$ ²². This controlled degradation by radiolysis is both convenient and reproducible, since the fracture reaction is insensitive to wide variations in radiation source-type (X , γ or e^-), dose rates (0.1–100 Mrad/h), atmosphere (air or *in vacuo*), or ambient source temperature (20°–40°C)²³. Furthermore, the G -value remains relatively constant up to doses of at least 40 Mrad (1 Mrad = 6×10^{19} eV/g)²⁴. A dose of a few Mrad transforms the initial distribution to a ‘most probable distribution’, for which $k = 1$ ²⁵. In such cases the number average molecular weight, \bar{M}_n , can be calculated from the value prior to irradiation, $\bar{M}_{n,0}$, (equation 4) in which R is the dose in Mrad:

$$\frac{1}{\bar{M}_n} = \frac{1}{\bar{M}_{n,0}} + \left[\frac{R \times G(F)}{9.6}\right] \times 10^{-5} \quad (4)$$

In a first approach it would suffice to calculate molecular weights from equation (4), but in the present work reliance was placed on experimentally determined limiting viscosity numbers, $[\eta]$. This allows the calculation of a viscosity molecular weight, \bar{M}_v , (equation 2) and derivation of a number average, \bar{M}_n , from equation (5):

$$\bar{M}_v = \frac{\bar{M}_n}{k} \left[\frac{\Gamma(1+k+\alpha)}{\Gamma(1+k)}\right]^{1/\alpha} \quad (5)$$

i.e.

$$\bar{M}_v = 1.89\bar{M}_n \text{ for } k = 1 \quad (6a)$$

and

$$\bar{M}_v = 1.45\bar{M}_n \text{ for } k = 2 \quad (6b)$$

Equation (6a) was used since the ‘most probable distribution’ is generated by random fracture^{25,26}.

The above considerations are the result of the simple fracture of PMMA molecules by irradiation. In polymers, however, fracture is usually accompanied by crosslinking reactions. PMMA is unusual in that it is degraded ‘without appreciable crosslinking’. Definitive evidence has been reported by Shultz *et al.*²⁷ for doses up to 11 Mrad. In the present work it is assumed provisionally that it is valid to even higher doses.

Radiolysis of PMMA is also known to cause other chemical reactions which are normally considered to be of secondary importance because they do not influence molecular size. Nevertheless, attention should be given to factors which might influence the measurements of fracture energy.

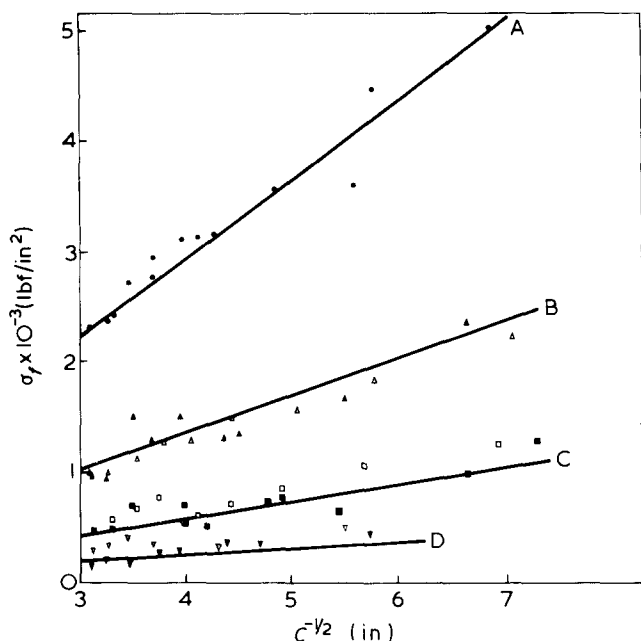


Figure 3 Influence of crack length (c) on tensile strength (σ_f) as a function of molecular weight (\bar{M}_v): A, $\gamma = 2.4 \times 10^5$ erg/cm², $\bar{M}_v = 1\,120\,000$, ● degassed specimens; B, $\gamma = 4.7 \times 10^4$ erg/cm², $\bar{M}_v = 52\,600$, ▲ degassed, △ not degassed specimens; C, $\gamma = 1.3 \times 10^4$ erg/cm², $\bar{M}_v = 29\,200$, ■ degassed, □ not degassed; D, $\gamma = 3.4 \times 10^3$ erg/cm²; $\bar{M}_v = 15\,000$, ▼ degassed, ▽ not degassed

By far the most important of these reactions is the G -value of gas formation. This subject will be pursued in a subsequent section.

Estimation of fracture energy

Values for γ , can be calculated from Griffith's equation (7) (plane strain)¹ in which σ_f is the tensile stress at fracture, c , the crack length, E , Young's modulus, and ν , Poisson's ratio:

$$\sigma_f = \left[\frac{2E\gamma}{\pi c(1-\nu^2)} \right]^{1/2} \quad (7)$$

This expression may be used since the ratio of the crack length to specimen width (c/w) is small (<0.1), which minimizes the interaction of the strain energy field near the crack tip with the specimen edge²⁸. The functional dependence of σ_f on c has been demonstrated previously for high molecular weight PMMA¹⁶ and is now shown for low molecular weights (Figure 3). Theoretically, Griffith's equation is only applicable to brittle materials but its use has been extended to other materials, e.g. PMMA, which conform empirically but which, nevertheless, are known to undergo localized plastic deformation in the vicinity of the crack tip. In such cases Griffith's equation may be used but the physical significance of γ is a matter of conjecture. In the case of metals, Orowan³ and Irwin⁵ independently suggested that γ be regarded as the sum of an elastic and plastic component. In the present work, γ comprises a contribution from the energy expended in generating surfaces by cleavage, γ_1 , and in causing localized plastic deformation, γ_2 , i.e.

$$\gamma = \gamma_1 + \gamma_2 \quad (8)$$

Values of γ were calculated from the slopes of Figure 3 in which $\nu = 0.32$ and $E = 3.8 \times 10^{10}$ dyn/cm². The value of E was measured as a flexural modulus which was found to be independent of molecular weight (Figure 4). Sisman

and Bopp²⁹ found that Young's modulus was unaffected when specimens of PMMA were exposed to radiation from an atomic pile ($E = 3.2 \times 10^{10}$ dyn/cm²). Furthermore from a plot of $\log P/\delta$ vs. $\log l$ on irradiated double cantilever beams, the intercept and slope, both of which are related to the elastic properties of the material, were insensitive to molecular weight change¹⁴. These observations are in contrast to Berry's report that E increases from 2.30×10^{10} to 3.06×10^{10} dyn/cm² as \bar{M}_v increases from 0.98×10^5 to 3.0×10^6 ¹¹. The present data is preferred, because, in principle, there is no reason why E should be dependent on the molecular weight range studied.

A number of factors might influence estimates of fracture energy. First, it is known that gases are formed on irradiation of PMMA with initial G -values (up to a dose of 6.5 Mrad) as follows: $G(\text{CH}_4) = 0.55$; $G(\text{CO}) = 0.44$; $G(\text{CO}_2) = 0.32$; $G(\text{H}_2) = 0.21$ and $G(\text{HCO}_2\text{H}) = 0.09$ ³⁰. This would correspond to a total gas formation of ~ 3 cm³ (STP)/cm³ polymer/Mrad. From the foaming phenomenon associated with heating the irradiated polymer, it is apparent that some of this gas remains trapped immediately after irradiation. This does not result in the formation of any flaws detectable to the naked eye; e.g. there is no turbidity. However, since cavitation is an important phenomenon in crazing, which occurs immediately ahead of the crack tip, there is some possibility that gas might influence fracture energy. A comparison of specimens which were degassed with those tested immediately after irradiation, shows that gas formation is unimportant (Table 1). This suggests that, similar to experiments describing the yielding in metals, moderate hydrostatic stresses do not, in the first approximation, affect the failure criterion of PMMA^{31,32}.

The second factor, which Griffith found important in his study of silicate glasses, was the influence of initial stress on fracture energy. For PMMA no significant effect was detected throughout the range of molecular weights

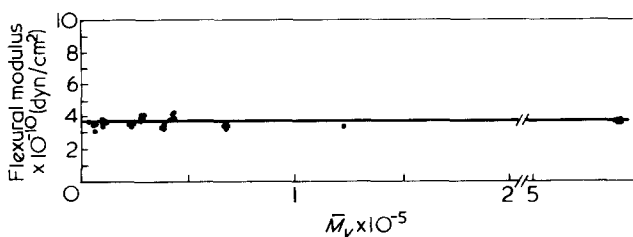


Figure 4 Influence of molecular weight (\bar{M}_v) on modulus of elasticity (E) in transverse bending

Table 1 Dependence of fracture energy (γ) on residual gas

Nominal dose R (Mrad)	\bar{M}_v	γ (erg/cm ²)*	
		degassed	not degassed
0	1 120 000	$2.5 (\pm 18) \times 10^5$	
		$2.4 (\pm 15) \times 10^5$	
5	193 000	$1.7 (\pm 16) \times 10^5$	$1.6 (\pm 25) \times 10^5$
10	112 000	$1.7 (\pm 20) \times 10^5$	$1.6 (\pm 17) \times 10^5$
17	75 000	$1.4 (\pm 30) \times 10^5$	$9.7 (\pm 29) \times 10^4$
25	52 600	$4.9 (\pm 30) \times 10^4$	$4.5 (\pm 7) \times 10^4$
32	42 100	$3.2 (\pm 28) \times 10^4$	$3.4 (\pm 18) \times 10^4$
40	33 500	$1.7 (\pm 31) \times 10^4$	$1.8 (\pm 20) \times 10^4$
50	29 200	$1.1 (\pm 38) \times 10^4$	$1.4 (\pm 20) \times 10^4$
65	21 700	$6.1 (\pm 38) \times 10^3$	$5.3 (\pm 34) \times 10^3$
80	15 000	$2.3 (\pm 41) \times 10^3$	$4.5 (\pm 49) \times 10^3$

* Mean (\pm SD) of ten specimens which were tested with saw notches (pre-irradiation notched) after annealing ($\dot{R} = 0.90$ Mrad/h). SD expressed as % of mean.

Table 2 Dependence of fracture energy (γ) on residual stress

Dose R(Mrad)	\bar{M}_v	γ (erg/cm ²)*	
		annealed	unannealed
0	1 160 000	2.4 (± 20) $\times 10^5$ (35)**	1.9 (± 15) $\times 10^5$ (15)
30.9 (\dot{R} = 0.90 Mrad/ h)	37 100	6.6 (± 15) $\times 10^3$ (5)	6.8 (± 28) $\times 10^3$ (5)
30.9 (\dot{R} = 2.1 Mrad/ h)	28 900	6.3 (± 32) $\times 10^3$ (5)	4.2 (± 18) $\times 10^3$ (5)

* Mean (\pm SD) of indicated number of specimens (***) which were tested with saw notches (pre-irradiation notched) after degassing. SD expressed as % of mean.

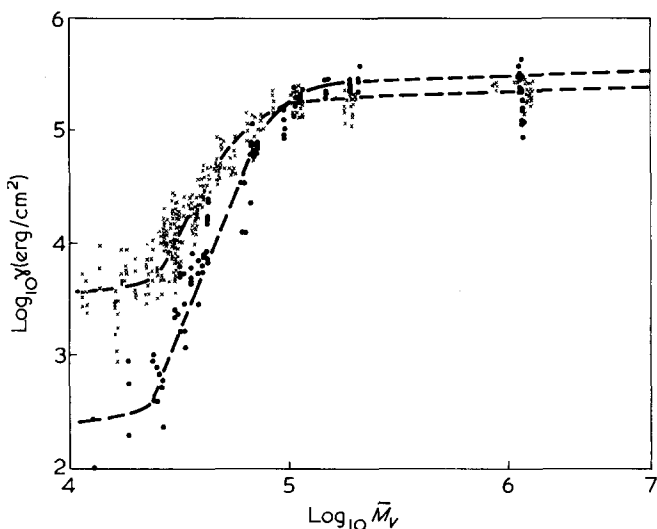


Figure 5 Comparison of fracture energy (γ) versus molecular weight (\bar{M}_v): x, saw notches; •, natural notches formed by driving in wedge. Specimens were pre-irradiation notched and tested in annealed and degassed condition

studied (Table 2). While it might be argued that PMMA tested at room temperature is sufficiently close to its glass transition temperature to relieve the residual stresses introduced from specimen preparation, it is more plausible that the residual stress is relieved in the vicinity of the crack tip by the applied stress field during testing. Andrews and Kazama³³ have suggested in unplasticized PVC that, with increasing stress, localized yielding occurs as the glass transition is reduced to the test temperature. Similarly, stress-induced annealing could occur in the proximity of the initial notch long before unstable fracture initiated. It is worthwhile to note that the glass transition temperature (105°C) does decrease as a function of molecular weight^{26,34}.

A third factor of concern in measuring fracture energy is the influence of crack tip geometry. For high molecular weight specimens, similar results were obtained whether a crude slot was introduced directly with a saw or whether a crack-craze combination was created by driving in a wedge (Figure 5). Apparently the time consumed in the buildup of stress prior to fracture, is sufficient to result in some typical crack-craze combination, which makes the initial notch geometry immaterial. In contrast the surface energy of more brittle specimens, of lower molecular weight, in which modification of the crack tip by crazing is expected to be less important, are influenced by the sharpness of the crack tip (Figure 5). For studying the influence of molecu-

lar weight on fracture energy, crack formation by driving in a wedge is preferred.

In order to put the present results in perspective, a comparison of surface energy of PMMA with previous work is shown (Figure 6). Comparisons are only possible for high molecular weight specimens. In agreement with Marshall *et al.*²⁸, a scatter of some $\pm 15\%$ is observed for the original (0 Mrad) material (Table 1 and 2) compared with $\pm 9\%$ for parallel cleavage bars. Also for a given molecular weight, cleavage tests give lower values of γ than do notched tensile bars. This is consistent with energy *versus* crack velocity data (the test method was immaterial), in which the high crack velocities of notched tensile specimens yield greater values of γ than do the slower crack velocities done in cleavage. Present experiments do not account for large variations in crack velocity which might perturb the results with respect to variations in molecular weight. Experiments on irradiated parallel cleavage specimens are in progress to investigate this factor.

A theoretical relationship for the dependence of fracture energy on molecular weight

Berry noted from his data that a marked decrease in γ did not occur until $\bar{M}_v < 4 \times 10^5$ ¹¹. He suggested that only molecules long enough to pass through the craze region immediately ahead of the crack tip, could act as stress bearing members between the two adjacent uncrazed boundaries. In his words, 'The contribution which any particular molecule makes to the surface energy will be determined by the length that is contained within this region. A sufficiently long molecule will start in the unyielded region, pass through the yielded region, and terminate once again in the unyielded region. Under these conditions, the contribution made by the molecule to the surface energy will be independent of its length. Correspondingly this energy should tend to a limiting value at high molecular weights, ...'¹¹. Berry's views may be expressed in quantitative terms by making the additional assumption, that the molecules above

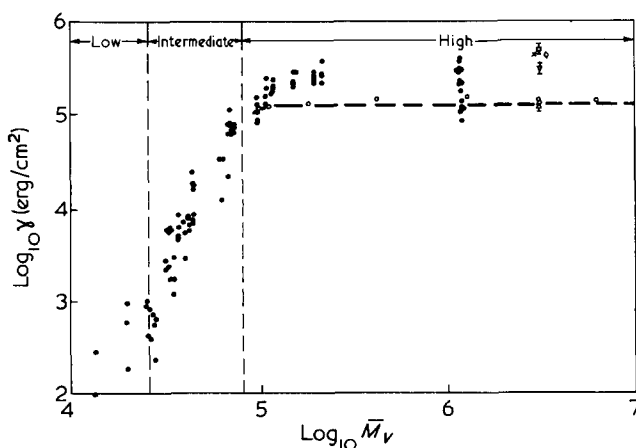


Figure 6 Influence of fracture energy (γ) on molecular weight (\bar{M}_v) for various investigators

Symbol	Investigators	Poly(methyl methacrylate) Designation	Test Method
□	Benbow & Roesler (35)	Perspex	Wedge Splitting
x	Irwin & Kies (5)	Plexiglas II	Central Notch
◇	Svensson (36)	Perspex	Wedge Splitting
▽	Berry (16)	Plexiglas II	Tensile Test
△	Berry (11)	Plexiglas II	Cleavage Test
◊	Broulman & Mc Garry (37)	Plexiglas II	Cleavage Test
•	Present Work, natural notches	Plexiglas G	Tensile Test

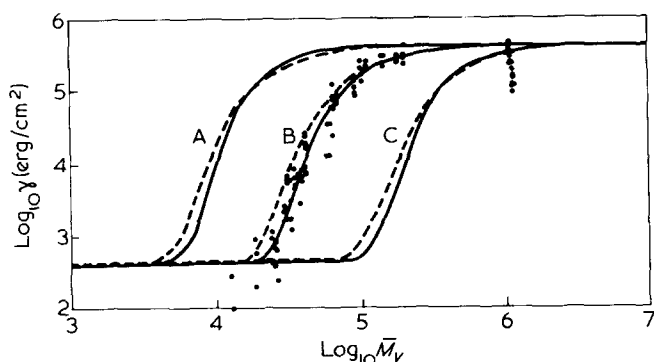


Figure 7 Influence of x and k on the theoretical relationship for fracture energy (γ). [Present experimental results, (●) are shown versus ———, $k = 1$; ———, $k = 2$]. A, $x = 2.5 \times 10^2$; B, $x = 1 \times 10^3$; C, $x = 5 \times 10^3$

a critical length contribute to the γ_2 term in proportion to their volume fraction. This procedure approximates to the 'rule of mixtures', a familiar empirical relationship. However, as a variation to this rule, it is physically more significant to assume that the γ_1 term is constant rather than proportional to the volume fraction of molecules below the critical length. In practice this variation is unimportant at higher average molecular weights since the γ_1 contribution is negligible.

On the assumption that only molecules with more than a critical number of monomer units (x) contribute to the work of plastic deformation, i.e. to the γ_2 term, and that γ_2 is equal to the product of the volume fraction of such molecules, v_2 , and a constant energy term, γ_c , equation 9 results:

$$\gamma = \gamma_1 + \gamma_2 = \gamma_1 + v_2 \gamma_c \quad (9)$$

For convenience equation (9) can be expressed in terms of the volume fraction of molecules with numbers of units (i.e. degree of polymerization) $\leq x$, v_1 , and by replacing volume fractions with corresponding weight fractions, i.e. w_1 for v_1 (equation 10). This last approximation is permissible as the density of PMMA is virtually independent of molecular weight.

$$\gamma \approx \gamma_1 + (1 - w_1) \gamma_c \quad (10)$$

The weight fraction of all molecules with up to x monomer units (equation 11) can be evaluated for the case of the 'most probable distribution' ($k = 1$) from the expression for $W(r)$ (see equation 3 and equation 12). Substitution of w_1 in equation (10) yields equation (13).

$$w_1 = \int_0^x W(r) dr \quad (11)$$

$$W(r) = \frac{r}{x_n^2} e^{-r/x_n} \quad (12)$$

$$\gamma \approx \gamma_1 + \gamma_c e^{-x/x_n} \left(1 + \frac{x}{x_n} \right) \quad (13)$$

Similar expressions can be evaluated for other molecular weight distributions, e.g. when $k = 2$ (see equation 3):

$$\gamma \approx \gamma_1 + \gamma_c e^{-\frac{2x}{x_n}} \left(1 + \frac{2x}{x_n} + \frac{2x^2}{x_n^2} \right) \quad (14)$$

Comparison of theory and experiment

The theory, as expressed by equation (13), agrees with experiment (Figure 6) by giving a sigmoidal dependence of γ on number average molecular weight, i.e. on $\bar{M}_n = x_n M_0$ or, equivalently, on $\bar{M}_v = 1.89 \bar{M}_n$ (M_0 is the molecular weight of the monomer unit, which equals 100 for PMMA). The limiting values for the sigmoid are as follows:

$$\lim_{x_n \rightarrow 0} \gamma = \gamma_1$$

$$\lim_{x_n \rightarrow \infty} \gamma = \gamma_1 + \gamma_c \approx \gamma_c, (\gamma_c \gg \gamma_1)$$

A theoretical value of $\gamma_1 = 450 \text{ erg/cm}^2$ has been calculated by Berry¹⁶ on the assumption that cleavage of a monolayer of covalent bonds occurs. The experimental value of $\gamma_1 = 450 \pm 250 \text{ erg/cm}^2$ is in agreement with this calculation, but the experimental data are too erratic to warrant further comment. No theoretical estimate is available for γ_c , although values fluctuate from $1.1\text{--}4.9 \times 10^5 \text{ erg/cm}^2$,^{15,16,28,35-37} the former considered to be the best at slow crack velocities²⁸, i.e. the isothermal state. However, a precise value is not a critical consideration at this stage and an empirical value was selected which best represented the present data (Figure 6), of $\gamma_c = 3.5 \times 10^5 \text{ erg/cm}^2$.

With values for γ_1 and γ_c determined, the dependence of γ on average molecular weight can be calculated from equation (13) for any selected critical degree of polymerization, x . Calculated curves for $x = 2.5 \times 10^2$, 1×10^3 , and 5×10^3 are shown in Figure 7, in which \bar{M}_v is expressed instead of \bar{M}_n to facilitate comparison with experimental data. In order to test the sensitivity of such plots to the extremes of molecular weight distribution, the foregoing procedure was applied for the case when $k = 2$ using equation (14). This factor is small in relation to changes caused by the selection of values of x . From the theoretical curves and experimental data in Figure 7, the critical value of x is near 1×10^3 , i.e. to a molecular weight of 1×10^5 .

A test of the theory would be to check whether the dependence of fracture energy on average molecular weight could be predicted for other distributions. A particularly challenging test would be to check whether or not, as theory would predict, a step function dependence of γ on molecular weight for monodisperse fractions (i.e. $\bar{M}_n = \bar{M}_v$) would result with $\gamma = \gamma_1$ for $M < 1 \times 10^5$ and $\gamma = \gamma_c$ for $M > 1 \times 10^5$. Information of this kind is not available for PMMA, but has been determined for approximately monodisperse specimens of polystyrene¹⁵. Robertson's data (Figure 1), point to an obvious inadequacy of the theory. The assumption that there is an unique boundary molecular chain length which determines an all or nothing contribution to the energy of plastic deformation, is an over simplification. In fact, the physical significance of this assumption is not entirely clear. According to Berry¹¹, a critical molecular chain length is required to bridge the craze layer immediately ahead of the crack tip (i.e. the 'crack opening displacement' in the Dugdale model). Direct observations on high molecular weight PMMA, however, indicate that this dimension is about $1 \times 10^4 \text{ \AA}$ ³⁸, whereas a fully extended molecule of molecular weight 10^5 is smaller by a factor of three. It would be more realistic to regard the craze as an extended network of polymer molecules held together by physical entanglements³⁹. Then the upturn in γ_1 at $\log \bar{M}_v \approx 4.3$ (Figure 7), could be interpreted as the molecular weight required for incipient net-

work formation due to entanglements. Bueche⁴⁰ has reported a range of values ($\log \bar{M}_v \approx 4.30-4.56$), for the molecular weight at which entanglements cause a sudden increase in bulk viscosity measurements of PMMA, plasticized with 75% diethyl phthalate (at 60°C). Naturally, the conditions are not strictly comparable since the craze is 'plasticized' not by solvent but by about 40% holes, 100 Å in diameter⁴¹. Despite the considerable attention given to entanglements with respect to viscosity measurements, no quantitative treatment for γ could be developed in these terms. For the moment then, the role which entanglements have must be limited to some form of negative skewing of the sigmoid.

CONCLUSIONS

(1) γ may be conveniently determined as a function of molecular weight by the radiolysis of PMMA.

(2) The Griffith theory is valid over the entire range of molecular weights studied from the straight line relationship of σ_f vs. $c^{-1/2}$.

(3) While the formation of gas and the presence of residual stresses have no significant effect on γ , notch geometry is critical with decreasing molecular weight ($\bar{M}_v \lesssim 10^5$).

(4) For notched tensile specimens varying from $\bar{M}_v = 1.5 \times 10^4 - 1.1 \times 10^6$, γ ranged from $4.5 \times 10^2 - 3.5 \times 10^5$.

(5) The dependence of γ on molecular weight was shown by partitioning γ into an elastic (γ_1) and plastic (γ_2) component and by assuming that only molecules greater than x , contribute to γ_2 . (a) Both theoretical and experimental data indicate that γ has a sigmoidal dependence on molecular weight. (b) Varying x greatly influences the sigmoid, while k has little effect. (c) The critical molecular chain length (x) corresponds to $\approx 1 \times 10^3$. (d) The crazed layer may be best described as a network of extended chains containing periodic entanglements. (e) The upturn of γ_1 at $\log \bar{M}_v \approx 4.3$ may be interpreted as the onset of entanglement networks.

ACKNOWLEDGEMENT

We are grateful to the Applied Radiation Division of NBS and the Physics Department at UNC for use of the ⁶⁰Co and ¹³⁷Cs facilities. We thank Mrs Beverly Lytwyn and Mr Gerald Thalken for assistance with the experimental work. This investigation was supported by NIH research grant number DE 02668 from the National Institute of Dental Research and by NIH grant number RR 05333 from the Division of Research Facilities and Resources.

REFERENCES

- 1 Griffith, A. A. *Philos. Trans. R. Soc. (A)* 1921, **221**, 163
- 2 Inglis, C. E. *Trans. Inst. Naval Arch.* 1913, **55**, 219
- 3 Orowan, E. *Z. Phys.* 1933, **82**, 239; *Welding J.* 1955, **34**, 1575; Felbeck, D. K., and Orowan, E. *Welding J.* 1955, **34**, 570
- 4 Obreimoff, J. W. *Proc. R. Soc. (A)* 1939, **127**, 290
- 5 Irwin, G. R. and Kies, J. A., *Welding J.* 1952, **31**, 995; 1954, **33**, 1935
- 6 Irwin, G. R., Kies, J. A., and Smith, H. L. *ASTM Proc.* 1958, **58**, 640
- 7 Gilman, J. *J. Appl. Phys.* 1960, **31**, 2208
- 8 Berry, J. P. *J. Polym. Sci.* 1961, **50**, 313
- 9 Marsh, D. M. *Proc. Roy. Soc. (A)* 1964, **279**, 420
- 10 Causton, B. E. *J. Dent. Res.* 1975, **54**, 339
- 11 Berry, J. P. *J. Polym. Sci. (A)* 1964, **2**, 4069
- 12 Kusy, R. P. and Turner, D. T. *Polymer* 1974, **15**, 394
- 13 Vincent, P. I. *Polymer* 1960, **1**, 425
- 14 Kusy, R. P. and Turner, D. T. unpublished work
- 15 Robertson, R. E. *ACS Polym. Symp.*, Toughness and Brittleness of Plastics, in press
- 16 Berry, J. P. *J. Polym. Sci.* 1961, **50**, 107
- 17 Loshaek, J. *Polym. Sci.* 1955, **15**, 391
- 18 Charlesby, A. "Atomic Radiation and Polymers", Pergamon Press, London 1960, Ch. 18; *Nucleonics* 1954, **12**, 18
- 19 Cernica, J. N. "Strength of Materials", Holt, Rinehart, and Winston, New York, 1966, Ch 4
- 20 Cantow, H. J. and Shultz, G. V. *Z. Phys. Chem.* 1954, **2**, 117
- 21 Peebles, L. H. "Molecular Weight Distributions in Polymers", Interscience, New York, 1971, Ch 1
- 22 Dole, M. "The Radiation Chemistry of Macromolecules", Academic Press, New York, 1973, Vol 2, Ch 6
- 23 Chapiro, A. "Radiation Chemistry of Polymeric Systems", Interscience, New York, 1962
- 24 Kusy, R. P. and Turner, D. T. *J. Polym. Sci.* 1974, **12**, 2137
- 25 Bovey, F. A. "The Effects of Ionizing Radiation on Natural and Synthetic High Polymers", Interscience, New York, 1958
- 26 Thompson, E. V. *J. Polym. Sci.* 1966, **4**, 199
- 27 Shultz, A. R., Roth, P. I. and Rathmann, G. B. *J. Polym. Sci.* 1956, **22**, 495
- 28 Marshall, G. P., Culver, L. E., and Williams, J. G. *Plast. Polym.* 1969, **37**, 75
- 29 Bopp, C. D. and Sisman, O. *Nucleonics* 1955, **13**, 28
- 30 Turner, D. T. *Macromol. Rev.* 1971, **5**
- 31 Polanyi, M. and Schmid, E. *Z. Phys.* 1923, **16**, 336
- 32 Bridgman, P. W. *Met. Technol. Tech. Pub.* 1782, 1944
- 33 Haward, R. N. "The Physics of Glassy Polymers", Applied Science, London, 1973, p.328
- 34 Beevers, R. B. and White, E. F. T. *Trans. Faraday. Soc.* 1960, **56**, 744
- 35 Benbow, J. J. and Roesler, F. C. *Proc. Phys. Soc.*, 1957, **70B**, 201
- 36 Svensson, N. L. *Proc. Phys. Soc.* 1961, **77**, 876
- 37 Broutman, L. J. and McGarry, F. J. *J. Appl. Polym. Sci.* 1965, **9**, 589
- 38 Kambour, R. P. and Barker, R. E. *J. Polym. Sci.* 1966, **4**, 359
- 39 Bueche, F. "Physical Properties of Polymers", Interscience, New York, 1962, Ch. 2 and 3.
- 40 Bueche, F. *J. Appl. Phys.* 1955, **26**, 738
- 41 Kambour, R. P. and Robertson, R. E. *G.E. Tech. Rep. 70-C-104*, 1970, p 65

Notes to the Editor

Optical anisotropy and orientation of structural units

P. Zoller

Kunststofflabor, Neu-Technikum Buchs, CH-9470 Buchs, Switzerland

(Received 11 July 1975; revised 21 August 1975)

A situation is considered, where the optical anisotropy of a polymer is caused exclusively by a non-random distribution of anisotropic structural units. A structural unit is thought to be some structure in the polymer which does not change its internal structure during orientation. Electrically it is characterized by the principal values α_{ii} ($i = 1, 2, 3$) of its polarizability tensor. The associated principal axes attached to the structural unit are designated by x'_i ($i = 1, 2, 3$). The optical anisotropy of the sample is specified by the three principal refractive indices n_i ($i = 1, 2, 3$) and the associated principal axes of the sample x_i ($i = 1, 2, 3$)¹.

The polarizability tensor b_{ij} of the sample, is diagonal ($b_{ij} = 0$, if $i \neq j$) when its components are referred to the x_i set of axes, and the diagonal components of b_{ij} can be related to the principal refractive indices in a good approximation by the Lorentz-Lorenz equations¹:

$$b_{ii} = \frac{3}{4\pi N} \times \frac{n_i^2 - 1}{n_i^2 + 2} \quad i = 1, 2, 3 \quad (1)$$

in which N is the number of structural units per unit volume. Therefore, $N = \delta N_0/M$, where δ is the density of the sample, N_0 is Avogadro's number ($6.02 \times 10^{-23} \text{ mol}^{-1}$) and M is the molecular weight of the structural unit.

Another way of expressing b_{ij} , is by transforming the polarizability tensor α_{ij} of each structural unit from the sets of axes x'_i , attached to the structural units, to the set of axes x_i , attached to the sample (in which its components are designated by α''_{ij}). Assuming additivity of the contributions from all structural units we obtain:

$$\begin{aligned} b_{11} &= \langle \alpha''_{11} \rangle = \langle t_{11}^2 \rangle \alpha_{11} + \langle t_{12}^2 \rangle \alpha_{22} + \langle t_{13}^2 \rangle \alpha_{33} \\ b_{22} &= \langle \alpha''_{22} \rangle = \langle t_{21}^2 \rangle \alpha_{11} + \langle t_{22}^2 \rangle \alpha_{22} + \langle t_{23}^2 \rangle \alpha_{33} \\ b_{33} &= \langle \alpha''_{33} \rangle = \langle t_{31}^2 \rangle \alpha_{11} + \langle t_{32}^2 \rangle \alpha_{22} + \langle t_{33}^2 \rangle \alpha_{33} \end{aligned} \quad (2)$$

The t_{nm} are the components of the transformation matrix between the x'_i and the x_i sets of axes:

$$\alpha''_{kl} = t_{k'l} \alpha_{ij} \quad k, l = 1, 2, 3 \quad (3)$$

and the brackets $\langle \rangle$ denote averaging over the distribution of structural units. Since the transformation is between sets of orthogonal coordinate systems the coefficients t_{nm} obey the orthonormality relations:

$$t_{im} t_{in} = \delta_{mn} = \begin{cases} 0 & \text{if } m \neq n \\ 1 & \text{if } m = n \end{cases} \quad (4)$$

From these equations the following relations can be deduced by taking averages:

$$\begin{aligned} \langle t_{11}^2 \rangle + \langle t_{12}^2 \rangle + \langle t_{13}^2 \rangle &= 1 & \langle t_{11}^2 \rangle + \langle t_{21}^2 \rangle + \langle t_{31}^2 \rangle &= 1 \\ \langle t_{21}^2 \rangle + \langle t_{22}^2 \rangle + \langle t_{23}^2 \rangle &= 1 & \langle t_{12}^2 \rangle + \langle t_{22}^2 \rangle + \langle t_{32}^2 \rangle &= 1 \\ \langle t_{31}^2 \rangle + \langle t_{32}^2 \rangle + \langle t_{33}^2 \rangle &= 1 & \langle t_{13}^2 \rangle + \langle t_{23}^2 \rangle + \langle t_{33}^2 \rangle &= 1 \end{aligned} \quad (5)$$

Note, that only five of these six equations are independent. Because of the orthonormality conditions, it is possible to express the t_{nm} through trigonometric functions of three angles (called the Euler angles, see e.g. Kashiwagi *et al.*²), such that the orthonormality relations are automatically met. We feel, however, that it is clearer to proceed with the usual meaning of the t_{nm} as direction cosines

$$t_{nm} = \cos(X_n, X'_m) \quad n, m = 1, 2, 3 \quad (6)$$

and keeping equations (5) as a set of auxiliary equations. Equations (2) and (5) form a set of nine linear, inhomogeneous equations for the quantities $\langle t_{nm}^2 \rangle$. Since only seven of the nine equations of the associated homogeneous system are linearly independent, the $\langle t_{nm}^2 \rangle$ can in general not be determined uniquely. Note also that the inhomogeneous system only has a solution if:

$$b_{11} + b_{22} + b_{33} = \alpha_{11} + \alpha_{22} + \alpha_{33} \quad (7)$$

We will proceed to investigate in a formal mathematical way, information about the $\langle t_{nm}^2 \rangle$ that can be obtained from equations (2) and (5). This will depend on the degree of optical symmetry that either the sample or the structural unit possesses. The following cases are possible:

The sample possesses orthorhombic optical symmetry

In this case, $b_{11} \neq b_{22} \neq b_{33} \neq b_{11}$ (or $n_1 \neq n_2 \neq n_3 \neq n_1$); this is the most general case for the optical anisotropy of the sample. The directions of the principal axes of the sample are completely determined.

The structural unit possesses orthorhombic optical symmetry

In this case, $\alpha_{11} \neq \alpha_{22} \neq \alpha_{33} \neq \alpha_{11}$; this is the most general case for the anisotropy of the polarizability of the structural unit. The directions of the principal axes of the polarizability tensor in the structural unit are completely determined.

Notes to the Editor

The sample is optically transversally isotropic

In this case, $b_{11} \neq b_{22} = b_{33} = b_T$ (or $n_1 \neq n_2 = n_3 = n_T$); the direction of only one principal axis in the sample is determined (x_1); the other two (x_2 and x_3) can be chosen at will, provided they form an orthogonal system of axes with x_1 .

The structural unit is transversally isotropic

In this case, $\alpha_{11} \neq \alpha_{22} = \alpha_{33} = \alpha_T$. The direction of only one principal axis of the polarizability tensor of the structural unit is determined (x'_1); the other two (x'_2 and x'_3) can be chosen at will, provided they form an orthogonal system of axes with x'_1 .

The sample is optically isotropic

In this case, $b_{11} = b_{22} = b_{33} = b$ (or $n_1 = n_2 = n_3 = n$). Any system of orthogonal axes in the sample is a system of principal axes.

The structural unit is isotropic

In this case, $\alpha_{11} = \alpha_{22} = \alpha_{33}$. Since an isotropic structural unit can only lead to an isotropic sample this case is pursued no further.

The solution derived below for different combinations of these cases could be written in somewhat different forms by making use of equation (7) to replace one of the three α_{ii} or one of the three b_{ii} , by the remaining α_{ii} and b_{ii} .

Transversally isotropic structural unit

The choice in the directions of x'_2 and x'_3 in each structural unit can clearly be used to make:

$$\langle t_{12}^2 \rangle = \langle t_{13}^2 \rangle, \langle t_{22}^2 \rangle = \langle t_{23}^2 \rangle, \langle t_{32}^2 \rangle = \langle t_{33}^2 \rangle \quad (8)$$

The only $\langle t_{nm}^2 \rangle$ with physical significance are the ones with the second index equal to one.

For a sample with orthorhombic optical symmetry we obtain from equations (2) and (5):

$$\begin{aligned} \langle t_{11}^2 \rangle &= \frac{b_{11} - \alpha_T}{\alpha_{11} - \alpha_T} \\ \langle t_{21}^2 \rangle &= \frac{b_{22} - \alpha_T}{\alpha_{11} - \alpha_T}, \quad \langle t_{31}^2 \rangle = \frac{b_{33} - \alpha_T}{\alpha_{11} - \alpha_T} \end{aligned} \quad (9)$$

If the sample is transversally isotropic the result is (for any choice of the x_2 and x_3 axes):

$$\begin{aligned} \langle t_{11}^2 \rangle &= \frac{b_{11} - \alpha_T}{\alpha_{11} - \alpha_T} \\ \langle t_{21}^2 \rangle = \langle t_{31}^2 \rangle &= \frac{b_T - \alpha_T}{\alpha_{11} - \alpha_T} \end{aligned} \quad (10)$$

If the sample is isotropic we immediately obtain:

$$\langle t_{11}^2 \rangle = \langle t_{21}^2 \rangle = \langle t_{31}^2 \rangle = 1/3 \quad (11)$$

for any choice of the x_1, x_2 and x_3 axes in the sample.

The cases of a transversally isotropic structural unit and either an orthorhombic or a transversally isotropic sample have been worked out by Kashiwagi *et al.*² using Euler angles to specify the orientation.

OPTICALLY ORTHORHOMBIC STRUCTURAL UNIT AND ORTHORHOMBIC OPTICAL SYMMETRY OF THE SAMPLE

The general solution for the $\langle t_{nm}^2 \rangle$ of our basic equations (2) and (5) contain two parameters λ_1 and λ_2 . One way of writing the solution is:

$$\begin{aligned} \langle t_{11}^2 \rangle &= \frac{\alpha_{22} - b_{11}}{\alpha_{22} - \alpha_{11}} + (\lambda_1 - \lambda_2) \frac{\alpha_{33} - \alpha_{22}}{\alpha_{22} - \alpha_{11}} \\ \langle t_{12}^2 \rangle &= \frac{b_{11} - \alpha_{11}}{\alpha_{22} - \alpha_{11}} - (\lambda_1 - \lambda_2) \frac{\alpha_{33} - \alpha_{11}}{\alpha_{22} - \alpha_{11}} \\ \langle t_{13}^2 \rangle &= \lambda_1 - \lambda_2 \\ \langle t_{21}^2 \rangle &= \frac{\alpha_{22} - b_{22}}{\alpha_{22} - \alpha_{11}} + \lambda_2 \frac{\alpha_{33} - \alpha_{22}}{\alpha_{22} - \alpha_{11}} \\ \langle t_{22}^2 \rangle &= \frac{b_{22} - \alpha_{11}}{\alpha_{22} - \alpha_{11}} - \lambda_2 \frac{\alpha_{33} - \alpha_{11}}{\alpha_{22} - \alpha_{11}} \\ \langle t_{23}^2 \rangle &= \lambda_2 \\ \langle t_{31}^2 \rangle &= \frac{\alpha_{33} - b_{33}}{\alpha_{22} - \alpha_{11}} - \lambda_1 \frac{\alpha_{33} - \alpha_{22}}{\alpha_{22} - \alpha_{11}} \\ \langle t_{32}^2 \rangle &= \frac{b_{33} - \alpha_{33}}{\alpha_{22} - \alpha_{11}} + \lambda_1 \frac{\alpha_{33} - \alpha_{11}}{\alpha_{22} - \alpha_{11}} \\ \langle t_{33}^2 \rangle &= 1 - \lambda_1 \end{aligned} \quad (12)$$

Any choice of the parameters λ_1 and λ_2 will give a solution to the system, and all possible solutions are obtained by varying λ_1 and λ_2 . However, only certain choices of λ_1 and λ_2 will give physically meaningful results, since, from the meaning of the $\langle t_{nm}^2 \rangle$ as averages of the squares of direction cosines, we must require:

$$0 \leq \langle t_{nm}^2 \rangle \leq 1 \quad n, m = 1, 2, 3 \quad (13)$$

This immediately puts the following conditions on λ_1 and λ_2 :

$$0 \leq \lambda_1 \leq 1, 0 \leq \lambda_2 \leq 1, \lambda_1 \geq \lambda_2 \quad (14)$$

In general the range of the allowed λ_1 and λ_2 , will be even more restricted by equation (13), but a certain finite range will remain for λ_1 and λ_2 and with it, through equations (12), a certain range for the $\langle t_{nm}^2 \rangle$. This calculation of the allowed ranges for the $\langle t_{nm}^2 \rangle$ is the maximum information which can be extracted from the optical anisotropy without additional assumptions. If this range is small for one or more of the $\langle t_{nm}^2 \rangle$ this knowledge constitutes valuable information.

An additional assumption which can be made to reach a complete solution, is that of random orientation of the x'_3 and x'_2 axes around the x'_1 axis in different structural units. Mathematically this implies:

$$\langle t_{12}^2 \rangle = \langle t_{13}^2 \rangle, \langle t_{22}^2 \rangle = \langle t_{23}^2 \rangle, \langle t_{32}^2 \rangle = \langle t_{33}^2 \rangle \quad (15)$$

These equations fix the values of λ_1 and λ_2 exactly, yielding the following solution for the $\langle t_{nm}^2 \rangle$:

$$\begin{aligned}
 \langle t_{11}^2 \rangle &= \frac{\alpha_{22} + \alpha_{33} - 2b_{11}}{\alpha_{22} + \alpha_{33} - 2\alpha_{11}} \\
 \langle t_{12}^2 \rangle = \langle t_{13}^2 \rangle &= \frac{b_{11} - \alpha_{11}}{\alpha_{22} + \alpha_{33} - 2\alpha_{11}} \\
 \langle t_{21}^2 \rangle &= \frac{\alpha_{22} + \alpha_{33} - 2b_{22}}{\alpha_{22} + \alpha_{33} - 2\alpha_{11}} \\
 \langle t_{22}^2 \rangle = \langle t_{23}^2 \rangle &= \frac{b_{22} - \alpha_{11}}{\alpha_{22} + \alpha_{33} - 2\alpha_{11}} \\
 \langle t_{31}^2 \rangle &= \frac{\alpha_{22} + \alpha_{33} - 2b_{33}}{\alpha_{22} + \alpha_{33} - 2\alpha_{11}} \\
 \langle t_{32}^2 \rangle = \langle t_{33}^2 \rangle &= \frac{b_{33} - \alpha_{11}}{\alpha_{22} + \alpha_{33} - 2\alpha_{11}}
 \end{aligned} \tag{16}$$

OPTICALLY ORTHORHOMBIC STRUCTURAL UNIT AND TRANSVERSALLY ISOTROPIC SAMPLE

For any choice of the x_2 and x_3 axes:

$$\langle t_{21}^2 \rangle = \langle t_{31}^2 \rangle, \langle t_{22}^2 \rangle = \langle t_{32}^2 \rangle, \langle t_{23}^2 \rangle = \langle t_{33}^2 \rangle \tag{17}$$

These equations put the additional condition $\lambda_1 + \lambda_2 = 1$ on our two parameters. Eliminating λ_2 yields:

$$\begin{aligned}
 \langle t_{11}^2 \rangle &= \frac{2\alpha_{22} - \alpha_{33} - b_{11}}{\alpha_{22} - \alpha_{11}} + 2\lambda_1 \frac{\alpha_{33} - \alpha_{22}}{\alpha_{22} - \alpha_{11}} \\
 \langle t_{12}^2 \rangle &= \frac{\alpha_{33} - 2\alpha_{22} + b_{11}}{\alpha_{22} - \alpha_{11}} - 2\lambda_1 \frac{\alpha_{33} - \alpha_{11}}{\alpha_{22} - \alpha_{11}} \\
 \langle t_{13}^2 \rangle &= 2\lambda_1 - 1 \\
 \langle t_{21}^2 \rangle = \langle t_{31}^2 \rangle &= \frac{\alpha_{33} - b_T}{\alpha_{22} - \alpha_{11}} - \lambda_1 \frac{\alpha_{33} - \alpha_{22}}{\alpha_{22} - \alpha_{11}} \\
 \langle t_{22}^2 \rangle = \langle t_{32}^2 \rangle &= \frac{b_T - \alpha_{33}}{\alpha_{22} - \alpha_{11}} + \lambda_1 \frac{\alpha_{33} - \alpha_{11}}{\alpha_{22} - \alpha_{11}} \\
 \langle t_{23}^2 \rangle = \langle t_{33}^2 \rangle &= 1 - \lambda_1
 \end{aligned} \tag{18}$$

Equation (13) again limits the range of λ_1 . From the third of equations (18) we get at once:

$$0.5 \leq \lambda_1 \leq 1 \tag{19}$$

but, as before, in general the range of λ_1 will be even more restricted. The resulting ranges in the $\langle t_{nm}^2 \rangle$ are again the maximum information obtainable from the optical anisotropy without further assumptions.

If we again make the assumption of random orientation of the x'_2 and x'_3 axes around the x'_1 axis, i.e. if we again require equations (15) to hold, we get the following unique solutions:

$$\begin{aligned}
 \langle t_{11}^2 \rangle &= \frac{\alpha_{22} + \alpha_{33} - 2b_{11}}{\alpha_{22} + \alpha_{33} - 2\alpha_{11}} \\
 \langle t_{12}^2 \rangle = \langle t_{13}^2 \rangle &= \frac{b_{11} - \alpha_{11}}{\alpha_{22} + \alpha_{33} - 2\alpha_{11}} \\
 \langle t_{21}^2 \rangle = \langle t_{31}^2 \rangle &= \frac{\alpha_{22} + \alpha_{33} - 2b_T}{\alpha_{22} + \alpha_{33} - 2\alpha_{11}} \\
 \langle t_{22}^2 \rangle = \langle t_{32}^2 \rangle = \langle t_{23}^2 \rangle = \langle t_{33}^2 \rangle &= \frac{b_T - \alpha_{11}}{\alpha_{22} + \alpha_{33} - 2\alpha_{11}}
 \end{aligned} \tag{20}$$

OPTICALLY ORTHORHOMBIC STRUCTURAL UNIT AND ISOTROPIC SAMPLE

We obtain at once the result that all $\langle t_{nm}^2 \rangle$ are equal for any choice of the x_1, x_2 and x_3 axes, which means:

$$\langle t_{nm}^2 \rangle = 1/3 \quad n, m = 1, 2, 3 \tag{21}$$

REFERENCES

- 1 Born, M. and Wolf, E. 'Principles of Optics', 4th Edn, Pergamon Press, Oxford, 1970
- 2 Kashiwagi, M., Cunningham, A., Manuel, A. J. and Ward, I. M. *Polymer* 1973, **14**, 111

Simple and direct assignment of the methylene and methine ^{13}C resonances in polystyrene

J. R. Ebdon and T. N. Huckerby

Department of Chemistry, University of Lancaster, Lancaster LA1 4YA, UK
(Received 29 September 1975)

There is considerable confusion in the recent literature concerning the assignment of ^{13}C resonances to the methylene and methine carbons in polystyrenes. In the original study¹ only the aromatic carbons were discussed, but in several subsequent papers it has been assumed that for the aliphatic signals the 'normal' order, i.e. $\delta\text{CH} > \delta\text{CH}_2$ was obeyed^{2,3}.

There is however, some indirect evidence⁴⁻⁶ not described in detail which would suggest that this intuitive assignment is incorrect. The importance of making a correct assignment is obvious, since past and future studies on homo- and co-polymers of styrene together with parallel work on α -methyl styrenes and similar compounds will all be affected.

Figure 1 illustrates 20 MHz proton noise decoupled carbon spectra, for 10% w/v solutions of atactic polystyrene and the corresponding β,β -dideutero derivative (with a degree of deuteration exceeding 95%). It is seen that the relatively sharp upfield signal remains almost unaffected in appearance upon deuteration apart from a small upfield isotope shift while the downfield resonance, which now bears C-D couplings and no longer benefits from the nuclear Overhauser effect, has almost disappeared. This therefore constitutes direct evidence for the assignment of the high field ($\delta \approx 40.5$ ppm) aliphatic resonance in polystyrene to the CH group. It would thus appear that although ring current effects due to aromatic groups are believed to be small and relatively unimportant in ^{13}C n.m.r.⁷, the suggestion⁶ that they may have considerable influence in this system does indeed seem to be justified.

REFERENCES

1 Johnson, L. E., Heatley, F. and Bovey, F. A. *Macromolecules* 1970, 3, 175

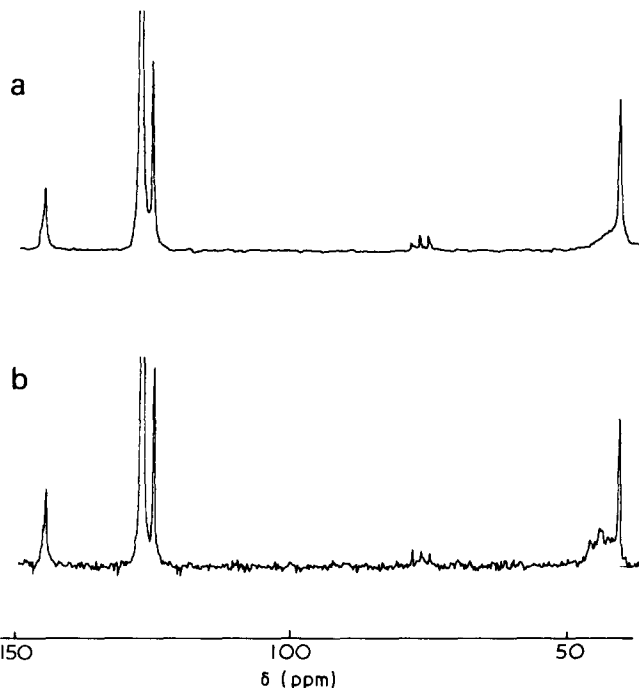


Figure 1 ^{13}C spectra for 10% w/v solutions of (a) atactic polystyrene and (b) β,β -dideutero derivative

- 2 Evans, D. C., Phillips, L., Barrie, J. A. and George, M. H. *J. Polym. Sci. (Polym. Lett. Edn)* 1974, 12, 199
- 3 Segre, A. L., Delfini, M., Conti, F. and Boicelli, A. *Polymer* 1975, 16, 338
- 4 Inoue, Y., Nishioka, A. and Chûjo, R. *Makromol. Chem.* 1972, 156, 207
- 5 Allerhand, A. and Hailstone, R. K. *J. Chem. Phys.* 1972, 56, 3718
- 6 Randall, J. C. *J. Polym. Sci. (Polym. Phys. Edn)* 1975, 13, 889
- 7 Levin, R. H. and Roberts, J. D. *Tetrahedron Lett.* 1973, p 135

Letters

Dependence of rate on monomer concentration in the radiation graft polymerization of styrene to polyethylene

Introduction

The radiation-initiated, free radical graft polymerization of styrene to polyethylene by the mutual irradiation technique has been extensively studied¹⁻⁶ but its kinetics have not been completely established, especially the dependence of grafting rate on monomer concentration. Various studies, although yielding interesting results, have been carried out in a manner precluding elucidation of the dependence of rate on monomer. Monomer concentration in a polyethylene sample has been varied in vapour phase grafting by suspending it in the vapour above a reservoir of liquid styrene for different time periods; subsequently, the polyethylene-styrene is irradiated while still suspended above liquid styrene. When polyethylene is placed directly in liquid styrene and the mixture irradiated, varying concentrations of monomer have been attained by diluting the styrene with a solvent such as methanol which does not itself swell polyethylene. The greater the relative amount of methanol employed, the greater the decrease in the concentration of styrene in the polyethylene. Using these approaches, Silverman and coworkers^{2,3} found the grafting rate increases initially with monomer concentration, reaches a maximum, and then decreases as monomer concentration increases further. The latter decrease has been attributed to a decrease in viscosity inside the polymer with increasing styrene concentration, resulting in an increased rate of termination relative to propagation. Similarly, Wilson⁴ found the grafting rate to increase in the order polyethylene > polypropylene > poly(4-methylpentene) while the styrene concentrations increased in the reverse order. We see here various experiments in which both monomer concentration and inside viscosity varied simultaneously, precluding elucidation of the dependence of rate on monomer.

Using styrene-benzene-alcohol mixtures, Wilson⁷ attempted to vary the monomer concentration while keeping viscosity constant by varying the alcohol used and its relative amount to obtain solutions having the same value of the Hildebrand solubility parameter. This promising approach was applied, however, by assuming the composition of styrene-benzene-alcohol absorbed inside a polyethylene sample ('inside' solution) to be the same as the composition of the solution in which the sample was placed ('outside' solution); further, that the amount of absorbed solution was independent of outside solution composition. Both assumptions are doubtful in view of previous work^{2,5} on the polyethylene-styrene-methanol system; in any case, experimental verification is needed. The most significant previous work is (for reasons which become clear below) probably that of Ballantine and coworkers⁸ who found the grafting rate to depend approximately on the 5/2-power of monomer concentration; the styrene concentration being varied by using styrene-benzene mixtures. In that study as in Wilson's, no attempt was made to determine the composition of the inside solution. This preliminary result, appearing without detailed experimental data and only as a brief paragraph in a Brookhaven

National Laboratory report, was overlooked for two decades by researchers who continued to assume¹⁻⁷ a first-power dependence of rate on monomer concentration. We report here the results of our study on the dependence of rate on monomer concentration for the polyethylene-styrene system.

Experimental and Results

Our experimental procedures were similar to those previously reported⁶. Styrene was washed with base followed by water, dried over sodium carbonate and magnesium sulphate and vacuum distilled; benzene was distilled at atmospheric pressure. Gulf Company 9614 polyethylene films (1 and 10 mil thick, both having density = 0.962 g/cm³; $\bar{M}_n = 19\ 000$, crystallinity of 79% as measured by density and d.s.c.) were washed with acetone and dried at 50°C under vacuum before use. To avoid problems associated with previous work on the dependence of rate on monomer concentration, it was necessary to choose the experimental system such that the inside styrene concentration could be varied without varying the inside viscosity. The use of benzene as a diluent for styrene was considered since benzene and styrene are very similar in solubility characteristics (the Hildebrand solubility parameters are 9.2 and 9.3 (cal/cm³)^{1/2}, respectively; the viscosity of benzene is 0.564 cP at 30°C, while that of styrene is 0.587 cP at 37.8°C)^{9,10}.

After equilibration with styrene or styrene-benzene mixtures at 25°C, 10 mil thick polyethylene samples were removed, blotted rapidly with absorbent paper to remove surface liquid and weighed to determine the amount of liquid absorbed by polyethylene. The extent of swelling of polyethylene by benzene-styrene was found to be 5.30% by wt independent of the benzene-styrene composition over the range 35-100 vol% styrene. (Although 1 mil films were used in the grafting experiments, the absorption studies were carried out with 10 mil films owing to the higher accuracy attainable with the thicker films. This did not introduce an error since both the 1 and 10 mil films have the same crystallinity and would have the same absorption characteristics; this was verified in a separate experiment.) To determine the composition of the inside solution, an equilibrated polyethylene sample was blotted, placed in a flask connected to a vacuum trap cooled by liquid nitrogen and the system evacuated to distill the inside solution into the cold trap. The composition of the inside solution, as determined by ultra-violet spectroscopy and refractive index measurements, was found to be exactly the same as the composition of the outside solution over the range of benzene-styrene compositions studied. Thus, the use of benzene-styrene mixtures allows one to vary the concentration of styrene inside the polyethylene while keeping constant the inside concentration of total liquid (benzene plus styrene). The inside viscosity is very close to being constant since the viscosity of benzene-styrene varies less than 10% over the range of compositions studied. An additional reason for choosing benzene as a diluent for styrene is that the *G* values for radical formation are similar for the two compounds¹¹. Thus, one expects the extent of homopolymerization relative to graft polymerization to be the same for

styrene–benzene mixtures as for styrene; further, the presence of benzene should not introduce appreciable energy transfer processes.

Graft polymerization was carried out as follows: 1 mil polyethylene samples were immersed in styrene or styrene–benzene in reaction tubes connected to a vacuum line, oxygen was removed by alternate freezing and thawing under vacuum, and the reaction tubes were sealed under vacuum. After equilibration at 25°C, the sealed reaction tubes were irradiated for specified periods at dose rates of 0.00076 and 0.037 Mrad/h using a J. L. Shepherd Mark I ¹³⁷Cs gamma source located in a room maintained at 23–25°C. The temperatures of the reaction mixtures rose slightly upon irradiation, usually to 26°C, as high as 27°C in a few instances. After irradiation, the polyethylene films were removed from the reaction tubes, washed with benzene followed by acetone, vacuum dried and weighed. The vacuum drying was carried out exhaustively (at 40–50°C at less than 1 mmHg pressure) until samples reached constant weight to ensure that all solvent and unreacted monomer was removed from the grafted polymer sample. The extent of graft polymerization in a sample was calculated as its percentage increase in weight. The results at the higher dose rate are shown in Figure 1; the course of the reaction at the lower dose rate was similar.

Initial rates were obtained by limiting grafting experiments to low conversions (10–15%) to avoid the auto-acceleration usually present in radical chain polymerization; high conversions would also involve significant changes in the nature of the polymer being grafted. The initial graft polymerization rates, determined by least-squares calculations, are shown in Table 1. Log–log plots of graft polymerization rate versus monomer concentration at the two dose rates are shown in Figure 2. Least squares calculations yielded slopes of 1.56 ± 0.04 and 2.61 ± 0.06 , at 0.00076 and 0.353 Mrad/h respectively.

In summary, we have established that the dependence of rate on monomer concentration for the radiation grafting of styrene to polyethylene is not first-order as previously assumed; the dependence is 3/2-order at the low dose rate and 5/2-order at the higher dose rate. Work is currently in progress in our laboratories to elucidate the mechanism(s) responsible for these effects, including a study of the rate dependence on monomer over a wider range of dose rates as well as the rate dependence on intensity. Further, since

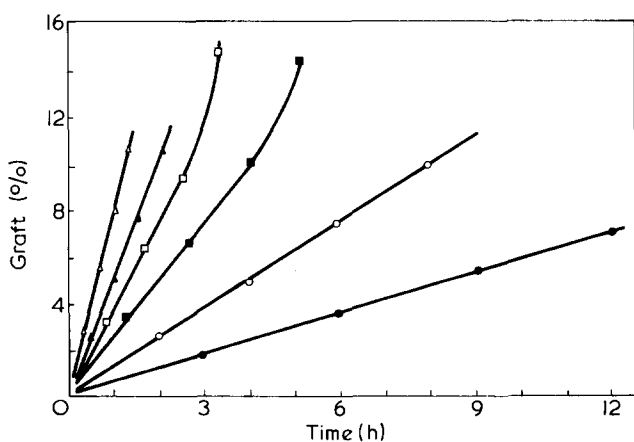


Figure 1 Degree of graft polymerization versus time for various styrene–benzene mixtures at a dose rate of 0.037 Mrad/h. Styrene concentrations: Δ , 100; \blacktriangle , 85; \square , 75; \blacksquare , 65; \circ , 50; \bullet , 35%

Table 1 Initial graft polymerization rates for different benzene–styrene mixtures

Composition of inside and outside solution (vol % styrene)	Inside monomer concentration (mol/l) ^a	Grafting rate (% graft/h) at	
		0.00076 Mrad/h	0.037 Mrad/h
100	2.55	1.37	7.95
85	2.18	0.993	5.10
75	1.94	0.863	3.78
65	1.68	0.700	2.51
50	1.30	0.451	1.24
35	0.917	0.271	0.564

^a mol styrene/l swollen amorphous polyethylene

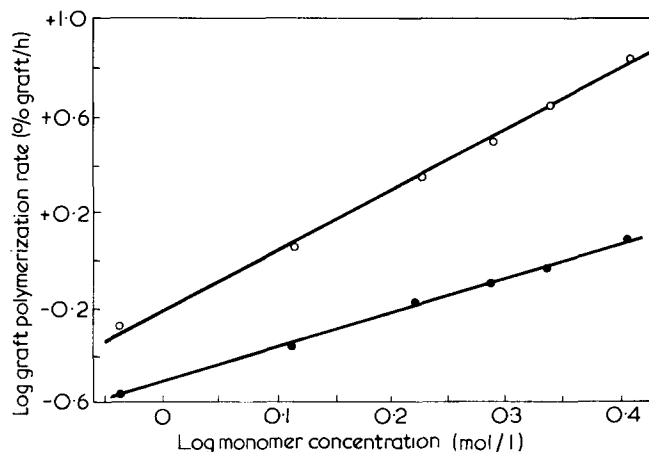


Figure 2 Log–log plot of graft polymerization rate versus monomer concentration at dose rates of 0.037 (○) and 0.00076 (●) Mrad/h. Slope: ○, 2.61; ●, 1.56

our measured extents of grafting like those of other investigators probably include appreciable amounts of the homopolymer formed inside the polyethylene film⁶, an effort will be made to determine and separate the kinetics applicable to homopolymerization occurring inside the polymer from the kinetics of the graft polymerization process. The kinetics of the two processes are not necessarily the same; the results should help clarify the mechanism(s) applicable to our present results.

Acknowledgements

The authors gratefully acknowledge the support of this research by the National Science Foundation under Grant ENG-75-05775 and the Research Foundation of the City University of New York under grants FRAP4-10193 and 06-11085.

George Odian

Chemistry Program, Richmond College of the City University of New York, Staten Island, NY 10301, USA

and Abdelgawad Rabie

Department of Chemistry, Faculty of Science, Ain Shams University, Cairo, Egypt

(Received 29 September 1975; revised 10 November 1975)

References

- 1 Chaprio, A. 'Radiation Chemistry of Polymeric Systems', Wiley-Interscience, New York, 1962, Ch XII
- 2 Machi, S., Kamel, I. and Silverman, J. *J. Polym. Sci. (A-1)* 1970, **8**, 3329
- 3 Kamel, I., Machi, S. and Silverman, J. *J. Polym. Sci. (A-1)* 1972, **10**, 1019
- 4 Wilson, J. E. *J. Macromol. Sci. (A)* 1971, **5**, 777
- 5 Odian, G., Sobel, M., Rossi, A. and Klein, R. *J. Polym. Sci.* 1961, **55**, 663
- 6 Odian, G., Henry, R., Koenig, R., Mangaraj, D., Trung, L. D., Chao, B. and Derman, A. *J. Polym. Sci. (Polym. Chem. Edn)* 1975, **13**, 623
- 7 Wilson, J. E. *J. Macromol. Sci. (A)* 1974, **8**, 733
- 8 Ballantine, D. S., Colombo, P., Glines, A., Manowitz, B. and Metz, D. J. *Brookhaven Nat. Lab. Progr. Rep. 414(T-81)* 1956
- 9 Brandrup, J. and Immergut, E. H. 'Polymer Handbook', 2nd Edn, Wiley-Interscience, New York, 1975, pp IV-341, VII-25
- 10 Shell Development Co. Technical Data Bulletin
- 11 Chapiro, A. 'Radiation Chemistry of Polymeric Systems', Wiley-Interscience, New York, 1962, Ch VII

Solubilization of bovine elastin by a formic acid + salt method

The importance of elastin as a component of the connective tissue has directed a good deal of attention to its isolation. Procedures have, in the main, relied on its insolubility to chemical treatment. In an early and well known series of experiments, Hass *et al.*¹ have examined the isolation of elastin by use of formic acid to remove all other tissue components. This method is not now used since it can be shown that at least 60% of elastin can be solubilized in 88% HCOOH at 45°C if treatment is prolonged².

Of several methods for the partial degradation and solubilization of elastin, treatment by reflux in 0.25 M oxalic acid is the most widely used³. It has also been shown that elastin can be hydrolysed by use of a salt + alcohol mixture, the inorganic component acting as an accelerator⁴. Ioffe and Sorokin⁵ have also obtained a soluble elastin by reaction of isolated elastin with a solution of the mixed salts, CuSO₄ and Ba(OH)₂ at 37°C for 60 h. The rate of reaction was greatly reduced in the absence of the copper ion. The use of salts in aiding the hydrolytic cleavage of elastin is of interest especially in its relationship to the study of atherosclerosis. Elastin has a high affinity for calcium ions⁶ and Hall⁷ has found that calcium which is bound to the elastin matrix can act both as a crosslinking agent and as an activator of elastolysis.

Earland and Raven⁸ have examined the use of salt + formic acid mixtures for the solubilization of silk. They were able to obtain a partial solubilization with a range of formic acid + salt combinations. Since both silk and elastin have some similarity with high glycine and alanine amino acid compositions and also show a high degree of swelling in formic acid this method was considered as worth trying for elastin. Preliminary experiments, choosing salt combinations with formic acid from the list given by Earland and Raven⁸, showed that for all combinations tested (about 15), complete solubilization of bovine elastin could be achieved.

A short report is given of the results of a more detailed investigation of the use of 0.25 M solutions of CaCl₂, MgCl₂ and (NH₄)₂SO₄ in 98% HCOOH and an examination of some properties of the corresponding elastin solutions.

Part of the isolated bovine elastin which was used as the starting material was also solubilized by the oxalic acid method³ and provided a basis for comparison.

The isolation of elastin from bovine ligament followed the usual procedure² material for this study (E10) being obtained from a 1.5 year old animal. Details of the solubilization procedures are given in *Table 1*. Amino acid analyses of the soluble elastins showed no significant differences between the preparations and a satisfactory agreement was obtained with published data for bovine elastin³. The soluble elastins have been characterized by measurement of the coacervation temperature, t_c ³ and the limiting viscosity number, $[\eta]$ determined in buffer solutions of different pH but constant ionic strength¹⁰. (Full experimental details can be supplied if requested.)

It has been found that soluble elastins can be prepared using the Earland and Raven⁸ formic acid method in a similar yield but with fewer stages of reflux than the oxalic acid procedure³. Details of the preparations and a summary of the properties of the soluble elastin solutions are given in *Table 1*. The oxalic acid preparation, used as a reference, is designated E10.PDA. Gel electrophoresis measurements¹¹ showed that all the formic acid preparations contained an appreciable proportion of high molecular weight material. Coacervation was observed in all solutions of the elastins. A significant dependence of t_c ($\pm 0.2^\circ\text{C}$) on protein concentration was observed. The agreement between results for the reference preparation and those of Partridge *et al.*³ is quite close.

Although amino acid determinations made on these preparations reveals no significant differences physical measurements show them to be not identical. There are differences between the protein concentration-independent values of t_c , as shown in *Figure 1*, and in the viscometric results shown in *Figure 2*. The values of $[\eta]$ for α and β elastin (separated by coacervation) as obtained by Ksiezny *et al.*¹⁰ for oxalic acid solubilized bovine elastin are indicated in *Figure 2* by the broken lines.

Results for E10.PDA, for which the α and β components have not been separated, conform with those of Ksiezny *et al.*¹⁰ (α -elastin being the major component) and show a minimum value of $[\eta]$ in the range pH 4 to 6. With the exception of preparation E10.NH₄ a similar pH dependence is shown by the formic acid solubilized elastins. However, values of $[\eta]$ for E10.Mg and E10.Ca are significantly reduced and for the most part they are lower than the corresponding values for β -elastin.

As reported, these solutions show coacervation and con-

Table 1 Details of the preparation and properties of the solubilized elastins

Code	Reagent system	Stages of reflux	Liquid/solid ratio	Yield (% w/w)	$[\eta]$ * (ml/g)	t_c † (°C)
E10.PDA**	(COOH) ₂	5	12	56	8.6§	28.7‡
E10.Ca	HCOOH + CaCl ₂	2	25	46	7.1	25.6
E10.Mg	HCOOH + MgCl ₂	3	50	46	5.8	30.0
E10.NH ₄	HCOOH + (NH ₄) ₂ SO ₄	4	25	61	8.3	26.1

* Determined at 20°C and pH 5

† Interpolated at $c = 10$ mg/ml

** Reference sample

‡ Partridge *et al.*³ obtained $t_c = 27.8^\circ\text{C}$ at $c = 7$ mg/ml

§ For α - and β -elastin values of $[\eta]$ are 9.3 and 7.2 ml/g

References

- 1 Chaprio, A. 'Radiation Chemistry of Polymeric Systems', Wiley-Interscience, New York, 1962, Ch XII
- 2 Machi, S., Kamel, I. and Silverman, J. *J. Polym. Sci. (A-1)* 1970, **8**, 3329
- 3 Kamel, I., Machi, S. and Silverman, J. *J. Polym. Sci. (A-1)* 1972, **10**, 1019
- 4 Wilson, J. E. *J. Macromol. Sci. (A)* 1971, **5**, 777
- 5 Odian, G., Sobel, M., Rossi, A. and Klein, R. *J. Polym. Sci.* 1961, **55**, 663
- 6 Odian, G., Henry, R., Koenig, R., Mangaraj, D., Trung, L. D., Chao, B. and Derman, A. *J. Polym. Sci. (Polym. Chem. Edn)* 1975, **13**, 623
- 7 Wilson, J. E. *J. Macromol. Sci. (A)* 1974, **8**, 733
- 8 Ballantine, D. S., Colombo, P., Glines, A., Manowitz, B. and Metz, D. J. *Brookhaven Nat. Lab. Progr. Rep. 414(T-81)* 1956
- 9 Brandrup, J. and Immergut, E. H. 'Polymer Handbook', 2nd Edn, Wiley-Interscience, New York, 1975, pp IV-341, VII-25
- 10 Shell Development Co. Technical Data Bulletin
- 11 Chapiro, A. 'Radiation Chemistry of Polymeric Systems', Wiley-Interscience, New York, 1962, Ch VII

Solubilization of bovine elastin by a formic acid + salt method

The importance of elastin as a component of the connective tissue has directed a good deal of attention to its isolation. Procedures have, in the main, relied on its insolubility to chemical treatment. In an early and well known series of experiments, Hass *et al.*¹ have examined the isolation of elastin by use of formic acid to remove all other tissue components. This method is not now used since it can be shown that at least 60% of elastin can be solubilized in 88% HCOOH at 45°C if treatment is prolonged².

Of several methods for the partial degradation and solubilization of elastin, treatment by reflux in 0.25 M oxalic acid is the most widely used³. It has also been shown that elastin can be hydrolysed by use of a salt + alcohol mixture, the inorganic component acting as an accelerator⁴. Ioffe and Sorokin⁵ have also obtained a soluble elastin by reaction of isolated elastin with a solution of the mixed salts, CuSO₄ and Ba(OH)₂ at 37°C for 60 h. The rate of reaction was greatly reduced in the absence of the copper ion. The use of salts in aiding the hydrolytic cleavage of elastin is of interest especially in its relationship to the study of atherosclerosis. Elastin has a high affinity for calcium ions⁶ and Hall⁷ has found that calcium which is bound to the elastin matrix can act both as a crosslinking agent and as an activator of elastolysis.

Earland and Raven⁸ have examined the use of salt + formic acid mixtures for the solubilization of silk. They were able to obtain a partial solubilization with a range of formic acid + salt combinations. Since both silk and elastin have some similarity with high glycine and alanine amino acid compositions and also show a high degree of swelling in formic acid this method was considered as worth trying for elastin. Preliminary experiments, choosing salt combinations with formic acid from the list given by Earland and Raven⁸, showed that for all combinations tested (about 15), complete solubilization of bovine elastin could be achieved.

A short report is given of the results of a more detailed investigation of the use of 0.25 M solutions of CaCl₂, MgCl₂ and (NH₄)₂SO₄ in 98% HCOOH and an examination of some properties of the corresponding elastin solutions.

Part of the isolated bovine elastin which was used as the starting material was also solubilized by the oxalic acid method³ and provided a basis for comparison.

The isolation of elastin from bovine ligament followed the usual procedure² material for this study (E10) being obtained from a 1.5 year old animal. Details of the solubilization procedures are given in *Table 1*. Amino acid analyses of the soluble elastins showed no significant differences between the preparations and a satisfactory agreement was obtained with published data for bovine elastin³. The soluble elastins have been characterized by measurement of the coacervation temperature, t_c ³ and the limiting viscosity number, $[\eta]$ determined in buffer solutions of different pH but constant ionic strength¹⁰. (Full experimental details can be supplied if requested.)

It has been found that soluble elastins can be prepared using the Earland and Raven⁸ formic acid method in a similar yield but with fewer stages of reflux than the oxalic acid procedure³. Details of the preparations and a summary of the properties of the soluble elastin solutions are given in *Table 1*. The oxalic acid preparation, used as a reference, is designated E10.PDA. Gel electrophoresis measurements¹¹ showed that all the formic acid preparations contained an appreciable proportion of high molecular weight material. Coacervation was observed in all solutions of the elastins. A significant dependence of t_c ($\pm 0.2^\circ\text{C}$) on protein concentration was observed. The agreement between results for the reference preparation and those of Partridge *et al.*³ is quite close.

Although amino acid determinations made on these preparations reveals no significant differences physical measurements show them to be not identical. There are differences between the protein concentration-independent values of t_c , as shown in *Figure 1*, and in the viscometric results shown in *Figure 2*. The values of $[\eta]$ for α and β elastin (separated by coacervation) as obtained by Ksiezny *et al.*¹⁰ for oxalic acid solubilized bovine elastin are indicated in *Figure 2* by the broken lines.

Results for E10.PDA, for which the α and β components have not been separated, conform with those of Ksiezny *et al.*¹⁰ (α -elastin being the major component) and show a minimum value of $[\eta]$ in the range pH 4 to 6. With the exception of preparation E10.NH₄ a similar pH dependence is shown by the formic acid solubilized elastins. However, values of $[\eta]$ for E10.Mg and E10.Ca are significantly reduced and for the most part they are lower than the corresponding values for β -elastin.

As reported, these solutions show coacervation and con-

Table 1 Details of the preparation and properties of the solubilized elastins

Code	Reagent system	Stages of reflux	Liquid/solid ratio	Yield (% w/w)	$[\eta]$ * (ml/g)	t_c † (°C)
E10.PDA**	(COOH) ₂	5	12	56	8.6§	28.7‡
E10.Ca	HCOOH + CaCl ₂	2	25	46	7.1	25.6
E10.Mg	HCOOH + MgCl ₂	3	50	46	5.8	30.0
E10.NH ₄	HCOOH + (NH ₄) ₂ SO ₄	4	25	61	8.3	26.1

* Determined at 20°C and pH 5

† Interpolated at $c = 10$ mg/ml

** Reference sample

‡ Partridge *et al.*³ obtained $t_c = 27.8^\circ\text{C}$ at $c = 7$ mg/ml

§ For α - and β -elastin values of $[\eta]$ are 9.3 and 7.2 ml/g

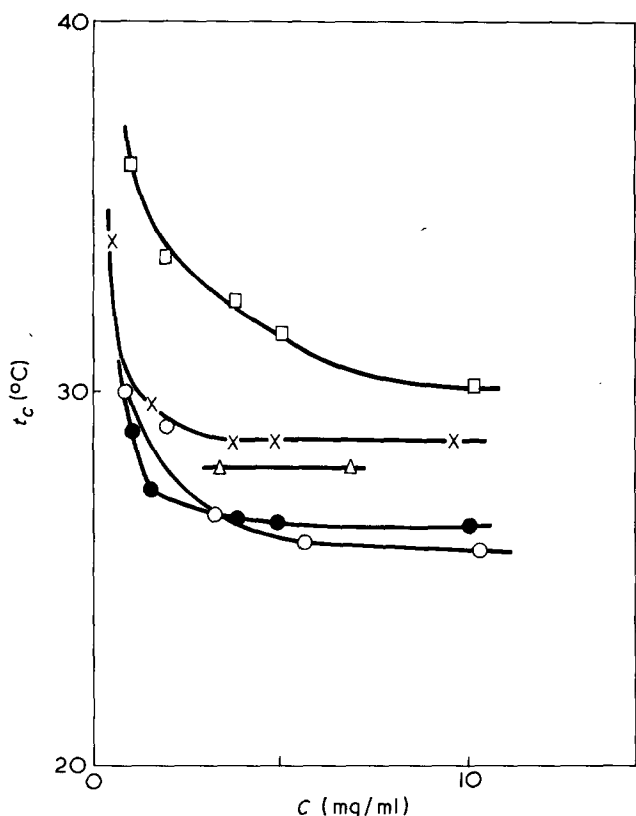


Figure 1 Dependence of the coacervation temperature on the concentration of the elastin solution as determined at pH 4.7 and an ionic strength of 0.05. \square , E10.Mg; \bullet , E10.NH₄; \circ , E10.Ca; \times , E10.PDA; \triangle , Partridge *et al.*³

tain appreciable amounts of high molecular weight material whereas β -elastin is non-coacervating and of low molecular weight (about 3000). Thus measurement of $[\eta]$ for elastin solutions cannot serve as an unambiguous guide to molecular size and, without more evidence, cannot be used to characterize the fractionation of soluble elastins¹². Differences in $[\eta]$ and t_c may well indicate conformational variation by the elastin molecule in solution. Further clarification of the mechanism of coacervation by the solubilized elastin molecules is necessary before determination of t_c also can provide a method of characterization³.

However, the main objective of this study was to try the Earland and Raven⁸ formic acid method with elastin and this has been achieved beyond expectations. The oxalic acid method, although widely used, has no possibility for variation whereas the success of the formic acid solubilization procedure now makes it possible to consider detailed study of the mechanism of interaction between inorganic ions and the elastin matrix⁷ through examination of the properties of the solubilized products.

R. B. Beevers

Belvoir Research Laboratory,
160 Chatham Road,
Eastwood, NSW 2122,
Australia
(Received 29 September 1975)

References

- 1 Ayer, J. P., Hass, G. M. and Philpott, D. E. *Arch. Pathol.* 1958, 65, 519
- 2 Jackson, D. S. and Cleary, E. G. *Methods Biochem. Anal.* 1967, 15, 25

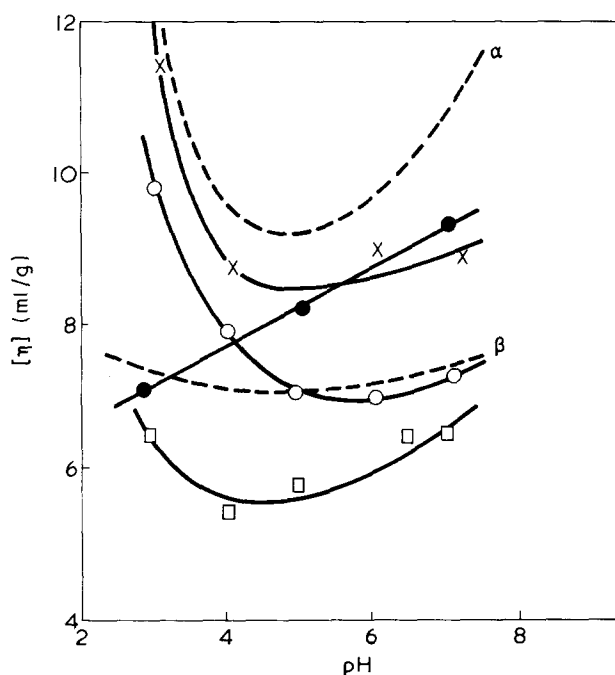


Figure 2 Dependence of the limiting viscosity number for the solubilized elastins on the pH of the buffer solution and at an ionic strength of 0.05. Measurements were made at 20°C to avoid coacervation of the solutions. Key as in Figure 1. -----, Ksiezny *et al.*¹⁰ data for α - and β -elastin

- 3 Partridge, S. M., Davis, H. F. and Adair, G. S. *Biochem. J.* 1955, 61, 11
- 4 Kornfeld, N. and Rebeyrotte, P. *Experientia* 1970, 26, 1064
- 5 Ioffe, K. G. and Sorokin, V. M. *Biokhimiya* 1954, 19, 652
- 6 Urry, D. W. *Proc. Nat. Acad. Sci. US* 1971, 68, 810
- 7 Hall, D. A. *Gerontologia* 1970, 16, 325
- 8 Earland, C. and Raven, D. J. *Nature* 1954, 174, 461
- 9 Lotan, N., Bixon, M. and Berger, A. *Biopolymers* 1967, 5, 69
- 10 Ksiezny, S., Ardelt, W., Budzynski, A. Z., Niedzwiecka-Namslowska, I. and Wojtecka-Lukasik, I. *Acta Biochim. Polon.* 1965, 12, 327
- 11 Shapiro, A. L., Vinuela, E. and Maizel, J. V. *Biochem. Biophys. Res. Commun.* 1967, 28, 815
- 12 Beevers, R. B. *Biochim. Biophys. Acta* 1971, 243, 102

Conference Announcement

Deformation, Yield and Fracture of Polymers

Cambridge, UK, 29 March to 1 April, 1976

The third international conference on Deformation, yield and fracture of polymers will be held at Churchill College, Cambridge from 29 March to 1 April 1976 and is being organized by the Plastics and Rubber Institute on behalf of a number of collaborating bodies. A programme of thirty two contributions has been arranged under the following sessions: creep and yielding, fracture, crazing, rubbers and selected topics, crystal deformation, and a general session on selected topics. Further details and application forms may be obtained from Mr J. N. Ratcliffe, Plastics and Rubber Institute, 11 Hobart Place, London SW1W 0HL, UK.

Book Reviews

IUPAC International Symposium on Macromolecules

Edited by E. B. Mano

Elsevier, Amsterdam, 1975. 463 pp. \$46.25

In July 1974 a symposium on polymer science and technology was organized by the Brazilian authorities in collaboration with IUPAC, the programme dealing with polymerization processes, physical chemistry, polymer technology and, to meet a wider range of interests, with biopolymers. Abstracts of the contributed papers were available at the meeting and doubtless there will be fuller publication in due course, but in keeping with the practice at many IUPAC symposia main lectures on special aspects were presented by invited speakers and the present volume contains the text of these.

In his opening address Sir Harry Melville reviewed some current trends in polymer science, drawing attention to a number of areas meriting continued study: precise control of molecular weight, tacticity and unit sequence, network systems, surface properties, dimensional stability, superconductivity, degradation, and liquid rubbers. It is perhaps unfortunate that the book does not contain also the closing plenary lecture, 'Polymers worldwide', given by Professor Herman Mark.

The papers on polymer chemistry are on inclusion polymerization with special reference to the use of perhydrotriphenylene as the host compound (Farina) and on photopolymerization and photoresponsive polymers (Smets); cyclopolymerization is discussed by Butler, Porri reviews developments in polymerizing conjugated dienes using new uranium-based catalysts, and Stille outlines the synthesis of rigid polyphenylphenylenes and polyanthrazolines. In the physical chemistry section are papers by Meares on transport phenomena and their relevance to membrane separation and by Szwarc reviewing anionic polymerization and applications of living polymer processes. Infra-red spectroscopy is applied to a study of crystalline polyethylene (Krimm) and high-resolution ^{13}C n.m.r. for investigation of stereochemical configurations in vinyl polymers (Bovey), while Guillet discusses the role of molecular mobility in photochemical processes.

Polymer technology has seven papers which include a review of polyethylenes and the provision of polymers of improved fabrication performance (Foster), segment deformation in glassy polymers (Yannas) and new thermally stable aromatic or heterocyclic copolycondensates (Fontan), which paper regrettably gives no references. Okamura reviews his work on the production of synthetic fibres from modified PVC dispersions, and Morton outlines advances made with synthetic elastomers, especially the *trans*-polypentenamer, thermoelastic block copolymers and liquid rubbers. Work on the effects of fine structure on the pyrolysis behaviour of cellulosic materials is discussed by Lewin, and Ranby has a paper on teaching technology in Sweden.

The seven papers in the final section on biopolymers deal with receptor proteins for neuroactive drugs (Robertis), adenovirus proteins (Pereira), and controlled synthesis in enzyme studies (Merrifield). Synthesis in bacterial genes is described by Khorana and the use of ^{13}C n.m.r. in a study of mucopolysaccharides by Perlin. Polymeric carriers and immobilization of enzymes is the subject of a paper by Manecke, and Dawes discusses the function of poly(β -hydroxybutyrate) in micro-organisms.

In all, these collected papers provide a good picture of developments in polymer science, showing particularly the many fields of activity and methods of scientific approach. From these invited lectures one is able to appreciate the depth of the studies in progress as well as the ultimate use of the findings in practical terms, whether this be in plastics, fibre or rubber technology, the medical world, or other fields of endeavour.

While the book is handsomely bound and produced, the text itself consists of the photo-reduced typescripts as received from the various authors and editing has been minimal. This perhaps contributes to the originality of the contributions but it is a little disconcerting to encounter different sets of type-face throughout the book, a lack of explanation to a few of the diagrams and abbreviations, and to have no index. However, such direct use of the authors' scripts has enabled the book to be produced without delay, and in a rapidly developing field like that of macromolecules

this is a decided advantage which will outweigh the minor faults noted above.

At the price quoted the volume may prove expensive for purchase by an individual but the many papers give it considerable merit and it could with some benefit be used by those who wish to have brief but authoritative reviews on particular aspects or more generally to read of developments outside their areas of immediate interest.

R. J. W. Reynolds

Advances in polymer science, Volume 15 Springer Verlag, Berlin, 1975, 155 pp. \$27.80

The book contains four review articles, Oligomerisation of ethylene with soluble transition-metal catalysts by G. H. Olivé and S. Olivé. Stereochemistry of propylene polymerisation by A. Zambelli and C. Tosi, Structures of copolymers of high olefins by Y. V. Kissin and Mercaption-containing polymers by C. D. S. Lee and W. H. Daly. All four articles are reasonably well written and present an interesting account of the subject described.

The article of Olivé and Olivé discusses Ziegler-based systems (transition metal compounds plus aluminium alkyl compounds) as catalysts for the oligomerization of ethylene. It is a useful collection of facts but lacks clarity and conviction when talking about the mechanism of the processes concerned. The basic difficulty in trying to disentangle the mechanism of Ziegler catalysts is that there are too many possible structural options for the reactive centre in any given system. This produces reviews which are catalogues of data with little unambiguous evidence as to what exactly is going on. In this review it is implied that although there may exist monometallic catalysts which can oligomerize ethylene they are in general lacking in activity and require a cocatalyst, aluminium alkyls, to give effective systems. This is, of course, not completely correct as it is known that the system $\text{Br}_3\text{ZrC}_3\text{H}_5$ (*Adv. Catalysis* 1973, 23, 263) oligomerize ethylene to give 60–100 residues per α -olefin chain at very high rates indeed.

The kinetic analysis of these reactions does not take account of the fact that in many of these systems large amounts of 1-butene is formed and the postulate of a six-centre transition state seems unnecessary to account for the β -hydrogen abstraction process. The industrial side of ethylene oligomerization is also poorly dealt with. Most industrial processes do not use this type of chemistry, wax cracking has until recently been the preferred process but in new plants this is being replaced by 'ethylene growth' using aluminium alkyl chemistry.

The stereochemistry of propylene polymerization is a well written description of the ideas of Professor Zambelli and his colleagues in which they attempt to use the four centre transition state to explain the chemistry of Ziegler-Natta catalysts and their ability to control the stereochemistry of the insertion process. The mechanism they describe may well have some relation to real behaviour in polymerizations initiated by transition metal alkyls since the latter are essentially monometallic catalysts. However, Ziegler-Natta systems are almost certainly bimetallic and the choice of aluminium alkyl as cocatalyst can have a profound effect on the ability of the centre to stereoregulate.

The final contribution on polyolefins is a paper by the Russian scientist Y. V. Kissin on the structure of copolymers of the higher olefins. This is a very interesting review and collects together information on 1:1 copolymers of the common olefins, with some data on their fine structure derived mainly from infra-red studies. In view of the known difficulties of making many of these copolymers it is surprising that such a wide variety of types are now available for study. The work of Dr Turner-Jones on the 4-methyl pentene-1 copolymers is treated in detail and serves to illustrate, for all crystalline polyolefins, the effect of copolymerization on crystallinity, melting points, and infra-red spectra. The observations divide themselves into three principal groups: copolymers in which the comonomer side chain is rejected by the host crystal lattice, in these cases quite small amounts of comonomer reduce the crystallinity drastically; copolymers such as 4-methyl pentene-1/hexene-1 for example where the comonomer side chains can crystallize with the host lattice and crystallinity persists over the whole range of compositions; the least known system and probably the most useful are

those in which the comonomer is incorporated as a series of blocks so that the microstructure is made up of discrete phases. It has been observed with the latter systems that unusual mechanical properties are obtained. It would have been helpful if some information of this kind could have been given, but mechanical behaviour is not discussed.

In conclusion the book will be of interest to polymer chemists in general and particularly those interested in polyolefins.

D. G. H. Ballard

Ionic polymers

Edited by L. Holliday

Applied Science, London, 1975, 416 pp, £14

The most familiar examples of ionic polymers, the so-called 'ionomers', have enjoyed considerable commercial success over the past few years, a factor which has undoubtedly assisted in generating enthusiasm in this area. Present trends in research, as reflected in this book, are directed towards a wider understanding of both the essentially organic and inorganic ion-containing materials. An initial step in this development is the recognition of materials such as inorganic oxide glasses, metal dicarboxylates and crystalline silicate and phosphate minerals as polymers. A useful exchange of the concepts and the considerable body of knowledge available within these hitherto discrete areas of study with the field of organic polymers may then follow. As the introductory chapter of the book intimates, in only one or two topics of study, such as the glass transition temperature, have unifying semi-empirical relationships and correlations been established. Much progress has yet to be made to consolidate a cohesive study of ionic polymers on such a broad base as it is presented here.

Following the introductory chapter, in which classifications and general properties of ionic polymers are presented in a clear and logical way, there are seven further chapters each dealing with different types of ionic material. These chapters have different authors and each chapter emphasizes a different aspect of its subject. The chapters concerned with ionomers, carboxylated elastomers and crystalline silicates and phosphates are thorough and systematic reviews of the extensive literature on these materials

whereas the chapter on rigid, highly carboxylated ionic polymers is, for the greater part, an authoritative account of recently developed dental cements. However, the conformational changes and ion-binding phenomena which are referred to in the opening section of this account apply to dilute solutions and are inappropriate when discussed in the context of the concentrated systems encountered in these cements. There are two shorter chapters on metal dicarboxylates and the technology of polyelectrolyte complexes and the final chapter by N. H. Ray describes an essentially novel approach to the structure of inorganic glasses.

Taken as a whole the book is somewhat heterogeneous, but as a first step it represents a welcome development and the individual contributions are very useful in themselves. The book will be of interest to research workers and could provide some novel ideas on presentation of course work for teachers in materials departments. The book is well presented but its price will probably restrict it to appropriate departmental libraries for which it will be a good investment.

P. V. Wright

The Proprietors of British Patent No. 1163502, for "Method for activating cycloaliphatic polyamines as curing agents for reaction with epoxide compounds", desire to enter into negotiations for the sale of the patent, or for the grant of licences thereunder. Further particulars may be obtained from Marks & Clerk, 57-60 Lincoln's Inn Fields, London WC2A 3LS.

RESOURCES POLICY

the economics, planning and use of mineral resources

**A QUARTERLY JOURNAL
DECEMBER 1975**

The impasse over Limits to Growth: a suggested course of research F. J. Wells

The geographic concentration of world mineral supplies M. H. Govett

Indonesia's mineral resources — performance and prospects B. Lloyd

United States uranium resources: the 1975—2000 outlook D. G. Brookins

Other sections

- . Current topics
- . Conference reports
- . Forthcoming meetings
- . Book reviews and announcements
- . Publications received

RESOURCES POLICY presents multi-disciplinary discussions at an upper management/academic level. The aim is to identify policy options for the future supply and demand of mineral resources. It encompasses the many disciplines and examines options as they affect industrial, commercial and social institutions at world and regional levels.

Published quarterly in March, June, September, December.

One-year subscription (four issues) £22.00 U.K. £25 (\$65.00) Overseas

For details apply to: IPC Business Press (Sales and Distribution Ltd.)

Oakfield House, Perrymount Road, Haywards Heath, Sussex, England RH6 3DH

Telephone Haywards Heath (0444) 53281 Telex: Bisnespress Ldn 25137

Book Reviews

IUPAC International Symposium on Macromolecules

Edited by E. B. Mano

Elsevier, Amsterdam, 1975. 463 pp. \$46.25

In July 1974 a symposium on polymer science and technology was organized by the Brazilian authorities in collaboration with IUPAC, the programme dealing with polymerization processes, physical chemistry, polymer technology and, to meet a wider range of interests, with biopolymers. Abstracts of the contributed papers were available at the meeting and doubtless there will be fuller publication in due course, but in keeping with the practice at many IUPAC symposia main lectures on special aspects were presented by invited speakers and the present volume contains the text of these.

In his opening address Sir Harry Melville reviewed some current trends in polymer science, drawing attention to a number of areas meriting continued study: precise control of molecular weight, tacticity and unit sequence, network systems, surface properties, dimensional stability, superconductivity, degradation, and liquid rubbers. It is perhaps unfortunate that the book does not contain also the closing plenary lecture, 'Polymers worldwide', given by Professor Herman Mark.

The papers on polymer chemistry are on inclusion polymerization with special reference to the use of perhydrotriphenylene as the host compound (Farina) and on photopolymerization and photoresponsive polymers (Smets); cyclopolymerization is discussed by Butler, Porri reviews developments in polymerizing conjugated dienes using new uranium-based catalysts, and Stille outlines the synthesis of rigid polyphenylphenylenes and polyanthrazolines. In the physical chemistry section are papers by Meares on transport phenomena and their relevance to membrane separation and by Szwarc reviewing anionic polymerization and applications of living polymer processes. Infra-red spectroscopy is applied to a study of crystalline polyethylene (Krimm) and high-resolution ^{13}C n.m.r. for investigation of stereochemical configurations in vinyl polymers (Bovey), while Guillet discusses the role of molecular mobility in photochemical processes.

Polymer technology has seven papers which include a review of polyethylenes and the provision of polymers of improved fabrication performance (Foster), segment deformation in glassy polymers (Yannas) and new thermally stable aromatic or heterocyclic copolycondensates (Fontan), which paper regrettably gives no references. Okamura reviews his work on the production of synthetic fibres from modified PVC dispersions, and Morton outlines advances made with synthetic elastomers, especially the *trans*-polypentenamer, thermoelastic block copolymers and liquid rubbers. Work on the effects of fine structure on the pyrolysis behaviour of cellulosic materials is discussed by Lewin, and Ranby has a paper on teaching technology in Sweden.

The seven papers in the final section on biopolymers deal with receptor proteins for neuroactive drugs (Robertis), adenovirus proteins (Pereira), and controlled synthesis in enzyme studies (Merrifield). Synthesis in bacterial genes is described by Khorana and the use of ^{13}C n.m.r. in a study of mucopolysaccharides by Perlin. Polymeric carriers and immobilization of enzymes is the subject of a paper by Manecke, and Dawes discusses the function of poly(β -hydroxybutyrate) in micro-organisms.

In all, these collected papers provide a good picture of developments in polymer science, showing particularly the many fields of activity and methods of scientific approach. From these invited lectures one is able to appreciate the depth of the studies in progress as well as the ultimate use of the findings in practical terms, whether this be in plastics, fibre or rubber technology, the medical world, or other fields of endeavour.

While the book is handsomely bound and produced, the text itself consists of the photo-reduced typescripts as received from the various authors and editing has been minimal. This perhaps contributes to the originality of the contributions but it is a little disconcerting to encounter different sets of type-face throughout the book, a lack of explanation to a few of the diagrams and abbreviations, and to have no index. However, such direct use of the authors' scripts has enabled the book to be produced without delay, and in a rapidly developing field like that of macromolecules

this is a decided advantage which will outweigh the minor faults noted above.

At the price quoted the volume may prove expensive for purchase by an individual but the many papers give it considerable merit and it could with some benefit be used by those who wish to have brief but authoritative reviews on particular aspects or more generally to read of developments outside their areas of immediate interest.

R. J. W. Reynolds

Advances in polymer science, Volume 15 Springer Verlag, Berlin, 1975, 155 pp. \$27.80

The book contains four review articles, Oligomerisation of ethylene with soluble transition-metal catalysts by G. H. Olivé and S. Olivé. Stereochemistry of propylene polymerisation by A. Zambelli and C. Tosi, Structures of copolymers of high olefins by Y. V. Kissin and Mercaption-containing polymers by C. D. S. Lee and W. H. Daly. All four articles are reasonably well written and present an interesting account of the subject described.

The article of Olivé and Olivé discusses Ziegler-based systems (transition metal compounds plus aluminium alkyl compounds) as catalysts for the oligomerization of ethylene. It is a useful collection of facts but lacks clarity and conviction when talking about the mechanism of the processes concerned. The basic difficulty in trying to disentangle the mechanism of Ziegler catalysts is that there are too many possible structural options for the reactive centre in any given system. This produces reviews which are catalogues of data with little unambiguous evidence as to what exactly is going on. In this review it is implied that although there may exist monometallic catalysts which can oligomerize ethylene they are in general lacking in activity and require a cocatalyst, aluminium alkyls, to give effective systems. This is, of course, not completely correct as it is known that the system $\text{Br}_3\text{ZrC}_3\text{H}_5$ (*Adv. Catalysis* 1973, 23, 263) oligomerize ethylene to give 60–100 residues per α -olefin chain at very high rates indeed.

The kinetic analysis of these reactions does not take account of the fact that in many of these systems large amounts of 1-butene is formed and the postulate of a six-centre transition state seems unnecessary to account for the β -hydrogen abstraction process. The industrial side of ethylene oligomerization is also poorly dealt with. Most industrial processes do not use this type of chemistry, wax cracking has until recently been the preferred process but in new plants this is being replaced by 'ethylene growth' using aluminium alkyl chemistry.

The stereochemistry of propylene polymerization is a well written description of the ideas of Professor Zambelli and his colleagues in which they attempt to use the four centre transition state to explain the chemistry of Ziegler-Natta catalysts and their ability to control the stereochemistry of the insertion process. The mechanism they describe may well have some relation to real behaviour in polymerizations initiated by transition metal alkyls since the latter are essentially monometallic catalysts. However, Ziegler-Natta systems are almost certainly bimetallic and the choice of aluminium alkyl as cocatalyst can have a profound effect on the ability of the centre to stereoregulate.

The final contribution on polyolefins is a paper by the Russian scientist Y. V. Kissin on the structure of copolymers of the higher olefins. This is a very interesting review and collects together information on 1:1 copolymers of the common olefins, with some data on their fine structure derived mainly from infra-red studies. In view of the known difficulties of making many of these copolymers it is surprising that such a wide variety of types are now available for study. The work of Dr Turner-Jones on the 4-methyl pentene-1 copolymers is treated in detail and serves to illustrate, for all crystalline polyolefins, the effect of copolymerization on crystallinity, melting points, and infra-red spectra. The observations divide themselves into three principal groups: copolymers in which the comonomer side chain is rejected by the host crystal lattice, in these cases quite small amounts of comonomer reduce the crystallinity drastically; copolymers such as 4-methyl pentene-1/hexene-1 for example where the comonomer side chains can crystallize with the host lattice and crystallinity persists over the whole range of compositions; the least known system and probably the most useful are

those in which the comonomer is incorporated as a series of blocks so that the microstructure is made up of discrete phases. It has been observed with the latter systems that unusual mechanical properties are obtained. It would have been helpful if some information of this kind could have been given, but mechanical behaviour is not discussed.

In conclusion the book will be of interest to polymer chemists in general and particularly those interested in polyolefins.

D. G. H. Ballard

Ionic polymers

Edited by L. Holliday

Applied Science, London, 1975, 416 pp, £14

The most familiar examples of ionic polymers, the so-called 'ionomers', have enjoyed considerable commercial success over the past few years, a factor which has undoubtedly assisted in generating enthusiasm in this area. Present trends in research, as reflected in this book, are directed towards a wider understanding of both the essentially organic and inorganic ion-containing materials. An initial step in this development is the recognition of materials such as inorganic oxide glasses, metal dicarboxylates and crystalline silicate and phosphate minerals as polymers. A useful exchange of the concepts and the considerable body of knowledge available within these hitherto discrete areas of study with the field of organic polymers may then follow. As the introductory chapter of the book intimates, in only one or two topics of study, such as the glass transition temperature, have unifying semi-empirical relationships and correlations been established. Much progress has yet to be made to consolidate a cohesive study of ionic polymers on such a broad base as it is presented here.

Following the introductory chapter, in which classifications and general properties of ionic polymers are presented in a clear and logical way, there are seven further chapters each dealing with different types of ionic material. These chapters have different authors and each chapter emphasizes a different aspect of its subject. The chapters concerned with ionomers, carboxylated elastomers and crystalline silicates and phosphates are thorough and systematic reviews of the extensive literature on these materials

whereas the chapter on rigid, highly carboxylated ionic polymers is, for the greater part, an authoritative account of recently developed dental cements. However, the conformational changes and ion-binding phenomena which are referred to in the opening section of this account apply to dilute solutions and are inappropriate when discussed in the context of the concentrated systems encountered in these cements. There are two shorter chapters on metal dicarboxylates and the technology of polyelectrolyte complexes and the final chapter by N. H. Ray describes an essentially novel approach to the structure of inorganic glasses.

Taken as a whole the book is somewhat heterogeneous, but as a first step it represents a welcome development and the individual contributions are very useful in themselves. The book will be of interest to research workers and could provide some novel ideas on presentation of course work for teachers in materials departments. The book is well presented but its price will probably restrict it to appropriate departmental libraries for which it will be a good investment.

P. V. Wright

The Proprietors of British Patent No. 1163502, for "Method for activating cycloaliphatic polyamines as curing agents for reaction with epoxide compounds", desire to enter into negotiations for the sale of the patent, or for the grant of licences thereunder. Further particulars may be obtained from Marks & Clerk, 57-60 Lincoln's Inn Fields, London WC2A 3LS.

RESOURCES POLICY

the economics, planning and use of mineral resources

**A QUARTERLY JOURNAL
DECEMBER 1975**

The impasse over Limits to Growth: a suggested course of research F. J. Wells

The geographic concentration of world mineral supplies M. H. Govett

Indonesia's mineral resources — performance and prospects B. Lloyd

United States uranium resources: the 1975—2000 outlook D. G. Brookins

Other sections

- . Current topics
- . Conference reports
- . Forthcoming meetings
- . Book reviews and announcements
- . Publications received

RESOURCES POLICY presents multi-disciplinary discussions at an upper management/academic level. The aim is to identify policy options for the future supply and demand of mineral resources. It encompasses the many disciplines and examines options as they affect industrial, commercial and social institutions at world and regional levels.

Published quarterly in March, June, September, December.

One-year subscription (four issues) £22.00 U.K. £25 (\$65.00) Overseas

For details apply to: IPC Business Press (Sales and Distribution Ltd.)

Oakfield House, Perrymount Road, Haywards Heath, Sussex, England RH6 3DH

Telephone Haywards Heath (0444) 53281 Telex: Bisnespress Ldn 25137

Universality approach to the expansion factor of a polymer chain

C. Domb

Wheatstone Physics Laboratory, King's College, Strand, London WC2R 2LS, UK

and A. J. Barrett

Department of Mathematics, Royal Military College, Kingston, Ontario, Canada

(Received 25 September 1975)

Attention is drawn to recent developments in the theory of critical point thermodynamics, which can be of great help in elucidating classical problems relating to the size and shape of a molecular chain, when intramolecular forces are taken into account. It is suggested that the two-parameter function used to describe the expansion factor, α^2 , of the end-to-end length of a polymer chain, is 'universal', i.e. the same for lattice and continuum models. Hence well-established numerical data of self-avoiding walks on lattices can be used to test various formulae which have been advanced for α^2 . By combining these numerical data with the well-known virial expansion, a new formula is proposed to represent the two-parameter function.

INTRODUCTION

A central problem in the theory of polymer chains in dilute solution is the effect of intramolecular forces, $V(r)$, on the shape and size of the chain. It is reasonable to represent the latter by a hard core repulsion and a longer range van der Waals type attraction; by analogy with a fluid we should then expect to find a 'gas-like' phase at sufficiently high temperatures, condensing into a 'liquid-like' phase at a sharply defined transition temperature¹. Special care is needed to explore the detailed behaviour in the transition region, and this has recently begun to attract increasing attention²⁻⁶.

In the 'gas-like' phase, the repulsive forces dominate and give rise to the excluded volume effect, which has been the object of much theoretical study for some 25 years. For this region, it has usually been assumed that the total intramolecular forces can (to a sufficient approximation) be replaced by a δ -function of appropriate strength $-\nu\delta(r)$, where:

$$\nu = \int [1 - \exp -\beta V(r)] dr, \quad (\beta = 1/kT) \quad (1)$$

and ν has the dimensions of volume. There has been little attempt to assess precisely how good is this approximation. Recent Monte Carlo work by Smith and Fleming⁷ has indicated that it may be significantly worse than is usually assumed. But as a first step, it would at least be useful, to have reliable information regarding the behaviour of this simplified model in which all the intramolecular forces are combined into a single parameter.

Unfortunately, the current theoretical picture of the behaviour of this model is very confused. At least twelve different formulae have been advanced, each claiming to represent the expansion factor in the end-to-end length:

$$\alpha^2 = \langle R_N^2 \rangle / \langle R_{N0}^2 \rangle = \langle R_N^2 \rangle / N \quad (2)$$

Some of these are illustrated in *Figure 1*, as a function of the dimensionless parameter:

$$z = \left(\frac{3}{2\pi a^2} \right)^{3/2} \nu N^{1/2} \quad (3)$$

where a , is the length of a unit of the chain. (This diagram follows Yamakawa⁸, except that α^2 is plotted rather than α^3 which has no direct physical significance.) All of the formulae assume that α^2 is a function of z only, say $\psi(z)$ (this is sometimes called the 'two-parameter theory'⁹). Such an assumption is rigorously valid in the limit $N \rightarrow \infty$, $\nu \rightarrow 0$, $\nu N^{1/2}$ finite, and there is evidence that it provides a reasonable general approximation for large N ¹⁰.

In this confused situation, it may seem presumptuous to put forward yet another formula for α^2 . We do so, only because we think that the remarkable progress in recent years in our understanding of critical point behaviour, has supplied general principles on which to base a reliable calculation of α^2 and other quantities related to the shape and size of the chain. Since many polymer theorists are unfamiliar with these developments we shall spend a few paragraphs discussing them.

CRITICAL POINT THERMODYNAMICS

There are a variety of physical phenomena associated with critical point or λ -point transitions, i.e. transitions involving no discontinuity in energy or entropy but discontinuities or singularities in higher derivatives of the free energy. The oldest and best known is the liquid-vapour critical point; other examples are the Curie point of a ferromagnet, and of an order-disorder transition in an alloy, the Néel point of an antiferromagnet, the λ -point of liquid helium, and the critical point for mixing of solutions. The transitions in solids involve regular crystal lattices, those in fluids have no lattice structure.

Despite the different types of microscopic interaction which give rise to critical points, the general behaviour follows a standard pattern. The most important characteristic, is a long range correlation just above the critical temperature T_c , and it is this correlation which provides an analogy with the mean square end-to-end length of a polymer chain (as will be elaborated shortly). For each particular system, an 'order parameter' is defined, in terms of which the detailed character of the long range correlation can be specified.

Theoretical models, introduced to represent particular systems, have been investigated in detail by several different

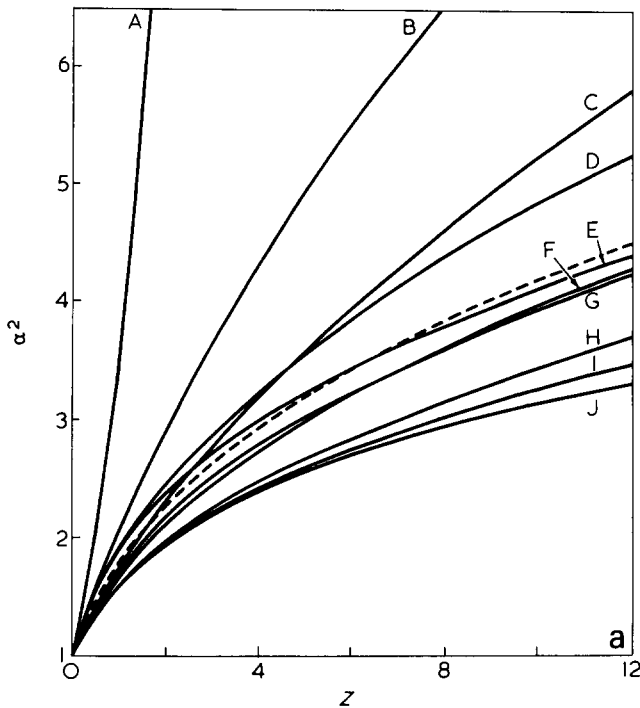


Figure 1a Some approximations to the expansion factor α^2 , for values of $z = 0-12$. A, Bueche-James: $\alpha^2 - 1 = 4\alpha z/3$; B, Fixman: $\alpha^3 = 1 + 2z$; C, Ptitsyn: $4.67\alpha^2 = 3.67 + (1 + 9.34z)^{2/3}$; D, Alexandrowicz-Kurata: $\alpha^5/5 + \alpha^3/3 - 8/15 = 4z/3$; E, Flory: $\alpha^5 - \alpha^3 = 3(3)^{1/2} z/2$; F, Yamakawa-Tanaka: $\alpha^2 = 0.572 + 0.428(1 + 6.23z)^{1/2}$; G, Fujita-Okita-Norisuye: $\alpha^5 - 0.4931\alpha^3 - 0.2499\alpha^{-1.332} \sin(1.073 \ln \alpha) - 0.5069\alpha^{-1.332} \cos(1.073 \ln \alpha) = 2.630z$; H, Bueche: $\alpha^4 - \alpha^2 = 48z(1 + 2/3\alpha^2 + 1/4\alpha^4)/69$; I, Modified Flory: $\alpha^5 - \alpha^3 = 4z/3$; J, Yamakawa: $\alpha^{6.67} = 1 + 4.45z$. z , is defined by equation (3). - - - -, is given by equation (20)

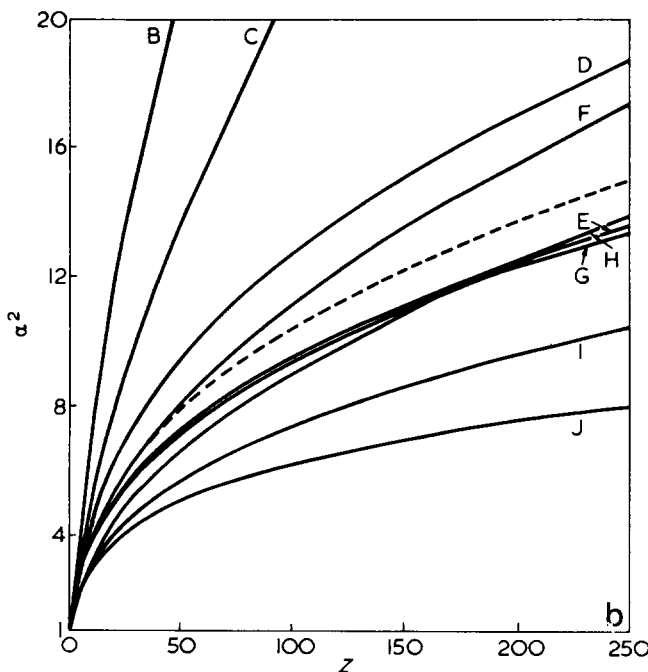


Figure 1b Some approximations to the expansion factor for values of $z = 0-250$. Curves B-J as for (a)

techniques. For a few models exact calculations have been possible, the best known being the classic solution of the two-dimensional Ising model by Onsager¹¹. For other models, numerical techniques have been developed which have proved highly effective¹², and good agreement with experiment has been achieved over a wide range. More recently, the renormalization group approach introduced

into the field by Wilson¹³ has provided a general theoretical framework for understanding the characteristic features of critical point behaviour. Numerical calculations using this approach agree well with the older more empirical calculations. Most theoretical and experimental workers in the field would subscribe to the view that, a basic understanding of the phenomena has been achieved, and reliable methods of calculation have been developed with which to calculate properties of interest and importance.

During the above investigations the idea of 'universality' has emerged, i.e. that certain features of critical behaviour are independent of the model for a variety of models. For example, it has been found that exponents which characterize critical behaviour and the function which specifies the equation of state in the critical region, do not depend on lattice structure for a given type of interaction. One might therefore reasonably expect such properties to apply equally to a continuum model.

A simple illustration of the above ideas is provided by the well-known properties of random walks on lattices, which correspond to a model of critical behaviour known as the Gaussian model. For a random walk of N steps on any lattice in any dimension, or in a continuum:

$$\langle R_N^2 \rangle = N \tag{4}$$

This is a property of wide universality, since it is independent both of lattice structure and dimension; it is related to the correlation length for the Gaussian model. A more typical result related to the specific heat near T_c , is the fraction of walks which are at the origin after N steps, given by:

$$p_N \sim AN^{-d/2} \tag{5}$$

Here the exponent is independent of lattice structure for a given dimension, although the amplitude depends on lattice structure. Likewise the shape of the walk¹⁵ for large N :

$$f(u) = \left(\frac{d}{2\pi} \right)^{d/2} \exp - \frac{d}{2} u^2 \tag{6}$$

is independent of lattice structure in a given dimension.

It might be of interest to specify in more detail how configurational properties, which are functions of N , are related to critical behaviour which depends on $(T - T_c)$. For any model of critical behaviour, an interaction parameter J must be specified, and if X is the thermodynamic property to be investigated and $\phi(N)$ an appropriate configurational property, it can readily be shown from elementary statistical mechanics that:

$$X(T) = \sum_{N=1}^{\infty} \phi(N) \exp - \beta NJ = \sum_{N=1}^{\infty} \phi(N) y^N \quad (y = \exp -\beta J) \tag{7}$$

Singular behaviour in $X(T)$ arises at a temperature T_c corresponding to the radius of convergence of this power series, and if the asymptotic behaviour of $\phi(N)$ is:

$$\phi(N) \sim N^{-h} \tag{8}$$

then that of $X(T)$ is:

$$X(T) \sim (T - T_c)^{-h-1} \tag{9}$$

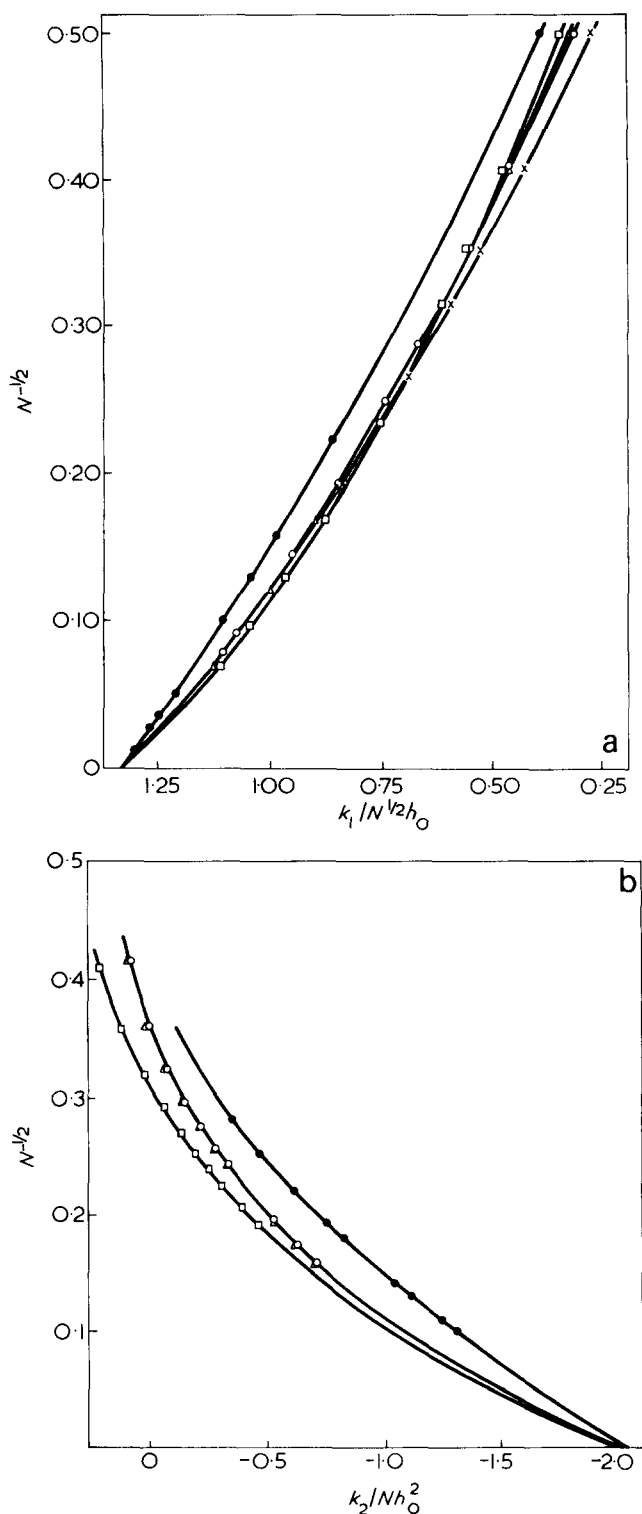


Figure 2 Convergence of virial coefficients for various lattices to two-parameter value. (a) $k_1/h_0N^{1/2}$ vs. $N^{-1/2}$, points shown are values computed numerically: ●, Gaussian continuum model; ○, s.c. lattice; △, b.c.c. lattice; □, f.c.c. lattice; x, diamond lattice. (b) k_2/Nh_0^2 vs. $N^{-1/2}$: ●, Gaussian model; ○, s.c. lattice; △, b.c.c. lattice; □, f.c.c. lattice. It will be seen that there is convergence to a single value as $N \rightarrow \infty$ (the two-parameter value)

When $\phi(N)$ represents a mean square end-to-end distance, $X(T)$ represents a range of correlation.

In a set of models of ferromagnetism which have been much studied by renormalization group methods¹³, the interacting units consist of classical vector spins in n dimensions, and the exponents have been calculated as a perturbation series whose coefficients are functions of n . $n = 1$

corresponds to the Ising model, and de Gennes¹⁶ pointed out that the case $n = 0$ corresponds exactly to the problem of a self-avoiding walk on a lattice; the estimates of the exponents are then in good agreement with those obtained by numerical studies¹⁴. This is of direct relevance to the polymer problem.

UNIVERSALITY IN A POLYMER CHAIN

We shall now endeavour to show that the expansion factor α^2 as a function of z introduced earlier, is a universal function as $N \rightarrow \infty$. We must first specify a lattice version of the problem, and this is available in the Domb–Joyce model¹⁷ of a random chain on the lattice with an intramolecular interaction $-w\delta_{ij}$ between any pair of points of any configuration, i and j being the lattice sites occupied by the i th and j th points of the walk. The Boltzmann factor associated with any configuration of the chain is the product:

$$\prod_{i=0}^{N-2} \prod_{j=i+2}^N (1 - w\delta_{ij}) \quad (10)$$

There is an interaction between any points of the chain occupying the same site, and the model is the direct analogue of the continuum chain discussed earlier. We note, however, that when $w = 1$, no site can be occupied more than once, and the walk is self-avoiding.

We can expand α^2 as a perturbation series in w , for any lattice^{17,18} and for any N :

$$\alpha^2 = 1 + k_1w + k_2w^2 + k_3w^3 + \dots \quad (11)$$

where the leading term in k_r is of order $N^{r/2}$. The continuum model (1) can be expanded likewise in powers of v , and in fact, there is no difference between the form of the expansion for a lattice model and that for a continuum; by the choice of an appropriate generating function for returns to the origin in the corresponding random walk, both can be expressed in the same mathematical form. The virial expansion for the function $\psi(z)$ results from ignoring all but the term of highest order, $N^{r/2}$.

Our claim to universality for $\psi(z)$ is based partly on the evidence that with the exception of a particular numerical constant for each lattice, the virial coefficients are identical for all lattices and for a continuum chain. We have verified this to the third order, but we suspect that a proof should be possible to all orders. We illustrate this property in Figure 2; the first two virial coefficients are plotted as functions of $N^{-1/2}$, and it will be seen that by choosing a suitable scale factor, h_0 , the reduced coefficients become identical as $N \rightarrow \infty$. For a lattice h_0 is given by:

$$h_0 = \left(\frac{3}{2\pi} \right)^{3/2} \frac{g}{a^3} \quad (12)$$

where g is the volume per unit of the lattice, and a the length of a step of the walk. For the s.c., b.c.c., and f.c.c. lattices, g/a^3 has the values 1, $4.3^{-3/2}$, $2^{-1/2}$ respectively; for the diamond lattice there are two atoms per unit cell and the corresponding g/a^3 is $8.3^{-3/2}$.

We therefore conjecture that if we take as variable:

$$z = h_0N^{1/2}w \quad (13)$$

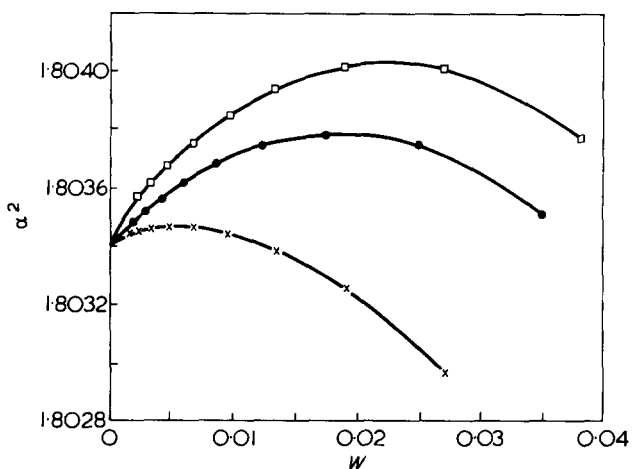


Figure 3 Convergence of numerical estimates for various lattices to the two-parameter value ($z = 1$). \square , f.c.c. lattice; \bullet , b.c.c. lattice; \times , s.c. lattice

the expansion factor α^2 is asymptotically the same function of z for all lattices. This can be tested by numerical estimates for various lattices^{10,18}, and a typical result is shown in Figure 3. The constant h_0 has been chosen to give the same function, $\psi(z)$, as that defined for a continuum earlier.

CALCULATION OF THE EXPANSION FACTOR

We now apply the above ideas to the estimation of $\psi(z)$. For small z , we can use the three known coefficients of the virial expansion⁸. We have recently recalculated these coefficients by an alternative method and have obtained a slightly different value for the third coefficient¹⁸ (details will be published elsewhere). However, even the knowledge of several more coefficients would be of little additional value, since the series is asymptotic and not convergent¹⁹. The physical basis for this is apparent, since the chain will collapse to a single link for an attractive force however small, i.e. for any negative ν or w .

Fortunately, we can make use of the lattice enumerations when $w = 1$, i.e. when the walk is self-avoiding. In this case the enumeration and extrapolation methods parallel those for the Ising model, for which great accuracy has been achieved; additional confirmation was supplied recently, when exact calculations for the susceptibility of the two-dimensional Ising model became available²⁰.

For the s.c., b.c.c., f.c.c., and diamond lattices the general asymptotic formula:

$$\langle R_N^2 \rangle \sim BN^{6/5} \quad (14)$$

has been conjectured¹⁴, the most accurate estimates of B being as follows^{21,22}:

$$\begin{aligned} B_{s.c.} &= 1.067, & B_{b.c.c.} &= 0.959, & B_{f.c.c.} &= 0.921 \\ B_{\text{diamond}} &= 1.283 \end{aligned} \quad (15)$$

We have pointed out that the existence of a single function $\psi(z)$ to describe α^2 is true only asymptotically as $N \rightarrow \infty$ and $w \rightarrow 0$. However, there is evidence^{10,18} that it is a reasonable approximation elsewhere, and we can furnish a numerical test when $w = 1$ using the values in equation (15). Equation (14) then implies that:

$$\psi(z) \sim bz^{2/5} \quad (16)$$

and combining with equation (13) we have:

$$b \approx Bh_0^{-2/5} \quad (17)$$

Estimates of b obtained from the data in equation (15) are given in Table 1, and the deviations from a constant value (less than 2%) provide an estimate of the error in the above approximation. We should note that because of the different values of h_0 for different lattices in relation (13), each lattice provides an estimate of $\psi(z)$ for a different range of z . The information available so far about this function is illustrated in Figure 4, and most of the approximations mentioned earlier differ markedly from the portion represented by the self-avoiding walks.

By using exact enumerations for small N for the above lattices and extrapolating¹⁰, it is possible to obtain an improved estimate of b , and we would like to suggest the value of 1.64, as providing the best fit to the data currently available. The portion of $\psi(z)$ corresponding to equation (16) is drawn in Figure 4, and it will be seen that there is little difficulty in interpolating the rest of the curve (shown dotted), to complete our estimate over the whole range.

When we come to compare our result with other estimates, we find that the closest fit over the whole range is provided by Flory's original formula²³:

$$\psi^{5/2} - \psi^{3/2} = \frac{3(3)^{1/2}}{2} z \quad (18)$$

Even though this does not give the correct value for any of the virial coefficients, the region covered by these coefficients is small. The subsequent modification by Flory and Fisk²⁴, in which the right-hand side of equation (18) is replaced by $9\sqrt{3}z/14$ so as to correct the first virial coefficient, is more seriously wrong in asymptotic behaviour. In fact, we consider that far too much attention has been paid to virial coefficients as a method of discriminating between the various closed form formulae.

To make our own numerical estimate more conveniently available, it is important to provide a closed form formula.

Table 1 Estimates of b from self-avoiding walk enumerations

Lattice	b
f.c.c.	1.648
b.c.c.	1.659
s.c.	1.663
diamond	1.682

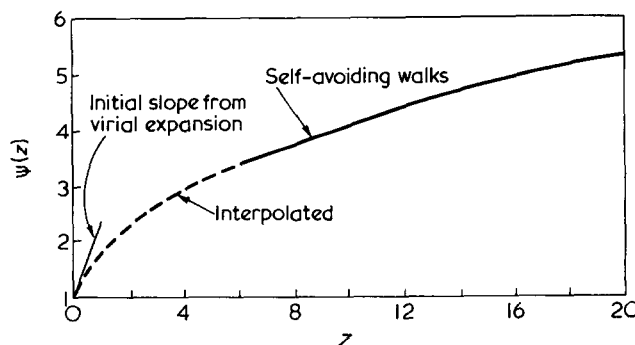


Figure 4 Estimation of $\psi(z)$ for the whole range of z : for small z , virial expansion $\psi \approx 1 + 4z/3$; for sufficiently large z , $\psi \sim 1.64z^{2/5}$; and interpolation in the intermediate range

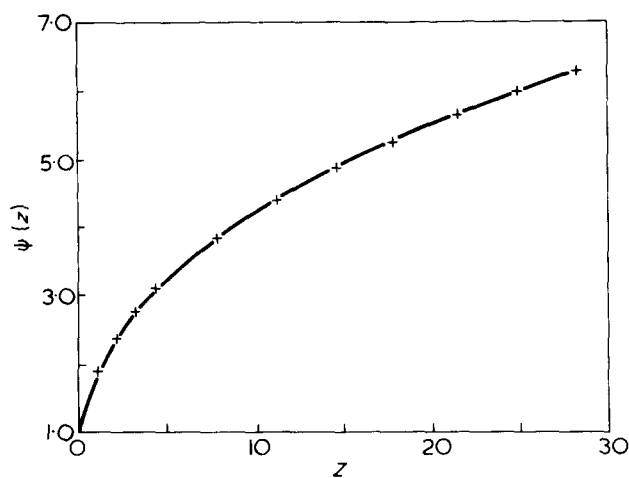


Figure 5 Formulae for $\psi(z)$

The crudest approximation involving only two parameters endeavours to take account correctly of the first virial coefficient and the asymptotic form, equation (16):

$$\psi^5 = 1 + \frac{20}{3}z + 4\pi z^2 \quad (19)$$

It is because two parameters are required for such a fit that, no modification of a Flory type formula, equation (18), involving only one adjustable parameter, can be adequate.

A more refined formula takes account of the three known virial coefficients as well as the asymptotic formula, equation (18):

$$\psi^{15} = \left[1 + 10z + \left(\frac{70}{9}\pi + \frac{10}{3} \right) z^2 + 8\pi^{3/2} z^3 \right]^2 \quad (20)$$

Both of these formulae are drawn in *Figure 5* and they are in good agreement with the best numerical estimates. Since the latter may themselves be subject to errors of one or two percent, we feel that the formulae (19) or (20) can be used in most practical situations.

Formulae (19) and (20) do not provide a correct analytical representation of $\psi(z)$ near $z = 0$, since they give rise to a convergent rather than an asymptotic series. To provide a representation which is analytically correct, we could make use of some well-known asymptotic series, such as those for Bessel functions, and seek a formula of the type:

$$\psi = z^{2/5} \exp(4/5z) \left[aI_0 \left(\frac{1}{z} \right) + bI_1 \left(\frac{1}{z} \right) + cI_2 \left(\frac{1}{z} \right) \right]^{-4/5} \quad (21)$$

However, since the point at issue is somewhat esoteric, we have not pursued numerical estimates of the parameters in equation (21).

RADIUS OF GYRATION

A property of greater significance than the end-to-end length is the radius of gyration, $\langle S^2_N \rangle$, and by analogy with

equation (2) we can define an expansion factor arising from intramolecular forces:

$$\alpha^2_S = \langle S^2_N \rangle / \langle S^2_{N0} \rangle = 6 \langle S^2_N \rangle / N \quad (22)$$

Various formulae have been advanced for α^2_S as for α^2 , and an illustration analogous to *Figure 1* has been given by Yamakawa⁸.

The ideas and methods which have been described in the previous sections can be applied equally to α^2_S . Exact enumerations for small N have been undertaken, but the results have not yet been processed²⁵. However, data for self-avoiding walks are available^{14,26}, and therefore a reasonable first approximation can be derived.

We prefer to concentrate on the ratio:

$$\alpha^2_S / \alpha^2 = 6 \langle S^2_N \rangle / \langle R^2_N \rangle = \theta(z) \quad (23)$$

since this has a simple pattern of behaviour and rapidly approaches a limiting asymptotic value. In fact, estimates of this quantity for self-avoiding walks on different lattices were so close, that it was suggested that it might be a universal constant²⁶. However, it is clear from the general argument above that this cannot be rigorously correct, and the proper conclusion to draw is that $\theta(z)$ varies little with z , once z is greater than a particular value z_0 .

Only two terms of the virial expansion for α^2_S are currently available, and from these we deduce that for small z :

$$\theta(z) \sim 1 - 0.057z - 0.069z^2 \quad (24)$$

Using as our limiting estimate for large z the value, 0.933, we approximate to $\theta(z)$ by the formula:

$$\theta(z) = 0.933 + 0.067 [\exp -(0.85z + 1.39z^2)] \quad (25)$$

Since we have not checked against exact enumerations we put forward this approximation more tentatively than equations (19) and (20).

CONCLUSIONS

As stated earlier, we believe that the δ -function model of intramolecular interactions has several limitations. However, before it is possible to investigate these limitations in more detail, one must clear up the confusion which exists in the literature about the properties of this model. We feel that the formulae we have advanced have a reliable basis, and it would be useful if they could be tested by some alternative approach. The natural test which suggests itself is that of Monte Carlo enumeration²⁷, since one can ensure that the model tested corresponds exactly to the theoretical model. A preliminary treatment yielded results in modest agreement with the numerical extrapolations on which our formulae are based. We feel, however, that there is scope for a more comprehensive investigation.

ACKNOWLEDGEMENTS

The authors are grateful to Professor Manfred Gordon for reading and commenting on the manuscript, and to Dr Melville Lax for helpful discussion and correspondence.

This research is supported (in part) by the European Research Office of the U.S. Army.

REFERENCES

- 1 Stockmeyer, W. H. *Makromol. Chem.* 1960, **35**, 54
- 2 Eizner, Yu. Ye. *Polym. Sci. USSR* 1972, **14**, 1695 (*Vysokomol. Soedin (A)* 1972, **14**, 1512)
- 3 Lifshitz, I. M. *Sov. Phys. JETP* 1969, **28**, 280 (*Zh. Eksp. Teor. Fiz.* 1968, **55**, 2408)
- 4 Domb, C. *Polymer* 1974, **15**, 259
- 5 de Gennes, P. *J. Phys. Lett.* 1975, **36**, L55
- 6 Massih, A. R. and Moore, M. A. *J. Phys. (A)* 1975, **8**, 237
- 7 Smith, N. C. and Fleming, R. J. *J. Phys. (A)* 1975, **8**, 929, 938
- 8 Yamakawa, H. 'Modern Theory of Polymer Solutions', Harper and Row, New York, 1971, Ch 3
- 9 Chikahisa, Y. *J. Chem. Phys.* 1970, **52**, 206
- 10 Domb, C., Barrett, A. J. and Lax, M. *J. Phys. (A)* 1973, **6**, L82
- 11 Onsager, L. *Phys. Rev.* 1944, **65**, 117
- 12 'Phase Transitions and Critical Phenomena', (Eds. C. Domb and M. S. Green), Academic Press, London, 1974, Vol 3
- 13 Wilson, K. G. and Kogut, J. B. *Phys. Rep. (C)* 1974, **12**, 75
- 14 Domb, C. *Adv. Chem. Phys.* 1969, **15**, 229
- 15 Domb, C. in 'Critical Phenomena in Alloys, Magnets and Superconductors', (Eds. R. E. Mills, E. Ascher and R. I. Jaffee), McGraw-Hill, New York, 1971, p 83
- 16 de Gennes, P. *Phys. Lett. (A)* 1972, **38**, 339
- 17 Domb, C. and Joyce, G. S. *J. Phys. (C)* 1972, **5**, 956
- 18 Barrett, A. J. *PhD Thesis* University of London (1975)
- 19 Edwards, S. F. *J. Phys. (A)* 1975, **8**, 1171
- 20 Barouch, E., McCoy, B. M. and Wu, T. T. *Phys. Rev. Lett.* 1973, **31**, 1409
- 21 Domb, C. *J. Chem. Phys.* 1963, **38**, 2957
- 22 Wall, F. T. and Hioe, F. T. *J. Phys. Chem.* 1970, **74**, 4416
- 23 Flory, P. J. *J. Chem. Phys.* 1949, **17**, 303
- 24 Flory, P. J. and Fisk, S. *J. Chem. Phys.* 1966, **44**, 2243
- 25 Lax, M. personal communication
- 26 Domb, C. and Hioe, F. T. *J. Chem. Phys.* 1969, **51**, 1915
- 27 Alexandrowicz, Z. and Accad. Y. *Macromolecules* 1973, **6**, 251

Influence of intra-chain *trans* double bonds on the melt crystallization of polyamides

G. Maglio, E. Martuscelli, R. Palumbo and I. Soldati

Laboratorio di Ricerche-su Tecnologia dei Polimeri e Reologia, CNR, Via Toiano 2, Arco Felice, Napoli, Italy

(Received 22 July 1975; revised 19 September 1975)

Melt crystallization kinetics of some aliphatic polyamides, with variable amounts of intra-chain double bonds, was investigated by d.s.c. technique. Crystallization isotherms fit the Avrami equation, yielding for the Avrami parameter, n , values independent from the polyamide composition and close to 4. The values of the calorimetric crystallization rate, in the proximity of the melting point, were analysed using the secondary nucleation theory of Hoffman and Lauritzen. The equilibrium melting temperatures, T_m^0 , were found to increase regularly with increase in the amount of unsaturation. The free energy of formation of a nucleus of critical dimensions and the surface free energies σ and σ_e of the lamellar crystals were determined. The values were correlated with the copolymer composition. Under the same undercooling, an increase in the rate of crystallization with the amount of double bonds in the chain, is observed. This result is related to surface effects; corresponding lowering in the free energy of folding σ_e is found.

INTRODUCTION

The purpose of this paper is to investigate the effect of increasing chain flexibility, obtained by introducing intra-chain double bonds, on the rate of isothermal melt crystallization of aliphatic polyamides. This research is part of a more general project on the influence of constitutional and configurational defects on the structure and on the properties of polymeric materials¹. It seemed interesting, both from fundamental and technological points of view, to relate the amount of double bond unsaturation within polyamide chains, with half time of crystallization, Avrami exponent and kinetic rate constant. Further, we were also interested to observe the dependence of the energy of formation of a nucleus of critical dimensions and of the surface free energy of lamellar fibrillae of spherulites, on the amount of double bonds along the main chain.

EXPERIMENTAL

Materials

The polymers were prepared by interfacial polycondensation from 1,6-diaminohexane and the acid chlorides using a chloroform *n*-hexane mixture (1:1 v/v) as organic phase and sodium hydroxide as acid acceptor². They are reported in Table 1, along with their composition and in-

Table 1 Composition and inherent viscosity of the prepared polyamide samples

Polyamide*	Name	Molar fraction of 4-OD	η_{inh} (dl/g)
SUB-HMD	A	0	2.5
SUB-HMD-4-OD	B ₁	0.12	2.4
SUB-HMD-4-OD	B ₂	0.24	2.3
SUB-HMD-4-OD	B ₃	0.46	2.0
SUB-HMD-4-OD	B ₄	0.61	1.1
SUB-HMD-4-OD	B ₅	0.79	1.4
4-OD-HMD	C	1.00	2.0

* SUB, suberic acid; HMD, 1,6-diaminohexane; 4-OD, *trans*-4-octen-1,8-dioic acid

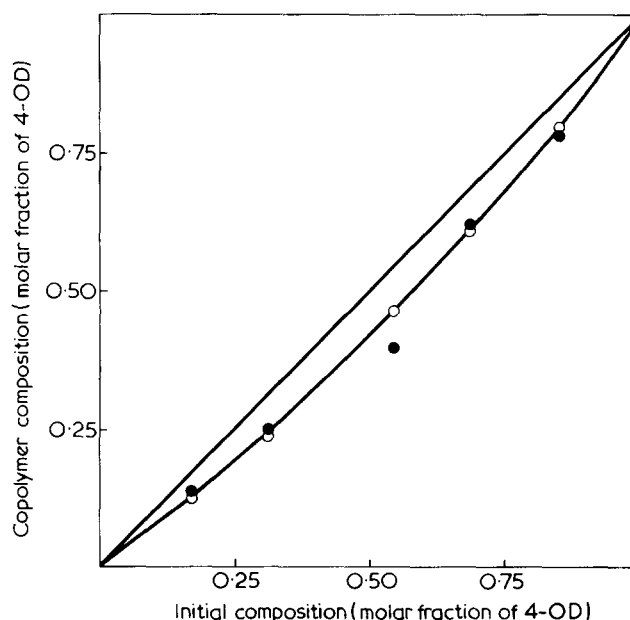


Figure 1 Composition of the copolymers, as average of i.r. and p.m.r. (●) analyses versus the composition of the initial mixture. ○, represent the values of copolymer composition used throughout the paper as interpolation of the experimental points

herent viscosities. The composition of the copolymers was determined by infra-red analysis, by using the absorbance ratio $A_{967\text{ cm}^{-1}}/A_{3300\text{ cm}^{-1}}$ of the *trans* double bond bending and of the N-H stretching respectively. The experimental ratios, were compared with those of calibration curve obtained with blends of the pure homopolymers (samples A and C in Table 1) of known composition. Alternatively, the composition was determined by analysis of the p.m.r. spectra of trifluoroacetic acid solutions of the copolymers. Peak area measurements of the olefinic protons at 5.62 δ and of the methylene protons adjacent to the nitrogen at 3.56 δ , were employed (tetramethylsilane as internal standard). The compositions determined by means of i.r. and p.m.r. techniques, agree fairly well. The average values are reported in Figure 1. The polymers of

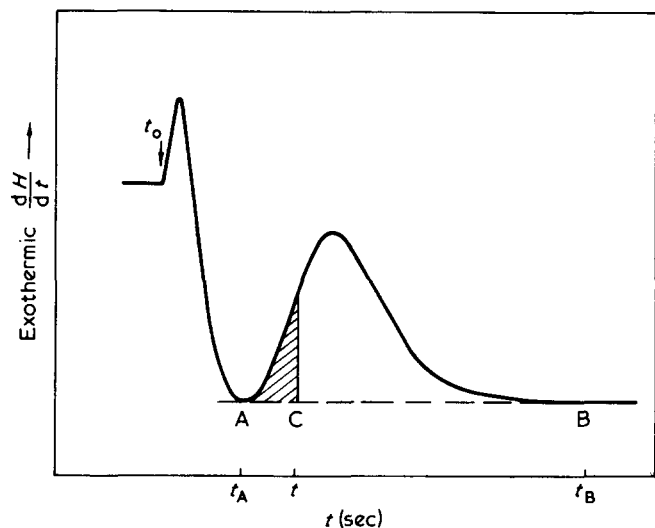


Figure 2 Typical crystallization isotherm obtained by means of d.s.c. technique (see text)

Table 2 Crystallinity, apparent enthalpy of fusion and thermodynamic enthalpy of fusion of nylon-6,8 and of unsaturated copolyamides

Sample	Molar fraction of 4-OD	ΔH_F^* (cal/g)†	X_c (%)	$\Delta H^o F$ (cal/g)
A	0	12	57	20
B ₁	0.12	11		
B ₂	0.24	11	61	19
B ₃	0.46	12	63	20
B ₄	0.61	13	64	21
B ₅	0.79	12	61	19
C	1.00	13	61	21

† The accuracy of ΔH_F^* is within 10%

Table 1 have comparable inherent viscosities (η_{inh} 2.0–2.5 in *m*-cresol at 25°C; *c*, 0.5 g/dl) except for samples B₄ and B₅, and show high molecular weight (\bar{M}_n 28 000 ± 1000 for sample C as determined by endgroup titration)³. Thus effects of the molecular weight on the crystallization kinetics should be negligible.

Thermal analysis

The isothermal crystallization kinetics was examined under a nitrogen atmosphere by means of a Perkin-Elmer DSC-1B differential scanning calorimeter using well dried polymer samples of 5–8 mg by wt. The following standard procedure was employed: the polymer sample, placed in the calorimeter cell was heated for 15–20 min to a temperature (T_1), 15–20 degrees above its melting temperature in order to destroy any traces of crystallinity. Subsequently the sample was rapidly cooled to the required crystallization temperature, T_c . The heat evolved was recorded as function of time and the weight fraction X_t of material crystallized at time t was calculated from the equation:

$$X_t = \frac{\int_0^t \left(\frac{dH}{dt} \right) dt}{\int_0^\infty \left(\frac{dH}{dt} \right) dt}$$

Zero time of crystallization was taken, as the time when the central light came on, indicating thermal equilibrium. A

typical curve of crystallization is shown in Figure 2. The apparent enthalpies of fusion, were calculated from the corresponding endotherm areas, by comparison with those of a weighted indium sample, which has a heat of fusion of 6.81 cal/g. The temperature scale was calibrated against high purity standards.

The maximum of d.s.c. endotherm of fusion, was assumed to be the melting temperature T_m of the polymer sample. In order to correlate melting and crystallization temperatures, T_m was determined for each of the samples after isothermal crystallization at T_c .

X-ray characterization

The X-ray diffraction patterns, in the wide angle region, were recorded by means of a diffractometer Philips 1050/25, using the $\text{CuK}\alpha$ radiation. As shown in Figure 3, the diffraction pattern has been numerically resolved into a broad diffuse halo and sharp diffraction. The mass crystallinity has been calculated in a traditional way, assuming the broad halo to be the amorphous contribution and the sharp peaks to be the crystalline contribution⁴. In the separation, we assume for the maximum of the amorphous halo, an angle of about 19 degrees. The thermodynamic enthalpy of melting, ΔH_F , has been determined by using the simplified relation:

$$\Delta H_F = \frac{\Delta H_F^*}{X_c} \quad (1)$$

where ΔH_F^* , the apparent enthalpy of fusion, is obtained by thermal measurements and X_c is the X-ray mass crystallinity. The values of X_c , ΔH_F^* and ΔH_F , as function of the composition of polyamides are reported in Table 2.

The two strongest reflections, observed in the traces of Figure 3, as deduced by X-ray spectra of oriented fibres, are equatorials being related to $(hk0)$ planes. The variations of the spacings d_1 and d_2 are shown in Figure 4, as function of the composition.

RESULTS AND DISCUSSION

Examples of crystallization isotherms of polyamides with different amounts of *trans* double bonds along the chain (samples B₄, B₅ and C of Table 1), are reported in Figure 5. From such curves the half time of conversion, $t_{1/2}$, of each polymer has been determined at various crystallization temperatures T_c .

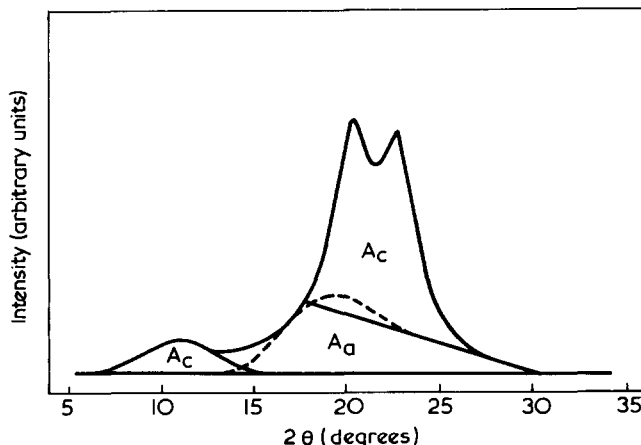


Figure 3 Typical X-ray diffraction traces of a sample of copolyamide. The method followed for the separation of the contributions of amorphous and crystalline is also shown (see text)

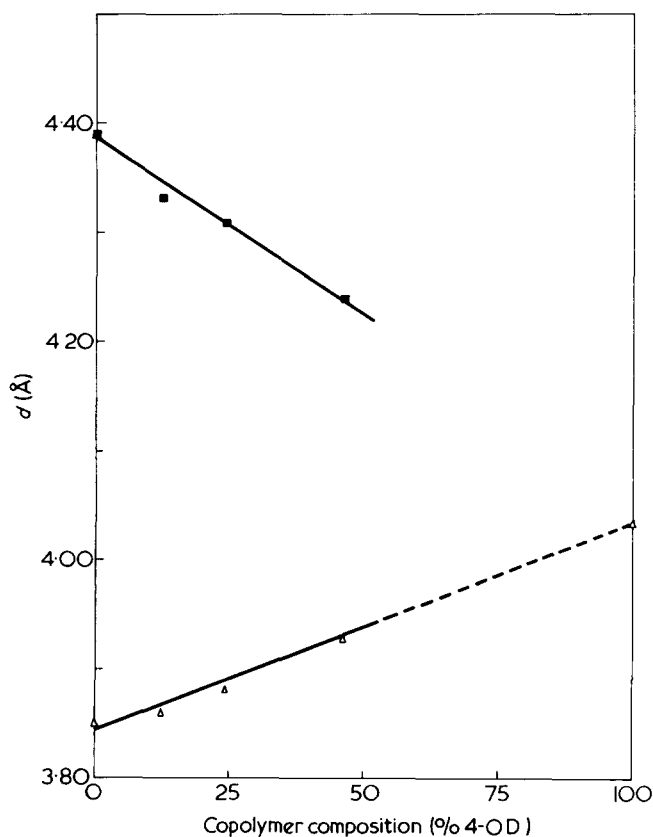


Figure 4 Variations of the spacing d_1 , (■); and d_2 , (△), of the strongest reflections observed in the X-ray traces of polyamides with the copolymer composition

In Figure 6, the variation of $t_{1/2}$ with T_c for each polymer is shown. It is well known that, crystallization curves of polymers can be analysed by means of the Avrami equation⁵:

$$(1 - X_t) = \exp(-Zt^n) \quad (2)$$

In logarithmic form equation (2) is written:

$$\log[-\log(1 - X_t)] = n \log t + \log \frac{Z}{2.3} \quad (3)$$

In equations (2) and (3), X_t is the weight fraction of crystallized material at time t , Z is the kinetic rate constant, and n the Avrami exponent.

The crystallization kinetics of our polyamides, follow equation (3) up to a high degree of conversion at almost all crystallization temperatures. This is shown in Figure 7 where the quantity, $\log[-\log(1 - X_t)]$, is reported against $\log t$ for samples B₁, B₃ and C. Deviations at the end of the process may be due to secondary crystallization phenomena.

The values of the Avrami exponent n , graphically calculated from the slopes of the curves $\log[-\log(1 - X_t)] \rightarrow \log t$ are reported in Table 3, together with the values of the rate constant Z calculated by means of the relation:

$$Z = \frac{\ln 2}{t_{1/2}^n} \quad (4)$$

As shown in Table 3, the values of the Avrami parameter n are almost independent of the crystallization temperature and of the composition of the samples, and are very close

to 4. According to the theory⁵, n should be a combined function of the number of dimensions in which growth takes place, and also of the order of the time dependence of the nucleation process. Accordingly, n should assume a value of 4 when three-dimensional spherulitic growth units, develop from nuclei whose amount increases linearly with time. The values of Z reported in Table 3, have been obtained by assuming for n an integer value of 4 for all the polymers investigated.

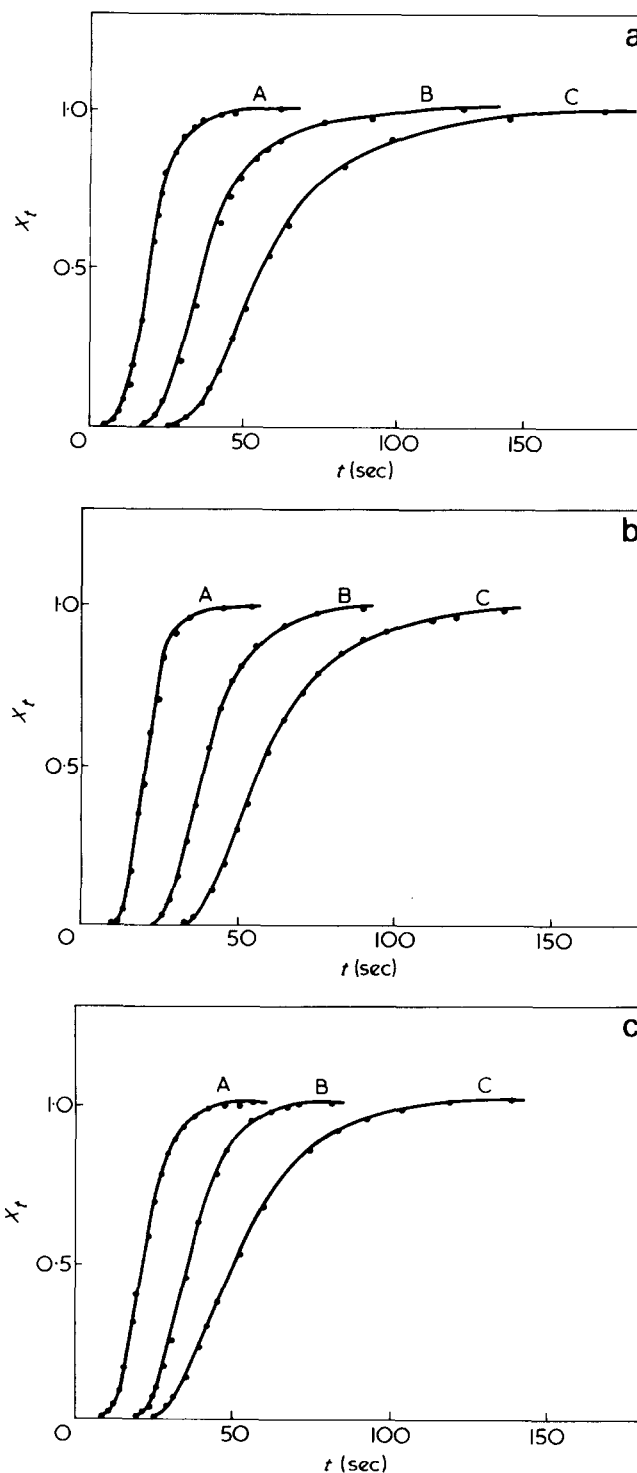


Figure 5 Crystallization isotherms of polyamides with different composition at various crystallization temperature: (a) sample B₄; crystallization temperatures: A, 495 K; B, 497 K; C, 501 K; (b) sample B₅; crystallization temperatures: A, 502 K; B, 506 K; C, 508 K; (c) sample C; crystallization temperatures: A, 504 K; B, 510 K; C, 512 K

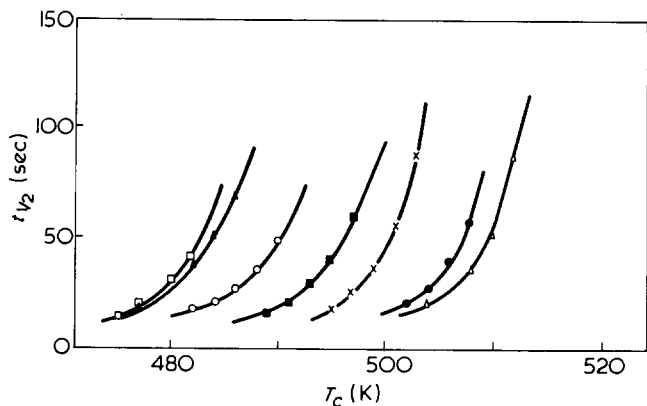


Figure 6 Variation of half time of crystallization $t_{1/2}$ with the crystallization temperature for samples: Δ , C; \bullet , B₅; X, B₄; \blacksquare , B₃; \circ , B₂; \blacktriangle , B₁; \square , A

The equilibrium melting temperatures T_m^0 have been determined from plots of T_m against the crystallization temperature T_c according to equation (5):

$$T_m = T_m^0 \left(\frac{\gamma - 1}{\gamma} \right) + \frac{T_c}{\gamma} \quad (5)$$

where γ is a constant⁶.

Examples of plots of T_m against T_c , are shown in Figure 8, for samples B₃ and B₅. A linear trend is observed for all the polyamides examined. T_m^0 is graphically obtained from such plots, by extrapolating the experimental line to the point where $T_m = T_c$.

The values of T_m^0 are reported in Table 3. They increase regularly with the amount of unsaturation along the chain. The half time of conversion $t_{1/2}$, for the same value of the undercooling $\Delta T = T_m^0 - T_c$, decreases with increasing the

number of *trans* double bond along the chain. This trend is shown in Figure 9. The effect of the double bond concentration is more relevant at low values of ΔT .

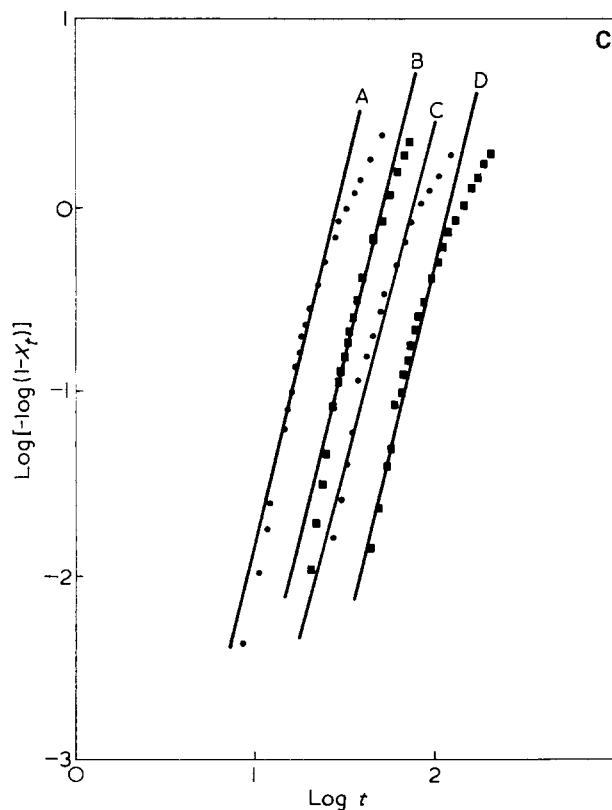
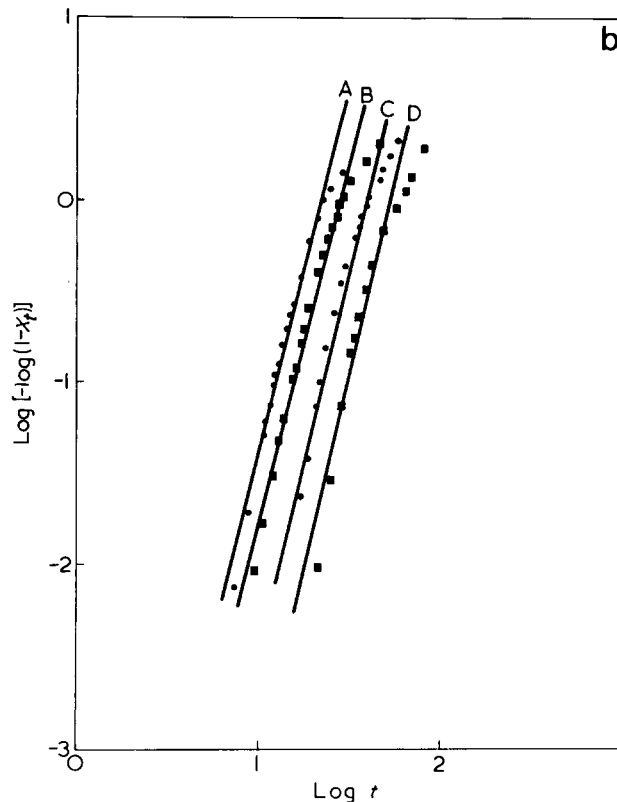


Figure 7 Avrami plots for copolyamides with different composition at various crystallization temperature: (a) sample B₁; crystallization temperatures: A, 477 K; B, 480 K; C, 482 K; D, 484 K; E, 486 K; (b) sample B₃; crystallization temperatures: A, 489 K; B, 491 K; C, 493 K; D, 495 K; (c) sample C, crystallization temperatures: A, 504 K; B, 508 K; C, 510 K; D, 512 K

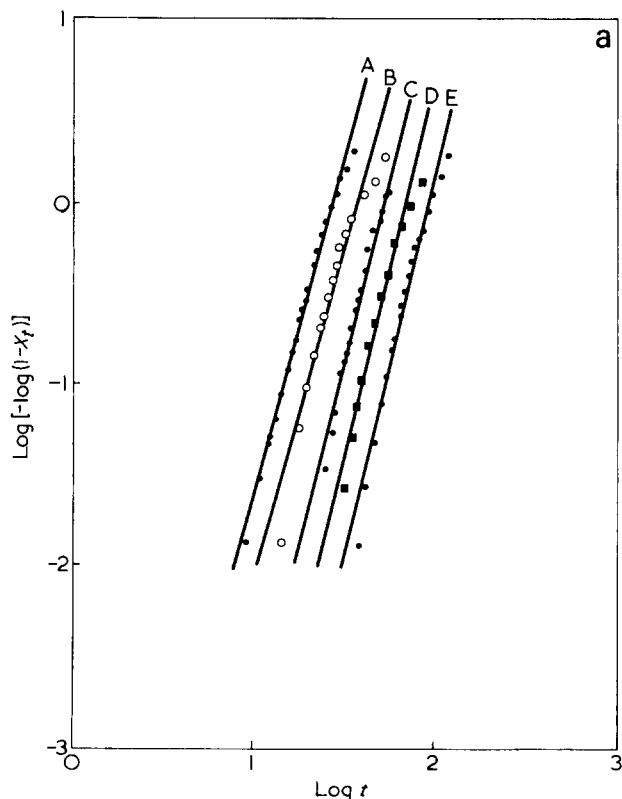


Table 3 Value of the exponent n of Avrami and of the rate constant Z , at various crystallization temperatures. The equilibrium melting temperature is also reported

Sample	Molar fraction of 4-OD	T_c (K)	n^*	$Z \times 10^{-6}$ (sec $^{-4}$)	T_m^0 (K)
SUB-HMD A	0	475	4.2	13.69	514
		477	4.1	4.33	
		480	5.0	0.85	
		482	4.0	0.27	
SUB-HMD-4-OD B ₁	0.12	477	4.0	6.60	518
		480	3.4	1.77	
		482	4.3	0.41	
		484	4.0	0.11	
SUB-HMD-4-OD B ₂	0.24	482	4.0	6.60	521
		484	4.2	4.33	
		486	4.4	0.85	
		488	4.2	0.46	
SUB-HMD-4-OD B ₃	0.46	489	4.0	8.29	525
		491	4.1	2.96	
		493	4.1	0.98	
		495	4.0	0.27	
SUB-HMD-4-OD B ₄	0.61	495	3.6	6.60	528
		496	3.7	1.77	
		499	4.0	0.46	
		501	4.2	0.01	
SUB-HMD-4-OD B ₅	0.79	502	3.7	4.33	530
		504	4.2	1.40	
		506	4.3	0.27	
		508	4.1	0.06	
4-OD-HMD C	1.00	504	4.1	4.33	533
		508	3.9	0.41	
		510	3.8	0.11	
		512	4.2	0.01	

* Estimated error in n is ± 0.4

According to the kinetic theory of polymer crystallization^{6,7}, the overall rate constant of crystallization Z , in the case of spherulitic growth units of lamellar type, may be obtained from the relation:

$$\frac{1}{3} \log Z + \frac{\Delta F^*}{2.3KT_c} = A_0 - \frac{\Delta\phi^*}{2.3KT_c} \quad (6)$$

In equation (6) ΔF^* , is the activation energy for the transport process at the liquid-crystal interface. ΔF^* is usually approximate to the activation energy of the viscous flow of melt polymer, ΔF_{WLF} . $\Delta\phi^*$ is the free energy of formation of a nucleus of critical dimensions, and K the Boltzmann constant.

When a coherent two-dimensional surface secondary nucleation process controls the radial growth of lamellar spherulites then $\Delta\phi^*$ may be expressed by the relation⁷:

$$\Delta\phi^* = \frac{4b_0\sigma\sigma_e T_m^0}{\Delta H_F \Delta T} \quad (7)$$

where σ and σ_e are the free energies per unit area of the surfaces parallel and perpendicular, respectively, to the molecular chain direction; ΔT is the undercooling; ΔH_F is the enthalpy of melting and b_0 is the distance of two adjacent fold planes. Plots of $(1/3) \log Z$ against $T_m^0/T_c \Delta T$, are shown in Figure 10, for some of the investigated polyamides. A linear trend is observed. According to equation

(6), this result indicates that the transport term is constant, in the proximity of the melting point, at least for the undercooling values investigated. The transport term ΔF^* was calculated by means of the approximate relation of Williams, Landel and Ferry⁸:

$$\Delta F^* = F_{WLF} = \frac{C_1 T_c}{C_2 + T_c - T_g} \quad (8)$$

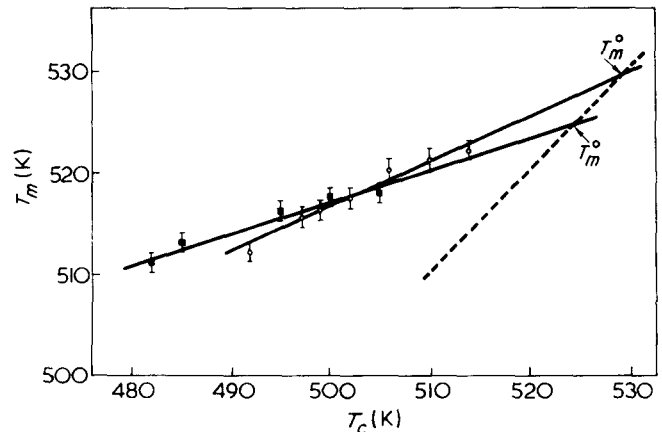


Figure 8 Examples of T_m against T_c plots for samples: ■, B₃; ○, B₅; ---, line $T_m^0 = T_c$

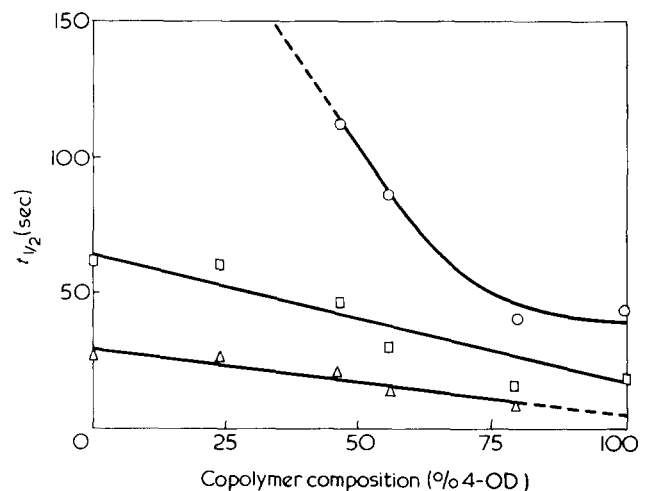


Figure 9 Variation of the half time of conversion $t_{1/2}$, under the same undercooling ΔT , with the copolymer composition: ○, $\Delta T = 25$ K; □, $\Delta T = 30$ K; △, $\Delta T = 35$ K

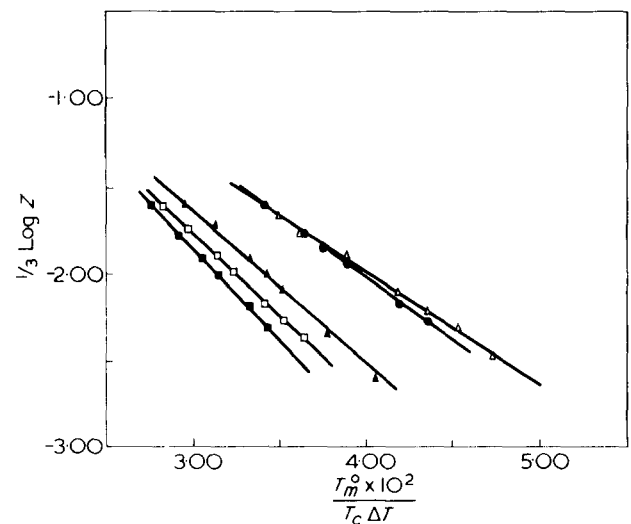


Figure 10 Plots $(1/3) \log Z$ against $T_m^0/T_c \Delta T$ for nylon-6,8 and some unsaturated copolyamides: ■, A; □, B₃; △, B₄; ●, B₅; △, C

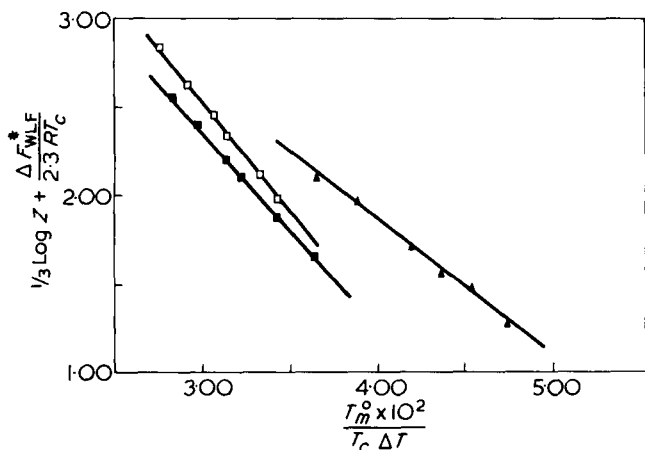


Figure 11 Plots of $(1/3) \log Z + \Delta F_{WLF} / 2.3RT_c$ against $T_m^0 / T_c \Delta T$ for samples A (□); B₃ (■); and C, (▲)

Table 4 Values of the quantity $4b_0\sigma\sigma_e / \Delta H_F$ obtained from the slopes of the lines of Figures 10 (A) and 11 (B)

Sample	Molar fraction of 4-OD	$4b_0\sigma\sigma_e / \Delta H_F \cdot 2.3K$	
		A	B
A	0	244	281
B ₁	0.12		
B ₂	0.24	212	256
B ₃	0.46	221	256
B ₄	0.61	206	255
B ₅	0.79	166	189
C	1.00	152	175

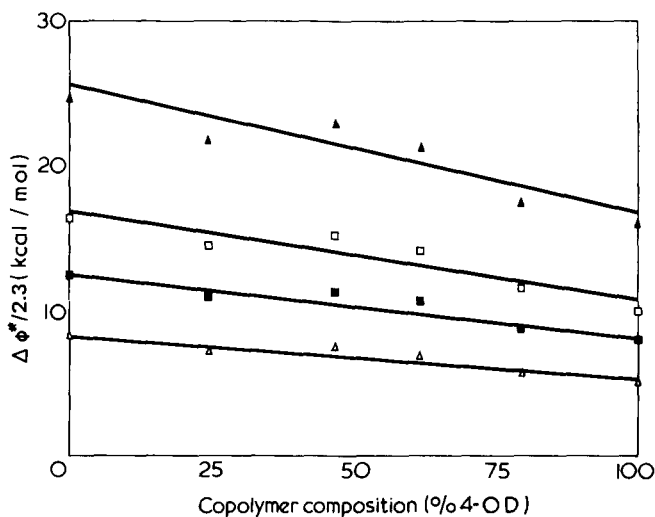


Figure 12 Variation of the free energy of formation $\Delta\phi^*$ of a nucleus of critical dimension as a function of the copolymer composition. The values are compared under the same value of ΔT : ▲, $\Delta T = 10 K$; □, $\Delta T = 15 K$; ■, $\Delta T = 20 K$; △, $\Delta T = 30 K$

Table 5 Values of ΔH_F , b_0 , $\sigma\sigma_e$, σ and σ_e for nylon-6,8 and for unsaturated copolyamides

Sample	ΔH_F (cal/cm ³)	b_0^* (Å)	$\sigma\sigma_e \ddagger$ (erg ² /cm ⁴)	$\sigma\sigma_e \uparrow$ (erg ² /cm ⁴)	σ (erg/cm ²)	$\sigma_e \ddagger$ (erg/cm ²)	$\sigma_e \uparrow$ (erg/cm ²)
A	24	3.84	511	586	3.9	131	151
B ₁		3.86					
B ₂	22	3.88	402	490	3.6	112	135
B ₃	23	3.93	441	511	3.9	113	131
B ₄	25	3.95	434	559	4.1	105	135
B ₅	23	3.98	320	363	3.8	83	95
C	26	4.02	320	370	4.3	75	86

* b_0 is assumed as equal to the d_2 spacing in the X-ray traces (see text)

‡ From the slopes of the curves $(1/3) \log Z$ against $T_m^0 / T_c \Delta T$

† From the slopes of the curves $(1/3) \log Z + \Delta F_{WLF} / 2.3RT_c$ against $T_m^0 / T_c \Delta T$

C_1 and C_2 are constants generally assumed equal to 4.12 Kcal/mol and 51.6 K respectively. For T_g we used for all polyamides the value of 323 K that is the glass transition of nylon-6,10⁹.

Plots of the quantity $(1/3) \log Z + \Delta F_{WLF} / 2.3RT_c$ against $T_m^0 / T_c \Delta T$, show for all samples a linear trend. Examples of such plots are reported in Figure 11, for A, B₃ and C polymers. The values of the quantity $4b_0\sigma\sigma_e / 2.3\Delta H_F$, calculated from the slopes of the lines of Figures 10 and 11, are reported in Table 4, for each of the polyamide examined. The two methods lead to differences in the value of the slopes of about 15%. This fair agreement, supports the assumptions made in the calculation of the transport term, ΔF^* .

The free energy of formation of a nucleus of critical dimensions $\Delta\phi^*$, calculated from the values of the slopes of Figure 10, continually decreases with the amount of unsaturation along the chain. This behaviour is shown in Figure 12 for various values of ΔT .

From the values of $4b_0\sigma\sigma_e / 2.3\Delta H_F$ reported in Table 4, the quantity σ_e can be calculated, if ΔH_F and b_0 are known. The estimation of b_0 , was based on the observation that in the case of nylon-6,8 the value of d_2 (3.84 Å) is close to the spacing of the (010) crystallographic fold planes of nylon-6,6. This strongly indicates that for our polyamides also, d_2 can be assumed as a measure of the distance between adjacent fold planes.

It is interesting to observe that d_2 increases with the amount of double bond along the chain as shown in Figure 4. The values of $\sigma\sigma_e$ are reported in Table 5 for each polyamide. The free energy σ of the lateral surfaces of the lamellar fibrillae was estimated by using the empirical relation:

$$\sigma = \alpha \Delta H_F b_0 \quad (9)$$

where the constant α is equal to 0.1 for all polymers⁶. From the values of $\sigma\sigma_e$ and σ , the folding free energy σ_e was calculated. The values of σ and σ_e are reported in Table 5.

As shown in Figure 13, σ_e drastically decreases with increase in the amount of unsaturations in the polyamide chain, whereas σ keeps practically constant. In fact, in the case of nylon-6,8 we found for σ_e an average value of 141 erg/cm², while for the completely unsaturated polyamide the value is lowered to 81 erg/cm². The value of σ is around 4 erg/cm², being about one tenth of σ_e .

CONCLUSIONS

The experimental results reported in the present paper show that the presence of intra-chain *trans* double bonds

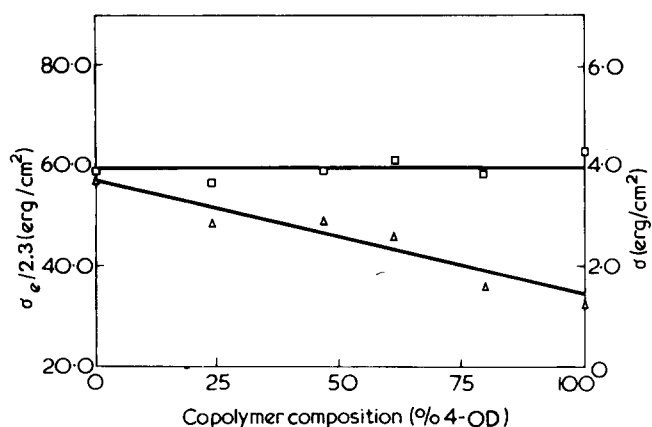
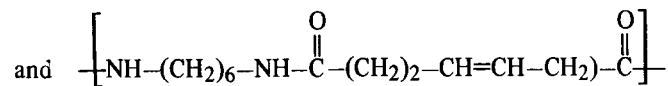
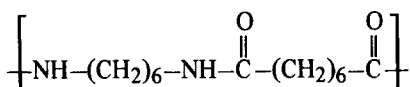


Figure 13 Effect of the copolymer composition on the value of σ_e and σ : □, σ ; △, σ_e

along a polyamide backbone, strongly influence some kinetic and thermodynamic parameters of melt crystallization. In fact the equilibrium melting point T_m^0 of nylon-6,8, increases with increasing amount of double bonds within the chain ($T_m^0 = 514$ K for nylon-6,8 and 533 K for the nylon obtained by polycondensation of 1,6-diaminohexane with *trans*-octen-1,8-dioic acid). However, the thermodynamic enthalpy of melting does not seem to be affected, in a systematic way, by the amount of unsaturation.

The spacings of the most intense X-ray equatorial reflections of nylon-6,8 continuously increase with the amount of unsaturations within the chain. These results can be only explained if repeat units of:



type are able to cocrystallize, even if in the resulting polymer, the double bonds are not regularly spaced along the polymer chain. Moreover, under the same undercooling the rate of crystallization drastically increases with increasing % unsaturated comonomer. This phenomenon must be attributed partly at least, to the corresponding lowering observed in the values of the free energy of formation $\Delta\phi^*$ of a nucleus of critical dimensions.

The last finding is mainly related to surface effects. In fact, the free energy of folding σ_e is lowered by 44%, going from nylon-6,8 to the completely unsaturated nylon. Probably entropic effects due to the higher flexibility of the more unsaturated chains¹¹ on the surface of the lamellar fibrillae, may explain this behaviour.

REFERENCES

- 1 Martuscelli, E. and Pracella, M. *Polymer* 1974, **15**, 306; Marchetti, A. and Martuscelli, E. *J. Polym. Sci. (A)* 1974, **12**, 1649; Amelino, L. and Martuscelli, E. *Polymer* 1975, **16**, 864
- 2 Lanzetta, N., Maglio, G., Marchetti, C. and Palumbo, R. *J. Polym. Sci. (A-1)* 1973, **11**, 913
- 3 Waltz, E. and Taylor, G. B. *Analyt. Chem.* 1947, **19**, 448
- 4 Hermans, P. H. and Weidinger, A. *Makromol. Chem.* 1961, **44-46**, 24; *Makromol. Chem.* 1961, **50**, 98
- 5 Sharples, A. 'Introduction to Polymer Crystallization', Arnold, London, 1966
- 6 Hoffman, J. D. *SPE Trans.* 1964, **4**, 315
- 7 Hoffman, J. D. and Weeks, J. *J. Chem. Phys.* 1962, **37**, 1723
- 8 Williams, M. L., Landel, R. F. and Ferry, J. D. *J. Am. Chem. Soc.* 1955, **77**, 3701
- 9 Brandrup, J. and Immergut, E. H. 'Polymer Handbook', Interscience, New York, 1966
- 10 Geil, P. H. 'Polymer Single Crystals', Interscience, New York, 1963
- 11 Martuscelli, E. *Acta Crystallogr.* 1967, **23**, 1086; Corradini, P., Frasci, A. and Martuscelli, E. *Chem. Commun.* 1969, 779; Martuscelli, E. and Frasci, A. *Acta Crystallogr. (B)* 1969, **25**, 2547

Persistent internal polarization studies in poly(*N*-vinylcarbazole)/trinitrofluorenone charge transfer complex

P. K. C. Pillai and R. C. Ahuja

Department of Physics, Indian Institute of Technology, New Delhi-110029, India
(Received 23 July 1975; revised 27 October 1975)

Studies on the persistent internal polarization in poly(*N*-vinylcarbazole) (PNVC)/trinitrofluorenone (TNF) charge transfer complex are reported. This complex is known to be photoconducting and in the present investigation, the photoelectret charge has been studied as a function of applied voltage, intensity of illumination and time of polarization. A saturation effect is observed in each case. Also the possibility of the use of PNVC/TNF complex in PIP electrophotography has been explored and a comparison of the results of this investigation is made with the results obtained for PNVC.

INTRODUCTION

Poly (*N*-vinylcarbazole) (PNVC) is reported to be one of the best photoconducting polymers known at present¹⁻⁷. It has also been reported that this polymer exhibits photo-induced discharge and that its photoresponse may be strongly improved by doping with a wide variety of electron acceptors². Recently it has been reported that the action spectrum of PNVC could be shifted to the visible range by doping it with 2,4,7-trinitrofluorenone (TNF)⁷. This PNVC/TNF charge transfer complex also exhibits a high photosensitivity⁷.

The present investigation deals with the photoelectret (photopolarization and depolarization) characteristics of the PNVC/TNF complex. Photoelectret state in a photoconductor results from the simultaneous application of electric field and exciting radiation. The photogenerated carriers undergo a directional trapping under the influence of the electric field and a polarization is set up which persists even after the removal of the electric field and illumination. A study of this persistent internal polarization gives an insight into the electronic processes taking place in the photoconductor and also helps in the selection of photoconductor for electrophotographic applications.

A comparison of the results obtained for the PNVC/TNF complex with those of pure PNVC⁹, shows that the doped PNVC layer could give a better performance, when used in PIP electrophotography.

EXPERIMENTAL

Specimen preparation

PNVC, supplied by BASF (West Germany), is a colourless granular material containing 3-4% vinylcarbazole and anthracene. To remove these and other monomeric impurities, PNVC was dissolved in benzene and was precipitated in methanol several times. The purified PNVC was then mixed with 2,4,7-trinitrofluorenone (1:1 molar ratio) and dissolved in tetrahydrofuran. Good quality films can be obtained by pouring this solution over aluminium sheets and allowing it to evaporate in an atmosphere saturated with tetrahydrofuran vapours. The film is dried in an air oven at 50°C to remove the residual solvent.

Measurement technique

The experimental arrangement has been shown in *Figure 1*. The PNVC/TNF film (1 cm × 1 cm × 0.01 cm) was pressed between an aluminium electrode and a conducting glass electrode with the aid of teflon sheets and screws. The sample holder was then put in an earthed metallic chamber with provision for illumination with a 200 W tungsten filament lamp.

One of the electrodes was connected to an electrometer for low current measurements, whereas the other could be connected to the positive of a battery or earthed. The sample was exposed to light through the upper electrode in a direction parallel to the electric field and was polarized by illuminating it in the presence of an electric field. At the end of this operation, the electrode (previously connected to the power supply) was earthed and the resulting depolarization current was measured with respect to time. The depolarization current reduced to zero after certain time. Thus the charge of photoelectret could be calculated by integrating depolarization current with respect to time.

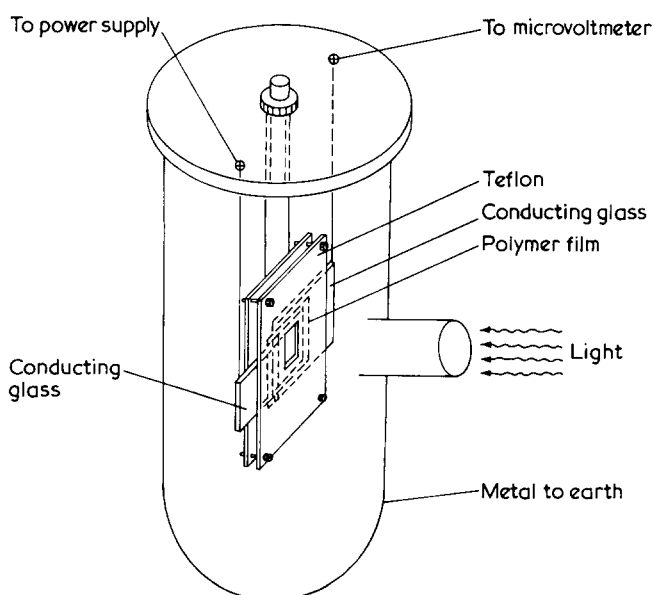


Figure 1 Experimental set up for photo and dark depolarization measurements

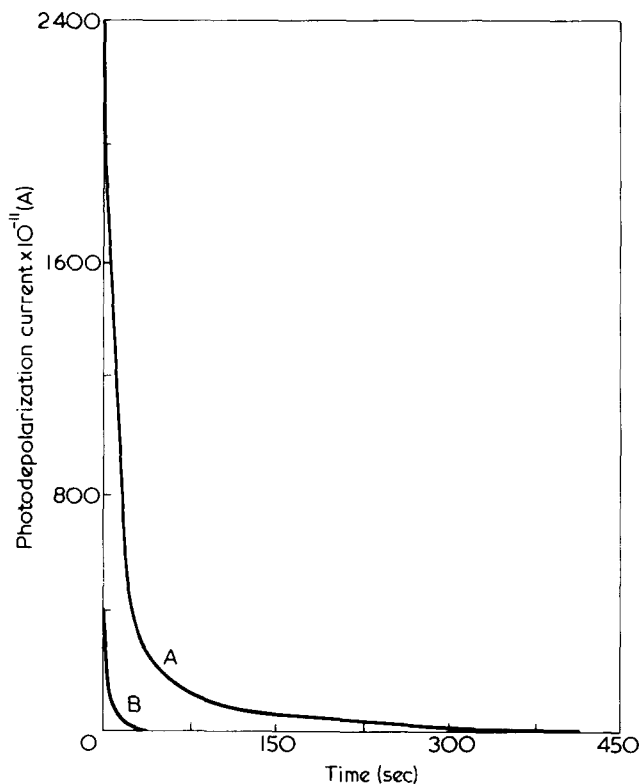


Figure 2 Depolarization characteristics of PNVC/TNF films for an applied electric field 50 kV/cm and time of polarization, $t_p = 1$ min. A, photo-depolarization, $I = 1000$ lux; B, dark depolarization

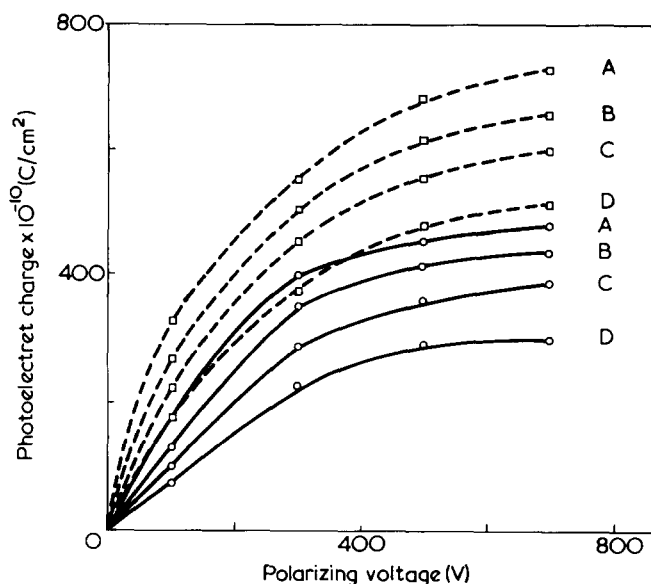


Figure 3 Photoelectret charge vs. polarizing voltage, $t_p = 15$ sec (—); $t_p = 4$ min (---): A, $I = 6500$ lx; B, $I = 1000$ lx; C, $I = 525$ lx; D, $I = 280$ lx

The photoelectret state of the PNVC/TNF has been studied under the following conditions: (a) time of polarization varying from 15 sec to 4 min; (b) polarizing voltage varying from 100 to 700 V; (c) intensity of illumination varying from dark to 6500 lx.

RESULTS

Figure 2 shows the dark and photodepolarization currents of PNVC/TNF film polarized for 1 min in an electric field of 50 kV/cm and at 1000 lx. The decay of charge is quite fast in dark and takes about 30 sec for the total decay. The

light decay is also quite fast initially but slows down afterwards, taking about 5 min for the current to reduce to zero. These characteristics help in determining the time of exposure required to obtain a particular image contrast, when the layer is to be used in PIP electrophotography.

Figure 3 shows the dependence of photoelectret charge (obtained by integrating the curves shown in Figure 2) on polarizing voltage. The charge increases linearly with voltage at low values and shows a tendency to saturate at higher values. However, the saturation effect is more noticeable at low intensities of light.

Figure 4 shows the variation of photoelectret charge with polarizing time. The initial variation is linear (for polarizing times up to 15 sec) but shows saturation effect for polarizing times beyond 1 min. The curves could approximately fit the relation:

$$P = P_{\max}(1 - e^{-t/\tau})$$

where t is the time of polarization and τ depends on the voltage and intensity of illumination during polarization.

Figure 5 shows the dependence of photoelectret charge on the intensity of illumination. Here, also the initial variation is linear (up to 50 lx) followed by saturation effect.

Figure 6 shows the dependence of $I_{\text{photo}}/I_{\text{dark}}$ on the applied field. It is seen that the value of $I_{\text{photo}}/I_{\text{dark}}$ is strongly field dependent. This is not surprising as the photogeneration efficiency in organic solids has been found to be strongly field dependent.

DISCUSSION

The charge transfer complex of poly(*N*-vinylcarbazole) with trinitrofluorenone is highly photoconducting throughout the visible spectrum⁷. The spectra of PNVC/TNF films show the appearance of new absorption bands which cannot be attributed to either PNVC or the dopant, indicating the formation of molecular complexes between carbazole rings and the dopant molecule¹⁰⁻¹¹.

Brackmann¹², Mulliken¹³, Briegleb¹⁴ and others have shown that molecular complex formation is due to charge transfer interaction between electron donor type molecules and electron acceptors. In the presence of radiation of the appropriate energy, an electron transfer occurs according to:

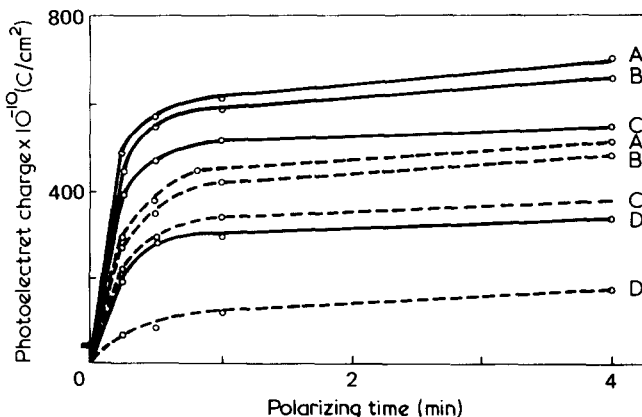
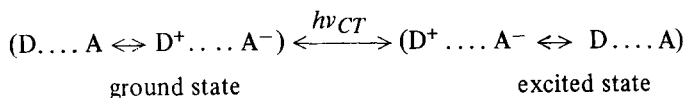


Figure 4 Photoelectret charge vs. polarizing time, $I = 6500$ lx (—); $I = 280$ lx (---). A, $V_p = 700$ V; B, $V_p = 500$ V; C, $V_p = 300$ V; D, $V_p = 100$ V

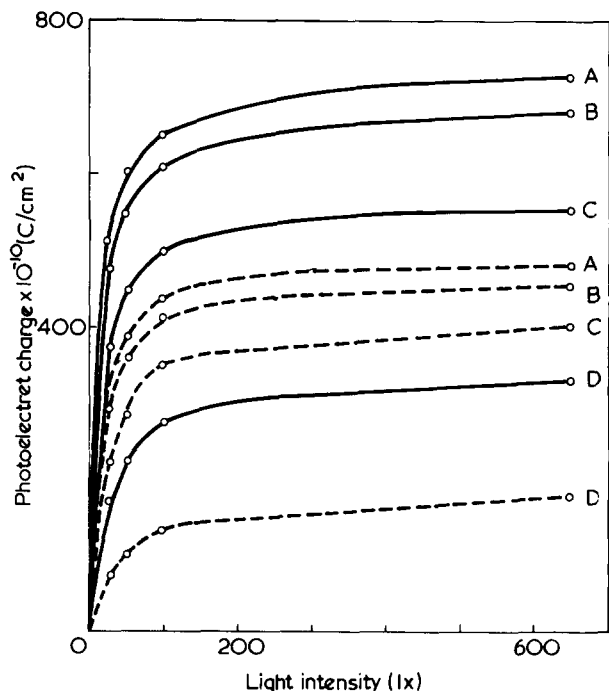


Figure 5 Photoelectret charge vs. intensity of illumination, $t_p = 4$ min (—); $t_p = 15$ min (---). A, $V_p = 700$ V; B, $V_p = 500$ V; C, $V_p = 300$ V; D, $V_p = 100$ V

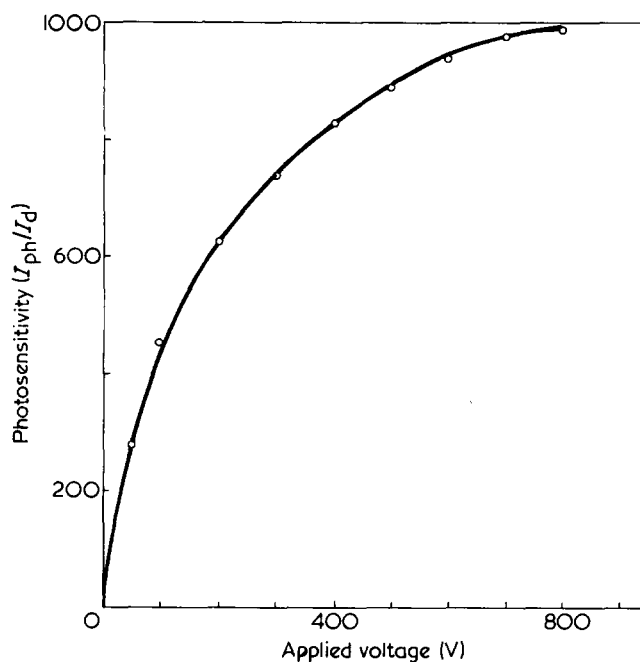


Figure 6 I_{photo}/I_{dark} vs. applied voltage

The CT band may be calculated from the relationship:

$$h\nu_{CT} = I_D - E_A + C$$

where I_D is the ionization energy of donor. E_A the electron affinity of acceptor and C corresponds to the Coulomb energy of D^+A^- ionic couple. Ionized molecules (the radical ions D^+ and A^-) are formed at the excited state in more or less high concentration, depending on the ionization potential of D and A.

Charge transport in PNVC has been the subject of a number of investigations¹⁵⁻²⁰. Holes have been shown to dominate the conduction and the hole drift mobility was found

to be extremely low and strongly field dependent. With the addition of TNF to PNVC, charge transfer complexing takes place introducing absorption bands in the visible region. At sufficiently high TNF concentrations, electron transport dominates the conductivity⁴⁻⁶. The low mobilities indicate a high degree of localization of the carriers, which in turn suggests some form of intermolecular 'hopping' as the transport mechanism. The photogeneration efficiency in organic solids may be viewed as a two-step process²¹. In the first step the absorbed photon excites the electron from its ground state to some excited bound state. From this excited bound state, the electron may undergo thermalization/autoionization into a continuum state where it can conduct or may fall back to the ground state. The yield of electrons in the continuum state per absorbed photon is found to be field dependent making the photogeneration of carriers and the I_{photo}/I_{dark} in organic solids as observed in our case, field dependent.

A comparison of the results obtained for pure PNVC⁹ with that of PNVC/TNF charge transfer complex shows that the latter shows more photoelectret charge than the former. The difference is almost one order of magnitude. This increase can be attributed to the increase in the number of photoexcited carriers in PNVC/TNF. The action spectrum also shifts in the visible range in PNVC/TNF case. Also it is seen that to obtain the same amount of photopolarization, the magnitude of applied field, time of polarization and intensity of illumination required in the case of PNVC/TNF complex, are considerably lower than that of pure PNVC. The value of Q_{PE}/Q_{dP} (taken as the image contrast) comes to be 500 in the case of PNVC/TNF while for pure PNVC it was found to be only 100.

ACKNOWLEDGEMENTS

The authors would like to thank Mr P. K. Nair for useful discussions. R. C. A. gratefully acknowledges the financial assistance given by CSIR India.

REFERENCES

- 1 Hisch, R. and Pohl, R. W. *Z. Phys.* 1933, 87, 78
- 2 Hoegl, H. *J. Phys. Chem.* 1965, 69, 755
- 3 Lardon, M., Doeller, E. L. and Weigl, J. W. *Mol. Crystallogr.* 1967, 2, 241
- 4 Seki, H. and Gill, W. D. *Proc. 2nd Int. Conf. Low Mobility Materials*, 1971
- 5 Gill, W. D. *J. Appl. Phys.* 1972, 43, 5033
- 6 Gill, W. D. *Proc. 5th Int. Conf. Amorphous and Liquid Semiconductors, Garmisch-Partenkirchen*, 1973
- 7 Schaffert, R. M. *IBM J. Res. Dev.* 1971, 15, 75
- 8 Chiu, T. T. and Hecht, J. K. *Tappi* 1971, 54, 391
- 9 Pillai, P. K. C. and Ahuja, R. C. *J. Polym. Sci. (Polym. Phys. Edn)* 1974, 12, 2465
- 10 Klopffer, W. *Macromol. Chem.* 1968, 115, 156
- 11 Kanazawa, K. K. *Bull. Am. Phys. Soc.* 1973, 18, 451
- 12 Brackmann, W. *Recl Trav. Chim. Pays Bas* 1949, 68, 147
- 13 Mulliken, R. S. *J. Chem. Phys.* 1951, 19, 514
- 14 Briegleb, G. 'Elektronen-Donator-Acceptor Komplexe', Springer, Berlin, 1961
- 15 Okamoto, K., Kusabayashi, S. and Mikawa, H. *Bull. Chem. Soc. Japan* 1973, 46, 1948
- 16 Klopffer, W. *J. Chem. Phys.* 1969, 50, 2337
- 17 Bauser, H. and Klopffer, W. *Chem. Phys. Lett.* 1970, 7, 137
- 18 Pai, D. M. *J. Chem. Phys.* 1970, 52, 2285
- 19 Mort, J. *Phys. Rev. (B)* 1972, 5, 3329
- 20 Hoegl, H., Barchietto, G. and Tar, B. *Photochem. Photobiol.* 1972, 16, 335
- 21 Melz, P. J. *J. Chem. Phys.* 1972, 57, 1694

Relaxation controlled (case II) transport of lower alcohols in poly(methyl methacrylate)

H. B. Hopfenberg*, L. Nicolais, and E. Drioli

Istituto di Principi di Ingegneria Chimica, Università di Napoli, Naples, Italy

(Received 12 August 1975; revised 6 October 1975)

The remarkably consistent long term absorption data of Andrews, are shown to obey relaxation controlled (case II) transport kinetics for the absorption of methanol, ethanol, n-propanol, isopropanol, and n-butanol in glassy poly(methyl methacrylate). Andrews' data were obtained by monitoring gravimetric absorption, in 1 mm sheet specimens, under controlled conditions, for a period of years until absorption equilibria were established. Activation energies for the relaxation controlled (zero-order) absorption kinetics were calculated to be ~ 17 kcal/g mol and the enthalpy of absorption varied regularly and explicity with carbon number of the alcohol and with solubility parameter of the homologous penetrants. The dramatic monotonic increase of sorption rate with decreasing carbon number is analysed in terms of the increased concentration gradient which presumably develops as carbon number is decreased, rather than the more attractive theory that increased absorption rate is a direct function of decreased molar volume of the penetrant. Since the absorption kinetics are completely controlled by osmotic stress induced relaxations, molecular size of the penetrant does not directly affect the observed kinetics of penetration.

INTRODUCTION

In 1966, Alfrey *et al.*¹ described a second limiting transport process, frequently controlling absorption of organic vapours and liquids in glassy polymers, wherein diffusion *per se* played no part in the rate determining transport mechanism. Alfrey termed this behaviour case II transport, in contrast to the well understood and often described Fickian diffusion, which is termed case I transport.

For Fickian transport, the rate of absorption in slab or film geometries decreases continuously with time, owing to the continuous decrease of the driving concentration gradient. Conversely, for many cases involving penetration of glasses by organic penetrants, relaxation at a sharp boundary between uniformly swollen and essentially unplasticized polymers, provides a constant, rate determining step for the absorption. An extremely steep concentration gradient develops at the sharp and discernable boundary² between swollen and unswollen polymer and, in turn, a large, osmotically induced stress gradient drives the rate determining relaxations occurring in the region of the large gradient. In this second limiting case, the absorption proceeds at a constant rate independent of time or position.

In the course of a literature search supporting a cooperative research program between this Institute and the Department of Chemical Engineering, North Carolina State University concerning tensile and torsional stress biased relaxation controlled transport in glassy polymers, a significant paper³ by Andrews, Levy, and Willis was reviewed. The Andrews *et al.* paper reports absorption kinetics and equilibria of methanol, ethanol, n-propanol, isopropanol, and n-butanol in 1 mm sheet specimens of poly(methyl methacrylate) (PMMA). The protracted absorption kinetics were observed, in many cases, over periods of years.

The dedication, embodied in their work, has reaped the reward of data describing both absorption kinetics and equilibria which are not only completely consistent but provide a most convincing exposition of a relaxation controlled (case II) absorption process. The Andrews' data are quite extensive, involving five homologous lower alcohols over a significant temperature range. The focus of the Andrews paper was directed towards the role of absorption on environmental crazing and, therefore, a detailed interpretation of the absorption kinetics and equilibria was not attempted. Their brief discussion concerning mechanism of absorption did not include consideration of relaxation controlled (case II) absorption kinetics and a rather conventional treatment, involving plots of volumetric swelling *versus* square root time were presented to characterize the absorption kinetics.

Replotting the Andrews data, considering the well accepted⁴⁻⁹ relaxation controlled transport processes, frequently controlling organic penetrant absorption in glassy polymers, revealed, in all cases, an excellent fit with case II transport theory. Moreover, the highly temperature dependent absorption kinetics, the consistent trends concerning temperature dependence of the equilibria (enthalpy of absorption), and the rational correlation between molar concentration of penetrant at equilibrium and the observed kinetics prompted this rather in depth re-analysis of the extremely valuable data of Andrews' *et al.*

ANDREWS' EXPERIMENTAL PROCEDURE

Plane sheet specimens of 1 mm thick PMMA (ICI Ltd) were prepared with the approximate major surface dimensions 30 × 7 mm. The specimens were dried under vacuum for two hours at 348 K, prior to weighing in a stoppered container on a microbalance sensitive to 10^{-8} kg. Batches of three such specimens were placed in flasks containing

* Department of Chemical Engineering, North Carolina State University, Raleigh, North Carolina 27607, USA

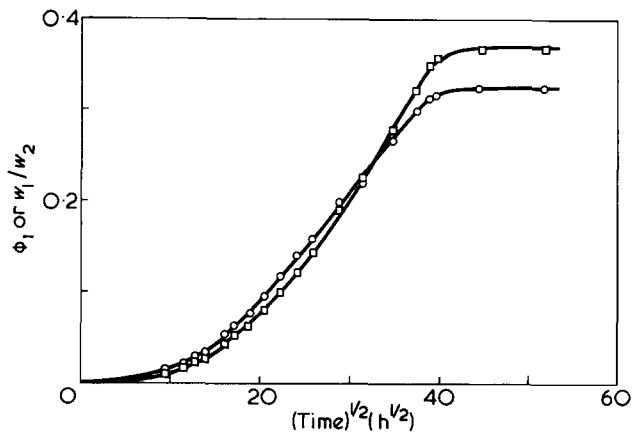


Figure 1 Anomalous Fickian kinetics of n-propyl alcohol absorption in poly(methyl methacrylate) sheets. [Volume fraction or weight ratio, w_1/w_2 , as a function of $t^{1/2}$ ($T = 318$ K)]. Volume fraction ϕ_1 , \circ ; weight ratio w_1/w_2 , \square

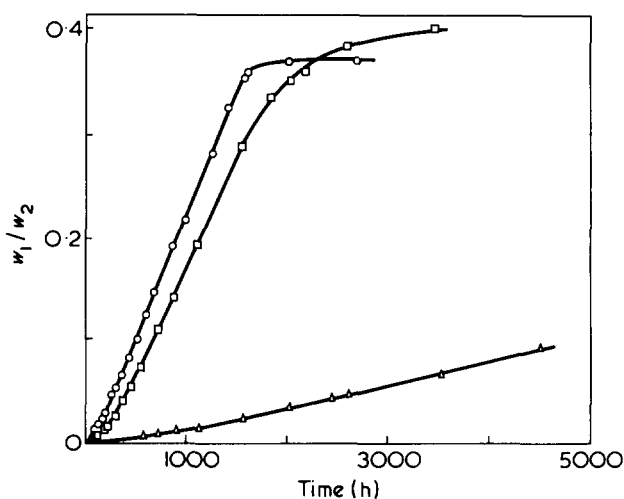


Figure 2 Case II kinetics of n-propyl, i-propyl and n-butyl alcohol absorption in poly(methyl methacrylate) sheets. [Weight of alcohol per original dry sheet weight, w_1/w_2 , versus t ($T = 318$ K)] \circ , n-propyl alcohol; \square , isopropyl alcohol; \triangle , n-butyl alcohol

methyl, ethyl, n-propyl, isopropyl, and n-butyl alcohol controlled at 293 and 318 K. The specimens were periodically removed from their flasks, rapidly dried with filter and tissue paper, and weighed in the stoppered container. After weighing, the specimens were immediately returned to their respective flasks.

The volume fraction, ϕ_2 , of polymer in the PMMA-alcohol mixture was calculated as:

$$\phi_2 = (1 - \phi_1) = (w_2/\rho_2) (w_1/\rho_1 + w_2/\rho_2)^{-1} \quad (1)$$

where w_1 and w_2 are, respectively, the weight of alcohol in the swollen mixture and the original (dry) weight of PMMA, and ρ_1 and ρ_2 are, respectively, the density of alcohol at the test temperature and the density of PMMA³.

For this reinterpretation of the kinetic and equilibrium data, the weight fractions, molar concentrations and, in turn, weight of penetrant per dry weight of polymer, were back calculated from the volume fraction data reported by Andrews *et al.*

The undefended assumptions embodied in equation (1), (viz no volume change on mixing), are, of course, implicit in calculated values of molar concentrations, however, the calculated value of w_1/w_2 or $w_1/(w_1 + w_2) = \Omega_1$ eliminate

this assumption since w_1 and w_2 were actually determined experimentally.

RESULTS AND DISCUSSION

Kinetics

The absorption kinetics of lower alcohols in PMMA, presented by Andrews, Levy, and Willis³ were presented in plots of ϕ_2 , volume fraction of polymer as a function of $[\text{time}(t)]^{1/2}$ measured in $(\text{h})^{1/2}$. Typical results are presented here again in Figure 1, for n-propanol in PMMA as $\phi_1 = (1 - \phi_2)$, volume fraction of alcohol as a function of $t^{1/2}$. A plot of w_1/w_2 (for n-propanol) versus $t^{1/2}$ is also included in Figure 1 for comparison. Clearly, the transport is non-Fickian⁷, however, their conclusions regarding the seemingly complex nature of these kinetic processes may be unduly complicated.

Alternatively, plots of the weight of penetrant absorbed per original dry sheet weight, w_1/w_2 , versus linear t are presented in Figure 2 for n-propanol, isopropanol, and n-butanol. A similar plot for ethanol is presented in Figure 3. The data for methanol were too compressed in the graphical presentation of Andrews to permit meaningful re-interpretation.

The use of ϕ_1 , as an ordinate tends to depress ordinate values of relatively high values of ϕ_1 . The alternate, and more conventional choice of w_1/w_2 (or related mass quantities) has several advantages. The normalized mass ordinate requires no assumptions regarding volume changes associated with mixing and the mass readings are not only a direct consequence of the actual experimental measurements but also provide an unequivocal means for monitoring the related absorption of penetrant in either mass or mol units.

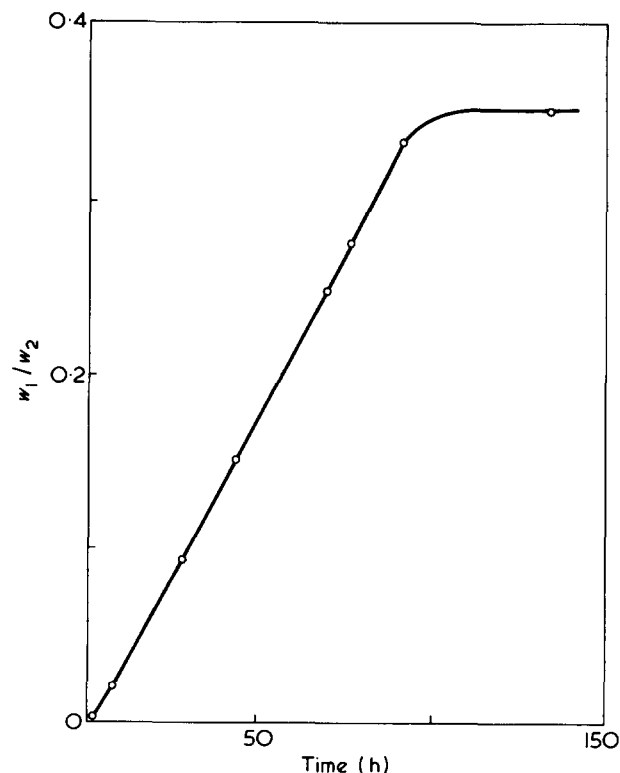
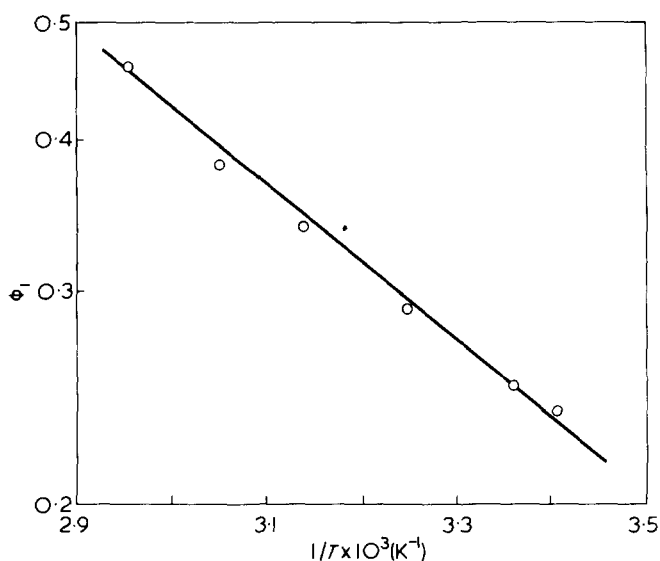


Figure 3 Case II kinetics of ethyl alcohol absorption in poly(methyl methacrylate) sheets. [Weight of ethanol per original dry sheet weight, w_1/w_2 , versus t ($T = 318$ K)]

Table 1 Activation energies for relaxation controlled transport of lower alcohols in PMMA

Alcohol	Activation Energy (kcal/g mol)
ethyl alcohol	17.6
n-propyl alcohol	17.4
isopropyl alcohol	16.7

**Figure 4** Van't Hoff plot of temperature dependence of absorption equilibria for ethanol in PMMA

The use of a w_1/w_2 ordinate would be preferred, especially for the analysis of presumed case II absorption since true linearity between amount of penetrant absorbed should only be observed on a plot of w_1/w_2 (rather than $w_1/(w_1 + w_2)$ or ϕ_1) versus t .

Moreover, use of the w_1/w_2 ordinate, in the case II (w_1/w_2 versus t plots), reveals an intriguing induction period which is maintained for approximately 4% of the total sorption. Ideal case II kinetics are maintained, thereafter, for ~90% of the total sorption period. In contrast, the plot of w_1/w_2 versus $t^{1/2}$ does not, in fact, fit true diffusion kinetics (e.g. w_1/w_2 versus $t^{1/2}$ linear) over any significant portion of the sorption history. The reduction in ordinate value associated with the use of ϕ_1 , rather than w_1/w_2 is apparent at the high swelling levels in *Figure 1*.

The brief induction period, apparent in *Figures 2* and *3* is, most likely, a manifestation of a relatively slow, diffusion controlled development of an ideal step concentration profile in the sheet specimen. Alternatively, this observed induction may be related to 'case-hardened' surface layers resulting from the specific thermal history imposed upon the specimens during sample preparation.

Activation energies for the apparently relaxation controlled transport process, were calculated by comparing the experimental times required to achieve an arbitrarily selected fractional sorption value at 293 K and 318 K. These calculations, of course, assume Arrhenius behaviour. This assumption, though well justified^{2,6,9} is required since sorption kinetics were reported for only these two temperatures. The results of these calculations are presented in *Table 1*.

These virtually identical activation energies are, in fact, much higher than typically reported activation energies for diffusion. This temperature dependence provides significant, independent support for the hypothesis that polymer

relaxations provide the rate determining step for absorption of the lower alcohols in PMMA. Moreover, the nearly identical values of the calculated activation energies are consistent with relaxations occurring in sheet specimens, swollen to essentially the same equilibrium penetrant volume fractions. The equilibrium concentration is maintained at the 'shoulder' of the concentration step. In contrast, activation energies for diffusion typically vary significantly with penetrant size.

Equilibria

Andrews *et al.*³ present a table of equilibrium volume fractions of the various alcohols in PMMA contacted with the liquid alcohols for 6 temperatures covering the temperature range, 293–338 K. If one makes the simplifying assumption that the enthalpy of mixing associated with the isothermal change of 1 mol of alcohol liquid dissolving in PMMA is constant and that Henry's law is obeyed over the temperature range studied, a value of the enthalpy of mixing may be extracted from the slope of semi-log of $\ln \phi_1$ versus $1/T$. These assumptions are exceedingly stringent and quantitatively unjustifiable, however, they permit a qualitatively comparative analysis of the temperature dependence of the equilibrium behaviour within this limited alcohol series.

Using these assumptions, the semi-log plots of $\ln \phi_1$ versus $1/T$ were constructed for the various alcohols. Typical results are presented for the case of ethanol in *Figure 4*. The calculated values of the enthalpy of mixing are presented in *Table 2* for the various alcohols.

The trend amongst these endothermic enthalpies of mixing is consistent with the theory that hydrogen bonding is the predominant intermolecular interaction in the bulk liquid and, furthermore, that hydrogen bonding is not the predominant intermolecular interaction involved with penetrant-polymer equilibration. Specifically, as carbon number of the alcohol is reduced, the hydrogen bonding in the liquid is presumably increased. In contrast, hydrogen bonding between alcohol and PMMA is relatively invariant amongst alcohols within this series, therefore, the enthalpy change between pure alcohol and swollen polymer increases as carbon number is reduced.

The theory that hydrogen bonding controls penetrant-polymer interactions, but plays a smaller role in the overall interaction between penetrant and polymer, is consistent with the observed trend of ΔH_{mix} as a function of carbon number of the alcohol as well as the observed correlation between ϕ_1 and $\Delta\delta$ (the solubility parameter difference between polymer and penetrant) for this alcohol series reported by Andrews, *et al.*³

In any event these equilibrium values should be considered with some reservation since the more rapidly equilibrating (higher temperature experiments) are presumably more reliable. The surprisingly large calculated values of

Table 2 Enthalpy of mixing lower alcohols in PMMA in the temperature range 293 to 338 K

Alcohol	ΔH_{mix} (kcal/g mol)
methyl alcohol	2.8
ethyl alcohol	2.6
n-propyl alcohol	2.1
isopropyl alcohol	2.1

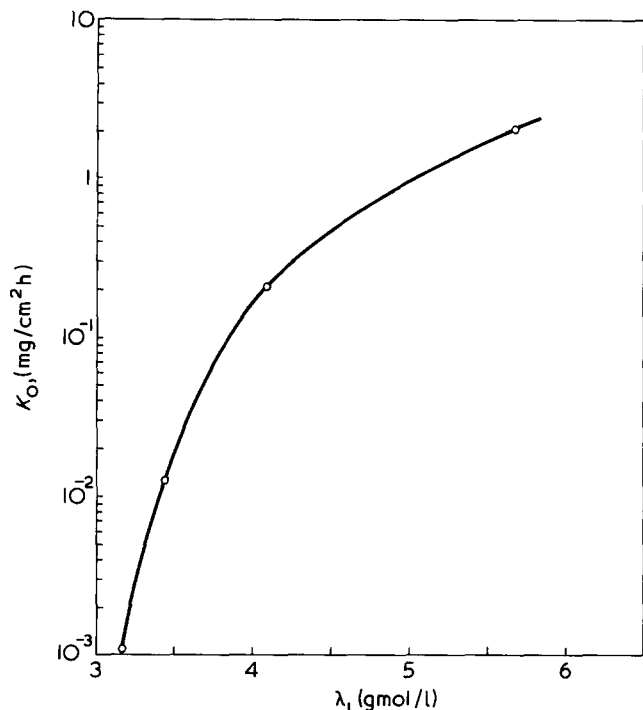


Figure 5 Log-log plot of absorption rate, k_0 , (mg/cm² h) versus molar concentration of the various alcohols. [$T = 318$ K]

ΔH_{mix} are consistent with the possibility that the low temperature data do not reflect true equilibrium.

Relationship between the kinetics and the equilibria of absorption

Although the equilibrium weight, weight fraction, or volume fraction of penetrant absorbed varies only slightly with carbon number of the alcohol, there is a significant and regular variation in equilibrium molar concentration of the various alcohols in PMMA. The osmotic stresses and more importantly, stress gradients, which develop consequent to the equilibration of the swollen shell, are related monotonically to the molar concentration (rather than weight fraction or volume fraction) of the penetrant in the polymer. The relaxation processes, responsible for the rate determining sorption step, are in turn, driven monotonically by these osmotic stress gradients. These identical effects have been observed^{6,9,11,12} under controlled conditions for a single penetrant in a single polymer by varying systematically the penetrant activity. There is no means, however, of determining the magnitude of the concentration gradient driving the relaxations. Quite possibly the qualitative and quantitative details of the steep concentration gradients, which develop at the 'step' differ from alcohol to alcohol as a consequence of differing sorption affinities and varying diffusional penetration into the essentially dry core⁵.

Jacques and Hopfenberg⁹ reported a 10,000-fold increase in the rate of case II penetration of polystyrene-poly(phenylene oxide) blends associated with only a two-fold increase in equilibrium penetrant concentration of the

same penetrant. In their study, the penetrant concentration was changed by varying either the penetrant activity or the blend composition. The relationship between absorption rate and the molar concentration of alcohol is presented in Figure 5 for the normal alcohol series. Presumably, the higher absorption rates observed as molecular weight of the alcohol is reduced is a coincidental analogue of a diffusion controlled process.

CONCLUSIONS

The detailed data of Andrews *et al.* describing penetration of PMMA by a homologous series of lower alcohols are best described by case II relaxation controlled transport preceded by a brief diffusion controlled induction period during which a step concentration profile is established. Analysis of the temperature dependence of the sorption equilibria suggests that hydrogen bonding between penetrant and penetrant is well developed in the liquid phase whereas hydrogen bonding is not primarily responsible for equilibrium penetrant-polymer interactions.

Analysis of sorption kinetics of organic penetrants in polymeric glasses is served best by selecting a w_1/w_2 ordinate rather than a ϕ_1 ordinate. Moreover, selection of a linear time abscissa is indicated for absorption experiments where case II kinetics may predominate.

ACKNOWLEDGEMENTS

The authors appreciate the financial support provided by the CNR. of Italy under Grant Number 74.00872.11. Professor G. Astarita stimulated valuable discussions between the authors.

REFERENCES

- 1 Alfrey, Jr. T., Gurnee, E. F. and Lloyd, W. G. *J. Polym. Sci. (C)* 1966, **12**, 249
- 2 Michaels, A. S., Bixler, H. J. and Hopfenberg, H. B. *J. Appl. Polym. Sci.* 1968, **12**, 991
- 3 Andrews, E. H., Levy, G. M. and Willis, J. *J. Mater. Sci.* 1973, **8**, 1000
- 4 Kwei, T. K. and Zupko, H. M. *J. Polym. Sci. (A-2)* 1969, **7**, 867
- 5 Peterlin, A. *Makromol. Chem.* 1969, **124**, 136
- 6 Hopfenberg, H. B., Holley, R. H. and Stannett, V. *Polym. Eng. Sci.* 1969, **9**, 242
- 7 Hopfenberg, H. B. and Frisch, H. L. *J. Polym. Sci. (B)* 1969, **7**, 905
- 8 Jacques, C. H. M. and Hopfenberg, H. B. *Polym. Eng. Sci.* 1974, **14**, 441
- 9 Jacques, C. H. M. and Hopfenberg, H. B. *Polym. Eng. Sci.* 1974, **14**, 449
- 10 Bernier, G. A. and Kambour, R. P. *Macromolecules* 1968, **1**, 393
- 11 Baird, B. R., Hopfenberg, H. B. and Stannett, V. *Polym. Eng. Sci.* 1971, **11**, 275
- 12 Hopfenberg, H. B., Stannett, V. and Jacques, C. H. M. *J. Appl. Polym. Sci.*, in press

Thermal stabilities of poly(*N*-alkyl maleimides)

S. Matui

Department of Industrial Chemistry, Fukui Technical College, Fukui, Japan

and H. Aida

Department of Industrial Chemistry, Faculty of Engineering, Fukui University, Fukui, Japan

(Received 24 June 1975; revised 18 September 1975)

The thermal stabilities of polymaleimide (PMI), poly(*N*-methyl maleimide) (PMMI), poly(*N*-ethyl maleimide) (PEMI), poly(*N*-*n*-propyl maleimide) (PNPMI) and poly(*N*-isopropyl maleimide) (PIPMI) were studied over the temperature range 300° to 400°C under a constant flow of nitrogen. At the initial stage of degradation the following results were obtained: (1) the main chain of PMMI is the most stable among the poly(*N*-alkyl maleimides); (2) the weight loss of PEMI, PNPMI and PIPMI is larger than that of PMI and PMMI; (3) the five-membered imide of PMI is the most unstable among the poly(*N*-alkyl maleimides); (4) the crosslinkages are formed more easily in PMI and PMMI than in PEMI, PNPMI and PIPMI.

INTRODUCTION

N-substituted maleimides polymerize easily by means of free radical initiators¹, anionic initiators¹, γ -ray² and ultraviolet irradiation³. The physical properties of poly(*N*-substituted maleimides) have been studied by many investigators. Cubbon¹ reported on the stereospecific configuration of poly(*N*-alkyl maleimides); Sheremeteva *et al.*⁴ on the solution properties of poly(*N*-isobutyl maleimide) and Walker *et al.*^{5,6} reported on the dielectric relaxation of poly(*N*-alkyl maleimides) and poly(*N*-aryl maleimides), and on the nuclear magnetic relaxation of poly(*N*-amyl maleimide) and poly(*N*-dodecyl maleimide). These results indicate that *N*-substituted maleimide polymers have high softening points, considerable chain rigidity and region of oriented structure. However, the thermal degradation behaviour has not previously been studied. We report on a study of the thermal stabilities of poly(*N*-alkyl maleimides) over the temperature range 300° to 400°C, under a constant flow of nitrogen. The volatile product, the scission of a main chain, the weight loss, the cleavage of a five-membered imide ring and the side reaction have been investigated, and the degradation mechanism was discussed on the basis of the results.

EXPERIMENTAL

Polymer preparations

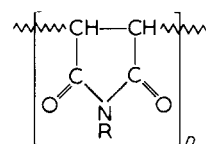
The *N*-alkyl maleimides except for maleimide were prepared from maleic anhydride by the method of Mehta *et al.*⁷ *N*-methyl maleimide was purified by recrystallization from ethyl ether; *N*-ethyl maleimide by sublimation under reduced pressure, and *N*-*n*-propyl maleimide and *N*-isopropyl maleimide by redistillation under reduced pressure. Maleimide was prepared from maleic anhydride by the method of Tawney *et al.*⁸ and purified by recrystallization from ethyl acetate.

The polymers were obtained by free radical polymerization, which was carried out in cyclohexanone as a solvent at 60°C for 5 h, in the presence of azobisisobutyronitrile as an initiator, under flow of nitrogen. After completion of

polymerization, the polymers were precipitated by pouring the solution into methanol, purified by fractional precipitation and dried *in vacuo* at 80°C. The solvent for polymerization of maleimide was dioxane and the precipitant was ethyl acetate.

The intrinsic viscosities of poly(*N*-ethyl maleimide) (PEMI), poly(*N*-*n*-propyl maleimide) (PNPMI) and poly(*N*-isopropyl maleimide) (PIPMI) were measured in acetone at 30°C by means of a Ubbelohde viscometer. Dimethylformamide was used for viscosity measurements of polymaleimide (PMI) and poly(*N*-methyl maleimide) (PMMI). The values of intrinsic viscosities are shown in Table 1.

The polymers have the following chemical structures.



R = H(PMI)
 = CH₃(PMMI)
 = CH₂CH₃(PEMI)
 = CH₂CH₂CH₃(PNPMI)
 = CH(CH₃)CH₃(PIPMI)

Table 1 Properties of samples

Imide	Monomer		Polymer	
	B.p.* (°C/ mmHg)	M.p.† (°C)	[η] (dl/g)	S.p.‡ (°C)
Maleimide		94.0	0.185	>340
<i>N</i> -methyl maleimide		96.2	0.155	>320
<i>N</i> -ethyl maleimide		46.0	0.149	253–265
<i>N</i> - <i>n</i> -propyl maleimide	—	—	0.145	238–248
<i>N</i> -isopropyl maleimide	75/10	—	0.156	—

* Boiling point

† Melting point

‡ Softening point

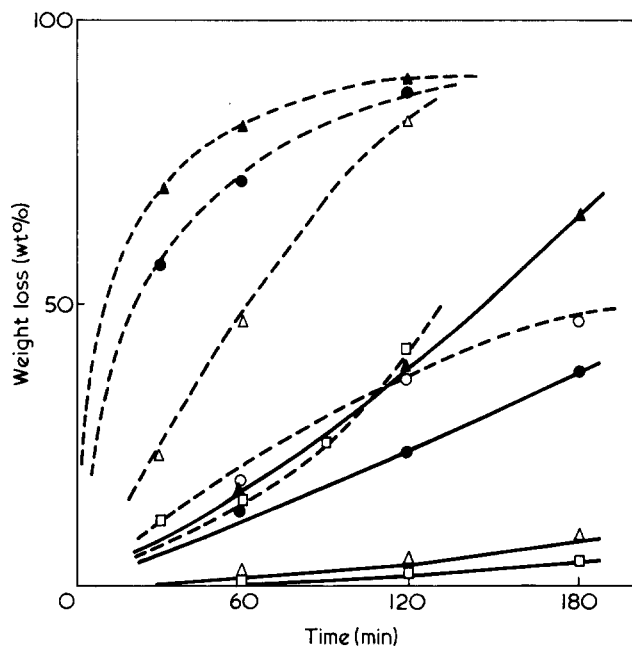


Figure 1 Weight loss vs. time at various temperatures. —, 320°C; ---, 360°C. □, PMI; ○, PMMI; ▲, PEMI; ●, PNPMI; △, PIPMI

Degradation experiments

A boat holding the sample was placed at the centre of a Pyrex reaction tube in a furnace controlled at a constant temperature over the range 300°–400°C. The polymer powder was moulded into the form of a disc 10 mm in diameter and ~1 mm in thickness, under 1 t/cm² pressure, as the powder is scattered from the boat, when nitrogen gas passes through the reaction tube. The reaction tube was evacuated with vacuum pump (5 mmHg) to remove air before admitting the nitrogen gas. The degraded residue in the boat was used for measurement of weight loss, viscosity and crosslinkage. The condensates on the wall of the reaction tube were collected and isolated by column chromatography (developing solvent: ethyl acetate/benzene/acetone = 3:6:1; silica gel column). After purification, the chemical structures of the isolated substances were determined on the basis of the elemental analysis, infra-red spectra, molecular weight (cryoscopic method), number of double bonds (bromination titration method) and boiling and melting points.

The gaseous products of degradation were condensed in the side tube of a sealed Pyrex reaction tube, and the condensates were analysed by use of infra-red spectroscopy and gas chromatography.

RESULTS AND DISCUSSION

Weight loss

Plots of weight loss against time of heating are shown in Figure 1. Further, the initial rates of weight loss and the weight loss after 1 h at various temperatures, are given in Table 2. The weight loss under the same conditions increases in the following order:



PMI and PMMI are more stable than the other polymers.

Crosslinkage

Original PMI and PMMI are soluble in dimethylformamide, and PEMI, PNPMI and PIPMI are soluble in acetone.

On the other hand, the degraded polymers are partly soluble in each solvent. Therefore, the degraded polymers were separated into two fractions by refluxing them with an excess of solvent for 72 h. The results are shown in Table 3, where the values are the weight % of the fraction insoluble in solvent per weight of the original polymer. The amount of the insoluble fraction at the initial stage of degradation increases in the following order:



This order is the reverse one of the weight loss. It is thought that the stabilities of the maleimide polymers increase with an increase in the number of crosslinkages.

Change in viscosity

The intrinsic viscosities of the solvent-soluble fraction of degraded polymers were measured at 30°C. Plots of $[\eta]_t/[\eta]_0$ against time of heating are shown in Figure 2, where $[\eta]_0$ is the intrinsic viscosity of the original polymer, and $[\eta]_t$ is that of the solvent-soluble fraction of degraded polymer heated for t h. The drop of viscosity at the initial stage of degradation increases in the following order:



This order corresponds to that of the weight loss except for PMI. It is thought that the weight loss is caused primarily by the elimination of low molecular substances from the end of polymer chains; the details will be presented

Table 2 Weight losses of poly(N-alkyl-substituted maleimides)

Polymer	Rate of weight loss (wt %/min) at 360°C	Weight loss (wt %) after 1 h				
		300°C	320°C	340°C	360°C	380°C
PMI	0.30	1.0	2.2	3.5	15.4	—
PMMI	0.30	—	—	1.2	19.3	36.2
PEMI	1.34	3.1	15.3	75.4	80.1	—
PNPMI	1.18	0	3.4	20.0	71.2	—
PIPMI	0.75	0	3.1	13.4	46.5	88.3

Table 3 Insoluble fractions of degraded samples at various temperatures

Heating temperature (°C)	Heating time (h)	Insoluble fraction (wt %)				
		PMI	PMMI	PEMI	PNPMI	PIPMI
320	1	0	—	0	0	0
	2	0	0	0	0	0
	3	0	0	0	0	0
340	1	0	2.3	0	0	—
	2	0.5	2.7	0	0	—
	3	1.3	4.1	0	0	—
360	0.5	0	—	0	0	0
	1	5.4	21.2	0	0	0
	1.5	9.9	27.1	—	0	2.9
	2	12.9	31.3	1.3	1.7	4.7
380	3	16.3	10.9	2.1	3.2	6.7
	0.5	—	17.8	2.3	—	1.3
	1	—	11.3	3.3	—	5.0
	2	—	6.3	2.9	—	8.2

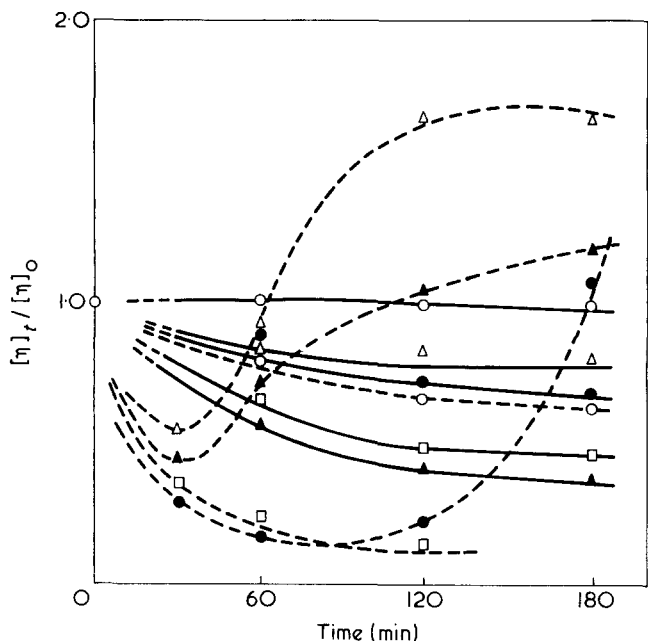


Figure 2 Change of viscosity with time. —, 320°C; ---, 360°C. □, PMI; ○, PMMI; ▲, PEMI; ●, PNPMI; △, PIPMI. $[\eta]_0$: intrinsic viscosity of original sample; $[\eta]_t$: intrinsic viscosity of solvent-soluble part after time t

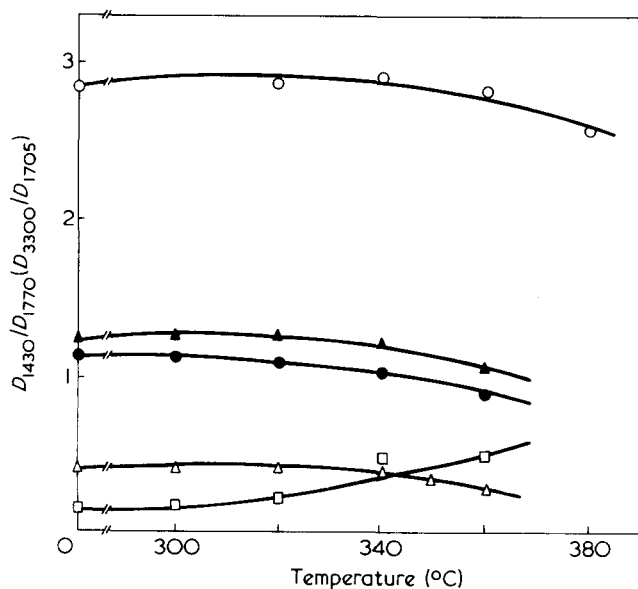


Figure 3 Relative changes in optical density of *N*-substituted group with that of imide ring at various temperatures (heating time, 2 h). □, PMI; ○, PMMI; ▲, PEMI; ●, PNPMI; △, PIPMI. $D(1430)$, optical density of 1430 cm^{-1} characteristic to methyl group; $D(1705, 1770)$, optical density of 1705, 1770 cm^{-1} characteristic to carbonyl group; $D(3300)$, optical density of 3300 cm^{-1} characteristic to amino group

later. The minima in the curves of PEMI, PNPMI and PIPMI seem to appear as a result of competition between the scission of main chains and the formation of crosslinkages.

Infra-red spectra of degraded polymers

The study of the infra-red spectra of the polymers degraded at 360°C shows that the characteristic bands⁹⁻¹¹ of five-membered imide ring of PMI (1770, 1710, 1370 and 1180 cm^{-1}) disappear, the intensities of the characteristic bands of PEMI (1790, 1700, 1350 and 1210 cm^{-1}) decrease remarkably, but those of PMMI (1770, 1710, 1370 and 1260 cm^{-1}); PNPMI (1790, 1710, 1350 and

1190 cm^{-1}) and PIPMI (1770, 1700, 1370 and 1220 cm^{-1}) scarcely decrease. When PMMI, PNPMI and PIPMI are degraded at 380°C, the intensities of the characteristic bands of PNPMI and PIPMI decrease remarkably, but those of PMMI scarcely decrease. From the above facts the stability of five-membered imide ring increases in the following order:



The five-membered imide ring of PMMI is the most stable in contrast to that of PMI.

The ratio of the optical density of characteristic band of five-membered imide ring to that of *N*-substituted group, against the degradation temperature is plotted in Figure 3. The *N*-substituted group of poly(*N*-alkyl maleimides) except for PMI, seems to break more easily than the five-membered imide ring with an increase in temperature above 340°C. On the other hand, PMI gives a reverse tendency, which suggests the unstability of its five-membered imide ring.

Formation of double bonds

The number of double bonds formed in the degradation products was estimated by use of bromination titration method. The results are shown in Table 4, where the values are the number of moles of double bond formed per 100 moles of the repeating unit. It was found that a few double bonds were formed in the chains of degraded polymers and volatilized substances.

Volatilized substances

The substances volatilized from polymers over the temperature range 300°–400°C, were analysed and the results are shown in Tables 5 and 6. At the initial stage of degradation below 360°C, *N*-substituted succinimide, dimer of *N*-substituted maleimide and trimer of *N*-substituted maleimide are chiefly produced from PMMI, PEMI, PNPMI and PIPMI. On the other hand, both succinimide and urea are chiefly produced from PMI. The result of PMI is the same as the results of poly(*N*-phenyl maleimide)¹², poly(*N*-*p*-tolyl maleimide)¹³ and poly(*N*-*p*-acetylphenyl maleimide)¹³, in which both *N*-aryl succinimide and urea compound are chief products. These facts show that the main chains of poly(*N*-alkyl maleimides) except for PMI, seem to break more easily than the side chains and the five-membered imide rings. Since no monomers were found in the degradation products, the end radicals of the polymer chains seem to be liable to abstract a hydrogen atom during de-

Table 4 Number of double bonds formed in the degraded products

Polymer	Residue* (mol %)	Dimer—trimer of <i>N</i> -alkyl maleimide† (mol %)
PMI	3.2–4.7	—
PMMI	—	12.0–15.4
PEMI	3.0–5.4	14.2–16.0
PNPMI	2.6–9.7	18.6–20.9
PIPMI	0–3.8	—

* Degradated at 340°C

† Volatilized at 320°–360°C

Table 5 Properties of volatilized substances

Polymer	Volatilized substance	M.p. [b.p.] (°C)	Molecular weight		Elemental analysis					
			Experimental	Calculated	C (%)		H (%)		N (%)	
					Experimental	Calculated	Experimental	Calculated	Experimental	Calculated
PMI	succinimide	125.0 (125.0)*	98	99	48.57	48.48	5.13	5.05	14.80	14.14
	dimer-trimer of maleimide	—	—	196-291	44.37	48.97-49.48	4.30	3.09-4.08	12.60	14.28-14.43
	urea	131.5 (132.7)*	60	60	20.69	20.00	6.71	6.60	45.36	46.67
PMMI	N-methyl succinimide	69.0(71.0)*	111	113	52.87	53.09	6.26	6.24	12.41	12.38
	dimer of MMI	—	223	224	52.10	53.57	5.43	5.36	12.39	12.50
	trimer of MMI	181.7-184.0(-)*	334	333	55.94	54.05	4.54	4.50	12.60	12.61
PEMI	N-ethyl succinimide	(243.0)(245.0)*	125	127	56.32	56.59	7.03	7.13	11.03	11.01
	dimer of EMI	—	229	252	57.03	57.14	6.46	6.35	10.51	11.11
	trimer of EMI	189.0-190.0(-)*	366	375	57.49	57.60	5.35	5.60	11.39	11.20
PNPMI	N-n-propyl succinimide	[240.0] (240.0)*	138	141	58.64	59.57	8.40	7.80	9.52	9.93
	dimer of NPMI	[>240.0] (-)*	283	282	60.37	60.00	7.54	7.14	9.10	10.00
	trimer of NPMI	190.0-190.8(-)*	405	417	60.20	60.43	6.51	6.47	10.04	10.07
PIPMI	N-isopropyl succinimide	68.0 (69.0)*	131	141	59.34	59.57	7.94	7.80	10.10	9.93
	dimer of IPMI	—	274	282	61.58	60.00	7.04	7.14	10.15	10.00
	trimer of IPMI	170.0-172.0(-)*	391	417	60.30	60.43	6.64	6.47	9.59	10.07

* Value for the authentic compound

Table 6 Volatilized substances

Polymer	Volatilized substances at 300-360°C	Volatilized substances at 380-400°C
PMI	succinimide, dimer-trimer of maleimide, urea, CO, CO ₂ , NH ₃ , NH ₄ OCN, (CONH) ₃	H ₂ , CO, CO ₂ , NH ₃ , urea, NH ₄ OCN, (CONH) ₃
PMMI	MSI*, dimer-trimer of MMI	H ₂ , CO, CO ₂ , CH ₄ , NH ₃ , NH ₄ HCO ₃
PEMI	ESI†, dimer-trimer of EMI, CO, CO ₂	H ₂ , CO, CO ₂ , CH ₄ , C ₂ H ₄ , C ₂ H ₆ , NH ₃ , NH ₄ HCO ₃
PNPMI	NPSI**, dimer-trimer of NPMI, CO, CO ₂	H ₂ , CO, CO ₂ , CH ₄ , C ₃ H ₆ , C ₃ H ₈ , NH ₃ , NH ₄ HCO ₃
PIPMI	IPSI‡, dimer-trimer of IPMI, CO, CO ₂	H ₂ , CO, CO ₂ , CH ₄ , C ₂ H ₆ , C ₃ H ₆ , C ₃ H ₈ , NH ₃

* N-methylsuccinimide
 ** N-n-propylsuccinimide
 † N-ethylsuccinimide
 ‡ N-isopropylsuccinimide

Table 7 Amount of carbon dioxide and carbon monoxide evolved at 320-360°C

Heat- ing temp- era- ture (°C)	Heat- ing time (h)	CO ₂ (wt %) [CO(ppm)] *				
		PMI	PMMI	PEMI	PNPMI	PIPMI
320	0.5	—	—	0[0]	0[0]	-[0]
	1	1.3	—	0.1	0	—
	2	2.2	—	0.4	0	—
340	0.5	—	0[0]	0.3[70]	0[25]	0[35]
	1	4.1	0	1.6	0	0.1
	2	7.5	0	1.7	0	0.1
360	0.5	3.6[300]	0[0]	0.9[200]	0[50]	0.3[200]
	1	4.8	0	2.4	0	1.2
	2	16.0	0	2.8	0	2.3
	3	27.5	0.6	—	—	—

* Amount of carbon monoxide produced in 1 min after 30 min heating

gradation. At elevated temperatures, above 380°C, the substances of low molecular weight are produced by the cleavage of side chains, by the cleavage of five-membered imide rings or by the secondary reactions.

The amount of carbon dioxide and carbon monoxide estimated by usual methods are shown in Table 7, where the amount of carbon dioxide was determined by use of a titration method and the amount of carbon monoxide by means of Kitagawa A-type CO detector. Since the evolu-

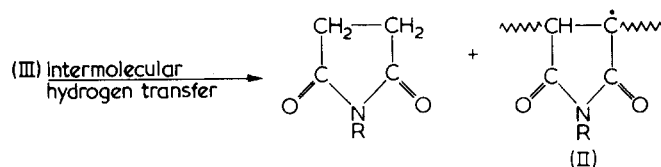
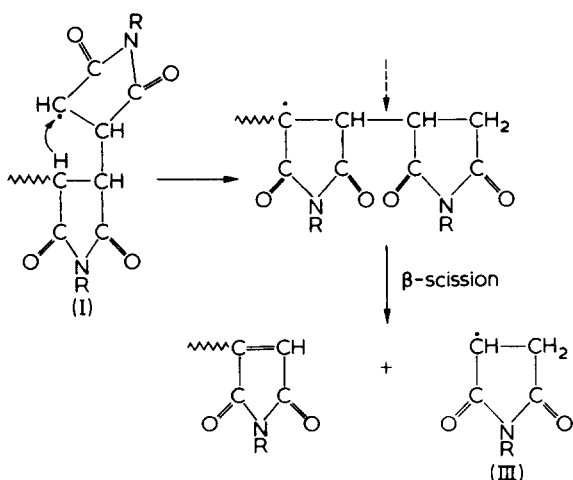
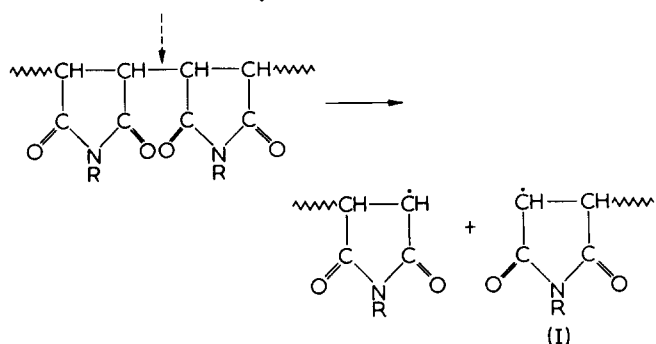
tion of carbon dioxide and carbon monoxide is caused by the cleavage of five-membered imide rings, it seems that the stability of five-membered imide ring increases in the following order:



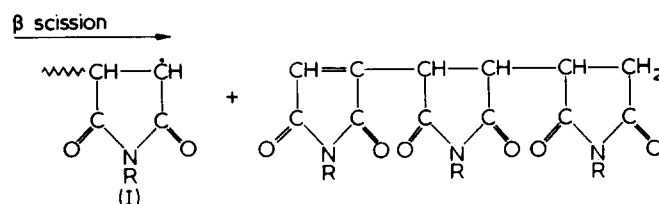
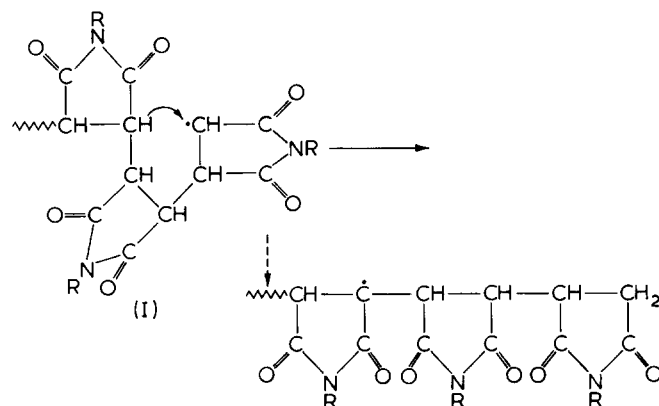
This order agrees with that obtained from infra-red spectra described previously.

Behaviour of degradation

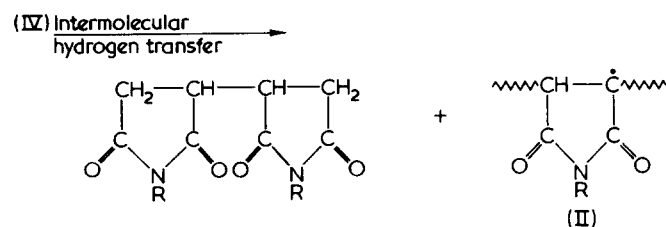
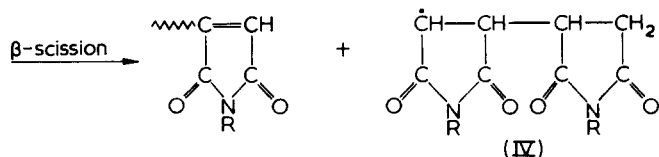
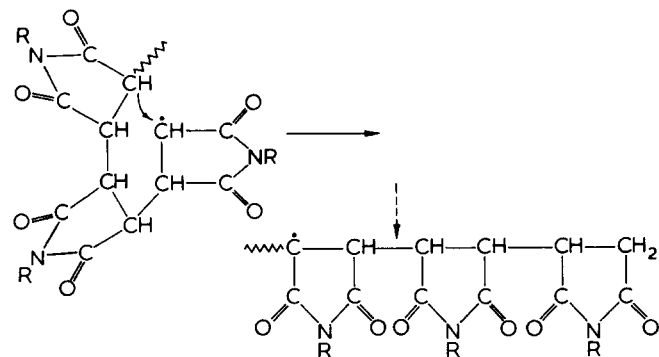
PEMI, PNPMI and PIPMI give a similar behaviour of degradation, in which the main chains break easily, the weight loss is large, but the number of crosslinkages is slight and the five-membered imide rings are stable. The molecular weight drops rapidly during the first few per cent of weight loss. The initial drop in molecular weight may be caused primarily by random scissions in the main chains. The carbon atoms in the main chains of poly(*N*-alkyl maleimides) are tertiary and the C—C bonds in the main chains are in β -position to carbonyl groups. Furthermore, the degradation products from PEMI, PNPMI and PIPMI chiefly consist of *N*-substituted succinimide, dimer of *N*-substituted maleimide and trimer of *N*-substituted maleimide. However, no monomers are isolated. From the above results, it is assumed that the thermal scission of the C—C bonds in the main chains at the β -position is accompanied by inter- and intra-molecular hydrogen transfers. The intramolecular hydrogen transfers are caused by back biting reaction, in which the hydrogen atoms attached to 4-, 5- and 6-position carbon are abstracted by the end radicals.



Abstraction of the hydrogen atom attached to 5-position carbon leads to the formation of trimer of *N*-substituted maleimide.

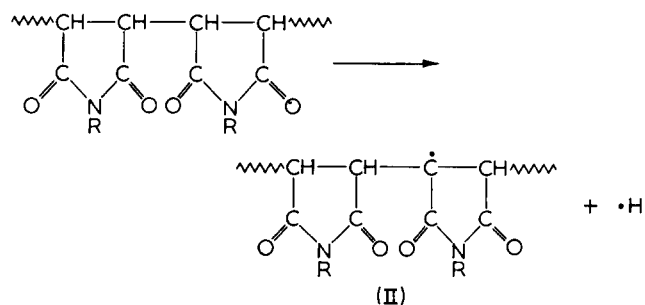


Abstraction of the hydrogen atom attached to 6-position carbon leads to the formation of dimer of *N*-substituted maleimide.



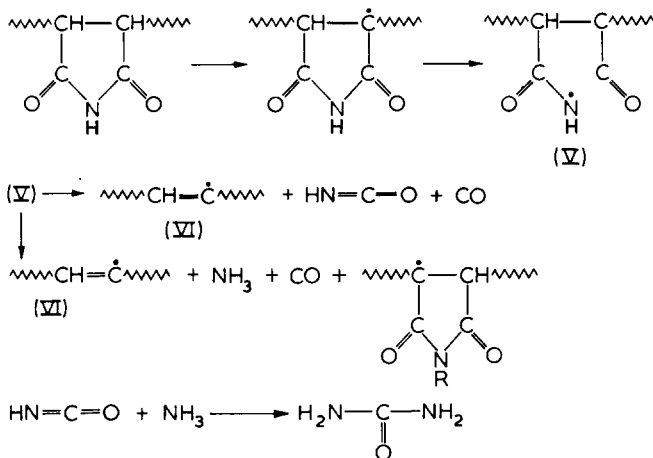
The degradation behaviour of PMI and PMMI is different from that of PEMI, PNPMI and PIPMI. In PMI and PMMI the number of crosslinkages are relatively large and the weight loss is slight. At 320°C, no crosslinkages are formed in both PMI and PMMI. When the viscosities of the polymers degraded at 320°C are compared, the molecular weight

of PMI drops rapidly, while that of PMMI scarcely drops. The imide ring of PMI is the most unstable among poly(*N*-alkyl maleimides). Therefore, the main chain and the imide ring of PMI break easily, while those of PMMI are difficult to break. From these results, in the case of PMMI, the dissociation of the hydrogen atom from the tertiary carbon in the main chain may predominantly occur and may result in the formation of intermolecular crosslinkage.

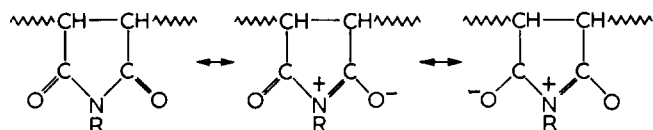


(II) + (II) → intermolecular crosslinking

In the case of PMI the scission of both C—C bonds and C—H bonds in the main chain is accompanied by the scission of the imide rings, which results in the formation of urea and crosslinkage.



Urea and ammonia are detected as shown in Table 6. The stability of the imide ring depends upon the interaction between *N*-substituted and carbonyl groups. Matuo¹⁰ suggests that an electron-donating substituent is preferred in stabilizing the ionic structures in the imide ring.



The extent of stabilization of the ionic structures due to a substituent, R, is expected to be in the following order:

alkyl group > hydrogen ≅ aromatic group

This effect strengthens the C—N—C bonds in the imide rings of *N*-alkyl-substituted maleimides. From these facts, it is thought that the five-membered imide rings of poly(*N*-alkyl maleimides) except for PMI are significantly stable in comparison with the main chains.

REFERENCES

- 1 Cubbon, R. C. P. *Polymer* 1965, 6, 419
- 2 Kagiya, T., Izu, M. and Fukui, K. *J. Polym. Sci. (B)* 1966, 4, 387
- 3 Kagiya, T., Izu, M. and Fukui, K. *J. Polym. Sci. (A-1)* 1967, 5, 1415
- 4 Sheremeteva, T. V., Larina, G. N., Tsvetkov, V. N. and Shtennikova, I. N. *J. Polym. Sci. (C)* 1968, 22, 185
- 5 Block, H., Groves, R. and Walker, S. M. *Polymer* 1972, 13, 527
- 6 Bailey, J., Block, H., Cowden, D. R. and Walker, S. M. *Polymer* 1973, 14, 45
- 7 Mehta, N. B. *et al. J. Org. Chem.* 1960, 25, 1012
- 8 Tawney, P. O. *et al. J. Org. Chem.* 1966, 25, 56
- 9 Uno, T. and Machida, K. *Bull. Chem. Soc. Japan*, 1962, 35, 276
- 10 Matsuo, T. *Bull. Chem. Soc. Japan* 1964, 37, 1844
- 11 Bellamy, L. J. 'The Infrared Spectra of Complex Molecules', John Wiley, New York, 1960
- 12 Urushizaki, M., Aida, H. and Matsui, S. *Kobunshi Kagaku* 1970, 27, 303, 474
- 13 Urushizaki, M., Aida, H. and Ikegami, A. *Kobunshi Kagaku* 1972, 29, 321, 40

Synthesis of narrow distribution polytetrahydrofuran

T. G. Croucher and R. E. Wetton

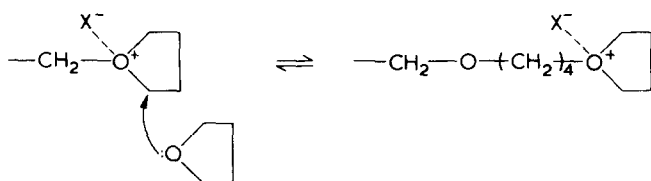
Department of Chemistry, Loughborough University of Technology, Loughborough, Leicestershire, LE11 3TU, UK

(Received 13 October 1975; revised 1 November 1975)

Bulk polymerizations of tetrahydrofuran (THF) have been studied kinetically at reaction temperatures in the range -10 to $+80^{\circ}\text{C}$ using *p*-chlorophenyldiazonium hexafluorophosphate initiator. Initiation has been studied to enable selection of a 'clean' initiation condition (95°C for 4 min). Factors causing broadening of the molecular weight distribution are discussed, the main causes of such broadening being chain transfer reactions and concurrent initiation with propagation. These could be minimized by using a low reaction temperature (-10°C). Molecular weight distributions were measured by gel permeation chromatography. Propagation rate constants were determined and found to increase with increasing temperature according to an Arrhenius expression giving an activation energy of 51 kJ/mol. The method will produce monodisperse samples of THF polymer over a wide molecular weight range from 5×10^3 to 10^6 .

INTRODUCTION

Tetrahydrofuran may be ring-opened using cationic initiators to give high molecular weight polymers of polytetrahydrofuran (PTHF); otherwise known as poly(tetramethylene oxide). The propagation stage is considered to proceed via a growing oxonium ion as follows:



Such reactions have been the subject of a number of original and review papers¹⁻⁴. It is well established that using PF_6^- as the counter-ion (X^-) in polar and aromatic solvents and in bulk enables high molecular weight products to be obtained, and a living system without termination can be observed⁵. A particularly facile initiator is *p*-chlorophenyldiazonium hexafluorophosphate⁶.

In this work we wished to prepare samples for model crystallization studies and it was a prerequisite that these should be monodisperse as well as cover a wide molecular weight range. The literature data on PTHF contain few records of the production of narrow distribution polymers despite the clear demonstration that the polymerization is a living system under rigorous conditions. Those that are mentioned are either low molecular weight products taken to low conversion⁷, or the very rapid dicationic systems of Smith and Hubin⁸.

It has been noted that the polydispersity ratio, which should commence as a Poisson distribution ($\bar{M}_w/\bar{M}_n < 1.1$ for low polymer) and broaden to the most probable distribution of 2 for a reversible polymerization at equilibrium, does in fact broaden much more rapidly than predicted⁵, and can attain a value much greater than 2.

The present work describes pertinent kinetic experiments which were undertaken to establish the origin of the high polydispersity ratio normally obtained for PTHF. These

results allow selection of initiation and growth conditions which lead to the production of narrow distribution polymers over a wide molecular weight range.

EXPERIMENTAL

All reactions were carried out under high vacuum, a pressure of 10^{-5} mmHg being generally obtained in a greaseless vacuum system. The reaction vessels were made of glass with a helical tube arrangement designed to maximize heat transfer to surrounding baths, and to allow good initial mixing (Figure 1). After cleaning with chromic acid the reactors were treated with a solution of dichlorodimethyl silane in chloroform (10% v/v), in order to minimize water pick up on the internal glass surfaces.

The initiator, *p*-chlorophenyldiazonium hexafluorophosphate, obtained commercially as Phosfluorogen A (Ozark-Mahoning Co., Tulsa, Oklahoma, USA), was purified by recrystallization from water as white plates⁶, and stored under vacuum. Tetrahydrofuran (Fison's SLR grade) was distilled under nitrogen, a middle cut being taken and stored under vacuum over calcium hydride. Before use it was vacuum distilled onto a complex of sodium/potassium alloy and α -methylstyrene to ensure complete removal of protonic species. Sodium ethoxide was prepared by the reaction of sodium metal upon ethanol in diethyl ether solution⁹.

Preparation of polymers

A given quantity of initiator was weighed into a reaction vessel such that its concentration would be 2×10^{-2} mol/l of monomer, and evacuated for several hours. A known volume of dry THF was distilled into the vessel at liquid nitrogen temperature. The reaction vessel was vacuum sealed and stored in liquid nitrogen until used.

Initiation followed the same procedure for all samples. The reactor was removed from liquid nitrogen and allowed to stand at room temperature for 4 min, by which time the monomer had melted. It was then transferred to a methanol bath at -10°C for 6 min with continual turning to en-

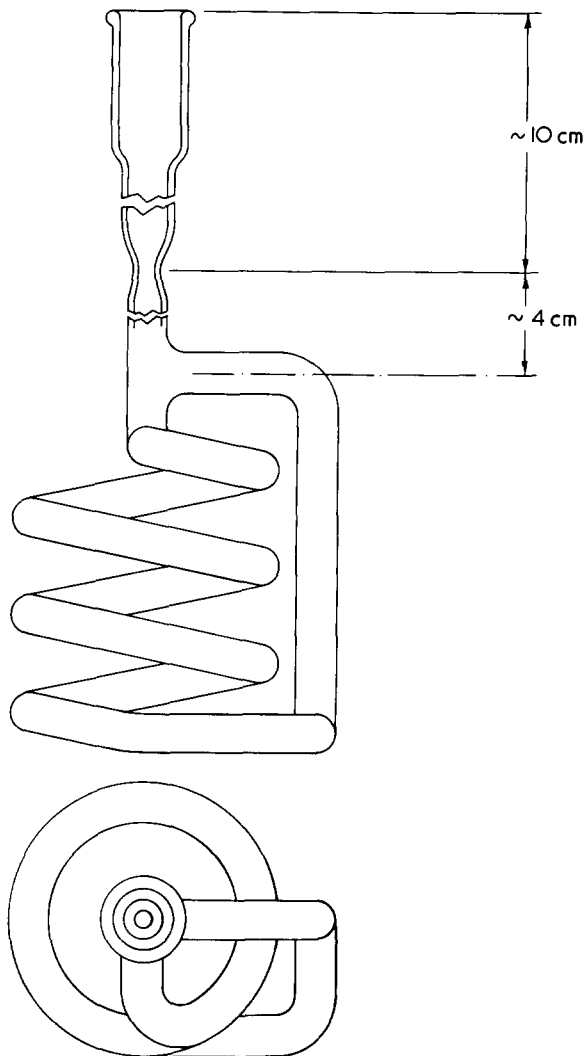


Figure 1 A helical glass reactor having an internal volume of approximately 40 ml, with a greaseless high-vacuum joint

sure homogeneous mixing of the reactants. Initiation was effected by placing the vessel in an oil bath at a high temperature for a specified time (usually 95°C for 4 min) during which time an intense purple colour developed. This active system was cooled rapidly in a bath at -10°C for 15 sec and then in liquid nitrogen for 15 sec, after which it was removed to a bath set at the required reaction temperature.

Termination was achieved by freezing the reactants rapidly in liquid nitrogen, opening the vessel and transferring the contents to a terminating solution. Initially this was a 10% (v/v) solution of acetic acid in THF, but in later reactions this was changed to a solution of sodium ethoxide in THF (5×10^{-2} mol/l).

Residual catalyst and catalyst fragments were isolated from the THF solution by adding distilled water, evaporating off the THF under a stream of nitrogen and extracting the polymer with benzene, thus removing any water soluble material. After removal of the benzene under nitrogen and drying for several days under vacuum, the weight of product was recorded. High molecular weight polymers could be isolated simply by precipitating with methanol, drying and weighing.

It should be noted that the coloration introduced at the initiation stage was still evident in the recovered products. It was assumed at first that this was caused by initiator residues, or by the formation of coloured by-products as suggested by Dreyfuss¹⁰. Accordingly a preparative gel per-

meation chromatograph was set up following the procedure of Mulder and Buytenhys¹¹ to purify the products further.

Purification of polymers

Preparative g.p.c. columns were set up using Bio-Rad SX-1 (high molecular weight) or SX-8 (low molecular weight) gels in toluene as solvent. The flow was gravity fed from a constant pressure reservoir; a syphon injection system was used together with infra-red monitoring of the effluent. A normal solute concentration of 5% (w/v) was injected. The gel was chosen so that the polymer molecular weight was above the exclusion limit of the gel, and was thus carried through the column in the excluded volume. Any low molecular weight impurities diffused into the substrate and were retained longer on the column.

This process was observed visually by the separation of the sample into two distinct bands, the coloured polymer band (red/purple) eluting first, followed by an orange/yellow band. U.v. and i.r. spectroscopy were performed on the polymer before and after this treatment, the traces being shown in Figure 2. The disappearance of the peak at $39\,000\text{ cm}^{-1}$ (256 nm) in the u.v. spectrum suggests removal of an aromatic species undergoing a $\pi \rightarrow \pi^*$ transition (local excitation of electrons in a benzene nucleus).

Molecular weight determinations

Average molecular weights were determined using a Waters Associates ALC/GPC 501 liquid chromatograph. Tetrahydrofuran was used as solvent at room temperature upon commercially available styragel columns. The instrument was calibrated with the familiar narrow distribution

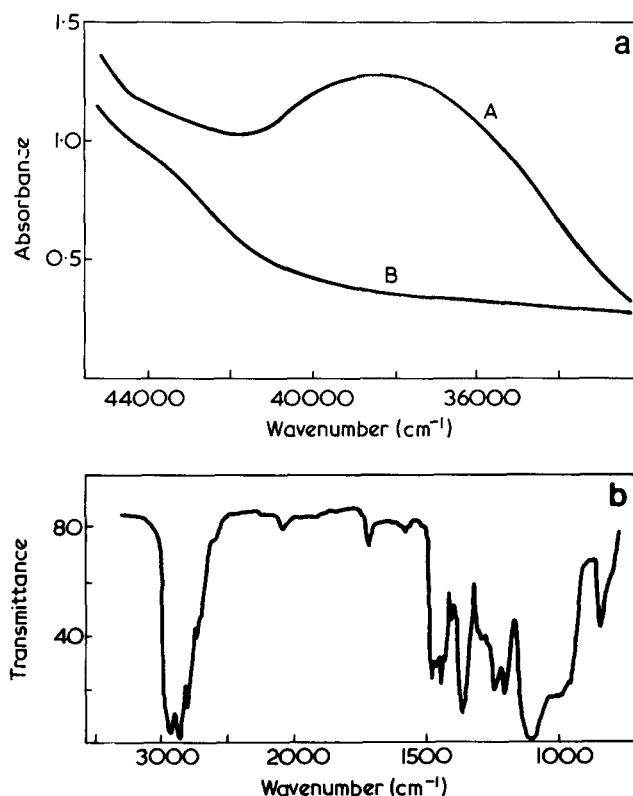


Figure 2 (a) U.v. spectra of polymer ($\bar{M}_n = 7000$) in solution in ethanol (0.01%) showing disappearance of peak at $39\,000\text{ cm}^{-1}$ (256 nm) after passage of polymer through preparative g.p.c. column. A, crude polymer; B, purified polymer. (b) i.r. spectrum of polymer ($\bar{M}_n = 7000$), cast from chloroform onto KBr disc, showing no difference before and after passage through preparative g.p.c. column

polystyrene standards, and a conversion factor was calculated based on the hydrodynamic volume procedure proposed by Benoit and coworkers¹². For polystyrene (PS) and polytetrahydrofuran (PTHF) in THF having identical hydrodynamic volumes

$$\log[\eta]_{\text{PTHF}} M_{\text{PTHF}} = \log[\eta]_{\text{PS}} M_{\text{PS}}$$

where $[\eta]$ is the intrinsic viscosity and M is the molecular weight. The intrinsic viscosity can be written in terms of the unperturbed end-to-end distance $[\overline{r_0^2}]^{1/2}$ and the expansion factor α , with ϕ the universal viscosity constant¹³

$$[\eta] = \phi \left(\frac{\overline{r_0^2}}{M} \right)^{3/2} M^{1/2} \alpha^3$$

substituting for $[\eta]$ yields

$$\frac{M_{\text{PTHF}}}{M_{\text{PS}}} = \left(\frac{\overline{r_0^2}}{M} \right)_{\text{PS}} \left(\frac{M}{\overline{r_0^2}} \right)_{\text{PTHF}} \left(\frac{\alpha_{\text{PS}}}{\alpha_{\text{PTHF}}} \right)^2$$

Assuming $(\alpha_{\text{PS}}/\alpha_{\text{THF}}) = 1$ for these two polymers in the g.p.c. solvent (as proposed by Dawkins¹⁴ and taking literature values for $[\overline{r_0^2}/M]$ ¹³ we calculate the value 0.592 as a conversion factor, i.e.

$$M_{\text{PTHF}} = 0.592 M_{\text{PS}}$$

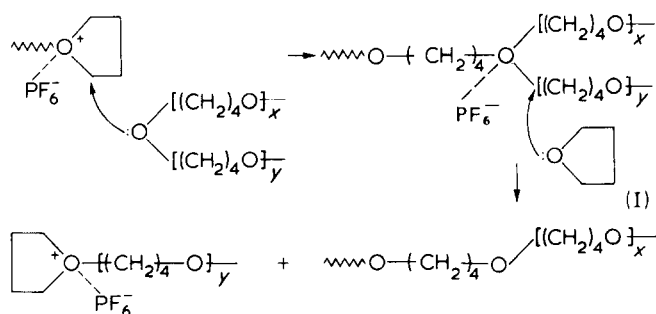
at a given elution volume. The determination of M_{PTHF} enables absolute molecular weights to be evaluated from the chromatogram.

An empirical correction for machine-broadening was made by comparing the $\overline{M}_w/\overline{M}_n$ ratios for polystyrene found from the instrument, to that given with these samples, and a plot of % correction *versus* log molecular weight made. Thus a correction for machine broadening could be made covering the entire molecular weight range of the instrument. A computer program was written to perform the tedious calculations, using the method of Pickett *et al.*¹⁵.

Factors causing molecular weight broadening

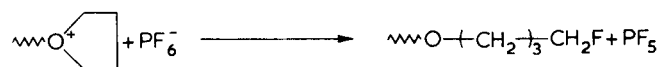
Equilibrium effects. Living PTHF chains eventually reach an equilibrium between monomer and polymer where the rates of propagation and depropagation become equal. The effect of having competing forward and backward reactions is, eventually, to spread the distribution of molecular weights until it reaches the Flory distribution ($\overline{M}_w/\overline{M}_n = 2$). Miyake and Stockmayer¹⁶ have calculated that for the anionic polymerization of styrene it will take 80 years to reach this polydispersity. Dreyfuss and Dreyfuss⁵ quote a corresponding value of 20 days for PTHF at 30°C. This reflects the fact that polymer is the favoured species at low temperature but as the ceiling temperature is approached the reverse reaction is progressively more favoured. Since broadening is observed even at low temperatures and to a higher degree than predicted the propagation-depropagation effect cannot be solely responsible.

Chain transfer reactions. Assuming a very low level of impurities in our rigorous system, the most likely chain transfer agents present are in-chain oxygens and counter ions.



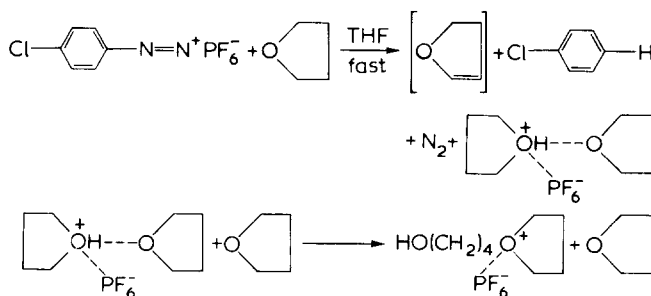
This example shows chain transfer to polymer oxygen, which is really a special case of a dialkyl ether. Dreyfuss⁶ has shown dialkyl ethers to be effective chain transfer agents, and as can be seen from the above scheme this reaction leads to a randomization of molecular weights with no decrease in the rate of polymerization. Rosenberg² has suggested that, in the later stages of polymerization when monomer is becoming scarce, species I increases in concentration leading to a very large rise in viscosity, although association of active ends would cause a similar effect. Problems of this type will grow in severity as the conversion increase so most of this work was performed with conversions below 10%.

With many systems, reaction of the growing chain-end with counter-ion is a termination reaction, and this becomes a difficult problem when relatively unstable counter-ions, such as BF_4^- , are used. However, with PF_6^- as counter-ion, the reaction between them is envisaged as follows¹:



The PF_5 itself may act as an initiator¹⁷ and thus a transfer, rather than termination, reaction occurs. The effect of such a transfer reaction will again be to broaden the distribution of molecular weights, but in this case with a delay in the chain reaction and an alteration of the counter ion.

Slow initiation reactions The mechanism of initiation by trityl or diazonium salts has been the subject of much controversy but has been proposed¹⁰ as follows for the diazonium salt:



Dehydrogenation of THF to a furan or dihydrofuran occurs, along with the formation of the free acid of the counter ion (HPF_6), which is stabilized by complexing with monomer (HPF_6 is normally found as its diethyl ether complex, $\text{HPF}_6 \cdot 2(\text{CH}_3\text{CH}_2)_2\text{O}$). The acid complex then reacts slowly with additional monomer to form the propagating species, which should have an hydroxyl end group. It is further suggested that the intense colours observed during the initiation are formed by the acid catalysed resinification of the furan or dihydrofuran by-products. In the present work, however, a high degree of colouration is observed in

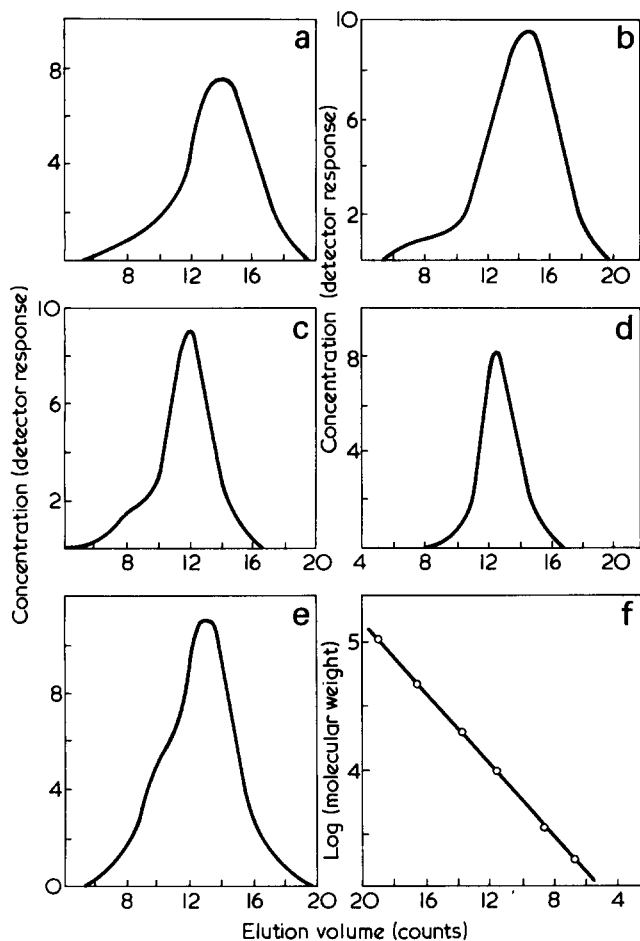
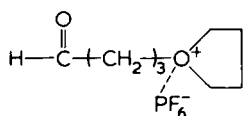


Figure 3 Gel permeation chromatograms (polymer concentration versus elution volume) showing effect of initiation temperature upon the molecular weight distribution. (a)–(c) initiated for 7.5 min; (d), (e) initiated for 5 min. (f) shows the calibration curve for the instrument (polystyrene standards). Initiation temperatures: (a) 85°C; (b) 90°C; (c) 95°C; (d) 95°C; (e) 100°C

the polymer even after preparative g.p.c., suggesting that the colour is chemically associated with the initiated chain end.

Ledwith and Sherrington³ have also suggested a homolytic decomposition reaction for the diazonium salt involving a chain reaction in the initiation process and leading to the aldehydic end group:

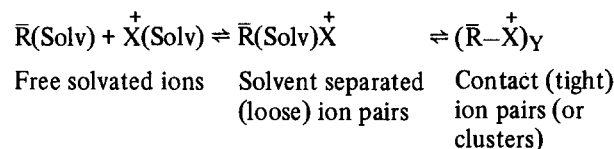


There is no conclusive evidence as to the chemical nature of the initiated chain-end.

Both of these reaction mechanisms involve a slow, rate-determining step, in line with the observed slow initiation at temperatures where the rate of propagation is reasonably fast. This will be a prime cause in broadening the molecular weight distribution, since centres initiated early in the reaction may grow to much longer chain lengths than those initiated later.

Ion pair structure. Whenever ions are present in solution their local environment will largely determine their rate of reaction. The following general scheme for the ions

R^- and X^+ in solution may be envisaged:



The order to reactivity of these ion pairs is expected to be: free solvated ions \geq loose ion pairs $>$ tight ion pairs.

Now consideration of the propagation reaction together with the knowledge that a ceiling temperature T_c exists for a given concentration of reactants such that ΔG (polymerization) = 0 at T_c , leads to:

$$k_p/k_B = A \exp[-\Delta H(T_c - T)/RT T_c] \quad (1)$$

and as ΔH is negative k_p/k_B decreases with increasing temperature, strongly near T_c . However, we observe the polymerization to increase in rate with temperature well below T_c thus signifying a progressive change from tight ion-pairing (or clustering) towards the free ion situation with increasing temperature.

The rate of addition of monomer is only approximately 1 monomer per chain per 6 sec at -10°C . Thus in the time taken to grow high polymer every chain end will fluctuate statistically between the various possible structures. Every chain will thus propagate at the same overall statistical rate and differences in ion pair structure will not lead to broadening with the present system.

RESULTS AND DISCUSSION

The preceding comments allow sensible interpretation of an initially complex pattern of results. Figure 3 shows the g.p.c. traces obtained for a series of bulk polymerizations with initiator concentrations of 1.75×10^{-2} mol/l identical in all respects except that they were initiated for 7.5 min (Figures 3a–3c) and 5 min (Figures 3d and 3e) at progressively higher temperatures before reacting at 0°C to approximately 2% conversion. A closely related series of experiments was carried out to investigate the effect of initiation time at each temperature. The results follow a similar pattern for all of the lower temperatures and are typified by the curves in Figure 4 for initiation at 60°C , followed by reaction at 0°C , to ~ 10 –15% conversion. The

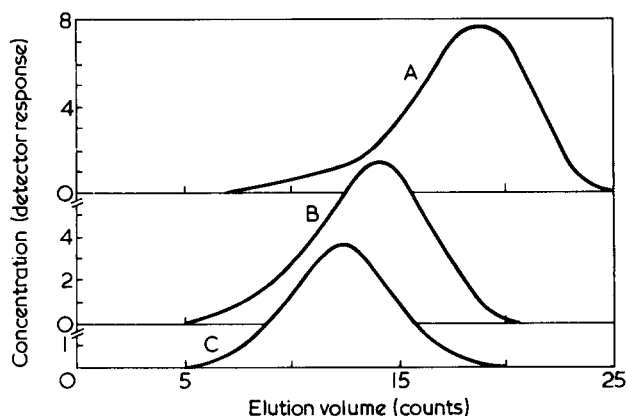


Figure 4 Gel permeation chromatograms showing samples initiated for different times at 60°C and reacted for the same time (30 min) at 0°C . The molecular weight and distribution increase with increasing initiation time. Initiation times: A, 30 min; B, 15 min; C, 7.5 min

Table 1 Kinetics of polymerization followed at a series of low temperatures

Reaction Temp. (°C)	Time (h)	Conversion (%)
-10	2	1.83
	4	2.85
	6	3.97
	8	5.16
0	1	1.98
	2	3.22
	2	3.43
	3	4.69
	4	5.99
	6	8.18
20	0.50	4.43
	0.75	6.38
	1.00	8.91
	1.25	11.16
	1.50	13.80

significance of these results will become clear as we consider further evidence, but empirically it is seen (*Figure 3d*) that initiation at 95°C for 5 min followed by rapid quenching to a low reaction temperature gives a nearly monodisperse polymer ($\bar{M}_w/\bar{M}_n = 1.08$).

Using the clean initiation conditions (95°C for 4 min) the kinetics of polymerization were followed at a series of low temperatures, viz. -10°C, 0°C and 20°C, with molecular weight averages being measured in each case. The kinetic results are given in *Table 1*. Now at the high initiation temperatures ($[I_0] - [I]$) mol/l of initiator decomposes and we will assume each gives rise to a living polymer chain which grows predominantly during the time held at the low polymerization temperature. Then at the polymerization temperature the rate of monomer consumption is

$$\begin{aligned} \frac{-dM}{dt} &= k_i [I] ([M] - [M_e]) \\ &+ (k_p/n) ([I_0] - [I]) ([M] - [M_e]) \end{aligned} \quad (2)$$

The terms $([M] - [M_e])$ are the effective concentrations¹⁸ under conditions where the equilibrium concentration would be $[M_e]$ and n is the number of initiators required to start one chain. The first term on the right allows for consumption of monomer in further initiation reactions at the polymerization temperature. At low polymerization temperatures k_i is small and we will neglect the first term giving

$$\frac{1}{[I_0]} \ln \frac{[M_0] - [M_e]}{[M] - [M_e]} = \frac{f}{n} k_p t \quad (3)$$

where $f = ([I_0] - [I])/[I_0]$ is the fraction of catalyst decomposed under the initiation conditions. These conditions were constant with f/n , known approximately from the relation:

$$\frac{f}{n} = \frac{\text{yield}}{\text{molecular weight } [I_0]}, \text{ being } \approx 0.1.$$

Plots of $(2.303/[I_0]) \log ([M_0] - [M_e])/([M] - [M_e])$ against time are shown in *Figure 5*. Good straight lines re-

sult at -10 and 0°C, but at 20°C a positive deviation is present. Values of $(f/n)k_p$ at each temperature were calculated from the initial slopes, and the k_p values are shown, together with the $[M_0]$ and $[M_e]$ ¹⁹ values used, in *Table 2*.

A plot of $\ln k_p$ against $1/T$, using the three lowest temperature values of k_p from *Table 2*, is shown in *Figure 6*, along with the results from a high temperature set of single point determinations, as described later. A straight line results showing k_p increasing with increasing temperature with an activation energy (probably for ion pair dissociation) of 51.3 kJ/mol.

Number average molecular weights (\bar{M}_n) are shown plotted against time in *Figure 7*. At -10°C this yields a straight line, but at 0°C the plot falls away from a linear relation with time, whereas the conversion increases linearly. The logical interpretation of these data is that chain transfer reactions become more significant at higher temperatures. Accordingly the polydispersity ratios are all narrow for polymers at -10°C, but begin to broaden with time at 0°C. These values are given in *Table 3*.

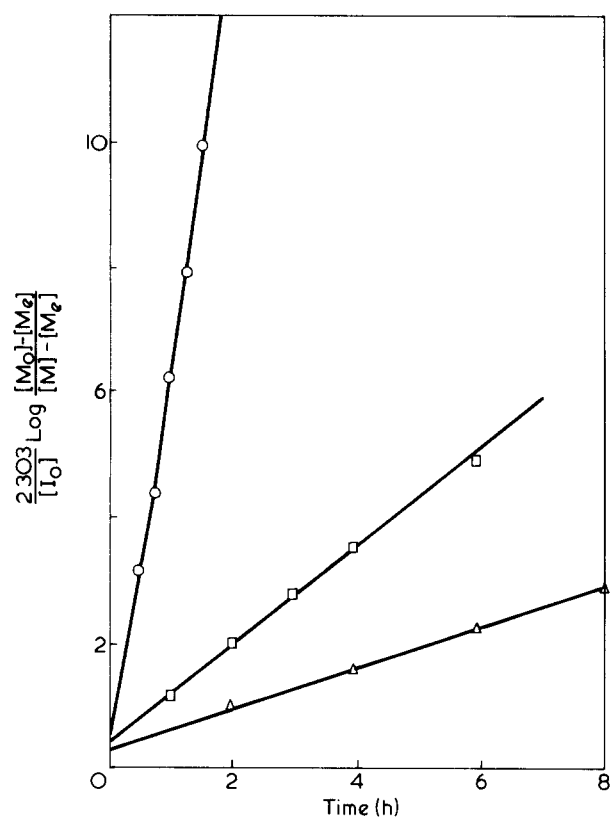


Figure 5 Plots of $(2.303/[I_0]) \log ([M_0] - [M_e])/([M] - [M_e])$ versus time to test equation (3), and also to allow calculation of fk_p/n and hence k_p at each temperature: \circ , 20°C; \square , 0°C; \triangle , -10°C

Table 2 Values of k_p calculated from *Figure 5* at various temperatures, together with $[M_e]$ and $[M_0]$ values

Temperature (°C)	$[M_e]^*$ (mol/l)	$[M_0]$ (mol/l)	k_p (l/mol sec)
-10	1.25	12.74	9.20×10^{-4}
0	1.70	12.60	2.20×10^{-3}
20	2.96	12.32	1.46×10^{-2}
50	5.93	11.90	1.29×10^{-1}
60	7.32	11.76	2.85×10^{-1}
70	8.94	11.63	5.19×10^{-1}
80	10.81	11.49	1.05×10^0

* $[M_e]$ values from Ofstead¹⁹

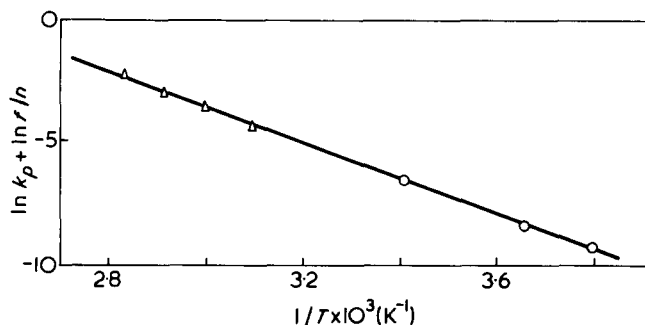


Figure 6 Plot of $\ln k_p + \ln f/n$ versus $1/T$. The low temperature values (\circ), are obtained from Figure 5, the high temperature values (Δ), are obtained from single point measurements at each temperature. This plot yields an activation energy of 51.3 kJ/mol

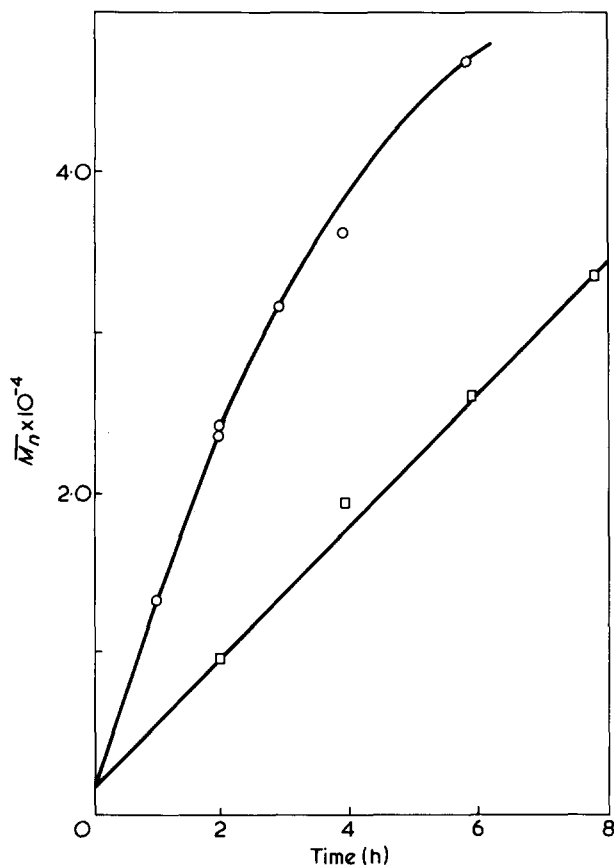
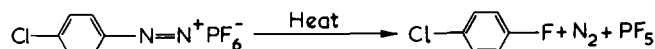


Figure 7 Increase of molecular weight (\bar{M}_n) with time at temperatures of -10°C (\square , linear) and 0°C (\circ , falls away from linear relation due to the onset of significant chain transfer reactions)

Another series of kinetic experiments was carried out using the clean initiation conditions (95°C for 4 min) followed by propagation reactions at a series of temperatures (50° , 60° , 70° and 80°C) for the same period of time (10 min). A plot of % conversion against propagation temperature is given in Figure 8, and this shows a clear maximum in the yield at a temperature of 65°C . This plot is closely followed by the theoretical line shown in Figure 8 calculated using equation (3). Since the overall rate of polymerization passes through this maximum on cooling, it is necessary to quench the samples as rapidly as possible after the initiation stage. Equation (3) was used to calculate k_p from the single point at each temperature, and these are also plotted in Figure 6 where they clearly show good agreement with the extrapolation of the low temperature data. A significant inference from this result is that the assumption made

in deriving equation (3) is valid and $k_i [I]$ must be small compared with $k_p ([I_0] - [I])$. This is reasonable since at 95°C the initiation will be rapid, with some 20–40% (depending on the mechanism) of initiator used in starting chains. In addition the initiator will tend to decompose thermally as follows:



In the solid state this occurs at 150°C , but in solution this temperature will be reduced. Thus we propose that only a small concentration ($\sim 20\%$) of the starting concentration of initiator remains unreacted after treatment at 95°C for 4 min.

At temperatures below T_c , Figure 4 shows that molecular weight broadening occurs more rapidly as initiation time increases. It is clear from the preceding discussion that this is caused by continuous initiation during propagation, as the two rates are similar at these temperatures.

The choice of 95°C as the temperature of initiation may be explained with reference to Figure 3. At temperatures below 95°C , initiation and growth are occurring simultaneously throughout the initiation reaction, with chain transfer also occurring at longer reaction times, thus giving a very broad molecular weight distribution. At 95°C , however, the temperature is sufficiently far above the ceiling temperature to prevent significant growth from occurring, thus upon cooling and subsequent propagation a narrow molecular weight distribution occurs. Above 95°C further polymerization occurs in sealed reactors due to the increase in pressure which will favour the polymerization reaction if this occurs with a decrease in volume (as in the present case). This is equivalent to an elevation of ceiling temperature with pressure²⁰.

Table 3 Polydispersity ratios at different temperatures and reaction times

Temperature ($^\circ\text{C}$)	Polydispersity ratio after stated reaction times					
	1 h	2 h	3 h	4 h	6 h	8 h
-10		1.08		1.08	1.08	1.10
0	1.17	1.26	1.31	1.36	1.75	

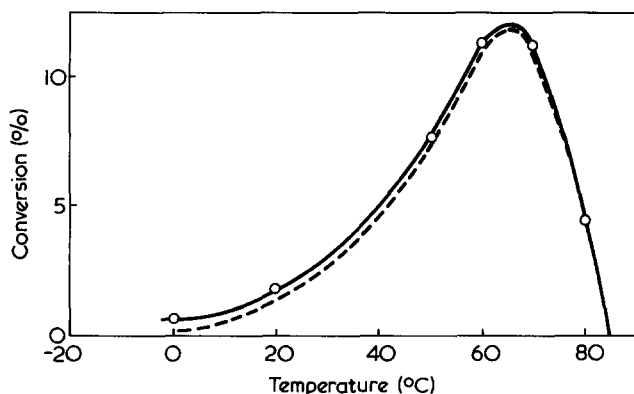


Figure 8 Plot of conversion versus temperature for reactions of the same time (10 min, \circ) and also the theoretical conversion (---) predicted by equation (3)

In considering the significance of the present results in terms of the factors, listed earlier, which could produce molecular weight broadening we see that changing ion pair structure may well be the reason for the increase in chain transfer over propagation reactions as the temperature is raised. Competing initiation and polymerization reactions occur if initiation is attempted below T_c , but conversely the effect of a reversible reaction on broadening is not important well below T_c and at low conversions.

The method outlined is excellent for producing near monodisperse high molecular weight polymers. In the present work polymers as low as 5000 molecular weight have been produced still with good monodispersity. The disadvantage with low polymers is the high catalyst concentration required ($\sim 1:1$ based on polymer produced) with the inevitable difficulties of adequate separation of catalyst residues from the polymer. In the low molecular weight range we have found triethyloxonium hexafluorophosphate more convenient⁵.

CONCLUSIONS

Bulk tetrahydrofuran at low conversions obeys second order reaction kinetics with reversibility and no termination under high vacuum conditions. The propagation rate constant increases with temperature according to an Arrhenius relation with activation energy = 51.3 kJ/mol. Initiation rates also increase with temperature, but because of the reversibility of the polymerization reaction, initiation at 95°C (above the ceiling temperature) gives rapid production of active chains, but little growth. Rapid quenching to low temperatures (-10°C) then allows growth without simultaneous initiation, giving a near monodisperse system (typically $\bar{M}_w/\bar{M}_n = 1.08$). Selection of low temperatures for growth is necessitated largely because chain transfer to polymer occurs more predominantly as the temperature is raised giving increased polydispersity. The procedures outlined are particularly useful in producing polymers in the thousands to million molecular weight range with good monodispersity.

ACKNOWLEDGEMENT

T.G.C. acknowledges receipt of a Science Research Council Studentship.

REFERENCES

- 1 Dreyfuss, P. and Dreyfuss, M. P. *Adv. Polym. Sci.* 1967, **4**, 528
- 2 Rosenberg, B. A., Ludvig, E. B., Gantmakher, A. R. and Medvedev, S. S. *J. Polym. Sci. (C)* 1967, **16**, 1917
- 3 Ledwith, A. and Sherrington, D. C. in 'Reactivity, Mechanism and Structure in Polymer Chemistry', (Eds. Jenkins, A. D. and Ledwith, A.), Wiley, London, 1974, Ch 9
- 4 Dreyfuss, P. *J. Macromol. Sci. (A)* 1973, **7**, 1361
- 5 Dreyfuss, P. and Dreyfuss, M. P. *Adv. Chem. Ser.* 1969, **91**
- 6 Dreyfuss, M. P. and Dreyfuss, P. *J. Polym. Sci. (A-1)* 1966, **4**, 2179
- 7 Stejny, J. *J. Macromol. Sci. (A)* 1973, **7**, 1435
- 8 Smith, S. and Hubin, A. J. *J. Macromol. Sci. (A)* 1973, **7**, 1399
- 9 Fieser, L. F. 'Experiments in Organic Chemistry', Heath, Boston, 1957
- 10 Dreyfuss, M. P., Westfahl, J. C. and Dreyfuss, P. *Macromolecules* 1968, **1**, 437
- 11 Mulder, J. L. and Buytenhuys, F. A. *J. Chromatogr.* 1970, **51**, 459
- 12 Grubisic, Z., Rempp, P. and Benoit, H. *J. Polym. Sci. (B)* 1967, **5**, 753
- 13 Flory, P. J. 'Statistical Mechanics of Chain Molecules', Wiley, New York, 1969
- 14 Dawkins, J. V. *Br. Polym. J.* 1972, **4**, 87
- 15 Pickett, H. E., Cantow, M. J. R. and Johnson, J. F. *J. Appl. Polym. Sci.* 1966, **10**, 917
- 16 Miyake, A. and Stockmayer, W. H. *Makromol. Chem.* 1965, **88**, 90
- 17 Sims, D. *Makromol. Chem.* 1966, **98**, 245
- 18 Vofsi, D. and Tobolsky, A. V. *J. Polym. Sci. (A)* 1965, **3**, 3261
- 19 Ofstead, E. A. *Polym. Prepr.* 1965, **6**, 674
- 20 Rahman, M. and Weale, K. E. *Polymer* 1970, **11**, 122

Analysis of relaxation processes in methacrylate polymers by thermally stimulated discharge

M. Kryszewski, M. Zielinski and S. Sapięha

Centre of Molecular and Macromolecular Studies, Polish Academy of Sciences, Łódź, Poland

(Received 1 August 1975; revised 7 October 1975)

An analysis of relaxation processes in poly(methyl methacrylate), poly(ethyl methacrylate), poly(isobutyl methacrylate) and poly(n-butyl methacrylate) by means of thermally stimulated discharge (t.s.d.), is presented. Distribution functions, calculated from the thermocurrent spectra using the Staverman-Schwarzl transform, are compared with semi-empirical distribution functions of Fuoss-Kirkwood and Havriliak-Negami. Distribution functions of β processes fit the first function very well and those of α processes fit the second distribution function. The distribution parameters are comparable with those in the literature. It is also demonstrated that the activation energy can be calculated from the initial rise by means of the Bucci, Fieschi and Guidi equation, if the proper correction coefficient is introduced, depending on the width of the distribution.

INTRODUCTION

In recent years the thermally stimulated currents (t.s.c.) and thermally stimulated depolarization (t.s.d.) techniques, applied to polymers, were used to evaluate trapping levels and other trap parameters in these materials. However, for dipolar polymers, t.s.d. is a very useful technique for elucidating their molecular parameters as relaxation frequencies, distribution functions and activation energies. Recent results of Van Turnhout¹ have shown, that it is possible to calculate these parameters from t.s.d. spectra. However, the authors did not focus their attention on the specific distribution functions for all relaxations¹⁻⁴, giving only examples^{1,2} of the calculation method, based on the simple, symmetric distributions of β and γ relaxations in PMMA.

All studies of dielectric properties of methacrylic polymers have led to the asymmetric distributions of relaxation times, at least in the glass transition temperature region. However, the shape of these distribution curves is still a subject for discussion. For this reason we have applied the t.s.d. method, which is considerably simpler, from the experimental point of view than other methods normally used, for determination of the characteristics of dipolar relaxation in polymers, giving some supplementary information related to the subject.

EXPERIMENTAL

Films of poly(methyl methacrylate) (PMMA), poly(ethyl methacrylate) (PEMA), poly(n-butyl methacrylate) (PnBMA) and poly(isobutyl methacrylate) (PiBMA) were investigated. Films were obtained by solvent evaporation from solution in chloroform, and their thickness was $\sim 20 \mu\text{m}$. After careful drying the solvent content in the polymer was negligible. The samples were then supplied with gold electrodes evaporated in a vacuum.

The t.s.d. measurements were carried out in a vacuum in the equipment described elsewhere⁵, at a constant heating rate, $4^\circ\text{C}/\text{min}$. The polarization field E_p and polarization time t_p , were constant for all experiments (150 kV/cm and 1 h respectively). The polarization temperature T_p was

altered depending on the T_g of the polymer. The influence of the heating rate on the t.s.d. peaks was in good agreement with theoretical predictions², and for our method the rate $4^\circ\text{C}/\text{min}$ was found most convenient. Because of the small thickness of the sample ($20 \mu\text{m}$), the temperature gradient across the sample was negligible.

The changes of temperature and field in the consecutive stages of the experiment: polarization, storage and t.s.d. measurements are presented in Figure 1.

RESULTS

T.s.d. spectra

Experimentally obtained spectra are discussed, assuming the Debye model of relaxation and a distribution in natural frequencies. For this type of relaxation one can obtain an

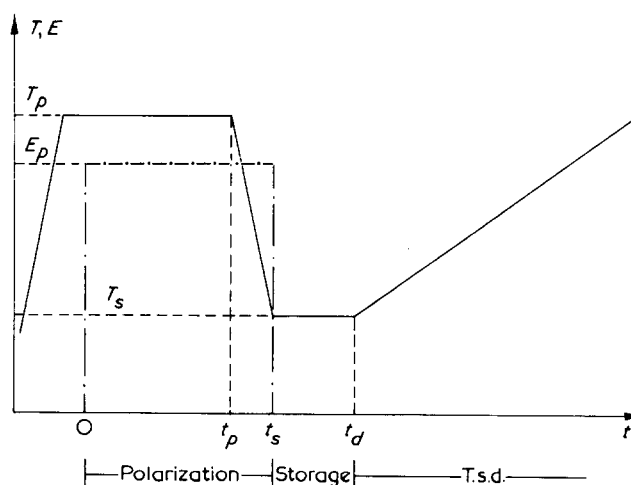


Figure 1 Time-temperature scheme of polarization, storage and t.s.d.: —, temperature changes; - - -, field changes

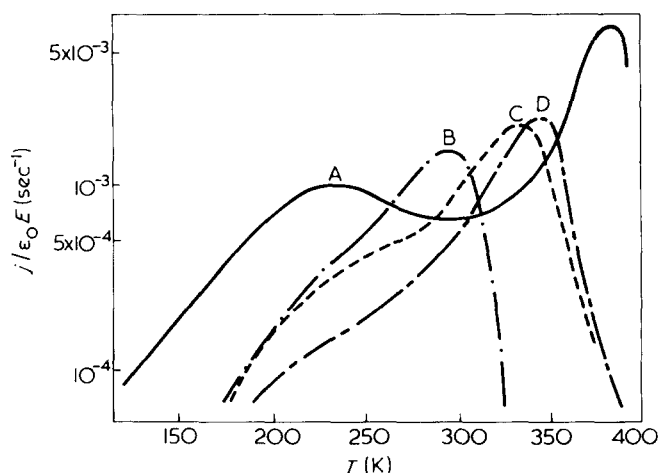


Figure 2 T.s.d. spectra of: A, PMMA; B, PnBMA; C, PiBMA; D, PEMA

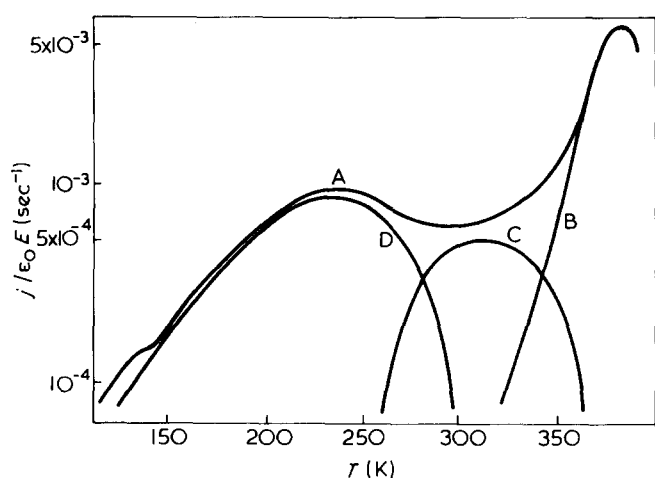


Figure 3 Thermal cleaning of the PMMA spectrum. A, an overall spectrum; thermally cleaned peaks: α , B; β , C; β' , D

equation for the released t.s.d. current density, j^2 :

$$j/\epsilon_0 E = (\epsilon_s - \epsilon_\infty) \times a(T) \int_0^\infty F(T, t) \times f(\alpha_r) \times \exp \left\{ -\alpha_r \xi(T_s, T) \right\} d\alpha_r \quad (1)$$

where: ϵ_0 permittivity of vacuum;
 ϵ_s static dielectric constant;
 ϵ_∞ high frequency dielectric constant;
 $a(T)$ the temperature shift of the dipolar relaxation frequency;
 $F(T, t)$ the filling state function;
 α_r the natural frequency of dipolar relaxation;
 $f(\alpha_r)$ distribution function;
 $\xi(T_s, T) = s \int_{T_s}^T a(T) dT$ is the so-called 'reduced time' an analogue of time in similar equation for isothermal discharge;
 T_s storage temperature;
 s reciprocal of heating rate.

The temperature shift of the dipolar relaxation frequency $a(T)$ is defined by the equation $\alpha(T) = \alpha_r a(T)$ where α_r is constant and $\alpha(T)$ is the relaxation frequency. In the simplest case of Arrhenius shift, $a(T)$ is equal to $\exp(-A/kT)$, where A is the activation energy and k is the Boltzmann constant. The distribution function $f(\alpha_r)$ is the one normally used in the theory of dielectrics.

The filling state function is given by the following equation²:

$$F(T, t) = \{1 - \exp[\alpha(T_p) t_p - \alpha_r \xi(T_p, T_s)]\} \exp[-\alpha(T_s)(t_d - t_s)] \quad (2)$$

where: t_s , total time of field application; t_d , time, when t.s.d. begins. This function, dependent both on polarization and storage conditions, characterizes the filling state of the polarized sample. If the polymer sample is polarized completely, then $F(T, t) = 1$, and the t.s.d. spectrum is determined by the heating rate and such material parameters as $(\epsilon_s - \epsilon_\infty)$, α_r , $a(T)$ and $f(\alpha_r)$. Model calculations of Van Turnhout², show, that this condition is fulfilled if the polarization temperature is $\sim 20^\circ\text{C}$ higher than the T_g (for α relaxation). In all our investigations these requirements have been taken into consideration.

The t.s.d. spectra of the investigated polymers are presented in Figure 2. One can see, that for PMMA the α and β peaks are well resolved (the nomenclature of the relaxation processes is according to McCrum *et al.*⁶), but for all the three remaining polymers (PEMA, PiBMA and PnBMA), the β peak exists only as a shoulder on a low temperature tail of the α peak. T.s.d., however, has an exceptional ability to resolve overlapping peaks and in Figures 3 and 4, the spectra are well resolved with 'thermal cleaning technique'^{3,7}. This technique involves a partial discharge of the first peak up to some temperature T_1 . The temperature T_1 should be carefully chosen and usually, it corresponds to the valley between two peaks. In the next run, while only the second polarization is filled, an unperturbed peak due to the second process can be seen, and the remaining part of the first peak can be obtained by subtraction. The β peak in PEMA, isolated by this technique from the whole spectrum, is depicted in Figure 4. However, in the case of PMMA, attempts to isolate the β and α peaks were unsuccessful, as another peak was always seen (or an inflection on the falling shoulder of the β peak or on the rising shoulder of the α peak), independent of the choice of T_1 , between

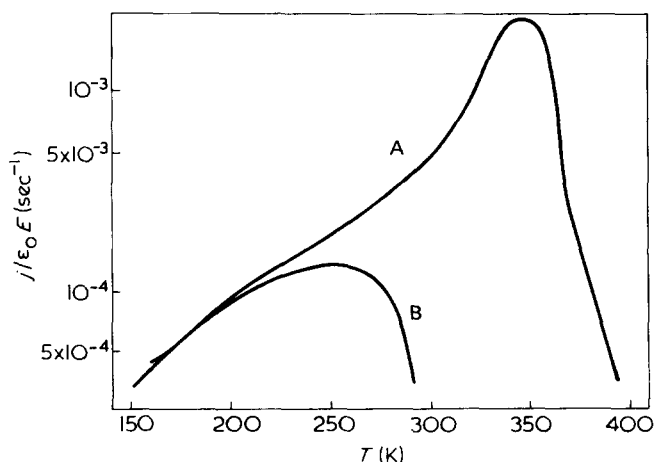


Figure 4 Thermal cleaning of the PEMA spectrum. A, the overall spectrum; B, the thermally cleaned peak β

the maxima of the β and α peaks. Thus, by successive applications of 'thermal cleaning' it was possible to isolate three different peaks; the α and β peaks and another one, β' , located between them, with a maximum temperature of $\sim 50^\circ\text{C}$. (Figure 3) A similar process was observed by Mikhailov *et al.*⁸ by means of a.c. measurements and by Wittman *et al.*⁹ by means of dilatometric measurements, and it is ascribed to the presence of heterotactic sequences in conventional PMMA [evidence from high resolution n.m.r. studies¹⁰ suggests, that conventional PMMA may contain a fairly high degree ($\leq 60\%$) of syndiotactic sequences]. Vanderschueren⁴ also observed such a process in t.s.d. investigations of PMMA, and found, that it follows monomolecular kinetics, which in our case, indicates that it could be ascribed to another dipolar process.

Activation energies and distribution functions

There are several methods of calculating activation energies from the t.s.d. spectra. One can take into consideration the initial rise of thermocurrent, the half-width temperatures of the peaks or the least squares fit¹¹. In this work we have used the method proposed by Bucci, Fieschi and Guidi⁷ (BFG), which leads to the following equation:

$$A = -k \frac{d \ln \alpha(T)}{d(1/T)} \quad (4)$$

where:

$$\alpha(T) = j/P_s(T) \text{ and } P_s(T) = -s \int_{T_u}^T j \, dT, \quad (5)$$

T_u is the ultimate temperature, when j reaches zero. Unfortunately all these methods hold only for non-distributed polarizations. It was demonstrated by Van Turnhout², that for a distribution in natural frequencies in the case of the initial rise of thermocurrent in t.s.d.:

$$k \frac{d \ln j}{d(1/T)} = -cA$$

where c is a constant. The same holds for the BFG equation. Taking into consideration some particular distribution functions, it can be proved, that $c = 1$ for Wagner and Gevers distribution, and $c = m$ for Fouss-Kirkwood and Cole-Cole distribution functions¹², where m is a parameter of these distributions.

It is a common procedure in evaluating dielectric and mechanical relaxation data to introduce a distribution function, for it allows us to fit them to the Debye relaxation model. To calculate the distribution functions from the t.s.d. data, we have used the Staverman and Schwarzl approximation¹³ of the inverse Laplace transform of equation (2), taking into consideration only the second-order approximation. We have introduced the logarithmic distribution function², normalized to the maximum value:

$$L \left(\frac{\tau_r}{\tau_0} \right) = f(\ln \tau_r/\tau_0)$$

where $\tau_r = 1/\alpha_r$; τ_0 is the most probable value of τ_r

$$\frac{L_1 \left(\frac{\tau_r}{\tau_0} \right)}{L_m} = \left[\frac{T^2 j(T)}{T_m^2 j_m} \right]_{c'=1}$$

$$\frac{L_2}{L_m} = \frac{L_1}{L_m} - \left[\frac{T^2 d \left(\frac{j(T)}{j_m} \right)}{s T_m^2 dT} \right]_{c'=0.5}$$

where:

$$\frac{\tau_r}{\tau_0} = \frac{c' T^2 a(T)}{T_{\max}^2 \alpha(T_{\max})}$$

T_m, j_m are the temperature and current density values for maximum of t.s.d. peak, and T_{\max} is a temperature maximum of Debye relaxation for τ_0 .

For our calculations we have assumed that $T_m = T_{\max}$. To compare the results obtained with those found in dielectric and mechanical loss measurements, we have taken two of the semi-empirical distribution functions derived for interpretation of dynamic measurements. These are, symmetrical Fuoss-Kirkwood distribution¹²:

$$f(u) = \frac{m \cos(m\pi/2) \times \cosh(mu)}{\cos^2(m\pi/2) + \sinh^2(mu)}$$

and the two parameter asymmetrical Havriliak-Negami¹⁴ function:

$$f(u) = \frac{1}{\pi} \sin(\beta\theta) \times \{1 + \exp[-2u(1-\alpha)] + 2 \exp[-u(1-\alpha)] \cos \pi(1-\alpha)\}^{-\beta/2}$$

where:

$$\theta = \tan^{-1} \left\{ \frac{\sin \pi(1-\alpha)}{\exp[(1-\alpha)u] + \cos \pi(1-\alpha)} \right\}$$

for both distributions $u = \ln(\tau_r/\tau_0)$ and m, α, β are parameters of these functions.

All the numerical calculations of these equations were performed on a digital computer.

DISCUSSION

Of all dipolar processes revealed by the t.s.d. spectra, the β process in PMMA, which could be separated clearly, has the broadest distribution of relaxation times, and is also the most symmetrical one. For this case we could apply the Fuoss-Kirkwood distribution function. Distributions calculated from the spectra fit the Fuoss-Kirkwood function very well as can be seen in Figure 5.

The distributions of relaxation times for α processes in all four polymers are less symmetrical, than for β processes, as would be expected from dielectric measurements⁶, and they do not fit the symmetrical Fuoss-Kirkwood function. For this case we tried to apply another distribution function, derived by Havriliak and Negami¹⁴, which is a generalization of the two known and well documented functions of

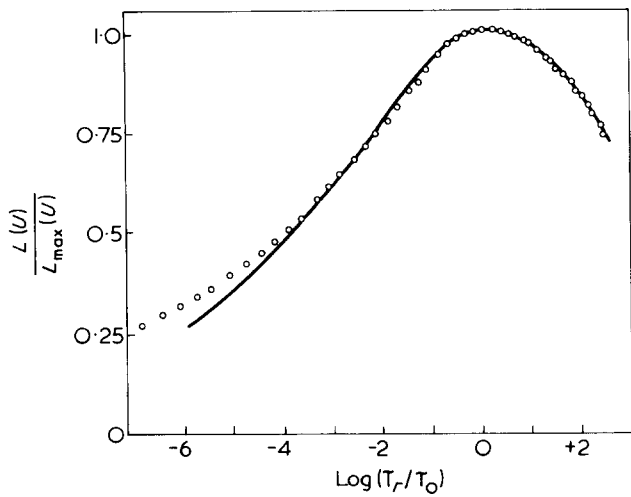


Figure 5 Distribution function for: β relaxation in PMMA, \circ ; Fuoss-Kirkwood fit, —

Cole^{15,16}. The fits of this function to the α relaxation time distributions of all four polymers are presented on Figure 6, and the distribution parameters are summarized in Table 1.

The values of the distribution parameters are generally in fairly good agreement with those obtained from dielectric measurements, but there are some discrepancies between the distribution parameters obtained by Havriliak and Negami, and those obtained in the present work.

In our case, however, the fit to the experimental data is very good. Thus, because of the temperature dependence of the distribution parameters observed by Havriliak and Negami, these differences can be explained by the fact that our measurements are non-isothermal and the equivalent temperature is different from the one used by these authors.

The t.s.d. spectra exhibit only peaks corresponding to α , and in the case of PMMA to β dipolar relaxation processes too. By the 'thermal cleaning' technique, the hidden β' processes in PMMA, and β process in other polymers can be

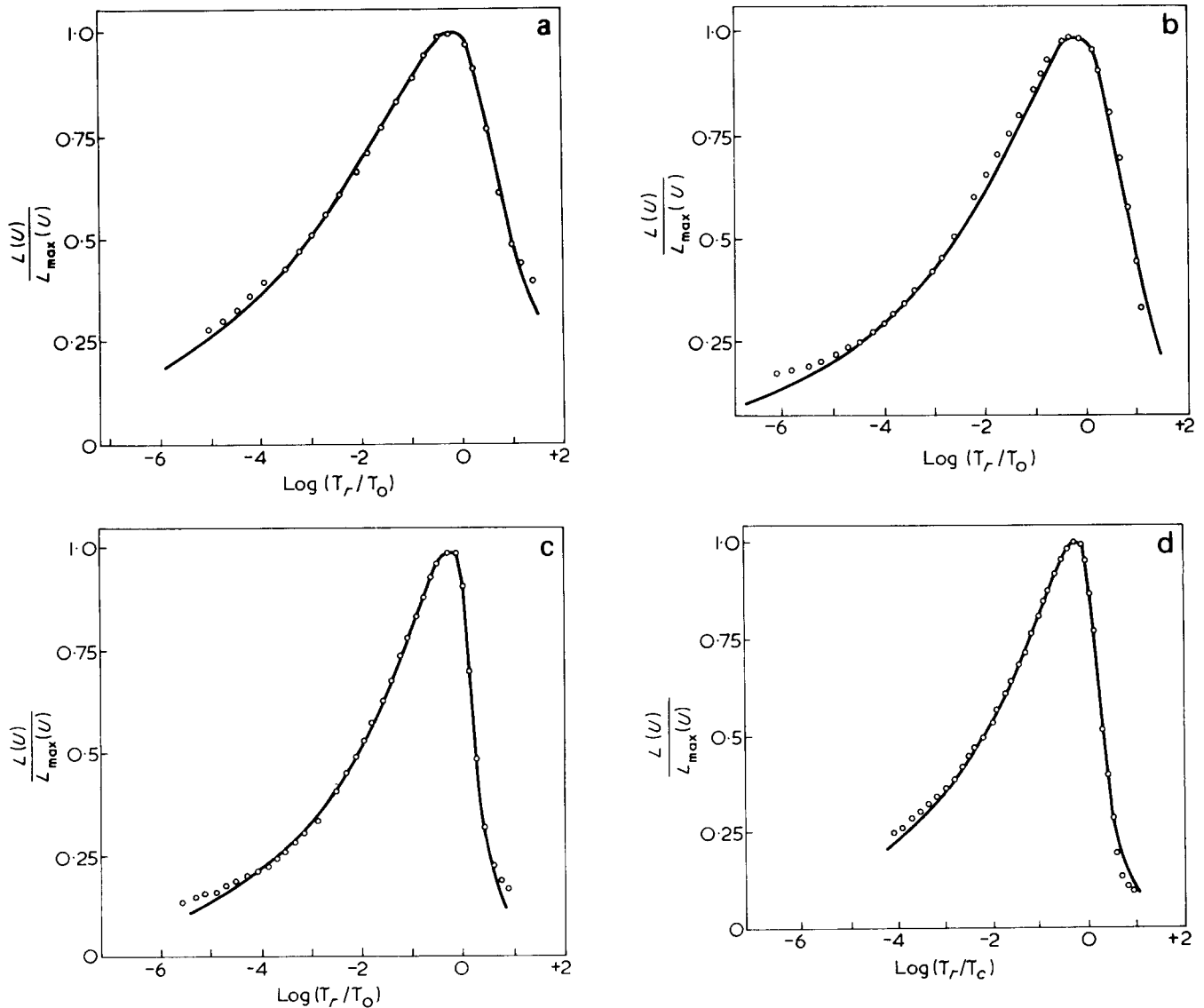


Figure 6 Distribution functions for α relaxation in four investigated polymers (\circ) and Havriliak-Negami fits (—). (a) PMMA, $\alpha = 0.50$, $\beta = 0.30$; (b) PEMA, $\alpha = 0.45$, $\beta = 0.32$; (c) PiBMA, $\alpha = 0.23$, $\beta = 0.26$; (d) PnBMA, $\alpha = 0.24$, $\beta = 0.24$

Table 1 Parameters α and β of the Havriliak–Negami distribution function obtained from the fit to distribution of relaxation times of α processes in investigated polymers

Polymer	Distribution parameters	
	α	β
PMMA	0.50	0.30
PEMA	0.45	0.32
PIBMA	0.23	0.26
PnBMA	0.24	0.24

Table 2 Apparent activation energies (mean values), calculated by means of BFG method for the investigated polymers

Polymer	Relaxation process (eV)			
	α	β'	β	γ
PMMA	1.05	0.42	0.11	0.026
PEMA	0.58	0.24	0.080	0.034
PIBMA	0.53	—	0.072	—
PnBMA	0.56	0.20	0.093	0.035

Table 3 Experimental (A_{BFG}), corrected (A), and literature (A_{lit}) values of activation energies for β relaxation process in PMMA

A_{lit}	A_{BFG}	Correction coefficient m (Fuoss–Kirkwood)	$A = \frac{A_{\text{BFG}}}{m}$
0.76	0.103	0.14	0.74
0.76	0.088	0.12	0.73

made evident. However, on an Arrhenius plot of $\ln [j/P_s(T)]$ vs. $1/T$, according to BFG, one can find more straight line segments, than the number of visible peaks on the spectrum, thus allowing us to calculate the following values of apparent activation energies (Table 2).

As it was expected, calculated values are much lower than the values obtained by conventional methods, and it is clear that the coefficient c must be introduced (equation 6). Literature values of activation energies for the β process in PMMA and those obtained in the present work are compared in Table 3.

One can see, that there is a very good agreement between the corrected values of activation energies calculated from the t.s.d. spectra and the literature values.

Although it is not possible in this way to check if in the case of other relaxation processes (e.g. α process), the activation energy is calculated correctly; considering the results obtained for the β process, one should expect the way in which broadening of the peaks affect the apparent activation energy, to be similar.

Assuming that all dipolar processes found in methacrylate polymers are distributed, we can ascribe the processes, whose activation energies are presented in Table 2, to α , β' , β and γ dipolar relaxations respectively.

CONCLUSIONS

The results obtained lead to the conclusion, that thermally stimulated depolarization, is a very suitable method for the analysis of relaxation processes in polar polymers. The Staverman–Schwarzl transform, although it is only an approximation, seems to be accurate enough for calculating the distributions of relaxation times.

Measuring the activation energy from the initial current rise, by means of the more accurate method of Bucci, Fieschi and Guidi, allows us to calculate the distribution parameter of a symmetrical distribution or the right value of activation energy, if the distribution is known.

If any relation between the asymmetrical distribution parameters α and β and the correction coefficient c is found, this method can be extended also to the cases, where only the asymmetrical distribution function can be applied.

ACKNOWLEDGEMENTS

This work was supported by the Polish Academy of Sciences under the project 03.1.2.

REFERENCES

- 1 Turnhout, J. V. *Polym. J.* 1971, **2**, 173
- 2 Turnhout, J. V. 'Thermally Stimulated Discharge of Polymer Electrets', Elsevier, Amsterdam, 1974
- 3 Creswell, R. A. and Perlman, M. M. *J. Appl. Phys.* 1970, **41**, 2365
- 4 J. Vanderschueren in 'Electrets, charge storage and transport in dielectrics', (ed. M. M. Perlman), Electrochemical Soc., New Jersey, 1974, p 155
- 5 Kryszewski, M., Kasica, H., Patora, J. and Piotrowski, J. *J. Polym. Sci. (C)* 1970, **30**, 243
- 6 McCrum, N. G., Read, B. E. and Williams, G. 'Anelastic and Dielectric Effects in Polymeric Solids', Wiley, London, 1967
- 7 Bucci, C., Fieschi, R. and Guidi, G. *Phys. Rev.* 1966, **148**, 816
- 8 Mikhaelov, G. P. and Borisova, T. I. *Vysokomol. Soedin.* 1960, **2**, 619
- 9 Witman, J. G. and Kovacs, A. J. *J. Polym. Sci. (C)* 1969, **16**, 4443
- 10 Bovey, F. A. and Tiers, G. V. *J. Polym. Sci.* 1960, **44**, 173
- 11 Cowell, T. A. T. and Woods, J. *Br. J. Appl. Phys.* 1967, 1045
- 12 Gross, B. 'Mathematical Structure of Theories of Viscoelasticity', Herman, Paris, 1953
- 13 Schwarzl, F. R. and Staverman, A. J. *J. Appl. Phys.* 1952, **23**, 838
- 14 Havriliak, S. and Negami, S. *Polymer* 1967, **8**, 161
- 15 Cole, K. S. and Cole, R. H. *J. Phys. Chem.* 1941, **9**, 341
- 16 Cole, R. H. *J. Phys. Chem.* 1955, **23**, 493

Radiochemical study of the radical copolymerization of styrene and methyl methacrylate

Giorgio Bontà, Bianca M. Gallo*, Saverio Russo and Claudio Uliana*

Centro Studi Chimico-Fisici di Macromolecole Sintetiche e Naturali del CNR, Via Pastore 3, 16132 Genova, Italy

(Received 15 September 1975)

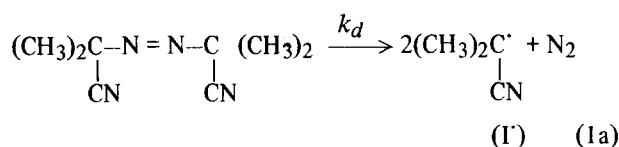
The rates of initiation for the copolymerization of styrene and methyl methacrylate at 50°, in different reaction media (bulk, acetone, dimethylformamide and dioxane) have been determined by using the isotopic labelling technique (¹⁴C - azobisisobutyronitrile). For all mixtures, except dioxane, the experimental data do not support the linear interpolation of the initiation rates, which is usually adopted in literature. In the whole range of monomer feed compositions, any modification of the reaction medium causes a relevant change of the initiation rate, so that the overall pattern is markedly modified. The strongest solvent effect is given by dioxane, which reduces the initiation rates for all monomer mixtures.

The radioactive tracer method also enables the determination of the modes of termination, which occur almost exclusively by combination for monomer feed compositions up to about 70 molar % of methyl methacrylate. The \bar{P}_w/\bar{P}_n ratios obtained by g.p.c. confirm the general trend of the termination mechanisms as a function of monomer mixture and reaction medium.

INTRODUCTION

In the past few years, we have undertaken a detailed study of the fundamental aspects of the radical copolymerization reaction¹⁻⁶, using, as a model, the pair styrene (S)-methyl methacrylate (MMA) polymerized in bulk^{3,4} and in solution^{5,6} [initiator, α , α' -azobisisobutyronitrile (AIBN)]. The aim of our study is to obtain a more precise knowledge of the kinetics and mechanisms which control the stages of initiation, propagation, and termination. Indeed, one of the less investigated features of radical copolymerization, which is still subject to a remarkable uncertainty, concerns the initiation reaction. On the other side, a deep knowledge of the kinetics of initiation is essential for any treatment of the overall copolymerization process. So far, it has usually been assumed⁷⁻¹², that the initiation rate R_i in catalyzed copolymerizations, is almost independent of the feed composition, although there is some evidence that for a few systems R_i is a function of the monomer mixture¹³⁻¹⁸.

As far as AIBN is concerned, the chemistry of its thermal, homolytic dissociation, is now well established¹⁹⁻²¹, whilst the role of the reaction medium on the decomposition rate, is still obscure. Earlier studies, showing insignificant variations of the decomposition rate constant in various solvents²²⁻²⁶, are conflicting with more recent reports²⁷⁻³³. The initiation stage in AIBN catalyzed thermal polymerizations can be depicted according to equations (1a) and (1b):



and the rate of initiation is given by equation (2):

$$R_i = 2fk_d[\text{I}] \quad (2)$$

where the initiator efficiency f , accounts for primary radical wastage, owing to the cage effect and, when present, to primary radical termination. Changes of monomers³⁴⁻³⁶, solvents³⁶⁻³⁸ and monomer concentrations³⁹, also in connection with actual changes in the viscosity of the medium⁴⁰⁻⁴³, cause significant variations of the initiation rate. Both k_d and f seem affected by the reaction medium. The physical interpretations of the kinetic deviations are based, among others, on cage effects⁴⁴, hot radical hypothesis⁴⁵ and complex formation²⁷⁻²⁹.

From the above considerations it follows that the modification of the reaction medium, owing to change of the solvent and/or to the variation of monomer feed composition, should affect the initiation rate of copolymerization in a considerable way. Influence of the reaction medium on the propagation stage⁵ and on the overall copolymerization rate⁶ for the system AIBN-S-MMA has already been found. A similar effect seems likely to be present also in the initiation step.

In order to clarify the kinetics of the initiation stage in radical copolymerization, we have carried out the present study using the radioactive tracer method, a technique which is widely utilized in the mechanistic studies of several polymerizations, but very seldom employed in copolymerization. Carbon-14 labelled azobisisobutyronitrile (AIBN-¹⁴C) was used as initiator and enabled determination of rates of initiation as well as modes of termination. Our copolymerization experiments were performed at 50°C either in bulk or in solution, and the solvents used were *p*-dioxane, acetone and *N,N'*-dimethylformamide (DMF).

* Istituto di Chimica Industriale, Università di Genova, 16132 Genova, Italy

Table 1 Values of $(fk_d) \times 10^6$ (sec⁻¹) at 50°C

		bulk	acetone	DMF	dioxane
S	a	1.44	1.42	1.31	0.97
	b	1.42	1.43	1.31	0.91
	c	1.46 1.46 ⁵⁴	1.45	1.31	0.93 1.00 ⁵⁵
MMA	a	1.01	1.03	1.48	0.94
	b	1.05	1.28	1.53	0.98
	c	1.11	0.97	1.42	0.93
		—	—	—	—

a Values calculated from equation (2)

b Values calculated from equation: $R_i = R_p^2 \delta_M^2 / [M]^2$, where δ_M represents the ratio $(2k_t/k_p^2)^{0.5}$, and the values for k_p , δ_M and $[M]$ are obtained from refs 4 and 6

c Values calculated from \bar{M}_n data⁵⁶ from equation: $R_i = R_p n m / \bar{M}_n$, where $n = 2$ for S and $n \sim 1.17$ for MMA (interpolated value)^{57,58}

EXPERIMENTAL

Materials

The purification of monomers, solvents and unlabelled initiator was carried out following previously described techniques^{4,5}. AIBN-¹⁴C was obtained through the courtesy of Professor S. Polowinski, Łódź, and possessed a specific activity of 0.476 mCi/g. A reverse isotope dilution analysis gave its radiochemical purity as $100 \pm 2\%$. The labelled product was suitably diluted with inactive AIBN and dissolved in acetone.

Polymerization procedure and polymer purification

All experiments were performed as described^{4,5}. In particular the ratios $[I]/[M]$ were kept sufficiently low to minimize any primary termination reaction or induced initiator decomposition. Solution polymerization was carried out using a monomer/solvent ratio equal to 1:2 (v/v). The polymerization temperature was $50^\circ \pm 0.05^\circ\text{C}$. Initiation due to photochemical reaction or to radiation from the isotope was carefully prevented. For all experiments the specific activity of the labelled initiator was equal to 2.06×10^{10} d/min mol. The polymers were precipitated twice using benzene or methyl ethyl ketone as solvents and methanol as precipitant⁵.

Characterization

Number average molecular weights, \bar{M}_n , were determined either by osmometry in toluene solution, using a Mechrolab mod. 501 high speed membrane osmometer operating at 30°C , or by g.p.c. in DMF solution at 80°C . The specific activities of initiator and polymers were assayed in toluene solution (20 ml) containing butyl PBD (0.5% w/v) as scintillator. Polymer concentration was in the range of 1–2%. A Packard Tri-Carb scintillation spectrometer type 3313 was employed. After subtraction of the background count, observed count rates were converted to dpm by the channels ratio method. Reproducibility was about $\pm 1.0\%$.

RESULTS AND DISCUSSION

Rates of initiation

The ratio between the specific activities of the labelled initiator, a_i , and the polymer, a_p , gives the kinetic chain

length ν , i.e. the number of monomer units per combined initiator fragment, given by equation (3):

$$\nu = a_i / 2ma_p \quad (3)$$

where the term 2 takes into account the fact that two primary radicals are produced from each molecule of initiator, and m is the molecular weight of the monomer. In copolymerization m is an average value, calculated on the basis of the molar composition of the copolymer⁹. Thus, rates of initiation can be unambiguously evaluated from the ratio between rate of polymerization and kinetic chain length:

$$R_i = (R_p/\nu) ([I]_0/[I]_{av}) \quad (4)$$

provided that initiator is not included in the polymer by other processes, such as chain transfer to initiator and primary radical termination, and proper corrections for any thermal initiation are considered. $[I]_{av}$ is the mean initiator concentration during the reaction period, and the ratio $[I]_0/[I]_{av}$ allows for the decrease in rate owing to initiator loss^{46,47}. At 50°C the thermal contribution to the copolymerization rate is sufficiently small to be disregarded in the whole range of monomer feed compositions^{4,6}. Also the primary radical termination reaction can be neglected in our experimental conditions, except for the system AIBN-S-acetone⁴⁸. On the other hand, literature data on the chain transfer constants to AIBN^{49–51}, can provide suitable corrections for the proper calculation of R_i .

As mentioned in previous papers^{4,6}, the overall rate of copolymerization, R_p , is strictly proportional to the square root of the initiator concentration and to the first power of total monomer concentration, except for the system styrene-acetone where a non-ideal kinetics has been found⁴⁸. Therefore the simplest kinetic scheme for radical polymerization⁵² and the derived relationships can be applied to our systems. In Figure 1, the initiation rates divided by the initial concentration of AIBN, are plotted as functions of monomer feed composition for the copolymerization experiments in (a) bulk; (b) acetone; (c) DMF and (d) dioxane; respectively.

From the patterns shown in Figure 1 it is evident that all reaction mixtures except dioxane, cause a complex variation of R_i , which does not follow the linear interpolation for monomer mixtures (broken lines) often suggested on literature^{4,16,53}. In fact, when bulk, acetone, and DMF are the reaction media, a more or less pronounced deviation from the broken lines is present. For dioxane, on the contrary, the differences between experimental points and the linear interpolation are very slight.

From the data of Figure 1 and using equation (2), it is possible to obtain the (fk_d) values, related to the homopolymerization of S and MMA in the various media, which are compared in Table 1 with literature data and other methods of evaluation.

The good agreement among the values of Table 1, obtained from the various equations, very strongly supports the reliability of the radiochemical method and its applicability to the copolymerization experiments. The data of Figure 1 and Table 1, show a remarkable influence of the reaction medium on the initiation rate in the polymerization of styrene and methyl methacrylate, as well as in their copolymerization. The $R_i/[I]_0$ values obtained in DMF solution are higher than those in the other media for the whole composition range, except for feeds very rich in styrene (95–100%), where the initiation rate in bulk gives the

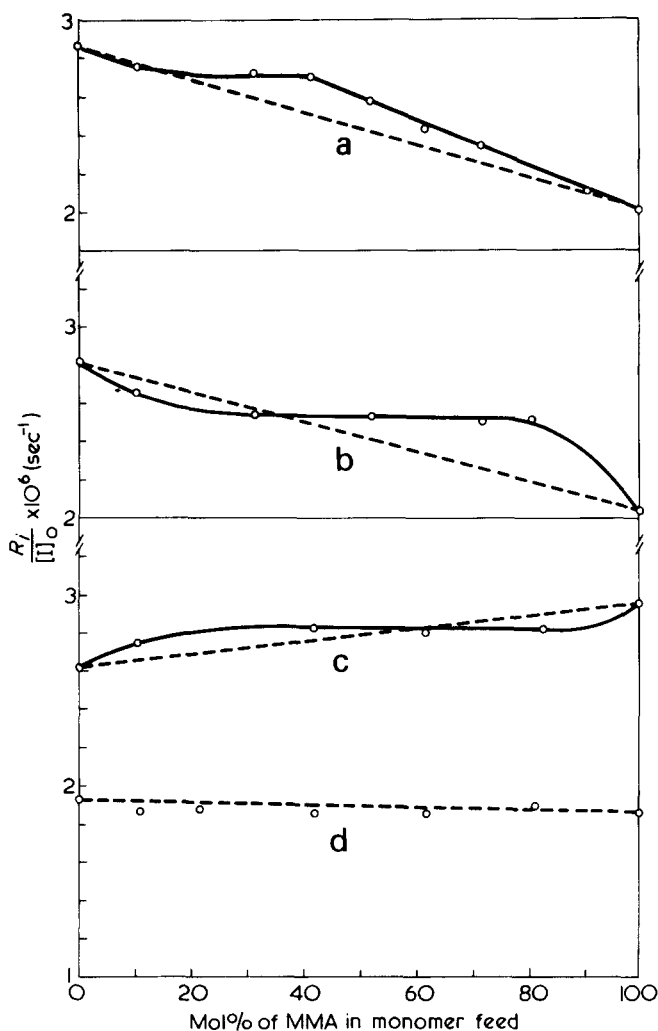


Figure 1 Initiation rate divided by the initial concentration of AIBN as a function of the monomer feed composition in the various media: (a) bulk (b) acetone (c) DMF; (d) dioxane.

highest values. The strongest solvent effect is exhibited by dioxane, which gives the lowest rate of initiation for all feed compositions. The behaviour of the initiation rates in bulk and in acetone is juxtaposed: for styrene rich feeds the $R_i/[I]_0$ values are higher in bulk than in acetone, whereas an opposite trend is present in MMA rich mixtures.

For all compositions, any change of the reaction medium causes a very strong variation of the initiation rate. No easy correlation with the medium fluidity has been found, and this fact suggests that diffusion phenomena are not the only factors involved in the initiation stage of the radical polymerization. As compared to bulk, all solvents depress the initiation rate of styrene polymerization, in the following order: bulk \sim acetone $>$ DMF \gg dioxane. The very strong effect of dioxane, already found in previous papers^{54,55}, is fully confirmed, as the agreement between experimental and literature data of Table 1 clearly shows. Recent results concerning solvent effects on the propagation rate constant⁶ show a somewhat similar behaviour:

$$k_{p \text{ bulk}} \sim k_{p \text{ dioxane}} > k_{p \text{ DMF}} > k_{p \text{ acetone}}$$

i.e. here again the k_p for styrene is higher in bulk than in solution, but now the order of the solvents is completely reversed.

As far as MMA is concerned, the initiation rates are in the following order: DMF \gg acetone \sim bulk $>$ dioxane.

This behaviour, if compared to the trend of the propagation rate constants⁶, show consistent differences; in fact, $k_{p \text{ bulk}}$ is always lower than $k_{p \text{ solution}}$ and in the following order:

$$k_{p \text{ DMF}} \sim k_{p \text{ dioxane}} > k_{p \text{ acetone}} > k_{p \text{ bulk}}$$

At present the exact nature of these differences cannot be fully understood. However, besides the different chemical reactivities of the various radicals, diffusion phenomena, which are present in the initiation stage and are irrelevant during propagation, can provide a further qualitative explanation of the aforesaid phenomenon. The complex dependence of f_{AIBN} on chemical and diffusion mechanisms has been recently pointed out by Mayer⁵⁹. Also k_d , as indicated previously, shows unequivocal correlations with medium viscosity; recent results of Yokota and Kondo³⁶ confirm a marked decrease of the decomposition rate by increasing the viscosity of the mixture.

However, besides the diffusion effects on k_d and f , other factors should be considered in order to explain the data of Figure 1 and Table 1; different monomer reactivity toward primary radicals, monomer and radical solvation, solvent complexation, etc.

Modes of termination

The average number of initiator fragments per polymer molecule, n , can be evaluated using equation (5):

$$n = \bar{P}_n/\nu = (2a_p\bar{M}_n)/a_i \quad (5)$$

and can be used to calculate the modes of termination, i.e. the extent of combination and disproportionation, by means of the simple relationship:

$$\lambda = (2 - n)/n \quad (6)$$

where λ is defined as the fraction of polymer radicals undergoing disproportionation. Limitations and errors associated with this method are well known^{47,51,60}. Limitations are connected with the relevance of transfer reactions to initiation, monomer, and solvent (besides other sources of initiation and primary radical termination, as already discussed), whereas errors arise from the polymer purification techniques and the accuracy in molecular weight determination.

In Figure 2 a plot of n as a function of the feed composition for the various reaction media is given. It is evident that also, at 50°C, termination occurs almost exclusively by combination in a very large range of monomer mixtures (from 0 to about 70% MMA), thus confirming previous findings at 60°C. It is also clear that the reaction medium does not play any relevant role on the termination mechanism.

These results, based on the radiochemical assay technique, are fully supported by our data of molecular weight distributions obtained by g.p.c.⁵⁶. As is well known, the ratio of \bar{P}_w to \bar{P}_n ranges from 1.5, if termination is solely by combination, to 2 for complete disproportionation of radicals. From the whole set of data it seems definitively confirmed, despite some recent arguments⁶¹, the general opinion that termination for styrene takes place solely by combination⁶². For MMA, the value of $\lambda \sim 0.71$, interpolated from the data of Bamford *et al.*^{57,58}, is still the most reliable among the many different values reported in literature.

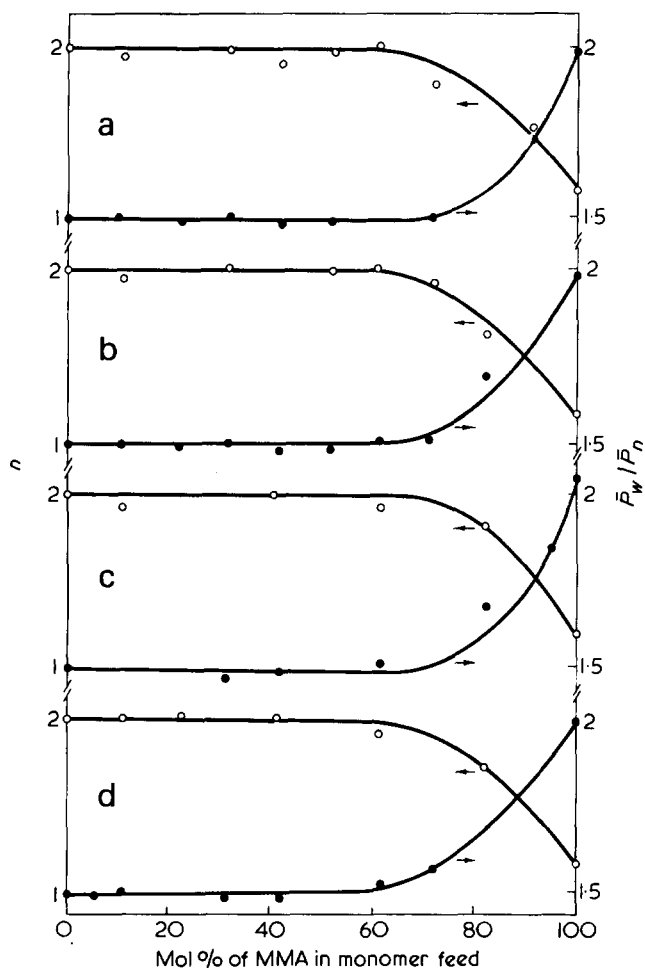


Figure 2 ○, n and ●, \bar{P}_w/\bar{P}_n values as functions of the monomer feed composition in the various media: (a); bulk, (b) acetone; (c) DMF; (d) dioxane.

ACKNOWLEDGEMENT

This work has been supported by the Italian CNR (project no. 22/73.00482.03)

REFERENCES

- 1 Russo, S. and Munari, S. *J. Macromol. Sci. (A)* 1968, **2**, 1321
- 2 Russo, S. and Munari, S. *Chim. Ind. (Milan)* 1969, **51**, 125
- 3 Russo, S., Gallo, B. M. and Bontà, G. *Chim. Ind. (Milan)* 1972, **54**, 521
- 4 Bontà, G., Gallo, B. M. and Russo, S. *J.C.S. Faraday Trans. I* 1973, **69**, 328
- 5 Bontà, G., Gallo, B. M. and Russo, S. *Polymer* 1975, **16**, 429
- 6 Bontà, G., Gallo, B. M. and Russo, S. *J.C.S. Faraday Trans. I* 1975, **71**, 1727
- 7 Walling, C. *J. Am. Chem. Soc.* 1949, **71**, 1930
- 8 Abkin, A. D., Medvedev, S. S., Khomikovskii, P. M. and Zabolotskaya, E. V. *Zh. Fiz. Khim.* 1953, **27**, 1516
- 9 Bevington, J. C., Melville, H. W. and Taylor, R. P. *J. Polym. Sci.* 1954, **14**, 463
- 10 Abkin, A. D. 'Voprosy khimicheskoi kinetiki, kataliza i reaktсионnoi sposobnosti', Izdatel'stvo Akademii Nauk SSSR, Moskva, 1955, p. 338
- 11 Tkachenko, G. V., Khomikovskii, P. M., Abkin, A. D. and Medvedev, S. S. *Zh. Fiz. Khim.* 1957, **31**, 242
- 12 Burnett, G. and Gersmann, H. *J. Polym. Sci.* 1958, **28**, 655
- 13 Melville, H. W. and Valentine, L. *Proc. R. Soc. (A)* 1950, **200**, 337, 358
- 14 Arlman, E. J. and Melville, H. W. *Proc. R. Soc. (A)* 1950, **203**, 301
- 15 Bonsall, E. P., Valentine, L. and Melville, H. W. *J. Polym. Sci.* 1951, **7**, 39

- 16 Bradbury, J. H. and Melville, H. W. *Proc. R. Soc. (A)* 1954, **222**, 456
- 17 Atherton, J. N. and North, A. M. *Trans. Faraday Soc.* 1962, **58**, 2049
- 18 Szaferko, J. and Turska, E. *Makromol. Chem.* 1972, **156**, 311
- 19 Hammond, G. S., Trapp, O. D., Keys, R. T. and Neff, D. L. *J. Am. Chem. Soc.* 1959, **81**, 4878
- 20 Hammond, G. S., Wu, C. H. S., Trapp, O. D., Warkentin, J. and Keys, R. T. *J. Am. Chem. Soc.* 1960, **82**, 5394
- 21 Ayrey, G., Evans, K. L. and Wong, D. J. D. *Eur. Polym. J.* 1973, **9**, 1347, and references quoted therein.
- 22 Lewis, F. M. and Matheson, M. S. *J. Am. Chem. Soc.* 1949, **71**, 747
- 23 Overberger, C. G., O'Shaughnessy, M. T., and Shalit, H. *J. Am. Chem. Soc.* 1949, **71**, 2661
- 24 Arnett, L. M. *J. Am. Chem. Soc.* 1952, **74**, 2027
- 25 Anderson, D. B., Burnett, G. M. and Gowan, A. C. *J. Polym. Sci. (A)* 1963, **1**, 1465
- 26 Burnett, G. M., Dailey, W. S. and Pearson, J. M. *Trans. Faraday Soc.* 1965, **61**, 1216
- 27 Leffler, J. E. and Hubbard, R. A. *J. Org. Chem.* 1954, **19**, 1089
- 28 Alder, M. G. and Leffler, J. E. *J. Am. Chem. Soc.* 1954, **76**, 1425
- 29 Cohen, M. D., Leffler, J. E. and Barbato, L. M. *J. Am. Chem. Soc.* 1954, **76**, 4169
- 30 Saad, I. A. and Eirich, F. R. *Polym. Prepr. Am. Chem. Soc.* 1960, **2**, 276
- 31 Petersen, R. C., Markgraf, J. H. and Ross, S. D. *J. Am. Chem. Soc.* 1961, **83**, 3819
- 32 Henrici-Olivé, G. and Olivé, S. *Makromol. Chem.* 1962, **58**, 188
- 33 Moroni, A. F. *Makromol. Chem.* 1967, **105**, 43
- 34 Arnett, L. M. and Peterson, J. H. *J. Am. Chem. Soc.* 1952, **74**, 2031
- 35 Chernobai, A. V. *Vysokomol. Soedin. (A)* 1968, **10**, 1716
- 36 Yokota, K. and Kondo, A. *Makromol. Chem.* 1973, **171**, 113
- 37 Walling, C. *J. Polym. Sci.* 1954, **14**, 214
- 38 Burnett, G. M., Cameron, G. G. and Zafar, M. M. *Eur. Polym. J.* 1970, **6**, 823
- 39 Bevington, J. C. *Trans. Faraday Soc.* 1955, **51**, 1392
- 40 Messerle, P. YE. and Gladyshev, G. P. *Vysokomol. Soedin.* 1966, **8**, 1818
- 41 Messerle, P. YE., Rafikov, S. R. and Gladyshev, G. P. *Dokl. Akad. Nauk. SSSR* 1966, **166**, 158
- 42 De Schrijver, F. and Smets, G. *J. Polym. Sci. (A 1)* 1966, **4**, 2201
- 43 Rafikov, S. R., Messerle, P. YE., Gladyshev, G. P. and Shaf-ranskaya, I. B. *J. Polym. Sci. (B)* 1967, **5**, 715
- 44 Matheson, M. S. *J. Chem. Phys.* 1945, **13**, 584
- 45 Tüdos, F. *Acta Chim. Acad. Sci. Hung.* 1965, **43**, 397
- 46 Bevington, J. C., Bradbury, J. H., and Burnett, G. M. *J. Polym. Sci.* 1954, **12**, 469
- 47 Ayrey, G., Levitt, F. G., and Mazza R. J. *Polymer* 1965, **6**, 157
- 48 Russo, S. *J. Macromol. Sci. (A)* in press
- 49 May, J. A. and Smith, W. B. *J. Phys. Chem.* 1968, **72**, 2993
- 50 Pryor, W. A. and Fiske, T. R. *Macromolecules* 1969, **2**, 62
- 51 Ayrey, G. and Haynes, A. C. *Makromol. Chem.* 1974, **175**, 1463
- 52 Flory, P. J. 'Principles of Polymer Chemistry', Cornell University Press, Ithaca, New York, 1953, Chap IV
- 53 Bonsall, E. P., Valentine, L. and Melville, H. W. *Trans. Faraday Soc.* 1952, **48**, 763
- 54 Ref. 45, p. 403f, and references quoted therein
- 55 Tüdos, F. *Acta Chim. Acad. Sci. Hung.* 1965, **44**, 403, and references quoted therein
- 56 Gallo, B. M., Palesi, B., Pedemonte, E. and Russo, S. to be published
- 57 Bamford, C. H., Eastmond, G. C. and Whittle, D. *Polymer* 1969, **10**, 771
- 58 Bamford, C. H., Dyson, R. W. and Eastmond, G. C. *Polymer* 1969, **10**, 885
- 59 Mayer, G. *Makromol. Chem.* 1974, **175**, 3495
- 60 Ayrey, G. and Moore, C. G. *J. Polym. Sci.* 1959, **36**, 41
- 61 Berger, K. C. and Meyerhoff, G. *Makromol. Chem.* 1975, **176**, 1983
- 62 Eastmond, G. C. 'Free Radical Polymerization' from 'Encyclopedia of Polymer Science and Technology', (Eds. H. F. Mark, N. G. Gaylord, and N. M. Bikales) Wiley, New York, 1967, vol. 7, p. 385 and references quoted therein

Studies on the formation of poly(ethylene terephthalate): 6. Catalytic activity of metal compounds in polycondensation of bis(2-hydroxyethyl) terephthalate

Kosuke Tomita

Research and Development Center, Unitika Ltd, 23 Kozakura, Uji, Kyoto 611, Japan

(Received 15 September 1975)

The rate parameters (p and d values) associated with the rate constants of propagation and thermal degradation reactions in the polycondensation process of bis(2-hydroxyethyl) terephthalate (BHET) in the presence of various metal compounds as catalysts at 283°C, calculated from the time dependence of the molecular weight of the formed polymer, were used to evaluate each metal compound in its catalytic activity. These logarithms of the p and d values were correlated by linear relationships (mountain-shaped) with the stability constants ($\log \beta_1$) of dibenzoyl methane (DBM) complexes of the corresponding metal species. Consequently, the stability constant of DBM complex of each metal species was found to be very useful in forecasting the catalytic activity of the metal compound. The compound of metal species with values of $\log \beta_1$ about 12 was most active as the catalyst on the propagation reaction and that of values about 11 was most active on the thermal degradation reaction.

INTRODUCTION

In the production of high molecular weight poly(ethylene terephthalate) (PET) by polycondensation of bis(2-hydroxyethyl) terephthalate (BHET), at a temperature of ~280°C under reduced pressure, the presence of a catalyst is essential.

A knowledge of the catalyst in the polycondensation of BHET is important for the polyester fibre industry, but at the present time little is known about the mode of catalytic activity, owing to difficulties in the kinetic treatment of the polycondensation.

The author¹ proposed a kinetic expression for the polycondensation process: p - d analysis, and in the present study, this method of analysis has been used to derive rules governing the catalytic activity of metal compounds in the BHET polycondensation process.

EXPERIMENTAL

Reagents

BHET was synthesized from dimethyl terephthalate (DMT) and ethylene glycol (EG), using a mole ratio (EG: DMT) of five, with sodium acetate (1×10^{-2} mol/mol DMT) as a catalyst at 200°C. Pure BHET (m.p. 109°C) was obtained by repeated recrystallization of the product from water.

All the catalysts were metal acetates. Commercial products (guaranteed reagent grade) were used without further purification. Antimony (III) acetate was synthesized according to the method of Nerdel and Kleinwächter², and aluminium acetate by the method of Pande and Mehrotra³.

Polycondensation

The reaction of 0.3 mol BHET and 3×10^{-5} mol metal acetate was carried out in an open system with stirring (120 rev/min) under reduced pressure (0.02–0.05 mmHg),

at a temperature maintained at 283°C using a dimethyl phthalate vapour bath. At suitable intervals reaction mixture was sampled.

Determination of molecular weight

The intrinsic viscosity $[\eta]$ was measured, using a phenol-tetrachloroethane (1:1 w/w) mixture as a solvent at 20°C. This was converted to molecular weight by means of the following relation⁴:

$$[\eta] = 7.55 \times 10^{-4} \bar{M}_n^{0.685}$$

EVALUATION OF CATALYTIC ACTIVITY

Zimmermann⁵ investigated polycondensation of BHET, and compared the activities of some catalysts from the value of the relative viscosity (η_{rel}) and the number of the carboxyl end group of the polymer formed after the definite reaction time. This is, however, too simple as a means of evaluation, and is insufficient to correlate catalytic activity with reaction mechanism.

Catalytic activity must be evaluated from a kinetic point of view and for the polycondensation process of BHET, the following rate equation, p - d analysis, was proposed in a previous paper¹:

$$n = \frac{1}{1 + pt} + dt \quad (1)$$

where n is a mole number (a reciprocal of degree of polymerization) of a polymer, p is a rate parameter for the propagation reaction and d is a rate parameter for the degradation reaction; p and d are associated with the rate constants of these two reactions, respectively. The author applied equation (1) to the polycondensation process of BHET with various metal acetates as catalysts, and calculated p and d

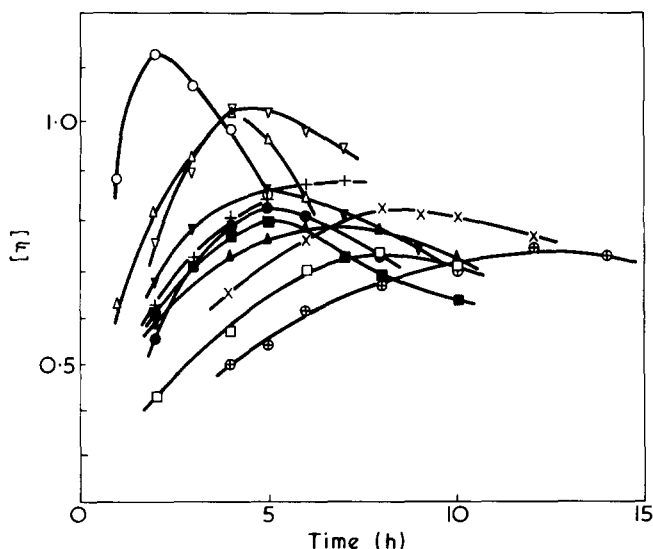


Figure 1 Polycondensation of BHET with various metal acetates as catalysts: ○, Ti; △, Sn; ▽, Sb; ■, Zn; +, Al; ●, Co; ▲, Pb; ▼, Ce; ×, Mn; □, Mg; ⊕ without catalyst

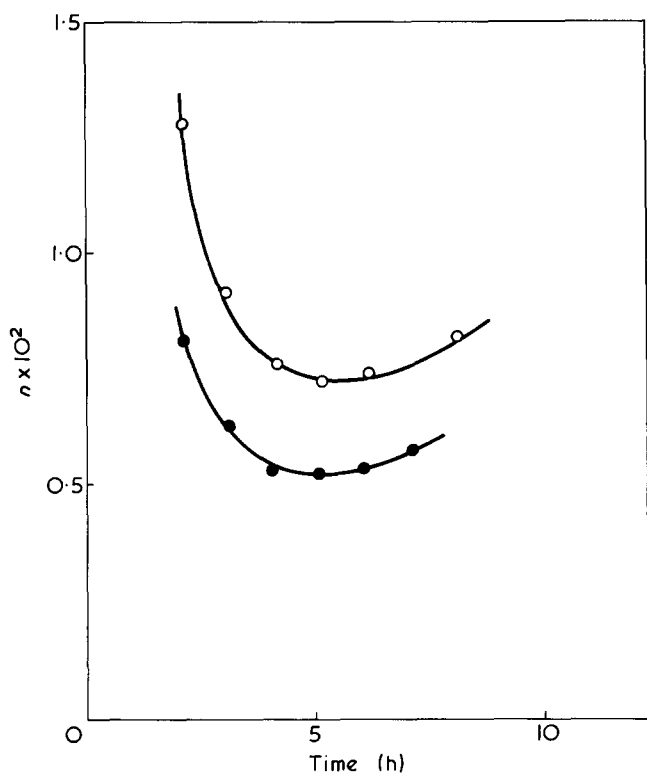


Figure 2 Application of $p-d$ analysis to data for cobalt acetate and antimony acetate in Figure 1: ○, Co; ●, Sb

values for each catalytic system. These values were regarded as kinetic parameters of the catalytic activity.

RESULTS AND DISCUSSION

Figure 1 shows that the time dependence of the molecular weight of the polymer formed with various metal acetate catalysts varies in a remarkable and complicated manner. As reported¹, the propagation reaction, (the polycondensation reaction), and the degradation reaction, (the pyrolysis reaction), occur simultaneously in the polycondensation process. By means of $p-d$ analysis the effect of metal species on both of the reactions can be clarified.

Application of $p-d$ analysis.

Some examples of the application of equation (1) to the experimental values in Figure 1 are shown in Figures 2-4. In these three Figures each point represents an experimental value and the full lines represent equation (1) after fitting the parameters p and d . From these Figures it is evident that equation (1) is in good agreement with the experimental results. The obtained p and d values are summarized in Table 1. The catalyst having a large p accelerates the propagation reaction, and that having a large d accelerates the degradation reaction. Accordingly, Table 1 shows the characteristics of each catalyst: e.g. titanium acetate markedly accelerates both reactions; antimony acetate considerably accelerates the propagation reaction and slightly accele-

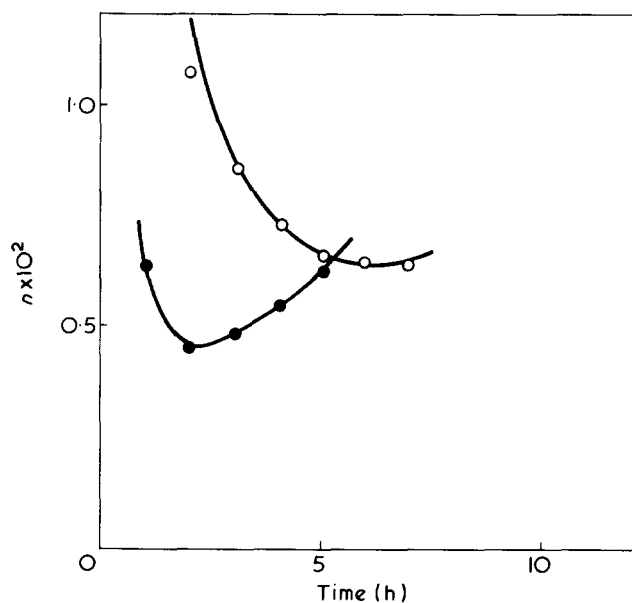


Figure 3 Application of $p-d$ analysis to data for aluminium acetate and titanium acetate in Figure 1: ○, Al; ●, Ti

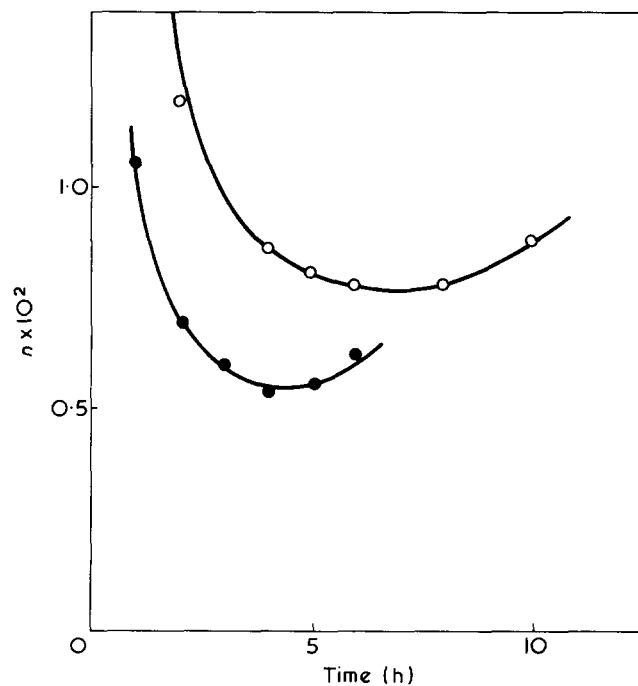


Figure 4 Application of $p-d$ analysis to data for plumbous acetate and stannous acetate in Figure 1: ○, Pb; ●, Sn

Table 1 Values of p and d in the polycondensation process of BHET with various metal acetates as catalysts

Metal species	p ($\text{mol}^{-1}\text{h}^{-1}$)	$d \times 10^4$ (h^{-1})
Mg	25	4.5
Mn	35	4.7
Pb	42	6.2
Co	51	7.0
Zn	55	8.3
Ce	65	7.8
Ti	210	11.2
Sn	89	6.6
Sb	76	5.5
Al	47	5.0
None	19	3.5

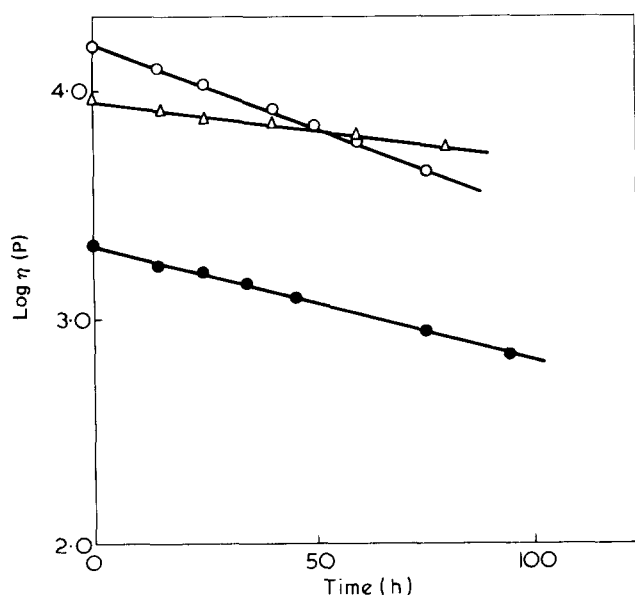


Figure 5 Time dependence of the melt viscosity of PET obtained with titanium acetate, antimony acetate or zinc acetate as a catalyst: \circ , Ti; \triangle , Sb; \bullet , Zn

rates the degradation reaction; zinc acetate forms a contrast to antimony acetate, etc.

Zimmermann⁵ by the means of evaluation mentioned above, concluded that titanium compound slightly accelerated the degradation reaction, in disagreement with the author's conclusion. In order to resolve this question, the melt viscosity of the polymer was investigated. According to Tuckett⁶, in a random degradation reaction a plot of $\log \eta$ (η is the melt viscosity) vs. time should be linear, and of slope related to the rate constant for the degradation reaction. For the purpose of comparison, the time dependence of the melt viscosity of the polymer obtained (with titanium acetate, zinc acetate or antimony acetate as a catalyst) was followed with a rheometer at 280°C (Figure 5). The results show that titanium acetate is a very active catalyst on the degradation reaction and lend support to the author's conclusion derived from the d value. This suggests that Zimmermann's means of evaluation of catalytic activity is incorrect.

Ordering of catalytic activity

The values of p and d in Table 1 make possible the evaluation of the catalytic activity of the metal compounds in the polycondensation process of BHET, and also a discussion of the ordering factor of catalytic activity.

The author⁷ found that the stability constant of dibenzoyl methane (DBM) complex of each metal species was an excellent ordering factor and was very useful in forecasting the catalytic activity of the metal compound in the transesterification of dimethyl terephthalate (DMT) with ethylene glycol (EG). This result was consistent with the proposed mechanism of catalytic action, especially with the reaction intermediate.

The ordering factor may be discussed from the same point of view. The propagation reaction proceeds by the nucleophilic attack of hydroxyl end groups upon ester carbonyl groups in 2-hydroxyethyl benzoate end groups. The reaction intermediate is regarded as a complex formed by coordination of the ester carbonyl group to the metal species. This coordination lowers the electron density of carbonyl carbon atom and facilitates the nucleophilic attack of the hydroxyl group upon this positively polarized carbon atom. This reaction scheme is essentially similar to that of the transesterification of DMT with EG⁷. On the other hand, in the degradation reaction, the reaction intermediate is also regarded as a complex formed by coordination of the ester, carbonyl group to the metal species. This coordination increases the positive character of the α methylene group adjacent to carboxylate group and facilitates 1,2-elimination reaction by E_i mechanism.

Consequently, the author considered adopting the degree of facility of coordination of ester carbonyl groups to metal species as the ordering factor of catalytic activity of metal compound⁷, and attempted to apply the stability constant of DBM complex to the ordering of catalytic activity of the metal compound in the polycondensation process of BHET. The stability constants of DBM complexes ($\log \beta_1$) were shown in ref 7 with respect to the metal species except for Ti. The value for Ti, 11.7, was calculated from the value of the rate constant in the transesterification of DMT with EG by titanium acetate as a catalyst (1×10^{-4} mol/mol DMT), since a linear relationship (mountain-shaped) exists between the logarithmic rate constants in the transesterification of DMT with EG by metal compounds as catalysts and $\log \beta_1$ of the corresponding metal species⁷. Such calculation is generally suitable for the determination of unknown σ value in Hammett relationship^{8*}, and is significant in view of the above hypothesis that the transesterification of DMT with EG and the polycondensation of BHET are similar in their reaction intermediates or in their mechanisms of catalytic action.

The p and d values after subtracting those for the reactions without catalyst are plotted as $\log p$ and $\log d$ against $\log \beta_1$ in Figures 6 and 7.

Consequently, it is concluded that the stability constant of DBM complex is the correct ordering factor of the catalytic activity of the metal compound in the polycondensation process of BHET, and this result supports the above view about the mechanism of catalytic action of the metal compound.

The straight lines in Figures 6 and 7 are mountain-shaped similarly to that in the transesterification of DMT with EG, and their peaks appear in $\log \beta_1$ about 12 for p , and 11 for d . These relationships suggest catalytic effect of so-called 'volcano-shaped activity order'¹⁰. The drop in catalytic activity is produced by the stronger or weaker bond between the catalyst and the reactant, and $\log \beta_1$ is

* The catalytic effect of the metal compound on the formative reaction of PET is the same as that due to an electron withdrawing substituent, and $\log \beta_1$ is regarded as corresponding to σ value in Hammett relationship⁹.

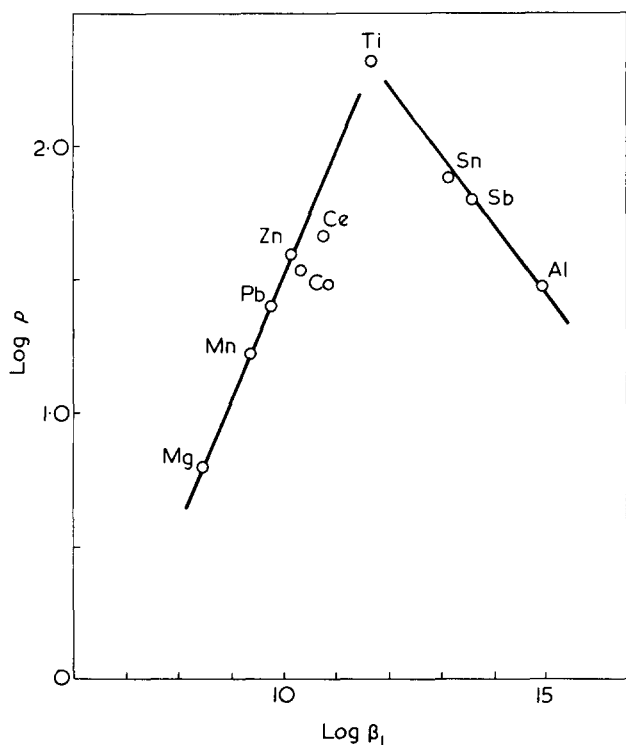


Figure 6 Values of p in the polycondensation process of BHET with various metal acetates as catalysts against $\log \beta_1$ of DBM complexes of the corresponding metal species

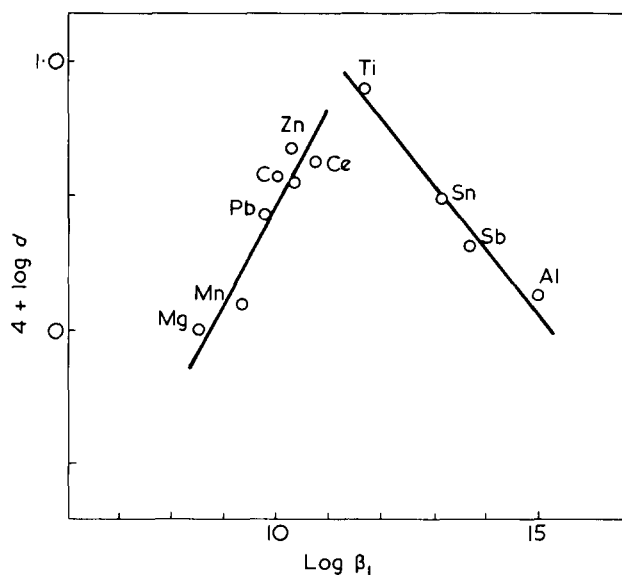


Figure 7 Values of d in the polycondensation process of BHET with various metal acetates as catalysts against $\log \beta_1$ of DBM complexes of the corresponding metal species

regarded as corresponding to the bond strength between metal species (catalyst) and benzoyl group (reactant). The optimum catalytic activity requires the optimum bond strength, that is, the optimum value of $\log \beta_1$.

The optimum values of $\log \beta_1$ for p and d differ from each other. Furthermore, as mentioned above, the transesterification of DMT with EG is a similar nucleophilic substitution reaction to the propagation reaction in the polycondensation process, but in the former the optimum value of $\log \beta_1$ was about 10 (see ref 7) and differs from that in the latter.

It is difficult to understand the cause for the above shifts in the optimum value of $\log \beta_1$ in detail, but this is most likely due to a difference in the bonding state of each reactant. For example, the comparison of BHET or its polycondensate to DMT in terms of their end groups suggests that the electron density of benzoate carbonyl group is lower in 2-hydroxyethyl benzoate group than in methyl benzoate group. This is as a result of the terminal hydroxyl group: electron withdrawing, and hydrogen bond effect. Accordingly, it may be concluded that the bond strength of methyl benzoate to the metal species is stronger, and that the optimum value of $\log \beta_1$ is lower in the transesterification of DMT with EG than in the propagation reaction of the polycondensation process of BHET.

ACKNOWLEDGEMENTS

The author wishes to thank Professors Seizo Okamura and Toshinobu Higashimura (Kyoto University) for their interest in this work and their helpful criticism of the manuscript, and Mr Hiroaki Ida (Unitika Ltd) for his powerful cooperation in this work.

REFERENCES

- 1 Tomita, K. *Polymer* 1973, **14**, 50
- 2 Nerdel, F. and Kleinwächter, J. *Chem. Ber.* 1957, **90**, 600
- 3 Pande, K. C. and Mehrotra, R. C. *Z. Anorg. Allg. Chem.* 1956, **286**, 291
- 4 Koepp, H. M. and Werner, H. *Makromol. Chem.* 1959, **32**, 79
- 5 Zimmermann, H. *Faserforsch. Textiltech.* 1962, **13**, 481
- 6 Tuckett, R. F. *Trans. Faraday Soc.* 1945, **41**, 351
- 7 Tomita, K. and Ida, H. *Polymer* 1975, **16**, 185
- 8 Leffler, J. E. and Grunwald, E. 'Rates and Equilibria of Organic Reactions', Wiley, New York, 1963, p 174
- 9 Tomita, K. *Nippon Kagaku Kaishi* 1975, 514
- 10 Balandin, A. A. *Adv. Cataly.* 1958, **10**, 120; 1969, **19**, 1

Polymerization of tetrafluoroethylene in acetic acid photoinitiated by metal carbonyls

C. H. Bamford and S. U. Mullik

Department of Inorganic, Physical and Industrial Chemistry, University of Liverpool, Liverpool, L69 3BX, UK

(Received 17 October 1975)

Tetrafluoroethylene may be polymerized in acetic acid at ambient temperatures and pressures close to atmospheric with photoinitiation by transition metal carbonyls, notably $\text{Mn}_2(\text{CO})_{10}$, $\text{Re}_2(\text{CO})_{10}$ and $\text{Os}_3(\text{CO})_{12}$. A kinetic study of the reaction photoinitiated ($\lambda = 435.8 \text{ nm}$) by $\text{Mn}_2(\text{CO})_{10}$ is presented. The rate of polymerization is proportional to the square root of the incident intensity and the order in tetrafluoroethylene concentration is ~ 1.4 , over the range $0.78\text{--}2.60 \text{ mol l}^{-1}$. The decay coefficient of $\text{Mn}_2(\text{CO})_{10}$ is linear in C_2F_4 over the range studied (up to 0.45 mol l^{-1}). These and other observations indicate that the dependence of the rate of initiation on $[\text{C}_2\text{F}_4]$ in acetic acid is much less 'sharp' than in other systems examined. Occlusion phenomena are not marked under the conditions used. Polymers prepared in this way show the infra-red absorption near 2000 cm^{-1} characteristic of $(\text{CO})_5\text{MnCF}_2\text{CF}_2$ —end-groups, confirming that the initiating radicals have the structure $(\text{CO})_5\text{MnCF}_2\dot{\text{C}}\text{F}_2$. In our experiments no evidence of chain-transfer to acetic acid could be found, a result which we attribute to the polar properties of the medium and the propagating radicals. The polymerization is powerfully retarded by benzene, which enters into addition and H-abstraction reactions with the fluorinated radicals; a simple kinetic treatment is presented. Photoinitiation by benzoyl peroxide is shown to be accompanied by retardation. Tetrafluoroethylene may also be copolymerized with the aid of the present technique and some results with ethylene and vinyl acetate are briefly described. It is noteworthy that in the copolymerization of C_2F_4 and C_2H_4 chain-transfer to acetic acid has been detected.

INTRODUCTION

Relatively little detailed information has been reported on the kinetics and mechanism of polymerization of tetrafluoroethylene. There are some obvious reasons for this: (1) the polymer is insoluble in common liquids, so that complications arising from occlusion phenomena would be expected during polymerization; (2) hydrogen-abstraction reactions between diluent and the highly reactive propagating radicals normally result in powerful retardation; (3) some conventional initiators cannot be used satisfactorily with tetrafluoroethylene and (4) the low boiling point of the monomer introduces practical difficulties in polymerization studies.

It has been reported¹ that the use of perfluorinated saturated media (e.g. perfluoro-methylcyclohexane) leads to relatively high reaction rates and polymer yields. Copolymerizations of C_2F_4 have also been carried out in these liquids². Initiation in such systems has been effected by azobisisobutyronitrile¹ or perfluorobutyryl peroxide². In some instances³, initiation by fluorinated peroxyacids prepared *in situ* by interaction of a fluorinated acid anhydride with hydrogen peroxide was used. Tabata and his colleagues⁴⁻⁷ have investigated the radiation-induced polymerization and copolymerizations of tetrafluoroethylene in fluorinated liquids such as $\text{CF}_2\text{ClCFCl}_2$, CF_2Cl_2 and CHF_2Cl .

The possibility of employing acetic and/or formic or sulphuric acids as reaction media together with redox initiation was reported by Bro and Schreyer⁸. With sulphuric and acetic acids, these workers used $\text{NaHSO}_3 + \text{KBrO}_3$ and $\text{TiCl}_3 + \text{NH}_2\text{OH}$, respectively, as initiators. Temperatures

in the range -40 to $+30^\circ\text{C}$ and pressures between 20 and 200 atmospheres were preferred.

Although polymerization in non-aqueous media is clearly feasible, the techniques commonly used are based on aqueous systems, generally with initiation by a peroxy disulphate and at super-atmospheric pressures⁹.

We have already reported¹⁰ the bulk polymerization of tetrafluoroethylene at -93°C photoinitiated by transition metal carbonyls, notably $\text{Mn}_2(\text{CO})_{10}$ and $\text{Re}_2(\text{CO})_{10}$. We have subsequently observed that polymerization can readily be carried out in acetic acid at ambient temperatures and pressures close to atmospheric with the same type of initiation. In the present paper we report a kinetic investigation of this polymerization with photoinitiation by manganese carbonyl. As far as we know, no other studies of the photoinitiated polymerization of tetrafluoroethylene in the liquid phase are described in the literature.

EXPERIMENTAL

Materials

Tetrafluoroethylene, methyl methacrylate, manganese carbonyl and rhenium carbonyl were purified as described in earlier publications¹⁰⁻¹². Molybdenum carbonyl and ruthenium carbonyl [$\text{Ru}_3(\text{CO})_{12}$] were sublimed in vacuum at room temperature and at 80°C , respectively. Tungsten carbonyl and osmium carbonyl [$\text{Os}_3(\text{CO})_{12}$] were used without purification. Acetic acid (AR), ethyl acetate (AR) and benzene (BDH Research Grade) were twice distilled in vacuum with retention of the middle fraction. Benzoyl peroxide was twice precipitated in methanol from chloroform and dried in vacuum at room temperature.

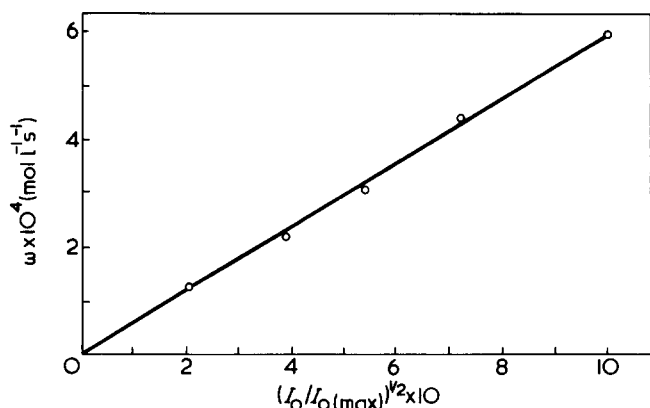


Figure 1 Photoinitiated polymerization of tetrafluoroethylene in acetic acid; dependence of rate on $I_0^{1/2}$. Initial concentrations (mol l^{-1}): C_2F_4 , 2.60; $Mn_2(CO)_{10}$, 1.03×10^{-3} . $\lambda = 435.8$ nm, $I_0(\max) = 3.58 \times 10^{-7}$ einstein $l^{-1}s^{-1}$, $25^\circ C$

Apparatus and techniques

All experiments were carried out in a laboratory illuminated by inactive (sodium) light. The optical system was virtually the same as that previously described¹⁰. The polymerization was studied gravimetrically at $25^\circ C$ in Pyrex reaction vessels (external and internal diameters 13 and 9 mm, respectively) of capacity 9.5 ml. Quantum inputs to the reaction mixture and rates of decay of manganese carbonyl under various conditions were measured as reported earlier¹¹.

Measurements of the solubilities of C_2F_4 and C_2H_4 in various solvents were made as described by Bamford and Mullik¹¹ to allow concentrations in the liquid phase to be calculated. Values of the absorption coefficient β defined by these authors were found to be at $25^\circ C$: tetrafluoroethylene-acetic acid, 2.23×10^{-2} mmHg $^{-1}$; tetrafluoroethylene-benzene, 2.49×10^{-2} mmHg $^{-1}$; tetrafluoroethylene-ethyl acetate, 1.31×10^{-2} mmHg $^{-1}$; ethylene-acetic acid, 8.60×10^{-2} mmHg $^{-1}$. A correction to allow for the increase in volume accompanying the solution of tetrafluoroethylene in acetic acid was made with the aid of density data for liquid C_2F_4 given by Sherratt¹³.

RESULTS AND DISCUSSION

Kinetics of polymerization

Manganese carbonyl has the same absorption spectrum in acetic acid, methyl methacrylate, ethyl acetate and benzene solutions, suggesting that no significant interactions occur with any of these solvents. Addition of C_2F_4 does not produce any change.

Figure 1 shows that at constant $[C_2F_4]$ (2.60 mol l^{-1}) the mean rate of polymerization ω is proportional to the square root of the incident intensity I_0 , as expected for an uncomplicated free radical polymerization obeying the relation:

$$\omega = k_p k_t^{-1/2} [M] \mathcal{I}^{1/2} \quad (1)$$

in which k_p , k_t are the rate coefficients of propagation and second-order termination, respectively, \mathcal{I} is the rate of initiation and M represents monomer. Thus, although the system becomes heterogeneous during polymerization, there do not seem to be any significant occlusion phenomena, which would increase the intensity exponent above 0.5¹⁴. The highly swollen condition of the polymer which is precipitated is probably responsible for this behaviour.

The order of the overall polymerization in monomer was determined for $[C_2F_4]$ in the range 0.78–2.60 mol l^{-1} . The data presented in Figure 2 are consistent with a value 1.4–1.5, which in the absence of occlusion effects implies a strong dependence of the rate of initiation on $[C_2F_4]$ over the range studied. In this respect the system is very different from the $Mn_2(CO)_{10} + C_2F_4$ system with methyl methacrylate as solvent, since in the latter the rate of initiation is only weakly dependent on $[C_2F_4]$ for $[C_2F_4] > 0.2$ mol l^{-1} , approximately¹¹. We shall return to this point later.

The rate of consumption of manganese carbonyl was measured spectrophotometrically as previously described¹¹ over a range of $[C_2F_4]$; in all cases good first-order rate coefficients k were obtained. They are plotted against $[C_2F_4]$ in Figure 3, which indicates that over the range studied ($[C_2F_4] < 0.45$ mol l^{-1}) k is linear in $[C_2F_4]$. This type of dependence is again very different from that encountered¹¹ in methyl methacrylate solution, for which k is shown as a function of $[C_2F_4]$ in Figure 3 (with k on a scale reduced by a factor 10). Clearly, for a given $[C_2F_4]$, k is much greater in methyl methacrylate solution and the approach to a plateau value found with this solvent is not apparent with acetic acid according to the data presented in Figure 3.

An order of 1.5 in $[C_2F_4]$ for the overall polymerization requires, according to equation (1), that $\mathcal{I} \propto [C_2F_4]$, or, since in all other systems studied $\mathcal{I} = k [Mn_2(CO)_{10}]$, that k should be directly proportional to $[C_2F_4]$. A long extrapolation of the straight line in Figure 3 to $[C_2F_4] = 2.60$ mol l^{-1} (the highest $[C_2F_4]$ in Figure 2) gives $k = 66.7 \times 10^{-4} s^{-1}$ (for $I_0 = 9.85 \times 10^{-6}$

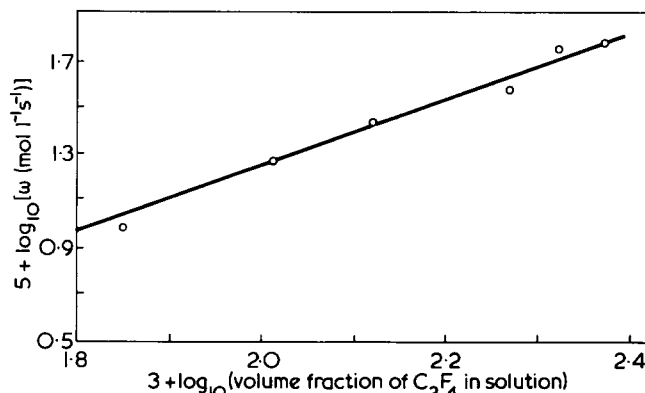


Figure 2 Photoinitiated polymerization of tetrafluoroethylene in acetic acid; order in $[C_2F_4]$. $[Mn_2(CO)_{10}] = 1.03 \times 10^{-3}$ mol l^{-1} initially. $\lambda = 435.8$ nm, $I_0 = 3.58 \times 10^{-7}$ einstein $l^{-1}s^{-1}$, $25^\circ C$

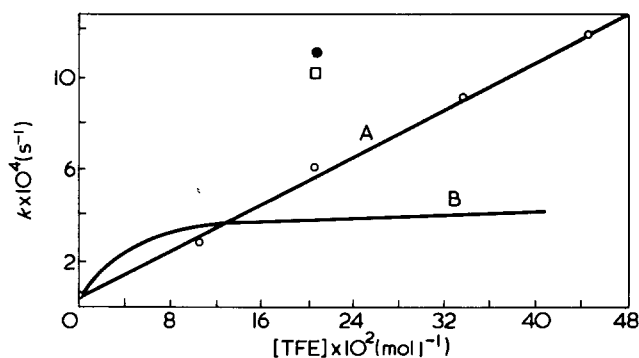


Figure 3 Dependence of decay coefficient of $Mn_2(CO)_{10}$ on $[C_2F_4]$. $[Mn_2(CO)_{10}] = 8.5 \times 10^{-4}$ mol l^{-1} , initially. $\lambda = 435.8$ nm, $I_0 = 9.85 \times 10^{-6}$ einstein $l^{-1}s^{-1}$, $25^\circ C$. A, acetic acid solution; B, methyl methacrylate solution¹¹ ($\times 10^{-1}$). Individual values: \bullet , benzene solution; \square , ethyl acetate solution

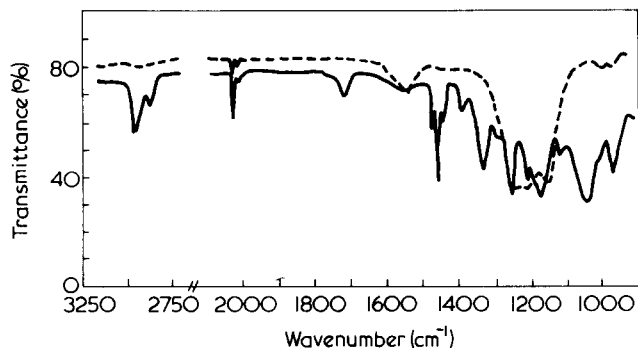


Figure 4 Infra-red absorption spectra of polymers prepared in acetic acid. ---, PTFE; —, copolymer $C_2F_4 + C_2H_4$ (no. 4, Table 3)

einstein $l^{-1}s^{-1}$). For the incident intensity in the experiments in Figure 2, $I_0 = 3.58 \times 10^{-7}$ einstein $l^{-1}s^{-1}$, this becomes $2.42 \times 10^{-4}s^{-1}$ (since k is normally proportional to I_0 for weak absorption¹¹). Thus the initial rate of consumption of $Mn_2(CO)_{10}$ for $I_0 = 3.58 \times 10^{-7}$ einstein $l^{-1}s^{-1}$, $[C_2F_4] = 2.60 \text{ mol } l^{-1}$ and $[Mn_2(CO)_{10}] = 1.03 \times 10^{-3} \text{ mol } l^{-1}$ should be, on this basis, $2.42 \times 10^{-4} \times 1.03 \times 10^{-3} = 2.50 \times 10^{-7} \text{ mol } l^{-1}s^{-1}$. However, the absorbed intensity in the experiments of Figure 2 is only 1.24×10^{-7} einstein $l^{-1}s^{-1}$. Hence this extrapolation would lead to a quantum yield of $[Mn_2(CO)_{10}]$ decay and initiation of polymerization close to 2. Although this would be possible in principle, a quantum yield of initiation exceeding unity has never been observed^{11,15,16}, so that we believe the linear extrapolation is inappropriate. We shall assume that in the experiments of Figure 2 the limiting value of k is reached at $[C_2F_4] = 2.60 \text{ mol } l^{-1}$ and is equal to $0.92 \times 10^{-4}s^{-1}$, corresponding to unit quantum yield of initiation. The highest $[C_2F_4]$ at which k can be measured directly with the equipment available is $0.45 \text{ mol } l^{-1}$ (Figure 3); here k adjusted for the conditions of Figure 2 is $3.2 \times 10^{-5}s^{-1}$. The behaviour of k in the range of $[C_2F_4]$ between 0.45 and $2.60 \text{ mol } l^{-1}$ is not known, but we may note that the dependence on $[C_2F_4]$ is given by a mean order (determined from the extremes) of 0.75. Since the rate of initiation would show the same order in $[C_2F_4]$, the polymerization reaction in the range we are considering should have a mean order of $1 + (0.75/2) = 1.38$. This is probably consistent with the data in Figure 2 within the limits of experimental error.

In interpreting the data in Figure 2 we have neglected the possibility of primary termination. This calls for comment, especially since rather low monomer concentrations were used in some of the experiments in Figure 2¹⁷. If primary termination were significant the true order in $[C_2F_4]$ would be lower than the value 1.4–1.5 deduced from Figure 2 and this would clearly have implications on the nature of the $\mathcal{J} - [C_2F_4]$ relation. In the experiments in Figure 2 the relatively low value of the incident intensity would minimize primary termination¹⁷. Further, conclusions about the unusual nature of the $\mathcal{J} - [C_2F_4]$ relation do not depend on Figure 2 alone since Figure 3 also indicates that this relation is markedly different from that in systems previously studied. Figure 1 shows that with $[C_2F_4] = 2.60 \text{ mol } l^{-1}$, the rate of polymerization is proportional to $I_0^{1/2}$, so that primary termination is not important under these conditions¹⁷. In our opinion, primary termination is not a significant process in these investigations.

These considerations illustrate the important role played by the solvent in photoinitiating reactions between $Mn_2(CO)_{10}$ and C_2F_4 . A few scattered data available for benzene and ethyl acetate solutions (Figure 3) also support this view.

From Figure 2 we see that with $[C_2F_4] = 2.60 \text{ mol } l^{-1}$ the rate of polymerization is $6.02 \times 10^{-4} \text{ mol } l^{-1}s^{-1}$ while \mathcal{J} , calculated on the basis of unit quantum yield as discussed above, is equal to $1.24 \times 10^{-7} \text{ mol } l^{-1}s^{-1}$. Inserting these values in equation (1) we find that at $25^\circ C$:

$$k_p k_t^{-1/2} = 0.66 \text{ mol}^{-1/2} l^{1/2} s^{-1/2}. \quad (2)$$

The mean kinetic chain length in the polymerization under these conditions is 4894, so that if transfer is negligible and termination occurs by combination the molecular weight of the polymer is 9.78×10^5 .

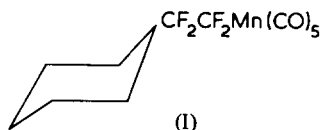
We now briefly consider the value of $k_p k_t^{-1/2}$ given in equation (2). This is greater than the corresponding value¹⁸ for methyl methacrylate (in bulk monomer) by a factor of 11, and for acrylonitrile¹⁹ in solution by a factor of 9, approximately. On the other hand, values of $k_p k_t^{-1/2}$ up to 0.69 and 0.72 $\text{mol}^{-1/2} l^{1/2} s^{-1/2}$ have been reported¹⁹ for methyl acrylate and ethyl acrylate, respectively. Thus the figure for C_2F_4 given in equation (2) does not appear unreasonable, especially when it is recalled that slight occlusion¹⁴ would reduce k_t and so increase $k_p k_t^{-1/2}$. Hisasue *et al.*⁷ have presented results from polymerization studies of C_2F_4 in chlorofluorocarbons from which a value of $k_p k_t^{-1/2} = 4.2 \text{ mol}^{-1/2} l^{1/2} s^{-1/2}$ at $0^\circ C$ may be deduced. This appears to be outside the range normally encountered in the free radical polymerization of olefinic monomers and may be unreliable owing to the intervention of unquantifiable occlusion phenomena (see below).

We believe that there is little chain-transfer in the polymerization of tetrafluoroethylene in acetic acid solution. No acetic acid residues could be detected in the polymers by infra-red spectroscopy. Such residues would lead to absorption near 1730 and 3000 cm^{-1} , but the spectrum of PTFE in Figure 4 shows no corresponding bands. On the other hand, when tetrafluoroethylene and ethylene are copolymerized in acetic acid solution the resulting copolymers show definite absorption at 1730 cm^{-1} (spectrum of a copolymer of $C_2F_4 + C_2H_4$ in Figure 4) suggesting the incorporation of acetic acid residues by chain-transfer involving radicals with terminal ethylene units. Further, in our experience, chain-transfer in the polymerization of C_2F_4 always appears to be accompanied by extensive retardation and very low polymer yields. These views are in agreement with the work of Bro and Schreyer⁸, who concluded that polytetrafluoroethylene of high molecular weight may be prepared in acetic acid.

The data presented above gain in significance when it is recalled²⁰ that hydrogen abstraction from hydrocarbons by perfluoroalkyl radicals is often faster than the corresponding reaction of alkyl radicals by a factor of $10^2 - 10^3$. It would seem that the relatively low reactivity of propagating polytetrafluoroethylene radicals towards acetic acid must be attributed in the main to the operation of polar factors²¹. Thus the presence of the strongly electronegative carboxyl in the molecule would discourage hydrogen abstraction from the CH_3 group by the propagating radicals which themselves bear a positive charge on the carbon atoms carrying the unpaired spins^{21,22}. In this connection it is interesting to contrast the behaviour of acetic acid with that of cyclohexane. Polymerization of C_2F_4 in the latter

Table 1 Retardation by benzene. $[C_2F_4] = 2.60 \text{ mol l}^{-1}$; $[Mn_2(CO)_{10}] = 1.03 \times 10^{-3} \text{ mol l}^{-1}$; $I_{abs} = 1.24 \times 10^{-7} \text{ einstein l}^{-1}\text{s}^{-1}$; $\lambda = 435.8 \text{ nm}$

$[benzene] \times 10^4$ (mol l ⁻¹)	$\omega \times 10^4$ (mol l ⁻¹ s ⁻¹)
0.00	6.12
0.14	4.82
1.36	4.12
2.27	3.18
4.55	2.66
6.83	2.08
11.40	0.88
22.80	0.53
100.00	0.18
500.00	0.032



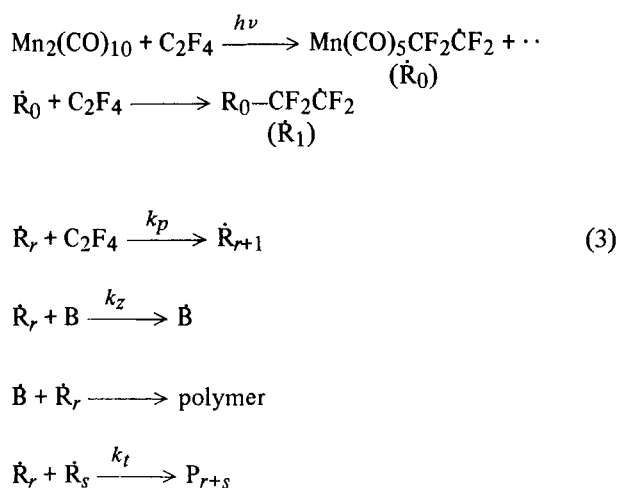
is virtually impossible on account of extensive chain-transfer and retardation. As will be reported subsequently²³, the compounds $(CO)_5MnCF_2CF_2H$ and (I) are major reaction products and clearly have their origin in hydrogen abstraction from cyclohexane by the primary radicals $(CO)_5MnCF_2\dot{C}F_2$.

Retardation by benzene

A remarkable feature of the polymerization of tetrafluoroethylene in acetic acid is its sensitivity to the presence of benzene, which acts as a powerful retarder. Observations are presented in Table 1.

It appears that a concentration of benzene as low as $2.5 \times 10^{-4} \text{ mol l}^{-1}$ reduces the rate of polymerization by a factor of 2, approximately. At concentrations of benzene higher than those given in Table 1 no polymer is formed. On removing the volatiles after reaction at high benzene concentration a viscous liquid product remains. The n.m.r. spectrum is consistent with the presence of several components originating from interactions between benzene and $(CO)_5MnCF_2\dot{C}F_2$ radicals involving both addition and H-abstraction²³. Since the radical products of these reactions are not sufficiently active to reinitiate polymerization strong retardation ensues. Evidently the reactions of the primary and propagating radicals, not only with cyclohexane but also with benzene, are strongly reminiscent of the behaviour of perfluoroalkyl radicals^{20,24,25}.

A simple kinetic scheme consistent with the data on retardation of benzene is given below.



The structure $(CO)_5MnCF_2\dot{C}F_2$ is assigned to the primary radicals (R_0) on the basis of earlier work^{10-12,15}. These radicals appear as terminal groups in the polymer and show characteristic infrared absorption near 2000 cm^{-1} as is evident from Figure 4. Details of the initiation process are not included since they are not necessary for present purposes. In relation (3) B, B represent benzene and a radical derived from benzene either by addition of a fluorocarbon radical or by hydrogen abstraction, respectively. It is assumed that the different types of B radical have similar reactivities.

Relation (4) is readily deduced from relation (3) by application of the steady-state hypothesis:

$$\frac{1}{\omega^2} = \frac{2k_z}{k_p[C_2F_4]\mathcal{J}} \frac{[B]}{\omega} + \frac{k_t}{k_p^2[C_2F_4]^2\mathcal{J}} \tag{4}$$

Figure 5 is a plot of $10^{-7}/\omega^2$ against $[B]/\omega$ and shows that relation (4) conforms to the experimental results fairly satisfactorily. From the slope of the straight line in Figure 5 we find that

$$\frac{2k_z}{k_p[C_2F_4]} = 9.09 \times 10^6 \text{ mol}^{-2}\text{l}^2\text{s}$$

Inserting the values $[C_2F_4] = 2.60 \text{ mol l}^{-1}$ and $\mathcal{J} = 1.24 \times 10^{-7} \text{ mol l}^{-1}\text{s}^{-1}$ we estimate that at 25°C :

$$\frac{k_z}{k_p} = 1.46 \tag{5}$$

Equation (5) illustrates quantitatively the high reactivity of benzene towards the propagating radicals.

It is to be expected that other aromatic compounds would behave as retarders in a similar way. This has been found to be so with benzoyl peroxide (Bz_2O_2) when employed as photoinitiator. Results are presented in Figure 6. Although a linear relation between ω and $[Bz_2O_2]^{1/2}$ is

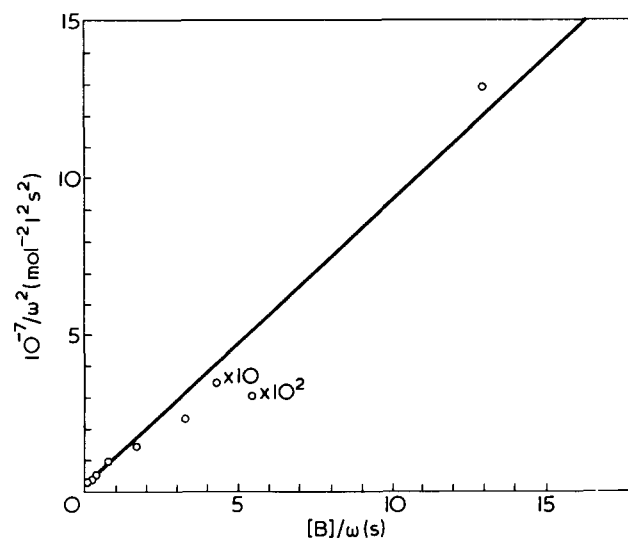


Figure 5 Retardation of photoinitiated polymerization of C_2F_4 in acetic acid by benzene (B). Plot of results in Table 1 according to equation (4). Initial concentrations (mol l⁻¹): C_2F_4 , 2.60; $Mn_2(CO)_{10}$, 1.03×10^{-3} . $\lambda = 435.8 \text{ nm}$. $I_{abs} = 1.24 \times 10^{-7} \text{ einstein l}^{-1}\text{s}^{-1}$, 25°C

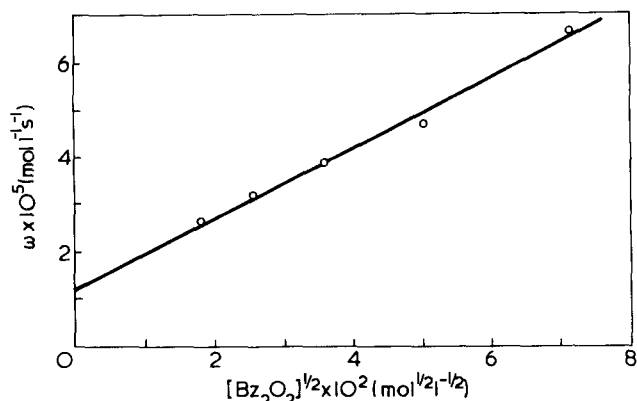


Figure 6 Polymerization of tetrafluoroethylene in acetic acid with benzoyl peroxide as photoinitiator. $[\text{C}_2\text{F}_4] = 2.60 \text{ mol l}^{-1}$ initially. Full light of mercury arc¹⁰, 25°C

Table 2 Photoinitiated polymerization of tetrafluoroethylene in acetic acid at 25°C. $\lambda = 365 \text{ nm}$; $I_0 = 2.01 \times 10^{-6} \text{ einstein l}^{-1}\text{s}^{-1}$; $[\text{C}_2\text{F}_4] = 2.06 \text{ mol l}^{-1}$

Carbonyl	Concentration $\times 10^3$ (mol l ⁻¹)	[CCl ₄] (mol l ⁻¹)	Time of irradiation (min)	$\omega \times 10^5$ (mol l ⁻¹ s ⁻¹)
Mo(CO) ₆	1.51	0	30	0.26
Mo(CO) ₆	1.51	0.01	30	1.64
Mo(CO) ₆	1.51	0.1	30	14.2
W(CO) ₆	2.83	0	30	0.13
W(CO) ₆	2.83	0.1	30	9.9
Re ₂ (CO) ₁₀	0.51	0	15	144.5
Os ₃ (CO) ₁₂	1.11	0	10	98.5
Ru ₃ (CO) ₁₂	0.63	0	30	1.25
Ru ₃ (CO) ₁₂	0.63	0.1	30	10.0

Table 3 Copolymerization in acetic acid at 25°C. Acetic acid, 1 ml; $[\text{Mn}_2(\text{CO})_{10}] = 1.03 \times 10^{-3} \text{ mol l}^{-1}$; $I_0 = 4.24 \times 10^{-7} \text{ einstein l}^{-1}\text{s}^{-1}$; $\lambda = 435.8 \text{ nm}$; time of irradiation 60 min

No.	Total weights of initial monomers (g)			Weight of polymer (g)
	C ₂ F ₄	C ₂ H ₄	VA	
1	0.44	0.062	—	0.113
2	0.44	0.124	—	0.136
3	0.33	0.093	—	0.056
4	0.22	0.124	—	0.046
5	0.88	—	0.24	0.315
6	0.44	—	0.28	0.294

obtained, the line does not pass through the origin. An increasing extent of retardation as $[\text{Bz}_2\text{O}_2]$ increases would explain this observation.

Earlier work on solution polymerization

We now discuss briefly the work of Tabata and colleagues⁴⁻⁷ to which reference has already been made. For the bulk polymerization Tabata *et al.*⁴ mention a 'remarkable post polymerization. . . even in the liquid phase' and comment that this is 'a rare case'. They also remark that 'there are large differences in activation energy between in-source

and postpolymerizations, as in the case of solid-state polymerization. Propagation may be accelerated through vibrational excitation by sub-excitation electrons during irradiation'. They state⁶ that in polymerization in solution in monochlorodifluoromethane 'propagation reactions are extremely different in in-source and postpolymerizations'. It is our opinion that the results obtained by Tabata and co-workers illustrate the operation of occlusion phenomena¹⁴, and can be completely interpreted in terms of such phenomena. Thus, postpolymerization in a system in which the polymeric product is insoluble is to be expected, and is certainly not 'a rare case'. The 'differences' between the propagation reactions in-source and out-of-source may also be readily accounted for by occlusion and we do not believe that the observations reflect any mechanistic change in the propagation processes. In a later paper⁷ Tabata *et al.* note that the 'remarkable after-effect' is due to occlusion. However, it is clear that in these papers, the essential point that, in polymerizations in which occlusion is important, the rate coefficients are not constant¹⁴, has not been appreciated, so that quantitative conclusions are suspect.

Photoinitiation by other transition metal carbonyls

An examination of the efficiencies of a number of transition metal carbonyls as photoinitiators for the polymerization of tetrafluoroethylene in acetic acid led to the results presented in Table 2.

The group VI carbonyls are relatively ineffective; their efficiency is greater in the presence of CCl₄, under which conditions CCl₃ is the initiating species²⁶. In group VII both Re₂(CO)₁₀ and Mn₂(CO)₁₀ are very active and, of the group VIII carbonyls, Os₃(CO)₁₂ is much more effective than Ru₃(CO)₁₂. The efficiency of the latter increases markedly in the presence of CCl₄.

Copolymerization of tetrafluoroethylene in acetic acid

A few experiments were carried out to examine the possibility of photoinitiated copolymerization of tetrafluoroethylene with ethylene and vinyl acetate (VA) in acetic acid. Results are presented in Table 3.

All the polymers were shown by infra-red spectroscopy to contain units of both monomers. The infra-red spectrum of copolymer no. 4 (Table 3) is shown in Figure 4.

These experiments show that the technique described is convenient for preparing copolymers of tetrafluoroethylene.

REFERENCES

- Bro, M. I. Ger. Pat. 1 044 410 (1958)
- Bro, M. I. US Pat. 2 943 080 (1960)
- Bro, M. I., Convery, R. J. and Schreyer, R. C. Br. Pat. 840 080 (1960)
- Tabata, Y., Ito, W. and Oshima, K. *J. Macromol. Sci. (A)* 1970, 4, 789
- Tabata, Y., Ishigure, K., Higaki, H. and Oshima, K. *J. Macromol. Sci. (A)* 1970, 4, 801
- Tabata, Y., Ito, W., Oshima, K. and Tagaki, J. *J. Macromol. Sci. (A)* 1970, 4, 815
- Hisasue, M., Ukihashi, H. and Tabata, Y. *J. Macromol. Sci. (A)* 1973, 7, 795
- Bro, M. I. and Schreyer, R. C. US Pat. 3 032 543 (1959)
- McCane, D. I. in 'Encyclopaedia of Polymer Science and Technology', (Ed. H. F. Mark and N. G. Gaylord), Interscience, New York, 1970, Vol 13, p 623
- Bamford, C. H. and Mullik, S. U. *Polymer* 1973, 14, 38

Polymerization of tetrafluoroethylene: C. H. Bamford and S. U. Mullik

- 11 Bamford, C. H. and Mullik, S. U. *JCS Faraday Trans. I* 1973, **69**, 1127
- 12 Bamford, C. H. and Mullik, S. U. *JCS Faraday Trans. I* 1975, **71**, 625
- 13 Sherrat, S. in 'Encyclopaedia of Chemical Technology', (Ed. A. Standen), Interscience, New York, 1966, Vol 9, p 805
- 14 Bamford, C. H., Barb, W. G., Jenkins, A. D. and Onyon, P. F. 'The Kinetics of Vinyl Polymerization by Radical Mechanisms', Butterworths, London, 1958
- 15 Aliwi, S. M., Bamford, C. H. and Mullik, S. U. *J. Polym. Sci. (C)* 1975, **50**, 33
- 16 Bamford, C. H. and Mullik, S. U. *JCS Faraday Trans. I*, 1976, **72**, 368
- 17 Bamford, C. H., Jenkins, A. D. and Johnston, R. *Trans. Faraday Soc.* 1959, **55**, 1451
- 18 Bamford, C. H., Crowe, P. A., Hobbs, J. and Wayne, R. P. *Proc. Roy. Soc. (A)* 1966, **292**, 153
- 19 Bamford, C. H., Dyson, R. W. and Eastmond, G. C. *Polymer* 1969, **10**, 885
- 20 Whytock, D. A., Clarke, J. D. and Gray, P. *JCS Faraday Trans. I* 1972, **68**, 689
- 21 Bamford, C. H., Jenkins, A. D. and Johnston, R. *Trans. Faraday Soc.* 1959, **55**, 418
- 22 Bamford, C. H. and Jenkins, A. D. *Trans. Faraday Soc.* 1963, **59**, 530
- 23 Bamford, C. H. and Mullik, S. U. in press
- 24 Charles, S. W. and Whittle, E. *Trans. Faraday Soc.* 1960, **56**, 794
- 25 Whytock, D. A., Clarke, J. D. and Gray, P. *JCS Faraday Trans. I*, 1974, **70**, 411
- 26 Bamford, C. H. in 'Reactivity, Mechanism and Structure in Polymer Chemistry', (Ed. A. D. Jenkins, and A. Ledwith), Wiley, New York, 1974, Ch. 3

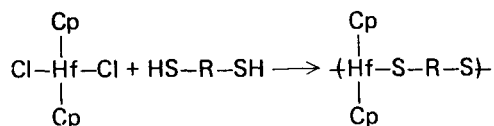
Synthesis and thermal characterization of hafnium polythioethers

Charles E. Carraher, Jr.

University of South Dakota, Department of Chemistry, Vermillion, South Dakota, 57069, USA

(Received 15 September 1975)

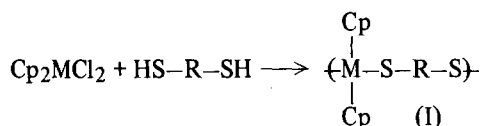
Hafnium polythioethers were synthesized utilizing both the aqueous solution and interfacial condensation techniques. Synthesis is general and fairly rapid being complete within 1 min.



Several products exhibit reasonably good weight retention (70% at 1000°C) but all show poor low temperature stabilities with degradation beginning about 100°C. Initial degradation to ~250°C is via an internal non-oxidative pathway where as degradation at higher temperatures occurs via an oxidative mode in air.

INTRODUCTION

We have been involved in the synthesis and characterization of metal containing polymers generally via the condensation of organometallic halides with Lewis bases^{1,2}. Recently we reported the synthesis of titanium polythioethers of form I where $M = \text{Ti}^{3-4}$. Here we report the initial synthesis of the corresponding hafnium polythioethers where $M = \text{Hf}$ and on preliminary thermal characterization of the products.



The synthetic routes chosen are the interfacial and aqueous solution techniques (i.e. low temperature condensation procedures) since the hafnium containing moiety, Cp_2HfCl_2 , is soluble in both a number of organic solvents and water and since many organometallic reactants and products are unstable at even moderately high temperatures resulting in many undesirable reactions occurring.

Synthesis of group IVB $M-S$ bonds is known and briefly reviewed in ref 3.

EXPERIMENTAL

Dicyclopentadienylnhafnium dichloride was obtained from Strem Chemicals, Inc., Danvers, Mass.; dimercaptopropionate (ethylene-bis-3-mercaptoacetate) from Evans Chemetics, Inc., Darlen, Conn.; all other dithiols were obtained from Aldrich Chemical Co., Milwaukee, Wis. and used without further purification.

Polymerization apparatus⁵ and procedures^{3,4} are analogous to those reported in detail elsewhere. Briefly, polymerizations were conducted utilizing a 1 qt (1.137 dm³) Kimex emulsifying jar set on a Waring Blendor. The phase containing the dithiol and added base were added through a hole in the jar lid using a large mouthed funnel to rapidly

stirred solutions containing Cp_2HfCl_2 in solution. Polymer precipitated rapidly as a white powdery solid.

Infra-red spectra were obtained using KBr pellets with Beckman IR-10 and Perkin-Elmer 273-B spectrophotometers. Bands characteristic of a repeating unit of form I are found. For instance all the spectra exhibit bands in the region of 1440, 1015 and 815 cm^{-1} , characteristic of the Cp group. Bands about 3000 to 2800 cm^{-1} characteristic of aliphatic C-H stretching are present derived, from the dithiol containing moiety. Spectra of dimercaptopropionate and dimercaptoacetate exhibit bands in the 1750–1735 cm^{-1} region, characteristic of the carbonyl stretching vibration. Spectra of the pure dithiols show bands about 2600–2500 cm^{-1} characteristic of the S-H stretch and about 720–680 cm^{-1} characteristic of the C-S stretching vibration. The former band is not present in spectra of polythioethers, and the latter band is shifted downward (~680–640 cm^{-1} , when detectable) consistent with observations made for bondings to metals by Lewis bases as diols. Elemental analysis is also consistent with a structure of form I. For instance for the product with 1,8-octanedithiol. Hf: calc, 37%; found, 39%.

Attempts were made to dissolve the polythioethers in numerous solvents by placing ~1 mg in a small test tube containing about 2 ml of solvent. As in the case of the analogous titanium polythioethers and many other similar organometallic polymers, solution was not effected in any solvent. Solvents tried included water, carbon tetrachloride, chloroform, DMF, DMSO, α -chlorotoluene, octane, 1-ethyl-2-nitrobenzene, triethyl phosphate, ethyl sulphide, *o*-dichlorobenzene, 2-nitropropane, dioxane, benzene, acetone, xylene and acetonitrile. This lack of solubility is unfortunate and presents a major obstacle to characterization of the products and evaluation of molecular weight. Even so it does not eliminate uses where solution is not necessary.

Thermal characterization was effected using the 950 Dupont TGA and a d.s.c. cell fitted onto a 900 Dupont Thermal Analyzer console. Air and nitrogen gas flows were maintained at 0.3 to 0.2 l/min. Samples were ground to

Table 1 Yield as a function of dithiol

Dithiol	Yield (%)	
	(interfacial)	(aqueous solution)
Dimercaptopropionate	78	35
Dimercaptoacetate	78	53
1,2-Ethanedithiol	51	57
1,3-Propanedithiol	59	
1,6-Hexanedithiol	58	31
1,8-Octanedithiol	29	

Reaction conditions: interfacial systems: Dithiol (0.50 mmol) with Et_3N (1.00 mmol) in 15 ml of water added to rapidly stirred ($\sim 23,000$ rev/min no load) solutions of Cp_2HfCl_2 (0.50 mmol) in 15 ml chloroform at 27°C for 1 min stirring time. Aqueous Solution Systems: as above except Cp_2HfCl_2 is contained in 15 ml of water instead of chloroform

fine powders to aid in obtaining reproducible results. A linear baseline compensator was used with the d.s.c. cell to ensure a constant energy baseline. A Mettler H20 semi-micro balance was employed for weighing the d.s.c. samples. D.s.c. measurements were made using samples contained in open aluminium cups, allowing free flow from the sample of volatilized gases thus more closely simulating the conditions under which t.g.a. measurements were made.

Visual thermal characterization was effected to 300°C using a Fisher-Johns melting point apparatus and what is called a static, open system where the sample is simply left in the open on a cover slide. This closely simulates conditions under which the d.s.c. and t.g.a. measurements (in air) were carried out. Observations were also made using what can be referred to as a dynamic, closed system, where about 10 p.s.i. is applied to samples placed between two cover slides. Conditions in the latter observations more closely simulate bulk and 'use' conditions and measurements obtained under inert atmospheres. The temperature at which colour change begins is similar for both systems but the colours vary markedly. Additionally the product from 1,8-octanedithiol melted using the dynamic, closed system. All materials were powders at 300°C .

RESULTS AND DISCUSSION

Reasons for using Cp_2HfCl_2 as the hafnium containing moiety are:

(1) Cp_2HfCl_2 is used as a catalyst or cocatalyst in certain commercial processes. Additionally, inclusion of the Cp_2Hf moiety generally imparts better u.v. stability to materials. Such properties might be imparted to polymers containing the Cp_2Hf unit.

(2) Cp_2HfCl_2 has been successfully condensed in analogous systems to form polyesters and polyethers.

(3) It is the only commercially available hafnium compound of the form R_2HfX_2 .

(4) It is stable in air, soluble in a number of organic solvents and hydrolyses in water to give $\text{Cp}_2\text{Hf}^{2+}$, which is active in condensations with Lewis bases⁶.

Condensation is general occurring in good to moderate yield for both the aqueous and interfacial systems (Table 1). Reaction, while rapid, reaching a plateau in yield ~ 1 min, is slower than for many similar condensations where reaction is complete within ~ 10 sec⁶.

The synthesis of hafnium polythioethers was also desired since other hafnium polymers synthesized by us have showed generally markedly better thermal stabilities than the

corresponding titanium products. Several titanium polythioethers exhibited moderate weight retention (less than 30% weight loss to $\sim 1000^\circ\text{C}$). Thus the analogous hafnium products might exhibit good weight retention.

D.s.c. and t.g.a. results appear in Figures 1-3. Several items should be noted.

(A) There appears to be no general trend with respect to weight retention as a function of atmosphere or dithiol.

(B) The products exhibited both kinetically and non-kinetically controlled weight retention plateaus. For instance, the plateau exhibited in the 600° to 800°C range (in nitrogen) for the product with dimercaptopropionate is not kinetically controlled (i.e. weight retention is time independent) whereas the weight retention in the 120° to 600°C range is kinetically controlled (i.e. weight retention is time and heating rate dependent).

(C) Several products showed 70% plus weight retention to 1000°C . This is considered fairly good. In considering weight retentions with many organometallic polymers the amount of organic material retained is important. The end thermal degradation product in air is HfO_2 . Table 2 shows values of '%- HfO_2 ' which is the % weight retention expected if only hafnium dioxide were left. The difference between the theoretical HfO_2 % weight retention and actual weight retention is taken to be a crude measure of organic material retained. Thus for the product with dimercaptopropionate at 650°C in air there is 70% actual weight retention compared to 39% HfO_2 theoretically possible, giving a gross organic weight retention of $\sim 31\%$ or about 45% of the remaining weight.

(D) Products begin to degrade at $\sim 50^\circ$ to 100°C , thus while they exhibit moderate high temperature (400° to

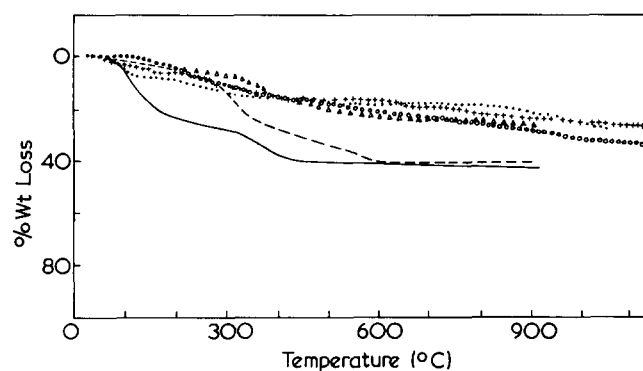


Figure 1 T.g.a. thermograms for products of Cp_2HfCl_2 with 1,2-ethanedithiol (●), 1,3-propanedithiol (○), 1,6-hexanedithiol (+), 1,8-octanedithiol —, dimercaptopropionate (Δ), and dimercaptoacetate --- in air with a gas flow of 0.3 l/min at a heating rate of $30^\circ\text{C}/\text{min}$

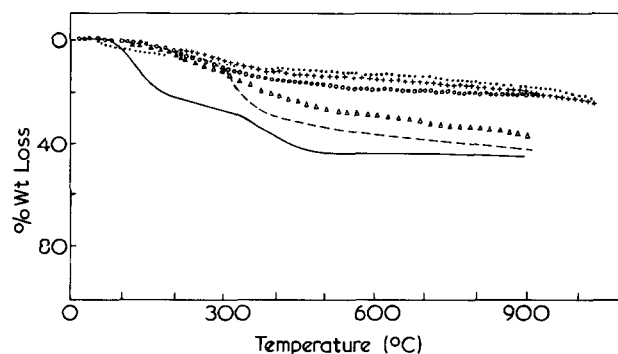


Figure 2 T.g.a. thermograms in nitrogen as described in Figure 1

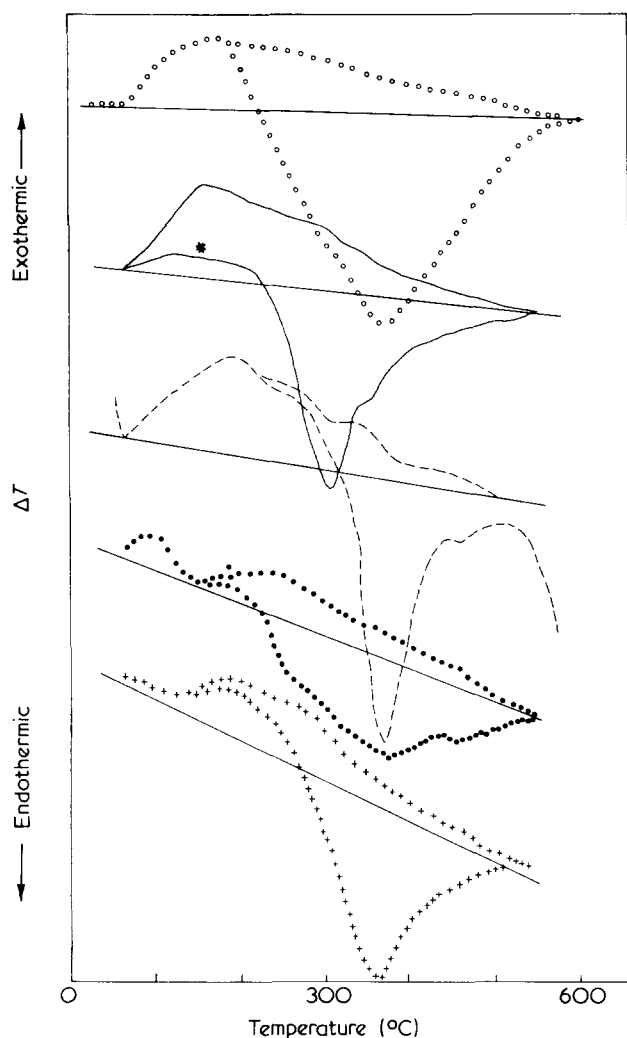


Figure 3 D.s.c. thermograms for products defined in Figure 1 in air-lower portion of plot and nitrogen-upper portion of plot at a gas flow rate of 3 l/min, heating rate of 30°C/min and a Y axis setting of 0.1°C/in (0.0040 mV/in) (except for sample * in air where the Y axis setting was 0.5°C/in) where the straight solid line represents $\Delta T = 0$

Table 2 Yield as a function of stirring time

Stirring time (sec)	Yield (%)	
	(interfacial)	(aqueous solution)
5	55	6
15	67	20
60	78	53
300	78	53

Reaction conditions are the same as Table 1 employing dimercaptoacetate at different stirring times

1100°C range) stability, they show poor low temperature stability. This weight loss is often accompanied by the production of a 'thiol-like' odour indicating loss of sulphur containing segments.

(E) Thermal degradation up 150° to 250°C appears to be identical in air and nitrogen, indicating an internal type of degradation via a non-oxidative mode(s). After this the degradation modes are quite dissimilar with degradation in air occurring via an oxidative mode(s).

Degradation probably occurs by a complex pathway(s) as indicated by the asymmetries and irregularities present in both the d.s.c. (mainly) and t.g.a. thermograms making quantitative measurements difficult to interpret. Thus ΔH values reported in Table 3 must be viewed as simply gross values indicative of composite, possibly only net, heat content change values.

Four endgroups are possible, they are: Hf-OH, Hf-Cl, R-SH and an endgroup formed from the condensation of Hf-Cl with Et₃N. All products exhibit bands in the 3600 to 3000 cm⁻¹ region characteristic of the Hf-OH group. The presence of S-H endgroups is not indicated because of the lack of bands in the 2600-2500 cm⁻¹ region. Presence of endgroups containing the Et₃N moiety is not indicated due to the absence of bands characteristic of this moiety. The assignment of bands characteristic of the

Table 3 Summary of thermal values

Dithiol	$\Delta H(\text{cal/g})^a$ atmosphere		Static (open) system	Dynamic (closed) system
	Air	Na		
1,2-Ethanedithiol	-0.018; 0.080	-0.080	260-270°C colour change to buff brown	250°-260°C colour change to buff brown
1,3-Propanedithiol	-0.031; 0.110	-0.096	230°C and upwards, progressive change to red-brown	220°-250°C colour change to brown
1,6-Hexanedithiol	-0.002; 0.089	-0.064	260°-270°C colour change to dark brown	250°-260°C colour change to brown
1,8-Octanedithiol	-0.038; 0.57	-0.20	270°C and upwards, colour change to light brown	Melts ~200°C, colour change to brown ~250°C
Dimercaptoacetate	-0.056; 0.095	-0.10	250°-270°C colour change to buff brown	Colour change to brown begins 250°C
Dimercaptopropionate			230°C begins progressive change to red-brown	220°-250°C change to brown

^a Convention utilized: exothermic values are reported as positive values, endothermic values as negative values

Hf-Cl unit is unsure, probably occurring about the 400 to 200 cm^{-1} range. Within this range the products exhibit a number of unassigned bands, thus identification is not presently possible. Thus there exists at least Hf-OH end-groups, indicative of the importance of Cp_2HfCl_2 hydroxylation.

ACKNOWLEDGEMENTS

The author is pleased to acknowledge support of this project by the American Chemical Society-Petroleum Research

Fund-Grant 7814-B1,3 and a grant from the University of South Dakota Research Fund.

REFERENCES

- 1 Carraher, C. and Lee, J. *J. Macromol. Sci. (A)* 1975, **9**, 191
- 2 Carraher, C. and Schroeder, J. *J. Polym. Sci. (B)* 1975, **13**, 215
- 3 Carraher, C. and Nordin, R. *J. Polym. Sci. (A-1)* 1972, **10**, 521
- 4 Carraher, C. and Nordin, R. *Makromol. Chem.* 1973, **164**, 87
- 5 Carraher, C. *J. Chem. Educ.* 1969, **46**, 314
- 6 Carraher, C. 'Interfacial Synthesis', (Eds. F. Millich and C. Carraher) Dekker, New York, 1975

New slit die rheometer: some results with a butadiene–styrene block copolymer*

Jean L. Leblanc

Chimie Industrielle Minérale, Faculté des Sciences Appliquées, Université de Liège, B-4000 Liège, Belgium

(Received 27 May 1975; revised 23 July 1975)

The slit die rheometer described, is a modification of the extrusion part of a Zwick rheometer (piston apparatus with constant applied pressure). The new slit has a variable depth, and pressure–temperature transducers are flush mounted at the die wall. The duct is 85 mm long and has a rectangular cross-section, 10 mm wide; four depths are available (0.50, 0.75, 1.00 and 1.50 mm). The hydraulic system gives pressures ranging from ~80 to 430 kg/cm², and the volumetric flow rate is determined by collecting extrudate samples. Some results are presented on Solprene 415, a butadiene–styrene block copolymer. Parabolic pressure profiles are accepted along the longitudinal distance of the die. A method is proposed to linearize the pressure gradient, in order to calculate the wall shear stress. A flow curve is obtained which is not strictly described by a power law relation.

INTRODUCTION

Extensive use has been made of the capillary rheometer, to determine the rheological properties of viscoelastic fluids, especially polymer melts. Because of the facility of analyzing experimental data and the possibility of achieving high levels of shear, the capillary rheometry has shown a growing development, for scientific studies as well as for industrial testing. Another geometry as simple as the capillary rheometer, is the system of two parallel plates of infinite width, in practice the geometry of a rectangular cross-section, with the so-called slit die rheometer.

Twelve years ago, several researchers^{1–3}, reported pressure and velocity profile measurements with slit dies. More recently, Han and coworkers^{4,8,9} constructed a slit type instrument with flush mounting of pressure transducers on the die wall. They demonstrated further^{5–7,10}, that the slit and capillary rheometers, produce essentially the same information and pointed out the existence of an ‘exit pressure’ during extrusion, from the measurements of wall normal stress distributions in the axial direction. With such measurements, Han was able to propose a method of determining the viscous and elastic properties of polymeric melts. This method consists essentially of obtaining the viscous property from the slope of the axial normal stress distribution, and the elastic property from the exit pressure. The exit pressure is the extrapolation value of wall normal stress to the exit of the die, from pressure readings within the duct.

In this connection, recent papers from Han and Drexler¹¹, describe rectangular slit dies with glass windows on either side, permitting the observation of stress birefringence patterns during extrusion. Their birefringence technique, together with measurements of wall normal stresses, give the stress distributions in the duct.

Some recent experimental studies have also been reported on the extrusion of polymer melts, through dies of rectangular cross-section^{12,13} and it is expected that the slit die

rheometry will show a similar development to capillary rheometry.

A SLIT DIE WITH VARIABLE DEPTH

The apparatus described here is a large modification of the extrusion part of a Zwick Z 4.1 C rheometer. In fact, we only use the hydraulic system of the Zwick rheometer, to provide and maintain the applied pressure to the piston. This piston is moving in a heated barrel of 30 mm diameter. A slit die of special design has been constructed which is connected to the end of the barrel.

The variable depth slit die is made of stainless steel and is composed of a main part and a cap separated by calibrated spacers, as shown in *Figure 1*. There is a set of spacers which enable the depth of the slot to be varied. The duct is 85 mm long and the rectangular cross-section, 10 mm wide; four depths are available: 0.50; 0.75; 1.00 and 1.50 mm. The cap has three pressure tap holes along the longitudinal axis. The dimensions of the slot and the positions of pressure–temperature transducers are indicated in *Figure 2*. The melt pressure transducers are ‘mounted flush’ with the slot wall, in such a manner that there is no ‘dead space’ between the tip of the transducer and the flow channel. This kind of mounting avoids flow disturbances, stagnations of the melt and possible hole effects. The main part and the cap are constructed in such a way that the slit has an entrance angle of 82 degrees, which prevents stagnation at the entry of the die. A general plan of the system is given in *Figure 3*.

The pressures and temperatures were measured with Dynisco TPT-432-A transducers. Pressure readings are recorded with a Riken Denshi model F-72T X–Y₁, Y₂ recorder, so that pressure–time curves are automatically plotted during the extrusion. Both the barrel and the die are electrically heated and especially insulated to prevent heat loss. The temperatures of the barrel and the die are separately checked with contact-thermometers or with thermocouples – Pyrectron KY(CORECI) indicating controllers. Both drive Thyristor-operated thermal regulators. The temperatures of the barrel and the die are controlled to remain within 1°C of the desired temperature.

* Part of this paper was presented at the British Society of Rheology meeting on Rheometry: methods of measurement and analysis of results, held at Shrivenham, April 1975.

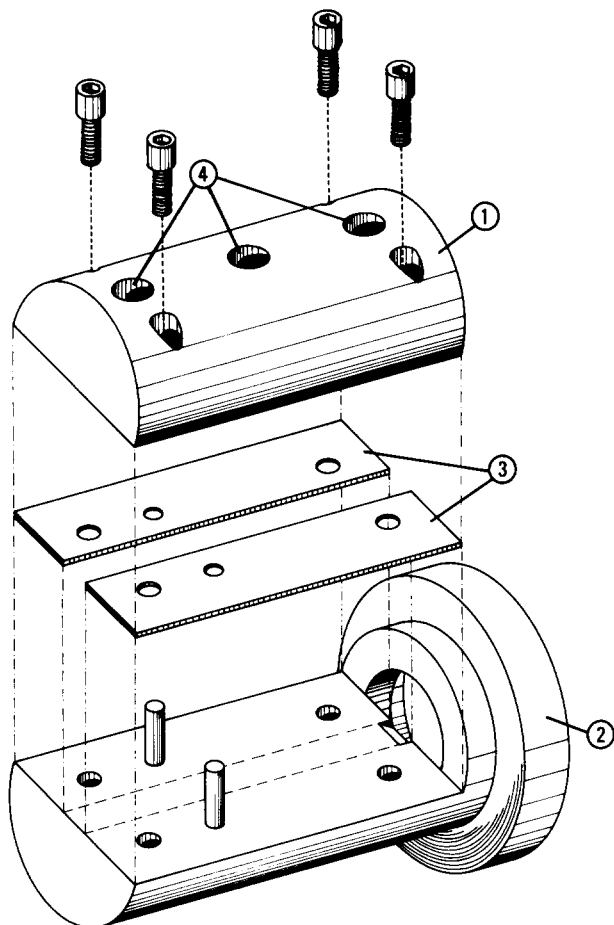


Figure 1 Extrusion slit die with variable depth. 1, Cap; 2, main part; 3, calibrated spacers (0.50, 0.75, 1.00 and 1.50 mm thick); 4, holes for pressure transducers

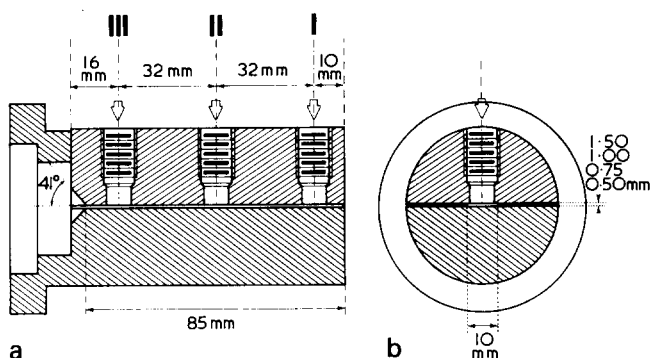


Figure 2 Slit dies dimensions and locations of pressure holes. (a) Longitudinal section; (b) transverse section

The hydraulic system of the Zwick rheometer provides pressures ranging from 80 to 430 kg/cm², and the volumetric flow rate is determined by collecting extrudate samples. This was later used to calculate apparent shear rate.

RESULTS AND DISCUSSION

Presented here are preliminary results with a butadiene-styrene block copolymer (Solprene 415 supplied by Phillips petroleum company). Characteristics of Solprene 415 are given in Table 1.

All results presented below, are obtained at a melting temperature of 175°C. Several experiments have been carried out with all the various depths and with the variation of the applied pressure, measuring the volumetric flow rate, and with automatic pressure recordings. Figures 4, 5, 6 and 7 show the axial pressure profiles in die of different depths, with the shear rate at the wall used as a parameter. In these Figures, values of the pressure plotted for a longitudinal distance of 95 mm (from the exit of the die), correspond to applied pressures in the barrel, and are not taken into account to draw axial pressure profiles. Thus, with no assumption about die entrance loss, it is possible to set out a parabolic curve for each set of three measured pressures, which responds to the general equation:

$$P = ax^2 + bx + P_0$$

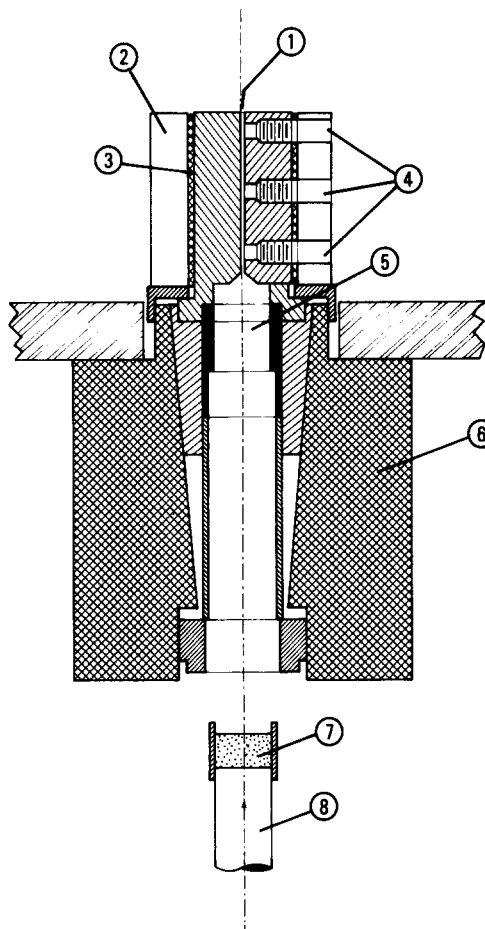


Figure 3 Modified Zwick rheometer with slit die. 1, Slit die; 2, thermal insulation; 3, heating element; 4, pressure-temperature transducers' holes; 5, compression chamber; 6, heating cylinder; 7, polymer; 8, piston

Table 1 Characteristics of the Solprene 415 sample¹⁴

butadiene (BD)/styrene ratio	60/40
styrene wt % (experimental)	40.5
butadienic microstructures (i.r.)	
<i>cis</i> -1,4 (%/BD phase)	32
<i>trans</i> -1,4 (%/BD phase)	49
vinyl(1,2) (%/BD phase)	11
total unsaturation (ICl method) (%)	95
specific gravity (g/cm ³)	0.957
[η] (dl/g) (toluene; 25°C)	0.97
[η] (dl/g) (THF; 25°C)	0.98
M_w (by g.p.c.)	153 000
M_n (by g.p.c.)	123 000
M_w/M_n	1.24

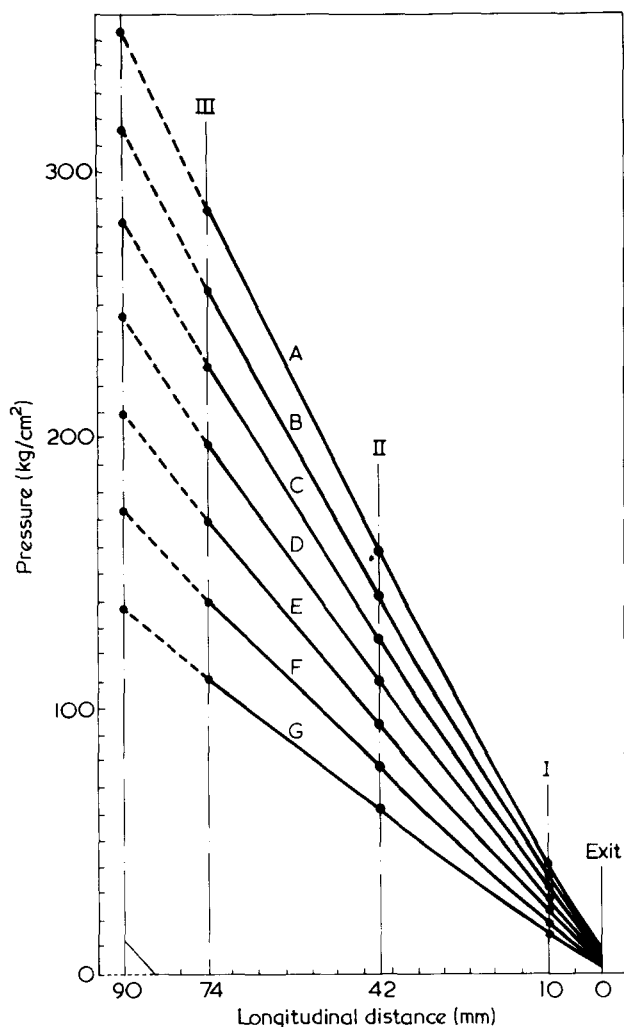


Figure 4 Axial pressure profiles in slit die for Solprene 415 at 175°C. Slit die: L , 85 mm; b , 10 mm; d , 0.5 mm. Values for $\dot{\gamma}$ (sec^{-1}): A, 6.58; B, 3.30; C, 2.38; D, 1.546; E, 0.995; F, 0.598; G, 0.299

where P is the pressure and x the longitudinal distance from the exit of the die. For each pressure profile, coefficients a and b are computed by making linear regression of $(P - P_I)/(x - x_1)$ versus $(x - x_1)$, where x_1 is taken equal to 10 (pressure transducer's position I) and P_I is the corresponding pressure. Straight lines are so obtained from which the slope gives a , and the zero intercept gives $(2ax_1 + b)$ and thus b . The third coefficient which corresponds to the 'exit pressure' P_0 is calculated by introducing experimental values. By using a Hewlett-Packard HP-55 programmable computer, great precision is obtained in determining the values of the coefficients and more accurate pressure profiles can be drawn. As an example, results are given in Table 2 for the slit die of 0.50 mm thickness.

The following observations can be made from Figures 4–7: (a) between measurement positions I and III, the pressure gradient is *not* strictly constant within the longitudinal distance; (b) the shape of the pressure profiles is clearly dependent on the flow rate, and varies with the die geometry; (c) non-zero 'exit pressures' are obtained by extrapolating the parabolic curves (i.e. by calculating the P_0 coefficient of the parabolic equation).

Concerning the shape of pressure profiles, it seems that the deeper the slot, the less 'linear' are the curves. Moreover, the pressure drop at the entry (largest part seems to be given by the difference between the applied pressure in

the barrel and the measured pressure in position III) is more important as the shear rate increases; but at constant shear rate, the pressure drop at the entry, increases as the slit depth decreases. These observations agreed very well with the results of Han and Charles for capillary flow of molten polymers¹⁵ and are well understood since the greater the cross-section of the capillary/cross-section of the barrel ratio, the smaller the pressure drop at the entry.

Inside the die, the pressure profiles are parabolic, but in such a manner that they become approximately linear as the longitudinal distance (from the exit of the die) decreases. Non-linear pressure profiles have also been reported for polystyrene at 200°C by Han, Charles and Philippoff in their first publication^{4(a)}. This was attributed to under developed flow; the criterion used to ascertain whether or not the flow is fully developed, being the constancy of the pressure gradient; but no explanation was given for these non-linear pressure profiles. It must be noted that for high viscosity materials such as polymer melts, it is doubtful as to whether fully developed flow can be achieved. Although flow birefringence observations in slit die¹¹ reveal that, at a distance of about twice the slit thickness from the die entrance, isochromatic fringe patterns become parallel to the slit wall (at least for the studied polymers, i.e. polyethylene, polypropylene and polystyrene). In the system we present here, the first pressure measurement after the die entrance (P_{III}) is at a distance of 22, 14.7, 11 and 7.3 times the slit thickness from the die entrance, for depths of 0.50, 0.75, 1.00 and 1.50 mm, respectively. However, it is pos-

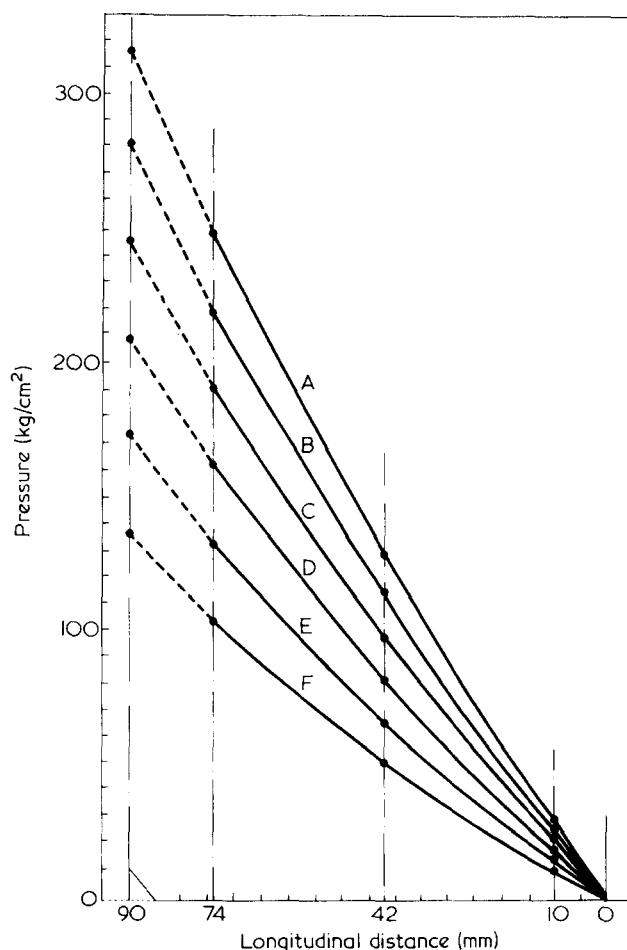


Figure 5 Axial pressure profiles in slit die for Solprene 415 at 175°C. Slit die: L , 85 mm; b , 10 mm; d , 0.75 mm. Values for $\dot{\gamma}$ (sec^{-1}): A, 39; B, 11.5; C, 3.84; D, 2.33; E, 1.28; F, 0.613

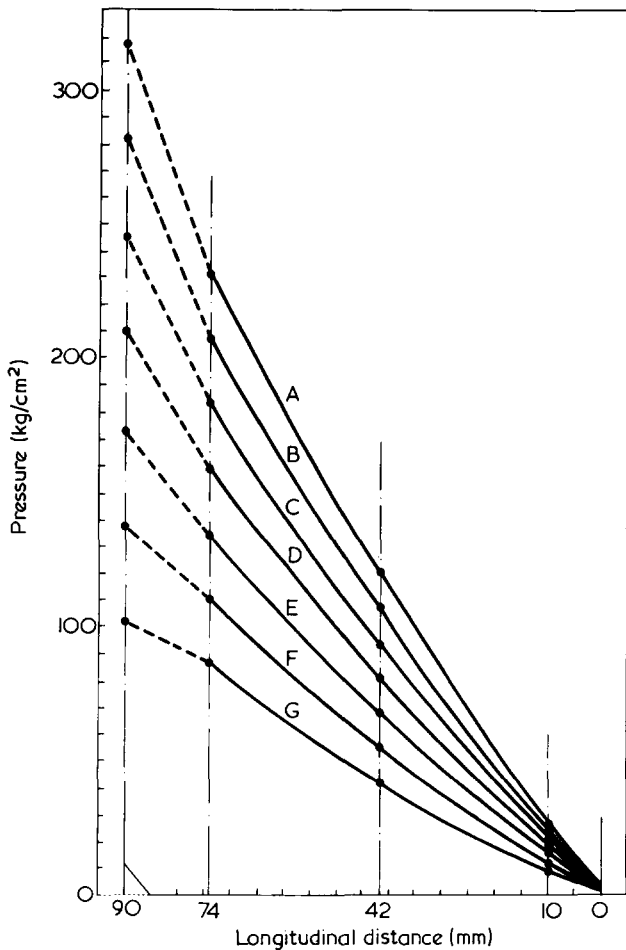


Figure 6 Axial pressure profiles in slit die for Solprene 415 at 175°C. Slit die: L , 85 mm; b , 10 mm; d , 1 mm. Values for $\dot{\gamma}$ (sec^{-1}): A, 105; B, 43.4; C, 21.6; D, 7.81; E, 3.26; F, 1.53; G, 0.723

sible that with the Solprene 415 butadiene-styrene block copolymer used, the importance of the elastic component of the material does not permit a fully developed flow to be achieved within a length equivalent to at least 22 times the slit die thickness. It is also possible that the parabolic shape of pressure profiles is typical of highly elastic polymer melts. With the parabolic equations, we compute for each pressure profile, in the manner described above, it is clear that the extrapolation to the exit of the die is reasonable, because at the present time no 'exit effects' have been shown off.

In spite of the extrapolation procedure used, it appears from Figures 4 to 7 that, at constant shear rate, the exit pressure increases while the depth of the slit decreases, and in conformity with the works of Han and coworkers⁴⁻⁹; who observed strict linearity in pressure profiles for slot of 0.13-0.25 mm depth, it seems that important 'exit pressures' are only available with a very thin slit.

The wall shear stress τ_{wc} in a slit die may be given, in a classical manner, by:

$$\tau_{wc} = \frac{bd}{2(b+d)} \cdot \left(\frac{\partial P}{\partial x} \right) \quad (1)$$

where $\partial P/\partial x$ is the pressure gradient along the axis, b the slit width and d the slit thickness¹⁶. This equation gives a mean corrected wall shear stress, including the edge correction, and if the pressure gradient is determined by pressure measurements inside the die, no Bagley correction (extrapo-

lation to zero pressure of plots of pressure versus L/d ratio at given shear rate) is necessary. When the slit becomes very thin, the wall shear stress is obviously given by.

$$\tau_w \approx \frac{d}{2} \cdot \left(\frac{\partial P}{\partial x} \right) \quad (2)$$

This simplified equation has been used by Han⁸ for slit dies of b/d ratios equal to 10 and 20.

Since, in our experiments, pressure profiles are not straight lines, a problem of linearization appeared in calculating wall shear stresses. A first approximate method is to assimilate the smooth pressure curves between P_I and P_{III} to straight lines and obtain the pressure gradient by:

$$\frac{\partial P}{\partial x} = \frac{P_{III} - P_I}{64} \quad (3)$$

since $x = 64$ mm between pressure transducers I and III. A more rigorous method is to use the parabolic equations we determine for each pressure profile. First derivative gives the pressure gradient by:

$$\frac{\partial P}{\partial x} = 2ax + b \quad (4)$$

at any fixed value of x . In this manner we compute the pressure gradient taking $x = 42$ (the transducer's position

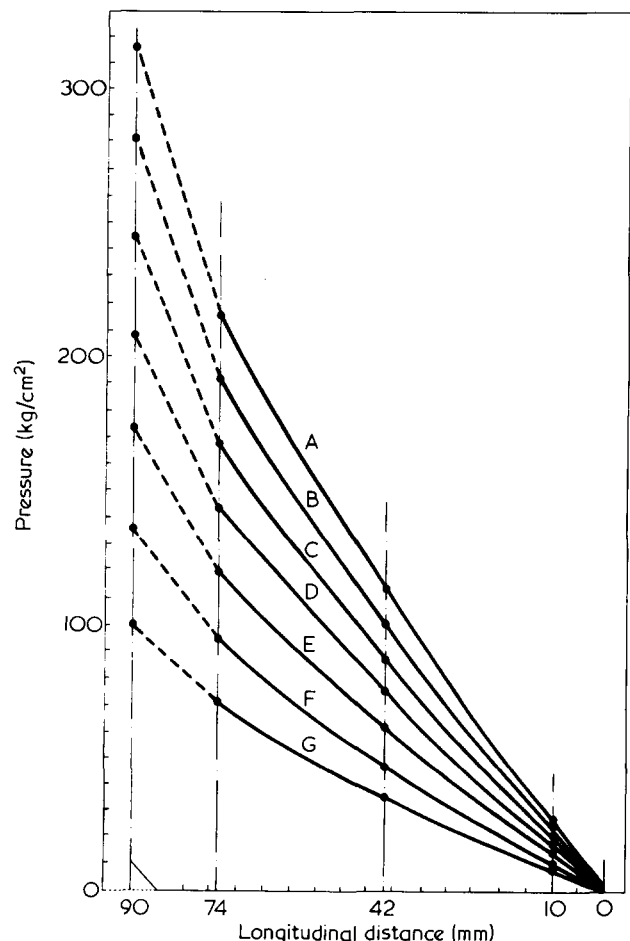


Figure 7 Axial pressure profiles in slit die for Solprene 415 at 175°C. Slit die: L , 85 mm; b , 10 mm; d , 1.5 mm. Values for $\dot{\gamma}$ (sec^{-1}): A, 15.5; B, 96.5; C, 57.7; D, 31.5; E, 13.2; F, 5.03; G, 1.42

Table 2 Pressure profiles for Solprene 415 at 175°C. Slit die: $L = 85$ mm; $b = 10$ mm; $d = 0.50$ mm; Parabolic pressure profiles: $P = ax^2 + bx + P_0$

Applied pressure (kg/cm ²)	P_I (kg/cm ²)	P_{II} (kg/cm ²)	P_{III} (kg/cm ²)	a (kg/cm ⁴)	b (kg/cm ³)	P_0 (kg/cm ²)
	$x = 10$	$x = 42$	$x = 74$			
137	15	61	110	0.00146	1.36133	1.240
173	19	77	139	0.00195	1.71094	1.695
209	23	93	168	0.00244	2.06055	2.150
245	27	109	197	0.00293	2.41016	2.605
281	32	125	226	0.00391	2.70313	4.578
317	37	141	255	0.00488	2.99606	6.551
353	42	157	284	0.00586	3.28906	8.523

Table 3 Pressure gradients for Solprene 415 at 175°C. Slit die: $L = 85$ mm; $b = 10$ mm; $d = 1.5$ mm

$\dot{\gamma}_{wa-1}$ (sec ⁻¹)	P_I (kg/cm ²)	P_{II} (kg/cm ²)	P_{III} (kg/cm ²)	$\frac{\partial P}{\partial x} = \frac{P_{III} - P_I}{64}$	$\frac{\partial P}{\partial x} = 2ax + b$ ($x = 42$)
0.679	9	36	71	0.96875	0.96907
2.4	12	49	95	1.29688	1.29649
6.3	15	62	119	1.62500	1.62476
15.0	18	75	143	1.95313	1.95303
27.5	21	88	167	2.28125	2.28130
46	24	101	191	2.60938	2.60957
74	27	114	215	2.93750	2.93784

Table 4 Wall shear stresses for Solprene 415 at 175°C

$L = 85$ mm; $b = 10$ mm; $d = 1.5$ mm				$L = 85$ mm; $b = 10$ mm; $d = 0.5$ mm			
$\dot{\gamma}_{wa-1}$ (sec ⁻¹)	$\frac{\partial P}{\partial x}$	τ_{wc} (kg/cm ²) [equation 1]	τ_w (kg/cm ²) [equation 2]	$\dot{\gamma}_{wa-1}$ (sec ⁻¹)	$\frac{\partial P}{\partial x}$	τ_{wc} (kg/cm ²) [equation 1]	τ_w (kg/cm ²) [equation 2]
0.679	0.96907	0.6320	0.7268	0.173	1.48397	0.3533	0.3710
2.4	1.29649	0.8455	0.9724	0.346	1.87474	0.4464	0.4687
6.3	1.62476	1.0596	1.2186	0.572	2.26551	0.5394	0.5664
15.0	1.95303	1.2737	1.4648	0.893	2.65628	0.6324	0.6641
27.5	2.28130	1.4878	1.7110	1.373	3.03157	0.7218	0.7479
46	2.60957	1.7019	1.9572	1.91	3.40601	0.8110	0.8515
74	2.93784	1.9160	2.2034	3.8	3.78130	0.9003	0.9453

II; halfway of the die) and the difference between pressure gradients calculated by the first or the second method appears only at the fourth decimal. As an example of corrections introduced by using equations (1) to (4), some results are given in Table 3 for the slit of 1.5 mm thick, for which the differences are the more important.

For the determination of shear stresses, we use pressure gradients as calculated by equation (4). Table 4 gives an idea of differences introduced by use of equation (1) (edge correction included) or equation (2) (no edge correction), for the slit die, 1.5 mm thick, and for the slit die, 0.5 mm. The error arising from use of equation (2) is 15% (of τ_{wc} values) for the 1.5 mm slit and 5% for the 0.5 mm slit. Edge effects are thus not negligible and use of the simplified equation (2) to calculate shear stresses can introduce serious errors in determining flow curves. We have thus used equation (1) to calculate the wall shear stress.

The apparent shear rate at the wall $\dot{\gamma}_{wa}$ has been calculated using:

$$\dot{\gamma}_{wa} = \frac{6Q}{bd^2} \quad (6)$$

where Q is the volumetric flow rate (mm³/sec) and b the slit width. Plots of $\log \tau_{wc}$ versus $\log \dot{\gamma}_{wa}$ are drawn and the slope is measured for each experimental apparent shear rate, in order to apply the Rabinowitsch correction, so that the true wall shear rate $\dot{\gamma}_w$ is given by:

$$\begin{aligned} \dot{\gamma}_w &= \dot{\gamma}_{wa} \left(\frac{2}{3} + \frac{1}{3} \cdot \frac{\partial \log \dot{\gamma}_{wa}}{\partial \log \tau_{wc}} \right) \\ &= \left(\frac{2n+1}{3n} \right) \dot{\gamma}_{wa} \end{aligned} \quad (7)$$

where $n = \partial \log \tau_{wc} / \partial \log \dot{\gamma}_{wa}$.

We have then constructed a flow curve by plotting τ_{wc} versus $\dot{\gamma}_w$. Figure 8 shows the flow curve of Solprene 415 melt at 175°C, plotted with extrusion data of the four slit geometries. It is clear that the different slit dies give consistent results, when edge corrections are included in the calculation of shear stresses. The flow curve in Figure 8 is the 'best' curve it is possible to draw through experimental data. In order to test the validity of a power law relation, to describe the behaviour of Solprene 415 in the studied

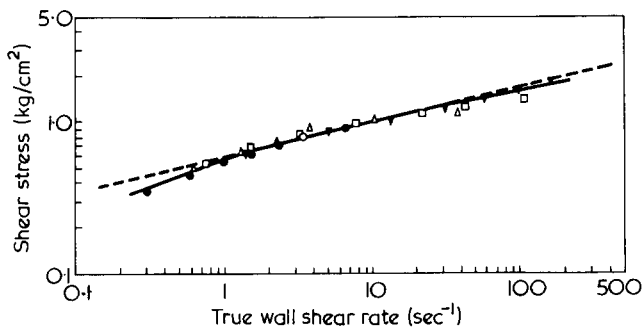


Figure 8 Flow curve of Solprene 415 at 175°C. ●, 0.50; △, 0.75; □, 1.00; ▼, 1.50 mm

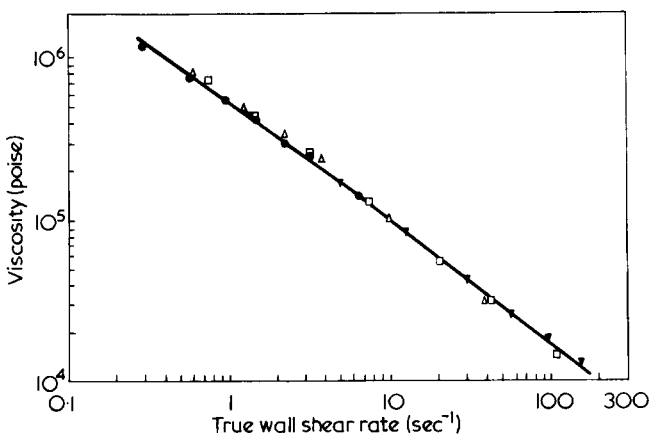


Figure 9 Melt viscosity versus shear rate for Solprene 415 at 175°C. ●, 0.50; △, 0.75; □, 1.00; ▼, 1.50 mm

range of shear rates, we compute by linear regression the power function:

$$\tau = k \cdot \dot{\gamma}^n$$

which may be adjusted to the set of experimental points $[(\dot{\gamma}_i, \tau_i), i = 1, 2, \dots, p]$. The power law index n is given by:

$$n = \frac{\sum (\ln \dot{\gamma}_i)(\ln \tau_i) - [(\sum \ln \dot{\gamma}_i)(\sum \ln \tau_i)]/p}{\sum (\ln \dot{\gamma}_i)^2 - [\sum (\ln \dot{\gamma}_i)^2]/p}$$

and k is given by¹⁷

$$k = \exp \left(\frac{\sum \ln \tau_i}{p} - n \frac{\sum \ln \dot{\gamma}_i}{p} \right)$$

We thus obtain a power law:

$$\tau = 0.5751 \dot{\gamma}^{0.2314}$$

which is plotted in Figure 8 (broken line). It seems that the behaviour of Solprene 415 is not strictly described by

a power law relation. In plotting the melt viscosity against shear rate, as shown in Figure 9, it may be seen that Solprene 415 is in the non-Newtonian flow regime over the range of studied shear rates.

CONCLUSIONS

The slit die rheometer with variable depths, constructed with a Zwick rheometer gives acceptable results in studying the melt flow properties of polymers. With the depths actually available, it is quite possible to obtain flow curves and viscosity functions for shear rates ranging from 10^{-1} to 10^2 sec^{-1} , hence in the non-Newtonian region. Moreover the apparatus permits to plot pressure profiles along the die, with the possibility to extrapolate up to exit pressure.

ACKNOWLEDGEMENTS

The author would like to thank Professor K. Gamski for helpful discussions and for the Zwick rheometer placed at his disposal. He is indebted to Mr C. Courard and coworkers for machining of the slit die. Thanks are also due to Mr R. Fayt for Gel permeation chromatography experiments, and to Miss D. Degeimbre for her support in determining characteristics of the sample. The author wishes to acknowledge the Phillips petroleum company (Technical Centre at Overijse, Belgium) for providing the Solprene sample.

REFERENCES

- 1 Eswaran, R., Janeschitz-Kriegl, H. and Schijf, J. *Rheol. Acta* 1963, 3, 83
- 2 Wales, J. L. S., den Otter, J. L. and Janeschitz-Kriegl, H. *Rheol. Acta* 1965, 4, 146
- 3 den Otter, J. L., Wales, J. L. S. and Schijf, J. *Rheol. Acta* 1967, 6, 205
- 4 (a) Han, C. D., Charles, M. and Philippoff, W. *Trans. Soc. Rheol.* 1969, 13, 455 (b) 1970, 14, 393 (c) 1970, 14, 409
- 5 (a) Han, C. D., Yu, T. C. and Kim, K. U. *J. Appl. Polym. Sci.* 1971, 15, 1149 (b) *idem, ibid.* 1971, 15, 1163
- 6 Han, C. D. and Kim, K. U. *Polym. Eng. Sci.* 1971, 11, 395
- 7 Han, C. D. and Yu, T. C. *Rheol. Acta* 1971, 10, 398
- 8 Han, C. D. *J. Appl. Polym. Sci.* 1971, 15, 2567, 2579, 2591
- 9 Han, C. D. and Charles, M. *Polym. Eng. Sci.* 1970, 10, 148
- 10 Han, C. D., Kim, K. U., Siskovic, N. and Huang, C. R. *J. Appl. Polym. Sci.* 1973, 17, 95
- 11 Han, C. D. and Drexler, L. H. *J. Appl. Polym. Sci.* 1973, 17, 2329, 2355, 2369
- 12 Ramsteiner, F. *Kunststoffe* 1971, 61, 943
- 13 Ehrmann, G., Robens, G. and Wagner, M. H. *Kunststoffe* 1974, 64, 463
- 14 Leblanc, J. L. *Trib. Cebedeau* 1975, 28, 231
- 15 Han, C. D. and Charles, M. *Trans. Soc. Rheol.* 1971, 15, 371
- 16 McKelvey, J. M. 'Polymer Processing', Wiley, New York, 1962
- 17 Brownlee, K. A. 'Statistical Theory and Methodology in Science and Engineering', Wiley, New York, 1965

Thermal analysis of heat set poly(ethylene terephthalate) fibres*

H.-J. Berndt and Adelgund Bossmann

Textilforschung Krefeld, D-4150 Krefeld, Frankenring 2, W. Germany

(Received 16 July 1975; revised 23 October 1975)

Differential thermal analysis (d.t.a.) has been used for characterization of the thermal history of poly(ethylene terephthalate) (PET) fibres. The latter were treated under a variety of temperatures and times in a manner similar to conditions employed in conventional textile processing. The d.t.a. revealed an endotherm at temperatures below the main melting peak of the fibre polymer, related directly to temperature and time of thermal treatment, even with yarns that were heat set for less than 0.2 sec (e.g. false twisting process). The maximum of this low temperature endotherm is a direct measure of the effective temperature (T_{eff}) that has been acquired by the PET fibres during the thermal processing. In practice, several thermal treatments are often involved in textile processing. Results of this work imply that PET fibres subjected to a second heat treatment will show an additional low temperature endotherm on d.t.a. scanning, provided that the structural characteristics formed in the first thermal process are not neutralized in the second thermal process and recrystallizable material is still present in the fibre polymer.

INTRODUCTION

In order to attain a PET yarn or fabric with certain properties, the drawn PET filament will be subjected to various processing steps while heat is applied. During these thermal mechanical processing operations, changes in the state of order in the polymer occur via a decrease in internal stresses and reorganization of polymer segments. A recrystallization and an after-crystallization will concurrently take place. The solid phase transitions in the PET fibre polymer can be detected by d.t.a. traces¹⁻⁴. Multiple melting peaks during d.t.a. scanning have been reported⁵⁻⁸ for annealed PET bulk polymer. The PET samples were heat treated for periods varying from several minutes (5 min) to several hours (24 h) at different temperatures to study the effect on thermograms in d.t.a. Between the glass transition temperature and the main melting peak at about 260°C, a low temperature endotherm was observed. The position of this low temperature endotherm is reported to be related to the temperature to which the PET polymer has been exposed prior to d.t.a. scanning⁵⁻⁷. An increase in time of treatment during annealing at a constant temperature causes an increase in the low temperature d.t.a. endotherm⁵.

Roberts⁵ ascribed this low temperature endotherm to melting of chain folded crystals, and the main melting peak to melting of bundle-like crystals. More recent work by Roberts⁹ and Holdsworth and Turner Jones⁸ discounted this chain folded and bundle-like crystal endotherms hypothesis because of the change in the relative areas of the two endotherms with change in d.t.a. heating rate. A change in heating rate from 4 to 64 K/min⁹ causes not only an increase in intensity of the low melting endotherm but also an increase in temperature on the d.t.a. trace. These changes are considered to be due to structural changes taking place during d.t.a. scanning according to the heating rate^{8,9}. These studies were mainly carried out on bulky polymer annealed for a fairly long time (from ~5 min to several hours).

Wiesener⁴ who investigated thermally treated drawn PET fibres, also found an increase in temperature of the low temperature endotherm when the PET fibres were subjected to increasing setting temperatures. However, also in this investigation the PET fibres were treated for 10 to 240 min.

Our concern is to investigate the changes of structure in PET fibres as brought about under the influence of various processing operations. For practical significance, time during the different heat setting processes varies from 0.2 sec (e.g. false twisting) to 4 h (e.g. heat setting of heavy technical fabrics). The feasibility of d.t.a. to define the thermal prehistory of PET fibres as produced under ordinary commercial thermal processing is, therefore, studied. Good understanding of the structural changes as generated in PET fibre polymer under various conditions would be useful to predict the specific parameters of the heat setting process; an aspect which is needed to attain desirable and reproducible quality.

EXPERIMENTAL

Material

The materials used in this study are exclusively commercial drawn PET filament yarns of different origins. The yarns were heat set at temperatures varying from 110° to 230°C under simultaneous constant tension (0.0–0.1 N/tex) during setting. The time of treatment varied from 0.5 sec to 240 sec in hot air and up to 90 min during a high temperature dyeing process. In order to meet these setting demands, special heat setting equipment was developed¹ to control the process parameters, temperature, tension and processing time.

False twisted textured yarns are also used to study in particular, the effect of heat setting for very short times on structural changes in PET fibres.

* Part XVII of a series on the heat setting of PET¹⁴

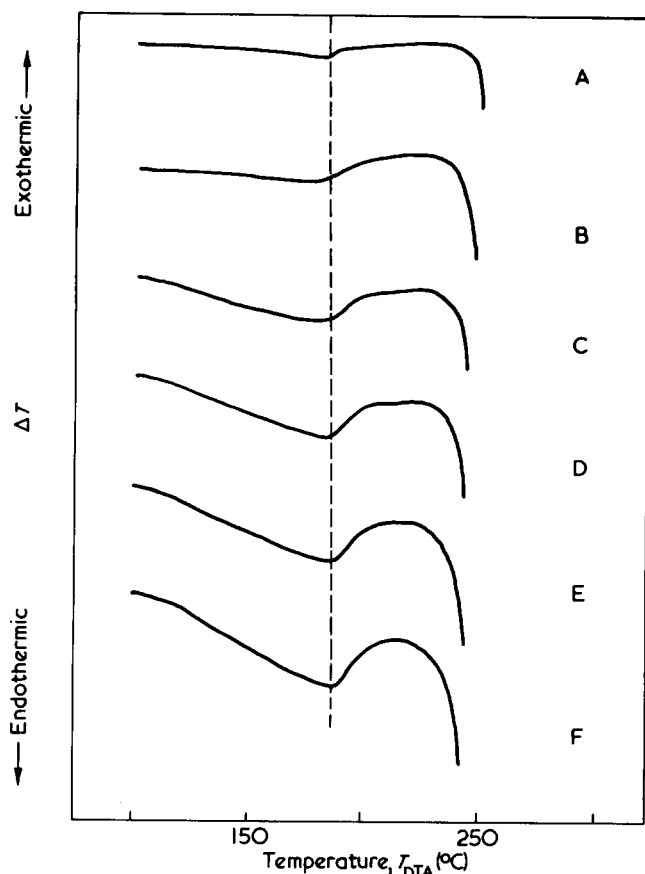


Figure 1 D.t.a. traces of PET fibres heat set at 180°C for 20 sec; d.t.a. heating rates (K/min): A, 5; B, 10; C, 15; D, 20; E, 25; F, 30

Differential thermal analysis

Samples (5–6 mg) of PET yarn were accurately weighed into an aluminium sample pan. The covers of the sample pans were provided with small holes to allow for evaporation of finishing agent and to maintain atmospheric pressure during d.t.a. scanning. The measurements were made with the sample in air, since prior tests have demonstrated that the heat of reaction is generally not influenced by atmospheric oxygen. The thermograms of the PET yarns samples were run on a Du Pont Differential Analyser, Type 900 using the d.s.c. cell. A good resolution was needed to observe the heat of fusion, which did not always appear as a peak rather than as a deflection in the slope of the d.t.a. trace. A heating rate of 30 K/min and a sensitivity range for ΔT of 0.1 or 0.2 K/in were chosen.

RESULTS AND DISCUSSION

Heating rate

The change of d.t.a. traces on increasing heating rate is shown in Figure 1. A PET yarn sample was isothermally treated at 180°C for 20 sec at zero tension and d.t.a. traces obtained at various heating rates. An increase in the partial melting peak temperature and a change in the low temperature endotherm are observed with increasing instrument heating rate. On running the fibre sample at a low heating rate (5 K/min), a small fusion endotherm with a poorly resolved maximum at 183°C is found, whereas a heating rate of 30 K/min leads to a fusion endotherm over a broad temperature range with its maximum at 190°C. This change in the endotherm and peak temperature is indicative of a reorganization taking place during scanning⁸.

The change on d.t.a. traces due to heating rate can be explained by the theory of Zachmann and Stuart¹⁰, who found that only imperfect crystals are formed at low crystallization temperatures (180°C, 20 sec). On heating, the perfection of the crystals formed at low temperatures increases owing to partial melting and recrystallization. At low heating rates a kinetic balance of melting and recrystallization will occur which is not detectable in the thermogram baseline. However, if the heating rate is high enough the faster melting process exceeds the slower recrystallization process, producing the increase in the low temperature endotherm. The increase in the partial melting peak temperature with increasing heating rate is apparently due to the fact that the crystals may be heated faster than the melt-crystal interface can progress towards the interior and the crystals melt at a higher temperature¹¹.

Heat setting temperature

D.t.a. traces of a PET yarn 10tex/36 filaments isothermally heat set at various temperatures are shown in Figure 2. The yarn samples were treated for 20 sec at zero tension. The thermograms were run at a sensitivity range of $\Delta T = 0.2$ K/in. They show a distinct partial melting peak prior to the main melting peak at 256°C. The partial melting peak appears 10°C above the machine temperature of thermal setting. With increasing machine temperature the maximum of this peak increases linearly on the d.t.a. temperature scale. These results suggest that the imperfect crystals in the fibre polymer melt on heating in the d.t.a. at a given heating rate just above the temperature at which they were formed during heat setting. The maximum of the partial melting endotherm is directly related to the setting temperature and is defined as the effective temperature T_{eff} .

If the PET fibre is exposed to a further heat process like a high temperature dyeing at 130°C for 90 min, an addi-

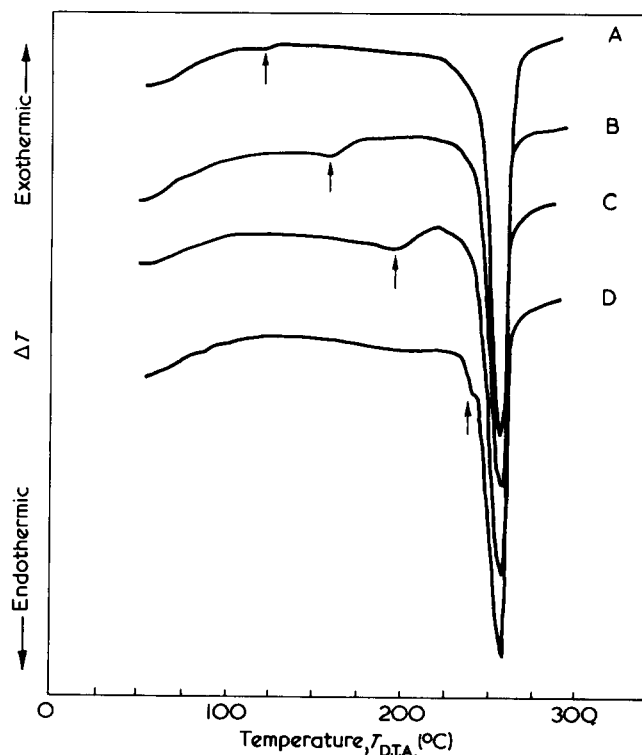


Figure 2 D.t.a. traces of PET fibres heat set for 20 sec at the various temperatures (°C): A, 110; B, 150; C, 190; D, 230

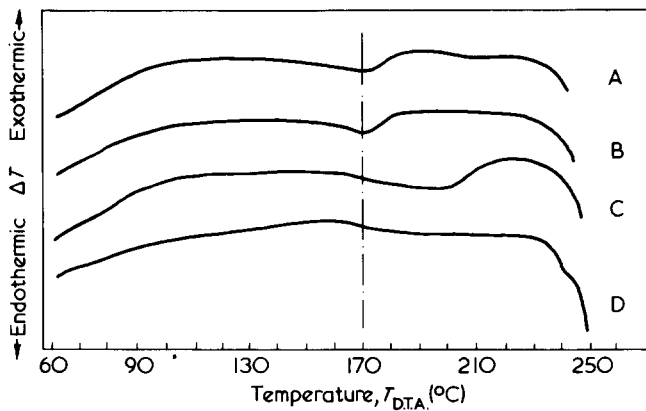


Figure 3 D.t.a. traces of PET fibres after heat setting at the various temperatures ($^{\circ}\text{C}$): A, 110; B, 150; C, 190; D, 230. High temperature-dyeing at 130°C for 90 min

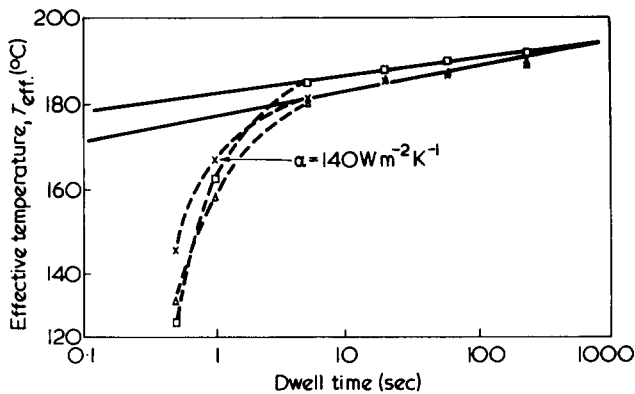


Figure 4 Effective temperature of PET fibres as a function of dwell time of heat setting at 180°C and zero tension. Standard type (X); chemical modification S-type (\square); physical modification S-type (\triangle)

tional low temperature endotherm in the d.t.a. trace is observed at a constant temperature of 170°C (Figure 3). The increase in temperature of 40°C on the d.t.a. temperature scale above the dyeing temperature is caused by the hydrothermal treatment. Schefer¹² found that a hydrothermal treatment causes a higher heat setting effect on PET than hot air does. The d.t.a. traces indicate that the partial melting peak due to the first thermal process, vanishes in cases where the T_{eff} of the succeeding process exceeds the T_{eff} of the first process. Only PET yarns which have adopted a T_{eff} in the first thermal process sufficiently above T_{eff} of the second thermal process (so as not to be masked by an overlapping effect) show a partial melting peak from the first thermal process and a second one from high temperature dyeing.

Repetitive measurements on replicate samples showed good agreement. The mean deviation from 3 or 4 values did not exceed $\pm 1^{\circ}\text{C}$. Results proved also to be instrument independent. Measurements carried out in other laboratories on different instruments were in good agreement and reproducible to $\pm 1^{\circ}\text{C}$.

Time of treatment

Commercial drawn PET yarns of different origin were heat set for various times (0.5 to 240 sec) at a constant temperature (180°C) using zero tension. The observed partial melting peaks (T_{eff}) are plotted as a function of log time in Figure 4. The results indicate that increasing the time of treatment from 0.5 to 5 sec is accompanied by a large difference between the effective temperature and the

machine temperature. That is, with such a short time of treatment the PET yarns do not adopt the machine temperature. Further prolongation of time caused a linear increase in the effective temperature with log time, owing to after-crystallization.

The dependence of the effective temperature on the heat setting temperature, dwell time and high temperature dyeing is shown in Figure 5. The heat setting temperature reveals a linear relation with T_{eff} . A change in dwell time causes a parallel shift on the ordinate indicating that a decrease in dwell time decreases T_{eff} . The effective temperature due to a high temperature dyeing process at 130°C is drawn as a horizontal line at 170°C . This indicates that this process wipes out any structural features of the fibre polymer which are due to thermal treatments with effective temperatures below that of the high temperature dyeing. It follows from this that the intensity of a thermal treatment should not be characterized by machine data but rather by its effective temperature which indicates changes in the state of order in the polymer brought about by thermal treatment.

Tension during heat setting

To study the effect of tension during heat setting, PET filament yarn was treated at different specific tensions varied from 0.0 N/tex to 0.1 N/tex. The setting temperature (200°C) and time (20 sec) were kept constant. The thermograms of these samples are shown in Figure 6a. It is observed that the tension during heat setting influences the partial melting peak. An increase from zero tension to 0.02 N/tex causes a decrease in temperature of the partial melting peak. The result leads to the assumption that the stresses developed in the non-crystalline regions during heat setting cause a less uniform crystal size distribution in the PET polymer, thereby lowering the partial melting peak temperature.

If the same material is subjected to a high temperature dyeing process an additional partial melting peak at 170°C is observed as shown in Figure 6b. In this case the premelting peak, at 170°C increases slightly on the d.t.a. tempera-

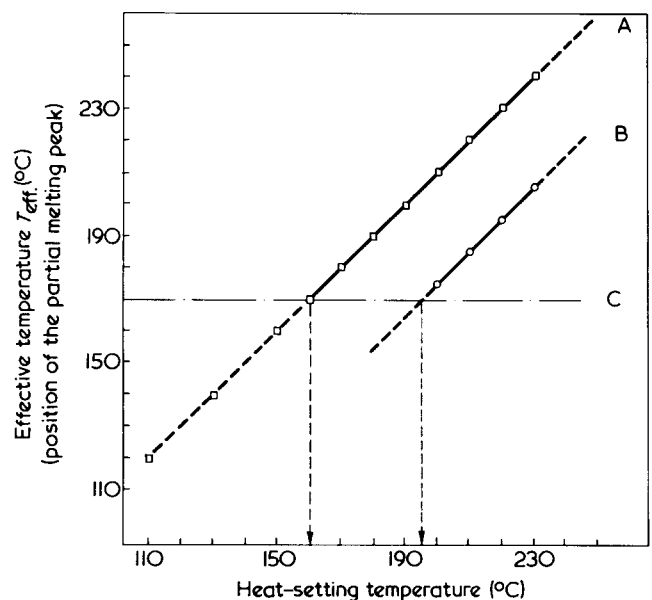


Figure 5 Influence of heat setting temperature, time of treatment and high temperature dyeing on the effective temperature. A, heat setting 20 sec in hot air (\square); B, heat setting 0.2 sec in hot air (\circ); C, high temperature dyeing at 130°C , 90 min (---)

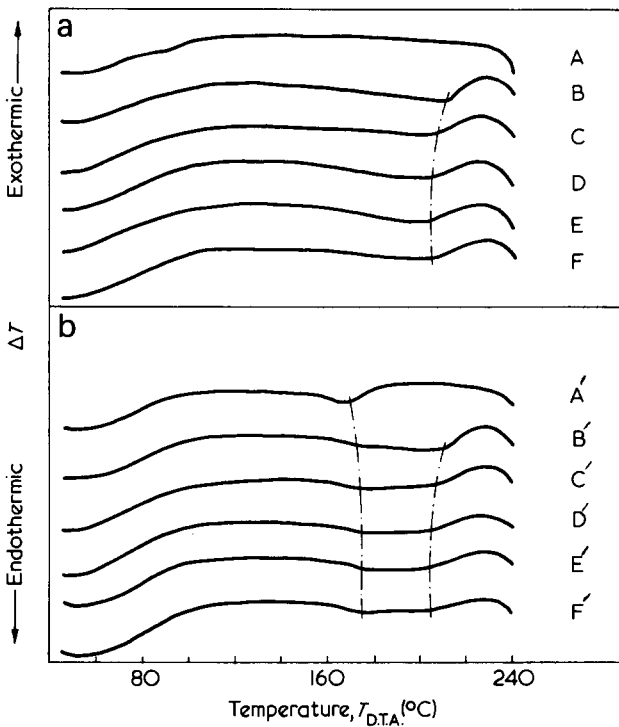


Figure 6 (a) D.t.a. traces of PET fibres heat set (hot air, 20 sec, 200°C) at the various indicated tensions (N/tex): A, original; B, 0.00; C, 0.01; D, 0.02; E, 0.05; F, 0.10. (b) As (a) and high temperature dyed (90 min, 130°C). Tensions (N/tex): A', original; B', 0.00; C', 0.01; D', 0.02; E', 0.05; F', 0.10

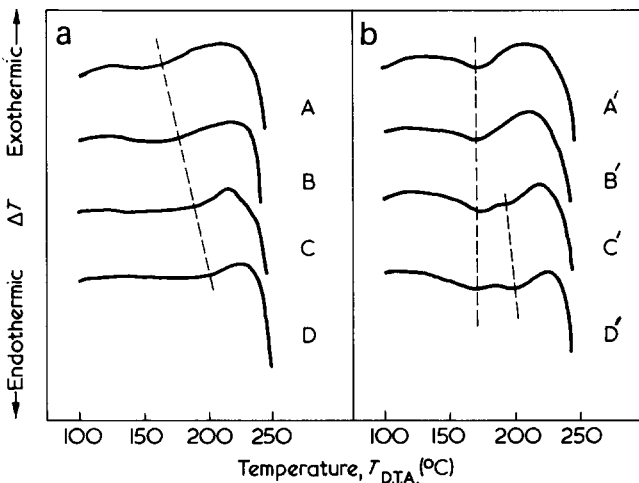


Figure 7 D.t.a. traces of PET yarns false twisted at the various indicated temperatures: (a) before steam setting, temperatures (°C): A, 200; B, 210; C, 220; D, 230 (b) after steam setting, temperatures (°C): A', 200; B', 210; C', 220; D', 230

ture scale with increasing tension. The slight increase in temperature of the endotherm leads one to speculate that the thermodynamically less stable lower melting structures brought about by thermo-setting under tension, melt and recrystallize under the conditions of the dyeing process, as a consequence they cause an improved crystal size distribution and increased molecular orientation in the non-dyed fibre.

This example illustrates that the d.t.a. method should not be used exclusively for identification of fault analysis to explain the cause of the structural changes of PET fibres. The results of d.t.a. measurements should be rather supported by other methods e.g. temperature dependent change of

length (t.m.a.)² or thermal shrinkage force¹³ to characterize the state of structural order.

Application of d.t.a. to fault analysis

Two further examples indicate the feasibility of fault analysis by the d.t.a. method.

Figure 7 shows d.t.a. traces of false twisted yarns heat set at the indicated temperatures for 0.2 sec. A less distinguished but still well detectable partial melting peak is observed at about 25°C below the machine temperature. A following steam setting process intensifies an endotherm at 170°C, in cases where the yarn was exposed to machine temperatures less than 210°C, whereas yarns false twisted at higher temperatures (220° or 230°C) show two separate partial melting peaks in the d.t.a. thermogram. While the first peak at 170°C reflects the effect of steaming, the second one could be associated with the false twisting process itself. In Figure 8 d.t.a. thermograms are shown of textured yarns from a streaky dyed fabric. The first d.t.a. trace demonstrates the behaviour of the lightly dyed material and the second one of the deeper dyed material. Comparing the two traces one can suppose that the lightly dyed material has a less broadened endothermal peak, indicating that during false twisting the yarn adopted a T_{eff} which is comparable with that of the high temperature dyeing. On the other hand the deeper dyed yarn adopted a T_{eff} during false twisting which is about 15°C higher. The difference in T_{eff} could be traced back to differences in heat transfer and/or differences in temperature of heating.

In another case difficulties were encountered when a heavy technical PET fabric were placed on a cylinder thermosetting machine. During thermal treatment the fabric began to drag. D.t.a. measurements made on the material showed (Figure 9) that the fabric did not adopt the same temperature throughout the whole width. As a result different shrinkage forces were developed in the various regions of the fabric and led to dragging. Checking the temperature distribution in the machine by direct measurements confirmed the d.t.a. results.

CONCLUSION

The results of this work illustrate the feasibility of using d.t.a. measurements as an aid to determine the temperature effect which influences the properties of a PET product.

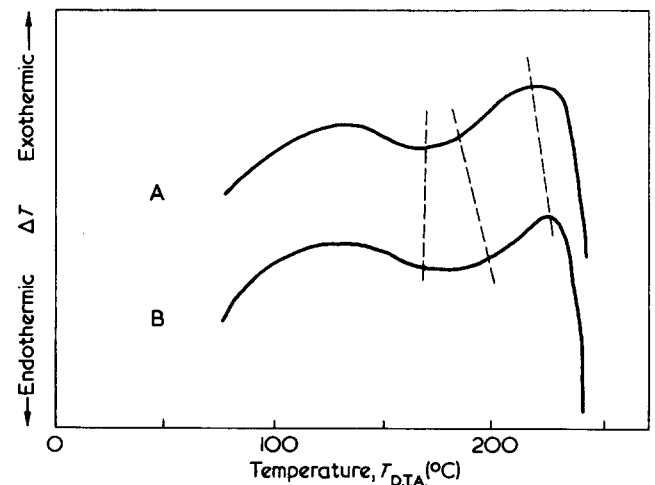


Figure 8 D.t.a. traces of false twisted dyed PET yarn. A, light shade; B, deep shade

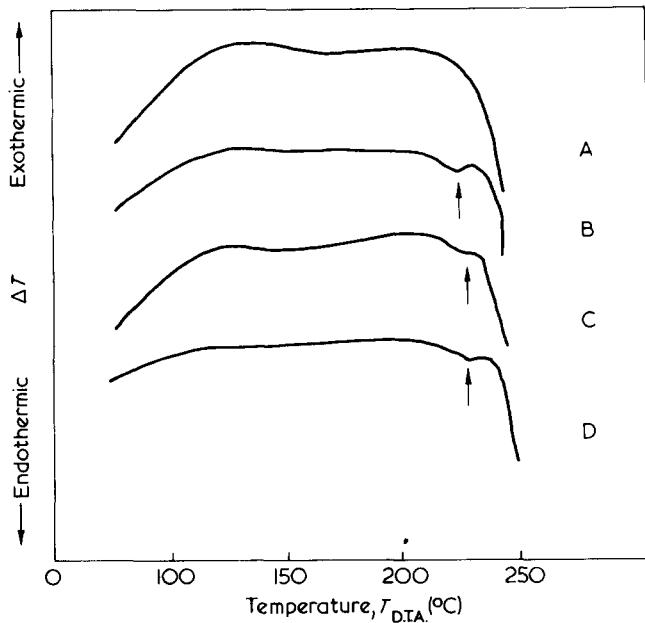


Figure 9 Effect of a temperature distribution in a cylinder thermo-setting machine on the d.t.a. traces of a PET technical fabric; heat set at a machine temperature of 220°C. Curve A, original material; B, right side of treated fabric; C, left side of treated fabric; D, middle of treated fabric

A partial melting peak prior to the main melting peak was observed on commercial PET fibres which were heat set at various temperatures and times, even if the latter were fractions of a second, as in a false twisting process. The position of the partial melting peak on the d.t.a. temperature scale determines the effective temperature (T_{eff}) of the PET fibre. This effective temperature corresponds to a structural feature which is generated by a thermal treatment of the material.

The effective temperature acquired by the PET material is not necessarily equal to the machine temperature since it relies on many different factors such as transfer of heat, medium, and dwell time.

However it cannot be said that d.t.a. should be used independently of other techniques to analyse the state of order of PET or to optimize the process technology.

ACKNOWLEDGEMENTS

This project is part of the programme of the process technology research group at the textile research centre at Krefeld. The authors acknowledge the experimental assistance by members of the group and are grateful to Professor Dr G. Valk and Dr G. Heidemann for valuable discussions.

REFERENCES

- 1 Berndt, H.-J. *Dissertation TH Aachen* (1971)
- 2 Berndt, H.-J. and Heidemann, G. *Dtsch. Färberkal.* 1972, **76**, 408
- 3 Heidemann, G. and Berndt, H.-J. *Chemiefasern Textilind.* 1974, **24**(76), 46
- 4 Wiesener, E. *Faserforsch. Textiltech.* 1968, **19**, 301
- 5 Roberts, R. C. *Polymer* 1969, **10**, 117
- 6 Lawton, E. L. and Cates, D. M. *Polym. Prepr.* 1968, **9**, 851
- 7 Ikeda, M. *Chem. High Polym.* 1968, **25**, 87
- 8 Holdsworth, P. J. and Turner Jones, A. *Polymer* 1971, **12**, 195
- 9 Roberts, R. C. *J. Polym. Sci.* 1970, **8**, 381
- 10 Zachmann, H. G. and Stuart, H. A. *Makromol. Chem.* 1960, **41**, 131
- 11 Wrasidlo, W. *Adv. Polym. Sci.* 1974, **13**
- 12 Schefer, W. *Textilveredlung* 1971, **6**, 69
- 13 Berndt, H.-J. and Heidemann, G. *Melliand Textilber.* 1974, **55**, 548
- 14 Valk, G., Heidemann, G., Berndt, H.-J. and Bossmann, A. *Lenzinger Ber.* 1975, **38**, 172 (Part XVI)

Stored elasticity in flowing solutions of polyisobutylene as measured by recoil

J. Schurz and H.-G. Müller*

*Institut für Physikalische Chemie der Universität Graz und Sonderforschungsbereich 41 (Chemie und Physik der Makromoleküle), A-8010 Graz, Austria
(Received 16 July 1975; revised 10 October 1975)*

Recoil measurements in capillary flow are performed with solutions of polyisobutylene in toluene and used to calculate a shear modulus G . The shear rate dependence of G is explained in terms of a stiffening function and a network destruction function, the first contribution dominating in the measured range. Good agreement is found for recoil in both the capillary and in a rotational viscometer.

INTRODUCTION

Concentrated solutions of high polymers are generally of the network type, in which a continuous network is formed by the molecular strands, by means of so-called 'entanglements'. The bonding at these crossing points may consist of geometrical entanglements of coils penetrating each other, or of secondary bonding at the interface of the molecular coils, which overlap at their periphery only. Further, the networks have to be regarded as temporary, the number of entanglement (resp. bonding) points being a function of the shear rate acting.

One of the most important properties of such a network solution, is its elasticity. The stored elasticity in a flowing solution can be measured via the normal force effects, or directly by means of recoil. Such recoil measurements are possible in both the rotational viscometer and the capillary viscometer. Unfortunately, there is little experience on how well measurements by various methods agree. Therefore, in this paper, we shall report some measurements with toluene solutions of technical (unfractionated) polyisobutylenes, using direct observation of recoil in the capillary and in the rotational viscometer.

EXPERIMENTAL

The substance

We used technical grade polyisobutylene (unfractionated), obtained from BASF-Ludwigshafen (Oppanol B). The sample Oppanol B 200 was used. Small pieces of the material were swollen in toluene for 24 h, then the remainder of the solvent was added and the solutions rotated on a turning wheel for several weeks. In this way, concentrations of 0.01 to 0.08 g/ml (1–8%) were prepared. Polyisobutylene/toluene solutions prepared in this way have excellent stability. No viscosity variations could be found even for two year old solutions.

The sample had a M_w of $3,55 \times 10^6$ and a M_n of 6×10^5 . Intrinsic viscosity in toluene was 575 ml/g at 25°C. All measurements described were carried out at 25°C.

Apparatus

Recoil measurements were carried out both in a rotational viscometer and in a capillary viscometer. For the

first mentioned method, a commercially available instrument was used (Haake Rotovisco, plus elasticity equipment); these measurements have been described in detail somewhere else¹. For capillary recoil, we used an instrument of our own design², which consisted of an attachment to our high pressure capillary viscometer, which has been amply described in the literature, and which is commercially available (Anton Paar K. G., Graz, Austria).

The connection between the viscometer unit and the horizontally positioned measuring capillary, is made by a three-way cock with a T-bore (see Figure 1). In position 1, it connects the pressure vessel containing the sample, with the measuring capillary; in position 2, it provides a connection between the measuring capillary and atmospheric pressure. The measuring capillary is fixed in such a way, that the moving liquid thread can be observed visually by means of a microscope, with 30 fold magnification (Messmikroskop no. 35496 by Zeiss, Jena). The microscope is mounted on an optical bench. It can be shifted in such a way as to follow the liquid thread, whereby small shifts are accomplished by operating the worm drive of the microscope stage; larger shifts are made by moving the microscope along the optical bench. The capillary is equipped with markings at 10, 20 and 30 cm length. For a measurement, the liquid is allowed to flow until its meniscus just touches one of the markings. Then the three-way cock is turned very quickly by 90°, so that the liquid thread is connected with atmospheric pressure at both ends; as a consequence it will recoil, i.e. the meniscus will retract. The amount of recoil can be measured by means of the crosslines in the microscope, which are shifted from the original position of the meniscus to the new one by means of the microscope rack and pinion, which has

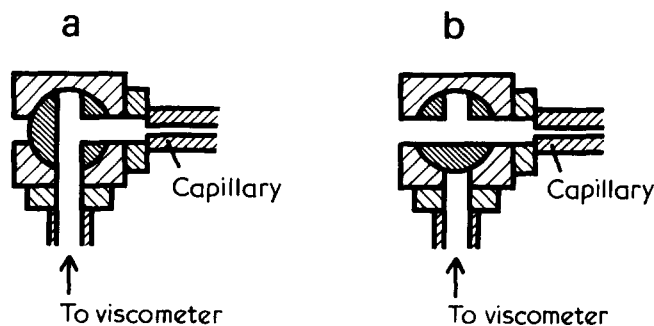


Figure 1 Recoil attachment, schematically. Three way cock: (a) position 1; (b) position 2

* Present address: Donnerburgweg 11, D-33 Braunschweig, West Germany.

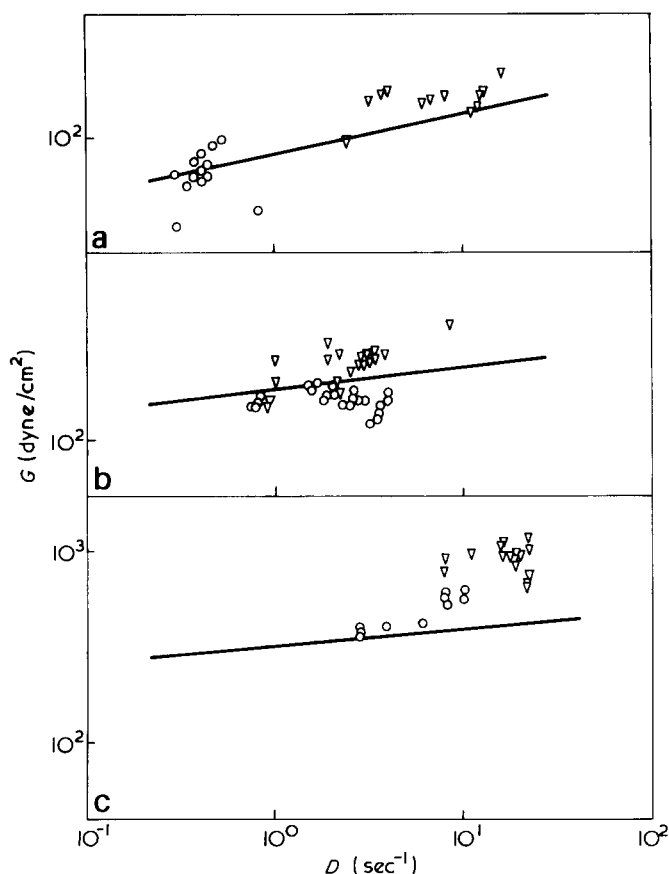


Figure 2 Shear modulus G calculated from recoil for polyisobutylene/toluene. —, recoil measurements in the rotational viscometer Rotovisco. (a) $c = 0.03$ g/ml, $\text{tg}\alpha = 0.22$; (b) $c = 0.04$ g/ml, $\text{tg}\alpha = 0.12$; (c) $c = 0.05$ g/ml, $\text{tg}\alpha = 0.1$

an accuracy of 1/100 mm. This construction allowed the recoil as a function of the length of the liquid thread in the capillary to be tested also. A possible source of error is the fact, that during recoil the shape of the meniscus in the capillary will change. It is slightly concave during flow at small shear rate; after cessation of the flow, the shape changes to a more pronounced concave one. With higher shear rate, the meniscus of the flowing liquid is planar, and only at rest the usual concavity is reformed. In all cases, the amount of recoil was determined at the centre of the profile, that is in the axis of the capillary. Furthermore, in these recoil experiments, the surface tension effects will provide an additional source of error. However, since the capillary is open to the air at both ends, we may expect similar effects at both free surfaces, so that they will cancel in a first approximation.

The evaluation of the data was carried out in the usual way⁴. The shear rate D and shear stress τ were calculated from:

$$D = \frac{4Q}{\pi R^3}; \tau = \frac{Rp}{2l}$$

where: R , radius of capillary; l , length of capillary; Q , flow volume per second; p , driving pressure.

No Weissenberg correction was applied. The recoil length Δl was used first to calculate the recoil volume $V = R^2 \times \pi \times \Delta l$, and this figure was used to derive the recoverable shear S according to Philippoff:

$$S = \frac{4 \times \Delta V}{\pi R^3}$$

From S , a shear modulus G was obtained according to:

$$G = \frac{\tau}{S} = \frac{R^2 p}{8l\Delta l}$$

The resolution of our recoil measurements was 10^{-2} mm. Smaller recoil effects could not be detected in our apparatus. The ratio τ/D is called apparent viscosity and designated by η' .

RESULTS

Dependence of recoil on the flowing volume

First, the amount of recoil was measured as a function of the length of the flowing liquid thread in the capillary, whereby this length was varied between 10 and 33 cm. By adjusting the driving pressure, we kept the shear rate constant for all experiments. It turned out that the amount of recoil is independent of the flowing volume, it is a constant figure and therefore not connected with any variation of the free volume of the flowing liquid, as perhaps caused by the pressure release. If that be the case, the recoil should rise with increasing length of the liquid thread. The absence of such an effect supports the view, that the recoil is caused by elastic effects.

Systematic recoil measurements

The results of our recoil measurements for the sample polyisobutylene B 200 in toluene, for different shear rates and the concentrations 0.03, 0.04 and 0.05 g/ml are shown in Figure 2. In this figure, our results from recoil measurements in the rotational viscometer Rotovisco are also included; they are drawn as solid lines. The shear rate represents the value calculated at the moment of pressure release, thus at the start of the recoil. The data are given in terms of a shear modulus G calculated according to the formulas given above, and presented as a log-log plot.

The results show, that this method of recoil measurement is obviously afflicted with very large inaccuracies, so that the scattering of the measuring points is considerable. Furthermore, these experiments showed that in this way, recoil can only be measured in a limited shear rate range. The reason for this limitation is, that only with a relatively slowly flowing liquid thread, is it possible to stop the flow exactly at the marking of the microscope, which is necessary for the evaluation of the recoil. Furthermore, the accuracy is reduced due to the variation of the shape of the meniscus during recoil.

In spite of all these shortcomings, we note that the measurements in both the rotational viscometer and in the capillary agree satisfactorily. In view of the fact, that agreement of elasticity measurements in instruments so different in measuring principle has hardly been observed so far, we regard this as a support of the general validity of our data. In the small shear rate range we could measure, the shear modulus varies with D^w , w being positive and having the values 0.22, 0.12 and 0.10 for the solutions with concentration 0.03, 0.04 and 0.05 g/ml.

DISCUSSION

The shear rate dependence of the shear modulus is governed by two effects, a stiffening factor $f_1(D)$, which takes into account incomplete relaxation of the network strands and thus will enhance G , and a factor $f_2(D)$, which lowers the

Table 1 Polyisobutylene B 200/Toluene

c(g/ml)	w	u	v
0.03	0.22	2	-1.78
0.04	0.12	2	-1.88
0.05	0.10	2	-1.90

modulus due to network destruction by hydrodynamic forces, which will reduce the number of network points. Thus we may write:

$$G = G_0 \times f_1(D) \times f_2(D) \quad G_0 \text{ value of } G \text{ when } D = 0 \\ \text{(modulus at rest)}$$

If we now use the following notations:

$$G = k \times D^w, \text{ experimental function;}$$

$$f_1(D) = A \times D^u, \text{ stiffening factor;}$$

$$f_2(D) = B \times D^v, \text{ network destruction factor;}$$

we must have:

$$w = u + v \text{ or } v = w - u$$

If we assume $u = 2$ (taken from the dynamic theory of Rouse), we arrive at the following results (see Table I).

Therefore, assuming $u = 2$ we obtain for v , negative values between -1.78 and -1.9 . That means, the network destruction takes place proportional to D^{-v} , whereby v is close to 2. In any event it can be stated, that the increasing function $f_1(D)$ predominates in this range, over the decreasing function $f_2(D)$, so that the overall picture shows a slight increase of the shear modulus G with increasing shear rate.

The level of the shear moduli measured in our D -range is about 10^2 to 10^3 dyn/cm², as seen in Figure 2. This is considerably lower than the G_0 values obtained in an elastoviscometer⁵ (10^4 to 10^5 dyn/cm²). This reflects the fact, that in the flowing solution, significant network destruction must take place.

REFERENCES

- 1 Müller, H.-G. and Schurz, J. *Angew. Makromol. Chem.* 1975, **44**, 119
- 2 Lederer, K. and Schurz, J. *Rheol. Acta* 1975, **14**, 252
- 3 Schurz, J. 'Viskositätsmessungen an Hochpolymeren', Kohlhammer, 1974
- 4 Schurz, J. *Rheol. Acta* 1975, **14**, 293
- 5 Lederer, K. and Schurz, J. *Kolloid. Z. Z. Polym.* 1969, **233**, 878

Effect of pressure on phase transition and morphology of bulk poly(*trans*-1,4-butadiene)

Tsuyoshi Kijima*, Mikio Imamura and Naoshi Kusumoto

Department of Industrial Chemistry, Faculty of Engineering, Kumamoto University, Kumamoto, Japan

(Received 28 August 1975)

The effect of pressure on the melting, solid–solid transition, and crystallization of poly(*trans*-1,4-butadiene) (PTBD) was investigated using the pressure range of 1–3000 kg/cm². D.t.a. measurements showed that, the melting and transition temperatures increase with increasing pressure, whose pressure coefficients are 38°C per 1000 kg/cm² and 22°C per 1000 kg/cm², respectively. These values were in fairly close agreement with those calculated from the Clausius–Clapeyron equation. Morphological studies using electron microscope and small-angle X-ray scattering method revealed that, the samples crystallized with relatively small supercoolings under normal or high pressure, are formed of distinct lamellae 400–800 Å thick. The lamellar thickness was inappreciably dependent on crystallization pressure. The significant effect of pressure on crystallization was recognized in a tendency of the crystallinity to increase, with increasing crystallization pressure. This pressure effect was explained by the mechanism that, the increased pressure might make the packing of molecular chains in liquid, more dense and that the secondary crystallization might be accelerated, to increase the lateral dimensions of lamellae.

INTRODUCTION

Poly(*trans*-1,4-butadiene) (PTBD) is known to have some marked features of structure, molecular motion, and chain flexibility. The molecular chains of this polymer are considered to have relatively high flexibility¹. PTBD undergoes the first-order solid–solid transition, from one crystalline modification (form I) to another form (form II)²; particularly form II, which is stable at temperatures above 76°C and under atmospheric pressure, and is a so-called plastic crystal, in which the molecular chains are free to move and rotate around the molecular axes^{2,3}. In connection with these basic features, a variety of interesting findings have been reported on the morphology^{4–6}, mechanical properties⁵, and calorimetric properties^{6,7}.

The morphology of PTBD single crystals has been studied by several authors by electron microscopy^{4,5}, n.m.r.^{5,6} and calorimetric measurements⁶. However, very few papers have been published concerning the super-structure of PTBD crystallized in bulk. In addition, the effect of pressure on the phase transition of PTBD is of interest if the above mentioned features of the polymer are taken into account. Although there is a report on the solid–solid transition of PTBD under high pressure⁸, no studies have been reported on the effect of pressure on the crystallization and melting.

Therefore, attempts were made to clarify the morphology of PTBD crystallized from the melt at various pressures, along with the pressure dependence of the melting and solid–solid transition temperatures.

EXPERIMENTAL

Material

PTBD was extracted from the original material of Ube Kosan Co. Ltd. with benzene and then precipitated with

methanol, which was filtered and dried to form an aggregate of the polymer. The aggregate was melt-pressed at 160°C and then slowly cooled to room temperature to form thin plate. The intrinsic viscosity of the PTBD in toluene solution at 30°C was 0.967, which yields $M_v = 2.8 \times 10^4$. The infra-red (i.r.) spectrum of this polymer gave >95% *trans* content.

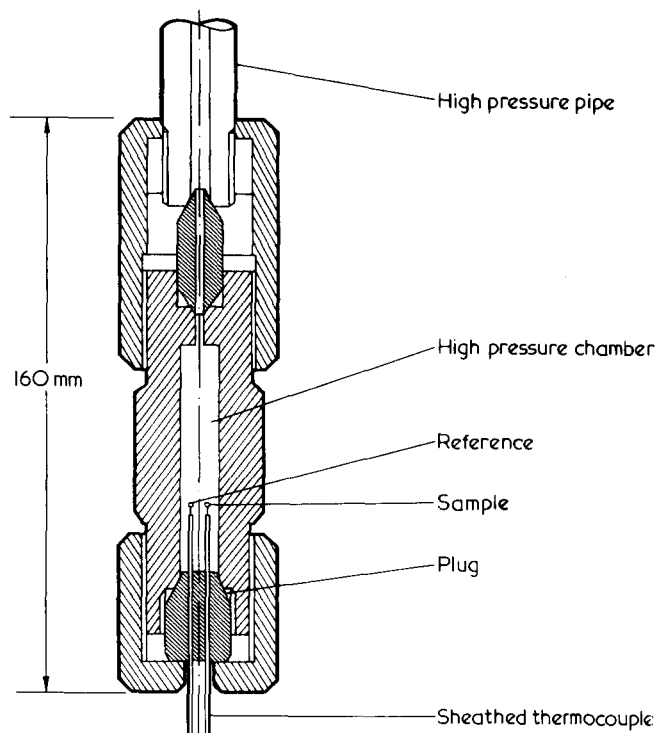


Figure 1 High pressure d.t.a. cell

* Present address: National Institute of Inorganic Materials, Tsukuba, Ibaragi, Japan.

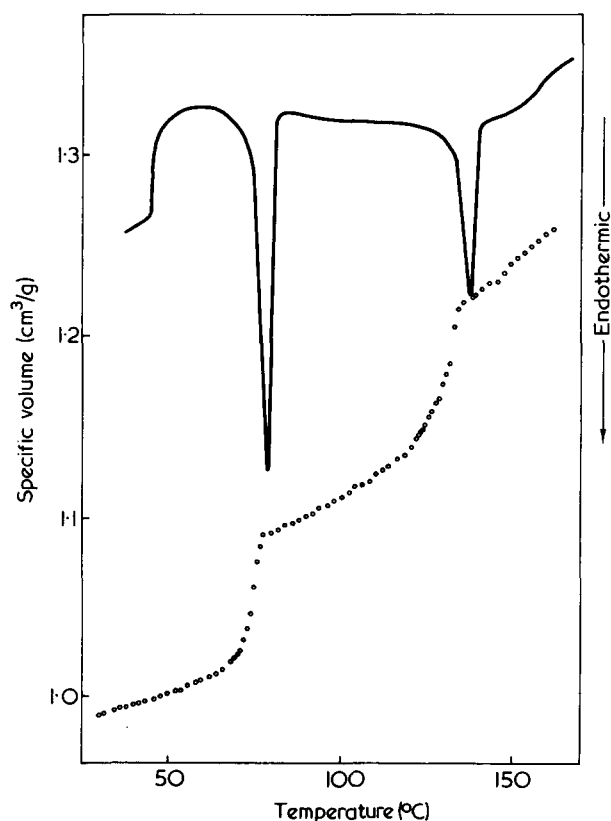


Figure 2 D.s.c. (—) and volume vs. temperature (O) curves of PTBD under normal pressure

Differential thermal analysis (d.t.a.) under elevated pressure

Figure 1 shows the d.t.a. cell, which was designed in a similar manner to that developed by Takemura *et al.*¹⁰. The cell has a chamber of 100 mm in length and 10 mm in diameter, with openings at both ends. One of the openings was connected with a pipe, which was led to the pressure intensifier; the other was closed by a plug containing two metal-sheathed chromel–alumel thermocouples. A few mg of fused PTBD sample were fixed to the junction of the element wires at one end of one of the thermocouples, and the epoxy resin (Araldite) was fixed to that of the other thermocouple, as a reference material. The PTBD was covered with epoxy resin to keep out the pressure transmitting fluid under elevated pressure and temperature. Silicone oil (Toshiba TSF 431) was used as the fluid. The temperature of the d.t.a. cell was controlled manually in an oil bath.

Measurements were conducted with the sample, crystallized from the melt under normal pressure by cooling from 160°C to room temperature at the rate of 1°–2°C/min, while the sample was being fixed to the thermocouple. The normal heating rate of 4°C/min and the pressure range of 1–3000 kg/cm² were used. Measurements in the cooling process were performed with a cooling rate of 1°–3°C/min.

Preparation of pressure crystallized samples

A sheet of the polymer was wrapped in Teflon film and coated with epoxy resin (Araldite), and then it was put into the d.t.a. cell filled with silicone oil. After being precompressed to an appropriate pressure, the sample was heated up to a prescribed temperature to bring about the molten state, and then the pressure was increased rapidly to a predetermined value and held for 3 h. The crystallization temperature was controlled within ±1°C. After gradual cooling to room temperature, the pressure was removed and the sample was taken out.

Some samples were prepared from the melt under normal pressure by isothermal crystallization at various temperatures.

Sample characterization

The characterization of the PTBD samples obtained was carried out by using various methods under normal pressure as follows. Density measurement was conducted by the flotation method, with an aqueous solution of calcium chloride at 25°C. The viscosity of samples in toluene solution was measured at 30°C and i.r. measurement was performed by the KBr pellet method, using a Hitachi/Perkin-Elmer Model 125 spectrophotometer at room temperature. Wide- and small-angle X-ray scattering patterns were taken by the usual method using CuK α rays at room temperature.

In order to determine some thermodynamic quantities upon melting and solid–solid transition, dilatometric and calorimetric measurements under normal pressure were conducted on the sample crystallized for 3 h at 125°C and at normal pressure (sample D). The density of this sample at 25°C was 1.017 g/cm³. This gave a value of 84.3% for the degree of crystallinity, by taking the density of the crystalline region as 1.037 g/cm³¹¹ and that of the amorphous region as 0.926 g/cm³¹². Dilatometry was performed with a heating rate of 1°C/min. Differential scanning calorimetry (d.s.c.) was carried out with a scanning rate of 5°C/min, by using a Rigaku Denki Thermoflex. The temperature and the peak areas were calibrated with indium standard.

RESULTS AND DISCUSSION

Thermodynamic quantities upon melting and transition under normal pressure

Figure 2 shows the dilatometric and the d.s.c. curves under normal pressure for sample D. Each curve exhibits two transitions. The one at the higher temperature side is the melting point and the other is the solid–solid transition (form I to form II). The volume, enthalpy and entropy of melting and those of transition were obtained from these data. Table 1 lists the values of these thermodynamic quantities without and with making crystallinity corrections.

Suehiro *et al.*¹³, reported that the fibre period of PTBD crystal, changes from 4.83 to 4.66 Å and the nearest inter-chain distance, from 4.65 to 4.90 Å at the transition point. These data give a value of 7.17×10^{-2} cm³/g for ΔV_{tr} , in close agreement with 8.05×10^{-2} cm³/g in Table 1.

Table 1 Thermodynamic quantities of transition and melting at normal pressure for PTBD

	Transition			
	T_{tr} (°C)	ΔV_{tr} $\times 10^{-2}$ (cm ³ /g)	ΔH_{tr} (cal/g)	ΔS_{tr} $\times 10^{-2}$ (cal/K g)
obs. ^a	78.0	6.79	26.4	7.52
corr. ^b	78.0	8.05	31.4	8.75
	Melting			
	T_m (°C)	ΔV_m $\times 10^{-2}$ (cm ³ /g)	ΔH_m (cal/g)	ΔS_m $\times 10^{-2}$ (cal/K g)
obs. ^a	136.0	6.14	14.3	3.50
corr. ^b	136.0	7.29	17.1	4.18

^a Values observed on the sample with 84.3% crystallinity

^b Values corrected for the degree of crystallinity

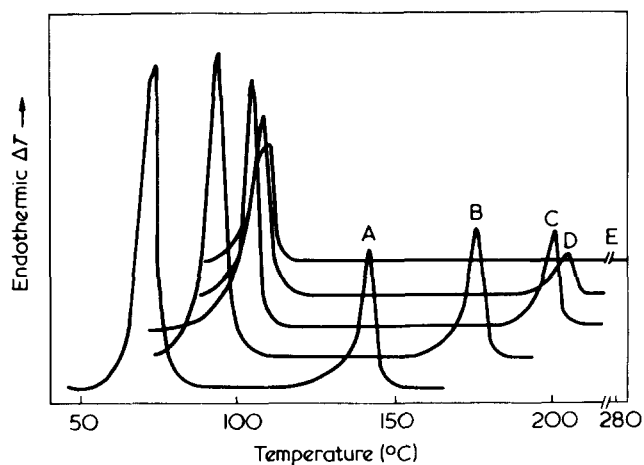


Figure 3 D.t.a. curves of PTBD at various pressures: A, 1; B, 1000; C, 2000; D, 2500; E, 3000 Kg/cm²

Stellman and Woodward⁶, obtained values of ΔH_{tr} , ΔH_m , ΔS_{tr} and ΔS_m for the bulk crystallized PTBD samples, the average values of which were 26.7 cal/g, 13.7 cal/g, 0.078 cal/K g, and 0.035 cal/K g, respectively. These values are in good accord with those uncorrected for the degree of crystallinity in Table 1, but 0.1–0.2 times smaller than the values for purely crystalline PTBD.

Pressure effect on melting and transition

Figure 3 shows the d.t.a. curves as a function of pressure for the sample crystallized by slow cooling under normal pressure. Each curve shows two endothermic peaks, one due to solid–solid transition and the other due to melting.

The melting and transition temperatures defined by each peak temperature are plotted against pressure in Figure 4. The values of dT_m/dP and dT_{tr}/dP , are 38°C per 1000 kg/cm² and 22°C per 1000 kg/cm², respectively, at normal pressure and they tend to decrease with increasing pressure. A value of 22°C per 1000 kg/cm² for dT_{tr}/dP is larger than 17.5°C per 1000 kg/cm², reported by Takemura *et al.*⁸.

The Clausius–Clapeyron, equation (1), for melting ($k = m$) or solid–solid transition ($k = tr$) enables us to calculate the values of dT_m/dP and dT_{tr}/dP using the data on volume and entropy changes:

$$\frac{dT_k}{dP} = \frac{\Delta V_k}{\Delta S_k} \quad (1)$$

The value of dT_m/dP for PTBD at normal pressure, was calculated as 41.1°C per 1000 kg/cm² using the data on ΔV_m and ΔS_m in Table 1. This value is fairly close to 38°C per 1000 kg/cm² experimentally obtained. The calculated value of dT_{tr}/dP at normal pressure was 21.1°C per 1000 kg/cm², in fair agreement with 22°C per 1000 kg/cm² directly measured.

The experimental value of dT_m/dP for PTBD is about 1.7 times larger than that of dT_{tr}/dP . Referring to the data of Table 1, the large difference between the values of dT_m/dP and dT_{tr}/dP for PTBD, can be explained by the fact that the entropy of melting is smaller than that of transition by about 53%, although the volume of melting is smaller than that of transition by only about 10%. The value of dT_m/dP for PTBD is also fairly large in comparison with that for the extended chain crystals of polyethylene (26°C per 1000 kg/cm²), according to one of the authors¹⁴. The values of ΔS_m and ΔV_m per mole of bond, for PTBD are

taken as 0.564 cal/K and 0.986 cm³, respectively, according to Table 1, and those for polyethylene are taken as 2.32 cal/K and 2.56 cm³, respectively¹⁴. Hence, the value of ΔV_m per bond for polyethylene is about 2.6 times as large as that for PTBD, whereas the values of ΔS_m per bond of the former is about 4.1 times as large as that of the latter. This fact is compatible with the large value of dT_m/dP for PTBD compared with that for polyethylene.

The d.t.a. traces for melting and transition of PTBD, showed a remarkable tendency to decrease in peak area with increasing pressure, as seen in Figure 3; the melting peak no longer appeared at 3000 kg/cm². This fact suggests that the enthalpy and entropy of melting and those of transition might decrease remarkably with an increase of pressure. This is not inconceivable, if the considerably small entropies of melting and transition per bond, at normal pressure for PTBD compared to the entropy of melting per bond of many other polymers¹⁵ are taken into account.

Lamellar structure of PTBD crystallized at normal and high pressures

Table 2 lists the density at 25°C, degree of crystallinity, and the melting and transition temperatures under normal pressure of PTBD samples crystallized for 3 h at various temperatures (T_c) and at various pressures (P_c); the melting temperature at 3000 kg/cm² was estimated as 210°C from the extrapolation of T_m – P curve indicated by a broken line in Figure 4. For reference, the recrystallization and retransition temperatures in the slow cooling process from the melt are plotted against pressure by solid circles in the same Figure. Some data on sample D were previously described.

Wide-angle X-ray scattering patterns (WAXS), were taken on the starting sample prepared from the melt by slow cooling under normal pressure and sample F crystal-

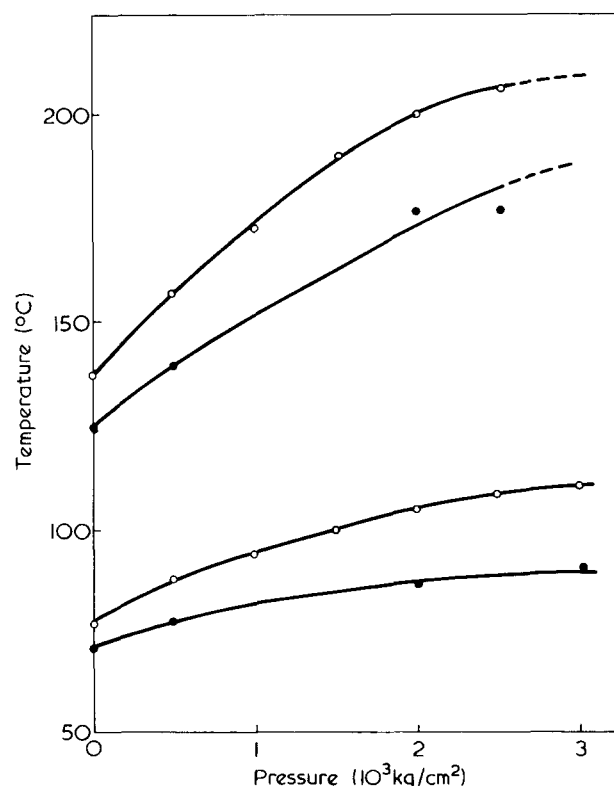


Figure 4 Plots of melting (○, upper); transition (○, lower); recrystallization (●, upper); and retransition (●, lower) temperatures against pressure for PTBD

Table 2 Crystallization condition of PTBD samples and their characterization

Sample	C	D	F	G
Crystallization pressure, P_c (kg/cm ²)	1	1	2000	3000
Crystallization temperature, T_c (°C)	65	125	170	200
Crystallization time, (h)	3	3	3	3
Degree of supercooling, $T_m - T_c$ (°C)	73	13	30	10
Density at 25°C at 1 atm (g/cm ³)	1.015	1.017	1.018	1.023
Degree of crystallinity (%)	82.6	84.3	85.1	89.3
T_{tr} at 1 atm (°C)	75.0	78.0	76.8	76.6
T_m at 1 atm (°C)	135.5	136.0	135.5	134.5
Lamellar thickness (Å)				
EM ^a	400–500	500–850	400–500	400–600
SAXS ^b (ib. average)	410–460 (435)	660–800 (730)	430–500 (465)	460–620 (540)

^a Determined from electron micrograph

^b Determined from SAXS pattern

Table 3 Values of d -spacing obtained from the WAXS patterns of (A) starting sample and (B) sample F in Table 2

d -spacing (Å)	
A	B
3.85	3.90
3.14	3.05
2.89	2.89
2.50	2.52
2.25	2.26
2.05	2.03

lized at 2000 kg/cm². The five reflections observed in both patterns were found to give nearly the same d -spacings, as shown in Table 3. This fact indicates that no new crystalline modification is formed by pressure crystallization. The i.r. spectra of pressure-crystallized samples, showed no significant changes against the starting sample, suggesting that the thermal deterioration of samples during the crystallization processes are negligible. The d.s.c. traces under normal pressure for samples F, G, and C were similar to that of sample D shown in Figure 1. The melting and transition temperatures, T_m and T_{tr} , determined from the peak positions in each d.s.c. curve are shown in Table 2.

Figure 5 shows, the electron micrograph of replica of a fracture surface of sample G crystallized at 3000 kg/cm² and at 200°C. In the micrograph, some sets of long lamellae of 400–600 Å in thickness, can be seen to extend in parallel or spheroidally. The lamellae are also noticed to be remarkably uniform in thickness, which suggests that sample G will yield a discrete small-angle X-ray scattering (SAXS) pattern. The SAXS pattern of sample G shows a discrete diffraction ring in the larger angle range, whereas a trace of a more intense diffraction ring is seen in the smaller angle range (around the centre). Provided that the discrete diffraction in the larger angle range is a first-order diffraction, the long period of 270 Å is obtained. This value, however,

is too small compared with the lamellar thickness observed above. On the other hand, if the large-angle diffraction is assumed to be the second order of the more intense diffraction found in the smaller angle range, it yields a value of 540 Å for the first period, in agreement with the lamellar thickness determined microscopically. The fact that the SAXS pattern of sample G exhibits a uniform ring, not a spotty one, suggests that the observed lamellae are constituent parts of spherulites. Similar lamellar structure is found on the surface replica of sample F crystallized at 170°C under 2000 kg/cm² (Figure 6) and that of sample D crystallized at 125°C under normal pressure (Figure 7). On the other hand, the lamellar structure of sample C crystallized at 65°C under normal pressure, is less distinct and the lamellae are shorter in lateral dimension and poorly oriented in comparison with samples crystallized with smaller supercoolings, as shown in Figure 8. Clearly the less developed lamellar structure of sample C is reflected in the relatively low crystallinity shown in Table 2. Sample C also gave a discrete SAXS pattern, and for each sample, the lamellar thickness observed by electron microscope and the long period determined from the SAXS pattern, were found to be consistent with each other, as shown in Table 2.

The above data and observations show some characteristics of melt-crystallized PTBD. The density data indicates that PTBD readily yields considerably high density or crystallinity by the melt-crystallization. The very high density

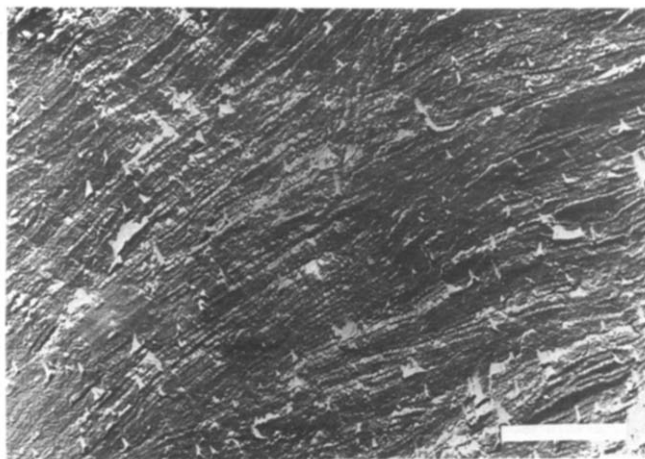


Figure 5 Electron micrograph of a fracture surface of PTBD crystallized at 3000 kg/cm² and at 200°C (sample G). Scale bar represents 1 μm



Figure 6 Electron micrograph of a fracture surface of PTBD crystallized at 2000 kg/cm² and at 170°C (sample F). Scale bar represents 1 μm

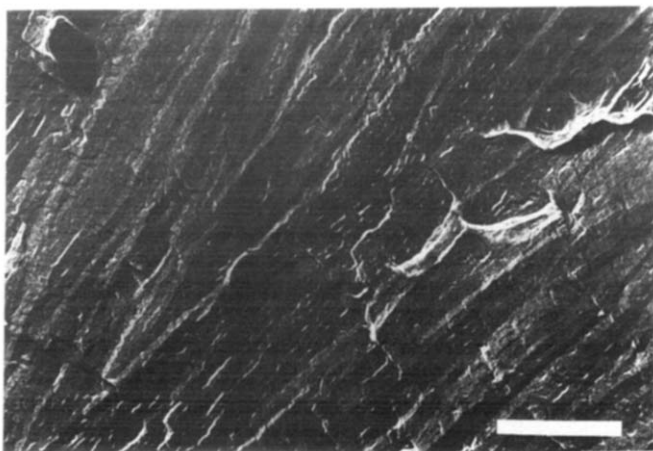


Figure 7 Electron micrograph of a fracture surface of PTBD crystallized at 125°C under normal pressure (sample D). Scale bar represents 1 μm

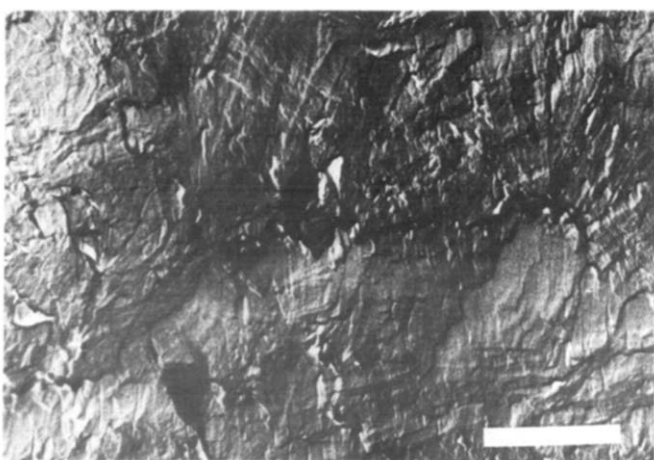


Figure 8 Electron micrograph of a fracture surface of PTBD crystallized at 65°C under normal pressure (sample C). Scale bar represents 1 μm

or crystallinity is also consistent with the fact that highly developed lamellar structure is observed as mentioned above. The PTBD samples crystallized at relatively small supercoolings, were found to be formed of distinct lamellae 400–800 Å thick. Such a distinct lamellar structure with the same order in thickness, was observed for the melt-crystallized polyethylene with low molecular weight, whose lamellae were found to be composed of extended chains¹⁶. The PTBD lamellae observed above, on the contrary, can be regarded as being composed of folded chains,

since the fully extended chain length of the PTBD with $M_v = 2.8 \times 10^4$, is about 2600 Å. The significant effect of pressure on crystallization of PTBD can be evidently found in the crystallinity data in Table 2; samples G and F crystallized at elevated pressure exhibit increased crystallinity, compared to sample D crystallized at normal pressure, although the lamellar thicknesses of the former two are rather smaller than that of the latter. The increase of crystallinity with increasing pressure, will be ascribable to the increase in lateral dimension of lamellae, as suggested by the morphology of sample C with low crystallinity in Figure 8. This may be explained by the mechanism that the increased pressure might make the packing of molecular chains in liquid more dense and thus the secondary crystallization might be accelerated to increase the lateral dimension of lamellae.

ACKNOWLEDGEMENT

We wish to thank Professor M. Takayanagi in Department of Applied Chemistry of Kyushu University for supplying the polymer and making the high pressure apparatus available.

REFERENCES

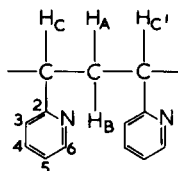
- 1 Swallow, J. C. *Proc. R. Soc. (A)* 1956, **1**, 238
- 2 Natta, G. and Corradi, P. *Nuovo Cimento* 1960, **15**, (Suppl. 1), 9
- 3 Iwayanagi, S. and Miura, I. *Rep. Prog. Polym. Phys. Japan* 1965, **8**, 303
- 4 Iwayanagi, S. and Miura, I. *Rep. Prog. Polym. Phys. Japan* 1965, **8**, 95
- 5 Tatsumi, T., Fukushima, I., Imada, K. and Takayanagi, M. *J. Macromol. Sci. (B)* 1967, **1**, 459
- 6 Stellman, J. M. and Woodward, A. E. *J. Macromol. Sci. (B)* 1973, **7**, 539
- 7 Daiton, F. S., Evans, D. M., Hoare, F. E. and Melia, T. P. *Polymer* 1962, **3**, 297
- 8 Ueno, H., Yasuniwa, M., Taki, S., Nakafuku, C., Hirakawa, S. and Takemura, T. *Technol. Rep. Kyushu Univ.* 1970, **42**, 798; Takemura, T. *Prog. Polym. Sci. Japan* 1974, **7**, 225
- 9 Takeda, M. and Endo, R. *Rep. Prog. Polym. Phys. Japan* 1963, **6**, 37
- 10 Takemura, T. *Prog. Polym. Sci. Japan* 1974, **7**, 225
- 11 Iwayanagi, S., Sakurai, I., Sakurai, T. and Seto, T. *J. Macromol. Sci. (B)* 1968, **2**, 163
- 12 Natta, G. and Moraglio, G. *Rubber Plast. Age* 1963, **44**, 42
- 13 Suehiro, K. and Takayanagi, M. *J. Macromol. Sci. (B)* 1970, **4**, 39
- 14 Takayanagi, M., Kijima, T., Imada, K. and Yoshizumi, T. *Proc. 4th Int. Conf. High Pressure, Kyoto* 1974, p 51
- 15 Manderkern, L. 'Crystallization of Polymers', McGraw-Hill, New York, 1964, Ch 5
- 16 Anderson, F. *J. Polym. Sci. (C)* 1963, **3**, 123

Notes to the Editor

Microstructure of poly(2-vinylpyridine): correlation between ^{13}C and ^1H n.m.r. determinations

M. Brigodiot, H. Cheradame, M. Fontanille* and J. P. Vairon†
Ecole Francaise de Papeterie, 44 Avenue Felix Viallet, 3800 Grenoble, France
(Received 10 October 1975)

First attempts of structure determination on poly(2-vinylpyridine) (P2VP) by 60 MHz p.m.r. led only to essentially qualitative conclusions: a broad peak with a low field shoulder was observed for α and β chain protons and the intensity of the shoulder increased with increasing isotactic content of the polymer^{1,2}.



Further examinations at 100 MHz of isotactic P2VP samples^{3,4} have shown that the low field peak corresponds to the isotactic H_C methine resonance. When the spectra were run at 140° – 160°C in *o*-dichlorobenzene, fine structures were observed leading to two multiplets centred at ~ 8.0 and 7.4τ , and assigned respectively to H_C and H_A, H_B . A theoretical spectrum was calculated using a single coupling constant between the α and β protons ($J_{AC} = J_{BC} = J_{AC'} = J_{BC'} = 7 \text{ Hz}$) and was in fair agreement with the two observed multiplets. Isotactic $\alpha, \text{trans-}\beta\text{-}d_2\text{-poly(2-vinylpyridine)}$ was also prepared and the H_C quintet disappeared from the spectrum, supporting thus the above assignment⁴.

$^{13}\text{C}\text{-}\{^1\text{H}\}$ resonance spectra of atactic and isotactic P2VP were recently published^{5,6}. One of these studies⁵ was devoted to relaxation times and side group motions and does not report on tacticity measurements. The other study⁶ showed that the quaternary carbon C_2 of the pyridyl ring was the most stereosensitive. The C_2 resonance line split into three peaks, which, according to the expected structures of polymers studied, were assigned to iso-, hetero- and syndio-tactic triads in the order of increasing field. We recently used the ^{13}C n.m.r. for tacticity determinations of different P2VP samples and some discrepancies appeared between preceding assignments and our results. It was thus interesting to correlate the ^1H and ^{13}C analyses in order to test the validity of the method. We report here on a careful re-examination of the 25.15 MHz $^{13}\text{C}\text{-}\{^1\text{H}\}$ and 250 MHz ^1H spectra of poly(2-vinylpyridine) samples of different tacticities.

EXPERIMENTAL

Polymer samples

Isotactic P2VP (A) was prepared by anionic polymeriza-

* Laboratoire de Recherches sur les Macromolécules de l'Université Paris-Nord, Place du 8 Mai 1945, 93206 Saint-Denis Cedex, France.

† Laboratoire de Chimie Macromoléculaire associé au CNRS, Université Pierre et Marie Curie-4, Place Jessieu, 75230 Paris Cedex 05, France.

tion in benzene solution with $\text{C}_6\text{H}_5 \text{Mg Br}$ as initiator. Atactic P2VP samples (B) and (C) were prepared anionically at -78°C in THF solution, using respectively Na^+ and K^+ as counter-ions. Atactic P2VP samples (D) and (E) were prepared by radical polymerization at 60°C using AIBN as initiator, either in bulk (D) or in 30% (v/v) methanol solution (E).

N.m.r. analysis

P.m.r. spectra were run at 250 MHz in CDCl_3 or CD_3OD solutions (10% w/v) at room temperature using a Cameca 250 MHz spectrometer. The $^{13}\text{C}\text{-}\{^1\text{H}\}$ spectra were observed at 25.15 MHz at room temperature in CD_3OD solution (observation of aromatic carbons) and CDCl_3 solution (observation of chain carbons) with noise proton decoupling and internal lock on deuterium using either Jeol PFT 100 or Varian XL 100-12 WG FT spectrometers. Tacticity measurements were done by integration for ^1H spectra and by cutting and weighing the paper for ^{13}C spectra. Overlapping peaks were hand resolved.

RESULTS AND DISCUSSION

As the proton spectrum of isotactic P2VP was run at room temperature we obtained only the envelopes of the two expected multiplets with a beginning of fine structure appearance (Figure 1). No fine structure at all was observed for the atactic samples as the resonance of (mr + rr) methine protons H_C overlap with (r + m) methylenic protons H_A and H_B . But, for all samples, the isotactic (mm) α -proton H_C triad is fairly well separated from the broad pattern due to CH_2 (m + r) dyads and CH (mr + rr) triads, allowing an easy measurement of peak areas and the determination of the isotactic triad content of the different polymers ($[\text{mm}] = 3a_I/(a_I + a_{II})$, see Figure 1).

Chain and pyridyl ring carbons are differently stereosensitive, depending on the solvent used. The best sensitivity was observed for the ring carbon C_2 in methanol solution and for the chain carbons in CDCl_3 solution, as was previously reported by Lukovkin *et al.*⁶

The C_2 triad pattern is sufficiently resolved to measure accurately the areas of the three main peaks. As shown in Figure 2 a comparison between isotactic and atactic P2VP spectra leads to an unequivocal triad assignment. Thus the triad content of each sample can be directly determined from the C_2 pattern. Each of these triad resonances exhibit pentad effects and a tentative assignment of pentad placements may be provided at least for iso and heterotactic sequences (Figure 2). In the isotactic polymer (A), the most probable mmmm pentad appears at the lowest field position of the mm resonance pattern and, in the atactic samples, the relative importance of the lowest field shoulder of the mr peak increases with increasing isotactic content of the

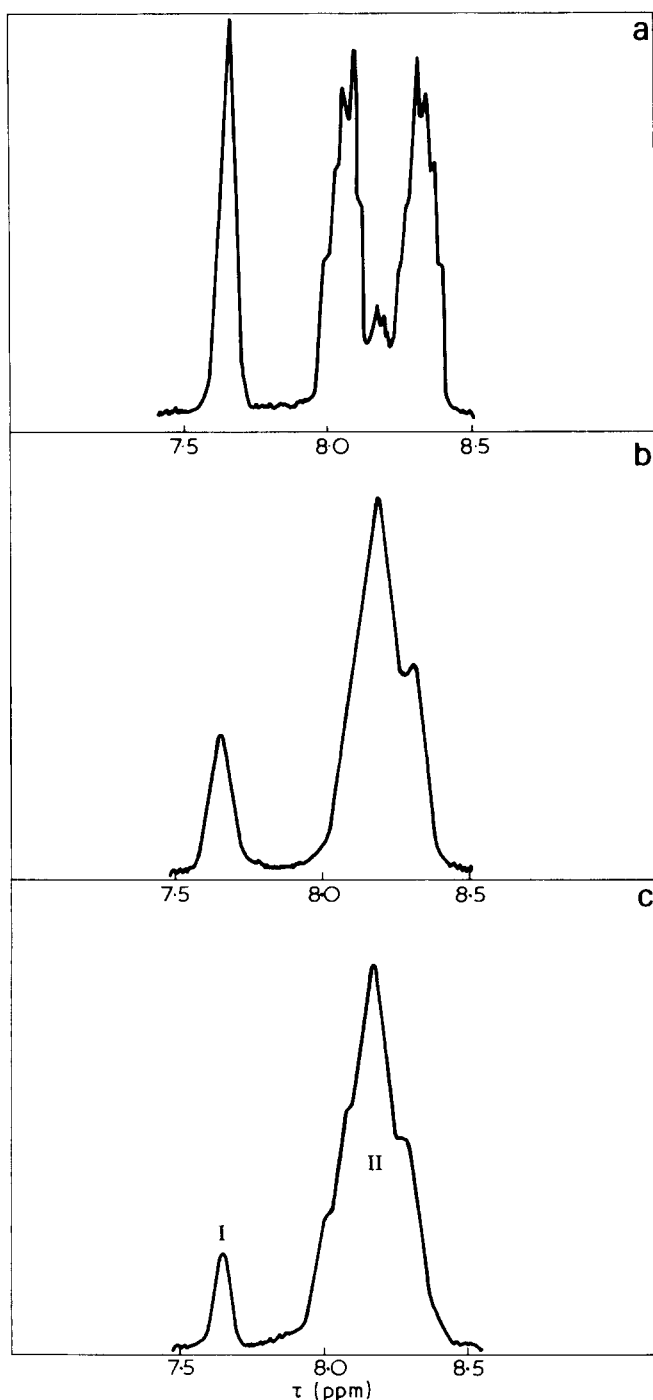


Figure 1 Chain protons 250 MHz spectra of (a) isotactic (sample A); (b) atactic (sample B) and (c) atactic (sample E) poly(2-vinylpyridines) (CD_3OD solution at 25°C)

polymer, leading to a mmmr assignment for this shoulder. The proposed order is more doubtful for syndiotactic pentads.

In the isotactic P2VP sample, CH and CH_2 chain carbons appear as two single and well separated resonance lines, whereas in atactic samples the corresponding peaks split into two multiplets (Figure 3). The CH patterns exhibit the expected triad effect, but the syndiotactic triad resonance overlaps the heterotactic one and cannot be accurately resolved. The complex multiplet corresponding to the methylenic chain carbon is so poorly resolved that we cannot provide, the mmm tetrad position apart, any reasonable assignment. It can be seen in Table 1 that the tacticity determinations by ^1H and ^{13}C n.m.r. are in good agreement, supporting thus the above assignments.

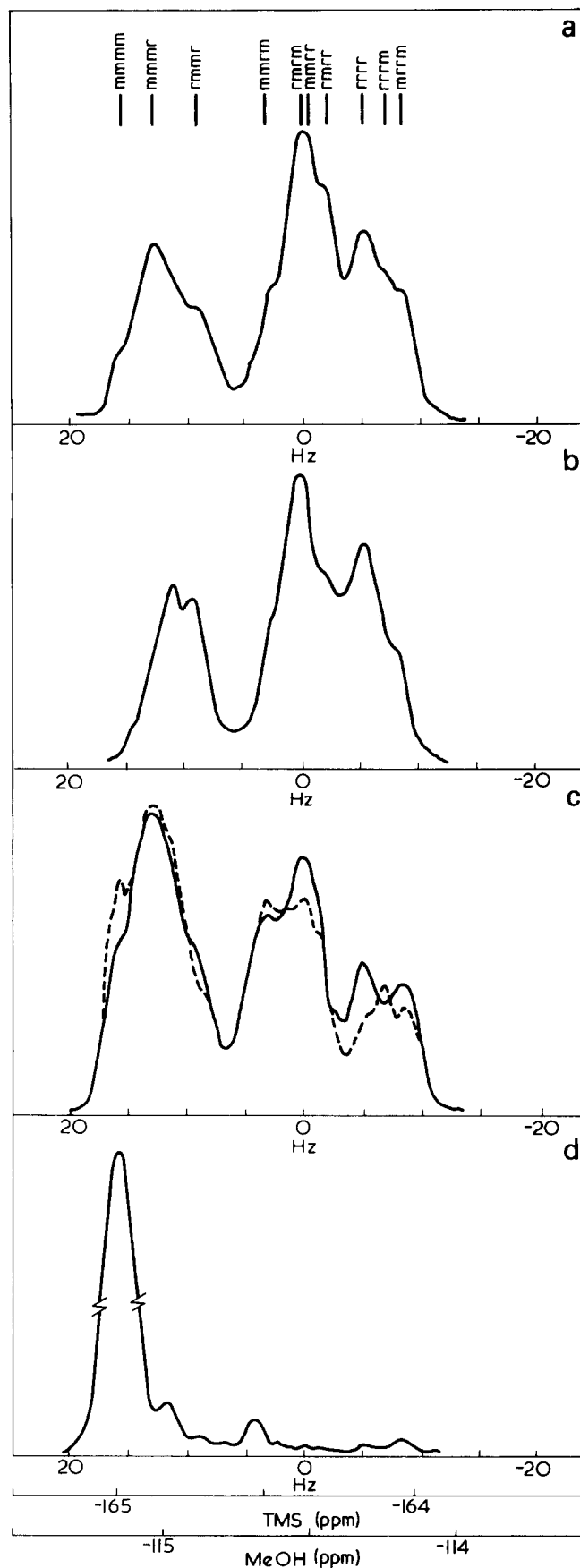


Figure 2 $^{13}\text{C}-\{^1\text{H}\}$ spectra of C_2 pyridyl ring carbon observed at 25.15 MHz in $\text{CD}_3\text{OD}/\text{CH}_3\text{OD}$ solution at 25°C (TMS and methanol as internal standards). (a), sample D; (b), sample E; (c) samples B (—) and C (---); (d), sample A

Table 1 Comparison between the ^1H (chain protons) and ^{13}C (ring carbon C2) n.m.r. determinations of P2VP tacticity

Samples	Polymerization conditions	$^1\text{H}^*$		$^{13}\text{C}-\{^1\text{H}\}^\dagger$			$4is$
		<i>i</i>	<i>h + s</i>	<i>i</i>	<i>h</i>	<i>s</i>	h^2
A	$\phi\text{MgBr}/\text{C}_6\text{H}_6$	0.89	0.11	0.89	~ 0.06	~ 0.05	—
B	$\text{Na}^+/\text{THF}/-78^\circ\text{C}$	0.43	0.57	0.47	0.38	0.15	1.95
C	$\text{K}^+/\text{THF}/-78^\circ\text{C}$	0.50	0.50	0.50	0.36	0.14	2.16
D	AIBN/bulk/ 60°C	0.27	0.73	(0.49)	(0.49)	(0.51)	—
E	AIBN/ $\text{Me}_2\text{OH}/60^\circ\text{C}$	0.25	0.75	0.28	0.48	0.24	1.07

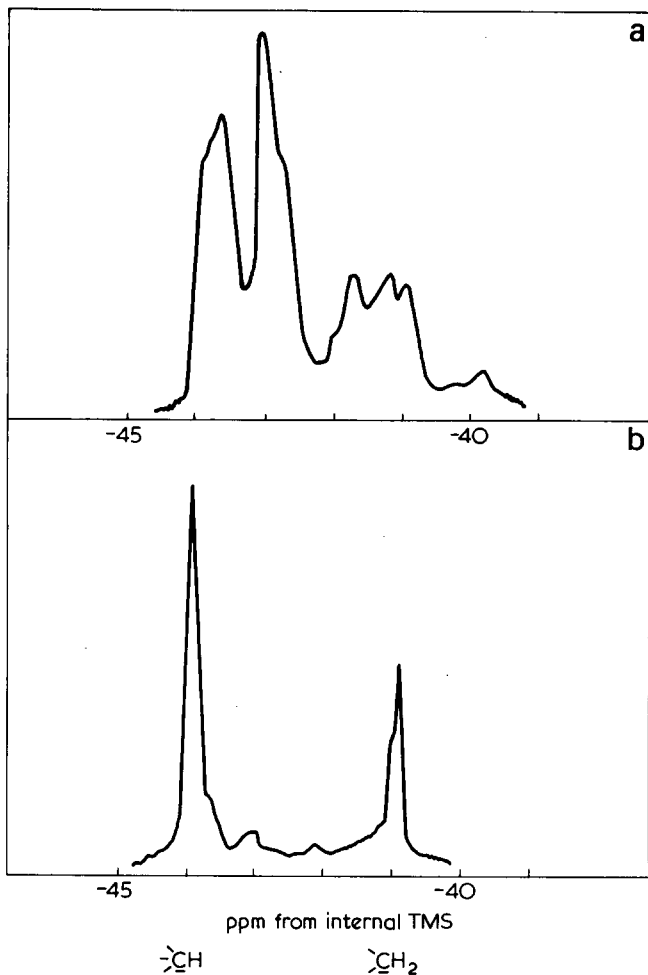
* Accuracy ± 0.02 † Accuracy ± 0.03 . Values in brackets are referred to determination on methine chain carbon

Figure 3 $^{13}\text{C}-\{^1\text{H}\}$ spectra of chain carbons of (a) atactic (sample C) and (b) isotactic (sample A) poly(2-vinylpyridines), observed at 25.15 MHz in CDCl_3 solution at 25°C

For radical polymerizations (in bulk or even in solution) propagation mechanisms appear to be controlled by a Bernoulli trial process ($4is/h^2 \sim 1$) whereas for anionic polymerization they deviate noticeably from Bernoullian statistics. Unfortunately the lack of resolution does not allow the determination of tetrads and pentads contents and Markov or Coleman-Fox statistics cannot be tested for the predominantly isotactic polymers.

The observed ^{13}C chemical shifts (see Figures 2 and 3) agree closely with those reported by Chachaty *et al.*⁵ but they are somewhat different (~ 1 ppm) from those given by Lukovkin *et al.*⁶. The major discrepancy with the results of these last authors concerns the assignment of the C_2

triad pattern. Their analysis of a polymer prepared in the same conditions as those used for our sample D (see Table 1) led to a predominantly syndiotactic Bernoullian distribution ($P_m = 0.22$) with a very low isotactic triad content (2%), in complete disagreement with our own analysis of the same type of polymer (sample D, $P_m = 0.53$). As in the spectrum published by Lukovkin the isotactic peak appears as a very weak shoulder, the assigned *h* peak might most probably be the true isotactic one. Thus the assigned *s* peak might be the overlapping of the hetero- and syndiotactic ones. We observed the same chemical shifts difference (~ 12 Hz) between the peaks we assigned *i* and *h* as between the peaks Lukovkin assigned *h* and *s*, whereas we observed a 6 Hz difference between the peaks we assigned *h* and *s*. This observation supports the above explanation.

In conclusion a good correlation is observed between the ^1H and ^{13}C n.m.r. determinations of poly(2-vinylpyridine) microstructure. The 25.15 MHz ^{13}C spectra allow the estimation of triad contents and the propagation of the 2VP radical polymerization appears to be controlled by a Bernoullian process. Higher field ^{13}C n.m.r. observation will probably lead to quantitative pentad and tetrad determinations and this will give information on the non-Bernoullian propagation of 2VP anionic polymerization. This is not only depending upon the active centres dissociation equilibrium but also upon an assumed specific penultimate solvation of the sodium counterion⁹ which might strongly influence the propagation statistics. We have presently undertaken a higher field re-examination of different anionic samples of P2VP.

ACKNOWLEDGEMENTS

The authors are indebted to the NMR centre of Grenoble and to the spectrochemical centre of P. and M. Curie University.

REFERENCES

- Geuskens, G., Lubikulu, J. C. and David, C. *Polymer* 1966, 7, 63
- Holt, P. F. and Lindsay, H. *J. Chem. Soc. (C)* 1969, p 1012
- Weill, G. and Hermann, G. *J. Polym. Sci. (A-2)* 1967, 5, 1293
- Matsuzaki, K. and Sugimoto, T. *J. Polym. Sci. (A 2)* 1967, 5, 1320
- Chachaty, C., Forchioni, A. and Ronfard-Haret, J. C. *Makromol. Chem.* 1973, 173, 213
- Lukovkin, G. M., Komarova, O. P., Torchilin, V. P. and Kirsh, Y. E. *Vysokomol. Soedin. (A)* 1973, 15, (2), 443
- Natta, G., Mazzanti, G., Dall'asta, G. and Longi, P. *Makromol. Chem.* 1960, 37, 160
- Natta, G., Mazzanti, G., Longi, P., Dall'asta, G. and Bernardini, F. *J. Polym. Sci.* 1961, 51, 487
- Tardi, M. and Sigwalt, P. *Eur. Polym. J.* 1972, 8, 151

Potential energy calculations about the chain folding of α (-)poly(L-alanine)

M. D'Alagni

Centro di Studio per la Chimica dei Recettori del CNR, c/o Università Cattolica, via Pineta Sacchetti 644, 00168 Roma, Italy

E. Giglio*

Istituto di Chimica-fisica, Università di Roma, 00185 Roma, Italy

and N. V. Pavel

Laboratori Ricerche di Base, Snam Progetti SpA, 00015 Monterotondo, Roma, Italy

(Received 9 September 1975)

Studies on the crystalline morphology of α -poly(L-alanine), (PA), clearly showed the existence of sheaves consisting of platelets about 150 Å thick, stacked on edge¹, so that it can be inferred that re-entrant folding must occur, owing to the length of a single macromolecule much greater than 150 Å. The same behaviour is displayed by other biopolymers²⁻⁴ and by a wide variety of synthetic polymers⁵⁻⁷. On the other hand, it is widely believed that a polypeptide chain folds in a physiological environment or, in general, in a solvent according to the laws of thermodynamics. In this connection high ΔH^0 values, achieved from potentiometric measurements, seemed to point to the presence of compact hydrophobic states, in the case of the sequential copolymers poly(L-leucyl-L-leucyl-L-aspartic acid)⁸ and poly(L-leucyl-L-leucyl-L-lysine)⁹. The experimental results agree with the formation of α -helical segments, strongly stabilized by hydrophobic interactions and suggest the existence of a rather ordered structure, which may be characterized by chains folding back and forth on themselves.

In order to gain information about possible models of folding, we undertook van der Waals energy calculations on PA, which has the advantage of possessing the hydrophobic methyl group, and no degrees of freedom in the side chain, if CH₃ is considered as one atom. Intramolecular¹⁰⁻¹⁴ as well as intermolecular^{15,16} potential energy calculations were previously performed for regular helical conformations of PA.

The crystal structure of the α -helical PA has been investigated by many researchers¹⁵⁻²⁰ and it has been found to be formed by 50% of 'up-pointing' and 50% of 'down-pointing' right-handed helices arranged in a hexagonal cell with $a = 8.55$ Å, $c = 70.3$ Å. The unit cell contains 47 alanine residues in 13 turns, and the C atoms of the methyl groups, belonging to the 'up' and 'down' chains, are displaced -0.52 Å and rotated 15.1 degrees²⁰. The unit height and twist are $h = 1.495$ Å and $t = 99.57$ degrees respectively,

and the helix is defined by the torsion angles $\phi = -57.4^\circ$, $\psi = -47.5^\circ$ and $\omega = -179.8^\circ$ in agreement with the convention of Klyne and Prelog²¹, which will be used later on.

First, we performed van der Waals energy calculations on the right-handed α -helix of PA built up with the coordinates of Parry and Suzuki²², given in Table 1 together with those of Arnott and Dover²⁰ in parentheses for comparison. The α -helix parameters are: $h = 1.5$ Å; $t = 100^\circ$; $\phi = -51.45^\circ$; $\psi = -52.74^\circ$; $\omega = 180^\circ$. The coefficients of the potentials employed in the generalized form:

$$V(r) = a \exp(-br)/r^d - cr^{-6}$$

were previously reported²³. The system taken into account is illustrated in Figure 1, where both A and C represent 18, 36 or 54 monomers in α -helical conformation and B is the part involved in the minimization procedure (see below), carried out as a function of five rotation angles $\psi_1 - \psi_5$. The van der Waals energy was computed by considering

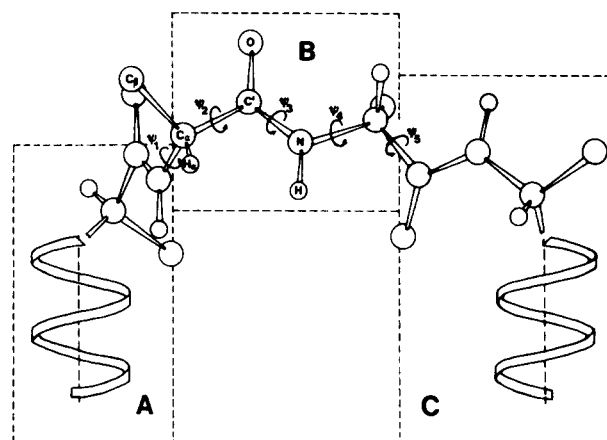


Figure 1 Scheme of the system considered in the calculations. C_β represents the methyl group

* To whom enquiries should be addressed.

Table 1 Atomic cylindrical coordinates and geometry of a monomer of PA following Parry and Suzuki. The values of Arnott and Dover are given in parentheses

Atom	$r(\text{Å})$	ϕ (degrees)	$z(\text{Å})$	Bond lengths (Å)		Bond angles (degrees)		
N	1.550	(1.548)	-28.69 (-27.35)	-0.873 (-0.906)	NC _α	1.47 (1.47)	C _α C'O	121.1 (121.0)
H	1.586	(1.539)	-20.63 (-18.57)	-1.847 (-1.878)	C _α C'	1.53 (1.53)	C _α C'N	114.0 (115.4)
C _α	2.280	(2.288)	0 (0)	0 (0)	C'N	1.32 (1.32)	NC'O	125.0 (123.6)
H _α	3.069	(3.013)	-13.17 (-13.54)	0.467 (0.485)	C'O	1.24 (1.24)	C'NC _α	123.0 (120.9)
C _β	3.218	(3.294)	18.65 (17.63)	-0.830 (-0.808)	NH	1.00 (1.00)	C'NH	123.0 (123.0)
C'	1.645	(1.664)	25.88 (27.16)	1.089 (1.054)	C _α C _β	1.53 (1.54)	C _α NH	114.0 (116.1)
O	1.858	(1.906)	18.15 (21.24)	2.288 (2.256)	C _α H _α	1.10 (1.07)	NC _α C'	109.5 (109.7)
							NC _α C _β	109.4 (109.5)
							C'C _α H _α	109.5 (109.4)
							C _β C _α H _α	109.5 (109.5)

- 6 Keller, A. *Rep. Prog. Phys.* 1968, **31**, 623
 7 Fraser, R. D. B. and MacRae, T. P. in 'Conformation in Fibrous Proteins' (Eds. B. Horecker, N. O. Kaplan, J. Marmur and H. A. Scheraga), Academic Press, New York, 1973
 8 Carità Morelli, M. and D'Alagni, M. *Polymer* 1972, **13**, 515
 9 Corsi, E., and D'Alagni, M. *J. Phys. Chem.* 1975, **79**, 1301
 10 De Santis, P., Giglio, E., Liquori, A. M. and Ripamonti, A. *Nature* 1965, **206**, 456
 11 Brant, D. A., Miller, W. G. and Flory, P. J. *J. Mol. Biol.* 1967, **23**, 47
 12 Ooi, T., Scott, R. A., Vanderkooi, G. and Scheraga, H. A. *J. Chem. Phys.* 1967, **46**, 4410
 13 Hoffman, R. and Imamura, A. *Biopolymers* 1969, **7**, 207
 14 Maignet, B., Pullman, B. and Dreyfus, M. *J. Theor. Biol.* 1970, **26**, 321
 15 Arnott, S. and Wonacott, A. J. *J. Mol. Biol.* 1966, **21**, 371
 16 Parry, D. A. D. and Suzuki, E. *Biopolymers* 1969, **7**, 199
 17 Brown, L. and Trotter, I. F. *Trans. Faraday Soc.* 1956, **52**, 537
 18 Elliott, A. and Malcolm, B. R. *Proc. R. Soc. (A)* 1959, **249**, 30
 19 Arnott, S. and Wonacott, A. J. *Polymer* 1966, **7**, 157
 20 Arnott, S. and Dover, S. D. *J. Mol. Biol.* 1967, **30**, 209
 21 Klyne, W. and Prelog, V. *Experientia* 1960, **16**, 521
 22 Parry, D. A. D. and Suzuki, E. *Biopolymers* 1969, **7**, 189
 23 Giglio, E. *Nature* 1969, **222**, 339
 24 Scott, R. A. and Scheraga, H. A. *J. Chem. Phys.* 1966, **44**, 3054
 25 Cernia, E., Conte, G., D'Ilario, L., Pavel, N. V. and Giglio, E. *J. Polym. Sci. (A-1)* 1975, **13**, 125
 26 Scott, R. A. and Scheraga, H. A. *J. Chem. Phys.* 1966, **45**, 2091
 27 Allegra, G., Benedetti, E. and Pedone, C. *Macromolecules* 1970, **3**, 727

Interaction between sequential polypeptides and sodium deoxycholate

E. Corsi, M. D'Alagni* and E. Giglio

Istituto di Chimica-fisica, Università di Roma, 00185 Roma, Italy
 (Received 9 September 1975; revised 23 October 1975)

The sequential copolymers poly(L-leucyl-L-leucyl-L-aspartic acid) (PLLAA) and poly(L-leucyl-L-leucyl-L-lysine) (PLLL) were previously studied in aqueous solution^{1,2} as well as in mixtures of water with an organic solvent³ by spectroscopic and potentiometric measurements. A conformational transition from a charged to an uncharged state was detected for both copolymers. The ΔH_{98}° and ΔS° values are 6173 cal/mol and 26.0 cal/deg mol for PLLAA and 2784 cal/mol and 11.7 cal/deg mol for PLLL. These high values seem to indicate the presence of compact macromolecules, characterized by α -helical segments and stabilized by hydrophobic forces evidenced, also, in both random⁴⁻⁶ and block⁷ copolymers.

The deoxycholic acid molecule shows a hydrophobic side with three protruding methyl groups, which give rise to a strong binding with apolar and highly polarizable moieties, and a polar side with two hydroxyl and one carboxyl groups, which are able to form a complicated network of hydrogen bonds in crystals of choleic acids⁸.

It is well known that the sodium deoxycholate (DCANa) is customarily used in order to solubilize biological membranes, interacting with both phospholipids⁹ and proteins^{10,11}.

We have investigated by circular dichroism (c.d.) spectra the PLLAA-DCANa and PLLL-DCANa aqueous solutions for the following reasons:

(a) Strong interactions can occur between the two copolymers and DCANa, owing to the presence in each compound of polar and apolar groups. The sequential polypeptides could be considered as simplified models of proteins, allowing us to gain some information on the solubilization mechanism exerted by the bile salt.

(b) The interactions between DCANa and PLLAA or PLLL may be competitive with the intramolecular ones in each copolypeptide. Thus conformational changes could be detected in the macromolecules.

First, we have recorded c.d. spectra of PLLAA and DCANa over a wide range of molar ratios without a significant variation in the molar ellipticity values. From the c.d. spectrum of an aqueous solution of PLLAA, $c = 1.4172 \times 10^{-4}$ mol/l and pH = 6.19, the presence of two negative maxima centred at about 220 nm and at 206 nm, and a cross-over at 198 nm are inferred. The molar ellipticity values, expressed as degree cm²/dmol, are $[\theta]_{220} = -9200$ and $[\theta]_{206} = -16400$. The c.d. spectrum of an aqueous solution of PLLAA-DCANa, 1:1 molar ratio, $c = 0.7086 \times 10^{-4}$ mol/l and pH = 6.62, shows the same characteristic cross-over and band positions with $[\theta]_{220} = -9100$ and $[\theta]_{206} = -16100$. At this pH in an aqueous solution of PLLAA the macromolecules are charged for about 20%¹. Since the two spectra nearly coincide, it is reasonable to conclude that the DCANa does not influence the PLLAA conformation. The solutions appear to be much more stable during the time than those of PLLAA.

Different behaviour at pH = 10.25 is displayed by PLLL-DCANa, as compared with PLLL, which at the same pH has about 15% of ionized groups². $[\theta]$ in the 198-230 nm region abruptly increases by adding DCANa and, at the same time, the negative dichroic characteristic bands of the α -helix are red shifted as well as the cross-over and the positive maximum, which, however, lie in a region where DCANa contributes (see *Figure 1*). Therefore, the remarkable decreasing of the α -helix content indicates a strong binding between PLLL and DCANa. Furthermore, the PLLL-DCANa solutions, after few hours, give rise to a precipitate, containing all the PLLL, since the supernatant solution does not show any appreciable dichroism above 200 nm. The above-mentioned conformational change, caused by DCANa, is reversible. The very similar, full and broken curves of *Figure 2* refer to solutions of PLLL and PLLL-DCANa, after removal of the bile salt, at similar pHs. The qualitative behaviour of PLLL is satisfied and the third curve of *Figure 2* shows that $[\theta]$ below 232 nm increases at pH ~ 9 , as already observed for PLLL².

* Centro di Studio per la Chimica dei Recettori del CNR, c/o Università Cattolica, via Pineta Sacchetti 644, 00168 Roma, Italy, and to whom enquiries should be addressed.

- 6 Keller, A. *Rep. Prog. Phys.* 1968, **31**, 623
 7 Fraser, R. D. B. and MacRae, T. P. in 'Conformation in Fibrous Proteins' (Eds. B. Horecker, N. O. Kaplan, J. Marmur and H. A. Scheraga), Academic Press, New York, 1973
 8 Carità Morelli, M. and D'Alagni, M. *Polymer* 1972, **13**, 515
 9 Corsi, E., and D'Alagni, M. *J. Phys. Chem.* 1975, **79**, 1301
 10 De Santis, P., Giglio, E., Liquori, A. M. and Ripamonti, A. *Nature* 1965, **206**, 456
 11 Brant, D. A., Miller, W. G. and Flory, P. J. *J. Mol. Biol.* 1967, **23**, 47
 12 Ooi, T., Scott, R. A., Vanderkooi, G. and Scheraga, H. A. *J. Chem. Phys.* 1967, **46**, 4410
 13 Hoffman, R. and Imamura, A. *Biopolymers* 1969, **7**, 207
 14 Maignet, B., Pullman, B. and Dreyfus, M. *J. Theor. Biol.* 1970, **26**, 321
 15 Arnott, S. and Wonacott, A. J. *J. Mol. Biol.* 1966, **21**, 371
 16 Parry, D. A. D. and Suzuki, E. *Biopolymers* 1969, **7**, 199
 17 Brown, L. and Trotter, I. F. *Trans. Faraday Soc.* 1956, **52**, 537
 18 Elliott, A. and Malcolm, B. R. *Proc. R. Soc. (A)* 1959, **249**, 30
 19 Arnott, S. and Wonacott, A. J. *Polymer* 1966, **7**, 157
 20 Arnott, S. and Dover, S. D. *J. Mol. Biol.* 1967, **30**, 209
 21 Klyne, W. and Prelog, V. *Experientia* 1960, **16**, 521
 22 Parry, D. A. D. and Suzuki, E. *Biopolymers* 1969, **7**, 189
 23 Giglio, E. *Nature* 1969, **222**, 339
 24 Scott, R. A. and Scheraga, H. A. *J. Chem. Phys.* 1966, **44**, 3054
 25 Cernia, E., Conte, G., D'Ilario, L., Pavel, N. V. and Giglio, E. *J. Polym. Sci. (A-1)* 1975, **13**, 125
 26 Scott, R. A. and Scheraga, H. A. *J. Chem. Phys.* 1966, **45**, 2091
 27 Allegra, G., Benedetti, E. and Pedone, C. *Macromolecules* 1970, **3**, 727

Interaction between sequential polypeptides and sodium deoxycholate

E. Corsi, M. D'Alagni* and E. Giglio

Istituto di Chimica-fisica, Università di Roma, 00185 Roma, Italy
 (Received 9 September 1975; revised 23 October 1975)

The sequential copolymers poly(L-leucyl-L-leucyl-L-aspartic acid) (PLLAA) and poly(L-leucyl-L-leucyl-L-lysine) (PLLL) were previously studied in aqueous solution^{1,2} as well as in mixtures of water with an organic solvent³ by spectroscopic and potentiometric measurements. A conformational transition from a charged to an uncharged state was detected for both copolymers. The ΔH_{98}° and ΔS° values are 6173 cal/mol and 26.0 cal/deg mol for PLLAA and 2784 cal/mol and 11.7 cal/deg mol for PLLL. These high values seem to indicate the presence of compact macromolecules, characterized by α -helical segments and stabilized by hydrophobic forces evidenced, also, in both random⁴⁻⁶ and block⁷ copolymers.

The deoxycholic acid molecule shows a hydrophobic side with three protruding methyl groups, which give rise to a strong binding with apolar and highly polarizable moieties, and a polar side with two hydroxyl and one carboxyl groups, which are able to form a complicated network of hydrogen bonds in crystals of choleic acids⁸.

It is well known that the sodium deoxycholate (DCANa) is customarily used in order to solubilize biological membranes, interacting with both phospholipids⁹ and proteins^{10,11}.

We have investigated by circular dichroism (c.d.) spectra the PLLAA-DCANa and PLLL-DCANa aqueous solutions for the following reasons:

(a) Strong interactions can occur between the two copolymers and DCANa, owing to the presence in each compound of polar and apolar groups. The sequential polypeptides could be considered as simplified models of proteins, allowing us to gain some information on the solubilization mechanism exerted by the bile salt.

(b) The interactions between DCANa and PLLAA or PLLL may be competitive with the intramolecular ones in each copolypeptide. Thus conformational changes could be detected in the macromolecules.

First, we have recorded c.d. spectra of PLLAA and DCANa over a wide range of molar ratios without a significant variation in the molar ellipticity values. From the c.d. spectrum of an aqueous solution of PLLAA, $c = 1.4172 \times 10^{-4}$ mol/l and pH = 6.19, the presence of two negative maxima centred at about 220 nm and at 206 nm, and a cross-over at 198 nm are inferred. The molar ellipticity values, expressed as degree cm²/dmol, are $[\theta]_{220} = -9200$ and $[\theta]_{206} = -16400$. The c.d. spectrum of an aqueous solution of PLLAA-DCANa, 1:1 molar ratio, $c = 0.7086 \times 10^{-4}$ mol/l and pH = 6.62, shows the same characteristic cross-over and band positions with $[\theta]_{220} = -9100$ and $[\theta]_{206} = -16100$. At this pH in an aqueous solution of PLLAA the macromolecules are charged for about 20%¹. Since the two spectra nearly coincide, it is reasonable to conclude that the DCANa does not influence the PLLAA conformation. The solutions appear to be much more stable during the time than those of PLLAA.

Different behaviour at pH = 10.25 is displayed by PLLL-DCANa, as compared with PLLL, which at the same pH has about 15% of ionized groups². $[\theta]$ in the 198-230 nm region abruptly increases by adding DCANa and, at the same time, the negative dichroic characteristic bands of the α -helix are red shifted as well as the cross-over and the positive maximum, which, however, lie in a region where DCANa contributes (see *Figure 1*). Therefore, the remarkable decreasing of the α -helix content indicates a strong binding between PLLL and DCANa. Furthermore, the PLLL-DCANa solutions, after few hours, give rise to a precipitate, containing all the PLLL, since the supernatant solution does not show any appreciable dichroism above 200 nm. The above-mentioned conformational change, caused by DCANa, is reversible. The very similar, full and broken curves of *Figure 2* refer to solutions of PLLL and PLLL-DCANa, after removal of the bile salt, at similar pHs. The qualitative behaviour of PLLL is satisfied and the third curve of *Figure 2* shows that $[\theta]$ below 232 nm increases at pH ~ 9 , as already observed for PLLL².

* Centro di Studio per la Chimica dei Recettori del CNR, c/o Università Cattolica, via Pineta Sacchetti 644, 00168 Roma, Italy, and to whom enquiries should be addressed.

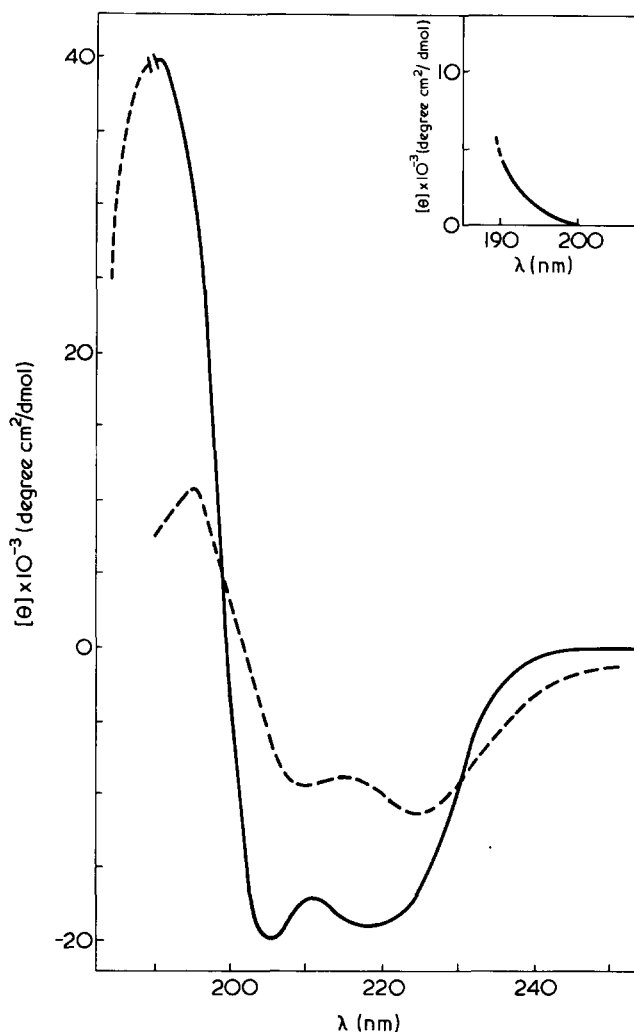


Figure 1 C.d. spectra of aqueous solutions of: —, PLL, $c = 1.8420 \times 10^{-4}$ mol/l, pH = 10.30; ----, PLL-DCANa (1:1 molar ratio), $c = 1.9640 \times 10^{-4}$ mol/l, pH = 10.25. The c.d. spectrum of DCANa, $c = 4.212 \times 10^{-4}$ mol/l, pH = 10.21, is shown in the right upper part of the Figure

The PLLAA-DCANa and PLL-DCANa systems have been studied within the range of about one pH unit around 6.8 and 9.8 respectively. In this range the percentage of ionized groups varies from about 14 to 62% for PLLAA¹ and 15 to 55% for PLL² at 25°C. Contemporaneously, the $[\theta]$ changes for the two systems are of the same order of magnitude as for PLLAA and PLL without DCANa at the same pHs.

The experimental data may be explained by supposing that the DCANa molecules interact in different ways with PLLAA and PLL. The bile salt molecules are mainly bonded to the leucyl residues of the acid copolymer with their hydrophobic side, while the charged carboxyl groups may repel each other. Thus the greater solubility of PLLAA-DCANa may be ascribed to the outer polar groups in contact with the aqueous environment. On the other hand the

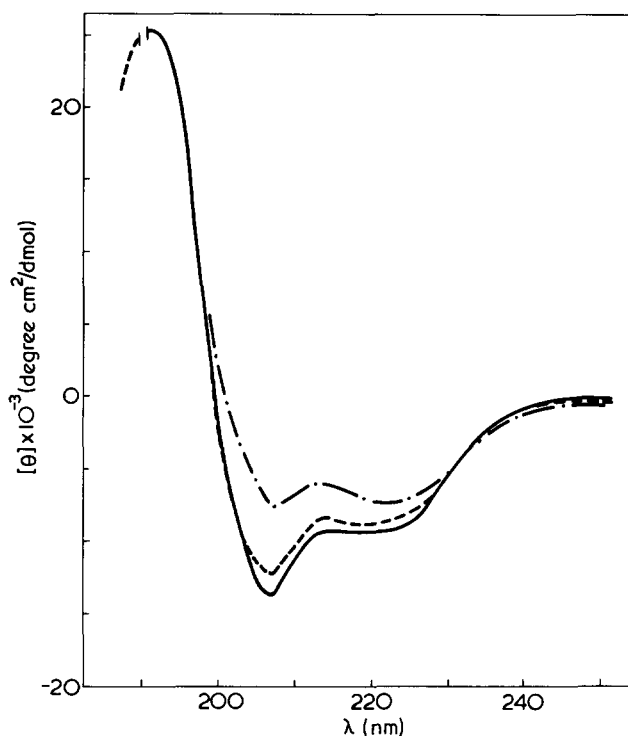


Figure 2 C.d. spectra of aqueous solutions of: —, PLL, $c = 1.9640 \times 10^{-4}$ mol/l, pH = 4.59; ----, PLL, $c = 1.9640 \times 10^{-4}$ mol/l, pH = 4.44, after interaction with DCANa and subsequent dialysis; - · - · - ·, as for the broken curve but pH = 9.00

NH_2 and NH_3^+ of PLL may form hydrogen bonds and electrostatic interactions with the hydrophilic side groups of the DCANa molecules, which protrude their apolar face towards the polar surrounding medium, causing precipitation.

ACKNOWLEDGEMENT

The authors acknowledge the Consiglio Nazionale delle Ricerche for financial support.

REFERENCES

- 1 Carità Morelli, M. and D'Alagni, M. *Polymer* 1972, **13**, 515
- 2 Corsi, E. and D'Alagni, M. *J. Phys. Chem.* 1975, **79**, 1301
- 3 D'Alagni, M. and Giglio, E. *Polymer* 1975, **16**, 382
- 4 Chou, P. Y., Wells, M. and Fasman, G. D. *Biochemistry* 1972, **11**, 3028
- 5 Snell, C. R. and Fasman, G. D. *Biopolymers* 1972, **11**, 1723
- 6 Mandel, R. and Fasman, G. D. *Biopolymers* 1975, **14**, 1633
- 7 Ostroy, S. E., Lotan, N., Ingwall, R. T. and Scheraga, H. A. *Biopolymers* 1970, **9**, 749
- 8 Candeloro De Sanctis, S., Giglio, E., Pavel, N. V. and Quagliata, C. *Acta Crystallogr. (B)* 1972, **28**, 3656
- 9 Philippot, J. *Biochim. Biophys. Acta* 1971, **225**, 201
- 10 Smart, J. E. and Bonner, J. *J. Mol. Biol.* 1971, **58**, 651
- 11 Visser, L., Robinson, N. C. and Tanford, C. *Biochemistry* 1975, **14**, 1194

Radiation curing of unsaturated polyester resin

K. Sędziński

Akademia Techniczno-Rolnicza, ul. Olszewskiego 20, 85-225 Bydgoszcz, Poland

(Received 29 September 1975; revised 11 November 1975)

Some tests on the influence of irradiation parameters on the properties of unsaturated polyester resins have been undertaken. A commercial resin (Polimal 109) which is a 35% styrene solution of unsaturated polyester, was used. Two radiation devices, the BK-6 equipment and the equipment for rating radiometers, were used to cure the resins. Radiation device BK-6 is equipped with 6 radiation sources of ^{60}Co gamma rays which are placed around the irradiated substance. The radiation device for rating radiometers is equipped with one source of ^{60}Co and a collimator which gives a parallel beam of gamma rays.

These tests¹ lead to the following conclusions:

(1) For radiation hardening of the Polimal 109 resin the delivery of 0.5×10^4 J/kg (0.5 Mrad of gamma rays energy) is necessary. This minimum dose does not, however, guarantee the hardening of the surface which is in contact with the air.

(2) The determined properties (hardness, compressive strength, bending strength, softening point determined by Vicat's method) of the Polimal 109 resin, hardened by radiation curing, do not depend fundamentally either on

the value of the absorbed dose of the gamma rays within the range 0.5×10^4 to 8.0×10^4 J/kg (from 0.5 to 8.0 Mrad) or on the value of the gamma rays dose rate within the range 0.0347 to 0.2778 W/kg (12.5 to 100 krad/h). This conclusion was arrived at by statistical analysis.

(3) The resin hardened in the radiation device BK-6 proved to have a 25% higher softening point, 8% higher compressive strength and 9.5% lower bending strength in comparison with resin hardened with parallel beam of gamma rays.

The difference in the properties of the same resin hardened in two radiation devices at the same dose rate of gamma rays can be explained by the different geometry of the absorption of the energy of the gamma rays, which is the result of the different 'source of radiation — irradiated substance' geometry systems.

REFERENCE

- 1 Sedziński, K. *Doctoral Thesis* 1974 (unpublished)

Book Reviews

Structure and properties of oriented polymers

Edited by I. M. Ward

Applied Science, Barking, 1975, 500 pp. £18

Partly as a result of commercial importance, there has been considerable activity and progress in studies of the structure and properties of oriented polymers. Clearly no one volume could account for all aspects of such systems, and the present volume is largely concerned with the fundamental aspects of orientation, its measurement and its interpretation in macroscopic and molecular terms. Professor Ward has obtained an excellent blend of contributions from leading scientists in industry, government research and university.

The book contains thirteen chapters, the first being a clear and concise introduction by Holliday and Ward to the occurrence and nature of orientation and the techniques which may be used in its elucidation. This is followed by an account by Peterlin of molecular aspects of crystallites and oriented material which, although brief, is rich in basic information. Having set the basis, there are three aspects of oriented polymers which are considered at length with great clarity which occupy the remainder of the book being: (i) molecular aspects as studied by spectroscopic and related methods (Ch 3 to 6, approximately one third of the book); (ii) macroscopic aspects of mechanical and viscoelastic behaviour (Ch 7 to 11, approximately one third of the book) and (iii) illustrative and up-to-date aspects of the production of oriented films and fibres and of ultra-high modulus organic fibres (Ch 12 and 13, approximately one sixth of the book). Whilst it is not possible to review here the details of any of these accounts, it is appropriate to indicate some of their aims. The chapter by Stein and Wilkes (92 pages) is mainly concerned with optical birefringence, X-ray and light scattering methods, beautifully illustrated with many examples (e.g. spheru-

lite deformation) and contains a valuable account of the theory of X-ray and light scattering processes. The chapters by Read (u.v. visible and infra-red dichroism) by Bower (fluorescence and Raman spectroscopy) and by Folkes and Ward (nuclear magnetic resonance) describe the current situation with regard to the understanding of orientation in molecular terms, are written with authority and clarity and set the stage for further work on this exciting topic. Holliday (Ch 7) deals with calculated values for chain stiffness and their relation to the experimental moduli for a wide range of polymers. Hadley and Ward (Ch 8) and Hadley (Ch 9) are concerned with low-strain mechanical properties of oriented polymers while Darlington and Saunders (Ch 10) discuss anisotropic creep behaviour and Duckett (Ch 11) anisotropic yield behaviour. All five chapters place considerable emphasis on experimental results and their interpretation in terms of the structure and texture of the various polymers. The Chapter by Schuur and Van der Vegt on the practical aspects of the orientation of films and fibrillation is a delight, its clarity and choice of contemporary material make it one highlight of many in this excellent book. Finally, Chapter 13 by Carter and Schenk describe the preparation of certain ultra-high modulus fibres (e.g. poly(*p*-benzamide)) which are also thermally stable materials. We note here that solutions of such polymers form liquid crystal phases and this aspect may open up new approaches to fibre formation. The editor and the authors are to be congratulated for arriving at a systematic and readable account of a class of material involving so many variables. Its readership spans fibre and film scientists, post-graduate polymer scientists and engineers, and post-graduate scientists involved with other oriented materials. One anticipates that this book will become the standard text on the fundamentals of oriented polymers and will stimulate further research work.

G. Williams

Comprehensive Chemical Kinetics
(Volume 14, Degradation of Polymers)
Edited by C. H. Bamford and C. F. H. Tipper
Elsevier, Amsterdam, 1975, 562 pp. \$83.50

The degradation of polymers is currently attracting a great deal of attention both for the continuing reason that new materials are constantly being developed and applied in even more hostile environments and also for a variety of rather novel reasons like the development of degradable polymers for the control of environmental pollution and the control of flammability in plastics for use as structural materials. It is therefore not unreasonable that in this series on chemical kinetics, of the two volumes in section 5 entitled 'Polymerisation Reactions', one volume should be devoted entirely to polymer degradation.

This book comprises four large chapters which are devoted to the fundamental rather than the technological aspects of four major aspects of polymer degradation and written by three authors who are highly regarded internationally for their current activities in the field. The first two chapters, on thermal and high energy degradation respectively, are written by Dr C. David of the Free University of Brussels, the third, on photodegradation by Professor G. Geuskens, also of the Free University of Brussels and the last, on oxidative degradation by Dr J. F. Rabek of the Royal Institute of Technology in Stockholm.

About 20% of the first chapter is devoted to a general discussion of experimental methods and the kinetics of thermal depolymerization and the remainder to the specific reactions of a wide variety of polymers. The second chapter begins with a description of some general aspects of polymer radiolysis, interaction of high energy radiation with matter and the theory of cross-linking and degradation. Thereafter individual polymers are discussed specifically from the point of view of trapped free radicals, chemical effects and mechanical properties. The structure of chapter 3 is similarly based on the discussion of the reactions of individual polymers together with sections on general principles of photochemistry, experimental methods, stabilization, and photophysics of polymers. In his conception of chapter 4, Dr Rabek took rather a different view. Thus after emphasizing the importance of hydroperoxides in the oxidation process he continues: 'This chapter is mainly concerned with the chemical and physical factors that are responsible for the formation of hydroperoxides during the induction period and that influence the mechanism of polymer oxidation. A detailed discussion of the oxidation of various polymers is not included since two excellent books dealing with this subject are published'.

These three authors have succeeded admirably in combining together to produce an authoritative, critical and very readable account of the major growth areas of polymer degradation. It is unfortunate that its price will preclude purchase by most individuals so that it will be largely confined to libraries rather than the desks of practicing scientists where it belongs.

N. Grassie

Advances in polymer science
Edited by Z. A. Rogovin
Wiley, New York, 1975, £14.70

This book is a translation of a collection of essays by Russian scientists on various aspects of polymer science.

The text tends to be written in a very wordy style which makes reading difficult. Some chapters appear to be out of date by as much as four years. For example, Dr Andrianova's chapter on Large Deformation in Crystalline Polymers makes no mention of the recent developments in the production of ultra high modulus PE via solid state cold drawing techniques as described by Professor Ward of Leeds University. Also there is no mention of the work of Wunderlich (USA) and Bassett (UK) on high pressure annealing of polyethylene. A second feature is that the range of subjects is extremely broad and includes the physical, chemical, biomedical and industrial aspects of polymer science. The advantages of such a book is that the previews include summaries of Russian work, which is not readily available, and enables an assessment to be made of Russian polymer science.

An interesting discussion by S. G. Entelis and others considers the problem of characterization of oligomers with functional groups according to their functionality. The review summarizes the basic

equations used and the role of the number average (f_n) and weight average (f_w) functionalities of Stockmayer which are derivable from these. Experimental methods of characterization are compared, including the measurements of f_w from gelation studies f_n from the cross-link density measurements, and the use of gel-permeation chromatography (g.p.c.). The latter, which is the most important method, is only described in a limited way by reference to the original Terry and Rodrigues paper in the Journal of Polymer Science published in 1968. Modern g.p.c. units with multichannel i.r. detectors are the most direct way of tackling this problem and merited more detailed discussion. Final sections in this chapter include a summary of some Russian work on relations between distribution of functionality and mechanical properties.

The article by E. F. Razvodovskii reviews the literature since 1962 on synthetic polymers in pharmacology. There is an interesting discussion of antisilicosis activity and structure of poly(*N*-oxides) including some Russian work in this field on the relationship between molecular weight of poly(2-vinyl pyridine *N*-oxide) and antisilicosis activity. Another group of biologically active polymers are the 'ionenes', – a class of polymers with a quarternary *N*-atoms in the main chain. These exhibit bactericidal properties, curane-like and antiheparin activity. One important aspect associated with putting drug molecules onto a polymer chain is that a reduction in toxicity occurs. This is not a new idea since it transpires that the arsenicals such as Salvarsan owe their low toxicity to the fact that they are substituted poly(arsenic oxides); a fact not appreciated at the time of their discovery.

The paper by Amerik and Krentsel on the Role of Anisotropic States in Polymerization Processes summarizes and compares work on polymerization in the crystalline and paracrystalline states and in liquid crystals and matrices of various kinds. In most cases polymerization prefers to occur at the interface of two phases or at temperatures close to a phase transition.

Finally two aspects of the use of spectroscopy to study polymers are discussed at some length. One of the more interesting of these is that of A. L. Buchachenko and others which is concerned with the use of stable radicals for studying molecular motions based on the line widths of electron paramagnetic resonance (e.p.r.) spectra due to rotary and translatory motions of the radicals. Using organic radicals differing in shape, dimensions and structure of their molecules but containing the same paramagnetic fragment $>N-O$ it has been shown that the diffusion depends on the glass transition temperature T_g , indicating a dependence on the segmental motion of the polymer molecules. The parameters which can be measured using this technique include: the temperature of unfreezing of the radicals (T_u); activation energies (E), and pre-experimental factors (V_0) of the rotational frequencies of radicals in polymers. Data for different radical types and their behaviour in amorphous, crystalline and cross-linked polymers are presented and discussed.

D. G. H. Ballard

Polymer Engineering
H. Leverne Williams
Elsevier, Amsterdam, 1975, 166 pp. £14.75

My first impression of this book, written for use by 'the young Chemical Engineer entering industry' was quite favourable. It is short, it is well bound, it is easy to read, there are plenty of bold line diagrams in the text, there are very few equations and the references are limited to major works. Above all during the early chapters the author is intent on pointing out that this effect is useful because rather than concentrating on problems.

Professor Williams carried me with him through the early chapters on the nature of high polymers and their morphology. This seemed just the sort of information which the young chemical engineer would find useful to aid his learning processes in an industrial environment. However when the author reached the sections on deformation and flow, the area in which the references claim that he has a special competence, he loses my sympathy entirely.

I suppose one can forgive an author for introducing his own notation rather than using one of the many types which have become standard. However, it is irritating to find that he changes notation from chapter to chapter (p 84, 127) and downright disturbing when the same nomenclature is used in sequential chapters (η in chapters 6 and 7) to mean different things (at least I hope that he means different things).

Then there are the contradictions like high molecular weight polymer increasing viscosity (when describing solution viscosities) and decreasing viscosity when considering drag reduction, and the gratuitous theoretical explanations of such effects which may sound alright when spoken quickly but do not bear being put into print in such a text especially when the concept of Reynolds turbulence (surely one of the most commonly used formulae in chemical engineering) receives not a word.

Finally, in a chapter on viscoelasticity there is the agony of statements like the reciprocal of Young's modulus is compliance (p 87) and the implication (p 91) that relaxation and retardation behaviour are the same thing by different names. Such things are not to be expected when the author cites Professor Ferry's treatise as his prime source, and it would be much better to say nothing at all rather than to suggest ideas which will subsequently be difficult to remove.

Thus in two chapters the author undid the confidence which his approach had shown in the early part of the book so that I cannot recommend it at all.

F. N. Cogswell

Polymer Chemistry — an Introduction

M. P. Stevens

Addison-Wesley, Reading, Mass., 1975, 458 pp.
\$17.50

In contrast to the situation of even five years ago, the lecturer giving a course in polymer science can now choose from several excellent course texts. The present book is intended as a text book for an introductory course in polymer chemistry at the undergraduate or postgraduate level, but differs in being written from the viewpoint of organic rather than physical chemistry.

The fifteen chapters of this book form three main sections. The first occupies 100 pages and is a brief discussion of the physical chemistry of polymerization reactions and of the physical properties of polymers. This is the weakest section and any realistic course would require supplementary reading. Its balance can also be criticized; for example, flame-retarding additives receive almost twice as much space as the discussion of glass-transition temperatures. The second section, occupying 109 pages, gives a concise and well written account of the addition polymerization of vinyl and diene monomers and of the chemical reactions of vinyl polymers. Most of the material in this section is covered in other standard texts. It is in the third section that the book really comes into its own. This section, covering 216 pages, is a discussion of non-vinyl polymers, beginning with polyethers, ending with natural polymers and covering every conceivable polymer type in between. It is well written, concise and readable and successfully avoids being a 'preparation and properties' catalogue. It is an excellent treatment of an area of polymer science which is much less well covered elsewhere.

Because of the strong bias towards organic chemistry I would find it difficult to consider this book as a primary course text but would give it strong recommendation as supplementary reading. The high price of even the paperback edition, implies that few students will buy it although it should be in any library associated with polymer science teaching. It would probably have been a more useful book if the first section had been omitted and the price reduced to correspond.

N. C. Billingham

Creep, viscoelasticity and creep fracture in solids

J. Gittus

Applied Science, Barking, 1975, 725 pp. £25

I think that this is a very good book indeed and illustrates the unity of the science of the behaviour of solid materials. Its subject matter, is to review comprehensively diffusion creep in crystals and polycrystals and to relate this to flow in glasses. This is followed by consideration of creep due to dislocation glide in metals and in non metals, with, for the latter, some histories of various important systems, e.g. various transition metal oxides and uranium carbide.

A relationship is then noted with creep within the earth's mantle. Irradiation induced deformation due to volume or length changes and the resultant creep under stress is next considered.

At this stage the author pauses and notes with truth 'today it is possible to become deeply involved with theories of dislocation creep in metals without having more than a hazy notion of the part played by elastic strains of various types. Of course the converse is also true and experts on the viscoelastic behaviour of polymers are only now beginning to be aware of the role which dislocation theory may play in helping to rationalize the behaviour of the materials with which they are concerned'. Dr. Gittus goes on to instruct these two types of scientist of materials and he is well equipped to do so having made contributions to irradiation creep. Nimonic alloys and to the flow of foundry sand, himself.

Succeeding chapters deal with viscoelastic models, which are very well explained, viscoelasticity in metals and in non metals; here the kinetic theory of rubber elasticity is dealt with and viscoelasticity in amorphous polymers with important ones, such as PVC, polystyrene, PMMA being dealt with in detail. Then metals and alloys of high creep strength are dealt with and the behaviour of Nimonic and specific refractory metals, e.g. W, Mo, Nb, dealt with individually.

Theory and experiment of superplastic effects which occur principally in metals and offer a low temperature forming process analogous to drawing of polymers consumes Chapter 11 and creep fracture Chapter 12 which includes among other things wedge cracks in crystalline materials and crazing in glassy polymers. Before a final discussion of a mechanical equation of state, a chapter is devoted to the effects of environment which includes oxidizing metals, segregation to grain boundaries, stress corrosion (environmental stress cracking) and effects of humidity on the creep of concrete.

As Sir Monty Finnieston says in his introduction, Gittus' courage must be admired in taking on so vast a task. I think both that and his success. Many may cavil at the treatment of their speciality but I think the sweep is right and the judgement good. A fine comprehensive and up-to-date work which should be on the shelves of all scientists of materials who can afford it.

A. Kelly

Organic polymeric semiconductors

Ya. M. Paushkin, T. P. Vishnyakovo, A. F. Lunin
and S. A. Nizova

Wiley, New York, 1975, 242 pp. £10.10

Experiments on small molecules had made it clear by 1955 that an increase in the number of conjugated double bonds induces increased semiconduction in crystalline organic substances, and shortly afterwards the enhancing effect of charge-transfer complexation was also established. Around 1959 the subject was taken up by Russian polymer scientists, who embarked on a large programme of synthesis of conjugated linear polymers, with the object of increasing the conductivity still further. By and large, this work may be criticized in that the products were amorphous and not well characterized, and the electrical conduction measurements were rather scrappy. This translation provides a valuable service in gathering together all the references, and reviewing all the results, previously only available in the Russian language. However, the whole book smacks of scissors and paste-pot, and as a scientific contribution it leaves much to be desired. Indeed, the reviewer makes so bold as to assert, that it falls far below the high standards established in this field by that great pioneer of organic semi-conductors, the Soviet scientist, Academician Terenin. Accordingly, it emphatically cannot be recommended to postgraduate students or anyone else who seek a scientifically intelligible and coherent account of conduction in polymers. But it will provide a valuable *vade mecum* for laboratories active in the field to this early Russian synthetic work, much of which will no doubt bear further consideration or even repetition, in the light of the rapid advances now occurring in the science of organic single crystals as metallic conductors. So it would perhaps be churlish not to thank the translators for their efforts, while chiding the authors for the absence of any coherent account of the physics of their problem, their lack of any grasp of the international literature, and the slips and other blemishes which the expert eye can detect in this book.

D. D. Eley

Comprehensive Chemical Kinetics
(Volume 14, Degradation of Polymers)
Edited by C. H. Bamford and C. F. H. Tipper
Elsevier, Amsterdam, 1975, 562 pp. \$83.50

The degradation of polymers is currently attracting a great deal of attention both for the continuing reason that new materials are constantly being developed and applied in even more hostile environments and also for a variety of rather novel reasons like the development of degradable polymers for the control of environmental pollution and the control of flammability in plastics for use as structural materials. It is therefore not unreasonable that in this series on chemical kinetics, of the two volumes in section 5 entitled 'Polymerisation Reactions', one volume should be devoted entirely to polymer degradation.

This book comprises four large chapters which are devoted to the fundamental rather than the technological aspects of four major aspects of polymer degradation and written by three authors who are highly regarded internationally for their current activities in the field. The first two chapters, on thermal and high energy degradation respectively, are written by Dr C. David of the Free University of Brussels, the third, on photodegradation by Professor G. Geuskens, also of the Free University of Brussels and the last, on oxidative degradation by Dr J. F. Rabek of the Royal Institute of Technology in Stockholm.

About 20% of the first chapter is devoted to a general discussion of experimental methods and the kinetics of thermal depolymerization and the remainder to the specific reactions of a wide variety of polymers. The second chapter begins with a description of some general aspects of polymer radiolysis, interaction of high energy radiation with matter and the theory of cross-linking and degradation. Thereafter individual polymers are discussed specifically from the point of view of trapped free radicals, chemical effects and mechanical properties. The structure of chapter 3 is similarly based on the discussion of the reactions of individual polymers together with sections on general principles of photochemistry, experimental methods, stabilization, and photophysics of polymers. In his conception of chapter 4, Dr Rabek took rather a different view. Thus after emphasizing the importance of hydroperoxides in the oxidation process he continues: 'This chapter is mainly concerned with the chemical and physical factors that are responsible for the formation of hydroperoxides during the induction period and that influence the mechanism of polymer oxidation. A detailed discussion of the oxidation of various polymers is not included since two excellent books dealing with this subject are published'.

These three authors have succeeded admirably in combining together to produce an authoritative, critical and very readable account of the major growth areas of polymer degradation. It is unfortunate that its price will preclude purchase by most individuals so that it will be largely confined to libraries rather than the desks of practicing scientists where it belongs.

N. Grassie

Advances in polymer science
Edited by Z. A. Rogovin
Wiley, New York, 1975, £14.70

This book is a translation of a collection of essays by Russian scientists on various aspects of polymer science.

The text tends to be written in a very wordy style which makes reading difficult. Some chapters appear to be out of date by as much as four years. For example, Dr Andrianova's chapter on Large Deformation in Crystalline Polymers makes no mention of the recent developments in the production of ultra high modulus PE via solid state cold drawing techniques as described by Professor Ward of Leeds University. Also there is no mention of the work of Wunderlich (USA) and Bassett (UK) on high pressure annealing of polyethylene. A second feature is that the range of subjects is extremely broad and includes the physical, chemical, biomedical and industrial aspects of polymer science. The advantages of such a book is that the previews include summaries of Russian work, which is not readily available, and enables an assessment to be made of Russian polymer science.

An interesting discussion by S. G. Entelis and others considers the problem of characterization of oligomers with functional groups according to their functionality. The review summarizes the basic

equations used and the role of the number average (f_n) and weight average (f_w) functionalities of Stockmayer which are derivable from these. Experimental methods of characterization are compared, including the measurements of f_w from gelation studies f_n from the cross-link density measurements, and the use of gel-permeation chromatography (g.p.c.). The latter, which is the most important method, is only described in a limited way by reference to the original Terry and Rodrigues paper in the Journal of Polymer Science published in 1968. Modern g.p.c. units with multichannel i.r. detectors are the most direct way of tackling this problem and merited more detailed discussion. Final sections in this chapter include a summary of some Russian work on relations between distribution of functionality and mechanical properties.

The article by E. F. Razvodovskii reviews the literature since 1962 on synthetic polymers in pharmacology. There is an interesting discussion of antisilicosis activity and structure of poly(*N*-oxides) including some Russian work in this field on the relationship between molecular weight of poly(2-vinyl pyridine *N*-oxide) and antisilicosis activity. Another group of biologically active polymers are the 'ionenes', — a class of polymers with a quarternary *N*-atoms in the main chain. These exhibit bactericidal properties, curane-like and antiheparin activity. One important aspect associated with putting drug molecules onto a polymer chain is that a reduction in toxicity occurs. This is not a new idea since it transpires that the arsenicals such as Salvarsan owe their low toxicity to the fact that they are substituted poly(arsenic oxides); a fact not appreciated at the time of their discovery.

The paper by Amerik and Krentsel on the Role of Anisotropic States in Polymerization Processes summarizes and compares work on polymerization in the crystalline and paracrystalline states and in liquid crystals and matrices of various kinds. In most cases polymerization prefers to occur at the interface of two phases or at temperatures close to a phase transition.

Finally two aspects of the use of spectroscopy to study polymers are discussed at some length. One of the more interesting of these is that of A. L. Buchachenko and others which is concerned with the use of stable radicals for studying molecular motions based on the line widths of electron paramagnetic resonance (e.p.r.) spectra due to rotary and translatory motions of the radicals. Using organic radicals differing in shape, dimensions and structure of their molecules but containing the same paramagnetic fragment $>N-O$ it has been shown that the diffusion depends on the glass transition temperature T_g , indicating a dependence on the segmental motion of the polymer molecules. The parameters which can be measured using this technique include: the temperature of unfreezing of the radicals (T_u); activation energies (E), and pre-experimental factors (V_0) of the rotational frequencies of radicals in polymers. Data for different radical types and their behaviour in amorphous, crystalline and cross-linked polymers are presented and discussed.

D. G. H. Ballard

Polymer Engineering
H. Leverne Williams
Elsevier, Amsterdam, 1975, 166 pp. £14.75

My first impression of this book, written for use by 'the young Chemical Engineer entering industry' was quite favourable. It is short, it is well bound, it is easy to read, there are plenty of bold line diagrams in the text, there are very few equations and the references are limited to major works. Above all during the early chapters the author is intent on pointing out that this effect is useful because rather than concentrating on problems.

Professor Williams carried me with him through the early chapters on the nature of high polymers and their morphology. This seemed just the sort of information which the young chemical engineer would find useful to aid his learning processes in an industrial environment. However when the author reached the sections on deformation and flow, the area in which the references claim that he has a special competence, he loses my sympathy entirely.

I suppose one can forgive an author for introducing his own notation rather than using one of the many types which have become standard. However, it is irritating to find that he changes notation from chapter to chapter (p 84, 127) and downright disturbing when the same nomenclature is used in sequential chapters (η in chapters 6 and 7) to mean different things (at least I hope that he means different things).

Then there are the contradictions like high molecular weight polymer increasing viscosity (when describing solution viscosities) and decreasing viscosity when considering drag reduction, and the gratuitous theoretical explanations of such effects which may sound alright when spoken quickly but do not bear being put into print in such a text especially when the concept of Reynolds turbulence (surely one of the most commonly used formulae in chemical engineering) receives not a word.

Finally, in a chapter on viscoelasticity there is the agony of statements like the reciprocal of Young's modulus is compliance (p 87) and the implication (p 91) that relaxation and retardation behaviour are the same thing by different names. Such things are not to be expected when the author cites Professor Ferry's treatise as his prime source, and it would be much better to say nothing at all rather than to suggest ideas which will subsequently be difficult to remove.

Thus in two chapters the author undid the confidence which his approach had shown in the early part of the book so that I cannot recommend it at all.

F. N. Cogswell

Polymer Chemistry — an Introduction

M. P. Stevens

Addison-Wesley, Reading, Mass., 1975, 458 pp.
\$17.50

In contrast to the situation of even five years ago, the lecturer giving a course in polymer science can now choose from several excellent course texts. The present book is intended as a text book for an introductory course in polymer chemistry at the undergraduate or postgraduate level, but differs in being written from the viewpoint of organic rather than physical chemistry.

The fifteen chapters of this book form three main sections. The first occupies 100 pages and is a brief discussion of the physical chemistry of polymerization reactions and of the physical properties of polymers. This is the weakest section and any realistic course would require supplementary reading. Its balance can also be criticized; for example, flame-retarding additives receive almost twice as much space as the discussion of glass-transition temperatures. The second section, occupying 109 pages, gives a concise and well written account of the addition polymerization of vinyl and diene monomers and of the chemical reactions of vinyl polymers. Most of the material in this section is covered in other standard texts. It is in the third section that the book really comes into its own. This section, covering 216 pages, is a discussion of non-vinyl polymers, beginning with polyethers, ending with natural polymers and covering every conceivable polymer type in between. It is well written, concise and readable and successfully avoids being a 'preparation and properties' catalogue. It is an excellent treatment of an area of polymer science which is much less well covered elsewhere.

Because of the strong bias towards organic chemistry I would find it difficult to consider this book as a primary course text but would give it strong recommendation as supplementary reading. The high price of even the paperback edition, implies that few students will buy it although it should be in any library associated with polymer science teaching. It would probably have been a more useful book if the first section had been omitted and the price reduced to correspond.

N. C. Billingham

Creep, viscoelasticity and creep fracture in solids

J. Gittus

Applied Science, Barking, 1975, 725 pp. £25

I think that this is a very good book indeed and illustrates the unity of the science of the behaviour of solid materials. Its subject matter, is to review comprehensively diffusion creep in crystals and polycrystals and to relate this to flow in glasses. This is followed by consideration of creep due to dislocation glide in metals and in non metals, with, for the latter, some histories of various important systems, e.g. various transition metal oxides and uranium carbide.

A relationship is then noted with creep within the earth's mantle. Irradiation induced deformation due to volume or length changes and the resultant creep under stress is next considered.

At this stage the author pauses and notes with truth 'today it is possible to become deeply involved with theories of dislocation creep in metals without having more than a hazy notion of the part played by elastic strains of various types. Of course the converse is also true and experts on the viscoelastic behaviour of polymers are only now beginning to be aware of the role which dislocation theory may play in helping to rationalize the behaviour of the materials with which they are concerned'. Dr. Gittus goes on to instruct these two types of scientist of materials and he is well equipped to do so having made contributions to irradiation creep. Nimonic alloys and to the flow of foundry sand, himself.

Succeeding chapters deal with viscoelastic models, which are very well explained, viscoelasticity in metals and in non metals; here the kinetic theory of rubber elasticity is dealt with and viscoelasticity in amorphous polymers with important ones, such as PVC, polystyrene, PMMA being dealt with in detail. Then metals and alloys of high creep strength are dealt with and the behaviour of Nimonic and specific refractory metals, e.g. W, Mo, Nb, dealt with individually.

Theory and experiment of superplastic effects which occur principally in metals and offer a low temperature forming process analogous to drawing of polymers consumes Chapter 11 and creep fracture Chapter 12 which includes among other things wedge cracks in crystalline materials and crazing in glassy polymers. Before a final discussion of a mechanical equation of state, a chapter is devoted to the effects of environment which includes oxidizing metals, segregation to grain boundaries, stress corrosion (environmental stress cracking) and effects of humidity on the creep of concrete.

As Sir Monty Finnieston says in his introduction, Gittus' courage must be admired in taking on so vast a task. I think both that and his success. Many may cavil at the treatment of their speciality but I think the sweep is right and the judgement good. A fine comprehensive and up-to-date work which should be on the shelves of all scientists of materials who can afford it.

A. Kelly

Organic polymeric semiconductors

Ya. M. Paushkin, T. P. Vishnyakovo, A. F. Lunin
and S. A. Nizova

Wiley, New York, 1975, 242 pp. £10.10

Experiments on small molecules had made it clear by 1955 that an increase in the number of conjugated double bonds induces increased semiconduction in crystalline organic substances, and shortly afterwards the enhancing effect of charge-transfer complexation was also established. Around 1959 the subject was taken up by Russian polymer scientists, who embarked on a large programme of synthesis of conjugated linear polymers, with the object of increasing the conductivity still further. By and large, this work may be criticized in that the products were amorphous and not well characterized, and the electrical conduction measurements were rather scrappy. This translation provides a valuable service in gathering together all the references, and reviewing all the results, previously only available in the Russian language. However, the whole book smacks of scissors and paste-pot, and as a scientific contribution it leaves much to be desired. Indeed, the reviewer makes so bold as to assert, that it falls far below the high standards established in this field by that great pioneer of organic semi-conductors, the Soviet scientist, Academician Terenin. Accordingly, it emphatically cannot be recommended to postgraduate students or anyone else who seek a scientifically intelligible and coherent account of conduction in polymers. But it will provide a valuable *vade mecum* for laboratories active in the field to this early Russian synthetic work, much of which will no doubt bear further consideration or even repetition, in the light of the rapid advances now occurring in the science of organic single crystals as metallic conductors. So it would perhaps be churlish not to thank the translators for their efforts, while chiding the authors for the absence of any coherent account of the physics of their problem, their lack of any grasp of the international literature, and the slips and other blemishes which the expert eye can detect in this book.

D. D. Eley

Recent advances in polymer science
(*Polymer Symposia No. 46*)
Wiley, New York, 1974, 366 pp. £9.75

This volume includes 23 papers read at a symposium held at Princeton in 1973, in memory of Professor Arthur V. Tobolsky. The volume also includes a short tribute and bibliography of Tobolsky's publications.

Tobolsky was a distinguished polymer scientist and an outstanding teacher, and the contributions to this volume are largely by his former students and coworkers. His major contribution to polymer science was to the subject of the relationship between properties and structure and in particular, the mechanical and viscoelastic behaviour of polymers. The latter subject forms the main theme of the symposium, which includes several papers on the synthesis and viscoelastic properties of block copolymers, the properties of cross-linked systems, dielectric relaxation, and also contribution of technical interest on adhesion, blown films and resin coatings. The volume is a fine tribute to an eminent scientist.

C. E. H. Bawn

Irradiation in Chemical Processes. Recent Developments

M. W. Ranney
Noyes Data, New Jersey, 1975, \$36

This book represents an attempt to supply detailed technical information which has been extracted from the more recent US patent literature in this field. An author's quote 'By indicating all the information that is significant and eliminating legal jargon and juristic phraseology, this book presents an advanced, technically oriented review of irradiation in chemical processes'.

On the whole the technical contents of the book support the authors' claim. There are many creditable aspects. It is unfortunate that there are also several features present which detract from the books' overall merit.

This volume is largely poorly presented. As an example, the first chapter which deals with general chemical synthesis contains, on average, one significant error every two pages. Indicative are incorrect formulae, incomplete sentences, meaningless terminology, inconsistency in units, and incorrect units (density measured as lb/ft). Chapter 2 contains the statement that the coefficient of linear expansion at 73°F of solid polytetrafluoroethylene has a value of 5.5×10^5 inches.

The method of processing used to produce this book, whilst undoubtedly cutting costs and providing useful information in a relatively short time, does so at the expense of the presentation. Data in the tables are difficult to read without very careful scrutiny. The depth of print is variable and the quality of paper unbecoming a book of this price. It is doubtful if any of the sections in the book have been proof read in a conscientious manner.

Despite these faults, the book has much to recommend it. The subjects are dealt with in six sections of varying length, depending on the importance of the technique of irradiation to the particular application. Each chapter contains a wealth of up-to-date material which should be of value to industrial and academic researchers alike. The detail given is such that this volume could provide the basis of many research programmes. The contents cover a range of interests from general chemical synthesis through polymer processes, coatings and printing inks, the application of radiation to composites and specific applications. Various types of irradiation procedure are covered in depth. Those sections which proved particularly useful to the reviewer included coatings and printing inks (in which radiation induced processes are becoming firmly established) and polymer grafting techniques where there are definite signs of future commercial exploitation.

On the basis of its contents this book deserves wide circulation. However, it is the unwarranted number of errors which will detract from its appeal. It is difficult to understand how any volume could have reached publication with so many mistakes in the text. The concept of abstracting the patent literature, properly presenting the information in a digestible form and maintaining continuity is an attractive one which could be adopted in other disciplines. One hopes that in such instances, the proof reading will be much more thorough than is the case here.

J. T. Guthrie

Conference Announcement

The Outlook for Polymer Science
UMIST, Manchester, 24 and 25 March 1976

The Sixth Biennial Manchester Polymer Symposium will be held at UMIST on 24 and 25 March 1976 and is being organized with the support of British polymer manufacturers to mark the retirement of Professor Geoffrey Gee CBE, FRS as Sir Samuel Hall Professor of Chemistry in the University of Manchester. The aim is to survey the achievements and assess prospects for future developments in four areas of polymer science with which Professor Gee has been associated: preparation of polymers with desirable structures; mechanisms of polymerization reactions; thermodynamics of polymer solutions; and mechanical properties of polymers in relation to their chemical structures. The programme will consist of the following lectures:

- Achievements and prospects in polymer science: introduction to the symposium
Professor G. Allen (Imperial College, London)
- Molecular design of polymers
Dr A. H. Willbourn (ICI Plastics Division, Welwyn Garden City)

- Some aspects of the stereoregulation in the stereospecific polymerization of vinyl monomers
Professor P. Pino (Federal Institute of Technology, Zurich)
- Intermolecular forces in polymer synthesis — from Lewis acid complexes to exciplexes
Dr A. Ledwith (University of Liverpool)
- Progress and problems in the thermodynamics of polymer solutions
Professor W. H. Stockmayer (Dartmouth College, USA)
- Mechanical motions in amorphous and semi-crystalline polymers
Dr R. F. Boyer (Midland Macromolecular Institute, USA)
- Structure and properties of multiphase polymer systems — perspectives on present status and future potential
Dr S. L. Aggarawal (General Tire, Akron, USA)
- Glassy polymers
Professor Sir S. F. Edwards (Science Research Council, London)

Texts of the lectures presented will be published in POLYMER later this year. Further details may be obtained from The Registrar, University of Manchester Institute of Science and Technology, PO Box 88, Manchester M60 1QD, UK.

Structure refinement of α -poly(L-methionine): X-ray and conformational analysis

F. Colonna-Cesari and S. Premilat

Laboratoire de Biophysique, Université de Nancy 1, Centre de premier Cycle, Case Officielle No. 140, 54037, Nancy Cedex, France

(Received 1 July 1975; revised 10 November 1975)

Using the agreement function between observed and calculated X-ray intensities of the fibre pattern as a constraint in the packing energy minimization, a structure is proposed for the α -helix of poly(L-methionine). This structure has a negative packing energy, is in good agreement with X-ray data, and consists of three different side chain conformations. A model for the packing of randomly up and down pointing polypeptide chains is proposed.

INTRODUCTION

In a previous paper¹, the unit cell of the crystalline lattice of poly(L-methionine) (PLM) (see Figure 1) in its α form was determined from X-ray fibre patterns, but no precise model could be proposed from these crystallographic data. As in the case of other α -helical polypeptides [poly(L-alanine), poly(γ -chloro-benzyl-L-aspartate). .] the existence of a strong meridional reflection near $1/4.4 \text{ \AA}^{-1}$ suggests that 3 consecutive side chains adopt different conformations^{2,3}. It would be of interest to know the extent to which these conformations differ. Takeda and coworkers³, using crystallographic methods only (without refinement) tried to establish a model with 3 distinct consecutive side chains for the α -helical form of poly(β -chlorobenzyl-L-aspartate), but their final model displays identical conformations for each of them. It might be thought that the method developed by Arnott and Wonacott⁴ would be powerful enough to solve this problem. As shown in the present paper, however, the determination of the twelve χ torsional angle values, is not possible with the help of X-ray data only; extra information is clearly needed.

This additional information may well be drawn from the necessity to obtain a structural model which corresponds to a minimum of the packing energy. On this basis, we have established a model for the side chains conformation of the α -helical form of PLM in the fibrous state.

EXPERIMENTAL

From a concentrated chloroform solution of PLM in which a few drops of dichloroacetic acid were added to avoid aggregates, very thin highly birefringent fibres are obtained by dipping and slowly removing a spatula. The most crystalline fibres are selected under a polarizing microscope, bundled into a super-fibre of 90 to 100 μm diameter and fixed to a metallic holder with araldite. The crystalline order is improved by annealing the sample *in vacuo* for 2 h at 150°C .

A cylindrical camera of 29 mm radius, evacuated with a rotary pump, is used with Ni filtered $\text{CuK}\alpha$ radiation ($\lambda = 1.542 \text{ \AA}$). Sets of 3 superposed films are exposed at a time for a period of 1 h to 15 days, in order to measure reflections in the entire density range. Integrated intensity measurements are achieved with a Joyce-Loeble densitometer.

For each diffraction arc a radial densitometer trace is obtained. The background contribution is estimated empirically and the observed integrated intensity is obtained by measuring with a planimeter the area between the densitometer trace and the background estimation. Corrections are then applied to obtain the I_{obs} values of the observed intensities directly comparable to the calculated values⁵.

X-RAY RESULTS

Figure 2 shows three X-ray diffraction patterns of the same sample taken under different experimental conditions. They consist of 62 measurable reflections whose corrected intensities I_{obs} are given in Table 5, and of strong streaks

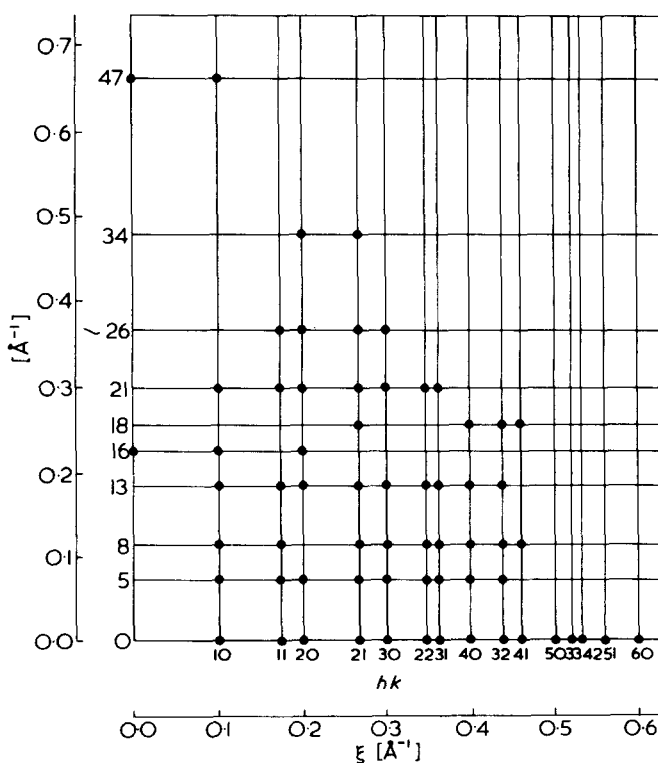


Figure 1 Reciprocal lattice rotation diagram of PLM

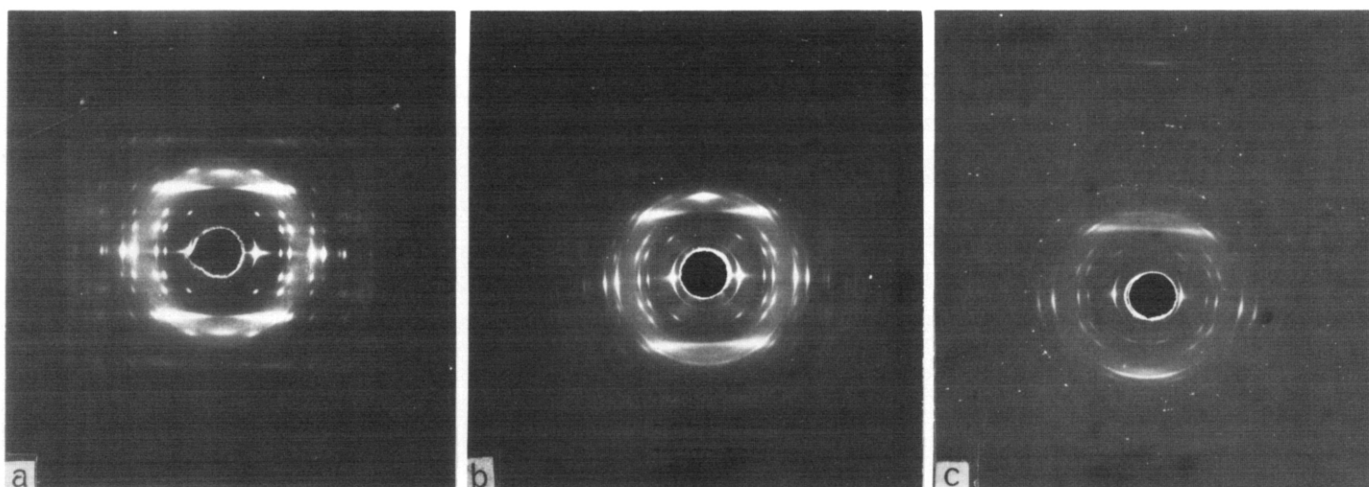


Figure 2 X-ray diffraction photograph of PLM; cylindrical camera of 29 mm radius (a) The fibre axis is vertical and normal to the beam; (b) the fibre axis is tilted 10° from the normal to the beam to show the intense 4.40 Å meridional reflection; (c) the fibre axis is horizontal and tilted 31° from the normal to the beam to show the 1.500 Å meridional reflection

on a few layer lines, suggesting some randomness of the chain sense²; their positions in the reciprocal space are reported in Figure 1. The unit-cell may thus be considered as statistical and contains one up pointing half helix and one down pointing half helix.

The equatorial spacings, together with the existence of two meridional reflections at 4.40 ± 0.01 Å and 1.500 ± 0.002 Å indicate a hexagonal lattice with $a = 11.490 \pm 0.005$ Å and $c = 70.5 \pm 0.1$ Å. The two meridional reflections may be indexed as (0 0 16) and (0 0 47) respectively as in poly(L-alanine). Thus the helical symmetry is 47/13. The (0 0 16) reflection being due to side chains, we may suppose that their structure can be well approximated by a 16/13 helix with the same c value as the 47/13 helix related to the peptidic backbone. In fact the 47/13 helix can also be approximated by a 18/5 helix. The only slight difference lies in the layer lines location, but nothing is changed as far as the Bessel function indices are concerned, since we only consider the first index for each layer line, as shown in Table 1. If the same approximation is made with the 16/13 helix we can consider, in agreement with Takeda and coworkers³ that the side chains pack roughly in a 6/5 helix, in order to accommodate the 6-fold symmetry of the packing interactions. In this approximation, the asymmetric unit of the 6/5 helix consists of exactly 3 consecutive side chains; it is, however, only an approximate model as $16 \times 3 = 48$ and not 47. The side chains helix does not have exactly the same periodicity as that of the peptidic backbone, as already shown by Elliott and Malcolm². As a consequence, the significant layer lines of the two systems may sometimes slightly differ (Table 1), but for the sake of simplicity we only consider the 47/13 helix significant layer line system. This will be taken into account when computing theoretical intensities (see Appendix).

From these crystallographic data we attempt to locate the sulphur atom with the cylindrical Patterson method of McGillavry and Bruins⁶. Contrary to Takeda and coworkers work, no information on the sulphur location is available as the sulphur peaks overlap those due to the second order of the α -helical backbone. Another attempt is then made with the electronic density projection method; but no resolution comparable to that given by Vainshtein⁷ for poly(γ -methyl glutamate) can be obtained. We are thus induced to build an *a priori* molecular model and to try

and accord the theoretical diffraction spectrum with the experimental data.

THE STRUCTURE REFINEMENT FROM X-RAY DATA

Molecular and crystal parameters

Each α -helix divides into two parts: first, the polypeptide backbone including the C_β atoms, which is assumed to keep the 47/13 symmetry and whose asymmetric unit is one peptide group $[-NH-C_\alpha H_\alpha - C_\beta - C' O -]$; secondly, the side chains. In a first approximation, we may suppose, as Takeda and coworkers did, that the side chain atoms also lie on 47/13 helices, which is what we call the 'pure' α -helical case. When 16/13 helices are considered, their asymmetric units consist of the three consecutive side chain sequences $[H_\beta H_\beta - C_\gamma H_\gamma H_\gamma - S_\delta - C_\epsilon H_\epsilon H_\epsilon]$.

The following parameters are needed to define the molecular model: (1) fixed molecular parameters, such as bond

Table 1 Bessel function indices contributing to measurable reflections (lower than 7) for the different symmetries. l , the layer line index for 47/13 and 16/13 symmetries, l' , for 18/5 and 6/5 symmetries. *47/13 significant layer line system corresponding to Figure 1

Layer line l	Symmetries				Layer line l'
	47/13	16/13	18/5	6/5	
0*	0	0	0	0	0
5*	4	—	4	—2	2
6	—	—2	—	—	—
7	—	3	—	—	—
8*	—3	—	—3	±3	3
9	—	—3	—	—	—
13*	1	1	1	1	5
16*	—6	0	—6	0	6
18*	5	—	5	—1	7
19	—	—1	—	—	—
21*	—2	—	—2	—2	8
22	—	—2	—	—	—
26*	2	2	2	2	10
34*	—1	—	—1	—1	13
35	—	—1	—	—	—
47*	0	—	0	0	18
48	—	0	—	—	—

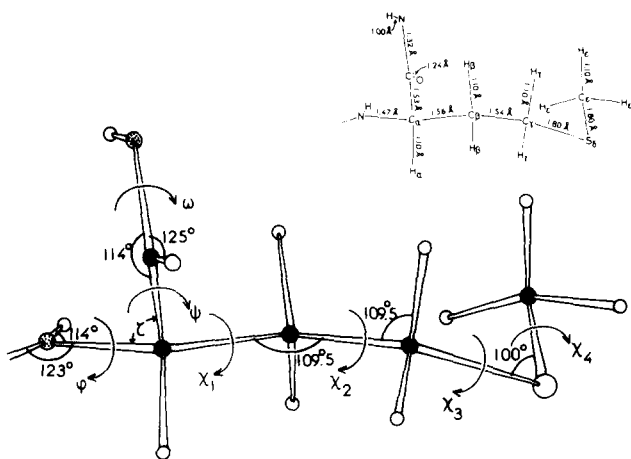


Figure 3 The structural parameters used for the methionyl residue

lengths and bond angles given by a mean on the data found in literature (Figure 3). (2) variable molecular parameters (Figure 3): the internal rotation angles ϕ , ψ , ω and χ_1 , χ_2 , χ_3 , χ_4 when only 47/13 symmetry is concerned or χ_i^j ($i = 1,4, j = 1,3$) when 16/13 symmetry is concerned, the bond angle $\tau = \angle \text{NC}_\alpha\text{C}'$. (3) variable packing parameters (Figure 4): the absolute rotation α of the two half up pointing and down pointing helices about the c axis ($\alpha = 0$ when the C_α up of the asymmetric unit is on the a axis, α sense is anticlockwise).

The relative rotation β of the down pointing helix with regard to the up pointing helix ($\beta = 0$ when the C_α of the up pointing and down pointing part of the asymmetric unit have the same equatorial projection, the β sense is clockwise). The relative translation t of the down pointing helix with regard to the up one ($t = 0$ when the two C_α of the up and down part have the same z coordinate, the positive t are along the down axis).

To these parameters we add two temperature factors: an overall temperature factor B_1 applied to every atom and an additional one B_2 applied only to the side chain atoms. In the most general case (47/13 plus 16/13 symmetries) we have to consider not less than 21 parameters.

Refinement procedure and results

Many authors choose the crystallographic R factor as a test function even when dealing with fibres; others⁴ prefer to derive a least square function. In this paper we choose the correlation factor ρ defined by:

$$\rho = \sum_i (|F_i^c| - |\bar{F}^c|) (|F_i^o| - |\bar{F}^o|) / \sigma_o \sigma_c$$

where i is running over all the reflections measured, $|F_i^c|$ is the modulus of the calculated structure amplitude for reflection i , $|F_i^o| = (I \text{ obs})^{1/2}$ for the same reflections. $|\bar{F}^c|$ and $|\bar{F}^o|$ are the means of these two sets, σ_o and σ_c their standard deviation. We want to minimize the function $\Phi = 1 - \rho^2$. This choice was carried out first, as ρ has a clear physical meaning and is now extensively used⁸ and secondly because no scaling factor needs to be introduced more or less artificially in the optimization process.

Contrary to Arnott's procedure no helical constraint is used in the optimization. The helical constraints are directly included in the helix building program by solving the Miyazawa's equations⁹ with a Newton procedure. The

values of ϕ and ψ are then automatically determined each time ω and τ vary in a region where the α -helix is defined. The helix is set up in its own coordinate system by a simple matrix transformation. The 8 helical parameters used by Arnott and Wonacott¹⁰ (ϕ , ψ , ω , τ , θ_x , θ_y , θ_z , D) are therefore reduced to ω and τ . However the derivatives with respect to ω and τ are not simple and must be evaluated numerically, but they are scarcely used in our problem. All the other derivatives are calculated analytically.

Instead of the simple least square matrix method, we use the conjugated gradient method of Fletcher and Powell¹¹, since our starting structures are too far from the optimum one.

Optimization of the Φ function leads to many possibilities in so far as the part of the information due to side chains is relatively weak in the X-ray diagram compared to that due to the α -helical backbone, as confirmed by the diffuse cylindrical Patterson function. This may be due to some necessary disorder affecting side chains included in interactions between helices of same polarity, as we shall show below. Since, on the other hand, the packing energy E is more sensitive to the conformation of the side chains than to that of the peptidic backbone, by optimizing the packing energy we should obtain some satisfactory starting structures for ulterior optimization of Φ .

CONFORMATIONAL ENERGY ANALYSIS

In fact simple empirical packing energy calculation seldom yields realistic structures. For example, Fu and coworkers¹² have determined several stable conformations for poly(β -chlorobenzyl-L-aspartate) by energy analysis. It turns out that the conformation derived from X-ray analysis by Takeda *et al.*³ has the less favourable energy.

In this work we obtained similar results with PLM; structures obtained by optimization of E only give poor Φ values and *vice versa*. The reason lies mainly in the difficulty to find all the minima of a several variable function. On the other hand, a coupled optimization of E and Φ at

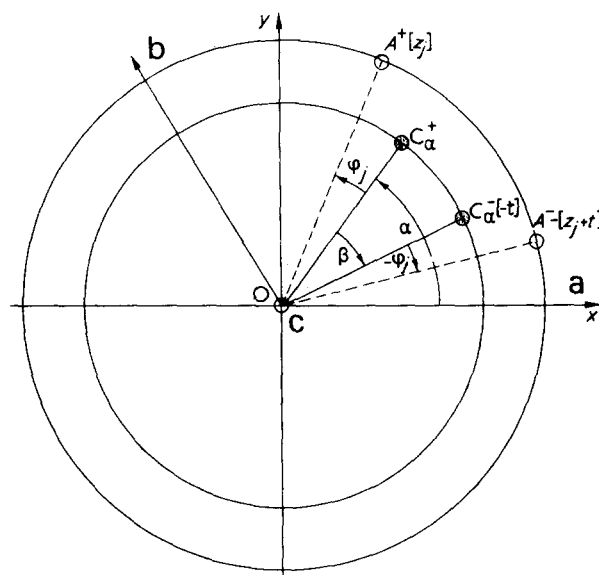


Figure 4 The parameters α and β and their rotation senses. $A^+(r_j, \phi_j, z_j)$ represents the equatorial projection of a given atom in the up pointing helix and $A^-(r_j, -\phi_j - \beta + \alpha, -z_j - t)$ the projection of the homologous of A^+ on the down pointing helix. C_α^+ and C_α^- are the origins respectively for the up and down helices; $-t$ is the translation of C_α^- relatively to C_α^+

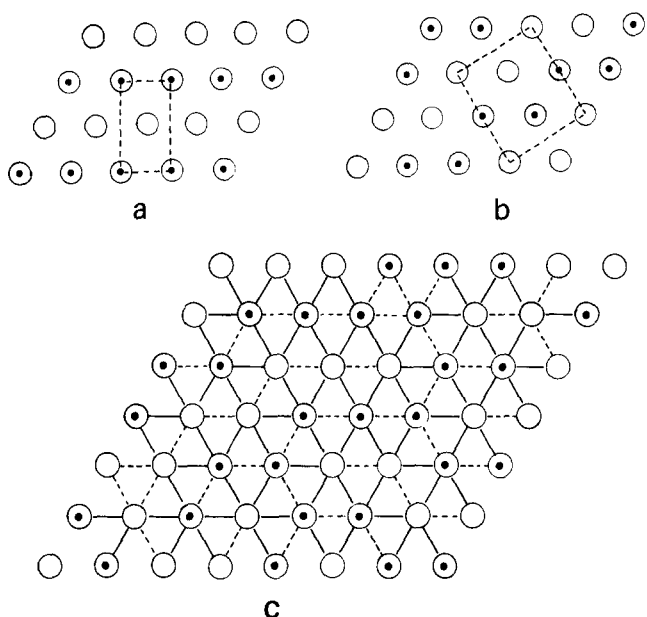


Figure 5 The different lattice models, with as many up pointing chains \odot as down pointing chains \circ . (a) model I: orthorhombic unit-cell with two helices; (b) model II: orthorhombic unit-cell with four helices; (c) possible real arrangement with hexagonal statistical unit-cell. Parallel interactions (---); antiparallel interactions (—)

the same time will certainly present much less minima. And it must yield a structure energetically favourable and in agreement with X-ray data.

Potentials

We use the 6–12 Lennard–Jones potentials published by Scheraga¹³, with increased van der Waals radii as used previously¹⁴. In the exploration phase a cut-off of 4 Å is used on these interactions to save computer time, and 7 Å in the final computations. Electrostatic interactions are calculated without cut-off with a dielectric constant of 1 and the partial charges of the monopole approximation are taken from the paper of Poland and Scheraga¹⁵. Torsional energy around covalent bonds and τ angle deformation energy are calculated from the values published by Scheraga¹³. The hydrogen bond potential is taken from Poland and Scheraga¹⁵.

Molecular packing model

At this step, it is necessary to suppose an hexagonal arrangement of the randomly up and down pointing chains corresponding to the X-ray model, simple enough to allow quick energy calculations.

Let us consider the interactions of a given up pointing helix with its 6 first neighbours. They divide into two types: parallel interactions when the up pointing helix interacts with other up pointing helices and antiparallel interactions when it interacts with down pointing helices. First, we can consider a model in which each site of the hexagonal lattice is randomly occupied by an up or a down pointing helix. In this case, interactions between helices are also randomly distributed; it is impossible to conceive a 6/5 helical symmetry for the side chains, induced by the hexagonal lattice, or some correlations in the helices orientations. The diffraction pattern would be similar to that of the tobacco mosaic virus¹⁶.

In fact, the existence of a hexagonal lattice and of a 6/5 helical symmetry for the side chains implies some local

order. In other words, one type of interaction must be more frequent than the other.

In this way, they are, on average, two consecutive helices with the same sense in the nearest neighbouring of a given helix: this is sufficient to ensure the existence of the (4.4 Å) reflection characteristic of the 16/13 or 6/5 helical symmetry. In addition, this predominant type of interaction, by imposing its own local order, ensures that the helices are correlated in orientation. This allows the existence of a crystalline order. This predominant type of interaction is therefore responsible for the X-ray diffraction pattern. As energy calculations show that electrostatic interactions between parallel helices are 10 kcal/mol-residue less favourable than those between antiparallel helices, we suggest that antiparallel interactions predominate in the helices arrangement. Regular lattices, with as many up as down pointing helices but in which antiparallel interactions are twice as numerous, can be built as shown in Figures 5a and 5b. Nevertheless these regular models give orthorhombic unit cells and are not consistent with the existence of streaks. So, we suggest that the actual lattice may look like that of Figure 5c, i.e. mixture of models I and II of Figure 5a and b, consistent with the hexagonal lattice and streaks. The necessary presence of parallel interactions implies some disorder in the conformation of the side chains involved. This type of lattice thus contains an important 'amorphous phase' which could be at the origin of the strong diffuse halo on the X-ray patterns.

As pointed out above, the antiparallel interactions alone are responsible for the Bragg reflections. The following model is then sufficient to undertake energy calculations: an up pointing helix surrounded by 6 down pointing helices. The antiparallel interactions alone are taken into account. We construct such an arrangement with the middle of an up pointing helix of 9 residues and 6 down pointing helices of 15 residues. Further, the first 3 residues of the up pointing helix are facing the middle residues of the down pointing helices.

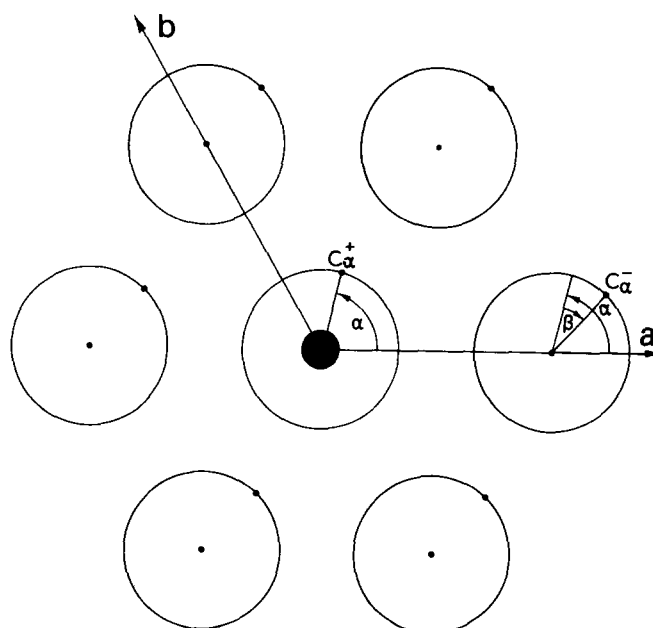


Figure 6 Arrangement of up and down pointing chains used for energy calculations

Table 2 Conformational parameters for the five areas of minimum intramolecular energy

	χ_1 (degrees)	χ_2 (degrees)	χ_3 (degrees)	χ_4 (degrees)	E_i (kcal/mol residue)
(1)	180	160	60	60	-11.38
(2)	180	40	60	20	-10.63
(3)	-160	-160	-60	60	-10.25
(4)	-100	-160	-60	-20	-7.96
(5)	-160	120	-60	20	-6.27

In the calculations, the packing energy E by residue is divided into two parts: (a) E_i the intramolecular energy of a helix, calculated as the energy of interaction of the 3 first residues of the middle helix with themselves and with the remaining residues divided by 3; (b) E_R the intermolecular energy calculated as the energy of interaction of the 3 first residues of the middle helix with the down pointing helices divided by 3.

The molecular parameters used as variables in the calculation of E are the same as those used for X-ray refinement (α , β and t being now defined as shown by Figure 6).

Given a set of parameters (ω , τ , χ_i^j , α , β , t , $B_1 B_2$) we can now calculate Φ , the test function for X-ray data, and E at the same time.

Results of energy calculations

To eliminate side chains conformations giving high intramolecular energies we first build energy maps of a pure 47/13 α helix where χ_1 and χ_2 are varied from 20° to 20° for values of χ_3 equal to 60° , 180° and -60° and χ_4 equal to 60° , 20° and -20° . We thus obtain five areas of negative intramolecular energy (see Table 2).

In order to eliminate very unfavourable conformations (such as extended side chains of very high intramolecular energy) a shallow optimization is performed on E starting from these areas, always with the pure α -helical conformation. As expected, no conformation gives a negative value for E associated with a good Φ value. Nevertheless they yield reasonable starting points for the coupled optimization and allow the elimination of unlikely structures.

COUPLED REFINEMENT

Method

As discussed above, if we do not want to go astray in local minima of E providing poor agreement with X-ray data, we must use a coupled or simultaneous minimization of E and Φ . The mathematical problem is therefore: to find a set of conformational and packing parameters so as to minimize E with the imperative condition that $\Phi \leq \sigma$ [or $\rho \geq \rho_\sigma = (1 - \sigma^2)^{1/2}$], where σ is a given positive number smaller than 1. This problem is very similar to the protein refinement problem. In this paper we prefer to deal with the constrain $\Phi \leq \sigma$ by a Lagrangian method, more powerful than the oversimplified penalty minimizations used in this type of work^{17,18}. For this purpose, we use the conjugated gradient method published by Haaroff and Buys¹⁹ to solve non-linear constrained minimization problems. A series of constrained optimizations is undertaken in which σ is lowered from 0.50 to 0.20 (or ρ_σ increased from about 0.70 to 0.90) by small steps, to drive the parameters gently towards regions leading to lower energies consistent with $\Phi \leq \sigma$.

Results

Starting from points obtained by the previous E optimization, the coupled optimization procedure is first applied to the 'pure' α -helical conformation.

When a conflict arises between Φ and E optimizations, the next step is carried out with side chains in the 16/13 symmetry. The optimization is stopped when a further decrease in σ leads to stationary values for E and Φ or conflicts with a further optimization of E .

As ρ reaches a values of 0.85, we refine B_1 and B_2 to obtain $B_1 = 9$ and $B_2 = 3$. We keep $B_1 = 9$ in the next steps but $B_2 = 0$ so that the role of side chains in the Φ optimization does not decrease too artificially.

A final refinement is made on ω and τ leading to some improvement, mainly in the intramolecular energy E . We verify too that no other values for α , β and t give new solutions. Finally, two conformations (Table 3) reached the final stage. For both of them $\rho = 0.88$, but one of them (b) is eliminated as it does not account for the small values of the (1 0 13) reflection, an important fact of the diffraction pattern (it also has the greater energy). So, we propose the conformation (a) of Table 3 as a probable structure for PLM α -helices in the fibrous state. The corresponding atomic coordinates of the asymmetric unit are given in Table 4. Figure 7 shows equatorial projection of this structure and Table 5 gives the calculated X-ray intensities.

DISCUSSION AND CONCLUSION

The examination of the results of Table 3 and 5 shows that the model we proposed is still coarse ($\rho = 0.88$, $R \approx 0.4$),

Table 3 Refined parameters for the two final structures. (a) and (b) correspond respectively to starting points (1) and (3) of Table 2. R factor is given for comparison

	(a)	(b)
ϕ	-57.0	-55.479
ψ	-48.225	-49.566
ω	180.880	180.770
τ	109.6	109.4
χ_1^1	179.3	-124.3
χ_2^1	152.4	177.7
χ_3^1	47.6	-76.0
χ_4^1	50.9	-16.4
χ_1^2	153.9	-120.2
χ_2^2	150.0	179.4
χ_3^2	48.4	-69.2
χ_4^2	52.2	-17.0
χ_1^3	147.6	-119.7
χ_2^3	165.2	172.1
χ_3^3	57.1	-82.5
χ_4^3	52.1	16.9
α	17.1	41.9
β	154.5	203.0
t	0.0	0.16
B_1	10.0	10.6
B_2	2.0	0.4
R^*	0.393	0.435
Φ	0.23	0.23
ρ	0.88	0.88
E	-11.32	-9.76
(kcal/mol residue)		

$$* R = \frac{\sum_i ||F_i^c| - |F_i^o||}{\sum_i |F_i^o|}$$

Table 4 Cylindrical atomic coordinates corresponding to the structure (a) of Table 3

	Residue 1			Residue 2			Residue 3		
	r(Å)	ϕ (degrees)	z(Å)	r(Å)	ϕ (degrees)	z(Å)	r(Å)	ϕ (degrees)	z(Å)
peptidic backbone									
N	1.53	-11.11	-0.87	1.53	88.46	0.63	1.53	-171.96	2.13
H	1.50	-1.57	-1.84	1.50	98.00	-0.34	1.50	-162.42	1.16
C $_{\alpha}$	2.29	17.10	0.0	2.29	116.67	1.50	2.29	-143.75	3.00
H $_{\alpha}$	3.06	3.56	0.47	3.06	103.13	1.97	3.06	-157.29	3.47
C $_{\beta}$	3.26	35.37	-0.85	3.26	134.94	0.65	3.26	-125.48	2.15
C $_{\gamma}$	1.68	43.39	1.09	1.68	43.39	2.59	1.68	-117.46	4.09
O	1.96	37.03	2.28	1.96	37.03	3.78	1.96	-123.82	5.28
side chain									
H $_{\beta}^1$	3.70	24.65	-1.62	4.01	124.15	0.21	4.07	-135.93	1.81
H $_{\beta}^2$	2.97	52.82	-1.33	2.84	146.60	-0.16	2.84	-115.71	1.28
C $_{\gamma}$	4.45	40.85	0.06	4.18	148.13	1.55	4.11	-110.42	3.01
H $_{\gamma}^1$	4.45	53.96	0.48	4.09	163.36	1.55	3.83	-95.11	3.13
H $_{\gamma}^2$	4.55	31.55	0.88	4.13	142.69	2.57	4.25	-116.76	4.00
S $_{\gamma}$	5.98	40.08	-0.88	5.86	145.80	0.93	5.72	-109.27	2.21
C $_{\epsilon}$	5.59	50.12	-2.32	5.61	149.56	-0.81	5.29	-101.51	0.63
H $_{\epsilon}^1$	6.49	50.51	-2.94	6.58	149.67	-1.32	6.23	-100.33	0.05
H $_{\epsilon}^2$	4.78	45.06	-2.91	5.02	140.81	-1.27	4.64	-109.42	0.06
H $_{\epsilon}^3$	5.42	60.91	-1.99	5.22	160.46	-0.90	4.92	-90.01	0.80

Table 5 Observed (I_{obs}) and calculated intensities corresponding to the structure (a) (Table 3), (I_{a}^c) and structure (b), (I_{b}^c). The last are given for comparison. Equatorial reflections from 200 to 310 are too weak for the (a) conformation

hkl	I_{obs}	I_{a}^c	I_{b}^c	hkl	I_{obs}	I_{a}^c	I_{b}^c
1 0 0	37.15	46.75	56.44	2 0 13	4.28	3.02	3.49
1 1 0	7.20	10.59	19.40	2 1 13	1.10	0.87	1.22
2 0 0	19.43	5.70	14.56	3 0 13	1.42	1.75	0.43
2 1 0	39.31	18.96	27.40	2 2 13	1.07	0.04	0.46
3 0 0	48.04	19.32	36.61	3 1 13	1.38	0.71	1.12
2 2 0	6.68	3.71	7.15	4 0 13	1.30	3.10	1.98
3 1 0	7.44	2.34	3.44	3 2 13	0.40	1.22	0.74
4 0 0	1.84	2.82	1.74	1 0 16	0.91	0.13	0.08
3 2 0	3.5	3.36	2.75	1 1 16	—	0.02	0.04
4 1 0	0.35	1.76	2.02	2 0 16	0.16	0.04	0.03
5 0 0	0.12	0.07	0.01	1 0 18	—	0.00	0.00
3 3 0	0.14	0.59	0.21	1 1 18	—	0.02	0.04
4 2 0	0.71	0.80	0.41	2 0 18	—	0.07	0.07
5 1 0	0.32	0.72	0.60	2 1 18	0.13	0.09	0.21
6 0 0	0.77	0.10	0.21	3 0 18	—	—	—
1 0 5	0.05	0.04	0.20	2 2 18	—	—	—
1 1 5	3.22	0.73	0.16	3 1 18	—	—	—
2 0 5	6.08	1.40	0.08	4 0 18	0.8	0.31	0.02
2 1 5	2.14	3.15	0.10	3 2 18	0.57	0.62	0.01
3 0 5	1.12	3.33	0.40	4 1 18	0.56	0.76	0.02
2 2 5	0.56	2.55	1.39	1 0 21	0.37	1.33	2.59
3 1 5	0.32	2.21	1.68	1 1 21	1.29	0.34	3.70
4 0 5	0.57	1.32	2.10	2 0 21	0.84	0.63	2.13
3 2 5	0.35	0.72	1.80	2 1 21	1.42	1.78	0.82
1 0 8	0.95	1.17	0.61	3 0 21	1.61	2.32	0.42
1 1 8	3.86	1.13	2.12	2 2 21	1.49	2.24	1.75
2 0 8	—	0.25	2.12	3 1 21	1.12	2.01	1.57
2 1 8	1.04	0.56	0.39	1 0 26	—	0.18	1.00
3 0 8	0.52	1.19	0.03	1 1 26	0.02	1.59	0.06
2 2 8	1.02	1.80	1.02	2 0 26	0.11	0.90	0.21
3 1 8	1.22	1.83	1.34	2 1 26	0.74	0.32	1.29
4 0 8	1.15	1.50	1.58	3 0 26	1.08	1.06	0.46
3 2 8	0.50	0.92	1.26	1 0 34	—	0.02	0.01
4 1 8	0.27	0.57	0.93	1 1 34	—	0.41	0.22
1 0 13	0.18	0.02	2.35	2 0 34	0.10	0.41	0.56
1 1 13	8.89	10.81	4.82	2 1 34	0.15	0.23	0.05
				1 0 47	0.03	1.06	0.81

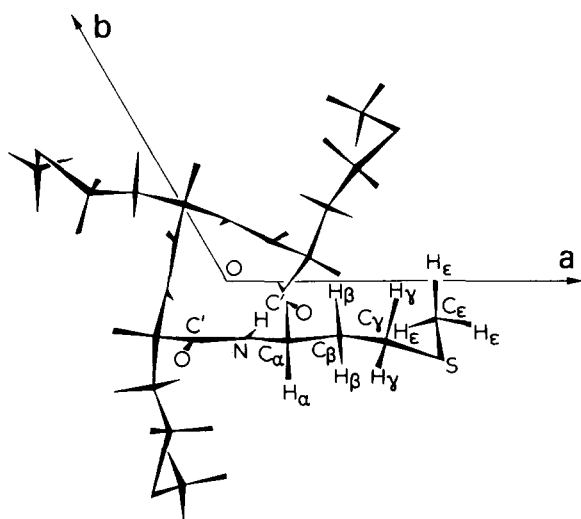


Figure 7 Equatorial projection of the structure (a) of Table 3

in particular the 200 reflection is too weak. This region of the reciprocal space is very sensitive to the position of the side chains atoms. A possible explanation of this discrepancy may be that in the actual asymmetric unit the 'up and down' half helices have different geometrical parameters in particular different χ angles. Thus, in the real structure, the S atoms, in particular, are not exactly, in the same relative position for the up and down pointing chains. This fact may affect the intensity of the reflections near the reciprocal space origin.

A second reason may be that we have not taken into account the postulated existence of an 'amorphous phase' for some side chains. As a consequence, the relative intensity due to the side chains is over estimated and must be a cause of error. We did not want to introduce these supplementary parameters which will make the calculations too unwieldy.

Nevertheless our results show that the hypothesis of a 16/13 (or more simply 6/5) symmetry for the side chains of an α -helix in the fibrous state is correct, since it allows an improvement of ρ and E as well. Besides, we show that, by considering the agreement function Φ as a constraint of the packing energy optimization problem we avoid the reefs found when separate optimizations are done or simple penalty methods used. We thus obtain a structure in rather good agreement with X-ray data and a good packing energy. We think that this procedure of constrained optimization could be applied to industrial synthetic polymers and perhaps to protein refinement problems.

Moreover, close examination of the packing mode of α -helices in hexagonal lattice shows that it is a rather complicated statistical array, including an amorphous phase which could only crystallize in lattice with orthorhombic unit cells. Analogous regular systems have been observed for mixture of poly(D and poly(L-benzyl-glutamates)²⁰ and ω helices of poly(β -benzyl-L-aspartate)²¹, but have never been observed in enantiomorphous α -helical lattices.

REFERENCES

- 1 Colonna-Cesari, F., Horn, P., Belhaj-Soulami, A., Marraud, M. and Neel, J. *J. Chim. Phys.* 1969, **66**, 2009

- 2 Elliott, A. and Malcolm, B. R. *Proc. R. Soc. (A)* 1959, **249**, 30
- 3 Takeda, Y., Itaka, Y. and Tsuboi, M. *J. Mol. Biol.* 1970, **51**, 101
- 4 Arnott, S. and Wonacott, A. J. *Polymer* 1966, **7**, 157
- 5 Arnott, S. *Polymer* 1965, **6**, 478
- 6 McGillavry, C. H. and Bruins, E. M. *Acta Crystallogr.* 1948, **1**, 156
- 7 Vainshtein, B. K. *Dokl. Akad. Nauk SSSR* 1961, **169**, 1347
- 8 Birktoft, J. J. and Blow, D. H. *J. Mol. Biol.* 1972, **68**, 187
- 9 Sugeta, H. and Miyazawa, T. *Biopolymers* 1967, **5**, 673
- 10 Arnott, S. and Wonacott, A. J. *J. Mol. Biol.* 1966, **21**, 371
- 11 Fletcher, R. and Powell, M. J. D. *Comput. J.* 1963, **6**, 163
- 12 Fu, Yi-Ch., MacGuire, R. F. and Scheraga, H. A. *Macromolecules* 1974, **7**, 4108
- 13 Scheraga, H. A. *Adv. Phys. Org. Chem.* 1968, **6**, 103
- 14 Colonna-Cesari, F., Premilat, S. and Lotz, B. *J. Mol. Biol.* 1974, **87**, 181
- 15 Poland, D. and Scheraga, H. A. *Biochemistry* 1967, **6**, 3791
- 16 Vainshtein, B. K. in 'Diffraction of X-rays by chain molecules', Elsevier, Amsterdam, 1966, p 322
- 17 Rasse, D., Warne, P. K. and Scheraga, H. A. *Proc. Nat. Acad. Sci. USA* 1974, **71**, 3736
- 18 Levitt, M. and Lifson, S. *J. Mol. Biol.* 1969, **46**, 269
- 19 Haaroff, P. C. and Buys, J. D. *Comput. J.* 1970, **13**, 178
- 20 Squire, J. M. and Elliott, A. *J. Mol. Biol.* 1972, **65**, 291
- 21 Baldwin, J. P., Bradbury, E. M., MacLuckie, I. F. and Stephens, R. M. *Macromolecules* 1973, **6**, 83
- 22 Cochran, W., Crick, F. H. C. and Vand, V. *Acta Crystallogr.* 1952, **5**, 581

APPENDIX

Fourier Transform of double helical symmetry chains with random up-down polarities

In the general case, the Fourier transform of a macromolecular helix, with ν asymmetric units in t turns, is yielded by the formula derived by Cochran *et al.*²²:

$$F(R, \psi, l/c) = \sum_n \sum_{j \in A} f_j J_n(2\pi R r_j) \exp \left\{ i[n(\pi/2 - \phi_j) + (2\pi l z_j/c)] \right\} \exp(in\psi)$$

$$\text{or } F(R, \psi, l/c) = \sum_n (A_n + iB_n) \exp(in\psi) \quad (\text{A1})$$

where r_j , ϕ_j , z_j are the cylindrical coordinates of the atom j of the asymmetric unit A , f_j the atomic scattering factor of the atom j , R , ψ , l/c are the cylindrical coordinates of a point in the reciprocal space and n is running over all the J_n Bessel function indices occurring on the layer line l and given by the selection rule:

$$l = nt + m\nu \quad (\text{A2})$$

where m is an integer.

We consider now a statistical unit cell with a half up helix superposed to a half down helix whose relative positions are defined by α , β and t as defined by Figure 3. For each atom u of the up helix whose coordinates are $(r_u, \phi_u + \alpha, z_u)$ there is a corresponding atom on the down helix whose coordinates are: $[r_u, -(\phi_u + \beta) + \alpha, -(z_u + t)]$

If we put $\Phi_u = -n\phi_u + 2\pi l z_u/c$

$$\gamma = n\beta - 2\pi l t/c$$

from (A1) we obtain:

$$A_n = \cos[n(\pi/2 - \alpha) + \gamma/2] \sum_{u \in U} f_u J_n(2\pi R r_u)$$

$$\cos(\Phi_u - \gamma/2)$$

$$B_n = \sin[n(\pi/2 - \alpha) + \gamma/2] \sum_{u \in U} f_u J_n(2\pi R r_u)$$

$$\cos(\Phi_u - \gamma/2)$$

where U is the asymmetric unit of the up-helix. Putting:

$$\Gamma = n(\pi/2 - \alpha) + \gamma/2$$

and

$$F_n = \sum_{u \in U} f_u J_n(2\pi R r_u) \cos(\Phi_u - \gamma/2)$$

we obtain:

$$\begin{aligned} F(R, \psi, l/c) &= \sum_n (A_n + iB_n) \exp(in\psi) \\ &= \sum_n F_n \exp[i(n\psi + \Gamma)] \end{aligned}$$

If the asymmetric unit consists of two different helices characterized in relation (A2) respectively by n_1 and n_2 , we obtain for (A1):

$$\begin{aligned} F(R, \psi, l/c) &= \sum_{n_1} F_{n_1} \exp[i(n_1\psi + \Gamma_1)] + \\ &\quad \sum_{n_2} F_{n_2} \exp[i(n_2\psi + \Gamma_2)] \end{aligned}$$

with

$$F_{nk} = \sum_{j \in U_k} f_j J_{nk}(2\pi R r_j) \cos(\Phi_j - \gamma_k/2)$$

where

$$\Phi_{jk} = -nk\phi_j + 2\pi lz_j/c$$

$$\gamma_k = nk\beta - 2\pi lt/c$$

$$\Gamma_k = nk(\pi/2 - \alpha) + \gamma_k/2$$

if first Bessel indices only are significant we obtain:

$$\begin{aligned} I = FF^* &= F_{n_1}^2 + F_{n_2}^2 + 2F_{n_1}F_{n_2} \cos[(n_1 - n_2)\psi \\ &\quad + \Gamma_1 - \Gamma_2] \end{aligned}$$

As in a fibre diagram we only measure $I^c = \langle FF^* \rangle_\psi$ the mean over ψ of FF^* , we thus have:

$$I^c(R, l/c) = \langle FF^* \rangle_\psi = F_{n_1}^2 + F_{n_2}^2 \text{ if } n_1 \neq n_2$$

[or if the layer lines systems are not exactly superposed on the layer line l (see text)]

$$= (F_{n_1} + F_{n_2})^2 \text{ if } n_1 = n_2$$

Morphological study of chain-extended growth in polyethylene:

1. Crystallization

D. C. Bassett and B. A. Khalifa*

J. J. Thomson Physical Laboratory, University of Reading, Reading RG6 2AF, UK

(Received 10 October 1975)

Polyethylene crystallizes from the melt at pressures of a few kbar as lamellar crystals whose thickness extends over at least two orders of magnitude from a few hundred of Å to μm . The average value in bulk unconstrained polymer in these experiments is ~ 4000 Å but this value progressively decreases to ~ 200 Å as thinner and thinner specimens are used. Morphological evidence shows no discontinuity of physical texture throughout this range but reveals, by the occurrence of parallel changes in the thinnest films and the bulk polymer, that the entire spectrum of lamellar thicknesses is associated with crystallization into the hexagonal phase. This implies on the one hand, that lamellar thickness is not a suitable measure to distinguish the so-called chain-extended and chain-folded modes of crystallization of polyethylene and, on the other, that the very large effect of constraints needs to be included in theories of polymeric crystallization.

INTRODUCTION

The problem presented by the crystallization of molten polyethylene at high pressure (~ 5 kbar) has been greatly changed by recent work. The main issue used to be to understand why growth under such conditions produced crystals so different, notably by being an order of magnitude thicker, from those formed at atmospheric pressure¹. Various possible reasons were suggested for this, among them a change from chain-folded to bundlelike nucleation², enhanced lamellar thickening³ and a continuous large increase of fold surface free energy with pressure⁴. However, all of these proposals were incompatible with the results of further work, in particular the demonstration that chain-extended crystallization of polyethylene is independent of chain-folded crystallization and is favoured by longer molecules^{5,6}. Instead the underlying reason, according to Bassett and Turner, is that at high pressures and moderate supercoolings polyethylene crystallizes into a new intermediate phase by chain-extended crystallization, and only transforms into the orthorhombic structure at low pressures and/or temperatures^{7,8}. By contrast, chain-folded crystallization is direct precipitation of orthorhombic polyethylene from the melt.

This hypothesis has now, in our view, been shown to be correct by the identification of the new (hexagonal) phase using high pressure, high temperature X-ray diffraction and the correlation of its formation with the characteristic appearance and properties of the chain-extended polymer⁹. It must be stated, nevertheless, that the original proposals of Bassett and Turner based on volumetric and d.t.a. data showing that fusion and recrystallization of polyethylene at 5 kbar proceeded in two stages have been questioned by other workers. Kanetsuna and coworkers have interpreted their volumetric data in terms of only part of the polymer forming a 'super-extended structure'¹⁰⁻¹². This seems to us incompatible with the X-ray evidence, and their more complex data^{11,12} to be a consequence of the complicated

fractionation between the two processes as chain-folded growth gives way to chain-extended with increasing pressure. On the other hand, Yasuniwa *et al.* do discuss their high pressure d.t.a. data in terms of a new phase, but again which only consists of a portion of the sample, and which they speculate may be a nematic high pressure phase¹³. This interpretation is refuted by the same objection as previously and, in particular, a nematic structure is inconsistent with the sharp X-ray line observed⁹.

The recognition that chain-extended growth of polyethylene is crystallization of a new phase immediately prompts the question of whether it is possible to describe both chain-folded and chain-extended crystallization as the same process modified only by the differing properties of the orthorhombic and hexagonal phases. Collected results show that, *prima facie*, this appears to be the case. Data for chain-extended polyethylene (CEPE)^{14,15} and also for PTFE¹⁶ conform to the formalism of kinetic theory as well as does chain-folded polyethylene, with the large lamellar thicknesses stemming essentially from the low entropies of fusion. The facts do not appear to support the contention of Wunderlich that there is one growth mechanism for chain-folded polymers and another for chain-extended¹⁷. Nevertheless, detailed study of both CEPE and PTFE has revealed important new aspects of behaviour which, if there is to be but one theory of polymeric growth, will need to be incorporated into kinetic theories. The new context in which we now see CEPE is, therefore, as a model system for the study of polymeric crystallization which, because of its great lamellar size, allows the study of new aspects of behaviour.

The purpose of this series of papers is to document certain of these new features and also to fill in more of the morphological record of chain-extended growth in polyethylene. Unlike most other topics in polymeric crystallization, our knowledge of CEPE owes comparatively little to morphological investigation, beyond the appreciation of the large crystal size. This is because the existence of the hexagonal phase leaves little other clear indication in the physical texture. Nevertheless a wide range of such studies

* Present address: Faculty of Science, Ain Shams University, Cairo, Egypt

has been made in this laboratory aimed initially at preparing isolated chain-extended crystals and more recently at clarifying aspects of chain-extended growth. The initial results of this work were often apparently confusing although at one point they contributed importantly to the deduction that chain-extended growth was independent of chain-folded⁵. Now, however, the features can be viewed in their new perspective. In this paper we are concerned with the morphological distinction between chain-folded and chain-extended growth not only in bulk but also in thin films and the demonstration that with suitable constraints lamellar thicknesses resulting from crystallization of hexagonal polyethylene can be depressed by an order of magnitude.

The second paper¹⁸ discusses the annealing of bulk polyethylene at high pressure, correcting certain mistakes in the literature; annealing in thin films is the subject of the third paper¹⁹. In a fourth paper²⁰ we present data from various techniques to illustrate the nature of chain-extended lamellae.

PRELIMINARY EXPERIMENTS

The experiments described in this series of papers had their beginnings as long ago as 1966 when a preliminary survey was undertaken into the practicability of preparing isolated 'extended-chain' crystals. The first approach²² was to co-crystallize polyethylene and $n\text{-C}_{32}\text{H}_{66}$ hoping that subsequent removal of the latter, in the manner of Keith *et al.*²¹ would leave behind relatively isolated chain-extended crystals. It turned out that behaviour at low concentrations was akin to that reported for other solutions and not until the polymer was in a proportion $>\sim 40\%$ did crystallization at several kbar produce the expected melting point of $\sim 140^\circ\text{C}$ ²²; these results are in agreement with a fuller investigation by Treiber *et al.*²³. At this concentration the texture was far too compact for ready microscopic examination so that this approach was taken no further until the thin film work described in Part 4 of this series²⁰.

Subsequently, following the discovery that high-pressure annealing transformed solution-grown polyethylene crystals (sedimented in mats) into lamellae 2000 Å and more in thickness^{24,25}, individual crystals of the same preparations, but suspended either in the supposed non-solvent 2-butoxy-ethanol or in silicone oil were also annealed at ~ 5 kbar (1 bar = 10^5 N/m²). Surprisingly this never gave thick (>1000 Å) lamellae; instead crystal thickening occurred to an extent reminiscent of atmospheric behaviour, with a legacy of oriented holes²², as described in the more detailed work of Roe *et al.*²⁶. This rather remarkable effect had no obvious explanation and parallel behaviour became apparent in unpublished work of Bassett and Phillips who examined thin films of three fractionated polyethylenes recrystallized at 5 kbar using techniques similar to our own. Once again while bulk samples acquired the high crystal thicknesses, melting points and densities expected at this pressure, for the thinnest films in the same runs, lamellar thicknesses remained at a few hundred Å. It was not then clear how, if at all, such thin layers, which clearly contained molecules having many folds, were related to the thick, chain-extended laminae found in the bulk polymer. At the same time, there had to be an increase in lamellar thickness for thicker films but examination of increasingly thick films to the maximum penetration of 100 kV electrons showed no obvious discontinuity in behaviour. Particular possible causes for recrystallized lamellae being so thin were then looked into, viz. the restricting effect of the sub-

strate and of the lack of appropriate nuclei. Thus, for the latter 'shish-kebab' structures were provided as possible promoters of chain-extended growth but in no case was the resulting lamellar thickness sufficiently influenced to account for the disparity. It appeared, therefore that a whole spectrum of crystal thicknesses was formed during high pressure crystallization, with thicknesses increasing for thicker specimens. This trend was definitely established for films 3 μm and more in thickness by replication of fracture surfaces²⁷. Moreover, because of a similarity in texture in the optical microscope it seemed that the whole spectrum of layer thicknesses down to hundreds of Å should be associated with chain-extended growth²⁷.

Prior to this time, however, the meaning of the term chain-extended polyethylene was not well defined especially as the conformational definition of containing fully-extended molecules was known not to apply¹⁴. It was then found that for crystallized (as opposed to annealed) samples, the combination of texture in the polarizing microscope and melting point gave a working distinction between specimens of 'chain-extended' and 'chain-folded' polyethylene². This in turn led to the demonstration that chain-folded and chain-extended growth are independent processes^{5,6} which we now recognize to be crystallization from the melt into the orthorhombic phase and into the hexagonal phase of polyethylene respectively⁷⁻⁹.

Using these definitions we now re-examine the thin film morphologies of pressure-crystallized polyethylene and find evidence which supports the contention that even layers only a few hundred Å thick result from crystallization into the hexagonal structure and so can properly be regarded as part of the chain-extended texture.

RESULTS

Samples of three commercial linear polyethylenes Rigidex 2 and Rigidex 9 (BP Chemicals Ltd) and Hifax 1900 (Hercules Powder Co.) in the forms of (a) bulk pellets, (b) thin (~ 3 μm) sections, (c) solvent-cast films, and (d) solution-grown crystals deposited on a substrate have been recrystallized under conditions listed in Table 1 while immersed in the pressure-transmitting silicone fluid inside the piston and cylinder apparatus described previously⁶. The oil penetrates specimens to a slight extent, but this is not responsible for the effects described because they are also found with different systems e.g. employing encapsulation in water.

The basic morphological difference between chain-folded and CEPE is illustrated in Figure 1, which shows four sections of Rigidex 9 initially 3 μm thick, recrystallized at high pressures and then viewed optically between crossed polars. These were specimens crystallized at 2.60 and 2.87 kbar where small changes in crystallization conditions cause a changeover from one growth régime to the other. The crystallization procedure was first to impose a pressure of 1.5–1.6 kbar, secondly to increase the temperature from ambient until it was controlled at the required value (which had to be above the melting point at the initial pressure used) and thirdly to increase the pressure to that chosen for crystallization. This third step produces adiabatic heating which can under suitable circumstances cause substantial rises in temperature²⁸; care was taken therefore to limit this transient rise to ~ 3 K. Finally, after the elapse of the chosen time (usually 2 h) heaters were switched off and the samples were cooled under pressure at an initial rate of ~ 2 K/min.

Table 1 Crystallization conditions

Run	Crystallization				Melting points (°C)		
	Pressure (kbar)	Time (h)	Temperature (°C)	Super-cooling (K)	Rigidex 9 bulk		PAF
PC88	2.87	2	190.25	20	134.2	139.1	0.1
PC89	2.87	2	200.5	10	130.5	141.3	0.6
PC109	2.60	2	193.5	11	133.5	141.0	0.25
PC110	2.60	2	185	20	133.9		0.0
PC121	5.5 ₃	1	240.5	16	122.8	129.7	
PC127	5.5 ₃	1	243.5	13	122.7	130.2	
PC128	5.5 ₃	1	241.5	15	122.5	128.8	
PC129	5.5 ₃	1	245.5	11	122.9	130.2	

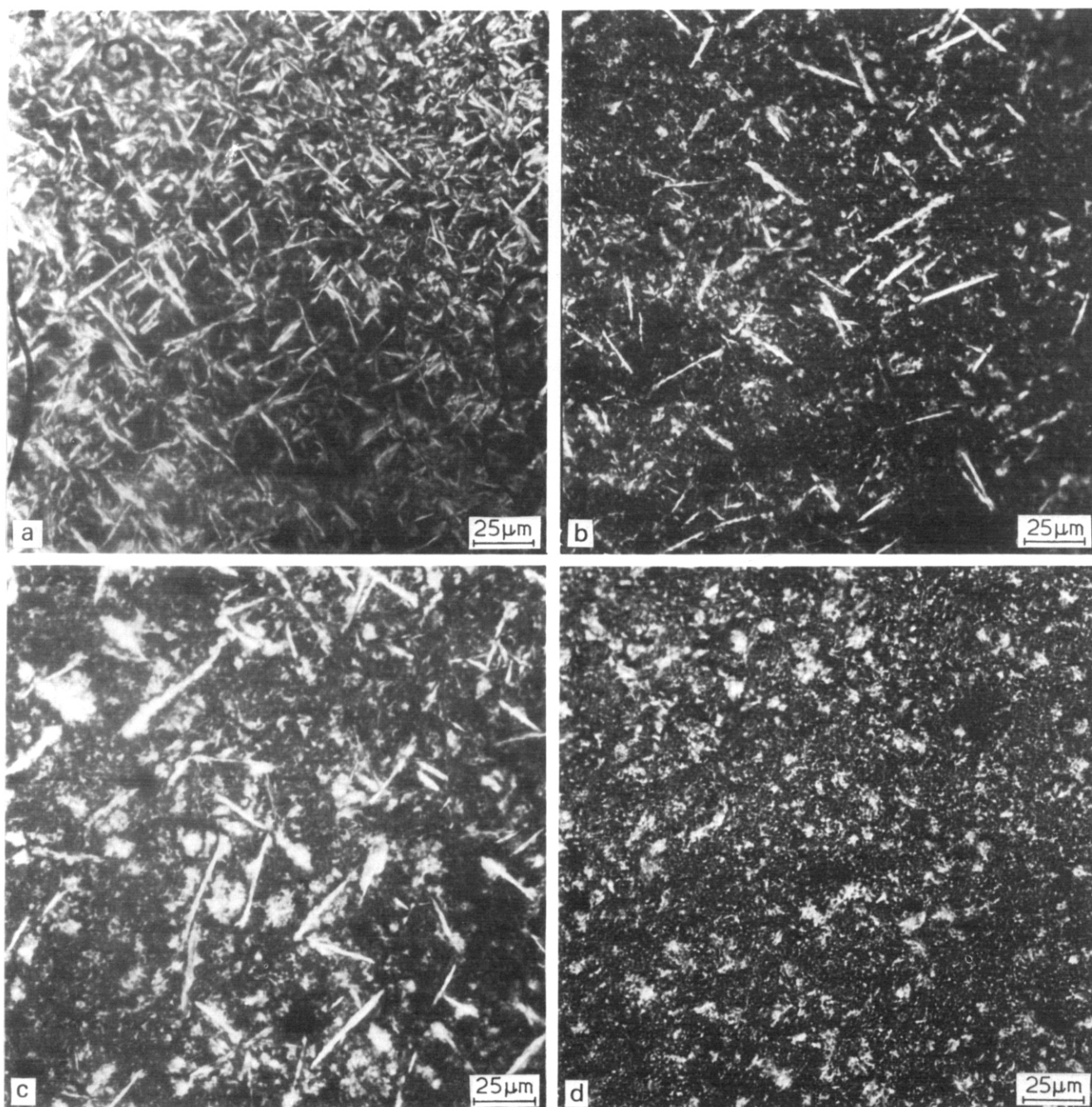


Figure 1 Optical distinction between chain-folded and chain-extended textures in polyethylene revealed between crossed polars. Samples of Rigidex 9 crystallized at: (a) 2.87 kbar and 200.5°C; (b) 2.87 kbar and 190°C; (c) 2.60 kbar and 193.5°C; (d) 2.60 kbar and 185°C. Sample (a) appears mostly chain-extended, (d) is entirely chain-folded while (b) and (c) are mixtures

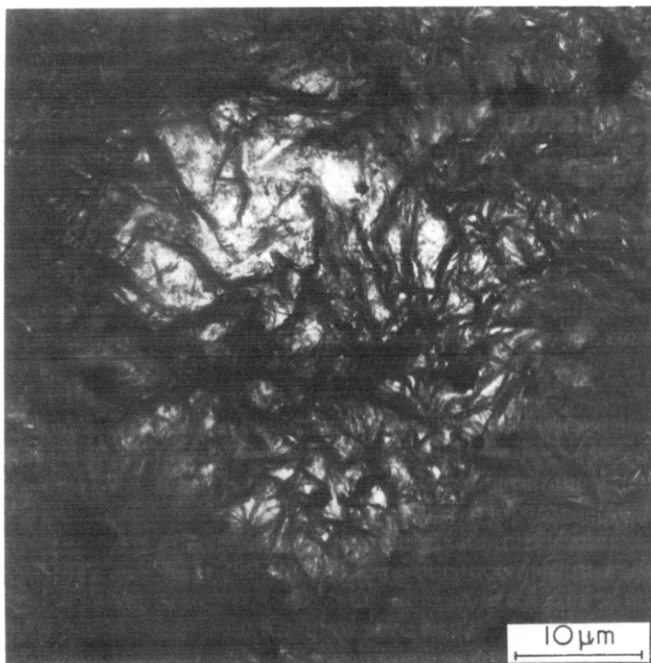


Figure 2 Transmission micrograph of a specimen as in Figure 1a taken with 1 MV electrons. Notice the development of contrast in the highly irradiated area

Figure 1a is of a 3 μm section of the linear polyethylene Rigidex 9 after recrystallization between glass cover slips. It has the coarse, spikey appearance of CEPE, although as the PAF (peak area fraction, approximately the fraction of chain-extended material⁶) of a bulk sample crystallized alongside was 0.6, it is likely to contain $\sim 40\%$ of chain-folded material also. By increasing the supercooling from 10 to 20 K at this pressure the PAF drops to 0.1 and Figure 1b is clearly a mixed product. So too is Figure 1c whose sample was grown at a supercooling of 11 K but at the lower pressure of 2.6 kbar; the PAF was 0.25. Figure 1d, however, is entirely chain-folded; the PAF is zero and the growth conditions are 2.6 kbar and 20 K supercooling.

At this optical level, the textural differentiation is unmistakable but this needs to be reconciled with the preliminary electron microscope observations. For this purpose, the 1 MV microscope was used, whose electron beam readily penetrates such 3 μm thick specimens as in Figure 1. Thus Figure 2 is a low-magnification image of the specimen of Figure 1a which shows similar contrast to that photograph but only within the area subjected to a high electron intensity. Evidently the contrast is a result of mass transport caused by radiation damage and relates only at second-hand to that originally present, behaviour which is similar to that known to occur in other systems²⁹. The intrinsic contrast in specimens appears initially to be zero and is always relatively low in such an energetic electron beam. Better contrast resulted when specimens were stained with a caesium salt. The results of this are seen in Figure 3.

The stainant used is unusual and originated from other work in this laboratory³⁰. It has been found possible chemically to attach chlorophosphoryl groups selectively to chain-folds of polyethylene lamellae, by reacting the suspended crystals with phosphorus chloride at 60°C through which oxygen was bubbling³¹. A similar technique was

used here, with the polyethylene sections immersed in the activated reagent for 6 h, washed with *o*-dichlorobenzene and then stored for 1 week in a solution of Cs metal in dry methanol.

With the improved contrast of such specimens, it is possible to see, as in Figure 3, details of lamellar arrangements in both chain-extended and chain-folded regions. Although the gross features of Figure 3a and 3b appear rather different, and obviously correspond to the differing optical appearances between crossed polars (Figures 1a and 1b) already in Figure 3c, the fine detail suggests that there is a continuous range of lamellar thicknesses present. At the same time, the comparison with Figure 3d is less distinctive and suggests how earlier difficulties in distinguishing transmission micrographs of chain-extended and chain-folded growth may have arisen. For comparison fracture surface replicas of these same samples are illustrated in Figures 3e and 3f. It is noteworthy in these how the thicker chain-extended layers are revealed in the mixed (but mainly chain-folded) sample in Figure 3f. This agrees with previous experience that the tendency is for chain-folded lamellae not to be evident in fracture surfaces¹⁴. For this reason measurements of lamellar thickness from fracture surfaces tend to be of the chain-extended component alone. In this case, the (number) average thickness parallel to *c*, measured in our standard way¹⁴, is 1770 and 2040 Å for samples PC88 and 89 (Table 1) respectively. Notice also the greater number of fibres pulled from the surface during replication in Figure 3f than in Figure 3e, an effect which in agreement with earlier observations is more prevalent for thinner layers of the same polymer¹⁴.

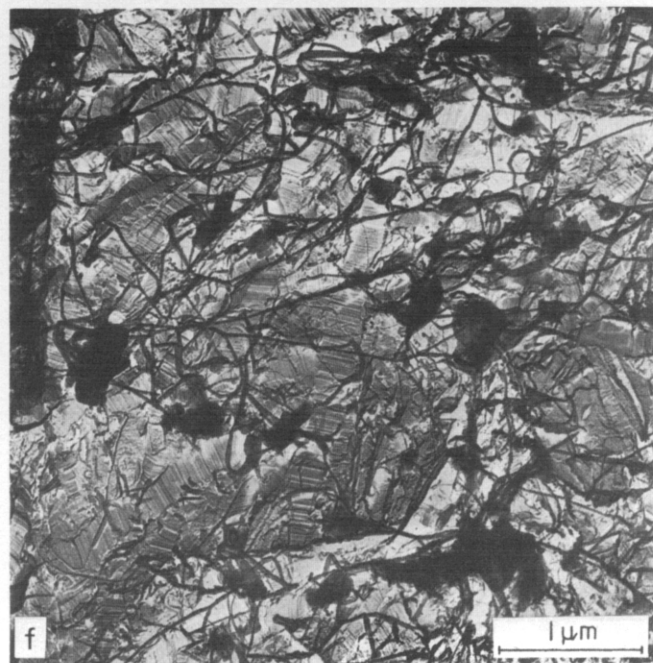
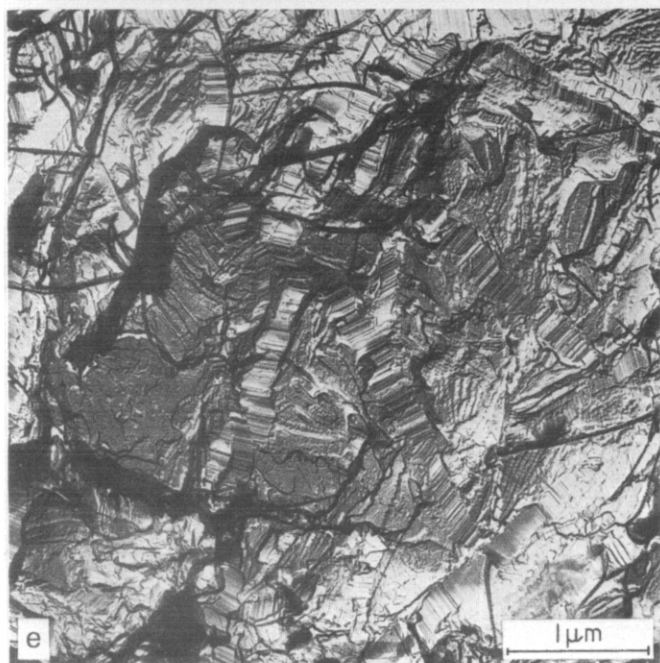
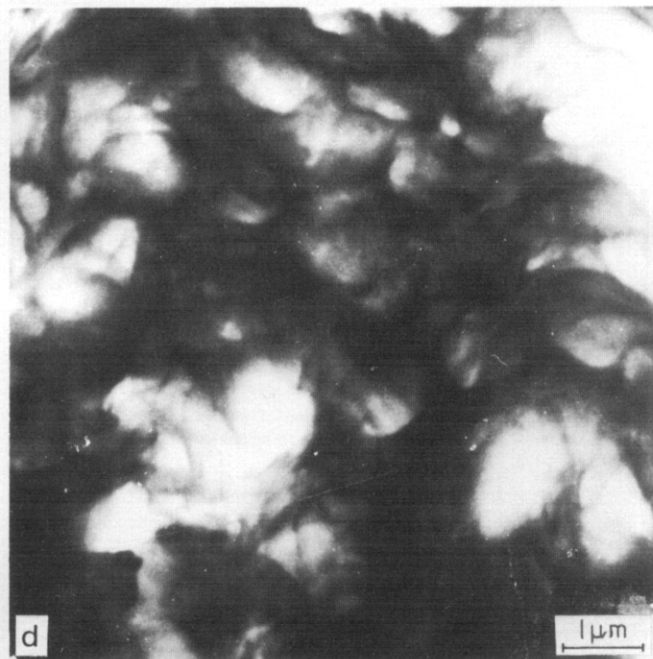
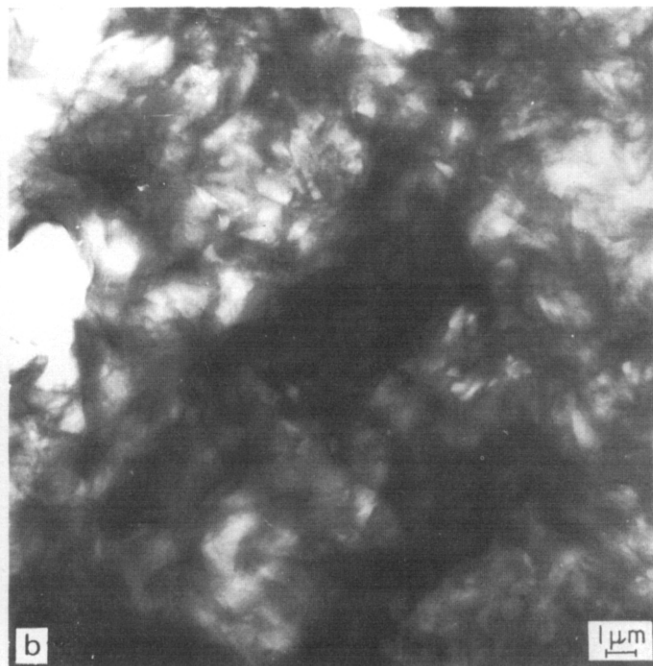
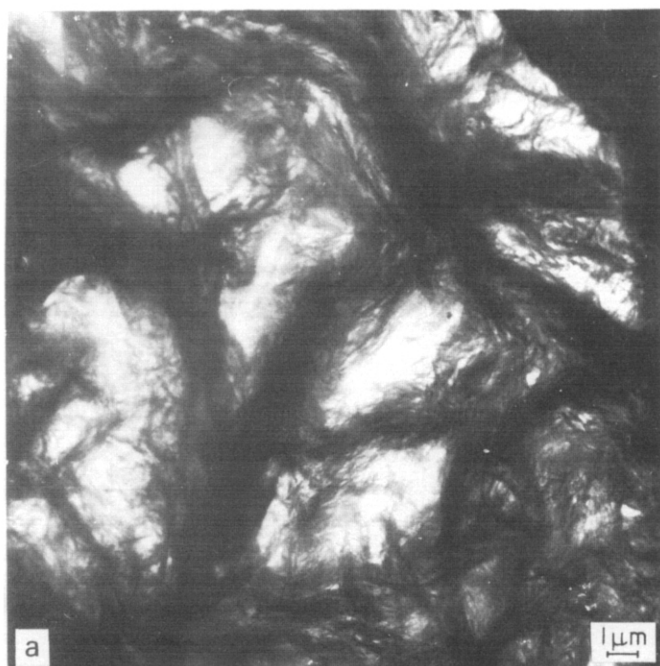
We turn now to crystallization in very thin films and in particular to the recrystallization on various substrates of solution-grown crystals. We consider in detail only monolayer crystals ~ 150 Å thick, although by the use of multilayer crystals, axialites and solvent-cast films, progressively thicker films have been prepared. These did not, however, appear to introduce any fundamentally new features.

The crystals shown in Figure 4 were grown from a solution of Rigidex 9 in xylene (fuller details are given in Part 3¹⁹) and sedimented on carbon-coated mica sheets which in turn were suspended alongside other specimens in runs PC121, 117, 128 and 129 (Table 1); metal shadowing was applied subsequently after washing off the remaining silicone oil with xylene. Figure 4 shows that recrystallization at 5.5 kbar produced similar features throughout the readily accessible crystallization range, i.e. from supercoolings of 11 to 20 K.

The resulting morphology is one of small islands, lying within the outline of the original crystals, with systematic changes in density (number/unit area). There are often, though not always, fewer in what were the original {100} sectors. In most cases the region of the central pleat where the hollow pyramidal lamellae have collapsed is more or less free of islands. But islands bounding these regions, and also those in the {100} sectors tend to be thicker than elsewhere; also, where lamellae overlap, or where there are growth pyramids, islands are fewer, thicker and many-layered.

In contrast, Figure 5 shows the results of recrystallization at 2.6 kbar and at the two supercoolings of 11 and 20 K in the same runs PC109 and 110 giving the specimens

Figure 3 Electron microscopic detail of chain-folded and chain-extended specimens similar to those in Figures 1a and 1b. (a) and (c) are detail of a stained predominantly chain extended sample; (b) and (d) refer to a mostly chain-folded one. Fracture surface replicas of the same samples are shown in (e) and (f)



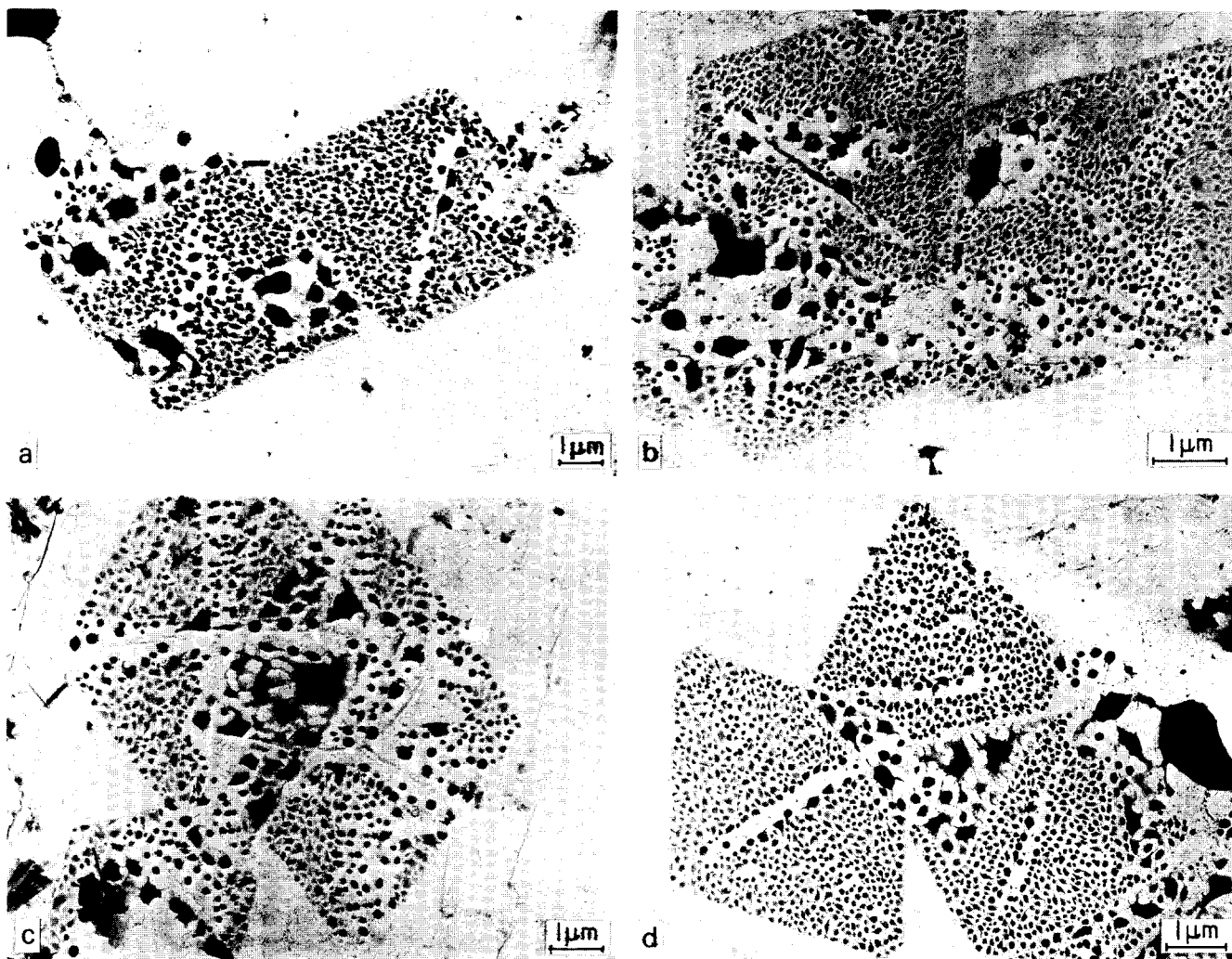


Figure 4 Results of recrystallizing solution-grown Rigidex 9 polyethylene lamellae on a substrate at 5.5 kbar and crystallization temperatures of: (a) 245.5°; (b) 243.5°; (c) 241.5°; (d) 240.5°C

in Figures 1c and 1d. Besides Rigidex 9, crystals of Rigidex 2, which has a wider molecular weight distribution than Rigidex 9 and in particular twice as many (5% as against 2.5%) in excess of 10^6 , and Hifax 1900 are shown for comparison. For bulk Rigidex 9, crystallization at the higher temperature gave 25% of chain-extended component, but none at 20 K of supercooling (Figures 1c and 1d). The molecular weights of Rigidex 2 and Hifax 1900 are higher than Rigidex 9, so that one would expect the proportion of CEPE to increase for constant crystallization conditions. In contrast to behaviour at 5.5 kbar where Figure 4 showed that morphology was insensitive to crystallization temperature, there are marked differences in Figure 5 with both temperature and molecular weight. It will be shown in the discussion how these are consistent with expectation.

DISCUSSION

It is a remarkable fact that of two polyethylene samples crystallized side by side at high pressure the one recrystallized as a thin film should contain lamellae an order of magnitude thinner than the average values for the other, recrystallized in bulk. Such an effect in polymers is unprecedented. We shall argue that it is a demonstration, in a suitable model system, of the very considerable influence constraints can exert on polymeric crystal growth.

Before the results can be taken at face value, however,

it has to be shown that in both cases the polymer crystallized into the hexagonal phase. Were it the case that for thin films the polymer precipitated as the orthorhombic form then thin layers would be expected, but at some film thickness there would have to be a substantial increase of lamellar thickness as crystallization switched to the hexagonal structure. Much effort has been spent looking for such a change without success; no evidence has been found for a discontinuity in lamellar thickness with specimen size. On the contrary there appears to be a continuous increase, with the fine structure of specimens a few hundred Å thick essentially similar to that of 3 μm slices of known chain-extended polymer (Figure 3). It appears, therefore, that the thin layers found for thin specimens are part of the spectrum of lamellar thicknesses produced by crystallization of the hexagonal phase, i.e. chain-extended growth in continuation of the trend previously found in thick films²⁷.

To a certain extent this conclusion can be substantiated by a study of the optical appearance of polyethylene films of varying thicknesses recrystallized at high pressure, showing a continuity in the characteristic chain-extended appearance in polarizing and phase-contrast images. What appears to us conclusive proof, however, is provided by the morphology of specimens as in Figures 4 and 5 where changes in the appearance of thin films alter in a predictable way to parallel changes in adjacent bulk samples when crystallization of the hexagonal structure gives way to the orthorhombic.

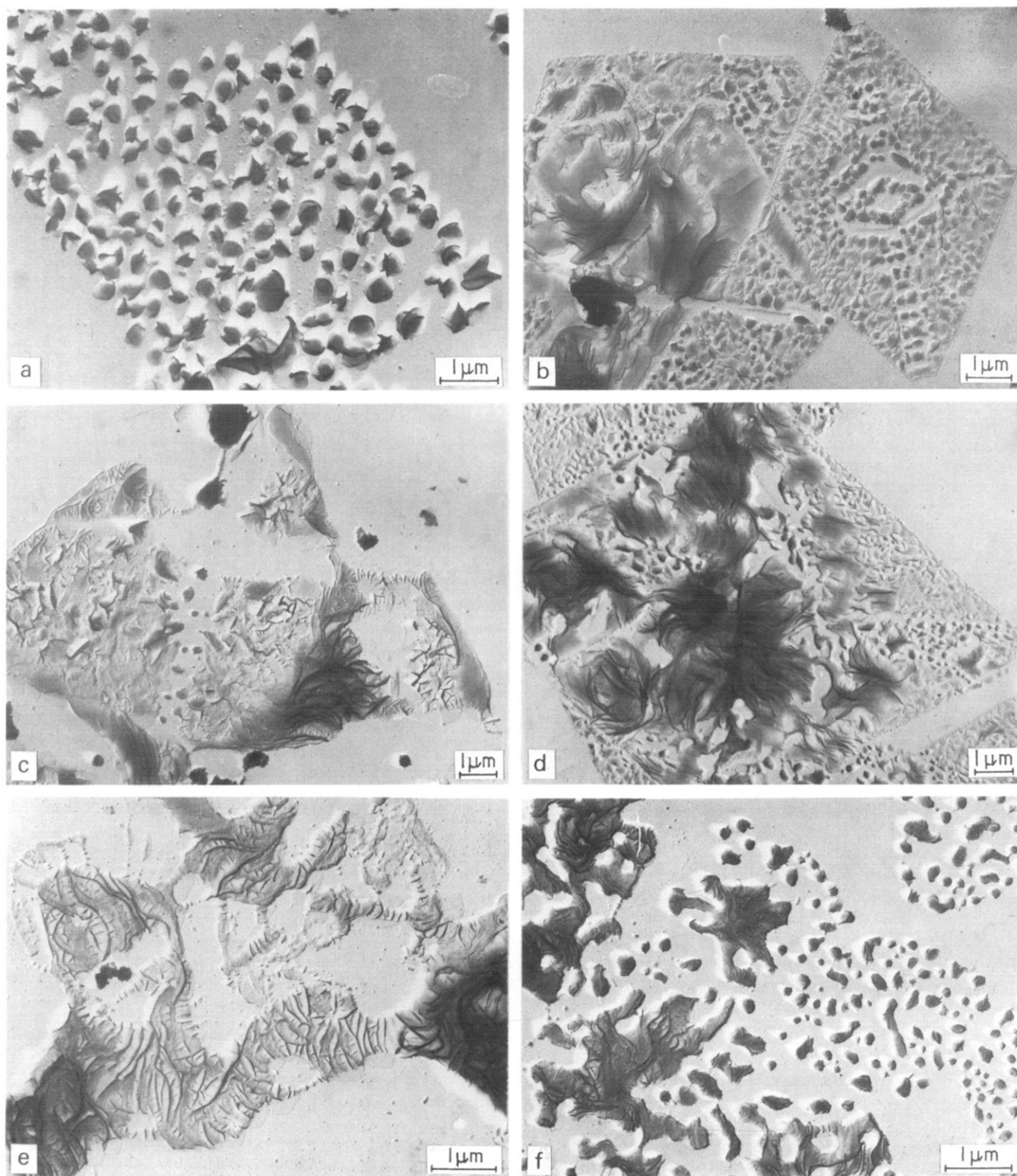


Figure 5 Results of recrystallizing various solution grown polyethylene lamellae on a substrate at 2.6 kbar and two temperatures. (a), (b) Rigidex 9; (c), (d) Rigidex 2; (e), (f) Hifax 1900. (a), (c) and (e) were recrystallized at 193.5°C and (b), (d) and (f) at 185°C

The morphology of thin polymer films crystallized on a substrate is undoubtedly influenced by the surface as e.g. the behaviour of the central pleat caused by collapse of the hollow pyramidal structure during sedimentation. Nevertheless such differences are not likely to vary substantially with changing conditions of recrystallization so that for such alterations in morphology we may look to details of nucleation and growth.

Previous work^{6,8} on the relationship between chain-folded and chain-extended growth in bulk polyethylene has shown

that the nucleation and growth rate of the hexagonal phase from the melt increases with molecular weight at a given pressure for the three polyethylenes studied here, while the lowest pressure at which the hexagonal phase forms from the melt decreases with molecular weight. In addition, there is a limit in the region of 4000 below which polymer does not appear capable of forming the hexagonal phase at 5 kbar. If we assume that these relationships also apply to recrystallization in thin films, then the nature of the observed changes in morphology can be accounted for.

At 5.5 kbar, practically all the molecules within Rigidex 9 are capable of crystallizing into the hexagonal phase and do so rapidly at the supercoolings of the experiments of *Figure 4*. One expects, therefore, a comparatively large number of nuclei of the hexagonal phase virtually independent of crystallization temperature within the range covered, and that many of these will be independent growth centres because of the constraining effect of the substrate. On going to lower pressures the anticipated trend should be fewer chain-extended nuclei and fewer growth islands initiated by them because with decreasing pressure only the longest molecules remain capable of nucleating the hexagonal phase. This is what is found in *Figure 5a*, though here one must seek to locate the ~75% of chain-folded material expected from the PAF of the bulk polymer. Although not every crystal in a population is identical, that shown in *Figure 5a* is typical. We infer, therefore, that any chain-folded growth must have occurred around the same centres as the chain-extended. Indeed these islands contain multiple lamellae and even growth pyramids which are not nearly so much in evidence in *Figure 4* and suggest different details of growth.

For *Figure 5b* we have a clear change of appearance — many fewer, and also thinner, islands. This is to be expected if growth is now chain-folded because the restrictions on nucleation will then be removed. We thus conclude that there are observable changes which are consistent with established trends of behaviour, even in lamellae only a few hundred Å in thickness produced by recrystallization at high pressures. This conclusion can, moreover, be reinforced by showing that the same trends in behaviour with molecular weight hold for thin films as for bulk polymer.

The high molecular weight Hifax polymer illustrated in *Figures 5e* and *5f* is known to be able to crystallize chain-extended at lower pressures than Rigidex 9. It is not surprising therefore, that *Figure 5f* should resemble *Figure 5a*, for, in terms of chain-extended nucleation, conditions are likely to be rather similar. In *Figure 5e*, we have still more extension as is clearly evident from the coarsely branched habit characteristically found in high molecular weight chain-extended polyethylene.

Rigidex 2, the polyethylene used in *Figures 5c* and *5d* is broader in distribution than Rigidex 9 encompassing both lower and higher molecular lengths than that polymer. We may, therefore, expect the high molecular tail to render *Figure 5d* intermediate in character between *Figures 5b* and *5f* and *Figure 5c* between *Figures 5a* and *5e*; this is clearly so. On the other hand, the low molecular weight tail is likely to be more fluid and crystallize last, with a tendency to fill interstices between growth centres. *Figures 5c* and *5d* give the impression that this may also be happening.

The conclusions we draw from the very wide spectrum of lamellar thicknesses given by crystallization with the hexagonal phase are three. First, it is evident that lamellar thickness alone is not sufficient to diagnose chain-extended as opposed to chain-folded crystallization of polyethylene. This is a point on which much confusion has arisen, stemming from the unfortunate initial description of polyethylene recrystallized at high pressures as 'extended-chain'. This is not true, in general, in a configurational sense as the typical product does contain folded molecules¹⁴. Moreover, although to have a thickness exceeding 2000 Å confers properties of melting point and density which are a reasonable approximation to those for fully-extended molecules³², this is not a useful distinction between low and high pressure phenomena. The distinction between these

two cases, as has been shown, is rather one of crystallization into different phases⁷⁻⁹. Nor is there any other length which can be used to divide off one form of crystallization from the other. We have here lamellar thicknesses for chain-extended samples of a few hundred Å, which is less than dimensions readily reached for chain-folded crystallization. Even for bulk samples, the average chain-extended crystal thickness has previously been shown to fall as low as 800 Å⁶, substantially less than figures measured for long term chain-folded crystallization at 1 bar³³.

Secondly, the range of lamellar thicknesses produced in these experiments by isothermal crystallization at 5 kbar by variation in specimen size is far wider than that previously reported for kinetically controlled (chain-folded) crystallization with any variable. It follows that, for chain-extended growth, lamellar thickness is a function of pressure, temperature, molecular weight⁸ and specimen size. It is not specified sufficiently by supercooling alone as is the case at atmospheric pressure. The spread of average values of lamellar thickness is in excess of 1 order of magnitude from ~4000 Å in bulk polyethylene to <400 Å for the crystals of *Figure 4* while a second order of magnitude is involved if one considers the thicknesses of individual lamellae which have long been known to reach 4 μm¹ while substantially thicker ones have been reported more recently¹⁰. Evidently constraints of a kind are involved which in this particular model system are able to reveal the extent of their influence, whereas in a more familiar system, e.g. chain-folded polyethylene, there is much less scope for depression of crystal sizes. It is difficult to state precisely what these constraints may be, but the factors are clearly not limited to the influence of a substrate as the thickness of lamellae in *Figures 4* and *5* persists into the higher layers present. One possibility might be memory effects in the melt, but recent studies using neutron scattering give little support to speculations of retention of order in molten polyethylene³⁴.

Finally, these results are not obviously compatible with existing theories of kinetically controlled growth which consider lamellar thickness as determined (except for relatively minor readjustments) when a molecule adds to the growth face of a lamellae. It is hard to see how such a process can be influenced by constraints associated with specimen size. As has now been shown directly⁹, however, the thickest chain-extended crystals grow outwards behind a narrowed edge, i.e. they only attain their final thickness at a roughly similar distance behind the growth face. This presumably involves a cooperative process and as such will, in principle, be susceptible to effects of specimen size. The scale of the effects actually revealed is, nevertheless, remarkable and shows a new facet to the character of kinetically controlled polymeric crystallization.

ACKNOWLEDGEMENT

The authors are indebted to Professor Sir Peter Hirsch, FRS, and his staff for use of the Oxford high voltage electron microscope.

REFERENCES

- 1 Geil, P. H., Anderson, F. R., Wunderlich, B. and Arakawa, T. *J. Polym. Sci. (A)* 1964, **2**, 3707
- 2 Kawai, T. *Kolloid-Z.* 1965, **201**, 15
- 3 Peterlin, A. *Polymer* 1965, **6**, 25
- 4 Calvert, P. D. and Uhlmann, D. R. *J. Polym. Sci. (A-2)* 1972, **10**, 1811

- 5 Bassett, D. C., Khalifa, B. A. and Turner, B. *Nature (Phys. Sci.)* 1972, **239**, 106
- 6 Bassett, D. C. and Turner, B. *Phil. Mag.* 1974, **29**, 285
- 7 Bassett, D. C. and Turner, B. *Nature (Phys. Sci.)* 1972, **240**, 146
- 8 Bassett, D. C. and Turner, B. *Phil. Mag.* 1974, **29**, 925
- 9 Bassett, D. C., Block, S. and Piermarini, G. *J. Appl. Phys.* 1974, **45**, 4146
- 10 Hatekayama, T., Kanetsuna, H. and Hashimoto, T. *J. Macromol. Sci. (B)* 1973, **7**, 411
- 11 Maeda, Y. and Kanetsuna, H. *J. Polym. Sci. (A-2)* 1974, **12**, 2551
- 12 Maeda, Y. and Kanetsuna, H. *ibid.* 1975, **13**, 637
- 13 Yasuniwa, M., Nakafuku, C. and Takemura, T. *Polym. J.* 1973, **4**, 526
- 14 Rees, D. V. and Bassett, D. C. *J. Polym. Sci. (A-2)* 1971, **9**, 385
- 15 Bassett, D. C. and Phillips, J. M. *Polymer* 1971, **12**, 730
- 16 Bassett, D. C. and Davitt, R. *Polymer* 1974, **15**, 721
- 17 Wunderlich, B. *Pure Appl. Chem.* 1972, **31**, 49
- 18 Bassett, D. C., Khalifa, B. A. and Olley, R. H. *Polymer* 1976, **17**, 284
- 19 Khalifa, B. A. and Bassett, D. C. *Polymer* 1976, **17**, 291
- 20 Bassett, D. C., Khalifa, B. A. and Mouis, R. B. to be published
- 21 Keith, H. D., Padden, F. J. and Vadimsky, R. G. *J. Polym. Sci. (A-2)* 1966, **4**, 267
- 22 Rees, D. V. *PhD Thesis* Univ. of Reading (1970)
- 23 Treiber, G., Melillo, L. and Wunderlich, B. J. *J. Polym. Sci. (B)* 1973, **11**, 435
- 24 Rees, D. V. and Bassett, D. C. *Nature* 1968, **219**, 368
- 25 Rees, D. V. and Bassett, D. C. *J. Polym. Sci. (B)* 1969, **7**, 273
- 26 Roe, R.-J., Gieniewski, C. and Vadimsky, R. G. *J. Polym. Sci. (A-2)* 1973, **11**, 1653
- 27 Bassett, D. C. and Khalifa, B. A. *Polymer* 1973, **14**, 390
- 28 Morris, R. B. and Bassett, D. C. *J. Polym. Sci. (A-2)* 1975, **13**, 1501
- 29 Grubb, D. T., Keller, A. and Groves, G. W. *J. Mat. Sci.* 1972, **7**, 131
- 30 Bedborough, D. S. *PhD Thesis* Univ. of Reading (1974)
- 31 Phillips, P. J. and MacKnight, W. J. *J. Polym. Sci. (B)* 1970, **8**, 87
- 32 Wunderlich, B. and Davidson, T. *J. Polym. Sci. (A-2)* 1969, **7**, 2043
- 33 Mandelkern, L., Price, J. M., Gopalan, M. and Fatou, J. M. *J. Polym. Sci. (A-2)* 1966, **4**, 385
- 34 Schelten, J., Wignall, G. D. and Ballard, D. G. H. *Polymer* 1974, **15**, 682

Morphological study of chain-extended growth in polyethylene:

2. Annealed bulk polymer

D. C. Bassett, B. A. Khalifa* and R. H. Olley

*J. J. Thomson Physical Laboratory, University of Reading, Reading RG6 2AF, UK
(Received 10 October 1975)*

The morphology of initially spherulitic, chain-folded polyethylene has been observed after specimens had been annealed at temperatures up to and including the melting point at 5.35 kbar. The pattern of the various phenomena corresponds to a transition from orthorhombic to hexagonal structures prior to melting in accordance with other recent work. Certain errors in the literature are corrected and additional evidence is provided for the view that the molecular mechanism of annealing in polyethylene is little different from local melting followed by recrystallization provided the effect of constraints is recognized.

INTRODUCTION

The discovery of the hexagonal phase of polyethylene and the demonstration that its crystallization from the melt is responsible for chain-extended growth¹ have important implications also for the understanding of high-pressure annealing of polyethylene. This is a topic which has been somewhat controversial partly because of certain errors in the supposed facts and partly because in ignorance of the existence of the hexagonal phase, the essential basis for understanding the various phenomena was not available. Nevertheless, previous work from this laboratory concerned with the annealing at 5 kbar of drawn polyethylene², was able to reconcile the conflicting factual records and also, by anticipating the existence of the new phase, to discuss the subject in its new perspective. In this paper we are similarly concerned with spherulitic polymer and reach conclusions which reinforce those of the earlier work. In addition, the stage is prepared for the microscopic investigation described in Part 3³ and further evidence is provided that lamellar thickening resulting from annealing polyethylene can be regarded as a consequence of localized melting followed by recrystallization provided the effect of environmental constraints is considered.

EXPERIMENTAL

The experiments have been carried out, using the equipment and procedures described previously², on the linear polyethylene Rigidex 9 (BP Chemicals Ltd). The results of annealing for 15 min at 5.35 kbar are summarized in Table 1. The temperatures quoted are the average ones over the period, with the maximum deviations from this figure. In the three cases where this was larger than 0.25K, the highest temperature occurred in the middle of runs PC43 and PC92 but at the end of experiment PC101; probably it is the maximum temperature attained which is significant.

The picture which emerges is one of steadily increasing lamellar thickness with increasing annealing temperature, in agreement with earlier work^{2,4,5}. (In retrospect it is quite clear that the reason why Fischer and Puderbach⁶ did not

observe large thicknesses in polyethylene annealed at high pressures is that they did not anneal to sufficiently high temperatures.) Associated with this thickening are parallel increases in density and atmospheric melting point which compare favourably with the earlier work on drawn Rigidex 2 (BP Chemicals Ltd). One minor difference related to the broader molecular weight distribution of Rigidex 2 is that there is only one low melting peak for Rigidex 9, at 124°C, involving a constant 7% of the polymer. This is known to be caused by shorter (and/or possibly defective) molecules and compares with two fixed and one variable peak found after annealing drawn Rigidex 2.

The morphological counterparts to these changes are illustrated in Figures 1 and 2. Figure 1a shows small lamellae just resolved in a fracture-surface replica at the lowest annealing temperature. (The drawn fibres are pulled from the sample during replication; their number decreases with increasing chain-extension.) Figures 1b to 1e are similar, showing thickening and widening of lamellae and (a characteristic feature of annealed as opposed to crystallized material) a zig-zagging of the fracture-induced striation along *c*. For Figures 1f and 1g the annealing temperatures fall within the span of the melting peak recorded by high pressure d.t.a. (Figure 3) and Figure 1h is of a sample which had been completely molten. Figure 1 has to be considered together with Figure 2 which shows the optical appearance between crossed polars of ~3 μm slices of Rigidex 9 which were annealed between glass coverslips alongside the samples of Figure 1. Figures 2(a) to 2d show that the familiar

Table 1 Properties of Rigidex 9 polyethylene after annealing at 5.35 kbar for 15 min

Run No.	T_a (°C)	\bar{L}_{FS} (Å)	$\bar{L}_{g.p.c.}$ (Å)	Density (Mg/m ³)	Atmospheric melting peaks (°C)
PC 43 (a)	238 ± 1.5	1134	720	0.985 ₇	135.0
PC 87 (b)	242 ± 0.2 ₅	1250	1563	0.992 ₄	124, 137.6
PC 90 (c)	244 ± 0.2 ₅	1501	1783	0.992 ₈	124, 138.0
PC 91 (d)	248 ± 0.2 ₅	1571	2086	0.993 ₀	124, 138.7
PC 96 (e)	250 ± 0.2 ₅	1702	2076	0.993 ₂	124 139.5
PC 92 (f)	253.2 ₅ ± 0.5	2222	2864	0.994 ₈	124 139.0
PC 99 (g)	254 ± 0.2 ₅	2113	2286	0.994 ₂	124 139.7
PC 101 (h)	256 ± 1	3581	3776	0.994 ₄	124 140.0

* Present address: Faculty of Science, Ain Shams University, Cairo, Egypt.

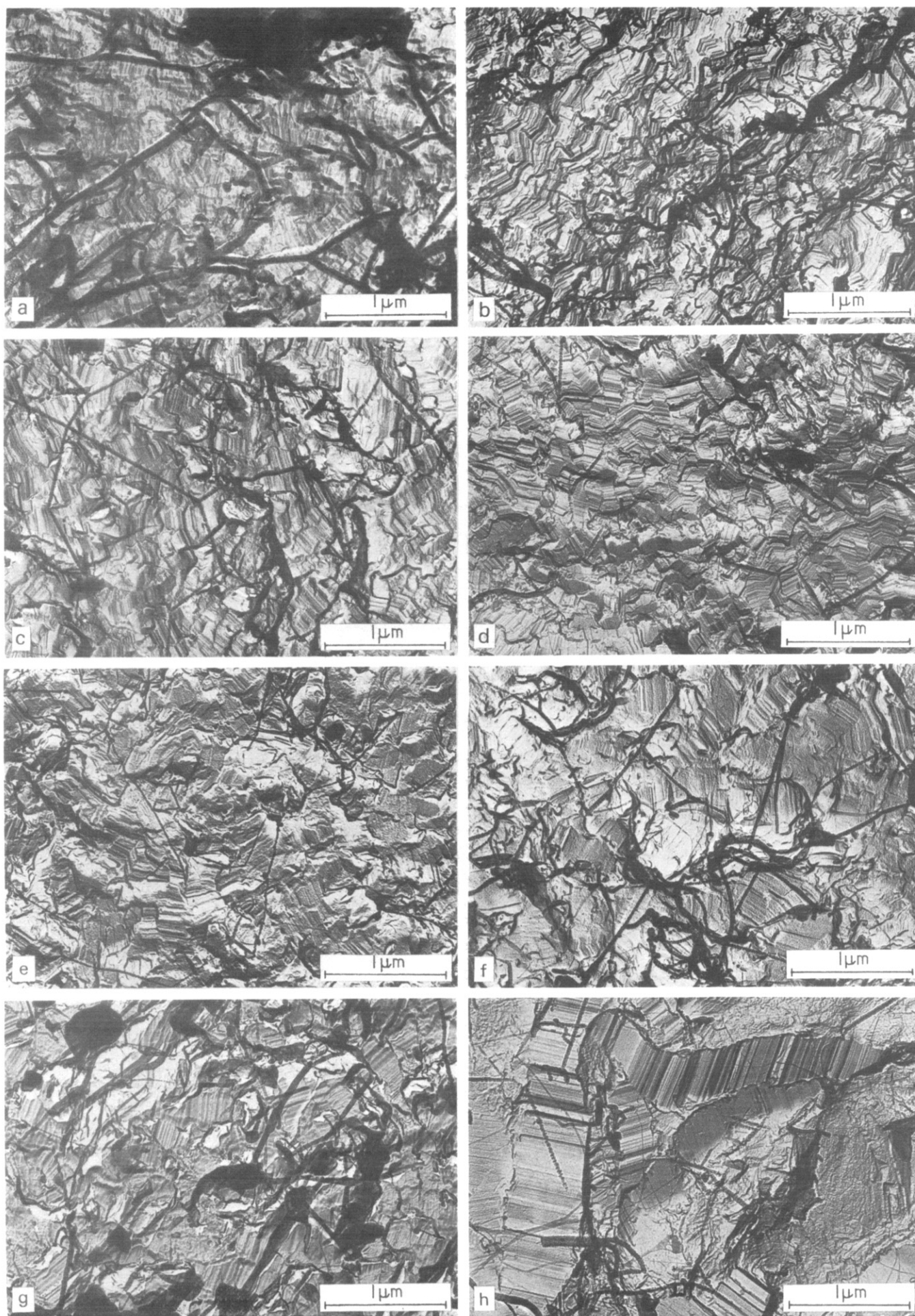


Figure 1 Fracture-surface morphologies of initially spherulitic polyethylene after 15 min annealing at 5.3 kbar and the following temperatures: (a) 238°C; (b) 242°C; (c) 244°C; (d) 248°C; (e) 250°C; (f) 253°C; (g) 254°C; (h) 256°C

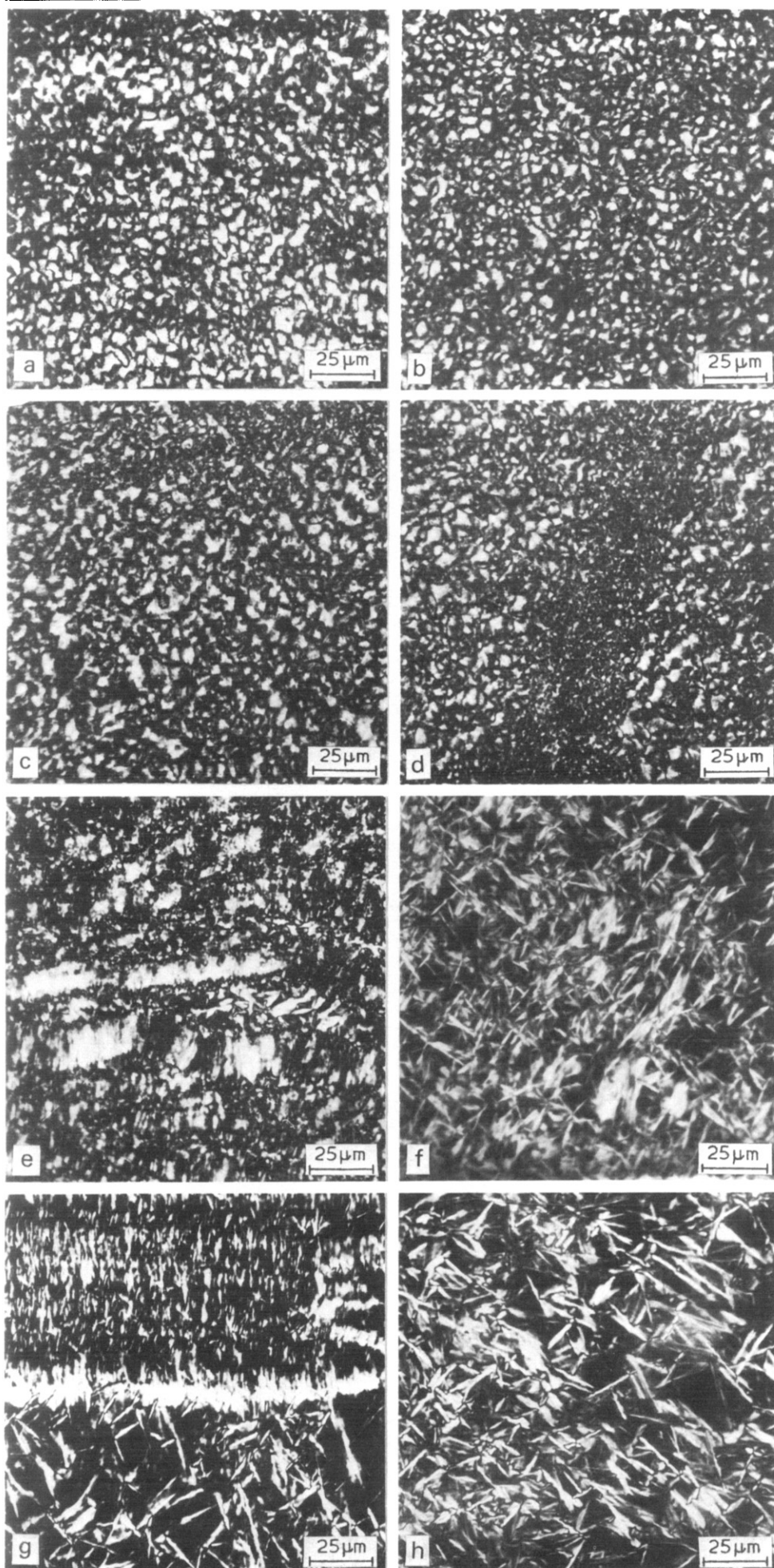


Figure 2 Optical texture seen between crossed polars of samples corresponding to those in Figure 1

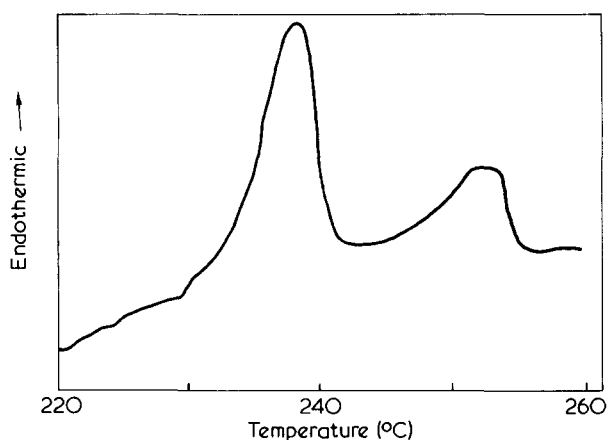


Figure 3 High pressure d.t.a. trace of the melting of the initially spherulitic polyethylene used, at 5.3₅ kbar and a heating rate of ~ 1.7 K/min

gross texture of small, banded spherulites is invariant to 248°C and only begins to alter towards the appearance of chain-extended, recrystallized polyethylene seen in Figure 2(h) when annealing takes place in the melting region (Figures 2e to 2g).

Figure 2 conflicts with the assumptions of Gruner *et al.*⁷ who did not test the point directly but believed that spherulitic texture and chain orientation were lost with the melting of chain-extended lamellae at 242°C at 5.1 kbar (equivalent to 246°C at 5.35 kbar) and that lamellae remained superheated for a further 3K rise in temperature. This is not true; for initially chain-folded Rigidex 9 Figure 3 shows a final (hexagonal) melting peak centred at 253.5°C. Instead, the work of this and previous papers substantiate fully the initial claim of Rees and Bassett^{4,5} that chain orientation and gross spherulitic texture persist when chain-extended polyethylene lamellae are formed by annealing chain-folded ones at high pressure.

A major innovation in the present work is that the lengths recorded in Table 1 have been derived not just from fracture surface data as in the past but also by the nitric acid/g.p.c. method. This is now a standard method in this laboratory and by providing an independent means of assessing chain extension is contributing importantly to the various aspects of work on chain-extended polyethylene. The experimental procedure follows the pioneering work of the Bristol group⁸ in applying the Palmer–Cobbold technique to polyethylene.

The technique used was to encapsulate polyethylene samples of 20–50 mg with 10 ml of fuming nitric acid in universal containers sealed with PTFE discs. Reaction was allowed for three days at 60°C after which samples were washed for several hours with water, 1:1 water–methanol, methanol and dichloromethane successively and then dried. Subsequently, molecular weights of the degraded products were determined by gel permeation chromatography (g.p.c.) using a Waters Associates 200 instrument with *o*-dichlorobenzene at 130°C as solvent and a system of four columns with nominal exclusion limits of 10⁶, 10⁵, 10⁴ and 10³ Å. Standard polystyrene fractions were used for calibration and samples were injected as 2 ml portions of 0.2% solutions in *o*-dichlorobenzene.

Figure 4b shows a typical g.p.c. trace of a nitrated sample and that it compares sensibly with the melting endotherm (Figure 4a) of the original sample. In Figure 5 the differential weight and number-average distributions derived from the g.p.c. data are superposed on the fracture surface

data for the same samples measured in our usual way⁹. The general agreement between the two techniques is good (this applies also to crystallized samples) and supports all previous conclusions on chain-extended polyethylene derived from fracture surface data alone. Agreement is best between the weight-average g.p.c. data and the number-average fracture surface histograms, but the fracture surface data do not generally show the longest or the shortest lengths recorded by the g.p.c. technique. The reasons for this are discussed in detail elsewhere¹⁰; here we merely observe that longer lengths than the crystal thickness will be measured by the g.p.c. if not all folds are cut during nitration, also the thinnest, least well-defined lamellae might be expected to be underrecorded in fracture surfaces. It is likely that only the thicker layers have been selected in Figure 5a where the fracture surface data are higher than the melting point and density would suggest, although in previous work with oriented samples² this difficulty did not obviously

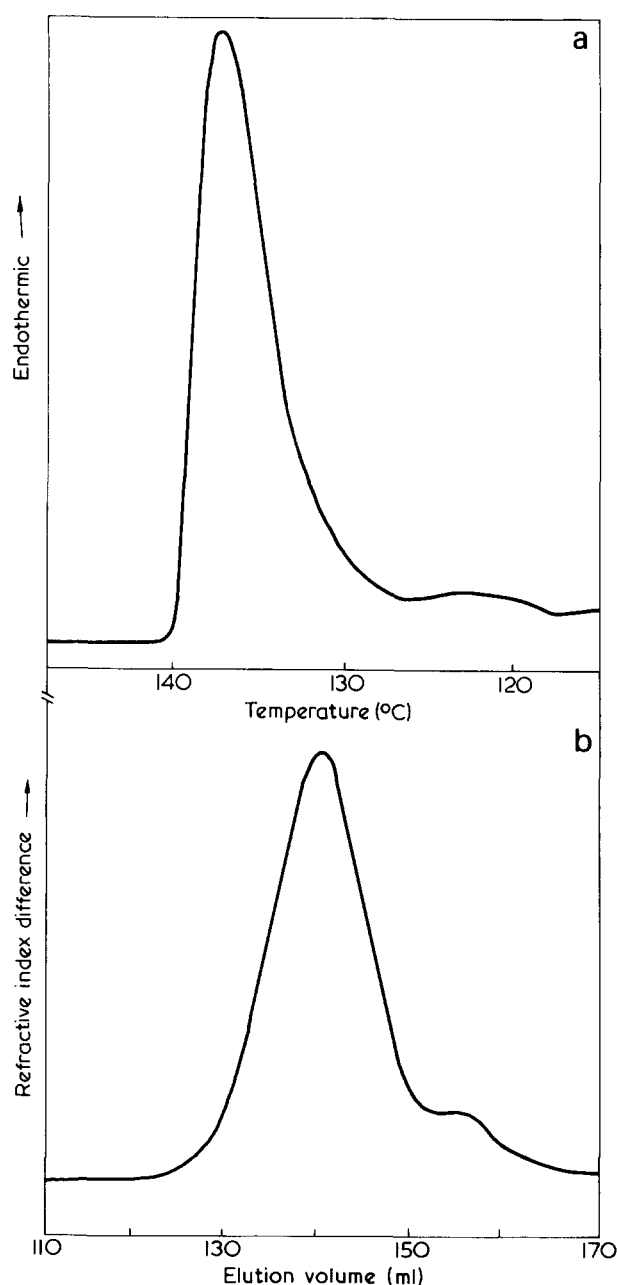


Figure 4 A comparison of (a) the d.s.c. melting endotherm with (b) the g.p.c. molecular length distribution of the sample of Figure 1d

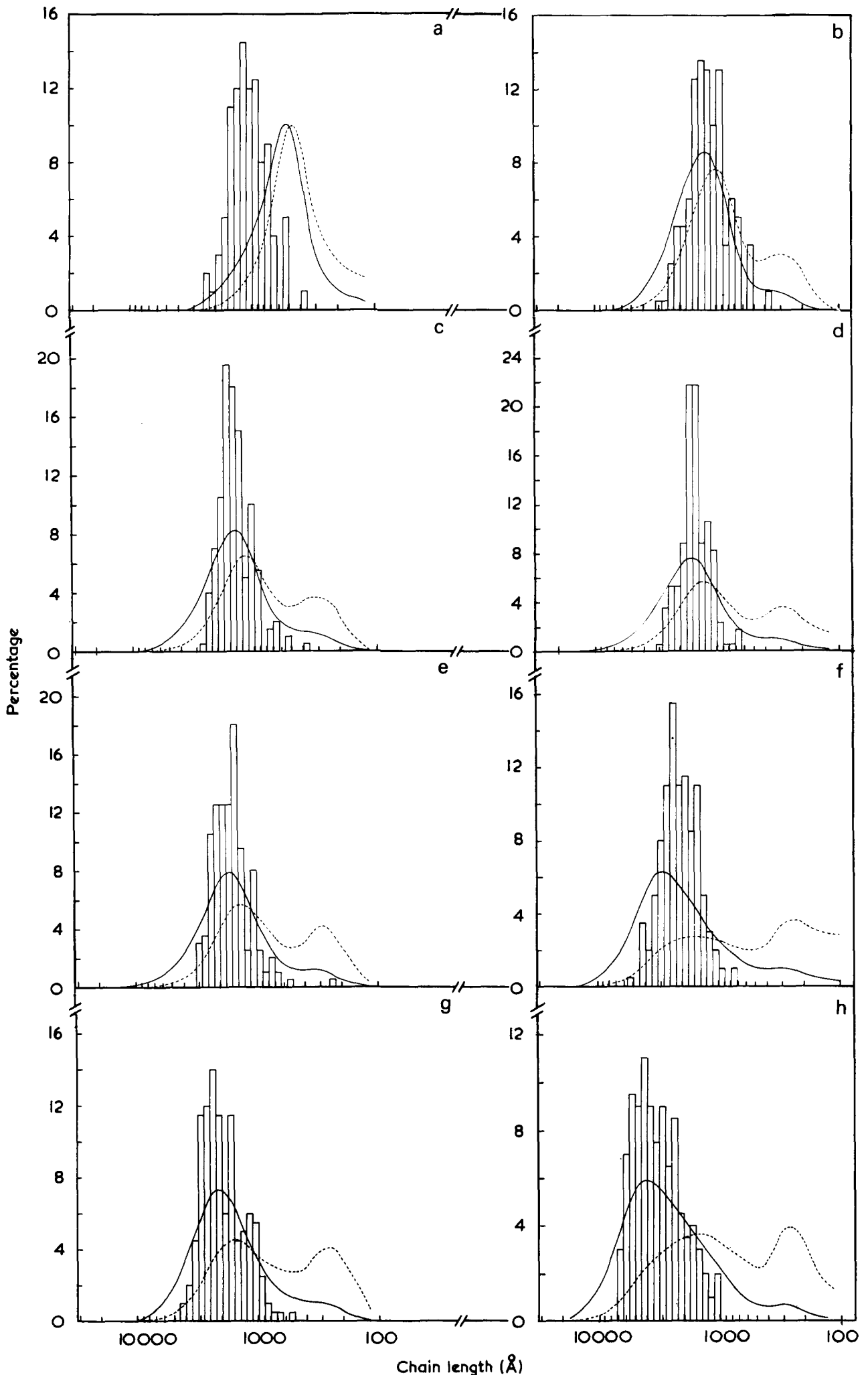


Figure 5 Chain extension of the eight samples of Figure 1 assessed in three ways. □ (histograms), fracture surface data; —, weight-average g.p.c. data of nitrated samples; ····, corresponding number-average data

arise. We thus have an illustration of how the nitric acid/g.p.c. method can be more reliable than that of fracture surfaces. Both techniques, however, are agreed in showing that run PC92 is out of sequence in that the lamellar thickness is apparently too high; this is, in fact, not unexpected for the temperature variation during annealing as will be discussed later. The run serves, therefore, as an example of how well the new and old techniques reinforce each other.

DISCUSSION

High pressure d.t.a. data show two endothermic peaks in the melting range of chain-folded Rigidex 9. At 5.35 kbar *Figure 3* shows that for the particular samples of these experiments, the maxima are at 241°C, which represents the phase change from orthorhombic to hexagonal and 253.5°C when the hexagonal structure melts. This knowledge places the topic in a new context, first discussed by Bassett and Carder², whose interpretation we shall follow.

Both endothermic peaks described are much wider than the instrumental broadening and both are noticeably skewed to lower temperatures; these effects are mainly consequences of the wide molecular weight distribution. Unpublished work (Morris and Bassett) has shown that for a series of coarse polyethylene fractions whose mode molecular weights increased from 10^4 to 10^5 , the maxima of the corresponding two endothermic peaks for chain-extended samples increased from 237° to 245°C and from 245° to 258°C respectively. Peak positions also vary with crystal thickness, but this is a smaller effect; previous work¹¹ measured an increase to 242.75°C in the lower temperature peak for chain-extended as opposed to chain-folded Rigidex 9, but no corresponding significant variation in the hexagonal melting temperature.

We may, accordingly, describe the effects of increasing the temperature of Rigidex 9 polyethylene through the annealing range at 5.35 kbar as follows. Until the temperature approaches within a few degrees of 240°C, the entire sample remains in the orthorhombic structure. It is not surprising, therefore, that annealing experiments confined to this range^{6,12} should find high-pressure behaviour to be similar to that at 1 bar. Above a temperature which depends upon the precise lower molecular weight tail of the sample but for these specimens is ~232°C according to *Figure 3*, the orthorhombic to hexagonal transition begins to occur, during which crystals of ~4000 molecular weight polymer and above transform, at successively higher temperatures, into the hexagonal structure. The shortest molecules, however, appear not to be capable of forming the hexagonal phase at this pressure. Instead they become molten, in this same region of temperature, and distribute themselves between the remaining lamellae. It is here that they recrystallize (as randomly oriented chain-folded lamellae) on the return to lower pressures and temperatures and where they have been shown to be responsible for brittle fracture in a slightly higher molecular weight polyethylene². As is to be expected, the proportion of material in the corresponding atmospheric low-melting peak at 125°C soon rises with annealing temperature to an effectively constant figure (of 7% of the total area under the peak). This proportion may be used to estimate that the shortest molecules which can form the hexagonal phase at this pressure are ~350 Å long. Assuming all molecules are linear, the lowest 7% of the molecular weight distribution of Rigidex 9 falls below 3800; for Rigidex 2 which has a similar mode but a broader overall distribution the corresponding pro-

portion is 11%. This latter figure is in agreement with melting endotherms observed in previous work on annealing drawn Rigidex 2 at 5.35 kbar where two additional atmospheric low-melting peaks were recorded which have not been observed in this work on Rigidex 9. It was shown that these were also due to short molecules² but the precise reason for the multiplicity has not been investigated. Nevertheless, with its approximately constant proportion of polymer, the atmospheric melting peak at $132 \pm 1^\circ\text{C}$ at 1 bar found for Rigidex 2 probably also consists of a particular species of short and/or defective molecules. The remaining peak which, with increasing annealing temperature above 247°C increases in proportion and also melting point (to a maximum of ~140°C) is particularly interesting. Such behaviour would be expected of molecules, probably with molecular weights from 4000 to 10 000, which had entered the hexagonal phase but then melted out in greater numbers and for longer lengths as the temperature rose. If they were then unable to recrystallize (into thicker crystals) at the annealing temperature but could do so, into the hexagonal phase, on subsequent cooling, the observed behaviour would follow. The higher the annealing temperature, the more material would be involved and because of its higher molecular weight, which would raise both the temperature of recrystallization and the ultimate thermodynamic melting point, the higher melting the final segregated product would be. All three low melting peaks never constituted more than 20% of the whole for Rigidex 2; our g.p.c. measurements show that 20% of this polymer lies below a molecular weight of 9500.

For the present experiments, little or no separation of low molecular weight polymer was detectable after annealing at 238°C, but the final value of 7% segregation is already present according to both d.s.c. and g.p.c. measurements after annealing at 242°C. Annealing is by then taking place in the hexagonal phase of lamellae interleaved with molten shorter molecules. This is a region of gradually increasing lamellar thickness, density and atmospheric melting point. By 244°C, when the orthorhombic to hexagonal phase transition is complete, few lamellae are less than 1000 Å thick (*Figure 5c*), the overall density exceeds 0.992 g/cm³ and the d.s.c. melting point is close to 140°C. Also as reported by Rees and Bassett⁴, and in agreement with high pressure optical microscopy, there is no change in the gross optical appearance of samples between crossed polars (*Figure 2*). This is now readily understandable because this texture depends on the orientation of the *c* axis and it has been shown that this is common to the two phases¹.

The first sign of a change in optical appearance comes with the beginning of final melting, i.e. the higher temperature peak in *Figure 3*. Thus portions of the sample annealed at 250°C (*Figure 2e*) resemble small elements of the coarse texture characteristic of polyethylene recrystallized into the hexagonal phase^{13,14}. Doubtless a proportion of the material is melting-regions of shorter molecules at lower temperatures and then recrystallizing, possibly slightly at the holding temperature but predominantly on subsequent cooling. This proportion evidently increases at still higher temperatures but, until melting is complete (by 256°C) recrystallization must occur in part into a matrix of solid polymer. As is still to be discussed, but is quite evident from *Figure 2g*, this is a process which depends sensitively upon the precise treatment given to a sample.

The molecular mechanisms induced by annealing crystalline polymers, particularly those responsible for the in-

crease in lamellar thickness are by no means generally agreed upon. Sensitive calorimetry at atmospheric pressure has detected the prolonged evolution of heat once samples are raised to temperatures above that at which they were prepared¹⁵ doubtless due to the improvement of crystalline order; indeed increased order of fold surfaces has been shown to result independently¹⁶. Still higher temperatures are needed before changes in X-ray long period are found¹⁷. These occur very rapidly, apparently in the solid state (hence 'solid state thickening') but with increasing temperatures the slower time-scales involved clearly show that in polyethylene there is first disorganization then reorganization¹⁸. Even the very beginning of lamellar thickening has been pointed out to behave as though it were being triggered by melting of the material¹⁶. This is the simplest hypothesis and we have argued that once the effect of constraints on crystallization is recognized, it is consistent with the available evidence^{2,19}. Because of what is now a considerable weight of evidence showing, we believe, that the molecular mechanism of annealing in polyethylene cannot be very different from local melting, possibly of only a few fold stems, followed by rapid recrystallization, to thicker (and stabler) layers, we shall consider them to be identical unless and until future evidence shows the hypothesis to be untenable. In so doing, however, we do not mean to exclude *a priori* other models based on an apparently similar picture, notably that of Sanchez *et al.*³⁰.

Work at high pressures brings much new evidence to support this point of view reinforcing, as it does, the close parallel between annealing and recrystallization behaviour even in conditions far removed from familiar work at 1 bar. At least three authors^{6,12,21} have drawn attention to the closely similar X-ray long periods of polyethylene after annealing in the orthorhombic phase at low and high pressures at the same temperature interval below the melting point. Moreover, once annealing occurs in the hexagonal phase, then lamellar thicknesses show substantial increases corresponding to those found for recrystallized chain-extended polyethylene. This is to be expected on a melting-recrystallization hypothesis, but does not obviously follow from other mechanisms proposed, e.g. solid-state thickening or fold-length doubling²² when a fold migrates through a crystal layer. Furthermore, there is the similar response of both processes to constraints shown by the investigation of thin films described in Part 1²³ and Part 3³.

The continuing increase of average lamellar thickness with annealing temperature is likely to result from a combination of several factors. The first is that melting and recrystallization occur at a higher temperature, which is well known to give thicker crystals. In addition, the higher the temperature the higher the molecular weight of polymer involved and this, according to studies of chain-extended crystallization, will tend to give thicker crystals¹⁴. The actual size of lamellae formed at a given temperature is, however, strongly dependent upon the physical environment, an effect we shall refer to briefly as due to constraints. Such constraints are likely to decrease with increasing annealing temperatures and this constitutes a third factor favouring increased lamellar thickness.

With runs (f) and (g), annealing occurs well within the final melting peak. Here samples will remain partly molten at the annealing temperature, although the longer they are held there, the greater the chance of some recrystallization at temperature. The remaining portion which will generally be of low molecular weight must recrystallize on cooling and it will do so within the constraints of a solid mat-

rix. The factors affecting lamellar thickness are those described above viz. molecular weight, temperature, time and fewer constraints; the actual value resulting is likely to depend sensitively on details of the treatment. Thus in run (f) the temperature reached its maximum after 5 min and then slowly decayed, in contrast to a uniform temperature in (g); under these conditions one might well expect (f) to have recrystallized at a higher temperature and with fewer constraints than (g) in keeping with the increase in lamellar thickness found.

The origin of the increased average thicknesses in (f) and (g) is the appearance of lamellae thicker than 3000 Å (Figure 5), then in (h), for material which was fully molten, still thicker lamellae to 7000 Å appear. The underlying factor here also appears likely to be constraints as is well illustrated in Figure 2g where lamellae growing with the constraint of pre-existing oriented nuclei are substantially smaller and thinner than those adjacent which formed from apparently unconstrained melt. Once such constraints disappear, lamellar thickness will take its full value. This effect of constraints is crucial to the interpretation of annealing as melting plus recrystallization; if it is neglected the thesis fails. Nevertheless, its effect has been clearly demonstrated e.g. in the previous²³ and following³ papers. Indeed that it should occur in both cases is yet further reinforcement of the view that the two processes are essentially the same.

The conclusions of this paper are therefore, twofold. First, that the apparently anomalous behaviour of polyethylene annealed at high pressures can be readily understood in terms of a transition to the hexagonal phase prior to melting. Secondly, that the high pressure evidence provides substantial support for considering the molecular mechanism of annealing as essentially local melting followed by recrystallization.

REFERENCES

- Bassett, D. C., Block, S. and Piermarini, G. J. *J. Appl. Phys.* 1974, **45**, 4146
- Bassett, D. C. and Carder, D. R. *Phil. Mag.* 1973, **28**, 513
- Khalifa, B. A. and Bassett, D. C. *Polymer* 1976, **17**, 291
- Rees, D. V. and Bassett, D. C. *Nature* 1968, **219**, 368
- Rees, D. V. and Bassett, D. C. *J. Polym. Sci. (B)* 1969, **7**, 273
- Fischer, E. W. and Puderbach, H. *Kolloid-Z.* 1969, **235**, 1260
- Gruner, C. L., Wunderlich, B. and Bopp, R. C. *J. Polym. Sci. (A-2)* 1969, **7**, 2099
- Williams, T., Alundell, D. J., Keller, A. and Ward, I. M. *J. Polym. Sci. (A-2)* 1968, **6**, 1613
- Rees, D. V. and Bassett, D. C. *J. Polymer Sci. A-2*, 1971, **9**, 385
- Bassett, D. C., Khalifa, B. A. and Olley, R. H. to be published
- Bassett, D. C. and Turner, B. *Phil. Mag.* 1974, **29**, 925
- Kijima, T., Imada, K. and Takayanagi, M. *Rep. Progr. Polym. Phys. Japan* 1970, **13**, 177
- Bassett, D. C., Khalifa, B. A. and Turner, B. *Nature (Phys. Sci.)* 1972, **239**, 106
- Bassett, D. C. and Turner, B. *Phil. Mag.* 1974, **29**, 285
- Richardson, M. J. *Trans. Faraday Soc.* 1965, **61**, 1876
- Balta-Calleja, F. J., Bassett, D. C. and Keller, A. *Polymer* 1963, **4**, 269
- Statton, W. O. and Geil, P. H. *J. Appl. Polym. Sci.* 1960, **3**, 357
- Fischer, E. W. and Schmidt, G. F. *Angew. Chem.* 1962, **74**, 551
- Bassett, D. C. and Khalifa, B. A. *Polymer* 1973, **14**, 390
- Sanchez, I. C., Colson, J. P. and Eby, R. K. *J. Appl. Phys.* 1973, **44**, 4332
- Rees, D. V. *PhD Thesis* University of Reading (1970)
- Dreyfuss, P. and Keller, A. *J. Macromol. Sci. (B)* 1970, **4**, 811
- Bassett, D. C. and Khalifa, B. A. *Polymer* 1976, **17**, 275

Morphological study of chain-extended growth in polyethylene:

3. Annealing of solution-grown lamellae

B. A. Khalifa* and D. C. Bassett

J. J. Thomson Physical Laboratory, University of Reading, Reading RG6 2AF, UK

(Received 10 October 1975)

Solution-grown lamellae of three commercial polyethylenes of differing molecular weight ranges have been annealed on substrates at high pressures. The polymers transform to the new high-pressure phase before melting but the new lamellar thicknesses reached remain much below those found for the bulk material. Electron diffraction patterns support the identification of the new phase as hexagonal and it is concluded that the effects of annealing polyethylene in an unusual context are close to those which would have been produced by local melting followed by rapid recrystallization.

INTRODUCTION

This paper presents observations made on solution-grown lamellae of three linear polyethylenes after annealing on a substrate at 5.35 kbar. It is shown that the initial orthorhombic structure transforms into the newly discovered hexagonal form prior to melting so that the detailed morphologies found are justifiably described as 'chain-extended'. Nevertheless, the lamellar thicknesses attained by annealing polyethylene lamellae initially ~ 150 Å thick on a substrate at high pressure are substantially less than those produced in adjacent unconstrained bulk polymer. This parallels behaviour found for recrystallization in thin films at high pressure which besides reinforcing the close similarity between the two processes provides a further illustration of the exceedingly large effects constraints can have on polymeric crystallization behaviour.

* Present address: Faculty of Science, Ain Shams University, Cairo, Egypt

EXPERIMENTAL AND RESULTS

All the experiments have been carried out on lamellar crystals of the three linear polyethylenes Rigidex 9 and Rigidex 2 (BP Chemicals Ltd) and Hifax 1900 (Hercules Powder Co. Inc.) as illustrated in *Figure 1*. These were grown from 0.01% solutions in xylene by a self-seeding technique whereby a suspension of previously grown crystals was heated to 103°C at 0.1 K/min and then transferred to an isothermal bath held at 85°C. The truncated lozenges thus formed were sedimented on carbon-coated mica substrates and annealed at 5.35 kbar alongside the bulk samples described in Part 2¹. The annealing conditions and procedures are, therefore, those set out in the previous paper except that annealing at the lowest temperature, 238.25 ± 0.25 °C for 15 min, was carried out in run PC86 rather than PC43.

Afterwards, the pressure-transmitting silicone fluid was washed off with xylene and crystals shadowed prior to electron microscopic study. The appearance of reasonably typical annealed morphologies for Rigidex 9, Rigidex 2 and

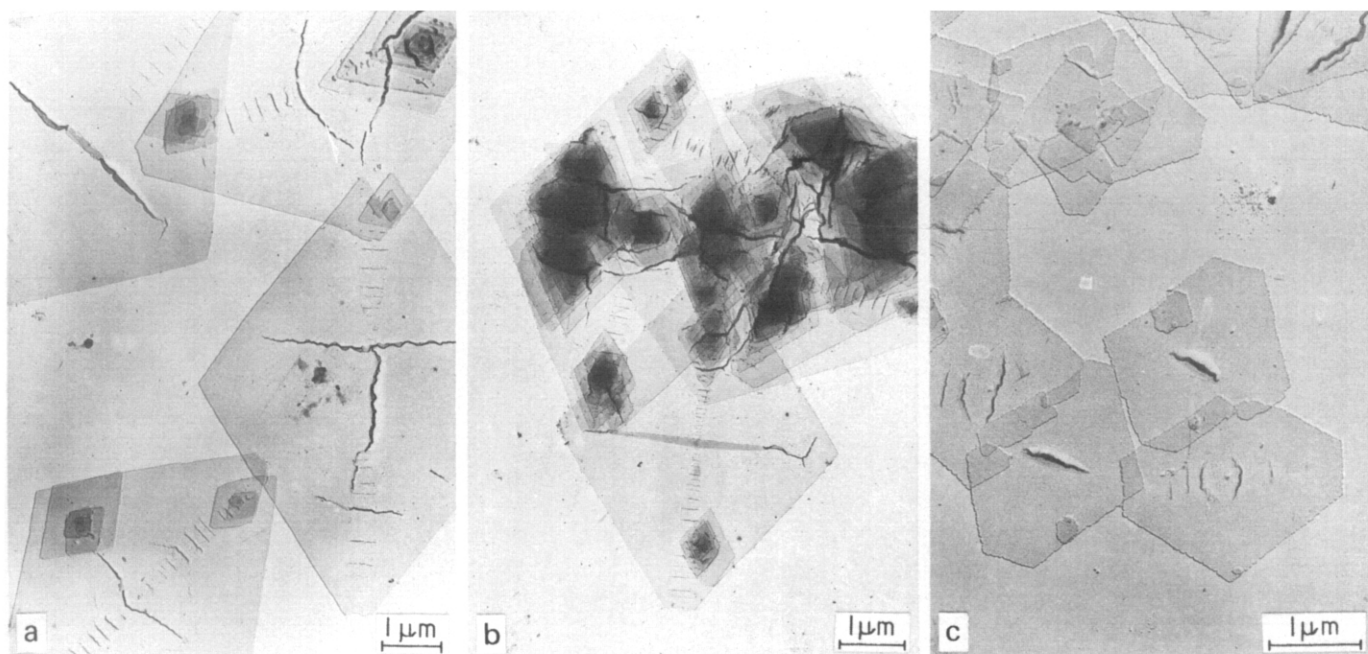


Figure 1 Examples of the truncated polyethylene lozenges used in the experiments. (a) Rigidex 9; (b) Rigidex 2; (c) Hifax 1900

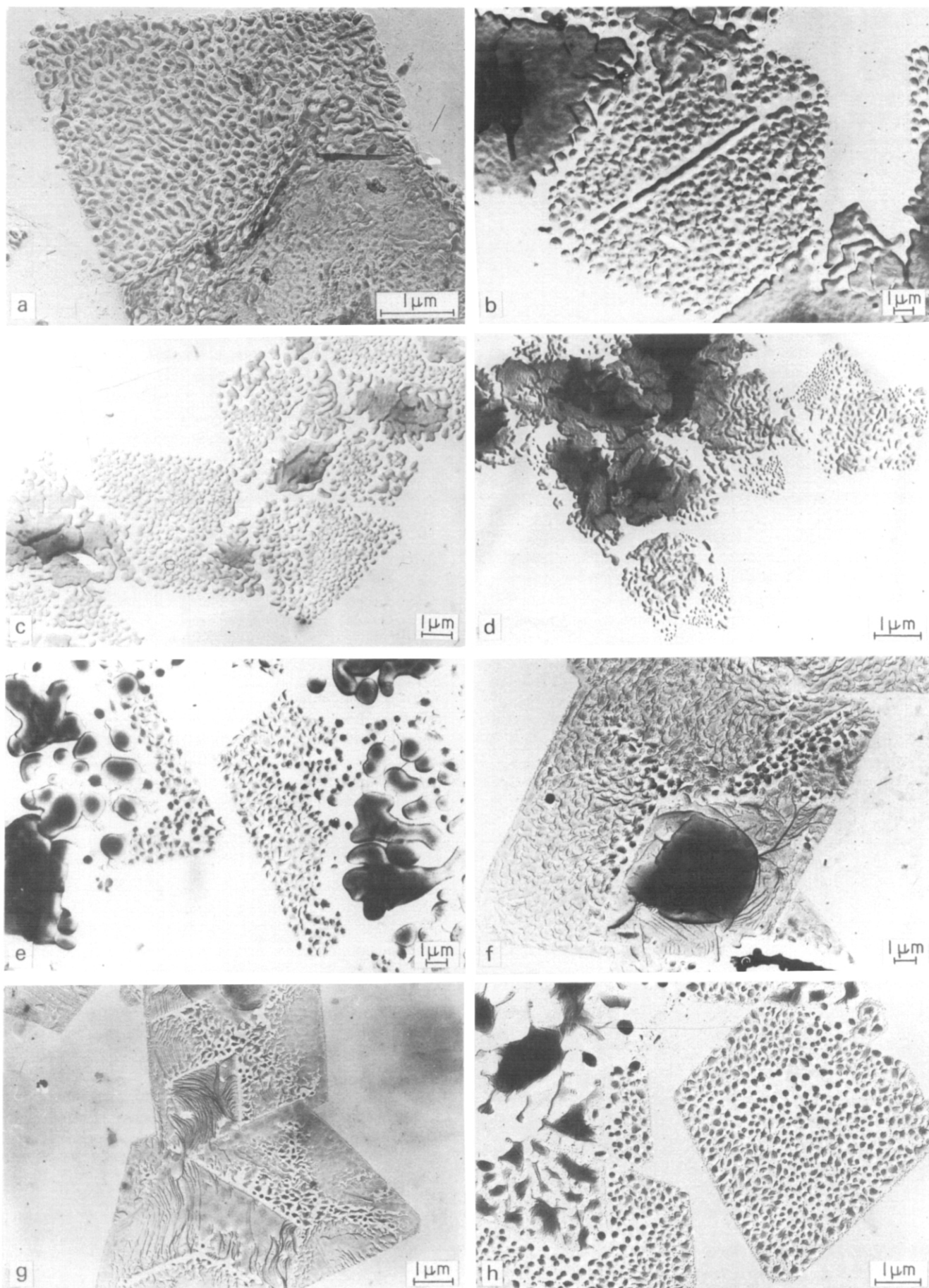


Figure 2 Typical morphologies after annealing Rigidex 9 crystals for 15 min at 5.3₅ kbar and the following temperatures: (a) 238°; (b) 242°; (c) 244°; (d) 248°; (e) 250°; (f) 253°; (g) 254°; (h) 256°C

Hifax 1900 at each annealing temperature is displayed in *Figures 2, 3 and 4* respectively. These should be compared not only with each other but also with *Figures 1 and 2* of Part 2¹ illustrating the bulk material. It should also be emphasized that, though not all crystals show exactly similar changes and the selection of one or even a few for illustration is necessarily subjective, the trends with temperature and molecular weight are unmistakable.

DISCUSSION

Studies of polymer lamellae annealed on solid surfaces generally reveal not only intrinsic properties of the crystals themselves but also features due to interaction with the substrate. It is apparent that crystal layers which touch the substrate behave differently from those which do not and, also, that smaller layers having proportionately larger surface energy/volume ratios undergo changes before their wider neighbours.

The major change effected by annealing polymer crystals is one of lamellar thickening² which can often be seen to proceed preferentially where there are differences in layer thickness, to be initiated at particular sites, e.g. at intralamellar steps and to leave a legacy of crystallographically oriented holes related to the original directions of fold packing. Additionally, in the presence of a substrate, there are effects due to the degree of mutual contact of crystal and underlying surface plus others due to deformation during deposition, especially that involving collapse of non-planar structures. Annealing in suspension can usefully avoid this last complication, indeed the lack of constraint has allowed the adoption of otherwise unknown habits^{3,4}. Nevertheless a substrate does have the advantage of retaining for examination small scale structures left when lamellae break up, which would quite possibly have been missed in suspension and certainly have lost their spatial relationships. So it is in this work where the changes seen go beyond those found for annealing in suspension⁵ and parallel those observed in bulk polymer annealed adjacently¹. They provide further evidence that lamellae 200–300 Å thick do transform into the hexagonal phase but show also that the constraints of a substrate and small specimen size depress the resulting average layer thicknesses by factors typically of 3 to 4.

The first marked changes in morphology are apparent after annealing at 230°C and 5.35 kbar, conditions under which these polyethylenes remain orthorhombic⁶. It is not surprising, therefore, that these changes, viz. lines perpendicular to the prism faces, are those which are well known at 1 bar³ and have also been observed in other work at high pressure confined to the orthorhombic phase⁵. The molecular orientation also behaves similarly in that 020 becomes the strongest reflection in diffraction patterns taken with the electron beam perpendicular to the specimen plane. This is characteristic of the well known rotation of the unit cell about the *b* axis which can also be seen in upper layers as crumples along *b* (*Figure 5c*)⁷.

Before discussing higher annealing temperatures in detail, it needs to be shown that for these thin lamellae just as for the bulk specimens of the previous paper, there is a transition into the hexagonal phase⁸ before melting. Two pieces of evidence show this. First, there is a clear change in morphology between 254°C and 256°C (in each of *Figures 2, 3 and 4*) corresponding to melting. This is at least 10K higher than would be expected for melting of the orthorhombic phase at this pressure even before taking into account crystal size effects but coincides with the melting point of

hexagonal bulk polymer for which depression due to lamellar thickness is known to be small⁶. Secondly, there is the characteristic three fold twin orientation shown in *Figure 5b* for a crystal of Rigidex 9 (*Figure 5a*) annealed at 245°C and 5.35 kbar in related experiments. This is an effect which was looked for previously in bulk polymer⁶ and is to be expected after the sequence orthorhombic → hexagonal → orthorhombic polyethylene.

What were the {110} and {200} planes in orthorhombic polyethylene become identical {10.0} planes in the hexagonal structure. For the reverse transformation there are, in consequence, three orientations of the orthorhombic cell available for each hexagonal {10.0} plane which are shown in *Figure 6* on the assumptions (i) that the *c* axis is invariant, and (ii) that the orientation of the plane considered remains unaltered. According to *Figure 6a*, 110 twinning will then lead to two additional unit cell orientations in the final orthorhombic texture with the new ⟨020⟩ directions OB' rotated by ±2α away from the original OB where 2α (=67°30') is the angle between (110) and (1 $\bar{1}$ 0) planes. Similarly *Figure 6b* shows that replacement of {110} by {200} or *vice versa* gives additional orientations of ⟨020⟩ at ±β where β (=56°15') is the complement of α. However, assumption (ii) cannot be exact for it can only hold for one set of planes in a particular region. In practice, therefore, one anticipates a spread of orientations for 020 spots around the 0° and ±60° rotations with respect to the original orthorhombic lamella; this is present in *Figures 5b and 5d*. These diffraction patterns also suggest that assumption (i) may not always hold either. Although high-pressure diffraction has shown that the *c* axis direction is common to orthorhombic and hexagonal phases in bulk polyethylene⁸, nevertheless there is also evidence that this is not always maintained locally. This is shown, in particular, by the characteristic zig-zagging of the *c* axis found in annealed bulk polymer¹ and adopted, perhaps, as a means of increasing chain-extension within a given lamellar thickness. So, whereas 020 has the expected three fold orientation, *Figures 5b and especially 5d* show that there can be a tendency for the only 110 and 200 spots present to be those of the initial orientation. As the 020 reflections are also the strongest, it is probable that the new unit cell orientations at ±60° have also undergone an additional rotation about *b*, causing *c* to move away from the lamellar normal. Such a rotation, familiar in other contexts^{7,9}, if of more than a few degrees would remove zero-layer reflections other than 0*k*0 from the patterns in the way observed. The evidence of *Figure 5*, therefore, supports the identification of the high-pressure polyethylene phase as hexagonal⁸ and indicates that in the new orientations the *c* axis tends to have been rotated away from the lamellar normal about *b*.

It follows that, notwithstanding the considerable morphological differences, the annealing of solution-grown polyethylene lamellae at high pressures passes through the same three stages as that of bulk material, viz. annealing in the orthorhombic phase, then in the hexagonal phase and finally melting. The first of these has already been discussed but the changeover to the second leaves no sharp alteration in the morphological record. There are no d.t.a. data to show directly when the phase transition occurs in thin films, but the appearance of the twinned diffraction pattern has been detected in the case of Rigidex 9 after annealing at temperatures as low as 236°C (*Figures 5c and 5d*). This is at the lower end of the d.t.a. peak for bulk material¹ and shows that, despite the difficulty of anticipating to what extent the effect of the substrate offsets the lowering of transition

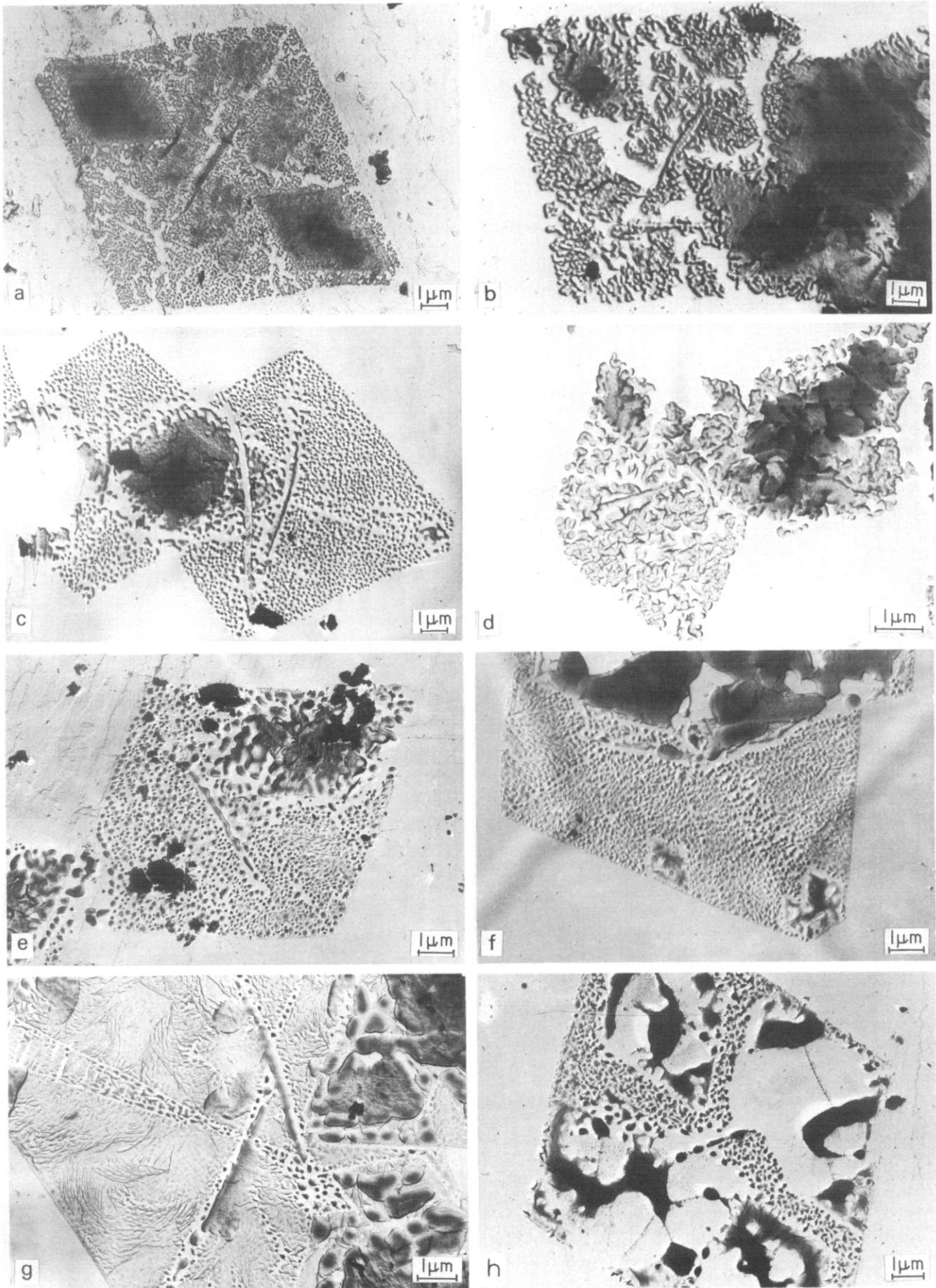


Figure 3 As Figure 2, but for Rigidex 2 crystals

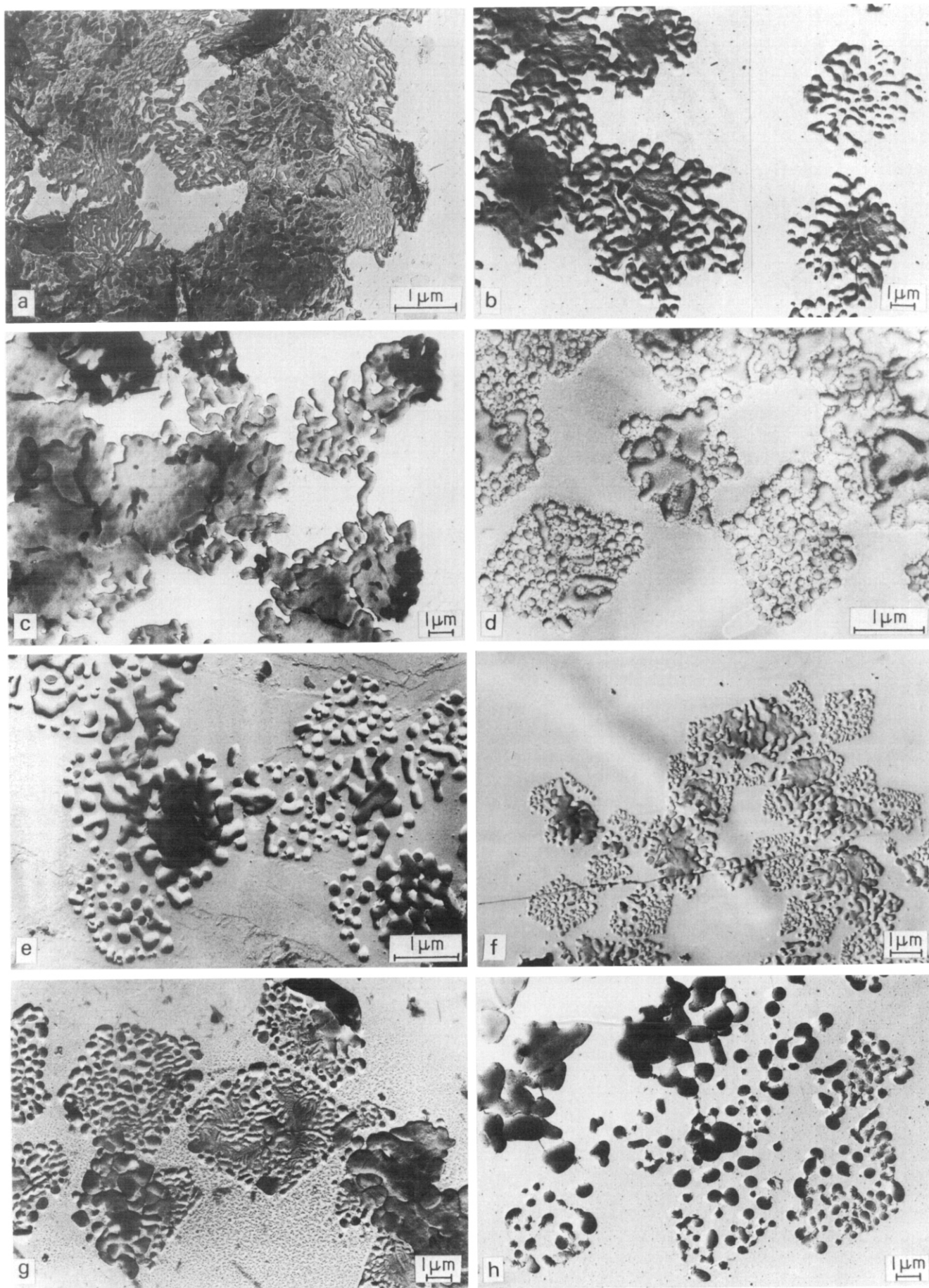


Figure 4 As Figure 2, but for Hifax crystals

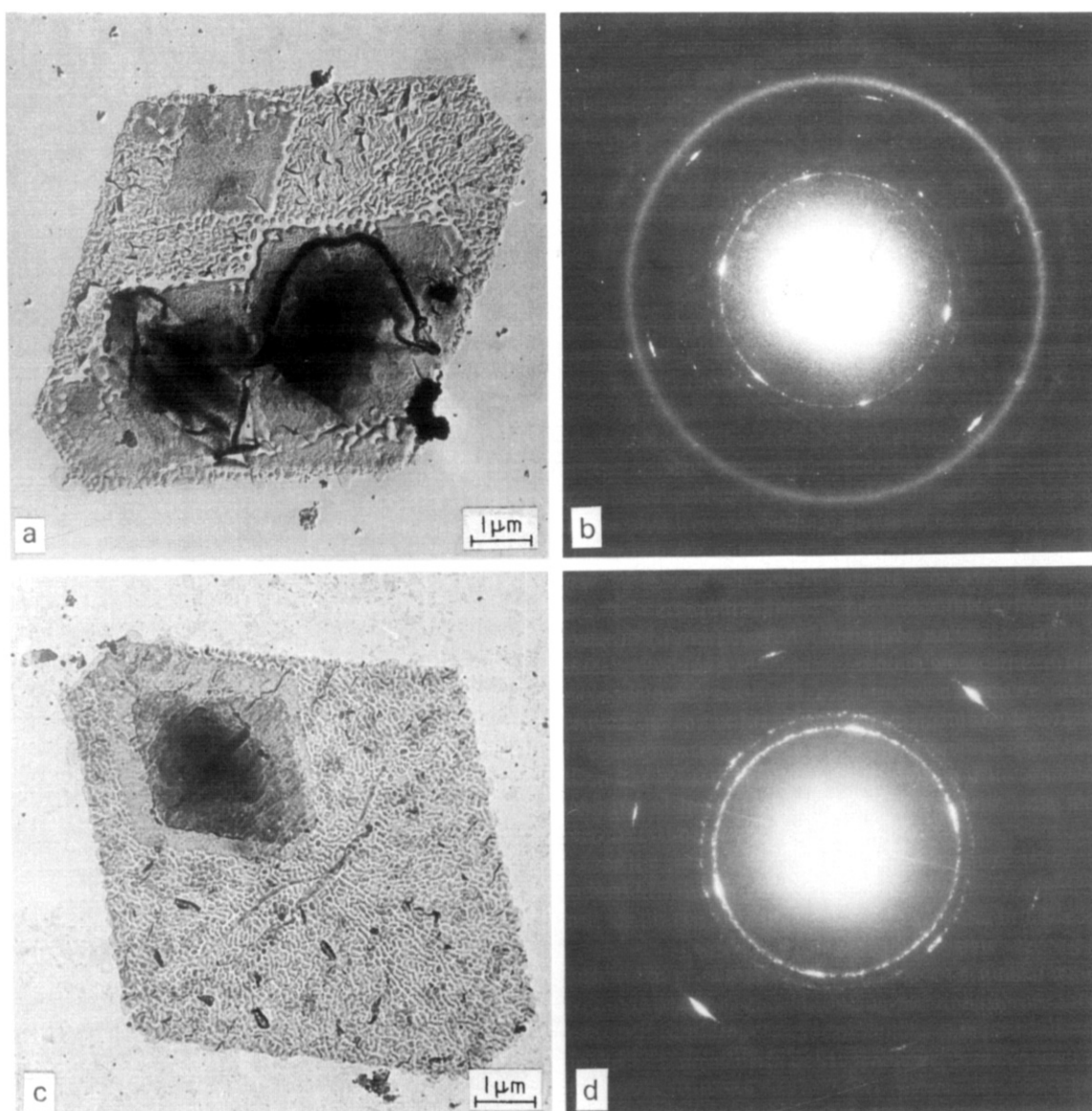


Figure 5 Morphology and electron diffraction patterns of Rigidex 9 crystals annealed for 15 min at 5.3₅ kbar at 245°C (a, b) and 236°C (c, d).

temperatures by lamellar thickness, the change to the hexagonal structure occurs, in these experiments, at approximately the same temperatures in thin layers as in bulk.

The main change in appearance in this region is the disintegration of once continuous lamellae into small islands confined within the original outlines but increasing in thickness, with intermediate stages of multiply connected shapes. According to Figures 2, 3 and 4 this transformation occurs, as would be expected, at slightly higher temperatures for higher molecular weight polymer. Once definitely within the hexagonal phase, at temperatures between 242° and 250°C, it is noticeable that where two layers overlap the islands are approximately twice as wide and that annealing of three or more overlying layers, as in the central pleat, gives a continuous sheet without holes. It follows, as shadow lengths confirm, that these islands are ~500 Å thick, although they are not generally flat-topped but rounded and thinnest at the edges. The outlines of higher layers are much softened with only the thickest pleats still readily discernible whereas annealing in the orthorhombic phase to say, 230°C (Figures 3a and 4a) leaves them much better defined.

It may be inferred from this that, on annealing, a system of lamellae will adopt a sufficient thickness, if necessary at

the expense of creating additional side surfaces (holes), but once this has been reached further thickening, which could give lamellae of at least the maximum thickness of the initial aggregate, is subordinated to the reduction of total energy which a uniform layer gives with its minimal side surfaces. The thickness adopted is considerably less than that found in thicker aggregates of identical lamellae treated similarly showing that for annealing, just as for recrystallization of polyethylene at high pressures¹⁰, specimen size exerts a considerable influence on lamellar thickness.

Such an effect is, perhaps, not so surprising in the case of annealing because most of the explanations suggested for lamellar thickening envisage it as a cooperative process. Following our previous work^{1,10}, it is also compatible with regarding annealing as local melting followed by rapid recrystallization because of the similar effect of specimen size which, in our view, is associated with the thickening of lamellae close to the growing edge.

The effect of local deformation on annealing behaviour is noticeable in subsidiary features, all of which are found in Figure 3c. Here material is denuded from an accidental scratch running vertically through the centre of the picture, from both {110} and {100} sector boundaries and around the edges of the central growth pyramid; the last two sites

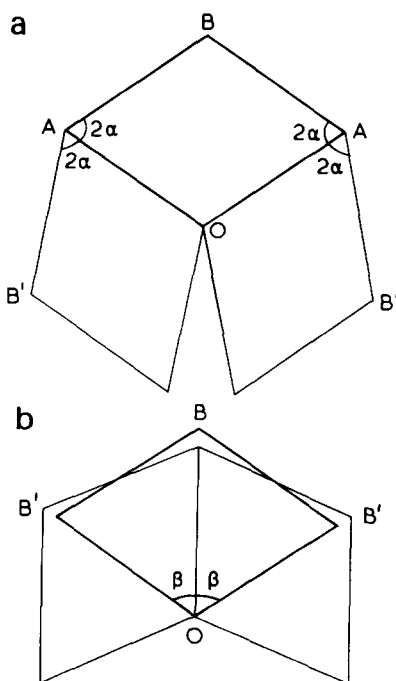


Figure 6 Possible twinning schemes for a polyethylene crystal undergoing the sequence of transitions orthorhombic \rightarrow hexagonal \rightarrow orthorhombic

are those where deformation will have been concentrated during sedimentation. As deformed regions will have lower melting points, material in them would be expected to become mobile earlier during annealing and so to move towards adjacent undeformed regions.

Finally, we come to the melting region. By 256°C all three polymers have melted and show the appropriate crystallized morphologies¹⁰ (Figures 2, 3 and 4). Of particular interest, however, is the transformation region revealed at 253° and 254°C, temperatures lying within the region of the final high pressure d.t.a. melting peak of each bulk polymer. Features here are a filling in of the original outline and the clear demarcation of what were once the {100} sectors in some, but not all, lamellae. Figure 3g shows that infilling growth has occurred around a very few centres and, moreover, at a thickness close to that of the original lamellae. These centres are almost certainly unmolten higher molecular weight material acting as nuclei for subsequent growth of shorter molecules during cooling in agreement with earlier work¹¹ and in a way familiar from atmospheric 'self-seeding'¹². In this way one can explain why Hifax alone, with its dearth of short molecules, fails to show the effect at 253°C and why Rigidex 9, having fewer very long molecules should have fewer nuclei and so be more 'filled in' than Rigidex 2 at 253°C.

The distinction of the {100} sectors at this stage is interesting and reminiscent of a well known effect at 1 bar ascribed to 'early melting or other transformation' related to lattice differences stemming from different directions of fold packing in different sectors^{13,14}. In the present case the demarcation appears due to the demarcation of sector boundaries already remarked on, which isolates various sectors in favourable conditions, plus a later melting of the {100} sectors. Thus in Figure 2f especially it can be seen that flow associated with melting has occurred in {110} domains but not in one {100} sector. This is consistent

with the greater thickness (and smaller number) of islands in the {100} sectors, though whether this itself is due to inherent differences between sectors or relates to details of lamellar collapse and contact with the substrate is not entirely clear. Eventually, however, flow does occur in these sectors too (Figure 3g) and then it leaves a pattern with lines parallel to *b*, in a similar way to collapse features in the {100} sectors (Figure 1) implying that the second suggestion may well be correct.

That the original crystal outline is virtually completely filled in during recrystallization shows the lamellar thickness is close to the original ~ 150 Å. Here, however, crystallization must have been into the hexagonal phase because, having shown that recrystallization from the melt at this pressure normally is into the new phase, then it follows that this must be also true of the more rapid self-seeded recrystallization occurring at a higher temperature during cooling. We have, therefore, still further evidence that the crystallization of hexagonal polyethylene at a given temperature and pressure encompasses layer thicknesses down to the 100 Å level. Conversely, the lamellar thickness is not determined mainly by the crystallization temperature but varies by at least an order of magnitude with specimen size and constraints.

In a similar way, we have abundant evidence that annealing thin polyethylene films at high pressures does not produce the thick lamellae characteristic of the bulk. Both effects deny us routes of preparing isolated thick chain-extended crystals of polyethylene. But at the same time, the parallel behaviour of both annealing and recrystallization treatments in an unusual context provides important reinforcement for the view that, at least in polyethylene, the changes produced by annealing are essentially those produced by local melting followed by rapid recrystallization. The other main conclusion of this paper is that electron diffraction patterns provide independent confirmation that the structure of the high-pressure phase of polyethylene is indeed hexagonal.

REFERENCES

- Bassett, D. C., Khalifa, B. A. and Olley, R. H. *Polymer* 1976, **17**, 284
- Statton, W. O. and Geil, P. H. *J. Appl. Polym. Sci.* 1960, **3**, 357
- Keller, A. and Bassett, D. C. *J. R. Microsc. Soc.* 1960, **79**, 243
- Bassett, D. C., Frank, F. C. and Keller, A. *Phil. Mag.* 1973, **8**, 1753
- Roe, R.-J., Gieniewski, C. and Vadimsky, R. G. *J. Polym. Sci. (A-2)* 1973, **11**, 1653
- Bassett, D. C. and Turner, B. *Phil. Mag.* 1974, **29**, 925
- Bassett, D. C. and Keller, A. *J. Polym. Sci.* 1959, **40**, 565
- Bassett, D. C., Block, S. and Piermarini, G. J. *J. Appl. Phys.* 1974, **45**, 4146
- Balta-Calleja, F. J., Bassett, D. C. and Keller, A. *Polymer* 1963, **4**, 269
- Bassett, D. C. and Khalifa, B. A. *Polymer* 1976, **17**, 275
- Rees, D. V. and Bassett, D. C. *J. Polym. Sci. (B)* 1969, **7**, 273
- Blundell, D. J. and Keller, A. *J. Macromol. Sci. (B)* 1968, **2**, 301
- Bassett, D. C., Frank, F. C. and Keller, A. *Nature* 1959, **184**, 810
- Bassett, D. C., Frank, F. C. and Keller, A. *Proc. Eur. Reg. Conf. Electron Microsc., Delft* 1960, **1**, 244

Theoretical estimation of the effect of solvent on unperturbed dimensions: 1. Isotactic poly(vinyl alcohol)*

T. Bleha and L. Valkot

Polymer Institute of the Slovak Academy of Sciences, Dúbravská cesta, 809 34 Bratislava, Czechoslovakia

(Received 22 July 1974)

The effect of the quality of solvent on the unperturbed chain dimensions \bar{r}_0^2 of perfectly isotactic poly(vinyl alcohol) (iso-PVA) was studied by means of some model calculations according to the matrix method of Flory *et al.* These investigations were based on the assumption that the quality of solvent affected mainly the energy of the intramolecular hydrogen bond, while the magnitude of the interactions between other groups, hardly varied with the change of solvent. The individual conformation energies in a chain of iso-PVA were estimated from the analysis of structurally similar polymers, as well as the results obtained with 2,4-pentandiol. It was found that the characteristic ratio $C = \bar{r}_0^2/nl^2$ increased in non-polar solvents, with energy of the intramolecular hydrogen bond stabilizing the stretched zig-zag conformation of chain. Conversely, the characteristic ratio, monotonously decreased with increasing polarity of solvent to the value of about 6, typical of a flexible random coil. The existence of an analogous relationship, valid for other polymers, able to form an intramolecular hydrogen bond in the chain, was also discussed.

INTRODUCTION

The study of the configurational characteristics of polymer chains, usually involves, explicitly, merely the dependence of these characteristics on temperature. At the same time it is assumed tacitly that these characteristics, for instance the unperturbed dimensions of chains, do not depend on the quality of solvent. This assumption seems to be fulfilled sufficiently for the non-polar polymer-solvent systems. With increasing interest in the study of polar synthetic polymers and biopolymers the experimental evidence¹⁻¹⁰, for the invalidity of this assumption in above systems, accumulates.

Provided fixed bond angles and bond lengths are assumed to be present in the skeleton of the chain, its dimensions are determined by the corresponding conformation energies. In general, at a given temperature, these conformation energies depend on intramolecular, as well as intermolecular interactions, with the solvent and other polymer chains. As for polar low-molecular compounds, this fact is well known and described in the literature¹¹⁻¹⁴. An analogous phenomenon may also be expected, in the case of polymer chains; while a small shift in the position of the potential minima of internal rotation about the bonds in the skeleton of the chain, may affect the unperturbed dimensions of this chain.

A formal description of the effect of solvent on unperturbed dimensions based on statistical mechanics, was developed formerly by Lifson and Oppenheim¹⁵. In other approaches to configurational statistics¹⁶⁻¹⁸, this effect was not taken into consideration explicitly, and the intramolecular origin of the conformation energies of the chain

was particularly emphasized. It is of interest to try to estimate the solvent effect for individual polymers theoretically, by using the recent matrix method of Flory¹⁸ based on statistical mechanics.

Poly(vinyl alcohol) with regular isotactic structure, is a convenient model for theoretical study of the effect of solvent on unperturbed dimensions. The possible formation of an intramolecular hydrogen bond providing a side backbone in the chain, with zig-zag stretched conformation, is the decisive factor which affects the set of stable conformations in the chain. But it is well known that the energy of an intramolecular hydrogen bond, depends very much on the polarity of solvent and therefore, the formation of intermolecular hydrogen bonds usually prevails in polar solvents. It may be concluded from this that the polarity of a solvent affects the competitive equilibrium between the formation of intramolecular and intermolecular hydrogen bond in the case of the iso-PVA chains, also. Therefore, this study is a theoretical investigation of the relationship between the unperturbed dimensions of iso-PVA and the parameter ω_2 , characterizing the magnitude of the interaction between two neighbouring OH groups in the chain. We suppose that such a simplified computation could give a true picture of the characteristic features of the effect of solvent on the unperturbed dimensions of the chains for real iso-PVA.

THEORETICAL

Model

The model of rotational-isomeric states, taking into account the interaction of the nearest neighbouring groups in a linear chain, was in the last decade, successfully applied to the correlation of various configurational properties of a great number of polymers¹⁸, including the dimen-

* Presented in part at the 9th Microsymposium on Thermodynamics of Interactions in Polymer Solutions, Prague, September, 1971

† Institute of Physical Chemistry of the Slovak Technical University, 880 37 Bratislava, Czechoslovakia.

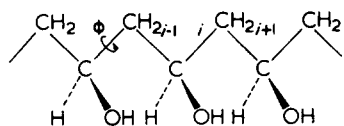


Figure 1 All-trans planar conformation of a portion of isotactic poly(vinyl alcohol) chain

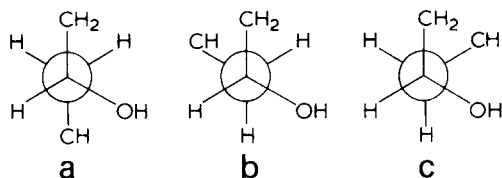


Figure 2 Newman projections of the three rotational states of skeletal bond i , and the associated statistical weight factors: (a) *trans* T (η); (b) *gauche*, G^+ (1); (c) *gauche*, G^- (τ)

sions of isotactic vinyl polymers^{18–24}. This approach may be also adapted, easily for iso-PVA (Figure 1) assuming fixed bond angles and bond lengths. Also, the set of rotational-isomeric states about single bonds in the skeleton and the corresponding conformation free energies must be specified for the calculation.

The usual set of the rotational isomeric states *trans*, *gauche* plus and *gauche* minus (T , G^+ , G^-), localized at the angles 0° , 120° , -120° were used. In view of the illustrative character of the calculations, we neglected the shift in the rotational isomeric states, which is usual in the case of vinyl polymers, owing to intramolecular steric interactions.

Following Flory¹⁸, the first order free energies depending on single rotational angle are referred to the G^+ state. Their representation and denotation are given in Figure 2 for iso-PVA. In general, it may be expected that the statistical weight τ is smaller than η , because of the coincident *syn* position of the groups with respect to the CH_3 as well as OH groups. The interactions of second order depend on the relative position of two bonds in skeleton and are denoted as ω , ω_1 and ω_2 ²⁵. Factor ω represents the interaction between the pairs of CH_2 or CH groups, ω_1 characterizes the interaction between CH_2 and OH groups. Statistical weight ω_2 , expresses the interaction between two OH groups and is, therefore, a function of the energy of the intramolecular hydrogen bond.

By means of statistical weights it is possible to specify two matrices which are necessary for the analysis of isotactic vinyl polymers^{18,25}:

$$U' = \begin{bmatrix} \eta & 1 & \tau \\ \eta & 1 & \tau\omega \\ \eta & \omega & \tau \end{bmatrix}; U''_m = \begin{bmatrix} \eta\omega_2 & \tau\omega_1 & 1 \\ \eta & \tau\omega_1 & \omega \\ \eta\omega_1 & \tau\omega_2\omega & \omega_1 \end{bmatrix}$$

Matrix U' is attributed to the bond of $\text{CHOH}-\text{CH}_2$ which belongs to an asymmetric centre and matrix U''_m corresponds to the bond of CH_2-CHOH in *meso*-*dd*-dyad. These statistical weights together with the geometrical parameters of the chain skeleton, enable us to calculate the configurational partition function and other conformation dependent properties as e.g. characteristic ratio for perfectly isotactic PVA. The characteristic ratio $C = \bar{r}_0^2/nl^2$ expresses the ratio of the mean square value of the distance between the unperturbed chain ends, to the analogous value valid for the model of freely connected chains.

By simulating the effect of solvent on unperturbed dimensions we shall examine the dependence of the charac-

teristic ratio C on the statistical weight ω_2 . We suppose that the quality of solvent affects the value of other statistical weights, only slightly. Thus it is possible to convert the study of an originally intermolecular effect, into the investigation of the dependence of this effect on intramolecular interaction free energy.

Estimation of the statistical weights for iso-PVA

The magnitude of individual statistical weights may be assessed for iso-PVA in two ways, i.e. from the literary data concerning structurally analogous polymers and n.m.r. results obtained for low molecular weight model compounds of PVA. In the study of configurational characteristics of poly(trimethylene oxide) $[(\text{CH}_2)_3-\text{O}]_n$, Mark^{26,27} assigned the statistical weight $\sigma' = 1.4 \pm 0.5$, at 25°C to one of the *gauche* positions occurring in the chain (Figure 3a). In the case of polymethylene (Figure 3b), Flory¹⁸ used the value $\sigma = 0.54$, at 140°C for the *gauche* position, which corresponds to $\sigma = 0.43$, at 25°C . These values of σ , referring to the unit statistical weight for *trans* conformation in the chain, corroborate the preferential occurrence of oxygen in *gauche* position¹⁸. Provided the statistical weight η is predominately determined by the interaction of neighbouring atomic groups, the comparison between the conformations represented in Figure 2 and Figure 3, gives $\eta = \sigma'/\sigma = 3.2 \pm 1.1$, at 25°C . This reasoning involves the assumption that the interactions $\text{O} \dots \text{CH}_2$ and $\text{OH} \dots \text{CH}$, are approximately equal.

Under analogous assumptions, analysis of the conformations of poly(tetramethylene oxide)^{26,27} gives the value 0.55 ± 0.3 for the statistical weight ω_1 at 25°C . The value $\omega = 0.034$ (25°C) is normally used for the statistical weight incident to the overlap of two groups. But the accuracy of the estimate of this value is probably over estimated. Reliable data available for the estimate of the statistical weight τ , are not abundant. From the earlier paper on the configurational statistics of vinyl polymers, it follows that the value of factor τ effected the characteristic ratio only slightly. The value of τ assessed, was found to be in the range $0.05-1$ ¹⁸.

Another independent way for the estimation of the statistical weights for iso-PVA is based on the experimental results of the n.m.r. measurements obtained by Fukurci *et al.*²⁸, for the model substance 2,4-pentanediol in different solvents as well as the theoretical analyses of these results performed by Moritani and Fujiwara²⁹. By using the set of the five statistical weights mentioned, it is possible to express the population of individual conformers in the *meso* as well as *racemic* isomer of 2,4-pentanediol. From the dependence on temperature of the vicinal spin-spin coupling constant, the values of statistical weights may be also determined. Moritani and Fujiwara present the following values: $\eta = 1.94$; $\tau = 0.5$; $\omega = 0.04$; and $\omega_1 = 0.24$. The value of the statistical weight ω_2 varied with the polarity of the solvent used from 0.28 for D_2O to 4.87 for CH_2Cl_2 .

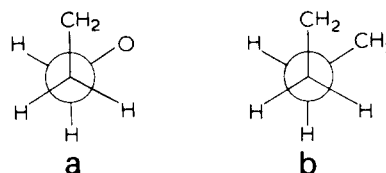


Figure 3 Newman representation of *gauche* position and the corresponding statistical weights for (A) poly(trimethylene oxide), $\sigma' = 1.4 \pm 0.5$; (B) poly-methylene at 25°C , $\sigma = 0.43$

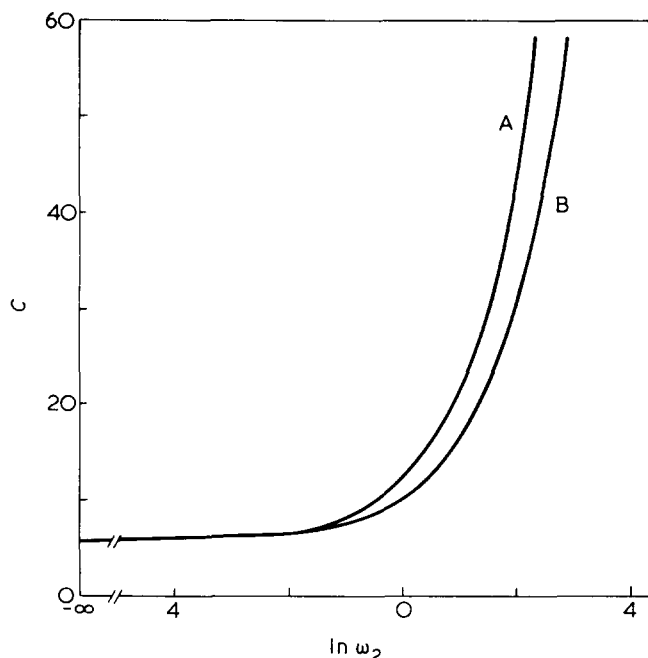


Figure 4 Dependence of the characteristic ratio C on the statistical weight ω_2 for iso-PVA. Two different values of the statistical weight η , $\tau = 1$, $\omega = 0.05$, $\omega_1 = 0.5$. Curve A, $\eta = 3.5$; B, $\eta = 2.5$

In conformity with the previous assumption for iso-PVA, Moritani and Fujiwara explained the observed solvent effect on the conformations of 2,4-pentanediol, merely by the variation of the statistical weight ω_2 , while other statistical weights did not change with solvent.

If both the methods of the estimation of statistical weights are compared, a difference appears especially in the case of the statistical weights η and ω_1 . This disagreement may be partly removed, if we modify the statistical weights estimation for 2,4-pentanediol²⁹ by the use of experimentally found relationship between η and ω_1 , (Figure 6e)²⁹. In this way, choosing $\omega_1 = 0.55$ it is possible to obtain a modified value of the statistical weight η of about 2.5. Then the agreement of both methods is sufficient, but it does not count to over estimate the accuracy of the estimation of individual statistical weights.

RESULTS AND DISCUSSION

Dependence of C on ω_2

Following Flory¹⁸, we used the value of 1.53 Å for the length of the C–C bond in the chain skeleton and the values of 112° for the bond angle $\angle CCC$. The dependence of the characteristic ratio C on ω_2 for two representative values of η (2.5 and 3.5), while $\tau = 1$, $\omega = 0.05$, and $\omega_1 = 0.5$, is presented in Figure 4. For comparison, some other values of C found by the variation of the individual statistical weights are listed in Table 1.

The calculated values of the characteristic ratio in Figure 4 and Table 1 correspond to an infinitely long chain. The matrix multiplication method¹⁸ was applied and the value of 0.02 was used as a convergence limit for the difference between two characteristic ratios in two successive cycles. The rate of convergence of C_n is represented in Figure 5 for different values of ω_2 . With increasing ω_2 , it is possible to obtain the limiting value of C_n for very long chains ($n \geq 100$), only.

For small values of ω_2 the value of C does not change necessarily with any statistical weight, but for $\omega_2 > 5$ the value of C depends strongly on all other statistical weights.

The final form of this relationship depends mainly on the reliability of the statistical weights used. It may be stated with certainty that $\eta > 1$, since oxygen atoms tend to stabilize the *gauche* position¹⁸. Contrary to expectation the form of relationship between C and ω_2 is sensitive also on the exact value of τ , e.g. approximately the same shape of curves as in Figure 4 may be obtained for $\tau = 1$ and $\tau = 0.3$ with $\eta = 2.5$, $\omega = 0.05$, $\omega_1 = 0.5$. As regards the second order interactions, Flory¹⁸ has already stressed that three kinds of ω must be distinguished in the case of PVA when $\omega_2 > 1$. Because of the illustrative character of our calculations we did not consider it necessary to analyse in more detail the effect of other statistical weights on the C versus ω_2 relationship. We assume that the used values of statistical weights, represent a reasonable estimate of the interactions in the chain. Another approach to the estimate of statistical weights is based on the semi-empirical methods of theoretical conformation analysis¹⁸. Though the method was also applied in the case of 2,4-pentanediol³⁰, the results cannot be used here since the contribution of the intra-

Table 1 Calculated values of the characteristic ratio for iso-PVA

η	τ	ω	ω_1	ω_2	C
1.5	1	0.05	0.5	1	7.27
2.5	1	0.05	0.5	0.6	7.85
2.5	1	0.05	0.5	5	22.59
2.5	1	0.05	0.5	10	37.06
2.5	1	0.05	0.5	50	105.18
2.5	1	0.05	0.5	250	162.53
2.5	1	0.05	0.5	0.1	6.02
2.5	1	0.05	0.5	0.01	5.77
2.5	1	0.05	0.5	0	5.60
2.5	1.5	0.05	0.5	10	28.27
2.5	1.5	0.05	0.5	0.1	5.55
2.5	0.3	0.05	0.5	10	53.54
2.5	0.3	0.05	0.5	0.1	6.98
2.5	1	0.2	0.5	10	25.37
2.5	1	0.05	0.8	10	31.39
2.5	1	0.05	0.35	10	40.73
3.5	1	0.05	0.5	10	54.80
3.5	1	0.05	0.5	0.5	8.65
3.5	1	0.05	0.5	0	5.83
5.0	1	0.05	0.5	10	81.18

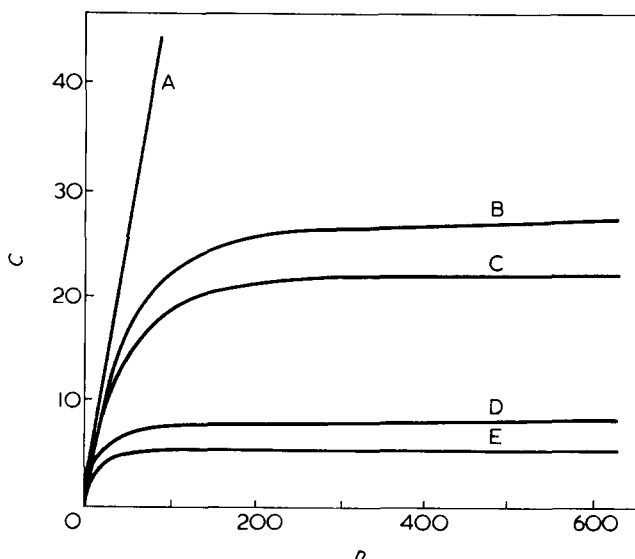


Figure 5 Dependence of the characteristic ratio on the number of C–C bonds in the chain of iso-PVA for different values of the statistical weight ω_2 : A, 50; B, 10; C, 5; D, 0.6; E, 0.0

molecular hydrogen bond was not explicitly taken into consideration.

By varying individual statistical weights about their average value, it is also possible using Boltzmann's factors to estimate very approximately the temperature coefficient $\text{dln } \bar{r}_0^2/\text{dT}$ of the unperturbed chain dimensions. This procedure is equivalent to the assumption that the details of the rotational potential function do not change in a narrow temperature range. The calculated value depends on the estimate of statistical weights. For instance, a relatively high negative value of the temperature coefficient (about -9×10^{-3} degree $^{-1}$) is obtained for $\eta = 2.5$, $\tau = 1$, $\omega = 0.05$, $\omega_1 = 0.5$ and $\omega_2 = 10$ at 25°C.

Solvent effect on ω_2

As it was to be expected, the characteristic ratio increases with the statistical weight ω_2 , because the population of the segments with a zig-zag stretched *trans* conformation stabilized by an intramolecular hydrogen bond in the chain increases. Provided the statistical weight ω_2 decreases, the characteristic ratio falls to the value of about 6 according to the choice of other statistical weights. This decrease is connected with a disruption of the intramolecular hydrogen bond and with an increase in the population of *gauche* conformations in the chain. It is clear from Figure 4 that the condition $\omega_2 = 0$, is not sufficient to provide a preference of the conformations of the type $(TG^+)_n$ or $(G^-T)_n$, forming 3_1 helices, which are characteristic for vinyl polymers. This would be manifested by the increase in C in Figure 4. Conversely, the values of C calculated for small values of ω_2 indicate a considerable flexibility of the chain forming a random coil in solution. The value of ω_2 particularly small may be expected for the aqueous solutions of iso-PVA.

Since the formation of intramolecular hydrogen bond depends on the polarity of medium, it may be concluded from Figure 4 that the characteristic ratio for iso-PVA, decreases with increasing polarity of the solvent. The results obtained for the *meso*-isomer of 2,4-pentanediol, confirm the decrease in the population of *TT* isomer with increasing polarity of the solvent^{28,31}. If we use the values of ω_2 estimated for 2,4-pentanediol as representative values for the chains of iso-PVA, then according to Figure 4, an increase in the characteristic ratio of about 15 or more, follows for the change of solvent from D₂O ($\omega_2 = 0.28$) to CH₂Cl₂ ($\omega_2 = 4.87$). It is evident that the attainment of such changes is limited in real polymer systems by the insolubility of iso-PVA in non-polar solvents and the experimental verification of the predicted relationship between the characteristic ratio and the quality of solvent, will be limited to a much narrower region of the polarity of solvents.

The manner in which the competitive equilibrium between intramolecular and intermolecular bond depends on the polarity of solvent, ensues from the results of analysis for 1,3-propanol³². While only 4.6% of the molecules of 1,3-propanol form an intramolecular hydrogen and almost the whole remainder forms two intermolecular hydrogen bonds in pure dioxane, in a less polar mixed solvent (dioxane/CCl₄ = 1:2), no less than 11.7% of molecules form an intramolecular hydrogen bond. The preferential formation of intermolecular hydrogen bond may be attributed to the fact that the linear system of atoms OH . . . X thus formed, is more energetically advantageous than a similar bent system containing an intramolecular hydrogen bond. Besides the molecules of solvent, the OH groups on neigh-

bour chain can form intermolecular hydrogen bonds. So in non-polar solvents the formation of intermolecular hydrogen bonds of the type polymer-polymer may modify the value of ω_2 , which may also vary with polymer concentration.

We have not found in the literature any experimental data concerning the solvent effect with respect to perfectly isotactic PVA. This effect was, however, found experimentally in the case of atactic PVA dissolved in mixed solvents³³. The use of mixed solvents or thermodynamically good solvents, complicates the analysis of the solvent effect on unperturbed dimensions^{5,6}. An attempt was also made to estimate the solvent effect from the measurements of elastic properties of a swollen polymer network³⁴. However, it may be expected that only the use of the methods more sensitive to the change in the local conformation of chain, will provide more reliable data concerning the magnitude of the solvent effect on the unperturbed dimensions of polymers. For instance by using n.m.r. it was possible to establish the solvent effect on the preference of stable conformations in the case of such non-polar polymer as polyethylene^{35,36}.

Now we shall try to extrapolate some conclusions from the presented calculation. Similarly as for the characteristic ratio, the solvent effect can be also simulated for other conformation dependent quantities of iso-PVA, such as mean square of dipole moment $\bar{\mu}_0^2$. In analogy with the characteristic ratio, a conspicuous solvent effect may be expected in this case, also. It follows from the study of model substances for perfectly syndiotactic PVA^{38,31}, that the *G*⁻*T* conformations are stabilized in non-polar solvents by intramolecular hydrogen bond. Because of a higher population of other conformations (*TT*, *G*⁺*G*⁻, *TG*⁺) a less distinct solvent effect may be expected for this polymer in comparison with the results obtained for iso-PVA.

Characteristic features of the model calculation of solvent effect in the case of iso-PVA, may be extended to other types of the polymers in which the formation of intramolecular hydrogen bond affects the stable conformations in the skeleton of the chain in a decisive way. For the refinement of the theoretical approach to the configurational statistics of polymers it will be, therefore, necessary in some cases to do away with the approximation involving the assumption that the relative energies of individual rotational isomers in the chain are independent of the quality of solvent.

ACKNOWLEDGEMENTS

The authors would like to thank Professor P. J. Flory for helpful discussion. They are also grateful to Dr K. Dusek for his valuable comments.

REFERENCES

- 1 Flory, P. J., Spurr, Jr. O. K. and Carpentier, D. K. *J. Polym. Sci.* 1958, **27**, 231
- 2 Ivin, K. J. and Ende, H. A. *J. Polym. Sci.* 1961, **54**, 517
- 3 Ivin, K. J., Ende, H. A. and Meyerhof, G. *Polymer* 1962, **3**, 129
- 4 Crescenzi, V. and Flory, J. P. *J. Am. Chem. Soc.* 1964, **86**, 141
- 5 Kurata, M. and Stockmayer, W. H. *Fortschr. Hochpolym. Forsch.* 1963, **3**, 196
- 6 Dondos, A. and Benoit, H. *Macromolecules* 1971, **4**, 279
- 7 Orofino, T. A. *J. Chem. Phys.* 1966, **45**, 4310
- 8 Bohdanecký, M., Petrus, V. and Kratochvil, P. *Collect. Czech. Chem. Commun.* 1969, **34**, 1168

Theoretical estimation of the effect of solvent on unperturbed dimensions (1): T. Bleha and L. Valko

- 9 Mattice, W. I. and Mandelkern, L. *J. Am. Chem. Soc.* 1971, **93**, 1769
- 10 Elias, H. G. and Ibrahim, F. W. *Makromol. Chem.* 1965, **89**, 12
- 11 Mizushima, S. I. 'Structure of Molecules and Internal Rotation', Academic Press, New York, 1954
- 12 Abraham, R. J. *J. Phys. Chem.* 1969, **73**, 1192
- 13 Govil, G. and Bernstein, H. J. *J. Chem. Phys.* 1968, **48**, 285
- 14 Heatley, F. and Allen, G. *Mol. Phys.* 1969, **16**, 77
- 15 Lifson, S. and Oppenheim, I. *J. Chem. Phys.* 1960, **33**, 109
- 16 Volkenstein, M. V. 'Konfiguratsionnaja Statistika Polimernykh Tsepei', Izdav. Akad. Nauk SSR, Moscow, 1959
- 17 Birshtein, T. M. and Ptitsyn, O. B. 'Konformatsii makromolekul', Nauka, Moscow, 1964
- 18 Flory, J. P. 'Statistical Mechanics of Chain Molecules', Wiley, New York, 1969
- 19 Abe, A. *Polym. J.* 1970, **1**, 232
- 20 Fujiwara, Y. and Flory, J. P. *Macromolecules* 1970, **3**, 280
- 21 Boyd, R. H. and Breitling, S. M. *Macromolecules* 1972, **5**, 279
- 22 Heatley, F. *Polymer* 1972, **13**, 219
- 23 Biskup, U. and Cantow, H. J. *Macromolecules* 1972, **5**, 546
- 24 Allegra, G., Calligaris, M., Randaccio, L. and Moraglio, G. *Macromolecules* 1973, **6**, 397
- 25 Flory, P. J. and Williams, A. D. *J. Am. Chem. Soc.* 1959, **91**, 3111
- 26 Mark, J. E. *J. Am. Chem. Soc.* 1966, **88**, 3708
- 27 Mark, J. E. *J. Polym. Sci. (B)* 1966, **4**, 825
- 28 Fukuroi, T., Fujiwara, Y., Fujiwara, S. and Fujii, K. *Anal. Chem.* 1968, **40**, 879
- 29 Moritani, T. and Fujiwara, Y. *J. Chem. Phys.* 1973, **59**, 1175
- 30 McMahon, P. B. and Tincher, W. C. *J. Mol. Spectrosc.* 1965, **15**, 180
- 31 Doskočilová, D., Štokr, J., Votavová, E., Schneider, B. and Lihn, D. *J. Polym. Sci. (C)* 1967, **16**, 2225
- 32 Toshiyasu, Y., Kimura, K. and Fujishiro, R. *Bull. Chem. Soc. Japan* 1970, **43**, 2676
- 33 Wolfram, E. and Nagy, M. *Kolloid Z. Z. Polym.* 1968, **227**, 86
- 34 Hoeve, C. A. J. and O'Brien, M. K. *J. Polym. Sci. (A-1)* 1963, **1**, 1947
- 35 Liu, K. J. *Polymer* 1969, **10**, 951
- 36 Ando, I. and Nishioka, A. *Makromol. Chem.* 1972, **152**, 7

Monoclinic macrolattice of quenched and cold-drawn sheets of isotactic polypropylene*

J. Loboda-Čačković, R. Hosemann and H. Čačković

Teilinstitut für Strukturforschung am Fritz-Haber-Institut der Max-Planck-Gesellschaft, Berlin, West Germany

and F. Ferrero and E. Ferracini

Consiglio Nazionale delle Ricerche, Bologna, Italy

(Received 3 July 1975; revised 18 December 1975)

The small angle scattering (SAXS) of quenched and cold drawn sheets of isotactic polypropylene (PP), has been analysed two-dimensionally. The appearance of equatorial SAXS reflections enabled a more detailed analysis of the size and arrangement of the microparacrystallites (*mPC*) in PP. These results confirm our earlier conclusions concerning polyethylene and polybutene, which were obtained without equatorial SAXS. Microparacrystals 50 Å wide and 40 Å long, build up a monoclinic macrolattice. The appearance of SAXS on the equator is explained by broadened lateral grain boundaries between the microparacrystallites of one layer in the direction of the sheet surface. This effect originates from plane stress fields generated in the necking zone of the stretched sheet.

INTRODUCTION

Most high polymers consist of paracrystalline microdomains. These microparacrystallites (*mPC*) aggregate to lamellae if the sample is hot stretched. They build up a more or less nematic-like super-lattice in the cold stretched state. These superlattices (tertiary structures) can be described by the paracrystalline theory, also. Bundles of microparacrystallites build up macroparacrystals (*MPC*)¹. They can be investigated quantitatively by a two-dimensional analysis of small angle scattering. A rapidly quenched, molten film of isotactic polypropylene (PP) consists of *mPC* with large distortions and is therefore, very poorly crystalline²⁻⁴. The different descriptions of this structure, for instance, 'smectic', 'non-crystalline', 'mesomorphic' or 'modification II', demonstrate that this structure is still quite unknown. It is the aim of this work to analyse the mutual arrangements of the *mPC* in the quenched and drawn PP-film, with the help of the paracrystalline theory; in other words, to analyse the structure of the *MPC* two-dimensionally, using the method that was developed for linear polyethylene and isotactic polybutene⁵⁻⁷. In this case the two-dimensional analysis of the SAXS is enhanced by the inclusion of SAXS equatorial reflections, corresponding to the macrolattice. These reflections were first observed by Hermans and Weidinger⁸.

EXPERIMENTAL

The samples were prepared by quenching 1 mm thick sheets of isotactic PP in an ice-water bath, which had previously been heated to the polymer melting point (176°C). The sheets were then cold drawn at 21°C to a stretching ratio of 9. The samples were investigated using a small angle X-ray camera, with pinhole collimation. The sample to film distance was 260.5 mm with the primary beam both paral-

lel and orthogonal to the PP sheet. The X-ray intensities were resolved with a Dupont 310 curve resolver.

TWO-DIMENSIONAL ANALYSIS OF THE SAXS MERIDIONAL REFLECTION

The SAXS pattern of the PP sample we used is shown in *Figure 1*. The meridional intensities observed with the specimen both perpendicular and parallel to the primary beam have the same shape. In contrast to Hermans and Weidinger⁸, we see only one SAXS reflection on the equator when the beam is orthogonal to the sheet. In the parallel position it is split into two relatively sharp spots. The analysis of the meridional reflection is performed in the manner described earlier⁵⁻⁷. The microphotometer curves are shown as full lines in *Figure 2* along the b_3 -axis which is parallel to the stretching direction, in *Figure 3* along the radial direction, b_r , parallel to the equator and through the maximum of the meridional reflection. The calculated points come from the theory of paracrystals⁹, applied to

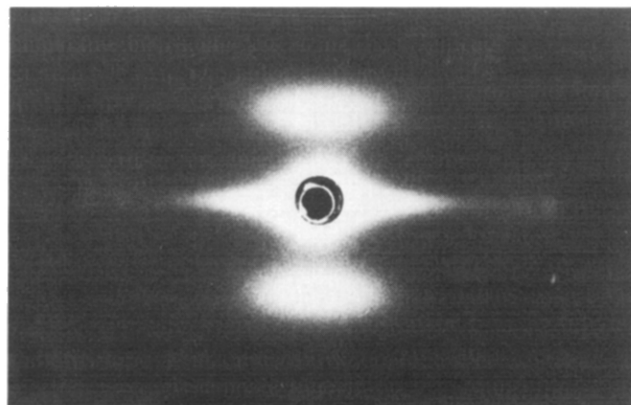


Figure 1 SAXS pattern of a foil of quenched and cold drawn isotactic PP. The drawing direction is vertical. X-ray beam parallel to platelet. On each side two discrete equatorial reflections can be seen

* Dedicated to Professor W. Menke, on the occasion of his 65th birthday.

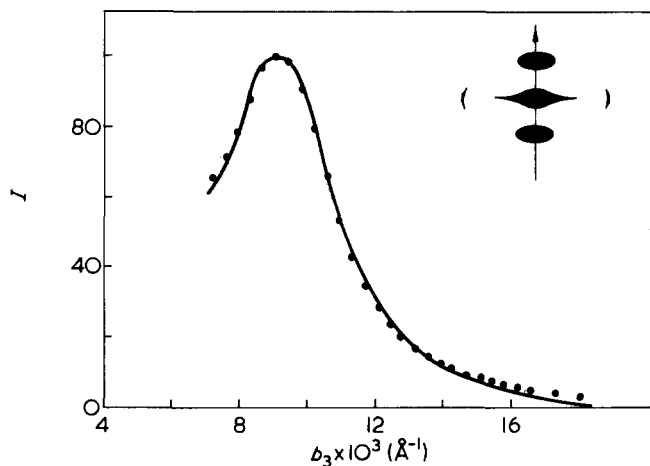


Figure 2 Intensity distribution $I(b_r, b_3)$ in meridional direction $b_3(b_r = 0)$. The microphotometer curve (—) is compared with calculated values (●) folded with the profile of the primary beam

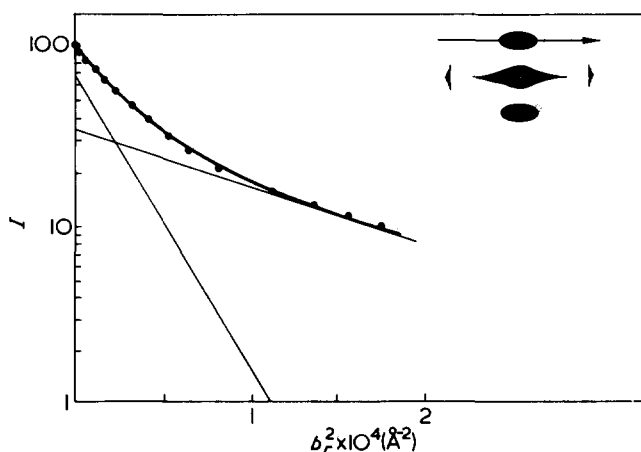


Figure 3 Intensity distribution $I(b_r, b_3)$ orthogonal to the meridian ($b_3 = \text{constant}$) through its maximum in a $\ln I - b_r^2$ plot. —, Experimental values; ●, calculated from theory and folded with the profile of the primary beam

the macrolattice, which is build up of microparacrystallites (*mPC*). The theoretical intensity function $I(b_r, b_3)$, then is folded with the shape of the primary beam. The agreement with the experimental values is very good. In Figure 2 $I(0, b_3)$, is plotted against b_3 ; in Figure 3 $\ln I(b_r, b_3 = \text{constant})$, is plotted against b_r^2 . This intensity can be separated into two Gaussian terms. The outer tail of the intensity defines the Gaussian term with the smaller slope. It gives the so called brick factor $f^2(b_r)$, which is the Fourier-transform of the shape of a *mPC* (brick) in the radial direction. It has a diameter of 50 Å. From a similar analysis of the continuous equatorial scattering (Figure 4), one obtains similar diameters (see later) for the bricks. This shows that the outer part in Figure 3 ($b_r \geq 9.5 \times 10^{-3} \text{ Å}^{-1}$), is really generated by the shape factor of the *mPC*, which build up the paracrystalline macrolattice. The inner part of Figure 3 (●), can be explained by the product of this shape factor, with the paracrystalline superlattice factor $Z^2 Z_3(b)$ ⁵⁻⁷. From this, the value g_{r3} of the macrolattice can be calculated (see Table 1). g_{r3} defines the relative statistical fluctuation of the lateral vector a_r of the macrolattice in the stretching direction 3 divided by the vector a_3 of the macrolattice in fibre direction. The *mPC* are so much shifted against each other in a direction that no lamellar structure exists. On the contrary, its relatively large value (40%) proves that the

macrolattice possesses a partially nematic-like character and bears little relation to a smectic phase.

The intensity along the meridian (Figure 2) shows the well known feature of cold stretched synthetic fibres; namely one diffuse maximum. From this one can calculate the relative statistical fluctuation g_{33} of a_3 in the direction 3 (see Table 1). In the outer part ($b_3 \geq 14 \times 10^{-3} \text{ Å}^{-1}$), $Z^2 Z_3$ again has reached the value 1. This part is therefore proportional to the brick factor $f^2(b_3)$ and gives a mean height H of 40 Å for the microparacrystallites in fibre direction (Table 1).

P is the so-called long period calculated from the position of the maximum of the meridional reflection. This value is again about 20% larger than the real superlattice cell a_3 in the fibre direction. Similar effects have been previously observed^{5,6}. Since $a_3 = 100 \text{ Å}$, the packing density in the meridional direction is $H/a_3 = 0.4$. Moreover one learns from the two-dimensional analysis that the cold drawn PP is similar to polyethylene and polybutene with rough fold-surfaces and no sharply defined boundaries between the paracrystalline and amorphous layer. They have an anomalously large value of 10 Å compared with H . This thickness of the transition region (given by the value of β) is 25% of the paracrystallite height H and so is relatively, much greater than in polyethylene (4%) and in polybutene (15%). The polydispersity g_H of the paracrystallite height H in chain direction, is $g_H = 0.25$. The shape of the meridional reflection parallel to the equator (Figure 3) is determined between the inner and outer part, discussed above, by the relative fluctuation g_{3r} of the vector a_3 , in radial direction also. It can be obtained, as mentioned in earlier papers^{6,7}, only with a relative uncertainty and is very large (40%). It demonstrates the lack of ultra-fibrillar character in the alignment of the microparacrystallites

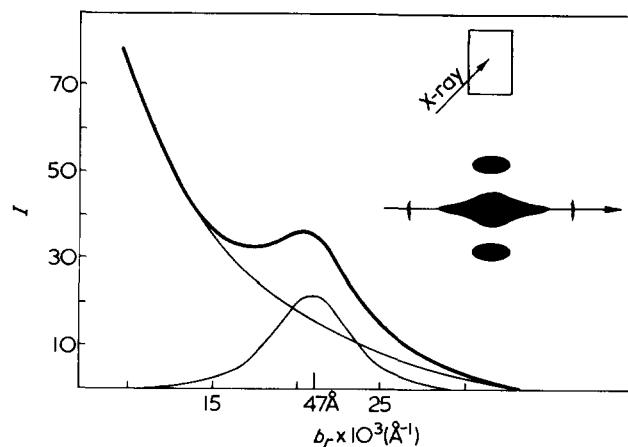


Figure 4 Intensity distribution $I(b_r, 0)$ along the equator, primary beam orthogonal to the PP sheet. The SAXS reflection (100) of the cell of the *MPC* is separated from the reflection (000) which gives rise to the so-called continuous SAXS

Table 1 Parameters of the paracrystalline superlattice (*MPC*) of cold drawn isotactic PP calculated from the meridian. P long period, a_3 and a_r cell edges of the *MPC* in fibre direction 3 and orthogonal direction r . H height and D diameter of the *mPC* in direction 3 and r , g_{ik} defined by equation (3). β , thickness of the transition region; g_H , polydispersity in chain direction

$P = 120 \text{ Å}$	$D = 50 \text{ Å}$	$g_H = 0.25$
$a_3 = 100 \text{ Å}$	$a_r = 50 \text{ Å}$	$g_{33} = 0.25$
$H = 40 \text{ Å}$		$g_{rr} = 0.23$
$\beta = 10 \text{ Å}$		$g_{r3} = 0.40$
		$g_{3r} \sim 0.40$

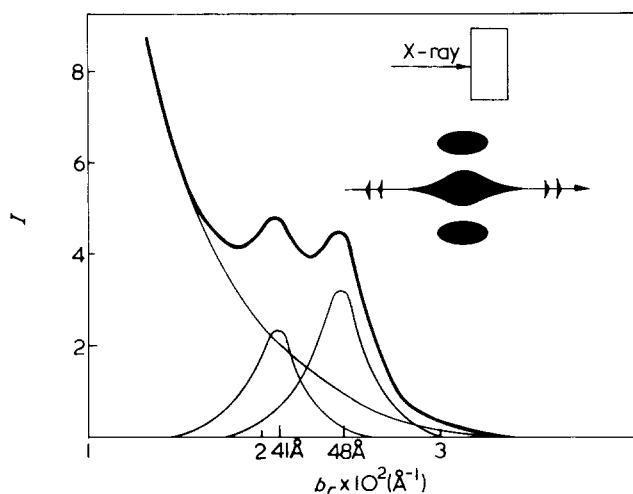


Figure 5 As for Figure 4, but the primary beam parallel to the sheet

along the stretching direction. Thus, there is no reason to speak of a smectic macrostructure, (as discussed above). It is to the advantage of the paracrystalline theory, that structures, which are neither smectic nor nematic, can be explained quantitatively.

ANALYSIS OF THE EQUATORIAL SAXS PATTERN

This is the first time that the two-dimensional SAXS analysis has been applied to a substance which shows SAXS-reflections on the equator. It is not surprising therefore that one can now obtain information directly about the macrolattice cell in the lateral direction. We will see moreover that the results obtained from the meridional reflection fit well to those obtained in this section.

The shape of the whole equatorial scattering is different when observed with the primary beam orthogonal (Figure 4) or parallel to the sheet (Figure 5). Orthogonal to the sheet, only one maximum at 47 Å exists. When parallel, there are two maxima at 48 and 41 Å. The analysis of the maxima was carried out by the Dupont curve resolver, taking Lorentzian squared profiles for the shape of the reflections. The $\ln I - b_r^2$ plot in Figure 6 shows the separation of the continuous particle scattering in two Gaussian curves. From the broader maximum one obtains a particle diameter, parallel to the film of 47 Å and from the same plot of the intensity in Figure 5, a diameter of 52 Å orthogonal to the sheet. These values agree well with the lateral paracrystallite size $D = 50$, obtained from the two-dimensional analysis of the meridional reflection, as mentioned previously. It proves directly that this outer tail of the meridional reflection, parallel to the equator, is given by the shape factor of the microparacrystals. The existence of the equatorial reflections gives evidence that the diameter of the microparacrystals are not only very similar (as in PE and PB), but that the paracrystallites are not fully closely packed within the layers and have a larger amount of amorphous material between them.

The integral width δb_{rr} of the equatorial SAXS reflections in the direction r is determined by the lateral sizes of the coherently scattering clusters of mPC and the g_{rr} value of their macrolattice. From a pure particle effect, one would obtain clusters of ~ 100 Å diameter, hence consisting of ~ 4 mPC . From the analysis of the meridional reflection we know⁶, that the particle effect is negligible in the SAXS of synthetic fibres and therefore δb_{rr} depends

also solely on the paracrystalline distortions. Further proof of this is given in a later section. Hence one obtains, as a first approximation for δb_{rr} and δb_{r3} :

$$\delta b_{rr} = \frac{1}{2d} (\pi g_{rr})^2; \delta b_{r3} = \frac{1}{a_3} (\pi g_{3r})^2 \quad (1)$$

from the theory⁶, d is the netplane distance (48 Å and 41 Å respectively). One obtains from the reflection from Figure 4, $g_{rr} = 0.24$ and from the two reflections from Figure 5, $g_{rr} = 0.19$ and 0.18. These three g_{rr} values are in good agreement with the value obtained from the meridional reflection $g_{rr} = 0.23$ (Table 1).

Another important advance in the two-dimensional SAXS analysis is the fact that one can now also measure the integral widths δb_{r3} of the SAXS equatorial reflections in the fibre direction. From this one obtains direct information concerning the smectic-like distortion g_{3r} of the macrolattice. It leads to a value $g_{3r} = 0.16$, which is much smaller than the g_{3r} value obtained from the middle section of Figure 3. The reason for this discrepancy is clearly explained by the bimodal statistics, $H_3(x)$, of the vector a_3 in r -direction*. In the calculation we use the fact that the SAXS is proportional⁵⁻⁷ to:

$$I \sim Z_3 Z_r^2 (h_r, h_3)$$

$$Z_3 = Re \frac{1 + F_3}{1 - F_3}; F_3(b) = \mathcal{F} H_3; \mathcal{F} = \int \exp(2\pi i b x) dx \quad (2)$$

$$|F_3| = \exp -2\pi^2 [g_{33}^2 h_3^2 + g_{3r}^2 h_r^2]; g_{ik}^2 = \overline{a_{ik}^2} / \overline{a_k^2} - 1 \quad (3)$$

In Figure 7 the inner part I of $|F_3(h_r)|$ is plotted for the large g_{3r} value, g_{3r} of Table 1, obtained from the meridional reflections. For the outer tail II of F_3 , a slope is used according to the value $g_{3r} = 0.16$ from the equatorial analysis. Furthermore two Gaussian components III and IV are plotted, whose sum gives the correct slope for the inner and outer part of $|F_3|$. Their slopes and weights, define a bimodal H_3 statistic in r direction, with values g'_{3r} and g''_{3r} given in Table 2, and occurring with the probability of 20 resp. 80%.

* In our previous papers⁵⁻⁷, similar bimodal statistics were found for the statistics $H_r(x)$ of the lateral vector a_r in fibre direction 3.

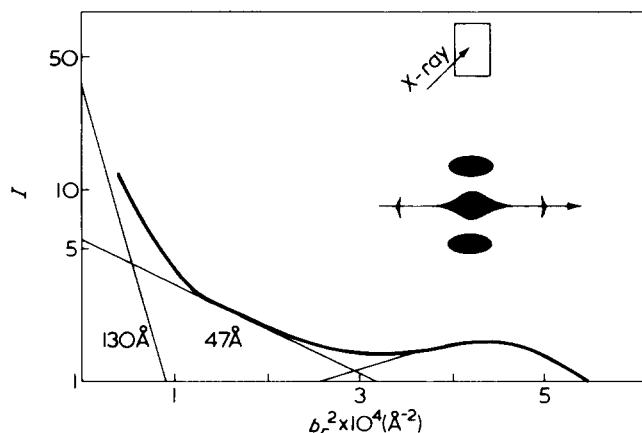


Figure 6 $\ln I - b_r^2$ plot of the intensity from Figure 4

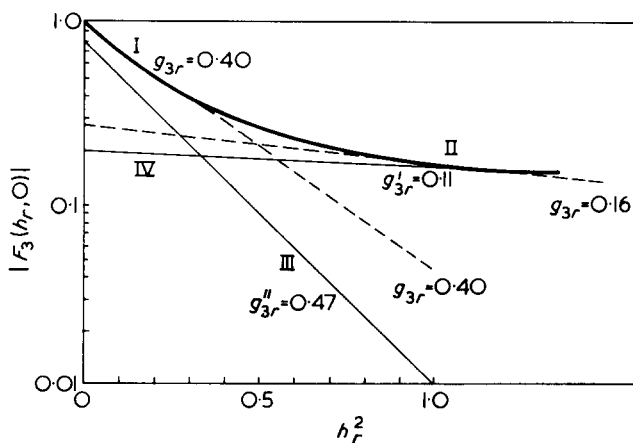


Figure 7 Modulus of the statistic factor $F_3(b)$ of the axial vector a_3 composed of two Gaussian terms III and IV. I and II, experimentally observed slopes

Table 2 Parameters of the paracrystalline macrolattice (MPC) of cold drawn isotactic PP calculated from the equator (see Figure 8)

$a_1 = 50,5 \text{ \AA}$	$d_a = 48 \text{ \AA}$	to the sheet
$a_2 = 59 \text{ \AA}$	$d_b = 41 \text{ \AA}$	
$\gamma = 54,2^\circ$	$D = \begin{cases} 47 \text{ \AA} & \text{parallel} \\ 52 \text{ \AA} & \text{orthogonal} \end{cases}$	to the sheet
	$g_{rr} = \begin{cases} 0.24 & \text{parallel} \\ 0.19 & \text{orthogonal} \end{cases}$	to the sheet
	$g'_{3r} = 0.11$ (20%)	
	$g''_{3r} = 0.47$ (80%)	

Now let us discuss the equatorial macrostructure. Since only the reflection at 48 \AA appears with the primary beam orthogonal to the sheet, a monoclinic deformed pseudo-hexagonal lattice with a certain degree of disorientation is indicated. The families of netplanes parallel to the surface are compressed somewhat orthogonally to these netplanes. Figure 8a gives the respective reciprocal lattice and Figure 8b a schematic drawing of the macrostructure. Both kinds of reflections of 48 \AA and 41 \AA appear in the pattern with the beam parallel to the sheet. This can be explained by a texture of MPC. The macrolattices of Figure 8b have only a finite size and show a variety of orientation, which give rise to the 'sickle' shaped reflection of Figure 8a. It corresponds to a change of the orientation of the MPC by rotation about an axis parallel to the stretching direction, of at least 60° . Thus one obtains parameters of the idealized macrolattice cell in the equatorial plane which is monoclinic (Figure 8b). In reality the single MPC are polydisperse and have a statistical fluctuation in their diameter, of the order of the value g_{rr} ($\approx 24\%$). In Figure 8b is plotted for convenience one MPC which is not tilted. All MPC are somewhat elongated, orthogonal to the sheet surface, according to results obtained from the continuous SAXS along the equator (Table 2).

The model in Figure 8b is also idealized from the point of view of order. In the real structure, the netplanes are wavy and the diameters of the MPC vary slightly from one to the other, thus generating paracrystalline distortions in the sense discussed before.

DISCUSSION

First, we calculate the packing density α of the paracrystallites in the macrolattice. From the two-dimensional analysis we obtained the meridional packing density (Table 1):

$$\alpha_3 = \frac{H}{a_3} = 0.40 \quad (4)$$

The packing density α_r in the equatorial plane can be calculated from the model from Figure 8b as the ratio of the ultrafibril cross-section $\pi(D/2)^2$ to the lattice cell area V_c . From the measured netplane distances d_a and d_b one obtains:

$$V_c = \frac{d_a d_b}{\left[1 - \left(\frac{d_a}{2d_b}\right)^2\right]^{1/2}} \quad (5)$$

The packing density then is given by:

$$\alpha = \alpha_3 \times \alpha_r = \frac{H}{a_3} \pi \frac{D^2}{2} \frac{\left[1 - \left(\frac{d_a}{2d_b}\right)^2\right]^{1/2}}{d_a d_b} \quad (6)$$

$$\alpha = 0.40 \times 0.81 = 0.32$$

Thus one can calculate the density of the amorphous phase. The density ρ_c of the 'crystalline phase', can be determined from the size of the molecular lattice cell ($\rho_c = 0.921 \text{ g/cm}^3$)¹⁰. The macroscopic density is $\bar{\rho} = 0.891 \text{ g/cm}^3$. Using the above calculated value of α for a two-phase model, one obtains a density for the amorphous parts: $\rho_a = 0.877 \text{ g/cm}^3$. This is larger than the density of atactic PP which is $\rho_a = 0.85 \text{ g/cm}^3$.

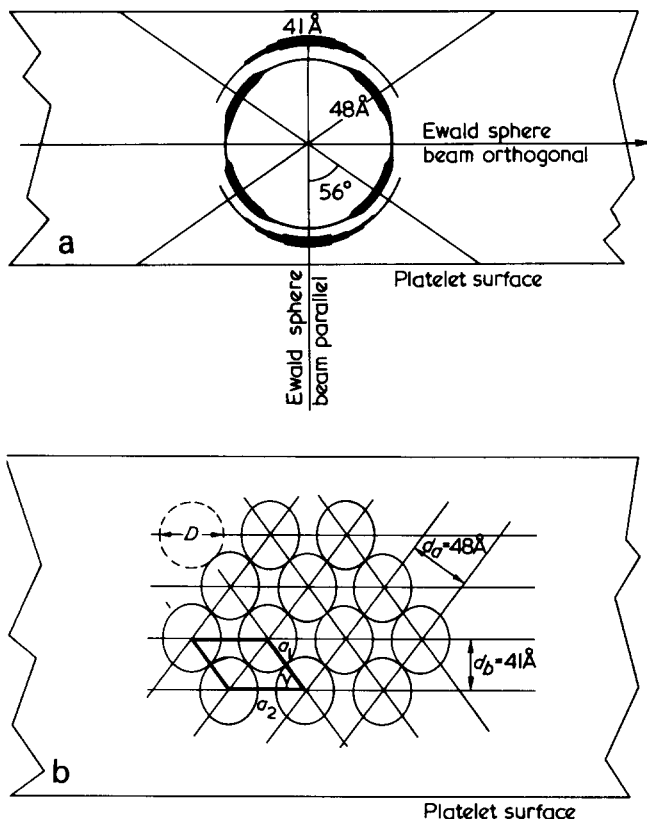


Figure 8 (a) Monoclinic reciprocal lattice cell in the equatorial plane with an angular fluctuation of at least 56° ; (b) idealized model of a monoclinic MPC of paracrystallites in a cross-section orthogonal to draw direction

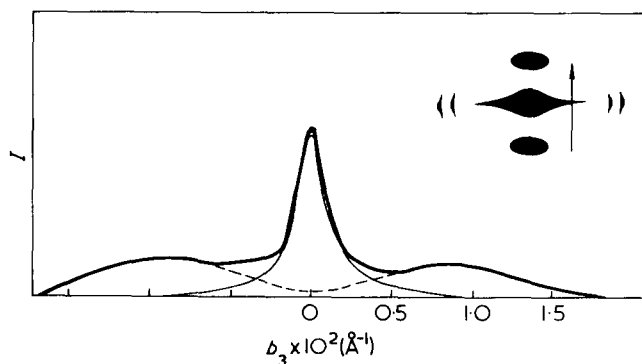


Figure 9 A microphotometer trace orthogonal through the equator at $b_r = 1.25 \times 10^{-2} \text{ \AA}^{-1}$. The outer maxima (---) are generated by crossing the meridional reflection

The dimension of the *MPC* in the chain direction, can be calculated from the integral width of the continuous equatorial scattering in the fibre direction analysed at various b_r values parallel to the meridian up to $1.5 \times 10^{-2} \text{ \AA}^{-1}$ (Figure 9). We obtain $M \sim 420 \text{ \AA}$ after correction for the primary beam. This indicates that on average, four *mPC* scatter coherently in the fibre direction. This agrees very well with the bimodal character of the statistics of a_3 in lateral directions. According to Table 2 the probability is only 20%, that one finds the neighbouring paracrystal with $g'_{3r} = 0.11$, in the fibre direction. It therefore makes no sense to consider ultrafibrils in this stretched material.

Another interesting fact can be deduced for the superstructure in these polymers. For the lattices of *mPC* one finds a relation between g and the number N_{\max} of maximum possible netplanes¹¹:

$$N_{\max} = (\alpha^*/g)^2 \quad (7)$$

where α^* is in the order of 0.07–0.23, for all samples investigated, up to now. This relation was explained by the fact that in a *mPC*, the distance fluctuation between the first and N th netplanes is given by $\Delta_N = (N)^{1/2} \Delta_1$, where Δ_1 is the distance fluctuation between adjacent netplanes with the mean distance d and Δ_1/d , hence the g value. If Δ_N reaches a value α^*d , the lateral binding forces within one netplane are so distorted that this netplane breaks.

In the case of *MPC*, α^* can be much larger because the nature of the 'crystalline' layers of assemblies of *mPC* is quite different from the netplanes within one *mPC*. From $g_{33} = 0.25$ (Table 1) and $N_{\max} = M/a_3 = 4.2$, one obtains:

$$\alpha^* = 0.25 (4.2)^{1/2} = 0.51 \quad (8)$$

This agrees well with electron microscopic pictures of PP, where bundles of lamellae and *mPC* can be seen directly. Here, they are much larger than they can be with $\alpha^* = 0.2$. Thus one can deduce an interesting result from the interpretation of line profiles: According to equation (1), the line width of the first order reflection is proportional to $(\pi g)^2$. Introducing equation (7), it becomes proportional to $1/N(\pi \alpha^*)^2$, whilst the particle size effect is proportional to $1/N$. Both effects add to each other quadratically,

to a first approximation. For molecular lattices $(\pi \alpha^*)^4 \ll 1$, for macrolattices $(\pi \alpha^*)^4 > 1$. For this one finds that the width of the first order SAXS reflection according to equation (1) is largely determined by the paracrystalline distortion of the *MPC* and the first order WAXS reflection has a width largely determined by the particle size of the *mPC*.

Another point of interest is that the equatorial SAXS reflection appears only if a sheet is stretched. A stretched rod shows no such reflections. In both cases the material is deformed according to an affined transformation¹². In the necking zone, the three-dimensional network is deformed in such a way that micro-necks are generated¹³. This can be explained by the schematic drawing in Figure 10. Each microdomain consists of a series of *mPC*, which are plastically deformed, in the necking zone. This necking process is isotropic for a rod, but quite anisotropic for a sheet, because its thickness is diminished by a much smaller amount than the width of the sheet. It is of no surprise, that parallel to the sheets, where the *mPC* have to change their lateral positions greatly during affined transformation, micro-necks may remain between them as shown in Figure 8b.†

Another point of interest is that the cold stretched sheet of PP still remains transparent but shows a remarkable equatorial SAXS. In all other cases of stretched polymers either they can be transparent and have no equatorial SAXS or they can become opaque and exhibit an equatorial SAXS. This anomalous behaviour can be explained by electron density inhomogenities, which are small comparable to the wave length of light. A similar phenomenon was observed for PE prepared under controlled shear conditions from the melt¹⁴.

† This kind of deformation is called plane stress.

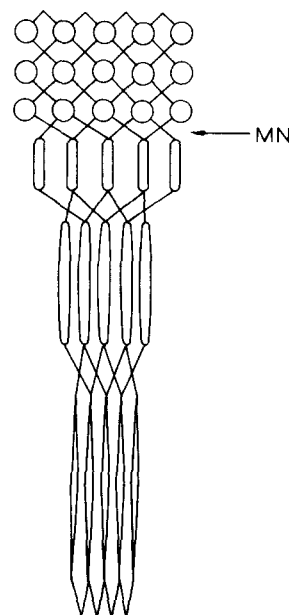


Figure 10 Necking process during stretching to the natural draw ratio. Before stretching the microdomains are schematically drawn by circles (above) with tie-molecules and transform affined into elongated domains (below). The three-dimensional network of tie-molecules is deformed within the neck which gives rise to micro-necks (MN)

ACKNOWLEDGEMENTS

The Deutsche Forschungsgemeinschaft kindly supported this work by a grant. We are grateful to Dr P. Bond for his careful review of the manuscript and to Miss Chr. Kunze for technical assistance.

REFERENCES

- 1 Yeh, G. S. Y., Hosemann, R., Loboda-Čačković, J. and Čačković, H. *Polymer* 1976, 17, 309
- 2 Natta, G., Corradini, P. and Cesari, M. *Atti. Acad. Naz. Lincei. Cl. Sci. Fis. Mat. Nat. Rend.* 1959, 27, 14
- 3 Natta, G. *Macromol. Chem.* 1960, 35, 94
- 4 Miller, R. L. *Polymer* 1960, 1, 135
- 5 Loboda-Čačković, J., Hosemann, R. and Čačković, H. *Kolloid-Z. Z. Polym.* 1971, 247, 824
- 6 Hosemann, R., Loboda-Čačković, J. and Čačković, H. *J. Polym. Sci.* 1973, 42, 563
- 7 Ferracini, E., Ferrero, A., Loboda-Čačković, J., Hosemann, R. and Čačković, H. *J. Macromol. Sci. (B)* 1974, 10, 97
- 8 Weidinger, A. and Hermans, P. H. *Makromol. Chem.* 1963, 62, 139
- 9 Hosemann, R. and Bagchi, S. N. 'Direct Analysis of Diffraction by Matter', North-Holland, Amsterdam, 1962
- 10 Loboda-Čačković, J. and Čačković, H. in press
- 11 Hosemann, R. *CRC Crit. Rev. Macromol. Sci.* 1972, 1, 351
- 12 Hosemann, R., Loboda-Čačković, J. and Čačković, H. *Ber. Bunsenges, Phys. Chem.* 1973, 77, 1044
- 13 Peterlin, A. 'Advance in Polymer Science and Engineering', (Eds. K. K. Pae, D. R. Morrow and Yu Chen), Plenum, New York, 1972
- 14 Krueger, D. L. and Yeh, G. S. Y. *J. Appl. Phys.* 1972, 43, 4339

Annealing effects of polymers and their underlying molecular mechanisms*

G. S. Y. Yeh

University of Michigan, Ann Arbor, Michigan 98104, USA

R. Hosemann, J. Loboda-Čačković and H. Čačković

Fritz-Haber-Institut der Max-Planck-Gesellschaft, Berlin, West Germany

(Received 3 July 1975)

This paper indicates that changes in chain mobility, heat capacity, WAXS crystallinity, SAXS long period, SAXS peak intensity, specific volume and morphology as a function of increasing temperature, occur in three fairly distinct annealing ranges (I, II and III) that are more or less the same for all crystallized polymers with a lamellar morphology. It is shown that none of the proposed molecular models to date, including the well-known fold surface premelting model, can satisfactorily account for all the experimental data. However, a new molecular interpretation, based primarily on electron microscopy and SAXS studies of changes such as lateral 'melting' from edges of microparacrystallites (*mPC*) within the lamellae seen at the annealing temperatures can account for the data. With our new molecular interpretation, the effect of temperature increase is established to result in a slight breakup of the laterally aligned *mPC* within the lamellae at low annealing temperatures in range I, and selective lateral 'melting' of the exposed *mPC* and recrystallization at higher annealing temperatures in ranges II and III, with the recrystallization being very limited in range III. Annealing effects seen in cold- or hot-drawn polymers with a fibrillar morphology can also be readily accounted for by this very general molecular mechanism occurring in the same annealing temperature ranges.

INTRODUCTION

The effects of annealing a semi-crystalline polymer with a lamellar morphology to near its melting point are fairly well known^{1-3,6}. Substantial changes can be detected in molecular mobility, morphology, physical and mechanical properties. These changes are not only important from a user's point of view, but also in determining optimum conditions under which solid state processing techniques can be applied to fabrication of polymer products. However, in spite of the numerous extensive studies on this very important and practical subject of annealing in the past 10-20 years, we are still not very clear about the underlying molecular mechanisms responsible for the various observed annealing effects. There have been several proposed molecular mechanisms, all apparently very different from one another², none of which is seen to be more satisfying in the explanation of annealing data than the other although all of them appear to have some degree of experimental justification.

One of the major difficulties in coming up with a better understanding of the annealing phenomena, is the dependency of observed changes on numerous factors such as annealing temperature, time and rate, prior thermal history and the physical state (drawn vs. undrawn or single crystal vs. bulk) of the sample, as well as its chemical structure and composition (molecular weight, degree of branching, etc.). These factors often contribute to a shifting and/or narrowing of the temperature ranges in which the changes may occur, to the degree of reversibility and to the magnitude of the observed changes which may lead to the various proposed molecular mechanisms. Another factor, which is less important but contributes to some degree of confusion,

lies in the choice of words in describing some of the changes occurring well below the melting point. For example, it was cautioned by Hoffman⁴ several years ago, that the word 'premelting' should be used with care in describing certain annealing phenomena allegedly associated with melting in polymers.

It is the purpose of this paper to show and discuss briefly, that most of the annealing changes occur in three more or less distinct temperature ranges, to examine more critically the three most popular proposed molecular mechanisms, to introduce and discuss the validity of some other annealing mechanisms based on direct morphological changes observed at the annealing temperature, and to see how they can be applied to the understanding of annealing phenomena which occur in cold or hot drawn systems.

Whenever possible, we shall discuss primarily the annealing changes measured on as-crystallized, well-equilibrated lamellar systems kept at the annealing temperatures. Discussions on measurements made on samples after quenching will be limited and pointed out in order to minimize sources of confusion. For the sake of clarity and brevity we shall restrict our present discussions to annealing phenomena which occur upon temperature increase. The many interesting effects which occur upon temperature decrease after annealing (at higher temperatures) will be discussed only for clarifying points raised.

SEPARATION OF ANNEALING CHANGES INTO THREE ANNEALING TEMPERATURE RANGES

As the annealing changes are very much dependent on a number of factors as pointed out in the introduction, it is difficult to make any precise separations of the changes

* Dedicated to Professor G. Manecke on the occasion of his 60th birthday

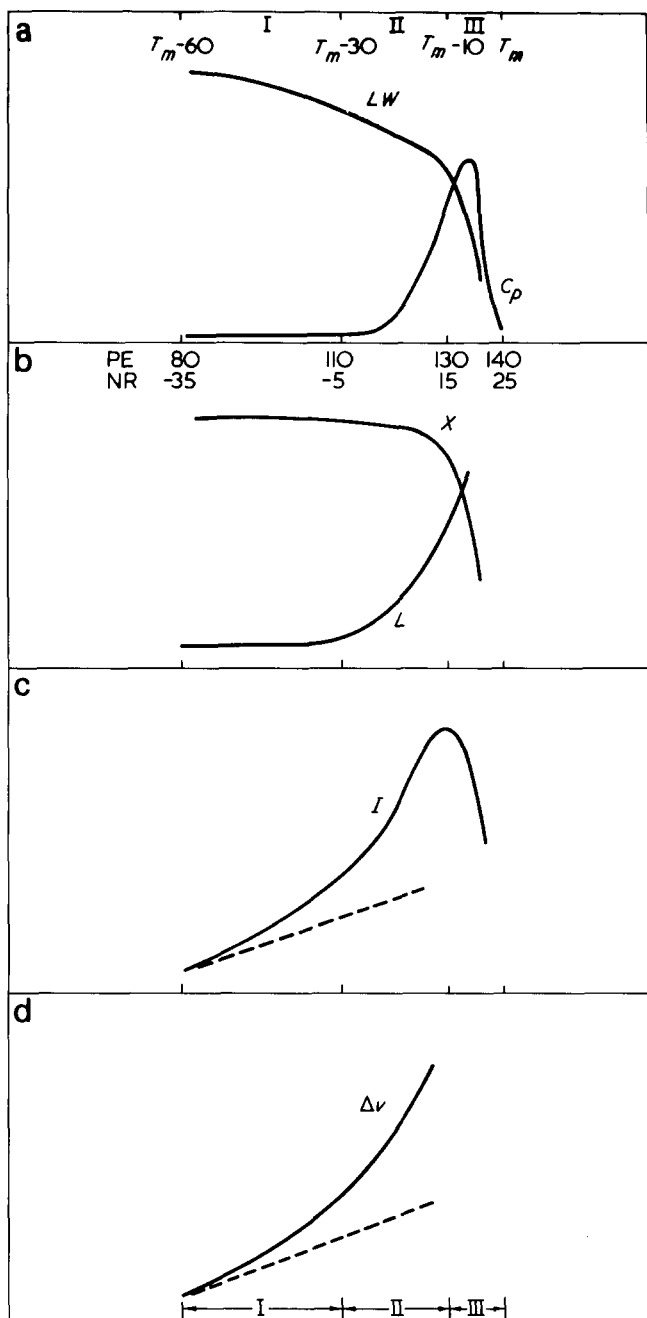


Figure 1 (a)–(d) are schematic drawings showing some well-known annealing effects in crystallized polymers upon heating to temperature ranges I, II and III. (a) n.m.r. line-width, LW (inversely proportional to molecular mobility) of the crystalline polymer component and specific heat, C_p ; (b) WAXS crystallinity, X , and SAXS long period, L ; (c) SAXS intensity, I ; (d) specific volume difference, ΔV

with annealing temperature. However, after examining numerous annealing data, we have come to the conclusion that there are certain distinct characteristics e.g. the magnitude of changes upon temperature increases or the degree of reversibility of changes upon temperature decrease, which allow us to assign the changes according to three annealing temperature ranges I, II and III.

Figures 1a–1d represent schematically the generally reported changes in chain mobility from n.m.r. linewidth (LW), specific heat (C_p), WAXS crystallinity (X), SAXS long period (L), SAXS intensity (I), and difference in specific volume (ΔV), and the three approximate temperature ranges in which the changes are observed to vary for most polymers when heated to near their melting points. The

lines (dotted) in Figures 1c and 1d are inserted to show the expected changes in SAXS intensity and specific volume, assuming no changes in the relative respective amounts of the two crystalline and non-crystalline components of the polymers, (see references 2 and 3).

The three approximate temperature ranges are: (I), from $\sim(T_m - 60)$ to $\sim(T_m - 30)$ (or to a temperature near the original crystallization temperature or to the first annealing temperature of a crystallized polymer); (II) from $\sim(T_m - 30)$ to $\sim(T_m - 10)$; and (III) from $\sim(T_m - 10)$ to $\sim T_m$ (the melting point). They are generally believed to be more or less the dividing temperature ranges in which the above mentioned annealing effects are characteristically seen to be changing in nearly all well-equilibrated, crystallized polymers with a lamellar morphology. For example, the range will be from $\sim 80^\circ$ to 110°C , $\sim 110^\circ$ to 130°C and $\sim 130^\circ$ to 140°C for polyethylene crystallized by slow cooling, and from $\sim -35^\circ$ to -5°C , $\sim -5^\circ$ to 15°C and $\sim 15^\circ$ to 25°C for natural rubber also when crystallized by slow cooling. The melting points are assumed to be 140°C and 25°C respectively for polyethylene and natural rubber crystallized under isotropic conditions.

In the annealing temperature range I as shown in Figures 1a–1d, practically no changes are observed in C_p , X or L while some small increases are already noticeable in degree of chain mobility as reflected in the decrease in LW from n.m.r. and in ΔV ; the specific volume increase¹ indicating an apparent decrease in volume crystallinity. There is also a noticeable increase in SAXS intensity over and above the expected increase due to the thermal expansions of the respective crystalline and amorphous components¹.

All the annealing effects including the morphological changes (to be discussed later) detected in range I, are generally found to be small and generally reversible with temperature, i.e. upon temperature decrease to the original starting temperature the changes disappear. This is quite different from the annealing phenomena seen in annealing temperature ranges II and III, where the degree of reversibility appears to be generally limited.

In annealing range II the higher temperatures generally bring about greater increases in the changes (LW , I and V_{sp}) started in range I. In addition, other very noticeable changes begin to show up in this temperature range, i.e. C_p and L (see Figures 1a and 1b). The crystallinity X as determined from WAXS, however, remains practically unaffected in this temperature range, after long annealing times. The effect of annealing time in this temperature range on X was first reported by Fischer and Schmidt on bulk and single crystals of polyethylene⁵. Their data showing a loss of WAXS peak intensities at early stages of annealing, indicated some type of melting, followed by some type of recrystallization, which resulted in the recovery of the WAXS peak intensities.

Similar interpretation of annealing time effects, noted above for WAXS peak intensity changes, has also often been made for density changes detected in bulk and single crystal samples of polyethylene after quenching to room temperature from annealing temperatures in range II. However, the interpretation of premelting and surface melting and recrystallization based on such density data alone, is less convincing than the X-ray results.

In annealing range III whatever partial (but real) melting process has started in range II, continues into the higher annealing temperature range. However, the 'recrystallization process', cannot be extended to too high a temperature because of the limited supercoolings (and therefore

smaller nucleation rate) at higher temperatures. Consequently, one can see in this temperature range, that there is a substantial change in molecular mobility as judged by the decrease seen in LW , increases in ΔV and L (due to recrystallization at smaller supercoolings), and decreases in WAXS crystallinity as well as SAXS intensity.

PRESENT STATUS CONCERNING UNDERLYING MOLECULAR MECHANISMS

The three most often cited molecular mechanisms to account for the annealing effects, in particular the lamellar thickness increase, are: A, refolding by 'solid state' diffusion; B, 'selective melting of thinner lamellae and recrystallization to thicker lamellae' and C, the fold surface 'premelting'. Their merits have been reviewed extensively by Fischer² and therefore will not be belaboured further here. Nevertheless, it is felt that a brief discussion of these three molecular models, in light of all the annealing effects cited above, is appropriate for any new concepts of annealing mechanisms to be introduced later.

'Solid state' diffusion

Refolding by a 'solid state' snaking type long chain diffusion process along the c -axis, was based mainly on the observation that the c -axis in thickened portions of polyethylene single crystals after annealing to 125°C, remains perpendicular to the lamellar surface when examined at room temperature⁶. As was originally proposed, this seemed a very probable process especially in the higher annealing temperature ranges, where molecular mobility may be sufficiently high and lattice sufficiently expanded, for such gliding movements. However, in light of the annealing time effects discussed earlier concerning WAXS intensity changes in annealing temperature range II for polyethylene single crystals or bulk polyethylene and the detectable changes in annealed morphology (to be discussed later), one questions the general validity and applicability, if one defines solid state diffusion as diffusion of atoms or molecular chain segments in a lattice which retains its 3-dimensional crystalline property. Some limited refolding by solid state diffusion, of course, can and probably does occur, e.g. in non-equilibrated systems, such as cold or hot drawn systems containing numerous highly stressed defective crystals. However, in such systems we may be dealing with numerous 'crystalline' regions, that can hardly be considered as solid to begin with and annealing of such systems even at temperatures below those in ranges II and III may lead to limited growth of crystallites by a pseudo-recrystallization process.

Selective melting of thinner lamellae

Since the lamellae in crystallized polymers generally consist of a distribution of thicknesses, the proposal that thinner lamellae melt first (and therefore selectively), within a stack of lamellae appears to be a reasonable one and is still considered by many, including Hoffman and Kilian⁴, together with some degree of recrystallization, to be the most reasonable explanation for the observed long period increase. Fischer's objection to this model centres entirely around the disagreement between experimental SAXS peak intensity measurements (see *Figure 1c*) and theoretically predicted values which should show a decrease rather than the observed increase, if melting of lamellae occurs selectively in a stack of lamellae that can scatter X-ray coherently. Al-

though this is a reasonable objection which will be amplified further later there is some indication that a modified form of selective melting, also to be discussed in later, may indeed be occurring in annealing temperature range III.

Fold surface 'premelting'

This model indicates that starting at some temperature, the fold surfaces 'premelting' gradually inwards towards the crystalline core along the chain axis, until the whole lamellar crystal is melted at the T_m . This premelting model appears to be able to account for nearly all the experimental evidences of annealing effects, in particular the evidence concerning the SAXS integrated and peak intensity increase with annealing temperatures as has been found in a number of polymeric systems⁵. However, even if it is a correct model, as was pointed out earlier by Luch and Yeh⁹, it can be applied to lamellar systems with only very little increase in lamellar thickness upon annealing, since the melting of fold surface does not directly lead to large increases in amorphous thicknesses, as have been observed in a number of cases in annealing temperature ranges II and III. Furthermore, for the model to apply, the polymers must have initial crystallinities of greater than 50%; otherwise, a predicted decrease in SAXS peak or integrated intensity will result. However, Luch and Yeh⁷ studied natural rubber which has a maximum crystallinity of well below 50% and showed the same kind of SAXS peak intensity changes (*Figure 1c*) with an initial increase followed by a decrease at annealing temperatures close to T_m .

It should be mentioned that the difficulty with the surface premelting model to explain large changes in lamellar thicknesses (in regions II and III), was not encountered when the model was originally conceived and applied⁸ to explain the SAXS intensity changes for polyethylene single crystals in annealing temperature range I where there is hardly any change in long period (*Figure 1b*). Therefore, it will be of interest in this respect to re-examine the experimental evidence that has led to the surface premelting model. The evidence is in the SAXS intensity change (*Figure 1c*). Nukushina, Itoh and Fischer⁸ using PE single crystal mats and Schultz, Robinson and Pound⁹ using bulk PE have noted reversible peak intensity changes up to four-fold with hardly any changes in long period L . Since this intensity increase was found to be much greater than could be accounted for by density changes owing to thermal coefficients of expansion of the two respective phases, (see lines (dotted) in *Figures 1c* and *1d*) it was, albeit incorrectly, suggested that the increase must be due to increase in the amorphous thickness (or in the decrease of volume fraction of crystals) and, therefore, melting from the lamellar fold surface inward at the expense of the crystalline core.

MOLECULAR MECHANISM(S) BASED ON MORPHOLOGICAL OBSERVATIONS

The above discussions, although brief, clearly indicate a degree of inadequacy existing in all the three proposed models, including surface 'premelting', to account for the various phenomena that appeared during annealing.

In addition to the shortcomings mentioned earlier, the premelting and the surface melting models, seldom discuss specifically whether and how a recrystallization process follows the 'melting' process in either range II or III. If a recrystallization process takes place, i.e. one to increase the crystal thickness of the remaining, unmelted lamellae

(or the unmelted crystalline cores in the case of Fischer's fold surface premelting model), one wonders how this crystal thickness increase comes about without greatly disturbing the crystalline lattice of the remaining, unmelted lamellae in a stack of well-packed lamellae. Any substantial disturbance will lead to melting of the whole stack of lamellae. Otherwise, one has to suggest some kind of 'solid state' diffusion process by which the molecules from the melt regions can participate in the thickening process of the previously unmelted crystalline core of the lamellae.

It seems that on the one hand we need to propose some sort of melting, albeit of a limited extent, to explain most of the observed phenomena; while on the other hand we seem to need also, some sort of 'solid state' diffusion process to explain how the crystal thickness increase takes place. As will be shown below, these problems quickly disappear when one finds that the suggested 'premelting' in annealing temperature range I, and the suggested partial melting/recrystallization process and the 'solid state' diffusion process in annealing temperature ranges II and III, may all appear to have taken place. Even though the underlying molecular mechanism(s) which gives rise to the annealing changes seen in ranges I, II and III, may be quite different from the proposed models.

The underlying molecular mechanism(s) to be discussed below is primarily based on direct observations of morphological changes in polymers annealed at the temperature. The starting polymer has the well-known lamellar texture, which is typical of well-equilibrated, well-crystallized systems, in either the oriented or unoriented state. Another point to be made here is that the basic crystalline units in crystallized polymers are not the lamellae, as had been gradually assumed over the years, but rather the smaller micro-paracrystallites (*mPC*) or nodules within the lamellae. This has been established independently by Hosemann¹⁰ using X-ray scattering techniques and Yeh using direct morphological observations¹¹. It is particularly useful to keep this fact in mind when one tries to evaluate the generality of the observations and the molecular mechanisms discussed below.

Direct morphological studies of unoriented polymers or single crystals after annealing in temperature range I and examined at room temperature, do not generally reveal any detectable changes. This can be due to a number of reasons, e.g. the problem with detecting changes from unoriented specimens or single crystals when examined from vertical positions perpendicular to the lamellar surface, or with recovered morphological changes when examined at room temperature, or with the degree of resolution due to proper examining techniques and specimen preparations, etc.

In our earlier studies^{12,13} of strain-crystallized natural rubber (*cis*-polyisoprene) and gutta percha (*trans*-polyisoprene), we were able to detect definite changes in morphology at the annealing temperature in range I by means of OsO₄ staining technique and examining the edges of stacks of well-oriented lamellae in a direction *perpendicular* to the *c*-axis. An example of the changes is reproduced here in *Figure 2b* for natural rubber when annealed to -15°C (in the annealing temperature range I) and OsO₄ stained at the annealing temperature. It shows a slight, but noticeable 'breakup' of the well-formed lamellae originally present in the sample (*Figure 2a*) into blocks of about 100 Å lateral size as deduced by the attained 'amorphous' boundaries in between the *mPC*. *Figures 3b* and *3c* show schematic representations of the *mPC* originally present within the lamellae and after their 'breakup'. We suggest

that the 'amorphous' boundaries arise from an increase in localized intrachain defects at the *mPC* grain boundaries upon reaching annealing temperature in range I. They could very well contribute to the α_1 type of molecular motions as detected and assigned by Takayanagi to be occurring within the mosaic block grain boundaries of polyethylene single crystals¹⁴ in the same annealing temperature range I. Since intrachain defects involve a contraction of chain segments at the mosaic crystal grain boundaries, the contraction will create vacancies at the lamellar fold surface. They contribute to a greater lowering of the density in the interfacial region, inbetween the crystalline lamellae than that of the crystalline lamellar cores, thereby leading to a larger difference in density ($\rho_c - \rho_a$ or $\Delta\rho$) between the two phases. Therefore over and above the values based on changes due only to thermal coefficients of expansion there exists an extra ΔV increase (*Figure 1d*). The SAXS intensity increase in this temperature range I (*Figure 1c*) is then the direct result of vacancies created at the fold surface boundary since intensity is proportional to $(\Delta\rho)^2$, somewhat similar to the origin of substantial SAXS intensity increase observed for *n*-paraffins upon annealing¹⁵.

This type of morphological change was observed to be reversible with temperature, i.e. upon cooling the lamellae were found to be coherent again, as long as the annealing temperature stays inside range I, which also explains why the changes in SAXS intensity and specific volume are also found to be reversible with temperature. Therefore, it is not necessary to have a surface 'premelting' type of molecular mechanism to explain either the SAXS intensity increase or its reversibility with temperature. Furthermore, one would not expect this kind of intrachain defect to cause any significant change in molecular mobility, specific heat, crystallinity or long period, as, indeed, is generally found to be the case (*Figures 1a* and *1b*).

Upon entering annealing temperature range II, an entirely different morphology arises. First, there is clear indication from direct observations^{12,13} that whole or parts of *mPC* or nodular crystallites melt *within* the lamellae. This is again deduced from careful examinations of stacks of well-oriented lamellae of natural rubber and *trans*-polyisoprene annealed and OsO₄ stained at the annealing temperatures. When held at the annealing temperatures for a sufficient length of time, the true melting process within the lamellae is followed by a recrystallization process, resulting in more stable, thicker (along the *c*-axis) *mPC* which then repack and realign with one another to form apparently smooth and filled* lamellae, at long annealing times. The lamellae now have thicker crystalline as well as thicker amorphous regions, as for example, shown in *Figure 4* for *trans*-polyisoprene. The relatively constant WAXS crystallinity (*Figure 1b*) can now be explained by nearly the same percentage increase of the crystal (l_c) and the amorphous (l_a) thicknesses. In an ideal two phase lamellar structure, the WAXS crystallinity should be the same as the linear crystallinity $l_c/(l_a + l_c)$ directly measured from the electron micrographs, if the lamellae are present throughout the volume as recently demonstrated by Yeh¹⁶. The true melting process (which continues in range III) also causes substantial molecular motion and increase in specific heat (*Figure 1a*), while the increase in SAXS long period is due

* Polyethylene single crystals when annealed to this temperature range, often showed holes within single lamellae after annealing and cooling to room temperature⁶. This is due to unavailability of neighbouring crystallites, above or below the lamella, for space filling.

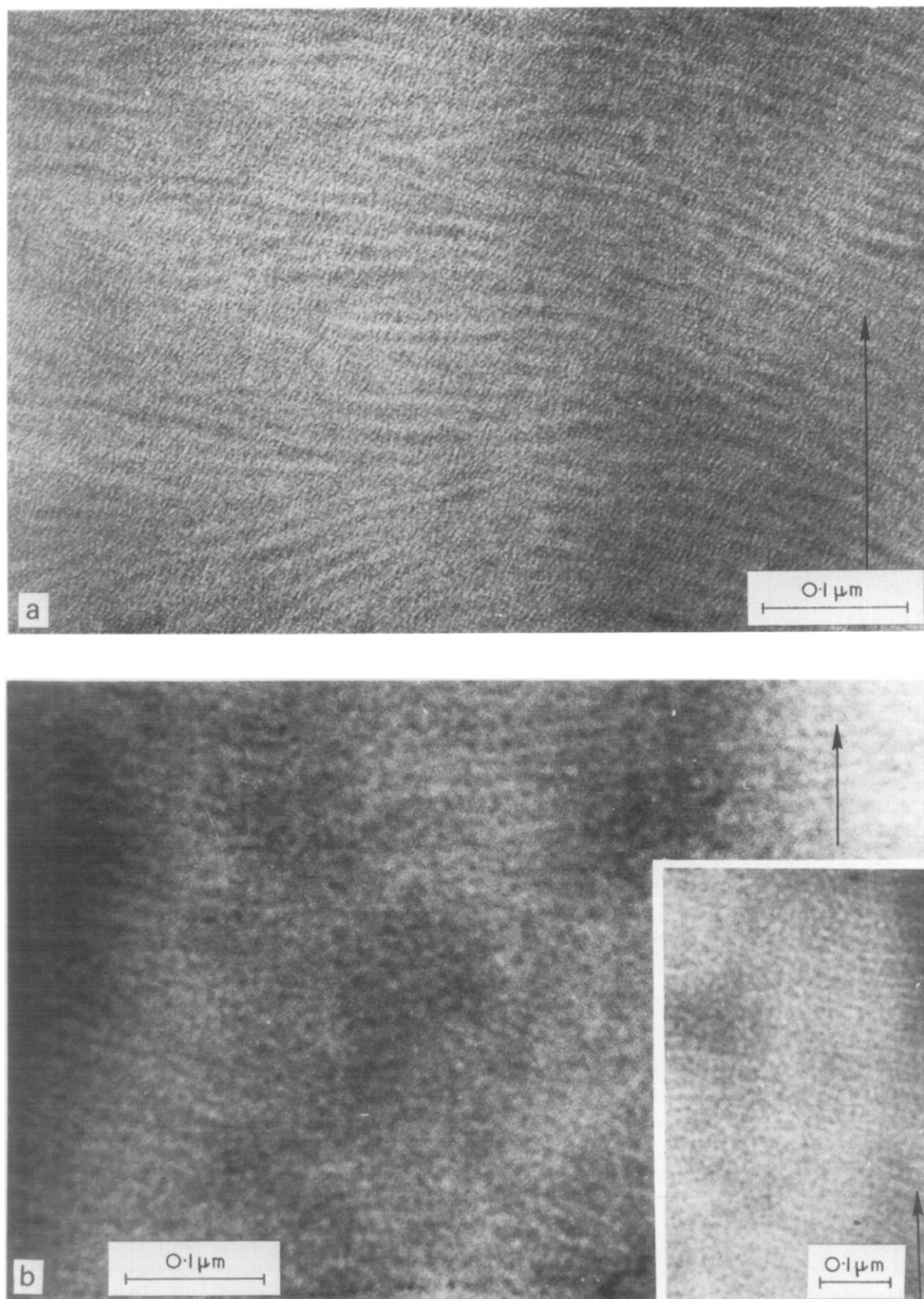


Figure 2 (a) Typical bundles of 'lamellae', seen edgewise in strain-crystallized natural rubber after OsO₄ staining at -28°C¹²; (b) Individual *mPC* seen within lamellae after annealing and OsO₄ staining at -15°C in range I¹²

to an increase in both l_a and l_c (Figure 4). If the melting involves melting of smaller or thinner *mPC* within the lamellae, as we believe it does, then a slightly modified selective *mPC*, rather than lamellar, melting model will apply very well here. This will be shown later. Nevertheless, one can safely eliminate the fold surface 'premelting' model involving longitudinal melting from the lamellar fold

surface inward, or the selective melting of the thinner lamellae within a stack of lamellae, since neither are observed^{12,13}. The basis for the objection to the fold surface premelting model in annealing temperature ranges II (and III) is therefore quite different from that in range I, where no substantial 'premelting' of the lamellae (either laterally or longitudinally) is observed.

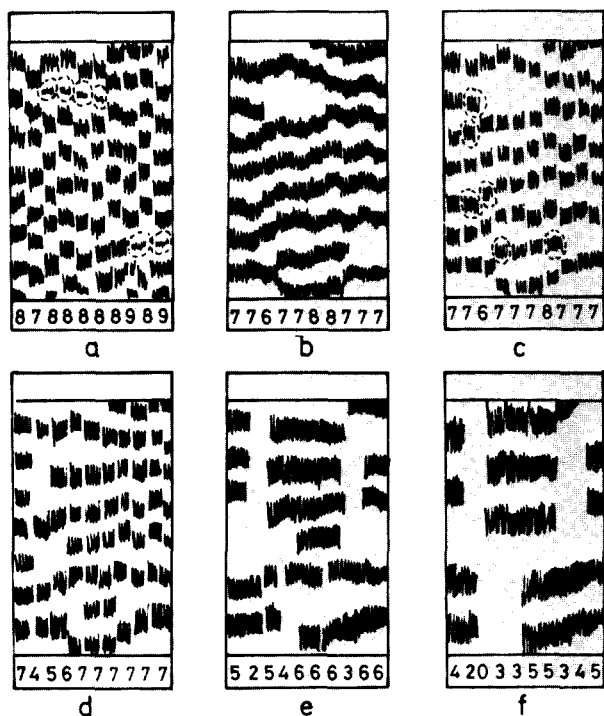


Figure 3 Structure of the *mPC* in the three temperature ranges. Schematically 10 columns of *mPC* extend over the whole picture. The numbers at the bottom give the number of *mPC* along the vertical direction. (a) Below range I in non-equilibrated drawn systems; the *mPC* are nematic-like; some of them can be very thin (circled). (b) Beginning of range I. The *mPC* are laterally aligned to form a smectic-like layer structure (originally present in well-equilibrated lamellae systems). Thin *mPC* are partially melted upon reaching range I in non-equilibrated drawn systems. (c) In range I the chain segments in lateral boundaries of *mPC* have higher mobilities, will begin to melt and contract to produce vacancies at the fold surface and unprotected lateral boundaries (circled). (d) In range II lateral melting of *mPC* may start at the unprotected lateral boundaries with simultaneous recrystallization to thicker *mPC*, resulting in the increase of long period. (e) At end of range II, after long annealing times, most of the melted regions have recrystallized epitaxially onto the more stable thicker *mPC*, which are now realigned to form smoother lamellae. (Only a few regions may still remain molten). (f) In range III, only thicker *mPC* can resist the melting process, while many other regions remain molten. The volume fraction γ of bundles and hence l , the crystallinity X and n.m.r. line-width LW decrease drastically; whereas the long period L may still keep on increasing

In annealing range III, the partial melting process of *mPC* which started in region II occurs with a much greater intensity at higher temperatures. However, the recrystallization process cannot be expected to extend to too high a temperature, since nucleation rate is a strong function of supercooling. Consequently, some of the melted regions remain selectively and permanently molten, contributing to substantial increases in molecular mobility (as judged by a substantial decrease in LW) and specific volume, and decreases in WAXS crystallinity, while other molten regions may still recrystallize into lamellae of greater thicknesses and therefore larger SAXS long periods consisting of substantially greater crystalline and amorphous thicknesses (Figure 4). An example is given in Figure 5 showing the presence of permanently molten regions as well as shorter segments of lamellae. A similar possibility of permanent melting and thickening of portions of lamellae, is seen from recrystallized morphology of polyethylene single crystals, observed at room temperature after annealing to higher temperatures in region III¹. The deduction of permanent melting in polyethylene single crystals occurring at the

annealing temperature was based on the observed disoriented fibrillar crystallites present within the lamellae at room temperature.

The permanently melted regions directly detected in Figure 5 can also explain the much lower volume crystallinity measured at annealing temperatures in region III, as reported earlier by Fatou and Mandelkern¹⁷ for polyethylene of various molecular weights.

Melting and recrystallization process

We believe that the melting starts at the grain boundaries between the *mPC* where the intrachain defects have become substantially increased upon heating to annealing temperature range I (Figure 3c). Because of their small size ($\sim 100 \times 100 \times 100 \text{ \AA}^3$), the much weakened exposed boundaries can be sources of instability and initial melting (Figure 3d). Eventually the melted region can recrystallize epitaxially onto the more stable, thicker *mPC* which had remained unmelted, with a greater lamellar thickness corresponding to a particular smaller supercooling (Figure 3e). The new crystals will have the same *c*-axis orientation as the old crystals upon which the new crystallites have nucleated. One can easily show that the melting and recrystallization can lead to a substantial reduction in total surface free energy. For example, an increase in lamellar thickness to 120 \AA from a 100 \AA thick cube, will result in a reduction in total surface free energy of about 12% owing to reduction of high energy fold surface area from $100 \times 100 \text{ \AA}^2$ to about $91 \times 91 \text{ \AA}^2$, assuming a reported¹⁸ end fold surface

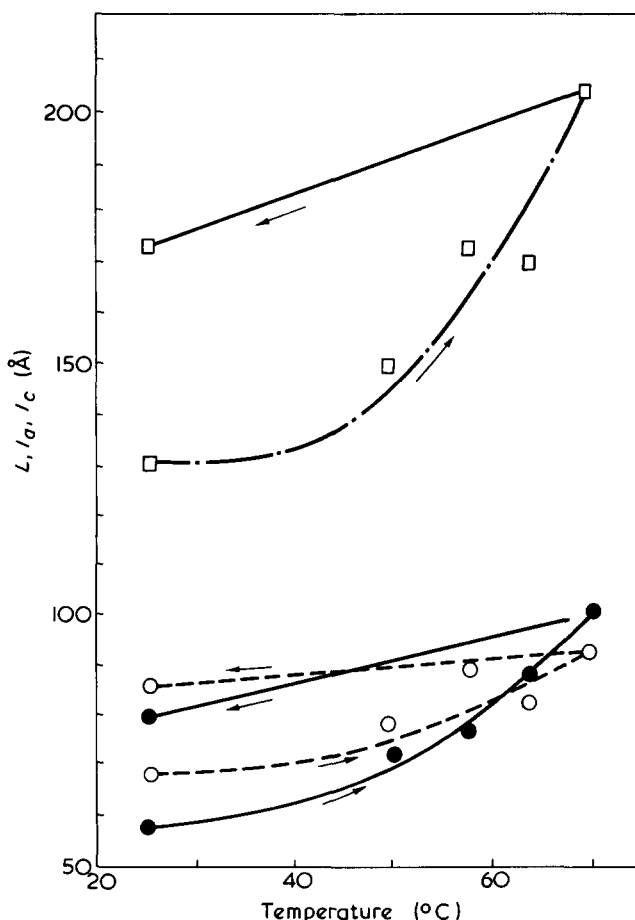


Figure 4 E.m. long period, L , plotted against annealing temperature for a strain-crystallized *trans*-polyisoprene¹³ (---). Variation in crystal thickness, l_c , (---) and variation in amorphous thickness, l_a (—)

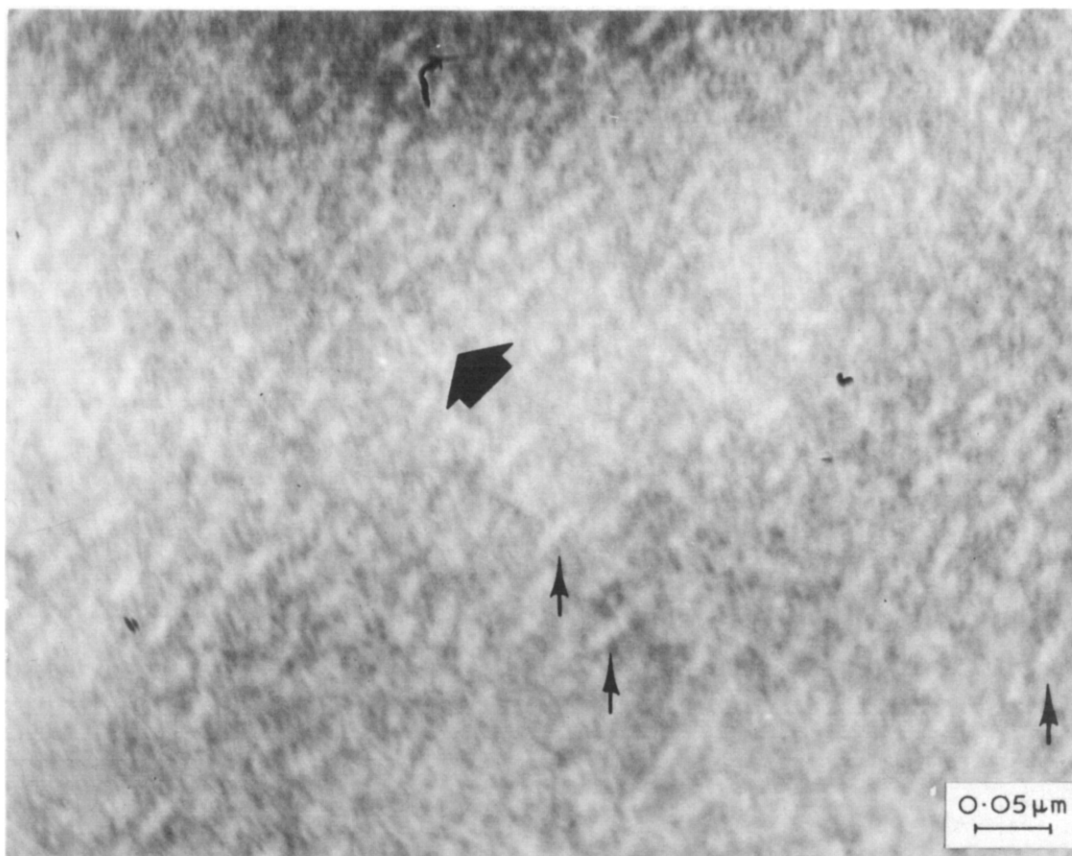


Figure 5 Typical bundles of lamellae seen edgewise in strain-crystallized *trans*-polyisoprene after annealing and OsO_4 staining at 70°C in range III¹³

free energy of about 80 ergs/cm^2 and a reasonable lateral side surface free energy of about 10 ergs/cm^2 . The new *mPC* can further reduce their total surface free energy through lateral alignment to form new lamellae consisting of some old and some new *mPC*.

Figures 3c and 3d schematically give an example of this melting and recrystallization process. Along columns 2, 3, 4 and 7 six *mPC* with unprotected lateral surfaces show up (circled) in Figure 3c upon annealing to range I. (Prior to reaching temperature I, the lamellae have the smooth fold surface as shown in Figure 3b.) Upon reaching temperature range II (Figure 3d), the *mPC* (circled) become molten in either column 2, 3, 4 or 7. Therefore the number of long periods in these columns has decreased in range II; column 3, 4 or 7 by one and column 2 by 3, from 7 to 4. The average number of long periods in the 10 columns has diminished from 70/10 or 7.0 in Figure 3c to 64/10 or 6.4 in Figure 3d. The average long period is therefore 9% larger in Figure 3d than in Figure 3c. Lateral alignment of the new and old *mPC* in further reduction of total surface free energy, is shown in Figures 3e and 3f.

With the type of lateral melting of *mPC* similar to the lateral melting proposed by Hosemann in 1962¹⁹, recrystallization and repacking, one can readily explain how the formation of new lamellae comes about, without resorting to nearly complete melting, as well as all the other annealing effects observed in annealing ranges II and III, including SAXS intensity and substantial long period increases, while the X-ray crystallinity remains relatively constant at long annealing times (Figure 1). Unlike the cause of SAXS intensity change in annealing range I which is due to greater differences of densities caused mainly by the vacancies introduced at the fold surface, the increase in SAXS peak intensity in annealing temperature ranges II and III, is

caused primarily by increases of the thickness of lamellae (due to increases in l_d and l_c) which is not discussed in the various idealized two-phase lamellar models in an earlier section. This process continues into annealing temperature range III. However, because of the limited driving force at higher temperature (smaller supercooling) substantial permanent melting will set in and lead to a reduction of the number of bundles (Figure 5), resulting in a substantial loss of crystallinity X and in the observed drop of SAXS intensity (Figures 1b and 1c). The following formulae give the quantitative expressions.

Peak intensity of SAXS

The formulae of SAXS for an idealized lamellar two-phase model, do not take into account the lateral boundaries existing between the adjacent *mPC* within a given lamella. Therefore they cannot adequately describe the changes in peak intensity I_p for many of the observed structures that may differ appreciably from an ideal lamellar two-phase model. However, it can be shown (see below), that with a slight modification of the basic formulae from the paracrystalline theory¹⁹ the changes in peak intensity for an oriented polymer can be readily accounted for by the changes in structure as a function of temperature. For example it has been demonstrated that a two-dimensional analysis of the SAXS of oriented samples can also give information about the shape of the *mPC* and their mutual positions²⁰⁻²², but this generally requires the use of a pin-hole-camera. But even with the use of a camera with a slit orthogonal to the fibre axis some information can still be obtained of the two phases whether or not unbounded lamellae exist.

Let $f(b)$ be the scattering amplitude of one *mPC* and $Z(b)$ the macroparacrystalline (*MPC*) lattice factor of an

unbounded assembly of *mPC* (if they are all pointlike). If $|S^2(b)|$ is the shape factor of the volume of a bounded assembly of *mPC*, the SAXS is given by:

$$I(b) = n[\bar{f}^2(b) - \bar{f}^{-2}(b)] + \frac{1}{v} \bar{f}^{-2}(b) \widehat{Z(b)} |S^2(b)| \quad (1)$$

n is the number of *mPC* in the assembly, which occupies the volume V and $v = V/n$ that of one *mPC*.

In the case of polymers having a lamellar structure there exist M bundles, each containing N lamellae in the average. If b_3 is the axis of one of these bundles in the reciprocal space, then $Z_3(b)$ is the intensity function of the centres of lamellae of an unbounded bundle:

$$Z_3(b) = R \exp \frac{1 + F_3(b)}{1 - F_3(b)}; F_3(b) = \mathcal{F}H_3(x) \quad (2)$$

$H_3(x)$ is the frequency distribution of a vector x between the centres of gravity of adjacent lamellae and $\mathcal{F} = [\int \exp - (2\pi i b x) dx]$ the symbol of Fourier-transform. The vector x expands the physical and b the reciprocal space. If l_c is the mean thickness of the lamellar crystalline cores and l_a that of the amorphous interlayer, the intensity of one bundle along the b_3 -axis of the reciprocal b -space is proportional to equation (1) with:

$$b \rightarrow b_3; v \rightarrow l_c + l_a; \widehat{Z(b)} |S^2(b)| \rightarrow \widehat{Z_3(b_3)} |S_3^2(b_3)|; \quad (3)$$

$$f(b) \rightarrow f_3(b_3) = \frac{\sin \pi l_c b_3}{\pi b_3}.$$

$f_3(b_3)$ is proportional to the scattering amplitude of one lamellae which consists of many *mPC* packed next to each other in the lateral direction. The symbol $\widehat{}$ stands for a convolution product. In equation (1) there is a three-dimensional convolution product of the three-dimensionally defined function Z and $|S^2|$; in equation (3) there is a one-dimensional convolution product of the one-dimensionally defined function Z_3 and $|S_3^2|$.

If all the lamellae are cylindrical discs with a diameter D and if $\Delta\rho$ is the electron density difference between the 'crystalline' and the 'amorphous' phase of a lamella one obtains for the integral intensity of the SAXS along a line, at a constant distance b_3 , parallel to the equator:

$$I(b_3) = \iint I(b_1, b_2, b_3) db_1 db_2 = (\Delta\rho)^2 \frac{\pi D^2}{4} \left(\frac{\sin \pi l_c b_3}{\pi b_3} \right)^2 \times \frac{1}{l_c + l_a} \widehat{Z_3} |S_3^2|. \quad (4)$$

For convenience the first term of equation (1) is neglected here, because it does not affect the final results very much²¹. The application of the paracrystalline theory to the macro-paracrystalline lattice of the lamellae will now be introduced. (It should be pointed out here that the exact one-dimensional solution of Hermans²³, often used by Tsvankin et al.²⁴ in avoiding statistical overlapping of adjacent lamellae cannot be generalized to a three-dimensional bundle of lamellae²⁵.)

Equation (2) shows that Z_3 has its first peak at $b_3 = 1/(l_a + l_c)$ with a maximum value:

$$Z_{3 \max} = \frac{1 + |F_3(b_{3m})|}{1 - |F_3(b_{3m})|}; b_{3m} = (l_c + l_a)^{-1} \quad (5)$$

Z_3 has an integral width δb_Z given by²⁵:

$$\delta b_Z = \frac{1}{2(l_c + l_a)} (1 - |F_3(b_{3m})|) \quad (6)$$

$|S_3^2|$ on the other hand has an integral width given by:

$$\delta b_s = \frac{1}{(l_a + l_c)N} \quad (7)$$

The peak intensity depends on the relative contributions of these two quantities and has extreme values as follows:

$$\frac{1}{l_a + l_c} \widehat{Z_3} |S_3^2| = \begin{cases} N^2 & \text{if } \delta b_Z < \delta b_s \\ NZ_3(b_{3m}) & \text{if } \delta b_Z > \delta b_s \end{cases} \quad (8a)$$

$$(8b)$$

Since the modulus of $F_3(b)$ in equation (5) can be approximated as:

$$|F_3(b_3)| \sim \exp(-2\pi^2 g^2 h^2) \quad (9)$$

where $g^2 = \frac{(l_c + l_a)^2}{(l_c + l_a)^2} - 1$; $h = b_3/(l_c + l_a)$

introducing this into equation (6) one obtains for the integral width of the first peak at $h = 1$ of Z_3 :

$$\delta b_Z = \pi^2 g^2 / (l_a + l_c) \quad (10)$$

g generally lies in the order of $\sim 20\%$ from a two-dimensional SAXS analysis of high oriented polymers²⁰⁻²². The product, $(l_a + l_c)\delta b_Z$, is therefore in the order of 0.4. From electron microscopy^{12,13} the number of lamellae in one bundle is generally found to be larger than 10. Therefore $\delta b_Z \gg \delta b_s$ and in all these cases equation (8b) should hold.

Now, to obtain the peak intensity $\iint I db_2 db_3$ of the bundle one must subtract the background of the SAXS. Part of the background is given by the first term of equation (1). The rest comes from $Z_3(b)$ and is given by:

$$Z_{3 \min} \cong \frac{1 - |F_3(b_{3m})|}{1 + |F_3(b_{3m})|} \quad (11)$$

The difference between equations (5) and (9) then gives the contribution of Z_3 to the peak intensity of the bundle:

$$Z_{3p} = \frac{4|F_3(b_{3m})|}{1 - |F_3(b_{3m})|^2} \quad (12)$$

The peak intensity of the first meridian reflection of an oriented sample in a microdensitometer with a slit parallel to the equator is therefore given by equation (4). If one introduces equations (8b) and (12) the result is:

$$\bar{I}_p = (\Delta\rho)^2 \frac{\pi D^2}{4} \left(\frac{\sin \pi l_c b_{3m}}{\pi b_{3m}} \right)^2 NZ_{3p} \quad (13)$$

Its position is approximately given in most cases by $h = 0.9$ since the peak of $Z_3(b_3)$ at $h = 1$ is multiplied with $\sin \pi l_c b_{3m} / \pi b_{3m}$, which in most cases decreases drastically with increasing b_3 in the region of this peak²². $|F_3(b_{3m})|$ is, according to the above mentioned value of g ($\sim 20\%$), in

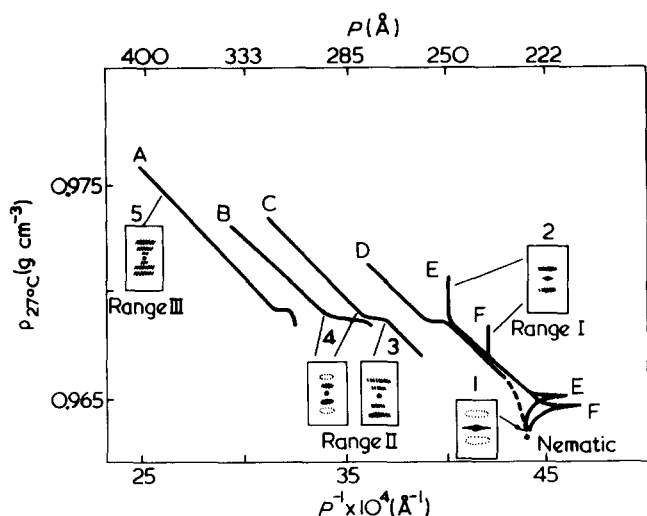


Figure 6 Density, ρ , of hot-drawn polyethylene (linear polyethylene LUPOLEN 6001H stretched) plotted against the reciprocal of long period for various annealing temperatures ($^{\circ}\text{C}$): A, 129; B, 126; C, 120; D, 110; E, 100; F, 95 and times²⁷ in the three temperature ranges and the respective SAXS pattern. P (long period) reaches a finite value after some days according to Figure 3b and grows unbounded in range III according to Figure 3f. Stretching temperature T_1 , 80°C , draw ratio 9.6x

the order of $1/2$, hence $4F_3(b_{3m})/1 - |F_3(b_{3m})|^2$ is in the order of 3.

If V is the irradiated volume of the sample, M the number of bundles and γ the volume fraction of bundles, then the volume occupied by the bundles is given by:

$$\gamma V = MN(l_a + l_c)\pi D^2/4 \quad (14)$$

Introducing this in equation (13) we finally obtain for the SAXS peak intensity:

$$\bar{I}_p = (\Delta\rho)^2 \gamma V \left(\frac{\sin\pi l_c b_{3m}}{\pi b_{3m}} \right)^2 \frac{l_c + l_a}{\pi} Z_{3p} \quad (15)$$

Equation (15) shows that \bar{I}_p is proportional to the square of the electron density difference (as seen in annealing range I), to the volume fraction of bundles (as seen in range III) and to Z_{3p} as defined by equation (12), or in the order of 3. At a given long period ($l_a + l_c$) it has a maximum for $l_a = l_c$, which is well-known. The next interesting result is the proportionality to $(l_a + l_c)$. Even if the volume fraction γ , l_a/l_c , g and $\Delta\rho$ are constant, \bar{I}_p increases if the thickness of the lamellae ($l_a + l_c$) increases uniformly as in annealing range II.

APPLICATION TO ANNEALING EFFECTS OBSERVED IN DRAWN SYSTEMS

In the case of cold or hot drawn systems, the lamellar morphology is often replaced by a typical fibrillar morphology at sufficiently high extensions (Figure 3a). When the highly drawn fibrillar systems is annealed in the different temperature ranges I, II and III and studied by means of electron microscopy (e.m.) at room temperatures²⁶, results suggest little or no morphological changes taking place at the annealing temperature in range I, but that a transformation from a fibrillar to a lamellar morphology must have taken place starting at some temperature in annealing temperature range I (Figure 3b). The generally accepted ex-

planation is that at high enough temperature additional molecular mobility allows the lateral alignment of crystallites in neighbouring fibrils as well as the additional growth of lamellar thickness by means of a solid state refolding process.

However, additional information can be obtained about the transformation process from two-dimensional analysis of SAXS patterns obtained at room temperatures of such systems after annealing at various temperatures for various times. Since the details of the SAXS studies have already been reported elsewhere²⁷, it is our purpose here to show how the annealing mechanisms described earlier can also be of direct application to the understanding of the annealing effects detected in such non-equilibrated drawn systems that are often encountered during normal fibre or film processings or any future applications of solid state forming processes.

Figure 6 shows a plot of density vs. the inverse of SAXS long period for an annealed hot drawn polyethylene. Both the density and the long period were measured at room temperature after quenching from the various annealing temperatures at the end of various annealing times. There are various interesting characteristics to the curves. When annealed to temperatures below 110°C (which we shall refer to as range I'), the observed changes are quite different from those seen after annealing between $\sim 110^{\circ}\text{C}$ and $\sim 130^{\circ}\text{C}$ (range II'). In range I, after 10^2 min, the SAXS long period stays nearly constant while ρ increases and finally reaches a limiting value. The voids originally present between the microfibrils as a result of the stretching process are now partially removed after the annealing step, which contributes to the observed increase in density to a limiting value. The limited mobility of the chain segments in range I (Figure 1a) explains the limited increase of long period as well as the lack of lateral alignment of mPC in neighbouring fibrils, from information provided by the SAXS patterns, which showed an mPC packing to be nearly the same as the one depicted in Figure 3b.

In range II', both the long period and density increase with time except for a small plateau, where density stays nearly constant and only long period increases. The extent of this plateau becomes shorter, but it takes place earlier with increasing annealing temperature. Two-dimensional analysis of the SAXS patterns indicates that in temperature range II', the morphology begins to change with annealing time going from a fibrillar to a lamellar structure. This is in complete agreement with similar electron microscopy studies²⁶, which not only showed the transformation but that it takes less and less time with increasing temperature after annealing between 110° and 130°C . The results from density measurements and SAXS and e.m. studies indicate that the fibrillar-to-lamellar morphological transformation can take place by a similar melting of the exposed small mPC (Figures 3a, 3c and 3d), and recrystallization process described earlier. However, because the recrystallization on crystallization from an oriented melt occurs at a much faster rate than recrystallization from an unoriented melt, the solidification process is most likely to have been completed within the annealing times or during quenching to room temperatures after annealing. This explains the differences seen in density changes with time for unoriented and oriented systems; the density for oriented systems generally increases with time whereas for unoriented systems it may show a drop initially before it proceeds to increase with time⁵. We suggest that if the density for our annealed oriented systems is measured fast enough at the

annealing temperature, we should be able to detect a decrease due to initial melting.

ACKNOWLEDGEMENTS

The authors gratefully acknowledge the generous support of this work by the Alexander von Humboldt-Stiftung and the Deutsche Forschungsgemeinschaft, Bonn. One of the authors (G. S. Y. Y.) was a recipient of a Senior US Scientist Award of the Alexander von Humboldt-Stiftung and wishes to give special thanks to the Foundation and his host (R. H.) for their generous hospitality.

REFERENCES

- 1 Fischer, E. W. *Kolloid-Z. Z. Polym.* 1969, **231**, 458
- 2 Fischer, E. W. *Pure Appl. Chem.* 1972, **31**, 113
- 3 Schultz, J. M. 'Polymer Materials Science' Prentice-Hall, New Jersey, 1974
- 4 Hoffman, J. D. see Fischer, E. W. *Kolloid-Z. Z. Polym.* 1969, **231**, 458; Kilian, H. G., *Kolloid-Z. Z. Polym.* 1969, **231**, 534
- 5 Fischer, E. W. and Schmidt, G. F. *Angew. Chem.* 1962, **1**, 488
- 6 Geil, P. H. 'Polymer Single Crystals', Interscience, New York, 1963
- 7 Luch, D. and Yeh, G. S. Y. *J. Macromol. Sci. (B)* 1973, **7**, 121
- 8 Nukushina, Y., Itoh, Y. and Fischer, E. W. *J. Polym. Sci. (B)* 1965, **3**, 383
- 9 Schultz, J. M., Robinson, W. H. and Pound, G. M. *J. Polym. Sci. (A)* 1967, **5**, 511
- 10 Hosemann, R., Wilke, W. and Baltá-Calleja, F. H. *Acta Crystallogr.* 1966, **21**, 118
- 11 Yeh, G. S. Y. and Geil, P. H. *J. Macromol. Sci. (B)* 1967, **1**, 235, 251; Yeh, G. S. Y. and Lambert, S. L. *J. Appl. Phys.* 1971, **42**, 4614, *J. Macromol. Sci. (B)* 1972, **6**, 599
- 12 Luch, D. and Yeh, G. S. Y. *J. Appl. Phys.* 1972, **43**, 4326
- 13 Hardin, I. R. and Yeh, G. S. Y. *J. Macromol. Sci. (B)*, 1973, **7**, 375
- 14 Takayanagi, M. *J. Macromol. Sci. (B)* 1974, **9**, 391
- 15 Strobl, S., Ewen, B., Fischer, E. W. and Piesecek, W. *J. Chem. Phys.* 1974, **61**, 5257
- 16 Yeh, G. S. Y. *J. Macromol. Sci. (B)*, 1973, **8**, 241
- 17 Fatou, J. G. and Mandelkern, L. *J. Phys. Chem.* 1965, **69**, 417
- 18 Illers, K. H. and Hendus, H. *Makromol. Chem.* 1968, **113**, 1
- 19 Hosemann, R. *Polymer* 1962, **3**, 349
- 20 Hosemann, R. *Ber. Bunsenges. Phys. Chem.* 1970, **74**, 755
- 21 Ferracini, E., Ferrero, A., Loboda-Čačković, J., Hosemann, R. and Čačković, H. *J. Macromol. Sci. (B)* 1974, **10**, 97
- 22 Loboda-Čačković, J., Hosemann, R. and Čačković, H. *Kolloid-Z. Z. Polym.* 1971, **247**, 824
- 23 Hermans, J. J. *Recl. Trav. Chim. Pays. Bas.* 1944, **63**, 5
- 24 Tsvankin, D. J. *Vysokomol. Soedin (A)* 1967, **9**, 2628
- 25 Hosemann, R. and Bagchi, S. N. 'Direct Analysis of Diffraction by Matter', North-Holland, Amsterdam, 1962
- 26 Yeh, G. S. Y. and Geil, P. H. *J. Mater. Sci.* 1967, **2**, 457
- 27 Loboda-Čačković, J., Hosemann, R. and Wilke, W. *Kolloid-Z. Z. Polym.* 1969, **235**, 1162

Phosphonitrilic chloride: 33. Cyclomatrixphosphazene polymers formed from hexachlorocyclotriphosphazene and metal acetates

M. Kajiwara and H. Saito

Department of Applied Chemistry, Faculty of Engineering, Nagoya University, Nagoya, Japan

(Received 18 November 1975)

Cross-linked polymers of the metaphosphomic type structure were prepared by the reaction of hexachlorocyclotriphosphazene with various divalent metal acetates in aqueous solution at 30°C. The poorly crystalline insoluble products swell in water and most organic solvents. The product containing barium was the most stable toward heat. The products were easily decomposed by dilute hydrogen chloride at 80°C.

INTRODUCTION

This paper describes cyclomatrixphosphazene polymers formed from the reaction of hexachlorocyclotriphosphazene (NPCl₂)₃ with metal acetates (CH₃COO)₂M in aqueous solution.

EXPERIMENTAL

Hexachlorocyclotriphosphazene, (NPCl₂)₃, was prepared by the modified method of Kajiwara¹. The pure trimer was obtained by repeated fractional recrystallization from light petroleum ether.

The reaction of (NPCl₂)₃ (3.4 g, 0.01 mol) of 28 mesh grain size added to a 200 ml aqueous solution containing

0.09 mol metal acetates, was carried out at 30°C with vigorous stirring. The extent of the reaction was measured by the amount of metal chloride formed. The reaction mixture was filtered, and the residue extracted with petroleum ether, acetone and after washing with water, was dried in air at 105°C for 24 h. Metal salts used were calcium, magnesium, barium, zinc, lead, nickel, cobalt, copper and tin acetate, respectively.

The infra-red spectra were recorded on a Shimadzu Model-450 type spectrometer in the region of 4000 cm⁻¹ to 200 cm⁻¹ using the pressed KBr disc technique. X-ray diffraction photographs were measured using a Shimadzu Co. VDF-1 type instrument and powder diffraction method. The thermal analysis was recorded on a Shimadzu Model-20B in air at 5°C/min.

Table 1 Yield of the products and the variations of pH in aqueous solution

(NPCl ₂) ₃ (g)	(CH ₃ COO) ₂ M		pH		Yield (g)	Appearance
	M	(g/200 cm ³)	Initial	Final		
3.46	Ca	14.227	7.8	4.3	2.67	White, amorphous solid
3.46	Mg	19.301	7.7	4.2	1.31	White, amorphous solid
3.46	Ba	24.609	6.7	4.1	4.03	White, crystalline solid
3.46	Pb	34.142	5.3	3.9	7.48	White, amorphous solid
3.46	Zn	19.755	5.3	4.4	2.44	White, crystalline solid
3.46	Cu	17.969	7.8	4.3	1.11	Blue, crystalline solid
3.46	Co	22.417	6.8	6.8	—	
3.46	Ni	22.396	6.6	6.6	—	
3.46	Sn	14.207	6.0	1.2	13.50	Brown, amorphous solid

Table 2 Chemical analysis of the products

M in (CH ₃ COO) ₂ M	Found (%)			Calculated* (%)		
	P	N	M	P	N	M
Ca	34.00	17.41	20.04	30.92	14.43	20.65
Mg	7.60	17.14	28.75	33.36	15.57	13.52
Ba	22.46	8.91	55.39	20.59	9.61	47.14
Pb	8.97	6.80	50.70	16.66	7.75	57.46
Zn	27.25	11.22	26.19	27.35	12.76	29.78
Cu	29.00	13.01	29.44	27.58	12.87	29.21

* P₃N₃H₃O₆M_{1.5} Z. Anorg. Allg. Chem. 1972, 387, 271

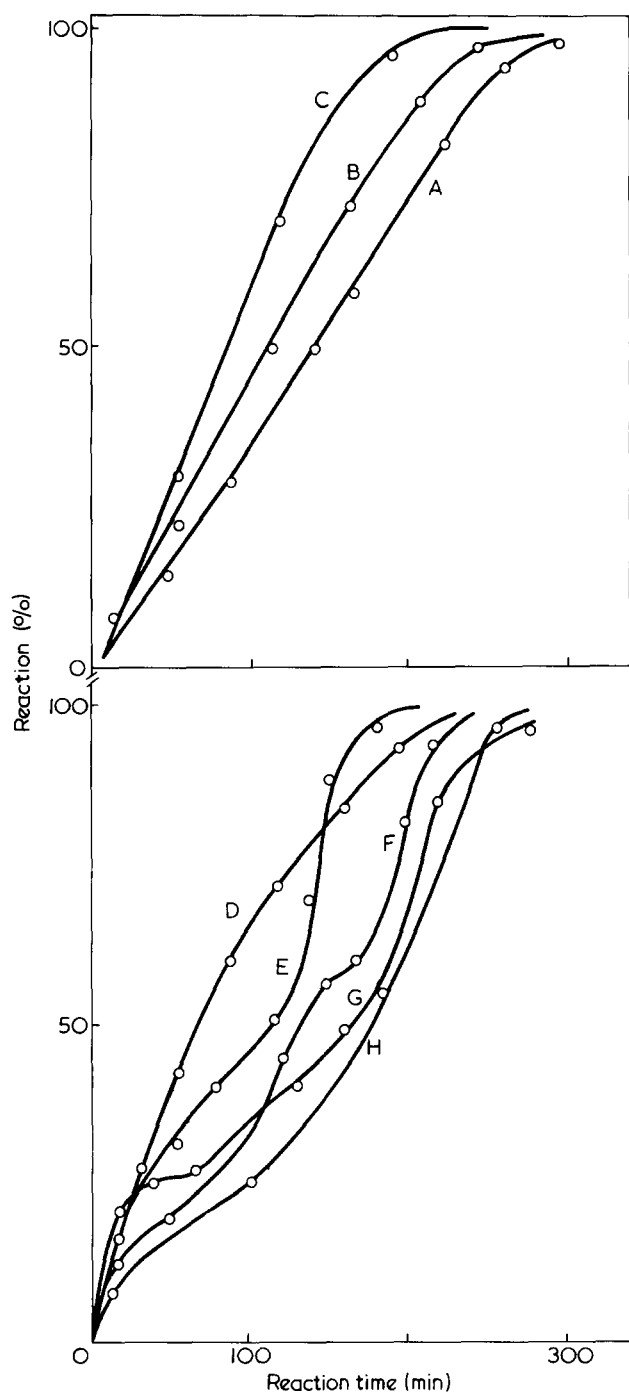


Figure 1 Amount of formed chlorine as a function of the reaction time. A, Mg; B, Ba; C, Ca; D, Zn; E, Ni; F, Co; G, Pb; H, Cu

RESULTS AND DISCUSSION

The reaction rate determined by the amount of metal chloride is shown in Figure 1.

The yield of the products and pH values of the reaction solution are summarized in Table 1. The acidity is due to HCl formed. Water soluble products were formed with cobalt or nickel acetates. The insoluble products which were highly crosslinked, swell in water, benzene and other organic solvents.

X-ray diffraction analysis showed that the products formed from barium, zinc and copper acetates gave well defined diffraction lines but showed no polarization under the polarizing microscope owing to poor lattice fit.

Infra-red absorption spectra of the products showed the NH frequency in the region of 3200 cm⁻¹ and P-N fre-

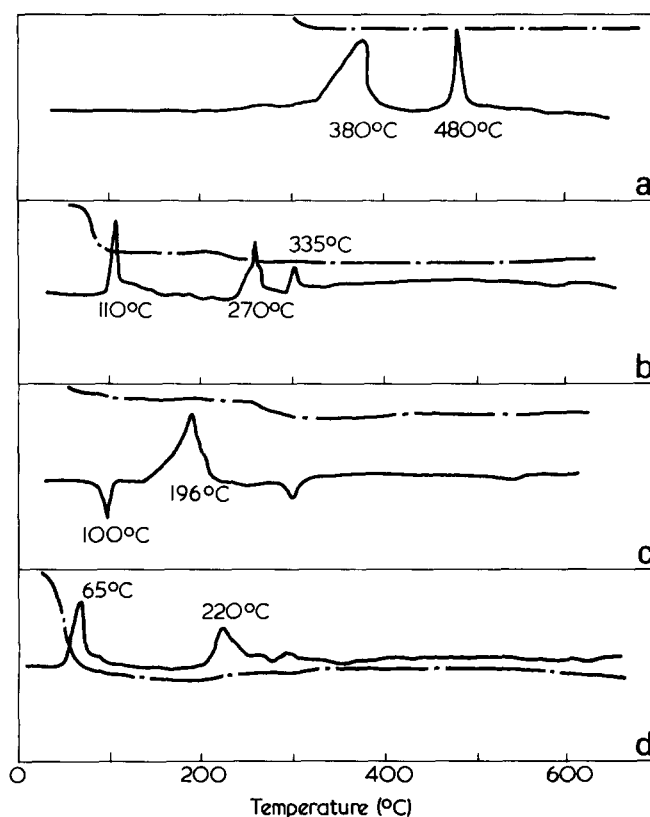
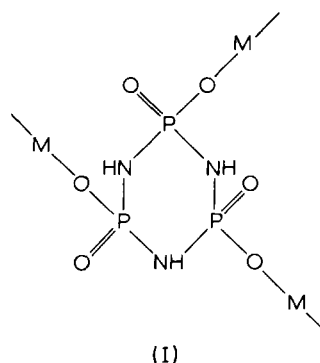


Figure 2 Thermal gravimetric (---) and differential thermal analysis (—) of the products formed by reaction between dichlorocyclophosphazene and metal acetate. (a), Ba; (b), Ca; (c), Cu; (d), Mg

quency in the region of 1200 cm⁻¹ and 1050 cm⁻¹, respectively.

Chemical analyses (Table 2) were in fair agreement with the calculated values for the metaphosphomic structure shown below.



Thermal decomposition temperatures as measured by differential thermal analysis and thermogravimetric analysis (Figure 2) show that the barium acetate product is very stable to heating. The products formed by heating were shown by gas chromatography to contain NH₃, H₂O or a trace of CH₃COOH. Ammonium and phosphate ions were detected as the products treated with dilute hydrogen chloride at 80°C for a few minutes.

REFERENCE

1 Saito, H. and Kajiwara, M. *J. Chem. Soc. Japan (Ind. Chem. Sect.)* 1963, 66, 618

New photoinitiating systems and photoactive polymers and their applications*

C. H. Bamford

Department of Inorganic, Physical and Industrial Chemistry, University of Liverpool, Liverpool, L69 3BX, UK

(Received 30 October 1975)

Two new types of photoinitiating systems based on transition metal carbonyls [mainly $\text{Mn}_2(\text{CO})_{10}$ and $\text{Re}_2(\text{CO})_{10}$] and free from abstractable halogen atoms are described. The first consists of a low concentration (typically $\sim 0.1 \text{ mol l}^{-1}$) of a fluoro-olefin, together with the metal carbonyl. Quantum yield data for photoinitiation by a number of these systems are presented; $\text{Re}_2(\text{CO})_{10}$ is generally more active than $\text{Mn}_2(\text{CO})_{10}$ and quantum yields near unity are obtainable. Polymers prepared with the aid of these initiators carry terminal groups in which the metal atom is covalently bound to the polymer chain through a fluoro-olefin unit. In the second type no halogen is present. The additive employed with the metal carbonyl is (a) acetylene or an acetylene derivative (e.g. acetylene dicarboxylic acid); or (b) an olefinic derivative carrying electron-attracting groups (e.g. diethyl fumarate). Mechanistically these photoinitiators resemble those based on fluoro-olefins; high quantum yields of initiation may be obtained and terminal groups containing covalently bound metal atoms are present in the polymers. Polymers prepared with either type of photoinitiator behave as macromolecular thermal initiators at higher temperatures (e.g. 100°C) and furnish a convenient route to block copolymers. A third type of photoinitiator, based on a vanadium (V) chelate, is also discussed. Chelates such as $\text{V}^{\text{V}}\text{OQ}_2$ or, where Q represents 8-quinolyloxo, have been shown to photolyse by scission of (OR)'. If R is a side chain attached to a polymer molecule, photolysis yields a macroradical capable of initiating grafting reactions. The behaviour and applications of these photoactive polymers are described.

INTRODUCTION

The photochemistry and photophysics of systems based on monomers and/or polymers currently attract much attention. In this lecture we shall be concerned mainly with photochemistry, but we may note that photophysical studies provide information about a number of processes of interest to the chemist, such as the migration of energy along polymer chains and the effects of polymer chain conformation on interactions of electronically excited chromophores with ground state species¹.

Interest in the photochemistry of these systems stems from a number of origins. A study of photoinitiation yields data about the nature and reactivities of intermediates and the mechanism of polymerization. Of great importance are the many practical applications of photoactive polymer-based systems, for example, in image and data storage and retrieval, and in the manufacture of printing plates and printed circuits. Increasing environmental pressures demand the development of systems free from organic solvents, so that there is a rapidly developing interest in all types of photocuring processes. Further, it is conceivable that such processes may displace some conventional fabrication technologies.

Since photoinitiation and photocuring are processes which are closely related there is an obvious incentive for work on photoinitiation. Some years ago we embarked on a study of photoinitiation of free-radical polymerization by transition metal complexes². After a very brief reference to early work (following section), our more recent results will be described.

SYSTEMS CONTAINING ABSTRACTABLE HALOGEN ATOMS²

Many transition metal complex/organic halide combinations are photoactive. Among the transition metal carbonyls which have been investigated in detail from this point of view are $\text{Mn}_2(\text{CO})_{10}$, $\text{Re}_2(\text{CO})_{10}$ and $\text{ArCr}(\text{CO})_3$. In all systems of this type, an active species produced photochemically enters into a redox reaction with the halide; as a result the metal atom (M) in the former acquires a higher oxidation state while the halide is converted into a free radical, e.g.



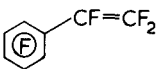
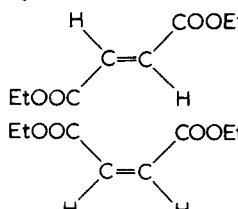
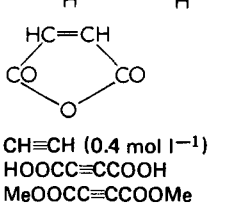
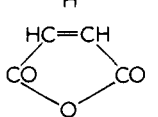
By replacing the simple halide by a preformed polyhalide, a wide variety of graft block and network copolymers have been synthesized and highly efficient photocrosslinking systems may be developed²⁻⁴.

SYSTEMS WITHOUT ABSTRACTABLE HALOGEN ATOMS

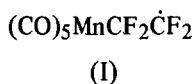
In 1972 we observed^{5,6} that manganese and rhenium carbonyls are very active photoinitiators for the polymerization of liquid tetrafluoroethylene at -92°C . Some other carbonyls [e.g. $\text{Os}_3(\text{CO})_{12}$ and $\text{Ru}_3(\text{CO})_{12}$] also photoinitiate, but are less active. Further, one of these carbonyls in the presence of a low concentration of C_2F_4 (e.g. 0.1 mol l^{-1}) was found to photoinitiate free-radical polymerization of common vinyl monomers at 25°C . In other words, C_2F_4 appeared able to function as halide component of systems such as those described². However, it

* Plenary lecture given at the 5th Int. Symp. 'Polymers 75', Varna, Bulgaria, October 1975.

Table 1 Quantum yields for photoinitiation of polymerization of methyl methacrylate at 25°C by $\text{Re}_2(\text{CO})_{10}$ ($\lambda = 365 \text{ nm}$) and $\text{Mn}_2(\text{CO})_{10}$ ($\lambda = 435.8 \text{ nm}$) in the presence of additives

Additive (Concentration: 0.1 mol l^{-1})	$\text{Re}_2(\text{CO})_{10}$	$\text{Mn}_2(\text{CO})_{10}$
none	~0.03	0
$\text{CF}_2=\text{CF}_2$	1.0	0.9
$\text{CF}_2=\text{CHF}$	1.0	0
$\text{CF}_2=\text{CFCl}$	0.87	0
$\text{CF}_2=\text{CH}_2$	0.35	0
$\text{CHF}=\text{CH}_2$	0.41	0
$\text{CF}_2=\text{CFCl}$	0.87	0.72
$\text{CF}_2=\text{CCl}_2$	0.65	0.06
$\text{CF}_3\text{CF}=\text{CF}_2$	1.0	0
$\text{CF}_2=\text{CF}-\text{CF}=\text{CF}_2$	1.0	0.23
	1.0	—
	0.77	0
	0.18	0
	0.09	0
$\text{CH}=\text{CH}$ (0.4 mol l^{-1})	0.90	0
$\text{HOCC}=\text{CCOOH}$	0.98	0.42
$\text{MeOCC}=\text{CCOOMe}$	0.98	0.61

seemed very unlikely that the fluorine atoms in C_2F_4 are abstractable under the experimental conditions, so that a mechanism different from that of equation (1) was indicated. In support of this, saturated fluorocarbons such as perfluorocyclohexane were found to be completely inactive. Two additional observations clarified the nature of the initiation process: (a) Analysis⁶ of the polymers obtained from the system methyl methacrylate + $\text{Mn}_2(\text{CO})_{10}$ + C_2F_4 revealed that the polymers carry covalently bound manganese atoms, the mean number per polymer chain being 1.23. This is close to the number expected (1.21) if each initiating radical contains one Mn atom, with combination of poly(methyl methacrylate) radicals constituting 34% of the total termination; (b) The polymers show infra-red absorption near 2000 cm^{-1} , very similar to that of model compounds such as $(\text{CO})_5\text{MnC}_2\text{F}_5$ ⁷. It therefore seems clear that the initiating radicals have the structure:



More recently⁷ a number of different fluoro-olefins have been shown to behave similarly to C_2F_4 . Detailed observations have been extended⁸ to $\text{Re}_2(\text{CO})_{10}$, which photoinitiates by the same type of mechanism as $\text{Mn}_2(\text{CO})_{10}$, but is more active. The quantum yields of initiation obtainable in these systems are presented in Table 1.

The rate of consumption of $\text{Mn}_2(\text{CO})_{10}$ has been measured spectrophotometrically and found to follow simple first-order kinetics^{6,7}. Comparison with the rate of initiation deduced from polymerization kinetics shows that for the photoinitiators $\text{Mn}_2(\text{CO})_{10}/\text{C}_2\text{F}_4$ and $\text{Mn}_2(\text{CO})_{10}/\text{C}_2\text{F}_3\text{Cl}$, each molecule of $\text{Mn}_2(\text{CO})_{10}$ consumed gives rise

to one initiating radical. Unfortunately, similar observations with $\text{Re}_2(\text{CO})_{10}$ are not feasible⁸ since the formation of a product with strong light absorption obscures the decreasing absorption attributable to the decay of $\text{Re}_2(\text{CO})_{10}$.

The results we have described demonstrate the great difference in behaviour between fluoro-olefins and 'conventional' monomers (e.g. methyl methacrylate) in these systems. We attribute the high activity of the former to the ability of the fluoroderivatives to form relatively strong metal-carbon bonds⁶. In fluoroalkyl-, compared to alkyl-, derivatives of transition metals, the metal-carbon bonds are relatively short, probably on account of back-donation from d_π metal orbitals to σ^* levels of fluoroalkyl⁹. The resulting increase in bond energy would play a decisive role in the formation of radicals such as structure (I).

SYSTEMS WITHOUT HALIDES

The observations on fluoro-olefins reported above suggested that other classes of additives which readily form ligands with transition metals might be active components of photoinitiating systems containing a Group VII metal carbonyl. Very recently¹⁰ we have demonstrated that this is the case. The additives studied include: (a) olefinic derivatives carrying electron-attracting groups e.g. diethyl fumarate, diethyl maleate, maleic anhydride; (b) acetylene and its derivatives acetylene dicarboxylic acid and the dimethyl ester of the latter. Thus, a new class of photoinitiators, free from halogen atoms, becomes available.

Mechanistically, these photoinitiators resemble systems based on fluoro-olefins. The kinetics indicate uncomplicated free-radical polymerization; Figure 1 presents the dependence of the rate of polymerization on additive concentration for selected systems. Quantum yields of initiation under 'plateau' conditions are given in Table 1; evidently with acetylene and its derivatives values close to unity are obtainable with $\text{Re}_2(\text{CO})_{10}$. The lower activity of $\text{Mn}_2(\text{CO})_{10}$, relative to $\text{Re}_2(\text{CO})_{10}$, is also clear from Table 1. Further, with $\text{Mn}_2(\text{CO})_{10}$ /acetylene dicarboxylic acid dimethyl ester systems, it has been shown that one initiating radical arises from each $\text{Mn}_2(\text{CO})_{10}$ consumed¹⁰

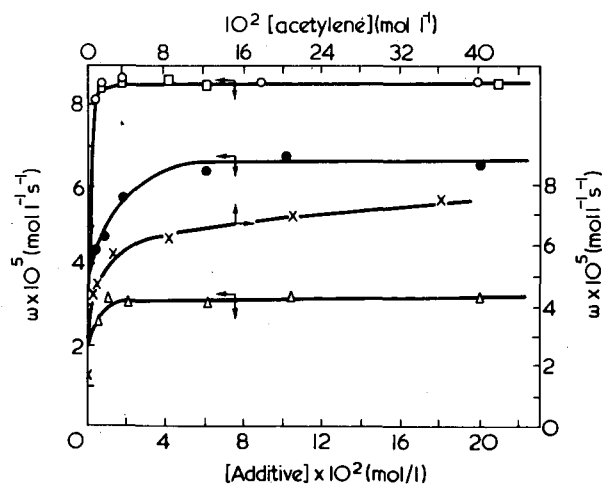


Figure 1 Dependence of rate of polymerization of methyl methacrylate at 25°C (ω) on [additive]. $[\text{Re}_2(\text{CO})_{10}] = 5.11 \times 10^{-4} \text{ mol l}^{-1}$, $\lambda = 365 \text{ nm}$. $10^8 I_{\text{abs}}$ (einstein $\text{l}^{-1} \text{ s}^{-1}$): X, 2.51 (acetylene); O, 2.72 (acetylene dicarboxylic acid); □, 2.72 (acetylene dicarboxylic acid dimethyl ester); ●, 2.03 (diethyl fumarate); △, 2.03 (diethyl maleate)

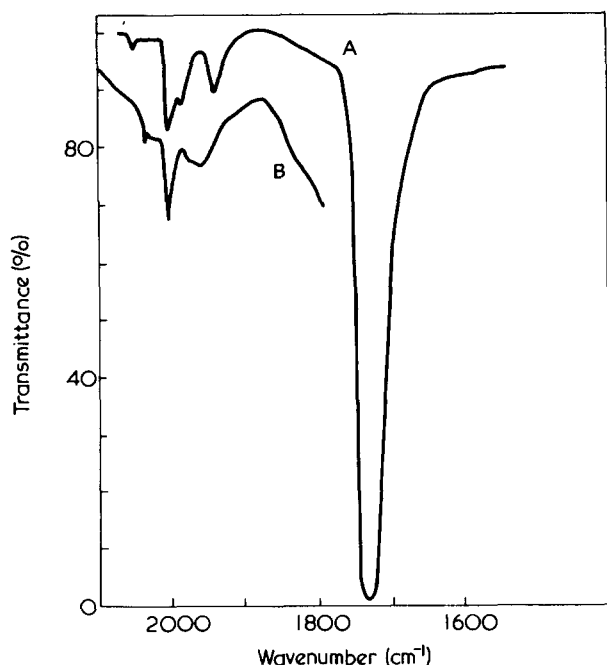
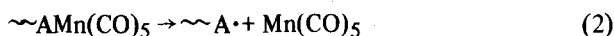


Figure 2 Infrared absorption of poly(methyl methacrylate) prepared by photoinitiation with $\text{Re}_2(\text{CO})_{10}$ + additive. A, additive: acetylene dicarboxylic acid dimethyl ester. B, additive: acetylene

Analysis of purified polymers obtained from methyl methacrylate with the aid of these initiators reveals the presence of Mn or Re atoms and the polymers show infra-red absorption near 2000 cm^{-1} , characteristic of end-groups such as $(\text{CO})_5\text{ReCH}=\text{CH}-$ and $(\text{CO})_5\text{Re}(\text{MeOOC})\text{C}=\text{C}(\text{COOMe})-$ (Figure 2).

In the light of these results we believe that the mechanism of initiation is substantially the same as with the fluoro-olefins. In our opinion these reactions may provide a useful method of introducing functional terminal groups into polymer chains. Acetylene derivatives, $\text{CX}\equiv\text{CH}$ or $\text{CX}\equiv\text{CY}$, where X or Y are functional groups, appear most appropriate for this purpose, in view of the reluctance of these derivatives to polymerize readily by free-radical reactions.

It is of interest that the polymers obtained with the aid of the photoinitiating systems described in this and the preceding section behave as thermal initiators at higher temperatures. As an example we may refer to the polymer obtained from methyl methacrylate with photoinitiation by $\text{Mn}_2(\text{CO})_{10}$ /acetylene dicarboxylic methyl ester, which we may designate as $(\text{CO})_5\text{MnA}\sim\sim$, where A is equivalent to $-(\text{MeOOC})\text{C}=\text{C}(\text{COOMe})-$. At 100°C in solution in a vinyl monomer, this polymer forms macroradicals by reaction (2):

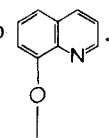


Propagation from $\sim\text{A}\cdot$ leads to the formation of a block copolymer. We have demonstrated the occurrence of this process and are examining its potential value as a general synthetic route to block copolymers¹⁷.

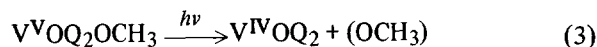
PHOTOCHEMISTRY OF V^{V} DERIVATIVES

In earlier papers^{11,12} we have reported investigations of the photochemistry of $\text{V}^{\text{V}}\text{O}(\text{acac})_2\text{Cl}$ and derivatives of the type $[\text{V}^{\text{V}}\text{O}(\text{acac})_2\text{D}]^+\text{Cl}^-$ obtained from $\text{VO}(\text{acac})_2\text{Cl}$ in the presence of an electron-donor D. More recently¹³, we have described studies of the vanadium chelate

$\text{V}^{\text{V}}\text{OQ}_2\text{OCH}_3$ where Q represents 8-quinolyloxo

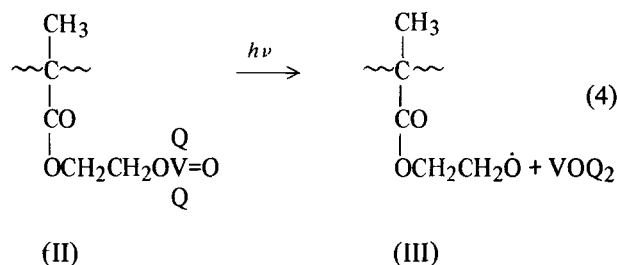


On irradiation with light of wavelength 365 nm, photolysis occurs according to equation (3).



The radical product of equation (3) can initiate free-radical polymerization giving an overall quantum yield 2×10^{-3} . Comparison of the rates of chelate decomposition and initiation of polymerization shows that each chelate molecule photolysed yields one initiating radical. Spin-trapping experiments with benzylidene-(*t*-butyl) amine *N*-oxide in benzene solution reveal the rapid isomerization of the primary $\text{CH}_3\dot{\text{O}}$ radical to CH_2OH . This isomerization is therefore not dependent on the presence of methanol, as some earlier workers suggested¹⁴ (see also ref.15). Photolysis of the chelate VOQ_2OR is a useful general method of producing (OR) radicals in non-aqueous solution.

For present purposes the main interest in these derivatives lies in their incorporation into polymer chains to yield photoactive polymers. Copolymers of methyl methacrylate and hydroxyethyl methacrylate with units (II) containing vanadium have been synthesized.



Photolysis of (II) ($\lambda = 365\text{ nm}$) proceeds by the mechanism described for VOQ_2OCH_3 (equation 4), with formation of a V^{IV} chelate and the macroradical (III) (which may be isomerized). Irradiation in a vinyl monomer therefore leads to graft polymerization and ultimate gelation. As a synthetic route to grafts and networks this technique has the advantage of not producing unwanted homopolymer; further, after reaction, excess vanadium may be removed by treatment with methanol.

The kinetics of photolysis of these photoactive polymers show unexpected complexities¹⁶. The possible dependence of the kinetic behaviour on chain conformation is being examined.

REFERENCES

- Bamford, C. H. in 'Reactions on Polymers', (Ed. J. A. Moore), Nato Advanced Study Institutes Series, Reidel, 1973, p 230
- Bamford, C. H. in 'Reactivity, Mechanism and Structure in Polymer Chemistry', (Eds A. Ledwith and A. D. Jenkins), Wiley, New York, 1973, Ch 3
- Bamford, C. H. and Eastmond, G. C. in 'Recent Advances in Polymer Blends, Grafts and Blocks', (Ed. L. H. Sperling), Plenum, London, 1974, p 165
- Bamford, C. H. and Eastmond, G. C. in 'Copolymers, Polyblends and Composites' (Ed. N. A. J. Platzer), Adv. Chem. Ser. 142, 1975, p 354

New photoinitiating systems and photoactive polymers: C. H. Bamford

- 5 Bamford, C. H. and Mullik, S. U. *Polymer* 1973, **14**, 38
- 6 Bamford, C. H. and Mullik, S. U. *J.C.S., Faraday Trans. I* 1973, **69**, 1127
- 7 Aliwi, S. M., Bamford, C. H. and Mullik, S. U. IUPAC 23rd Int. Symp. *Macromolecules, Madrid*, 1974; *J. Polym. Sci. (C)* 1975, **50**, 33
- 8 Bamford, C. H. and Mullik, S. U. *J.C.S., Faraday Trans. I* 1975, **71**, 625
- 9 Cotton, F. A. *Inorg. Chem.* 1964, **3**, 702; Cotton, F. A. and McCleverty, J. A. *J. Organomet. Chem.* 1965, **4**, 490
- 10 Bamford, C. H. and Mullik, S. U. *J.C.S. Faraday Trans. I* 1976, **72**, 368
- 11 Aliwi, S. M. and Bamford, C. H. *J.C.S. Faraday Trans. I* 1974, **70**, 2092
- 12 Aliwi, S. M. and Bamford, C. H. *J.C.S. Faraday Trans. I* 1975, **71**, 52
- 13 Aliwi, S. M. and Bamford, C. H. *J.C.S. Faraday Trans. I* 1975, **71**, 1733
- 14 Ledwith, A., Russell, P. J. and Sutcliffe, L. H. *Proc. Roy. Soc. (A)* 1973, **322**, 151
- 15 Berdnikov, V. M., Bazhin, N. M., Fedorov, V. K. and Polyakov, O. V. *Kinet. Catal.* 1972, **13**, 986
- 16 Aliwi, S. M. and Bamford, C. H. unpublished results
- 17 Bamford, C. H. and Mullik, S. U. *Polymer* 1976, **17**, 94

Chemorheology of irradiation-cured natural rubbers: 2. Stress relaxation mechanisms of sulphur-containing cured systems in air

Saburo Tamura and Kenkichi Murakami

Chemical Research Institute of Non-aqueous Solutions, Tohoku University, Sendai, Japan
(Received 4 November 1975)

Stress relaxation mechanisms in air were investigated for irradiation-cured natural rubbers (NR) containing the various levels of sulphur, in relation to the crosslinked structure. All the stress relaxation curves of these vulcanizates except the sulphur-free sample were the sum of two exponential terms. The relaxation rate in the long time region increased with increasing sulphur contents, in spite of having the same initial chain density. This behaviour could be explained by introducing the assumption, that this system has two independent networks, i.e. one ($N_p(O)$) based on the polysulphide crosslinkages and another ($N_{c,m}(O)$) based on the mono- and di-sulphide linkages and the carbon-carbon bonds. $N_p(O)$ increased with increasing sulphur contents and $N_{c,m}(O)$ decreased with increasing sulphur contents. The $q_{m,c}(t)$ (the number of moles of main chain scission) were in agreement with each other, independent of the sulphur contents. However, this value was larger than that of the sulphur-free sample. This was similar to irradiation-cured tetramethylthiuram disulphide NR, in which the crosslinking sites consisted of mono- and di-sulphides and carbon-carbon bonds.

INTRODUCTION

In part 1¹, stress relaxation mechanisms were investigated for various curing systems of natural rubber in air, specially the complex crosslinking irradiation-cure systems containing tetramethylthiuram disulphide (TMTD) or sulphur (S) at high temperature. In the case of irradiation-TMTD cures, the stress decay was based on the oxidative scission of the main chain. The number of moles of main chain scission was independent of the ratio, ρ , of initial chain density $N_c(O)$, based on the carbon-carbon crosslinkages, to $N_m(O)$ based on the mono- and di-sulphide linkages. The stress relaxation curve (the relative stress) of irradiation-sulphur cures in air was expressed by the sum of two exponential terms, i.e.:

$$f(t)/f(O) = A \exp(-k_A t) + B \exp(-k_B t) \quad (1)$$

where, $f(O)$ is the initial stress and $f(t)$ is the stress at time t . We suggested that the stress relaxation of these curing systems could be explained by both the interchange reaction of polysulphide linkages (rate constant k_B) and the random scission on the main chain (k_A). However, we did not carry out the quantitative discussion of the relaxation mechanism of these curing systems.

In the present paper, we will attempt to investigate quantitatively, the chemical relaxation of irradiation cured natural rubbers, with varying sulphur contents, in air.

EXPERIMENTAL

Thin sheets (~0.5 mm) of non-crosslinked natural rubber (RSS No 1), were made by cold milling with 0.0, 0.1, 0.25, 0.5, 0.75, 1.0, 2.0, and 3.0 phr of sulphur, and pressing at 145°C. The sheets were cured by exposure to γ -rays from ⁶⁰Co. Total dose of γ -irradiation was 28.8 Mrad. All the samples were extracted with hot acetone for 48 h, in order to eliminate the impurities and the residual sulphur, and were dried *in vacuo*.

Details of stress relaxation methods have been described in a previous paper¹. Stress relaxation was measured (in most cases) at 100°C in air.

RESULT AND DISCUSSION

Crosslinking structure of sulphur irradiation-cured NR

The initial chain density, $N(O)$ (mol/ml) of samples used in this study, was estimated by the statistical theory of rubber-like elasticity. The relation of $N(O)$ and sulphur content (from 0.0 to 2.0 phr) is shown in Figure 1. It can

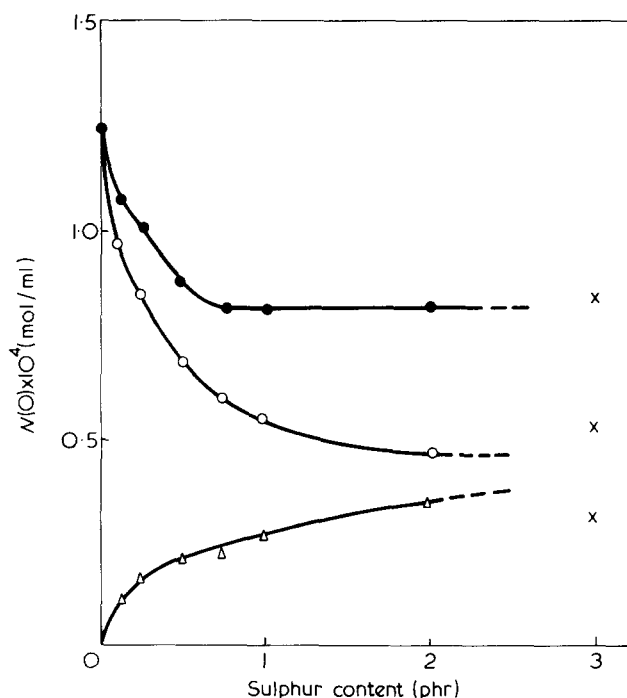


Figure 1 Relation between initial chain density $N(O)$ and sulphur content. ●, $N(O)$; ○, $N_{c,m}(O)$; △, $N_p(O)$

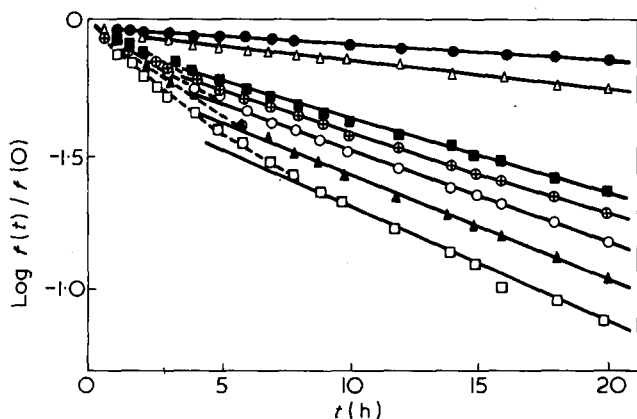


Figure 2 Stress relaxation of irradiation-cured NR containing various levels of sulphur in air at 100°C: ●, free; △, 0.1 phr; ■, 0.25 phr; ⊕, 0.5 phr; ⊙, 0.75 phr; ▲, 1.0 phr; □, 2.0 phr

be seen from this Figure that, as the sulphur level is increased to 0.75 phr, the $N(O)$ value gradually decreases and the value for samples containing 0.75 phr sulphur or more is almost independent of sulphur content. In this Figure, the $N(O)$ value of the sample containing 3.0 phr sulphur (mark X in Figure 1) obtained in the previous paper, is also represented and is slightly larger than others. In the case of γ -irradiation curing, if the sample was prepared at different times, even though the sulphur content was the same and the curing condition the same; good reproducibility of $N(O)$ could not be obtained. Therefore, the comparison between 3.0 phr sample and others is not correct.

The crosslinking site, in these samples, except for the sample not containing sulphur, will consist of carbon-carbon bonds, and mono-, di- and polysulphide linkages.

Figure 2 shows the stress relaxation curves [the logarithm of relative stress $\log f(t)/f(O)$ versus time t (h)] of these samples in air at 100°C. The relaxation curve of the sulphur-free sample ($S = 0$) is represented by a straight line over the range of observation time and is based on the random scission of the main chain, as is well-known¹⁻³. However, the others, i.e. the stress relaxation of sulphur-containing samples, decay rapidly in a short time and then become linear after a longer time. All these curves can be expressed by equation (1). The rapid relaxation at the initial stage increases with increasing sulphur content. This relaxation was discussed in connection with the interchange reaction of polysulphide linkages at length elsewhere^{1,4-6}. On the other hand, the rate of relaxation at a later stage, also increases with increasing sulphur content, despite having the same value of $N(O)$ at 0.75 phr sulphur or more. This behaviour cannot be explained by Tobolsky's theory², related with $N(O)$ only.

The investigation of the relaxation mechanism of these curing systems in the longer time region, will be attempted in some detail. For the discussion, it is necessary to have quantitative information of the crosslinking structures. The carbon-carbon bonds, and mono- and di-sulphide linkages of crosslinkages as mentioned above, seem to be stable for thermal oxidation at this temperature^{1,7}. Now, we define the initial chain density based on these crosslinkages as $N_{c,m}(O)$ and that based on the polysulphide crosslinkages, which are thermally unstable, as $N_p(O)$. Therefore, $N(O)$ is expressed by equation (2):

$$N(O) = N_{c,m}(O) + N_p(O) \quad (2)$$

The initial stress, $f(O)$ and that at time t , $f(t)$, are related to $N(O)$ and to the chain density at time t , $N(t)$, respectively by the following equations²:

$$f(O) = N(O)RT(\alpha - \alpha^{-2}) \quad (3)$$

$$f(t) = N(t)RT(\alpha - \alpha^{-2}) \quad (4)$$

Where, R is the gas constant, T the absolute temperature and α the extension ratio. From equations (2), (3) and (4) we obtain:

$$f(t)/f(O) = N(t)/N(O) = N_{c,m}(t)/N(O) + N_p(t)/N(O) \quad (5)$$

If the stresses associated with $N_{c,m}$ and N_p are $f_{c,m}$ and f_p , respectively, then:

$$\begin{aligned} f(t)/f(O) &= N_{c,m}(t)/N(O) + N_p(t)/N(O) \\ &= f_{c,m}(t)/f(O) + f_p(t)/f(O) \end{aligned} \quad (6)$$

Also, from equations (1) and (6), if $N_{c,m}$ and N_p are presumed to be independent of each other and can be separated into two networks, the following two relations will be valid:

$$f_{c,m}(t)/f(O) = A \exp(-k_A t) \quad (7)$$

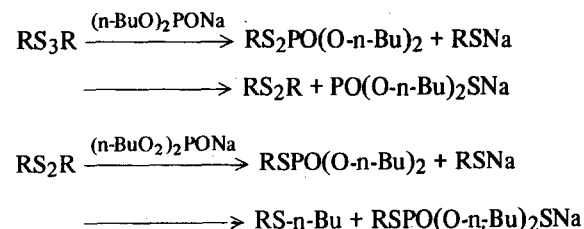
$$f_p(t)/f(O) = B \exp(-k_P t) \quad (8)$$

When $t = 0$:

$$f_{c,m}(O)/f(O) = N_{c,m}(O)/N(O) = A \quad (9)$$

The A value can be estimated directly by extrapolation of $\log f(t)/f(O)$ versus t plot. Therefore, the initial chain density $N_{c,m}(O)$ based on carbon-carbon crosslinkages, mono- and di-sulphide linkages can be calculated from equation (9), and the $N_p(O)$ based on polysulphide linkages is also obtained from equation (2).

For the irradiation-sulphur curing systems, the results estimated by the above method are shown in Figure 1. The value of $N(O)$ of samples containing 0.75 phr sulphur or more, is almost independent of sulphur content, while the $N_{c,m}(O)$ gradually decreases with sulphur content until 2 phr. The question may be raised, whether the above treatment, in particular, the assumption that $N_{c,m}$ and N_p are independent of each other, is correct. As described in the previous paper¹, the value of A [i.e. $N_{c,m}(O)$] estimated from the stress relaxation in air, is in good agreement with that in nitrogen. Therefore, this treatment appears probably, to be correct. If it is not correct, as each relaxation at the later stage is based on the distinct chemical actions (in air as compared with in nitrogen), the A value should be different. In order to confirm the above theory further, we carried out the following experiment. Moore and Trego⁸ reported that poly- and di-sulphide crosslinkages were cleaved in a benzene solution of sodium di-*n*-butyl phosphite, as follows:



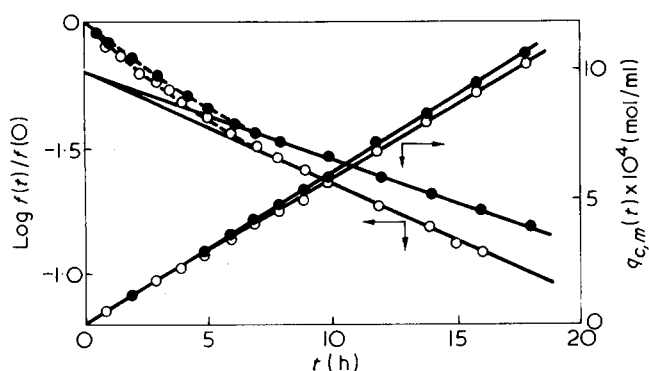


Figure 3 Stress relaxation of irradiation-cured NR, containing 3.0 phr of sulphur having different initial chain density and relation between the number of moles of main chain scission $q_{c,m}(t)$ and time t : \circ , irradiation dose 28.8 Mrad, $N(O) = 0.84 \times 10^{-4}$ mol/ml, and $N_{c,m}(O) = 0.54 \times 10^{-4}$ mol/ml; \times , 43.2 Mrad, $N(O) = 1.13 \times 10^{-4}$ mol/ml, and $N_{c,m}(O) = 0.71 \times 10^{-4}$ mol/ml

The sample containing 3 phr of sulphur, was placed into 0.14 mol/l benzene solution of sodium di-n-butyl phosphite. After nitrogen was passed through the solution for about 10 min, the mixture was sealed *in vacuo*. The reaction was carried out by heating for 24 h at 25°C and then for 4 h at 80°C. After that, the sample was extracted with benzene for 24 h and was dried *in vacuo*. The effective chain density $N'_{c,m}(O)$ of this sample, was estimated by stress-strain measurement, to result in 0.36×10^{-4} mol/ml. The difference between $N'_{c,m}(O)$ and $N_{c,m}(O)$ (0.53×10^{-4} mol/ml) is somewhat large; however if one considers that $N_{c,m}(O)$ is the effective chain density due to carbon-carbon crosslinkages, and mono- and di-sulphide linkages as defined above, it seems to be comparable. Therefore, the above mentioned assumption seems to be correct. In order to confirm our treatment, further, it is necessary to have a detailed knowledge of crosslinking structure in this system.

Chemical stress relaxation of sulphur-irradiation-cured NR

Initially, it is necessary to investigate the stress relaxation of samples having the same sulphur content and having different initial chain density. Though the stress relaxation of such samples, containing 3 phr of sulphur was reported in the previous paper, quantitative results were not concluded. Figure 3 shows some of the results of the previous work. The samples having different initial chain density $N(O)$, were prepared by the alternation of irradiation dose. In that curing system, since the rate of relaxation at a later stage was dependent on $N(O)$, the stress decay was probably based on the oxidative scission of the main chain. The value of $N_{c,m}(O)$ estimated by the above method, was 0.54 mol/ml for 28.8 Mrad irradiation-sample and 0.72 mol/ml for 43.2 Mrad irradiation-sample, respectively. Now, if this sample was assumed to have carbon-carbon, mono- and di-sulphide crosslinkages but not polysulphide linkages, then the stress relaxation will be expressed by:

$$f_{c,m}(t)/f_{c,m}(O) = A' \exp(-k'_A t) \quad (10)$$

In the case of undergoing the random scission on the main chains in the system, the number of moles of main chain scission, $q_{c,m}(t)$, is represented by equation (11), which was proposed by Tobolsky²:

$$q_{c,m}(t) = -N_{c,m}(O) \ln f_{c,m}(t)/f_{c,m}(O) \quad (11)$$

Hence, $q_{c,m}(t)$ can be obtained directly from a stress relaxation measurement. The relation between $q_{c,m}(t)$ and t is also shown in Figure 3. The $q_{c,m}(t)$ is almost independent of $N_{c,m}(O)$. This suggests that the stress decay at the later stage of this sample, is based on the random scission of only the main chain.

Next, we investigate the effect of sulphur content on $q_{c,m}(t)$, which is obtained from Figure 2. The result is shown in Figure 4. It can be seen that the $q_{c,m}(t)$ are almost equivalent, regardless of the sulphur contents, except for the 0.1 phr and the sulphur free samples. This is independent of the ρ values which were defined, in Part 1, as the ratio of the effective chain density $N_c(O)$ based on the carbon-carbon bonds, to $N_m(O)$ based on mono- and di-sulphide linkages and probably varies with sulphur content. Further, this supports the validity of our assumption in Part 1, relating to the result of tetramethylthiuram disulphide (TMTD)-irradiation cured NR having carbon-carbon, mono- and di-sulphide crosslinkages. Both results, however, are not in agreement, i.e. the $q_{c,m}(t)$ estimated from the relaxation of TMTD-irradiation cured NR is significantly larger than that of the sulphur-irradiation cure (Figure 4). Though we are unable to explain the difference definitely, the following two reasons can be considered: (a) in the case of the latter, the gloval network was considered as two independently separated networks (giving rise to $N_{c,m}(O)$ and $N_p(O)$). Consequently, the number of moles of main chain scission which occurred in the $N_p(O)$ network was not estimated. On the other hand, the former case exhibited only the scission of main chain; (b) there is a distinction of stress relaxation mechanisms between both curing systems, i.e. the latter follows the interchange reaction of polysulphide, resulting in the mono- and/or di-sulphide linkages, and the formation of these crosslinkages probably affects somewhat the continuous stress relaxation⁹, while during the former, little crosslinking reaction is considered to occur.

Temperature dependence of the chemical stress relaxation

The temperature dependence of the rate of chemical stress relaxation in air, for all the samples used here, was investigated. The measurements were carried out at 100°, 110° and 120°C. The rate constants of the main chain scission K_A can be obtained from the gradients of stress relaxation at the later stage, and is expressed by the Arrhenius equation:

$$K_A = A \exp(-E_a/RT) \quad (12)$$

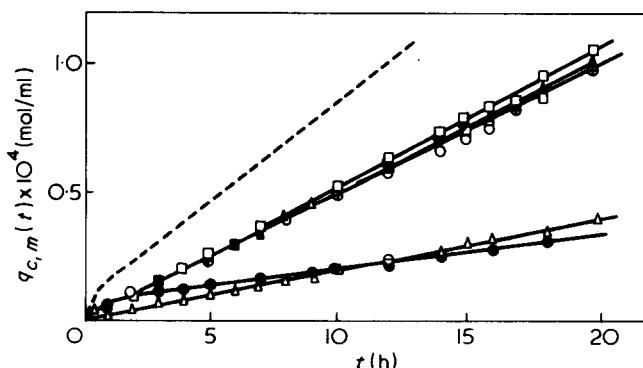


Figure 4 Relation between $q_{c,m}(t)$ and t of irradiation sulphur-cured NR and irradiation-TMTD-cured NR (---); Sulphur: \circ , free; \triangle , 0.1 phr; \square , 0.25 phr; \oplus , 0.5 phr; \odot , 0.75 phr; \blacktriangle , 1.0 phr; \blacksquare , 2.0 phr

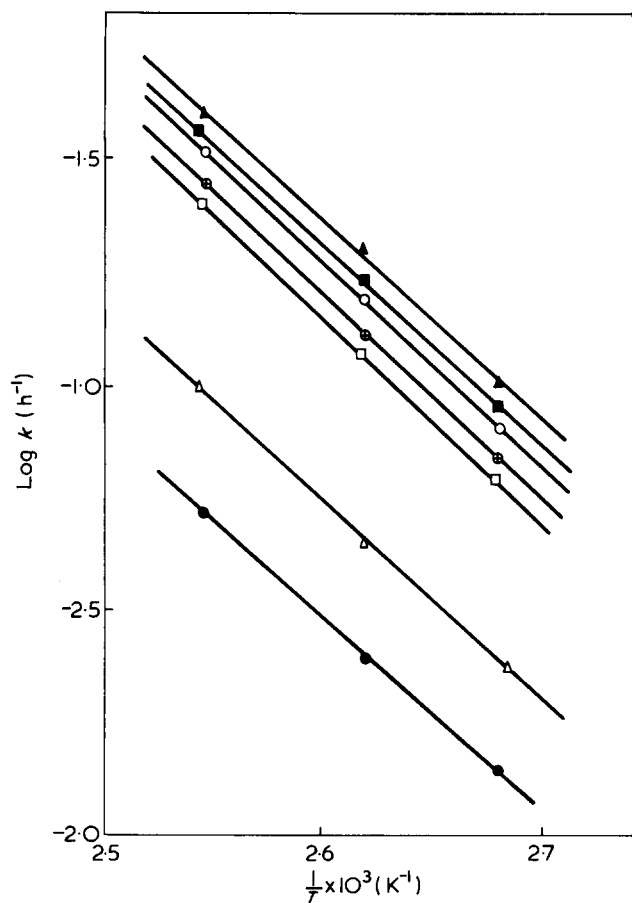


Figure 5 Plot of $\log K$ versus $1/T$ for each sample containing various sulphur levels: ●, free; △, 0.1 phr; □, 0.25 phr; ⊕, 0.5 phr; ○, 0.75 phr; ■, 1.0 phr; ▲, 2.0 phr

where E_a is the apparent activation energy (kcal/mol) for main chain scission reaction. The relation of $\log K_A$ (h^{-1}) and $1/T$ (K) is shown in Figure 5. From the Figure, we find that the value of K_A in this system becomes larger as the sulphur content increases. This result is different from the one related to EPDM¹⁰ or EPR¹¹. In the case of EPDM, the relaxation rate in the longer time region decreases with increasing the sulphur content. The value of E_a for all the samples used here was estimated to be ~ 21 kcal/mol. This value also differs from the one for TMTD-irradiation-cured NR, which was 27 kcal/mol as mentioned in Part 1.

REFERENCES

- 1 Tamura, S. and Murakami, K. *Polymer* 1973, 14, 569
- 2 Tobolsky, A. V. 'Properties and Structure of Polymers', Wiley, New York, 1962
- 3 Tamura, S. and Murakami, K. *J. Appl. Polym. Sci.* 1972, 16, 1149; Dunn, J. R., Scanlan, J. and Watson, W. F. *Trans. Faraday Soc.* 1959, 55, 667
- 4 Murakami, K. and Tamura, S. *J. Polym. Sci. (A-1)* 1971, 9, 423
- 5 Tobolsky, A. V. *J. Polym. Sci. (B)* 1964, 2, 823
- 6 Beevers, R. B. *J. Colloid Sci.* 1964, 19, 40
- 7 Takahashi, Y. and Tobolsky, A. V. *Polym. J.* 1971, 2, 457
- 8 Moore, C. G. and Trego, B. R. *J. Appl. Polym. Sci.* 1964, 8, 1957
- 9 Tobolsky, A. V. and Naganuma, S. *Polym. J.* 1972, 3, 60
- 10 Tamura, S. and Murakami, K. *J. Appl. Polym. Sci.* 1972, 16, 2803
- 11 Dunn, J. R. *J. Macromol. Chem.* 1966, 1, 739

Time dependent effects of pressure on the shear modulus of polypropylene

R. A. Duckett and S. H. Joseph

Department of Physics, University of Leeds, Leeds LS2 9JT, UK

(Received 15 September 1975)

The time dependent changes in the shear modulus of polypropylene have been followed subsequent to both step and ramp changes in pressure for pressures up to 400 MN/m². Although the changes in pressure (*P*-jumps) are accompanied by transient heating effects which complicate the interpretation of the results; large changes in modulus can be seen at times of up to three hours after the pressure change. At these times the effects of temperature changes would be expected to be negligible. The results are consistent with the expected changes of free volume occurring during the dilatational creep under pressure, and lend no support to the 'microstress' theory recently proposed.

INTRODUCTION

It is now well established that hydrostatic pressure can have a considerable effect on the physical properties of polymers. This has stimulated interest in relating the effects of pressure to those of temperature and time or frequency. Considerably less effort has so far been invested in studying the transient response of the polymer to changes in pressure, although this is also of considerable significance. There have recently been suggestions regarding the possible forms of the response to changes in pressure. One proposal¹⁻³ is that a change in pressure, the same as a change in temperature, induces a volume change which is accompanied by the generation of microstresses around structural heterogeneities such as crystallites. These microstresses combined with the usual type of non-linear behaviour produce an anomalously low value of the modulus. As the microstresses decay with time the modulus rises steadily towards the linear value appropriate to the new conditions, regardless of whether the change in temperature or pressure is positive or negative. A completely different approach suggests that changes in pressure cause changes in the free volume in the polymer, as the dilatational creep progresses. These free volume changes will also affect most physical properties of the material and furthermore the 'sense' of the changes would be expected to depend on whether the pressure is increased or decreased.

There are thus distinct qualitative differences between these two approaches. In an attempt to discern which of these applies to polypropylene we have investigated the time dependence of the large changes in the shear modulus following positive and negative changes in hydrostatic pressure (*P*-jumps) by performing torsion tests at constant twist rate, at different elapsed times from the *P*-jump. It turns out that the results of these experiments are complicated by the concomitant changes in temperature induced by the changes in pressure, in both the pressure transmitting fluid and in the polymer. In order to investigate the contribution to this temperature rise by the polymer itself, temperature changes due to adiabatic compression of polypropylene were studied using a constrained uniaxial compression cell. An alternative approach to the investigation of the time dependent shear modulus, involving the use of hydrostatic pressure increasing at constant ramp rates, was also used. This results in a closer approximation to iso-

thermal conditions, and provides more accurate temperature control.

Although little previous work has been carried out directly on time dependent modulus changes following changes in pressure or temperature¹⁻³, the changes in modulus on the free volume scheme are expected to relate to total volume changes under such conditions. Such time dependent volume measurements have been made following small changes in temperature and pressure⁴ and following large changes in temperature⁵ in amorphous polymers near their dilatational glass transition temperature (*T_g*). Volume creep in several polymers has also been investigated at high pressures^{6,7}. There are more data available on the static effects of hydrostatic pressure on both shear and bulk moduli; such data have been reviewed⁸ and we refer especially here to torsion pendulum data for polypropylene⁹.

EXPERIMENTAL

Torsion tests

Full details of the apparatus and specimens will be presented elsewhere¹⁰ so here we give only a brief description. The apparatus is a modified version of that previously described¹¹. Right solid cylindrical specimens of isotropic isotactic polypropylene (PP), density 909.5 ± 0.1 kg/m³, are subjected to a constant rate of twist whilst under hydrostatic pressure applied via Plexol 201 lubricant (diethyl dihexyl sebacate). The specimen design minimizes the magnitude of end effects, thus enabling the strain in the specimen to be deduced accurately from the angle of twist of the grips, which can be monitored outside the pressure vessel. Torque is also continuously monitored via an angular transducer mounted on the torque tube, and the torque-twist curve for the specimen for small angles of twist is recorded on an X-Y recorder. From this curve the stress-strain curve for small strains under constant strain rate conditions may be deduced¹⁰. The vessel temperature is governed by a water bath controlled to ±0.3°C surrounding the vessel.

The first two testing programmes followed the pressure schedule shown in *Figure 1*. Each step in pressure corresponded to 30 MN/m² in the first programme and to 100 MN/m² in the second. The specimen was loaded into the vessel and allowed to come to equilibrium at the testing

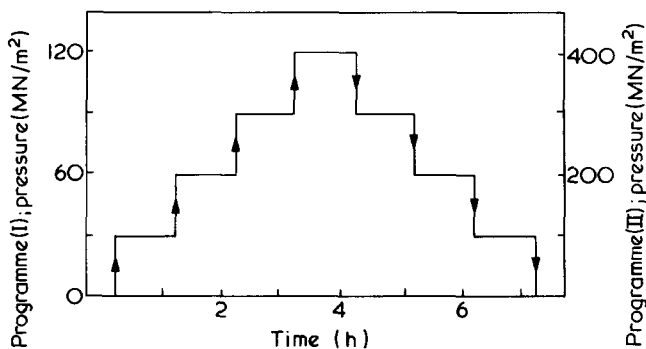


Figure 1 Pressure schedule for the first two testing programmes (I) and (II). In each case step length, approximately 3600 sec. Pressure 'step-height' (I) 30 MN/m²; (II) 100 MN/m²

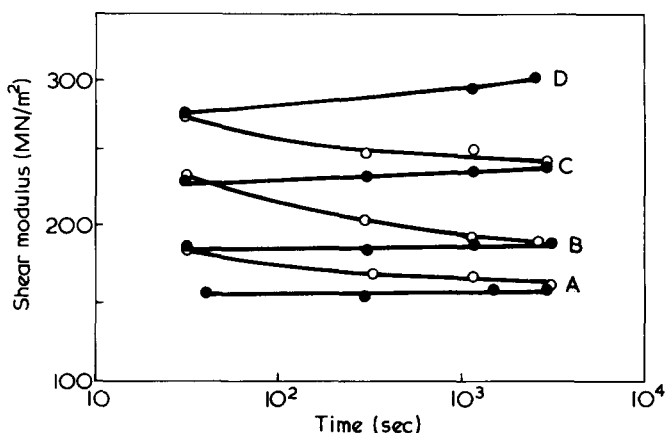


Figure 2 Shear modulus vs. time under pressure (logarithmic scale) according to testing programme (I), (see Figure 1). Pressures: A, 30 MN/m²; B, 60 MN/m²; C, 90 MN/m²; D, 120 MN/m². ●, pressure increasing; ○, pressure decreasing

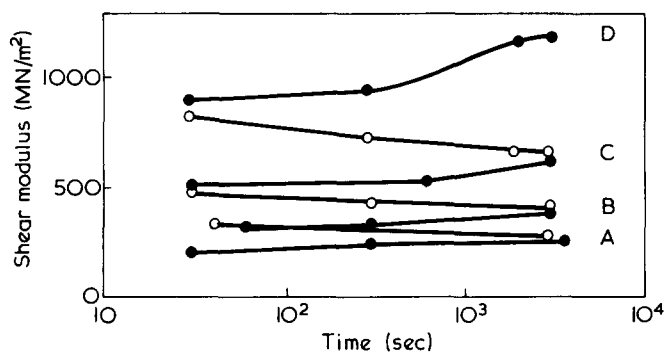


Figure 3 Shear modulus vs. time under pressure (logarithmic scale) according to testing programme (II), (see Figure 1). Pressures: A, 100 MN/m²; B, 200 MN/m²; C, 300 MN/m²; D, 400 MN/m². ●, pressure increasing; ○, pressure decreasing

temperature for at least 12 h at atmospheric pressure. A torsion test was then performed at a rate equivalent to a strain rate of 1.1×10^{-3} /sec, up to a maximum strain of 2.5×10^{-2} . The specimen was immediately unloaded to zero torque and allowed to recover for 300 sec. The pressure was then changed to the first in the schedule (30 MN/m² for the first programme), at a rate of 5 MN/m² sec and a sequence of the above torsion tests performed at convenient logarithmically spaced times, i.e. at about 30 sec, 300 sec, 1000 sec, 3000 sec after the achievement of the new pressure. Then, after a further recovery period of 300 sec from the final test in the sequence, the pressure was changed to the next on the schedule, and the same sequence of torsion tests performed again, under the new constant

pressure. In this way the whole of the pressure schedule is completed. The results, 2% secant modulus values against elapsed time, at 58°C, are plotted in Figures 2 and 3.

In the second pair of testing programmes the effects of starting at atmospheric pressure and increasing directly to constant pressures of 100, 200, 300 and 400 MN/m² were examined (see Figure 4) at 39°C and 58°C. After application of the hydrostatic pressure the above time sequence of tests was performed; graphs of the modulus vs. elapsed time are shown in Figures 5 and 6.

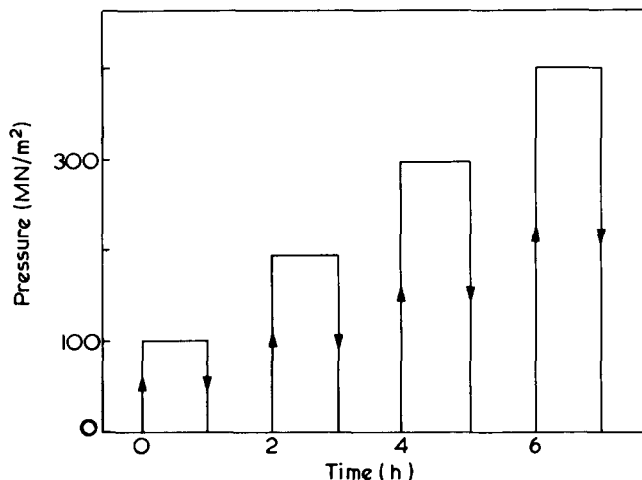


Figure 4 Second pressure schedule, showing the pressure increased rapidly from atmospheric to each of 100, 200, 300 and 400 MN/m² in turn. The time at atmospheric pressure between tests was approximately 3600 sec

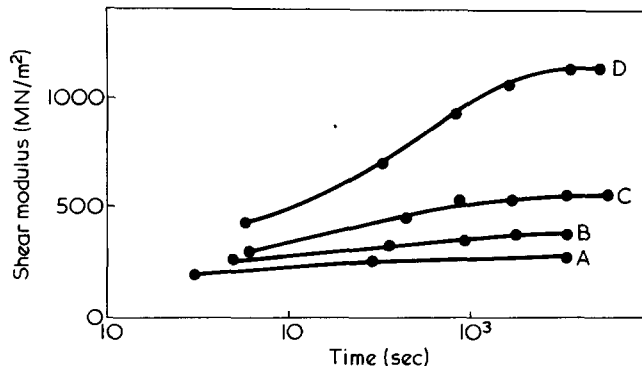


Figure 5 Shear modulus vs. time under pressure (logarithmic scale) according to second pressure schedule (see Figure 4). Pressures: A, 100 MN/m²; B, 200 MN/m²; C, 300 MN/m²; D, 400 MN/m². Nominal temperature 58°C

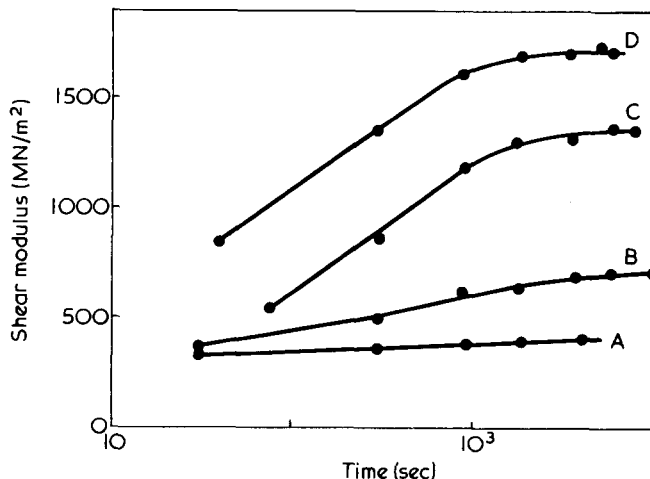


Figure 6 Shear modulus vs. time under pressure according to second pressure schedule. Pressures as in Figure 5. Nominal temperature 21°C

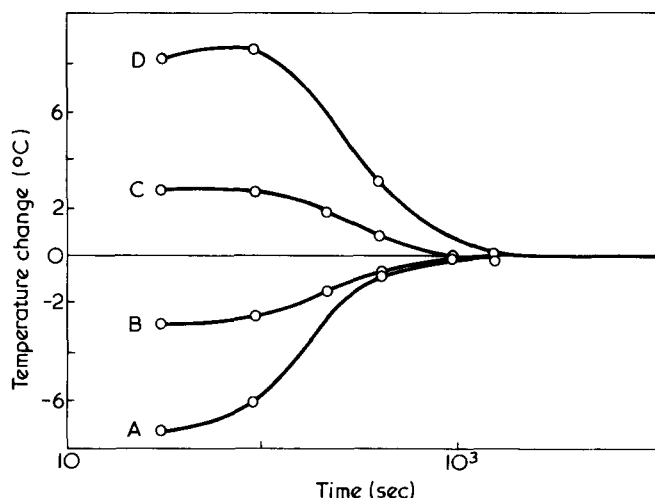


Figure 7 Temperature changes due to P -jumps. The temperature was measured at the surface of the specimen using copper resistance thermometry. Pressure changes involved are: A, -100 MN/m^2 ; B, -30 MN/m^2 ; C, $+30 \text{ MN/m}^2$; D, $+100 \text{ MN/m}^2$

Temperature effects

In the hydrostatic fluid system. Findley, Reed and Stern⁶ have pointed out the need to consider temperature changes caused by adiabatic compression of hydrostatic pressure fluid. The temperature changes in our system are shown in Figure 7 for changes in pressure of $\pm 100 \text{ MN/m}^2$ and $\pm 30 \text{ MN/m}^2$. The temperature was found to rise at the rate of $0.09^\circ\text{C} (\text{MN/m}^2)^{-1}$ at pressures of up to 100 MN/m^2 , the rate dropping slightly to about $0.06^\circ\text{C} (\text{MN/m}^2)^{-1}$ for pressures above 200 MN/m^2 . This resulted in temperature changes of up to 25°C for a 400 MN/m^2 change in pressure. At all pressures, the temperature rise decayed with a time constant of approximately 340 sec as the centre of the vessel came into equilibrium with the bath.

The temperatures above were measured using the change in resistance in a copper coil of resistance approximately 20 ohms wound in a single layer on a PP former. Thus the temperature measured was at the PP-fluid surface. In order to check that a significant amount of the polymer also experienced these temperatures, the temperature measurement was repeated after coating the coil with latex to a thickness of 1.5 mm. Similar temperature-time profiles were found as before, but delayed in time by about 40 sec. The resistance thermometry was checked against mercury-in-glass thermometers at atmospheric pressure, and had absolute accuracy better than $\pm 0.5^\circ\text{C}$. The pressure coefficient of resistance of copper¹² is such that the error in temperature measurement due to pressure changes with this method is less than $0.005^\circ\text{C} (\text{MN/m}^2)^{-1}$. Thus with this method we are able to find the temperature changes that have occurred within the specimen after the P -jump experiments.

Within the polymer. In the case of PP, as with polymers in a rubbery state, the bulk modulus and density are of the same magnitude to those of oils, and there is a considerable temperature change on the application of pressure. It is readily shown¹³ that for a reversible adiabatic change:

$$\left(\frac{\partial T}{\partial P}\right)_s = \frac{\alpha VT}{C_p} \quad (1)$$

where α , V and C_p are the coefficient of cubical expansion, specific volume and specific heat at constant pressure respectively.

Using appropriate engineering data values* for PP we get:

$$\left(\frac{\partial T}{\partial P}\right)_s = 0.06^\circ\text{C} (\text{MN/m}^2)^{-1} \text{ at } 20^\circ\text{C}$$

To examine this for PP we constructed, to fit an Instron compression/tension test machine, a simple pressure cell in which the specimen is restrained from lateral expansion during axial compression (see Figure 8). The highest pressure used was 150 MN/m^2 . The specimens were 13 mm diameter \times 15 mm long and had a 34 swg chromel-alumel thermocouple inserted into a 0.9 mm diameter axial hole filled with grease, so that the junction was centrally placed within the specimen.

In this mode of deformation the effective modulus of the specimen M can be shown to be:

$$M = K + \frac{4}{3}G \quad (2)$$

where K is the bulk modulus and G the shear modulus. To check the operation of the cell, load deflection curves were plotted at low strain rate ($6.4 \times 10^{-5}/\text{sec}$) to ensure isothermal conditions, and the experimental value of M found for pressures less than 45 MN/m^2 was in good agreement with estimates based on published values of K and G at atmospheric pressure^{7,10}. Above this pressure, M was seen to rise, an effect we attribute to an increase in K and G at high pressures offset by the slight decrease in G at high shear strains. (For very low loads, corresponding to pressures less than 15 MN/m^2 , there is a region of low modulus where the specimen is effectively under unconstrained uniaxial compression before play is taken up and lateral strain is eliminated).

To investigate the adiabatic heating effect intrinsic to the polymer, the following sequence of tests was performed: a nearly static load was applied to the specimen, and load cell and thermocouple outputs continuously recorded.

* $\alpha = 3.3 \times 10^{-4} (\text{C}^\circ)^{-1}$ at 20°C and $C_p = 1.8 \text{ kJ/kg}$

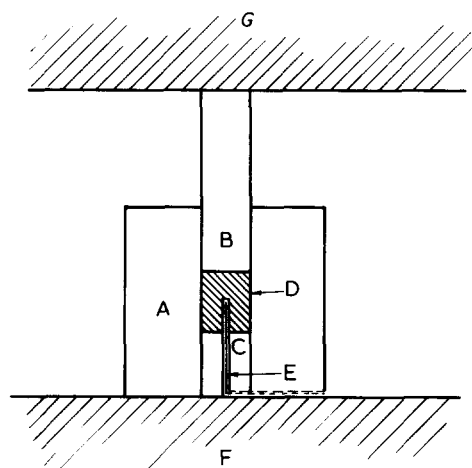


Figure 8 The constrained uniaxial compression cell used in conjunction with an Instron machine for compression beneath the crosshead. A, mild steel cylinder; B and C, mild steel push-rods; D, polypropylene specimen; E, thermocouple; F, Instron compression load-cell anvil; G, anvil attached to underside of moveable crosshead

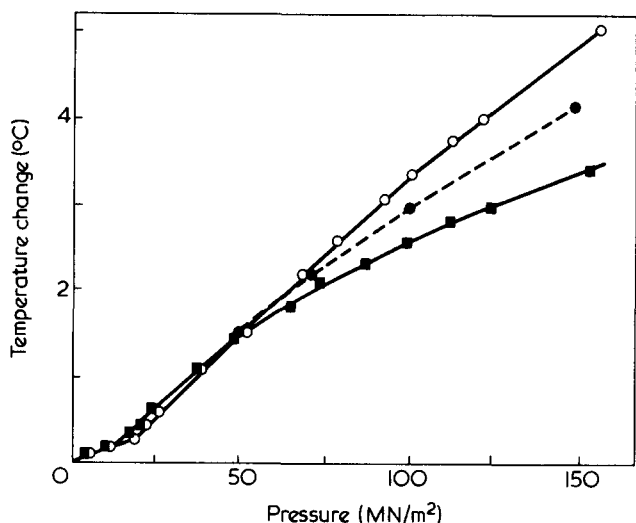


Figure 9 Temperature changes measured using the constrained uniaxial compression cell. ○, compression; ■, decomposition; ●, calculated from decompression curve corrected for viscous work done (see text)

Loading was achieved through a nominal strain rate of 6×10^{-3} /sec corresponding to a maximum loading time of 10 sec. When the temperature once again became static (after approximately 1000 sec) the load was rapidly removed (unloading time ~ 0.1 sec). In Figure 9 the peak temperature change is plotted against the pressure change for both unloading and loading. We see a region at low stress corresponding to unconstrained uniaxial compression. Then for pressures greater than 15 MN/m² the temperature changes are linearly dependent on pressure, and equal and opposite for compression and decompression, with a temperature coefficient of $0.04^\circ\text{C}(\text{MN}/\text{m}^2)^{-1}$. There is a discrepancy between the temperature coefficient found here and that calculated above using standard engineering data values for C_p and α . This may be merely due to differences between samples of polypropylene, but may also reflect the shorter times involved in this experiment compared with those usually involved in measurements of α and C_p .

Using the measured value of $(\partial T/\partial P)_s = 0.04^\circ\text{C}(\text{MN}/\text{m}^2)^{-1}$ the low stress region of Figure 9 has also been analysed and the measured temperature changes are consistent with the interpretation of unconstrained uniaxial deformation.

At stresses greater than 50 MN/m² the temperature changes for compression, $|\Delta T_+|$, exceed those observed for decompression, $|\Delta T_-|$. Further tests indicate that the values approach each other at low strain rates, extending the pressure range for which $|\Delta T_+| \sim |\Delta T_-|$.

To assess the possibility that the divergence between $|\Delta T_+|$ and $|\Delta T_-|$ is due to temperature changes arising from viscous work done, which being positive in sign, will increase $|\Delta T_+|$ but decrease $|\Delta T_-|$, we have calculated the temperature change ΔT_v expected for a standard linear solid. Assuming that K is elastic, that the shear modulus G has an unrelaxed value $G_u = 2100 \text{ MN}/\text{m}^2$ and a relaxed value $G_r = 450 \text{ MN}/\text{m}^2$, and that the load is changed in a time very much smaller than the creep relaxation time, we find that $\Delta T_v = 3.5 \times 10^{-5} (\Delta P)^2 (\text{C})$, where ΔP is the pressure change in MN/m². Values of $|\Delta T_-| + |\Delta T_v|$ are plotted in Figure 9 and are seen to lie approximately midway between the two curves for $|\Delta T_+|$ and $|\Delta T_-|$. Although the excellent agreement obtained may be somewhat fortuitous in view of the simplicity of the model assumed, it does seem to indicate that the difference between $|\Delta T_+|$ and $|\Delta T_-|$ is due to viscous heating.

If we write $|\Delta T_{\pm}| = |\pm\Delta T_p + \Delta T_v|$, then it can be seen from Figure 9 that $\Delta T_p/\Delta P$ decreases at higher pressures. This is as expected from the changes in α and C_p as pressure increases and the β transition is approached.

Pressure ramp experiments

We have shown that the rapid changes in pressure involved in the P -jump experiment necessarily implies transient heating effects of up to 25°C for P -jumps of $400 \text{ MN}/\text{m}^2$. In the next section we discuss the additional complexities of interpretation arising from this temperature change. To observe changes in modulus under more nearly isothermal conditions we have performed tests in which the pressure is increased at a constant rate and the modulus is measured at convenient intervals of pressure. (We refer to these as a pressure ramp experiments). In these experiments an initial rise in temperature of the vessel is seen, but the constant heat input due to the ramp results in an equilibrium temperature being obtained within 500 sec, at which temperature losses from the fluid to the surrounding water bath are equal to the heat input. Thus by presetting the bath temperature slightly below the desired experimental temperature by an amount calculable from the thermal characteristics of the vessel, we can achieve a well defined temperature which is effectively constant throughout the pressure ramp.

With this pressure ramp experiment we have attempted to detect the effects of varying ramp rate within the range 67 and $1200 \text{ MN}/\text{m}^2 \text{ h}$. At the higher rates it is possible that the pressure can be applied in times less than the volumetric creep relaxation time, whereas at low rates the polymer might be able to creep sufficiently fast to remain in equilibrium with the pressure at all times. In Figure 10 the results of such ramp experiments are shown, at tem-

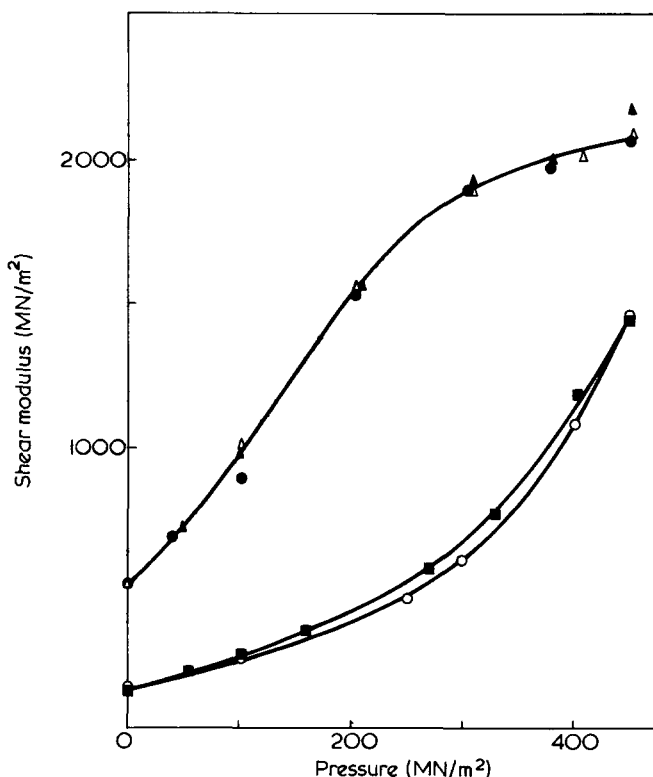


Figure 10 Shear modulus vs. pressure, from pressure ramp experiments. At temperature = 21°C : ▲, $67 \text{ MN}/\text{m}^2 \text{ h}$; ●, $400 \text{ MN}/\text{m}^2 \text{ h}$; △, $1207 \text{ MN}/\text{m}^2 \text{ h}$. At temperature = 58°C : ■, $67 \text{ MN}/\text{m}^2 \text{ h}$; ○, $400 \text{ MN}/\text{m}^2 \text{ h}$

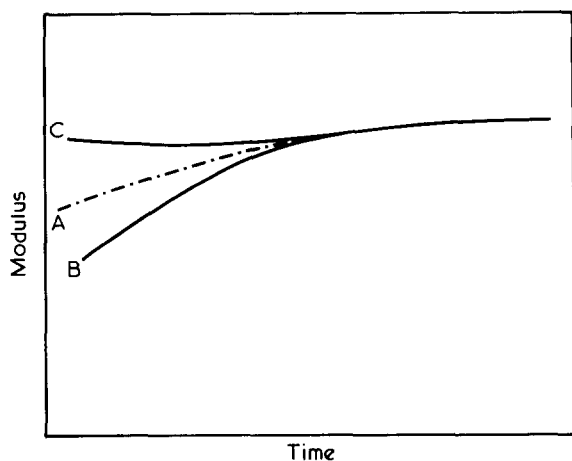


Figure 11 Modulus changes expected following step changes in pressure according to the microstress theory. A, (— · —) compression or decompression assuming no temperature change; B, compression, allowing for initial temperature rise; C, decompression allowing for initial fall in temperature

peratures of 58°C and 21°C. (Where necessary small corrections for errors in temperature setting have been made.) It can be seen that at both temperatures the modulus increases with increasing pressure, and that there is a qualitative similarity to the effects of increasing frequency. Also, to within experimental accuracy, the only detectable effect of ramp rate has been at 58°C and below 400 MN/m² pressure, although the rate effects might have been expected to be more apparent in the glass transition region, say at 30°C, 200 MN/m².

DISCUSSION

Modulus changes on pressurization

The data in Figures 2, 4, 5, 6 and 10 show clearly the development in time of the changes in shear modulus of PP subsequent to changes in pressure. The curves indicate that the hydrostatic pressure is taking the polymer through its glass (β) transition. The data show that the changes in modulus are quantitatively consistent with the idea that the modulus is closely related to the volume of the specimen during loading and unloading; i.e. the application of pressure reduces free volume, and hence lengthens the relaxation times in the polymer.

For $P\uparrow$ steps the fraction of the modulus change that occurs in the time interval 30 to 3000 sec increases with pressure, as one would expect on the basis that the higher pressures cause slowing down of the bulk creep process and hence the modulus change. The $P\downarrow$ steps show marked asymmetry compared to the $P\uparrow$ steps in that the process appears slower for pressure release than for pressure increase.

However, the temperature changes resulting from the P -jump complicates any interpretation of the results. For times less than 1000 sec from the pressure change some sort of temperature correction is required. Findley *et al.*⁵ corrected their hydrostatic creep data for temperature effects using the instantaneous temperatures and the coefficient of volume expansion. The efficacy of such a correction in our case is doubtful, both because of the increased theoretical complexity involved in dealing with dynamic pressure and temperature changes and their effects on modulus in the transition region, and also because of their

findings of its inability to describe the results from partial release of pressure experiments.

Hutchinson and McCrum¹ proposed an alternative mechanism for time dependent changes in modulus in crystalline polymers following jumps in temperature or pressure. They proposed that the relaxation of microstresses generated by P -jumps would lead to a time dependent hardening as shown in Figure 11, curve A. However if we allow for the appropriate temperature changes we would expect curves B and C for $P\uparrow$ and $P\downarrow$ respectively. Comparison with Figure 2 indicates no support for the microstress hypothesis. It should be pointed out that PP does not show microstress effects in T -jump experiments either, unlike the polyethylene used by Hutchinson and McCrum^{1,3}.

A more helpful way of interpreting the P -jump results is to consider the temperature rise as partially negating the compression effects for a period up to 1000 sec. We can therefore attempt to interpret the data on the basis of an isothermal experiment in which the pressure is applied fairly gradually, and look to see if there are any changes in the modulus at times long compared with the effective rise time of the pressure. The data in Figures 2 and 3 show that as pressure increases, there is an increase both in the rate of change of modulus with pressure, and in the fraction of modulus change that takes place in the observed time interval, independent of the sign of the pressure change. This is consistent with the onset of the β transition as pressure increases. In Figures 5 and 6 we see the large modulus changes involved in the transition region, and also definite evidence of time dependence of modulus not only at times greater than 1000 sec but even at a time of 3 h, thus showing the need for working at a consistent time under pressure when investigating the dependence of modulus on pressure. A more quantitative analysis of these data is difficult in view of the temperature changes, not only as they instantaneously affect the modulus but also because temperature history can affect the modulus at a later time¹. However, the results here qualitatively agree with the ideas of temperature dependent bulk-viscosity as applied by Kovacs^{5,14} to his data on volume changes following a temperature change. As a transition temperature is approached (in the case of Kovacs, T_g for PVAC) the bulk processes slow down, as do shear processes, until bulk relaxation times are of the order of experimental times. If we further assume that the free volume affects the relaxation time and hence the modulus as in the WLF approach, then changes in modulus following P -jumps will become larger and slower with increasing pressure, as found in the present investigation.

However, when we look at the pressure ramp experiments in this light, we would expect to find that as pressure rises the bulk relaxation time should increase until at a pressure P_1 it becomes greater than the time allowed by the ramp rate. At pressures greater than P_1 the volume and hence the modulus should depend on the ramp rate, modulus being higher for lower ramp rate due to the greater degree of bulk contraction allowed by the longer times involved. Thus a bulk dispersion region should be revealed by these modulus measurements. Despite the slight dispersion seen at 58°C (Figure 10) there is none in the measurements at 21°C for which one would expect to see a higher dispersion as the transition region is swept through. Thus we conclude that at the rates we are able to employ, the shear dispersion region occurs at a lower pressure than the bulk dispersion region. This agrees with available evidence on bulk and shear relaxation times in glass forming liquids¹⁵ and poly(vinyl

acetate) (PVAC)^{16,17} which show that shear relaxation times are greater than bulk relaxation times. That is, in terms of the pressure ramp experiment, the bulk processes are relaxed throughout the shear β transition region.

Adiabatic heating

The adiabatic heating effect is of much greater experimental importance in studying modulus changes following a pressure jump than it is in studying volume changes. The adiabatic heating has been correctly ignored in volume measurements⁴. This is justified for PP as follows: equal changes in volume are produced by $\sim 1 \text{ MN/m}^2$ pressure change and 1°C temperature change at 20°C . However, the adiabatic heating effect produces only 0.04°C temperature change for 1 MN/m^2 pressure change. If the change in volume due to change in temperature following a P -jump is ΔV_θ , and the total change in volume consequent on the jump is ΔV , then $\Delta V_\theta \simeq 0.04\Delta V$. In volume change experiments⁴ the volume seen to relax in the experimental time scale is greater than $0.4 \times \Delta V$, i.e. an order of magnitude larger than ΔV_θ . However, in the case of modulus measurements the situation is different: equal changes of modulus are produced by 10 MN/m^2 and 1°C ⁸, and the adiabatic heating produces a temperature change of 0.4°C for 10 MN/m^2 pressure change. Thus the difference between shear modulus changes resulting from adiabatic or isothermal pressure changes is much more significant than the difference between adiabatic and isothermal bulk moduli.

The experimental precision achieved here in studying the adiabatic heating phenomenon could be much improved by the use of a pure hydrostatic pressure apparatus^{6,7}. This would enable the bulk processes in transition regions to be investigated via the temperature changes produced by application of pressure. Such investigations would hope to reveal both thermodynamic effects of changes in specific heat and thermal expansion coefficient as included in equation (1) on passing through the transition, and also viscous heating effects associated with the bulk compression.

CONCLUSIONS

Considerable changes in the shear modulus of isotropic polypropylene have been observed subsequent to changes in

hydrostatic pressure. In qualitative terms the effects on the shear modulus of increasing pressure are similar to those of decreasing temperature and take the polymer through its glass transition. The increases in modulus, which can occur over periods up to three hours after the pressure change, are consistent with a relaxation of free volume during the period of hydrostatic creep. The data lend no support to the 'microstress' hypothesis recently proposed.

Subsidiary experiments have revealed that the pressure changes are also accompanied by significant temperature changes; no reliable method of correcting the data for these temperature changes can be proposed.

ACKNOWLEDGEMENTS

S. H. J. was supported by a Science Research Council studentship throughout this work. We are grateful to Dr J. S. C. Parry of Bristol University for the design and construction of the basic torsion apparatus.

REFERENCES

- 1 Hutchinson, J. M. and McCrum, N. G. *Nature* 1974, **252**, 295
- 2 Parry Jones, E. and Tabor, D. *J. Mater. Sci.* 1974, **9**, 289
- 3 Hutchinson, J. M., Mathews, J. F. and McCrum, N. G. (1973). *Proc. 2nd Int. Conf. on Yield deformation and Fracture of Polymers, Cambridge, 1973*
- 4 Rehage, G. and Goldbach, G. *Ber. Bunsenges. Phys. Chem* 1966, **70**, 1144
- 5 Kovacs, A. J. *Adv. Polym. Sci.* 1963, **3**, 394
- 6 Findley, W. N., Reed, A. M. and Stern, P. *Mod. Plast.* 1968, **45**, 141
- 7 Mallon, P. J. and Benham, P. P. *Plast. Polym.* 1972, **40**, 77
- 8 Jones Parry, E. and Tabor, D. *J. Mater. Sci.* 1973, **8**, 1510
- 9 Jones Parry, E. and Tabor, D. *Polymer* 1973, **14**, 617
- 10 Duckett, R. A. and Joseph, S. H. to be published
- 11 Rabinowitz, S., Ward, I. M. and Parry, J. S. C. *J. Mater. Sci.* 1970, **5**, 29
- 12 'International Critical Tables', McGraw-Hill, New York, 1935, Vol 6, p 137
- 13 Zemansky, M. W. 'Heat and Thermodynamics', McGraw Hill, New York, 4th Edn. 1957, p 248
- 14 Kovacs, A. J. *Trans. Soc. Rheol.* 1961, **5**, 285
- 15 Litovitz, T. A. and Davies, C. M. in 'Physical Acoustics' (Ed. Warren P. Mason) 1965, Vol 2, p 281
- 16 McKinney, J. E. and Belcher, H. V. *J. Res. Nat. Bur. Stand. (A)* 1963, **67**, 43
- 17 Williams, M. L. and Ferry, J. D. *J. Colloid Sci.* 1954, **9**, 479

Craze growth and crack growth in poly(vinyl chloride) under monotonic and fatigue loading

N. J. Mills and N. Walker

Department of Physical Metallurgy and Science of Materials, University of Birmingham, Birmingham, B15 2TT, UK

(Received 9 October 1975; revised 10 December 1975)

Cracks in poly(vinyl chloride) sheet were loaded to known stress intensity factors and the craze length measured. These measurements, and the craze thickness profile, were compared with the Dugdale model of crack tip yielding. The fracture toughness of poly(vinyl chloride) was measured, and an analysis made of circular 'advance fractures' that occur on the fracture surface. Fatigue crack growth studies confirmed that crack growth occurs discontinuously once every few hundred cycles, and showed that the craze fracture mechanism is quite different from the monotonic loading failure mechanism.

INTRODUCTION

This research forms part of a fracture mechanics programme on glassy polymers. By studying the brittle fracture processes, and analysing them using fracture mechanics, it is hoped both to produce design data, and to aid the analysis of more complex situations, such as notched impact tests.

In an early investigation¹ of fracture surfaces of poly(vinyl chloride) (PVC), no evidence for crazing was found. However subsequent research has shown that PVC under tensile stress will craze from the surface^{2,3}. It has also been found that the process of notching PVC can produce a bundle of crazes at the notch tip⁴. Therefore any treatment of crack tip plasticity in PVC should take into account the possibility of crazing.

Elinck *et al.*⁵, in their study of fatigue crack growth in PVC, observed regular striations on the fracture surface. They used the Dugdale model⁶ of plasticity at a crack tip, to relate the striation spacing to the ratio of maximum applied stress to the yield stress. They were unable to observe crack tip events since they used red pigmented PVC, but they established that the number of striations was approximately one two hundredth of the number of cycles of loading. A subsequent investigation with transparent PVC⁷ showed that craze growth at the crack tip was continuous during fatigue, and that the crack tip advanced discontinuously. The fatigue crack growth tests^{5,7} covered only a limited range of the stress intensity range ΔK , and did not investigate the effect of the mean stress intensity K_m on the growth rate. It was felt that a more comprehensive investigation was justified, in view of the deviation from the usual rule of one cycle per striation.

Kambour⁸ observed the thickness profiles of crazes that grew at a crack tip under monotonic loading, and Cotterell⁹ subsequently applied the Dugdale model to these data. More recently¹⁰, the complete shape of a craze at a crack tip in poly(methyl methacrylate) has been shown to fit the Dugdale model. If this can also be shown to be true for PVC it would give further support for the use of the Dugdale model to interpret fatigue crack growth. Since Rice¹¹, has extended the model to deal with loading/unloading situations, it should be possible to relate the observed reverse plastic zone size to the stress-strain behaviour of the craze.

THEORY

Application of the Dugdale model of yielding at a crack to crazing

Dugdale⁶ considered the problem of a central slit in a thin sheet of material, with an applied tensile stress σ perpendicular to the slit (*Figure 1*). He assumed that: (a) the plastic zone is confined to the line of the slit; (b) the stress in the yielded zone has a constant value σ_0 ; (c) at the extremity of the yielded zone there is no stress singularity. He applied the elastic stress field methods of Muskhelishvili¹² and found that the plastic zone length R is related to the crack half length a , and to the applied stress by:

$$R/a = \sec(\pi\sigma/2\sigma_0) - 1 \quad (1)$$

$$\simeq \frac{1}{2}(\pi\sigma/2\sigma_0)^2 \text{ for } \sigma < 0.3 \sigma_0$$

The conditions when this last approximation can be used are usually referred to as small scale yielding. Under these conditions, Rice¹¹ used Westergaard stress functions to calculate the plastic zone face separation δ as a function of the distance x from the crack tip:

$$\delta = \frac{(\kappa + 1) \sigma_0 R}{\pi G} \left[\xi - \frac{x}{2R} \log \left(\frac{1 + \xi}{1 - \xi} \right) \right] \quad (2)$$

where $\kappa = (3 - \nu)/(1 + \nu)$ for plane stress deformation or $(3 - 4\nu)$ for plane strain and ν is Poisson's ratio, G is the shear modulus, and $\xi = (1 - x/R)^{1/2}$. The variation of the normalized separation δ/δ_0 with distance is shown in *Figure 2*. Crazing at a crack tip can be considered as a plane strain

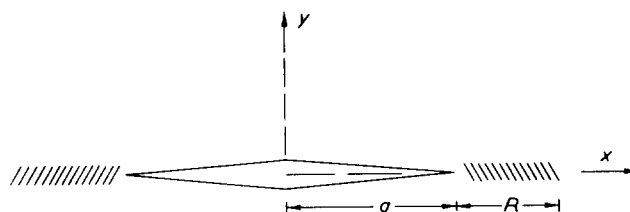


Figure 1 Dugdale model of crack tip plasticity

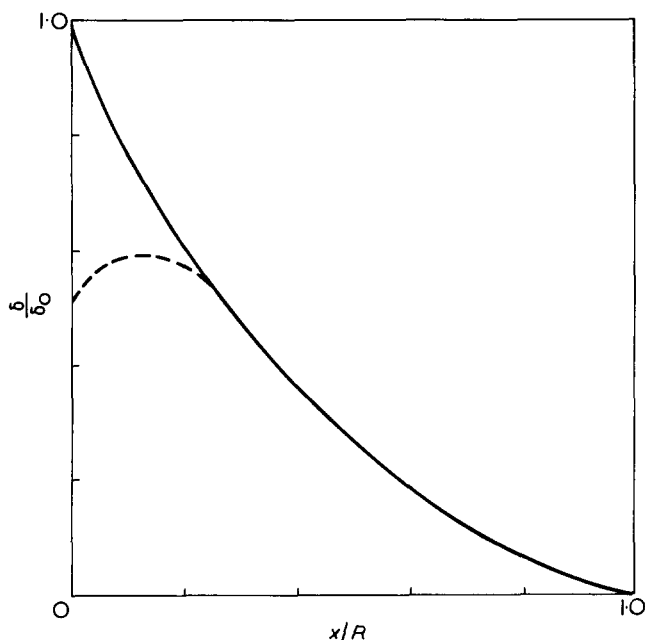


Figure 2 Separation of the plastic zone faces versus distance from the crack tip for the loaded Dugdale model — equation (2); and the unloaded model - - - - equation (4)

process, if there is no yielding outside the craze. The craze thickness is far smaller than the usual sheet thickness, and no significant through thickness plastic strain occurs.

Although the Dugdale model does not consider the criterion for fracture, it can be combined with the suggestion of Wells¹³ that fracture occurs when a critical crack opening displacement (COD) is exceeded. The COD can be identified with the value of δ_0 at the crack tip. Recently a critical COD criterion has been suggested for crack growth in drawn poly(ethylene terephthalate) film¹⁴ and toughened polystyrene¹⁵. In both these polymers the plastic zone size is large compared with the crack length at fracture. If however the only form of yielding before fracture is a single craze at the crack tip, the craze length is usually much smaller than either the crack length or any specimen dimension, and the elastic stress field around the crack can still be adequately described by Irwin's stress intensity factor K ^{16,17}. In these cases either a critical stress intensity K_c or a critical COD fracture criterion can be used. The two quantities are related, as can be seen by combining equations (1) and (2) in the case of small scale plane stress yielding, and using the Young's modulus E instead of shear modulus G :

$$\delta_0 = \sigma^2 \pi a / E \sigma_0$$

$$\text{then } \delta_{0c} = K_c^2 / E \sigma_0 \quad (3)$$

Existing knowledge of the conditions for craze initiation, and of the stresses in crazes, should be considered before applying the Dugdale model indiscriminately. Experiments on craze initiation in unnotched polymers have used biaxial stress fields. It has been shown that crazing occurs when the largest principal stress in poly(methyl methacrylate)¹⁸ or the largest principal strain in polystyrene¹⁹ reaches a critical value, which is dependent on the hydrostatic tension component of the total stress. There has been very little research with notched polymers, where a triaxial stress can occur ahead of the notch. Recent work with polycarbonate²⁰, showed that both a tensile stress greater than the conventional yield stress, and a hydrostatic ten-

sion are required to initiate internal crazes. There has been no similar experimental analysis of crack tip conditions, but recent theoretical results²¹ confirm the Prandtl slip line field solution for the stresses in a plane strain plastic zone at a crack tip. Thus conventional plane strain yielding will lead to a high triaxial tension ahead of a crack tip, which should be able to nucleate a craze in most glassy polymers. Once the craze has formed, the question remains as to whether the stresses at its boundaries are of the same nature as those in the Dugdale model. In the model, if the applied stress at infinity is a uniaxial stress $\sigma_{yy} = \sigma$, then the stresses at the yielded zone boundary are $\sigma_{yy} = \sigma_0$, $\sigma_{xx} = \sigma_0 - \sigma$. For materials with a Tresca or Von Mises type of yield criterion, conventional yielding will then occur under plane stress conditions, i.e. with $\sigma_{zz} = 0$. If crazing occurs, then the yielding is plane strain, but some doubt remains over the stress conditions at the craze/bulk boundary. It is possible that the void formation in crazing largely relaxes the hydrostatic tension component of stress, and hence also the through thickness stress. We have assumed this in some later calculations. Another problem may be that the stresses vary with position in the craze. If this is the case, the thickness profile of equation (2) will differ from the craze thickness profile.

Dugdale model and fatigue crazes

Rice¹¹ has calculated the yielded zone thickness for the strip yield model on complete unloading, on the assumption that the compressive yield stress in the zone is $-\sigma_0$. The length of the reverse yielded zone is one quarter of the original yielded zone, and within it the thickness varies according to:

$$\delta = \frac{(\kappa + 1) \sigma_0 R}{\pi G} \left[\xi - \frac{x}{2R} \log \left(\frac{1 + \xi}{1 - \xi} \right) - \frac{\phi}{2} + \frac{x}{R} \times \log \left(\frac{1 + \phi}{1 - \phi} \right) \right] \quad (4)$$

where the symbols are as in equation (2) and $\phi = (1 - 4x/R)^{1/2}$. Figure 2 shows that on unloading, the major changes in δ occur very close to the crack tip, and the value of δ_0 is halved.

If however the yielded zone had a zero yield stress for compression back to zero plastic strain, then the Dugdale model would predict $\delta = 0$ for the whole zone i.e. the reverse yielded zone would be the same length as the original plastic zone, and there would be no residual elastic stresses on unloading. Kambour²² has shown that crazes in polycarbonate, grown in a solvent environment to extend right across a tensile specimen, exhibit considerable hysteresis in a loading-unloading cycle, and that the foam-like craze structure does not collapse back to the original density on unloading. Hence, although during the initial unloading we can approximate the craze behaviour by a zero compressive yield stress, there is a stable craze strain beyond which a very large compressive stress is required for further contraction. This stable unloaded craze will exist on both crack faces, and will lead to compressive stresses across the crack faces in an unloaded specimen. Such crack closure stresses have been observed after fatigue crack growth in polycarbonate²³, which is a more sensitive photoelastic material than PVC. Thus we expect the whole craze to be cyclically strained in low frequency fatigue, with however

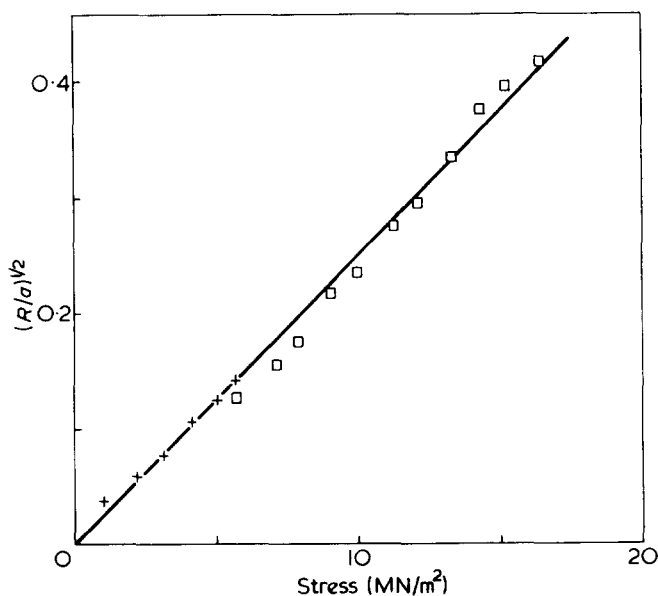


Figure 3 Ratio of craze to crack length versus applied tensile stress for 6 mm thick PVC sheet. +, $a = 19.68$ mm; □, $a = 3.14$ mm

a residual δ_0 even if the load reduces to zero, because of crack face closure.

In high frequency fatigue it is possible that the craze resists compression, and the stress must fall by an amount $\Delta\sigma$ before reverse yielding starts. If this is the case Rice¹¹ shows that the reverse yielded zone length R' is related to the fall in the stress intensity factor ΔK by:

$$R' = \frac{\pi}{8} \left(\frac{\Delta K}{\Delta\sigma} \right)^2 \quad (5)$$

for small scale yielding.

EXPERIMENTAL

Sample preparation

The rigid PVC used was ICI Darvic 025 in 1, 2, 3 and 6 mm sheets. No information on the molecular weight was available. It is assumed that the stabilizer/lubricant system is of the liquid type since the polymer does not stress whiten when it yields in a tensile test. Other PVC samples which incorporate insoluble stabilizers do stress whiten, and differ in their fracture toughness from Darvic 025. 8 in \times 3 in specimens were milled from the sheet and double edge notched (*DEN*). The machined V-notch was then sharpened by inserting a new razor blade, and then the PVC given a thermal history of either: (a) 1 h at 65°C, 5 h at 50°C and 16 h at 40°C; (b) 30 min at 90°C, then 15 min at 0°C. Treatment (a) was intended, by annealing below the glass transition temperature of about 65°C, to obtain a material with the highest possible yield stress. Treatment (b), of rapidly cooling through the glass transition was intended to effectively remove the yield stress maximum in a tensile test. Further discussion of how these thermal treatments affect plane stress yielding from a crack is given in ref 24. The treated PVC was stored at 23°C and 50% relative humidity before monotonic loading with an Instron tensile testing machine.

For fatigue crack growth tests single edge notched (*SEN*) specimens, and compact tension specimens were cut from 6 mm Darvic sheet. The former were used with a 0.4 ton

Amsler Vibrophore testing machine to obtain fatigue crack growth data at a frequency of about 67 cycles/sec. The latter were fatigue loaded on a small electromagnetic shaker driven machine to obtain sharp fatigue cracks, and then used for fracture toughness tests. Critical stress intensity factors (K_c) were obtained from fracture loads at low Instron crosshead speeds (0.05 cm/min) using corrections for the finite specimen width²⁵, for single edge notched and for compact tension specimens²⁶.

Craze growth during monotonic loading of cracks

First, the craze length was observed at known stress intensities. *DEN* samples machined from 6 mm thick Darvic 025 sheet were annealed (thermal history a). They were then loaded at an overall strain rate of $5 \times 10^{-5} \text{ sec}^{-1}$, in a temperature (23°C) and relative humidity (50%) controlled room. The craze growth was observed with a low power binocular microscope, using obliquely transmitted light. This method was devised by Kambour²⁷ who found that with the correct choice of the angle of incidence, total internal reflection occurs at the crack surface but not at the polymer/craze interface. Figure 3 shows the variation of craze length with applied stress. The data has been normalized, and using equation (1) the slope of the fitted straight line through the origin gives a value $\sigma_0 = 46 \text{ MN/m}^2$.

Secondly the craze thickness profile was investigated, although in this case the stress field intensity was unknown. *SEN* specimens of 6 mm thick Darvic 025 sheet were fatigued in a Amsler Vibrophore at 67 cycles/sec until several mm of crack growth had occurred. The specimens were then cut and polished parallel to the crack plane to give a specimen 6 mm deep containing the crack. The crack in the resulting slice was opened by driving a metal wedge into the machined part of the crack, using a hand operated compression cage on the stage of an optical microscope. The craze that formed was viewed by normal incidence using approximately monochromatic green light (maximum intensity at 0.54 nm and half width of 0.04 nm). The growth of a particular craze is shown in Figure 4. After each wedging open of the crack, the craze grew rapidly in length at first, but tended to an equilibrium length after about a minute. The effect of unloading on the fringe pattern was investigated, and in some cases, when the crack propagated and the craze wedge was left intact on one fracture surface, the fringe pattern of a craze on a free surface recorded. For unbroken crazes the thickness δ is related to the fringe number f (counting dark fringes from the zeroth fringe at the craze tip), the refractive index of the craze n_c , and the wavelength λ by:

$$\delta = f\lambda/2n_c \quad (6)$$

If equation (6) is to be used for crazes viewed on fracture surfaces, the fringes should be numbered $\frac{1}{2}$, $1\frac{1}{2}$ etc, since there is a phase change of π , only when light is reflected into a medium of lower refractive index. The shape of crazes in unloaded PVC and on fracture surfaces is shown in Figure 5. The craze tip is cusp-like, but the main portion of the craze is a uniform wedge, in contrast to the unloaded Dugdale model of Figure 2.

The refractive index of an unloaded craze was determined by Kambour's method of determining the critical angle for total internal reflection at the craze/matrix interface²⁷. The critical angle of incidence i at the sheet surface

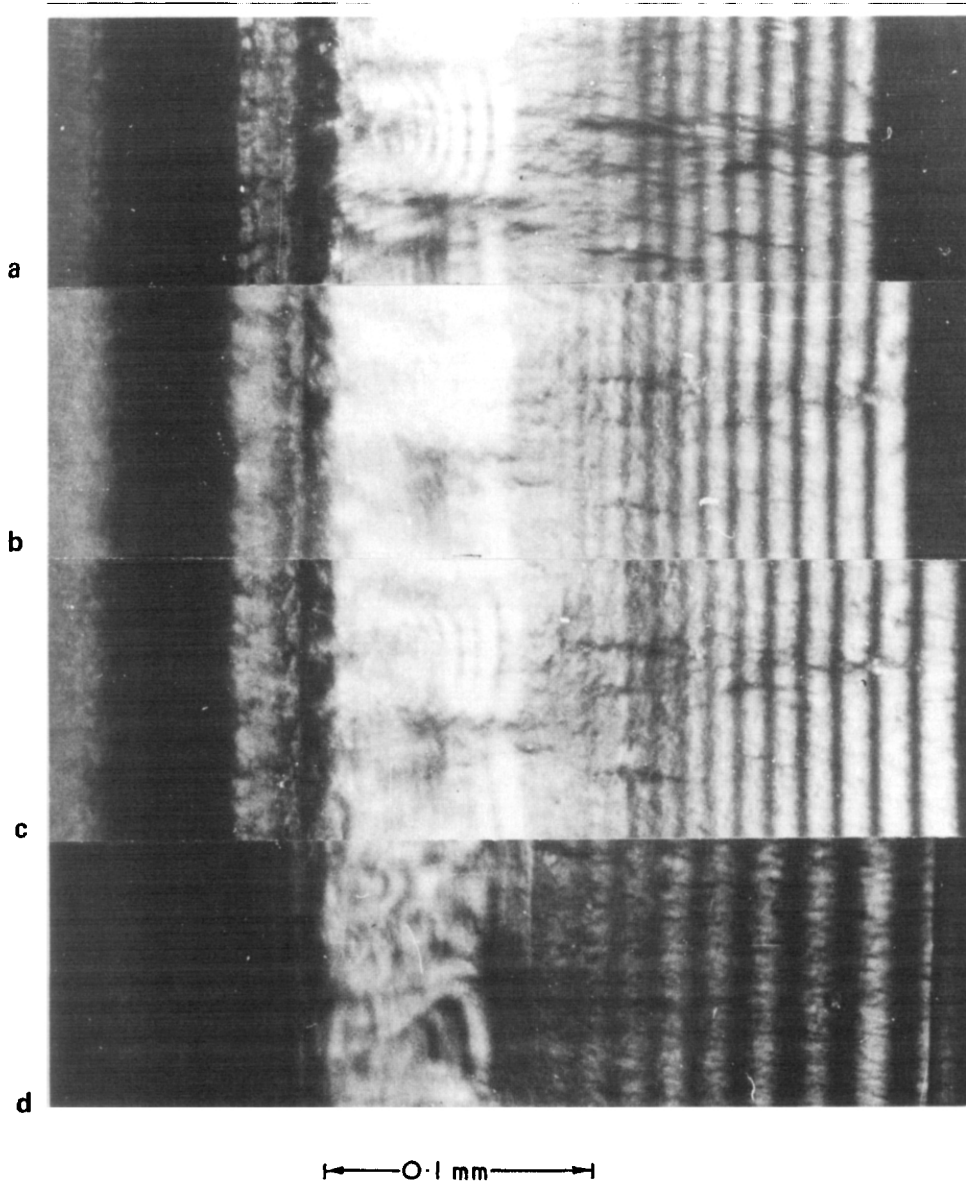


Figure 4 Sequence of optical micrographs of a craze taken at time intervals of a, 30 sec; b, 90 sec; c, 300 sec of loading a crack; d, unloaded. The equally spaced lines on the left are the fatigue crack growth striations

was found to be $59 \pm 5^\circ$. Use of the relationship:

$$n_c^2 = n_m^2 - \sin^2 i$$

together with a matrix refractive index of $n_m = 1.56 \pm 0.01$, lead to a value for the unloaded craze refractive index of $n_c = 1.30 \pm 0.03$.

In order to convert the fringe pattern of a loaded PVC craze into a thickness profile, the refractive index of the loaded craze n_L , must be found. This is carried out by assuming that very little birefringence occurs in the craze, so that the Lorentz-Lorenz relationship applies before and after loading.

$$\frac{n^2 - 1}{n^2 + 2} = p\rho; \quad \frac{n_c^2 - 1}{n_c^2 + 2} = p\rho_c \quad (7)$$

where p is a material constant and ρ is the density. The craze deformation is a plane strain process, so if the polymer content of the craze is constant the product of craze thickness and density also remains constant. Denoting the

ratio of the loaded thickness to the unloaded thickness by r , we have from equation (6):

$$r = \frac{fn_c}{f_0n} \quad (8)$$

where f_0 is the unloaded and f the loaded fringe number. Eliminating n between equations (8) and (7) leads to the cubic in r :

$$r^3 + 2Ar^2 - Br + AB = 0 \quad (9)$$

where $A = (n_c^2 - 1)/(n_c^2 + 2)$ and $B = (n_c f/f_0)^2$. The one solution of this cubic with value >1 is used. The ratio of f/f_0 was plotted versus the distance from the craze tip in Figure 6. The ratio falls in the range 1.43 ± 0.03 , except at the very tip of the craze. Substituting this value in equation (9) gives $r = 1.57$. Further application of the above analysis to the observed values of refractive index for the original PVC and the unloaded craze leads to the result that the unloaded craze has an extension ratio of 1.72 compared

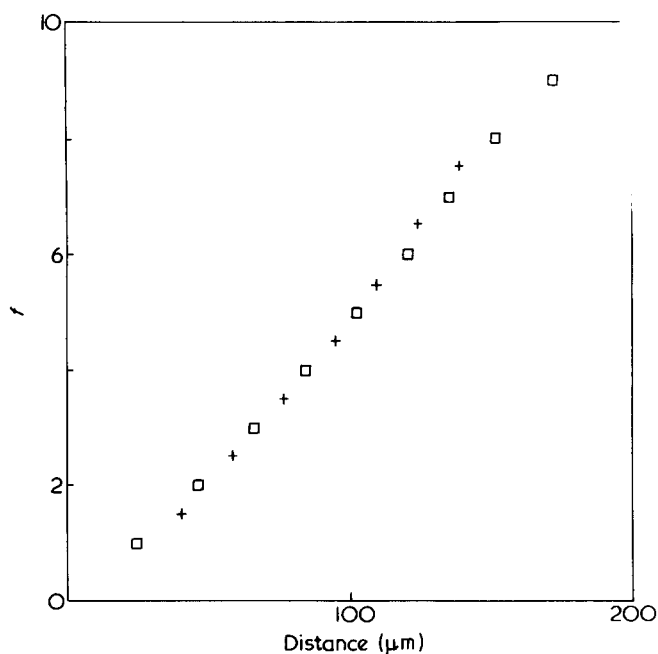


Figure 5 Thickness profiles of unloaded crazes. □, an unbroken sample; +, on a fracture surface. The thickness in fringes is plotted against the distance from the craze tip

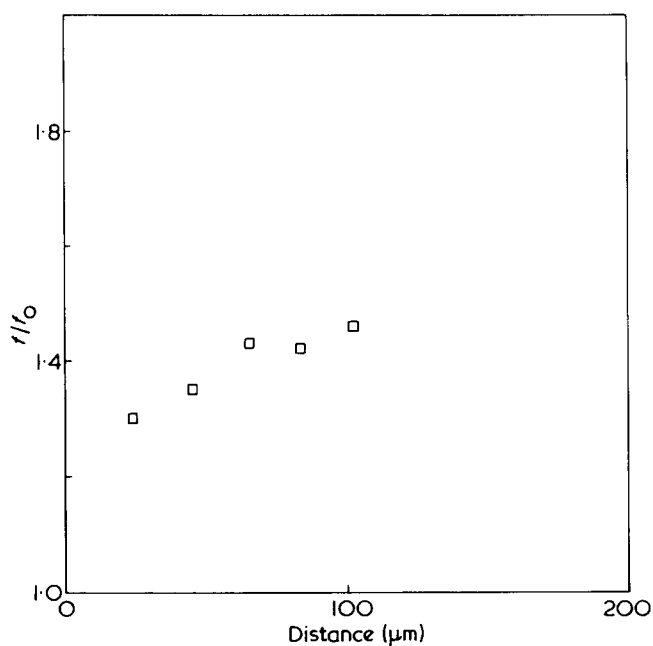


Figure 6 Ratio of the fringe number for a loaded craze to the unloaded value versus the distance from the craze tip

with the original polymer. Both these values are independent of the position in the craze, excluding the craze tip. Since the craze was observed to grow in length with a constant wedge angle, it can be concluded that it does so by drawing in more polymer, rather than by further straining material already in the craze. On the other hand, on unloading this new material does not revert to the uncrazed state.

The maximum thickness of unloaded crazes at the crack tip was estimated by linearly extrapolating craze thicknesses to the observed position of the crack tip (the thickness fringes are obscured near the crack tip). Values of 4.0 to 5.7 μm were obtained. Using the calculated value of r , we can calculate the crack tip thickness of loaded crazes to have a maximum value of 6.3 to 8.9 μm .

Fracture toughness measurements

Two main sets of fracture toughness measurements were made. In the first the effect of sheet thickness on the validity of the plane strain K_C test was investigated. It is recommended²⁵ that the sheet thickness should exceed $2.5 (K_C/\sigma_0)^2$ for a valid test. In this set DEN samples were used and the machined notches were sharpened by a cut of ~ 0.05 mm with a new razor blade, before heat treatment. Table 1 shows the results.

R_C is the length on the fracture surface from the original crack tip to the end of the flat craze region (see next section). σ_0 is the plane strain tension lower engineering yield stress; this has been shown to be the yield stress relevant to the Dugdale model (a localized neck forms in the plane of the crack if very thin sheet is tested) and the values are taken from ref.24. Finally in the last column a plain strain fracture toughness of $K_C = 2.0 \text{ MN/m}^{3/2}$ is used to calculate the recommended sample thickness.

From Table 1 it can be seen that the recommended thickness requirements are somewhat conservative. For 'valid' fracture toughness tests the thermal history has no significant effect on the K_C values observed.

The second set of tests were made in view of the results of Marshall *et al.*²⁸, who found that the method of notching in polystyrene strongly affected the observed K_C values, in particular slow razor notching produced a craze bunch at the notch tip and a high K_C value, whereas cracks grown by fatigue at 30 cycles/sec, had a single craze at their tip and gave a low K_C value. Even though we did not observe craze bunches with razor notched specimens, there was a chance that fatigued specimens would give a smaller K_C value. Table 2 shows the fracture toughness values obtained on loading compact tension (CT) specimens at a crosshead speed of 0.05 cm/min. The two typical fatigue crack surface appearances have been described for polycarbonate²⁹. The conventional fatigue striations parallel to the crack tip occur if the crack grows in the plane perpendicular to the applied load. However, in some cases, the crack twisted about its growth direction by about 12° . In this case, the

Table 1 DEN fracture toughness tests

Thermal history	Sheet thickness (mm)	No. of samples	K_C (MN/m ^{3/2})	R_C (mm)	σ_0 (MN/m ²)	Recommended thickness (mm)
b + 1 h	2	4	2.57 ± 0.24	0.55 ± 0.2	47 ± 2	4.5
b + 1 h	3.6	4	1.95 ± 0.16	0.53 ± 0.2	47 ± 2	4.5
b + 21 days	2,3,6	9	1.94 ± 0.17	0.46 ± 0.1	51 ± 1	3.9
a	1,2,3,6	12	2.00 ± 0.20	0.51 ± 0.1	not available	—

Table 2 CT fracture toughness tests

Fatigue surface appearance	No. of samples	K_C (MN/m ^{3/2})	R_C (mm)
Striations // to crack tip	8	1.84 ± 0.09	(~ 0.3)
Cylinders \perp to crack tip	6	2.9 ± 0.4	—

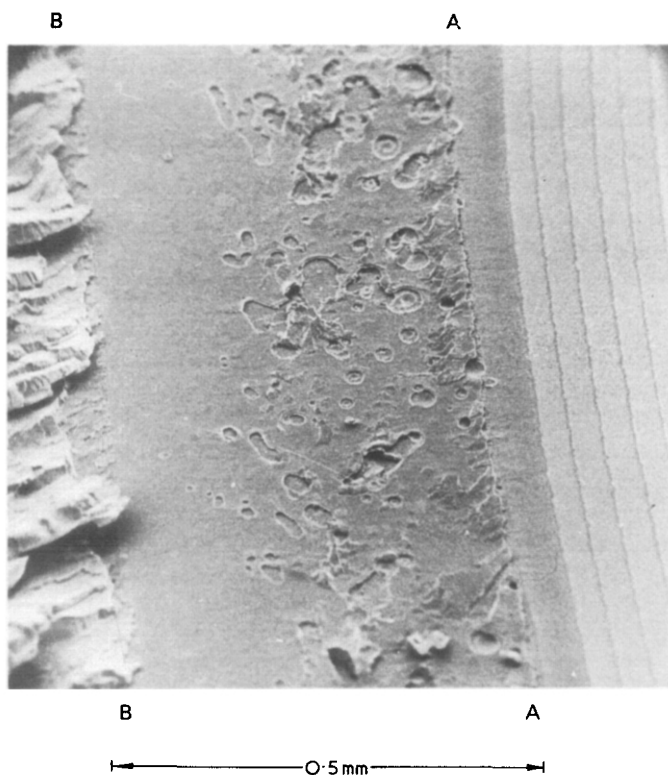


Figure 7 Scanning electron micrograph of a PVC fracture surface. AA is the boundary of the fatigue crack growth, and BB of the craze grown in monotonic loading

crack front splits up into a large number of small crack fronts on slightly different layers, and where these fronts overlap and intersect cylindrical pieces of polymer are detached. It is suspected that this latter type of fatigue crack growth, is a result of a slight misalignment of the load points, and that the greater effective crack front leads to a higher K_c value. It can be noted that the K_c values for the conventional fatigue surface appearance are not significantly different to those for the *DEN* tests, so craze bunch formation in the type of PVC used cannot be a problem.

Having obtained a fracture toughness value, it is instructive to use the Dugdale model and equation (3) to calculate a critical crack opening displacement. Using $K_c = 1.84 \text{ MN/m}^{3/2}$, $\sigma_0 = 46 \text{ MN/m}^2$, and literature values of 100 sec for the creep modulus at 20°C and 1% strain of 3.0 GN/m^2 ³⁰, and Poisson's ratio of for other glassy plastics of 0.42³¹, we obtain $\delta_{0c} = 20 \text{ }\mu\text{m}$, which is approximately double the observed maximum craze thickness.

Fracture surface appearance

The fracture surface of 6 mm thick Darvic fracture toughness specimens shows no evidence of slow crack growth, rather there is a flat region about 0.5 mm wide where a craze had developed on loading, followed by a rough fast fracture region (Figure 7). If the flat region is observed by normally incident light, it will be found that one fracture surface has interference bands parallel to the end of the craze, and the other has no bands. Since the craze thickness fringes are identical to those for unloaded crazes in an unbroken specimen, it follows that the craze has broken on one of its interfaces with the uncrazed material. Circular holes are visible in the craze in Figure 7, and on another fracture surface where the craze has detached, some circular remnants remain (Figure 8). This suggests that 'penny' shaped cracks have developed in the craze be-

fore the craze/bulk interface has fractured. Close to the crack tip, the density of these $\sim 10 \text{ }\mu\text{m}$ radius 'penny' shaped cracks, may be so great that they coalesce (Figure 8) into a larger crack, which would appear to be the fracture source. With the razor notched specimens the crack usually propagates rapidly from this source either above or below the craze, so the flat craze areas only appear at the sides of the fracture surface. With the fatigue cracked specimens the fracture usually follows the initial craze. The craze/bulk interface must split much more rapidly than the penny shaped cracks are growing, otherwise the latter would have non-circular outlines.

Mechanism of fatigue crack growth

Fatigue crack growth was observed both as a function of the stress field intensity range ΔK , and the *R* ratio of $K_{\text{max}}/K_{\text{min}}$. Whereas previous workers^{5,7} had used *R* ratios of 0.1 or smaller, this greater range of experiments enabled the following observations to be made:

(a) It is confirmed that the crack grows discontinuously. The number of cycles of loading at the natural frequency of the Amsler of about 67 cycles/sec being about 1400 at ΔK values of $0.5 \text{ MN m}^{-1.5}$, decreasing to about 200 cycles at $\Delta K = 1.2 \text{ MN m}^{-1.5}$ for each fatigue striation.

(b) It is confirmed that craze growth occurs continuously⁷ at the crack tip. This is a single craze, and not a double craze as inferred⁷, where the surface of the sheet was examined. It is suggested that the two parallel markings on the sheet surface are a result of the shear lip that occurs at the surface.

(c) Except at very low *R* ratios, the crack does not jump the full length of the existing craze when it grows. Figure 9 shows clearly that the crack only advances a fraction of the craze length. The previous observation⁷ that for *R* = 0.1, the crack jumped approximately the full craze length is consistent with this.



Figure 8 As Figure 7, but for a razor notched specimen, showing more detail of the coalescence of 'penny' shaped cracks

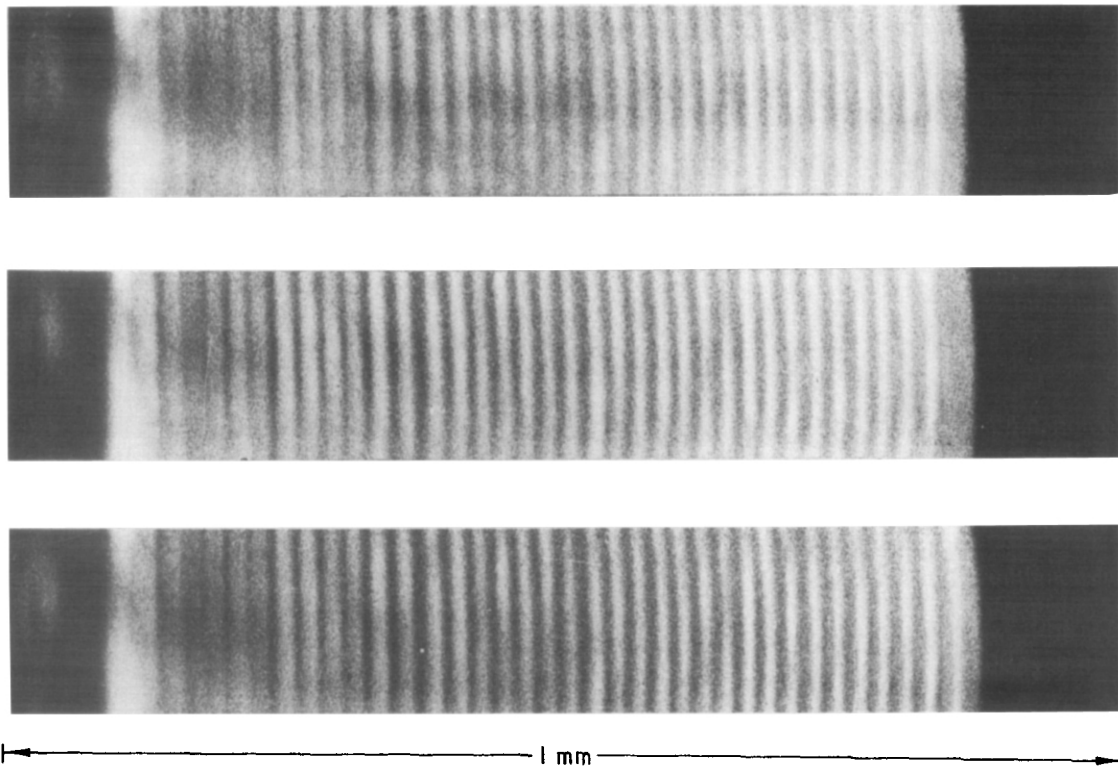


Figure 9 Series of photographs of the crack tip during fatigue at 67 cycles/sec

(d) If the striation spacing s is plotted against ΔK , the results of many experiments can be correlated well (see Figure 10). If however K_{\max} is used, the correlation is much poorer.

(e) The fatigue crack growth rate also correlates well with ΔK (Figure 11), but not with K_{\max} .

Observations (c) and (d) strongly suggest that the crack jumps the length of the reversed plastic zone, which should be proportional to ΔK^2 on Rice's strip yield model (equation 5), rather than the full length of the craze, which might be expected to vary with either the maximum or the mean value of K . Since static loading experiments have shown that craze growth is time dependent for at least 1 min, it is not surprising that an equilibrium craze length is not reached in the 2 to 20 sec between crack jumps. The slope of the log striation spacing versus log ΔK (Figure 10) is only 1.35. On the strip yield model of a rigid-plastic material, whatever the ratio of the reverse to the forward yield stress, the reverse yielded zone should be proportional to ΔK^2 . The discrepancy may be due either to a further viscoelastic effect or to a change in the stress-strain behaviour of the craze as its size increases.

Examination of the fatigue surfaces showed that the craze structure is visible inbetween the striation bands (Figure 12). The cellular holes in the craze, just ahead of the crack arrest band, are only about $0.2 \mu\text{m}$ in diameter. There is no obvious change in the size of these holes between one arrest band and the next ($20 \mu\text{m}$ apart in this case). This conflicts with observations of fatigue surface replicas⁷ which suggest that 'equiaxed dimples' on the surface decrease in size from about $2 \mu\text{m}$ in front of one arrest band to about $0.2 \mu\text{m}$ behind the next band. It may reasonably be concluded that the craze fails near its mid-section rather than near the craze bulk interface, and that it is a fast 'brittle' failure; hence the audible clicks when growth occurs.

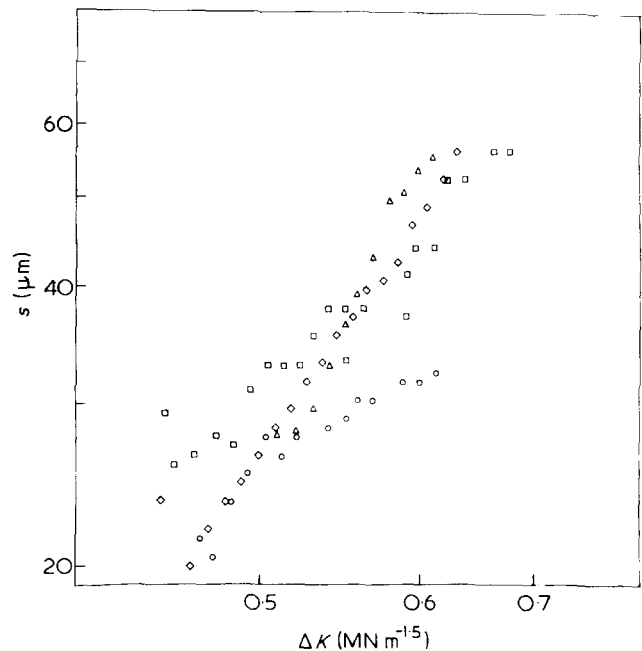


Figure 10 Fatigue striation spacing versus stress intensity range for R ratios of \square , 0.05; \circ , 0.2; \square , 0.33; \triangle , 0.5

DISCUSSION

The first area of discussion is the usefulness of the Dugdale model in describing craze formation at a loaded crack in PVC. The form of the craze is far closer to the Dugdale's assumed plastic zone shape than is the equivalent plane stress plastic zone in thin sheets. Time dependent craze growth is a problem, but an equilibrium length is reached either after several minutes at each load, or on very slow continuous loading. Brown and Ward¹⁰, found that the

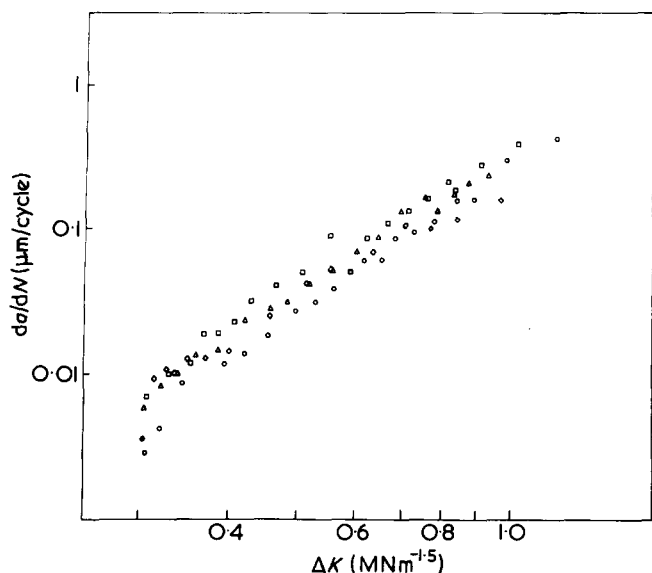


Figure 11 Fatigue crack growth rate versus stress intensity range for *R* ratios of □, 0.05; ○, 0.2; ◇, 0.33; △, 0.5

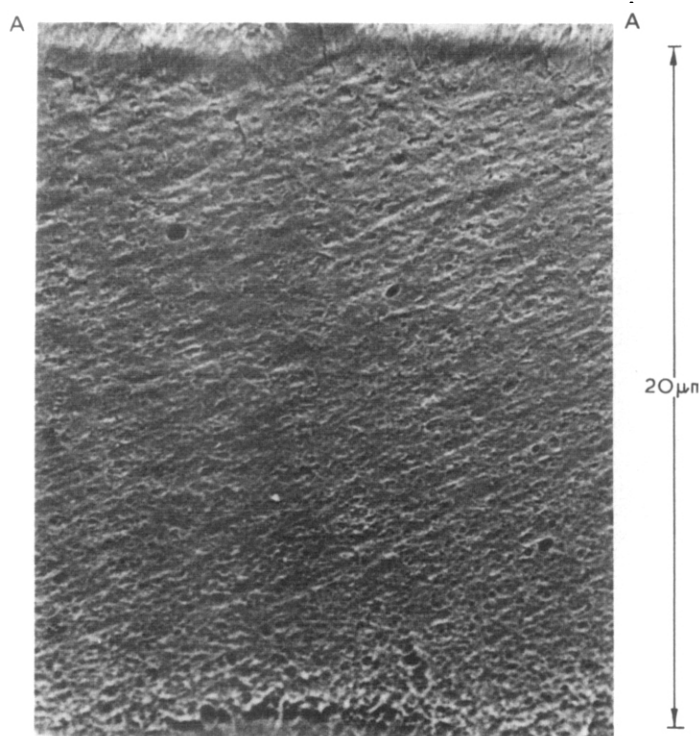


Figure 12 Scanning electron micrograph of a fatigue fracture surface. AA is a crack arrest line

thickness profile of loaded crazes in poly(methyl methacrylate) (PMMA) was in good agreement with the Dugdale model, but in PVC the profile has been found to be much closer to a uniform wedge. This may be related to the much greater length of crazes in PVC than in PMMA (see Table 3).

It is useful to see whether information obtained by applying the Dugdale model to crazes in PVC, is in accord with independent information on the crazing and fracture behaviour. By observing the craze length versus the applied stress (Figure 3), a value of $\sigma_0 = 46 \text{ MN/m}^2$ for the stress at the boundary of the yielded zone was obtained. This stress is slightly lower than the estimated lower plane strain tension yield stress of 55 MN/m^2 for annealed PVC. As the

density of a loaded craze is only 37% of that of the bulk polymer, the true stress in the highly oriented craze fibrils, must be about 124 MN/m^2 . It must be supposed that the orientation hardening in the craze fibrils is such that, rather than the fibrils yielding further, the craze thickens by advancing the craze-bulk boundary. The observation that the craze grows with a constant wedge angle (Figures 4 and 5), shows that the ratio of crack opening displacement to craze length δ_0/R remains constant. From the Dugdale model equations (1) and (3) we have:

$$\delta_0/R = 8\sigma_0/\pi E \tag{10}$$

At the boundary of the plastic zone the stresses are $\sigma_{xx} = \sigma_{yy} = \sigma_0$ and $\sigma_{zz} = 0$ (the model assumes uniform biaxial loading at infinity, which is not too different from the actual small uniaxial tension), so the elastic strains are $e_{xx} = e_{yy} = \sigma_0(1 - \nu)/E$; $e_{zz} = -2\nu\sigma_0/E$.

Substituting in equation (10) we then have:

$$\delta_0/R = 8e_{yy}/\pi(1 - \nu) \tag{11}$$

Equation (11) has been used to calculate the tensile strain e_{yy} at the boundary of the craze from our δ_0/R values, and from literature values for other glassy polymers, using $\nu = 0.42$. These are compared in Table 3 with e_{cr} , the critical strain below which crazing does not appear in long time ($\sim 24 \text{ h}$) tensile creep tests on unnotched glassy polymers.

If it is assumed that flaws on the surface of tensile creep specimens initiate craze growth if the tensile strain is great enough, then the correspondence between this strain and the value deduced from the Dugdale model is reasonable. In the case of PVC where σ_0 is known independently (Brown and Ward only calculated a value for PMMA by measuring the specimen compliance, and hence effective Young's modulus E^*), we can calculate $\sigma_0(1 - \nu)/e_{yy}$ to get a value of 6.5 GN/m^2 for the Young's modulus. This is about twice the experimental creep modulus³⁰. The discrepancy may be due to some yielding occurring above and below the craze. σ_0 is of the same order as the conventional yield stress, and if this additional yielding occurs, the craze would not need to be so thick, and e_{yy} would be underestimated by equation (11). It would also explain why the earlier calculation of a critical crack opening displacement of $20 \mu\text{m}$, from the Dugdale model and the measured K_{Ic} value, is greater than the observed value in Table 3.

The second area of discussion is the mechanism of craze failure in monotonic loading. We can start with the comment³² that the occurrence of circular 'advance fractures' in polystyrene shows that it is incorrect to use Griffith's approach to fracture (or the modification by Orowan³⁴ to include the plastic deformation of a surface layer) for polystyrene. We have observed for PVC both similar craze dimensions to those in polystyrene, and circular 'advance fractures'. Since we have suggested that the Dugdale model is more suitable for the crack/craze situation than the purely elastic situation investigated by Griffiths, we must

Table 3 Maximum craze dimensions, and strains

Polymer	δ_0 (μm)	<i>R</i> (μm)	e_{yy}	e_{cr}
PMMA ³³	1.73	24.2	0.016	0.008 ³²
Polystyrene ⁸	6*	550	—	0.0035 ³³
PVC	9	500	0.0041	0.007 ²

* For an unloaded craze

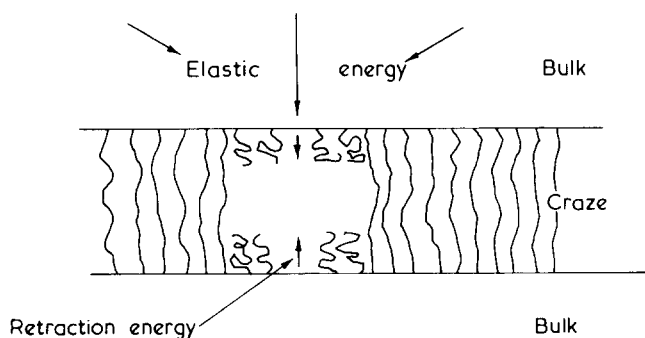


Figure 13 Model of the energy transfer in the formation of an advance fracture in a craze

investigate whether it is consistent with the formation of 'advance fractures'. In the model, the stresses in the yielded zone are uniform, whereas 'advance fractures' are observed to occur in the thickest part of the craze nearest the crack. We now estimate the amount of energy released when an 'advance fracture' forms. This consists of contributions from both within the craze, and from the surrounding uncrazed polymer (Figure 13). If the craze material is sufficiently anisotropic for the oriented strands bridging the craze to be able to break without load transfer to the neighbouring strands, then the energy released when a circular feature of radius c appears in the craze of thickness δ is the relaxed volume $\pi c^2 \delta$ multiplied by the elastic energy density released on unloading the craze. Such data are only available for specially thick crazes in polycarbonate²², so we assume that the craze unloads linearly from a stress of 46 MN/m² to 0.65 of its loaded thickness. Thus the recoverable energy density in the loaded craze is 8 MJ/m³. If a crack of radius 10 μm appears in a 8 μm thick craze, the energy released is 2×10^{-8} J. A second contribution from the uncrazed material is estimated as follows: we assume that a 'penny' shaped crack of radius C appears in a material that initially had a uniform stress $\sigma_0 = 46$ MN/m² normal to the plane of the crack. Sneddon³⁵ has shown that the reduction in the stored elastic energy of the solid is given by $8(1 - \nu^2) \sigma_0^2 C^3 / 3E$, which for $C = 10 \mu\text{m}$, $\nu = 0.42$ and $E = 3.0$ GN/m² gives a value of 0.15×10^{-8} J. The actual amount will be rather less because the stresses in the Dugdale model decrease away from the yielded zone rather than remaining constant. Even though the effect of the craze plane on the result is unknown, this suggests that energy release from within the craze is an order of magnitude greater than that from the surrounding uncrazed material for $C = 10 \mu\text{m}$. Since the former term is proportional to the craze thickness, we have provided a necessary explanation of the advance fracture appearing in the thickest part of the craze. However it is not sufficient, since the mechanism of the fracture initiation is unknown.

It has been common practice to quote 'surface energies' for the fracture of polymers, using Orowan's modification of Griffith's approach. If this is carried out for PVC we obtain a critical strain energy release rate ($2 \times$ the surface energy) of $G_c = K_c^2/E$ or 1300 J/m². The danger of presenting the fracture information in this way is that, it implies that PVC behaves in accord with the Griffiths model i.e. that if a testpiece of the correct geometry is used (so that the strain energy release rate is constant as the crack grows) then stable slow crack growth is possible for a value of G just exceeding G_c , with a uniformly thick craze layer being left on the crack surfaces. However the real situation is quite different. If our analysis of advance fracture forma-

tion is correct, this is a low surface energy process with a G_c of $8 \text{ MJ/m}^3 \times 8 \mu\text{m} = 64 \text{ J/m}^2$. When a number of these fractures have coalesced, cleavage at the craze boundary occurs, which again should be a low surface energy process. The crack immediately accelerates to about 500 m/sec⁴, at which speed crack bifurcation and other processes occur and absorb the 1300 J/m² of strain energy release. The difficulties of using G_c can be avoided entirely by using the critical stress intensity factor K_c , since this represents the critical elastic stress field, outside the yielded zone, that is necessary to initiate crack growth. Green and Pratt⁴ have shown that a stress intensity factor K of 2 MN/m^{3/2} is sufficient to maintain crack speeds of 500 m/sec in a similar PVC. Thus this PVC grade differs from PMMA, where it has been shown that K is an increasing function of crack speed for crack speeds less than 0.025 m/sec³⁶. Since advance fracture formation does not occur ahead of a slowly moving crack in PMMA, it seems likely that this low surface energy process is responsible for the absence of slow crack propagation in PVC.

Turning finally to the fatigue crack growth results, it is evident that the Dugdale model is less successful here than for the static craze growth experiments. Although Elinck *et al.*⁵ calculated values of σ_0 in the Dugdale model from their observed striation spacings, their experiments only covered a limit range of stress intensities. It is apparent that the striation spacing does not have a ΔK^2 dependence for our more extensive tests, so it is impossible to calculate σ_0 . The continuous craze growth during high frequency fatigue is most likely to be a viscoelastic process, with the craze having insufficient time to reach its equilibrium length before further crack growth occurs. If this is the case it is not very helpful to apply crack growth theories developed for metals which behave as elastic-plastic solids. Investigation of the cyclic stress strain behaviour of PVC crazes to see if they work harden or soften would be necessary before any further analysis of the crack growth process could be made. Observation of the fatigue fracture surfaces showed no 'advance fractures'. This is not surprising if the mechanism proposed for their formation is valid; the crazes fracture in fatigue when they are only 20–80 μm long, and if they have the same wedge angle as static crazes they will be too thin to contain sufficient elastic energy. In the fatigue fracture the craze appears to fail near its centre plane with relatively little damage to the open celled craze structure. The key to the fatigue growth rate probably lies in the material at the crack tip during each crack arrest. This material is left on the fracture surface as a distinctive band. The material survives a decreasing number of cycles as the stress intensity range increases, but at present the reasons for its eventual failure are unknown.

ACKNOWLEDGEMENTS

The authors are grateful to the Science Research Council for support.

REFERENCES

- 1 Kambour, R. P. *J. Polym. Sci. A-2* 1966, **4**, 17
- 2 Gotham, K. V. *Plast. Polym.* 1969, **37**, 309
- 3 Cornes, P. L. and Haward, R. N. *Polymer* 1974, **15**, 149
- 4 Green, A. K. and Pratt, P. L. *5th Int. Conf. Stress Analysis, Udine* 1974

Craze growth and crack growth in poly(vinyl chloride): N. J. Mills and N. Walker

- | | |
|---|--|
| <p>5 Elinck, J. P., Bauwens, J. C. and Homes, G. <i>Int. J. Fract. Mech.</i> 1971, 7, 277</p> <p>6 Dugdale, D. S. <i>J. Mech. Phys. Solids</i> 1960, 8, 100</p> <p>7 Hertzberg, R. W. and Manson, J. A. <i>J. Mater. Sci.</i> 1973, 8, 1554</p> <p>8 Kambour, R. P. <i>J. Polym. Sci. (A-2)</i> 1966, 4, 359</p> <p>9 Cotterell, B. <i>Int. J. Fract. Mech.</i> 1968, 4, 209</p> <p>10 Brown, H. R. and Ward, I. M. <i>Polymer</i> 1973, 14, 469</p> <p>11 Rice, J. R. <i>Proc. 1st Int. Conf. Fracture Sendai</i>, 1966, 1, 283</p> <p>12 Muskhelishvili, N. I. 'Theory of Elasticity', Noordhoff, Leiden, (1953)</p> <p>13 Wells, A. A. <i>Proc. Conf. Crack Propagation, Cranfield</i> 1961</p> <p>14 Ferguson, R. J. and Williams, J. G. <i>Polymer</i> 1973, 14, 103</p> <p>15 Ferguson, R. J., Marshall, G. P. and Williams, J. G. <i>Polymer</i> 1973, 14, 451</p> <p>16 Green, A. K. and Pratt, P. L. <i>Eng. Fract. Mech.</i> 1974, 6, 7</p> <p>17 Gales, R. D. R. and Mills, N. J. <i>Eng. Fract. Mech.</i> 1974, 6, 93</p> <p>18 Sternstein, S. S. and Ongchin, L. <i>Am. Chem. Soc. Polym. Prepr.</i> 1969, 10, 117</p> <p>19 Oxborough, R. J. and Bowden, P. B. <i>Phil. Mag.</i> 1973, 28, 547</p> <p>20 Mills, N. J. <i>J. Mater. Sci.</i> 1976, 11, 363</p> | <p>21 Levy, N., Marcal, P. V., Ostergren, W. J. and Rice, J. R. <i>Int. J. Fract. Mech.</i> 1971, 7, 143</p> <p>22 Kambour, R. P. <i>Polym. Eng. Sci.</i> 1968, 8, 281</p> <p>23 Walker, N. to be published</p> <p>24 Mills, N. J. <i>Eng. Fract. Mech.</i> 1974, 6, 537</p> <p>25 Brown, W. F. and Srawley, J. E. 'Plane strain crack toughness testing', ASTM STP 410, 1966</p> <p>26 ASTM Annual Book of Standards, Part 31, E399-72</p> <p>27 Kambour, R. P. <i>Polymer</i> 1964, 5, 143</p> <p>28 Marshall, G. P., Culver, L. E. and Williams, J. G. <i>Int. J. Fract. Mech.</i> 1973, 9, 295</p> <p>29 Jacoby, G. and Cramer, C. <i>Rheol. Acta.</i> 1968, 7, 23</p> <p>30 Turner, S. <i>Br. Plast.</i> 1964, No. 12, p30</p> <p>31 Powers, J. M. and Caddell, R. M. <i>Polym. Eng. Sci.</i> 1972, 12, 432</p> <p>32 Doyle, M. J., Mancini, A., Orowan, E. and Stork, S. T. <i>Proc. R. Soc. (A)</i> 1972, 329, 137</p> <p>33 Kambour, R. P. <i>J. Polym. Sci. Macromol. Rev.</i> 1973, 7, 1</p> <p>34 Orowan, E. <i>Trans. Inst. Eng. Shipbuild. Scotl.</i> 1945, 89, 165</p> <p>35 Sneddon, I. N. <i>Proc. R. Soc. (A)</i> 1946, 187, 229</p> <p>36 Marshall, G. P., Culver, L. E. and Williams, J. G. <i>Plast. Polym.</i> 1969, 37, 75</p> |
|---|--|

Determination of chain branching in low density polyethylene by ^{13}C nuclear magnetic resonance and infra-red spectroscopy

M. E. A. Cudby and A. Bunn

ICI Plastics Division, Welwyn Garden City, Hertfordshire, UK
(Received 27 August 1975, revised 5 December 1975)

Pulsed Fourier transform ^{13}C n.m.r. studies clearly demonstrate the presence of ethyl, butyl and longer chain branches in commercial low density polyethylene. The most suitable conditions for the measurement of the relative intensities of the resonance in the ^{13}C spectrum, were determined using a standard linear long chain hydrocarbon. The ^{13}C spectra of polyethylenes obtained using these parameters, in conjunction with a total methyl content by infra-red spectroscopy allow a quantitative measurement of the number of each branch type to be made.

INTRODUCTION

It is now well established¹⁻⁸ that many physical properties of low density polyethylene are dependent upon the nature and number of both short and long chain branches. As a result the study of branching in polyethylene has received considerable attention⁹⁻¹⁷. The early work on this problem by Willbourn⁹ made use of infra-red spectroscopic examination of model compounds such as branched polymethylenes and of the mass spectroscopic analysis of the products of irradiation of deuterated branched polymethylene. He found that low density polyethylene contained ethyl and butyl short chain branches, and the measurements which he reported, gave a ratio of 2:1 in favour of the ethyl branch.

Other authors¹⁸ then produced results which in general agreed, that ethyl and butyl branches were present in low density polyethylene but offered small variations on the ethyl to butyl ratio. This general picture was accepted until Bovey¹⁹ produced his ^{13}C n.m.r. data, and stated 'that for all practical purposes only n-butyl branches are present in commercial high pressure polyethylene'.

The work reported in this paper demonstrates the validity of the original claim that both ethyl and butyl branches are present in low density polyethylene and we have shown that quantitative determination of the number of these branches by ^{13}C n.m.r. is feasible under controlled experimental conditions. However, we also show that the ratio of ethyl to butyl branches can vary over a wide range and we believe this to depend on the reactor conditions used during the manufacture of the polymer being studied. Nevertheless, the present measurements generally indicate much lower ethyl/butyl ratios than those reported by Willbourn. A re-examination of the data in Willbourn's paper, in the light of subsequent work, suggests that the absolute values of the ethyl/butyl ratios may well be in error. Owing to the relatively small number of samples then available with known branching characteristics, assumptions had to be made both in relation to extinction coefficients and band overlap. The effect of these assumptions was to introduce a systematic error in the measurement of ethyl/butyl ratio. We also show furthermore, that the presence of longer chain branches is revealed by the ^{13}C n.m.r. examination and that the concentration of these branches may be determined also.

INSTRUMENTATION AND EXPERIMENTAL CONDITIONS

The ^{13}C n.m.r. spectra were obtained on a Varian XL-100-15 pulsed Fourier transform spectrometer controlled by a Varian 620i 16K computer. Concentrated solutions (~50% w/v) of polymers and eicosane were prepared in *o*-dichlorobenzene and the spectra obtained at ~140°C. A deuterium field/frequency lock is required for the operation of the XL-100-15 spectrometer and 1,1,2,2-tetraethoxyethylene glycol proved satisfactory at elevated temperatures. The D_4 ethylene glycol was contained in a 5 mm o.d. n.m.r. tube held centrally in a 12 mm o.d. n.m.r. tube containing the polymer solution. The chemical shifts were initially related to tetramethylsilane (TMS) but consistency was obtained by internal reference to the $-(\text{CH}_2)_n$ resonance in polyethylene at 29.9 ppm.

In order to achieve a signal to noise ratio adequate to determine the type and extent of branching in low density polyethylene, it is necessary to use the pulsed Fourier transform (*FT*) technique. This will result in a signal enhancement due to the Nuclear Overhauser Effect (*NOE*)²⁰⁻²². However, it is known that small differences in the *NOE* factor may be observed between for example methyl and methylene carbons²³. Thus, in the experiments described comparisons are only made between like ^{13}C species where the *NOE* factor is assumed to be constant. Further difficulties in quantitative analysis are experienced with *FT* experiments because of differences in the relaxation times of ^{13}C nuclei in different chemical environments. Therefore a series of experiments were devised using a pure sample of the linear hydrocarbon eicosane as a standard in which the instrumental parameters pulse width, pulse delay and acquisition time were varied. The best conditions were determined by measurement of the peak heights of the resonances due to the various carbon atoms of eicosane obtained with different instrument parameters. The instrumental conditions which produced the optimum relationship between the methylene carbon atoms were then used in the subsequent experiments with low density branched polyethylenes. All polyethylene spectra were therefore run with a pulse width of 40 μsec equivalent to a 30° tip angle, pulse delay of 3.0 sec and an acquisition time of 1.0 sec.

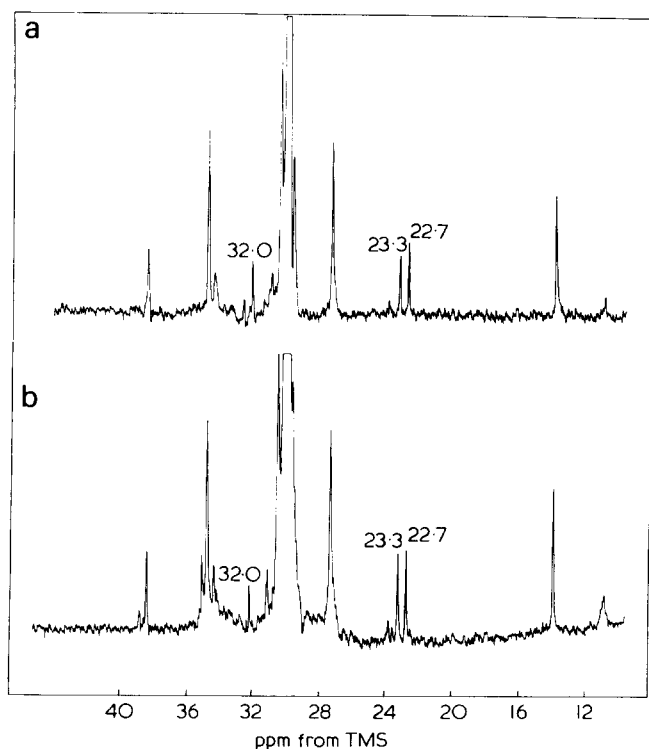


Figure 1 ^{13}C n.m.r. spectra obtained from low density commercial polymers (a) polymer A; (b) polymer B

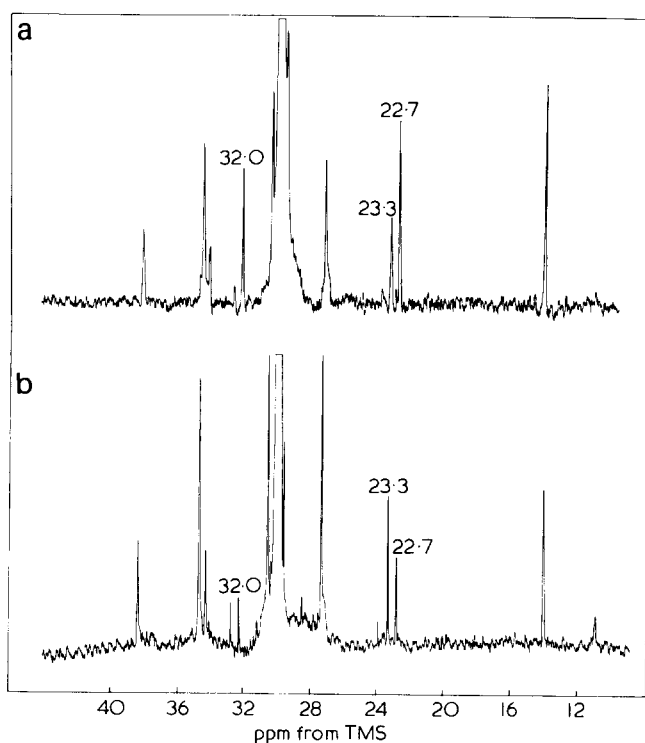


Figure 2 ^{13}C n.m.r. spectra obtained from low density commercial polymers C and D. (a) polymer C; (b) polymer D

Representative spectra of the commercial low density polyethylene samples which are the subject of this paper are shown in Figures 1 and 2. The total methyl group contents of these materials were determined by the standard infra-red method²⁴ and the results are shown in Table 1.

It can be seen from the spectra of the low density polymers used, that resonances are clearly observed at 11.2 and 14.0 ppm from TMS. These correspond respectively to the methyl carbons in ethyl branches and butyl plus greater

length branches²⁵. In addition it is expected from observation of the spectra published by Randall²⁵ that the α -methylene carbon, i.e. that carbon adjacent to the terminal methyl group, will have a recognizably different chemical shift for n-butyl branches and for branches of longer linear methylene sequences. We find these resonances to occur at 23.3 and 22.7 ppm from TMS, respectively, in the spectra of the low density polyethylenes examined. Whilst we do not question the appearance of resonances at 32.02 and 32.58 ppm (Randall shifts) in the spectrum of low density polyethylene, we are not convinced that the assignment of the 32.58 ppm resonance to amyl branches is consistent with the data presented. For example, from the data listed for copolymers, the methyl carbon for amyl branches at 14.72 ppm should be observably different from the methyl carbon of longer branches at 14.29 ppm; a difference of 0.43 ppm. However, these are not observed as separate resonances in Randall's spectrum of low density polyethylene in which he claims to recognise the presence of both amyl and longer chain branches. The 3 methylene carbons (Randall) show a much smaller chemical shift difference in the same copolymers, 0.08 ppm. This is now apparently observed in the spectrum of polyethylene with a 0.56 ppm difference. Unlike Randall therefore, we cannot claim to be able to recognise separately the presence of the amyl branch.

In his paper, Bovey¹⁸ draws particular attention to the absence of a resonance in his spectra due to the β -methylene carbon, β to the terminal methyl of a long chain branch. However, it is possible to observe a resonance at 32.0 ppm in low density polyethylene under our specified experimental conditions which we attribute to the β -methylene carbon in question found in long chain branches. Thus, it is possible to distinguish resonances due separately to the presence of ethyl, n-butyl and longer chain branches in low density polyethylene.

The concentrations of ethyl, n-butyl and longer chain branches in the tabulated low density polymers were determined using the specific parameters indicated and the total methyl content per 1000 C atoms were determined by infra-red spectroscopy. The ratio of ethyl to butyl, plus longer branches is determined from area measurements of the resonances due to the end methyl carbons. This is justified since the measurement involves only carbon atoms where the NOE is similar. The ratio of butyl to longer branches is determined from the respective methylene carbons and are therefore also comparable in this analysis. The results are given in Table 1.

Because of the low molecular weight of polymer C the value for branches longer than n-butyl will be enhanced because of a significant contribution from the end group methyl. In the original paper by Willbourn⁹ on the branch-

Table 1

Representative samples of commercial polymer	Infra-red methyl content per 1000 C atoms	Ethyl	n-Butyl	Longer chain
Polymer A	28	3-4	11	13
Polymer B	37	11/11*	13/14*	14/12*
Polymer C	32	<1	10	21
Polymer D	23	4	12	8

* Repeat sample

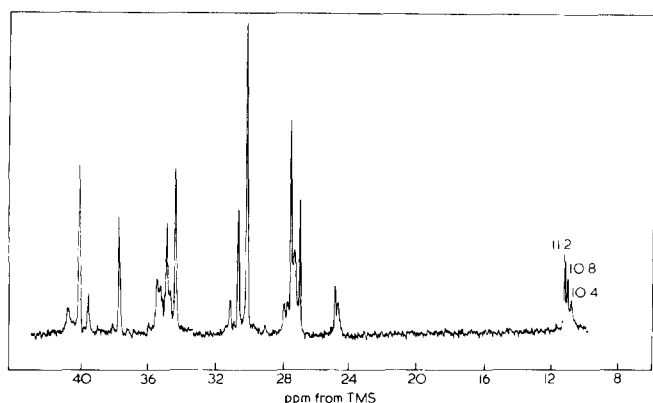


Figure 3 ^{13}C n.m.r. spectrum of an ethylene/butene-1 copolymer containing approximately 30 mol% butene-1

ing in polyethylene by infra-red spectroscopy a ratio of ethyl to n-butyl branches was given as 2:1 for a number of commercially available polymers. It is apparent from our ^{13}C n.m.r. data, that the ratio of n-butyl to ethyl branches can vary considerably in low density polyethylenes. The activation energy for formation is much higher for ethyl branches than for butyl branches and thus depending upon reactor conditions polymers produced will have different ethyl to butyl branch ratios. However, it would seem from the present examination that the number of n-butyl branches generally exceeds the number of ethyl branches in low density polyethylene.

Nevertheless, contrary to Bovey *et al.*¹⁸ it is clear that certain commercially available low density polyethylenes do contain a marked proportion of ethyl branches. The ratio of ethyl to n-butyl branches now observed, although different to that proposed by Willbourn, does not invalidate his comments on the branching mechanism. The new ratios indicate that there is less bunching of short chain branches than was originally thought to be the case. It may be noted that the resonance due to the methyl carbon of the ethyl branch is considerably more broad than the methyl carbon resonance of the n-butyl branch. Figure 3 is the spectrum of an ethylene/butene-1 copolymer containing approximately 30 mol% butene-1. The methyl carbon of the ethyl branch is now seen as three separate resonances arising from ethyl branches in different environments. These, we believe will be associated with (a) isolated butene units, giving rise to a resonance at 11.2 ppm; (b) adjacent butene-1 units as *meso* and *racemic* dyads, giving rise to resonances at 10.8 and 10.4 ppm respectively. Such variations may also be possible in the environment of ethyl branches in polyethylene, in combination with other structural possibilities such as the 2-ethyl hexyl branch. Thus, it would be reasonable to expect sufficient variations in the chemical shift of the terminal methyl carbon which could contribute to the observed broadening of the resonance. Although it is possible that n-butyl and longer branches also exist as *m* and *r* dyads it is unlikely that the methyl carbon resonance will show similar broadening since there is a greater distance and therefore less interaction between the methyl carbon and the main chain carbons than is the case for the ethyl branch.

CONCLUSION

There is no doubt that the ^{13}C n.m.r. spectrum demonstrates the presence of ethyl, n-butyl and longer branches in a number of unfractionated commercially available low density polyethylenes. Furthermore, the quantitative estimation of the number of branches of each type may be achieved provided the correct conditions for the Fourier transform experiment pertain.

ACKNOWLEDGEMENTS

The authors wish to acknowledge the useful discussions with Dr H. A. Willis and Dr R. A. Jackson, both of ICI Plastics Division during the preparation of this paper.

REFERENCES

- 1 Boghetich, L. and Kratz, R. E. *Trans. Soc. Rheol.* 1965, **9**, 255
- 2 Bastein, I. J., Ford, R. W. and Mak, H. D. *J. Polym. Sci. (B)* 1966, **4**, 147
- 3 Sperat, C. A., Franta, W. A. and Starkweather, H. W. *J. Am. Chem. Soc.* 1953, **75**, 6127
- 4 Asbach, G. I. *Faserforsch. Textiltech.* 1967, **18**, 127
- 5 Ram, A. and Miltz, J. *Int. J. Polym. Mater.* 1972, **2**, 39
- 6 Shirayama, K., Kita, S. and Watabe, D. *Makromol. Chem.* 1972, **151**, 97
- 7 Mortimer, G. A. *J. Appl. Polym. Sci.* 1971, **15**, 1231
- 8 Kline, D. E., Sauer, J. A. and Woodward, A. E. *J. Polym. Sci.* 1956, **22**, 455
- 9 Willbourn, A. H. *J. Polym. Sci.* 1959, **34**, 569
- 10 Tirpak, G. A. *J. Polym. Sci. (B)* 1966, **4**, 111
- 11 Shirayama, K., Okada, T. and Kita, S. *J. Polym. Sci. (A)* 1965, **3**, 907
- 12 Tirpak, G. A. *J. Polym. Sci. (B)* 1965, **3**, 371
- 13 Roedel, M. J. *J. Am. Chem. Soc.* 1953, **75**, 6110
- 14 Drott, E. E. and Mendelson, R. A. *Polym. Prepr.* 1971, **12**, 276
- 15 Otocka, E. P. *et al. Polym. Prepr.* 1971, **12**, 274
- 16 Kamath, P. M. and Barlow, A. *J. Polym. Sci. (A-1)* 1967, **8**, 2023
- 17 Teranishi, K. and Sagahara, K. *Kobunshi Kagaku* 1966, **23**, 512
- 18 Boyd, D. R. J., Voter, R. C. and Bryant, W. M. D. *Abstr. 132nd Meet. of Am. Chem. Soc.* 1957, p 8T
- 19 Dorman, D. E., Otocka, E. P. and Bovey, F. A. *Macromolecules* 1972, **5**, 574
- 20 Doddrell, D., Glushko, V. and Allerhand, A. *J. Chem. Phys.* 1972, **56**, 3683
- 21 Kuhlmann, K. F. and Grant, D. M. *J. Am. Chem. Soc.* 1968, **90**, 7355
- 22 Kuhlmann, K. F., Grant, D. M. and Harris, R. K. *J. Chem. Phys.* 1970, **52**, 3439
- 23 Lyerla, J. R. and Grant, D. M. *J. Phys. Chem.* 1972, **76**, 3213
- 24 Haslam, J., Willis, H. A. and Squirrell, D. C. M. 'Identification and Analysis of Plastics', Iliffe, London, 1972
- 25 Randall, J. C. *J. Polym. Sci. (Polym. Phys. Edn.)* 1973, **11**, 275

Notes to the Editor

Glass transition temperature determination of poly(ethylene sulphide), poly(isobutylene sulphide) and their random copolymers

E. Sorta and A. De Chirico

*Snamprogetti SpA., Direzione Ricerca e Sviluppo, 20097 San Donato Milanese, Milano, Italy
(Received 20 October 1975)*

INTRODUCTION

In the course of further physicochemical characterization of copolymers made from ethylene sulphide (ES) and isobutylene sulphide (IBS) having very high crystallization rates, a method of very fast quenching was developed, following a suggestion reported in Wrasidlo's review¹.

This fact allowed us to obtain homopolymers and copolymers sufficiently amorphous to allow their glass transition temperature (T_g) to be determined. For poly(ethylene sulphide), it was not possible to find a direct measurement of T_g in the literature.

An attempt was made² to obtain the T_g of poly(ethylene sulphide) as a result of extrapolation from the T_g values of amorphous copolymers ethylene sulphide-propylene sulphide. The results, in this respect, were not sufficiently reliable and a direct experimental confirmation is required. The same techniques were used to determine the T_g of ES-IBS copolymers, obtained by means of polymerization with a low degree of conversion, which previously gave uncertain experimental values owing to the high degree of conversion. Hence every examined copolymer shows a T_g , which may be correlated, following existing theories, to its composition and to the homopolymer T_g .

EXPERIMENTAL

Materials

Homo- and co-polysulphides were prepared by methods described elsewhere⁶.

Besides poly(ethylene sulphide) (PES), and poly(isobutylene sulphide) (PIBS), four completely random copolymers with different comonomer ratio were prepared and then the random character tested by means of nuclear magnetic resonance⁴. The compositions are reported in Table 1.

Table 1 Copolymer compositions and glass transition temperatures

Sample	ES content (mol %)	T_g (°C)
IBS	0	-14
ES-IBS 18	17.7	-24
ES-IBS 32	32.0	-31
ES-IBS 40	40.0	-35
ES-IBS 58	58.0	-42
ES	100	-50

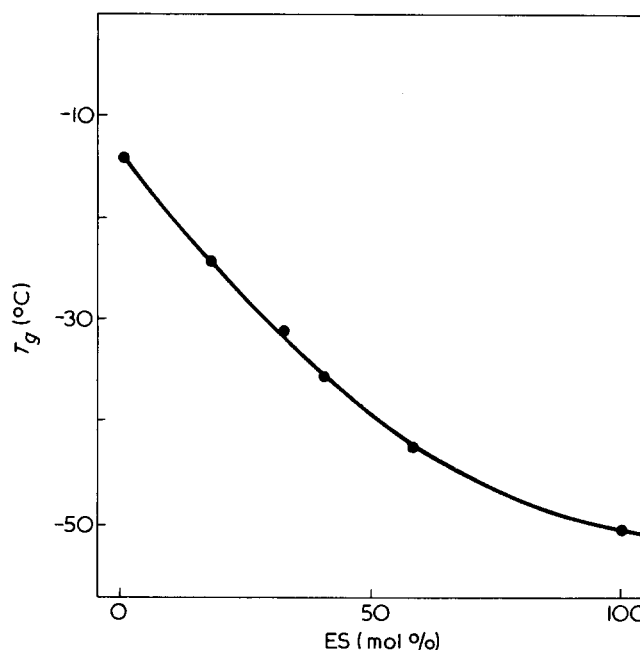


Figure 1 Glass transition temperatures vs. ethylene sulphide content (mol %) in the copolymer ethylene sulphide-isobutylene sulphide

Differential thermal analysis

Differential thermal analyses measurements were carried out using a model 900 Du Pont instrument in the d.s.c. version with a heating rate of 10°C/min.

The samples were heated at 30°C above their melting temperature for 10 min and then quenched between two metallic plates previously cooled at -190°C. The thermograms showed a typical glass transition, followed by a sharp cold crystallization peak. The glass transition temperatures were measured by the initial departure of the base line⁵.

RESULTS AND DISCUSSION

The experimental T_g values of the homopolymers (PES, PIBS) and copolymers (PES-PIBS) are reported in Table 1.

Figure 1 shows the relationship between T_g and the content of ethylene sulphide expressed in mol %. The behaviour is typical for random copolymers. This fact enables us to analyse the results following the theory of

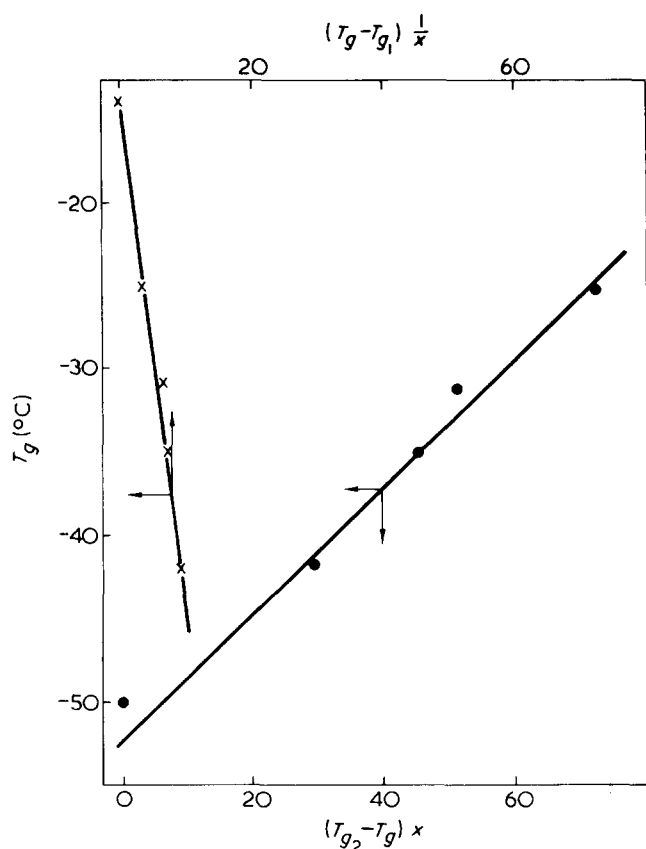


Figure 2 Glass transition temperatures vs. $M_2 n_2 / M_1 n_1 (T_{g2} - T_g)$ and $M_1 n_1 / M_2 n_2 (T_{g1} - T_g)$ according to the Gordon-Taylor representation

Gordon-Taylor shown by Wood³. According to these authors, the glass transition temperature, T_g of the copolymer, can be represented by a function of the glass transition of the homopolymers T_{g1} and T_{g2} made from the respective constituents PES(1) and PIBS(2), in the following manner:

$$T_g = KX(T_{g2} - T_g) + T_{g1} \text{ or } T_g = \frac{1}{K} \frac{1}{X} (T_g - T_{g1}) + T_{g2} \quad (1)$$

where $T_{g2} > T_g > T_{g1}$; K is a constant of the materials and $X = n_2 M_2 / n_1 M_1$ with n_1, n_2 molar fractions of the comonomers having molecular weight M_1 and M_2 .

We obtain two straight lines which satisfy with good approximation, equation (1) as shown in Figure 2. The straight lines were drawn with the mean square method, without taking into consideration the homopolymers' experimental T_g values. Experimentally, the glass transition temperature of PIBS and PES were found to be -14° and -50° C, respectively. These values are in accordance with those extrapolated from copolymers and differ slightly from those predicted earlier².

REFERENCES

- 1 Wrasidlo, W. *Fortschr. Hochpoly. Forsch.* 1974, 13, 21
- 2 De Chirico, A. and Zotteri, L. *Eur. Polym. J.* 1975, 11, 487
- 3 Wood, L. A. *J. Polym. Sci.* 1958, 28, 319
- 4 Corno, C. and Roggero, A. to be published
- 5 Ke, B. 'Newer Methods of Polymer Characterization', Interscience, London, 1964, p 396
- 6 Roggero, A. *et al.* *Eur. Polym. J.* in press

Configuration of low molecular weight polystyrene in deuterated cyclohexane

D. G. H. Ballard and M. G. Rayner

Imperial Chemical Industries Limited, Corporate Laboratory, Runcorn, Cheshire, UK

and J. Schelten

Institut für Festkörperforschung, KFA, Jülich, West Germany
(Received 15 August 1975; revised 1 December 1975)

The radius of gyration of low molecular weight polystyrene in cyclohexane has been measured using the small-angle scattering facility at Jülich. The purpose of these measurements was to investigate how the molecular weight dependence of $\langle s_0^2 \rangle^{1/2}$ deviates from the $M^{0.5}$ law which holds for high molecular weights. The solvent was deuterated to provide the dissolved molecules with a larger scattering amplitude in a scattering experiment with slow neutrons. In a small-angle X-ray scattering experiment, the small difference between the electron density along the dissolved molecules and that of the solvent provides a low contrast. Hence, it would become extremely difficult to measure the coherent scattering from the low molecular weight polystyrene in the presence of a large background. Solutions with 5% and 1% narrow distribution polystyrene of 4000, 2100 and 600 molecular weight have been prepared and measured with neutrons of 7 \AA wavelength with

a sample-to-detector distance of 1 and 2 m. The measurements were performed at the θ -temperature, $T = 38^\circ$ C, in order to avoid long range interaction effects.

The coherent scattering from the solution of 1% polystyrene of the highest molecular weight, $M = 4000$, was, at zero scattering angle, about the same as the background scattering caused by the incoherent scattering cross-section of deuterium in the solvent and of hydrogen in the solute. This demonstrates that the background corrections had to be handled carefully, especially for the lowest molecular weight $M = 600$, where for background reasons experiments with a 1% solution were not feasible. A typical result of the coherent scattering from the dissolved polystyrene is shown in Figure 1 as a plot I_0/I versus K^2 .

The radii of gyration $\langle s_0^2 \rangle_2^{1/2}$ and $\langle s_0^2 \rangle_1^{1/2}$ obtained from the 2 m and 1 m runs, respectively, for the 5% and 1% solutions and their mean values, (giving the 2 m runs

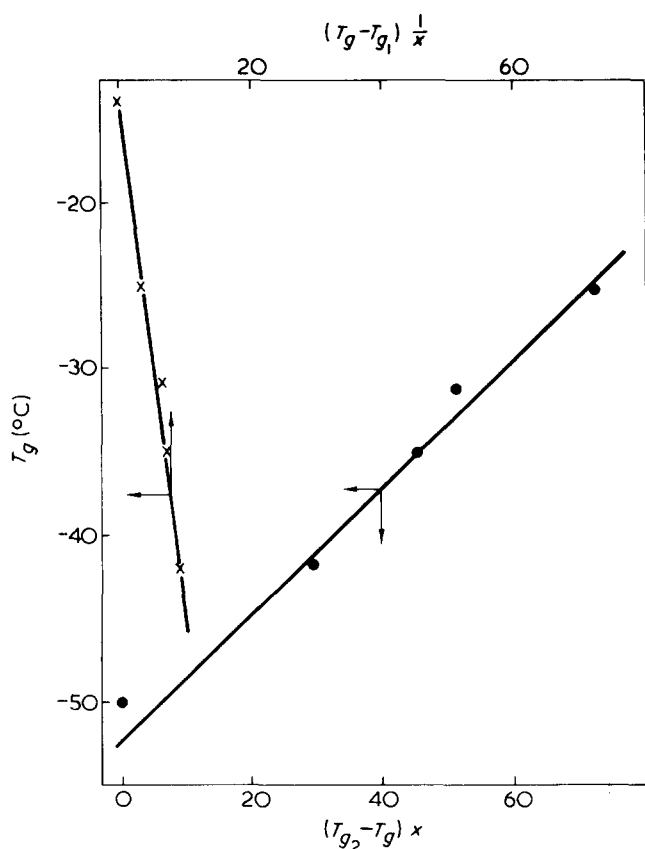


Figure 2 Glass transition temperatures vs. $M_2 n_2 / M_1 n_1 (T_{g2} - T_g)$ and $M_1 n_1 / M_2 n_2 (T_{g1} - T_g)$ according to the Gordon-Taylor representation

Gordon-Taylor shown by Wood³. According to these authors, the glass transition temperature, T_g of the copolymer, can be represented by a function of the glass transition of the homopolymers T_{g1} and T_{g2} made from the respective constituents PES(1) and PIBS(2), in the following manner:

$$T_g = KX(T_{g2} - T_g) + T_{g1} \text{ or } T_g = \frac{1}{K} \frac{1}{X} (T_g - T_{g1}) + T_{g2} \quad (1)$$

where $T_{g2} > T_g > T_{g1}$; K is a constant of the materials and $X = n_2 M_2 / n_1 M_1$ with n_1, n_2 molar fractions of the comonomers having molecular weight M_1 and M_2 .

We obtain two straight lines which satisfy with good approximation, equation (1) as shown in Figure 2. The straight lines were drawn with the mean square method, without taking into consideration the homopolymers' experimental T_g values. Experimentally, the glass transition temperature of PIBS and PES were found to be -14° and -50°C , respectively. These values are in accordance with those extrapolated from copolymers and differ slightly from those predicted earlier².

REFERENCES

- 1 Wrasidlo, W. *Fortschr. Hochpoly. Forsch.* 1974, 13, 21
- 2 De Chirico, A. and Zotteri, L. *Eur. Polym. J.* 1975, 11, 487
- 3 Wood, L. A. *J. Polym. Sci.* 1958, 28, 319
- 4 Corno, C. and Roggero, A. to be published
- 5 Ke, B. 'Newer Methods of Polymer Characterization', Interscience, London, 1964, p 396
- 6 Roggero, A. *et al. Eur. Polym. J.* in press

Configuration of low molecular weight polystyrene in deuterated cyclohexane

D. G. H. Ballard and M. G. Rayner

Imperial Chemical Industries Limited, Corporate Laboratory, Runcorn, Cheshire, UK

and J. Schelten

Institut für Festkörperforschung, KFA, Jülich, West Germany

(Received 15 August 1975; revised 1 December 1975)

The radius of gyration of low molecular weight polystyrene in cyclohexane has been measured using the small-angle scattering facility at Jülich. The purpose of these measurements was to investigate how the molecular weight dependence of $\langle s_0^2 \rangle^{1/2}$ deviates from the $M^{0.5}$ law which holds for high molecular weights. The solvent was deuterated to provide the dissolved molecules with a larger scattering amplitude in a scattering experiment with slow neutrons. In a small-angle X-ray scattering experiment, the small difference between the electron density along the dissolved molecules and that of the solvent provides a low contrast. Hence, it would become extremely difficult to measure the coherent scattering from the low molecular weight polystyrene in the presence of a large background. Solutions with 5% and 1% narrow distribution polystyrene of 4000, 2100 and 600 molecular weight have been prepared and measured with neutrons of 7 \AA wavelength with

a sample-to-detector distance of 1 and 2 m. The measurements were performed at the θ -temperature, $T = 38^\circ\text{C}$, in order to avoid long range interaction effects.

The coherent scattering from the solution of 1% polystyrene of the highest molecular weight, $M = 4000$, was, at zero scattering angle, about the same as the background scattering caused by the incoherent scattering cross-section of deuterium in the solvent and of hydrogen in the solute. This demonstrates that the background corrections had to be handled carefully, especially for the lowest molecular weight $M = 600$, where for background reasons experiments with a 1% solution were not feasible. A typical result of the coherent scattering from the dissolved polystyrene is shown in Figure 1 as a plot I_0/I versus K^2 .

The radii of gyration $\langle s_0^2 \rangle_2^{1/2}$ and $\langle s_0^2 \rangle_1^{1/2}$ obtained from the 2 m and 1 m runs, respectively, for the 5% and 1% solutions and their mean values, (giving the 2 m runs

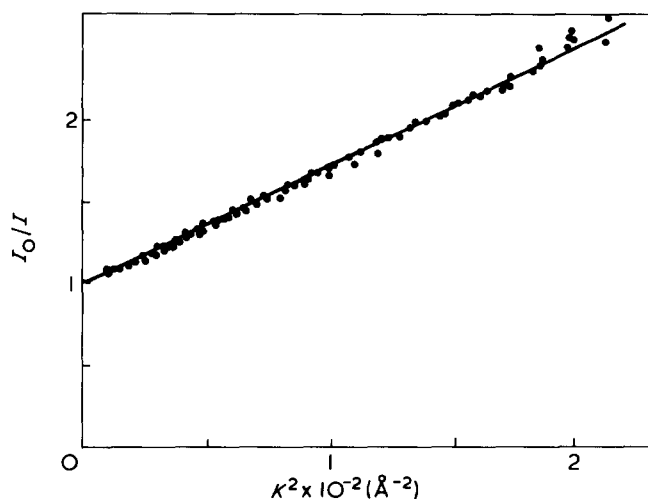


Figure 1 The reciprocal of the coherent neutron scattering I from the 5% polystyrene molecules of $M = 2100$ in deuterated cyclohexane, normalized to its forward scattering value I_0 as a function of the square of the scattering vector K^2

Table 1 Radii of gyration obtained with 5% and 1% solutions

M	$\langle s_0^2 \rangle_2^{1/2}$		$\langle s_0^2 \rangle_1^{1/2}$		Mean $\langle s_0^2 \rangle^{1/2}$
	5%	1%	5%	1%	
4000	15.6	15.4	16.5	16.0	15.7 ± 1
2100	10.2	10.0	12.1	12.2	10.8 ± 1
600	4.0	—			4.0 ± 0.5

twice the statistical weight of the 1 m runs), are given in Table 1. Within experimental errors, both the forward scattering normalized to the same concentration and the radius of gyration were found to be concentration independent.

The tabulated mean $\langle s_0^2 \rangle^{1/2}$ values are plotted versus the molecular weight in Figure 2 in order to compare the experimental results with various models. The uncertainties in measurement at different molecular weights are shown by error bars.

For high molecular weight polystyrene in a θ -solvent, it has been established that the unperturbed radius of gyration is related to molecular weight by the following expression¹:

$$\langle s_0^2 \rangle^{1/2} = \beta M^{0.5} \quad (1)$$

where $\beta = 0.272 \text{ \AA}$. This relationship is plotted in Figure 2 (solid line). As expected the measured $\langle s_0^2 \rangle^{1/2}$ are considerably below this line but they approach it asymptotically at higher molecular weights.

At very low molecular weights it is anticipated that a rigid-rod model should apply. The radius of gyration for such a model is determined by the total length L of the molecule:

$$\langle s_0^2 \rangle^{1/2} = L/(12)^{1/2} \quad (2)$$

where $L = l_b M/M_b$ and l_b and M_b are the length and the molecular weight of the repeat unit C_8H_8 . Using $l_b = 2.6 \text{ \AA}$ we find:

$$\langle s_0^2 \rangle^{1/2} = \gamma M \quad (3)$$

where $\gamma = 0.0072 \text{ \AA}$. This relationship is also plotted in Figure 2 for comparison with the experimental results. In this case the measured $\langle s_0^2 \rangle^{1/2}$ are below the line drawn for this model but they approach it asymptotically at low molecular weights.

A possible model for chain molecule configurations should yield an expression for $\langle s_0^2 \rangle^{1/2}$ which approaches equation (3) for very small M and equation (1) for very large M . Such a model has been proposed by Porod and Kratky and is frequently referred to as the worm-like chain^{3,4}. The expression for the radius of gyration is:

$$\langle s_0^2 \rangle = \frac{aL}{3} \left\{ 1 + \frac{3a}{L} + 6 \left(\frac{a}{L} \right)^2 - 6 \left(\frac{a}{L} \right)^3 \times [1 - \exp(-L/a)] \right\} \quad (4)$$

The persistence length, a , is determined from the requirement that for large L , equation (4) should approach equation (1) i.e.

$$\frac{aL}{3} = \beta^2 M \quad (5)$$

which yields $a = 8.8 \text{ \AA}$.

The molecular weight dependence of $\langle s_0^2 \rangle^{1/2}$ from equation (4) is shown in Figure 2. The experimental values are close to this line. Taking into account that the $\langle s_0^2 \rangle^{1/2}$ are z -averages which have to be lowered by less than 4% according to the equation⁵:

$$\langle s_0^2 \rangle_w^{1/2} = \langle s_0^2 \rangle_z^{1/2} \left(\frac{1+U}{1+2U} \right)^{1/2} \quad (6)$$

where $U = (\bar{M}_w/\bar{M}_n) - 1 \leq 0.1$ for these polymers, the result of this experiment is that the molecular weight dependence of $\langle s_0^2 \rangle^{1/2}$ is satisfactorily described by the Porod-Kratky model.

These results may be compared with those described in Figure 1 of Kirste's paper⁶, obtained for low molecular weight poly(methyl methacrylate) in acetone, by small-

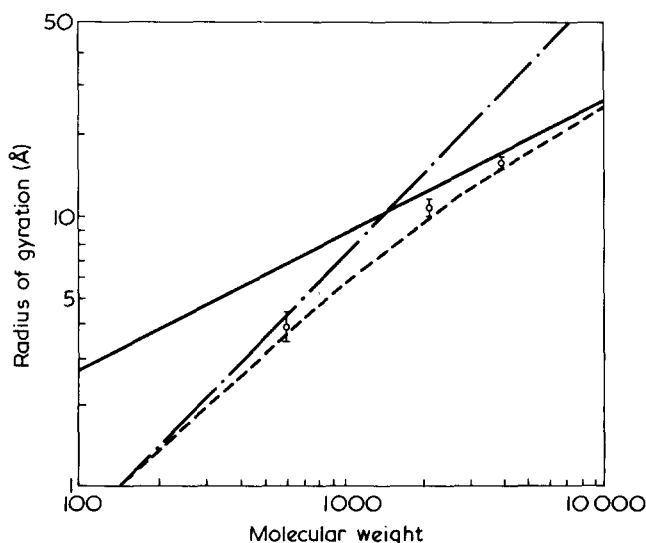


Figure 2 Radius of gyration $\langle s_0^2 \rangle^{1/2}$, as a function of molecular weight on a log-log scale. Neutron scattering results, I ; (—), $\langle s_0^2 \rangle^{1/2} = \beta M^{0.5}$; (- - -), $\langle s_0^2 \rangle^{1/2} = \gamma M$; (- · - · -), Porod-Kratky model $\langle s_0^2 \rangle^{1/2} = f(a, L)$

angle X-ray scattering. In contrast with the present data, Kirste reported serious deviations between his experimental data and those predicted by equation (4). He attempted to explain these deviations in terms of the finite cross-section of the chain but concluded that deviations from the Porod-Kratky model were responsible for the differences. The contribution of the finite cross-section of the chains is in the case of neutron scattering, about 15% of the smallest measured $(s_0^2)^{1/2}$ value and less than 2% for the others. It would seem from our data that in the critical region equation (4) is correct for polystyrene.

Reaction between lithium polystyryl and iodinated polystyrene

J. Pannell

Research Department, ICI Plastics Division, Welwyn Garden City, Herts, UK
(Received 3 November 1975; revised 1 December 1975)

INTRODUCTION

The successful preparation of comb-type branched polystyrenes has been reported by several authors¹⁻⁵. In all cases 'living' polystyrene (the branch precursor) was allowed to react with appropriate functional groups incorporated in another polystyrene chain (the backbone). The most commonly used functional group was the chloromethyl group substituted in the aromatic rings *para* to the carbon chain¹⁻⁴, although the ester group has also been used⁵, incorporated into the backbone by copolymerizing methyl methacrylate with styrene. In this method of preparation the branched polymer forms part of a mixture also containing linear polymer, which is produced by termination of the living polymer by impurities in the system. A study of the properties of these branched polymers therefore necessitates either a fractionation to remove this linear homopolymer^{2a,3} or some way of making allowance for it^{2b}. An alternative method of preparing branched polymers, and one that can in principle be used to prepare graft copolymers also, is the addition of a monomer to a multifunctional polymeric initiator. However, this type of initiator has not so far been prepared free of a monofunctional species, which competes for the monomer to give linear homopolymer.

In considering alternative methods for preparing branched polymers and graft copolymers, a study was made of the reaction between low molecular weight lithium polystyryl* and iodinated polystyrene. The preparation of the latter⁶ was found to be easily controlled and reproducible and not accompanied by undesirable side reactions, factors which make it preferable to the introduction of chloromethyl groups into polystyrene by classical chloromethylation. The results of this study are reported here.

EXPERIMENTAL

Iodination of polystyrene

A purified commercially available sample of polysty-

* Now more commonly known as polystyryl lithium but changed here for consistency with earlier work².

REFERENCES

- 1 Flory, P. J. 'Statistical Mechanics of Chain Molecules', Interscience, New York, 1969, p 40
- 2 Wecker, S. M., Davidson, Th. and Cohen, J. B. *J. Mater. Sci.* 1972, 7, 1249
- 3 Heine, S., Kratky, O. and Porod, G. *Makromol. Chem.* 1961, 41, 682
- 4 Flory, P. J. 'Statistical Mechanics of Chain Molecules' Interscience, New York, 1969, p 403
- 5 Altgelt, K. and Schulz, G. V. *Makromol. Chem.* 1960, 36, 209
- 6 Kriste, R. G. 'Characterisation of Macromolecular Structure', Nat. Acad. Sci., Washington DC, 1968, p 74

rene ($\bar{M}_n = 1.14 \times 10^5$), was partially iodinated in nitrobenzene solution at 90°C using a procedure described by Braun⁶. After 12 h the solution was cooled and the polymer precipitated by adding to a large volume of methanol. The pale yellow polymer was re-precipitated from tetrahydrofuran (THF) into methanol and dried. The iodine content, determined by the oxygen flask combustion method, was 28.9% by weight. This result, together with the infra-red spectrum of the product, shows that one in three of the aromatic rings contain iodine substituted exclusively *para* to the carbon chain of the polymer.

Preparation of lithium polystyryl

Low molecular weight lithium polystyryl was prepared using n-butyl lithium as initiator, employing techniques described elsewhere² and was used in the reaction with partially iodinated polystyrene shortly after its preparation. A small portion was terminated with methanol and characterized. The solvent used in the preparation of lithium polystyryl was either benzene or a mixture of THF and benzene (80:20 v/v).

Reactions

The reaction between lithium polystyryl and the iodinated polystyrene was carried out at room temperature in an inert atmosphere of argon using techniques similar to those described previously². Three experiments were performed.

(i) A solution containing 3 g iodinated polystyrene in 150 cm³ THF was added slowly to a stirred solution of lithium polystyryl in THF/benzene mixture. A slightly yellow granular precipitate formed immediately and the addition of the iodinated polystyrene was continued until no more precipitate formed. At this stage the solution was amber-coloured but became colourless immediately on the addition of methanol.

(ii) A solution of 18.5 g lithium polystyryl in 80 cm³ benzene was added slowly to a stirred solution of 1 g iodinated polystyrene in 150 cm³ THF. A turbidity developed during the addition of about two-thirds of the living poly-

angle X-ray scattering. In contrast with the present data, Kirste reported serious deviations between his experimental data and those predicted by equation (4). He attempted to explain these deviations in terms of the finite cross-section of the chain but concluded that deviations from the Porod-Kratky model were responsible for the differences. The contribution of the finite cross-section of the chains is in the case of neutron scattering, about 15% of the smallest measured $(s_0^2)^{1/2}$ value and less than 2% for the others. It would seem from our data that in the critical region equation (4) is correct for polystyrene.

Reaction between lithium polystyryl and iodinated polystyrene

J. Pannell

Research Department, ICI Plastics Division, Welwyn Garden City, Herts, UK
(Received 3 November 1975; revised 1 December 1975)

INTRODUCTION

The successful preparation of comb-type branched polystyrenes has been reported by several authors¹⁻⁵. In all cases 'living' polystyrene (the branch precursor) was allowed to react with appropriate functional groups incorporated in another polystyrene chain (the backbone). The most commonly used functional group was the chloromethyl group substituted in the aromatic rings *para* to the carbon chain¹⁻⁴, although the ester group has also been used⁵, incorporated into the backbone by copolymerizing methyl methacrylate with styrene. In this method of preparation the branched polymer forms part of a mixture also containing linear polymer, which is produced by termination of the living polymer by impurities in the system. A study of the properties of these branched polymers therefore necessitates either a fractionation to remove this linear homopolymer^{2a,3} or some way of making allowance for it^{2b}. An alternative method of preparing branched polymers, and one that can in principle be used to prepare graft copolymers also, is the addition of a monomer to a multifunctional polymeric initiator. However, this type of initiator has not so far been prepared free of a monofunctional species, which competes for the monomer to give linear homopolymer.

In considering alternative methods for preparing branched polymers and graft copolymers, a study was made of the reaction between low molecular weight lithium polystyryl* and iodinated polystyrene. The preparation of the latter⁶ was found to be easily controlled and reproducible and not accompanied by undesirable side reactions, factors which make it preferable to the introduction of chloromethyl groups into polystyrene by classical chloromethylation. The results of this study are reported here.

EXPERIMENTAL

Iodination of polystyrene

A purified commercially available sample of polysty-

* Now more commonly known as polystyryl lithium but changed here for consistency with earlier work².

REFERENCES

- 1 Flory, P. J. 'Statistical Mechanics of Chain Molecules', Interscience, New York, 1969, p 40
- 2 Wecker, S. M., Davidson, Th. and Cohen, J. B. *J. Mater. Sci.* 1972, 7, 1249
- 3 Heine, S., Kratky, O. and Porod, G. *Makromol. Chem.* 1961, 41, 682
- 4 Flory, P. J. 'Statistical Mechanics of Chain Molecules' Interscience, New York, 1969, p 403
- 5 Altgelt, K. and Schulz, G. V. *Makromol. Chem.* 1960, 36, 209
- 6 Kriste, R. G. 'Characterisation of Macromolecular Structure', Nat. Acad. Sci., Washington DC, 1968, p 74

rene ($\bar{M}_n = 1.14 \times 10^5$), was partially iodinated in nitrobenzene solution at 90°C using a procedure described by Braun⁶. After 12 h the solution was cooled and the polymer precipitated by adding to a large volume of methanol. The pale yellow polymer was re-precipitated from tetrahydrofuran (THF) into methanol and dried. The iodine content, determined by the oxygen flask combustion method, was 28.9% by weight. This result, together with the infra-red spectrum of the product, shows that one in three of the aromatic rings contain iodine substituted exclusively *para* to the carbon chain of the polymer.

Preparation of lithium polystyryl

Low molecular weight lithium polystyryl was prepared using n-butyl lithium as initiator, employing techniques described elsewhere² and was used in the reaction with partially iodinated polystyrene shortly after its preparation. A small portion was terminated with methanol and characterized. The solvent used in the preparation of lithium polystyryl was either benzene or a mixture of THF and benzene (80:20 v/v).

Reactions

The reaction between lithium polystyryl and the iodinated polystyrene was carried out at room temperature in an inert atmosphere of argon using techniques similar to those described previously². Three experiments were performed.

(i) A solution containing 3 g iodinated polystyrene in 150 cm³ THF was added slowly to a stirred solution of lithium polystyryl in THF/benzene mixture. A slightly yellow granular precipitate formed immediately and the addition of the iodinated polystyrene was continued until no more precipitate formed. At this stage the solution was amber-coloured but became colourless immediately on the addition of methanol.

(ii) A solution of 18.5 g lithium polystyryl in 80 cm³ benzene was added slowly to a stirred solution of 1 g iodinated polystyrene in 150 cm³ THF. A turbidity developed during the addition of about two-thirds of the living poly-

mer solution but beyond this, a slightly yellow granular precipitate settled out. The addition of lithium polystyryl was continued until a definite orange colouration persisted and then a few drops of methanol were added, giving a colourless solution.

(iii) Experiment (ii) was repeated, except that the iodinated polystyrene was in solution in benzene. A slight turbidity formed during the reaction but no precipitate separated.

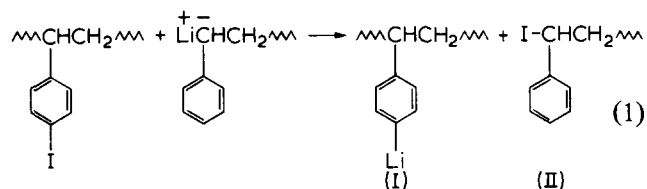
The precipitate which formed in experiments (i) and (ii), was separated by centrifuging and was washed repeatedly with THF until the washings were colourless. The soluble polymer in all three experiments was recovered by precipitation into methanol, followed by re-precipitations into water and methanol.

RESULTS AND DISCUSSION

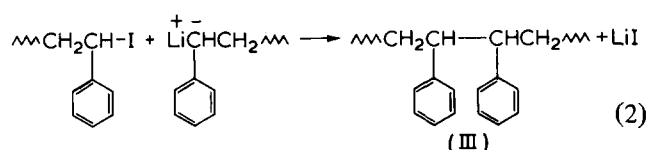
Characterization of the soluble polymer recovered after the reaction between lithium polystyryl and partially iodinated polystyrene shows that its molecular weight is nearly double that of the lithium polystyryl (see Table 1).

G.p.c. also shows that the molecular weight of the soluble polymer recovered after the reaction, although still low compared with that of the polystyrene used for iodination, is higher than that of the lithium polystyryl precursor. Furthermore the chromatograms show that the molecular weight distribution of the soluble product is less skewed than that of the precursor. (Figure 1).

These results suggest that during the title reaction the lithium polystyryl was involved in a chain extension reaction rather than a coupling reaction with the iodinated polystyrene. (During the reaction some of the living polymer is terminated by impurities and it is this which makes the apparent molecular weight of the soluble product somewhat less than twice that of the precursor). The simplest mechanism which can explain these results involves two distinct steps. In the first step the lithium polystyryl and the partially iodinated polystyrene undergo lithium-halogen exchange:



The iodo-capped polymer (II) then couples with lithium polystyryl to give the soluble product polymer with a head-to-head linkage:



The lithium-halogen exchange reaction is known to occur between both poly(*p*-bromostyrene) and poly(*p*-iodostyrene) and *n*-butyl lithium⁶⁻⁸ and evidence has been presented (Altares *et al.*¹) which suggests that the more ionic lithium polystyryl can also take part in an exchange reaction (with chlorine in 1, 2, 4, 5-tetrachloromethylbenzene), although this occurs to a lesser extent than the coupling or displacement reaction. If lithium polystyryl

Table 1 Molecular weight measurements by ebulliometry

	\bar{M}_n , terminated living polymer	\bar{M}_n , soluble polymer isolated after reaction
Experiment (ii)	4700 ± 100	8750 ± 200
Experiment (iii)	4600 ± 200	8000 ± 200

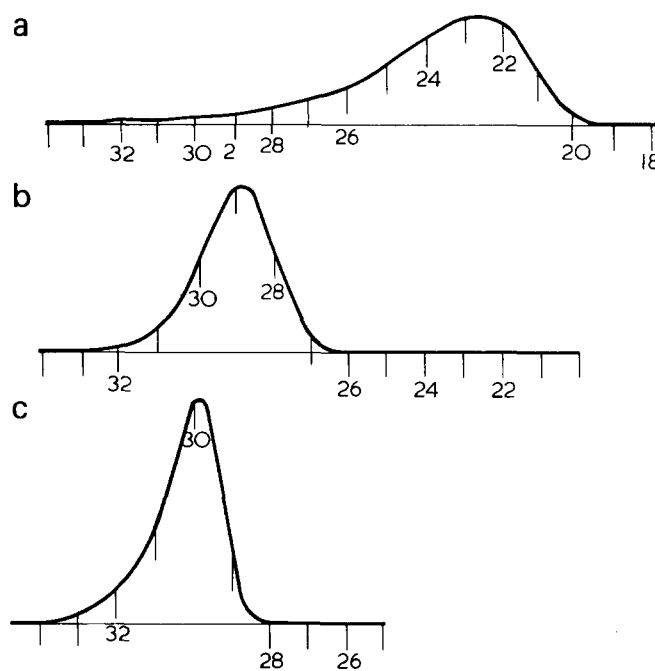


Figure 1 The g.p.c. chromatograms: (a) polystyrene used for iodination; (b) soluble product polymer from reaction (2); (c) proton-terminated lithium polystyryl used in reaction (2). The samples were injected into a Waters Associates chromatograph at 308 K using chloroform as solvent; their concentration was 1/4% by wt. Four columns (each 122 cm long and 0.95 cm in diameter) containing 'Styragel' were used in series (10^6 , 10^5 , 10^4 , and 10^3 Å respectively)

is capable of participating in lithium-halogen exchange with an organic chloride, then it is more likely to do so with an organic iodide e.g. poly(*p*-iodostyrene).

The chain extension reaction shown in equation (2), also occurs in the reaction of the disodium salts of the dianions of both polystyrene and the α -methyl styrene tetramer with iodine^{9,10} and in the reaction between potassium polystyryl and bromine¹¹.

The polymer that was recovered from the reaction carried out in benzene, was largely the chain-extended polymer, but a turbidimetric titration confirmed the presence of a small proportion of a high molecular weight component which before protonation was the lithiated polystyrene (I).

Additional evidence in support of the proposed mechanism was sought by looking for differences in the accumulated ¹³C n.m.r. spectra of the proton-terminated precursor and the chain extended polymer(III). The spectra of both polymers (Figure 2) show weak resonances at 13.8, 22.2, 26.9 and 31.7 ppm (relative to the resonance from the internal standard tetramethylsilane) not present in the spectrum of free radical polystyrene¹²; they are assigned to the carbon

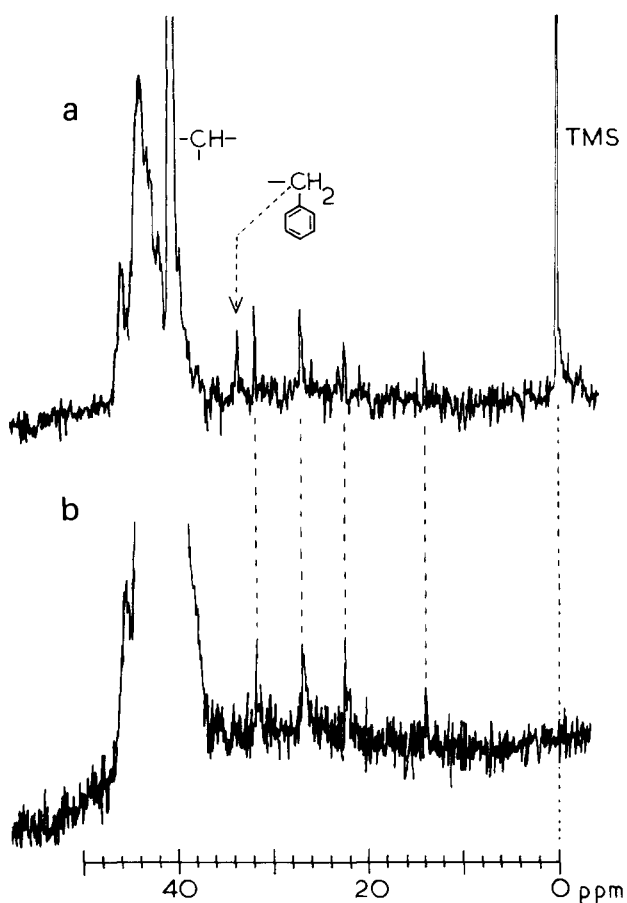


Figure 2 Part of the accumulated ^{13}C n.m.r. spectra of (a) proton-terminated lithium polystyryl and (b) the soluble product polymer from the reaction of lithium polystyryl with iodinated polystyrene. The spectra were recorded on a Varian XL100 spectrometer at 25.2 MHz with the polymers dissolved in CDCl_3

atoms in the *n*-butyl end groups derived from the initiator. However, an additional weak resonance at 33.7 ppm appears in the spectrum of the proton-terminated living polymer and this is thought to be due to the $-\text{CH}_2-$ carbon in the terminal $-\text{CH}_2-(\text{Ph})$ group, a group not present in the chain-extended polymer (III). The resonance from the corresponding methylene carbon in some model compounds (ethyl-, *n*-butyl-, dodecyl- and *n*-propyl benzene) appears at 29.3, 35.9, 36.2 and 38.3 ppm respectively¹³.

A resonance attributable solely to the methine carbons of the head-to-head linkage $-\text{CH}(\text{Ph})-\text{CH}(\text{Ph})-$ in the chain extended polymer was not observed, probably because of overlap with the much stronger resonance at 40.5 ppm from the methine carbons of the repeat units in the chain.

The lithiated polystyrene (I) which formed as a result of the lithium-iodine exchange reaction (1), and which precipitated from the mixed benzene/THF system, became protonated on the addition of methanol but remained insoluble thereafter. The infra-red spectrum of this insoluble polymer shows that not all the iodine in the original iodinated polystyrene had exchanged with lithium; about one in nine of the aromatic rings of the repeat units still contained iodine *para* to the carbon chain. This is about one third of the iodine content of the original iodinated polystyrene.

One of the consequences of the lithium-iodine exchange reaction in the system described here is that species are

present which might conceivably crosslink and this could be the reason for the formation of an insoluble polymer from the THF/benzene mixture used in two of the experiments. However, the granular form of the original precipitate was unlike that of a typical crosslinked polystyrene and an insoluble polymer did not form when the reaction was carried out in benzene. It seems more likely, therefore, that differences in solubility of the lithiated polystyrene, either alone or as a complex with lithium iodide, accounts for the formation of a precipitate from THF/benzene but not from benzene alone. If this is so then the reason why the precipitate that formed in the THF/benzene system remained insoluble on protonation, is that crosslinking occurred subsequently i.e. during isolation of the polymer.

CONCLUSION

When low molecular weight lithium polystyryl reacts with iodinated polystyrene, lithium-iodine exchange occurs to give a lithiated polystyrene and a chain extended polymer derived from the lithium polystyryl. The lithiated polystyrene precipitates from a THF/benzene mixture when approximately 22% of the aromatic rings are lithiated, i.e. before all the iodine has exchanged. When the reaction is carried out in benzene by the addition of lithium polystyryl to the iodinated polystyrene the lithiated polymer remains in solution and can be prepared free of excess living polymer. Thus a multifunctional anionic initiator may be made for the preparation of branched polymers or graft copolymers free of an excess of a monofunctional species which can cause homopolymerization of the added monomer. This method of preparing lithiated polystyrene therefore appears to have a distinct advantage over that which uses (a) *n*-butyl lithium in a similar lithium-halogen exchange reaction^{6,7} or (b) the *n*-butyl lithium/TMEDA* complex for direct metalation of polystyrene¹⁴. Further experimental work will be necessary to confirm this.

ACKNOWLEDGEMENTS

The author is grateful to Mr A. Titterton for experimental assistance and to Mr A. Bunn for recording the n.m.r. spectra.

REFERENCES

- 1 Altares, T., Wyman, D. P., Allen, V. R. and Meyerson, K. *J. Polym. Sci. (A)* 1965, **3**, 4131
- 2 (a) Pannell, J. *Polymer* 1971, **12**, 558; (b) 1972, **13**, 2
- 3 Fujimoto, T., Narukawa, H. and Nagasawa, M. *Macromolecules* 1970, **3**, 57
- 4 Candau, F. and Franta, E. *Makromol. Chem.* 1971, **149**, 41
- 5 Decker, D. *Makromol. Chem.* 1969, **125**, 136
- 6 Braun, D. *Makromol. Chem.* 1959, **30**, 85
- 7 Leavitt, F. C. and Matternas, L. H. *J. Polym. Sci.* 1960, **45**, 249
- 8 Melby, L. R. and Strobach, D. R. *J. Am. Chem. Soc.* 1967, **89**, 450
- 9 Richards, D. H., Salter, D. A. and Williams, R. L. *Chem. Commun.* 1966, **2**, 38
- 10 Richards, D. H. and Salter, D. A. *Polymer* 1967, **8**, 139
- 11 Candau, F. and Rempp, P. *C.R. Acad. Sci. (C)* 1968, **267**, 601
- 12 Inoue, Y., Niskioka, A. and Chujo, R. *Makromol. Chem.* 1972, **156**, 207
- 13 Randall, J. C. *J. Polym. Sci. Polym. Phys. Ed.* 1975, **13**, 889
- 14 Evans, D. C., George, M. H. and Barrie, J. A. *J. Polym. Sci. Polym. Chem. Ed.* 1974, **12**, 247

* TMEDA = *N, N, N', N'*-tetramethylethylenediamine.

Raman scattering from the longitudinal acoustic mode in crystalline poly(ethylene oxide)

Low-frequency Raman bands have been observed in solid n-paraffins. These bands which have fundamental frequencies inversely proportional to chain length¹ have been assigned as the longitudinal acoustic (LA) accordion-like vibration of the chain. If the chain is treated as a continuum the fundamental frequency ν (cm^{-1}) is given by:

$$\nu = \frac{1}{2lc} \left(\frac{E}{\rho} \right)^{1/2} \quad (1)$$

where E is the Young's modulus of the chain, l is the chain length and ρ the density. Analogous LA modes in single crystals of polyethylene^{2,3} and in bulk melt-crystallized polyethylene⁴⁻⁶ have also been reported. Here, we report the first observation of the LA mode in well-characterized α,ω -hydroxy-poly(ethylene oxide) fractions of molecular weights from 1000 to 20 000 and in a series of α,ω -alkoxy-poly(ethylene oxide) fractions.

Poly(ethylene oxide) samples, obtained from the sources listed in Table 1, were precipitated from benzene solution by addition of iso-octane and dried. These fractions, with very narrow molecular weight distributions (see Table 1), were melt-crystallized at the temperatures indicated in Table 1. Raman spectra from 6 cm^{-1} to 100 cm^{-1} were obtained using a Cary 82 spectrometer and an argon ion laser operating at 5145 \AA with 600 mW power. A typical spectrum is shown in Figure 1. Three distinct peaks were obtained for the crystalline polymers, two of which are illustrated in Figure 1. None of these peaks are present in the spectrum of the melt. Lamella spacings were determined by small-angle X-ray scattering by means of a Rigaku-Denki camera as described elsewhere⁷.

The lowest peak frequencies (ν) and the lamellar spacings (l_x) are listed in Table 1. For samples of $\bar{M}_n < 3000$, which are known⁷ to crystallize in chain-extended form when melt-crystallized at 25°C , the frequencies show a smooth shift to lower values corresponding to the gradual increase in lamellar thickness. Therefore, we assign these peaks to the fundamental LA accordion-like modes in

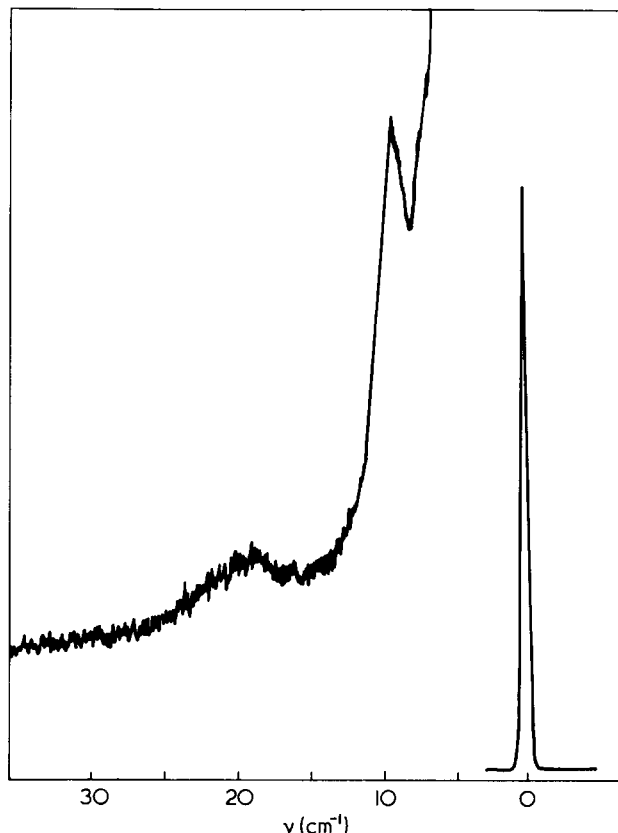


Figure 1 Low-frequency Raman spectrum for crystalline poly(ethylene oxide) of $\bar{M}_n = 2000$. The Rayleigh scattered peak is recorded on reduced scale

poly(ethylene oxide). The second peaks, which are broader and of lower intensity, have frequencies greater than those of the fundamentals by a factor of approximately 2.3, rather than 3.0 as would be expected of a third overtone. The third peak centered at 84 cm^{-1} , is very broad and does not change with lamellar thickness.

On the basis of the Raman and X-ray evidence it can be concluded that for a crystallization temperature of 25°C , poly(ethylene oxide) of $\bar{M}_n = 2000$ or less crystallizes in the chain-extended form and that of $\bar{M}_n = 4000$ or higher in the chain-folded form. Fraction 3000 contains both types of crystal. Its low-angle X-ray diffraction pattern shows two maxima of similar intensities corresponding to repeat distances of 19.3 and 9.9 nm. The Raman peak at 12.0 cm^{-1} , which is close to that of fraction 1500, is indicative of the presence of the once-folded crystal in fraction 3000. Unfortunately, the LA mode frequency for the chain-extended crystal is too low to be observable by the present technique. Fraction 3000 crystallized at 35°C was found to give a weak Raman peak at 12.0 cm^{-1} , reflecting a decrease in the proportion of the once-folded material. These findings are in accordance with previous conclusions derived from crystallization rate and melting point data^{7,8}.

A simple stacked lamella model with alternating crystalline and non-crystalline layers can be used to describe the crystalline state of poly(ethylene oxide)⁹. There is evi-

Table 1 Experimental results for poly(ethylene oxide)

\bar{M}_n	Source	\bar{M}_w/\bar{M}_n	T_c (K)	ν (cm^{-1})	l_x (nm)	ν/l_x
1000	a	1.05	25	18.0	7.1	127.8
1500	a	1.05	25	12.5	9.8	122.5
1750	b	1.04	33	10.5	11.0 ^b	115.5
2000	c	1.06	25	9.0	13.2	118.8
3000	d	1.06	25	12.0	19.3, 9.9	118.8 ^e
3000	d	1.06	35	12.0	19.5	—
4000	a	1.06	25	8.0	15.4	123.2
20 000	c	1.20	25	7.0	16.8	117.6

a, Shell Chemical Co. Ltd; b, Ref. 9; c, Hoechst Chemical Ltd; d, Fluka AG; e, for once-folded crystal

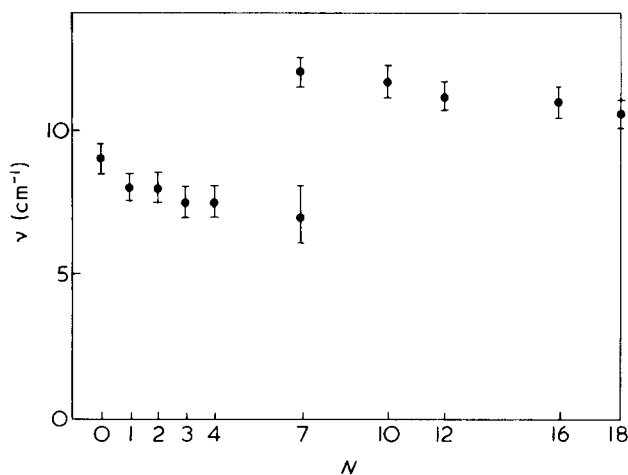


Figure 2 Raman peak frequency of the LA mode in α,ω -alkoxy-poly(ethylene oxide) plotted against N the number of carbon atoms in the alkane chain

dence⁹ that the crystalline lamella thickness (l_c) is proportional to the lamella spacing (l_x) obtained from X-ray scattering. The constant of proportionality for chain-extended crystals of poly(ethylene oxide) fractions has been estimated⁹ to be about 0.67. A value of $\nu l_x = 121 \times 10^{-7}$ (see Table 1) leads to a value of νl_c of 81×10^{-7} and so, taking the density of perfectly crystalline poly(ethylene oxide) to be 1.12 g/cm^3 , to a value of the elastic modulus of the crystalline helical poly(ethylene oxide) chain of $E = 2.7 \times 10^{10} \text{ N/m}^2$ as compared with the value of $1.0 \times 10^{10} \text{ N/m}^2$ found from lattice extension measurements¹⁰. However, we must be cautious in this interpretation since it is not clear from our present data whether the Raman peak is associated with l_c or l_x .

We have also studied the Raman spectra of a series of fractions with a constant central poly(ethylene oxide) block of $\bar{M}_n = 2000$ and with symmetrical alkoxy-end-groups ranging in chain lengths from 1 (methoxy-) to 18 (octadecoxy-) carbon atoms. The samples were prepared from α,ω -hydroxy-poly(ethylene oxide) by a modified Williamson ether synthesis recommended by Dr D. R. Cooper. The LA mode frequencies for these fractions melt-crystallized at 25°C , are plotted against the numbers of carbon atoms in the alkoxy-end-group in Figure 2. These results indicate that the lower members of the series crystallize in chain-extended form whereas the higher members crystallize in chain-folded form; the sample with heptoxy-end-groups (C7) forms both types of crystals. These findings are confirmed by small-angle X-ray scattering and melting point measurements¹¹. A further feature of interest in these data is a slight decrease in the product νl_x as the alkane chain length is increased. Various diblocks, triblocks and mixtures of poly(ethylene oxide) are currently under investigation.

Acknowledgements

We thank the Science Research Council for financial support.

A. Hartley, Y. K. Leung, C. Booth and
I. W. Shepherd

Departments of Physics and Chemistry,
Brunswick Street,
University of Manchester,
Manchester M13 9PL. UK
(Received 20 January 1976)

References

- Schaufele, R. F. and Shimanouchi, T. *J. Chem. Phys.* 1967, **47**, 3605
- Peticolas, W. L., Hibler, G. W., Lippert, J. L., Peterlin, A. and Olf, H. G. *Appl. Phys. Lett.* 1971, **18**, 87
- Peterlin, A., Olf, H. G., Peticolas, W. L., Hibler, G. W. and Lippert, J. L. *J. Polym. Sci. (B)* 1971, **9**, 583
- Olf, H. G., Peterlin, A. and Peticolas, W. L. *J. Polym. Sci. (B)* 1974, **12**, 359
- Koenig, J. L. and Tabb, D. L. *J. Macromol. Sci. (B)* 1974, **9**, 141
- Folkes, M. J., Keller, A., Stejny, J., Goggin, P. L., Fraser, G. V. and Hendra, P. J. *Colloid Polym. Sci.* 1975, **253**, 354
- Beech, D. R., Booth, C., Dodgson, D. V., Sharpe, R. R. and Waring, J. R. S. *Polymer* 1972, **13**, 73
- Kovacs, A. J., Gonthier, A. and Straupe, C. *J. Polym. Sci. Polym. Symp.* 1975, **50**, 283
- Ashman, P. C. and Booth, C. *Polymer* 1975, **16**, 889
- Sakurada, F., Ito, T. and Nakamae, K. *J. Polym. Sci. (C)* 1966, **15**, 75
- Leung, Y. K., Cooper, D. R. and Booth C. to be published

Intermolecular forces and the Raman spectrum of crystalline PVC

In a recent paper¹, Moore and Krimm have presented the results of a vibrational analysis of crystalline syndiotactic poly(vinyl chloride). The calculation was based on a general valence force field derived from an analysis of the spectra of small secondary chloride molecules and it included an intermolecular force field chosen to reproduce correctly the infra-red band observed at 64 cm^{-1} in both secondary chlorides and highly syndiotactic PVC. This band has been assigned previously^{2,3} to a vibration whose potential energy is distributed between an intramolecular torsional vibration and an intermolecular motion and the intermolecular interaction is taken to be hydrogen-bonding of the form C—H...Cl—C.

The results of the calculation are compared with the i.r. results of Krimm *et al.*⁴ and the Raman results of Koenig and Druedow⁵ and the overall agreement appears to be good. In particular, the calculation predicts that the A_1 and B_1 C—Cl stretching modes, observed in the infra-red at 640 and 604 cm^{-1} , should each be split, because of correlations between the motions of the two chains in the unit cell, into two components with significant separation. The four predicted frequencies are shown in Table 1, together with their spectral activity and the frequencies observed by Krimm *et al.* and by Koenig and Druedow.

We are at present involved in a detailed study of the vibrational spectra (more particularly the Raman spectra) of various samples of PVC with a view to characterizing their tacticity, conformational distribution and molecular orientation distribution. We are studying the C—Cl stretching region in great detail because of its sensitivity to these structural parameters and the frequency that we observe for the B_{3g} Raman-active mode of highly syndiotactic urea-canal complex PVC does not agree very well with that of Koenig and Druedow, as is shown in the last column of Table 1. Also shown in this column are our values for the frequencies of the A_g Raman active mode and the B_{1u} and B_{2u} infra-red active modes, which agree quite well with the earlier results.

The Raman spectra were obtained from powder samples of urea-canal complex PVC held in the open ends of capillary tubes. The laser beam was focused into the open end and the Raman light was collected at 90° to the direc-

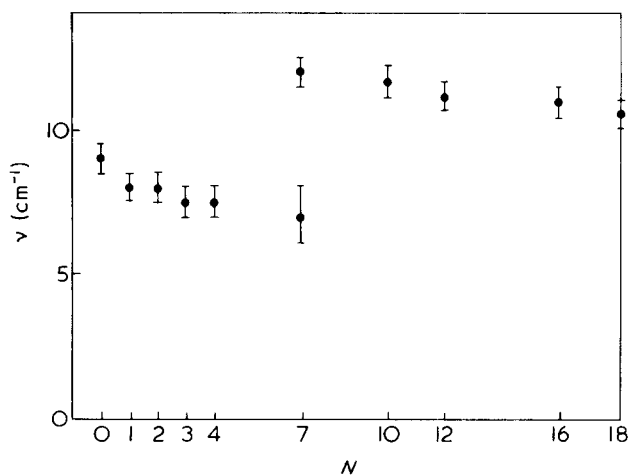


Figure 2 Raman peak frequency of the LA mode in α,ω -alkoxy-poly(ethylene oxide) plotted against N the number of carbon atoms in the alkane chain

dence⁹ that the crystalline lamella thickness (l_c) is proportional to the lamella spacing (l_x) obtained from X-ray scattering. The constant of proportionality for chain-extended crystals of poly(ethylene oxide) fractions has been estimated⁹ to be about 0.67. A value of $\nu l_x = 121 \times 10^{-7}$ (see Table 1) leads to a value of νl_c of 81×10^{-7} and so, taking the density of perfectly crystalline poly(ethylene oxide) to be 1.12 g/cm^3 , to a value of the elastic modulus of the crystalline helical poly(ethylene oxide) chain of $E = 2.7 \times 10^{10} \text{ N/m}^2$ as compared with the value of $1.0 \times 10^{10} \text{ N/m}^2$ found from lattice extension measurements¹⁰. However, we must be cautious in this interpretation since it is not clear from our present data whether the Raman peak is associated with l_c or l_x .

We have also studied the Raman spectra of a series of fractions with a constant central poly(ethylene oxide) block of $\bar{M}_n = 2000$ and with symmetrical alkoxy-end-groups ranging in chain lengths from 1 (methoxy-) to 18 (octadecoxy-) carbon atoms. The samples were prepared from α,ω -hydroxy-poly(ethylene oxide) by a modified Williamson ether synthesis recommended by Dr D. R. Cooper. The LA mode frequencies for these fractions melt-crystallized at 25°C , are plotted against the numbers of carbon atoms in the alkoxy-end-group in Figure 2. These results indicate that the lower members of the series crystallize in chain-extended form whereas the higher members crystallize in chain-folded form; the sample with heptoxy-end-groups (C7) forms both types of crystals. These findings are confirmed by small-angle X-ray scattering and melting point measurements¹¹. A further feature of interest in these data is a slight decrease in the product νl_x as the alkane chain length is increased. Various diblocks, triblocks and mixtures of poly(ethylene oxide) are currently under investigation.

Acknowledgements

We thank the Science Research Council for financial support.

A. Hartley, Y. K. Leung, C. Booth and
I. W. Shepherd

Departments of Physics and Chemistry,
Brunswick Street,
University of Manchester,
Manchester M13 9PL. UK
(Received 20 January 1976)

References

- Schaufele, R. F. and Shimanouchi, T. *J. Chem. Phys.* 1967, **47**, 3605
- Peticolas, W. L., Hibler, G. W., Lippert, J. L., Peterlin, A. and Olf, H. G. *Appl. Phys. Lett.* 1971, **18**, 87
- Peterlin, A., Olf, H. G., Peticolas, W. L., Hibler, G. W. and Lippert, J. L. *J. Polym. Sci. (B)* 1971, **9**, 583
- Olf, H. G., Peterlin, A. and Peticolas, W. L. *J. Polym. Sci. (B)* 1974, **12**, 359
- Koenig, J. L. and Tabb, D. L. *J. Macromol. Sci. (B)* 1974, **9**, 141
- Folkes, M. J., Keller, A., Stejny, J., Goggin, P. L., Fraser, G. V. and Hendra, P. J. *Colloid Polym. Sci.* 1975, **253**, 354
- Beech, D. R., Booth, C., Dodgson, D. V., Sharpe, R. R. and Waring, J. R. S. *Polymer* 1972, **13**, 73
- Kovacs, A. J., Gonthier, A. and Straupe, C. *J. Polym. Sci. Polym. Symp.* 1975, **50**, 283
- Ashman, P. C. and Booth, C. *Polymer* 1975, **16**, 889
- Sakurada, F., Ito, T. and Nakamae, K. *J. Polym. Sci. (C)* 1966, **15**, 75
- Leung, Y. K., Cooper, D. R. and Booth C. to be published

Intermolecular forces and the Raman spectrum of crystalline PVC

In a recent paper¹, Moore and Krimm have presented the results of a vibrational analysis of crystalline syndiotactic poly(vinyl chloride). The calculation was based on a general valence force field derived from an analysis of the spectra of small secondary chloride molecules and it included an intermolecular force field chosen to reproduce correctly the infra-red band observed at 64 cm^{-1} in both secondary chlorides and highly syndiotactic PVC. This band has been assigned previously^{2,3} to a vibration whose potential energy is distributed between an intramolecular torsional vibration and an intermolecular motion and the intermolecular interaction is taken to be hydrogen-bonding of the form C—H...Cl—C.

The results of the calculation are compared with the i.r. results of Krimm *et al.*⁴ and the Raman results of Koenig and Druedow⁵ and the overall agreement appears to be good. In particular, the calculation predicts that the A_1 and B_1 C—Cl stretching modes, observed in the infra-red at 640 and 604 cm^{-1} , should each be split, because of correlations between the motions of the two chains in the unit cell, into two components with significant separation. The four predicted frequencies are shown in Table 1, together with their spectral activity and the frequencies observed by Krimm *et al.* and by Koenig and Druedow.

We are at present involved in a detailed study of the vibrational spectra (more particularly the Raman spectra) of various samples of PVC with a view to characterizing their tacticity, conformational distribution and molecular orientation distribution. We are studying the C—Cl stretching region in great detail because of its sensitivity to these structural parameters and the frequency that we observe for the B_{3g} Raman-active mode of highly syndiotactic urea-canal complex PVC does not agree very well with that of Koenig and Druedow, as is shown in the last column of Table 1. Also shown in this column are our values for the frequencies of the A_g Raman active mode and the B_{1u} and B_{2u} infra-red active modes, which agree quite well with the earlier results.

The Raman spectra were obtained from powder samples of urea-canal complex PVC held in the open ends of capillary tubes. The laser beam was focused into the open end and the Raman light was collected at 90° to the direc-

Table 1 C-Cl stretching modes

Symmetry species single chain	Symmetry species crystal	Activity	Frequency (cm ⁻¹)			
			calc.	obs. (ref 4)	obs. (ref 5)	obs. (present investigation)
B ₁	B _{3g}	R	602		599	608 ± 1
B ₁	B _{1u}	i.r.	604	604		601 ± 1
A ₁	B _{2u}	i.r.	637	640		639 ± 1
A ₁	A _g	R	642		638	639 ± 1

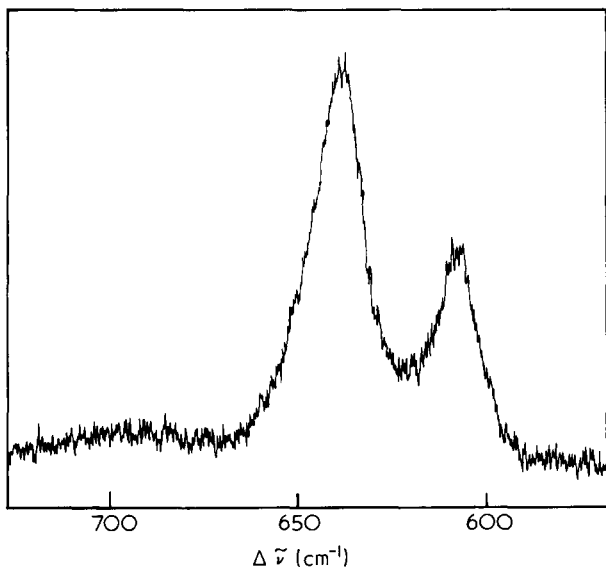


Figure 1 Stokes Raman spectrum of urea-canal complex powder in C-Cl stretching region run on Coderg PHO spectrometer. Exciting wavelength 488 nm

tion of the incident beam and analysed by means of a Coderg PHO Raman spectrometer. The spectrometer was calibrated by means of a neon discharge-tube and the frequencies are believed to be accurate to ± 1 cm⁻¹.

Figure 1 shows the C-Cl stretching modes which are much more clearly resolved in our spectrum than in that of Koenig and Druedow. As part of our detailed study of the C-Cl stretching region, the spectra of the various samples in the range 550 cm⁻¹ to 750 cm⁻¹ have been recorded digitally on paper tape and analysed into a set of overlapping Lorentzians and a linear background. It is necessary to use at least four Lorentzians to fit this region of the urea-canal complex PVC spectrum, the two most intense of which correspond to the observed peaks at 608 and 639 cm⁻¹. A broad weak peak centred at 695 cm⁻¹ is to be interpreted as being due to vibrations of non-crystalline bent syndiotactic conformations and possibly isotactic structures. This region of the i.r. spectrum has been discussed in detail by Krimm and his coworkers⁶. The fourth Lorentzian corresponds to a small peak centred near 645 cm⁻¹ and this feature cannot be interpreted, as far as we can see, as a C-Cl stretching mode. It appears to be present in all our samples of PVC and further study of its intensity relative to the other peaks in the C-Cl region is being undertaken with a view to understanding its origin.

The present results suggest that the predicted correlation splitting of the B₁ species is too small and that the predict-

ed order in frequency of the components is wrong. This in turn suggests that the interchain force field used may not be entirely satisfactory, although both the observed and predicted splittings are quite small, so that the test is not very sensitive. Similar but larger correlation splittings are predicted for the A₁ and B₁ C-C-Cl bending vibrations. The calculated and observed frequencies for the C-C-Cl bending vibrations between 300 and 400 cm⁻¹ are given in Table 2 and the Raman spectrum is shown in Figure 2. For the A₁ and B₁ vibrations the observed Raman and infra-red frequencies show splittings of only 1 or 2 cm⁻¹, whereas the predicted splittings of the A₁ and B₁ species are 16 and 6 cm⁻¹ respectively. We do not observe any Raman peak at 330 or 345 cm⁻¹.

A more direct test of the force-field would be provided by the observation of the predicted low-frequency modes which depend more directly on the intermolecular force field and we therefore attempted to obtain good spectra in the region of the Raman spectrum below 200 cm⁻¹, which was not reported by Koenig and Druedow. Spectra were obtained down to ~ 50 cm⁻¹ on the Coderg double spectrometer and down to ~ 7 cm⁻¹, on a Carey 82 triple spectrometer. Both Stokes and anti-Stokes spectra were run on the Carey 82 and Figure 3 shows the results from 15 cm⁻¹ to 200 cm⁻¹.

A very strong peak is observed at 88 ± 1 cm⁻¹, which

Table 2 C-C-Cl bending modes

Symmetry species single chain	Symmetry species crystal	Activity	Frequency (cm ⁻¹)			
			calc.	obs. (ref 4)	obs. (ref 5)	obs. (present investigation)
B ₁	B _{3g}	R	315		310	316 ± 1
B ₁	B _{1u}	i.r.	321	315		
B ₂	B _{3u}	i.r.	330	345		
B ₂	B _{1g}	R	330		345	
A ₁	A _g	R	360		363	361 ± 1
A ₁	B _{2u}	i.r.	376	358		

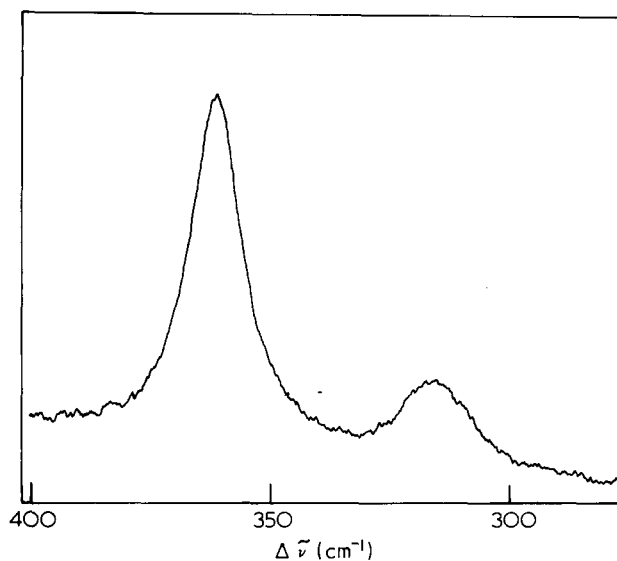


Figure 2 Stokes Raman spectrum of urea-canal complex powder in C-C-Cl bending region run on Carey 82 spectrometer. Exciting wavelength 514.5 nm

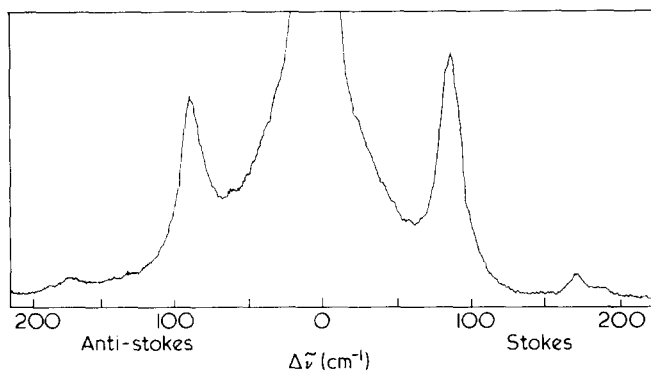


Figure 3 Low-frequency Raman Spectrum of urea-canal complex PVC run on Carey 82 spectrometer. Exciting wavelength 514.5 nm. An arbitrary displacement has been made on the intensity scale between the Stokes and anti-Stokes spectra

clearly corresponds to the peak observed² at 89 cm^{-1} in the infra-red and predicted at 86 cm^{-1} in the Raman. Peaks of moderate strength are observed at 170 and 185 cm^{-1} and a very weak peak at 60 cm^{-1} . There are no predicted Raman-active modes within 10 cm^{-1} of any of these, the nearest possible assignment being that of the 60 cm^{-1} peak to the predicted B_{3g} mode at 45 cm^{-1} . There is no sign of peaks in the predicted positions 39 , 45 , 80 and 134 cm^{-1} , the first three of which would be particularly sensitive to the intermolecular potential. It is possible that the modes predicted at 39 and 134 cm^{-1} are too weak to be observed, and that the two modes predicted at 80 cm^{-1} are of low intensity and are lost beneath the peak at 88 cm^{-1} , which has a half width of $\sim 13\text{ cm}^{-1}$.

The two peaks observed at 170 and 185 cm^{-1} are not easily accounted for. Tasumi and Shimanouchi⁷ have observed an absorption in the infra-red spectrum of an oriented highly syndiotactic sample at 180 cm^{-1} which shows parallel polarization and a weaker shoulder at about 160 cm^{-1} . They were unable to predict vibrations in this frequency region from their single-chain analysis and suggested that it was likely that the absorption at 180 cm^{-1} arises from a mode in which internal rotation is coupled with a lattice vibration, whereas Moore and Krimm⁸ have subsequently suggested that vibrations in the vicinity of 180 cm^{-1} should be assigned to conformations other than the planar zig-zag. The weakness of the observed Raman peaks for the urea-canal complex polymer does not allow us to deny the possibility that they may originate from disordered chains, but we have observed that in the Raman spectrum from a less ordered sample (Montecatini-Edison fibre-forming grade PVC) there is only what appears to be a single peak about 40 cm^{-1} wide centred near 160 cm^{-1} , which is somewhat more intense relative to the peak at 88 cm^{-1} than the 170 and 185 cm^{-1} peaks are for the urea-canal complex sample. This observation suggests that the vibrations due to disordered conformations may occur predominantly at lower frequencies than 170 and 185 cm^{-1} . Another possibility for the origin of these two peaks is that they are due to overtones or combinations of the four modes predicted by Moore and Krimm¹ at 80 , 80 and 86 cm^{-1} in the Raman and 90 cm^{-1} in the infra-red, but bands due to overtones and combinations are usually too weak to be observed in the Raman spectrum.

Polarization studies might be expected to help in the interpretation of the spectrum, since the only bands due to the crystalline material that should not be totally depolarized are those corresponding to A_g symmetry. One of the modes predicted at 80 cm^{-1} has this symmetry, and so do any first overtone bands. The only other predicted A_g mode in the low frequency region is that at 39 cm^{-1} . Unfortunately, we have only very small quantities of the urea-canal complex polymer in powder form so that we have been unable to make polarization studies on it. We have, however, looked for variations in the depolarization of bands in the low frequency Raman spectrum of sheets pressed from Montecatini-Edison fibre-forming grade PVC (which is more syndiotactic than the usual commercial PVCs but less syndiotactic than urea-canal PVC) but without success. All bands appeared to be depolarized to approximately the same degree.

We conclude that the observed low frequency Raman spectrum offers no confirmation of the intermolecular force-field used by Moore and Krimm¹. The only observed frequency which coincides closely with a predicted frequency is that at 88 cm^{-1} , which corresponds directly to that at 86 cm^{-1} in the infra-red. The internal torsional force constant was based essentially on the corresponding frequencies for secondary chlorides. None of the frequencies predicted for the lattice modes have been observed, unless the peak observed at 60 cm^{-1} corresponds to the B_{3g} mode predicted at 45 cm^{-1} , and peaks observed at 170 and 185 cm^{-1} are not satisfactorily accounted for. The low frequency region would thus repay further study, particularly if larger quantities of highly syndiotactic polymer were available.

Acknowledgements

We should like to thank the Department of Chemistry at the University of Manchester, for allowing us to use the Carey 82 spectrometer, Montecatini-Edison SpA., for supplying us with a sample of their fibre-forming grade of PVC and B. F. Goodrich Co. for providing the sample of urea-canal complex PVC. We are grateful to the SRC for granting a CASE studentship to M.E.R.R.

M. E. R. Robinson and D. I. Bower

Department of Physics,
University of Leeds,
Leeds LS2 9JT, UK

W. F. Maddams

British Petroleum Company Ltd,
Epsom Division Group Research and Development Department,
Epsom, UK
(Received 23 December 1975)

References

- 1 Moore, W. H. and Krimm, S. *Makromol. Chem. Suppl.* 1975, 1, 491
- 2 Warriar, A. V. R. and Krimm, S. *J. Chem. Phys.* 1970, 52, 4316
- 3 Warriar, A. V. R. and Krimm, S. *Macromolecules* 1970, 3, 709
- 4 Krimm, S., Folt, V. L., Shipman, J. J. and Berens, A. R. *J. Polym. Sci. (A)* 1963, 1, 2621
- 5 Koenig, J. L. and Druesdow, D. *J. Polym. Sci. (A-2)* 1969, 7, 1075
- 6 Krimm, S. *Pure Appl. Chem.* 1968, 16, 369
- 7 Tasumi, M. and Shimanouchi, T. *Polym. J.* 1971, 2, 62
- 8 Moore, W. H. and Krimm, S. *Spectrochim. Acta. (A)* 1973, 29, 2025

On the structure of 3,4-/*cis*-1,4-polyisoprene by ^{13}C n.m.r.

Introduction

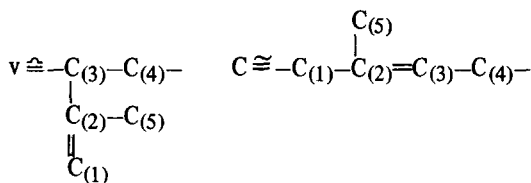
^1H n.m.r. and infra-red spectroscopic studies on polyisoprenes with different microstructure have given information only on the content but not on the arrangement of isomeric units¹. Although ^{13}C n.m.r. spectroscopy has been proven to be a powerful tool for the elucidation of the sequence structure of polybutadienes^{2,3}, only a little work has been carried out on polyisoprene by this method since the pioneering ^{13}C n.m.r. study of Duch and Grant⁴. A recent study on *cis-trans* isomerized 1,4-polyisoprene⁵ showed that the distribution of *cis-cis*, *cis-trans* and *trans-trans* linkages can be determined by ^{13}C n.m.r. The purpose of this communication is to report that ^{13}C n.m.r. spectroscopy gives detailed information on the sequence structure of a binary polyisoprene with 3,4- and *cis*-1,4 structural units.

Experimental

The polymer was prepared with $\text{Ti}(\text{O}-n\text{-C}_3\text{H}_7)_4$ $\text{Al}(\text{C}_2\text{H}_5)_3$ catalyst⁶ in toluene at 0°C . The conversion was low. The sample contained 64% 3,4- and 36% *cis*-1,4-units as determined by ^{13}C and ^1H n.m.r.

Results and Discussion

In order to label the position of a particular carbon atom in a given sequence the i 'th C-atom of 3,4-units (v) and *cis*-1,4-units (c), is marked by v_i and c_i respectively ($i = 1, 2, 3, 4, 5$) where the carbon atoms are numbered according to the following scheme:



Throughout head-to-tail enchainment of the structural units is assumed. In a sequence of symbols the enchainment of the corresponding units is head-to-tail from right-to-left. Thus the notation v_3c_4 , for instance, means the tertiary C-atom, C^x , of the central v -unit in the following chain segment:

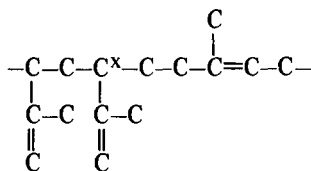


Figure 1 shows the ^{13}C n.m.r. spectrum of 3,4-/*cis*-1,4-polyisoprene. In the olefinic region (a), particularly the resonances of olefinic α -C-atoms, v_2 , of 3,4-units and olefinic β -C-atoms, c_3 , of *cis*-1,4-units show fine structure due to different isomeric structure of neighbouring units. Of the methyl groups in the aliphatic part of the spectrum (b), only the resonance of the methyl carbon v_5 in the vinyl side group of 3,4-units is split into several signals. The highest informational content, however, is contained in the region between 26 and 50 ppm which contains 12

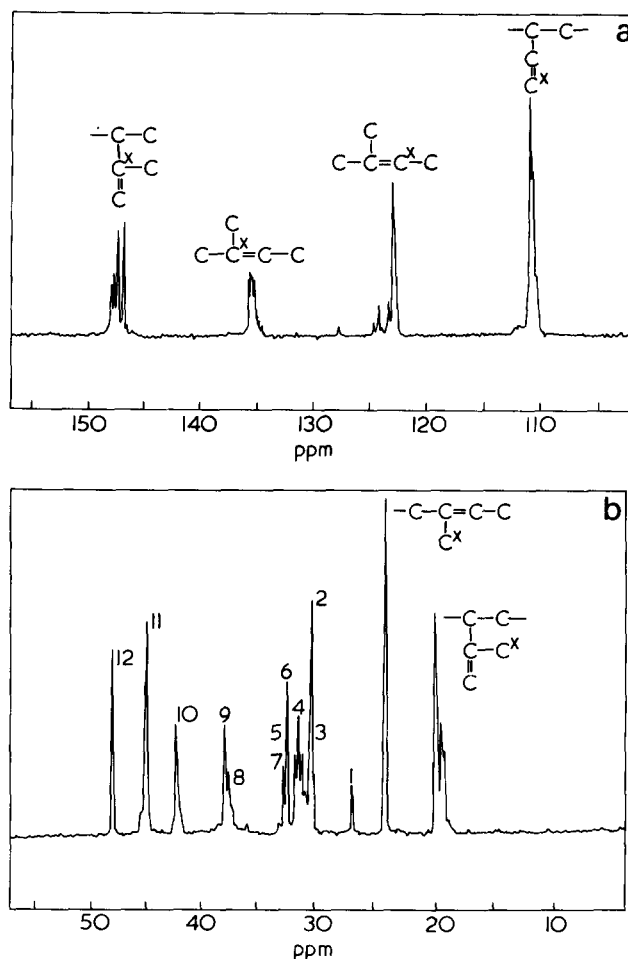


Figure 1 ^{13}C n.m.r. spectrum (22.63 MHz) of 3,4-/*cis*-1,4-polyisoprene; (a), olefinic region; and (b) aliphatic region

resonances of methylene C-atoms c_1 and c_4 of *cis*-1,4-units, of methylene C-atoms v_4 of 3,4-units and of methine C-atoms v_3 of 3,4-units. The analysis of the present communication is restricted to this region.

By comparison with the spectrum of pure *cis*-1,4 polyisoprene, the signals of methylene C-atoms c_1 and c_4 in *cis*-1,4-block sequences can be localized at once at 26.2 ppm (1) and at 32.4 ppm (7). Although the ^{13}C n.m.r. spectrum of pure 3,4-polyisoprene is not available at present it will be shown that the resonances of secondary C-atoms v_4 and tertiary C-atoms v_3 in 3,4-block sequences must be assigned to signal 9 at 37.8 ppm and to signal 10 at 42.1 ppm.

For linear saturated hydrocarbons the chemical shift δ_k of the k 'th C-atom can be expressed by the following relation

$$\delta_k = B + \sum_l A_l n_{kl} \quad (1)$$

The constant B is almost equal to the chemical shift of methane, -2.6 ppm⁷, n_{kl} is the number of carbons in the l 'th position relative to the k 'th carbon and A_l is the chemical shift parameter assigned to the l 'th C-atom. The five A_l values: α , β , γ , δ and ϵ found by regression analysis of the chemical shifts of linear alkanes, are given in Table 1. The chemical shifts of polyisoprene evaluated on the basis of these parameters by means of relation (1) are far from being in agreement with the experimental values. The calculated set, however, has two important features. First, the calculated values can be classified into 12 groups of closely

Table 1 Chemical shift parameters (ppm) for the calculation of chemical shifts in 3,4-*cis*-1,4-polyisoprene

Values for linear alkanes ⁷		Correction parameters ^a	
α	9.1	$c_1(\alpha)$	-7.5
β	9.4	$c_4(\alpha)$	1.0
γ	-2.5	$3 \times (2^\circ)$	-6.2
δ	0.3	$2^\circ (3 \times)$	-1.1
ϵ	0.1		

^a symbols as explained in the text

spaced signals corresponding to the observed signals 1–12. Secondly, the three highest predicted shifts are obtained for the tertiary C-atoms of 3,4-units in the central position of triads. The differences between these values are essentially due to the γ -shift induced by the tertiary centre of the flanking v-units in these triads. The observed shift differences of the 3 low field signals of the aliphatic spectrum (b) in *Figure 1* are of similar magnitude indicating corresponding structural differences. The best absolute agreement of predicted and observed shifts of these signals is obtained by using an improved parameter set for tertiary C-atoms in branched alkanes⁸. With this set one finds 39.5 ppm (vv_{3v}), 44.2 ppm (vv_{3c}, cv_{3v}) and 46.3 ppm (cv_{3c}) as compared with the experimental positions of 42.1 ppm (10), 44.7 ppm (11) and 47.9 (12).

Even with the best available parameter sets for branched alkanes⁸, it is not possible to obtain perfect agreement either between predicted and postulated signal positions of tertiary C-atoms v₃ in 3,4-block sequences or between predicted and known positions of the methylene C-atoms c₁ and c₄ in the *cis*-1,4-homopolymer. Therefore we use the 5 shift parameters for linear alkanes only and determine new experimental correction parameters for polyisoprene from the differences of observed and evaluated signal positions of the block sequences. From the difference of the experimental shift 32.4 ppm and the predicted value 39.9 ppm of the signal cc_{1c} the parameter c₁(α) is obtained, which means the correction for methylene C-atoms with 1,1 disubstituted olefinic C-atom in α -position. From the difference of 26.2 ppm and 25.2 ppm for experimental and calculated positions of the c_{4c} signal the parameter c₄(α) is determined, which means a correction for methylene C-atoms with a monosubstituted olefinic C-atom in α -position. For the signal of tertiary C-atoms vv_{3v} in 3,4-block sequences the difference of the postulated position at 42.1 ppm and the predicted position at 54.5 ppm yields the parameter $3 \times (2^\circ)$, which means the correction for tertiary C-atoms with an olefinic vinyl C-atom in α -position bound to a secondary C-atom. The values of c₁(α), c₄(α) and $3 \times (2^\circ)$ are contained in *Table 1*. Now the shifts of all C-atoms c₁ and v₃ in other than block sequences are calculated by means of relation (1) and the experimentally determined correction terms. The corresponding sequences are assigned to the spectral positions (2), (6) and (11), (12) as shown in *Table 2*. One is left with the secondary C-atoms v₄ of 3,4-units and secondary C-atoms c_{4v} of *cis*-1,4-units adjacent to the tertiary centre of a neighbouring 3,4-unit. The maximum predicted shift, 40 ppm, of these signals is evaluated for the methylene C-atoms in 3,4-block sequences. Therefore, of the remaining signals, the signal 9 at lowest field at 37.8 ppm is assigned to these C-atoms. From the difference of the postulated and calculated positions a further parameter $2^\circ (3 \times)$ is determined, which means a correction for secondary C-atoms adjacent to tertiary centres, with olefinic vinyl C-atoms in α -position. By means

of the complete set of correction parameters of *Table 1*, the chemical shifts of the remaining carbon resonances are recalculated and assigned to the spectral positions 3, 4, 5 and 6. Considering the complete assignment given in *Table 2* one notices that the predicted shifts assigned to the positions 2–6 exceed the experimental values by 0.2–0.4 ppm, which is the order of separation between the observed signals in this region. Actually, an almost perfect coincidence between experimental and calculated shifts could be achieved if the assignment of the positions 3–6 is displaced by one position towards lower field and the empty position at (3) is filled by some of the calculated signals assigned to position (2). This would, however, not be in agreement with the observed relative signal intensities.

The probability $P(v)$ of finding a 3,4-unit in the polymer can be estimated according to the relation:

$$\frac{1}{2} P(v) = I_{10} + I_{11} + I_{12} \quad (2)$$

where I_{10} , I_{11} , I_{12} are the relative intensities of the signals 10, 11 and 12 normalized with respect to the total intensity of the signals 1–12. The factor 1/2 on the left hand side of equation (2) arises because the total intensity is proportional to twice the total number of structural units. From equation (2) and the experimental intensities the value $P(v) = 0.64$ is obtained. The conditional probability of finding a v-unit, given an adjacent c-unit, can be estimated from:

$$\frac{1}{2} [1 - P(v)] P_{cv} = \frac{1}{2} I_{11} + I_{12} \quad (3)$$

The correspondingly defined conditional probability P_{vc} is determined from the equation:

$$\frac{1}{2} P(v) [1 - P_{vc}] = I_{10} + \frac{1}{2} I_{11} \quad (4)$$

Table 2 Chemical shift data and relative intensities in 3,4-*cis*-1,4-polyisoprene

Signal	Carbon atom and sequence ^a	Chemical shift (ppm)		Relative intensities		
		Calc.	Exp.	Calc. ^b	Calc. ^c	Exp.
1	c _{4c}	26.2	26.2	0.065	0.025	0.023
2	cv _{c1c}	30.2				
	vv _{c1c}	30.3	30.0	0.114	0.157	0.172
	cv _{c1v}	30.3				
	vv _{c1v}	30.4				
3	cv _{4c}	31.1	30.8			
4	vv _{4c}	31.5	31.1	0.155	0.232	0.231
5	c _{4vc}	32.5	31.5			
6	c _{4vv}	32.5	32.1	0.137	0.106	0.118
	cc _{1v}	32.5	32.1			
	cc _{1c}	32.4	32.4			
8	cv _{4vc}	37.0	37.5	0.204	0.163	0.134
	cv _{4vv}	37.4	37.5			
	vv _{4vc}	37.4	37.8			
9	vv _{4vv}	37.8	37.8			
	cv _{3vc}	42.0				
	vv _{3vc}	42.0	42.1	0.131	0.083	0.080
10	vv _{3vv}	42.0				
	vv _{3vv}	42.1				
	cv _{3c}	44.1				
	vv _{3c}	44.2	44.7	0.146	0.160	0.170
11	cv _{3vc}	44.1				
	cv _{3vv}	44.2				
	cv _{3c}	44.2				
12	cv _{3c}	46.3	47.9	0.041	0.076	0.071

^a Symbols as explained in the text; ^bcalculated for a Bernoullian distribution; ^ccalculated for first order Markov statistics.

From (3) and (4) the values $P_{CV} = 0.86$ and $P_{VC} = 0.49$ are obtained. These values indicate that the distribution of structural units does not follow Bernoullian chain statistics but statistics with a tendency towards alternation of structural units. This can also be seen qualitatively by comparing the relatively strong intensity of the signal cv_3c (12) of triads with alternating structure with the intensity of the signal vv_3v (10) of block triads.

By means of the statistical parameters determined from the spectrum the relative intensities of all signals were evaluated assuming first order Markov statistics as well as Bernoullian chain statistics. Table 2 shows that for all signal groups, the intensity of which can be measured with sufficient accuracy, the best agreement between predicted and experimental intensities is found for the Markov model. To explain these results further investigations are being carried out on this system.

W. Gronski, N. Murayama and H.-J. Cantow

Institut für Makromolekulare Chemie,
Universität Freiburg,
D-78 Freiburg i. Br., West Germany

T. Miyamoto

Institute for Chemical Research,
Kyoto University,
Kyoto, Japan
(Received 14 January 1976)

References

- 1 Tanaka, Y., Takeuchi, Y., Kobayashi, M. and Tadamoro, H. *J. Polym. Sci. (A-2)* 1971, 43
- 2 Elgert, K. F., Quack, G. and Stützel, B. *Polymer* 1975, 16, 154
- 3 Elgert, K. F., Quack, G. and Stützel, B. *Makromol. Chem.* 1974, 175, 1955
- 4 Duch, M. W. and Grant, D. M. *Macromolecules* 1970, 3, 165
- 5 Tanaka, Y., Sato, H. and Seimiya, T. *Polym. J.* 1975, 7, 264
- 6 Natta, G., Pori, L. and Carbonaro, A. *Makromol. Chem.* 1964, 77, 126
- 7 Grant, D. M. and Paul, E. G. *J. Am. Chem. Soc.* 1964, 86, 2984
- 8 Lindeman, L. P. and Adams, J. Q. *Anal. Chem.* 1971, 43, 1245

Book Reviews

The Physics of Rubber Elasticity (third edition)

L. R. G. Treloar

Clarendon Press, Oxford, 1975, pp 310, £14.00

The first edition of this book was published some twenty five years ago. It deservedly won respect from physicists and chemists of the time for its lucid exposition of a subject which was widely regarded until then as being unamenable to scientific discipline. The second edition appeared in 1958. It maintained the same high standard but in order to allow an adequate updating of the major themes some peripheral topics were curtailed. This process is continued in the third edition to the point where the chapters on the dynamic mechanical properties and on crystallization have been dropped completely. The book is still about the same length as of previous editions, but it is now devoted entirely to the equilibrium properties of rubbers and to the rubbery state of matter. The treatment of this narrower field is refined and very much up-to-date. It sets a standard of presentation rarely equalled in monographs of this kind.

The first nine chapters deal with general phenomena, statistics of a single chain, network statistics and the experimental examination of the predictions of theory which includes the thermodynamics of dry and swollen rubbers and photoelasticity. Extraneous information has been carefully pruned from the earlier texts and the main arguments are clarified and amplified. The author is at pains to point out where opinions differ and where he stands with respect to these opinions.

The remainder of the book deals with recent developments in the phenomenology of general strain, the theory of large deformations and thermoelastic studies. These chapters are new and two at least – 'alternative forms of the strain-energy function' and 'thermoelastic analysis of the Gaussian network' – are gems.

Treloar's personal qualities include a clear mind and a facility for designing simple pertinent experiments. These qualities shine through the book. It will be enjoyed by research workers, teachers and students whether or not they are familiar with the subject.

One sad comment: The elasticity of caoutchouc is exceeded only by the elasticity shown by the publishers in stretching the price of the third edition. In 1960, the second edition cost £2-5-0.

G. Allen

Mechanics of Polymers

R. G. C. Arridge

Clarendon Press, Oxford, 1975, £6.50

A wide coverage of topics make this book suitable as a course book on mechanics of polymers. It may also be useful to researchers requiring information on aspects of polymer mechanics related to their work. Chapter 1 provides a good general introduction to polymers and plastics. Viscoelasticity is outlined in some detail in Chapter 3. The relationships between the relaxation and retardation spectra and between the stress relaxation, creep and dynamic moduli and compliances have also been discussed. However the useful approximate conversion equations are dealt with rather briefly (p 75), although reference is made to a good source. Perhaps some examples of their use and graphical representation of typical data could have been given following the descriptions of lab methods in Chapter 4. Here, although the torsion pendulum is described in adequate detail, creep and stress relaxation testing is described very briefly. A brief discussion of the tensile test would be here appropriate. Values of frequencies used in Figures 4.2, 4.5, 4.8 should be quoted and discussed in relation to the investigated temperature range.

The subject of secondary transitions is also dealt with rather briefly considering the important effects these have upon polymer properties. On the other hand stress and strain are dealt with at length and this is available in many books on strength of materials.

The subject of anisotropy is well treated and is of practical importance. Also yield, cold drawing, work hardening and softening is treated thoroughly and had a close relationship to fracture. The reviewer finds the subject of fracture being dealt with rather briefly. The compliance method of measuring fracture toughness should have been described in detail. Some of the more widely used fracture toughness specimen types with their K calibration formulae could have been included so that non specialists could carry out fracture toughness measurements without further information. Alternatively reference could have been made to suitable texts (such as ASTM) on this extensive and important subject. Apart from some basic references on fracture mechanics, a few more important papers on fracture toughness of specific plastics (e.g. Ehrlich, Knaus, Wnuk, Retting) could be quoted. Similarly, a brief description of the modern approach to fatigue (Hirschberg, Manson) and stress corrosion (Scully) would be useful in providing a simple link between physics and engineering.

The effort made in the book to compare and contrast polymer behaviour with that of metals and ceramics is useful. Similarly the treatment of properties on an atomic (or molecular), micro and macro scale is valuable. However students might find that there was a lack of practical examples compared to the theoretical content while the book's usefulness to other users e.g. researchers, would be much improved if the book had a much higher content of up-to-date data on the properties of the more important polymers (e.g. see McCrum-Read-Williams book).

J. C. Radon

From (3) and (4) the values $P_{CV} = 0.86$ and $P_{VC} = 0.49$ are obtained. These values indicate that the distribution of structural units does not follow Bernoullian chain statistics but statistics with a tendency towards alternation of structural units. This can also be seen qualitatively by comparing the relatively strong intensity of the signal cv_3c (12) of triads with alternating structure with the intensity of the signal vv_3v (10) of block triads.

By means of the statistical parameters determined from the spectrum the relative intensities of all signals were evaluated assuming first order Markov statistics as well as Bernoullian chain statistics. Table 2 shows that for all signal groups, the intensity of which can be measured with sufficient accuracy, the best agreement between predicted and experimental intensities is found for the Markov model. To explain these results further investigations are being carried out on this system.

W. Gronski, N. Murayama and H.-J. Cantow

Institut für Makromolekulare Chemie,
Universität Freiburg,
D-78 Freiburg i. Br., West Germany

T. Miyamoto

Institute for Chemical Research,
Kyoto University,
Kyoto, Japan
(Received 14 January 1976)

References

- 1 Tanaka, Y., Takeuchi, Y., Kobayashi, M. and Tadamoro, H. *J. Polym. Sci. (A-2)* 1971, 43
- 2 Elgert, K. F., Quack, G. and Stützel, B. *Polymer* 1975, 16, 154
- 3 Elgert, K. F., Quack, G. and Stützel, B. *Makromol. Chem.* 1974, 175, 1955
- 4 Duch, M. W. and Grant, D. M. *Macromolecules* 1970, 3, 165
- 5 Tanaka, Y., Sato, H. and Seimiya, T. *Polym. J.* 1975, 7, 264
- 6 Natta, G., Pori, L. and Carbonaro, A. *Makromol. Chem.* 1964, 77, 126
- 7 Grant, D. M. and Paul, E. G. *J. Am. Chem. Soc.* 1964, 86, 2984
- 8 Lindeman, L. P. and Adams, J. Q. *Anal. Chem.* 1971, 43, 1245

Book Reviews

The Physics of Rubber Elasticity (third edition)
L. R. G. Treloar
Clarendon Press, Oxford, 1975, pp 310, £14.00

The first edition of this book was published some twenty five years ago. It deservedly won respect from physicists and chemists of the time for its lucid exposition of a subject which was widely regarded until then as being unamenable to scientific discipline. The second edition appeared in 1958. It maintained the same high standard but in order to allow an adequate updating of the major themes some peripheral topics were curtailed. This process is continued in the third edition to the point where the chapters on the dynamic mechanical properties and on crystallization have been dropped completely. The book is still about the same length as of previous editions, but it is now devoted entirely to the equilibrium properties of rubbers and to the rubbery state of matter. The treatment of this narrower field is refined and very much up-to-date. It sets a standard of presentation rarely equalled in monographs of this kind.

The first nine chapters deal with general phenomena, statistics of a single chain, network statistics and the experimental examination of the predictions of theory which includes the thermodynamics of dry and swollen rubbers and photoelasticity. Extraneous information has been carefully pruned from the earlier texts and the main arguments are clarified and amplified. The author is at pains to point out where opinions differ and where he stands with respect to these opinions.

The remainder of the book deals with recent developments in the phenomenology of general strain, the theory of large deformations and thermoelastic studies. These chapters are new and two at least – 'alternative forms of the strain-energy function' and 'thermoelastic analysis of the Gaussian network' – are gems.

Treloar's personal qualities include a clear mind and a facility for designing simple pertinent experiments. These qualities shine through the book. It will be enjoyed by research workers, teachers and students whether or not they are familiar with the subject.

One sad comment: The elasticity of caoutchouc is exceeded only by the elasticity shown by the publishers in stretching the price of the third edition. In 1960, the second edition cost £2-5-0.

G. Allen

Mechanics of Polymers

R. G. C. Arridge

Clarendon Press, Oxford, 1975, £6.50

A wide coverage of topics make this book suitable as a course book on mechanics of polymers. It may also be useful to researchers requiring information on aspects of polymer mechanics related to their work. Chapter 1 provides a good general introduction to polymers and plastics. Viscoelasticity is outlined in some detail in Chapter 3. The relationships between the relaxation and retardation spectra and between the stress relaxation, creep and dynamic moduli and compliances have also been discussed. However the useful approximate conversion equations are dealt with rather briefly (p 75), although reference is made to a good source. Perhaps some examples of their use and graphical representation of typical data could have been given following the descriptions of lab methods in Chapter 4. Here, although the torsion pendulum is described in adequate detail, creep and stress relaxation testing is described very briefly. A brief discussion of the tensile test would be here appropriate. Values of frequencies used in Figures 4.2, 4.5, 4.8 should be quoted and discussed in relation to the investigated temperature range.

The subject of secondary transitions is also dealt with rather briefly considering the important effects these have upon polymer properties. On the other hand stress and strain are dealt with at length and this is available in many books on strength of materials.

The subject of anisotropy is well treated and is of practical importance. Also yield, cold drawing, work hardening and softening is treated thoroughly and had a close relationship to fracture. The reviewer finds the subject of fracture being dealt with rather briefly. The compliance method of measuring fracture toughness should have been described in detail. Some of the more widely used fracture toughness specimen types with their K calibration formulae could have been included so that non specialists could carry out fracture toughness measurements without further information. Alternatively reference could have been made to suitable texts (such as ASTM) on this extensive and important subject. Apart from some basic references on fracture mechanics, a few more important papers on fracture toughness of specific plastics (e.g. Ehrlich, Knaus, Wnuk, Retting) could be quoted. Similarly, a brief description of the modern approach to fatigue (Hirschberg, Manson) and stress corrosion (Scully) would be useful in providing a simple link between physics and engineering.

The effort made in the book to compare and contrast polymer behaviour with that of metals and ceramics is useful. Similarly the treatment of properties on an atomic (or molecular), micro and macro scale is valuable. However students might find that there was a lack of practical examples compared to the theoretical content while the book's usefulness to other users e.g. researchers, would be much improved if the book had a much higher content of up-to-date data on the properties of the more important polymers (e.g. see McCrum-Read-Williams book).

J. C. Radon

Persistence length of cellulose tricarbaniolate by small-angle neutron scattering

A. K. Gupta, J. P. Cotton*, E. Marchal, W. Burchard† and H. Benoit

Centre de Recherches sur les Macromolécules CNRS, 6, rue Boussingault, 67083 Strasbourg Cedex, France

(Received 12 December 1975)

Small-angle neutron scattering measurements were made on cellulose tricarbaniolate in dioxane at different temperatures. The persistence length evaluated from the Kratky plot was found to be 110 Å at room temperature. A decrease in persistence length with increasing temperature was observed.

INTRODUCTION

Cellulose tricarbaniolate (CC) has been shown to have a rather rigid conformation in dioxane solution. Its conformation is usually described by the Kratky–Porod model¹ for which the rigidity is characterized by a quantity, a , called ‘persistence length’. A variation of persistence length with temperature was noticed^{2,3} for CC and was shown to be related to a change from one conformational state to another². Usually, persistence lengths are determined by studying one quantity as function of molecular weight. If the conformation, and thus a , depends on molecular weight, which is the case for CC², these methods cannot be used in a straightforward manner. Thus, those investigations which allow the determination of a on a single sample are of utmost interest.

Small-angle neutron scattering (SANS) or X-ray scattering provide such methods. The X-ray technique has been applied with success to CC in acetone at 20°C⁴. It is interesting to compare the two techniques. We report SANS results on CC in dioxane at various temperatures. The previous two studies^{5,6} on the application of this technique for the determination of a were made on systems in which independent determinations of a had not been carried out. For the present system, the values of a determined from various techniques have been reviewed in a recent publication².

Two sets of experiments were performed in order to cover a wide range of wave vectors, using different wavelengths of incident neutron beams and different sample-detector separations. Identical results were obtained from both sets of experiments. However, at the larger sample-detector separation an important scatter of experimental points was found at higher scattering angles (due to a smaller difference between signal and background). The extrapolations carried out on these data were ascertained by comparison with theoretical scattering curves. The persistence length was evaluated using the Kratky procedure⁷, which is described below in brief.

It is well known that the scattering envelope can be divided into different domains depending on the relative values of the wavevector q [$q = (4\pi/\lambda) \sin \theta/2$, λ being the wavelength and θ the scattering angle] and the dimensions of the coil:

(1) If $q \leq 1/R$, R being molecular radius of gyration, we are in the Guinier domain and a plot of I^{-1} or $\log I$ (I being scattered intensity) as a function of q^2 allows the determination of R .

(2) When q increases, the scattering envelope can be described by the Debye formula⁸:

$$I = \frac{2KcM}{(q^2R^2)^2} [q^2R^2 - 1 + \exp(-q^2R^2)] \quad (1)$$

if the chain is Gaussian. Here K is the optical constant of the system, c the concentration in g/ml. This formula is valid as long as $q < 1/a$. If $(R^2)^{1/2}$ is much longer than a there is a domain of q :

$$\frac{1}{R} \leq q \leq \frac{1}{a}$$

where the asymptotic law $I \sim q^{-2}$ is valid.

(3) If $1/a < q < 1/r$, r being the radius of gyration of a cross-section of the chain or a characteristic distance of the repeating unit of the polymer, the chain behaves like a rod of length L and the asymptotic expression:

$$I = Kc \frac{M}{L} \pi q^{-1} \quad (2)$$

can be used⁹.

It is usual to represent the results using the Kratky procedure, i.e. plotting Iq^2 versus q . If the three quantities R , a and r are very different, one should obtain a graph similar to that plotted in Figure 1. Part 1 is the Guinier range; part 2 the Debye domain, where Iq^2 reaches an asymptotic value; part 3 the rod-like behaviour domain, where Iq^2 is proportional to q and part 4 the domain where the internal structure of the monomeric units has to be taken into account.

The most interesting feature in this representation is the transition between domains 2 and 3. Under favourable circumstances there is a sharp transition between the horizontal domain (part 2) and the sloping straight line (part 3) at a value q^* of q related to the persistence length by:

$$a = A/q^* \quad (3)$$

The constant A is easily calculated by equating the limiting

* Service de Physique du Solide et de Résonance Magnétique, Centre d'Etudes Nucléaires de Saclay, BP 2, 91190 Gif-sur-Yvette, France.

† Institut für Makromolekulare Chemie, Universität Freiburg, Freiburg i-Br, West Germany.

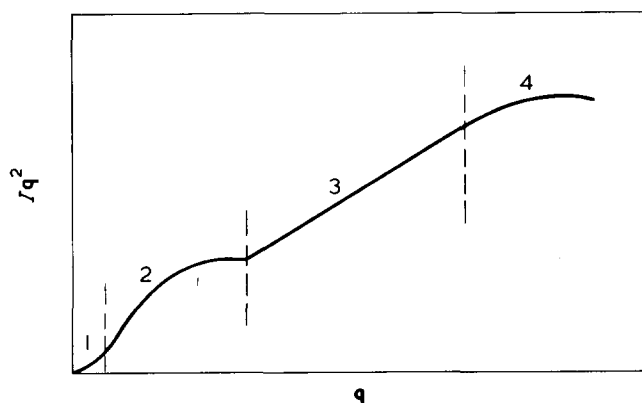


Figure 1 Schematic representation of a Kratky plot showing the four parts of the scattering pattern for stiff chains

intensity in equation (1) at high q and that of equation (2). Using the expression for radius of gyration of worm-like chain in the limiting case $L \gg a$ ($R^2 = aL/3$), this value is $A = 6/\pi \sim 1.91$.

This ideal situation is not often encountered and various authors^{4,10} have made calculations to see the exact shape of the scattering curve in the regions 2 and 3 when the above equations are not fulfilled. More specifically, if R is not very large compared to a , the Debye branch (part 2) is no longer horizontal in the Iq^2 vs. q plot and q^* lies in the region where the curvature goes through a maximum. The value of the constant A may differ from the ideal value 1.91; in fact values of $A = 2.23$ ¹⁰ and $A = 2.87$ ⁴ have been reported as upper limits. A lower value of $A = 1.7$ is obtained from des Cloizeaux's¹¹ treatment of an infinite Kratky–Porod chain. The approximation used by some authors⁵, which consists in using $A = 1$, seems to be an over-simplification. In the case of an infinitely large Gaussian coil the horizontal line would lie below the curve obtained for real chains.

EXPERIMENTAL

Apparatus

Neutron scattering experiments were made on the small-angle apparatus of the Leon Brillouin Laboratory using the neutron flux produced by the reactor EL3 (CEN, Saclay). The detector used is the multidetector of (ρ, θ) type¹². The principle of the set up is very similar to that described elsewhere¹³. Here the incident beam is collimated by two holes (3 mm diameter) separated by a distance of 1.20 m. The effects of the large incident wavelength distribution ($\Delta\lambda/\lambda \sim 30\%$) are corrected for by taking for the mean wavelength¹³:

$$\langle \lambda \rangle = \frac{1}{I_0} \int \lambda i(\lambda) d\lambda$$

which is valid in the range of q where equation (2) holds. The mean wavelength of neutron beam 7.05 Å and sample detector distance of 3.75 m provided measurements in the range $0.007 < q < 0.07 \text{ Å}^{-1}$ for the first set of experiment (experiment I). For the second set of experiments (experiment II) a range of q values $0.004 < q < 0.04 \text{ Å}^{-1}$ was obtained by using a neutron beam of wavelength 8.72 Å and a sample-detector distance of 5 m. A 5 mm thick quartz cell was employed for holding the sample. The tempera-

ture of the sample was kept constant to within $\pm 0.1^\circ\text{C}$ by enclosing the sample in a thermostatically controlled chamber.

Materials

The CC sample of weight-average molecular weight 130 000 was used in this study. Details of its preparation and characterization are given elsewhere². Deuterated dioxane (from Carl Roth OHG Karlsruhe) was used without redistillation, to obtain better contrast between intensity scattered from solvent and solute. Concentration of the solution was maintained at $\sim 8 \times 10^{-3} \text{ g/ml}$, which was within the range where no intermolecular effects are observed².

RESULTS AND DISCUSSION

Experiment I

The scattering data of experiment I are shown in Figure 2 in the form of Iq^2 vs. q plots at different temperatures. Because of the finite molecular weight of the sample, the horizontal straight line corresponding to the Debye branch (of ideal case) is not observed. However, there are inflection points in the expected regions on these experimental curves. They are very similar to the theoretical curves described⁴ for finite chains. They allow a rather precise determination of q^* and thus of the persistence length. These values are recorded in Table 1.

Values of persistence length obtained from this experiment are in agreement with those reported in previous studies. For CC in dioxane at 25°C its value as obtained from dielectric measurements² is 108 Å. Some other known values for the same system are: 136 Å at 20°C from light scattering¹⁴; 80 Å at 25°C from translational diffusion coefficient measurements¹⁵; and 129 Å at 25°C from stress–optical coefficient measurements³. In other solvents the values reported are: 77 Å in benzophenone at 55°C ¹⁶; 108 Å* in acetone at 20°C from low-angle X-ray scattering

* This value was obtained with $A = 2.87$; when using $A = 1.91$, a smaller persistence length of $a = 72 \text{ Å}$ is found for CC in acetone.

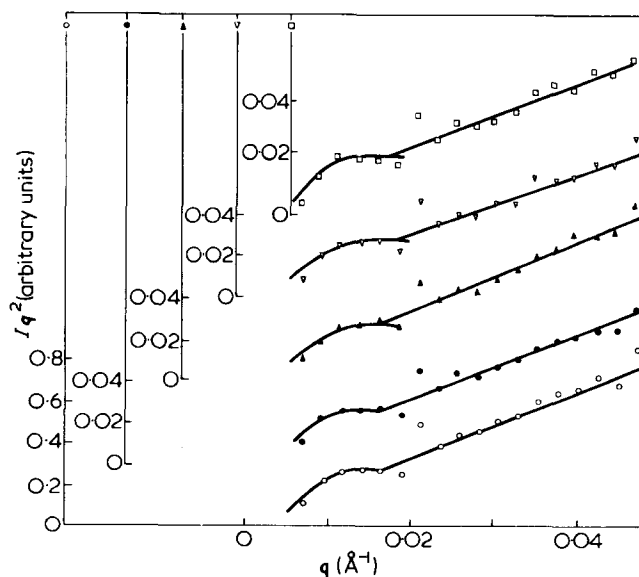


Figure 2 Iq^2 vs. q plots at different temperatures from the scattering data of experiment I on CC in dioxane. The origin on the ordinate is shifted, as shown, in order to separate each curve: □, 85.5°C ; ▽, 66.1°C ; ▲, 53.0°C ; ●, 34.1°C ; ○, 21.5°C

Table 1 Results from scattering data of experiment I

$T(^{\circ}\text{C})$	$q^*(\text{\AA}^{-1})$	$a(\text{\AA})$
21.5	0.0165	116
34.1	0.0170	112
53.0	0.0170	112
66.1	0.0180	106
85.5	0.0183	104

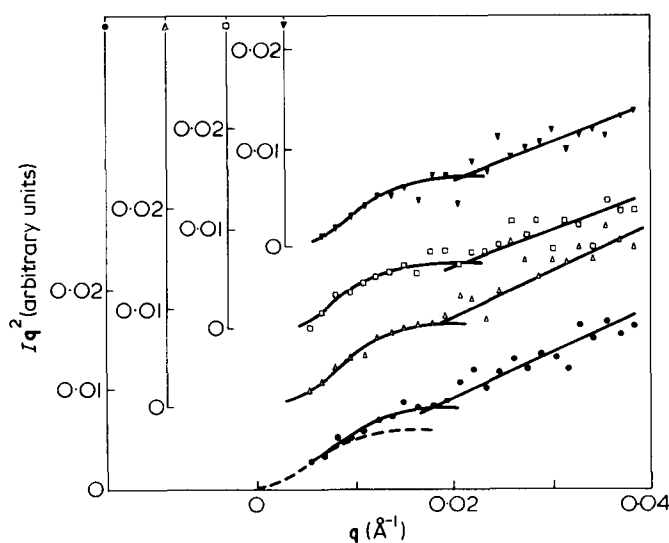


Figure 3 Iq^2 vs. q plots at different temperatures from the scattering data of experiment II on CC in dioxane. The origin on the ordinate is shifted, as shown, in order to separate each curve. ---, calculated Debye curve as described in the text. ∇ , 80.2°C; \square , 62.6°C; \triangle , 40.9°C; \bullet , 22.0°C

measurements⁴. Slight disagreement of these values, except for the last one, has been attributed to the molecular weight range studied or the incomplete degree of substitution of the samples used.

The variation with temperature of persistence length is, however, less reliable in this set of experiments. This is due to low precision in locating the inflection point which lies near the boundary of the experimental range.

Experiment II

The scattering data of experiment II are shown in Figure 3 in the form of Iq^2 vs. q plots at different temperatures. Even though a dispersion of the data occurs in both experiments the inflection points are again apparent around the same q -values. Values of the wavevector, q^* , corresponding to the characteristic inflection points as well as the persistence lengths deduced from these, are recorded in Table 2.

The q^* values in experiment II are relatively more precise since the domain of experimental q values is more favourable. Variation of persistence length with temperature also becomes well apparent in this case. The agreement of temperature variation of persistence length obtained in this experiment is better in comparison to that obtained from stress-optical coefficient data³ than to that from dielectric data² (also shown in Table 2).

In order to check the self consistency of these results and thus to ascertain the extrapolations for different branches of the scattering curve we proceed in the following way. From the slope of the ascending straight line branch and the mass per unit length one can obtain the

Table 2 Results from scattering data of experiment II with some other reported values of persistence length

$T(^{\circ}\text{C})$	$q^*(\text{\AA}^{-1})$	$a(\text{\AA})$		
		scattering data of experiment II	stress-optical data ³	dielectric data ²
22.0	0.0172	111	—	—
25.0	—	—	129	108
35.0	—	—	—	90
40.9	0.0186	103	—	—
50.0	—	—	109	73
62.6	0.0200	95	—	—
75.0	—	—	109	57
80.2	0.0210	91	—	—
90.0	—	—	99	50

value of optical constant K from equation (2). In this calculation we have used for monomer length the value 5.15 Å determined from X-ray crystallographic data on cellulose¹⁷ and found $K = 1.55 \times 10^{-3}$. Further, we tried to fit the results at smaller angles with the Debye scattering function (equation 1) using this value of K . One such calculated Debye curve along with the experimental data is shown in Figure 3 (by the broken line), where the agreement is good upto $q \sim 0.01 \text{ \AA}^{-1}$. Above this q range the tendency of deviation from ideal horizontal Debye curve becomes apparent. It is clear that in this range neither of the ideal expressions hold, as already mentioned.

At this stage we wish to point out that all calculations for the persistence lengths from SANS were made with an A -constant of 1.91 which refers to the idealized model discussed above. The persistence lengths so calculated, may be considered as lower limits. By the use of $A = 2.87$, which was found from the Daniels approximation, one would obtain persistence lengths 1.5 times larger than reported here. These values would agree with an interpretation of light scattering data¹⁴. Since the question of the correct A -value does not seem to be fully settled in theory, we confine ourselves to reporting these two limits (it is probable that A depends on the chain stiffness, i.e. the number of repeating units per persistence length, and on the ratio L/a of the contour length to the persistence length).

The relatively good internal fit makes the determination of persistence length more reliable. Furthermore, the value $a = 110 \text{ \AA}$ found by SANS at room temperature agrees with those found by other methods. These measurements thus justify the applicability of SANS technique for the determination of characteristic parameters of the Kratky-Porod chain. Because of the large contrast which can be obtained by the use of deuterated solvents and the large domain of q -values obtainable if besides the Saclay apparatus one uses the one at ILL Grenoble, it is clear that experiments are much faster and much easier with neutrons than with X-rays, if one does not take into account the price of the equipment.

REFERENCES

- 1 Kratky, O. and Porod, G. *Recl. Trav. Chim. Pays-Bas* 1949, 68, 1106
- 2 Gupta, A. K., Marchal, E. and Burchard, W. *Macromolecules* 1975, 8, 843

Persistence length of cellulose tricarbaniolate: A. K. Gupta et al.

- 3 Noordermeer, J. W. M. *Thesis*. Technische Hogeschool, Delft (1974); Noordermeer, J. W. M., Darganani, R. and Janeschitz-Kriegl, H. *Polymer* 1975, **16**, 359
- 4 Burchard, W. and Kajiwara, K. *Proc. R. Soc. (A)* 1970, **316**, 185
- 5 Moan, M., Wolff, C. and Ober, R. *Chem. Phys. Lett.* 1974, **28**, 505; Moan, M. and Wolff, C. *Polymer* 1975, **16**, 776
- 6 Wignall, G. D., Ballard, D. G. H. and Schelten, J. *Eur. Polym. J.* 1974, **10**, 861
- 7 Kratky, O. *Pure Appl. Chem.* 1966, **12**, 483
- 8 Debye, P. *J. Phys. Colloid Chem.* 1947, **51**, 18
- 9 Kratochvil, P. 'Light Scattering from Polymer Solutions', (Ed. M. B. Huglin), Academic Press, London, 1972
- 10 Heine, S., Kratky, O. and Roppert, J. *Makromol. Chem.* 1962, **56**, 150
- 11 des Cloizeaux, J. *Macromolecules* 1973, **6**, 403
- 12 Allemand, R., *et al.* *Nucl. Instrum. Methods* 1975, **126**, 29
- 13 Cotton, J. P., *et al.* *Macromolecules* 1974, **7**, 863
- 14 Burchard, W. *Br. Polym. J.* 1971, **3**, 214
- 15 Tsvetkov, V. N., Rjuntsev, E. I., Andreeva, L. N., Pogodina, N. V., Levrenko, P. N. and Kutsenko, L. I. *Eur. Polym. J.* 1974, **10**, 563
- 16 Janeschitz-Kriegl, H. and Burchard, W. *J. Polym. Sci. (A-2)* 1968, **6**, 1953
- 17 Meyer, K. H. and Misch, L. *Ber. Dtsch. Chem. Ges. (B)* 1937, **70**, 226

Note added in proof

A recent re-examination of previous light scattering measurements¹⁴, assuming $l = 5.15 \text{ \AA}$ and taking into account the chain length dependence of persistence length leads to $a = 113 \text{ \AA}$ for the sample in concern, which is in very satisfactory agreement with SANS and dielectric relaxation measurements.

Some morphological aspects of AB crosslinked polymers

G. C. Eastmond and E. G. Smith*

*Department of Inorganic, Physical and Industrial Chemistry, University of Liverpool, PO Box 147, Liverpool L69 3BX, UK
(Received 28 November 1975)*

The structures of multicomponent species present in AB crosslinked polymers (ABCPs) formed by the random introduction of crosslinks of polymer B into an assembly of chains of polymer A are described for different extents of crosslinking. Microphase separation has been observed in solvent cast samples of ABCPs prepared by crosslinking poly(vinyl trichloroacetate) and a styrene copolymer (A-components) with polychloroprene (B-component). The morphologies of the polymers at low and high degrees of crosslinking are presented. Polychloroprene domain sizes have been determined for various crosslink lengths and crosslink densities. Domain sizes and their variation with molecular weight of the B-chains are discussed in terms of the structures of the multicomponent species present in the ABCPs and with theoretically predicted domain sizes in linear block copolymers. Distributions of domain sizes have been determined and compared with the molecular weight distributions of the B-chains.

INTRODUCTION

The term AB crosslinked polymers (ABCPs) refers to polymers in which chains of polymer A are connected by long crosslinks of a chemically different polymer B. This terminology can be used to describe materials ranging from simple structures with low degrees of crosslinking to infinite network structures with high degrees of crosslinking.

Previous papers¹⁻⁴ described a general method of preparing ABCPs of known structure by reacting a preformed polymer (the A-component) having reactive halogen in side chains with a metal carbonyl in the presence of a monomer. The metal carbonyl specifically removes halogen atoms (at a predetermined rate in a thermal or photochemical reaction) from the preformed polymer to produce radical sites on the side groups of the A-chains. These macroradicals initiate polymerization of the monomer to produce growing chains of polymer B attached to the A-chains. Combination termination of the propagating grafts produces B-crosslinks, while disproportionation termination generates B-branches on A-chains. The specificity of the initiating system ensures that, in the absence of chain transfer, no homopolymer of B is formed. However, as prepared, ABCPs always contain some unreacted A homopolymer in addition to the multi-component species. By careful control of the reaction kinetics it is possible to achieve random crosslinking, (thus avoiding excessive intramolecular crosslinking of A-chains) and to control number average degrees of polymerization of the crosslinks. Conditions for achieving random crosslinking in these systems have been presented elsewhere¹.

The normal incompatibility of chemically different polymers leads to phase separation in most polyblends and to microphase separation in block and graft copolymers. In both cases, molecular reorganization occurs readily in solution or in the melt allowing like chains to aggregate and to exclude unlike chains from their vicinity. At low crosslink densities ABCPs contain, in addition to homopolymer

A, only simple crosslinked structures (e.g. two A-chains crosslinked by one B-chain) and it might be anticipated that they could readily undergo microphase separation. However, at high crosslink densities ABCPs contain infinite network structures and, although the ABCPs are normally prepared in dilute solution, it is not immediately apparent that microphase separation will be observed in the solid polymer since molecular reorganization could be restricted by the comparative immobility of junction points in the network structures.

Preliminary electron microscope studies of thin cast films demonstrated that microphase separation can occur in ABCPs of poly(vinyl trichloroacetate) (PVTCA) crosslinked with polychloroprene (PCP), designated PVTCA/PCP⁵. Indirect evidence for microphase separation in highly crosslinked ABCPs of PVTCA crosslinked with polystyrene (PS) or with poly(methyl methacrylate) (PMMA) has been obtained from dilatometric studies of the solid polymers⁶.

In this paper we report the results of an electron microscope study of thin sections of some ABCPs, providing information on the morphological features of the bulk polymers. The ABCPs used were PVTCA/PCP and a copolymer of styrene and *p*-vinyl benzyl-trichloroacetate (PS*) crosslinked with PCP (designated PS*/PCP). In both cases the crosslinks were the minor component. The morphological features of these materials are discussed in terms of the structures and compositions of the ABCPs.

EXPERIMENTAL

Materials

Methyl methacrylate and manganese carbonyl were purified as described previously⁷. Chloroprene was washed free of inhibitor with aqueous sodium hydroxide, dried, prepolymerized and vacuum distilled before use. PVTCA (\bar{P}_w of trichloroacetate residues was 4140) was prepared by trichloroacetylation of poly(vinyl alcohol) (\bar{M}_n 124 000) as described previously¹. The polystyrene copolymer PS* (\bar{M}_n 130 000) incorporating 7% (mol/mol) *p*-vinylbenzyl-

* Present address: Unilever Research Port Sunlight Laboratory Port Sunlight, Wirral, Merseyside, L62 4XN.

trichloroacetate, was prepared from polystyrene homopolymer⁸.

ABCs were prepared by reacting preformed polymer in chloroprene solution using photoinitiation with manganese carbonyl ($\lambda = 436 \text{ nm}$) at 25°C . Small concentrations of benzene, as cosolvent, were used to ensure dissolution of the preformed polymer. Degrees of polymerization of crosslinks were determined by the manganese carbonyl concentration and light intensity employed. Crosslinking indices of the ABCs were controlled by the reaction time; reaction times required for gelation were ascertained in separate experiments performed under the same conditions.

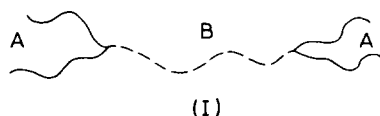
PVTCA/PCP ABCs of low crosslink density (reaction stopped prior to gelation) were precipitated into petroleum ether. Samples of higher crosslink density were isolated by removing excess monomer under high vacuum. PS*/PCP ABCs were initially isolated by evaporation of volatiles under high vacuum.

Electron microscopy

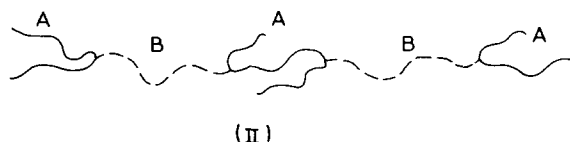
Samples of ABCs of low crosslink density were cast as films (0.5–1 mm thick) from dilute solutions in appropriate solvents. Samples of higher crosslink density were prepared by drying pieces of polymer swollen by solvent. Pieces of the dry ABCs were mounted on epoxy-resin blocks. PVTCA/PCP and PS*/PCP ABCs were stained and hardened for ~ 4 days in an aqueous solution of osmic acid [$\sim 1\%$ solution (w/v)]. Ultra-thin sections ($\sim 100 \text{ nm}$ thick) were cut on an ultramicrotome (LKB Mk III) and examined using a JEM 7 transmission electron microscope.

NATURE OF MULTICOMPONENT SPECIES IN ABCs

In the preparation of an ABC the initial reaction mixture contains an assembly of homopolymer A-chains with a distribution of molecular weights. Crosslinks of polymer B are then introduced randomly. Because of their higher functionality, high molecular weight A-chains are preferentially incorporated into multicomponent species in the early stages of reaction. If the propagating B-chains terminate exclusively by combination (e.g. when chloroprene is used to form the crosslinks) the first multicomponent species to be formed have structure (I), reminiscent of an ABA block copolymer but with two terminal blocks at each end of the



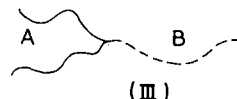
central block, i.e. an A_2BA_2 block copolymer. Continued reaction generates more species with structure (I), the reaction gradually involving a larger proportion of the shorter A-chains. Simultaneously, A-chains already incorporated into multicomponent species react further to produce species such as (II)



and even more complex species; again reaction preferentially involves long A-chains. Eventually the reaction mixture gels as infinite network structures are formed; the reaction mixture then contains a gel fraction comprised of

attached A- and B-chains and a sol fraction consisting of simpler multicomponent species together with unreacted A-chains. Further reaction then incorporates more B-chains and species from the sol fraction into the infinite structure.

If propagating B-chains could terminate exclusively by disproportionation, only B-branches would be formed on A-chains. In the early stages of reaction, species such as (III)



would be formed (an A_2B block copolymer) and subsequently more complex branched structures would be produced. In cases where termination proceeds by both combination and disproportionation (e.g. when using methyl methacrylate to form crosslinks) a mixture of branches and crosslinks of polymer B will be incorporated into multicomponent species, their relative proportions depending on the relative rates of the two termination reactions.

For random crosslinking in an assembly of monodispersed polymer chains, Flory calculated⁹ the weight fractions of crosslinked species of different complexity as a function of crosslink density. Stockmayer¹⁰ considered random crosslinking of a polydispersed polymer but to the best of our knowledge the relative proportions of crosslinked species of different complexity and molecular weight have not been determined quantitatively. Exactly the same principles as used by Flory and Stockmayer apply to the formation of ABCs but with the complication that the crosslinks themselves have a distribution of degrees of polymerization determined by the kinetics of the crosslinking polymerization. Prior to gelation, the crosslinks formed have a molecular weight distribution characterized by $\bar{M}_w/\bar{M}_n = 1.5$; branches have a most probable distribution. Following gelation, the rate of polymerization of certain monomers accelerates (at constant rate of initiation) owing to an increase in chain length; the molecular weight distribution of crosslinks formed under such conditions is not known at present but the average degree of polymerization can be calculated from kinetic data. At the present time, therefore, we are unable to give a quantitative description of the numbers of multicomponent species of different complexity in ABCs but we calculate the number of crosslinks and the crosslinking index in these materials. (We define the relative crosslinking index γ_r as the ratio of the true crosslinking index to that at the gel point; γ_r is the number of crosslinking units per weight-average A-chain and is proportional to the number of crosslinks in the system.) Following the arguments of earlier workers we may predict that prior to gelation the population of multicomponent species with different numbers of A-chains decreases with increasing numbers of A-chains. Also, as reaction proceeds the average length of unreacted A-chains and of A-blocks in multicomponent species decreases.

In the present study no attempt has been made to separate multicomponent species from unreacted A-chains. Consequently the morphologies reported are those of blends of AB crosslinked species and unreacted A-chains.

RESULTS AND DISCUSSION

General morphological features

Table 1 presents structural parameters for ABCs having polychloroprene crosslinks as the minor component.

Table 1 Structural parameters of some ABCPs

ABCP	Polychloroprene (% w/w)	\bar{P}_n of PCP crosslinks	γ_r
PVTCA/PCP 1	4	900	0.4
PVTCA/PCP 2	6	900	0.8
PVTCA/PCP 3	8	900	1.2
PVTCA/PCP 4	25	3720	8-9
PS*/PCP 1	~5	1064-2800	0.67
PS*/PCP 2	15	5900	0.83

Figure 1 is a representative selection of electron micrographs of the above samples cast from various solvents illustrating the occurrence of microphase separation. Samples with low crosslinking index ($\gamma_r \leq 1.2$) exhibit well-defined spherical PCP domains randomly distributed within the matrix of the A-component. ABCP, PVTCA/PCP4 (Figure 1c), with high crosslinking index ($\gamma_r \sim 8$), contains highly-crosslinked network structures and exhibits a more confused morphology of very small domains; some aggregates of small domains are apparent in the micrograph.

Low crosslink density. For $\gamma_r \ll 1$ the volume fraction of crosslinks is very small, the predominant multicomponent species have structure (I) and a large proportion of A-chains remain unreacted. Assuming complete microphase separation with a narrow interface, the PCP chains which aggregate to form the domains will have both ends located at the domain-matrix interface with the attached A-chains in the matrix, as schematically represented in Figure 2a. While we shall show later that domain diameters may be related to the degree of polymerization of the B-chains, the average inter-domain distance will be determined by the overall composition and not by the structural parameters of the A-chains; the domains are distributed randomly in a matrix of A-chains. Any species such as (II), or more complex species, which are present will have both B-chains in the same domain (Figure 2b) with the central A-chain forming a loop on the domain surface (this A-chain will normally be too short to traverse the distance between neighbouring domains). Thus, inter-domain linkages (Figure 2c) will be infrequent.

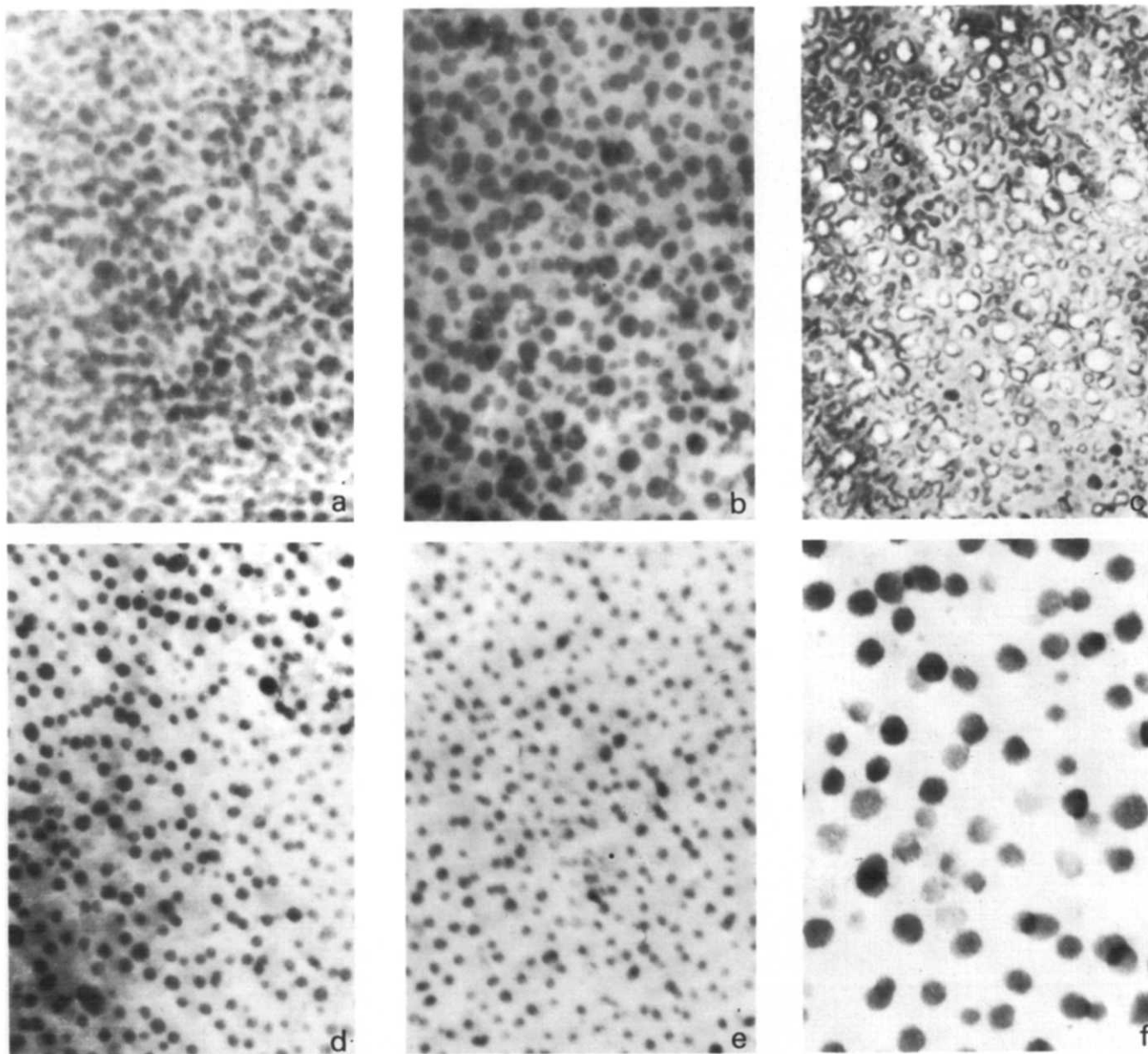


Figure 1 Representative electron micrographs illustrating microphase separation in ABCPs; (a) PVTCA/PCP 1; (b) PVTCA/PCP 3; (c) PVTCA/PCP 4; (d) PS*/PCP 1 cast from benzene solution; (e) PS*/PCP 1 cast from chloroprene/benzene (4:1 v/v); (f) PS*/PCP 2 cast from chloroform solution. Magnification 60 000 X

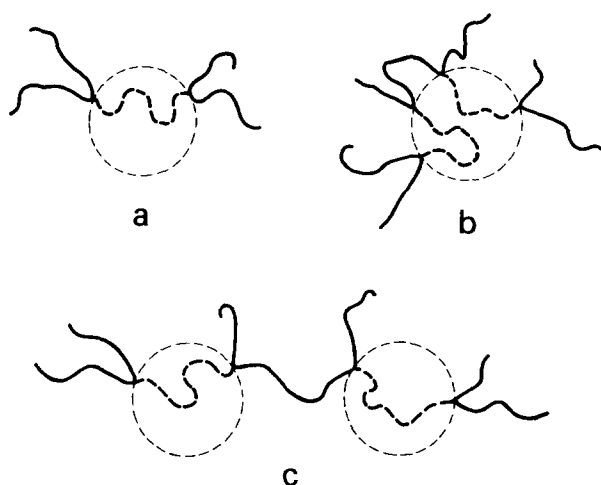


Figure 2 Schematic representation of microphase separation in ABCPs for species with structures (I) and (II), as discussed in text. —, A; ---, B component, broken circles represent the domain-matrix interface

As γ_r increases ($\gamma_r < 1$) the volume fraction of B-chains and the proportion of A-chains in multicomponent species (and to some extent the complexity of those species) increases. Consequently the inter-domain separation must decrease and it might be anticipated that some increase in long-range order would be observed under appropriate conditions. However, at higher degrees of crosslinking this latter event may be overtaken by the increasing complexity of the system. A reduction in inter-domain separation will also allow an increase in inter-domain connections (Figure 2c).

High crosslink density. Under conditions $\gamma_r > 1$ the ABCPs contain infinite network structures which must restrict molecular reorganization and may affect microphase separation. For γ_r slightly in excess of unity, the ABCPs contain a large sol fraction capable of diffusing through the swollen gel and minimizing constraints on microphase separation as the swollen gel collapses during sample preparation; Figure 1b is an electron micrograph of PVTCA/PCP 3 with $\gamma_r = 1.2$, which exhibits the same morphological features as more lightly crosslinked samples. At high values of γ_r (Figure 1c is a micrograph of PVTCA/PCP 4, $\gamma_r \sim 8$) the sol fraction is negligible. Aggregation requires the relative movement of network junctions and may be restricted. Additionally, most A-chains will have multiple junctions, so that the average block length of A-chains between the junctions will be short and inter-domain separations must be small. This view is consistent with the relatively small PCP domains in Figure 1c (ABCPs PVTCA/PCP 3 and 4; \bar{P}_n for crosslinks are 900 and 3720, respectively) and a more confused morphology.

Domain size analysis

In this section we consider domain sizes in ABCPs where γ_r is small and the morphology is not dominated by network constraints. Electron micrographs of ABCPs PVTCA/PCP 1–3 and PS*/PCP 1 and 2, show distributions of domain sizes which are wide compared with those obtained from linear block copolymers with narrow molecular weight distributions. Any natural distribution of domain sizes in the sample is complicated by the sectioning process since domains with centres outside the section, but within one domain radius of the section surface, will be cut during sectioning leaving an apparently small domain in the sec-

tion (assuming domains are not torn out during sectioning). This effect, which apparently enhances the number of small domains, increases with decreasing section thickness.

In analysing size distributions we measured the diameters of between 200 and 340 domains for each sample and corrected observed distributions for effects of sectioning assuming a section thickness of 100 nm (microtome settings were 80–100 nm). Figures 3a and 3b show, respectively, the uncorrected and corrected distributions for PS*/PCP 2 cast from chloroform. [For comparative purposes all corrected distributions have been normalized to a count of 250 domains (positive)]. The negative portion of the corrected distribution probably reflects errors in counting small domains which may be slightly underestimated as a result of domain overlap or lack of contrast (some domains show relatively poor contrast for their diameters probably because they are fragments of domains left on sectioning). We shall assume the positive portions of the distributions provide adequate descriptions of the true distributions.

Casting solvent. Figures 3b and 3c are the corrected distributions for PS*/PCP 2 cast from chloroform and benzene, respectively; the mean radii and their standard deviations are very similar (Table 2). Corrected distributions for PS*/PCP 1 cast from various solvents are shown in Figure 4 and their mean radii and standard deviations are given in Table 2. Again, the distributions are very similar. For both ABCPs, domain radii for samples cast from

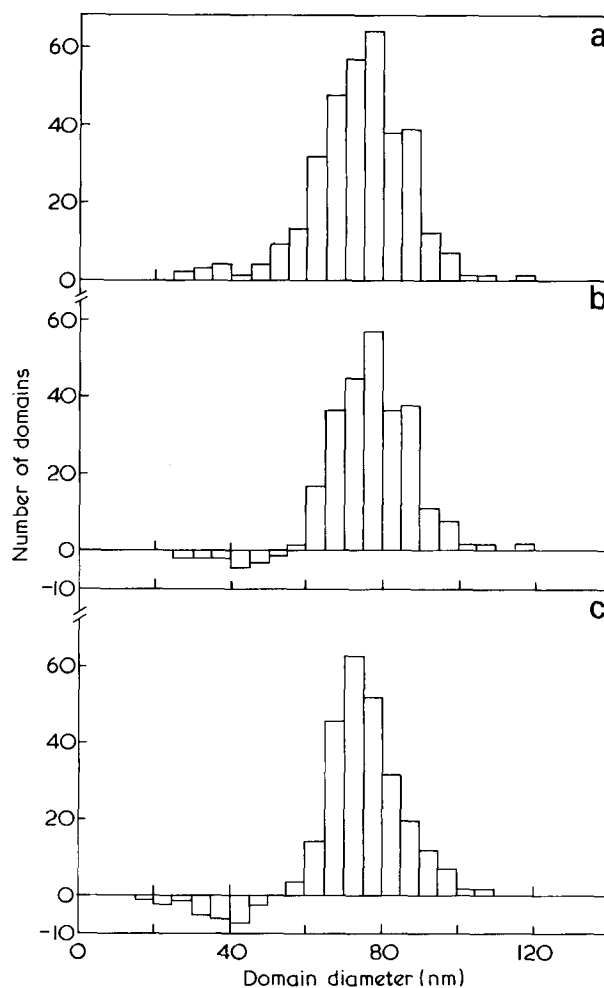


Figure 3 Domain size distributions in ABCP, PS*/PCP 2. (a), (b) are uncorrected and corrected distributions, respectively, for a sample cast from chloroform solution, (c) corrected distribution for a sample cast from benzene solution

Table 2 Domain size analysis for some ABCPs

ABCP	Casting solvent	Mean domain radius (nm)	Standard deviation (nm)
PVTCA/PCP 1	Benzene	18.38	3.25
PVTCA/PCP 2	Benzene	19.99	5.06
PVTCA/PCP 3	Benzene	19.50	4.71
PS*/PCP 1	Benzene	15.25	2.83
PS*/PCP 1	Chloroform	16.42	3.67
PS*/PCP 1	Chloroprene/ benzene (4:1 v/v)	13.53	2.38
PS*/PCP 1	Compression moulded	15.1	3.20
PS*/PCP 2	Benzene	38.17	4.56
PS*/PCP 2	Chloroform	40.24	4.93

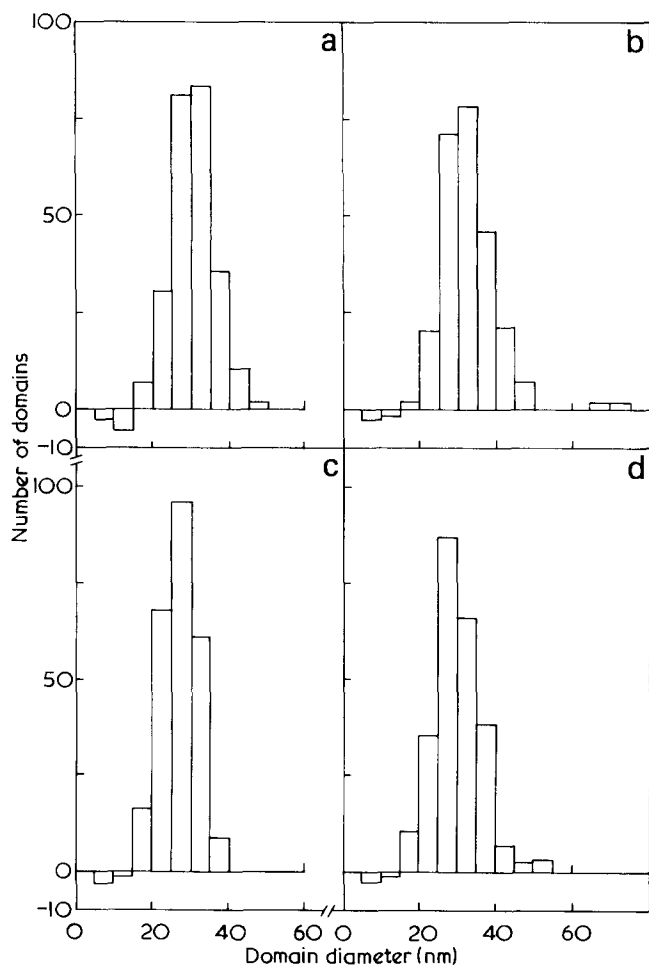


Figure 4 Corrected domain size distributions for ABCP, PS*/PCP 1. Samples cast from: (a) benzene; (b) chloroform; (c) chloroprene benzene (4:1 v/v); (d) refers to a compression moulded sample

chloroform are slightly greater than for those cast from benzene. Whether or not the minor variations observed reflect true changes with casting solvent cannot be ascertained from the limited data available.

Crosslink density. Variations in domain size distribution with crosslinking index (at constant crosslink length) were examined using ABCPs PVTCA/PCP 1–3 cast from benzene solution; corrected distributions are shown in Figure 5. Small differences in domain diameter and standard deviations are observed. Perhaps the most significant differences are the changes in shape of the distributions and the increase in proportion of small domains in PVTCA/

PCP 3 ($\gamma_r = 1.2$) which possibly reflects a tendency for highly crosslinked structures to produce large numbers of very small domains (Figure 1c).

Influence of crosslink molecular weight. We now consider domain sizes in relation to the molecular weights of the domain-forming chains. Using a space-filling model aimed at achieving uniform segment densities within the domains and within the matrix, Meier considered the morphologies of AB block copolymers^{11,12} and predicted that characteristic morphological features would be given by equations of the type:

$$r = k\alpha CM^{1/2} \quad (1)$$

For spherical domains, r is the domain radius, k is a constant characteristic of the morphology (1.33 for spheres), C is the constant relating unperturbed root mean square end-to-end chain dimensions to the molecular weight M of the domain forming chains and α is a perturbation parameter equal to the ratio of the perturbed to unperturbed chain dimensions. The calculations assumed that the sizes of statistical segments of A- and B- components were equal, that the chains conformed with random flight statistics and that the blocks were monodispersed with respect to molecular weight.

The mean diameters \bar{r} of the PCP domains in ABCPs: PVTCA/PCP 1–3 and PS*/PCP 2 are consistent with an equation of the same type as equation (1), viz.:

$$\bar{r} \approx 0.06\bar{M}_n^{1/2} \quad (2)$$

Unfortunately, the number-average molecular weight of the PCP chains in PS*/PCP 1 is uncertain but if it is at the lower end of the possible range, domain sizes in this sample are consistent with equation (2) which is also substantiated by data¹³ from recent micrographs of other samples of PS*/PCP.

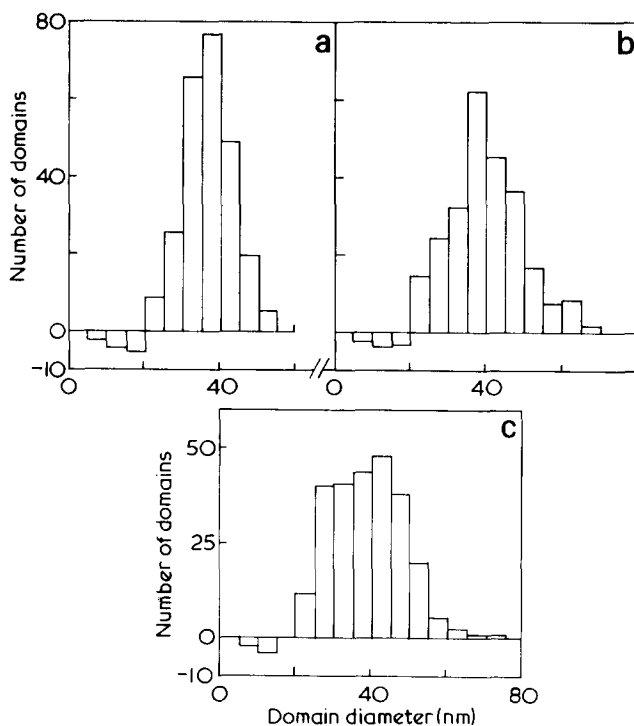


Figure 5 Corrected domain size distributions for ABCPs: (a) PVTCA/PCP 1; (b) PVTCA/PCP 2; (c) PVTCA/PCP 3

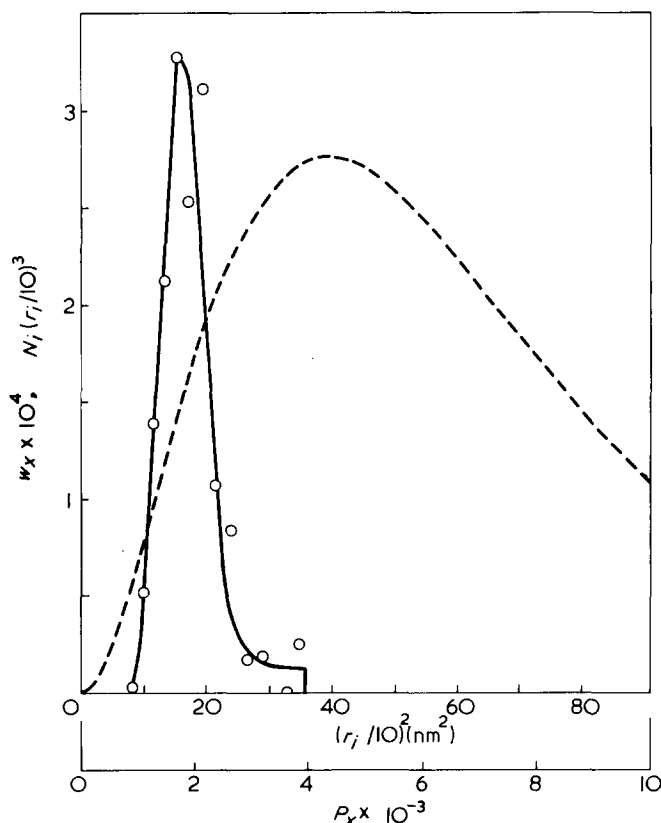


Figure 6 Variation in the total relative volumes of domains $[N_i(r_i/10)^3]$ of radius r_i with r_i^2 (—) and the variation in weight fraction w_x with degree of polymerization P_x for a polymer with $\bar{P}_n = 5900$ and $\bar{M}_w/\bar{M}_n = 1.5$ (---). Curves normalized as described in text

To compare relations (1) and (2), we assume a value of $C = 0.08$ nm, a reasonable value for polydienes¹⁴. Appropriate values of α for PCP domains in a PVTCA or PS* matrix are unknown, but Meier estimated¹¹ a value between 1.3 and 2.6 for polystyrene in a polydiene matrix (molecular weights $\sim 10^5$) and predicted that for spherical domains values of α relating to domain and matrix components should be approximately equal¹². We assume a value of $\alpha = 2$ when relation (1) becomes:

$$r = 0.21M^{1/2} \quad (3)$$

which predicts domain sizes considerably in excess of those observed for ABCPs.

A basic structural difference between ABCPs and AB block copolymers is that in the former both ends of the B-chains are attached to A-chains. For B-chains in domains, in an AB block copolymer only one end of the B-chain is restricted to the domain-matrix interface and the other end is free to occupy any point within the domain. In ABCPs both ends of the B-chains are restricted to points on the interface. Consequently, for equal chain lengths, B-chains in ABCPs cannot occupy sites as far removed from the interface as in AB block copolymers and smaller domains must ensue. To estimate the magnitude of this effect we may assume that structures such as (I) behave as two $A_2B_{1/2}$ copolymers; i.e. B-chains behave as if they were half their true length, reducing the predicted domain diameter by a factor of $(2)^{1/2}$. This estimate compares favourably with Meier's predicted value of $k = 1.0$ for ABA block copolymers with B-domains¹⁵ for which similar considerations apply.

ABCPs and ABA block copolymers differ structurally

in that in the former case two A-chains are attached to each end of the B-chains but only one in the latter. In ABCPs two A-chains occupy area at the surface of the domains for each junction point and it is to be expected that the surface area occupied by the two A-chains will be greater than if they were a single chain of the same total degree of polymerization. Meier's prediction that, for AB block copolymers with spherical domains, the values of α for both components are approximately equal and independent of chain lengths, was based on the assumption that the number of A- and B-chains per unit area of the interface are equal¹². This assumption is not true for ABCPs for which there are two A-chains attached to one B-chain at each junction point. By analogy with arguments presented by Meier for calculating α_A/α_B for lamellar morphologies in AB block copolymers¹⁵ we may expect that for spherical domains in ABCPs, $\alpha_B = \alpha_A/2$. Unless α_A (the perturbation factor for the matrix component) is increased by 2, α_B will be smaller in ABCPs than in AB block copolymers and this effect will also contribute to a reduction in domain size.

ABCPs as prepared and examined here contain homopolymer A. Although it is now known that the amount of homopolymer A present can influence the gross morphology of the ABCPs¹⁶, it is not yet known if the sizes of B-domains are influenced by homopolymer A.

Molecular weight distribution of crosslinks. Hoffmann *et al.*¹⁷ reported that mixtures of two AB block copolymers, differing only in molecular weights of the blocks, produced domains of two different sizes, i.e. fractionation according to molecular weight occurred during microphase separation. It might be anticipated that domain-size distributions in ABCPs arise as a result of fractionation of the B-chains. Figure 6 contains a plot of the relative volumes of domains $[N_i(r_i/10)^3]$, where N_i is the number of domains of radius r_i of different sizes as a function of the square of the domain radii for ABCP, PS*/PCP 2; i.e. effectively as a function of degree of polymerization assuming $r \propto P^{1/2}$. Also presented in Figure 6 is a plot of the weight fraction distribution for a polymer with \bar{P}_n 5900 prepared by free-radical polymerization with combination termination. The abscissae have been normalized by calculating a degree of polymerization corresponding to r assuming Meier's formula for ABA block copolymers (B domains) applies with $\alpha = 1$ and making \bar{r}^2 coincident with this value of P on the weight fraction distribution. Obviously the volume fraction distribution of domain sizes is much narrower than the weight fraction distribution (similar distributions are obtained with other ABCPs). From these data there is no evidence of fractionation in the ABCPs. It can also be concluded that high molecular weight crosslinks are incorporated into smaller domains than if they were in linear block copolymers with a narrow molecular weight distribution; α for these chains must be small.

Theoretical calculations of domain sizes for multicomponent polymers with distributions of block lengths have not been reported and it is uncertain as to which average of the molecular weight distribution should be used in attempting to employ relations developed for simple systems to more complex materials. A large proportion of the weight fraction of the polymer is in chains with molecular weights greater than \bar{M}_n and the tendency for such chains to adopt random flight statistics would tend to expand the domains. On the other hand, short chains introduce a relatively large number of junction points into the interface and such chains will have a disproportionately large effect on the surface energy of the domains.

CONCLUSIONS

ABCPs prepared by crosslinking PVTCA or PS* with PCP (the crosslinks being the minor component) have been shown to exhibit microphase separation in the bulk polymer at both low and high degrees of crosslinking. While highly crosslinked polymers show a somewhat confused morphology of very small domains because of network constraints hindering the development of domains, lightly crosslinked materials contain well-defined spherical domains of PCP crosslinks.

For lightly crosslinked polymers, and within the limited range of conditions employed in these experiments, no significant variations in domain diameters were observed with changes in the casting solvent or crosslink density. Domain diameters appear to be proportional to the square root of the degree of polymerization of the domain-forming chains.

Diameters of domains of the B-component in ABCPs are smaller than those predicted for AB and ABA block copolymers with B-chains of the same degree of polymerization. It is proposed that the relatively small sizes of the domains arise since both ends of the B-chains are located at the domain-matrix interface and since each end of such a chain is attached to two chains of the A-component.

Although ABCPs exhibit a distribution of diameters of B-domains those distributions are narrow compared with the molecular weight distributions of the domain-forming chains and no evidence for fractionation with respect to the molecular weights of the B-chains was observed.

ACKNOWLEDGEMENTS

The authors wish to thank the Department of Metallurgy and Materials Science for providing the electron micro-

scope facility, Dr J. Ashworth for the provision of the PS*/PCP ABCPs, British Petroleum Limited for a gift of chloroprene, Unilever Research for financial assistance to E.G.S. and Science Research Council for funds to purchase the ultramicrotome.

REFERENCES

- 1 Bamford, C. H., Dyson, R. W. and Eastmond, G. C. *J. Polym. Sci. (C)* 1967, **16**, 2425
- 2 Bamford, C. H., Dyson, R. W., Eastmond, G. C. and Whittle, D. *Polymer* 1969, **10**, 759
- 3 Bamford, C. H., Eastmond, G. C. and Whittle, D. *Polymer* 1969, **10**, 771
- 4 Bamford, C. H., Dyson, R. W. and Eastmond, G. C. *Polymer* 1969, **10**, 885
- 5 Ashworth, J., Bamford, C. H. and Smith, E. G. *Polymer* 1972, **13**, 52
- 6 Bamford, C. H., Eastmond, G. C. and Whittle, D. *Polymer* 1975, **16**, 377
- 7 Bamford, C. H., Eastmond, G. C. and Robinson, V. J. *Trans. Faraday Soc.* 1964, **60**, 751
- 8 Bamford, C. H. and Lindsay, H. *Polymer* 1973, **14**, 330
- 9 Flory, P. J. *J. Phys. Chem.* 1942, **46**, 132
- 10 Stockmayer, W. H. *J. Chem. Phys.* 1944, **12**, 125
- 11 Meier, D. J. *J. Polym. Sci. (C)* 1969, **26**, 81
- 12 Meier, D. J. *Polym. Prepr.* 1970, **11**, 400
- 13 Hughes, E. O. unpublished data
- 14 Kurata, M., Iwama, M. and Kamada, K. in 'Polymer Handbook' (Eds. J. Brandrup and E. H. Immergut), Interscience, New York, 1966
- 15 Meier, D. J. in 'Block and Graft Copolymers' (Ed. J. Burke), Syracuse University Press, Syracuse, 1973, p 105
- 16 Eastmond, G. C. and Phillips, D. G. unpublished results
- 17 Hoffmann, M., Kampf, G., Kromer, H. and Pampus, G. *Adv. Chem. Ser.* 1971, **99**, 351

Thermodynamics of α,ω -methoxy-poly(ethylene oxide)/*n*-alkane systems by gas – liquid chromatography

Yu-Kwan Leung

Department of Chemistry, University of Manchester, Manchester M13 9PL, UK

(Received 16 October 1975; revised 29 December 1975)

The gas–liquid chromatographic method has been used to measure the thermodynamic parameters of low molecular weight α,ω -methoxy-poly(ethylene oxide) with C_5 – C_{12} *n*-alkanes. High positive values of the solution interaction parameters and reduced residual enthalpies are obtained. The signs of the reduced residual entropies at infinite dilution of solvent can be predicted by the Flory–Orwoll–Vrij theory.

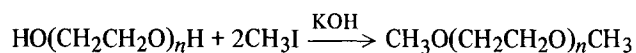
INTRODUCTION

The morphology and melting behaviour of α,ω -alkoxy-poly(ethylene oxide) samples are currently being investigated in this laboratory. In order to assess the effect of mixing of end and mid-chain segments on the process of melting, it is desirable to investigate the thermodynamics of mixing of the corresponding pure substances, i.e. PEO and *n*-alkanes. To avoid complications due to specific interaction of the hydroxy-end-groups of commercially available samples of poly(ethylene oxide) it is necessary to substitute less polar groups. In this work a Williamson synthesis, as modified by Dr D. R. Cooper, has been used to substitute methoxy end-groups. Since *n*-alkanes are in fact very poor solvents for PEO, conventional methods of experimental solution thermodynamics are not applicable. Recently the technique of gas–liquid chromatography (g.l.c.) has been developed and shown to be reliable in obtaining thermodynamic information on concentrated polymer solutions^{1–5}. In this paper, we report the results of g.l.c. measurements of several *n*-alkanes in two α,ω -methoxy-poly(ethylene oxide) fractions of molecular weight 2000 and 1000.

EXPERIMENTAL

Preparation

Hydroxy-ended poly(ethylene oxide) of MW 1000 and 2000 were obtained from Shell Chemical Company Ltd and Hoechst Chemical Ltd respectively. The Williamson ether synthesis was used for the transformation of the terminal hydroxy-groups of PEO to methoxy-groups:



Details of the method will be published elsewhere⁶. Two samples, designated PEO-1000M and PEO-2000M, were prepared.

Laboratory reagent (BDH) *n*-pentane, *n*-heptane, *n*-octane, *n*-decane and *n*-dodecane or Spectrosol reagent *n*-hexane were used as received.

Characterization

The degree of methoxylation of PEO was estimated by comparison of the intensities of the hydroxyl stretching

band at $\sim 3500\text{ cm}^{-1}$ for the starting polymer and the product. The C–H stretching peak at $\sim 2900\text{ cm}^{-1}$ was taken as reference to account for variation of film thickness. At least 95% replacement of hydroxy- by methoxy-groups was achieved.

Number-average molecular weights of the samples, determined by vapour pressure osmometry (Mechrolab, benzene at 25°C), were close to the nominal *MW* of their parent polymers and therefore the nominal values were adopted for subsequent calculation. Gel permeation chromatography was used to monitor the molecular weight distribution of the polymers⁷. The PEO did not exhibit detectable degradation during the preparation and the value of M_w/M_n was near to 1.06.

Specific volumes (v_{sp}) and thermal expansion coefficients (α) of the polymers were determined by pycnometry. The pycnometers have been described elsewhere⁸. For PEO-2000M, $v_{sp} = 0.9196\text{ cm}^3/\text{g}$ (55.8°C) and $\alpha = 7.2 \times 10^{-4}/\text{K}$ (55° – 70°C); for PEO-1000M, $v_{sp} = 0.9100\text{ cm}^3/\text{g}$ (46.1°C) and $\alpha = 7.4 \times 10^{-4}/\text{K}$ (40° – 55°C). Melting points, measured by hot-stage microscopy, were found to be 52.6°C and 36.8°C for PEO-2000M and PEO-1000M respectively.

Gas–liquid chromatography

The experimental procedures of g.l.c. and column preparation have been described fully elsewhere³. The stationary phase was coated onto Chromosorb W(45/60) from solution in benzene. The % weight of polymer on the solid support was determined by Soxhlet extraction with benzene for duplicate samples. The coated particles were packed into a stainless-steel tube, 1 m long and 4 mm i.d. Two columns were prepared, one with 1.302 g PEO-2000M (24.2% by wt) and the other with 0.768 g PEO-1000M (17.9% by wt).

The apparatus used was a Perkin-Elmer Model 452 Gas Chromatograph with a thermal-conductivity detector. Column temperatures were controlled to $\pm 0.05\text{ K}$. Hydrogen was chosen as carrier gas. A soap-bubble flowmeter located at the outlet of the instrument was used to measure flow rate with an accuracy of $\pm 1\%$. Flow rates, commonly in the range of 15 – $30\text{ cm}^3/\text{min}$, were controlled by adjusting an upstream pressure regulator. Inlet pressures of $\sim 17 \times 6984.76\text{ N/m}^2$ were measured by a pressure gauge.

Table 1 Experimental thermodynamic quantities of interaction in α,ω -methoxy-poly(ethylene oxide) of *MW* 2000

	57.0°C			66.7°C			κ	$\bar{S}_1^R/R\phi_2^2$
	χ_v	χ_s	ν_{1b}	χ_v	χ_s	ν_{1b}		
n-C ₅	1.90	2.06	0.085	1.82	2.00	0.096	2.0	-0.0 ₃
n-C ₆	2.02	2.16	0.074	1.94	2.09	0.083	2.4	+0.2 ₇
n-C ₇	2.15	2.26	0.063	2.06	2.18	0.071	2.8	+0.5 ₈
n-C ₈	2.30	2.39	0.053	2.19	2.29	0.062	3.7	+1.3
n-C ₁₀	2.67	2.74	0.035	2.51	2.59	0.042	5.3	+2.6
n-C ₁₂	3.04	3.09	0.023	2.84	2.90	0.029	6.4	+3.4

The outlet pressure was atmospheric pressure. Liquid *n*-alkanes (C₅–C₈, C₁₀, C₁₂) mixed with air were injected into the carrier gas stream. The retention time for the solvent was taken to be the difference between the elution times of the solvent and the air. Retention volumes of n-C₅ to n-C₈ did not alter with the injected amount over the range 0.01–0.3 mm³ while that of n-C₁₀ and n-C₁₂ increased considerably. Therefore the retention volume was extrapolated (approximately linearly) to zero concentration for n-C₁₀ and n-C₁₂. For the rest, retention volumes corresponding to sample size of 0.02 mm³ were measured. For this sample size, a rough estimation of the peak area places the volume fraction of solvent near 10⁻⁴. Also, variation of retention volume with the flow rate in the stated range was insignificant.

RESULTS AND DISCUSSION

The Flory–Huggins solution parameter χ_v using volume fraction (ν) as composition variable is related to the net retention volume V_N as follows³:

$$\chi_v = \ln(RTV^L/V_1^0 p_1^0 V_N) - (B_{11} - V_1^0) p_1^0 / RT - 1 + 1/r + (2B_{13} - \bar{V}_1^\infty) p_o J_3^4 / RT \quad (1)$$

where V^L is the volume of the polymer (designated as 2), V_1^0 , p_1^0 and B_{11} are the molar volume, the vapour pressure and the gas-phase second virial coefficient of pure solvent (designated as 1) at the column temperature T (K), \bar{V}_1^∞ is the partial molar volume of solvent at infinite dilution, B_{13} is gas-phase mixed second virial coefficient for solvent vapour and carrier gas, r is the ratio of molar volumes of polymer and solvent. The J_3^4 pressure factor is defined as $(3/4)[(p_i/p_o)^4 - 1]/[(p_i/p_o)^3 - 1]$ where p_i and p_o are inlet and outlet pressures across the column respectively. The last term in equation (1) is included to correct for the effect of the finite column pressure upon the retention volumes⁹ and its magnitude is ~ 0.006 for hydrogen carrier gas and *n*-alkane solvents.

The Flory–Huggins theory is based upon a quasi-lattice model of the liquid mixture. More satisfactory approaches^{10–12} take account of the differing properties of the component liquids. The Flory, Orwoll and Vrij theory^{10,11}, which has been widely applied to a number of polymer/solvent systems, leads to an interaction parameter based on segment fraction (ϕ) given by:

$$\chi_s = \chi_v + \ln(\bar{\nu}_1/\bar{\nu}_2) \quad (2)$$

where $\bar{\nu}_i$ is the reduced volume of component i . The reduced partial molar residual enthalpy ($\kappa = \bar{H}_1^R/RT\phi_2^2$) is obtained from the temperature dependence of χ , viz.:

$$\kappa = -(\partial\chi_s/\partial\ln T)_{\phi_1=0} = -(\partial\chi_v/\partial\ln T)_{\phi_1=0} + T(\alpha_2 - \alpha_1) \quad (3)$$

Consequently, the reduced partial molar residual entropy is:

$$\bar{S}_1^R/R\phi_2^2 = \kappa - \chi_s \quad (4)$$

in the limit $\phi_1 = 0$. Experimental values of χ , κ and $\bar{S}_1^R/R\phi_2^2$ are recorded in *Tables 1* and *2* for PEO-2000M and PEO-1000M respectively. The estimated uncertainties of χ , κ and $\bar{S}_1^R/R\phi_2^2$ are 1%, 25% and 25% respectively. Constants of *n*-alkanes used for calculation have been reported earlier¹³. Temperature variations of κ are omitted because of limited data.

In order to verify that the solution formed during the elution of alkane vapour is homogeneous, it is necessary to investigate the miscibility gaps of the mixtures. If a system containing a polymer and a very poor solvent separates into two phases, then each of the phases contains one of the components virtually in its standard state. The condition for equilibrium of the solvent is:

$$\ln\nu_{1b} + (1 - 1/r)\nu_{2b} + \chi_v\nu_{2b}^2 = 0 \quad (5)$$

where subscript b denotes the binodial compositions. Volume fractions ν_{1b} in the highly concentrated polymer phase were obtained by numerical solution of equation (5) using the experimental χ_v values (assuming χ_v to be independent of concentration). These values are also entered in *Tables 1* and *2*. They indicate that the concentration range ($\nu_1 \approx 10^{-4}$) studied by g.l.c. is orders of magnitude smaller than the solubility limit. Therefore homogeneity of solutions is assured.

Several features of the data are noteworthy. The systems investigated show high positive values of the interaction parameters (χ_v , χ_s) as expected for polymer/poor solvent systems. Secondly, despite the larger combinatory entropy gain for the lower *MW* polymer during the mixing process, it can be seen, by comparing ν_{1b} values in *Tables 1* and *2*, that a given alkane molecule appears to be a better solvent for the higher *MW* polymer. Thirdly, the residual entropies change sign and become increasingly positive as the solvents increase in chain length from *n*-pentane to its higher analogues.

These features can be further analysed in terms of the Flory, Orwoll and Vrij (FOV) theory. According to the FOV theory, the contact interaction parameter X_{12} denoting the energy change for the formation of contacts between unlike species at the expense of contacts between like species is evaluated from the experimental χ_s data, as follows:

$$X_{12} = RT(\bar{\nu}_2/V_1^*)\chi_s - P_1^* \bar{\nu}_2 \{3\bar{T}_1 \ln[(\bar{\nu}_1^{1/3} - 1)/(\bar{\nu}_2^{1/3} - 1)] + (\bar{\nu}_1^{-1} - \bar{\nu}_2^{-1})\} \quad (6)$$

Table 2 Experimental thermodynamic quantities of interaction in α,ω -methoxy-poly(ethylene oxide) of *MW* 1000

	42.1°C			56.8°C			κ	$\bar{S}_1^R/R\phi_2^2$
	χ_v	χ_s	ν_{1b}	χ_v	χ_s	ν_{1b}		
n-C ₅	2.50	2.65	0.043	2.39	2.56	0.049	2.0	-0.6
n-C ₆	2.84	2.95	0.030	2.68	2.80	0.036	3.3	+0.4
n-C ₇	3.05	3.14	0.024	2.87	2.98	0.029	3.6	+0.5
n-C ₈	3.31	3.39	0.018	3.09	3.18	0.023	4.6	+1.3

Table 3 Contact interaction parameters and reduced partial molar residual entropies calculated by the Flory-Orwoll-Vrij theory

	PEO-2000 M			PEO-1000 M		
	X_{12} (cal/cm ³)		$\bar{S}_1^R/R\phi_2^2$	X_{12} (cal/cm ³)		$\bar{S}_1^R/R\phi_2^2$
	57.0°C	66.7°C	at 57.0°C	42.1°C	56.8°C	at 56.7°C
n-C ₅	15.7	15.3	-0.10	20.4	20.4	-0.03
n-C ₆	14.6	14.3	-0.04	20.3	20.0	+0.18
n-C ₇	13.8	13.5	+0.10	19.3	19.0	+0.33
n-C ₈	13.3	13.0	+0.18	18.8	18.3	+0.43
n-C ₁₀	13.0	12.5	+0.37			
n-C ₁₂	12.6	12.1	+0.50			

where V_1^* is the characteristic molar volume. (Characteristic quantities are denoted by an asterisk.) The reduced partial molar residual entropy can then be calculated from:

$$\begin{aligned} \bar{S}_1^R/R\phi_2^2 = & - (P_1^*V_1^*/R) \{3(T_1^*)^{-1} \ln[(\bar{v}_1^{1/3} - 1)/ \\ & (\bar{v}_2^{1/3} - 1)] - \alpha_2\bar{v}_2^{-1}(T_2^*/T_1^* - 1) + \alpha_2V_1^*X_{12}/R\bar{v}_2 \} \end{aligned} \quad (7)$$

by employing the corresponding X_{12} values. Predicted values of $\bar{S}_1^R/R\phi_2^2$ are recorded in Table 3, together with the values found for X_{12} .

Comparison of contact parameters between different polymer fractions indicates that the interaction of a given solvent molecule with terminal segments of PEO-M is more repulsive than that with mid-chain segments. This is consistent with the molecular geometry of the α,ω -methoxy-poly(ethylene oxide) chain: the fraction of the surface area attributable to sp^2 oxygen is greater in the methoxy end-group than in the mid-chain segment.

The trend of the residual entropies is reproduced by the theory. Examination of equation (7) reveals that the sign of the residual entropy is determined by the balance between the negative contribution from the equation-of-state terms and the positive contribution from the contact energy term. The magnitude of the latter are, in most cases, larger than those of the former because of the large positive exchange energy term. Quantitative agreement between theory and experiment is unsatisfactory. There is some

difficulty in making the comparison because of the experimental problems of measuring small changes in χ with T . However, overall it seems that theory underestimates \bar{S}_1^R by a factor of about 5.

As pointed out previously⁴, the residual entropy of mixing in the concentration range near pure polymer might yield valuable information concerning the conformation of polymers in the amorphous state. The poly(ethylene oxide) mixtures with n-pentane exhibit a negative \bar{S}_1^R , whereas the observed positive residual entropies for higher n-alkanes are the direct consequence of their large positive contact interaction parameters. Therefore no dissipation of order with dilution of low MW α,ω -methoxy-poly(ethylene oxide) is discernable in the present data.

ACKNOWLEDGEMENTS

The author wishes to thank Dr C. Booth for many helpful discussions and for a critical reading of the manuscript and Dr D. R. Cooper for recommending the procedure of sample preparation.

REFERENCES

- 1 Tewari, Y. B. and Schreiber, H. P. *Macromolecules* 1972, 5, 329; Schreiber H. P., Tewari, Y. B. and Patterson, D. *J. Polym. Sci. (A-2)* 1973, 11, 15
- 2 Smidsrød, O. and Guillet, J. E. *Macromolecules* 1969, 2, 272; Lavoie, A. and Guillet, J. E. *Macromolecules* 1969, 2, 443
- 3 Leung, Yu-Kwan and Eichinger, B. E. *J. Phys. Chem.* 1974, 78, 60; *Rubber Chem. Technol.* 1975, 48, 108
- 4 Leung, Yu-Kwan and Eichinger, B. E. *Macromolecules* 1974, 7, 685; *Rubber Chem. Technol.* 1975, 48, 119
- 5 Olabisi, O. *Macromolecules* 1975, 8, 316
- 6 Cooper, D. R. to be published
- 7 Booth, C., Bruce, J. Malcolm and Buggy, M. *Polymer* 1972, 13, 475
- 8 Ashman, P. C. and Booth, C. *Polymer* 1975, 16, 889
- 9 Cruickshank, A. J. B., Windsor, M. L. and Young, C. L. *Proc. R. Soc. (A)* 1966, 295, 259, 291
- 10 Flory, P. J., Orwoll, R. A. and Vrij, A. *J. Am. Chem. Soc.* 1964, 86, 3507
- 11 Eichinger, B. E. and Flory, P. J. *Trans. Faraday Soc.* 1968, 64, 2035
- 12 Delmas, G., Patterson, D. and Somcynsky, T. *J. Polym. Sci.* 1962, 57, 79
- 13 Orwoll, R. A. and Flory, P. J. *J. Am. Chem. Soc.* 1967, 89, 6814

Melt rheology of some aliphatic polyamides

P. Parrini, D. Romanini and G. P. Righi

Montedison SpA, Centro Ricerche Ferrara, 44100 Ferrara, Italy

(Received 13 October 1975; revised 16 January 1976)

The melt rheology of nylon-6, nylon-6,6, nylon-6,10 and nylon-11, has been investigated by different techniques. It has been found that their behaviour is quite similar and almost Newtonian regarding both the flow curves and the elastic and instability properties. The samples show rather different viscous flow activation energies, although their values approach each other at high shear rate. The critical shear stresses of such materials are compared with those of other known polymers.

INTRODUCTION

The rheological properties of polyamides in the molten state have received little study, although these polymers are among the best known and most extensively used, especially as synthetic fibres.

The literature gives very little information on polycaprolactam (nylon-6). Publications are of a general type¹, or concern the processes of transformation². Pezzin and Gechele³ studied the behaviour of such a polymer by capillary rheometer, over a wide range of molecular weights and shear stresses.

On the other hand, no literature exists on other polyamides, such as poly(hexamethylene adipamide) (nylon-6,6) and poly(ω -undecanamide) (nylon-11) and poly(hexamethylene sebacamide) (nylon-6,10), which are used on an industrial scale.

Therefore, the purpose of this paper is to investigate the rheology of nylon-6 using both capillary rheometers of different types and cone and plate rotational viscometers to obtain information on normal stresses, and to study the behaviour of the other nylons. It is thus possible to obtain a general picture of the properties of an entire class of polymers, especially regarding the influence of the temperature and the elastic properties of the materials.

EXPERIMENTAL

Polymers

Measurements were made on commercial polymers. Poly(hexamethylene adipamide) (nylon-6,6), polycaprolactam (nylon-6) and poly(hexamethylene sebacamide) (nylon-6,10) were produced by Montedison; poly(ω -undecanamide) (nylon-11) was produced by Organico and sold under the trade name of Rilsan. Table 1 shows the characteristics of the investigated samples. Melting temperatures and corresponding enthalpies, ΔH , (cal/g) were detected by differential calorimetry using a Perkin-Elmer DSC-IB apparatus. Densities (g/cm³) were measured using a gradient column (ASTM-D-1505/68).

Intrinsic viscosities in *m*-cresol at 30°C were measured and molecular weights were calculated from the $[\eta] - M$ relationships given in the literature⁴. The melt indices were determined according to the ASTM 1238/71 standard, condition *K* for nylon-6,6 and condition *Q* for the other samples. Before measurement, all the polymers were carefully

dried at 110°C for 8 h under a nitrogen stream to give a water content of not more than 100 ppm.

Rheological measurements

Capillary rheometer under constant pressure. Using a viscometer (obtained from Ceast, Turin) the amount of extruded material in the unit of time was measured. Shear stress τ and shear rate $\dot{\gamma}$ at the wall are calculated from the known relations:

$$\tau = \frac{PR}{2L} \text{ (dyne/cm}^2\text{)} \quad (1)$$

$$\dot{\gamma} = \frac{4Q}{\pi R^3} \text{ (sec}^{-1}\text{)} \quad (2)$$

where P is the applied pressure (dyne/cm²); Q is the amount of extruded polymer (cm³/sec); R is the capillary radius (cm), L its length (cm).

With this type of viscometer, were determined: the flow constancy in the time, the existence or the absence of wall slipping and the end correction. An interchangeable series of capillaries having the geometrical properties shown in Table 2 were used. Capillary diameters are given with an error of about 1%, lengths with an error lower than 1%.

By using spinnerets with a different L/D ratio, possible inlet phenomena were investigated, whereas by using capillaries with the same L/D ratio but with different diameters, the existence of wall slipping was sought. By this device, a shear rate range from 10 to 2×10^4 sec⁻¹ was considered. Temperatures to within $\pm 1^\circ$ were maintained. Melt densities of the polymers at the different temperatures were measured via dilatometry⁵.

Table 1 Chemical and physical properties of the nylons used

Sample	Melting temperature (°C)	Density 23°C (g/cm ³)	$[\eta]$ at 30°C in <i>m</i> -cresol (dl/g)	Molecular weight <i>M</i>	Melt index ΔH (g/10 min) (cal/g)
Nylon-6	226	1.146	1.02	17 000	32.3 16
Nylon-6,6	266	1.144	1.09	14 000	16 15.5
Nylon-6,10	226	1.070	1.07	12 200	10.7 16.5
Nylon-11	190	1.035	0.84	21 000	33.1 10

Table 2 Geometrical characteristics of the flat entrance capillaries used in the rheometer under constant pressure

Capillary	Diameter (mm)	Length (mm)	L/D ratio
1	0.15	0.75	5.0
2	0.3	0.9	3.0
3	0.3	1.5	5.0
4	0.3	1.0	3.3
5	0.5	1.0	2.0
6	0.5	2.5	5.0
7	1.0	1.0	1.0
8	1.0	5.0	5.0

Capillary rheometer at constant rate (MCR). Using an Instron capillary rheometer the applied stress was measured by a load cell placed at the top of the piston pushing the molten polymer into the capillary. The shear stress and shear rate at the wall are again given by relations (1) and (2).

The apparent viscosity η may be calculated, with a good approximation, by the Poiseuille equation, since the flow curves do not considerably differ from those corrected according to the Rabinowitsch law⁶, for these materials.

With this rheometer the flow curves of nylons at different temperatures and the activation energies of viscous flow were determined, using one capillary having a diameter of 0.734 mm and length of 25.56 mm ($L/D = 34.82$).

A shear rate range from 20 to $2 \times 10^4 \text{ sec}^{-1}$ was employed. By using this capillary, the corrections due to entrance effect are eliminated. Using a capillary having a diameter of 0.25 mm and length of 5 mm ($L/D = 20$), the flow instability conditions have been investigated.

Cone and plate rotational viscometer (WRG). By this rheometer, (Weissenberg rheogoniometer model R-18 of Sangamo Control Ltd) the shear rate is given by:

$$\dot{\gamma} = \frac{\omega}{\alpha} \quad (3)$$

where ω is the rotational velocity of the bottom plate and α is the cone-angle.

The shear stress at any point of the fluid is given by:

$$\tau = \frac{3M}{2\pi r^3} \quad (4)$$

where M is the torque transmitted from the material to the top plate and r is the plate and cone radius.

The apparent viscosity η is again obtained from the relation:

$$\eta = \frac{\tau}{\dot{\gamma}} \quad (5)$$

Because of the considerable fluidity of the polymers, the experimental studies by rheogoniometer have been carried out at temperatures slightly above the melting point, by using a plate and cone having a diameter of 5 cm and an angle $\approx 4^\circ$. The range of shear rates explored was between 10^{-1} and 10^2 sec^{-1} . By this apparatus, also the first normal stress difference $P_{11} - P_{22}$ (indicated by σ) has been measured as a function of $\dot{\gamma}$. Temperatures within $\pm 2^\circ\text{C}$ were kept constant.

Outline of measurements. The test temperatures have been selected on the basis of the apparatus used and the melting point of materials examined (see Table 3).

Determination of the rheological parameters at very low shear rates require quite long measurement times; therefore, knowledge of thermal stability material is required in order to avoid possible decomposition effects and consequent variation in molecular weight and molecular weight distribution. By volumetric flow measurements at different residence times (using constant-pressure rheometer), the polymers should remain stable at least for 30 min, a necessary condition for this investigation.

RESULTS AND DISCUSSION

By using the constant-pressure rheometer and interchanging the capillaries (see Table 2), flow curves ($\tau-\dot{\gamma}$) have been determined. The curves obtained are practically coincident with values contained over a very narrow range, although the capillaries used have very low L/D ratios. Therefore, it can be stated that the nylons studied do not give rise to any entrance and wall slipping effects.

Typical flow curves

Using the apparatus described we determined the flow curves of the four nylons so as to acquire a greater knowledge of the rheological behaviour of such materials and to study their optimum use in the transformation processes.

Figures 1-4 give $\eta-\dot{\gamma}$ curves of the samples examined at different temperatures in a very wide range of shear stresses or shear rates. As it may be seen, nylons exhibit a Newtonian behaviour up to $\sim 10^2 \text{ sec}^{-1}$ depending on the test temperature. To obtain a direct comparison among the samples examined, the rheological parameters must be expressed as a function of reduced variable normalizing the temperature effect. For this purpose, we record in Figure 5 the values of shear stress obtained using the MCR and the WRG rheometers, at different temperatures as a function of the product $\eta_0\dot{\gamma}$ for all the four nylons. η_0 is the Newtonian viscosity of the material at the test temperature.

Table 3 Test temperatures

Polymer	Rheometer under constant pressure	Test temperature ($^\circ\text{C}$)		
		Rheometer at constant speed	Flow curves	Flow instability
Nylon-6	240	240	240	230
		260		
		280		
Nylon-6,6	275	270	280	270
		280		
		290		
		300		
		300		
Nylon-6,10	240	240	240	240
		260		
		280		
Nylon-11	210	220	210	210
		240		
		260		
		280		

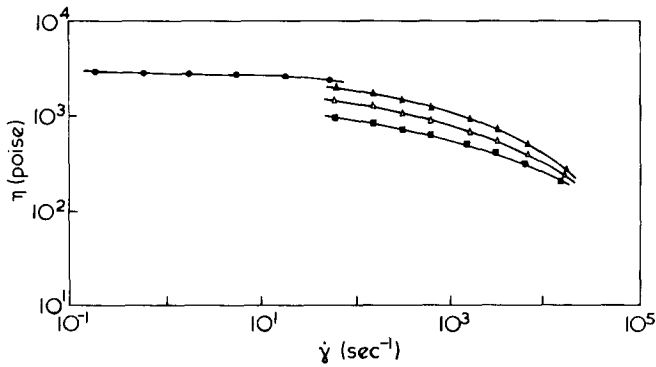


Figure 1 Melt viscosity η versus shear rate $\dot{\gamma}$ of the nylon-6 for several extrusion temperatures. MCR: \blacktriangle , 240°; \triangle , 260°; \blacksquare , 280° C. WRG: \bullet , 230° C

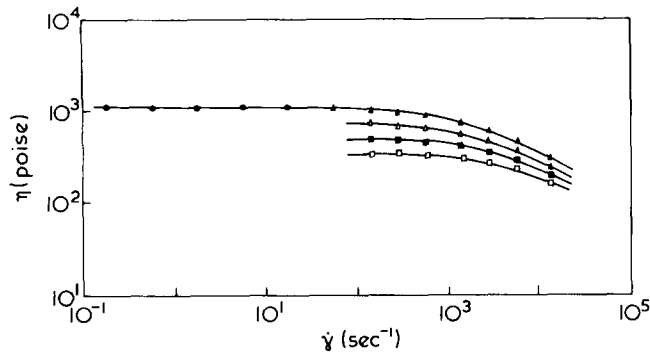


Figure 2 Melt viscosity η versus shear rate $\dot{\gamma}$ of the nylon-6,6 for several extrusion temperatures. MCR: \blacktriangle , 270°; \triangle , 280°; \blacksquare , 290°; \square , 300° C. WRG: \bullet , 270° C

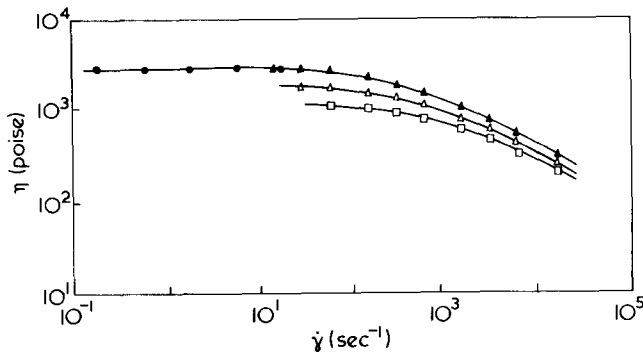


Figure 3 Melt viscosity η versus shear rate $\dot{\gamma}$ of the nylon-6,10 for several extrusion temperatures. MCR: \blacktriangle , 240°; \triangle , 260°; \blacksquare , 280° C. WRG: \bullet , 240° C

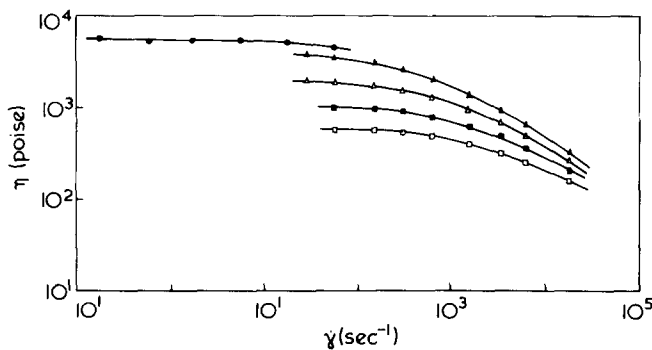


Figure 4 Melt viscosity η versus shear rate $\dot{\gamma}$ of the nylon-11 for several extrusion temperatures. MCR: \blacktriangle , 220°; \triangle , 240°; \blacksquare , 260°; \square , 280° C. WRG: \bullet , 210° C

Similarly, Figure 6 shows the behaviour of the η/η_0 ratio as a function of the product $\eta_0\dot{\gamma}$. On examining the two Figures, it appears to be evident that all the polyamides investigated exhibit essentially the same rheological behaviour, independent of the temperature effect. They are Newtonian up to values greater than 10^5 dyne/cm². In order to represent the rheological behaviour of the polymers investigated by single relation we may write with a good approximation:

$$\log \tau = -2.88 + 2.18 \log \eta_0 \dot{\gamma} - 0.121 (\log \eta_0 \dot{\gamma})^2 \quad (6)$$

which is valid between 10^2 and 10^8 dyne/cm². Equation (6) has been calculated by regression analysis.

Viscous flow activation energy

From flow curves at different temperatures, we obtain $(E - \log \tau)$ and the $(E - \log \dot{\gamma})$ relations; the viscous flow activation energies E of investigated polymers are markedly different. In the examined shear stress field, the values of E are constant and are shown in Table 4, whereas the curves $(E - \log \dot{\gamma})$ are shown in Figure 7.

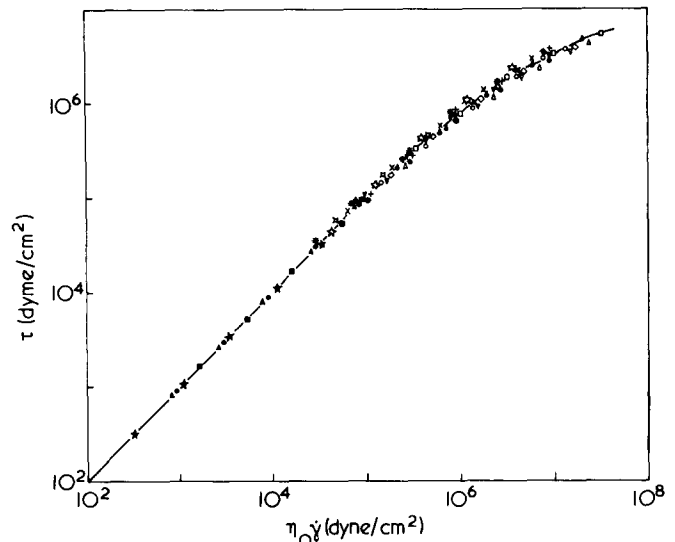


Figure 5 Melt shear stress τ versus $\eta_0 \dot{\gamma}$ product for the four nylons at different test temperatures. Nylon-6—MCR: \bullet , 240° C; \circ , 260° C; \oplus , 280° C. WRG: \bullet , 230° C. Nylon-6,6—MCR: $+$, 270° C; \times , 280° C; \star , 290° C; \ast , 300° C. WRG: \star , 270° C. Nylon-6,10—MCR: \triangle , 240° C; ∇ , 260° C; \blacktriangledown , 280° C. WRG: \blacktriangle , 240° C. Nylon-11—MCR: \square , 220° C; \diamond , 240° C; \blacklozenge , 260° C; \blacksquare , 280° C. WRG: \blacksquare , 210° C

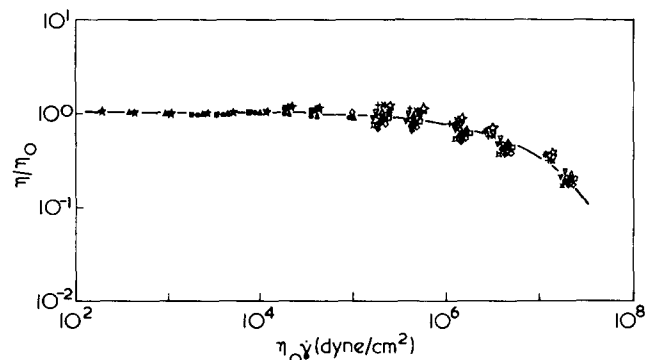


Figure 6 η/η_0 ratio versus $\eta_0 \dot{\gamma}$ product for the four nylons at different test temperatures. Nylon-6—MCR: \bullet , 240° C; \circ , 260° C; \oplus , 280° C. WRG: \bullet , 230° C. Nylon-6,6—MCR: $+$, 270° C; \times , 280° C; \star , 290° C; \ast , 300° C. WRG: \star , 270° C. Nylon-6,10—MCR: \triangle , 240° C; ∇ , 260° C; \blacktriangledown , 280° C. WRG: \blacktriangle , 240° C. Nylon-11—MCR: \square , 220° C; \diamond , 240° C; \blacklozenge , 260° C; \blacksquare , 280° C. WRG: \blacksquare , 210° C

Table 4 Activation energies E for the nylons in the shear stresses field between 1×10^5 and 1×10^7 dyne/cm²

	Nylon-6	Nylon-6,6	Nylon-6,10	Nylon-11
E (kcal/mol)	11.3	23.9	13.7	17.3

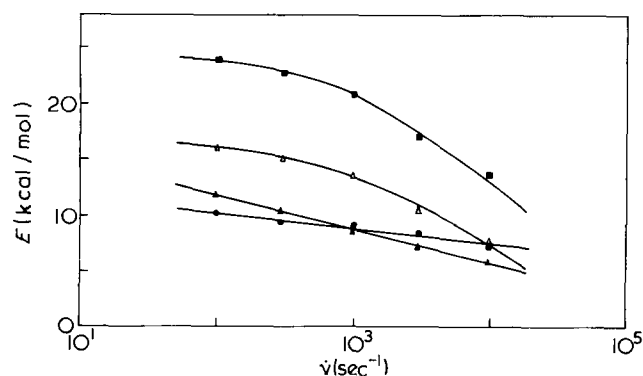


Figure 7 Activation energy E at constant shear rate versus shear rate $\dot{\gamma}$ for the samples examined: ●, nylon-6; ■, nylon-6,6; ▲, nylon-6,10; ▽, nylon-11

This plot shows the activation energy considerably decreasing with increasing $\dot{\gamma}$ for nylon-6 and nylon-11, whereas far less markedly for the other samples. All curves are converging at fairly close energy values. The differences observed do not considerably influence processing of such polyamides, since both spinning and extrusion moulding shear rates are fairly high, of the order of $10^4 - 10^5 \text{ sec}^{-1}$.

Elastic properties

The first normal stress difference σ (dyne/cm²) on varying the shear rate for the different test temperatures, was determined using WRG. Figure 8 shows the values of σ as a function of the reduced variable $\eta_0 \dot{\gamma}$ for the different polymers; as may be seen, all the experimental points fall on the same curve within the experimental error.

This means that, the shear stress being the same (the product $\eta_0 \dot{\gamma}$ has the dimensions of dyne/cm²), by excluding the temperature effect, the four nylons examined have almost the same values of the first normal stress difference. With good approximation, the following relation (obtained by regression analysis) may be given:

$$\log \sigma = -2.706 + 1.43 \log \eta_0 \dot{\gamma} \quad (7)$$

which is valid in a $\eta_0 \dot{\gamma}$ range between 10^3 and 10^6 dyne/cm². The σ/τ ratio, obtained at the same shear rate (sec^{-1}), is directly connected to the elastic recovery and hence to the material swelling. For the examined samples, σ/τ ratio keeps at extremely low values, within the shear field investigated, as shown in Figure 9 where σ/τ is reported as a function of the reduced variable $\eta_0 \dot{\gamma}$. Polyolefins, in the same measurement range, assume σ/τ values of 2–3 units.

Because of the extreme fluidity of the polyamides under examination, the extrudate swelling could not be determined.

Flow instability

The flow instability of the four nylons, by use of the Instron rheometer, has been investigated up to fairly high extrusion rates ($\sim 7 \times 10^4 \text{ cm/min}$). The flow instability parameters of such materials are reported in Table 5.

This Table shows the excellent performance of the nylons examined at high deformation rates; the flow instability appears at very high shear rates for all the samples, excluding the nylon-11 which has been extruded at quite low temperatures. Therefore the $\dot{\gamma}_c \eta_0$ product takes it into the values field of the other samples.

The τ_c (critical shear stress) $\times \bar{M}$ (molecular weight) products of the four investigated nylons, assume fairly close results, within $1.1 - 1.5 \times 10^{11}$ range. (The \bar{M} values have been taken from Table 1.)

The above products have been obtained excluding the test temperature effect on the τ_c determination. Such effect, in the temperature field employed, has little influence on the $\tau_c \times \bar{M}$ product.

A comparison between the critical flow conditions of some of the best known polymers and the nylons is made in Table 6, where the critical shear stress values determined by the authors⁷ and drawn from the literature⁸⁻¹² are reported.

Even by taking into account the approximation of such measurements, it appears that the excellent rheological behaviour of the polyamides, is quite favourable in processes involving high shear rates.

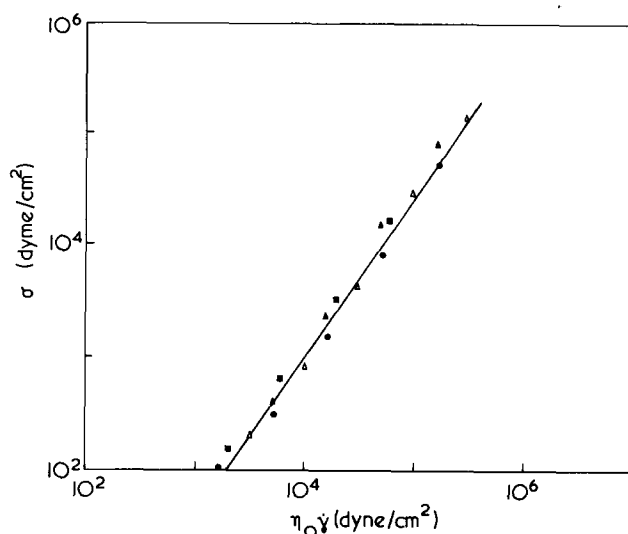


Figure 8 First normal stress difference σ versus reduced variable $\eta_0 \dot{\gamma}$, measured by rheogoniometer: ●, nylon-6 at 230°C; ■, nylon-6,6 at 270°C; ▲, nylon-6,10 at 240°C; ▽, nylon-11 at 210°C

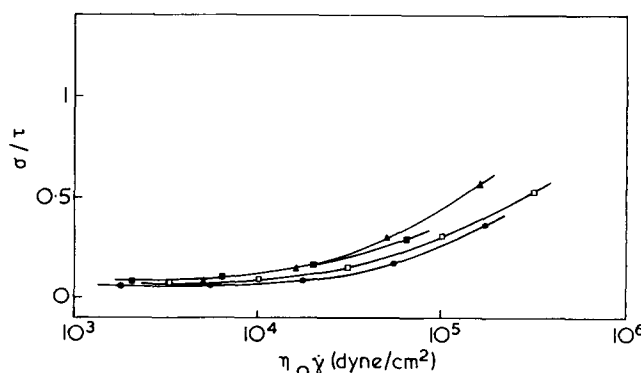


Figure 9 Elastic recovery σ/τ versus $\eta_0 \dot{\gamma}$ product, carried out by rheogoniometer: ●, nylon-6 at 230°C; ■, nylon-6,6 at 270°C; ▲, nylon-6,10 at 240°C; □, nylon-11 at 210°C

Table 5 Critical flow conditions

Sample	Extrusion temperature (°C)	Critical extrusion rate (cm/min)	Critical shear rate $\dot{\gamma}_c$ (sec ⁻¹)	Critical shear stress τ_c (dyne/cm ²)	Critical volumetric flow rate Q_c (cm ³ /min)	$\dot{\gamma}_c \times \eta_0$	$Q_c \times \eta_0$
Nylon-6	240	6.6×10^4	3.5×10^5	9.0×10^6	32.2	8.0×10^8	7.4×10^4
Nylon-6,6	280	7.2×10^4	3.84×10^5	8.6×10^6	35.3	2.7×10^8	2.5×10^4
Nylon-6,10	240	2.1×10^4	1.1×10^5	9.0×10^6	10.2	3.1×10^8	2.9×10^4
Nylon-11	210	5.8×10^3	3.1×10^4	7.0×10^6	2.9	1.7×10^8	1.5×10^4

Table 6 Critical shear stresses of different polymers

Sample	Temperature (°C)	Critical stress (dyne/cm ²)
Nylon-6	240	9.0×10^6
Nylon-6,6	280	8.6×10^6
Nylon-6,10	240	9.0×10^6
Nylon-11	210	7.0×10^6
Polyacetals (copolymers)	190	$7-8 \times 10^6$
Poly(methyl methacrylate) ([η] = 0.46)	170	5.0×10^6
Poly(ethylene terephthalate) ([η] = 0.67)	270	$1-1.6 \times 10^7$
HDPE ($M_l = 2.1$)	150-240	$1.5-2 \times 10^6$
LDPE	130-230	$0.8-1.3 \times 10^6$
Polypropylene ([η] = 1/3)	200-300	$0.8-1.4 \times 10^6$
Polystyrene	200-250	$1.2-1.4 \times 10^6$
Polytetrafluoroethylene	360	$1-2 \times 10^6$

CONCLUSIONS

Nylons exhibit quite negligible inlet and wall slipping effects in the capillaries and have essentially the same rheological behaviour. Their pseudo-plastic behaviour is very small. Activation energies of viscous flow are rather different depending on the type of polymer; however this does not seem to influence processing since a flattening of the curves is observed at the shear rates used. Melt elastic recovery of such polymers is quite low, much lower than that of the polyolefins, but the polyamides examined show an unstable flow onset at very high shear stresses.

The work indicates that the rheological behaviour of these materials make them very suitable for transformation techniques requiring high output rates and high precision geometries.

ACKNOWLEDGEMENTS

We wish to express our appreciation for the help given with the experimental work by Mrs B. Barboni and Mr L. Ceron.

REFERENCES

- Snider, O. E. and Richardson, R. J. 'Encyclopedia of Polymer Science and Technology', Interscience, New York, 1969, Vol 10, pp 347-460
- Bernhardt, E. C. 'Processing of thermoplastic materials', Reinold, New York, 1959
- Pezzin, G. and Gechele, G. B. *J. Appl. Polym. Sci.* 1964, 8, 2195
- Sweeny, W. and Zimmerman, J. 'Encyclopedia of Polymer Science and Technology', Interscience, New York, 1969, Vol 10, pp 483-597
- Parrini, P. and Corrieri, G. *Makromol. Chem.* 1963, 62, 83
- Rabinowitsch, B. *Z. Phys. Chem. (A)* 1929, 145, 1
- Parrini, P., Righi, G. P. and Romanini, D. *Atti del 2nd Convegno Società Italiana di Reologia, Siena* 1973, p 291
- Cappuccio, V., Coen, A., Bertinotti, F. and Conti, W. *Chim. Ind. (Milan)* 1962, 44, 463
- Tordella, J. P. *J. Appl. Phys.* 1956, 27, 454
- Tordella, J. P. *Trans. Soc. Rheol.* 1957, 1, 203
- Tordella, J. P. 'Rheology', Academic Press, New York, 1969, Vol 5, pp 57-92
- Vlachopoulos, J. and Alam, M. *Polym. Eng. Sci.* 1972, 12, 184

Ion-clustering and viscoelastic properties in poly(butadiene–styrene–4-vinylpyridine) crosslinked by nickel chloride

C. T. Meyer* and M. Pineri

Centre d'Études Nucléaires de Grenoble, Département de Recherche Fondamentale, Section de Physique du Solide, BP 85, 38041 Grenoble Cedex, France

(Received 20 October 1975; revised 12 January 1976)

A butadiene–styrene–4-vinylpyridine terpolymer was crosslinked by coordination of the pyridine side-groups with nickel chloride. Previous studies have shown that the complexes cluster together, although some complexes remain isolated, especially at low metal concentration. Thermoreversibility of the crosslinking is studied by stress relaxation and internal friction. Superposition of two relaxation mechanisms occurs; up to a temperature $T \approx 20^\circ\text{C}$ the shift factor follows the usual WLF equation. For higher temperatures $\log a_T$ obeys an Arrhenius equation with an activation energy of 28 kcal. This secondary relaxation mechanism is attributed to exchange reactions between complexes of the clusters. This behaviour is similar to that of other polymers with microphase separation. Influence of the concentration is studied by internal friction. At low concentration breakdown of the modulus takes place in two steps corresponding to the onset of intermolecular bonding lability, first in isolated complexes and then in clustered complexes. At higher concentration clustered complexes are sufficiently numerous to prevent the first flow.

INTRODUCTION

Ion-containing polymers have been intensively studied during the past decade¹. Particular attention was given to ionomers, statistical copolymers containing a small percentage of salt groups such as neutralized carboxylic acid². Microphase separation occurs by clustering of the ionic groups as a result of the electrostatic interactions between them. These clusters may be considered as crosslinks, which contrary to usual covalent crosslinks, are thermoreversible.

Polymers crosslinked by coordination complexes may be considered as very similar to ionomers. Crosslinking is achieved by complexing pyridine side-groups, statistically distributed along the polymer chain, by a transition metal chloride. The first experiments on these polymers have shown that they have the same properties as ionomers: microphase separation and thermoreversibility of the crosslinking.

Clustering of these complexes has been shown by electron microscopy³, small-angle X-ray (SAXS) or small angle neutron scattering (SANS)⁴, and Mössbauer effect⁵. The size distribution is very broad but most of the clusters are less than 100 Å in diameter. The clusters still exist at very high temperatures because no change in the SAXS curve is found up to 200°C.

Salt concentration has been shown to play an important role; at low concentration, (less than one metal for two pyridine) the complexes are predominantly isolated but at high concentration most of the complexes are in clusters. However, the two kinds of complexes are present whatever the concentration. The exact nature of the crosslinks is not clear. In particular complexes involving only one pyridine, i.e. only one polymer chain, may possibly exist⁴. They cannot be crosslinks in the true sense of the word. We must thus consider that crosslinking is due to the clustering of complexes. However, it does not exclude

that the isolated complexes, if involving more than one pyridine, can constitute true chemical crosslinks.

The mechanical properties of these polymers are characterized by the thermoreversibility of the crosslinking⁶, indicating some lability of the intermolecular bonding.

A study of their mechanical properties was undertaken here by stress relaxation and dynamic mechanical measurements, to explain the mechanism of the thermoreversibility and to determine what is the influence of microphase separation on the viscoelastic response. In these polymers there is the same problem as in ionomers, i.e. the validity of the time–temperature superposition principle. Inapplicability of time–temperature superposition in the treatment of viscoelastic data has been reported for many amorphous polymers, thus defined as thermorheologically complex. This behaviour can be attributed to the existence of a secondary relaxation mechanism operating simultaneously with the usual diffusional process⁷. This secondary relaxation mechanism may be for example, side chain motion as in poly(alkyl methacrylate)⁸, bond interchange as in polymeric sulphur⁹.

Ionomers have been reported as thermorheologically complex. Eisenberg *et al.*¹⁰ have shown that in styrene–sodium methacrylate copolymers the viscoelastic response is characterized by two relaxation mechanisms. A breakdown in time–temperature superposition has been observed. The shift factors corresponding to the short time superposition obeyed the WLF equation¹¹ with some increase in the C_1 and C_2 values due to the increased cohesion introduced by the electrostatic interactions. The shift factors corresponding to the secondary master curve, fit an Arrhenius type equation from which an activation energy of 25 kcal has been obtained. This secondary mechanism exists only for concentrations in ionic groups higher than 6 mol %, when clustering occurs. For lower concentration superposition is possible and the shift factors fit a WLF equation.

* Present address: Laboratoire d'Électrostatique, CNRS, 38042 Grenoble Cedex, France.

However, other thermorheologically complex systems, where microphase separation occurs, show good superposition, although two relaxation processes are operating. This behaviour is observed for example in triblock copolymers such as styrene–butadiene–styrene. The shift factors have been shown to obey a WLF equation for temperatures near the glass transition of the butadiene phase. For higher temperatures an Arrhenius dependence is found¹². This good time–temperature superposition has been shown to be only apparent¹³ and could be explained by the large separation in temperature or frequency of the two relaxation mechanisms.

In this paper we shall attempt to answer the following questions: (a) is time–temperature superposition possible that is to say how does the presence of complexes affect the usual diffusional process, in particular does it introduce a secondary relaxation mechanism? (b) what is the influence of concentration, do the isolated complexes play the same role as the clustered complexes do?

EXPERIMENTAL

Samples

The polymer used in this study is an amorphous terpolymer, butadiene–styrene–4-vinylpyridine. The percentage of monomer units are respectively 85, 10 and 5%.

This polymer has been synthesized by free radical polymerization in emulsion by ATO*. Addition of the vinyl pyridine monomer during the reaction was progressive to take into account the different reactivity factors of the monomers. Nitrogen concentration of the latex during polymerization remains constant. Thus due to polymerization conditions, this polymer may be considered as statistical.

The number-average molecular weight is of the order of 80 000, the polydispersity being 4. In order to prevent any degradation a small amount (1%) of antioxidant (*N*-phenyl-*N'*-cyclohexyl-*p*-phenylenediamine) is added. A careful purification has been performed so as to eliminate impurities coming from polymerization.

The transition metal salt used for coordination is NiCl₂·6H₂O. Coordination is achieved in solution: a concentrated methanolic solution of nickel chloride is added slowly to a 3% polymer solution in benzene under vigorous stirring. No precipitation takes place. The solvents are then taken off by vacuum pumping to constant weight. Samples are designated by *x*, the number of nickel ions per pyridine side-group.

Stress relaxation

The experiments were performed with type IFC relaxometers¹⁴.

Two different relaxometers were used, depending on the temperature range (–33°C to room temperature and 30°C to 140°C), the temperature being correct to ±0.2°C. The samples have a cross-section of 1 × 2 mm² and are 18 mm long. They have been taken from films obtained by compression at 150°C.

The deformation in length is 10% and achieved very quickly (some 1/10 sec) with an oleopneumatic jack.

In order to keep measurable stress values, the experiments have been limited to 1 h (3.5 decades of time in seconds) and a temperature of 90°C.

Internal friction

The experiments were performed by using a free oscillation torsion pendulum in a frequency range around 1 Hz¹⁵. The shear modulus is calculated by:

$$G(T) = \frac{K}{P^2}$$

where *P* is the period of the oscillations; *K* is a constant depending on the geometry¹⁷. The relative energy loss $\Delta W/W$ during one period was obtained from:

$$\Delta W/W = 1 - \exp \left(-\frac{2}{n} \log \frac{\theta_1}{\theta_{n+1}} \right)$$

where θ_1 is the amplitude for the first oscillation and θ_{n+1} that of the (*n* + 1) oscillation.

The samples (25 mm long × 3 mm wide) used were taken from films obtained by compression moulding at 150°C. A thickness of 2 mm has been chosen so that the period above *T_g* remains between 1 and 10 sec. So experiments of temperatures lower than *T_g* are impossible because of the very small value of the period.

STRESS RELAXATION

Results

Relaxation experiments have been realized with the sample *x* = 1.23. This high concentration was chosen in order to have the best conditions to see the influence of clusters: at this concentration complexes are mostly clustered.

Figure 1 represents the log $E(\rho_0 T_0 / \rho T)$ values plotted against log *t* for different temperatures. The values of the modulus have been corrected from the variations of density, ρ , when changing the temperature. The reference temperature *T₀* has been chosen as –31.4°C, which is the lowest temperature at which the experiments have been carried out.

We can see that some of the curves intersect. This fact may be due to the systematic error introduced when calculating the modulus from the stress as a result of ill-defined parameters. If we suppose an error of 2% in the section, 0.2% in the strain, then the systematic error in the modulus value is 6% i.e. 0.03 in log *E*. Because of this error in the log *E* values, a vertical shift is necessary to obtain a good fit when operating superposition of the curves. The best vertical shift factor is calculated with a computation program derived from that employed by King¹⁶ for the determination of the horizontal shift factor. The superposition of two curves is achieved for different values of the vertical shift factor log *f*. For each value the horizontal shift factor is calculated:

$$A = \frac{\sum \alpha_i}{N}$$

where α_i are the different distances between the two curves and *N* the number of values. The accuracy of the fit is

* ATO, Aquitaine Total Organico, Centre de Recherche d'Orsay, BP 25, 91400 Orsay, France.

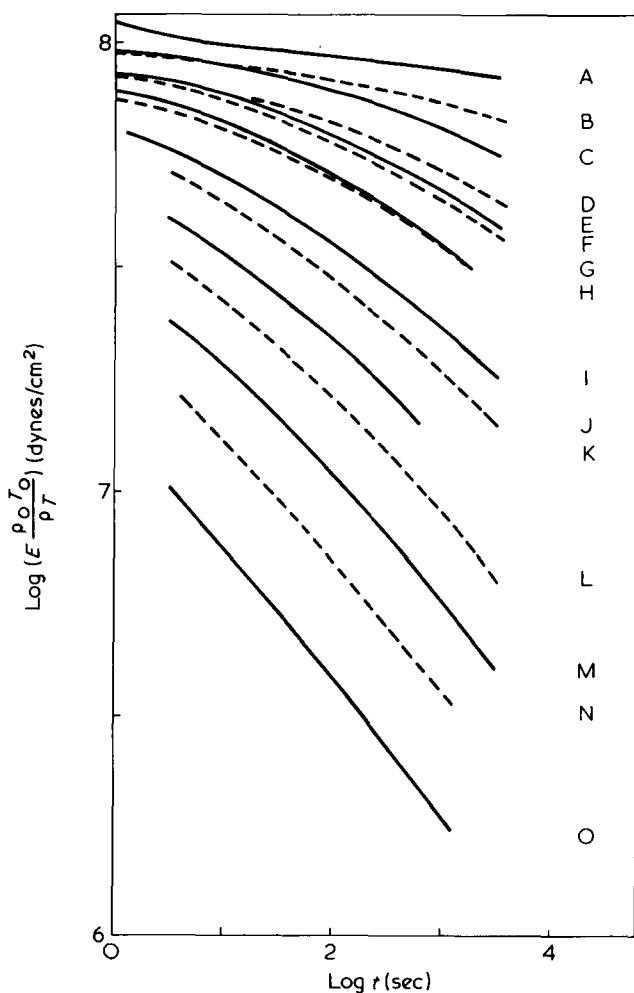


Figure 1 Stress relaxation curves (sample $x = 1.23$). Temperatures ($^{\circ}\text{C}$): A, -31.4; B, -20; C, -10; D, 0.2; E, 7.5; F, 8.6; G, 16; H, 19.4; I, 25.7; J, 30; K, 40; L, 50; M, 60; N, 75; O, 90

Table 1 Vertical shift factors $\log f$ and horizontal shift factors $\log a_T$, used for master curve construction

$T(^{\circ}\text{C})$	$\log f$	$\log a_T$	$\chi^2 \times 10^4$
-31.4		0	
-20	0.01	-1.385	6
-10	-0.025	-2.454	2
0.2	0.005	-3.055	3
7.5	-0.025	-3.631	6
8.6	-0.02	-3.737	3
16	0.01	-4.196	3
19.4	-0.02	-4.309	3
25.7	0.015	-5.103	1
30	0	-5.640	0
40	0	-6.314	2
50	0	-6.829	2
60	0	-7.528	2
75	0	-8.222	3
90	0	-9.118	1

characterized by:

$$\chi^2 = \frac{\sum(\alpha_i - A)^2}{N}$$

The best vertical shift factor corresponds to the lowest χ^2 values. Table 1 gives the horizontal and vertical shift factors and χ^2 values. The vertical shift factors vary at random

with temperature and are smaller than the possible error in $\log E$.

Figure 2 gives the master curve obtained by this procedure. Its shape shows clearly that the complexes do not give stable crosslinking; a breakdown of the modulus is observed, contrary to covalent crosslinking, with which a constant modulus is obtained.

Figure 3 represents the variation of the experimental shift factors $\log a_T$ with temperature. $T = 20^{\circ}\text{C}$ appears as a critical temperature. For temperatures lower than 20°C , $\log a_T$ fits a WLF equation:

$$\log a_T = \frac{-C_1(T - T_0)}{C_2 + T - T_0}$$

with constants $C_1 = 11.3$ and $C_2 = 82.3$. If $T_g = 217\text{ K}$, as determined by internal friction, is chosen as reference temperature, C_1 and C_2 are found to be 16 and 59.3, i.e. very similar to the usual constants⁷.

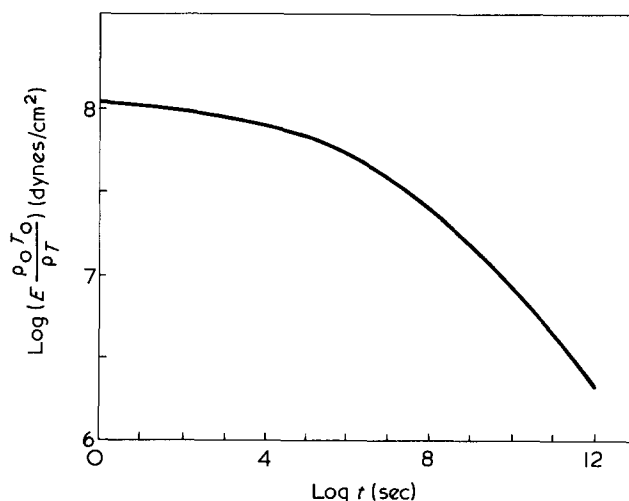


Figure 2 Master curve (sample $x = 1.23$), $T_0 = 31.4^{\circ}\text{C}$

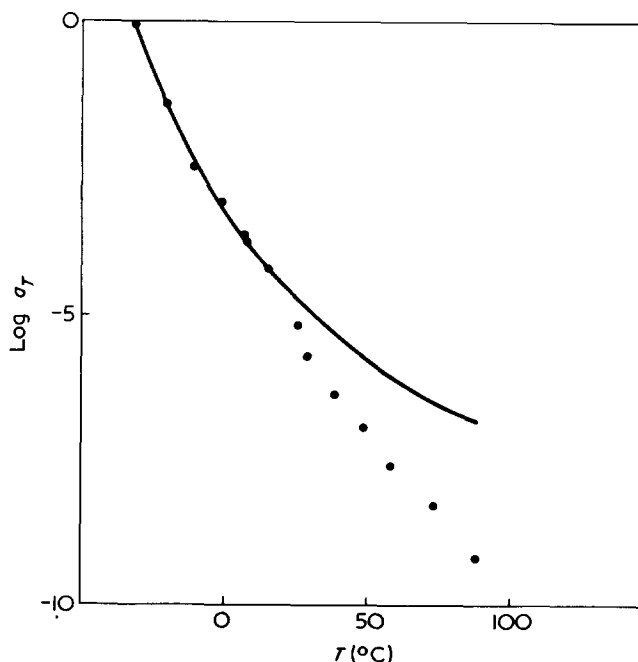


Figure 3 Shift factors $\log a_T$ versus temperature and WLF curve corresponding to the low temperature experimental points

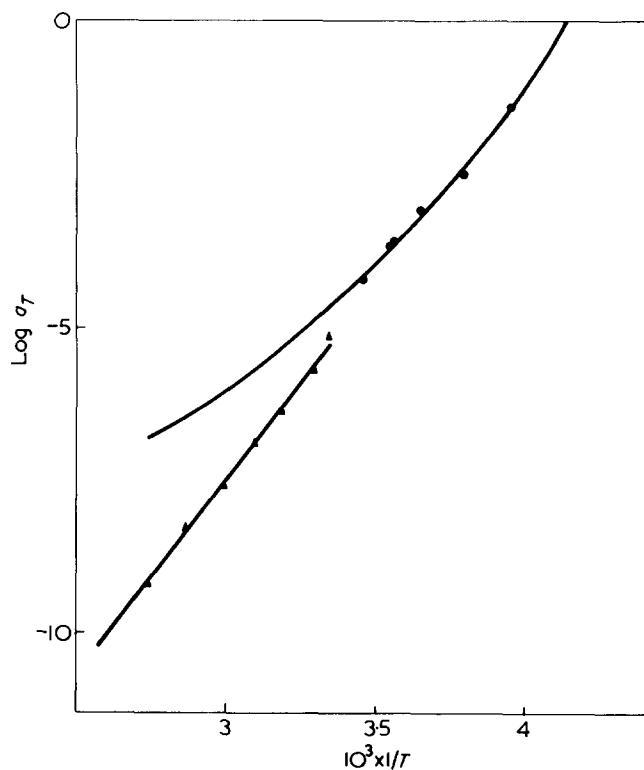


Figure 4 Shift factors $\log a_T$ versus $1/T$ with the corresponding WLF curve (●) for low temperatures and Arrhenius curve (▲, $\Delta H = 28$ kcal/mol) for high temperatures

For temperatures above 20°C the experimental shift factors deviate clearly from the WLF curve which best fits the experimental shift factors below 20°C . Therefore an additional relaxation mechanism takes place and must be related to the breakdown of the temporary crosslinks formed by the complexes.

Figure 4 gives the curve of $\log a_T$ versus $1/T$. Above 20°C this curve is a straight line, indicating a constant activation energy for the process. Thus this secondary relaxation mechanism obeys an Arrhenius equation:

$$a_T = a_0 \exp \left(-\frac{\Delta H}{RT} \right)$$

with an activation energy ΔH of 28 kcal.

The distribution of relaxation time is plotted in Figure 5. $H_1(\tau)$ is calculated with the first approximation of Alfrey:

$$H_1(\tau) = E(t) \left[\frac{d \log E(t)}{d \log t} \right]_{t=\tau}$$

A broad maximum related to the second mechanism of relaxation is observed.

Discussion

The first fact to note is that the relaxation operates by two processes. The first one is predominant at temperatures below 20°C . Because of the WLF dependence on the shift factor, this process must be related to the usual diffusional process above the glass transition. In the distribution of relaxation times, it corresponds to the initial decrease with a slope of the order of $-1/2^7$.

At higher temperatures the relaxation is completely dominated by the breaking of high energy crosslinks, this

process follows an Arrhenius law. Owing to the previously shown existence of clusters with high density of complexes, it is logical to relate this relaxation process to this phase. An exchange reaction, breaking and reforming of crosslinks must be supposed because the clusters are stable up to very high temperatures, as it has been shown in SAXS⁴.

The observed superposition agreement must be only apparent. The relaxation times having a WLF and an Arrhenius dependence must be affected to a different degree by a change in temperature. Failure of the time-temperature superposition would be observed if the measurements were realized during more than 3.5 decades. In our thermorheologically complex polymer, the relaxation behaviour is completely dominated by one phase (with a WLF dependence) or by the other (with an Arrhenius dependence).

INTERNAL FRICTION

Results

Figure 6 represents $\log G$ and $\Delta W/W$ plotted against temperature for samples with different nickel concentration. For increasing nickel concentration, we note for the modulus: an increase in the values of the modulus associated with the rubbery plateau, and an increase in the temperature amplitude of this rubbery plateau.

For the $\Delta W/W$ against temperature curves, we note a decrease in the minimum value of $\Delta W/W$ related to the rubbery plateau for the modulus and the disappearance in samples $x = 0.645$ and $x = 1.25$ of a peak located around 280 K in samples $x = 0.296$ and $x = 0.176$.

Modulus and damping curves in the transition zone give the same transition temperature for all samples i.e. 217 ± 3 K. This result is in agreement with that of differential enthalpic analysis³. The fact that glass transition does not shift after coordination has been attributed to microphase separation; the observed glass transition concerns a phase containing no or few crosslinks.

Discussion

The modulus and $\Delta W/W$ curves can be explained by the presence of temporary crosslinks. The same behaviour has been observed in non-crosslinked polymers when changing the molecular weight¹⁷. The increase of the number of entanglements gives an increase of the modulus associated to the rubbery plateau, wider temperature range of this plateau, a decrease in the damping minimum value.

In samples $x = 0.176$ and $x = 0.296$ simultaneous presence of two kinds of temporary crosslinks are clearly

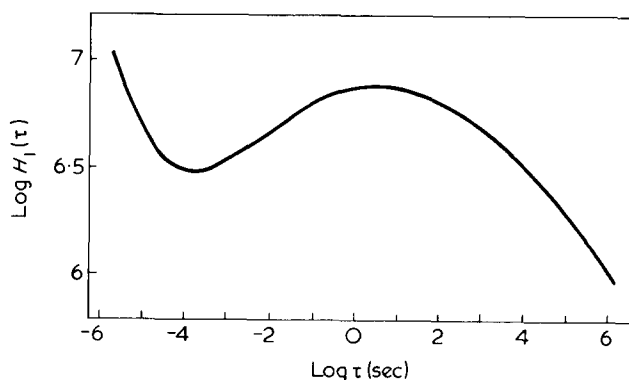


Figure 5 Relaxation time distribution, $T_0 = 30^\circ\text{C}$

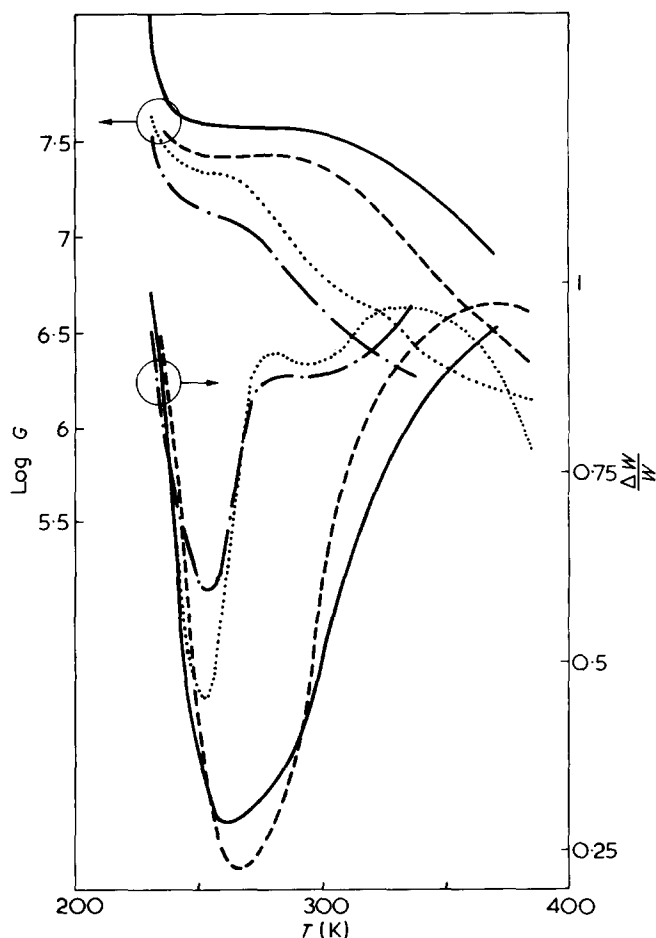


Figure 6 Modulus G and damping $\Delta W/W$ versus temperature curves for various nickel concentrations: $x = 0.176$ (- · - · - ·); $x = 0.296$ (·····); $x = 0.645$ (---); $x = 1.25$ (—)

shown. A first $\Delta W/W$ maximum associated with the beginning of the decrease of the modulus, is observed around 280 K and must be related to breakdown of temporary crosslinks. These crosslinks slow down the polymer chains diffusion much more than entanglements do; for the uncoordinated polymer the beginning of the flow is already observed at 245 K.

The existence of another maximum in $\Delta W/W$ against temperature curve after the beginning of viscous flow reveals the presence of other, higher energy, temporary crosslinks. The number of these crosslinks is not large enough to prevent the beginning of the flow at a lower temperature.

In samples $x = 0.645$ and $x = 1.25$ the high energy crosslinking density is large enough to avoid an initial flow. The plateau region covers a wider temperature range and the decrease of modulus is associated with breaking and

reforming of high energy crosslinks. A maximum in the damping curves is associated with the fall of the modulus.

Thus the first crosslinks to break must be the isolated complexes, predominant for low concentrations. The crosslinks which break at higher temperature are constituted by the clustered complexes predominant at high concentration.

CONCLUSION

These experiments of stress relaxation and internal friction give some answer to the questions. Relaxation of the polymer chains operate by two mechanisms: the usual diffusional process and a secondary mechanism obeying an Arrhenius equation with an activation energy of 28 kcal. This mechanism corresponds to exchange between complexes and is related to the second phase constituted by the clusters.

Isolated complexes enable relaxation before clustered complexes but their role is only seen at low concentrations.

REFERENCES

- 1 Eisenberg, A. and Hoover, M. F. 'Ion containing polymers', Am. Chem. Soc. Washington, D.C., 1972
- 2 Otocka, E. P. *J. Macromol. Sci. (C)* 1971, 5, 275
- 3 Pineri, M., Meyer, C. T. and Bourret A. *J. Polym. Sci. (A-2)* 1975, 13, 1881
- 4 Meyer, C. T. and Pineri, M. to be published
- 5 Meyer, C. T. and Pineri, M. *J. Polym. Sci. (A-2)* 1975, 13, 1057
- 6 Minoux, J. *Inf. Chim.* 1974, 130, 191
- 7 Ferry, J. D. 'Viscoelastic properties of polymers', Wiley, New York, 1970
- 8 Ferry, J. D., Child, W. C. Jr, Zand, R., Stern, D. M., Williams, M. L. and Landel, R. F. *J. Colloid Sci.* 1957, 12, 53; Child, W. C. Jr, and Ferry, J. D. *J. Colloid Sci.* 1957, 12, 327, 389
- 9 Eisenberg, A. and Teter, L. A. *J. Phys. Chem.* 1967, 71, 2332
- 10 Eisenberg, A. and Navratil, M. *J. Polym. Sci. (Polym. Lett. Edn)* 1972, 10, 537; Eisenberg, A. and Navratil, M. *Macromolecules* 1973, 6, 604; Eisenberg, A., King, M. and Navratil, M. *Macromolecules* 1973, 6, 734
- 11 Williams, M. L., Landel, R. F. and Ferry, J. D. *J. Am. Chem. Soc.* 1955, 77, 3701
- 12 Fielding-Russel, G. S., Fitzhugh, R. L. *J. Polym. Sci. (A-2)* 1972, 10, 1625; Lim, C. K., Coehn, R. E. and Tsehoeigl, N. M. *Adv. Chem. Ser.* 1971, 99
- 13 Fesko, D. G. and Tsehoeigl, N. W. *J. Polym. Sci. (C)* 1971, 35, 51
- 14 Chasset, R. *Colloques internationaux du CNRS no 231. Obernai*, 1973
- 15 Pineri, M., Bonjour, E., Gerard, P. and Martin D'hermont, F. *Plast. Mod.* 1972, p 156
- 16 King, M. *PhD Thesis* McGill University, Montreal (1972)
- 17 Nielsen, L. 'Mechanical properties of polymers', Reinhold, New York, 1961

Dissolution of polypropylene in organic solvents: 1. Partial dissolution

D. A. Blackadder and G. J. Le Poidevin*

Department of Chemical Engineering, University of Cambridge, Cambridge CB2 3RA, UK

(Received 8 January 1976)

The dissolution of polypropylene in organic solvents has been investigated in detail. The complete study will provide an interesting comparison with the literature concerning the dissolution of amorphous polymers. Under appropriate conditions polypropylene dissolves at a steady rate, but there is a preliminary induction period. The results reported here concern this period, and provide the foundation for later parts of the work. It was necessary to study solvent sorption by polymer as well as the partial or fractional dissolution characteristic of the induction period. The Hildebrand solubility parameter proved useful in understanding the behaviour of polypropylene soaked in various solvents over a range of temperatures. Factors controlling the partial dissolution have been identified and analysed.

INTRODUCTION

In a series of papers¹⁻⁷ Ueberreiter and his collaborators have provided a detailed description of the dissolution of polystyrene, a typical amorphous polymer, in organic solvents. Among the factors identified as having a bearing on the rate of dissolution were: the nature and molecular weight of the polymer; the viscosity and size of the solvent molecules; the compatibility of polymer and solvent; and the temperature and conditions of agitation in the system. Hitherto, relatively little has been reported concerning the dissolution of semi-crystalline polymers where one would expect the crystallinity to have some effect and, less obviously perhaps, where some material and some regions are more soluble than the remainder under given conditions. The dissolution of polypropylene has now been studied in detail.

The present paper, Part 1 of a series, describes the effect of soaking polypropylene film in organic solvents at various temperatures up to 110°C. It will be shown in a later paper that bulk specimens of this polymer can be made to dissolve at a constant rate at temperatures from 110°C upwards, once an induction period has been completed. This induction period arises because the penetration of polymer by solvent is a prerequisite for dissolution and it takes time to establish a situation in which characteristic events are occurring at different depths of penetration. Clearly there will be a gradation in composition and properties between dry bulk polymer to which no solvent has penetrated and the boundary layer of liquid adjacent to the swollen surface of the solid.

In order to understand the induction period it is necessary to investigate the general effects of solvents on the polymer under conditions where total dissolution does not occur. This involves measurement of the amount of polymer dissolved and the amount of solvent imbibed under various conditions, and the interpretation of the results in the light of thermodynamics and kinetics. It is already known that fractional dissolution of polyethylene can occur at temperatures well below the melting point⁸ and the material dissolved is of low molecular weight. When steric fac-

tors are of importance, as for polypropylene, the extracted material may consist mainly of low molecular weight isotactic chains and also of atactic chains, not necessarily of low molecular weight⁹⁻¹¹.

At temperatures well below their melting points, semi-crystalline polymers do not dissolve wholly in organic solvents. This is because the positive entropy changes associated with fusion and mixing do not sufficiently offset the large heat of fusion and the overall free energy change for crystallite dissolution is therefore positive. However, even at low temperatures, *most* solvents can penetrate the non-crystalline regions to some degree, resulting in the solvation of individual segments of polymer chains and overall swelling of the specimen. At the equilibrium swollen state, the osmotic pressure associated with the mixing of solvent and polymer is just balanced by the elastic retractive forces supplied by a network of interlamellar tie-molecules.

EXPERIMENTAL

Materials

Polymer. The polypropylene used was a homopolymer, GXM 43, kindly supplied by ICI Plastics Division. The amount of atactic material present was estimated to be about 2 wt %, and the polymer contained the usual small amounts of antioxidant and stabilizer. In view of the relatively high temperatures used in some of the present experiments these additives were welcome and no attempt was made to remove them. The polymer was quoted as having a melt flow index of 2.16 and a melt viscosity of 5.0×10^3 Nsec/m at 190°C.

Solvents. The *p*-xylene was a 99% product obtained from ICI. The other organic solvents, of SR or AR grade, were used as received.

Procedures

Preparation of film specimens. To investigate the effect of soaking polymer in solvent it is convenient to use film rather than thicker specimens. Polypropylene chips were compression moulded between platens at 220°C for 4 min.

* Now at the Electricity Council Research Centre, Capenhurst, Chester, UK.

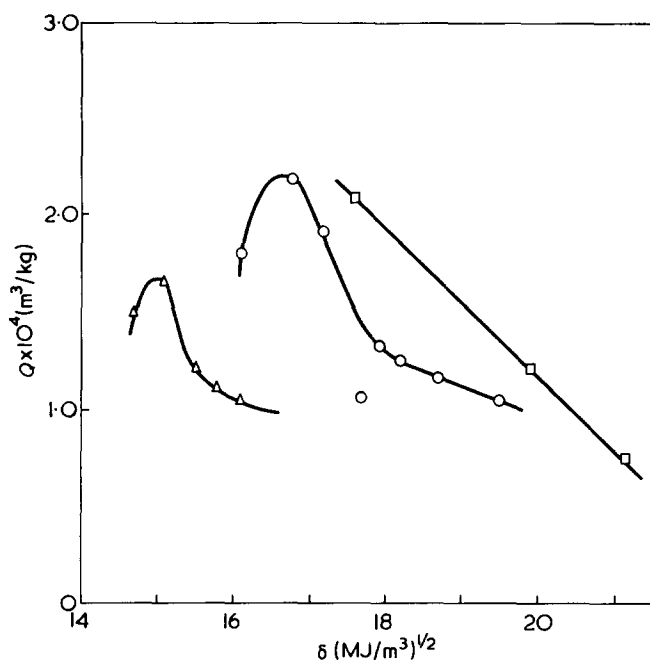


Figure 1 Relationship between solubility parameter and equilibrium solvent uptake by polypropylene at 25°C: □, chlorinated solvents; ○, aromatic and naphthenic solvents; △, n-alkanes

The resulting films were quench cooled by immersion in cold water. The thickness was about 0.3 mm, and rectangular pieces measuring 50 mm by 16 mm were cut as required. The average thickness of each strip was determined from ten micrometer measurements spaced along both of the long sides. The density of strips was adjusted when necessary by annealing for 2 h in a vacuum oven at an appropriate temperature.

Solvent sorption. Several dry strips of film were weighed to 0.05 mg and then transferred simultaneously to tubes of solvent held in a thermostat controlled to $\pm 0.05^\circ\text{C}$. After a suitable immersion time a strip was removed from the liquid, lightly pressed between tissues, and hung from one arm of a balance. A second stopwatch was started as the strip was removed from the liquid and the total mass of polymer and imbibed solvent was noted at 30 sec intervals over a period of 3 min. A graph of mass against time permitted extrapolation to the moment of removal, thus giving the true mass of solvent imbibed per unit mass of dry polymer after a known period of immersion¹². The time for attainment of equilibrium at 25°C varied from a few hours to several days but all equilibrium values were based on the uptake after 7 days, using the original mass of dry polymer as a basis, irrespective of the amount of polymer dissolved while solvent was imbibed. At higher temperatures it is quite possible that equilibrium was not always attained, but the results were instructive nevertheless. The error in measuring the uptake was estimated to be only $\sim 1\%$ at 25°C, rising to at least 5% at 100°C. It was often convenient to convert the measured uptake into units of volume sorbed per unit mass of polymer.

Soluble fraction. Strips of film, as described above, were vacuum dried at 80°C for 12 h before weighing. For initial densities between 908 and 918 kg/m³, this treatment was shown to cause no detectable change in density. Strips were soaked for 7 days in solvents at chosen temperatures, with a solvent: polymer ratio of 250:1 to avoid any possibility of saturating the solvent with soluble species. After removal from solvent, specimens were wiped dry and left in air for 24 h. A period of 12 h in a vacuum oven at 60°C

completed the drying process by removing residual solvent. The final mass of the specimen was used to calculate the percentage of the original material which had been dissolved out.

Density and crystallinity. Densities were measured in a density gradient column at 25°C using *p*-xylene and chlorobenzene as column liquids. Fragments of polymer film were cut so as to have a specific surface of less than 10 m²/kg, as recommended by Blackadder and Keniry¹³. In general they reached equilibrium in the column in less than 24 h. It can be shown that loss of soluble material to the column liquids requires a small correction to the observed density, which would otherwise be overestimated. With the correction, values are reliable to 0.2 kg/m³. When required, crystallinities were calculated from densities using Natta's formula¹⁴:

$$(1 - \lambda) = \frac{983 + 0.90(T - 93) - (10^6/d)}{0.48(T - 93)} \quad (1)$$

where $(1 - \lambda)$ is the weight fraction of crystalline material, commonly written as w_c , and d is the density (kg/m³) at T (K).

RESULTS AND DISCUSSION

Solubility of polypropylene in various solvents

In order to interpret polymer solubility in thermodynamic terms, it is natural to turn to well-tried parameters which have enjoyed some success in characterizing simpler systems. The strength of the non-valence or secondary bonding in a liquid system is related to the cohesive energy density, $\Delta E_v/V$, where ΔE_v is the molar energy of vaporization and V is the molar volume. It is better to predict and interpret solubilities in terms of the square root of the cohesive energy density, known as the Hildebrand solubility parameter¹⁵ given by:

$$\delta = \left(\frac{\Delta E_v}{V} \right)^{1/2} \quad (2)$$

Liquids with like values of δ tend to be equally good solvents for a given solute and to be mutually compatible. This leads to indirect methods of measuring δ for a polymer where $\Delta E_v/V$ cannot be evaluated. Michaels *et al.*¹⁶ have measured the equilibrium sorption of various solvent vapours by polypropylene at 25°C, and found that the equilibrium sorption (mass of solvent vapour sorbed by unit mass of dry polymer) reached a maximum for cyclohexane which had a solubility parameter of 16.8 (MJ/m³)^{1/2}. Since the thermodynamic dissolution temperature of the polymer, T_s , was a minimum in the same solvent, it was suggested that polypropylene had a solubility parameter of ~ 16.8 (MJ/m³)^{1/2}. Other authors¹⁷ have pointed out that the viscosity of solutions of a polymer in various solvents at a given temperature and concentration shows a maximum when the polymer and solvent have most nearly the same δ value. The maximum arises because the polymer chains are most uncoiled in solvents of high compatibility.

Figure 1 shows Q , the equilibrium volume of solvent imbibed per unit mass of dry polypropylene at 25°C, plotted against literature values^{15,18} of the solubility parameters of the various solvents, calculated from the heats of vaporization and the molar volumes. The density of the poly-

Table 1 Effect of solubility parameter, δ , on the equilibrium swelling, Q , of polypropylene at 25°C

Solvent	Solvent type	$Q \times 10^4$ (m ³ /kg)	δ (MJ/m ³) ^{1/2}
Benzene	Aromatic	1.16	18.7
Toluene	Aromatic	1.24	18.2
<i>p</i> -Xylene	Aromatic	1.30	17.9
Cumene	Aromatic	1.06	17.7
Cyclohexane	Hydroaromatic	2.20	16.8
Methylcyclohexane	Hydroaromatic	1.80	16.1
Tetrahydro-naphthalene	Naphthenic	1.04	19.5
Decahydro-naphthalene	Naphthenic	1.91	17.2
α -Chloro-naphthalene	Chlorinated naphthenic	0.74	21.1
Chlorobenzene	Chlorinated hydrocarbon	1.22	19.9
Carbon tetrachloride	Chlorinated hydrocarbon	2.08	17.6
<i>n</i> -Dodecane	<i>n</i> -Alkane	1.06	16.1
<i>n</i> -Decane	<i>n</i> -Alkane	1.10	15.8
<i>n</i> -Octane	<i>n</i> -Alkane	1.21	15.5
<i>n</i> -Heptane	<i>n</i> -Alkane	1.66	15.1
<i>n</i> -Hexane	<i>n</i> -Alkane	1.48	14.7

propylene used was 907.7 kg/m³ at 25°C. In good agreement with Michaels *et al.*¹⁶ the maximum uptake of solvent for the naphthenic and aromatic solvents occurs at a value of δ between 16.5 and 16.8 (MJ/m³)^{1/2}. There is a separate curve for *n*-alkanes, and signs of yet another for chlorinated hydrocarbons. The swelling data appear in Table 1. It is significant that for alkanes the maximum occurs at a lower δ value than for the naphthenics and aromatics; Hildebrand¹⁹ and other workers have noted anomalies in binary solutions where one component is a paraffin. In particular Hildebrand²⁰ evaluated δ values by means of regular solution theory and showed that they were consistently higher than values obtained from equation (2). He quoted isooctane and *n*-heptane as having δ values 2.0 and 1.2 (MJ/m³)^{1/2} higher, respectively, than those determined from ΔE_v and V , whereas the value for cyclohexane was much the same for both methods of evaluation. This reinforces the argument that δ for polypropylene is indeed very close to 16.8 (MJ/m³)^{1/2}, and there is a case for correcting alkane values by ~ 1.7 (MJ/m³)^{1/2}, an amount which would make the maximum of the alkane curve on Figure 1 coincide with that of the other curve.

It is noteworthy that cumene falls between the aromatic–naphthenic curve and the *n*-alkane curve. This may be because cumene has a fairly bulky aliphatic side chain, which confers some alkane character without being large enough to overshadow the effect of the benzene ring. If the abscissa of the point for cumene is indeed too small it would account for the observed displacement.

Repeating the above experiments at 50°C gave the results shown on Figure 2, which includes data discussed in the following section.

Soluble fraction

It was mentioned in the introduction that atactic and some low molecular weight isotactic material might be expected to dissolve at temperatures substantially lower than the dissolution temperature of the bulk polymer. An attempt was made to correlate the densities of 3 distinct polypropylene specimens with the weight losses recorded after soaking in 4 different solvents for 7 days at 25°C. No

correlation could be established, though shorter soak times might have shown up some dependence on crystallinity¹². At least the results suggest that the material soluble at 25°C is essentially non-crystalline. The lowest recorded weight loss was 0.11% in 1-chloronaphthalene and even this was probably more than mere antioxidant removal. Further experiments were devised to test the hypothesis that the 1.1% or so dissolved by *p*-xylene, the best solvent used, was polymeric and mostly atactic.

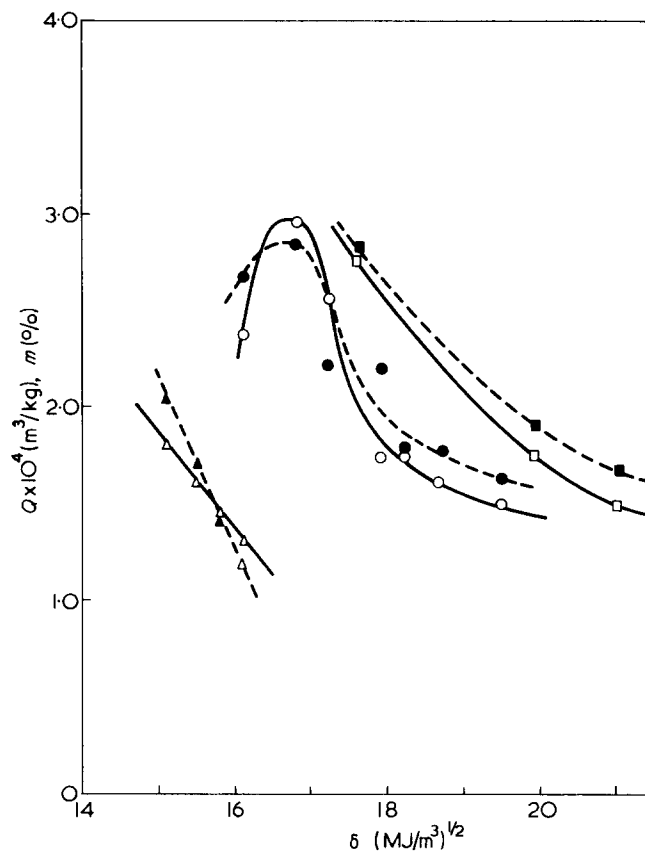


Figure 2 Relationship between solubility parameter, equilibrium solvent uptake and mass percentage loss of soluble material for polypropylene at 50°C: \square , \blacksquare chlorinated solvents; \circ , \bullet aromatic and naphthenic solvents; \triangle , \blacktriangle *n*-alkanes. Equilibrium solvent uptake (—); mass percentage loss (---)

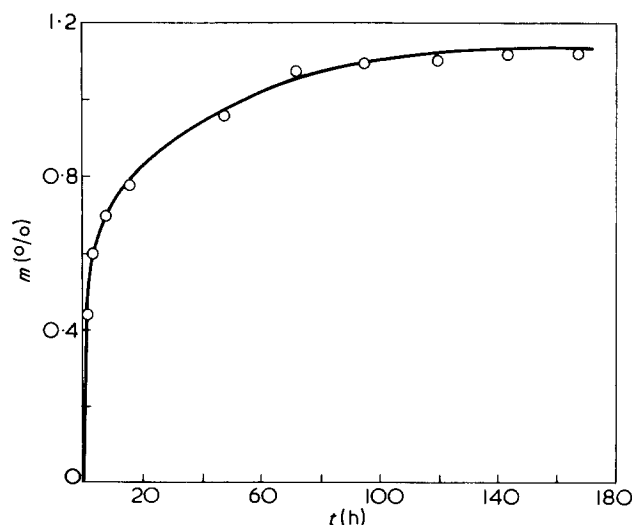


Figure 3 Loss of soluble material (wt%) plotted against time for polypropylene film density 908 kg/m³ immersed in *p*-xylene at 25°C

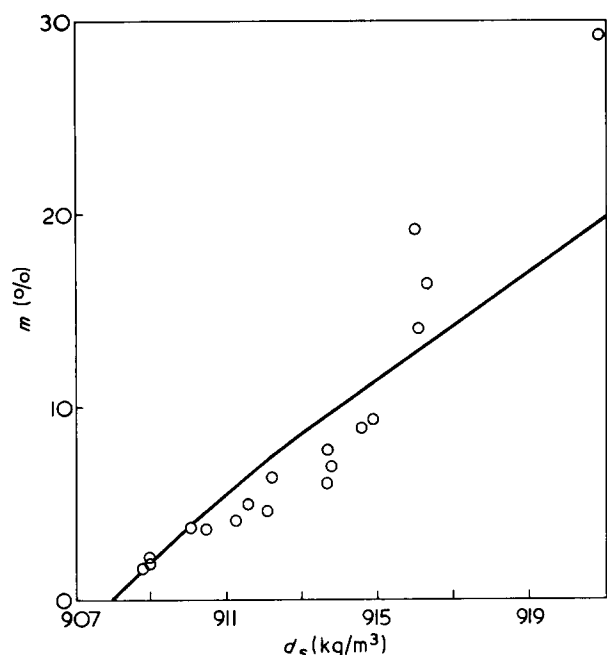


Figure 4 Loss of soluble material (wt%) plotted against density of polypropylene after treatment with various solvents (initial density 908 kg/m^3): \circ , measured values; —, calculated values assuming soluble material is leached only from non-crystalline regions of the bulk polymer

Figure 3 shows one consequence of soaking polypropylene film in *p*-xylene at 25°C . Several selected strips of uniform thickness ($0.300 \pm 0.010 \text{ mm}$) and density 907.7 kg/m^3 were weighed and separately immersed in *p*-xylene. Samples were removed after appropriate times and dried as described earlier, so that the soluble fraction might be calculated at various intervals over a period of 7 days. After a steep initial rise the curve flattened off to become effectively horizontal after about 90 h. It is possible to test directly whether the soluble material being removed had about the same density as amorphous polypropylene. Suppose that a specimen is soaked as above for 7 days, dried, and a fragment released into the density gradient column at the same time as an unsoaked fragment of identical shape and size. The pre-soaked specimen will settle fairly quickly to its final density since there is no more material to be dissolved, but the other will behave differently. According to Figure 3 about 0.68 wt% will go into solution in the first 7 h, assuming that the mixture of column liquids behaves like pure *p*-xylene. (This is a reasonable assumption on two counts: the column liquid adjacent to the specimen after 7 h is 83% *p*-xylene by volume, and separate experiments have shown that the weight loss after 7 days is the same in pure chlorobenzene as in pure *p*-xylene.) In the period between 7 h and 7 days after insertion of the test fragments into the column, the unsoaked piece will still be losing atactic or low crystallinity isotactic material and will continue to fall as its density increases.

The above argument was tested by cutting 4 samples, 2 mm square, from film previously soaked in *p*-xylene at 25°C for 7 days, then dried, and 4 similar samples were cut from unsoaked film. Figure 3 predicts that unsoaked specimens should lose about 0.44% in weight between 7 h and 7 days, and equation (1) permits the calculation of the corresponding increase in overall crystallinity. A crystallinity change of 0.30% corresponds to a displacement of 3.7 mm in the density gradient column, which compares well with the observed value of $3.9 \pm 0.5 \text{ mm}$. The implication is that

the dissolved material had an *in situ* density of between 848 and 860 kg/m^3 , limits which enclose Natta's value¹⁴ of 857 kg/m^3 for the density of wholly amorphous polypropylene at 25°C . Since the atactic content of the polymer is $\sim 2\%$, it seems that the 1.12% lost to *p*-xylene in 7 days is very probably wholly atactic.

Having demonstrated that at 25°C the overall density of a polypropylene specimen increased as soluble material was leached from the non-crystalline regions, it was appropriate to investigate higher temperatures and other solvents, always with a view to understanding the induction period preceding steady total dissolution at higher temperatures still. Figure 2 shows that at 50°C there is a rather close correspondence between solvent uptake and weight loss in the same period, and the solubility parameter correlates both properties effectively, bearing in mind the possible corrections to the δ values for some solvents. Figure 4 gives the measured weight loss for various temperatures and solvents plotted against the appropriate density after soaking for the usual 7 days. The intercept corresponds to unsoaked film and the solid curve is the relationship expected if: (a) all the material dissolved had the density of amorphous polypropylene; and (b) the soaking treatment left the remainder totally unaffected. The curve was obtained as follows. Equation (1) relates $(1 - \lambda)_u$ to d_u as well as $(1 - \lambda)_s$ to d_s , where the subscripts *u* and *s* denote unsoaked and soaked specimens. If the mass of crystalline material is indeed unaffected by any soaking treatment then it follows that:

$$\frac{(1 - \lambda)_u \times 100}{100 - m} = (1 - \lambda)_s \quad (3)$$

Evidently the percentage loss in weight, *m*, can be calculated from this expression if d_s and d_u can be measured. It is clear from Figure 4 that there are marked deviations from the theoretical curve, and these deviations prove to be very informative.

Comparison of columns 4 and 5 in Table 2 will show that for all solvents the significant deviations arise for soak temperatures in excess of 50°C . It appears that up to ~ 4 wt% of the soluble material has a density like that of amorphous polypropylene, as required by the theoretical curve. Some of the 4% is evidently isotactic yet non-crystalline. For weight losses between 4 and 12% the points lie to the right of the curve, which is evidence for a structural reorganization process during the soaking, the result being a density increase over and above that caused by dissolution of low density material. At very high temperatures and when the weight loss exceeds 12%, the points start to fall above the curve and another new feature requires explanation.

To interpret Figure 4 it is necessary to recall certain morphological features of semi-crystalline polymers. During the crystallization of polyethylene from the melt there is some segregation of low molecular weight material^{21,22} and this tends to persist in part in uncrystallized form located within and between the spherulites. Hofmann and Lauritzen²³ have shown that the disappearance of crystallinity at temperatures well below the melting point²⁴⁻²⁶ may be attributed to the early melting of the smallest crystallites. Baddour *et al.*²⁷ have pointed out that such effects are accentuated by the presence of solvent acting as a diluent to reduce the melting points of crystallites of any size below their 'dry' value. If the smaller crystallites also tend to contain more of the lower molecular weight

Table 2 Effect of soak temperature on the density of polypropylene

Solvent	Soak temperature (°C)	Measured % weight loss	Measured d_s (kg/m ³)	d_s calculated from equation (3) (kg/m ³)	Δd_s (kg/m ³)
<i>p</i> -Xylene	50	2.20	909.0	909.3	-0.3
Cumene	50	1.62	908.8	908.9	-0.1
Chlorobenzene	50	1.92	909.0	909.1	-0.1
Decahydro-naphthalene	50	2.22	909.0	909.3	-0.3
<i>p</i> -Xylene	75	4.12	911.3	910.4	0.9
Cumene	75	3.80	910.1	910.2	-0.1
Decahydro-naphthalene	75	4.83	911.6	910.8	0.8
Cumene	95	4.59	912.1	910.6	1.5
Decahydro-naphthalene	95	7.68	913.7	912.5	1.2
<i>n</i> -Octane	95	6.27	912.2	911.5	0.7
<i>p</i> -Xylene	100	8.88	914.6	913.2	1.4
Cumene	100	6.87	913.8	912.0	1.8
Decahydro-naphthalene	100	29.4	920.8	931.8	-11.0
<i>n</i> -Octane	100	6.00	913.7	911.5	2.2
1-Chloro-naphthalene	100	3.68	910.5	910.0	0.5
Cumene	107	19.22	916.0	920.8	-4.8
<i>n</i> -Octane	107	9.29	914.9	913.6	1.3
Cumene	110	16.34	916.3	918.5	-2.2
<i>n</i> -Octane	110	14.06	916.1	916.9	-0.8

material, then the deviations from the curve in Figure 4 may be interpreted in terms of three parallel processes: (a) removal of amorphous material having the same density as amorphous polypropylene; (b) melting out and dissolution of small crystallites or crystallites containing notable amounts of low molecular weight polymer; (c) inclusion of material described in (a) and (b) into existing crystallites with a consequent increase in overall density, or possibly the creation of new crystallites large enough to resist solvent.

Process (a), on which the theoretical curve in Figure 4 is exclusively based, evidently covers the lower temperatures of soaking and weight losses up to ~4%. Suppose that at temperatures of 75°C upwards, the consequences of soaking were covered by processes (a) and (b) only. Although m would continue to rise with d_s , the points would lie above the curve, because the dissolved material would include some polymer from the crystalline regions. The density of the soaked polymer would therefore be lower than if all the soluble material had come from non-crystalline regions. (Indeed if a high enough proportion were leached from the crystalline regions it would even be possible for d_s to fall with increasing m , though this was not observed.) Figure 4 shows that the points concerned actually lie below the curve, and this positively requires the operation of process (c) in addition to (a) and (b) for values of m from 4 to 12%. The process is presumably similar to that induced in pure bulk crystallized polymer on dry annealing at elevated temperatures, but with solvent present, the reorganization occurs at much lower temperatures. At temperatures in excess of 100°C it can be seen that the experimental points lie well above the curve on Figure 4, and this may be interpreted in terms of the increasing dominance of process (b). It does not mean that

process (c) becomes less important in absolute terms, as the following observations confirm.

Consider a polypropylene specimen which had been soaked at 100°C in decahydronaphthalene (well above the curve in Figure 4) and another soaked in *p*-xylene at the same temperature (below the curve). After removing all the imbibed solvents these dried specimens were re-immersed in separate tubes containing fresh *p*-xylene at 25°C. The results are shown in Table 3. The sample pre-treated in *p*-xylene is seen to have absorbed more than twice as much of this same solvent at 25°C as the sample pre-treated in decahydronaphthalene. Even on the basis of C^* (volume of liquid sorbed per unit volume amorphous polymer) the uptake at 25°C is much higher for the sample pre-treated in *p*-xylene. This is the opposite of what is generally found for specimens not subjected to pre-treatment, as it will be shown later that C^* normally increases with the density of dry but annealed specimens. The decrease in C^* with increased density cannot be explained in terms of void formation caused by the loss of soluble polymer, since the percentage loss is considerably higher for decahydronaphthalene pre-treatment, yet the amount of *p*-xylene finally imbibed at 25°C is lower.

A possible explanation is that the interlamellar tie-lengths in the two specimens are different after pre-treatment, and these lengths determine the extent to which re-swelling can occur. The specimen pre-treated in decahydronaphthalene would have to have the shorter tie-molecules and this could arise if some of the inter-lamellar chains originally present were incorporated into the crystalline lattice structure as a result of soaking in this good solvent. Re-swelling at 25°C would then give a low result.

Blackadder and Keniry⁸ have shown that if polyethylene film is soaked in liquid *p*-xylene at 50°C then dried, it absorbs a greater amount of *p*-xylene vapour at 30°C than

Table 3 Effect of solvent pretreatment at high temperatures on subsequent reswelling at 25°C in *p*-xylene

Temperature (°C)	Solvent pre-treatment			Reswelling in <i>p</i> -xylene at 25°C		
	Solvent	Equilibrium swelling $\times 10^4$ (m ³ /kg)	Percentage weight loss	d_s † (kg/m ³)	Equilibrium swelling $\times 10^4$ (m ³ /kg)	C^*
100	<i>p</i> -Xylene	7.0	8.88	914.6	5.53	1.92
100	Decahydro-naphthalene	12.7	29.4	920.8	2.46	1.05

† d_s for both specimens was 908.0 kg/m³

Table 4 Effect of liquid pre-treatment on percentage weight loss of soluble material

Solvent	Pre-treatment		Percentage weight loss		
	Temperature (°C)	Time (Days)	True % weight loss	Calculated from d_s	Calculated from swelling
<i>p</i> -Xylene	75	7	4.12	5.70	5.0
<i>p</i> -Xylene	100	7	8.88	10.8	24.6
Decahydro-naphthalene	100	7	29.4	19.5	8.15

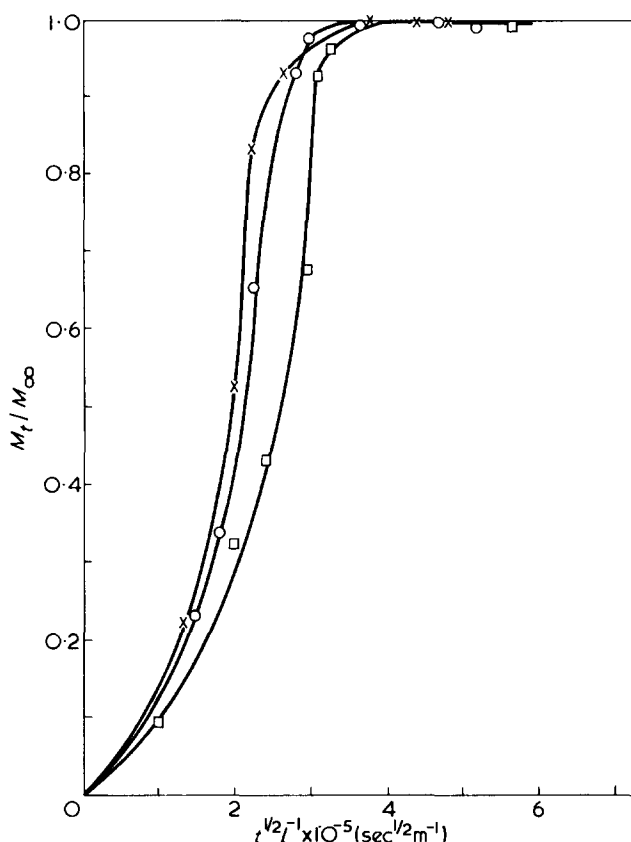


Figure 5 Reduced sorption curves for polypropylene and liquid *p*-xylene at 25°C. Initial densities: □, 907.7; ○, 914.1; ×, 917.9 kg/m³

does untreated film, whatever the vapour activity. Indeed by extrapolating the relevant isotherms to unit activity it emerged that the increased volumetric uptake exactly compensated for the volumetric loss of soluble material in the pre-treatment. Experiments along similar lines would appear to offer another method of establishing when the dissolution of soluble material from polypropylene is accompanied by reorganization of the crystalline and non-crystalline regions.

For this work liquid uptakes were measured rather than vapour isotherms. Specimens of polypropylene film of density 908.0 kg/m³ were immersed in *p*-xylene (at 75° or 100°C) or decahydronaphthalene (at 100°C). After 7 days the specimens were removed from their respective liquids, dried, reweighed and the losses determined. They were then re-immersed in separate 50 cm³ quantities of *p*-xylene at 25°C. Unsoaked control specimens were also treated in this way. After 24 h the equilibrium uptakes were determined and, without exception, samples which had been pre-treated at temperatures above 25°C imbibed more solvent than did untreated specimens. The increased liquid uptake was used to estimate the equivalent weight lost during the pre-treatment on the assumption that the soluble material had a density of about 860 kg/m³ at 25°C. The results appear in Table 4, together with the true weight losses and values calculated from d_s .

For the samples pre-treated in *p*-xylene at 75°C it is noteworthy that the weight losses arrived at by all three methods are much more comparable than for the other pre-treatment procedures. This suggests that for this 75°C treatment the material removed is largely from non-crystalline regions and any induced reorganization is small. The wide spread in the loss values for treatment at 100°C in

p-xylene, can be explained as follows. The fact that the true weight loss is less than the value calculated from d_s points to some incorporation of previously non-crystalline material into crystallites, while the much larger loss calculated from the swelling data points to a considerable lengthening of the average interlamellar tie length above the untreated value. Blackadder and Keniry⁸ showed that sorption of vapour at quite low activity and temperature by polyethylene film resulted in a permanent increase in the average length of interlamellar ties. This can arise because bulk crystallized polymer has a wide distribution of tie-lengths. On the way to sorption equilibrium some of the shorter ties might be pulled out or even fractured, and this process can hardly be reversed on removing the solvent, thus resulting in a permanent increase in the average length of the interlamellar ties. The sorption of liquid *p*-xylene by polypropylene at 100°C has a more drastic effect, as seen by the very large difference between the measured weight loss and that calculated from swelling data.

The situation when polypropylene is pre-treated in decahydronaphthalene at 100°C is quite different. The much lower percentage loss calculated from swelling measurements is presumably the result of some recrystallization, yet at 100°C untreated polymer absorbs almost twice as much decahydronaphthalene as *p*-xylene. This fits perfectly with the expectation that the former solvent would penetrate the polymer to a greater extent than the latter and recrystallization would be easier under the conditions of the pre-treatment.

Sorption kinetics

Studies of sorption kinetics are likely to be relevant to polymer dissolution. Unlike microcrystalline substances, amorphous polymers swell prior to dissolution²⁸, and it will be shown in Part 2 that polypropylene also swells. One of the factors determining the rate of dissolution might thus be the rate of movement of the diffusing solvent front as it penetrates the non-crystalline material before affecting the crystallites.

For a plane sheet of polymer, thickness l , immersed in a liquid, it is a standard result that:

$$D = \frac{0.0419}{(t_{1/2}/l^2)} \quad (4)$$

where D is a diffusion coefficient and $t_{1/2}$ is the time required for the amount of liquid imbibed to reach half of its equilibrium value. The intrinsic error in this approximate formula is negligible, but a more serious objection is that it assumes a constant diffusion coefficient. In fact D will depend on concentration (among other things) and the use of equation (3) will generate some sort of average value for the range of concentrations present in the film during the measurements.

Reduced plots for the sorption of liquid *p*-xylene into polypropylene films of different densities are presented in Figure 5, which refers to 25°C. M_t/M_∞ is expressed as a function of t/l^2 , M_t being the uptake at time t , and M_∞ is the final equilibrium uptake. The curves have sigmoid shapes as observed by Rogers *et al.*²⁹ for the sorption of organic vapour into polyethylene at high vapour activities. Figure 5 shows that liquid is imbibed more rapidly for the higher densities, and Table 5 indicates that there is a reduced equilibrium uptake at the higher densities. Note that appropriate film densities were obtained by annealing, and

Table 5 Effect of density on diffusion coefficient and equilibrium uptake of *p*-xylene at 25°C

Anneal temperature (°C)	Density (kg/m ³)	$D \times 10^{12}$ (m ² /sec)	Equilibrium uptake (w/w%)
120	907.7	0.75	10.70
150	914.1	1.08	9.57
163	918.1	1.28	9.05

the temperatures concerned appear in Table 5. It has been shown by McCrum³⁰, Michaels *et al.*³¹ and by Keniry³² that for bulk polymer, D increases with annealing temperature for experiments with low activity solvent vapours and polyethylene. In the present work on polypropylene and where the solvent activity is unity (pure liquid), it is again evident that the value of D increases with the annealing temperature.

Michaels *et al.*^{31,33} have expressed the diffusion coefficient of a penetrant in a semi-crystalline polymer in the form:

$$D = D^*/\tau\beta$$

where D^* refers to the same penetrant in wholly amorphous polymer, τ is a tortuosity factor to allow for the increased path length when diffusion occurs round crystallites, and β is a chain immobilization factor to account for the restraining effect of crystallites on segmental mobility. It is known that annealing leads to an increase in fold length which, in turn, causes a decrease in the width to thickness ratio of crystalline lamellae and hence a decrease in tortuosity (for a given volume fraction of obstructive material tortuosity is increased least by spheres and most by rods). This would appear to explain the increase in D with annealing temperatures noted here.

Figure 6 shows the sorption data plotted on the basis of C^* , the volume of liquid sorbed per unit volume of non-crystalline polymer (assuming the two phase model), rather than M_t/M_∞ , and it can be seen that C^* increases with density. The explanation of this interesting observation lies in a comparison of the morphology of semi-crystalline polymer with that of crosslinked amorphous polymer. The latter swells much less than the unlinked form of the same polymer because the links restrain the uncoiling of chains which accompanies sorption. In polypropylene the non-crystalline regions might thereby be expected to have a lower sorptive capacity than wholly amorphous polypropylene, volume for volume. Ochiai *et al.*³⁴ measured the equilibrium uptake of two liquids by polypropylene film and found that C^* increased with density as in the present work. Their explanation virtually constituted a denial of the simple two-phase model, and the suggestion made by Keniry in the context of polyethylene³² appears more convincing. It hinges on the observation that mats of agglomerated single crystals swell more than bulk crystallized polymer, the obvious inference being that tie-molecules inhibit the swelling of the latter and are absent in single crystal agglomerates. Furthermore, the sorptive capacity of unit volume of non-crystalline material was highest for single crystals, and bulk polymer tended towards this only as the density was increased by annealing. An increase in the fraction of non-crystalline material in the form of chain folds rather than miscellaneous tangle would appear to favour high absorption.

CONCLUSIONS

(1) The Hildebrand solubility parameter for polypropylene is $16.7 \text{ (MJ/m}^3)^{1/2}$. This quantity is obtainable by plotting the swelling caused by various solvents against calculated values of the parameter for these solvents and noting the position of the maximum. A correction must be applied to values for *n*-alkanes obtained from the cohesive energy density. When suitably corrected the solubility parameters correlate well with the amount of polypropylene dissolved by each solvent at 50°C and with the amount of solvent imbibed by the polymer.

(2) At 25°C the density of polypropylene films cannot be correlated with the amount of polymer dissolved by soaking at that temperature. This suggests that the material soluble at 25°C is not removed from the crystalline regions, a view for which other evidence is available. It is noteworthy that polypropylene samples immersed in a density gradient column suffer from loss of soluble material, and this source of error should be allowed for when necessary.

(3) Soaking of polypropylene film in solvents at temperatures from 25° to 75°C involves dissolution of soluble material from the non-crystalline regions only, at least for a polymer density of 908 kg/m³. Up to 4 wt% of the samples is thought to be a mixture of atactic material and isotactic material, all excluded from crystallites. At temperatures from 75° to 100°C solvent soaking brings about considerable reorganization of the general morphology, previously non-crystalline chains or parts thereof being incorporated into new or existing crystallites. In the high temperature range of 100° to 110°C (just bordering on that

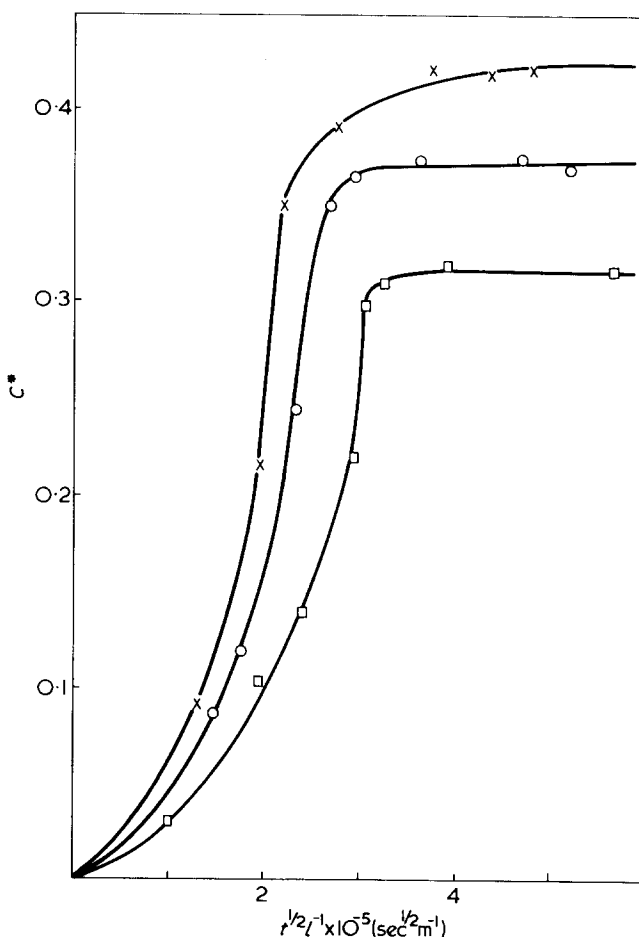


Figure 6 Sorption curves for polypropylene and liquid *p*-xylene at 25°C. Initial densities: □, 907.7; ○, 914.1; X, 917.9 kg/m³

required for total dissolution) the reorganization is overshadowed by the destruction and dissolution of the smaller crystallites. It appears that there are irreversible changes in the average lengths of the interlamellar ties.

(4) Sorption kinetics show that at 25°C liquid *p*-xylene swells polypropylene most rapidly at high sample density, and in addition more liquid is then imbibed per unit volume of non-crystalline material. This is explained in terms of morphology.

(5) The results of this paper form the foundation for the investigation of the conditions under which total, and not merely fractional, dissolution of polypropylene occurs. In particular the present results relate to the induction period preceding steady state dissolution.

ACKNOWLEDGEMENTS

One of the authors (G. J. Le P.) is indebted to the Science Research Council for a Studentship.

REFERENCES

- 1 Ueberreiter, K. and Asmussen, F. *J. Polym. Sci.* 1957, **23**, 75
- 2 Ueberreiter, K. and Asmussen, F. *Makromol. Chem.* 1961, **43**, 324
- 3 Ueberreiter, K. and Asmussen, F. *J. Polym. Sci.* 1962, **57**, 187
- 4 Asmussen, F. and Ueberreiter, K. *J. Polym. Sci.* 1962, **57**, 199
- 5 Asmussen, F. and Ueberreiter, K. *Makromol. Chem.* 1962, **52**, 164
- 6 Asmussen, F. and Ueberreiter, K. *Kolloid-Z.* 1962, **185**, 1
- 7 Asmussen, F. and Ueberreiter, K. *Kolloid-Z.* 1968, **223**, 6
- 8 Blackadder, D. A. and Keniry, J. S. *J. Appl. Polym. Sci.* 1972, **16**, 1261
- 9 Natta, G., Mazzanti, G., Crespi, G. and Moraglio, G. *Chim. Ind. Milan* 1957, **39**, 275
- 10 Natta, G. *J. Polym. Sci.* 1959, **34**, 531
- 11 Natta, G., Pasquon, I., Zambelli, A. and Gatti, G. *Makromol. Chem.* 1964, **70**, 191
- 12 Blackadder, D. A. and Vincent, P. I. *Polymer* 1974, **15**, 2
- 13 Blackadder, D. A. and Keniry, J. S. *Makromol. Chem.* 1971, **141**, 211
- 14 Danusso, F., Moraglio, G. and Natta, G. *Ind. Plast. Mod.* 1958, **10**, 40
- 15 Hildebrand, J. H. and Scott, R. L. 'Solubility of Non-electrolytes', Reinhold, New York, 1950
- 16 Michaels, A. S., Vieth, W. R. and Alcalay, H. H. *J. Appl. Polym. Sci.* 1968, **12**, 1621
- 17 Cowie, J. M. G., Ranson, R. J. and Burchard, W. *Br. Polym. J.* 1969, **1**, 187
- 18 Brandrup, J. and Immergut, E. I. 'Polymer Handbook', Interscience, New York, 1966
- 19 Hildebrand, J. H., Prausnitz, J. M. and Scott, R. L. 'Regular and Related Solutions', Reinhold, New York, 1970
- 20 Hildebrand, J. H. *J. Chem. Phys.* 1950, **18**, 1337
- 21 Keith, H. D. and Padden, F. J. *J. Polym. Sci.* 1961, **51**, S4
- 22 Lindenmeyer, P. H. *Science* 1965, **147**, 1256
- 23 Hofmann, J. D. and Lauritzen, J. I. *J. Res. Nat. Bur. Stand. (A)* 1961, **65**, 297
- 24 Turner-Jones, A., Aizlewood, J. M. and Beckett, D. R. *Makromol. Chem.* 1964, **75**, 134
- 25 Farrow, G. *Polymer* 1963, **4**, 191
- 26 Wilkinson, R. W. and Dole, M. *J. Polym. Sci.* 1962, **58**, 1089
- 27 Baddour, R. F., Michaels, A. S., Bixler, H. J., de Filippi, R. P. and Barrie, J. A. *J. Appl. Polym. Sci.* 1964, **8**, 897
- 28 Ueberreiter, K. in 'Diffusion in Polymers' (Eds J. Crank, and G. S. Park), Academic Press, London, 1968
- 29 Rogers, C. E., Stannett, V. and Szwarc, M. *J. Polym. Sci.* 1960, **45**, 61
- 30 McCrum, N. G. *Polymer* 1964, **5**, 319
- 31 Michaels, A. S., Bixler, H. J. and Fein, H. L. *J. Appl. Phys.* 1964, **35**, 3165
- 32 Keniry, J. S. *PhD Thesis* University of Cambridge (1971)
- 33 Michaels, A. S. and Bixler, H. J. *J. Polym. Sci.* 1961, **50**, 413
- 34 Ochiai, H., Gekko, K. and Yamamura, H. *J. Polym. Sci. (A-2)* 1971, **9**, 1629

Configurational and dynamic flexibility of polymer chains

M. G. Brereton and A. Rusli*

Department of Physics, University of Leeds, Leeds LS2 9JT, UK
(Received 27 October 1975; revised 22 January 1976)

The frequency of collisions between the end-groups of a polymer molecule is a useful measure of the dynamic flexibility of the molecule. An exact expression for this quantity is given in terms of the various distribution functions which characterize the polymer and the result compared with the experiments of Szwarc *et al.* on polymethylene chains in solution. The implication of some of the results for normal mode models of polymers is also discussed.

INTRODUCTION

There are two measures of molecular flexibility that are useful in the study of polymers. The first may be termed 'configurational flexibility' and arises from the multitude of conformations available to a polymer molecule. The second is 'dynamic flexibility' and comes about because, in thermal equilibrium in say a solvent, the molecule is not static but will be undergoing continual conformational changes. The rate at which these changes are occurring is clearly a reflection of the dynamic flexibility. As a measure of the configurational flexibility of a polymer we may take the probability of contact being made between the ends of the molecule (i.e. a ring closure). This, however, gives no indication of the rate at which end-to-end contacts are being made. We will use this latter quantity as a measure of the dynamic flexibility of the molecule.

In an attempt to quantify the concept of dynamic flexibility, Szwarc and Shimada^{1,2} have made a series of experiments designed to measure the frequency of collisions between the end groups of a polymethylene chain in solution. Furthermore, they were able to investigate the dependence of the collision frequency on the chain length, solvent viscosity and temperature. In this paper we will formulate the problem and give an exact expression for the frequency of the expected number of end-to-end collisions in terms of the various distribution functions which characterize the polymer molecule. The results of Szwarc and Shimada will then be discussed in the light of our results.

EXPECTED FREQUENCY OF END GROUP COLLISIONS

In Figure 1, the configuration of a polymer chain at some instant of time, t , is shown, together with a schematic sketch of the time dependence of the square of the end-to-end vector, $R(t)$. The forces governing the behaviour of $R(t)$ will be sufficiently complex to ensure that $R^2(t)$ may be regarded as a stochastic process. The problem of calculating the frequency of end-group collisions may then be formulated as finding the frequency of zeros in the stochastic process described by $R(t)$. In fact in the experiment of Szwarc *et al.* the collision of the end groups was detected using e.s.r. techniques by the transference of an electron between the end groups. In this experiment the end groups

needed only to be within a certain minimum distance, d , for the electron to be transferred. We are therefore interested in the frequency with which the stochastic process $R^2(t)$ crosses the level d^2 . This problem arises in many diverse fields of study, e.g. in electronics, fatigue studies, speech analysis etc. and is generally known as the level crossing problem. A solution was first given by Rice³, but the derivation we will use follows that given by Bendat⁴.

If we put $A(t) = R^2(t)$, then the expected number of level crossings of $A(t)$ through the interval $R^2, R^2 + dR^2$ for a given value of $dA/dt = \beta$ is:

$$\frac{f(R^2, \beta)dR^2d\beta}{|dt|} \quad (1)$$

where $f(R^2, \beta)dR^2d\beta$ is the probability that $R^2 < A(t) < R^2 + dR^2$ and $\beta < \dot{A} < \beta + d\beta$, and $|dt|$ is the time to cross dR^2 , i.e. $|\beta| = dR^2/|dt|$. The total number of crossings/unit time ν is then given by:

$$\nu = \int_{-\infty}^{\infty} |\beta| f(R^2, \beta)d\beta \quad (2)$$

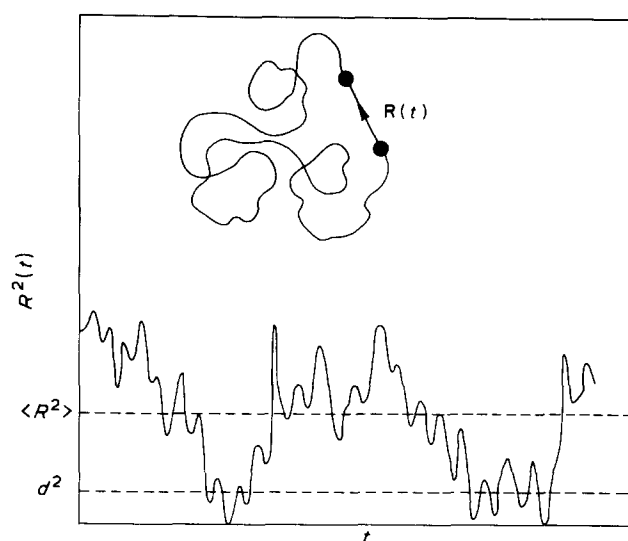


Figure 1 Schematic sketch of the time dependence of the end-to-end vector $R(t)$

* Permanent address: Physics Department, The Institute of Technology, Bandung, Indonesia.

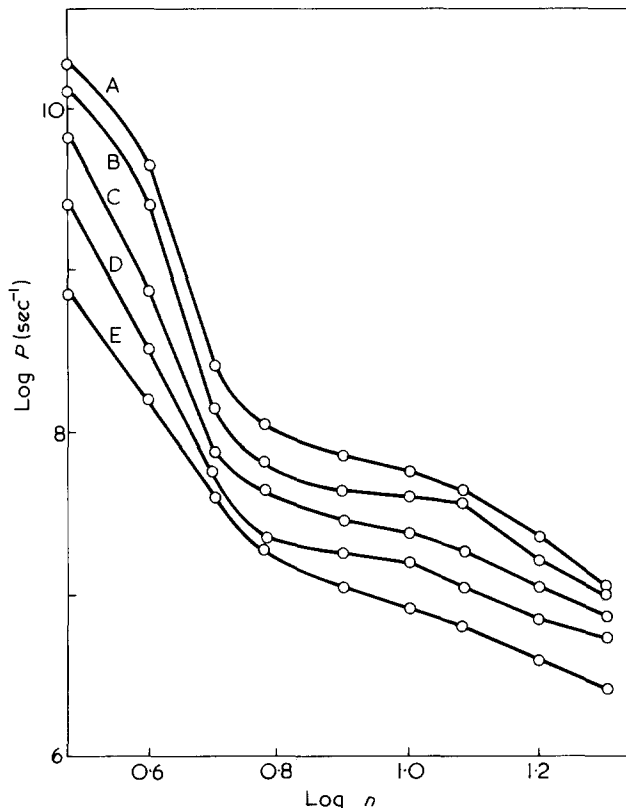


Figure 2 Log (electron transfer frequency, P) as a function of log (no. of monomers, n) for various temperatures: A, 40°C; B, 30°C; C, 15°C; D, 0°C; E, -15°C. Solvent HMPA

In thermal equilibrium $A(t) = R^2(t)$ constitutes a stationary process, i.e. the correlation $\langle A(t)A(t + \tau) \rangle$ is independent of the time t . Therefore:

$$\frac{d}{dt} \langle A(t)A(t + \tau) \rangle = \langle \dot{A}(t)A(t + \tau) \rangle + \langle A(t)\dot{A}(t + \tau) \rangle = 0 \quad (3)$$

in which case $A(t)$ and $\dot{A}(t)$ are uncorrelated and consequently $f(R^2, \beta)$ can be written as:

$$f(R^2, \beta) = g(R^2)h(\beta) \quad (4)$$

$g(R^2)$ is related to the usual probability density $p(R, L)$, that the end-to-end distance of a chain of length L is equal to R by:

$$g(R^2)dR^2 = p(R, L)4\pi R^2 dR$$

or

$$g(R^2) = 2\pi R p(R, L) \quad (5)$$

Using equations (4) and (5) we can write the frequency with which the stochastic process $R^2(t)$ crosses the level d^2 as:

$$\nu = 2\pi d p(d, L) \int_{-\infty}^{\infty} |\beta| h(\beta) d\beta \quad (6)$$

The integral in equation (6) is just by definition $\langle |\beta| \rangle$ and since:

$$\beta = |\dot{A}|_{R=d} = |2R\dot{R}|_{R=d} = 2d\dot{R} \quad (7)$$

we finally obtain that the number of end-to-end 'collisions' ($R < d$) is given by:

$$\nu = \frac{1}{2} 4\pi d^2 p(d, L) \langle |\dot{R}| \rangle \quad (8)$$

This is the main result of the paper; if ν is taken as a measure of dynamic flexibility and $p(d, L)$ as a measure of configurational flexibility, then equation (8) indicates that they are related primarily by the term $\langle |\dot{R}| \rangle$, i.e. the speed of the end-to-end separation.

In the next section we will discuss some aspects of the result and give a comparison with the experiment of Szwarc and Shimada.

COMPARISON WITH EXPERIMENT

In the experiment of Szwarc and Shimada they measured, using electron spin resonance techniques, the frequency P of intramolecular electron exchange in $N-(CH_2)_n-N^{\cdot-}$ in the solvent HMPA (hexamethylphosphoric triamide) where N denotes an α -naphthyl moiety. In this system, for $n \geq 5$ the frequency of electron transfer when the end groups are together, is much faster than the frequency ν with which the end groups actually come together. In other words there was a one-half probability that an electron on one end group before the encounter would be on the other end group after the encounter. Hence $P = \frac{1}{2}\nu$. The principal results of this experiment are shown in Figure 2 where $\log P$ is plotted as a function of $\log n$ for various temperatures.

In the previous section we showed (equation 8) that there are three factors which determine the collision frequency ν and hence P . They are: (a) an effective scattering cross-section $4\pi d^2$; (b) the probability $p(d, L)$ of an end-to-end separation d for a chain of length L ; and (c) the average speed $\langle |\dot{R}| \rangle$ of the end-to-end vector $\mathbf{R}(t)$. Of these factors, $p(d, L)$ is expected to depend most strongly on n . For a Gaussian chain of n links, each of length l we have that:

$$p(d, L) = \left(\frac{3}{2\pi n l^2} \right)^{3/2} \exp \left(-\frac{3d^2}{2nl^2} \right) \quad (9)$$

and the slope of $\ln(p)$ versus $\ln(n)$ is given by:

$$\frac{d \ln(p)}{d \ln(n)} = -\frac{3}{2} \left(1 - \frac{d^2}{nl^2} \right) \quad (10)$$

For large n we get a limiting slope of $-3/2$ characteristic of the Gaussian model. This is confirmed by Szwarc for the temperatures -15° , 0° and 15° C by plotting $\log(Pn^{3/2})$ versus $\log n$. The results are shown in Figure 3. For smaller values of n , equation (10) indicates that the slope should flatten and become zero when:

$$\langle R^2 \rangle = nl^2 = d^2 \quad (11)$$

i.e. when the root mean square, end-to-end distance is equal to the distance over which the electron can be transferred. Qualitatively the slope in Figure 2 does decrease as

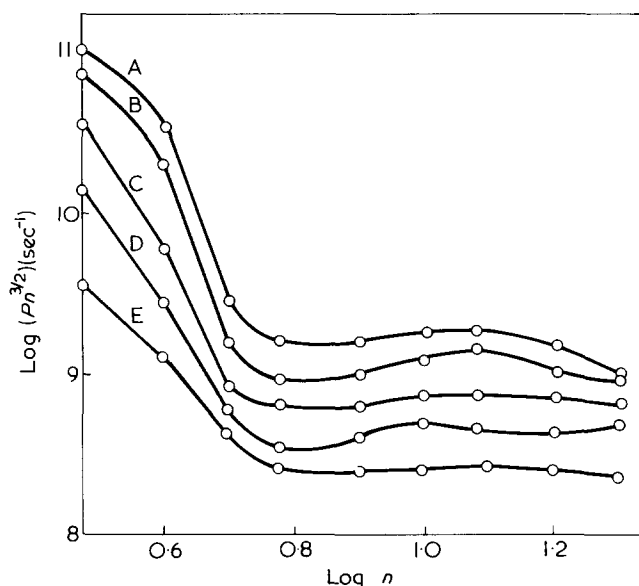


Figure 3 $\text{Log}(Pn^{3/2})$ as a function of $\text{log } n$ for various temperatures; A, 45°C; B, 30°C; C, 15°C; D, 0°C; E, -15°C

n decreases and for $n \approx 10$ is approximately flat. In the experiment, d was estimated to be of the order of 7–9 Å, which gives using equation (11) for the link length l of the chain $l \sim 2.3\text{--}3$ Å. For polymethylene chain this estimate is about right. A much faster increase of P with n for $n < 5$ comes about because for these short chains the end-groups are always in the vicinity of each other for the electron to be transferred.

In general we might expect that $p(d, L)$ will be inversely proportional to the 'volume' $4\pi/3\langle R^2 \rangle^{3/2}$ of the polymer. The Gaussian result gives $\langle R^2 \rangle \sim n$, but if excluded volume effects are also included then for large n (strictly speaking $n \rightarrow \infty$) we have $\langle R^2 \rangle \sim n^{6/5}$. Therefore we would have that:

$$\nu \sim p(d, L) \sim n^{9/5} = n^{1.8}$$

In Figure 4 we have plotted $\text{log } Pn^{1.8}$ as a function of $\text{log } n$; however the experimental results do not appear to be sufficiently accurate to distinguish an exponent of 1.8 from 1.5.

Szwarc and Shimada also showed that the electron transfer frequency P and hence the end-group collision frequency ν was an activated process. For chains of more than five monomers the 'activation energy' was approximately 5 kcal/mol and independent of the length of the chain. This has important implications for the kind of theoretical model most appropriate for the description of the dynamic of the polymer molecules. The only factor in our expression (8) for ν likely to contain any strong temperature dependence is the term $\langle |\dot{R}| \rangle$, i.e. the average relative speed of the end-groups. However, any model of a polymer molecule which describes the motion in terms of normal modes will inevitably lead to a temperature dependence of $\langle |\dot{R}| \rangle$ of the form:

$$\langle |\dot{R}| \rangle \sim \left(\frac{kT}{m} \right)^{1/2} \quad (12)$$

where m is the mass of a segment. This result comes from the equipartition of energy, where for each normal mode

coordinate k_n , we have that:

$$\langle |\dot{k}|^2 \rangle \sim \frac{kT}{m} \quad (13)$$

The end-to-end vector can be obtained as a linear combination of normal modes and so we obtain equation (12). This result holds under considerably wide circumstances⁵ and in particular when chain stiffness and internal viscosity factors are included. Even though these factors may be regarded as activated processes, the use of normal modes is the overriding consideration and leads to the stated result for $\langle |\dot{R}| \rangle$. Thus Edwards and Goodyear⁶ considered a model where the motion of the polymer was dominated by potential barriers between conformations; however, as a result of reducing their model to a Rouse form their work contains the result (12). This indicates that for a discussion of the frequency of end-group collisions the dynamics of the polymer chain need to be treated in greater detail. This is being currently investigated and will be reported later.

CONCLUSION

A measure of the dynamic flexibility of a polymer chain is given by the collision frequency ν of the end-groups. In this paper we have shown that ν depends on three factors: (a) an effective cross-section $4\pi d^2$; (b) the probability of an end-to-end separation d ; and (c) the average speed of the end-to-end separation. In the experiments of Szwarc *et al.* the dependence of ν on the length of the chain is reasonably well accounted for by a Gaussian distribution function, although excluded volume effects could not entirely be ruled out. The most difficult factor to account for was the average speed $\langle |\dot{R}| \rangle$ of the end-to-end separation. A preliminary investigation based on the idea of normal modes

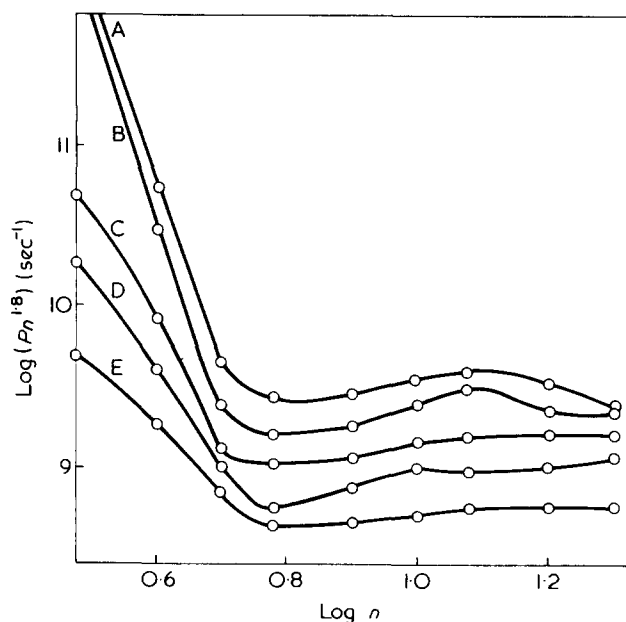


Figure 4 $\text{Log}(Pn^{1.8})$ as a function of $\text{log } n$ for various temperatures; A, 45°C; B, 30°C; C, 15°C; D, 0°C; E, -15°C

and the equipartition of energy indicates that the $\langle |\dot{R}| \rangle$ should depend on $(T)^{1/2}$. Experiments, however, show that the collision frequency is an activated process. Work is in progress to resolve this issue.

ACKNOWLEDGEMENTS

A. R. would like to acknowledge a Technical Assistance Award from the British Council.

REFERENCES

- 1 Szwarc, M. and Shimada, K. *J. Polym. Sci. Polym. Symp.* 1974, **46**, 193
- 2 Shimada, K. and Szwarc, M. *J. Am. Chem. Soc.* 1975, **97**, 3313, 3321
- 3 Rice, S. O., *Bell Syst. Tech. J.* 1944, **23**, 282; 1945, **24**, 46
- 4 Bendat, J. S. 'Principles and Applications of Random Noise Theory', Wiley, New York, 1958
- 5 Brereton, M. G. and Rusli, A. unpublished work
- 6 Edwards, S. F. and Goodyear, A. G. *J. Phys. (A)* 1972, **5**, 965

Molecular motion of poly(methyl methacrylate), polystyrene and poly(propylene oxide) in solution studied by ^{13}C n.m.r. spin-lattice relaxation measurements: effects due to distributions of correlation times

F. Heatley and Afrozi Begum

Chemistry Department, University of Manchester, Manchester M13 9PL, UK

(Received 11 November 1975)

The ^{13}C n.m.r. spin lattice relaxation times and Nuclear Overhauser Enhancements have been measured for solutions of poly(methyl methacrylate) (PMMA) in *o*-dichlorobenzene, polystyrene (PS) in pentachloroethane and poly(propylene oxide) (PPO) in CDCl_3 as a function of temperature. For PS and PMMA a T_1 minimum is observed close to ambient temperature. The single correlation time theory of relaxation is inadequate to explain the relaxation data, but within experimental error, the data can be interpreted in terms of either the Cole–Cole distribution of correlation times, the $\log -\chi^2$ distribution or a conformational jump model of chain dynamics.

INTRODUCTION

Several workers in recent years^{1–7} have used ^{13}C n.m.r. relaxation time measurements to study polymer motion in solution, and the topic has also been the subject of some theoretical investigation^{8–12}. In most work of this type, it has been assumed that the single correlation time model^{8,9} of segmental re-orientation is valid, but there is clear evidence^{10,11} that this is not necessarily so. Schaefer¹⁰ was obliged to use a distribution of correlation times to explain spin–lattice (T_1) and spin–spin (T_2) relaxation times and Nuclear Overhauser Enhancements (*NOE*) for both bulk and dissolved polymers. However, these results whilst of considerable importance, were limited to only a single temperature. This point was also noted by Hermann and Weill¹¹ who made an extensive series of ^1H , ^2H and ^{13}C relaxation measurements over a range of temperature for poly(ethylene oxide). Again the single correlation time theory was found inadequate but they chose to use a correlation function which was the sum of two exponentials, observing that a distribution of (single) correlation times is indistinguishable experimentally from a non-exponential correlation function. They assumed the anisotropic rotation model¹³ of relaxation but purely as a formal way of expressing a non-exponential correlation function. The results were satisfactorily interpreted by a self-consistent set of parameters, though each nucleus required a different set. This is surprising if the model is to be realistic, since the ^{13}C and ^2H relaxation times depend on exactly the same auto-correlation function viz that for the orientation of the C–H bond, and should therefore have the same set of parameters. The significance of this model is therefore doubtful.

At normal temperatures, poly(ethylene oxide) is a very flexible polymer, and it seemed likely that measurements on less flexible molecules could be more informative. We therefore have determined values of ^{13}C , T_1 and *NOE* for poly(methyl methacrylate) (PMMA) in *o*-dichlorobenzene (ODCB), polystyrene (PS) in pentachloroethane (PCE) and poly(propylene oxide) (PPO) in CDCl_3 over a wide temperature range. (These solvents were chosen for their large liquid range and lack of conflicting ^{13}C signals rather than

for thermodynamic reasons). These polymers provide a wide range of motional variety from the very flexible PPO ($T_g = 198\text{ K}$) to the stiff PMMA ($T_g = 298\text{ K}$), and contain side groups with varying amounts of freedom, from the mobile CH_3 groups in PPO to the highly restricted aromatic rings in PS. The observed relaxation data was interpreted in terms of three models: (I) the empirical Cole–Cole distribution^{14,15} used in analysis of dielectric relaxation^{16,17}; (II) the $\log -\chi^2$ distribution used by Schaefer¹⁰ referred to above; (III) the non-exponential correlation function deduced by Monnerie *et al.*¹² for a conformational jump model of polymer dynamics.

The necessary theoretical formulae are outlined in the Theory section, together with the results of trial calculations, and this is followed by a discussion of the experimental results.

EXPERIMENTAL

^{13}C relaxation times were measured on a Varian Associates XL-100 spectrometer at 25.14 MHz using the standard $\pi - \tau - \pi/2$ inversion recovery technique. The values of *NOE* were measured by comparing the integrals of spectra recorded first with complete proton noise decoupling and then with the decoupler offset 30 kHz in *cw* mode. This procedure eliminated sample temperature changes due to switching the decoupler on or off. Measurements were made for solutions of 100 and 400 mg polymer/ml solvent. The solutions were not degassed as the relaxation times of interest rarely exceed 500 msec. The theoretical maximum value of *NOE* was observed in a number of cases showing that the effect of paramagnetic impurities was indeed negligible.

The PMMA was a predominantly syndiotactic sample of $M_n = 90\,000$ supplied by the Rubber and Plastics Research Association, Shrewsbury, England. Two PS samples of $M_n = 10\,000$ and 110 000 with $M_w/M_n = 1.06$ were supplied by Pressure Chemical Co., Pittsburgh, Pa. Both samples were found to be atactic. The PPO was a sample of $M_n = 2020$ supplied by Waters Associates, Framingham, Mass.

THEORY

The ^{13}C spin-lattice relaxation time, T_1 , and Nuclear Overhauser Enhancement Factor, η , for a $^{13}\text{CH}_n$ group, are given in terms of spectral densities $J_n(\omega)$ by the formulae⁸ (in SI units)

$$\frac{1}{T_1} = \frac{\mu_0^2 \gamma_C^2 \gamma_H^2 h^2}{40\pi^2 r_{\text{CH}}^6} \{J_0(\omega_H - \omega_C) + 3J_1(\omega_C) + 6J_2(\omega_H + \omega_C)\} \quad (1)$$

$$\eta = 3.976 \left[\frac{6J_2(\omega_H + \omega_C) - J_0(\omega_H - \omega_C)}{J_0(\omega_H - \omega_C) + 3J_1(\omega_C) + 6J_2(\omega_H + \omega_C)} \right] \quad (2)$$

γ_H and γ_C are the magnetogyric ratios of ^1H and ^{13}C respectively, and r_{CH} is the C-H bond length. It is assumed that ^{13}C relaxation occurs solely by intramolecular dipole-dipole interaction with the attached protons, and this is undoubtedly true for motions of the time scale encountered in polymers. The spectral densities $J_n(\omega)$ are the Fourier transforms of the normalized autocorrelation functions of the second-order spherical harmonics of the C-H bond orientation angles:

$$J_n(\omega) = \int F_n^2(\tau) F_n^2(0) e^{i\omega\tau} d\tau \quad (3)$$

For an exponential autocorrelation function with a single correlation time τ_c (isotropic rotation), then:

$$J_n(\omega) = \frac{\tau_c}{1 + \omega^2 \tau_c^2} \quad (4)$$

For a distribution of correlation times, with distribution function $G(\tau_c)$ then equation (4) becomes:

$$J_n(\omega) = \int_0^\infty \frac{G(\tau_c) \tau_c}{1 + \omega^2 \tau_c^2} \cdot d\tau_c \quad (5)$$

Because n.m.r. correlation times may cover a very wide range, it is more convenient to use a logarithmic scale. Defining a new variable S by:

$$S = \ln(\tau_c/\tau_0)$$

the Cole-Cole distribution function of S , $L(S)$, is given by¹⁵:

$$L(S) dS = \frac{1}{2\pi} \cdot \frac{\sin \gamma \pi}{\cosh \gamma S + \cos \gamma \pi} \cdot dS \quad (6)$$

where the width parameter γ lies in the range 0 to 1. $\gamma = 1$ reduces to the single correlation time case. The expression for $J_n(\omega)$ is:

$$J_n(\omega) = \frac{1}{2\omega} \left[\frac{\cos(1 - \gamma)\pi/2}{\cosh(\gamma \ln \omega \tau_0) + \sin(1 - \gamma)\pi/2} \right] \quad (7)$$

In the log $-\chi^2$ distribution employed by Schaefer¹⁰, the logarithmic time scale (of adjustable base b) is defined by:

$$S = \log_b [1 + (b - 1)\tau_c/\tau_0]$$

and the distribution function $H(S)$ by:

$$H(S) dS = \frac{1}{\Gamma(p)} (pS)^{p-1} \exp(-pS) \quad (8)$$

where p is the width parameter. In addition to the time constant τ_0 , two parameters, p and b , are needed to specify this distribution. However, Schaefer has pointed out that it is really necessary to fix p and τ_0 , provided that b is sufficiently large. The larger p , the narrower the distribution; for $p \geq 100$, the distribution is so narrow as to be indistinguishable from the single correlation time case. The spectral density function is given by the integral:

$$J_n(\omega) = \int_0^\infty \frac{\tau_0 H(S) [\exp_b S - 1] dS}{(b - 1) \{1 + \omega^2 \tau_0^2 [(\exp_b S - 1)/(b - 1)]^2\}} \quad (9)$$

which was evaluated numerically.

In both distributions, τ_0 is the average correlation time but whereas the Cole-Cole distribution is symmetrical, the log $-\chi^2$ distribution is unsymmetrical with a tail towards longer correlation times. Other symmetrical distribution functions which have been briefly applied¹⁵ to n.m.r. relaxations include the Gaussian and Fuoss-Kirkwood distributions¹⁸, but these are very similar in effect to the Cole-Cole. The Davidson-Cole distribution^{15,19} is an unsymmetrical distribution which has been applied to dielectric relaxation. Here the tail is to shorter correlation times, but this does not seem physically reasonable for n.m.r. relaxation in polymers (see ref. 10 and the Discussion).

The third model employed is the non-exponential correlation function obtained by Monnerie *et al.*¹² for relaxation by conformation jumps of a polymer chain on a diamond lattice. This model is of course a highly simplified picture of the conformation freedom of a real polymer chain, which is generally considerably restricted by steric interactions. However, it is felt that it may be sufficiently realistic to be of some value in interpreting experimental observations. The same correlation function was obtained by Hunt and Powles²⁰ for a defect diffusion model of relaxation in supercooled liquids and glasses, but they found it necessary to include also an exponential term to take account of molecular rotation. The same approach was followed here, since polymer motion in solution is undoubtedly a combination of conformational jumps and overall molecular tumbling. The correlation function used is:

$$\overline{F_n^2(\tau) F_n^2(0)} = \exp\left(-\frac{\tau}{\tau_0}\right) \exp\left(-\frac{\tau}{\tau_D}\right) \left[1 - \operatorname{erf}\left(\frac{\tau}{\tau_D}\right)\right]^{1/2} \quad (10)$$

where τ_0 and τ_D are correlation times characterizing molecular tumbling and conformation transitions respectively. The spectral density function for this correlation function

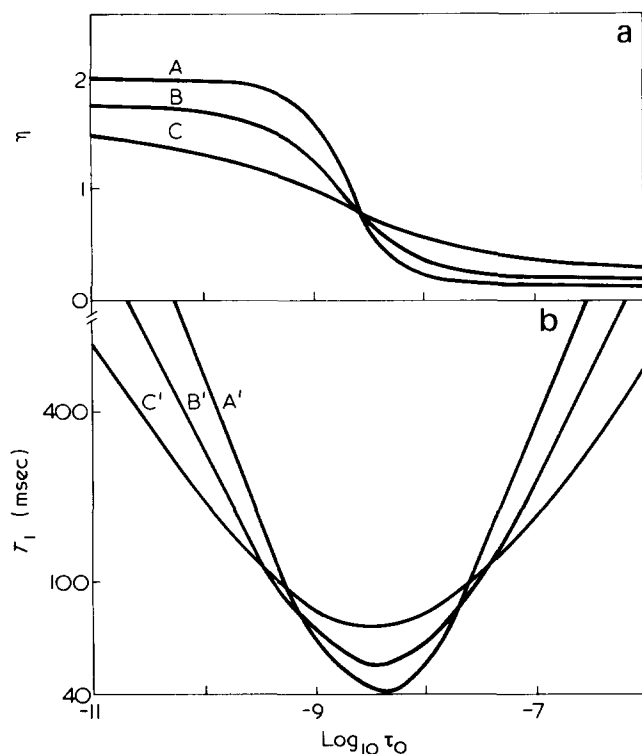


Figure 1 Plots of (a) η and (b) T_1 vs. τ_0 for a CH group with a Cole-Cole distribution of correlation times, $r_{\text{CH}} = 1.1 \text{ \AA}$. Values of γ : A, A', 1.0; B, B', 0.8; C, C', 0.6

is given by¹²:

$$J_n(\omega) = \frac{\tau_0 \tau_D (\tau_0 - \tau_D)}{(\tau_0 - \tau_D)^2 + \omega^2 \tau_0^2 \tau_D^2} \left\{ \left(\frac{\tau_0}{2\tau_D} \right)^{1/2} \left[\frac{1 + \omega^2 \tau_0^2}{1 + \omega^2 \tau_D^2} \right]^{1/2} + \left(\frac{\tau_0}{2\tau_D} \right)^{1/2} \frac{\omega \tau_0 \tau_D}{(\tau_0 - \tau_D)} \left[\frac{(1 + \omega^2 \tau_0^2)^{1/2} - 1}{1 + \omega^2 \tau_0^2} \right]^{1/2} - 1 \right\} \quad (11)$$

By using equations (1), (2), (7), (9) and (11), the relaxation times and Overhauser enhancements are easily calculated as a function of correlation times and width parameters. Selected results are shown in Figures 1, 2 and 3. Such calculations of relaxation times have already been presented for the Cole-Cole distribution by Connor¹⁵, but these were given in reduced form and not specifically for ^{13}C relaxation. The effect of such a distribution on the Overhauser enhancement has not previously been studied. The results for the log $-\chi^2$ distribution have of course been published by the originator¹⁰, but are included here for convenient comparison with the others. The most prominent feature in Figures 1 and 2 is the raising and broadening of the T_1 minimum as the distribution increases in width. If the minimum can be observed, its value immediately determines the width parameter at that point. Furthermore, the sharp increase in η in the vicinity of the T_1 minimum is moderated. Equally notable is the decrease in effective activation energy for T_1 with increasing width of distribution. For the Cole-Cole distribution, Connor¹⁵ has shown that the effective activation energy for $T_1(E^*)$ is related to the true activation energy for $\tau_0(E)$ by:

$$E^* = \gamma E$$

For the conformation jump model (Figure 3) the crucial factor is the ratio τ_D/τ_0 . If $\tau_D/\tau_0 \geq 10$, the correlation decay is dominated by τ_0 , and the model reduces effectively to the single correlation time case. As τ_D becomes comparable to, or less than τ_0 , the T_1 minimum is raised and broadened, as in Figures 1 and 2, and also markedly shifted on the log τ_D scale.

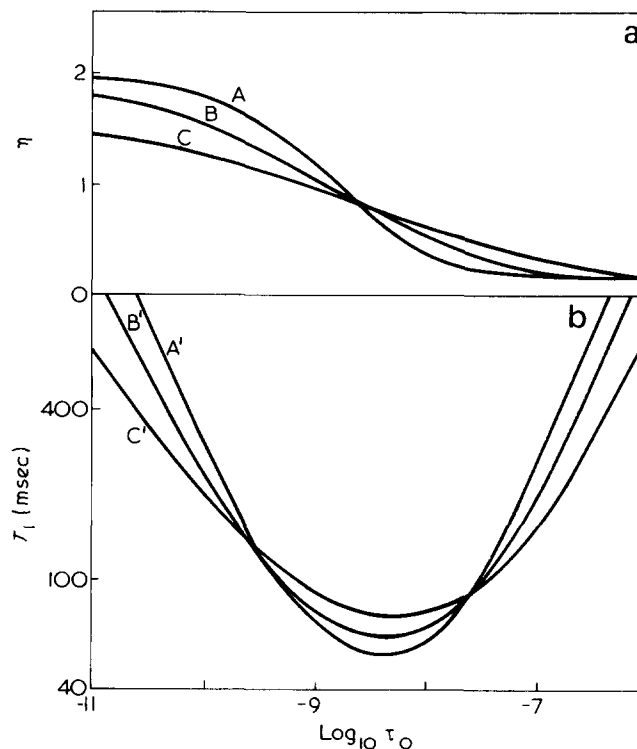


Figure 2 Plots of (a) η and (b) T_1 vs. τ_0 for a CH group with a log $-\chi^2$ distribution of correlation times, $b = 1000$, $r_{\text{CH}} = 1.1 \text{ \AA}$. Values of p : A, A', 40; B, B', 20; C, C', 10

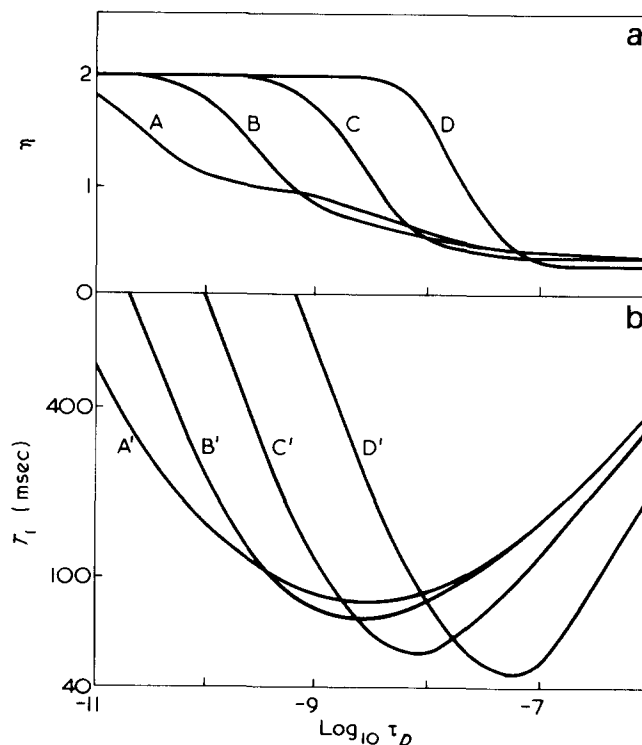


Figure 3 Plots of (a) η and (b) T_1 vs. τ_D for a CH group with a correlation function given by the conformational jump model (see text), $r_{\text{CH}} = 1.1 \text{ \AA}$. Values of τ_D/τ_0 : A, A', 0.01; B, B', 0.1; C, C', 1.0; D, D', 10.0

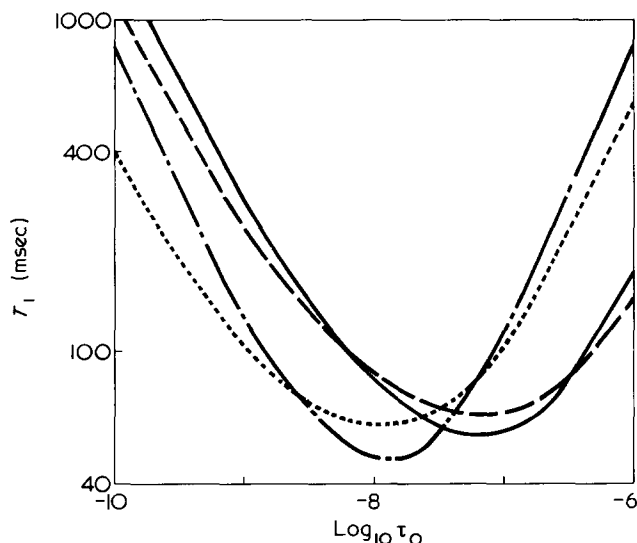


Figure 4 Plot of T_1 vs. τ_0 for a CH group undergoing simultaneous overall and internal rotation with a log $-\chi^2$ distribution of correlation times. (—), $\tau_g/\tau_c = 0.1$, τ_g same distribution as τ_c , $\rho = 40$; (---), $\tau_g/\tau_c = 0.1$, τ_g same distribution as τ_c , $\rho = 20$; (·····), $\tau_g/\tau_c = 1.0$, τ_g same distribution as τ_c , $\rho = 20$; (-·-·-), $\tau_g/\tau_c = 1.0$, τ_g independent of τ_c , $\rho = 20$

It would normally be expected that τ_0 and τ_D would vary with temperature according to the Arrhenius equation, and the calculated curves should therefore also correspond to $\log T_1$ vs. $1/T$ plots. However, it is quite likely that in the case of the distributions the width parameter varies with temperature, and in the case of the jump model τ_D and τ_0 have different activation energies so that the ratio varies with temperature. In practice therefore the temperature dependence of T_1 and η may be quite complicated.

For the $^{13}\text{CH}_3$ groups in PPO and PMMA, an additional relaxation process arises from internal rotation. Formula for the spectral densities for a nucleus undergoing simultaneous overall and internal rotation have been given by Woessner²¹. In the case of a three-fold potential well, the spectral density is:

$$J_H(\omega) = \frac{1}{4} \left[(1 - 3 \cos^2 \alpha)^2 \cdot \frac{\tau_c}{1 + \omega^2 \tau_c^2} + 3(\sin^2 2\alpha + \sin^4 \alpha) \times \frac{\tau'_c}{1 + \omega^2 \tau_c'^2} \right] \quad (12)$$

where:

$$\frac{1}{\tau'_c} = \frac{1}{\tau_c} + \frac{3}{2\tau_g}$$

τ_g is the lifetime of any of the three equivalent methyl positions and α is the angle between the CH bond and the rotation axis. For a polymer with a distribution of correlation times there are two extreme relationships between τ_g and τ_c . In the first case, exemplified by PPO⁶, τ_g is essentially independent of τ_c and is constant throughout the distribution. In the second case, exemplified by polyisobutylene⁶, τ_g is proportional to τ_c and therefore has the same distribution function. The appropriate versions of equations (1), (2), (5) and (12) can be used to calculate T_1 and η for each case and some results for the log $-\chi^2$ distribution are shown in Figure 4. Broadening the distribution raises and flattens

the T_1 minimum as for the backbone carbons, but its position on the τ_0 scale and its depth are much affected by the ratio τ_g/τ_0 . The relaxation times also depend a great deal on whether τ_g is independent of or proportional to τ_c , so it is important to choose the correct relationship for the particular polymer under investigation.

RESULTS AND DISCUSSION

The ^{13}C spectra of all polymers studied here have been presented elsewhere^{6,20}. For PMMA, the CH_2 and OCH_3 peaks lie close together and overlap strongly at the lower temperatures, limiting the accuracy of T_1 and particularly *NOE* measurements. Fine structure due to sequences of different tacticity is observed in the CH_2 region at the higher temperatures, but all peaks relaxed identically within experimental error. The $\alpha\text{-CH}_3$ region clearly showed three peaks due to syndiotactic, heterotactic and isotactic triads. The last one was very weak, but it proved possible to measure individual T_1 for the syndiotactic and heterotactic peaks, though not individual *NOE*. The results for two solutions of 100 and 400 mg/ml are shown in Figure 5. It is seen that in both cases a minimum in T_1 for the backbone $^{13}\text{CH}_2$ group is observed at about 30°C for the more dilute solution and 60°C for the more concentrated. The relaxation time at the minimum is in each case approximately twice as long as expected from the single correlation time theory, which is a clear imperative for the adoption of a more complicated relaxation theory. In addition, it is noteworthy that the activation energy for the CH_2 value of T_1 at the higher temperatures is apparently less for the 400 mg solution than for the 100 mg solution. This result is opposite to that expected intuitively, and points to the existence of a distribution of correlation times. The values of *NOE* for the CH_2 group increase as T_1 increases and are higher for the more dilute solution, as expected. The $\alpha\text{-CH}_3$ relaxation times are somewhat longer than the CH_2 values because of additional mobility conferred by internal rotation. It is noticeable that the T_1 of the heterotactic peak is greater than that of the syndiotac-

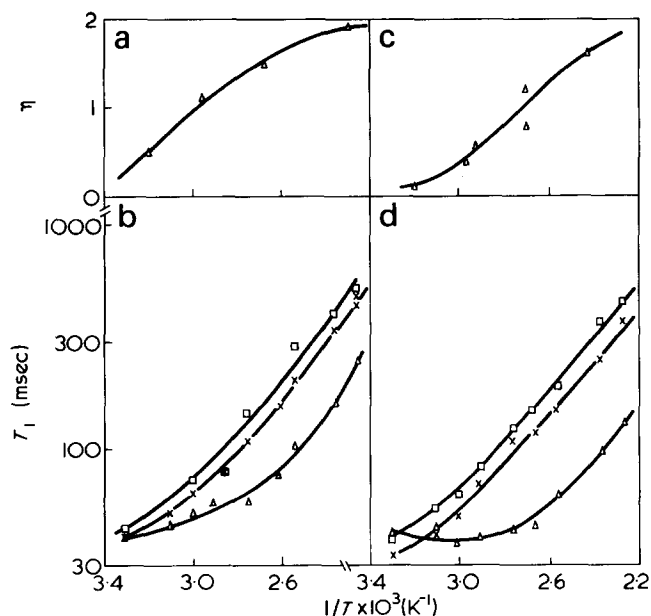


Figure 5 ^{13}C T_1 and η for PMMA in *o*-dichlorobenzene. (a), (b), 100 mg/ml solvent; (c), (d), 400 mg/ml solvent. Δ , CH_2 ; X, syndiotactic $\alpha\text{-CH}_3$; \square , heterotactic $\alpha\text{-CH}_3$

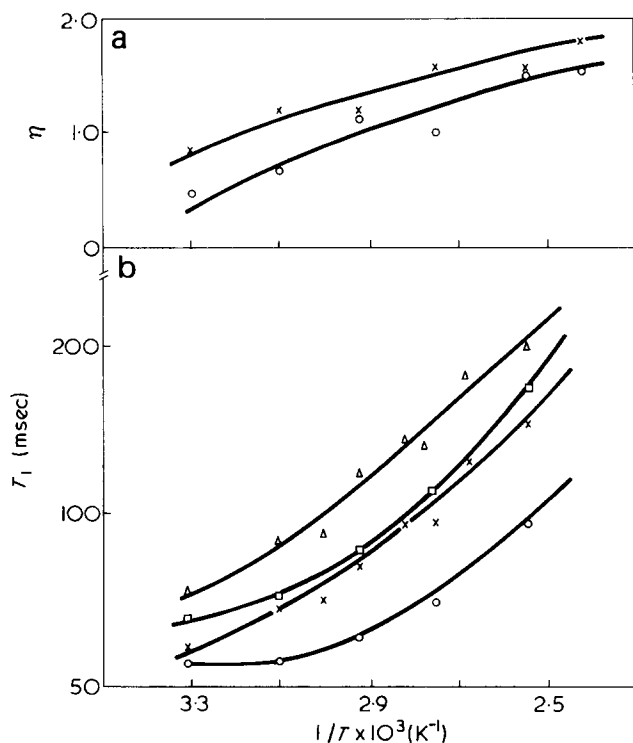


Figure 6 ^{13}C T_1 and η for PS (MW 10000) in CDCl_3 . (a) X, backbone CH + CH_2 100 mg/ml solvent; O, backbone CH + CH_2 400 mg/ml solvent. (b) X, backbone CH, 100 mg/ml solvent; O, backbone CH, 400 mg/ml solvent; Δ , aromatic $\text{C}_{2,3,5,6}$, 100 mg/ml solvent; \square , aromatic $\text{C}_{2,3,5,6}$, 400 mg/ml solvent

tic peak, suggesting faster internal rotation and a lower torsional barrier. This observation is in agreement with a neutron scattering measurement of barriers in PMMA²¹ which gave 34.3 kJ/mol for the syndiotactic $\alpha\text{-CH}_3$ barrier and 16.7 kJ/mol for the isotactic isomer.

The values of T_1 for the $-\text{OCH}_3$, backbone $-\text{C}-$ and $\text{C}=\text{O}$ carbons in PMMA are considerably longer than those of the CH_2 and $\alpha\text{-CH}_3$ peaks, in the first case because of high internal flexibility of the $-\text{COOCH}_3$ side group and in the last two cases because of the absence of directly bonded protons. These T_1 values were not measured, as the substantial additional experimental time was not supported by a confident interpretation of the values obtained.

For polystyrene, the backbone CH and CH_2 peaks lie very close together, the former being much sharper in atactic polystyrene²⁰. The *ortho* (C_2C_6) and *meta* (C_3C_5) aromatic carbons also overlap, but the *para* (C_4) carbon is fairly well resolved at all temperatures except the very lowest in the more concentrated solutions. The C_1 carbon is well separated from $\text{C}_2\text{-C}_6$ to low field but its T_1 value was not measured for the same reasons as the $-\text{C}-$ and $\text{C}=\text{O}$

carbons in PMMA. Also the CH_2 resonance is broadened so much by the effects of tacticity that its relaxation time is difficult to measure accurately. The results in Figures 6 and 7 therefore comprise relaxation times for the backbone CH, and aromatic C_2 , C_3 , C_5 and C_6 combined. The values of *NOE* reported are for backbone CH and CH_2 combined and for aromatic C_2 to C_6 combined. A clear minimum for T_1 for the backbone CH, at about 50°C is observed only for the 400 mg/ml solution, though it is obvious that the minimum for the 100 mg/ml solution is just beyond the lower limit of the temperature range covered here at about 15°C . As for PMMA, the T_1 at the minimum is roughly

twice the value expected for the single correlation time theory. The values of T_1 for the aromatic and backbone carbons lie on approximately parallel curves, with the aromatic carbons having slightly longer T_1 . The aromatic ring is therefore highly restricted compared to the $\alpha\text{-CH}_3$ group in PMMA, but still retains a small degree of oscillatory freedom. There is no variation of T_1 with molecular weight, in agreement with results reported some time ago by Allerhand and Hailstone¹.

In PPO, there is no difficulty in resolving the proton-decoupled CH, CH_2 and CH_3 signals, though in the uncoupled spectra, the CH doublet and CH_2 triplet overlap. Individual values of T_1 are therefore reported but only a combined CH + CH_2 value for *NOE* (Figure 8). PPO is a much more flexible polymer than PMMA or PS and only tentative indications of a minimum in T_1 were observed even at -60°C . The apparent activation energies increase with concentration, unlike PMMA, and since this is entirely reasonable, there is no obvious indication of a distribution of correlation times for this polymer. To elucidate such details, it is necessary to fit the observed values of T_1 and *NOE* to each model. However, before presenting the relaxation model parameters applicable to the experimental data discussed above, there are several points worth discussing concerning the accuracy with which such parameters can be obtained.

It is clearly necessary that both T_1 and the *NOE* be dependent of the model parameters. There are two regions where this is not so. The first is in the vicinity of the T_1 minimum, where T_1 is only slightly dependent on τ_0 (or τ_D). The minimum value of T_1 itself is quite strongly dependent on the parameters γ , p and τ_D/τ_0 , as Figures 1-3 show, but the usual uncertainty of at least 5% in T_1 does not permit an accuracy in τ_0 in this region of less than a factor of 2 or so (i.e. an error in $\log \tau_0$ of ± 0.3). It is true that the region of the T_1 minimum is where the *NOE* is most sensitive to τ_0 , but because the *NOE* is approximately propor-

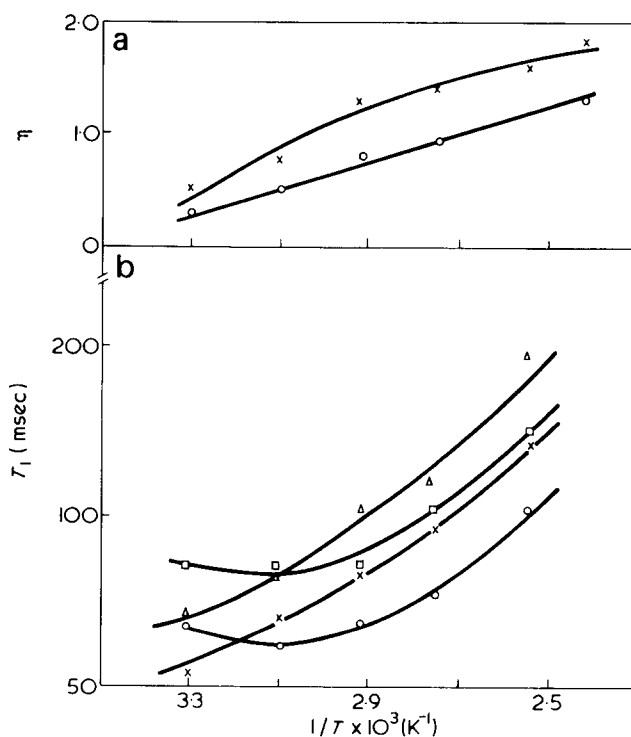


Figure 7 ^{13}C T_1 and η for PS (MW 110000) in CDCl_3 . Legend as for Figure 6

tional to $\log \tau_0$, the experimental error of say ± 0.1 in the *NOE* leads to factor of 2 uncertainty in τ_0 .

The second region giving an imprecise interpretation of experimental data is to the high temperature (short correlation time) side of the T_1 minimum, where the *NOE* is approaching its limiting value. For the $\log -\chi^2$ distribution and the conformational jump model, the curves for all values of the parameters p and τ_D/τ_0 respectively approach the value 1.988 at varying rates, but below some critical correlation time the *NOE* becomes insensitive to the model parameters. T_1 here is strongly dependent on τ_0 , so if a value for p or τ_D/τ_0 is assumed, the corresponding value of τ_0 can be determined to the same accuracy. However, the

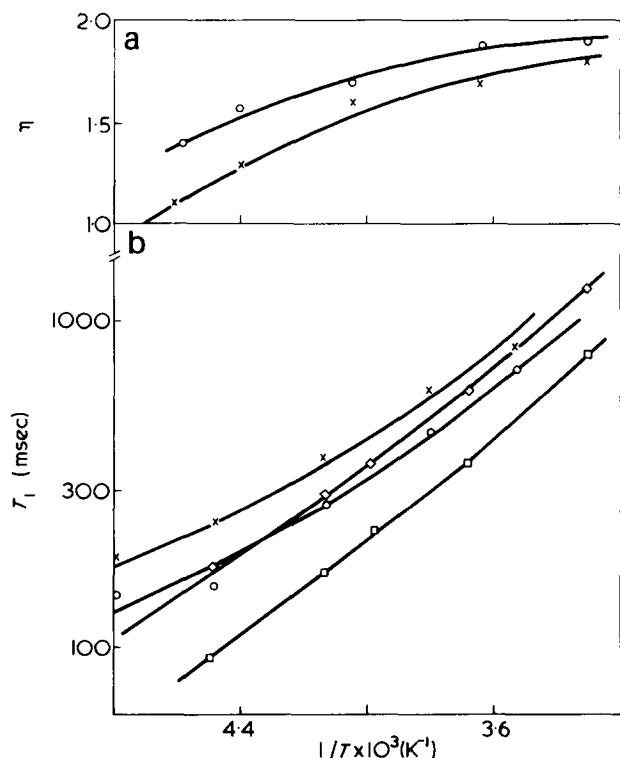


Figure 8 ^{13}C T_1 and η for PPO in CDCl_3 . (a) \circ , CH + CH_2 , 100 mg/ml solvent; \times , CH + CH_2 , 400 mg/ml solvent. (b) \circ , CH, 100 mg/ml solvent; \times , CH_3 , 100 mg/ml solvent; \square , CH, 400 mg/ml solvent; \diamond , CH_3 , 400 mg/ml solvent

NOE at that point cannot be used to distinguish between different values of p or τ_D/τ_0 (and hence different correlation times) except between wide limits. Figure 1 shows that this second structure does not apply to the Cole–Cole distribution where the limiting values of the *NOE* are strongly dependent on the width parameter γ . In practice, some limitation on the range of uncertainty may be placed by the need for physical coherence. For instance it may reasonably be expected that τ_0 will (at least approximately) follow the Arrhenius equation, and that γ and p will vary consistently with temperature.

With these restrictions in mind, the experimental data given above has been interpreted in terms of the parameters at the three models, and the results are presented in Tables 1 to 4. Values especially subject to the uncertainties described are placed in parentheses. It is estimated that the errors in the remaining parameters are approximately $\pm 20\%$.

There was little difficulty in fitting most of the data to any of the three models. Problems were encountered for the lowest temperatures of the more concentrated PS and PMMA solutions where the calculated values of *NOE* were consistently higher than the observed values of *NOE* for any reasonable model parameters, but no explanation has been found as yet. The discrepancy was common to all models, and there is little reason on the basis of these measurements to prefer one model over another. The experimental data certainly requires a distribution of correlation times, or its equivalent but the exact form is immaterial provided it has the flexibility to cover a wide range. The conformational jump model yields values for the ratio τ_D/τ_0 of less than unity, which is reasonable since it is expected that the correlation time for small-scale, limited local motions will be less than that for larger scale re-orientation. However, the conformity to reasonable physical behaviour may be no more than coincidence. It could well be that the non-exponential part of the jump model auto-correlation function, dominant since $\tau_D < \tau_0$, is simply a satisfactory representation of a certain distribution of correlation times of which τ_D is the average value. It is significant that for any system and temperature, the three models give values of τ_0 and τ_D which rarely differ by more than a factor of 2, and usually by much less. The temperature dependence of τ_D/τ_0 is erratic, in some cases increasing with temperature e.g. PMMA, and in others decreasing

Table 1 Correlation times and width parameters for PMMA in *o*-dichlorobenzene. Model I, the Cole–Cole distribution, Model II, the $\log -\chi^2$ distribution and Model III the conformational jump model

Model	Parameter	$10^3/T$ (K^{-1})					
		3.3	3.1	2.9	2.7	2.5	2.3
(a) Concentration = 100 mg polymer/ml solvent							
I	$-\log \tau_0$	(8.8)	9.1	9.37	9.64	9.95	10.21
	γ	0.57	0.57	0.6	0.65	0.7	0.8
II	$-\log \tau_0$	(8.6)	9.05	9.34	9.63	9.87	(10.25)
	p	8	10	15	20	30	(30)
III	$-\log \tau_D$	(9.04)	9.25	9.44	9.64	9.93	(10.26)
	τ_D/τ_0	0.04	0.04	0.06	0.1	0.1	(0.1)
(b) Concentration = 400 mg polymer/ml solvent							
I	$-\log \tau_0$	(8.1)	(8.35)	(8.7)	9.17	9.58	9.89
	γ	0.55	0.55	0.58	0.6	0.7	0.8
II	$-\log \tau_0$	(7.85)	(8.2)	(8.6)	9.05	9.55	9.92
	p	8	8	10	12	20	30
III	$-\log \tau_D$	(8.15)	(8.50)	(9.10)	9.40	9.62	10.0
	τ_D/τ_0	0.025	0.025	0.04	0.06	0.1	0.1

For discussion of values in parentheses see text

Table 2 Correlation times and width parameters for PS (MW 10 000) in pentachloroethane. Models I–III as in Table 1

Model	Parameter	$10^3/T$ (K $^{-1}$)				
		3.3	3.1	2.9	2.7	2.5
(a) Concentration = 100 mg polymer/ml solvent						
I	$-\log \tau_0$	8.6	8.93	9.15	9.36	9.57
	γ	0.75	0.75	0.8	0.8	0.85
II	$-\log \tau_0$	8.68	8.96	9.2	9.38	9.62
	ρ	30	30	40	40	40
III	$-\log \tau_D$	8.30	8.57	8.80	9.20	9.55
	τ_D/τ_0	1.5	1.0	0.8	0.4	0.25
(b) Concentration = 400 mg polymer/ml solvent						
I	$-\log \tau_0$	(8.25)	(8.50)	8.85	9.08	9.37
	γ	0.72	0.75	0.8	0.8	0.8
II	$-\log \tau_0$	(8.25)	(8.5)	8.84	9.12	9.39
	ρ	30	30	40	40	40
III	$-\log \tau_D$	(7.87)	(8.23)	8.41	8.73	9.17
	τ_D/τ_0	1.0	1.0	1.0	0.7	0.4

For discussion of values in parentheses see text

Table 3 Correlation times and width parameters for PS (MW 110 000) in pentachloroethane. Models I–III as in Table 1

Model	Parameter	$10^3/T$ (K $^{-1}$)				
		3.3	3.1	2.9	2.7	2.5
(a) Concentration = 100 mg polymer/ml solvent						
I	$-\log \tau_0$	(8.35)	8.80	9.07	9.28	9.48
	γ	0.72	0.72	0.72	0.8	0.85
II	$-\log \tau_0$	(8.35)	8.75	9.10	9.3	9.55
	ρ	20	20	25	30	30
III	$-\log \tau_D$	(8.4)	8.7	8.92	9.09	9.32
	τ_D/τ_0	0.4	0.4	0.4	0.4	0.4
(b) Concentration = 400 mg polymer/ml solvent						
I	$-\log \tau_0$	(8.15)	(8.35)	8.75	9.1	9.45
	γ	0.72	0.72	0.72	0.72	0.72
II	$-\log \tau_0$	(8.0)	(8.3)	8.65	9.15	9.45
	ρ	20	20	20	20	20
III	$-\log \tau_D$	(8.10)	(8.40)	8.70	9.13	9.49
	τ_D/τ_0	0.4	0.4	0.4	0.2	0.1

For discussion of values in parentheses see text

Table 4 Correlation times and width parameters for PPO solutions in CDCl_3 . Models I–III as in Table 1

Model	Parameter	$10^3/T$ (K $^{-1}$)						
		4.6	4.4	4.2	4.0	3.8	3.6	3.4
(a) Concentration = 100 mg polymer/ml solvent								
I	$-\log \tau_0$	9.67	9.79	9.91	10.03	10.15	10.27	10.39
	γ	0.7	0.75	0.8	0.8	0.9	0.9	0.95
II	$-\log \tau_0$	9.68	9.82	9.96	10.1	10.24	(10.38)	(10.52)
	ρ	20	25	30	35	35	(40)	(40)
III	$-\log \tau_D$	9.70	9.87	10.01	10.18	10.33	(10.48)	(10.64)
	τ_D/τ_0	0.1	0.1	0.1	0.1	0.1	(0.1)	(0.1)
(b) Concentration = 400 mg polymer/ml solvent								
I	$-\log \tau_0$	9.05	9.36	9.67	9.92	10.1	10.25	10.4
	γ	0.7	0.7	0.7	0.75	0.8	0.8	0.85
II	$-\log \tau_0$	9.07	9.4	9.7	9.96	10.22	10.44	(10.66)
	ρ	20	20	20	20	20	20	(20)
III	$-\log \tau_D$	9.0	9.44	9.7	10.1	10.39	10.85	(11.08)
	τ_D/τ_0	0.4	0.1	0.1	0.05	0.025	0.01	(0.01)

For discussion of values in parentheses see text

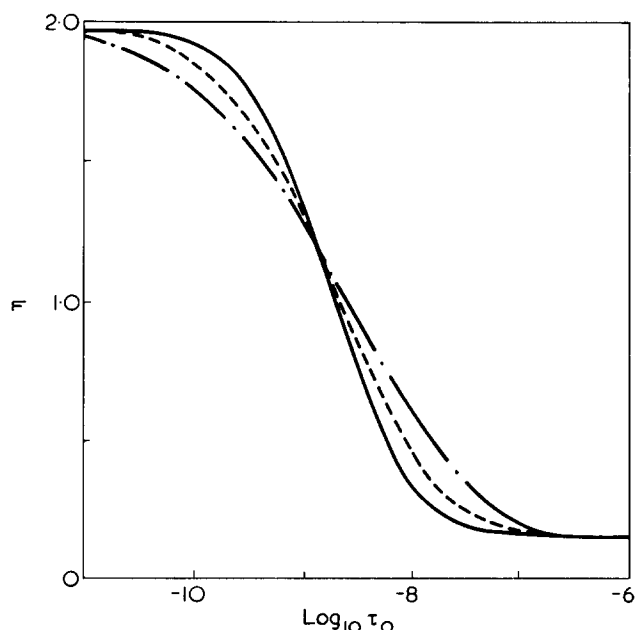


Figure 9 $\hat{\eta}$ calculated according to equation (13) for $\log -\chi^2$ distribution. (—), $\rho = 40$; (---), $\rho = 20$; (- · - ·), $\rho = 10$. $b = 1000$ in all cases

e.g. PS. It is difficult to understand why PS and PMMA, two polymers of similar flexibility, should differ in this respect, and this anomaly does call the physical basis of the model into question.

The temperature dependence of the width parameters for the other two models is consistent for all systems, the distribution narrowing as the temperature increases; this is as expected. Greater thermal activity will lead to greater independence of successive units and less inequality between the time constants for different types of motion. The decrease in width is in most cases quite rapid at the lower temperatures, near the T_1 minimum, and there are indications that the distribution width tends to stabilize at the higher temperatures, though the evidence is not conclusive.

The distribution width appears to depend mainly on the chemical structure of the polymer and the temperature, but does not differ a great deal between the two concentrations. This is particularly true near the T_1 minimum where the appreciable decrease of T_1 with concentration arises from an increase in the correlation time. At higher temperatures, the variation of correlation time with concentration is less since the more concentrated solution has a higher activation energy. In some cases, notably PPO, the correlation times for the two solutions are very close and the observed decrease in T_1 with concentration arises from a small increase in the distribution width. The variation of molecular weight for PS has a greater effect on the width than on the correlation time, especially for the higher concentration. Experimentally the increase in width affects the *NOE* rather than the T_1 , the former decreasing with concentration to a greater extent than the latter.

The origin of the distribution of correlation times is difficult to decide. The evidence from the present data is that the distribution arises from intramolecular rather than intermolecular effects. Thus the fact that the distribution width is relatively independent of concentration, even though the bulk viscosity changes by an order of magnitude indicates an intramolecular origin. The environment

affects the correlation time and its activation energy but not the nature of the polymer motion. Further circumstantial evidence arises from calculations of the *NOE* by a different approach to equations (2) and (5). The distribution of correlation times may arise from a distribution of environments due to small-scale inhomogeneity of the polymer solution, or alternatively as an effective way of expressing a non-exponential correlation function. Substitution of equation (5) into (2) is correct in the latter case and also in the former case when the rate of environmental fluctuation is rapid compared to the average decay of the autocorrelation function. More probably, the fluctuation rate is slower than the autocorrelation function decay, in which case the expression for the *NOE* should be averaged, and averaged spectral densities should not be used.

The appropriate equation for the *NOE* is:

$$\hat{\eta} = \int_0^{\infty} G(\tau_c)\eta(\tau_c)d\tau_c \quad (13)$$

Since the expression for $1/T_1$ is linear in the spectral densities, there is no change in this expression. Figure 9 shows $\hat{\eta}$ calculated using equation (13) for the $\log -\chi^2$ distribution. Comparing with Figure 2, the *NOE* is much less sensitive to the distribution width, and in fact it proved impossible to fit the majority of experimental results to this model. It is probable therefore that the use of a distribution is necessary to represent a non-exponential correlation function arising from the character of polymer motion. The nature of this motion has been discussed by Schaefer¹⁰ and others¹¹ who conclude it is likely to consist of a rapid short range process leading to partial loss of correlation of the C-H vector followed by a slower, longer range process leading to complete loss of correlation. The less effective the initial process, or the greater the disparity in correlation times, the wider is the distribution. The rate of each process is strongly affected by the chemical structure of the chain, as is obvious from the fact that the correlation time appropriate to the T_1 minimum in the strongly hindered PS and PMMA molecules occurs at about 30°C, whereas that in PPO occurs at a much lower temperature, estimated at about -90°C. It is interesting however that the distribution width for PPO at the lower temperatures is comparable to the widths for PS and PMMA in the vicinity of the T_1 minima. It seems that the balance between short and long-range processes expressed by the width parameter correlates in roughly the same way for all polymers with the average correlation time. The correlation is not exact, as can be seen from the fact that the distribution width for PMMA is larger than for PS at the T_1 minima even though both polymers have similar flexibilities. There is however a major conformational difference between the two polymers which may explain this and indirectly support the above explanation of the distribution origin. PS possesses accessible conformations in which steric interactions are very small or non-existent whereas all conformations of PMMA contain some degree of irreducible steric conflict. The additional interactions in PMMA need not lead to higher barriers to rotation, as might be expected, provided the energies of both stable conformations and transition states between conformations are affected to the same extent. (This effect has been observed in dielectric relaxation of substituted polystyrenes¹⁶.) However the strong

Table 5 Correlation times for internal rotation of the $\alpha\text{-CH}_3$ groups in PPO and PMMA

(a) PMMA (100 mg/ml solvent)

$1/T$ (K^{-1})	Syndiotactic CH_3		Heterotactic CH_3	
	$-\log \tau_g$	τ_g/τ_0	$-\log \tau_g$	τ_g/τ_0
3.1	9.53	0.33	9.87	0.15
2.9	9.86	0.3	10.19	0.14
2.7	10.11	0.33	10.45	0.15
2.5	10.33	0.35	10.57	0.20
2.3	10.50	0.45	10.71	0.35

(b) PPO

$1/T$ (K^{-1})	Concentration = 100 mg/ml solvent		Concentration = 400 mg/ml solvent	
	$-\log \tau_g$	τ_g/τ_0	$-\log \tau_g$	τ_g/τ_0
4.6	9.98	0.5	10.03	0.11
4.4	10.04	0.6	10.12	0.19
4.2	10.15	0.65	10.17	0.34
4.0	10.2	0.8	10.41	0.45
3.8	10.34	0.8	10.37	0.7
3.6	10.45	0.85	10.49	0.9
3.4	—	—	10.63	1.1

Table 6 Activation energies for backbone motions and internal rotation of $\alpha\text{-CH}_3$ groups. Models I–III as in Table 1

Polymer	Concentration (mg/ml solvent)	Activation energies for Backbone motions (kJ/mol)			Internal rotation of $\alpha\text{-CH}_3$ groups
		Model I	Model II	Model III	
PMMA	100	28 ± 5	31 ± 6	23 ± 6	$25 \pm 6^*$, $20 \pm 5^\dagger$
	400	35 ± 8	42 ± 7	37 ± 7	
PS (10 000)	100	24 ± 5	21 ± 4	30 ± 7	—
	400	31 ± 5	29 ± 6	31 ± 6	—
PS (110 000)	100	27 ± 5	27 ± 6	21 ± 5	—
	400	32 ± 6	35 ± 7	33 ± 6	—
PPO	100	12 ± 1	14 ± 3	15 ± 3	9.3 ± 2
	400	21 ± 6	25 ± 5	35 ± 8	9.3 ± 2

* Syndiotactic CH_3 † Heterotactic CH_3

interactions will lead to a greater degree of correlation between the motions of successive segments and hence a wider distribution of correlation times. It is interesting to compare distribution parameters obtained for PMMA from dielectric relaxation¹⁷. The Cole–Cole parameter for PMMA in dilute solution in CCl_4 at 25° to 50°C is approximately 0.75, rather higher than the values given here. However, the two values are not strictly analogous, since the present value applies to backbone motion only while the dielectric value must also incorporate a contribution from internal motions within the ester group in which the dipole moment resides. Such motions will tend to reduce the effective distribution width, though not eliminate it completely.

The $\alpha\text{-CH}_3$ relaxation times for the two PPO solutions and the less concentrated PMMA solution have been analysed using the extension of the relaxation theory outlined earlier for the $\log -\chi^2$ distribution. For PPO, it was assumed that τ_g is independent of τ_c , following previous work on this system⁶. For PMMA it was assumed that τ_g is proportional to τ_c because of the similarity in basic structure between PMMA and polyisobutylene for which this

has been found to be approximately true⁶. Knowing the correlation times and distribution widths for the backbone, it is straightforward to determine the value of τ_g reproducing the observed $^{13}\text{CH}_3$ value for T_1 . A graphical interpolation method was employed, giving the values in Table 5. For almost all cases, τ_g is less than τ_0 , though on average the ratio τ_g/τ_0 is comparable for the two polymers. The factors which determine the magnitude of τ_0 are also important in determining τ_g . It is interesting to note that the values of τ_g at the same temperature for the two PPO solutions are practically identical, though τ_0 differs considerably. This observation, surprisingly consistent in view of the propagation of experimental errors in the lengthy analysis, confirms a previous conclusion⁶ that the internal rotation of methyl groups in PPO is truly an internal process and is independent of the rate of molecular tumbling. PMMA on the other hand resembles polyisobutylene where the rate of methyl rotation correlates with the rate of molecular rotation. τ_g for the heterotactic $\alpha\text{-CH}_3$ group is shorter than τ_g for the syndiotactic group, indicating greater freedom of movement, though this is not revealed so clearly by the activation energies which are given in Table 6. The values of the $\alpha\text{-CH}_3$ barrier obtained here are similar to the value of 32.7 kJ/mol for syndiotactic PMMA reported by Higgins *et al.* from neutron scattering²³. In that work a value of 16.7 was given for isotactic PMMA, but unfortunately this isomer could not be obtained for the present work. The $\alpha\text{-CH}_3$ barrier in PPO is rather lower than the values of 11 kcal/mol from neutron scattering²³. It is significant that in PPO the $\alpha\text{-CH}_3$ barrier is appreciably less than the backbone activation energy, whereas in PMMA, the two quantities are comparable. This is further evidence that in PPO side group and chain motion are essentially independent while in PMMA the motions are linked. The backbone activation energy for PPO increases by a greater relative amount on increasing the concentration than the backbone activation energies for PS and PMMA. Presumably the viscoelastic properties of the polymer environment exert a greater influence on the backbone motion when the intramolecular barriers are small. The necessity of taking correlation time distributions into account is seen clearly by comparing the activation energies for the two solutions in Table 6 with the slopes of the T_1 plots in Figure 1. A cursory inspection of the T_1 data suggests that the activation energy decreases with concentration whereas the opposite is in fact true.

To progress further in studies of this kind, the first requirement is additional experimental relaxation data. The spin–spin relaxation time is measurable from the n.m.r. linewidth, if it is sufficiently short to dominate other line broadening processes, but unfortunately in the present polymers there is an unknown contribution to line broadening from chemical shift dispersion due to irregular tacticity. Further data could be obtained from measurements made at different resonance frequencies, and the possibilities in this direction are worth investigation.

ACKNOWLEDGEMENTS

The authors acknowledge with gratitude the financial support of the SRC and the benefit of discussions with Professor G. Allen and Mr R. F. Warren of this Department.

REFERENCES

- 1 Allerhand, A. and Hailstone, R. K. *J. Chem. Phys.* 1972, **56**, 3718
- 2 Chachaty, C., Forchioni, A. and Ronfard-Haret, J. C. *Makromol. Chem.* 1973, **173**, 213
- 3 Inoue, Y., Nishioka, A. and Chujo, R. *Makromol. Chem.* 1973, **168**, 163
- 4 Inoue, Y., Nishioka, A. and Chujo, R. *J. Polym. Sci. Polym. Phys. Ed.* 1973, **11**, 2237
- 5 Schaefer, J. *Macromolecules* 1972, **5**, 427
- 6 Heatley, F. *Polymer* 1975, **16**, 493
- 7 Heatley, F. *Polymer* 1975, **16**, 489
- 8 Schaefer, J. and Natusch, D. F. S. *Macromolecules* 1972, **5**, 416
- 9 Doddrell, D., Glushko, V. and Allerhand, A. *J. Chem. Phys.* 1972, **56**, 3683
- 10 Schaefer, J. *Macromolecules* 1973, **6**, 882
- 11 Hermann, G. and Weill, G. *Macromolecules* 1975, **8**, 171
- 12 Valur, B., Jarry, J. P., Geny, F. and Monnerie, L. *J. Polym. Sci. Polym. Phys. Ed.* 1975, **13**, 667, 675
- 13 Woessner, D. E. *J. Chem. Phys.* 1962, **37**, 647
- 14 Cole, K. S. and Cole, R. H. *J. Chem. Phys.* 1941, **9**, 341
- 15 Connor, T. M. *Trans. Faraday Soc.* 1964, **60**, 1574
- 16 North, A. M. *Chem. Soc. Rev.* 1972, **1**, 49
- 17 Mashimo, S., Chiba, A. and Shinohara, K. *Polym. J.* 1974, **6**, 170
- 18 Fuoss, R. M. and Kirkwood, J. G. *J. Am. Chem. Soc.* 1941, **63**, 385
- 19 Davidson, D. W. and Cole, R. H. *J. Chem. Phys.* 1950, **18**, 1417; 1951, **19**, 1484
- 20 Hunt, B. I. and Powles, J. G. *Proc. Phys. Soc.* 1966, **88**, 513
- 21 Woessner, D. E., Snowden, B. S. and Meyer, G. H. *J. Chem. Phys.* 1969, **59**, 719
- 22 Johnson, L. F., Heatley, F. and Bovey, F. A. *Macromolecules* 1970, **3**, 175
- 23 Higgins, J. S., Allen, G. and Brier, P. N. *Polymer* 1972, **13**, 157

New solid state polyamidation process

Emmanuel M. Kampouris

Faculty of Chemical Engineering, National Technical University of Athens, 42 Patission Street, Athens 147, Greece

(Received 15 October 1975)

Solid state polymerization reactions are of considerable scientific and industrial interest. In some cases nylon salts can be converted to polyamides through intermediates of lower melting point, involving a solid—melt—solid sequence which is incompatible with known solid state polyamidation processes. A new solid state polyamidation process is described for use with salts, prepolymers, or amino acids which provides good temperature control and the avoidance of agglomeration of particles. The process comprises: (a) suspension of the particles of raw material (salt, amino acid or prepolymer) in an inert solvent; (b) reaction at the boiling point of the solvent with continuous distillation and feeding of solvent; (c) reactions at higher temperatures by feeding with the correct solvent; (d) separation of the formed granules of polymer by centrifugation, and (e) washing and drying. This process was tested for the solid state polymerization of hexamethylenediammonium maleate, which polymerizes through intermediates of lower melting point, and the following factors were examined: (a) presence and amount of dispersing agents; (b) nature of inert solvent; (c) grain size of salt; (d) distillation rate; (e) the ratio of salt: inert solvent and (f) temperature and time.

INTRODUCTION

Polyamides can be prepared by a variety of methods. Of these only three have been found of importance for industrial application. These are melt reaction, ring-opening polymerization, and low temperature solution polymerization with acid chlorides.

The method of melt reaction is the one exclusively used in the case of polyamides prepared from diamines and diacids. The method is inapplicable in the case of diamines or diacids sensitive to the high temperatures of the melt reaction, and also when undesirable side reactions, such as cyclization, can proceed. Solid state reactions proceed generally at lower temperatures and can be topochemically controlled. Thus when the reaction is compatible with the geometry of arrangement of molecules in the solid state, the polymerization can be followed and cyclization excluded.

The proposed processes for solid state polyamidation generally include: (a) heating in an inert gas flow¹⁻³, and (b) heating in an inert solvent⁴. The first has been proposed for use in the case of further polymerization of given prepolymers, and the second for the polymerization of nylon salt.

In non-catalysed solid state polymerizations the reaction rate is strongly affected by the temperature and thus the reaction is generally studied in a narrow temperature range close to the melting point of the monomer⁵⁻⁷. In this case, the narrower the range the greater the need for satisfactory temperature control, in order to avoid the possibility of hot spots in which the melt phase forms and the particles tend to agglomerate. Experience in solid state polymerizations of a number of salts indicate that in some cases the conversion, from the solid salt to a polymer of higher melting point, passes through intermediates of lower melting points. In these cases and soon after the early stages of the reaction the solid particles become sticky and the reaction partly proceeds through a semi-solid or melt state. This state continues until formation of a product of higher melting point. After that the reaction occurs in the solid state. To avoid the semi-solid state, in the case of reactions close to the melting point, and to overcome the tendency

to agglomerate, in the case of lower melting point products formed during the course of the reaction, a suitable process is needed.

This paper presents a new solid state polymerization process designed for use with nylon salts, prepolymers and amino acids. It is also designed to secure the required temperature control and overcome tendency of semi-solid particles to agglomerate. The process is based on the principle of suspension polymerization and shows basic differences from that already proposed⁴. These include different methods of temperature control, ability to effect reaction at lower temperatures, ability to continue reaction for long times at a given temperature, and ability to overcome the tendency for agglomeration. The process comprises: (a) dispersion of the ground salt, prepolymer or amino acid, in an inert solvent with or without the presence of a suitable dispersion agent. The requirements for the inert solvent include non-solvent action for the raw materials, the intermediates and the polymer and a boiling point equal to the desired temperature of reaction; (b) reaction under continuous distillation and introduction of additional inert solvent, for the required time; (c) change of the reaction temperature by feeding with another suitable solvent; (d) separation of the product by filtration (centrifugation); (e) washing and drying.

In order to examine the various factors affecting the process, the polymerization of hexamethylenediammonium maleate was studied as an interesting example. The factors examined were: (a) the presence and amount of dispersion agents; (b) the nature of inert solvent; (c) the grain size of the salt; (d) the distillation rate; (e) the ratio of salt:inert solvent; (f) the temperature and time.

EXPERIMENTAL

Preparation of hexamethylenediammonium maleate

Hexamethylenediamine (250 g) was added in portions to a stirred solution of maleic acid (250 g) in water (300 ml), while cooling to maintain the temperature at ~40°C. Stirring was continued for 1 h, after the addition of all the

Table 1 Effectiveness of dispersing agents

Type of dispersing agent	Dispersing agent (% w/v)								
	0.1	0.4	0.6	0.8	1	2	3	4	5
1	p	p	p	g	g	g	g	g	g
2	p	p	p	g	g	g	g	g	g
3	p	p	p	g	g	g	g	g	g
4	p	p	p	p	g	g	g	g	g
5	p	p	p	p	g	g	g	g	g
6	p	p	p	p	p	p	p	p	p
7	p	p	p	p	p	p	p	p	p
8	p	p	p	p	p	p	p	p	p

1, Crude montana wax; 2, decolourized montana wax; 3, bleached montana wax; 4, carnauba wax; 5, sodium stearate; 6, fatty acid poly(ethylene glycol) ester; 7, fatty alcohol poly(ethylene glycol) ether; 8, alkyl phenol poly(ethylene glycol) ether; p, poor results; g, good results

Table 2 Effect of the nature of the inert solvent

Inert solvent	Reaction temperature (°C)	NH ₂ content (%)	Product on no. 30 sieve (%)
Tetrachloroethylene	121	7.5	7.7
n-Octane	125	7.3	7.2
n-Nonane	151	2.6	9.0
Cumene	152	2.4	9.3

hexamethylenediamine, and the reaction mixture was cooled to assist deposition of the salt formed. The separated product was filtered off and dried, over CaCl₂, to give 410 g (76%) of hexamethylenediammonium maleate monohydrate. Recrystallization from water gave prisms, melting point 130°–131°C. (Found: H₂O, 7.7%; C₁₀H₂₀N₂O₄·H₂O requires H₂O, 7.2%.) Dilution of the mother liquors with an equal volume of methanol and cooling produced more product, to give a total yield of 95%. The anhydrous salt was obtained by drying the monohydrate over P₂O₅ *in vacuo* at room temperature. Recrystallization from ethanol gave the anhydrous form, melting point 150°–151°C. (Found: C, 51.4; H, 8.4; N, 12.3; and NH₂, 13.9%. C₁₀H₂₀N₂O₄ requires: C, 51.7; H, 8.6; N, 12.1; and NH₂, 13.8%.) The salt was soluble in water (pH of 1% solution, 7.8), slightly soluble in the lower alcohols, and insoluble in paraffinic, aromatic and chlorinated hydrocarbons.

Polymerization

50 g of screened anhydrous salt were suspended in 500 ml of the selected non-solvent, contained in a four-necked 1.5 l flask. The flask was equipped with side condenser, stirrer, inert gas inlet, and separating funnel, and was heated by an oil bath. The stirred mixture was de-aerated, blanketed with a weak flow of N₂ and the reaction was carried out at the boiling point of the inert solvent with a continuous feed of de-aerated solvent, to equalize the amount distilling. The water formed was continuously eliminated with the distilling solvent. At the end of the reaction, the mixture was cooled, and the product was separated, washed with hexane, and dried under vacuum. When dispersing agents were used, the calculated amount was dissolved in the inert solvent before the addition of the salt.

Characterization

The characterization of the products obtained was based on end-group analysis, melting point determination, and i.r. spectroscopy. End-group analysis was by NH₂ determination⁸ and parallel determinations for carboxyl groups indicated no considerable differences, indicating that only a little amine was eliminated during the process. I.r. spectra, obtained with KBr discs, showed a successive change from the salt to a polyamide structure⁹.

RESULTS AND DISCUSSION

Presence and amount of dispersion agents

The polymerization of hexamethylenediammonium maleate is one of the better examples of the process taking place through lower melting point intermediates. Even at 120°C, i.e. 30°C below the melting point of the salt, the particles soon become sticky and tend to agglomerate to a semi-solid mass. Suspension throughout the course of the reaction was assured by the use of a dispersing agent. The suitability of the following agents was examined: (a) montana wax (crude, decolourized, and bleached); (b) carnauba wax; (c) sodium stearate; (d) fatty acid poly(ethylene glycol) ester; (e) fatty alcohol poly(ethylene glycol) ether; and (f) alkyl phenol poly(ethylene glycol) ether.

The efficiency of the dispersion agents was tested at 125°C (n-octane) under the following conditions: (a) reaction time, 4 h; (b) salt to non-solvent ratio, 1:10 w/v; (c) salt grain size, 30 to 40 mesh (US Sieve Series); and (d) amount of dispersion agent, 0.1 to 5% w/v on the inert solvent.

As a measure of the efficiency of dispersion agents, the reaction product, was collected, on the 30 mesh sieve. The greater the efficiency of the dispersion agent, the lower the amount of product collected. The results obtained are given in Table 1 where 'good' signifies an amount on the sieve no greater than 10%, and 'poor' indicates greater percentages. As the data indicate montana wax (crude, decolourized, or bleached) can be satisfactorily used for concentrations of 0.8% and higher. Carnauba wax and sodium stearate were found good enough for concentrations greater than 1%. The other agents failed for all concentrations up to 5%. Accordingly decolourized montana wax was used, in 1% w/v concentration of the inert solvent.

Nature of the inert solvent

Paraffinic, aromatic, and chlorinated hydrocarbons were examined for use as inert solvents (non-solvents for the salt and the reaction products). Two pairs of solvents having similar boiling points were compared: (a) n-octane (125°C) and tetrachloroethylene (121°C) and (b) n-nonane (151°C) and cumene (152°C). The reaction was carried out for 4 h, in the presence of 1% montana wax (on non-solvent), for salt to non-solvent ratio 1:10 w/v, for salt grain size 30 to 40 mesh, and for a distillation rate of 400 ml/h. The results from Table 2 indicate no visible difference between a n-paraffin and a chlorinated hydrocarbon, also between a n-paraffin and an aromatic hydrocarbon, when the differences in boiling points are small. These results enable us to conclude that, at least between the experimental limits used, the nature of the non-solvent does not affect the polymerization process.

Table 3 Effect of the grain size of salt

Grain size (mesh)	NH ₂ content (%)
20-25	7.8
30-35	7.5
40-45	7.2
50-60	7.4

Table 4 Effect of the distillation rate

Distillation rate (ml/h)	NH ₂ content (%)
100	7.4
250	7.2
500	7.6
750	7.3
1000	7.3

Grain size of salt

The effect of the grain size of salt upon the polymerization rate was examined for grain sizes 20 to 25 mesh, 30 to 35 mesh, 40 to 45 mesh, and 50 to 60 mesh (US Sieve Series). The conditions of the reaction were: temperature 125°C (n-octane); duration, 4 h; distillation rate, 400 ml/h; ratio of salt to non-solvent, 1:10 w/v; and montana wax, 1% on non-solvent. The results obtained are given in Table 3. As the data indicate, the NH₂ content varies between 7.2 and 7.8%, thus there is no visible effect of the grain size upon the reaction rate. These results indicate that the reaction rate is not controlled by the diffusion process by which the water formed is eliminated from the grain. Similar results have been published for the solid state polymerization of nylon-6,6 prepolymers¹⁰.

Distillation rate

The effect of the distillation rate of non-solvent upon the polymerization process was examined for rates from 100 to 1000 ml/h. The conditions were; temperature, 125°C (n-octane); salt grain size, below 50 mesh; montana wax 1%; salt to non-solvent ratio, 1:10 w/v; and duration, 4 h. The results obtained are given in Table 4. As the data indicate there is no appreciable differences in NH₂ content, thus the distillation rate does not affect the reaction rate, at least not in the case studied.

Ratio salt: inert solvent

This effect was examined for n-octane (125°C) and cumene (152°C), and for the ratios 1/20; 1/15; 1/10 and 1/5 w/v. The two non-solvents were selected to have boiling points below and equal to the melting point of the salt. In all cases the concentration of montana wax was 1% of the non-solvent (w/v), the grain size of the salt 50 to 60 mesh, the distillation rate 400 ml/h, and the time 4 h. The results obtained are given in Table 5. As the data indicate the value of the ratio, at least between the limits used, does not affect the polymerization process or the effectiveness of the dispersing agent.

Temperature and time

The effect of temperature was examined in the range 125° to 180°C and that of time for 14 h. The non-solvents used were n-octane, cumene, mesitylene, and *o*-dichloro-

benzene. The grain size of the salt was below 50 mesh (US Sieve Series), the concentration of montana wax 1% w/v, the ratio salt to non-solvent 1/10 w/v, and the distillation rate 250 ml/h. In the case of reactions at 164°C (mesitylene) and 180°C (*o*-dichlorobenzene), the salt was first suspended in cumene and once the distillation started was continuously fed with the correct non-solvent. In these cases the ability of the method to proceed at various temperatures was tested, and the final temperatures were reached after about 3 h. The results obtained (Table 6) indicate in all cases that the polymerization proceeds through intermediates of melting points lower than that of salt. The case of n-octane represents a typical solid state reaction (the melting point of product being always higher than the boiling point of the non-solvent), while in the other cases the reaction starts in the melt and changes to a solid state polymerization (the melting point of product being at the early stages lower and then greater than the boiling point of the non-solvent).

All the products obtained, were in the form of small spheres, free flowing, and containing microscopic bubbles. The reaction rate and the conversion, as the examination of the amine group content indicates, were low at 125°C and increased both with temperature and time. The low molecular weight products of high NH₂ content, were soluble in water and 70% alcohol and highly hygroscopic. Solubility and hygroscopicity decreased with increase of molecular weight, and the high molecular weight products became non-hygroscopic and insoluble. Search for a satisfactory solvent, among the common polyamide solvents e.g. DMF, DMSO, trifluoroacetic acid etc. was unsuccessful and small amounts dissolved only in concentrated sulphuric acid. The melting point increases sharply from 145°–150°C to more than 300°C (discoloration beginning from about 250°C), but the products can be formed into sheets by pressing at 180°–200°C. The insolubility and infusibility, followed by formability under pressure, may be due to the polyamide structure rather than to possible reactions, such as crosslinking through the maleate double bonds. Analogous behaviour has been reported for the case of poly(hexamethylene fumaramide)¹¹ prepared by interfacial polycondensation from hexamethylenediamine and fumaroyl chloride. The consistency of the products of polymerization changed from brittle, in the case of low molecular weights, to stiff difficult to break, and hot-press formable, in the case of the high molecular ones.

The i.r. spectra, obtained with KBr discs, showed the characteristic polyamide bands at 1630 cm⁻¹ and 1540 cm⁻¹. The identification of the maleamide groups by i.r. analysis is quite difficult. In polyesters it is possible to distinguish between maleic acid and fumaric acid units, the

Table 5 Effect of the ratio salt: inert solvent

Ratio (w/v)	NH ₂ content (%)	Effectiveness of dispersion agent
	n-octane	
1/20	7.4	good
1/15	7.8	good
1/10	7.3	good
1/5	7.5	good
	cumene	
1/20	2.5	good
1/15	2.4	good
1/10	2.6	good
1/5	2.7	good

Table 6 Effect of temperature and time

Time (days)	n-octane			cumene			mesitylene			o-dichlorobenzene		
	NH ₂ (%)	m.p. (°C)	70% alcohol	NH ₂ (%)	m.p. (°C)	70% alcohol	NH ₂ (%)	m.p. (°C)	70% alcohol	NH ₂ (%)	m.p. (°C)	70% alcohol
2	9.6	140-5	soluble	5.1	140-5	soluble	2.8	140-5	soluble	1.1	145-50	soluble
4	7.8	140-5	soluble	2.6	140-5	soluble	1.4	145-50	soluble	unde- terminated	150-5	insoluble
6	7.2	140-5	soluble	2.0	140-5	soluble	unde- terminated	>300	insoluble	unde- terminated	>300	insoluble
8	6.8	135-40	soluble	1.5	145-50	soluble	unde- terminated	>300	insoluble	unde- terminated	>300	insoluble
10	6.5	130-5	soluble	1.1	145-50	soluble	unde- terminated	>300	insoluble	unde- terminated	>300	insoluble
12	6.2	135-40	soluble	unde- terminated	200	insoluble	unde- terminated	>300	insoluble	unde- terminated	>300	insoluble
14	6.0	135-40	soluble	unde- terminated	>300	insoluble	unde- terminated	>300	insoluble	unde- terminated	>300	insoluble

former showing absorption bands at $7.17 \mu\text{m}$ (1400 cm^{-1}) and $7.45 \mu\text{m}$ (1350 cm^{-1}) and the latter at $8.42 \mu\text{m}$ (1175 cm^{-1}) and $7.52 \mu\text{m}$ (1330 cm^{-1}), but usually these bands overlap with other absorptions in the spectra⁹. Earlier literature for the case of polyamides has not been found except for the case of fumaramides¹¹. In our spectrograms bands were found at 1400 cm^{-1} and 1380 cm^{-1} , possibly characterizing maleic acid units. No bands characteristic of fumaric acid units were found.

REFERENCES

- 1 Flory, P. J. US Pat. 2 172 374 (1939)
- 2 Monroe, G. C. US Pat. 3 031 433 (1962)
- 3 Bruck, S. D. *Ind. Eng. Chem. Prod. Res. Dev.* 1963, 2, 119
- 4 California Research Corp. Br. Pat. 852 672 (1960)
- 5 Colonge, J. and Guyot, P. *C. R. Acad. Sci.* 1951, 233, 1604
- 6 Volokhina, V. A., Kudryavtsev, G. I., Skuratov, M. S. and Bonetskaya, K. A. *J. Polym. Sci.* 1961, 53, 289
- 7 Khripkov, E. G., Kharitonov, V. M. and Kudryavtsev, G. I. *Khim. Volonka* 1970, 6, 63
- 8 Waltz, E. J. and Taylor, B. G. *Anal. Chem.* 1947, 19, 448
- 9 Hummel, D. and Scholl, F. 'Infrared Analysis of Polymers, Resins, and Additives. An Atlas'. Wiley-Interscience, New York, 1971, Vol 1, Ch 8.3, 8.4, 8.5
- 10 Chen, C. F., Griskey, G. R. and Beyer, H. G. *AIChE J.* 1969, 15, 680
- 11 Mortillaro, L., Russo, M., Credali, L. and Guidotti, V. *Makromol. Chem.* 1969, 126, 239

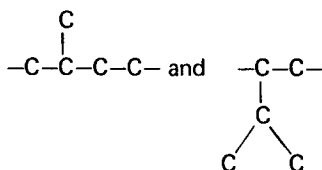
Sequence distribution of polyisoprenes

Yasuyuki Tanaka and Hisaya Sato

Department of Textiles and Polymer Science, Faculty of Technology, Tokyo University of Agriculture and Technology, Koganei, Tokyo 184, Japan

(Received 20 November 1975)

The ^{13}C n.m.r. spectra of hydrogenated polyisoprenes were investigated. Polyisoprenes were prepared with $n\text{-BuLi-Et}_2\text{O}$, $\text{Ti}(\text{OBu})_4\text{-AlEt}_3$, $\text{CoI}_2\text{-ROH-PhMgBr}$, Alfin, and radical catalysts. These polymer were hydrogenated with *p*-toluenesulphonylhydrazide. ^{13}C n.m.r. signals were assigned for triad sequences of



arising respectively from 1,4- and 3,4-units. Signals due to head-to-head and tail-to-tail linkages of 1,4- and 3,4-units were also assigned. It is disclosed that 1,4- and 3,4-units were randomly distributed in $n\text{-BuLi-Et}_2\text{O}$, $\text{CoI}_2\text{-ROH-PhMgBr}$, and radical catalysed polyisoprenes, rather alternating in $\text{Ti}(\text{OBu})_4\text{-AlEt}_3$ catalysed polyisoprene, and slightly in blocks in Alfin polyisoprene. It is also confirmed that Alfin, radical, and cobalt catalysed polyisoprenes contained significant amounts of head-to-head and tail-to-tail linkages of 1,4- and 3,4- units. Signals due to the tacticity of the polyads of 3,4-units were also discussed.

INTRODUCTION

Isoprene can be polymerized into four types of isomeric structures; *cis*-1,4, *trans*-1,4, 3,4, and 1,2, depending on catalysts and polymerization conditions. So far, the difference of mechanical and thermal properties among polyisoprenes has been discussed chiefly on the basis of amounts of these isomeric structures. However, it is quite reasonable to expect that the polymer properties are affected not only by the composition of isomeric structures but also by the distribution of isomeric structures, the arrangement of head and tail linkages, and the degree of branching. This idea was adopted by Hackathorn and Brock as an explanation of the poor crystallizability of lithium polyisoprene; i.e. head-to-head and/or tail-to-tail linkages of 1,4- and 3,4-units prevented the crystallization of the polymer¹.

Pyrolysis-gas chromatography has been applied to the investigation of the sequence distribution of 1,4- and 3,4-units in polyisoprenes^{2,3}. This method is based on the structural relationship between the isoprene dimers and the dyad sequences of 1,4- and 3,4-units. However, it is difficult to discuss the slight differences in the yield of each dimer because the absolute amount of the dimers is small (~30%) compared to the isoprene monomer (~65%). Ozonolysis has been used to measure the amount of head-to-head, head-to-tail, and tail-to-tail linkages of the 1,4-unit in polyisoprenes^{4,5}. This method, however, is limited to the detection of these linkages of 1,4-unit.

In a previous paper, we have investigated ^{13}C n.m.r. spectra of chicle and *cis-trans* isomerized polyisoprenes and determined the sequence distribution of *cis*-1,4- and

trans-1,4-units in these polymers⁶. We have also studied ^{13}C n.m.r. spectra of hydrogenated polyisoprenes prepared with $n\text{-BuLi-Et}_2\text{O}$ catalysts and found that 1,4- and 3,4-units were distributed randomly along the polymer chains regardless of the amounts of 3,4-unit⁷. In the present investigation we prepared various types of polyisoprenes and discussed the distribution of 1,4- and 3,4-units, arrangements of head and tail linkages, the branches of polymer chains, and the tacticity of polyads of 3,4-unit by the use of ^{13}C n.m.r. spectra of hydrogenated polyisoprenes.

EXPERIMENTAL

Materials

Polyisoprenes were prepared with $n\text{-BuLi-Et}_2\text{O}$, $\text{Ti}(\text{OBu})_4\text{-AlEt}_3$, Alfin, and $\text{CoI}_2\text{-MeOH-PhMgBr}$ catalysts, and a radical initiator (emulsion polymerization) in the conventional methods. Isomeric structures of the polymers were determined by ^1H n.m.r. and i.r. studies. Polymerization conditions and isomeric structures of the polymers are listed in Table 1. Isoprene-piperylene copolymer was prepared by adding isoprene dropwise into a pentane solution of piperylene after the addition of $n\text{-BuLi}$ as an initiator. Polyisoprenes and isoprene-piperylene copolymer were hydrogenated by the use of *p*-toluenesulphonylhydrazide in xylene according to the method of Sanui *et al.*⁸. Hydrogenation was carried out twice in order to reduce the residual unsaturation to less than 2%. The absence of cyclization of polymer chain during the hydrogenation was confirmed by the ^{13}C n.m.r. spectrum of

Table 1 Microstructure of polyisoprenes

Catalyst (mole ratio)	Solvent	Microstructure (%)		
		1,4-	3,4-	1,2-
(a) BuLi-Et ₂ O (1:24)	Pentane	51	48	1
(b) Ti(OBu) ₄ -AlEt ₃ (1:6)	Toluene	39	60	1
(c) Alfin	Hexane	72	23	5
(d) Radical	Water (emulsion)	89	7	4
(e) CoI ₂ -MeOH-PhMgBr (1:2:2.2)	Toluene	37	62	1

hydrogenated natural rubber. Poly(3-methylbutene-1) was prepared with TiCl₄-AlEt₃ catalyst according to the method of Natta *et al.*⁹. The crude polymer was washed with methanol and extracted with benzene in order to remove the amorphous fraction.

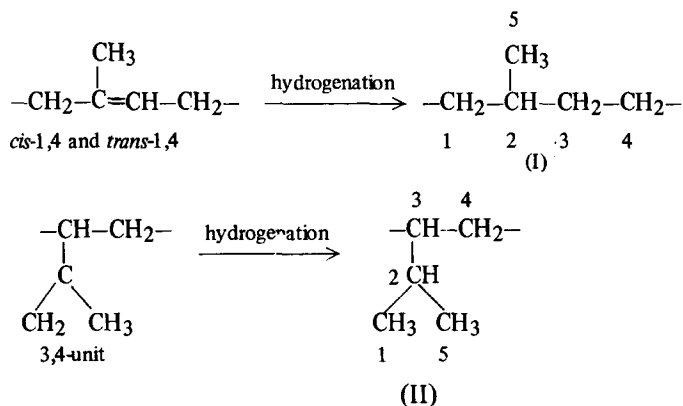
¹³C n.m.r. measurements

The ¹³C n.m.r. spectra were obtained at 25.1 MHz by using a JEOL JNM-PS 100 spectrometer equipped with a Fourier transfer accessory at room temperature or 60°C. About 25% w/v CDCl₃ solution was used for the hydrogenated polyisoprenes and the copolymer. In the case of poly(3-methylbutene-1), ¹³C n.m.r. measurement was carried out for a swollen polymer in CS₂ containing 5% of CDCl₃. Chemical shifts were referred to tetramethylsilane, added as an internal standard. All the spectra were proton noise decoupled and obtained with multiple scans at a pulse repetition time of 2.0 sec.

RESULTS AND DISCUSSION

Sequences of 1,4- and 3,4-units

Polyisoprenes containing *cis*-1,4-, *trans*-1,4-, and 3,4-units exhibit complicated ¹³C n.m.r. resonances resulting from various types of carbon atoms in different sequences. After hydrogenation *cis*-1,4- and *trans*-1,4-units are converted into the same structure (I), and 3,4-unit becomes the structure (II). Therefore, hydrogenated polyisoprenes containing only a slight amount of 1,2-unit can be regarded as copolymers consisting of structures (I) and (II).



The chemical shift of each carbon atom in the hydrogenated polymer can be predicted by using the empirical equations for branched and linear alkanes proposed by Paul and Grant¹⁰ or Lindeman and Adams¹¹.

Figure 1 shows ¹³C n.m.r. spectra of hydrogenated polyisoprenes prepared with n-BuLi-Et₂O and Ti(OBu)₄-AlEt₃ catalysts [polymers (a) and (b), respectively]. Both polymers exhibited sixteen main signals as indicated by symbols A to P in the spectra. These signals have been assigned to the carbon atoms in the central monomer unit of a triad sequence of the structures (I) and (II) as listed in Table 2⁷.

Signals due to head-to-head and tail-to-tail linkages

Figure 2 shows ¹³C n.m.r. spectra of hydrogenated polyisoprenes prepared with Alfin and radical catalysts [polymers (c) and (d), respectively]. In these spectra characteristic signals were observed at 34.41 (signal E') and 27.42 ppm (signal L'), which were scarcely observed in the polymers (a) and (b). These new signals are assigned to C₁ and C₄ carbon atoms of structure (I) in head-to-head (4,1-1,4) and tail-to-tail (1,4-4,1) linkages, respectively, from a comparison of the observed chemical shifts with the predicted values. It is also disclosed that C₂ carbon atom in head-to-head linkage resonated at 33.25 ppm, which is overlapped with the signal of C₂ carbon atom in structure (I) adjacent to structure (II) (Table 3).

An isoprene-piperylene (1,3-pentadiene) copolymer was prepared as a model polymer containing head-to-head (4,1-1,4) and tail-to-tail (1,4-4,1) linkages of polyisoprene. It was confirmed that the copolymer prepared with n-BuLi consisted of predominantly 1,4-addition for both monomers by ¹H n.m.r. and i.r. studies. Therefore, the hydrogenated copolymer corresponds to a hydrogenated polyisoprene containing significant amounts of head-to-head and tail-to-tail linkages as illustrated below.

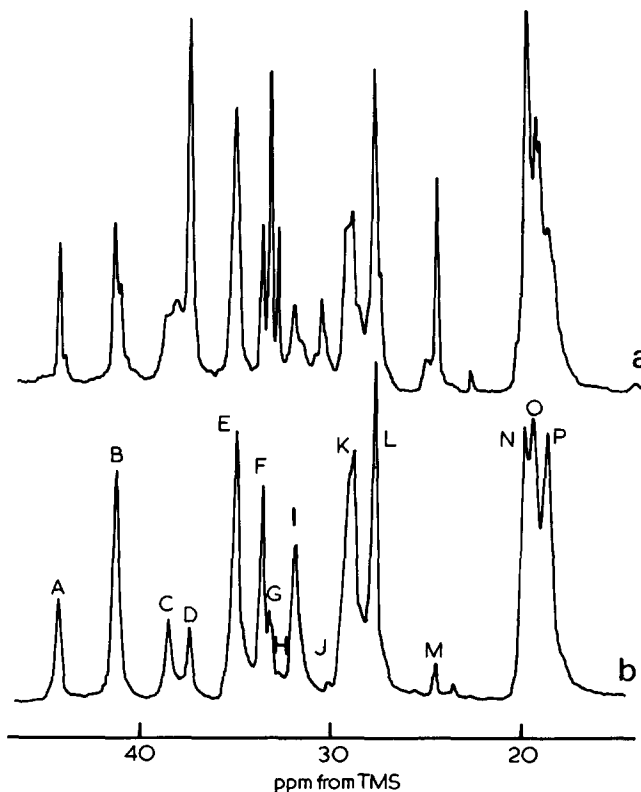
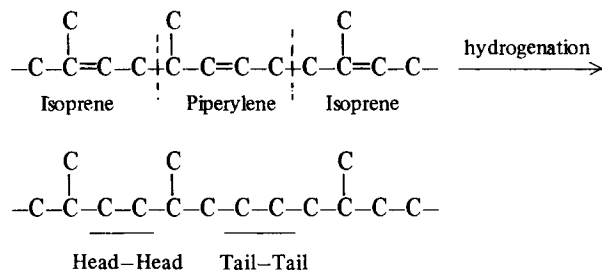
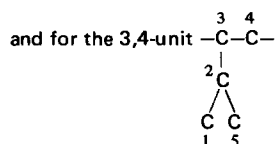
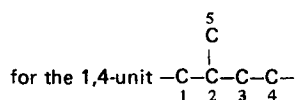


Figure 1 ¹³C n.m.r. spectra of hydrogenated polyisoprenes prepared with (a) n-BuLi-Et₂O and (b) Ti(OBu)₄-AlEt₃ catalysts

Table 2 ^{13}C n.m.r. signal assignments

Triad sequence	Carbon atom	Signal	δ (ppm)	Triad sequence	Carbon atom	Signal	δ (ppm)
1,4-1,4-1,4	1	D	37.47	1,4-3,4-1,4	1,5	O	19.34
	2	H	32.84		2	K	29.32
	3	D	37.47		3	A	44.39
	4	M	24.51		4	L	27.84
	5	N	19.83				
1,4-1,4-3,4	1	D	37.47	1,4-3,4-3,4	1,5	P	18.61
	2	G	33.25		2	K	29.32
	3	E	35.09		3	B	41.43
	4	L	27.84		4 ^a	I	31.96
	5	N	19.83				
3,4-1,4-1,4	1	E	35.09	3,4-3,4-1,4	1,5	P	18.61
	2	G	33.25		2	K	29.32
	3	D	37.47		3	B	41.43
	4	M	24.51		4	L	27.84
	5	N	19.83				
3,4-1,4-3,4	1	E	35.09	3,4-3,4-3,4	1,5	P	18.61
	2	F	33.64		2	K	29.32
	3	E	35.09		3	C	38.13
	4	L	27.84		4 ^a	I	31.96
	5	N	19.83				

^a The signal split into two peaks
Carbon atoms are denoted as follows:



The ^{13}C -n.m.r. spectrum of the hydrogenated copolymer displayed the signals at 34.41, 33.25, and 27.42 ppm corresponding to head-to-head and tail-to-tail linkages of 1,4-unit in hydrogenated polyisoprene. It has been reported that the central methylene carbon of squalene, which corresponds to tail-to-tail 1,4-linkage, resonated at 27.5 ppm characteristic of this linkage¹². These findings indicate the validity of the signal assignments described above.

In a previous paper the predominance of head-to-tail arrangement was confirmed for n-BuLi catalysed polyisoprenes regardless of the amounts of 3,4-unit⁷. Polymers having 4,1-3,4 (head-to-head) and 1,4-4,3 (tail-to-tail) linkages are expected to have characteristic signals around 38 and 25 ppm, respectively (Table 3). In the ^{13}C n.m.r. spectra of polymers (a), (c) and (d), a small signal was observed at 25.00 ppm (signal M'), which is assigned to the C₄ carbon atom of the structure (I) in 1,4-4,3 linkage. Polymer (d) exhibited also a small signal at 38.1 ppm (signal C'), which can be assigned to the C₁ carbon atom of the structure (I) in 4,1-3,4 linkage. In the case of polymers (a) and (d), however, no distinct signal corresponding to C' was observed.

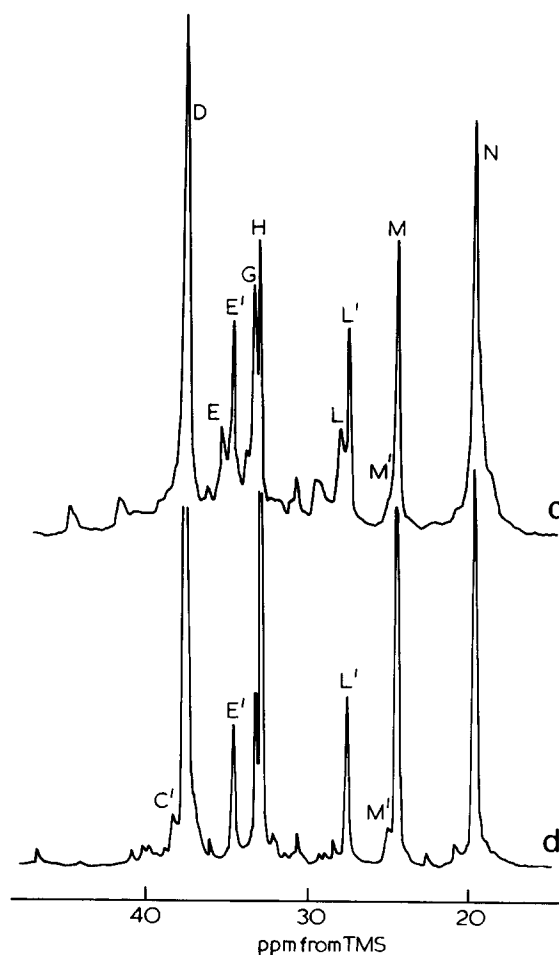


Figure 2 ^{13}C n.m.r. spectra of hydrogenated polyisoprenes prepared with (c) Alfin and (d) radical catalysts

Table 3 Signals due to head-to-head and tail-to-tail linkages

Structure	Linkage	Carbon atom	Signal	Chemical shift (ppm)	
				Obs.	Calc.
$\begin{array}{ccccccc} & & \text{C} & & \text{C} & & \\ & & & & & & \\ -\text{C}-\text{C}-\text{C}-\text{C}-\text{C}-\text{C}- & & & & & & \\ & & 2 & 1 & 1 & 2 & \end{array}$	4,1-1,4 head-to-head	C ₁ C ₂	E' G	34.41 33.25	34.22 32.52
$\begin{array}{ccccccc} & & \text{C} & & & & \text{C} \\ & & & & & & \\ -\text{C}-\text{C}-\text{C}-\text{C}-\text{C}-\text{C}- & & & & & & \\ & & 4 & 4 & & & \end{array}$	1,4-4,1 tail-to-tail	C ₄	L'	27.42	27.52
$\begin{array}{ccccccc} & & \text{C} & & & & \\ & & & & & & \\ -\text{C}-\text{C}-\text{C}-\text{C}-\text{C}- & & & & & & \\ & & 1 & & & & \\ & & & & & & \\ & & \text{C} & & & & \\ & & & & & & \\ & & \text{C} & & & & \end{array}$	4,1-3,4 head-to-head	C ₁	C'	38.1	38.48
$\begin{array}{ccccccc} & & \text{C} & & & & \\ & & & & & & \\ -\text{C}-\text{C}-\text{C}-\text{C}-\text{C}- & & & & & & \\ & & 4 & & & & \\ & & & & & & \\ & & \text{C} & & & & \\ & & & & & & \\ & & \text{C} & & & & \end{array}$	1,4-4,3 tail-to-tail	C ₄	L'	25.00	25.08

Figure 3 shows ^{13}C n.m.r. spectrum of hydrogenated polyisoprene prepared with $\text{CoI}_2\text{-ROH-PhMgBr}$ catalyst. This polymer also exhibited signals E', L', and M', indicating that it contained head-to-head and tail-to-tail linkages of 1,4- and 3,4-units.

Distribution of isomeric structures

In a previous paper triad sequence distributions of 1,4- and 3,4-units in BuLi catalysed polyisoprenes were analysed using the signals F, G, and H, and also A, B, and C. In the case of polyisoprenes containing head-to-head and tail-to-tail linkages some of these signals were overlapped with the signals due to these linkages. In these cases distributions of 1,4- and 3,4-units, including head and tail arrangements, were determined as dyad sequences by using the signals M, L, E', L', M', and C', which arise from C₁ and C₄ carbons. On the basis of these assignments the fractions of dyad sequences were measured according to the following equations by using the relative intensities of signals:

$$\begin{array}{ll} 1,4-1,4 & \text{linkage} = M/\Sigma \quad (\text{head-to-tail}) \\ 4,1-1,4 & \text{linkage} = E'/2\Sigma \quad (\text{head-to-head}) \\ 1,4-4,1 & \text{linkage} = L'/2\Sigma \quad (\text{tail-to-tail}) \\ \left. \begin{array}{l} 1,4-3,4 \\ 3,4-1,4 \end{array} \right\} & \text{linkage} = L/\Sigma \quad (\text{head-to-tail}) \\ 1,4-4,3 & \text{linkage} = M'/\Sigma \quad (\text{tail-to-tail}) \\ 4,1-3,4 & \text{linkage} = C'/\Sigma \quad (\text{head-to-head}) \\ \left. \begin{array}{l} 3,4-3,4 \\ 4,3-3,4 \\ 3,4-4,3 \end{array} \right\} & \text{linkage} = [K - (L + M' + C')/2]/\Sigma \end{array}$$

where, $\Sigma = M + K + (L + E + L' + M + C')/2$

The results are listed in Table 4.

In the polyisoprene prepared with n-BuLi-Et₂O catalyst, a random distribution of 1,4- and 3,4-units with predominantly head-to-tail linkage is also demonstrated in this experiment. On the other hand, Hackathorn and Brock suggested that a 3,4-unit was incorporated into the polymer chain chiefly with 1,4-4,3 linkage, in the case of alkyl lithium catalysed polymerization, on the basis of crystal-

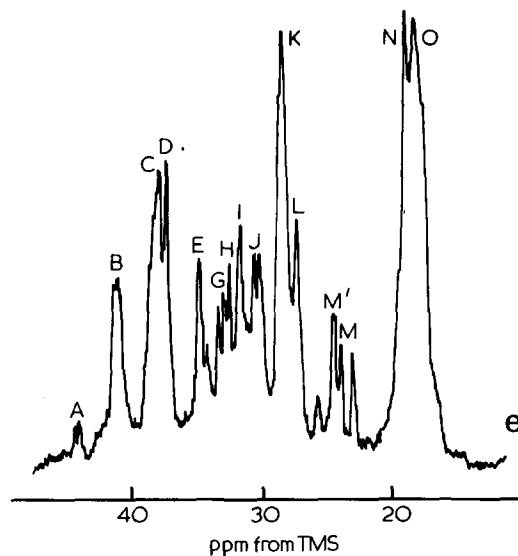


Figure 3 ^{13}C n.m.r. spectrum of hydrogenated polyisoprene prepared with (e) $\text{CoI}_2\text{-ROH-PhMgBr}$ catalyst

lization and ozonolysis studies¹. In our experiment, however, only a small signal due to 1,4-4,3 linkage was observed, while signals due to 1,4-3,4 and 3,4-1,4 linkages were clearly observed. Therefore, it may be necessary to take into account other factors to interpret the poor crystallizability of lithium polyisoprenes.

$\text{Ti}(\text{OBu})_4\text{-AlEt}_3$ system was reported to be a catalyst providing 3,4-polyisoprene from the i.r. spectrum of the polymer¹³. In our experiment the polyisoprene prepared with this catalyst contained only 60% of 3,4-unit. Furthermore, it is revealed that distribution of 1,4- and 3,4-units is rather alternating with exclusively head-to-tail linkage in this polymer.

It is ascertained that polyisoprenes prepared with Alfin and radical catalysts contained about 20% of head-to-head and tail-to-tail linkages of 1,4- and 3,4-units. It is also disclosed that 1,4- and 3,4-units were distributed slightly in blocks in Alfin polyisoprene and almost randomly in emulsion polyisoprene.

Table 4 Sequence distribution of polyisoprenes

Linkage ^a	Signal	BuLi-Et ₂ O	Ti(OBu) ₄ -AlEt ₃	Alfin	Emulsion	CoI ₂ -ROH-PhMgBr
1,4-1,4	M	25	6	35	60	10
4,1-1,4 (H)	E'	0	0	16	14	6
1,4-4,1 (T)	L'	0	0	12	14	2
1,4-3,4						
3,4-1,4	L	50	61	19	0	25
4,1-3,4 (H)	C'	—	—	—	6	—
1,4-4,3 (T)	M'	3	0	5	6	13
3,4-3,4 etc.		22	33	13	0	44
1,4-1,4 ^b		25(27)	6(13)	63(56)	88(88)	18(14)
1,4-3,4 ^b		53(50)	61(47)	24(38)	12(12)	38(46)
3,4-3,4 ^b		22(23)	33(40)	13(6)	0(0)	44(40)

^a (H), head-to-head; (T), tail-to-tail

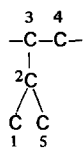
^b Sequence distribution regardless of head and tail arrangements

Values in parantheses represent calculated values assuming a random distribution of 1,4- and 3,4-units

Table 5 Signal assignments of poly(3-methylbutene-1) and structure (II)

Carbon ^a	Signal	Chemical shift (ppm)		Dyad tacticity
		Obs.	Calc.	
C ₃	C	38.13	39.52	
C ₄	I	31.96	33.60	meso
	J	30.58	33.60	racemic
C ₂	K	29.32	30.46	
C ₁ , C ₅	P	18.61	19.63	

^a Carbon atoms are denoted as follows:



CoI₂-ROH-PhMgBr system was reported as a catalyst providing equibinary polyisoprene composed of equal amounts of *cis*-1,4- and 3,4-units¹⁴. An alternating sequence of 1,4- and 3,4-units was expected by Teyssié *et al.* for this equibinary polyisoprene on the basis of polymerization mechanism. It is clearly demonstrated in Table 4 that the equibinary polyisoprene had a rather random distribution of 1,4- and 3,4-units along the chain with significant amounts of head-to-head and tail-to-tail linkages of these units. In Table 4 the discrepancy between the amounts of head-to-head and tail-to-tail linkages is probably owing to the fact that the amounts of 4,1-3,4 (head-to-head), 4,3-3,4 (head-to-head), and 3,4-4,3 (tail-to-tail) linkages were not separately determined in this measurement.

Configurational sequences of 3,4-polyads

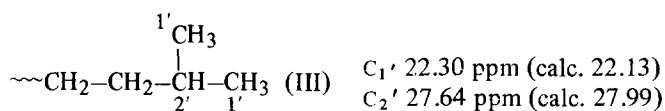
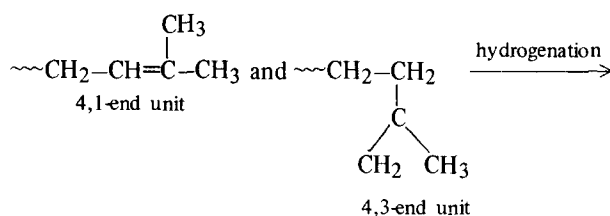
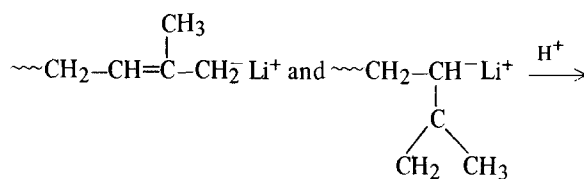
The signals due to carbon atoms in the polyads of structure (II) are expected to display splitting because of the tacticity. In a previous paper signals I and J were assigned to the central methylene carbon (C₄) in the dyad of structure (II) on the basis of the finding that the intensity ratio of I and J signals did not vary with changing the ratio of structures (I) and (II) for *n*-BuLi-Et₂O catalysed polyisoprenes⁷. The detailed assignment of the signals I and J was carried out by using isotactic poly(3-methylbutene-1) prepared with TiCl₄-AlEt₃ catalyst as a model

compound of an isotactic sequence of structure (II). Four signals were observed by the measurement of a swollen polymer in carbon disulphide, though the spectrum was not well resolved owing to the poor solubility of the polymer¹⁵. These signals are assigned as shown in Table 5.

Signals I and J are assigned to methylene carbons in meso and racemic dyad of structure (II) from the comparison of the chemical shift of methylene carbon (C₄) in hydrogenated polyisoprene with that of poly(3-methylbutene-1). In the case of Ti(OBu)₄-AlEt₃ catalysed polyisoprene, the intensity ratio of the signals I and J was about 9 to 1, indicating the highly isotactic configuration of 3,4-unit in the polymer. The polyisoprenes prepared with *n*-BuLi-Et₂O, CoI₂-ROH-PhMgBr, and Alfin catalysts were less stereoregular.

Signals due to end groups

Low molecular weight polymers and highly branched polymers are expected to display signals due to carbon atoms in the end groups. It has been reported that almost all monomer units are incorporated into polymer chain by 4,1- or 4,3-addition in BuLi catalysed polymerization¹⁶. In such a case the terminal units become structure (III) after hydrogenation regardless of the isomeric structure of the end units:



The terminal methyl (C_{1'}) and methine (C_{2'}) carbon atoms are expected to resonate around 22 and 28 ppm, respectively.

Polymer (a) exhibited small signals at 22.30 and 27.64 ppm indicating that this polymer had measurable amount of the end groups. Furthermore, this polymer displayed a signal around 14 ppm attributed to the methyl carbon in n-butyl group derived from the initiator. The amounts of terminal group (III) and residual butyl group of the initiator were found to be 0.7 and 0.6 units, respectively, per hundred monomer units, demonstrating that this polymer had few branches. The absence of branches was also confirmed by the molecular weight measurement. The number of the end group obtained by vapour pressure osmometric measurement was found to be 1.1 units per hundred monomer units which is comparable to the values determined by ¹³C n.m.r.

Polymer (d) also showed a small signal at 22.3 ppm corresponding to the terminal methyl carbon. The degree of polymerization for this polymer was found to be about 300 by osmometric measurement, hence it is concluded that some part of this signal had arisen from end groups in branches. In the case of polymers (b), (c) and (e), no signal due to end groups was detected. This may be due to the fact that the molecular weight of these polymers was too high to detect end groups.

ACKNOWLEDGEMENT

The authors are very grateful to Dr Koei Komatsu of Japan

Synthetic Rubber Co. for preparing Alfin and emulsion polyisoprenes.

REFERENCES

- 1 Brock, M. J. and Hackathorn, M. J. *Rubber Chem. Technol.* 1972, **45**, 1303
- 2 Hackathorn, M. J. and Brock, M. J. *J. Polym. Sci. (Polym. Lett. Edn)* 1970, **8**, 617
- 3 Galin, M. J. *Macromol. Sci. (A)* 1973, **7**, 873
- 4 Hackathorn, M. J. and Brock, M. J. *Rubber Chem. Technol.* 1972, **45**, 1295
- 5 Hackathorn, M. J. and Brock, M. J. *J. Polym. Sci. (Polym. Chem. Edn)* 1975, **13**, 945
- 6 Tanaka, Y. and Sato, H. *Polymer* 1976, **17**, 113
- 7 Tanaka, Y., Sato, H., Ogura, A. and Nagoya, I. *J. Polym. Sci. (Polym. Chem. Edn)* in press
- 8 Sanui, K., MacKnight, W. J. and Lentz, R. W. *J. Polym. Sci. (Polym. Lett. Edn)* 1973, **11**, 427
- 9 Natta, G., Pino, P., Mazzanti, G., Corradini, P. and Gianini, U. *Rend. Accad. Naz. Lincei* 1955, **19**, 397
- 10 Grant, D. M. and Paul, E. G. *J. Am. Chem. Soc.* 1964, **86**, 2984
- 11 Lindeman, L. P. and Adams, J. Q. *Anal. Chem.* 1971, **43**, 1245
- 12 Tanaka, Y. and Hatada, K. *J. Polym. Sci. (Polym. Chem. Edn)* 1973, **11**, 2057
- 13 Natta, G., Porri, L. and Carbonaro, A. *Makromol. Chem.* 1964, **77**, 126
- 14 Dawans, F. and Teyssié, Ph. *Makromol. Chem.* 1967, **109**, 68
- 15 Tanaka, Y. and Sato, H. *J. Polym. Sci. (Polym. Lett. Edn)* to be published
- 16 Morton, M., Sanderson, R. D., Sakata, R. and Falvo, L. A. *Macromolecules* 1973, **6**, 186

Laser flash photolysis investigations on primary processes of the sensitized polymerization of vinyl monomers:

1. Experiments with benzophenone

R. Kuhlmann and W. Schnabel

Hahn-Meitner-Institut für Kernforschung Berlin GmbH, Bereich Strahlenchemie,
1 Berlin 39, Germany

(Received 30 September 1975; revised 19 December 1975)

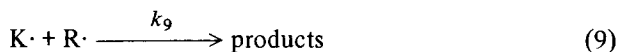
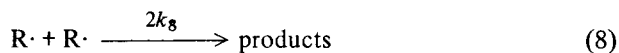
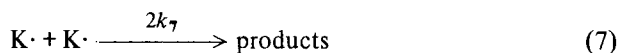
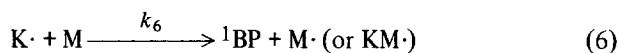
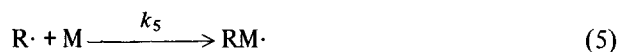
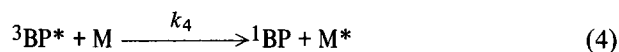
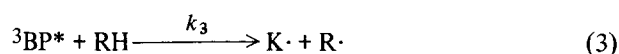
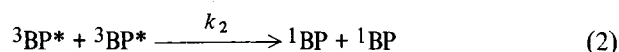
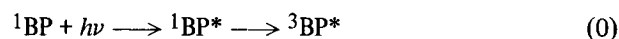
The laser flash photolysis technique was used in order to evaluate kinetic parameters concerning the efficiency of benzophenone (BP) as a photosensitizer for polymerizations. Rate constants (in $M^{-1} \text{sec}^{-1}$) of the reaction of triplet BP with monomers were measured (e.g. styrene, 3.3×10^9 ; methyl methacrylate, 6.9×10^7 ; acrylonitrile, 3.4×10^7 ; vinyl acetate, 5.4×10^6). The rate constant of the reaction of triplet BP with tetrahydrofuran is $3 \times 10^6 M^{-1} \text{sec}^{-1}$. From these results it can be derived, for example, that the BP photosensitized polymerization of styrene is not feasible. Ketyl radicals of BP were found to react relatively slowly with vinyl acetate ($5.5 \times 10^3 M^{-1} \text{sec}^{-1}$), acrylonitrile ($3.8 \times 10^3 M^{-1} \text{sec}^{-1}$) and methyl methacrylate ($9.0 \times 10^3 M^{-1} \text{sec}^{-1}$). Based on these data it was estimated that benzpinacol should not be formed as a major reaction product at relatively low incident light intensities and at monomer concentrations greater than 1 mol/l.

INTRODUCTION

During recent years the photosensitized polymerization of vinyl compounds has attracted attention for its applicability for technical processes¹. Besides other groups of compounds aromatic carbonyl compounds are used frequently as sensitizers. There are, however, limitations concerning the general usability of a certain compound as sensitizer. Benzophenone (BP) for example, was reported by Heine *et al.*² not to initiate the polymerization of styrene since it was assumed that styrene acts as a quencher for triplet excited benzophenone molecules ($^3\text{BP}^*$). Thus, the formation of polymerization-initiating radicals (by the reaction of $^3\text{BP}^*$ with hydrogen donor compounds present in the system) is inhibited. Slightly controversial to this are findings of Block *et al.*³ that BP and 3,3', 4,4'-tetramethoxycarbonyl benzophenone photosensitized the polymerization of styrene when the latter was irradiated in a 50% (v/v) solution in tetrahydrofuran.

Evidence of the triplet quenching ability of another vinyl monomer (methyl acrylate) was obtained recently⁴ from measurements of the quantum yield of the photoreduction of benzophenone by t-butanol and benzhydrol.

Questions concerning the influence of sensitizer triplet quenching by monomer molecules on the initiation of polymerization could in principle be readily answered if the respective kinetic parameters were available. It was the aim of our investigation to collect relevant information. In this paper we wish to report mainly on the reaction of several vinyl monomers with benzophenone triplets and ketyl radicals. We considered benzophenone as an appropriate substance to start our studies with, since its photochemistry has been investigated rather thoroughly before⁵⁻¹³. It appears to be useful to represent the elementary reactions this work is dealing with, in the following scheme:



EXPERIMENTAL

Materials

Benzene (Merck, 99.5%) was shaken several times with concentrated H_2SO_4 , washed with distilled water, dried over CaCl_2 and CaH_2 and distilled over a splitting tube column. Tetrahydrofuran (Merck, 99.5%) was treated with CaH_2 , distilled over a Vigreux column, dried over sodium wire and distilled again from KOH. The monomers contained stabilizers and were treated before use as follows: methyl methacrylate (MMA), acrylonitrile (AN), styrene (St) and α -methylstyrene (α -MSt) were washed with NaOH solution and water, dried over CaCl_2 and CaH_2 and distilled over a 1 m Vigreux column. Vinyl pyrrolidone (VP)

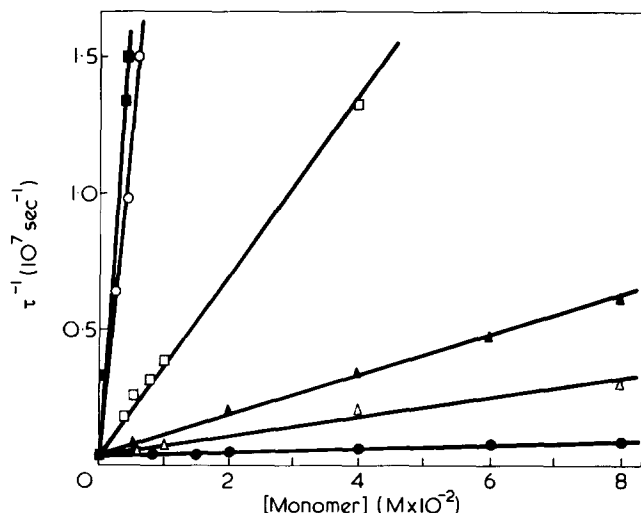


Figure 1 First order life time of the decay of the absorption at $\lambda = 532 \text{ nm}$ as a function of monomer concentration. St, \blacksquare ; α -MSt, \circ ; VP, \square ; MMA, \blacktriangle ; AN, \triangle ; VAC, \bullet . [BP] = $7.4 \times 10^{-4} \text{ M}$. Absorbed dose per flash $7 \times 10^{-5} \text{ einstein/l}$. Solvent: benzene

Table 1 Quenching of benzophenone triplets by vinyl monomers

Monomer	$k_4 \text{ (M}^{-1} \text{ sec}^{-1}\text{)}$
Styrene	$(3.3 \pm 0.3) \times 10^9$
α -Methylstyrene	$(2.7 \pm 0.3) \times 10^9$
Vinyl pyrrolidone	$(3.6 \pm 0.4) \times 10^8$
Methyl methacrylate	$(6.9 \pm 0.7) \times 10^7$
Acrylonitrile	$(3.4 \pm 0.3) \times 10^7$
Vinyl acetate	$(5.4 \pm 0.5) \times 10^6$

was stabilized with 0.1% NaOH and therefore washed with aqueous H_2SO_4 , washed and dried over CaH_2 and subsequently distilled. Vinyl acetate (VAC) was treated as methyl methacrylate except that it underwent a 48 h treatment with NaHSO_3 immediately before distillation in a nitrogen atmosphere³. Benzophenone (Aldrich, 99%) was twice recrystallized from heptane (melting point 48.0°C).

Irradiation of samples

Solutions were de-aerated by bubbling with purified Ar. The oxygen content in the solutions was less than 3 ppm. Samples were irradiated in rectangular cells with 347.1 nm light flashes (25 nsec) of a frequency doubled ruby laser (Korad model K1QS2). Schott BG23 filters were used to reduce the incident intensity of light. A xenon lamp (Osram XBO450W) was used as light source for the analysing light. Further details have been given before¹⁴.

Actinometry

The dose absorbed per flash was measured with a potassium ferrioxalate actinometer¹⁵ ($\phi[\text{Fe}^{2+}] = 1.20$). Normal laser operation yielded $\sim 4 \times 10^{16}$ photons per flash. In calculating concentrations of triplets a quantum yield of 1.0, taken from the literature^{16,17} was used.

RESULTS AND DISCUSSION

Reaction of benzophenone triplets with vinyl monomers

With benzene solutions of BP ($7.4 \times 10^{-4} \text{ M}$), the well known^{9,12,13} T-T absorption spectrum of benzophenone was recorded by measuring the optical absorption of the

solution at the end of the laser flash. In the absence of added substances this spectrum decayed according to a first order law with life times between 3 and 12 μsec depending on the intensity of incident light. At a constant intensity corresponding to an absorbed dose per flash of $10^{-5} \text{ einstein/mol}$ ([BP] = $7.4 \times 10^{-4} \text{ M}$), the variation of first order life times with the concentration of added monomer was measured. Results are shown in Figure 1. Since the monomer concentration hardly changed during these experiments, the rate constant of the quenching reaction (4) could be evaluated by use of equation (10):

$$\frac{1}{\tau} = \Sigma k(1) + k_4[M] \quad (10)$$

where $\Sigma k(1)$ is the rate constant of decay of ${}^3\text{BP}^*$ in the absence of monomer. Values of k_4 are compiled in Table 1, which shows that the quenching effectiveness decreases in the sequence: styrene > α -methylstyrene > vinyl pyrrolidone > methyl methacrylate > acrylonitrile > vinyl acetate.

Reaction of ${}^3\text{BP}^*$ with tetrahydrofuran (THF)

The reaction of ${}^3\text{BP}^*$ with THF was studied by adding small amounts of THF to $7.4 \times 10^{-4} \text{ M}$ BP solutions in benzene. The decay of the T-T absorption of ${}^3\text{BP}^*$ at 532 nm was recorded as a function of time. Figure 2a shows a typical oscilloscope trace. The initial decay is due to benzophenone triplets which are converted to ketyl radicals by reaction (3). The absorption of the radicals is represented by the slowly decaying branch of the trace. Values of k_3 were obtained either from a plot of reciprocal life times of ${}^3\text{BP}^*$ versus [THF] as shown in Figure 2b by use of equation (11):

$$\frac{1}{\tau} = \Sigma k(1) + k_3[\text{THF}] \quad (11)$$

($\Sigma k(1)$ = rate constant of decay of ${}^3\text{BP}^*$ in the absence of THF) or from the optical density (OD) of $\text{K}\cdot$ at $t = 3 \mu\text{sec}$

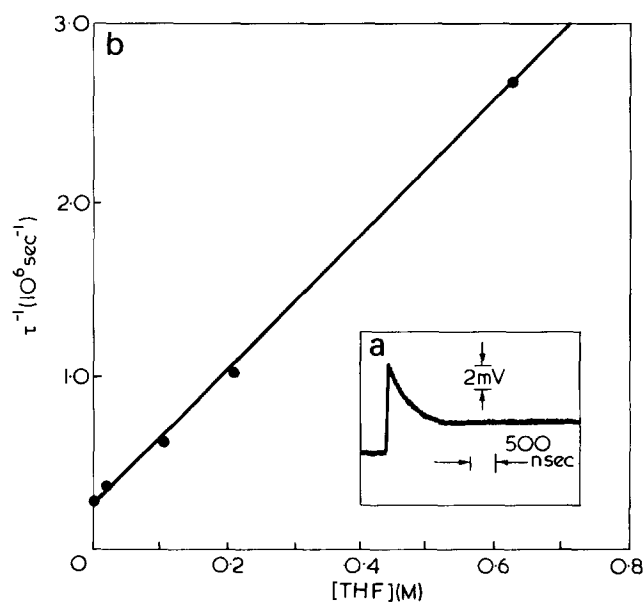


Figure 2 (a) Oscilloscope trace demonstrating the variation of optical absorption at $\lambda = 532 \text{ nm}$ with time. (b) Reciprocal first order life times of the initial decay of the absorption at $\lambda = 532 \text{ nm}$ versus the concentration of tetrahydrofuran

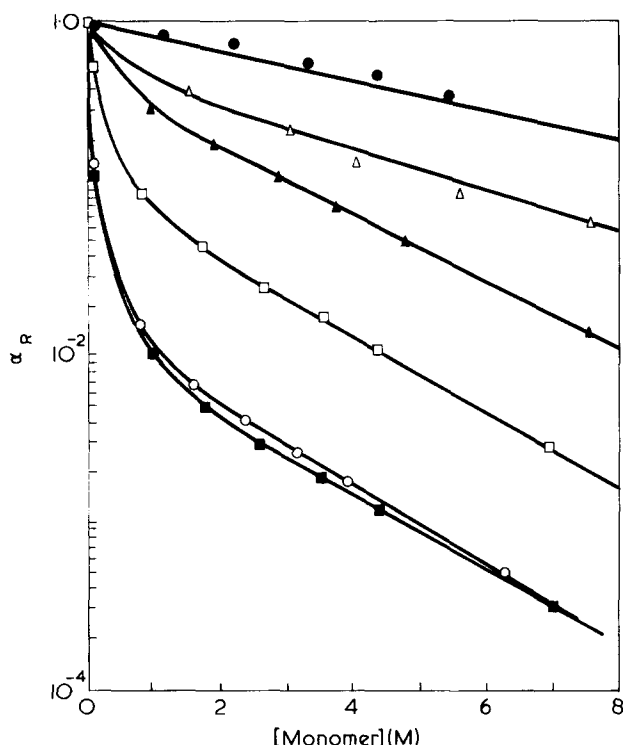


Figure 3 Probability α_R for the formation of radicals capable of inducing polymerization versus the monomer concentration according to equation (13). VAC, ●; AN, △; MMA, ▲; VP, □; α -MSt, ○; St, ■. Competition of reactions (3) and (4) for the decay of ${}^3\text{BP}^*$ is assumed

after the flash recorded as a function of [THF] according to equation (12):

$$\frac{OD(S)}{OD} = 1 + \frac{\Sigma k(1)}{k_3[\text{THF}]} \quad (12)$$

$OD(S)$ denotes the saturation value of the optical density observed at high THF concentrations, i.e. when all triplets react according to reaction (3).

$k_3(\text{THF}) = (3 \pm 1) \times 10^6 \text{ M}^{-1} \text{ sec}^{-1}$ was obtained which is about as high as the rate constant for the reaction of ${}^3\text{BP}^*$ with isopropanol ($k_3(\text{isopropanol}) = 1.3 \times 10^6 \text{ M}^{-1} \text{ sec}^{-1}$) determined by Beckett and Porter⁵.

From a formal treatment, the probability α_R for the formation of radicals capable of initiating the polymerization of a monomer M dissolved in the solvent RH, may be derived. If a relatively simple case is considered where reactions (3) and (4) are the only competing reactions, equation (13) is obtained:

$$\alpha_R = \frac{k_3(\text{RH})[\text{RH}]}{k_3(\text{RH})[\text{RH}] + k_4[\text{M}]} \quad (13)$$

It is presumed here that all ${}^3\text{BP}^*$ particles are converted to pairs of ketyl and solvent radicals in the absence of monomer. If M is present in the solution a fraction of ${}^3\text{BP}^*$ is quenched by M according to reaction (4).

Figure 3 shows the probability α_R as a function of monomer concentration expected for THF solutions. α_R was calculated with the values of k_4 given in Table 1 and the value of $k_3(\text{THF})$ given above. It is hereby assumed that the rate constants determined in benzene are also valid for THF as the solvent. It results that for a typical

monomer concentration of 2 mol/l, radicals capable of initiating the polymerization of the monomer are hardly formed in styrene solutions whereas in the case of vinyl acetate polymerization appears to be feasible. With the other monomers intermediate situations are expected. Experimental results relevant to this subject were obtained by Block *et al.*^{3a}. They reported a sensitizing effect of BP in THF for St, AN and MMA. The rate of polymerization of VAC was retarded by BP in THF and accelerated of BP in toluene. The inability of BP to sensitize the polymerization of VAC in THF is according to these authors due to the fact that THF radicals are incapable of adding to VAC. A sensitizing effect of BP on the rate of polymerization of styrene is not expected according to the respective curve in Figure 3. It may be noted that the importance of the data by Block *et al.* is somewhat reduced by the fact that remarkable rates of polymerization were observed in certain cases already in the absence of sensitizer, a fact which pertains especially to the case of vinyl acetate.

Reaction of ketyl radicals with vinyl monomers

Since the reaction of ${}^3\text{BP}^*$ with the solvent yields solvent radicals as well as ketyl radicals the question arises as to whether or not ketyl radicals can initiate the polymerization of vinyl monomers via reaction (6). It is frequently assumed that ketyl radicals are deactivated essentially by reaction (7). However, it has been shown by Hutchinson *et al.*^{3b} that semi-pinacol radicals act as terminators during the free radical polymerization of MMA. The possibility that semi-pinacol radicals act as initiators of the polymerization of MMA has been pointed out by the same authors^{3b}. By monitoring the slow decay of the absorption at $\lambda = 532 \text{ nm}$ and plotting the respective values of the reciprocal optical density versus time we found by using $\epsilon_K(532 \text{ nm}) = 5.1 \times 10^3 \text{ M}^{-1} \text{ cm}^{-1}$; $k'_7 = 6.4 \times 10^7 \text{ M}^{-1} \text{ sec}^{-1}$, which agrees fairly well with the value reported by Beckett and Porter ($2k_7 = 5.9 \times 10^7 \text{ M}^{-1} \text{ sec}^{-1}$)⁵. k'_7 may differ from $2k_7$ [rate constant of reaction (7), since reaction (9) may also be involved in the observed second order decay (compare equation (15))].

In order to determine k_6 experimental conditions were chosen such that the competing reactions (7) and (9) could be neglected. In this case the optical density due to ketyl radicals decayed according to pseudo first-order kinetics with a rate constant proportional to the monomer concentration:

$$k_{(\text{pseudo } 1)} = k_6[\text{M}] \quad (14)$$

This procedure of determination of k_6 could, however, only be applied for monomers with relatively low values of k_4 . Therefore, styrene ($k_4 = 3.3 \times 10^9 \text{ M}^{-1} \text{ sec}^{-1}$, α -methylstyrene ($k_4 = 2.7 \times 10^9 \text{ M}^{-1} \text{ sec}^{-1}$) and vinyl pyrrolidone ($k_4 = 3.6 \times 10^8 \text{ M}^{-1} \text{ sec}^{-1}$) were not included in this series of experiments, since in order to be allowed to neglect reactions (7) and (9) monomer concentrations must be kept relatively high. With styrene, α -methylstyrene and vinyl pyrrolidone thus, situations would be encountered where no ketyl radicals are formed owing to quenching of practically all triplets according to reaction (4).

Typical pseudo first-order plots are shown in Figure 4. Corresponding data are presented in Table 2 which shows that k_6 is relatively high in the case of vinyl acetate. The efficacy of ketyl radicals as polymerization-inducing agents in the presence of solvent radicals depends, of course, on

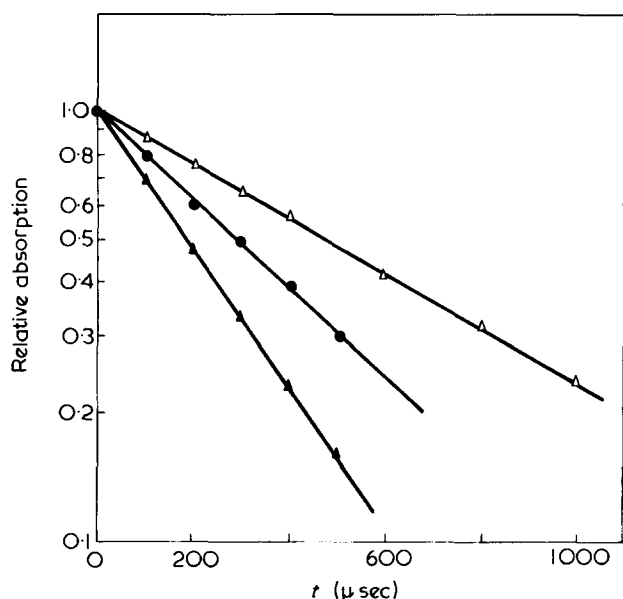


Figure 4 Semilogarithmic plot of the optical absorption at $\lambda = 532$ nm versus time for various monomers dissolved in THF: MMA, Δ ; VAC, \bullet ; AN, \triangle . Monomer concentrations are given in Table 2. [BP] = 7×10^{-4} M. The absorption was normalized relative to an absorbed dose per flash of 3.5×10^{-5} einstein/l

Table 2 Reaction of ketyl radicals with vinyl monomers for the determination of k_6 (see Figure 4)

Monomer	[M] (M)	$k_6 \times 10^{-3}$ ($M^{-1} \text{sec}^{-1}$)
Vinyl acetate	0.4	(5.5 \pm 1.5)
Acrylonitrile	0.4	(3.8 \pm 1.0)
Methyl methacrylate	0.4	(9.0 \pm 2.0)

Table 3 Numerical presentation for the estimate concerning the formation of benzpinacol, which is possible if $k_7' [\text{K}\cdot] \gg k_6 [\text{M}]$ (based on $k_6 = 3.8 \times 10^3 M^{-1} \text{sec}^{-1}$)

[M] mol/l	$[\text{K}\cdot]_{\text{St}^*}$ mol/l	$k_7' [\text{K}\cdot]$ (sec^{-1})	$k_6 [\text{M}] \times 10^{-3}$ (sec^{-1})
0.5	10^{-5}	6.4×10^2	1.9
	10^{-6}	6.4×10^1	1.9
	10^{-8}	6.4×10^{-1}	1.9
	10^{-10}	6.4×10^{-3}	1.9
2.0	10^{-5}	6.4×10^2	7.6
	10^{-6}	6.4×10^1	7.6
	10^{-8}	6.4×10^{-1}	7.6
	10^{-10}	6.4×10^{-3}	7.6

* Stationary concentration

the ratio $k_6 [\text{K}\cdot] / k_5 [\text{R}\cdot]$, which is equal to k_6 / k_5 since $[\text{K}\cdot] = [\text{R}\cdot]$. However, since k_5 is not known the fraction of polymer molecules generated by an initiation via reaction (6) cannot be predicted.

Knowing the values of k_6 and k_7 it can be estimated that at stationary concentrations of $[\text{K}\cdot] < 10^{-6}$ mol/l, the mutual deactivation of ketyl radicals must be negligible at sufficiently high monomer concentrations ($[\text{M}] > 0.5$ mol/l). This follows from equation (15) according to which the rate of decay of ketyl radicals is equal to the sum of the rates of reactions (6), (7) and (9):

$$-\frac{d[\text{K}\cdot]}{dt} = k_6 [\text{K}\cdot] [\text{M}] + 2k_7 [\text{K}\cdot]^2 + k_9 [\text{K}\cdot] [\text{R}\cdot] \quad (15)$$

$$= k_6 [\text{K}\cdot] [\text{M}] + (2k_7 + k_9) [\text{K}\cdot]^2$$

A predominant decay of $\text{K}\cdot$ according to reaction (6) is to be expected if $k_6 [\text{M}] \gg (2k_7 + k_9) [\text{K}\cdot] = k_7' [\text{K}\cdot]$. Some typical numerical data are given in Table 3. Under conditions frequently applied $[\text{K}\cdot]_{\text{stationary}}$ is certainly very small, which implies that benzpinacol should not be formed at monomer concentration of e.g., 2 mol/l.

REFERENCES

- Barzynski, H., Penzien, R. and Volkert, O. *Chem. Ztg.* 1972, 96, 545; Phillips, D. *Photochemistry* 1974, 5, 691
- Heine, H. C., Rosenkranz, H. J. and Rudolph, H. *Angew. Chem.* 1972, 84, 1032
- (a) Block, H., Ledwith, A. and Taylor, A. R. *Polymer* 1971, 12, 271; (b) Hutchinson, J., Lambert, M. C. and Ledwith, A. *Polymer* 1973, 14, 250
- Sandner, M. R., Osborn, C. L. and Trecker, D. W. *J. Polym. Sci. (A-1)* 1972, 10, 3173
- Beckett, A. and Porter, G. *Trans. Faraday Soc.* 1963, 59, 2038
- Ledger, M. B. and Porter, G. *JCS Faraday. Trans.* 1972, 68, 539
- Porter, G. and Wilkinson, F. *Trans. Faraday Soc.* 1961, 57, 1686
- Bell, J. A. and Linschitz, H. *J. Am. Chem. Soc.* 1963, 85, 528
- Buettner, A. V. and Dedinas, J. *J. Phys. Chem.* 1971, 75, 187
- Schuster, D. A. and Weil, T. M. *Chem. Commun.* 1971, p 1212; *Mol. Photochem.* 1974, 6, 69
- Adams, G. E. and Willson, R. L. *JCS Faraday. Trans.* 1973, 69, 719
- McClure, D. S. and Hanst, P. L. *J. Chem. Phys.* 1955, 23, 1772
- Porter, G. and Windsor, M. W. *Proc. R. Soc. (A)* 1958, 245, 238
- Beck, G., Dobrowolski, G., Kiwi, J. and Schnabel, W. *Macromolecules* 1975, 8, 9; Kiwi, J. and Schnabel, W. *Macromolecules* 1975, 8, 430
- Calvert, J. G. and Pitts, J. N. 'Photochemistry', Wiley, New York, 1967
- Lamola, A. A. and Hammond, G. S. *J. Chem. Phys.* 1965, 43, 2129
- Engel, P. S. and Monroe, B. M. *Adv. Photochem.* 1971, 8, 245

Cobalticinium-bridged polybenzazoles: 1. Low temperature solution polymerization

Eberhard W. Neuse, Gernot Horlbeck, Heinz W. Siesler, and Kleantes Yannakou

Department of Chemistry, University of the Witwatersrand, Johannesburg, South Africa

(Received 10 November 1975)

The low temperature solution polymerization of 1,1'-bis(chlorocarbonyl)-cobalticinium hexafluorophosphate/chloride with 3,3'-diaminobenzidine in aprotic media furnishes linear, soluble polymeric intermediates, the recurring unit of which comprises the 1,1'-cobalticinium nucleus linked with the (diamino-substituted) biphenyl system by an amide bridge. The analogous interaction of the cobalticinium salt with 3,3'-dimercaptobenzidine produces corresponding polymers containing both amide and thioester links. Because of the heterogeneous nature of the reactions, the degrees of polymerization attained in both types of reaction are low ($\eta_{inh} = 10\text{--}20$ ml/g). A solid-state heat treatment at temperatures up to 300°C converts the pre-polymers to polyheterocyclics essentially composed of alternating cobalticinium-1,1'-diyl and 6,6'-bibenzazole-2,2'-diyl units, the heterocycle being, respectively, of the imidazole and thiazole type. Structural imperfections in the end products are indicated by their insolubility and by a t.g.a. performance (in both air and nitrogen) inferior to that of common phenylene-bridged bibenzimidazole polymers. Thermal instability of the PF_6^- counter ion at the conversion temperatures employed may be a factor contributing to the unsatisfactory t.g.a. performance observed.

INTRODUCTION

The excellent resistance of the cobalticinium ion to oxidative and thermal attack² prompted suggestions, many years ago³, that cobalticinium-based polymeric compounds should display outstanding performance in materials applications requiring high thermo-oxidative stability. Several reports of cobalticinium polymer preparations have since appeared in the literature. Thus, oligomethylene-bridged cobalticinium polymers were synthesized from α,ω -dicyclopentadienylalkanes (via their sodium salts) and hexamminecobalt (II) chloride⁴; several polyesters were prepared from diols and 1,1'-bis(chlorocarbonyl)- or 1,1'-bis(carboxy)cobalticinium salts^{5,6}, and a series of tin-, titanium-, and zirconium-containing polyesters were obtained by interfacial polymerization of cobalticinium dicarboxylate dianion with the appropriate reactants⁷⁻¹⁰. While most of the polymers described were of quite low molecular mass, one of the titanium-containing products⁹ exhibited a reduced viscosity value as high as 45 ml/g and showed excellent thermal stability in thermogravimetric analysis (t.g.a.) tests.

In an effort to obtain all-aromatic polymers devoid of functional groups in the bridging moieties between cobalticinium units, we have investigated synthetic routes leading to linear polymer structures in which cobalticinium-1,1'-diyl units alternate along the backbone with heterocyclic groupings of the bibenzimidazolyl and bibenzothiazolyl types. As part of this effort, the present communication is concerned with a polymerization study involving conditions of low temperature solution polycondensation.

EXPERIMENTAL

Melting points, uncorrected, were taken in sealed capillaries. Infra-red spectra, on KBr pellets, were recorded with a Perkin-Elmer, Model 521, spectrophotometer. Proton magnetic resonance spectra were obtained with a Var-

ian A-60 NMR Spectrometer at 60 MHz on CF_3COOH solutions (chemical shifts, δ , in ppm relative to internal TMS). Inherent viscosities were determined in Cannon-Fenske viscometers at 30°C (0.5% w/v in 98% formic acid); in order to minimize acidolysis, the period required for dissolution, filtration and thermal equilibration was restricted to 20-25 min. Microanalyses were performed by Robertson Laboratory, Florham Park, NJ, USA. Thermogravimetric analysis traces were obtained in the laboratories of the Polymers & Plastics Department, Westinghouse Electric Corporation, with a Du Pont Thermogravimetric Analyzer, Model 950, at a heating rate of 10°C/min and a gas (N_2 , air) flow rate of 0.2 l/min.

Materials

3,3'-Diaminobenzidine. The compound, prepared by the method of Vogel and Marvel¹⁶ and purified by sublimation¹⁷, melted at 178°-179°C; it was kept under N_2 in the dark until used.

3,3'-Dimercaptobenzidine. Preparation of the base in pure form presented appreciable experimental difficulties. Although synthesized by many workers^{12,17-23}, the oxidatively unstable base has preferably been used in the form of its dihydrochloride, for which analytical findings are available^{17,19}. The free compound, on the other hand, has never been unambiguously described in the literature. Dokoshi *et al.*²², while publishing the found (correct) elemental composition, listed a melting point of 287°C for the base. Rabilloud and coworkers²³ described the compound as infusible. Both groups of authors obviously had in their hands a polymeric disulphide of the base, which, according to Hergenrother²⁴, possesses about the same elemental composition and melts with decomposition at 273°C. In our work, preparation by the standard procedure¹⁸ failed to give a product pure enough for subsequent successful polymerization. Satisfactory purification was eventually

achieved by repetitive fractional precipitation of the compound from alkaline solution with acetic acid. To this end, the crude dipotassium salt, obtained as described¹⁸, was dissolved in water (150 ml/10 g of salt), and the free base was regenerated from the filtered solution by acidification with glacial acetic acid. The precipitated product was redissolved in 1 M aqueous potassium hydroxide (500 ml/10 g of base). Slow addition of acetic acid to the filtered, rapidly stirred solution produced a precipitate of yellow impurities (largely the polymeric disulphide²⁴) as the point of neutrality was approached. Following removal of the impurities by filtration, the addition of acid was continued to pH 5–6 whereupon the base separated as almost colourless and reasonably air-stable, fine crystals, m.p. 156°–160°C. Two more reprecipitations by the same procedure, followed by drying for 24 h at 50°C/0.1 mmHg, furnished a product with m.p. 158°–161°C* in an overall yield of 35–40%. No further narrowing of the melting range was observed upon additional reprecipitations. All operations described were performed under a blanket of nitrogen, and the solvents were meticulously degassed prior to use.

Calculated for C₁₂H₁₂N₂S₂: C, 58.03; H, 4.87; N, 11.28; S, 25.82%. Found: C, 58.36; H, 5.02; N, 11.25; S, 25.26%.

I.r. (KBr, prominent bands only): 3425, 3342 ($\nu_{\text{N-H}}$), 2544 ($\nu_{\text{S-H}}$), 1615 ($\delta_{\text{N-H}}$, $\nu_{\text{C-C}}$), 1480–1490 ($\delta_{\text{C-H}}$), 1272, 1280 ($\nu_{\text{C-N}}$), 875, 815 ($\delta_{\text{C-H}}$).

1,1'-Bis(chlorocarbonyl)cobalticinium hexafluorophosphate/chloride. 1,1'-Dimethylcobalticinium hexafluorophosphate, obtained from methylcyclopentadiene and anhydrous cobaltous bromide⁵ or, alternatively, from thallium (I) methylcyclopentadienide and cobaltous chloride hexahydrate²⁵, was oxidized as described previously^{5,11}. The crude oxidation products, precipitated as the hexafluorophosphate salts, were thoroughly extracted with hot acetone for removal of monocarboxy compound¹¹, leaving the dicarboxylic acid hexafluorophosphate as yellow, fluffy fine needles. The compound gave ¹H n.m.r. absorptions as reported previously¹¹, and no resonances due to monosubstituted or incompletely oxidized products were observed.

The dicarboxylic acid was chlorinated with freshly distilled thionyl chloride (10 ml/1 g of acid) for 24 h at the reflux temperature with moisture protection. (Heating periods of 6 h, corresponding to the literature value⁵, gave product contaminated with starting material or monochloride as indicated by i.r. absorption near 1725 cm⁻¹.) The dichloride, which crystallized from the cooled (0°C) solution, was separated by filtration, washed with dry benzene, and dried for 24 h at 60°C/0.1 mmHg. Yields in the chlorination step amounted to 80–87%. The compound gave the same i.r. bands as reported by the earlier authors⁵. Chlorine determinations on the hydrolysis products of samples from several runs indicated variable Cl⁻ contents generally 15–30% by wt in the anion moiety, (see, however, first footnote in results section); for stoichiometric calculations, throughout this work, the anion composition of the dichloride was taken to be 80% PF₆⁻, 20% Cl⁻. The extreme moisture sensitivity of the compound necessitated rigorous precautions, including the use of dry-box techniques, in handling and transfer manipulations.

* In a personal communication, for which we are most indebted, Mr P. M. Hergenrother, Whittaker Corporation, has recently brought to our attention some results of unpublished work in his laboratory on the synthesis of the free base, which was found to melt at about the same temperature as in our study.

Intermediate polymer I from 3,3'-diaminobenzidine and 1,1'-bis(chlorocarbonyl)cobalticinium salt

In this and all subsequent polymerization experiments, all glass ware was flamed and flushed with dry N₂. Solvent media were redistilled *in vacuo*, stored over Molecular Sieves, type 4A, and degassed prior to use. Transfer operations involving monomers were performed in the dry-box, and the poly-condensation reactions were conducted under an argon blanket with rigorous moisture protection.

In a 100 ml three-neck flask equipped with mechanical stirrer and fitted with gas in- and out-let tubes, 0.54 g (2.5 mmol) of pre-dried diaminobenzidine was briefly shaken under a rapid stream of dry argon and was dissolved in 15 ml of *N*-methylpyrrolidone. To the solution, cooled to -5°C, was added dropwise, with stirring, 1.09 g (2.5 mmol) of bis(chlorocarbonyl)cobalticinium salt, dissolved in 45 ml of acetonitrile. Throughout the addition period (45 min) and another 3 h thereafter, the temperature was maintained at -5 ± 3°C and was subsequently allowed to rise to 22 ± 3°C. Stirring was continued at that temperature for 15 h. The mixture remained heterogeneous throughout, as oligomeric condensation products began to precipitate shortly after the addition of the cobalticinium salt was started. Product precipitation was completed at the end of the reaction period by the addition of 300 ml of dry ether, and the separated dark reddish-brown polymer I was collected by filtration, briefly washed with methanol (low-molecular mass constituents partly extracted), and dried for 2 days over P₂O₅ at 60°C/0.1 mmHg; yield, 0.98 g (71.8%, based on A⁻ = 50% PF₆⁻, 50% Cl⁻, by wt). The polymer was soluble in water and formic acid, but insoluble in aprotic solvents. In acidic solutions, rapid chain degradation was indicated by viscosity reductions to nearly one-half the initial values upon standing for 40–60 min at ambient temperature.

For regeneration of the PF₆⁻ anion, a 0.20 g sample of the crude polymer was rapidly dissolved in 2 ml of 98% formic acid containing 0.1 g of NH₄PF₆. The filtered solution was stirred dropwise into 30 ml of diethyl ether/ethanol (1:1) saturated with NH₄PF₆, and the precipitated polymer I (A⁻ = PF₆⁻), after rapid separation by filtration, was washed successively with diethyl ether (50 ml), diethyl ether/ethanol (1:1) saturated with NH₄PF₆ (50 ml), and ethanol (200 ml). After drying for 50 h at 65°C/0.2 mmHg over P₂O₅, the reddish-black polymer weighed 0.11 g, corresponding to an overall yield of 39.5% (based on monomers). The product, while now insoluble in water, showed solubility in dimethylformamide and other aprotic solvents.

The reaction variables for the described polymerization run are summarized in Table 1 (experiment 1), which also lists analytical data for the crude and reprecipitated I.

Intermediate polymer III from 3,3'-dimercaptobenzidine and 1,1'-bis(chlorocarbonyl)cobalticinium salt

To the solution of 0.60 g (2.4 mmol) of the dimercaptobenzidine in 30 ml of hexamethylphosphoramide, rapidly stirred and precooled to -5°C, was added 1.05 g (2.4 mmol) of solid bis(chlorocarbonyl)cobalticinium salt. Following 1 h of stirring at -5 ± 3°C, the temperature was allowed to rise to 22 ± 3°C and was there maintained for another 48 h with continued stirring. Heterogeneity of the mixture obtained throughout the reaction period. The work up method as described in the preceding section gave 1.2 g (86.2%, based on A⁻ = 50% PF₆⁻, 50% Cl⁻, by wt) of crude, brownish-black polymer (III), which was partly soluble in

Table 1 Intermediate polymers I and III from benzidine derivatives and 1,1'-bis(chlorocarbonyl)cobalticinium salt

Ex- peri- ment No.	Reac- tants ^a	Sol- vent ^b	Heat treat- ment ^c	Polymer yield ^d (%)	Found ^f (%)								η_{inh}^g (ml/g)
					after repreci- tation ^e	Polymer I			Polymer III				
				crude	C	H	N	C	H	N	S		
1	DAB + BCC	NMP/ MeCN (1:3)	3 h at -5°C, 72 then 15 h at 22°C	39	(a) 53.57 (b) 48.69	4.02 3.07	11.12 ^h 9.70 ⁱ					12	
2	DMB + BCC ^j	HMP	1 h at -5°C, 86 then 48 h at 22°C ^k	44				(a) 50.10 (b) 45.87	3.12 2.93	4.71 4.52	10.24 ^l — ^m	20	
3	DMB + BCC	HMP	4 h at -5°C, 88 then 96 h at 20°C	—				(a) 49.77	3.20	4.50	10.72 ⁿ	9	
4	DMB + BCC	MeCN/ Py (2:1)	4 h at -5°C, 79 then 15 h at 20°C, 2 h at 60°C	—				(a) 50.99	3.05	5.45	10.49 ^o	10	

- a Employed in equimolar quantities. Concentrations, mol/l: 0.042 (experiment 1); 0.08 (experiments 2 and 3); 0.05 (experiment 4). DAB = 3,3'-diaminobenzidine; DMB = 3,3'-dimercaptobenzidine; BCC = 1,1'-bis(chlorocarbonyl)cobalticinium salt ($A^- = 80\% PF_6^-, 20\% Cl^-$)
- b NMP = *N*-methylpyrrolidone; MeCN = acetonitrile; HMP = hexamethylphosphoramide; Py = pyridine. Ratios by volume
- c Temperature variation $\pm 3^\circ C$, ~ 2 h period to reach ambient temperature
- d Calculated for $A^- = 50\% PF_6^-, 50\% Cl^-$ (by wt) in crude polymer; for $A^- = PF_6^-$ in reprecipitated polymer
- e Crude polymer reprecipitated from formic acid solution in the presence of NH_4PF_6 (see text)
- f Line (a), crude polymer; line (b), reprecipitated polymer (footnote e). All values are averages of at least two determinations
- g At $30^\circ C$; 0.5% (w/v) in 98% formic acid, on reprecipitated polymer (footnote e) in experiments 1 and 2; on crude polymer in experiments 3 and 4. Measurements made within 30 min following dissolution. Value in experiment 2 drops to 11 (9) ml/g after 40 (60) min standing in solution
- h Calculated for I, $A^- = 40\% PF_6^-, 60\% Cl^-$: C, 53.53; H, 3.72; N, 11.15%
- i Calculated for I, $A^- = PF_6^-$: C, 48.01; H, 3.36; N, 9.33%
- j No significant changes in composition or degree of polymerization at DMB/BCC molar ratios of either 0.9 or 1.1
- k No significant changes in degree of polymerization after 1 h at $-5^\circ C$, followed by 8 h at $20^\circ C$ and 15 h at $60^\circ C$
- l Calculated for III, $A^- = 45\% PF_6^-, 55\% Cl^-$: C, 50.20; H, 3.16; N, 4.88; S, 11.16%
- m Calculated for III, $A^- = PF_6^-$: C, 45.43; H, 2.86; N, 4.42%
- n Calculated for III, $A^- = 50\% PF_6^-, 50\% Cl^-$: C, 49.73; H, 3.13; N, 4.83; S, 11.06%
- o Calculated for III, $A^- = 40\% PF_6^-, 60\% Cl^-$: C, 50.68; H, 3.19; N, 4.93; S, 11.27%

water and alkanols and completely soluble in formic acid, but essentially insoluble in aprotic solvents. Similar sensitivity to acidolytic chain scission was observed as with the polyamide I.

Regeneration of the PF_6^- anion was accomplished by rapid reprecipitation from formic acid solution in the presence of NH_4PF_6 as described for I. Polymer III ($A^- = PF_6^-$) so obtained in a yield corresponding to 43.6% (based on monomers) was insoluble in water, but moderately soluble in dimethylformamide.

The experimental variables and analytical results for both the crude and the reprecipitated polymer III are compiled in Table 1 (experiment 2).

A polymerization run conducted as above, except that the temperature was maintained for 4 h at $-5^\circ C$ followed by 96 h at $20^\circ C$, is summarized in Table 1 as experiment 3. A further run, employing the solvent system acetonitrile/pyridine (2:1 v/v), is tabulated as experiment 4; in this run, the dichloride was added as a 2.2% solution in acetonitrile. No reprecipitations were performed in the last-named two experiments, and the analytical data listed accordingly refer to the crude polymer products possessing mixed Cl^-/PF_6^- anions. Summarized results for additional polymerization experiments are found in footnotes j and k of the same Table.

Polyazoles, II and IV by thermal advancement of intermediate polymers I and III

Samples (0.05 g) of I and III, both crude ($A^- = PF_6^-/Cl^-$) and after reprecipitation from formic acid/ NH_4PF_6 ($A^- =$

PF_6^-), were placed in Schlenk tubes and were subjected to heating cycles as exemplified in Table 2. The samples were employed either in the solid, powdery state or else as films cast from aqueous solutions (crude I) or from dimethylformamide solutions (reprecipitated I and III). Because of the low degrees of polymerization attained, the films generally were quite brittle and tended to crumble on handling. Throughout the heating period, the pressure was reduced to 0.05 mmHg. Alternatively, in a few experiments, heating was conducted under a blanket of deoxygenated argon. The cooled tubes, on opening after completed heat treatment, were found to contain acidic (pH 3–4) vapours of pungent odour reminiscent of phosphorus fluorides. The brownish-black polyazoles obtained were insoluble in all common organic solvents and mineral acids. Analytical data on representative samples are collected in Table 2. Selected polymers, as marked in the Table, were used for the t.g.a. scans.

RESULTS AND DISCUSSION

Intermediary polyamides and polythioesters

The synthetic approach chosen for the preparation of polymers with bibenzimidazolyl backbone constituents comprised the low temperature solution condensation of 3,3'-diaminobenzidine and 1,1'-bis(chlorocarbonyl)cobalticinium hexafluorophosphate/chloride in *N*-methylpyrrolidone/acetonitrile. The analogous procedure selected for the synthesis of polymers with bibenzothiazolyl units in the backbone involved the low temperature solution con-

Table 2 Polyazoles II and IV by thermal advancement of intermediate polymers I and III

Starting material	Heat treatment ^a	Found ^b (%)							
		polybenzimidazole II			polybenzothiazole IV				
		C	H	N	C	H	N	S	
Polymer 1:									
crude (A ⁻ = PF ₆ ⁻ /Cl ⁻) ^c	5 h at 100–180°C, 1 h at 250°C, 2 h at 290°C	(a)	57.31	3.91	11.05 ^{d,k}				
		(b)	57.44	3.78	11.00				
reprecipitated (A ⁻ = PF ₆ ⁻) ^e	5 h at 120–200°C, 1 h at 250°C, 2 h at 300°C	(a)	51.46	3.67	9.62 ^{f,k}				
		(c)	52.07	3.48	9.75				
Polymer 3:									
crude (A ⁻ = PF ₆ ⁻ /Cl ⁻) ^g	12 h at 100–180°C, 2 h at 250°C, 2 h at 300°C	(a)	54.72	2.71	5.74	11.05 ^{h,k}			
reprecipitated (A ⁻ = PF ₆ ⁻) ⁱ	12 h at 100–180°C, 2 h at 250°C, 2 h at 300°C	(a)	49.70	2.82	4.74	10.06 ^j			
		(c)	50.13	2.96	4.96	10.33			

^a Performed at 0.05 mmHg unless marked to the contrary

^b Line (a), advanced as powder; line (b), advanced as film cast from aqueous solution; line (c), advanced as film cast from DMF solution. All values are averages of at least two determinations

^c Crude polymer I from experiment 1, Table 1

^d Found for sample advanced under Ar: C, 57.50; H, 3.94; N, 11.07%; for sample advanced as tabulated, but additionally heated for 0.5 h at 380°C: C, 57.22; H, 3.53; N, 11.17%. Calculated for II, A⁻ = 40% PF₆⁻, 60% Cl⁻: C, 57.37; H, 3.19; N, 11.95%

^e Reprecipitated polymer I from experiment 1, Table 1

^f Found for sample heated under Ar: C, 52.33; H, 3.27; N, 9.65%. Calculated for II, A⁻ = PF₆⁻: C, 51.08; H, 2.86; N, 9.93%

^g Crude polymer III from experiment 4, Table 1

^h Found for sample heated under Ar: C, 54.11; H, 2.82; N, 11.21%. Calculated for IV, A⁻ = 40% PF₆⁻, 60% Cl⁻: C, 54.64; H, 2.68; N, 5.31; S, 12.16%

ⁱ Reprecipitated polymer III from experiment 2, Table 1

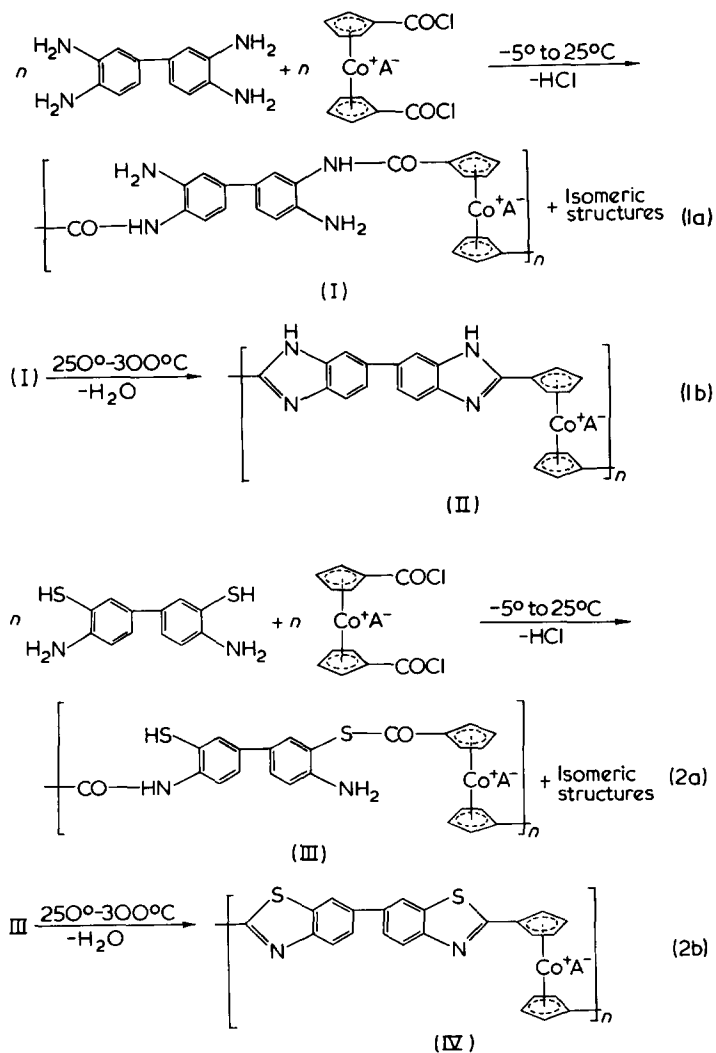
^j Calculated for IV, A⁻ = PF₆⁻: C, 48.17; H, 2.36; N, 4.68; S, 10.72%

^k Sample employed in t.g.a. test

densation of 3,3'-dimercaptobenzidine with the same cobalticinium compound; the medium used was hexamethylphosphoramide, which in this case proved slightly superior to the methylpyrrolidone/acetonitrile mixture. Advancement to an acceptably high degree of polymerization called for utmost purity of the starting materials, a requirement presenting appreciable experimental difficulties with both the cobalticinium salt and the dimercapto compound (see experimental). The former compound was prepared as the mixed PF₆⁻/Cl⁻ salt⁵, a variable*, minor portion of the PF₆⁻ counter ion originally present in the dicarboxy-cobalticinium salt having undergone exchange with Cl⁻ anion in the course of chlorination in accord with earlier observations⁵. The two reactant pairs were allowed to undergo polycondensation at -5° to 25°C in the respective media (equations 1a and 2a).

Experimental conditions are summarized in Table 1 for two typical runs each employing equimolar reactant quantities (experiments 1 and 2). Insolubility in the aprotic solvents caused immediate partial precipitation of the product salts in both cases; for this reason, propagation largely proceeded in a heterogeneous system, and the degrees of polymerization attained were correspondingly low ($\eta_{inh} = 10\text{--}20\text{ ml/g}$). Product precipitation was completed at the end of the specified reaction periods by the addition of excess ether, use of this precipitant being dictated by the partial solubility of the products in water and, to a lesser extent, in lower alkanols. The separated polymeric intermediates gave C, H, N (S) microanalytical results (Table 1) in agreement with structures I and III respectively, having anion compositions of 40–50% PF₆⁻ and 60–50% Cl⁻.

* Although chlorine determinations indicate replacement of PF₆⁻ by Cl⁻ generally to be limited to 15–30%, halogen (F, Cl) and phosphorus analyses in the combination of elements present (notably Co) proved highly erratic and hence could not be used in our work for quantitative evaluation.



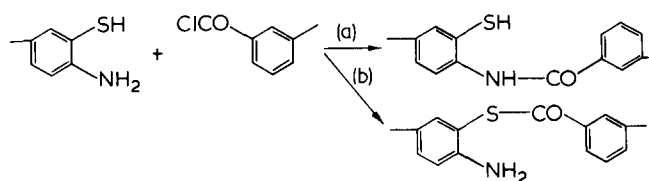
While a portion of this chloride anion percentage in both I and III is attributable to the cobalticenium salt reactant, the major part evidently resulted from anion exchange in the presence of the hydrogen chloride liberated in the propagation reaction. Such exchange was earlier observed by Pittman, Sheats, and collaborators⁵, but could not be verified quantitatively by a complete elemental analysis because of unreproducible results in the halogen determinations due to interference by the cobalt present†. We encountered the same analytical problems in our work, the experimentally found Cl and F contents generally adding up to 25–30% of the total (as against a maximum of 20.20%, calculated for $A^- = PF_6^-$ in I). Although, for this reason, we were unable to confirm the postulated anion compositions by halogen (and phosphorus) determinations, we found corroboration in the i.r. spectra. The spectrum of crude I, as isolated in these reactions, while showing in the expected intensities the common absorption patterns of the substituted biphenyl system and the 1,1'-disubstituted cobalticenium cation^{5,8} as well as the N–H and C–N stretching bands near 3350 and 1270 (sh) cm^{-1} associated with the primary amino groups and the amide I, II and III bands at about 1660, 1525, and 1305 cm^{-1} , displayed only weak absorption in the P–F stretching region of 830–840 cm^{-1} (partially merging with the benzene- and cobalticenium-aromatic C–H out-of-plane deformation bands at 810 and 860–870 cm^{-1}) and showed the typical 560 cm^{-1} peak of the PF_6^- complex‡ with appreciably lower intensity. The spectrum of crude III was characterized by a similarly attenuated P–F absorption in the two regions.

In order to regenerate the PF_6^- anion quantitatively, the crude polymers I and III were each reprecipitated from formic acid solution by ether/ethanol saturated with ammonium hexafluorophosphate. The polymers' extreme sensitivity to chain scission in contact with strong acids necessitated fast operation in this reprecipitation step. The C, H, N (S) contents of the polymers so treated conformed, respectively, to structures I and III with $A^- = PF_6^-$, and the i.r. spectra now featured the broad P–F stretching band system in the same dominating intensity as commonly observed with non-polymeric cobalticenium hexafluorophosphates and showed a strongly enhanced 560 cm^{-1} peak‡. Analytical data and inherent viscosities for the reprecipitated polymers are presented in Table 1.

Several polycondensations involving the reactant pair of equation (2a) were conducted over appreciably prolonged reaction periods under otherwise unchanged conditions in an attempt to raise both the conversion and the degree of polymerization in these largely heterogeneous reaction systems. Experiment 3 (Table 1), performed over a 96 h period, exemplifies this effort. In another experiment, the reaction temperature was gradually increased from -5° to $60^\circ C$. In still other polycondensation experiments, either the cobalticenium salt or the dimercapto compound was employed in a 5–10% molar excess over the respective reaction partner. In no case did an increase in conversion or polymer viscosity result from such modifications (footnotes j and k, Table 1). Changing to the solvent system acetonitrile/pyridine, at temperatures ultimately reaching $60^\circ C$ (experiment 4, Table 1), likewise proved of

no benefit in this respect. These findings rather conclusively point to the inhomogeneity of the reaction system as the principal hindrance to the attainment of high molecular masses and show the need for further scrutiny of the polymer solubility problem.

While the polyamide backbone structure of the intermediary polymer I can be regarded as established on the basis of the synthetic conditions, as well as the elemental analytical and i.r. spectroscopic findings discussed, the structural details of the analogous polymer III are by no means obvious. Hergenrother and Levine¹², discussing the two possible reaction paths originating from the condensation of isophthaloyl chloride with 3,3'-mercaptobenzidine, concluded from i.r. data that the principal reaction sequence leading to the intermediate polymer involved amide formation (path a), although preferred thioester formation (path b) was expected on the basis of relative nucleophilicity considerations. In the present case, i.r. evidence is inconclusive.



The spectra of polymers from different experiments invariably displayed the S–H stretching band near 2550 cm^{-1} (path a) in almost negligible intensities or failed to show it altogether, and the N–H stretching and bending vibrations of the primary amino group (path b) could not be detected in existing envelopes of other bands. While absorption was observed at the positions of the amide I, II and III bands, suggesting the existence of amide links, the amide I band appeared broadened, with a maximum emerging at 1670 cm^{-1} assignable to the thioester carbonyl stretching mode. We conclude that polyamide and polythioester structures both were formed under the conditions of our experiments, and the (idealized) representation polymer III takes account of these two isomeric types.

Polybenzazoles

The polymeric intermediates I and III, in both the crude ($A^- = PF_6^-/Cl^-$) and the reprecipitated ($A^- = PF_6^-$) forms, were subjected to thermal solid-state heat treatment under reduced pressure or under an argon blanket for cyclodehydration to the heterocyclic end-products, II and IV (equations 1b, 2b). Although preliminary checks by i.r. and elemental analyses had shown such cyclization to set in below $250^\circ C$, we employed temperatures in the vicinity of $300^\circ C$ to ensure optimal ring closure. (Higher temperatures still, up to $380^\circ C$, entailed no further changes in the spectral behaviour and elemental composition.) The heat treated, brownish-black polyheterocyclics were no longer soluble in organic solvents or mineral acids. Confirming substantially accomplished cyclodehydration, the i.r. spectrum of II featured the absorption characteristic of the aromatic benzimidazole system^{13–15} with maxima near 1625 (s), 1610 (m), 1505 (w), 1445–1470 (m–s, multiplet), 1280 (m–s), 1080–1130 (w–m, broad multiplet), 860 (m, partially merging with cobalticenium C–H deformation band), and 800 (s) cm^{-1} , as similarly shown by the benzene-aromatic polybenzimidazoles of Marvel's work¹⁶. The C–N stretching and amide I, II and III peaks, on the other hand, vanished in the envelopes of the adjacent benzimidazole absorptions. Analogously, the spectrum of IV was charac-

† Difficulties with P, F, Cl analyses have also been reported in studies involving other polymeric and non-polymeric cobalticenium hexachlorophosphates/chlorides^{9,11}.

‡ We found the band invariably at 550–570 cm^{-1} in the spectra of a large number of inorganic and organometallic hexafluorophosphates studied.

terized by absorption reasonably assignable to the benzothiazole unit at 1600–1590 (s), 1510 (s), 1445 (s), 1380 (m, shoulder on 1395 cm^{-1} cobalticinium band), 1270 (w–m), 865 (m, partly coalescing with cobalticinium band), and 815 (s) cm^{-1} , whereas the thioester and amide bands disappeared in the envelopes of these absorptions. The weak carboxyl end group absorption shown at 1720 cm^{-1} in the spectra of several samples also vanished upon the heat treatment, obviously as a result of thermal decarboxylation. 1,1'-Dicarboxycobalticinium hexafluorophosphate undergoes complete decarboxylation (concomitant with partial degradation of the PF_6^- counter ion) after 4 h at 250°C and 0.1 mmHg.

In further confirmation of substantially cyclized product structures, the C, H, N (S) microanalytical results (Table 2) obtained on polybenzazoles that were derived from the crude ($\text{A}^- = \text{PF}_6^-/\text{Cl}^-$) intermediary polymers agreed with structures II ($\text{A}^- = \text{PF}_6^-/\text{Cl}^-$) and IV ($\text{A}^- = \text{PF}_6^-/\text{Cl}^-$), respectively. Similarly, benzazole polymers obtained from the reprecipitated ($\text{A}^- = \text{PF}_6^-$) intermediates gave C, H, N (S) analytical data reasonably well in accord with product structures possessing $\text{A}^- = \text{PF}_6^-$, although the slightly higher C, H values found suggest a corresponding minor loss of fluorine and, perhaps, phosphorus contents. (For the reasons outlined further above, F and P could not be determined reproducibly and in any degree of reliability to verify such losses.) At the same time, the P–F stretching absorption in the i.r. spectra of the last named two polyazole types appeared in drastically reduced intensities relative to their precursor polymers with $\text{A}^- = \text{PF}_6^-$, clearly exposing the aforementioned C–H deformation bands of the cobalticinium and benzazole systems in this region. The weak evolution of acidic vapours observed during the heat treatment suggests rather limited thermal stability of the PF_6^- counterion in these polysalts, phosphorus fluorides being eliminated in the process. Conceivably, then, the cyclization steps in equation (1b) and (2b) were accompanied by a partial breakdown of PF_6^- into F^- and PF_5 , and the latter halide, being an aggressive fluorinating agent at these high temperatures, caused partial ring fluorination. Evidence for carbon-bonded fluorine in the products can indeed be found in the i.r. spectra, which invariably showed broad absorption at 1100–1150 cm^{-1} , whereas, not unexpectedly, this absorption was very weak or virtually absent in the spectra of polyazoles obtained from crude polymers I and III with grossly reduced PF_6^- contents. The PF_3 liberated in the fluorination step could partially escape and, to some extent, might also be re-incorporated into the polymers, e.g., through phosphorylation of amino groups. The various hexafluorophosphate degradation and ring fluorination reactions would account for both the considerably weakened 840 cm^{-1} i.r. absorption and the minor deviations of the C, H, N-contents from the calculated values in the hexafluorophosphate polysalts.

The loss of solubility accompanying the heat treatment of both I and III points to minor imperfections in the structural build-up of II and IV, including incomplete cyclization, branching, and crosslinking via functional groups escaping the ring-closing steps, and it remains to be studied to what extent these structural imperfections are caused and affected by the hexafluorophosphate counter ion and its inherent instability at the cyclization temperatures employed. As an immediate consequence of structural defects, the polyazoles, whether derived from precursors with $\text{A}^- = \text{PF}_6^-$ or from those with $\text{A}^- = \text{PF}_6^-/\text{Cl}^-$, showed a performance distinctly inferior to that of the

common all-aromatic polybenzimidazoles in thermogravimetric analysis. The thermograms of both II and IV recorded at a heating rate of 5°C/min, indicated weight loss to set in near 350°C in air and at 400–450°C in a nitrogen atmosphere. In the air runs, the relative weight loss at 500°, 650°, and 800°C was in the range of 45–55, 70–75, and 72–76%, respectively. In N_2 , the corresponding weight loss ranges were 10–15, 30–40, and 55–65%.

We are currently studying polymerizations in a more homogeneous phase as realized, for example, in polyphosphoric acid or ethylated polyphosphoric acid media. The consequences of replacing hexafluorophosphate by chloride and other anions in the intermediate polymers will also be examined.

ACKNOWLEDGEMENTS

This work was generously supported by the South African Atomic Energy Board with grants for both an assistantship and running expenses. The authors are also much indebted to Dr L. W. Frost and his staff, Westinghouse Electric Corporation, who kindly scanned the t.g.a. thermograms.

REFERENCES

- 1 Metalocene Polymers XXXI. For Part XXX, see E. W. Neuse, *J. South Afr. Chem. Inst.* 1975, 28, 365
- 2 Fischer, E. O. and Herberich, G. E. *Chem. Ber.* 1961, 94, 1517
- 3 Neuse, E. W. *Adv. Macromol. Chem.* 1968, 1, 1; Neuse, E. W. and Rosenberg, H. *Metalocene Polymers*, Marcel Dekker, New York, 1970.
- 4 Ito, T. and Kenjo, T. *Bull. Chem. Soc. Japan* 1968, 41, 614
- 5 Pittman, Jr. C. U., Ayers, O. E., McManus, S. P., Sheats, J. E. and Whitten, C. E. *Macromolecules* 1971, 4, 360
- 6 Pittman, Jr. C. U., Ayers, O. E., Suryanarayanan, B., McManus, S. P. and Sheats, J. E. *Makromol. Chem.* 1974, 175, 1427
- 7 Carraher, Jr. C. E., Peterson, G. F. and Sheats, J. E. *Prepr. ACS Div. Org. Coat. Plast. Chem.* 1973, 33, 427
- 8 Carraher, Jr. C. E., Peterson, G. F., Sheats, J. E. and Kirsch, T. *J. Macromol. Sci. (A)* 1974, 8, 1009; *Makromol. Chem.* 1974, 175, 3089
- 9 Carraher, Jr. C. E. and Sheats, J. E. *Prepr. ACS Div. Org. Coat. Plast. Chem.* 1973, 33, 634; *Makromol. Chem.* 1973, 166, 23
- 10 Sheats, J. E., Carraher, Jr. C. E., Bruyer, D. and Cole, M. *Am. Chem. Soc. Div. Org. Coat. Plast. Chem. Prepr.* 1974, 34, 474
- 11 Sheats, J. E. and Rausch, M. D. *J. Org. Chem.* 1970, 35, 3245
- 12 Hergenrother, P. M. and Levine, H. H. *J. Polym. Sci. (A-1)* 1966, 4, 2341
- 13 Morgan, K. J. *J. Chem. Soc.* 1961, 2343
- 14 Rabiger, D. J. and Joullié, M. M. *J. Chem. Soc.* 1964, 915; *J. Org. Chem.* 1964, 29, 482
- 15 Iwakura, Y., Uno, K. and Imai, Y. *J. Polym. Sci. (A)* 1964, 2, 2605
- 16 Vogel, H. and Marvel, C. S. *J. Polym. Sci.* 1961, 50, 511, *J. Polym. Sci. (A)* 1963, 1, 1531 and subsequent publications from that group
- 17 Kokelenberg, H. and Marvel, C. S. *J. Polym. Sci. (A)* 1970, 8, 3199
- 18 Houben-Weyl, *Methoden der Organischen Chemie*, (Ed. E. Miller), Georg Thieme Verlag, Stuttgart, 1955, Vol IX, p 39
- 19 Imai, Y., Taoka, I., Uno, K. and Iwakura, Y. *Makromol. Chem.* 1965, 83, 167
- 20 Hergenrother, P. M., Wrasidlo, W. and Levine, H. H. *J. Polym. Sci. (A-1)* 1965, 3, 1665
- 21 Okada, M. and Marvel, C. S. *J. Polym. Sci. (A-1)* 1968, 6, 1774
- 22 Dokoshi, N., Tohyama, S., Fujita, S., Kurihara, M. and Yoda, N. *J. Polym. Sci. (A-1)* 1970, 8, 2197
- 23 Rabilloud, G., Sillion, B. and de Gaudemaris, G. *Makromol. Chem.* 1971, 146, 215
- 24 Hergenrother, P. M. unpublished results 1974
- 25 Sheats, J. E. and Kirsch, T. *Synth. Inorg. Met. Org. Chem.* 1973, 3, 59

Syntheses and conformational studies of poly(γ -*N*-alkyl-L- α , γ -diaminobutyric acids) and their carbobenzoxy derivatives

Hiroyuki Yamamoto, Miho Miyazaki and Tadao Hayakawa

Institute of High Polymer Research, Faculty of Textile Science and Technology, Shinshu University, Ueda 386, Japan

(Received 5 November 1975)

Three types of high molecular weight poly(γ -*N*-methyl, γ -*N*-carbobenzoxy-L- α , γ -diaminobutyric acid), poly(γ -*N*-ethyl, γ -*N*-carbobenzoxy-L- α , γ -diaminobutyric acid), and poly(γ -*N*-benzyl, γ -*N*-carbobenzoxy-L- α , γ -diaminobutyric acid) were synthesized by the *N*-carboxyanhydride method. The helix-coil transition of these poly(γ -*N*-alkyl, γ -*N*-carbobenzoxy-L- α , γ -diaminobutyric acids) in chloroform-dichloroacetic acid was followed by optical rotation measurements. The introduction of a methyl, an ethyl, or a benzyl group to the side chain of the carbobenzoxyated derivative of poly(L- α , γ -diaminobutyric acid) appeared to weaken the helical conformation at 25°C and altered the direction of the temperature induced helix-coil transition from a 'normal' to an 'inverse'. For water-soluble poly(γ -*N*-alkyl-L- α , γ -diaminobutyric acids), the coil-to-helix transition was little observed even when the polypeptides were uncharged at pH 12. At sufficiently high methanol concentration, however, the polypeptides underwent a complete transition from the random coil to the α -helical conformation even at pH 3.

INTRODUCTION

In aqueous solution at 25°C uncharged PLL* is known to exist in a helical form, uncharged PLO is only partly helical, and uncharged PLD is almost a random coil structure¹⁻⁴. The only difference among the three polypeptides is that PLD has one less methylene group in the side chain than PLO and two less than PLL. To study further the chain length effect of the non-polar alkyl group on the conformational stability, we have reported the syntheses and conformational studies of poly(ϵ -*N*-alkyl-L-lysine), poly(δ -*N*-alkyl-L-ornithine), and their carbobenzoxyated derivatives in previous papers⁵⁻⁸.

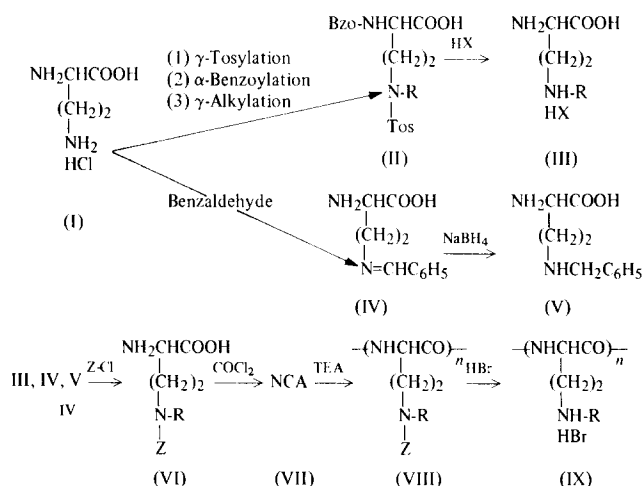
We now extend our investigations by introducing a methyl, an ethyl (aliphatic alkyl), or a benzyl (aromatic alkyl) group to the γ -amino group of the side chain, noting that γ -*N*-methyl-L- α , γ -diaminobutyric acid is an isomer of L-ornithine and γ -*N*-ethyl-L- α , γ -diaminobutyric acid is an isomer of L-lysine. In the present paper we report the

syntheses and conformational studies of PMLD, PELD, and PBLD and their carbobenzoxyated derivatives, PCMLD, PCELD, and PCBLD. The helix-coil transitions of the carbobenzoxyated polypeptides in mixed organic solvents of chloroform-DCA and the deprotected water-soluble polypeptides in aqueous solutions were followed by optical rotation and circular dichroism measurements.

EXPERIMENTAL

Polypeptides

PLD was prepared according to the method of Fasman *et al.*⁹. Three kinds of poly(γ -*N*-alkyl-L- α , γ -diaminobutyric acids) were synthesized according to the following scheme:



* Abbreviations used in this work: PLL, poly(L-lysine); PLO, poly(L-ornithine); PLD, poly(L- α , γ -diaminobutyric acid); PMLD, poly(γ -*N*-methyl-L- α , γ -diaminobutyric acid); PELD, poly(γ -*N*-ethyl-L- α , γ -diaminobutyric acid); PBLD, poly(γ -*N*-benzyl-L- α , γ -diaminobutyric acid); PCLL, poly(ϵ -*N*-carbobenzoxy-L-lysine); PCLO, poly(δ -*N*-carbobenzoxy-L-ornithine); PCLD, poly(γ -*N*-carbobenzoxy-L- α , γ -diaminobutyric acid); PCMLL, poly(ϵ -*N*-methyl, ϵ -*N*-carbobenzoxy-L-lysine); PCBLL, poly(ϵ -*N*-benzyl, ϵ -*N*-carbobenzoxy-L-lysine); PCMLO, poly(δ -*N*-methyl, δ -*N*-carbobenzoxy-L-ornithine); PCELO, poly(δ -*N*-ethyl, δ -*N*-carbobenzoxy-L-ornithine); PCBLO, poly(δ -*N*-benzyl, δ -*N*-carbobenzoxy-L-ornithine); PCMLD, poly(γ -*N*-methyl, γ -*N*-carbobenzoxy-L- α , γ -diaminobutyric acid); PCELD, poly(γ -*N*-ethyl, γ -*N*-carbobenzoxy-L- α , γ -diaminobutyric acid); PCBLD, poly(γ -*N*-benzyl, γ -*N*-carbobenzoxy-L- α , γ -diaminobutyric acid); DCA, dichloroacetic acid, o.r.d. optical rotatory dispersion; c.d., circular dichroism.

Tos = *p*-CH₃C₆H₄SO₂-; Bzo = C₆H₅CO-; Z = C₆H₅CH₂OCO-; TEA = triethylamine. In compounds II–III; R = CH₃- or C₂H₅-. In compounds VI–IX, R = CH₃-, C₂H₅-, or C₇H₇-.

γ -N-tosyl, α -N-benzoyl-L- α , γ -diaminobutyric acid

γ -N-tosyl-L- α , γ -diaminobutyric acid was prepared from L- α , γ -diaminobutyric acid monohydrochloride (I) and *p*-toluenesulphonyl chloride, as described in a previous paper⁶. The yield was 59%; melting point 209°–210°C; $[\alpha]_D^{25^\circ\text{C}} = 25.8$ ($c = 0.93\%$ in 6 N hydrochloric acid). Calculated for C₁₁H₁₆N₂O₄S: C = 48.52%; H = 5.92%; N = 10.29%; found: C = 48.43%; H = 6.01%; N = 10.10%. γ -N-tosyl, α -N-benzoyl-L- α , γ -diaminobutyric acid was prepared from γ -N-tosyl-L- α , γ -diaminobutyric acid and benzoyl chloride according to the Schotten–Baumann method⁶. This was recrystallized from ethanol and water; yield, 99%; melting point 141°–143°C; $[\alpha]_D^{25^\circ\text{C}} = -33.8$ ($c = 1.07\%$ in acetic acid). Calculated for C₁₈H₂₀N₂O₅S: C = 57.43%; H = 5.36%; N = 7.44%; found: C = 57.37%; H = 5.30%; N = 7.25%.

γ -N-tosyl, γ -N-methyl (or ethyl), α -N-benzoyl-L- α , γ -diaminobutyric acid (II)

To a solution of γ -N-tosyl, α -N-benzoyl-L- α , γ -diaminobutyric acid (32.7 g) in 32 ml of 33% sodium hydroxide, was added 12.4 ml of dimethyl sulphate. The mixture was stirred at room temperature for 3 h and at 50°C for 1 h. It was acidified to 'Congo' red with 3 N hydrochloric acid. An oily product separated which was extracted with ethyl acetate. The organic layer was washed with water and dried over anhydrous sodium sulphate, the solvent was removed under reduced pressure, and the residue was solidified as an amorphous foam from *n*-hexane; yield, 35.7 g (100% as mono-hydrate). The dicyclohexylamine salt, prepared from a 1.0 g sample in ethyl acetate, was recrystallized twice from ethyl acetate and *n*-hexane; yield, 1.24 g (86.4%); melting point 144°C; $[\alpha]_D^{25^\circ\text{C}} = 17.4$ ($c = 1.10\%$ in methanol). Calculated for C₃₁H₄₅N₃O₅S, H₂O: C = 63.13%; H = 8.03%; N = 7.12%; found: C = 62.87%; H = 7.85%; N = 7.05%.

The corresponding ethyl derivative was prepared as above from γ -N-tosyl, α -N-benzoyl-L- α , γ -diaminobutyric acid (31.4 g) and diethyl sulphate (16.3 ml); yield, 35.0 g (100% as mono-hydrate). A part of the amorphous foam was converted to the dicyclohexylamine salt; yield, 90.0%; melting point 78°–80°C; $[\alpha]_D^{25^\circ\text{C}} = 17.3$ ($c = 1.08\%$ in methanol). Calculated for C₃₂H₄₇N₃O₅S, H₂O: C = 63.63%; H = 8.18%; N = 6.96%; found: C = 63.86%; H = 7.91%; N = 7.12%.

γ -N-methyl (or ethyl)-L- α , γ -diaminobutyric acid hydrohalides (III)

A suspension of γ -N-methyl, γ -N-tosyl, α -N-benzoyl-L- α , γ -diaminobutyric acid (13.3 g) in 115 ml of 47% hydrobromic acid, was refluxed for 3 h at 150°C and cooled to 0°C. After filtration, the benzoic acid was removed by extraction with ether. The aqueous solution was then evaporated to dryness under reduced pressure. The oily residue was dissolved in ethanol and the solution neutralized to pH 6 with pyridine. The precipitate, γ -N-methyl-L- α , γ -diaminobutyric acid hydrobromide, was filtered and recrystallized from water and ethanol; yield, 4.0 g (62.6%); melting point 195°–196°C; $[\alpha]_D^{25^\circ\text{C}} = 19.8$ ($c = 1.04\%$ in 6 N hydrochloric acid). Calculated for C₅H₁₃N₂O₂Br: C =

28.18%; H = 6.15%; N = 13.15%; found: C = 27.95%; H = 6.02%; N = 12.99%.

γ -N-ethyl-L- α , γ -diaminobutyric acid hydrochloride was prepared from γ -N-ethyl, γ -N-tosyl, α -N-benzoyl-L- α , γ -diaminobutyric acid (30.5 g) and 180 ml of 12 N hydrochloric acid. The mixture was heated for 24 h at 100°C and treated in the same manner described above; yield, 4.2 g (30.5%); melting point 192°C; $[\alpha]_D^{25^\circ\text{C}} = 5.6$ ($c = 0.95\%$ in 6 N hydrochloric acid). Calculated for C₆H₁₅N₂O₂Cl, H₂O: C = 35.91%; H = 8.54%; N = 13.96%; found: C = 36.06%; H = 8.33%; N = 14.32%.

γ -N-benzylidene-L- α , γ -diaminobutyric acid (IV)

γ -N-benzylidene-L- α , γ -diaminobutyric acid was prepared from I (15 g) and benzaldehyde (10.3 ml) as described in a previous paper⁵; yield, 14.7 g (73.4%); melting point 173°C; $[\alpha]_D^{25^\circ\text{C}} = -4.0$ ($c = 0.50\%$ in 0.5 N sodium hydroxide). Calculated for C₁₁H₁₄N₂O₂: C = 64.06%; H = 6.84%; N = 13.58%; found: C = 63.88%; H = 6.65%; N = 13.23%.

γ -N-benzyl-L- α , γ -diaminobutyric acid (V)

γ -N-benzylidene-L- α , γ -diaminobutyric acid (14 g) in 68 ml of 1 N sodium hydroxide, was hydrogenated by sodium borohydride (3.9 g in 50 ml of water) as described in a previous paper⁵. The product was recrystallized from water (50 ml) and methanol (100 ml)—ethanol (10 ml); yield, 3.5 g (21.0%); melting point 200°C; $[\alpha]_D^{25^\circ\text{C}} = 8.7$ ($c = 0.58\%$ in 0.5 N sodium hydroxide). Calculated for C₁₁H₁₇N₂O₂Cl: C = 53.99%; H = 7.00%; N = 11.45%; found: C = 53.71%; H = 6.84%; N = 11.44%.

γ -N-alkyl, γ -N-carbobenzoxy-L- α , γ -diaminobutyric acids (VI)

γ -N-alkyl, γ -N-carbobenzoxy-L- α , γ -diaminobutyric acids were prepared by the usual procedure using carbobenzoxy chloride and cupric carbonate⁵ and recrystallized from 2 N hydrochloric acid and 2 N ammonium hydroxide (methyl and ethyl derivatives) or dilute acetic acid (benzyl derivative). γ -N-methyl, γ -N-carbobenzoxy-L- α , γ -diaminobutyric acid; yield, 82.1%; melting point 198°C; $[\alpha]_D^{25^\circ\text{C}} = -5.2$ ($c = 1.0\%$ in glacial acetic acid). Calculated for C₁₃H₁₈N₂O₄: C = 58.64%; H = 6.81%; N = 10.52%; found: C = 58.65%; H = 6.73%; N = 10.27%. γ -N-ethyl, γ -N-carbobenzoxy-L- α , γ -diaminobutyric acid; yield, 37.3%; melting point 200°C; $[\alpha]_D^{25^\circ\text{C}} = -2.3$ ($c = 1.0\%$ in glacial acetic acid). Calculated for C₁₄H₂₀N₂O₄: C = 59.99%; H = 7.19%; N = 9.99%; found: C = 59.65%; H = 6.94%; N = 10.17%. γ -N-benzyl, γ -N-carbobenzoxy-L- α , γ -diaminobutyric acid; yield, 51.1%; melting point 179°–180°C; $[\alpha]_D^{25^\circ\text{C}} = 2.1$ ($c = 1.17\%$ in glacial acetic acid). Calculated for C₁₉H₂₂N₂O₄: C = 66.65%; H = 6.48%; N = 8.18%; found: C = 66.69%; H = 6.60%; N = 7.90%.

γ -N-alkyl, γ -N-carbobenzoxy-L- α , γ -diaminobutyric acid N-carboxyanhydrides (NCA) (VII)

The NCAs were prepared by the usual procedure using phosgene for 1 h at 40°C in ten-fold dry dioxane. The crude NCAs were dissolved in dry acetone and then passed through a dry charcoal–silver oxide column to purify them. The acetone was evaporated to dryness under reduced pressure. γ -N-alkyl, γ -N-carbobenzoxy-L- α , γ -diaminobutyric acid NCAs were obtained as syrups and used for immediate polymerization. The three NCAs showed double absorp-

Table 1 Molecular weight of PCLD, PCMLD, PCELD, and PCBLD

Polypeptide	$[\eta]_{\text{DCA}}^{25^\circ}$	DP*	Molecular weight
PCLD	0.355	210	50 000
PCMLD	0.790	690	172 000
PCELD	0.194	90	23 000
PCBLD	0.257	130	43 000

* Degree of polymerization

tion peaks at 1785–1788 and 1853–1855 cm^{-1} due to the cyclic anhydride.

Poly(γ -*N*-alkyl, γ -*N*-carboboxy-L- α , γ -diaminobutyric acids) (VIII)

High molecular weight polypeptides (VIII) were prepared by polymerizing the NCAs in ten-fold dioxane for a week at room temperature and for 2 h at 100°C using triethylamine as an initiator (A/I = 100). The polypeptides were precipitated with water and filtered. PCMLD: yield, 80.6% (from the methyl derivative of VI). Calculated for $(\text{C}_{13}\text{H}_{16}\text{N}_2\text{O}_3)_n$: C = 62.89%; H = 6.50%; N = 11.28%; found: C = 62.44%; H = 6.23%; N = 11.19%. PCELD: yield, 95.6% (from the ethyl derivative of VI). Calculated for $(\text{C}_{14}\text{H}_{18}\text{N}_2\text{O}_3)_n$: C = 64.11%; H = 6.92%; N = 10.68%; found: C = 64.49%; H = 6.64%; N = 10.63%. PCBLD: yield, 88.1% (from the benzyl derivative of VI). Calculated for $(\text{C}_{19}\text{H}_{20}\text{N}_2\text{O}_3)_n$: C = 70.35%; H = 6.21%; N = 8.63%; found: C = 70.49%; H = 6.17%; N = 8.59%.

Poly(γ -*N*-alkyl-L- α , γ -diaminobutyric acid) hydrobromides (IX)

The polypeptide hydrobromides were prepared from VIII by the usual procedure using hydrogen bromide in glacial acetic acid¹⁰. The polypeptides were re-precipitated from water (2 ml) and ethanol (20 ml)–ether (25 ml). PMDL, HBr: yield, 95.2%. Calculated for $(\text{C}_5\text{H}_{10}\text{N}_2\text{O}, \text{HBr})_n$: C = 30.79%; H = 5.69%; N = 14.36%; found: C = 30.97%; H = 5.51%; N = 14.37%. PELD, HBr: yield, 86.5%. Calculated for $(\text{C}_6\text{H}_{12}\text{N}_2\text{O}, \text{HBr}, \text{H}_2\text{O})_n$: C = 31.73%; H = 6.66%; N = 12.33%; found: C = 31.34%; H = 6.47%; N = 12.50%. PBLD, HBr: yield, 96.0%. Calculated for $(\text{C}_{11}\text{H}_{14}\text{N}_2\text{O}, \text{HBr})_n$: C = 48.72%; H = 5.58%; N = 10.33%; found: C = 48.94%; H = 5.33%; N = 9.94%.

Methods

O.r.d. and c.d. were measured with a Jasco ORD/UV-5 spectro-polarimeter under constant nitrogen flush. Constant temperature was maintained by circulating water or ethanol (cooled by dry ice) through the jacket of a specially designed cell holder from a Haake constant temperature bath. The temperature of the solution in the cell was measured on a Takara thermistor. The experimental data were expressed in terms of specific rotation $[\alpha]$ or reduced mean residue rotation $[m']$ (degree cm^2/dmol) for o.r.d. and mean residue ellipticity $[\theta]$ (degree cm^2/dmol) for c.d. The refractive indexes of the chloroform–DCA and water–methanol mixtures were assumed to be the average of solvent composition of that of each solvent.

The intrinsic viscosities were measured in DCA at 25°C using an Ubbelohde viscometer. The molecular weights were estimated from an empirical equation $\log DP = 1.47 \log [\eta] + 2.99$, in DCA at 25°C for ϵ -*N*-carboboxy-lyllysine⁴ and listed in Table 1.

RESULTS AND DISCUSSION

Poly(γ -*N*-alkyl, γ -*N*-carboboxy-L- α , γ -diaminobutyric acids)

Conformation. The o.r.d. above 340 nm for PCLD, PCMLD, PCELD, and PCBLD was fitted with the Moffitt–Yang equation¹¹. The b_0 values were large and negative in a helix-promoting solvent, e.g. dioxane or chloroform, and close to zero in a coil-promoting solvent, e.g. DCA (Table 2). The b_0 value –400 of PCLD in chloroform–DCA (95:5 v/v) at 25°C, was in good agreement with the reported value of Hatano⁴. In the ultra-violet region, the o.r.d. of the three γ -*N*-alkyl polypeptides showed a 233 nm trough in dioxane or chloroform and their helical contents based on the 233 nm trough coincided well with that based on the b_0 values. Therefore, PCMLD is mostly helical (right-handed) in dioxane or chloroform but PCELD and PCBLD are less helical (about 50%) in the same solvent. This difference of the helical contents might arise from the difference of the bulkiness in the side chain.

Solvent induced transition. Figure 1 shows the helix–coil transition of PCLD, PCMLD, PCELD, and PCBLD in chloroform–DCA mixed solvents at 25°C with midpoints at 40, 10, 10, and 4% (v/v) DCA, respectively. Thus, the introduction of an alkyl group to the γ -*N*-amino group in the side chain appears to weaken the helical conformation at 25°C. For comparison, the transition points for ω -*N*-carboboxylylated poly(basic L-amino acids) and their ω -*N*-alkylated polypeptides are listed in Table 3. Less DCA is required to destroy the helical conformation of PCMLD than its isomer PCLO and PCELD than PCLL.

Temperature induced transition. PCLO and PCLL are known to display an ‘inverse’ temperature induced transition in mixed solvents, i.e. high temperature favours the helical form and low temperature the coiled form^{12–15}. As contrasted with its higher homologues, only PCLD displays a ‘normal’ temperature induced transition. This fact suggests that the number of methylene groups in the side chain markedly influences the direction of the temperature induced transition. As listed in Table 3, in the previous papers^{6,8} we have shown that all the ϵ -*N*- and δ -*N*-alkylated polypeptides underwent an ‘inverse’ transition and the introduction of an alkyl group did not alter the direction of the transition.

Table 2 Values of $[m']_{233}$, a_0 , and b_0 for PCLD, PCMLD, PCELD, and PCBLD in various solvents at 25°C

Polymer	Solvent	$[m']_{233}$ (degree cm^2/dmol)	a_0 (degree cm^2/dmol)	b_0 (degree cm^2/dmol)
PCLD*	Chloroform– DCA(95:5 v/v)		50	–400
	DCA		–260	0
PCMLD	Dioxane	–12 800	30	–570
	Chloroform	–11 100	–30	–440
PCELD	DCA		–430	25
	Dioxane	–5700	20	–260
	Chloroform	–5500	0	–240
PCBLD	DCA		–240	15
	Dioxane	–6200	10	–250
	Chloroform	–6000	–10	–200
	DCA		–370	–10

* Insoluble in dioxane or chloroform

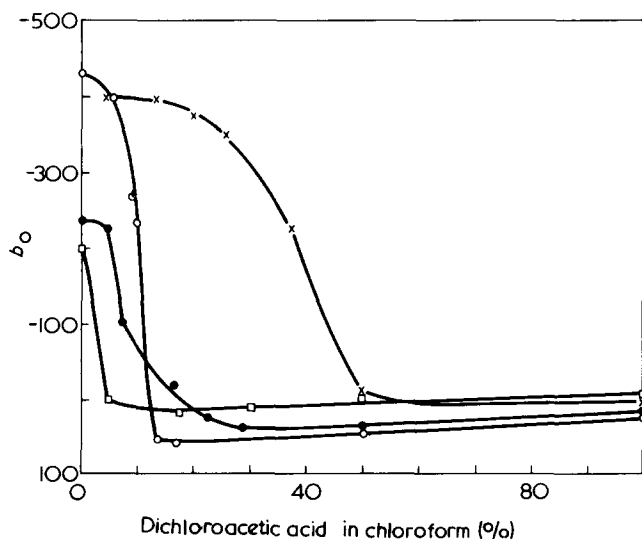


Figure 1 Helix-coil transition of PCLD (x); PCMLD (O); PCELD (●) and PCBLD (□) in chloroform-DCA mixtures at 25°C

One of the interests of the present study is whether a γ -*N*-alkyl group alters the direction or not. Figure 2 shows the temperature dependence of the rotation for PCMLD, PCELD, and PCBLD in the transition region (Figure 1) with 11, 11, and 5% DCA, respectively. At high temperature the three polypeptides decreased the negative rotation. Since $[\alpha]_{450}$ were smaller negative values (in magnitude) for the helical form than for the coiled form, PCMLD, PCELD, and PCBLD underwent an 'inverse' temperature induced transition. Thus, as contrasted with their ω -*N*-alkylated derivatives of PCLL and PCLO, the γ -*N*-alkylated derivatives of PCLD alter the direction of the transition from a 'normal' to an 'inverse'.

Poly(γ -*N*-alkyl-L- α , γ -diaminobutyric acids)

Conformation. PLD, PMLD, and PELD are soluble in water, 0.1 M sodium chloride solution, and up to 95:5 (v/v) methanol-water at all pH. PBLD hydrobromide is insoluble in water; below pH 7, however, it can be solubilized in 0.1 M sodium chloride solution by heating at 50°C (concentration less than 0.05%). Table 4 lists the $[m']_{233}$ values for the four polypeptides. The positions and the magnitudes of the trough suggested that the uncharged polypeptides (except PBLD) at pH 12 were within a few per cent of helix and the charged polypeptides at pH 3 were in a coiled conformation (see also Figure 5).

Charge induced transition. Figure 3 shows the changes in optical rotations at 233 nm with pH for the four polypeptides in 0.1 M sodium chloride solution at 25°C. PLD, PMLD, and PELD did not undergo a sharp charge induced coil-to-helix transition and judging from the magnitudes of $[m']_{233}$ the three polypeptides showed a very slight change from a random coil to within a few per cent of helix even at pH 12. At pH 12, unlike PLL (completely α -helical with $[m']_{233} = -12\,000$ to $\sim -14\,700^{1,16}$), its isomer PELD had a $[m']_{233} = -2050$ and, unlike PLO (25 to $\sim 35\%$ helical with $[m']_{233} = -5400$ to $\sim -6700^{1,3}$), its isomer PMLD a $[m']_{233} = -3400$. Thus, the conformation of PMLD or PELD differs completely from that of its isomer PLO or PLL. It is difficult to explain why PELD is less helical than PMLD, which has one less methylene group in the side chain than the former.

PBLD showed a marked tendency to increase its rotation but, because of its poor solubility, no data were obtained above pH 7.

Solvent induced transition. Figure 4 and Table 4 show the $[m']_{233}$ values for PLD, PMLD, PELD, and PBLD in mixed solvents of water and methanol at pH_{app} 3 and pH_{app} 12. At pH_{app} 3 the coil-to-helix transition of charged four polypeptides began sharply at ~ 70 to $\sim 75\%$ (v/v) methanol content. The four polypeptides became completely helical

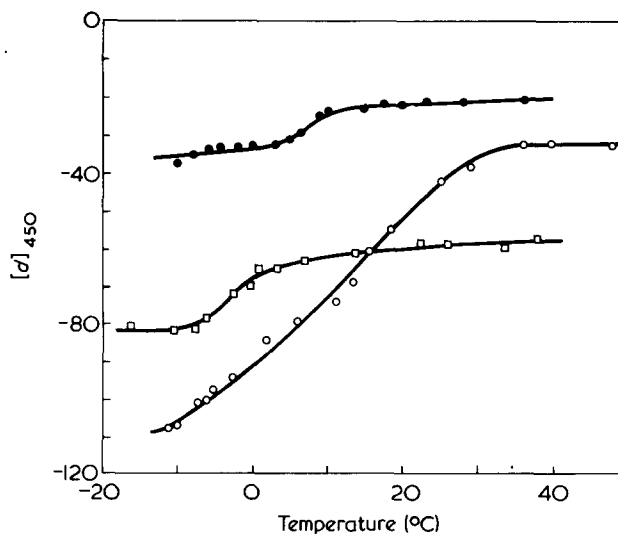


Figure 2 Change in optical rotation with temperature for PCMLD (O); PCELD (●) and PCBLD (□) in the coil-to-helix transition region in chloroform-DCA mixtures. DCA concentration: 11% for PCMLD, 11% for PCELD and 5% for PCBLD

Table 3 Temperature induced helix-coil transition of poly(basic amino acids) in mixed organic solvents

Polypeptide	Side chain	Solvent transition, % DCA in chloroform	Direction of transition	Reference
PCLD	ZNH(CH ₂) ₂ -	51, 40	Normal	12-14
PCMLD	ZN(CH ₃)(CH ₂) ₂ -	10	Inverse	present paper
PCELD	ZN(C ₂ H ₅)(CH ₂) ₂ -	10	Inverse	present paper
PCBLD	ZN(C ₇ H ₇)(CH ₂) ₂ -	4	Inverse	present paper
PCLO	ZNH(CH ₂) ₃ -	35, 38	Inverse	12, 13
PCMLO	ZN(CH ₃)(CH ₂) ₃ -	12	Inverse	6
PCELO	ZN(C ₂ H ₅)(CH ₂) ₃ -	30	Inverse	6
PCBLO	ZN(C ₇ H ₇)(CH ₂) ₃ -	12	Inverse	8
PCLL	ZNH(CH ₂) ₄ -	37	Inverse	15
PCMLL	ZN(CH ₃)(CH ₂) ₄ -	10	Inverse	6
PCBLL	ZN(C ₇ H ₇)(CH ₂) ₄ -	8	Inverse	8

Table 4 Values of $[m']_{233}$ for PLD, PMLD, PELD, and PBLD at 25°C

pH	PLD		PMLD		PELD		PBLD	
	3	12	3	12	3	12	3	7
	In water*							
	-1400	-2300	-1270	-3400	-1270	-2050	-20	-720
	In 90~95% methanol:							
	-11 000	-11 000	-12 100	-12 200	-11 600	-11 800	-12 300	

* In 0.1 M sodium chloride solution

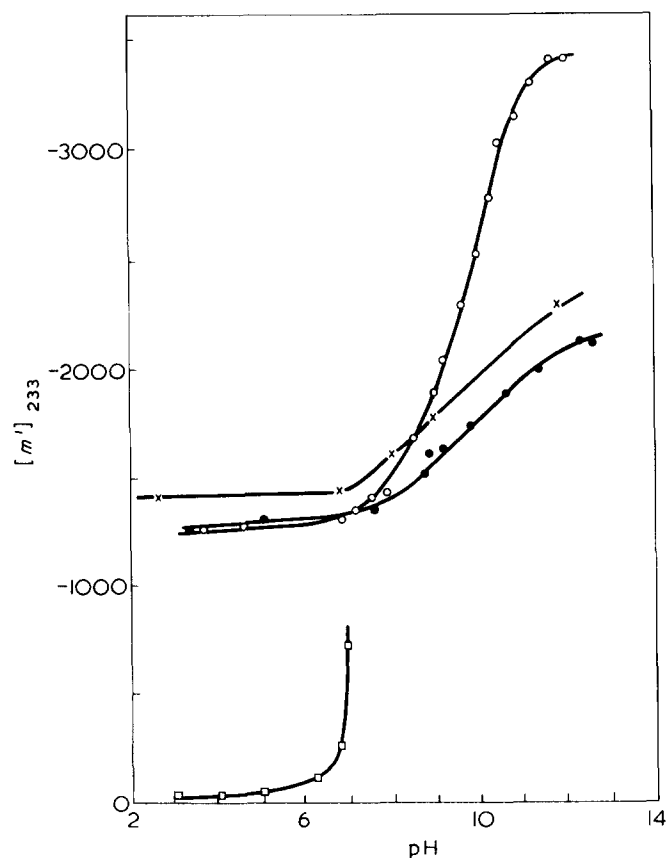


Figure 3 Change in optical rotation with pH for PLD (x); PMLD (O); PELD (●) and PBLD (□) in 0.1 M sodium chloride solution at 25°C

with $[m']_{233} = -11\,000$ to $\sim -12\,300$ in 90 to $\sim 95\%$ methanol at 25°C, showing no racemization during the syntheses. At $\text{pH}_{\text{app}} 12$ the partly ordered structure-to-helix transition of uncharged PLD, PMLD, and PELD began broadly at about 40% methanol. Since the three polypeptides are partially helical even in zero methanol content, the transition is not sharp. At above 80% methanol content, the polypeptides would have been in the helical conformation over the entire range of pH. Such was the case of PLL in 95% methanol or 76% 2-propanol^{17,18} and poly(δ -*N*-benzyl-L-ornithine) in 90% 1-propanol⁸.

Temperature induced transition. The $[\theta]$ in Figure 5 shows the temperature dependence of the ellipticity for PLD and PMLD. Lowering the temperature from 25°C to 4°C, enhanced the helicities of PLD and PMLD; PLD, $[\theta]_{220} = -2800$ (25°C) and $-10\,000$ (4°C), and PMLD, $[\theta]_{220} = -3100$ (25°C) and $-12\,300$ (4°C). In analogy to protein denaturation, both PLD and PMLD became helical at low

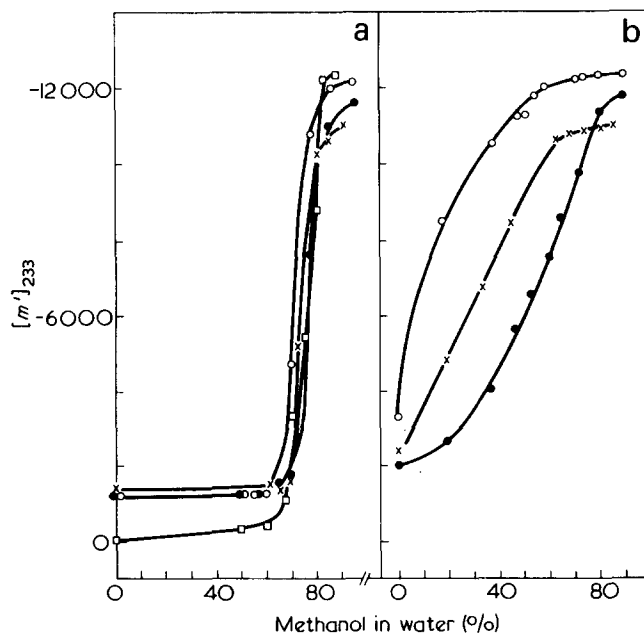
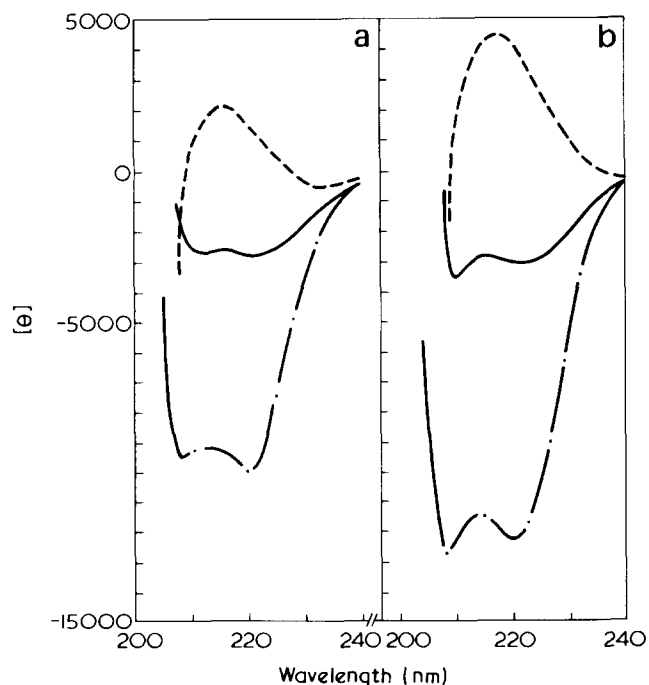
Figure 4 Effect of methanol content on $[m']_{233}$ of PLD (x); PMLD (O); PELD (●) and PBLD (□) at 25°C: (a) at pH 3 (b) at pH 12

Figure 5 C.d. spectra of (a), PLD and (b), PMLD in aqueous solution at indicated pH and temperature: random coil (---), at pH 3 and 25°C; partial helix (—), at pH 12 and 25°C; partial helix (- · - ·), at pH 12 and 4°C

temperature and disordered at high temperature. PLL and PLO showed also the same tendency¹.

To summarize, three kinds of new poly(γ -*N*-alkyl-L- α , γ -diaminobutyric acids) and their carbobenzoxyated derivatives were synthesized and the effect of the side chain was investigated. PCLD and PCMLD fold a complete helix in organic solvents, while PCELD and PCBLD, which have the bulkier alkyl groups, fold a partial helix. The three carbobenzoxyated γ -*N*-alkyl polypeptides alter the direction of the temperature induced transition from a 'normal' to an 'inverse'. The water-soluble polypeptides, PMLD and PELD, undergo a helix-coil transition slightly by increasing the pH of the solution. PMLD, an isomer of PLO, or PELD, that of PLL, behaves like PLD rather than PLO or PLL showing no increased alkyl effect. This suggests that the helical stability depends not only on the total number of methylene group in the side chain, but also on the steric arrangement of alkyl group around the ω -amino or imino group.

REFERENCES

- 1 Grouke, M. J. and Gibbs, J. H. *Biopolymers* 1971, **10**, 795

- 2 Blauer, G. and Alfassi, Z. B. *Biochim. Biophys. Acta* 1967, **133**, 206
- 3 Chaudhuri, S. R. and Yang, J. T. *Biochemistry* 1968, **7**, 1379
- 4 Hatano, M. and Yoneyama, M. *J. Am. Chem. Soc.* 1970, **92**, 1392
- 5 Yamamoto, H. and Hayakawa, T. *Biopolymers* 1972, **11**, 1259
- 6 Yamamoto, H. and Yang, J. T. *Biopolymers* 1974, **13**, 1093
- 7 Yamamoto, H. and Yang, J. T. *Biopolymers* 1974, **13**, 1109
- 8 Yamamoto, H., Hayakawa, T. and Yang, J. T. *Biopolymers* 1974, **13**, 1117
- 9 Fasman, G. D., Idelson, M. and Blout, E. R. *J. Am. Chem. Soc.* 1961, **83**, 709
- 10 Ben-Ishai, D. *J. Org. Chem.* 1952, **17**, 1564
- 11 Moffitt, W. and Yang, J. T. *Proc. Natl. Acad. Sci. USA* 1956, **42**, 596
- 12 Gaskin, F., Kubota, S. and Yang, J. T. *J. Am. Chem. Soc.* 1969, **91**, 6526
- 13 Gaskin, F. and Yang, J. T. *Biopolymers* 1971, **10**, 631
- 14 Giacometti, G., Turolla, A. and Verdini, A. *J. Am. Chem. Soc.* 1971, **93**, 3092
- 15 Karasz, F. E., O'Reilly, J. M. and Bair, H. E. *Biopolymers* 1965, **3**, 241
- 16 Davidson, B. and Fasman, G.D. *Biochemistry* 1967, **6**, 1616
- 17 Epand, R. F. and Scheraga, H. A. *Biopolymers* 1968, **6**, 1383
- 18 Liem, R. K. H., Poland, D. and Scheraga, H. A. *J. Am. Chem. Soc.* 1970, **92**, 5717

Response of macromolecular structure to shear gradients

B. Hlavacek and H. P. Schreiber

Department of Chemical Engineering, Ecole Polytechnique, Montreal, Canada
(Received 15 September 1975; revised 7 January 1976)

The response of macromolecular structure to increasing shear gradients is considered. It is suggested that the coiled configuration, characteristic of the macromolecule at zero shear gradient, persists far into the region of non-linear viscous response. The increase in recoverable shear, normal stress and related parameters of elastic response in this range of shear gradients is attributed to shifts in the orientation of the principal stress axis, the polymer coil remaining characterized by the gyration radius at zero shear. Uncoiling of the macromolecule is postulated only at shear gradients greater than that corresponding to the onset of flow instability, such as structural turbulence. Literature data for a variety of polymer solutions are used to confirm the postulates of the present model.

INTRODUCTION

This paper presents a simple model for the behaviour of macromolecular fluids (solutions and melts) at high gradients of shear. The problem treated here is of long standing concern. The interest stems from inter-relationships between molecular structure and the shear response of polymer molecules and equally from phenomena such as flow instability or melt fracture¹, which impose high shear limits on the commercial processing of polymer fluids. Ram² has summarized the current situation, noting that the commonest interpretations of non-Newtonian behaviour relate the reduction of viscosity to the gradual orientation and disentanglement of chain segments as the polymer chains deform and orient under the influence of a shear gradient. The concept of chain entanglement is a subtle one, however, experimental evidence indicating^{3,4} that viscous and elastic responses in polymers are probably due to short- and long-range associations owing to entanglement, respectively.

Existing theories for the behaviour of polymers in high shear fields generally do not differentiate between segmental and longer-range (domain) entanglements. Among the most familiar of these theories are the soft dumbbell approaches of Zimm⁵ and Bueche⁶, and non-linear viscoelastic flow models such as those of Meister and Biggs⁷ and Bird and Carreau⁸. These latter theories particularly, differ substantially in their handling of the variation of entanglement density with shear gradient, yet they tend to be non-discriminating in their goodness-of-fit to experimental data. Consequently it seems reasonable to avoid the complexity inherent in considerations of entanglements at the sub-chain (segment) level, and to attempt a rationalization of polymer fluid behaviour under high shear gradients via a simple method based on deformations at the supra-molecular level.

THEORETICAL CONSIDERATIONS

A convenient starting point for our argument is the assumed presence in polymers of supra-molecular structures of the type discussed by Busse⁹, or of 'viscoelastic drops', as introduced previously by Hlavacek *et al.*^{10,11}. In considering the response of these large structures to shear gra-

dients, we expect to gain information on the change with shear gradients of the number of interaction (entanglement) points at the domain level but, inherently, little detail can be expected about the situation at the sub-chain (segmental) level. Since interactions at the domain level relate more specifically to elastic than to purely viscous properties of polymer fluids^{3,4}, it is in the former area that relevant tests of the model must be sought.

We begin with two basic concepts:

(a) Following Bueche¹², at zero gradient the flexible macromolecule is subject to Brownian movement and is distributed uniformly about a centre of mass. In this state, assuming shear-thinning characteristics, its viscosity is at a maximum, η_{\max} , corresponding to the upper Newtonian limit, and a direct correlation can be expected between η_{\max} and the unperturbed gyration radius of the unit $(\bar{r}^2)_0$.

(b) At finite gradients in the range $0 < \dot{\gamma} < 1/\tau_{\max}$, where $\dot{\gamma}$ is the shear rate and τ_{\max} is the maximum relaxation time, the polymer structure should remain effectively unchanged. Consequently, the existence of relationships is called for between the principal stress and the quantities, $\eta_{\max} \dot{\gamma}$; $G'(\omega)$ and $G''(\omega)$, where the latter are the real and imaginary parts of dynamic moduli at rotational velocity ω . At gradients $\dot{\gamma} > 1/\tau_{\max}$, we should expect variations in these three parameters.

Introducing θ as the angle of orientation for the principal stress axis, and $\delta = 90 - \theta$, the following simple expression can be written:

$$(\eta_{\max} + \delta \eta_{\max}) \times \dot{\gamma} \cos \delta = [(P_{11} - P_{22})^2 + (2P_{12})^2]^{1/2} \quad (1)$$

where $P_{11} - P_{22}$ is the normal stress. Equation (1) is essentially a restatement of Philippoff's expression¹³ to which the dynamic component $\cos \delta$ in the response of the macromolecule to the shear gradient, has been added.

In the above equation, we note that:

$$\cos \delta = \frac{2P_{11}}{[(P_{11} - P_{22})^2 + (2P_{12})^2]^{1/2}}$$

It is surprising that for many polymer solutions at varying concentrations the relationship of equation (1) is well obeyed over 4–5 decades of shear^{10,11}.

In a majority of cases for which experimental results are available, simple relationships can be found between G' , G'' and $P_{11} - P_{12}$ ($\omega = \dot{\gamma}$) and P_{12} ($\omega = \dot{\gamma}$). Consequently, we can rewrite equation (1) in the form:

$$\frac{\eta_{\max} \times \dot{\gamma}}{F(\alpha)} \times \frac{\alpha G''}{[(\alpha^2 \times G')^2 + (\alpha G'')^2]^{1/2}} = [(2\alpha^2 G')^2 + (2\alpha G'')^2]^{1/2} \quad (2)$$

where $\alpha = \left(\frac{P_{11} - P_{22}}{2G'} \right)_{\omega = \dot{\gamma}}^{1/2}$

$$\simeq \frac{\eta(\dot{\gamma})}{\eta'(\omega = \dot{\gamma})} \quad (3)$$

Whilst $F(\alpha)$ is, in principle, a weak function of $\dot{\gamma}$, we find for many polymers^{10,11} that $F(\alpha) \simeq \alpha$, though for lower molecular weight systems such as polystyrene ($M \simeq 10^4$) and aluminium soap, $F(\alpha) = 1$, i.e. the macromolecular structure remains virtually undeformed over the entire shear gradient studied.

Further, in spite of the possible shear gradient dependence of the relationship:

$$\left(\frac{P_{11} - P_{22}}{2G'} \right)^{1/2} \simeq \frac{\eta(\dot{\gamma})}{\eta'(\omega = \dot{\gamma})}$$

equations (1)–(3) fit experimental data very well^{10,11} in the range $\dot{\gamma} > 1/\tau_{\max}$.

The emphasis in this paper is on the structural connotations of the above, particularly on the use of the expression:

$$\eta_{\max} + \Delta\eta_{\max} = \frac{\eta_{\max}}{F(\alpha)} \quad (4)$$

as a means for interpreting the shear response of viscoelastic drops or molecular domains. As noted already, η_{\max} reflects the number of entanglement points per unit structure and their distribution about a centre of mass. Further, according to the well-known Bueche theory¹², η_{\max} is proportional to the molecular weight of the polymer and to a friction coefficient, f_0 , per monomer unit. Any change in η_{\max} at gradients $\dot{\gamma} > 1/\tau_{\max}$ can therefore be construed as a change in the effective geometry of the structure, i.e. with some effective value of the gyration radius, such that: $(\bar{r}^2)_{\text{eff}} \neq (\bar{r}^2)_0$. Restating the point, only when changes in η_{\max} are observed following application of a shear gradient, can a corresponding change in the 'entanglement density', characteristic of the structure, be postulated. (We note that although our reference is the supra-molecular domain, an analogous set of statements can be made in terms of simple macromolecules and entanglements at the sub-chain level.) Experimental tests of these concepts are outlined in the following section.

EXPERIMENTAL TESTS AND DISCUSSION

Region of laminar flow

The experimental data of Carreau and coworkers¹⁴ and of others quoted by Carreau¹⁵, were used for the present

requirements. The former consider the behaviour, over a wide range of shear, of 7% aluminium laurate in decalin/*m*-cresol, (system I) and of a 2% solution of polyisobutylene in Primol 355 (system II) while the latter provides data for 4% polystyrene solutions in Aroclor 1248 (system III).

First, we consider the result of applying equation (1) to systems (I) and (III). The necessary parameters (η_{\max} , $P_{11} - P_{22}$, P_{12} , G' and G'') are given by the authors^{14,15}, making feasible a calculation of $F(\alpha)$ and hence of the sum ($\eta_{\max} + \Delta\eta_{\max}$). For convenience of presentation, we introduce the identity $\eta^+ \equiv (\eta_{\max} + \Delta\eta_{\max})$, and plot $\log \eta^+ / \eta_{\max}$ vs. $\log \dot{\gamma}$ in Figures 1 and 2. Since both systems (I) and (III) satisfy the demands of equation (3), it is reasonable to use data in our computation from both the linear and non-linear range of viscoelastic behaviour. Indeed over the 4 decades (approximately) of $\dot{\gamma}$ in which laminar flow persists, while the net solution viscosities vary by factors of about 10^3 , it is evident that the 'structural' viscosity, η_{\max} , varies by no more than a factor of 2–3. Thus, only minor changes can have occurred in the entanglement densities at the segmental level, and the large responses in the observed viscosity, a viscoelastic property, must be due to elastic effects at the domain or supra-molecular level.

We suggest that these elastic responses represent a shift from shear to normal stress effects as the principal stress axis of the flow units orients in the direction of flow. The situation can be inferred from a Mohr's circle argument¹⁶.

The instructive results of applying present concepts to system II, are shown as curves *A* and *A'* of Figure 3. Sec-

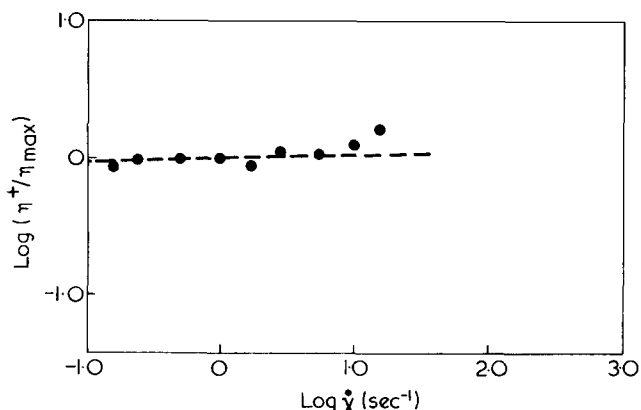


Figure 1 Dependence of 'structural' viscosity on shear rate, 7% Al soap solution. Data of Carreau et al.¹⁴

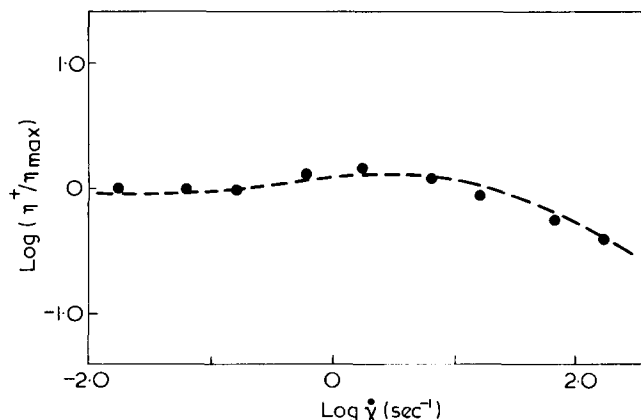


Figure 2 Dependence of 'structural' viscosity on shear rate, 4% polystyrene solution. Data of Carreau et al.¹⁴

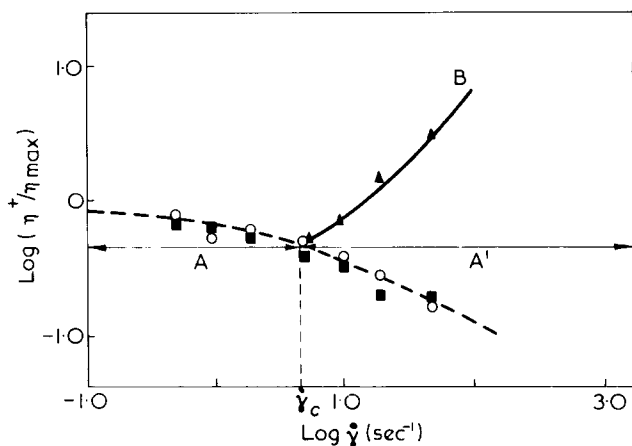


Figure 3 Dependence of 'structural' viscosity on shear rate, 2% PIB solutions. Data of Carreau¹⁵. A, Calculations of structural viscosity using data from linear range and equation (2) (○); from non-linear range and equation (1) (■); B, calculation based on data from range of turbulent flow (▲)

tion A of the curve can be obtained by two alternative methods: the use of equation (2) and G' , G'' data from the linear range of behaviour, or by using equation (1) with $(P_{11} - P_{22})$ and P_{12} data calculated from the expression given by Bird and Carreau⁸. It is evident that in section A of Figure 3, the two approaches yield equivalent results. Application of the Bird and Carreau expression for calculations of $P_{11} - P_{22}$, P_{12} , etc. in the range $\dot{\gamma} > \dot{\gamma}_c$ yields section A' of Figure 3. This deviates sharply from curve B, denoting the fact that real and calculated normal stress data produce very different values of 'structural' viscosity in the range of unstable flow. The point is discussed further in the following section.

Thus, for diverse polymer solutions with highly non-Newtonian properties no major changes in the geometry of the macromolecule can be substantiated at shear gradients corresponding to laminar flow of the systems. For any individual macromolecule then, $(\bar{r}^2)_{\text{eff}} \approx (\bar{r}^2)_0$. Accepting the fundamental evidence for rotational motion of coiled macromolecules under shear gradients^{17,18}, we suggest that the frequency of changes in compressional and elongational force fields (proportional to $\dot{\gamma}$) is such as to require no significant change in the spacial arrangement of chain segments populating a given domain (viscoelastic drop). Therefore, in $0 < \dot{\gamma} < \dot{\gamma}_c$ (where $\dot{\gamma}_c$ is the shear rate for onset of elastic melt-fracture¹ or structural turbulence as defined by Ram²), we can find little reason for believing that individual polymer molecules uncoil, the principal mode of deformation residing instead at the interdomain level. Here, elastic energy is stored owing to the shift of the principal stress axis, as already noted above.

The slight deviations from η_{max} which can be seen in Figures 1–3, may in fact be due to changes in the density of segmental entanglements. Various causes may contribute to this relatively minor effect, including the gradual loss of solvent from the internal volume of the coiled macromolecule, as $\dot{\gamma}$ rises and the hydrodynamic volume of the coil tends to a minimum¹⁹.

Region of flow instabilities

The effects of structural turbulence² and elastic melt fracture, occurring deep in the non-linear flow regime of polymer solutions and melts, have been discussed frequently^{1,2,7,20}. Using a notation of recoverable shear strain

and working with polymer melts²⁰, Bagley noted a discontinuity in this parameter at the onset of flow turbulence and identified this flow defect as elastic in nature. A limiting value of recoverable shear (7–14 units), was found to depend essentially on the flexibility of the macromolecular chain. Philippoff²¹, working with polymer solutions, noted a similar discontinuity at the onset of turbulent flow in optical birefringence data and further noted a sharp increase in birefringence effects at very high shear strains. He attributed this feature to an uncoiling of the polymer chain.

Significantly the correlations arising from the use of our equations (1)–(3) break down for data collected in the shear gradient range $\dot{\gamma} > \dot{\gamma}_c$. As shown schematically in Figure 4, the parameters $P_{11} - P_{22}$ and P_{12} have distinct inflection points associated with this critical value of the shear gradient^{7,8,14,15}. Of the existing theories for flow behaviour at high shear gradients, only that of Meister and Biggs⁷ seems to have coped with this problem realistically. For $\dot{\gamma} < \dot{\gamma}_c$, these authors stipulate a rotational velocity $\omega = \dot{\gamma}/2$, a requirement which, they state, breaks down for $\dot{\gamma} > \dot{\gamma}_c$. A fundamental change in the rotational motion of the system's structural units apparently occurs. In the present context, the data for system (II) extend into the appropriate range of shear rate. The requirements of equation (3) are satisfied approximately, and equation (2) holds for $F(\alpha) \approx \alpha$. This time introducing real rather than calculated values of $(P_{11} - P_{22})$, P_{12} into equation (1), we now generate η^+ values which are shown in Figure 3 as curve B.

Evidently, for $\dot{\gamma} > \dot{\gamma}_c$, a major (nearly 10-fold) increase in the 'structural' viscosity η_{max} must be taken into account. From our previously introduced stipulates therefore, $(\bar{r}^2)_{\text{eff}} > (\bar{r}^2)_0$. Where primarily elastic effects associated with deformations at the level of domains were operative at $\dot{\gamma} < \dot{\gamma}_c$, it now appears that important deformations at the molecular level also occur, the individual macromolecules becoming more widely distributed about their centre of mass. We therefore suggest, in keeping with Philippoff's concept²¹, that only in the region of turbulent flow does the rotational motion of macromolecules result in significant changes of entanglement density at the level of individual chain segments.

CONCLUSIONS

(1) A simple supra-molecular domain, or viscoelastic drop model accounts for the behaviour of polymer fluids

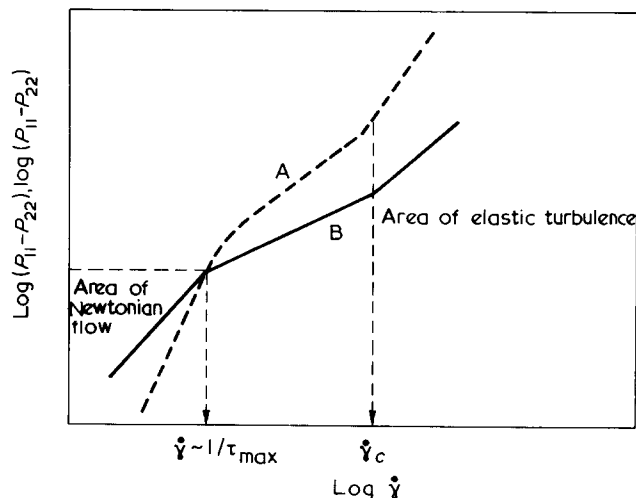


Figure 4 Schematic view of shear rate dependence of $P_{11} - P_{22}$, (A) and P_{12} (B)

under shear gradients extending well into the region of non-linear viscoelasticity.

(2) The parameters η_{\max} , G' and G'' which characterize the systems in the region of linear viscoelastic behaviour, vary only slightly with $\dot{\gamma}$, following the correlations $2G' \rightarrow P_{11} - P_{22}$ and $G'' \rightarrow P_{12}$. Only in the area of structural turbulence (or elastic flow instability) does the η_{\max} value become a strong function of $\dot{\gamma}$ ($> \dot{\gamma}_c$). Uncoiling of the molecule, or similar deformations leading to a change in the density of segmental entanglements, is postulated for this region.

(3) In the region of steady, laminar shear flow, elastic deformations at the domain level of associations are postulated, the number of entanglement points on a molecular level being only weakly dependent, or independent of $\dot{\gamma}$.

ACKNOWLEDGEMENTS

We thank the National Research Council of Canada for financial support, and Dr P. J. Carreau for stimulating and helpful discussions.

REFERENCES

- 1 Tordella, J. P. in 'Rheology' (Ed. F. R. Eirich), Academic Press, New York, 1969, Vol 5
- 2 Ram, A. in 'Rheology', (Ed. F. R. Eirich), Academic Press, New York, 1967, Vol 4
- 3 Schreiber, H. P., Rudin, A. and Bagley, E. B. *J. Appl. Polym. Sci.* 1965, **9**, 887
- 4 Newlin, T. E., Lovell, S. E., Saunders, P. R. and Ferry, J. O. *J. Colloid Sci.* 1962, **17**, 10
- 5 Zimm, B. H. *J. Chem. Phys.* 1956, **24**, 269
- 6 Bueche, F. *J. Appl. Phys.* 1959, **30**, 1114
- 7 Meister, B. J. and Biggs, R. D. *AIChE J.* 1969, **15**, 643
- 8 Bird, R. B. and Carreau, P. J. *Chem. Eng. Sci.* 1968, **23**, 427
- 9 Busse, W. F. *J. Polym. Sci. (A-2)* 1967, **5**, 1261
- 10 Hlavacek, B., Seyer, F. A. and Stanislav, J. *Kolloid Z. Z. Polym.* 1973, **251**, 474
- 11 Hlavacek, B., Seyer, F. A. and Stanislav, J. *Can. J. Chem. Eng.* 1973, **51**, 412
- 12 Bueche, F. 'Physical Properties of Polymers', Wiley, New York, 1962
- 13 Philippoff, W. *Trans. Soc. Rheol.* 1968, **12**, 85
- 14 Carreau, P. J., MacDonald, I. F. and Bird, R. B. *Chem. Eng. Sci.* 1968, **23**, 901
- 15 Carreau, P. J. *Trans. Soc. Rheol.* 1972, **16**, 99
- 16 Reiner, M. in 'Rheology', (Ed. F. R. Eirich), Academic Press, New York, 1954, Vol 1
- 17 Goldsmith, H. L. and Mason, S. G. *Nature* 1961, **190**, 1095; *J. Colloid Sci.* 1962, **17**, 448
- 18 Philippoff, W. *J. Appl. Phys.* 1965, **36**, 3033
- 19 Subirama, J. A. *J. Chem. Phys.* 1964, **41**, 3852
- 20 Bagley, E. B. *Trans. Soc. Rheol.* 1961, **5**, 355
- 21 Philippoff, W. *Trans. Soc. Rheol.* 1966, **10**, 1; Philippoff, W. and Gaskins, F. H. *Trans. Soc. Rheol.* 1958, **2**, 263

Craze kinetics for PMMA in liquids

I. D. Graham*, J. G. Williamst and E. L. Zichy‡

(Received 9 May 1975; revised 12 January 1976)

Observations are reported on the growth of crazes in PMMA immersed in a range of alcohols, some less active crazing agents and some mixtures of methanol and inactive agents. When there is substantial plasticization of the craze, the growth is adequately described by the fluid flow model. Mixtures are also explicable in these terms since the active agent is preferentially absorbed. For lower degrees of plasticization, the craze growth is small and probably relaxation controlled.

INTRODUCTION

Several previous papers¹⁻⁴ have described a model for the growth of crazes in polymers in the presence of plasticizing environments. The criteria of craze initiation and growth rates were described in terms of stress intensity factors K involving both stress level σ and initial crack size a . The most recent work⁴ postulates that the governing factor in determining growth rate is the slower either of the relaxation processes of the polymer or the flow of the crazing fluid within the porous craze structure. The nature of the processes involved results in the initial behaviour being flow controlled while subsequent growth is relaxation controlled⁴.

For flow controlled growth the craze length x is given by:

$$x = \left(\frac{(1-m)P.C}{(1+m+n)6\mu\sigma_0 E_0} \right)^{1/2} \times K \times t^{1/2 + \frac{m+n}{2}} \quad (1)$$

where P = the pressure drop within the craze; usually atmospheric pressure 0.1 MN/m^2 ; μ = fluid viscosity. The yield stress and modulus are described as power laws of time in the form:

$$\sigma = \sigma_0 t^{-m} \text{ and } E = E_0 t^{-n} \quad (2)$$

where σ_0 and E_0 are unit time values.

The model proposes that the void area within the craze is determined by the deformation of the ligaments between void sites in the craze. If these sites have a spacing l_0 and the craze is strained to an extension ratio λ (deformed length/original length), then the void area is given by:

$$A = l_0^2 [\lambda - (\lambda)^{1/2}]$$

The void content of the craze is:

$$V = (1 - \lambda^{-1})$$

If the craze subsequently swells by a volume factor S then l_0 becomes $S^{1/3}l_0$ so that:

$$A = S^{2/3}l_0^2 [\lambda - (\lambda)^{1/2}]$$

while V remains unchanged.

λ may be estimated from the displacement applied at the craze tip:

$$u = K^2/\sigma E \quad (3)$$

and the original crack tip diameter d_0 so that:

$$\lambda = 1 + u/d_0$$

In the model described here, crazes are always formed in unplasticized (and unswollen) material so that λ is predetermined and so is V . It seems probable, therefore, that V will not change with S which will change with the fluid used, while A may well do so.

For small values of λ (i.e. < 2) we may write:

$$\begin{aligned} A &\approx S^{2/3}l_0^2 u/2d_0 \\ &= C \times u \end{aligned}$$

where

$$C = S^{2/3}l_0^2/2d_0 \quad (4)$$

Relaxation controlled growth has the form:

$$x = \frac{\pi}{8} \cdot \frac{K^2}{\sigma_0^2} (1-m)^2 \times t^{2m} \quad (5)$$

Since $m \approx n \approx 0.1$ for most polymers, we expect flow controlled growth with $x \propto t^{0.6}$ and relaxation control with $x \propto t^{0.2}$.

The craze is modelled as a line plastic zone so that the length implies an average craze stress for a given length given by:

$$\frac{a}{a+x} = \cos \left(\frac{\pi}{2} \times \frac{\sigma}{\sigma_c} \right) \quad (6)$$

so that σ_c may be determined for combinations of σ , a and x .

Previous work has used these models to describe the poly(methyl methacrylate) (PMMA)–methanol system, since it was convenient to use. In this work the ideas are explored for PMMA in various liquids; i.e. several alcohols, a set of relatively inactive liquids and then some mixtures of methanol and inert liquids.

* Ciba-Geigy (UK) Limited, Duxford, Cambridge, UK.

† Department of Mechanical Engineering, Imperial College, London SW7 2BX, UK.

‡ ICI Plastics Division, Welwyn Garden City, UK.

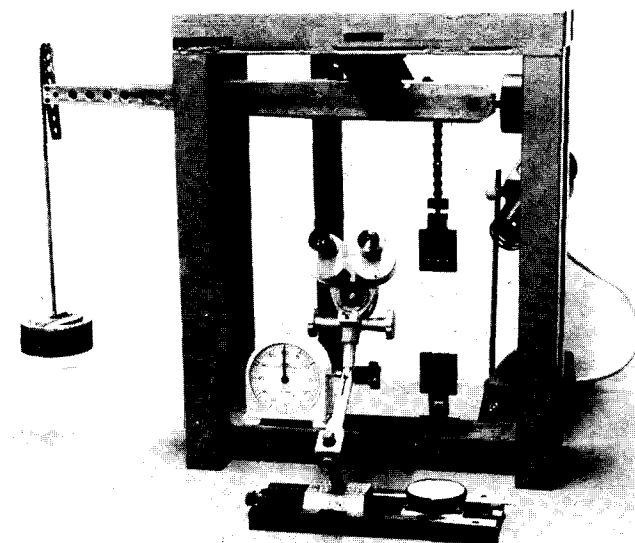


Figure 1 Experimental arrangement

EXPERIMENTAL

The technique used has been described previously¹, and consisted of loading rectangular specimens $150 \times 50 \times 1.6$ mm thick in dead loading machines and measuring the craze growth from an initial flaw inserted in the side of the specimen. The environment was applied by means of small tanks made from microscope slides stuck onto the specimen using silicone grease and filled with a hypodermic syringe. The arrangement is shown in Figure 1. Craze growth was measured using a travelling microscope looking through the tank wall and all tests were performed at 20°C and 50% R.H.

The alcohol series methanol, ethanol, propanol and butanol, was first considered. Methanol was used originally because it gave a single craze with no evidence of surface crazing. As the series was used, the occurrence of surface crazing increased. In addition, bifurcations became more prevalent and of the form, 2 for ethanol, about 5 for propanol and 10 in butanol. It was observed that in both propanol and butanol there were coloured fringes clearly visible in the craze indicating very thin craze material.

All the crazes had a uniform silvery appearance and at low K levels growth at decreasing rates resulted in convex craze fronts as observed in methanol previously. At high K levels constant speeds could be induced with a concave craze front as described for methanol¹ and attributed to flow through the specimen sides. No description of constant speed growth will be given here other than to note its occurrence.

The relatively inert liquid series used was water, ethylene glycol, paraffin and white spirit. The last two are mixtures but of sufficient industrial interest as common crazing agents to be included. White spirit behaved as if it were just further up the alcohol scale than butanol giving 10 bifurcations and surface crazing. The other liquids all gave considerable bifurcation with many crazes formed but no evidence of surface crazing. No constant speed growth was observed and fringes were seen on all crazes.

Mixtures of 25, 50 and 75% methanol in both water and ethylene glycol were tested and there was a general trend towards the methanol behaviour as the methanol content increased. Constant speed behaviour was only found with the 25% water mixtures but with ethylene glycol, 50% mix-

tures gave some constant speed behaviour. A notable effect was that all the crazes grown in mixtures had very uneven craze fronts and a scaly appearance as opposed to the even silvery appearance in pure liquids.

VOID CONTENTS

The void content of dry crazes has been measured using changes of refractive index previously by Kambour⁵ but it was considered reasonable to observe any variation with crazing liquid. The void content may be deduced by assuming the Lorentz-Lorenz equation relating refractive index and density and if θ is the angle of total internal reflection then the void content V is given by:

$$V = \frac{\rho_0}{\rho_0 - \rho_1} \times \frac{3N}{N-1} \frac{1 - \sin^2\theta}{N \sin^2\theta + 2} \quad (7)$$

where ρ_0 = the density of the polymer; ρ_1 = the density of the liquid; N = the refractive index of the polymer. The experimental method for determining θ was a refinement of that used⁵ and consisted of a long thin tube, through which the craze was viewed, which was pivoted about an axis in the line of the craze. A protractor was also mounted on the axis and when the tube was rotated until the illuminated craze was observed to go dark, the angle of rotation could be measured. The test was performed by viewing the craze from both above and below and an average value of θ taken. Loaded crazes were used in all the liquids and at various loading levels and no appreciable variation was found with an average value of 50% as given by Kambour⁵. This indicates a similarity in craze structure independent of environment in accordance with the idea of a craze formed in unswollen material as mentioned previously.

MODELLING OF CRAZE KINETICS

In the liquids used there were clearly two types of behaviour. Water, ethylene glycol and paraffin produced very short crazes indicating high craze stresses and thus a low degree of plasticization. When craze growth was observed, the time power was generally in the region 0.2–0.3 with very rapid initial growth followed by the slow relaxation growth indicated by these powers. Careful observation was necessary to detect any flow controlled growth since the craze lengths were short ($\approx 20 \mu\text{m}$) and changing rapidly. By recording the growth on videotape it was possible to make some measurements and these gave approximately $t^{1/2}$ behaviour. The short time results, however, are not very accurate and should be treated with caution.

For the remaining liquids and mixtures the craze growths were much larger indicating considerable plasticization and in fact very good $t^{1/2}$ data was obtained indicating $m = n = 0$ followed by complete arrest of the craze. Figure 2 shows some typical data for ethanol. This is in line with Andrews' observation⁶ that the crazed polymer is swollen to a rubbery state with heavy plasticization so eliminating any viscoelastic behaviour. Figure 3 shows some data for craze arrest lengths plotted versus stress in accordance with equation (6) indicating good agreement with the line zone model. Table 1 lists the craze stress values for the liquids used and suggests that a decrease of σ_c from the air value of 100 MN/m^2 to around 33 MN/m^2 is sufficient to produce this effect.

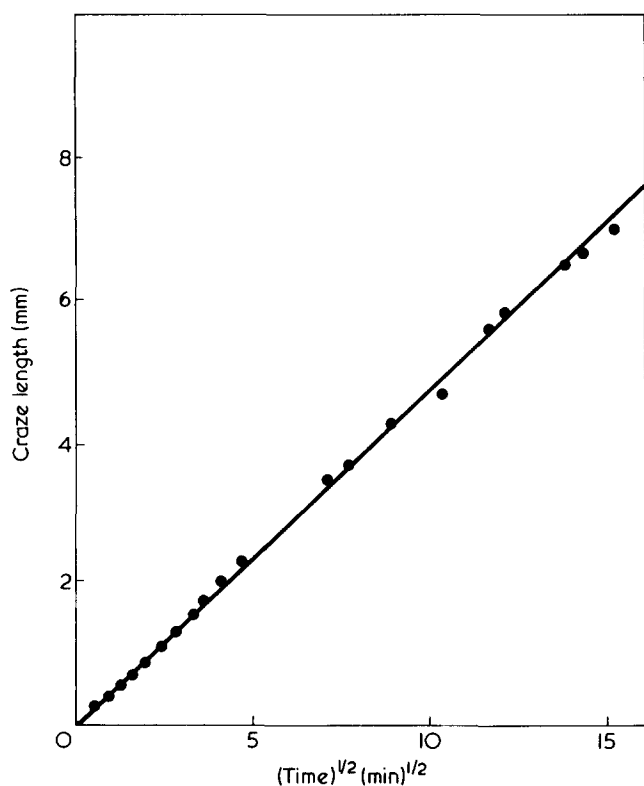


Figure 2 Craze growth in ethanol

Table 1 also gives the slopes of the K versus $x(t)^{1/2}$ lines, the derived values of $C = S^{2/3}l_0^2/2d_0$, equation (4), and the initiation value K_m , of K . There is a clear correlation of K_m and σ_c and this is shown in Figure 4, which gives a value for the craze size at initiation from equation (6) of $11.5 \mu\text{m}$ for all fluids. This is the initial value, the condition for craze growth is that sufficient load must be applied to overload the softened craze for new craze material to form. The new craze material is then plasticized further; repetition of this sequence results in craze growth.

The newly formed voids appear in unplasticized material ahead of the softened craze and when C is calculated from equation (1), σ_0 and E_0 must refer to the unplasticized material. The data in Table 1 referring to methanol

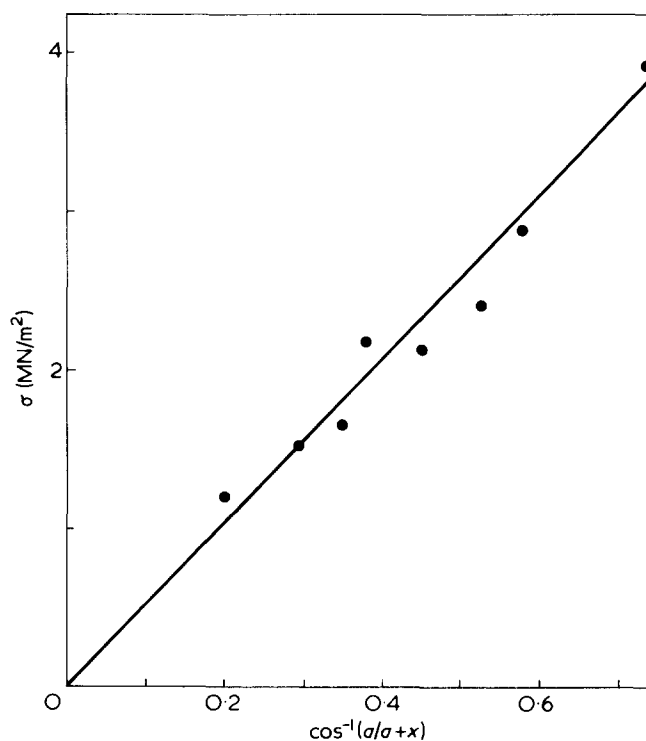


Figure 3 Craze arrest lengths as a function of applied stress according to equation (6)

and its mixtures with water and ethylene glycol show that this concept is essentially valid assuming that in the mixtures methanol is the more active agent and controls S giving values of C between $2.41-3.15 \times 10^{-10} \text{ m}$. This indicates a practically constant material composition at the craze tip; by contrast the craze stress varies in tune with the proportion of the ingredients of the mixture.

Different C values are obtained for crazing agents other than methanol. As a first approximation one may expect a variation of C roughly parallel to the equilibrium swelling of PMMA in the crazing liquid as reflected in S . This view finds support in the observation that the ratio of C for the alcohols to C for water or hydrocarbon liquids given in Table 1 is about the same as the ratio of equilibrium swelling of PMMA in these liquids. However, this approach fails on closer examination because of its inherent oversimplification.

Table 1 Craze stress values for liquids used

Environment	σ_c (MN/m ²)	$K/x/(t)^{1/2} \times 10^3$ (MN sec ^{1/2} /m ^{5/2})	K_m (MN/m ^{3/2})	μ (cP)	$C(S^{2/3}l_0^2/2d_0)$ (Å)
Methanol	7.0	6.3	0.05	0.59	2.71
Ethanol	5.2	6.5	0.02	1.22	5.19
Propanol	5.3	10.1	0.01	2.95	3.96
Butanol	9.6	9.6	0.07	2.95	5.73
Water	86.4	41.1	0.40	1.00	0.11
Ethylene glycol	35.3	43.4	0.14	19.70	1.90
White spirit	15.2	28.9	0.09	0.87	0.29
Paraffin	40.8	37.2	0.22	1.16	0.15
Water/Methanol:					
0.75:0.25	31.4	9.7	0.17	1.54	2.96
0.50:0.50	22.0	10.5	0.15	1.76	2.86
0.25:0.75	14.9	8.7	0.12	1.33	3.15
Ethylene glycol/methanol:					
0.75:0.25	24.6	21.3	0.12	7.33	2.93
0.50:0.50	16.2	15.7	0.09	3.38	2.41
0.25:0.75	9.7	9.6	0.06	1.29	2.58
Air	100.0	—	0.70		

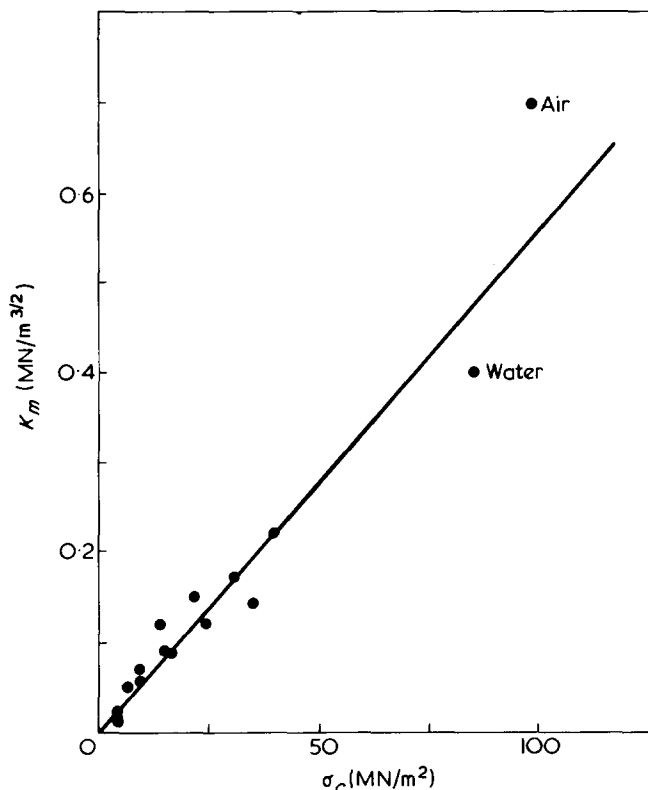


Figure 4 Correlation of initiation K and craze stress

Polymers made up of ester groups along a hydrocarbon chain are essentially amphiphilic, they can react with liquids by hydrogen bonding at the ester–oxygen functions or by van der Waals forces along the hydrocarbon chain. PMMA is a good example of such behaviour as shown by the variety of liquids which can cause crazing and swelling. For example, H-bonding alcohols as well as hydrocarbons like paraffin and white spirit, which interact by van der Waals forces alone. The effect of the two interactions on the structure of the swollen polymer is not expected to be the same, because they affect different parts of the molecule. This differentiation should manifest itself especially clearly in the series of the lower alcohols, because of the gradual change of the balance between H-bonding and van der Waals interactions.

One sees accordingly considerable variations in C with the four lower alcohols. It is probably significant that the variations do not follow the sequence of the number of carbon atoms. Clearly we do not have a sufficiently detailed understanding of the polymer–liquid interactions taking place in these systems, nor of the influence on those of stress and strain. Without this knowledge any further discussion of the observed variations of C with the different

alcohols would be pointless. We have to limit ourselves to the first approximation, i.e. that C is broadly parallel to equilibrium swelling, if liquids are compared in which the equilibrium swelling of PMMA shows great differences.

The mechanical model used in fracture mechanics served us well in explaining craze propagation as long as one single crazing agent or a mixture of this agent with much less active liquids was used. The experiments reported here have shown that the material constant C is not a parameter characteristic of the polymer alone, but of the polymer liquid system. Fracture mechanics is not the framework in which the interaction of a polymer with different liquids can be discussed.

CONCLUSIONS

The use of liquids of various degrees of plasticization capacity has shown that provided there is a sufficient reduction in the craze stress (to about 1/3) then the fluid flow model is an adequate description of the behaviour. For mixtures of active and inactive liquids preferential absorption takes place of the active one. Thus there is good consistency for methanol and its mixtures. For other alcohols there is very similar behaviour but a difference in void spacing is apparent and this seems likely to be due to differences in swelling behaviour. The evidence of craze stresses and initiation behaviour is strong support for the concept that already formed crazes are softened by the liquids and that this leads to propagation.

For liquids which are less active in plasticizing the craze the experiments are difficult to perform because the crazes are very short. The growth curves are not, in general, $t^{1/2}$ and are probably relaxation controlled. The few values obtained for $t^{1/2}$ data indicate low values of void size consistent with low swelling as expected but the data are far from conclusive.

REFERENCES

- 1 Marshall, G. P., Culver, L. E. and Williams, J. G. *Proc. R. Soc. (A)* 1970, **319**, 165
- 2 Graham, I. D., Marshall, G. P. and Williams, J. G. 'Proc. Int. Conf. Dynamic Crack Propagation', Noordhoff, Leyden, 1972, p 261
- 3 Williams, J. G., Marshall, G. P., Graham, I. D. and Zichy, E. L. *Pure Appl. Chem.* 1974, **39**, 275
- 4 Williams, J. G. and Marshall, G. P. *Proc. R. Soc. (A)* 1975, **342**, 855
- 5 Kambour, R. P. *J. Polym. Sci. (A)* 1964, **2**, 4159
- 6 Andrews, E. H., Levy, G. M. and Willis, J. *J. Mater. Sci.* 1973, **8**, 1000

Melting of polymers in narrow annular shear devices

B. Yi and R. T. Fenner

Department of Mechanical Engineering, Imperial College of Science and Technology, London SW7 2BX, UK

(Received 24 July 1975; revised 31 December 1975)

The melting process of a compacted solid bed of polymer forced through a narrow annular shear cell has been investigated. This melting device is used in a continuous ram extruder¹, where melting rates are independent of throughput rates and are governed mainly by the tangential shear rates and heat conducted from surrounding walls. Theoretical results show that increasing shear rates promotes faster melting, but the rate at which melting accelerates slows down significantly at excessive shear rates. This is due to the reduction in polymer melt viscosity as shear rates and temperature increase in the melt film where most of the energy for melting is generated by viscous dissipation. A comparison with melting in a single screw extruder of similar size and capacity indicates that the present device may have superior performance.

INTRODUCTION

Polymers supplied to the processing industry are generally in the form of small particles. To manufacture the products, the polymer is first melted, then shaped and finally solidified. Screw extruders and screw plasticating units are the most commonly used devices for melting. The mechanism of melting in screw devices has been extensively studied² and under certain circumstances the process becomes unstable³. Screw extruders also act as melt conveyors. This pumping and the melting functions are interdependent to such an extent that often one of these functions is sacrificed for the other in commercial production.

A continuous ram extruder has been described by the authors¹ where a different method of melting and pumping polymers is employed in which these two functions can be made virtually independent of each other. The purpose of such a development was to provide a more flexible and versatile extruder, to overcome one of the major disadvantages of screw extruders. The technique relied on a positive ram conveying system for forcing material continuously through a narrow annular shear cell formed by an externally heated barrel with a concentric plasticating shaft rotating inside. The material was melted by the shear action of the shaft and heat supplied through the barrel. The plasticating action was controlled independently of the pumping system by adjusting the barrel wall temperature and the shaft speed.

A theoretical analysis of the melting process described above is developed here as a design tool with the aim of predicting the length of the shear cell necessary for melting completely the solid polymer pumped through. The theoretical model is also used for studying the effects of operating conditions on melting. It can be used for studying melting of polymers in any similar device using the same principle.

MELTING MECHANISM

Figure 1 shows a sectional view of the annular shear cell made up to the barrel with the rotating shaft inside forming a narrow annular channel. The solid polymer bed for-

med by compacted small particles is forced through the cell by an axial pressure gradient, and as it moves from left to right in the diagram, melt films are formed at the surfaces of contact with the barrel (which is heated) and the plasticating shaft. Melting is initiated by heat conducted through the barrel wall and heat generated by friction of solid polymer against the metal walls. Once the films have formed, their thicknesses increase as a result of further material melting off by heat conduction across and viscous dissipation in the melt, particularly in the film adjacent to the shaft. The molten polymer is conveyed downstream by the dragging action of the solid bed and also by pressure gradient in the polymer melts.

ASSUMPTIONS

To reduce the complexity of the problem, a rectangular coordinate system is used to describe the geometry rather

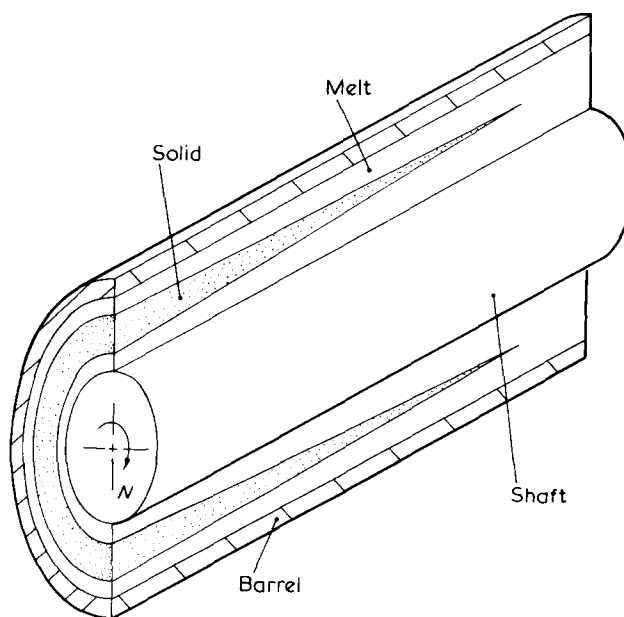


Figure 1 Annular shear cell

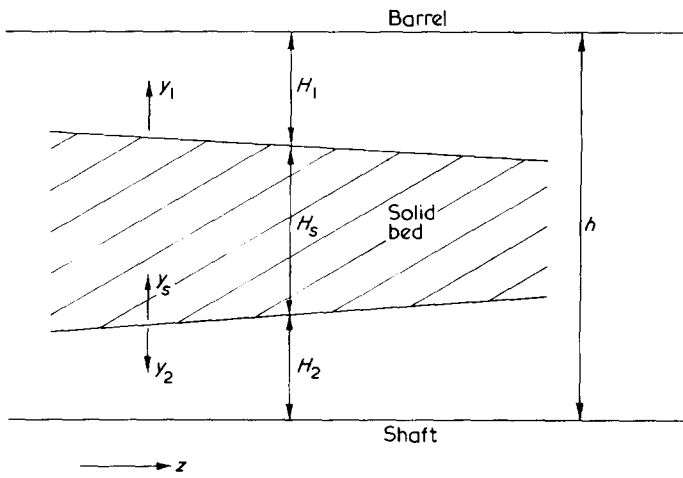


Figure 2 Rectangular geometry considered in theoretical model

than the more natural cylindrical coordinate system. The annulus is therefore regarded as a rectangular slit and the flow confined between two flat plates. This assumption is reasonable and errors are small provided the annulus is narrow, that is $h/D \ll 1$, where D is the internal barrel and h is the annular gap.

Figure 2 shows the geometry considered, in which the rotational speed of the shaft is replaced by an equivalent velocity V_x , in the x -direction (perpendicular to the plane of the diagram), for the lower plate.

In addition the following assumptions are made: (a) a steady state melting process prevails; (b) the polymer has a sharp melting point and linear relationships between enthalpy and temperature in the solid and the melt phases; (c) material properties other than viscosity are independent of temperatures and pressure; (d) the polymer melt is represented by a 'power-law' fluid constitutive equation with temperature dependent viscosity; (e) pressure varies in the downstream direction only and is therefore uniform across any downstream section; (f) the solid bed is assumed to be rigid enough to withstand shearing forces and moves as a plug in the downstream direction without rotating (it is, however, allowed to deform freely in the downstream direction). This assumption was later confirmed on the prototype continuous ram extruder to be valid⁴.

MATHEMATICAL MODEL

Considering a spatial element of infinitesimal length δz , conservation of mass in the film adjacent to the barrel requires that:

$$\frac{d\dot{m}_1}{dz} = \frac{C}{\Delta E_1} \left[k_m \left(\frac{\partial T_1}{\partial y_1} \right)_{y_1=0} - k_s \left(\frac{\partial T_s}{\partial y_s} \right)_{y_s=H_s} \right] \quad (1)$$

and for the film adjacent to the shaft:

$$\frac{d\dot{m}_2}{dz} = \frac{C}{\Delta E_2} \left[k_m \left(\frac{\partial T_2}{\partial y_2} \right)_{y_2=0} + k_s \left(\frac{\partial T_s}{\partial y_s} \right)_{y_s=0} \right] \quad (2)$$

where ΔE_1 and ΔE_2 are the changes in enthalpy given by:

$$\Delta E_1 = \lambda + c_s(T_m - \bar{T}_s) + c_m(\bar{T}_1 - T_m)$$

and

$$\Delta E_2 = \lambda + c_s(T_m - \bar{T}_s) + c_m(\bar{T}_2 - T_m)$$

Overall mass continuity requires that:

$$M - \dot{m}_1 - \dot{m}_2 - \dot{m}_s = 0 \quad (3)$$

The model is then completed by an equation expressing the equilibrium of forces acting in the z -direction on the solid bed:

$$\tau_1 + \tau_2 + \frac{dp}{dz} H_s = 0 \quad (4)$$

Equations (1) to (4) describe the melting process. An additional set of secondary equations must also be solved to provide values for the terms appearing in equations (1) to (4).

The temperature gradients are obtained from the temperature distribution in the material which for the melt films are given by (neglecting conduction in z -direction):

$$\rho_m c_m v_z \frac{\partial T}{\partial z} = k_m \frac{\partial^2 T}{\partial y^2} + \tau_{yz} \frac{dv_z}{dy} + \tau_{xy} \frac{dv_x}{dy} \quad (5)$$

The shear stresses and the velocity gradients in equation (5) are given by the equations of motion:

$$\begin{aligned} \frac{d}{dy} \left(\mu \frac{dv_x}{dy} \right) &= 0 \\ \frac{d}{dy} \left(\mu \frac{dv_z}{dy} \right) &= \frac{dp}{dz} = P_z \end{aligned} \quad (6)$$

where:

$$\begin{aligned} \mu &= \mu_0 \left[(dv_z/dy)^2 + (dv_x/dy)^2 \right]^{1/2} / \gamma_0 \eta^{n-1} \times \\ &\exp[-b(T - T_0)] \end{aligned}$$

Note that no subscript 1 or 2 has been used in equations (5) and (6) as they apply to both melt films. The initial and boundary conditions for these equations are (with the appropriate subscripts):

(a) for the film adjacent to the barrel:

$$T_1(y_1, 0) = T_1^*(y_1)$$

$$T_1(0, z) = T_m$$

$$T_1(H_1, z) = T_b(z)$$

$$v_{x_1}(y_1) = v_{z_1}(H_1) = 0$$

$$v_{z_1}(0) = V_{sz}$$

(b) for the film adjacent to the shaft:

$$T_2(y_2, 0) = T_2^*(y_2)$$

$$T_2(0, z) = T_m$$

$$\frac{\partial T_2(H_2, z)}{\partial y_2} = 0 \text{ (see footnote)}$$

$$v_{x_2}(0) = v_{z_2}(H_2) = 0$$

$$v_{x_2}(H) = V_x$$

$$v_{z_2}(0) = V_{sz}$$

The temperature distribution in the solid bed is given by:

$$\rho_s c_s V_{sz} \frac{\partial T_s}{\partial z} = k_s \frac{\partial^2 T_s}{\partial y_s^2} \quad (7)$$

with

$$T_s(y_s, 0) = T_s^*(y_s)$$

$$T_s(0, z) = T_s(H_s, z) = T_m$$

The solution of equations (5) to (7) provides the temperature and velocity profiles in the material. From the velocity profiles in the melt films, the flow rates are obtained as:

$$\dot{m}_i = \rho_m C \int_0^{H_i} v_{z_i} dy_i \quad (8)$$

and the shear stresses:

$$\tau_i = \mu_i \left(\frac{dv_{z_i}}{dy_i} \right)_{y_i=0} \quad (9)$$

Noting that v_{z_i} depends on V_{sz} , P_z and H_i , equations (8) and (9) may be expressed as:

$$\dot{m}_i = \dot{m}_i(V_{sz}, P_z, H_i) \quad (10)$$

and

$$\tau_i = \tau_i(V_{sz}, P_z, H_i) \quad (11)$$

In equations (8) to (11), $i = 1$ and 2 respectively for the melt film adjacent to the barrel and to the shaft.

METHOD OF SOLUTION

Using equations (10) and (11), equations (3) and (4) are expressed as:

$$f_1(V_{sz}, P_z, H_1, H_2) = 0 \quad (12)$$

The thermal boundary condition at $y_2 = H_2$ is difficult to establish without a complete analysis of the melt/metal heat transfer coupling effect. The condition used is:

$$\frac{\partial T_2(H_2, z)}{\partial y_2} = 0$$

which has been shown to be a valid assumption by Martin⁵ for Newtonian flows with the geometry and conditions considered in the present work.

and

$$f_2(V_{sz}, P_z, H_1, H_2) = 0 \quad (13)$$

If, in addition to \dot{M} , \dot{m}_1 and \dot{m}_2 are also known, then a set of values of the variables V_{sz} , P_z , H_1 and H_2 can be found to satisfy equations (12), (13) and:

$$\dot{m}_1 = \dot{m}_1(V_{sz}, P_z, H_1) \quad (14)$$

and

$$\dot{m}_2 = \dot{m}_2(V_{sz}, P_z, H_2) \quad (15)$$

which come from equation (10) with $i = 1$ and 2 .

An iterative procedure was used for calculating the values of V_{sz} , P_z , H_1 and H_2 . At the start of the solution, values for \dot{m}_1 and \dot{m}_2 were assumed. These were typically of the order of $\dot{m} \approx 0.001 \dot{M}$.

Having obtained the solution of equations (12) to (15) which also gives the solution of equations (6), the bulk mean temperatures in the expressions for ΔE are obtained as:

$$\bar{T} = \frac{\int_0^H v_z T dy}{\int_0^H v_z dy}$$

The temperature gradients are evaluated from the initially specified temperature profiles T^* and hence equations (1) and (2) integrated numerically to give a new set of values for \dot{m}_1 and \dot{m}_2 at a suitably small δ_z increment. The parabolic equations (5) and (7) are then solved using a finite-difference method and hence the temperature profiles at the same axial location are obtained. A new set of values of V_{sz} , P_z , H_1 and H_2 is calculated and the procedure is repeated until the material is completely molten when $H_s = 0$.

Starting conditions are somewhat difficult to define because at the initiation of melting, a different mechanism operates. The melt formed does not accumulate into a film until it has filled the gaps in the layers of the solid bed near the barrel and shaft. The values of $\dot{m} \approx 0.001 \dot{M}$ for starting were found to work well with the method of solution used. In fact, the general results are little affected by the initial values for \dot{m} provided these are kept relatively small, which they are in reality when the melting mechanism studied begins to function.

The initial temperature profiles assumed in the melt films were:

$$T^* = T_m + (T_r - T_m) \frac{y}{H} + \frac{\bar{\mu} V_r^2}{2k_m H} \left(1 - \frac{y}{H} \right)$$

where, for the film adjacent to the barrel:

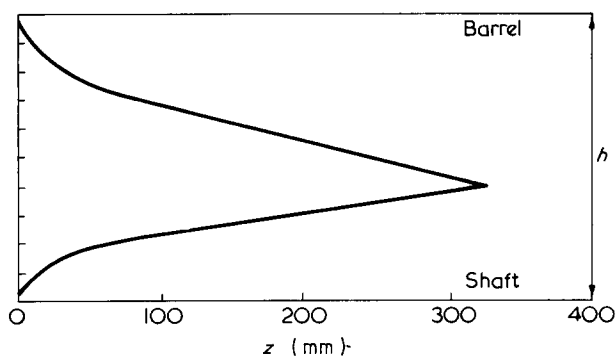
$$T_r = T_b \text{ and } V_r^2 = V_{sz}^2$$

and for the film adjacent to the shaft:

$$T_r = \frac{\bar{\mu}_2 V_r^2}{2k_m} + T_m \text{ and } V_r^2 = V_{sz}^2 + V_x^2$$

Table 1 Material properties for low density polyethylene

Material property	Value
b	0.0054
c_m	2428 (J/kg °C)
c_s	2512 (J/kg °C)
k_m	0.268 (J/msec °C)
k_s	0.268 (J/msec °C)
n	0.423
T_0	145°C
γ_0	1 sec ⁻¹
λ	209.35 × 10 ³ (J/kg)
μ_0	6274 (N sec/m ²)
ρ_m	780 (kg/m ³)
ρ_s	880 (kg/m ³)

Figure 3 Solid bed profile for $\dot{M} = 20$ kg/h, $T_b = 200^\circ\text{C}$ and $N = 120$ rev/min

T^* is the temperature profile in the drag flow of a Newtonian melt and is suitable for starting purposes.

The initial temperature profile in the solid bed T_s^* was assumed to be linear, varying from T_a at $y_s = H_s/2$ to T_m at the melting interfaces.

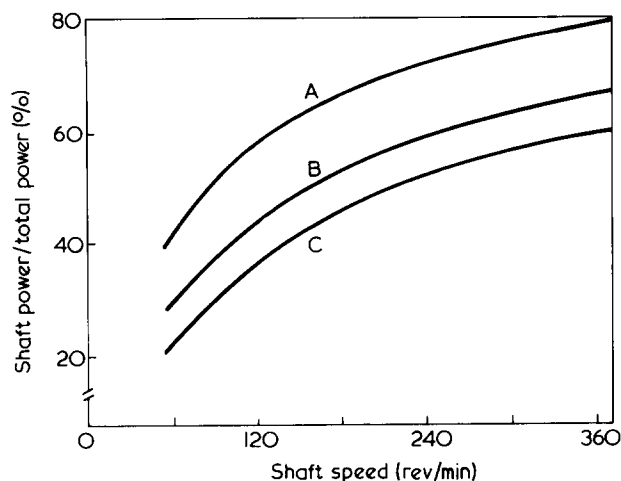
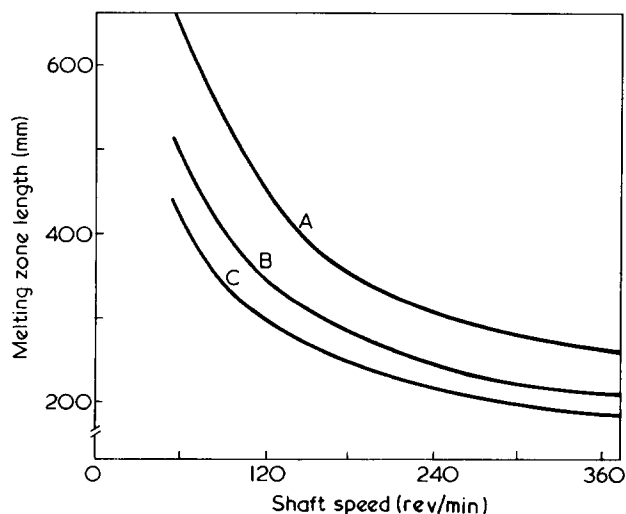
RESULTS

The annular shear cell size selected for performing the calculations was a 44.5 mm diameter barrel with a 3.18 mm annular gap. These are based on the prototype continuous ram extruder which has been operated successfully¹. The material properties supplied to the computer program were those for a grade of granulated low density polyethylene, and are given in Table 1. A typical throughput rate of 20 kg/h for this size of channel was assumed.

Figure 3 shows the predicted profile for the solid bed when the shaft is rotated at 120 rpm and the barrel temperature is uniform at 200°C. At this relatively high barrel temperature, the contribution of heat conduction from the barrel to melting is as significant as the heat generated by the rotating shaft. Figure 4 shows the variation of the ratio of shaft power to the total power input (shaft power + heat conducted from barrel) with operating conditions. The curves tend to flatten out with increasing shaft speed. This is due to the non-Newtonian nature and the temperature sensitivity of the polymer melt viscosity in that at higher shear rates and associated higher temperatures, the viscosity reduces and hence the amount of heat generated increases at a slower rate. Thus, for a given polymer/machine system, there is a shaft speed above which increased shear rates do not lead to corresponding increases in melting rates, and therefore resulting in little improvement to melting performance.

This aspect becomes more clear in Figure 5 where the length of channel required for the completion of melting is plotted against the shaft speed. It decreases rapidly as speed is increased from 60 rev/min, but above 240 rev/min, further increase in shaft speeds produces only a minor reduction in the melting length. Figure 6 shows that the melting length increases almost linearly with output rate.

An interesting exercise is to compare melting in the present situation with that occurring in a single screw plasticating extruder. Melting in the screw is inherently efficient in that the melt film across which most of the heat is generated and conducted for melting is kept thin by the continuous deformation of the solid bed of polymer. For this comparison, the melting model provided in ref 3 was used and the performance of a screw extruder of equivalent physical size was simulated. Details of this extruder are given in Table 2. Melting was assumed to start at the beginning of the transition zone and a barrel temperature of 200°C was assumed. To yield an output rate of 20 kg/h, a screw speed of 54 rev/min was selected to give a dimensionless flow rate of 0.5, which is a practical value found with many extruders. The dimensionless flow rate is defined as volumetric flow rate/(cross-sectional area of screw

Figure 4 Variation of power consumption ratio with shaft speed for $\dot{M} = 20$ kg/h. Curve A, $T_b = 150^\circ\text{C}$; B, $T_b = 200^\circ\text{C}$; C, $T_b = 250^\circ\text{C}$ Figure 5 Variation of melting zone length with shaft speed for $\dot{M} = 20$ kg/h. Curve A, $T_b = 150^\circ\text{C}$; B, $T_b = 200^\circ\text{C}$; C, $T_b = 250^\circ\text{C}$

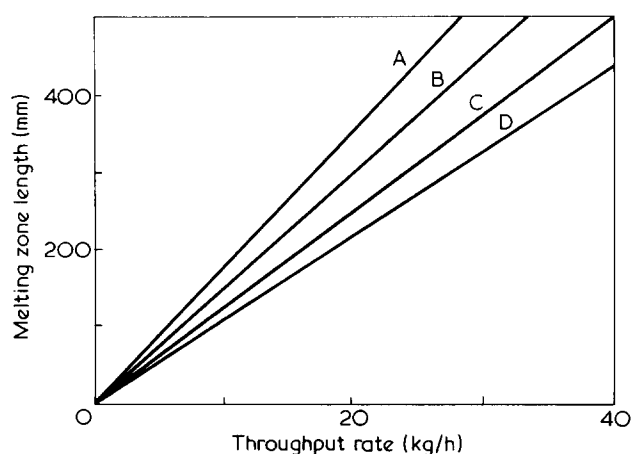


Figure 6 Variation of melting zone length with throughput rate. Curve A, $T_b = 200^\circ\text{C}$, $N = 120$ rev/min; B, $T_b = 250^\circ\text{C}$, $N = 120$ rev/min; C, $T_b = 200^\circ\text{C}$, $N = 240$ rev/min; D, $T_b = 250^\circ\text{C}$, $N = 120$ rev/min

Table 2 Details of screw extruder simulated

Barrel diameter	= 44.5 mm
Length of feed section	= 5 diameters
Length of compression section	= 5 diameters
Length of metering section	= 10 diameters
Depth of feed section	= 9.5 mm
Depth of metering section	= 3.18 mm
Radial clearance	= 0.04 mm
Flight width	= 4.45 mm
Lead	= 44.5 mm
Number of starts	= 1
Helix angle	= 17.7°
Channel width	= 37.9 mm

channel in metering zone \times velocity component parallel to the screw flights of barrel relative to screw). The simulation has shown that the melting process in the screw is likely to become unstable at an axial location of 12 diameters where about 25% of the polymer remains unmelted. This instability is manifested in the breaking up of the solid bed producing surges in the output rate, and is detected in the simulation by a rapid acceleration of the solid bed.

Simulation of melting in the annular cell of the same material with $T_b = 200^\circ\text{C}$, $N = 54$ rev/min and $M = 20$ kg/h, shows that at an axial location of about 11 diameters from the beginning of melting, the polymer is completely molten and no significant acceleration of the solid bed occurs thus indicating that a stable melting process prevails. It should also be noted that in this case the output rate is independent of the shaft speed, whereas in the case of the screw extruder output rates are almost linearly proportional to the screw speed. The speed of 54 rev/min chosen for the shaft was to provide a shear rate of the same order of magnitude as that in the metering zone of the comparative screw extruder, and is completely independent of output rate.

CONCLUSIONS

In this work, the melting of a compacted bed of polymer particles moving through a narrow annulus subjected to tangential shear was studied. The mathematical model has been kept as simple as possible yet retaining the important features of the process. It can be applied as a powerful design tool, but solutions must be obtained numerically on a digital computer.

The melting mechanism described operates in a limited number of processing devices as yet. Basically the process is equally if not more efficient than melting in single screw extruders and should also be more stable. In addition, the independence of melting rates from throughput rates adds considerable flexibility to the process. As a consequence, it is envisaged that wider application of this method will be found in the processing industry.

NOMENCLATURE

b	temperature coefficient of viscosity
c_m, c_s	specific heats of melt and solid
C	mean circumference of annulus
D	diameter of barrel
f_1, f_2	functions in equations (12) and (13)
h	annular gap size
H	thickness of material
k_m, k_s	thermal conductivities of melt and solid
\dot{m}	mass flow rate
\dot{M}	overall throughput rate
n	power law index
N	shaft speed
p	pressure
P_z	pressure gradient
T	temperature in material
T_a	ambient temperature
T_m	melting point of polymer
T_0	reference temperature
T_r	temperature used in specifying T^*
T^*	initial temperature profile
\bar{T}	bulk mean temperature
v_x, v_z	velocities in x and z directions
V_{sz}	solid bed velocity
V_x	velocity of shaft
x, y, z	rectangular coordinates
γ_0	reference shear rate
ΔE	change in enthalpy
λ	latent heat of fusion
$\underline{\mu}$	viscosity
$\bar{\mu}$	mean viscosity
μ_0	effective viscosity at γ_0 and T_0
ρ_m, ρ_s	densities of melt and solid
τ	shear stress at melting interface
τ_{xy}, τ_{yz}	transverse and downstream shear stresses

Subscripts

1	variables related to melt film adjacent to barrel
2	variables related to melt film adjacent to shaft
s	variables related to the solid bed

ACKNOWLEDGEMENTS

The present work was carried out as part of a general project on new methods of processing polymers financially supported by the Science Research Council.

REFERENCES

- 1 Yi, B. and Fenner, R. T. *Plast. and Polym.* 1975, **43**, 224
- 2 Tadmor, Z. and Klein, I. 'Engineering Principles of Plasticating Extrusion', Van Nostrand/Reinhold, New York, 1970
- 3 Edmondson, I. R. and Fenner, R. T. *Polymer* 1975, **16**, 49
- 4 Yi, B. *PhD Thesis* London University (1975)
- 5 Martin, B. 'Heat Transfer Coupling Effects Between a Dissipative Fluid Flow and its Containing Metal Boundaries', Report for the European Working Party on Polymer Processing, 1970

Molecular motions and segmental size of vulcanized natural and acrylonitrile-butadiene rubbers by the spin-probe method

N. Kusumoto, S. Sano*, N. Zaitso† and Y. Motozato‡

Department of Industrial Chemistry, Faculty of Engineering, Kumamoto University, Kumamoto 860, Japan

(Received 26 November 1975)

Nitroxide radicals were dispersed as paramagnetic probes in natural and acrylonitrile-butadiene rubbers, differing in the content of combined sulphur, and their molecular motions were investigated through the motion of the probe inspecting e.s.r. spectra. Broad e.s.r. spectra at low temperatures changed into sharp ones around or above T_g of the rubbers, showing the rapid narrowing of the extreme line separation of triplet spectra. From the activation energy of the rotational motion of the probe, calculated from the temperature dependence of the rotational correlation frequency, it was deduced that the self-diffusion of the probe through polymer matrices and polymer segments had occurred around or above T_g . The temperature narrowing of the line separation was correlated to the glass transition of the rubbers and a relation between the temperature narrowing, T_g and the molar volume ratio of the segment to the probe on the basis of the hole theory, was proposed. From this theory, the size of segments of the rubbers was estimated.

INTRODUCTION

The spin-probe method detects molecular motions of solid polymers through e.s.r. spectra of paramagnetic probes which are usually stable nitroxide radicals embedded in polymer matrices. Although this method is an indirect observation, it has been found by Strukov¹ that e.s.r. spectra enable us to study the molecular motions of host polymers since the motion of the probe is dominated by that of polymer matrices.

Further, Rabold² reported that this method was useful for characterizing polymers. Since then, studies have been made on the transition of rubbers³, blend polymers⁴, the crystallization of poly(ethylene terephthalate)⁵, styrene-butadiene block and random copolymers⁶, the distribution and motions of probes in polymer matrices⁷⁻⁹, latexes¹⁰, drawing^{11,12} and annealing¹³ effects on polyethylene and the surface problem of polyethylene single crystals¹⁴.

In this method, two kinds of parameters have been used to represent the motion of the probe. One of these, for instance, is the correlation frequency of tumbling motion of the probe, which can be estimated by use of the Kivelson theory¹⁵. However, the frequency range, for which this theory is valid is confined to a range of 10^9 – 10^{11} cycles/sec and the analysis of spectra often becomes difficult in practice. Another parameter is the extreme line separation of a triplet spectra of the nitroxide radical. This line separation varies with the motion of the probe owing to the averaging of the anisotropic hyperfine interaction and the anisotropy of the g -value. In almost all cases this narrowing of the line separation takes place rapidly, and the temperature at which the line separation crosses 50

gauss is defined as T_n which characterizes the polymer matrix².

Meanwhile, the motional mode of the probe in polymer matrices has not yet been clarified. In many cases the motion has been supposed to be isotropic, but in some cases it is anisotropic⁷. In a previous paper¹⁴, one of the authors has suggested that the probe possibly jumps from a hole to an adjacent one in the same manner as polymer segments do, and this jumping might be related to the narrowing of the extreme line separation mentioned above. In the present study, the motional mode of the probe was carefully taken into consideration and a theory was given on the relation between the temperature narrowing of line separation (T_n), glass transition temperature (T_g) of polymers and the volume ratio of the segment to the probe on the basis of the hole theory of the glass transition. Attempts were made to estimate the segmental size of the polymers.

EXPERIMENTAL

Materials

Natural (NR) and acrylonitrile-butadiene (NBR, nitrile content 35%, Nihon Synthetic Rubber Co.) rubbers were chosen as materials. The vulcanizing conditions are listed in Table 1. The samples contain 1 wt. % of 2-mercaptobenzothiazole and phenyl- β -naphthylamine as vulcanizing accelerator and antioxidant, respectively.

Introduction of paramagnetic probe

2,2,6,6-Tetramethyl-4-piperidinol-1-oxyl was employed as a paramagnetic probe. This was prepared as described in a previous paper¹⁴. The rubber specimens were soaked in 0.1 wt. % of xylene solution of the probe at 20°C for 10 h for specimens No. 1–4 and 24 h for No. 5–7, respectively. After soaking, the surface of specimens was lightly washed by methanol and then dried under reduced pressure for 2–3 weeks.

* Present address: Mitsubishi Jushi Co., Hiratsuka, Japan

† Present address: Bridge Stone Tire Co., Tokyo, Japan

‡ Department of Synthetic Chemistry, Faculty of Engineering, Kumamoto University, Kumamoto 860, Japan

Table 1 Vulcanization conditions and sulphur content

No.	NR				NBR			
	Temperature (°C)	Time (h)	S_m (%)	S_c (%)	Temperature (°C)	Time (h)	S_m (%)	S_c (%)
1	140	2	2	1.1	140	2	2	2
2	140	2	4	1.9	140	2	4	3.8
3	140	2	8	3.2	140	2	8	7.2
4	140	3	14	7.5	140	3	14	11.9
5	140	4.5	20	11.2	140	4.5	20	17.5
6	140	4.5	25	—	140	4.5	25	—
7	140	4.5	32	15.1	140	4.5	32	23.4

S_m , mixed sulphur; S_c , combined sulphur

Measurements

E.s.r. spectra were recorded on a Nihon Denshi JES-3BSX e.s.r. spectrometer using X-band and 100 kHz field modulation. Temperature was varied from -160° to 100°C using the JES-VT-3A temperature controller and the JES-UCT-2A gas flow cryostat. The sample temperature was measured by a thermocouple inserted into a sample tube during the e.s.r. measurements. For exact estimation of theoretical correlation frequency of the probe from the linewidth of e.s.r. spectra, the modulation width and the microwave power level were carefully controlled to decrease the line broadening and the power saturation, respectively, while maintaining necessary sensitivity of the spectrometer.

The glass transition temperature of the samples was measured by the dilatometry at the rate of temperature elevation, $0.5^\circ\text{C}/\text{min}$.

RESULTS AND DISCUSSION

Line shape of e.s.r. spectra

Figure 1 shows the e.s.r. spectra of NBR at various temperatures. At liquid nitrogen temperature, both NR and NBR show similar broad asymmetric triplet spectra caused by the interaction of an unpaired electron with a nitrogen atom, the broad line shape indicating that the probe is in a rigid matrix. These broad spectra change into sharp ones with narrower line separation with increasing temperature, indicating that the probes begin to move at higher temperatures. A small subsplitting appears at around -90°C , increasing in intensity as temperature is increased for both NR and NBR. This aspect seems to be superposition of two kinds of spectra with broad and narrow line separation. The broad spectral component narrows almost simultaneously with increase in intensity of the narrow component, and the spectral shape finally changes into a sharp triplet.

This multiplicity of spectra has already been interpreted in two ways as described before¹⁴. One of them is the superposition of a broad and a narrow spectra caused by the inhomogeneity of fine structure of a matrix. Another may intrinsically occur by the partial averaging of anisotropic hyperfine interaction and g -value in an intermediate frequency range¹⁶. As far as the present data are concerned at least the former case may be conceivable since the effect of fine structure of the polymer on the spectra is observed; namely the higher the content of combined sulphur of the samples the clearer the separation of two peaks in the intermediate temperature becomes, as shown for NR in Figure 2.

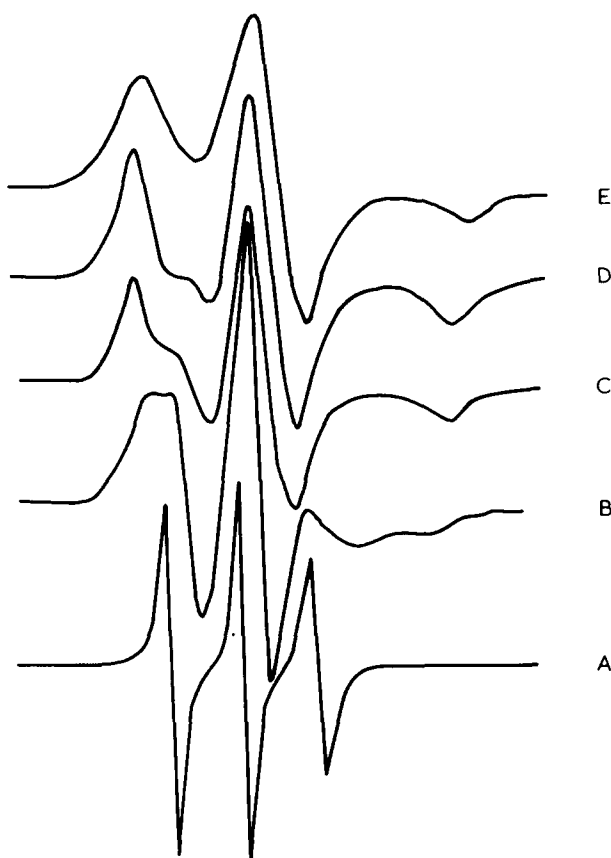


Figure 1 E.s.r. spectra of NBR at various temperatures: A, 75°C ; B, 25°C ; C, -20°C ; D, -90°C ; E, -180°C

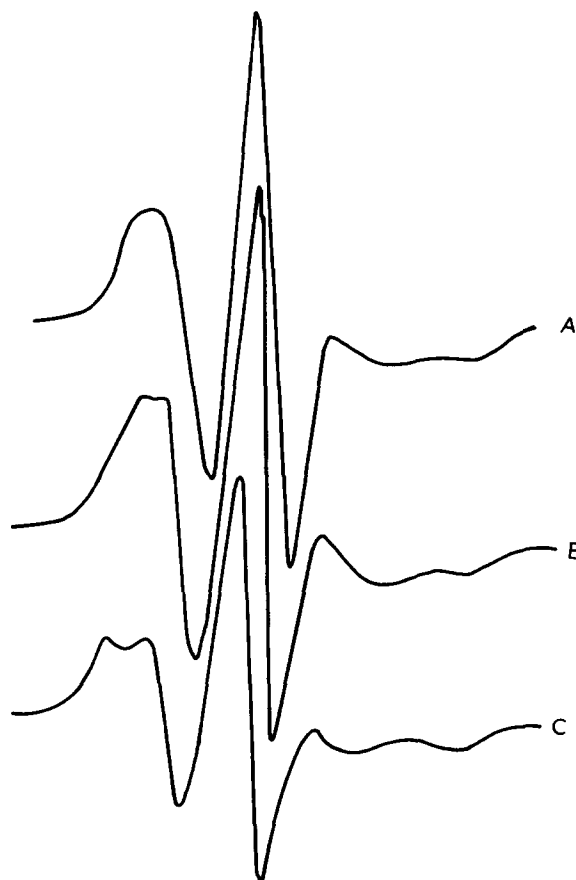


Figure 2 E.s.r. spectra of NR at around T_g . A, $S_c = 1.1\%$ at 16°C ; B, $S_c = 7.5\%$ at 25°C ; C, $S_c = 15.1\%$ at 33°C

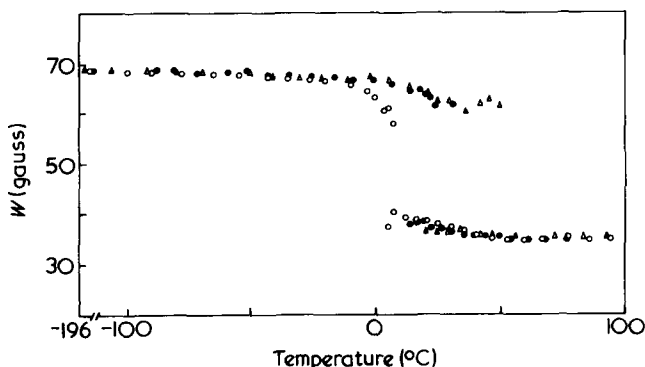


Figure 3 Temperature dependence of line separation for NBR. \circ , $S_C = 2\%$; \bullet , $S_C = 11.9\%$; \triangle , $S_C = 23.4\%$

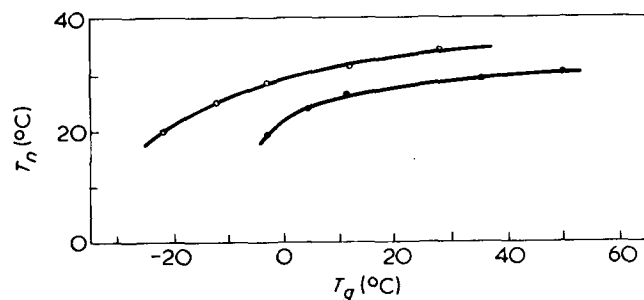


Figure 4 Relations between T_n and T_g , \circ , NR; \bullet , NBR

Moreover, it has been reported¹⁷ that vulcanized *cis*-1,4-polybutadiene rubber showed the increase of microstructural inhomogeneity with increasing sulphur content. The increase in the peak separation with increasing combined sulphur content may be similarly related.

Variation of extreme line separation with temperature

It has been proposed as mentioned before, that extreme line separation of a triplet pattern, W , can be used as a measure of the motion of the probe. Figure 3 shows the variation of W with temperature for NBR samples. The line separation is about 69 gauss at liquid nitrogen temperature and shows rapid narrowing above the glass transition. Since the spectra show a complex pattern, the Figure shows the line separation of two components. The temperature difference of the two narrowing temperatures is found to increase with increase in the content of combined sulphur in accordance with the increasing double peak separation (Figure 2).

For convenience, the average temperature narrowing at which the intensity of the two peaks becomes equal as shown in Figure 2 is taken as the temperature narrowing, T_n . The relation between T_n and T_g is shown in Figure 4, indicating a correlation between T_n and T_g . T_n is found to increase with increasing T_g . From these curves it can be deduced that T_n will coincide with T_g at 34°C for NR and 28°C for NBR, respectively, and T_n exceeds T_g above 23°C for NBR. These relations between T_n and T_g will be discussed later.

Correlation frequency of tumbling motion of probes

When temperature is increased to cause enough sharpening of the line width, the correlation time of isotropic tumbling motion of the probe can be calculated using the Kivelson theory¹⁵ viz.:

$$\tau_c = W_0[(h_0/h_1)^{1/2} - (h_0/h_{-1})^{1/2}]C \quad (1)$$

$$\tau_c = W_0[(h_0/h_1)^{1/2} + (h_0/h_{-1})^{1/2} - 2]C' \quad (2)$$

where W_0 is the maximum slope line width of central peak of the three line spectrum, h is the peak height, whose subscript represents the nuclear quantum number of nitrogen atom, C and C' are constants determined by experimental conditions such as the hyperfine interaction characteristic of the probe and the magnitude of a static magnetic field. These equations are mathematically equal, but accuracy in employment has been discussed by Strukov¹. In this theory the rate conditions mentioned in a previous paper¹⁴ must be fulfilled.

Figure 5 shows the plots of the logarithmic correlation frequency ($1/\tau_c$) versus the reciprocal of observation temperature. The correlation frequency increases with increasing combined sulphur content over the whole temperature range indicating that the polymer matrix is immobilized by the increase of combined sulphur. Slight upward departure in the frequency from the linear plot at low temperatures is found for NR samples with low sulphur content (No. 1-3), and progressive decrease in the frequency at higher temperatures is seen also for NR samples with high sulphur content (No. 5-7).

On the other hand, for NBR the upward departure can be found and, in turn, a progressive decrease at higher temperatures is seen for all samples. The decrease becomes larger with increasing sulphur content.

The activation energy of the motion of the probe is calculated by the equation:

$$E = R \ln(1/\tau_c) / d(1/T) \quad (3)$$

The linear parts of the curves of Figure 5 are shown in Table 2.

For NR samples which show two linear relations, the activation energy at higher, E_1 , and lower temperatures, E_2 were estimated. The values of E_1 and E_2 are comparable to those of bulk polyethylene¹³, although much higher than those estimated from the Arrhenius plots of the lower temperature region of polyethylene single crystals¹⁴.

As has been suggested in a previous paper¹⁴, this relatively large activation energy E_2 may possibly be associated with the jumping mode of the probe into adjacent holes. Andrew¹⁵ has shown by the measurements of second moment of wideline n.m.r. that cyclohexane molecules begin to diffuse through the crystal lattice between -53° and -33°C. In this case, the activation energy of molecular motion was estimated as 8 kcal/mol, which is supposed to be two-thirds of the lattice energy, suggesting the occurrence of the self-diffusion of cyclohexane molecules. This explanation provides a valuable indication of the existence of the self-diffusion of the probe in the rubbers. The value of 9-11 kcal/mol in the present study and the fact that the activation energy is almost independent of the sulphur content, implies that the probe is not restricted in a local potential barrier in a polymer matrix so-called cavity model but diffuses through polymer matrix.

At low temperatures the probe is in a rigid state and begins restricted rotational oscillation, and then free rotation as the temperature increases. The rotational oscillation and the free rotation may possibly average out the anisotropic hyperfine interaction and g -value, causing the narrowing of the line separation until the self-diffusion takes place. However, appearance of the narrowing depends on the rotational frequency of the probe, the narrowing being recognized only when the frequency exceeds the e.s.r. frequency of 10^{7-8} cycles/sec. Since the motional mode of the probe and its frequency depends on the nature of the probe such as size, shape and the aspect of

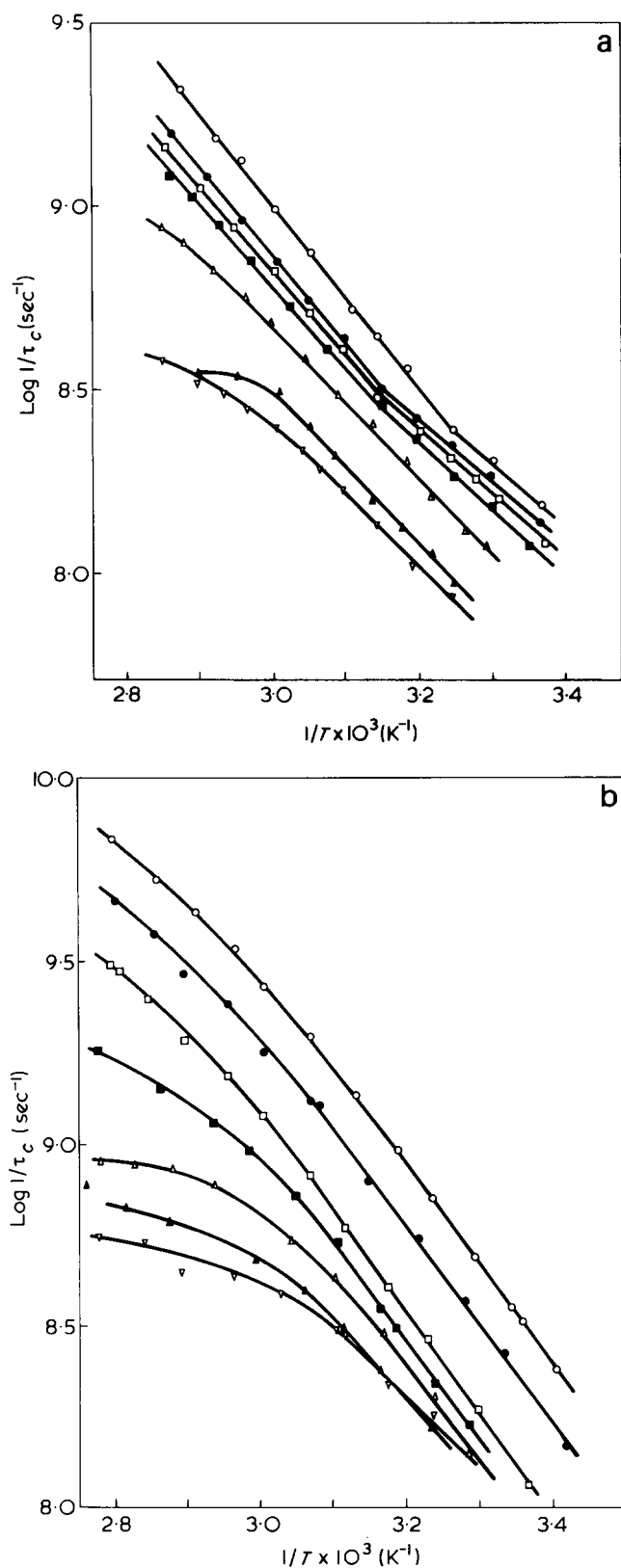


Figure 5 Arrhenius plots of correlation frequency. (a) \circ , NR with $S_c = 1.1\%$; \bullet , NR with $S_c = 1.9\%$; \square , NR with $S_c = 3.2\%$; \blacksquare , NR with $S_c = 7.5\%$; \triangle , NR with $S_c = 11.2\%$; \blacktriangle , NR with $S_m = 25\%$; ∇ , NR with $S_c = 15.1\%$; (b) \circ , NBR with $S_c = 2\%$; \bullet , NBR with $S_c = 3.8\%$; \square , NBR with $S_c = 7.2\%$; \blacksquare , NBR with $S_c = 11.9\%$; \triangle , NBR with $S_c = 17.5\%$; \blacktriangle , NBR with $S_m = 25\%$; ∇ , NBR with $S_c = 23.4\%$

interaction with the polymer, the cause of the narrowing is not always the same.

However, when the narrowing occurs by the rotational mode, the activation energy will be ~ 10 kcal/mol. The

energies below 6 kcal/mol obtained for the low temperature region in polyethylene^{13,14} may be associated with this mode.

In the present study, the appearance of the break point around 50°C in the Arrhenius relations in Figure 5a suggests that the rotational mode of the probe is mixed and leads to a change in the slope of the curves in the low temperature region.

Theoretical treatment of the relation among T_n , T_g and the molar volume ratio of the segment to the probe

As has been discussed in the previous section the motional mode of the probe in NR in the highest temperature range can be the self diffusion of the probe in the polymer matrix. Further, the correlation between T_n and T_g implies that this self-diffusion takes place in a similar manner to the segmental diffusion of the polymer above glass transition.

In terms of the hole theory, the segments of polymer molecules begin to jump into adjacent holes formed by displacement of the segment and the thermal expansion of polymer matrix around T_g . At the same time, if the probe has a comparable size to a segment it will jump into an adjacent hole as well as the polymer segment. According to the theory by Bueche¹⁹ let us consider a polymeric system which consists of polymer molecules with n segments, probes and the free volume, V_f as shown in Figure 6. V_f is supposed to be the summation of packets with the volume of v_f :

$$V_f = n \times v_f \quad (4)$$

Table 2 Activation energy of the tumbling motion of the probe

No	NR		
	E_1 (kcal/mol)	E_2 (kcal/mol)	E_1 for NBR (kcal/mol)
1	7.8	11	12
2	7.4	11	12
3	7.2	10	12
4	7.6	10	12
5	—	10	12
6	—	10	10
7	—	9	10

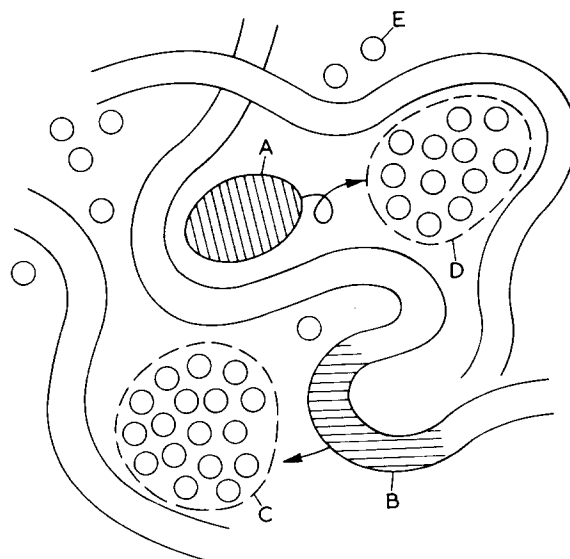


Figure 6 Schematic model of jumping of probe and segment: A, probe (volume v_p); B, segment (volume v_f); C, hole (volume $v_f > v_m^*$); D, hole (volume $v_f > v_p^*$); E, packet (volume v_f)

Provided that q packets are gathered to form a hole with the volume of v_f' in the vicinity of a segment or probe, the segment or the probe will jump into this hole when v_f' exceeds the activation volume for jumping, v_m^* and v_p^* , which are for the segment and the probe, respectively. In this system, the probability that q packets are gathered around a certain segment is given by:

$$p(q) = (1 - 1/n)^{n-q} (1/n)^q [n!/q!(n-q)!] \quad (5)$$

This calculation is comparable to the case where a person throws n balls towards n boxes and has the possibility of getting q balls in a certain box. The ball corresponds to the hole and the box to the segment. Let us consider the case where a few of the boxes are replaced by ones differing in size and having q balls in one of them. This corresponds to the case where q balls are gathered around the probe in a polymer matrix. In this case, the difference in interaction between the probe and the segment and inter-segments is ignored. When the number of the probe is negligibly small compared with that of segments, the probability of q holes around the probe may approximately be given rewriting equation (5) as:

$$p(q) = (1 - v_p/nv_m)^{n-q} (v_p/nv_m)^q [n!/q!(n-q)!] \quad (6)$$

where v_p and v_m denote the molar volume of the probe and the segment, respectively. In equation (5) the possibility of a hole around a segment is $1/n$, therefore, this possibility is modified in equation (6) as being proportional to the volume ratio of the segment to the probe.

Assuming $n \gg q$ and using:

$$\lim_{n \rightarrow \infty} (1 - v_p/nv_m)^n = \exp[-v_p/nv_m]$$

and

$$n!/q!(n-q)! = n(n-1) \cdots (n-q+1)/q! \approx nq/q!$$

equation (6) is rewritten as:

$$p(q) = \exp[-v_p/v_m] \times (v_p/v_m)^q (1/q!) \quad (7)$$

While the gamma function $\Gamma(2)$ is: $\Gamma(n+1) = n!$ and from the Stirling formula: $\lim_{n \rightarrow \infty} (n+1)/(2n\pi)^{1/2} (n/e)^n = 1$.

Therefore, when q is not so small:

$$1/q! = (2\pi q)^{-1/2} \times (q/e)^{-q} \quad (8)$$

Substituting equation (7) into equation (8):

$$p(q) = (2\pi q)^{-1/2} (v_m q/v_p)^{-q} \times \exp(q - v_p/v_m) \quad (9)$$

$q = v_f'/v_f$, therefore the probability that the probe encompasses the free volume of v_f' :

$$p(v_f') = (2\pi v_f'/v_f)^{-1/2} \exp[-(\beta + \ln v_m/v_p) v_f'/v_f - v_p/v_m] \quad (10)$$

where $\beta = \ln(v_f'/v_f) - 1$.

The probe jumps into the hole when $v_f' \geq v_f^*$, therefore the probability is:

$$\int_{v_p^*}^{\infty} p(v_f') dv_f' \approx (\text{const.}) \exp[-(\beta^* + \ln v_m/v_p) v_p^*/v_f - v_p/v_m] \quad (11)$$

The jumping frequency is:

$$\Phi = \Phi_0 \exp[-(\beta^* + \ln v_m/v_p) v_p^*/v_f - v_p/v_m] \quad (12)$$

The microscopic free volume v_f changes with temperature above T_g :

$$v_f = v_{fg} + v_{mg} \Delta\alpha (T - T_g) \quad (13)$$

where, v_{fg} and v_{mg} are the free volume and the occupied volume of a segment at T_g , respectively. $\Delta\alpha$ is the difference between thermal volume expansion coefficients above and below T_g . This relation is valid in a temperature range $T_g \leq T \leq T_g + 120^\circ\text{C}$.

Substituting equation (13) into equation (12) and rearranging the formula we obtain:

$$T - T_g = \left\{ \frac{[\ln(v_m/v_p) + \beta^*] v_p^* v_{fg} v_m^*}{\ln(\Phi_0/\Phi) \times v_{fg} \times v_m^* - v_p v_m^* v_{fg}/v_m} \right\} v_{mg} \Delta\alpha \quad (14)$$

The Doolittle relations: $v_{fg}/v_{mg} \Delta\alpha = 52$ and $v_m^*/v_{fg} = 40$ and $\beta^* \approx 1$ are substituted into equation (14) and assuming $\ln\Phi/\Phi_0 \gg f$, we obtain:

$$T - T_g = 52 [40f(\ln 1/f + 1)/\ln\Phi_0/\Phi - 1] \quad (15)$$

where $f = v_p^*/v_m^* = v_p/v_m$.

$\Phi_0 = 10^{14}$ is assumed according to Bueche¹⁹. The narrowing of line separation may occur at $\Phi = 10^8$. This supposition is satisfactory since the extrapolation of almost all curves in Figure 4 to the narrowing temperatures is of the order of 10^8 . Thus, we obtain the simple formula:

$$T_n - T_g = 52 [2.9(\ln 1/f + 1) - 1] \quad (16)$$

When T_n and T_g are determined experimentally and the molar size of the probe is known the segmental size of polymer can be estimated using equation (16).

Figure 7 shows the value of $T_n - T_g$ as a function of f , calculated from equation (16). $T_n - T_g$ has a maximum at $f = 1$. This may mean physically that the probe is not able to jump at T_g , when the size of the probe exceeds that of the segment. The maximum value of $T_n - T_g$ is 98.8°C , indicating that this equation is valid on the supposition $0 \leq T_n - T_g \leq 120^\circ\text{C}$. On the other hand, $T_n - T_g$ becomes negative as mentioned in the previous section. This may occur when the probe is considerably smaller than the segment and the jumping mode occurs by the local motion of the segment. For instance, this will occur in the system which has a wide distribution of segmental size because of the inhomogeneity of a matrix. The deduction that the inhomogeneity of the matrix becomes larger with increasing content of combined sulphur may explain this phenomenon. This may also occur by the local relaxation mode. In such a case, macroscopic volume expansion and total increase in free volume, is not necessary for the displacement of the probe. The diffusion of the probe due to the displacement of the local free volume may afford the narrowing of e.s.r. pattern. The case where $T_n - T_g < 0$ is also seen in a polymeric system which has large side groups such as polystyrene. For this polymer it was found²⁰ that $T_n - T_g$ is -15°C when di-*t*-butylnitroxide $(\text{CH}_3)_3\text{C}(\text{NO})\cdot$ $\text{C}(\text{CH}_3)_3$ is used as a probe, while it is 35°C for the probe used in this study. The molar volume of di-*t*-butylnitroxide

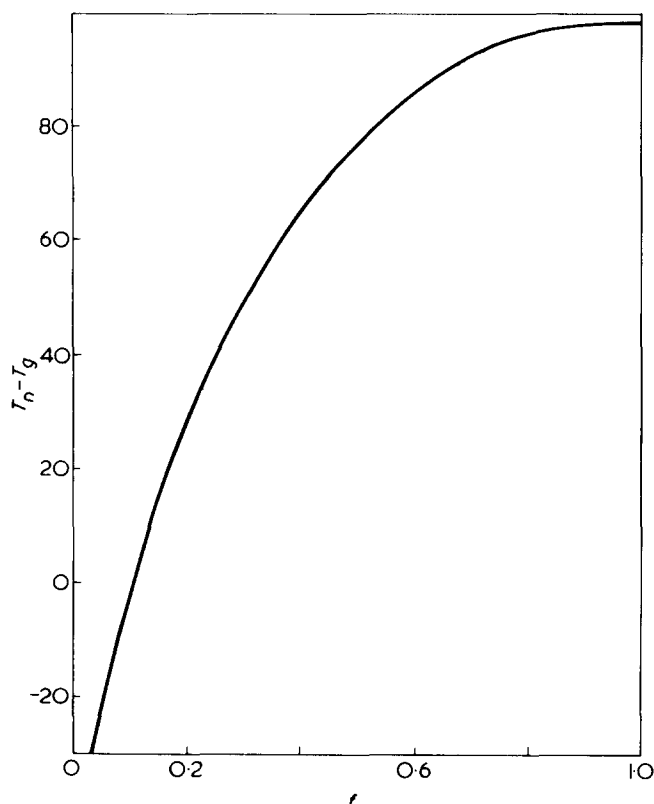

 Figure 7 Relation between $T_n - T_g$ and f

Table 3 Calculated size of the segment

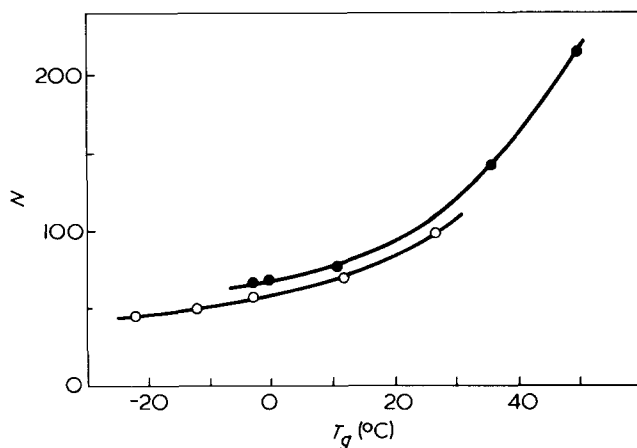
No.	T_n (°C)	T_g (°C)	ΔT (°C)	f	v_m (cm ³ /mol)	d_m (Å)	v'_m (Å ³)	d'_m (Å)	N
NR									
3	20	-22	42	0.268	876	14.0	660	10.8	45
4	25	-12	37	0.246	955	14.5	719	11.1	50
5	28	-3	31	0.219	1073	15.0	808	11.5	56
6	31	12	19	0.175	1609	15.1	1011	12.4	70
7	33	27	6	0.125	1880	15.3	1416	13.9	98
NBR									
3	19	-3	22	0.182	1291	16.0	973	12.3	65
4	24	4	20	0.175	1343	16.2	1011	12.4	68
5	26	11	15	0.156	1505	16.8	1135	13.3	76
6	29	36	-7	0.090	2611	17.1	1966	15.5	142
7	30	41	-11	0.055	4273	23.8	3218	18.3	215

$\Delta T = T_n - T_g$, v_m and d_m are from atomic volume at boiling point²¹, v'_m and d'_m are calculated by the Slonimskii's method²², N is the number of backbone atoms of the segment

is 88% of the latter, accordingly the narrowing can occur at lower temperatures. The effect of the probe size is well interpreted by equation (16). The details of the data will be reported elsewhere.

From Figure 7 we can estimate the segmental size of polymers above glass transition measuring T_n and T_g since the molar volume of the probe is known. Table 3 lists the estimated values of f , the molar volume of the segment, the number of backbone atoms of the segment and the diameter of the segment, calculated assuming the spherical shape of the segment.

For calculation of v_m and v'_m the atomic volume at boiling point²¹ and the Slonimskii's method²² were employed.


 Figure 8 Relation between the number of backbone atoms of the segment and T_g . ○, NR; ●, NBR

The latter case includes only the excluded volume of the segment, therefore this may be the smallest value estimated. The number of backbone atoms of the segment was estimated by multiplying the number of backbone atoms of the repeating unit of the polymers to the excluded volume ratio of the repeating unit to the segment. Thus, 45–98 and 65–215 backbone atoms are included in the segment of NR and NBR, respectively depending upon the content of combined sulphur. For this calculation, sulphur is not taken into consideration. However, the values are almost coincident with those estimated by dividing the number of backbone atoms of the probe (12) by f within $\pm 2\%$, therefore the number estimated may be valuable as a first approximation. These values may be comparable to the case of polypropylene ($T_g = -10^\circ\text{C}$), where the size of the segment has been estimated as 30 monomeric units corresponding to 90 backbone atoms, estimated from viscoelastic data²³.

Figure 8 shows the number of backbone atoms as a function of T_g . The values of NBR are found to be located above the T_g of NR. When the segmental size of NBR is the same as that of NR T_g is about 5–15°C higher than that of NR. This fact may be due to the cohesive energy of NBR molecule being larger than that of NR.

REFERENCES

- Strukov, V. B. and Rosantzev, E. G. *Vysokomol. Soedin. (A)* 1968, **10**, 626
- Rabold, G. P. *J. Polym. Sci. (A-1)* 1969, **7**, 1203
- Kovarskii, A. L., Vassermann, A. M. and Buchachenko, A. L. *Dokl. Akad. Nauk SSSR* 1970, **193**, 132
- Kovarskii, A. L., Arkina, S. N. and Vassermann, A. M. *Vysokomol. Soedin. (B)* 1970, **12**, 38
- Kovarskii, A. L., Vassermann, A. M. and Buchachenko, A. L. *Vysokomol. Soedin. (B)* 1970, **12**, 211
- Kovarskii, A. L., Burkova, S. G., Vassermann, A. M. and Morozov, Yu. L. *Dokl. Akad. Nauk SSSR* 1971, **196**, 383
- Kovarskii, A. L., Vassermann, A. M. and Buchachenko, A. L. *Vysokomol. Soedin. (A)* 1971, **13**, 1647
- Vassermann, A. M., Buchachenko, A. L., Kovarskii, A. L. and Neiman, M. B. *Eur. Polym. J.* 1969 (Supplement), 473
- Kovarskii, A. L., Vassermann, A. M. and Buchachenko, A. L. *Dokl. Akad. Nauk SSSR* 1971, **201**, 1385
- Rabold, G. P. *J. Polym. Sci. (A-1)* 1969, **7**, 1203
- Kusumoto, N. and Mukoyama, H. *Rep. Prog. Polym. Phys. Japan* 1972, **15**, 581

Vulcanized and acrylonitrile-butadiene rubbers studied by the spin-probe method: N. Kusumoto et al.

- | | | | |
|----|--|----|---|
| 12 | Kusumoto, N. and Mukoyama, H. <i>Rep. Prog. Polym. Phys. Japan</i> 1973, 16 , 555 | 18 | Andrew, E. R. 'Nuclear Magnetic Resonance', University Press, Cambridge, 1955 |
| 13 | Kusumoto, N. and Mukoyama, H. <i>Rep. Prog. Polym. Phys. Japan</i> 1973, 16 , 551 | 19 | Bueche, F. 'Physical Properties of Polymers', Wiley, New York, 1962 |
| 14 | Kusumoto, N., Yonezawa, M. and Motozato, Y. <i>Polymer</i> 1974, 15 , 793 | 20 | Kusumoto, N., Sano, S. and Kijima, T. unpublished work |
| 15 | Kivelson, D. <i>J. Chem. Phys.</i> 1960, 33 , 1094 | 21 | Perry, J. H. 'Chemical Engineer's Handbook', McGraw-Hill, New York, 1950, p 538 |
| 16 | Itokowitz, M. S. <i>J. Chem. Phys.</i> 1967, 46 , 3048 | 22 | Slonimskii, G. L., Askadskii, A. A. and Kitaigorodskii, A. I. <i>Vysokomol. Soedin. (A)</i> 1970, 12 , 494 |
| 17 | Yamamoto, S., Kitamura, K. and Takayanagi, M. <i>Zairyo</i> 1970, 19 , 380 | 23 | Muus, L. T. <i>SPE J.</i> 1959, 15 , 368 |

Letter

Determination of concentration dependence of the hydrodynamic dimensions by differential g.p.c.

The decrease in hydrodynamic dimensions of macromolecules with increasing concentration is a well established phenomena¹⁻³. The elution volume of macromolecules in gel permeation chromatography is a measure of the hydrodynamic radius of such molecules⁴⁻⁶. Measurement of hydrodynamic volumes as a function of concentration has been done only in a limited number of cases^{7,8}. Rudin⁹ determined molecular dimensions at finite concentrations using gel permeation chromatography to confirm calculations based on dilute solution viscosity measurements. In this case the calculated values were compared against those determined experimentally by varying the concentration of the polymer injected into the gel permeation chromatograph. This requires the assumptions that the sample is injected instantaneously onto the column so that the initial concentration is applicable to the hydrodynamic volume of the solute in the column and that the samples are monodisperse in terms of molecular weight. These assumptions probably do not affect the results. A further assumption that the longitudinal diffusion is negligible may be an over simplification and cause appreciable uncertainty in the results, as suggested by Rudin.

The method of differential gel permeation chromatography (g.p.c.) involves dissolving a polymer in the solvent so that solvent contains a known concentration of polymer. The g.p.c. measurements are then made in the usual way. This method was introduced by Chuang and Johnson¹⁰ who used it to determine small differences in molecular weight distributions. The method appears to overcome the assumptions made by Rudin and to be able to directly determine molecular dimensions as a function of concentration.

Results and Discussion

The data used in this report were taken from Chuang and Johnson¹⁰. Calculations of the hydrodynamic volume from viscosity parameters, densities and molecular weight were carried out in the same manner using the same constants as Rudin. The hydrodynamic dimensions were calculated based on zero concentration or infinite dilution for samples containing no polymer in the solvent, although the concentrations were in actuality 0.016 mg/ml with an injection

volume of 0.318 ml. Calibration curves were then determined by plotting the log of the hydrodynamic radii vs. the elution volume. Elution volumes determined at finite concentrations of polymer using the differential method were then used with the equation resulting from the previously described plots to calculate hydrodynamic radii. The results are shown in *Table 1*. The values at concentrations of 0.667 mg/ml are in reasonable agreement with those calculated by the method of Rudin. At the higher concentration of 4.10 mg/ml, the values are appreciably lower. It should be emphasized that the polymer used to establish the known concentration was that of a moderately broad distribution polystyrene having a \bar{M}_w of 424 000 and a \bar{M}_w/\bar{M}_n of 1.8.

From this we conclude that the values are reasonable and that this appears to be a convenient, reasonably precise way of determining the change of the hydrodynamic dimensions as a function of concentration. Further measurements are in progress and will be reported in the near future.

Acknowledgement

A portion of this work was supported by the National Science Foundation through grant number MPS75-01915.

Edward G. Bartick and Julian F. Johnson

*Institute of Materials Science
and Department of Chemistry,
University of Connecticut,
Storrs, Connecticut 06268, USA
(Received 3 February 1976; revised 27 February 1976)*

References

- 1 Yamakawa, H. *J. Chem. Phys.* 1961, **34**, 1360
- 2 Grimly, T. B. *Trans. Faraday Soc.* 1961, **57**, 1974
- 3 Fixman, M. and Peterson, J. M. *J. Am. Chem. Soc.* 1964, **86**, 3524
- 4 Benoit, H. *et al. J. Chim. Phys.* 1966, **63**, 1507
- 5 Dawkins, J. V. and Maddock, J. W. *Eur. Polym. J.* 1971, **7**, 1537
- 6 Chan, R. K. S. *Polym. Eng. Sci.* 1971, **11**, 152
- 7 Debye, P., Chu, B. and Woermann, D. *J. Chem. Phys.* 1962, **36**, 1803
- 8 Maron, S. H. *et al. J. Polym. Sci.* 1959, **37**, 1
- 9 Rudin, A. *J. Polym. Sci. (A-1)* 1971, **9**, 2587
- 10 Chuang, J. Y. and Johnson, J. F. *J. Appl. Polym. Sci.* 1973, **17**, 2123

Table 1

Molecular weight	Conc. $\times 10^3$ (g/ml)	Elution volume (counts)	$V \times 10^{18}$	g_x	ϵ_x	ϵ_0	ϵ	Theoretical $R \times 10^6$ (cm)	Experimental $R \times 10^6$ (cm) (from plot)	% Difference from theoretical
670 000	0	11.97	1.070	0.110	4.79	82.35	82.35	2.76		
	0.667	12.12						2.68	2.53	5.6
	4.10	12.51						2.36	2.25	4.7
498 000	0	12.41	0.7950	0.125	4.23	65.61	65.61	2.32		
	0.667	12.53						2.26	2.23	1.3
	4.10	13.07						2.04	1.88	7.8
411 000	0	12.75	0.6261	0.134	3.94	56.63	56.63	2.04		
	0.667	12.97						2.00	1.94	3.0
	4.10	13.45						1.82	1.66	8.8
200 000	0	13.97	0.3193	0.162	3.25	32.62	32.62	1.35		
	0.667	14.25						1.34	1.32	1.5
	4.10	14.90						1.26	1.07	15.1

Book Reviews

Natural & Synthetic Polymers An Introduction

Henry I. Bolker

Marcel Dekker, New York, 1974, \$29.75

This is a book written for students of polymer chemistry wherein the author makes the novel approach of treating knowledge of natural and synthetic polymers in a unified manner. To achieve his objective he has of necessity had to restrict his coverage to organic and biological material and to exclude any physical concepts.

Following a short introductory chapter in which polymers and macromolecules are defined, polymers of life and commerce are introduced, some basic definitions given and sufficient history of a range of big molecules presented to whet the appetite.

The author divides his book into 3 Parts subdivided into 12 chapters and an Appendix. Part I is concerned with linear homopolymers and its first chapter is an essay on linear polysaccharides, 60% of which is devoted to cellulose. From the wide literature on this remarkable molecule, the author condenses a truly vast amount of information into an essay which makes really exciting reading for the students. The account of the uses of cellulose is particularly timely. A very brief introduction is given to the molecules of amylose, amylopectin, chitin etc. and to the nucleosides involved in the synthesis of polysaccharides.

Chapter 3 gives an account of synthetic condensation polymers and covers polyesters, polyamides, polysiloxanes, polycarbonates and a great deal of information all clearly crowded into a small compass. Interfacial polycondensation and the theoretical aspects of condensation polymerization are well done.

Addition or chain-growth polymers are next considered beginning with an account of the methods of polymerization, plastication and stabilization. All the well known polymers such as poly(vinyl chloride), polystyrene, polyethylene, the acrylics, fluoro polymers, etc. receive attention with important aspects such as initiation, propagation and termination being adequately described.

The two succeeding chapters, (nearly one quarter of the book), we are given full accounts of the stereo regularity in addition polymers, the story of branched homopolymers both natural and synthetic, and of natural hetero polymers – mainly polysaccharides and nucleic acids. Then there is a sharp jump to the consideration of copolymers and copolymerization, to cross linking mainly in synthetic polymers and back again we come to learn about polypeptide and proteins with a courageous summary of the Genetics code and the chemical and biosynthesis of peptides, and thence to a study of lignins. Finally, we are given an important if brief introduction to the methods used for measuring the molecular weight of polymers.

Conference Announcement

Theoretical Methods in Polymer Physics

Leeds, 5–7 July 1976

The Institute of Physics Polymer Physics Group is organizing a conference on Theoretical methods in polymer physics at the University of Leeds from 5 to 7 July 1976. The programme will consist of invited lectures given by: Professor Sir Samuel Edwards; Professor C. Domb; Dr M. A. Moore; Professor P. G. de Gennes; Professor M. Gordon; Professor W. H. Stockmayer; Dr M. G. Brereton; and Professor G. J. Morgan, together with a number of contributed papers. Further information and registration forms may be obtained from the Meetings Officer, Institute of Physics, 47 Belgrave Square, London SW1X 8QX, UK.

When the late Sir Norman Haworth (whose contribution to polysaccharides are rather neglected in the book) favourably reviewed a book he would write, 'I have had this book at my elbow for 6 weeks', and one can follow him by saying that graduate students of polymer chemistry will greatly benefit by having this book at hand throughout their courses and afterwards. It contains a wealth of well sifted information and achieves the author's objective of presenting a new comprehensive approach to the study of macromolecules.

The book is in typescript reproduced by a photolithographic process – quite adequate for a student text.

M. Stacey

Characterization of Materials in Research: Ceramics and Polymers

Edited by John J. Burke and Volker Weiss

Syracuse University Press, Syracuse, New York, 1975, 566 pp. \$32.00

This volume contains the proceedings of the 20th Sagamore Army Materials Research Conference, held during September 1973. It comprises eighteen review Chapters dealing with methods for characterizing the structure of ceramic or polymeric materials in relation to their behaviour and applications.

There can be little doubt about the importance of adequately characterizing materials. This is frequently essential for obtaining conclusive research data, for the preparation of standards and specifications, and for more efficient design with existing materials. A discussion of these points, together with comments on the waste of effort resulting from negligence in characterization, is included in an Introductory Chapter by N. E. Promise on the Concept of Characterization. In the case of polymers, F. W. Billmeyer later emphasizes the difficulties associated with specifying all aspects of structure, and the probable need for compromise. In view of the expanding efforts in materials research and development, the theme of the proceedings is timely and important.

The proceedings are arranged into five sections dealing, respectively, with the Physics of Nonmetallic Solids, Ceramic Characterization, Molecular Characterization of Polymers, Characterization of Polymers in Bulk and Case Histories. The polymer sections contain reviews on molecular weight measurements (J. B. Kinsinger), sequence distribution and tacticity (H. J. Harwood), statistical properties (J. E. Mark), morphology of semicrystalline polymers (L. Mandelkern), characterization of bulk polymer morphology by optical methods (S. B. Clough), rheological characterization (W. W. Graessley) and characterization of molecular and crystalline orientation (C. R. Desper). A chapter by H. K. Herglotz on the characterization of polymers by unconventional X-ray techniques is included in the section of nonmetallic solids, as is a review of amorphous solids by D. R. Uhlmann which includes some reference to polymeric glasses. A discussion by F. R. Barnet and M. K. Norr on the structure of etched carbon fibres, as revealed by the scanning electron microscope, should be of interest to workers in the field of polymer composites. The Chapters relating to ceramics include several informative descriptions of experimental techniques which should interest those concerned with various aspects of polymer structure.

In general, the aims and principles of the different methods of characterization are clearly presented, the methods are well-illustrated with critical discussions of selected data, and comments on recent developments are frequently included. Each Chapter contains a comprehensive list of up-to-date references. The book is carefully and attractively produced with few apparent errors. It should be a useful reference for practical research workers, lecturers and advanced students of polymer or materials science, and for organizations concerned with the development of materials standards and specifications.

B. E. Read

Chain-extended polyethylene in context: a review*

D. C. Bassett

*J. J. Thomson Physical Laboratory, University of Reading, Whiteknights, Reading RG6 2AF, UK
(Received 19 December 1975)*

The subject of crystallization of polyethylene at high pressures, commonly known as chain-extended crystallization, is reviewed. An historical approach is taken for the topics of molecular conformation, the relationship to chain-folded growth and the responsibility of the hexagonal phase. With the identification of this new phase and the demonstration that chain-extended growth is crystallization of hexagonal polyethylene, the basis of understanding is established. The field is then surveyed in this new context with discussion of high pressure annealing and molecular mechanisms involved, implications for the understanding of kinetically controlled growth in general and the use of chain-extended polyethylene as a model for crystal growth and mechanical behaviour.

INTRODUCTION

Recent work has brought the understanding of high-pressure crystallization of polyethylene, widely known as chain-extended crystallization, into the context of chain-folded polymers and suggests that this apparently esoteric subject may have important implications for polymeric crystallization in general.

THE PROBLEM

1964 saw the publication of two papers on the interior morphology of bulk polyethylene (PE) as revealed on fracture surfaces. Both showed lamellae fractured in planes containing the *c* axes, a consequence in linear polyethylene of having little or no molecular folding. In one¹, fractions of up to 12 000 molecular weight had been crystallized for up to ten days at 128°C *in vacuo* and formed lamellae approximately equal in thickness to their molecular lengths. The other² showed a similar appearance but of lamellae increased dramatically in thickness (the maximum observed being ~3 μm) to dimensions commensurate with typical molecular lengths. This sample had been crystallized from the melt around 5 kbar. The molecular conformation in the first case was seemingly one of full extension in what were thus denoted as 'extended-chain' lamellae in contrast to the thinner folded-chain crystals produced in similar circumstances with higher molecular weight polymer. This nomenclature seemed appropriate also to the high pressure case and it has become common usage to identify the product of high pressure crystallization as 'extended-chain polyethylene' although this now needs qualification and the alternative 'chain-extended' has been adopted in recent work. The problem presented by chain-extended polyethylene (CEPE) falls into three parts: to understand why the use of high pressures should so alter the morphology of PE crystallized from the melt, but not from solution nor for polymers in general, to describe what that morphology actually is and to explain how it comes about.

With a topic requiring specialized apparatus and, therefore, still limited to only a few laboratories, it was inevitable that the experimental background should be slow to

be established. Nevertheless possible explanations of the effect were soon forthcoming based on the facts as they then appeared to be. In the early papers^{3,4} it was assumed that PE had either crystallized as chain-folded or as 'extended-chain' lamellae i.e. that there were two alternative crystallization processes. Kawai⁵ suggested specifically that these involved folded and bundle-like nucleation respectively and went on to propose detailed explanations^{6,7} generalizing, as we now know incorrectly, from Anderson's atmospheric data¹ that shorter molecules more readily formed chain-extended lamellae at a given pressure. An alternative hypothesis advanced by Peterlin⁸ sought to explain the situation in terms of enhanced lamellar thickening whereby folded-chain crystals formed initially would, under appropriate conditions, undergo an 'avalanche-like long period growth' and transform into extended-chain crystals. The experimental evidence, which merely suggested that one morphological form was appearing at the expense of the other³, could not then decide between these two proposals. Indeed the basic issue of whether there were two independent processes operating at low and high pressures respectively or merely one, suitably modified, remained unresolved for ten years and a major difficulty in clarifying the situation.

Molecular Conformation

The evidence of the very first papers suggested that PE molecules could have become fully extended after high pressure crystallization. Samples crystallized at 5 kbar³ had densities up to 0.994 Mg/m³, maximum melting points of 140°C and were full of lamellae much thicker than any encountered previously, the spectrum of thicknesses extending to 3 μm, with an average value of 2500 Å². The *c* axis direction, identified by electron diffraction and optical birefringence, is parallel to a characteristic striation on fracture surfaces² and is sometimes along but more often moderately inclined to the lamellar normal in similar ways to the oblique structures encountered in chain-folded PE. For full extension, the lamellar thicknesses along *c* must agree with values expected from the molecular weight of the sample; in the case cited² this was $\bar{M}_n = 1.1 \times 10^4$ and $\bar{M}_w = 1.25 \times 10^5$ so that at least the lamellar dimensions were of the right order. However, doubt was expressed⁴ as

* Presented at the Polymer Physics Group (Institute of Physics) Biennial Conference, Shrivenham, September 1975.

to whether extension could be complete after crystallization at 5 kbar because a substantial increase in molecular weight (by comparing polymethylene with Marlex 6050) produced only a marginal increase in crystal thickness. A proper test of this point required a detailed comparison of the distribution of crystal thickness and molecular weight. The first of such was published by Wunderlich and Melillo⁹ followed by similar ones from Prime and Wunderlich¹⁰. From the statistics of fracture surfaces computed for a variety of chain-extended polyethylenes ranging from whole Marlex 50 through fractions of polydispersities from 3.5 to 5.3 to polymethylene it was inferred that the shortest molecules ($\leq 10^4$ in weight) did attain full extension in a separated population of crystals. The remaining molecules crystallized together producing lamellae which were thicker for longer crystallization times¹¹ and for increasing molecular weight, although a rise of 1000 in molecular length only produced a tenfold increase of crystal thickness. In this, the great majority of the material, at least the longest molecules had to be folded to some extent⁹⁻¹².

All the above samples had, however, been treated so as to try and maximize their molecular extension. When the effect of changing crystallization conditions was examined by Rees and Bassett¹³, using fractions of polydispersity 1.14 it was discovered that the lamellar thickness of CEPE increased not only with the molecular length and crystallization time but also, and most markedly, with crystallization temperature. For example, for a 5×10^4 MW fraction crystallized at 4.9 kbar for 30 min, average thicknesses over the attainable range of temperatures increased from 2000 to 3300 Å, whereas the average molecular length was close to 5000 Å. It followed that full molecular extension was the exception rather than the rule and that the conformations of all molecules in CEPE, not just the longest, were generally folded¹³.

All measurements on lamellar thickness at this time came from fracture surfaces, a method which is always under suspicion of bias. However, the data produced can now be seen to have been much more reliable than might have been feared. In fact the most evident bias actually improves the measurement because low-melting (chain-folded) lamellae are much under-recorded¹³ so that fracture surfaces tend to select the chain-extended component from the mixture of chain-folded and chain-extended crystals typically produced by crystallizing whole polymer at 5 kbar. Particular care was taken to establish the reliability of fracture surface measurements by guarding against errors due to chain axes being inclined to the fracture surfaces and by testing for statistical significance. It was found that the fracture surface method gave repeatable values for the same sample and that for example the increases found between samples crystallized at progressively higher temperatures were real¹³. Further confidence in the method came with excellent correlations found between fracture surface measurements and density, melting point and low-angle X-ray data measured on PE annealed at high pressure¹⁴. Most recently the introduction of the entirely different method of nitration followed by g.p.c. analysis which correlates well with fracture surface data over the entire range of molecular weights and pressure treatments¹⁵ shows clearly that statistics derived from fracture surfaces are a reliable means of measuring molecular extension in chain-extended crystals of linear PE. The fracture surface method is not available for chain-extended branched polyethylenes, however, as these generally fracture between lamellae and do not expose the relevant surfaces. For these, the nitration/g.p.c. method

is the only one so far available.

Qualitatively, the change in layer thicknesses of CEPE resembles those found for chain-folded crystallization *in vacuo*. Further examination showed that both conformed to the temperature dependence of kinetic theory formalism connecting lamellar thickness l to supercooling ΔT by the equation:

$$l = \frac{2\sigma_e}{\Delta s_f} \times \frac{1}{\Delta T} + \delta l$$

where σ_e is the fold surface free energy, Δs_f the entropy of fusion and δl is a small length. Indeed, data for CEPE and for chain-folded crystals of low molecular weight material (chosen to have a similar number of folds per molecule) have a common reduced plot of fractional change in crystal thickness against supercooling¹⁶. The implication is that lamellae in CEPE are essentially large-scale copies of chain-folded layers, a conclusion which is reinforced by the similar logarithmic time dependence of long period during annealing at both high and low pressures¹⁷. In view of the most recent developments, this conclusion seems a natural one, but at the same time it carries with it implications concerning the nature of melt growth in general.

Another recent finding is that full chain-extension does not seem to be the upper limit of layer thickness. Two pieces of evidence indicate that, given the right conditions, molecules will fit end-to-end inside one crystal in fully extended conformation. Hatakeyama, Kanetsuna and Hashimoto¹⁸ found that prolonged crystallization of 50 000 MW PE at 237°C and 4.8 kbar for 200 h gave lamellae up to 40 μm thick, with over 20% thicker than 10 μm , whereas only 1.2% of molecules were longer than 10 μm . In a similar way, detailed comparison of fracture surface data, molecular weight measurements and g.p.c. analysis after nitration¹⁵ indicates that the proportion of long molecules in ordinary CEPE samples is often quite insufficient to account for the comparatively large number of thick lamellae present. Having lamellae more than one molecule thick might be anticipated by current thinking on chain-extended growth, and could be expected to occur for prolonged crystallization at low supercoolings. It does, however, raise interesting questions as to how the observed wide variation of crystal thickness with molecular weight under given crystallization conditions comes about if lamellar thickness is not limited by molecular length.

Morphological investigations

From the outset, the morphology of CEPE has been carefully scanned looking for clues to its formation. Almost all studies have been confined to fracture surface replication, a technique which is particularly suited to these often brittle materials. In linear PE fracture is predominantly along prism faces but occasionally basal surfaces are also exposed; both are present in *Figure 1*. The prism faces possess a characteristic striation parallel to c ; this is confined to fracture surfaces and whereas there had been early speculation² that it represented a structural feature, detailed investigation concluded that it did not, but was created at the moment of fracture¹⁹.

Because of exposed side surfaces^{19,20} such striations begin to melt as low as 100°C at 1 bar. By 120°C, a pronounced 'ripple' develops very rapidly (<10 sec), as chain-folded lamellae form as oriented overgrowths on the underlying chain-extended polymer^{9,19}. The importance of this is that

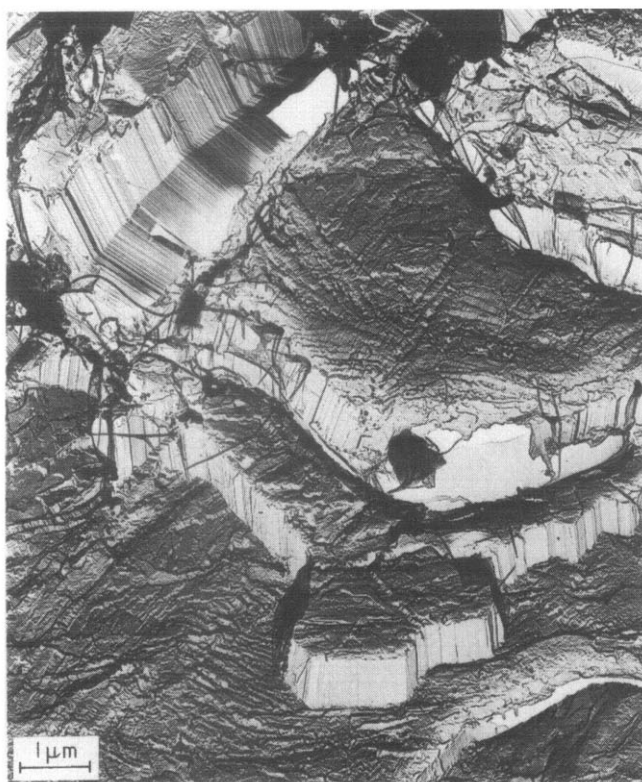


Figure 1 Thick lamellae characteristic of CEPE (D. C. Bassett and B. A. Khalifa, unpublished)

it shows that notwithstanding primary nucleation with highly-extended conformation, lamellar thickness is determined by secondary nucleation at the growing surface^{9,19,21,22}. This is in agreement with observations on solution growth²³ and of the foundations of kinetic theory. Moreover, even with careful annealing at 1 bar such lamellae cannot be thickened to the dimensions of the underlying substrate⁹. This fact, too, is readily understood in terms of recent work.

Replicas of CEPE and the morphologically similar PTFE^{24,25} often reveal a number of threads pulled from the surface. These appear to be produced when specimens are stripped from the backing film during two-stage replication; stripping at a suitably low temperature where the polymer is entirely brittle avoids the phenomenon. The extent of the drawing is intimately related to the degree of folding in a sample, thus in whole polymer threads are pulled preferentially from the thinnest lamellae¹¹; using sharp fractions their number increases for lower crystallization temperatures¹³ (which give thinner lamellae) and the effect can be so pronounced for high molecular weight that it can obscure practically all surface detail.

The most interesting result of morphological studies is, however, that they clearly show lamellae increasing their thicknesses with time. The same lamella is found to become thicker in positions further away from its primary nucleus or branch point⁹. Above all, where they impinge, one on another, the thickest lamellae always show a tapered profile, within which lamellar thickness decreases from perhaps 1 μm or even less^{9,13}. From this and other evidence, Wunderlich^{9,26} concluded that lamellae in CEPE grow by adding molecules to their edges at dimensions of ~1000 Å, i.e. in folded conformation after which there is thickening towards the thermodynamically most stable extended-chain

conformation. Wunderlich and coworkers saw no principle difference between atmospheric and high pressure crystallization but considered that whereas chain-extension is kinetically hindered at 1 bar it is very much enhanced at high pressures. This was thought to be partly due to the pressure but even more to the high temperatures involved. In both cases the driving force for extension was the reduction, as chain-extension increased, of the number of folds introduced by secondary nucleation at the growth face. Wunderlich has also proposed that such a mechanism is responsible for the formation of a class of extended-chain crystals within which he includes PTFE, PCTFE and selenium²⁷. The existence of such a class grown by a distinct mechanism has, however, been disputed²⁵ and does not seem required by recent work.

Faced with rather similar evidence, Rees and Bassett¹³ deduced that the tapered profiles of thick chain-extended lamellae were not due to special circumstances but indicated that in general molecular extension and lamellar thickness increased rapidly behind the growth front. They also had direct evidence from fracture surface statistics of increasing average lamellar thicknesses with time over the longer term and the very marked effect of crystallization temperature. They, therefore, stressed the analogy with chain-folded crystallization at 1 bar, left open the implications of growth proceeding behind a narrowed edge and concluded by remarking that the relationship of lamellar thickening to crystallization and the attainment of high chain extension under pressure are probably different aspects of the same problem. This still appears to be true, the relevant problem being kinetically controlled (i.e. chain-folded) growth from the melt.

The evidence of tapered tips was discounted by Calvert and Uhlmann²⁸, who pointed out correctly that crystals of many kinds grow in this fashion. There are, however, additional implications from molecular connectedness if this shape resembles the profile of a growing edge. In the event, direct observation of the growth of thick chain-extended lamellae has confirmed that they do indeed grow behind a narrowed edge²⁹. These authors also proposed an alternative theory of chain-extended growth²⁸ whereby growth at 5 kbar was similar to that at 1 bar but gives thicker crystals because of a large fold surface free energy, the value of this parameter increasing considerably with pressure. Unfortunately a central part of their argument involved combining two sets of data from the literature which have not been reproduced in subsequent work. Moreover, their basic premise of a continuous change of behaviour from 1 bar to 5 kbar turned out to be incorrect.

The sum of all the work so far described and carried out on CEPE after return to atmospheric pressure was to leave the situation still confused and with no consensus as to what essentially was going on. Although it had been shown that full chain-extension was not the general rule, the question of whether chain-extended growth was independent of or an extrapolation of chain-folded growth was not answered; one did not then know why solution growth did not reproduce the high thicknesses found in the melt³⁰, and explanations of the large increase in thickness of CEPE were still rather speculative. Furthermore, high pressure annealing experiments carried out contemporarily³¹⁻³³ had added to the problems by showing that this was also a means of producing CEPE. In these circumstances increased attention began to be paid to the monitoring of high pressure crystallization of PE *in situ*; it was from these experiments that the essential new information came.

HIGH PRESSURE MEASUREMENTS

Early measurements in which the melting and recrystallization of PE under high pressure were monitored by dilatometric or d.t.a. means were those of Matsuoka³⁴ (to 4 kbar), Osugi³⁵ (to 30 kbar), Baltenas and Igonin³⁶ (to 3 kbar) and Baer and Kardos³⁷ (to 3 kbar). Though not entirely consistent one with another, all the papers showed an apparently unchanging pattern of behaviour from atmospheric conditions into the pressure region where CEPE formed. Above all, Davidson and Wunderlich³⁸ had made high pressure d.t.a. observations to 4.2 kbar, (compared to 2.8 kbar for the first formation of CEPE) without finding any new feature to associate with chain-extended growth.

CEPE had even been watched growing directly in a high-pressure diamond-anvil optical cell by Jackson, Hsu and Brasch³⁹. They observed the formation of what is a characteristic appearance of CEPE by the growth of what they interpreted as rod-like crystals but which are really oriented lamellae viewed edge-on of the same dimensions as lamellae measured in CEPE by Rees and Bassett¹³. Although the pattern of growth was quite different from normal spherulitic growth, no specific indication of its cause or difference from atmospheric behaviour was noted.

The prospects of *in situ* high pressure measurements revealing anything very new about chain-extended growth thus seemed remote but the continuing need to clarify the relationship between chain-folded and chain-extended growth prompted a second look at what Wunderlich and Arakawa³ called the intermediate pressure region, where the high melting points and thick lamellae had begun to appear.

Once it was appreciated that full molecular extension was not a characteristic of CEPE, the meaning of the term had to be redefined. Wunderlich had done this empirically by choosing 2000 Å as the minimum thickness of a chain-extended layer⁴⁰. This is a conformational definition such that basic properties approach sufficiently closely to their ultimate values, e.g. the melting point depression is $< \sim 1\text{K}$. Though this might correspond to a suitable minimum level of thickening in a monotonic approach to infinity, in practice there is a natural pattern of behaviour for which this description is quite unsuitable.

It was shown by Wunderlich and Arakawa³ that PE crystallized between 2.8 and 3.8 kbar at a supercooling of 10K showed two atmospheric melting peaks, the lower apparently continuous with the single peak observed at lower pressures and the higher with the main peak at higher pressures, although the maximum melting points are almost continuous through the pressure range. This behaviour is, *prima facie*, compatible with either a change-over to a different crystallization mechanism or with an 'avalanche-like long period growth'⁸ as is familiar from annealing studies on solution-grown lamellae at 1 bar⁴¹. It is, however, natural to associate the higher melting peak with chain-extended layers and the lower one with chain-folded as was done in early papers⁴. The distinction was carried further when it was noted that for each PE studied there were two non-overlapping ranges of melting point for crystals grown at moderate supercoolings, though these varied with molecular weight so much that there was no one melting point, nor, correspondingly, one crystal thickness, which could always be said to divide off chain-folded from CEPE. Nevertheless, Bassett, Khalifa and Turner⁴² showed that material in the two melting peaks could always be distinguished by their characteristic textures as seen in the polarizing microscope. The lower peak or chain-folded material,

was clearly spherulitic, with rounded or polygonal outlines and sometimes banding, whereas chain-extended material of the higher melting peak had a coarse spikey sheaf-like appearance previously noted at 5 kbar⁹ which while possibly due to embryonic spherulites would nowadays be regarded as similar to the morphology produced by regime 1 crystallization at low supercoolings⁴³. This gave a working distinction between chain-folded and chain-extended material produced by recrystallization at high pressures. It played a significant role in the subsequent advance in the subject but has now been superseded by a fundamental definition following recent work. One of the consequences of using it, however, was a realization that the language chain-extended/chain-folded is not well suited to the description of what actually occurs with high pressure crystallization. For example, with decreasing molecular weight, lamellar thicknesses associated with the chain-extended melting peak drop, and average values as low as 800 Å have been recorded for a 20 000 MW fraction⁴⁴, considerably less than values recorded for chain-folded lamellae of similar molecular weight polymer in other circumstances¹. The absurdity of the terminology has increased following studies of crystallization in thin films showing that lamellae as thin as 100–200 Å should also be regarded as chain-extended^{45,46}. The underlying reason for this is now clear, but the scientific case for a change in nomenclature is extremely strong notwithstanding the current widespread usage.

The first consequence of using this new definition was the demonstration that it is easier for longer molecules to become chain-extended than for shorter ones⁴⁴. This somewhat paradoxical conclusion shows that it is not possible to generalize Anderson's observations at ambient pressure¹ to high pressure behaviour, thus negating theories proposed by Kawai^{6,7}. The relevant observations were that the change-over from chain-folded to chain-extended behaviour for sharp fractions occurs over a narrow temperature range (5K) at a suitable constant pressure and at lower pressures for longer molecules.

The second conclusion was that chain-folded and chain-extended growth are independent processes. The different textures of chain-folded and CEPE had already cast doubts on a thickening hypothesis because it had also been shown that thickening lamellae ten-fold to over 2000 Å on average by high pressure annealing left the gross physical texture unaltered³¹. The conclusion was established, however, following high pressure d.t.a. observations. These showed that at a cooling rate of $\sim 1\text{K}/\text{min}$, crystallization of a 50 000 MW fraction occurred at characteristic supercoolings of $\sim 16\text{K}$ for chain-folded crystallization and $\sim 12\text{K}$ for chain-extended⁴⁷. In the region where both morphologies resulted, two d.t.a. peaks were detected having the characteristic super-coolings and widths measured on either side of this region⁴⁴. There was thus no evidence for a modification of either process when they overlapped, but an indication that both were occurring independently. Finally it was shown that under particular isothermal, isobaric conditions chain-extended polymer formed before chain-folded material⁴⁴. The conclusion is, therefore, that chain-extended material could not in this case have formed by a reorganization of chain-folded material but must have formed independently. This has since been verified by direct optical observation of high pressure crystallization²⁹.

Support for the independence of chain-folded and chain-extended growth also came from the studies of Kanetsuna and coworkers⁴⁸. They, too, observed the sharp change from a chain-folded to a chain-extended product with a

change of a few degrees in the temperature of isothermal crystallization at a fixed pressure of 3 kbar and decided that this was most likely to be a consequence of a different growth mechanism, possibly involving a bundle-like nucleus. Subsequently Maeda and Kanetsuna⁴⁹ reported volumetric data showing the same phenomenon observed with high pressure d.t.a., namely that when crystallization during cooling gave a mixed product, the chain-extended component formed first, at a higher temperature, before the onset of chain-folded growth. Accordingly they supported the conclusion of the Reading group that there were two growth processes involved.

At this stage the subject was in a curious state. The discontinuity in behaviour ruled out the hypotheses of Peterlin⁸, of Calvert and Uhlmann²⁸ and of Wunderlich²⁶ (at least in the form in which it has so far been expressed). The facts showed that there were two independent crystallization processes each producing lamellae containing folded molecules with only a difference of scale between them. The nature of these two processes was, for a while, still obscure but was soon suggested following further *in situ* high pressure measurements.

New phenomena at high pressures

The first reports of a change in the customary pattern of crystallization behaviour came in 1972. Bassett and Turner⁵⁰ reported that at 4.10 kbar and higher pressures an additional high temperature endothermic d.t.a. peak appeared during melting of PE. The change was reversible and a corresponding exothermic peak was detected at 4.3 kbar and higher pressures. The same high pressure d.t.a. phenomena were also reported by Yasuniwa, Nakafuku and Takemura⁵¹ during melting at 4.0 kbar and above and during crystallization at 6.0 kbar. These authors simply referred to the peaks as due to the melting and crystallization of an unknown structure. Bassett and Turner⁵⁰, however, also reported corresponding dilatometric changes and concluded from criteria of reversibility, stability and accord with the Clausius–Clapeyron equation that the changes were first-order transitions into and out of a new high pressure phase intermediate in properties between orthorhombic solid and melt. A phase diagram was published based on melting data for thick crystals and an ‘excellent correlation’ claimed between the formation of chain-extended polymer and the occurrence of the new exotherm during crystallization. It was proposed, in consequence, that crystallization of orthorhombic PE from the melt gave the customary chain-folded polymer while chain-extended polymer resulted, strictly when the sequence melt → intermediate phase → orthorhombic occurred, but was likely simply to be crystallization of the new phase, inferred to be either liquid crystalline or solid, from the melt. This hypothesis explained the main features of chain-extended growth in a straightforward manner, notably the specificity of the phenomenon to melt crystallization of PE, and its absence in dilute solution or for polymers in general and the relationship with chain-folded growth. In particular a substantial increase of thickness would be expected for the chain-extended polymer according to kinetic theories of crystallization because the entropy of fusion of the intermediate phase is reduced below that of the orthorhombic phase by a factor of approximately four.

These two sets of authors were then joined by Maeda and Kanetsuna who reported extensive dilatometric data^{49,52}. While the actual results of the three groups are in good

agreement, the respective interpretations were quite different.

Maeda and Kanetsuna at first doubted⁴⁹, then rejected⁵², the interpretation in terms of a new phase. Partly this was because of their experience of the effect of thermal history of a sample in the moderate pressure region where chain-folded growth gives way to chain-extended and where widespread and delicate fractionation causes great complication. Most of all, though, these authors considered that the additional d.t.a. peak and related volume change concerned not the whole sample as Bassett and Turner believed, but only a part. This part they termed highly-extended-chain crystals in contrast to ordinary extended-chain crystals. These were thought to be present above 4.7 kbar when the additional peaks were well-resolved and were taken to be composed of the crystals ~2 μm thick which are the dominant cause of the characteristic texture of chain-extended polyethylene in the polarizing microscope. They believed that such crystals resulted from reorganization of ordinary extended-chain crystals in a similar way to the reorganization of folded-chain into extended-chain polymer known to occur under high pressure annealing³¹ and confirmed by their own data. This reorganization would not necessarily be detected as a peak in either d.t.a. or volumetric measurements in the same way that a secondary d.s.c. peak is often not recorded during melting of polymer crystals at 1 bar even though reorganization and crystal thickening undoubtedly occur⁴¹. Finally in support of their arguments, Maeda and Kanetsuna reported a distinct population of crystal lengths of order 2 μm, representing about 10% of a sample, when crystal thicknesses are measured by the nitric acid/g.p.c. method. It should be noted, however, that the corresponding peak is not present in the raw g.p.c. data, but only appears after correction to allow for instrumental broadening⁵³.

The interpretation of Yasuniwa, Nakafuku and Takemura⁵¹ is in many ways similar to that of Maeda and Kanetsuna. They also found that on slow cooling at ~3 kbar chain-extended crystals formed before chain-folded and were able to identify the two processes by direct observation with the diamond-anvil optical cell. Moreover, they too, showed that folded-chain crystals can reorganize into extended-chain crystals during the melting of initially chain-folded PE and a continuation of this process is apparently the model for formation of their unknown structure which is said to form later in the sequence by recrystallization after melting of extended-chain crystals. Conversely, during slow cooling at 6 kbar, the two high pressure d.t.a. peaks are said to be of ‘an unknown structure and an extended-chain crystal’. This interpretation also considers the additional d.t.a. peak as relating to only part of a sample as is confirmed firstly, by the listing of separate melting (and crystallization) temperatures for both extended-chain crystals and the unknown structure, secondly, by the (unsuccessful) attempt to isolate the appropriate morphology by pressure quenching a sample from the crystallization temperature of the unknown structure and, thirdly, by the (allegedly successful) demonstration of extended-chain crystals growing directly at their ‘crystallization temperature’. Evidently the unknown structure is taken to be additional to the extended-chain crystals and is only considered to occur above 4 kbar where the additional d.t.a. peaks are observed. The nature of the unknown structure was left open with the statement that ‘it may be a nematic liquid crystal phase — but we have no proof’.

Both the Japanese interpretations are inconsistent with the previously published proposals of Bassett and Turner

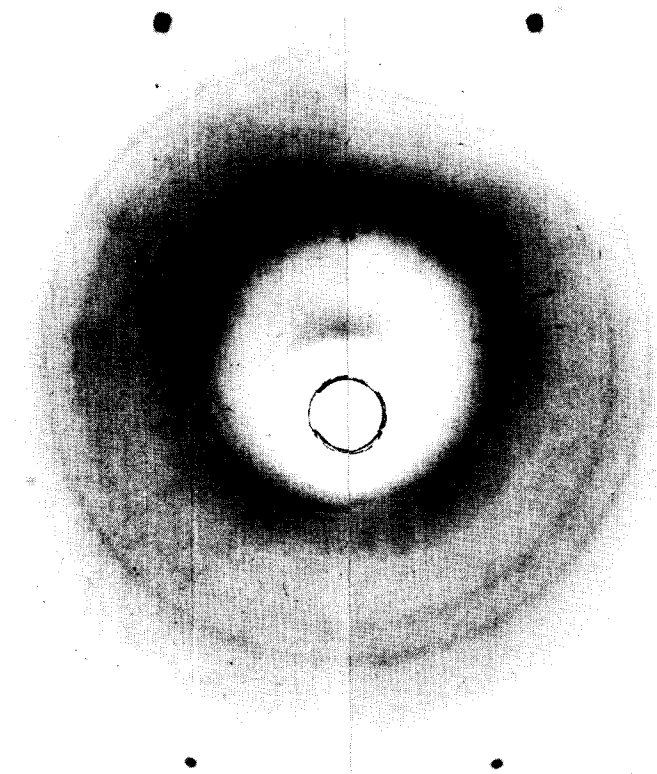


Figure 2 X-ray patterns of PE recorded at high pressure and temperature²⁹ showing, on the left, the 110 and 200 orthorhombic rings, and on the right, the single 100 hexagonal ring to which they give way before the polymer melts

based on experiments reported in detail in a full paper⁴⁷. The two major differences are that these authors considered the additional d.t.a. peaks as due to the whole and not merely a part of a sample (neglecting the segregation of the lowest molecular weights) and claimed that even though the extra peak on crystallization could not be resolved below 4 kbar it was still present and necessarily involved in the formation of chain-extended polymer to below 3 kbar where crystallization switched to the chain-folded mode. Regarding the first point, Bassett and Turner had the advantage of working with fractionated polymer (polydispersity 1.14) but despite thorough searching could find no inhomogeneity at atmospheric pressure to correspond to the extra d.t.a. peak at 5 kbar. They thus were forced to conclude that the two high pressure peaks were sequential processes involving the entire sample and did not involve different components within it. Fundamental to their case, also, was the correlation between the formation of CEPE (defined by optical texture and d.s.c. melting point)^{42,44} with the two d.t.a. peaks on cooling. This came from a study of the supercoolings of the beginnings and the maxima of all d.t.a. crystallization peaks as a function of pressure. It was shown that the two separate peaks observed at 5 kbar draw closer together before merging at about 4 kbar into a single peak (assumed to be the unresolved sum of the previous two) which at first was suitably wider, then extrapolated smoothly back to the onset of chain-extended growth when a discontinuous change to the conditions for chain-folded growth occurred⁴⁷.

The situation in which three groups of authors interpreted essentially the same facts in three different ways was resolved by the discovery of the high pressure intermediate phase postulated by Bassett and Turner⁵⁰. This was achieved by Bassett, Block and Piermarini²⁹ using the gasketed

diamond-anvil cell, a device similar to that used in previous optical studies of high pressure crystallization³⁹. The 110 and 200 lines of orthorhombic polyethylene were observed to give way to a single spacing of 4.23 Å before melting at ~6 kbar (Figure 2). Although only one line was recorded this, nevertheless, compares favourably with an earlier view that it is 'not possible to observe the X-ray pattern of a polymer sample with this system'⁵⁴. The new phase was identified as hexagonal and having the prescribed properties i.e. that there was a discontinuous change from orthorhombic to hexagonal then from hexagonal to melt, and that the average chain axis direction c was preserved in the orthorhombic to hexagonal transition. Moreover, a direct correlation was established of the hexagonal X-ray pattern with the optical appearance of chain-extended polymer under the same conditions. The formation of chain-folded polymer correlated similarly with the orthorhombic X-ray pattern. The proposals of Bassett and Turner^{47,50}, were thus confirmed in their essentials. It is the hexagonal phase which causes the changed pattern of behaviour when PE crystallizes from the melt at high pressures. Crystallization of orthorhombic PE from the melt is what has been termed chain-folded growth whereas crystallization of hexagonal PE (followed by a transition to the orthorhombic structure during reduction of pressure and/or temperature) is chain-extended growth.

Hexagonal polyethylene

Although only one X-ray reflection of the new phase was detected²⁹, this was shown to be of $hk0$ type in a uniaxial structure. Knowledge of the volume change during the transition⁴⁷ then eliminated the possibility of a tetragonal structure with a hexagonal/trigonal structure as the only alternative. Since then further confirmation has come from finding the anticipated threefold twinning resulting after an orthorhombic \rightarrow hexagonal \rightarrow orthorhombic sequence of transitions⁵⁵.

There is the well-known precedent of the n -paraffins in which a hexagonal structure also intervenes between the orthorhombic form and the melt. However, whereas the hexagonal form of the paraffins is a well-ordered solid, closer in properties to the orthorhombic phase than to the melt⁵⁶, this does not seem to be the case for PE. The single sharp X-ray line, while incompatible with a nematic liquid crystalline structure merely defines a close-packing of rods. The spacing of these rods is significantly wider for PE (the relevant X-ray spacing is 4.23 Å compared to 4.11 Å for n -C₂₄H₅₀) yet the respective increases in specific volume over the orthorhombic phase are not so different. The value for PE according to Bassett and Turner⁴⁷ is 0.085 cm³/g (more recent values of Maeda and Kanetsuna⁵² suggest a slightly lower figure which, however, probably needs revising upwards because of the presence of a chain-folded component in the samples). This is an increase of only 8.5%, whereas the increase in cross-sectional area per chain is from 18.2 to 20.6 Å², i.e. 13%. It was suggested, therefore, that the average c axis spacing per ethylene unit had to decrease from the presumed 2.53 of an all *trans* configuration to 2.45 Å and shown that this was most unlikely to occur by the adoption of a uniform helix. Hexagonal PE thus seems to have lost the all *trans* configuration and to include a proportion of *gauche* bonds along the chain, so that it is probably not a fully-ordered solid. It is certainly much closer to the melt in its specific volume and enthalpy than to the orthorhombic form as is commonly found in

liquid crystals but is not the case for the hexagonal form of the n-paraffins. This is intuitively reasonable because its formation is favoured by increasing pressure⁵⁰ whereas the hexagonal forms of paraffins are not stable above a few kbar⁵⁶.

High pressure annealing

The effects produced by annealing PE at high pressures are intimately related to the crystallization phenomena, although their role in the development of the subject has been mostly to raise questions rather than to provide many of the answers. Thus the discovery by Rees and Bassett^{31,32} that chain-folded PE in various forms: single crystal mats, drawn fibres, spherulitic films, could be converted into chain-extended, with maintained molecular orientation and gross texture but gradually increasing lamellar thicknesses, by high pressure annealing appeared, at the time, to support the proposal that enhanced lamellar thickening was responsible for the formation of CEPE. It certainly showed that a range of conformations could be produced and not merely that of full molecular extension. These results have now been confirmed by many groups^{14,49,51,58,59} but further work showed that although there is some increase in thickening rate (i.e. the gradient of a plot of crystal thickness against log time) at 5 kbar compared to 1 bar, this was insufficient to account for the large thicknesses of CEPE which were already established at short times¹⁷. They did, however, prompt work looking for the time (and temperature) dependence of lamellar thickness during high pressure crystallization which brought out the similarity in pattern with chain-folded crystallization¹³.

Early criticism of this work was misguided, as is now quite evident. Fischer and Puderbach⁶⁰ were unable to reproduce the high extensions reported by Rees and Bassett, but this was simply because they had not annealed to sufficiently high temperatures and the polymer had not entered the hexagonal phase. Gruner, Wunderlich and Bopp³³, on the other hand, did find the high extensions, but mistook the orthorhombic-hexagonal transition for a change in molecular mechanism from solid-state thickening to 'partial melting' and recrystallization. They also considered, wrongly and without testing the point, that molecular orientation would not be maintained beyond this transition. The first discussion of high pressure annealing in terms of the hexagonal phase was that of Bassett and Carder¹⁴ on drawn sheets, but the behaviour of other samples is essentially the same and the case of spherulitic PE has also recently been placed in this context⁵⁹.

Annealing in the hexagonal phase produces high thicknesses in bulk polymer; these then increase gradually with temperature and time until the final melting of the hexagonal phase which results in a substantial further increase typically from ~2000 Å average to ~4000 Å, achieved mainly by the appearance of very thick lamellae^{14,59}. Annealing which is confined to the orthorhombic phase tends to reproduce phenomena found at 1 bar. Thus X-ray long period gives approximately a common reduction in terms of supercooling for 5 kbar and 1 bar⁶⁰⁻⁶², while the morphology of solution-grown lamellae annealed at high pressures^{61,63} shows features already familiar from atmospheric experiments²³.

It is a strong argument in favour of regarding the effects of annealing as due to a sequence of melting then recrystallizing (at a higher and more stable thickness) part of a sample, perhaps only a few fold stems in the early stages, that

annealing in the hexagonal phase should also give layer thicknesses approaching but lower than those produced by crystallization into this phase, thereby reproducing a pattern familiar in many polymers⁶⁴. Even though the more open structure of the hexagonal phase will tend to assist postulated molecular mechanisms such as solid-state thickening, the rate of thickening actually measured is not large enough to account for the high thicknesses produced¹⁷. The interpretation in terms of local melting followed by recrystallization has been strongly canvassed in several recent papers from Reading^{14,45,55,59}, although in earlier research Rees and Bassett¹³ were not then able to support this point of view because of the known effect of sample prehistory on annealed specimens^{13,65}, a factor which should not have influenced melting/recrystallization according to facts then known. Soon afterwards, however, it was reported that the thicknesses produced in chain-extended samples decreased with sample size. Recent papers show that crystallization of hexagonal PE from the melt and annealing of hexagonal PE can both give lamellae only 100 Å or so thick in the thinnest films whereas bulk specimens treated alongside acquire lamellar thicknesses one to two orders greater^{46,55}.

This phenomenon removes, in principle, the objection based on sample prehistory by allowing local melting of a smaller part of a sample to produce a lower lamellar thickness on recrystallization⁴⁵. A side-effect of work on CEPE has thus been to provide what appears to be a consistent explanation of this second long standing problem in polymer crystallization.

CURRENT STATUS

Pattern of crystallization

The current status of research on CEPE is that the hypothesis of Bassett and Turner^{50,47} allows a simple understanding of the main features within the framework of ideas developed for chain-folding, but that many of the detailed points need thorough testing. At the same time the generalization of behaviour found in CEPE to chain-folded growth as a whole sheds interesting light on some old problems.

Because the hexagonal phase is specific to molten polyethylene, one has a simple answer to the mystery of why crystallization under pressure does not greatly affect the behaviour of other polymers nor indeed the growth of polyethylene from solution^{30,61,66}. Even when new phases do appear with pressure as e.g. in *cis*-polyisoprene⁶⁷ one would not expect these to produce pronounced increases in lamellar thickness unless, as for hexagonal PE, the new phase has a correspondingly reduced entropy of fusion, i.e. it is closer to the melt in properties than to the normal solid.

The independence of chain-folded and chain-extended growth is inherent in this scheme, but the manner in which one gives way to the other is of particular interest. At 5 kbar the expected behaviour is for CEPE to form at low supercoolings and for chain-folded growth to set in at higher supercoolings corresponding to the pattern of the phase diagram. This is observed in practice^{13,48,68}, although crystallization of the hexagonal phase frequently occurs at sufficiently high supercoolings to make it metastable⁴⁷. In a similar way, CEPE is still formed isothermally at temperatures and pressures a little below the estimated orthorhombic/hexagonal/melt triple point^{44,47}. It can also be formed by rapid application of pressure beginning at temperatures

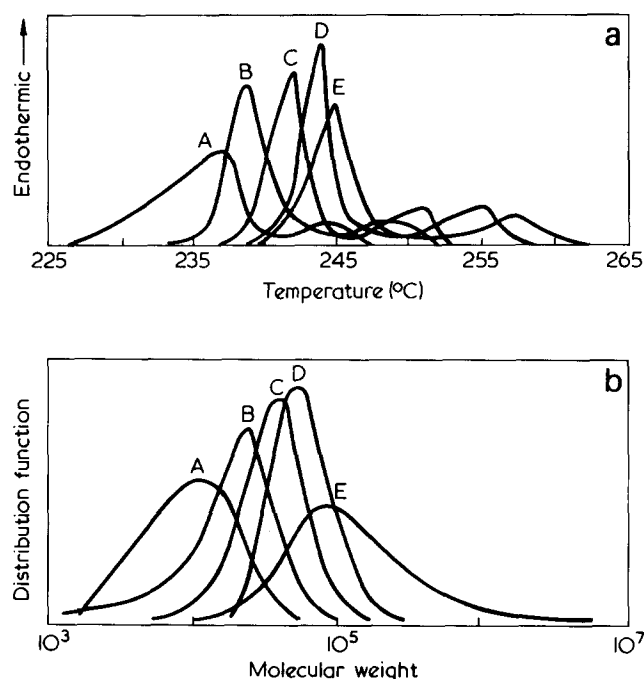


Figure 3 (a) High pressure d.t.a. traces of PE fractions having the molecular weight distributions shown in (b). All samples had previously been crystallized into the hexagonal phase at 4.9 kbar. (R. B. Morris and D. C. Bassett, unpublished)

as low as 170°C for high molecular weight polymer³, but this is merely a consequence of temperature rising during the pressure quenching to conditions close to those where isothermal crystallization occurs⁶⁹. Such temperature rises can be substantial (8K/kbar has been estimated for molten PE in the range 1–4 kbar⁶⁹) and as pressure crystallization has mostly been carried out by the rapid imposition of pressure at a given temperature it is probable that in at least some of the experiments in the literature, crystallization actually occurred at higher temperatures than those reported.

The change from chain-folded to chain-extended growth is very dependent on molecular weight^{42,44,48}. In part this is a consequence of kinetics, but it also reflects the sensitivity of the triple point, the orthorhombic–hexagonal transition and the melting point to this parameter⁴⁷. Unpublished estimates from this laboratory place the extrapolated triple point as low as 2.7 kbar for very high molecular weight linear polyethylene whereas it is above 5 kbar for molecular weights of a few thousand. Figure 3a taken from unpublished work by Morris and Bassett shows that the orthorhombic to hexagonal transition temperature increases at 5.35 kbar from 237° to 245°C and the hexagonal melting point from 245° to 258°C, all samples having previously been crystallized by slow cooling at 4.9 kbar, with average molecular weight rising from 10⁴ to 10⁵. (The effect of increasing the branch content is qualitatively the same as lowering the molecular weight of linear polymer). Inevitably, therefore, fractionation is widespread during high pressure crystallization^{2,4,13}. At 5 kbar, obvious fractionation can be avoided by removing molecules below 10⁴ molecular weight^{70,71,14}, although the impression gained by direct observation of crystallization is that fractionation on a fine-scale still persists with a change in habit and branching frequency with molecular weight; this is in accord with the facts cited above and observations on the

progress of melting through a sample⁷¹. Near the triple point, however, even tolerably good fractions (polydispersity 1.14) undergo internal fractionation⁴⁷ and mixed samples of disparate molecular lengths separate out⁷² because the higher crystallizes into the hexagonal phase and the lower into the orthorhombic. In addition there are time effects, altogether making for a complicated situation whose details remain to be elucidated.

Segregation of lower molecular weight material is responsible for separate low melting peaks of thinner crystals which appear not only in recrystallized PE but also in specimens annealed at high pressures^{14,33,70,71}. The number of such peaks and their explanation vary. There is always at least one clearly attributable to direct crystallization into the orthorhombic phase i.e. chain-folded polymer. The triclinic structure has also been detected⁷³. In addition there is often a peak of intermediate melting point, rising in certain circumstances to ~140°C at 1 bar^{14,33,71}, whose origin was once claimed to be the onset of molecular motion at 1 bar⁴ similar to that of the orthorhombic–hexagonal transition in n-paraffins. Alternatively it was suggested that it referred to PE of intermediate molecular weight in either folded-chain or fully-extended conformation^{33,71}. Most recently it has been proposed⁵⁹ that this is material which is unable to crystallize into the hexagonal phase at the treatment temperature but does so on cooling, thereby being differentiated from the shortest molecules which are incapable of forming the hexagonal phase at the pressure used. Here, too, the details need clarification although they are not likely to affect the broad understanding of chain-extended growth.

Lamellar thickness

Knowing of the existence of the hexagonal phase, it is a natural assumption that the differences between chain-extended and chain-folded growth reflect the properties of the two phases rather than a change in the crystallization process itself, i.e. that chain-extended growth is just kinetically controlled ('chain-folded') growth of the hexagonal phase. There is support for this view in the dependence of lamellar thickness on supercooling¹⁶ and the entropy of fusion^{50,47}, in the similar ratio of σ_{eff} needed to fit the kinetic theory formalism to σ_e , the surface free energy derived from melting points²⁵ and in the similarity to PTFE²⁵. On this basis the lamellar thicknesses produced by chain-extended growth should be higher than those of chain-folded polymer because of the lower entropy of fusion. At pressures ~3 kbar where both forms of PE can be produced at the same temperature, the ratio of lamellar thicknesses of chain-folded and CEPE is about 4⁴⁴, a value consistent with the relative entropies of fusion estimated when they can be resolved i.e. at 5 kbar⁴⁷. This behaviour is that expected from kinetic theory, but for CEPE crystallized at higher pressures (at constant supercooling) there is a large increase of crystal thickness with pressure of ~750 Å/kbar for 50 000 molecular weight polymer⁴⁴. The variation of thickness of chain-folded crystals with pressure has hardly been studied either experimentally or theoretically. A modest increase has been found⁷⁴ for chain-folded PE (~50 Å/kbar) of a magnitude anticipated from the increase with pressure associated with the density deficit of chain-folds in the surface free energy¹³ and little change observed for *cis*-polyisoprene⁷⁵. It is possible, however, that a substantial increase of lamellar thickness might be anticipated on existing theories of chain-folding from the melt.

In his early formulation, Hoffman⁷⁶ found the observed thickness of a melt-grown lamella to be:

$$l = \gamma \left[\frac{2\sigma_e}{\Delta h_f} \times \frac{T_m^0}{\Delta T} + \delta l \right]$$

where $\delta l = kT/b\sigma$, γ expresses the effect of isothermal thickening, b is the lattice translation and the remaining symbols have their previous meaning. Later, Lauritzen and Passaglia⁷⁷ obtained a similar expression:

$$l = \frac{2\sigma_{\text{eff}}}{\Delta h_f} \times \frac{T_m^0}{\Delta T} + \delta l(T)$$

which removes γ , replaces σ_e by σ_{eff} which is a function of temperature and δl by $\delta l(T)$. The latter expression was used by Bassett and Davitt²⁵, with the assumption that $\delta l(T)$ was small, to show that the ratio $\sigma_{\text{eff}}/\sigma_e \approx \gamma$ was approximately the same (~ 2.5) for PTFE, for chain-folded PE and for CEPE in making a case for a common crystallization process. Concerning the increase of lamellar thickness with pressure, Hoffman (personal communication) has pointed out that, in addition to the large increase in l due to the small enthalpy of fusion of the hexagonal phase, δl in the first expression should also increase for CEPE firstly because σ , the lateral surface free energy, is expected to be proportional to Δh_f , the enthalpy of fusion, and so will be proportionately lowered for the hexagonal phase. There should, moreover, be a second and even greater effect because σ is liable to decrease with pressure, in a parallel way to its decrease with falling temperature, as the hexagonal phase and melt become closer in properties. In addition, the theory of lamellar thickening relating to the factor γ predicts⁷⁶ a logarithmic increase with time of a magnitude inversely proportional to σ^2 , so that the initial rate of thickening might become quite large, conceivably accounting for a projectile shaped profile for the growth front as has been observed.

Experimental facts against which to judge any such proposals are still meagre but it has been shown that lamellar thickness increases approximately with inverse supercooling at a given pressure¹⁶, with pressure at a fixed supercooling⁴⁴, with molecular weight (between 2×10^4 and 5×10^4) at a fixed temperature^{4,10,13,44} and pressure and, most markedly of all, with specimen size below $\sim 100 \mu\text{m}$ ^{45,46}. This last parameter can depress lamellar thicknesses by more than an order of magnitude and yet, for lamellae away from a free surface, would not be expected to have much influence in the thickness of a simple molecular strip adding to a crystal in the model envisaged by kinetic theories, but would have a significant role in any subsequent lamellar thickening⁴⁵. It is noteworthy that, in comparison, the factor γ is only ~ 2.5 ²⁵. Secondly, in terms of the rationalization of γ in terms of lamellar thickening, all data have been measured away from the growing edge of lamellae and may well, therefore, not be related to the tapered profiles now observed. It should also be pointed out that these profiles and the effect of specimen size have led to questioning of the basis of kinetic theories^{25,46}. To clarify all these points there is an urgent need for further data which hopefully may be forthcoming from direct observation of chain-extended crystallization in the diamond-anvil cell.

Kinetics

The kinetics of chain-extended growth have been little studied until recently and should be capable of adding sig-

nificantly to our understanding of its nature. Although Davidson and Wunderlich³⁸ reported that both crystallization and melting rates are retarded under elevated pressure, other workers have found the opposite. Thus Kyotani and Kanetsuna⁷⁹ found an increase of crystallization rate with pressure throughout the range from 0 to 5 kbar. In this and other work from this group⁸⁰, dilatometric data obtained for varying molecular weights, pressures and temperatures were analysed in terms of the Avrami equation. Whereas at lower pressures the Avrami exponent was ~ 2 , there was an abrupt change at pressures where CEPE occurred. Data at these higher pressures were interpreted in terms of a single process, whereas we now know that two are involved.

The high pressure d.t.a. data of Bassett and Turner⁴⁷ also show an increasing rate of crystallization with pressure from 1 to 5 kbar. They show, in addition, that this is true of the crystallization of the hexagonal phase just as for the orthorhombic, but that the rate of the hexagonal to orthorhombic transition is more or less constant with pressure. The effect of increasing molecular weight from 5×10^4 to 2×10^6 was to increase the rates of hexagonal crystallization and hexagonal to orthorhombic transition but to decrease the rate of chain-folded (i.e. orthorhombic) crystallization at 2 kbar and below. These authors also presumed that in a given set of crystallization conditions the actual product was the result of kinetic competition between crystallization into orthorhombic and hexagonal phases. In this connection, they pointed out that the observed changeover between chain-folded and CEPE occurred below the triple point by a pressure approximately that needed to alter the melting points sufficiently to offset the difference in rates measured by the relative supercoolings at the triple point. The whole question of kinetic competition is an interesting one which remains to be investigated.

Chain-extended polyethylene as a model system

CEPE is an interesting material in its own right because of its large lamellar thicknesses and the consequent approach to fully crystalline properties. This large lamellar thickness also makes it of particular value as a model system because at least the thickest lamellae can be individually resolved in the optical microscope. So far advantage has been taken of this in two ways, the direct observation of lamellae growing from the melt and the study of mechanical properties in relation to physical texture⁸¹.

The first observations of CEPE forming under pressure by Jackson, Hsu and Brasch³⁹ have been referred to briefly. Further studies of a similar kind have now been reported by Bassett, Block and Piermarini²⁹ and, most fully, by Yasuniwa and Takemura⁷⁸. These have shown the hexagonal-orthorhombic transition and, most significantly, confirmed directly that at least the thickest lamellae of CEPE do grow outwards behind a narrowed edge as had been inferred from observations of fracture-surfaces^{13,21,26} and thin films (e.g. *Figure 4*). This establishes that the final lamellar thickness only appears after very substantial lamellar thickening. The suppression of lamellar thicknesses with decreasing specimen size has also been claimed as evidence of a cooperative process, involving a number of molecules, being involved in the attainment of the familiar large thicknesses⁴⁶. Furthermore, arguments have been brought to bear suggesting that this is likely to be true also of thin-

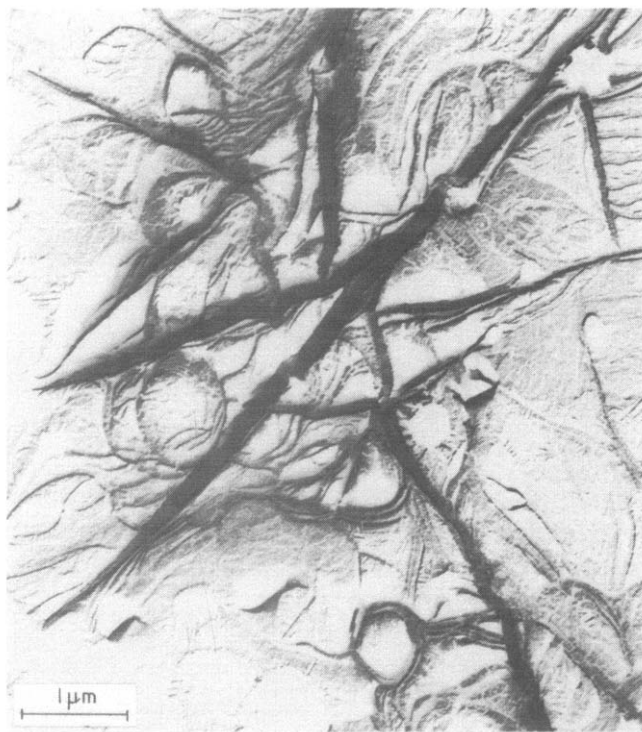


Figure 4 Thick lamellae with highly-tapered edges viewed edge-on, produced by crystallization of a thin film of a PE fraction ($M_w = 5 \times 10^5$) at 5 kbar. (D. C. Bassett and J. M. Phillips, unpublished)

ner lamellae in CEPE^{13,21} and of lamellae produced by kinetically controlled growth in general²⁵.

Such a process appears to be at variance with the concepts of the LP kinetic theory⁷⁷, which envisages a single strip laid on a substrate as establishing layer thickness with, presumably, only σ_{eff} to look to to account for systematic variations in thickness. In terms of the earlier Hoffman theory⁷⁶, if it can be shown that the thickness at the tip is nucleation controlled, then the observations concern the theory of the factor γ . To date the theory of γ has generalized the logarithmic time dependence observed for thicknesses away from lamellar edges; whether this is relevant to the profile of the edge is not known. As has also been pointed out previously, however, the value of γ for PE is estimated at ~ 2 ⁷⁶ or ~ 2.5 ²⁵, whereas the suppression of thickness by specimen size is at least an order of magnitude.

Mechanical properties

As first prepared, CEPE was notorious for its brittleness² so that its mechanical properties did not seem especially interesting. Even the brittleness, however, is revealing because whereas for the linear polymer CEPE characteristically fractures in $\{hk0\}$ planes, only a small proportion of short-chain branching effects a striking change to fracture between the basal lamellar surfaces. It was subsequently shown by Bassett and Carder⁸¹ that, in an oriented sample, brittleness in tension along the chain axis disappeared if short chains (less than a few thousand Å long) were removed, otherwise they segregate between the large lamellar surfaces. Subsequent investigation has shown that the polymer remains brittle for other directions of stress. This, however, is a matter of molecular weight and in recent work Attenburrow and Bassett⁸² report that Hifax polyethylene (molecular weight in excess of 2×10^6) can be drawn about 5 times at 80°C; at room temperature the material shows ductile fracture.

The first paper on mechanical properties of CEPE was that of Bassett and Carder⁸¹ who investigated the change in chain-axis modulus as a function of annealing temperature at 5.35 kbar. They showed that towards the end of the chain-folded region, the polymer behaved, according to its morphology, melting point, density and stiffness, as a series composite of crystal and intercrystalline regions while average lamellar thickness increased from 500 to 1000 Å. Once in the chain-extended region this simple model broke down, as is not unexpected, in view of the sensitive fractionation indicated by Figure 3.

The modulus parallel to c of CEPE is of particular interest in the quest for attainment of the theoretical stiffness of polymers; for PE this is ~ 300 GN/m², rather more than that for steel⁸³. It is now widely appreciated that it is the interruption by fold surfaces of the sequence of covalent carbon-carbon bonds which leads to the observed chain-axis modulus of PE being often at least 100 times lower than the maximum. To increase the modulus one must, therefore, ensure good orientation, stiffen interlamellar connections and reduce the number of interfaces by increasing chain-extension^{83,84}. Bassett and Carder⁸¹ studied the compromise between the last two factors resulting when drawn fibres, with stiff interfaces but low chain-extension, gradually had their chain-extension increased but simultaneously, their interfaces softened. It was shown that interface stiffening is much more important to modulus than is chain-extension. This is the factor which has now been exploited in the attainment of moduli of order 100 GN/m², through the use of very high draw ratios⁸⁵.

The mechanism of drawing has itself been the subject of much study but its understanding is severely handicapped by the difficulties of establishing the facts in chain-folded systems, especially those concerning the fate of lamellae which cannot, in general, be examined directly. This is no longer the case for CEPE where at least the larger lamellae can be directly observed in bulk specimens in the optical microscope. A second advantage is that whether melting (or quasi-melting) occurs during drawing, a hypothesis which continues to receive support, can be checked very simply. If this were to happen at atmospheric pressure, it could not reproduce the large crystal thicknesses (and high melting point) because these are a legacy of crystallization into (or annealing in) the hexagonal phase and so crystal thicknesses would drop to a few hundred Å and melting points fall to $\sim 130^\circ\text{C}$. In fact Attenburrow and Bassett⁸² have shown that melting does not occur in five-fold drawing and that lamellae survive this process at essentially constant thickness but become highly sheared along c . CEPE is thus proving valuable in yet another context to illuminate major problems in polymer physics.

CONCLUSIONS

The study of CEPE can be summarized as having led to four main conclusions:

(1) In the case of PE, chain-extended growth is crystallization of the hexagonal phase. The chain-folded/chain-extended terminology is confusing; it is probably best avoided and replaced by reference to the orthorhombic and hexagonal phases respectively.

(2) The mechanism of lamellar thickening during annealing of polyethylene can be regarded as due to (it is certainly very little different from) local melting, initially perhaps of only a few fold stems, followed by recrystallization.

(3) There is probably one mechanism of polymeric crystallization with molecular folding common to chain-folded and chain-extended polyethylene as well as to PTFE and other polymers. This process is cooperative, being more than the deposition of a single molecule on a substrate and leads to observed lamellar thicknesses being approximately inversely proportional to the entropy of fusion and to supercooling.

(4) CEPE is a valuable model system particularly in so far as it allows observation of individual lamellae being formed during crystallization and being deformed mechanically.

REFERENCES

- 1 Anderson, F. R. *J. Appl. Phys.* 1964, **35**, 64
- 2 Geil, P. H., Anderson, F. R., Wunderlich, B. and Arakawa, T. *J. Polym. Sci. (A)* 1964, **2**, 3707
- 3 Wunderlich, B. and Arakawa, T. *J. Polym. Sci. (A)* 1964, **2**, 3697
- 4 Kardos, J. L., Baer, E., Geil, P. H. and Koenig, J. L. *Kolloid Z.* 1965, **204**, 1
- 5 Kawai, T. *Kolloid Z.* 1965, **201**, 15
- 6 Kawai, T. *Makromol. Chem.* 1965, **84**, 294
- 7 Kawai, T., Ehara, K., Sasano, H. and Kamide, K. *Makromol. Chem.* 1968, **111**, 271
- 8 Peterlin, A. *Polymer* 1965, **6**, 25
- 9 Wunderlich, B. and Melillo, L. *Makromol. Chem.* 1968, **118**, 250
- 10 Prime, R. B. and Wunderlich, B. *J. Polym. Sci. (A-2)* 1969, **7**, 2061
- 11 Davidym, T. and Wunderlich, B. *J. Polym. Sci. (A-2)* 1969, **7**, 2051
- 12 Arakawa, T. and Wunderlich, B. *J. Polym. Sci. (C)* 1967, **16**, 653
- 13 Rees, D. V. and Bassett, D. C. *J. Polym. Sci. (A-2)* 1971, **9**, 385
- 14 Bassett, D. C. and Carder, D. R. *Phil. Mag.* 1973, **28**, 513
- 15 Bassett, D. C. and Olley, R. H. unpublished data
- 16 Bassett, D. C. and Phillips, J. M. *Polymer* 1971, **12**, 730
- 17 Bassett, D. C. and Carder, D. R. *Polymer* 1973, **14**, 387
- 18 Hatakeyama, T., Kanetsuna, H. and Hashimoto, T. *J. Macromol. Sci. (B)* 1973, **7**, 411
- 19 Wunderlich, B., Melillo, L., Cormier, C. M., Davidson, T. and Snyder, G. *J. Macromol. Sci. (B)* 1967, **1**, 485
- 20 Ingram, P. *Polymer* 1967, **8**, 488
- 21 Wunderlich, B. and Melillo, L. *Science* 1966, **154**, 1329
- 22 Wunderlich, B. and Cormier, C. M. *J. Phys. Chem.* 1966, **70**, 1844
- 23 Keller, A. and Bassett, D. C. *J. R. Micros. Soc.* 1960, **79**, 243
- 24 Melillo, L. and Wunderlich, B. *Kolloid Z.* 1972, **250**, 417
- 25 Bassett, D. C. and Davitt, R. *Polymer* 1974, **15**, 721
- 26 Wunderlich, B. *J. Polym. Sci. (B)* 1967, **5**, 7
- 27 Wunderlich, B. *Pure Appl. Chem.* 1972, **31**, 49
- 28 Calvert, P. D. and Uhlmann, D. R. *J. Polym. Sci. (A-2)* 1972, **10**, 1811
- 29 Bassett, D. C., Block, S. and Piermarini, G. J. *J. Appl. Phys.* 1974, **45**, 4146
- 30 Wunderlich, B. *J. Polym. Sci. (A)* 1963, **1**, 1245
- 31 Rees, D. V. and Bassett, D. C. *Nature* 1968, **219**, 368
- 32 Rees, D. V. and Bassett, D. C. *J. Polym. Sci. (B)* 1969, **7**, 273
- 33 Gruner, C. L., Wunderlich, B. and Bopp, R. C. *J. Polym. Sci. (A-2)* 1969, **7**, 2099
- 34 Matsuoka, S. *J. Polym. Sci.* 1962, **57**, 569
- 35 Osugi, J. and Hara, K. *Rev. Phys. Chem. Japan* 1966, **36**, 28
- 36 Baltenas, R. A. and Igonin, L. A. *Dokl. Akad. Nauk SSSR* 1965, **163**, 917
- 37 Baer, E. and Kardos, J. L. *J. Polym. Sci. (A)* 1965, **3**, 2827
- 38 Davidson, T. and Wunderlich, B. *J. Polym. Sci. (A-2)* 1969, **7**, 377
- 39 Jackson, J. F., Hsu, T. S. and Brasch, J. W. *J. Polym. Sci. (B)* 1972, **10**, 207
- 40 Wunderlich, B. and Davidson, T. *J. Polym. Sci. (A-2)* 1969, **7**, 2043
- 41 Bair, H. E., Salovey, R. and Huseby, T. W. *Polymer* 1967, **8**, 9
- 42 Bassett, D. C., Khalifa, B. A. and Turner, B. *Nature (Phys. Sci.)* 1972, **239**, 106
- 43 Lauritzen, J. I. and Hoffman, J. D. *J. Appl. Phys.* 1973, **44**, 4340
- 44 Bassett, D. C. and Turner, B. *Phil. Mag.* 1974, **29**, 285
- 45 Bassett, D. C. and Khalifa, B. A. *Polymer* 1973, **14**, 390
- 46 Bassett, D. C. and Khalifa, B. A. *Polymer* 1976, **17**, 275
- 47 Bassett, D. C. and Turner, B. *Phil. Mag.* 1974, **29**, 925
- 48 Kanetsuna, H., Mitsuhashi, S., Iguchi, M., Hatakayama, T., Kyotani, M. and Maeda, Y. *J. Polym. Sci. (C)* 1973, **42**, 783
- 49 Maeda, Y. and Kanetsuna, H. *J. Polym. Sci. (A-2)* 1974, **12**, 2551
- 50 Bassett, D. C. and Turner, B. *Nature (Phys. Sci.)* 1972, **240**, 146
- 51 Yasuniwa, M., Nakafuku, C. and Takemura, T. *Polym. J.* 1973, **4**, 526
- 52 Maeda, Y. and Kanetsuna, H. *J. Polym. Sci. (A-2)* 1975, **13**, 637
- 53 Maeda, Y. and Kanetsuna, H. *USA-Japan meeting on Thermal Analysis*, 1974
- 54 Van Valkenburg, A. and Powers, J. *J. Appl. Phys.* 1963, **34**, 2433
- 55 Khalifa, B. A. and Bassett, D. C. *Polymer* 1976, **17**, 291
- 56 Nelson, R. R., Webb, W. and Dixon, J. A. *J. Chem. Phys.* 1960, **33**, 1756
- 57 Muller, A. *Proc. R. Soc. (A)* 1932, **128**, 514
- 58 Zubov, Yu. A., Selikhova, V. I., Konstantinopolskaya, M. B., Sukhov, F. F., Slovokhotova, N. A., Bakeyev, N. F., Kruykov, A. V., Sokolsky, V. A. and Belov, G. P. *J. Polym. Sci. (C)* 1972, **38**, 459
- 59 Bassett, D. C., Khalifa, B. A. and Olley, R. H. *Polymer* 1976, **17**, 284
- 60 Fischer, E. W. and Puderbach, H. *Kolloid Z.* 1969, **235**, 1260
- 61 Rees, D. V. *PhD Thesis* University of Reading (1970)
- 62 Kijima, T., Imada, K. and Takayanagi, M. *Rep. Prog. Polym. Phys. Japan* 1970, **13**, 177
- 63 Roe, R.-J., Gieniewski, C. and Vadimsky, R. G. *J. Polym. Sci. (A-2)* 1973, **11**, 1653
- 64 Blais, J. J. B. P. and Manley, R. St. J. *J. Macromol. Sci. (B)* 1967, **1**, 525
- 65 Balta Calleja, F. J., Bassett, D. C. and Keller, A. *Polymer* 1963, **4**, 269
- 66 Treiber, G., Melillo, L. and Wunderlich, B. *J. Polym. Sci. (B)* 1973, **11**, 435
- 67 Edwards, B. C. and Phillips, P. J. *J. Mater. Sci.* 1975, **10**, 1233
- 68 Calvert, P. D. and Uhlmann, D. R. *J. Polym. Sci. (B)* 1970, **8**, 165
- 69 Morris, R. B. and Bassett, D. C. *J. Polym. Sci. (A-2)* 1975, **13**, 1501
- 70 Prime, R. B. and Wunderlich, B. *J. Polym. Sci. (A-2)* 1969, **7**, 2073
- 71 Prime, R. B., Wunderlich, B. and Melillo, L. *J. Polym. Sci. (A-2)* 1969, **7**, 2091
- 72 Kardos, J. L., Li, H.-M. and Huckshold, K. A. *J. Polym. Sci. (A-2)* 1971, **9**, 2061
- 73 Holdsworth, P. J. and Keller, A. *J. Macromol. Sci. (B)* 1967, **1**, 595
- 74 Bedborough, D. S. *PhD Thesis* University of Reading (1974)
- 75 Phillips, P. J. and Edwards, B. C. *J. Polym. Sci. (A-2)* 1975, **10**, 1233
- 76 Hoffman, J. D. *SPE Trans.* 1964, **4**, 1
- 77 Lauritzen, J. I. and Passaglia, E. *J. Res. Nat. Bur. Stand. (A)* 1967, **71**, 261
- 78 Yasuniwa, M. and Takemura, T. *Polymer* 1974, **15**, 661
- 79 Kyotani, M. and Kanetsuna, H. *J. Polym. Sci.* 1974, **12**, 2331
- 80 Hatakayama, T., Kanetsuna, H., Kaneda, H. and Hashimoto, T. *J. Macromol. Sci. (B)* 1974, **10**, 359
- 81 Bassett, D. C. and Carder, D. R. *Phil. Mag.* 1973, **28**, 535
- 82 Attenburrow, G. E. and Bassett, D. C. *J. Mater. Sci.* 1976
- 83 Frank, F. C. *Proc. R. Soc. (A)* 1970, **319**, 127
- 84 Bassett, D. C. *Spectrum.* 1975, **128**, 10
- 85 Capaccio, G. and Ward, I. M. *Polymer* 1975, **16**, 239

Study of crystallization and isothermal thickening in polyethylene using SAXD, low frequency Raman spectroscopy and electron microscopy*

J. Dlugosz, G. V. Fraser, D. Grubb, A. Keller and J. A. Odell
H. H. Wills Physics Laboratory, University of Bristol, Bristol BS8 1TL, UK

and P. L. Goggin

Department of Chemistry, University of Bristol, Bristol, BS8 1TL, UK
(Received 16 February 1976)

This study contains a combined application of three different techniques for the study of polyethylenes crystallized from the melt under different circumstances, small-angle X-ray diffraction (SAXD), low frequency Raman spectroscopy to examine the longitudinal acoustic (*LA*) mode, and electron microscopy. In particular, the combination of SAXD and Raman methods enables the separation of the situation where there is only one lamellar structure which displays several orders in the SAXD pattern, from that where there is more than one type of lamellar thickness present. The superior power of the Raman method, which does not depend on the regularity in the lamellar stacking, becomes apparent. The multiplicity of the lamellar population could be associated with lamellae formed isothermally at the preselected crystallization temperature and with lamellae which originated from material which has remained uncrystallized at this temperature and formed subsequently with smaller lamellar thickness during cooling of the sample. The existence of the corresponding double lamellar population could be made directly visible using electron microscopy on freeze-cut and stained sections. The thinner lamellae in the double population could be extracted by solvents, removing the corresponding SAXD and Raman peaks, and leaving blank image areas in place of the thin lamellae in the electron-micrographs. These extracted thinner lamellae correspond to lower molecular weights as assessed by g.p.c. Thus molecular segregation during crystallization is involved. Furthermore the segregated texture units and their arrangement within the full morphology could now be identified. Pronounced changes in lamellar thickness with crystallization time were observed throughout and were associated in the early stages of crystallization with molecular fractionation and in the later stages with thickening of lamellae already present. An unexpected interrelation between nucleation density and the final lamellar thickness through the agency of isothermal lamellar thickening has been established. Examples are quoted which are contrary to the expected trend of lamellar thickness with crystallization temperature, but which are interpretable nevertheless in the light of the effect of isothermal lamellar thickening. The potential significance of all these findings and of this kind of approach for the characterization of crystalline bulk polymers is made throughout.

INTRODUCTION

It has been established that the Raman active longitudinal acoustic mode of vibration (*LA* mode) can be used as a measure of the straight chain length in lamellar crystals of polyethylene¹⁻³. A greater part of the recent discussion involving the Raman method has centred around correlations of the Raman derived chain length with the lamellar spacing determined from small-angle X-ray diffraction. The motivation for this has been to obtain a better description of the lamellar morphology in terms of the crystalline core and an amorphous fold surface. At a quantitative level there are several problems to this approach. In the Raman spectrum a vibrational frequency is observed and the problem becomes one of interpreting this frequency in terms of a chain length. This is usually carried out by using the following relationship developed for the *n*-paraffins⁴: $\nu = (m/2L)E/\rho^{1/2}$ where ν is the vibrational frequency of the

LA mode, *m*, the order of the vibration, *L* the length of the vibrating chain, *E* the Young's modulus and ρ the density. A rigorous treatment however, would require the special features associated with polyethylene for example chain branches and fold surfaces to be taken into account⁵. These effects are known to be small but their precise values on which clearly a meaningful comparison with other techniques depends is as yet unknown. By contrast both SAXD and electron microscopy are established techniques in this field. However, there are still uncertainties surrounding the values of lamellar thickness for melt crystallized polyethylene. Authors differ in their treatment of the SAXD data which in turn affects the long spacings determined. Furthermore in cases where more than one SAXD maximum is observed there is disagreement about which one represents the lamellar spacing^{6,7}. Generally observations by electron microscopy have not shown good agreement with the expectations of lamella thickness given by SAXD⁸.

While pursuing these problems, in particular the relationship of SAXD to Raman data, new information has

* Presented at the Polymer Physics Group (Institute of Physics) Biennial Conference, Shrivenham, September 1975.

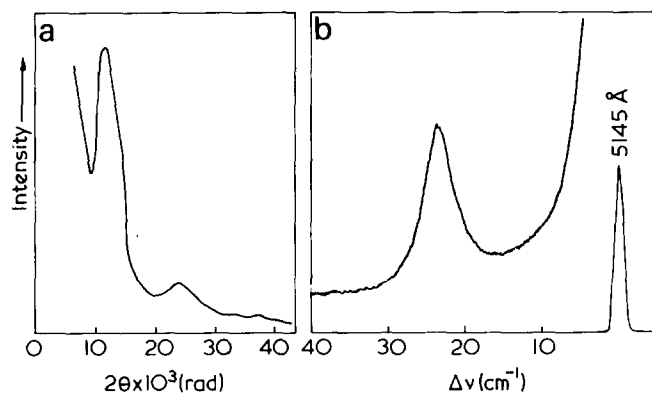


Figure 1 Typical (a) SAXD pattern and (b) Raman spectrum of PE single crystals (Marlex 6002, T_c 85°C)

become available on the dependence of the lamellar thickness on the time of crystallization and on the effect of nucleation density when crystallization is carried out from the melt including a tie-up with the wider field of molecular weight segregation during crystallization. These results are presented in this paper and the interrelation of crystallization time, temperature and nucleation density is discussed. In an attempt to confirm deductions made from the Raman spectra about the crystallization process the electron microscope has been used. Here it is possible to show that information obtained from the Raman spectrum on the distribution of lamellar thicknesses is directly related to the fine structure observable using the electron microscope, hence showing the complementary nature of these techniques.

The wider implications of this work are in the control of the structure and properties of polyethylene formed by the process of crystallization from the melt.

EXPERIMENTAL

Raman spectroscopy

Raman spectra were obtained at room temperature using a triple monochromator spectrometer, a Coderg model T800. Laser excitation was provided by a CRL model 52 argon ion laser which was set to give a power of 100 mW at the sample.

In all spectra the *LA* modes appear against a sloping background which tends to distort the band-heads to lower frequencies. In order to minimize this error it is desirable to obtain well resolved peaks when subtraction of a background has only a small effect on the peak frequencies. This was attempted using small slit widths typically 1 cm^{-1} and occasionally 0.5 cm^{-1} for recording spectra below $\Delta\nu = 5 \text{ cm}^{-1}$. Noise on the trace also creates an uncertainty in peak position, although nowadays this is generally not a problem since signal to noise ratios better than 20:1 can be achieved. On this basis we were able to locate strong *LA* mode peaks to better than $\pm 0.5 \text{ cm}^{-1}$ depending upon the individual conditions. The error bars for Raman chain length quoted in this paper correspond to the uncertainty in the frequencies of the *LA* modes.

The frequency shift of a peak with respect to the exciting radiation is denoted by $\Delta\nu$ and expressed in cm^{-1} throughout the text. Values of $\Delta\nu$ were converted into values of chain length using the relationship derived by Schaufele and Shimanouchi⁴. In certain spectra there are two low frequency peaks. In these cases the peak with the lower value of ν is referred to as peak 1 and that with the higher value as peak 2.

Small-angle X-ray diffraction (SAXD)

SAXD photographs were taken at room temperature using a Frank's point focusing X-ray camera. An exposure time of 17 h was used for all samples with a specimen to film distance of 9 cm. On a number of occasions a point collimating Rigaku-Denki camera and rotating anode X-ray generator were used whereby the exposure time could be reduced to 4 h using a specimen to film distance of 30 cm. Experience with the results obtained showed that these cameras were very similar in terms of resolving power and background scatter.

Densitometer traces of the X-ray plates were recorded using a Joyce and Loebel two beam microdensitometer. Bragg's law was applied to the maxima to determine the lamellar long spacings. When two distinct maxima are observed in the SAXD pattern, the one at the smaller angle is referred to as θ_1 and that at the larger angle as θ_2 in accordance with the usual convention.

Recently some discussion has centred around the need to apply a Lorentz-geometric correction to SAXD intensity curves^{7,8}. The Lorentz correction was originally introduced as an intensity correction for wide angle X-ray rotation photographs and allows for the different times for which crystallographic planes are in the reflecting condition. In a randomly oriented sample it should be applied to correct for the different probability of planes being in the reflecting condition. At low angles the combined Lorentz-geometric correction takes the form of a θ^2 multiplication factor.

The application of this correction to SAXD curves from single crystal material (Figure 1), or from bulk material with well defined peaks (Figure 2) creates no problems, and the effect is to shift the peaks only slightly towards a lower spacing. In Figure 1, for example, the peak is moved from 124 to 114 Å, by the application of this correction.

The situation has been found to be rather more complicated in the case of some isothermally crystallized bulk materials. In addition to any background scatter from the instrument or from the air, which can be subtracted from the intensity curve, such materials produce a strong intrinsic background scatter at very small angles. Since we believe that this scatter does not originate from the basic lamellar periodicity, it must be subtracted before the Lorentz correction can properly be applied.

The exact form of the background scatter is unknown, but subtracting various trial backgrounds and then applying the Lorentz correction has the effect of reducing the

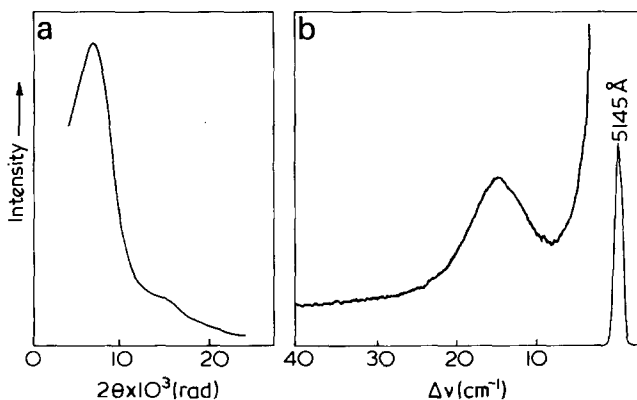


Figure 2 (a) SAXD pattern and (b) Raman spectrum of quenched PE (Rigidex 50 as supplied) with two maxima in the SAXD pattern and with one first order *LA* mode in the Raman spectrum

Table 1 SAXD and Raman parameters for polyethylene samples

Figure number	Sample description	SAXD layer thickness*, L_x (Å)		Raman chain† length, L_R (Å)	
		θ_1	θ_2	peak 1	peak 2
1	Single crystals of Marlex 6002, T_c 85°C	124(114)	—	135	—
2	Bulk Rigidex 50, as supplied	219(190)	112(93)	208 ± 5	—
3	Bulk Marlex 50, T_c 122.9°C	320(260)	170(140)	397 ± 17	—
4	Bulk Carlona 65045, T_c 128.4°C	—	—	601 ± 50	—
5	Bulk Unifes 7006, T_c 126.0°C	231(205)	—	370 ± 17	204 ± 5
6	Bulk Unifes 7006, T_c 127.9°C	220(185)	—	531 ± 35	253 ± 8

* Values in parentheses are those for Lorentz-geometric corrected long spacings

† The error bar arises from the uncertainty in the peak position, for a discussion of the errors in the SAXD long spacings, see text.

measured lamellar periodicity of curves 3 to 6 by ~20%. Whilst the effect is not strongly dependent on the particular background which is subtracted, this introduces an uncertainty in the values of long period estimated by SAXD of about 10%. Because of the uncertainties involved, the SAXD spacings shown in Table 1 are uncorrected, with corrected values shown in parentheses.

Electron microscopy

Some of the specimens were treated so as to make the lamellar structure visible in the electron microscope. The technique used was recently discovered by Kanig^{9,10}, independently of previous similar work by Körösy and Zeiger-son¹¹. Small pieces of the polyethylene were put into chlorosulphonic acid and left at 60°C for 9 h. After washing in concentrated sulphuric acid and then distilled water the samples were left for 3 h in a 0.7% aqueous solution of uranyl acetate. Thin sections were then cut from these stained blocks at temperatures below 150K, using an ultramicrotome with a diamond knife and liquid nitrogen cooling system. The chlorosulphonic acid attacks polyethylene, and it diffuses preferentially into the disordered interlamellar material, and not into the crystalline lamellae. In the reaction with polyethylene, polar groups are substituted for hydrogens, and these polar groups attract the heavy metal ions from the staining solutions. Thus the amorphous or disordered regions are made very electron dense. In the electron microscope at focus, the image seen is the projected electron density distribution in the section, so that when a crystalline lamella extends through the section, it appears as a light, electron transparent region.

Another important effect of the acid treatment on polyethylene is to introduce crosslinks between chains, making the sample rigid. It is then very much less susceptible to the large distortions which are otherwise produced by mechanical damage during cutting and radiation damage during observation in the electron microscope. Because of this stability, no special techniques are required in the actual microscopy, and it is possible to assert confidently that the structures observed are representative of those existing in the bulk material.

Samples

Samples were taken from a range of high density polyethylenes of Marlex, Rigidex, Unifes and Carlona types. Specimens were prepared by pressing pellets between thin microscope coverslips on a hot bench at 180°C and held at this temperature for several minutes to allow any orientation in the material to disappear. The thin discs so formed (~0.1 mm thick × 0.5 cm in diameter) were then cooled to about 150°C on the hot bench and then quickly transferred to a thermostat containing silicone oil at the crystallization temperature. The temperature of the oil bath was constant to within ±0.1°C.

For samples of special interest solvent extractions were carried out in *p*-xylene, the details of which are described later. The results of the extraction were analysed in terms of the molecular weight distribution using a Waters analytical g.p.c. apparatus.

RESULTS AND DISCUSSION

Scope and limitations of the techniques available

Since the techniques of SAXD, low frequency Raman spectroscopy and electron microscopy examine different properties of the material, meaningful comparisons of the results can only be made by bearing in mind how the information is obtained. The difference in density between crystalline lamellae and the disordered interlamellar material is detected directly by X-rays, but a prerequisite for the appearance of a discrete maximum in the small angle region is the regular stacking one upon another of lamellae of reasonably uniform size. The position of the peak then indicates the average repeat distance in the stacks of lamellae.

The Raman active *LA* mode depends upon the average length of the extended chains within the lamellae. This will not necessarily be the same as the thickness of the lamellae because the chains may not be perpendicular to the lamellar surface as earlier work has shown¹². Furthermore the *LA* mode will clearly not depend on how the lamellae are arranged in stacks.

The electron microscope looks at density variations but these are not the density variations that originally existed within the material. They have been artificially induced by staining and so reflect the permeability variations within the material. Low permeability is associated with crystalline order and thus high original density. Again, observation of a lamellar thickness does not depend on regular stacking, indeed the arrangement of lamellae may be observed directly.

In Figures 1–6 we give illustrative examples of typical SAXD patterns and Raman spectra of polyethylene. The values of X-ray long spacings and Raman chain lengths are given in Table 1.

For mats of polyethylene single crystals which are well ordered and consist of fairly small crystals the SAXD pattern gives well resolved peaks and several orders of diffraction as shown in Figure 1. For melt crystallized polyethylene in general the position is not so good. The SAXD maxima in Figures 2–4 tend to be obscured by the intense background scatter. Consequently it is difficult or in some cases impossible to measure or even resolve them. In the Raman spectra the *LA* mode peaks also get nearer to the main beam (in this case the intense laser line) as the lamellar thickness increases. However, the recent introduction of triple monochromators has made it generally possible to

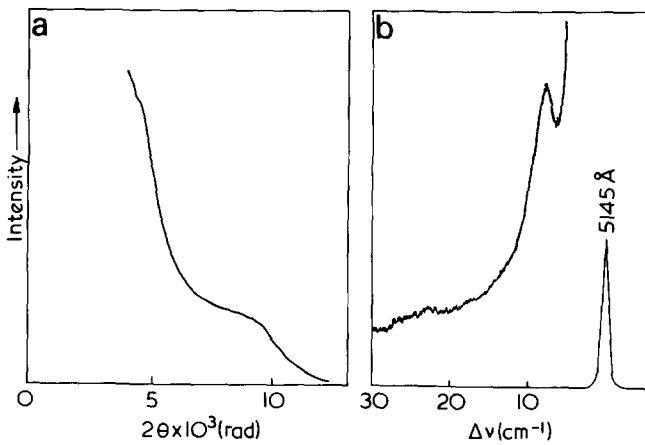


Figure 3 (a) SAXD pattern and (b) Raman spectrum of isothermally crystallized bulk PE (Marlex 50, T_c 122.9°C) with two maxima in the SAXD pattern and with one first order LA mode and a weak corresponding third order in the Raman spectrum

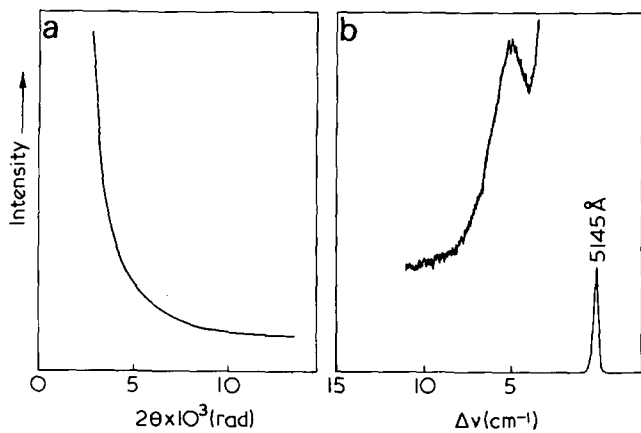


Figure 4 (a) SAXD pattern and (b) Raman spectrum of isothermally crystallized bulk PE (Shell Carlon 65045, T_c 128.4°C) without a maximum in the SAXD pattern but with a well defined LA mode in the Raman spectrum

obtain well defined peaks for melt crystallized material, and peaks can be detected even when the corresponding chain lengths are over 500 Å as illustrated in Figure 4. SAXD patterns from material containing such large lamellae give little or no indication of a maximum. Greater intensity and thus finer collimation may be obtained using slit collimated cameras, but to avoid slit height corrections we have concentrated our efforts on point collimation.

Since the electron microscope looks at lamellae in real space the accuracy is not limited by the lamellar size. However, the accuracy is never high for the following reasons: the possibility of distortion of the specimen during preparation; the very small volume of the sample which is observed; and the difficulty of calibrating the microscope accurately.

To summarize, therefore, the Raman technique can give information on a routine basis in circumstances when the SAXD method cannot, at least not without time consuming procedures. To compare these two techniques quantitatively requires knowledge of the chain obliquity which can be obtained independently using wide angle X-ray diffraction for oriented samples only. By using the two methods together there exists the possibility of distinguishing effects due to individual lamellae and those due to the stacking of lamellae. Electron microscopy gives direct visual information about the stacking and arrangement of lamellae as well as about lamellar size but the procedure is

time consuming and the accuracy for the latter purpose is more limited.

Values for lamellar thicknesses

Since L_R is a measure of the straight chain portion, then it might be expected to be smaller than the total lamellar thickness which is considered to be sub-divided into a crystalline and a more or less disordered (amorphous) surface layer. In previous works³, nevertheless, L_R was found to be larger than L_X . This could be accounted for by the fact that the chains are inclined with respect to the layer surface. In cases where the chain inclination could be assessed L_R was found to be close to $L_X/\cos\phi$ (ϕ = angle between straight chain direction and lamellar normal). This implies that L_R is a measure of the appropriately inclined straight chain traverse across the full layer. As laid out previously³ this leaves little room for amorphous material such as does not partake in the vibration contributing to the Raman peak, a point of potential consequence for the visualization of a polymer crystal. It means that, contrary to much other experimental evidence, there is either

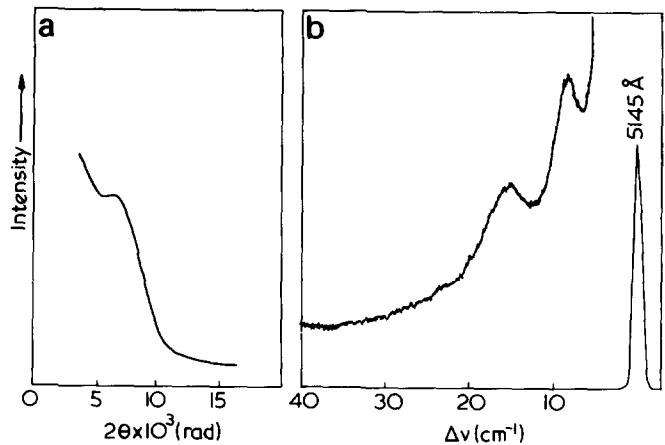


Figure 5 (a) SAXD pattern and (b) Raman spectrum of isothermally crystallized bulk PE (Unifex 7006, T_c 126°C) with one maximum in the SAXD pattern and with two first order LA modes in the Raman spectrum

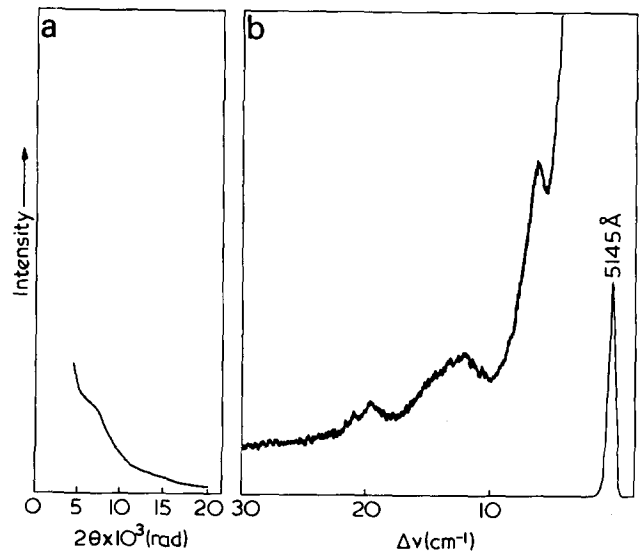


Figure 6 (a) SAXD pattern and (b) Raman spectrum of isothermally crystallized bulk PE (Unifex 7006, T_c 127.9°C) with one maximum in the SAXD pattern and with two first order LA modes and a weak third order in the Raman spectrum

no appreciable amount of amorphous material at the crystal surface or the amorphous material has some special structure and orientation. While we shall not take this issue further in the present paper we must state that the results to be described will further emphasize this point.

Single crystal mats. Single crystal mats give clear results which are comparatively easy to interpret. They are being used here as control specimens. Three orders are visible in the SAXD pattern and a clear primary *LA* mode in the Raman spectrum as shown by *Figure 1*. As seen from the corresponding entry in *Table 1*, the Raman chain length L_R is larger than the X-ray long period L_X . With reference to the preceding paragraph we may invoke chain inclination as an explanation and test for the relation $(L_X/L_R) = \cos\phi$ which as stated above implies that the entire oblique traverse length partakes in the vibration. We find that $\phi = 25^\circ$ or 32° for the uncorrected and corrected values of L_X respectively. These are within the range for crystals grown at 85°C^{13} .

Melt-crystallized polyethylene. *Figures 2–6* show examples of SAXD patterns and Raman spectra from various melt-crystallized samples. They show that two X-ray peaks may appear when only one Raman peak appears as in *Figures 2* and *3* and that two or more Raman peaks may appear when only one X-ray peak is present as in *Figures 5* and *6*. The new observation of multiple Raman peaks is discussed fully later. Here we will confine the discussion to cases where one Raman peak and two X-ray peaks are observed. We find this behaviour for samples which have essentially fully crystallized at one temperature.

When there is only one Raman peak the chain length is closest to the larger of the two X-ray spacings as shown by *Table 1*. This agrees with the results of Koenig and Tabb². For a rapidly quenched sample, as in *Figure 2*, L_R is closely equal to the uncorrected value of L_X while it is slightly larger than the corrected L_X value. In the latter case the chain inclination, considering again the oblique traverse across the full layer, would be 24° . As the precise temperature at which this sample was crystallized is not known such a tilt could be reasonable; for a quenched sample it is unlikely to be larger¹⁴.

For an isothermally crystallized sample, as in *Figure 3*, $L_R > L_X$, both for the corrected and uncorrected L_X values. This is consistent with the expectation of increasing chain tilt with crystallization temperature as documented in earlier electron diffraction work. For the bulk sample in *Figure 3* this yields tilts of 36° and 49° for uncorrected and corrected L_X values respectively, again taking the oblique traverse as running across the full layer. While the latter may appear on the high side it is still within the range of practical experience in cases where the tilt angle could be directly assessed³. It is to be noted that a traverse length shorter than that across the full layer would require still higher tilt angles.

The observation of two low angle maxima has been reported many times previously. Since in many cases the ratio of the spacings has not been 2:1 they have been interpreted as two independent first orders of diffraction arising from two different lamellar periodicities^{6,7}. Support for this has been found using the electron microscope where different types of lamellae have been observed¹⁵. However, recently it has been shown that if the X-ray data obtained using slit collimated cameras are rigorously corrected then the ratio of spacings becomes closer to 2:1 thus favouring an interpretation based on two orders of diffraction from the same lamellar periodicity.

Multiple SAXD spacings may be due either to higher orders of diffraction from a single lamellar periodicity or the two distinct sets of lamellae. Clearly the observation of a single, primary *LA* mode together with two SAXD maxima in *Figures 2–4* indicate that at least in these cases only one lamellar periodicity is present, consequently the SAXD maxima are 1st and 2nd orders of the same spacing. Even if we did not go to such lengths on the effect of the exact corrections to the L_X values as some other authors⁸ the entries in *Table 1* are certainly in support of this plausible assignment.

This is in contrast to *Figures 5* and *6* where two *LA* modes but only one broad SAXD maximum are observed. As will be apparent below the two *LA* modes correspond to two types of lamellae. Accordingly, the single SAXD maximum may arise either from one set of lamellae only, that due to the second not being resolved, or may result from the superposition of the maxima arising from two sets of lamellae. In any event in this case we find that the Raman effect is the more informative and shall proceed to follow its behaviour more closely.

Observation and interpretation of the multiple Raman peaks in melt crystallized polyethylene

First we have to examine the possibility that a Raman peak appearing at a higher wavenumber than peak 1 corresponds to a higher order vibration of the first Raman peak. The second order *LA* mode is not Raman active but an active third order *LA* mode is predicted in the Raman spectrum and this has been observed previously for melt crystallized polyethylene¹². Occasionally we have observed such a peak at approximately three times the wavenumber shift of the first peak as shown in *Figures 3* and *6*. However, in most cases the higher order is readily distinguishable from peak 2 as shown in *Figure 6*. Furthermore, the wavenumber shifts of peaks 1 and 2 bear no simple numerical relationship to one another. Thus one can say that peaks 1 and 2 are of different origin.

The frequencies of peaks 1 and 2 have been measured for a variety of crystallization temperatures. *Figure 7* shows the data obtained for Rigidex 50. In this and later figures it is assumed in the first instance that both peaks are primary *LA* modes and their frequencies have been converted into Raman chain lengths. Here the data strongly suggest a dependence of the frequency of peak 1 upon the time of crystallization. Hence Raman spectra were measured as a function of time at a constant crystallization temperature of 126°C . This information is given in *Figures 8* and *9* which show the Raman chain lengths and relative intensities of peaks 1 and 2 as a function of crystallization time. The major observations concerning the assignment of these peaks are:

(a) The length corresponding to peak 1 (the longer chain length) increases as a function of crystallization temperature as shown by the upper curve in *Figure 7*.

(b) The length corresponding to peak 2 is largely independent of crystallization temperature as shown by the lower points of *Figure 7*. The length is generally in the range 200–250 Å although we have found that it can be lower for samples which have been cooled rapidly from the isothermal crystallization temperature by quenching into an ice/water mixture.

(c) For a given crystallization temperature peak 2 decreases in intensity relative to peak 1 as the time allowed for crystallisation increases. At long times peak 2, although very weak, is still detectable as shown in *Figure 9*.

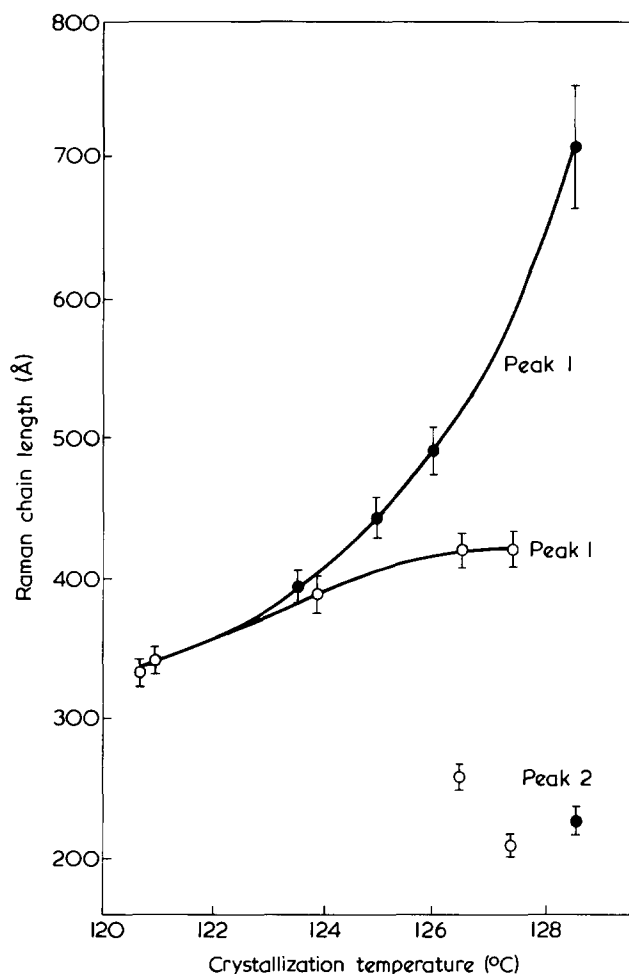


Figure 7 Raman chain length as a function of crystallization temperature for Rigidex 50. \circ , data for a crystallization time of 1 h; \bullet , data obtained for more complete crystallization. The times used for the latter were at 123.6°C, 20 h; 125.0°C, 53 h; 126.0°C, 1 day; and 128.6°C, 2½ days

From this we conclude that peak 1 corresponds to an LA vibration in material which crystallized isothermally at the temperature of the oil bath and that peak 2 is an LA vibration in material which remained uncrystallized at the end of the 'crystallization time' and crystallized subsequently while the sample was cooled to room temperature. At longer isothermal crystallization times more material has crystallized and so peak 2 weakens. Eventually after several days all the material crystallizable at the particular bath temperature has crystallized isothermally and consequently peak 1 predominates.

The persistence of peak 2 at long crystallization times suggests that there remains a portion of the material which is able to crystallize only on cooling. During the course of this work our attention was drawn to a recent paper by Mehta and Wunderlich¹⁷ in which a study of molecular segregation during crystallization from the melt was made. Here it was shown that for a given crystallization temperature material below a critical molecular weight does not crystallize. On this basis it is anticipated that a small portion of uncrystallized material will remain when isothermal crystallization is complete. This would crystallize on cooling and would give rise to an additional LA mode such as peak 2. The possibility of making a connection between the structure of the resulting crystals and the process of molecular segregation is explored later.

The immediate implication from the Raman results in Figures 8 and 9 is that polyethylene can be crystallized

from the melt containing two different sets of lamellae. The SAXD patterns of this type of sample commonly contain one maximum only. This can be explained by referring back to the need for regular stacking of lamellae to give a distinct SAXD maximum. Clearly if lamellae of two different sizes are mixed, SAXD will not be able to distinguish them. Decisive further evidence for the existence of two kinds of lamellae and their relative arrangement was sought at this stage using electron microscopy.

Samples were chosen from the series prepared for the Raman study of chain length as a function of crystallization time so that a direct comparison of the results obtained from these different techniques could be made.

A micrograph of material which gives two Raman peaks is shown in Figure 10b. This is a stained section of Rigidex 50 crystallized at 126°C for 78 min. For comparison in Figure 10a a micrograph is shown of the same material crystallized for a longer time of 24 h so that the Raman

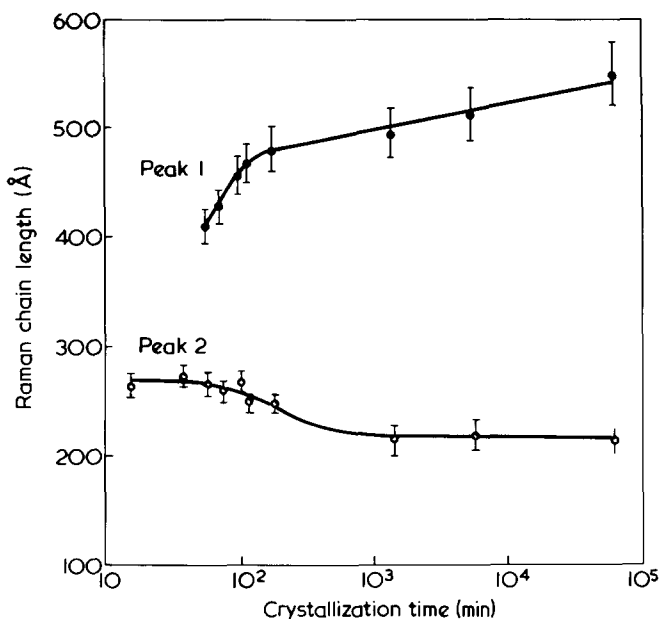


Figure 8 Raman chain length as a function of crystallization time for Rigidex 50 crystallized at 126°C. The data were obtained from spectra of the type shown in Figures 5 and 6 and recorded at room temperature. \bullet , peak 1, refers to the LA mode observed at the lower wavenumber shift (larger L_R); \circ , peak 2, refers to the LA mode observed at the higher wavenumber shift (smaller L_R)

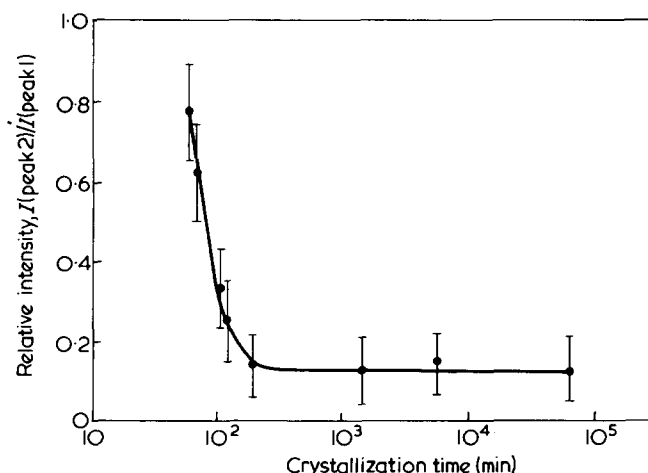


Figure 9 Relative intensities of Raman peaks 1 and 2 as a function of crystallization time for Rigidex 50 crystallized at 126°C



Figure 10 Electron micrographs of stained sections of Rigidex 50 crystallized at 126°C all the same magnification. (a) Sample crystallized for 24 h showing predominantly one layer thickness; (b) sample crystallized for 78 min showing a bimodal distribution of lamellar thicknesses. The thinner (light) central area is assumed to contain lamellae whose normals are oblique to the plane of the section; (c) solid residue from the sample in (b) after solvent extraction, showing removal of the thinner lamellae

peak 2 is very weak. In *Figure 10b* two types of lamellae are clearly distinguishable. Some lamellae are thick, long and quite straight while others are much thinner and occur in groups surrounded by the thicker lamellae. Faint tracks or confused areas occur where the lamellar normals do not lie in the plane of the section. By comparison for a longer crystallization time of 24 h the lamellae are all very thick,

long and straight and occur in large parallel bundles as shown in *Figure 10a*. The order in these is sufficiently good for one to be able to distinguish edge and screw dislocations in the lamellar arrangement.

These visual impressions are borne out by measurements of the distributions of lamellar thicknesses which for *Figure 10b* give two peaks at 316 ± 35 and 190 ± 20 Å. Similar measurements for material in *Figure 10a* give a single peak at 437 ± 70 Å. The errors given indicate the sharpness of the peaks, but there is an additional error of 10% due to the magnification calibration of the electron microscope. The corresponding Raman measurements are 425 and 259 Å for the sample giving two peaks and 489 Å for the sample giving one predominant peak. If the difference between these results is to be explained by chain tilt, the angle must be $40 \pm 14^\circ$, $41 \pm 13^\circ$, $25 \pm 25^\circ$ in the three cases. These are very inaccurate results for ϕ , but they are consistent with previous measurements giving $\phi = 35^\circ$ for bulk polyethylene¹⁴. In any case the quantitative aspects of electron microscopy are not so important. What is important is that the presence of two kinds of lamellae are clearly indicated, supporting the original assumption that both peaks in the Raman spectra are due to LAM vibrations. Further, the arrangement of the lamellae strongly supports the hypothesis that the larger grew first, unimpeded, at the higher isothermal crystallization temperature and the smaller lamellae filled in the gaps between the larger on cooling. An area as at the centre right of *Figure 10b* where the large lamellae are further apart contains between them piles of lamellae of a smaller more uniform size, which will have formed later in the cooling process.

Molecular weight and lamellar morphology

As shown in *Figure 7* the relative intensities of the two Raman peaks on storing at the temperature of the oil bath suggest that some form of fractionation occurs during crystallization from the melt. In the past there have been several reports of molecular fractionation especially during crystallization from solution^{18–20} and indications that a similar process may occur during crystallization from the melt^{14,21,22}. It has been suggested that this leads to rejection of the lower molecular weight molecules which may or may not crystallize subsequently.

Mehta and Wunderlich¹⁷ used solvent extraction to remove material which had crystallized on cooling from the isothermal crystallization temperature¹⁷. In order to examine the material constituting the different sets of lamellae observed in our experiments, we carried out similar extractions on samples selected from the series crystallized at 126°C. Samples which had been crystallized for times of 78 and 108 min were chosen since both showed two Raman peaks and for the time of 78 min the lamellar structure had also been observed using the electron microscope as in *Figure 10b*. Specimens of these were placed in *p*-xylene at 102.5°C and held for 50 h. The solid residues left behind and the polymer extracted in solution were then separated by filtration.

The Raman spectra of the solid residues of the 78 min sample and the 108 min sample showed peak 1 only. These appeared at the same frequencies as in the starting materials. This suggested that the thinner lamellae had been dissolved during the extraction. Supporting evidence was found by examining the solid residues of the 78 min sample left behind using the electron microscope. The result is shown in *Figure 10c*. Here it is seen that only the thicker

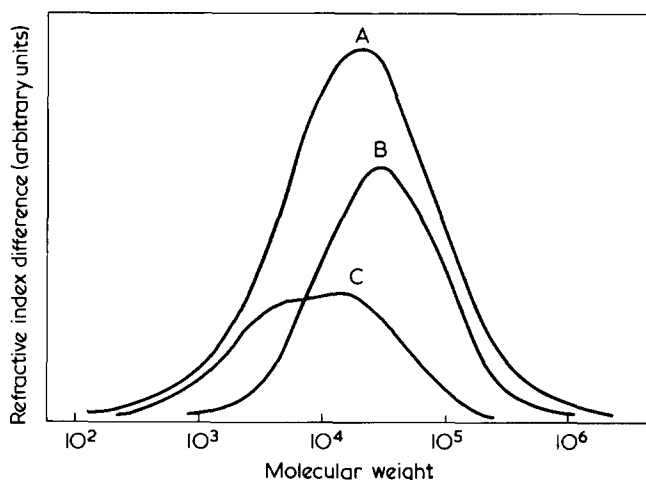


Figure 11 G.p.c. traces of Rigidex 50 crystallized at 126°C for 108 min before and after solvent extraction in *p*-xylene at 102.5°C for 50 h. A, starting material before extraction; B, solid residue left behind after extraction; C, material dissolved and removed by extraction

lamellae remain and that there is a large number of void spaces which by comparison with *Figure 10b* are likely to have been occupied by the thinner lamellae.

Because the supply of sample crystallized for 78 min had been exhausted by the preparations for the microscopy, g.p.c. analysis was carried out on the 108 min sample. It will be remembered that this sample also showed the removal of peak 2 by the solvent extraction. The results are given in *Figure 11* which, even by inspection, show that, by comparison with the starting material (curve A), the solid residue (curve B) consists of the high molecular weights and that the lower molecular weights have been extracted (curve C). The values of the weight- and number-average molecular weights have been calculated from these curves and are given in *Table 2*. Values of dispersivity so given indicate that the extraction has produced two narrower fractions than the starting material; one of high and one of lower molecular weight corresponding respectively to the solid residues and the extracted material. No attempt was made to optimize the extraction procedure and it appears that the extraction conditions were more rigorous than strictly necessary since curve C also contains some high molecular weights.

We are now in a position to correlate the results of the g.p.c. analysis with the previous electron microscopy and Raman results. The removal of the thinner lamellae in conjunction with the loss of the lower molecular weights both caused by the solvent extraction strongly supports the idea that the thinner lamellae are composed mainly of lower molecular weight material. Since all the evidence indicates that the thinner lamellae crystallized on cooling rather than isothermally this in turn favours the operation of a fractionation process during crystallization from the melt. In addition to showing this we have identified the lamellar thicknesses associated with the segregated material and illustrated their arrangement and location within the overall texture.

Time dependence of lamellar thickness

The upper curve in *Figure 8* gives a direct indication that isothermal thickening occurs upon storage at the crystallization temperature. There are two regions in this plot where thickening occurs. Initially there is rapid thickening at times up to 100 min followed by a slower rate of thicken-

ing which appears to operate even at times greater than ten days. Observations of the thickening of lamellae at the crystallization temperature have been made previously by Kawai²², by Hoffman and Weeks²³ and by Kawai and Keller²⁴. We will now examine our Raman data in the light of the theories of thickening put forward by these authors and also discuss the varying magnitudes of thickening which have been reported.

Hoffman and Weeks explain the increase in X-ray long spacing by the annealing of lamellae after they have crystallized whereas Kawai²² suggests a mechanism involving molecular fractionation during crystallization.

According to Kawai²² the higher molecular weight species crystallize first giving rise to thinner lamellae and with time the lower molecular weight species crystallize with a lower degree of supercooling giving rise to thicker lamellae. Assuming that molecular fractionation operates in this way it should be a simple matter to determine its influence on the lamellar thickness by examination of the Raman data. If, as proposed by Kawai²², molecular fractionation controls lamellar thickness then it is expected that the number of lamellae of a given thickness never decreases. Consequently the distribution of thicknesses should broaden continually in the direction of thicker lamellae. As far as it is possible to determine from the spectra obtained this expectation is not fulfilled, since, when peak 1 shifts to lower frequencies (longer chain lengths), it does so without retention of its previous intensity on the higher side of the peak (shorter chain lengths). This suggests that molecular fractionation may not be totally responsible for the observed thickening.

Further evidence of the complex nature of isothermal thickening is given in *Figure 8*. The form of the curve of lamellar thickness as a function of time suggests a discontinuity at around 150 min. This occurs at about the same time as peak 2 decreases in intensity to a small constant value, as shown in *Figure 9*. Thus when crystallization is essentially complete the lamellae continue to thicken on storing at the crystallization temperature. In this region therefore the evidence favours strongly a thickening mechanism based on annealing as proposed by Hoffman and Weeks²³.

The implications are, therefore, that molecular segregation, coupled with isothermal thickening of the lamellae once they have formed, are responsible for the period of initial rapid thickening, while the continued thickening after crystallization is complete is caused by chain refolding alone.

In so far as it is possible to compare the results of different authors using different experimental procedures a number of comments on the scale of thickening can be made. The results of Kawai and those presented in this work were both obtained on samples examined at room temperature. The scale of thickening indicated by the Raman results is, however, much greater than that in the SAXD study of Kawai. It is notable, however, that in our studies of samples giving two Raman peaks one SAXD maximum only is observed.

Table 2 Molecular weight determinations on Rigidex 50 crystallized at 126°C for 108 min before and after solvent extraction

Sample	\bar{M}_w	\bar{M}_n	Dispersivity \bar{M}_w/\bar{M}_n
Starting material	62 000	10 000	6.2
Solid residue	59 000	18 000	3.3
Material extracted	18 000	5 000	3.6

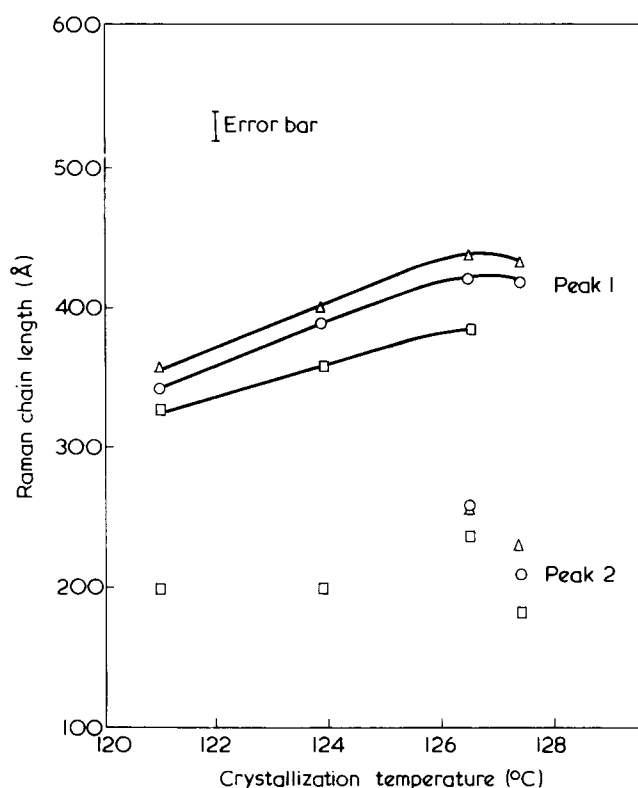


Figure 12 Raman chain length as a function of crystallization temperature for samples of bulk PE with different nucleation densities. A crystallization time of 1 h was used for all samples. Out of the samples chosen Shell Carlona 65045 (Δ) had the highest nucleation density, and Unifex 7006 (\square) had the lowest nucleation density while that of Rigidex 50 (\circ) was intermediate

Thus the presence of two sets of lamellae and hence the nature of the thickening mechanism remained undetected to us using the SAXD technique. Hoffman and Weeks, however, obtained their SAXD data at the temperature of crystallization and so should have detected only lamellae growing at the crystallization temperature. They observed two maxima but chose the smaller spacing as the lamellar periodicity. This may explain why they obtained much smaller values of lamellar thicknesses than in the experiments reported in this paper.

For a direct comparison with Hoffman and Weeks we have attempted to follow this effect by observing the behaviour of the *LA* mode at the crystallization temperature. This has not been entirely successful due to the smeared-out appearance of the *LA* mode peak at elevated temperatures. We have some indication that thickening occurs in these experiments but precise location of the peaks is not possible. An examination of the behaviour of *LA* mode peaks at high temperatures is to be reported elsewhere²⁵.

Nucleation density

When crystallization takes place isothermally the nucleation density has a dramatic effect on the time required for the completion of crystallization. For example at $T_c = 122^\circ\text{C}$ different samples require between 20 min and several hours before crystallization is complete²⁶. Thus for a range of materials with different nucleation densities crystallized at the same temperature for the same time the average age of lamellae can vary significantly. Consequently the degree of thickening is expected to vary accordingly, and it is anticipated that older lamellae will have thickened more. This effect has indeed been observed as shown by the spread of results for peak 1 in Figure 12. The relative

nucleation densities of these polymers were determined from observations of spherulitic structures in the optical microscope²⁶. The samples with the higher nucleation densities consistently produce thicker lamellae for the same crystallization conditions. Typically the range of variation of spacings is in the region 50–100 Å. Although the effect is usually small it has been observed consistently. Initially we propose that lamellae in all samples are of the same thickness. Subsequently the sample with the larger number of growth centres contains more crystalline material and has on average thickened more than the sample with the smaller number of growth centres.

The greatest effect we have observed is for the sample with the lowest nucleation density (see Figure 12) where peak 1 is not detectable after crystallization for 1 h at 127.4°C . Peak 2, however, is of large intensity which indicates that this sample crystallized mainly on cooling. The value of chain length obtained from peak 2 is ~ 230 Å. This behaviour contrasts with that for samples having higher nucleation densities (Figure 12) where peak 1 is the most intense peak. It appears therefore that for higher nucleation densities under these crystallization conditions the greater proportion of the material crystallized isothermally. Accordingly a higher value of chain length of ~ 420 Å is given.

It will be seen in Figure 7 that using the same crystallization time of 1 h the chain length for a sample crystallized at 127.4°C is almost identical to that for a sample of the same nucleation density crystallized at the lower temperature of 126.5°C . This trend is also shown for other samples with different nucleation densities in Figure 12. This is contrary to expectations based on the usually observed dependence of the lamellar thickness upon the supercooling whereby crystallization at the higher temperature produces the larger lamellar thickness, hence longer chain traverse lengths.

The following explanation for this anomaly is proposed. The larger thickness observed is that arising during primary crystallization followed by subsequent thickening. As the latter is a function of time, its magnitude at a given temperature will depend on the age of the lamellae. At any given instant during crystallization we have a spectrum of ages. At a comparatively short time of crystallization, say at time t_x in Figure 13, the majority of the lamellae present will have formed towards the end of the time interval $t_x - t_0$ in the case of the crystallization conducted at high temperatures (curve 1). Thus the corresponding lamellae will be young in comparison to the average of those formed by further crystallization at a lower temperature (curve 2) by the same time t_x . This means that they have had less time to thicken and although formed with an initially larger chain length the actual value of this length as measured at time t_x can be equal or even lower. We see that we can envisage a situation where thickening can compensate for, or even reverse, the differences in lamellar thicknesses arising due to different crystallization temperatures, particularly at the early stages of crystallization. This particular influence of lamellar thickening to counteract the established trend due to the crystallization temperature itself should diminish with increasing crystallization time. This in fact is observed as shown in Figure 7. For crystallization times of 1 h the data in the lower curve were obtained. For crystallization times much larger than 1 h under the present conditions the data shown in the upper curve followed the commonly observed rapid upsweep of chain length with increasing crystallization temperature.

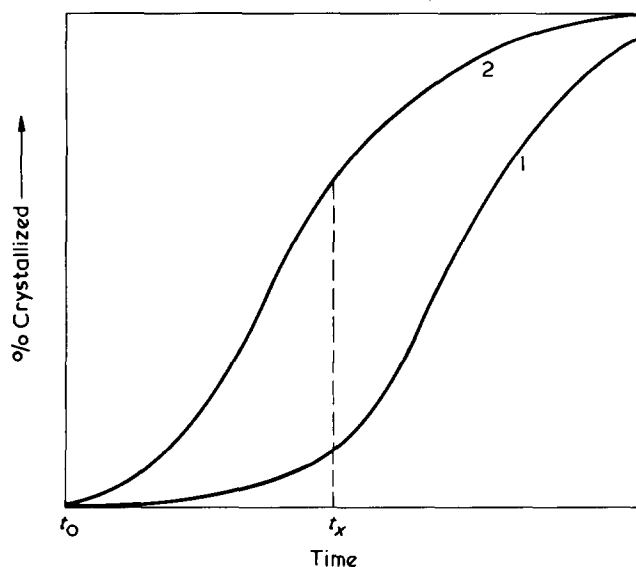


Figure 13 Schematic diagram of percentage of polymer crystallized as a function of crystallization time. Curve 1 represents crystallization at a higher temperature than curve 2. Curves 1 and 2 illustrate the situation where at a relatively short time of crystallization, t_x , more material has crystallized in case 2 than in case 1

We conclude therefore that nucleation density, through the agency of isothermal thickening, affects the lamellar thickness. This relationship is rarely noted and may go some way towards explaining the comparatively large variations in the values of lamellar thickness reported by various authors using polyethylene from different sources.

CONCLUSION

The power of the combined application of the different structure methods has been demonstrated. The Raman method has proved superior in registering lamellae and identifying their true origin while the more conventional low-angle X-ray scattering method is capable of giving information on their mode of stacking. Electron microscopy, involving novel sample preparation methods, can then provide the visual image corresponding to these diffraction and spectroscopic effects thus providing direct confirmation of the structural units involved and of their arrangements in the overall texture.

The important part played by isothermal thickening has been highlighted. This, together with other factors including nucleation density, determines the measured lamellar thickness and is thus pertinent to the problem of interpreting lamellar thicknesses in terms of the crystallization temperature.

The effect of molecular segregation on crystallization is forcefully brought out by these studies whereby the structural entities comprising the segregated materials have been identified and their lamellar thicknesses measured.

ACKNOWLEDGEMENTS

During the course of this work G.V.F. and D.G. have been supported by the Science Research Council and J.A.O. by the Ministry of Defence. We also wish to acknowledge the assistance of the Science Research Council for the partial provision of the Raman spectrometer. We are indebted to P. Volans for the supply of samples and to Dr J. Stejny, who with the assistance of Mrs A. Halter carried out the g.p.c. analysis.

REFERENCES

- 1 Olf, H. G., Peterlin, A. and Peticolas, W. L. *J. Polym. Sci. (Polym. Phys. Edn)* 1974, **12**, 359
- 2 Koenig, J. L. and Tabb, D. L. *J. Macromol. Sci. (B)* 1974, **9**, 141
- 3 Folkes, M. J., Keller, A., Stejny, J., Fraser, G. V., Hendra, P. J. and Goggin, P. L. *Colloid Polym. Sci.* 1975, **13**, 341
- 4 Schaufele, R. F. and Shimanouchi, T. *J. Chem. Phys.* 1967, **47**, 3605
- 5 Fanconi, B. M. and Crissman, J. *J. Polym. Sci. (Polym. Lett. Ed.)* 1975, **13**, 241
- 6 Brown, R. G. and Eby, R. K. *J. Appl. Phys.* 1964, **35**, 1156
- 7 Crist, B. and Morosoff, N. *J. Polym. Sci. (Polym. Phys. Edn)* 1973, **11**, 1023
- 8 Burmester, A. F. and Geil, P. H. in 'Advances in Polymer Science and Engineering', (Eds K. D. Pae, D. R. Morrow and Yu Chen), Plenum Press, New York, 1972, pp 43-100
- 9 Kanig, G. *Kolloid Z. Z. Polym.* 1973, **251**, 782
- 10 Kanig, G. *Kunststoffe* 1974, **64**, 470
- 11 de Körösy, F. and Zeigerson, E. *J. Appl. Polym. Sci.* 1967, **11**, 909
- 12 Fraser, G. V., Keller, A. and Pope, D. P. *J. Polym. Sci. (Polym. Lett. Ed.)* 1975, **13**, 341
- 13 Bassett, D. C. and Keller, A. *Phil. Mag.* 1963, **8**, 1753
- 14 Keller, A. and Sawada, S. *Makromol. Chem.* 1964, **74**, 190
- 15 Anderson, F. R. *J. Appl. Phys.* 1964, **35**, 64
- 16 Fraser, G. V., Hendra, P. J., Cudby, M. E. A. and Willis, H. A. *J. Mater. Sci.* 1974, **9**, 1270
- 17 Mehta, A. and Wunderlich, B. *Colloid Polym. Sci.* 1975, **253**, 193
- 18 Peterlin, A. and Meinel, G. *J. Polym. Sci. (B)* 1964, **2**, 751
- 19 Prime, R. B. and Wunderlich, B. *J. Polym. Sci. (A-2)* 1969, **7**, 2021
- 20 Sadler, D. M. *J. Polym. Sci. (A-2)* 1971, **9**, 779
- 21 Gruner, C. L., Wunderlich, B. and Bopp, R. C. *J. Polym. Sci. (A-2)* 1969, **1**, 2099
- 22 Kawai, T. *Kolloid-Z.* 1967, **229**, 116
- 23 Hoffman, J. D. and Weeks, J. J. *J. Chem. Phys.* 1965, **42**, 4301
- 24 Kawai, T. and Keller, A. *Phil. Mag.* 1966, **14**, 132
- 25 Fraser, G. V. and Keller, A. to be published
- 26 Fraser, G. V., Odell, J. A. and Keller, A. to be published

Diffusion of large molecules in polymers: a measuring technique based on microdensitometry in the infra-red*

J. Klein and B. J. Briscoe

Physics and Chemistry of Solids, Cavendish Laboratory, University of Cambridge, Cambridge CB3 0HE, UK

(Received 18 December 1975)

A technique based on infra-red microdensitometry has been developed for studying the centre-of-mass translational diffusion of large additive molecules in polymeric matrices. In this technique the diffusion broadening with time of a known initial concentration profile of the additive within the bulk polymer is monitored. The shape of the concentration profile after diffusion broadening readily yields D , the diffusion constant; it may also yield the concentration dependence of D where this is significant. The technique is found to be reasonably flexible, and applicable to a number of polymer-additive combinations. Values of D in the range 10^{-5} to 10^{-10} cm²/sec and initial additive concentrations of down to 0.3% may be studied. The technique is viable over a wide range of temperatures and pressures. Some results obtained by this technique are presented, for the case of various linear long-chain amides diffusing in low density polyethylene.

INTRODUCTION

The diffusion of small molecules through polymers has been extensively studied in the past. Several well established techniques for such studies exist and are described in detail elsewhere¹. Studies of the diffusion of large molecules, including polymeric self-diffusion, have been far less common. In this context 'small' molecules refer to those in the gaseous, vapour or liquid phase at room temperature and pressure and 'large' molecules are those forming solids under these conditions. Bueche *et al.*² first described the use of radioactively labelled polymers in the determination of self-diffusion coefficients in polymers. Their technique, with slight variations, has since been used with some success in studying the diffusion of smaller (though still 'large' in this context) additive molecules through various polymeric matrices³⁻⁵. These techniques involving radioactive labelling of the diffusant are, generally speaking, faced with two major shortcomings in addition to the necessity of having to obtain the required labelled material: they fail for the case of diffusants which are surface active with respect to the polymer matrix, and they may also involve significant interfacial resistance which the method does not readily reveal. Nuclear magnetic resonance (n.m.r.) has also been used to determine diffusion coefficients in polymers, as for example by McCall *et al.*⁶. These measurements are limited to the melt or liquid phases of the polymer. Furthermore the n.m.r. technique is limited¹ to measuring values of D , the diffusion coefficient, greater than about 3×10^{-7} cm²/sec. Autoradiographical determination of D for large molecules is at present not a viable technique¹.

We have developed a simple technique for the measurement of the translational diffusion of large molecules in polymeric matrices, based on microdensitometry in the infra-red (i.r.). A preliminary outline of this technique has already appeared⁷. The purpose of the present paper is to describe the procedure and underlying principles in more detail.

THEORY

The principles underlying the technique are simple. When a step function in the concentration of a diffusant is set up within a host matrix it will broaden with time under diffusion, the driving force being the concentration gradient. The shape of the resulting concentration profile is established, as a solution of Fick's equations⁸ with the appropriate boundary conditions, and is expressed in terms of x (the distance along the diffusion direction), D and t , the time over which diffusion broadening has taken place. D may itself depend significantly on the diffusant concentration, C .

Figure 1 shows the diffusion broadening where D is independent of C .

In essence the technique involves setting up a step function in additive concentration within the bulk polymer, allowing this to broaden under diffusion at the required temperature and pressure, terminating the process at a known time t , and comparing the resulting broadening concentration profile with the theoretical case. D is thus readily evaluated.

EXPERIMENTAL

The procedure for setting up a step function in additive concentration within the bulk polymer is illustrated in Figure 2. The concentration C_0 of additive in specimen I is typically 0.5% w/w but values as low as 0.3% w/w of additive have been used. Actual joining (Figure 2b) is effected by local melting of the adjacent surfaces in vacuum for a very short duration and pressing them together. We find this to result in an interface which generally presents little or no resistance to diffusion, and at the same time only negligibly distorts the initial step function (see later, also Figure 5). Dimensions of the specimens are such that the final broadening of the initial distribution is small in comparison, to minimize end effects in the case of surface active additives. After joining, diffusion broadening of the initial step function is allowed to occur at the desired temperature and pressure for a time t , when it is effectively terminated by

* Presented at the Polymer Physics Group (Institute of Physics) Biennial Conference, Shrivenham, September 1975.

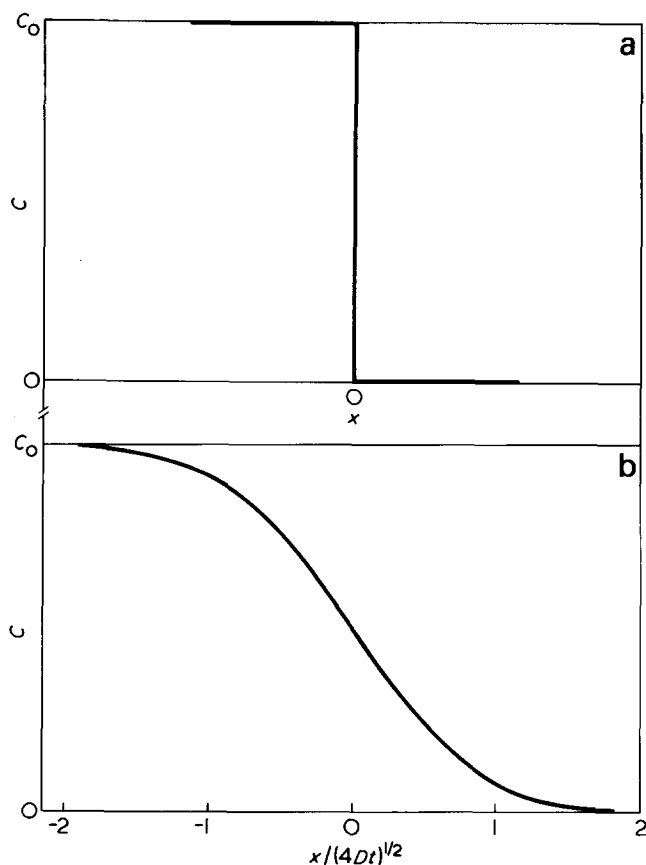


Figure 1 Concentration profiles. (a) Initial step function; (b) calculated⁸ diffusion-broadened step function after time t . D constant

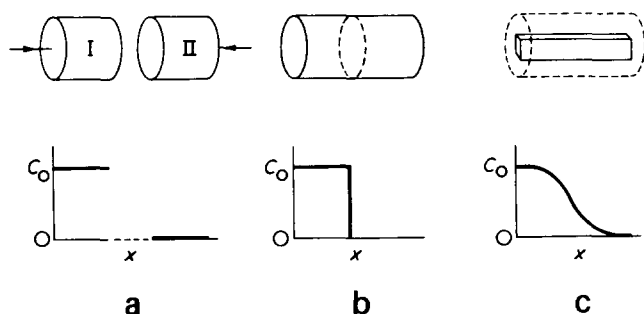


Figure 2 Setting up a step-function. (a) Specimen I: polymer containing a concentration C_0 ($\sim 0.5\%$) of additive uniformly dispersed; specimen II: additive-free polymer. Adjacent surfaces melted in vacuum and pressed together; (b) composite immediately after join has been made; (c) slice removed from centre of composite, after diffusion has occurred, and monitored in the microdensitometer. The concentration profiles corresponding to the different stages are also shown

quenching. A thin (typically $150\ \mu\text{m}$) slice is representative of the centre of the specimen removed by microtoming as shown in Figure 2c, and the concentration of additive $C(x)$, along its length x , is monitored.

In order to obtain a measure of the diffusant concentration it is necessary that it absorb at some i.r. frequency unaffected by the bulk polymer. When scanning through the frequency spectrum a sharp absorption peak is observed at this 'labelling' frequency of the additive, and this is shown in Figure 3.

The lateral scanning of the thin slice is then carried out at this 'labelling' frequency. A commercial double beam i.r. spectrometer (Perkin-Elmer 157) has been adapted for this

purpose, and a slit of width $90 \pm 10\ \mu\text{m}$ mounted at the focus of the sample beam. This represents the limiting value of the spatial resolution of the 'microdensitometer'. The spectrometer is then fixed at the labelling frequency, and the slice slowly traversed across the slit on a motorized translation stage.

If I_0 is the incident intensity of the sample beam reaching the slice, then the intensity I passing through the slice at a point x may be written (neglecting the small diffraction effect):

$$I/I_0 \propto \exp \{-\epsilon_0 d(x)C(x)\} \quad (1)$$

if the Beer's relation applies. ϵ_0 is the absorptivity of the additive at the scan frequency ν_0 , d is the slice thickness at x and $C(x)$ is the additive concentration at x . The proportionality factor represents such effects as the polymer matrix absorption at the scan frequency, the reflectivity of the slice and also some instrument effects. If d is constant and $C \ll 1$, however, the proportionality factor in equation (1) may be taken as constant for a given run. We have found d to be constant within 1–2% typically, by micro-meter measurements along the slice.

Taking logarithms, we have:

$$-\log \left\{ \frac{I}{I_0} \right\} \equiv -\log T(x) = \text{constant} + A\epsilon_0 C(x) \quad (2)$$

for constant d , where A is constant. By making up a composite (as in Figure 2) consisting of five layers of known different concentrations and scanning a slice through this composite, we have shown that, within error, (Figure 4):

$$-\log(T(x)) = \text{constant} + A'C(x) \quad (3)$$

thus ϵ_0 , for the additives and concentrations we have used, is independent of concentration.

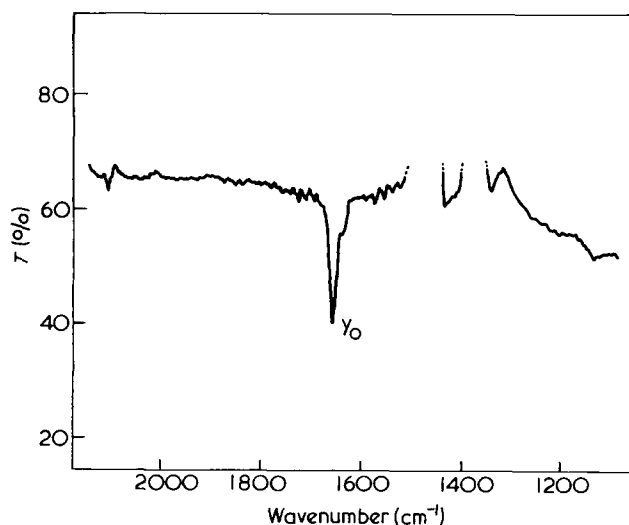


Figure 3 Spectrogram of a polymer-additive sample in the region of the labelling absorption frequency, ν_0 . T is the percentage transmission through the microdensitometer slit. The sample is a slice $\sim 160\ \mu\text{m}$ thick of low density polyethylene containing 0.5% w/w stearamide. ν_0 corresponds to a wavenumber of $1660\ \text{cm}^{-1}$, an amide absorption peak. (A similar but additive free slice of polyethylene is in the reference beam for compensation, and the inverse-absorption peaks near $1500\ \text{cm}^{-1}$ are due to overcompensation.)

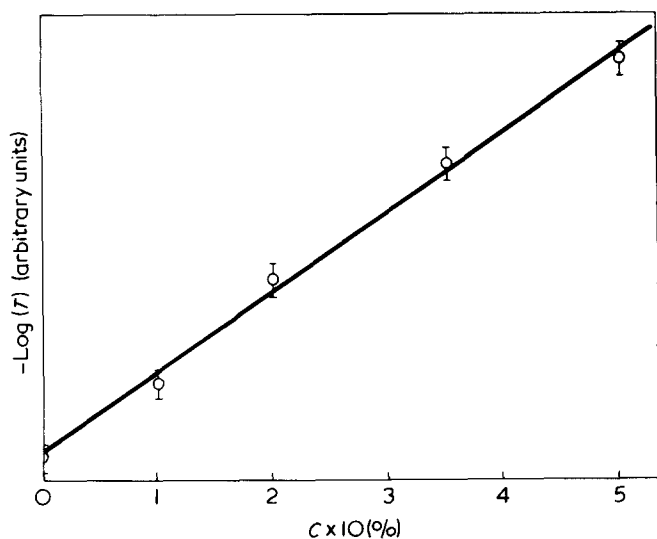


Figure 4 Variation of $\log T$ vs. concentration of stearamide in low density polyethylene. Scan frequency corresponds to 1660 cm^{-1} (see Figure 3)

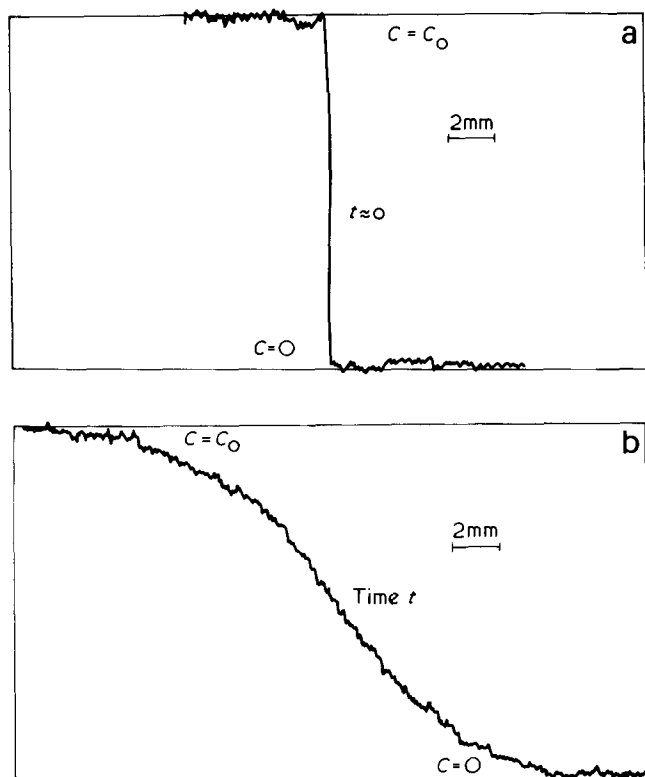


Figure 5 Observed concentration profiles. (a) $t \approx 0$ (initial step function; $t = 54 \text{ sec}$, $C_0 = 0.5\% \text{ w/w}$ stearamide in low density polyethylene; (b) after time t ($t = 5.22 \times 10^4 \text{ sec}$, $T = 130^\circ \text{C}$, C_0 as in (a)). Both profiles scanned at 1660 cm^{-1} , an amide absorption frequency

The output of the i.r. spectrometer as the slice is traversed along the slit is fed via a linear-to-log converter to the y-axis of an X-Y recorder, the X axis of which is coupled to the lateral traverse of the slice, i.e. x in our notation. This yields concentration profiles directly. Figure 5 shows (on the same scale) both the initial step function and the diffusion-broadened profile for a typical run. Comparison with Figure 1 shows the agreement between Fickian predictions and experiment to be good, and compatible with a D independent of C . The actual value of D is readily evaluated by comparison of observed and calculated curves.

It is possible to calculate the concentration dependence of D , where this is significant, by the Matano-Boltzmann⁸ procedure. If any resistance to diffusional flow across the interface between the two halves exists, it can be detected by predictable⁸ discontinuities in the broadened concentration profile, as in Figure 6.

With the present resolution of the technique we can measure values at D in the range of 10^{-5} to $10^{-10} \text{ cm}^2/\text{sec}$ in times of the order of 1–30 days. Estimated errors are of order 15%.

DISCUSSION AND SOME RESULTS

It is possible to anneal the composite sample after joining its two halves, but prior to measuring the diffusion – this would involve a slightly different procedure for evaluating D .

Preliminary experiments with a number of additives and different polymers indicate that the technique is quite flexible. For example, by suitably labelling molecules of the polymer itself, say by deuteration, self-diffusion constants may be obtained. The labelling frequency here would be that of the C–D bond as against the C–H background.

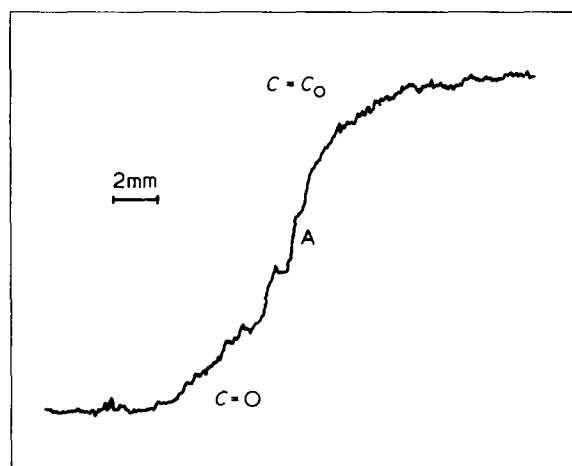


Figure 6 Concentration profile showing a discontinuity (at A) indicating resistance to diffusional flow at the interface. $C_0 = 0.5\%$ in low density polyethylene

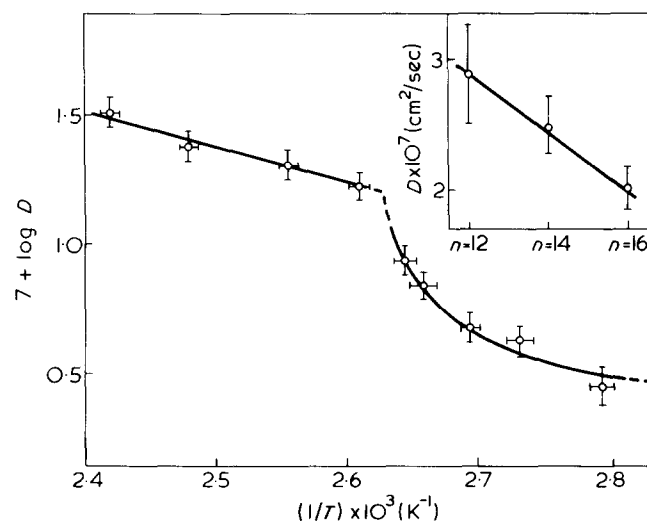


Figure 7 Variation of the diffusion constant D of stearamide in low density polyethylene as a function of temperature T , about the melting point of the polymer. Inset: diffusion constants D of $\text{CH}_3(\text{CH}_2)_n\text{CONH}_2$ in LDPE as a function of n , at 118°C . D decreases as diffusant length increases

We have studied the diffusion of various long chain n-alkyl amides in low density polyethylene (LDPE) about the melting point of the polymer at atmospheric pressure. The additives were incorporated into the bulk polymer by mixing the powders in the required proportions, then milling at 125°C for 20 min. The cylindrical specimens (Figure 2) were prepared by hot pressing in a die *in vacuo*. Their diameter was 30 mm and each half was 30 mm in length. Some results for temperature and chain length dependence are presented in Figure 7. The variation in slope of the Arrhenius plot is probably due in part to the breakdown of crystalline lamellae in the polythene, which at temperatures below about 80°C comprise some 60% of the polymer⁹; this leads to a decrease in the tortuosity of the path taken by the chains in the amorphous polymer regions, over and above the usual temperature dependence. (However, it appears that this variation in slope is not solely due to lamellar breakdown — effects due to annealing of the bulk polymer¹⁰ and to association of the stearamide probably also play a part.) D.s.c. studies show that the discontinuity in the slope of the Arrhenius plot at $T \approx 107^\circ\text{C}$ corresponds, within experimental error, to the melting point of the polythene.

The activation energy in the melt region is 6.2 ± 0.2 kcal/mol. This compares with the activation energies for self-diffusion of 5.3 ± 0.8 and 5.6 ± 0.3 kcal/mol for a low MW (4100) polyethylene fraction and n-C₃₂H₆₆ respectively, as obtained from n.m.r. studies⁶.

The diffusional behaviour of longer molecules, including polymeric self-diffusion, is being explored.

ACKNOWLEDGEMENTS

We thank ICI Plastics Division (Welwyn) for preparing the materials, and one of us (J. K.) thanks Dow Corning Chemicals for a maintenance grant. We are also very grateful to Professor D. Tabor for encouragement.

REFERENCES

- 1 Crank, J. and Park, G. S. 'Diffusion in Polymers' (Eds J. Crank and G. S. Park), Academic Press, London, 1968, Ch 1, pp 1–39
- 2 Bueche, F., Cashin, W. M. and Debye, P. *J. Chem. Phys.* 1952, **20**, 1956
- 3 Auerbach, I., Miller, W. R., Kuryla, W. C. and Gehman, S. D. *J. Polym. Sci.* 1958, **28**, 129
- 4 Jackson, R. A., Oldland, S. R. D. and Pajaczkowski, A. *J. Appl. Polym. Sci.* 1968, **12**, 1297
- 5 Westlake, J. F. and Johnson, M. *J. Appl. Polym. Sci.* 1975, **19**, 319
- 6 McCall, D. W., Douglass, D. C. and Anderson, E. W. *J. Chem. Phys.* 1959, **30**, 771
- 7 Klein, J. and Briscoe, B. J. *Nature* 1975, **257**, 386
- 8 Crank, J., 'Mathematics of Diffusion', 2nd edn., Oxford University Press, London, 1975
- 9 Ke, B. *J. Polym. Sci.* 1960, **42**, 15
- 10 Michaels, A. S., Bixler, H. J. and Fein, H. L. *J. Appl. Phys.* 1964, **35**, 3165

Radial distribution functions from molten polyethylene by X-ray diffraction*

G. W. Longman†, G. D. Wignall‡ and R. P. Sheldon§

(Received 22 January 1976)

The short range ordering in molten polyethylene has been investigated by radial distribution function (*RDF*) methods. The intramolecular distances resolved are consistent with the presence of *gauche* conformations, whilst no long *trans* sequences are resolved. Broad peaks at ~5, 10 and 15 Å are attributed to intermolecular ordering, which is greater than that observed in glassy amorphous polymers. The results are not inconsistent with the polymer chains adopting a random coil configuration over distances greater than ~20 Å.

INTRODUCTION

Few radial distribution function studies have been made concerning ordering in molten polymers, and almost none have been by X-ray methods. Ovchinnikov and Markova¹ and Ovchinnikov, Markova and Kargin² made extensive studies of molten polyethylene between 136° and 211°C by means of radial distribution functions (*RDF*) derived from electron diffraction. Some of the peaks in the *RDF* curves (i.e. 1.3, 2.3 and 3.7 Å) were attributed to intramolecular distances. Other distinct peaks were observed at 4.8 and 5.8 Å, especially at temperatures near the melting point. These distinct peaks were attributed to intermolecular distances and became more diffuse with increasing temperature. The observed peaks were compared with those occurring in crystalline polyethylene and in an array of hexagonally packed parallel chain segments. On the basis of this comparison the authors proposed that molten polyethylene consisted of ordered regions ~50 Å in diameter, within which the chains were essentially parallel.

Subsequently these experimental findings were challenged by Fischer *et al.*³ and Voigt-Martin and Mijlhoff⁴ who also measured *RDF* curves from molten linear polyethylene at 140° and 200°C. They observed a broad intermolecular peak in the region 4–6 Å with intramolecular peaks at 1.16, 1.53, 2.18, 2.56, 2.99, 3.57, 3.95, 4.51 and 5.08 Å. They criticized the previous work on the grounds that: 'not only is the CH distance missing and the C–C and C–C–C distance in the wrong place and incorrectly weighted, but there are considerable termination and background ripples on the *RDF* curve'³. They concluded 'that there is a distribution of atomic distances between 4–6 Å, rather than tightly packed bundles with a well defined intermolecular distance' as postulated by the Russian workers. The discrepancies between the different data sets derived from electron diffraction, and the conclusions which have been built on the disputed features, point to the need for very careful data correction procedures. These procedures are discussed in detail by Voigt-Martin and Mijlhoff⁴ for the case of electron diffraction. In principle the same *RDF* functions can be obtained from X-ray dif-

fraction measurements though the experimental details naturally differ between the two techniques.

The main experimental problems and procedures necessary to remove artefacts in the X-ray technique have been discussed by Wignall⁵. In an effort to resolve the above discrepancies in the measured *RDF* curves from electron diffraction, we have performed complementary *RDF* measurements on polyethylene by X-ray techniques.

EXPERIMENTAL

The experimental methods employed have already been described in detail⁶. Measurements were performed on a Picker Automatic 4 Circle Diffractometer within the range $0.11 < s < 16.1 \text{ \AA}^{-1}$ where $s = (4\pi/\lambda)\sin\theta$; 2θ is the scatter angle and $\lambda = 0.7107 \text{ \AA}$ is the wavelength of the incident molybdenum K_α radiation. The sample was ~0.125 cm thick and was held in a heated cell and constrained by thin Melinex film (~18 μm thick). The sample was maintained at $160^\circ\text{C} \pm 2^\circ\text{C}$ by tungsten heaters embedded in mica plates and placed each side of the sample. Windows ~1 cm² allowed the passage of the incident and diffracted beams, the irradiated sample volume being ~1 mm³.

The scattered data were corrected for incoherent scattering, absorption in the sample and Melinex cell walls, double scattering and polarization of the scattered beam. The methods for performing these corrections, and for choosing the collimation limits, monochromatizing the incident beam etc. are described in ref 6. The data were normalized using the dispersion corrected form factors of Berghius⁷ and Stewart⁸, and incoherent scattering factors of Keating and Vineyard⁹. The resulting *RDF*, $H(r)$, was calculated from

$$H(r) = \frac{1}{2\pi^2\bar{\rho}r} \int_{s_{\min}}^{s_{\max}} si(s) \sin sr ds \quad (1)$$

where $\bar{\rho}$ is the atomic density (atoms/unit volume) of the sample, and $s_{\min} = 0.11 \text{ \AA}^{-1}$ and $s_{\max} = 16.1 \text{ \AA}^{-1}$. $H(r)$ for molten high density polyethylene is shown in Figure 1, whilst the second moment of the *RDF*, $4\pi\bar{\rho}r^2H(r)$ is shown in Figure 2.

DISCUSSION

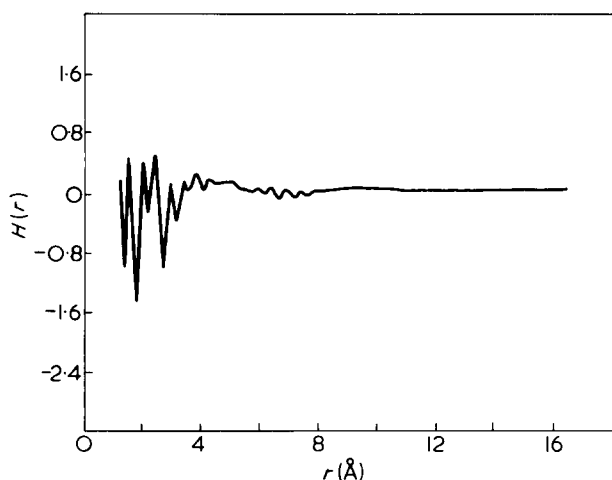
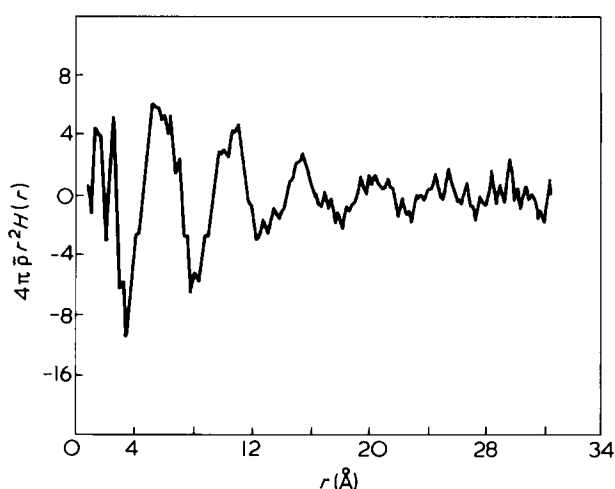
The main peaks in the *RDF* of Figure 1 are listed in Table 1 together with those observed previously^{1,4}. The peak posi-

* Presented at the Polymer Physics Group (Institute of Physics) Biennial Conference, Shrivensham, September 1975.

† ICI Corporate Laboratory, The Heath, Runcorn, Cheshire WA7 4QE, UK.

‡ ICI Europa Ltd, Everslaan 45, B-3078 Everberg, Belgium.

§ School of Polymer Science, University of Bradford, Bradford, BD7 1DP, UK.


 Figure 1 The RDF, $H(r)$ vs. r for molten high density polyethylene

 Figure 2 The second moment of the RDF, $4\pi\bar{\rho}r^2H(r)$ vs. r for molten high density polyethylene

tions are very similar to those observed by Voigt-Martin and Mijlhoff (VMM). In particular we observe a peak at ~ 3.0 Å, which was attributed by VMM to a high concentration of *gauche* bonds, but was absent from the previous work of Ovchinnikov and Markova (OM). There are no resolvable peaks in the RDF consistent with the presence of extended sequences in the *trans* configuration, neither do we see the strong features at 4.8 Å and 5.8 Å reported by OM.

No correction has been made to the data of Figure 1 for truncation errors, but the close agreement obtained with the work of VMM suggests that truncation errors are not a serious problem in the region $1 < r < 6$ Å. This is particularly so in view of the wide differences in truncation limits used in the present work and those used by VMM ($s_{\min} = 1 \text{ \AA}^{-1}$, $s_{\max} = 25 \text{ \AA}^{-1}$) as truncation features generally have a frequency inversely proportional to the truncation limits. The positions of the main RDF peaks of VMM are within a few percent of those resolved in this work, which suggests strongly that the observed peaks are real and not truncation features.

At higher values of r one would not expect to resolve sharp peaks in the RDF, due to the increasing number of overlapping interatomic distances. The small oscillations in the RDF of Figure 1 above ~ 7 Å probably represent residual truncation features, as they have a frequency given approximately by $2\pi/s_{\max} \approx 0.4$ Å. These are small in $H(r)$, but when plotting $4\pi\bar{\rho}r^2H(r)$ (Figure 2) the r^2 weight-

ing factor considerably magnifies these features, and hence the data of Figure 2 have been 'damped' by inclusion of a damping factor $\exp(-\alpha^2s^2)$ in equation (1) before transformation. The value of $\alpha = 0.112$ was chosen to eliminate most of the high frequency oscillations (~ 0.4 Å), whilst leaving the lower frequency structural features unchanged. The high frequency oscillations at ~ 24 Å are probably the residue of these truncation features, and should not be taken as evidence of long range ordering.

The second moment of the RDF (Figure 2) exhibits broad maxima with a period ~ 5 Å. The first broad maximum between 4–7 Å is very similar to that reported by VMM, and supports their conclusion that 'there is a distribution of atomic distances between 4–6 Å', rather than the sharp distinct peaks at 4.8 and 5.8 Å observed by OM. This broad peak is similar to peaks observed for amorphous polycarbonate⁶, and amorphous polystyrenes¹⁰, and has been attributed to interchain packing.

Further broad peaks at 10 and 15 Å (and possibly 20 Å) suggest that there is considerable liquid like order caused by the packing of polymer chains with an effective diameter of ~ 5 Å. Odajima *et al.*¹¹ have derived an RDF for the amorphous regions of solid polyethylene from X-ray diffraction data, and have observed similar broad oscillations with maxima at 5, 10 and 15 Å. These broad oscillations have been compared with a paracrystalline model based on the methods of Hosemann and Bagchi¹². Starting with a pseudo-hexagonal lattice as an initial structure, the positions of atoms were disordered to create a paracrystalline arrangement of atoms. To obtain the RDF, $D(r) = 4\pi r^2 \bar{\rho} H(r)$, a summation was taken over all atoms in a spherical shell about each atom. Odajima *et al.* chose a disorder parameter which gave the best fit to the observed oscillations in solid polyethylene. The amplitude of the oscillation at ~ 5 Å in Figure 2 is ~ 5 compared to a value of ~ 3 observed in amorphous polyethylene and a value of ~ 4 predicted from the model. Thus the amplitude and area of the first peak are consistent with the polymer molecules being arranged in a pseudo-crystalline lattice with parallel packing of chains¹³ and as suggested by OM. A similar conclusion concerning polystyrene was reached by Wecker, Davidson and Cohen¹⁰, from an analysis of RDF plots derived from X-ray diffraction studies of amorphous polystyrenes.

The broad oscillations seen in Figure 2 are fairly rapidly damped and cannot be resolved clearly beyond ~ 15 Å. It therefore appears that any pseudo-crystalline parallel ordering of polymer chains does not persist over large distances.

Table 1 Positions of the main peaks in the RDF plots from molten polyethylene

Ovchinnikov and Markova ¹ ($T = 136^\circ\text{C}$)	Voigt-Martin and Mijlhoff ⁴ ($T = 140^\circ\text{C}$)	This work ($T = 160^\circ\text{C}$)	Predicted from short range intramolecular order ⁴
	1.16		1.14
1.4	1.53	1.58	1.53
	2.18	2.10	2.10
2.5	2.56	2.50	2.54
	2.99	3.05	2.99
	3.57	3.50	3.45
3.8	3.95	3.92	3.90
4.84	4.51	4.44	4.39
	5.08	5.15	5.07

Complementary neutron scattering measurements have been performed on molten polyethylene^{14,15}. The polymer molecule adopts an overall conformation such that the radius of gyration of the molecule is very close to that measured in θ solvents, and is that predicted by the random coil model¹⁶. Furthermore, analysis of the full neutron scattering curve¹⁵ indicates that the polymer molecule obeys random statistics above 20 Å. These findings are consistent with the *RDF* measurements, which do not resolve interatomic distances associated with extended sequences in the *trans* configuration. The existence of some nearest neighbour intermolecular peaks over short ranges would be expected simply in terms of the geometrical packing of polymer chains with a diameter ~ 5 Å. This packing mechanism is the basis of much of the short range order in liquids, and the existence of this kind of short range liquid like order is not inconsistent with the random coil concept. This may be regarded as being particularly so in the case of polyethylene where the cross-sectional dimensions of the polymer chain are approximately the same in different directions, irrespective of whether the carbon backbone is in the *trans* or *gauche* configuration. It is probable that the chain packing is enhanced by this uniformity of the chain dimensions. Certainly the level of intermolecular ordering observed in molten polyethylene is greater than that observed in glassy amorphous polycarbonate⁶ and poly(ethylene terephthalate)¹⁷. The molecular chains in these latter polymers are both stiffer than polyethylene and the cross-sectional dimensions are different along each of the axes perpendicular to the chain backbone. Apparently, even for molten polyethylene the ordering does not persist beyond ~ 30 Å perpendicular to the polymer molecules, and for distances less than ~ 20 Å along the chains. This level of short range ordering does not conflict with results that show that over larger distances the molecule adopts a random configuration.

ACKNOWLEDGEMENTS

The authors wish to acknowledge valuable discussions with Professor A. Odajima (Hokkaido University) and Professor E. W. Fischer (University of Mainz).

REFERENCES

- 1 Ovchinnikov, J. K. and Markova, G. S. *Vysokomol. Soedin (A)* 1967, **9**, 449
- 2 Ovchinnikov, J. K., Markova, G. S. and Kargin, V. A. *Polym. Sci. USSR (A)* 1969, **11**, 329
- 3 Fischer, E. W. *et al. J. Macromol. Sci.*, to be published
- 4 Voigt-Martin, I. and Mijlhoff, F. C. J. *Appl. Phys.* 1975, **46**, 1165
- 5 Wignall, G. D. 'Recent Advances in Fibre Science', Academic Press, New York, 1976, ch 7
- 6 Wignall, G. D. and Longman, G. W. *J. Mater. Sci.* 1973, **8**, 1439
- 7 Berghuis, J. *et al. Acta Crystallogr.* 1966, **21**, 478
- 8 Stewart, R. F. and Davidson, E. R. *J. Chem. Phys.* 1965, **42**, 3175
- 9 Keating, D. T. and Vineyard, G. H. *Acta Crystallogr.* 1956, **9**, 895
- 10 Wecker, S. M., Davidson, T. and Cohen, J. B. *J. Mater. Sci.* 1972, **7**, 1249
- 11 Odajima, A. *et al. Prog. Poly. Phys. Japan* 1975, **18**
- 12 Hosemann, R. and Bagchi, S. N. 'Direct Analysis of Diffraction by Matter', North Holland, Amsterdam, 1962
- 13 Odajima, A. Personal communication
- 14 Schelten, J., Wignall, G. D. and Ballard, D. G. H. *Polymer* 1974, **15**, 682
- 15 Lieser, G., Fischer, E. W. and Ibel, K. *J. Polym. Sci. (Polym. Lett. Edn)* 1975, **13**, 39
- 16 Flory, P. J. 'Principles of Polymer Chemistry', Cornell University Press, Ithaca, 1953
- 17 Longman, G. W., Sheldon, R. P. and Wignall, G. D. *J. Mater. Sci.* to be published

Analysis of wide-angle X-ray diffraction patterns of aligned glassy polymers with particular references to polystyrene*

Richard Lovell and Alan H. Windle

Department of Metallurgy and Materials Science, University of Cambridge, Cambridge CB2 3QZ, UK
(Received 19 December 1975)

Improvement of WAXD patterns from aligned glassy polymers by a numerical desmearing technique is reported. This gives a fibre type diffraction pattern that can be more easily interpreted than radial or cylindrical distribution functions. Application to atactic and quenched isotactic polystyrene shows that the molecular conformations that are found are in agreement with those deduced from i.r. and n.m.r. spectroscopy. For isotactic polystyrene there is significant agreement between the fibre pattern of the aligned glassy polymer and that of the drawn crystalline polymer.

INTRODUCTION

The conformation and packing of molecules in solid glassy polymers is not fully understood. Much of the conformational data on these materials has been derived from infrared (i.r.) spectroscopy, the powerful methods of high resolution nuclear magnetic resonance (n.m.r.) analysis being readily applicable only to polymer solutions.

Careful small-angle X-ray and neutron scattering experiments^{1,2} have failed to reveal any density fluctuations on a scale greater than 50 Å which can be attributed to specific microstructural features. Wide-angle X-ray diffraction (WAXD) produces the familiar diffuse peaks. The traditional approach to their analysis is to prepare radial distribution functions (*RDF*) which essentially plot the distribution of the interatomic vector lengths. However, in the case of fairly complicated materials such as most polymers where it is the actual structure which is in doubt, it appears that *RDF* are of limited value only and do not always enable interchain and intrachain distances to be separately identified.

A slightly different approach to the problem of structure determinations is to align the glassy polymer by extension at a temperature a few degrees below its glass transition. This alignment is reflected in the concentration of some of the WAXD halos at particular azimuthal angles which can reveal whether they are of inter- or intra-molecular origin. Ohlberg *et al.*³ have attempted to derive a measure of the molecular orientation from the azimuthal profile of a halo that intensified on the equator although their conclusions have since been queried^{4,5}, and Brady and Yeh⁶ have used measurements of the loss of alignment in WAXD patterns as an indication of the structural reorganization which occurs on annealing glassy polymers. It must be emphasized though, that the observation of optical phenomena⁷ such as birefringence and i.r. dichroism as well as n.m.r. effects⁸ are also established techniques for the measurement of molecular orientation in glassy polymers. However WAXD alignment, where it can be observed, has the possible advantage that it is not controlled by the polarizability or absorption of specific parts of the molecule.

It also gives information as to the distances between adjacent molecular chains.

Cylindrical distribution functions (*CDF*) can be prepared from the WAXD patterns of aligned specimens with fibre symmetry⁹. They are, however, difficult to calculate and interpret. Milberg and Daly¹⁰ have used a difference-*CDF* which shows only the contributions due to orientation. Since it needs few corrections to the measured intensities, it is easier to calculate but the problems of interpretation remains.

In the work reported here we have concentrated on improving the apparent alignment in the diffraction pattern and then approaching its analysis in much the same way as one would a crystalline fibre diagram. In this way we have extracted additional information about the polymer structure from the positions of and intensity distributions along the layer lines.

In this paper we describe in some detail the analytical technique of desmearing developed to improve the azimuthal resolution of the diffraction patterns as well as its application to atactic polystyrene (a-PS) and quenched isotactic polystyrene (i-PS). Polystyrene is a particularly suitable candidate for this technique as its first diffraction halo concentrates only on the equator and hence provides a quantitative measure of the orientation distribution in the aligned specimens.

EXPERIMENTAL

The two polymers investigated were atactic polystyrene (BP Rigidex KLP 35) and quenched isotactic polystyrene (prepared by Dr N. Overbergh at the H. H. Wills Physics Laboratory, Bristol, and kindly loaned to us for these initial experiments. It is the same material as that used by the Bristol group for their gelation-crystallization studies¹¹). For each polymer a degree of chain alignment was obtained by multiple extrusion in a channel die at 85°C. The technique was to extrude to two or three times the original length, then to cut in half and repeat with one half on top of the other. Any one specimen was extruded up to four times in this way, although the improvement in alignment for the stages subsequent to the first was comparatively small.

* Presented at the Polymer Physics Group (Institute of Physics) Biennial Conference, Shrivenham, September 1975.

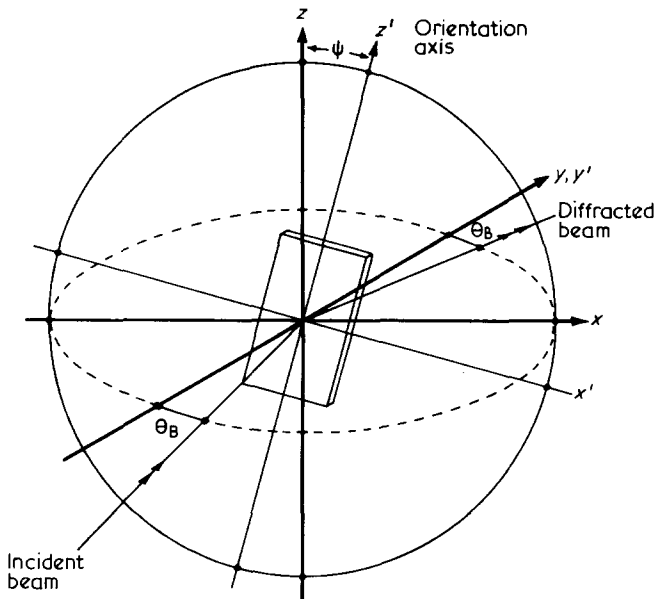


Figure 1 Relationship between diffractometer coordinate axes (xyz) and specimen coordinate axes ($x'y'z'$). y and y' axes are always coincident i.e. specimen is rotated with the orientation axis (z') in the $x-z$ plane

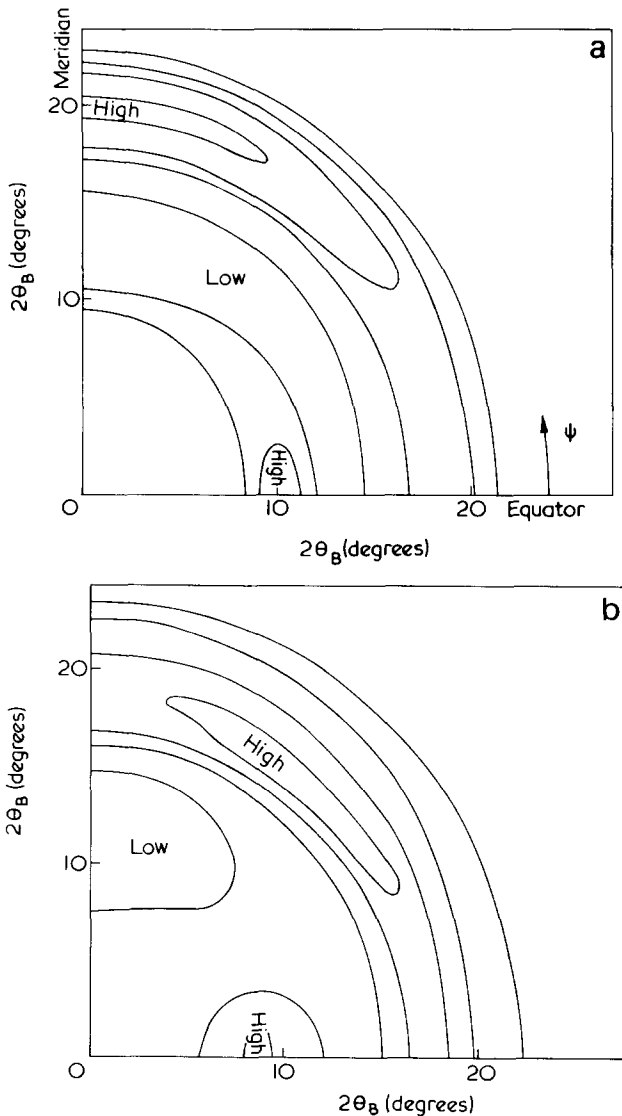


Figure 2 Experimental intensity patterns for (a) aligned atactic polystyrene, a-PS and (b) aligned, quenched isotactic polystyrene, i-PS. The intensity is in arbitrary units and the contours are at equal intervals

X-ray diffraction measurements were made using a texture goniometer set up with the symmetrical transmission geometry as sketched in Figure 1. At each particular $2\theta_B$ setting, the specimen was rotated about the y axis and the azimuthal distribution of scattered intensity plotted on a chart recorder. Figures 2a and 2b show the intensity patterns built up for a-PS and i-PS respectively. No corrections have been made for absorption, polarization, double diffraction or incoherent scattering. The radiation was $\text{CuK}\alpha$.

In view of the fact that n.m.r. has shown a-PS to be predominantly syndiotactic¹² it is perhaps surprising that the WAXD patterns of unaligned a-PS and i-PS are very similar¹³. However, a significant difference is apparent between the aligned diagrams (Figure 2) in that the second halo of a-PS is at maximum intensity on the meridian while that of i-PS shows maxima in the region of $\psi = \pm 45^\circ$.

With fibre patterns from crystalline polymers it is normal to view equatorial and meridional peaks as corresponding to inter- and intra-chain correlations respectively. In order to check that this assumption was valid in the case of glassy a-PS, the positions of the diffuse halos were measured as a function of temperature. The results are plotted in Figure 3. For the first (equatorial) halo at $2\theta_B = 10^\circ$, there was a marked shift towards lower angles (longer spacings) as the temperature was increased, especially above T_g , which appears to confirm that the halo is attributable to interchain spacings. (These results are in agreement with those of Kilian and Boueke¹⁴.) The shift of the second halo as a function of temperature is not nearly as distinctive as in the case of the first. This reflects the appearance of the second halo on alignment where it shows no clear predisposition to concentrate exclusively on either the equator or meridian.

AZIMUTHAL SHARPENING OF ALIGNED WAXD PATTERNS

Aims and assumptions

In this work the interpretation of WAXD patterns from aligned glassy polymers is approached in the same way as for the familiar fibre diagrams of a drawn crystalline polymer. However, in the case of an aligned glassy polymer one has to contend with not only a lack of long range order and

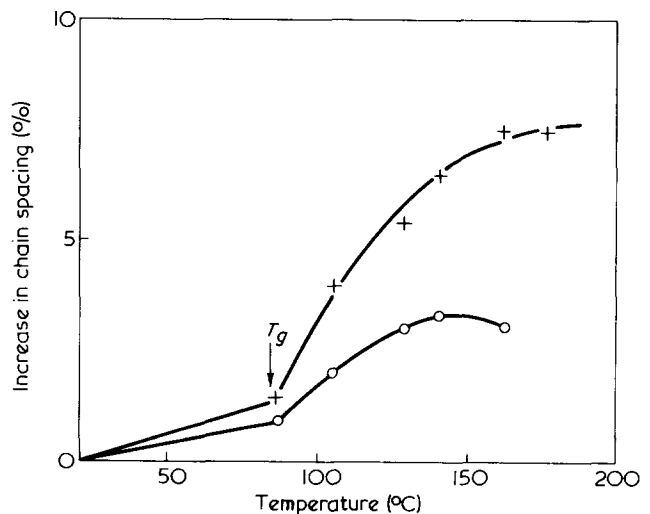


Figure 3 Change in chain spacing as a function of temperature determined from the positions of the first (+) and second (o) halos of unaligned atactic polystyrene

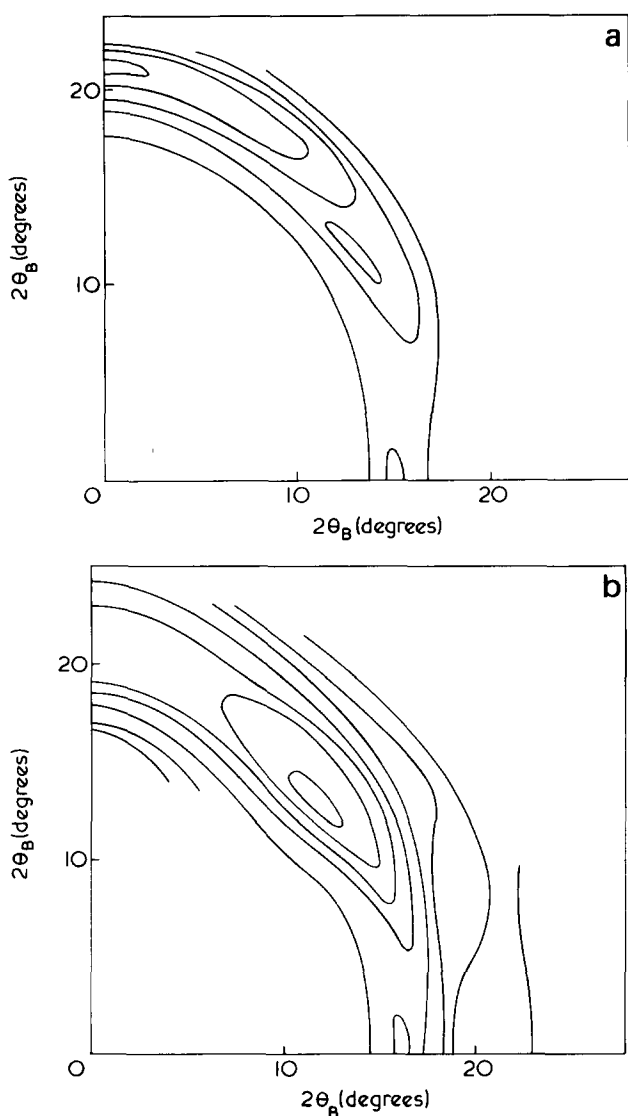


Figure 4 Experimental intensities as in Figure 2, azimuthally deconvolved with the profile of the first halo. (a), a-PS; (b), i-PS

hence diffraction maxima with a half width of several degrees or more, but also with the relatively poor degree of fibre orientation which is the best so far achieved. The analytical method outlined here has been developed to improve the apparent fibre orientation by azimuthally sharpening the X-ray diffraction pattern.

The aligned glassy polymer is treated as containing many entities each with its own fibre symmetry. The axes of the fibre entities are distributed in angle about the macroscopic fibre axis of the sample which we call the orientation axis; (z' axis lying in $z-x$ plane of Figure 1). The individual diffracting domains may not have fibre symmetry, however we are viewing a fibre entity as a collection of all domains which share a common molecular orientation. Thus each fibre entity will contribute to the diffraction pattern according to its angular position in relation to the orientation axis (z'). For the purposes of this analysis it is best to consider the fibre axis of an entity as having two components of 'misorientation' with respect to the orientation axis: one about y' ($\equiv y$) in the $x'-z'$ plane and another about x' in the $y'-z'$ plane. We can assume that the projections of the overall distribution of fibre entities about the orientation axis onto the $x'-z'$ and $y'-z'$ planes are identical. We style the projected distribution $D(\alpha)$ where α is measured from the orientation axis.

First stage desmearing

The projected distribution $D(\alpha)$ on the $x'-z'$ plane can be thought of as azimuthally smearing that diffraction pattern which would be recorded if all the fibre entities were aligned into the $y'-z'$ plane. For a particular $2\theta_B$ we will refer to this pattern as $I_2(\psi)$. Hence we can write that the experimental intensity $I_1(\psi)$ is the convolution of $I_2(\psi)$ and $D(\alpha)$ expressed as $D(\psi')$, i.e.

$$I_1(\psi) = \int_0^{\pi/2} I_2(\psi - \psi') D(\psi') d\psi' \quad (1)$$

For equatorially centred reflections from the fibre entities the distribution $D(\alpha)$ in the $x'-z'$ plane is the only contribution to the smearing which is therefore fully described by the above relation, and $I_2(\psi)$ is the true intensity distribution $I(\psi)$. Hence in the case of PS and other polymers which possess a halo which alignment concentrates onto the equator alone, $D(\alpha)$ can be obtained directly from the halo's azimuthal profile. It must of course be kept in mind that any significant extension of the equatorial maxima in the meridional direction, resulting perhaps from the small size of diffracting domains in this direction or from significantly curved molecules, will complicate the determination of the true $D(\alpha)$. However, in the case of PS, azimuthal smearing is so obviously the dominant factor, that the working approximation has been made that the azimuthal profile of the equatorial peak is equivalent to $D(\alpha)$. For PS therefore, the first stage of azimuthal sharpening is to remove the effect of the $x'-z'$ distribution function by deconvolution with the profile of the inner halo. (With some other glassy polymers such as poly(methyl methacrylate) and polycarbonate where no halo is uniquely equatorial the determination of $D(\alpha)$ will present additional problems.)

Several methods of deconvolution are applicable¹⁵, and one based on iterative procedures has been selected for this work. The convolution of two functions is written:

$$f(x) = g(x) * h(x) \quad (2)$$

Deconvolution is the solution of this equation for $g(x)$ where $h(x)$, the smearing function, is known. The iterative method used is based on a scheme to improve an approximation to $g(x)$.

This is:

$$g_{n+1}(x) = g_n(x) + [f(x) - g_n(x) * h(x)] \quad (3)$$

The first approximation to $g(x)$, $g_1(x)$, is taken as equal to $f(x)$.

The results of azimuthally deconvolving the profile of the equatorial peaks from the experimental intensities, at values of $2\theta_B$ which include the 2nd halo, for a-PS and i-PS are shown in Figures 4a and 4b. This procedure of course totally eliminates azimuthal spread from the first halo which is not represented in the Figures.

Second stage desmearing

For all but equatorial reflections, the distribution in the $y'-z'$ plane smears the diffracted information towards the meridian. Figure 5 shows the construction for calculating the nature of the smearing by considering a 'reflection' at

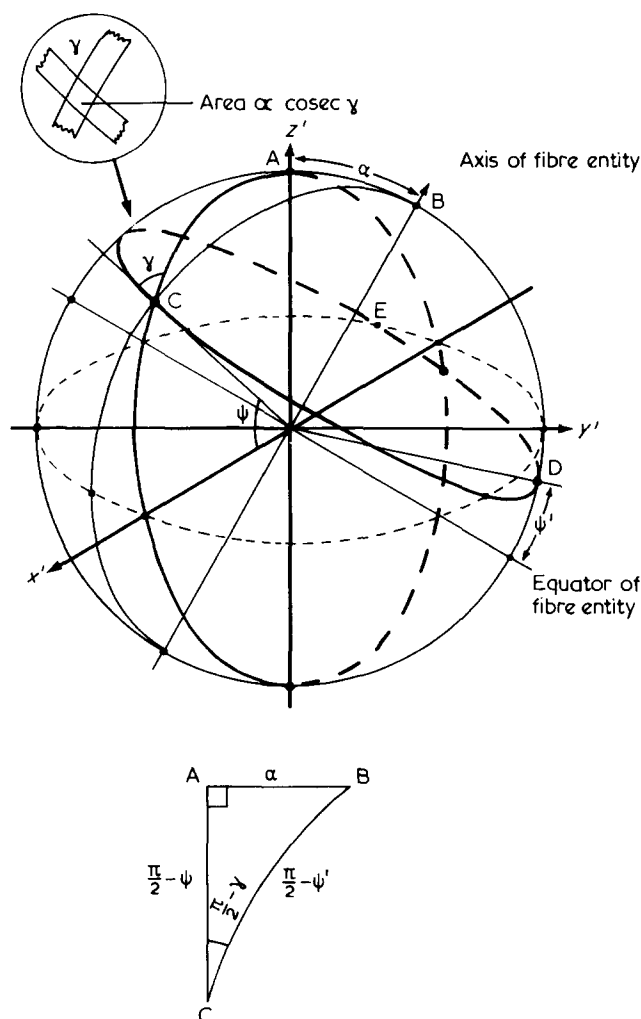


Figure 5 Construction in reciprocal space for calculating the position and intensity of a reflection from a fibre entity lying in the $y'-z'$ plane. The axis of the entity makes an angle α with the orientation axis (z') and the reflection makes an angle ψ' with the equator of the entity

the angle ψ' to the equator of a fibre entity. In reciprocal space this reflection is derived from the intersection of the small circle (CDE) and the 'reflection' plane, $x'-z'$ at C. If the axis of the entity is tilted away from the orientation axis by an angle α , in the $y'-z'$ plane, then the reflection will appear at an azimuthal angle ψ with its integrated intensity increased according to $\text{cosec } \gamma$. We now have to relate γ to ψ and ψ' , and obtain an expression which relates an increment of α , $\Delta\alpha$, in the $y'-z'$ plane, to an increment of ψ , $\Delta\psi$; in fact the value of $d\alpha/d\psi$. These relations can be obtained with reference to the spherical triangle ABC on Figure 5.

From ABC:

$$\cos\left(\frac{\pi}{2} - \psi'\right) = \cos\left(\frac{\pi}{2} - \psi\right) \cos\alpha + \sin\left(\frac{\pi}{2} - \psi\right) \times \sin\alpha \cos\frac{\pi}{2}$$

$$\text{Therefore: } \cos\alpha = \frac{\sin\psi'}{\sin\psi} \quad (4)$$

$$\text{and } \frac{d\alpha}{d\psi} = \frac{\cos\psi \sin\psi'}{\sin\psi(\sin^2\psi - \sin^2\psi')^{1/2}} \quad (5)$$

And also,

$$\cos\alpha = \cos\left(\frac{\pi}{2} - \psi\right) \cos\left(\frac{\pi}{2} - \psi'\right) + \sin\left(\frac{\pi}{2} - \psi\right) \times \sin\left(\frac{\pi}{2} - \psi'\right) \cos\left(\frac{\pi}{2} - \gamma\right)$$

Therefore:

$$\cos\alpha = \sin\psi \sin\psi' + \cos\psi \cos\psi' \sin\gamma \quad (6)$$

and using equation (4):

$$\text{cosec}\gamma = \frac{\tan\psi}{\tan\psi'} \quad (7)$$

Hence the distribution $D(\alpha)$ in the $y'-z'$ plane will smear intensity around the azimuthal circle according to the function:

$$D\left[\alpha = \cos^{-1}\left(\frac{\sin\psi'}{\sin\psi}\right)\right] \times \frac{\tan\psi}{\tan\psi'} \times \frac{\cos\psi \sin\psi'}{\sin\psi(\sin^2\psi - \sin^2\psi')^{1/2}} \quad (8)$$

The second two terms of this function simplify to:

$$\frac{\cos\psi'}{(\sin^2\psi - \sin^2\psi')^{1/2}}$$

which is plotted for $\psi' = 30^\circ$ in Figure 6.

The function $I_2(\psi)$ (equation 1) obtained after the first deconvolution is therefore the true azimuthal distribution $I(\psi)$ smeared by the function (8). It can be represented by a transform integral of the type:

$$I_2(\psi) = \int_0^{\pi/2} I(\psi - \psi') \times D\left[\cos^{-1}\left(\frac{\sin\psi'}{\sin\psi}\right)\right] \times \frac{\cos\psi' \cdot d\psi'}{(\sin^2\psi - \sin^2\psi')^{1/2}} \quad (9)$$

This is not strictly a convolution because the smearing function changes shape with ψ ; however, it can still be solved for the true distribution $I(\psi)$ using the iterative method. The convolution operation in the final term of equation (3) becomes now strictly one of smearing which nevertheless can still be performed numerically.

The results of this second stage desmearing are shown in the contour plots of Figure 7 (for a-PS and Figure 8 (for i-PS). Comparison with Figures 2 and 4 indicate that the second stage process leads to a smaller improvement in azimuthal sharpness than the first, although its application does emphasize the presence of a discrete meridional maximum at $2\theta_B = 21^\circ$ in the i-PS pattern.

DISCUSSION

In simple terms, a fibre diffraction pattern can provide information as to the structural and residue repeat distances along the chain, the mode of packing of the molecules and

the incidence of longitudinal register between adjacent molecules (as indicated by sampling of the layer lines other than the equator).

If the intensity distributions of Figures 7 and 8 are viewed as fibre patterns then it should be possible to ex-

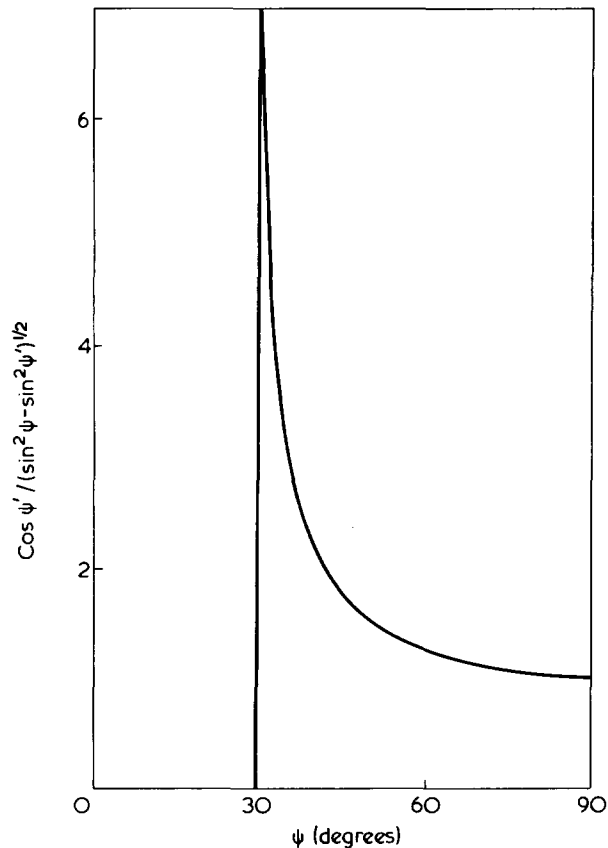


Figure 6 Plot of $\cos \psi' / (\sin^2 \psi - \sin^2 \psi')^{1/2}$ for $\psi' = 30^\circ$

tract some at least of this structural information. However, compared with diffraction from a crystalline fibre, the patterns from the glassy polystyrenes present additional problems. There is of course considerable disorder along the molecular chains as well as in their packing which is responsible for the general lack of definition in the pattern. In addition it is very probable that there is no unique chain conformation, so that the pattern may have to be treated as the superposition of two or more separate patterns.

In attempting to analyse the diffraction from a-PS and i-PS, we have started by narrowing down the number of possible conformations for isotactic and syndiotactic configurations. We have considered mainly those based on staggered bonds, although one particular possibility involving eclipsed bonds is also included. The relevant bond rotation angles for the carbon backbone are defined in Table 1. In Table 2 the possible conformations with repeats less than 8 Å based on combinations of rotation angles are listed. Conformations which we have successfully constructed from CPK models without undue intrachain steric hindrance are indicated with a + and those which satisfy Natta and Corradini's equivalence principle¹⁶ are marked in addition with an ε. The chain repeat distances for the various conformations are essentially those of Bunn¹⁷ for an unencumbered carbon backbone but modified slightly on the basis of observations of the CPK molecular models to take account of some measure of steric hindrance. In addition the distances only refer to the structures which can be readily built (i.e. those marked with +). The figure of 6.65 Å for $(tg)_3$ is simply the repeat shown by crystalline i-PS (The corresponding Bunn figure is 6.20 Å).

Atactic polystyrene

There is strong evidence that a-PS is predominantly syndiotactic¹². For this reason the analysis of the sharpened diffraction pattern of a-PS (Figure 7) is viewed initially in terms of the possible syndiotactic conformations listed in

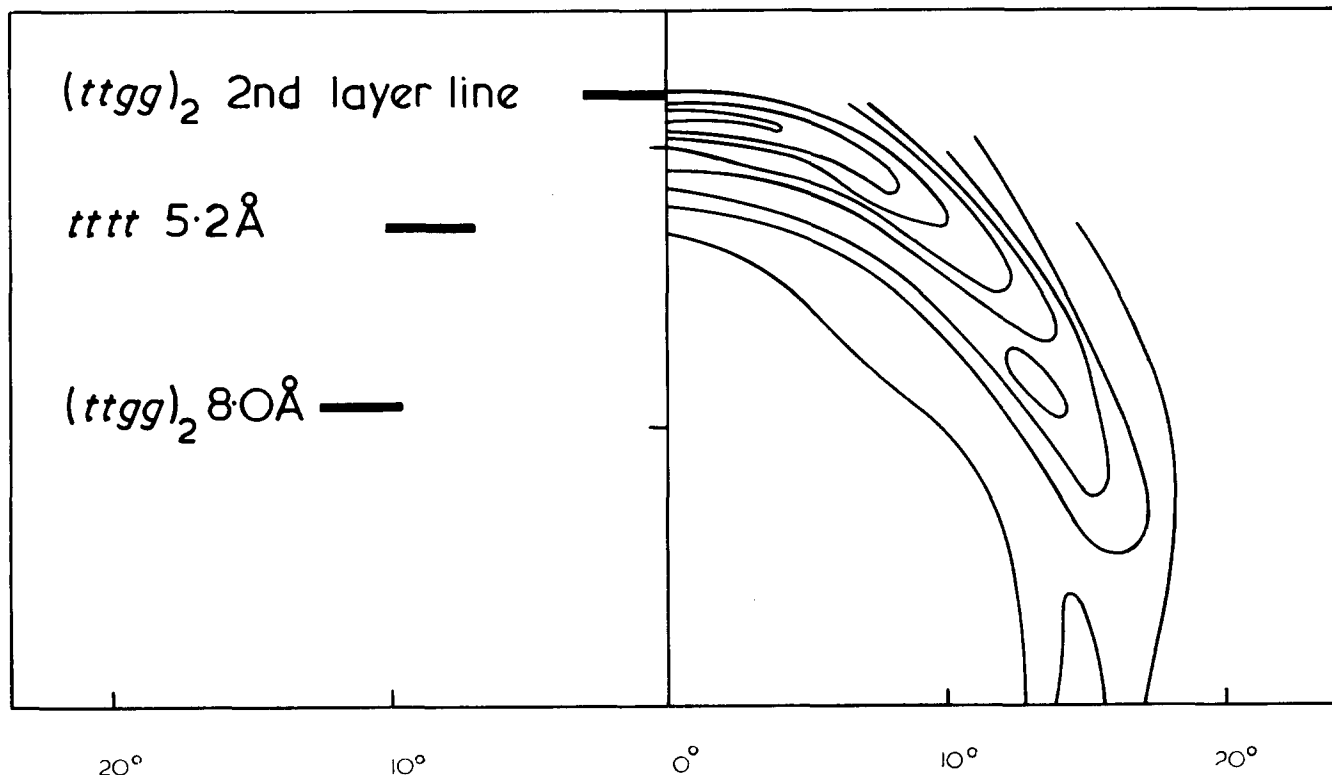


Figure 7 Result of second stage desmearing for aligned atactic polystyrene. The calculated positions of the regions of high intensity on the 1st layer line of $(tttt)$ and on the 1st and 2nd layer lines of $(ttgg)_2$ are shown on the left

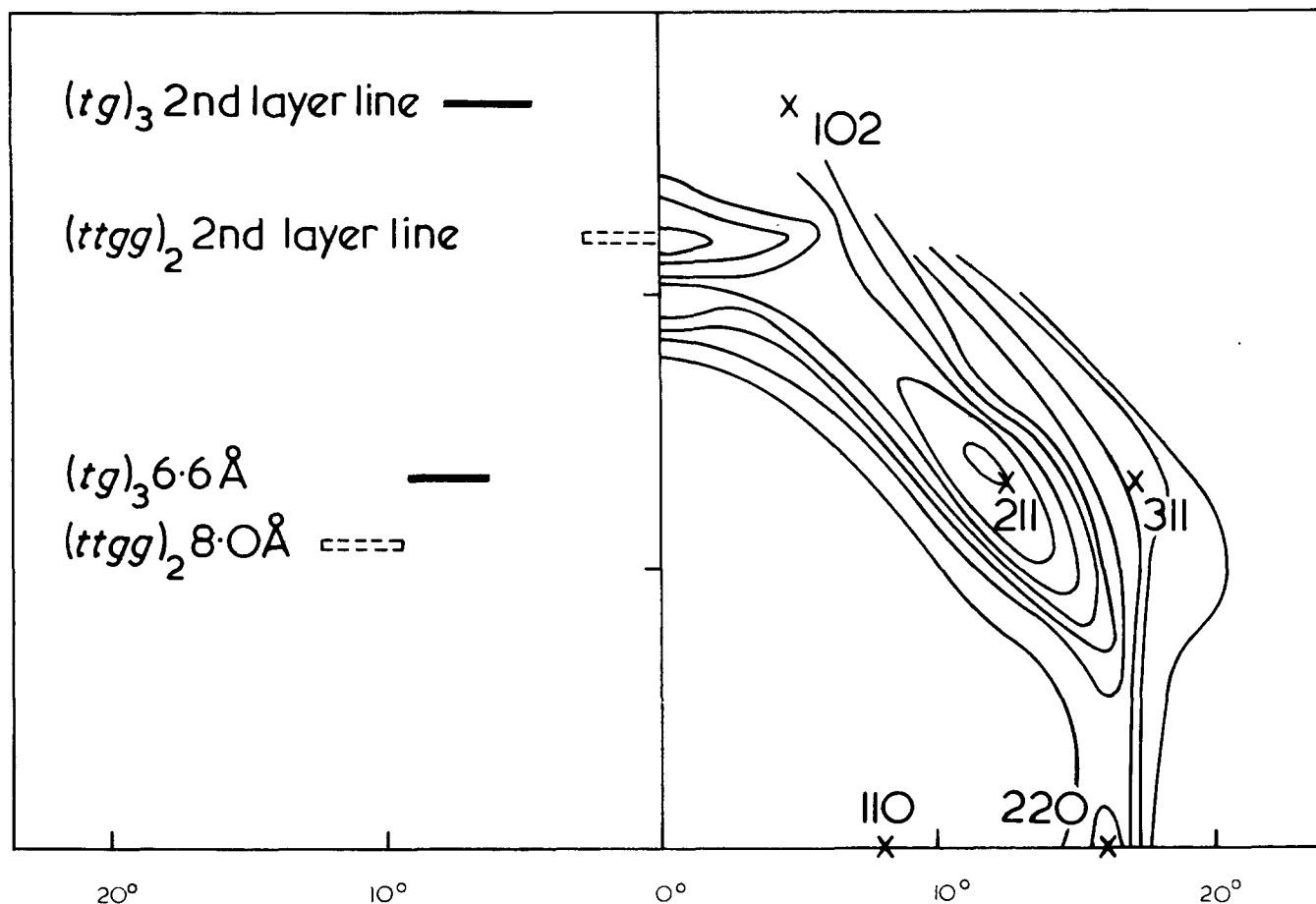


Figure 8 Result of second stage desmearing for aligned, quenched isotactic polystyrene. The calculated positions of maximum intensity for the 1st and 2nd layer lines of $(tg)_3$ and $(ttgg)_2$ are shown on the left. The crosses mark the positions of the most intense reflections for aligned crystalline isotactic polystyrene

Table 1 Internal rotation angles

	ϕ (degrees)	
Trans, <i>t</i>	0	} Staggered
Gauche, $g(\bar{g})$	120 (-120)	
Skew, $s(\bar{s})$	60 (-60)	} Eclipsed
Cis, <i>c</i>	180	

Table 2 Possible conformations for polystyrene

Conformation	Chain repeat (Å)	i-PS	s-PS
$g\bar{4}$	4.0	ϵ	ϵ
$tg\bar{t}g$	4.4	—	+ ϵ
$tst\bar{s}$	4.8	+	+ ϵ
$tttt$	5.2	ϵ	+ ϵ
$(tg)_3$	6.65	+ ϵ	—
$(ttgg)_2$	7.8	+	+ ϵ

+, indicates a conformation which does not lead to undue steric hindrance

ϵ , indicates a conformation which satisfies equivalence i.e. each monomer unit has a similar environment

Table 2. The pattern shows equatorial maxima at ($2\theta_B = 10^\circ, \psi = 0^\circ$) and ($15^\circ, 0^\circ$), a small peak at ($17.5^\circ, 40^\circ$) and a broad arc centred on the meridian at ($21^\circ, 90^\circ$).

The peak at ($17.5^\circ, 40^\circ$) corresponds to a chain repeat distance of 7.5–8.0 Å. If we are to interpret this in terms of $(ttgg)_2$ which has a repeat of 7.8 Å, then there should be a second layer line intersecting the meridian at $2\theta_B = 22$ – 23° with its maximum intensity on the meridian. This appears to correspond to the central region of the broad arc.

The calculated positions of the intensity maxima on the first two layer lines of the transform of a s-PS chain in $(ttgg)_2$ conformation (i.e. a 2/1 helix) are represented on the left side of Figure 7. The large azimuthal spread of the ($21^\circ, 90^\circ$) arc appears to deny the effectiveness of the desmearing procedures already applied. An alternative approach however is to consider the 'wings' of the arc as representing off meridional intensity maxima on a layer line intersecting the meridian at $2\theta \approx 18^\circ$, i.e. about 5 Å. Such an intensity disposition would correspond fairly well to the $(tttt)$ planar zig-zag conformation as indicated on the left of Figure 7. The data therefore suggest that atactic polystyrene contains substantial syndiotactic sequences in both $(tttt)$ and $(ttgg)$ conformations, both conformations being present in roughly equal proportions. However, we cannot exclude the possibility of $(tg\bar{t}g)$ which would also lead to an intensity maximum close to the meridional peak at ($21^\circ, 90^\circ$). No other experimental technique has provided direct evidence for the chain conformation in bulk a-PS (or for that matter in s-PS which has not apparently been synthesized) so it is not possible to confirm our predictions. However, it is most encouraging to note that n.m.r. measurements on syndiotactic triphenylheptane (a model for s-PS) in solution have shown that it has equal preference for the conformations $(tttt)$ and $(ttgg)$ ¹⁸. Moreover calculations¹⁹ have shown that for s-PS the two conformations are energetically equivalent. Further support is given to the reasonableness of the prediction of $(tttt)$ and $(ttgg)_2$ by observations of the crystal structure of syndiotactic polypropylene. Two structures are reported, one²⁰ based on $(tttt)$ with a chain repeat of 5.05 Å and the other²¹

based on $(ttgg)_2$ with a chain repeat of 7.4 Å. Since the repeat distance of the 3/1 helix of i-PS is ~3% greater than that of i-PP, we can perhaps expect distances of 5.2 Å for $(tttt)$ s-PS and 7.6 Å for $(ttgg)_2$ s-PS.

It should also be possible, on the basis of the equatorial X-ray data, to make proposals as to the chain packing, which of course should be in line with the predicted conformations. Such studies are in progress but not reported here.

Isotactic polystyrene

Perhaps the most striking feature of the sharpened diffraction pattern from glassy i-PS (*Figure 8*) is the correspondence between some of the maxima and the 'reflection' positions in a corresponding fibre diagram from crystallized and aligned material. That glassy i-PS contains chains in the $(tg)_3$ conformation (3/1 helices) is not particularly surprising as evidence for this conformation in solutions of the polymer has been obtained from infra-red^{22,23} and ultra-violet²⁴ spectroscopy and it is of course present in the crystal²⁵. What is intriguing however is that the correspondence of the patterns implies longitudinal register between adjacent molecules in the glassy phase; that is, some measure of three-dimensional order. Further confirmation of longitudinal register can be obtained by comparing the position of the first maxima on the 6.65 Å layer line of the sharpened pattern, with the calculated position for the maximum on this layer line corresponding to an isolated 3/1 helix. (*Figure 8*) (Its position is not significantly changed if an enantiomeric pair of helices is considered). The two maxima are at different distances from the meridian. This indicates that the first layer line of the glassy polymer is sampled by a reciprocal lattice with the implication of three-dimensional order. It is not clear at this stage whether the glassy structure should be viewed as crystals with a high degree of paracrystalline disorder, as exceptionally small crystallites or as some combination of both.

There is, however, a maximum at $(21^\circ, 90^\circ)$ which, lying between the first and second layer lines of the crystal pattern, implies that a conformation other than $(tg)_3$ is also present. It is difficult to interpret this maximum. Perhaps the best explanation is that it is the second layer line of the isotactic equivalent of $(ttgg)_2$, already proposed for the syndiotactic material, but which does not satisfy the equivalence principle. If this is the case there should also be maximum on a first layer line corresponding to a repeat of about 8 Å. It is just possible that the 'lobes' extending downwards from the prominent peaks on the 6.65 Å layer lines (3/1 helix) represent these maxima.

CONCLUSIONS

Wide-angle X-ray diffraction is a promising technique for the investigation of the structure of oriented glassy polymers.

The fact that it is not possible to obtain a very high level of fibre orientation by mechanical extension has led to the development of a numerical technique to enhance the azimuthal resolution of the aligned diffraction patterns.

The polystyrene results presented are from our first series of experiments only. They do however permit several conclusions to be drawn as to the structure of a-PS and i-PS in the aligned glassy state. For the atactic material there is evidence that the conformations $(tttt)$ and $(ttgg)_2$ are present in roughly equal proportions, whereas the iso-

tactic samples contain some three-dimensional order based on the 3/1 helices, although the diffraction halos still remain broad.

In the light of these results it appears that a useful approach to the problem of the microstructure of glassy polymers may well be through X-ray structural studies of aligned samples.

The structural information derived by these methods is of course only directly applicable to polymers in the aligned state. However, experiments of Colebrooke and Windle²⁶ suggest that as far as chain conformation and packing are concerned, the extra information which can be extracted from the diffraction patterns of the aligned material is also relevant to the normal unaligned material.

ACKNOWLEDGEMENTS

The authors would like to thank Professor R. W. K. Honeycombe for the encouragement given to this work in the Department of Metallurgy and Materials Science at Cambridge. Thanks are also due to Professor J. G. Ball and Mr F. Huggins for the provision and maintenance of facilities at Imperial College where much of the experimental work was carried out. As mentioned in the text, the isotactic polystyrene was prepared by Dr N. Overbergh in Professor Keller's group at Bristol. We acknowledge with many thanks the loan of a sample of this material. We thank the Science Research Council for a grant which enabled this work to be carried out.

REFERENCES

- 1 Kirste, R. G., Kruse, W. A. and Ibel, K. *Polymer* 1975, **16**, 120
- 2 Wendorff, J. H. and Fischer, E. W. *Kolloid Z. Z. Polym.* 1973, **251**, 876
- 3 Ohlberg, S. M., Alexander, L. E. and Warrick, E. L. *J. Polym. Sci.* 1958, **27**, 1
- 4 Milberg, M. E. *J. Appl. Phys.* 1962, **33**, 1766
- 5 Alexander, L. E. 'X-ray Diffraction Methods in Polymer Science' Wiley, New York, 1969, p 198
- 6 Brady, T. E. and Yeh, G. S. Y. *J. Macromol. Sci. (B)* 1973, **7**, 243
- 7 Stein, R. S. and Read, B. E. *Appl. Polym. Symp.* 1969, **8**, 255
- 8 Kashiwagi, M., *et al.* *Polymer* 1971, **12**, 697
- 9 Norman, N. *Acta Crystallogr.* 1954, **7**, 462
- 10 Milberg, M. E. and Daly, M. C. *J. Chem. Phys.* 1963, **39**, 2966
- 11 Girolamo, M., Keller, A., Miyasaka, S. and Overbergh, N. *J. Polym. Sci. (Polym. Phys. Edn)* 1976, **14**, 39
- 12 Brownstein, S., Bywater, S. and Worsfield, D. J. *Makromol. Chem.* 1961, **48**, 127
- 13 Wecker, S. M., Davidson, T. and Cohen, J. B. *J. Mater. Sci.* 1972, **7**, 1249
- 14 Kilian, H.-G. and Boueke, K. *J. Polym. Sci.* 1962, **58**, 311
- 15 Jones, A. F. and Misell, D. L. *J. Phys. (A)* 1970, **3**, 462
- 16 Natta, G. and Corradini, P. *Nuovo Cimento Suppl.* 1960, **15**, 9
- 17 Bunn, C. W. *Proc. R. Soc. (A)* 1942, **180**, 67
- 18 Pivcová, H., Kolínský, M., Lím, D. and Schneider, B. *J. Polym. Sci. (C)* 1969, **22**, 1093
- 19 Borisova, N. P. and Birshtein, T. M. *Polym. Sci. USSR* 1964, **6**, 1360
- 20 Natta, G. *et al.* *Makromol. Chem.* 1964, **75**, 215
- 21 Corradini, P., Natta, G., Ganis, P. and Temussi, P. A. *J. Polym. Sci. (C)* 1967, **16**, 2477
- 22 Onishi, T. and Krimm, S. *J. Appl. Phys.* 1961, **32**, 2320
- 23 Kobayashi, M., Tsumara, K. and Tadokoro, H. *J. Polym. Sci. (A-2)* 1968, **6**, 1493
- 24 Longworth, J. W. *Biopolymers* 1966, **4**, 1131
- 25 Natta, G., Corradini, P. and Bassi, I. W. *Nuovo Cimento Suppl.* 1960, **15**, 68
- 26 Colebrooke, A. and Windle, A. H. *J. Macromol. Sci. (B)*, in press

Effect of sample geometry on the measurement of mechanical properties of anisotropic materials*

R. G. C. Arridge and M. J. Folkest

*H. H. Wills Physics Laboratory, University of Bristol, Bristol BS8 1TL, UK
(Received 15 December 1975; revised 2 February 1976)*

Experimental observations have been made of the effect of sample geometry on the mechanical properties of anisotropic polymer systems. The non-uniform stresses at the sample ends, arising from the method of clamping are found to persist over much greater distances than in isotropic materials, as judged by their effect on the tensile and torsional modulus. The Principle of St. Venant does not appear to be applicable to anisotropic materials. This is further supported by results obtained using finite element methods. The results raise serious doubts concerning current practice in determining the mechanical properties of anisotropic materials.

INTRODUCTION

In the practical determination of the elastic constants of solids, the most commonly used test methods involve tension, bending or torsion either under dead loading or dynamic conditions. In all of these methods, it is usually assumed that stress concentrations imposed at the ends of the sample as a result of the particular clamping arrangement can be neglected in the calculation of the elastic constants. In practice, the approach has been either to choose appropriate sample dimensions or to measure deformations of the sample by means of strain gauges attached to the surface. There are other limitations to be considered in the experiment namely time effects if the material is viscoelastic and non-linear effects such as are found in many polymers. These problems are not, however, our concern here although they may well interact with the effects of sample end constraint, which is the main subject of this present paper.

The ability to neglect sample end effects in suitably shaped samples rests upon the validity of the so-called Principle of St. Venant proposed by the French elastician in 1855. This states (we quote Love¹) 'the strains that are produced in a body by the application to a small part of its surface of a system of forces statically equivalent to zero force and zero couple, are of negligible magnitude at distances which are large compared with the linear dimensions of the part'. In practice this means that the irregular stress distribution arising from the particular method employed to transfer an external force to the sample, becomes uniform at a distance away from the points of application equal to about one lateral dimension of the sample, and that from this distance further only the *resultant* forces and couples need to be considered.

The irregularity of the stress distribution can be shown to decay away exponentially with distance from the sample ends so that, strictly, end effects are always present. However in the case of isotropic materials, they are usually found to be negligible about one specimen width away from

the sample ends compared to the other errors incurred in the measurement of any mechanical property. This means that in practice, depending on how far one is prepared to go in order to eliminate end effects, a specimen length/width ratio of 10 is sufficient.

Recently, Folkes and Arridge² reported observations made on highly anisotropic material in the form of a polymeric microcomposite, which showed end effects in torsion persisting over very much greater sample lengths compared to those for isotropic materials. Subsequent studies in this laboratory have shown that similar effects exist in other polymeric materials, namely high density polyethylene which has been either extruded in the solid state or drawn to a high draw ratio. All of these observations cast serious doubt on the validity of St. Venant's Principle when applied to anisotropic materials.

It is the purpose of this paper first to summarize the findings of Folkes and Arridge² and then to describe preliminary results on ultra-high modulus polyethylene together with theoretical studies using the finite element method for a two dimensional model of anisotropic material in tension.

The authors feel that the results to be reported have important implications in the accurate measurement of the mechanical properties of anisotropic materials in general and may require current testing standards to be modified.

THEORETICAL DEVELOPMENTS OF ST. VENANT'S PRINCIPLE

The Principle of St. Venant in the form stated in the introduction is not universally true for, as Toupin³ shows, the stresses in a beam of dumbbell cross-section loaded at one end by couples whose resultant is zero will persist far along the beam. St. Venant in fact, stated the principle as being valid for perfect cylinders only, not necessarily for those of arbitrary cross-section. For this reason, mathematicians have recently sought a more general principle and in addition, have examined the case of anisotropic materials.

A criterion based upon elastic stored energy has been proposed by Toupin³ and when applied to anisotropic materials by Horgan⁴ led to the concept of a characteristic decay length for the stored elastic energy. This in turn led

* Presented at the Polymer Physics Group (Institute of Physics) Biennial Conference, Shrivenham, September 1975.

† Present address: Department of Materials, Cranfield Institute of Technology, Cranfield, Bedford MK43 0AL, UK.

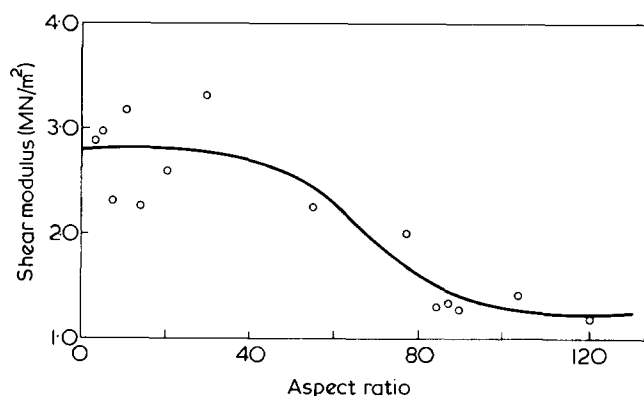


Figure 1 Dependence of shear modulus in torsion of S-B-S 'single-crystal' on sample aspect (length/width) ratio. Curve indicates probable trend

to an exponential decay for the stress irregularity at interior points. For anisotropic materials Horgan⁴ showed that this decay length was always greater than it was for an isotropic material and was of the form $\lambda = b(E/G)^{1/2}$ where b is the maximum lateral dimension of the sample, E is Young's modulus along the axis of the specimen and G the shear modulus, for shear which includes that direction, the so-called longitudinal shear modulus.

Now for isotropic materials E/G lies between 2.6 and 3.0, so λ is $\sim 1.6-1.7b$. For very anisotropic materials e.g. the microcomposite studied by Folkes and Arridge², E/G can reach values as high as 280 so that λ may be as high as $16.7b$. In such cases, therefore, neglect of the stress distribution at the points of loading becomes quite unjustifiable and only two alternatives remain. One is to determine the stress distribution for the particular method of sample clamping employed, solve the elastic equations of equilibrium and hence derive the elastic constants. The other is to choose a sample length/width ratio so large that the end effect may still be ignored.

The first alternative is extremely difficult; not only are the stresses (or displacements) difficult to determine in practice but the solution of the elastic problem for an anisotropic body is a formidable task even for simple geometries. Pagano and Halpin⁵ have considered this for tensile loading of an anisotropic material in directions at an angle to the symmetry axes and derive an explicit expression for the Young's modulus along these directions as a function of the length/width ratio of the sample. Their analysis breaks down, however, when the applied load acts along an axis of symmetry.

The second alternative seems at present the better one, provided sufficient sample material is available, which may not always be the case, for example, with minute 'whisker' crystals of inorganic or organic substances, or those samples as used in the classical measurements of the elastic constants of crystals of various symmetry classes.

EXPERIMENTAL OBSERVATIONS

In this section we report on studies of end effects in two highly anisotropic materials, one in torsion and the other in tension.

Block copolymer microcomposite

The material used for our investigations was Kraton 102, an S-B-S block copolymer, which by suitable processing can be obtained in 'single-crystal' form, consisting of a hexagonal array of polystyrene cylinders embedded in a

matrix of polybutadiene, with the cylinder axes uniaxially aligned⁶. The mechanical properties of this material have been studied in simple tension^{7,8} and torsion² and the results compared using the following approach.

If we consider the elastic properties of an anisotropic material having transverse isotropy, then the Young's modulus E_θ measured at any angle θ to the symmetry axis is given by the usual transformation equation:

$$\frac{1}{E_\theta} = S_{11} \sin^4\theta + (2S_{13} + S_{44}) \sin^2\theta \cos^2\theta + S_{33} \cos^4\theta$$

where the coefficients S_{ij} are the two-suffix compliances (see e.g. Hearmon⁹) and the symmetry axis is taken as the 3 direction.

The measured values of Young's modulus for the 'single-crystal' samples of Kraton 102 have been fitted to the above equation using the method of least squares, from which one derives values for S_{11} , S_{33} and $(2S_{13} + S_{44})$. In a previous paper⁸, it was shown on theoretical grounds that $S_{13} \sim 10^{-3}S_{44}$ and hence Young's modulus anisotropy provides values for S_{11} , S_{33} and S_{44} , the latter being inversely proportional to the longitudinal shear modulus G .

The shear modulus G can of course, be directly measured by a torsion test about the symmetry axis on a long sample². It should be noted, however, that any end effects are expected to be much less pronounced in deriving G from the tensile data in view of the fact that this quantity is primarily determined by the Young's modulus corresponding to off axis loading where the ratio E/G is much less than for loading along the symmetry axis.

Values of S_{44} or $G = 1/S_{44}$ from tensile measurements can be compared with those from torsion tests. When this is done it is found that G , derived from tensile measurements, is about one half of the value measured by a direct torsion experiment. At the time of a previous paper by the authors⁸ no explanation could be proposed for this discrepancy, but later it became apparent that end effects in torsion may mean that the usual assumptions implicit in the classical theory of torsion are unjustified. Accordingly, torsion measurements were made on samples of varying aspect (length/width) ratio up to about 120 with the results given in Figure 1. It appears from the results that the discrepancy referred to above is resolved only when very long samples are used, in fact greatly exceeding those normally used in torsion measurements.

As stated earlier, end effects are expected to persist for a length of the order of $b(E/G)^{1/2}$, which for Kraton 102 is about 16-17 sample widths from each end. Hence we would expect that the measured shear modulus should show a decrease commencing near a length/width value of about 32, as observed.

The fact that short samples give higher values of shear modulus is attributed to the constraint imposed by the sample clamping, which prevents a portion of the sample length from undergoing pure torsion. In our experiments, here, the end surfaces of the specimen were constrained to remain plane by glueing the specimens onto tufnol blocks or by inserting them in exactly matching blocks of glue so that the specimens were free to slide vertically but not able to rotate (their cross-sections were rectangular). Since Kraton 102 is a relatively soft material, this form of sample clamping is simple to arrange and gives a well defined end constraint. This may not always be possible and in fact preliminary experiments with carbon-fibre reinforced epoxy

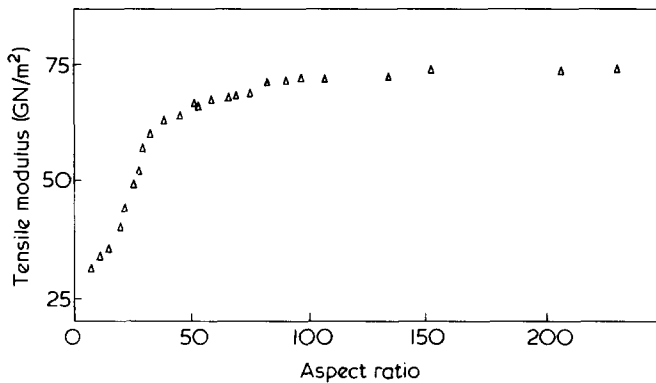


Figure 2 Apparent tensile modulus of linear polyethylene film (draw ratio 28) as function of length/width ratio

resin specimens indicate that constraint of such materials, which can be stiffer than steel, requires very careful experimental design. More often than not, the sample clamping technique involves gripping the ends of the sample directly in the jaws of a mechanical testing machine. In this case, although the stresses still decay with a characteristic length $b(E/G)^{1/2}$, the form of the end constraint is very different.

High modulus polyethylene

End effects can also be expected in tensile and bending tests since, again, the distribution of stresses at points of application of loads does not become negligible until a length of the order of $b(E/G)^{1/2}$ is reached. Tensile specimens therefore need to be at least $2b(E/G)^{1/2}$ in length before uniformity of stress over the sample cross-section can be assumed and a three-point bend test specimen would need to be $4b(E/G)^{1/2}$ in length before the simple beam equation could be assumed correct. As stated earlier, the effect is most pronounced along the direction of highest Young's modulus. Evidence for such a slow decay in stress concentration during tensile testing is afforded by another polymeric system exhibiting a large mechanical anisotropy, represented by the ultra-high modulus polyethylene, at present the subject of extensive research in many laboratories. Figure 2 shows a plot (from ref 10) of Young's modulus versus aspect ratio for polyethylene, drawn to a draw ratio of 28, with the tensile stress applied along the symmetry axis. Sample preparation has been given elsewhere¹¹. Two important points here should be emphasized. First, it can be seen that very long samples are required before a plateau is reached on the curve and secondly the Young's modulus is seen to rise with increase in aspect ratio of sample. The latter arises from the fact that the samples were held in cylindrical collars in the jaws of the tensometer and the load is therefore applied to the sample via shear from the surface to interior points. For short samples, therefore, the load is applied to only a fraction of the sample cross-section, producing an abnormally large strain and hence under-estimating the Young's modulus for the sample as a whole. The values of Young's modulus were obtained using estimated sample strain¹⁰ assuming homogeneous stress and allowing for testing machine compliances (see Figure 9). The effect is particularly pronounced in very anisotropic materials and is supported by theoretical work using finite element methods as shown below.

If one takes the theoretical values for E and G for a polyethylene single crystal as given by Odajima and Maeda¹², then $(E/G)^{1/2} = 15.1$. This shows that the end effects should start to decrease for aspect ratios of about 30, which

is in satisfactory agreement with the experimental results in Figure 2.

Finite element calculations

The issues raised above are further illustrated in Figures 3–8 obtained using finite element models in plane strain but it should be emphasized, they are models only. Figures 3 and 4, show end effects in tension in an isotropic beam loaded at the corners only. The symbols on the diagrams represent the relative magnitudes and directions of the principal stresses. The effect of stresses introduced there is seen to approach a uniform resultant within 1–2 sample widths away from the ends. Analysis of the stresses at the centre line in these models shows, in fact, that for a length/width ratio of 5 the stress is uniform at the centre section and remains so up to 2 widths from each end. Similarly for the beam of aspect ratio 10. This is therefore consistent with the statement of St. Venant's Principle.

This is certainly not true for anisotropic beams similarly loaded, however, as Figures 5–8 show. The values of E and G used in these calculations were those calculated for polyethylene crystals by Odajima and Maeda¹². It can be seen that the applied tensile load is almost entirely concentrated in the surface layers and analysis shows that the beam has to have an aspect ratio of about 40 before the stress at the centre cross-section becomes uniform to within 1%. It is still non-uniform for about 14 widths from each end, in very good agreement with the theory of Horgan⁴, discussed earlier. Finite element calculations for beams in which the two outer surface nodes at each end and on each side are given identical displacements yield very similar results to those of Figures 5–8. This loading corresponds to the case of a soft material bonded directly on its lateral surfaces at each end to a much stiffer material.

Of great significance to the experimentalist is the fact that not until an aspect ratio of 40:1 is reached is there a region of uniform stress across the specimen. This means that not even by using strain gauges will a correct value of tensile modulus be deduced, since the surface strain is not representative of the sample as a whole. Figure 9 shows the predictions of the apparent tensile modulus deduced from the finite element model for specimens with the same degree of mechanical anisotropy as used above. One curve shows results when the movement of the points of loading is used as a measure of the sample strain while the other uses surface strain as would be measured by a suitable strain gauge. It is apparent that erroneous values will be obtained unless the specimen is long enough to ensure uniform strain at its centre. There is qualitative agreement with the experimental curve of Figure 2. Quantitative experimental results using strain gauges or other means of measuring surface strain on high-drawn polyethylene have not yet been obtained. The strains are very difficult to measure on the very small specimens available.

Evidence for a slow decay in stress concentrations due to point loads in glass-fibre reinforced material has been obtained by photoelastic means by Bold¹³, but in this material the anisotropy is much less marked, though still apparent.

CONCLUSIONS

Experimental measurements on torsion and in tension on two highly anisotropic materials show that end effects produced by various means of clamping persist further into the specimen than would be expected using the conventional

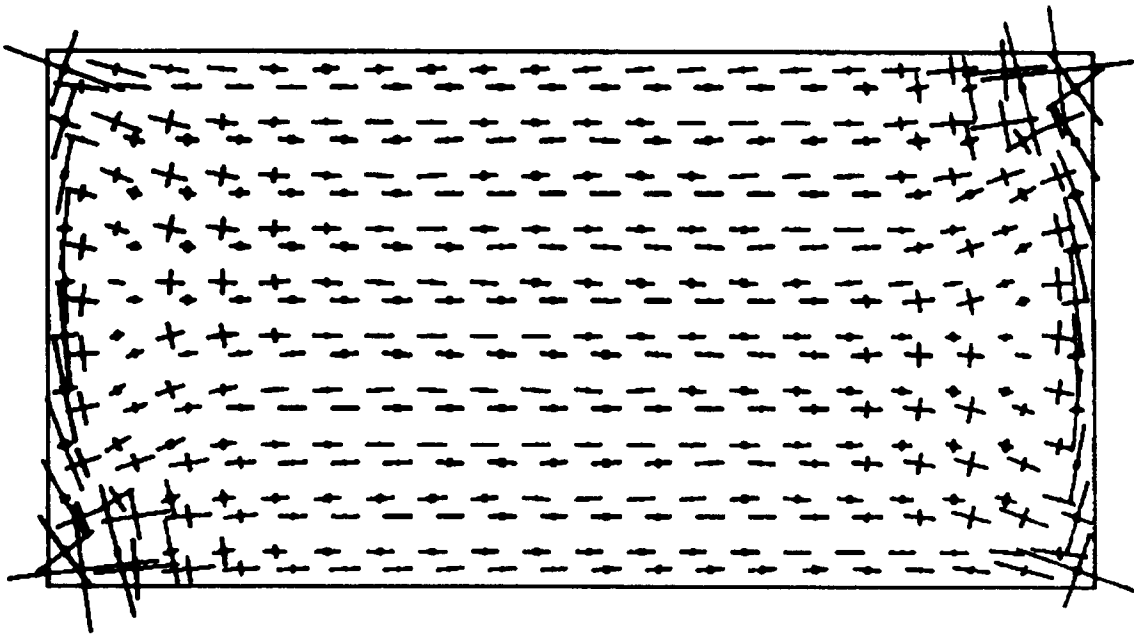


Figure 3 Principal stress values for isotropic rectangular bar loaded in plane strain at the four corners; length/width ratio 5

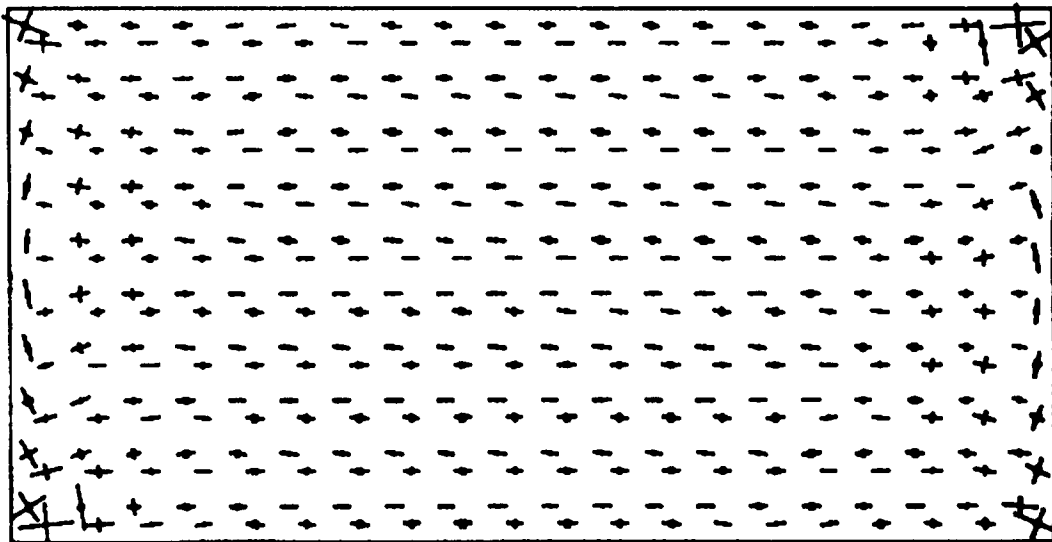


Figure 4 As in Figure 3 but length/width ratio 10

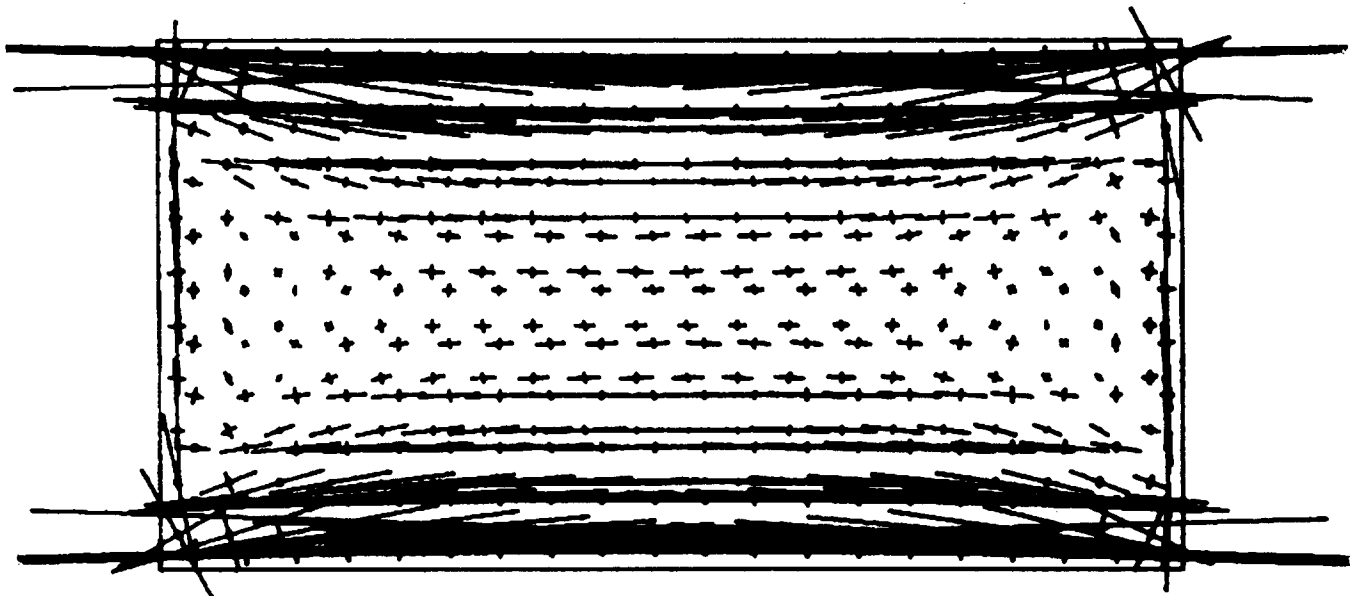


Figure 5 Principal stress values for anisotropic rectangular bar loaded in plane strain at the four corners. $(E/G)^{1/2} = 15.1$; length/width ratio 5

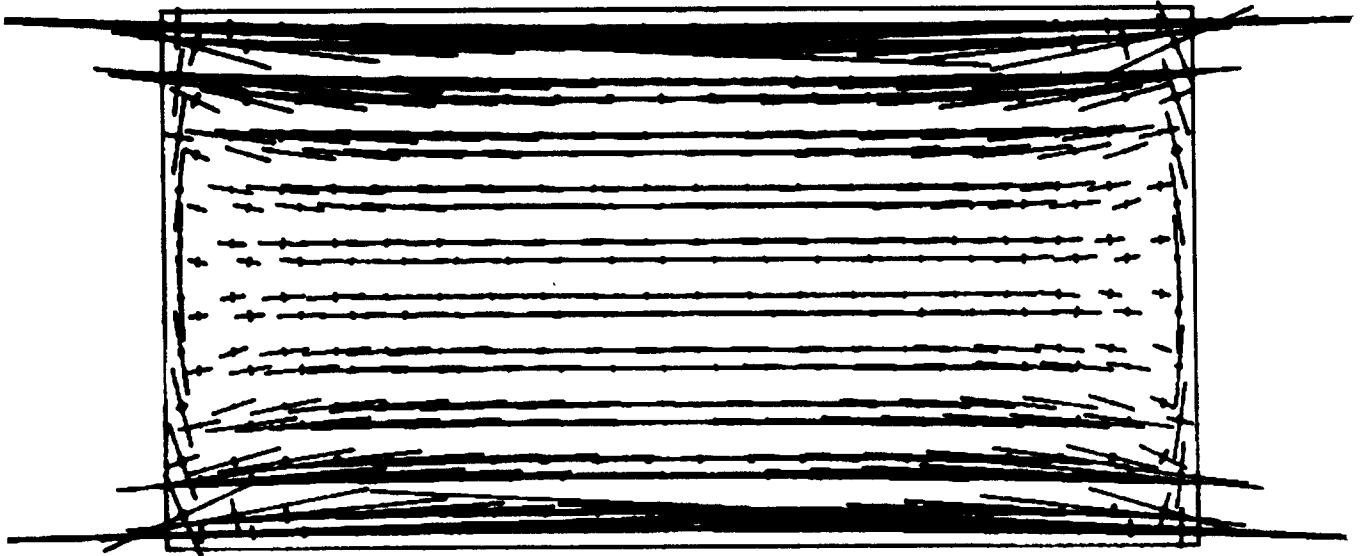


Figure 6 As for Figure 5 but length/width ratio 10

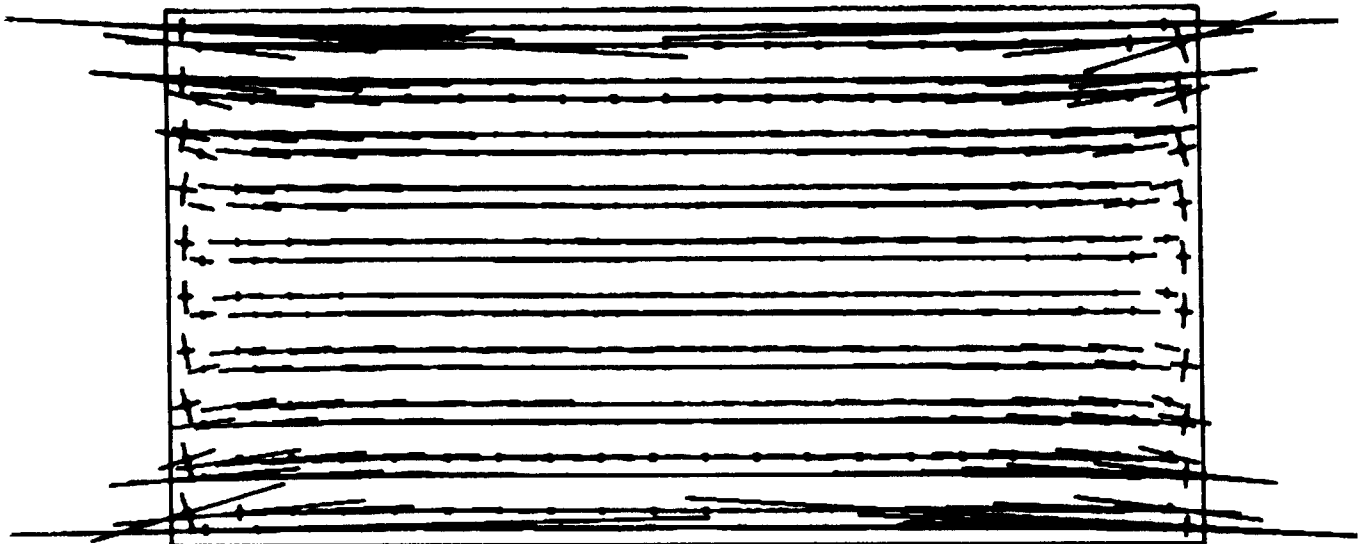


Figure 7 As for Figure 5 but length/width ratio 20



Figure 8 As for Figure 5 but length/width ratio 40

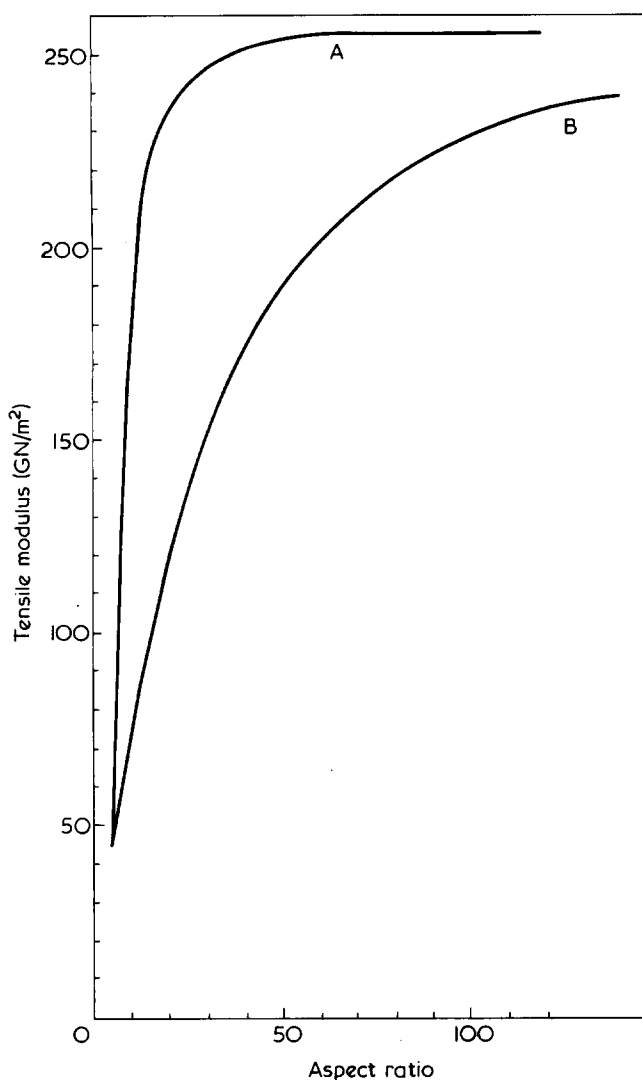


Figure 9 Calculated Young's modulus for bar of Figures 5-8. See text for explanation of terms used. A, surface strain; B, overall strain

Principle of St. Venant. There is good agreement with the prediction of Horgan that such effects persist for a distance $b(E/G)^{1/2}$ and consequently specimens need to be long enough for this enhanced end effect to be ignorable.

In principle the finite element method enables calculation to be made of the stress distributions due to any system of loading. In practice this is not possible since we have no means of measuring the distribution of stresses at the points of attachment of the clamps to the specimen. The practical conclusion therefore is that measurements of any elastic moduli on anisotropic materials need to be repeated on specimens of increasing length/width ratio until consistent results are obtained. This may mean length/width ratios up to 100 for very anisotropic materials.

ACKNOWLEDGEMENT

We would like to acknowledge the assistance of Mr F. A. Lovett in the computing work.

REFERENCES

- 1 Love, A. E. H. 'Mathematical Theory of Elasticity', Dover Reprints, New York, 1944
- 2 Folkes, M. J. and Arridge, R. G. C. *J. Phys. (D)* 1975, 8, 1053
- 3 Toupin, R. A. *Arch. Ration. Mech. Anal.* 1965, 18, 83
- 4 Horgan, C. O. *J. Elasticity* 1972, 2, 169, 335; *Int. J. Solids Struct.* 1974, 10, 837
- 5 Pagano, N. J. and Halpin, J. C. *J. Compos. Mater.* 1968, 2, 18
- 6 Keller, A., Pedemonte, E. and Willmouth, F. M. *Nature* 1970, 225, 538; *Kolloid Z.* 1970, 238, 385
- 7 Folkes, M. J. and Keller, A. *Polymer* 1971, 12, 222
- 8 Arridge, R. G. C. and Folkes, M. J. *J. Phys. (D)* 1972, 5, 344
- 9 Hearmon, R. F. S. 'An introduction to Applied Anisotropic Elasticity', Clarendon Press, Oxford, 1961
- 10 Arridge, R. G. C., Barham, P. J., Farrell, C. J. and Keller, A. *J. Mater. Sci.* in the press
- 11 Barham, P. J. and Keller, A. *J. Mater. Sci.* in the press
- 12 Odajima, A. and Maeda, T. 1966, *J. Polym. Sci. (C)* 1966, 15, 55
- 13 Bold, S. *MSc Thesis* Bristol University (1973)

Multi-pass Fabry–Perot spectroscopy of polymers*

S. M. Lindsay, A. J. Hartley and I. W. Shepherd

Physics Department, University of Manchester, Manchester M13 9PL, UK

(Received 25 November 1975)

The potential utility of multi-pass Fabry–Perot spectroscopy in the study of polymers is demonstrated. A triple-pass system is described and the performance is discussed. Preliminary results in three areas are presented: (1) a study of anisotropy in oriented poly(methyl methacrylate); (2) hyper-sonic viscoelastic behaviour of poly(propylene oxide) and poly(dimethyl siloxane); (3) the effect of crosslinking in poly(dimethyl siloxane) on the high frequency elastic properties and on phonon absorption.

INTRODUCTION

In this paper we wish to describe a relatively new technique, multi-pass Fabry–Perot spectroscopy (*MPFPS*), and to indicate possible applications to the study of polymers. We also present some of the early results obtained on our triple-pass equipment at Manchester.

In this work the Fabry–Perot (*FP*) is used to analyse the spectrum of laser light scattered from polymers. It is thus one of many techniques employed in scattering experiments and it is helpful to place it in context. Scattering of many types has played an important part in physics over many years, ranging in time and complication from the classical Rutherford and Compton scattering experiments to the modern work using high-flux reactors which produce intense neutron beams. These diverse experiments all have a common basis: an incident particle having momentum $\hbar\mathbf{k}_i$ and energy $\hbar\omega_i$ is scattered in the medium to emerge with changed momentum and energy $\hbar\mathbf{k}_s$ and $\hbar\omega_s$. An excitation of momentum $\hbar\mathbf{K}$ and energy $\hbar\Omega$ is created (or annihilated) in the medium. Conservation of energy and momentum requires that:

$$\omega_i - \omega_s = \pm\Omega \quad (1)$$

and

$$\mathbf{k}_i - \mathbf{k}_s = \mathbf{K} \quad (2)$$

where the positive and negative signs in equation (1) refer to creation and annihilation of an excitation. It is clear

* Presented at the Polymer Physics Group (Institute of Physics) Biennial Conference, Shrivenham, September 1975.

from these simple but basic considerations that if the incident beam is well-defined, measurement of the frequency and momentum of the scattered particle will yield information about \mathbf{K} and Ω which in turn can give information about the medium itself. Equations (1) and (2) also show that the range of momentum and energy transfer, i.e. the range of \mathbf{K} and Ω that is measurable, will depend on the incident momentum and energy. These incident beam parameters will depend on the nature of the particles, and *Table 1* and *Figure 1* show the regions of $\mathbf{K} - \Omega$ space that are covered by several different techniques. The precise shapes of the blocks in *Figure 1* are affected by experimental resolution, and in drawing the diagram criteria have been adopted that are possible to realize using modern equipment. In the interest of simplicity the range of Ω has been limited to that covered by visible light scattering, so that 'high energy' particle scattering is excluded. The most striking features of this plot are the wide open spaces not covered by any presently available techniques. In other words, this type of experiment is only grazing the surface. The second most striking features are the very wide frequency range covered by visible light scattering and the very narrow momentum range. The so-called Brillouin region, which covers the gap between Rayleigh line-width and Raman is covered by the Fabry–Perot technique. The narrow momentum range is the most serious limitation of the method, and is of course due to the fact that $|\mathbf{k}_i|$ for a visible photon is only of the order 10^5 cm^{-1} . Equation (2) then shows that the maximum $|\mathbf{K}|$ possible is $2|\mathbf{k}_i|$ or approximately $2 \times 10^5 \text{ cm}^{-1}$. This is very much less than the reciprocal of an interatomic spacing in a solid or a liquid, and so light scattering studies are effectively limited to zone centres. This limitation does not apply to the neutron, which is a massive particle for which momenta of

Table 1 Range of energy and momentum parameters in a number of scattering experiments

Radiation	Wavelength (Å)	Momentum (Å ⁻¹)	Energy (eV)	Energy transfer (eV)
Neutrons	0.2–10	5–0.1	0.1–0.002	0.1–0.002
Electrons	0.01–100	100–0.01	$\sim 5 \times 10^4$ –0.1	Wide
X-ray	1	1	$\sim 10^4$	Wide
Visible light:				
Raman	5×10^3	2×10^{-4}	3	0.5 – 5×10^{-4}
Brillouin	5×10^3	2×10^{-4}	3	10^{-3} – 10^{-6}
Rayleigh linewidth	5×10^3	2×10^{-4}	3	10^{-8} – 10^{-14}

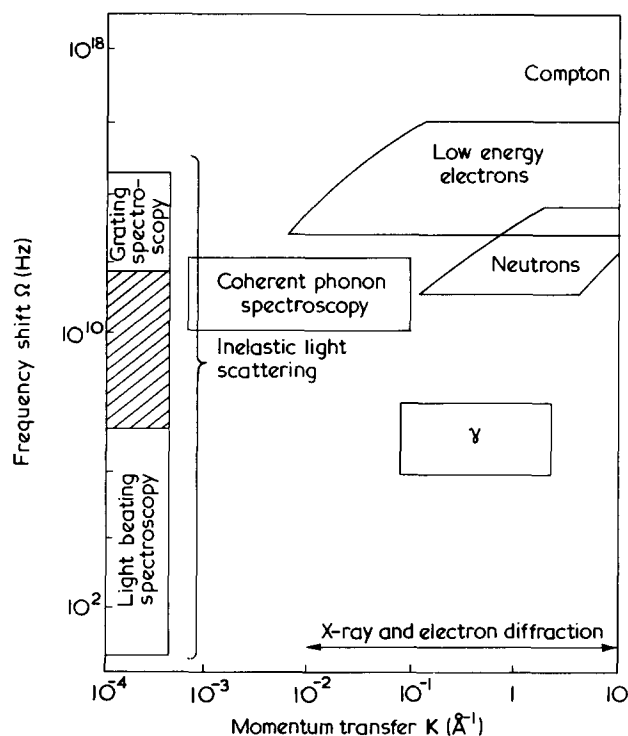


Figure 1 The regions of frequency-momentum space covered by several scattering techniques. The shaded area represents the region covered by Fabry-Perot spectroscopy

$|\mathbf{k}_i| \sim 10^8 \text{ cm}^{-1}$ are readily obtainable. Advantages of light scattering in general and Brillouin in particular, other than the wide energy range, are not apparent from Figure 1. They are: (a) Good sensitivity. (b) High resolution (10^7 – 10^8 Hz in Brillouin). (c) Sample preservation. Except in extreme circumstances the experiments are non-destructive. (d) Possibility of observing transient effects. Very fast pulse techniques may allow the observation of transient effects down to a time resolution of 10^{-7} sec.

Particular contributions that may be made to the study of polymers using the *FP* are suggested in Table 2. There is a somewhat arbitrary division in this Table between Brillouin scattering and low frequency Raman scattering. Historically Brillouin's name is associated with scattering from propagating pressure waves, i.e. sound waves, so the items in this column make use of the waves at hypersound frequencies to give information about the materials. The velocity of sound, v , is connected with the measured frequency shift by:

$$\frac{\Omega}{\omega_0} = \frac{2n\nu}{c} \sin \frac{\theta}{2} \quad (3)$$

where ω_0 is the incident frequency, n the refractive index and θ the angle of scatter. The width of the Brillouin peaks gives information about the attenuation or lifetime of the waves, and thus about the structure over a range of 0.1–20 μm . Where phonon-phonon scattering makes an important contribution, absorption measurements will also yield information about the high frequency (10^9 – 10^{12} Hz) dynamics of the network. The generic term 'Raman' is used for the other light scattering phenomena. The method of detection is, of course, the same in either case. Otherwise Table 2 is self-explanatory. When it is realized that the list is only a selection of possible experiments it is clear that the technique is potentially of great value.

INSTRUMENT DESCRIPTION

The spectral range we wish to cover is roughly between 10^7 and 10^{11} Hz. Visible laser sources are normally used and therefore the required resolving power is high, of the order 10^7 . The only practical possibility in these circumstances is to use a *FP* etalon which achieves high resolving power by the interference of beams multiply reflected between two highly reflecting plates. The response function¹ of the etalon for a monochromatic beam of intensity I_0 incident at 90° to the plates is given by:

$$\frac{I(\delta)}{I_0} = \frac{1}{1 + (2F_R/\pi)^2 \sin^2 \frac{1}{2}\delta} \quad (4)$$

where the phase parameter $\delta = 2d|\mathbf{k}|$; d is the plate separation and $|\mathbf{k}| = 2\pi\lambda^{-1}$ the light wavevector. F_R is the reflectivity finesse and is defined in terms of the reflection coefficient r as $\pi^{1/2}(1-r)^{-1}$. It has been assumed that the finesse is determined solely by the reflectivity. In practice other factors, such as plate flatness, can be important and decrease the finesse to an actual value F which is below the theoretical reflectivity value. The response is plotted in Figure 2 for spectral orders n and $N+1$. The parameters of experimental importance are indicated in the Figure. They are: (1) the free spectral range $\Delta\nu$, which determines the accessible region of the spectrum free of overlap between orders; (2) the instrumental linewidth $\delta\nu$, which determines the smallest measurable linewidth; (3) the contrast C , which is the ratio between the maximum and minimum intensities; (4) the resolving power $R = \nu/\delta\nu$. The free spectral range is determined by plate separation and, in frequency units, is given by $\Delta\nu = c/2d$, where c is the velocity of light. It can be adjusted between the approximate limits of 10^8 and 10^{12} Hz to suit experimental requirements. Stability problems are enhanced by the large plate separations at the lower limit and make lower values of $\Delta\nu$ extremely difficult to obtain. If it is not necessary to have an adjustable free spectral range, greater stability can be obtained by using a confocal arrangement². It is not, in general, important to increase the upper limit, because 10^{12} Hz

Table 2 Selection of possible applications of multi-pass Fabry-Perot spectroscopy to the study of polymers

Brillouin scattering	Low frequency Raman (0.03 → 30 cm^{-1})
Only method for:	(e) 'Accordion modes'
(a) High frequency viscoelastic measurements 10^9 – 10^{11} Hz.	A study of very low frequencies in chain-folded materials may resolve X-ray/Raman anomalies.
(b) Thermodynamic and elastic studies of microcrystals and thin films (studies of the amorphous state)*	(f) Determination of moduli in big regular molecules, e.g. TMV, collagen.
Convenient for:	(g) Measurement of 'super' lattice modes in block copolymers, e.g. SBS.
(c) Many thermodynamic studies e.g. volumetric measurements, glass transitions, Grüneisen parameters. (sample volume down to 10^{-7} cm^{-3})	(h) Rotations of polymer side-groups.
(d) Structural determinations: directly 0.1–20 μm indirectly 0.1–0.001 μm	(i) Low frequency modes in n-alkanes.

* Dr G. Patterson, Bell Telephone Labs, Murray Hill, New Jersey, USA, is using the thin film technique to obtain amorphous materials.

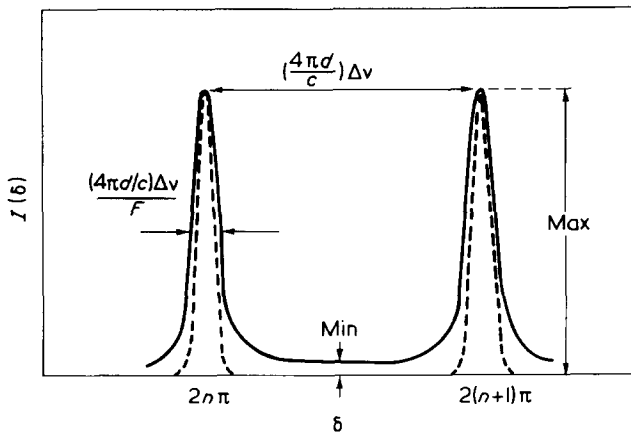


Figure 2 Response function of an etalon with monochromatic input. F is the finesse, d the plate separation, δ the phase factor $4\pi d/\lambda$, n the order and $\Delta\nu$ the free spectral range in frequency units. (---) represents the effect of passing the beam through three times (triple-pass)

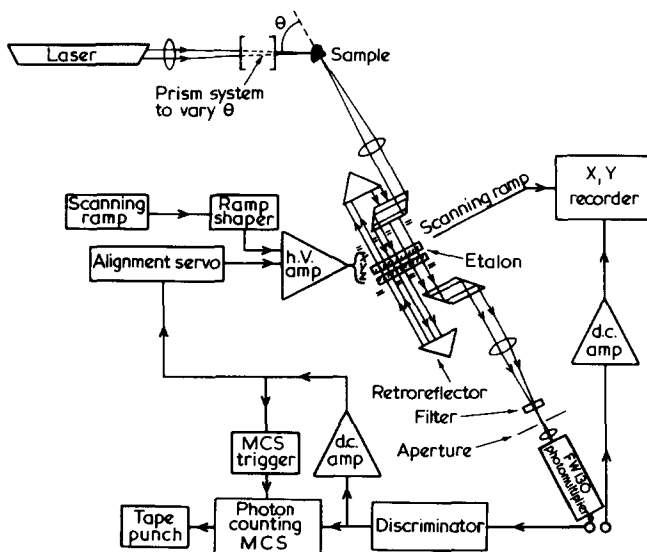


Figure 3 Schematic diagram of a triple-pass Fabry-Perot etalon system incorporating piezoelectric scanning and digital detection

is already well within the range of modern grating spectrometers. Under the assumption that the mirror reflectivity is the limiting factor in performance, other parameters can be expressed in terms of $\Delta\nu$ and F as $\delta\nu = \Delta\nu F^{-1}$, $C \approx 4F^2\pi^{-2}$ and $R = \nu F/\Delta\nu$. Normally finesse values of between 40 and 50 are attainable, corresponding to reflectivity of about 95% with plates flat to about $\lambda/100$. Values of C are then $\sim 10^3$, which are sufficient for samples of high optical quality that do not produce a large random scattering intensity. Unfortunately many polymers are of poor quality, and the Brillouin spectra may be unobservable because the peaks are much smaller than the minimum intensity in $I(\delta)$. This problem can be overcome by operating the etalon in a 'multi-pass' mode in which the beam is reflected back through m times, where m has experimentally optimum values of 3 or 5. In this configuration the output function is determined by raising the function in equation (4) to the m 'th power, and in this way contrasts up to 10^8 can be obtained. The effect of 'triple-passing' the instrument is indicated by the broken line in Figure 2; the important point is that the minimum is significantly suppressed. A schematic diagram of the experimental equipment is shown in Figure 3. The incident laser light from an argon ion laser ($\lambda = 5145 \text{ \AA}$) is scattered through an angle θ and

then collimated into the etalon. The beam is returned three times by corner-cube retro-reflectors and emerges through a filter to be detected by a photomultiplier tube. The signal is then recorded using multichannel scaling techniques. Line shape analysis is carried out using an off-line computer. The etalon plates are scanned piezoelectrically and Figure 3 includes a block diagram of the electronic control system. More detailed descriptions of this system can be found in refs 4 and 5.

The enormous improvements to be obtained by multi-passing are illustrated in Figure 4 where we present Brillouin spectra of a crosslinked rubber, poly(dimethyl siloxane). In Figure 4a the spectrum is shown after a single pass and the Brillouin peaks are only just visible above the background. Figure 4b shows the same system after three passes when the Brillouin peaks seem to be completely resolved and quantitative analysis of line shapes is possible. From this data it is clearly possible to determine to a high accuracy the sound velocity from the frequency shift and attenuation from the line width of the phonon bands. Finally, the limit of performance is shown in Figure 5 where the Brillouin spectra obtained by surface scattering from

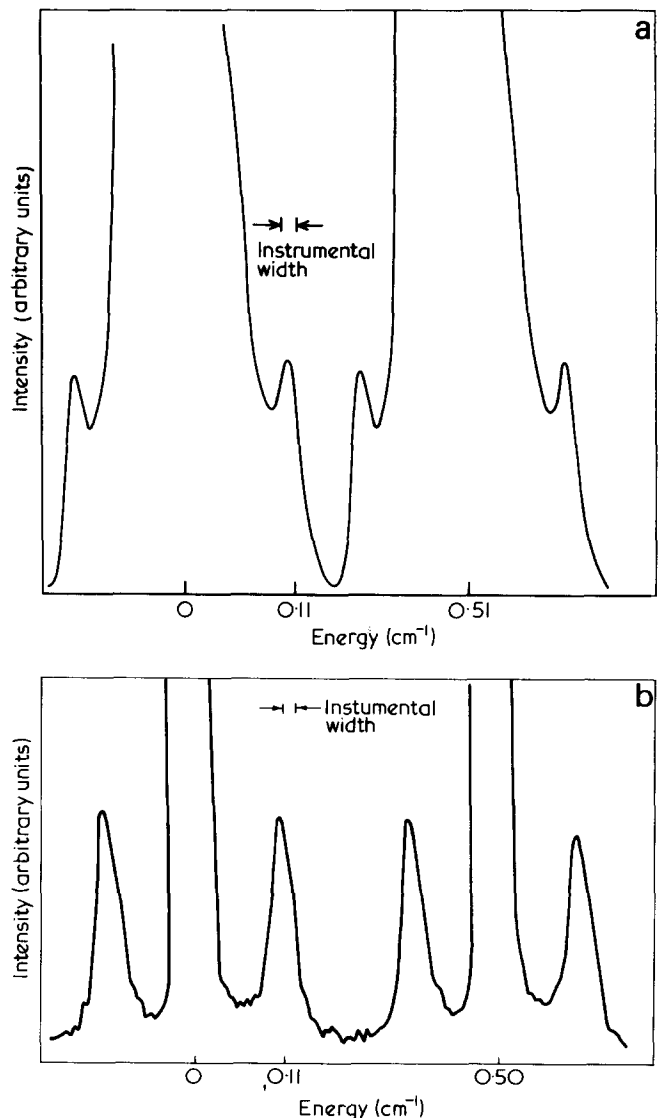


Figure 4 Brillouin spectra of poly(dimethyl siloxane) rubber networks at 30°C (a) after a single pass through the etalon, $\theta = 90^\circ$ (b) after three passes, $\theta = 90^\circ$. The Landau-Placzek ratio, the ratio of the central peak intensity to the sum of the side band intensities, in this case is 3000

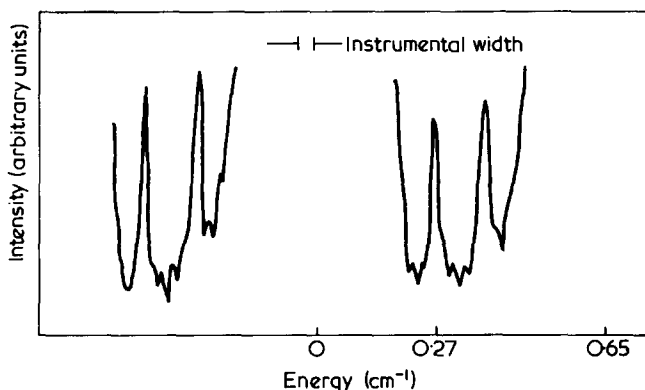


Figure 5 Brillouin spectra obtained by surface scattering in poly(methyl methacrylate), $\theta = 56^\circ$. The Landau-Placzek ratio is $>10^8$, showing that a contrast of at least this magnitude has been obtained.

poly(methyl methacrylate) is shown. In this case the ratio of central to side band intensities is greater than 10^8 indicating that a contrast of this magnitude has been obtained.

EXPERIMENTAL RESULTS

The data presented above have shown that extremely high contrasts of 10^8 can be obtained with a triple-pass etalon system. This implies a qualitative change in the study of polymer systems. Previously only samples of extremely high optical quality could be studied, which limited activity to clean liquids, optical quality quartz and carefully prepared poly(methyl methacrylate) blocks plus a very few other similar systems. Now, with multi-passing, samples can be chosen for study because of their intrinsic interest, and it is even possible to study entirely opaque materials by back scattering⁶. In this section we present preliminary measurements in three areas of interest.

Measurements in oriented poly(methyl methacrylate) (PMMA)

The purpose of this experiment was to measure the anisotropy of the high frequency elastic modulus in strained samples by observing the variation of sound speed as a function of the propagation direction with respect to the draw axis. This can be accomplished using Brillouin techniques with a volume resolution of 10^{-6} cm^3 . We also attempted to observe dispersion effects by varying the scattering angle and hence the sound wavelength and frequency.

Samples of ICI Perspex were drawn just above T_g and quenched. Further details of the sample preparation may be found in ref 7. The samples were then shaped into discs with the orientation axis in the plane. The scattering geometry is illustrated in Figure 6a where the incident and scattered beams, the orientation and the phonon are all in the same plane. The angle between phonon direction and orientation axis, ϕ , could be varied by rotation of the sample. Within the experimental error it appears that the phonon line width is independent of propagation direction, indicating that the phonon attenuation is independent of orientation. This is in substantial agreement with low temperature thermal conductivity studies⁸ which have found no measurable anisotropy in conductivity. The measured values of sound velocity v , as a function of ϕ are shown in Figure 6b for three different strained samples and an annealed sample. The degree of strain was characterized by the optical birefringence, Δn , and this parameter had the values -24 , -9 and -4×10^{-4} in the three cases. The func-

tional form of the data in each case is similar and follows closely the expression:

$$V(\phi) = V_0(1 - \Delta \sin^2\phi) \quad (5)$$

where V_0 is the velocity in the annealed sample, which shows no variation with ϕ , Δ is the appropriate anisotropy. It is interesting to note that the values of $V(\phi)$ are always less than V_0 , indicating that the observed sound waves are propagating in regions of high density. This contrasts with the ultrasonic work of Wright *et al.*⁹ on the same samples where considerable increase in velocity along the draw direction is observed (see Figure 8). These regions are probably separated by voids and this heterogeneity causes the large random scattering in the sample evidenced by the strong central peak that prevents such a study using a single pass system. The values of anisotropy, Δ , that give the best fit to data shown in Figure 6b are plotted as a function of birefringence, Δn in Figure 7; the dependence is apparently linear.

If the structure of the strained PMMA indeed includes regions of high density separated by voids then it may be possible to observe dispersion effects when the sound wavelength, Λ , is of the same order as the dimensions of these regions. We therefore made measurements of sound

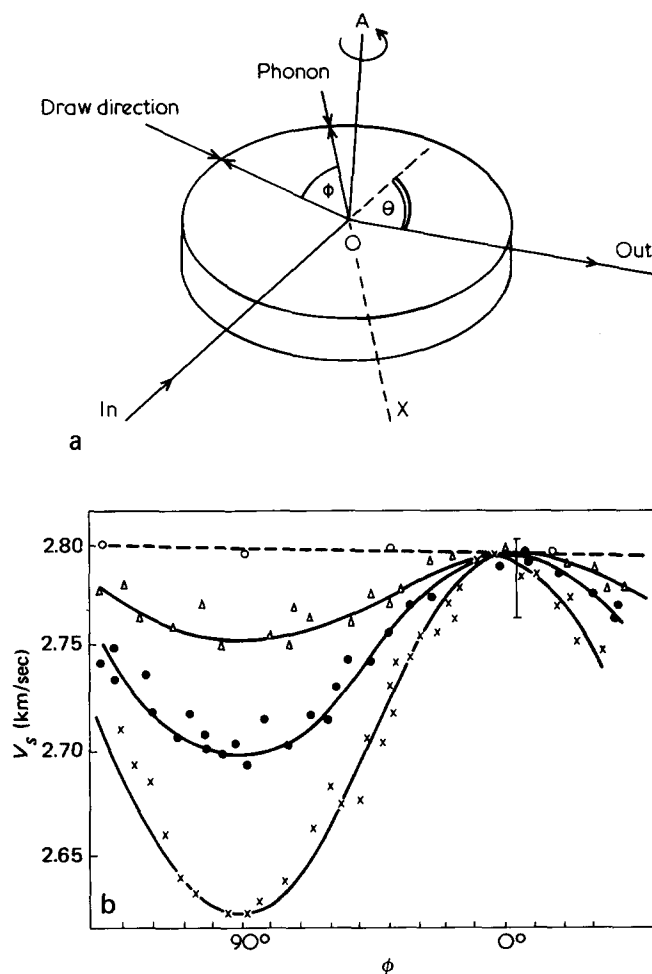


Figure 6 (a) The sample and scattering geometries for a uniaxially oriented sample (b) The measured values of longitudinal sound velocity in PMMA as a function of propagation direction ϕ relative to orientation axis. All points taken with scattering angle $\theta = 90^\circ$. The values of birefringence Δn : X, -24×10^{-4} ; ●, -9×10^{-4} ; Δ, -4×10^{-4} ; ---, represents the value of V for the annealed sample; —, represents fits to the form of equation (5)

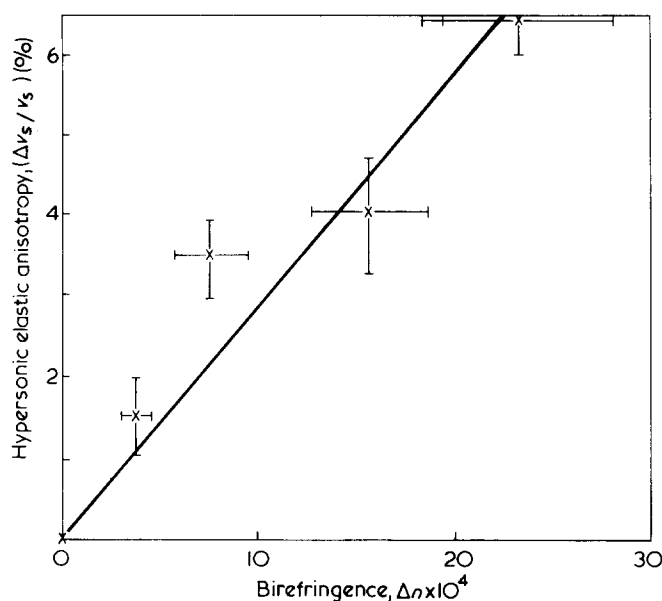


Figure 7 Values of elastic anisotropy in oriented PMMA, obtained as best fits to the data in Figure 6b, plotted against birefringence

velocity as a function of the scattering angle θ which is connected with Λ by:

$$\Lambda = \frac{\lambda}{2n} \left(\sin \frac{\theta}{2} \right)^{-1} \quad (6)$$

where λ is the incident light wavelength.

The results are shown in Figure 8 for the sample having $\Delta n = -24 \times 10^{-4}$ at ϕ values of 0 and 90° . Also shown are measurements on an annealed sample and data taken at the lower frequency of 4 MHz. No dispersive effects are observed over the range of Λ values from 0.2 to 0.8 μm . However the data taken at $\phi = 0^\circ$ at hypersonic frequency deviate significantly from the measurement at 4 MHz and this suggests that the average dimension of the structure is larger than the largest value of Λ that we have yet attained by varying θ . In fact the lowest angle of scatter we have used is $\theta = 25^\circ$ and with care it should be possible to extend the range to $\theta = 5^\circ$ and hence cover Λ values up to 5 μm . By making use of incident radiation of longer wavelength, for instance from a helium-neon laser ($\lambda = 6328 \text{ \AA}$) a further increase in Λ of 25% can be obtained and it is then very possible that the dispersion region will be reached. This would then yield valuable information about the strained structure.

High frequency relaxations in polymer fluids

The purpose of this work was to try and observe relaxations in the hypersonic frequency range and to obtain some information about the glass transition at these high frequencies. In order to conduct the experiments at a convenient temperature it is necessary to choose a polymer sample with a very flexible chain. The first choice was therefore poly(dimethyl siloxane) (PDMS) and measurements were made of sound velocity and attenuation as a function of temperature at 3.5 GHz (using the FP) and at 35 MHz (using ultrasound equipment). These data proved quite featureless. There was no sign of any relaxation over the range $240 < T < 340\text{K}$ at either frequency and the velocities at the two frequencies were identical within the experimental errors as is α/f^2 (α is the sound absorption

coefficient, f the frequency). Since it is unlikely that the α relaxation is above 340K at 35 MHz (see Figure 10) we deduce that even at 3.5 GHz the PDMS is still in a rubbery state and above the main glass transition. The fact that PDMS crystallizes at 223K makes it difficult to extend the measurements to lower temperatures and we are left with the supposition that T_g even at gigahertz frequencies is at a temperature near to, or lower than, the crystallization point for this material.

The second material chosen for this study was poly(propylene oxide) (PPO). While working on this material, of molecular weight $M_w \sim 1500$, (Shell PPG 1500), we became aware of recent work¹⁰ on a low molecular weight material ($M_w = 425$) in which a relaxation was observed at gigahertz frequencies. Our data for both sound attenuation and velocity are shown in Figure 9. A break in the gradient of the graph of V versus temperature at $\sim 187\text{K}$ is attributed¹⁰ to the glass transition. It is important to note that the value of T_g measured in this way in fact reflects changes in quasi-static parameters, such as the Gruneisen parameter, γ , and the coefficient of volume expansion, α , and does not represent a determination of T_g at hypersonic frequencies. We believe the relaxation at $\sim 310\text{K}$ to be the main α -relaxation. Accordingly this value of T_g is plotted for a frequency of 5 GHz in Figure 10 which shows the frequency dependence of the glass transition for PPO by plotting $1/T_g$ against the logarithm of frequency. Mechanical and dielectric measurements over a range of frequency from 10^{-3} to 10^7 Hz¹¹ and ultrasound measurements at 10^7 Hz as well as the present data are included. The dependence is clearly not linear implying that a single activation energy is insufficient to describe this complicated transition. The dearth of points in the high frequency region (10^7 – 10^9 Hz) can be remedied by making Brillouin measurements at low scattering angles, giving measurement frequencies in the region of 10^8 Hz. Such measurements would enable a good estimate of the activation energy appropriate to the high frequency transition to be obtained. Apart from a 50% discrepancy in the values of V our data are in reasonable agreement with the measurements of Huang and Wang¹⁰. Their measurements on a low molecular weight material did not show evidence of the secondary relaxation apparent in our data in the vicinity of 260K (Figure 9b). This is consistent with ultrasound measurements on this polymer which indicate

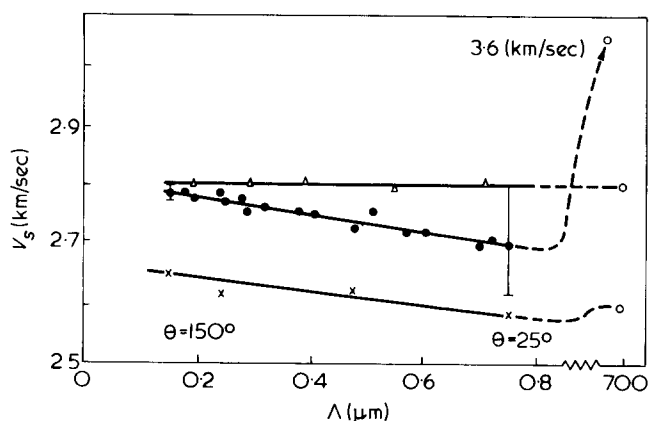


Figure 8 Values of longitudinal sound velocity, v , plotted as a function of sound wavelength $\Lambda = (\lambda/2n) (\sin \theta/2)^{-1}$ in strained samples with propagation direction parallel and perpendicular to the strain axis. Data is also shown for an annealed sample. \bullet , strained sample $\phi = 0^\circ$; \times , strained sample $\phi = 90^\circ$; Δ , annealed sample; \circ , ultrasound data 4 MHz. The scattering angles θ corresponding to extreme Λ values are indicated

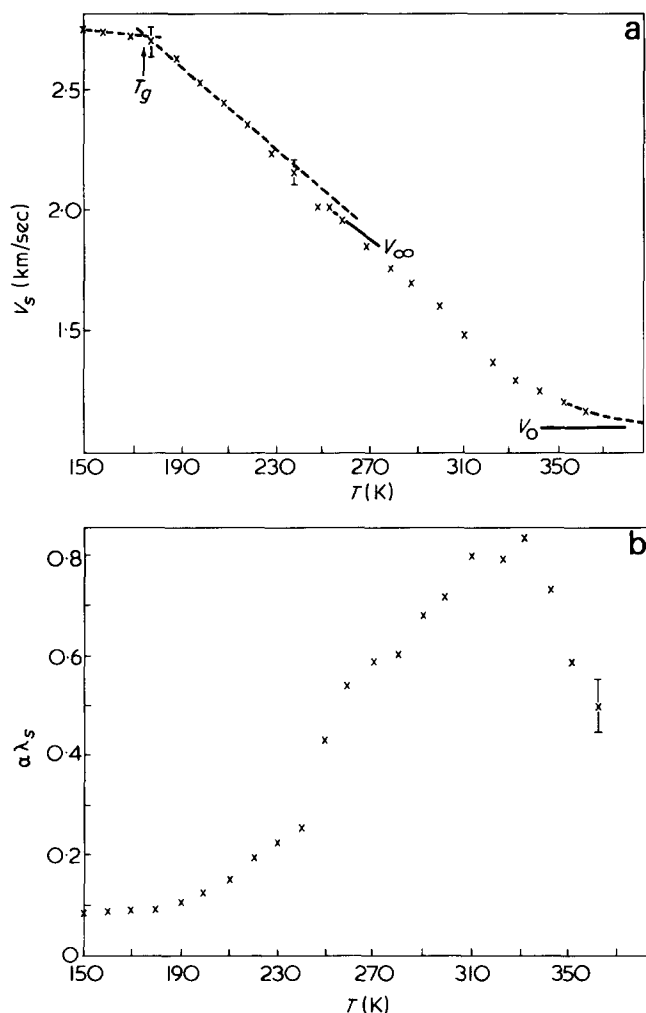


Figure 9 (a) Longitudinal sound velocity and (b) attenuation measured at 5 GHz in poly(propylene oxide) as a function of temperature. ($M_w = 1500$). The observed dispersion is attributed to the main α -relaxation (V_∞ and V_0 are the infinite and low frequency limiting values of velocity respectively)

that low molecular weight PPO shows no specific polymeric relaxational behaviour¹². The reduced data are a reasonable fit to a two relaxational time model with $\tau_1 = 0.09 \tau_M$ and $\tau_2 = 0.002 \tau_M^5$. (τ_M is the Maxwellian relaxation time given by $\eta_s J_\infty$ where η_s is the shear viscosity and J_∞ the infinite frequency shear compliance.) Between 220 and 260K the material behaves like a non-relaxing fluid with $(\rho V^2 - k_0) J_\infty$ constant as a function of temperature (k_0 is the zero frequency bulk modulus). Between 200K and the quasi-static glass transition the material behaves like a solid with $\partial V/\partial T$ constant as a function of temperature. The measured velocity-temperature coefficient in this range corresponds to a volume expansion coefficient of 7×10^{-4} and a Gruneisen parameter of +4.5. Away from the relaxation the mechanism of phonon absorption is not understood. The value of $\alpha \lambda_s$ (~ 0.1) is consistent with that predicted for phonon-phonon scattering in long phonon lifetime limit ($\omega \tau_p \gg 1$) although estimates of phonon lifetimes from quantities such as the thermal diffusivity indicate that $\omega \tau_p \ll 1^5$.

The preliminary results of this project are encouraging. First it is extremely easy to prepare samples for multi-pass Fabry-Perot spectroscopy, and it should be possible to study a wide range of samples. Secondly, the existence of relaxation in the GHz region has already been established in one polymer (and initial measurements suggest they exist

in others), whereas only recently it was doubted that relaxations at these frequencies existed at all¹³. There should be much more information forthcoming about the α -relaxation using this technique.

Studies in rubber networks

The purpose of these studies was to investigate the constraints imposed on chain motion by crosslinking. PDMS samples of $M_w = 7 \times 10^4$ were crosslinked by γ -irradiation and the shear modulus, G , measured by the quasi-static method of ball-bearing indentation. The average crosslink density, N , was obtained from Charlesby's critical gel dose point data^{14,15} and in the samples used the average number of monomer units between crosslinks, $\langle n \rangle$, ranged from 109 to 14. The value of G increases monotonically with $\langle n \rangle^{-1}$ over the range 0.7 to 3×10^7 N/m². The extrapolated value with zero crosslinking was 0.3×10^7 N/m². and is attributed to the effect of entanglements. Values of G calculated from $G = NkT$ were an order of magnitude lower than the measured values. This disagreement may reflect uncertainty in the gel dose point due to the distribution of chain lengths between links. Measurements of the longitudinal sound velocity were made at two frequencies 5 MHz and 3.5 GHz. PDMS is in a rubbery state at these frequencies, but may sustain shear because of the crosslinks. The effective modulus is given by:

$$M = \rho V^2 = k_0 + \frac{4}{3} G \tag{7}$$

where $k_0 = \rho V_0^2$ (V_0 is the velocity in the uncrosslinked sample). Sample density increased from 9751 kg/m³ in the fluid to 9941 kg/m³ in the most highly crosslinked sample. The Brillouin and ultrasound velocity measurements are

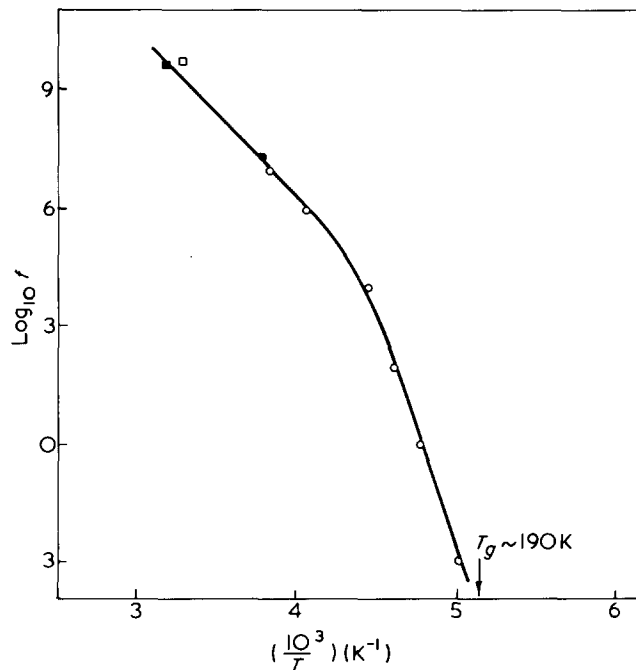


Figure 10 A plot of $(T_g)^{-1}$ for PPO as a function of the logarithm of the frequency. The dependence is not linear, indicating that a single activation energy is insufficient to describe the relaxation. \circ , Dielectric and mechanical loss measurements (high M_w)¹¹; \blacktriangle , ultrasound measurements (M_w 400); \bullet , ultrasound measurements (M_w 4000); \blacksquare , hypersound measurements (M_w 1500) present work; \square , hypersound measurements (M_w 425)¹⁰

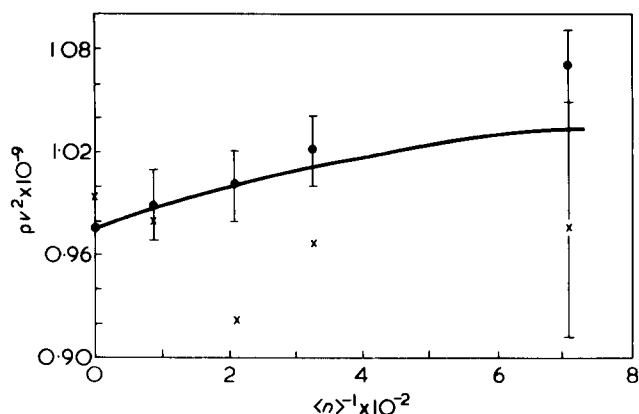


Figure 11 The product of density ρ and the square of the longitudinal sound velocity v^2 measured in PDMS at 3.5 GHz (●) and 5 MHz (x) versus the crosslink density $\langle n \rangle^{-1}$. —, corresponds to values of ρv^2 calculated from equation (7) using the static values of the shear modulus

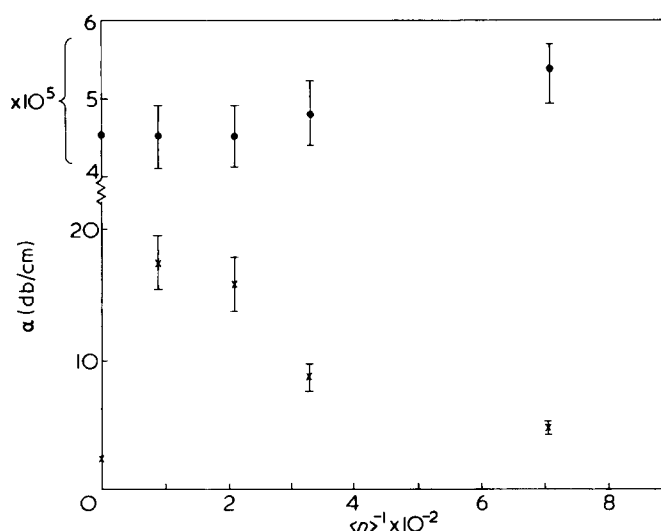


Figure 12 Phonon attenuation, α , in PDMS measured at 3.5 GHz (●) and 5 MHz (x) versus the inverse of the crosslink density

summarized in Figure 11 in which ρv^2 is plotted with $\langle n \rangle^{-1}$. The solid line is calculated according to equation (7) using the measured values of G . Whilst uncertainty in the ultrasound data points precludes any comment on their crosslink density dependence the Brillouin data is a good fit to the predictions of equation (7). Clearly the elastic behaviour of the network over distances $\sim 0.3 \mu\text{m}$ mirrors the macroscopic elastic behaviour.

The absorption data show more distinct features: (a) There is a marked difference between the crosslinked and the uncrosslinked but entangled material in the ultrasound case. At Brillouin frequencies no difference is apparent. (b) Ultrasound absorption falls as a function of crosslink density above the gel point whilst Brillouin absorption rises.

These results are not understood in detail; however, it may be that the difference between the crosslinked and uncrosslinked material in the two cases reflects relaxational motions by entanglements which are 'frozen in' at Brillouin

frequencies. If this is true then the entanglements must relax with a characteristic time which lies between a microsecond and a nanosecond. At ultrasonic frequencies crosslinking below the gel point has the effect of increasing the molecular weight while leaving the chains mobile. The viscosity, and therefore the absorption, increases. Above the gel point decreasing chain mobility restricts the contributions of chain motion to the viscous loss process and so reduces acoustic losses. It may be that the increase in absorption at high crosslink density in the Brillouin case is caused by the introduction of a high frequency relaxation between crosslinks, possibly an LA mode of the free chains lengths. Extension of the experimental work to a wider range of frequencies and samples with other $\langle n \rangle^{-1}$ values is in hand.

CONCLUSION

We have suggested that the techniques of MPFPS can be used to great advantage in the study of many polymer properties and have described the construction of a triple-pass system. In addition preliminary data in three fields have been presented: (1) the study of anisotropy in strained samples; (2) the observation of the α -relaxation at hypersonic frequency; (3) the study of the constraints imposed by crosslinks on high frequency relaxations. These experiments are incomplete as yet, and in each case we are actively engaged in extending the work. However, these examples already show clearly the power of the technique in making measurements that have until now been impossible.

ACKNOWLEDGEMENTS

The authors wish to acknowledge Mr Evans of Salford University for help in preparing the PDMS rubber samples; Dr R. A. Pethrick, Department of Chemistry, University of Strathclyde and Dr Morrell of RAPRA for the use of their ultrasonic equipment; and Dr E. F. T. White of UMIST for the use of his sample preparation facilities. The work was supported by the SRC Polymer Committee.

REFERENCES

- 1 e.g. James, J. F. and Sternberg, R. S. 'The design of Optical Spectrometers', Chapman and Hall, London, 1969
- 2 Hercher, M. *Appl. Opt.* 1968, 7, 951
- 3 Sandercock, J. *Opt. Commun.* 1970, 2, 73
- 4 Lindsay, S. M. and Shepherd, I. W. *J. Phys. (E)* submitted
- 5 Lindsay, S. M. *PhD Thesis* Manchester University (1976)
- 6 Sandercock, J. *Phys. Rev. Lett.* 1972, 28, 237
- 7 Spells, S. J. and Shepherd, I. W. *J. Chem. Phys.* to be published
- 8 Reese, W. J. *Appl. Phys.* 1966, 37, 864
- 9 Wright, H., Faraday, C. S. N., White, E. F. T. and Treloar, L. R. G. *J. Phys. (D)* 1971, 4, 2002
- 10 Huang, Y. Y. and Wang, C. H. *J. Chem. Phys.* 1975, 62, 120
- 11 McCrum, N. G., Read, B. I. and Williams, G. 'Anelastic and Dielectric Effects in Polymeric Solids' Wiley, New York, 1967, p 573 and references therein
- 12 Barlow, A. J. and Erginsav, A. *Polymer* 1975, 16, 110
- 13 Goldstein, M. *J. Chem. Phys.* 1969, 51, 3728
- 14 Charlesby, A. *Proc. R. Soc. (A-2)* 1952, 5, 187
- 15 Charlesby, A. *Nature* 1954, 173, 679

Electric birefringence of aqueous solutions of methyl cellulose*

A. R. Foweraker and B. R. Jennings

Physics Department, Brunel University, Uxbridge, Middlesex, UK

(Received 15 December 1975; revised 16 February 1976)

Electric birefringence studies have been conducted on six samples of methyl cellulose in the molecular weight range 3×10^4 to 1.5×10^5 . Using pulsed electric fields, both the amplitudes and rates of the transient birefringence induced in these solutions have been analysed. For molecular weights below 2×10^3 , the molecules are represented by rigid rods. Above this value increasing flexibility is evident. This can conveniently be seen through reduced electrical parameters, defined herein, which are obtained from a combination of the electrical and geometrical properties of the molecules. These parameters are apparently very sensitive to flexibility in the near-rod regime. It demonstrates the utility of electro-optic experiments in which both the electrical and geometrical data are obtained simultaneously. The persistence length concept does not appear to be adequate when rotary relaxation times are interpreted through it using current equations.

INTRODUCTION

Cellulose is insoluble in water owing to its strong intramolecular hydrogen bonding. Water soluble derivatives can be produced by introducing methyl, carboxymethyl, ethyl, hydroxyethyl or hydroxypropyl groups into the cellulose molecule at one or more of the available hydroxyl groups of the cellobiose units. As the degree of etherification increases so too does the water solubility of the cellulose derivative. The products so obtained have wide commercial utility in the adhesives, cosmetics, food stuffs, oil drilling and paint industries.

In this communication we report an electric birefringence study on six different molecular weight samples of methyl cellulose in aqueous solution. The electric birefringence technique was employed in order to study both the electrical and hydrodynamical properties of the solute molecules. Measurements were made on each sample as a function of the applied field strength. The majority of macromolecules are optically anisotropic. In dilute solution, with no intermolecular interactions, each macromolecule adopts a random orientation. The bulk solution is then optically isotropic. However, on application of an electric field, any molecular electric dipoles interact with this field and cause the suspended molecules to orientate, deform and align. The bulk solution then partially exhibits the optical anisotropy of the individual molecules. It is by measuring the changes in the optical properties of the solution that we can monitor the average rotary behaviour of the constituent molecules. The *amplitude* of the changes can be interpreted in terms of the magnitudes of the electrical dipoles, whilst the *rates* of change indicate the molecular relaxation times (τ) and hence the particle sizes.

In this work, electrically induced birefringence (Δn) is measured. This is defined¹ as the difference in refractive indices parallel and perpendicular to the applied field direction for the bulk solution. It is related directly to the differences in refractive index (or optical polarizability, g) along the major axes of a molecule of cylindrical segmental symmetry. The property is measured by recording the

changes ΔI in the light intensity transmitted through an optical assembly consisting of a polarizer, a cell containing the test solution and an analyser. The electric field is applied at 45° to the azimuth of the polarizer and the analyser is crossed with the polarizer and then offset by a small angle σ . The basic theory for the birefringence of the solution in terms of the light penetrating such a system² together with details of the apparatus and its mode of operation³ have been described in detail elsewhere.

EXPERIMENTAL

All samples were kindly supplied by British Cellanese Ltd, of Spondon, Derbyshire, under their trade name Celacol. Each sample was dissolved by continuous stirring for 24 h in de-ionized water at room temperature and at a concentration of 1×10^{-3} g/ml. All optical measurements were made with light of 546 nm wavelength (*in vacuo*).

RESULTS AND DISCUSSION

The molecular orientation relaxation times (τ) were obtained by analysis of the birefringence decay rates following the termination of the applied electric field pulse. Conventional semi-logarithmic plots³ were drawn of the normalized birefringence amplitudes as a function of time and τ were evaluated from the initial slopes. Such τ values were interpreted using three molecular models, namely, the rigid rod model⁴, the weakly bending rod⁵ and the worm-like chain model⁶. The molecular parameters derived for each of these three structures are given in Table 1. The parameter L is the hydrodynamic extended length. It was calculated assuming each monomer unit to be of 0.69 nm length as indicated by X-ray data⁷. Hence, a polymer of Z degree of polymerization has $L = 0.69 Z$ nm. The equivalent rod length (l_r) is the length obtained from the experimental value of τ using the Broersma equation⁴ as for a rigid rod particle exhibiting end-over-end tumbling rotation. A parameter which has been used to indicate molecular flexibility is the 'persistence length'. This has been defined as the projection of an infinitely long molecular chain in the direction of the first segment. It can be calculated from τ using an equation for

* Presented at the Polymer Physics (Institute of Physics) Biennial Conference, Shrivenham, September 1975.

Table 1 Geometrical parameters for methyl cellulose

$M \times 10^{-3}$	Z	L (nm)	l_r (nm)	q_{WBR} (nm)	q_{WLC} (nm)
34	185	128	47	1.80	1.05
58	315	218	62	1.57	1.02
92	500	346	60	0.62	0.57
110	597	414	78	0.95	0.81
132	717	497	79	0.51	0.54
150	815	565	78	0.54	0.58

Z is the degree of polymerization for molecules of molecular weight M . The length parameters are L for an extended rod and l_r for the equivalent rod length obtained from the relaxation time as for a rigid rod. The 'persistence lengths', q , have been evaluated from the weakly bending rod (WBR) and the worm-like chain (WLC) models respectively

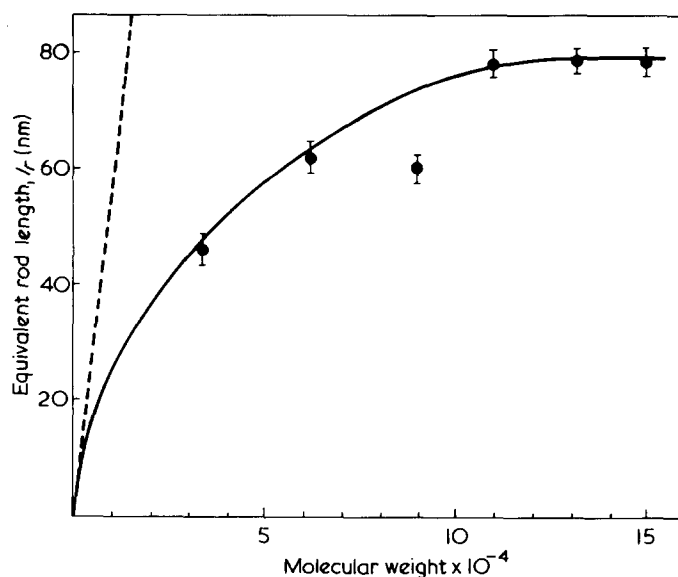


Figure 1 Variation of the equivalent rod length (l_r) with molecular weight calculated using a molecular diameter of 0.35 nm^{10} . ---, indicates the behaviour of the extended length (L). Data from relaxation times for solutions of $1 \times 10^{-3} \text{ g/ml}$ concentration

a weakly bending rod (WBR)⁵, hence q_{WBR} , or by using an equation for a worm-like chain (WLC)⁵, hence q_{WLC} . Under the concepts of each of the appropriate models, these two last mentioned parameters q_{WBR} and q_{WLC} should remain constant with Z or M .

In Figure 1 we compare both l_r and L as functions of the molecular weight. If the molecules were always rigid rods, then one would expect these curves to remain coincident. Departure from such behaviour shows this not to be the case. That they are coincident at low molecular weight does indicate rigid rod like behaviour for samples of low Z .

Values for q , whether obtained from the weakly bending rod or the worm-like chain equations are not constant with Z . Furthermore, they tend to assume a value which is of the order of the length of the cellobiose unit at high Z . We agree with Dev *et al.*⁸ that the concept of q ceases to be credible in such a situation. Hence, although q is often used as a flexibility parameter for samples intermediate between rigid rod and flexible coil conformations, we do not find it to be very satisfactory when derived through the relaxation time equations.

Finally, to complete the analysis of τ , we considered the modified form of Hearst's equation⁵ as presented by Tsvetkov *et al.*⁹ for slightly curved rods in the low molecular weight range. Following their procedure and incorporating

the relevant data in their equation leads to values of $\lambda = 3.0 \pm 0.2 \times 10^{-8}$ and $S = 222 \pm 15$ respectively. In the words of Tsvetkov *et al.* ' λ is the projection of the monomer unit on the direction of the molecular chain and S is the number of monomer units in a Kuhn segment'. Our values for these parameters for methyl cellulose compare well with those evaluated by Tsvetkov *et al.*⁹ for polychlorohexylisocyanates. However, we have reservations about their validity as we feel that the derivation of Tsvetkov's *et al.* equation is incompatible with that of Hearst⁵.

A typical plot of the dependence of the birefringence amplitude on field strength is shown in Figure 2. Similarly linear plots were obtained for each sample of methyl cellulose. The initial slope of these plots [$\lim_{E \rightarrow 0} (\Delta n/E^2)$] is a function of both the optical and electrical parameters of the solvent molecules. The optical polarizability difference ($g_1 - g_2$) is independent of molecular weight and molecular concentration. By using the same concentration for each sample, the initial slope as given in Table 2 was directly proportional to the molecular electrical parameters. The experimental values for each sample as listed in Table 2 are therefore taken as being directly indicative of the relative amplitudes of the electrical orientation function.

The magnitudes of the initial slope values suggest that molecular orientation is attained as a result of interaction between the applied electric field and the induced electrical polarizability anisotropy. As discussed elsewhere³ this parameter is expected to be proportional to the molecular

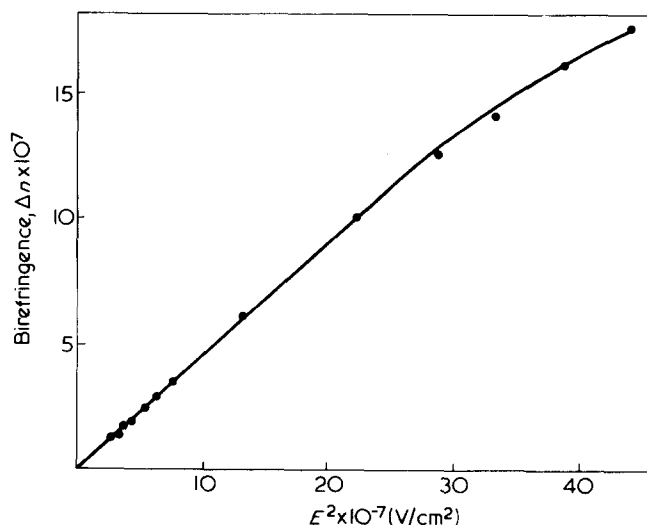


Figure 2 Dependence of the birefringence on the square of the applied electric field for a solution of $1 \times 10^{-3} \text{ g/ml}$ of methyl cellulose in water. For this sample, $M = 1.1 \times 10^5$

Table 2 Electrical parameters for methyl cellulose

$M \times 10^{-3}$	$\Delta n/E^2 \times 10^{15}$ ($\text{cm}^2 \text{ V}^{-2}$)	$\beta/\beta_{M \rightarrow 0}$	$\gamma/\gamma_{M \rightarrow 0}$
34	1.64	1.2	0.44
58	2.43	1.44	0.41
92	3.27	1.88	0.32
110	4.48	1.97	0.35
132	4.86	2.13	0.33
150	4.64	2.04	0.28

The parameters β and γ are given by $(\Delta n/l_r E^2)$ and $(\Delta n/L E^2)$ respectively, where Δn is the birefringence measured in an electric field of amplitude E . For a true rigid rod, the ratios in columns 3 and 4 would be equal for all rows of the Table

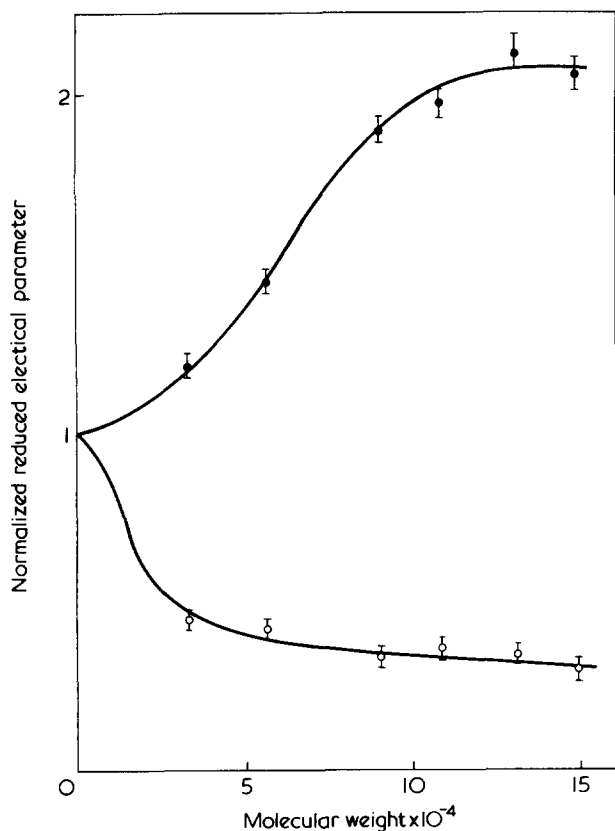


Figure 3 Variation of the reduced electrical parameters $\beta/\beta_{M \rightarrow 0}$ (●) and $\gamma/\gamma_{M \rightarrow 0}$ (○) with molecular weight. These parameters are defined in Table 2

length for rigid and flexible rod-like molecules. Hence in accordance with previous work^{2,3} the values obtained were reduced to unit length values and normalized to the intersection value as M approached zero. If we define the parameters β and γ as $(\Delta n/l_r E^2)$ and $(\Delta n/LE^2)$ respectively, then we have plotted the functions $\beta/\beta_{M \rightarrow 0}$ and $\gamma/\gamma_{M \rightarrow 0}$ in Figure 3 as a function of molecular weight. Here again, departure from a constant value indicates departure from rod-like behaviour with increasing molecular weight, whilst the common intercept on the ordinate indicates rod behaviour at low M .

CONCLUSIONS

- (1) The parameters β and γ are very sensitive indicators of the degree of flexibility, especially when plotted as functions of molecular weight. They indicate departure from rod-like behaviour with increasing M and may be used numerically as empirical parameters for flexibility.
- (2) At low M , methyl cellulose behaves as a rigid rod particle in an electric field.
- (3) Methyl cellulose departs significantly from such rod-like behaviour for molecular weights exceeding 2×10^3 .
- (4) That the persistence length (q) does not appear to be a satisfactory parameter for the indication of flexibility of this molecular system at least when evaluated from rotary relaxation data.

ACKNOWLEDGEMENTS

One of us (B.R.J.) wishes to thank Unilever Research Ltd, for the award of grant, under the terms of which A.R.F. was employed as a postdoctoral fellow.

REFERENCES

- 1 Peterlin, A. and Stuart, H. A. 'Handbuch and Jahrbuch der Chemischen Physik' Becker and Erler, Leipzig, 1943, Vol 8, Section 1B
- 2 Foweraker, A. R. and Jennings, B. R. *Polymer* 1975, 16, 720
- 3 Foweraker, A. R. and Jennings, B. R. *Adv. Mol. Relaxation Processes* 1974, 6, 241
- 4 Broersma, S. *J. Chem. Phys.* 1960, 32, 1626
- 5 Hearst, J. *J. Chem. Phys.* 1963, 38, 1062
- 6 Kratky, D. and Porod, G. *Rec. Trav. Chim. Pays Bas Belg.* 1949, 68, 1106
- 7 Rundle, R. E. *J. Am. Chem. Soc.* 1947, 69, 1769
- 8 Dev, S. B., Lockhead, R. Y. and North, A. M. *Discuss. Faraday. Soc.* 1970, 49, 244
- 9 Tsvetkov, V. N., Rjuntsev, E. I., Pogodina, N. V. and Shtenonikova, I. N. *Eur. Polym. J.* 1975, 11, 37
- 10 Jennings, B. R. and Schweitzer, J. F. *Eur. Polym. J.* 1974, 10, 459

Optical anisotropy of polyisobutene*

J. V. Champion, A. Dandridge, D. Downer, J. C. McGrath and G. H. Meeten

Department of Physics, Sir John Cass School of Science and Technology, City of London Polytechnic, London EC3N 2EY, UK

(Received 19 December 1975; revised 15 January 1976)

The distribution of chemical bonds in polyisobutene results in a theoretically zero optical and electrical anisotropy of the polymer according to bond polarizability additivity principles as conventionally applied, irrespective of polymer chain conformation. Non-zero values of the segmental anisotropy ($\sim 4.4 \times 10^{-40} \text{ C}^2 \text{ m}^2/\text{J}$) derived from strain-optical birefringence on the polymer in the rubbery state have been recently reported by Liberman *et al.* who suggest qualitatively that severe crowding of the chemical groups in the polymer affects the anisotropies of the group polarizabilities and gives the observed non-zero segmental anisotropy. We have measured optical, electrical and magnetic anisotropies for the pure liquid polymer using techniques of flow birefringence, depolarized light scattering, electro-optic birefringence and magneto-optic birefringence. Segmental optical anisotropies so derived agree with those measured by Liberman *et al.* and results of the above measurements taken as a whole lead to an origin for the observed anisotropy which requires locality dependent values of optical and electrical bond polarizability anisotropies to be used in the calculation of the polyisobutene polarizability anisotropy. Our explanation of the polarizability locality dependence differs from the steric overlap suggestion of Liberman *et al.* and depends upon the electric field interaction between dipoles induced in polarizable bonds.

INTRODUCTION

Evaluation of the optical anisotropy of polyisobutene using the bond polarizability tensor additivity scheme has been made by Volkenstein¹ and Liberman *et al.*² Both calculations show that the assumption of tetrahedral bond angles produces a zero anisotropy for any conformation of the polyisobutene chain. Measurements of the optical anisotropy of the statistical segment by flow birefringence³ in polyisobutene solutions, and by strain-optical measurements^{1,2} in dry and swollen butyl rubber, have shown that an optical anisotropy exists comparable with that of polyethylene. Calculations of the segmental optical anisotropy by Liberman *et al.*², which allow for possible non-tetrahedral bond angles, give a value which is an order of magnitude smaller than measured by strain or flow birefringence. Volkenstein¹ quotes similar results.

We have made measurements of the flow birefringence, depolarized light scattering, electro-optic Kerr effect and magneto-optic Cotton–Mouton effect for low molecular weight polyisobutene ($M_n \approx 300\text{--}3000$), which is liquid at room temperature. In the molecular theories of all the above phenomena, the measured quantities can be related to some form of polymer chain optical anisotropy, each of which are examined in detail in the discussion. Meanwhile it is useful to point out that the various measurement techniques have a different effect on the molecule. Whereas strain and flow birefringence measurements involve considerable degrees of molecular strain and orientation, this does not occur in light scattering, Kerr effect and Cotton–Mouton effect measurements. The applied electric and magnetic field forces in these latter measurements have a negligible or very small effect on the molecular conformation or orientation. Hence a comparison of the optical anisotropy measured using such a range of techniques is of value in determining its origin.

EXPERIMENTAL

Materials

The polyisobutene liquids used for all measurements were derived from commercial samples donated by the Post Office Research Station (Dollis Hill), BP Chemicals Ltd and BASF Ltd. These were cleaned of dust using Millipore filters and their molecular weights, densities, viscosities and refractive indices determined. Their structure was examined by i.r. and n.m.r. spectroscopy and all samples were linear polyisobutene. No evidence was found for strongly anisotropic or dipolar impurities which could contribute disproportionately to the measured optical anisotropy. All samples were polydisperse with $M_w/M_n \approx 2$. The polymer end-groups are not uniquely defined by the polymerization process and chemical analysis showed some end-groups to possess a CC double bond.

Flow birefringence

The apparatus and techniques used have been described previously^{4,5}. For all liquids the flow birefringence Δn was positive, proportional to the velocity gradient G and the angle of extinction χ was $45^\circ \pm 0.2^\circ$. The liquid viscosities η were independent of G in the range of velocity gradients used to measure Δn . The maximum velocity gradient used for each liquid ranged from $\sim 10^4 \text{ sec}^{-1}$ for the lowest molecular weights ($\eta \approx 0.015 \text{ Pa sec}$) to 1 sec^{-1} for the highest ($\eta \approx 600 \text{ Pa sec}$).

The stress-optical coefficient $\nabla = \Delta n/\eta G$ may be related to the average optical anisotropy $\langle \Delta \alpha \rangle$ of the undisturbed polymer chain. $\Delta \alpha$ is defined as $\alpha_l - \alpha_r$ where α_l and α_r are the polarizabilities for optical wave fields parallel and perpendicular respectively to the end-to-end distance of the chain. An expression for ∇ for long chains has been developed by Peterlin⁶ and Lodge⁷:

$$\nabla = \frac{(n^2 + 2)^2}{45kT\epsilon_0 n} \langle \Delta \alpha \rangle \quad (1)$$

* Presented at the Polymer Physics Group (Institute of Physics) Biennial Conference, Shrivenham, September 1975.

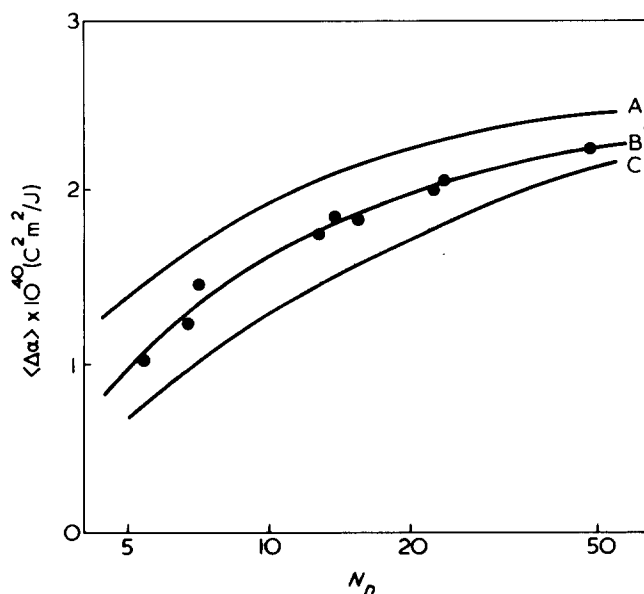


Figure 1 Flow birefringence value of $\langle \Delta\alpha \rangle$ versus number-average monomer units per molecule. —, Calculated from the theory of Gotlib and Svetlov for A, 2; B, 4; C, 6 monomer units per persistence length

where n is the refractive index of the liquid, ϵ_0 is the permittivity of free space and $\langle \Delta\alpha \rangle$ is the Kuhn statistical segment anisotropy when the molecule is perturbed by the flow. For long chains:

$$\langle \Delta\alpha \rangle_\infty = \frac{3}{5} \Delta a$$

Figure 1 shows $\langle \Delta\alpha \rangle$ calculated from experimental ∇ values using equation (1), plotted with the number-average of monomer units per molecule N_n . Since the polyisobutene chains do not contain sufficient monomer units for long chain polymer statistics to be applied, equation (1) is not strictly valid; $\langle \Delta\alpha \rangle$ is not constant but tends to an asymptotic $\langle \Delta\alpha \rangle_\infty$. A plot of $\log_{10} (10^{40} \times \langle \Delta\alpha \rangle) (\text{C}^2\text{m}^2/\text{J})$ versus N_n^{-1} was found to be linear (Figure 2) from which $\langle \Delta\alpha \rangle_\infty = 2.52 \times 10^{-40} \text{C}^2\text{m}^2/\text{J}$ at $N_n^{-1} = 0$. This extrapolated value compares closely with the value $2.72 \times 10^{-40} \text{C}^2\text{m}^2/\text{J}$ derived from the results of Liberman *et al.*² who gave $\langle \Delta\alpha \rangle = (4.55 \pm 0.1) \times 10^{-40} \text{C}^2\text{m}^2/\text{J}$ measured by strain-optical birefringence in crosslinked butyl rubber. We conclude from this comparison that the origin of the optical anisotropy is the same in both short and long polyisobutene chains.

Gotlib and Svetlov's theory of flow birefringence of short polymer chains gives an expression for ∇ in terms of $\langle \Delta\alpha \rangle$ and a parameter $x = L/a$, a being the persistence length of a worm-like chain and L the polymer contour length, obtaining:

$$\nabla = \frac{(n^2 + 2)^2}{75kTn\epsilon_0} \langle \Delta\alpha \rangle \frac{x\phi_1}{\phi_2} \quad (2)$$

where ϕ_1 and ϕ_2 are complex numerical functions of x only. Figure 1 shows the fit between our experimental results and this short chain theory, obtaining $\langle \Delta\alpha \rangle$ at $N_n^{-1} = 0$ from Figure 2. A persistence length corresponding to 4 monomer units gives the closest agreement with the experimental points.

Depolarized light scattering

Measurements of the depolarized scattered light Rayleigh ratio R_{Hu} were made using a Sofica photogoniometer. The incident light was linearly polarized in the scattering plane and R_{Hu} was calculated from the total scattered intensity at 90° . For isolated anisotropic scatterers the optical anisotropy function which determines R_{Hu} is the polarizability tensor invariant:

$$\gamma^2 = \frac{1}{2} [(\alpha_1 - \alpha_2)^2 + (\alpha_2 - \alpha_3)^2 + (\alpha_3 - \alpha_1)^2]$$

where α_i are principal polarizabilities of the polymer chain about the end-to-end distance. For flexible molecules, where γ^2 depends on the molecular conformation, it may be shown⁹ that:

$$R_{Hu} = \frac{400\pi^2\rho N_A}{27\lambda^4 M\epsilon_0^2} \left(\frac{n^2 + 2}{3} \right)^2 \langle \gamma^2 \rangle \quad (3)$$

where the angled brackets $\langle \rangle$ represent the ensemble average with no externally applied perturbing forces, ρ is the density of the scatterers and M their molecular weight. Thus R_{Hu} is zero if the polyisobutene polymer is optically isotropic. For polymer chains which are closely packed as in the liquid state, angular correlations¹⁰ between nearby chains will modify $\langle \gamma^2 \rangle$ which is then not only a function of the anisotropy of an isolated scatterer, but of neighbouring scatterers also. Thus $\langle \gamma^2 \rangle$ in equation (3) is to be regarded as an effective value for a polymer chain in its liquid environment. Figure 3 shows that $\langle \gamma^2 \rangle / N_n$ calculated from equation (3) and our experimental values of R_{Hu} , is independent of N_n within experimental error. The slight increase of $\langle \gamma^2 \rangle / N_n$ with decreasing N_n is surprising since $\langle \Delta\alpha \rangle$ decreases by a factor of 2 in the same molecular weight

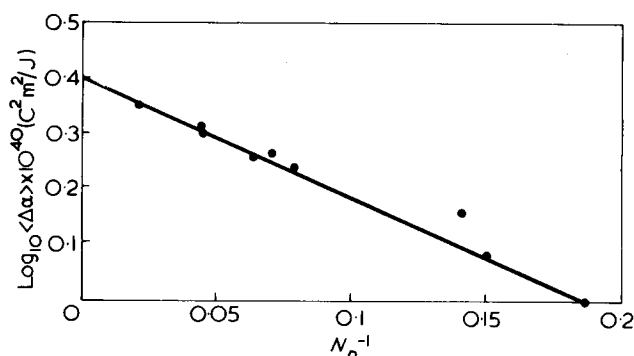


Figure 2 $\log_{10} \langle \Delta\alpha \rangle \times 10^{40} (\text{C}^2\text{m}^2/\text{J})$ versus N_n^{-1}

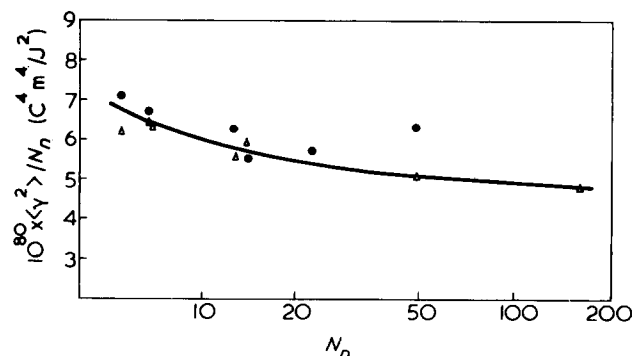


Figure 3 $\langle \gamma^2 \rangle / N_n$ versus N_n . Δ , Kerr effect; \bullet , depolarized light scattering

range. Hence it was felt necessary to use another experimental technique, the electro-optic Kerr effect, to give an alternative method of determining $\langle\gamma^2\rangle$.

Electro-optic Kerr effect

The basic measurement techniques and apparatus used for liquids having a small Kerr constant has been described previously^{11,12}. For our measurements on the polyisobutene liquids, the visual end-point determination was replaced with the Badoz photometric linear detection method¹³, increasing the apparatus sensitivity by about 100 times.

The polyisobutene birefringence Δn was proportional to the square of the applied electric field E , typical of the behaviour of small molecules or flexible polymers. The Kerr constant $B = \Delta n/\lambda E^2$ was measured over a range of molecular weights. Two major mechanisms contribute to B in non-dipolar liquids^{11,12}. One is due to the preferred orientation of anisotropically polarizable molecules, B^{an} . The other is due to hyperpolarizability, B^{hy} , and has been calculated for polyisobutene from the bond hyperpolarizability data of liquid n-alkanes¹². Thus $B^{an} = B - B^{hy}$ and B^{an} is related to $\langle\gamma^2\rangle$ by¹¹:

$$B^{an} = \frac{3\pi\rho N_A}{4\pi\epsilon_0 n \lambda M} \left(\frac{n^2 + 2}{3}\right) \left(\frac{\epsilon_r + 2}{3}\right) \left(\frac{\epsilon_r - 1}{n^2 - 1}\right) \frac{\langle\gamma^2\rangle}{45kT} \quad (4)$$

where ϵ_r is the zero frequency relative permittivity of the liquid. $\langle\gamma^2\rangle/N_n$ versus N_n is plotted with the light scattering results in Figure 3 which shows that the two sets of data are in close agreement for all polyisobutene samples. The value of $\langle\gamma^2\rangle$ derived from Kerr effect measurements includes the influence of angular correlations as in depolarized light scattering assuming that the static field induced dipole-induced dipole interaction is negligible. The anisotropy of the end-group CC double bond has a value $\Delta\alpha \approx 3 \times 10^{-40} \text{ C}^2\text{m}^2/\text{J}$. Although its effect would be negligible in high molecular weight polyisobutene, it could account for the increase of $\langle\gamma^2\rangle/N_n$ with decreasing N_n as observed.

Magneto-optic Cotton-Mouton effect

The measurement technique and apparatus used for small Cotton-Mouton constant liquids have been described⁵. A birefringence Δn was easily measurable using this apparatus with other low molecular weight polymers such as n-alkanes, poly(ethylene glycol) and poly(propylene glycol), Δn being proportional to the square of the applied magnetic field H . The smallest measurable Cotton-Mouton constant $C = \Delta n/\lambda\mu_0^2 H^2$ was about $\pm 2 \times 10^{-5} \text{ m}^{-1} \text{ T}^{-2}$ where $\mu_0 = 4\pi \times 10^{-7} \text{ H/m}$, the permeability of free space. The birefringence of polyisobutene was undetectable and hence its Cotton-Mouton constant was less than $\pm 2 \times 10^{-5} \text{ m}^{-1} \text{ T}^{-2}$. The Cotton-Mouton constant is related¹⁰ to the polymer chain magneto-optic anisotropy $\langle\gamma_m^2\rangle$ by:

$$C = \frac{(n^2 + 2)N_A\rho}{270nkT\lambda\epsilon_0\mu_0} \langle\gamma_m^2\rangle \quad (5)$$

where $2\gamma_m^2 = (\alpha_1 - \alpha_2)(\chi_1 - \chi_2) + (\alpha_2 - \alpha_3)(\chi_2 - \chi_3) + (\alpha_3 - \alpha_1)(\chi_3 - \chi_1)$ and α_i and χ_i ($i = 1, 2, 3$) are the principal values of optical and diamagnetic polarizability of a polymer chain.

Since the optical polarizability difference terms $(\alpha_i - \alpha_j)$ are not zero as shown by a finite $\langle\gamma^2\rangle$, then the near-zero

Cotton-Mouton constant implies that the $(\chi_i - \chi_j)$ terms are correspondingly small, as would result from the application of the diamagnetic bond polarizability anisotropy scheme to tetrahedrally bonded polyisobutene. An alternative explanation of $C \approx 0$ is that there is cancellation between terms of opposite sign in γ_m^2 . We regard this as unlikely since negative Cotton-Mouton constants are never found experimentally in organic liquids.

DISCUSSION

Bond polarizability additivity

The bond polarizability additivity scheme as originally proposed by Wang¹⁵ and Denbigh¹⁶ for calculating the optical polarizability of a molecule from the polarizabilities of its constituent bonds assumed that the components of the bond polarizability tensors were independent of the location of the bond within the molecule or from one molecular type to another. On this basis, tables of experimental polarizabilities for several chemical bonds have been given by Denbigh¹⁶, Vuks¹⁷, Le Fevre¹⁸ and Clement *et al.*^{19,20}. For any particular bond these tables show a large variation in the anisotropy of polarizability but when used in strongly anisotropic groups such as benzene, fair agreement is obtained. Le Fevre's results show the variation of bond polarizability anisotropy for the same bond from one molecular type to another. By contrast, the above-cited values show a good agreement for values of the mean bond polarizability. Thus it is clear experimentally that bond polarizability anisotropy may be regarded as a locality dependent quantity which varies from one environment to another, but that mean bond polarizability can be regarded as locality independent to a good approximation.

Several authors have recognized the above situation and have attempted to explain it and to examine or re-establish the rules of bond polarizability additivity.

Pitzer²¹ used the Silberstein²² model describing an anisotropically polarizable bond of two induced point dipoles having a separation r . Pitzer showed that the anisotropy of such a bond varied strongly with r but the mean polarizability was nearly constant, as found experimentally.

Matossi²³ has modified the Silberstein model by introducing screening factors to account for lack of agreement between the model and experiment. Using this model of an anisotropically polarizable bond both the anisotropy and mean polarizability would vary strongly with r unless the screening factors of the bonded atoms were equal. Matossi's modification is thus of doubtful value.

Rowell and Stein²⁴ have studied the effect of induced dipole interaction between the bonds in ethane. A considerable distortion of the electric field exists whereby the field polarizing any particular bond is the sum of the field E applied to the molecule and the field E' from the induced dipole moments of the other bonds in the molecule. They explored the range of bond polarizability tensor components which provided values of mean molecular polarizability $\bar{\alpha}$ and optical anisotropy γ^2 close to those obtained from experiment.

The CC and CH bond mean polarizabilities thus obtained were (0.54 ± 0.03) and $(0.77 \pm 0.04) \times 10^{-40} \text{ C}^2\text{m}^2/\text{J}$ respectively, where the uncertainties show the domain over which a fit between theory and experiment was possible. These values agree closely with mean bond polarizabilities listed in the tables cited above. By contrast, CC and CH bond polarizability anisotropies were not well defined and

formed a large domain of about 1 to 3×10^{-40} , and 0.3 to $8 \times 10^{-40} \text{ C}^2\text{m}^2/\text{J}$ respectively. It was thus possible to obtain consistent values of $\bar{\alpha}$ and γ^2 over a wide range of combinations of the means and anisotropies of bond polarizabilities.

Teixeira-Dias and Murrell²⁵ have calculated the polarizability tensor of methane, ethane and propane from molecular orbital theory. Using their calculated data, they show that the mean polarizabilities are bond-additive but the polarizability anisotropies are not, which they attribute to the large internal fields from bond polarizations within the molecule and also to the flow of electrons between bonds.

Mortensen²⁶ has generalized the approach of Rowell and Stein, and within the approximation afforded by the neglect of interactions between induced bond quadrupoles and higher moments has shown that the polarizability tensor of a molecule may be regarded as the sum of bond polarizability tensors. In this theory the locality independent bond polarizability tensors are replaced by a locality dependent value, wherein the apparent polarizability tensor of a bond is dependent upon the degree of distortion of the uniform applied field caused by the polarization of all other bonds in the molecule. Thus the polarizability anisotropy of a bond generally will vary according to the location of the bond within the molecule, or from one molecular type to another.

We may summarize as follows. Two effects have been neglected by most workers in deriving experimental bond polarizabilities from experimental molecular polarizability data. These are the interactions between the induced dipoles of the bonds and the flow of electrons between bonds. The former can be accounted for while still preserving bond-additivity as shown by Mortensen²⁶, where the bond polarizabilities are now locality dependent. The latter removes the identity of a bond as a polarizable unit and hence the principle of any sort of additivity. The relative proportions of these effects is not generally known. Although the molecular orbital calculations of Teixeira-Dias and Murrell²⁵ were able to reproduce mean molecular polarizabilities to within a few percent, their estimate of the optical anisotropy of ethane was a factor of four lower than experiment. Thus their anisotropy results and conclusions drawn therefrom can be regarded only as qualitative. The experimental fact of locality independent mean bond polarizabilities which are capable of being summed to give mean molecular polarizabilities to within a few percent²⁷ implies that the bond has a meaningful identity as a polarizable unit and the electron flow effect of Teixeira-Dias and Murrell is small compared with the effect of dipole or higher interactions between bonds.

Polyisobutene

The principles outlined above are applicable to polyisobutene and are capable of explaining the finite optical anisotropy and near zero diamagnetic anisotropy of this polymer.

No bond angle distortion from tetrahedral is required to explain the finite optical anisotropy of the chain. Like methane, each monomer unit possesses tetrahedral symmetry of bonds and so the locality independent bond polarizability tensor additivity scheme predicts a zero anisotropy for both. This symmetry disappears when dipole interactions are allowed between bonds. Methane remains isotropic²⁸ since its bond induced dipole interac-

tions are symmetric. The polyisobutene monomer is influenced by the polarization of the rest of the bonds in the chain, principally by those in neighbouring monomer units. This dipole interaction is not spherically symmetric and the monomer unit hence becomes anisotropic as observed.

The Cotton-Mouton constant of liquid polyisobutene is very small ($C < \pm 2 \times 10^{-5} \text{ m}^{-1}\text{T}^{-2}$) compared with other short chain hydrocarbon polymers, e.g. $C = 27 \times 10^{-5} \text{ m}^{-1}\text{T}^{-2}$ for n-tetradecane¹⁴. This result is also explicable in terms of induced dipole interactions between bonds. An electric field E induced a dipole field $E' \approx E\alpha/4\pi\epsilon_0r^3$ at a distance r from the centre of a bond of electric polarizability α . Inserting typical values: $\alpha \approx 1 \times 10^{-40} \text{ C}^2\text{m}^2/\text{J}$; $r \approx 10^{-10} \text{ m}$, gives $E' \approx E$. This shows the necessity to allow for induced dipole-induced dipole interactions in molecules. For a magnetic field, $H' \approx H\chi/4\pi r^3$ and inserting typical values: $\chi \approx 1 \times 10^{-34} \text{ m}^3$; $r \approx 10^{-10} \text{ m}$, gives $H' \approx 10^{-5} \text{ H}$. Thus for applied magnetic fields there is negligible distortion of the field at any particular bond due to the magnetic dipoles induced in nearby bonds. The diamagnetic bond tensors are thus almost locality independent and the tetrahedral symmetry of the polyisobutene molecule ensures a near-zero Cotton-Mouton constant, as observed.

The calculation of the optical anisotropy for polyisobutene could be carried out in principle by the method used for ethane by Rowell and Stein²⁴. This would be extremely complex. Accordingly, we have devised an empirical approach to this end as below.

We assign a different optical polarizability anisotropy to the skeletal and side-arm CC bonds. These are denoted $\Delta\alpha^{\text{CC}^*}$ and $\Delta\alpha^{\text{CC}}$ respectively and are assumed to differ by reason of their different locations in the chain and the consequently differing induced dipole field distortions. Simple analysis assuming tetrahedral bond angles and neglecting any difference between the skeletal and side-arm CH bond anisotropies then gives $\Delta\alpha^{\text{CC}^*} - \Delta\alpha^{\text{CC}} = \Delta\alpha_e$ for the monomer unit optical anisotropy, the polarizability tensor being diagonal for coordinate axes parallel and perpendicular to the skeletal CC bond.

Estimates of $\Delta\alpha_e$ are available from measurements of the optical anisotropy γ^2 in small molecules such as branched alkanes. A suitable molecule having no rotational isomers and similar branching to polyisobutene is 2,2-dimethylbutane for which $\gamma^2 = 2.52 \times 10^{-80} \text{ C}^4\text{m}^4/\text{J}$ as measured in the liquid state by Clement and Bothorel^{29,30}. These workers found that the measured value of γ^2 for some highly branched alkanes was larger than the value predicted by the application of the locality independent optical bond polarizability tensor additivity scheme, where the bond polarizability parameters had been derived from linear n-alkanes. We regard this discrepancy as resulting from the locality dependence of bond anisotropies and we have re-analysed the optical anisotropy of 2,2-dimethylbutane assuming that the most deeply buried CC bond has the anisotropy $\Delta\alpha^{\text{CC}^*}$. 2,2-dimethylbutane is thus $(\text{CH}_3)_3\text{C}^*\text{CH}_2\text{CH}_3$ where the asterisk denotes the CC* bond. With the assumption of tetrahedral bond angles, the addition of bond tensors gives:

$$\begin{aligned} \gamma^2 = & \Delta\alpha^{\text{CC}^*2} + \frac{8}{3} \Delta\alpha^{\text{CC}2} - \frac{8}{3} \Delta\alpha^{\text{CC}^*} \cdot \Delta\alpha^{\text{CC}} \\ & - \frac{16}{3} \Delta\alpha^{\text{CC}} \cdot \Delta\alpha^{\text{CH}} + \frac{4}{3} \Delta\alpha^{\text{CC}^*} \cdot \Delta\alpha^{\text{CH}} + 4\Delta\alpha^{\text{CH}2} \end{aligned}$$

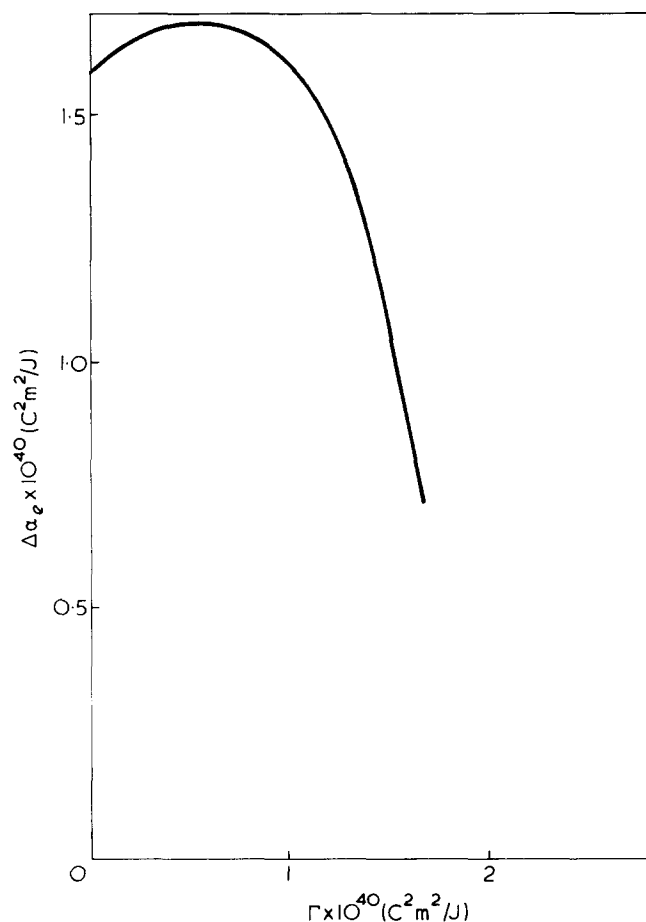


Figure 4 Dependence of effective back-bone C-C bond anisotropy $\Delta\alpha_e$ on $\Gamma = \Delta\alpha_{CC} - 2\Delta\alpha_{CH}$

from which:

$$\Delta\alpha_e = \Delta\alpha^{CC*} - \Delta\alpha^{CC} = \frac{1}{3} \Gamma \pm (\gamma^2 - 8/9\Gamma^2)^{1/2} \quad (6)$$

where Γ is the bond polarizability parameter $\Delta\alpha^{CC} - 2\Delta\alpha^{CH}$. Figure 4 shows the positive values of $\Delta\alpha_e$ calculated from equation (6). Negative $\Delta\alpha_e$ values are ruled out by the sign of flow birefringence in polyisobutene, which was always positive. Figure 4 shows that $\Delta\alpha_e \approx 1.6 \times 10^{-40} \text{ C}^2 \text{ m}^2/\text{J}$ over the whole range of Γ existing in the literature³¹, 0.6 to $1.2 \times 10^{-40} \text{ C}^2 \text{ m}^2/\text{J}$.

No theory at present exists which realistically estimates $\langle\Delta\alpha\rangle$ or $\langle\gamma^2\rangle$ from $\Delta\alpha_e$ for polyisobutene in the liquid state. As well as the usual features of the rotation-isomeric approach¹ any theory must also include intermolecular interactions, angular correlations and the effect of the strong intramolecular steric interference between the side-groups. Conformational measurements³² and calculations³³, as well as space-filling molecular models, show that steric interference is dominant in determining polyisobutene conformation and hence conformationally dependent parameters such as $\langle\Delta\alpha\rangle$ and $\langle\gamma^2\rangle$.

However, $\Delta\alpha_e$ can be estimated from the polyisobutene flow birefringence results and a comparison made with the value of $\Delta\alpha_e \approx 1.6 \times 10^{-40} \text{ C}^2 \text{ m}^2/\text{J}$ provided by our analysis of 2,2-dimethylbutane. Tsvetkov's flow birefringence theory³⁴ relates the Kuhn statistical segment anisotropy $\langle\Delta\alpha\rangle_\infty$ to the number of monomer units per segment S by

$\langle\Delta\alpha\rangle_\infty = S\Delta\alpha_e'$ ($\Delta\alpha_e'$ is the monomer unit anisotropy referred to axes parallel and transverse to the backbone direction of the fully extended chain.) Thus $\Delta\alpha_e' = \frac{1}{2}\Delta\alpha_e$ if bond angles are tetrahedral. S is given by $2 \times$ persistence length³⁵ = 8 monomer units per segment. From our flow birefringence value of $\langle\Delta\alpha\rangle_\infty = 4.2 \times 10^{-40} \text{ C}^2 \text{ m}^2/\text{J}$ (Figure 2) this gives $\Delta\alpha_e' = 1 \times 10^{-40} \text{ C}^2 \text{ m}^2/\text{J}$ compared with $1.6 \times 10^{-40} \text{ C}^2 \text{ m}^2/\text{J}$ derived from 2,2-dimethylbutane.

CONCLUSION

The optical polarizability tensor of a bond depends on the location of that bond within the molecule due to fields set up by the polarizations of the other bonds in the molecule. The additivity of optical bond anisotropies remains valid provided that the same bonds in different locations are assigned different anisotropies. Additivity of mean optical bond polarizabilities remains unaffected to an accuracy of a few percent, as does additivity of diamagnetic bond anisotropies where the magnetic induced dipoles and dipole fields are very weak. The effect of locality dependent optical bond anisotropies may be small for strongly anisotropic molecules but will be dominant in near-symmetric cases where the molecular anisotropy is the small difference between a number of large terms such as for polyisobutene. We propose that induced dipole interactions between bonds causes the observed optical anisotropy in polyisobutene and that anisotropy calculations of weakly anisotropic molecules using locality independent optical bond anisotropies may be subject to large errors. This proposal is substantiated by the fair agreement between the polyisobutene monomer unit effective anisotropy $\Delta\alpha_e$ derived from flow birefringence data and $\Delta\alpha_e$ derived from a similarly branched small molecule 2,2-dimethylbutane.

Liberman *et al.*² propose to explain the finite observed optical anisotropy of polyisobutene by the steric overlaps prevailing in the polymer chain which alter the polarizabilities of groups or bonds, thus producing locality dependent bond polarizabilities. This suggestion would also predict a finite diamagnetic anisotropy of the chain, contrary to our results. Although we agree with the proposals of Liberman *et al.* that the finite anisotropy of polyisobutene is the result of locality dependent bond polarizabilities, we suggest that the locality-dependence arises predominantly from the electric field interaction between the dipoles induced in the bonds rather than steric overlaps between bonds.

REFERENCES

- 1 Configurational Statistics of Polymeric Chains, (Ed. M. V. Volkenstein), Interscience, New York, 1963
- 2 Liberman, M. H., Debolt, L. C. and Flory, P. J. *J. Polym. Sci. (Polym. Phys. Ed.)* 1974, 12, 187
- 3 Frisman, E. V. and Davivanyan, A. K. *J. Polym. Sci. (Polym. Phys. Ed.)* 1967, 16, 1001
- 4 Champion, J. V. *Proc. Phys. Soc.* 1960, 75, 421
- 5 Champion, J. V., Desson, R. A. and Meeten, G. H. *Polymer* 1974, 15, 301
- 6 Peterlin, A. *J. Polym. Sci.* 1954, 12, 45
- 7 Lodge, A. S. *Nature* 1955, 176, 838
- 8 Gotlib, Y. Y. and Svetlov, Y. E. *Dokl. Akad. Nauk. SSSR* 1966, 168, 621
- 9 Erenburg, E. G., Piskareva, E. P. and Poddubuyi, I. Y. *Vysokomol. Soedin. (A)* 1970, 12, 2996
- 10 Bothorel, P. *J. Chim. Phys.* 1974, 71, 1133
- 11 Champion, J. V., Meeten, G. H. and Whittle, C. D. *Trans. Faraday Soc.* 1970, 66, 2671

- 12 Champion, J. V., Meeten, G. H. and Southwell, G. *J.C.S. Faraday Trans. 2* 1975, **71**, 225
- 13 Badoz, J. *J. Phys. Radium* 1956, **17**, 143
- 14 Meeten, G. H. *J. Chim. Phys.* 1972, **69**, 1175
- 15 Wang, S. N. *J. Chem. Phys.* 1939, **7**, 1012
- 16 Denbigh, K. G. *Trans. Faraday Soc.* 1940, **36**, 936
- 17 Vuks, M. F. *Opt. Spektrosk.* 1957, **2**, 494
- 18 Le Fevre, R. J. W. *Adv. Phys. Org. Chem.* 1965, **3**, 1
- 19 Clement, C. and Bothorel, P. *J. Chim. Phys.* 1964, **61**, 1282
- 20 Clement, C. and Seurin, R. *J. Chim. Phys.* 1971, **68**, 22
- 21 Pitzer, K. *Adv. Chem. Phys.* 1959, **2**, 59
- 22 Silberstein, L. *Philos. Mag.* 1917, **33**, 92, 215, 521
- 23 Matossi, F. *J. Chem. Phys.* 1952, **20**, 1934
- 24 Rowell, R. L. and Stein, R. S. *J. Chem. Phys.* 1967, **47**, 2985
- 25 Teixeira-Dias, J. J. C. and Murrell, J. N. *Mol. Phys.* 1970, **19**, 329
- 26 Mortensen, E. M. *J. Chem. Phys.* 1968, **49**, 3732
- 27 Vickery, B. C. and Denbigh, K. G. *Trans. Faraday Soc.* 1949, **45**, 61
- 28 Rudder, R. R. and Bach, O. R. *J. Opt. Soc. Am.* 1968, **58**, 1260
- 29 Clement, C. and Bothorel, P. *J. Chim. Phys.* 1964, **61**, 1262
- 30 Clement, C. and Bothorel, P. *J. Chim. Phys.* 1964, **61**, 1282
- 31 Champion, J. V. and Meeten, G. H. *Trans. Faraday Soc.* 1968, **64**, 238
- 32 Bunn, C. *Chem. Br.* 1975, **11**, 171
- 33 Flory, P. J. 'Statistical Mechanics of Chain Molecules', Interscience, New York, 1969
- 34 Tsvetkov, V. N. 'Newer Methods of Polymer Characterisation', (Ed. Ke), Interscience, New York, 1964
- 35 Tsvetkov, V. N., Eskin, V. E. and Frenkel, S. Y. 'Structure of Macromolecules in Solution', Moscow, 1964, Vol 1

Elastic modulus in the crystalline region of poly(*p*-phenylene terephthalamide)

R. J. Gaymans, J. Tijssen, S. Harkema and A. Bantjes

Department of Chemical Technology, Technological University of Twente, The Netherlands
(Received 13 January 1976)

Fibres from aromatic polyamides have a much higher Young's modulus than fibres from aliphatic polyamides. In order to contribute to the explanation of this observed difference we looked at one of the ultimate properties, the elastic modulus in the crystalline region in the chain direction ($E_{cr//}$). We carried out measurements on a bundle of filaments of PRD 49 fibre, which we identified by i.r. and X-ray analyses as poly(*p*-phenylene terephthalamide). With the X-ray technique we determined the lattice extensions under loading and from these data the $E_{cr//}$ was calculated. The $E_{cr//}$ was found to be 20×10^{11} dyne/cm² which is in good agreement with the calculated $E_{cr//}$, but not very different from that of nylon-6,6. The Young's modulus was found to be 11×10^{11} dyne/cm².

INTRODUCTION

Aromatic polyamides form a class of polymers which have thermal and mechanical properties that are quite different from those of the aliphatic polyamides. Fibres of aromatic polyamides have a much higher Young's modulus than corresponding aliphatic ones.

Aromatic polyamides are thought to be very good materials for reinforcing fibres¹⁻⁴. The properties of these polyamides have been reviewed by Black⁴. He states that a possible explanation for the extraordinary properties of these polymers is due to the extended orientation rather than to the high crystallinity. Since aromatic polyamide chains are much stiffer than those of aliphatic polyamides, chain folding is less likely and a fully extended chain is obtained much easier.

Both the crystallinity and the orientation seem to be very high for these aromatic polyamide fibres. Northolt and Van Aartsen⁵ suggest that poly(*p*-phenylene terephthalamide) (PpPT) has a paracrystalline structure with a long order. They did not observe any periodicity up to 250 Å with small-angle scattering.

Dulmage and Contois⁶ developed a model for the calculation of the Young's modulus from the moduli of the amorphous and crystalline phases and the degree of crystallinity, assuming the crystalline phase to be fully oriented and the amorphous phase to be unoriented.

Holliday and White⁷ have given a review on the present status of the factors governing the Young's modulus and the techniques available for measuring them.

One of these basic properties is the modulus in the crystalline region in the chain direction ($E_{cr//}$). The experimentally determined values of $E_{cr//}$ agree on the whole fairly well with the calculated values.

Fielding Russell⁸ has calculated the $E_{cr//}$ for PpPT using the method of Treloar with assumed chain dimensions and found a value of 20×10^{11} dyne/cm², which we also found with the now available cell dimensions⁵.

EXPERIMENTAL

Sample preparation

The elastic modulus was determined using an industrial fibre from Du Pont (PRD 49). In order to prepare a film

for i.r. analysis the Du Pont product was dissolved in chlorosulphonic acid and precipitated in cooled methanol (-60°C). A fine suspension of gelly particles was obtained by warming up under vigorous stirring. Filtration of the suspension gave a fairly homogeneous film. After washing and drying an i.r. spectrum of the film was taken, and compared with the spectra of poly(*p*-phenylene terephthalamide) and poly(*p*-benzamide) synthesized in our laboratory (Figure 1). As can be seen the i.r. spectra of PRD 49 and poly(*p*-phenylene terephthalamide) are identical.

The X-ray diffraction pattern of PRD 49 fibre gave the same reflections as Northolt and van Aartsen⁵ obtained on PpPT. From these results and the literature data³ we assumed PRD 49 to be poly(*p*-phenylene terephthalamide).

One filament of the fibre was too thin to obtain strong enough reflections so a bundle of 25 filaments was used. In order to be sure that all the filaments were equally well stressed both ends of the bundle were kit together while each filament was under a preload of 1.3 g. The ends were imbedded in such a way that easy clamping was possible. The length of the bundle of filaments between the imbedded areas was 4 cm.

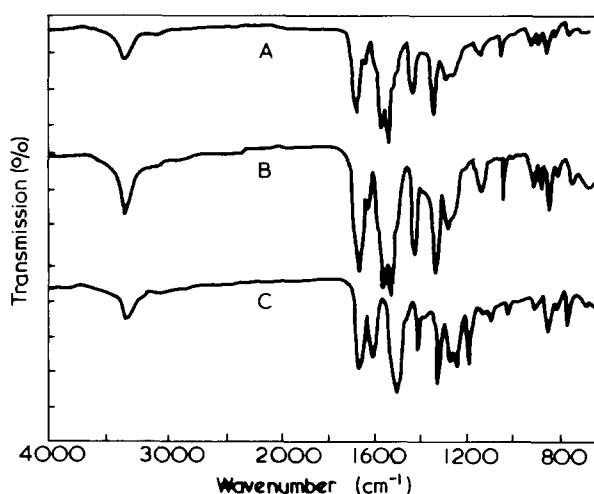


Figure 1 Infra-red spectra of polymer films of A, PRD 49; B, poly(*p*-phenylene terephthalamide) and C, poly(*p*-benzamide)

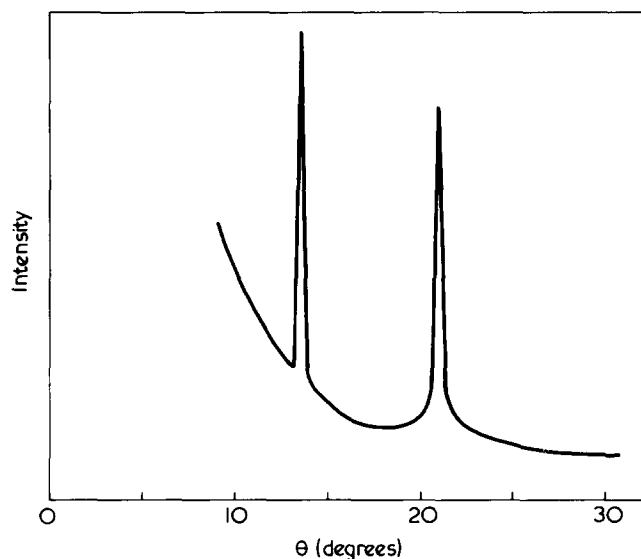
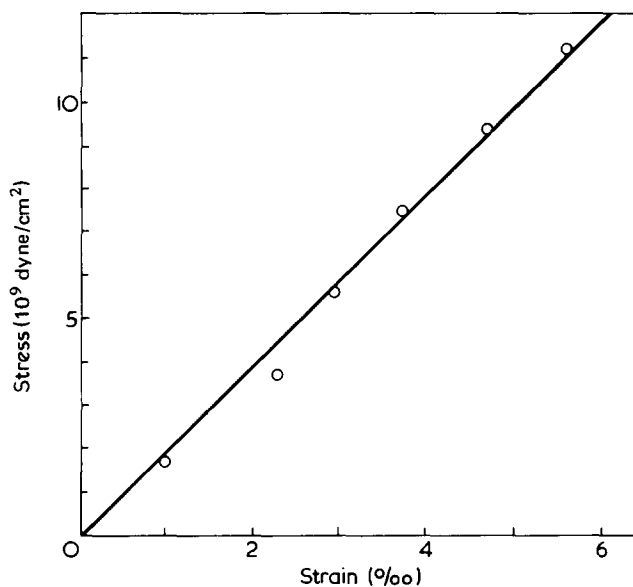
Figure 2 X-ray intensity curve in the 00*l*-plane

Figure 3 Applied stress versus lattice extension

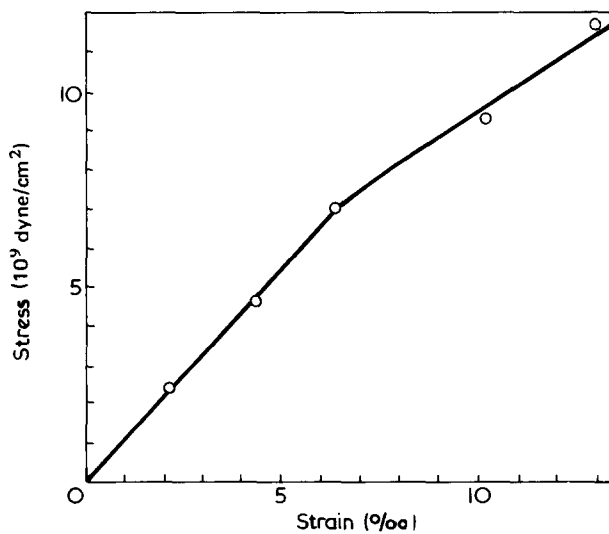


Figure 4 Applied stress versus macroscopic strain

Apparatus

The X-ray method was chosen for the determination of the $E_{cr//}$. Sakurada⁹ gives a detailed set-up for determining the lattice extensions. A Nonius diffractometer with a nickel filtered $\text{CuK}\alpha$ -beam was used.

We measured, at any one time, an angular range of $\theta \pm 0.12^\circ$. Reflections were scanned by steps of 0.1° with a counting time for each point of 4000 sec. From these intensities the centre of gravity of the reflection curve was calculated. The samples were loaded with dead weights and from the shifts of the gravity point the lattice extensions were calculated. Friction losses in the loading set-up were less than 5 g. The macroscopic stress-strain curve was obtained by loading a bundle of filaments and measuring the lengthening with a kathetometer. The load was increased each hour.

RESULTS AND DISCUSSION

The crystal structure of PpPT is given by Northolt and Van Aartsen⁵ as monoclinic with the cell dimensions $a = 7.87 \text{ \AA}$, $b = 5.18 \text{ \AA}$, $c = 12.9 \text{ \AA}$, and $\gamma = 90^\circ$. The space group is Pn or $P2_1/n$. For the determination of $E_{cr//}$ the reflections from the 00*l*-planes were measured. The normals of these planes are parallel to the chain axis. The intensity curve is measured from a bundle of filaments as a function of θ (Figure 2). In the intensity curve the reflections 004 and 006 can be seen. The reflections 00*l* etc., where *l* is odd, are expected extinctions. The 006 plane reflection was chosen to be measured.

It is quite important to note that in the measured region the structure factor is not very dependent on θ . Therefore the reflection maximum coincides with the lattice factor maximum so that we can use the Bragg law.

The stress-lattice extension data are given in Figure 3. The $E_{cr//}$, calculated from the slope of the curve, is $20 \times 10^{11} \text{ dyne/cm}^2$.

The macroscopic stress-strain data are given in Figure 4. Young's modulus determined from these data is $11 \times 10^{11} \text{ dyne/cm}^2$. As can be seen the calculated and the experimental $E_{cr//}$ agree very well and these values are not very different from those obtained on nylon-6,^{6,11}

So the higher Young's modulus of these aromatic polyamide fibres cannot be explained by the ultimate property, the elastic modulus in the crystalline region in the chain direction.

REFERENCES

- 1 Rothuizen, J. H. *Text. Inst. Ind.* 1973, **11**, 142
- 2 Wilfong, R. E. and Zimmerman, J. *J. Appl. Polym. Sci.* 1973, **17**, 2039
- 3 Gan, L. H., Blais, P., Carlsson, D. J., Suprunchuk, T. and Wiles, D. M. *J. Appl. Polym. Sci.* 1975, **19**, 69
- 4 Black, L. B. *J. Macromol. Sci. (A)* 1973, **7**, 99
- 5 Northolt, M. G. and van Aartsen, J. J. *Polym. Lett.* 1973, **11**, 333
- 6 Dulmage, W. J. and Contois, L. E. *J. Polym. Sci.* 1958, **28**, 275
- 7 Holliday, L. and White, J. W. *Pure Appl. Chem.* 1971, **26**, 545
- 8 Fielding-Russell, G. S. *Text. Res. J.* 1971, **41**, 861
- 9 Sakurada, I., Nukushina, Y. and Ito, T. *J. Polym. Sci.* 1962, **57**, 651
- 10 Wallner, L. G. *Monatsh. Chem.* 1948, **79**, 279
- 11 Dumbleton, J. H. and Buchanan, R. *Polymer* 1968, **9**, 601

Coordinate polymerization of heterocycles: 1. Oligomerization of epichlorohydrin by TiCl_4

M. Kučera, A. Zahradníčková, K. Majerová

Research Institute of Macromolecular Chemistry, 656 49 Brno, Czechoslovakia

(Received 2 June 1975; revised 28 January 1976)

The polymerization of epichlorohydrin proceeds via the $\text{TiCl}_4 \cdot 2\text{EPC}$ complex provided the concentration of epichlorohydrin is twice as high as that of TiCl_4 . The oligomerization process requires supposedly the existence of a complex in which the epichlorohydrin is coordinate through a Cl—Ti bond. Diethyl ether has an inhibiting effect on the reaction. The oligomerization rate is increased in the presence of acetyl chloride, diethyl ether having no effect this time. The transformation of epichlorohydrin to polymer is always kinetically non-stationary, the number of active centres decreasing with time. Both the initiation and propagation steps proceed through a rearrangement following the coordination of monomer to the activating ligands. No polymerization active free ions have been found to be present in the system. The intermediate and final products were analysed employing spectral, chromatographic, kinetic, and conductivity measurements. The reaction mechanism of oligomerization has been suggested.

INTRODUCTION

The Ziegler–Natta polymerization of olefins can be regarded as a typical example of coordinate polymerization having considerable industrial importance. The propagating centres are almost exclusively believed to be an ‘anionic’ coordinate character^{1,2}. Epoxides can also polymerize by ‘cationic’ or ‘anionic’ coordinate mechanisms³. Cyclic ethers with more than three members in a ring can be polymerized only in the presence of strong acids. Some of these initiators facilitate the coordination of monomer prior to ring opening^{4,5}; the mechanism of these polymerizations is not well understood. The coordinate mechanism has, however, not been considered.

The character of polymerization of four- and multi-membered oxygen heterocycles strongly suggests that the ‘cationic’ coordinate polymerization might be involved. We have been interested in the nature of active centres of this kind. For this reason TiCl_4 was selected as Lewis acid for the initiation, tetrahydrofuran (THF) being the monomer. Tetrahydrofuran, however, will oligomerize in the presence of TiCl_4 only when a ‘promotor’, e.g. epichlorohydrin (EPC), is simultaneously present. We have focused our attention towards the system containing TiCl_4 and epichlorohydrin. In some cases also another promotor of THF polymerization, acetyl chloride, (AcCl), was added.

EXPERIMENTAL

Chemicals

Epichlorohydrin (a Lachema product, purissimum grade) was rectified several times, the 391.1K fraction being collected. The fraction, which was at least 99.9% pure (analysed by g.l.c.) was stored over CaH_2 in a storage bulb attached to a vacuum line.

TiCl_4 (a Fabrique de produits chimiques de Thann et de Mulhouse product) was distilled into an ampoule attached to a vacuum line. After the de-aeration, the product was

distilled into a storage bulb from where it could be transferred into a calibrated pipette. The amount required could then be transferred to a spectrometer cell or a dilatometer.

Dichloromethane (a Lachema product, analytical grade) was shaken with concentrated H_2SO_4 for several days. After washing with water until neutral the product was refluxed for 6 h in the presence of AlCl_3 , then distilled, refluxed again in the presence of P_2O_5 and rectified. The fraction containing more than 99.98% of CH_2Cl_2 was collected and stored over P_2O_5 in a storage vessel attached to a vacuum line. The connection of the storage vessel with the vacuum line was effected by a high-vacuum stainless steel valve.

Diethyl ether (Et_2O) (a Lachema product, u.v. spectroscopic grade) was dried with Na and stored over Na in a vacuum line storage bulb.

Sodium ethanolate was prepared from $\text{C}_2\text{H}_5\text{OH}$ and sodium. The stoichiometric ratio of components was selected to give a solution with a 3 mol/dm^3 concentration. This solution was stored in the dark at low temperature.

Other chemicals used (hexyl chloride, acetyl chloride) were of analytical grade.

Instruments and procedures

Polymerization: closed system. A schematic diagram of the dilatometer used for measurements is presented in *Figure 1*. The dilatometers were sealed to a vacuum line. After 1–2 days pumping the required amounts of epichlorohydrin as well as other components (dichloromethane, acetyl chloride, diethyl ether) were transferred to the dilatometer by a bulb-to-bulb distillation. The volume of each liquid component was measured using calibrated pipettes. The part containing the liquid mixture was then sealed off under vacuum. The TiCl_4 was transferred into the dilatometer using the same procedure.

Polymerizations were carried out under stirring at a constant temperature. Both dilatometer parts were first tem-

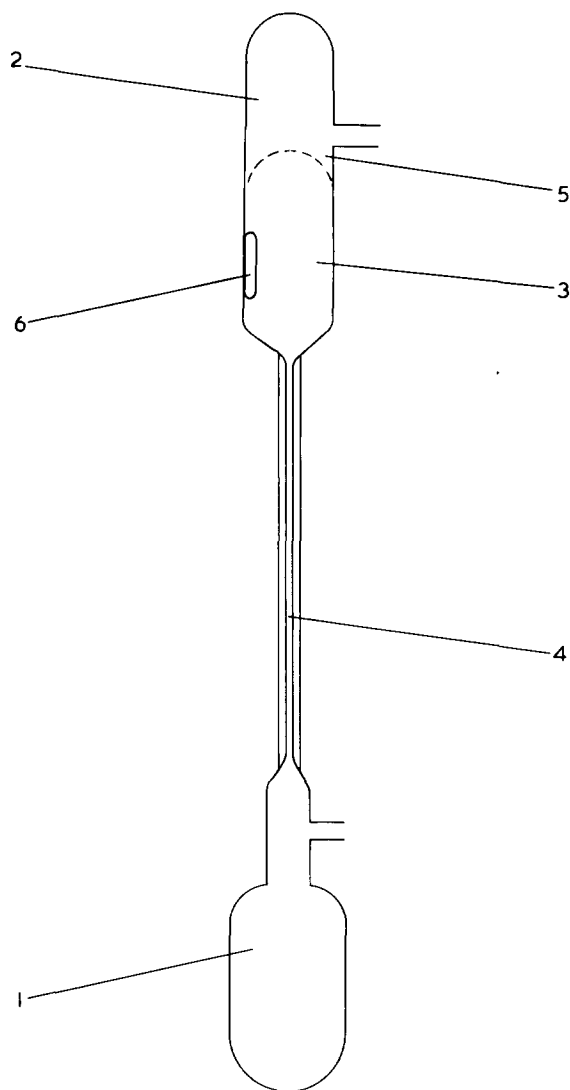


Figure 1 Vacuum dilatometer: 1, space for epichlorohydrin, dichloromethane and acetylchloride; 2, space for initiator; 3, dilatometer bulb; 4, capillary i.d. 2.53 mm; 5, break seal; 6, breaker

perature-equilibrated and then the seals were broken. After a certain time the dilatometer was opened so that the polymerization could be stopped by adding an excess of sodium ethanolate (double the quantity with regard to $TiCl_4$), an aliquot sample was taken and dried *in vacuo* to constant weight. The polymer was isolated from the residual part in the following way: approximately 1 h after the polymerization had been stopped by sodium ethanolate an excess of 1 N HCl was added, the acid-containing layer was extracted with toluene and the toluene extract was extracted with water. The solvent contained in the toluene layer was evaporated and the polymer was dried *in vacuo* at ambient temperature to constant weight. The polymer content in other layers was negligible.

Polymerization: open system. The polymerizations of epichlorohydrin in the presence of water were carried out in glass dilatometers⁶ capable of holding 13.5 and 16 ml of liquid, respectively. A millimeter scale was etched on the dilatometer capillary. The dilatometers were positioned in a cylinder which was maintained at a constant temperature of $293.0 \pm 0.1K$.

The water concentration in individual components of the polymerization mixture was determined using a coulometrically modified Fischer method⁷.

The calculated volumes of initiator ($TiCl_4$) and solvent (CH_2Cl_2) were transferred into a dilatometer flask. After reaching an equilibrium temperature, monomer and other components (epichlorohydrin, acetyl chloride, diethyl ether) were added. Neither surface nor the rate of stirring showed any influence on the polymerization. The heat due to the interaction of $TiCl_4$ with ethers was dissipated into the constant temperature bath within the first 70 sec (measured by a thermocouple). The first reading was taken 90 sec after mixing the components. The reproducibility of polymerization runs was satisfactory.

The same method as that described for the closed system was used to stop the polymerization and to isolate the polymer. The conversion achieved during each run was determined gravimetrically and tested by g.l.c.

The comparison of results from closed system with those from open system has shown that water has no significant effect upon the oligomerization even when present at concentrations as high as several hundred $mmol/dm^3$. Most of the kinetic measurements were thus performed in the open system at a constant concentration of water ($25 mmol/dm^3$) in the reaction mixture.

Each of the curves shown in the results is representative of a series of curves⁸ (e.g. at various monomer concentrations). Although all experimental curves have been interpreted and conclusions drawn, only some of the curves are presented here.

Chromatography

After the completion of the polymerization run, 5 ml of the reaction mixture were degassed on a vacuum line. The residual monomer together with low molecular reaction products were transferred into a liquid nitrogen cooled ampoule by a bulb-to-bulb distillation. The volatiles were then analysed on a Perkin-Elmer F 11 chromatograph fitted with a thermal conductivity detector; a stainless steel column 2 m long \times 3 mm i.d., was packed with Chromosorb W 60/80 mesh with 20% of silicon rubber E 301 as a stationary phase. Ar was used as a carrier gas.

Molecular weight determination

Number-average molecular weight, \bar{M}_n , was determined by the v.p.o. method using a VPO ÚMCH ČSAV instrument. The deviation method was employed, bromoform, naphthalene and diphenyl ether respectively being the standards. Acetone, dichloromethane and in some cases ethanol were the solvents used.

Conductivity measurements

The conductivity of samples was measured using a Radiometer A/S-DK-2400 Copenhagen NV-Emdrupvej 72 instrument.

In all cases the conductivity was followed as a function of polymerization time. Most of the measurements were carried out in a stopcock apparatus but no vacuum was applied. From the experiments performed in the strict absence of water under high vacuum it was established that the amount of water which can get into the open system has no significant influence upon the time dependence of conductivity changes⁸.

N.m.r. spectra

A/VMR Tesla BS 487A-80 MHz spectrometer was used to measure n.m.r. spectra. The samples were placed in ground tubes 5 mm o.d. using an external capillary standard

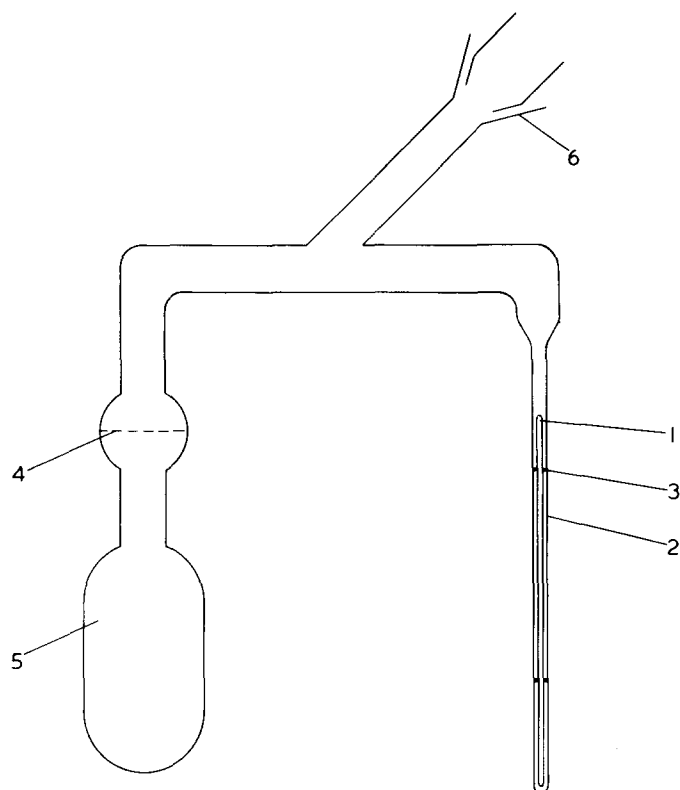


Figure 2 Apparatus for filling n.m.r. tubes: 1, capillary standard containing HMDS alone or in mixture with chloroform; 2, ground tube 5 mm diameter; 3, teflon rings; 4, sintered glass S 2; 5, bulb with reaction components; 6, ground joint connecting the apparatus to vacuum line. The n.m.r. tube is filled by tipping the apparatus

(hexamethyldisiloxane alone or mixed with CHCl_3 at 1:1 ratio). All the sample tubes were filled under high vacuum using an apparatus shown in Figure 2. The spectra were taken at room temperature as well as at 253 and 233K. No band shift or intensity changes were observed.

U.v. spectra

U.v. spectra were measured employing a double beam spectrophotometer Optica Milano CF-4 DR. The spectrophotometer cells (QS, $l = 1$ mm) were filled with sample under vacuum and sealed off. The differential method was used for obtaining the spectra, the samples being contained in cells shown schematically in Figure 3.

The spectrum of TiCl_4 in CH_2Cl_2 was taken first using CH_2Cl_2 in a reference beam. The break-seal separating the spectrometer cell from the storage bulb containing epichlorohydrin was then broken and the spectrum measured, using the CH_2Cl_2 solution of the same component as a reference.

I.r. spectra

The spectra were measured on an UR-10 instrument in standard cells at $308.0 \pm 0.5\text{K}$.

RESULTS

The character of epichlorohydrin oligomerization is apparent from Figure 4. At higher concentrations of diethyl ether ($>1.0 \text{ mol/dm}^3$) the polymerization of epichlorohydrin is completely inhibited. When acetyl chloride is present, however, then the contraction is increased by ether. The polymerization proceeds in a non-stationary fashion. When more epichlorohydrin is added after the end of polymeriza-

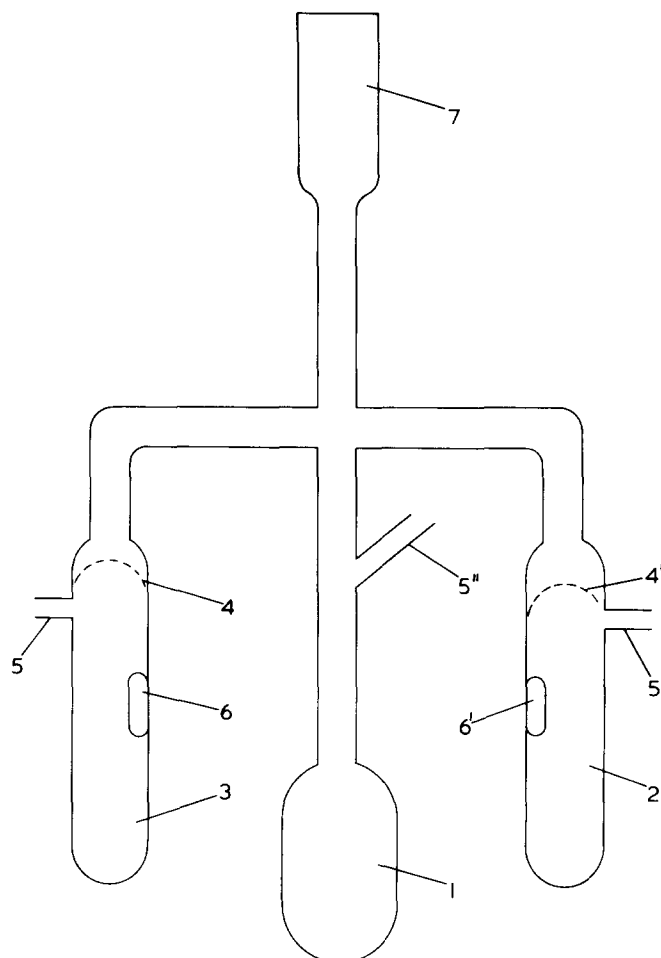


Figure 3 Measuring cell: 1, space for sampling dichloromethane solution of TiCl_4 ; 2, sampling of tetrahydrofuran; 3, sampling of epichlorohydrin; 4, 4', break seals; 5, 5', 5'', connections to vacuum line; 6, 6', stirrers; 7, quartz cell (pathlength = 1 mm)

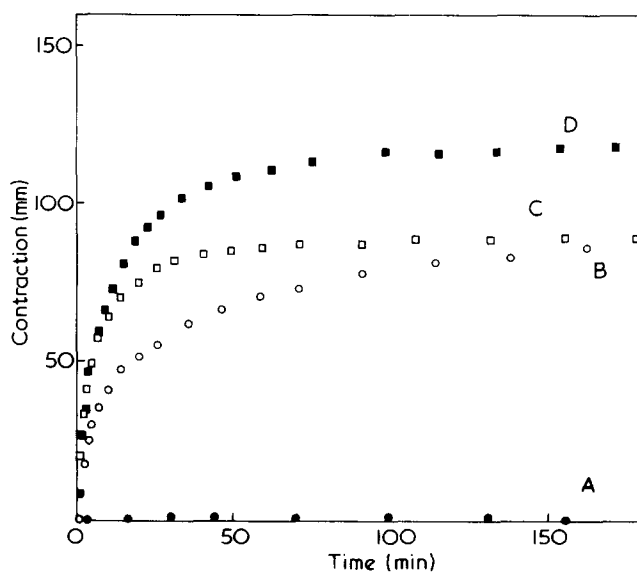


Figure 4 Contraction curves of epichlorohydrin polymerization. Temperature 293.1K; $[\text{TiCl}_4] = 0.5 \text{ mol/dm}^3$; concentration of components (mol/dm^3): A, $[\text{EPC}] = 6.43$, $[\text{Et}_2\text{O}] = 2.9$; B, $[\text{EPC}] = 6.43$; C, $[\text{EPC}] = 6.43$, $[\text{Et}_2\text{O}] = 0$, $[\text{AcCl}] = 2.5$; D, $[\text{EPC}] = 6.43$, $[\text{Et}_2\text{O}] = 2.9$, $[\text{AcCl}] = 2.5$

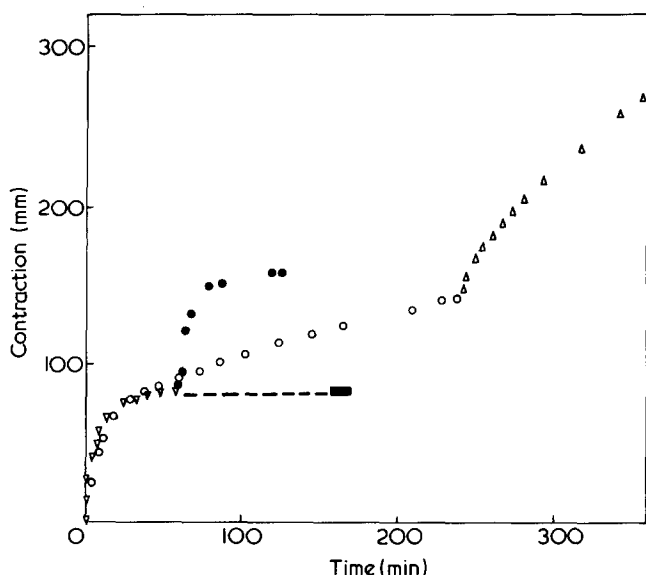


Figure 5 Contraction curves of epichlorohydrin polymerization. Temperature 293.1K, $[\text{TiCl}_4] = 0.5 \text{ mol/dm}^3$, $[\text{EPC}] = 6.43 \text{ mol/dm}^3$. Addition of components: \circ , EPC; \triangle , EPC added, 6.43 mol/dm^3 ; ∇ , EPC + AcCl; \bullet , after 60 min AcCl added, 2.5 mol/dm^3 ; \blacksquare , after 180 min TiCl_4 added, 0.5 mol/dm^3

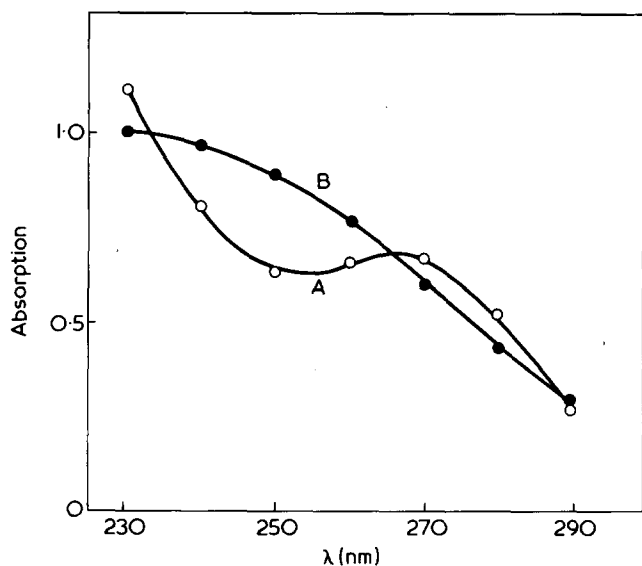


Figure 6 Absorption curves of TiCl_4 and epichlorohydrin- TiCl_4 systems. Solvent dichloromethane; temperature 298.1K; $[\text{TiCl}_4] \sim 10^{-3} \text{ mol/dm}^3$, $[\text{EPC}] = 1.7 \text{ mol/dm}^3$. A, TiCl_4 in CH_2Cl_2 vs. CH_2Cl_2 ; B, TiCl_4 in CH_2Cl_2 and EPC vs. CH_2Cl_2 with EPC

tion (provided no acetyl chloride was present) then a new, slower oligomerization commences. The addition of acetyl chloride can restart the polymerization, which had already ceased, to the full extent while further addition of TiCl_4 does not show this effect (Figure 5).

Calculated from initial rates, the oligomerization is of the first order with regard to TiCl_4 and apparently of the second order with regard to monomer. The latter value, however, is questionable because the effect of the increasing dielectric constant, this being a consequence of increasing the epichlorohydrin concentration, cannot be neglected. Since no sufficiently inert solvent possessing physical properties of epichlorohydrin is available the question of the reaction order cannot be unequivocally answered. The reaction order with regard to monomer is equal to zero in the presence of acetyl chloride. The same value with regard to acetyl chloride is equal to two. Epichlorohydrin

starts to polymerize at concentrations higher than 1 mol/dm^3 (epichlorohydrin concentration $\geq 2 [\text{TiCl}_4]$).

U.v. spectra of TiCl_4 and epichlorohydrin in dichloromethane are shown in Figure 6.

In order to judge the interaction between TiCl_4 and CH_2Cl_2 the i.r. spectrum of TiCl_4 in the mixture of CH_2Cl_2 and hexyl chloride was taken. Apart from originally present TiCl_4 (495 cm^{-1} and 615 cm^{-1}) and C-Cl (650 cm^{-1}) bands a new weak band at 625 cm^{-1} was recorded. Here the newly formed absorption band was attributed to TiCl_4 to which hexyl chloride is coordinated via chlorine atoms.

The composition of both monomer and polymer phase, concentration of components, and their structure, was determined using i.r. spectrometry and gas chromatography. The amount of monomer determined by g.l.c. was in agreement with the gravimetry. Both methods were also used for the calibration of the contraction-conversion relationship. This dependence is strictly linear in the whole interval of measurement. The conversion $([\text{EPC}]_0 - [\text{EPC}]) / [\text{EPC}]_0$ can be thus calculated by multiplying the contraction (mm) by the constant $2.75 \times 10^{-3} (\text{mm}^{-1})$.

I.r. spectra of polymers are presented in Figure 7.

Table 1 summarizes the results of analyses of products

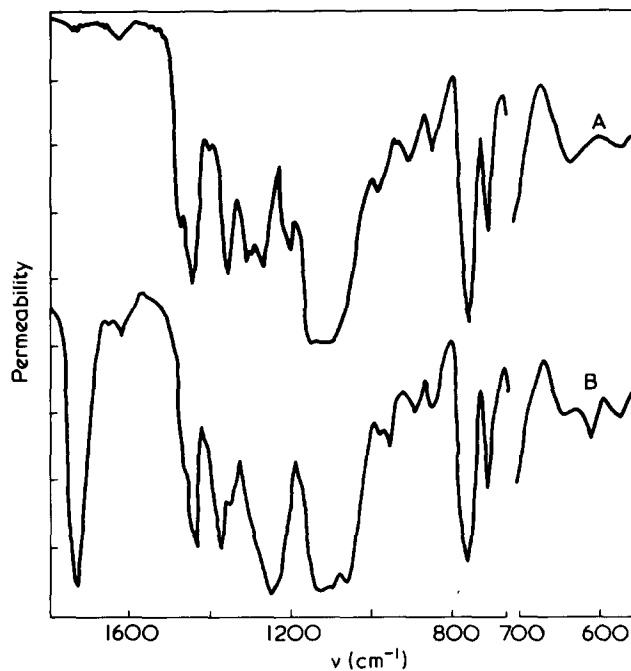


Figure 7 I.r. spectra of polymers isolated from polymerization systems. Temperature of polymerization 293.1K, temperature during spectral measurements $308 \pm 0.5 \text{ K}$. Concentration of components (mol/dm^3): $\text{TiCl}_4 = 0.5$; A, EPC = 6.43; B, EPC = 6.43, AcCl = 2.5

Table 1 Structure and relative yields of products during the oligomerization of epichlorohydrin

System	Product	Relative yield (%)
Epichlorohydrin	$\text{HO}-\text{CH}_2-\text{CH}(\text{CH}_2\text{Cl})-\text{O}-\text{CH}_2-\text{CH}(\text{CH}_2\text{Cl})-\text{O}-\text{CH}_2-\text{CH}(\text{CH}_2\text{Cl})-\text{O}-\text{CH}_2-\text{CH}(\text{CH}_2\text{Cl})-\text{H}$ $n = 5-20$	100
Epichlorohydrin, acetyl chloride	$\text{CH}_3\text{C}(\text{O})-\text{CH}(\text{CH}_2\text{Cl})-\text{CH}_2-\text{CH}_2-\text{CH}(\text{CH}_2\text{Cl})-\text{O}-\text{CH}_2-\text{CH}(\text{CH}_2\text{Cl})-\text{O}-\text{CH}_2-\text{CH}(\text{CH}_2\text{Cl})-\text{H}$	60
	$\text{HO}-\text{CH}(\text{CH}_2\text{Cl})-\text{CH}_2-\text{O}-\text{CH}(\text{CH}_2\text{Cl})-\text{CH}_2-\text{O}-\text{CH}(\text{CH}_2\text{Cl})-\text{CH}_2-\text{O}-\text{CH}(\text{CH}_2\text{Cl})-\text{CH}_2-\text{O}-\text{CH}(\text{CH}_2\text{Cl})-\text{H}$	40

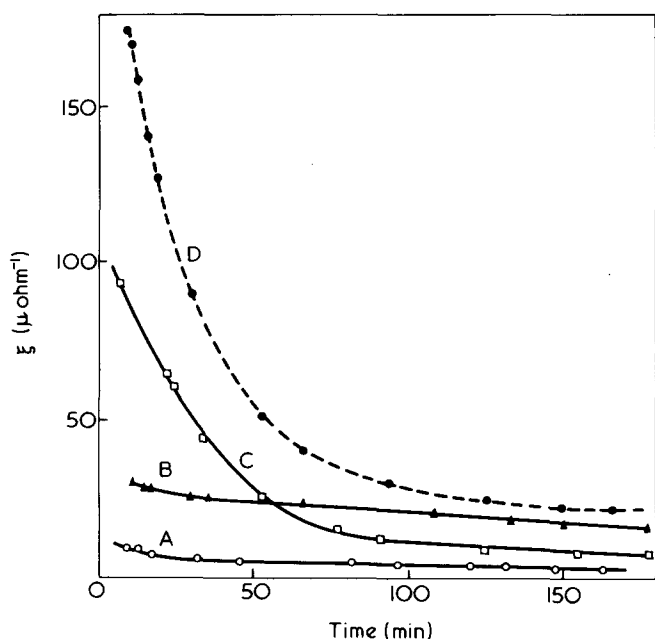


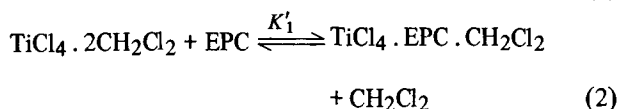
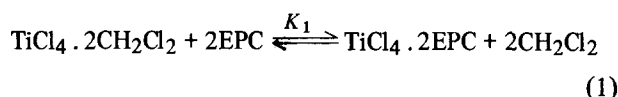
Figure 8 Time dependence of electric conductivity during the polymerization of epichlorohydrin. Temperature 293.1K; concentration of components (mol/dm³): TiCl₄ = 0.5, EPC = 6.43. Curve A, EPC alone; B, AcCl = 2.5; C, AcCl = 2.5; Et₂O = 2.9; D, Et₂O = 2.9 mol/dm³

formed by interaction between epichlorohydrin and TiCl₄ or epichlorohydrin, TiCl₄ and acetyl chloride.

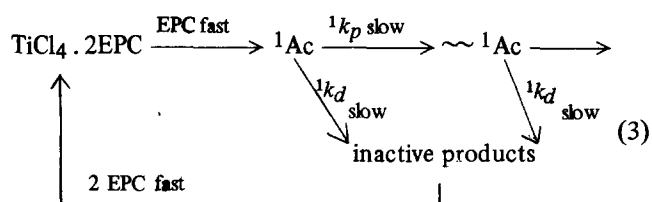
The conductivity measurements were carried out in a conductivity cell in which epichlorohydrin was polymerized. The results of these experiments are summed up in Figure 8. All experimental curves of ξ (specific electric conductivity) vs. t are monotonous. The highest conductivity was observed in medium in which polymerization was not proceeding. These results suggest that free ions do not play a significant role during the polymerization.

DISCUSSION

The concentration of free TiCl₄ will be practically zero in the presence of donor compounds. Thus following equilibria will be established at the beginning of polymerization of epichlorohydrin:



Epichlorohydrin starts to polymerize at concentrations that are at least twice as high as that of TiCl₄. The TiCl₄ · 2EPC complex is thus the centre to which the monomer is coordinated; TiCl₄ · EPC · CH₂Cl₂ is kinetically insignificant. Neither inhibition nor induction periods were observed; all active centres are formed immediately after mixing the components. The reaction order towards TiCl₄ is one which means that the active centre reacts with free non-complexed monomer to give polymer chain or it is deactivated to inactive derivatives and new forms of TiCl₄ capable of being activated:



The material balance of TiCl₄ can be expressed as:

$$[\text{TiCl}_4]_0 = \text{}^1\text{Ac} ([\text{CH}_2\text{Cl}_2]^2 + K_1[\text{EPC}]^2) / (K_1[\text{EPC}]^2) \quad (4)$$

If the supply of monomer to the TiCl₄ · 2EPC is faster than the propagation or deactivation rearrangement, the propagation will be of zero order with regard to epichlorohydrin. This case was observed in tetrahydrofuran oligomerization⁹. The rate of epichlorohydrin disappearance can be then expressed as:

$$-\frac{d[\text{EPC}]}{dt} = \text{}^1k_p \text{}^1\text{Ac} = \text{}^1k_p [\text{TiCl}_4]_0 (K_1[\text{EPC}]^2) / ([\text{CH}_2\text{Cl}_2]^2 + K_1[\text{EPC}]^2) \quad (5)$$

Active centres, however, also disappear in the course of polymerization. Their disappearance cannot be simply expressed as a dependence on EPC concentration according to equation (4). Judging from Figure 4, some other reaction is involved. According to equation (3) it holds:

$$-\frac{d[\text{}^1\text{Ac}]}{dt} = \text{}^1k_d [\text{}^1\text{Ac}] \quad (6)$$

When equation (5) is divided by expression (6) then the following expression results:

$$\frac{d[\text{EPC}]}{d[\text{}^1\text{Ac}]} = \frac{\text{}^1k_p}{\text{}^1k_d} \times \frac{[\text{TiCl}_4]_0 K_1 [\text{EPC}]^2}{[\text{CH}_2\text{Cl}_2]^2 + K_1 [\text{EPC}]^2} \times \frac{1}{[\text{}^1\text{Ac}]} \quad (7)$$

The actual concentration of active centres expressed as a function of EPC concentration can be obtained by integrating equation (7), assuming that $[\text{CH}_2\text{Cl}_2]^2 \ll K_1[\text{EPC}]_0 \times [\text{EPC}]$

$$[\text{}^1\text{Ac}] = [\text{}^1\text{Ac}]_0 \exp \left[-\frac{\text{}^1k_d}{\text{}^1k_p [\text{TiCl}_4]_0} ([\text{EPC}]_0 - [\text{EPC}]) \right] \quad (8)$$

Inserting equation (8) into (5) and integrating within corresponding limits the following expression is obtained:

$$[\text{EPC}]_0 - [\text{EPC}] = \frac{\text{}^1k_p}{\text{}^1k_d} [\text{TiCl}_4]_0 \ln \left(1 + \frac{\text{}^1k_d}{[\text{TiCl}_4]_0} \times [\text{}^1\text{Ac}]_0 \right) \quad (9)$$

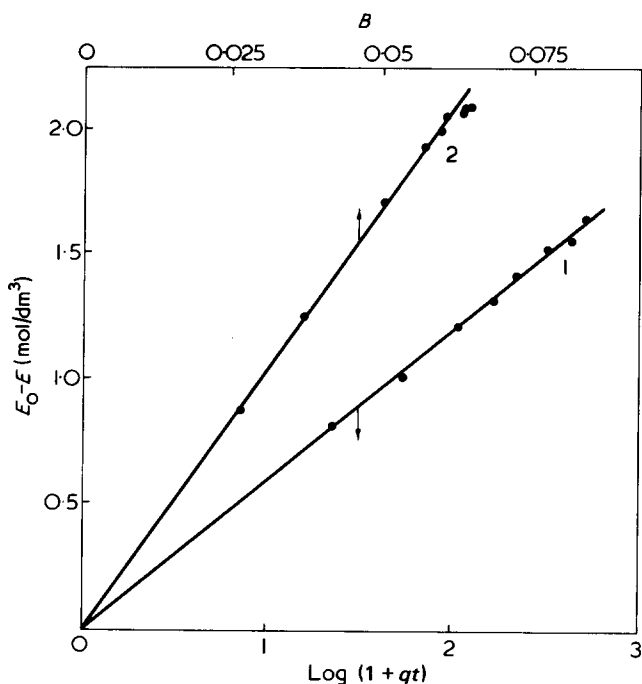


Figure 9 The dependence of $E_0 - E$ as a function of measured variables and constants. Temperature 293.1K; concentration (mol/dm³): $\text{TiCl}_4 = 0.5$, $\text{EPC} = 6.43$. Curve A, dependence of $E_0 - E$ on $\log(1 + qt)$; $q = [^1\text{Ac}]_0 \cdot ^1k_d$; $[\text{AcCl}] = [\text{Et}_2\text{O}] = 0$; Curve B, dependence of $E_0 - E$ on B , where

$$B = \frac{[\text{TiCl}_4]_0}{^5k_d} \frac{K_2[\text{AcCl}]_0}{K_1[\text{EPC}]_0^2 + K_3[\text{Et}_2\text{O}]^2} \times \left(1 - \frac{1}{1 + [\text{AcCl}]_0 \cdot ^5k_d t} \right)$$

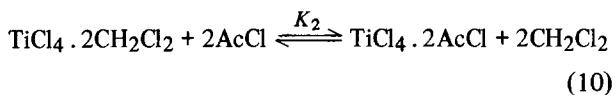
$[\text{AcCl}]_0 = 2.5 \text{ mol/dm}^3$; $[\text{Et}_2\text{O}] = 2.9 \text{ mol/dm}^3$

The values of K_1 , 1k_p and $^1k_d^*$ can then be calculated from equation (9) using experimental data.

Equation (9) can be plotted as a straight line (curve A in Figure 9). Experimental data presented in Figure 4 (curve B) were used for plotting.

Oligomerization of epichlorohydrin in the presence of acetyl chloride

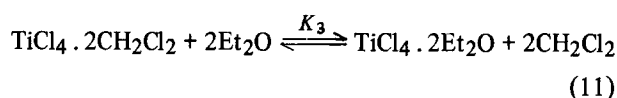
Besides equilibria (1) and (2) the formation of complexes with acetyl chloride and diethyl ether, should also be considered. No complexes containing mixed ligands, other than Cl, were found to be formed. Therefore



* $E_0 - E = k \ln(1 + qt)$. The most suitable values of q are found by approximation of experimental values of $E_0 - E$ and t . The values of q_1 and q_2 are derived from two different values of $[E]_0$. Then K_1 can be expressed:

$$K_1 = \frac{\{[\text{CH}_2\text{Cl}_2]_2^2 - [\text{CH}_2\text{Cl}_2]_1^2\}}{[E_{01}]^2[E_{02}]^2} \left([E_{01}]^2 - \frac{q_1}{q_2} [E_{02}]^2 \right) \times \frac{q_2}{q_2 - q_1}$$

The value of K_1 is used to calculate $^1k_d [^1\text{Ac}]_0$ from equation (4) into which the initial concentration of EPC was inserted. 1k_p is then evident from the slope of the plotted function (9).



Reaction orders with regard to components together with the effect of component additions, mainly, however, the identical initial course of the oligomerization in the presence and absence of diethyl ether, suggest that out of two possible types of active centres only that type should be considered whose existence is determined by the presence of acetyl chloride. The reaction scheme of oligomerization presented in equation (3) can thus be applied for this case:

$$-\frac{d[\text{EPC}]}{dt} = ^1k_p[^1\text{Ac}] + ^2k_p[^2\text{Ac}] \approx ^2k_p[^2\text{Ac}] \quad (12)$$

The concentration $[^2\text{Ac}]$, which is kinetically manifested in form $\text{TiCl}_4 \cdot 2\text{AcCl}$, can be expressed using relationships for material balance of TiCl_4 (equations 1, 10 and 11):

$$[^2\text{Ac}] = [\text{TiCl}_4]_0 \times \frac{K_2[\text{AcCl}]^2}{[\text{CH}_2\text{Cl}_2]^2 + K_1[\text{EPC}]^2 + K_2[\text{AcCl}]^2 + K_3[\text{Et}_2\text{O}]^2} \quad (13)$$

Oligomerization of epichlorohydrin in the presence of acetyl chloride and in the absence of diethyl ether. The polymerization ceases at low conversions. Thus at first approximation the initial concentration of epichlorohydrin can be used instead of the actual one in the denominator of expression (13). Direct determinations of actual concentrations of acetyl chloride during tetrahydrofuran oligomerization have revealed that the rate of acetyl chloride disappearance depends on the value of deactivation constant k_d and time according to relationship: $[\text{AcCl}] = [\text{AcCl}]_0 (1 - [\text{AcCl}]_0 k_d t)^{-1}$ (see refs 8 and 9). The parallelism of effects caused by acetyl chloride concentration changes allows one to assume that a similar mechanism of acetyl chloride disappearance from the reaction zone is operative at oligomerization of epichlorohydrin. The n.m.r. method could not be used to measure the disappearance of acetyl chloride in epichlorohydrin medium. If the equation for the concentration of acetyl chloride is inserted into equation (13) (k_d being denoted 2k_d now) the following expression is obtained upon rearrangement and integration:

$$[\text{EPC}]_0 - [\text{EPC}] = \frac{^2k_p[\text{TiCl}_4]_0}{^2k_d[\text{AcCl}]_0} \times \frac{1}{\gamma} \times \{ \arctan \gamma (1 + [\text{AcCl}]_0 \times ^2k_d t) - \arctan \gamma \} \quad (14)$$

If donor numbers of components¹⁰ are taken into account then it can be considered that $\gamma^2 c^2 \gg 1$. In this case the following equation can be used to calculate the difference between the initial and actual concentration of epichlorohydrin:

$$[\text{EPC}]_0 - [\text{EPC}] = \frac{^2k_p}{^2k_d} \frac{[\text{TiCl}_4]_0}{[\text{AcCl}]_0} \frac{1}{\gamma^2} \left(1 - \frac{1}{c} \right) \quad (15)$$

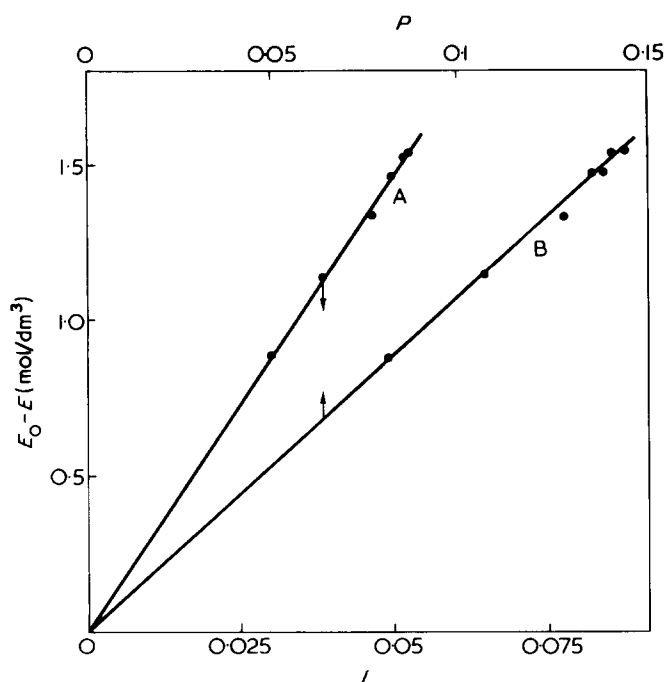


Figure 10 Dependence of $E_0 - E$ upon values of L and P . Temperature 293.1K; concentration of components (mol/dm³): $TiCl_4 = 0.5$; $AcCl = 2.5$; $EPC = 6.43$. Curve A, dependence of $E_0 - E$ on L ;

$$L = \frac{[TiCl_4]_0}{2k_d[AcCl]_0} \times \{\arctan \gamma c - \arctan \gamma\};$$

Curve B, dependence of $E_0 - E$ on P ;

$$P = \frac{1}{\gamma^2} \frac{[TiCl_4]_0}{2k_d[AcCl]_0} \left(1 - \frac{1}{c}\right);$$

where

$$\gamma^2 = \frac{[CH_2Cl_2]^2 + K_1[EPC]_0^2}{K_2[AcCl]_0^2}; c = 1 + [AcCl]_0^2 k_{dt}$$

When the right hand sides of equations (14) and (15) are compared for the same $[EPC]_0 - [EPC]$ then the following relationship is obtained:

$$\gamma[\arctan \gamma c - \arctan \gamma] \doteq 1 - \frac{1}{c} \quad (16)$$

The values of c and γ † can be computed from equations (15) and (16) using experimental data. Subsequently the values of K_2 , $2k_p$ and $2k_d$ are obtained.

Figure 10 shows the agreement between experimental data and equations (14) and (15) containing constants calculated in the way just described.

Oligomerization of epichlorohydrin in the presence of acetyl chloride and diethyl ether. Since the sum $K_2[AcCl]^2 + [CH_2Cl_2]^2$ can be neglected with regard to other terms

† The values of $[EPC]_0$ ($t = 0$), $[EPC]_1$ (t_1) and $[EPC]_2$ (at_1) are determined from the contraction curve. At $t > 10$ min it holds that $c \approx [AcCl]_0^2 k_{dt}$. At time t , $c = c_1$ while at time at , $c = ac_1$. Thus two equations containing two unknown variables can be set up allowing one to calculate c for a given difference $[EPC]_0 - [EPC]$.

in denominator of relationship (13) the rate of disappearance of epichlorohydrin can be expressed as:

$$-\frac{d[EPC]}{dt} = 2k_p[Ac] = 2k_p[TiCl_4]_0 \times \frac{K_2[AcCl]^2}{K_1[EPC]^2 + K_3[Et_2O]^2} \quad (17)$$

Inserting the concentration of acetyl chloride $[AcCl]$ into this equation (k_d being denoted 5k_d now) and integrating, the following equation results:

$$[EPC]_0 - [EPC] = \frac{2k_p}{5k_d} [TiCl_4]_0 \times \frac{K_2[AcCl]_0}{K_1[EPC]^2 + K_3[Et_2O]^2} \times \left(1 - \frac{1}{1 + [AcCl]_0^5 k_{dt}}\right) \quad (18)$$

The insertion of known values of K_1 , K_2 and $2k_p$ allows one to calculate K_3 and 5k_d . The agreement between experimental and calculated values is shown in Figure 9 (curve B).

The values of equilibrium and kinetic constants are summarized in Table 2.

Mechanism of oligomerization

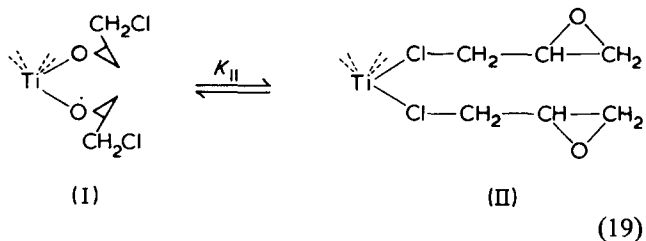
The low values of conductivity, even in a relatively polar medium indicate that no free ions are involved in the reaction. Ion-pairs are not likely to be active species in this case either, because the conductivity is not increasing with the increasing dielectric constant of the reaction medium. High concentration of $TiCl_4$, mono-molecular rearrangement of the active centre leading to higher or diminished activity, and no response towards the presence of water in the reaction mixture, are the most important observations that are suggestive of the coordinate mechanism of oligomerization.

The stability of $TiCl_4$ complexes with heterocyclic ligands coordinated to Ti atom through oxygen indicates that the polymerization of monomers bonded in this way will be difficult. If we dismiss the participation of ions in the growth reaction and assume the participation of zwitterions as a little probable one, it is very difficult to imagine the rise of a trimer and higher polymers (PO does not form high polymers in the presence of $TiCl_4$ ¹¹).

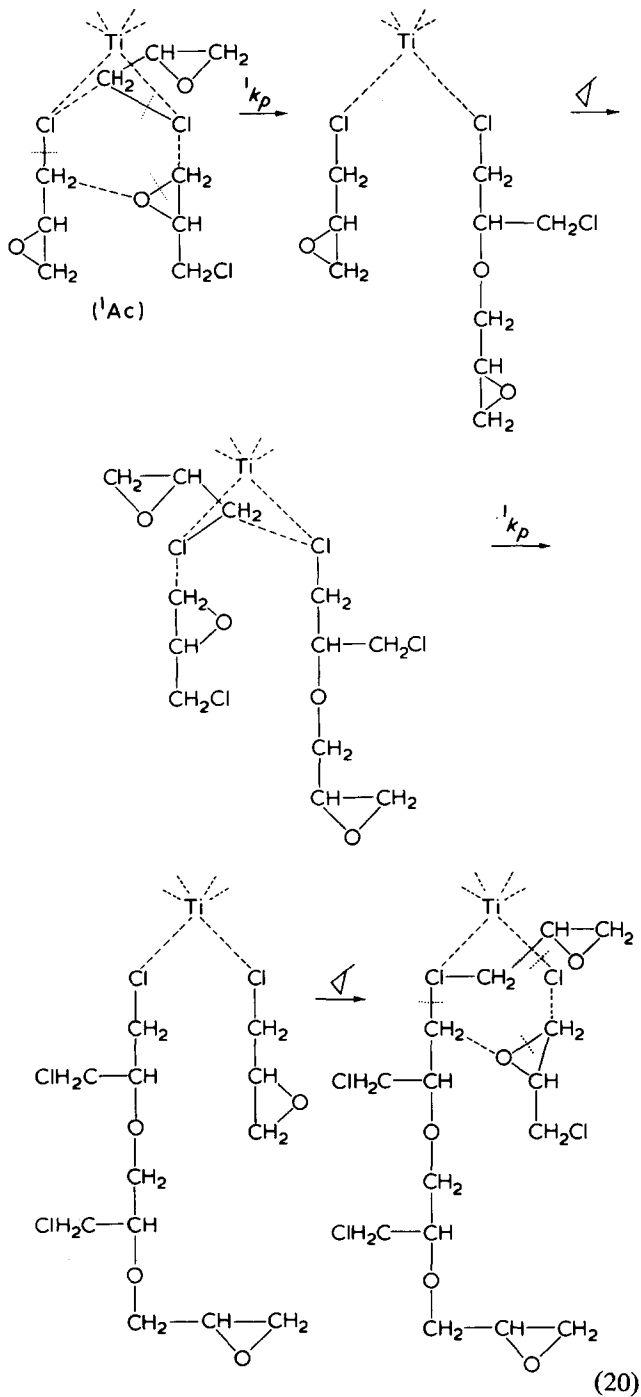
Table 2 Values of equilibrium and kinetic constants

Constant	Value	Rate constant	$k \times 10^2 [\text{sec}^{-1}]$
K_1	5	$1k_p$	4.90
K_2	1	$2k_p$	48.70
K_3	20	$1k_d$	9.33
		$2k_d$	0.17
		$5k_d$	0.08

Even though we have not succeeded in getting direct proof let us assume the existence of an equilibrium:



According to this conception the complex (I) is kinetically inactive. Only complex (II) can start the polymerization:

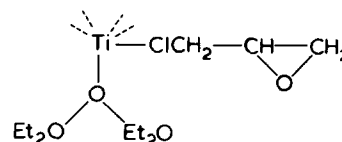


The active centre of propagation is very unstable. Its activity may disappear either by a change of coordination mode (equation 19) or by splitting off the growing chain

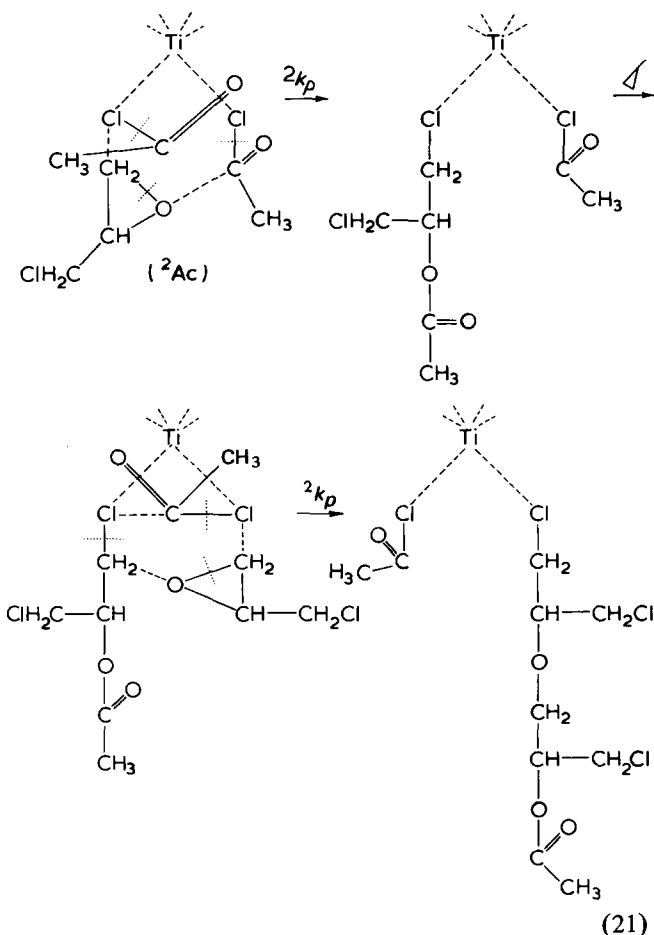
or exchanging the growing ligand for the polymeric ligand which will be coordinated to Ti via some of its oxygen atoms present in the backbone. The transfer occurs when the growing ligand is exchanged for epichlorohydrin.

This simplified picture is to be understood as a first approximation to the elucidation of the mechanism, e.g. n.m.r. spectra clearly indicate that HCl is eliminated from the epichlorohydrin molecule. The HCl thus evolved may play an important role in termination and transfer processes.

The inhibiting effect of diethyl ether can be accounted for by the coordination of the latter to Ti. Such an addition would preclude further polymerization.



The accelerating effect of acetyl chloride is probably due to the increased number of Ti-Cl-C- bonds. The coordination of acetyl chloride to Ti via chlorine atom is not excluded¹²:



This hypothesis is supported by finding the values of 2k_d lower than 1k_d and by the ability of acetyl chloride additions to restart the polymerization. When the growing ligand is detached together with Cl atom then an ester, whose presence has been detected, is formed. The other product is chlorohydrin which may be formed by the hydrolysis of the ester during the isolation of a dimer.

REFERENCES

- 1 Boor, J. Jr. in 'Macromolecular Reviews', (Ed. A. A. Peterlin, M. Goodman, S. Okamura, B. H. Zimm and H. F. Mark), Interscience, New York, 1967, Vol 2, p 115; *Ind. Eng. Chem. (Prod. Res. Dev.)* 1970, 9, 437
- 2 Rodrigues, L. A. M. and van Looy, H. M. *J. Polym. Sci.* 1966, 4, 1951, 1971 and previous work of these authors; Armstrong, D. R., Perkins, P. G. and Steward, J. J. D. *J. Chem. Soc.* 1972, 18, 1972
- 3 Ishii, Y. and Sakai, S. in 'Ring-opening Polymerization', (Ed. K. C. Frisch, S. L. Reegen) Marcel Dekker, New York, 1969, pp 31
- 4 Saegusa, T., Ueshima, T., Imai, H. and Furukawa, J. *Makromol. Chem.* 1964, 79, 221
- 5 Imai, H., Saegusa, T., Ohsugi, S. and Furukawa, J. *Makromol. Chem.* 1965, 81, 119
- 6 Kučera, M., Hladký, E. and Majerová, K. *J. Polym. Sci. (A-1)* 1968, 6, 527
- 7 Příbyl, M. and Slovák, Z. *Mikrochim. Acta* 1964, 1097
- 8 Zahradníčková, A. *Thesis* Research Institute of Macromolecular Chemistry, Brno (1974)
- 9 Kucera, M., Zahradníčková, A. and Majerová, K. *Polymer*, 1976, 17, 528
- 10 Gutmann, V. 'Coordination Chemistry in Non-Aqueous Solutions', Springer Verlag, Wien, 1968, p 19
- 11 Kučera, M., Zahradníčková, A. and Majerová, K. to be published
- 12 Chevrier, B. and Weiss, R. *Angew. Chem.* 1974, 86, 1, 12

Coordinate polymerization of heterocycles: 2. Oligomerization of tetrahydrofuran by TiCl₄ in the presence of acetyl chloride or epichlorohydrin

M. Kučera, A. Zahradničková, and K. Majerová

Research Institute of Macromolecular Chemistry, 656 49 Brno, Czechoslovakia

(Received 2 June 1975; revised 28 January 1976)

Both acetyl chloride and epichlorohydrin facilitate the opening of the tetrahydrofuran ring in the presence of TiCl₄. Electrical conductivity and spectral measurements indicate that the process is not of a cationic character. The solvent, however, exhibits a strong influence upon the reaction. An equilibrium in the ligand field of Ti atom will be established depending on the medium; this equilibrium then determines the character of the active centre and thus its ability to polymerize tetrahydrofuran or epichlorohydrin. The kinetic analysis of polymerization was made possible by using a simple relationship between the rate and actual concentration of acetyl chloride, the latter being directly measurable by n.m.r. The values of equilibrium and rate constants have been calculated.

INTRODUCTION

The data on the polymerization of tetrahydrofuran (THF) considerably enhance our knowledge of cationic polymerization and the mechanism and the kinetics of polymerization of cyclic ethers. It is generally believed that the polymerization will proceed only if the propagating centre is in the form of a trialkyloxonium ion or a salt. This opinion is expressed explicitly in a review by Dreyfuss¹ but it occurs implicitly also in later papers². To our knowledge, the coordinate mechanism of tetrahydrofuran polymerization has not been considered to account for the observed results.

Tetrahydrofuran reacts with TiCl₄ to give a stable yellow complex. In order to enhance the fission of the tetrahydrofuran ring, promoters were added accelerating polymerization in other than TiCl₄ induced cases. Such a promoter is e.g. epichlorohydrin (EPC), which is capable of generating trialkyloxonium ion *in situ*³ or acetyl chloride (AcCl) which increases the concentration of carboxonium ions⁴.

Each of these promoters, when combined with TiCl₄, induces the tetrahydrofuran ring opening to give low molecular weight products. Employing the common methods of macromolecular chemistry we attempted to elucidate the mechanism and kinetics of oligomerization.

EXPERIMENTAL

The purity of most chemicals used, working procedures and apparatus have been presented in the first paper of this series⁵.

Tetrahydrofuran (a VEB Laborchemie Apolda product, pure) was distilled several times in the presence of metallic sodium, then in the presence of potassium permanganate to remove peroxides, until no reaction with ferrous sulphate occurred. The product was finally rectified several times using a ~4 TP column. Purity, checked by gas chromatography, was found to be better than 99.9%. 1,4-Dioxane (Lachema, analytical grade), purity checked by gas chromatography, was better than 99%.

The actual concentration of acetyl chloride during the oligomerization was determined by measuring n.m.r. spectra at various time intervals. The signals at 7.35 τ (from the methyl group in acetyl chloride) and at 8.0 τ (acetyl group in the form of acetic acid ester CH₃COOCH₂~) are typical for the spectrum. The concentration of acetyl chloride could be calculated by integrating the spectrum (*Figure 1*).

The conversion could be determined from the resonance intensity decrease of α , β hydrogens of tetrahydrofuran and from the resonance intensity increase at 8.3 τ , 6.55 τ and 5.86 τ . The agreement with conversion determined gravimetrically and by g.l.c. was satisfactory. These three methods verified that the relation between a measured contraction and an actual conversion is strictly linear. The product of an observed contraction and of a constant of proportionality yields a conversion $\pi = ([M_0] - [M])/[M_0]$.

During all experiments in the open system the concentration of water was constant (25 mmol/dm³).

RESULTS

The oligomerization of tetrahydrofuran in the presence of acetyl chloride is a strongly non-stationary process. The reaction subsides before a complete depletion of the monomer. A typical reaction course is shown in *Figure 2*, which presents a dilatometric record of contraction vs. time, the proportionality constant (mm⁻¹) being 0.175×10^{-2} for curves A, B, D, 0.33×10^{-2} for curve C and 0.55×10^{-2} for curve E. The initial rate of oligomerization is independent of concentration of water within the concentration interval $0 \leq [H_2O] \leq 0.8$ mol/dm³.

The reaction order with regard to tetrahydrofuran is low, near to zero in CH₂Cl₂ and equal to two in ether (Et₂O). The reaction is, however, strongly retarded in the presence of ether. Since, under these conditions, the diethyl ether presence made up for the decreasing concentration of tetrahydrofuran, the observed reaction rate decrease was evidently due to the increasing concentration of ether; not even CH₂Cl₂ would be inert. When 1,4-dioxane is used as a solvent then, indeed, the reaction order with regard to

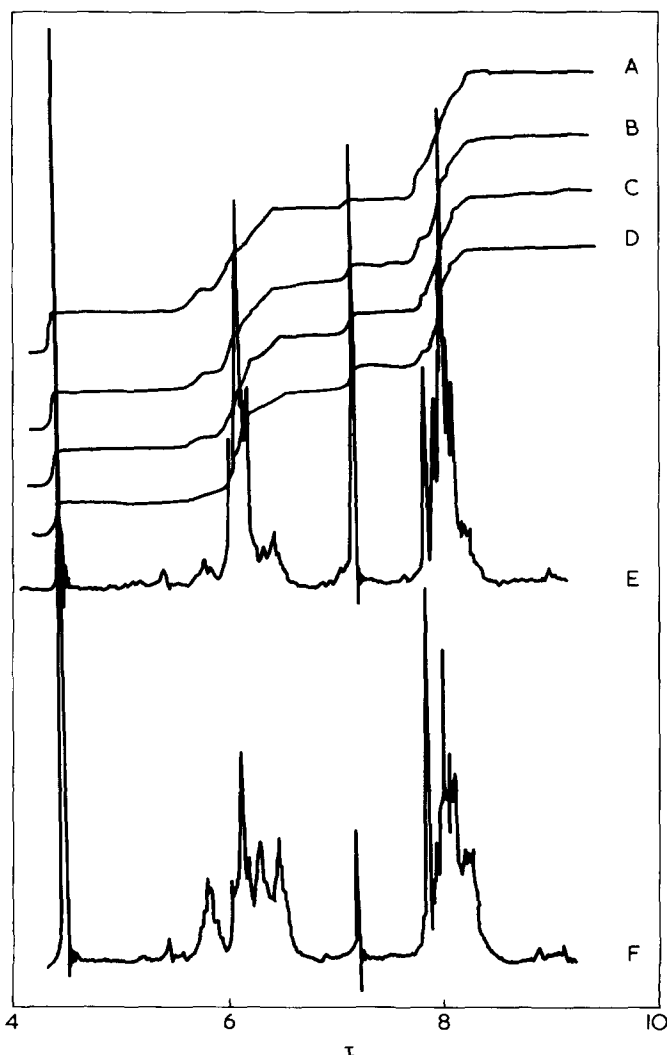


Figure 1 N.m.r. spectra and their integrals measured on the system tetrahydrofuran, acetyl chloride, TiCl_4 at various time intervals. Solvent CH_2Cl_2 ; temperature 298.1K; concentration of components (mol/dm^3): $[\text{THF}]_0 = 6.1$; $[\text{AcCl}]_0 = 2.5$; $[\text{H}_2\text{O}]_0 = 0.035$. Time, t (min): A, 149; B, 69; C, 19; D, 9; E, 6; F, 150

tetrahydrofuran is unequivocally zero. The order with regard to acetyl chloride (calculated from initial rates) is ~ 2.0 and that with regard to TiCl_4 , 1.0. Neither the addition of fresh monomer nor TiCl_4 is able to restart the reaction once it has subsided. The addition of fresh acetyl chloride to such a system can, however, restart the polymerization, the latter being initiated by the second generation of active centres (Figure 3).

The concentration of acetyl chloride is therefore directly determining the concentration of active centres. N.m.r. spectra make it possible to determine the actual concentration of acetyl chloride at any stage of oligomerization. It follows from Figure 4 that the disappearance of acetyl chloride strictly obeys the relationship valid for the second-order reactions. No presence of polymerization active free ions was observed during the oligomerization; the specific electric conductivity being generally lower than in non-polymerizing systems⁵.

Differential u.v. spectra of TiCl_4 in dichloromethane (measured according to the procedure described in a previous paper⁵) are shown in Figure 5. The yellow complex $\text{TiCl}_4 \cdot 2\text{THF}$ shows an absorption at 300 nm. In the presence of EPC tetrahydrofuran is substituted in the ligand sphere of the Ti atom which results in a lowering of this absorption.

Typical oxonium ions formed in the presence of other Lewis acids, as reported by Meerwein⁶, are not formed in our case, even in the presence of acetyl chloride (Figure 6).

The infra red spectrum of a $\text{TiCl}_4 \cdot 2\text{THF}$ complex taken in the solid state is also changed by addition of a small amount of epichlorohydrin, a new band being observed at 640 cm^{-1} . The formation of other bands seen in the OH region at 3350 cm^{-1} is suggestive of the THF ring opening.

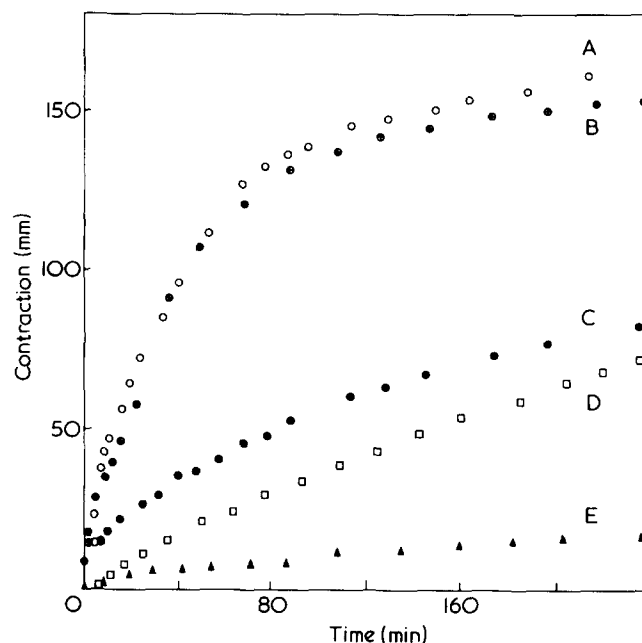


Figure 2 Oligomerization of tetrahydrofuran in the presence of acetyl chloride and epichlorohydrin, respectively. Temperature 293.1K; $[\text{TiCl}_4] = 0.5 \text{ mol}/\text{dm}^3$. Concentration of components (mol/dm^3): A, THF = 6.1; AcCl = 2.5; EPC = 0; $\text{CH}_2\text{Cl}_2 = 4.1$; B, THF = 6.1; AcCl = 2.5; EPC = 0; $\text{CH}_2\text{Cl}_2 = 1.49$; 1,4-dioxane = 2.3; C, THF = 6.1; AcCl = 0; EPC = 4.0; $\text{CH}_2\text{Cl}_2 = 2.4$; D, THF = 6.1; AcCl = 2.5; EPC = 0; $\text{CH}_2\text{Cl}_2 = 0.46$; $\text{Et}_2\text{O} = 2.9$; E, THF = 3.6; AcCl = 0; EPC = 4.0; $\text{Et}_2\text{O} = 3.9$; $\text{CH}_2\text{Cl}_2 = 0.6$

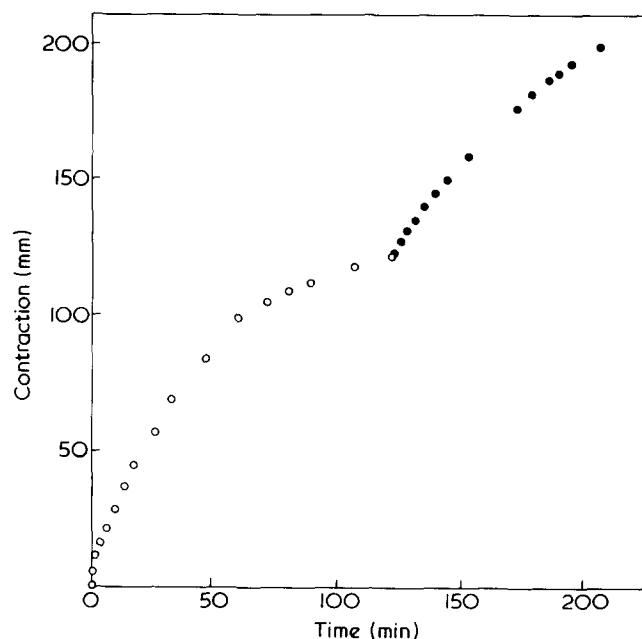


Figure 3 The second oligomerization of tetrahydrofuran induced by a fresh addition of acetyl chloride. Temperature 293.1K; concentration of components (mol/dm^3): THF = 6.1; AcCl = 2.5; $\text{TiCl}_4 = 0.5$; $[\text{H}_2\text{O}]_0 = 0.56$; after 120 min AcCl added ($2.5 \text{ mol}/\text{dm}^3$)

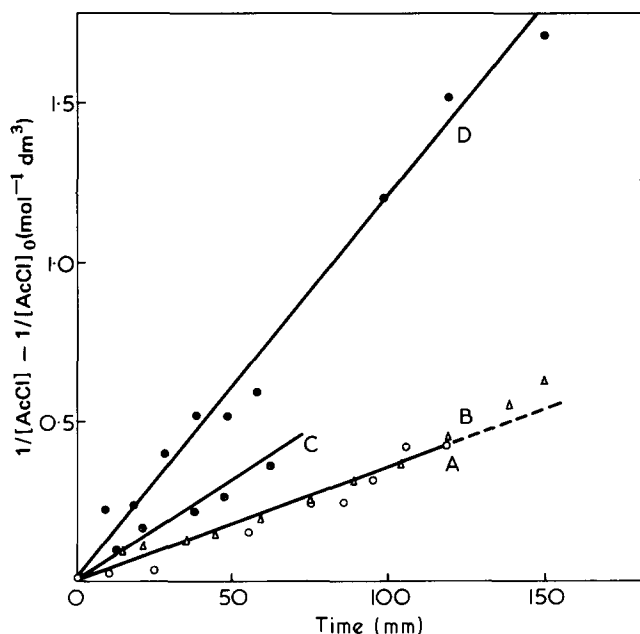


Figure 4 The disappearance of acetyl chloride during oligomerization. Temperature 293.1K; component concentration (mol/dm³): AcCl = 2.5; TiCl₄ = 0.5. A, THF = 6.1; Et₂O = 2.9; B, THF = 8.54; Et₂O = 0.97; C, THF = 1.83; D, THF = 6.1

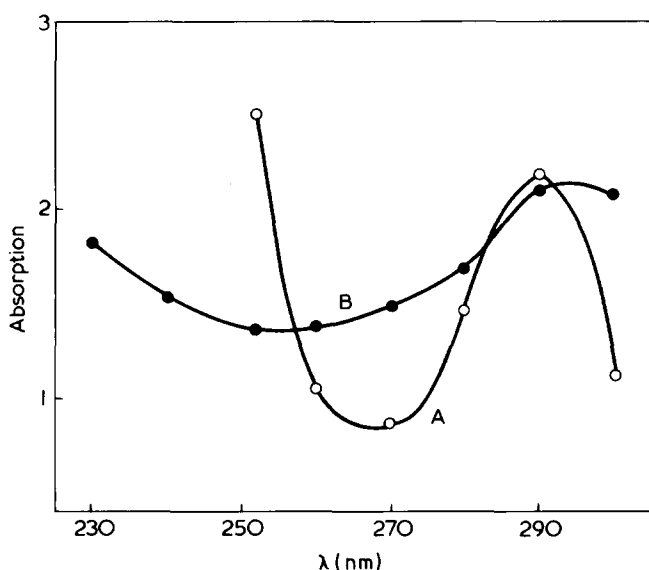


Figure 5 Absorption curves of TiCl₄ and its mixture with tetrahydrofuran. Solvent CH₂Cl₂; temperature 298.1K; [THF] = 1 mol/dm³, [TiCl₄] ~ 10⁻³ mol/dm³. A, TiCl₄ in CH₂Cl₂ ~ CH₂Cl₂; B, TiCl₄ in CH₂Cl₂ with THF ~ CH₂Cl₂ + THF

The solid complex TiCl₄ · 2THF is dissolved by a greater amount of epichlorohydrin. Thus a new pronounced absorption band is seen at 615 cm⁻¹ accompanied by less intense bands at 625 and 645 cm⁻¹, instead of the original absorption due to TiCl₄ at 495 cm⁻¹. Simultaneously the maximum of OH bands is increasing at 3370 cm⁻¹.

N.m.r. spectra of the product of tetrahydrofuran oligomerization in the presence of acetyl chloride or epichlorohydrin are presented in Figures 7 and 8. I.r. spectra are shown in Figure 9.

The \bar{M}_n of oligomers formed is 230–450. Gas-chromatographic analysis⁷ together with the results of spectral measurements suggest the composition of products given in Table 1.

DISCUSSION

Oligomerization of THF in the presence of acetyl chloride.

The following equilibria should be considered to be present in the reaction system containing TiCl₄, tetrahydro-

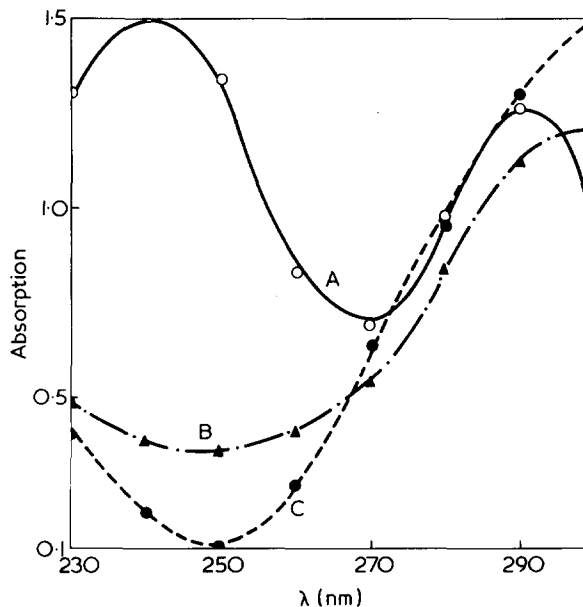


Figure 6 U.v. spectra of TiCl₄ and its mixtures with AcCl and with acetyl chloride and tetrahydrofuran. Solvent CH₂Cl₂, temperature 298.1K; [TiCl₄] ~ 10⁻³ mol/dm³, [THF] = 0.95 mol/dm³, [AcCl] = 0.6 mol/dm³. A, TiCl₄ in CH₂Cl₂ ~ CH₂Cl₂; B, TiCl₄ in CH₂Cl₂ + AcCl ~ CH₂Cl₂ + AcCl; C, TiCl₄ in CH₂Cl₂ + AcCl + THF ~ CH₂Cl₂ + AcCl + THF

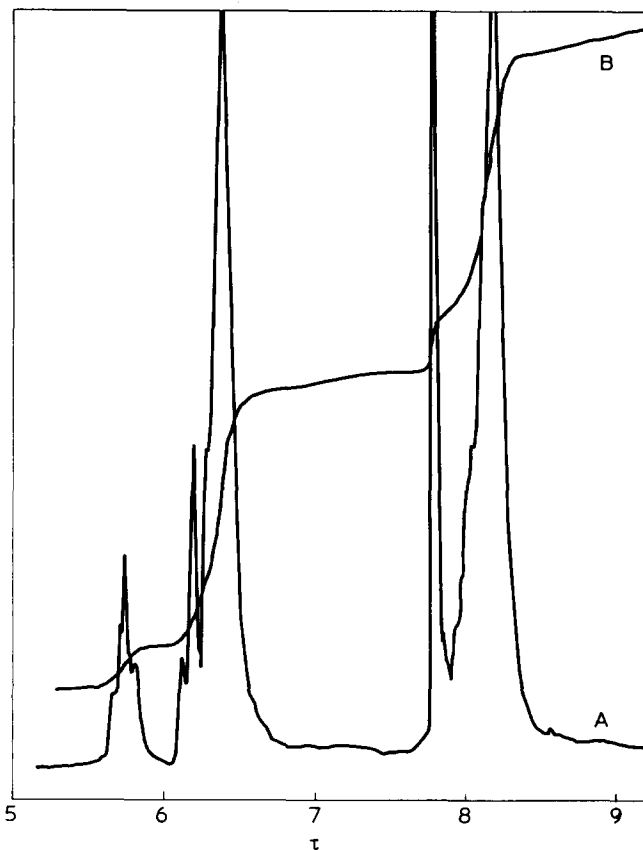


Figure 7 N.m.r. spectrum of polymer formed in the system tetrahydrofuran-acetyl chloride-TiCl₄. Temperature 293.1K, concentration of components (mol/dm³): THF = 8.54; AcCl = 2.5; TiCl₄ = 0.5. A, the spectrum taken at 323.1K; B, integral

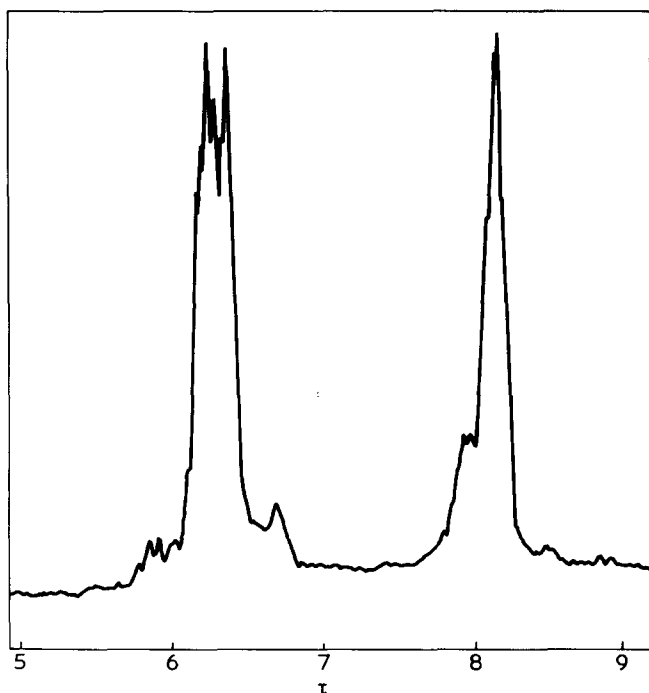


Figure 8 N.m.r. spectra of polymer formed in the system tetrahydrofuran–epichlorohydrin. Temperature of polymerization 293.1K, temperature of measurement 298.1K; concentration of components in the polymerization system (mol/dm³): THF = 6.1; EPC = 4; [H₂O]₀ = 0

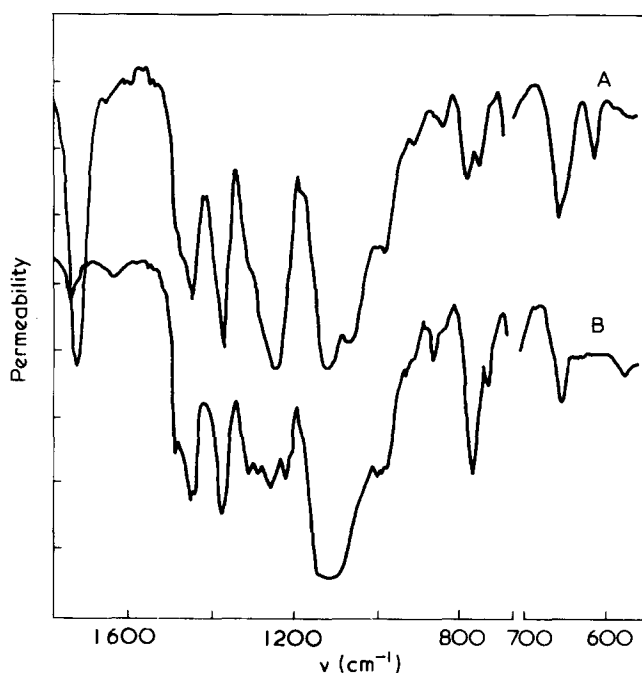
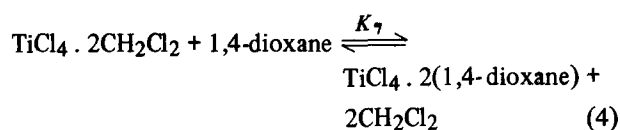
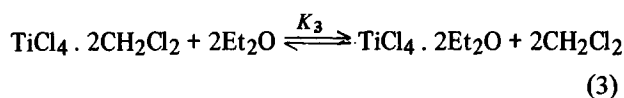
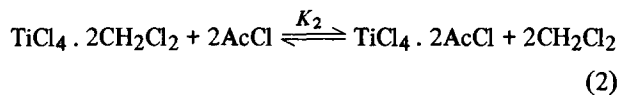
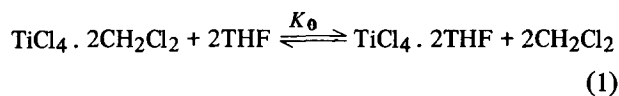
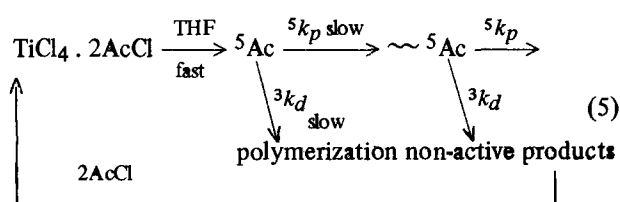


Figure 9 I.r. spectra of polymers isolated from polymerization systems. Temperature of polymerization 293.1K; temperature of measurement 308.0 ± 0.5K; concentration of components in the system (mol/dm³): A, THF = 8.54; AcCl = 2.5; B, THF = 6.1; EPC = 4

furan, dichloromethane and 1,4-dioxane or diethyl ether:



None of the reaction orders found, suggests the existence of complexes containing mixed ligands (e.g. TiCl₄ · AcCl · Et₂O). Therefore such complexes are not considered to be kinetically important species. The rate of oligomerization is directly proportional to the square of acetyl chloride concentration while the zero order with regard to the monomer indicates that the reaction of tetrahydrofuran with active centre is not the rate controlling step. Let us assume that the opening of the tetrahydrofuran ring is effected via a slow rearrangement of the active centre. The disappearance of centre activity, during which TiCl₄ is regenerated, is a competitive reaction:



It follows from the material balance ([⁵Ac] = [TiCl₄ · 2AcCl]) that:

$$[\text{}^5\text{Ac}] = [\text{TiCl}_4]_0 \times \frac{K_2[\text{AcCl}]^2}{[\text{CH}_2\text{Cl}_2]^2 + K_0[\text{THF}]^2 + K_3[\text{Et}_2\text{O}]^2 + K_7[1,4\text{-dioxane}]^2 + K_2[\text{AcCl}]^2} \quad (6)$$

The rate of tetrahydrofuran disappearance follows from scheme (5):

$$-\frac{d[\text{THF}]}{dt} = 5k_p[{}^5\text{Ac}] \quad (7)$$

The actual concentration of acetyl chloride is, according to Figure 4, expressed by the relationship:

$$[\text{AcCl}] = [\text{AcCl}]_0 / (1 + [\text{AcCl}]_0 3k_d t) = [\text{AcCl}]_0 / c \quad (8)$$

The dependence of tetrahydrofuran rate of disappearance upon measurable parameters is obtained when equations (8) and (6) are used to express equation (7). Since the oligomerization ceases at low conversions the initial

Table 1 Products of tetrahydrofuran oligomerization

System	Product	% of total
THF, AcCl	$\text{CH}_3\text{-}\overset{\text{O}}{\underset{\text{O}}{\text{C}}}\text{-(O+(CH}_2)_4)_3\text{-H}$	66
	$\text{Cl-(CH}_2)_4\text{O-(CH}_2)_4\text{-OH}$	34
THF, EPC	$\text{H-O-CH}_2\text{-CH}_2\text{-}[\text{-O-(CH}_2)_4\text{]}_n\text{-Cl}$	100

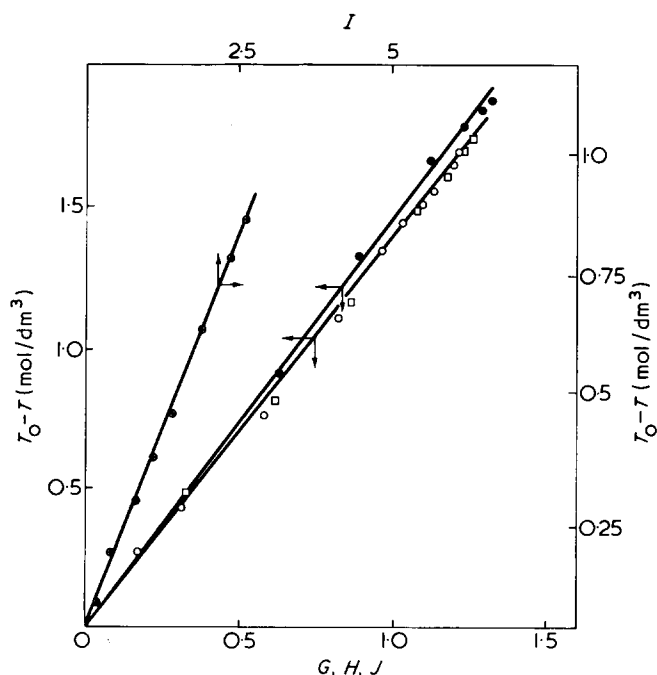


Figure 10 The dependence of difference between initial and actual concentration of tetrahydrofuran as a function of equilibrium and rate constants and time. O, data from curve A, Figure 2, processed according to equation (11) ($G = \{[\text{TiCl}_4]_0 / \alpha [\text{AcCl}]_0\} \times [\arctan \alpha c - \arctan \alpha]$); □, data from curve A, Figure 2, processed according to equation (13) ($H = \{[\text{TiCl}_4]_0 / [\text{AcCl}]_0\} \times (1/\alpha^2)(1 - 1/c)$); ⊕, data from curve D, Figure 2, processed according to equation (15) ($I = \{[\text{TiCl}_4]_0 / k_d \beta\} \times [(\arctan \beta c' / [\text{AcCl}]_0) - (\arctan \beta / [\text{AcCl}]_0)]$); ●, data from curve B, Figure 2, processed according to equation (11) (similarly to curve A) but with modified α :

$$\alpha'^2 = \frac{[\text{CH}_2\text{Cl}_2 + K_0([\text{THF}]^2 + k_7[1,4\text{-dioxane}]^2)}{K_2[\text{AcCl}]_0^2}$$

$$\left(J = \frac{[\text{TiCl}_4]_0}{\alpha' [\text{AcCl}]_0} \times [\arctan \alpha' c - \arctan \alpha'] \right)$$

concentration of tetrahydrofuran can be used instead of the actual concentration.

Oligomerization in dichloromethane. Thus to the first approximation:

$$-\frac{d[\text{THF}]}{dt} = 5k_p[\text{TiCl}_4]_0 \frac{1}{1 + \alpha^2 c^2} \quad (9)$$

$$\alpha^2 = \frac{[\text{CH}_2\text{Cl}_2]^2 + K_0[\text{THF}]_0^2}{K_2[\text{AcCl}]_0^2} \quad (10)$$

The expression for the difference between initial and actual concentration of monomer is obtained by the integration of equation (9):

$$[\text{THF}]_0 - [\text{THF}] = \frac{5k_p}{3k_d} [\text{TiCl}_4]_0 \frac{1}{\alpha [\text{AcCl}]_0} \times [\arctan \alpha c - \arctan \alpha] \quad (11)$$

Taking into account the values of donor numbers of tetrahydrofuran and acetyl chloride⁸ it holds:

$$\alpha^2 c^2 \gg 1 \quad (12)$$

Equation (9) then assumes the form:

$$[\text{THF}]_0 - [\text{THF}] = \frac{5k_p}{3k_d} \frac{[\text{TiCl}_4]_0}{[\text{AcCl}]_0} \frac{1}{\alpha^2} \left(1 - \frac{1}{c} \right) \quad (13)$$

Comparing expressions (11) and (13) the equation $1 - 1/c = \alpha(\arctan \alpha c - \arctan \alpha)$ is obtained; it consists of α and of directly measurable values $[\text{AcCl}]_0$, $3k_d$ and t ; the values of α can be calculated. Knowing K_2 (see ref 5), the value of K_0 can easily be calculated from α .

Oligomerization in the presence of diethyl ether. The values of concentrations of reactants present in the denominator of equation (6) were comparable. Since K_3 is more than an order of magnitude higher than other constants⁵ the expression for ${}^5\text{Ac}$ can be simplified:

$$-\frac{d[\text{THF}]}{dt} = 5k_p[\text{TiCl}_4]_0 \frac{K_2[\text{AcCl}]^2}{K_3[\text{Et}_2\text{O}]^2 + K_2[\text{AcCl}]^2}$$

$$= 5k_p[\text{TiCl}_4]_0 \frac{[\text{AcCl}]_0^2}{\beta^2 c'^2 + [\text{AcCl}]_0^2} \quad (14)$$

Where:

$$\beta = \frac{K_3^{1/2} [\text{Et}_2\text{O}]}{K_2^{1/2}}$$

$$c' = (1 + [\text{AcCl}]_0^4 k_d t)$$

4k_d being directly measurable (see Figure 4).

Integrating equation (14), an expression is obtained in which all values are known from previous measurements and thus it can be used for the verification of derived constants.

$$[\text{THF}]_0 - [\text{THF}] = \frac{5k_p}{4k_d} [\text{TiCl}_4]_0 \frac{1}{\beta} \times \left(\arctan \frac{\beta c'}{[\text{AcCl}]_0} - \arctan \frac{\beta}{[\text{AcCl}]_0} \right) \quad (15)$$

The observed reaction order with regard to tetrahydrofuran follows directly from equation (15). During this measurement the tetrahydrofuran concentration decrease was compensated by the increase in diethyl ether concentration. The latter is accompanied by the decrease in overall rate because of high value of K_3 .

Oligomerization in the presence of 1,4-dioxane. The sum of concentrations of tetrahydrofuran and dioxane was maintained constant. The value of denominator in right hand term of equation (6) will be constant if $K_0 \approx K_7$. The polymerization will be of zero-order with regard to monomer up to relatively high conversions. This was confirmed experimentally.

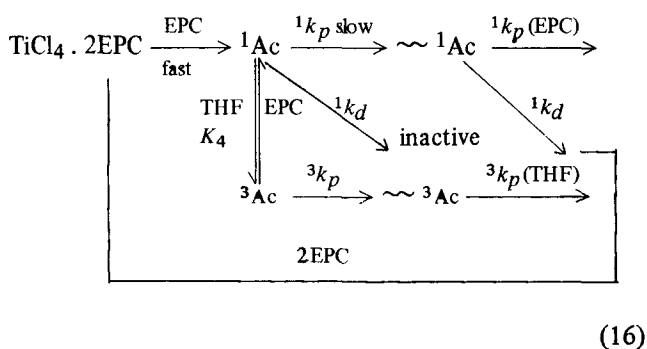
The graphical confrontation of experimental results with expressions derived here is presented in Figure 10.

Table 2 Values of equilibrium and rate constants (other constants have been taken from ref 7)

Constant	Value	Rate constant	$k_p(d) \times 10^3$ (sec ⁻¹)
K_0	1.3	3k_p	0.45
K_4	1.0	5k_p	22.67
K_7	1.3	3k_d	0.20
		4k_d	0.017

Oligomerization of THF in the presence of EPC

Only two kinds of active centres can be involved in this case: $\text{TiCl}_4 \cdot 2\text{EPC} \cdot \text{EPC}$ denoted by ${}^1\text{Ac}$ and $\text{TiCl}_4 \cdot 2\text{EPC} \cdot \text{THF}$ denoted by ${}^3\text{Ac}$. The formation of the latter should obey the following equilibria:



According to the notion ${}^1\text{Ac}$ is transformed to ${}^3\text{Ac}$ by the exchange of epichlorohydrin for tetrahydrofuran (equation 16) and *vice versa*. Therefore the consumption of tetrahydrofuran is indicative of its oligomerization on ${}^3\text{Ac}$ while the reaction of epichlorohydrin involves ${}^1\text{Ac}$. The character of ${}^1\text{Ac}$ has been known from the studies concerning the polymerization of epichlorohydrin⁵. These species are unstable, their activity disappearing with time. Judging from curve shapes in Figure 2 (curves C and E), it seems that ${}^3\text{Ac}$ centres are considerably stable. Let us assume, in the first approximation, that the value of k_d for their disappearance is zero (see also ref 5):

$$\begin{aligned}
 -\frac{d[\text{THF}]}{dt} &= {}^3k_p[{}^3\text{Ac}]_0 \\
 -\frac{d[\text{EPC}]}{dt} &= {}^1k_p[{}^1\text{Ac}] = {}^1k_p[{}^1\text{Ac}]_0 \times \\
 &\quad \exp\left(\frac{{}^1k_d}{{}^1k_p} \frac{[\text{EPC}]_0 - [\text{EPC}]}{[\text{TiCl}_4]_0}\right) \quad (17)
 \end{aligned}$$

The sum of both equations upon integration gives the relationship describing the course of oligomerization (M denotes the sum of monomers):

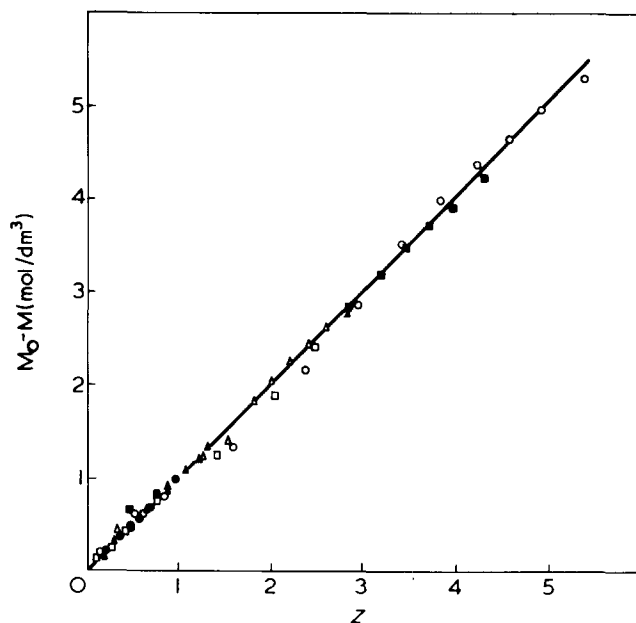
$$\begin{aligned}
 [M]_0 - [M] &= {}^3k_p[{}^3\text{Ac}]_0 t + \frac{{}^1k_p[\text{TiCl}_4]_0}{{}^1k_d} \times \\
 &\quad \ln(1 + {}^1k_d[{}^1\text{Ac}]_0 t) \quad (18)
 \end{aligned}$$

The expression for concentration of ${}^3\text{Ac}$ can be derived from equilibria (1), (3), (16) and (1) in ref 5 taking into account TiCl_4 balance:

$$\begin{aligned}
 [{}^3\text{Ac}] &= [\text{TiCl}_4]_0 \times \\
 &\quad \frac{K_1 K_4 [\text{THF}] [\text{EPC}]}{[\text{CH}_2\text{Cl}_2]^2 + K_0 [\text{THF}]^2 + K_1 [\text{EPC}]^2 + K_3 [\text{Et}_2\text{O}]^2} \quad (19)
 \end{aligned}$$

K_4 is the only unknown in this expression. We do not know of a direct method of its determination. If we presume that the rates of coordination of tetrahydrofuran or epichlorohydrin to the ligands are similar, than $K_4 \approx 1$. When this value is used then $[{}^3\text{Ac}]$ can be calculated from equation (19) (because of low conversions the initial concentrations of monomers can be used instead of actual ones) and 3k_p obtained from equation (18). The agreement between equation (18) and experimental results represented by curves C and E in Figure 2 is shown in Figure 11. The values of constants are summarized in Table 2.

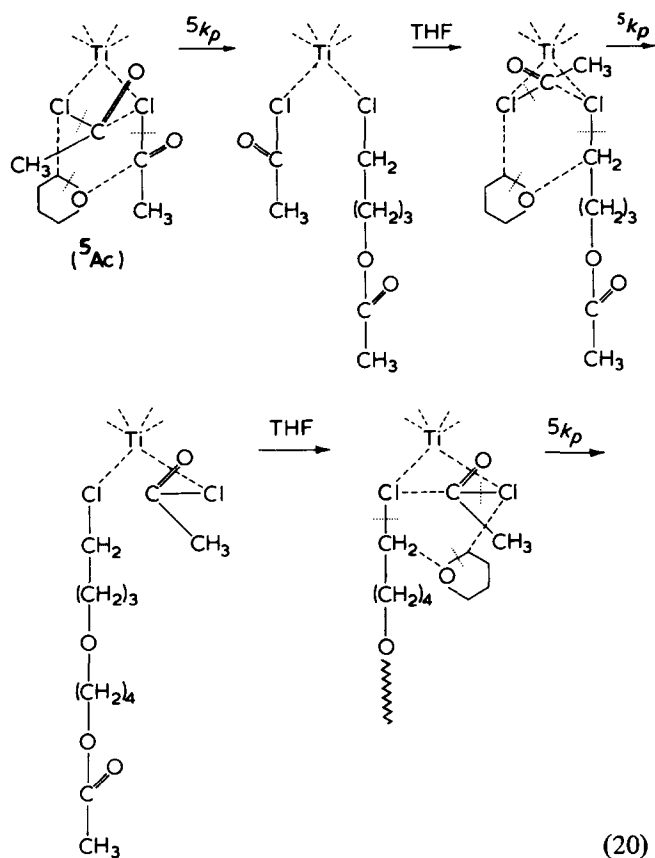
Mechanism. The results of spectral and kinetic studies suggest the mechanism of this reaction. The coordination of acetyl chloride to TiCl_4 via chlorine is not excluded⁹. The oligomerization of tetrahydrofuran in the presence of acetyl chloride can again be visualized as a coordination of monomer to activating ligands:


 Figure 11 The dependence of $M_0 - M$ upon Z (tetrahydrofuran-epichlorohydrin system).

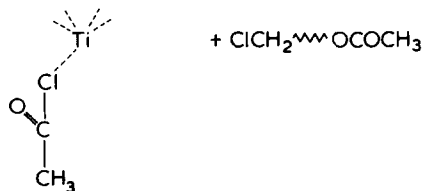
$$M_0 - M = ([\text{THF}]_0 + [\text{EPC}]_0) - ([\text{THF}] + [\text{EPC}]).$$

$$Z = 4k_p[{}^3\text{Ac}]_0 t + \frac{{}^3k_p[\text{TiCl}_4]_0}{{}^3k_d} \ln(1 + {}^3k_d[{}^2\text{Ac}]_0 t).$$

Temperature 293.1K; $\text{TiCl}_4 = 0.5 \text{ mol/dm}^3$; constant concentration of epichlorohydrin, 4 mol/dm^3 ; tetrahydrofuran concentration (mol/dm³): \circ , 8.54; \triangle , 6.1; \oplus , 3.66; \bullet , 1.83. Constant concentration of tetrahydrofuran, 6.1 mol/dm^3 ; epichlorohydrin concentration (mol/dm³): \blacksquare , 5; \blacktriangle , 3; \square , 2

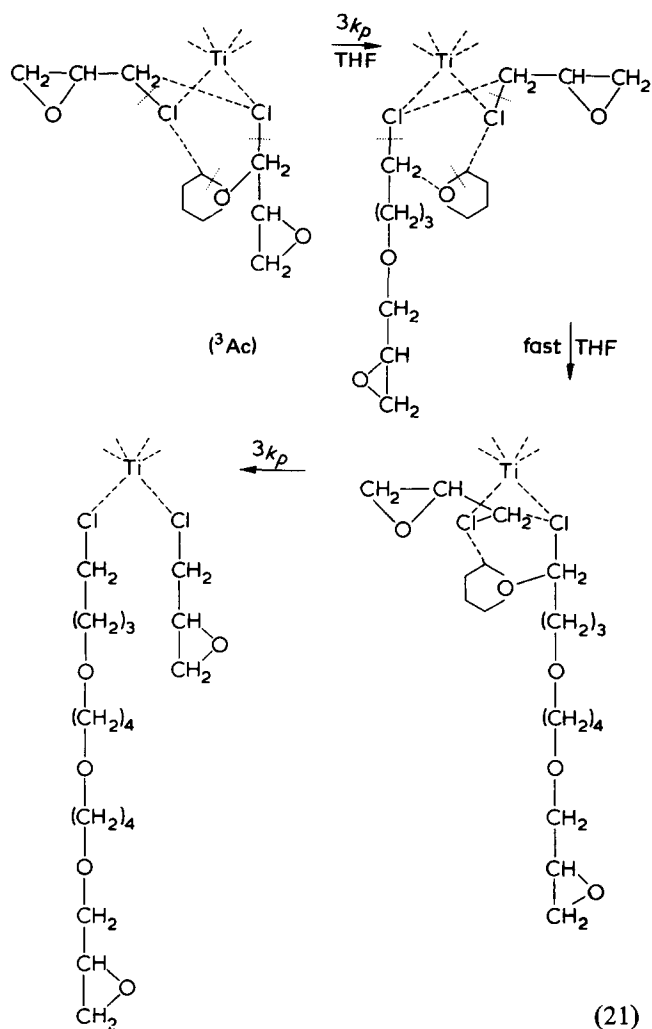


The termination may take place when the growing ligand is split off:



or by coordination of monomer or polymer to the Ti atom via oxygen.

A similar mechanism may be suggested when epichlorohydrin is used as a promotor:



Also in this case the termination occurs probably by splitting off the growing ligand or by coordination of monomer or polymer to titanium via oxygen.

REFERENCES

- 1 Dreyfuss, P. and Dreyfuss, M. P. 'Ring-Opening Polymerization', (Eds K. C. Frisch and S. L. Reegen), Marcel Dekker, New York, 1969, pp 129
- 2 Kobayashi, S., Danda, H. and Saegusa, T. *Macromolecules* 1974, 7, 415
- 3 Dreyfuss, P. and Dreyfuss, M. P. *Adv. Polym. Sci.* 1967, 4, 528
- 4 Lyudwig, E. B., Rozenberg, B. A., Zvereva, T. M. and Medvedev, S. S. *Vysokomol. Soedin.* 1965, 7, 269
- 5 Kučera, M., Zahradníčková, A. and Majerová, K. *Polymer* 1976, 17, 519
- 6 Meerwein, H., Delfs, D. and Morshel, H. *Angew. Chem.* 1960, 72, 927
- 7 Zahradníčková, A. *Thesis* Research Institute of Macromolecular Chemistry, Brno (1974)
- 8 Gutmann, V. 'Coordination Chemistry in Non-Aqueous Solutions', Springer Verlag, Vienna, 1968, p 19
- 9 Chevrier, B. and Weiss, R. *Angew. Chem.* 1974, 86, 1, 12

Coordinate polymerization of heterocycles: 3. Oligomerization of tetrahydrofuran induced by TiCl_4 in the presence of acetyl chloride and epichlorohydrin

M. Kučera, A. Zahradníčková, and K. Majerová

Research Institute of Macromolecular Chemistry, 656 49 Brno, Czechoslovakia

(Received 2 June 1975; revised 28 January 1976)

When a strong and a weak donor are present as promoters in the oligomerization of tetrahydrofuran then under certain conditions a pronounced stabilization of active centres occurs. The formation of centres is governed by equilibrium reactions during which the monomer and promoters are coordinated to Ti atom. The coordination ability is determined by the donor numbers. The dependence of oligomerization reaction rate on the molar fraction of tetrahydrofuran exhibits a minimum. At the concentration conditions corresponding to this minimum, especially in the presence of diethyl ether, the active centres do not lose their reactivity and the oligomerization becomes stationary to high conversions. The results suggest that the classification of coordinate polymerizations to cationic and anionic coordinate polymerizations is meaningless. Coordinate polymerizations belong to a separate group of polyreactions similarly as e.g. radical polymerizations.

INTRODUCTION

In our previous communications we analysed the oligomerization of epichlorohydrin (EPC) and tetrahydrofuran (THF) in the presence of acetyl chloride (AcCl) or epichlorohydrin. All these polymerizations are strongly non-stationary. In the presence of diethyl ether (Et_2O) and at low concentrations of epichlorohydrin the constants controlling the disappearance of activity of centres are decreasing. The question arises whether a suitable combination of conditions, namely the varying composition of the reaction mixture, cannot preclude the destruction of centres.

It is commonly believed, with a few exceptions¹ that the tetrahydrofuran ring can be opened only via a cationic process. The processes which have been shown to proceed through the coordinate mechanism are usually called cationic² or anionic (e.g. Ziegler–Natta polymerization of olefins³) coordinate processes. In the systems which we have studied so far no polymerization active free ions have been observed⁴. The strong donors which were present in the studied media would act as catalyst poisons in the case of Ziegler–Natta polymerizations.

Therefore, it seems useful to compare both cationic and anionic coordinate mechanisms and to decide how justified is the use of the attributed 'cationic' or 'anionic' in the case of coordinate polymerizations.

EXPERIMENTAL

The purification of chemicals, the method of following the course of oligomerization, measuring electric conductivity, identification of intermediates and reaction products by spectral and g.l.c. methods have been described in our previous papers⁴. The chlorine content in polymers isolated from the reaction mixture was determined by elemental analysis.

RESULTS

An example of tetrahydrofuran oligomerization in the presence of a constant amount of acetyl chloride and various concentrations of epichlorohydrin is shown in *Figure 1* where contraction is plotted against time. In all cases the contraction is directly proportional to conversion⁴. The

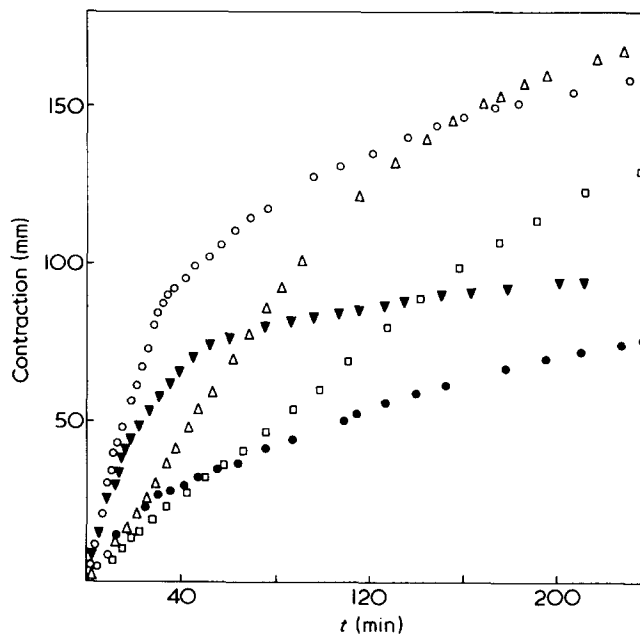


Figure 1 Contraction curves of tetrahydrofuran oligomerization in the presence of both promoters. Temperature 293.1K; concentration of components (mol/dm^3): $\text{TiCl}_4 = 0.5$; $\text{THF} = 6.1$; $\text{AcCl} = 2.5$. Concentration of EPC (mol/dm^3): Δ , 0.5; \circ , 0.25; \square , 1; ∇ , 3; \bullet , 2. The proportionality constant (mm^{-1}) for (Δ) and (\circ) 0.2×10^{-2} ; (\square) 0.22×10^{-2} ; (∇) 0.29×10^{-2} ; (\bullet) 0.25×10^{-2}

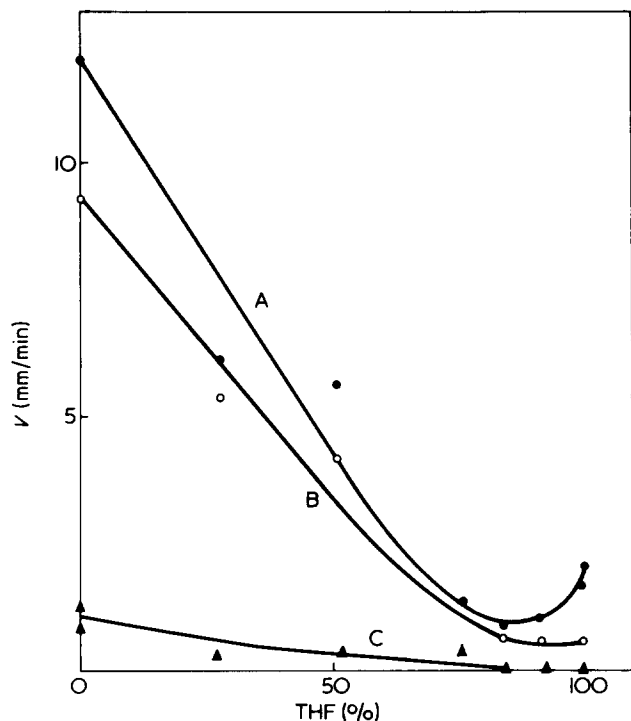


Figure 2 Dependence of initial rate on mol % tetrahydrofuran in monomer mixture. Temperature 293.1K; concentration of components (mol/dm³): TiCl₄ = 0.5; AcCl = 2.5; Et₂O = 2.9. Polymerization systems: A, THF-EPC-AcCl; B, THF-EPC-AcCl-Et₂O; C, THF-EPC

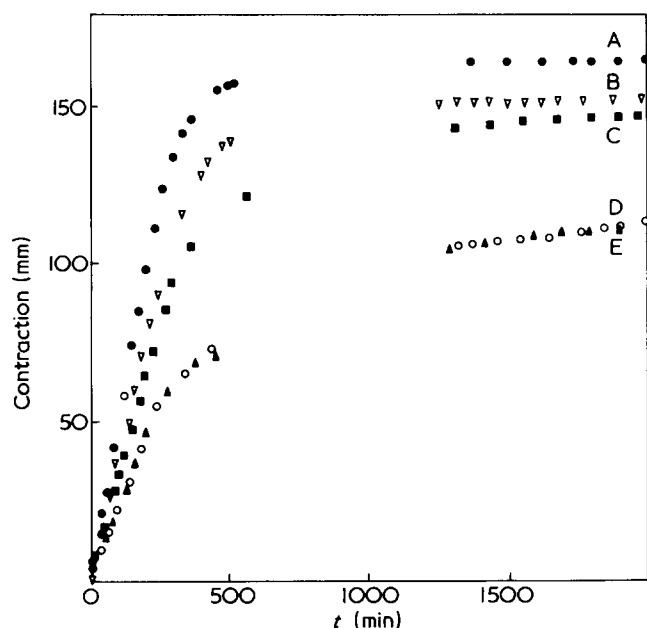


Figure 3 Stationary long time polymerizations of THF-EPC-AcCl-Et₂O system. Temperature 293.1K; concentration of components (mol/dm³): TiCl₄ = 0.5; AcCl = 2.5; EPC = 1. Concentration of THF and Et₂O (mol/dm³): A, 7.32 and 0.97; B, 6.1 and 1.94; C, 3.66 and 3.88; D, 1.83 and 5.34; E, 1.83 and 5.34

dependence of initial rate on the percentage of tetrahydrofuran in the mixture of monomers X_{THF} exhibits a minimum (Figure 2).

The shape of contraction curves is suggestive of a considerable influence of the reaction mixture composition upon the stationarity of oligomerization. This influence is in accordance with previous observations of the deactivation constant (k_d) changes⁴. If this influence is enhanced

by the selection of component concentration and by additions of diethyl ether then k_d may be practically zero and the oligomerization will proceed at constant concentration of centres. Such stationary oligomerizations are shown in Figure 3.

Under the conditions described above both the internal and external order of reaction with regard to tetrahydrofuran is equal to zero; the oligomerization rate is directly proportional to the concentration of acetyl chloride, being in reciprocal dependence upon diethyl ether concentration. As in previous observations⁴ the presence of polymerization active free ions in the oligomerizing system has not been detected.

The quantitative analysis of monomers has been carried out using gas chromatography. The chromatograms revealed the presence of another two components the elution times of which are identical to those of CH₃COO(CH₂)₄Cl and Cl-(CH₂)₄-OH (Figure 4).

N.m.r. spectroscopy of solid oligomerization products (Figure 5) enabled us to establish the concentration ratio of tetrahydrofuran/epichlorohydrin, the kind of monomer

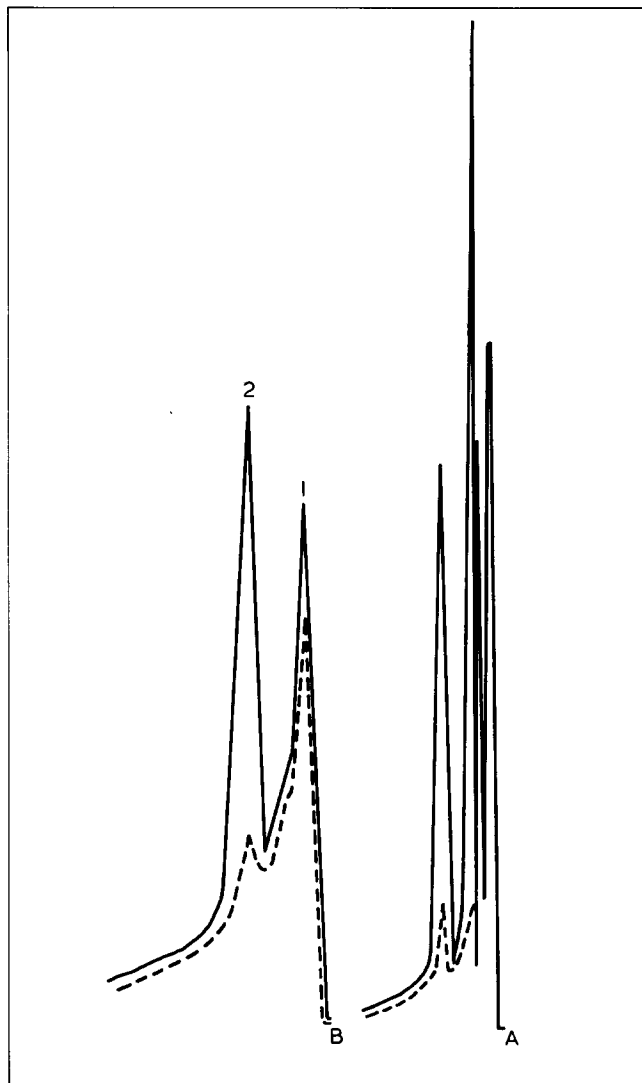


Figure 4 Chromatograms of monomer phase. Concentration of components (mol/dm³): 1, THF = 6.1; EPC = 3; AcCl = 2.5; 2, THF = 3.66; EPC = 3; AcCl = 2.5; Et₂O = 2.4. Temperature: A, 313.1K (6 min); B, 413.1K

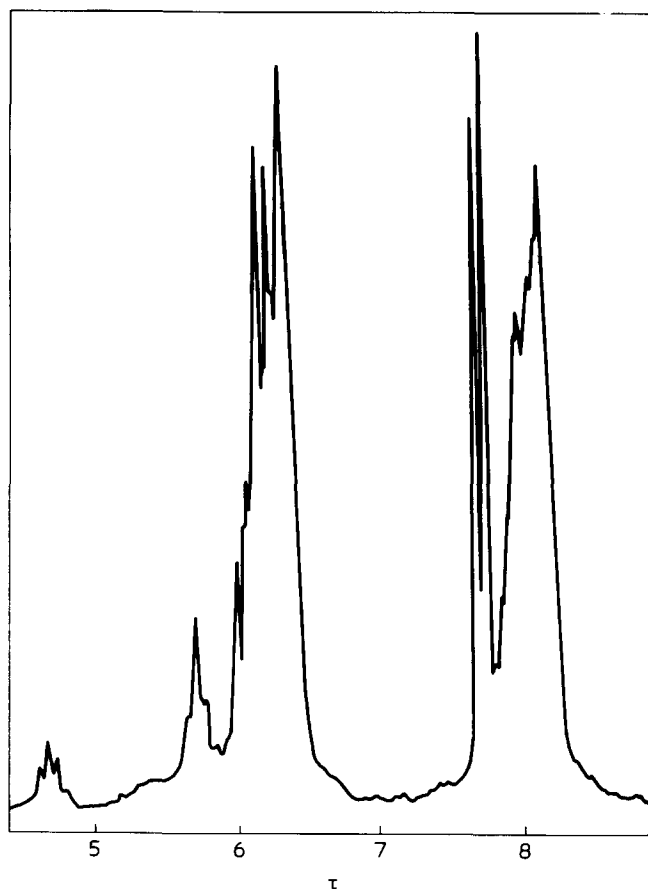
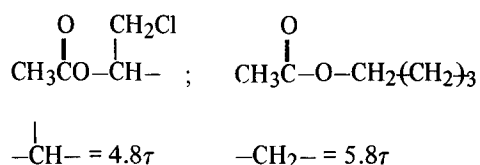


Figure 5 N.m.r. spectra of polymers obtained from tetrahydrofuran-epichlorohydrin-acetyl chloride system. Temperature of polymerization 293.1K, temperature of measurement 298.1K. Concentrations of components (mol/dm³): TiCl₄ = 0.5; THF = 6.1; EPC = 1; AcCl = 2.5

bonded to the acetyl group:



and an approximate number of bonded monomer units. The percentage of epichlorohydrin and the band intensity of C=O and -OH groups was measured by means of i.r. spectroscopy (Figure 6). The -OH groups content was determined indirectly from i.r. spectra of polymers containing additions of 1,4-chlorobutanol. There is a shift of the -OH band from 3450 cm⁻¹ towards 3350 cm⁻¹ which increases with the concentration of chlorobutanol (H-bonds). The areas of absorption bands, measured planimetrically, when inserted into the Lambert-Beer plot gave a straight line dependence. The extrapolation of the linear dependence to the origin enabled us to calculate the concentration of -OH end-groups as a percentage of added 1,4-chlorobutanol. These values were in good agreement with those obtained by elemental analysis, molecular weight measurements and n.m.r. spectroscopy.

The spectra of polymers prepared in the 'dry' system on the vacuum line were not different from those of polymers prepared in the presence of 200 mmol/dm³ H₂O. Thus the -OH groups observed in chlorohydrin were probably formed from ester CH₃CO-O- groups when alcoholic C₂H₅ONa,

containing water, was added to stop the reaction. In some cases, however, the -OH bands were observed in spite of the absence of acetyl chloride in the system. Thus the active centres containing epichlorohydrin can give -OH groups by alkaline fission of the oxirane ring taking place during the neutralization of the reaction mixture.

The approximate composition of the polymers isolated from the systems was deduced on the bases of the data presented above and is shown in Table 1.

DISCUSSION

The change in tetrahydrofuran-epichlorohydrin ratio in the presence of acetyl chloride leads to radical changes in the course of oligomerization. The oligomerization rate in the presence of a small amount of epichlorohydrin is even lower than in the absence of epichlorohydrin, the decrease of reaction rate with time being, however, small. The excess of epichlorohydrin exhibits similar effects as those observed during the polymerization of epichlorohydrin in the presence of acetyl chloride.

It follows from Figure 2 that it would be misleading to consider observed overall reaction orders in terms of molecularity. Moreover, the dielectric constant is decreasing with the increasing abscissa. Also the attempt to find a relationship describing these processes would be of no practical importance. The behaviour of systems at a certain concentration ratio of tetrahydrofuran and epichlorohydrin can, however, be analysed. At $X_{\text{THF}} = 0$ and $X_{\text{THF}} = 100$ the relationship derived in our previous papers⁴ will be valid. The most interesting, however, is the region around the minimum where the oligomerization exhibits a stationary behaviour.

In the systems containing both promoters the following centres may be present: [¹Ac], [⁵Ac], [³Ac] and TiCl₄.

EPC · AcCl, the complex from which [⁴Ac] results by a fast

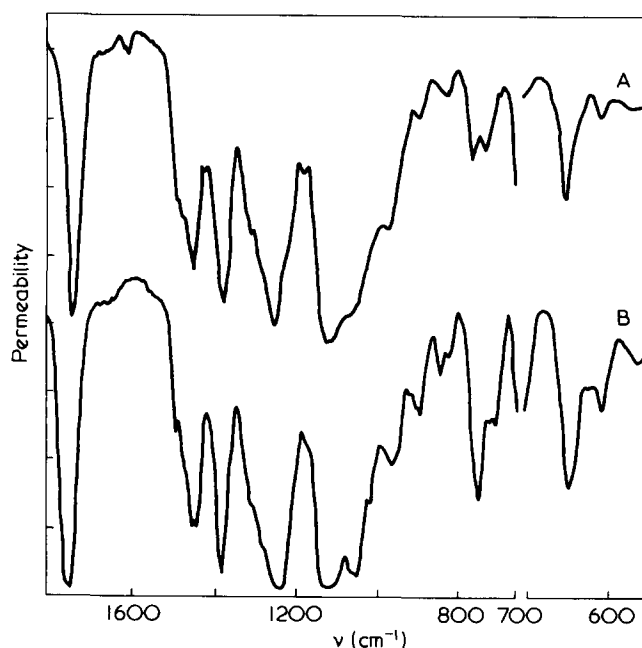
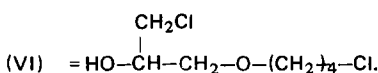
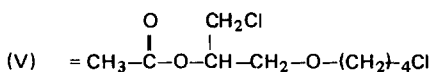
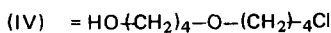
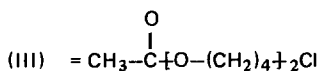
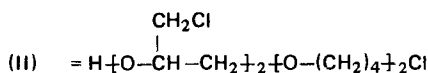
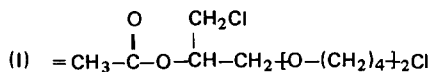


Figure 6 I.r. spectra of polymers isolated from polymerization systems containing tetrahydrofuran-epichlorohydrin-acetyl chloride. Temperature of polymerization 293.1K, temperature of measurement 308 ± 0.5K. Concentration of components (mol/dm³): TiCl₄ = 0.5; EPC = 3; AcCl = 2.5; (A) THF-EPC-AcCl-Et₂O: THF = 3.66, Et₂O = 2.4; (B) THF-EPC-AcCl: THF = 6.1

Table 1 The properties of polymers formed in systems containing 6.1 mol/dm³ tetrahydrofuran, 0.5 mol/dm³ AcCl + Y + CH₂Cl₂ (filling up to the mark); oligomerization temperature 293.1K

No.	Y (mol/dm ³)	Cl (%)	\bar{M}_n	Formula	Content (%)
1	3 EPC	27.9	340	(I)	50
				(II)	50
2	1 EPC	21.5	233	(I)	33
				(III)	50
				(IV)	17
3	1 EPC + 1.9 Et ₂ O	23.4	200	(III)	50
				(V)	20
				(IV)	15
				(VI)	15

Where:



addition of tetrahydrofuran. The presence of ¹Ac need not be considered in the region of the minimum because even epichlorohydrin alone does not polymerize at corresponding concentration. Therefore:

$$-\frac{d[\text{THF}]}{dt} = 5k_p[{}^5\text{Ac}] + 3k_p[{}^3\text{Ac}] + 4k_p[{}^4\text{Ac}] \quad (1)$$

The concentration of both ⁵Ac and ³Ac can be determined⁴. In order to determine the value of ⁴Ac a following equilibrium is considered:



The constant K_6 is not directly accessible. It can be estimated from the values of K_1 and K_2 ; to the first approximation the value 2×10^{-2} was used. In simple cases the ⁴Ac can be expressed as:

$$[{}^4\text{Ac}] = \frac{[\text{TiCl}_4]_0 K_1 K_6 [\text{EPC}] [\text{AcCl}]}{[\text{CH}_2\text{Cl}_2]^2 + K_0 [\text{THF}]^2 + K_1 [\text{EPC}]^2 + K_2 [\text{AcCl}]^2 + K_3 [\text{Et}_2\text{O}]^2 + K_1 K_6 [\text{EPC}] [\text{AcCl}]} \quad (3)$$

When the values of ⁵Ac and ³Ac (see ref 4) are inserted and ⁴Ac from equation (3)*, neglecting small

* At low conversions the value of [THF] can be considered as [THF]₀ and [EPC] as [EPC]₀. The actual concentration of acetyl chloride was expressed using the previously verified expression⁴: [AcCl] = [AcCl]₀ / (1 + [AcCl]₀³k_dt).

terms in denominators, then a following equation is obtained upon integration:

$$[\text{THF}]_0 - [\text{THF}] = [\text{TiCl}_4]_0 \left\{ \frac{([\text{EPC}]_0) / (K_0 [\text{THF}]_0^2 + K_1 [\text{EPC}]_0^2)}{[{}^3k_p K_1 K_4 [\text{THF}]_0 + {}^4k_p K_1 K_6 [\text{AcCl}]_0] t + [{}^5k_p K_2^{1/2} / ({}^3k_d K_0^{1/2} [\text{THF}]_0)} \right\} \left[\arctan (K_0^{1/2} [\text{THF}]_0) (1 + [\text{AcCl}]_0^3 k_d t) / (K_2^{1/2} [\text{AcCl}]_0) - \arctan (K_0^{1/2} [\text{THF}]_0) / (K_2^{1/2} [\text{AcCl}]_0) \right] \quad (4)$$

Equation (4) appears to be very complicated. All quantities are, however, known, the value of ⁴k_p being the only exception. The agreement of experimental results, represented by curves in Figure 4, with the interpretation according to equation (4) is apparent from Figure 7.

The rate of oligomerization becomes constant till high conversions when diethyl ether is present in the system (see Figure 3). The term $K_3 [\text{Et}_2\text{O}]^2$ in the denominator of equation (3) will outweigh other terms in most cases so that equation (4) assumes the form:

$$[\text{THF}]_0 - [\text{THF}] = [\text{TiCl}_4]_0 \left\{ \frac{[\text{EPC}]_0}{K_0 [\text{THF}]_0^2 + K_1 [\text{EPC}]_0^2 + K_3 [\text{Et}_2\text{O}]^2} \times [{}^3k_p K_1 K_4 [\text{THF}]_0 + {}^4k_p K_1 K_6 [\text{AcCl}]_0] t + [{}^5k_p K_2^{1/2} / ({}^3k_d K_3^{1/2} [\text{Et}_2\text{O}])] \times \left[\arctan \frac{K_3^{1/2} [\text{Et}_2\text{O}] (1 + [\text{AcCl}]_0^3 k_d t)}{K_2^{1/2} [\text{AcCl}]_0} - \arctan \frac{K_3^{1/2} [\text{Et}_2\text{O}]_0}{K_2^{1/2} [\text{AcCl}]_0} \right] \right\} \quad (5)$$

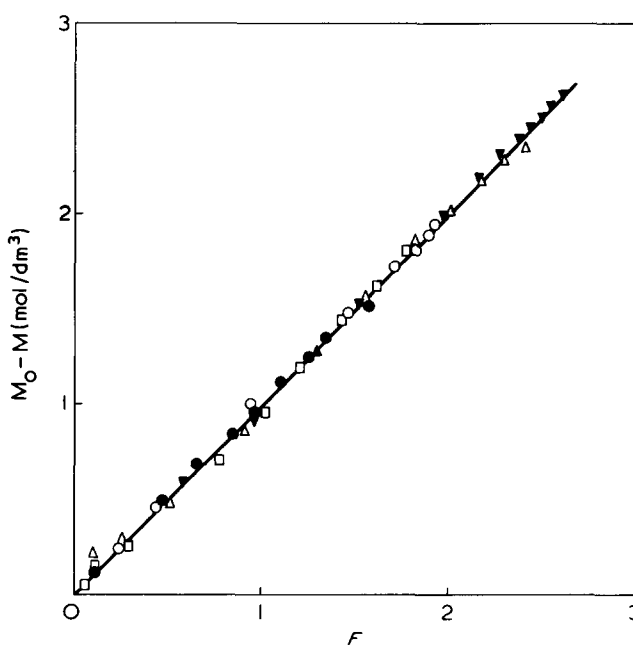
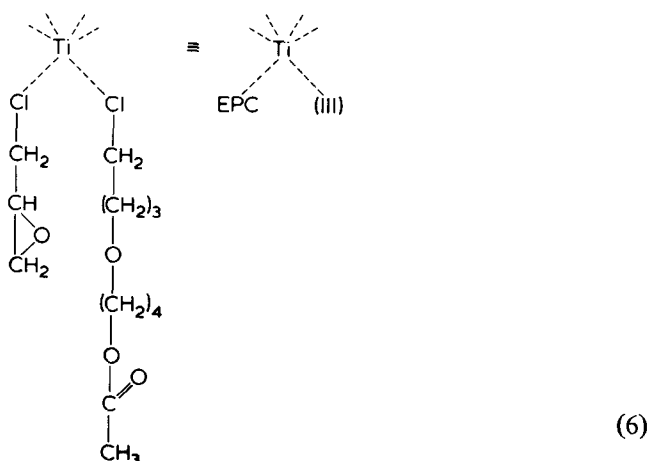
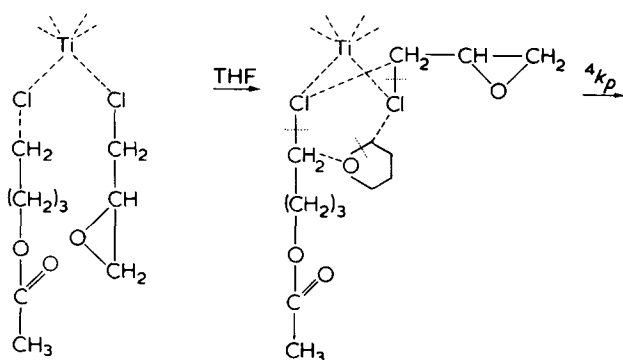
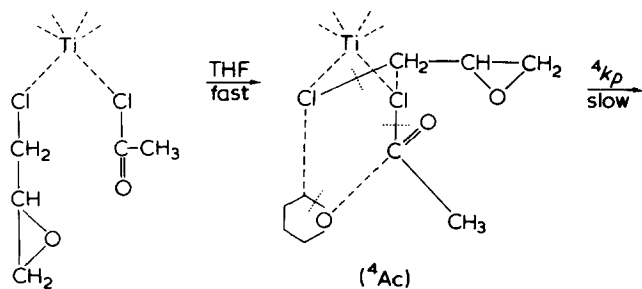


Figure 7 Dependence of $M_0 - M$ on F . $M_0 - M = ([\text{THF}]_0 + [\text{EPC}]_0) - ([\text{THF}] + [\text{EPC}])$. $F =$ right hand side of equation (4). The designation of point corresponds to Figure 1

The agreement between experimental data (Figure 3) and equation (5) is also satisfactory and is shown in Figure 8.

The analyses have revealed that more than 85% of the products were formed on ⁵Ac and ⁴Ac centres containing AcCl. The oligomerization on ⁴Ac centres is again visualized as a mutual substitution of ligands to which tetrahydrofuran is coordinated:



Another explanation accounting for the presence of products (II) and (VI) (see Table I) is offered by scheme (21) in a previous paper⁴.

The rearrangement of the complex following a relatively fast coordination of tetrahydrofuran is the rate controlling step of this reaction. The minimum reaction rate observed when changing the tetrahydrofuran–epichlorohydrin ratio (Figure 2) is due to the varying concentration of individual active centres with different rate controlling steps. The role of diethyl ether will probably lie in its ability to lower the equilibrium concentration of (⁵Ac) centres by displacing acetyl chloride from complexes. The lowering of concentration of centres whose activity is

diminishing or their complete elimination will direct the process to a kinetically stationary region. The termination of chain growth may be effected either by a detachment of the growing ligand (e.g. product (III) from Table I) or by coordination of the heterocycle or diethyl ether (or the product) to the Ti atom via oxygen. The rate constant of the rate controlling step of stationary oligomerization was determined on the basis of experimental data: ${}^4k_p = 0.04$ (sec^{-1}) at 293.1K.

It is practically impossible to meet the requirement of having only one variable when studying the behaviour of systems containing various amounts of the monomer. The quality of the medium is changing in those categories which are difficult to be assessed quantitatively (polarity, solvation ability, etc.). It is thus difficult to compare the values of k_p and k_d obtained at various concentration ratios of individual components. The dependence of k_p and k_d (obtained under a variety of conditions in this and previous works⁴) upon the reciprocal of dielectric constant indicates that such a comparison is feasible (Figure 9). It follows from the figures that: (a) the values of 4k_p and 5k_p are identical as to their magnitude and dependence on the dielectric constant; (b) the same as above will hold for 2k_d , 3k_d and 5k_d ; (c) the increasing dielectric constant causes the increase in k_p only in the case of epichlorohydrin oligomerization.

The rate of rearrangement of ⁵Ac and ⁴Ac during the oligomerization of tetrahydrofuran will be equal. Diethyl ether has no effect on the rate of disappearance of ²Ac during the epichlorohydrin oligomerization. In the polymerization of tetrahydrofuran, however, it acts as a strong retarder of centre disappearance.

CONCLUSION

The studied oligomerizations of tetrahydrofuran and epichlorohydrin are examples of coordinate polymerizations. It* seems that the different features in the reaction mech-

* In our opinion the active centre has its origin in the coordination of the monomer to activating ligands.

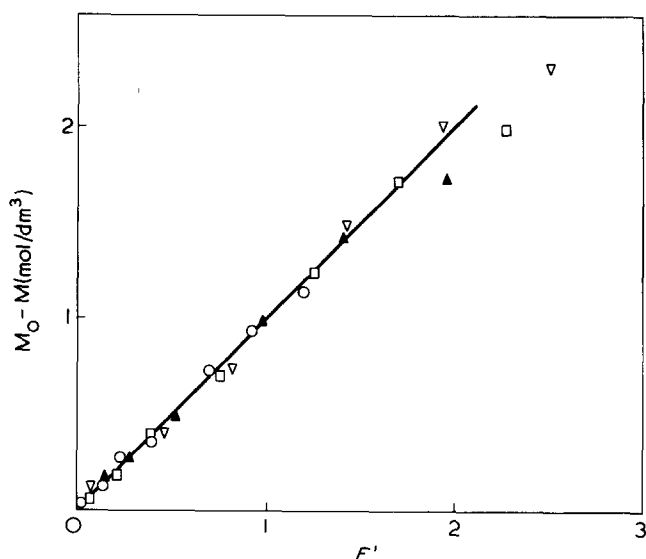


Figure 8 Dependence of M_0-M on F' (system THF–EPC–AcCl–Et₂O). $M_0-M = ([\text{THF}]_0 + [\text{EPC}]_0) - ([\text{THF}] + [\text{EPC}])$. F' = right hand side of equation (5). Temperature 293.1K, component concentration in (mol/dm^3): $\text{TiCl}_4 = 0.5$; $\text{AcCl} = 2.5$; $\text{EPC} = 1$. Concentration of THF and Et₂O respectively (mol/dm^3): \circ , 1.8 and 5.35; \blacktriangle , 3.6 and 3.88; \square , 6.1 and 1.94; ∇ , 7.3 and 0.97

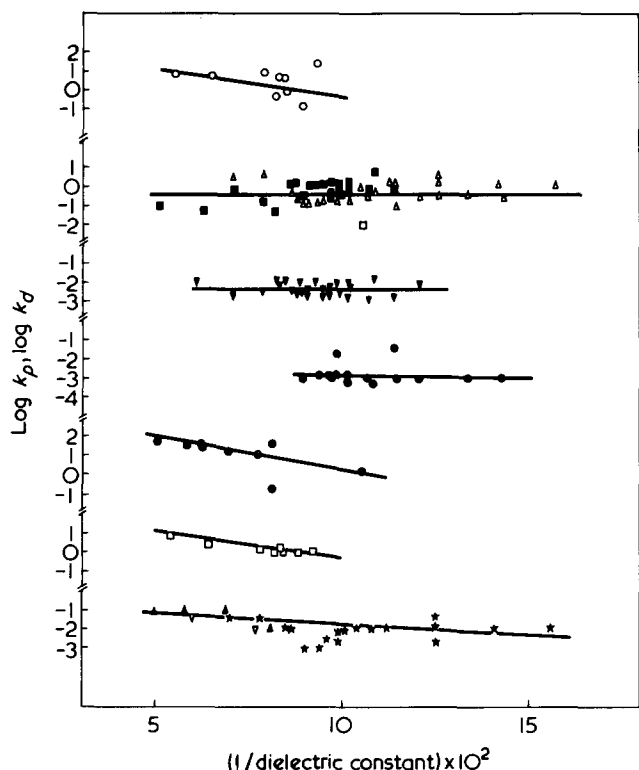


Figure 9 Dependence of k_p and k_d on the dielectric constant EPC system: \square , 1k_p ; \circ , 1k_d . System EPC-AcCl: \oplus , 2k_p ; \blacktriangle , 2k_d ; ∇ , 5k_d . System THF-AcCl: \triangle , 5k_p ; \star , 3k_d ; \bullet , 4k_d . System THF-EPC: \blacktriangledown , 3k_p . System THF-EPC-AcCl: \blacksquare , 4k_p

anism, when comparing with Ziegler–Natta anionic coordinate polymerizations³, may be accounted for by the basicity of donors (monomers). Strong donors, which act as catalyst poisons in Ziegler–Natta polymerization, may, in our case, participate in the formation of ligand sphere of the Ti atom. We believe that it is of no advantage to distinguish between ‘anionic’ and ‘cationic’ coordinate mechanism. This opinion is in agreement with conclusions of Italian authors who examined the Ziegler–Natta polymerization⁵.

According to our notions the coordinate polymerizations belong to an independent class of polymerizations comparable e.g. with the class of radical polymerizations.

REFERENCES

- 1 Szwarz, M. ‘Carbanions, Living Polymers and Electron-Transfer processes’, Interscience, New York, 1968, p 658
- 2 Colclough, R. O. and Wilkinson, K. *J. Polym. Sci. (C)* 1963, 4, 331
- 3 Boor, J. Jr. *Macromol. Rev.* 1967, 2, 115; *Ind. Eng. Chem. Prod. Res. Dev.* 1970, 9, 437; Rodrigues, L. A. M. and van Looy H. M. *J. Polym. Sci.* 1966, 4, 1951, 1971 and previous works of these authors.
- 4 Kučera, M., Zahradníčková, A. and Majerová, K. *Polymer* 1976, 17, 519, 528
- 5 Cesca, S., Bertolini, G., Santi, G. and Roggero, A. *J. Macromol. Sci. (A)* 1973, 7, 475
- 6 Zahradníčková, A. *Thesis* Research Institute of Macromolecular Chemistry, Brno (1974)

Influence of intrachain double bonds on the properties of solution grown single crystals of polyethylene

C. Mancarella, E. Martuscelli and M. Pracella

Laboratorio di Ricerche su Tecnologia dei Polimeri e Reologia, CNR, 80072 Arco Felice (Napoli), Italy
(Received 1 December 1975)

The influence of intrachain *trans* double bonds, statistically distributed along a polyethylene chain, on the structure and behaviour of chain-folded single crystals has been studied. The dependence upon the percentage of double bonds of dissolution and thermal properties, external crystal habit, X-ray diffraction in the wide- and low-angle regions, of solution grown single crystals of ethylene-butadiene copolymers may be interpreted by assuming that a certain amount of $-\text{CH}_2-\text{CH}=\text{CH}-\text{CH}_2-$ units are incorporated in the lattice as defects. The results of the bromination of single crystals of a sample of ethylene-butadiene copolymers show that about the 56% of double bonds, not accessible to bromine, are situated not on the fold surface but in the inner part of the crystals.

INTRODUCTION

The effect of chemical groups statistically spaced along a polymer chain is of considerable interest. The properties of linear polyethylene may be drastically changed by introducing along the chain a small amount of units with different chemical structure. Modifications may be carried out through various chemical reactions of which chlorination and chlorosulphonation are of technological importance because the derivatives constitute a series of thermoplastic and elastomeric materials¹.

Foreign units may also be introduced along the chain of polyethylene by means of reaction of copolymerization. The properties of copolymers, obtained by reaction of ethylene and α -olefins and ethylene and carbon monoxide have been extensively studied by the authors². In a previous paper³ the effect of intrachain double bonds on the crystallization of polyethylene from the melt was investigated. *Trans* double bonds were statistically introduced in the chain of polyethylene by means of a reaction of copolymerization of ethylene and butadiene⁴. We focused our attention on copolymers with low butadiene/ethylene ratios since they can have very important technological applications different from those of linear polyethylene.

In the present paper we are mainly interested in investigating the influence of the concentration of *trans* double bonds on the crystallization of polyethylene from dilute solution; therefore the morphology, the structure, the melt properties and the bromination of solution grown single crystals of ethylene-butadiene copolymers have been examined.

EXPERIMENTAL

Materials

The experiments reported here were carried out on unfractionated samples of random ethylene-butadiene copolymers (1,4-enchainment) and of linear polyethylene (Vestolen 6013 and Marlex 6009).

The copolymers were synthesized in the laboratories of Eni-Snam Progetti, Milano (Italy) by using vanadium based catalysts. This process of polymerization leads to

samples of copolymers with a rather sharp distribution of molecular weight⁴.

The composition of the polymer samples, determined by i.r. and some melt rheological properties related to the molecular weight and to their distribution are reported in Table 1. Vestolen and ethylene-butadiene copolymers are comparable in both distribution and average molecular weight whereas Marlex has a higher average molecular weight. The presence of an appreciable number of butadiene units in *cis* configuration, in the chains of copolymers, is excluded by i.r. analysis.

Solution grown single crystals

Single crystals of linear polyethylene and of ethylene-butadiene copolymers were isothermally grown from 0.08% w/w xylene solutions. Crystallization temperatures T_c of 75°, 80° and 85°C were used. The self-seeding technique⁵ was applied throughout. The crystallization conditions used are summarized in Table 2, where precrystallization, T_{pc} , apparent dissolution T_d and seeding temperatures T_s are indicated together with the crystallization temperature T_c . For all preparations the same rate of heating to T_s and the same time of dissolution at T_s of 15 min were used. The external habit of single crystals was examined by means of a Philips EM 300 transmission electron microscope. Low-angle X-ray diffraction patterns of dried orien-

Table 1 Composition, melting flow index (MFI) and viscosity-average molecular weight of samples of ethylene-butadiene copolymers

Sample	Composi- tion (mol % buta- diene)	MFI _{2,16} (g/10 min)	MFI _{21,6} (g/10 min)		Viscosity average molecular weight
			MFI _{2,16} (g/10 min)	MFI _{21,6} (g/10 min)	
Marlex 6009	0.0	0.85	—	—	128 000
Vestolen 6013	0.0	2.0	30	—	80 000
EB1 copolymer	0.7	3.0	20	—	75 000
EB2 copolymer	1.0	2.6	20	—	70 000
EB3 copolymer	1.7	3.0	22	—	75 000
EB4 copolymer	2.85	3.0	34	—	75 000

^a In decalin at 135°C.

Table 2 Crystallization conditions used to grow from solution single crystals of ethylene-butadiene copolymers and of linear polyethylene (see text for explanation)

Sample	Solution concentration, C (% w/w)	T_{pc} ($^{\circ}$ C)	T_D ($^{\circ}$ C)	T_s ($^{\circ}$ C)	T_c ($^{\circ}$ C)
Marlex 6009	0.08	60	98.5	99.5-101.5-102.5-103.5	75,80,85
Vestolen 6013	0.08	60	98.5	99.5-101.5	75,80,85
EB1	0.08	60	96	97-99-100-101	75,80,85
EB2	0.08	60	95	96-98-99-100	75,80,85
EB3	0.08	60	94	95-97-98-99-100	75,80,85
EB4	0.08	60	93	94-96-97-98-100	75,80,85

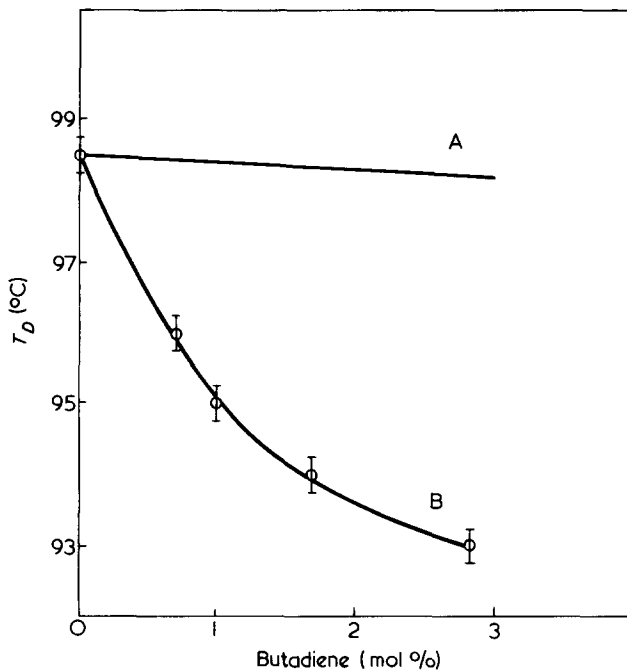


Figure 1 A, Dissolution temperature calculated according to the Flory equation (see text); B, variation of the apparent dissolution temperature of single crystals of polyethylene and of ethylene-butadiene copolymers as function of the composition

ted mats of single crystals were recorded by using a pinhole collimated Rigaku-Denki camera. The X-ray diffractions patterns, in the wide-angle region, were recorded by means of a Philips 1050/25 diffractometer using the Cu α radiation.

The density of single crystals was measured by flotation at 29 $^{\circ}$ C. Melting temperature and apparent enthalpy of fusion were determined with a Perkin-Elmer DSC-2 by using standard methods².

Bromination of single crystals

Crystals suspended in xylene were exchanged by 10 or 11 washes into CCl₄. The addition of bromine to the double bonds of sample EB4 of ethylene-butadiene copolymers was accomplished by adding 2 ml of a solution of bromine (in CCl₄, 1% by volume) to a suspension of single crystals (containing about 100 mg of polymer in 200 ml of CCl₄). The reaction proceeded in the dark at 0 $^{\circ}$ C. Time zero was taken as the instant of mixing, and samples (50 ml) were taken at appropriate intervals of time. The samples were rapidly filtered and the brominated single crystals were washed with distilled acetone to remove any traces of free bromine. The percentage of double bonds brominated was determined by i.r. absorption using a Perkin-Elmer 257 spectrophotometer.

RESULTS AND DISCUSSION

Dissolution and morphology of single crystals

The apparent dissolution temperature, T_D , of single crystals of ethylene-butadiene copolymers, defined as the clearing point of suspensions, is reported in Figure 1, where B is plotted against % butadiene. The same precrystallization temperature of 60 $^{\circ}$ C in dilute xylene and the same concentration were used for all samples. As shown in Figure 1, by increasing the butadiene content in the chains, crystals with markedly lower stability are obtained.

According to the theory of Flory⁶ the dependence of T_D on the concentration of crystallizable units in a random copolymer is given by:

$$\frac{1}{T_D} - \frac{1}{T_D^0} = -\frac{R}{\Delta H_F} \ln N \quad (1)$$

In equation (1) T_D^0 is the dissolution temperature of the pure homopolymer, N the mole fraction of crystallizable units and ΔH_F the melting enthalpy per mole of the homopolymer repeating unit. Equation (1) can be used for elucidating the dissolution temperature depression of single crystals of ethylene-butadiene copolymers. The value of T_D^0 theoretically calculated by equation (1), assuming for T_D^0 the experimental value of 98.5 $^{\circ}$ C and $\Delta H_F = 970$ cal/mol CH₂⁷, are higher than the values experimentally measured; their variation with % butadiene is shown in Figure 1, curve A. A plot of $1/T_D$ versus $-\log N$ is given in Figure 2. In our case N is the mole fraction of ethylene units. It is seen that the points for the copolymers lay fairly well on a

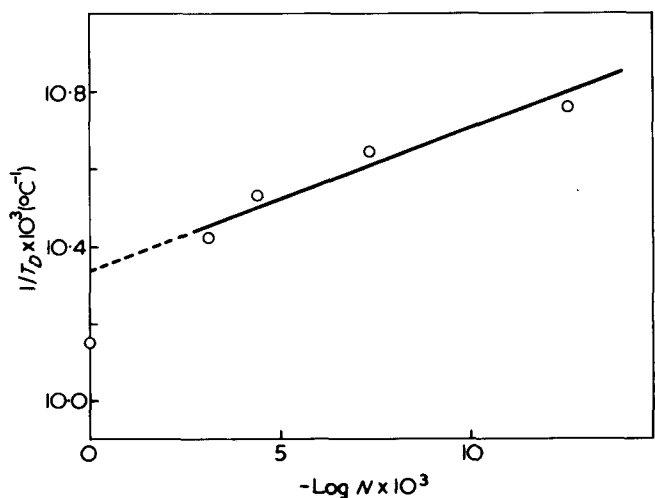


Figure 2 Reciprocal apparent dissolution temperature versus $-\log N$ (N = mol fraction of crystallizable units for ethylene-butadiene copolymers)

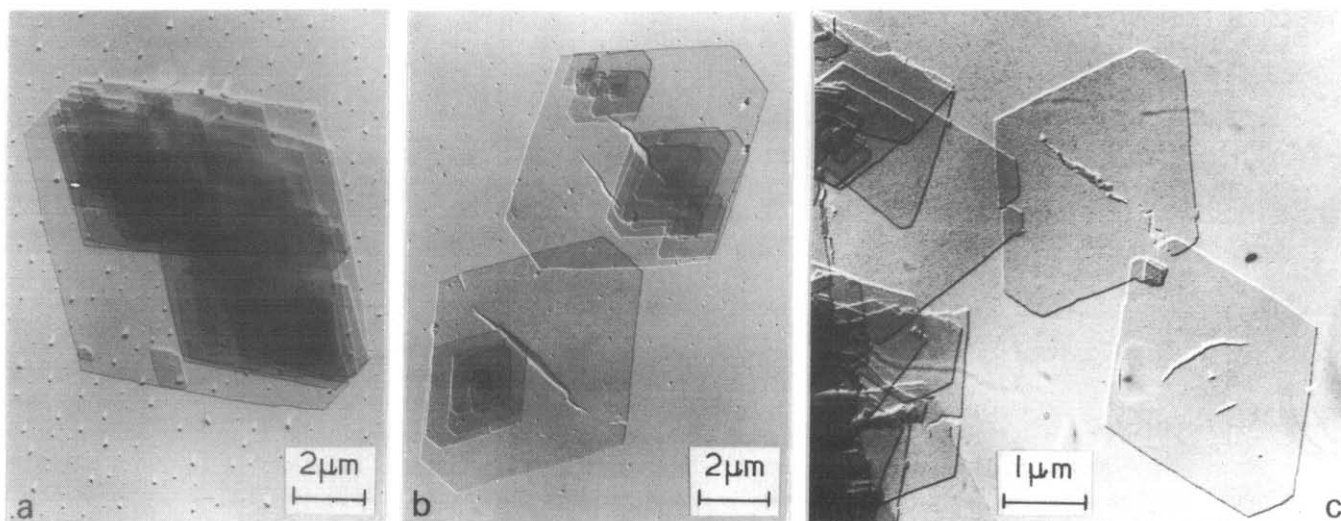


Figure 3 Single crystals of ethylene-butadiene copolymers grown from xylene at 75°C. (Electron micrographs). (a) Sample EB1, $\Delta T_s = 3^\circ\text{C}$; (b) EB2, $\Delta T_s = 3^\circ\text{C}$; (c) EB4, $\Delta T_s = 3^\circ\text{C}$

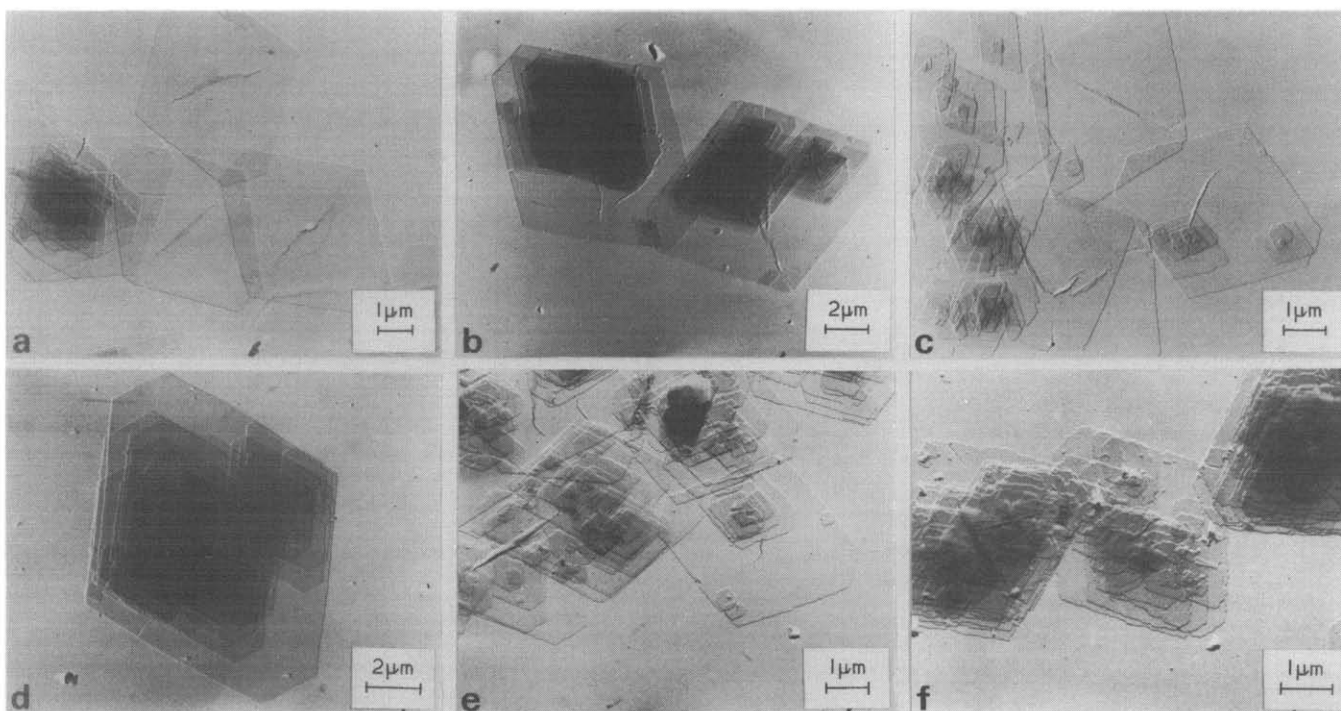


Figure 4 Single crystals of ethylene-butadiene copolymers grown from xylene at 80°C. (Electron micrographs). (a) Sample EB1, $\Delta T_s = 1^\circ\text{C}$; (b) EB1, $\Delta T_s = 3^\circ\text{C}$; (c) EB2, $\Delta T_s = 1^\circ\text{C}$; (d) EB2, $\Delta T_s = 3^\circ\text{C}$; (e) EB4, $\Delta T_s = 1^\circ\text{C}$; (f) EB4, $\Delta T_s = 3^\circ\text{C}$

line. The extrapolation to $-\log N = 0$ gives for T_D^0 a value of 96.5°C while the experimental value measured for Marlex and Vestolen is 98.5°C .

These results are an indication that the crystal lattice of ethylene-butadiene copolymers is somehow different from that of linear polyethylene. The difference is likely to be due to the incorporation of $-\text{CH}_2-\text{CH}=\text{CH}-\text{CH}_2-$ units in the lattice of polyethylene as defects.

In Figures 3, 4 and 5 electron micrographs of single crystals of polyethylene and ethylene-butadiene copolymers, grown at various crystallization conditions, are shown.

The crystals in all cases are truncated lozenges similar in shape to that of linear polyethylene. For the same crystallization temperature, seeding temperature and composition they result uniform in size indicating that the self-

seeding technique applies to ethylene-butadiene copolymers as well.

A slightly larger tendency to form terraced overgrowth is observed in the case of single crystals of the copolymers with higher butadiene content. The external crystal habit of truncated lozenges may be described by the quantities D , d , t , D_1 and α , defined in Figure 6 and by the thickness L of the lamellae as measured by low-angle X-ray diffraction analysis.

For a given butadiene concentration the dimensions of the crystals increases continuously increasing the seeding temperature T_s . The trend is shown in Figures 7 and 8 where the quantities $\log D$ and $\log D_1$ are plotted against $\Delta T_s = (T_s - T_D)$. It can be seen that increasing the seeding temperature $\log D$ and $\log D_1$ increases with an almost linear trend. The rate of variation as measured by the

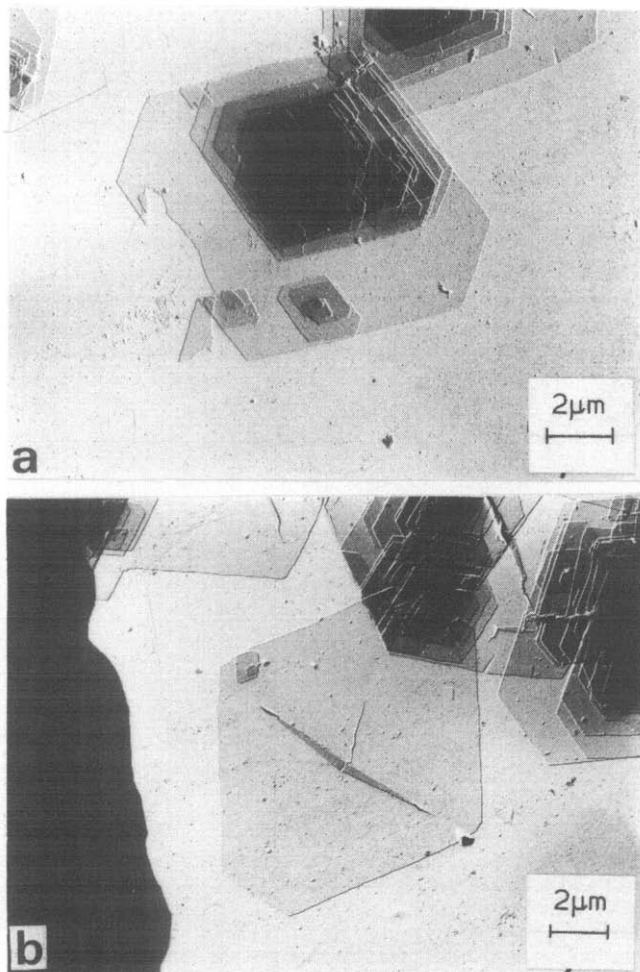


Figure 5 Single crystals of ethylene-butadiene copolymers grown at 85°C from xylene (Electron micrographs). (a) Sample EB1, $\Delta T_s = 3^\circ\text{C}$; (b) EB2, $\Delta T_s = 3^\circ\text{C}$

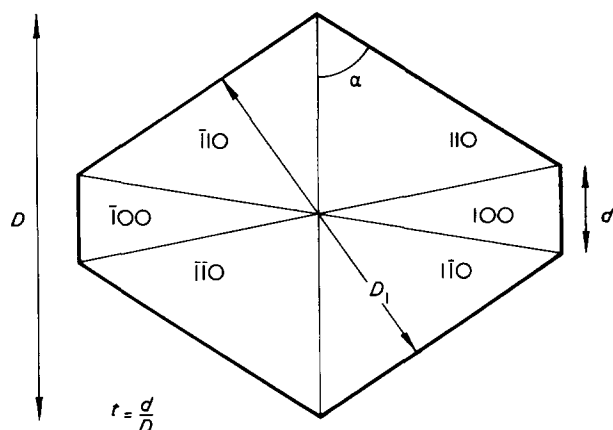


Figure 6 Diagrammatic plan of a pyramidal crystal of polyethylene indicating the various sectors. The quantities D , D_1 , d , r , α , are also specified

slopes of the curves of Figures 7 and 8 is plotted versus the composition of the samples in Figure 9. The points lay on the same curve. A drastic reduction in the values of the rates $d[\log D, (D_1)]/d(\Delta T_s)$ with increasing amounts of double bonds in the chain of polyethylene is observed.

As shown in Figure 10, for single crystals of ethylene-butadiene copolymers, the values of D , measured under the same ΔT_s , and at $T_c = 80^\circ\text{C}$ monotonically decrease with % butadiene.

The effect seems to be more drastic at higher values of ΔT_s . The values of D of single crystals of linear polyethylene (Marlex and Vestolen) are also reported in Figure 10. They lay outside the curves of the copolymer points. For $\Delta T_s = 1^\circ$ and 3°C the values of D for single crystals of Marlex and Vestolen are lower than that of single crystals of samples EB1, EB2, EB3 and EB4.

Assuming that the mass of polymer crystallized at T_c is the same, we have to conclude that in the series of samples of ethylene-butadiene copolymers increasing % butadiene under the same T_{pc} , T_c , T_s and c , a larger number of nuclei are present in solution. Overgrowing effects observed on some of the single crystals with a larger concentration of butadiene units and differences in the lamellar

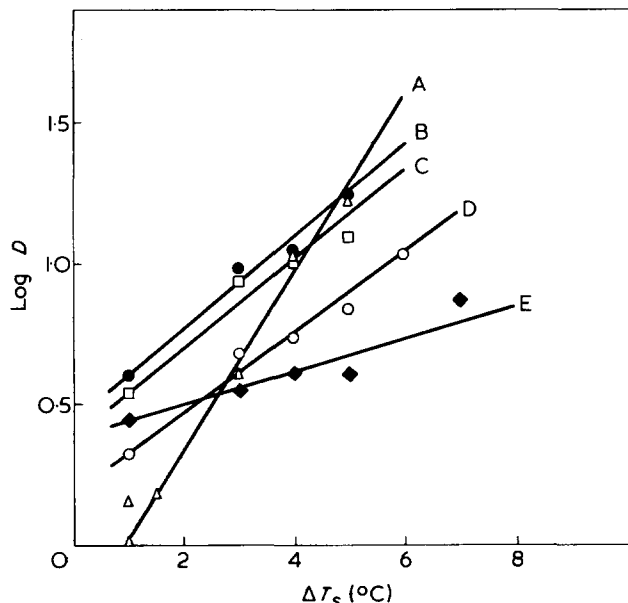


Figure 7 $\log D$ versus $\Delta T_s = T_s - T_D$ for single crystals of ethylene-butadiene copolymers and of linear polyethylene (Marlex and Vestolen) grown from xylene at 80°C . A, PE; B, EB1; C, EB2; D, EB3; E, EB4

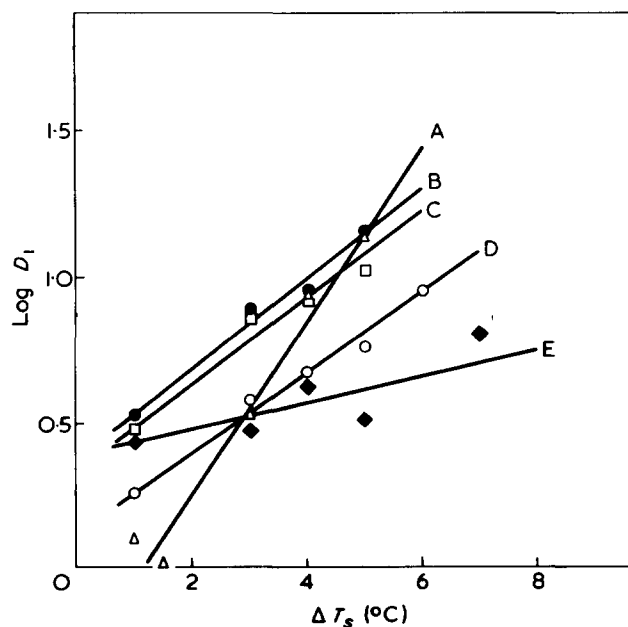


Figure 8 $\log D_1$ versus $\Delta T_s = T_s - T_D$ for single crystals of ethylene-butadiene copolymers and of linear polyethylene (Marlex and Vestolen) grown from xylene at 80°C . A, PE; B, EB1; C, EB2; D, EB3; E, EB4

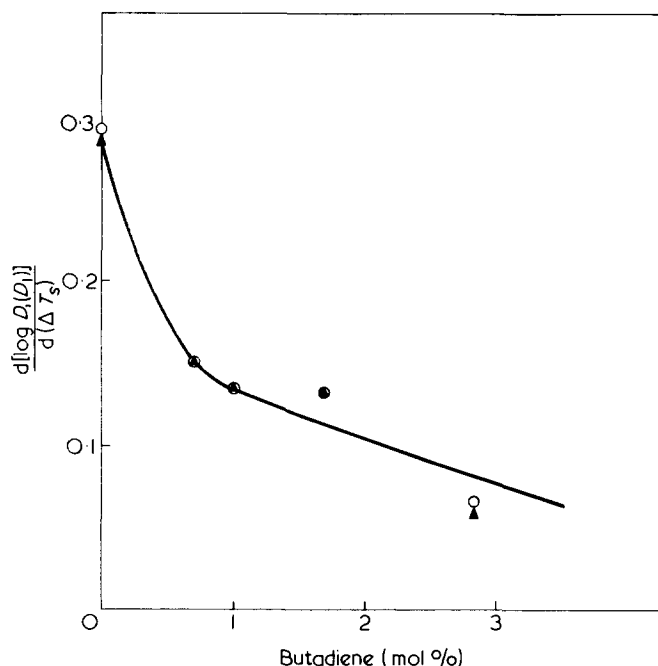


Figure 9 The rate $d[\log D, (D_1)] / d(\Delta T_s)$ versus % butadiene for single crystals of polyethylene and ethylene-butadiene copolymers grown at 80°C . \circ , from $\log D$ against T_s curve; \blacktriangle , from $\log D_1$ against T_s curve

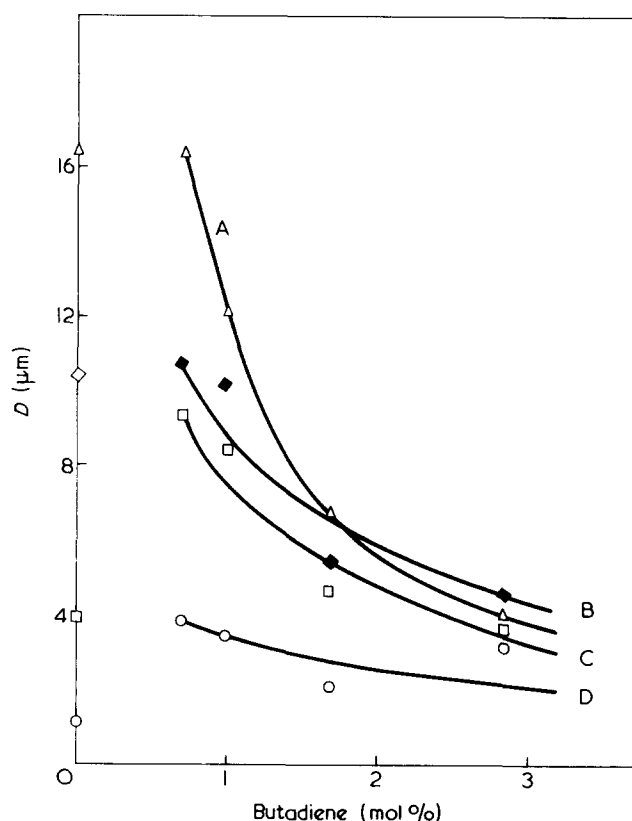


Figure 10 The dimensions of the crystals measured by D versus the composition of the polymer. The comparison is made under the same value of ΔT_s and at $T_c = 80^\circ\text{C}$. Marlex and Vestolen points are practically coincident. A, $\Delta T_s = 5$; B, $\Delta T_s = 4$; C, $\Delta T_s = 3$; D, $\Delta T_s = 1^\circ\text{C}$

thickness (see below) have to be taken also into consideration.

The effect of the crystallization temperature on D is shown in Figure 11 where D is plotted as function of the composition for $T_c = 85^\circ, 80^\circ$ and 75°C , at $\Delta T_s = 3^\circ\text{C}$.

The trend of the curves is the same. A slight increase in D with T_c is observed. The values of ΔT_s for growing single crystals of ethylene-butadiene copolymers with the same dimension D were found to increase linearly with increasing amounts of unsaturations. The extrapolation of these lines (see Figure 12) gives for the pure homopolymer values of ΔT_s close to zero whereas the experimental values are about 3°C .

As shown in Table 3 the values of $\tan \alpha$, measured on single crystals of polyethylene and of ethylene-butadiene copolymers, increase with the percentage of unsaturations in the chain. For Marlex we found for $\tan \alpha$ a value of 1.54 (crystallographic value 1.485) and for EB4, 1.68. This result is probably related to an expansion of the unit cell caused by the inclusion of some $-\text{CH}_2-\text{CH}=\text{CH}-\text{CH}_2-$ units as defects. This conclusion is in agreement with the

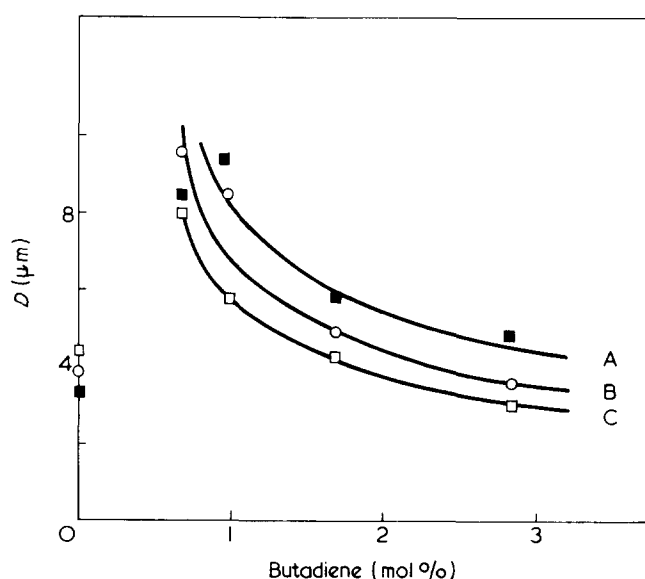


Figure 11 D versus the composition of the polymer at different crystallization temperature and for $\Delta T_s = 3^\circ\text{C}$. A, $T_c = 85$; B, $T_c = 80$; C, $T_c = 75^\circ\text{C}$

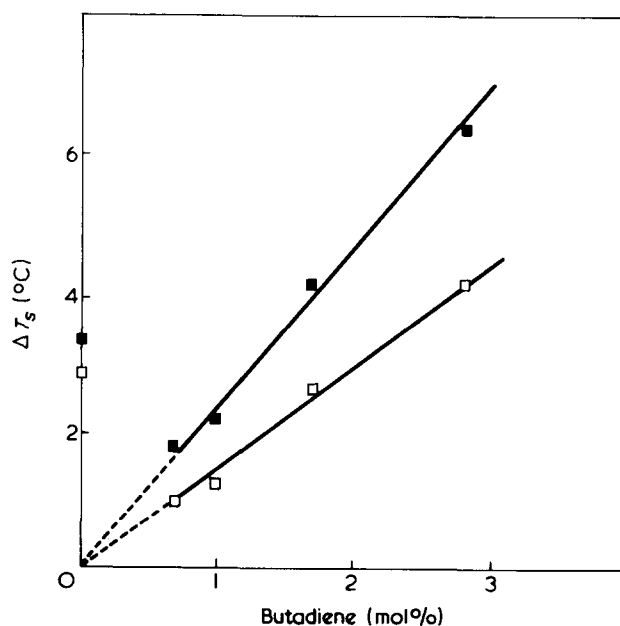


Figure 12 Dependence of ΔT_s upon the composition of the polymer to grow crystals with the same values of D . \blacksquare , $D = 6$; \square , $D = 4$

Table 3 Values of $\tan \alpha$ and of the truncation ratio for single crystals of polyethylene and ethylene-butadiene copolymers ($T_c = 80^\circ\text{C}$)

Sample	$\tan \alpha$	Truncation ratio, t
Marlex 6009	1.54 (± 0.04)	0.23 (± 0.02)
EB1	1.58	0.20
EB2	1.64	0.21
EB3	1.65	0.205
EB4	1.68	0.21

finding that, an increase of about 1% in the spacing of (200) and (110) wide-angle X-ray reflections had been found in the case of bulk EB4 copolymer.

From literature data⁸ it is well known that for single crystals of linear polyethylene the size of {100} sectors and the outline shape depends on the crystallization conditions, the sectors being more pronounced for higher polymer concentration and lower undercooling.

The truncation ratios of single crystals of ethylene-butadiene copolymers, crystallized at 80°C , range from 0.20 to 0.21 and are lower than that of linear polyethylene (0.23 for Marlex and 0.25 for Vestolen) crystallized under the same conditions and therefore at larger undercooling. The values of t are reported in *Table 3*. This last result is in contrast with the quoted literature data⁸ and seems to indicate that the chemical structure of the polymer and not only the undercooling affect the value of t . It is likely that in the case of copolymers the mobility of the chain in solution, increased by the presence of the double bonds along the chain⁹, is responsible for this behaviour, partly at least. This should indicate that the truncation phenomenon in single crystals of polyethylene cannot be simply interpreted on a crystallographic basis but perhaps better on a thermodynamics basis. The same conclusions were also reached by Pedemonte and others¹⁰ starting from different and independent observations.

Melt properties and bromination of single crystals

Density, melting temperature and apparent enthalpy of fusion of single crystals aggregates of polyethylene and ethylene-butadiene copolymers grown at 80°C are reported in *Table 4* together with the lamellar thickness measured by X-ray low-angle diffraction.

Melting temperatures of single crystals of copolymers range from 125° to 127°C and are lower than that of linear polyethylene 129.5°C . No systematic variation in the values of density and apparent enthalpy of fusion of single crystals are observed.

A significative and continuous increase with the percentage of unsaturation is found in the values of the long

spacing L . In fact, for linear polyethylene $L = 110 \text{ \AA}$ while for sample EB4 $L = 131 \text{ \AA}$. This result is in agreement with the findings of Martuscelli and others¹¹ that, under the same crystallization conditions, thicker crystals are obtained when polymers having a larger concentration of chain defects along the chains are allowed to crystallize from dilute solutions. The bromination of single crystals of sample EB4 of ethylene-butadiene copolymers was followed qualitatively and quantitatively by i.r. analysis in the wavelength region of 625 to 4000 cm^{-1} . *Figure 13* shows the intensity of the i.r. 970 cm^{-1} band, normalized with respect to the 735 cm^{-1} (*Figure 13a*) and 1475 cm^{-1} (*Figure 13b*) $-\text{CH}_2-$ bands, as function of the time of reaction. It can be seen that the absorbance due to the double bonds first drops very rapidly then a steady state is reached indicating that the reaction is terminated.

The percentage of double bonds accessible to bromine, on the fold surface of the crystals, calculated from the decay in the i.r. absorbance is about 44%.

These results are convincing evidence that a certain amount of double bonds is situated, in the core of the crystals in agreement with the findings and the experimental results reported above in the present paper.

CONCLUSIONS

The analysis of the solution properties and of some important morphological parameters shows that single crystals of ethylene-butadiene copolymers and of linear polyethylene have a different behaviour. Further a certain number of double bonds are incorporated in the crystal lattice as defects.

In the case of EB4 copolymer about 56% of double

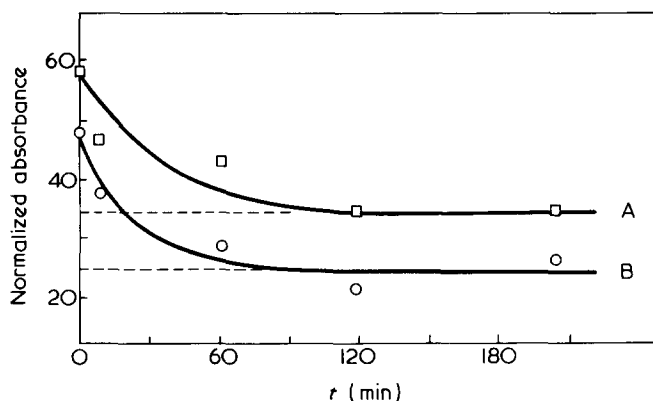


Figure 13 Intensity of i.r. 970 cm^{-1} double bond peak of EB4 single crystals versus the time of bromination at 0°C . A, normalized with respect to 735 cm^{-1} $-\text{CH}_2-$ band; B, normalized with respect to 1475 cm^{-1} $-\text{CH}_2-$ band

Table 4 Thickness, density, apparent enthalpy of fusion, and melting temperature of single crystals of polyethylene and of ethylene-butadiene copolymers grown at 80°C

Sample	Crystallization temperature, T_c ($^\circ\text{C}$)	Long spacing (\AA)	Density ^a (g/cm^3)	Apparent enthalpy of fusion, ΔH^* (cal/g)	Melting temperature, T_m ($^\circ\text{C}$)
Marlex 6009	80	110	0.965 ± 0.005	45 ± 2	129.5 ± 0.5
EB1	80	122	0.970 ± 0.001	43	125
EB2	80	—	0.976 ± 0.002	43	125.5
EB3	80	128.5	0.97 ± 0.01	36	126
EB4	80	131	0.970 ± 0.001	45	127

^a at 29°C

bonds are not accessible to bromine. This should indicate that during crystallization from dilute solution a larger part of double bonds are not rejected from the crystal lattice. The decrease in the rate of crystallization and the drastic increase in the value of the free energy of formation of a nucleus of critical dimensions with increasing number of double bonds, observed when the samples of ethylene-butadiene copolymers are allowed to crystallize isothermally from the melt³, together with the different behaviour of single crystals and of their solution properties as reported in the present paper may be related to the following observations:

(a) The mobility of the chain is increased by the presence of double bonds because of the lower energy barrier that hinders the rotation around the single C-C bonds adjacent to the C=C groups⁹.

(b) The crystalline lattice of crystals of ethylene-butadiene copolymers is perturbed by the inclusions of double bond as reticular defects.

REFERENCES

- 1 Väino, A. Erä. *Makromol. Chem.* 1974, **175**, 2191
- 2 Martuscelli, E. and Pracella, M. *Polymer* 1974, **15**, 306; Alfonso, G. C., Fiorina, L., Martuscelli, E., Pedemonte, E. and Russo, S. *Polymer* 1973, **14**, 373
- 3 Amelino, L. and Martuscelli, E. *Polymer* 1975, **16**, 864
- 4 Cucinella, S. and Mazzei, A. *Chim. Ind. (Milan)* 1971, **53**, 748
- 5 Blundell, D. J. and Keller, A. *J. Macromol. Sci. (B)* 1968, **2**, 301
- 6 Flory, P. J. *J. Chem. Phys.* 1949, **17**, 223
- 7 Jackson, J. B., Flory, P. J. and Chiang, R. *Trans. Faraday Soc.* 1963, **59**, 1906
- 8 Blundell, D. J. and Keller, A. *J. Macromol. Sci. (B)* 1968, **2**, 337; Kawai, T. and Keller, A. *Phil. Mag.* 1965, **11**, 1165
- 9 Martuscelli, E. *Acta Crystallogr.* 1967, **23**, 1086; Corradini, P., Frasci, A. and Martuscelli, E. *Chem. Commun.* 1969, p 779; Martuscelli, E. and Frasci, A. *Acta Crystallogr. (B)* 1969, **25**, 2547
- 10 Valenti, B. and Pedemonte, E. *Chim. Ind. (Milan)* 1972, **54**, 112
- 11 Martuscelli, E. *J. Macromol. Sci. (B)* 1975, **11**, 1

Monomer sequence distribution in butene/propylene copolymers by ^{13}C nuclear magnetic resonance

A. Bunn and M. E. A. Cudby

*ICI Plastics Division, Welwyn Garden City, Hertfordshire, UK
(Received 27 January 1976)*

We wish to report the determination of monomer sequence distribution in butene/propylene copolymers by ^{13}C nuclear magnetic resonance (^{13}C n.m.r.). This is an established technique for the measurement of stereoregularity in homopolymers¹⁻¹⁰ and the measurement of sequence distributions in copolymers¹¹⁻²¹. However, to our knowledge, the only reports of ^{13}C n.m.r. measurements of α -olefin copolymers concern the systems ethylene/ α -olefin¹⁵ and propylene/ethylene¹⁶⁻¹⁸. The proton magnetic resonances in polyolefins are severely overlapped and this limits the structural information obtainable. As the resonances in the ^{13}C n.m.r. spectra of polyolefins occur over a range of about 40 ppm we expect this technique to produce more information than proton magnetic resonance. This is indeed the situation for polypropylene⁵⁻⁷, polyethylene^{15,22,24} and propylene/ethylene copolymers¹⁶⁻¹⁸. Calculated chemical shifts from Lindeman and Adams data²³ predict that the ^{13}C n.m.r. chemical shifts in butene/propylene copolymers would be sensitive to monomer sequence distribution. In this Note, we report ^{13}C n.m.r. data on butene/propylene copolymers including random and block distributions and a copolymer which has a mixture of block and random distributions. The observed resonances are assigned to dyad, triad and tetrad monomer sequences.

The natural abundance ^{13}C n.m.r. spectra of polypropylene, polybutene and butene/propylene copolymers were measured in *o*-dichlorobenzene solution at 140°C. The 25.2 MHz spectra were recorded on a Varian XL100-15 spectrometer equipped with a proton-noise decoupler and a standard VFT-100X Fourier transform system. A 2 sec acquisition time and a 90 μsec pulse width (tip angle $\sim 70^\circ$) were used to acquire data. Field-frequency stabilization was provided by D_6 -dimethyl sulphoxide contained in a 5 mm o.d. n.m.r. tube held centrally in a 12 mm o.d. tube which contained the copolymer solution.

Figure 1 shows ^{13}C n.m.r. spectra of polybutene and polypropylene. The assignments of the resonances are also shown on the Figure. Those for polypropylene are known and those for polybutene were determined from predicted values (Lindeman and Adams data) and an off-resonance experiment. Our own work on poly(α -olefins) higher than polybutene shows that backbone methine and methylene carbon resonances are the most sensitive to tacticity changes and that in the spectra of non-isotactic polymers these resonances are broader than the remaining resonances. As the resonances in the ^{13}C n.m.r. spectra of butene/propylene copolymers examined were equally sharp and in co-

polymers with long propylene sequences the propylene α -methyl carbon resonance was a singlet and had a chemical shift the same as that found in isotactic polypropylene we feel justified in making the assumption that only a meso addition of either monomer to the polymer chain is made.

Copolymers prepared with a wide range of composition and with differing monomer sequence distributions were examined. Representative spectra of the materials are shown in Figures 2 and 3. The resonances in the ^{13}C n.m.r. spectra of these copolymers were assigned by reference to the spectra of the homopolymers, predicted values from Lindeman and Adams's data²³ and by checking that the relative intensities of the resonances were self consistent. Table 1 lists the chemical shift data of the ^{13}C n.m.r. spectra of these copolymers, our proposed assignments and the monomer sequences characterized by each resonance. The letters P and B denote propylene and butene units with any two forming a meso dyad. Thus a PPB triad would contain a

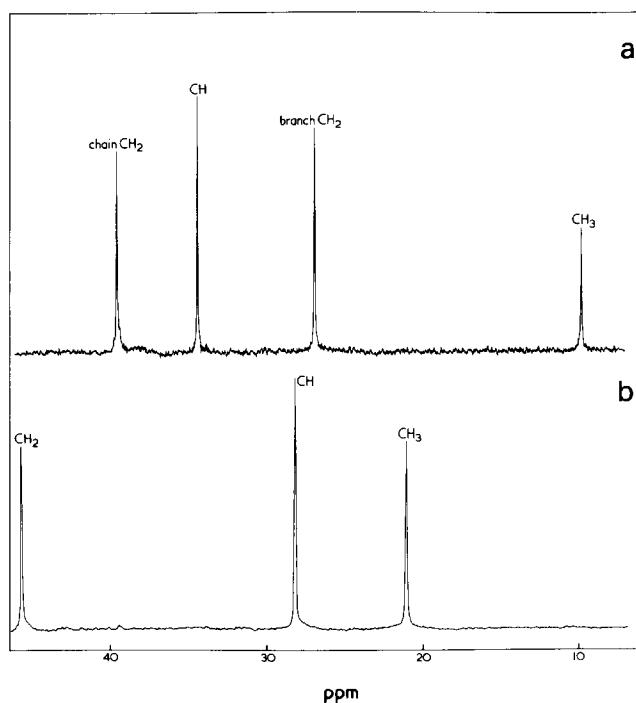


Figure 1 ^{13}C n.m.r. spectra of (a) polybutene (b) polypropylene

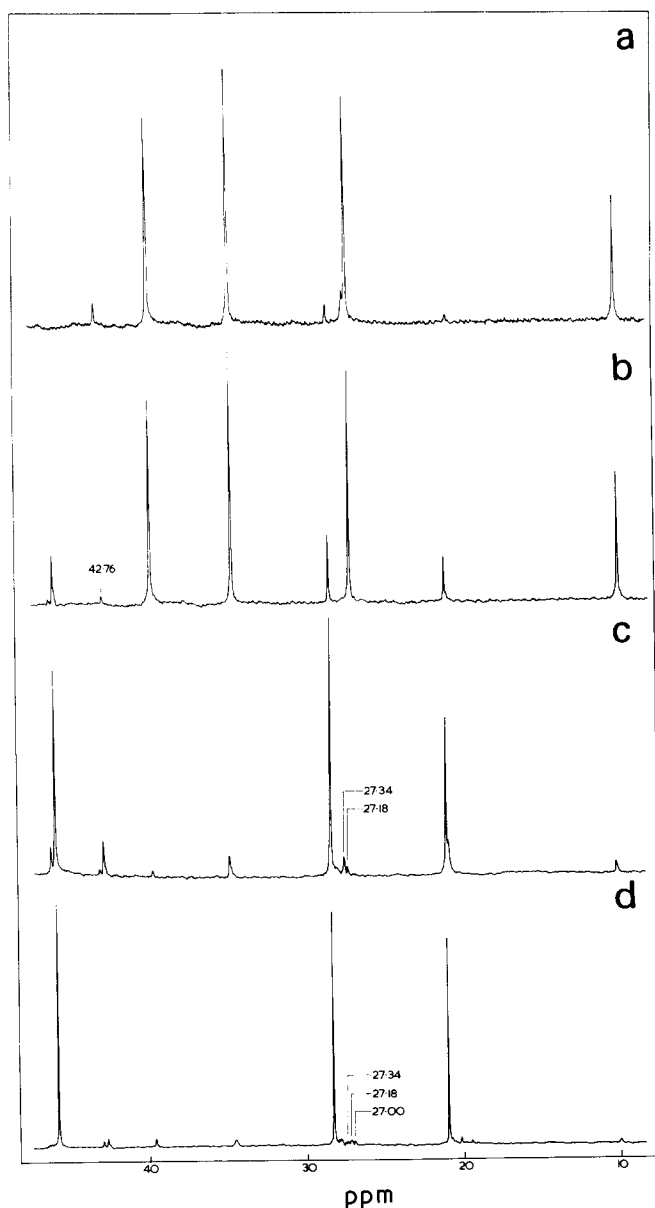
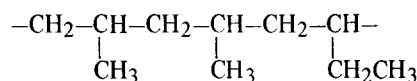


Figure 2 ^{13}C n.m.r. spectra of butene/propylene copolymers (a) 10 molar % propylene as isolated units; (b) 10 molar % propylene as propylene blocks; (c) 10 molar % butene as random copolymer; (d) 10 molar % butene with some butene blocks

PP and a PB meso dyad:



Figures 2a–2d show ^{13}C n.m.r. spectra of four copolymers denoted by A–D. Copolymer A is rich in butene and contains isolated propylene units only i.e. BPB. In contrast, copolymer B, although approximately the same overall composition as copolymer A, contains long propylene sequences. The few interchange units give rise to a resonance at 42.76 ppm from the backbone methylene carbon atom. Copolymers C and D are propylene rich and contain approximately 10 molar % butene. Copolymer C has the majority of butene units adjacent to propylene units, i.e. PBP, with the required number of adjacent butene units as is appropriate to a random monomer distribution²⁵. For copolymer D, the relative intensities of the methylene carbon reso-

nances characteristic of PP, PB and BB dyads show that there are more adjacent butene units than would be predicted for a random copolymer. The presence of three or more adjacent butene units in the copolymer chain is responsible for the 27.00 ppm resonance. The branch-methylene group carbon resonances at 27.00 ppm, 27.18 and 27.34 ppm are characteristic of BBB, BBP and PBP sequences and indicate the blockiness or otherwise of the butene units.

Figures 3a–3c show spectra of copolymers E to G. These copolymers contain roughly equal amounts of butene and propylene, E and F have spectra with resonance intensities which show that the copolymers are fairly random. The intensities of the resonances in the spectrum of copolymer G (Figure 3c) show that the copolymer does not have a random monomer distribution; this is expected, as its method of preparation would produce long sequence of adjacent propylene units. Features to note in the spectra shown in Figures 3a–3c are the resonances at 27.00 ppm, 27.18 ppm and 27.34 ppm which are characteristic of the three possible butene centred triads, and the three propylene methyl group carbon resonances around 20.7 ppm which are characteristic of the propylene centred triads i.e. PPP, PPB and BPB at 20.96 ppm, 20.74 ppm and 20.60 ppm respectively.

Tetrad sequences for propylene/propylene centred units, BPPB, PPPB, PPPP are observed from the backbone methylene carbon resonances at 45.86, 46.10 and 46.40 ppm respectively. The lack of structure on the methine carbon resonances of both butene and propylene units is somewhat surprising, especially as the butene methyl group carbon

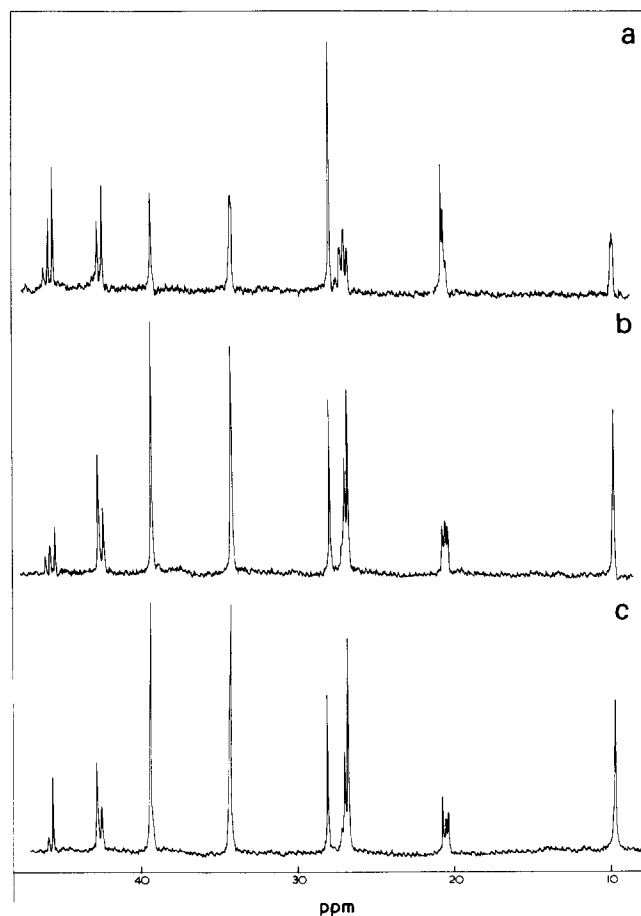


Figure 3 ^{13}C n.m.r. spectra of butene/propylene copolymers with approximately equal amounts of propylene and butene. Copolymer G (Figure 3c) contains blocks of propylene together with random material

Note to the Editor

Table 1 Chemical shift data of the ^{13}C n.m.r. spectra of the copolymers examined

Chemical shift from tetramethylsilane (ppm)	Assignment, carbon marked with *	Polymer sequences characterized
9.92	*CH ₃ -CH ₂ -CH	BBB, BBP, PBP
20.60	*CH ₃ -CH	BPB
20.74	*CH ₃ -CH	BPP
20.96	*CH ₃ -CH	PPP
27.00	CH ₃ -*CH ₂ -CH	BBB
27.18	CH ₃ -*CH ₂ -CH	BBP
27.34	CH ₃ -*CH ₂ -CH	PBP
28.29	CH ₃ -*CH	PPP, PPB, BPB
34.47	CH ₃ -CH ₂ -*CH	BBB, BBP, PBP
39.64	-CH-*CH ₂ -CH Et Et	BBBB, BBBP, PBBP
42.76	-CH ₂ -CH-*CH ₂ -CH Et Me	PBPP
43.04	-CH ₂ -CH-*CH-CH Et Me	BBPB, BBPP and probably also PBPB
45.86	-CH-*CH ₂ -CH Me Me	PPPP
46.10	-CH-*CH ₂ -CH- Me Me	PPPB
46.40	-CH-*CH ₂ -CH- Me Me	BPPB

resonances show well defined shoulders in some of the spectra. These facts indicate to us that the origin of the chemical shift observed on the butene methyl group carbon is not a through bond effect.

In conclusion, the above data show that ^{13}C n.m.r. spectroscopy can be used to characterize butene/propylene copolymers in terms of dyad and triad sequences. Well resolved resonances were also observed for propylene/propylene centred tetrads.

REFERENCES

- Schaefer, J. *Macromolecules* 1971, 4, 110
- Carman, C. J., Tarpley Jr. A. R. and Goldstein, J. H. *Macromolecules* 1971, 4, 445
- Inoue, Y., Nishioka, A. and Chujo, R. *Polym. J.* 1971, 2, 535
- Matsuzaki, K., Kanai, T. and Matsumoto, S. *J. Polym. Sci. (Polym. Chem. Edn)* 1974, 12, 2377
- Randall, J. C. *J. Polym. Sci. (Polym. Phys. Edn)* 1974, 12, 703
- Inoue, Y., Nishioka, A. and Chujo, R. *Makromol. Chem.* 1972, 152, 15
- Zambelli, A., Dorman, D. E., Brewster, A. I. and Bovey, F. A. *Macromolecules* 1973, 6, 925
- Inoue, Y., Nishioka, A. and Chujo, R. *Makromol. Chem.* 1972, 156, 207
- Lapeyre, W., Cheradame, H., Spassky, N. and Sigwalt, P. *J. Chim. Phys.* 1973, 70, 838
- Boileau, S. *et al. C. R. Acad. Sci. (C)* 1972, 275, 535
- Whipple, E. B. and Green, P. J. *Macromolecules* 1973, 6, 38
- Schaefer, J. *Macromolecules* 1969, 2, 210
- Delfini, M., Seagre, A. L. and Conti, F. *Macromolecules* 1973, 6, 456
- Schaefer, J. *Macromolecules* 1971, 4, 107
- Randall, J. C. *J. Polym. Sci. (Polym. Phys. Edn)* 1973, 11, 275
- Crain, W. O., Zambelli, A. and Roberts, J. D. *Macromolecules* 1971, 4, 330
- Zambelli, A., Gabbi, G., Sochi, C., Crain, W. O. and Roberts, J. D. *Macromolecules* 1971, 4, 475
- Carman, C. J. and Wilkes, C. E. *Rubber Chem. Technol.* 1971, 781
- Cornu, C., Roggaro, A. and Salvation, T. *Eur. Polym. J.* 1974, 10, 525
- Wu, T. K., Ovenall, D. W. and Reddy, G. S. *J. Polym. Sci. (Polym. Phys. Edn)* 1974, 2, 901
- Stejskal, E. O. and Schaefer, J. *Macromolecules* 1974, 7, 14
- Dorman, D. E., Otocka, E. P. and Bovey, F. A. *Macromolecules* 1972, 5, 574
- Linderman, L. P. and Adams, J. Q. *Anal. Chem.* 1971, 43, 1245
- Cudby, M. E. A. and Bunn, A. in press
- Schaefer, J. *J. Phys. Chem.* 1966, 70, 1975

ERRATUM

'Sequence distribution of *cis*-1,4 and *trans*-1,4 units is polyisoprene' by Yasuyuki Tanaka and Hisaya Sato, *Polymer* 1976, 17, 113-116.

Page 113, right hand column, line 6:
for 15.0 MHz
read 20.0 MHz

We apologise for this error.

Note to the Editor

Table 1 Chemical shift data of the ^{13}C n.m.r. spectra of the copolymers examined

Chemical shift from tetramethylsilane (ppm)	Assignment, carbon marked with *	Polymer sequences characterized
9.92	*CH ₃ -CH ₂ -CH	BBB, BBP, PBP
20.60	*CH ₃ -CH	BPB
20.74	*CH ₃ -CH	BPP
20.96	*CH ₃ -CH	PPP
27.00	CH ₃ -*CH ₂ -CH	BBB
27.18	CH ₃ -*CH ₂ -CH	BBP
27.34	CH ₃ -*CH ₂ -CH	PBP
28.29	CH ₃ -*CH	PPP, PPB, BPB
34.47	CH ₃ -CH ₂ -*CH	BBB, BBP, PBP
39.64	-CH-*CH ₂ -CH Et Et	BBBB, BBBP, PBBP
42.76	-CH ₂ -CH-*CH ₂ -CH Et Me	PBPP
43.04	-CH ₂ -CH-*CH-CH Et Me	BBPB, BBPP and probably also PBPB
45.86	-CH-*CH ₂ -CH Me Me	PPPP
46.10	-CH-*CH ₂ -CH- Me Me	PPPB
46.40	-CH-*CH ₂ -CH- Me Me	BPPB

resonances show well defined shoulders in some of the spectra. These facts indicate to us that the origin of the chemical shift observed on the butene methyl group carbon is not a through bond effect.

In conclusion, the above data show that ^{13}C n.m.r. spectroscopy can be used to characterize butene/propylene copolymers in terms of dyad and triad sequences. Well resolved resonances were also observed for propylene/propylene centred tetrads.

REFERENCES

- Schaefer, J. *Macromolecules* 1971, 4, 110
- Carman, C. J., Tarpley Jr. A. R. and Goldstein, J. H. *Macromolecules* 1971, 4, 445
- Inoue, Y., Nishioka, A. and Chujo, R. *Polym. J.* 1971, 2, 535
- Matsuzaki, K., Kanai, T. and Matsumoto, S. *J. Polym. Sci. (Polym. Chem. Edn)* 1974, 12, 2377
- Randall, J. C. *J. Polym. Sci. (Polym. Phys. Edn)* 1974, 12, 703
- Inoue, Y., Nishioka, A. and Chujo, R. *Makromol. Chem.* 1972, 152, 15
- Zambelli, A., Dorman, D. E., Brewster, A. I. and Bovey, F. A. *Macromolecules* 1973, 6, 925
- Inoue, Y., Nishioka, A. and Chujo, R. *Makromol. Chem.* 1972, 156, 207
- Lapeyre, W., Cheradame, H., Spassky, N. and Sigwalt, P. *J. Chim. Phys.* 1973, 70, 838
- Boileau, S. *et al. C. R. Acad. Sci. (C)* 1972, 275, 535
- Whipple, E. B. and Green, P. J. *Macromolecules* 1973, 6, 38
- Schaefer, J. *Macromolecules* 1969, 2, 210
- Delfini, M., Seagre, A. L. and Conti, F. *Macromolecules* 1973, 6, 456
- Schaefer, J. *Macromolecules* 1971, 4, 107
- Randall, J. C. *J. Polym. Sci. (Polym. Phys. Edn)* 1973, 11, 275
- Crain, W. O., Zambelli, A. and Roberts, J. D. *Macromolecules* 1971, 4, 330
- Zambelli, A., Gabbi, G., Sochi, C., Crain, W. O. and Roberts, J. D. *Macromolecules* 1971, 4, 475
- Carman, C. J. and Wilkes, C. E. *Rubber Chem. Technol.* 1971, 781
- Cornu, C., Roggaro, A. and Salvation, T. *Eur. Polym. J.* 1974, 10, 525
- Wu, T. K., Ovenall, D. W. and Reddy, G. S. *J. Polym. Sci. (Polym. Phys. Edn)* 1974, 2, 901
- Stejskal, E. O. and Schaefer, J. *Macromolecules* 1974, 7, 14
- Dorman, D. E., Otocka, E. P. and Bovey, F. A. *Macromolecules* 1972, 5, 574
- Linderman, L. P. and Adams, J. Q. *Anal. Chem.* 1971, 43, 1245
- Cudby, M. E. A. and Bunn, A. in press
- Schaefer, J. *J. Phys. Chem.* 1966, 70, 1975

ERRATUM

'Sequence distribution of *cis*-1,4 and *trans*-1,4 units is polyisoprene' by Yasuyuki Tanaka and Hisaya Sato, *Polymer* 1976, 17, 113-116.

Page 113, right hand column, line 6:
for 15.0 MHz
read 20.0 MHz

We apologise for this error.

Multiple endotherms in polyepichlorohydrin

Multiple endotherms have been reported in the literature for several polymers, e.g. polyesters^{1,2}, polyethylenes (linear³, branched⁴, and extended chain⁵), isotactic polystyrene⁶, polytetrafluoroethylene⁷ and natural rubber⁸. However comparatively few investigations of multiple melting behaviour in multicomponent systems have been reported^{9,10}. This is understandable since the question of multiple melting in homopolymers itself has presented many problems in interpretation. We wish to report some preliminary investigations on multiple melting in polyepichlorohydrin (PECH) homopolymer and multicomponent systems containing crystalline PECH.

Crystalline PECH homopolymer was prepared in the laboratory according to the method of Hsieh¹¹ with a few minor changes in experimental procedure¹². Samples of homopolymer thus prepared ($T_g = -20^\circ\text{C}$, $T_m = +107^\circ\text{C}$) were heated to 200°C and kept for 10 min at this temperature to destroy previous morphology. They were then taken out of the heating chamber, the d.s.c. cell of a Du Pont 900 Thermal Analyzer, cooled to room temperature (i.e. quench cooled), allowed to crystallize for one day at room temperature and scanned in the Du Pont 900 Analyser at $30^\circ\text{C}/\text{min}$. A typical trace is shown in *Figure 1*. Two distinctly separate endotherms are noticeable. One of these with a melting peak at about 40°C was separated from the other which had a maximum peak at 100°C . This latter endotherm always showed a minor endotherm at 70°C and in addition in some batches a well-defined endotherm appeared at 90°C . (The endotherms will be designated by peak temperatures.) Experimental investigations of 70° , 90° and 100°C endotherms involving manipulation of an-

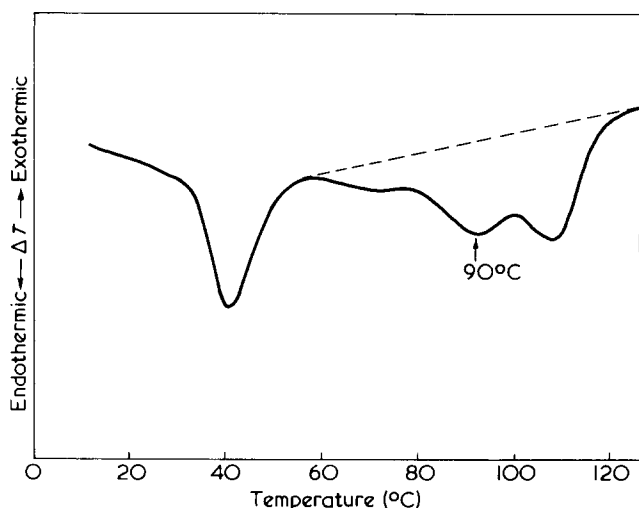


Figure 1 D.t.a. trace of crystalline polyepichlorohydrin showing multiple endotherm

nealing and rates of heating on the lines of Bell^{1,13} and Roberts¹⁴ showed that the three endotherms were not interdependent i.e. the higher melting endotherms were not formed by melting and recrystallization of lower melting endotherms during d.t.a. scanning. The following observations on the 90°C endotherm were noted. The 90°C endotherm was detected only in batches of PECH prepared under conditions such that there was initial fast polymerization¹². Batches thus prepared had to be melted in a two-roll mill and crystallized from the melt for the 90°C endotherm to be recorded. Unmilled samples crystallized from the melt or milled samples not crystallized from the melt failed to show the 90°C endotherm. Within the limits of experimental and sampling error ($\pm 10\%$) the total area (enclosed by the broken base line in *Figure 1*) of samples in which the 90°C endotherm was resolved was equal to areas of samples which failed to record this endotherm.

Crystalline PECH possessed elastomeric properties and hence multicomponent systems could be prepared by two-roll milling with other commercially available elastomers and fillers. Batches of PECH possessing the 90°C endotherm were milled with reinforcing (ISAF black, Vulcan 6—Cabot) and inert (clay, whiting) fillers. In all cases the area of the 90°C endotherm decreased with increasing filler content although the total area essentially remained constant equal to that of the unfilled homopolymer.

The effect of blending a second elastomer, without filler, on the 90°C endotherm depended on the nature of the second elastomer. Thus when natural rubber, amorphous PECH (Herclor H, Hercules) and propylene oxide rubber (Parel 58, Hercules) were used for blending, the 90°C endotherms and total areas were somewhat reduced when compared with crystalline PECH batches used but remained constant over a wide range of composition. However when more polar rubbers were used for blending, the 90°C endotherm was not recorded at the 1:1 (by weight) composition; chlorosulphonated polyethylene, nitrile and acrylic rubbers belonged to this group and blending was presumably accompanied by a very large reduction of total crystallinity.

In the case of unfilled blends, retention of the 90°C endotherm would indicate poor miscibility and compatibility as in the cases of natural rubber and the cyclic ether rubbers; disappearance of the endotherm in the blends with more polar rubbers would imply better dispersion and compatibility.

Our investigations show that observations of multiple melting in multicomponent systems could prove to be a useful diagnostic tool in the interpretation of multiple melting in homopolymer and compatibility effects in blends. Two difficulties which stand in the way of a quantitative approach need mention. One concerns difficulties in estimation of d.t.a. areas of individual endotherms; the other concerns sampling variations due to the nature of the small amount of material used in dynamic calorimetric methods.

Acknowledgements

We wish to thank Dr Marianne Gilbert for several valuable discussions and suggestions in the course of this work.

Leslie P. Mendis

Present address:

Department of Scientific and Industry Research,
Colombo,
Sri Lanka

and Claude Hepburn

Institute of Polymer Technology,
Loughborough University of Technology,
Loughborough
Leicestershire LE11 3TU, UK

(Received 19 May 1975; revised 26 February 1976)

References

- 1 Bell, J. P. and Dumbleton, J. H. *J. Polym. Sci. (A-2)* 1969, 7, 1033
- 2 Gilbert, M. and Hybart, F. J. *Polymer* 1974, 15, 407
- 3 Harland, W. G., Khadr, M. M. and Peters, R. H. *Polymer* 1972, 13, 13
- 4 Holden, W. W. *J. Polym. Sci. (C)* 1964, 6, 53
- 5 Prime, R. B., Wunderlich, B. and Melillo, L. *J. Polym. Sci. (A-2)* 1969, 7, 2091
- 6 Pelzbauer, Z. and Manley, R. St. J. *J. Polym. Sci. (A-2)* 1970, 8, 649
- 7 Bassett, D. C. and Davitt, R. *Polymer* 1974, 15, 721
- 8 Kim, H.-G. and Mandelkern, L. *J. Polym. Sci. (A-2)* 1972, 10, 1125
- 9 Buszard, D. L. *PhD Thesis* Loughborough University of Technology (1973)
- 10 Sato, T. and Takahashi, M. *J. Appl. Polym. Sci.* 1969, 13, 2665
- 11 Hsieh, H. L. *J. Appl. Polym. Sci.* 1971, 15, 2425
- 12 Mendis, L. P. *PhD Thesis* Loughborough University of Technology (1975)
- 13 Sweet, G. E. and Bell, J. P. *J. Polym. Sci. (A-2)* 1972, 10, 1273
- 14 Roberts, R. C. *J. Polym. Sci. (B)* 1970, 8, 381

Book Reviews

Advances in Polymer Science

Volume 17: Polymerization

Springer-Verlag, Berlin, 1975, 103 pp. \$23.00

This volume in the series covers mechano-chemical initiation of copolymerization and the polymerization of thioaldehydes, thioketones and related compounds. It would be difficult to find two more widely different facets of polymer science. The first contribution, by Casale and Porter, includes processes of commercial importance whilst the second, by Sharkey, has yet to find industrial usage. Mechano-chemistry, as the authors ably illustrate, is applicable to an extremely wide range of polymer-monomer systems which can be activated by an extensive choice of 'bond-breaking' processes. On the one hand, the coextrusion of two viscoelastic polymers can lead to high yields of block copolymers having properties differing from simple blends, whilst on the other hand, esoteric materials can be synthesized for laboratory evaluation by vibromilling or even simple solvent swelling techniques. All reported aspects of mechano-chemical reactions leading to block and graft copolymerization are discussed in depth and there are extensive references to original publications.

The synthesis of polymers by polymerization through the carbon-sulphur double bond is a very specialized field which is treated in depth by Sharkey in this book with more extensive reference to recent publications, in particular the patent literature, than the mechano-chemical section. By virtue of its specialized nature, the latter section will have a rather limited interest more or less con-

finied to production and research personnel directly involved with condensation polymerization and ring opening reactions. The first section, because of its more general nature, will appeal to practically everyone involved in the research, development, production and application of copolymers at all levels.

Apart from some missing 'free radicals' on pages 9 and 22 and a pentavalent carbon atom on page 30, the book is relatively free of typographical errors. At \$23.00 it is expensive for approximately a hundred pages but it does give a thorough review of two topics for which much of the available data is published in languages other than English. The contribution by A. Cassale, R. H. Porter and W. H. Starkey maintains the high standard which we expect from this series and it will, therefore, take its rightful place in polymer libraries throughout the world.

R. J. Ceresa

Reinforced Thermoplastics

W. V. Titow and B. J. Latham

Applied Science, Barking, 1975, 294 pp. £10

'Reinforced Thermoplastics' is the first book to be published on this subject and its contents well meet the aim of its authors, which is 'to present a reasonably unified account of the technology and properties' of this class of plastics materials.

The description which the book provides is essentially technological in nature but it touches on some commercial problems. Thus, it ranges from a very useful list of commercially available reinforced thermoplastics and their producers, through a discussion of their principal applications to methods of processing and to material properties and there is also an appendix devoted to relevant patents.

The book is self-contained in that it includes a description of the polymeric materials which form the basis of reinforced thermoplastics and of their properties as well as that of fibrous and particulate fillers before dealing with the two in combination. The properties of reinforced thermoplastics are dealt with primarily in terms of short term data but the importance of long term behaviour is clearly recognised. In view of the inevitable lapse of time between the completion of a manuscript and publication, the discussion of properties does not include the results of research published during the past year or two. However, it is surprising to find virtually no mention of anisotropy, even though the authors have not attempted to deal in depth with what might be termed the more scientific aspects of reinforced thermoplastics, as they clearly state in the Preface. Nevertheless, their book should be of considerable interest and of value to anyone concerned with reinforced thermoplastics.

R. M. Ogorkiewicz

Conference Announcement

Structure and Uses of Biopolymers

Cleveland, Ohio, USA, 11-16 October 1976

The first Cleveland Symposium on Macromolecules will be held during the week of October 11-16th, 1976 with the topic of Structure and uses of biopolymers. The week-long conference will be organized around fifteen invited international presentations in three areas: fundamental structure of biopolymers; materials properties; and medical applications, and will involve local social functions. Contributions of short papers to be presented at the meeting in the above areas are solicited. Prospective contributors, attendees and interested persons should write for further information to: Professor Alan G. Walton, Department of Macromolecular Science, Case Western Reserve University, Cleveland, Ohio 44106, USA.

Acknowledgements

We wish to thank Dr Marianne Gilbert for several valuable discussions and suggestions in the course of this work.

Leslie P. Mendis

Present address:

Department of Scientific and Industry Research,
Colombo,
Sri Lanka

and Claude Hepburn

Institute of Polymer Technology,
Loughborough University of Technology,
Loughborough
Leicestershire LE11 3TU, UK

(Received 19 May 1975; revised 26 February 1976)

References

- 1 Bell, J. P. and Dumbleton, J. H. *J. Polym. Sci. (A-2)* 1969, 7, 1033
- 2 Gilbert, M. and Hybart, F. J. *Polymer* 1974, 15, 407
- 3 Harland, W. G., Khadr, M. M. and Peters, R. H. *Polymer* 1972, 13, 13
- 4 Holden, W. W. *J. Polym. Sci. (C)* 1964, 6, 53
- 5 Prime, R. B., Wunderlich, B. and Melillo, L. *J. Polym. Sci. (A-2)* 1969, 7, 2091
- 6 Pelzbauer, Z. and Manley, R. St. J. *J. Polym. Sci. (A-2)* 1970, 8, 649
- 7 Bassett, D. C. and Davitt, R. *Polymer* 1974, 15, 721
- 8 Kim, H.-G. and Mandelkern, L. *J. Polym. Sci. (A-2)* 1972, 10, 1125
- 9 Buszard, D. L. *PhD Thesis* Loughborough University of Technology (1973)
- 10 Sato, T. and Takahashi, M. *J. Appl. Polym. Sci.* 1969, 13, 2665
- 11 Hsieh, H. L. *J. Appl. Polym. Sci.* 1971, 15, 2425
- 12 Mendis, L. P. *PhD Thesis* Loughborough University of Technology (1975)
- 13 Sweet, G. E. and Bell, J. P. *J. Polym. Sci. (A-2)* 1972, 10, 1273
- 14 Roberts, R. C. *J. Polym. Sci. (B)* 1970, 8, 381

Book Reviews

Advances in Polymer Science

Volume 17: Polymerization

Springer-Verlag, Berlin, 1975, 103 pp. \$23.00

This volume in the series covers mechano-chemical initiation of copolymerization and the polymerization of thioaldehydes, thioketones and related compounds. It would be difficult to find two more widely different facets of polymer science. The first contribution, by Casale and Porter, includes processes of commercial importance whilst the second, by Sharkey, has yet to find industrial usage. Mechano-chemistry, as the authors ably illustrate, is applicable to an extremely wide range of polymer-monomer systems which can be activated by an extensive choice of 'bond-breaking' processes. On the one hand, the coextrusion of two viscoelastic polymers can lead to high yields of block copolymers having properties differing from simple blends, whilst on the other hand, esoteric materials can be synthesized for laboratory evaluation by vibromilling or even simple solvent swelling techniques. All reported aspects of mechano-chemical reactions leading to block and graft copolymerization are discussed in depth and there are extensive references to original publications.

The synthesis of polymers by polymerization through the carbon-sulphur double bond is a very specialized field which is treated in depth by Sharkey in this book with more extensive reference to recent publications, in particular the patent literature, than the mechano-chemical section. By virtue of its specialized nature, the latter section will have a rather limited interest more or less con-

finned to production and research personnel directly involved with condensation polymerization and ring opening reactions. The first section, because of its more general nature, will appeal to practically everyone involved in the research, development, production and application of copolymers at all levels.

Apart from some missing 'free radicals' on pages 9 and 22 and a pentavalent carbon atom on page 30, the book is relatively free of typographical errors. At \$23.00 it is expensive for approximately a hundred pages but it does give a thorough review of two topics for which much of the available data is published in languages other than English. The contribution by A. Cassale, R. H. Porter and W. H. Starkey maintains the high standard which we expect from this series and it will, therefore, take its rightful place in polymer libraries throughout the world.

R. J. Ceresa

Reinforced Thermoplastics

W. V. Titow and B. J. Latham

Applied Science, Barking, 1975, 294 pp. £10

'Reinforced Thermoplastics' is the first book to be published on this subject and its contents well meet the aim of its authors, which is 'to present a reasonably unified account of the technology and properties' of this class of plastics materials.

The description which the book provides is essentially technological in nature but it touches on some commercial problems. Thus, it ranges from a very useful list of commercially available reinforced thermoplastics and their producers, through a discussion of their principal applications to methods of processing and to material properties and there is also an appendix devoted to relevant patents.

The book is self-contained in that it includes a description of the polymeric materials which form the basis of reinforced thermoplastics and of their properties as well as that of fibrous and particulate fillers before dealing with the two in combination. The properties of reinforced thermoplastics are dealt with primarily in terms of short term data but the importance of long term behaviour is clearly recognised. In view of the inevitable lapse of time between the completion of a manuscript and publication, the discussion of properties does not include the results of research published during the past year or two. However, it is surprising to find virtually no mention of anisotropy, even though the authors have not attempted to deal in depth with what might be termed the more scientific aspects of reinforced thermoplastics, as they clearly state in the Preface. Nevertheless, their book should be of considerable interest and of value to anyone concerned with reinforced thermoplastics.

R. M. Ogorkiewicz

Conference Announcement

Structure and Uses of Biopolymers

Cleveland, Ohio, USA, 11-16 October 1976

The first Cleveland Symposium on Macromolecules will be held during the week of October 11-16th, 1976 with the topic of Structure and uses of biopolymers. The week-long conference will be organized around fifteen invited international presentations in three areas: fundamental structure of biopolymers; materials properties; and medical applications, and will involve local social functions. Contributions of short papers to be presented at the meeting in the above areas are solicited. Prospective contributors, attendees and interested persons should write for further information to: Professor Alan G. Walton, Department of Macromolecular Science, Case Western Reserve University, Cleveland, Ohio 44106, USA.

Interesterification of starch with methyl palmitate

M. L. Rooney

CSIRO, Division of Food Research, Food Research Laboratory, North Ryde, New South Wales, Australia

(Received 19 December 1975)

Thermoplastic polymers derived from natural products have been prepared by interesterifying starch with methyl palmitate. The degree of substitution (*DS*) of the esters has been found to be strongly dependent upon catalyst concentration and the ratio of methyl palmitate to starch, but is largely independent of temperature and starch concentration over the range studied. Replacement of methyl palmitate with methyl esters of shorter chain acids does not appear to affect the *DS*. These observations are interpreted from the results of studies on the effect of *DS* on the solubility parameter, the nature of the interchain bonding and the specific gravity of the polymers.

INTRODUCTION

Most polymers isolated from natural products and subsequently modified retain the hydrophilic characteristic of the base polymer, whereas polysaccharide esters of long chain fatty acids have been shown to be more hydrophobic^{1,2}. Recently several authors have proposed uses for such esters. Amylose esters of a variety of fatty acids have some properties sought in dip coatings for foods², while starch esters can be used as reactive bases for polyurethane resins³ or as an artificial skin⁴. Starch esters may ultimately prove useful as low cost resins and replace some of those currently derived from petroleum.

Fatty acid esters of starch are usually prepared in the laboratory using the acid chloride-pyridine method⁵. However, this method is of little commercial value because of the cost of acid chlorides⁶. Direct esterification using the acid gives unsatisfactory yields while the anhydrides are not readily available. Interesterification has been used extensively in the preparation of biodegradable detergents from sucrose and fatty acid methyl esters⁶⁻⁸. Latetin *et al.*⁹ reacted cellulose heterogeneously with methyl stearate in dimethylformamide to a maximum degree of substitution (*DS*) of 0.38 compared with a theoretical maximum of 3. The interesterification of starch with the methyl esters of higher fatty acids has not been reported, although it is of particular interest since starch, unlike cellulose, is soluble in such solvents as dimethylsulphoxide (DMSO).

The present work was undertaken to determine the conditions under which starch could be interesterified with the methyl esters of long chain fatty acids, and to obtain data indicating the *DS* at which useful properties might be obtained. These studies include an examination of the effects of temperature, the concentrations of starch, methyl palmitate and potassium methoxide as well as the chain length of the fatty acid, on the *DS* of the resultant esters. The effects of *DS* on the specific gravity, solubility parameter and infra-red spectra of each of the esters were also determined.

EXPERIMENTAL

Materials

Wheat starch (Fielders Ltd, Sydney) was defatted and dried to a moisture content of 2.1%. The methyl esters

of palmitic, lauric and octanoic acids were greater than 98% pure and had water and free fatty acid contents less than 0.05%. Methyl n-butanoate had water and free fatty acid contents of 0.38% and 0.17% respectively. Methanolic potassium methoxide solution, 1.5 M, was used as a catalyst. Dimethylsulphoxide (Ajax Chemicals, Sydney) was dried by vacuum evaporation of 15% of its volume¹⁰.

Interesterification

The method of interesterification was similar to that used with sucrose⁷, although the starch and methyl ester solutions (dried to less than 0.02% water) were not mixed until the catalyst had been added to the starch solution and the methanol removed. The reaction was allowed to continue for 6 h after which the starch ester was precipitated with aqueous ethanol, extracted for 3 days both with boiling water and ethanol and then dried under vacuum at 80°C for 6 h.

Analyses

Water analyses were carried out using Karl Fischer reagent. Acyl contents of starch esters of palmitic and lauric acids were determined using the method of Berni *et al.*¹¹ for cellulose esters, except that after 48 h hydrolysis the starch formed was precipitated with methanol.

Aliquots (0.5 μ l) of the fatty acid salt solution were chromatographed on a Perkin-Elmer FII gas chromatograph with flame ionization detector and a column, 2 m \times 3.2 mm o.d. packed with SE 30, 5% on Chromosorb W with a nitrogen carrier flow rate of 22 ml/min. The column and injection block temperatures were 238°C and 370°C respectively, the latter being necessary to pyrolyze the quaternary ammonium salts to methyl esters. At least two samples of each ester were hydrolysed for 48 h and a minimum of four aliquots of each were chromatographed.

Acyl contents of octanoate and n-butanoate esters were determined by the alcoholic alkali method¹².

Specific gravity

The specific gravity of the polymers was measured¹³ by displacement of water and/or light petroleum ether (b.p. 100°–120°C). Water was used only for esters of *DS* greater than 0.6 while light petroleum ether was used for all esters of lower *DS* and for spot checking some esters of higher *DS*.

Table 1 Starch palmitates prepared* at various catalyst concentrations

KOHCH ₃ concentration (mol/mol starch)	DS†	Precipitation‡		Yield‡ (%)
		Alkoxide	Ester	
0.001	0.03	—	—	67
0.010	0.18	—	—	65
0.025	0.60	—	+	90
0.050	0.86	+	+	88
0.100	1.10	+	+	93
0.200	0.98	+	+	94

* Reaction Conditions: Temperature 100°C; starch/DMSO ratio 9.5×10^{-3} ; methyl palmitate/starch ratio 3.0; time 6 h

† The value 0.98 is not significantly different ($P = 0.05$) from values of 1.10 and 0.86

‡ Precipitate formed (+); no precipitate formed (—)

‡ Calculated from the weight of starch in esterified form compared with the original weight of starch

Infra-red Spectra

Films less than 20 μm thick for i.r. studies were prepared by means of a laboratory heat sealer and dried over phosphorus pentoxide. I.r. spectra were recorded using a JASCO IRA-1 spectrophotometer (Tosco, Sydney).

RESULTS AND DISCUSSION

Starch concentration

The mole ratio of starch* to DMSO was varied in four steps from 4.7×10^{-3} to 2.8×10^{-2} at 100°C, while the mole ratios of catalyst and methyl palmitate to starch were held at 0.1 and 3.0 respectively. The DS of the resulting esters was independent ($P = 0.05$) of the starch concentration and so a starch to DMSO ratio of 0.5×10^{-3} , an experimentally convenient value, was chosen for subsequent studies.

The reaction was also attempted using a dispersion of starch in pyridine⁵ but no starch ester could be isolated.

Catalyst concentration

The effects of raising the mole ratio of potassium methoxide to starch from 0.001 to 0.200 are shown in Table 1. The DS increased significantly ($P = 0.05$) with catalyst concentration up to a catalyst to starch mole ratio of 0.100. Based on the present data however, the DS value at the highest catalyst to starch ratio of 0.200 was not significantly different ($P = 0.05$) from the DS values at ratios of 0.050 and 0.100.

The reaction occurred homogeneously or partly heterogeneously depending upon the catalyst to starch ratio (Table 1). Two factors may explain both this behaviour and the effect of catalyst to starch ratio on DS. These factors are the removal of catalyst by reaction with traces of water and the insolubility of highly esterified starch.

The initial water content in each preparation was less than or equal to 0.02%, which is equivalent to one hundred times the catalyst concentration when the catalyst to starch ratio was 0.001. The very low DS value (0.03) obtained under these conditions was probably a result of catalyst destruction by water. The same probably applied to a decreasing degree as the catalyst to starch ratio was increased to 0.10, at which point the maximum possible water content equalled the catalyst concentration.

* In this report anhydroglucose, the starch repeat unit, was used as the basis for calculation of the number of moles of starch.

The precipitation of starch ester gel at catalyst to starch ratios of 0.025 or greater may be understood by reference to Figure 1a which shows the effect of DS on the Hildebrand solubility parameter (δ) obtained from measured specific gravities¹⁴. Esters of solubility parameter less than about 11 should be insoluble in DMSO¹⁵ (solubility parameter 12.93) since a difference between the solubility parameters of solute and solvent of less than 1.7 to 2 is a critical requirement for solubility¹⁶. This difference rule is probably modified by the specific reaction between DMSO¹⁷ and carbohydrates and hydrogen bonding within the polymer¹⁶. The lowest DS ester which was precipitated (Table 1) had a solubility parameter of 10 which is 2.93 less than that of the solvent.

The fact that the maximum DS obtained was 1.10 instead of 3.0 leads to the suggestion that as the DS increased the solubility parameter decreased, and in the presence of DMSO, the gel became less accessible to dissolved catalyst and methyl palmitate.

The same two factors which affected the DS also affected the yield. Removal of catalyst from solution, by means of formation of starch alkoxide immobilized on gel molecules, prevented further reaction. In this way dissolved starch did not come into contact with the catalyst and the reaction stopped. A second catalyst addition after gel precipitation might have resulted in higher yields. At low catalyst concentrations the catalyst removal by water would also have reduced yields.

Potassium carbonate was also used as a catalyst but gave results similar to those obtained using the methoxide.

Reagent ratio

The reverse reaction of methanol with starch palmitate was inhibited by distillation of the methanol formed and by increases in the ratio of methyl palmitate to starch as

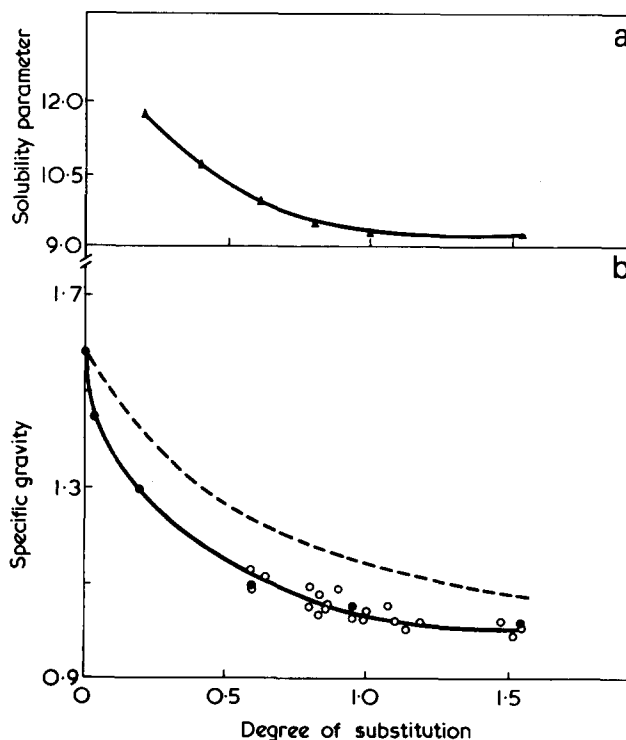


Figure 1 (a) Solubility parameter of starch palmitates versus degree of substitution. (b) Specific gravity of starch palmitates versus degree of substitution: ●, petroleum spirit; ○, water; as immersion liquid

Table 2 Starch palmitates prepared* at various reagent ratios

Methyl palmitate/ starch (mol/mol)	DS	Yield‡ (%)
1	0.59	75
3	1.10	93
5	1.48	82
10	1.52	71
15	1.54	67

* Reaction Conditions: Temperature 100°C; catalyst/starch ratio 0.10; starch/DMSO ratio 9.5×10^{-3} ; time 6 h

‡ Calculated from the weight of starch in esterified form compared with the original weight of starch

Table 3 Degree of substitution of starch palmitates prepared at various temperatures

Temperature (°C)	DS
80	0.71
90	0.90
100	1.08
110	0.86

shown in Table 2. The DS increased significantly ($P = 0.01$) as the reagent ratio was increased to a value of 10. Based on the present data, the DS value at the highest reagent ratio of 15 was not significantly different ($P = 0.01$) from the DS values at ratios of 5 and 10. This form of relationship is similar to those reported for cellulose stearate⁹ and sucrose palmitate⁸ formation.

Temperature

The effect of increasing the reaction temperature, from 80° to 110°C, on the DS of starch palmitate is shown in Table 3. This temperature ranged from the boiling point of DMSO at the vacuum used to the temperature above which starch degradation may become serious. All DS values were significantly different ($P = 0.05$) except those for 90° and 110°C. The differences between DS values for 100° and 110°C on the one hand and 80° and 100°C on the other are significant at $P = 0.01$. This very small effect of temperature on DS largely supports the findings of Latetin *et al.*⁹ for cellulose esterification.

Length of the fatty acid

The methyl esters of lauric, octanoic and butanoic acids were reacted with starch to establish whether or not the length of the fatty acid determined the maximum DS attainable at 100°C. The mole ratios of catalyst to starch, methyl palmitate to starch and starch to DMSO were 0.10, 9.5×10^{-3} and 5.0 respectively. Methanol was removed from the methyl butanoate reaction by means of a stream of nitrogen since the low boiling point of the methyl butanoate precluded use of refluxing under vacuum.

The DS values of the esters of octanoic, lauric and palmitic acids formed under these conditions were 1.53, 1.47 and 1.47 respectively. Such small differences could be attributed to similar relationships between solubility and DS for each of the fatty acid esters. The highest DS obtained for starch butanoate was 0.38 and this is attributed to the inadequate removal of methanol by the nitrogen stream.

This apparent independence of DS on length of the acid, at least for acids from C₈ to C₁₆, is in agreement with the

results of Gros and Feuge² for esterification using acid chlorides.

Infra-red spectra

The effect of DS on the hydrogen bonding in starch esters was studied by measurement of i.r. spectra. Esters of DS 0.6 or greater gave quite distinct spectra with many resolved bands, while the spectrum of an ester of DS 0.19 was quite similar to that of starch except for the carbonyl absorption. At DS values less than 0.19, polymer films were not prepared due to the failure of the polymers to melt.

The principal features of these spectra are the profile and wavelength of maximum absorption of the hydroxyl fundamental around 3400 cm⁻¹, as shown in Figure 2 for esters of DS 0.19, 0.64 and 1.54. This band is markedly influenced by DS, being (a) totally unresolved from that of the CH stretch at a DS of 0.19; (b) an asymmetrical band of maximum absorbance centering at 3340 cm⁻¹ at a DS of 0.64 and (c) a more symmetrical band with maximum absorbance at 3460 cm⁻¹ at a DS of 1.54. The result of partial acetylation of an ester of DS 1.52 is shown in Figure 2.

The hydroxyl absorption in the solution spectrum of an ester of DS 1.54 (0.02 M in carbon tetrachloride) was a composite of bands at 3460 cm⁻¹ and 3550 cm⁻¹. The latter band disappeared as the concentration was increased, until a saturated solution gave a spectrum similar to that of the solid polymer.

The spectral results may be interpreted as follows. As the DS increases from 0.19 to 0.54 the predominant form of hydrogen bonding changes from polymeric to dimeric¹⁸. Acetylation provides a free environment for some hydroxyls and allows mainly dimer formation for the rest. Solution in

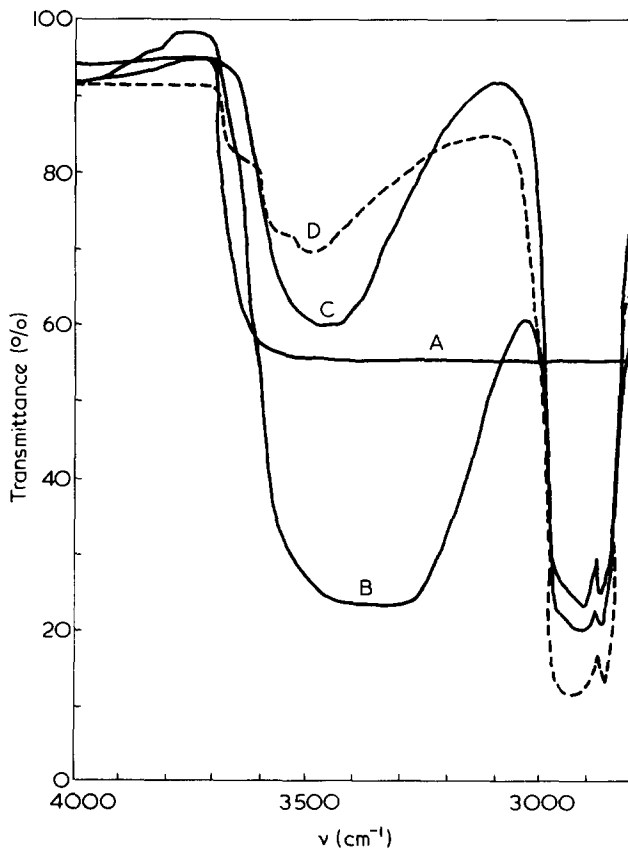


Figure 2 Absorption frequency of hydroxyl fundamental: A, DS = 0.19; B, DS = 0.64; C, DS = 1.54; D, DS = 1.52 then acetylated

carbon tetrachloride causes disruption of interchain hydrogen bonds leading to an increased proportion of dimers on dilution. Polymeric hydrogen bonding would probably involve hydroxyls on several chains or segments whereas dimers can be formed between hydroxyls at C₂ and C₃ on adjacent anhydroglucose units.

The frequencies of maximum absorbance (ν) of the hydroxyl fundamental in the spectra of all of the esters prepared have been fitted to the equation:

$$\nu = 3238 + 135 \times DS$$

with a standard error of estimate of 14.6 and a correlation coefficient of 0.94. The scatter of the results is attributed to the flatness of the absorption band as would be expected when several closely spaced bands overlap. Thus the frequency of maximum absorbance of this band provides a measure of the *DS* of the ester. There is also a sharp band near 720 cm⁻¹ which is probably due to the methylene rocking vibration of palmitate chains. The intensity of this band increases markedly with increasing *DS* and may also offer some scope for quantitative analysis of these and related esters.

Starch octanoate of *DS* 1.53 and the laurate of *DS* 1.47 both had their hydroxyl fundamental maximum at 3405 cm⁻¹, which is more than two standard errors lower than the frequencies for the corresponding palmitates. This would be expected with shorter chain fatty acid esters which would interfere less with hydrogen bonding.

Specific gravity

Figure 1*b* shows the effect of *DS* on the specific gravity (*SG*) at 23°C of starch palmitates. The broken curve was calculated using the linear combination of specific gravities of starch and palmitic acid. The disruption of optimal packing of molecules in both of the free components is reflected in the lower specific gravity values of the esters over the range studied. This is consistent with the i.r. results which indicate disruption of interchain hydrogen bonding.

The apparent approach of the experimental results to a limiting *SG* of around 1.01 is supported by the reported value² of 1.022 (at 30°C) for amylose palmitate of *DS* 2.02. The octanoate of *DS* 1.53 has a specific gravity of 1.115 compared with 1.119 reported² for amylose octanoate of *DS* 2.25. Similarly the starch laurate of *DS* 1.47 has a specific gravity of 1.056 compared with 1.059 reported² for amylose laurate of *DS* 2.49. It appears that these esters

may also have limiting specific gravity values independent of *DS* over a range similar to that for the palmitates.

Since the specific gravity of the palmitate esters appears to be fairly constant over the *DS* range from 1 to 2 approximately, it is possible that some of the valuable properties reported² for the high *DS* esters might be found in esters of much lower *DS* also. This suggestion is supported by the nature of the solubility parameter versus *DS* curve in Figure 1*a*.

ACKNOWLEDGEMENTS

The author wishes to thank Mr E. G. Davis and Dr R. V. Holland for their helpful advice; Mr D. J. Best for carrying out statistical analyses and Mr A. J. Shorter for his valuable technical assistance.

REFERENCES

- 1 Malm, C. J., Mench, J. W., Kendall, D. L. and Hiatt, C. D. *Ind. Eng. Chem.* 1951, **43**, 684
- 2 Gros, A. T. and Feuge, R. O. *J. Am. Oil Chem. Soc.* 1962, **39**, 19
- 3 Otey, F. H., Westhoff, R. P. and Mehlretter, C. L. *Staerke* 1972, **24**, 107
- 4 Laden, K., Sokol, P. E., Tsai, Hu-Chu and Rogers, B. A., *Germ. Pat.* 1 926 068 (1970)
- 5 Pacsu, E. and Mullen, J. W. *J. Am. Chem. Soc.* 1941, **63**, 1487
- 6 'Sucrose Ester Surfactants', Sugar Research Foundation, New York, 1960
- 7 Bares, M. and Zajic, J. *Sb. Vys. Sk. Chem. Technol. Prazhe Potraviny (E)* 1968, **21**, 55
- 8 Weiss, T. J., Brown, M. and Zeringue, H. J. *J. Am. Oil Chem. Soc.* 1972, **49**, 524
- 9 Latetin, A. J., Gal'braikh, L. S. and Rogovin, Z. A. *Polym. Sci. USSR* 1968, **10**, 761
- 10 Cohen, E. and Zilkha, A. *J. Polym. Sci. (A-1)* 1969, **7**, 1881
- 11 Berni, R., Soignet, D. and Ward, T. *Text. Res. J.* 1969, **39**, 887
- 12 Genung, L. B. and Mallatt, R. C. *Ind. Eng. Chem. Anal. Ed.* 1941, **13**, 369
- 13 ASTM Annual Book of Standards, Part 35, Standard Method D792-66, 1974
- 14 Hoy, K. L. *J. Paint. Technol.* 1970, **42**, 76
- 15 Hansen, C. M. and Skaarup, K. *J. Paint Technol.* 1967, **39**, 511
- 16 Billmeyer, F. W. 'Textbook of Polymer Science' 2nd Edn, Wiley Interscience, New York, 1971, p 25
- 17 Rao, V. S. R. and Foster, J. F. *J. Phys. Chem.* 1965, **69**, 656
- 18 Phillips, J. B. 'Spectra-Structure Correlation', Academic Press, New York, 1964, p 69

Differential scanning calorimetric studies on phase transition of glucose and cellulose oligosaccharides

Tatsuko Hatakeyama

Research Institute for Polymers and Textiles, Sawatari, Kanagawa-ku, Yokohama, Japan

and Hiroshi Yoshida*, Chikage Nagasaki† and Hyoe Hatakeyama

Industrial Products Research Institute, Shimomaruko, Ota-ku, Tokyo, Japan

(Received 29 August 1975; revised 30 January 1976)

The phase transitions of D-glucose and an homologous series of cellulose oligosaccharides up to cello-tetraose have been studied using a differential scanning calorimeter. A detailed comparison of our experimental results with those reported by other workers has been made in order to derive precise information on melting and glass transitions of carbohydrates. Particular attention has been given to the static values of melting temperature of D-glucose and cellobiose. It has also been found that cellulose oligosaccharides which have more than three anhydroglucose units decompose below melting temperature.

INTRODUCTION

In the course of the studies of the phase transition of glucose and an homologous series of cellulose oligosaccharides in solid state, information on precise values of phase transition temperatures such as melting and glass transition temperatures are undoubtedly necessary. Pigman *et al.*¹ reported melting temperatures of D-glucose in different crystal forms. Wolfrom and Dacons² reviewed the values of transition temperatures of glucose and cellulose oligosaccharides up to celloheptaose. Alfthan *et al.*³ tried to estimate glass transition temperatures of several oligosaccharides from cellulose and xylan.

However, those values reported seem to contain some errors from the thermodynamic point of view, since the values were not obtained under carefully defined thermal conditions and time factors. Therefore, in this study, we have re-examined phase transitions of D-glucose and cellulose oligosaccharides up to cello-tetraose by the use of a differential scanning calorimeter. The isothermal melting of the carbohydrates which have melting points was carried out and attempts were made to obtain the static values of melting temperature. At the same time glass transition temperatures of glassy samples of glucose and cellulose oligosaccharides were evaluated.

EXPERIMENTAL

Sample Preparation

D-glucose monohydrate obtained commercially from Merck AG was ground to a fine powder and was dissolved into hot, absolutely dry ethanol. The solution was then placed for one night at room temperature. Anhydrous α -D-glucose separated out as crystals.

The D-glucose, above (obtained commercially) was also dissolved into water. The solution was placed for 48 h in a refrigerator. Crystals of α -D-glucose monohydrate separated out.

β -D-glucose was obtained commercially from Tokyo Chemical Industry Co. Ltd and contained 7.7% of α -D-glucose as determined from a gas chromatogram obtained under the following conditions using a Shimadzu GC-4AIT gas chromatograph: the column was a stainless tube packed with 5% silicone SE-30/Celite; temperature, 200°C; carrier gas, He 30 ml/min; TCD detector, 3 mV full scale.

Cellobiose was obtained commercially from Merck AG. The crystal forms of the above compounds were examined from X-ray diffractograms⁴⁻⁷.

According to the procedure reported by Miller *et al.*⁸, cellulose oligosaccharides containing more than three anhydrous glucose units were prepared as follows. First cellulose was acetylated with a mixture of glacial acetic acid, acetic anhydride and concentrated sulphuric acid. Then the acetylated oligosaccharides produced were separated into two portions, the anhydrous methanol soluble portion was deacetylated with sodium methylate. The free oligosaccharides obtained were separated by ethanol-water gradient elution from a chromatographic column composed of stearic acid treated mixtures of charcoal and Celite. Each separated fraction was concentrated with a rotary vacuum evaporator and dried *in vacuo*. Purification of the samples was carried out by re-chromatographic treatment and the purity examined by thin layer chromatography⁹. Characterization of the samples was carried out by measuring the molecular weight with a Hitachi model 115 molecular weight apparatus.

Amorphous glucose and cellulose oligosaccharides were prepared by freeze-drying their aqueous solution¹⁰. First small amounts of the samples were dissolved in water. The solution was then frozen quickly using liquid nitrogen as a refrigerant, and dried *in vacuo* so as to drive the solvent off. Amorphous materials obtained were dried thoroughly *in vacuo* for more than two days. Amorphous glucose was also prepared by rapid cooling from the molten state.

* Present address: Tokyo Metropolitan University, Faculty of Technology, Setagaya-ku, Tokyo, Japan.

† Present address: Tokyo University of Agriculture and Technology, Faculty of Technology, Koganei, Tokyo, Japan.

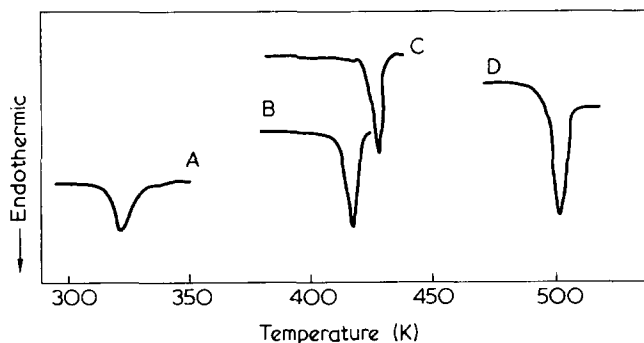


Figure 1 D.s.c. melting curves of glucose and cellobiose. A, α -D-Glucose monohydrate; B, α -D-glucose anhydride; C, β -D-glucose; D, cellobiose. Heating velocity, $1^{\circ}\text{C}/\text{min}$

Measurements

A Perkin-Elmer differential scanning calorimeter, DSC-II was used throughout this experiment, low temperature equipment being attached to the DSC-II when the glass transition of D-glucose was measured. Temperature was calibrated at all scanning velocity ranges using the melting temperature of indium as a standard. At low temperature regions, melting of spectrograde benzene was used for the calibration. In both cases, the foot temperature of a melting peak observed in a differential scanning calorimetric (d.s.c.) curve was taken as the melting temperature according to the procedure recommended as a common calibration method in the manual for DSC-II¹¹.

Samples were sealed into d.s.c. pans for volatile samples as this eliminates the effect of humidity. Sample weight used as in this study was from 2 to 3 mg. Heating velocity was varied from 0.63 to $20^{\circ}\text{C}/\text{min}$. When crystalline samples were measured by dynamic method at the desired heating velocity, peak temperature was adopted as a criterion of melting for a matter of convenience¹². We mixed some samples with copper powder (1:1 in weight) and pressed into thin, small plates to increase the thermal conductivity, as the samples used were rather bulky. These mixed samples were also tested and compared with unmixed ones.

The following isothermal melting was carried out using the DSC-II, in order to measure the equilibrium melting temperatures of D-glucose and cellobiose. At first the sample was heated to the melting temperature which was roughly estimated from the value extrapolated to zero heating velocity from dynamic measurements carried out at different heating velocities. The heat change was recorded while the sample was maintained above the melting temperature. After keeping the sample at the temperature for a certain time, the sample was reheated to ascertain whether any crystals remained. The equilibrium melting temperature was thus determined by successively changing temperatures in the vicinity of the supposed equilibrium temperature.

The glass transition temperature was defined as the point when the extension of the base line intersects with a line tangent to the maximum slope of the endothermic peak.

RESULTS AND DISCUSSION

Figure 1 shows the d.s.c. curves of α -D-glucose having different crystal forms, anhydride and monohydrate; β -D-glucose and cellobiose respectively. Melting temperatures of these compounds measured at the heating velocity of $1^{\circ}\text{C}/\text{min}$ are not very different from the temperature reported pre-

viously². Melting curves of glucose and cellobiose were broad compared with those of other materials used as calibration standards such as benzene, benzoic acid and indium. The initial melting temperature of the above carbohydrates was difficult to estimate precisely from the foot temperature of a melting peak because of a gradual change in specific heat occurring from a temperature far lower than that of melting. Therefore, peak temperature was adopted in this study as a criterion of melting as described previously. In the case of cellobiose, the specific heat change was observed as a deflection in the base line of a d.s.c. curve before and after melting. Partial decomposition seems to be masked with the melting peak¹³.

Figure 2 shows the relation between the temperature of a peak and heating velocity for the samples of α -D-glucose anhydride and β -D-glucose. The melting temperature increased with increasing heating velocity. The change of peak temperatures was remarkable compared to known values of organic compounds. Similar results were also obtained in the case of α -D-glucose monohydrate and cellobiose.

Hellmuth *et al.*¹⁴ suggested that super heating was taking place after considering the special character of the structure of these organic compounds. On the other hand, Ichihara¹⁵ suggested that the heat conductivity of an organic compound could not be ignored when the heating velocity dependency was discussed even if the sample weight was very small. Iguchi¹⁶ and Hatakeyama¹⁷ obtained good agreement with the results of Ichihara¹⁵ by using extended chain-type polyoxymethylene crystal and high molecular

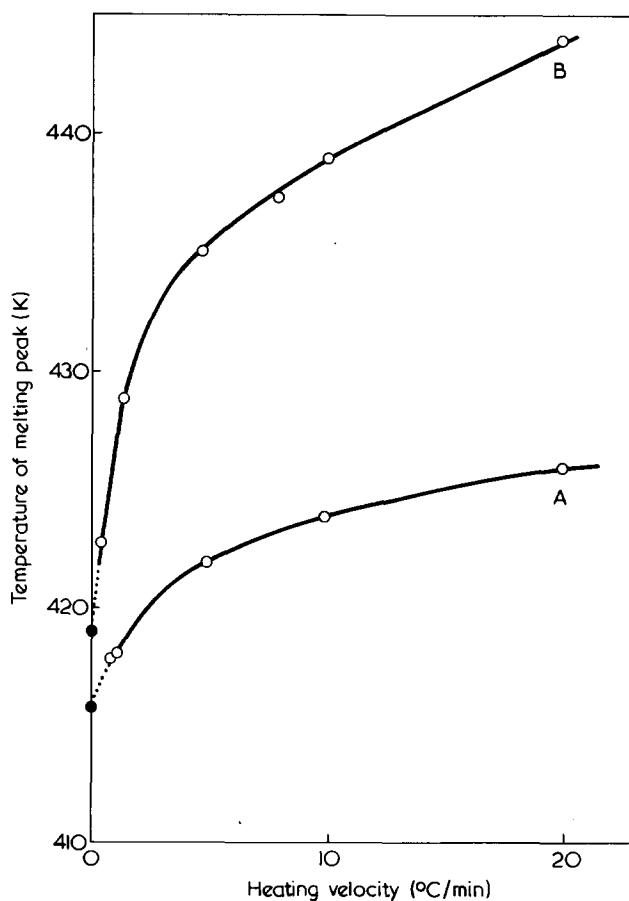


Figure 2 Heating velocity dependency of melting peak temperature for α -D-glucose anhydride and β -D-glucose. A, α -D-Glucose anhydride; B, β -D-glucose

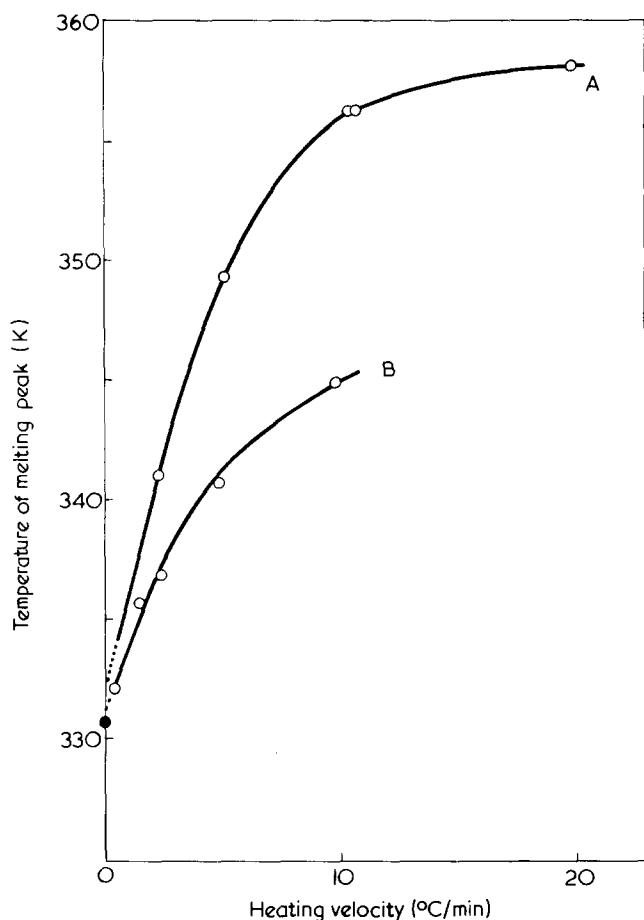


Figure 3 Heating velocity dependency of melting peak temperature for α -D-glucose monohydrate. A, α -D-Glucose monohydrate; B, α -D-glucose monohydrate with Cu powder

weight polyethylene as samples. In order to clarify the effect of super heating and/or heat conductivity on the melting of carbohydrates, the melting temperature of α -D-glucose monohydrate was compared with that mixed with copper powder, as described earlier. As shown in Figure 3, the melting temperature of α -D-glucose monohydrate was affected seriously by the conditions of the sample in the high heating velocity region. This fact suggests that the heat conductivity of a sample played an important part in heating velocity dependency.

It was difficult to evaluate the melting temperature of the compounds from the data obtained by dynamic measurements, since the melting peak temperatures of glucose and cellobiose depended on heating velocity. Therefore, we tried to measure the equilibrium melting temperatures from melting curves obtained by the procedure described earlier.

Figure 4 shows the isothermal melting curves of α -D-glucose monohydrate. From this Figure, it is shown that the melting of the sample takes place over a very long time interval. The same melting behaviour was observed in the case of cellobiose. The large heating velocity dependency of glucose and cellobiose seemed due to the above features of the compounds. Isothermal melting was carried out for all samples having melting temperatures. The cellulose oligosaccharides having more than three anhydroglucose units decomposed without melting. It is possible to redraw the endotherms shown in Figure 4 into accumulation type melting curves as a function of time as shown in Figure 5. From these curves, we could estimate the half-time of melting at various temperatures. The half-time thus evalu-

ated is shown in Figure 6 for the case of α -D-glucose monohydrate.

As described above, the half-time of melting shown in Figure 6 was calculated from the isotherm of a sample which remained isothermal until it melted completely. In this case, however, if the temperature at which a sample is kept isothermally approaches an ideal equilibrium melting temperature, the time interval for melting is also expected to approach infinity, which cannot be attained in the experimental time interval. Moreover, the sensitivity of the d.s.c. is not sufficient to follow such a small amount of heat in unit time, since the transition occurs over a long period. However, the difference between the maximum and minimum temperatures where isothermal melt could occur in a sample converged within $\pm 0.5^\circ\text{C}$ by holding a

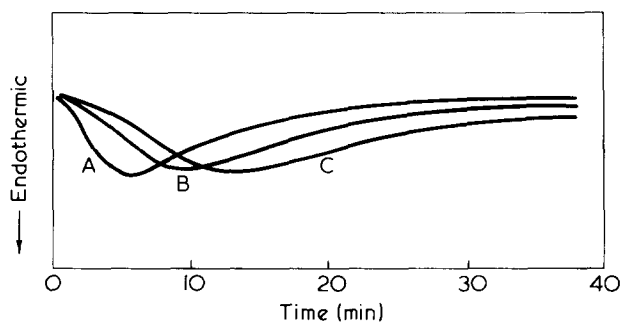


Figure 4 Isothermal melting curves of α -D-glucose monohydrate. A, 336K; B, 334K; C, 333K

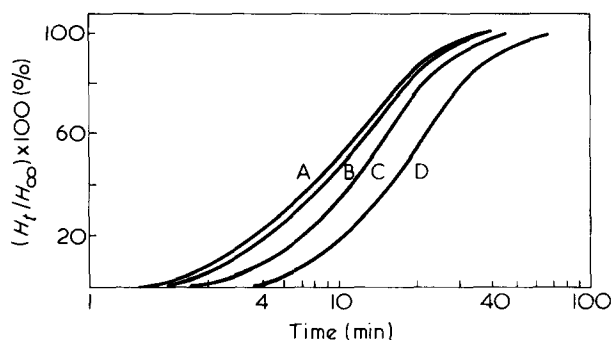


Figure 5 Accumulation type of melting curves for α -D-glucose monohydrate; where H_t is the heat of fusion at time t and H_∞ is the final heat of fusion. A, 336K; B, 335K; C, 334K; D, 333K

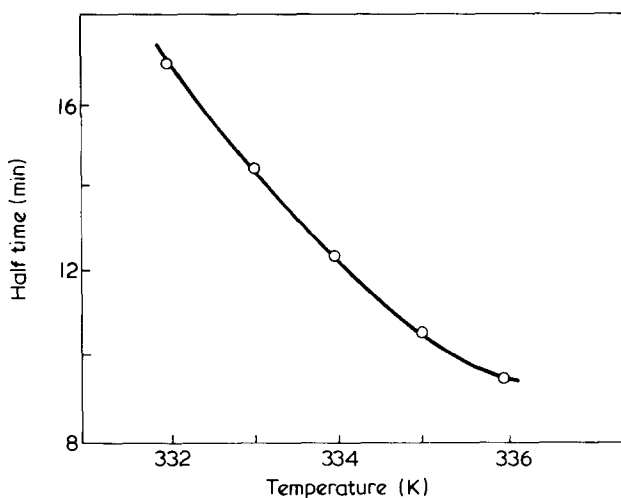


Figure 6 Relationship between half-time of melting and the temperature for α -D-glucose monohydrate kept in an isothermal state

Table 1 Melting (T_m) and glass transition (T_g) temperatures of cellulose oligosaccharides

Sample	T_m (K)		T_g (K)	
	This work*	Reference 2	This work*	Reference 3
α -D-Glucose monohydrate	331	356		
α -D-Glucose anhydride	416	419	284	—
β -D-Glucose	419	421–428		
Cellobiose	505	521	335	397
Cellotriose	—		364	—
Cellotetraose	—		355	431

* In this work, T_m was determined by isothermal melting and T_g was estimated from a d.s.c. curve at the heating velocity of $10^\circ\text{C}/\text{min}$

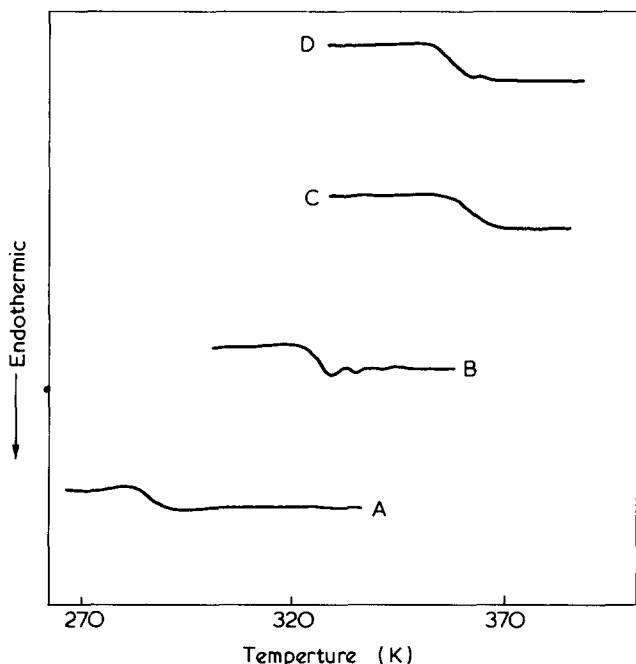


Figure 7 D.s.c. curves of amorphous glucose, cellobiose, cellotriose and cellotetraose near the glass transition temperature. A, D-Glucose; B, cellobiose; C, cellotriose; D, cellotetraose. Heating velocity, $10^\circ\text{C}/\text{min}$

sample successively at different temperatures. The isothermal melting temperature obtained by the above method coincided well with that obtained by extrapolating values from the dynamic measurements shown in Figures 2 and 3. Table 1 shows phase transition temperatures obtained in this experiment and those reported in the literatures.

Amorphous samples of D-glucose and cellulose oligosaccharides were prepared following the method described earlier. X-ray diffractograms of the samples showed the typical amorphous pattern. It was possible for crystallization to take place by conditioning amorphous samples under an atmosphere with a very small amount of water at a suitable crystallization temperature. Crystallization of amorphous samples has been discussed in another report¹⁸. Crystallization was never observed by d.s.c. or X-ray diffraction measurement, if a sample was completely dried and handled in water free conditions. Figure 7 shows the d.s.c. heating curves of amorphous samples measured at the heating velocity of $10^\circ\text{C}/\text{min}$ near the glass transition temperatures. The specific heat change was seen clearly for all

samples. The glass transition temperatures were determined from the curves in Figure 7. The temperature errors of glass transition were within $\pm 1^\circ\text{C}$ among the runs made using different samples. No serious effects of temperature cycling was observed among the runs carried out in the temperature range from 270K to 400K.

The melting and glass transition temperatures estimated above are all listed in Table 1 together with the data obtained previously. From Table 1 it can be seen that the melting temperatures estimated in the present study are rather low as a whole compared with data reported previously. This is because the effect of time factor on phase transition process is taken into consideration.

As seen in Table 1 the glass transition temperatures of oligosaccharides increase with increasing degree of polymerization except for cellotetraose which might be contaminated by small amounts of impurities. The glass transition temperatures measured in the present study are quite different from those obtained by Alfthan *et al.*³, even after considering the different techniques used. They estimated the glass transition by torsional brake analysis and the maximum temperature of damping was adopted as the criterion of the glass transition temperature. As is well known, dynamic loss in viscoelasticity does not correspond only to the main motion but also to other phase transition, such as crystallization and local mode relaxations. On the other hand, by the thermal analysis, the glass transition is observed as the specific heat change, which is clearly distinguishable from the other first order transitions. Judging from the results obtained in this study, the glass transition temperatures reported by Alfthan *et al.*³ seem to coincide rather well with the cold crystallization temperatures which were detected in d.s.c. curves when the amorphous samples contained small amounts of water.

REFERENCES

- 1 Pigman, W. W. and Coepp Jr., R. M. 'Chemistry of the Carbohydrates, Academic Press, New York, 1948
- 2 Wolfrom, M. L. and Dacons, J. C. *J. Am. Chem. Soc.* 1952, 74, 5331
- 3 Alfthan, E., Ruvo, A. and Brown, W. *Polymer* 1973, 14, 329
- 4 McDonald, T. R. R. and Beevers, C. A. *Acta. Crystallogr.* 1952, 5, 654
- 5 Kiliean, R. C. G., Ferrier, W. G. and Young, D. W. *Acta. Crystallogr.* 1962, 15, 911
- 6 Ferrier, W. G. *Acta. Crystallogr.* 1963, 16, 1023
- 7 Jacobsson, R. A. *Acta. Crystallogr.* 1961, 14, 598
- 8 Miller, G. L., Dean, J. and Blum, R. *Arch. Biochem. Biophys.* 1960, 91, 21
- 9 Becker, E. S., Hamilton, J. K. and Lucke, W. E. *Tappi* 1965, 48, 60
- 10 Mann, J. *Proc. Wood Chem. Symp. Montreal, Canada 1961* p 91
- 11 Perkin Elmer Manual for DSC-II.
- 12 Seki, S. *et al.* 'Jikken Kagaku Koza' (Eds M. Otake *et al.*), Maruzen, Tokyo, 1958, Vol 5, pp 324
- 13 Shafizadeh, F. and Lai, Y. Z. *Carbohydr. Res.* 1973, 31, 57
- 14 Hellmuth, E. and Wunderlich, B. *J. Appl. Phys.* 1956, 36, 309; Hellmuth, E., Wunderlich, B. and Rankin Jr., J. M. *Appl. Polym. Symp.* 1966, 2, 101
- 15 Ichihara, S. *Proc. 5th Semin. Therm. Anal. Japan, Tokyo, Japan 1975*; Ichihara, S. *Proc. 23rd Meet. Polym. Sci. Japan, Tokyo, Japan 1974* p 515
- 16 Iguchi, M. *Makromol. Chem.* in press
- 17 Hatakeyama, T. *Sen'i Gakkaishi* 1965, 31, 289
- 18 Hatakeyama, H., Yoshida, H. and Nakano, J. *Proc. 25th Meet. Wood Chem. Japan, Fukuoka, Japan 1975* p 116

Interaction between carboxylic acids and the peptide group

R. M. Stephens and E. M. Bradbury

Biophysics Laboratories, Portsmouth Polytechnic, Portsmouth PO1 2QG, UK
(Received 22 September 1975; revised 26 February 1976)

The interaction between the peptide group and carboxylic acids is one of either protonation or hydrogen bonding. Both interactions will affect the vibrational frequency of the peptide group, resulting in changes in the characteristic amide vibrations. Infra-red spectroscopy has been used to examine the change in the amide I and II absorption bands of the model compound *N*-methylacetamide (NMA) when it is dissolved in deuteriochloroform and various deuteriochloroform/carboxylic acids, such as acetic, formic, dichloroacetic and trifluoroacetic acid. The results indicate that the interaction is one of hydrogen bonding except when NMA is dissolved in the strongest acid used, trifluoroacetic acid (TFA). Studies on the interaction between TFA and the peptide group of poly(L-alanine) various poly(DL-alanines) and poly(γ -benzyl-L-glutamate) show that the hydrogen bond interaction occurs, with little evidence of protonation taking place. In poly(γ -benzyl-L-glutamate) it was found that the TFA interacted both with the peptide group and the side chain carboxyl group.

INTRODUCTION

Helix-random coil transitions of polypeptides can be induced by varying the proportion of polar and non-polar components in a mixed solvent. The polar solvents are normally trifluoroacetic acid (TFA) or dichloroacetic acid (DCA) and the interaction between these acids and the peptide group are not fully understood. The interactions that can occur between TFA and the peptide group can be illustrated by examining the interaction between *N*-methylacetamide (NMA) and TFA where it can be seen that either (a) protonation or (b) hydrogen bonding can occur, (see Figure 1).

Klotz and coworkers¹⁻³ have investigated this interaction by examining the overtone region of the infra-red spectra of *N*-methylacetamide dissolved in TFA and other non-polar solvents. The first overtone of the N-H stretching vibration was observed at 6557 cm⁻¹ when NMA was dissolved in carbon tetrachloride, dioxane and water. For low concentrations of NMA in TFA two peaks were observed, one at 6620 cm⁻¹ the other at 6557 cm⁻¹ with a shoulder at 6711 cm⁻¹. The 6620 cm⁻¹ band observed for NMA in TFA was identified as that due to the overtone of the N-H group of the amide in the protonated state, and the one at 6637 cm⁻¹ due to additional hydrogen bonding between N-H groups of the protonated series and either undissociated acid or the acid anion. It was also suggested that the shoulder of 6711 cm⁻¹ observed from NMA in TFA and the band at 6734 cm⁻¹ from NMA in acetic acid was due to amide N-H hydrogen bonded to the carboxyl groups of the acid. Measurements made in the 1800 cm⁻¹ to 1500 cm⁻¹ region for NMA in TFA showed bands at 1736 cm⁻¹, 1655 cm⁻¹ and 1613 cm⁻¹. These were interpreted as being due to the C=O vibration from the COOH group in TFA, to the amide I vibrations of the peptide group and to the presence of COO⁻ ions which would have an anti-symmetric stretching vibrational frequency at about 1613 cm⁻¹. The amide II vibration which occurs at 1563 cm⁻¹ in NMA was not seen. The results obtained from the near infra-red studies of poly(L-alanine), poly(L-leucine) and poly(γ -benzyl-L-glutamate) in CHCl₃/

TFA solutions showed that as the acid concentration increased there was a decrease in absorption at 6630 cm⁻¹ with a corresponding increase in absorption of 6711 cm⁻¹ showing that the number of protonated groups increase with the proportion of acid content. Similar infra-red studies on the interaction between ethylene dichloride/DCA mixtures and the peptide group of poly(γ -benzyl-L-glutamate), poly(L-alanine) and poly(L-methionine) suggested that the interaction was one of protonation of the peptide group even at low acid concentration⁴. Volchek has investigated the interaction between DCA, TFA and the peptide group of different model amides including NMA by monitoring the changes that occur in the amide I region of the infra-red spectra for different acid/chloroform concentration⁵. The concentration of the solution was defined as $X_k = N_k(N_0 + N_k)$ where N_k is the molarity of acid in chloroform. N_0 the molarity of the model amide in chloroform was kept constant at 0.2 M. The results show that for NMA in TFA/CHCl₃ solutions, a strong absorption band occurs at the approximately 1615 cm when $X_k < 0.5$, and shifts to approximately 1632 cm⁻¹ when $X_k > 0.5$. These bands are attributed to a hydrogen bonding interaction and protonation respectively. Similar results were obtained when other model amides were dissolved in either DCA/CHCl₃ or TFA/CHCl₃ solutions and it was concluded

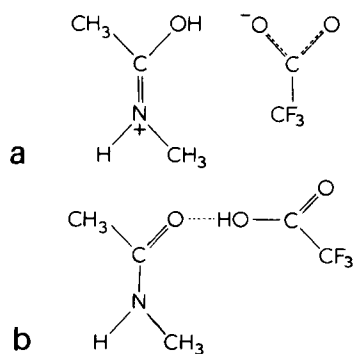


Figure 1 (a) Protonation; (b) hydrogen bonding

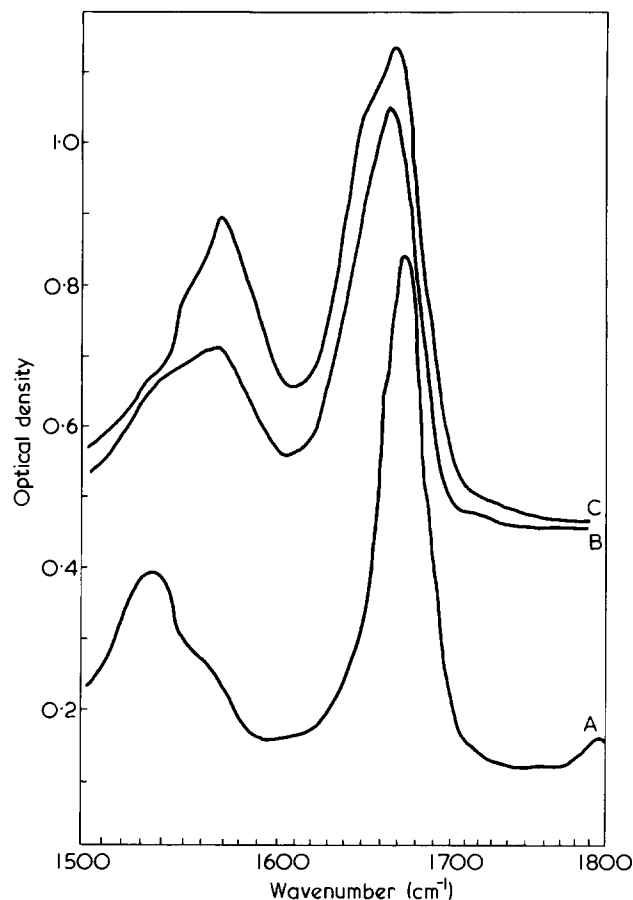


Figure 2 I.r. spectra of NMA in deuteriochloroform solutions. A, 0.2 M NMA in CDCl_3 ; B, 2 M NMA in CDCl_3 ; C, liquid NMA

that a hydrogen bonding interaction took place between the acid and the peptide group when $X_k < 0.5$ and protonation of the peptide group occurred when $X_k > 0.5$. Other investigations, using infra-red spectroscopy, of the interaction between the peptide group and TFA, concluded that the interaction was one of hydrogen bonding and not protonation^{6,7}. Mandelkern and coworkers have studied the nuclear magnetic resonance spectra obtained from poly(L-alanine) and poly(DL-alanine) NMA and *N,N*-dimethylacetamide, in TFA/ CDCl_3 solvents and concluded that whereas protonation of the peptide group occurred in the model compounds there was no evidence of a similar interaction between polypeptides and carboxylic acids^{8,9}. Quadrioglio and Urry using circular dichroism techniques also concluded that protonation did not occur in helical poly(γ -benzyl-L-glutamate) in 3.65 M DCA in CDCl_3 solution¹⁰.

The aim of this investigation is to examine and to establish the nature of the interaction between NMA and carboxylic acids having different acidities, and use the results to interpret the type of interaction taking place between several polypeptides and TFA. Infra-red spectroscopy has been used to record changes that occur in the characteristic vibrational frequencies of the peptide group when an interaction occurs between this group and other molecules; in this case carboxylic acids. If the hydrogen bonding interaction occurs the vibrational frequency of the amide I (80% C=O stretching) is lowered with little change in the amide II frequency (60% N-H in plane bending, 40% C-N stretching). If protonation of the peptide group occurs then the amide I is replaced by a new absorption band which comes from the anti-symmetrical stretching vibration of the charged carboxyl group and this occurs at a con-

siderably lower frequency. The characteristic amide II vibration will no longer occur.

EXPERIMENTAL

The concentration N_0 of water free NMA or polypeptides in deuteriochloroform was kept constant at 0.2 M and the molarity N_k of the carboxylic acid/ CDCl_3 solution of NMA was varied by adding the required amount of acid to the NMA/ CDCl_3 solution. Analar grade reagents were used and the purity of the CDCl_3 was 99.8%. The infra-red spectra of the solutions were recorded using a Grubb Parsons Spectromaster. The cells contained barium fluoride windows and had a path length of 0.05 cm. The scanning speed of the instrument was 1 $\mu\text{m}/4$ min.

RESULTS

NMA in deuteriochloroform

Figure 2 shows the infra-red spectra of liquid NMA and various solutions of NMA in deuteriochloroform (CDCl_3) at room temperature. For the pure liquid NMA the amide I occurs at 1663 cm^{-1} with a broad shoulder at 1649 cm^{-1} . The amide II also shows asymmetry with a peak at 1566 cm^{-1} and shoulders on the low frequency side. The amide I vibration is due mainly to carboxyl stretching and the amide II to N-H in plane bending and C-N stretching, and the pronounced asymmetries are due to hydrogen bonding, between NMA molecules involving the peptide group. For a dilute solution of 0.2 M NMA in CDCl_3 the amide I and II sharpen considerably and occur at 1672 cm^{-1} and 1536 cm^{-1} , indicating that very little hydrogen bonding is taking place. As the concentration of NMA in CDCl_3 increases the amide I shifts to a lower frequency and broadens and the amide II moves to a higher frequency. At 4.0 M NMA in CDCl_3 the amide I and II bands occur at 1653 cm^{-1} and 1570 cm^{-1} with very little asymmetry in either band. This indicates that very strong hydrogen bonding is taking place at this concentration.

NMA in acetic acid/deuteriochloroform

For NMA in dilute acetic acid/deuteriochloroform ($\text{CH}_3\text{COOH}/\text{CDCl}_3$) solution two distinct amide I absorption bands are seen at 1670 cm^{-1} and 1651 cm^{-1} with a broad amide II at $\sim 1537\text{ cm}^{-1}$ (Figure 3). At the higher acid concentration of 2.0 M only two bands can be seen, one at 1649 cm^{-1} , the other at 1558 cm^{-1} . If there was another higher frequency band present it could not be observed due to the intense background from the acid peak. Examination of the solvent spectra for this acid concentration shows that there is no strongly absorbing band at 1558 cm^{-1} and thus the 1558 cm^{-1} is due completely to the amide vibration. Therefore it seems likely from the intensity and position of the peaks observed for 0.2 M NMA in 2.0 M $\text{CH}_3\text{COOH}/\text{CDCl}_3$ that the interaction between acetic acid and NMA is one of hydrogen bonding.

NMA in formic acid/deuteriochloroform

For NMA in formic acid/deuteriochloroform solution, the amide I absorption occurs at 1670 cm^{-1} with a shoulder at 1643 cm^{-1} which becomes well resolved in 0.1 M formic acid (Figure 4). The amide II band is broad and centred about 1538 cm^{-1} . These results indicate that hydrogen bonding is taking place. However, at 0.75 M formic acid the amide I is broad with a peak at 1639 cm^{-1} .

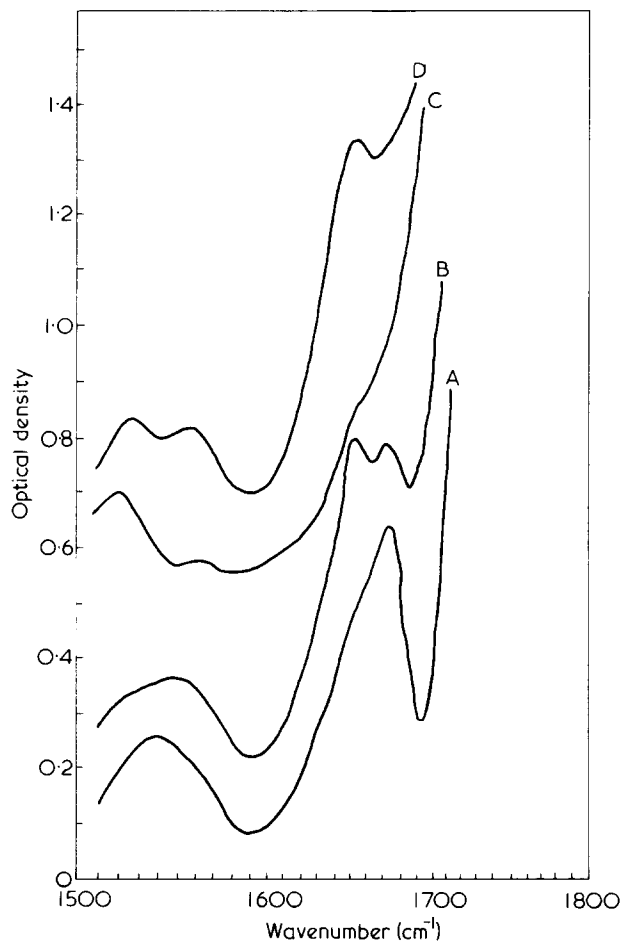


Figure 3 I.r. spectra of 0.2 M NMA in acetic acid/ CDCl_3 solutions. A, NMA in 0.2 M acetic acid in CDCl_3 ; B, NMA in 0.7 M acetic acid in CDCl_3 ; C, 2 M acetic acid/ CDCl_3 solvent; D, NMA in 2.0 M acetic acid in CDCl_3

The amide II occurs at 1558 cm^{-1} with a shoulder at 1565 cm^{-1} , and may have lost some of its intensity. If this region of the spectrum is compared with the corresponding solvent spectrum it is seen that there are no solvent peaks present. Thus there may be two different interactions between formic acid and NMA; hydrogen bonding and a small amount of protonation at the higher acetic acid concentration.

NMA in dichloroacetic acid/deuterochloroform

When NMA is dissolved in dichloroacetic acid/deuterochloroform ($\text{Cl}_2\text{CHOOH}/\text{CDCl}_3$) at an acid concentration of 0.1 M the amide I is sharp and occurs at 1670 cm^{-1} , the amide II absorbs at 1544 cm^{-1} and 1559 cm^{-1} , and the interaction band occurs at 1628 cm^{-1} (Figure 5). At an acid concentration of 0.2 M, the interaction band increases in intensity, and is accompanied by a decrease in intensity of the amide I band. At the higher acid concentration of 1.0 M, the interaction band has shifted to 1610 cm^{-1} and the amide I absorption band is not observed. In the amide II region there is a band at 1565 cm^{-1} but when the spectrum of the solvent is examined it is seen that there is an absorption band present near this position, indicating that the amide II absorption band has greatly reduced intensity. This suggests that protonation of the peptide group in NMA is occurring at 1.0 M DCA in CDCl_3 .

NMA trifluoroacetic acid/deuterochloroform

With NMA dissolved in trifluoroacetic acid/deuterochloroform ($\text{CF}_3\text{COOH}/\text{CDCl}_3$) and interesting effect is observed. Below an acid concentration of 0.25 M and above a concentration of 7.5 M the solution of NMA and TFA/ CDCl_3 is clear but between these two acid concentrations the solution is cloudy at room temperature, but can be made transparent by gentle heat. The infra-red spectrum at the high acid concentration (Figure 6), shows a strong interaction band at 1620 cm^{-1} with asymmetry on the high frequency side, and a band at 1558 cm^{-1} . Examination of the solvent spectrum at this acid concentration shows that the band at 1558 cm^{-1} is due to solvent, and thus the amide absorption band has disappeared indicating that only one interaction is taking place between NMA and TFA at this concentration. For the 0.25 M acid solution the interaction band occurs at 1610 cm^{-1} with a pronounced shoulder on the high frequency side, and absorption band at 1560 cm^{-1} . As the acid concentration is 30 times lower than previously this band must be due to the amide II vibration. Its intensity however, is low, similar to that observed for the 1.0 M DCA in CDCl_3 solvent which

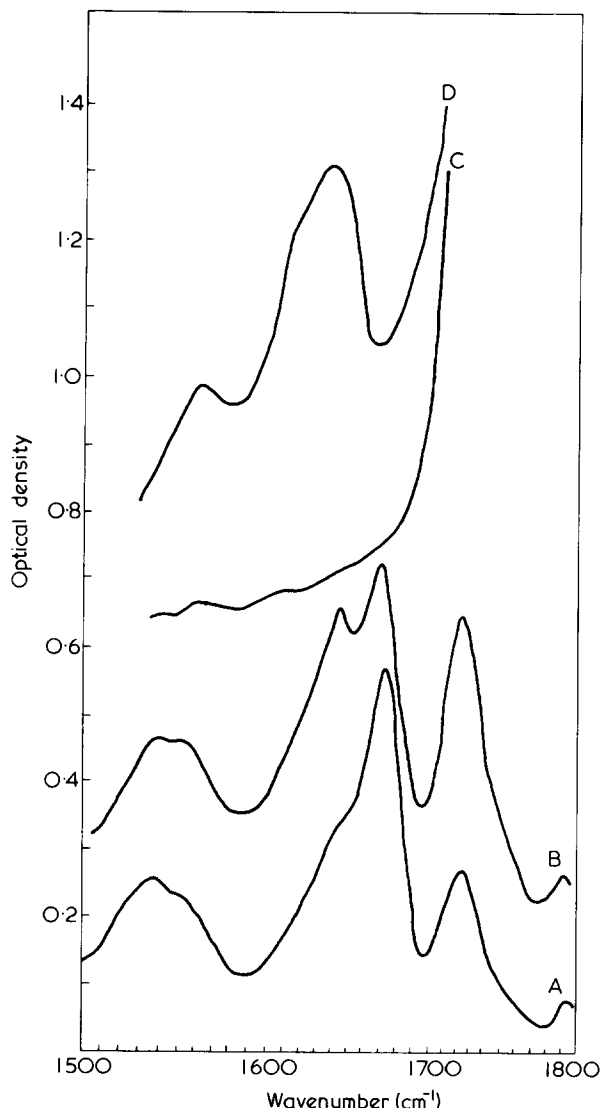


Figure 4 I.r. spectra of 0.2 M NMA in formic acid/ CDCl_3 solution. A, NMA in 0.05 M formic acid in CDCl_3 ; B, NMA in 0.1 M formic acid in CDCl_3 ; C, 0.75 M formic acid in CDCl_3 solvent; D, NMA in 0.75 M formic acid in CDCl_3

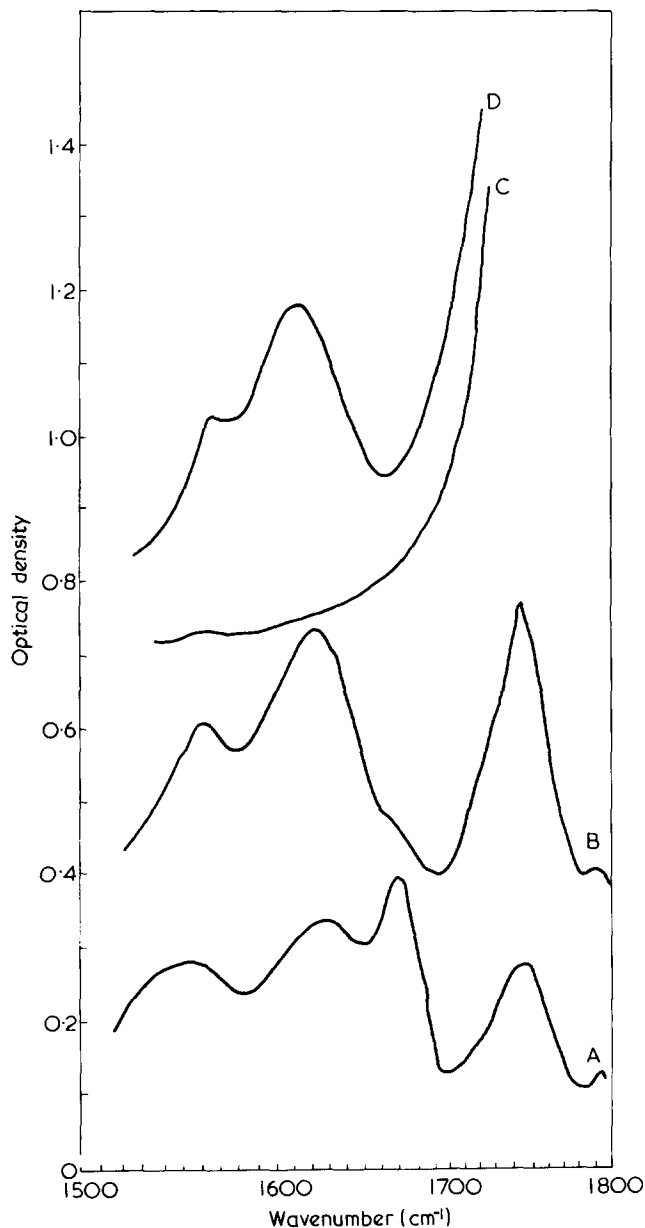


Figure 5 I.r. spectra of 0.2 M solutions of NMA in DCA/CDCl₃ solution. A, NMA in 0.1 M DCA in CDCl₃; B, NMA in 0.2 M DCA in CDCl₃; C, 1 M DCA in CDCl₃ solvent; D, NMA in 1 M DCA in CDCl₃

suggests that at 0.25 M TFA in CDCl₃ two interactions are taking place between the NMA and TFA. If deuterated TFA is used, the interaction band occurs at 1620 cm⁻¹ at an acid concentration of 0.25 M (Figure 7). This is 10 cm⁻¹ higher than the corresponding band when the hydrogenated acid interacts with NMA and the intensity of the band at 1566 cm⁻¹ is lower than that observed using ordinary TFA. This additional decrease in the intensity of the amide II is due to deuteration of the amide hydrogen but as the acid concentration (0.25 M) is similar to the NMA concentration (0.2 M) only 50% of the amide hydrogens are deuterated. At the higher deuterated acid concentration (7.5 M) the interaction band occurs at 1636 cm⁻¹. If the interaction at this high acid content were due to hydrogen bonding between the amide carboxyl group and the acid, deuteration of the hydrogen bond would shift this interaction band to a slightly lower frequency (due to the fact that the interaction band would arise from a modified carboxyl stretching vibration).

POLYPEPTIDES IN TRIFLUOROACETIC ACID/DEUTEROCHLOROFORM

Poly(L-alanine) in TFA/CDCl₃

To see if hydrogen bonding or protonation occurs between the acid and the peptide group for poly(L-alanine) in TFA/CDCl₃ solutions its infra-red spectra have been examined. Figure 8 shows the spectrum of a solution of poly(L-alanine) in 5.4 M TFA in CDCl₃. It can be seen that the amide I and II bands occur at 1658 cm⁻¹ and 1556 cm⁻¹ respectively, and that an interaction band of almost the same intensity as the amide I occurs at 1623 cm⁻¹. For the same polymer in 5.4 M deuterated TFA in CDCl₃ the amide I occurs at 1653 cm⁻¹ and due to deuteration of the amide hydrogen, the amide II has shifted to a much lower frequency. The interaction band occurs at 1621 cm⁻¹ and is 2 cm⁻¹ lower than that which was observed when the polymer was dissolved in the hydrogenated acid. It is unlikely from these results that protonation is taking place at this acid concentration as the intensity of the amide II is lower when the acid is deuterated (as would be expected when hydrogen bonding takes place). O.r.d. results have shown that poly(L-alanine) in 5.4 M TFA in CDCl₃ is mainly helical²⁰.

Poly(DL-alanines) in TFA/CDCl₃

To see if a similar interaction takes place between TFA and randomly coiled polyalanine, the infra-red spectra of solutions of various poly(DL-alanines) in 7.4 M TFA in CDCl₃ were recorded. It can be seen from Figure 9 that when L/D = 39 a strong acid interaction band is present at

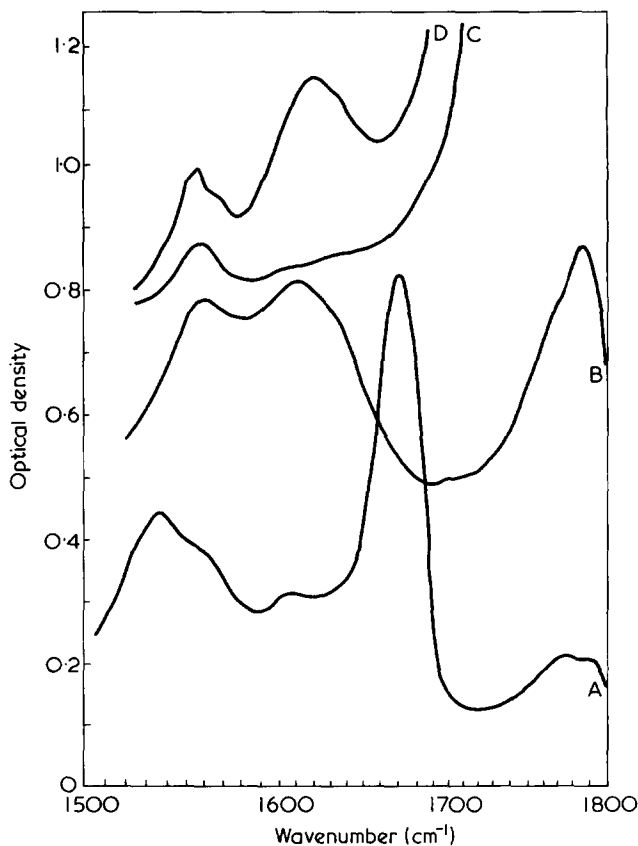


Figure 6 I.r. spectra of 0.2 M NMA in TFA/CDCl₃ solutions. A, NMA in 0.05 M TFA in CDCl₃; B, NMA in 0.25 M TFA in CDCl₃; C, 7.5 M TFA in CDCl₃ solvent; D, NMA in 7.5 M TFA in CDCl₃

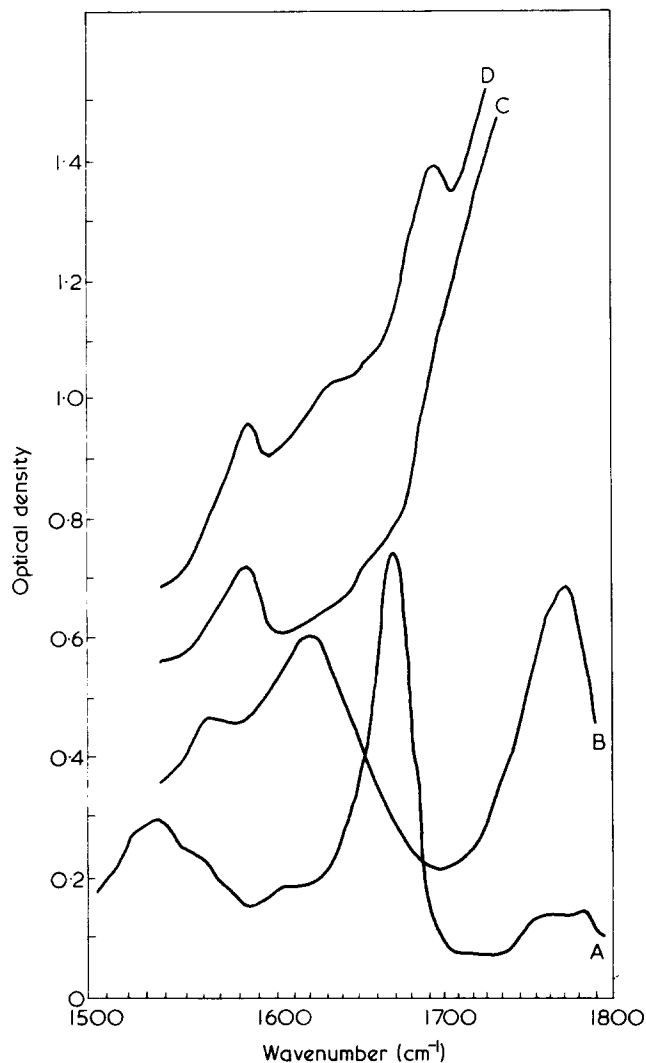


Figure 7 I.r. spectra of 0.2 M NMA in deuterated TFA/CDCl₃ solutions. A, NMA in 0.05 M deuterated TFA in CDCl₃; B, NMA in 0.25 M deuterated TFA in CDCl₃; C, 7.5 M deuterated TFA in CDCl₃ solvent; D, NMA in 7.5 M deuterated TFA in CDCl₃

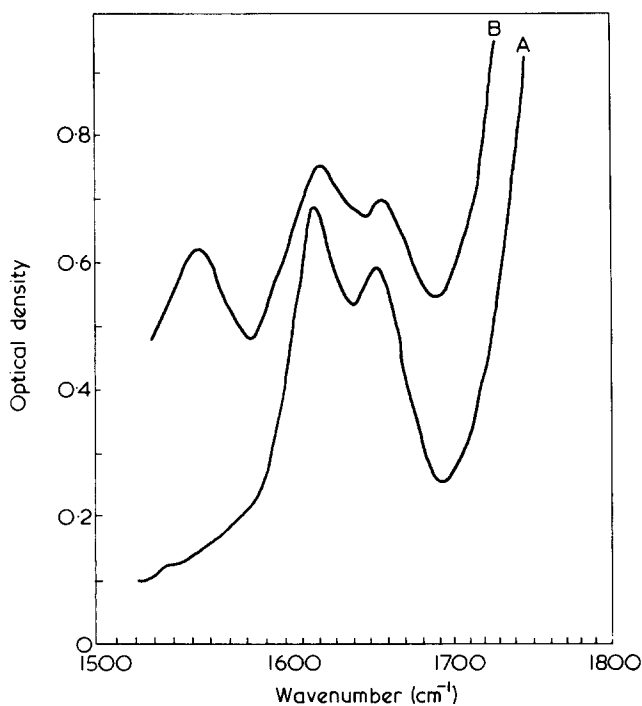


Figure 8 I.r. spectra of 0.2 M solutions of poly(L-alanine) in A, 5.4 M deuterated TFA in CDCl₃; B, 5.4 M TFA in CDCl₃

1626 cm⁻¹ which is absent when L/D = 1.25. In the latter case the amide I band is broad and occurs at 1637 cm⁻¹ indicative of the acid solvated random coil form. For the polymer with L/D = 39 the amide I occurs at 1656 cm⁻¹ indicating that this polymer is helical. The conformations of the poly(DL-alanines) in 7.4 M TFA in CDCl₃ has been confirmed using o.r.d. techniques²⁰. However, irrespective of the ratio of L:D i.e. the helicity of the polymer the intensity of the amide II band remains almost constant with the result that very little protonation is taking place.

Poly(γ -benzyl-L-glutamate) in TFA/CDCl₃

Figure 10 shows the infra-red spectra of solutions of poly(γ -benzyl-L-glutamate) in TFA/CDCl₃. It can be seen that at an acid concentration of 0.34 M TFA two changes have occurred in its infra-red spectrum compared with that obtained from the polypeptide in deuteriochloroform. The first is the appearance of a weak band at 1613 cm⁻¹ which is in a similar position to the interaction band that is seen when poly(L-alanine) is dissolved in TFA/CDCl₃ solution. Secondly the intensity of the ester C=O at 1736 cm⁻¹ has diminished with the appearance of a new band at 1713 cm⁻¹. It can be seen that as the acid concentration increases the intensity of the band at 1713 cm⁻¹ increases steadily and the one at 1736 cm⁻¹ decreases, until at an acid concentration of 2.0 M only a band at 1713 cm⁻¹ can be seen. Meanwhile the intensity of the weak band at 1610 cm⁻¹ has reduced as the acid concentration increased and as the conformation of the polymer changed from helical to random coil as indicated by the changes in the amide I and II bands.

DISCUSSION

Infra-red spectroscopy has been used to investigate the type of interaction taking place between carboxylic acids

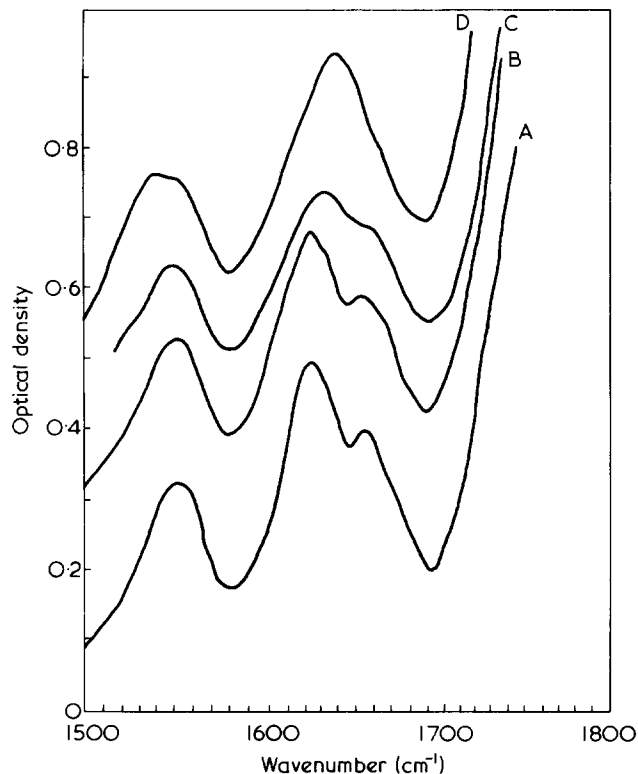


Figure 9 I.r. spectra of 0.2 M solutions of poly(DL alanine) in 7.4 M TFA in CDCl₃. A, poly(L-alanine); B, L:D 39; C, L:D 9; D, L:D 1.25

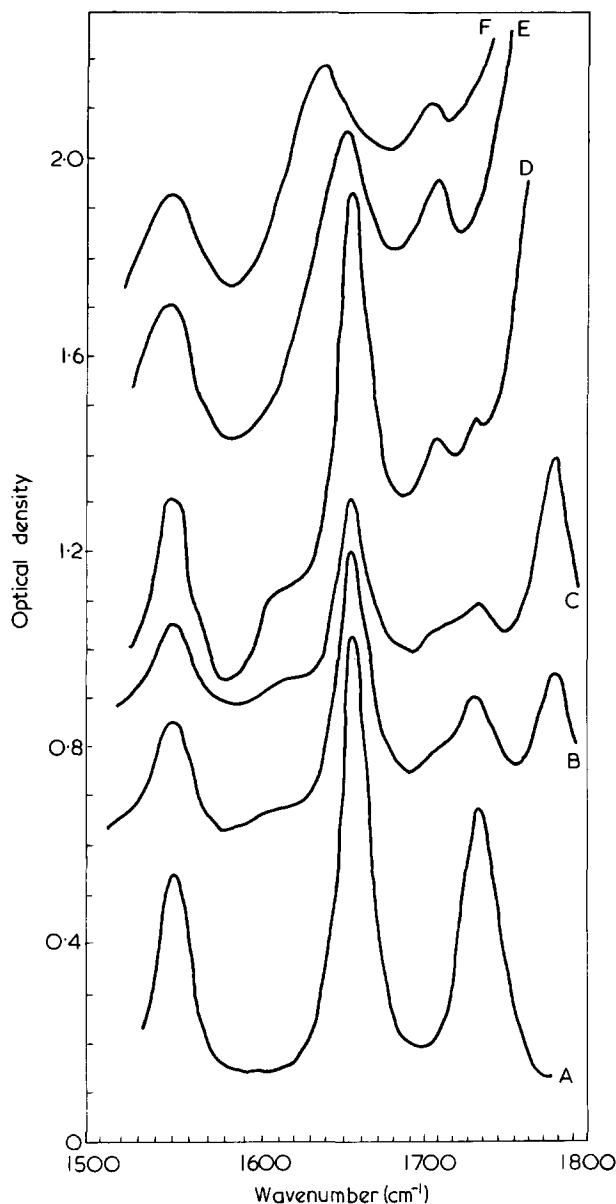


Figure 10 I.r. spectra of 0.2 M solutions of poly(γ -benzyl-L-glutamate) in A, CDCl_3 ; B, 0.34 M TFA in CDCl_3 ; C, 0.67 M TFA in CDCl_3 ; D, 1.35 M TFA in CDCl_3 ; E, 2.0 M TFA in CDCl_3 ; F, 2.73 M TFA in CDCl_3

and the peptide group of NMA and various polypeptides. The interaction may be either (a) hydrogen bonding or (b) protonation. The former causes a reduction in the stretching frequency of the affected group whilst the latter gives rise to the presence of a charged COO^- stretching vibration accompanied by the disappearance of the amide II vibration.

This investigation of the interaction between NMA and various carboxylic acids, show that two types of interaction may occur. For relatively weak acids like acetic or formic acids, $K_a = 1.75 \times 10^{-5}$ and 1.77×10^{-4} respectively, hydrogen bonding between the acid and NMA is present at quite high acid concentrations, with possibly only a little protonation occurring. Protonation is only likely to occur with the stronger carboxylic acids.

When hydrogen bonding is taking place between the acid and NMA the frequency of the interaction band occurs between 1651 cm^{-1} and 1649 cm^{-1} for acetic acid ($MW 60$) and between 1645 cm^{-1} to 1639 cm^{-1} for formic acid ($MW 46$). The frequency of the hydrogen bonded interaction band should depend to some extent upon the mass

of the hydrogen bonded molecule. Thus the fact that the interaction band frequencies are lower for the lowest molecular weight acid (formic acid) indicates that the hydrogen bonding is stronger in formic acid than in acetic acid. This is to be expected when one compares the magnitude of their acidity constants K_a . The fact that the hydrogen bonded interaction band is at 1649 cm^{-1} for pure liquid NMA ($MW 73$) means that the hydrogen bonding interactions between NMA molecules is weaker than between these carboxylic acids and NMA. Any hydrogen bonding occurring between DCA ($K_a = 5 \times 10^{-2}$) and NMA is likely to be stronger than that for acetic and formic acid. Consequently the frequency of the hydrogen bonded carboxyl stretching band should be even lower than that observed when formic acid hydrogen bonds to NMA. The interaction band for low dichloroacetic acid concentrations (0.1 M) is broad and has a peak at 1628 cm^{-1} . It sharpens and occurs at 1620 cm^{-1} when the acid concentration is 1 M. The amide II vibration is present at the lowest acid concentration but absent at the higher one. Thus when DCA/ CDCl_3 is used as a solvent for NMA it appears that the interaction is mainly one of hydrogen bonding at low acid concentration but with increasing amounts of protonation as the acid concentration increases.

For NMA dissolved in 0.05 M TFA in CDCl_3 the amide I and II absorption bands are present and a weak interaction band occurs at 1610 cm^{-1} . In 7.5 M TFA in CDCl_3 only two bands can be seen one at 1620 cm^{-1} the other at about 1555 cm^{-1} . This latter band is due to absorption from the solvent, indicating that the amide II absorption is absent. It appears then that at an acid concentration of 7.5 M the interaction is one of almost complete protonation. In 0.05 M TFA in CDCl_3 the interaction between the acid and NMA is likely to be hydrogen bonding. Even so protonation cannot be ruled out as the acid concentration is low and any observable effect would be small.

In view of the above conclusions, that complete protonation of NMA only occurs with high concentration of TFA and not with the weaker acids, the interactions between polypeptides and carboxylic acids has been restricted to that between polypeptides and TFA.

With poly(L-alanine) in 5.4 M TFA in CDCl_3 the infrared spectra show that an interaction band occurs at 1623 cm^{-1} with amide I and II bands at 1658 cm^{-1} and 1555 cm^{-1} respectively. When deuterated TFA is used the interaction band occurs at a slightly lower frequency and it appears likely that hydrogen bonding takes place between TFA and helical poly(L-alanine). From the studies made on various poly(DL-alanines) at an acid concentration of 7.4 M in CDCl_3 , hydrogen bonding occurs between the peptide group and TFA when $L/D = 39$ (as the interaction band occurs at 1626 cm^{-1} and the amide II band is present). When $L/D = 1.25$ the resultant spectrum is indicative of the acid solvated random coil form.

When the interaction between TFA and the polypeptide containing an ester group [poly(γ -benzyl-L-glutamate)] is examined, two interaction bands occur which were not present when the polypeptide was dissolved in deuteriochloroform. For an acid concentration of 0.34 M, apart from the expected amide I, II and ester $\text{C}=\text{O}$ stretching vibration absorption bands, two weak bands occurred at 1610 cm^{-1} and 1713 cm^{-1} . As the acid concentration increased, the polypeptide becomes more random (as indicated by the shape of the amide bands), the band at 1610 cm^{-1} remained practically unchanged in intensity, whilst the band at 1713 cm^{-1} increased in intensity. When the acid concen-

tration is 2.0 M TFA in CDCl_3 the spectrum is that from the acid solvated random coil form of poly(γ -benzyl-L-glutamate) with the interaction band at 1610 cm^{-1} absent and the one at 1713 cm^{-1} very strong. Thus it seems that the main interaction occurs between TFA and the side chain ester group in poly(γ -benzyl-L-glutamate), and is one of hydrogen bonding. Very few TFA molecules appear to interact with the peptide group of this polypeptide.

CONCLUSIONS

The results above indicate that protonation of NMA occurs when strong carboxylic acids such as DCA and TFA are used as solvents. Hydrogen bonding occurs between NMA and weaker carboxylic acids (acetic and formic acid) and at low acid concentrations of NMA in DCA/ CDCl_3 solutions. Protonation of the peptide group is not observed for the polypeptides studied when they are dissolved in TFA/ CDCl_3 solutions; the interaction is one of hydrogen bonding between the peptide group of helical polymers and the acid. If the polypeptide contains an ester group in its side chain, such as poly(γ -benzyl-L-glutamate), there is good evidence that the carboxylic acid will hydrogen bond to the side chain ester group.

These conclusions are in agreement with the experimental and theoretical studies which support the ideas of a hydrogen bond interaction^{5-7,9,12-19}, and disagree with previous studies supporting protonation¹⁻⁴. The different conclusions may be due to the difficulty in characterizing

changes that were observed in the overtone region of the infra-red spectrum.

REFERENCES

- 1 Klotz, I. M., Russo, D. F., Hanlon, S. and Stake, M. A. *J. Am. Chem. Soc.* 1964, **86**, 4774
- 2 Hanlon, S., Russo, S. F. and Klotz, I. M. *J. Am. Chem. Soc.* 1963, **85**, 2024
- 3 Hanlon, S. and Klotz, I. M. *Biochemistry* 1965, **4**, 37
- 4 Hanlon, S. *Biochemistry* 1966, **5**, 2049
- 5 Volchek, B. Z. and Purkina, A. V. *Vysokomol. Soedin (A)* 1967, **9**, 1257
- 6 Coubelas, M. P. and Garrigou-Lagrange, C. *C.R. Acad. Sci.* 1971, **272**, 153
- 7 Coubelas, M. P. and Garrigou-Lagrange, C. *Spectrochim. Acta (A)* 1974, **30**, 550
- 8 Glick, R. E., Mandlekern, L. and Stewart, W. E. *Biochim. Biophys. Acta* 1966, **120**, 302
- 9 Stewart, W. E., Mandlekern, L. and Glick, R. E. *Biochemistry* 1967, **6**, 143
- 10 Quadrioglio, F. and Urry, D. W. *J. Phys. Chem.* 1967, **71**, 2364
- 11 Doty, P. and Yang, J. T. *J. Am. Chem. Soc.* 1956, **78**, 498
- 12 Bradbury, E. M. and Rattle, H. W. E. *Polymer* 1968, **9**, 201
- 13 Ferretti, J. A. and Paolillo, L. *Biopolymers* 1969, **7**, 155
- 14 Bovey, F. A. *Pure Appl. Chem.* 1968, **16**, 417
- 15 Schellmann, J. A. *J. Phys. Chem.* 1958, **62**, 1485
- 16 Bixon, M. and Lifson, S. *Biopolymers* 1966, **4**, 815
- 17 Peller, L. *J. Phys. Chem.* 1959, **63**, 1194
- 18 Gibbs, J. H. and Dimarzio, E. A. *J. Chem. Phys.* 1959, **30**, 271
- 19 Lapp, C. and Marchal, J. *J. Chim. Phys.* 1965, **62**, 1032
- 20 Cary, P. D. *PhD Thesis* University of London (1975)

Viscosity-molecular weight concentration relationships beyond the critical region in polymer solutions and melts

N. M. Chaurasia, Anil Kumar and Santosh K. Gupta

Department of Chemical Engineering, Indian Institute of Technology, Kanpur-208016, India

(Received 23 December 1975)

A multivariate regression analysis of viscosity—molecular weight—concentration data is presented which is superior to the methods currently used. Four sets of data from the literature are analysed to show the efficacy of the method.

INTRODUCTION

The flow properties of concentrated polymer solutions and melts are of great importance in the study of their processing characteristics and molecular structure. A considerable amount of experimental work has been reported in the literature¹⁻⁷ on the dependence of the zero shear viscosity, η_0 , of polymer solutions and melts on the molecular weight of the polymer, M , and its concentration, c , or density, ρ . The experimental data show a dependence of η_0 on $M^{3.4}$. However, the dependence of η_0 on the concentration appears to vary from system to system. Graessley⁸ has recently reviewed the theoretical developments^{3,8-11} in this area but most of the theories seem to be in contradiction with experimental behaviour.

It has been found empirically that log-log plots of η_0 versus M at different c and η_0 versus c at different M are superimposable by horizontal shifts and on this basis the following equation has been suggested for regions beyond the critical point⁸:

$$\eta_0 = Kc^\alpha M^\beta \quad (1)$$

where K , α and β are constants. Several methods have been used in the literature to evaluate α and β . In the first method¹², α and β are assumed to be 5.0 and 3.4 respectively (i.e. $\beta/\alpha = 0.68$) and a plot of $\log \eta_0$ versus $(3.4 \log M + 5.0 \log c)$ is made. The deviation of experimental points from a straight line of slope unity at high values of the abscissa indicate deviations from equation (1). This method has the drawback in that excessive experimental scatter does not indicate whether the functionality in equation (1) is wrong or whether incorrect values of α and β have been chosen. The same experimental data have been replotted¹³ and β/α has been found to be 0.54 instead of 0.68 assumed earlier. Recently a variation of this method has been used⁷ and $\log \eta_0$ has been plotted as a function of $\log (cM^{0.625})$ as well as $\log (cM^{0.68})$. Analysis of data on polystyrene in toluene reveals that it is impossible to decide which of the two exponents, 0.625 and 0.68, is really applicable. A similar insensitivity has been reported by Graessley⁸ who shifted $\log \eta_0$ versus $\log (cM)$ and $\log \eta_0$ versus $\log (cM^{0.68})$ plots vertically.

Plots of $\log \eta_0$ versus $\log M$ for various values of c as well as $\log \eta_0$ versus $\log c$ for various values of M have been made¹³ and these curves shifted horizontally to super-

pose on any reference concentration, c_0 , or molecular weight, M_0 . The shift factors $a_c (\equiv \log c/c_0)$ and $a_m (\equiv \log M/M_0)$ are related to β and α as:

$$a_c = -\frac{\beta}{\alpha} \times a_m \quad (2)$$

and a plot of a_c versus a_m gives β/α . This method has the drawback that the superposition of plots by visual methods leads to a loss of precision. Besides, this method is far too cumbersome to use.

The insensitivity of the various methods of analysing experimental viscosity data and the loss of precision by visual shifts necessitates a more reliable method of analysis. In this paper, a multivariate regression analysis is suggested and some representative data existing in the literature are analysed to give the 'best-fit' values of K , α and β in equation (1). This method has the advantage of being amenable to computer calculations.

METHOD OF ANALYSING DATA

Above the critical region, equation (1) can be written as:

$$\log \eta_0 = \log K + \alpha \log c + \beta \log M \quad (3)$$

or, in simplified notation:

$$y = A + \alpha x_1 + \beta x_2 \quad (4)$$

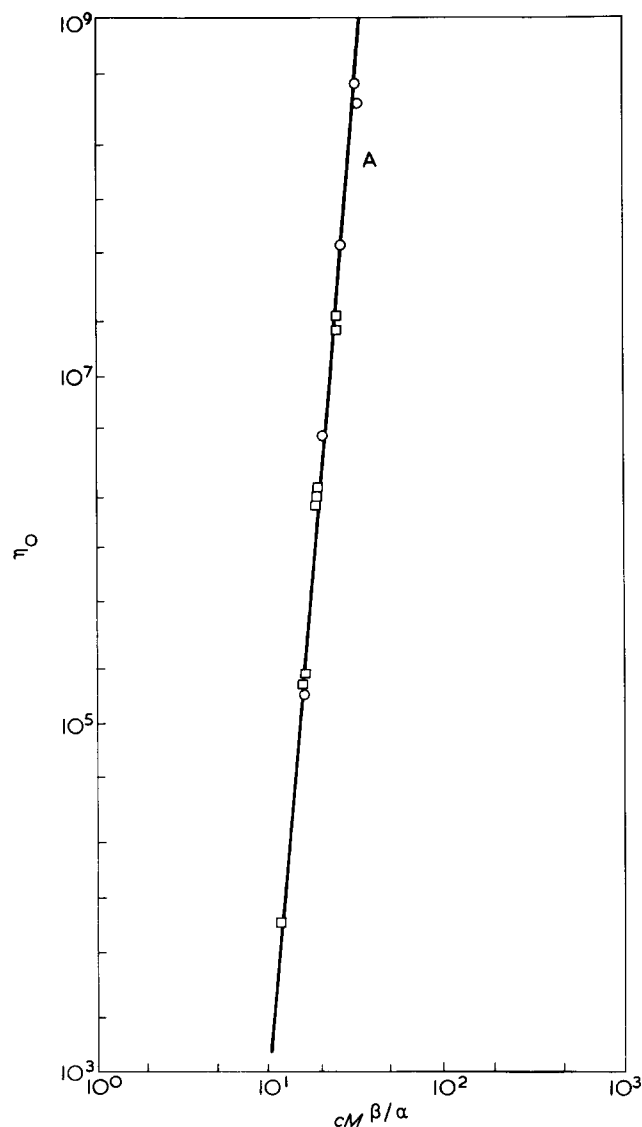
A multivariate regression analysis for the case of two independent variables leads to a set of three simultaneous algebraic equations in the three unknowns, A , α and β ¹⁴:

$$\begin{aligned} An + \alpha \sum x_{1,i} + \beta \sum x_{2,i} &= \sum y_i \\ A \sum x_{1,i} + \alpha \sum x_{1,i}^2 + \beta \sum x_{1,i}x_{2,i} &= \sum x_{1,i}y_i \\ A \sum x_{2,i} + \alpha \sum x_{2,i}x_{1,i} + \beta \sum x_{2,i}^2 &= \sum x_{2,i}y_i \end{aligned} \quad (5)$$

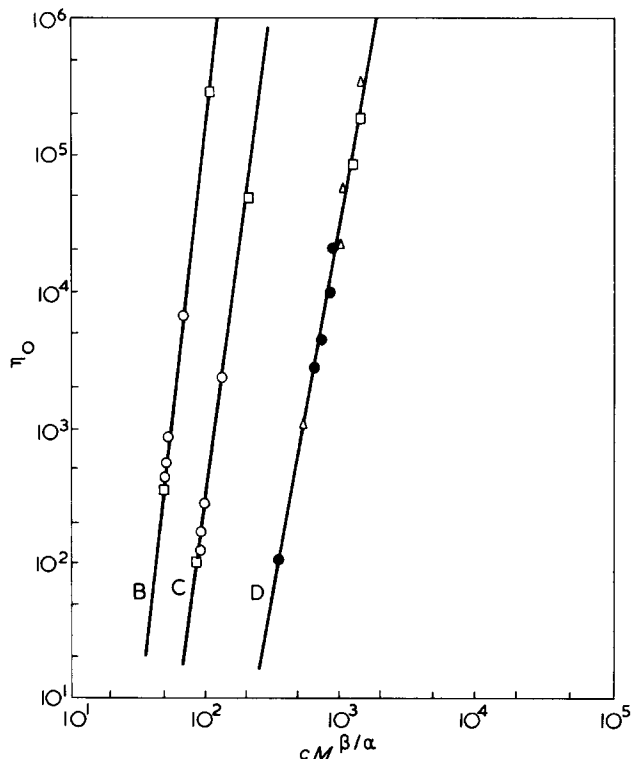
where n is the number of data points, $x_{1,i}$, $x_{2,i}$ and y_i are

Table 1 Values of $\log K$, α and β for viscosity data obtained using the regression analysis

System	Log K	α	β	β/α	Curve no.
Polystyrene—DOP ¹⁷	-17.3	10.795	3.269	0.3028	A
PMMA in diethyl-phthalate ¹⁶ at 30°C	-31.13	9.454	4.240	0.4485	B
PMMA in diethyl-phthalate at 60°C	-33.596	8.423	4.180	0.4963	C
PVAc in diethyl-phthalate ¹⁵	-28.518	5.599	3.411	0.6092	D


Figure 1 η_0 vs. $cM^{\beta/\alpha}$ for polystyrene in DOP¹⁷ (curve A): \square , 40%; \circ , 30%

the values of $\log c$, $\log M$ and $\log \eta_0$ for the i th data point and the summations are over all values of i from 1 to n . Cramer's rule can now be used to obtain the three best-fit values for the parameters.


Figure 2 η_0 vs. $cM^{\beta/\alpha}$ for PMMA in DEP¹⁶ at 30°C (Curve B) and at 60°C (Curve C): \square , $c = 0.226$; \circ , $c = 0.113$. Curve D represents η_0 vs. $cM^{\beta/\alpha}$ for PVAc in DEP¹⁵: \bullet , $c = 0.171$; \triangle , $c = 0.26$; \square , $c = 0.325$

DISCUSSION

The multivariate regression analysis has been applied to four sets of data beyond the critical region, taken from the current literature¹⁵⁻¹⁷. *Table 1* lists the values of K , α and β for the cases studied. It is observed that there is a considerable variation in the values of α . Such variations have already been reported¹⁸⁻²⁰. The values of β are all found to be around 3.4 except in the case of PMMA. *Figures 1* and *2* show plots of $\log \eta_0$ as a function of $\log (cM^{\beta/\alpha})$ using the values of β/α listed in *Table 1*, along with the best-fit lines.

This method of analysis of data does not have the drawback of insensitivity nor does it require any visual shifts of data which would lead to loss of precision. Moreover, the regression analysis minimizes the standard deviation.

It should be mentioned here that workers in this area usually plot $\log \eta_0$ versus $\log M$ and $\log \eta_0$ versus $\log c$ for different c and M and obtain β and α from the slopes of these plots above the critical region, respectively. As few as four to five points are normally used in the evaluation of β and α . As opposed to this, in the regression analysis presented here, the number of data points used is much larger because data for different M and c can be used simultaneously.

REFERENCES

- 1 Fox, T. G., Gratch, S. and Loshaek, S. 'Rheology', (Ed. F. R. Eirich), Academic Press, 1956, Vol 1 p446
- 2 Berry, G. C. and Fox, T. G. *Adv. Polym. Sci.* 1968, 5, 261
- 3 Bueche, F. 'Physical Properties of Polymers', Wiley, New York, 1962

- 4 Middleman, S. 'The Flow of High Polymers', Interscience, New York, 1968, Ch 5
- 5 Bueche, F. *J. Chem. Phys.* 1952, **20**, 1959; 1956, **25**, 599; 1964, **40**, 484
- 6 Chikahisha, Y. *J. Phys. Soc. Japan* 1964, **19**, 92
- 7 Gandhi, K. S. and Williams, M. C. *J. Polym. Sci. (C)* 1971, **35**, 211
- 8 Graessley, W. W. *Adv. Polym. Sci.* 1974, **16**, 1
- 9 Williams, M. C. *AIChEJ.* 1966, **12**, 1064
- 10 Williams, M. C. *AIChEJ.* 1967, **13**, 534
- 11 Williams, M. C. *AIChEJ.* 1967, **13**, 955
- 12 Chinai, S. N. and Schneider, W. C. *J. Polym. Sci. (A)* 1965, **3**, 1359
- 13 Onogi, S., Kimura, S., Kato, T., Masuda, T. and Miyanaga, N. *J. Polym. Sci. (C)* 1966, **15**, 381
- 14 Draper, N. R. and Smith, H. 'Applied Regression Analysis', Wiley, New York, 1966, Ch 2-4
- 15 Uy, W. C. and Graessley, W. W. *Macromolecules* 1971, **4**, 458
- 16 Graessley, W. W. and Pennline, H. W. *J. Polym. Sci. (Polym. Phys. Edn)* 1974, **12**, 2347
- 17 Gupta, D. and Forsman, W. C. *Macromolecules* 1969, **2**, 304
- 18 Onogi, S., Kobayashi, T., Kojima, Y. and Taniguchi, Y. *J. Appl. Polym. Sci.* 1963, **1**, 847
- 19 Bueche, F. *J. Appl. Phys.* 1953, **24**, 423
- 20 Onogi, S., Kimura, S., Kato, T., Masuda, T. and Miyanaga, N. *J. Polym. Sci. (C)* 1966, **15**, 381

Brillouin scattering study of gelatin gel using a double passed Fabry-Perot spectrometer

D. S. Bedborough and D. A. Jackson

Physics Laboratory, University of Kent, Canterbury, Kent CT2 7NR, UK

(Received 4 November 1975; revised 16 February 1976)

The Brillouin spectrum of gelatin gels has been recorded at room temperature as a function of concentration of gelatin, using a double passed Fabry-Perot spectrometer. It was found that both the Brillouin shifts and line-widths increase linearly with concentration. In the case of the line-widths it was shown that the rate of increase was sensitive to the thermal history of the gels, being greater for gels cooled slowly. Explanation of the results in terms of a relaxation phenomenon is improbable. The observations can however be explained in terms of the structure of the gel. Expressing this structure as a number density of crosslinks, which is dependent on the concentration of gelatin, the increase in Brillouin shift is consistent with the change in bulk properties. The increase in line-width is shown to be caused by the crosslinks scattering the sound waves in the gel.

INTRODUCTION

A common form for a polymeric material is that of a gel. This state is characterized by a low but finite rigidity and high incompressibility. These properties are directly related to the gel structure which usually incorporates both high and low molecular weight material. The high molecular weight material forming a semi-rigid three-dimensional network with the low molecular weight material (usually a liquid) pervading this network. An important part of the elucidation of the nature of a gel is the determination of the structure of the crosslinks between the polymer molecules forming the network. Another interesting feature of gels concerns the dynamics of the network. Both of these problems have been investigated by light scattering. Information on the structure is obtained by conventional elastic light scattering¹ and on the dynamics by the more recent technique of analysis of the quasi-elastic scattered light (Rayleigh line) by correlation and spectrum analysis methods². Raman scattering from molecular vibrations has also given information on the crosslinking structure³. However, to our knowledge the technique of Brillouin scattering, which measures the frequency and damping of sound waves in a system, has not been applied to the study of gels.

BRILLOUIN SCATTERING THEORY

Brillouin scattering⁴ arises when light is scattered with a change in frequency by sound waves in the system under study. Physically we may picture this as the sound wave giving rise to a spatially periodic compression and rarefaction of the medium which then acts as a moving diffraction grating; the frequency shift, essentially a Doppler shift, arises from the motion of the sound wave.

In the quantitative evaluation of Brillouin scattering experiments two central results are needed. One relating the wavelength of the sound wave (λ_p) being studied to the geometry of the experiment i.e.:

$$\frac{2\pi}{\lambda_p} = 2\nu \times \frac{2\pi}{\lambda_i} \sin \frac{\theta}{2} \quad (1)$$

where λ_i is the wavelength of the incident light, ν the velocity of sound in the medium under study and θ the angle between incident and observed light.

The equation (2) relates the change in frequency of the scattered light (ω_p) to the velocity of sound in the medium:

$$\omega_p = 2 \times \frac{n\nu}{c} \omega_i \sin \frac{\theta}{2} \quad (2)$$

where ω_i is the frequency of the incident light, n the medium refractive index and c is the velocity of light in vacuum.

More important than the frequency shifts in this work are the widths of the Brillouin lines (Γ_B) which are related to the lifetime of a phonon before it is scattered or absorbed. If we view the sound wave as spatially damped according to $\exp(-\alpha x)$ then the Brillouin width at half height in Hz is given by:

$$\Gamma_B = \frac{\alpha\nu}{\pi} \quad (3)$$

In many fluid systems (although we believe not in our case) a viscous mechanism is responsible for the line width⁵. However, we speculate below that the crosslinking regions of the gel under study, scatter the sound waves travelling in the liquid of the gel and give rise to broader Brillouin lines.

EXPERIMENTAL

Light scattering system

A conventional experimental system consisting of a Coherent Radiation Laboratories 52B Laser operated at a single frequency and 200 mW power, piezoelectrically scanned Fabry-Perot⁶ spectrometer plus d.c. detection of the light scattered at 90° was used except for one important feature not hitherto applied to polymer systems. This feature, made fairly standard in semi-conductor physics⁷, consists of passing the scattered light through the Fabry-

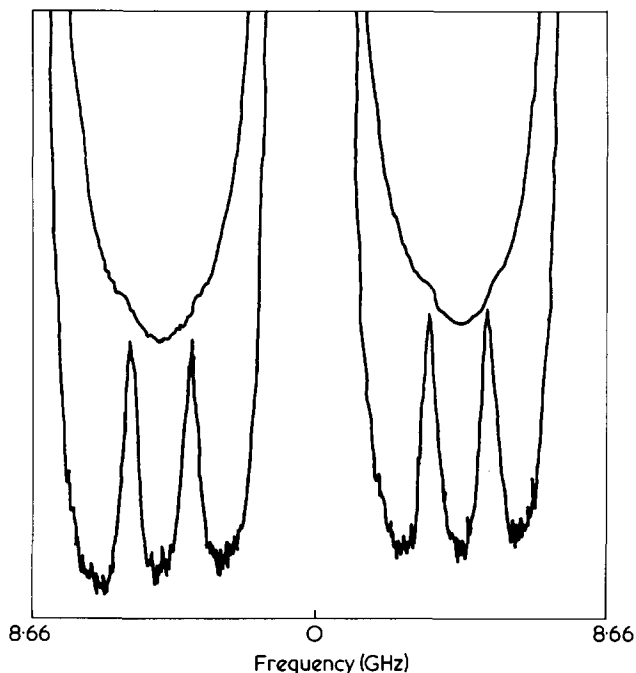


Figure 1 Typical Brillouin Spectra of gels of low gelatin concentration. The upper trace is a single pass Fabry-Perot (98% mirrors) and the lower spectra obtained by the double pass technique

Perot twice. This enables the weak scattered light to be detected in the presence of very much stronger elastically scattered light, i.e. it increases the contrast of the Fabry-Perot.

The reflectivities of the Fabry-Perot mirrors were chosen as 92% at the exciting wavelength of 5154 Å. The free spectral range⁶ of the instrument was 8.66 GHz which with a finesse of ~40 gave a resolution of 200 MHz. A typical spectrum is shown in Figure 1 along with a single passed spectrum taken using higher reflectivity plates (~98%) in the Fabry-Perot (contrast increases with plate reflectivity⁶). These spectra clearly demonstrate the need for a multipassed system. It is not clear whether the Tyndall light is inherent in the nature of the gel or merely due to impurities such as dust etc. In obtaining the line-widths, allowance was made for the convoluting effect of the instrument function.

Gels

The gelatin gels in this study were made from Eastman Gelatin (purified pigskin). A range of gels were made by dissolving appropriate quantities in 0.15 M NaCl solution which had been previously made using distilled water. The salt solution was used because it is known^{1,8} that the nature of a gel is dependent upon the ionic nature of the solvent and the presence of a significant amount of NaCl should make the effects of impurities less important.

The solutions were prepared by heating to not more than 60°C. The samples were then allowed to cool naturally to room temperature at a rate of ~0.5°C/min or transferred directly from the water bath at 60°C to a bath at 0°C (quenched samples).

RESULTS

The shift and width of the Brillouin lines were measured at room temperature (~20°C) for eight concentrations between zero and 0.2 g/cm³. The first set of results were taken from gels cooled slowly to room temperature (~1°C/

min). During an attempt to study the time dependent behaviour of the Brillouin spectra while a sample gelled, it was noted that the line width of the final sample was significantly lower. In view of the expected structure of the gel (see Discussion) and known phenomena of crystallization of polymers (crystalline regions decrease in size with increasing cooling rate) it was speculated that this change in line width was due to the rate at which the gel was cooled. Thus eight more samples were prepared and quenched in ice water and a significant drop in Brillouin line width was noted. The shifts and widths are displayed for the two cooling rates in Figures 2 and 3.

In view of the fact that the changes in the Brillouin Spectrum on gelling for the low concentrations are small and that the higher concentrations gel relatively rapidly it was found necessary to delay a dynamic study of the gelling process to a later date.

DISCUSSION

There are two possible interpretations to the observed Brillouin spectra. One phenomenological explanation is that changes in the spectra are brought about by the change

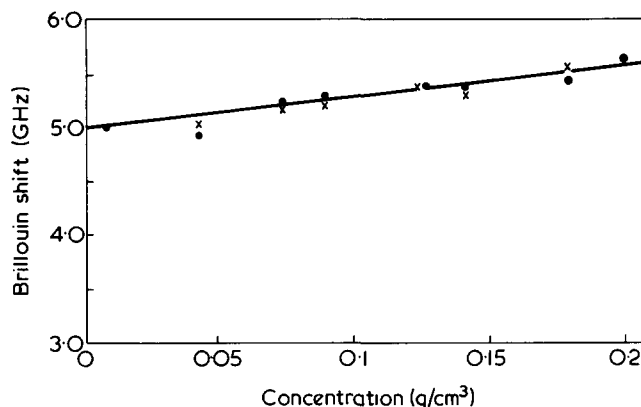


Figure 2 The graph of Brillouin shifts versus concentration of gelatin. X, gel cooled slowly (0.5°C/min); ●, gels quenched cooled to 0°C

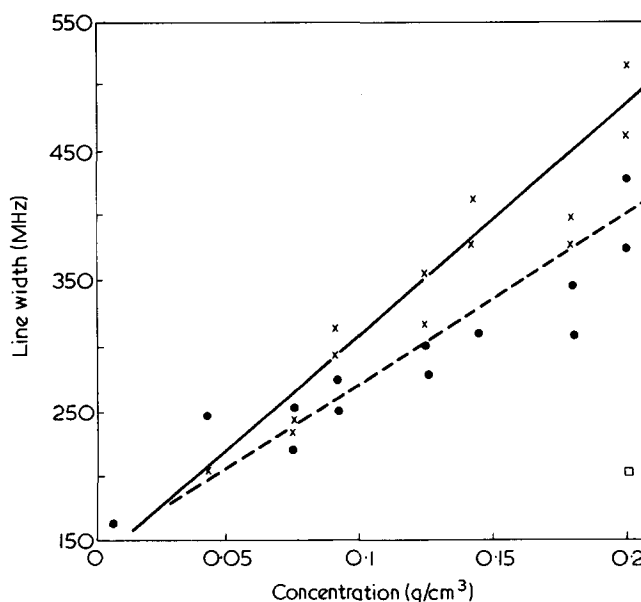


Figure 3 The graph of Brillouin line width versus concentration of gelatin. X, gels quench cooled slowly (0.5°C/min); ●, gels quenched to 0°C; □, line-width of the gel in the molten state

in concentration affecting the relaxation frequency of the gel and the other that the structure of the gel scatters the thermal phonons in the gel and therefore affects their frequency and lifetime. We briefly consider first the relaxational interpretation.

Relaxational interpretation

There are essentially two effects observed in these experiments, the small (~20%) increase in velocity of sound in the medium (*Figure 2*) and the large (~300%) increase in the widths of the Brillouin lines (*Figure 3*) which in turn mean a large decrease in the life-time of the sound wave.

Considering the equations describing Brillouin scattering in a relaxing medium⁴ under the very common approximation of a single relaxation time necessary to make the equations tractable, we investigate the possibility of the above two features being explained by a relaxational model.

It was found, however, that the only parameters physically variable in such a model i.e. the low frequency elastic modulus and the relaxation time, had to change in a physically unrealistic manner. The modulus for instance had to decrease with increasing gel concentration. Therefore it was concluded that a relaxational mechanism is very unlikely to be responsible for the observed effects.

However, stronger evidence against relaxational interpretation can be inferred from the effect on the Brillouin line-width of changing the exciting line from 5145 Å to 4880 Å. If a relaxation mechanism is present a decrease in line-width should be observed after correction for the inverse quadratic dependence of Γ_B on λ . However, on performing this experiment the width increases significantly. An accurate quantitative estimation of the dependence of width on frequency was not attempted since the resolution of the Fabry-Perot decreased with wavelength because of the nature of mirror coatings.

Structural scattering

Since a relaxational process would not appear to explain the experimental observations we investigate an alternative mechanism which might be responsible for the observed Brillouin line-widths i.e. that of the scattering of phonons by stationary objects.

Scattering interpretation

Taking as our model for the structure of the gel one in which the crosslinks between the polymer molecules are the triple helices⁹ of the parent collagen molecule we consider the regions of helices as cylindrical scattering entities. In this case the problem of the scattering of sound waves by such a system is closely analogous to that of the propagation of sound in a fog¹⁰. In the case of fog the scattering entities are spherical water droplets whereas in the gel they are the triple helix of a portion of the native collagen molecule which are cylindrical in shape. In principle it should be possible to interpret the Brillouin shifts and widths in terms of expressions derived from scattering from finite cylindrical scattering centres. Unfortunately, it appears that this problem has not been treated theoretically, however, it is justifiable to use the expression derived for spherical scatterers to demonstrate an order of magnitude for the effect.

Brillouin shift

The velocity of sound in a system of N spheres of radius a_n embedded in a medium is given by¹⁰:

$$v^2 = \frac{1}{K_R \rho_R} \quad (4)$$

$$K_R = K_0 + \sum_{n=1}^N \frac{4}{3} \pi a_n^3 (K_n - K_0) \quad (5)$$

$$\rho_R = \left[\frac{1}{\rho_0} + \sum_{n=1}^N \pi a_n^3 \left(\frac{1}{\rho_n} - \frac{1}{\rho_0} \right) \right]^{-1}$$

where K_R and ρ_R are the appropriate mean compressibility and density of the total system. The density and compressibility of the spheres and medium are ρ_n , K_n and ρ_0 , K_0 respectively. We know from our results that K_R and ρ_R increase only slightly. Therefore we may consider the effect of such small changes on equation (4) we have:

$$\frac{dv}{v} = -\frac{1}{2} \left| \frac{d\rho}{\rho} + \frac{dK}{K} \right|$$

Evaluating $d\rho/\rho$ and dK/K from (5) using ρ_n and K_n , 1.3 g/cm³ and $K = 10^{-11}$ cm² dyne¹¹ respectively and approximating the scattering centre as a sphere of radius 25 Å we calculate the value of N required to give the observed 10% increase in Brillouin shifts. This yields a value of $N \sim 10^{20}$ cm⁻³ which gives a value for inter-crosslink distance of the order 20 Å. This value would appear to be rather low but probably should not be interpreted too literally since equation (5) is derived assuming the interparticle distance is greater than the wavelength, and this would not appear to hold. It is worth noting however, that the above figures would predict approximately a 50% solution of gelatin, which is of the same order of magnitude as that used.

Brillouin widths

The expression for Brillouin widths arising from the scattering of phonons by the spheres can be derived from $\Gamma_B = \alpha v/\pi$ using a value of α . This can be shown to be¹⁰ $N\Sigma_s$ where Σ_s is the scattering cross-section of one of the spheres and is given by:

$$\Sigma = \frac{4}{3} \pi a^2 (\kappa a)^4 \left[\left| \frac{K_n - K_0}{K_0} \right|^2 + \left| \frac{\rho_n - \rho_0}{2\rho_n - \rho_0} \right|^2 \right]$$

Using the above values of K , ρ , n etc., and equation (3) to related spatial decay rate of a sound wave to Brillouin line width the calculated line width is ~100 MHz, giving a good order of magnitude agreement with observation. Thus it would appear that the Brillouin spectrum of the gel may be explained in terms of the scattering of sound waves by the structure of the gel, i.e. the crosslinking regions.

A further test that presents itself is the behaviour of the line width when the gel is melted. Melting the gel destroys the network and thus the line widths should decrease. We see from the single point of the graph, *Figure 3*, that this did in fact occur which further supported the scattering interpretation.

Correlation with ultrasonic results

An alternative experimental method of probing the properties of a gel using sound waves is by ultrasonic methods. However only scant data appears to be available. Koinito¹² reports no change in absorption on gelling at a frequency of 1 MHz. Mikhailor and Tarutina¹² report an increase in absorption up to a concentration of 3% and thereafter a constant absorption. This observation is consistent with the scattering interpretation since the wavelength (λ) of sound in ultrasonic experiments is very much larger than that in Brillouin scattering. For λ very much larger than the inter-crosslink distance the scattering is expected to be small in agreement with Koinito's results at high concentration. If the inter-crosslink distance decreases with increasing concentration then the behaviour described by Mikhailor and Tarutina may be expected. A convincing test would be effectively to increase the wavelength of the sound giving rise to the Brillouin scattering until it overlapped that of Mikhailor and Tarutina, however, this requires an unattainably small scattering angle.

Variation of line width and thermal treatment

An interesting result obtained from the Brillouin scattering measurements is the way that different thermal treatments affect the line-width. Quench cooling always resulting in a reduction in this width. These results are indicated in *Figure 3*.

If the increase in line width of the gel over that of water is accepted as due to scattering by the crosslinks in the gel then the explanation of the difference between slow cooled and quenched gel can be indicative of (a) differences in the size (probably the length) of the scattering units or (b) differences in the concentration of the scattering units. In reality, both probably occur and it is difficult, on the basis of the present inelastic light scattering data to distinguish between the two.

CONCLUSIONS

We have reported what we believe to be the first Brillouin scattering investigation of material of biological origin. This

was made possible due to the high contrast available from multipassed Fabry-Perot techniques. The results have been interpreted in terms of scattering of sound waves by the structure of the gel under study and parameters inferred from the study are in good agreement with the accepted structure of the gel.

ACKNOWLEDGEMENTS

Acknowledgement is due to the Science Research Council for a Fellowship for one of us (D.S.B), and to R. G. C. Povey for experimental assistance.

REFERENCES

- 1 Janus, J. W., Tabor, B. E. and Darlow, R. L. R. *Kolloid Z. Z. Polym.* 1965, **205**, 134; Boedtaker, H. and Doty, P. *J. Phys. Chem.* 1954, **58**, 968
- 2 Tanaka, T., Hoeker, L. O. and Benedek, G. B. *J. Chem. Phys.* 1973, **59**, 5151; Wun, K. L., Feke, G. T. and Prins, W. *Faraday Discuss. Chem. Soc.* 1974, **57**, 146; McAdam, J. D. G. King, T. A. and Knox, A. *Chem. Phys. Lett.* 1974, **26**, 64; French, M. J., Angus, J. C. and Walton, A. G. *Biochim. Biophys. Acta* 1971, **251**, 320
- 3 Frushour, B. G. and Koenig, J. L. *Biopolymers.* 1975, **14**, 379
- 4 Fleury, P. A. and Boon, J. P. *Adv. Chem. Phys.* 1973, **24**, 1
- 5 Hertzfeld, K. F. and Litovitz, T. A. 'Absorption and Dispersion of Ultrasonic Waves', Academic Press, New York, 1959
- 6 Born, M. and Wolf, E. 'Principles of Optics', Pergamon, Oxford, 1965
- 7 Sandercock, J. R. *Opt. Commun.* 1970, **2**, 76; Sandercock, J. R. in 'Light Scattering in Solids', (Ed. M. Balkinski), Flammarion, Paris, 1971
- 8 Stainsby, G. *Faraday Discuss. Chem. Soc.* 1974, **57**, 207
- 9 Traub, W. and Piez, K. A. *Adv. Protein Chem.* 1971, **25**, 243; Sifter, S. and Gallop, P. M. in 'The Proteins', (Ed. H. Neurath), Academic Press, New York, 1966, Vol 4
- 10 Morse, P. M. and Uno Ingard, K. 'Theoretical Acoustics', McGraw-Hill, New York, 1968
- 11 Harkness, R. D. in 'Treatise on Collagen', (Ed. B. S. Gould), Academic Press, New York, 1968, Vol 2
- 12 Dunn, F., Edmonds, P. D. and Fry, W. J. in 'Biological Engineering', (Ed. H. P. Schwan), McGraw-Hill, New York, 1969

A sonic pulse propagation study of phase separation in certain block copolymers

A. Beamish and D. J. Hourston

Department of Chemistry, University of Lancaster, Bailrigg, Lancaster LA1 4YA, UK
(Received 20 January 1976)

A pulse propagation technique has been used to measure the longitudinal sonic velocities (C_L) of both linear ABA and 4-arm star block copolymers of styrene and butadiene. When homo-polystyrene and homo-polybutadiene are added to vary the styrene content a plot of C_L against vol % polystyrene (V_G) results in a smooth curve whose equation can be represented empirically as $C_L = 6.9 \times 10^{-2} + 9.95 \times 10^{-4} V_G^{1.4}$. It is found that neither the star copolymer nor ABA poly(styrene-*b*-isoprene) lie on this curve. The latter material appears to give a lower and approximately parallel curve. The experimental curve cannot so far be predicted by equations of mixing including that attributed to Urick.

INTRODUCTION

A considerable number of papers concerned with the internal structures resulting from phase separation in ABA block copolymer systems, where A is a glassy and B a rubbery block, have now been published¹⁻⁵. Meier⁶⁻⁸ has deduced theoretically all the morphological possibilities. Part of this work has been devoted to the study of the influence of processing temperature¹ or casting solvent⁹ on the resulting structure, showing that both of these variables can influence the internal structure considerably.

To date the two techniques which have dominated morphological studies of this kind are electron microscopy and low-angle X-ray diffraction. The deduction of structure by both of these techniques is somewhat time consuming and, in the case of electron microscopy, some skill is also required in the sectioning of these rubbery materials. This latter difficulty is sometimes avoided by solvent-casting the polymer onto electron microscope grids, but as it is known that both the solvent, as already mentioned, and the evaporation rate⁹, at least for certain solvents, can influence the structure, it is an unsatisfactory approach if information on bulk structure of heat processed material is required.

As a more rapid method of achieving even only qualitative information about composition, structure and orientation in these systems would be welcome, a sonic pulse propagation technique has been applied in an attempt to achieve this end. This paper is a preliminary report on this work.

This technique has been applied to both homogeneous and heterogeneous polymer systems for some considerable time^{10,11}, but has mainly been used with semi-crystalline materials¹⁰⁻¹² often in an attempt to measure orientation in the amorphous phase^{12,13} which has a lower sonic velocity than the crystalline phase. In the case of styrene-butadiene-styrene and styrene-isoprene-styrene copolymers the individual homopolymers which comprise the blocks also have widely differing sonic velocities so that it would seem very probable that both copolymer composition and bulk structure should markedly influence the overall sonic velocity. For example, a system where the two phases are continuous should differ substantially in terms of sonic velocity from a system of the same compo-

sition where the glassy blocks are regularly dispersed as spheres in a rubbery matrix.

Craver and Taylor¹⁴ have discussed the theory of propagation of plane longitudinal sound waves through materials. In the case of a planar isotropic body, the sonic modulus (E_s) is related to the longitudinal wave velocity (C_L) by equation (1):

$$E_s = \rho C_L^2 (1 - \mu^2) \quad (1)$$

where ρ is the density of the sheet and μ is the Poisson's ratio.

The equivalent expression for the sonic shear modulus (G_s) is given by equation (2):

$$G_s = \rho C_T^2 \quad (2)$$

where C_T is the transverse sonic velocity. By the combination of equations (1) and (2), plus the relation $E_s = 2G_s(1 + \mu)$, the following expression for Poisson's ratio is obtained:

$$\mu = 1 - \left(\frac{2C_T^2}{C_L^2} \right) \quad (3)$$

Thus, by the measurement of longitudinal and transverse velocities it is possible to calculate Poisson's ratio and sonic moduli so long as the sample is isotropic.

Composition as well as structure should influence sonic velocity, but the form of such a dependence for this type of system is not known. The following equation for mixtures which is due to Urick¹⁵ has been applied as has a simple mixing equation, but neither fits the observed results:

$$C_L = \frac{1}{(\rho_0 K_0)^{1/2}} = \left\{ \frac{1}{[\rho_2 \beta + \rho_1 (1 - \beta)] [K_2 \beta + K_1 (1 - \beta)]} \right\}^{1/2} \quad (4)$$

where ρ_0 and K_0 , ρ_1 and K_1 and ρ_2 and K_2 are the density

Table 1 Characterization data for polymers used in this study

Sample	Styrene ^a (vol %)	$\bar{M}_n \times 10^{-3}$	Configurational analysis ^a			
			cis (%)	trans (%)	1,2-(%)	3,4-(%)
SBS-1	28.5	86	38	57	6	—
SBS-2	22.9	67	38	57	5	—
SIS-1	13.2	140	70	25	—	5
SIS-2	25.0	183	70	25	—	5
Star-1	34.6	210	—	—	—	—
Star-2	24.9	250	—	—	—	—
Polystyrene	100	124	—	—	—	—
Polybutadiene	—	105	34	51	15	—

^aFrom proton n.m.r.

and bulk compressibility of the composite, the matrix and the dispersed glassy phase respectively. β is the volume percent of the particulate phase.

EXPERIMENTAL

The four linear tri-block copolymers used in this study were unfractionated commercial polymers (Cariflex) manufactured by Shell Chemical Company. Both ABA poly(styrene-*b*-butadiene) (SBS) and ABA poly(styrene-*b*-isoprene) (SIS) were included. Two samples of a styrene-butadiene star copolymer (4 arms) were kindly supplied by Phillips Petroleum-UK Ltd. Details of these materials and of the polystyrene and polybutadiene homopolymers used in the compositional study are given in Table 1.

A Mechrolab Membrane Osmometer (Model 501) was used to determine number-average molecular weight and the configurational analysis was achieved by means of 220 MHz proton n.m.r.

All the systems investigated were fabricated into sheet by casting onto glass plates using re-distilled toluene as solvent. The rate of evaporation was kept low so that it could be eliminated as a factor influencing morphology.

A Morgan Dynamic Modulus Tester (PPM-5R) supplied by H. M. Morgan Co. Inc., Cambridge, Massachusetts, USA was used to measure sonic velocity. This instrument transmits a pulse of sound at a frequency of around 10 kHz from one piezoelectric transducer to another and directly measures the time elapsed between transmission and reception of the pulse. By changing the orientation of both transducers by 90° it is possible to measure the longitudinal and transverse sonic velocities.

Samples for electron microscopy were cast from very dilute toluene solutions onto a clean mercury surface and collected on nickel grids. The samples were stained by suspending the grids over a 1% aqueous solution of osmium tetroxide. The grids were examined using a Siemens Elmiskop 1A electron microscope.

RESULTS AND DISCUSSION

Applicability of the technique

The data in Table 2, which are for sheet prepared by hot pressing, show that the technique is sensitive to structural anisotropy. It was found that when these polymers were cast from toluene the resulting sheet was isotropic. The sonic velocity values for solvent cast samples of SBS-1 and SIS-2 were 0.161, 0.162 and 0.157 km/sec and 0.111, 0.109 and 0.111 km/sec respectively in the three previously

defined directions. For these cast samples, as shown in Table 3, Poisson's ratio was found to be close to 0.5. At low strains this is the expected result for a structure where the glassy phase is discontinuous and embedded in a rubbery matrix. This structure has been shown to be the correct one (see Figure 1a). This clearly shows a spherical or possibly a cylindrical polystyrene domain structure in a rubbery matrix.

Influence of polystyrene content on C_L

Figure 2 shows the influence of vol % polystyrene on C_L , indicating that when various amounts of polystyrene and polybutadiene homopolymers were added to SBS-1 a smooth curve (A) which also passes through the point representing pure polybutadiene results. Furthermore, it was found that the data for SBS-2 and SBS-2 with added polystyrene also fitted the same curve, but that the data for SIS-1 and SIS-2 did not fall on the curve, but seem to lie on a lower, and, approximately parallel, curve. In the case of the two styrene-butadiene star polymers the sonic velocities lay considerably above curve A.

Table 2 Sonic velocity and dynamic storage modulus (E') data illustrating the sensitivity of the technique to sample anisotropy

Sample	Direction ^a	C_L (km/sec)	$E' \times 10^{-7}$ (N/m ²) at 10°C ^b
SBS-1	1	0.236	3.9
	2	0.221	3.4
	3	0.242	4.5
SIS-2	1	0.318	6.7
	2	0.109	0.83
	3	0.182	2.0

^aDirections 1 and 2 were arbitrarily chosen to be mutually at right angles and direction 3 is at 45° to both directions 1 and 2; ^bmeasured using a Rheovibron Dynamic Viscoelastometer, Model DDV-II, at 110 Hz

Table 3 Poisson's ratio (μ) for samples cast from toluene

Sample	Direction ^a	μ^b
SBS-1	1	0.56 ± 0.06
	2	0.57 ± 0.06
	3	0.52 ± 0.04
SIS-2	1	0.50 ± 0.04
	2	0.51 ± 0.04
	3	0.49 ± 0.04

^aAs defined in Table 2; ^baverage of at least 5 determinations

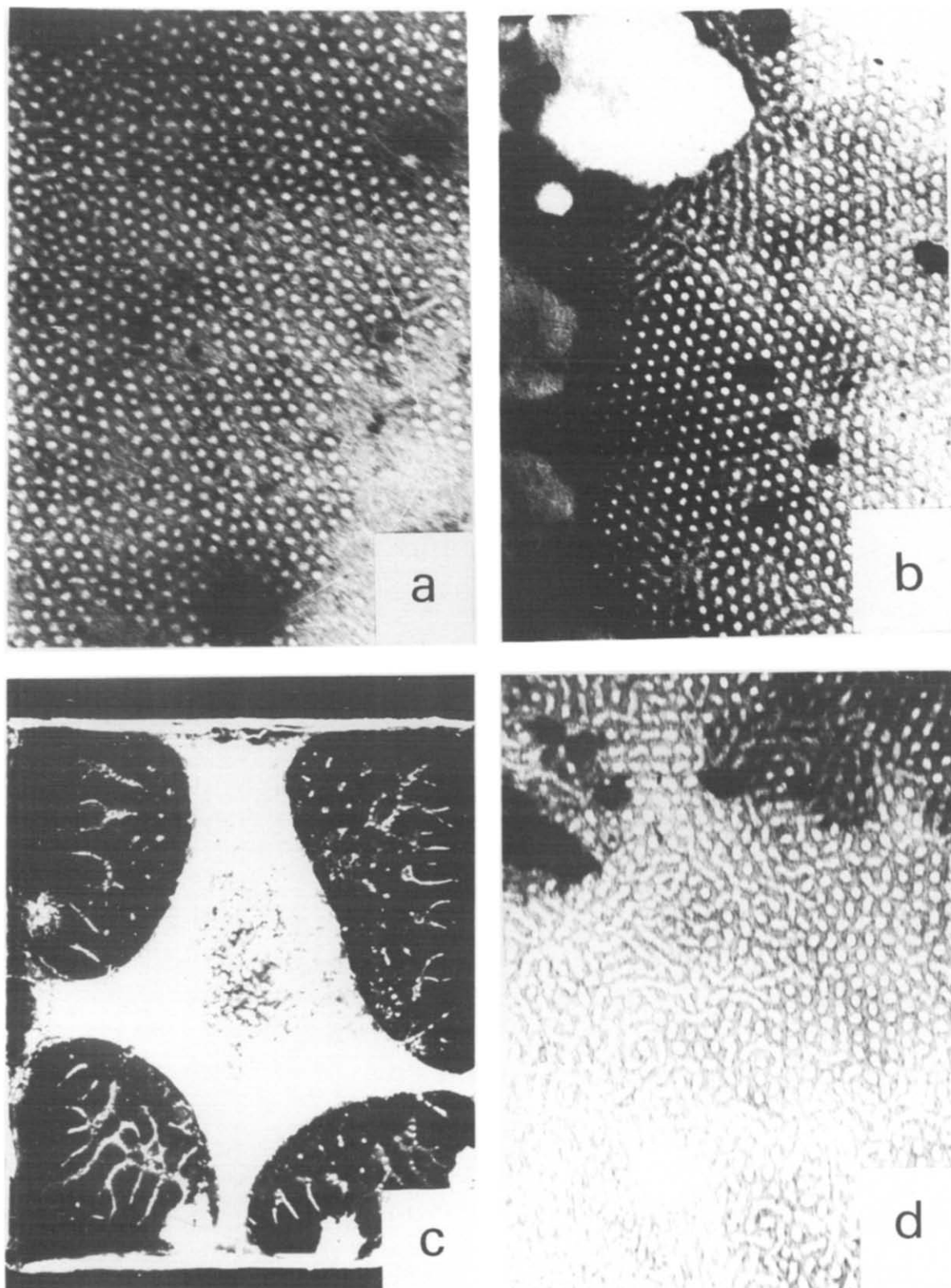


Figure 1 (a) Electron micrograph of SBS-1 cast from toluene. Magnification: 71 500x; (b) electron micrograph of SBS-1 plus 10% (w/w) added polystyrene (light areas). Cast from toluene. Magnification: 56 000x; (c) SBS-1 plus 50% (w/w) added polystyrene (dark areas). Magnification: 0.57x; (d) electron micrograph of Star-2 polymer cast from toluene. Magnification: 72 000x

The polystyrene added to the SBS rubbers had a considerably higher molecular weight than that of the end-blocks. A consequence of this, which was recognized in advance, was that some or even the bulk of the added homopolymer would not be accommodated in the domains,

but would rather form macrodomains of pure polystyrene. Such occluded polystyrene macrodomains were observed for all levels of added polystyrene. Figure 1b shows a typical structure which also shows that the regularity of domain structure is largely retained. If the volume per-

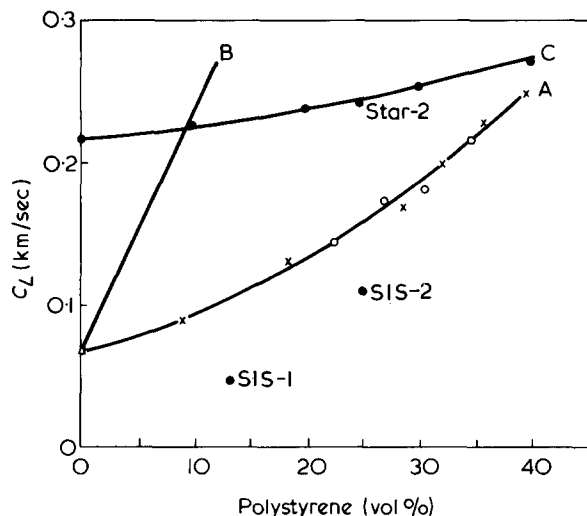


Figure 2 Longitudinal sonic velocity (C_L) versus vol % polystyrene. Curve A: \circ , SBS-2 and SBS-2 plus added polystyrene, \times , SBS-1 and SBS-1 plus added polybutadiene or polystyrene; Δ , polybutadiene. Curve B, equation (5). Curve C, equation (4)

centage of polystyrene exceeded $\sim 40\%$ the result was phase separation on a massive scale (see Figure 1c).

The polybutadiene which was added to lower the polystyrene content had a very similar microstructure and molecular weight to that of the mid-blocks of both SBS-1 and SBS-2, and would certainly be located in the matrix. The fact that all the points lie on a smooth curve would seem to a first approximation to indicate that the overall sonic velocity is sensitive only to the volume percent of the glassy phase and not to whether it is all incorporated into the pre-existing glassy domains or whether macrodomains result. In either case it is assumed that the polystyrene phase remains discrete. This tentative conclusion will be tested by using polystyrene of much lower molecular weight.

It has been reported¹⁶ that styrene-butadiene star copolymers have higher elastic moduli than their equivalent linear counterparts. As the densities of the two systems are very similar an inevitable consequence of this is that the sonic velocities will also be higher. In the case of Star-1 where the vol % polystyrene was 34.6, the sonic velocity was 0.540 km/s. The result for Star-2 is shown in Figure 2. Figure 1d shows that although the domains are somewhat less regular for the cast star polymer the rubbery phase is the continuous one.

Because of the non-linearity of curve A (Figure 2) simple equations of mixing such as equation (5) cannot be expected to fit the observed data precisely.

$$C_L = \nu_G C_G + (1 - \nu_G) C_R \quad (5)$$

Where ν_G is the volume fraction of glassy polymer and C_G and C_R are the longitudinal sonic velocities of the glassy and rubbery phases respectively. However, in fact, expressions of this type result in very poor fits as is illustrated by curve B (Figure 2). An experimentally determined value of 0.069 km/sec was used for the longitudinal sonic velocity

of polybutadiene. It is now clear that in such systems there will be boundary regions¹⁷ where an admixture of polystyrene and polybutadiene coexist. By considering this third phase it should be possible to improve, somewhat, the fit of such equations of mixing. At the moment however, it is not clear what composition should be used for this mixed phase.

The curve predicted by Urick's equation (equation 4) is shown as curve C (Figure 2), and, again, this curve bears no relation to the observed results. In the calculation of this curve the densities of the glassy and rubbery phases were taken as 0.899 and 1.05 g/cm³ respectively, whilst Poisson's ratios for these two phases were assumed to be 0.33 and 0.49 respectively. The bulk compressibilities were calculated from experimental values of dynamic storage modulus. This relation is very sensitive to the values chosen for Poisson's ratio for the rubber, but changes in this parameter, and, also the addition of a third mixed phase, only results in somewhat lower, and parallel, curves.

At this stage of the work it is necessary to resort to the empirical equation shown below.

$$C_L = 6.9 \times 10^{-2} + 9.95 \times 10^{-4} V_G^{1.4} \quad (6)$$

where V_G is the vol % polystyrene.

In conclusion, it can be stated that equation (6) relates C_L to vol % polystyrene specifically for linear SBS systems, and, that a similar relation will probably hold for SIS polymers. Acceptance of such relations would allow rapid estimation of polystyrene content.

ACKNOWLEDGEMENT

A. B. wishes to acknowledge, with gratitude, an Science Research Council Research Studentship.

REFERENCES

- 1 Pedemonte, E., Cartasegna, S., Devatta, P. and Turturro, A. *Chim. Ind.* 1973, **55**, 861
- 2 Holden, G., Bishop, E. T. and Legge, W. R. *J. Polym. Sci. (C)* 1969, **26**, 287
- 3 Hendus, H., Illers, K. H. and Rupte, E. *Kolloid-Z.* 1967, **216**, 110
- 4 Matsuo, M., Sagae, S. and Asai, H. *Polymer* 1969, **10**, 79
- 5 Matsuo, M. *Japan. Plast.* 1968, **2**, 6
- 6 Meier, D. J. *J. Polym. Sci. (C)* 1969, **26**, 81
- 7 Meier, D. J. *Polym. Prepr.* 1970, **11**, 400
- 8 Meier, D. J. *US-Japan Jt. Semin. Polym. Solid State, Case Western Reserve, USA, October 1972*
- 9 Miyamoto, T., Kodama, K. and Shibayama, K. *J. Polym. Sci. (A-2)* 1970, **8**, 2095
- 10 Charch, W. H. and Moseley Jr., W. W. *Text. Res. J.* 1959, **29**, 525
- 11 Moseley Jr., W. W. *J. Appl. Polym. Sci.* 1960, **3**, 266
- 12 Morgan, H. M. *Text. Res. J.* 1962, **32**, 865
- 13 Dumbleton, J. H. *J. Appl. Polym. Sci. (A-2)* 1968, **6**, 795
- 14 Craver, J. K. and Taylor, D. L. *Tappi* 1965, **48**, 142
- 15 Urick, R. J. *J. Appl. Phys.* 1947, **18**, 983
- 16 Bi, L.-K., Fetters, L. J. and Morton, M. *Polym. Prepr.* 1974, **15**, 157
- 17 Leary, D. F. and Williams, M. C. *J. Polym. Sci.* 1973, **11**, 345

Microstructure of directionally solidified poly(ethylene oxide)

Andrew J. Lovinger, Chi-Ming Lau and Carl C. Gryte

Department of Chemical Engineering and Applied Chemistry, Columbia University, New York 10027, USA

(Received 17 December 1975; revised 18 March 1976)

Poly(ethylene oxide), zone solidified within a temperature gradient, has been examined by electron microscopy and X-ray diffraction. Longitudinal fracture replicas show the lamellae to be oriented parallel to the direction of solidification, with no observable order in the transverse direction. These results are also substantiated by X-ray diffraction. In contrast to a drawn fibre, the crystallites are not oriented in a single direction, but rather parallel to the $\{100\}$ planes. This is consistent with growth on the $\{120\}$ faces. These are inclined by 45° with respect to the a^* axis, which is parallel to the direction of solidification and to the direction of the temperature gradient.

INTRODUCTION

During the past two decades, the zone solidification technique¹ developed by Pfann² has found widespread applications in the production of single crystals of metals³ and inorganic⁴ and organic⁵ compounds, in the oriented growth of alloys⁶, and in the purification of chemical substances^{7,8}. This technique involves passage of a rod of the material at a steady state through a zone heater where the temperature is high enough to cause melting. The melt–solid interface is steady, so that crystallization proceeds at a constant growth rate equal to the velocity of the rod.

This method has also been used to produce directionally oriented polymer crystals from the melt in the works of Fujiwara^{9,10} and Crissman^{11,12} on polyethylene and polypropylene, as well as Stein *et al.*¹³ on films of poly(butene-1). A review of these and other methods^{14,15} of inducing uniaxial growth of polymers has been given elsewhere¹⁶.

The microstructure of uniaxially crystallized material is expected to be similar to that in a narrow radial sector of ordinary spherulites. The divergence of the radii from a nucleation point requires a certain branching, but that does not affect the nearly parallel growth of adjacent fibrils. Price and Kilb¹⁷ have confined poly(ethylene oxide) (PEO) in a small capillary, and have in fact used the resulting morphology as a model for spherulitic microstructure. Also, the diffraction pattern of a small sector of a type III polypropylene spherulite, as shown by use of a micro-X-ray beam¹⁸, is very similar to that of a zone solidified sample¹⁰.

Poly(ethylene oxide) rods have been directionally solidified¹⁶ to produce uninterrupted lamellae that extend throughout the full length of the material. The morphology, as determined by polarizing optical microscopy, indicates a spherulitic macrostructure in the form of an uninterrupted matrix of parallel lamellar fibrils practically devoid of primary nuclei. These large specimens are thus ideally suited for microstructure evaluation by electron microscopy of fracture surfaces and by X-ray diffraction. It is the purpose of this report to use these techniques to determine the orientation of the PEO lamellae within a zone solidified rod, and to indicate their organization in planes parallel and normal to the direction of oriented growth.

EXPERIMENTAL

Poly(ethylene oxide), (Union Carbide WSR-205, molecular weight 600 000), was injection moulded to produce cylindrical rods, 10 cm in length and 1 cm in diameter. The rods were then placed into glass tubes that were subsequently evacuated, filled with dry nitrogen, and sealed. Zone solidification of the polymer was effected by passing the rods through an annular heater and cooler, as has previously been described¹⁶. The temperature gradient between these was substantially linear at $3^\circ\text{C}/\text{mm}$, and the solid–melt interface was observed to remain stationary during the procedure. At speeds below $400\ \mu\text{m}/\text{min}$, the directionally solidified sample was composed of spherulites slightly elongated in the direction of motion. When rates below $15\ \mu\text{m}/\text{min}$ were employed, the initially nucleated spherulites extended into the entire length of the polymer rod, and birefringence indicated that fibrils were oriented in the longitudinal direction, parallel to the cylinder axis¹⁶.

From the zone solidified samples, longitudinal and transverse sections, 1–2 mm thick, were cut to be used for X-ray studies. The same procedure was carried out on randomly crystallized rods, as well as on fibres; these were used for comparison purposes. As PEO is water soluble, the samples were stored under vacuum in a desiccator.

Diffraction patterns were recorded on X-ray film (Kodak Type AA-2) using a well collimated beam from a $\text{CuK}\alpha$ source. A lead beam stop was placed on the film, which was at a distance of 5.56 cm from the sample.

Electron micrographs were made of replicas produced from fracture surfaces in both the longitudinal and transverse directions of the rods. Clean breaks could be made only after cooling the samples to liquid nitrogen temperatures. As ordinary carbon replicas showed very little contrast, gold shadowing at an angle of about 30° was used prior to carbon deposition. The replicas were then isolated by dissolution of the polymer in water, and placed on 200-mesh grids or bar grids for bright field studies.

RESULTS AND DISCUSSION

Electron microscopy

Poly(ethylene oxide) crystallizes in the form of lamellae

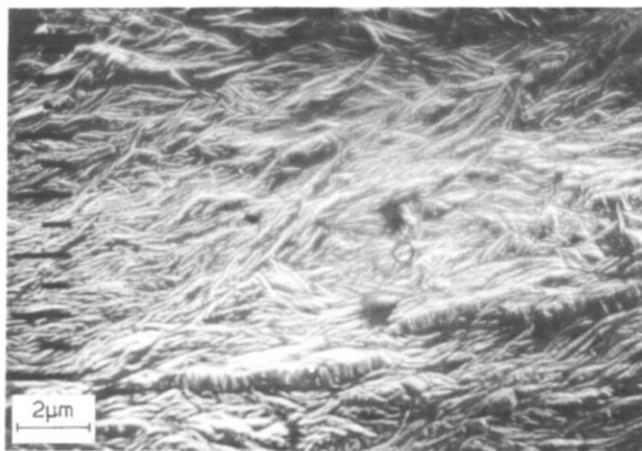


Figure 1 Fracture surface from a longitudinal section of directionally solidified PEO. Zone velocity = 15 $\mu\text{m}/\text{min}$

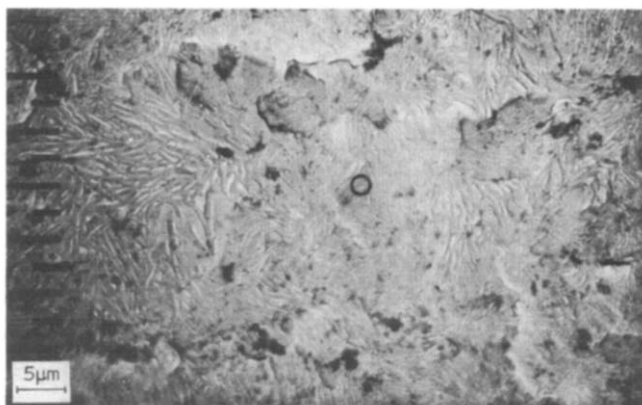


Figure 2 Fracture surface from a transverse section of directionally solidified PEO. Zone velocity = 15 $\mu\text{m}/\text{min}$

about 100 Å thick and several microns in lateral dimensions¹⁹. The clear lamellar structure of this polymer is seen in *Figure 1*, obtained from a surface replica in the longitudinal direction of a sample zone solidified at 15 $\mu\text{m}/\text{min}$. A distinct orientation of the lamellae from left to right is evident. Of course, the high magnification and consequent narrow field do not permit any general conclusions regarding overall orientation to be reached from a single micrograph. However, it has been conclusively observed by use of numerous electron micrographs taken from different areas of each replica, as well as from other longitudinal sections of the same and of similar samples, that for any given rod all lamellae are indeed oriented in the same direction. Use of bar grids has shown that this also coincides with the direction of zone solidification.

Examination of the transverse cross-section can be made on the electron micrograph of *Figure 2*. In order to be able to observe the overall structure, the magnification has been reduced so that the field of view is now about eight times larger than in *Figure 1*. Here, no unique orientation is apparent; practically all possible directions are represented in this micrograph. Similar results obtained from other transverse sections indicate that there is indeed no overall orientation normal to the direction of solidification. These observations are consistent with the optical birefringence data¹⁶ on the same materials, for which the transverse sections were found to be birefringent but without orientation when viewed between crossed polarizers.

Nevertheless, despite the lack of overall orientation, adjacent fibrils, as seen in small regions of *Figure 2*, do

adopt parallel directions. This is due to the space filling requirement of efficient packing of individual lamellae within the fibrillar texture. This is seen more clearly in *Figure 3*, which presents a part of the preceding photograph at a higher magnification. In addition, a number of very thin links are observed to connect many adjacent lamellae. Such links have been absent in all longitudinal replicas. These void-like areas may be caused by dimensional changes of the material during zone solidification. Their absence in the longitudinal direction would then be due to the fact that in this case all crystal boundaries are parallel to that direction.

X-ray diffraction

Figures 4a and *4b* show the diffraction patterns obtained from bulk crystallized PEO and from a drawn fibre of this polymer. By use of such diffraction patterns, several investigators^{17,20-24} have determined the unit cell parameters. In this study, the most recent values of Takahashi and Tadokoro²⁴ were used, postulating a monoclinic unit cell ($a = 8.05 \text{ \AA}$, $b = 13.04 \text{ \AA}$, $c = 19.48 \text{ \AA}$, $\beta = 125.4^\circ$) with a considerable distortion from the D_7 helical symmetry that had been previously observed.

Figures 5a and *5b* contain the diffraction patterns shown by two longitudinal sections of the directionally crystallized PEO, while the major inner reflections are indexed in *Figure 5c*. In all cases the direction of solidification is vertical. The sample of *Figure 5a* was zone solidified at 200 $\mu\text{m}/\text{min}$, forming numerous spherulites, all distinctly elongated in the direction of motion¹⁶. The full circles seen in the bulk crystallized specimen of *Figure 4a* now begin to partly break up into arcs, indicating the start of limited orientation. A much more highly oriented structure is exhibited in the diffraction pattern of *Figure 5b*, where very distinct arcs are now apparent. This photograph was obtained from a sample crystallized at 15 $\mu\text{m}/\text{min}$, representing uninterrupted growth of PEO lamellae in a temperature gradient.

When the X-ray beam is directed parallel to the sample axis through a transverse cross-section, the pattern of *Figure 5d* is obtained. Full circles are again formed, indicating the lack of any preferred orientation normal to the direction of oriented growth of the spherulitic fibrils. The molecular chains thus adopt all possible directions about the rod axis.

Comparison of the diffraction patterns from the bulk crystallized sample (*Figure 4a*) and from the transverse section (*Figure 5d*) shows a striking difference. Although

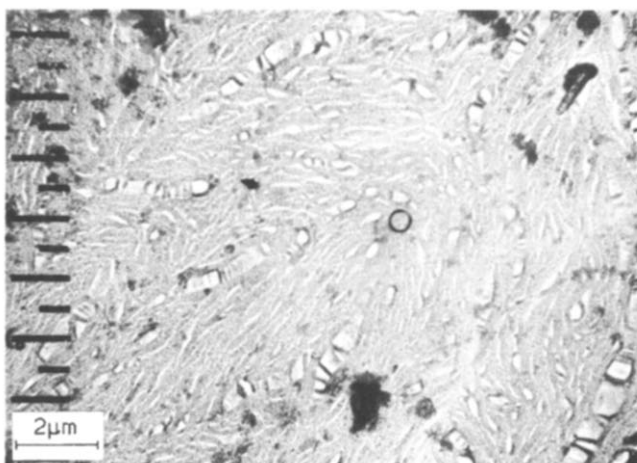


Figure 3 Higher magnification of the fracture surface of *Figure 2*

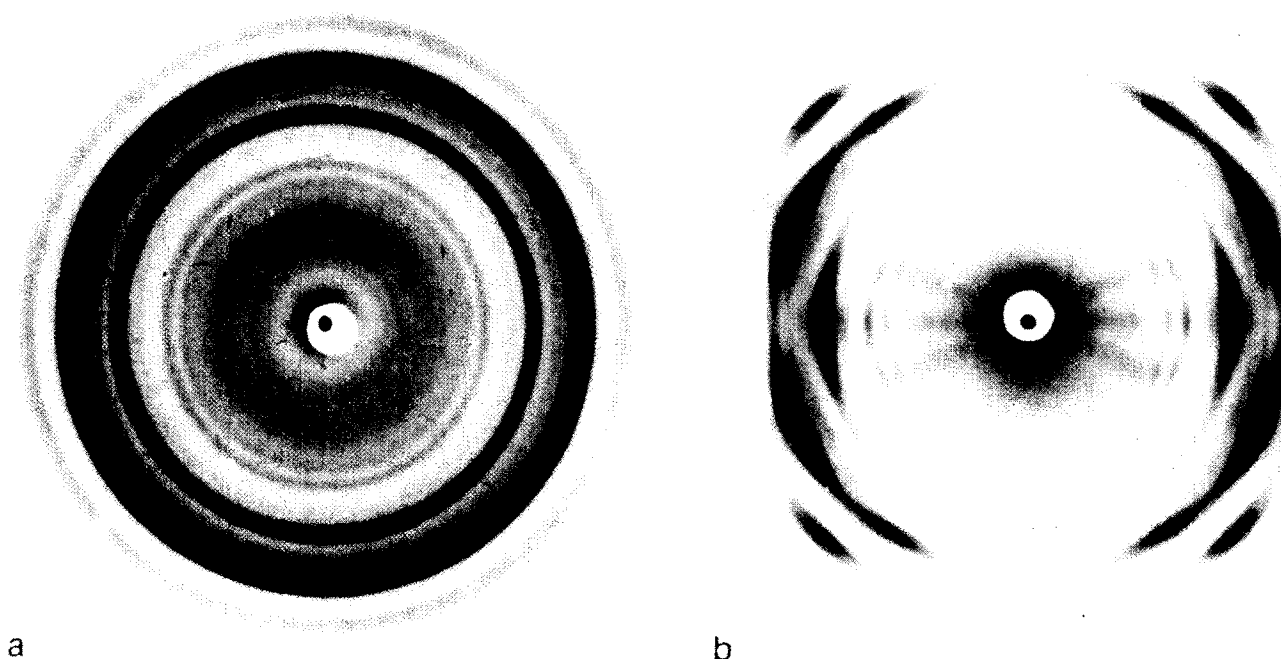


Figure 4 X-Ray diffraction patterns of PEO. (a) Bulk crystallized sample; (b) drawn fibre; fibre axis vertical

the strong outer ring of *Figure 4a* (composed chiefly of the 032 and $\bar{1}32$ reflections) is also present in *Figure 5d*, the strongest individual reflection, i.e. the 120 seen as the intense inner ring in *Figure 4a*, is almost totally absent in *Figure 5d*. This implies that orientation in the transverse cross-section is not totally random, since in no case do the $\{120\}$ planes adopt a Bragg angle of 9.6° required for their reflection.

The treatment of Sisson²⁶ regarding the various types of orientation can be used to explain the differences in the diffraction patterns of *Figures 4b* and *5b*. The former is the ordinary type of axial orientation²⁵ (or fibre formation) obtained by mechanical drawing, in which case the *c*-axes lie parallel to the fibre direction. In the zone solidified sample of *Figure 5b*, the crystallites lie parallel to a transverse plane¹⁶, but can otherwise have all possible directions on this plane.

In this case the X-ray photograph shows row lines parallel to a rotation axis. Layer lines are absent since the principle planes of the reciprocal lattice are now inclined with regard to the equator²⁵. Such row lines are clearly seen in *Figure 5b* and *5c* in the vertical direction. In these *Figures* the reflections on each specific row line have identical *k* indices. A transformation of the row lines using a Bernal diagram²⁷ indicates equatorial spacings of $13.1 \pm 0.2 \text{ \AA}$ which are indeed characteristic of the length of the *b*-axis of the PEO unit cell. Small individual deviations occur in each row line (e.g. in the 020 and the 021 reflections) when the *l* values of the reflections are different. In this case the *c*-axes to which these indices correspond are inclined with respect to the axis of rotation in the monoclinic cell.

A similar diffraction pattern was obtained by Price and Kilb¹⁷ from a PEO spherulite grown isothermally within a very fine capillary. They found crystal orientation consistent with rotation about the (401) plane normal, while Walter and Reding²⁸ had previously concluded that rotation occurs about the *b*-axis of the unit cell. However,

indexing of the diffraction pattern of *Figure 5b* shows that Price and Kilb¹⁷ are right in rejecting the *b*-axis. Nevertheless, the *b*-axis is still a very special direction within the unit cell; it is perpendicular to both the *a* and *c*-axes, as well as to the true rotation axis of the zone solidified polymer.

The present data tend to question also the $[401]^*$ axis proposed by Price and Kilb¹⁷. It is true that their axis is consistent with the experimental data, and the interplanar angles as calculated from the formula for monoclinic unit cells are in close agreement with those predicted from the observed azimuthal angles (see *Table 1*). However, it is equally true that this axis is physically awkward, resulting in an anomalous growth mode. This is seen in *Figure 6*, a perspective drawing of the PEO unit cell, and in *Figure 7*, which depicts two sections of this cell, viewed along the (010) and $(10\bar{4})$ plane normals. The $[401]^*$ axis is inclined at an angle of 4.6° with respect to the normal to the (100) plane, causing the *c*-axes of the unit cell to be positioned at an angle of 85.4° away from the $[401]^*$ direction.

A much more attractive choice for a rotation axis is the $[100]^*$, i.e. the *a** axis, which is normal to the *c*-axis, allowing the molecular chains to crystallize perpendicular to the growth direction and parallel to the melt–solid interface (see *Figures 6* and *7*). Not only is this axis also consistent with the diffraction pattern of *Figure 5b*, but a comparison of the observed and calculated interplanar angles gives a closer agreement for the $[100]^*$ axis than for the $[401]^*$, as is seen in *Table 1*.

The precise growth front is most likely composed of parallel lamellae, growing on their $\{120\}$ faces in a manner similar to that depicted in *Figure 8*. There is substantial evidence in the literature that the (120) is by far the favoured growth plane in the PEO crystals²⁹. Investigations of the unit cell structure^{17,20–24} show that the $\{120\}$ planes are the most closely packed in the lattice. In fact, the latest unit cell proposed by Takahashi and Tadokoro²⁴ causes the $\{120\}$ planes to be even more closely packed than had pre-

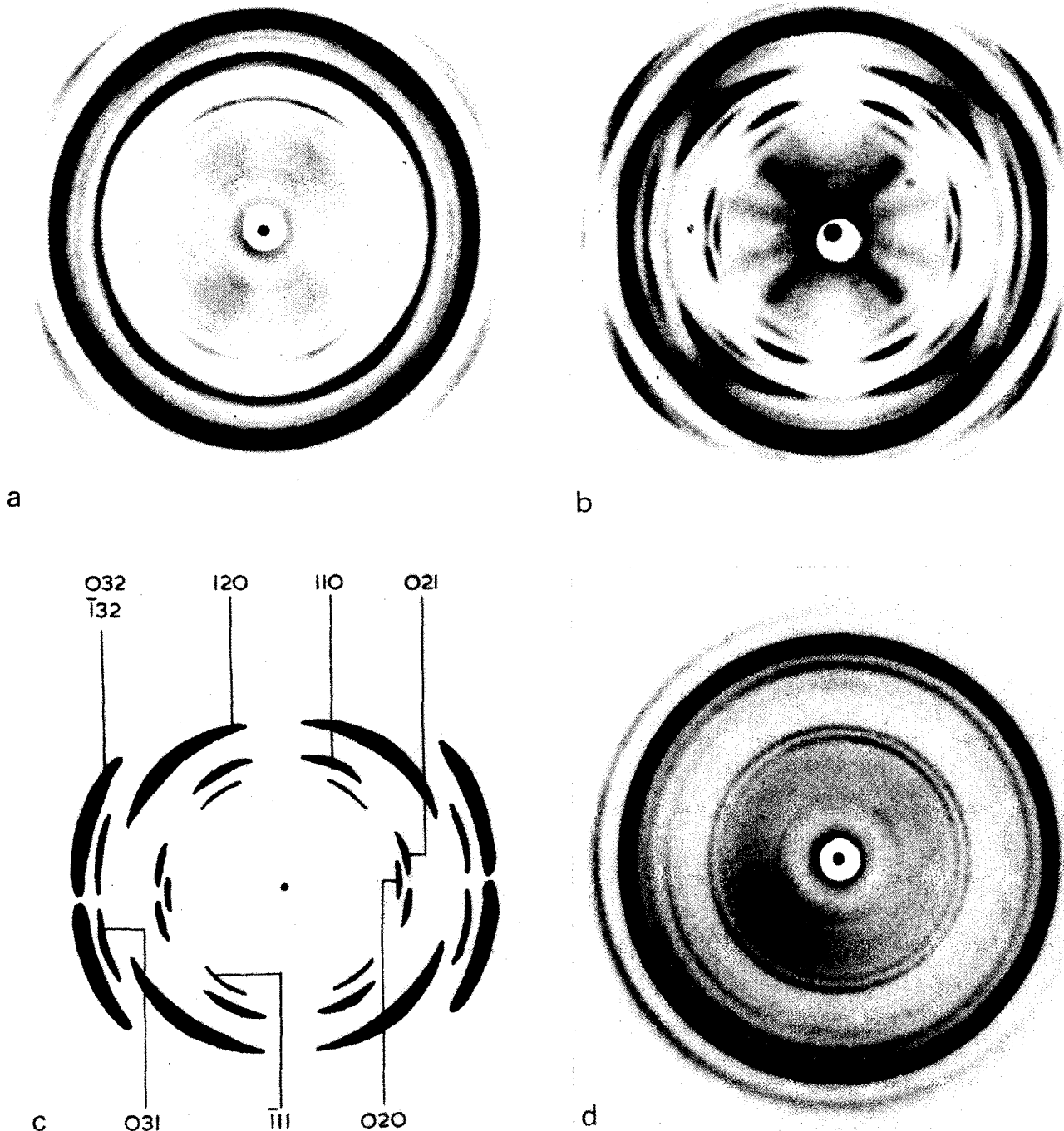


Figure 5 X-Ray diffraction patterns of zone solidified PEO. (a) Longitudinal section; axis vertical; zone velocity = 200 $\mu\text{m}/\text{min}$; (b) longitudinal section; axis vertical; zone velocity = 15 $\mu\text{m}/\text{min}$; (c) indices of the major inner reflections of Figure 5b; (d) transverse section; zone velocity = 15 $\mu\text{m}/\text{min}$

viously been thought. Barnes and Price¹⁹ have observed growth spirals and terraces typical of (120) growth on single crystals of PEO. Lotz and Kovacs³⁰ have isolated single crystals of PEO, which in most cases appear as nearly perfect squares whose four sides are (120) planes, while their diagonals are parallel to a^* and b^* . Thus, the above growth model also accounts for the striking absence of the strongest single reflection from the diffraction pattern of the transverse section in zone solidified PEO (Figure 5d). As this reflection is caused by the {120} planes which are inclined at a constant angle of 45.4° to the proposed $[100]^*$ axis (see Figure 6), the 9.6° Bragg angle required for reflection

can never be attained. As seen from the above discussion, this type of growth results in a conical orientation of the {120} planes. The base of the cone is a common (100) plane, and its axis is $[100]^*$ or a^* , which coincides with the direction of the oriented growth and the temperature gradient.

It should be noted that the model proposed is not in disagreement with the branching of spherulitic fibrils reported in the treatment of Keith and Padden³¹. However, as is also seen in Figure 1, directional growth geometrically constrains the extent of the branches produced, and thus the X-ray pattern should show no significant orientation other than around the rotation axis.

Table 1 Comparison of calculated and observed interplanar angles for the [401]* and [100]* axes

Reflection	<i>d</i> (Å)	Obs. δ (degrees)	Obs. ϕ (degrees)	Calc. ϕ [401]*	Calc. ϕ [100]*	Deviation (%)	
						[401]*	[100]*
210	3.1952	0	13.5	15.0	14.3	11.1	5.9
221	3.2122	160	147.4	155.2	148.6	3.3	0.8
040	3.2475	90	90.0	90.0	90.0	0.0	0.0
131	3.2984	50	51.3	50.5	51.3	1.6	0.0
224	3.3366	119	118.2	116.5	120.5	1.4	1.9
211	3.5548	160	157.1	157.8	160.8	0.4	2.4
201	3.6959	0	168.6	164.4	169.0	2.5	0.2
032	3.7854	73	73.4	71.6	73.4	2.5	0.0
031	4.1721	78	78.2	79.9	80.9	2.2	3.5
120	4.6269	45	45.8	45.6	45.4	0.4	0.9
110	5.8791	26	27.0	27.3	26.9	1.1	0.4
021	5.9957	78	78.1	75.5	76.9	3.3	1.5
020	6.4950	90	90.0	90.0	90.0	0.0	0.0
111	6.8070	145	144.5	138.1	140.8	4.4	2.6

Average difference [401]* = 2.28%; average difference [100]* = 1.34%

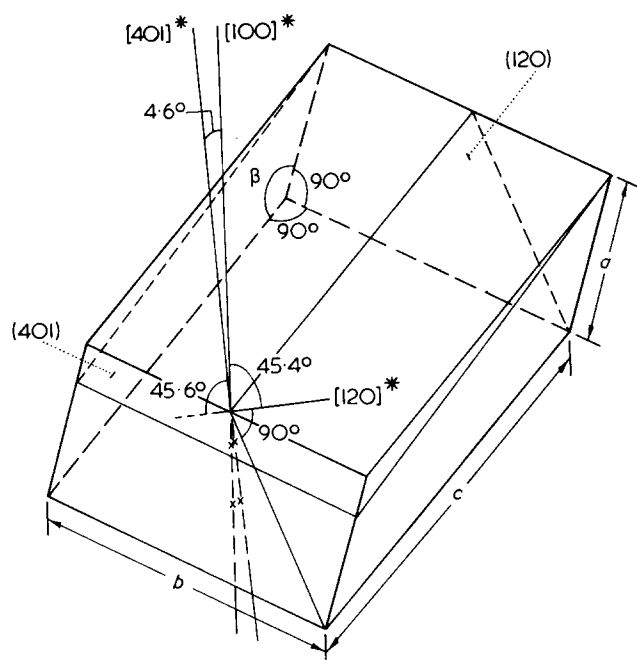


Figure 6 PEO unit cell, showing the two possible axes of rotation

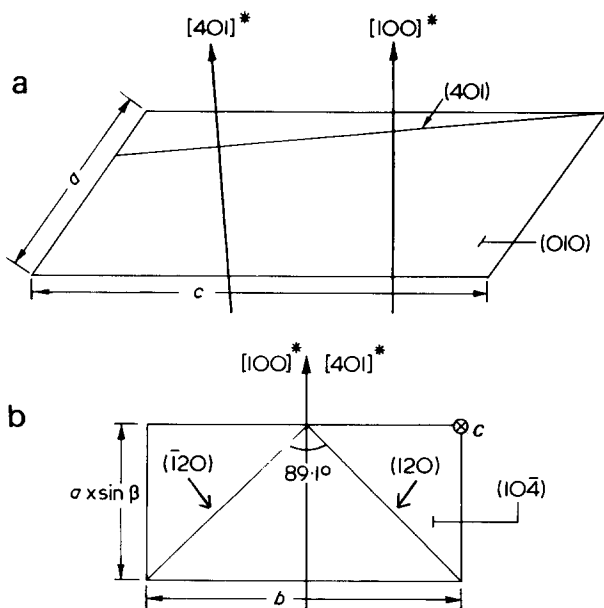


Figure 7 Two specific sections of the PEO unit cell. (a) View along (010) normal; (b) view along (104) normal

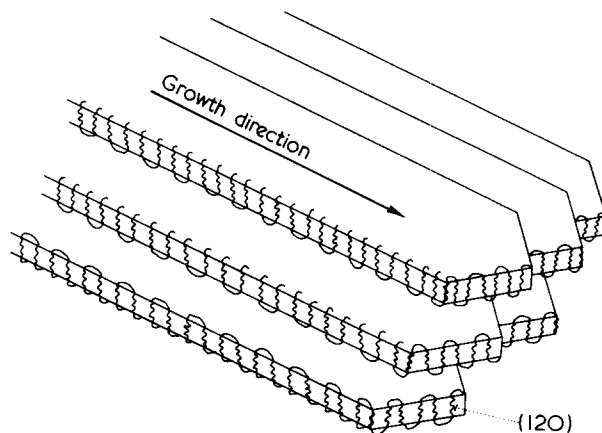


Figure 8 Proposed mode of growth of the PEO lamellar fibrils during zone solidification

ACKNOWLEDGEMENT

The support of the donors of Petroleum Research Fund, administered by the American Chemical Society, is appreciated.

REFERENCES

- Pfann, W. G. 'Zone Melting', 2nd Edn, Wiley, New York, 1966
- Pfann, W. G. *J. Met.* 1952, 4, 747, 861
- Pfann, W. G. and Olsen, K. M. *Phys. Rev.* 1953, 89, 322
- Keck, P. H. and Golay, M. J. *J. Phys. Rev.* 1953, 89, 1297
- Herington, E. F. G. 'Zone Melting of Organic Compounds', Blackwell, London, 1963
- Chadwick, G. A. in 'Eutectic Solidification', (Ed. B. Chalmers), Pergamon, London, 1963, Vol 12
- Beynon, J. H. and Saunders, R. A. *Br. J. Appl. Phys.* 1960, 11, 128
- Zief, M. in 'Fractional Solidification', (Eds. M. Zief and W. R. Wilcox), Marcel Dekker, New York, 1967, pp649-678
- Tanaka, K., Seto, T. and Fujiwara, Y. *Rep. Progr. Polym. Phys. Japan* 1963, 6, 285
- Fujiwara, Y. *Kolloid Z. Z. Polym.* 1968, 226, 135
- Crissman, J. M. and Passaglia, E. *J. Res. Nat. Bur. Stand. (A)* 1966, 70, 225
- Crissman, J. M. *J. Polym. Sci. (A-2)* 1968, 6, 389
- Sasaguri, K., Yamada, R. and Stein, R. S. *J. Appl. Phys.* 1964, 35, 3188
- Von Jenckel, E., Teege, E. and Hinrichs, W. *Kolloid Z. Z. Polym.* 1952, 129, 19
- Schonhorn, H. *J. Polym. Sci. (B)* 1964, 2, 465

- 16 Lovinger, A. J. and Gryte, C. C. *Macromolecules* 1976, **9**, 247
- 17 Price, F. P. and Kilb, R. W. *J. Polym. Sci.* 1962, **57**, 395
- 18 Samuels, R. J. and Yee, R. Y. *J. Polym. Sci. (A-2)* 1972, **10**, 385
- 19 Barnes, W. J. and Price, F. P. *Polymer* 1964, **5**, 283
- 20 Fuller, C. S. *Chem. Rev.* 1940, **26**, 143
- 21 Richards, J. R. *PhD Thesis* University of Pennsylvania (1961); *Diss. Abstr.* 1961, **22**, 1029
- 22 Danusso, T. and Gianotti, G. *Makromol. Chem.* 1963, **61**, 139
- 23 Tadokoro, H. *J. Polym. Sci. (C)* 1966, **15**, 1
- 24 Takahashi, Y. and Tadokoro, H. *Macromolecules* 1973, **6**, 672
- 25 'X-Ray Diffraction by Polycrystalline Materials', (Eds. H. S. Peiser, H. P. Booksby and A. J. C. Wilson), Institute of Physics, London, 1955, pp 361–362, 489–493
- 26 Sisson, W. A. *J. Phys. Chem.* 1936, **40**, 343
- 27 Alexander, L. E. 'X-Ray Diffraction Methods in Polymer Science', Wiley-Interscience, New York, 1969, p 60
- 28 Walter, R. E. and Reding, F. P. *133rd Nat. Meet. ACS, San Francisco* 1958, Abstr. No. 14R35
- 29 Wunderlich, B. 'Macromolecular Physics', Academic Press, New York, 1973, Vol 1, p 237
- 30 Lotz, B. and Kovacs, A. J. *Kolloid Z. Z. Polym.* 1966, **209**, 97
- 31 Keith, H. D. and Padden, F. J. *J. Appl. Phys.* 1963, **34**, 2409

Differential refractometry and light scattering on nylon-6 and poly(methyl acrylate) in mixed solvents

M. B. Huglin and R. W. Richards*

Department of Chemistry and Applied Chemistry, University of Salford, Salford M5 4WT, UK
(Received 21 January 1976; revised 23 February 1976)

Investigations have been made of solvent systems for potential use in characterizing nylon-6/poly(methyl acrylate) copolymers. To this end, measurements involving differential refractometry (at constant composition and also constant chemical potential of solvents) and light scattering have been conducted on solutions of nylon-6, poly(methyl acrylate) and a mixture of these two polymers. From refractometric and solubility considerations the most suitable solvents are binary mixtures of *o*-chlorophenol (*o*-CP) and 2, 2', 3, 3'-tetrafluoropropanol. In particular, the binary solvent containing 73% (by volume) of *o*-CP yields the molecular weight of the nylon-6 constituent of the polymer mixture directly, since the light scattering from the other polymer constituent is thereby eliminated. Preferential adsorption of *o*-CP occurs to both polymers, the maximum extents corresponding to 1 mol *o*-CP/1.4 segments nylon and 1 mol *o*-CP/5.7 segments poly(methyl acrylate). This is attributed to a breakdown of intramolecular hydrogen-bonding in *o*-CP and subsequent formation of hydrogen bonds with the carbonyl groups in the polymers.

INTRODUCTION

Previous communications¹⁻⁵ have been devoted to the kinetics of the γ -radiation initiated grafting of acrylic acid to nylon-6. A continuation of this work is the correlation of these kinetics with the chain lengths of the grafts and of the nylon/poly(acrylic acid) copolymer produced, the latter being freed from homopolymer and ungrafted substrate⁶. From solubility considerations it is found convenient to handle the grafts in their methylated form⁶, i.e. as poly(methyl acrylate). In the present communication we investigate the potentialities of some solvent systems with a view to optimizing a future characterization of methylated copolymers. To obviate any possible confusion it should be noted that no data on copolymers are reported here, and the measurements relate solely to solutions of nylon-6, poly(methyl acrylate) and a mixture of these two polymers.

CONDITIONS, UNITS AND ABBREVIATIONS

The temperature for all measurements was 303K and the wavelength of light *in vacuo* for refractometry, differential refractometry and light scattering was 436 nm. SI Units are used throughout so that molecular weights are quoted in kg/mol, these values consequently being smaller by a factor of 10^3 than those expressed more conventionally in the non-SI units of g/mol. These considerations apply equally to the heterogeneity parameters *P* and *Q*. The following abbreviations and symbols are adopted:

NY (also subscript A) nylon-6,
PMA (also subscript B) poly(methyl acrylate),
subscript AB mixture of polymers A and B,
o-CP (also subscript 1) *o*-chlorophenol,

TFP

M_A, M_B

M_{AB}, M_{AB}^*

$\langle S_A^2 \rangle, \langle S_B^2 \rangle$

$\langle S_{AB}^2 \rangle$

W_A, W_B

\tilde{n}_0

ϕ_1

ν

ν_ϕ, ν_μ

$[\eta]$

λ_0

2, 2', 3, 3'-tetrafluoropropanol, true weight-average molecular weights of polymers A and B, true and apparent weight-average molecular weights of mixture comprising polymers A and B, true *z*-average mean square radii of gyration of polymers A and B, apparent *z*-average mean square radius of gyration of mixture comprising polymers A and B, weight fractions of A and B in mixture comprising polymers A and B, refractive index of pure or mixed solvent, volume fraction of solvent 1 in mixed solvent comprising solvents 1 and 2, notation for specific refractive index increment in general (also denoted commonly elsewhere by $d\tilde{n}/dc$), specific refractive index increments at constant composition and constant chemical potential respectively, limiting viscosity number, wavelength of light *in vacuo*.

EXPERIMENTAL

Materials

NY film was Soxhlet extracted with methanol for 24 h, dissolved in freshly distilled *m*-cresol and precipitated in chilled diethyl ether. After filtering and washing, the powder was dried at 313K under vacuum.

* Present address: Department of Chemical Engineering and Chemical Technology, Imperial College of Science and Technology, London SW7 2AZ, UK.

PMA was prepared at 323K by polymerizing under nitrogen a solution of freshly distilled methyl acrylate in acetone (60% w/w) using azobisisobutyronitrile (0.4% w/w) as initiator. Reaction was carried out for 100 min (~10% conversion) and the PMA was isolated by precipitation in petroleum ether (b.p. 333–353K). The polymer was then dissolved in methyl ethyl ketone, reprecipitated as before and dried at 313K under vacuum. *o*-CP, as well as the methyl ethyl ketone required for physico-chemical measurements, were dried over anhydrous MgSO₄ and distilled at atmospheric pressure, the boiling points being 448.0 and 352.7K respectively.

Samples of TFP, obtained from three different commercial sources, were combined; the major portion (~90%) was an Eastman Kodak product. Purification was effected according to the procedure recommended by the Du Pont de Nemours Company⁷, viz. the crude TFP was mixed with 1/5 of its volume of water and 1/20 of its weight of sodium metabisulphite, left to stand for 24 h and then distilled rapidly at atmospheric pressure. Sufficient anhydrous lithium chloride was added to the distillate to saturate its aqueous portion and to thereby salt out the TFP as a lower layer. This separated layer was distilled, the residual water in it being removed as an azeotrope* with 71% (v/v) TFP at 366–368K. After isolation of more portions of TFP by salting out and distillation, all the products were combined, dried over anhydrous magnesium sulphate and redistilled through a Hempel Column. The major fraction distilling within the range 365–383K was retained, utilized and referred to in subsequent sections as TFP. The yield of product of reported* b.p. 380K would have been very low. In view of the boiling point range taken, the final product must certainly have contained impurities such as other fluorinated alcohols of similar physical properties. Reported values⁸ at 298K and $\lambda_0 = 546$ nm for \bar{n}_0 and $\nu_{\phi A}$ in the mixture LiCl/TFP/H₂O are 1.3217 and 0.185 dm³/kg respectively. The characteristics of the TFP used in the present work are b.p. 365–383K, $\bar{n}_0 = 1.3247$ and specific refractive index increment ($\nu_{\phi A}$) of NY in TFP = 0.186 dm³/kg, the last two quantities relating to 303K and $\lambda_0 = 436$ nm. When the solvent was reclaimed after use for further experiments, the procedure outlined was adhered to exactly (after removal of polymer present) and the properties quoted above were taken to characterize the reclaimed TFP.

Refractometry

Refractive indices of pure and mixed solvents were measured with a Pulfrich refractometer fitted with an external circulatory thermostat. Specific refractive index increments were measured in a Brice Phoenix differential refractometer maintained similarly at constant temperature. Values of ν_{ϕ} were obtained in pure and mixed solvents. Values of ν_{μ} for polymers in mixed solvents were measured at dialysis equilibrium of solution with mixed solvent of the same composition. This condition was achieved by the use of simple dialysis cells described previously⁹. However, to obtain good reproducibility, the dialysis bags were not allowed to dry, the water in the Visking tubing being extracted by repeated rinsing with methanol, which was then removed by successive washings with the mixed solvent. The time for dialysis equilibrium was 24 h.

Light Scattering

Measurements were made on a Sofica photometer maintained at constant temperature as above and calibrated with highly purified toluene, taking $R_{90} = 58.1 \times 10^{-4} \text{ m}^{-1}$ for this calibrant, as calculated from the Einstein–Cabannes equation¹⁰. Solutions and solvents were clarified by centrifugation at 1600 rev/min followed by filtration through Gelman ‘Solvinert’ filters. Data were analysed via Zimm plots. The molecular weights of the PMA and NY samples were determined separately using methyl ethyl ketone as solvent for the former and a mixture⁸ of TFP/LiCl/H₂O as solvent for the latter. Measurements were also made on solutions comprising a NY–PMA mixture in which $W_A = 0.573$ (to correspond to the composition of a copolymer, which it is intended to study later). These solutions were made up by weighing NY and PMA individually into graduated flasks and then adding the desired mixed solvent.

RESULTS

Refractive index increments and selection of solvent medium

In principle, light scattering measurements on a solution of a binary polymer system can be used to obtain its molecular parameters. For a copolymer comprising species A and B these parameters are the molecular weight (M_{AB}) of the copolymer as well as the molecular weights (M_A and M_B) of the A-portion and the B-portion. When the solute consists of a mixture of two polymers A and B, the derived quantities M_{AB} , M_A and M_B signify respectively the molecular weights of the mixture and of the separate polymers A and B. In practice, however, complications arise due to compositional heterogeneity of the sample, the effect being particularly pronounced for a mixture. This is manifested by an observed dependence of the molecular weight of the copolymer or mixture on the refractive index of the solvent. Hence the measured quantity has an apparent value (M_{AB}^*), only, and special procedures are necessary to evaluate the true molecular weights.

Among these is the expedient of conducting separate experiments using solvents of different indices, which in turn afford values of ν_A , ν_B and ν_{AB} that vary according to the solvent. The expression relating the experimental quantities M_{AB}^* , ν_A , ν_B and ν_{AB} to the desired molecular parameters of the systems can then be solved via simultaneous equations. Since there are three desired parameters (i.e. molecular weights), it is necessary to obtain data relating to at least three different solvent media. Alternatively, it is often possible to cover a larger range of values of the experimental quantities by using several solvents, which encompass a wide span of refractive indices. In this case the previously mentioned expression is not solved, since it is simpler to treat it graphically. The appropriate plot of the expression is parabolic and the desired parameters may be located on it from a knowledge of certain fixed co-ordinates. The form of the expression as well as full details of the procedures are given later.

These comments, directed at the general reader rather than the specialist, have been included to emphasize the necessarily more complex procedure involved when using light scattering to determine the molecular weight of a copolymer compared with that required for a polymer. In particular it will be evident that, in order to obtain true molecular parameters of a binary polymer system (co-

* We are indebted to Dr P. Kratochvíl (Institute of Macromolecular Chemistry, Prague) for this procedure.

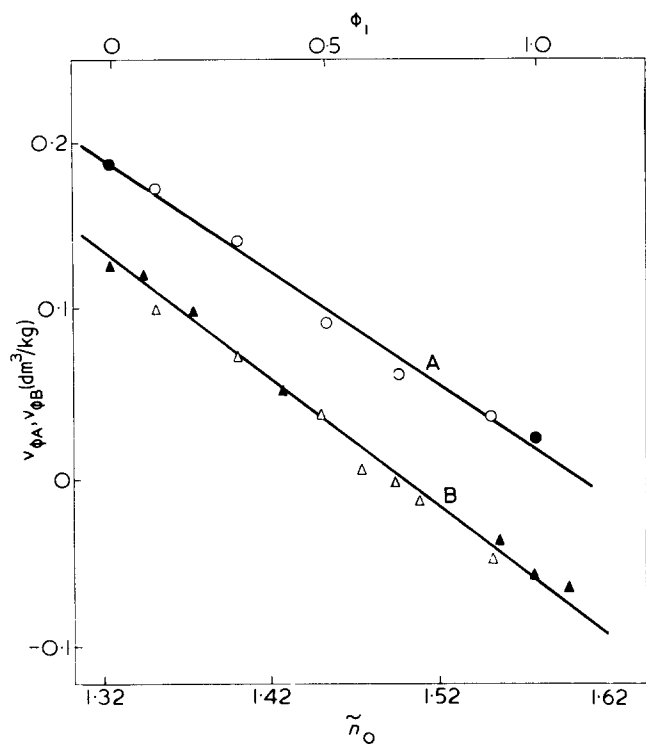


Figure 1 Specific refractive index increment at constant solvent composition as a function of refractive index of solvent. ●, ▲ single solvents; ○, △ binary *o*-CP/TFP solvent mixtures of composition indicated on upper abscissa scale. Curve A, NY; B, PMA

polymer or polymer mixture), certain criteria have to be met with regard to the values of the specific refractive index increments of species A and B. For maximum sensitivity of the molecular weight determinations, the following convenient summary of the optimum conditions has been proposed by Tuzar *et al.*¹¹:

$$|\nu_A| = |\nu_B| \text{ and both large, to obtain } M_{AB} \quad (1)$$

$$|\nu_A| \text{ large and } \nu_B = 0, \text{ to obtain } M_A \quad (2)$$

$$|\nu_B| \text{ large and } \nu_A = 0, \text{ to obtain } M_B \quad (3)$$

Since the refractive indices of NY and PMA are markedly different (~ 1.61 and 1.49 respectively), it is clear that condition (1) in terms of ν_ϕ cannot be realized. This is demonstrated also in Figure 1, where values of $\nu_{\phi A}$ and $\nu_{\phi B}$ in pure and mixed solvents are plotted as a function of \tilde{n}_0 . (Some of the data for PMA in single solvents were obtained here by Mr K. Harvey and have been included elsewhere^{12,13} as part of a compendium of ν_ϕ values for polymers). Condition (2) holds, although $\nu_{\phi A}$ is only moderately large ($0.069 \text{ dm}^3/\text{kg}$) when $\nu_{\phi B} = 0$. Interpolation shows that in order for condition (3) to hold (i.e. for $\nu_{\phi A} = 0$), the corresponding $\nu_{\phi B}$ would be moderately large in value ($\sim -0.077 \text{ dm}^3/\text{kg}$), but the appropriate solvent would have to be one of the few liquids having a high refractive index (~ 1.60).

The expedient of using mixed solvents and the resultant values of ν_μ can often induce changes which are sufficiently great to accommodate relationships (1)–(3). However, the refractometric nature of the solvent must be coupled closely with considerations of polymer solubility. Thus, whilst several solvents exist for NY and PMA individually, exploratory tests revealed only three liquids capable of dissolving NY–PMA copolymers, viz. TFP, dichloroacetic acid and molten chloral hydrate. The last two of these were

discounted on the grounds of possible degradation^{14,15} of the NY portion. The value of \tilde{n}_0 for TFP is very low (1.325) and hence the second component of a mixed solvent must be of extremely high refractive index (≥ 1.61). The inclusion of a large proportion of 1-bromonaphthalene ($\tilde{n}_0 = 1.69$), whilst suitable in principle, was not found to be feasible in practice, since addition of this liquid at low concentration to a solution of NY–PMA copolymer in TFP caused instantaneous precipitation of polymer. Consequently, recourse was made to the use of *o*-CP ($\tilde{n}_0 = 1.578$) in conjunction with TFP as mixed solvent. These two liquids are completely miscible and allow solubility of copolymer or polymer mixture over the whole range of solvent composition. As already noted from values of ν_ϕ for NY and PMA in such mixtures, the refractive index of *o*-CP is still not high enough to allow condition (3) to be fulfilled, but measurements of ν_μ were made to ascertain if a favourable change could be induced at constant chemical potential of mixed solvent.

In Figure 2 the values of ν_μ as a function of ϕ_1 (and \tilde{n}_0) are shown for solutions of NY and PMA in *o*-CP/TFP mixtures. In no case is condition (1) realized. Relation (2) does hold at $\phi_1 = 0.73$ (i.e. in a mixed solvent of $\tilde{n}_0 = 1.497$) and here, when $\nu_{\mu B} = 0$, the value of $\nu_{\mu A}$ is $0.100 \text{ dm}^3/\text{kg}$, which is rather larger than the corresponding value of $0.069 \text{ dm}^3/\text{kg}$ found for $\nu_{\phi A}$. However, even at the highest concentration of *o*-CP ($\phi_1 = 0.90$), the value of $\nu_{\mu A}$ is still not reduced to zero and hence condition (3) remains unfulfilled.

For PMA, $|\nu_{\mu B}| > |\nu_{\phi B}|$ except for the one mixture in which these two quantities are equal in magnitude. For NY, $|\nu_{\mu A}| > |\nu_{\phi A}|$ over most of the composition range, this relation being reversed only at high contents of *o*-CP, that is, at ϕ_1 greater than ~ 0.80 . Comparison of refractive increments at constant composition and constant chemical potential in mixed solvents is, in fact, one of the methods available for quantifying selective adsorption of one of the solvent components. Although they are of secondary importance to the main theme of selecting the most suitable solvent medium, we report also the findings on preferential adsorption. The fact that in general ν_ϕ is not equal to ν_μ

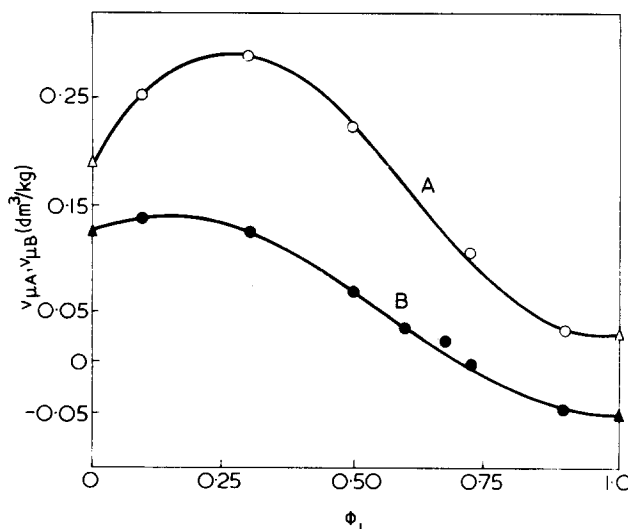


Figure 2 Dependence of specific refractive index increment at constant chemical potential of solvents on composition of *o*-CP/TFP mixed solvents. ▲, △ represent values relating to constant solvent composition for solutions in pure *o*-CP and pure TFP. Curve A, NY; B, PMA

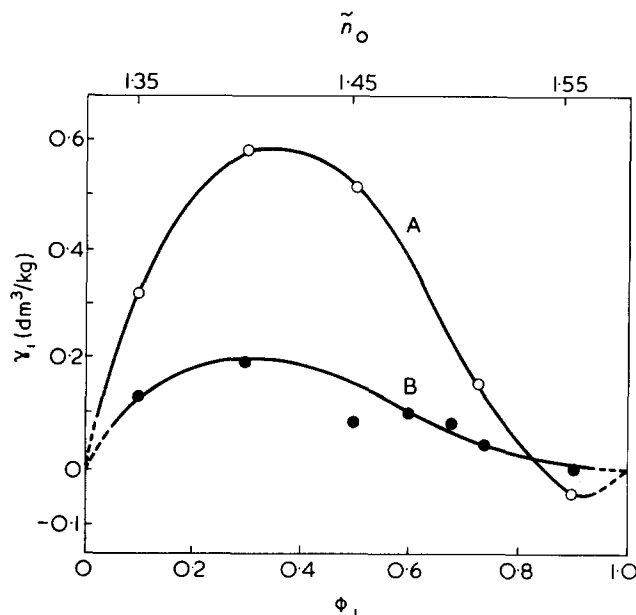


Figure 3 Parameter characterizing selective adsorption of *o*-CP as a function of composition of *o*-CP/TFP, mixed solvent. Refractive index of solvent indicated on upper abscissa scale. Curve A, NY; B, PMA

indicates finite values of the preferential adsorption coefficient γ_1 in equation (4)^{16,17}:

$$\gamma_1 = (\nu_\mu - \nu_\phi) / (d\tilde{n}_0/d\phi_1) \quad (4)$$

Here, $d\tilde{n}_0/d\phi_1$ expresses the dependence of the refractive index of the mixed solvent on the volume fraction ϕ_1 of *o*-CP in it. Measurements of the refractive index of *o*-CP/TFP mixtures over a range of composition showed a linear variation, thus:

$$\tilde{n}_0 = 1.325 + 0.253\phi_1$$

Hence the value of $d\tilde{n}_0/d\phi_1$ is 0.253 for all values of ϕ_1 . Values of the selective adsorption coefficient γ_1 have been calculated via equation (4) from experimental values of ν_μ and ν_ϕ for each of the two polymers in *o*-CP/TFP mixtures. The dependence of γ_1 on ϕ_1 is shown in Figure 3, where there is seen to be positive adsorption of *o*-CP to NY and to PMA except in solvents very rich in *o*-CP.

Light scattering

Estimation of molecular parameters from light scattering measurements is made via the following two equivalent expressions¹⁸ (equations 5 and 6), which have been referred to in general terms:

$$M_{AB}^* = (\nu_{\mu A} \nu_{\mu B} / \nu_{\mu AB}^2) M_{AB} + [\nu_{\mu A} (\nu_{\mu A} - \nu_{\mu B}) / \nu_{\mu AB}^2] \times \\ W_A M_A - [\nu_{\mu B} (\nu_{\mu A} - \nu_{\mu B}) / \nu_{\mu AB}^2] (1 - W_A) M_B \quad (5)$$

$$M_{AB}^* = M_{AB} + 2P[(\nu_{\mu A} - \nu_{\mu B}) / \nu_{\mu AB}] + \\ Q[(\nu_{\mu A} - \nu_{\mu B}) / \nu_{\mu AB}]^2 \quad (6)$$

In equation (6), P and Q are parameters characterizing the heterogeneity in composition of an A-B copolymer or, as in the present instance, a mixture of polymers A and B. The maximum heterogeneity is attained in a mixture. When using mixed solvents, as in the present situation, the appro-

priate refractive increments are those relating to constant chemical potential of solvents. Kratochvíl and coworkers¹¹ have demonstrated the validity of equations (5) and (6) expressed in terms of ν_μ instead of the ν_ϕ terms adopted in single solvents. To afford a range of ν_μ values, measurements were made using mixed solvents in which $\phi_1 = 0.1, 0.5$ and 0.7 . In each case the solute was the polymer mixture of previously quoted composition, and the values of $\nu_{\mu AB}$ were calculated from equation (7):

$$\nu_{\mu AB} = \nu_{\mu A} W_A + \nu_{\mu B} W_B \quad (7)$$

Solution of expressions (5) and (6) by simultaneous equations yielded values of M_{AB}, M_A, M_B, P and Q . An additional experiment was conducted in the mixed solvent of $\phi_1 = 0.73$ since, as already noted, the scattering due to PMA is thereby eliminated and equation (5) reduces to equation (8):

$$M_{AB}^* = (\nu_{\mu A}^2 / \nu_{\mu AB}^2) W_A M_A \quad (8)$$

As a means of comparison, directly measured values of M_A and M_B are available. Insertion of these into equation (9) allows M_{AB} for the mixture to be calculated:

$$M_{AB} = M_A W_A + M_B W_B \quad (9)$$

Similarly, if the directly measured values of M_A and M_B are inserted into equations (10), the parameters P and Q may be estimated¹⁸:

$$P = W_A W_B (M_A - M_B) \\ Q = W_A W_B (M_A W_A + M_B W_B) \quad (10)$$

All measured and calculated data are reported in Table 1.

The plot according to equation (5) is given in Figure 4. Included in this are the data points corresponding to the known values of M_A and M_B as well as that of M_{AB} calculated from equation (9). Thus¹⁸, for abscissae of $0, 1/W_A$ and $-1/W_B$, the corresponding ordinates are $M_{AB}, M_A/W_A$ and M_B/W_B . These points fall smoothly on the parabola

Table 1 Molecular parameters from light scattering for NY, PMA and NY/PMA mixture

	M_A	M_B	M_{AB}	P	Q
Direct measurement on solution of polymer	49.7	838			
Polymer mixture in three mixed solvents; simultaneous equations (5)	48.5	692	341		
Polymer mixture in the mixed solvent giving $\nu_{\mu B} = 0$	47.4				
Polymer mixture in three mixed solvents; simultaneous equations (6)			346	-163	101
Calculated from equation (9) using directly measured M_A and M_B			389		
Calculated from equations (10) using directly measured M_A and M_B				-193	123
From estimated minimum of parabola (Figure 4)				-178	104

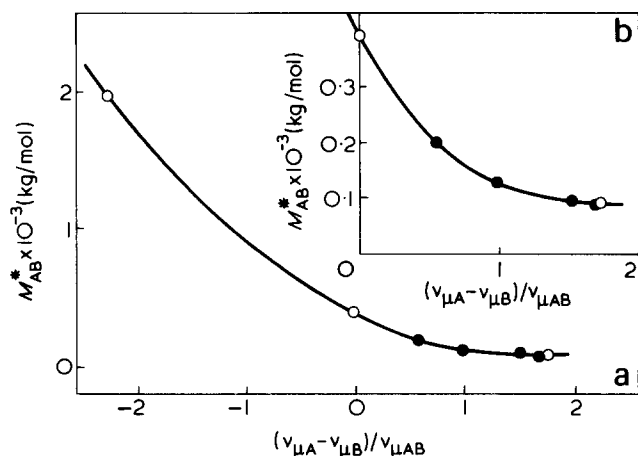


Figure 4 (a) Plot according to equations (5) and (6) for the polymer mixture in *o*-CP/TFP binary solvents. ●, experimental data; ○, points corresponding to known molecular weights of the individual polymers and the polymer mixture. (b) Enlargement of the section for positive values of abscissa

together with the four experimental data points. Because the abscissae do not extend to high enough positive values, it is not possible to locate the minimum of the curve with any degree of certainty. At the minimum the ordinate and abscissa correspond to $(M_{AB} - P^2/Q)$ and $(-P/Q)$ respectively¹⁸. The values of P and Q derived from the estimated minimum, in conjunction with the value of M_{AB} calculated from equation (9), are included in Table 1.

In addition to yielding an apparent molecular weight of the polymer mixture, light scattering gives an apparent value, $\langle S_{AB}^2 \rangle$, for the mean square radius of gyration in each mixed solvent. The relevant equation differs in form from that for a copolymer and is expressed by^{18,19}:

$$M_{AB}^* \langle S_{AB}^2 \rangle = (M_A \langle S_A^2 \rangle / W_A) y^2 + (M_B \langle S_B^2 \rangle / W_B) (1 - y)^2 \quad (11)$$

where $y \equiv W_A \nu_{\mu A} / \nu_{\mu AB}$

The plot of the left-hand side of equation (11) as a function of y should be parabolic and of upward curvature. Since W_A remains constant in value at 0.573, variations in y are effected solely via changes in solvent composition, i.e. effectively through differences in the refractive index increments. The situations $y = 1$ and $y = 0$ correspond to NY and PMA respectively and the values of $\langle S_A^2 \rangle$ and $\langle S_B^2 \rangle$ were measured individually for each of these samples. Consequently these constitute two additional points on the curve (Figure 5). Similarly, the minimum value of the ordinate, y_{\min} , can be calculated readily and, from equation (12), it is clear that this value must lie between 0 and 1:

$$y_{\min} = 1 / [1 + (M_A \langle S_A^2 \rangle W_B) / (M_B \langle S_B^2 \rangle W_A)] \quad (12)$$

The value of y_{\min} calculated from equation (12) and the corresponding minimum ordinate $M_{AB}^* \langle S_{AB}^2 \rangle$ obtained thereby from equation (11) are 0.99 and $4.2 \times 10^{-14} \text{ m}^2 \text{ kg/mol}$ respectively. The minimum of the smooth curve through the four experimental data points relating to *o*-CP/TFP solvent mixtures indicates values of 0.97 and $8.1 \times 10^{-14} \text{ m}^2 \text{ kg/mol}$ for these quantities. A value of 0.97 is actually obtained for y_{\min} from equation (12), if errors of $\pm 5\%$ and $\pm 10\%$ are assumed for the constituent molecular weights and mean square radii of gyration respectively, the signs of the errors being selected so as to maximize the

denominator in equation (12). However, under these conditions, the resultant minimum value of $M_{AB}^* \langle S_{AB}^2 \rangle$ is not significantly different from 4.2×10^{-14} (actually $4.3 \times 10^{-14} \text{ m}^2 \text{ kg/mol}$).

Further discussion is deferred to the next section. With regard to Figure 5 we wish to emphasize here that (1) the curve is of the form predicted theoretically and (2) the points relating to the two individual polymers alone ($y = 0$ and $y = 1$) do not fall on the curve.

DISCUSSION

Refractive index increments and selective adsorption

Assuming the value of $d\tilde{n}_0/d\phi_1$ to be subject to negligible error, the accuracy of γ_1 calculated via equation (4) is dictated solely by the errors in ν_{μ} and ν_{ϕ} . If the minimum absolute error in each of these is taken as $\pm 0.001 \text{ dm}^3/\text{kg}$ and the sign of each error is selected to maximize the total error, then the coefficient of selective adsorption is $\gamma_1 \pm (0.002/0.253)$, i.e. approximately $\gamma_1 \pm 0.01$, where γ_1 is the reported uncorrected value. This order of error in each datum point has a virtually undetectable effect on the curves in Figure 3. However, if the prime concern had been the absolute values of each adsorption coefficient, then the relative errors in γ_1 would have been reflected in a less favourable light, viz. ranging from $\sim 1\%$ (for high γ_1) to $\sim 20\%$ (for low γ_1).

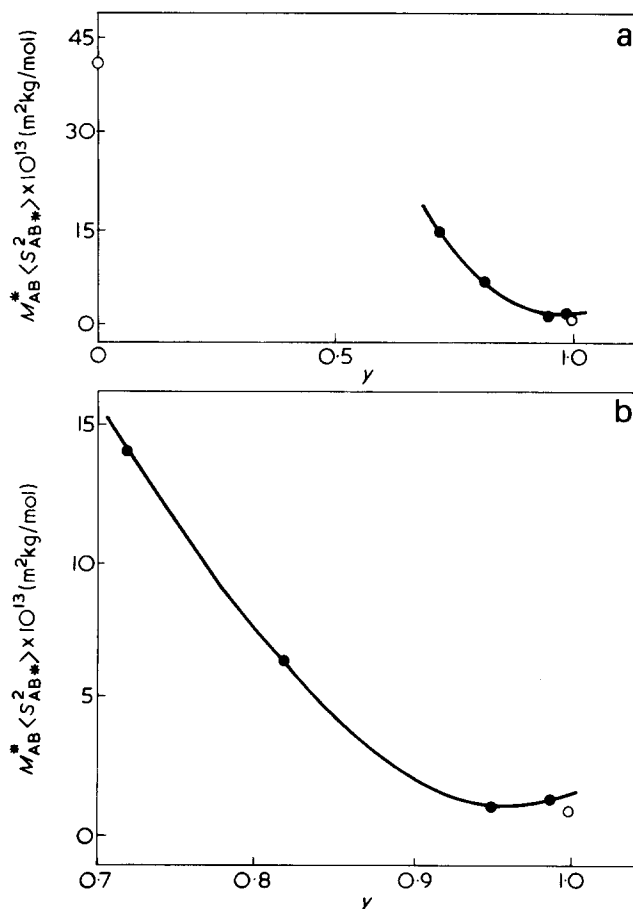


Figure 5 (a) Plot according to equation (11) for the polymer mixture in *o*-CP/TFP binary solvents. ●, experimental data; ○, points corresponding to known molecular weights and radii of gyration of the individual polymer. (b) Enlargement of the section for $y = 0.7-1.0$

With reference to equation (4), it is apparent that maximum or minimum values of γ_1 occur when $d\gamma_1/d\phi_1 = 0$, that is, when:

$$d\nu_\mu/d\phi_1 = d\nu_\phi/d\phi_1 \quad (13)$$

For both NY and PMA, comparison of the constant Gladstone–Dale slope in *Figure 1* with the various slopes in *Figure 2* indicates that:

(a) Relation (13) holds in the mixed solvent for which ϕ_1 is approximately 0.2–0.3, which is actually the region of maximum γ_1 in *Figure 3*.

(b) There is unlikely to be an abrupt change in the form of γ_1 versus ϕ_1 in the region $\phi_1 = 0$ to $\phi_1 = 0.1$, i.e. where there are no experimental data.

(c) The observed minimum in γ_1 versus ϕ_1 for solutions of NY suggests that there must be a value of ν_μ (in the region $\phi_1 = 0.9$ –1.0), which is of smaller magnitude than the lowest value obtained experimentally (i.e. at $\phi_1 = 0.9$).

Selective adsorption may be envisaged more readily when expressed in terms of the number (n_1) of *o*-CP molecules adsorbed preferentially per segment of polymer, thus¹⁶:

$$n_1 = \gamma_1 M_0 / \bar{V}_1 \approx \gamma_1 M_0 / V_1 \quad (14)$$

Here, M_0 is the molecular weight of the polymer segment and \bar{V}_1 and V_1 are respectively the partial molar volume and molar volume of *o*-CP. The maximum extents of selective adsorption are calculated from equation (14) to be equivalent to 1 molecule *o*-CP/1.4 segments NY and 1 molecule *o*-CP/5.7 segments PMA. The one negative value of γ_1 observed for NY indicates a preferential adsorption of TFP with a selective adsorption coefficient γ_2 , where $\gamma_2 = -\gamma_1$. In this situation equation (14) becomes

$$n_2 \approx -\gamma_1 M_0 / V_2$$

where V_2 is the molar volume of TFP and n_2 is the number of molecules of TFP adsorbed per segment of NY. This yields a selective adsorption of 1 molecule TFP/21 segments NY, when the solvent medium is very rich in *o*-CP ($\phi_1 = 0.9$).

The curves of preferential adsorption coefficient versus composition of mixed solvent (*Figure 3*) are of a similar form to those observed for other systems^{16,20,21}. Expressions have been derived^{16,22,23} for γ_1 in terms of ϕ_1 , but these involve the Flory–Huggins interaction parameters χ_{ij} , the values of which are not available for the present systems. In certain instances²⁴ the approach of calculating the values of the χ_{ij} terms from Hildebrand–Scott solubility parameters has met with some limited success, but here again the relevant values are not known. Consequently, we restrict our comments to a purely phenomenological discussion of the selective adsorption of *o*-CP.

Apart from the molecular weight²⁵ and the structure^{26,27} of the polymer, the most critical factor affecting the sign and magnitude of γ_1 is the nature of the two liquids comprising the binary solvent, as exemplified by their solvent power, polarity, associative capacity and molecular size. In the present system the two liquids exhibit similar solvent power for NY. Thus the values of $[\eta]$ (m^3/kg) in *o*-CP and TFP are 0.14 and 0.18 respectively. Moreover for PMA solutions, $[\eta] = 0.31$ for both solvents. A simple molecular size effect can be discounted, because V_1 and V_2 are of a very similar magnitude (0.093 and 0.104 dm^3/mol respectively).

Combela *et al.*²⁸ have studied the preferential adsorption by polyacryloylpiperidine of trifluoroethanol in admixture with carbon tetrachloride; hydrogen bonding between the alcoholic –OH groups and the $>\text{C}=\text{O}$ groups in the polymer was proposed. More recently Chaufer *et al.*²⁹ and Lety-Sistel *et al.*³⁰ have discussed selective adsorption in systems already reported, and they have themselves made a comprehensive investigation involving light scattering and infra-red analysis of selective adsorption occurring in the systems poly(vinyl pyrrolidone)/halogenated solvent/proton donating solvent. Dependent on the solvent composition, adsorption of either of the solvents was observed. In the case of preferential adsorption of the proton donating liquid, hydrogen bonding to the $>\text{C}=\text{O}$ group of the polymer, followed by further induced auto-association of the proton donor, was proposed. A rationale was also afforded for the preferential adsorption of the halogenated solvent. No such detailed infra-red analysis has been performed on the present system, but it is reasonable to infer that hydrogen-bonding prevails here also. The situation is complicated, however, by the facts that (a) *o*-CP, as opposed to the halogenated hydrocarbon, is itself capable of hydrogen-bonding and (b) consequently, the known hydrogen-bonding tendencies of *o*-CP and TFP separately may alter, when one liquid is in the presence of the other. Discussion is confined to some qualitative observations.

Infra-red spectra of *o*-CP and TFP reveal that there is intramolecular³¹ bonding between adjacent –OH and Cl groups, whereas in the latter there is intermolecular³² bonding between –OH groups. If entropic effects are neglected and realization is made about the uncertainty in reported values³³ of hydrogen-bond enthalpies (ΔH), then the following simplified picture emerges. The value of ΔH between –OH groups in alcohols is 21 kJ/mol, but the same amount of energy is liberated on reforming these bonds with $>\text{C}=\text{O}$ groups in the polymer chain (NY or PMA); hence there is no net decrease in energy. In contrast, the value of ΔH for intramolecular bonding in *o*-CP is –16 kJ/mol. Rupture of this bond followed by bonding between the –OH group in *o*-CP and $>\text{C}=\text{O}$ groups in the polymer would yield a net energy change of $(+16 - 21) = -5$ kJ/mol, i.e. a fall in energy, which would render bonding between polymer and *o*-CP more favourable than bonding between polymer and TFP. Moreover constructions with molecular models of a molecule of *o*-CP and a segment of NY suggest that the bonding may well be yet more energetically favourable. Thus, when the –OH group in *o*-CP is made to coincide with the $>\text{C}=\text{O}$ group in the polymer, the Cl group in *o*-CP coincides with the $>\text{NH}$ group separated by five carbon atoms. Hence it is feasible, at least, to envisage two forms of bonding of *o*-CP to NY with a net energy change of $(+16 - 21 - 16) = -21$ kJ/mol. This accords with the observed, higher values of γ_1 for NY than for PMA.

Light scattering

We consider now the parameters listed in *Table 1*. Although the three values obtained for M_A via different routes are in excellent agreement, this may be fortuitous to some extent in view of the errors which can be reasonably expected in light scattering. Of course, accuracy can rarely be ascertained for a molecular weight determination, since there is no basis for comparison in absolute terms. Hence it is more correct to indicate the good consistency and to note that the use of a mixed *o*-CP/TFP solvent of $\phi_1 = 0.73$

would be a reliable means of obtaining the molecular weight of the NY portion of a NY/PMA copolymer. The difference of ~17% between the directly measured value of M_B and the one derived indirectly via the use of three solvents exceeds the error expected from a single molecular weight determination. This large difference arises from the cumulative effect of the operations involved in solving simultaneous equations coupled with the errors in the molecular weights and refractive index increments contained therein. The accord among the values for M_{AB} may be considered satisfactory.

The parameter P correlates the molecular weight of the mixture with its composition and, although there are no limits to its numerical value, it must be of negative sign here, as follows from the definition in equations (10). The more commonly adopted ratio P/M_{AB} ranges slightly in magnitude from -0.47 to -0.50 depending on whether the values of P and M_{AB} taken together are those obtained experimentally from measurements in three solvents or are estimated from the known individual values of M_A and M_B .

The parameter Q quantifies the heterogeneity in composition of the mixture, and is expressed commonly per unit molecular weight as Q/M_{AB} . The value of this ratio is zero for a completely homogeneous sample, whereas the maximum value attainable for a mixture is $W_A W_B$, as seen in equations (10). As before, the value obtained for Q/M_{AB} depends on whether the values of Q and M_{AB} taken together are those determined experimentally in three solvents or are estimated from known individual values of M_A and M_B . In the former and latter instances respectively, Q/M_{AB} is 0.29 and 0.32, both of which exceed the theoretical maximum of $0.573 \times 0.427 = 0.245$. The expedient of combining the experimental $Q (=101)$ with the calculated $M_{AB} (=389)$ reduces Q/M_{AB} to a more acceptable value of 0.26. Effectively, this is equivalent to regarding the calculated value of M_{AB} as the correct one. This approach has been adopted by others such as Kratochvíl and coworkers who obtained the following experimental (and theoretical) values for mixtures in which the magnitudes of W_A and W_B were similar to those here: 0.25 (0.24) for poly(ethylene glycol methacrylate) + poly(methyl methacrylate)¹¹; 0.22 (0.25) for polystyrene + polybutadiene³⁴. The inherent errors mentioned in the determination of M_B apply equally to Q , when data relating to three solvents are employed. The value of Q/M_{AB} determined here would seem to be as accurate as allowed by this particular technique.

With regard to the minimum values of γ and $M_{AB}^* \langle S_{AB}^2 \rangle^*$ (equation 12 and Figure 5), the uncertainty in these is quite considerable, because in the present system $M_B \gg M_A$ and γ is generally very large. Moreover, the error in $\langle S_A^2 \rangle$ must be greater than that normally encountered when estimating the mean square radius of gyration from a limiting slope (at zero concentration) in a Zimm plot; indeed, it was a matter of some surprise that we were actually able to determine the value of $\langle S_A^2 \rangle$ in view of the low molecular weight of the NY sample (a molecular weight of ~200 kg/mol is considered³⁵ as an approximate lower limit for this purpose). The fact that the data points for the individual polymers fall outside the curve in Figure 5 is not disturbing, since the solvents used in the determination of $\langle S_A^2 \rangle$ and $\langle S_B^2 \rangle$ were different from each other and also different from those used for the solutions of the polymer mixture.

In connection with future work on graft copolymers of NY/PMA, the anticipated heterogeneity should be lower than that deliberately introduced here for the mixture. Consequently, any over-estimate in the value of Q will be

of greater relative significance. We note that such over-estimates in copolymer heterogeneity have been discussed in detail by Vorlíček and Kratochvíl³⁶, who concluded that a meaningful measure of Q in a copolymer is only possible by light scattering provided that certain critical conditions be fulfilled with respect to molecular weight and $|\nu_A - \nu_B|$.

ACKNOWLEDGEMENTS

The authors thank the Science Research Council for financial support and provision of a maintenance grant (to R. W. R.). The sample of nylon-6 was kindly donated by Vereenigde Plastic-Verkoopkantoor n.v. (Plasttrading Ltd), Zeist, Holland.

REFERENCES

- Huglin, M. B. and Johnson, B. L. *J. Polym. Sci. (A-1)* 1969, 7, 1379
- Huglin, M. B. and Johnson, B. L. *J. Appl. Polym. Sci.* 1972, 16, 921
- Huglin, M. B. and Johnson, B. L. *Kolloid Z. Z. Polym.* 1971, 249, 1080
- Huglin, M. B. and Johnson, B. L. *Eur. Polym. J.* 1972, 8, 911
- Huglin, M. B., Johnson, B. L. and Richards, R. W. *Eur. Polym. J.* 1973, 9, 519
- Collins, R., Huglin, M. B. and Richards, R. W. *Eur. Polym. J.* 1975, 11, 197
- 'Primary Fluorolcohols', new product information, Du Pont Organic Chemicals Department, E. I. Du Pont de Nemours and Co., Wilmington 98, Delaware, USA
- Tuzar, Z., Kratochvíl, P. and Bohdanecký, M. *J. Polym. Sci. (C)* 1967, 16, 693
- Guthrie, J. T., Huglin, M. B. and Phillips, G. O. *Angew. Makromol. Chem.* 1971, 149, 309
- Kerker, M. 'Scattering of Light and Other Electromagnetic Radiation', Academic Press, New York, 1969, p 496
- Tuzar, Z., Kratochvíl, P. and Straková, D. *Eur. Polym. J.* 1970, 6, 1113
- Huglin, M. B. in 'Light Scattering from Polymer Solutions', (Ed. M. B. Huglin), Academic Press, London and New York, 1972, Ch 6
- Huglin, M. B. in 'Polymer Handbook', (Eds. J. Brandrup and E. H. Immergut), Wiley, New York, 1974, pp IV-267 to IV-308
- Tuzar, Z. and Kratochvíl, P. *Collect. Czech. Chem. Commun.* 1967, 32, 2255
- Huglin, M. B. and Richards, R. W. *Angew. Makromol. Chem.* 1974, 38, 207
- Strazielle, C. in 'Light Scattering from Polymer Solutions', (Ed. M. B. Huglin), Academic Press, London and New York, 1972, Ch 15
- Cowie, J. M. G. *Pure Appl. Chem.* 1970, 23, 355
- Benoit, H. and Froelich, D. in 'Light Scattering from Polymer Solutions', (Ed. M. B. Huglin), Academic Press, London and New York, 1972, Ch 11
- Leng, M. and Benoit, H. *J. Chim. Phys.* 1961, 58, 480
- Tuzar, Z. and Kratochvíl, P. *Collect. Czech. Chem. Commun.* 1967, 32, 3358
- Cowie, J. M. G. and Bywater, S. *J. Macromol. Sci.* 1966, 1, 581
- Read, B. E. *Trans. Faraday Soc.* 1960, 56, 382
- Strazielle, C. and Benoit, H. *J. Chim. Phys.* 1961, 58, 678
- Cowie, J. M. G., Dey, R. and McCrindle, J. T. *Polym. J.* 1971, 2, 88
- Hert, M., Strazielle, C. and Benoit, H. *Makromol. Chem.* 1973, 172, 169
- Hert, M., Strazielle, C. and Benoit, H. *Makromol. Chem.* 1973, 172, 185
- Poděšva, J. and Kratochvíl, P. *Eur. Polym. J.* 1972, 8, 1179

- 28 Combelas, P., Cruege, F., Lascombe, J., Quivoron, C., Rey-Laffon, M. and Sebillé, B. *Spectrochim. Acta. (A)* 1970, **26**, 1323
- 29 Chaufer, B., Sebillé, B. and Quivoron, C. *Eur. Polym. J.* 1975, **11**, 683, 695
- 30 Lety-Sistel, C., Chaufer, B., Sebillé, B. and Quivoron, C. *Eur. Polym. J.* 1975, **11**, 689
- 31 Pimental, G. C. and McClellan, A. L. 'The Hydrogen Bond', Freeman, San Francisco and London, 1960
- 32 Barnes, A. J. University of Salford, personal communication
- 33 Pimental, G. C. and McClellan, A. L. 'The Hydrogen Bond', Freeman, San Francisco and London, 1960, Appendix B, p 348
- 34 Kratochvíl, P., Sedláček, B., Straková, D. and Tuzar, Z. *Makromol. Chem.* 1971, **148**, 271
- 35 Kratochvíl, P. in 'Light Scattering from Polymer Solutions', (Ed. M. B. Huglin), Academic Press, London and New York, 1972, Ch 7
- 36 Vorlíček, J. and Kratochvíl, P. *J. Polym. Sci. (Polym. Phys. Edn)* 1973, **11**, 855, 1251

Branched poly(ethylene terephthalate) correlations between viscosimetric properties and polymerization parameters

P. Manaresi*, P. Parrini, G. L. Semeghini and E. de Fornasari

Montedison Spa, Centro Ricerche Ferrara, 44100 Ferrara, Italy

(Received 13 October 1975; revised 20 January 1976)

Samples of poly(ethylene terephthalate) (PET) modified with small amounts of trimesic acid groups and hence containing long chain branching have been prepared. From the content of trifunctional modifier and from the experimental value of the extent of reaction, the weight-average molecular weight \bar{M}_w and branching density \bar{B}_w have been calculated, assuming that all the end-groups are equally reactive and intramolecular reactions are absent. The values of \bar{M}_w and \bar{B}_w have been correlated with the experimental values of intrinsic viscosity $[\eta]$ and the Newtonian melt viscosity η_0 . General relations of the following type have been obtained:

$$f_1([\eta], \bar{M}_w, \bar{B}_w) = 0; \quad f_2(\eta_0, \bar{M}_w, \bar{B}_w) = 0;$$

$$f_3(\eta_0, [\eta], \bar{B}_w) = 0; \quad f_4(\eta_0, [\eta], \bar{M}_w) = 0$$

In particular, $[\eta]$ and η_0 increase on increasing \bar{M}_w and decrease on increasing \bar{B}_w , but, at equal $[\eta]$ values, η_0 increases with \bar{B}_w . Through the last relation, the reliability limits of which should be experimentally checked, and from measurements of $[\eta]$ and η_0 , it is possible to calculate \bar{M}_w of a branched PET.

INTRODUCTION

One problem that is most frequently met in the technological development of polymers is obtaining slight property variations after carrying out operations on the structural parameters. Among them long chain branching, together with the molecular weight and chemical structure, are some of the most important.

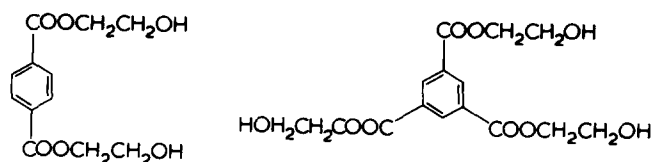
In the case of a polycondensate, branching may easily be obtained by using a comonomer having functionality higher than two: this may lead to the formation of a tri-dimensional network. The basic theoretical concepts concerning polyfunctional polycondensation and the criteria for gel formation were established several years ago by Carothers¹, Flory²⁻⁵ and Stockmayer^{6,7}. In recent years the topic has been studied thoroughly and partly revised, especially from a theoretical point of view⁸⁻¹⁷. However, apart from patent literature, no data have been published on branched poly(ethylene terephthalate) (PET) even though this polymer is quite important for the production of fibres.

Therefore we thought it interesting to prepare PET samples modified with small amounts (<2%) of a trifunctional comonomer, and to examine the relationships between the various viscometric quantities as a function of the extent of reaction and the content of modifier. This study was carried out in the light of theories concerning polyfunctional polycondensation and the influence of long chain branching on properties.

EXPERIMENTAL

Preparation of PET samples

PET samples were prepared from dimethylterephthalate and ethylene glycol with the desired amount of trimethyl-trimesate as the trifunctional modifier. The reaction was carried out in two consecutive steps, ester-interchange and polycondensation, according to the general procedure described in a previous paper¹⁸. After the ester-interchange step, only one type of functional group remains, the OH groups of glycolic esters, i.e.



and polycondensation proceeds with evolution of ethylene glycol.

Viscometric measurements

Intrinsic viscosity was measured in *o*-chlorophenol at 25°C. Melt viscosity was measured at 280°C by the capillary method¹⁸. The values of the flow gradient being low, the melt viscosity measured by this method practically corresponds to the Newtonian one.

Determination of the extent of reaction

Conversion *p* (extent of reaction) was obtained by separately determining the number of OH and COOH end-

* Istituto Chimico, Facoltà di Ingegneria, Università di Bologna, Bologna, Italy.

groups, the latter being present in small amounts. Carboxyl content was determined according to Pohl¹⁹, using freshly distilled aniline (instead of benzyl alcohol) as solvent. Hydroxyl content was determined according to the Conix method²⁰. E_{OH} and E_{COOH} being the number of equivalents of OH and COOH end-groups per 10⁶ g of polymer, the sum of the two $E = E_{OH} + E_{COOH}$ was considered in order to calculate p .

Conversion is given by:

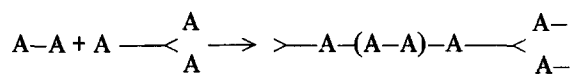
$$p = 1 - \frac{E}{10^6} \left[\frac{M_b}{2} - \rho \left(\frac{M_b}{2} - \frac{M_t}{3} \right) \right]$$

The significance of ρ , M_b and M_t is given below (in this particular case $M_b = 192.17$ and $M_t = 249.20$).

THEORETICAL

Polyfunctional polycondensation

In the case considered here after the first reaction step there is only one type of functional group, and the polymerization may be shown schematically as follows:



Let ρ be the composition parameter, i.e.:

$$\rho = \frac{\text{number of groups of initial trifunctional units}}{\text{number of total initial functional groups}} = \frac{3N_t}{3N_t + 2N_b} \quad (1)$$

where N_t = number of initial trifunctional molecules and N_b = number of initial bifunctional molecules.

By assuming that all functional groups have the same reactivity and by neglecting the intramolecular reactions, Flory² obtained for the branching coefficient α :

$$\alpha = \frac{p\rho}{1 - p(1 - \rho)} \quad (2)$$

where p is the extent of reaction. For $\alpha = 0.5$ gelation becomes possible; at this point the extent of reaction (critical value) is $p_c = 1/(1 + \rho)$.

The number-average degree of polymerization \bar{x}_n will be given by:

$$\bar{x}_n = \frac{N_t + N_b}{(N_t + N_b) - (3N_t/2 + N_b)p}$$

where the second term of the denominator represents the number of bonds formed. By introducing equation (1) we obtain:

$$\bar{x}_n = \frac{3 - \rho}{3 - \rho - 3p} \quad (3)$$

The number-average molecular weight is given by:

$$\bar{M}_n = \bar{x}_n M_0$$

where M_0 is the molecular weight of the average monomeric unit. If M_b and M_t are the molecular weights respectively of the bi- and tri-functional monomer units (in this case 192.17 and 249.20), then:

$$M_0 = \frac{M_b N_b + M_t N_t}{N_b + N_t} = \frac{3M_b + \rho(2M_t - 3M_b)}{3 - \rho}$$

Hence:

$$\bar{M}_n = \frac{3M_b + \rho(2M_t - 3M_b)}{3 - \rho - 3p} \quad (4)$$

Therefore \bar{M}_n depends on the extent of reaction and to a lower extent on the trifunctional units content: the latter, instead, extensively affects \bar{M}_w . In the case considered here, the distribution function obtained by Stockmayer⁶ is:

$$m_{n,l} = 3N_t \rho^{(n-1)} (1 - \rho)^l p^{(n+l-1)} (1 - p)^{(n+2)} \times \frac{(2n + l)!}{n! l! (n + 2)!} \quad (5)$$

where $m_{n,l}$ is the number of polymeric molecules consisting of n trifunctional units and of l bifunctional units. From the definition of \bar{M}_w :

$$\bar{M}_w = \frac{\sum_{n,l} m_{n,l} (M_b l + M_t n)^2}{N_b M_b + N_t M_t}$$

and from equations (1) and (5) is obtained:

$$\bar{M}_w = \frac{6(1 - p)^2}{p(2\rho M_t + 3M_b - 3\rho M_b)} \times \sum_{\substack{n,l=0 \\ (n+l \geq 1)}}^{\infty} \left\{ (M_b l + M_t n)^2 \times \frac{[p\rho(1 - p)]^n [p(1 - \rho)]^l (2n + l)!}{n!(n + 2)! l!} \right\} \quad (6)$$

[if the trifunctional group is absent, the usual relations are valid: $\bar{M}_n = M_b/(1 - p)$; $\bar{M}_w = M_b(1 + p)/(1 - p)$].

With the help of a computer the summation in equation (6) may be evaluated; since such a calculation must be generally carried out to very high values of l , we have applied the equation in a form that may be easily drawn from the previous one, i.e.

$$\bar{M}_w = \frac{6(1 - p)^2}{p(2\rho M_t + 3M_b - 3\rho M_b)} \times \sum_{\substack{n,l=0 \\ (n+l \geq 1)}}^{\infty} \left\{ (M_b l + M_t n)^2 [p\rho(1 - p)]^n [p(1 - \rho)]^l \frac{(l + 1)(l + 2) \dots (l + 2n)}{n!(n + 2)!} \right\} \quad (7)$$

Table 1 Linear and branched poly(ethylene terephthalates): polymerization parameters, viscosities and related properties

ρ	ρ	$[\eta]$ (dl/g)	η_0 (Poise)	$\bar{M}_n \times 10^{-4}$	$\bar{M}_w \times 10^{-4}$	α	\bar{B}_w	$[\eta]_b/[\eta]_l$	$\eta_{0,b}/\eta_{0,l}$
0	0.9735	0.275	50	0.73	1.43	0	0	1	1
0	0.9790	0.360	110	0.92	1.81	0	0	1	1
0	0.9815	0.380	290	1.04	2.06	0	0	1	1
0	0.9850	0.440	380	1.28	2.54	0	0	1	1
0	0.9880	0.510	1 100	1.60	3.18	0	0	1	1
0	0.9895	0.600	1 750	1.83	3.64	0	0	1	1
0	0.9910	0.640	2 900	2.14	4.25	0	0	1	1
0	0.9920	0.660	4 000	2.40	4.79	0	0	1	1
0	0.9940	0.850	9 600	3.20	6.39	0	0	1	1
0.00748	0.9690	0.290	70	0.67	1.55	0.190	0.60	1.00	0.93
0.00748	0.9785	0.420	380	1.01	2.60	0.254	1.01	0.93	0.80
0.00748	0.9800	0.440	500	1.10	2.90	0.269	1.13	0.91	0.71
0.00748	0.9850	0.530	2 200	1.54	5.01	0.330	1.95	0.74	0.45
0.00748	0.9860	0.550	3 900	1.67	5.76	0.344	2.24	0.69	0.49
0.00748	0.9870	0.565	4 600	1.83	6.76	0.363	2.63	0.63	0.34
0.00748	0.9875	0.630	8 000	1.92	7.37	0.372	2.87	0.66	0.43
0.00748	0.9885	0.680	8 700	2.13	9.00	0.392	3.51	0.62	0.23
0.00748	0.9890	0.710	14 000	2.26	10.00	0.403	3.89	0.59	0.25
0.01121	0.9780	0.280	60	1.05	3.40	0.333	1.99	0.52	0.050
0.01121	0.9860	0.420	510	1.86	11.80	0.442	6.91	0.31	0.0050
0.01121	0.9870	0.470	1 000	2.06	19.00	0.461	11.1	0.25	0.0020
0.01121	0.9880	0.610	4 700	2.31	39.00	0.481	22.0	0.19	0.0007
0.01121	0.9895	0.650	6 500	2.82	NC	0.515	NC	NC	NC
0.01121	0.9910	0.820	17 500	3.62	NC	0.554	NC	NC	NC
0.01493	0.9720	0.280	60	0.84	2.83	0.341	2.20	0.59	0.095
0.01493	0.9775	0.330	150	1.10	4.95	0.393	3.85	0.46	0.033
0.01493	0.9820	0.490	1 600	1.48	11.00	0.448	8.55	0.39	0.0210
0.01493	0.9840	0.580	7 000	1.75	20.00	0.479	15.6	0.29	0.0110
0.01493	0.9845	0.640	8 000	1.83	26.00	0.486	20.1	0.27	0.0050
0.01493	0.9860	0.675	9 300	2.13	NC	0.513	NC	NC	NC
0.01493	0.9920	0.720	13 000	6.39	NC	0.648	NC	NC	NC
0.02233	0.9665	0.250	40	0.73	3.25	0.392	3.81	0.48	0.039
0.02233	0.9740	0.340	200	1.03	8.70	0.455	10.2	0.32	0.0060
0.02233	0.9790	0.460	820	1.41	NC	0.510	NC	NC	NC
0.02233	0.9820	0.500	1 900	1.81	NC	0.549	NC	NC	NC
0.02233	0.9835	0.620	8 000	2.11	NC	0.571	NC	NC	NC
0.02233	0.9845	0.710	13 000	2.37	NC	0.587	NC	NC	NC
0.02233	0.9860	0.750	16 000	2.90	NC	0.611	NC	NC	NC

NC = not calculated, as $\alpha > 0.5$ ($\rho > \rho_c$).

From equation (7) it is possible to calculate the summation terms as long as the values of n are not too high. For values of n higher than 30, the equation has been transformed, through the Stirling approximation formula, into the following equation of easier use:

$$\bar{M}_w = \frac{3e^2(1-p)^2}{\pi p(2\rho M_t + 3M_b - 3\rho M_b)} \times \sum_{n,l} \left\{ \left(\frac{M_b l + M_t n}{n+2} \right)^2 \frac{1}{[n(n+2)]^{1/2}} \times \left[\frac{p\rho(1-p)e^2}{n(n+2)} \right]^n [p(1-\rho)]^l (l+1)(l+2) \dots (l+2n) \right\} \quad (8)$$

Table 1 shows the results of such calculations, carried out in some cases to values of $n = 300$ and $l = 30\,000$: when the extent of reaction gets near to the critical value p_c , \bar{M}_w rapidly approaches infinity, whereas \bar{M}_n stays relatively low.

Number of branches

The number of branches may also be theoretically deduced and may be quite significant for a correlation with

the experimental data. The number-average branching density, i.e., the average number of branches per molecule \bar{B}_n , is given by:

$$\bar{B}_n = \frac{N_t}{(N_t + N_b) - (3N_t/2 + N_b)p} \quad (9)$$

From equation (1) it follows:

$$\bar{B}_n = \frac{2\rho}{3 - \rho - 3p} \quad (10)$$

It is often more useful to consider the so-called weight-average branching density \bar{B}_w . The value of \bar{B}_w is related to that of \bar{B}_n and to the molecular weight distribution; in polycondensates, if the Stockmayer statistical distribution is assumed, the relation:

$$\bar{B}_w = \frac{3}{2} \bar{B}_n \bar{M}_w / \bar{M}_n \quad (11)$$

was proved to be valid²¹. While \bar{B}_n simply 'counts' the branches, \bar{B}_w 'weights' them in the larger molecules more than in the smaller ones. Evidently \bar{B}_w approaches infinity when p gets near to the p_c value.

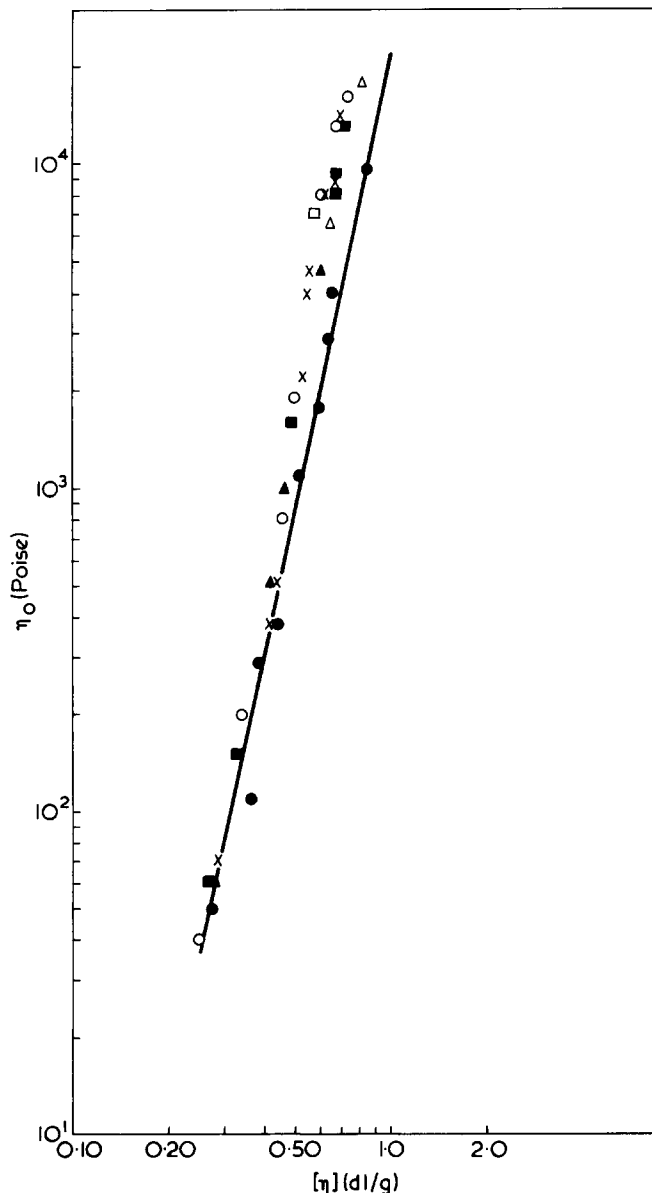


Figure 1 Dependence of the melt viscosity on intrinsic viscosity for various PET. —, linear PET; ●, $\rho = 0$ (linear PET); X, $\rho = 0.00748$; ▲, $\rho = 0.01121$; ■, $\rho = 0.01493$; ○, $\rho = 0.02233$

Analysis of the viscometric data

As is well known, the intrinsic viscosity of branched macromolecules is lower than that of linear ones with the same molecular weight, the volume of the former in solution being smaller^{22,23}.

The ratio $[\eta]_b/[\eta]_l$ between the intrinsic viscosities of the branched polymer and of the linear one, of the same molecular weight, has been frequently used as an experimental index of the degree of branching. In a θ solvent such a ratio should be a function of g only, i.e. of the corresponding ratio of the mean-square radii of gyration.

In the practical case of branched and polydispersed polymers, a comparison among intrinsic viscosities should be made, using convenient average quantities taking into account the 'viscosity exponent' in the Mark-Houwink equation^{21,24}. Semi-empirically and for sake of simplicity we chose to consider the \bar{M}_w values, the intrinsic viscosity being nearly a weight-average quantity. Our choice has also

been supported by the remarks reported in literature²⁵ according to which a correlation curve between $[\eta]$ and \bar{M}_w constitutes one of the most sensitive methods for evidencing the presence of branches.

The Newtonian melt viscosity also extensively depends on the presence of long branches. Their influence may be quite complex, but in general the final result is a decreased viscosity²⁶⁻²⁸. Therefore, even in that case, the ratio $\eta_{0,b}/\eta_{0,l}$ between Newtonian viscosities of branched and linear polymers, at the same value of \bar{M}_w , may supply an experimental index of the degree of branching.

RESULTS AND DISCUSSION

Table 1 shows the experimental values of ρ , $[\eta]$ and η_0 for linear PET's and those branched with different amounts of trimethyltrimesate. In this Table are also reported the calculated values of \bar{M}_n , \bar{M}_w , α and \bar{B}_w . Evidently, as the polymerization is statistical, the values of the conversion high and the trifunctional comonomer contents low, branches are few and long.

Correlations have been attempted between $[\eta]$, η_0 and \bar{M}_w : an approximate linearity on a bi-logarithmic scale was observed (Figures 1, 2 and 3). In all branched polymer, at equal \bar{M}_w values, $[\eta]$ and η_0 are significantly lower and, at equal $[\eta]$ values, η_0 is significantly higher than in the linear ones.

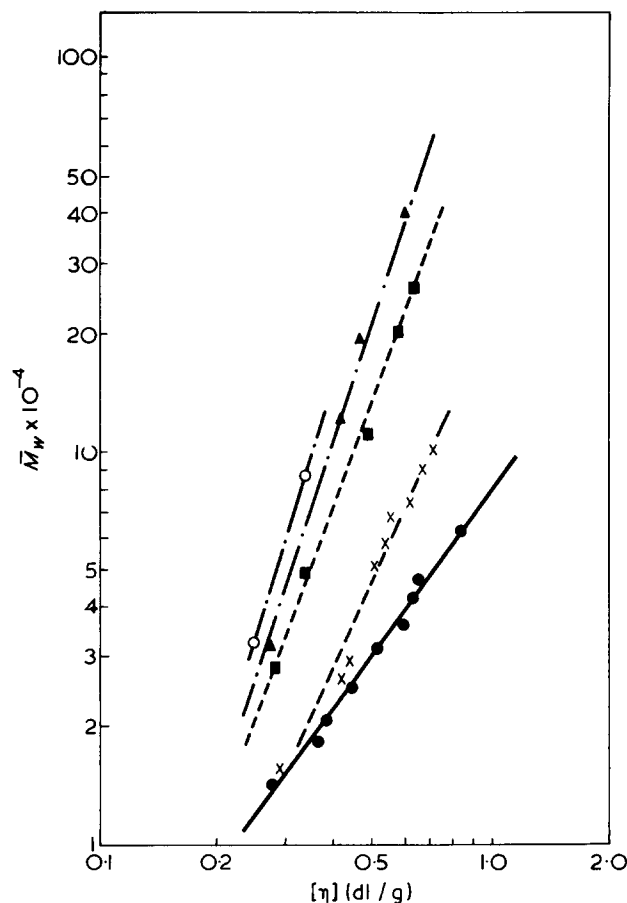


Figure 2 Dependence of the intrinsic viscosity on \bar{M}_w for various PET. ●, $\rho = 0$ (linear PET); X, $\rho = 0.00748$; ▲, $\rho = 0.01121$; ■, $\rho = 0.01493$; ○, $\rho = 0.02233$

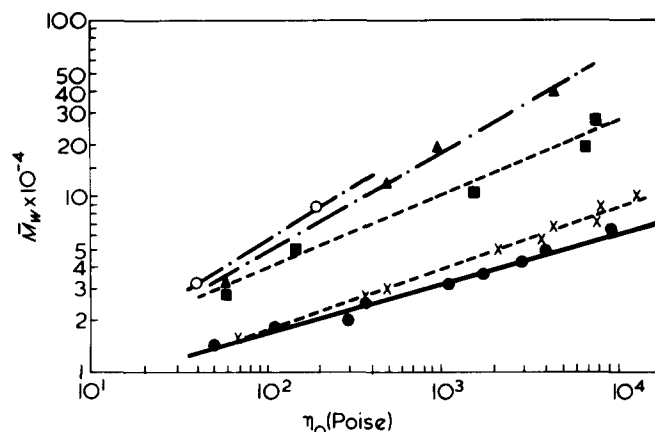


Figure 3 Dependence of the melt viscosity on \bar{M}_w for various PET. ●, $\rho = 0$ (linear PET); X, $\rho = 0.00748$; ▲, $\rho = 0.01121$; ■, $\rho = 0.01493$; ○, $\rho = 0.02233$

For the linear PET, the following relations have been obtained:

$$\log \eta_{0,1} = 4.36 + 4.78 \log [\eta]_1 \quad (12)$$

$$\log [\eta]_1 = -3.62 + 0.74 \log \bar{M}_w \quad (13)$$

$$\log \eta_{0,1} = -12.96 + 3.54 \log \bar{M}_w \quad (14)$$

in agreement with previous results by the authors¹⁸ and Gregory¹⁹.

Using relations (13) and (14) we calculated, for each branched sample, the values of $[\eta]_1$ and $\eta_{0,1}$ (at equal \bar{M}_w values), and then the ratios $[\eta]_b/[\eta]_1$ and $\eta_{0,b}/\eta_{0,1}$ reported in Table 1. These ratios, always below unity, decrease on increasing the trifunctional unit content and the extent of reaction, and a good correlation exists among them.

Since such 'viscosity indexes' must be related to the parameters that theoretically define the amount of branching, attempts have been made to correlate them with α , \bar{B}_n and \bar{B}_w . A satisfactory linear correlation has been obtained on a semi-logarithmic scale especially in the case of \bar{B}_w , apart from a few points corresponding to polymers with very high ρ values. The following equations have thus been derived:

$$\log [\eta]_b/[\eta]_1 = -0.06 \bar{B}_w \quad (15)$$

$$\log \eta_{0,b}/\eta_{0,1} = -0.25 \bar{B}_w \quad (16)$$

By combining equations (15) and (16) with (13) and (14) respectively, we obtained the following equations:

$$\log [\eta] = -3.62 + 0.74 \log \bar{M}_w - 0.06 \bar{B}_w \quad (17)$$

$$\log \eta_0 = -12.96 + 3.54 \log \bar{M}_w - 0.25 \bar{B}_w \quad (18)$$

Finally, by combining equations (17) and (18), two further ones are obtained:

$$\log \eta_0 = 4.36 + 4.78 \log [\eta] + 0.037 \bar{B}_w \quad (19)$$

$$\log \eta_0 = 2.13 + 4.17 \log [\eta] + 0.456 \log \bar{M}_w \quad (20)$$

All these relations are valid for both branched and linear PET. In Figures 4 and 5 curves corresponding to these equations are compared with experimental data: the relationships are valid for all values of ρ and p .

Thus both viscosities decrease, at equal \bar{M}_w values, on increasing \bar{B}_w , while the melt viscosity increases, at equal $[\eta]$ values, on increasing \bar{B}_w . This essentially occurs independently of the single values of ρ . Through equation (20) it is possible to calculate the value of \bar{M}_w for a branched (as well as linear) PET from solution and melt viscosity measurements.

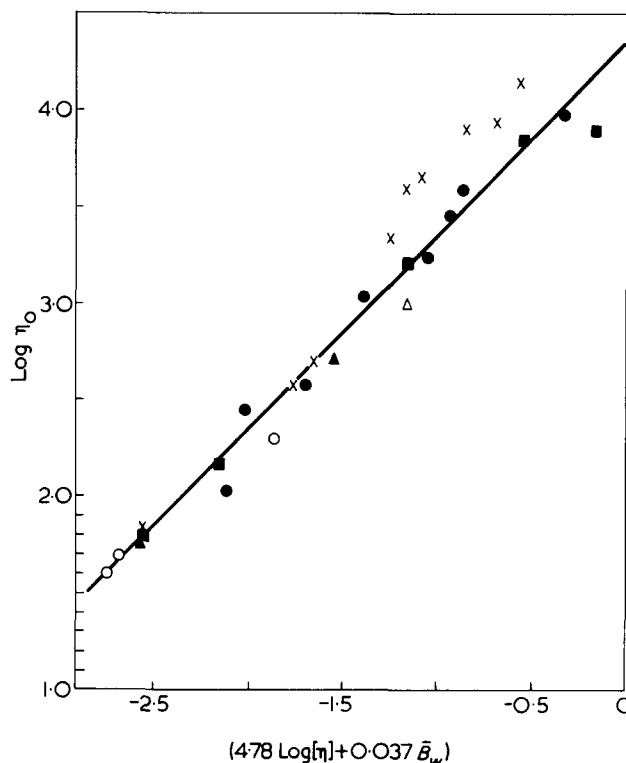


Figure 4 Melt viscosity as a function of intrinsic viscosity and branching density for various PET. —, corresponds to equation (19); ●, $\rho = 0$ (linear PET); X, $\rho = 0.00748$; ▲, $\rho = 0.01121$; ■, $\rho = 0.01493$; ○, $\rho = 0.02233$

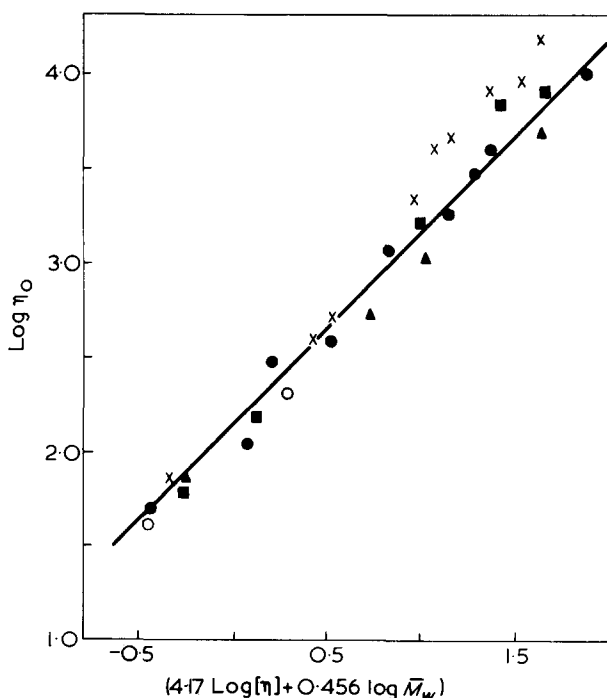


Figure 5 Melt viscosity as a function of the intrinsic viscosity and \bar{M}_w for various PET. —, corresponds to equation (20); ●, $\rho = 0$ (linear PET); X, $\rho = 0.00748$; ▲, $\rho = 0.01121$; ■, $\rho = 0.01493$; ○, $\rho = 0.02233$

Similar results had been obtained by Peticolas and co-workers^{30,31} and by Schreiber and coworkers³² in the case of polyethylenes with long branches. They found that η_0 at fixed temperature and given \bar{M}_w appears to be primarily a function of long branching, and they give for unfractio-nated polyethylenes relationships of the same form as equation (18)

More recently Ram and Miltz³³, by a careful character-ization of several samples of commercial free-radical poly-ethylenes, found that by using the variable $([\eta]_b/[\eta]_l)^2 \bar{M}_w$ most rheological parameters can be correlated into single straight lines on a bi-logarithmic scale. From Ram's data it is possible to obtain a general relation between η_0 , \bar{B}_w and \bar{M}_w of the same form as equation (18).

Finally, it must be noted that the values of \bar{M}_w have been calculated from those of p and ρ , by assuming that all end-groups have the same reactivity and intramolecular reactions are absent: it is certain that this last condition is no longer valid in proximity of the gel point. The most recent theories on gel formation, such as the stochastic graph theory, instead, suggest that this is due to the formation of cyclic structures as a result of intramolecular reactions¹³. Hence, in our opinion, one of the most important results achieved by this work is that the existence is suggested, with regard to branched (and linear) PET, of a general relation between η_0 , $[\eta]$ and \bar{M}_w such as equation (20). The reliability limits of such a relation should be checked by direct experimental measurements of \bar{M}_w .

REFERENCES

- 1 Carothers, W. H. *Trans. Faraday Soc.* 1936, **32**, 39
- 2 Flory, P. J. *J. Am. Chem. Soc.* 1941, **63**, 3083
- 3 Flory, P. J. *J. Am. Chem. Soc.* 1941, **63**, 3091
- 4 Flory, P. J. *J. Am. Chem. Soc.* 1941, **63**, 3096
- 5 Flory, P. J. *Chem. Rev.* 1946, **39**, 137
- 6 Stockmayer, W. H. *J. Chem. Phys.* 1943, **11**, 45
- 7 Stockmayer, W. H. *J. Polym. Sci.* 1952, **9**, 69
- 8 Good, I. J. *Proc. R. Soc. (A)* 1963, **292**, 54
- 9 Dobson, G. R. and Gordon, M. *J. Chem. Phys.* 1964, **41**, 2389
- 10 Tanaka, Y. and Kakiuchi, H. *J. Polym. Sci. (A)* 1965, **3**, 3279
- 11 Gordon, M., Malcom, G. N. and Butler, D. S. *Proc. R. Soc. (A)* 1966, **295**, 29
- 12 Yoshida, T. *Kobunshi Kagaku* 1966, **23**, 107
- 13 Bruneau, C. M. *Ann. Chim.* 1966, **1**, 273
- 14 Andrianov, K. A. Fromberg, M. B. and Belkina, T. M. *Vysokomol. Soedin. (A)* 1967, **9**, 2254; *Polym. Sci. USSR* 1967, **9**, 2550
- 15 Pavlova, S. A., Korshak, V. V. and Ciernomordik, Ju. A. *Vysokomol. Soedin. (B)* 1968, **10**, 411
- 16 Amemija, A. and Saito, O. *J. Phys. Soc. Japan* 1969, **26**, 1264
- 17 Pis'men, L. M. and Kuchanov, S. I. *Vysokomol. Soedin. (A)* 1971, **13**, 791; *Polym. Sci. USSR* 1971, **13**, 890
- 18 Manaresi, P., Giachetti, E. and de Fornasari, E. *J. Polym. Sci. (C)* 1968, **16**, 3133
- 19 Pohl, H. A. *J. Am. Chem. Soc.* 1951, **73**, 5660
- 20 Conix, A. *Makromol. Chem.* 1958, **26**, 226
- 21 Graessler, W. W. and Mittelhauser, H. M. *J. Polym. Sci. (A-2)* 1967, **5**, 431
- 22 Zimm, B. H. and Stockmayer, W. H. *J. Chem. Phys.* 1949, **17**, 1301
- 23 Zimm, B. H. and Kilb, R. W. *J. Polym. Sci.* 1959, **37**, 19
- 24 Nagasubramanian, K., Saito, O. and Graessler, W. W. *J. Polym. Sci. (A-2)* 1969, **7**, 1955
- 25 Thurmond, C. D. and Zimm, B. H. *J. Polym. Sci.* 1952, **8**, 477
- 26 Busse, W. F. and Langworth, R. *J. Polym. Sci.* 1962, **58**, 48
- 27 Fujimoto, T., Narukawa, H. and Nagasawa, M. *Macromolecules* 1970, **3**, 57
- 28 Pannell, J. *Polymer* 1971, **12**, 558
- 29 Gregory, D. R. *J. Appl. Polym. Sci.* 1972, **16**, 1479
- 30 Peticolas, W. L. and Watkins, J. M. *J. Am. Chem. Soc.* 1957, **79**, 5083
- 31 Peticolas, W. L. *J. Polym. Sci.* 1962, **58**, 1405
- 32 Schreiber, M. P. and Bagley, E. B. *J. Polym. Sci.* 1962, **58**, 29
- 33 Ram, A. and Miltz, J. *23rd International Symposium on Macromolecules Madrid* 1974, **2**, 748

Equilibrium ring concentrations and the statistical conformations of polymer chains: 14. Calculation of the concentrations of medium sized cyclics in poly(dimethyl siloxane) equilibrates

L. E. Scales* and J. A. Semlyen

Department of Chemistry, University of York, Heslington, York YO1 5DD, UK
(Received 29 December 1975; revised 10 February 1976)

Theoretical molar cyclization equilibrium constants K_x for dimethyl siloxane cyclics $[(CH_3)_2SiO]_x$ in undiluted poly(dimethyl siloxane) equilibrates are calculated for values of x in the range $7 < x < 13$. The Jacobson and Stockmayer theory is used for the calculations and K_x values are computed by finding the statistically weighted fraction of the 3^{2x-3} conformations [defined by the Flory, Crescenzi and Mark (FCM) rotational isomeric state model of poly(dimethyl siloxane)] that have terminal atoms in close proximity for ring formation. The FCM model gives theoretical K_x values in good agreement with experiment for $x = 8, 9, 10$ but yields a K_{11} value that is nine times greater than that found experimentally. This result is discussed in terms of the molecular structure of dimethyl siloxane chains. The effect on the calculated K_x values of modifying the FCM model by assigning a smaller value to the Si–O–Si bond angle is explored.

INTRODUCTION

It has been customary in developing theories in polymer science to assume that random-coil linear macromolecules obey Gaussian statistics. These statistics were established by Kuhn and others¹⁻⁴ over forty years ago and they have been applied to interpret a wide range of polymer properties and behaviour. However, it has always been realized that Gaussian statistics would not necessarily apply to flexible random-coil molecules of finite length. In general, as the lengths of molecules decrease, deviations from Gaussian behaviour would be expected to become greater.

Until recently, experimental data providing a close insight into the relationship between the statistical properties of chain molecules and their chain lengths have not been available. However, in the past few years experimental data have been obtained⁵ that give a unique opportunity of assessing the deviations from Gaussian statistics shown by chains of finite length. In particular, experimental molar cyclization equilibrium constants K_x have been measured with a considerable degree of precision for dimethyl siloxane cyclics $[(CH_3)_2SiO]_x$ with eight to as many as five hundred skeletal bonds⁶⁻⁸. Measurements were carried out for ring-chain equilibration reactions in the bulk polymer^{7,8} as well as in solution in toluene^{6,8} and in diglyme⁸. Plots of $\log K_x$ against $\log x$ exhibit well defined minima in the region $x = 12$ and these minima are followed by definite maxima located at values of $x \cong 15$.

One of the aims of this paper is to find a theoretical explanation for these experimental observations. To this end, the molar cyclization equilibrium constants for dimethyl siloxane rings have been calculated using the

Flory, Crescenzi and Mark⁹ rotational isomeric state model for poly(dimethyl siloxane). The computational procedures involve finding the statistically weighted fraction of the 3^{2x-3} conformations of the open chain molecules $[(CH_3)_2SiO]_x$ defined by the rotational isomeric state model that have terminal atoms in juxtaposition for ring formation. The calculations have been carried out for cyclics containing up to twenty four skeletal bonds. They are an extension of some calculations which were carried out for smaller dimethyl siloxane cyclics in an earlier study¹⁰.

ROTATIONAL ISOMERIC STATE MODEL OF POLY(DIMETHYL SILOXANE)

The rotational isomeric state model of poly(dimethyl siloxane) was set up by Flory, Crescenzi and Mark (FCM model)⁹. It was based on a critical examination of all the available molecular structure data. Their model takes each skeletal Si–O bond to be of length 1.64 Å, each Si–O–Si skeletal bond angle to be 143° and each O–Si–O skeletal bond angle to be 110°. The FCM model assigns each skeletal bond to one of three rotational isomeric states at $\phi = 0^\circ$ (*trans*), 120° (*gauche*⁺) and 240° (*gauche*⁻) positions. The statistical weight matrix U' that takes account of the mutual interdependence of adjacent pairs of skeletal bonds centred on silicon atoms is as follows:

$$U' = \begin{matrix} & \begin{matrix} t_i & g_i^+ & g_i^- \end{matrix} \\ \begin{matrix} t_{i-1} \\ g_{i-1}^+ \\ g_{i-1}^- \end{matrix} & \begin{bmatrix} 1 & \sigma & \sigma \\ 1 & \sigma & 0 \\ 1 & 0 & \sigma \end{bmatrix} \end{matrix} \quad (1)$$

* Present address: The Computer Laboratory, University of Liverpool, PO Box 147, Liverpool L69 3BX, UK.

The corresponding statistical weight matrix U'' that takes account of the mutual interdependence of adjacent pairs of skeletal bonds centred on oxygen atoms is:

$$U'' = \begin{matrix} & t_{i+1} & g_{i+1}^+ & g_{i+1}^- \\ \begin{matrix} t_i \\ g_i^+ \\ g_i^- \end{matrix} & \begin{bmatrix} 1 & \sigma & \sigma \\ 1 & \sigma & \delta \\ 1 & \delta & \sigma \end{bmatrix} \end{matrix} \quad (2)$$

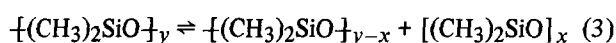
The parameters σ and δ of the FCM model were assigned values so as to reproduce the experimental characteristic ratio $\langle r^2 \rangle_0 / nl^2$ of linear poly(dimethyl siloxane) and the temperature coefficient $d(\ln \langle r^2 \rangle_0) / dT$ (where $\langle r^2 \rangle_0$ is the mean-square end-to-end distance of the unperturbed chain of n bonds each of length l in the limit $n \rightarrow \infty$)^{11,12}. The statistical weight parameters σ and δ are Boltzmann factors $\exp(-\Delta E / RT)$ where ΔE is the difference in energy between its associated conformation and the all-*trans* conformation, and R is the gas constant. At the temperature of 383K that is relevant to the calculations to be described here, the values of the FCM model parameters are $\sigma = 0.327$ and $\delta = 0.082$.

As will be discussed below, the greatest uncertainty in the assignment of a structural parameter in the FCM model is probably the value of 143° for the Si-O-Si skeletal bond angle. In the direct computations of cyclic concentrations to be described here, an alternative assignment was made for this bond angle. The statistical weight parameters were adjusted accordingly so as to reproduce the experimental values for the characteristic ratio and the temperature coefficient $d(\ln \langle r^2 \rangle_0) / dT$ of poly(dimethyl siloxane).

CALCULATION OF MOLAR CYCLIZATION EQUILIBRIUM CONSTANTS

Experimental and theoretical molar cyclization equilibrium constants

The equilibrium between ring and chain molecules of poly(dimethyl siloxane) may be represented thus:



This equilibrium can be set up in the bulk polymer^{7,8}, or in solution in toluene^{6,8} or diglyme⁸. In all these cases, there is a most probable distribution of chain lengths. It follows that the molar cyclization equilibrium constants K_x for cyclic dimethyl siloxanes are related to the extent of reaction of functional groups in the chain polymers p by:

$$K_x = [(\text{CH}_3)_2\text{SiO}]_x / p^x \quad (4)$$

In this paper, experimental K_x values used to compare with theory refer to undiluted equilibrates at 383K. Similar K_x values are found in diglyme⁸ but substantially larger K_x values were obtained for the smallest cyclics in toluene up to cyclics with $x < \sim 8$. These higher K_x values for the small rings have been discussed elsewhere^{7,8}.

The Jacobson and Stockmayer theory^{13,14} provides the following expression for K_x values (in mol/dm³) for cyclics produced by the forward step of equation (3):

$$K_x = \bar{W}_x / 2N_A x \quad (5)$$

where \bar{W}_x represents the density of end-to-end vectors \mathbf{r} in the region $\mathbf{r} \cong 0$ (in molecules/dm³) for an x -meric chain and N_A is the Avogadro constant.

As in the previous study¹⁰, no account is taken of the expected correlations between terminal bonds in the intramolecular cyclization processes, and K_x values are calculated using equation (5) by simply computing the statistically weighted fraction of the total number of conformations that have the centres of terminal atoms within small spheres of radius r . In this connection it is noted that there is no molecular structural information available as yet which could be used to define a solid angle within which the termini of siloxane chains must meet to form a bond.

Calculation of molar cyclization equilibrium constants for cyclic dimethyl siloxanes

In the previous paper¹⁰, molar cyclization equilibrium constants K_x for small cyclic dimethyl siloxanes $[(\text{CH}_3)_2\text{SiO}]_x$ were calculated using the FCM rotational isomeric state model by determining the statistically weighted fraction of the 3^{2x-3} discrete conformations of the corresponding open chain molecules which adopt highly coiled conformations corresponding to ring formation. The chains were assumed to be unperturbed by excluded volume effects and the calculations were carried out for cyclics with $x = 4-9$. Excellent agreement between experiment and theory was found for the cyclic octamer and nonamer. Furthermore, the failure of the FCM model to predict K_x values for the smaller cyclics and in particular the cyclic tetramer, pentamer and hexamer was rationalized by making a small but necessary adjustment to the FCM model so as to make it applicable to the calculation of the K_x values of small siloxane rings¹⁰.

The close agreement between experimental K_x values for the smaller cyclic siloxanes and those predicted by the FCM model has encouraged the calculations reported here, whereby K_x values for cyclics with $x > 9$ are computed. As will be seen, such an extension of the calculations has made it possible to explore the $\log K_x$ values in the region $x \cong 12$, where there is a well defined minimum rising to a maximum at $x \cong 15$ before the values decrease again (see Figure 1 for the experimental K_x values).

The calculations were carried out as before¹⁰. Probability densities \bar{W}_x required by equation (5) were calculated by dividing the sum z_r of the statistical weights for all chain conformations with their terminal atoms separated by less than r Å, by the volume $(4/3)\pi r^3$ and by the total sum Z of the statistical weights of all 3^{2x-3} conformations. Z is the conformational partition function of the x -meric chain and is given by:

$$Z = [1 \ 0 \ 0] (\mathbf{U}' \mathbf{U}')^{x-2} \mathbf{U}'' \begin{bmatrix} 1 \\ 1 \\ 1 \end{bmatrix} \quad (6)$$

and

$$\bar{W}_x = z_r / Z (4/3)\pi r^3 \quad (7)$$

The value of r , the radius of the sphere within which termini of siloxane chains meet to form a bond, is treated as an adjustable parameter. This radius is expected to be small but finite and in previous calculations it was assigned

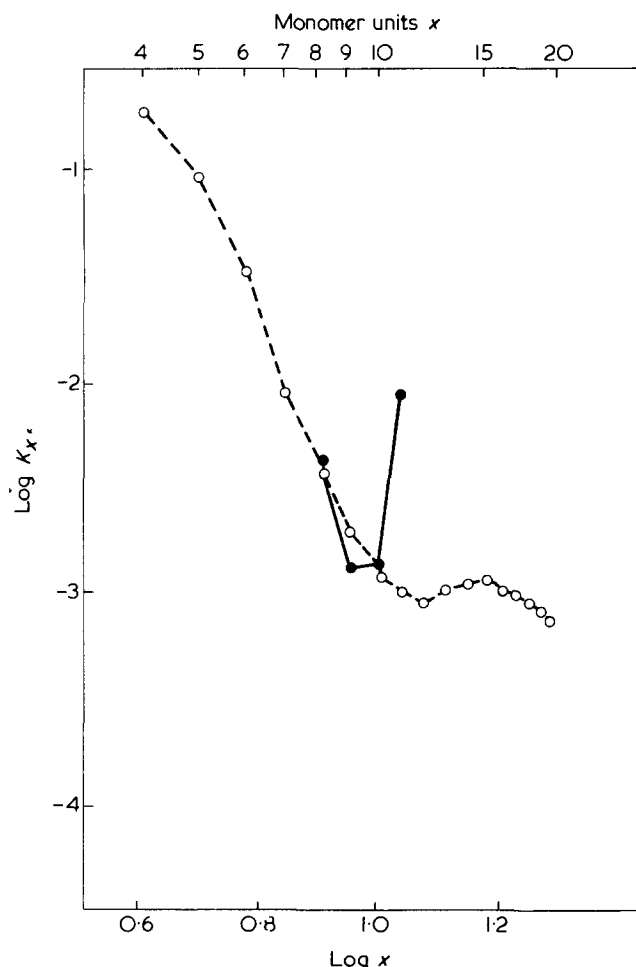


Figure 1 Theoretical molar cyclization equilibrium constants K_x for cyclic dimethyl siloxanes at 383K calculated by the direct computational method using the FCM model and assuming that $r = 2 \text{ \AA}$ (\bullet). They are compared with the experimental K_x values for an undiluted poly(dimethyl siloxane) equilibrate (\circ)

the value 3 \AA . For the calculations to be described here, smaller values have been assigned to r . In this connection it is noted that as the chains are built up and calculations of end-to-end distances are carried out, tests can be made at shorter chain lengths to discover whether the ends of the full length chain can ever fall within the volume of radius r . If they cannot, there is no further need to continue adding further skeletal bonds. Naturally, the smaller the value of r the greater will be the saving of computational time. Provided that r is not too small, the values of \bar{W}_x are found to be relatively insensitive to its precise value and the general conclusions reached in this paper are not dependent on the values chosen for r in particular calculations.

In Figure 1, K_x values for cyclics with $x = 8-11$ calculated by equations (5)–(7) using the FCM model and with $r = 2 \text{ \AA}$ are compared with experimental values for an undiluted poly(dimethyl siloxane) equilibrate at 383K. It is found that there is a close correspondence between experimental and theoretical K_8, K_9 and K_{10} values but a complete failure of the FCM model to calculate the experimental K_{11} value. Thus, the calculated K_8, K_9 and K_{10} values agree within experimental error with the corresponding experimental values, whereas the calculated K_{11} value is nearly nine times greater than the experimental value.

The reason for the sharp increase at $x = 11$ may be appreciated if the chain geometry is considered. The

poly(dimethyl siloxane) chain consists of a regular alternation of bond angles of unequal magnitude centred on silicon and oxygen atoms. Consequently, the planar all-*trans* conformation will correspond to a closed loop after a definite number of monomer units. For the bond angles chosen by Flory, Crescenzi and Mark⁹ chain closure occurs at eleven monomer units (see Figure 2). Hence, for $x = 11$ there are a total of 1 162 261 467 conformations and 296 357 of these have the centres of their terminal atoms within 2 \AA . The total statistical weight of these highly coiled conformations is approximately 17.4 and the all-*trans* conformation alone contributes a statistical weight of unity. Hence, the FCM model does predict a well defined minimum in the $\log K_x$ versus $\log x$ plot for dimethyl siloxane cyclics as is found experimentally but this minimum is not centred at $x = 12$. In the section to follow the FCM model is modified in order to explore whether even better correspondence between experiment and theory can be achieved.

Modification of the FCM model

The structural parameter of the poly(dimethyl siloxane) chain that is open to most doubt in the FCM model is the Si–O–Si bond angle. The value of 143° assigned to it is that observed in the cyclic tetramer $[(\text{CH}_3)_2\text{SiO}]_4$. Now, the Si–O–Si bond angle is known to be flexible and to adopt different values in different silicone and silicate structures¹⁵. For example, a bond angle of $130 \pm 10^\circ$ has been observed in hexamethyl disiloxane $[(\text{CH}_3)_2\text{Si}]_2\text{O}$ ^{16,17}. Hence a new value of 138° was assumed for the Si–O–Si bond angle, 5° less than that in the FCM model. This value corresponds to the first appearance of a planar all-*trans* cyclic conformation at $x \cong 13$. The statistical weight parameters of the FCM model were assigned new values of $\sigma = 0.22$ and $\delta = 0.10$ at 383K so as to reproduce the experimental characteristic ratio of poly(dimethyl siloxane) and the temperature coefficient of its unperturbed dimensions. The $\log K_x$ versus $\log x$ plot obtained using this

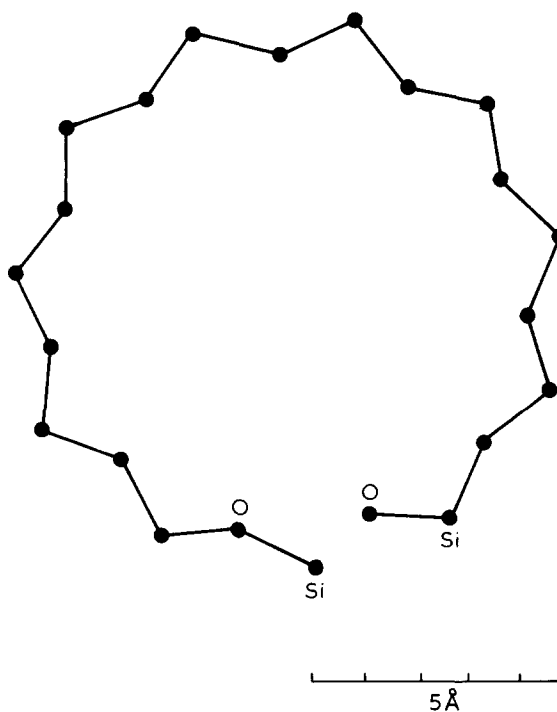


Figure 2 Diagram of the dimethyl siloxane chain in the planar, all-*trans* conformation

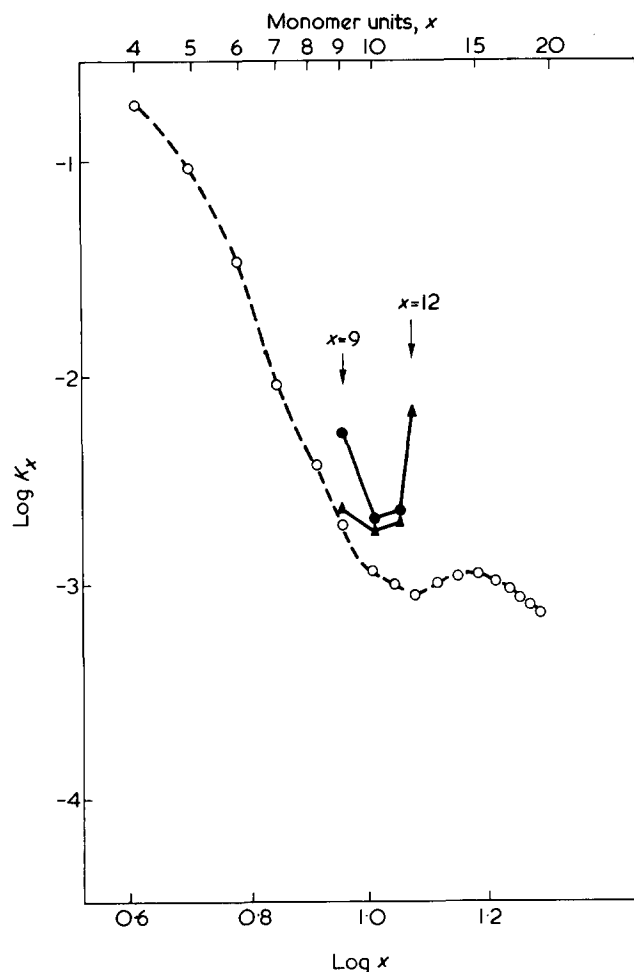


Figure 3 Theoretical molar cyclization equilibrium constants K_x for cyclic dimethyl siloxanes at 383K calculated by the direct computational method using the modified FCM model and assuming that $r = 1 \text{ \AA}$ (▲) and $r = 2 \text{ \AA}$ (●). They are compared with the experimental K_x values for an undiluted poly(dimethyl siloxane) equilibrate (O)

modified model predicts a minimum in the region $x \cong 10$ followed by a sharp increase at $x = 12$ (see Figure 3). Less complete calculations showed that the K_x value for $x = 13$ is also considerably higher than the experimental value. Furthermore, Monte Carlo calculations for even larger cyclics suggest that theoretical K_x values decrease as x increases. Hence a good rationalization of the experimental K_x values has been obtained.

CONCLUSIONS

The main conclusion of this study is that the FCM model gives a good qualitative understanding of the molar cyclization equilibrium constants for dimethyl siloxane cyclics but it does not predict K_x values for all the individual rings.

A small modification of the model by making a 5° decrease in the Si—O—Si bond angle moves the minimum in the $\log K_x$ versus $\log x$ plot but gives K_{12} and K_{13} values that are much higher than those observed experimentally.

These calculations provide a most exacting test of the FCM rotational isomeric state model and it is believed that it is the discrete nature of the model (with fixed bond angles and only three rotational isomeric states about each bond) that is responsible for the failure to predict theoretically the smooth changes in the $\log K_x$ versus $\log x$ plot that are observed experimentally.

ACKNOWLEDGEMENTS

We are indebted to the Science Research Council for a Research Studentship (to L.E.S.). We thank the Department of Computer Science of the University of York for providing extensive computational facilities and Dr M. S. Beevers for carrying out some preliminary calculations.

REFERENCES

- 1 Kuhn, W. *Kolloid-Z.* 1934, 68, 2
- 2 Guth, E. and Mark, H. *Monatsch. Chem.* 1934, 65, 93
- 3 Kuhn, W. *Kolloid-Z.* 1936, 76, 258
- 4 Kuhn, W. *Kolloid-Z.* 1939, 87, 3
- 5 Parts 1–13 of this series published in *Polymer* (1969–1974): Semlyen, J. A. and Wright, P. V. *Polymer* 1969, 10, 543; Semlyen, J. A. and Walker, G. R. *Polymer* 1969, 10, 597; Wright, P. V. and Semlyen, J. A. *Polymer* 1970, 11, 462; Walker, G. R. and Semlyen, J. A. *Polymer* 1970, 11, 472; Beevers, M. S. and Semlyen, J. A. *Polymer* 1971, 12, 373; Semlyen, J. A. *Polymer* 1971, 12, 373; Andrews, J. M. and Semlyen, J. A. *Polymer* 1972, 13, 142; Beevers, M. S. and Semlyen, J. A. *Polymer* 1972, 13, 385; Cooper, D. R. and Semlyen, J. A. *Polymer* 1972, 13, 414; Beevers, M. S. and Semlyen, J. A. *Polymer* 1972, 13, 523; Cooper, D. R. and Semlyen, J. A. *Polymer* 1973, 14, 185; Andrews, J. M., Jones, F. R. and Semlyen, J. A. *Polymer* 1974, 15, 420; Jones, F. R., Scales, L. E. and Semlyen, J. A. *Polymer* 1974, 15, 738
- 6 Brown, J. F. and Slusarczuk, G. M. J. *J. Am. Chem. Soc.* 1965, 87, 931
- 7 Semlyen, J. A. and Wright, P. V. *Polymer* 1969, 10, 543
- 8 Wright, P. V. *J. Polym. Sci. (Polym. Phys. Edn.)* 1973, 11, 51
- 9 Flory, P. J., Crescenzi, V. and Mark, J. E. *J. Am. Chem. Soc.* 1964, 86, 146
- 10 Beevers, M. S. and Semlyen, J. A. *Polymer* 1971, 12, 373
- 11 Crescenzi, V. and Flory, P. J. *J. Am. Chem. Soc.* 1964, 86, 141
- 12 Mark, J. E. and Flory, P. J. *J. Am. Chem. Soc.* 1964, 86, 138
- 13 Jacobson, H. and Stockmayer, W. H. *J. Chem. Phys.* 1950, 18, 1600
- 14 Flory, P. J. and Semlyen, J. A. *J. Am. Chem. Soc.* 1966, 88, 3209
- 15 Wells, A. F. 'Structural Inorganic Chemistry', 3rd Edn, Clarendon Press, Oxford, 1962
- 16 Yamasaki, K., Kotera, A., Tokoi, M. and Ueda, Y. *J. Chem. Phys.* 1950, 18, 1414
- 17 Yokoi, M. *Bull. Chem. Soc. Japan* 1957, 30, 100, 105

Comparison of the unperturbed dimension of polystyrene for endothermal and exothermal heats of dilution within the same system

B. A. Wolf and H. F. Bieringer*

*Institut für Physikalische Chemie der Universität Mainz, D-65 Mainz, Germany (*and Sonderforschungsbereich Makromoleküle, Mainz-Darmstadt, Germany)*

and J. W. Breitenbach

Institut für Physikalische Chemie der Universität Wien, A-1090 Wien, Austria (Received 8 December 1975; revised 26 February 1976)

Light scattering measurements for two samples of polystyrene (I, $M_w = 2.15 \times 10^5$; II, $M_w = 2.5 \times 10^6$) were performed in the iso-refractive mixed solvent dimethoxymethane–diethyl ether. For sample I the temperature dependence of the second osmotic virial coefficient A_2 was determined for three constant compositions of the mixed solvent. In the range -30° to $+25^\circ\text{C}$ the three curves run practically parallel and exhibit a maximum at approximately -10°C . For the volume fraction of 0.7 diethyl ether in the mixed solvent, an endothermal theta-temperature θ_+ was found at $-27.0^\circ \pm 1.5^\circ\text{C}$ and θ_- , the exothermal theta-temperature, at $-5.0 \pm 1^\circ\text{C}$. The investigation of sample II in the above-mentioned solvent confirmed the observed θ_- -temperature and displayed a higher exothermicity compared with I. Similarly to the temperature variation of A_2 , the chain dimensions of II, determined from the angular dependence of the scattered light, run through a maximum. The unperturbed dimensions in the mixed solvent are found to be: $r_w = 448 \pm 5 \text{ \AA}$ at $\theta_+ = -27^\circ\text{C}$ and $r_w = 443 \pm 5 \text{ \AA}$ at $\theta_- = -5^\circ\text{C}$, as compared with $r_w = 420 \pm 10 \text{ \AA}$ at $\theta_+ = +33^\circ\text{C}$ in cyclohexene. The inter-relation of the chain expansion coefficient and A_2 is quantitatively described by the Zimm–Stockmayer–Fixman equation over the entire range of heats of dilution.

INTRODUCTION

A lot of work has been dedicated to the question of whether the unperturbed dimensions of dissolved polymers, as determined by light scattering, depend on the particular conditions under which pseudo-ideality is achieved^{1–7}. Practically all systems studied so far were more or less endothermal and only in a few rare exceptions exothermal theta conditions were investigated^{8,9}. The quintessence of these studies is that when a polymer is examined in a series of endothermal solvents, showing different θ -temperatures and different heats of dilution, the unperturbed dimensions normally do not differ widely and there is no systematic dependence on either of these two parameters or on the chemical nature of the solvent.

To our knowledge no attempt has hitherto been made to compare the unperturbed dimensions of a given polymer for positive and negative heats of dilution and to eliminate chemical influences by using a solvent which exhibits both, endothermal and exothermal theta conditions. The present work is therefore concerned with this problem.

The requirement that the two θ -temperatures should lie within the normal operation range of a light scattering instrument is rarely met by a binary polymer–solvent system. From our investigation on mixed solvents for polystyrene^{10,11} it was clear, however, that a mixture of diethyl ether and a proper second component should serve the purpose, since the ether exhibits its maximum solvent power, which still does not mean complete miscibility, at approximately -10°C ¹². By adding a suitable amount of a better solvent, the desired θ_+ ($< -10^\circ\text{C}$) and θ_- ($> -10^\circ\text{C}$) condi-

tions^{13,14} could then be realized. For the determination of the unperturbed dimensions by means of light scattering measurements, the solvent had to meet a second condition, namely iso-refractivity with diethyl ether (DEE). Fortunately dimethoxymethane (DMOM) not only fulfills this requirement* in addition its mixing behaviour with DEE deviates only slightly from ideality, as can be seen from vapour pressure measurements¹⁵.

The system DMOM/DEE/PS is thus highly suited for a study of the purely thermodynamic influences on chain dimensions of dissolved polymers.

EXPERIMENTAL

Materials

Both samples of PS were anionically prepared. The low MW product is the main fraction of the lot S 111 provided by the Dow Chemical Co. The molecular weight of the main fraction prepared according to Breitenbach and Streichsbier¹⁶ was found to be $M_w = 2.15 \times 10^5$ as determined from its intrinsic viscosity and the viscosity–molecular weight relationship¹⁷. Its non-uniformity $U = M_w/M_n - 1$ is less than 0.1¹⁶. The corresponding values for the high molecular weight product, which was a commercial sample from the Pressure Chemical Co., are $M_w = 2.5 \times 10^6$ and $U \sim 1.0$; these results, which have been confirmed by measurements in different solvents (cyclohexane and

* We are grateful to our previous coworker J. K. Rigler for drawing our attention to this iso-refractive system and its possibilities.

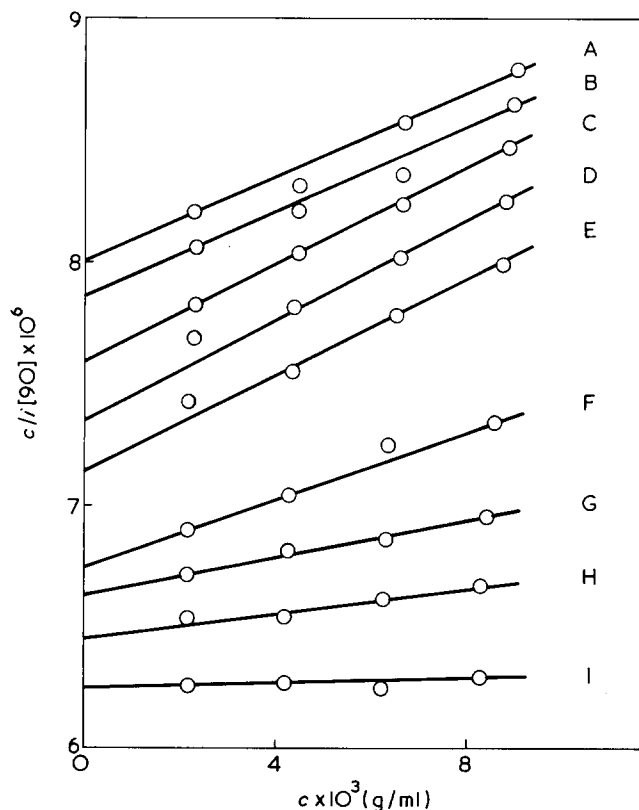


Figure 1 Evaluation of the light scattering data according to equation (2) for $\bar{M}_w = 2.15 \times 10^5$ and 66.6 vol % DEE (20°C) in the mixed solvent OTMF/DEE; $P^{-1}(90) = 1.08$. A, -30° ; B, -26° ; C, -20° ; D, -14° ; E, -7.5° ; F, 2.5° ; G, 9° ; H, 15° ; I, 21° C

t-decalin) and by different experimentalists are in disagreement with the data given by the producers, namely $M_w = 2.0 \times 10^6$ and $U \sim 0.2$.

The solvents were p.a. products, which we merely dried before use. The refractive indices n (at 15°C , 435.8 nm) of DMOM and DEE are 1.36356 and 1.36375, respectively and their thermal expansion coefficients at 0°C , $1.49 \times 10^{-3} \text{K}^{-1}$ and $1.52 \times 10^{-3} \text{K}^{-1}$ respectively.

Apparatus and procedure

Since DEE and DMOM are very volatile compounds, we had to construct special closed cells which are sealed by means of a spherical grind and teflon foils. The clasps by which the two parts of the grind are pressed together are made entirely of brass and fit exactly into the holding device of the commercially available light scattering instrument Sofica PGD 42000 in order to prevent the entrance of external light. A further consequence of the high volatility of our solvents was the necessity to clear the solutions by filtration instead of centrifugation. The use of relatively tight teflon coated cellulose filters, produced by Millipore Corp., Mass. USA (diameter $0.5 \mu\text{m}$), was possible because of the low viscosity of the solutions even at the working temperature of 0°C .

The light scattering apparatus itself also had to be adapted for low temperatures, since small ice particles forming in the bath result in a strong increase in light scattering, and water condensing on the window transmitting the light into the bath disturbs the geometry of the primary beam. The first difficulty was overcome by using a bath liquid miscible with water; the only substance meeting the additional requirement of approximately the same refractive index as glass (in order to keep the errors introduced by reflection small) was α -methylpyridine. The second problem was

solved by ventilating the window with a stream of dried nitrogen. For very low temperatures we had to stir the bath in order to prevent the formation of temperature gradients. All measurements were performed with unpolarized light of 435.8 nm.

EVALUATION

In order to avoid the laborious measurement of refractive index increments for polystyrene in our mixed solvent, we have used the evaluation procedure described by Kirste and Schulz¹⁸. Instead of the well known equation (1) of Debye:

$$\frac{K_\lambda c}{R} = \frac{1}{P(\theta)M_w} + 2A_2c + \dots \quad (1)$$

we start from the modified expression (2):

$$\frac{K_\lambda^* c}{i_\theta} = \frac{1}{P(\theta)M_w} + 2A_2c + \dots \quad (2)$$

in which i_θ , the difference in the galvanometer reading between solution and solvent observed at the angle θ replaces the Rayleigh-ratio R_θ . Consequently K_λ^* comprises the geometric constants of the apparatus and the correction for the reflected light in addition to the refractive index and refractive index increment (and some other quantities, constant for one measuring series) already contained in K_λ .

Zimm-like diagrams can now be constructed on the basis of equation (2), by plotting c/i_θ vs. $\sin^2 \theta/2 + \text{constant } c$. For known molecular weight M_w of the polymer, the constant K_λ^* is accessible from the twofold extrapolated ratio:

$$\left[\frac{c}{i_\theta} \right]_{\substack{c=0 \\ \theta=0}} = \frac{1}{M_w K_\lambda^*} \quad (3)$$

since $P(\theta) = 1$ for $\theta = 0$; once K_λ^* is known, the rest of the evaluation can be performed in the usual manner.

RESULTS AND DISCUSSION

Second osmotic virial coefficients

Figures 1–3 give the results for three different ratios of solvent and non-solvent. The evaluation of these data according to the procedure described in the experimental section, yields the temperature dependence of A_2 depicted in Figure 4.

For the highest DEE content the curve runs below $A_2 = 0$ over the entire temperature range. When the content of DMOM is increased a practically parallel shift towards higher A_2 -values is observed. For a volume fraction of $\phi_{\text{DEE}} \sim 0.71$ in the mixed solvent the maximum of the temperature dependence of A_2 would touch the abscissa at approximately -10°C , i.e. a theta condition would be created for the first time. Because $\partial A_2/\partial T$ becomes zero as well as A_2 , the corresponding θ -temperature belongs to an athermal heat of dilution.

For still higher DMOM contents of the mixed solvents the above mentioned athermal θ -temperature separates into an endothermal (θ_+) and an exothermal (θ_-) theta-temperature which drift apart as the mixed solvent becomes richer in the solvent component. The corresponding composition dependence of the θ -temperatures looks similar

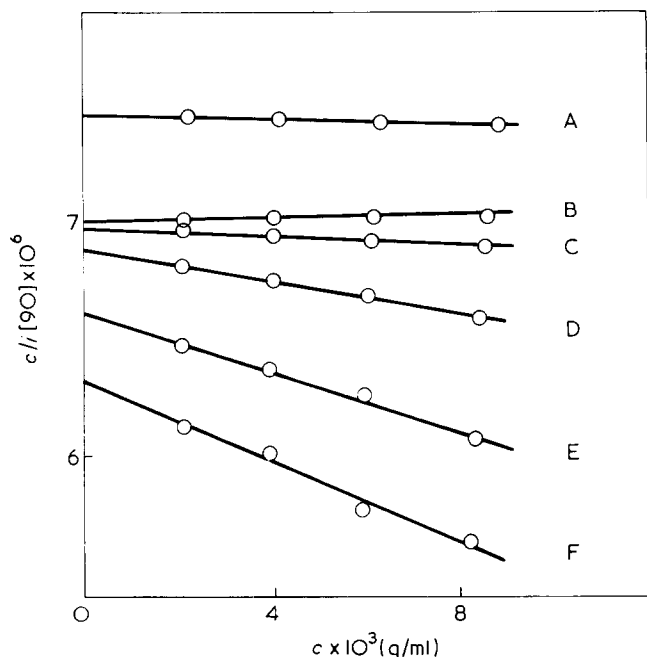


Figure 2 Evaluation of the light scattering data according to equation (2) for $\bar{M}_w = 2.15 \times 10^5$ and 70 vol % DEE (20°C) in the mixed solvent OTMF/DEE; $\bar{P}^{-1}(90) = 1.08$. A, -22°; B, -90°; C, 0°; D, 6.5°; E, 14°; F, 21°C

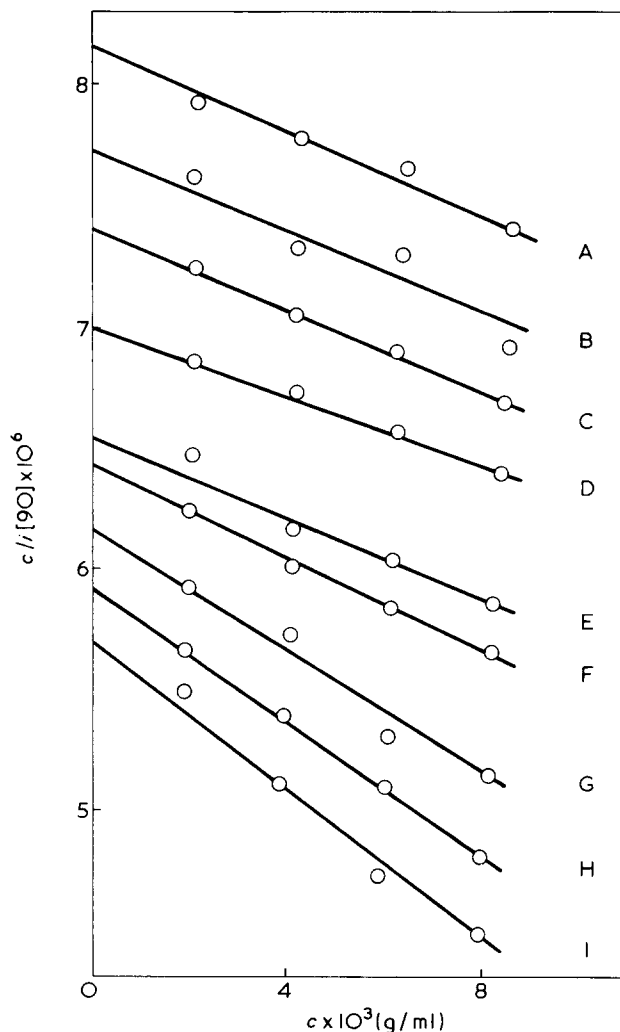


Figure 3 Evaluation of the light scattering data according to equation (2) for $\bar{M}_w = 2.15 \times 10^5$ and 75.0 vol % DEE in the mixed solvent OTMF/DEE; $\bar{P}^{-1}(90) = 1.08$. A, -22°; B, -18°; C, -12°; D, -8°; E, 1°; F, 6°; G, 12°; H, 20°; I, 25°C

to the binodal edges determined from phase equilibria¹¹, in fact it constitutes the critical line for infinite molecular weight of the polymer ($c_{pol} = 0$).

To our knowledge the present system is the first for which the complete transition from endothermal to exothermal θ -conditions could be followed by light scattering. It was thus interesting to check whether the theoretically calculated character of the interdependence of entropy and enthalpy contributions to the second osmotic virial coefficient¹⁹, hitherto only comparable to a limited range of heats of dilution¹⁹, is experimentally substantiated.

The required subdivision of A_2 into its enthalpy contribution $A_{2,H}$ and its entropy contribution $A_{2,S}$ ²⁰:

$$A_2 = -\frac{\Delta G_1^E}{RTc_2^2V_1} = -\frac{\Delta H_1}{RTc_2^2V_1} + \frac{\Delta S_1^E}{Rc_2^2V_1}$$

$$= A_{2,H} + A_{2,S} \quad (4)$$

was performed by means of its temperature dependence according to:

$$A_{2,H} = T \left(\alpha A_2 - \frac{\partial A_2}{\partial T} \right) \quad (5)$$

where α denotes the thermal expansivity of the solvent. Figure 5 shows the thus obtained interdependence of $A_{2,S}$ and $A_{2,H}$, which confirms the picture given by the Prigogine-Patterson theory¹⁹. In a diagram such as Figure 5, θ -conditions correspond to points on the diagonal, and it is clear that at a proper constant composition of the mixed solvent some curve should run through the origin of this graph. One could think that a perfect solution is created under these conditions ($\Delta S_1^E = \Delta H_1 = 0$), but this is not the case because of a non-zero ΔV_1 value, which must be anticipated from our pressure experiments on the similar system acetone/DEE/PS²¹.

For one mixed solvent ($\phi_{DEE} = 0.7$) the molecular weight influence on A_2 was also investigated. The corresponding results, as obtained from several Zimm-plots (an example of which is shown in Figure 6) are entered in Figure 4. Owing to the limits of experimental error (A_2 can be determined with an accuracy of approximately $\pm 5 \times 10^{-6} \text{ cm}^3 \text{ mol/g}^2$

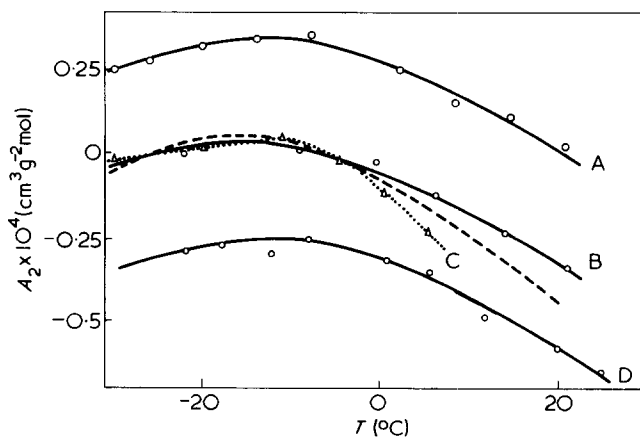


Figure 4 Temperature dependence of the second osmotic virial coefficient A_2 for the indicated molecular weights and compositions of the mixed solvent. ---, calculated according to the equations (6)–(8) as described in the text; \circ , $\bar{M}_w = 2.15 \times 10^5$; \triangle , $\bar{M}_w = 2.5 \times 10^6$. Curve A, $\phi_{DEE} = 0.666$; B, $\phi_{DEE} = 0.7$; C, $\phi_{DEE} = 0.7$; D, $\phi_{DEE} = 0.75$

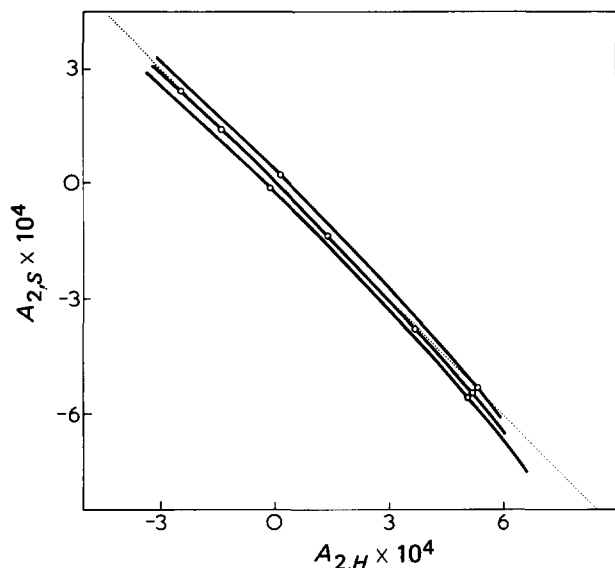


Figure 5 Interdependence of the enthalpy and the entropy contributions to the second osmotic virial coefficient for the indicated compositions of the mixed solvent for $\bar{M}_w = 2.15 \times 10^5$ with increasing temperature from left (endothermal) to right (exothermal) on the curves: A, $\phi_{DEE} = 0.66$; B, $\phi_{DEE} = 0.7$; C, $\phi_{DEE} = 0.75$

in the present case) there is some uncertainty as to the precise shape of the curve below -15°C . There is however no doubt that the temperature dependence of A_2 on the two molecular weights under investigation cross at θ_- and that the higher molecular weight sample exhibits the *more exothermal* heat of dilution. Since it is well established on the other hand, that a similar common point of intersection exists at θ_+ , which, however, is characterized by the fact that the higher MW sample exhibits *less endothermal* behaviour²², one should conclude, that the $A_2(T)$ functions intersect in the region $A_2 > 0$ and that a given solvent reaches its maximum solvent power for different molecular weights of the polymer at different temperatures.

As is generally known, a theoretical description of the temperature dependence of A_2 explaining the occurrence of θ_+ and θ_- in the same system, must in some way or other include free volume effects. In the application of all these theories at least one parameter is adjustable, we have thus chosen the simplest method for the calculation of the dependence of the Flory-Huggins interaction parameter χ on the variables of state. This is equation (6) which was introduced by Patterson and Delmas²³:

$$\chi = -\frac{\tilde{U}_1}{\tilde{T}_1} a + \frac{\tilde{c}_{p1}}{2} b \quad (6)$$

In this equation tildes, $\tilde{}$, indicate reduced quantities and the index 1 stands for the solvent. U represents the internal heat of vaporization and c_p its temperature derivative. The latter two quantities are calculated using Flory's equations of state²⁴:

$$\tilde{U} = -\tilde{V}^{-1} \quad (7)$$

and

$$\tilde{T} = \tilde{V}^{-1} - \tilde{V}^{-4/3}; \tilde{p} = 0 \quad (8)$$

Although, the system specific parameters a and b can in principle be calculated theoretically, a is normally adjusted

to the experiment. Since in addition, equation (6) constitutes an excellent analytical expression for the reproduction of measured dependencies, when both system specific parameters are adjusted^{21,25}, it seemed interesting to check, whether this equation can describe $A_2(T)$, when a and b are determined from the fact that according to:

$$A_2 = \left(\frac{1}{2} - \chi \right) \frac{1}{\rho_2^2 V_1} \quad (9)$$

χ must become 0.5 at θ_+ and θ_- , respectively.

Treating the mixed solvent (which shows negligible preferential solvation¹⁵) as one component, whose reduction temperature and reduction volume is calculated from the corresponding thermal expansivity to be:

$$T^* = 4070\text{K}, \text{ and } V^* = 72.2 \text{ cm}^3,$$

we arrived at the dependence shown in Figure 4 by the broken line.

Similar to the previous findings the dependence calculated from equations (7) and (8) is very close to the measured one even at relatively large distances from the points of adjustment. It is also noteworthy that the observed influences of molecular weight on A_2 cannot be explained theoretically by equations (6)–(9), unless either the θ -conditions are treated to be slightly dependent on molecular weight or the equations (6) and (9) are modified.

Radii of gyration

Chain dimensions as a function of temperature were determined for $M_w = 2.5 \times 10^6$ in the mixed solvent containing 70 vol% DEE (at 20°C). Under these conditions the unperturbed dimensions can be observed at $\theta_+ = -27^\circ \pm 2.5^\circ\text{C}$ and at $\theta_- = -5^\circ \pm 1^\circ\text{C}$. As an example for the Zimm-plots obtained, Figure 6 gives the result for -11°C , at which temperature the solvent power of the mixed solvent achieves its maximum.

The z-average of the radius of gyration was obtained from the initial slope of P_θ^{-1} vs. $\sin^2 \theta/2$ (which is found to be constant in the whole range in agreement with theoretical prediction for values of the non-uniformity near unity²⁶) according to²⁷:

$$P_\theta^{-1} = 1 + \frac{16\pi^2 r_z^2}{3\lambda^2} \sin^2 \frac{\theta}{2} + \dots \quad (10)$$

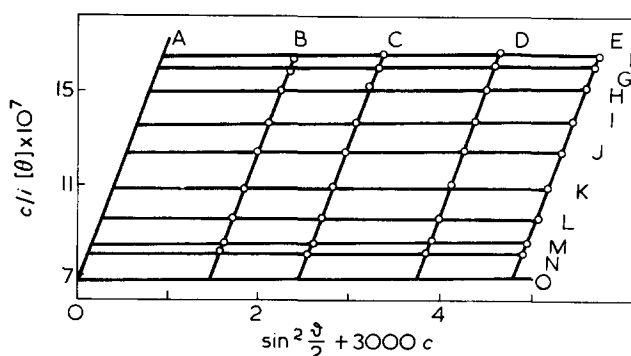


Figure 6 Evaluation of the light scattering data according to equation (2) for $\bar{M}_w = 2.5 \times 10^6$, 70.0 vol % DEE (20°C) in the mixed solvent OTMF/DEE and -11°C . A, $c = 0$; B, $c = 0.489 \times 10^{-3}$; C, $c = 0.813 \times 10^{-3}$; D, $c = 1.24 \times 10^{-3}$; E, $c = 1.6 \times 10^{-3}$; g/ml; F, $\theta = 142.5^\circ$; G, $\theta = 135^\circ$; H, $\theta = 120^\circ$; I, $\theta = 105^\circ$; J, $\theta = 90^\circ$; K, $\theta = 75^\circ$; L, $\theta = 60^\circ$; M, $\theta = 45^\circ$; N, $\theta = 37.5^\circ$; O, $\theta = 0^\circ$

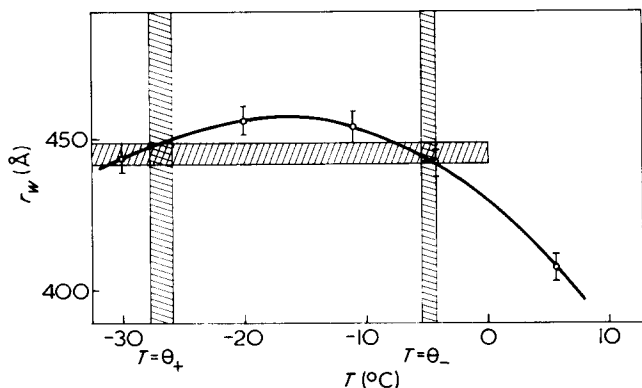


Figure 7 Temperature dependence of the radius of gyration for $M_w = 2.5 \times 10^6$ and 70.0 vol % DEE (20°C) in the mixed solvent OTMF/DEE. The shaded areas mark the limits of experimental reproducibility in the determination of the unperturbed dimensions

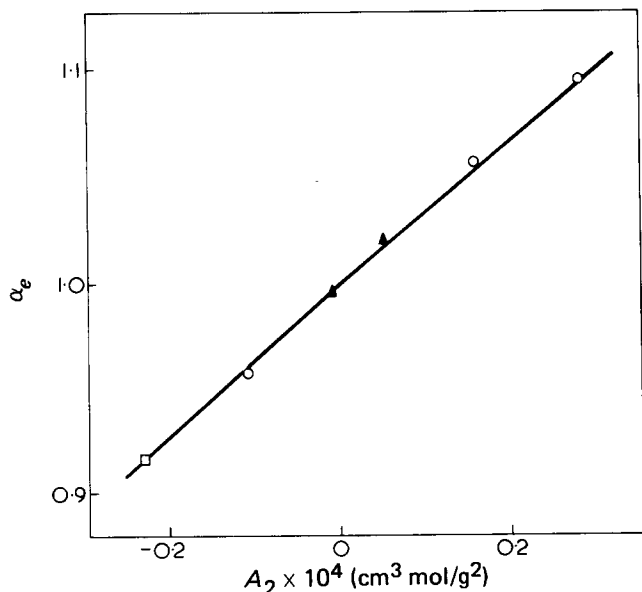


Figure 8 Dependence of the chain expansion coefficient α_e on the second osmotic virial coefficient A_2 for $M_w = 2.5 \times 10^6$. \circ, \square correspond to endothermal solutions; \blacktriangle , exothermal and endothermal points coincide; —, calculated from the theoretical equation (12); \blacktriangle, \square DMOM/DEE/PS; \circ , cyclohexane/PS

where $\lambda (= \lambda_0/n)$ is the wavelength of the light in the medium and r_z the z -average $r_z = (\overline{r_z^2})^{1/2}$ of the radius of gyration.

The conversion of r_z to the weight-average radius of gyration $r_w = (\overline{r_w^2})^{1/2}$ was performed by means of the relation given by Schulz²⁸:

$$r_w = r_z \left(\frac{1+U}{1+2U} \right)^{1/2} \quad (11)$$

The obtained values of r_w are on average in better agreement than $\pm 1.5\%$ with the results obtained by the evaluation of the corresponding dissymmetry data by means of tables²⁹, directly yielding r_w .

Figure 7 shows how r_w depends on temperature. As is immediately obvious from the shaded areas, the unperturbed dimensions in the endo- and exothermal solution are identical within experimental scattering i.e.:

$$r_w = 448 \pm 5 \text{ \AA at } \theta_+ = -27^\circ\text{C:}$$

$$r_w = 443 \pm 5 \text{ \AA at } \theta_- = -5^\circ\text{C}$$

Since it seems interesting to compare this value with that obtained for the same polymer sample in a conventional one component (with a much larger heat of dilution) θ -solution, we also determined the unperturbed dimensions in cyclohexane and arrived at $r_w^{\text{CH}} = 420 \pm 10 \text{ \AA}$ at $\theta_+ = +33^\circ\text{C}$. This result lies within the normal scattering of the unperturbed dimensions in different single solvents.

The conclusion can therefore readily be drawn that the enthalpy conditions as such stay inconsequential on the chain dimensions resulting for a pseudo-ideal Gibbs free energy of dilution of the solvent ($A_2 = 0$).

Chain expansion and second osmotic virial coefficient

The observed correlation of the chain expansion coefficient $\alpha_e = r/r_\theta$ with the second osmotic virial coefficient A_2 was compared with the theoretical expression reported in literature. Best agreement is obtained when the Zimm–Stockmayer–Fixman³⁰ equation:

$$A_2 M_w^{1/2} = 4N_L (\pi K'_\theta)^{3/2} a_1^{-1} (\alpha_e^2 - 1) \quad (12)$$

with the experimentally determined value $K'_\theta = r_{w,\theta}^2/M_w = 7.9 \times 10^{-18} \text{ (cm}^2\text{mol/g}^2\text{)}$ and $a_1 = 134/105$ is inserted.

Other theoretical equations give deviations up to 40%. The dependence of α_e on A_2 , calculated from equation (12), is shown in Figure 8 together with the experimental points. It is noteworthy that equation (12) is equally suited for the representation of slightly endo- and exothermal conditions of the mixed solvent and of the highly endothermal solution of PS in cyclohexane.

The fact that the K'_θ value for the mixed solvent is in good agreement with the mean value of 7.9×10^{-18} for several single solvents⁴ and in particular with the value of 7.2×10^{-18} obtained for our polymer in cyclohexane is a further indication that the mixed solvent really behaves like one component.

CONCLUSION

Because it is possible to tailor the thermodynamic quality of a solvent by selecting the proper ratio of its components, the entire typical dependence of A_2 on temperature could be followed. It was thus possible to compare the unperturbed dimensions r_θ for endothermal and exothermal conditions without changing the system. The observed independence of r_θ on the particular thermodynamic conditions under which pseudo-ideality of the solution is achieved, indicates that the variations of r_θ reported in literature are exclusively the result of some local, solvent specific interactions which influences the stability of the different conformers and/or temperature.

In addition, the abnormal molecular weight dependence encountered in the vicinity of the exothermal theta conditions makes it once more clear that the theoretical concept of the dimensionless intermolecular excluded volume function $h(z)$ must at least be modified, to cover all thermodynamic facts existing.

ACKNOWLEDGEMENT

One of us (H. F. B.) gratefully acknowledges a grant from the Deutscher Akademischer Austauschdienst.

REFERENCES

- 1 Krigbaum, W. R. and Carpenter, D. C. *J. Phys. Chem.* 1955, **59**, 1166
- 2 McIntyre, D., Wims, A., Williams, L. C. and Mandelkern, L. *J. Phys. Chem.* 1962, **66**, 1932
- 3 Burchard, W. *Makromol. Chem.* 1962, **56**, 239
- 4 Schulz, G. V., Baumann, H. and Darskus, R. L. *J. Phys. Chem.* 1966, **70**, 3647
- 5 Inagaki, H., Suzuki, H., Fujii, M. and Matsuo, T. *J. Phys. Chem.* 1966, **70**, 1718
- 6 Berry, G. C. *J. Chem. Phys.* 1966, **44**, 4550
- 7 Strazielle, C. in 'Light Scattering from Polymer Solutions', (Ed. M. B. Huglin), Academic Press, London and New York, 1972
- 8 Delmas, G. and Patterson, D. *Polymer* 1966, **7**, 513
- 9 Cowie, J. M. G. and McEwen, I. J. *Macromolecules* 1974, **7**, 291
- 10 Wolf, B. A., Breitenbach, J. W. and Senftl, H. *J. Polym. Sci. (C)* 1970, **31**, 345
- 11 Wolf, B. A., Breitenbach, J. W. and Rigler, J. K. *Angew. Makromol. Chem.* 1973, **34**, 177
- 12 Siow, K. S., Delmes, G. and Patterson, D. *Macromolecules* 1972, **5**, 29
- 13 Wolf, B. A. *Ber. Bunsenges. Physik. Chem.* 1971, **75**, 924
- 14 Wolf, B. A. *Adv. Polym. Sci.* 1972, **10**, 109
- 15 Wolf, B. A., Breitenbach, J. W. and Bieringer, H. F. to be published
- 16 Breitenbach, J. W. and Streichsbier, O. *Kolloid-Z.* 1962, **182**, 35
- 17 Breitenbach, J. W., Gabler, H. and Olaj, O. F. *Makromol. Chem.* 1965, **81**, 32
- 18 Kirste, R. G. and Schulz, G. V. *Z. Phys. Chem. (Frankfurt)* 1961, **27**, 301
- 19 Wolf, B. A. *J. Polym. Sci. (A-2)* 1972, **10**, 847
- 20 Schulz, G. V., Inagaki, H. and Kirste, R. G. *Z. Phys. Chem. (Frankfurt)* 1960, **24**, 390
- 21 Wolf, B. A. and Blaum, G. *Makromol. Chem.* in press
- 22 Schulz, G. V., Haug, A. and Kirste, R. G. *Z. Phys. Chem. (Frankfurt)* 1963, **38**, 1
- 23 Patterson, D. and Delmas, G. *Trans. Faraday Soc.* 1969, **65**, 708
- 24 Flory, P. J., Orwoll, R. A. and Vrij, A. *J. Am. Chem. Soc.* 1964, **86**, 3507, 3515
- 25 Wolf, B. A. and Blaum, G. *J. Polym. Sci. (A-2)* 1975, **13**, 1115
- 26 Greschner, G. S. *Makromol. Chem.* 1973, **170**, 203
- 27 Debye, P. *J. Phys. Colloid Chem.* 1947, **51**, 18
- 28 Schulz, G. V. and Altgelt, K. *Makromol. Chem.* 1960, **36**, 209
- 29 Beattie, W. H. and Booth, C. *J. Polym. Sci.* 1960, **44**, 81
- 30 Zimm, B. H., Stockmayer, W. H. and Fixman, H. *J. Chem. Phys.* 1953, **21**, 1716

Studies on the curing of a loaded unsaturated polyester binder

R. M. V. G. K. Rao* and A. Pourassamy*

Propulsion Division, National Aeronautical Laboratory, Bangalore-17, India
(Received 2 February 1976)

Experimental studies were made to determine the effect of loading and particle size on the gel-time of an unsaturated polyester binder filled with crystalline potassium chloride powder. The filler chosen was found to exhibit neither absorbing nor catalytic effect on the curing system in the time scale of these studies. While the gel-time decreased with increased solid (filler) loading and with decreased particle size, the gel-temperature essentially remained constant. A surface area mechanism is proposed to explain the observed results.

INTRODUCTION

Filler behaviour in thermosetting formulations is different from that with thermoplastic resins. While the thermoplastics render themselves processible through a physical change (e.g. melting, solidification etc.) thermosets do so through a chemical reaction resulting in the extension and crosslinking of the molecular chains. The filler, then has a direct effect on the curing parameters such as gel-time and gel-temperature, in a manner that depends on whether it has a tendency to absorb or adsorb the resin or whether it has any catalytic effect on the system. Curing in the presence of an absorptive filler presents all the complexities of a bulk process, while in the case of an adsorptive filler, the resin is taken up over a few layers of the filler giving rise to a surface mechanism. In such a case increased filler loading or decreased particle size for the same loading, means an increase in the surface area of the curing mass. Further, when the chosen filler is non-catalytic, the curing reaction becomes based on the surface area of the filler and the concentration of the chosen curing agents (catalyst and accelerator). This analysis was applied to explain the observed behaviour, as the chosen filler was found to exhibit no absorptive and catalytic effects on the system within the time scale of these experiments.

EXPERIMENTAL

General purpose polyester resin (Grade HSR 8111) was employed in these experiments in combination with the catalyst (methyl ethyl ketone peroxide) and the accelerator (cobalt naphthanate), all supplied by Bakelite Hylam (India) Ltd. The filler chosen was white crystalline potassium chloride powder (Analar grade) and it was classified into three different particle sizes, viz. 74, 53 and 44 μm . All the studies were conducted at a constant room temperature of $25 \pm 1^\circ\text{C}$.

In each experiment 50 g of resin were cured using 1 cm^3 of accelerator and 1 cm^3 of catalyst (2 $\text{cm}^3/100$ g resin). The time-temperature history was noted, from the instant of complete addition of solids, the reaction mass having been continuously stirred.

Gel-time was noted as the point, when the reaction mass became just rubbery enough and the corresponding temperature was defined as gel-temperature. This procedure was repeated for loadings ranging from 10–100 phr

* Present address: Materials Science Division, NAL, Bangalore-17, India.

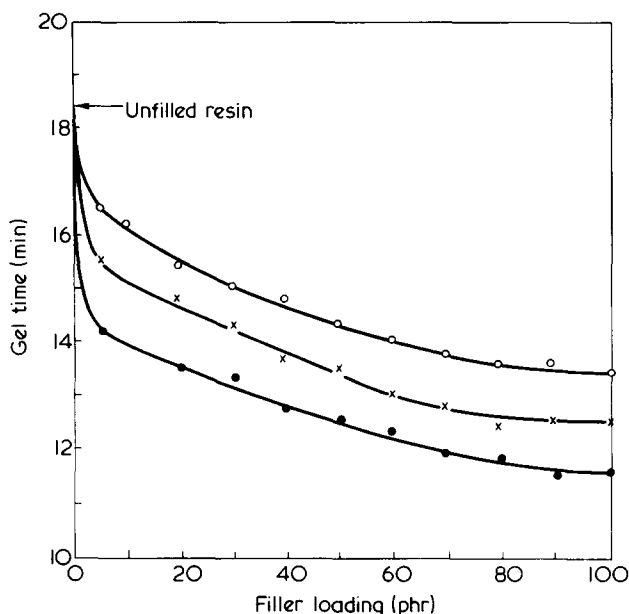


Figure 1 Relationship between gel-time and the filler loading for various particle sizes: \circ , 74 μm ; \times , 53 μm ; \bullet , 44 μm

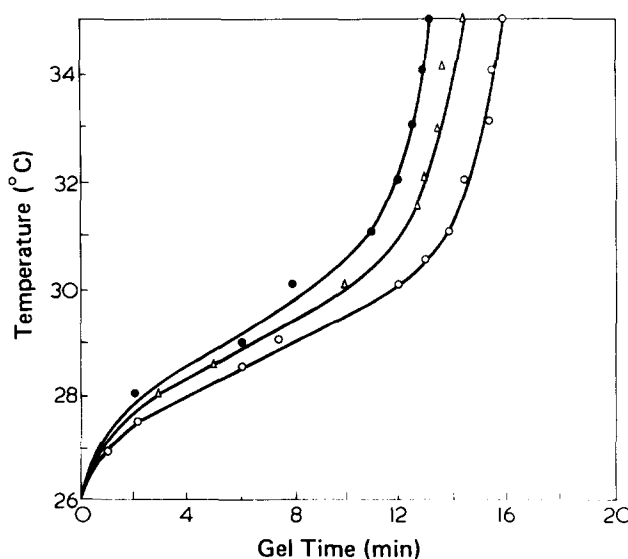


Figure 2 Relationship between time and temperature for particle size 53 μm at various filler loadings: \circ , 5 phr; \triangle , 50 phr; \bullet , 100 phr

and for three different particle sizes, viz. 74, 53 and 44 μm . The results have been presented in *Figures 1* and *2*.

RESULTS AND DISCUSSION

The relationship between gel-time and the filler loading for various particle sizes is shown in *Figure 1*.

Any curve in the diagram can be divided into three regions as marked in the Figure at a loading of 5 and 80 phr. The steep decline in gel-time from a value of 18.5 min for the unfilled resin to its value of 5 phr loading, occurs because of the sudden availability of surface area for the curing mass as a result of the incorporation of the first batch of the filler. Then there is further decrease in gel-time with increased loading upto 80 phr. The change, however, is gradual, since the resin/filler ratio decreases with progressing filler loading, leading to a resin-lean condition. Between the values of 80 and 100 phr the change in gel time is small, probably because all the resin is adsorbed by the filler and additional loading results only in a resin-deficient formulation. A similar effect is observed for different particle sizes, but for a particular loading. Here again, the gel-time decreases as the particle size diminishes.

Thus the occurrence of the same effect in both cases viz. increased filler loading and decreased particle size, both resulting in an increased surface area available to the curing mass, indicates the effect on the curing rate, of the surface area as evidenced by the decreased gel-times in these cases.

Referring to *Figure 2*, it can be seen that a steep rise in the slope of the curves beyond a value of 30°C occurs in all three cases, indicating the onset of gelling. This is characterized by a sudden change in the specific volume, temperature and viscosity of the mass. The onset of gelling is advanced with the increased filler loading as shown in the Figure. This is again a consequence of the surface area increase due to increased filler content.

The more or less constant temperature of gelling (33°–34°C) in all the cases tells us something about the relation between the heat release and the proportionality between the curing rate and the surface area. Thus, it may be expected that with an increase in the surface area of the filler, the curing rate increases, decreasing the gel-time, in order to give rise to a constant heat release.

CONCLUSIONS

Gel-time decreases with increased surface area of the non-absorbing and non-catalytic filler, as a result of progressive loading or decreased particle size for the same loading. Studies made on the system chosen indicate no absorbing or catalytic tendency of the filler towards the polymeric binder.

Curing rate increases with the increased surface area of the filler. Curing essentially occurs at a constant temperature in all cases indicating some constancy in the heat release, and this appears to explain why the gel-time decreases with increased curing rates.

In view of the problems associated with mixing at higher solid loadings, as experienced in these experiments, it seems desirable as far as possible to work with lower filler loadings but with finer filler particles.

A more comprehensive study would involve investigation of the effects of the filler's shape and its cohesive and adhesive tendencies, and the particle size distribution which affects the surface area change phenomenon under the above situation.

ACKNOWLEDGEMENTS

The authors are very grateful to the Head of Propulsion Division and the Director of this laboratory for providing the facilities to conduct the experiments and forwarding the paper.

REFERENCES

- 1 Wake, W. C. 'Fillers for Plastics', (Ed. W. C. Wake), Iliffe, London, 1971
- 2 Barre're, M., Jaumotte, A., De Veubeke, B. F. and Vandenkerckhove, J. 'Rocket Propulsion', Elsevier, Amsterdam, 1960
- 3 Langton, N. H. 'Rocket Propulsion', London University Press, London, 1970, Vol 2
- 4 'Encyclopedia of basic materials for plastics' (Eds Herbert R. Simmonds and James M. Church), Reinhold, New York, 1967
- 5 Maslia, L. 'The role of Additives in Plastics', Edward Arnold, London 1974

Polymerization of ethylene by n-butyl lithium

J. N. Hay, D. S. Harris and M. Wiles*

Department of Inorganic and Physical Chemistry, University of Birmingham, PO Box 363, Birmingham B15 2TT, UK

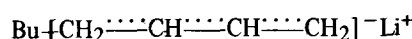
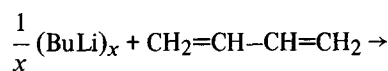
(Received 5 January 1976)

The polymerization of ethylene with butyl lithium activated with tetramethyl ethylene diamine (TMEDA) has been investigated, and the mechanism proposed by McCabe *et al.* substantially vindicated. The active initiating species is considered to be free monomeric butyl lithium, unchelated to TMEDA, and the mechanism of propagation of olefin insertion between the metal-carbon bond, probably involving an intermediate π -complex between olefin and metal alkyl.

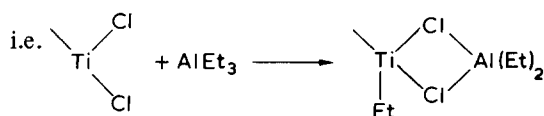
INTRODUCTION

The addition of metal alkyls to olefins is an important source of polymerization reactions, originally being studied as models of the heterogeneous coordination anionic catalyst, but also in their own right. They have been used to:

(1) initiate the anionic polymerization of dienes and α -olefins¹

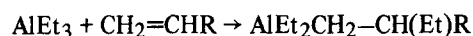


(2) study the coordination anionic catalyst²,

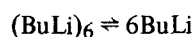


By analogy, aluminium triethyl dimers and 1:1 complexes have been studied in their reactivity to α -olefins;

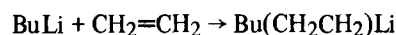
(3) oligomerize olefins³⁻⁶ by the insertion reaction:



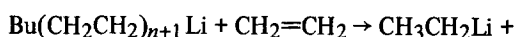
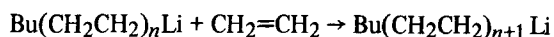
n-Butyl lithium has been observed to polymerize ethylene³ by an insertion mechanism, but high molecular weight polymer is produced only at high ethylene pressures. This is due to the competition of an elimination with the insertion reaction, and the polymerization is also inhibited by association of butyl lithium (hexamer) since only the monomer is reactive to addition, i.e.



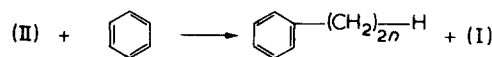
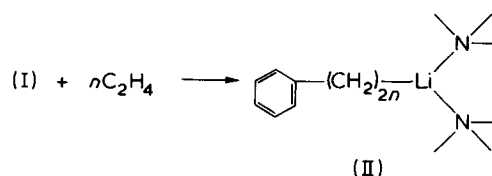
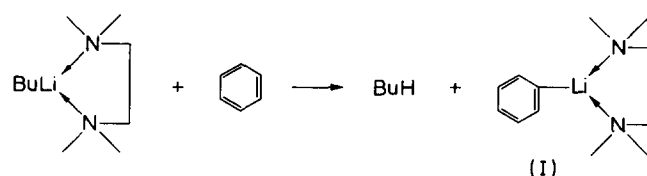
(this dissociation equilibrium is certainly over-simplified).



Polyethyl lithium species are also associated, but unassociated species in general are reactive to further addition:

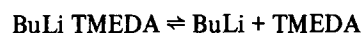


Various chelating agents have been found to have startling effects on the reactivity of n-butyl lithium. In particular, Eberhardt and Butte⁷, found that certain tertiary diamine, e.g. tetramethyl ethylene diamine and sparteine would telomerize ethylene in the presence of aromatic hydrocarbons. The following mechanism was proposed:



Later work⁸, in n-octane as solvent, was interpreted in terms of a 1:1 chelate polymerizing ethylene to a linear product. Langer^{9,10} has extended this to consider the effect of a number of bifunctional agents on the polymerization of ethylene with butyl lithium, and established that *N,N,N',N'*-tetramethyl ethylene diamine (TMEDA) was the most effective. Molecular weights up to 10^5 were reported at pressures of 5×10^3 lbf/in².

McCabe *et al.*^{11,12} have studied the kinetics of the ethylene polymerization and established that although the dominant species in solution is the 1:1 complex at BuLi:TMEDA molar ratios below 1:1, the rate of polymerization is independent of the chelate concentration over a wide molar ratio range. Accordingly the 1:1 complex could not be the active polymerizing species. It was suggested that the action of the chelating agent was to reduce the degree of association of the butyl lithium, encouraging the formation of unchelated butyl lithium monomer. Zero-order in chelating agent followed if it were required to reduce the association, and it complexed with the monomer,



It has been suggested that this mechanism is inconsistent since it would require the chelating agent to act as an

* Present address: Vinyl Products Ltd, Carshalton, Surrey, UK.

Table 1 Polymerization characteristics

Serial No.	Pressure (atm)	Polymer yield (mol)	BuLi (mol × 10 ⁻³)	Time (h)
Low pressure 0–2 atm, at 0°C				
V6	2	0.03	2.0	24
V7	2	0.03	2.5	48
V8	2	0.01	2.0	48
V9	2	0.04	2.7	48
V10	2	0.05	2.7	48
Pressure 5–100 atm, at 20°C				
P1	5	0.070	2.5	70
P2	5	0.040	2.5	70
P3	5	0.005	1.0	24
P4	10	0.15	5.0	100
P5	17	0.25	5.4	120
P6	15	0.06	2.7	50
P7	30	0.27	5.4	140
HP5	50	2.00	100.0	24
HP12	70	0.25	20.0	4

inhibitor for the polymerization¹³. Instead, an ionic mechanism was postulated in which the presence of the chelating agent encourages the formation of loose ion-pairs.

Accordingly, it is interesting to reconsider this ethylene polymerization further, particularly in the light of the three mechanisms, anionic, complex formation and monomer insertion, invoked previously.

EXPERIMENTAL

De-aromatized *n*-hexane and tetramethyl ethylene diamine (TMEDA) were used after distilling *in vacuo* from *n*-butyl lithium. Ethylene (Cambrian Chemical Co. Ltd) was used after drying; mass spectroscopic and g.l.c. analyses indicated that it was at least 99.5% pure.

Polymerizations were carried out in all glass apparatus with ethylene pressures up to 3 atm, and in a stainless-steel reaction vessel up to 100 atm. The extent of reaction, in the latter, was followed with a pressure transducer. Polymerization characteristics are listed in Table 1.

Low molecular weight hydrocarbon products were analysed by gel permeation chromatography, using a Waters Associates Model 100, with ten columns of crosslinked polystyrene gels with permeabilities in the range 13–15 nm. 1.6% w/v solutions in tetrahydrofuran, stabilized with 2,6-di-*t*-butyl-*p*-cresol, were used at a flow rate of 1 cm³/min at 295K.

Number-average molecular weights, \bar{M}_n , of the polyethylene samples in the range 500–10 000, were determined by ebulliometry using *p*-xylene as solvent. *n*-Tetracontane and naphthalene were used as calibrants. Higher molecular weights were determined by temperature drop turbidimetry.

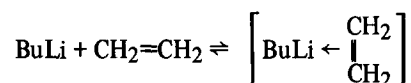
RESULTS

Lower pressure studies

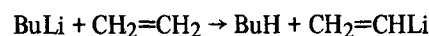
Rate measurements. McCabe *et al.*^{11,12} have studied the kinetics of polymerization from the overall ethylene pressure change. They established that a constant rate of ethylene uptake occurred only after an initial period of more rapid uptake of ethylene. The excess volume of ethylene absorbed in this period, over that absorbed at constant rate, corresponded with one mole of ethylene per mole of butyl lithium irrespective of the molar ratio of BuLi:TMEDA.

The nature of this initial rapid uptake of ethylene was further investigated by following pressure changes over a time scale consistent with first 2% conversion (moles of ethylene/moles of BuLi) of the slower constant rate of polymerization. The system was then degassed, ethylene re-admitted and the uptake of ethylene recorded as before. This was repeated (4 to 5 times) and in each case the ethylene uptake was the same. This adsorption was 25 times larger than ethylene solubility and corresponded to one mole per mole of *n*-butyl lithium present.

The initial rapid adsorption of ethylene was clearly reversible and dependent on butyl lithium concentration to first-order, consistent with McCabe's^{11,12} conclusions of a π -complex, i.e.:



Analyses of the products of the addition reaction indicated that little or no insertion of ethylene had taken place, and clearly metallation of the ethylene must be excluded since it cannot account for the reversible nature of the adsorption, i.e.:



The constant rate of ethylene consumption was first order in ethylene and butyl lithium and zero order in TMEDA. In the absence of TMEDA no reaction took place, at least below 330K, and at atmospheric pressure, even in the presence of tertiary amines. The effect of molar ratio was investigated over the range 100:1 to 1:30 (BuLi:TMEDA) from the observed rate constant, k :

$$-d/dt[\text{C}_2\text{H}_4] = kK_s p_{\text{C}_2\text{H}_4} [\text{BuLi}]_0$$

where K_s is the solubility constant of ethylene in hexane, and $p_{\text{C}_2\text{H}_4}$ the partial pressure of ethylene. At ratios above 100:1 no reaction was observed. With increasing TMEDA concentrations the observed rate constant increased to a value which remained constant over the range 10:1 to 1:10; at higher ratios the rate constant decreased (Figure 2).

Molecular weight changes. The molecular weight distributions of the products of the reaction broadened with increasing conversion, which is also with increasing time (see Table 2). Soluble products, up to chain lengths of 20, were monodispersed, and so termination or transfer reactions were not considered important. At higher chain lengths the polymerization became heterogeneous and the rate decreased. The broadening of the dispersities was not

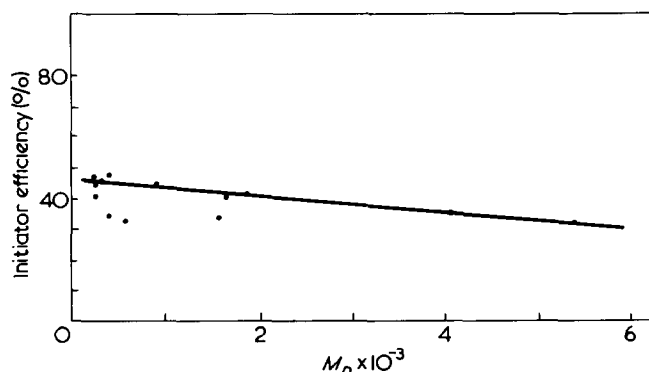


Figure 1 Variation of initiator efficiency with molecular weight

Table 2 Molecular weight characteristics

Serial No.	Molecular weight*, $M_n \times 10^{-3}$	D^\dagger
P4	1.70 ± 0.25	1.4
P5	4.10 ± 0.70	1.7
P7	5.40 ± 0.65	1.9
V6	1.40 ± 0.05	2.0
V7	0.90 ± 0.07	1.1
V8	0.60 ± 0.06	1.1
V9	1.14 ± 0.07	1.1
V10	1.50 ± 0.10	1.4
HP5	30.0†	1.90†
HP6	44.0	2.66
HP7	26.0	2.19
HP9	20.0	1.68
HP16	22.0	1.41
HP17	25.0	1.43

$D = \bar{M}_w/\bar{M}_n$, * measured by ebulliometry; † by g.p.c. characterized turbidimetry

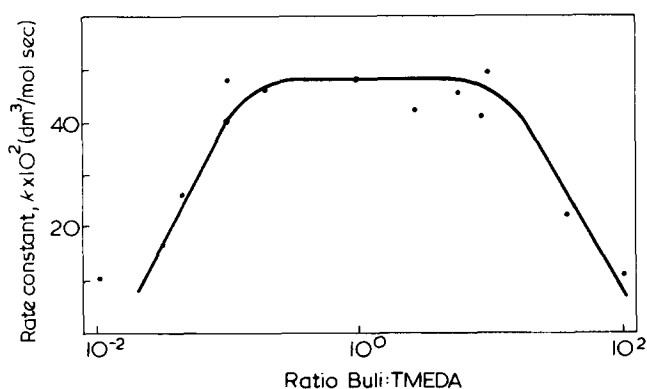


Figure 2 Effect of BuLi:TMEDA ratio on polymerization rate

inconsistent with the heterogeneous nature of the polymerization.

Number-average molecular weights of the products were greater than calculated assuming no transfer (or termination) and each mole of BuLi initiating. Indeed, based on these assumptions BuLi was 30–50% efficient, but decreased with conversion (which is also molecular weight) (see Figure 1). Extrapolation to low conversion did not exceed 50%, and there is evidence of catalyst decreasing in activity with time.

The 50% efficiency cannot readily be explained unless growth proceeds from both ends of the chain. Accordingly the number of active sites per chain was determined by terminating with excess benzoyl chloride and determining the phenyl ketone by the u.v. absorption band at 240 nm. 1.1–1.2 end-groups per chain were detected, (see Table 3). Hydrogen was also used to terminate the polymerization. Langer has shown that the 1:1 complex of BuLi:TMEDA reacts with hydrogen with the precipitation of lithium hydride. With a molar ratio of BuLi:TMEDA less than 1:2, 1 mole of hydrogen was absorbed per mole of BuLi initially present. Accordingly there was no loss of alkyl lithium bonds on initiation of the ethylene polymerization, although half the bonds were involved in initiating. McCabe *et al.*^{11,12} have also shown that polyethyl lithium will initiate the polymerization of butadiene, but with the same 50% efficiency in producing the block copolymer. Block lengths were consistent with this efficiency.

Polymerizations at higher pressure

Polymerizations were carried out in a stainless-steel vessel agitated by rocking. Despite this polymer was observed to form a crust on the liquid surface, and agitation was not sufficient to prevent the rate of solution of the ethylene determining the rate of polymerization. The observed kinetic parameters were considered atypical and experiments were restricted to a study of initiator activity.

In general, the yield of polymer increased with pressure, time and concentration of BuLi. Some of the scatter in experimental results was due to a part of the BuLi being used to purge the reaction system.

Langer^{9,10} studied the polymerization at similar ethylene pressures, and concluded that a more reactive initiator was formed on ageing by a slow reaction of polyethyl lithium and TMEDA to produce a $\sim\text{CH}_2-\text{N}(\text{CH}_2)_2\text{Li}^+$



species. This new initiator produced a higher molecular weight product. Langer's experiments were repeated by ageing (*in vacuo*) the TMEDA:BuLi (2:1 molar ratio) complexes for varying periods up to a week, before being used to polymerize ethylene for a fixed period of time at a constant ethylene pressure. The weight of polymer decreased with ageing period, (Table 4). Higher molecular weight materials were obtained, but this was considered more appropriate to a reduced initiator concentration, in that the rate of dissolution of ethylene became less rate controlling, and there was a decrease in competition between propagating centres for the available ethylene in solution, (see Table 4). The initiator decomposed to inactive material rather than to more reactive material (see Table 4).

Table 3 End-group determination

Serial No.	End group per molecule	Molecular weight			Catalyst efficiency (%)
		(a)	(b)	(c)	
V11	1.2	386	281	113	40
V12	1.1	378	273	127	46

(a) measured by v.p.o.; (b) calculated as RH from RCOPh assuming 1 CPh per chain; (c) calculated as $[\text{C}_2\text{H}_4]$ consumed/ $[\text{BuLi}]$

Table 4 Polymerization characteristics

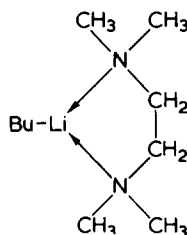
Serial No.	Ageing period (days)	Polymerization period (h)	Yield of polymer (mol)	Molecular weight $\times 10^3$	Initiator concentration (mol/dm ³)
Ageing of the initiator					
HP7	0	24	1.71	26 ± 5	0.10
HP5	1	24	1.30	30	0.10
HP6	3	24	0.63	34	0.10
HP8	6	24	0.20	27	0.10
Initiator concentration effect*					
HP1	0	5	0.09	20	0.020
HP2	0	5	0.50	—	0.20
HP3	0	5	1.04	—	0.60
Polymerization time†					
HP11	0	2	0.02	—	0.013
HP14	0	27	0.26	—	0.013
HP17	0	480	0.25	—	0.013

* 50 atm ethylene pressure; † 70 atm ethylene pressure

Polymerizations carried out over an extended period exhibited a similar decrease in initiator efficiencies (see Figure 2 and Table 4).

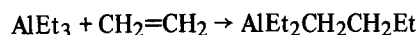
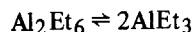
DISCUSSION

Langer⁹ has interpreted the reactivity of butyl lithium in the presence of TMEDA to the formation of a 1:1 complex, i.e.



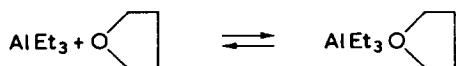
particularly since the n.m.r. chemical shift of the α -protons of the butyl lithium increased progressively up to this ratio. Indeed, molecular weight studies¹² in cyclohexane indicate a progressive decrease in association of butyl lithium, such that it is monomeric at a ratio of 1:1. If the reactivity can then be attributed to the decreased association and the increased ionic character of the Li-alkyl bond complex to TMEDA, maximum reactivity would then be achieved at a molar ratio of 1:1. This was observed by Langer^{9,10} in the hydrogenolysis of butyl lithium. Efficiencies studies also indicate that the same species is not involved in the hydrogenolysis and ethylene polymerization reactions. McCabe *et al.*¹⁴ have also shown, in the anionic polymerization of butadiene and isoprene, that a 1:2 molar ratio is required for maximum efficiency. This involved the propagating species, $\text{CH}=\text{CH}-\text{CH}_2\text{Li}^+(\text{TMEDA})_2$. No simple relationship between molar ratio and catalyst efficiency exists in the present polymerization studies; indeed a constant maximum polymerization rate is observed over the molar ratio 10:1 to 1:10, which covers the molar ratios required for all the predicted BuLi/TMEDA complexes, i.e. 4:1; 2:1; 1:1; 1:2, etc.

McCabe *et al.*¹² have argued that since the polymerization rate is first order in BuLi concentration, monomeric butyl lithium is involved in the initiating species. Also, by analogy TMEDA cannot be involved, other than to break up the degree of association. They invoked Zeigler's mechanism³ of olefin insertion into alkyl metal bond which is inhibited by association of the alkyl metal, since monomer is alone active, i.e.

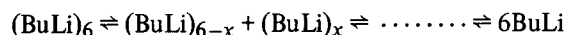


TMEDA accordingly accelerates the lithium alkyl reaction by reducing the degree of association, and increasing the stationary concentration of monomeric butyl lithium.

Allen *et al.*¹³ have indicated that this mechanism cannot be correct since chelating agents, e.g. cyclic ethers, will inhibit the addition reactions of aluminium triethyl, i.e.

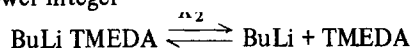


By analogy TMEDA should inhibit the reaction of BuLi monomer. While this indeed may be the case for a simple dimer/monomer equilibrium, it is by no means proved for a hexameric/monomer one, since:



$$[\text{BuLi}] = K^{1/n} [(\text{BuLi})_6]^{1/n}$$

where K is the overall dissociation constant, and n is 6 or a lower integer



$$[\text{BuLi}] = K_2 [\text{BuLi} + \text{TMEDA}] / [\text{TMEDA}]$$

If $K_1^{1/n} \ll K_2 / [\text{TMEDA}]$ the reaction will be accelerated over that of $(\text{BuLi})_6$.

These reactions are oversimplified; there is clear evidence for several BuLi:TMEDA complexes^{7-12,14}, and for each of these one can envisage the general reaction:

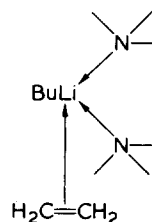


which assist the formation of BuLi monomer, so

$$[\text{BuLi}] = \sum_{x=1}^6 K_x \frac{[(\text{BuLi})_x \text{TMEDA}]}{[(\text{BuLi})_{x-1} \text{TMEDA}]} \quad (1)$$

The presence of these equilibria would have the effect of buffering the inhibition by TMEDA, until it is present in large excess. With a large excess of TMEDA there is indeed a decrease in rate. The presence of TMEDA complexes on either side of the equilibria will reduce the dependence of dissociation on its concentration, and so account for the apparent zero-order dependence. If on the average $x = 2$, the 50% efficiency may be explained.

Allen *et al.*¹³ have further proposed that the reactive species is a TMEDA-BuLi complex and the presence of TMEDA increases the concentration of looser (more reactive) ion-pairs, thereby increasing the overall reaction rate. If this were the case, the reaction would not be inhibited at higher TMEDA concentrations. It would appear that the reactive species is the unlikely monomeric BuLi, uncomplexed. BuLi:TMEDA complexes will form π -complexes to ethylene,



in a reversible equilibrium, which must have an effect on the dissociation reactions.

REFERENCES

- 1 Hsieh, H. L. *J. Polym. Sci. (A)* 1964, 3, 163
- 2 Roha, M., Kreider, L. C., Frederick, M. R. and Beears, W. L. *J. Polym. Sci.* 1959, 38, 51
- 3 Ziegler, K. and Gellert, H. *Ann. Phys.* 1950, 567, 195
- 4 Hay, J. N., Hooper, P. G. and Robb, J. C. *Trans. Faraday Soc.* 1970, 66, 2045; *J. Organomet. Chem.* 1971, 28, 193

- 5 Allen, P. E. M., Hay, J. N., Jones, G. R. and Robb, J. C. *Trans. Faraday Soc.* 1967, **63**, 1636
- 6 Allen, P. E. M. and Byers, A. E. *Trans. Faraday Soc.* 1971, **67**, 618; Allen, P. E. M., Byers, A. E. and Lough, R. M. *JCS Dalton Trans.* 1972, 479
- 7 Eberhardt, G. G. and Butte, W. A. *J. Org. Chem.* 1964, **29**, 2928
- 8 Eberhardt, G. G. and Davis, W. A. *J. Polym. Sci. (A)* 1965, **3**, 3753
- 9 Langer, A. W. *Trans. NY Acad. Sci.* 1965, **27**, 741
- 10 Langer, A. W. *Polym. Prepr.* 1966, **7**, 132
- 11 McCabe, J. F. *PhD Thesis* University of Birmingham (1972)
- 12 Hay, J. N., McCabe, J. F. and Robb, J. C. *JCS Faraday Trans. 1* 1972, **68**, 1227
- 13 Allen, P. E. M. and Lough, R. M. *JCS Faraday Trans. 1* 1973, **69**, 2087; 1973, **69**, 849
- 14 McCabe, J. F., Hay, J. N. and Robb, J. C. *JCS Faraday Trans. 1* 1972, **68**, 1

Stereospecific anionic polymerization and copolymerization of 1, 1-diphenylethyl methacrylate

Heimei Yuki, Yoshio Okamoto, Yoshiki Shimada, Koji Ohta and Koichi Hatada

Department of Chemistry, Faculty of Engineering Science, Osaka University, Toyonaka, Osaka, Japan
(Received 26 January 1976)

1,1-Diphenylethyl methacrylate (DPEMA), which is a new methacrylic ester, was synthesized and polymerized by *n*-butyllithium (*n*-BuLi) in toluene and THF. The triad tacticity of the polymers was determined from the n.m.r. spectrum of poly(methyl methacrylate) (PMMA) which was derived from them. A highly stereoregular polymer was not formed either in toluene or in THF by *n*-BuLi between -78° and 30° C. In toluene, the tacticity depended very much on the polymerization temperature, and unexpectedly, the polymer obtained at -78° C was rich in syndiotacticity. The polymers obtained in THF were atactic regardless of the temperature. A highly isotactic polymer was formed with Grignard reagents. DPEMA (M_1) was also copolymerized with methyl methacrylate (MMA), diphenylmethyl methacrylate (DPMMA), and trityl methacrylate (TrMA) (M_2) in toluene and THF with *n*-BuLi; the tacticity of the copolymers was determined. Generally, the stereoregularity of the copolymers was lower than those of the M_2 homopolymers. In the copolymerization with MMA monomer reactivity ratios were also determined.

INTRODUCTION

Stereospecific polymerizations of methyl and other methacrylates have been studied extensively and the effect of ester groups on the tacticity of polymers has been reported by many authors. Radical polymerizations of methacrylates have been investigated by Sakaguchi *et al.*¹, Niezette *et al.*², and Matsuzaki *et al.*³, who showed the relationship between the bulkiness of ester groups and the syndiotacticity of polymers. Since the stereoregulation in the anionic polymerizations of methacrylates is influenced by many factors such as propagation species, counter-ion, ester group and penultimate unit, there still exist several unresolved problems in the polymerization.

In a previous paper⁴, we reported the stereospecific polymerizations of very bulky methacrylates, diphenylmethyl methacrylate (DPMMA) and trityl methacrylate (TrMA), which formed quite different tactic polymers with *n*-BuLi in THF. The former gave a highly syndiotactic polymer, while the latter gave a highly isotactic one.

In the present study, a new monomer, 1,1-diphenylethyl methacrylate (DPEMA) was synthesized and polymerized by using *n*-BuLi in toluene and THF in order to clarify the steric effect of the ester group on the tacticity of the polymer. The bulkiness of the ester group of this monomer lies between those of the above two monomers. The stereoregularity of the copolymers of DPEMA with MMA, DPMMA, and TrMA was also investigated.

EXPERIMENTAL

Materials

DPEMA was prepared from silver methacrylate and 1,1-diphenylethyl chloride in diethyl ether. The chloride was produced by the reaction of equimolar amounts of diphenylmethylcarbinol (50 g, 0.25 mol) and HCl gas in benzene-petroleum ether (1:1) mixture (350 ml) at 0° C⁵. The chloride contained 1,1-diphenylethylene which was formed simultaneously, but was used without the separation of the olefin as the separation was found to be diffi-

cult. The yield of the chloride was found by n.m.r. analysis to be 69% (0.17 mol). The chloride and silver methacrylate (39 g, 0.20 mol) were allowed to react in 500 ml of diethyl ether for 3 h under reflux. Etheral solution was separated from precipitates by filtration, and ether, methacrylic acid, and 1,1-diphenylethylene were removed by distillation under reduced pressure. The residues contained DPEMA, the carbinol, 1,1-diphenylethylene, and a small amount of polymer which was produced thermally during the above treatment. These were poured into a large amount of petroleum ether in order to separate the polymer by filtration. The filtrate was then left at $\sim -20^{\circ}$ C for a few days to crystallize the monomer. The crude monomer thus obtained was recrystallized from petroleum ether; yield 11 g, 17%; m.p. 34.0° – 35.0° C. Found for $C_{18}H_{18}O_2$: C, 81.03%; H, 6.73%; calculated: C, 81.17%; H, 6.81%. The monomer is decomposed at $\sim 100^{\circ}$ C to give 1,1-diphenylethylene and methacrylic acid.

TrMA was prepared from silver methacrylate and trityl chloride in diethyl ether⁶; m.p. 102° – 104° C (literature value⁶ 101° – 103° C).

DPMMA was prepared by the reaction of methacryloyl chloride with diphenyl carbinol in the presence of triethylamine in diethyl ether; m.p. 80° – 82° C (literature value⁴ 78° – 79° C).

MMA was purified in the usual way and stored over CaH_2 . It was redistilled under vacuum just before use.

Toluene was purified and dried over sodium. The solvent was mixed with a small amount of *n*-BuLi and redistilled under high vacuum just before use. Tetrahydrofuran (THF) was purified in the usual way and was distilled onto lithium aluminium hydride, where it was stirred and redistilled under reduced pressure just before use. *n*-BuLi was prepared from *n*-butyl chloride and lithium metal in *n*-heptane.

Phenylmagnesium bromide (PhMgBr), cyclohexylmagnesium bromide ($C_6H_{11}MgBr$), and isobutylmagnesium bromide (iso-BuMgBr) were prepared from the corresponding bromides and magnesium in diethyl ether and most of the ether was replaced with toluene by distillation. Diethylaluminium diphenylamide (Et_2AlNPh_2) was prepared by

Table 1 Polymerization of DPPEMA by n-BuLi^a

Solvent	Temperature (°C)	Yield (%)	η_{sp}/C (dl/g)	Tacticity (%)			4IS/H ²
				I	H	S	
Toluene	-78	18	—	23	28	49	5.8
Toluene	-40	90	0.45	57	29	14	3.8
Toluene	0	90	0.21	52	37	11	1.7
Toluene	30	88	—	34	47	19	1.2
THF	-78	94	0.07	21	46	33	1.3
THF	-40	95	0.06	24	45	31	1.5
THF	0	94	0.07	17	48	35	1.0
THF	30	90	0.09	20	49	31	1.0
Toluene/THF ^b	-78	94	0.40	18	33	49	3.2
Toluene/THF ^c	-78	96	0.07	11	33	56	2.3

^aMonomer 1.88 mmol, solvent 10 ml, n-BuLi 0.094 mmol, time 24 h;

^btoluene 10 ml, [THF]/[n-BuLi] = 2; ^ctoluene 9 ml, THF 1 ml

the reaction of triethyl aluminium and diphenylamine in toluene at 60°C⁷.

Polymerization

The polymerization was carried out in a dry glass ampoule. The solid monomer was first placed in the ampoule under dry nitrogen. The ampoule was then evacuated and flushed with nitrogen gas. This procedure was repeated at least twice. Then, a solvent and a liquid comonomer, if necessary, were added with hypodermic syringes. A catalyst solution was added with a syringe to the ampoule which had been placed in a thermostat bath.

Monomer reactivity ratio

Monomer reactivity ratios were calculated by use of Fineman–Ross equation for the initial copolymer.

Conversion of poly(1,1-diphenylethyl methacrylate) to PMMA

Poly(1,1-diphenylethyl methacrylate) (DPPEMA) was completely hydrolysed to poly(methacrylic acid) (PMAA) by refluxing in methanol containing a small amount of hydrochloric acid. However, the DPPEMA obtained by the Grignard reagents was not completely hydrolysed under the above condition. These polymers and a copolymer of DPPEMA with DPMMA were converted to PMAA by the reaction with hydrogen bromide in toluene solution. The PMAA thus obtained was converted to PMMA with diazomethane in benzene–diethyl ether solution. The triad tacticity of the original polymer was determined from the n.m.r. spectrum of PMMA thus derived. In the hydrolysis of the copolymer of DPPEMA and MMA by hydrochloric acid in methanol, only the DPPEMA unit was hydrolysed quantitatively.

Measurement

N.m.r. spectra were obtained with a JEOL (JNM–MH–100) spectrometer at 100 MHz. The spectrum of PMMA was measured in 8–10% CDCl₃ solution at 60°C using tetramethylsilane as an internal reference. The copolymer composition was calculated from a n.m.r. spectrum of the copolymer which was measured in a 10% CCl₄ solution at 60°C using tetramethylsilane as an internal reference. The composition of the copolymer of MMA and PMAA derived from copolymer MMA/DPPEMA by hydrolysis was determined from an n.m.r. spectrum in a 10% pyridine-*d*₅ solution at 100°C using hexamethyldisiloxane as an internal reference.

The solution viscosity of a polymer was measured in toluene ($C = 0.5$ g/dl) at 30.0°C by using an Ubbelohde type viscometer.

RESULTS

Homopolymerization of DPPEMA

The polymerizations of DPPEMA by n-BuLi were carried out in toluene and THF. The results are shown in Table 1. Surprisingly, the DPPEMA obtained in toluene at -78°C was rather syndiotactic. This result is very unexpected, so the polymerization was repeated under the same reaction conditions taking care that there was no contamination from polar substances. However, the polymer obtained still had the same tacticity. The tacticity of the polymer was influenced by the polymerization temperature in toluene; i.e. syndiotactic at -78°C, isotactic at -40°C and atactic at 30°C, although the differences in tacticities were not remarkable. At -78°C the addition of twice as much THF as n-BuLi (mol/mol) did not induce a considerable change in tacticity, but the yield of the polymer was much greater than that in the absence of THF. However, the highest syndiotacticity was attained by adding ~10% THF to toluene. In THF atactic polymers were formed regardless of the temperature.

In Table 2 are shown the results of polymerizations by PhMgBr, C₆H₁₁MgBr, iso-BuMgBr, Et₂AlNPh₂, and AIBN in toluene. Highly isotactic polymers were obtained with Grignard reagents regardless of the organic moiety. The isotactic polymers were not completely hydrolysed to PMAA by methanolic hydrochloric acid, probably because of the highly regular structure. It is known that the polymerizations of methacrylates by Et₂AlNPh₂ usually produce syndiotactic polymers^{7,8}. DPPEMA also gave a syndiotactic polymer by this catalyst, although the syndiotactic content was low. The radical polymerization by AIBN gave an atactic polymer.

Anionic copolymerizations of DPPEMA (M₁) with MMA, TrMA, and DPMMA (M₂)

Monomer reactivity ratios, r_1 and r_2 were determined in the copolymerizations of DPPEMA (M₁) with MMA (M₂) by n-BuLi in toluene and in THF at -78°C. The copolymer composition curves are shown in Figure 1. The monomer reactivity ratios were found to be $r_1 = 0.56 \pm 0.36$ and $r_2 = 7.45 \pm 1.53$ in toluene, and $r_1 = 1.62 \pm 1.00$ and $r_2 = 1.13 \pm 0.35$ in THF.

Table 2 Polymerization of DPPEMA in toluene by various catalysts^a

Catalyst	Temperature (°C)	Yield (%)	η_{sp}/C (dl/g)	Tacticity (%)		
				I	H	S
PhMgBr	0	85	0.12	97	3	0
PhMgBr	-78	99	0.07	88	9	3
C ₆ H ₁₁ MgBr	0	87	0.12	91	8	1
C ₆ H ₁₁ MgBr	-78	95	0.06	88	9	2
iso-BuMgBr	0	92	0.09	92	6	1
iso-BuMgBr	-78	85	0.06	89	9	2
AIBN ^b	60	66	0.08	19	49	32
Et ₂ AlNPh ₂ ^c	-40	98	0.05	12	34	54

^aMonomer 1.88 mmol, catalyst 0.094 mmol, toluene 10 ml, time 24 h; ^bcatalyst 0.091 mmol; ^ctime 48 h

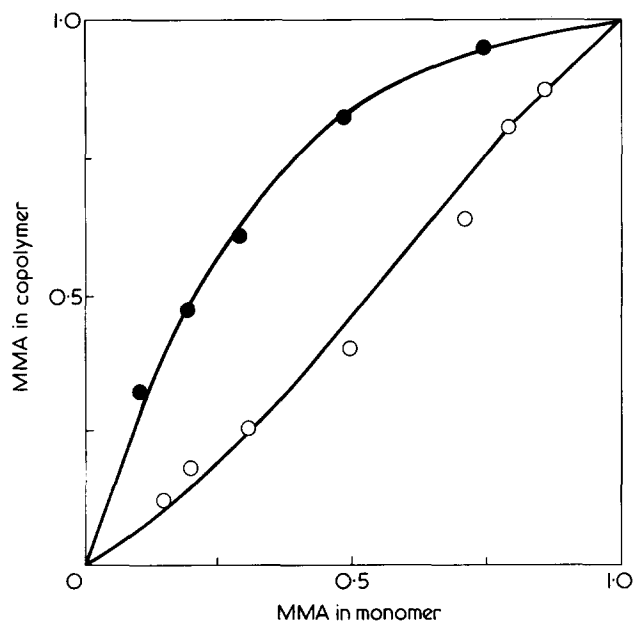


Figure 1 Copolymer composition curves for anionic copolymerizations of DPEMA (M_1) and MMA (M_2) by n -BuLi at -78°C . ●, in toluene; ○, in THF

Table 3 Copolymerization of DPEMA (M_1) with MMA (M_2) by n -BuLi^a

Solvent	Temperature ($^\circ\text{C}$)	Yield (%)	M_2/M_1^b	η_{sp}/C (dl/g)	Tacticity (%)		
					I	H	S
Toluene	-78	26	4.3	0.23	60	27	13
Toluene	-40	85	0.94	0.45	56	31	13
Toluene	0	90	1.0	0.17	56	31	13
Toluene	30	58	1.2	0.12	57	31	12
THF	-78	97	1.0	0.29	10	36	54
THF	-40	91	0.82	0.50	12	38	50
THF	0	46	0.54	0.07	17	42	41
THF	30	21	0.50	-	16	45	39

^a $[M_1]_0, [M_2]_0$ 1.88 mmol, solvent 7.5 ml, n -BuLi 0.188 mmol, time 24 h; ^bmolar ratio in copolymer

Anionic copolymerization of equimolar DPEMA and MMA was carried out for a prolonged time in toluene and THF with n -BuLi at various temperatures. The results are summarized in Table 3. In toluene the yield of the copolymer was highest at 0°C and lowest at -78°C . The composition of the copolymer obtained at -78°C was rich in MMA unit as expected from the r_1 and r_2 values. When the copolymers obtained in toluene were hydrolyzed in methanol containing a small amount of hydrochloric acid, methanol soluble and insoluble parts were separated. The results are summarized in Table 4. The methanol-insoluble part was

almost the homopolymer of MMA and the soluble part contained nearly equal amounts of MMA and DPEMA. The tacticity of the copolymers prepared in toluene was rich in isotactic triad and independent of the polymerization temperature. On the other hand, the copolymers obtained in THF at higher temperatures were rich in DPEMA unit. As the temperature increased, the syndiotacticity slightly decreased.

The polymerizations of DPEMA (M_1) with equimolar amounts of TrMA and DPMMMA (M_2) were also carried out in toluene and THF with n -BuLi at -78°C . The results are shown in Table 5. In the Table, besides the tacticity of the copolymers, that of the M_2 homopolymers prepared under the same reaction conditions is also shown. The reactivity of DPEMA in toluene was comparable to that of TrMA and much lower than that of DPMMMA. The stereoregularity of all the copolymers was much lower than that of the corresponding M_2 homopolymers and a great deal different from that of PDPEMA shown in Table 1.

DISCUSSION

It is well known that MMA forms an isotactic polymer by n -BuLi in a non-polar solvent at low temperatures⁹⁻¹¹. Various alkyl methacrylates and some acrylates whose α -position were substituted with alkyl or phenyl group also gave isotactic polymers under the same reaction conditions^{12,13}. The polymerization of DPEMA may be the first example which yielded a polymer rich in syndiotacticity by n -BuLi in a non-polar solvent.

The values of $4IS/H^2$ from which the penultimate effect in the polymerization can be estimated¹⁴ are given in Table 1. The values in toluene at low temperatures deviated from unity, indicating that the process of the polymerization cannot be explained by the Bernoulli trials.

The tacticity of PDPEMA was compared with those of PTrMA and PDPMMMA which have similar ester groups to PDPEMA (Table 6). It has already been observed that TrMA formed a highly isotactic polymer with n -BuLi not only in toluene but also in THF and DPMMMA gave a highly isotactic polymer in toluene and a syndiotactic one in THF⁴. In the polymerization of DPEMA a highly stereoregular polymer was not obtained either in toluene or THF by n -BuLi. On the other hand, these monomers behaved in quite a different manner in the polymerizations with PhMgBr in toluene. DPEMA formed a highly stereoregular polymer, DPMMMA gave an atactic polymer, and TrMA formed no polymer⁴. These results indicate that the small difference in ester group has a large influence on the tacticity of the polymer and the effect of the ester group can be varied a great deal by the nature of the counter-ion.

In the polymerization of MMA in toluene by n -BuLi it is postulated that the lithium counter-ion can coordinate with

Table 4 Fractionation of copolymers of DPEMA (M_1) with MMA (M_2) obtained by n -BuLi in toluene

Temperature ($^\circ\text{C}$)	Soluble Part in Methanol					Insoluble Part in Methanol				
	% w/w	M_2/M_1	Tacticity (%)			% w/w	M_2/M_1	Tacticity (%)		
			I	H	S			I	H	S
-78	54	1.6	56	32	13	46	24	63	24	13
-40	91	1.0	53	35	11	9	10	38	32	30
0	91	0.85	56	33	11	9	5.7	41	29	30
30	98	1.3	56	33	11	2	∞	79	13	8

Table 5 Copolymerizations of DPMEA (M_1) with TrMA and DPMMA (M_2) by *n*-BuLi at -78°C^a

M_2	Solvent	Yield (wt %)	M_2/M_1 (in copolymer)	η_{sp}/C (dl/g)	Tacticity (%)					
					Copolymer			M_2 homopolymer		
					I	H	S	I	H	S
TrMA ^b	Toluene	17	1.0	0.24	27	37	36	96	2	2
TrMA	THF	97	1.0	0.06	51	34	15	94	4	2
DPMMA	Toluene	57	4.3	0.26	66	22	12	99	1	0
DPMMA	THF	92	1.0	0.16	8	28	64	2	11	87

^a $[M_1]_0$, $[M_2]_0$ 1.88 mmol, solvent 7.5 ml, *n*-BuLi 0.188 mmol, time 24 h; ^btime 48 h

Table 6 Tacticity of PDPEMA, PDPMMA, and PTrMA

Monomer	Ester group	Temperature ($^\circ\text{C}$)	<i>n</i> -BuLi						PhMgBr			
			in toluene (%)			in THF (%)			Temperature ($^\circ\text{C}$)	in toluene (%)		
			I	H	S	I	H	S		I	H	S
DPMEA	$\begin{array}{c} \text{Ph} \\ \\ \text{CH}_3-\text{C}- \\ \\ \text{Ph} \end{array}$	-78	23	28	49	21	46	33	-78	88	9	3
		0	52	37	11	17	48	35	0	97	3	0
DPMMA	$\begin{array}{c} \text{Ph} \\ \\ \text{H}-\text{C}- \\ \\ \text{Ph} \end{array}$	-78	99	1	0	2	11	87	20	28	36	36
		0	93	4	3	2	31	67				
TrMA	$\begin{array}{c} \text{Ph} \\ \\ \text{Ph}-\text{C}- \\ \\ \text{Ph} \end{array}$	-78	96	2	2	94	4	2	30	Polymerization did not proceed		
		0	93	4	3	81	13	6				

the carbonyl oxygen of the penultimate monomer unit in the growing chain and the resulting cyclic intermediate dominates the conformation of the incoming monomer toward the lithium cation to give an isotactic polymer^{15,16}. It is expected from a molecular model that in the polymerization of TrMA, the bulkiness of a trityl group may prevent the syndiotactic placement and the monomer prefers to take the isotactic placement with a helical conformation⁴. This may be one of the reasons why TrMA forms an isotactic polymer even in THF. The very low stereoregularity of PDPEMA obtained by *n*-BuLi probably demonstrates that the bulkiness of the ester group is not enough to force the monomer to take the isotactic configuration, and the coordination to lithium ion may be weakened by the bulky ester group.

In previous papers^{17,18}, we reported the copolymerizations of various methacrylates (M_1) and MMA (M_2) with *n*-BuLi at -78°C , and the relative reactivity of the methacrylates towards MMA^- anion was correlated with the electron density on the β -carbon, accordingly the polar effect of the ester group of monomer. The plots of $\log(1/r_2)$ vs. the $^{13}\text{C}_\beta$ or $^1\text{H}_a$ (*cis* to carbonyl) n.m.r. chemical shifts of the monomers are shown in Figures 2 and 3, respectively.

The $\log(1/r_2)$ values in toluene and THF were practically identical for many methacrylates and many were situated near the straight line. However, the plots for DPMEA as well as TrMA and dimethylbenzyl methacrylate in toluene were quite different from those in THF because of the extremely low reactivity of those monomers in toluene. It

has been found that in the cases of TrMA and dimethylbenzyl methacrylate, not only the copolymers containing nearly equal amounts of M_1 and M_2 , but isotactic MMA homopolymers were also formed^{17,19}. Similar results were

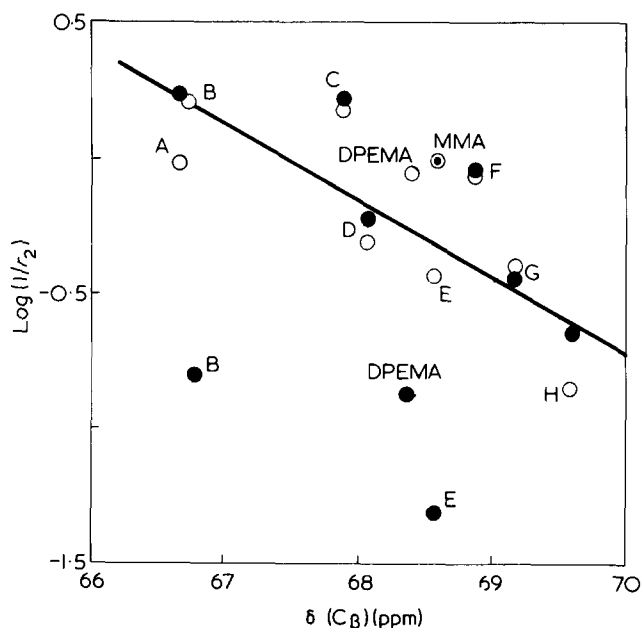


Figure 2 Plots of $\log(1/r_2)$ vs. $^{13}\text{C}_\beta$ chemical shift of methacrylates; ●, in toluene; ○, in THF. A, diphenylmethyl; B, trityl; C, benzyl; D, α -methylbenzyl; E, α,α -dimethylbenzyl; F, ethyl; G, isopropyl; H, *t*-butyl

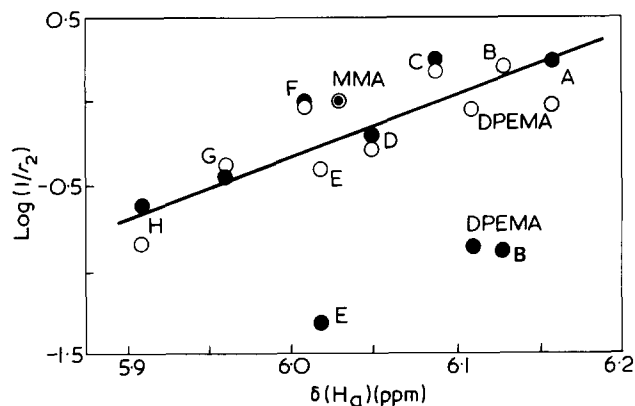


Figure 3 Plots of $\log(1/r_2)$ vs. $^1\text{H}_\alpha$ chemical shift of methacrylates; ●, in toluene; ○, in THF. A–H as in Figure 2

obtained in the hydrolysis of the copolymers of MMA with DPEMA, as shown in Table 4. These results suggest that there exist, at least, two kinds of propagating species, one which predominantly polymerizes MMA and the other which yields a copolymer. Consequently, the monomer reactivity ratios determined in toluene should be taken as mean values for these two propagating species; one leads to $r_1 = 0, r_2 \gg 1$ and the other leads to $r_1 \approx r_2 \approx 1$. In THF, however, only the species forming the copolymer may exist. This is probably one of the reasons for the extremely low reactivity of these monomers in toluene, and this suggests that the bulky tertiary ester monomers cannot add to the growing MMA chain end with subsequent long MMA sequences in toluene because of steric hindrance.

The isotacticity of the copolymer DPEMA/MMA obtained in toluene by *n*-BuLi lies between those of PMMA and PDPEMA obtained under the same conditions (Table 3). Similar results have been found in the copolymerizations of MMA with various methacrylates²⁰. The tacticity of the copolymers of DPEMA with TrMA and DPMMA obtained in THF seems to be close to the mean values of those of the homopolymers (Table 5). However, the isotacticity of the copolymer DPEMA/TrMA obtained in toluene was very low. Since this copolymer consists of equal amounts of DPEMA and TrMA, the distribution of the monomers in the copolymer may be rather at random. The isotacticity of the copolymer DPEMA/DPMMA prepared in toluene was also

rather low judging from the copolymer composition. It seems that DPEMA lowers the stereoregularity in the copolymerizations with these bulky monomers in toluene.

ACKNOWLEDGEMENTS

The authors are very grateful to Mr H. Okuda for the measurements of ^{13}C n.m.r. spectra. Part of this work was supported by the Grant-in-aid for scientific research from the Ministry of Education.

REFERENCES

- 1 Nishino, J., Nakahata, H. and Sakaguchi, Y. *Polym. J.* 1971, **2**, 555
- 2 Niezette, J. and Desreux, V. *Makromol. Chem.* 1971, **149**, 177
- 3 Matsuzaki, K., Kanai, T., Yamawaki, K. and Samre Rung, K. B. *Makromol. Chem.* 1973, **174**, 215
- 4 Yuki, H., Hatada, K., Niinomi, T. and Kikuchi, Y. *Polym. J.* 1970, **1**, 36
- 5 Brown, H. C. and Rei, Min-Hon. *J. Org. Chem.* 1966, **31**, 1090
- 6 Adrova, N. A. and Prokhorova, L. K. *Vyskomol. Soedin.* 1961, **3**, 1509
- 7 Murahashi, S., Niki, T., Obokata, T., Yuki, H. and Hatada, K. *Kobunshi Kagaku* 1967, **24**, 198
- 8 Murahashi, S., Obokata, T., Yuki, H. and Hatada, K. *Kobunshi Kagaku* 1967, **24**, 309
- 9 Fox, T. G., Garrett, B. S., Goode, W. E., Gratch, S., Kincaid, J. F., Spell, A. and Stroupe, J. D. *J. Am. Chem. Soc.* 1958, **80**, 1768
- 10 Miller, R. G. J., Mills, B., Small, P. A., Turner-Jones, A. and Wood, D. G. M. *Chem. Ind. (London)* 1958, 1323
- 11 Goode, W. E., Owens, F. H., Fellmann, R. P., Snyder, W. H. and Moore, J. E. *J. Polym. Sci.* 1960, **46**, 317
- 12 Yuki, H., Hatada, K., Niinomi, T. and Miyaji, K. *Polym. J.* 1970, **1**, 130
- 13 Yuki, H., Hatada, K., Niinomi, T., Hashimoto, M. and Ohshima, J. *Polym. J.* 1971, **2**, 629
- 14 Chujo, R. *J. Phys. Soc. Japan* 1966, **21**, 2669; *Makromol. Chem.* 1967, **107**, 142
- 15 Cram, D. J. and Kopecky, K. R. *J. Am. Chem. Soc.* 1959, **81**, 2748
- 16 Glusker, D. L., Lysloff, I. and Stiles, E. *J. Polym. Sci.* 1961, **49**, 315
- 17 Yuki, H., Okamoto, Y., Ohta, K. and Hatada, K. *J. Polym. Sci. (Polym. Chem. Edn)* 1975, **13**, 1161
- 18 Yuki, H., Hatada, K., Ohta, K. and Okamoto, Y. *J. Macromol. Sci. (A)* 1975, **9**, 983
- 19 Yuki, H., Ohta, K., Hatada, K., Okamoto, Y., Kamanaru, K., Obayashi, K. and Mochida, M. *J. Polym. Sci. (Polym. Chem. Edn)* to be published
- 20 Yuki, H., Okamoto, Y., Ohta, K. and Hatada, K. *Polym. J.* 1974, **6**, 573

Transition metal impurities in crystalline conjugated polymers

G. C. Stevens*, D. J. Andot†, D. Bloor and J. S. Ghotra

Department of Physics, Queen Mary College, London E1 4NS, UK
(Received 26 January 1976)

Two disubstituted diacetylene monomers and their corresponding polymers were found to contain transition metal impurities, the presence of which may be associated with the observation of anomalous e.s.r. absorption spectra. Copper complex impurities are considered responsible for the observed paramagnetism which is thought to arise from their inclusion at specific sites within the monomer crystal.

INTRODUCTION

Anomalous magnetic properties, including the occurrence of broad line e.s.r. absorption spectra, have been observed in natural macromolecules^{1,2} and synthetic conjugated polymers^{3,4}. The observed e.s.r. absorption lines were asymmetric, exceedingly broad ($\Delta H_{pp} \sim 500$ to 1500 Gauss; 1 Gauss = 10^{-4} Tesla) and of high integrated intensity; many spectra contained zero-field absorptions and *g*-values ranged from 2.1 to 3.0. Three possible explanations were proposed⁵ viz.: (a) presence of ferromagnetic inclusions; (b) presence of paramagnetic ions participating in collective interactions mediated by the hosts crystal and electronic structure and (c) unusual properties of unpaired electrons, a consequence of specific chemical and structural features of organic systems.

It soon became clear that these observations could be attributed to transition metal impurities, particularly iron⁶. Conjugated polymers prepared so as to minimize these impurities were found to contain 10 to 500 ppm of iron and one to three orders of magnitude less of cobalt, nickel and chromium⁶. The chemical nature of the impurities was not clear and the presence of ferromagnetic oxides in interstitial or colloidal form was invoked to explain the observations.

This problem has not been considered very important until recently when the possibility of preparing crystalline conjugated polymers by solid state polymerization⁷⁻⁹ required that it be reconsidered. These polymers allow the fundamental properties of the conjugated polymer chain, free from major morphological defects, to be investigated. The presence of transition metal impurities may be significant in this situation, not only in producing impurity e.s.r. absorption spectra but also by the unknown effects of these impurities on other physical properties, e.g. electrical conductivity. The impurities will be introduced during the growth of monomer crystals from solution and the degree of impurity inclusion can be assessed by a number of techniques¹⁰. Under these circumstances it is the purity of this initial monomer solution which is important in determining the final impurity content of the polymer.

EXPERIMENTAL

Two disubstituted diacetylene monomers were chosen for this study: 2,4-hexadiyne-1,6-diol (HD) and the diester, bis(*p*-toluenesulphonate) of 2,4-hexadiyne-1,6-diol (TSHD), derived from it. HD polymerizes to an amorphous polymer¹¹ in contrast to TSHD which retains its complete crystal structure during solid state polymerization^{10,12}. The monomer and polymer molecular structures of HD and TSHD are shown in *Figure 1*.

HD, 'Purum' grade (Fluka AG), was purified by recrystallization from redistilled 'Aristar' grade toluene (BDH Chemicals), the latter having a specified assay of less than 0.01 ppm for iron, cobalt, manganese and nickel and less than 0.02 ppm for cadmium, copper, lead and zinc. Purification was also achieved by vacuum sublimation. 'Pure' TSHD monomer was prepared by the Wegner method¹³ using diol as purified above and 'Analar' grade reagents (BDH Chemicals). 'Ultra-pure' TSHD monomer was prepared by the same method, using the following reagents: diol, purified as above; *p*-toluenesulphonyl chloride, 'Puriss' grade (Fluka AG), minimum assay 99% (typically 35 ppm iron, 5 ppm copper, other transition metals absent); tetrahydrofuran, 'Analar' grade (BDH Chemicals), minimum assay 99.5%; acetone, 'Aristar' grade (BDH Chemicals), general metal impurities ≤ 0.1 ppm; potassium hydroxide, 'Aristar' grade (BDH Chemicals), general metal impurities ≤ 250 ppm; demineralized water (resistivity $> 4 \times 10^5 \Omega \text{ cm}$).

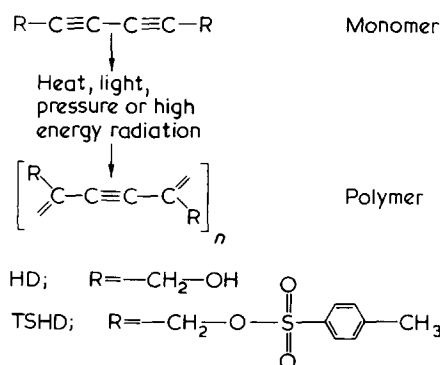


Figure 1 TSHD and HD monomer and polymer structure

* Present address: Central Electricity Research Laboratories, Leatherhead, Surrey, UK.

† To whom correspondence should be addressed.

Table 1 Sensitivities of metallic ions as determined by atomic absorption spectroscopy

Element	Sensitivity (ppm)
Fe	0.05
Cu	0.026
Co	0.035
Cr	0.04
Mn	0.02
Ni	0.038

Table 2 Iron concentrations of a single HD batch

Material as received (ppm)	Recrystallized material (ppm)			Sublimed material
	1X	2X	3X	
45	17	125	271	30

Samples of 'pure' TSHD for e.s.r. measurements were prepared by repeated freezing and melting of 'Analar' acetone solutions under vacuum and oxygen free argon to remove oxygen; polycrystalline samples of both TSHD and HD were placed in quartz sample tubes and evacuated to less than 10^{-3} Torr¹⁴. Monomer single crystals of 'ultra-pure' TSHD were grown from seeds by sub-ambient cooling of saturated 'Aristar' acetone solutions in an argon gas atmosphere.

Metallic ion impurity analysis was carried out by atomic absorption spectroscopy using a Pye Unicam SP-1950 machine, which allowed detection of required metallic ions to an accuracy of $\pm 2\%$, with sensitivities as shown in *Table 1*. E.s.r. spectra were recorded with a Varian E-9, X-band spectrometer incorporating an E-101 microwave bridge, as described previously¹⁴.

RESULTS AND DISCUSSION

2,4-Hexadiyne-1,6-diol

Iron and copper content varied in the 'as received' commercial HD; in most cases copper was absent or present in small traces with cobalt, chromium, manganese and nickel below the limits of detection. Typical iron concentrations for a single HD batch subjected to recrystallization and sublimation are shown in *Table 2*. A single recrystallization gave the best reduction in iron content; indeed, with care, single recrystallized samples were obtained with as little as 1 ppm concentration of iron.

The increase in impurity content on subsequent recrystallizations is unusual. 'As received' HD always contained some polymer which was extracted prior to recrystallization so that the first recrystallized monomer solution is essentially polymer free. Polymerization is slow and subsequent monomer solutions may contain small dispersed quantities of low molecular weight polymer. These chains may absorb or react with impurity species and be included in growing crystals allowing impurities to accumulate with repeated recrystallization.

E.s.r. observation of HD polycrystalline monomer samples taken from a single batch containing 1 ppm of iron by analysis did not reveal any spectra directly attributable to iron. This is to be expected since the corresponding impurity spin concentration of about 10^{16} spins per gram of

monomer would be difficult to detect in 50 mg samples and spectral linewidths of the order of 10^3 Gauss (*Figure 2*). However, monomer-batch impurity analysis can be misleading if the impurities are not homogeneously distributed. This is illustrated by the iron and copper content of an HD polymer sample, exhibiting no impurity e.s.r. absorption, from the high purity monomer-batch after thermal polymerization at 373K. The monomer-batch and polymer-sample iron contents were 1 and 54 ppm respectively; the copper levels were 0 and 18 ppm respectively. This variation in monomer-polymer impurity concentration will be discussed further below.

Bis(*p*-toluenesulphonate) of 2,4-hexadiyne-1,6-diol

Figures 2a and *2b* illustrate some typical broad impurity e.s.r. absorption spectra with $g \approx 2$ and $g \neq 2$ respectively for samples of 'pure' polycrystalline TSHD. For all samples observed it has been found that the impurity absorption spectra are present in the monomer and do not change in intensity, shape or position during thermal polymerization. The narrow $g = 2$ absorptions in *Figure 2* arise during polymerization and have been associated with defect centres in the 'as formed' polymer¹⁴. Some polycrystalline monomer-batch and resultant e.s.r. polymer-sample iron and copper impurity concentrations are listed in *Table 3*; all other common transition metals were absent. The polymer-sample impurity spin concentrations $N_s(\text{Fe})$ and $N_s(\text{Cu})$, calculated assuming one spin per impurity atom, may be compared with the observed spin concentration N_{OBS} , calculated from the observed first derivative spectra by double numerical integration and comparison with a Varian strong pitch reference standard ($3 \times 10^{15} \pm 15\%$ spin/cm)¹⁴.

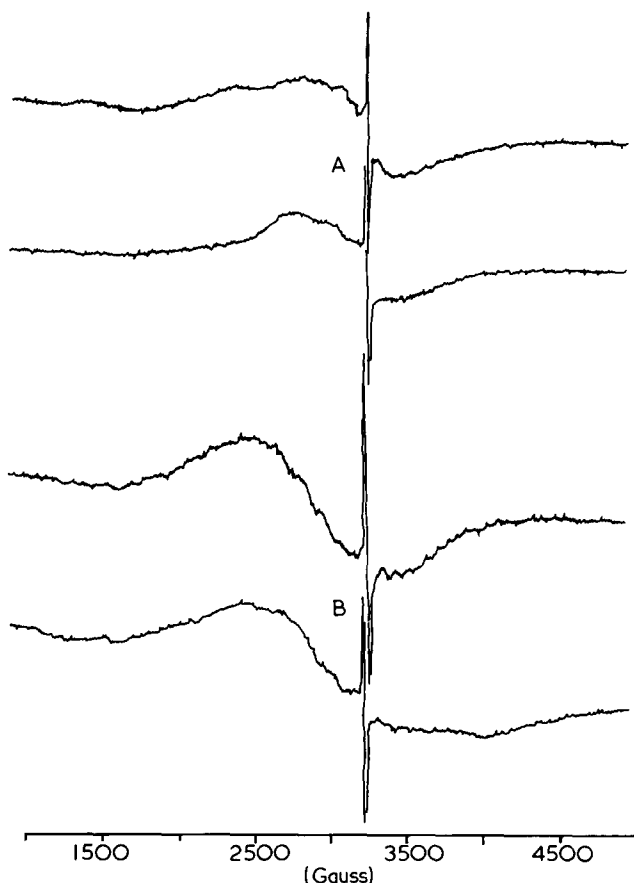


Figure 2 TSHD impurity e.s.r. absorption spectra. (A) $g \approx 2$; (B) $g \neq 2$

Table 3 Polycrystalline TSHD monomer-batch and polymer-sample iron and copper impurity concentrations and spin concentrations compared with observed sample spin concentration. All other metals absent

Sample	Batch Fe (ppm)	Batch Cu (ppm)	Sample Fe (ppm)	$N_S(\text{Fe})^a$	Sample Cu (ppm)	$N_S(\text{Cu})^a$	N_{OBS}^a
TSA1	79	32	0	0	83	7.9×10^{17}	5.8×10^{18}
TSA2	79	32	0	0	177	1.69×10^{18}	1.3×10^{18}
TSA8	190	320	1540	1.66×10^{19}	87	8.3×10^{17}	3.3×10^{18}
TSA10	90	0	350	3.78×10^{18}	2870	2.75×10^{19}	2.8×10^{18}
TSA12	90	0	440	4.75×10^{18}	18	1.74×10^{17}	2.5×10^{18}

^aspins/g of sample.

Inspection of *Table 3* indicates the inconsistent nature of the monomer-batch and polymer-sample impurity results. It is clear that both decreases and increases in individual impurity atom content occur in comparing the monomer-batch and polymer-sample results. This suggests that inhomogeneous impurity distribution occurs, post-recrystallization contamination is unlikely in view of the precautions taken during sample handling. However, the very large variation in polymer-sample impurity content is not reflected in the observed spin concentration which is typically about 3×10^{18} spins per gram of polymer sample. This result suggests that only a part of the total metallic impurities present actually contribute to the observed e.s.r. absorption; the TSA1 polymer-sample result suggests also that there is not necessarily a single spin per impurity atom contribution to the observed spectrum.

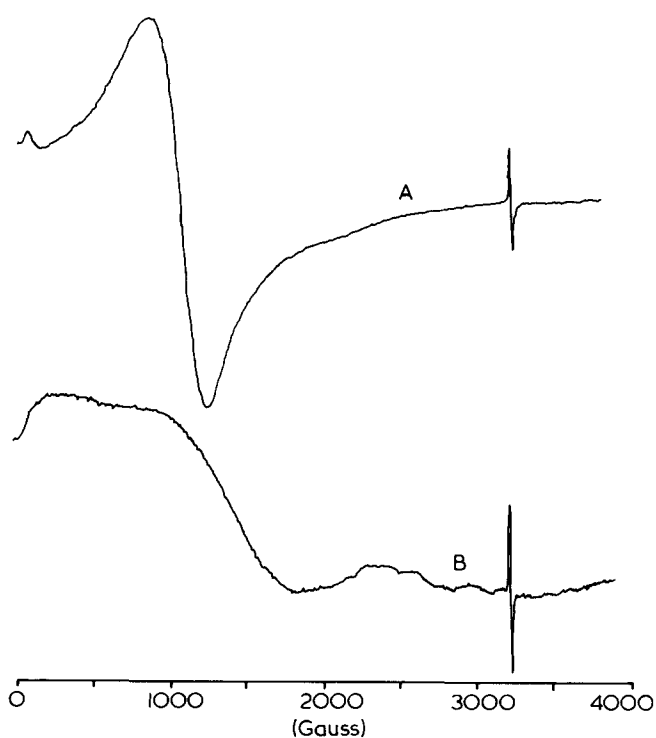
The above results and the need to investigate purer TSHD single crystals led to the preparation of an 'ultra-pure' monomer, as described earlier. Analysis of the monomer-batch sample revealed iron and copper concentrations of 34 ppm each, all other common transition metals being absent. In comparison, typical impurity concentrations of TSHD single crystals grown from this monomer were, copper between 50 and 120 ppm, with iron and all other common metals absent. E.s.r. observations of four single crystals gave no absorption spectra which could not be accounted for from other sources, e.g. sample tube.

However, anomalous e.s.r. absorptions do occur in polycrystalline TSHD samples with only copper contamination. *Figure 3* illustrates two very intense low field absorptions obtained from two polycrystalline samples, TSA4 and TSA9, whose monomer-batch analysis was that of TSA1 and TSA10 respectively. Both polymer samples contained only copper impurities, TSA4 approximately 168 ppm and TSA9 150 ppm. The strong zero-field absorptions in *Figure 3* are in agreement with the results of Blumenfel'd et al.³. They found that complexes of polyaminoquinones with copper gave broad absorption spectra and increasing copper content increased the intensity of the broad absorption already present and induced a strong zero-field absorption also. Thus, in associating the observed e.s.r. absorption spectra with a metallic or a corresponding metallic complex impurity, the results indicate, in the case of TSHD, that it is probably copper.

The formation of a copper-monomer complex involving the acetylenic bonds, such that unpaired electrons occupy the ground state of the complex, seems reasonable. However, the constancy of N_{OBS} in *Table 3* and the absence of absorption spectra in copper-containing single crystals require explanation. Two factors are important in determining impurity content of the monomer crystals. These are: (a) crystal morphology and (b) the presence of oligomeric species. Crystal morphology has a strong influ-

ence on impurity inclusion. For slow crystal growth, well faceted monomer single crystals are obtained containing minimal included impurity. Polycrystalline samples will contain some crystallites with irregular non-crystallographic facets which are much less effective in rejecting impurities¹⁰. Impurity inclusion at such faces may be either into the crystal lattice or into voids containing impurity rich solvent. In addition more of the final impurity rich solution will be trapped in the spaces between crystallites in polycrystalline samples. We can also conclude from the behaviour of HD, reported above, that repeated recrystallization as used in preparing polycrystalline samples leads to an enhancement of impurity content, possibly by the formation of impurity oligomer complexes which are included in the monomer crystal. These factors contribute to the large variations in impurity content from sample to sample. Our observation of a nearly constant e.s.r. spin density in spite of these variations can be explained in terms of diamagnetic impurity complexes some of which become paramagnetic by inclusion at particular sites, i.e. the close proximity of the complex to surrounding monomer or oligomer molecules with a specific geometry favours a reaction whose product is paramagnetic.

The results are not conclusive but it is suggested that explanation (b) in the introduction is the most acceptable

**Figure 3** TSHD impurity anomalous e.s.r. absorption spectra. A, TSA9; B, TSA4

for TSHD at the present time. However, the variety of e.s.r. absorption spectra observed for polycrystalline samples prohibit a more complete interpretation, in which the roles of copper and iron impurity complexes are clearly displayed. The degree of impurity control in diacetylene polymers is much greater than in most other polymer systems and this should allow more selective experiments, such as doping, to be pursued in conjunction with other techniques capable of identifying the impurity complex unambiguously.

ACKNOWLEDGEMENTS

We thank Mr S. Adams for performing the atomic absorption experiments. This work was supported by a Science Research Council grant and one of us (G.C.S.) thanks the Science Research Council for a studentship.

REFERENCES

- 1 Blumenfel'd, L. A., Kalmenson, A. E. and P'ei-Ken, Sheng. *Dokl. Akad. Nauk. SSSR* 1959, **124**, 1144
- 2 Blumenfel'd, L. A. *Biofizika* 1959, **4**, 515
- 3 Blumenfel'd, L. A., Berlin, A. A., Matveeva, N. G. and Kalmanzon, A. E. *Vysokomol. Soedin* 1959, **1**, 1647
- 4 Blumenfel'd, L. A., Berlin, A. A., Slinkin, A. A. and Kalmanzon, A. E. *Zh. Strukt. Khim.* 1960, **1**, 103
- 5 Blumenfel'd, L. A., Benderskii, V. A. and Kalmanzon, A. E. *Biofizika* 1961, **6**, 631
- 6 Blumenfel'd, L. A. *Dokl. Akad. Nauk. SSSR* 1963, **148**, 361
- 7 Wegner, G. and Schermann, W. *Colloid Polym. Sci.* 1974, **252**, 655
- 8 Baughman, R. H. *J. Polym. Sci. (Polym. Phys. Edn)* 1974, **12**, 1511
- 9 Wegner, G. *Z. Naturforsch (B)*. 1969, **24**, 824
- 10 Bloor, D., Koski, L. and Stevens, G. C. *J. Mater. Sci.* 1975, **10**, 1689
- 11 Baughman, R. H. *J. Appl. Phys.* 1972, **43**, 4362
- 12 Bloor, D., Koski, L., Stevens, G. C., Preston, F. H. and Ando, D. J. *J. Mater. Sci.* 1975, **10**, 1678
- 13 Wegner, G. *Makromol. Chem.* 1971, **145**, 85
- 14 Stevens, G. C. and Bloor, D. *J. Polym. Sci. (Polym. Phys. Edn)* 1975, **13**, 2411

Crack growth in plastic panels under biaxial stress

P. S. Leever, J. C. Radon and L. E. Culver

Department of Mechanical Engineering, Imperial College, London SW7 2BX, UK
(Received 12 January 1976; revised 18 February 1976)

It is commonly considered by theoreticians and practitioners of fracture mechanics that the behaviour of a crack is determined only by loads causing a stress singularity at its tip. However, evidence is accumulating which indicates that this may not be entirely so, and that stresses parallel to the crack can affect fracture toughness and cyclic propagation rates. More extensive investigation of these effects involves experimental difficulties. Testing equipment described in this article offers the solution of these problems in a simple way without any significant sacrifice in experimental accuracy. Preliminary tests on poly(methyl methacrylate) are described to demonstrate the machine itself and the phenomena which it is being used to investigate; the results suggest that, for this material at least, the effects of transverse stresses are indeed slight.

INTRODUCTION

The concepts and techniques of fracture mechanics are now widely used for predicting and analysing the behaviour of flawed components. The mathematical and physical models of the fracture process which are in common use generally concentrate on uniaxial-stress situations, in which the crack propagates normally to the applied load. Within the last ten years or so considerable effort has been directed towards the problem of the 'angled crack'¹, whose behaviour is significantly modified by superposed remote shear stresses. Situations in which the crack is subject to additional direct stress along its line have been much less widely investigated; if any consequent change in fracture behaviour is admitted at all, it is usually considered to be negligible.

This may be an optimistic over-simplification. Experiments and analyses have variously suggested that tensile transverse stresses can enhance^{2,3}, reduce⁴ or have no effect⁵ on fracture toughness; increase⁶, reduce⁷ or have little effect³ on fatigue crack growth rates; can cause instability of the path direction of the crack⁸, and can change slow-crack-growth rates in viscoelastic materials⁹. These effects are of obvious importance. Flaws in most service structures may be expected to initiate and propagate continuously along a minor principal stress trajectory^{10,11}, but the ratio between the two principal stresses can vary considerably during propagation. Since this is also the situation in many fracture specimen geometries, a parameter such as the stress intensity factor K may be inadequate to characterize the testing environment.

Clearly the field offers considerable scope for further investigation. Two interacting deterrents have contributed to its neglect: the lack of a substantial theoretical framework within which to treat data, and experimental difficulties. If conventional tensile and fatigue testing machines were equipped or readily adaptable for biaxial loading, much more data would be available; since they are not, investigators are required to design and construct their own. A recent publication¹² has described the development of a purpose-built biaxial fatigue testing rig. Capable of a wide range of biaxiality ratios, cyclic waveforms and frequencies, this type of system would be eminently suitable for

biaxial fracture testing. Unfortunately, it is correspondingly complex and expensive. For their own work in this field, the present authors have designed and constructed a system which represents a simple and cheap solution to the requirements of the planned test programme: a series of biaxial-stress static-load and fatigue fracture tests on various polymers. The essential features of the system are described in the present paper and results are presented from a series of exploratory tests, designed to demonstrate the suitability of the machine and the general character of the phenomena which it is being used to investigate.

SPECIMEN AND MACHINE DESIGN

Specimens and loading shackles

The logical starting point in the design of such a system is the selection of a suitable specimen geometry for biaxial-stress testing. Most previous examples of these are rendered unsuitable by the special requirements of a fracture mechanics approach, which weight the choice in favour of a conventional pre-cracked flat plate type, for which material is normally readily available. Of these, the classical centre notched (CN) configuration offers the advantages of a long usable propagation path which can vary freely in direction, and along which K can be assessed from existing analyses. Furthermore, a significant quantity of data from uniaxial-stress tests on such specimens is available for comparative purposes.

Some modifications to this simple geometry are required to maintain acceptably uniform stress biaxiality and symmetry in the working area. These have been specially investigated elsewhere^{13,14} and are implicit in an arrangement previously used¹⁵ for biaxial creep testing; the design arrived at for the present work (*Figure 1*) derives partly from all three sources. Load is applied to the central region, which is considered for analysis to be a square plate of 190 mm width under uniform normal boundary stresses, through four longitudinally-slotted extensions on each side. The longer and more laterally compliant these extensions are, the less will strain along the side affect the applied stress

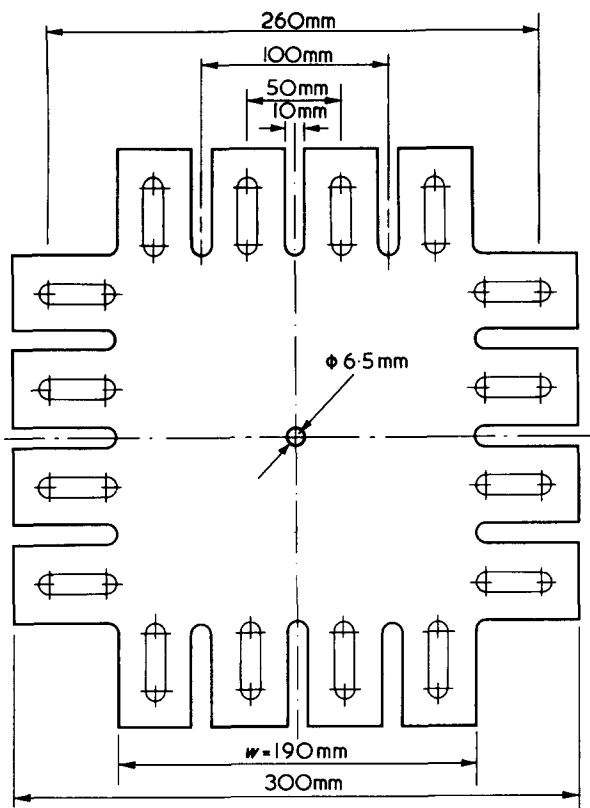


Figure 1 Biaxial-stress fracture specimen design

normality, and the less will the difference between uniform-load and uniform-displacement boundary conditions affect the crack tip stress field. However, a practical limit is imposed by material and machining costs. A convenient compromise can be achieved by the use of 'whipple-tree' loading shackles, which can accommodate extensive deformation or initial misalignment of the loading points on the specimen while maintaining equal and normal loads on them.

Figure 2 shows a specimen mounted in its shackles on the straining frame to be described below. The uniformity of the central stress field was checked *in situ*, using a full-size 6 mm thick Araldite CT200 replica of the specimen and a specially built photoelastic bench. Photographs of representative isochromatic fringe patterns for uniaxial and biaxial loading are shown in Figure 3. Analysis of isochromatics and isoclinics showed that within a central square of 75% of the plate width w , the local biaxiality ratio varied by less than 5% and principal plane directions were within 3° of the centrelines. These conditions in the uncracked specimen justify the assumption that cracks of lengths normally used in fracture testing (less than $0.5w$) will behave similarly to those in a square plate of width w under uniform, normal stresses on its boundaries.

Fatigue loading rigs: the design alternatives

The specimen and shackle design, having been adopted, constituted the primary constraint on the machine design. A system was required to apply two normal in-phase loads of independently-variable magnitude and ratio, either constantly or varying monotonically or cyclically with time. Easy visual access to the specimen was necessary for crack monitoring and transmission photoelastic work. Most important, simplicity, reliability and low cost were to be maintained.

A few investigators whose technical requirements have been similar have devised rigs of widely varied sophistication. Arrangements for transverse dead-weight loading have been added to conventional fatigue machines^{3,10}. In this situation the non-singular part of the crack-tip stress field varies cyclically and, if the crack path curves, so might the singular part, rendering analysis difficult. True biaxial fatigue fracture tests have been accomplished by eliminating transverse strain in a uniaxially fatigued *CN* plate³; the biaxiality ratio was therefore immutably equal to the Poisson ratio.

In a purpose-built rig¹⁶ for testing Mönch-Galster type specimens under static biaxial stresses, load was applied by two pairs of opposed hydraulic rams, each pair backed by an independent hydraulic system. This is a difficult arrangement to modify for in-phase fatigue loading. A similar straining frame has been used¹⁷ for strain cycling cruciform specimens by interconnecting the hydraulic systems to eliminate phasing errors, but thereby restricting load biaxiality ratios to 1, 0 and -1.

The same machine has subsequently been extensively developed¹² to overcome this difficulty. In its current form, each pair of hydraulic jacks is controlled by a servo-hydraulic valve, which forms part of a closed control loop working from load or strain feedback. Capable of a wide range of frequencies, cyclic waveforms and biaxiality ratios, this machine represents an ideal for the fracture tests which are now envisaged; unfortunately this flexibility demands a high capital outlay. The machine to be described below offers performance of a standard suitable for fracture testing at a fraction of the cost and complexity.

A simple biaxial fatigue machine

The machine applies in-phase tensile loads to both axes of the specimen, using a single hydraulic actuator; load biaxiality is stepwise variable. The output of two 15 kN capacity strain gauge load cells is used to measure (on an x/y plotter) and control (using a limit switching device) the load cycle. The electro-hydraulic interface is a direct solenoid-operated direction control valve, which implements an essentially triangular load/time characteristic whose rise and fall rates are independently controlled by flow control valves. The entire system is outlined schematically in Figure 4.

Mechanical system. The straining frame is constructed on a substantial welded *I*-beam base. As can be seen in Figure 2, the specimen is freely accessible, and there is

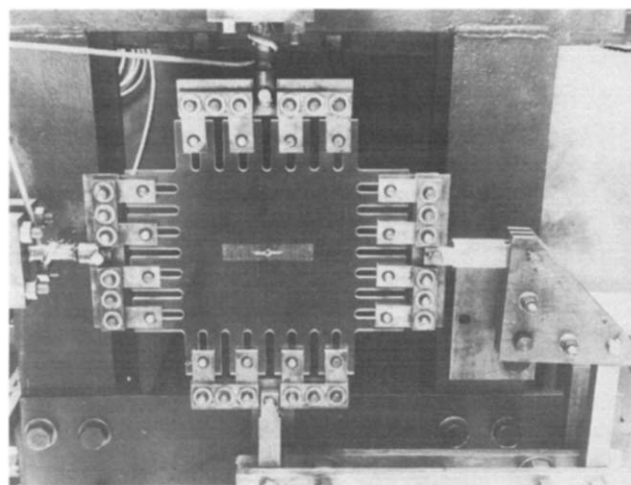


Figure 2 General view of specimen in straining frame

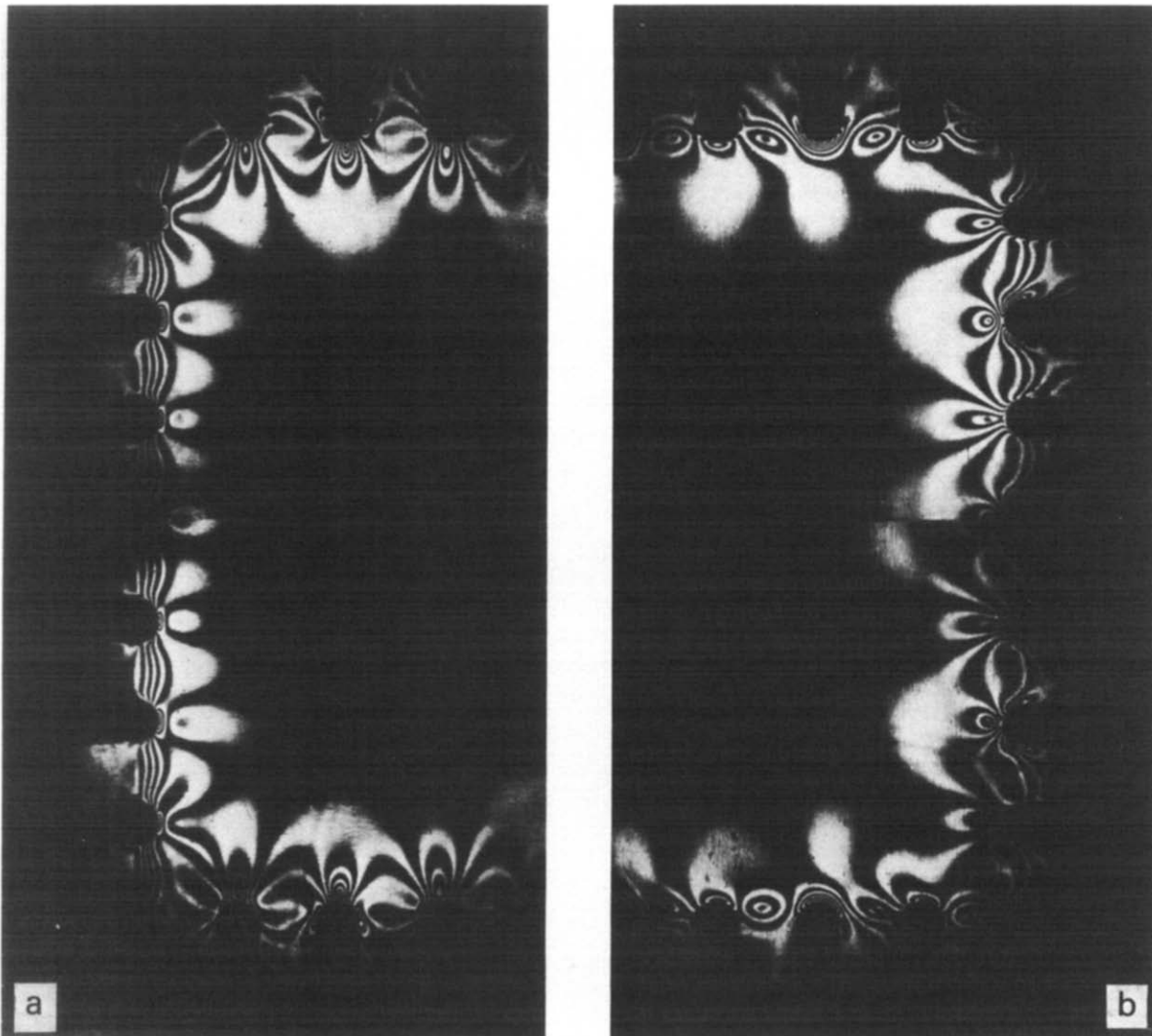


Figure 3 Isochromatic fringes in fracture specimen. Mercury vapour arc light, circularly polarized. (a) $B = 0$ (uniaxial), $P_y = 7.85$ kN, 4th order fringe at centre; (b) $B = 2.06$, $P_y = 7.60$ kN, 2nd order fringe at centre

ample room to fit a temperature controlled cabinet if required. One of each facing pair of shackles is connected to the frame via a pin-jointed load cell, and the two moving shackles are linked (in one case through a right-angle crank) to the ends of a single crosshead about 350 mm long. The point of load application on this crosshead determines the load biaxiality ratio B , defined as transverse load P_x divided by normal load P_y . In the present arrangement one of a limited number of nominal ratios B_n (0, 1, 1.5, 2, 3, 4) is selected by moving the hydraulic cylinder, but a similar system allowing infinite variability is clearly feasible.

The mechanical system is mounted in the horizontal plane. This takes the weight of the numerous pin-jointed linkages off the specimen, allowing their free self-alignment. Where necessary, heavy moving parts (e.g. the crosshead) are supported on rollers.

Electronic control system. Each load cell consists of a full strain gauge bridge (four TML type PL-3 120 Ohm foil gauges) mounted on a waisted tubular core of En24 steel. Calibration indicated 2% linearity in both cells up to 15 kN; 0.1% unbalance in each active gauge corresponded to 8.03 and 8.22 kN load. A.c. excitation and output signal amplification are achieved by a twin channel transducer converter (SE Labs Ltd, type SE 905), which has the useful ability to propagate a calibration step, corresponding to 0.1% change in active gauge resistance, through the control system.

The x/y plotter (Bryans Ltd, type 201 080/8) is calibrated on this basis to indicate both orthogonal loads, P_x and P_y , simultaneously. Alternatively, it can be used to plot the load/time characteristic, so that loading rates and the cyclic waveform can be accurately monitored at the frequencies of which the machine is capable (0.05 to 0.5 Hz).

The control loop is closed by a limit switching millivoltmeter. In the form used here (Messcontactor type 2023/P542, made by Gossen GMBH of West Germany), this is a 600 mV meter on whose scale two movable pointers set the desired cyclic maximum and minimum readings. Travel of the indicating pointer beyond each limit is sensed inductively and triggers a corresponding relay; this latches a simple relay bistable in the appropriate hydraulic direction control valve solenoid circuit. Since similar units are available with up to eight separate limit pointers, the system can be extended to apply programmed loading.

Hydraulic circuit. In essence, the hydraulic circuit is a simple meter-out configuration controlling flow from each side of an area-balanced double-acting cylinder. Line pressure, as set by the relief valve V3 (Figure 4), can be temporarily reset to tank pressure by operation of the tank return valve V1. This is operated by overtravel limit switches on the crosshead tracks, or from a control panel push-button, via a relay latch circuit. The solenoid-operated direc-

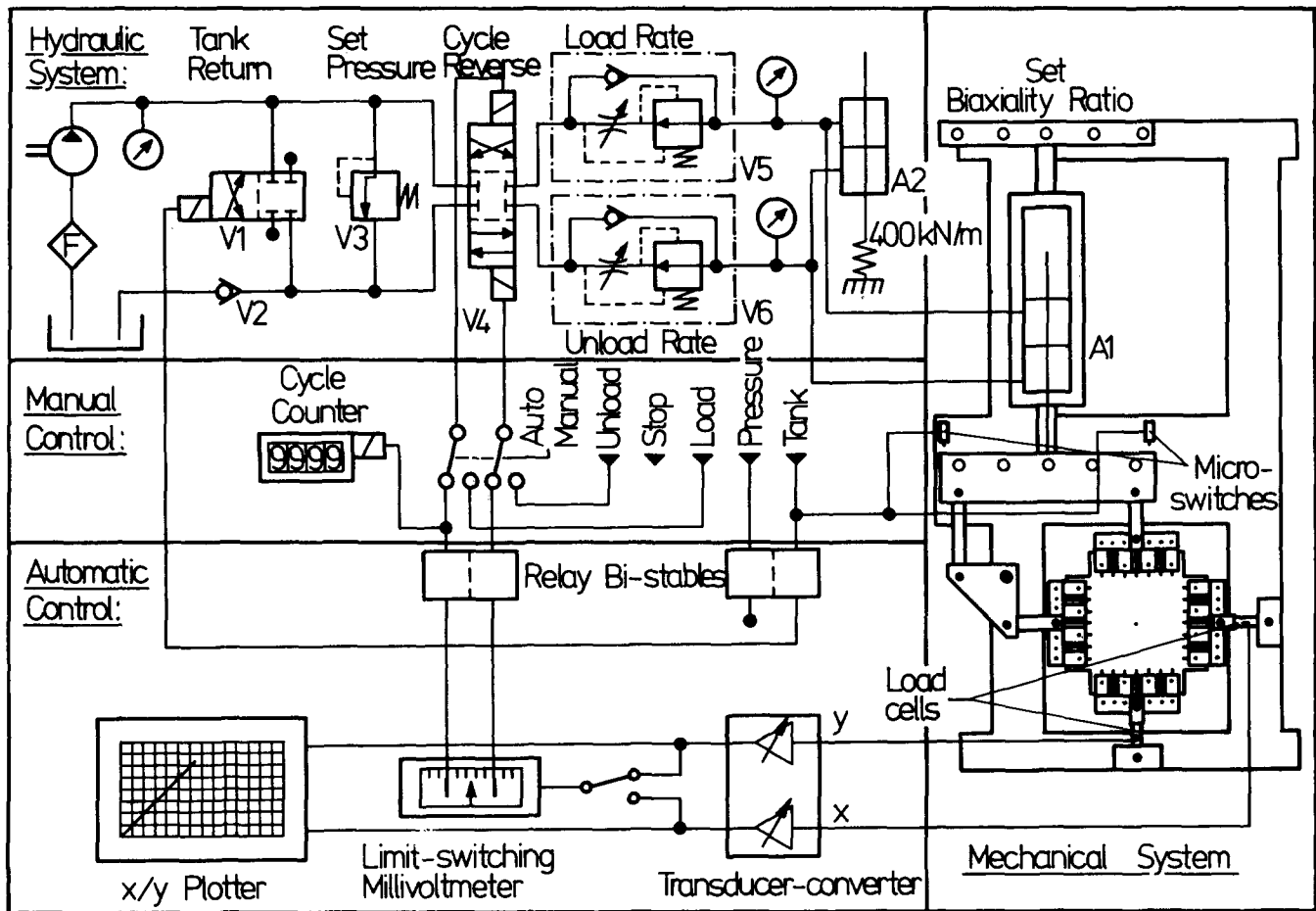


Figure 4 Biaxial-stress fatigue rig and operating system

tion control valve V4 reverses flow through the actuator at pre-set load limits; forward and reverse flow rates are set by pressure and viscosity compensated flow control valves V5 and V6.

The second actuator, A2, was connected in parallel with the first after initial performance inadequacies had been noted. The high stiffness of the machine reduced oil flow rates to levels which were difficult to control. Loading rates were erratic and the valves tended to jam with oil impurities; furthermore, transient leakage through the flow valve compensating spools at flow reversal caused shock unloading of the specimen at the peak point (Figure 5a) which was considered highly detrimental to valid testing. These problems were alleviated by increasing the hydraulic compliance of the load. Actuator A2 (identical to A1) acts against a 400 kN/m spring, raising flow rates by at least fifteen times, the factor depending on the degree of biaxiality. This has virtually eliminated sensitivity to hydraulic line shock, oil impurities and specimen stiffness variations, and has softened the machine response, as can be seen by the plateau at each load cycle limit (Figure 5b). These are significant advantages in a load-cycling testing machine.

MACHINE EVALUATION AND EXPLORATORY TESTS

The rig described above is initially to be used for measurement of fracture toughness, fatigue crack growth rates and fracture path stability in polymers under varying stress biaxiality. To assess the general character of these problems and the suitability of the machine for their investigation, some exploratory tests have been carried out on

poly(methyl methacrylate) (PMMA). This quasi-brittle thermoplastic, used here in the form of 6.35 mm thick ICI Perspex sheet, has been the subject of extensive previous work; much data on its fracture behaviour in established testing modes is therefore already in existence (see, for example, reference 10).

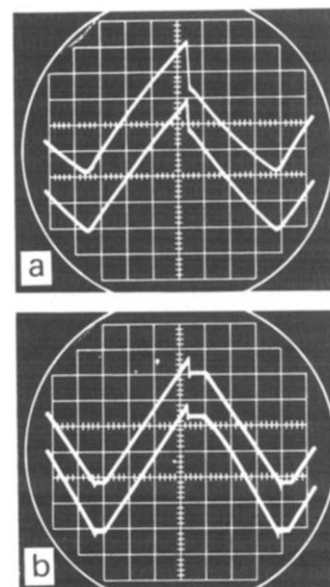


Figure 5 Oscillograms of load cycle waveform. Frequency = 0.1 Hz. Upper trace P_x , lower trace P_y . (a) without additional hydraulic accumulator; (b) with additional hydraulic accumulator

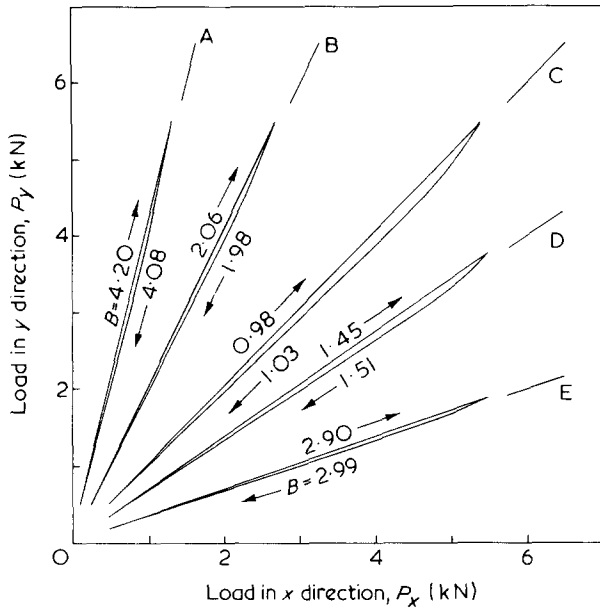


Figure 6 Cyclic traces of P_y versus P_x . Frequencies 0.1 to 0.5 Hz. Characteristic values of load biaxiality ratio B are shown for loading and unloading, for comparison with the nominal value B_n : A, 4; B, 2; C, 1; D, 1.5; E, 3

If the stress intensity factor K characterizes crack tip strain components, its true derivative dK/dt governs strain rates. For materials as highly strain-rate sensitive in their fracture behaviour as polymers^{18,19}, it seems desirable to compare results from different loading environments on a basis of similar time dependence of the governing conditions at the crack tip. A feature of the planned programme of tests, which involves only linear or triangular load/time (and hence, at constant crack length, K/time) histories, is therefore to be the adoption of a fixed value of dK/dt . Implementing this condition in fatigue tests involves increasing the cycle time linearly with ΔK , so that the frequency must be appropriately reduced as the crack propagates across the plate under a constant load range.

To gauge the effects, if any, of this variation in frequency on the shape of the cyclic crack growth rate da/dn versus ΔK curve, comparative tests have been performed at constant frequency (0.1 Hz) and at constant dK/dt ($0.2 \text{ MN}^{3/2}/\text{sec}$). These are convenient values for the particular material and for the machine. Using the same value of dK/dt , monotonic-load fracture toughness tests were performed at various biaxiality ratios.

Fatigue tests

30 mm long symmetrical centre cracks were produced by cutting 25 mm notches with a hacksaw and forcing a razor blade into each tip. Uniaxial fatigue loading for 1 or 2 kcycles was then used to straighten the crack fronts before the first readings were taken. A simple method of crack length measurement was devised to cover cases in which the crack path would curve, making the use of a travelling microscope difficult. A 100 mm square measuring grid, graduated in millimetre divisions, was cut from self-adhesive pre-printed acetate sheet (Letraset Letratone type LT159) and fixed centrally to one face of the specimen. Location of the crack tips on this grid by eye was judged to be accurate to ± 0.1 mm, and the accuracy of the sheet itself is better than 1%. The former error hardly affects crack growth curves for paths tens of millimetres long, while the latter is insignificant in comparison with the nor-

mal scatter band for this kind of test, and is correctable by grid calibration.

Fatigue tests were carried out at constant frequency and constant dK/dt at a load range of 3.5 kN, at a stress ratio of 0.1 and under uniaxial and equibiaxial stress ($B_n = 0$ and 1). Figure 6 shows an x/y plotter trace of P_x versus P_y during fatigue cycling at various nominal biaxiality ratios. It can be seen that the true-load biaxiality ratio B is affected by friction in the transverse loading linkage, mainly in the crank pivot, a PTFE-lined bush on a mild steel shaft. On the loading edge of the cycle B is constant up to the peak load, this being the point for which a characterizing value is defined. After load reversal friction elevates B , an upper-shelf value being attained at 60–70% of the load amplitude and then maintained downwards. Since the maximum and minimum values of B are not symmetrically disposed about B_n , geometrical errors in the linkage are indicated; viscous or inertial effects, however, appear to be negligible, the same plot being characteristic of a range of frequencies from 0.1 to 0.5 Hz.

The machine ran continuously for periods of up to 100 h during which the cycle time, at a constant frequency of 0.1 Hz, was maintained to within 5% on the initial flow valve settings. The response speed of the limit switching equipment and solenoid valve was found to be 0.2 sec; this caused limit overshoot. In variable frequency tests adjustments were necessary to maintain the required load limits of 0.4 and 3.9 kN (± 0.05 kN as measured on the x/y plotter) each time the frequency was adjusted, at about 1 mm crack growth increments.

Crack lengths at very high growth rates were measured from striations on the exposed surface after specimen fracture; these cycle-by-cycle measurements were then matched with those previously taken at intervals with a corresponding cycle counter reading. Figure 7 shows da/dn versus ΔK curves for PMMA in the high growth-rate region for the various conditions tested. It is clear that within the rather narrow range of conditions investigated, neither modification of the frequency nor superposition of in-phase transverse stress noticeably affects growth rates.

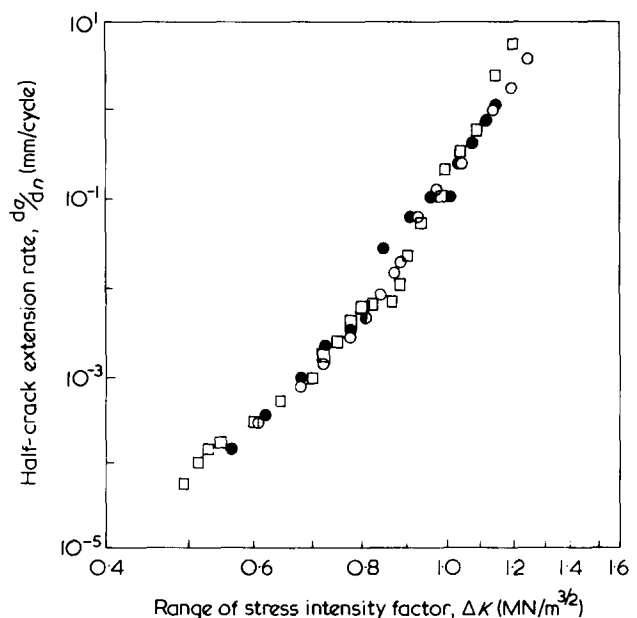


Figure 7 Fatigue crack growth rates: PMMA in air. \circ , $B = 0.9$, $dK/dt = 0.2 \text{ MN}^{3/2}/\text{sec}$; \bullet , $B = 0.9$, $f = 0.1 \text{ Hz}$; \square , $B = 0$, $f = 0.1 \text{ Hz}$

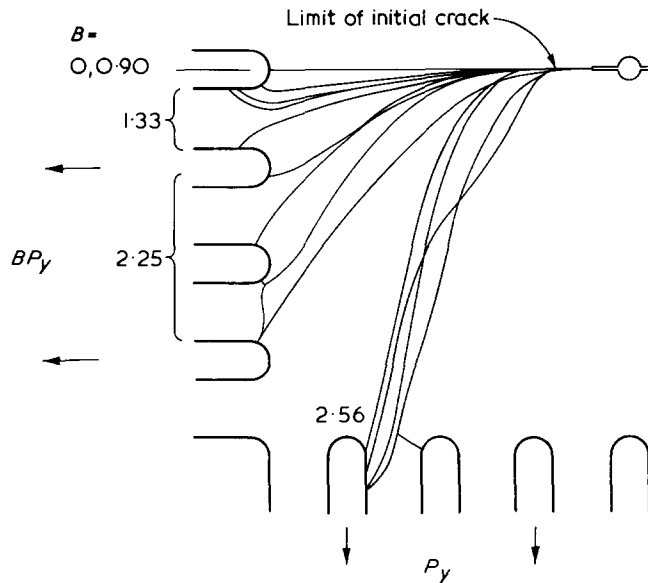


Figure 8 Fracture paths under biaxial, monotonically applied stress

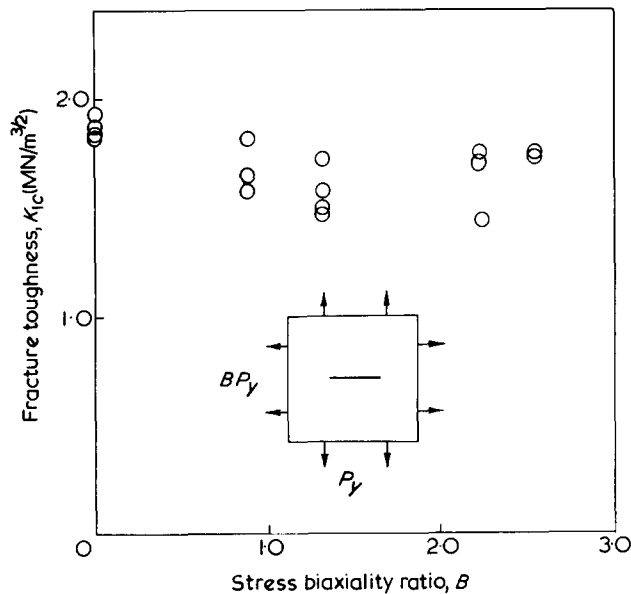


Figure 9 Fracture toughness, K_{Ic} , of PMMA in air, as a function of stress biaxiality B

Quasi-static tests

For these tests, the length of the initial crack was about 40 mm. For eleven of the thirteen specimens used, no attempt was made to straighten the crack tips by fatigue extension, since it is customary to base fracture toughness calculations on the crack length at the initiation of fast fracture, at which point slow crack extension has already taken place. A further two specimens, which were uniaxially fatigued prior to testing, showed similar toughness and path stability characteristics. The resulting fracture trajectories in all cases were straight at low stress biaxiality ratios and S-shaped (or, in one case, arch-shaped) at higher ones (Figure 8). No particular orientation was observed relative to the machine, the paths tending to veer off in the direction of the initial crack tip angle. The general shape of

these trajectories does not, however, seem to be so strongly influenced by the initial tip misorientation as by the biaxiality ratio. The possibility of correlating these path geometries with the stress biaxiality ratio will be discussed in a forthcoming paper.

Crack growth normally followed a smooth path from the initial crack tip, through a slow-growth region, and into fast fracture; only occasionally (more often at low transverse stress levels) was an 'angled crack' type path discontinuity observed. When this did occur, slow growth was generally suppressed, suggesting that perhaps the other tip had already reached the free surface before the first began to move. Fast fracture toughness values, K_{Ic} , for cracks in which preliminary slow growth had occurred are shown in Figure 9 as a function of stress biaxiality, which does not appear to exert any powerful influence. K_{Ic} was evaluated using the horizontal crack length after slow growth; curvature of the slow growth path was always less than 10° . Although the data is too scarce to support firm conclusions, a slight decrease in fracture toughness due to tensile transverse stress is indicated, rather than the large increase (up to 25%) previously reported³.

NOMENCLATURE

a	half crack length,
da/dn	rate of half-crack growth per cycle,
B	biaxiality ratio (P_x/P_y),
B_n	nominal value of B ,
f	fatigue loading frequency,
K	Mode I stress intensity factor,
K_{Ic}	value of K at initiation of unstable fracture,
ΔK	cyclic variation in K ,
P_x	load on specimen parallel to crack,
P_y	load on specimen normal to crack,
w	effective width of specimen.

REFERENCES

- Williams, J. G. and Ewing, P. D. *Int. J. Fract. Mech.* 1972, 8, p441
- Hilton, P. D. *Int. J. Fract.* 1973, 9, 149
- Kibler, J. J. and Roberts, R. *J. Eng. Ind.* 1970, 92, 727
- Smith, S. H. *Conf. Prospects Fract. Mech., Delft, Netherlands.* 1974
- Sih, G. C. and Liebowitz, H. *Int. J. Solids Struct.* 1967, 3, 1
- Joshi, S. R. and Shewchuck, J. *J. Exp. Mech.* 1970, 10, 529
- Adams, N. J. I. *Eng. Fract. Mech.* 1973, 5, 983
- Cotterell, B. *Int. J. Fract. Mech.* 1966, 2, 526
- Laheru, K. L., Hufferd, W. L. and Jacobs, H. R. *Int. J. Fract.* to be published
- Arad, S. *PhD Thesis* London University (1972)
- Klein, G. *J. Mater. Technol.* 1975, 6, 30
- Parsons, M. W. and Pascoe, K. J. *J. Strain Anal.* 1975, 10, 1
- Mönch, E. and Galster, D. *Br. J. Appl. Phys.* 1963, 14, 810
- Cridland, L. and Wood, W. G. *Int. J. Fract. Mech.* 1968, 4, 277
- Johnson, A. E. and Khan, B. in 'Machines for Materials and Environmental Testing', Inst. Mech. Eng., London, 1966
- Fessler, H. and Musson, J. K. *J. Strain Anal.* 1969, 4, 22
- Pascoe, K. J. and de Villiers, J. W. R. *J. Strain Anal.* 1967, 6, 117
- Johnson, F. A. and Radon, J. C. *J. Polym. Sci. (Polym. Chem. Edn)* 1973, 11, 1995
- Radon, J. C. and Culver, L. E. *Polymer* 1975, 16, 539

Association of stereoregular poly(methyl methacrylates): 3. Thermal behaviour and composition of stereocomplex

A. de Boer and G. Challa

Department of Polymer Chemistry, State University of Groningen, Groningen, The Netherlands
(Received 14 January 1976)

Stereocomplexes of isotactic and syndiotactic poly(methyl methacrylate) (i- and s-PMMA) were prepared by mixing dilute i- and s-PMMA solutions in acetone or DMF at different temperatures. At 50°C the rate of complex formation is larger than at 20° or 70°C. Differential scanning calorimetry and X-ray powder diffraction measurements were performed on the material crystallized from mixed solutions. The thermograms showed 3 endotherms at temperatures not depending on the i-/s-PMMA ratio of the sample. The endotherm at ~280°C is caused by degradation of PMMA, the maximum at ~210°C by melting of the stereocomplex and the endotherm at ~185°C by melting of solvent stabilized s-PMMA. By comparing X-ray powder diffraction patterns of s-PMMA crystallized from borderline solvents with those of stereocomplexes of i-/s-PMMA with different drying histories it is concluded that the reflection at $2\theta = 4^{\circ}10'$ belongs to a solvent stabilized s-PMMA structure. Partial association of i- and s-PMMA chains in an i-/s-PMMA ratio of about 1:1 and crystallization of solvent rich s-PMMA is proposed as a mechanism for the complex formation under the present conditions.

INTRODUCTION

In 1958 Fox *et al.*¹ reported for the first time that gelation occurred by mixing solutions of isotactic and syndiotactic poly(methyl methacrylate) (i- and s-PMMA). This gelation process can be explained by the formation of stereocomplexes of i-/s-PMMA. Stereocomplex formation may be regarded as a general property of stereoregular polymers. The driving force in the complex formation of i- and s-PMMA is the structural complementarity of both tactic polymers. This has also been proven by the template polymerization of MMA in the presence of i-PMMA, resulting in the formation of s-PMMA².

Basic questions concerning the composition and structure of the formed stereocomplexes remained unanswered. The stereocomplex formation of i- and s-PMMA has been investigated by viscometry and turbidimetry³⁻⁶, light scattering^{7,8}, high resolution and broad line n.m.r.^{9,10}, sedimentation in an ultracentrifuge^{8,11}, calorimetry^{12,13}, and by dynamic mechanical^{13,14} and dielectric measurements¹⁵.

Viscosity and turbidity measurements in dilute solutions have pointed out that complex formation of i- and s-PMMA can occur at concentrations far below that with homogeneous segmental distribution³. As the solvents have different influence on complex formation we divided them into three types: (a) strongly complexing; (b) weakly complexing, and (c) non-complexing solvents. Buter *et al.*¹⁶ and Gons *et al.*¹⁷ found that the effect of solvent on the stereochemistry and kinetics of the template polymerization of MMA in the presence of i-PMMA is in line with its complexing ability. The heats of complex formation of i- and s-PMMA as reported by Biroš *et al.*¹² are also in agreement with this classification.

N.m.r. measurements⁹ showed that the mobility of the methoxy protons of stereocomplexes is strongly decreased by mixing concentrated i- and s-PMMA solutions in CCl₄ or CD₃CN. Pyrlík *et al.*¹⁴ also found by dynamic mechanical measurements that complex formation can occur in very

concentrated solutions. In a previous paper¹³ we concluded from calorimetric and dynamic mechanical measurements that complex formation of i-/s-PMMA can even occur in bulk. We found that the complex formation rate was maximal at 140°C and that within a few minutes, more than half of the complex has been formed. From the fact that annealed and non-annealed samples had the same value of the storage modulus (G') above the glass transition temperature, we concluded that the main process taking place in bulk during annealing comprises growth of complex crystallites. Liquori *et al.*¹⁸ have proposed a model for the stereocomplex in the form of 5₁ helices of i-PMMA in the grooves of which the flat chains of s-PMMA lie so that the α -methyl groups of both macromolecules become situated at van der Waals distance from each other, stabilizing the stereocomplex in polar solvents by hydrophobic interaction. In this model the syndiotactic chains are tilted ~60° with respect to the isotactic helical chain. We find it difficult to understand the phenomena of the template polymerization of MMA in the presence of i-PMMA using this model. In this case one would expect that the isotactic and syndiotactic chains are aligned parallel to one another in some way. Moreover, we have shown that samples obtained by template polymerization behave like material crystallized from mixed dilute solutions of i- and s-PMMA³.

The most frequently quoted composition of the stereocomplex is an i-/s-PMMA ratio of 1:2, but other results have been presented^{4,6} in favour of an i-/s-PMMA ratio of 1:1 and lately also a ratio of 1:1.5^{9,12}. On the other hand, Chiang *et al.*⁸ concluded from ultracentrifuge measurements that complex formation of i- and s-PMMA does not proceed necessarily in a fixed stoichiometric ratio.

In order to elucidate the structure of the stereocomplex of i-/s-PMMA, it is necessary to know the real i-/s-PMMA ratio of the associated regions. Therefore we prepared stereocomplexes by mixing very dilute solutions of i- and s-PMMA in the strongly complexing solvents DMF or acetone at dif-

Table 1 Data of polymers used

	Triads I-H-S	$[\eta]$ (dl/g)	$\bar{M}_v \times 10^{-3}$
i-PMMA 107	91- 6-3	1.99	600
s-PMMA 106	4- 8-88	1.37	370
s-PMMA 113	4- 9-87	1.71	490
s-PMMA 119	1-11-88	0.14	22

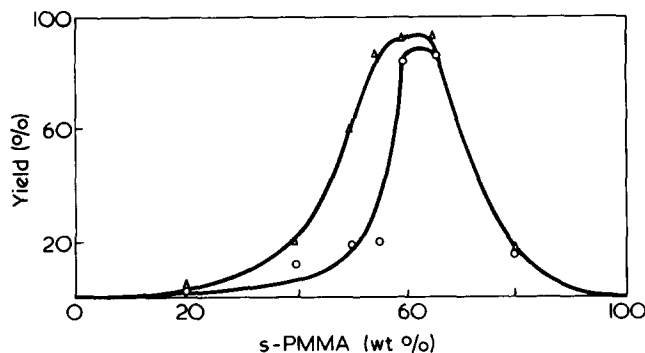


Figure 1 Yield of crystallized material (%) versus wt% s-PMMA for mixtures of i- and s-PMMA in DMF at 20°C (O) and 50°C (Δ). The total polymer concentration is always 0.2 wt%

ferent i/s-PMMA ratios. The results of calorimetric, X-ray and n.m.r. measurements on the crystallized material are described and discussed in this paper.

EXPERIMENTAL

The polymers i- and s-PMMA were prepared according to known procedures^{19,20}. The data of the polymers used are summarized in Table 1. The tacticities of PMMA were measured on 5 wt% solutions in *o*-dichlorobenzene at 160°C²¹ by 60 MHz n.m.r. spectroscopy with a Jeol C-60 HL apparatus. Values of $[\eta]$ for the PMMA samples were determined in chloroform at 25°C. For the calculation of \bar{M}_v we used the relationship²² $[\eta] = 4.8 \times 10^{-5} \bar{M}_v^{0.8}$. Stereocomplexes were prepared by mixing 0.2 wt% i- and s-PMMA solutions in DMF or acetone. The mixed solutions were kept in thermostatically controlled baths at 20° and 50° ± 0.1°C for 20 days. At 70°C no complex formation could be observed after 20 days. Therefore the solutions were kept 70 days at 70°C. The solvents DMF and acetone (Merck) were used without further purification. The crystallized material was separated from the solution in a centrifuge with an acceleration of 25 000 × *g* and then dried *in vacuo* at 70°C for 64 h.

The melting behaviour of i- and s-PMMA and their stereocomplex was studied with a differential scanning calorimeter (Perkin-Elmer DSC 1B). The temperature scale was calibrated with high purity metal standards. Normally a heating rate of 8°C/min and sealed pans were used, unless otherwise indicated.

Thermogravimetric measurements were performed with a Mettler DTA/TGA apparatus with a heating rate of 10°C/min. X-ray powder diffraction patterns were recorded by a Philips diffractometer with a scan speed of 0.5°/min and angle aperture of 1/2 or 1/6°. Ni-filtered CuK α radiation was applied. Triad contents of the crystallized material were measured in the same way as described for the PMMA samples. It is known^{3,14,23} that the stereocomplex is completely dissociated at 160°C.

RESULTS

Crystallization of i- and s-PMMA

For a better understanding of the thermal behaviour and structure of the stereocomplex we required first data on crystalline i- and s-PMMA. For i-PMMA the crystal growth in bulk showed a maximum rate at 120°C and produced a substantial melting endotherm at 155°C after 5 days²⁴. For s-PMMA only data are reported on crystallization from borderline solvents^{1,25-27}. We were also unsuccessful with bulk crystallization of s-PMMA and tried to achieve crystallization by cooling hot solutions of s-PMMA in borderline solvents. The precipitates isolated from heptanone-4 or methyl isobutyrate solutions at room temperature showed an endotherm at ~190°C in the d.s.c. and a reflection at $2\theta = 4^\circ 30'$ in the X-ray powder diffractogram. After drying at 70°C this reflection disappeared, while the melting endotherm was lost after drying at higher temperatures, e.g. 150°C *in vacuo*. The same phenomena were observed with the needle-like crystals of s-PMMA grown from toluene at -20°C. So, it seems that some crystalline structure of s-PMMA is stabilized by solvent and is destroyed by drying. Careful drying of a toluene solution in a desiccator above paraffin for 2 months at room temperature produced s-PMMA with an endotherm at about 200°C, which did not disappear after prolonged drying.

Stereocomplex of i/s-PMMA

In Figure 1 the yield of crystallized material is plotted versus wt% s-PMMA for DMF solutions at 20° and 50°C. Complex formation from acetone produced a similar picture. The results of DMF solutions at 70°C are not presented in this Figure because in this case the material was separated only after 70 days.

From n.m.r. measurements it appeared that the gross composition of the material crystallized from DMF or acetone at 20°C is about the same as the composition of PMMA in the starting solution.

Thermograms of crystallized material with different i/s-PMMA ratios obtained from DMF solutions at 20°C are represented in Figure 2. The peak temperatures of the

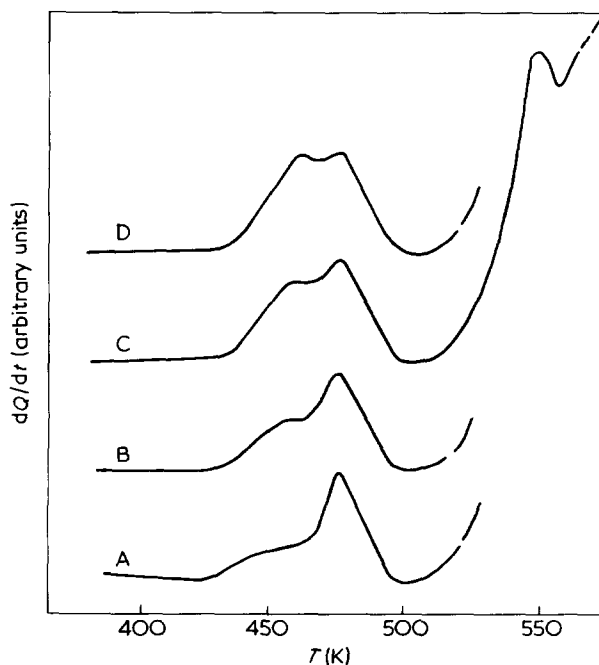


Figure 2 Thermograms of samples crystallized at 20°C from 0.2 wt% DMF solutions with different i/s-PMMA ratios: A, 60:40; B, 50:50; C, 33:67; D, 20:80

Table 2. Melting temperatures recorded by d.s.c. ($^{\circ}\text{C}$) of samples crystallized from acetone or DMF solutions with different i-/s-PMMA ratios at 20° , 50° and 70°C (T_c)

i-/s-PMMA ratio in the starting solution	Acetone				DMF					
	$T_c = 20^{\circ}\text{C}$		$T_c = 50^{\circ}\text{C}$		$T_c = 20^{\circ}\text{C}$		$T_c = 50^{\circ}\text{C}$		$T_c = 70^{\circ}\text{C}$	
	T_{m1}	T_{m2}	T_{m1}	T_{m2}	T_{m1}	T_{m2}	T_{m1}	T_{m2}	T_{m1}	T_{m2}
60:40	175	205	190	210	180	205	190	210		
50:50	185	205	190	215	185	205	190	214		222
33:67	185	205	190	215	185	205	190	215		226
20:80	189	209	195	213	186	207	190	215		

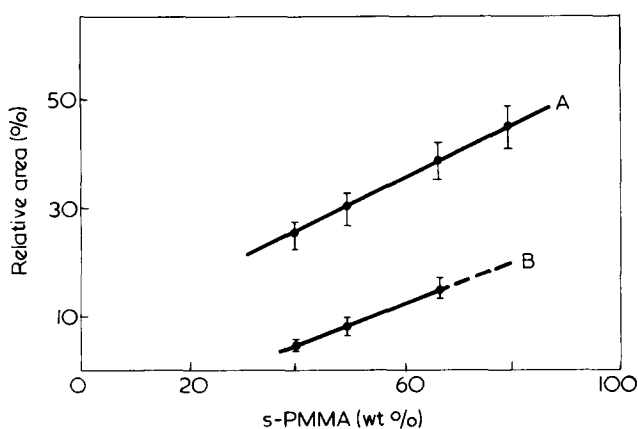


Figure 3. Relative area of the endotherm at $\sim 185^{\circ}\text{C}$ (T_{m1}) versus wt% s-PMMA for samples crystallized from DMF and acetone at 20°C (A) or 50°C (B), relative area = $T_{m1}/(T_{m1} + T_{m2})$

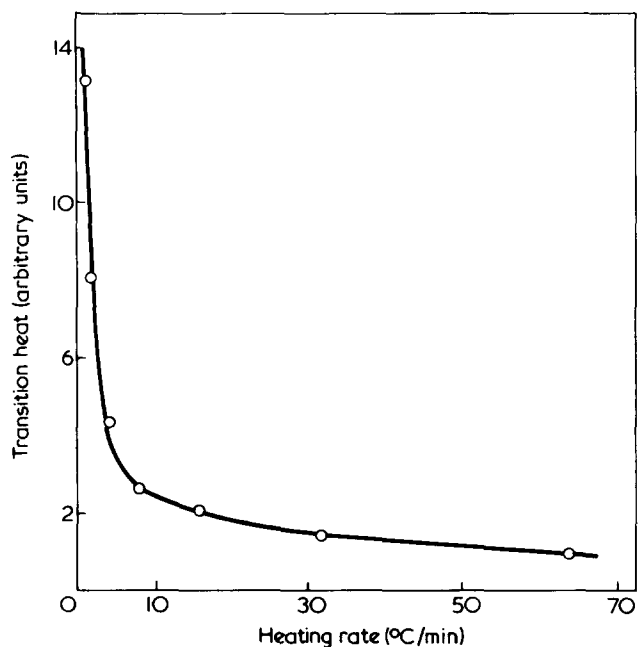


Figure 4. Area of the endotherm at $\sim 285^{\circ}\text{C}$ (T_{m3}) recorded by d.s.c. versus heating rate for samples crystallized from mixed solutions of i- and s-PMMA in DMF with i-/s-PMMA ratios of 1:2 or 1:1

endotherms at about 185° , 210° and 280°C are designated as T_{m1} , T_{m2} and T_{m3} respectively. In Table 2 values of T_{m1} and T_{m2} are compiled for products isolated from PMMA solutions with different i-/s-PMMA ratios in acetone and DMF at 20° , 50° and 70°C . T_{m1} could not be observed in samples obtained from DMF solutions at 70°C . In Figure 3 the relative area of the endotherm at 185°C (T_{m1}) is plotted versus wt% s-PMMA for products obtained

from acetone and DMF at 20° and 50°C . These Figures show that the relative area of the endotherm at T_{m1} increases with increasing s-PMMA content and is much larger for material prepared at 20° than at 50°C .

In Figure 4 the area under the endotherm at T_{m3} is plotted versus heating rate in the d.s.c. We see a strong decrease of transition heat with increasing heat rate, whereas the peak temperature T_{m3} itself increases from 270° to 335°C . These phenomena are less important for our present study of stereocomplex formation and can be explained by thermal depolymerization of PMMA. According to thermogravimetric analysis the weight loss started at 280°C , so that the volatile monomer can escape from the nonsealed pans at T_{m3} . At a lower heating rate more monomer can diffuse out of sample and pan at a given temperature which leads to the increase of the area and lowering of the peak temperature. When a sample is kept at 240°C for 10 min a fully amorphous X-ray powder diffraction pattern results. This also indicates that T_{m3} is not related to the stereocomplex.

X-ray powder diffraction patterns for different i-/s-PMMA ratios are presented in Figure 5. This Figure shows that the reflection in i-PMMA at $2\theta = 8^{\circ}10'$ which is a (110) or (200) reflection²⁸ is not present in the stereocomplex. The intensity of the reflection at $2\theta = 4^{\circ}10'$ which is a (hko) reflection¹⁸ increases with increasing s-PMMA content. As mentioned above this reflection also occurs in solvent stabilized 'crystalline' s-PMMA. The effect of drying on the X-ray powder diffractogram of a sample with an i-/s-PMMA ratio of 1:2 crystallized from DMF at 70°C is shown in Figure 6. A strong decrease of intensity of the reflection at $2\theta = 4^{\circ}10'$ is observed, but in this case the reflection does not fully disappear after prolonged drying. Samples crystallized at 20°C behave like s-PMMA and lose the reflection completely.

DISCUSSION

From Figure 1 it is clear that more crystalline material has been formed at 50° than at 20°C . By measuring the yield after 10 days, it was observed that the complex formation rate in a solution with i-/s-PMMA ratio of 1:1 is higher at 50° than at 20°C .

Spěvák and Schneider²⁹ have shown by n.m.r. measurements that self-association may occur in i-PMMA solutions. However, by varying the dissolution temperature of i- and s-PMMA in DMF no influence could be established on the amount and quality of the material crystallized from the mixed solutions at 20° and 50°C . Hence, the difference between the amounts of crystalline material formed at 20° and 50°C shown in Figure 1 cannot be ascribed to self-association and has to be explained in terms of a complex

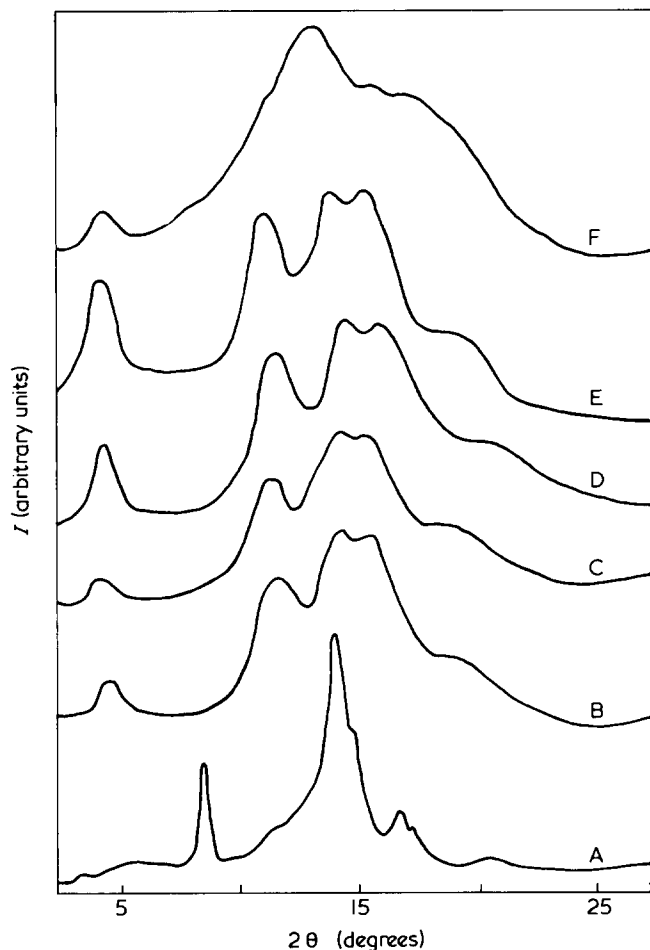


Figure 5 X-ray diffraction intensity (I) versus diffraction angle 2θ (degrees) for samples with different *i*-/*s*-PMMA ratios: A, 100:0; B, 60:40; C, 50:50; D, 33:67; E, 20:80; F, 0:100. Curve F relates to *s*-PMMA containing some solvent

formation which is closer to the equilibrium state at 50°C than at 20° or 70°C. The broadening of the yield curve at 50°C in Figure 1 towards lower *s*-PMMA contents indicates that *i*- and *s*-PMMA do not form stereocomplexes in a fixed stoichiometric *i*-/*s*-PMMA ratio of 1:2.

Figures 2 and 3 showed that the relative area of the endotherm T_{m1} increases with increasing *s*-PMMA content. The same trend is observed for the intensity of the reflection at $2\theta = 4^\circ 10'$ (Figure 5). From Figure 6 it is clear that the material crystallized from mixed solutions of *i*- and *s*-PMMA exhibits in some way the same behaviour as solvent stabilized 'crystalline' *s*-PMMA. Hence we conclude that the endotherm at about 185°C (T_{m1}) as well as the reflection at $2\theta = 4^\circ 10'$ can be attributed to solvent stabilized 'crystalline' *s*-PMMA. Experiments carried out with *s*-PMMA 119 showed that the molecular weight of *s*-PMMA does not affect the thermal behaviour and X-ray powder diffraction pattern of the crystallized material.

So far we have attributed T_{m3} to thermal degradation and T_{m1} to *s*-PMMA, leaving T_{m2} as the melting point for the stereocomplex. By partial scan and the effect of scan speed on T_{m2} ³⁰ we have shown that this endotherm is an independent one and does not result from the endotherm at T_{m1} by recrystallization. From the foregoing we derive the following mechanism: isotactic and syndiotactic PMMA chains partly associate in an *i*-/*s*-PMMA ratio of about 1:1. When these associates crystallize from the solution, non-associated isotactic and syndiotactic chains are dragged from the solution and the *s*-PMMA chains crystallize in a

solvent stabilized 'crystalline' structure. Indeed it appeared also possible to crystallize *i*-PMMA chain segments. Annealing a sample crystallized from an acetone solution with an *i*-/*s*-PMMA ratio of 1.5:1 for 5 days at 120°C an extra endotherm arose at about 170°C and the reflection at $2\theta = 8^\circ 10'$ could also be detected with the X-ray diffractometer. We know that the growth rate of *i*-PMMA crystals is maximal at 120°C²⁴ and that the rate of complex formation in bulk equals zero at this temperature¹³.

The proposed mechanism is partly in accordance with that of Miyamoto and Inagaki³¹ who performed ultra centrifuge and thin layer chromatography measurements on the complex formation of *i*- and *s*-PMMA in acetone. According to these authors a primary complex formation occurs yielding stereocomplexes with an *i*-/*s*-PMMA ratio of 1:1. In a second step these complexes are transformed in stereocomplexes with an *i*-/*s*-PMMA ratios of 2:1 or 1:2. However, Table 2 shows that the *i*-/*s*-PMMA ratio has no influence on the melting temperature (T_{m2}) of the stereocomplex. The melting temperature (T_{m2}) depends only on the temperature T_c of complex formation. So, in our opinion it is more likely that complex formation occurs

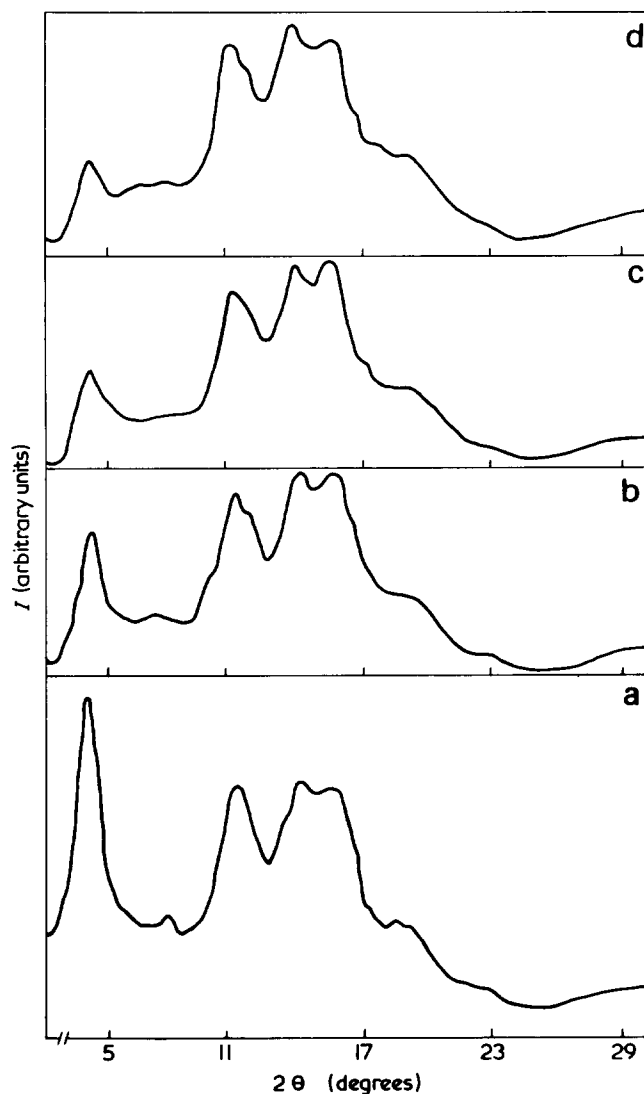


Figure 6 X-ray diffraction intensity (I) versus diffraction angle 2θ (degrees) for a sample crystallized at 70°C from a DMF solution with an *i*-/*s*-PMMA ratio of 1:2 subsequently dried at 70°C *in vacuo* for 64 h (A); at room temperature for 3 months (B); at 150°C *in vacuo* for 19 h (C); and at 150°C *in vacuo* for 120 h (D)

only in an i-/s-PMMA ratio of 1:1 and that at the same time some liquid induced crystallization of s-PMMA occurs. Under the prevailing conditions of solvent and temperature s-PMMA has a stronger tendency to crystallize than i-PMMA. This may explain why the yield curves in *Figure 1* are shifted towards higher s-PMMA content.

Finally, we have estimated the degree of crystallinity of the stereocomplex from X-ray powder diffraction patterns applying the method proposed by Challa *et al.*³². Stereocomplexes with an i-/s-PMMA ratio of 1:2 obtained from DMF at 70°, 50° and 20°C showed a crystallinity of 40, 30 and 15% respectively. In our opinion this is in line with our view that association of stereoregular PMMAs occurs only partially.

REFERENCES

- 1 Fox, T. G., Garret, B. S., Goode, W. E., Gratch, S., Kincaid, J. F., Spell, A. and Stroupe, J. D. *J. Am. Chem. Soc.* 1958, **80**, 1768
- 2 Buter, R., Tan, Y. Y. and Challa, G. *J. Polym. Sci. (A-1)* 1972, **10**, 1031
- 3 Challa, G., de Boer, A. and Tan, Y. Y. *Int. J. Polym. Mater.* 1976, **4**, 239
- 4 Liu, H. Z. and Liu, K. J. *Macromolecules* 1968, **1**, 157
- 5 van der Berg, W. B., Hijmans, B., Piet, P. and Heikens, D. *Nature* 1968, **217**, 449
- 6 Borchard, W., Pyrlík, M. and Rehage, G. *Makromol. Chem.* 1971, **145**, 169
- 7 Liquori, A. M., de Santis, P., Savino, M. and D'Alagni, M. *J. Polym. Sci. (B)* 1966, **4**, 943
- 8 Chiang, R., Burke, J. J., Threkeld, J. O. and Orofino, T. A. *J. Phys. Chem.* 1966, **70**, 3591
- 9 Spěvák, J. and Schneider, B. *Makromol. Chem.* 1974, **175**, 2939
- 10 Spěvák, J. and Schneider, B. *Makromol. Chem.* 1975, **176**, 729
- 11 Dayantis, J., Reiss, C. and Benoit, H. *Makromol. Chem.* 1968, **120**, 113
- 12 Biró, J., Mása, Z. and Pouchlý, J. *Eur. Polym. J.* 1974, **10**, 629
- 13 Feitsma, E. L., de Boer, A. and Challa, G. *Polymer* 1975, **16**, 515
- 14 Pyrlík, M., Borchard, W., Rehage, G. and Uerpman, E. P. *Angew. Makromol. Chem.* 1974, **36**, 133
- 15 Borchard, W., Kalawrytinis, G., Mohadjer, B., Pyrlík, M. and Rehage, G. *Angew. Makromol. Chem.* 1973, **29/30**, 471
- 16 Buter, R., Tan, Y. Y. and Challa, G. *J. Polym. Sci. (Polym. Chem. Edn.)* 1973, **11**, 2975
- 17 Gons, J., Vorenkamp, J. E. and Challa, G. *J. Polym. Sci. (Polym. Chem. Edn.)* 1975, **13**, 1699
- 18 Liquori, A. M., Anzuino, G., Coiro, V. M., D'Alagni, M., de Santis, P. and Savino, M. *Nature* 1965, **206**, 358
- 19 Goode, W. E., Owens, F. H., Feldmann, R. P., Snijder, W. H. and Moore, J. H. *J. Polym. Sci.* 1960, **46**, 317
- 20 Abe, H., Imai, K. and Matsumoto, M. *J. Polym. Sci. (C)* 1968, **23**, 469
- 21 Ramey, K. C. *J. Polym. Sci. (B)* 1967, **5**, 859
- 22 Bischof, J. and Desreux, V. *Bull. Soc. Chim. Belg.* 1952, **61**, 10
- 23 Spěvák, J. and Schneider, B. *J. Polym. Sci. (Polym. Lett. Edn.)* 1974, **12**, 349
- 24 de Boer, A., Alberda van Ekenstein, G. O. R. and Challa, G. *Polymer* 1975, **16**, 930
- 25 Kawasaki, A., Furukawa, J., Tsuruta, J., Inoue, S. and Ito, K. *Makromol. Chem.* 1960, **36**, 260
- 26 Fox, T. G., Goode, W. E., Gratch, S., Hugget, C. M., Kincaid, J. F., Spell, A. and Stroupe, J. D. *J. Polym. Sci.* 1958, **31**, 173
- 27 Miller, R. G. J., Mills, B., Small, P. A., Turner-Jones, A. and Wood, D. G. M. *Chem. Ind.* 1958, **11**, 1323
- 28 Roerdink, E. R. unpublished results
- 29 Spěvák, J. and Schneider, B. *Makromol. Chem.* 1975, **176**, 3409
- 30 Lemstra, P. J., Kooistra, T. and Challa, G. *J. Polym. Sci. (A-2)* 1972, **10**, 823
- 31 Miyamoto, T. and Inagaki, H. *Polym. J.* 1970, **1**, 46
- 32 Challa, G., Weidinger, A. and Hermans, P. H. *Makromol. Chem.* 1962, **56**, 169

Optical rotatory dispersion of crotamine: effect of denaturants

Oscar G. Hampe

Departamento de Fisiologia, Farmacologia e Biofísica, UFRGS 90.000, Porte Alegre, Brazil

and José M. Goncalves

Instituto de Energia Atômica, Setor de Radiobiologia, Cidade Universitaria, São Paulo, Brazil
(Received 9 December 1975; revised 23 February 1976)

The amino-acid sequence of crotamine, a toxin found in the venom of the south Brazilian snake *Crotalus durissus terrificus* was recently determined by Laure¹. It is a miniprotein with 42 amino-acid residues and a minimum molecular weight of about 5000. This molecule contains among others, 6 half-Cys, 2 Trp, 1 Tyr and 2 Phe residues which can contribute to the behaviour of the optical rotatory dispersion measured in the ultraviolet region of the spectra.

The present communication reports studies on the ultra-violet o.r.d. of crotamine and the effect of denaturants on the protein. The pure protein used in the experiments was obtained from the snake venom purified on a column of SP-Sephadex G-25 with a gradient of 0.5 to 3.0 M NaCl in 0.05 M ammonium formate, pH 3.2, after gel filtration in Sephadex G-75 with 0.05 M ammonium formate buffer pH 3.4. The purified material showed only a single component by disc electrophoresis in polyacrylamide gel².

O.r.d. measurements of the pure toxin, were carried out in a Fica Spectropol I Spectropolarimeter with a thermostated cell and the reduced mean residue rotation values, $[m']$, were expressed in degrees cm^2/dmol .

The infra-red spectrum of crotamine was obtained with a Perkin-Elmer Model 225 Spectrophotometer in a pressed potassium bromide disc.

Figure 1 shows the o.r.d. curve of native crotamine dissolved in unbuffered distilled water pH 5.5 over a wavelength range of 197 to 325 nm. This anomalous spectrum is due to several Cotton effects caused by the

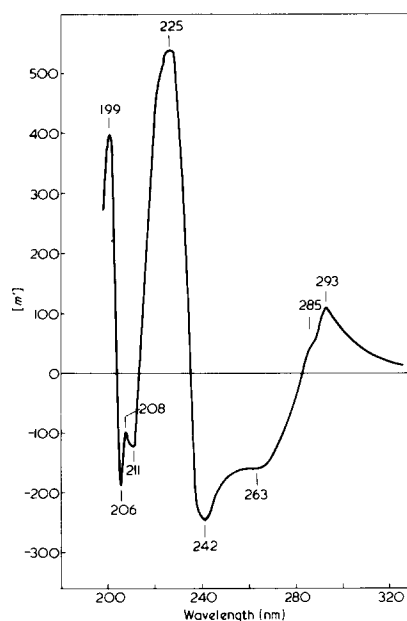


Figure 1 Optical rotatory dispersion of crotamine dissolved in unbuffered distilled water pH 5.5 at 25°C. The $[m']$ values from 325 to 237 nm are the average of those obtained for 0.25, 0.50, 0.75, 1.00, 1.25, and 1.50 mg/ml of protein using a 0.1 dm quartz cell, and those below 237 nm were obtained from 0.025 and 0.050 mg/ml of protein concentration using a 0.05 dm quartz cell

protein chromophores. The positive band found between 283 to 325 nm shows a peak at 293 nm which is related to the Trp residue. Besides the peak, a shoulder at 285 nm appears to the Tyr Cotton effect³. The very asymmetric negative band from 240 to 283 nm has two troughs centred at 263 and 242 nm. The first trough, indicates the participation of Phe³, and disulphide bridges⁴ in the anomalous o.r.d. spectrum of crotamine. The other one, can be related to β -II structure⁵. It is very

difficult, if not impossible to determine which chromophores of the toxin are responsible for each Cotton effect found below 283 nm, mainly below 235 nm through the o.r.d. spectrum. Nevertheless, the presence of disulphide bridges can perturb some of the other Cotton effects of the protein⁶.

Evidence of the presence of β -structure was obtained through the infra-red spectrum of the protein as shown in Figure 2. The peaks found at 1625 cm^{-1} of amide-I band and at 1533 cm^{-1} of amide-II band can be regarded as due to the presence of this structure in the molecule^{7,8}. The $[m']$ values of +400 at 199 nm shown in Figure 1, and of -1460 at 232 nm of Figure 3, are not enough to postulate significant helical content in this macromolecule, despite the fact that sodium dodecyl sulphate at the concentration of 6.5×10^{-3} M changes the very anomalous o.r.d. curve to one characteristic of helical like structure with a trough at 232 nm (Figure 3, curve A).

The effect of chemical denaturant urea at a concentration of 8 M on the crotamine spectrum is shown in Figure

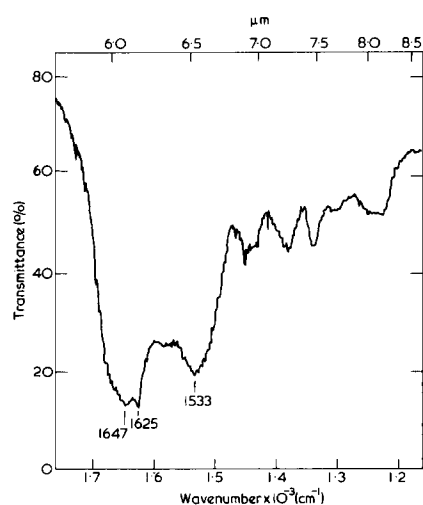


Figure 2 Infra-red spectrum of crotamine measured from 1.16×10^{-3} to 1.76×10^{-3} cm^{-1} . The spectrum was obtained using a pressed disc of 4 mg of protein with 200 mg of potassium bromide

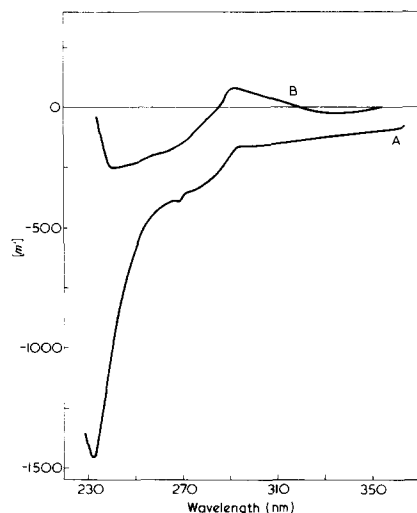


Figure 3 Effect of denaturants on the conformation of crotonamine. O.r.d. measurements of crotonamine solution with a concentration of 1 mg/ml in 6.5×10^{-3} M sodium dodecyl sulphate were carried out between 230 and 360 nm (curve A) and of the same concentration of protein in 0.1 M acetate buffer pH 5.5 containing 8.0 M urea, between 230 and 350 nm (curve B)

3, curve B. There are no significant changes in the spectrum from 235 to 350 nm which indicates a high resistance of the protein molecule to urea denaturation. The o.r.d. spectrum remained the same, even when a solution of crotonamine in 0.1 M acetate buffer pH 5.5 containing 8 M urea was left at room temperature for twenty days and then heated at 60°C for two hours. However, the protein must have significant tertiary structure, since the reduction of the disulphide bridges by 2-mercaptoethanol in the presence of 8 M urea in 0.1 M tris-HCl buffer pH 8.6 abolishes the anomalous o.r.d. spectrum of the molecule between 250 and 320 nm.

The high resistance to conformational modifications of crotonamine in the presence of concentrated urea solution combined with a very low intrinsic viscosity of 1.2 ml/g at pH 5.5, indicates that at tertiary structure level, the mini-protein is maintained very compact having an axial ratio close to the unity.

ACKNOWLEDGEMENTS

The authors thanks Dr Aida Hasson Volloch from the Instituto de Biofísica da UFRJ, for the use of the Spectropolarimeter, and Dr M. M. Vozári-Hampe for the critical analysis of the manuscript.

REFERENCES

- 1 Laure, C. J. *Hoppe-Seyler's Z. Physiol. Chem.* 1975, **356**, 213
- 2 Reisfeld, R. A., Lewis, V. J. and Williams, K. E. *Nature* 1972, **195**, 281
- 3 Myers, D. V. and Edsall, J. T. *Proc. Natl. Acad. Sci. USA* 1965, **53**, 169
- 4 Rosenberg, A. *J. Biol. Chem.* 1966, **241**, 5119
- 5 Fasman, G. D. and Potter, J. *Biochim. Biophys. Res. Commun.* 1967, **27**, 209
- 6 Coleman, D. L. and Blout, E. R. *J. Am. Chem. Soc.* 1968, **90**, 2405
- 7 Davidson, B. and Fasman, G. D. *Biochemistry* 1967, **6**, 1616
- 8 Krimm, S. *Proc. Natl. Acad. Sci. USA* 1962, **4**, 528

Structure of a compatible mixture of two polymers as revealed by low-angle neutron scattering

This letter reports results of a brief investigation made, using low-angle neutron scattering measurements, of the extent of segregation and dimensions of polymer molecules in a compatible mixture of two polymers. In recent years, the technique of low-angle neutron scattering has been developed to study molecular dimensions in amorphous polymers in the solid state¹⁻⁴. This method relies on the large difference in the coherent scattering length for neutron diffraction between hydrogen and deuterium atoms to provide the required contrast. For example, the neutron scattering pattern from a perdeutero polymer tagged with say 5% protopolymer, depending on molecular weight, may be compared with the scattering from a perdeutero polymer blank. Using this technique it is possible to examine the size of the molecules and, at the same time, check that the tagged molecules are statistically distributed within the sample and not clustered together. The technique has also been applied to semi-crystalline polymer systems both in the melt^{5,6} and solid state⁷ as well as to studies of polymer solutions^{8,9}. In addition, Kirste *et al.*⁸ have reported an initial result for an incompatible mixture of two homopolymers, poly(methyl methacrylate) and poly(α -methylstyrene). They deduce from the scattering results that, for this system, the poly(α -methylstyrene) formed spherical aggregates each containing about sixteen molecules (weight-average). However, as yet nothing is known about the distribution or dimensions of polymer molecules in an apparently compatible mixture: do the molecules adopt their unperturbed configuration as in an amorphous homopolymer or are the dimensions of the molecules affected by neighbouring unlike molecules? Are the molecules statistically distributed or is there any clustering of like molecules? The purpose of the experiments reported here was to attempt to elucidate the structure in a compatible polymer mixture.

The polymer system selected for

this investigation was polystyrene/poly(α -methylstyrene). At high molecular weights this system is reported to be incompatible but, in the lower molecular weight region we have used, compatible mixtures have been observed¹⁰. In addition, calculations made using the procedure described by Krause¹¹, based upon the Flory-Huggins theory of polymer solutions, have indicated that the polymer mixtures described below should be compatible.

The neutron scattering samples were prepared using polymers produced by anionic polymerizations: molecular weights obtained by gel permeation chromatography and compositions of the mixtures are shown in *Table 1*. The polydeuterostyrene was 98% deuterated. The concentration of tagged molecules, polyprotostyrene, in the samples was restricted to 5% which was low enough to ensure 'dilute solution' scattering behaviour¹². Mixtures were prepared by dissolving in chloroform and precipitating into methanol.

Each mixture appears to be a compatible system according to the differential scanning calorimetry data shown in *Table 1*. These data were obtained at a heating rate of 20°C/min. The

mixtures showed only broad transitions with no detectable transition corresponding to any of the homopolymers.

Low-angle neutron scattering experiments were performed at Jülich using a sample to detector distance of 3 m and a neutron wavelength of 7.2 Å. Guinier plots were constructed from the corrected scattering patterns obtained for each tagged sample and the intercept and slope used to derive the weight-average molecular weight, \bar{M}_w and the z-average radius of gyration, $\langle s^2 \rangle_z^{1/2}$, respectively. Both tagged samples gave a value for the polyprotostyrene \bar{M}_w of $54\,000 \pm 5000$ and for $\langle s^2 \rangle_z^{1/2}$ of 61 ± 2 Å. It will be seen from *Table 1* that the weight-average molecular weight derived from neutron scattering is identical with the g.p.c. datum. Because of this excellent agreement, a Zimm plot procedure was not considered necessary. This result clearly shows that in a compatible mixture of two polymers the molecules are statistically distributed. This contrasts with Kirste's result for an incompatible system where clustering was observed.

The weight-average radius of gyration, $\langle s^2 \rangle_w^{1/2}$, obtained from neutron scattering after correction for polydis-

Table 1 Compositions and d.s.c. data for polymer mixtures used in neutron scattering experiments

Polymers	G.p.c. \bar{M}_w	T_g (°C)	
		Onset	Finish
A Polyprotostyrene	54 000	103	110
B Polydeuterostyrene	128 000	102	109
C Poly(deutero- α -methylstyrene)	32 000	170	178

Mixtures	Composition (wt %)			T_g (°C)	
	A	B	C	Onset	Finish
6 (blank for 7)		10	90	155	172
7	5	5	90	154	173
8 (blank for 9)		5	95	156	171
9	5		95	162	174

persity was $54 \pm 2 \text{ \AA}$. This may be compared with a value of $63 \pm 3 \text{ \AA}$ calculated for an unperturbed system using $\langle s_0 \rangle_w^{1/2} = 0.660 \bar{M}_w^{1/2} / (6)^{1/2}$. The measured radius of gyration is thus near to, or slightly less than, the unperturbed value. If the uncertainties in the measurements are as low as indicated there is a small reduction in radius of gyration below that of the unperturbed value. Similar behaviour has been both observed¹³ and described theoretically¹⁴ for a single phase polymer solution in a poor solvent below the theta-temperature, when the second virial coefficient will be negative.

The main conclusion from the results of this work is that it is possible to produce a truly compatible mixture of two polymers in which the molecules are statistically distributed. This result may be used to clarify what is meant by the term 'polymer compatibility' and to impose a new criterion for establishing compatible polymer systems.

Acknowledgements

We wish to thank Mr P. Cheshire for synthesizing the polymers used in these experiments and Mr T. L. Crowley for computational assistance.

D. G. H. Ballard
and M. G. Rayner

ICI Ltd, Corporate Laboratory,
The Heath, Runcorn, Cheshire WA7 4QE,
UK

and J. Schelten

Institut für Festkörperforschung der
Kernforschungsanlage GmbH,
D-5170 Jülich 1, Postfach 1913,
Germany
(Received 4 March 1976)

References

- 1 Kirste, R. G., Kruse, W. A. and Schelten, J. *Makromol. Chem.* 1972, **162**, 299
- 2 Ballard, D. G. H., Wignall, G. D. and Schelten, J. *Eur. Polym. J.* 1973, **9**,

- 3 Benoit, H., Cotton, J. P., Decker, D., Farnoux, B., Higgins, J. S., Jannink, G., Ober, R. and Picot, C. *Nature* 1973, **245**, 13
- 4 Wignall, G. D., Ballard, D. G. H. and Schelten, J. *Eur. Polym. J.* 1974, **10**, 861
- 5 Schelten, J., Wignall, G. D. and Ballard, D. G. H. *Polymer* 1974, **15**, 682
- 6 Lieser, G., Fischer, E. W. and Ibel, K. *J. Polym. Sci.* 1975, **13**, 39
- 7 Schelten, J., Ballard, D. G. H., Wignall, G. D., Longman, G. and Schmatz, W. to be published
- 8 Kirste, R. G., Kruse, W. A. and Ibel, K. *Polymer* 1975, **16**, 120
- 9 Ballard, D. G. H., Rayner, M. G. and Schelten, J. *Polymer* 1976, **17**, 349
- 10 Dunn, D. J. and Krause, S. *J. Polym. Sci. (Polym. Lett. Edn)* 1974, **12**, 591
- 11 Krause, S. *J. Macromol. Sci. (C)* 1972, **7**, 251
- 12 Cotton, J. P., Farnoux, B. and Jannink, G. *J. Chem. Phys.* 1972, **57**, 290
- 13 Outer, P., Carr, C. I. and Zimm, B. H. *J. Chem. Phys.* 1950, **18**, 830
- 14 Flory, P. J. 'Principles of Polymer Chemistry', Cornell University Press, Ithaca, 1953

Optically active vinyl polymers containing fluorescent groups: 1. Synthesis and properties of copolymers of *N*-vinylcarbazole with optically active monomers

Introduction

Chiroptical properties of copolymers of vinylaromatic monomers with optically active α -olefins¹⁻³ have been useful in helping to define the conformational requirements of aromatic moieties inserted in a regular conformational environment. Studies of the same properties in copolymers of *N*-vinylcarbazole with optically active monomers could, in principle, permit a valuable approach to the correlation of luminescence and photoelectrical properties of poly(*N*-vinylcarbazole) with the stereochemical arrangement of monomeric units. In the present paper we report preliminary results of copolymerization experiments of *N*-vinylcarbazole (NVC) with optically active monomers (α -olefins, alkyl vinyl ethers, acrylates and methacrylates) in the presence of different catalytic systems.

Results and Discussion

Copolymerizations of NVC with optically active comonomers have been carried out in the presence of various catalytic systems which are capable of polymerizing NVC and/or the selected comonomers. In Table 1 data are collected for those reactions giving poly-

mer yields in excess of 10%. In all cases regular linear enchainment of monomeric units is substantiated by n.m.r. and i.r. spectroscopy which show the presence of bands characteristic of only unsubstituted carbazole rings. By using a conventional cationic catalyst (EtAlCl_2) and experimental conditions which are claimed to give stereoregular poly(alkyl vinyl ethers)⁴ and poly(*N*-vinylcarbazole)⁵, three different alkyl vinyl ethers having an asymmetric carbon atom in the β -position with respect to the double bond (BVE, TPVE, MVE) and one (MBVE) having the chiral centre γ to the double bond, have been copolymerized with NVC (Runs C1-C5). In one case (Run C6) a complex catalyst based on $\text{Al}(\text{iso-C}_4\text{H}_9)_3$ and H_2SO_4 was used⁶. (Full structures of the alkyl vinyl ether monomers are given later.)

Moderately high molecular weight polymers ($\bar{M}_n < 2 \times 10^4$) were obtained and, in the runs where the overall conversion is lower than 90%, the polymerization rate of NVC is always larger than that of alkyl vinyl ethers except Run C1 where BVE is polymerized more quickly than NVC. The solubility characteristics of the copolymerization products (polymers con-

taining appreciable amounts of NVC units are soluble to an extent greater than 90% in cyclohexane, which is a very poor solvent for poly(*N*-vinylcarbazole) as well as measurements of optical rotation and differential dichroic absorption ($\Delta\epsilon$) indicate the formation of copolymer macromolecules. In fact in all cases c.d. spectra show the presence of two complex dichroic bands at about 300 and 260 nm having practically the same rotatory strength ($\theta \approx 5 \times 10^3/\text{mol NVC unit}$), and it is particularly interesting that no dichroic band can be observed corresponding to the u.v. band at 350 nm associated with the ${}^1L_b \leftarrow {}^1A$ transition in the carbazole ring⁷.

Copolymerization of NVC with (*S*)-4-methyl-1-hexene, in the presence of the $\text{Al}(\text{iso-C}_4\text{H}_9)_3/\text{TiCl}_4$ catalytic system, which is claimed to polymerize NVC^{8,9} as well as α -olefins¹⁰ by an anionic coordinated mechanism, yielded only a mixture of the two homopolymers, supporting previous conclusions¹¹ that these types of monomers polymerize by independent routes. Therefore earlier assumptions of polymerization of NVC by an anionic coordinated mechanism seem to be questionable.

persity was $54 \pm 2 \text{ \AA}$. This may be compared with a value of $63 \pm 3 \text{ \AA}$ calculated for an unperturbed system using $\langle s_0 \rangle_w^{1/2} = 0.660 \bar{M}_w^{1/2} / (6)^{1/2}$. The measured radius of gyration is thus near to, or slightly less than, the unperturbed value. If the uncertainties in the measurements are as low as indicated there is a small reduction in radius of gyration below that of the unperturbed value. Similar behaviour has been both observed¹³ and described theoretically¹⁴ for a single phase polymer solution in a poor solvent below the theta-temperature, when the second virial coefficient will be negative.

The main conclusion from the results of this work is that it is possible to produce a truly compatible mixture of two polymers in which the molecules are statistically distributed. This result may be used to clarify what is meant by the term 'polymer compatibility' and to impose a new criterion for establishing compatible polymer systems.

Acknowledgements

We wish to thank Mr P. Cheshire for synthesizing the polymers used in these experiments and Mr T. L. Crowley for computational assistance.

D. G. H. Ballard
and M. G. Rayner

ICI Ltd, Corporate Laboratory,
The Heath, Runcorn, Cheshire WA7 4QE,
UK

and J. Schelten

Institut für Festkörperforschung der
Kernforschungsanlage GmbH,
D-5170 Jülich 1, Postfach 1913,
Germany
(Received 4 March 1976)

References

- 1 Kirste, R. G., Kruse, W. A. and Schelten, J. *Makromol. Chem.* 1972, **162**, 299
- 2 Ballard, D. G. H., Wignall, G. D. and Schelten, J. *Eur. Polym. J.* 1973, **9**,

- 3 Benoit, H., Cotton, J. P., Decker, D., Farnoux, B., Higgins, J. S., Jannink, G., Ober, R. and Picot, C. *Nature* 1973, **245**, 13
- 4 Wignall, G. D., Ballard, D. G. H. and Schelten, J. *Eur. Polym. J.* 1974, **10**, 861
- 5 Schelten, J., Wignall, G. D. and Ballard, D. G. H. *Polymer* 1974, **15**, 682
- 6 Lieser, G., Fischer, E. W. and Ibel, K. *J. Polym. Sci.* 1975, **13**, 39
- 7 Schelten, J., Ballard, D. G. H., Wignall, G. D., Longman, G. and Schmatz, W. to be published
- 8 Kirste, R. G., Kruse, W. A. and Ibel, K. *Polymer* 1975, **16**, 120
- 9 Ballard, D. G. H., Rayner, M. G. and Schelten, J. *Polymer* 1976, **17**, 349
- 10 Dunn, D. J. and Krause, S. *J. Polym. Sci. (Polym. Lett. Edn)* 1974, **12**, 591
- 11 Krause, S. *J. Macromol. Sci. (C)* 1972, **7**, 251
- 12 Cotton, J. P., Farnoux, B. and Jannink, G. *J. Chem. Phys.* 1972, **57**, 290
- 13 Outer, P., Carr, C. I. and Zimm, B. H. *J. Chem. Phys.* 1950, **18**, 830
- 14 Flory, P. J. 'Principles of Polymer Chemistry', Cornell University Press, Ithaca, 1953

Optically active vinyl polymers containing fluorescent groups: 1. Synthesis and properties of copolymers of *N*-vinylcarbazole with optically active monomers

Introduction

Chiroptical properties of copolymers of vinylaromatic monomers with optically active α -olefins¹⁻³ have been useful in helping to define the conformational requirements of aromatic moieties inserted in a regular conformational environment. Studies of the same properties in copolymers of *N*-vinylcarbazole with optically active monomers could, in principle, permit a valuable approach to the correlation of luminescence and photoelectrical properties of poly(*N*-vinylcarbazole) with the stereochemical arrangement of monomeric units. In the present paper we report preliminary results of copolymerization experiments of *N*-vinylcarbazole (NVC) with optically active monomers (α -olefins, alkyl vinyl ethers, acrylates and methacrylates) in the presence of different catalytic systems.

Results and Discussion

Copolymerizations of NVC with optically active comonomers have been carried out in the presence of various catalytic systems which are capable of polymerizing NVC and/or the selected comonomers. In Table 1 data are collected for those reactions giving poly-

mer yields in excess of 10%. In all cases regular linear enchainment of monomeric units is substantiated by n.m.r. and i.r. spectroscopy which show the presence of bands characteristic of only unsubstituted carbazole rings. By using a conventional cationic catalyst (EtAlCl_2) and experimental conditions which are claimed to give stereoregular poly(alkyl vinyl ethers)⁴ and poly(*N*-vinylcarbazole)⁵, three different alkyl vinyl ethers having an asymmetric carbon atom in the β -position with respect to the double bond (BVE, TPVE, MVE) and one (MBVE) having the chiral centre γ to the double bond, have been copolymerized with NVC (Runs C1-C5). In one case (Run C6) a complex catalyst based on $\text{Al}(\text{iso-C}_4\text{H}_9)_3$ and H_2SO_4 was used⁶. (Full structures of the alkyl vinyl ether monomers are given later.)

Moderately high molecular weight polymers ($\bar{M}_n < 2 \times 10^4$) were obtained and, in the runs where the overall conversion is lower than 90%, the polymerization rate of NVC is always larger than that of alkyl vinyl ethers except Run C1 where BVE is polymerized more quickly than NVC. The solubility characteristics of the copolymerization products (polymers con-

taining appreciable amounts of NVC units are soluble to an extent greater than 90% in cyclohexane, which is a very poor solvent for poly(*N*-vinylcarbazole) as well as measurements of optical rotation and differential dichroic absorption ($\Delta\epsilon$) indicate the formation of copolymer macromolecules. In fact in all cases c.d. spectra show the presence of two complex dichroic bands at about 300 and 260 nm having practically the same rotatory strength ($\theta \approx 5 \times 10^3/\text{mol NVC unit}$), and it is particularly interesting that no dichroic band can be observed corresponding to the u.v. band at 350 nm associated with the ${}^1L_b \leftarrow {}^1A$ transition in the carbazole ring⁷.

Copolymerization of NVC with (*S*)-4-methyl-1-hexene, in the presence of the $\text{Al}(\text{iso-C}_4\text{H}_9)_3/\text{TiCl}_4$ catalytic system, which is claimed to polymerize NVC^{8,9} as well as α -olefins¹⁰ by an anionic coordinated mechanism, yielded only a mixture of the two homopolymers, supporting previous conclusions¹¹ that these types of monomers polymerize by independent routes. Therefore earlier assumptions of polymerization of NVC by an anionic coordinated mechanism seem to be questionable.

Table 1 Copolymerization of vinylcarbazole (M_1) with optically active comonomers (M_2) in the presence of different catalytic systems

Run	Polymerization conditions				Conversion (%)	Polymeric product			
	Comonomer (M_2)		Molar ratio M_2/M_1 (mol/mol)	Catalyst		Molar ratio ^a M_2/M_1 (mol/mol)	$\bar{M}_n \times 10^{-3}$ ^b	$[\alpha]_D^{25}$ ^c	$[\alpha]_D^{0d}$
	Type	Amount (mmol)							
C1	BVE	15.5	3	EtAlCl ₂	46	5.0	—	+157	+204
C2	BVE	12.2	1		94	1.1	10.8	+ 53	+ 89
C3	TPVE	1.2	1		94	1.1	14.1	+ 83	+ 90
C4	MVE	23.3	3		17	2.1	17.6	-128	-133
C5	MBVE	16.0	1		32	0.36	9.9	+0.76	+0.70
C6	MBVE	16.0	1	Al(iso-C ₄ H ₉) ₃ /H ₂ SO ₄	19	0.58	5.5	+1.21	+1.15
ZN1	4ME	13.0	1	Al(iso-C ₄ H ₉) ₃ /TiCl ₄	65	0.1	—	+218 ^e	+245
RA1	MA	13.3	2	AIBN	88	1.7	0.28 ^f	- 74	- 53
RM1	MMA	7.8	2	AIBN	44	2.0	0.20 ^f	- 69	- 67

^aDetermined by n.m.r. spectroscopy and/or elemental analysis; ^bby vapour pressure osmometry in benzene at 37°C; ^cin CHCl₃ ($c = 1-5$ g/dl); ^devaluated for homopolymer mixture having the same composition as the corresponding copolymerization product; ^erelated to the fraction extracted with cyclohexane containing 88% of NVC monomeric units; ^fintrinsic viscosity in benzene at 25°C

In the presence of a conventional radical initiator (AIBN) NVC has been copolymerized with menthyl acrylate and methacrylate. The relative polymerization rate of the comonomers seems to be very similar, and formation of copolymers was established on the basis indicated above.

Finally in the presence of a conventional anionic catalyst (C₆H₅MgBr) both the comonomer mixtures gave polymers in very poor yield (conversion $\leq 5\%$), and which at the present have not been further characterized.

Studies are in progress to prepare copolymers of NVC with optically active alkyl vinyl ethers, acrylates and methacrylates in order to investigate the correlations between physico-optical properties on the one hand, with chemical composition, distribution of monomeric units, and stereoregularity of the copolymerization products.

Conclusions

Copolymers of optically active alkyl vinyl ethers, menthyl acrylates or methacrylates with *N*-vinylcarbazole can be obtained by copolymerization in the presence of conventional cationic catalyst or radical initiator respectively. Extraction of the polymeric products with boiling solvents, as well as their optical rotation and differential dichroic absorption demonstrates the formation of copolymer macromolecules rather than mixtures of homopolymers.

Attempts to copolymerize NVC with α -olefins, menthyl acrylate or methacrylate in the presence of anionic coordinated or anionic catalysts were unsuccessful.

Experimental

Monomers. (*S*)-4-methyl-1-hexene

(4 ME), $[\alpha]_D^{25} - 2.82$ (neat), optical purity 93.0%¹² was prepared according to the procedure already described¹².

[(*S*)-1-methylpropyl]-vinyl ether (BVE), $[\alpha]_D^{25} + 12.5$ (neat), optical purity 87.1%¹³; [(*S*)-2-methylbutyl]-vinyl ether (MBVE), $[\alpha]_D^{25} - 5.82$ (neat), optical purity 100%¹⁴; [(*S*)-1,2,2-trimethylpropyl]-vinyl ether (TPVE), $[\alpha]_D^{25} - 8.00$ (neat), optical purity 78.0%¹⁵ and (-)-menthyl vinyl ether (MVE), $[\alpha]_D^{25} - 73.6$ (neat), optical purity 100%^{13,16} have been prepared by transvinylolation¹⁷ starting from the corresponding optically active alcohols.

(-)-Menthyl acrylate (MA), $[\alpha]_D^{25} - 89.9$ (benzene), optical purity 97.0%¹⁸ was prepared by the reaction of methyl acrylate with menthoxymagnesium bromide¹⁹. (-)-Menthyl methacrylate (MMA), $[\alpha]_D^{25} - 91.8$ (neat), optical purity 99% was prepared as already reported¹⁵.

N-vinylcarbazole (NVC) (commercial grade purity) was purified by crystallization from *n*-hexane (m.p. 65°C)²⁰.

Catalysts. AIBN and TiCl₄ analytical grade purity were used without further purification. EtAlCl₂ and Al(iso-C₄H₉)₃ were distilled at reduced pressure prior to use. Al(iso-C₄H₉)₃/H₂SO₄ catalyst was prepared by adding H₂SO₄ (100%) dropwise to a solution of Al(iso-C₄H₉)₃ in *n*-heptane [Al(iso-C₄H₉)₃/H₂SO₄ = 4.5 mol/mol^{6,21}].

Copolymerization of NVC with (*S*)-4-methyl-1-hexene. The run was carried out in a glass vial under dry nitrogen. Equimolecular comonomer mixture was added at 0°C to the catalytic slurry obtained by reacting TiCl₄ with Al(iso-C₄H₉)₃ in toluene, comonomers/

TiCl₄ = 50 mol/mol, [Al(iso-C₄H₉)₃/TiCl₄ = 3 mol/mol]⁸. The run which was stopped after 70 h by addition of methanol, gave a polymeric product (68.4% yield evaluated as weight of polymer/weight of the starting comonomer mixture) constituted mainly (95%) of poly(*N*-vinylcarbazole).

Copolymerization of NVC with (-)-menthyl acrylate and methacrylate. Both runs were carried out in vials sealed under vacuum in the presence of AIBN at 70°C. 1 M solutions of comonomers in benzene were used and the polymerization were interrupted after 6 h.

Copolymerization of NVC with alkyl vinyl ethers. The copolymerization runs were carried out in glass vials at -78°C and -15°C when EtAlCl₂ and Al(iso-C₄H₉)₃/H₂SO₄ catalyst was used respectively. 1 M toluene solutions of comonomers were used.

Characterization of copolymerization products. The crude polymeric products, after reprecipitation from methanol, were characterized as unfractionated materials, but in some cases were fractionated by extraction with boiling solvents under nitrogen in Kumagawa extractors²² by using methanol, acetone, cyclohexane, and toluene or chloroform in that order. Chemical compositions of polymeric products were determined by elemental analysis and/or n.m.r. spectroscopy using a Varian T60 or a Jeol JNM-PS-100 spectrometer. Optical rotatory measurements were performed on a Perkin-Elmer Model 141 with sensitivity $\pm 0.003^\circ$ using chloroform solutions having a concentration in the range 0.5-5 g/dl. C.d. and u.v. spectra were measured for solutions in the range 240-400 nm using a Jouan II dichrograph and a Cary Model 14 Spectrophotometer.

Acknowledgement

The authors are grateful to the Science Research Council for the award of a Senior Research Assistantship (R. S.)

E. Chiellini, R. Solaro and
M. Palmieri

Centro di Studio del CNR per le
Macromolecole Stereoordinate ed
Otticamente Attive, Istituto di
Chimica Organica Industriale,
Universita di Pisa, Pisa, Italy

A. Ledwith

Department of Industrial Physical and
Inorganic Chemistry,
University of Liverpool, Liverpool,
L69 3BX, UK
(Received 26 March, 1976)

References

- Pino, P., et al. *J. Am. Chem. Soc.* 1968, **90**, 5025
- Ciardelli, F., Salvadori, P., Carlini, C. and Chiellini, E. *J. Am. Chem. Soc.* 1972, **94**, 6536
- Carlini, C. and Chiellini, E. *Makromol. Chem.* 1975, **176**, 519
- Natta, G., Dall'Asta, G., Mazzanti, G., Giannini, U. and Cesca, S. *Angew. Chem.* 1959, **71**, 205
- Dall'Asta, G. and Casale, A. *Rend. Acc. Naz. Lincei, Ser. VIII* 1965, **39**, 291
- Christman, D. L. and Vandenberg, E. J. US Pat. 3 025 282 (1962)
- Johnson, G. E. *J. Phys. Chem.* 1974, **78**, 1512
- Heller, J., Tieszen, D. O. and Parkinson, D. B. *J. Polym. Sci. (A)* 1963, **1**, 125
- Solomon, O. F., Dimonie, M., Ambroz, K. and Tomesku, M. *J. Polym. Sci.* 1961, **52**, 205
- Pino, P. *Adv. Polym. Sci.* 1965, **4**, 393
- Chiellini, E. and Nocci, R. *J. Polym. Sci. (Polym. Chem. Edn)* 1973, **11**, 493
- Pino, P., Lardicci, L. and Centoni, L. *Gazz. Chim. Ital.* 1961, **91**, 428
- Chiellini, E. *Gazz. Chim. Ital.* 1972, **102**, 830
- Lorenzi, G. P., Benedetti, E. and Chiellini, E. *Chim. Ind. (Milan)* 1964, **46**, 1474
- Lazzaroni, R. unpublished results
- Chiellini, E. *Macromolecules* 1970, **3**, 527
- Watanabe, W. H. and Conlon, L. E. *J. Am. Chem. Soc.* 1957, **79**, 2828
- Schulz, R. C. and Kaiser, F. *Makromol. Chem.* 1965, **86**, 80
- Frank, R. L., Davis, H. R., Drake, S. S. and McPherson, J. B. *J. Am. Chem. Soc.* 1944, **66**, 1509
- Natsuume, T., Nishimura, M., Fujimatsu, M., Shimizu, M., Shirota, Y., Kusabayashi, S. and Mikawa, H. *Polym. J.* 1970, **1**, 181
- Vandenberg, E. J., Heck, R. F. and Breslow, D. S. *J. Polym. Sci.* 1959, **41**, 519
- Natta, G., Pino, P. and Mazzanti, G. *Gazz. Chim. Ital.* 1957, **87**, 528

Novel synthesis of 2-vinylanthraquinone

Introduction

We have recently concentrated some attention on the synthesis, characterization and evaluation of various potentially intrinsically useful polymers. One system which appears to offer particular promise concerns poly(2-vinylanthraquinone). Earlier syntheses^{1,2} of a vinyl polymer containing the anthraquinone system were aimed at the production of materials containing redox groups and generally took the form of 2-vinylanthraquinone/styrene/divinylbenzene crosslinked networks. However, in recent years, the photochemistry and the stereochemistry of polymers containing large pendant π -systems has gained much interest. *N*-vinylcarbazole deserves particular mention in this respect³. Our interest in 2-vinylanthraquinone concerns its role as an intermediate in the synthesis of polymers having both novel and useful characteristics including intrinsic colour.

More recent syntheses of 2-vinylanthraquinone involve the use of high temperatures and catalysts, and require that the reacting species be in the vapour phase^{4,5}. Consequently yields are irreproducible and the products difficult to purify. Using this type of procedure Manecke⁶ has reportedly achieved yields of 2-vinylanthraquinone of the order of 83%. We have not been able to obtain yields at this level and

the reaction product composition was found to be un-reproducible as were the final yields.

Fernandez-Refojo *et al.*⁷ have devised an alternative route to 2-vinylanthraquinone which involves synthesis of anthraquinone-2-aldehyde, conversion to the 2-acrylic acid derivative which is subsequently decarboxylated to the vinyl compound (yield 25.7%).

Here we report details of an alternative, novel and reproducible route to 2-vinylanthraquinone, which results in significantly higher yields of the monomer, and involves forming the vinyl derivative from the aldehyde via the Wittig reaction.

The reaction of anthraquinone-2-aldehyde with the ylid, produced from methyl-triphenyl phosphonium bromide and phenyl lithium, did not give the corresponding expected 2-vinylanthraquinone but instead gave a stable blood-red complex. This was probably an ion-pair formed from interaction between the intermediate betaine and lithium bromide which is produced in the synthesis of the ylid⁸. Subsequently the stronger base, potassium *t*-butoxide (as a 1:1 complex with *t*-butanol in tetrahydrofuran) was employed. The reaction gave 2-vinylanthraquinone in high purity and allowed recovery of the unreacted aldehyde. This was then available for use in subsequent syntheses, thus ensuring mini-

mal losses of important intermediates.

Experimental

For ease of replication, full experimental details are presented.

Reagents. *t*-Butanol was distilled from fresh sodium. Tetrahydrofuran (THF) previously stored over sodium, was freshly distilled from lithium aluminium hydride prior to use. Benzene was dried over sodium after distillation from sodium. With the exception of potassium *t*-butoxide, which was stored in the cold, organic solids were dried to constant weight in a vacuum oven at 50°C. Nitrogen (oxygen-free) was dried by passing through sulphuric acid and calcium chloride.

Synthesis. A vigorously stirred suspension of 4.47 g (0.0135 mol) of methyl-triphenyl phosphonium bromide in 100 ml of benzene under a nitrogen atmosphere was treated to slow addition of a THF solution of 1.66 g (0.0148 mol) potassium *t*-butoxide complexed with 1.03 g (0.0148 mol) of *t*-butanol. The mixture was allowed to stand for 3/4 h, filtered and the filtrate added dropwise (over 2 h) to a refluxing, stirred solution of 3 g (0.135 mol) of anthraquinone-2-aldehyde in 80 ml of benzene under an atmosphere of nitrogen (the aldehyde was prepared, following the method of Fernandez-Refojo⁷ *et al.*, in 48% yields). The solution volume

Acknowledgement

The authors are grateful to the Science Research Council for the award of a Senior Research Assistantship (R. S.)

E. Chiellini, R. Solaro and
M. Palmieri

Centro di Studio del CNR per le
Macromolecole Stereoordinate ed
Otticamente Attive, Istituto di
Chimica Organica Industriale,
Universita di Pisa, Pisa, Italy

A. Ledwith

Department of Industrial Physical and
Inorganic Chemistry,
University of Liverpool, Liverpool,
L69 3BX, UK
(Received 26 March, 1976)

References

- Pino, P., et al. *J. Am. Chem. Soc.* 1968, **90**, 5025
- Ciardelli, F., Salvadori, P., Carlini, C. and Chiellini, E. *J. Am. Chem. Soc.* 1972, **94**, 6536
- Carlini, C. and Chiellini, E. *Makromol. Chem.* 1975, **176**, 519
- Natta, G., Dall'Asta, G., Mazzanti, G., Giannini, U. and Cesca, S. *Angew. Chem.* 1959, **71**, 205
- Dall'Asta, G. and Casale, A. *Rend. Acc. Naz. Lincei, Ser. VIII* 1965, **39**, 291
- Christman, D. L. and Vandenberg, E. J. US Pat. 3 025 282 (1962)
- Johnson, G. E. *J. Phys. Chem.* 1974, **78**, 1512
- Heller, J., Tieszen, D. O. and Parkinson, D. B. *J. Polym. Sci. (A)* 1963, **1**, 125
- Solomon, O. F., Dimonie, M., Ambroz, K. and Tomesku, M. *J. Polym. Sci.* 1961, **52**, 205
- Pino, P. *Adv. Polym. Sci.* 1965, **4**, 393
- Chiellini, E. and Nocci, R. *J. Polym. Sci. (Polym. Chem. Edn)* 1973, **11**, 493
- Pino, P., Lardicci, L. and Centoni, L. *Gazz. Chim. Ital.* 1961, **91**, 428
- Chiellini, E. *Gazz. Chim. Ital.* 1972, **102**, 830
- Lorenzi, G. P., Benedetti, E. and Chiellini, E. *Chim. Ind. (Milan)* 1964, **46**, 1474
- Lazzaroni, R. unpublished results
- Chiellini, E. *Macromolecules* 1970, **3**, 527
- Watanabe, W. H. and Conlon, L. E. *J. Am. Chem. Soc.* 1957, **79**, 2828
- Schulz, R. C. and Kaiser, F. *Makromol. Chem.* 1965, **86**, 80
- Frank, R. L., Davis, H. R., Drake, S. S. and McPherson, J. B. *J. Am. Chem. Soc.* 1944, **66**, 1509
- Natsuume, T., Nishimura, M., Fujimatsu, M., Shimizu, M., Shirota, Y., Kusabayashi, S. and Mikawa, H. *Polym. J.* 1970, **1**, 181
- Vandenberg, E. J., Heck, R. F. and Breslow, D. S. *J. Polym. Sci.* 1959, **41**, 519
- Natta, G., Pino, P. and Mazzanti, G. *Gazz. Chim. Ital.* 1957, **87**, 528

Novel synthesis of 2-vinylanthraquinone

Introduction

We have recently concentrated some attention on the synthesis, characterization and evaluation of various potentially intrinsically useful polymers. One system which appears to offer particular promise concerns poly(2-vinylanthraquinone). Earlier syntheses^{1,2} of a vinyl polymer containing the anthraquinone system were aimed at the production of materials containing redox groups and generally took the form of 2-vinylanthraquinone/styrene/divinylbenzene crosslinked networks. However, in recent years, the photochemistry and the stereochemistry of polymers containing large pendant π -systems has gained much interest. *N*-vinylcarbazole deserves particular mention in this respect³. Our interest in 2-vinylanthraquinone concerns its role as an intermediate in the synthesis of polymers having both novel and useful characteristics including intrinsic colour.

More recent syntheses of 2-vinylanthraquinone involve the use of high temperatures and catalysts, and require that the reacting species be in the vapour phase^{4,5}. Consequently yields are irreproducible and the products difficult to purify. Using this type of procedure Manecke⁶ has reportedly achieved yields of 2-vinylanthraquinone of the order of 83%. We have not been able to obtain yields at this level and

the reaction product composition was found to be un-reproducible as were the final yields.

Fernandez-Refojo *et al.*⁷ have devised an alternative route to 2-vinylanthraquinone which involves synthesis of anthraquinone-2-aldehyde, conversion to the 2-acrylic acid derivative which is subsequently decarboxylated to the vinyl compound (yield 25.7%).

Here we report details of an alternative, novel and reproducible route to 2-vinylanthraquinone, which results in significantly higher yields of the monomer, and involves forming the vinyl derivative from the aldehyde via the Wittig reaction.

The reaction of anthraquinone-2-aldehyde with the ylid, produced from methyl-triphenyl phosphonium bromide and phenyl lithium, did not give the corresponding expected 2-vinylanthraquinone but instead gave a stable blood-red complex. This was probably an ion-pair formed from interaction between the intermediate betaine and lithium bromide which is produced in the synthesis of the ylid⁸. Subsequently the stronger base, potassium *t*-butoxide (as a 1:1 complex with *t*-butanol in tetrahydrofuran) was employed. The reaction gave 2-vinylanthraquinone in high purity and allowed recovery of the unreacted aldehyde. This was then available for use in subsequent syntheses, thus ensuring mini-

mal losses of important intermediates.

Experimental

For ease of replication, full experimental details are presented.

Reagents. *t*-Butanol was distilled from fresh sodium. Tetrahydrofuran (THF) previously stored over sodium, was freshly distilled from lithium aluminium hydride prior to use. Benzene was dried over sodium after distillation from sodium. With the exception of potassium *t*-butoxide, which was stored in the cold, organic solids were dried to constant weight in a vacuum oven at 50°C. Nitrogen (oxygen-free) was dried by passing through sulphuric acid and calcium chloride.

Synthesis. A vigorously stirred suspension of 4.47 g (0.0135 mol) of methyl-triphenyl phosphonium bromide in 100 ml of benzene under a nitrogen atmosphere was treated to slow addition of a THF solution of 1.66 g (0.0148 mol) potassium *t*-butoxide complexed with 1.03 g (0.0148 mol) of *t*-butanol. The mixture was allowed to stand for 3/4 h, filtered and the filtrate added dropwise (over 2 h) to a refluxing, stirred solution of 3 g (0.135 mol) of anthraquinone-2-aldehyde in 80 ml of benzene under an atmosphere of nitrogen (the aldehyde was prepared, following the method of Fernandez-Refojo⁷ *et al.*, in 48% yields). The solution volume

was reduced by 50% by distillation and the residue allowed to reflux for 1 h. By this time the blood-red colour of the betaine intermediate had almost disappeared. The resulting mixture was poured slowly into a 3 fold excess of ligroin (60°–80°C) and the precipitate of triphenyl phosphine oxide separated. Residual solvents were removed and the yellow residue (aldehyde–vinyl anthraquinone mixture) partly dissolved in benzene/ligroin (3:1). The insoluble residue of unreacted aldehyde was recovered for recycling. The crude 2-vinylanthraquinone was purified by column elution with 4:1 ligroin/benzene. Recrystallization from 3:1 benzene/methanol gave pale yellow needles, melting point 176°–177°C, in 61% yield. Such yields have been maintained on repeated preparations. Analysis calculated for C₁₆H₁₀O₂: C, 82.05; H, 4.30. Found: C, 82.08; H, 4.50. The infra-red spectrum was found to be identical with the product

of the method of Manecké^{1,2}.

In forming vinyl compounds from aldehydes using the Wittig reaction the more customary addition of the aldehyde had to be reversed in order to reduce reaction at the 9,10-quinone positions. Any reaction in the 9,10-quinone positions of the anthraquinone nucleus gives 9,10-dimethylanthracene derivatives as highly fluorescent and unwanted side-products. It is the production of vinyl compounds, from a precursor containing both aldehyde and ketonic groups, by making use of the greater reactivity of the aldehyde group, which gives this preparation its originality, within the present context and creates a route for the production of many similar compounds.

Work is at present being carried out by one of us (A. J. G.) concerning the γ -ray, thermal, chemical and ionic routes to polymers based on vinylanthraquinones and their derivatives. Our immediate interest lies in the photo-

chemical, thermal and stereochemical properties of the monomers and resultant polymers.

References

- 1 Manecké, G. and Storck, W. *Macromol. Chem.* 1964, 75, 159
- 2 Manecké, G. *Angew. Makromol. Chem.* 1968, 2, 86
- 3 Okamoto, K., Ibayashi, A. and Kusabayashi, S. *Chem. Lett.* 1974, 1167
- 4 Etienne, A., Izoret, G. and Moritz, F. *C. R. Acad. Sci.* 1959, 249, 708
- 5 Etienne, A., Arditte, G. and Chuelevsky, A. *C. R. Acad. Sci.* 1968, 256, 2429
- 6 Manecké, G. and Storck, W. *Chem. Ber.* 1961, 94, 3239
- 7 Fernandez-Refojo, M., Pan, Y., Kun, K. A. and Cassidy, H. G. *J. Org. Chem.* 1960, 25, 416
- 8 Schlosser, M. and Christmann, K. F. *Angew. Chem.* 1964, 76, 683

A. J. Gradwell and J. T. Guthrie

Department of Colour Chemistry,
University of Leeds,
Leeds LS2 9JT, UK
(Received 12 April 1976)

Ultra-high modulus polyethylene by high temperature drawing

In this note we wish to report some remarkable new results obtained recently during an investigation now in progress on the high temperature drawing of linear polyethylene (LPE). This study forms a natural extension of our previous work on the preparation and properties of ultra-high modulus oriented polymers^{1–5}. It also attempts to re-examine, in the light of results for different drawing conditions, the conclusions of recent investigations^{1–4,6} on the inter-relationship between molecular parameters and processing conditions for LPE drawn at 75°C. In particular, our proposal^{2,6} that the drawing behaviour of a semi-crystalline polymer may be interpreted in terms of a network structure having crystalline domains and molecular entanglements as junction points – hence the vital role played by the non-crystalline material – can receive further support or be disproved by the temperature dependence of the drawing process.

We report here results for two grades of LPE: H020-54P (BP Chemicals International, $\bar{M}_w = 312\,000$, $\bar{M}_n = 33\,000$) and Hostalen GUR (Farbwerke Hoechst AG, $\bar{M}_w \sim 3\,500\,000$). Isotropic samples were produced by compression moulding at 160°C and either slow cooling to 110°C and quenching into water at room tem-

perature (160/110/W) or quenching directly into water (160/W), as described previously^{1,2}. Dumb-bell specimens of 2 cm gauge length were then drawn in air at different temperatures in an Instron Tensile Testing Machine using a crosshead speed of 10 cm/min.

The results of these drawing experiments were remarkable in two respects. First, it was found that effective drawing (drawing which produces ultra-high modulus material) can be achieved at temperatures very close or apparently even above the crystalline melting point of the polymer, provided that appropriately high molecular weight polymer is used. Secondly, the ultra-high modulus materials produced at high drawing temperatures can exhibit properties and structural features which are significantly different from those found in products from drawing at 75°C.

In Figure 1 the variation of the draw ratio λ in the plastically deformed region with draw time (t_d) is shown for samples drawn at 115° and 75°C, the results for 75°C being obtained in a previous investigation⁶. Despite some scatter in the present results, there does not appear from these data to be any difference in kind between drawing at 115°C and drawing at 75°C. The increased draw temperature does

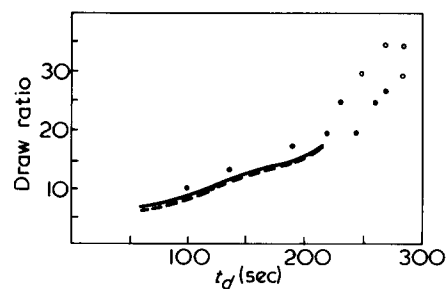


Figure 1 Local draw ratio (λ) as a function of time of draw (t_d) for sample H020-54P. $T_d = 115^\circ\text{C}$: \circ , 160/W; \bullet , 160/110/W. $T_d = 75^\circ\text{C}$: —, 160/W; —, 160/110/W

however result in an extension of the curve obtained for 75°C, allowing the production of much higher draw ratios before failure occurs.

When the properties of the drawn materials are examined, the results are more unusual. The 10 sec isochronal stress–strain curve (see Figure 2) for a sample of draw ratio 34 confirms that very high Young's moduli are still obtained from high temperature drawing. Although the value of 47.5 GN/m² at a strain of 10^{–3} is marginally lower than that for low molecular weight LPE drawn at 75°C, these high molecular weight drawn materials show much superior long term creep pro-

was reduced by 50% by distillation and the residue allowed to reflux for 1 h. By this time the blood-red colour of the betaine intermediate had almost disappeared. The resulting mixture was poured slowly into a 3 fold excess of ligroin (60°–80°C) and the precipitate of triphenyl phosphine oxide separated. Residual solvents were removed and the yellow residue (aldehyde–vinyl anthraquinone mixture) partly dissolved in benzene/ligroin (3:1). The insoluble residue of unreacted aldehyde was recovered for recycling. The crude 2-vinylanthraquinone was purified by column elution with 4:1 ligroin/benzene. Recrystallization from 3:1 benzene/methanol gave pale yellow needles, melting point 176°–177°C, in 61% yield. Such yields have been maintained on repeated preparations. Analysis calculated for C₁₆H₁₀O₂: C, 82.05; H, 4.30. Found: C, 82.08; H, 4.50. The infra-red spectrum was found to be identical with the product

of the method of Manecké^{1,2}.

In forming vinyl compounds from aldehydes using the Wittig reaction the more customary addition of the aldehyde had to be reversed in order to reduce reaction at the 9,10-quinone positions. Any reaction in the 9,10-quinone positions of the anthraquinone nucleus gives 9,10-dimethylanthracene derivatives as highly fluorescent and unwanted side-products. It is the production of vinyl compounds, from a precursor containing both aldehyde and ketonic groups, by making use of the greater reactivity of the aldehyde group, which gives this preparation its originality, within the present context and creates a route for the production of many similar compounds.

Work is at present being carried out by one of us (A. J. G.) concerning the γ -ray, thermal, chemical and ionic routes to polymers based on vinylanthraquinones and their derivatives. Our immediate interest lies in the photo-

chemical, thermal and stereochemical properties of the monomers and resultant polymers.

References

- 1 Manecké, G. and Storck, W. *Macromol. Chem.* 1964, 75, 159
- 2 Manecké, G. *Angew. Makromol. Chem.* 1968, 2, 86
- 3 Okamoto, K., Ibayashi, A. and Kusabayashi, S. *Chem. Lett.* 1974, 1167
- 4 Etienne, A., Izoret, G. and Moritz, F. *C. R. Acad. Sci.* 1959, 249, 708
- 5 Etienne, A., Arditte, G. and Chuelevsky, A. *C. R. Acad. Sci.* 1968, 256, 2429
- 6 Manecké, G. and Storck, W. *Chem. Ber.* 1961, 94, 3239
- 7 Fernandez-Refojo, M., Pan, Y., Kun, K. A. and Cassidy, H. G. *J. Org. Chem.* 1960, 25, 416
- 8 Schlosser, M. and Christmann, K. F. *Angew. Chem.* 1964, 76, 683

A. J. Gradwell and J. T. Guthrie

Department of Colour Chemistry,
University of Leeds,
Leeds LS2 9JT, UK
(Received 12 April 1976)

Ultra-high modulus polyethylene by high temperature drawing

In this note we wish to report some remarkable new results obtained recently during an investigation now in progress on the high temperature drawing of linear polyethylene (LPE). This study forms a natural extension of our previous work on the preparation and properties of ultra-high modulus oriented polymers^{1–5}. It also attempts to re-examine, in the light of results for different drawing conditions, the conclusions of recent investigations^{1–4,6} on the inter-relationship between molecular parameters and processing conditions for LPE drawn at 75°C. In particular, our proposal^{2,6} that the drawing behaviour of a semi-crystalline polymer may be interpreted in terms of a network structure having crystalline domains and molecular entanglements as junction points – hence the vital role played by the non-crystalline material – can receive further support or be disproved by the temperature dependence of the drawing process.

We report here results for two grades of LPE: H020-54P (BP Chemicals International, $\bar{M}_w = 312\,000$, $\bar{M}_n = 33\,000$) and Hostalen GUR (Farbwerke Hoechst AG, $\bar{M}_w \sim 3\,500\,000$). Isotropic samples were produced by compression moulding at 160°C and either slow cooling to 110°C and quenching into water at room tem-

perature (160/110/W) or quenching directly into water (160/W), as described previously^{1,2}. Dumb-bell specimens of 2 cm gauge length were then drawn in air at different temperatures in an Instron Tensile Testing Machine using a crosshead speed of 10 cm/min.

The results of these drawing experiments were remarkable in two respects. First, it was found that effective drawing (drawing which produces ultra-high modulus material) can be achieved at temperatures very close or apparently even above the crystalline melting point of the polymer, provided that appropriately high molecular weight polymer is used. Secondly, the ultra-high modulus materials produced at high drawing temperatures can exhibit properties and structural features which are significantly different from those found in products from drawing at 75°C.

In Figure 1 the variation of the draw ratio λ in the plastically deformed region with draw time (t_d) is shown for samples drawn at 115° and 75°C, the results for 75°C being obtained in a previous investigation⁶. Despite some scatter in the present results, there does not appear from these data to be any difference in kind between drawing at 115°C and drawing at 75°C. The increased draw temperature does

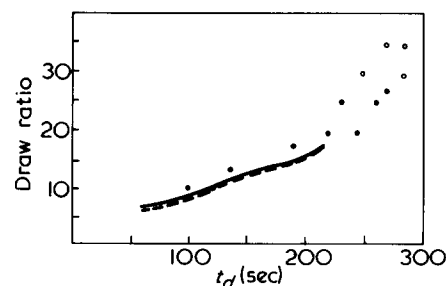


Figure 1 Local draw ratio (λ) as a function of time of draw (t_d) for sample H020-54P. $T_d = 115^\circ\text{C}$: \circ , 160/W; \bullet , 160/110/W. $T_d = 75^\circ\text{C}$: —, 160/W; —, 160/110/W

however result in an extension of the curve obtained for 75°C, allowing the production of much higher draw ratios before failure occurs.

When the properties of the drawn materials are examined, the results are more unusual. The 10 sec isochronal stress–strain curve (see Figure 2) for a sample of draw ratio 34 confirms that very high Young's moduli are still obtained from high temperature drawing. Although the value of 47.5 GN/m² at a strain of 10^{–3} is marginally lower than that for low molecular weight LPE drawn at 75°C, these high molecular weight drawn materials show much superior long term creep pro-

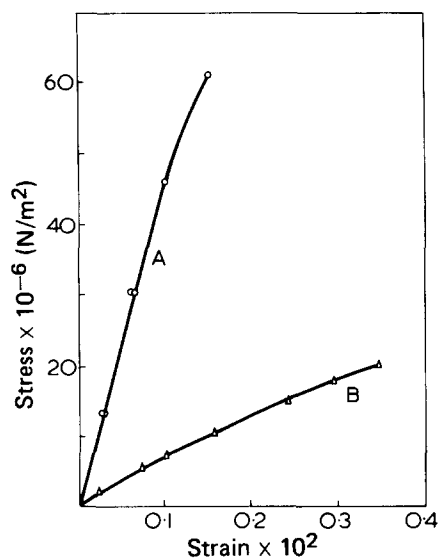


Figure 2 Room temperature 10 sec isochronal stress-strain curves for highly drawn samples of (A) H020-54P, $\lambda = 34$, $T_d = 115^\circ\text{C}$; (B) Hostalen GUR, $\lambda = 17$, $T_d = 135^\circ\text{C}$

erties⁷. These materials are more elastic in their behaviour, and this more than outweighs the slightly lower level of initial modulus.

The ultra-high molecular weight Hostalen GUR could not be drawn to high λ at 115°C . In order to achieve high draw ratios and explore fully the temperature boundaries for effective drawing, the deformation was therefore performed at an air temperature of 135°C i.e. above the melting point of isotropic material. Under these conditions the samples could be drawn to $\lambda = 17$ and the drawn materials exhibited interesting and novel properties. Previously, the draw ratios of this polymer appeared to be limited to about 4 with little or no increase in stiffness over isotropic material. Figure 2 shows that a value of 7 GN/m^2 is obtained for the Young's modulus, and that the stress-strain curve is remarkably linear.

The melting behaviour of these samples reveals very interesting structural differences with the lower molecular weight materials drawn at lower temperatures. The d.s.c. traces for both samples are shown in Figure 3. An unprecedentedly high melting temperature for drawn LPE of 141.5°C is recorded for the H020-54P grade, indicating the extremely high degree of order and continuity of the crystalline phase. On the other hand, the drawn Hostalen GUR shows a double peak with the higher T_m at 139.5°C . Wide-angle X-ray diffraction patterns

for these samples throw light on these differences. That for a drawn samples of the H020-54P grade, shown in Figure 4a, indicates a sharpness for the reflections similar to that obtained previously for ultra-high modulus materials drawn at $T_d = 75^\circ\text{C}$. The photograph for the Hostalen GUR samples is, however, remarkable in showing indications of poorly oriented material in addition to the sharp reflections which can be attributed to highly oriented crystalline material (Figure 4b). A possible explanation of the d.s.c. and X-ray diffraction data is that the high temperature peak and the sharp X-ray reflections arise from material crystallized under stress while the low temperature peak (Hostalen GUR) corresponds to poorly oriented material which crystallizes on cooling down to room temperature.

These results show that the preparation of ultra-high modulus LPE can be successfully extended to higher molecular weight polymers provided that drawing is carried out at high temperatures. For high molecular weight polymers the initial thermal treatment does not appear to influence the drawing process (Figure 1). We have suggested^{2,5} that this is because the high molecular weight material now plays a decisive role in the network structure which undergoes deformation in the drawing process. This idea receives con-

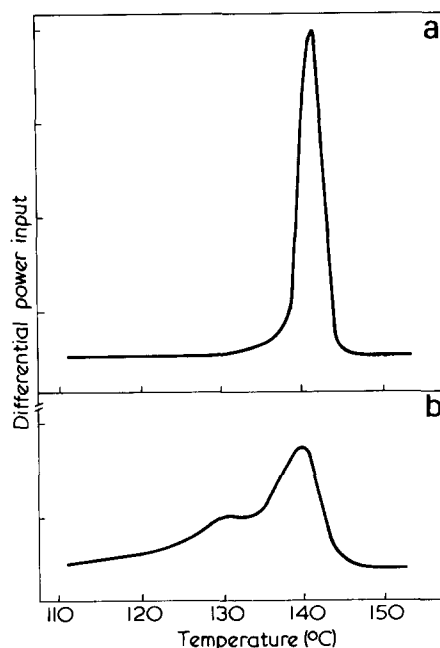


Figure 3 D.s.c. melting curves for highly drawn samples of (a) H020-54P, $T_d = 115^\circ\text{C}$; $\lambda = 25$; (b) Hostalen GUR, $T_d = 135^\circ\text{C}$; $\lambda = 17$.

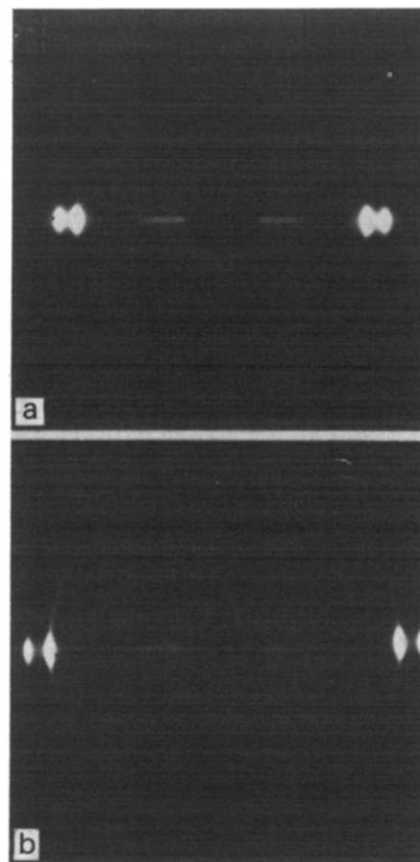


Figure 4 Wide-angle X-ray diffraction patterns for a sample of (a) H020-54P drawn to $\lambda = 25$ and (b) a sample of Hostalen GUR drawn to $\lambda = 17$

firmation from the present results. It is clear that drawing can be carried out even at temperatures close to or apparently above the crystalline melting point, provided that the molecular entanglements of high molecular weight material are available to guarantee continuity for the network structure.

G. Capaccio, T. A. Crompton and
I. M. Ward

Department of Physics,
University of Leeds,
Leeds LS2 9JT, UK

(Received 17 March; revised 8 April)

References

- 1 Capaccio, G. and Ward, I. M. *Nature Phys. Sci.* 1973, **243**, 130, 143; *Polymer* 1974, **15**, 233
- 2 Capaccio, G. and Ward, I. M. *Polymer* 1975, **16**, 239
- 3 Capaccio, G., Chapman, T. J. and Ward, I. M. *Polymer* 1975, **16**, 469
- 4 Smith, J. B., Davies, G. R., Capaccio, G. and Ward, I. M. *J. Polym. Sci. (Polym. Phys. Edn)* 1975, **13**, 2331
- 5 Ward, I. M., Capaccio, G. and Cansfield, D. L. M. *PRI Proc. Int. Conf. Polypropylene Text.* York 1975
- 6 Capaccio, G., Crompton, T. A. and Ward, I. M. *J. Polym. Sci.* in press
- 7 Wilding, M. A., Capaccio, G. and Ward, I. M. in preparation

On the field dependent photoconduction in poly(*N*-vinylcarbazole)

The photogeneration of carriers and their transport in poly(*N*-vinylcarbazole) (PNVC) has been the subject of many investigations¹⁻⁶. The photoconduction in PNVC is the result of a field enhanced carrier generation, explained on the basis of 'geminate recombination'³ of the electron-hole pairs produced and a field assisted drift mobility arising from the hopping mechanism² of the photogenerated holes. In the case of positive electrode illumination with strongly absorbed light (350 nm), the $I - V$ characteristics of PNVC (in a sandwich-cell configuration) is found to be linear for low values of V , but becomes superlinear (with a slope 2 in the double log plot) at higher values⁵ (~ 15 kV/cm). The origin of the superlinearity has been attributed to the following reason.

During their transit across the film towards the negative electrode, the photogenerated holes undergo repeated trapping and release from shallow and intermediate traps, whereas those trapped in deep levels remain bound to the trapping site. Since the trapping probability is proportional to the product of the number of unoccupied trapping sites and the number of free holes available, the field assisted carrier generation results in increased trapping at higher fields. As more and more traps become occupied, the trapping probability decreases, thereby increasing the number of holes available for conduction. The 'knee-point' in the $I - V$ plots should therefore correspond to the onset of trap-filling. Since only intermediate and deep traps are responsible for the above phenomenon (shallow traps being in thermal equilibrium with the valence band), the argument appears to be feasible in the case of PNVC, where the density of deep traps have been estimated to be very small⁶ ($\sim 10^{12}/\text{cm}^3$).

The purpose of the present note is to examine the validity of the above argument, which suggests that the photoelectret charge (Q), obtained by the time integration of the dark depolarization current⁷ (i_{dd}), should increase initially and approach a saturation value near the voltage corresponding to the knee-point in the $I - V$ plot.

The photoconduction and photoelectret measurements were carried out at room temperature (30°C) in a sandwich structure (Al-PNVC-NESA), fabricated by vacuum depositing Al

onto a PNVC layer (100 μm) cast on the NESA glass substrate. The sample was illuminated from the NESA side using a 125 W u.v. lamp, by keeping the NESA electrode positive. The values of photocurrents observed at different times after the commencement of the photopolarization are given in Figure 1 along with the level of dark currents observed at the end of 5 min dark polarization. It is seen that the onset of non-linearity (knee-

point) shifts towards lower voltage as the polarizing time increases. Figure 2 shows the i_{dd} values observed at different times and the photoelectret charge Q ($Q = \int_0^\infty i_{dd} dt$) for the different polarizing voltages. The values of i_{dd} and Q are found to exhibit a maximum for $V = 800$ V, which roughly corresponds to the knee-point in the $I - V$ plot. The broken lines in Figure 2 show that an expression $i_{dd}(t) \propto t^{-1}$ is valid for the i_{dd} decay

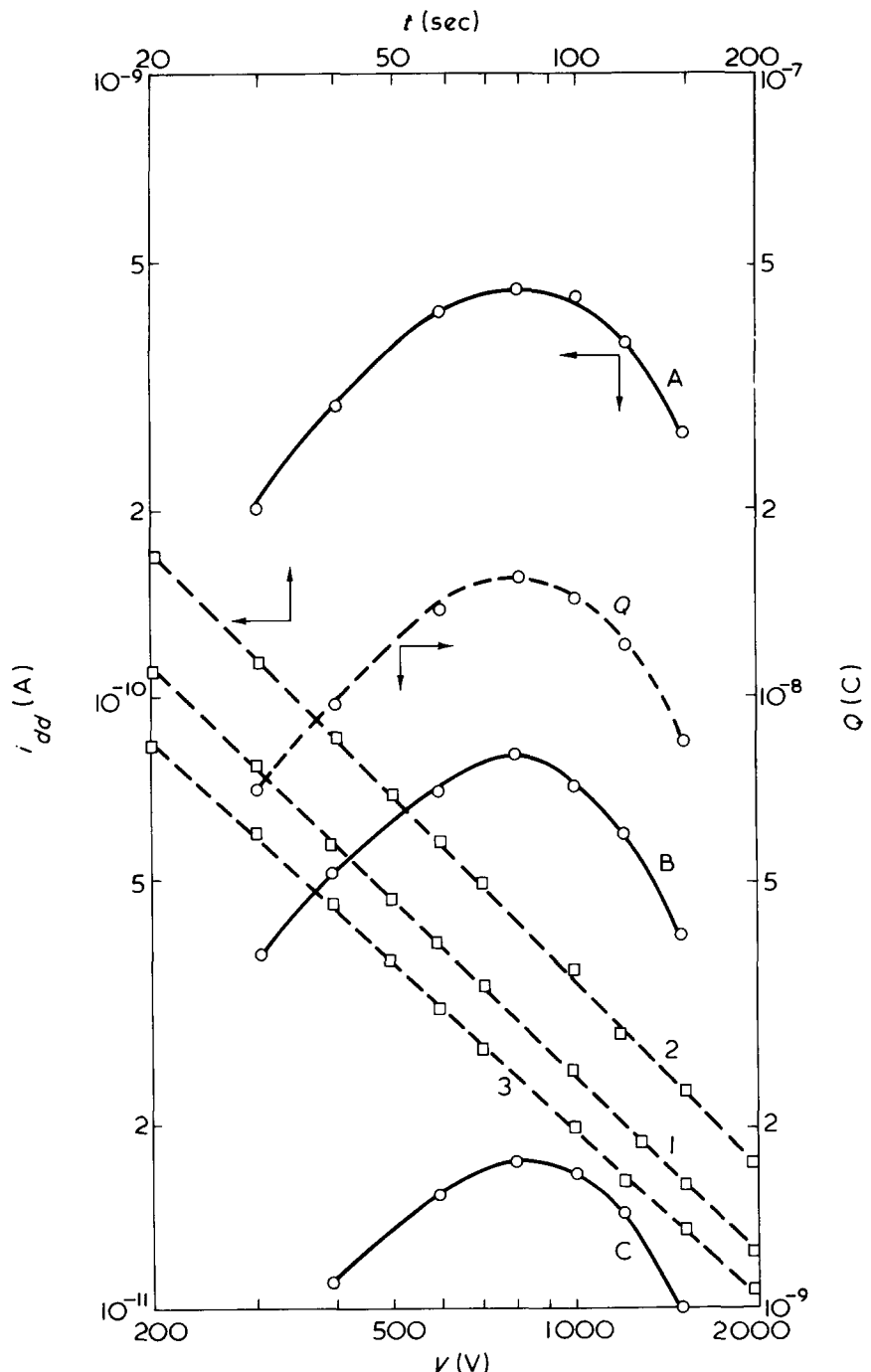


Figure 1 The photocurrents (i) in PNVC observed at an interval of A, 5 sec; B, 40 sec; C, 5 min after the application of polarizing voltage (V). ----, denotes the level of 5 min dark currents

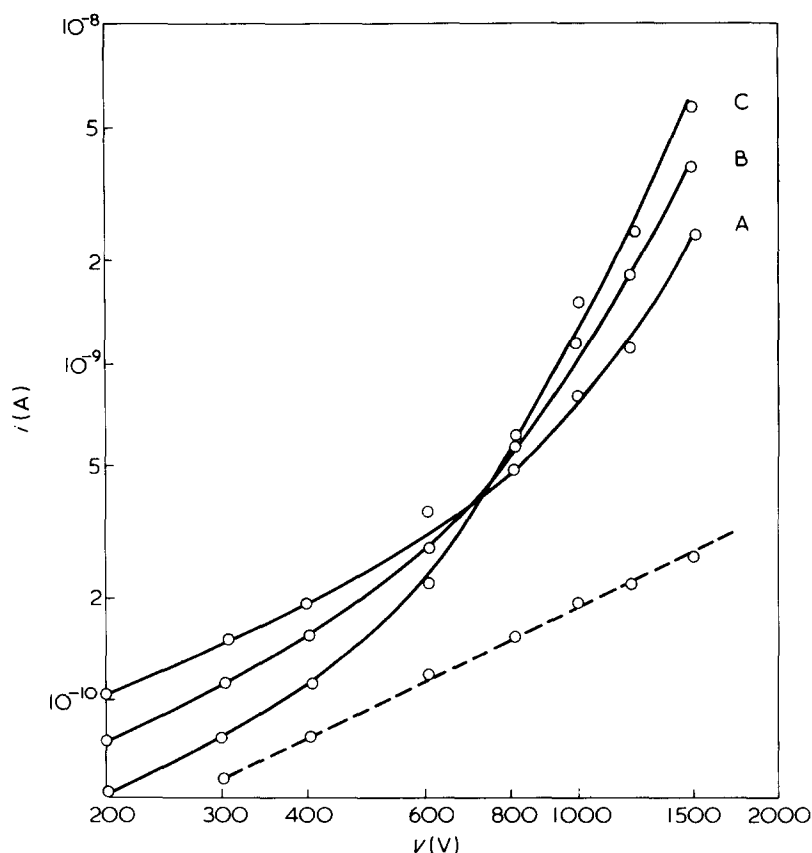


Figure 2 Dark depolarization currents (i_{dd}) observed after an interval of A, 5 sec; B, 45 sec; C, 3 min for different polarizing voltage (V) and the PE charge (Q) obtained by $Q = \int_0^{\infty} i_{dd} dt$. 1, 2 and 3 represent typical decay curves for the i_{dd} , for $V = 400$ V, 800 V and 1500 V respectively

with time on both sides of the maximum.

The photoelectret charge observed in the case of organic and inorganic semiconductors usually shows an initial increase with voltage, followed by a saturation⁸ though in the case of anthracene, the $Q - V$ plots (corresponding to the $i_{dd} - V$ plots) exhibited a maximum⁹. The observation of this maximum in the case of anthracene has been explained on the basis of homocharge formation at higher fields due to air breakdown in the sample-electrode interface, since the occurrence of a maximum was absent when an insulating spacer was introduced in this interface⁹. This possibility has to be ruled out in the present case, as there is no gap between the sample and the NESA or Al electrodes.

However, an explanation based on a field assisted detrapping seems to be plausible because of the correspondence between the knee-point in the

$I - V$ plot and the maximum in the $Q - V$ plot. In materials such as PNVC, characterized by a charge transport limited by the release from localized (trapping) states, where this release also is highly field dependent, it is possible that a charge could be trapped at a given state, when the next state is inaccessible at a particular field. However, for a higher applied field, the same state may not act as a trap due to a field enhanced release probability. This has been proved by 'thermally stimulated current' (TSC) experiments in PNVC², which has shown that the TSC peak shift towards lower temperature as the polarizing field is increased, indicating the decreased contribution to the total charge from the deeper traps at elevated fields.

Since trapping centres at considerable depth are either very few or absent in the case of PNVC, as concluded from the 'time of flight'⁶ and photoel-

ectret¹⁰ experiments, it can be assumed that a field as low as 10 kV/cm is able to influence even the deepest trapping sites with a meaningful abundance. It should be noted that such a case cannot arise in materials with an appreciable density of deep-lying traps, as the applied fields cannot influence such deeper levels, thereby explaining the absence of a maximum in the $Q - V$ plots of ordinary photoelectret materials.

From the present results on the photoconductivity in PNVC, it can therefore be concluded that the superlinearity in the $I - V$ plots is not only a consequence of a field enhanced carrier generation and a field assisted hopping transport, but also is due to a significant contribution from the field assisted release from the trapping centres. Further work on the spectral, temperature and illumination intensity dependence of the $Q - V$ characteristics is in progress.

Acknowledgement

One of the authors (SKA) gratefully acknowledges the financial support given by CSIR, Government of India.

P. K. C. Pillai, S. K. Agarwal and
P. K. Nair

Department of Physics,
Indian Institute of Technology,
New Delhi, India
(Received 16 March 1976)

References

- 1 Regensburger, P. J. *Photochem. Photobiol.* 1968, 8, 429
- 2 Pai, D. M. *J. Chem. Phys.* 1970, 52, 2285
- 3 Melz, P. J. *J. Chem. Phys.* 1972, 57, 1694
- 4 Reucroft, P. J. and Ghosh, S. K. *Phys. Rev. (B)* 1973, 8, 803
- 5 Okamoto, K., S. Kusabayashi, S. and Mikawa, H. *Bull. Chem. Soc. Japan* 1973, 46, 2324
- 6 Reucroft, P. J. and Takahashi, K. *J. Non Cryst. Solids* 1975, 17, 71
- 7 Pillai, P. K. C. and Goel, M. *Phys. Status Solidi (A)* 1971, 6, 9
- 8 Fridkin, V. M. 'Physics of Electrophotography', Focal Press, 1973, Ch 1 and 2
- 9 Belyaev, L. M., Golovin, B. M. and Zheludev, I. S. *Trans. II All-Union Conf. Phys. Dielectr. Izv Akad. Nauk SSSR* 1960
- 10 Pillai, P. K. C. and Ahuja, R. C. *J. Polym. Sci. (Polym. Phys. Edn)* 1974, 12, 2465

Book Reviews

Block and Graft Copolymerization Volume 2

Edited by R. J. Ceresa

Wiley, London, 1976, 402pp £16.50

Over seventy per cent of the text of this book is devoted to the synthesis, properties and applications of block copolymer polycol surfactants by L. G. Lundsted and I. R. Schmolka. These block copolymers based on poly(ethylene oxide) were first produced in 1950 and have been marketed since then by the Wyandotte Chemical Corporation under the trade names of Pluronic and Tetronics. From the references to patents and publications, both authors have been actively involved in the development of polyol surfactants at Wyandotte. Lundsted was one of the authors of the paper on the synthesis of ABA poly(ethylene oxide-*b*-propylene oxide) in 1951.

Chapter one on preparation and properties covers similar ground to a review by Schmolka published in 1967 on the nonionic surfactant properties of poly(alkylene oxide) block copolymers. More details on block copolymer synthesis have been included in the present book. Chapter two describes the applications of block copolymer surfactants under twenty seven headings. The applications are very wide-ranging. The uses of these surfactants appear to be continually expanding; over a quarter of the references are to papers and patents published from 1970 onwards. Polymer chemists will be particularly interested in the sections on emulsion polymerization, paint, plastics and polymers, polyurethanes, rubber and textiles. These two chapters illustrate that block and graft copolymers often have valuable interfacial properties, the study of which has received less attention than the use of these copolymers as thermoplastic elastomers and impact modifiers.

The remainder of the book is concerned with poly(vinyl chloride). In chapter three the editor reviews the synthesis of block and graft copolymers. In his preface he apologizes for any major omissions in this chapter which is concerned mainly with chemical

and irradiation grafting procedures, either by a monomer to a poly(vinyl chloride) backbone or by vinyl chloride to another polymeric backbone. Thus the work of J. P. Kennedy on cationic grafting is only briefly mentioned and references to his work published during the last three years are not included. The text is less than forty pages long and almost ninety per cent of the literature cited was published before 1970.

In chapter four on the properties and applications of graft copolymers of poly(vinyl chloride) by D. Hardt, less than six per cent of the references were published from 1970 onwards. Consequently, the recent developments in microphase separation in block and graft copolymers and their importance in poly(vinyl chloride) systems are not discussed in detail.

In summary, the first two chapters give a very comprehensive and authoritative review of poly(alkylene oxide) block and graft copolymers. The book should be bought by libraries serving polymer chemists and those interested in polymers at interfaces in colloidal systems. Workers concerned only with poly(vinyl chloride) obtain poor value, because of the high price, £16.50 for 130 pages, and because recent developments are not reviewed owing to the delay in publication. A list of 60 references published from 1971 onwards is included in an addendum.

J. V. Dawkins

Photodegradation, Photo-oxidation and Photostabilization of Polymers

B. Ranby and J. F. Rabek

Wiley, London, 1975, 573 pp. £16.50

Polymer chemists and technologists have for long been preoccupied by the deteriorative effects of light on their products. This interest has diversified in various directions over the years to include mechanisms of photolysis and photo-oxidation, photosensitization and photostabilization. In the meantime, rapid advances have been made in understanding the fundamental principles of photochemical and photophysical processes in materials generally.

This book, which is intended for experimental investigators in polymer chemistry, begins by explaining clearly and concisely the general fundamental principles of photochemistry and of the mechanism and kinetics of photodegradation and photooxidation. There follows a long chapter (134 pages) in which the specific reactions of a large variety of polymers are described in detail. A good deal of space is also devoted to photosensitized reactions of polymers, the stabilization of polymers to ultra-violet light and practical methods in the photochemistry of polymers. Interspersed with these longer chapters the overall picture is completed by shorter treatments of such diverse topics as singlet oxygen mechanism of polymer photo-oxidation, energy transfer in polymers, photochemistry of polymers in reactive gases (ozone, sulphur dioxide, nitrogen dioxide and chlorine), the role of photodegradable polymers in the packaging industry and finally weatherability of plastics materials.

The reviewer would confirm the authors' belief that this is the first monograph in which the fundamental photochemical reactions involved in the photodegradation of polymers has been thoroughly discussed. They have admirably succeeded in producing a comprehensive and critical yet easily readable account of the subject and the textual material is supported by a very complete bibliography of 2334 references for those who may require further information on a specific topic.

Scientists with any interest in photoreactions of polymers will wish to and will also find this volume very easy to read from cover to cover. Those more intimately concerned with research and development will find it a valuable source of information and a useful catalyst for the development of new approaches to their subject.

N. Grassie

Conference Announcement

The Science and Technology of Water Soluble Polymers

UWIST, Cardiff, 21–23 September 1976

A group representing various societies are holding a symposium on *The Science and Technology of Water Soluble Polymers* at UWIST Cardiff on the 21, 22 and 23 September 1976. The symposium is intended as an international meeting point for academic and industrial scientists interested in water soluble polymers. Some 20 papers will be presented which will include communications from Czechoslovakia, Switzerland, Norway, USA, Hungary, Belgium, France, Britain and Ireland. The topics covered include fundamental science and applications in the food, cosmetics, polymers, textiles, medical, pharmaceutical and photographic fields. Full programmes and application forms are available from The Short Courses Secretary, Planning Section, UWIST, King Edward VII Avenue, Cardiff CF1 3NU, UK.

Electro-optic Kerr birefringence of polystyrenes in dilute solutions

J. V. Champion, G. H. Meeten and G. W. Southwell

Department of Physics, Sir John Cass School of Science and Technology, City of London Polytechnic, London EC3N 2EY, UK

(Received 13 February 1976; revised 19 March 1976)

The electro-optic Kerr effect has been measured for styrene and several high molecular weight polystyrenes in dilute solution in carbon tetrachloride. The results for styrene clearly show free rotation of the phenyl group. The results for polystyrene are in accord with the predictions of the Stuart and Peterlin independently orientating segment theory, and also in agreement with the results to be expected from currently available estimates of the segmental anisotropy provided that the segmental dipole is orthogonal to the segmental end-to-end distance.

INTRODUCTION

Two models have been used to describe the electro-optic Kerr effect in flexible polymer chains. One of these describes the chain as a sequence of dipolar and anisotropically polarizable chemical bonds and enables calculation of the appropriate averages of optical polarizability anisotropy from the conformation and orientation of the chain in an applied strong field. The other describes the chain as a sequence of freely jointed segments having segmental dipolarity and polarizability anisotropy. These segments behave as independently orientating units in the applied strong field. The former model is exemplified by the calculations of Kluk¹, Volkenstein², Dows³, and Nagai⁴ who express the Kerr constant in terms of clearly defined bond parameters, i.e. the number of bonds and their polarizability tensors, dipole moments, bond angles and energies of rotational isomerism. They assume the validity of the bond polarizability tensor additivity scheme and the vectorial addition of bond dipole moments. Both assumptions may be questioned even as first order approximations but the model is applicable to chains of any length.

The segmental model of Stuart and Peterlin⁵ does not express the Kerr constant in terms of clearly defined bond parameters but employs segmental polarizability anisotropies and dipole moments, these being a conformational average of bond anisotropies and moments over a small number of bonds in a sequence. The model is only capable of describing chains having a sufficiently large number of monomer units to analyse statistically, but is not dependent on the assumptions of additivity of bond polarizability tensors and bond dipole moments. Segmental anisotropies are also derivable from flow birefringence, strain-optical birefringence and depolarized Rayleigh light scattering experiments. They provide useful knowledge about the conformational flexibility of the chain in a given solvent. Segmental dipole moments are of similar use. It will be shown that the Kerr constant of a dipolar polymer interpreted with the Stuart-Peterlin theory relates the segmental dipole vector to the axes of the segmental polarizability tensor.

Le Fevre *et al.*⁶ have made Kerr effect measurements of styrene and polystyrene in carbon tetrachloride solution. They found the specific Kerr constant to show a considerable molecular weight dependence in the molecular weight

range 900 to 250 000, and interpreted their data in terms of the re-orientation of the whole polymer chain behaving as a rigid unit under the influence of the applied electric field. This interpretation has subsequently been criticized by Dows³ who showed theoretically that the specific Kerr constant is related to the properties of a segment rather than the whole chain.

Since the molecular weight dependence of specific Kerr constants as found by Le Fevre indicates that the polymer chains are too short to be considered as being composed of a large number of segments, the aim of this work was to repeat the Le Fevre measurements using higher molecular weight polystyrenes, where an interpretation of results in terms of segmental properties should be valid.

EXPERIMENTAL

Material

Samples of polystyrene were used with weight-average molecular weights $M_w = 1, 2.1, 2.8, 8.8$ and 35×10^5 . The first three were obtained from Monsanto, Shell and BDH Ltd, the last two were made by the slow room temperature polymerization of styrene using benzoyl peroxide as a catalyst. The samples were all polydisperse with $M_w/M_n \approx 2$, as shown by g.p.c. measurements. M_w was determined by the techniques of light scattering and dilution viscometry. The solvent used for all samples was Analar grade carbon tetrachloride (Hopkin and Williams). The styrene was supplied by Hopkin and Williams as styrene monomer stabilized by about 0.001% *p*-*t*-butyl catechol. This was regarded as a negligible impurity as contributing to the measured Kerr effect.

Procedure

The apparatus and procedure have been described previously^{7,8}. Measurements were made at $\sim 25^\circ\text{C}$. All solutions were filtered before use with Millipore glass fibre pre-filters. For all solutions the birefringence Δn was proportional to the square of the applied field E , a least squares fit of Δn to E^2 giving the solution Kerr constant $B = \Delta n/\lambda E^2$, λ being 546 nm for the light used in all measurements. B was measured for several concentrations of polystyrene less than 100 kg/m^3 , the excess Kerr constant over the solvent, $B - B_1$, being proportional to the polystyrene

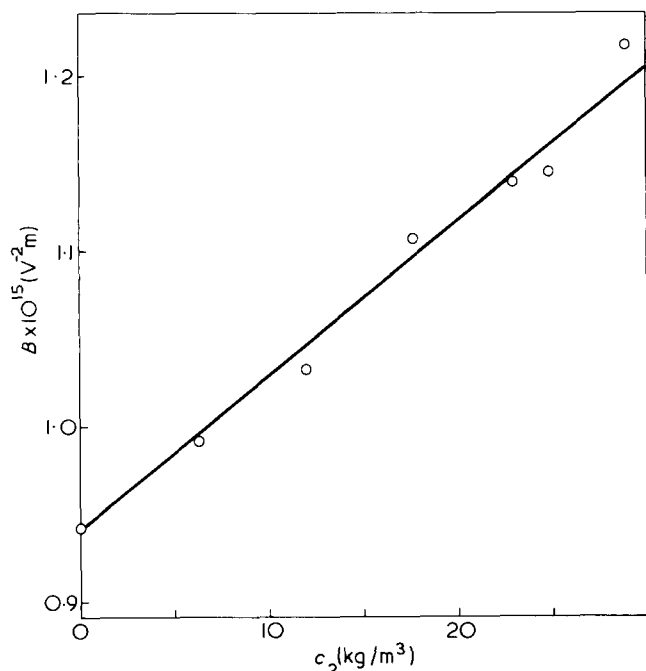


Figure 1 Variation of Kerr constant B with solution concentration c_2 of polystyrene, $M_w = 1 \times 10^5$

concentration c_2 within experimental error. A least squares fit of $B - B_1$ to c_2 then gave the specific incremental Kerr constant dB/dc_2 . Figure 1 shows a typical plot of B versus c_2 . Measurements of the specific incremental relative permittivity $d\epsilon/dc_2$ at low concentrations were made using a Wayne-Kerr B221A bridge and a temperature controlled capacitor. Specific refractive index increments dn/dc_2 were measured using a precision Abbé refractometer.

Results

Table 1 shows values of dB/dc_2 with weight-average molecular weight. Values of $d\epsilon/dc_2$ and dn/dc_2 of $0.4 \times 10^{-3} \text{ m}^3/\text{kg}$ and $0.15 \times 10^{-3} \text{ m}^3/\text{kg}$ were found for all polystyrene solutions, $d\epsilon/dc_2$ being calculated from dn/dc_2 as described previously⁷. For styrene, values of $d\epsilon/dc_2 = 0.235 \times 10^{-3} \text{ m}^3/\text{kg}$ and $dn/dc_2 = 0.118 \text{ m}^3/\text{kg}$ were obtained.

Systematic errors in dB/dc_2 arising from errors in the applied strong field (up to 10^7 V/m) and Kerr cell geometry amounted to about $\pm 2\%$. Random errors in dB/dc_2 measurements were about 10%, including errors in the concentration, the optical compensation and in observation.

THEORY AND DISCUSSION

Theory

The Kerr constant of the solute is defined as $B_2^* = \Delta n_2 / \lambda E^2$ where Δn_2 is that part of the electrically induced solution birefringence arising from the solute when a field of E is applied to the solution. The specific Kerr constant is then given in SI units by⁹:

$$\frac{B_2^*}{c_2} = \frac{750N_A}{n\epsilon_0\lambda M_2} \left(\frac{\epsilon + 2}{3} \right) \left(\frac{n^2 + 2}{3} \right)^2 (\theta_\alpha + \theta_\mu) \quad (1)$$

where

$$45kT\theta_\alpha = (\alpha_{xx} - \alpha_{yy})^2 + (\alpha_{yy} - \alpha_{zz})^2 + (\alpha_{zz} - \alpha_{xx})^2 + 6\alpha_{xy}^2 + 6\alpha_{yz}^2 + 6\alpha_{zx}^2$$

and

$$45k^2T^2\theta_\mu = (\mu_x^2 - \mu_y^2)(\alpha_{xx} - \alpha_{yy}) + (\mu_y^2 - \mu_z^2)(\alpha_{yy} - \alpha_{zz}) + (\mu_z^2 - \mu_x^2)(\alpha_{zz} - \alpha_{xx}) + 6\alpha_{xy}\mu_x\mu_y + 6\alpha_{yz}\mu_y\mu_z + 6\alpha_{zx}\mu_z\mu_x$$

In equation (1), M_2 is the molecular weight of the solute, θ_α is the term describing molecular re-orientation due to the interaction between the molecular polarizability tensor components α_{ij} and the applied field. θ_μ is the dipole term describing molecular re-orientation due to the interaction between the molecular dipole components μ_i and the applied field. In correspondence with recent work, (Vuks¹⁰, Zamkov¹¹, Kuball *et al.*¹²⁻¹⁴, Göb *et al.*¹⁵, and Proutiere *et al.*¹⁶) the factor $[(\epsilon + 2)/3]$ is of the first power rather than the second as was originally used for solutions and liquids by many workers. This change results from distinguishing between the internal polarizing field and the field responsible for the orientational couple acting on a molecule. When the solvent specific Kerr constant cannot be neglected with respect to the solute and it may be assumed that solute-solute interactions are absent at low concentrations, then the solution birefringence is the sum of the component birefringences weighted according to their respective number densities. It follows that:

$$\frac{B_2^*}{c_2} = \frac{dB}{dc_2} - \frac{3B_1}{(\epsilon_1 + 2)} \times \frac{d\epsilon}{dc_2} - \frac{B_1}{n_1} \left(\frac{3n_1^2 - 2}{n_1^2 + 2} \right) \times \frac{dn}{dc_2} + B_1 \bar{v}_2 \quad (2)$$

where the differentials are all limiting values as $c_2 \rightarrow 0$. \bar{v}_2 is the solute partial specific volume given by $1/c_1 [1 - (dc/dc_2)]$. Values of B_2^*/c_2 are shown in Table 1.

Styrene

For styrene, the experimental results will be used to determine the mutual orientation of the C=C bond and the phenyl ring. This mutual orientation is described by the orthogonal torsional angle ϕ between the normal N to the ring and the plane containing the C=C bond and the ring axis of rotation, as described by Figure 2. The axis of rotation of the ring makes an angle $\phi (< 90^\circ)$ to the x axis. The bond polarizability tensor additivity scheme gives the molecular tensor components α_{ij} in terms of the tensor components of the constituent bonds or groups. The anisotropy $\Delta\alpha^{JK}$ of a JK bond is the difference between the tensor components parallel and perpendicular to the length of the bond. All bonds have diagonal polarizability tensors for axes parallel and perpendicular to the bond length. Polar-

Table 1 Experimental values of dB/dc_2 and B_2^*/c_2

Solute	M_w	$(dB/dc_2) \times 10^{18}$ ($\text{V}^{-2} \text{ m}^4 \text{ kg}^{-1}$)	$(B_2^*/c_2) \times 10^{18}$ ($\text{V}^{-2} \text{ m}^4 \text{ kg}^{-1}$)
Styrene	104.1	13.4	14.2
Polystyrene	1×10^5	9.0	9.7
Polystyrene	2.1×10^5	9.3	10.0
Polystyrene	2.8×10^5	7.1	7.7
Polystyrene	8.8×10^5	8.8	9.5
Polystyrene	35×10^5	7.9	8.6

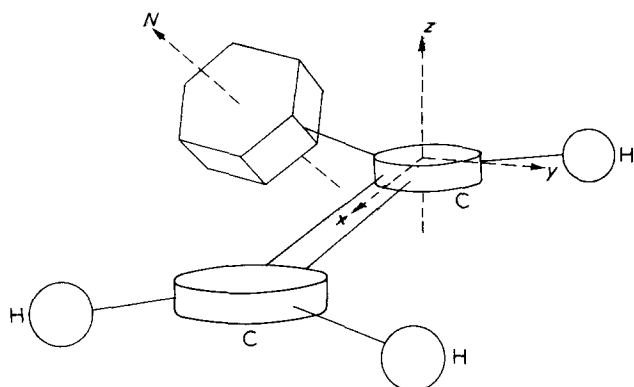


Figure 2 Styrene: the x axis lies parallel to the $C=C$ bond and the z axis normal to the xy plane containing the $C=C$ bond, the ring rotation axis and the CH bonds. The ring orientation is described by the torsional angle ϕ between the ring normal N and the xy plane

izability symmetry around the bond length axis is assumed for all bonds and for the phenyl ring, where N is the symmetry axis polarizability and $\Delta\alpha^b$ is the ring anisotropy. These assumptions give:

$$\alpha_{xx} - \alpha_{yy} = X - Y + [(N - M) \cos^2 \phi - (N - L)] \cos 2\theta$$

$$\alpha_{yy} - \alpha_{zz} = Y - Z + (N - L) \cos^2 \theta + (M - N) \times (1 + \cos^2 \theta) \cos^2 \phi + (L - M)$$

$$\alpha_{zz} - \alpha_{xx} = Z - X - (M - N) (2 - \cos^2 \theta) \cos^2 \phi + (N - L) \cos^2 \theta + (M - N)$$

$$\alpha_{xy} = (N - L) \sin \theta \cos \theta + (M - N) \sin \theta \cos \theta \cos^2 \phi$$

$$\alpha_{yz} = (N - M) \cos \theta \cos \phi \sin \phi$$

$$\alpha_{zx} = (N - M) \sin \theta \cos \phi \sin \phi$$

where

$$X - Y = \Delta\alpha^{C=C} - 4\Delta\alpha^{CH}(1 - 2 \cos^2 \theta)$$

$$Y - Z = 4\Delta\alpha^{CH} \sin^2 \theta$$

$$Z - X = -\Delta\alpha^{C=C} - 4\Delta\alpha^{CH} \cos^2 \theta$$

$$L - M = \Delta\alpha^{CC} - 2\Delta\alpha^{CH}$$

$$M - N = -\Delta\alpha^b$$

$$N - L = \Delta\alpha^b - \Delta\alpha^{CC} + \Delta\alpha^{CH} \quad (3)$$

The dipole moment μ is assumed to lie parallel to the axis of rotation of the phenyl ring so that:

$$\mu_x = \mu \cos \theta, \mu_y = -\mu \sin \theta, \mu_z = 0 \quad (4)$$

The functions θ_α and θ_μ in equation (1) are then given by:

$$45kT\theta_\alpha = (L - M + Y - Z)^2 + (M - N + Z - X)^2 + (N - L + X - Y)^2 - 6(M - N)(X - Y) \cos^2 \theta \cos^2 \theta - 6(M - N)(Z - X) \cos^2 \phi - 6(N - L)(X - Y) \cos^2 \theta$$

and

$$45k^2T^2\theta_\mu = \mu^2[(X - Y)(3 \cos^2 \theta - 1) + (Y - Z) + (L - M) + (L - N)] \quad (5)$$

Values of $\Delta\alpha^b = -6.67$, $\Delta\alpha^{CH} = 0.33$, $\Delta\alpha^{CC} = 1.58$, $\Delta\alpha^{C=C} = 3.34 \times 10^{-40} \text{ C}^2\text{m}^2/\text{J}$ for $\lambda = 0.546 \text{ nm}$ have been obtained from depolarized light scattering measurements on liquids and solutions¹⁷. Values $\mu = 1.17$ and $1.24 \times 10^{-30} \text{ C m}$ have been given^{6,18} for styrene dissolved in carbon tetrachloride. Graphs of B_2^*/c_2 versus the phenyl ring rotation angle ϕ are shown in Figure 3 for various values of μ and the $=C$ semi-dihedral angle θ , calculated from equations (1), (3) and (4). The experimental value for styrene of $B_2^*/c_2 = 14.2 \times 10^{-18} \text{ V}^{-2} \text{ m}^3 \text{ kg}^{-1}$ indicates $\phi \approx 45^\circ$. A probable explanation of this result is that $\cos^2 \phi = 0.5$ which indicates free rotation of the phenyl ring relative to the rest of the styrene molecule.

Polystyrene

Figure 4 shows B_2^*/c_2 plotted with M_w^{-1} . The near-independence of B_2^*/c_2 with molecular weight shows that the segmental values of θ_α and θ_μ are also molecular weight independent. This is a justification of the basic assumption in the Stuart and Peterlin theory of a large number of orientationally independent segments per polymer chain. Small tacticity deviations from atactic could explain the slight molecular weight dependence of B_2^*/c_2 , as iso- and syndiotactic chains possess markedly different optical anisotropies¹⁹.

The expression given by Stuart and Peterlin⁵ in their theory of the Kerr effect for flexible polymers may be derived from equation (1) where θ_α and θ_μ refer to segmental properties. They assumed the segment to be a polarizability ellipsoid of revolution about its end-to-end distance

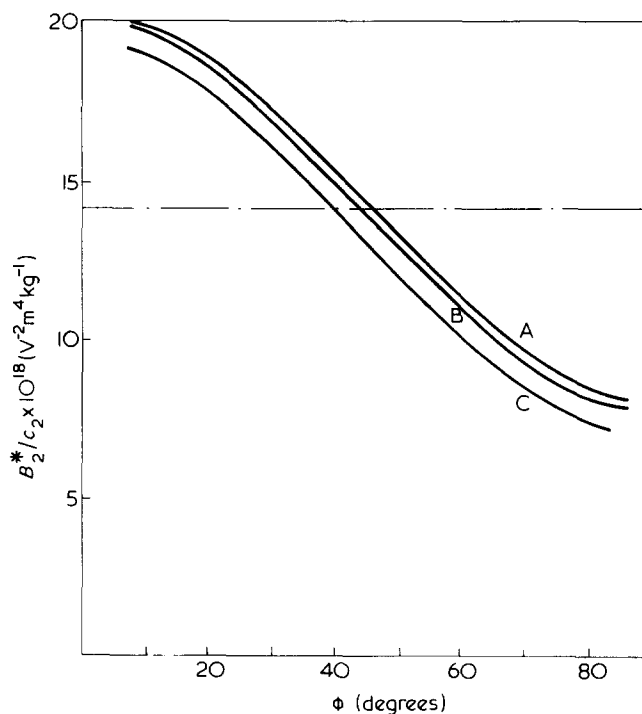


Figure 3 Solute specific Kerr constant versus torsional angle ϕ of phenyl ring in styrene. Units of μ are 10^{-30} C m . A, $\theta = 54^\circ$, $\mu = 1.24$; B, $\theta = 54^\circ$, $\mu = 1.17$; C, $\theta = 57^\circ$, $\mu = 1.17$. ----, measured value of B_2^*/c_2

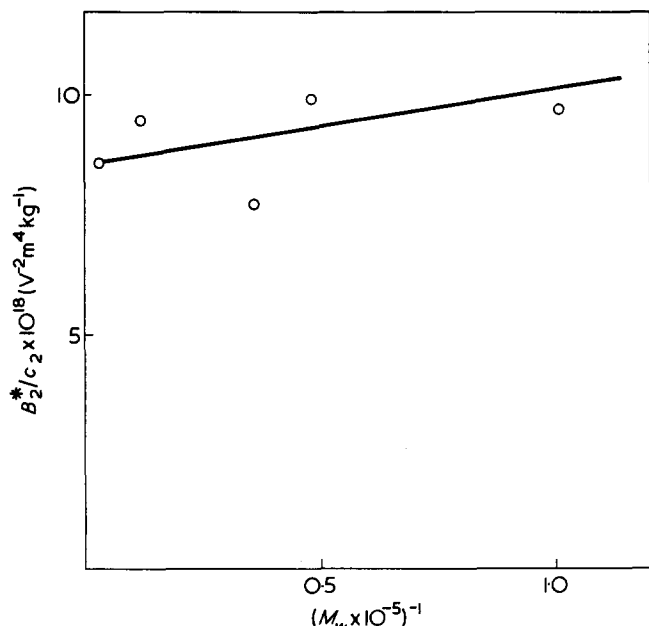


Figure 4 $(B_2^*/c_2) \times 10^{18}$ versus $(M_w \times 10^{-5})^{-1}$ for polystyrene

and to have a permanent dipole moment parallel to this distance. In polystyrene a dipole moment perpendicular to the segment end-to-end distance is expected from the direction of the moments associated with the phenyl groups. Both cases are covered by writing equation (1) in the form:

$$\frac{B_2^*}{c_2} = \frac{750N_A}{n\epsilon_0\lambda M_0} \left(\frac{\epsilon + 2}{3}\right) \left(\frac{n^2 + 2}{3}\right)^2 \times \left[\frac{2(\alpha_l - \alpha_r)^2}{45kTS} \pm \frac{\mu_s^2(\alpha_l - \alpha_r)}{45k^2T^2S} \right] \quad (6)$$

where α_l and α_r are the polarizabilities parallel and perpendicular to the segment end-to-end distance and μ_s is the segmental dipole moment. M_0 is the monomer unit molecular weight and S the number of monomer units per segment which is a parameter describing chain flexibility. The magnitude of μ_s^2 may be derived from available dielectric data since for the whole polymer chain the dipole moment $\langle \mu^2 \rangle = \Phi N_0 \mu_0^2$, where the angular brackets denote a statistical mechanical average of the chain dipole moment over all possible conformations of the polymer chain. Φ is a conformationally dependent parameter which is characteristic of a particular polymer-solvent pair²⁰ and μ_0 is the monomer unit dipole moment. N_0 and N_s are the number of monomer units and segments respectively per polymer chain. Since $S = N_s/N_0$, μ_s^2 may be written as $S\Phi\mu_0^2$ in equation (6), Φ and μ_0 being 0.65 and 1.17×10^{-30} C m respectively for polystyrene in carbon tetrachloride²⁰.

Flow birefringence measurements²¹ show that $(\alpha_l - \alpha_r)$ is negative. Thus the \pm sign in equation (6) is decided according to whether μ_s is perpendicular (+) or parallel (-) to the segment length. Figure 5 shows B_2^*/c_2 calculated from equation (6) plotted with $(\alpha_l - \alpha_r)$ for several values of S , with μ_s parallel or perpendicular to the segment length.

Values of $(\alpha_l - \alpha_r)$ for atactic polystyrene derived from flow birefringence^{21,22} and depolarized light scattering measurements^{22,24,25} demonstrate a solvent dependence as shown in Table 2. This dependence may have a conformational origin since different solvent-solute interactions

will generally produce different segmental lengths. It may also originate optically since the segmental anisotropy is influenced by angular correlation between monomer units and solvent molecules²⁶. The data in Table 2 represents the possible spread in value of $(\alpha_l - \alpha_r)$. Since $S \approx 8^{22,23}$ Figure 5 shows that there is good agreement between experimental and theoretical values of B_2^*/c_2 when the segmental dipole moment is orthogonal to the segment length. For the segmental dipole moment to be parallel to the segment length then $S \leq 5$ which is well outside the range of acceptability²².

CONCLUSION

The experimental values for the specific Kerr constants of various molecular weight polystyrenes in solution with carbon tetrachloride has been compared with the theoretical result as given by the Stuart and Peterlin theory. Using literature values of segmental parameters such as optical anisotropy, number of monomer units per segment and segmental dipole moment, the experimental and theoretical values of specific Kerr constant agree provided that

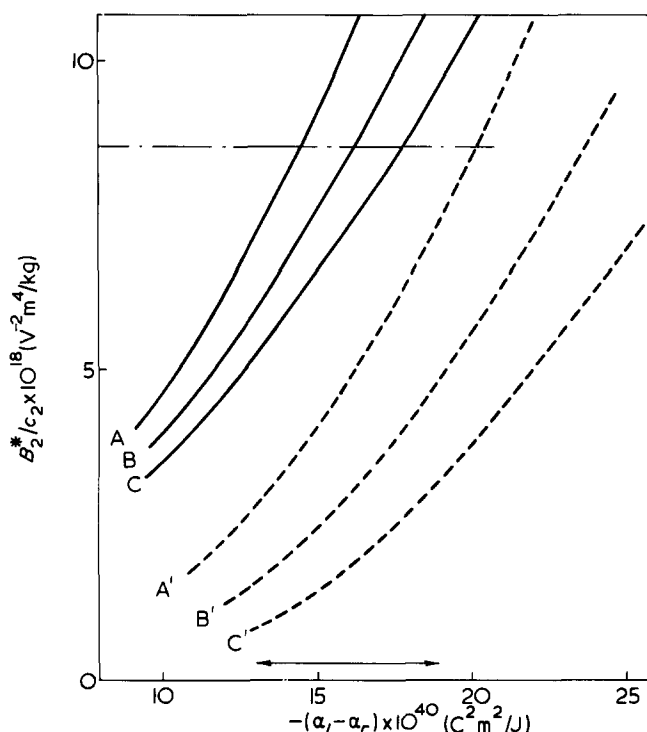


Figure 5 Theoretical specific Kerr constant versus segmental anisotropy for polystyrene with values of S : A, A', 6; B, B', 8; C, C', 10; calculated from equation (6). — — —, μ_s parallel to segment; — — —, μ_s perpendicular to segment; · · · · · measured value. The horizontal arrow denotes the spread of experimental $(\alpha_l - \alpha_r)$ values

Table 2 Experimental values of segmental anisotropy at 546 nm

Solvent	$(\alpha_l - \alpha_r) \times 10^{40}$ (C ² m ² /J)	Technique
Bromoform	-16.1	Flow birefringence ^{21,23}
Benzene	-15.0	Flow birefringence ²²
Benzene	-15.0	Light scattering ²²
Methylal	-18.9	Light scattering ²²
Cyclohexane	-17.2	Light scattering ²²
Bromoform	-15.0	Light scattering ²²
Chlorobenzene	-13.3	Light scattering ²⁴
—	-18.9	Strain birefringence ²⁶

the direction of the segmental dipole moment is assumed to be orthogonal to the segment length. We regard this agreement, together with the near-independence of specific Kerr constant upon molecular weight, as indicating the validity of the Stuart and Peterlin segmental model in the molecular weight range examined.

Bond polarizability based rotational isomeric state calculations have been made¹⁹ for polystyrene of the optical anisotropy γ^2 which is equal to $\frac{1}{2}\theta_\alpha$ if dispersion of the bond polarizability parameters is neglected. No similar calculations exist for θ_μ and hence B_μ^*/c_2 and therefore no comparison is yet possible between our experimental results and non-segmental theories of the Kerr effect.

REFERENCES

- 1 Kluk, E. *Acta. Phys. Pol.* 1962, **22**, 249
- 2 Volkenstein, M. V. 'Configurational Statistics of Polymeric Chain', Interscience, New York, 1963
- 3 Dows, D. A. *J. Chem. Phys.* 1964, **41**, 2656
- 4 Nagai, K. *J. Chem. Phys.* 1969, **51**, 1091
- 5 Stuart, H. A. and Peterlin, A. *J. Polym. Sci.* 1950, **5**, 551
- 6 Le Fevre, C. G., Le Fevre, R. J. W. and Parkins, G. M. *J. Chem. Soc.* 1958, 1468
- 7 Champion, J. V., Meeten, G. H. and Southwell, G. W. *JCS Faraday Trans. II* 1975, **71**, 225
- 8 Champion, J. V., Meeten, G. H. and Whittle, C. D. *Trans. Faraday Soc.* 1970, **66**, 2671
- 9 Le Fevre, C. G. and Le Fevre, R. J. W. 'Physical Methods of Chemistry', Interscience, New York, 1972, Vol 1, part IIIC, p 441
- 10 Vuks, M. F. *Opt. Spectros.* 1967, **21**, 383
- 11 Zamkov, V. A. *Opt. Spectros.* 1963, **15**, 355
- 12 Kuball, H.-G. and G6b, R. *Z. Naturforsch (A)* 1967, **22**, 737
- 13 Kuball, H.-G. and G6b, R. *Z. Phys. Chem.* 1968, **62**, 237
- 14 Kuball, H.-G. and G6b, R. *Z. Phys. Chem.* 1969, **63**, 251
- 15 G6b, R. and Kuball, H.-G. *Z. Phys. Chem.* 1970, **72**, 153
- 16 Proutiere, A., Baudet, J. G. R. and Camail, M. *J. Chem. Phys.* 1974, **71**, 1439
- 17 Clement, C. and Seurin, R. *J. Chem. Phys.* 1971, **68**, 22
- 18 McClellan, A. L. 'Tables of experimental dipole moments', Freeman, San Francisco, 1963
- 19 Tonelli, A. E., Abe, Y. and Flory, P. J. *Macromolecules* 1970, **3**, 303
- 20 Krigbaum, W. R. and Dawkins, J. V. 'Polymer Handbook', (Eds. J. Brandrup and E. H. Immergut), Interscience, New York, 1966
- 21 Tsvetkov, V. 'Newer Methods of Polymer Characterisation', (Ed. B. Ke), Interscience, New York, 1964
- 22 Ehrenburg, E. G., Piskareva, E. P. and Poddubnyi, I. Ya. *J. Polym. Sci. (Polym. Symp.)* 1973, **42**, 1021
- 23 Tsvetkov, V. N. *Rubber Chem. Technol.* 1967, **36**, 337
- 24 Tsvetkov, V. 'Polymer Handbook', (Eds. J. Brandrup and E. H. Immergut), Interscience, New York, 1966
- 25 Piskareva, E. P., Erenburg, E. G. and Poddubnyi, I. Ya. *Dokl. Akad. Nauk. SSSR* 1968, **180**, 470
- 26 Frisman, E. V. and Dadivanyan, A. K. *J. Polym. Sci.* 1967, **16**, 1001
- 27 Abe, Y., Tonelli, A. E. and Flory, P. J. *Macromolecules* 1970, **3**, 294

^{13}C n.m.r. spectra of some poly(*N*-acyliminoalkenes)

K. J. Ivin, L. C. Kuan-Essig, E. D. Lillie and P. Watt

Department of Chemistry, The Queen's University of Belfast, Belfast BT9 5AG, UK

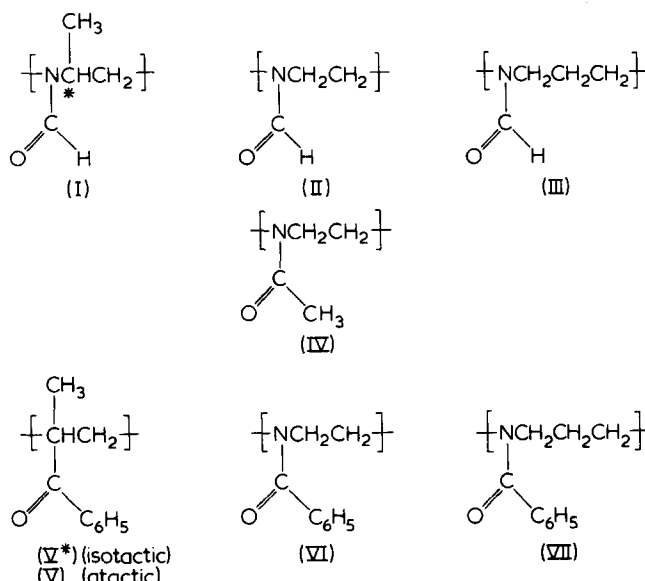
(Received 3 March 1976)

^{13}C n.m.r. spectra are reported for six poly(*N*-acyliminoalkenes), $-\{N(\text{COR})(\text{CH}_2)_n\}-$ ($n = 2, \text{R} = \text{H}, \text{CH}_3, \text{C}_6\text{H}_5; n = 3, \text{R} = \text{H}, \text{C}_6\text{H}_5$), and $-\{N(\text{COC}_6\text{H}_5)\text{CH}(\text{CH}_3)\text{CH}_2\}-$ (isotactic and atactic), and compared with that for poly(*N*-formyliminopropylene). These linear polymers were made by the isomerization polymerization of the appropriate oxazoline or oxazine derivatives. For the polymers with *N*-formyl or *N*-acetyl side groups the spectra of the main chain carbons show fine structure resulting from restricted rotation about the two nearest N-COR bonds. This fine structure shows a small temperature dependence and in some cases there are indications of the influence of a third N-COR group at the lower temperatures. For the polymers with *N*-benzoyl side groups the rotation of these groups is less restricted than for *N*-formyl and *N*-acetyl and at 120°C no fine structure is observed except that resulting from tacticity in atactic poly(*N*-benzoyliminopropylene), where the carbonyl and main-chain carbons exhibit partly resolved triad structure. At lower temperatures some of the lines broaden because of restricted rotation. In the model compound *N*-ethyl-*N*-methylbenzamide all eight types of carbon atom give two lines at -30°C (in CDCl_3), the two conformers being present in the approximate ratio 58:42. The pairs of lines coalesce in turn as the temperature is raised to 50°C . Spin-lattice relaxation times were measured for the carbon nuclei in poly(*N*-formyliminoethylene), in *N*-ethyl-*N*-methylformamide and in *N*-isopropyl-*N*-*n*-propylformamide. T_1 values increase by two orders of magnitude in going from the polymer to dimethylformamide. ^{13}C chemical shifts are recorded for seven oxazoline and two oxazine derivatives as well as for six model compounds of the polymers.

INTRODUCTION

It has recently been shown¹ that the $^{13}\text{C}\{^1\text{H}\}$ n.m.r. spectrum of isotactic* poly(*N*-formyliminopropylene)² (I), [poly(*N*-formylpropylenimine)] exhibits fine structure which may be interpreted in terms of restricted rotation about the N-CHO bonds. Each main-chain carbon gives four chemical shifts, according to whether the two nearest formyl groups take up *syn* or *anti*-conformations. However the spectrum of this polymer is complicated by two factors: first, there is overlap between the fine structure for the CH and CH_2 carbons; second, the methyl side group causes unequal populations of *syn* and *anti* conformers.

We now report the spectra of poly(*N*-formyliminoethylene) (II), poly(*N*-formyliminotrimethylene) (III) and poly(*N*-acetyliminoethylene) (IV), where these complications are not present; also the spectra of the *N*-benzoyl analogues of I, II and III namely V, VI and VII respectively, and of some model compounds of the *N*-benzoyl analogues.



EXPERIMENTAL

Polymers II to VII were prepared by the isomerization polymerization of the corresponding oxazoline or 1,3-oxazine derivatives II' to VII', using the cationic initiator and conditions listed in Table 1. ^{13}C shifts for these monomers are recorded in Appendix I. The molecular weights

of these polymers, where estimated from viscosity measurements, were found to be low (1000–10 000), as reported in the literature^{3–7}, but in no case were they so low as to reveal end effects in the ^{13}C n.m.r. spectra.

The sources of the monomers were as follows. II' and III' were prepared by Saegusa's method³ in which the appropriate amino-alcohol is reacted with *t*-butyl isonitrile, in the presence of silver cyanide. IV' was a commercial sample (Aldrich).

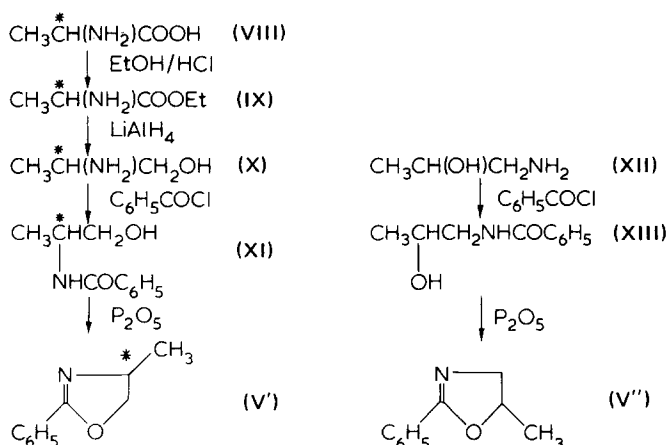
* In this paper the term 'tacticity' relates to the sequence of configurations about the asymmetric carbon atoms.

Table 1 Polymerization conditions

Compound number	Monomer	Conditions				Reference
		Initiator ^a	Temperature (°C)	Time (h)	Yield (%)	
II'	Oxazoline	3% A	70	4	65	4
III'	5,6-Dihydro-4H-1,3-oxazine	3% A	120	2	32	5
IV'	2-Methyloxazoline	0.7% A	80	50	~60	6
V'	L-2-Phenyl-4-methyloxazoline	0.6% B	100	18	70	this work
V''	2-Phenyl-5-methyloxazoline	1% C	135	160	30	this work
VI'	2-Phenyloxazoline	5% A	120	3	100	6
VII'	2-Phenyl-5,6-dihydro-4H-1,3-oxazine	4% A	150	3	97	7

^aInitiators: A, dimethyl sulphate; B, perchlorate of monomer; C, *p*-toluenesulphonic acid. (mol %)

V' and V'' were prepared by the following series of reactions:



The final stage in each case was carried out by adding a 50% excess of P₂O₅ to molten XI or XIII, the cooled mass then being treated with 10% sodium hydroxide solution. The product separated as an oil, which was extracted with ether, dried over magnesium sulphate and distilled under reduced pressure. For V' the yield was 25%; b.p. 86°C at 3 mmHg; $[\alpha]_{589}^{21.4} = 60.4^\circ$ (neat); -84.3° (10.8 g/100 cm³ in CHCl₃). ¹H n.m.r. (CDCl₃): δ 1.35 (*d*, 3, CH₃), 3.9–4.7 (*m*, 3, CH₂ and CH), 7.45 (*m*, 3, *m*- and *p*- aromatic H), 7.5 (*m*, 2, *o*-aromatic H). In the presence of 25 mol % of the shift reagent Eu(fod)₃ the two CH₂ and the CH signals were separated: δ 2.25 (*d*, 3, CH₃), 4.7 (*t* or *q*, 1, CH₂), 5.19 (*t* or *q*, 1, CH₂), 5.85 (*m*, 1, CH), 7.47 (*m*, 3, *m*- and *p*- aromatic H), 8.8 (*m*, 2, *o*- aromatic H). The geminal splitting constant was 9 Hz and the two vicinal constants 7.5 and 8.0 Hz. Infra-red absorption bands: 1650 cm⁻¹ (>C=N-) and 1260 cm⁻¹ (-C-O-C). This compound appears not to have been prepared before.

For V'' the yield was 61%, b.p. 95°C at 0.5 mmHg; picrate, yellow needles m.p. 166°–167°C. ¹H n.m.r. (CDCl₃): δ 1.4 (*d*, 3, CH₃), 3.85 (*m*, 2, CH₂), 4.77 (*m*, 1, CH), 7.43 (*m*, 3, *m*- and *p*- aromatic H), 7.95 (*m*, 2, *o*- aromatic H). In the presence of 79 mol % of the chiral shift reagent Eu(tfc)₃ only the methyl signal was split as the result of the presence of the two enantiomers. Downfield shifts were observed as follows: CH₂ (3.0), CH (2.1) and *o*- aromatic H (1.9), CH₃ (1.0), *m*- and *p*-H (0.07 ppm).

VI' was prepared as described by Matsuda and Kagiya⁸. VII' was prepared by cyclodehydration of *N*-(3-hydroxypropyl) benzamide using phosphorus pentoxide, as for the preparation of V' and V''. The benzamide derivative was prepared by reaction of benzoyl chloride with propanolamine.

The yield of VII was 25% based on propanolamine; b.p. 72°C at 0.05 mmHg.

N-methylbenzamide and *N,N*-dimethylbenzamide were commercial samples. *N*-ethyl-*N*-methylbenzamide was prepared by Fones' method¹⁰, starting from *N*-methylbenzamide and reacting it first with sodium hydride and then with ethyl iodide; m.p. 25°C.

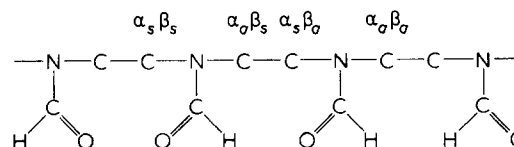
¹³C n.m.r. spectra were obtained with a WH90 Bruker spectrometer operating at 22.63 MHz in the pulsed Fourier transform mode, with decoupling from protons by broadband irradiation. The free induction decay was recorded at 8K points, transforming to a spectrum with 4K (4096) points. For aqueous (D₂O) solutions dioxane was added as a reference signal, its chemical shift being taken as 69.15 ppm relative to TMS; this value is somewhat arbitrary, being slightly dependent (± 1 ppm) on the medium. For solutions in DMSO-*d*₆, the chemical shift of the centre line of the solvent was taken as 39.67 ppm relative to TMS. For solutions in CDCl₃, chemical shifts were measured directly relative to TMS. Other details are given with each spectrum. Differences in chemical shifts have a precision of ± 0.02 ppm when determined using a sweep width of 2000 Hz.

*T*₁ measurements were carried out using the 180°- τ -90° pulse method and a built-in computer programme giving a least-squares fit to the equation $\ln(1 - A/A_\infty) = \tau/T_1 + \ln 2$. *A*_∞ was determined using a delay time of at least 5*T*₁. Values of *T*₁ were calculated from both areas and intensities and an average value taken.

RESULTS AND DISCUSSION

Poly(*N*-formyliminoethylene) II

The spectrum shown in Figure 1 is for a solution in D₂O at 35°C. The carbonyl carbon gives a single peak at 168.3 ppm. The main-chain carbons give two pairs of peaks, at 47.90 and 47.06, and at 42.77 and 41.86 ppm, which may be assigned to the four possible situations depicted in the following chain (see Figure 1).



The symbols α_s , α_a denote whether the carbon atom is *syn* (*s*) or *anti* (*a*) to the oxygen atom of the formyl group attached to the α -nitrogen atom; similarly for β_s , β_a . The chemical shift differences, $\alpha_a - \alpha_s$, etc. are as expected from small molecules¹ (see Table 4). The total probability of finding a carbon in the $\alpha_o \beta_s$ or $\alpha_a \beta_a$ situation is equal to

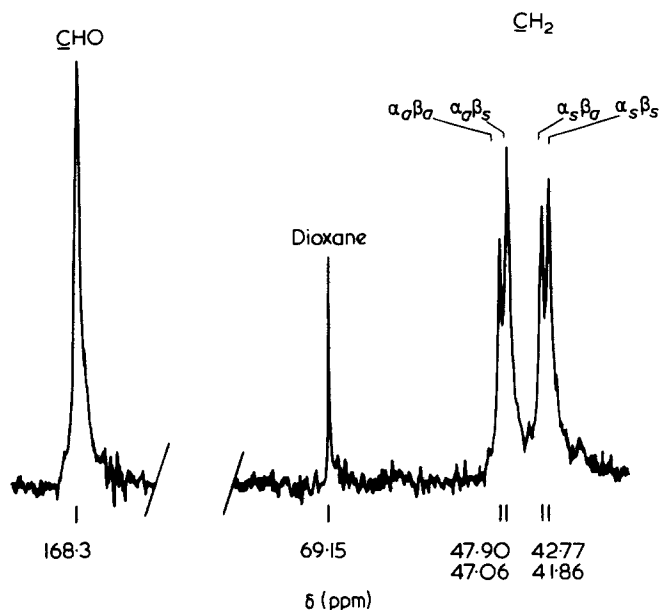


Figure 1 ¹³C{¹H} n.m.r. spectrum of $\text{-(N(CHO)CH}_2\text{CH}_2\text{)-}$. 20% solution in D₂O at 35°C. 16320 scans, sweep width 6024 Hz, acquisition time 0.679 sec, pulse width 6 μsec

that of finding it in the $\alpha_s\beta_s$ or $\alpha_s\beta_a$ situation, but the individual probabilities can only be equal either if the formyl groups are randomly oriented or if they take up certain non-random sequences of orientations. An attempt was made to determine the individual probabilities as follows. The spin-lattice relaxation times were first determined using a set of ten τ values between 0.05 and 10.0 sec, with the following results: CHO 0.4 ± 0.2 sec; CH₂ $\alpha_a\beta_a$ 0.3 ± 0.1 sec, $\alpha_a\beta_s$ 0.2 ± 0.1 sec, $\alpha_s\beta_a$ 0.15 ± 0.05 sec, $\alpha_s\beta_s$ 0.25 ± 0.1 sec. The limits of error cover the values of T_1 determined separately from both areas and peak heights. No significant difference between the T_1 values for the main-chain carbons was detected. With gated decoupling and a delay time of 30 sec between pulses the intensity pattern was not greatly changed although one would have expected a symmetrical intensity pattern to emerge ($\alpha_a\beta_s = \alpha_s\beta_a$; $\alpha_a\beta_a = \alpha_s\beta_s$) as a result of elimination of nuclear Overhauser and T_1 effects. The spectrum obtained without decoupling and with a time delay of 4 sec showed too much overlap of the fine structure ($J_{\text{CH}} = 140$ Hz, $J_{\text{CHO}} = 202$ Hz) for a clearcut answer to be obtained but was not inconsistent with equal populations of $\alpha_a\beta_a$, $\alpha_a\beta_s$, $\alpha_s\beta_a$ and $\alpha_s\beta_s$ structures.

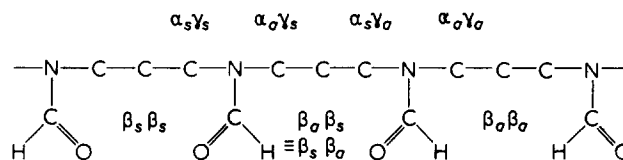
Raising the temperature to 80°C caused a downfield shift for the main-chain carbons, the downfield pair moving by about 0.2 ppm and the upfield pair by about 0.4 ppm, i.e. a net decrease in $\alpha_a - \alpha_s$; at the same time the peaks sharpened a little. The converse effect was found on cooling to 5°C, and between 15° and 5°C the fine structure due to the β -splitting disappeared. This effect is presumably connected with an increasing ease of rotation about the main-chain bonds as the temperature is raised.

Poly(N-formyliminotrimethylene) III

The spectrum shown in Figure 2 is for a solution in D₂O at 80°C. The carbonyl carbon gives a single peak at 167.7 ppm. Main-chain carbons adjacent to nitrogen show two pairs of peaks as for II, but the secondary splitting is now smaller since it arises from the conformation of the formyl group attached to the γ -nitrogen. If $\gamma_a - \gamma_s$ is negative, as in *N*-isopropyl-*N*-*n*-propylformamide¹, the line order is (downfield to upfield) $\alpha_a\gamma_s$, $\alpha_a\gamma_a$, $\alpha_s\gamma_s$, $\alpha_s\gamma_a$. The

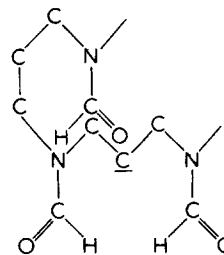
chemical shift differences $\alpha_a - \alpha_s$ etc. are as expected from small molecules (see Table 4).

The central methylene carbons give the expected 1:2:1 pattern with the assignments indicated on Figure 2 and the formula below.



The $\beta_a - \beta_s$ values are of the magnitude expected¹ (see Table 4).

On reducing the temperature all the peaks move slightly upfield (relative to dioxane), but while the upfield pair of α_s peaks remain well resolved, even at 3°C, the downfield pair of α_a peaks at first show signs of further fine structure, imperfectly resolved at 30°C, which then merges into a single broad peak at 3°C. This suggests that at low temperature the main-chain takes up a conformation which brings a third nitrogen close enough to the α_a carbon so that the conformation of the formyl group about this nitrogen can influence the chemical shift by a through-space effect. The sort of structure which might be involved is indicated below, the relevant carbon atom being underlined. Why this effect should not operate for both α -carbons is not clear, though possibly highly significant.



The intensity distribution in the fine structure is consistent with a random orientation of the formyl groups (compare with polymer II).

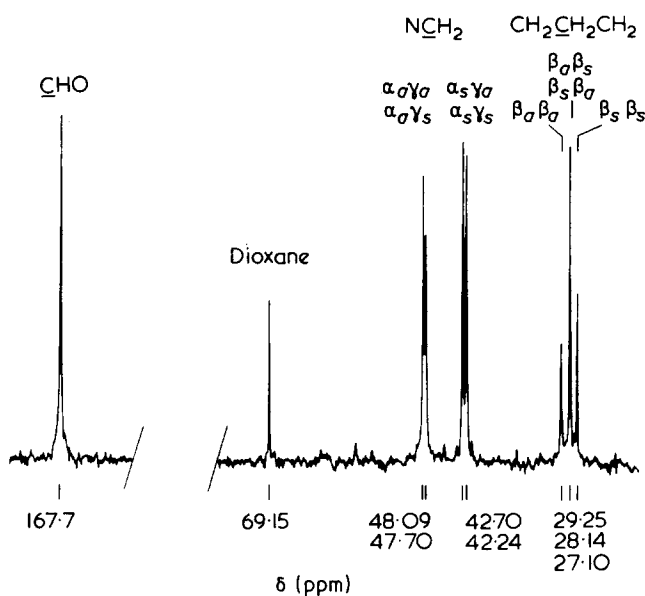


Figure 2 ¹³C{¹H} n.m.r. spectrum of $\text{-(N(CHO)CH}_2\text{CH}_2\text{CH}_2\text{)-}$. 10% solution in D₂O at 80°C. 29530 scans; other conditions as in Figure 1

Poly(N-acetyliminoethylene) IV

The spectrum shown in Figure 3 is for a solution in D₂O at 35°C. The carbonyl carbons give a single peak at 176.6 ppm; the methyl carbons also give a single peak, at 22.75 ppm. The methylene carbons give four peaks, with the upfield pair sharper and better resolved than the downfield pair. The assignments are as for II, with methyl replacing hydrogen. There is good reason^{11,12} to believe that the upfield pair corresponds to methylene *syn* to carbonyl, as in II. The differences $\alpha_a - \alpha_s$ are smaller than in the corresponding formamide, again as expected from small molecules¹¹; (see Table 4). It is notable that the average chemical shift for CH₂ in the acetyl compound IV is 3 ppm downfield compared with the formyl compound II and this again parallels the behaviour of model compounds¹³. Any additional steric effect caused by the introduction of the methyl group (which might have caused an upfield shift) is evidently outweighed by an electronic effect.

On raising the temperature to 80°C all the methylene peaks move about 0.3 ppm downfield relative to dioxane but the methyl peak is unaffected. In contrast to II the resolution of the downfield pair of methylene peaks did not improve.

Miron and Morawetz¹⁴ observed that in the ¹H n.m.r. spectrum of IV the methylene protons showed no splitting but the acetyl protons were split into two lines separated by 7 Hz, coalescing at 79°C. A higher temperature would be needed to cause coalescence of the β -splitting (18–26 Hz) in the CH₂ spectrum or of the α -splitting (62–70 Hz).

Poly(N-benzoyliminoethylene) VI

In DMSO-*d*₆ at 120°C single sharp lines were obtained for each carbon: CO, 170.43; C₁ (aromatic) 135.79; C₄, 128.71; C_{2,3}, 127.73, 125.78; CH₂ 44.41 ppm. The absence of fine structure indicates that at 120°C rotation about the N–CO bond is fast on the n.m.r. time scale (>100 Hz) and faster for N–COPh than for N–CHO. This accords with the observed behaviour of small molecules containing these groupings¹⁵; the conjugated PhCO system evidently reduces

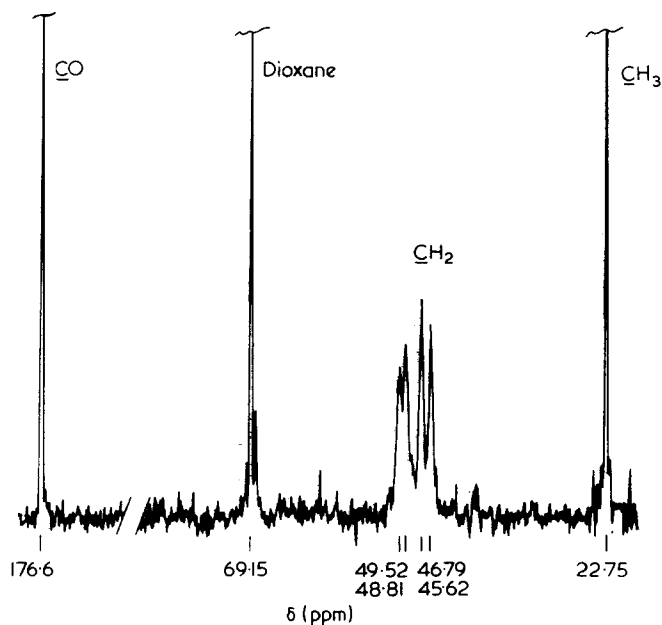


Figure 3 ¹³C{¹H} n.m.r. spectrum of $[-N(COCH_3)CH_2CH_2-]$. 30% solution in D₂O at 35°C. 2500 scans; other conditions as in Figure 1

the double-bond character of the N–CO bond. In CDCl₃ at 55°C the peaks remain sharp except for the main-chain carbon which splits into two broad peaks separated by about 3 ppm. At 5°C the aromatic peaks have broadened to the extent that the middle two have merged. This behaviour indicates that for the individual conformations about the N–CO bond the largest chemical shift difference occurs for the main-chain carbons, as expected.

Poly(N-benzoyliminotrimethylene) VII

In DMSO-*d*₆ at 120°C single sharp lines were obtained for each carbon, in the following positions: CO, 170.11; C₁, 136.70; C₄, 128.32, C_{2,3}, 127.67, 125.65; α CH₂, 43.76; β CH₂, 26.35 ppm. Again the rotation about the N–CO bond is fast on the n.m.r. time scale. In CDCl₃ at 32°C the α CH₂ signal is split into two broad peaks separated by about 4.5 ppm, the upfield peak showing secondary splitting of about 0.7 ppm. The β CH₂ signal is broadened into an incipient triplet but the aromatic and carbonyl peaks remain sharp. The behaviour is thus akin to that of poly(N-formyliminotrimethylene) (Figure 2) but with much lower coalescence temperatures.

*Poly(N-benzoyliminopropylene) V and V**

The spectrum of the isotactic polymer V* in DMSO-*d*₆ at 120°C is shown in Figure 4a. Single lines are observed for each carbon, with slight broadening of the main-chain carbon peaks. At room temperature all the lines are broadened, the main-chain carbons being barely distinguishable above the base line. The effect of temperature is similar to that for VI and VII. The spectrum for the atactic polymer in DMSO-*d*₆ at 120°C is shown in Figure 4b. Fine struc-

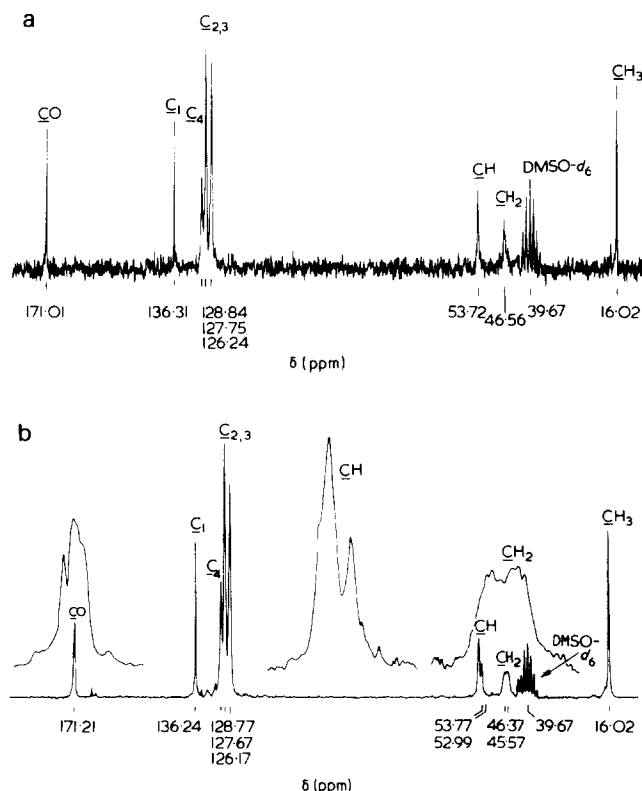


Figure 4 ¹³C{¹H} n.m.r. spectrum of $[-N(COC_6H_5)CH(CH_3)CH_2-]$ (a) Isotactic polymer, 20% in DMSO-*d*₆ at 120°C. 4000 scans; other conditions as in Figure 1. (b) Atactic polymer, 40% in DMSO-*d*₆ at 120°C. 82826 scans; other conditions as in Figure 1. The CO, CH and CH₂ regions are also shown in expanded form

Table 2 Tentative assignment of fine structure in ¹³C spectrum of atactic $\text{-N(COPh)CH(CH}_3\text{)CH}_2\text{-}$

CO	171.40	<i>rr</i>	CH ₂	46.56	* <i>mm</i>	
	171.21	<i>mr rm</i>		46.37		<i>mr (or rm)</i>
	171.01 (sh)	<i>mm</i>		45.67		<i>rm (or mr)</i>
				45.48	<i>rr</i>	
CH	54.03 (sh)	<i>rm (or mr)</i>				
	53.77	<i>mm mr</i>				
	52.99	<i>rr</i>				

sh, shoulder; * unresolved

ture may be seen for the CO, CH and CH₂ resonances and this must arise from tacticity effects with respect to the main-chain carbons (CH). The relative intensities may be interpreted in terms of a completely atactic structure with the groupings of lines and tentative assignments to dyad structures shown in Table 2. The *mm* (isotactic) assignments may be made with reasonable certainty, since there is agreement of the aromatic peak positions in Figures 4a and 4b within one channel (0.06 ppm). The rest are made by assuming a gradation of chemical shifts from *mm* to *rr* as normally found in polymers. The direct detection of triad structure in this polymer is made possible by the rapid rotation of the benzoyl groups at 120°C. This is in contrast to poly(*N*-formyliminopropylene) where it was necessary first to remove the formyl groups by hydrolysis before tacticity could be determined^{1,9}. An attempt was made to hydrolyse V for the same purpose but this did not prove successful.

Benzamide derivatives as model compounds of V, VI and VII

The spectra of *N*-methylbenzamide (XIV), *N,N*-dimethylbenzamide (XV), and *N*-ethyl-*N*-methylbenzamide (XVI), were examined. In CDCl₃ or DMSO-*d*₆ XIV showed a single set of sharp lines at all temperatures from -40° to 100°C, probably indicating the presence of a single conformer with CO-NH in the *anti* (*trans*) conformation¹⁵. For XV in DMSO-*d*₆ or CDCl₃ two broadened methyl peaks are observed at 33°C, separated by 91 Hz, which collapse into one sharp peak at 100°C. A coalescence temperature of about 36°C may be predicted from the ¹H n.m.r. spectrum¹⁶.

The spectrum of XVI in CDCl₃ at -30°C is shown in Figure 5. Every carbon atom gives two peaks of unequal intensity. The line positions, separations and approximate coalescence temperatures are shown in Table 3. Assignments to NCH₂ and NCH₃ were made by an off-resonance experiment. The relative intensities were derived from the print-out of areas. A plot of log Δδ against the reciprocal of the coalescence temperature gives a line whose slope corresponds to an activation energy of about 48 kJ/mol (11.5 kcal/mol), somewhat lower than the barrier reported¹⁶ for *N,N*-dimethylbenzamide (14.0 ± 0.25 kcal/mol). The variation in the relative intensities of the pairs of peaks from carbon to carbon is caused by differential nuclear Overhauser effects and differential spin-lattice relaxation times. The average intensity ratio for the eight pairs is 58:42 which is probably close to the actual relative populations of the two conformers. In order to make the assignment to the individual conformers we must make the same assumption as that for IV, namely that the upfield NCH₃ and NCH₂ peaks correspond to a *syn* conformation with

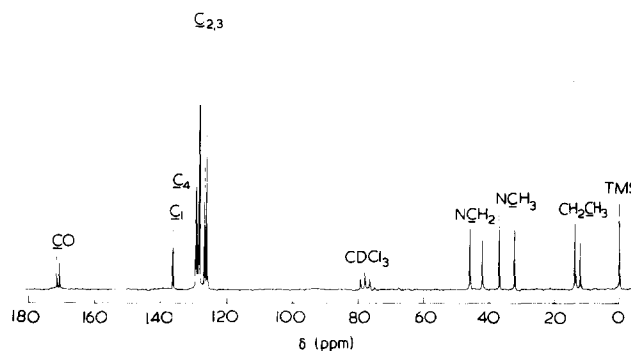
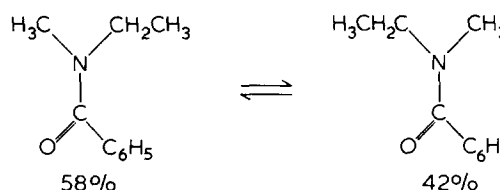


Figure 5 ¹³C{¹H} n.m.r. spectrum of C₂H₅N(COC₆H₅)CH₃. 50% solution in CDCl₃ at -30°C. 512 scans, acquisition time 0.679 sec, post-delay 2 sec, pulse width 11 μsec. In original spectrum each carbon shows 2 distinct lines

respect to the carbonyl oxygen¹ i.e.



The $\alpha_a - \alpha_s$ values are then as shown in Table 4.

Summary of ¹³C chemical shift differences for *syn* and *anti* conformations

The various values which we have determined are brought together in Table 4. It should be noted that $\alpha_a - \alpha_s$ for NCH₃ in *N*-ethyl-*N*-methylformamide was originally assigned a negative value¹. A further experiment using gated decoupling, with a delay time of 75 sec between pulses, has shown that this assignment was incorrect and that $\alpha_a - \alpha_s$ for NCH₃ has in fact a positive value. The spin-lattice relaxation times of the *syn* and *anti* carbons are substantially different and of such a magnitude (see below) that if the spectrum is taken with a short delay time between pulses the relative intensity of the two lines is reversed. The proportions of the two conformers determined from the gated decoupling experiment were 62% and 38%, good agreement being found for the four pairs of lines.

¹³C spin-lattice relaxation times in *N*-isopropyl-*N*-*n*-propylformamide and *N*-ethyl-*N*-methylformamide

For the former these were determined using a 50% solution in D₂O at 35°C. Fourteen sets of data were accumulated, with delay times τ ranging from 0.1 to 6.0 sec. For the latter, 7 sets of data were accumulated with delay times ranging from 1 to 75 sec for a 50% solution in CDCl₃ at 35°C. The results are shown below and compared with published results on dimethylformamide and di-*n*-butylformamide¹³, as well as with those reported above for poly(*N*-formyliminoethylene).

The assignment of the γ -carbons in *N,N*-di-*n*-butylformamide is the reverse of that given in the original paper in order to make $\gamma_a - \gamma_s$ negative as seems more likely - see earlier discussion. It is interesting to note that in *N*-isopropyl-*N*-*n*-propylformamide the relaxation times in the less abundant conformer are mostly longer than those in

Table 3 N-ethyl-N-methylbenzamide, ¹³C chemical shifts. Solvent CDCl₃, -30°C

Carbon atom	δ relative to TMS (±0.03) (ppm)		Δδ (±0.7) (Hz)	Coalescence temperature (±5°) (°C)
	Major peak	Minor peak		
CO	171.51(55)	170.66(45)	19.1	10
Aromatic C ₁	136.35(67)	136.22(33)	2.9	-20
Aromatic C ₄	129.20(55)	129.33(45)	-2.9	-10
Aromatic C _{2,3}	128.36(58)	128.23(42)	2.9	-10
	126.08(55)	126.80(45)	-16.0	25
NCH ₂	45.82(62)	41.92(38)	88.3	35
NCH ₃	32.11(56)	36.72(44)	-104.4	40
CH ₂ CH ₃	13.58(61)	11.96(39)	36.8	30
Average	(58)	(42)		

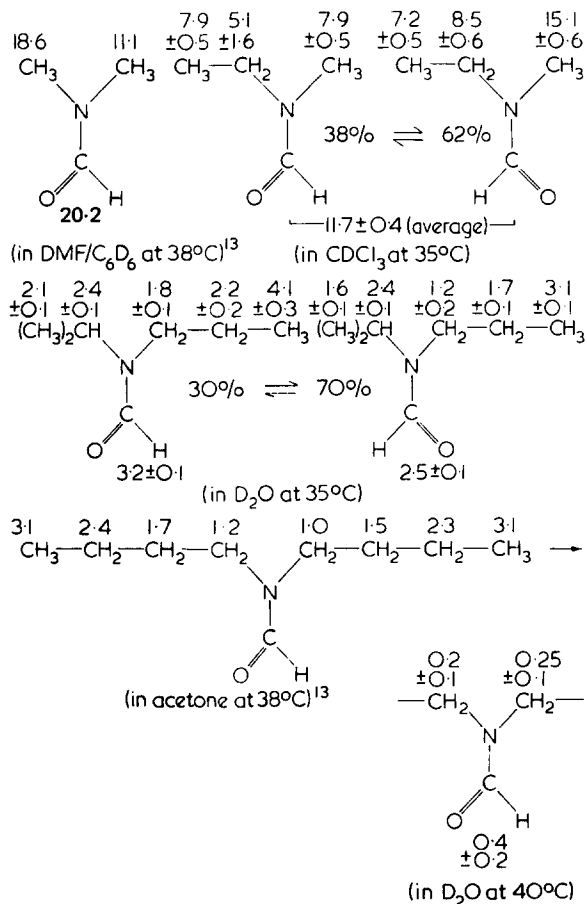
Values in parentheses represent relative intensities

Table 4 ¹³C chemical shift differences (ppm) of *syn* and *anti* carbons in some N,N-substituted amides and related polymers. (*Syn* and *anti* are defined with respect to the carbonyl oxygen)

Compound	Solvent	α _a - α _s	β _a - β _s	γ _a - γ _s
$\begin{array}{c} \text{CH}_3\text{NCH}_3 \\ \\ \text{HCO} \end{array}$	CDCl ₃ /35°C	5.07		
$\begin{array}{c} \text{CH}_3\text{NCH}_2\text{CH}_3 \\ \\ \text{HCO} \end{array}$	CDCl ₃ /35°C	5.13 (CH ₃) ^a 5.53 (CH ₂)	2.31	
$\begin{array}{c} \text{CH}_3\text{CH}_2\text{CH}_2\text{NCH}(\text{CH}_3)_2 \\ \\ \text{HCO} \end{array}$	CDCl ₃ /35°C	4.03 (CH ₂) 5.20 (CH)	2.34 (CH ₂) 1.95 (CH ₃)	-0.46
$\begin{array}{c} \text{-(CH}_2\text{NCH}_2\text{)-} \\ \\ \text{HCO} \end{array}$	D ₂ O/35°C	5.13 (β _a pair) 5.20 (β _s pair)	0.84 (α _a pair) 0.91 (α _s pair)	
$\begin{array}{c} \text{-(CH}_2\text{NCH}_2\text{CH}_2\text{)-} \\ \\ \text{HCO} \end{array}$	D ₂ O/80°C	5.46 (γ _a pair) 5.39 (γ _s pair)	1.11 (β _a pair) 1.04 (β _s pair)	-0.39 (α _a pair) -0.46 (α _s pair)
$\begin{array}{c} \text{-(CH}_2\text{NCH}(\text{CH}_3)\text{)-} \\ \\ \text{HCO} \end{array}$	D ₂ O/33°C	5.46	1.37	
$\begin{array}{c} \text{CH}_3\text{NCH}_3 \\ \\ \text{CH}_3\text{CO} \end{array}$	CDCl ₃ /35°C	3.06		
$\begin{array}{c} \text{-(CH}_2\text{NCH}_2\text{)-} \\ \\ \text{CH}_3\text{CO} \end{array}$	D ₂ O/35°C	2.73 (β _a pair) 3.19 (β _s pair)	0.71 (α _a pair) 1.37 (α _s pair)	
$\begin{array}{c} \text{CH}_3\text{NCH}_3 \\ \\ \text{C}_6\text{H}_5\text{CO} \end{array}$	CDCl ₃ /35°C	4.03		
$\begin{array}{c} \text{CH}_3\text{NCH}_2\text{CH}_3 \\ \\ \text{C}_6\text{H}_5\text{CO} \end{array}$	CDCl ₃ /-30°C	4.61 (CH ₃) 3.90 (CH ₂)	1.62	
$\begin{array}{c} \text{-(CH}_2\text{NCH}_2\text{)-} \\ \\ \text{C}_6\text{H}_5\text{CO} \end{array}$	CDCl ₃ /55°C	~3		
$\begin{array}{c} \text{-(CH}_2\text{NCH}_2\text{CH}_2\text{)-} \\ \\ \text{C}_6\text{H}_5\text{CO} \end{array}$	CDCl ₃ /32°C	~4.5		

^aSee text

the more abundant conformer, suggesting that the less abundant form can take up a more spherical and faster-rotating shape. There is the usual decrease in T_1 as one proceeds from the end to the centre of a short-chain molecule, and also as one goes from small to large molecules. The low T_1 values for the carbon nuclei in the polymer indicate a chain length high enough for the values of T_1 to be determined by the rate of rotation of segments of the chain.



CONCLUSIONS

The ¹³C n.m.r. spectra of all the polymers are as expected from the spectra of simple N-substituted formamides, acetamides and benzamides. Fine structure arises in two ways: first, because of restricted rotation about N-COR bonds; and second, when asymmetric carbons are present, from tacticity effects. The former is always present when R = H or CH₃ (up to 80°C) but can be eliminated when R = C₆H₅ by the use of a sufficiently high temperature (120°C). The

effect of restricted rotation about the N-COR bond is largest for the α-carbon, less for the β-carbon but still significant for the γ-carbon. In the polymers the chemical shifts for the main-chain carbons were governed by the conformation about the two nearest N-COR bonds, with a slight influence of a third, more remote, NCOR group in some cases. For poly(N-benzoyliminopropylene) the tacticity effect can be studied by itself by working at 120°C, but for poly(N-formyliminopropylene) this is not possible and the polymer must first be hydrolysed⁹.

ACKNOWLEDGEMENTS

We thank the Science Research Council for a postdoctoral fellowship (LCK), and Dr L. C. Waring (Belfast) and Dr I. A. Stenhouse (PCMU Harwell) for the ¹³C n.m.r. spectra.

REFERENCES

- 1 Hamilton, J. G., Ivin, K. J., Kuan-Essig, L. C. and Watt, P. *Macromolecules* 1976, **9**, in press
- 2 'Polymer Handbook', (Eds J. Brandrup and E. H. Immergut), 2nd Edn, Wiley-Interscience, New York 1975, pl-1
- 3 Saegusa, T., Kobayashi, S. and Ishiguro, M. *Macromolecules* 1974, **7**, 958
- 4 Saegusa, T., Ikeda, H. and Fujii, H. *Polym. J.* 1972, **3**, 176
- 5 Saegusa, T., Nagura, Y. and Kobayashi, S. *Macromolecules* 1973, **6**, 495
- 6 Saegusa, T., Ikeda, H. and Fujii, H. *Polym. J.* 1973, **4**, 87
- 7 Saegusa, T., Kobayashi, S. and Nagura, Y. *Macromolecules* 1974, **7**, 272
- 8 Matsuda, T. and Kagiya, T. *J. Macromol. Sci. (A)* 1971, **5**, 1265
- 9 Hamilton, J. G., Ivin, K. J., Kuan-Essig, L. C. and Watt, P. *Polymer* 1975, **16**, 763
- 10 Fones, W. S. *J. Org. Chem.* 1949, **14**, 1099
- 11 Dorman, D. E. and Bovey, F. A. *J. Org. Chem.* 1973, **38**, 1719
- 12 McFarlane, W. *JCS Chem. Commun.* 1970, 418
- 13 Levy, G. C. and Nelson, G. L. *J. Am. Chem. Soc.* 1972, **94**, 4897
- 14 Miron, Y. and Morawetz, H. *Macromolecules* 1969, **2**, 162
- 15 Stewart, W. E. and Siddall, T. H. *Chem. Rev.* 1970, **70**, 517
- 16 Reeves, L. W., Shaddick, R. C. and Shaw, K. N. *Can. J. Chem.* 1971, **49**, 3683
- 17 Meyers, A. I. and Collington, E. W. *J. Am. Chem. Soc.* 1970, **92**, 6676

Note added in proof

With improved resolution the spectrum of II (Figure 1) shows fine structure of the carbonyl peak (two lines of equal intensity) and splitting of each of the α_sβ_a and α_sβ_s lines into two equal components (cf. behaviour of α_aβ_a, α_aβ_s peaks of III). In the ¹H 220 MHz spectrum of II in D₂O at 22°C the formyl proton also shows fine structure (three lines, just resolved, spanning 0.03 ppm); the methylene protons give a single peak.

APPENDIX I

Table A1 ¹³C n.m.r. shifts for some oxazolines and 5,6-dihydro-4H-1,3-oxazines, ppm relative to TMS. Solvent CDCl₃, 35°C

Compound number	Formula	C ₂	C ₄	C ₅	C ₆	Aromatic (C _{1'} - C _{4'})			
II'		155.39	53.81	66.16					
I'		154.22 (157.99)	60.83 61.94	72.59 75.19	21.45 22.75) ^a				
XVII'		152.92	66.55	77.73	28.40				
IV'		165.27	54.85	67.52	13.71				
VI'		164.20	54.96	67.43		131.06 (C _{1'} + C _{4'})		128.13 (C _{2'} + C _{3'})	
V'		163.39	62.07	74.02	21.45	131.22 (C _{1'} + C _{4'})		128.29 (C _{2'} + C _{3'})	
V''		163.74	61.68	76.10	21.06	131.08 (C _{1'} + C _{4'})		128.22 (C _{2'} + C _{3'})	128.10
III'		149.61	41.59	22.75	64.34				
VII'		155.20	42.63	21.97	65.06	134.33 (C _{1'})	130.18 (C _{4'})	127.97 (C _{2'} + C _{3'})	126.93

^aValues in D₂O taking dioxane as 69.15 ppm

Note 1

Monomer XVII' was prepared by Saegusa's method³ from 2-amino-2-methylpropan-1-ol. Its polymerization was attempted but the product appeared to be oligomeric as judged from its n.m.r. spectrum. The monomer has previously been prepared by another method¹⁷.

Note 2

Three features of the spectra of the aromatic derivatives V', V'' and VI' are of particular interest. The first is the coincidence of the chemical shifts for C_{1'} and C_{4'} in all three cases. Second is the coincidence or near-coincidence of the chemical shifts for C_{2'} and C_{3'} in all three cases. Third is the second order splitting effect observed in off-resonance experiments for C₄ and C₅ in both V' and VI'; also for C_{1'} in all three compounds.

Note 3

The usual rules concerning the effects of substituents on the shifts are obeyed, as exemplified below:

Table A2

		α shift		β shift	
II'	→	I'	C ₄ 7.0	C ₅	6.4
VI'	→	V'	C ₄ 7.1	C ₅	6.6
VI'	→	V''	C ₅ 8.7	C ₄	6.6
I'	→	XVII'	C ₄ 5.7	C ₅	5.1
				C ₆	7.0

APPENDIX II

Summary of ¹³C n.m.r. shifts for poly(N-acyliminoalkenes) and model compounds

For ease of reference these shifts are summarized here, giving only *average* values for those cases where there is fine structure resulting from restricted rotation or tacticity.

Shifts are in ppm relative to TMS, using the following sub-standards where necessary: dioxane (in D₂O), 69.15; DMSO-*d*₆ 39.67; TSP (in D₂O), 0.

Table

Compound number	Polymer formula	Chemical shift	Solvent	Compound number	Model formula	Chemical shift	Solvent
II		a 44.9 b 168.3	D ₂ O/30°C	XVIII		a 33.7 b 162.4	CDCl ₃ /30°C
I		a 19.0 b 49.1 c 56.2 d 168.4	D ₂ O/33°C	XIX		a 11.4 b 21.6 c 23.1 d 43.8 e 48.4 f 162.4	CDCl ₃ /40°C
III		a 28.1 b 45.2 c 167.7	D ₂ O/80°C	XX		a 13.3 b 32.2 c 42.5 d 163.2	CDCl ₃ /35°C
IV		a 22.8 b 47.7 c 176.6	D ₂ O/35°C	XXI		a 21.5 b 36.4 c 170.2	CDCl ₃ /40°C
VI		a 44.4 b 125.8 c 127.7 d 128.7 e 135.8 f 170.4	DMSO/120°C	XV		a 37.3 b 127.0 c 128.2 d 129.4 e 136.4 f 171.4	CDCl ₃ /32°C
V		a 16.0 b 46.0 c 53.6 d 126.2 e 127.7 f 128.8 g 136.1 h 171.2	DMSO/120°C	XVI		a 12.9 b 34.1 c 44.2 d 126.4 e 128.3 f 129.3 g 136.3 h 171.2	CDCl ₃ /-30°C
VII		a 26.4 b 43.8 c 125.7 d 127.7 e 128.3 f 136.7 g 170.1	DMSO/120°C				

The usual rules concerning the effect of substituents are again obeyed, as exemplified below:

II	-	I	CH α shift	= 11.3
			CH ₂ (β + γ) shift	= 4.2
II	→	IV	CO α shift	= 8.3
XVIII	→	XXI	CO α shift	= 7.8
VI	→	V	CH α shift	= 9.2
			CH ₂ (β + γ) shift	= 1.6
XVIII	→	XX	CH ₂ α shift	= 8.8
			CH ₃ γ shift	= -1.5

It is also a general rule that the chemical shifts are higher for the aliphatic carbons in the polymers than in the corresponding model compounds. This may be regarded as a consequence of progressive substitution to form the long chains.

Comparison of the dielectric and viscoelastic properties of two poly (propylene glycol) liquids

Turhan Alper, A. John Barlow and R. Walter Gray

Department of Electronics and Electrical Engineering, University of Glasgow, Glasgow G12 8QQ, UK
(Received 22 January 1976; revised 15 March 1976)

The complex relative permittivities of two poly(propylene glycol) liquids, of molecular weights 380 and 3030, have been determined. Measurements were made in the frequency range 60 Hz to 200 MHz and at temperatures from -64° to $+25^{\circ}$ C. The lower molecular weight liquid showed only one relaxation region, which could be described by the Williams–Watts function with $\beta = 0.51$. The higher molecular weight liquid exhibited a similar main relaxation region and a secondary relaxation, of smaller amplitude, at lower frequencies. The relaxation times and their temperature dependencies are compared with previously determined viscoelastic relaxation and retardation times for the same liquids, and with the results from earlier dielectric studies by Baur and Stockmayer, and by Williams. The differences between the dielectric and mechanical times are discussed.

INTRODUCTION

A previous article¹ described the viscoelastic behaviour of two poly(propylene glycol) liquids, designated P400 and P4000. In general, the complex compliance, $J^*(j\omega)$, of a liquid may be described by:

$$J^*(j\omega) = J'(\omega) - jJ''(\omega) = J_{\infty} + 1/j\omega\eta + J_r^*(j\omega)$$

where J_{∞} ($= 1/G_{\infty}$) is the limiting high frequency compliance, ω the angular frequency of the applied shearing stress, η the steady flow viscosity and $J_r^*(j\omega)$ the complex retardational compliance. The product $J_{\infty}\eta$ is commonly termed the Maxwell relaxation time τ_M . For both poly(propylene glycol) liquids, J_r^* could be described by equation:

$$J_r^*(j\omega) = J_1(\omega) - jJ_2(\omega) = J_r/(1 + j\omega\tau_r)^{\beta}$$

which is analogous to the equation:

$$\epsilon_r^*(j\omega) = (\epsilon_0 - \epsilon_{\infty})/(1 + j\omega\tau_D)^{\beta D}$$

used by Davidson and Cole² in their studies of dielectric relaxation. For P400, the lower molecular weight liquid, ($M_n \sim 380$), the retardational compliance $J_r = 17.4 J_{\infty}$, the parameter $\beta = 0.45$ and the characteristic retardation time τ_r increased with decreasing temperature, reaching a limit of $170 \tau_M$ near 0° C. The viscoelastic behaviour of P400 is similar to that of many non-polymeric organic liquids. For the higher molecular weight liquid, P4000 ($M_n \sim 3030$), the viscoelastic properties were described by the same equation but with $J_r = 85 J_{\infty}$, $\beta = 0.76$ and $\tau_r = 15.4 \tau_M$, remaining constant at least over the temperature range from $+79.5^{\circ}$ to 0° C.

The dielectric behaviour of poly(propylene glycol) liquids has been investigated by several authors. In particular, Baur and Stockmayer³ investigated four liquids of nominal (number-average) molecular weights from 1025 to about 3700, and Williams⁴ has studied an amorphous sample of high molecular weight, $M_n > 10^5$. Other prop-

erties of high molecular weight material have also been determined and have been summarized by McCrum, Read and Williams⁵.

The present work supplements previous studies of dielectric properties by extension of the measurement range to lower molecular weights and to higher frequencies. In addition, since the samples P400 and P4000 used are the same as employed before¹, a quantitative comparison of the viscoelastic retardation and dielectric behaviour is possible.

EXPERIMENTAL

Details of the P400 and P4000 liquids used have been given previously¹. Measurements of the complex relative permittivity, $\epsilon^* = \epsilon' - j\epsilon''$, were made in two frequency ranges, 60 Hz to 200 kHz and 3 to 200 MHz, using conventional bridge techniques. In the lower frequency range a transformer ratio arm capacitance bridge was used, (General Radio, Model 1615A), with a matching generator and detector, together with a two terminal cell. Measurements were made with the cell immersed in a constant temperature bath. The estimated errors in the measurements made using this system are $\pm 1\%$ in ϵ' and $\pm 2\%$ in ϵ'' up to 10 kHz, above this frequency the accuracy decreases slightly. In the higher frequency range an R–X meter was used, (Hewlett Packard Type 250B) with a coaxial cell of capacitance (when empty) of 1.1 pF. The calibration of this cell was checked using liquids of known permittivities. The experimental errors in measurements made up to 100 MHz are estimated to be $\pm 1\%$ in capacitance and $\pm 3\%$ in conductance. Above 100 MHz the accuracy achieved was less because of the distributed impedance of the strips connecting the cell to the meter. The readings were corrected assuming a simple lumped circuit model for the connections. For this cell temperature stabilization was ensured by circulating a liquid at the desired temperature through a jacket around the cell. Temperatures were determined using platinum resistance thermometers and are estimated to be accurate to within $\pm 0.05^{\circ}$ C. Measurements in the high frequency range were made of P400 at temperatures from $+20^{\circ}$ to -22.8° C, and of P4000 from $+16.3^{\circ}$ to -64° C.

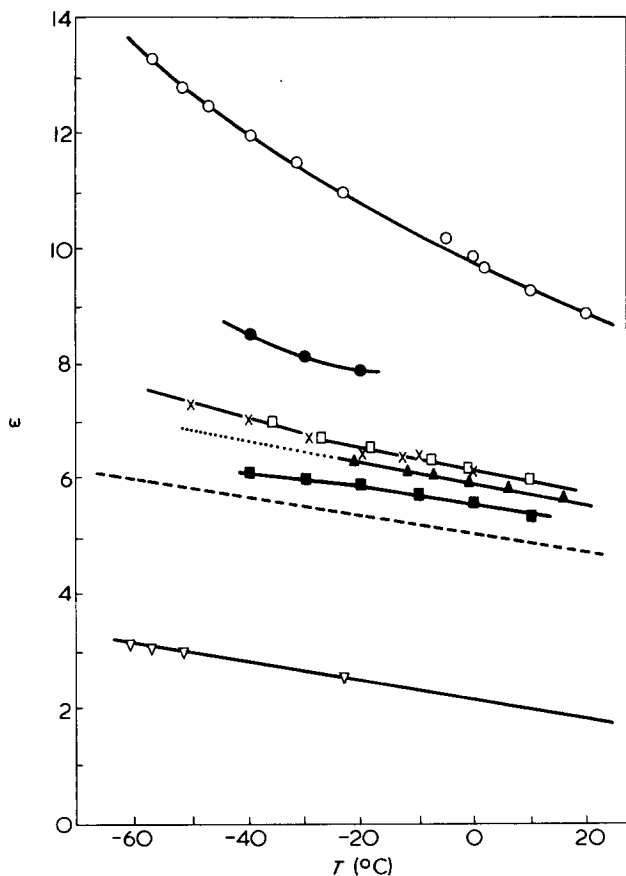


Figure 1 Temperature dependence of ϵ_0 for a range of poly(propylene glycol) liquids and of ϵ_∞ for the liquid of lowest molecular weight

	M_n nominal	M_n measured	Reference
▽	ϵ_∞ 400	380	P400, this work
○	ϵ_0 400	380	P400, this work
●	ϵ_0 1025	900 ± 100	Baur and Stockmayer, 1965
□	ϵ_0 2000		This work
X	ϵ_0 2025	1800 ± 300	Baur and Stockmayer, 1965
▲	ϵ_0 4000	3030	P4000, this work
■	ϵ_0 'HMW'	3700 ± 600	Baur and Stockmayer, 1965
---	ϵ_0 >10 ⁵		Williams, 1965

A few measurements were also made of a third poly(propylene glycol) liquid, P2000, which was obtained from the same source and processed in the same manner as the other two liquids¹. This liquid has a nominal (number-average) molecular weight of 2000. The dielectric behaviour of this liquid was found to be intermediate between that of P400 and P4000, and showed evidence of two relaxation processes which, however, were not sufficiently separated to allow useful analysis. Accordingly, measurements were limited to the low frequency region and to the temperature range +9.9° to -56°C.

RESULTS AND ANALYSIS

The data were sufficient to define the low frequency limit ϵ_0 for P400 over the range +20° to -61°C, and ϵ_0 for P4000 from +20° to -20°C. The results are shown in Figure 1, together with the variation of ϵ_0 found for other poly(propylene glycol) materials by Baur and Stockmayer³ and by Williams⁴. The high frequency limit ϵ_∞ for P400 was also defined in the range -22° to -61°C, the variation was linear and values at higher temperatures have been obtained by extrapolation.

Considering first P400, at each temperature the component ϵ'' was normalized with respect to its maximum value ϵ''_{\max} , and plotted as a function of $\omega\tau_\alpha$, where τ_α is the reciprocal of the angular frequency at the peak of the ϵ'' curve. The data reduced to a single curve as shown in Figure 2. Similarly, the ϵ' data were plotted as $(\epsilon' - \epsilon_\infty)/(\epsilon_0 - \epsilon_\infty)$ and combined to a single curve by shifting. Figure 3 shows the result plotted in terms of $\omega\tau_\alpha$. The temperature dependence of τ_α is given in Figure 4. For comparison with the viscoelastic retardation behaviour, the time τ_f , defined as the reciprocal of the angular frequency at the peak of the $J_2(\omega)$ curve, is also given in this Figure. A plot of $\epsilon''/(\epsilon_0 - \epsilon_\infty)$ against $(\epsilon' - \epsilon_\infty)/(\epsilon_0 - \epsilon_\infty)$, combining results obtained at three temperatures, is shown in Figure 5.

For P4000, the results showed the presence of two relaxation processes, as found by Baur and Stockmayer³ for a similar liquid. The minor secondary or β -peak of ϵ'' , occurring at lower frequencies than the α -peak, was suffi-

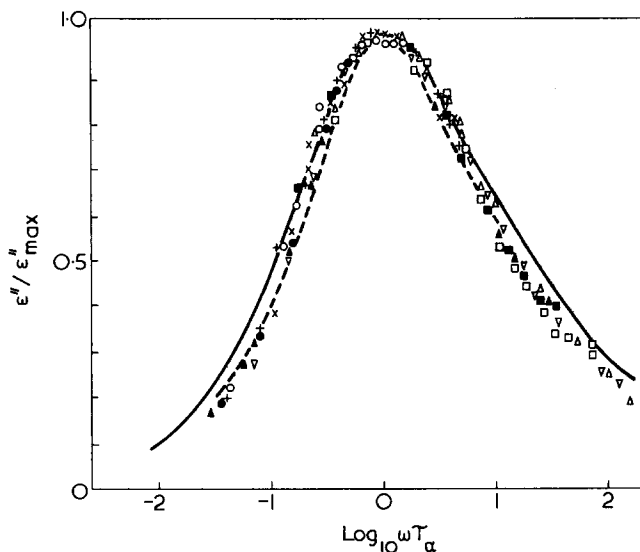


Figure 2 Values of $\epsilon''/\epsilon''_{\max}$ plotted against $\log_{10} \omega\tau_\alpha$ for poly(propylene glycol) P400 ($M_n \approx 380$): ○, +10.5°C; X, -0.1°C; □, -22.8°C; +, -46.9°C; △, -60.8°C; ▽, -57.0°C; ▲, -51.6°C; ●, -39.9°C; ■, -15.2°C. For comparison, results obtained by Williams (1965) for $M_n > 10^5$ (—) and by Baur and Stockmayer (1965) for $M_n \approx 1025$ (---), are also shown

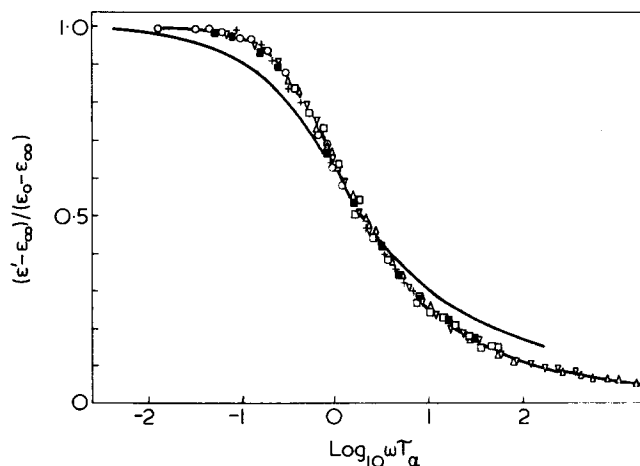


Figure 3 Values of $(\epsilon' - \epsilon_\infty)/(\epsilon_0 - \epsilon_\infty)$ for poly(propylene glycol) P400 ($M_n \approx 380$) plotted against $\log_{10} \omega\tau_\alpha$: ○, +20.0°C; □, -22.8°C; +, -46.9°C; ■, -51.6°C; ▽, -57.0°C; △, -60.8°C. —, the corresponding variation found by Williams (1965) for $M_n > 10^5$

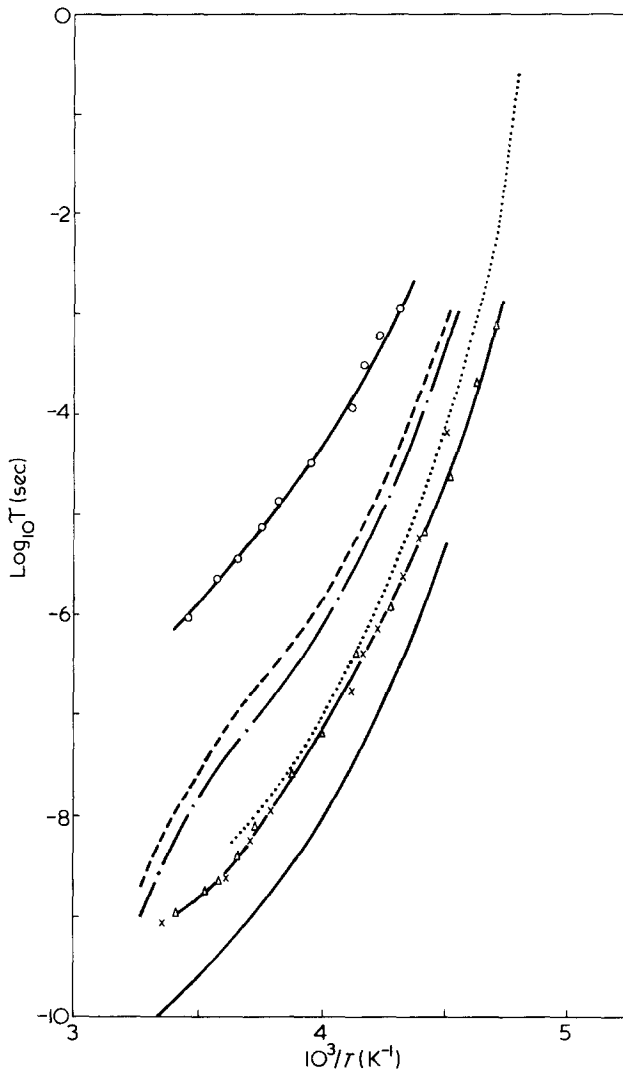


Figure 4 Temperature dependence of dielectric relaxation, viscoelastic retardation and viscoelastic relaxation times. P400 ($M_n \approx 380$): Δ , τ_α ; \cdots , τ_J ; $---$, τ_R ; $---$, τ_M . P4000 ($M_n \approx 3030$): X , τ_α ; \circ , τ_β ; \cdots , τ corresponding to the peak of the loss curve given by Williams (1965)

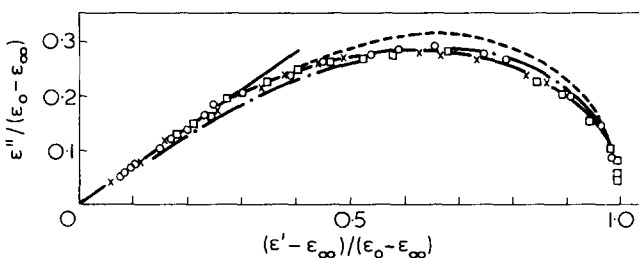


Figure 5 Plot of $\epsilon''/(\epsilon_0 - \epsilon_\infty)$ against $(\epsilon' - \epsilon_\infty)/(\epsilon_0 - \epsilon_\infty)$ for P400: \square , -51.6°C ; \circ , -57.0°C ; X , -60.8°C . $---$, derived from the William-Watts equation with $\beta = 0.51$; $---$, plotted using the Davidson-Cole equation with $\beta = 0.39$; \cdots , plotted using the Davidson-Cole equation with $\beta = 0.35$

ciently small and separated from the main α -peak to allow comparison of the α -peak with the single process found for P400. Figure 6 shows $\epsilon''/\epsilon''_{\max}$ for P4000 as a function of $\omega\tau_\alpha$. At the lowest frequencies the data for ϵ'' showed a frequency dependent loss attributable to d.c. conductivity and the results given in Figure 6 have been corrected for this effect; the corrections were significant only in the region $\log_{10} \omega\tau_\alpha < -3.5$. The data defining the main peak reduce to the same curve as found for P400. Accordingly,

the ratio of ϵ''_{\max} for the α -relaxation to the permittivity ϵ_α contributed by this process to ϵ_0 has been assumed to be the same, 0.283, as $\epsilon''_{\max}/(\epsilon_0 - \epsilon_\infty)$ for P400. ϵ_α can then be determined and deducted from ϵ_0 to give the sum of ϵ_∞ and ϵ_β , the permittivity for the secondary relaxation.

The ϵ'' curves for the secondary process are not well defined experimentally, they are similar to those obtained by Baur and Stockmayer³. They imply a distributed, but narrow, relaxation spectrum. The best estimate of the maximum value of ϵ'' for the β -process to ϵ_β is 0.4. If this ratio is assumed constant, then ϵ_β may be determined and hence ϵ_∞ . Figure 7 shows the temperature dependence of ϵ_0 , ϵ_α , ϵ_β and ϵ_∞ for P4000, the variation of ϵ_∞ deduced in this manner is linear and the extrapolated value at -64°C is in good agreement with the only measured value for this liquid. The ratio $\epsilon_\alpha/\epsilon_\beta$ is approximately 8, the corresponding value for P2000 is about 18.

The time τ_α and τ_β defined by the main and secondary peaks of the ϵ'' curves for P4000 have also been determined and are included in Figure 4.

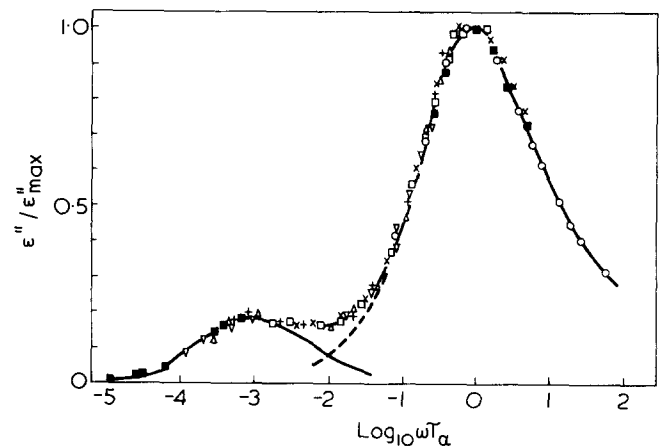


Figure 6 Values of $\epsilon''/\epsilon''_{\max}$ plotted against $\log_{10} \omega\tau_\alpha$ for P4000: \circ , -51.5°C ; X , -45.7°C ; \square , -42.2°C ; $+$, -37.0°C ; Δ , -33.0°C ; ∇ , -31.0°C ; \blacksquare , -10.0°C . $---$, the corresponding variation for P400

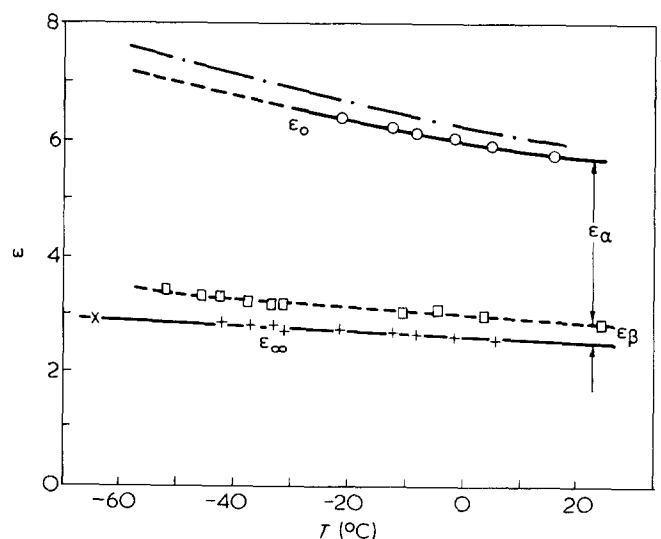


Figure 7 Temperature dependence of ϵ_0 and ϵ_∞ for P4000, showing the contributions of the main (α) and the secondary (β) processes. \circ , ϵ_0 measured; X , ϵ_∞ measured; \square , $\epsilon_\infty + \epsilon_\beta$ deduced; $+$, ϵ_∞ deduced. \cdots , represents the measured variation of ϵ_0 for a poly(propylene glycol) liquid of $M_n \approx 2000$ and is included for comparison

Table 1 Properties of poly(propylene glycol) liquids at 0°C

	Viscoelastic relaxation times (μsec)	Viscoelastic retardation times (μsec)	Dielectric relaxation times (μsec)
P4000	$\tau_1 = 4.1^*$ $\tau_2 = 1.0^*$ $\tau_M = 0.009$ $\tau_G = 0.001$	$\tau_a = 1.8^*$ $\tau_b = 0.6^*$ $\tau_r = 0.14$ $\tau_J = 0.1$	$\tau_\alpha = 0.0045$ $\tau_\beta = 3.6$
P400	$\tau_M = 0.0006$ $\tau_G = 0.0002$	$\tau_r = 0.1$ $\tau_J = 0.05$	$\tau_\alpha = 0.0045$

* Derived assuming the Rouse modes to be given by $\tau_p = 6\eta M/\pi^2 p^2 \rho RT$

DISCUSSION

The results (Figure 1) for P400 and P4000 confirm the previous findings of a decrease of ϵ_0 , and its temperature dependence, with increasing molecular weight. Stockmayer and Burke⁶ note that for both linear and branched poly(propylene oxide) ϵ_0 is an almost linear function of hydroxyl content. This is substantiated by the present results, a plot of ϵ_0 against $1/M_n$ is fitted by a straight line within the experimental error limits of molecular weight determination, e.g. at -20°C , $\epsilon_0 = 5.35 + 2220/M_n$. Plots of ϵ_0 against molecular weight or its inverse therefore provide a means of checking relative molecular weights. For P4000, M_n is clearly less than that of the *HMW* sample of Baur and Stockmayer³, for which $M_n \approx 3700$, and the measured value of $M_n \approx 3030$ is compatible with previous results to within about 10%.

Figures 2 and 3 show that the normalized dielectric relaxation curves for $\epsilon''/\epsilon''_{\text{max}}$ and $(\epsilon' - \epsilon_\infty)/(\epsilon_0 - \epsilon_\infty)$ are similar to those found by Williams⁴ for a very high molecular weight polymer. Although Baur and Stockmayer³ comment that the relaxation region broadens with increasing molecular weight there is no difference, within the limits of experimental accuracy, between their results and the present ones for P400 (and for P4000), and only a small increase in the width of the relaxation region as M_n increases to more than 10^5 . The plot of Figure 5 shows a skewed curve, which is not fitted by a Davidson–Cole² distribution of relaxation times – the best fit varying from $\beta = 0.39$ at high frequencies to 0.35 or less at low frequencies. However, the results can be described by the Williams–Watts function⁷, which is defined by the dielectric decay function $\gamma(t) = \exp(-t/\tau_0)^\beta$, where $0 < \beta \leq 1$ and τ_0 is a relaxation time. For P400, the data are fitted within the limits of experimental error by the corresponding frequency – dependent complex permittivity with the parameter $\beta = 0.51$. Williams, Watts, Dev and North⁸ have previously noted that this function describes the dielectric relaxation of a very high molecular weight poly(propylene oxide)⁴, and of the principal relaxation region of several other polymers. The main (α) relaxation process for P4000 (Figure 6) is the same as for P400, and is independent of molecular weight. Figure 4 and Table 1 show that at a given temperature the relaxation times, τ_α , for P4000 and P400 are the same; the value differs only slightly from that found by Williams⁴ for the polymer of $M_n > 10^5$. This similarity of the values of τ_α is accompanied by a comparable lack of dependence of the glass transition temperature T_g on molecular weight in the range 400 to $>10^5$, the values of T_g being within a few degrees of -75°C . The same physical process is clearly involved in the different

polymers, and local segmental motion of the polymer chain has been suggested³. Since τ_α for P400, with only 5 repeat units, is the same as for longer chain polymers, then any particular segmental motion must involve very few bonds, otherwise end effects would have a significant influence. Rather than making any such specific ascription, it is more realistic to regard the form of the α -relaxation as a general characteristic of the co-operative nature of local rearrangements⁹, and due to intermolecular rather than intramolecular movements.

For P400, the proportion of the relaxing permittivity due to end-groups is relatively large, yet their contribution to the relaxation process is in no way different from that of main chain elements. Johari and Goldstein¹⁰ and others¹¹, have pointed out the general similarity of the α -relaxation in amorphous polymers and in supercooled, small molecule liquids. The present results for P400 provide direct confirmation, within the same molecular species, of a common process being responsible; P400 may be regarded either as a very short chain polymer or more realistically, as a supercooled liquid with dielectric and viscoelastic properties similar to those of a non-polymeric liquid¹¹. In this context, it may be noted that the value $\beta = 0.51$, in the Williams–Watts function describing the α -relaxation, defines a stress relaxation curve which is very similar to that predicted theoretically from a relaxation model based upon a defect-diffusion mechanism^{12,13}.

The secondary dielectric dispersion in poly(propylene oxide) has been attributed by Baur, Burke and Stockmayer^{3,6} to the cumulative effect along the chain of the dipole moment (0.18 *D*) of each repeat unit. Since polymerization occurs by head-to-tail additions to the chain, more or less symmetrically about an initiator site, the resultant polarization has a (+ ··· · – ··· · +) form. The measured dielectric relaxation time of the secondary dispersion, its temperature variation and dependence on molecular weight were found to be similar to the corresponding properties of the second normal mechanical relaxation mode of the chain, calculated using the assumption of free-draining conditions as proposed by Rouse¹⁴. However, the apparently satisfactory numerical agreement with the Rouse theory is subject to some reservations. Firstly, the secondary dielectric dispersion is distributed and the longest relaxation time, τ_d , in such a spectrum is, in general, longer than that defined by the peak of the ϵ'' curve, τ_β . For P4000, τ_d may be up to 1.5 τ_β . Secondly, Stockmayer and coworkers compare the dielectric relaxation time and the viscoelastic relaxation time, instead of with the formally analogous retardation time. A spectrum of discrete relaxation times, as postulated in the Rouse theory, implies a spectrum of discrete retardation times, on a time scale these are interleaved between the relaxation times. The first retardational mode τ_a occurs at about 0.45 of τ_1 , the first relaxation mode, and the second retardational mode τ_b lies at about 0.6 of τ_2 , the second relaxational mode. The measured time for the secondary dielectric dispersion may therefore be up to 2.5 times the predicted viscoelastic retardation time. If the non-free-draining approach of Zimm¹⁵ is assumed, then the ratio is greater since this theory gives shorter predicted times¹⁶. In the present work a similar discrepancy is found, $\tau_\beta/\tau_b \approx 6$, (Table 1). Therefore, whilst the accepted explanation of the secondary dielectric dispersion may be correct in general, there are obvious short-comings in the detailed predictions of the theory. If instead of using the macroscopic dielectric times in these comparisons, a microscopic time is calculated using, for example, the factor proposed by Powles¹⁷, then

the discrepancies between mechanical and dielectric times are greater. Connor, Blears and Allen¹⁸ suggest that hydrogen bonding between end-groups increases the effective chain length, and this may account for τ_β being greater than τ_b . It may also be partly responsible for the absence of a secondary dielectric dispersion in very high molecular weight poly(propylene oxide), although random reversals of polarization along the chain and entanglements¹⁹ have also been suggested as possible explanations. An attempt has been made, by extending the range of previous viscoelastic measurements of P4000 to lower frequencies, to see if a mechanical retardation process occurs corresponding to the secondary dielectric dispersion. No separate process was found*.

Williams^{4,5} has shown that the mechanical loss peak of the dynamic shear modulus at the glass-rubber transition which was observed by Saba, Sauer and Woodward²⁰ at 0.37 Hz and -62°C , corresponds to the main (α) dielectric relaxation process in an amorphous high molecular weight poly(propylene glycol). At such a low temperature ($10^3/T \sim 4.7$) both mechanical and dielectric times are greatly affected by small variations in temperature, and any difference between them may be masked. The present results in Table 1 show that there is an appreciable difference between τ_α and the analogous mechanical retardation time τ_J . For P400, $\tau_J \approx 10 \tau_\alpha$ and for P4000, $\tau_J \approx 20 \tau_\alpha$. (For comparison, the time τ_G defined by the peak in the loss component G'' of the shear modulus is also given in the Table.) Whilst it remains possible that the relevant mechanical and dielectric losses have their origins in a common physical mechanism it is clear that there is no close numerical equivalence between τ_J and τ_α .

* However, subject to the uncertainty due to increasing experimental errors at lower frequencies, there is an indication of a gradual increase of the ratio J_p/J_∞ at temperatures above 0°C .

ACKNOWLEDGEMENTS

The authors are grateful to Professor J. Lamb for his help and encouragement of this work. Support for this research has been provided by the Science Research Council.

REFERENCES

- 1 Barlow, A. J. and Erginsav, A. *Polymer* 1975, **16**, 110
- 2 Davidson, D. W. and Cole, R. H. *J. Chem. Phys.* 1951, **19**, 1484
- 3 Baur, M. E. and Stockmayer, W. H. *J. Chem. Phys.* 1965, **43**, 4319
- 4 Williams, G. *Trans. Faraday Soc.* 1965, **61**, 1564
- 5 McCrum, N. G., Read, B. E. and Williams, G. 'Anelastic and dielectric effects in polymeric solids', Wiley, London, 1967, Ch 14, pp 568-574
- 6 Stockmayer, W. H. and Burke, J. J. *Macromolecules* 1969, **2**, 647
- 7 Williams, G. and Watts, D. C. *Trans. Faraday Soc.* 1970, **66**, 80
- 8 Williams, G., Watts, D. C., Dev, S. B. and North, A. M. *Trans. Faraday Soc.* 1971, **67**, 1323
- 9 Williams, G., Cook, M. and Hains, P. J. *JCS Faraday Trans. 2* 1972, **68**, 1045
- 10 Johari, G. P. and Goldstein, M. *J. Chem. Phys.* 1971, **55**, 4245
- 11 Williams, G. and Hains, P. J. *JCS Faraday Symp.* 1973, **6**, 14
- 12 Shears, M. F., Williams, G., Barlow, A. J. and Lamb, J. *JCS Faraday Trans. 2* 1974, **70**, 1783
- 13 Phillips, M. C., Barlow, A. J. and Lamb, J. *Proc. Roy. Soc. (A)* 1972, **329**, 193
- 14 Rouse, P. E. *J. Chem. Phys.* 1953, **21**, 1272
- 15 Zimm, B. H. *J. Chem. Phys.* 1956, **24**, 269
- 16 Ferry, J. D. 'Viscoelastic Properties of Polymers', Wiley, New York, 1961, Ch 10
- 17 Powles, J. G. *J. Chem. Phys.* 1953, **21**, 633
- 18 Connor, T. M., Blears, D. J. and Allan, G. *Trans. Faraday Soc.* 1965, **61**, 1097
- 19 Stockmayer, W. H. *Pure Appl. Chem.* 1967, **15**, 539
- 20 Saba, R. G., Sauer, J. A. and Woodward, A. E. *J. Polym. Sci.* 1963, **1**, 1483

Dimensions of poly(trimethylene oxide) chains in a theta-solvent

D. S. Chiu, Y. Takahashi* and J. E. Mark

Department of Chemistry and the Macromolecular Research Center, University of Michigan, Ann Arbor, Michigan, 48109, USA

(Received 26 February 1976)

Fractions of poly(trimethylene oxide) $\text{--}[(\text{CH}_2)_3\text{--O}]_x\text{--}$ of relatively high degree of polymerization x were studied in liquid-liquid phase equilibria in the poor solvent cyclohexane. The results thus obtained indicate that the ideal or theta-temperature for this system is $27.0 \pm 0.5^\circ\text{C}$. Intrinsic viscosities measured under these conditions were used to obtain a value for the characteristic ratio $\langle r^2 \rangle_0/nl^2$ of the unperturbed dimensions of these chains relative to the number of skeletal bonds and the average square of their length. The resulting value, 3.86 ± 0.08 , is unusually low, a fact which may be attributed to the high degree of conformational randomness in this chain molecule. Consideration of poly(trimethylene oxide) to be an alternating copolymer of ethylene and oxymethylene provides some additional information of interest. It clearly demonstrates that a chemical copolymer can have configuration-dependent properties which are vastly different from those of its parent homopolymers.

INTRODUCTION

Poly(trimethylene oxide) $\text{--}(\text{CH}_2\text{--CH}_2\text{--CH}_2\text{--O})_x\text{--}$ is one of the most interesting chain molecules which may be studied with regard to its spatial configurations in the random-coil state. The polymer may be prepared to relatively high degrees of polymerization x^1 , and has a rather low melting point (35°C)²; its characterization from the experimental point of view should therefore be straightforward. In addition, its investigation³⁻⁵ in terms of the rotational isomeric state theory⁴ of chain configurations is facilitated by two important features of this polyoxide chain. Its repeat unit has a very simple structure and most of the intramolecular interactions occurring in this molecule also occur in other members of the $\text{--}[(\text{CH}_2)_y\text{--O}]_x\text{--}$ series, several of which have now been extensively studied with regard to their configuration-dependent properties⁴⁻⁶. Finally, preliminary evidence¹ indicates that poly(trimethylene oxide) in the random-coil state is an unusually compact chain molecule, judging from approximate values of its unperturbed dimensions as estimated from viscosity measurements in a thermodynamically good solvent.

For the above reasons, the present study was undertaken to determine a reliable experimental value of the characteristic ratio $\langle r^2 \rangle_0/nl^2$ of poly(trimethylene oxide), where $\langle r^2 \rangle_0$ is the chain dimension as unperturbed by excluded volume effects^{1,7}, n is the number of skeletal bonds, and l^2 is the average square of their length. The approach taken, the study of the molecules in a theta (θ) solvent, where excluded volume interactions are known to be nullified⁷, is probably the most reliable method presently available for this purpose. The temperature at which a suitably poor solvent acts as a θ -solvent for poly(trimethylene oxide) will be located by measurements of the critical solution temperatures for liquid-liquid phase equilibria of solutions of the polymer, obtained as a function of its degree of polymerization⁷. Intrinsic viscosities measured in this solvent at the θ -temperature thus established then

directly yield values of the unperturbed dimensions and the characteristic ratio, without the need for approximate corrections for chain expansion due to excluded volume interactions.

Since there has been a considerable amount of interest in the configuration-dependent properties of chemical copolymers⁸⁻¹², it should be noted that poly(trimethylene oxide) may be thought of as an alternating copolymer of ethylene and oxymethylene. It is therefore obviously of considerable interest to compare its statistical properties with those of polyethylene⁴ and polyoxymethylene^{4,13,14}

EXPERIMENTAL

The five fractions of poly(trimethylene oxide) employed in the present study were among those studied previously in a thermodynamically good solvent, and their preparation is thus described elsewhere¹. Their number-average molecular weights M_n , which had been determined by osmometry in benzene at 30°C ¹, are listed in Table I.

A preliminary survey of solvents indicated that cyclohexane should serve as a θ -solvent⁷ for poly(trimethylene oxide) in the vicinity of room temperature. Precipitation temperatures, T_p , for liquid-liquid separations in the reagent-grade solvent were therefore determined for the five fractions listed in Table I, augmented by two others (F1 and F7¹, having values of $M_n \times 10^{-3}$, 53.5 and 153.0, res-

Table I Experimental results on poly(trimethylene oxide)

Fraction ^a	$M_n \times 10^{-3b}$	$[\eta]^c$ (dl/g)	$\langle r^2 \rangle_0/nl^2$
F2	65.1	0.275	3.78
F3	87.5	0.316	3.76
F4	109.1	0.380	3.95
F8	161.1	0.465	3.97
F10	292.5	0.591	3.82
			Average 3.86 ± 0.08

^aDetailed information on these fractions is given in ref 1. ^bObtained from osmotic pressure measurements in benzene at 30°C ; see ref 1. ^cIn the θ -solvent, cyclohexane, at 27.0°C ; present results

* Permanent address: Faculty of Science, Osaka University, Toyonaka, Osaka 560, Japan.

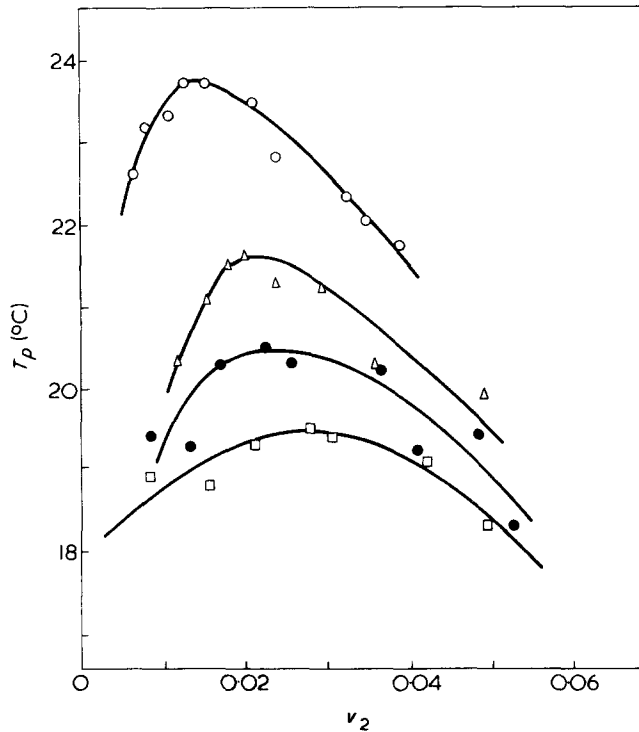


Figure 1 Some typical binodials characterizing liquid-liquid separations in the poly(trimethylene oxide)-cyclohexane system. The fractions represented are described in Table 1, and in a previous study¹: \circ , F10; \triangle , F7; \bullet , F4; \square , F2

pectively). Values of T_p were determined as a function of composition, for all seven fractions, using simple visual inspection, in the usual manner¹⁵. The volume fraction v_2 of polymer in each solution at 23°C was obtained from the weights of polymer and solvent, and the specific volumes at this temperature. Values of v_2 thus obtained were in good agreement with direct pycnometric measurements on the solutions themselves.

Viscosities of the poly(trimethylene oxide) fractions in the cyclohexane were determined in a Cannon-Ubbelohde viscometer. Each fraction was studied at a minimum of four concentrations, in the range 0.03 to 2.17 g/dl, and values of the relative viscosity ranged from 1.02 to 2.03.

RESULTS AND DISCUSSION

The binodials for the liquid-liquid phase separations were obtained by plotting values of the precipitation temperature against composition. Typical results are shown in Figure 1. The maximum of each binodal is the critical solution temperature T_c at that particular degree of polymerization x . Although some of the data scatter somewhat, presumably because of the relatively low molecular weights of some of the fractions, the values of T_c obtained are probably accurate to $\pm 0.2^\circ\text{C}$. Their reciprocals were plotted against the molecular size function indicated by theory, in the usual manner⁷. The results are presented in Figure 2, where the line shown was located by least-squares analysis. The intercept gives the value of T_c in the limit of infinite chain length, which is the θ -temperature of the system. We thus obtain $\theta = 27.0^\circ\text{C}$, with an uncertainty estimated to be $\sim \pm 0.5^\circ\text{C}$. The entropy of dilution parameter ψ_1 ⁷, obtained from the slope of this curve, was found to have the relatively large value 1.0.

Values of the intrinsic viscosity $[\eta]$ of the poly(trimethylene oxide) fractions in cyclohexane at 27.0°C were obtained from the solution viscosities in the usual manner⁷;

the results are given in Table 1. They are plotted logarithmically against the number-average molecular weight in Figure 3, and were found by least-squares analysis to be represented by the relationship:

$$[\eta] = 8.89 \times 10^{-4} M_n^{0.519} \quad (1)$$

The fact that the exponent on the molecular weight is one-half⁷ within experimental error confirms cyclohexane to be a θ -solvent for poly(trimethylene oxide) at 27.0°C . Values of the unperturbed dimensions $\langle r^2 \rangle_0$ are therefore directly calculable from the equation:

$$[\eta] = \Phi (\langle r^2 \rangle_0 / M_n)^{3/2} M_n^{1/2} \quad (2)$$

which is applicable to any random-coil polymer in a θ -solvent⁷; under these conditions, the constant Φ has the value 2.5×10^{21} dl/mol cm^3 ^{7,16}. The unperturbed dimensions thus obtained were expressed relative to nl^2 , with $n = 4(M_n/M_0)$, where $M_0 = 58.08$ is the molecular weight of the repeat unit, and $l^2 = 2.19 \text{ \AA}^2$ ¹. The resulting values of the characteristic ratio are given in Table 1 and are seen to be independent of molecular weight, as expected^{4,7}.

The average value $\langle r^2 \rangle_0 / nl^2 = 3.86 \pm 0.08$ is in excellent agreement with the value 3.94 ± 0.17 obtained from viscometric and osmometric measurements in a thermodynamically good solvent, benzene at 30°C ¹. The agreement may be somewhat fortuitous, however, in that it is frequently

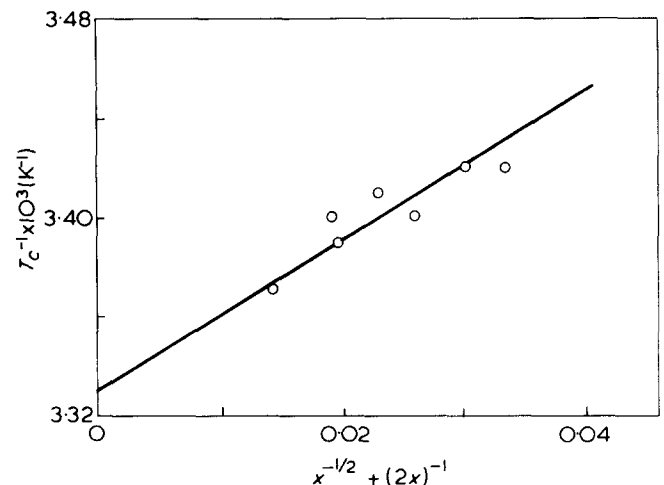


Figure 2 Extrapolation of reciprocal critical solution temperatures to obtain the θ -temperature for the poly(trimethylene oxide)-cyclohexane system.

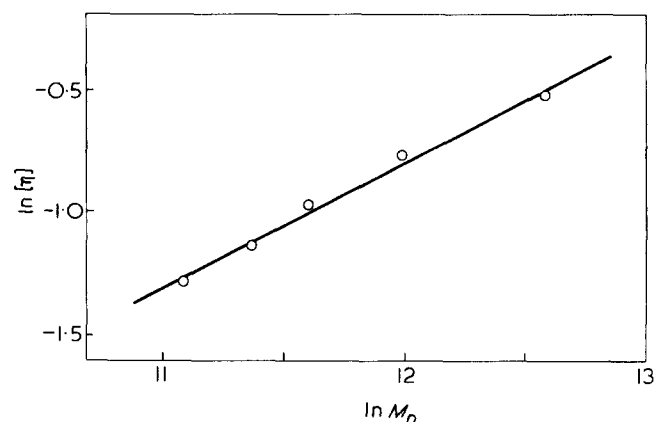


Figure 3 The intrinsic viscosity-molecular weight relationship for poly(trimethylene oxide) in cyclohexane at the θ -temperature, 27.0°C

Table 2 Some characteristics of polyethylene, polyoxymethylene, and their alternating copolymer poly(trimethylene oxide)

	PE	POM	POM ₃
Repeat unit	—CH ₂ —CH ₂ —	—CH ₂ —O—	—CH ₂ —CH ₂ —CH ₂ —O—
$\langle r^2 \rangle_0/nl^2$	7.6 ^{a,b}	12 ^c	3.9 ^e
$10^3 d(\ln \langle r^2 \rangle_0)/dT$	-1.1 ^a	-6 ^d	0.1 ^f

^aThe pertinent experimental studies are cited in ref 4. ^bThe actual experimental result is 6.7 at 140°C; it was corrected to the vicinity of 25°C by means of the coefficient $d(\ln \langle r^2 \rangle_0)/dT$. ^cApproximate value estimated from intrinsic viscosities¹³ obtained in a thermodynamically good solvent at 25°C, using a value of 2.1×10^{21} for the hydrodynamic constant $\Phi^{1,16}$. ^dVery approximate value estimated from intrinsic viscosities obtained in two thermodynamically good solvents at 25° and 90°C, respectively^{13,14}. ^ePresent study. ^fRef 1

very difficult to correct satisfactorily for the excluded volume effects present in thermodynamically good solvents^{17,18}. In any case, the characteristic ratio found for poly(trimethylene oxide) is unusually small, and is probably the smallest of those^{2,4} which are reliably known, to a high degree of accuracy†. This compactness of the poly(trimethylene oxide) chain is due to its high conformational randomness; two of the skeletal bonds of the repeat unit have a preference for *gauche* rotational states, whereas the other two have a preference for the alternative *trans* states^{1,3,5}.

In addition, it is of instructional value to note that poly(trimethylene oxide) may be considered an alternating copolymer of ethylene and oxymethylene units, and it is thus of interest to compare its configuration-dependent properties with those of its parent homopolymers polyethylene $(\text{—CH}_2\text{—CH}_2\text{—})_x$ and polyoxymethylene $(\text{—CH}_2\text{—O—})_x$. Pertinent results are given in Table 2. Polyethylene is seen to have a relatively high value, 7.6¹⁴, for the characteristic ratio in the vicinity of 25°C; polyoxymethylene, at the same temperature, has one of the highest values^{1,13}, 12‡, reported to date. This is due to the fact that these two homopolymeric chains exhibit a preference for conformations of high spatial extension; in polyethylene the preference is for *trans* or planar zig-zag conformations⁴, and in polyoxymethylene it is for *gauche* states giving rise to helical sequences⁴. High spatial extension is *not* preserved, however, upon mixing the two types of units, in alternating sequence, to give poly(trimethylene oxide). The characteristic ratio of poly(trimethylene oxide) is in fact very much smaller than the corresponding value for either homopolymer, since *gauche* states cause disruption of the planar *trans* sequences, while *trans* states likewise disrupt the helical *gauche* sequences. Similarly, the large negative values reported for the temperature coefficient $d(\ln \langle r^2 \rangle_0)/dT$ of the unperturbed dimensions of polyethylene and polyoxymethylene are of course a direct result of the fact that the spatially extended conformations in these chains are of relatively low energy⁴. Again, destruction of the conformational regularity in polyethylene and in polyoxymethylene by the intermixing of these two repeat units in poly(trimethylene oxide) has the marked effect of reducing its value of $d(\ln \langle r^2 \rangle_0)/dT$ essentially to zero¹. These compari-

† It is of course important to use the same conventions in calculating values of the characteristic ratio in comparisons of this type. In polypeptides, for example, 'virtual bonds' of length 3.80 Å are frequently used to replace three consecutive skeletal bonds, of lengths 1.53, 1.32, and 1.47 Å, respectively^{4,8}. For uniformity, therefore, characteristic ratios thus calculated would have to be multiplied by the factor $[3.80^2/(1.53^2 + 1.32^2 + 1.47^2)] = 2.31$.

‡ Stockmayer and Chan¹³ calculate the somewhat lower value 10.5 ± 1.5 , using $\Phi = 2.5 \times 10^{21}$ rather than the value 2.1×10^{21} we used to obtain $\langle r^2 \rangle_0/nl^2 \cong 12^1$. We consider the uncertainty associated with this assignment to be minor compared with other uncertainties^{19,20} inherent in the use of such extrapolation methods²¹ in the interpretation of viscometric data.

sons strikingly illustrate the very large error which may be introduced by use of the assumption⁹ that a chemical copolymer should have statistical properties intermediate to those of its parent homopolymers.

ACKNOWLEDGEMENTS

The authors are pleased to acknowledge financial support from the Ministry of Education of Japan, the National Science Foundation, and the Macromolecular Research Center of the University of Michigan.

REFERENCES

- 1 Takahashi, Y. and Mark, J. E. *J. Am. Chem. Soc.* 1976, **98**, 000
- 2 'Polymer Handbook', (Eds. J. Brandrup and E. H. Immergut), 2nd Edn, Interscience, New York, 1975
- 3 Mark, J. E. *J. Polym. Sci. (B)* 1966, **4**, 825
- 4 Flory, P. J. 'Statistical Mechanics of Chain Molecules', Interscience, New York, 1969
- 5 Abe, A. and Mark, J. E. *J. Am. Chem. Soc.* in press
- 6 Mark, J. E. *Acc. Chem. Res.* 1974, **7**, 218
- 7 Flory, P. J. 'Principles of Polymer Chemistry', Cornell University Press, Ithaca, 1953
- 8 Brant, D. A., Miller, W. G. and Flory, P. J. *J. Mol. Biol.* 1967, **23**, 47, 67
- 9 Cirlin, E. H. et al. *J. Macromol. Sci. (A)* 1971, **5**, 981; Chen, T. Y., Ristica, P. and Shen, M. *ibid.*, 1973, **7**, 889
- 10 Hallman, G. M. and Whittington, S. G. *Macromolecules* 1973, **6**, 386
- 11 Mark, J. E. *J. Polym. Sci. (Polym. Phys. Edn)* 1974, **12**, 1207
- 12 Mark, J. E. in 'Characterization of Materials in Research; Ceramics and Polymers', (Eds J. J. Burke and V. Weiss), Syracuse University Press, Syracuse, 1975
- 13 Stockmayer, W. H. and Chan, L.-L. *J. Polym. Sci. (A-2)* 1966, **4**, 437
- 14 Kokle, V. and Billmeyer, F. W. Jr. *J. Polym. Sci. (B)* 1965, **3**, 47
- 15 Mark, J. E. and Flory, P. J. *J. Am. Chem. Soc.* 1965, **87**, 1423
- 16 McIntyre, D. et al. *J. Phys. Chem.* 1962, **66**, 1932; Berry, G. C. *J. Chem. Phys.* 1967, **46**, 1338
- 17 Orofino, T. A. and Flory, P. J. *J. Chem. Phys.* 1957, **26**, 1067
- 18 Fujita, H. and Norisuye, T. *J. Chem. Phys.* 1970, **52**, 1115
- 19 Flory, P. J. *Makromol. Chem.* 1966, **98**, 128
- 20 Bluestone, S., Mark, J. E. and Flory, P. J. *Macromolecules* 1974, **7**, 325
- 21 Kurata, M. and Stockmayer, W. H. *Adv. Polym. Sci.* 1963, **3**, 196

Note added in proof

Also pertinent with regard to the statistical properties of chemical copolymers is the fact that the unperturbed dimensions of poly(vinylidene fluoride) $[\text{CF}_2\text{—CH}_2\text{—}]_x$ are quite different from those of polytetrafluoroethylene $[\text{CF}_2\text{—CF}_2\text{—}]_x$ and polyethylene $[\text{CH}_2\text{—CH}_2\text{—}]_x$ (Tonelli, A. E. *Macromolecules* submitted).

Mechanism of polysilazane thin film formation during glow discharge polymerization of hexamethylcyclotrisilazane

A. M. Wróbel, M. Kryszewski and M. Gazicki

Centre of Molecular and Macromolecular Studies, Polish Academy of Sciences, Łódź, Boczna 5, Poland

(Received 13 February 1976; revised 31 March 1976)

Preparation of thin polymer films by the glow discharge polymerization of hexamethylcyclotrisilazane has been studied. The effect of basic parameters of the process, such as time, pressure and current density on the polymer deposition kinetics has been established. It has been found that the curves of polymer deposition rate *versus* monomer vapour pressure have the same shape as the adsorption isotherms. The experimental relationships $R = f(p)$ have been analysed by means of the adsorption equations BET and HJ. A good agreement between the experimental results and adsorption equations suggests an adsorption mechanism of the polysilazane film formation. The effect of polymerization conditions on the properties and morphology of thin polysilazane films has been also investigated.

INTRODUCTION

In recent years there has been an increasing interest in the formation of thin polymer films by the polymerization of monomer vapours initiated by a glow discharge. The polymer films obtained by this technique on suitable substrates may find wide and various applications in modern technology¹⁻⁶ because of their interesting mechanical, thermal and electrical properties. Much attention has been given to the preparation of thin films from organosilicon monomers. The polymer films from these monomers have a high electric resistance, high dielectric strength and high thermal stability⁷⁻⁹.

The present paper reports the results of a study of the effect of some of the parameters of the glow discharge polymerization of hexamethylcyclotrisilazane, such as time, pressure and current density on the polymer film deposition rate. The results show a close relationship between the polymerization conditions and properties and morphology of thin films giving at the same time a partial explanation of the physical mechanism of film deposition. Using hexamethylcyclotrisilazane as monomer with Si-N bonds, we wished to verify the possibility of using the glow discharge process for preparation of thin polymer films of extremely high thermal stability as indicated in our previous paper¹⁰.

EXPERIMENTAL

The glow discharge polymerization was carried out in an electrode static system. A schematic diagram of the apparatus used in this study is shown in *Figure 1*. The discharge chamber consisted of a 20 dcm³ glass bell jar with two parallel electrodes, made of stainless steel, fixed inside. Freshly rectified hexamethylcyclotrisilazane placed in a feeder was thoroughly degassed by freezing-thawing evacuation cycles until the pressure was less than 10⁻⁵ Torr. Before starting the polymerization the chamber was evacuated to 5 × 10⁻⁶ Torr and then monomer vapour from the feeder

was admitted until the pressure inside the chamber reached a fixed value. The pressure inside the chamber was measured by means of a differential micromanometer filled with silicon oil DC-704. An electric field was then applied to the electrodes whereupon a glow discharge took place and as a result a polymer thin film was deposited on the electrodes. The polymerizations were carried out at an electrode temperature of 20°C for 30 sec, the monomer vapour pressure being varied over the range 0.05–0.5 Torr. Discharge current densities were 0.2–7.1 mA/cm² at a

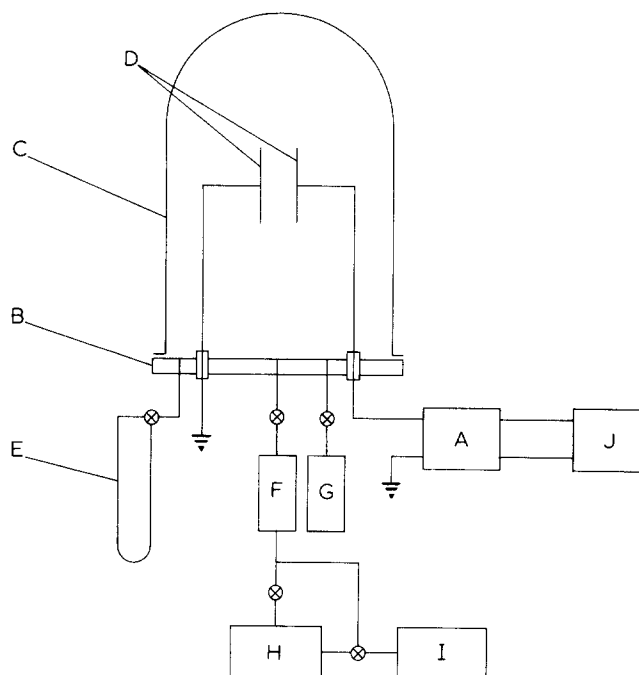


Figure 1 Schematic diagram of glow discharge apparatus: A, amplifier; B, base plate; C, bell jar; D, electrodes; E, differential micromanometer; F, cold trap; G, monomer feeder; H, oil diffusion pump; I, rotating pump; J, generator of frequency

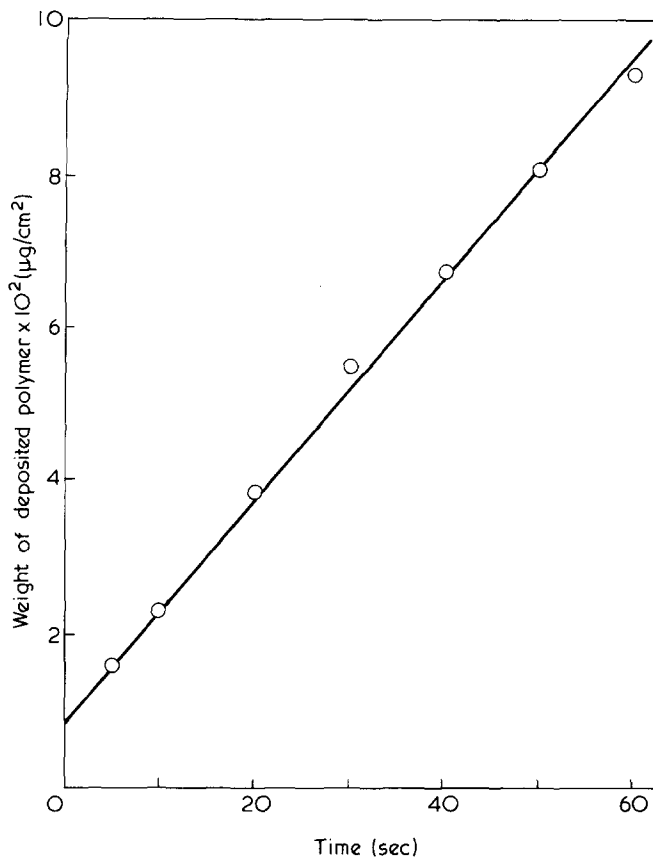


Figure 2 Weight of deposited polymer as a function of deposition time. Current density, 2 mA/cm²; pressure, 0.4 Torr

fixed frequency of 20 kHz and a fixed electrode separation of 3 cm.

The polymer film deposition rates were calculated from the amount of polymer deposited on the electrodes measured gravimetrically. A series of at least five experiments was made in order to calculate an average value of the deposition rate (R), and to find a point for the kinetic relationship curves.

Hexamethylcyclotrisilazane was purified by rectification using a Perkin-Elmer column, Model 151, with teflon spinning band and then the purity tested by gas chromatographic analysis.

RESULTS AND DISCUSSION

Effect of deposition time

The relationship between weight of polymer deposited on the electrode and duration of discharge was found for constant monomer vapour pressure 0.4 Torr and constant current density 2 mA/cm². As can be seen from Figure 2 the amount of polymer deposited increases linearly with the discharge time. This would suggest that the deposition rate is constant over the time range under investigation. The deposition rate calculated from the gradient is $R = 14.6 \mu\text{g}/\text{cm}^2 \text{ sec}$. The straight line extrapolated to zero time does not go through the origin, but intersects the polymer weight axis. This is probably connected with the change in conditions of the monomer adsorption resulting from the alteration of substrate by the polymerization process. As soon as the first layer of monomer molecules adsorbed on the metal surface of electrode is polymerized, adsorption of new monomer molecules takes place on a polymer layer already formed. Hence, the conditions of adsorption for the first layer are different from those for the next layers.

A similar phenomenon was observed in the polymerization of toluene by Tuzov *et al.*¹¹ who suggested a catalytic influence of the substrate.

Effect of monomer vapour pressure

Dependence of deposition rate on the monomer vapour pressure for polysilazane film was determined for various current densities: 0.6, 1.1 and 2.3 mA/cm². The curves obtained are shown in Figure 3. They are completely different from curves of an analogous relationship reported by other authors¹²⁻¹⁷. The different shapes of curves may result from the relatively low saturated vapour pressure of hexamethylcyclotrisilazane ($p_0 = 0.7$ Torr at 20°C) in comparison with considerably higher p_0 values for other monomers used in kinetic studies of glow discharge polymerization (for example, p_0 for styrene 4.8 Torr). It is interesting to note, that the curves of polysilazane deposition rate vs. vapour pressure have similar shapes to the adsorption isotherms of II type according to Brunauer^{18,19}. It can be seen in Figure 3 that within the range 0.05–0.3 Torr the deposition rate increases with pressure, reaching a saturation state over a certain pressure value. The course of the curves within this pressure range is explained by the fact that the number of monomer molecules adsorbed on the electrodes increases with increase in pressure. Over certain pressure values, for a given current density when all the active electrons present in the discharge zone take part in the initiation of polymerization, the film deposition rate reaches a constant value independent of pressure and limited only by the current density. This explains the appearance of distinct plateau in the curves (Figure 3) at current densities 0.6 and 1.1 mA/cm². The increase in deposition rate observed over the range 0.3–0.4 Torr may be due to a rapid increase in monomer adsorption since the range of these pressures is close to saturated vapour pressure p_0 of hexamethylcyclotrisilazane, and under these conditions a partial vapour con-

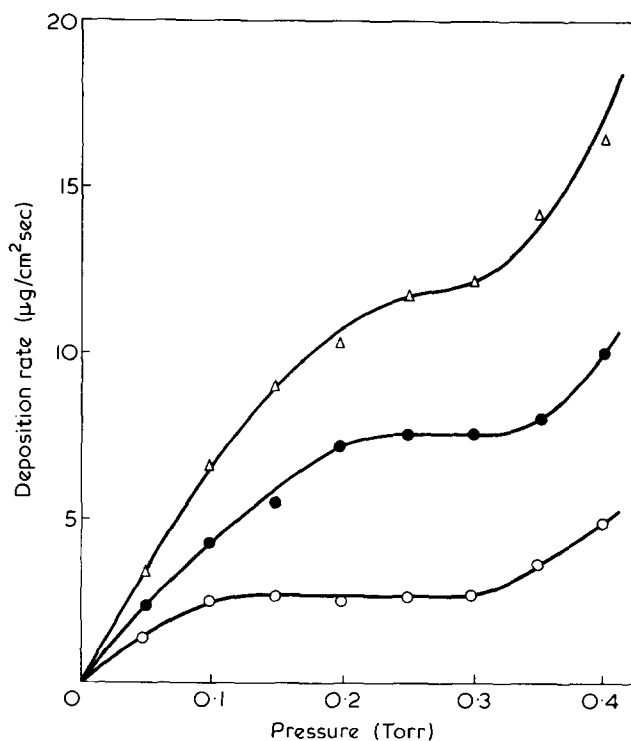


Figure 3 Polymer deposition rate at various current density as a function of monomer vapour pressure; deposition time 30 sec. Δ , 2.3; \bullet , 1.1; \circ , 0.6 mA/cm²

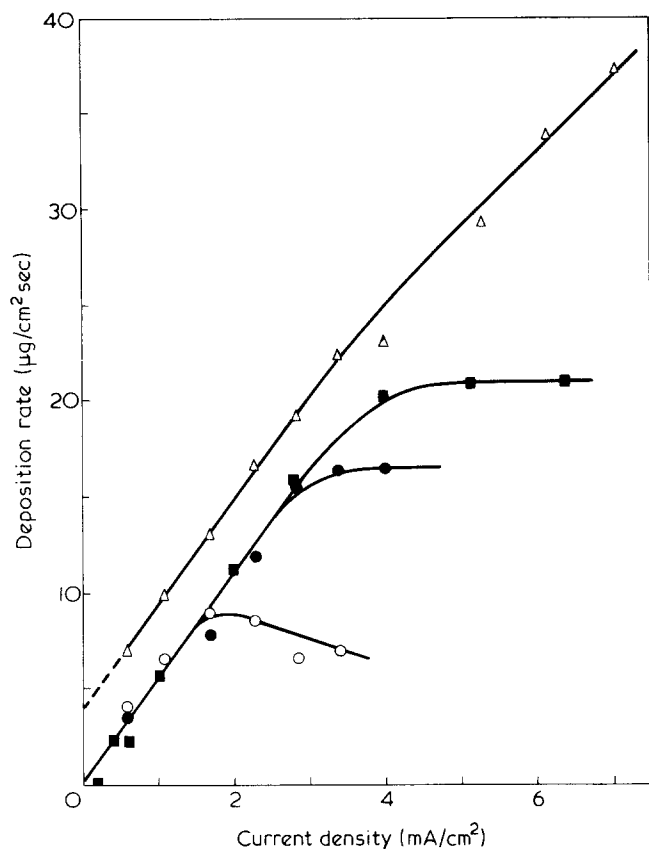


Figure 4 Polymer deposition rate at various pressure as a function of current density; deposition time 30 sec. Δ , 0.4; \blacksquare , 0.3; \bullet , 0.2, \circ , 0.1 Torr

condensation is likely to occur. In accordance with adsorption isotherms^{18,19}, the volume of molecules adsorbed increases asymptotically to infinity if $p \rightarrow p_0$, hence for p close to p_0 a multimolecular quasi-liquid layer of the adsorbate may be produced on the substrate. Therefore, the glow discharge polymerization of hexamethylcyclotrisilazane at pressure $p > 0.3$ Torr may be initiated in the quasi-liquid phase. This would cause the process yield to increase considerably and would explain the increase in the film deposition rate within this pressure range. The results show that adsorption of monomer plays a significant part in the mechanism of polysilazane film formation as initiated by the glow discharge.

Effect of discharge current density

The dependence of polysilazane film deposition rate on current density (j) (Figure 4) was determined at various monomer vapour pressures: 0.1, 0.2, 0.3 and 0.4 Torr. The relationships obtained at pressures 0.1, 0.2 and 0.3 Torr are consistent with data from the literature^{14,17,20,21} describing analogous relations for other monomers. It can be seen in Figure 4 that the deposition rate increases with the discharge current density and reaches a constant value over a current density defined for the given pressure. Some decrease in the deposition rate observed at 0.1 Torr and over 1.7 mA/cm^2 may be due to partial degradation of the polymers formed. The films obtained under these conditions, were cracked and badly adhered to the substrate. The relationship $R = f(j)$ for a pressure 0.4 Torr is completely different, and as is seen in Figure 4, the increase in the deposition rate is observed over the whole range of current densities used. The relationship is linear over the range $0.6\text{--}3.4 \text{ mA/cm}^2$, and when extrapolated to zero

current density, intersects the R axis. This different course of the relationship at 0.4 Torr pressure is probably due to the initiation of polymerization in a multimolecular quasi-liquid layer of monomer which at this pressure may be produced on the substrate as a result of partial vapour condensation. This fact explains the rapid rise in the deposition rate observed within the whole range of current densities used and the distinct curve shift from the origin of coordinates. The results are in agreement with the curves $R = f(p)$ for $p > 0.3$ Torr and confirm the correctness of our assumption on the initiation of polymerization in a quasi-liquid phase.

Properties and morphology of polysilazane thin films

It was found that the appearance of films and their properties depend to a great extent on the polymerization parameters. As the pressure increased at a constant current density the film became softer and much more adhesive to the substrate but when the current density increased at a constant monomer vapour pressure the film properties changed in the reverse direction. Solubility measurements showed that polysilazane films contained a small fraction soluble in non-polar solvents such as benzene or carbon tetrachloride but they were completely insoluble in acetone. The films prepared at constant pressure and low current densities ($\approx 1 \text{ mA/cm}^2$) contained about 16% by wt soluble fraction. The soluble fraction content decreased with increasing current density and the films obtained over 4 mA/cm^2 were completely insoluble. Insolubility of the films is a result of crosslinking taking place in the glow discharge polymerization. The degree of crosslinking increases with the current density as indicated by the loss of the soluble fraction in films obtained at higher current densities.

It was observed that under certain conditions homogeneity of the films was affected by powder products. Over 2 mA/cm^2 the powders were observed almost over the whole range of pressure used. At $1\text{--}2 \text{ mA/cm}^2$ the powder appeared at higher pressures while below 1 mA/cm^2 the films were transparent. It was also found that at constant current density and pressure the powder regions grew with the discharge duration. Figures 5 and 6 show electron micrographs of surfaces both of homogeneous film and powder region, respectively. In the powder region (Figure 6) one can easily observe distinct spheres on the film surface. The powder formation, also reported by other authors²¹⁻²⁸, is a typical feature of the glow discharge polymerization and according to a generally accepted opinion it is due to initiation of the process in the gas phase.

Mechanism of film formation

The results presented suggest that adsorption is a determining factor in the mechanism of polysilazane film formation. Nevertheless it should be noted, that the mechanism of film formation is not as simple as that of the adsorption process. During the film formation a continuous renewing of the substrate surface takes place resulting from growing film thickness. While in classic adsorption at a constant temperature and pressure a dynamic equilibrium state exists characterized by a constant volume of adsorbed molecules, here the equilibrium state can be determined by the volume adsorbed within the time unit because of the continuous renewal of substrate surface. It is clear that this volume depends not only on temperature and pressure but also on the film deposition rate, and thus on the current density.

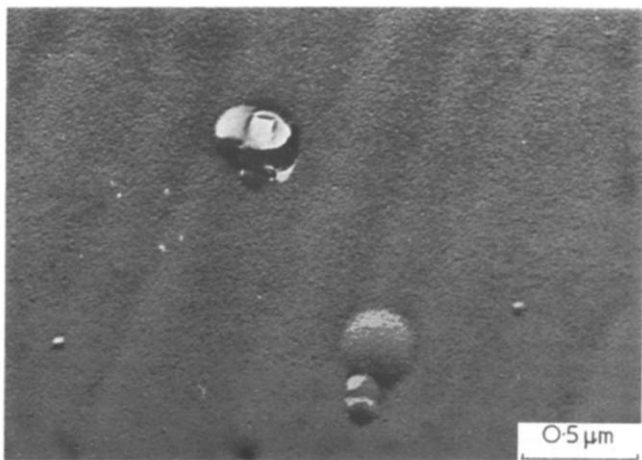


Figure 5 Electron micrograph of homogeneous polysilazane film formed at 1 mA/cm², 0.3 Torr

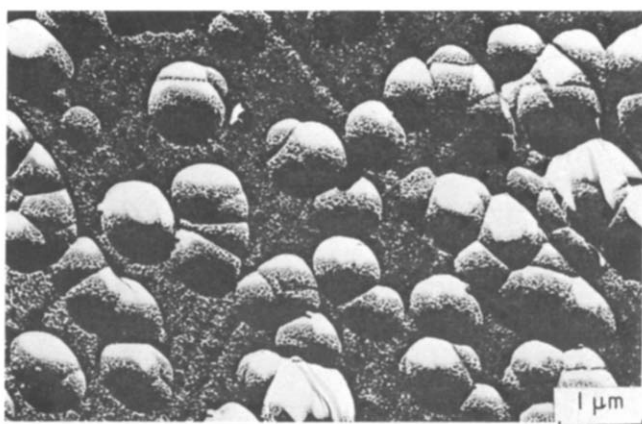


Figure 6 Electron micrograph of powder region in polysilazane film formed at 3 mA/cm², 0.3 Torr

Accepting such an assumption, one can verify whether the experimental relationship between polymer deposition rate and pressure is consistent with the Brunauer, Emmett and Teller (BET) multi-layer adsorption equation²⁹:

$$\frac{p}{\nu(p_0 - p)} = \frac{1}{c\nu_m} + \frac{1 - c}{c\nu_m} \frac{p}{p_0} \quad (1)$$

where ν is the volume of adsorbed gas, ν_m is the volume of monolayer, p is the pressure in the system, p_0 is the saturated vapour pressure of the adsorbate and c is a constant. The equation is a linear function of relative pressure p/p_0 . If one assumes that the polymer deposition rate is proportional to the volume of adsorbed monomer ($R \propto V$), the experimental relationships $R = f(p)$ (Figure 3) can be expressed in the form $p/R(p_0 - p) = f(p/p_0)$ according to the BET equation. These relationships as determined by equation (1) are shown in Figure 7. The curves obtained have similar shapes to those of typical BET isotherms^{18,19}. One can say that to an approximation the relationships for current densities 1.1 and 2.3 mA/cm² are linear only for $p/p_0 \leq 0.2$. This narrow linear range is a characteristic feature of BET isotherms as the multilayer adsorption equation is not free from some imperfections. The dependence of polysilazane film deposition rate on pressure, $R = f(p)$,

can be also described by the Harkins–Jura³⁰ (HJ) equation:

$$\ln \frac{p}{p_0} = B - \frac{A}{\nu^2} \quad (2)$$

which expresses the linear relationship $\ln(p/p_0) = f(1/\nu^2)$. Using previous assumptions, experimental relationships $R = f(p)$ were verified in the system $\ln(p/p_0) = f(1/R^2)$ according to equation (2). The linear relationships observed almost over the whole pressure range (Figure 8) show that the HJ equation describes the experimental results well.

A good agreement of the experimental relationships $R = f(p)$ with the adsorption equations would confirm the accuracy of our hypothesis on the adsorption nature of polysilazane film formation mechanism. It should be noted, however, that in the case of glow discharge polymerization, the adsorption phenomenon is a very complex one. In comparison to the classic adsorption dealing with a homogeneous gas, here we have a gas mixture, produced by monomer fragmentation, which consists of components of various adsorption constants. Therefore, the use of classic adsorption equations to describe the formation mechanism of polymer film is a certain simplification of this complex process.

An attempt was also made to verify the quantitative model of mechanism for glow discharge polymerization postulated by Denaro *et al.*¹³. Their theory put forward a radical mechanism of polymerization and linear relationship $1/R = f(1/p)$. The non-linear nature of this relation found by us in the case of polymerization of hexamethyl-

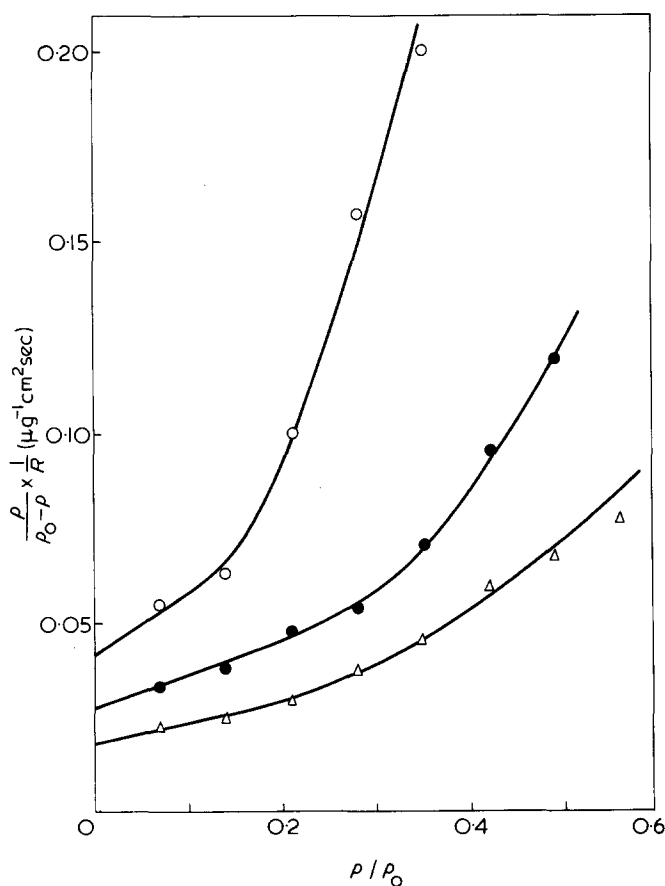


Figure 7 Experimental relationships $R = f(p)$ treated by BET equation²⁹. ○, 0.6; ●, 1.1; △, 2.3 mA/cm²

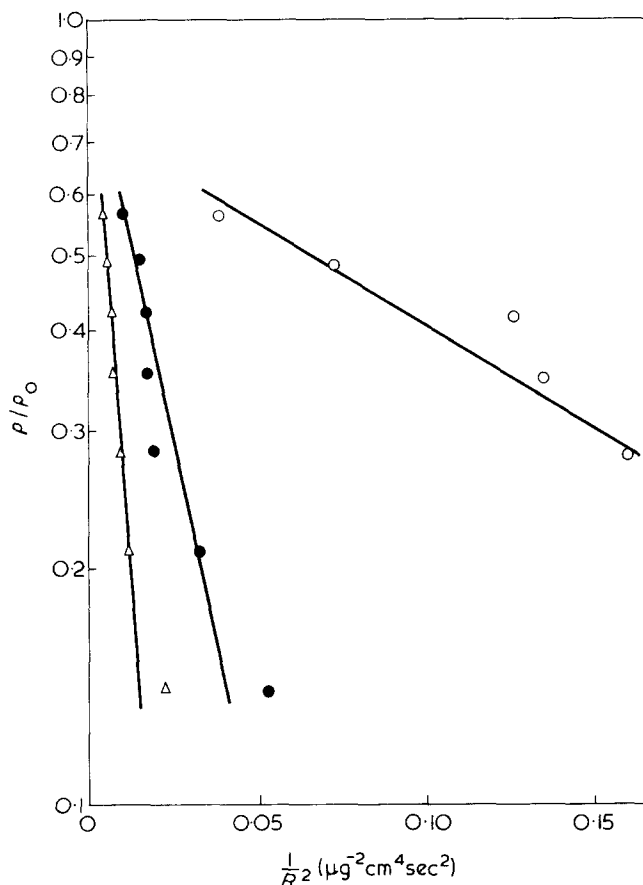


Figure 8 Experimental relationships $R = f(p)$ treated by HJ equation³⁰. ○, 0.6; ●, 1.1; △, 2.3 mA/cm²

cyclotrisilazane points out a limited application of the Denaro model for interpretation of glow discharge polymerization mechanism.

ACKNOWLEDGEMENTS

This work was supported by the Polish Academy of Sciences under the project Nr 03.1.2.

REFERENCES

- Allam, D. S. and Stoddard, C. T. H. *Chem. Br.* 1965, 1, 410
- Gregor, L. V. 'Advances in Research and Development', (Eds G. Hass and R. E. Thuned), Academic Press, New York, 1966
- Kolotyrykin, V. M., Gilman, A. B. and Tsapuk, A. K. *Russ. Chem. Revs.* 1967, 36, 579
- Gregor, L. V. *IBM J. Res. Dev.* 1968, 12, 140
- Mearns, A. M. *Thin Solid Films* 1969, 3, 201
- Millard, M. in 'Techniques and Applications of Plasma Chemistry', (Eds J. R. Hollahan and A. T. Bell) Wiley, New York, 1974, Ch 5
- Shchurov, A. N., Tuzov, L. S., Gilman, A. B., Kolotyrykin, V. M. and Tunitskij, N. N. *Vysokomol. Soedin. (A)* 1969, 11, 582
- Tuzov, L. S., Kolotyrykin, V. M. and Tunitskij, N. N. *Vysokomol. Soedin. (A)* 1970, 12, 849
- Tkachuck, B. V., Perova, L. V. and Kolotyrykin, V. M. *Vysokomol. Soedin. (A)* 1971, 13, 828
- Wróbel, A. M. and Kryszewski, M. *Bull. Acad. Pol. Sci. Ser. Sci. Chim.* 1974, 22, 471
- Tuzov, L. S., Gilman, A. B., Szurov, A. N. and Kolotyrykin, V. M. *Vysokomol. Soedin. (A)* 1967, 9, 2414
- Williams, T. and Hayes, M. W. *Nature* 1966, 209, 796
- Denaro, A. R., Owens, P. A. and Crawshaw, A. *Eur. Polym. J.* 1968, 4, 93; 1969, 5, 471; 1970, 6, 483
- Westwood, A. R. *Eur. Polym. J.* 1971, 7, 363
- Vasile, M. J. and Smolinsky, G. *J. Electrochem. Soc.* 1972, 119, 451
- Lippold, U., Poll, H. U. and Wickleder, K. H. *Eur. Polym. J.* 1973, 9, 1107
- Carchano, H. *PhD Thesis* University of P. Sabatier, Toulouse (1973)
- Brunauer, S. 'The Adsorption of Gases and Vapours', Princeton University Press, Princeton, 1945, Vol 1
- Adamson, A. W. 'Physical Chemistry of Surfaces', Interscience, New York, 1960
- Poll, H. U. *Z. Angew. Phys.* 1970, 29, 260
- Thompson, L. F. and Mayhan, K. G. *J. Appl. Polym. Sci.* 1972, 16, 2317
- Thompson, L. F. and Smolinsky, G. *J. Appl. Polym. Sci.* 1972, 16, 1179
- Liepins, R. and Sakaoku, K. *J. Appl. Polym. Sci.* 1972, 16, 2633
- Kobayashi, H., Bell, A. T. and Shen, M. *J. Appl. Polym. Sci.* 1973, 17, 885
- Kobayashi, H., Shen, M. and Bell, A. T. *J. Macromol. Sci. (A)* 1974, 8, 373
- Kobayashi, H., Bell, A. T. and Shen, M. *Macromolecules* 1974, 7, 277
- Neiswender, D. D. *Adv. Chem. Ser.* 1969, 80, 388
- Häfer, D., Tiller, H. J. and Mayer, K. *Plaste Kautsch* 1972, 19, 354
- Brunauer, S., Emmett, P. H. and Teller, E. *J. Am. Chem. Soc.* 1938, 60, 309
- Harkins, W. D. and Jura, G. *J. Am. Chem. Soc.* 1944, 66, 1366

Structure of glow discharge polysilazane thin films

A. M. Wróbel, M. Kryszewski and M. Gazicki

Centre of Molecular and Macromolecular Studies, Polish Academy of Sciences, Łódź, Boczna 5, Poland

(Received 13 February 1976)

Thin polysilazane films have been prepared by glow discharge polymerization of hexamethylcyclotrisilazane in an electrode static system. An increase in pressure in the reaction system observed during polymerization indicated that the monomer underwent fragmentation in the glow discharge. The structures of thin polysilazane films prepared at various current densities have been determined by elementary analysis, infra-red spectroscopy and gas chromatography. It has been found that fragmentation of hexamethylcyclotrisilazane takes place mainly through the cleavage of Si—C bonds and that methyl group content in the polymer film structure decreases with increasing current density. The mechanisms of reactions leading to polysilazane film formation have been discussed.

INTRODUCTION

Attention has been given to the use of the glow discharge technique for polymerization of organosilicon compounds in order to prepare thin polymer films with good dielectric properties and high thermal stability. Many investigations reported in the literature were carried out to study the properties and structure of polysilazane films¹⁻⁵. Among the great number of organosilicon compounds organosilazanes deserved particular attention. Polymers prepared from these compounds by a conventional polymerization have much higher thermal stability than polysiloxanes⁶. Using organosilazane monomers in the glow discharge process one can produce polymer films with good electrical properties⁷ and very high thermal stability⁸.

The aim of the present paper was to study the chemical structure of thin polysilazane films prepared by the glow discharge polymerization of hexamethylcyclotrisilazane and to establish a relation between polymerization conditions and polymer structure. However, one should be aware of the fact that examination of chemical structure of thin polymer films prepared by glow discharge in monomer vapour is difficult because of the complex mechanism of polymerization. Monomer molecules in the glow discharge undergo fragmentation by collisions with accelerated electrons or ions. In the gas phase several segments of molecules are formed which have definite probabilities of polymer film formation. Various molecule segments have different polymerization rate constants and different adsorption constants. Their contribution to the polymerization mechanism is difficult to establish, as the quantity of them in the total number of reactive molecules is not always known. Thus, the glow discharge polymerization can be considered as a copolymerization of numerous segments with different functions giving a polymer with a highly crosslinked structure. It is clear, that the chemical structure and properties of the polymer film will be closely related to the parameters of glow discharge.

EXPERIMENTAL

Glow discharge polymerizations of hexamethylcyclotrisilazane were carried out by means of the electrode static

system. Details of the apparatus used for this study have been reported previously⁹. Polysilazane samples were prepared in a glow discharge operating at 20 kHz. Polymer was formed as a thin film on the surfaces of two parallel stainless steel electrodes with the electrode separation fixed at 3 cm. Polymerization was carried out at an electrode temperature of 20°C and a constant discharge time of 30 sec with a fixed monomer vapour pressure of 0.3 Torr. Current density applied was within the range 0.2–6.4 mA/cm².

Infra-red spectra of the polymers were obtained by removing the polymers from the metal surface and dispersing in KBr discs. The spectra were run on a Unicam Model SP 1200 spectrophotometer.

Pyrolysis of the polymers was carried out in a Jeol pyrolyzer unit, Model PL 723. A polymer sample of 0.2 mg placed in the pyrolyzer was heated at 750°C for 15 sec. The volatile components of the pyrolysis products were directed immediately to the injection part of a Jeol, Model JGC 1100, gas chromatograph, equipped with a flame ionization detector. The stainless steel separation column 1 m × 3 mm i.d. was filled with a 5A 60/80 mesh molecular sieve. The column was heated at a constant rate of 10°C/min starting from the initial temperature of 40°C. Nitrogen was used as a carrier gas and the flow rate was 60 cm³/min.

Hexamethylcyclotrisilazane was purified as described previously⁹.

RESULTS AND DISCUSSION

Effect of glow discharge on pressure variation

It was observed that during glow discharge polymerization of hexamethylcyclotrisilazane a considerable increase in pressure took place in the reaction system. In order to obtain a quantitative picture of this phenomenon, measurements of pressure increase were made at various current densities. Increases in pressure, Δp , were measured after 30 sec of discharge and were calculated in relation to the initial monomer vapour pressure, p_M . To avoid an error caused by a pressure increase due to desorption of gases adsorbed on walls of the bell jar, a series of discharges were carried out in nitrogen under the same conditions. In this

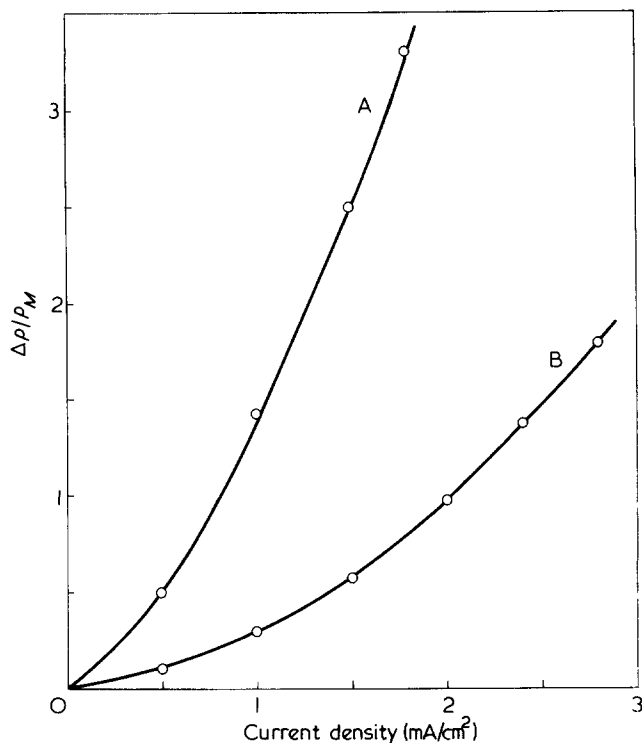


Figure 1 Effect of discharge current density on the relative pressure increase in the reaction system. Monomer vapour pressure $p_M = 0.1$ (A) and 0.3 Torr (B), discharge time 30 sec, frequency 20 kHz

way the relative pressure increase calculated from measurements was below 1%.

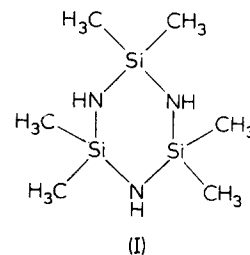
Relationships between the relative pressure increase, $\Delta p/p_M$, and current density, found for two various monomer vapour pressures 0.1 and 0.3 Torr are shown in Figure 1. It can be seen, that the pressure increase in the reaction system rises with increasing current density.

The phenomenon of pressure increase in the reaction system results from the monomer molecule fragmentation taking place during the glow discharge. Due to high energies of glow discharge reaching several electron volts, and even more, the initiation of polymerization proceeds spontaneously. This can lead to bond cleavages in the monomer molecule resulting in the formation of several segments in the gas phase and followed by pressure increase in the system. Higher pressure increases observed at lower monomer vapour pressure ($p_M = 0.1$ Torr) are connected with the fact that the kinetic energy of plasma particles increases with decreasing pressure as a result of increased mean free path. Hence, at lower pressures, as a result of collisions of monomer molecules with plasma particles of considerably higher energy, fragmentation of the monomer proceeds to a greater extent than at higher pressures. This explains the steeper shape of the curve for $p_M = 0.1$ torr (Figure 1). In accordance with the curves in Figure 1 one can draw a conclusion that the degree of fragmentation of hexamethylcyclotrisilazane depends strictly on the discharge conditions and increases with current density.

Interesting data on the pressure variation during glow discharge polymerization are reported by Yasuda *et al.*¹⁰⁻¹². These authors in their studies on polymerization of numerous aliphatic and aromatic compounds have found that fragmentation of monomer manifested by the pressure increase depends only on the structural features of the monomer¹². Pressure increase was observed during polymerization of almost all the saturated hydrocarbons used. High

hydrogen content in the gas phase indicated that most fragmentations of these compounds proceeded with C-H bonds cleavage.

Analysing the bond energy in a hexamethylcyclotrisilazane molecule (I) one can state that the Si-C bond has the lowest energy equal to 3.3 eV¹³ as compared with 3.6 eV for a Si-N bond¹⁴.



This would suggest that fragmentation of the compound in glow discharge proceeds most easily through Si-C bonds cleavage with the methyl groups splitting off. One may assume, that the fragmentation of monomer, resulting in a significant change of the gas phase composition, affects the chemical structure of the polymer films. The observed relationship between pressure increase and current density (Figure 1), being in close relation to fragmentation of hexamethylcyclotrisilazane, shows that the chemical structure of polysilazane films should depend to a great extent on the discharge parameters.

Composition of thin films

In order to examine the effect of polymerization conditions on the composition of glow discharge polysilazanes, elementary analysis of polymer films prepared at various current densities was carried out. Silicon, carbon, hydrogen and nitrogen contents were determined with oxygen content being calculated by difference. The results are given in Table 1. It can be seen, that the polymer contains less carbon, hydrogen and nitrogen than the monomer. The results of chemical analysis in terms of molar contents of particular elements in relation to silicon versus current density are illustrated in Figure 2. It can be seen, that molar contents of carbon and hydrogen in polysilazane decrease linearly with increasing current density.

The straight lines of C/Si and H/Si extrapolated to zero value of current density pass through the points representing contents of these elements in the monomer (C/Si = 2 and H/Si = 7). The decrease of carbon and hydrogen contents in the polymer observed with increasing current density proves, that hexamethylcyclotrisilazane is subject to strong fragmentation which results in cleavage of Si-C

Table 1 Composition of glow discharge polysilazane thin films formed with different current densities and at 20 kHz, 0.3 Torr, 30 sec

Current density (mA/cm ²)	Molecular formula				
	Si	C	H	N	O
0*	3	6	21	3	—
2.0	3	4.31	17.30	2.56	2.10
2.0	3	4.61	19.13	2.48	0.84
2.8	3	3.96	16.84	2.68	2.81
3.0	3	3.96	15.92	2.47	1.73
4.0	3	3.13	13.78	2.50	2.55
5.1	3	2.49	12.27	1.97	3.20
6.4	3	2.98	14.26	2.58	2.47

*Composition of hexamethylcyclotrisilazane

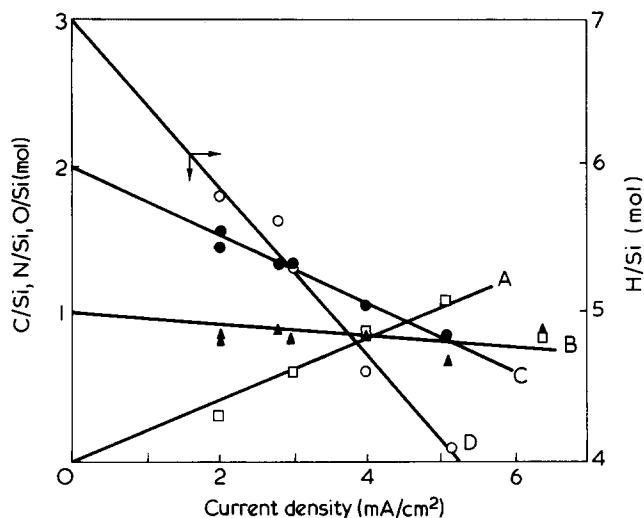


Figure 2 Effect of discharge current density on the composition of polysilazane thin film. Polymerization parameters: 20 kHz, 0.3 Torr, 30 sec. A, O/Si; B, N/Si; C, C/Si; D, H/Si

bonds and the methyl groups splitting off. Consequently, the number of the fragmentation products in the gas phase increases with current density causing a pressure increase in the system, which is consistent with the results shown in Figure 1.

A slight decrease of nitrogen content in the polymer (Figure 2) may be a result of the partial hydrolysis of Si-N bonds devoid of sufficient steric hindrance because of the methyl groups splitting off and therefore more susceptible to the action of hydrolytic agents. However, one can not exclude fragmentation of silazane ring leading to Si-N bonds cleavage.

From the elementary analysis it can be seen that glow discharge polysilazanes contain a certain amount of oxygen. As is seen in Figure 2, the oxygen content increases with current density. The presence of oxygen in glow discharge polymers has been reported by numerous authors¹⁵⁻¹⁹ and ascribed to the reaction of free radicals trapped in films with air oxygen. The polymer films prepared by these authors¹⁵⁻¹⁹ contained a certain amount of unsaturated bonds and as a result of this they showed high reactivity with oxygen or water vapour after exposure to the atmosphere. It should be noted that the monomers normally used to prepare thin polymer films contained unsaturated groups and hence one can understand the presence of a great number of unsaturated products in the polymer structure. The presence of oxygen in glow discharge polysilazane structure is a more complex problem because of the rather different chemical structure of monomer (absence of unsaturated bonds). As was already noted the presence of oxygen may be a result of the partial hydrolysis of Si-N bonds leading to the formation of Si-OH or Si-O-Si groups. On the other hand however, polysilazane films, similar to other glow discharge polymer films, may contain free radicals generated during glow discharge, which readily react with air oxygen. The presence of oxygen in the structure of glow discharge polysilazane seems likely to be due to both the processes mentioned. In order to obtain general information on the fragmentation products in the gas phase the change of H/C ratio in the polymer composition was analysed. Figure 3 shows the change of H/C ratio in glow discharge polysilazane as a function of current density. As can be seen the H/C ratio in the polymer grows linearly with current density and the value

of H/C found by extrapolation to zero current density is in a good agreement with the respective ratio for monomer, where H/C = 3.5.

The change in H/C ratio observed proves, that as the current density increases the carbon content in polysilazane decreases to a greater extent than the hydrogen content. This means that the gas phase is expected to contain fragmentation products in the form of unsaturated hydrocarbons such as ethylene or acetylene. The amount of these components in the gas mixture should increase with current density according to the plot in Figure 3. It might be interesting to quote results obtained by Kabayashi, Bell and Shen^{19,20} who investigated the composition of glow discharge polymers prepared from saturated and unsaturated hydrocarbons. They found that each of the polymers studied was hydrogen deficient in comparison to its respective monomers. This suggested that the polymers were highly crosslinked and contained significant amounts of unsaturation. The observed carbon deficiency in the case of glow discharge polysilazane would lead to the conclusion that the polymer can be expected to possess a highly saturated structure.

Chemical structure of thin films

In order to examine the effect of polymerization conditions on the polymer structure infra-red analysis was performed using polysilazane prepared at various current densities within the range 0.2–6.4 mA/cm² with the remaining parameters being constant. It followed from qualitative estimation that the i.r. spectra of glow discharge polysilazane are similar within the whole range of current densities used. A comparison of the i.r. spectra of glow discharge and conventional polysilazanes revealed the existence of analogous absorption bands²¹. A typical spectrum of glow discharge polysilazane and a spectrum of hexamethylcyclotrisilazane are shown in Figure 4. Both in the monomer spectrum and in that of the polymer there is a strong absorption of Si-NH-Si group revealed in the bands at 3400, 1170 and 930 cm⁻¹.

The bands correspond to $\nu(\text{NH})$, $\delta(\text{NH})$ and $\nu_{\text{as}}(\text{SiNSi})$ vibrations respectively. The presence of Si(CH₃)₂ groups in the polymer is characterized by the strong, sharp band at 1250 cm⁻¹ corresponding to $\delta_{\text{s}}(\text{CH}_3)$ vibration. The appearance of intense absorption bands in the polymer spectra at 2140 and 1030 cm⁻¹ which are absent in the monomer spectrum is interesting. The first of them at 2140 cm⁻¹ corresponds to $\nu(\text{SiH})$ vibrations. This group may be form-

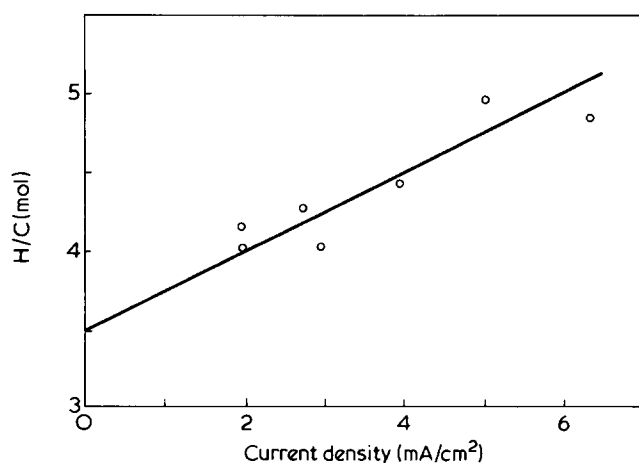


Figure 3 Hydrogen-carbon ratio in polysilazane film as a function of current density

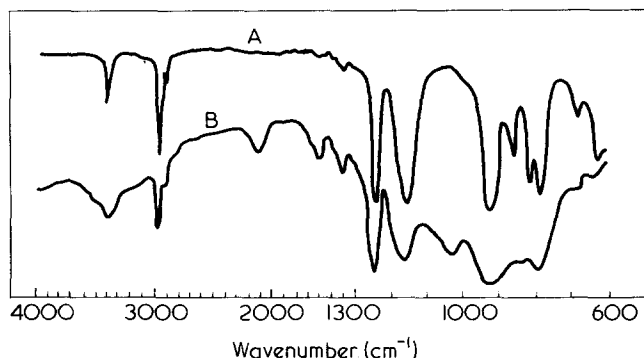


Figure 4 Infra-red spectra of hexamethylcyclotrisilazane (A) and polysilazane formed at 2 mA/cm², 20 kHz, 0.3 Torr, 30 sec (B)

ed as a result of monomer fragmentation connected with cleavage of Si–C and C–H bonds. The second absorption band at 1030 cm⁻¹ is a typical one for methylene groups between two silicon atoms and corresponds to $\omega(\text{CH}_2)$ vibration. The presence of Si–(CH₂)₁ or ₂–Si bonds was confirmed also in the structure of glow discharge polysiloxanes prepared from octamethylcyclotetrasiloxane²² by mass spectrometry. The absorption within the range 1100–1000 cm⁻¹ is also characteristic for $\nu_{\text{as}}(\text{SiOSi})$ vibration. This bond, as noted previously, may be formed as a result of hydrolysis of Si–N–Si bond. The appearance of a wide and non-symmetrical absorption band in this range in the polysilazane spectra is because of the overlap of signals from Si–CH₂–Si and Si–O–Si bonds present in the polymer structure. A very weak absorption band at 840 cm⁻¹ in the polymer spectrum is due to the presence of Si(CH₃)₃ groups in the polymer structure and corresponds to $\nu(\text{SiC})$ and $\rho(\text{CH}_3)$ vibrations. These groups confirm the fragmentation of silazane ring caused by the cleavage of Si–N bonds.

The results presented only give a qualitative picture of the chemical structure of thin polysilazane films. Much more information has been provided by quantitative interpretation of the i.r. spectra of polymers prepared at various current densities. Using this method, a change in relative intensity of absorption bands at 2140 and 1250 cm⁻¹, corresponding to SiH and SiCH₃ groups respectively, has been observed. It may be assumed that the absorption peak area at 2140 cm⁻¹, A_{SiH} , corresponds to the number of Si–H bonds in the polymer structure which enables the loss of methyl groups at the silicon atoms to be determined, while the absorption peak area at 1250 cm⁻¹, A_{SiCH_3} , corresponds to the total number of the methyl groups linked to silicon atoms. Hence the ratio $A_{\text{SiH}}/A_{\text{SiCH}_3}$ is a factor which characterizes, to some extent, the loss of methyl groups due to the monomer fragmentation. The plot of $A_{\text{SiH}}/A_{\text{SiCH}_3}$ ratio versus current density is shown in Figure 5. It can be seen that the deficiency of methyl groups in the polysilazane structure increases linearly with the current density. It should also be noted that the straight line (Figure 5) when extrapolated to zero current density passes through the origin of the coordinate system, which is consistent with the fact that an absorption band corresponding to the Si–H bond does not exist in the monomer spectrum. The above relationship has a similar course to that shown in Figure 3 and confirms the results of elementary analysis. Making a similar assumption, a change in relative intensity of absorption bands at 1170 and 930 cm⁻¹, corresponding to N–H and Si–N bonds respectively, has been analysed. If A_{NH} and A_{SiN} represent the areas determined from the absorption peaks in these bands, thus ratio $A_{\text{NH}}/$

A_{SiN} is a factor which characterizes the –NH– group content in the polymer structure. A plot of this ratio as a function of current density is shown in Figure 5. The value of $A_{\text{NH}}/A_{\text{SiN}}$ at zero current density was calculated from the monomer spectrum. As can be seen from Figure 5 the ratio $A_{\text{NH}}/A_{\text{SiN}}$ decreases with increasing current density, which means that there is a loss of –NH– groups in the polysilazane structure. This process may be due only to a transition of secondary nitrogen into tertiary through elimination of hydrogen from –NH– groups and formation of (>Si)₃N groups. Such groups have been identified by Krüger²¹ and Andrianov²³ in the structure of conventional polysilazane prepared from hexamethylcyclotrisilazane. The presence of Si–CH₂–Si and (>Si)₃N groups proved by i.r. analysis suggests that the structure of glow discharge polysilazane thin films is highly crosslinked which would explain the insolubility of the films observed previously⁹.

Interesting information about the structure of glow discharge polymers can be gained by examination of its pyrolysis products with the aid of gas chromatography. Samples of polysilazane prepared at different current densities were pyrolyzed at 750°C in nitrogen, with the gas products passing through a chromatographic column. The identification of peaks in the chromatograms pointed out that methane was a main component of the pyrolysis products. Ethylene was also found as well as small amounts of ethane, propane, acetylene and propylene. A typical chromatogram of the pyrolysis products is shown in Figure 6. Relative contents of the pyrolysis products expressed by a ratio of the peak area of particular components to methane, for polysilazane prepared at 1 mA/cm², are listed in Table 2. The data in Table 2 suggest, that besides methane the remaining components may be formed as a result of secondary reactions. The appearance of methane in the pyrolysis products is a result of the homolytic decomposition of Si–CH₃ groups. The methyl radicals formed in this way recombine with hydrogen radicals detached from the polymer structure, thus giving methane. This high methane content in the pyrolysis products confirms the results of elementary analysis which pointed out a high H/C ratio in glow discharge polysilazane.

Mechanism of polymerization

The results presented show that the chemical structure of polysilazane film is a very complex one and is formed

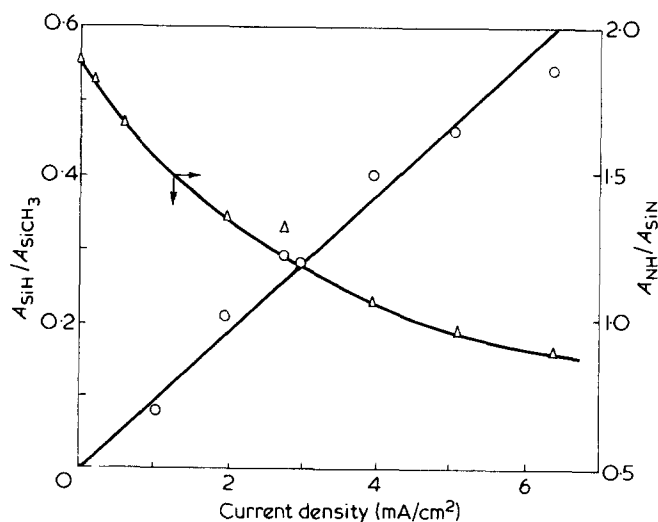


Figure 5 Relative i.r. absorption intensities: ○, $A_{\text{SiH}}/A_{\text{SiCH}_3}$; △, $A_{\text{NH}}/A_{\text{SiN}}$, as a function of current density

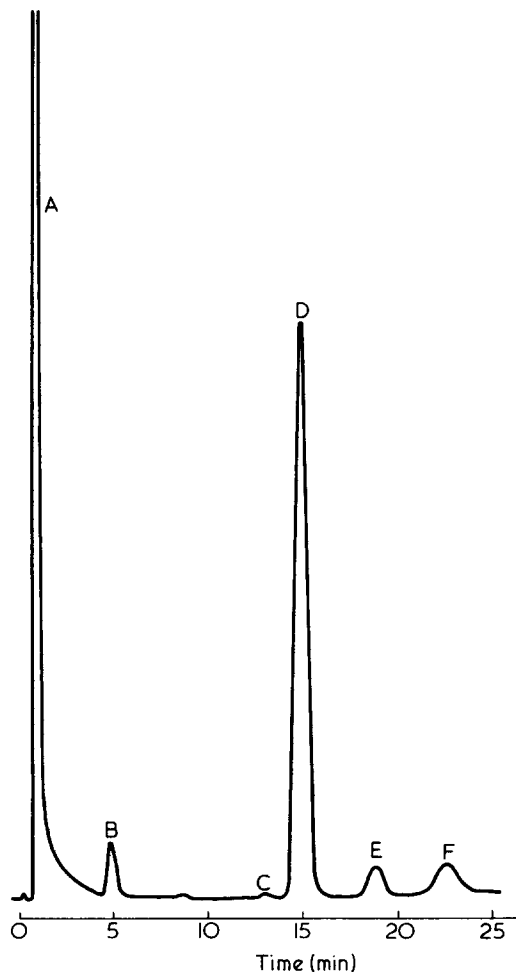
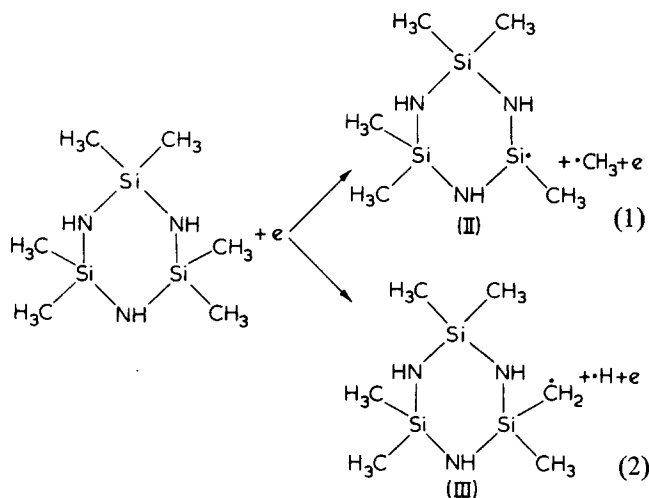


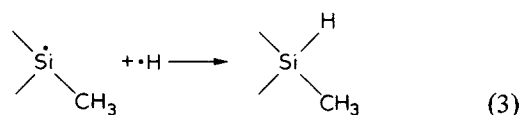
Figure 6 Chromatographic pyrolysis pattern of glow discharge polysilazane formed at 1 mA/cm², 20 kHz, 0.3 Torr, 30 sec. Pyrolysis conditions: temperature 750°C, heating time 15 sec, sample size 0.2 mg. A, methane; B, ethane; C, propane; D, ethylene; E, acetylene; F, propylene

as a result of the large number of various reactions initiated in the glow discharge. Detailed mechanism of glow discharge polymerization is difficult to elucidate, and opinions on this subject found in the literature are often inconsistent. According to the theory of Denaro *et al.*¹⁷, concerning the polymerization of styrene and its derivatives, the process is initiated mainly by free radicals generated by collisions of free electrons present in the plasma with monomer molecules. Yasuda¹² and Kabayashi^{19,20}, who have examined the polymerization of various hydrocarbons, have also concluded that the process proceeds according to a free-radical mechanism. A completely different conclusion has been drawn from the studies of Thompson and Mayhan²⁴ on styrene polymerization. Their results have shown that positive ions play a significant part in the initiation process. In spite of these different opinions on the nature of glow discharge polymerization it is most likely that two initiation mechanisms may occur simultaneously: a radical and an ionic. Such a hypothesis is supported by the fact that electrons present in plasma have some energy distribution and consequently by collision with monomer molecules may produce both radical and ionic species capable of initiating the polymerization. It is still a problem to establish the contribution of particular species in the whole initiation process. This contribution seems to be dependent not only on the electron energy distribution but also on the structural features of monomer.

Accepting such a consideration it is possible to describe the mechanism of some reactions leading to form identified structure fragments of glow discharge polysilazane. As a result of collision with accelerated electrons or ions of plasma, monomer molecules can be converted to an excited state. These excited molecules may then fragment into radical or ionic active species capable of propagating polymerization. According to the radical mechanism the fragmentation of hexamethylcyclotrisilazane molecule may proceed as follows:



Methyl and hydrogen radicals formed in the above reactions may produce methane and ethane by a suitable recombination in the gas phase. These compounds may then be converted by plasma to various gas products such as ethylene, acetylene as well as hydrogen, methyl, ethyl and vinyl radicals^{19,20}. The radicals (II) formed in reaction (1) by recombination with atomic hydrogen (reaction 3) may produce Si-H bonds identified in the polymer structure,



Monomer molecules by collision with accelerated electrons of plasma may also fragment according to ionic mechanism (4),

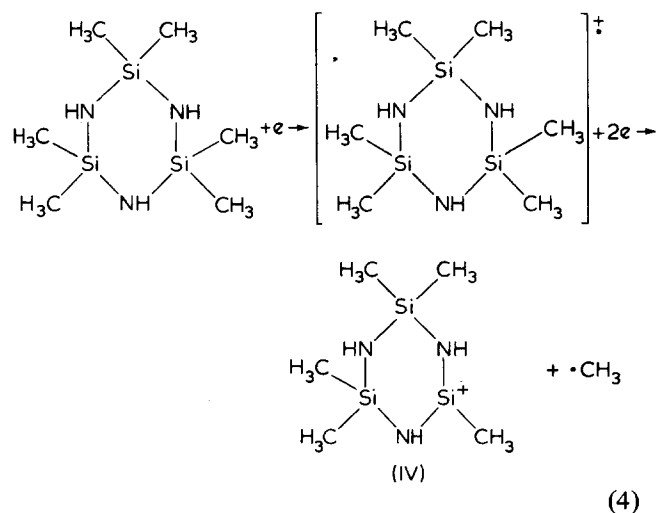
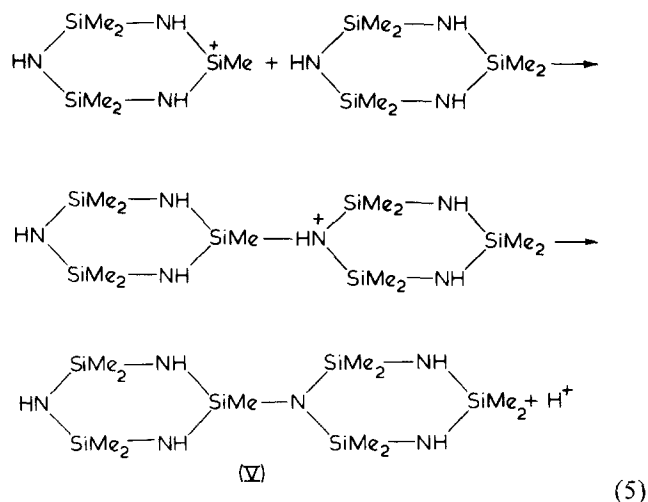


Table 2 Volatile pyrolysis products of glow discharge polysilazane formed at 1 mA/cm², 20 kHz, 0.3 Torr, 30 sec, determined by gas chromatography. Pyrolysis temperature 750°C

Component	Relative content (%)
Methane	100.0
Ethane	1.8
Propane	0.1
Ethylene	15.8
Acetylene	1.0
Propylene	1.5

Reaction (4) is a typical fragmentation which takes place in a mass spectrometer^{25,26}. The peak corresponding to cation (IV) has been found²⁶ to be present in mass spectra of hexamethylcyclotrisilazane, independent of the electron beam energy used, within the range 10–70 eV. Taking into consideration that plasma electrons have similar energies as those in the mass spectrometer²⁴ it is very probable that the ionization of hexamethylcyclotrisilazane molecules in the glow discharge may occur according to reaction (4)

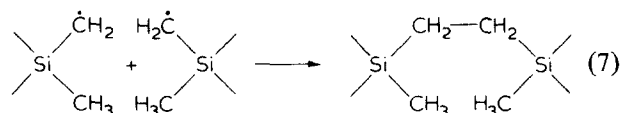
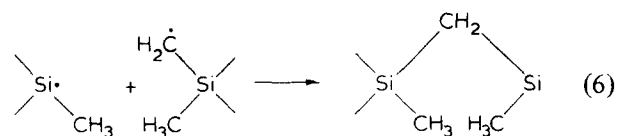
Cations (IV) produced by the ionization of monomer may initiate the polymerization as follows:



Dimer (V) may be ionized further and produce trimer through reaction with the next monomer molecule, and so on. Further growth of the macromolecule may take place also by a reaction of dimer (V) with cations (IV) present in the gas phase. The polymerization proceeding according to the mechanism presented is accompanied by transition of secondary nitrogen into tertiary and formation of (\geq Si)₃N groups in the polymer structure. This is confirmed by a decrease in the number of –NH– groups in the polymer as illustrated in Figure 5. The mechanism is also supported by the fact that a peak corresponding to dimer of structure (V) was found in mass spectra of the soluble fraction of glow discharge polysilazane²⁶. It is worth noticing that a similar mechanism was first proposed by Andrianov²³ for conventional polymerization of hexamethylcyclotrisilazane. It should be noted that polymerization according to reaction (5) may lead to the formation of branched and highly crosslinked polymer.

Crosslinking may also take place through the recombination of macroradicals type (I) and (III) to produce Si–(CH₂)₁ or 2–Si groups identified in the polymer structure.

The process may proceed as follows:



The reaction mechanism presented here may be considered only as a part of such a complex process as the glow discharge polymerization. We hope that the studies started by us on polymer structure and gas phase composition by means of gas chromatography and mass spectrometry will allow better elucidation of the mechanism of glow discharge polysilazane formation.

CONCLUSIONS

(1) The fragmentation of hexamethylcyclotrisilazane in glow discharge predominantly occurs through Si–C bond cleavages with the methyl groups splitting off.

(2) A decrease in methyl group content in glow discharge polysilazanes with increasing current density proves that polymers contain a significant amount of inorganic structure.

(3) Carbon deficiency in glow discharge polysilazanes by comparison with monomer points out that polymers are highly saturated.

(4) A decrease in NH group content in glow discharge polysilazane with increasing current density, suggests that the polymerization of hexamethylcyclotrisilazane may proceed through Si–N linking with cleavage of N–H and Si–C bonds. This process leads a highly crosslinked polymer being formed.

ACKNOWLEDGEMENTS

The authors wish to thank Dr P. Kowalski for help in gas chromatographic analysis. This work was supported by the Polish Academy of Sciences under the project Nr 03.1.2.

REFERENCES

- 1 Tkachuk, B. V., Bushin, V. V., Kolotyrykin, V. M. and Smetankina, N. P. *Vysokomol. Soedin. (A)* 1967, **9**, 2018
- 2 Tkachuk, B. V. and Kolotyrykin, V. M. *Vysokomol. Soedin. (B)* 1968, **10**, 24
- 3 Schuröv, A. N., Tuzov, L. S., Gilman, A. B., Kolotyrykin, V. M. and Tunitskij, N. N. *Vysokomol. Soedin. (A)* 1969, **11**, 582
- 4 Tuzov, L. S., Kolotyrykin, V. M. and Tunitskij, N. N. *Vysokomol. Soedin. (A)* 1970, **12**, 849
- 5 Tkachuk, B. V., Perova, L. V. and Kolotyrykin, V. M. *Vysokomol. Soedin. (A)* 1971, **13**, 828
- 6 Fink, W. *J. Paint Technol.* 1970, **42**, 220
- 7 Sapięha, S., Kryszewski, M., Cygler, M. and Wróbel, A. M. *Conf. Org. Solid State, Güstrov, GDR* 1973, p 59
- 8 Wróbel, A. M. and Kryszewski, M. *Bull. Acad. Pol. Sci., Ser. Sci. Chim.* 1974, **22**, 471
- 9 Wróbel, A. M., Kryszewski, M. and Gazicki, M. *Polymer* 1976, **17**, 673
- 10 Yasuda, H. and Lamaze, C. E. *J. Appl. Polym. Sci.* 1973, **17**, 1519
- 11 Yasuda, H. and Lamaze, C. E. *J. Appl. Polym. Sci.* 1973, **17**, 1533

Structure of glow discharge polysilazane thin films: A. M. Wróbel et al.

- 12 Yasuda, H., Bumgarner, M. O. and Hillman, J. J. *J. Appl. Polym. Sci.* 1975, **19**, 531
- 13 Eaborn, C. 'Organosilicon Compounds', Butterworths, London, 1960, p 90
- 14 Aylett, B. J. *Organometal. Chem. Rev.* 1968, **3**, 151
- 15 Kronick, P. L., Jeseh, K. F. and Bloor, J. E. *J. Polym. Sci. (A-1)* 1969, **7**, 767
- 16 Neiswender, D. D. *Adv. Chem.* 1969, **80**, 338
- 17 Denaro, A. R., Owens, P. A. and Crawshaw, A. *Eur. Polym. J.* 1968, **4**, 93; 1969, **5**, 471; 1970, **6**, 483
- 18 Westwood, A. R. *Eur. Polym. J.* 1971, **7**, 277
- 19 Kobayashi, H., Bell, A. T. and Shen, M. *Macromolecules* 1974, **7**, 277
- 20 Kobayashi, H., Shen, M. and Bell, A. T. *J. Macromol. Sci. (A)* 1974, **8**, 373
- 21 Krüger, C. R. and Rochow, E. C. *J. Polym. Sci. (A)* 1964, **2**, 3179
- 22 Denes, F., Ungurenasu, C. and Haiduc, J. *Eur. Polym. J.* 1970, **6**, 1155
- 23 Andrianov, K. A. and Rumba, G. Ya. *Vysokomol. Soedin.* 1962, **4**, 1060
- 24 Thompson, L. F. and Mayhan, K. G. *J. Appl. Polym. Sci.* 1972, **16**, 2317
- 25 Silbiger, J., Lifshitz, C., Fuchs, J. and Mandelbaum, A. *J. Am. Chem. Soc.* 1967, **89**, 4308
- 26 Gazicki, M., Wróbel, A. M. and Kryszewski, M. *J. Appl. Polym. Sci.* in press

Upper and lower critical solution temperatures in poly (ethylene glycol) solutions

Susumu Saeki, Nobuhiro Kuwahara, Mitsuo Nakata, and Motozo Kaneko

Department of Polymer Science, Hokkaido University, Sapporo, Japan

(Received 7 January 1976; revised 19 March 1976)

Upper and lower critical solution temperatures have been determined for solutions of poly(ethylene glycol) in t-butyl acetate and water over the molecular weight range of $M_n = 2.18 \times 10^3$ to $\sim 1020 \times 10^3$. The phase diagram for solutions of poly(ethylene glycol) ($M_n = 719 \times 10^3$) in t-butyl acetate was expressed as the 'hour glass' type, while the phase diagram for solution of poly(ethylene glycol) ($M_n = 2.18 \times 10^3$ to $\sim 2.29 \times 10^3$) in water was expressed as the 'closed loop' type. The value of the pressure dependence of the lower critical solution temperature $(dT/dP)_c$ in the poly(ethylene glycol) ($M_n = 1020 \times 10^3$)/water system over the pressure range of 0 to ~ 50 atm was negligibly small and positive.

INTRODUCTION

Investigation of the phase separation behaviour of polymer solutions over a wide range of molecular weights gives useful information on the dependence of the reduced residual chemical potential or the χ parameter on temperature, pressure, and concentration. The expression of χ_1 as a function of temperature derived by Patterson *et al.*¹⁻⁶ and Flory *et al.*⁷⁻¹⁰ has predicted the occurrence of phase separations at the lower critical solution temperature (*LCST*) and the upper critical solution temperature (*UCST*) in non-polar polymer solutions¹¹⁻²⁰ and the continuous change from the endothermic behaviour near the *UCST* to the exothermic near the *LCST* passing through the athermal condition in the intermediate temperature region between the *UCST* and the *LCST*¹⁴. The χ_1 parameter represented by a parabolic-like function of temperature with a minimum has been correlated with the polymer chain dimension in the dilute polymer solution with a maximum in the intermediate temperature region between θ_u and θ_l ²⁰⁻²², in which θ_u and θ_l are respectively the Flory temperatures for the *UCST* and *LCST*. The phase diagram of the 'closed loop' type with both the *UCST* and *LCST* in aqueous solutions e.g. nicotine-water²³, butyl glycol-water²⁴, poly(ethylene glycol)-water²⁵, and poly(riboadenylic acid)-water²⁶ has been distinguished from that in non-polar polymer solutions, e.g. polystyrene solutions^{13,16,17} and polyethylene solutions¹⁸. The behaviour of phase separation for the aqueous solutions has been explained by the existence of a special interaction, e.g. the hydrogen bond, which is beyond the scope of usual solution thermodynamics. A theoretical prediction for the phase diagram of the 'closed loop' type has been suggested by Barker and Fock²⁷ with the introduction of the molecular interaction depending on the relative orientation and by Scatchard and Wilson^{28,29} with the expression for the excess free energy of mixing. The temperature dependence of the second virial coefficient A_2 of a poly(riboadenylic acid) solution at neutral pH in 1 to ~ 1.33 mol sodium chloride²⁶ is represented by a parabolic-like curve with a minimum at 40°C in harmony with the parabolic-like temperature dependence of the mean square radius of gyration $\langle s^2 \rangle$ with a minimum

at 40°C . The behaviour of A_2 or $(1/2 - \chi_1)$ and $\langle s^2 \rangle$ over the temperature range of θ_u to $\sim \theta_l$ in the poly(riboadenylic acid) solutions is in extreme contrast to the temperature dependence of χ_1 and $\langle s^2 \rangle$ in the non-polar polymer solutions¹⁹⁻²¹. The phase separation behaviour of the *LCST* and the temperature dependence of A_2 for solutions of cellulose-, amylose-, and polyvinyl-carbanilate in polar solvents reported by Burchard³⁰ are also remarkably different from those for the non-polar polymer solutions and also for the aqueous solutions.

The *LCST* for solutions of poly(ethylene glycol) in methyl, ethyl, n-propyl, and iso-butyl acetate, acetone, and methyl ethyl ketone were observed in our preliminary experiments. However, we are interested in the appearance of both *UCST* and *LCST* in poly(ethylene glycol) solutions, which is a very general phenomenon in polymer solutions. In this paper the typical phase diagrams of the 'hour glass' type and of the 'closed loop' type with solutions of poly(ethylene glycol) in t-butyl acetate and water, are presented. We have also examined the pressure dependence of the *LCST* for solutions of poly(ethylene glycol) in water.

EXPERIMENTAL

Poly(ethylene glycol) [Union Carbide, Chemical Division Product Polyox WSR 301: $M = 4000 \times 10^3$; Wako Pure Chemical Industries, Product poly(ethylene glycol) 4000: $M = 3000$ and Nakarai Chemicals, Product poly(ethylene glycol) 20 000: $M = 15 \times 10^3$ to $\sim 25 \times 10^3$] were fractionated into seven fractions for the Polyox WSR 301, seven fractions for the poly(ethylene glycol) 4000, and thirteen fractions for the poly(ethylene glycol) 20 000. Fractionation was carried out by the solution fractionation technique called the coacervation method. After adding n-heptane to the poly(ethylene glycol)/benzene solution (concentration < 0.10 g/dl) the solution was kept for a day at 40°C in a water bath controlled to $\pm 0.01^\circ\text{C}$. After complete attainment of the liquid/liquid phase equilibrium for solutions of the Polyox WSR 301 and the poly(ethylene glycol) 20 000 or liquid/solid equilibrium for solutions of the poly(ethylene glycol) 4000, the dilute solution, in which

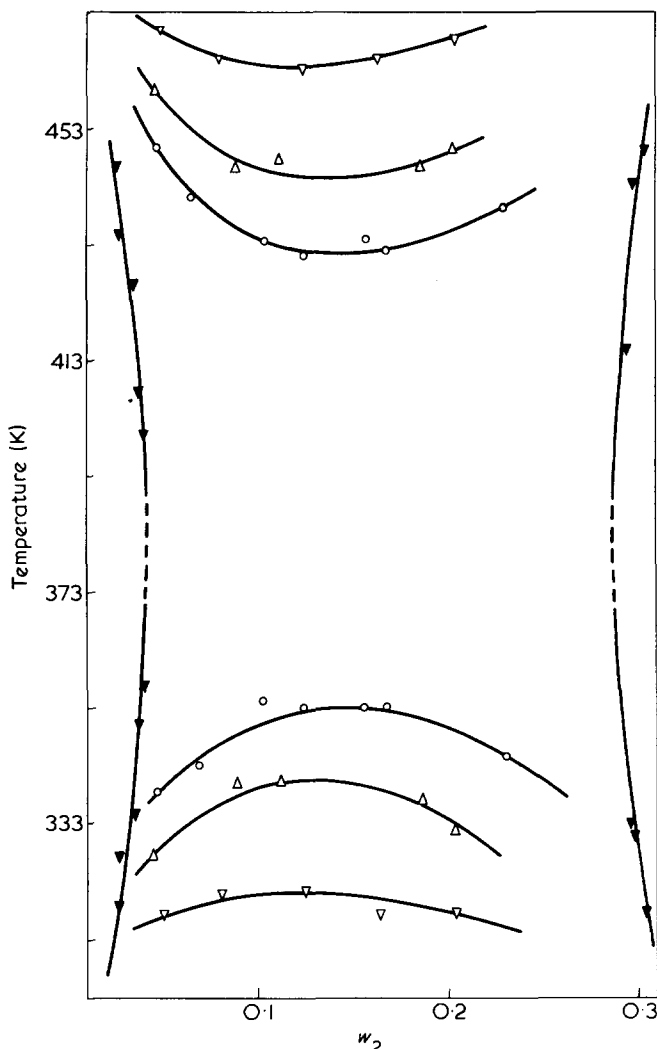


Figure 1 Temperature/weight fraction phase diagram for the poly(ethylene glycol) samples in t-butyl acetate: ∇ , $M_n = 719 \times 10^3$; \circ , $M_n = 21.2 \times 10^3$; \triangle , $M_n = 14.4 \times 10^3$; ∇ , $M_n = 8.0 \times 10^3$

lower molecular weight poly(ethylene glycol) is richer, was carefully separated from the concentrated solution phase. A fractionated poly(ethylene glycol) was obtained from the dilute phase and the concentrated phase was redissolved in a mixture of benzene and n-heptane for further fractionation. The fractionated samples were dried for more than two weeks at 40°C under vacuum. Reagent grade t-butyl acetate (500 g) was refluxed for 2 h over ~ 15 g of acetic anhydride and dried over anhydrous potassium carbonate. The dried solvent was fractionally distilled using a column 100 cm in length and 10 mm in diameter packed with stainless steel helices. Fractionally distilled water was obtained using a specially designed distillation apparatus, which was repeatedly washed by steam for seven years.

Several solutions of each polymer sample were prepared in t-butyl acetate and water for cloud point curve determinations, in the concentration range 0.3 to ~ 43 wt% and flame sealed under dry nitrogen gas in 7 mm i.d. cylindrical cells. Cloud point temperatures for the UCST and LCST were optically¹⁷ determined with an accuracy of $\pm 0.1^\circ\text{C}$ in a silicon oil bath over the temperature range 40° to $\sim 240^\circ\text{C}$. After measuring the precipitation temperatures for the LCST, the thermal degradation of poly(ethylene glycol) was examined by the reproducibility of the precipitation temperature for the UCST. Errors caused by thermal degradation are estimated to be 1.5° to $\sim 2.0^\circ\text{C}$ for the poly(ethylene glycol)/t-butyl acetate system, while no thermal

degradation was observed for solutions of poly(ethylene glycol) ($M_n = 2.18 \times 10^3 \sim 2.29 \times 10^3$) in water. Cloud point temperatures under pressure have been measured over 0 to ~ 50 atm using the pressure apparatus described in detail elsewhere³¹. Solutions for the cloud point temperature measurements under pressure were stirred with a magnetic stirrer for at least 24 h and then sealed using pure mercury inside the solution cells.

The molecular weights of the poly(ethylene glycol) samples were determined from the values of the limiting viscosity number $[\eta]$ for solutions of poly(ethylene glycol) in benzene at 20° and 25°C , according to the equation^{32,33}:

$$[\eta] = 4.8 \times 10^{-4} M^{0.68}$$

at 20°C ³² for $0.1 < M \times 10^{-3} < 20$

and $[\eta] = 3.97 \times 10^{-4} M^{0.686}$

at 25°C ³³ for $80 < M \times 10^{-3} < 5200$

Viscosity measurements were carried out with negligible kinetic energy corrections with an Ubbelohde-type viscometer with the aid of a water bath controlled to within $\pm 0.02^\circ\text{C}$. The concentration of solutions was determined by evaporating a known volume to dryness and weighing the residue. Viscosity data were treated by double extrapolation of η_{sp}/C and $\ln \eta_r/C$ against C to determine the limiting viscosity number, where η_{sp} and η_r are respectively the specific and the relative viscosity and C is the concentration (g/dl).

RESULTS

Phase diagrams of solutions of poly(ethylene glycol) in t-butyl acetate and water are shown in Figures 1 and 2, where w_2 is the weight fraction of the polymer. Complete miscibility of the poly(ethylene glycol) ($M_n = 719 \times 10^3$)/t-butyl acetate system occurs at concentrations < 4 wt% and > 29 wt% of the polymer. Although the maximum and minimum points of the cloud point curves for the low molecular weight poly(ethylene glycol) in t-butyl acetate and poly(ethylene glycol) in water systems deviate slightly from the critical points depending on the polydispersity of the samples, the deviation from the critical points should be quite small as the polymer samples were obtained by the solution fractionation technique^{34,35}. Since we are mainly interested in semi-quantitative features of miscibility, the maximum and minimum temperatures in the phase diagrams are taken as the critical solution temperatures for UCST and LCST, respectively. Values of UCST and LCST under saturated vapour pressure for the systems are compiled in Table 1. Coalescence of the UCST and LCST in the t-butyl acetate system would occur at $\sim M_n = 41 \times 10^3$, while both the UCST and LCST in the water system would disappear at $\sim M_n = 2.14 \times 10^3$ giving complete miscibility over the whole concentration range.

The pressure dependence of the cloud point temperatures at four concentrations in the vicinity of the critical concentration for the LCST in the poly(ethylene glycol) ($M_n = 1020 \times 10^3$)/water system is shown in Figure 3, where the value of $(dT/dP)_c$ for the LCST is pointed out to be negligibly small and positive ($0.004^\circ\text{C}/\text{atm}$). The cloud point curves of the poly(ethylene glycol)/water system were obtained under a solution vapour pressure of 20 to ~ 30 atm for the UCST and 1 to ~ 10 atm for the

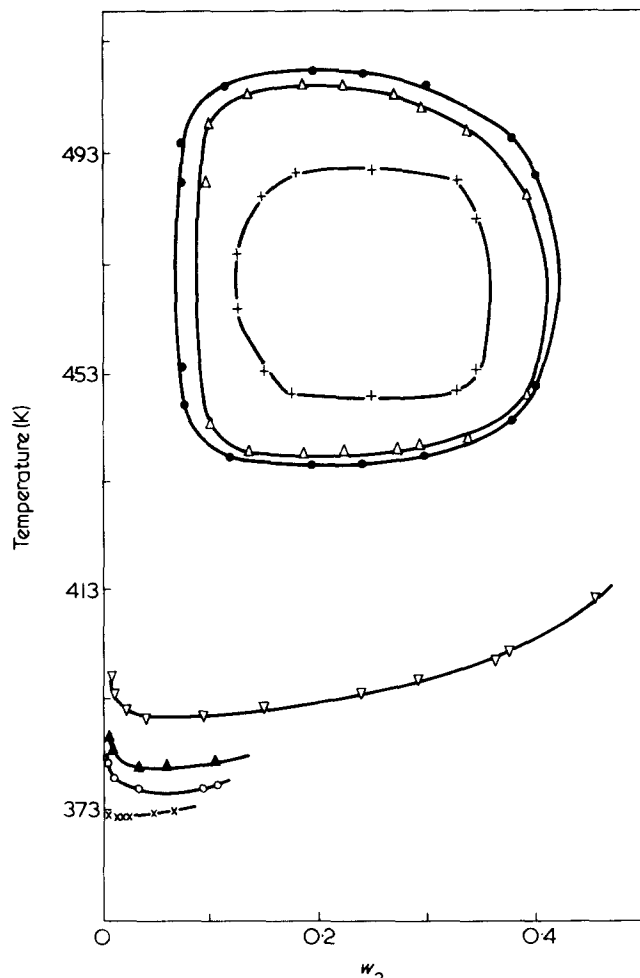


Figure 2 Temperature/weight fraction phase diagram for the poly(ethylene glycol) samples in water: X, $M_n = 1020 \times 10^3$; O, $M_n = 21.2 \times 10^3$; A, $M_n = 14.4 \times 10^3$; V, $M_n = 8.0 \times 10^3$; B, $M_n = 2.29 \times 10^3$; D, $M_n = 2.27 \times 10^3$; +, $M_n = 2.18 \times 10^3$

LCST, depending on the molecular weight of the samples. Corrections of the LCST to the zero pressure condition for aqueous solutions would be small, while the corrected values of the LCST for the t-butyl acetate solutions would be lower than the observed ones by $0.4 \sim 0.6^\circ\text{C}/\text{atm}$ depending on the solution vapour pressures³⁶⁻⁴⁰.

DISCUSSION

According to the Patterson-Delmas theory of corresponding states the polymer-solvent interaction parameter of χ_1 is expressed by¹⁻⁶:

$$\chi_1 = -(U_1/RT)v^2 + (C_{p,1}/2R)\tau^2 \quad (1)$$

where U_1 and $C_{p,1}$ are the configurational energy and configurational heat capacity of the solvent respectively, R is the gas constant, and both the v^2 parameter and the τ parameter are the temperature independent molecular parameters. The v^2 parameter is related to the cohesive energy and segment size of the solution components, while the τ parameter is determined from the characteristic temperature reduction parameters (T^*) of the solvent (1) and polymer (2). It is convenient to rewrite equation (1) when applying it to polymer solutions using thermodynamic relations such as the thermodynamic equation of state and the difference relation between the heat capacities at constant pressure (C_p) and at constant volume (C_v)⁴:

$$-U_1 = \gamma_{v,1}V_1T \quad (2)$$

and

$$C_{p,1} = \gamma_{v,1}V_1T\alpha_1 \quad (3)$$

where $\gamma_{v,1}$ is the thermal pressure coefficient, α_1 is the thermal expansion coefficient, and V_1 is the molar volume of the solvent. The χ_1 expression coupled with equations (2) and (3) is independent of the model used for the configurational energy of the liquid. The calculated curve for χ_1 against temperature for the poly(ethylene glycol)/t-butyl acetate system using equation (1) coupled with the equation of state of the van der Waals model⁷, the experimental values of α_1 for t-butyl acetate over the temperature range of 20° to 95°C ²⁰ and extrapolated values of α_1 over 95° to 160°C is shown in Figure 4, where the values of the configurational energy (v^2 term), the configurational heat capacity (τ^2 term) in equation (1), and values of the χ_1 (crit) are also included. Values of the v^2 , τ^2 , and c_1 parameters, and the characteristic reduction parameters such as P^* , T^* , and V^* for the poly(ethylene glycol)/t-butyl acetate system are listed in Table 2. The values of the χ_1 (crit) are determined by neglecting $\chi_2\phi_2$ and higher terms in the χ parameter¹⁰ and are given by:

$$\chi_1(\text{crit}) = (1/2)(1 + r^{-1/2})^2 \quad (4)$$

where r is the ratio of the characteristic molar volume reduction parameter (V^*) of the polymer and solvent. The parabolic-like temperature dependence of χ_1 with a mini-

Table 1 Critical solution temperatures for solutions of poly(ethylene glycol) in t-butyl acetate and water

System	Sample	$M_n \times 10^{-3}$ (g. mol. wt)	UCST (K)	LCST (K)
Poly(ethylene glycol)/ t-butyl acetate	B-1	8.00	321.2	464.2
	B-2	14.4	340.2	446.2
	B-3	21.2	353.2	431.2
Poly(ethylene glycol)/ water	C-1	2.18	489.7	448.7
	C-2	2.27	505.2	437.2
	C-5	2.29	507.7	435.7
	B-1	8.00		389.4
	B-2	14.4		380.7
	B-3	21.2		376.8
	A-3	719.0		372.3
A-4	1020.0		371.8	

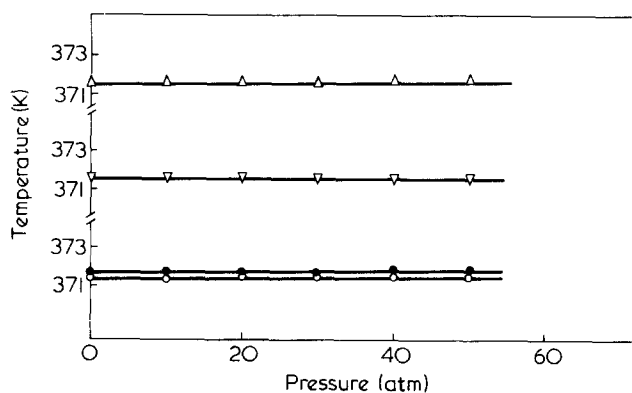


Figure 3 Pressure effect of cloud point temperatures for the poly(ethylene glycol) ($M_n = 1020 \times 10^3$)/water system at various concentrations (w_2): A, 0.01746; V, 0.01321; B, 0.01001; O, 0.02162

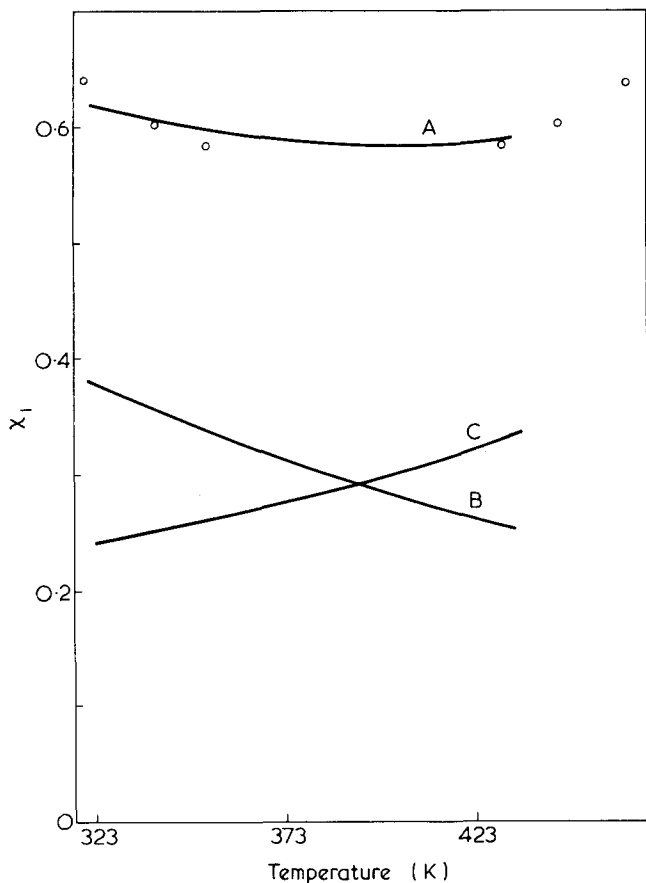


Figure 4 Interaction parameter χ_1 (A), ν^2 (B) and τ^2 (C) vs. temperature plots for the poly(ethylene glycol)/t-butyl acetate system. \circ , represent χ_1 (crit) from equation (4)

Table 2 Parameters of the system poly(ethylene glycol)/t-butyl acetate

Parameter	Value
T_1^* (K)	4728 ^a
V_1^* (cm ³ /mol)	105.0 ^a
P_1^* (atm)	5038 ^b
C_1	1.40 ^b
ν^2	0.0249
τ^2	0.0724

^aFrom ref 20; ^bfrom ref 40. $T_2^* = 6469\text{K}$ and $\nu_{sp,2}^* = 0.7532\text{ cm}^3/\text{g}$ for poly(ethylene glycol) were taken from ref 46. The values of T_1^* and V_1^* for t-butyl acetate are the average value over a temperature range of 40° to ~95°C

imum in the t-butyl acetate system is brought about by both an increasing contribution of the τ^2 term and decreasing contribution of the ν^2 term with increase in temperature.

The direct prediction of the temperature dependence of χ_1 in the poly(ethylene glycol)/water system by equation (4) is represented by the parabolic-like temperature dependence with a maximum. The temperature dependence of $\gamma_{v,1}$ for water^{41,42} is expressed by the parabolic-like temperature dependence with a maximum at ~150°C. This is contrary to the theoretical prediction from the reduced equation of state of the van der Waals model, which predicts a monotonous decrease of γ_v with an increase in temperature. The experimental values of γ_v for many liquids such as methane, n-heptane, benzene⁴², etc., monotonously decrease with increasing temperature. The increase of $\gamma_v = (\partial S / \partial V)_T$ with an increase in temperature observed in

water reflects the fact that the ratio of entropy change to enlargement of volume increases as the temperature increases. This behaviour is consistent with a contribution to the entropy originating from the break down of the structure of the water caused by an increase in temperature. In the light of these facts it is suggested that the phenomenon of the UCST and LCST in the poly(ethylene glycol)/water system is brought about by essentially different interactions from that of non-polar polymer solutions.

The value of $(dT/dP)_c$ for the LCST in the poly(ethylene glycol)/water system is related by^{43,44}:

$$\left(\frac{dT}{dP}\right)_c = \lim_{\substack{T \rightarrow T_c \\ \phi_2 \rightarrow \phi_c}} \frac{T(\partial^2 V / \partial \phi_2^2)_{T,P}}{(\partial^2 H / \partial \phi_2^2)_{T,P}} \quad (5)$$

where H and V are the enthalpy and the volume per mole mixture and ϕ_2 is the concentration of the polymer. The negligibly small and positive value of $(dT/dP)_c$ for the LCST in the aqueous solution corresponds to the negligibly small and positive value of $(\partial^2 V / \partial \phi_2^2)$ or the small negative excess volume of mixing because of the positive value of $(\partial^2 H / \partial \phi_2^2)$ in the vicinity of the LCST. The present value of $(dT/dP)_c$ for the LCST of the aqueous solution is consistent with the negative excess volume of mixing observed in the poly(ethylene glycol) ($M_n = 5 \times 10^3$)/water system at 65°C over the wide concentration range²⁵. The value of $(dT/dP)_c$ for the LCST in the poly(ethylene glycol)/water system (0.004°C/atm) is extremely small compared to the values of $(dT/dP)_c$ for the LCST in non-polar polymer solutions³⁶⁻⁴⁰, e.g. polystyrene/methyl acetate (0.45°C/atm)³⁷ and polystyrene/t-butyl acetate (0.65 ~ 0.70°C/atm)⁴⁰.

In this work it is emphasized that the phenomenon of the UCST and LCST and the pressure dependence of the LCST in the poly(ethylene glycol)/water system are caused by a special interaction between the poly(ethylene glycol) and water beyond the scope of van der Waals interactions, while the appearance of the UCST and LCST in the t-butyl acetate system can be explained by the recent theories of polymer solution thermodynamics by Patterson and Flory. It is also suggested from the temperature dependence of χ_1 estimated by equation (4) that the sign of the excess partial molar heat capacity⁴⁵ is negative for the t-butyl acetate system and positive for the water system.

ACKNOWLEDGEMENTS

The authors thank Dr Y. Miyake of Department of Polymer Science, Hokkaido University for the supply of distilled water.

REFERENCES

- Delmas, G., Patterson, D. and Somcynsky, T. *J. Polym. Sci.* 1962, **57**, 79
- Patterson, D. *J. Polym. Sci. (C)* 1968, **16**, 3379
- Delmas, G. and Patterson, D. *Int. Symp. Macromol. Chem. Toronto* 1968
- Patterson, D. and Delmas, G. *Trans. Faraday Soc.* 1969, **65**, 708
- Patterson, D. and Delmas, G. *Discuss. Faraday Soc.* 1970, **49**, 98
- Biros, J., Zeman, L. and Patterson, D. *Macromolecules* 1971, **4**, 30
- Flory, P. J., Orwoll, R. A. and Vrij, A. *J. Am. Chem. Soc.* 1964, **86**, 3507
- Flory, P. J., Orwoll, R. A. and Vrij, A. *J. Am. Chem. Soc.* 1964, **86**, 3515

- 9 Flory, P. J. *J. Am. Chem. Soc.* 1965, **87**, 1833
- 10 Eichinger, B. E. and Flory, P. J. *Trans. Faraday Soc.* 1968, **64**, 2035
- 11 Freeman, P. I. and Rowlinson, J. S. *Polymer* 1960, **1**, 20
- 12 Barker, C. H., Brown, W. B., Gee, G., Rowlinson, J. S., Stubbley, D. and Yeadon, R. E. *Polymer* 1962, **3**, 215
- 13 Allen, G. and Barker, C. H. *Polymer* 1965, **6**, 181
- 14 Liddell, A. H. and Swinton, F. L. *Discuss. Faraday Soc.* 1970, **49**, 115
- 15 Cowie, J. M. G., Maconnachie, A. and Ranson, R. J. *Macromolecules* 1971, **4**, 57
- 16 Siow, K. S., Delmas, G. and Patterson, D. *Macromolecules* 1972, **5**, 29
- 17 Saeki, S., Kuwahara, N., Konno, S. and Kaneko, M. *Macromolecules* 1973, **6**, 246, 589
- 18 Kuwahara, N., Saeki, S., Chiba, T. and Kaneko, M. *Polymer* 1974, **15**, 777
- 19 Saeki, S., Konno, S., Kuwahara, N., Nakata, M. and Kaneko, M. *Macromolecules* 1974, **7**, 521
- 20 Konno, S., Saeki, S., Kuwahara, N., Nakata, M. and Kaneko, M. *Macromolecules* 1975, **8**, 799
- 21 Kuwahara, N., Saeki, S., Konno, S. and Kaneko, M. *Polymer* 1974, **15**, 66
- 22 Delmas, G. and Patterson, D. *Polymer* 1966, **7**, 513
- 23 Fowler, R. T. *J. Soc. Chem. Ind.* 1950, **69**, 565
- 24 Cox, H. L. and Cretcher, L. H. *J. Am. Chem. Soc.* 1926, **48**, 451
- 25 Malcolm, G. N. and Rowlinson, J. S. *Trans. Faraday Soc.* 1957, **53**, 921
- 26 Eisenberg, H. and Felsenfeld, G. *J. Mol. Biol.* 1967, **30**, 17
- 27 Barker, J. A. and Fock, W. *Discuss. Faraday Soc.* 1953, **15**, 188
- 28 Wilson, G. M. *J. Am. Chem. Soc.* 1964, **86**, 127
- 29 Scatchard, G. and Wilson, G. M. *J. Am. Chem. Soc.* 1964, **86**, 133
- 30 Burchard, W. *Polymer* 1969, **10**, 467
- 31 Saeki, S., Kuwahara, N., Nakata, M. and Kaneko, M. *Polymer* 1975, **16**, 445
- 32 Sadron, C. and Rempp, P. *J. Polym. Sci.* 1958, **29**, 127
- 33 Allen, G., Booth, C., Hurst, S. J., Jones, M. N. and Price, C. *Polymer* 1967, **8**, 391
- 34 Koningsveld, R., Kleintjens, L. A. and Shultz, A. R. *J. Polym. Sci. (A-2)* 1970, **8**, 1261
- 35 Kuwahara, N., Nakata, M. and Kaneko, M. *Polymer* 1973, **14**, 415
- 36 Ehrlich, P. and Kurpen, J. J. *J. Polym. Sci. (A-1)* 1963, **1**, 3217
- 37 Myrat, C. D. and Rowlinson, J. S. *Polymer* 1965, **6**, 645
- 38 Zeman, L., Biro, J., Delmas, G. and Patterson, D. *J. Phys. Chem.* 1972, **76**, 1206
- 39 Zeman, L. and Patterson, D. *J. Phys. Chem.* 1972, **76**, 1214
- 40 Saeki, S., Kuwahara, N. and Kaneko, M. *Macromolecules* 1976, **9**, 101
- 41 'National Engineering Laboratory, Steam Table', (Ed. Bain, R. W.), HMSO, Edinburgh, 1964
- 42 Rowlinson, J. S. 'Liquid and Liquid Mixtures', 2nd Edn, Butterworths, London, 1969
- 43 Prigogine, I. and Defay, R. 'Chemical Thermodynamics', Longmans, London, 1954
- 44 Schneider, G. M. *Adv. Chem. Phys.* 1970, **16**, 1
- 45 Eichinger, B. E. *J. Chem. Phys.* 1970, **53**, 561
- 46 Booth, C. and Devoy, C. J. *Polymer* 1971, **12**, 309

Anomalous diffusion of water in glassy polymers

G. A. Pogany

Koninklijke/Shell Laboratorium, Amsterdam (Shell Research b.v.) The Netherlands
(Received 12 November 1975; revised 7 April 1976)

Anomalous diffusion of water has been observed in polystyrene and in epoxy resin. Sudden changes in the boundary conditions can cause the absorbed water to agglomerate and form a second phase within these polymers. The agglomerated water can force the polymer segments apart and create permanent crazes. The diffusion of water in crazed polymers is non-Fickian. The solubility becomes a function of the total pressure and the amount of water taken up from liquid water is much more than that absorbed in saturated water vapour.

INTRODUCTION

Many diffusion processes can be adequately described by Fick's first and second laws¹. However, deviations from Fickian diffusion in polymers have been observed². In these cases the diffusion coefficient becomes dependent not only on temperature, but also on time and concentration. Non-Fickian diffusion is usually explained by some kind of interaction between polymer and penetrant³⁻¹¹.

In the past special attention was paid to the anomalous diffusion of water in glassy polymers^{12,13}. More recently, this behaviour has been attributed to the presence of voids in the polymer¹⁴⁻¹⁸.

This paper presents the results of some experiments concerning the absorption of water by polystyrene and by epoxy resin. A qualitative explanation is given of the observed anomalies.

EXPERIMENTAL

Materials

The following materials were used: a pure, commercial, high molecular weight polystyrene homopolymer ('Carinex' HR), and a somewhat lower molecular weight polystyrene containing about 0.1 wt% of a finely dispersed (~1 μm), non-compatible, polymeric additive. Both samples were compression moulded into sheets of 1 and 3 mm thickness and cut into squares of approximately 10 × 10 cm.

In addition, samples of epoxy phenolic lacquers cast on tin plates were examined.

Technique

The dried and weighed polystyrene samples were immersed in water baths kept at 20°, 50°, 80° and 100°C, with an accuracy of ±1°C. At different intervals a sample was removed, plunged into ice-cold water, removed, dried of surface water with blotting paper, weighed on an analytical balance and returned to the bath. The whole procedure took about 30 sec. The purpose of using ice-cold water was to quench the sample and lower the diffusion constant so as to reduce the loss of absorbed water during weighing.

This process has been described by Braden¹⁹, except for the use of ice-cold water. Static electric charges sometimes developed during the surface drying of the samples, causing erratic weighing results. This problem was overcome by

ionizing the air with a spark from a Tesla coil inside the balance chamber²⁰.

The maximum solubility was found from a plot of the weight increase versus the logarithm of time. The diffusion constant can be calculated from such a curve using the relationship:

$$D = \frac{0.049L^2}{t_{1/2}}$$

where, D = diffusion constant in cm²/sec; L = thickness of the specimen in cm; $t_{1/2}$ = half-time of saturation in sec.

In addition to measuring the diffusion and solubility constants, we made use of an optical and an electron microscope.

RESULTS

Compression moulded sheets of pure, high molecular weight polystyrene immersed in water at temperatures up to 80°C (their approximate glass-transition temperature, T_g) absorbed water according to the sigmoid curves shown in Figure 1. These results proved reproducible after a number of absorption-desorption cycles. Sometimes, however, it was impossible to obtain a well-defined plateau of maximum absorption within the experimental time.

Figure 2 shows that the low molecular weight polystyrene, with a small amount of non-compatible polymeric additive dispersed in it, kept on increasing in weight at the same temperatures. Figure 3 shows that the pure, high molecular weight polystyrene behaved similarly at 100°C.

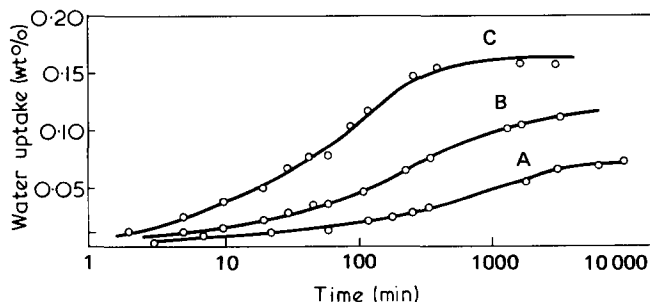


Figure 1 Absorption of water by pure polystyrene, $L \approx 3$ mm. A, 22°C; B, 50°C; C, 80°C

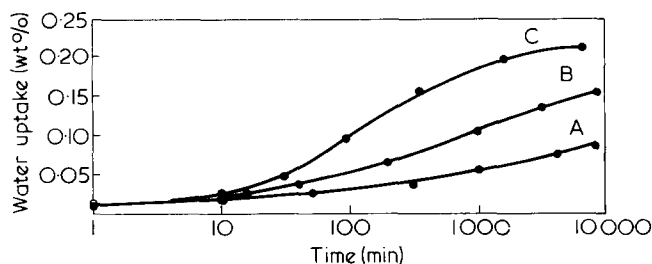


Figure 2 Absorption of water by polystyrene with additive, $L = \sim 3$ mm. A, 22°C; B, 50°C; C, 80°C

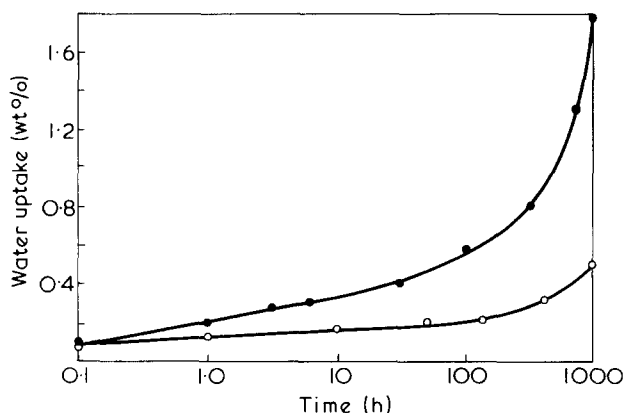


Figure 3 Absorption of water by polystyrene at 100°C, $L = \sim 1$ mm. ●, With additive; ○, pure

(Note the increased scales on both axes and the reduction in sample thickness from 3 to 1 mm.) Even more significant is the 100°C absorption curve of the lower molecular weight polystyrene, also depicted in Figure 3.

Solubility values and diffusion constants calculated from Figures 1 and 2 are presented in Table 1. The values for the non-pure polymer are based on the assumption that equilibrium has been reached in 10 000 min.

On the basis of the results given in Figures 1 and 2 one might expect a higher maximum weight to be reached at 100°C, since the saturated vapour pressure of water (driving force) increases with temperature faster than the solubility decreases. Moreover, the diffusion constant increases with temperature, so that the new maximum should be attained quicker. However, the uptake of water by the samples in Figure 3 shows no sign of reaching a maximum, in spite of the very long times involved.

In the 100°C experiment we observed that as long as the pure polystyrene samples were immersed in the hot water, they were transparent. On removal and cooling they turned opaque. On being returned to the hot water, they again became transparent. Opacity first developed on the outer faces of the test plate and moved inwards with time. We further observed that the opacity did not disappear with the complete removal of the absorbed water at room temperature, but faded away quickly when the dried sample was heated above its glass-transition temperature. The heated sample then became transparent again and remained so at all temperatures.

We induced opacity in a pure polystyrene sample by keeping it in a water bath at 100°C for 168 h. After removal of all the absorbed water *in vacuo* at room temperature, we repeated the 80°C absorption experiment. The still opaque sample proved to absorb much more water than the original, transparent one, as shown in Figure 4, which should be compared with Figure 1, curve C.

The additive-containing polystyrene sample was already opaque to start with. Whereas the pure polystyrene gave reproducible results at temperatures up to and including 80°C, this polymer took up increasingly large quantities of water on repeated absorption at 80°C (not shown). This material, too, was kept in a 100°C water bath for 168 h, along with the pure polymer. After drying at room temperature now it took up as much water at 80°C as the pure polystyrene (see Figure 4).

A transparent sample of pure polystyrene and two samples of the same material made opaque by prolonged immersion in hot water were allowed to absorb water at 80°C. They were then subjected to a series of experiments involving the consecutive use of vacuum, water, air saturated with water vapour, and saturated water vapour only (no air) at 50°C. Each condition was maintained for at least 48 h (2880 min), which – according to Figure 1 – is sufficiently long for equilibrium to be reached. Figure 5 shows the equilibrium values obtained, connected by straight lines, which serve as visual aids only.

Table 1 Solubility values and diffusion constants for pure polystyrene and polystyrene with additive

Unit	Temperature (°C)	Pure polystyrene	Polystyrene with additive
Solubility (cm ³ /cm ³ /cmHg)	22	0.385	0.533
	50	0.141	0.205
	80	0.053	0.073
Diffusion constant (cm ² /sec × 10 ⁷)	22	1.7	0.9
	50	5.6	3.1
	80	16.0	9.6

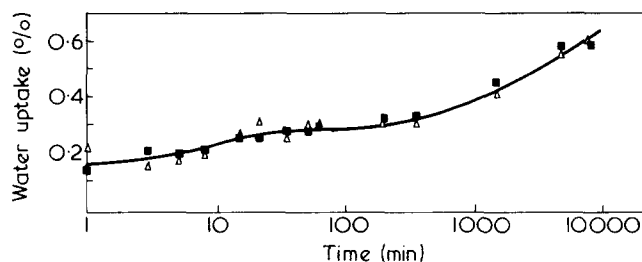


Figure 4 Reabsorption of water by polystyrene at 80°C after 168 h in 100°C water (to induce crazing) and desorption, $L = \sim 1$ mm. ■, Pure; △, with additive

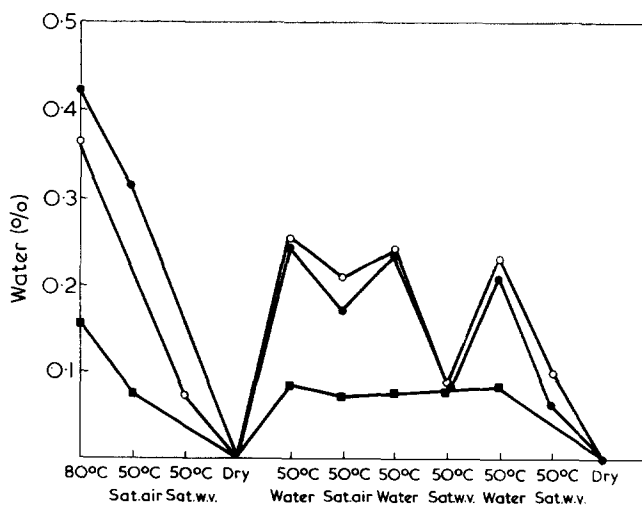


Figure 5 Water absorption and desorption experiments with compression moulded polystyrene (HR) plates. Each step measured after 48 h. ○, opaque; ●, opaque; ■, transparent

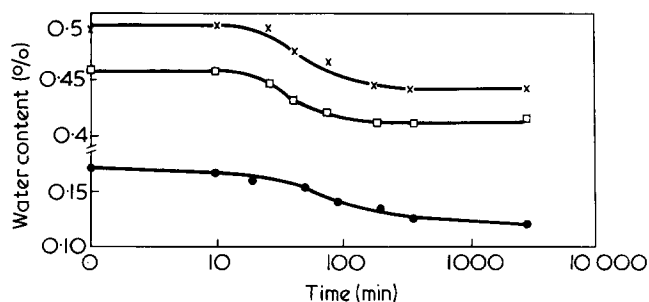


Figure 6 Desorption of water at 50°C from polystyrene sheets after immersion in water at 80°C for 50 h. X, Opaque; □, slightly opaque; ●, transparent

There seemed to be a difference between the equilibrium conditions of the transparent and the opaque samples. For the latter, a further difference was observed between samples submerged in the liquid water and those exposed to saturated water vapour only. The total amount of water retained in the opaque samples was no longer proportional to the partial pressure of water vapour, but proved to be a function of the total absolute pressure.

Three samples of pure polystyrene, one transparent, one slightly opaque and one opaque, were immersed in water at 80°C for two days and then transferred to a 50°C bath. The resultant weight loss as a function of time is shown in Figure 6. Interestingly, although the starting points were widely different, the three samples lost about equal amounts of water and reached a new equilibrium in about equal times.

Another glassy polymer, epoxy phenolic lacquer, is regularly subjected to hot water in practice. As coating material in tin cans it has to withstand sterilization. In certain cases (e.g. inadequate cure) white spots appear on the lacquer, a phenomenon known to the industry as 'blushing'. It is known that the part submerged in the water (100°C or higher but still below its T_g of about 140°C) exhibits more blushing than the part just above the water level, which is still in contact with the saturated vapour (see Figure 7).

Using an optical and an electron microscope we found that blushing is a result of the development of a large number of small voids (see Figure 8). These voids are not inherently present in the polymer but develop on sterilization. We have further established that just as with the polystyrene samples, as reported above, these voids appear on cooling the sample after its removal from the hot water. The voids remain after drying but heal if the sample is heated above its T_g .

DISCUSSION

It is evident from these experiments, that under certain conditions the diffusion of water in glassy polymers, such as polystyrene, can become non-Fickian. That is to say that the absorption curve is no longer sigmoid in shape, and an apparent diffusion constant, which could be calculated, would depend on the amount of water already absorbed (see Figure 4). This kind of behaviour has been recognized as such in the literature and many an explanation has already been offered. In the most general cases some kind of polymer/penetrant interaction²⁻⁶ or even swelling⁷⁻¹⁰ is postulated, whereas in others the general term 'active sites' is used¹¹. However, none of these theories can be applied to the polystyrene/water system.

It is more likely that in our systems the active site is nothing but a void^{14,17,18}. The existence of a submicroscopic network and free volume in glassy polymers is well established²¹⁻²³. There is further evidence to suggest the presence of local order and disorder²⁴⁻²⁶. To accommodate a water molecule, this hole must have a diameter of at least 3 Å. Since we observed no opacity in the pure polystyrene up to 80°C the diameter of the voids must be below 300 Å. Sarbolouki²⁷ measured the diffusion of water through cellulose acetate membranes of different porosities. He concluded that for 'true' diffusion the pore size should be 3-5 Å, and that above this value the diffusion constant should increase abruptly. However, using pore sizes up to 74 Å, he did not find any evidence of non-Fickian behaviour.

In our experiments the anomalous diffusion coincided with sample opacity, which we think points to the presence of discontinuities having a size of at least 300 Å. Anomalous diffusion and opacity have been linked before by others¹². Opacity or crazing in glassy polymers can be induced by mechanical stress²⁸⁻³⁰ or by a solvent^{8,9,31-33}. Drioli *et al.*¹⁵ induced crazing during diffusion measurements by applying pressure and measured its effect. If crazing is induced e.g. by creep even permanent gases behave anomalously in subsequent diffusion experiments¹⁶. Barrer and Barrie reported¹³ that crazing can result from clustering of water molecules during the experiment.

The term crazing is usually used to describe cavitation in the material due to local weakness as a result of tensile stress. It has been demonstrated that in glassy polymers these crazes contain, besides voids, continuous (oriented) polymeric material. The presence of such oriented matter in our samples has not been established, thus the use of the term craze in this context may be incorrect. Since the term 'solvent crazing' is so widely used, however, we felt justified in using the same term here.

In a non-homogeneous system permeability should be proportional to the concentration and the permeability of the individual components. This was confirmed for some systems³⁴ but not for others^{35,36}. Presumably, the adhesion and continuity at the interface play an important role. For the polystyrene with the polymeric additive we found that while the diffusion constant decreased the solubility had increased to values far above the level expected from its composition. We conclude that the dispersed particles had increased the voids content of the sample.

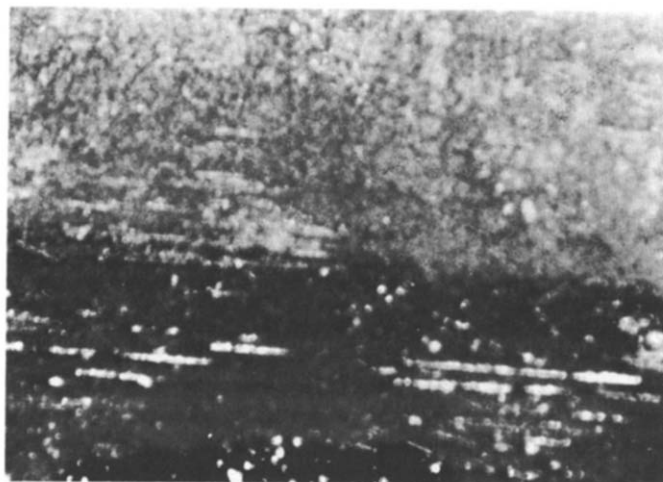


Figure 7 Optical micrograph of the border line in blushing lacquer. The darker part was submerged in liquid water, the lighter part was in contact with the saturated vapour only

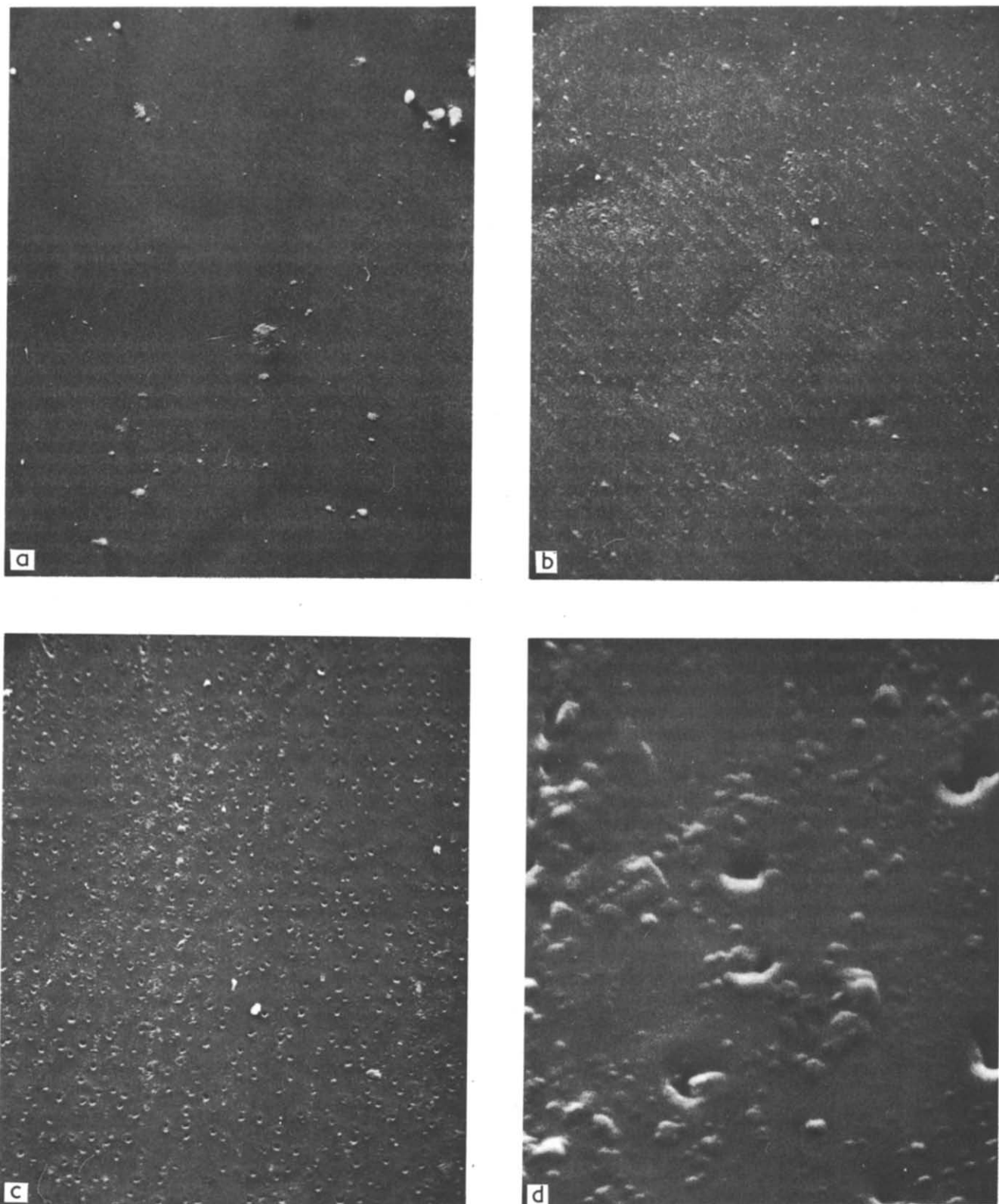


Figure 8 Electron micrographs of an undercured epoxy phenolic lacquer before and after sterilization in hot water. (a) Before sterilization, magnification 1000X; (b) after sterilization not submerged in water, magnification 1000X; (c) after sterilization submerged in water, magnification 1000X; (d) as for (c), magnification 10 000X

We further confirmed Barrer and Barrie's finding that crazing is caused by clustering of water in the pure polystyrene and epoxy resin samples. Our observations suggest the following mechanism: first the hot, absorbed water is dispersed in the polymer in units smaller than 300 \AA , then on rapid cooling the vapour pressure drops and the polymer attempts to eject the excess amount of water it holds. However, desorption is slow and in the meantime the surplus

water forms a second phase within the polymer. It agglomerates in places of least resistance and in near spherical shape to minimize its surface area. The holes created by the clusters remain as long as the polymer is in the glassy state.

It is known that mechanically crazed samples of polymers 'heal' when heated above their glass-transition temperature³⁷. We found the same to be true for 'absorption-

crazed' polymers. Above their glass transition temperature the mobility of polymer segments is restored and if the obstruction (i.e. absorbed water) has been removed the holes created by the forced deformation close permanently. If water is still present, it re-disperses and the sample becomes temporarily transparent again.

If the cycle of immersion in hot water and cooling is repeated some permanent damage is bound to occur, resulting in the creation of new holes and an increased water uptake in subsequent measurements. Thus *Figure 3* probably represents a polymer with a continuously increasing degree of crazing and solubility. As evidence in support of this hypothesis, we can report that some of the samples eventually developed visible cracks and broke up during an extended test.

It is difficult to be certain about where the non-Fickian process begins. In the pure polystyrene we first observed the development of a cobweb-like network of crazes. We believe this to represent the grain boundaries of individual polymer particles (extruded nibs) which were subsequently compression moulded. Evidently, the compression moulding process did not fully destroy the protection given by the oriented surface of the extruded particles.

The diffusion of water from the voids into the polymer remains Fickian, but the continuously increasing solubility suggests the overall process to be non-Fickian. The water in the crazes, whatever its quantity, is in thermodynamic equilibrium with its surroundings. The flow in and out of them is controlled by hydrostatic pressure differences and not by differences in partial pressure alone. This model may be used to explain the results of other workers^{38,39} who reported differences between diffusion of liquids and their vapours.

REFERENCES

- 1 Crank, J. 'The Mathematics of Diffusion', Clarendon Press, Oxford, 1957
- 2 Crank, J. and Park, G. S. 'Diffusion in Polymers', Academic Press, London, 1958, Ch 5
- 3 Narisawa, I. *J. Polym. Sci. (A-2)* 1972, **10**, 1789
- 4 Blackadder, D. A. and Keniry, J. S. *J. Appl. Polym. Sci.* 1973, **17**, 351

- 5 Jacques, C. H. M., Hopfenberg, H. B. and Stannett, V. *Polym. Eng. Sci.* 1973, **13**, 81
- 6 Clark-Monks, C. and Ellis, B. *J. Colloid Interface Sci.* 1973, **44**, 37
- 7 Yasuda, H. and Peterlin, A. *J. Appl. Polym. Sci.* 1973, **17**, 433
- 8 Deeg Jr, G. *Bell Lab. Rec.* 1947, **25**, 227
- 9 Russel, E. W. *Nature* 1950, **165**, 91
- 10 Chang, Y. J., Chen, C. T. and Tobalsky, A. V. *J. Polym. Sci. (Polym. Phys. Edn)* 1974, **12**, 1
- 11 Skirrow, G. and Young, K. R. *Polymer* 1974, **15**, 771
- 12 Crank, J. and Park, G. S. 'Diffusion in Polymers', Academic Press, London, 1968, Ch 8
- 13 Barrer, R. M. and Barrie, J. A. *J. Polym. Sci.* 1958, **28**, 377
- 14 Paul, D. R. *J. Polym. Sci. (A-2)* 1969, **7**, 1811
- 15 Drioli, E., Nicolais, L. and Ciferri, A. *J. Polym. Sci. (Polym. Chem. Edn)* 1973, **11**, 3327
- 16 Hosoi, H. and Findley, W. N. *Polym. Eng. Sci.* 1973, **13**, 225
- 17 Steen, S. A., Sen, S. K. and Rao, A. K. *J. Macromol. Sci. (B)* 1974, **10**, 507
- 18 Miyagi, Z. and Tanaka, H. *Polymer* 1975, **16**, 441
- 19 Braden, M. *Plast. Inst. Trans.* 1963, 83
- 20 Pogany, G. A. *J. Phys. (E)* 1968, **1**, 587
- 21 Ferry, J. 'Viscoelastic Properties of Polymers', Wiley, New York, 1961, p 411
- 22 Machin, D. and Rogers, C. E. *Makromol. Chem.* 1972, **155**, 269
- 23 Vieth, W. R. and Eilenberg, J. A. *J. Appl. Polym. Sci.* 1972, **16**, 945
- 24 Kargin, V. A. *J. Polym. Sci.* 1958, **30**, 247
- 25 Yeh, G. S. Y. *J. Macromol. Sci. (B)* 1972, **6**, 451
- 26 Brady, T. E. and Yeh, G. S. Y. *J. Macromol. Sci. (B)* 1973, **7**, 243
- 27 Sarbolouki, M. N. *J. Appl. Polym. Sci.* 1973, **17**, 2407
- 28 Berry, J. P. 'Fracture Processes in Polymeric Solids', (Ed. B. Rosen), Interscience, New York, 1964, Ch 2
- 29 Kambour, R. P. *J. Polym. Sci. (A-2)* 1966, **4**, 349
- 30 Menges, G. *Kunststoffe* 1973, **63**, 95
- 31 Andrews, E. H. and Bevan, L. *Polymer* 1972, **13**, 337
- 32 Earl, B. L., Lomeragen, R. J., Johns, J. H. T. and Crook, M. *Polym. Eng. Sci.* 1973, **13**, 390
- 33 Kambour, R. P., Aruner, C. L. and Romagosa, E. E. *J. Polym. Sci. (Polym. Phys. Edn)* 1973, **11**, 1879
- 34 Manson, J. A. and Chiv, E. H. *J. Polym. Sci. (Polym. Symp.)* 1973, **41**, 95
- 35 Clark-Monks, C. and Ellis, B. *J. Polym. Sci. (Polym. Phys. Edn)* 1973, **11**, 2089
- 36 Pritchard, G. and Taneja, N. *Composites* 1973, 199
- 37 Spurr, O. K. and Niegisch, W. D. *J. Appl. Polym. Sci.* 1962, **6**, 585
- 38 Yasuda, H. and Stannett, V. *J. Polym. Sci. (B)* 1963, **1**, 289
- 39 Sivadjian, J. and Ribeiro, D. *J. Appl. Polym. Sci.* 1964, **8**, 1403

Polyethylene and polytetrafluoroethylene crystals: chain folding, entropy of fusion and lamellar thickness

Alan E. Tonelli

Bell Laboratories, Murray Hill, New Jersey 07974, USA

(Received 14 January 1976; revised 17 February 1976)

Chain folding in polyethylene (PE) and in polytetrafluoroethylene (PTFE) crystallites is simulated on the computer in an attempt to determine if the large disparity in their lamellar thicknesses has its origin in any differences between their inherent abilities to fold. PE and PTFE chains of 6 to 15 carbon atoms are permitted to adopt each of their many rotational isomeric state (RIS) conformations, and each is checked for the presence of a chain fold. The conformational energetics of both polymers are used to calculate the probabilities of generating both randomly and adjacently re-entering chain folds. Depending on the RIS model adopted for PTFE, calculated probabilities for generating randomly re-entering folds are found to be comparable in PE and PTFE. Adjacently re-entering folds, however, are much more easily formed in PE than in PTFE. Despite the greater ease of folding PE chains, the relative energies required to create a unit area of chain fold are estimated to be nearly the same for both polymers in agreement with results obtained from the kinetic theory of chain folding. Consequently, in agreement with the recent proposal of Bassett and Davitt, it is concluded that the greater lamellar thickness of PTFE crystals is attributable exclusively to their lower entropy of fusion. An analysis of the possible reasons for the low entropy of fusion of PTFE is also presented.

INTRODUCTION

Melt crystallized polytetrafluoroethylene (PTFE) is unusual among crystalline polymers¹ with regard to its thick lamellae. Lamellar thicknesses of 1000–2500 Å are typically observed for PTFE, while by comparison polyethylene (PE) crystallized from the melt normally consists of lamellae 300–400 Å in thickness.

The disparity in lamellar thicknesses observed between melt crystallized PTFE and PE and its origin were recently the subjects of a study reported by Bassett and Davitt². They concluded that both polymers obey the kinetic theory of chain folding³, and PTFE derives its unusually thick lamellae from its low entropy of fusion.

The motivation for the present study of the inherent ability to fold PTFE and PE chains stems from the work of Bassett and Davitt². By comparing the probabilities of generating folds in PTFE and PE it is hoped that the underlying basis for the low entropy of fusion of PTFE, which results in a high melting temperature as well as thick lamellae, could be determined.

CALCULATION OF FOLD PROBABILITIES

Identical C–C bond lengths (1.53 Å) and C–C–C valence angles of 112° for PE and 116° for PTFE are adopted⁴ for PTFE and PE chains containing from 6 to 15 carbon atoms. The usual rotational isomeric state (RIS) model for PE is employed⁵. Each of the three staggered rotamers about each bond is permitted, with the two *gauche* rotational states ($g^\pm = \pm 120^\circ$) assigned an energy of $E_g^\pm = 500$ cal/mol higher than the *trans* state ($t = 0^\circ$). Neighbouring *gauche* states of opposite sign ($g^\pm g^\mp$) are allowed, but at a cost of $E_{gg}^\pm = 2.0$ kcal/mol.

Two different RIS models developed by Bates and Stockmayer^{6–8} for PTFE are adopted. The three-state model is identical to that described for PE except that $E_g^\pm = 700$ –1400 cal/mol and $E_{gg}^\pm > 4.0$ –5.0 kcal/mol. In the four-state model the *trans* rotational state is replaced by two states t^\pm symmetrically displaced by $\pm 15^\circ$ from the planar zig-zag. The $t^\pm g^\mp$, $g^\pm t^\mp$, and $g^\pm g^\mp$ states for neighbouring bonds are disallowed, and the $t^\pm g^\pm$, $g^\pm g^\pm$, and $t^\pm t^\mp$ states are assigned energies of 950, 950 and 1750 cal/mol, respectively, relative to the $t^\pm t^\pm$ and $g^\pm t^\pm$ states.

The RIS model of PE has been successful in predicting the dimensions and their temperature dependence⁵ and the constant volume entropy of fusion for PE⁹, the depolarized light scattering of n-alkanes¹⁰, and the dipole moments of the terminally substituted dibromo-n-alkanes¹¹ $\text{Br}-(\text{CH}_2)_n\text{Br}$. Because of the insolubility of PTFE experimental determination of the conformational characteristics of isolated PTFE chains is difficult. Instead, Bates and Stockmayer⁷ have measured the dipole moments of α,ω -dihydroperfluoroalkanes, $\text{H}-(\text{CF}_2)_n\text{H}$, with $n = 4, 6, 7, 8$ and 10. Their three- and four-state RIS models of PTFE, which were described above, successfully reproduce the experimental dipole moments of these α,ω -dihydroperfluoroalkanes.

A right-handed Cartesian coordinate system is defined with origin at the first carbon atom of the chain and the X-direction (same as C-axis in crystal) taken perpendicular to the H–C₁–H or F–C₁–F planes in the PE and PTFE chains, respectively. The positions of carbon atoms C₃ through C₁₅ in this reference frame are calculated for each of the RIS conformations generated. If the component of the C₆–C₁₅ position vectors along the X-axis is smaller than 0.3 to 0.5 Å, then a randomly re-entering fold is

assumed to have been formed provided the X -coordinates of the intervening atoms C_3-C_{14} are at least 1.0–1.3 Å above C_1 . This ensures that none of the atoms C_2-C_{n-1} in a C_1-C_n fold penetrate, or approach too closely, the crystal surface.

Each randomly re-entering fold generated above is tested further to determine whether or not it also belongs to the subgroup of adjacently re-entering folds. If the sum of the Y^2 and Z^2 components of the C_6-C_{15} position vectors is $\geq [ID - (0.3 \text{ to } 0.5 \text{ Å})]^2$ or $\leq [ID + (0.3 \text{ to } 0.5 \text{ Å})]^2$, where ID is the interchain separation in the crystal ($ID = 5.0 \text{ Å}$ for PE and 5.6 Å for PTFE)¹², then the fold formed is termed adjacently re-entering.

The 0.3 to 0.5 Å tolerances permitted in generating folds presumably corrects, at least partly, the artificial built in rigidity of the PE and PTFE chain models employed, i.e. the rigid valence angles and the perfect staggering of the rotational states.

A probability is calculated for each of the randomly and adjacently re-entering folds so generated. This is achieved by multiplying the pairwise dependent rotational state statistical weights $\mu_{\alpha\beta}$, where for bond i in state β and bond $i - 1$ in state α , $\mu_{\alpha\beta} = \mu_{i-1=\alpha, i=\beta} = \exp(-E_{\alpha\beta}/RT)$, for each of the $n - 2$ bond rotations in the n carbon atom

folds. This product of statistical weights is then divided by the sum of the products of statistical weights for every conformation (fold plus non-fold) possible for an n carbon atom chain, which is the configurational partition function. The resulting number is the fractional probability of forming a particular fold of n carbon atoms in length. The melting temperatures of PE and PTFE (140° and 330°C , respectively) are used in the calculation of the fold probabilities.

RESULTS AND DISCUSSION

Tables 1 and 2 contain the calculated fractional probabilities for forming folds of from 6 to 15 carbon atoms in PE and PTFE chains which re-enter the crystal surface in either a random or adjacent manner, respectively. The relative probabilities of forming randomly re-entering folds in PE and PTFE chains depend markedly on the RIS model adopted for PTFE. When the three-state RIS model is assumed for PTFE, the resulting fold probabilities are comparable to those calculated for randomly re-entering PE. On the other hand, the four-state model of PTFE leads to randomly re-entering fold probabilities much reduced from those calculated for PE.

Table 1 Fold probabilities for randomly re-entering PE and PTFE chains

Number of carbon atoms in fold	PE		PTFE			
	$\Delta X \leq 0.3 \text{ Å}$	$\Delta X \leq 0.5 \text{ Å}$	$\Delta X \leq 0.3 \text{ Å}$		$\Delta X \leq 0.5 \text{ Å}$	
			Three-state RIS model	Four-state RIS model	Three-state RIS model	Four-state RIS model
6	0.0243	0.0243	(0.0114–0.0281)	0.0	(0.0114–0.0281)	0.0
7	0.0165	0.0173	(0.0075–0.0152)	0.0	(0.0075–0.0152)	0.0
8	0.0164	0.0504	(0.0080–0.0172)	0.0	(0.0371–0.0501)	0.0
9	0.0135	0.0190	(0.0066–0.0131)	0.0018	(0.0090–0.0176)	0.0054
10	0.0089	0.0288	(0.0051–0.0093)	0.0009	(0.0233–0.0276)	0.0018
11	0.0093	0.0219	(0.0059–0.0094)	0.0029	(0.0160–0.0216)	0.0053
12	0.0064	0.0222	(0.0035–0.0062)	0.0016	(0.0216–0.0222)	0.0028
13	0.0060	0.0159	(0.0036–0.0059)	0.0031	(0.0127–0.0153)	0.0047
14	0.0053	0.0110	(0.0036–0.0052)	—	(0.0088–0.0105)	—
15	0.0052	0.0097	(0.0033–0.0052)	—	(0.0076–0.0093)	—

The range of probabilities in parentheses correspond to the range in $E_g^\ddagger = 700\text{--}1400 \text{ cal/mol}$

Table 2 Fold probabilities for adjacently re-entering PE and PTFE chains

Number of carbon atoms in folds	PE		PTFE			
	$\Delta X \leq 0.3 \text{ Å}^a$	$\Delta X \leq 0.5 \text{ Å}^b$	$\Delta X \leq 0.3 \text{ Å}^a$		$\Delta X \leq 0.5 \text{ Å}^b$	
			Three-state RIS model	Four-state RIS model	Three-state RIS model	Four-state RIS model
6	0.0243	0.0241	(0.0)	0.0	(0.0)	0.0
7	0.0	0.016	(0.0)	0.0	(0.008–0.014)	0.0
8	0.0010	0.0010	(0.0)	0.0	(0.0)	0.0
9	0.0021	0.0060	(0.000 06–0.000 08)	0.000 66	(0.001–0.002)	0.000 66
10	0.0031	0.0041	(0.0)	0.0	(0.0)	0.000 50
11	0.000 49	0.0020	(0.000 44–0.000 71)	0.0	(0.000 60–0.001 20)	0.0
12	0.000 63	0.000 82	(0.0)	0.000 010	(0.000 04–0.000 20)	0.000 19
13	0.000 51	0.0012	(0.000 22–0.000 34)	0.000 059	(0.000 22–0.000 31)	0.000 07
14	0.000 51	0.0010	(0.000 000 1– 0.000 000 4)	—	(0.000 54–0.000 68)	—
15	0.000 31	0.000 50	(0.000 23–0.000 32)	—	(0.000 29–0.000 41)	—

^a $(Y^2 + Z^2) \leq (ID + 0.3)^2$ or $\geq (ID - 0.3)^2$; ^b $(Y^2 + Z^2) \leq (ID + 0.5)^2$ or $\geq (ID - 0.5)^2$.

* The range of probabilities in parentheses correspond to the range $E_g^\ddagger = 700\text{--}1400 \text{ cal/mol}$

Table 3 Comparison of the entropies of fusion* of PE and PTFE

Polymer	ΔS_f	$(\Delta S_f)_v$	ΔS_v	ΔS_{conf}
PE	2.34	1.82	0.52	1.76
PTFE	1.14	0.77	0.37	1.60

* All entropies are given in eu/mol of repeat units (CH_2 or CF_2)

In contrast to the behaviour of the randomly re-entering folds, the probabilities of forming adjacently re-entering PE folds are considerably greater than the probabilities calculated for adjacently re-entering PTFE folds. This disparity in adjacently re-entering fold probabilities is independent of the *RIS* model adopted for PTFE.

Since it is becoming increasingly evident^{3,12-15} that the primary mode of folding in polymer chain crystals is the adjacent re-entry of portions of the same polymer chain, we restrict our attention to the probabilities calculated for adjacently re-entering folds. If the disparity in the fold probabilities calculated for PE and PTFE chains is interpreted in terms of differences in fold energy, q , in kcal/mol of folds, then it is possible to conclude from the probabilities presented in Table 2 that $q(\text{PTFE}) \geq 1.5q(\text{PE})$. This conclusion is based on the assumption that the fold probability is proportional to the Boltzmann factor of q at the melting temperature.

The fold energy, or work required to form a fold, q constitutes an important ingredient in the kinetic theory of chain folding³. Of direct concern here is the relation between the lamellar thickness l and the fold energy q . In the kinetic theory of chain folding³:

$$l = \frac{2\sigma_{\text{eff}}}{\Delta S_f \Delta T} + \delta l \quad (1)$$

and

$$\sigma_{\text{eff}} = \sigma + \frac{q}{2A_0} \quad (2)$$

where ΔS_f is the entropy of fusion per unit volume of the crystal, ΔT is the undercooling, σ is to a good approximation the lateral surface free energy of the polymer crystal, δl is nearly constant at 10–40 Å, and A_0 is the cross-sectional area of a chain in the crystal. Since for most polymer crystals³ $\sigma \ll q/2A_0$:

$$l \approx \left(\frac{q}{A_0 \Delta S_f \Delta T} \right) \quad (3)$$

From an analysis of lamellar thickness *versus* undercooling data, fold energies of 5 and 7.5 kcal/mol of fold have been obtained for PE and PTFE³, respectively. In other words it was found that $q(\text{PTFE}) = 1.5q(\text{PE})$ in kcal/mol of fold which is not inconsistent with the difference in fold energies derived here from the calculated fold probabilities.

Division of q by the cross-sectional area of a chain in the crystal A_0 leads to nearly identical ratios q/A_0 for PE and PTFE. As stressed by Bassett and Davitt² this means (see equation 3) that at a given undercooling the difference in the lamellar thicknesses observed for PE and PTFE crys-

tals grown in the bulk is directly attributable to the difference in their per unit volume entropies of fusion i.e. $\Delta S_f(\text{PE}) \approx 3.0 \Delta S_f(\text{PTFE})$. Thus, even though the inherent abilities of PE and PTFE to fold in adjacently re-entering fashion differ greatly, when they are translated into fold energies q and divided by fold area $2A_0$ the closely similar values of $(q/2A_0)$ obtained for both polymers eliminates them as the principal source of the disparity in lamellar thicknesses.

Turning finally to the difference in the entropies of fusion of PE and PTFE, which Bassett and Davitt² and we believe to be the sole source of the disparity in their lamellar thicknesses, it may be worthwhile to devote a few comments to the most likely sources of this entropy difference. When the entropies of fusion¹⁶ for PE and PTFE expressed per mole of repeat units, i.e. 2.34 and 1.14, respectively, are converted to a per unit of crystalline volume basis, the two-fold disparity is further magnified to over a three-fold difference, i.e. 0.167 eu/cm³ (PE) and 0.0502 eu/cm³ (PTFE). Even if the molar entropies of fusion were identical for PE and PTFE, the smaller molar density of the PTFE crystal would still result in a smaller volume entropy of fusion for PTFE and larger lamellae according to equation (3).

The entropy of fusion ΔS_f may be divided into two separate contributions¹⁷, the constant volume $(\Delta S_f)_v$ and the volume expansion ΔS_v entropies of fusion. Each of these contributions for PE and PTFE is listed in Table 3. Furthermore it has been demonstrated^{9,18} for a wide variety of polymers that the constant volume contribution $(\Delta S_f)_v$ is closely approximated by the gain in intramolecular (intra-chain) conformational entropy ΔS_{conf} experienced by each polymer chain upon melting. ΔS_{conf} can be calculated^{9,18} from the *RIS* model of a polymer chain, such as the three- and four-state models used to calculate the fold probabilities of PE and PTFE, by assuming that each polymer chain in the crystal is restricted to a single conformation. When applied to PE and PTFE the conformational entropies obtained are those shown in the final column of Table 3.

For PE $(\Delta S_f)_v \approx \Delta S_{\text{conf}}$, while for PTFE $(\Delta S_f)_v \approx \frac{1}{2}(\Delta S_{\text{conf}})$. Upon melting, half of the conformational entropy gain expected for the PTFE chains is not realized resulting in a total entropy of fusion significantly lower than that of PE and a larger lamellar thickness as well. Either the PTFE chains in the melt are partly ordered, preventing the complete achievement of the *RIS* entropy, or some conformational disorder exists in the crystal resulting in a non-zero conformational entropy for the crystalline PTFE chains. Based on statistical thermodynamic arguments¹⁹ and recently reported suggestions²⁰ of conformational isomorphism in PTFE crystals, we believe that conformational disordering* of the crystalline PTFE chains to be the most probable cause of the observed loss in conformational entropy upon melting.

In combination, the lower molar density of and probable conformational disorder in PTFE crystals are sufficient to cause the necessary reduction in the per unit volume entropy of fusion which leads to their increased lamellar thickness.

* Conformational disordering of the PTFE chains in the crystal is to be distinguished from the rotation and/or translation of rigid chains known²¹⁻²⁴ to occur in PTFE crystals below the melting point which serve to reduce the volume expansion entropy of fusion ΔS_v , but not the constant volume contribution $(\Delta S_f)_v$.

ACKNOWLEDGEMENT

Thanks are due to H. Schonhorn for bringing the subject of this paper to the author's attention.

REFERENCES

- 1 Bunn, C. W., Cobbold, A. J. and Palmer, R. P. *J. Polym. Sci.* 1959, **9**, 385
- 2 Bassett, D. C. and Davitt, R. *Polymer* 1974, **15**, 721
- 3 Hoffman, J. D., Davis, G. T. and Lauritzen, J. I. 'Treatise of Solid State Chemistry', (Ed. N. B. Hannay), Plenum Press, New York, 1976, Vol 3, Ch 6
- 4 Bowen, H. T. M. and Sutton, L. E. 'Tables of Interatomic Distances and Configurations in Molecules and Ions', The Chemical Society, London, 1958; Supplement, 1965
- 5 Abe, A., Jernigan, R. L. and Flory, P. J. *J. Am. Chem. Soc.* 1966, **88**, 631
- 6 Bates, T. W. *Trans. Faraday Soc.* 1967, **63**, 1825
- 7 Bates, T. W. and Stockmayer, W. H. *J. Chem. Phys.* 1966, **45**, 2321; *Macromolecules* 1968, **1**, 12
- 8 Stockmayer, W. H. and Bates, T. W. *Macromolecules* 1968, **1**, 17
- 9 Tonelli, A. E. *J. Chem. Phys.* 1970, **52**, 4749
- 10 Patterson, G. D. and Flory, P. J. *Trans. Faraday Soc.* 1972, **68**, 1098
- 11 Leonard, W. J., Jernigan, R. L. and Flory, P. J. *J. Chem. Phys.* 1965, **43**, 2256
- 12 Wunderlich, B. 'Macromolecular Physics', Academic Press, New York, 1973, Vol 1, Ch 3
- 13 Bank, M. J. and Krimm, S. *J. Polym. Sci. (A-2)* 1969, **7**, 1785
- 14 Ching, J. H. C. and Krimm, S. *Macromolecules* 1972, **5**, 209; *ibid* 1975, **8**, 894; *Bull. Am. Phys. Soc.* 1975, **20**, 283; *Polym. Prepr.* 1975, **16**, 407
- 15 Krimm, S. 'Proc. Symp. Macromolecules, Rio de Janeiro, July 1974'. (Ed. E. B. Mano), Elsevier, New York, 1974, p 107
- 16 Starkweather, Jr. H. W. and Boyd, Jr. R. H. *J. Phys. Chem.* 1960, **64**, 410
- 17 Mandelkern, L. 'Crystallization of Polymers', McGraw-Hill, New York, 1964, Ch. 6
- 18 Tonelli, A. E. 'Analytical Calorimetry', (Eds. R. S. Porter and J. F. Johnson), Plenum Press, New York, 1974, Vol 3, p 89
- 19 Flory, P. J. *Proc. R. Soc. (A)* 1965, **234**, 60
- 20 Corradini, P. *J. Polym. Sci. Polym. Symp.* 1975, **50**, 327; *ibid* 1975, **51**, 1
- 21 Slichter, W. P. *J. Polym. Sci.* 1957, **24**, 173
- 22 Hyndman, D. and Origlio, G. F. *J. Appl. Phys.* 1960, **31**, 1849
- 23 McBrierty, V. J., McCall, D. W., Douglass, D. C. and Falcone, D. R. *J. Chem. Phys.* 1970, **52**, 512; *Macromolecules* 1971, **4**, 584
- 24 McCall, D. W. *Acc. Chem. Res.* 1971, **4**, 223

Composition of rubber/resin adhesive films: 1. Surface composition as determined by ATR spectroscopy

R. S. Whitehouse and P. J. C. Counsell
Evode Holdings Ltd, Stafford ST16 3EH, UK

and G. Lewis

Department of Physical Sciences, Wolverhampton Polytechnic, Wolverhampton WV1 1LY, UK
(Received 5 March 1976)

Determination by ATR infra-red spectroscopy of the chemical composition of the surfaces of rubber/resin adhesive films is described. An excess concentration of resin at the surfaces compared with the bulk is found, this being shown to be dependent on the solvent, the overall bulk concentration of resin, the thickness of the film and time of equilibration. A proposed qualitative mechanism explains the appearance of the concentration profile in terms of the solubility characteristics of the system and the evaporation rate of the solvent.

INTRODUCTION

Modern adhesive systems of the pressure sensitive type are based on mixtures of several components, the exact formulations generally being based on empirical knowledge. The compatibility of the components is largely unknown and the phase structure of such systems has received comparatively little study¹⁻⁵. In addition, many of these adhesives are solvent based, i.e. the adhesive components are dissolved in a solvent which is used as a carrier to assist in the application of a thin film of the adhesive to the substrate. The solvent subsequently evaporates leaving the adhesive film on the substrate. Although the system may be a homogeneous solution at the normal solvent concentrations, during the evaporation stage any incompatibility within the mixture will become evident, and the nature of the solvent and the evaporation conditions might be expected to influence the final structure of the adhesive film. Incompatibility between the components in the adhesive might be expected to lead to a surface composition which is not identical with that of the bulk. Recent evidence⁶ has shown that solvent evaporation from thin films can give fractionation of incompatible components. A knowledge of the surface composition of adhesive films seems fundamental to an understanding of the mechanism of adhesive bond formation and failure, since it is the surface properties of the films which are of critical importance in this context.

A two component adhesive system was chosen, closely approximating to current industrial practice, consisting of natural rubber and a commercially available tackifying resin (glycerol ester of partly hydrogenated wood rosin). The function of the resin is to plasticize the rubber, and enable the adhesive to adhere easily to a wide variety of substrates. The maximum ability to adhere as measured by the tack energy⁷ may be developed in this type of adhesive with high loadings of the resin (up to 80% by volume). The pure resin is a brittle, glassy solid. The rubber and resin mixtures were dissolved in a variety of solvents, films were cast and the solvent allowed to evaporate; the chemical

composition of the film at the air/adhesive and adhesive/substrate interfaces was examined by internal reflection infra-red spectroscopy (ATR).

ATR has been used extensively to study qualitatively the chemical composition of surfaces of polymeric materials such as paint films^{8,9} and the chemical reactions occurring at the surfaces of such films under the influence of various environments¹⁰⁻¹². One of the problems inherent with quantitative analysis by ATR is obtaining consistent contact efficiency between the surface of the film and the internal reflection crystal. To overcome this, an internal standard was used, thus calibration curves were prepared by relating the intensity of a concentration dependent absorption to the intensity of an absorption which was not sensitive to changes in composition.

An examination of the fundamentals of the theory of ATR¹³ shows that the totally reflected beam from the crystal/adhesive interface penetrates the adhesive film, and the depth of penetration (dp), perpendicular to the interface, of the evanescent wave is given by Harrick¹³ as:

$$dp = \frac{\lambda}{2\pi n_1} (\sin^2\theta - n_{21}^2)^{-1/2} \quad (1)$$

where λ is the wavelength of the radiation in air, θ is the angle of incidence and n_{21} is the ratio of the refractive indices of the crystal (n_1) and the sample (n_2). The evanescent wave is selectively attenuated according to the infra-red activity of the sample in the region from the surface to a depth dp . Thus by varying θ or λ different depths of penetration into the sample may be achieved, and hence the variation of chemical composition of surface layers of varying thickness may be examined.

EXPERIMENTAL

Materials

Natural rubber. $\bar{M}_n = 736\,800$ g/mol; $\bar{M}_w = 927\,600$ g/mol; relative density = 0.900 at 293K.

Purification technique. The rubber was dissolved in

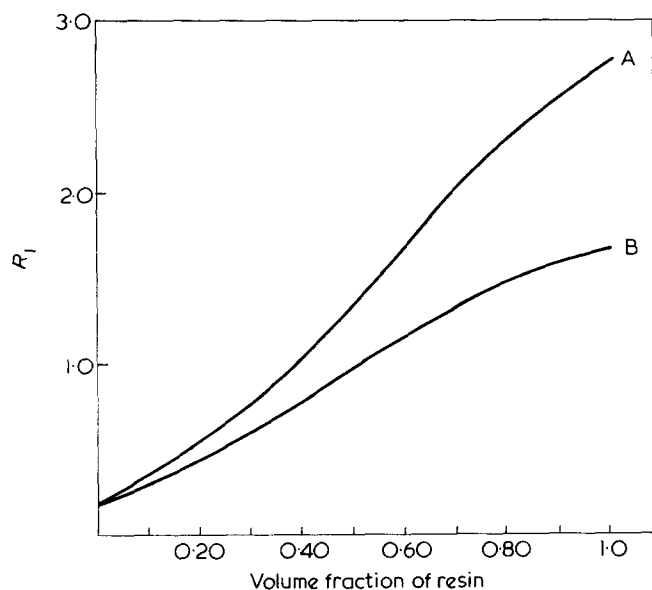


Figure 1 Ratio R_1 of absorption intensities at $5.78 \mu\text{m}$ (A) and $8.13 \mu\text{m}$ (B) to the internal standard absorption at $6.90 \mu\text{m}$ plotted against volume fraction of resin on the crystal surface

toluene (1–2 mass percent concentration), filtered through a No. 4 glass sinter to remove insoluble impurities. The natural rubber was then precipitated by adding excess acetone, filtered and dried to constant mass in a vacuum desiccator at 5 Torr and $293 \pm 2\text{K}$.

Resin. Staybelite Ester 10 (Hercules Powder Co.) glycerol ester of partly hydrogenated wood rosin which consisted of approximately 84% diester and 16% triester. $\bar{M}_n = 993 \text{ g/mol}$; relative density 1.066 at 293K ; softening point (Ring and Ball¹⁴) 358.5K .

Solvents. Analar grade reagents used without further purification.

ATR INFRA-RED SPECTRA

Spectra of the adhesive surfaces were obtained by use of a Perkin–Elmer model 457 grating infra-red spectrophotometer fitted with a Wilks model 9 multiple internal reflectance attachment. A KRS-5 crystal (eutectic mixture of thallos bromide and iodide) of width 20 mm and length 50 mm was used, having a 45° entrance and exit face, giving up to 25 reflections. This system gave a maximum transmission through the internal reflectance attachment corresponding to 35–45% of the intensity of the unattenuated reference beam. All spectra were obtained using a medium scan rate, which required approximately 15 min to scan from 4000 cm^{-1} ($2.5 \mu\text{m}$) to 250 cm^{-1} ($40 \mu\text{m}$).

The method was calibrated by casting separate films of pure rubber and pure resin in toluene onto adjacent areas of the same crystal. The solvent was allowed to evaporate completely under ambient temperature conditions ($293 \pm 2\text{K}$). By varying the length of the rubber and resin films (constant film width of 20 mm) various area ratios could be obtained. Thus spectra corresponding to the whole composition range were recorded. Two concentration-dependent absorptions were selected, at 1730 cm^{-1} ($5.78 \mu\text{m}$) and 1230 cm^{-1} ($8.13 \mu\text{m}$), both associated with the ester linkage of the resin. An absorption at 1450 cm^{-1} ($6.90 \mu\text{m}$) was selected as the internal standard, since the intensity of this absorption (due to the methyl, methylene and methyne bending vibrations, present in both resin and rubber) was not significantly concentration-dependent. The ratios R ,

of the absorption intensities at 1730 cm^{-1} and 1230 cm^{-1} to the internal standard absorption intensity at 1450 cm^{-1} are plotted against the percentage by area of resin on the crystal surface in Figure 1. The standard deviations in R , are within $\pm 0.2\%$.

The compositions of the adhesive films at the adhesive/substrate interface were examined by casting mixtures of rubber and resin dissolved in solvent (2.3% by mass) directly onto the KRS-5 crystal and allowing the product to evaporate completely under ambient conditions ($293 \pm 2\text{K}$). By controlling the concentration and volume of the solutions used for a given area of crystal, a constant dry film thickness of $5.20 \mu\text{m}$ was produced, and used for all measurements except where otherwise stated. The spectrum of the adhesive film was scanned as soon as all the solvent had evaporated from the film, usually within 20 min (the retained solvent concentration was less than $10^{-3}\%$). The ratios of the absorption intensities at 1730 cm^{-1} and 1230 cm^{-1} to the absorption intensity at 1450 cm^{-1} were calculated and hence the volume fraction of resin in the surface layer was found by reference to the calibration curves (Figure 1).

The compositions of the adhesive films at the adhesive/air interface were examined by casting the adhesive solutions onto an inert support film and laminating the dry film to the KRS-5 crystal. The intensity of the spectrum obtained in this manner was significantly affected by the modulus of the film and the lamination pressure, but the use of an internal standard removed the problems normally associated with variable contact efficiency.

Measurements were made using an internal reflection angle of 45° . The refractive indices of rubber and resin were measured by the usual methods in the visible region of the electromagnetic spectrum and equation (1) used to calculate the depth of penetration, dp . The depths of penetration dp corresponding to the concentration-dependent absorption at wavelengths, λ , of $5.78 \mu\text{m}$ (1730 cm^{-1}) and $8.13 \mu\text{m}$ (1230 cm^{-1}), were calculated to be $1.33 \mu\text{m}$ and $1.87 \mu\text{m}$ respectively.

Since the refractive indices of the rubber and resin may vary with the wavelength of the radiation, the depth of penetration was confirmed experimentally. Films of rubber of known thickness were cast onto a poly(ethylene terephthalate) support film and laminated onto the crystal face. The spectrum of the backing film was visible at $5.78 \mu\text{m}$ (ester absorption) when viewed through a $1.30 \mu\text{m}$ thick rubber film, but was not visible through a $1.35 \mu\text{m}$ thick film. This indicated that the depth of penetration at a wavelength of $5.78 \mu\text{m}$ was between $1.30 \mu\text{m}$ and $1.35 \mu\text{m}$; which is in good agreement with the theoretical value of $1.33 \mu\text{m}$.

All experimental data represent the mean of twelve spectra recorded for each composition. This procedure was used to compensate for random variations in the spectrum due to fluctuations in environmental conditions.

RESULTS AND DISCUSSION

The system was dissolved in toluene and investigated most thoroughly since this is a solvent often used in industrial practice. In all cases, adhesive films prepared from toluene solutions gave spectra which indicated a higher concentration of resin at the surface than the overall resin concentration for the whole film, based on the known masses of rubber and resin in the initial solution. The results are most

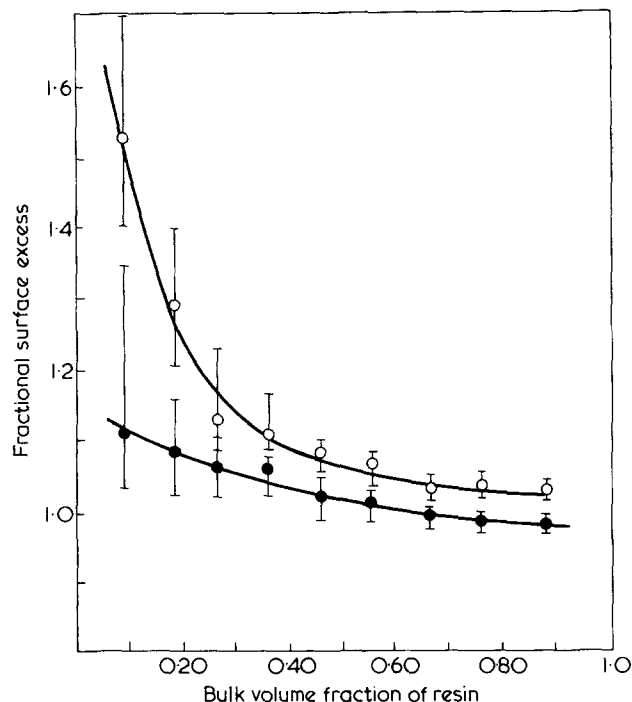


Figure 2 Fractional surface excess of resin for 5.2 μm films cast from toluene solutions for two depths of penetration: 1.33 μm (○); 1.87 μm (●)

easily displayed by defining a fractional surface excess i.e.

fractional surface excess =

$$\frac{\text{observed surface layer volume fraction of resin}}{\text{overall bulk volume fraction of resin}} \quad (2)$$

Figure 2 shows the variation in fractional surface excess with bulk volume fraction of resin for films cast from toluene solutions, using two depths of penetration of the radiation. Representative mean deviations are shown. The results were identical, within experimental uncertainties, for both the adhesive/substrate and the air/adhesive interfaces. It can be seen (a) that the fractional surface excess decreases as the bulk volume fraction of resin increases; (b) that the fractional surface excess decreases as the depth of penetration of the radiation increases.

These observations are consistent with the view that at the surface itself, there is an excess of resin for all compositions. It must be appreciated that the ATR technique is giving concentration data characteristic of surface layers of thicknesses which are not negligible compared with the total thickness of the adhesive film (5.20 μm). The results presented in Figure 2 suggest that in the dry adhesive film there exists a concentration gradient of resin varying from a maximum at each interface to a minimum at the centre of the film.

Figures 3 and 4 show the results obtained for the fractional surface excess of resin as a function of the bulk volume fraction of resin for films of increased thickness (11.40 μm), compared to the previous data of Figure 2. As the film thickness is increased, so the surface excess concentration of resin decreases.

The possibility that interactions between the rubber and resin cause changes in absorption intensities or the ratio of absorption intensities was investigated. Films of known thickness of pure resin and pure rubber were cast from

toluene solution onto each face of a rock salt plate. The transmission spectrum of this combination was recorded and compared with the transmission spectrum of a mixture of rubber and resin cast from solutions onto a single face of the rock salt plate. Both spectra thus measured the absorptions of identical amounts of rubber and resin, in one case without any possible interactions and in the other case with interactions possible. The spectra were identical within experimental uncertainties, showing that interactions between rubber and resin in the dry film do not cause spurious effects which might have suggested an excess of resin at the interface.

In order to assess the influence of the chemical and physical properties of the solvents on the composition of the surface layer of adhesive films, the volume fraction in the surface layers was measured for a wide range of solvents for five overall bulk resin compositions at two depths of penetration (Table 1) for 5.20 μm thick films. In all cases the data refer to both adhesive/substrate and air/adhesive interfaces, with no significant differences in composition being

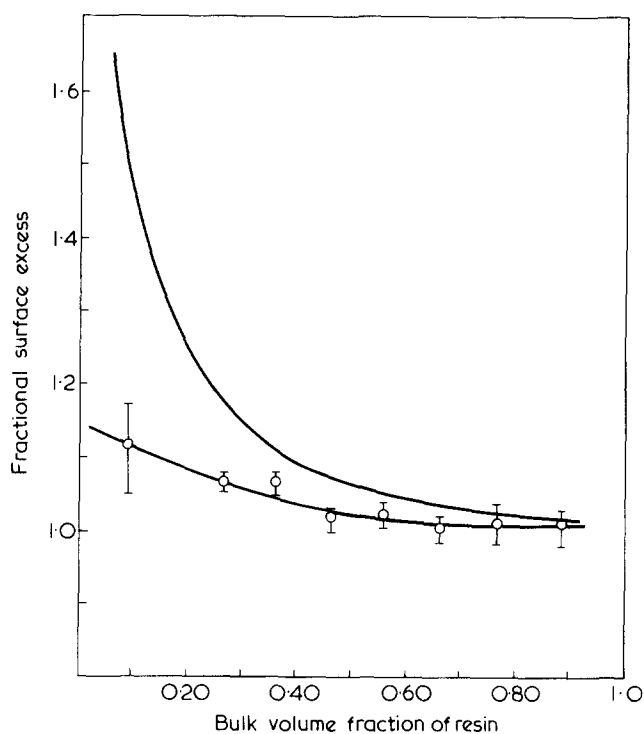


Figure 3 Fractional surface excess for 11.4 μm films cast from toluene solutions, for the depth of penetration 1.33 μm (○). —, represent results obtained for the 5.2 μm films

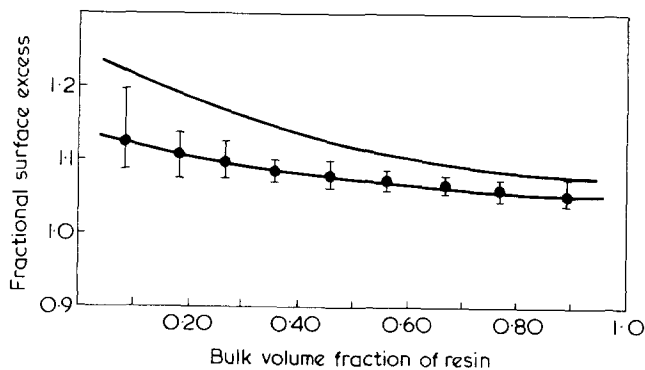


Figure 4 Fractional surface excess for 11.4 μm films cast from toluene solutions for the depth of penetration 1.87 μm (●). —, represent the results obtained for the 5.2 μm films

Table 1 Effect of various solvents on the concentration of resin in the surface layers for two depths of penetration

Solvent	Depth of penetration (μm)	Observed volume fraction of resin in surface layer for overall volume fractions of resin				
		0.086	0.266	0.458	0.664	0.884
Dichloromethane	1.33	0.121	0.361	0.569	0.771	0.947
	1.87	0.098	0.332	0.524	0.732	0.842
Chloroform	1.33	0.102	0.312	0.524	0.762	0.937
	1.87	0.081	0.265	0.466	0.623	0.860
Carbon tetrachloride	1.33	0.096	0.267	0.506	0.723	0.927
	1.87	0.079	0.226	0.457	0.622	0.843
Benzene	1.33	0.117	0.337	0.512	0.757	0.981
	1.87	0.090	0.301	0.437	0.640	0.819
Toluene	1.33	0.132	0.290	0.513	0.689	0.934
	1.87	0.095	0.286	0.466	0.659	0.884
Xylene	1.33	0.101	0.321	0.537	0.762	0.974
	1.87	0.080	0.274	0.440	0.609	0.781
Chlorobenzene	1.33	0.110	0.313	0.521	0.753	0.974
	1.87	0.090	0.265	0.460	0.626	0.781
Trichloroethylene	1.33	0.098	0.303	0.511	0.729	0.950
	1.87	0.086	0.277	0.450	0.628	0.832
1,2-Dichloroethane	1.33	0.142	0.351	0.543	0.745	0.972
	1.87	0.111	0.307	0.485	0.651	0.809
1,1,1-Trichloroethane	1.33	0.120	0.349	0.544	0.744	0.987
	1.87	0.087	0.295	0.473	0.648	0.840
1,1,2,2-Tetrachloroethane	1.33	0.102	0.307	0.490	0.759	0.914
	1.87	0.078	0.272	0.458	0.643	0.862

shown between the two interfaces. The general pattern of the results followed those shown in *Figure 1* for toluene. At least for the lower depth of penetration, all systems show an excess of resin in the interfacial layer, with the fractional surface excess of resin decreasing with increasing overall volume fractions of resin in the mixture. The absolute values of the fractional surface excesses of resin and their dependence on the overall concentration of the mixture are seen to be dependent on the solvent used in the film forming operation.

Since it has been shown that the fractional surface excess of resin is identical at either interface, and that it decreases with increasing depth of the surface layer, the volume fraction of resin, y , may be assumed to follow a simple parabolic relationship as a function of film thickness, x , having a minimum at $x = 0$, the centre of the film, and maxima at the film interfaces $-x_{\text{min}}$ and $+x_{\text{max}}$ (*Figure 5*). It may be seen from *Figure 4* that the experimentally observed volume fractions y_1, y_2, y_1^1 and y_2^1 represent the mean volume fractions with layers of thickness $(x_{\text{max}} - x_1), (x_{\text{max}} - x_2)$ etc. The mean bulk concentration for the film is y_{av} . The simplest equation for this parabolic relationship is:

$$y = ax^2 + b \quad (3)$$

where a and b are constants. Integration with respect to x gives:

$$\int y dx = \int (ax^2 + b) dx \quad (4)$$

Now

$$\int_{x_1} y dx = y_1(x_{\text{max}} - x_1) \quad (5)$$

Hence:

$$\int_{y_1}^{x_1} (x_{\text{max}} - x_1) = \left[\frac{ax^3}{3} + bx \right]_{x_1}^{x_{\text{max}}} \quad (6)$$

A further two equations may be obtained by considering the integrals between x_{max} and x_2 , and x_{max} and x_1 . Insertion of the known values of y_{av}, x_1, x_2 and x_{max} and the experimentally determined values of y and y_2 yield three equations and two unknowns a and b . Optimum values of a and b are thus calculated, from which may be calculated the volume fraction of resin at the interfaces y_{max} , and at

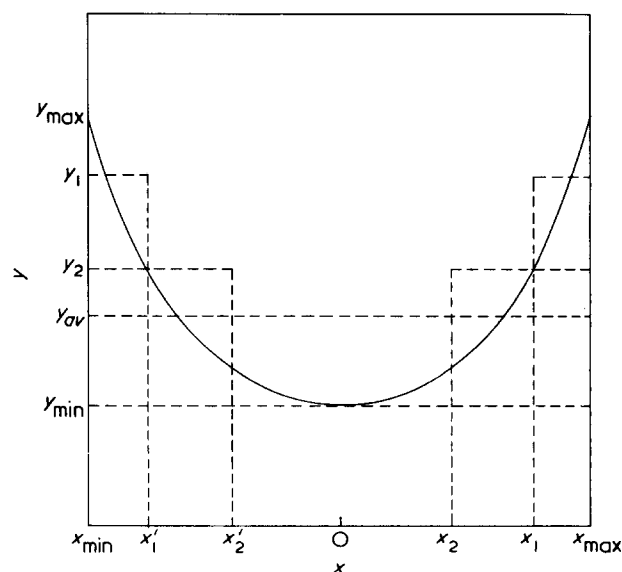


Figure 5 Variation of volume fraction of resin, y , as a function of the distance, x , from the central plane of the film

Table 2 Surface (y_{\max}) and centre (y_{\min}) volume fractions of resin for various mean compositions (y_{av}) related to solvents and their properties

Solvent	Vapour pressure (mmHg)	Cohesive energy density $\times 10^8$ (J/m ³)		y_{av}				
				0.086	0.266	0.458	0.664	0.884
Dichloromethane	437	406	y_{\max}	0.192	0.475	0.743	0.929	1.119
			y_{\min}	0.026	0.191	0.332	0.550	0.638
Chloroform	194	349	y_{\max}	0.154	0.437	0.685	0.998	1.083
			y_{\min}	0.036	0.151	0.312	0.400	0.736
Carbon tetrachloride	115	308	y_{\max}	0.130	0.374	0.584	0.815	1.102
			y_{\min}	0.051	0.153	0.382	0.550	0.704
Benzene	95	349	y_{\max}	0.167	0.461	0.652	0.966	1.304
			y_{\min}	0.040	0.170	0.317	0.455	0.554
Toluene	29	332	y_{\max}	0.207	0.334	0.601	0.746	1.048
			y_{\min}	0.019	0.236	0.377	0.606	0.801
Xylene	8	324	y_{\max}	0.140	0.410	0.708	1.060	
			y_{\min}	0.046	0.185	0.287	0.360	
Chlorobenzene	12	376	y_{\max}	0.149	0.389	0.620	0.992	1.386
			y_{\min}	0.051	0.192	0.363	0.422	0.458
Trichloroethylene	76	352	y_{\max}	0.117	0.365	0.615	0.925	1.220
			y_{\min}	0.068	0.213	0.355	0.464	0.614
1,2-Dichloroethane	82	400	y_{\max}	0.238	0.498	0.685	0.906	1.308
			y_{\min}	0.009	0.150	0.338	0.505	0.540
1,1,1-Trichloroethane	125	384	y_{\max}	0.173	0.489	0.683	0.911	1.264
			y_{\min}	0.035	0.149	0.332	0.498	0.604
1,1,2,2-Tetrachloroethane	8	394	y_{\max}	0.148	0.373	0.540	0.963	1.018
			y_{\min}	0.039	0.206	0.409	0.461	0.777

the centre of the film y_{\min} .

The maximum and minimum resin concentrations for 5.20 μm films, calculated in the manner described above, are presented in Table 2, in which the vapour pressure and cohesive energy densities of the solvents are also tabulated. Within the limits of the assumption of a parabolic dependence of y on x , the y_{\min} and y_{\max} values are estimated to be accurate to within $\pm 2\%$ of y . The calculated resin concentration at the interface often exceeds a volume fraction of unity for an average resin concentration of 0.884. This suggests that the surface of the film consists entirely of resin to some depth.

The results in Table 2 confirm that there are considerable differences in the composition of the interfaces of an adhesive film compared with the composition of the central plane of the film when first produced. However, when the films were allowed to equilibrate for approximately 500 days, the surface compositions of the film became identical to the overall bulk compositions. This indicates that the heterogeneity of such adhesive films is a consequence of the solvent evaporation stage, and that subsequent diffusion within the film will equalize the composition throughout the film. It can therefore be appreciated that adhesive properties of such films are likely to be appreciably time-dependent if equilibration has not been attained subsequent to film formation. Under the normal industrial conditions in which such adhesives are used, it is unlikely that they will be left for such a period before being used for bonding purposes. It is therefore necessary to propose a mechanism of film formation by solvent evaporation which would account for the concentration profile. The initial solution, containing solvent, rubber and resin may be assumed to be homogeneous. As the solvent is lost, the concentration of rubber and resin increases. As the resin has a higher cohesive energy density ($4.16 \times 10^8 \text{ J/m}^3$ compared with $2.94 \times 10^8 \text{ J/m}^3$) it is likely that the rubber and resin are incompatible to some extent. Hence the resin will act as a non-solvent for the rubber. Under these conditions, the rubber-rich phase is

likely to precipitate out of solution first, as a consequence of the lower contribution to the free energy of mixing with the solvent for a given volume of high molar mass rubber compared with an equal volume of low molar mass resin. Since the density of the natural rubber is less than that of the resin any tendency to settling out will favour movement of the resin plus solvent phase downwards towards the substrate interface, leading to an excess of resin at this interface. However, the movement of the rubber-rich phase is likely to be restricted in view of the high viscosity of this phase. The solvent evaporation process involves transport of solvent from the bulk of the drying film to the air/adhesive interface by spontaneous convection currents¹⁵⁻¹⁷ and subsequent loss of solvent to the atmosphere. Since the solvent is resin rich, this process will transport the mobile resin molecules to the air/adhesive interface, where solvent molecules are lost leaving an excess concentration of resin at the adhesive/air interface. Loss of solvent from the evaporating film is fast enough to prevent the resin diffusing back into the bulk of the film; essentially freezing the concentration profile for the film with surface excess of resin at both interfaces. The lower fractional surface excess of resin observed for the 11.4 μm thick films is consistent with the longer drying time required for a thicker film, leading to more diffusion of resin back into the bulk of the film. The concentration dependence of the fractional surface excess of resin may be caused by the variation in resin mobility with volume fraction of resin within the film. At low volume fractions of resin, the resin will exhibit maximum mobility, since the solubility limit of resin in solvent will not be reached until the final stages of the drying process. At high volume fractions of resin, the resin will exhibit minimum mobility, since the solubility limit of resin in solvent will be reached at an earlier stage of the drying process. Thus the fractional surface excess of resin should decrease with increasing overall volume fraction of resin in the mixture. The qualitative mechanism outlined, suggests that the surface excess of resin depends on the solubility characteristics of the ternary rubber/resin/solvent system and the

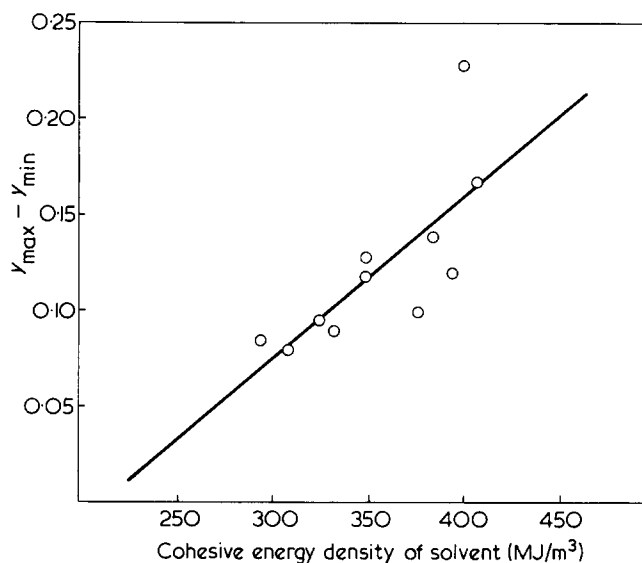


Figure 6 The degree of film heterogeneity measured by $\gamma_{\max} - \gamma_{\min}$ plotted against cohesive energy density of solvent, at an overall bulk volume fraction of resin of 0.086, for a variety of solvents. Dry film thickness $5.2 \mu\text{m}$

film drying time. The latter variable may also affect the temperature of the drying film and hence the solubility characteristics. The cohesive energy densities of the three components may be compared as a guide to the likely solubility characteristics for the system and the vapour pressures of the solvents may be compared as an indication of the rate of film formation. It is clear from a consideration of the data in Table 2 that no single overall correlation exists between the surface concentrations of resin and the cohesive energy densities and vapour pressures of the solvents over the whole concentration range of adhesive formulations. In general, however, the highest surface concentrations of resin tend to be shown by solvent systems having cohesive energy densities which are furthest removed from that of the rubber, and having high vapour pressures. These are the systems which would show minimum mobility for the rubber, due to fast drying times. A general trend can be discerned. If the heterogeneity of the films measured as $\gamma_{\max} - \gamma_{\min}$ (at 0.086 overall volume fraction of resin, where the resin excess is most pronounced) are plotted against cohesive energy density of the solvent, the heterogeneity increases as the cohesive energy density of the solvent increases from a value corresponding to that of the natural rubber up to a value corresponding to that of the resin (Figure 6). This is consistent with the idea that maximum mobility of the resin plus solvent phase and minimum mobility of the rubber-rich phase leads to highest values for the resin concentration at the interfaces of the adhesive film.

The heterogeneous nature of the rubber plus resin adhesive films, when cast from solvents, and the dependence of the degree of heterogeneity on the solvent, thickness of film and time for equilibration have demonstrated that the study

of adhesive properties of such films must take those parameters into account, since the surface properties of such adhesives are usually thought to be of vital importance in the adhesive bonding process.

CONCLUSIONS

Adhesive films consisting of natural rubber and a resin (glycerol ester of partly hydrogenated wood rosin), when cast from solvent, contain a concentration variation throughout the film, with maximum resin concentrations at the air/adhesive and adhesive/substrate interfaces. The magnitude of the fractional surface excess depends on the solvent, the overall bulk resin concentration, the thickness of the film and the time for equilibration after the film has dried. The concentration variation may be represented by a parabolic function, and hence the concentration of resin at the interfaces may be estimated. The resin excess appears to be related to the mechanism of the film forming process in which the solubility characteristics and rate of evaporation of the solvent are important parameters.

ACKNOWLEDGEMENTS

The authors would like to thank Evode Holdings Ltd, for sponsoring this research programme and allowing the publication of the data obtained. They would also like to thank the Wolverhampton Polytechnic for the use of their spectroscopic facilities.

REFERENCES

- Hock, C. W. *J. Appl. Polym. Sci. (C)* 1971, **15**, 483
- Dlvogsz, J. *5th Int. Congr. Electron Microscopy BB11* 1962
- Hock, C. W. and Abbott, A. N. *Rubber Age* 1957, **82**, 471
- Kamagata, K., Kosako, H., Hino, K. and Toyama, M. *J. Appl. Polym. Sci.* 1971, **15**, 483
- Toyama, M., Ito, T., Hino, K., Nakatsuko, H. and Ishikwa, T. *J. Appl. Polym. Sci.* 1973, **17**, 3495
- Brunn, J., Castanedo, N. and Doerfel, K. *Jena Rev.* 1974, **19**, 290
- Bates, R. *PhD Thesis* City University (1974)
- Rheineck, A. E., Peterson, R. H. and Sastry, P. *J. Paint Technol.* 1967, **39**, 484
- Kinkelaar, E. W., Rozsa, J. T. and Vavniska, L. J. *J. Paint Technol.* 1974, **46**, 63
- Campbell, G. G., Schurr, G. G., Slawikowski, E. D. and Spense, J. W. *J. Paint Technol.* 1974, **46**, 59
- Taham, M. *J. Paint Technol.* 1974, **46**, 35
- Taham, M. and Tighe, B. J. *J. Paint Technol.* 1974, **46**, 48
- Harrick, N. J. 'Internal Reflection Spectroscopy', Interscience, New York, 1967
- Institute of Petroleum Standards method IP 58/56
- Anand, J. N. and Balwinski, R. Z. *J. Colloid Interface Sci.* 1969, **31**, 196
- Anand, J. N. *J. Colloid Interface Sci.* 1969, **31**, 203
- Anand, J. N. and Karam, H. J. *J. Colloid Interface Sci.* 1969, **31**, 208

Modification of the fastness properties of dyed wool through grafting*

N. S. Batty, A. J. Gradwell and J. T. Guthrie

Department of Colour Chemistry and Dyeing, University of Leeds, Leeds LS2 9JT, UK
(Received 22 December 1975; revised 26 March 1976)

Methods are described whereby the light fastness and wash fastness properties of dyed wool can be improved through grafting small quantities of acrylonitrile onto the wool. Four dye classes are covered together with six techniques of copolymerization. Preliminary data from studies of the fading of dyes in solution with and without acrylonitrile are presented. These show that acrylonitrile reduces the rate of fading of most of the dyes investigated, irrespective of the chromophore structure. Radiation induced processes are more successful than those based on chemical initiation whilst post-irradiation induced grafting of acrylonitrile onto wool, followed by conventional dyeing offers particular promise for effectiveness and industrial exploitation.

INTRODUCTION

Recent work in this department has dealt with intrinsically coloured polymers¹⁻³. One of the many systems investigated involved the 'copolymerization' of acrylonitrile with vinylsulphonyl dyestuffs by high energy γ -radiation induced processes¹⁻². In this work it was noticed that solutions of dye containing acrylonitrile were markedly more stable to radiation than were those exposed without acrylonitrile. The more academic aspects of this observation are still under investigation. Here we are concerned with the applied aspects, more specifically with possible improvements to the light fastness (*LF*) and wash fastness (*WF*), acquired through the application of acrylonitrile, of wool treated with dyes from various classes. Also of interest are the effects of acrylonitrile on the fading characteristics of these dyes in aqueous solution.

Much work has been devoted to improving the physical properties of wool by grafting with acrylic monomers. The complex nature of the substrate makes any truly quantitative approach difficult, if not impossible. Thus, although many of the improvements have been substantiated, the mechanism of action is usually far from well understood. The characteristics of fading and the wash fastness of dyes on wool have also been extensively covered but many points require consideration. In fading, these include concepts such as energy transfer within the substrate which could lead to chromophore stability, the role of oxygen in the fading process, protection against damage by the use of additives, relationships between chromophore constitution and resistance to fading and the dye-concentration dependence of fading. Equally, the fundamental aspects of fastness to washing are noteworthy. These include the physical state of the dye during removal from the fabric, the mechanism of removal, the possible simultaneous removal of low molecular weight species from the matrix and so on. Ideally, any attempt at improving a particular aspect of wool's performance must not reduce its other qualities, though this is often difficult to achieve.

There have been several reports concerned with the radiation induced modification of wool⁴⁻⁶. It is opportune to consider whether or not the expertise gained might be extended. This point is of importance to the present survey of possible improvements to the light fastness and wash fastness of dyed wool, though other facets such as crease resistance, drape, shrinkage resistance and so on can be dealt with in this context.

We have investigated three dye classes namely basic dyes, acid dyes and reactive dyes, in terms of their fading and wash fastness on wool. Basic dyes are not used with wool because of their very poor light fastness properties although examples showing moderate wash fastness do exist. However, basic dyes are known to exhibit satisfactory light fastness on substrates based on polyacrylonitrile^{7,8}. Thus, a combination of wool and polyacrylonitrile should exhibit improved light fastness relative to wool alone, though other properties might be adversely affected. The position regarding other dye types was less certain. Two types of acid dye were considered, acid levelling dyes and acid milling dyes. The former show intermediate light fastness but poor wash fastness. Acid milling dyes have both good light and wash fastness so one might anticipate little improvement through grafting. The Remazol dyes, based on the vinylsulphonyl system show good wash fastness but variable light fastness. Previous experience with these dyes suggested that polyacrylonitrile would enhance their light fastness though the position regarding the wash fastness was uncertain.

The general approach to this work is one of simplicity in operation, geared to existing techniques with slight modifications. Little emphasis is placed on the deposition of acrylic monomers on wool using chemical initiators, other than azobisisobutyronitrile, although a variety of such systems does exist. These have been adequately dealt with elsewhere⁸ and need not be considered further here.

EXPERIMENTAL

Reagents

Acrylonitrile was supplied by BDH Ltd, UK. The inhibitor was removed and the monomer purified by standard

* Presented at the 5th International Wool Textile Research Conference, Aachen, 1975; published as special issue of *Schriftenreihe Deutsche Wollforschungsinstitute an der Technischen Hochschule Aachen*, 1976.

Table 1 Variation in light fastness and wash fastness WF/LF of samples of dyed wool with method of preparation

Dye	Code								Dyeing depth (%)
	A	B	C	D	E	F	G	H	
Methylene blue	1-2	1	1-2	1-2	1-2	2	2	3	1
Rhodamine B	1	1-2	2	2-3	2	2-3	2	2	
Magenta PNS	2-3	3	3	2-3	3	4	4	4	1
Methyl Violet	1-2	1-2	3	3	2-3	3	3	3	
Astra	2-4	2-4	2	2	2	3-4	4	4	1
Diamond Green	1	1-2	3	3	3	3-4	3	3	
Astrazone Blue BG	3-4	3	2-4	3-4	3	4	4	3	1
Astrazone Yellow	1	1-2	2-3	2-3	2	3	2	2-3	
7GLL	2-3	3	3-4	3	3	5	4	3	1
Astrazone Red BBL	1	1-2	2-3	2-3	2-3	3	3	3	
Tartrazine N200	-	3	5	4-5	3	5	4	4-5	1
Naphthalene Dark green	-	2	2-3	3	2-3	4	4	3	1
Solway Ultra Blue	2	2	3-4	3-4	2-3	4-5	4-5	4	
Naphthalene Red JS	2-3	2-3	2-3	2	2-3	4	4	2	0.6
Carbolan	4-5	3-4	6	6	6	6-7	6	6	
Yellow 3GS	4	4	3-4	4	3-4	5	4	4	0.6
Coomassie Violet 2RS	3	4	4-5	4-5	4-5	5-6	5	5	
Coomassie Blue BL200	4-5	4	5	5	5	6	3-4	5	0.6
Coomassie Fast	4-5	4-5	5	5	5	5	5	4	
Scarlet BS	4	4	5	4-5	4	6	3	5	1
Remazol Golden	-	4	4	5	3	5	5	5	
Yellow G	-	4-5	5	6-7	4	6-7	5	5	1
Remazol Red B	-	4-5	4	5	3	5	5	5	
Remazol Brilliant Blue B	3	3	4-5	5-6	3-4	6	4	5-6	1
Remazol Red 3B	-	3-4	4	5	3-4	5	5	5	
	-	4-5	4-5	6	4	6	5	6	1
	-	4-5	5	4	3-4	5	5	5	
	-	4	4-5	6	4	5-6	4-5	5	1

methods. With the exception of the Remazol dyestuffs (Hoechst-Cassella Dyestuffs Ltd, Manchester, UK) all the dyes were used as supplied by the manufacturer. Remazol dyestuffs were converted to the free vinyl form, as described in an earlier publication¹, before use. Azobisisobutyronitrile (AIBN) was used as supplied, though *N,N*-dimethylformamide (DMF) was distilled before use. Commercially available carbonized wool flannel was used as the substrate, after soxhlet extraction with ethanol and ether and prolonged washing with distilled water. Before exposure to either dye or dye/monomer solutions, the wool was soaked in boiling water for 15 min, allowed to cool, and always maintained in a moist condition.

It is fully appreciated that the previous history of the wool and its origin are important factors in any subsequent modifications. This point provides an extension to the present work and will be covered in a later publication.

Dye solutions

The dye solutions were formulated to satisfy the wt % dye on wool stated in Table 1. The wool substrates were

dyed from a 50/1 liquor/wool ratio and invariably exhaustion of the dye bath was observed. Basic dyes were applied from baths containing 0.5% acetic acid (based on the weight of wool), acid levelling and acid milling dyes from baths containing 2-3% sulphuric acid (based on the weight of wool) whilst the reactive dyes were applied from neutral aqueous solution.

Monomer solutions

Throughout this work the concentration of acrylonitrile in aqueous solution was maintained at 3% v/v which gave a weight of acrylonitrile in solution approximately equal to the weight of wool. For irradiations carried out in the presence of dye/acrylonitrile mixtures, the monomer solution constituted the liquor for the dye.

Procedures

In order to investigate various aspects of the influence of polyacrylonitrile on the physical properties of wool, several methods of grafting were applied. These are coded in

Table 1 and in the Results. Both chemical and physical methods of initiation were used. The details are as follows:—

(A) Information relating to the wash fastness and light fastness of the dyestuffs on wool, as supplied by the manufacturer of the dyes.

(B) Information acquired from our application of the dyes to carbonized wool flannel using conditions specified by the dye manufacturer. This treatment varies slightly depending on the dyestuff.

(C) Wool, dye and acrylonitrile used simultaneously in water with AIBN (applied as 0.1 g in 5 cm³ of methanol) as initiator and heated to 90°C on a rotary dyer for 1 h.

(D) Wool was treated with acrylonitrile from aqueous solution and water/DMF mixtures with AIBN (applied as 0.1 g in 5 cm³ of methanol), at 90°C for 1 h before dyeing.

(E) The wool was dyed, then grafted using AIBN (0.1 g in 5 cm³ of methanol), aqueous solutions of acrylonitrile, and at temperature of 90°C for 1 h.

(F) Wool, after exposure to high energy γ -radiation (16 h at a dose rate of 1.65×10^{-2} Mrad/h), was treated with aqueous solutions of acrylonitrile at 60°C in a rotary dyer. The modified samples were then dyed.

(G) Simultaneous irradiation of wool in aqueous solutions of acrylonitrile using the conditions outlined in procedure (F), before dyeing.

(H) Simultaneous irradiation of wool in aqueous solutions containing acrylonitrile and the dyestuff under conditions given in procedure (F). Irradiation was followed by heating at 90°C in a rotary dyer for 1 h.

(I) As conditions used in procedures (C) to (H), without the acrylonitrile. These systems act as standards so that the effects of the initiation processes alone on the light fastness of the dyed wool could be assessed.

Dyeing procedure

Samples of acrylonitrile grafted wool, standard wool and wool grafted with acrylonitrile in the presence of the dye, were all treated at 90°C \pm 2°C for 1 h on a rotary dyer to ensure efficient, level dyeing.

Pre-polymerization procedure

Simultaneous. Chemical initiation: the monomer solution (with or without dye) was made up as specified and 0.1 g of AIBN in 5 cm³ of methanol added. Tared, water equilibrated wool was added and the mixture shaken thoroughly before heating on a rotary dyer at 90°C, for 1 h.

Physical initiation: the monomer solution (with or without dye) containing tared, pre-swollen wool was irradiated at ambient temperatures (19° \pm 2°C) using the 10 000 Ci ⁶⁰Co radiation facility, located in the Department of Physical Chemistry at the University of Leeds, Leeds, UK

Post-irradiation

The time elapsing between cessation of irradiation and subsequent processing was approximately 10 min.

In post-irradiation processes samples of pre-swollen wool were irradiated in sealed tubes. These were then exposed to the dilute aqueous monomer solution for 30 min before dyeing.

All polymerizations were carried out in air using conventional dyeing tubes equipped with efficient screw sealing caps. Identical treatments were applied to the standards (Condition I) but in the absence of acrylonitrile.

Post-polymerization procedure

Copolymerization under conditions (C)–(H) gives rise to attendant homopolymerization of acrylonitrile. Polyacrylonitrile, being insoluble in the monomer solution, precipitates from solution. Attempts to remove homopolymer and unreacted monomer involved washing with water/DMF (5/95) mixtures. Whilst this treatment removes the monomer and loosely attached homopolymer, truly grafted polymer will be unaffected. Problems with homopolymer should not arise in method (F), though the same procedure was applied in order to remove any unreacted monomer. Water assists the swelling of the wool substrate and thus facilitates removal of any occluded homopolymer. However, as aqueous/DMF mixtures are prone to aggregation effects the use of these as washing media should be closely defined. The above ratio of water/DMF (5/95) was reached after previous experimentation.

Light fastness

A standard¹⁰ method for assessing the light fastness of wool was applied. A fading lamp, Microscal Ltd, based on a mercury–tungsten fluorescent bulb was used throughout the samples exposed until the contrast between the exposed and covered portions of the wool sample was equal to Grade 3 on the grey scale¹¹. Light fastness standards, 1–8, were exposed under identical conditions to the wool specimens and assessment of fastness made.

Wash fastness

Samples were assessed for wash fastness using the ISO 2¹² procedure with two modifications. (a) Staining was not assessed hence the dyed sample was free in the test solution. (b) Restrictions on sample size limited the specimen available for assessment. Consequently each dyed piece (5 cm \times 4 cm) was treated alongside undyed wool flannel of identical dimensions.

Fading of dyes in solution

Solutions of each of the dyes in water and water/acrylonitrile (95/5) were used. The dye concentration was arranged to give an optical density between 1.4 and 1.9 for the unexposed solution. Sealed tubes containing the dye solution were exposed using the Microscal light source. Fading was assessed over twenty days at regular intervals. Measurements were made on a Unicam SP800A spectrophotometer.

RESULTS AND DISCUSSION

The results in terms of changes in the light fastness and wash fastness of dyed wool specimens arising from treatment given are listed in Table 1 together with general observations. Preliminary investigations involved extensive grafting (up to 25% based on the original weight of wool). This level of grafting gave poor wash fastness results. Hence for this work the level of grafting was considerably reduced by using solutions of lower monomer concentration.

Studies of the level of grafting, obtained using the wool/acrylonitrile system with 3% v/v aqueous monomer solutions, indicated the difficulties associated with quantitative assessments of the extent of grafting using gravimetric techniques. These arise mainly from differences in equilibrium moisture content, removal of soluble fractions from the wool and the presence of occluded homopolymer, where relevant.

Attempts to reduce errors included the use of blanks, treated similarly but in the absence of acrylonitrile, condi-

tioning of the wool before and after treatment, careful handling during experimentation to avoid losses and attempted extraction of homopolymer and unreacted monomer. The levels of grafting recorded (as seen through weight changes in the wool after suitable correction), using the conditions (C)–(H), were always in the range of 1–2% based on the original weight of wool. These values must be treated with caution since no information is available relating to the uniformity of grafting. However the weight of acrylonitrile involved, grafted onto the wool, is similar to the weight of dye deposited on the fibre. Each experimental procedure was repeated four times in this preliminary investigation.

Initiation of polymerization under simultaneous conditions using dye/acrylonitrile mixtures produced coloured homopolymers. With the exception of the Remazol dye-stuffs, the colour strength of the homopolymeric species was weak, hence the homopolymer did not compete with the wool for the dye in solution. Remazol dyestuffs gave highly coloured homopolymer and so competition between the wool and homopolymer for the dye in solution resulted in weaker dyeings on wool. Generally the depth of shade was lower than was observed with untreated wool and acrylonitrile-grafted wool.

From *Table 1* the following observations can be made:

(i) Use of acrylonitrile grafted wool with basic dyes leads to slight improvements in the wash fastness but significant improvements in light fastness. Particular benefits appear from radiation induced processes – especially post-irradiation grafting of acrylonitrile, followed by dyeing (F). The basic dye standards (methylene blue, Rhodamine B, Magenta P and Methyl Violet), although showing less improvement in light fastness than the Astrazone Basic Dye-stuffs, are worthy of further consideration, because of their superior wash fastness.

(ii) Marked improvements to the light fastness of acid levelling dyes were noted though the wash fastness was unchanged. Radiation induced processes show particular promise in this series.

(iii) Acid milling dyes on wool show good wash fastness and reasonable light fastness without any modification. Use of acrylonitrile modified wool yields a product with very slightly improved wash fastness (except H) though moderate improvements to the light fastness are apparent.

(iv) Remazol reactive dyes show good wash fastness on wool which is maintained with the modified varieties [except for (E)]. Moderate improvements to the light fastness are apparent throughout.

(v) Results relating to conditions (C)–(H), in the absence of acrylonitrile were monitored with regard to light fastness and wash fastness (Code I). These results were then compared with those shown in *Table 1*.

The following points are relevant: (a) No changes in any of the wash fastness characteristics of the dyed wool samples were observed. In instances involving chemical initiation non-reproducibility of colour, shade and depth was observed. No changes in dyeing characteristics were observed for samples subjected to high energy radiation.

(b) Improvements to light fastness were marginal in most instances though in no case was the light fastness reduced as a consequence of exposure to the processes outlined. However with certain systems, using high energy irradiation, a noticeable improvement in the light fastness was observed. Whilst these improvements did not match those observed using polyacrylonitrile grafts, any improvement is significant. Post-irradiation was more effective in this respect.

Those dye-wool composites showing improvement are Rhodamine BN, Methyl Violet, Astra Diamond Green, Naphthalene Red JS and Coomassie Blue.

Fading of dyes in solution

The fading of aqueous dye solutions in the presence of acrylonitrile, compared with those irradiated in the absence of acrylonitrile, has been observed. With three exceptions (including Astrazone Yellow 7GLL) acrylonitrile reduced the rate of fading. Protection by the acrylonitrile was shown to be a property of the solution and not the result of a filtering action, since irradiation of dye solutions in tubes contained in slightly larger tubes with acrylonitrile – to provide a film of acrylonitrile around the inner tube – showed no reduction in the rates of fading. Two dyes (Astrazone Blue BG and Remazol Golden Yellow) showed no change in their rate of fading when mixed in solution with acrylonitrile. With these exceptions, all dyes were given appreciable protection. It is worth noting that apart from the Remazol dyes, all dyes monitored for fading in solution were used as supplied by their manufacturer, without further purification. This makes any interpretation of the fading characteristics difficult because of the complexity of the dye system. However the improvements imparted by acrylonitrile have been demonstrated in a realistic manner.

GENERAL DISCUSSION

The concept of radiation induced modification of textiles has been the subject of much interest though recently attention has been placed on the industrial use of accumulated expertise. This technique is at a more advanced stage in the packaging industry and in modification of cellulose^{13–15}. Improvements to physical properties of textiles by chemically initiated processes, involving the initiator, the monomer and the substrate simultaneously, are used to some extent but give rise to problems. These include secondary reactions arising from initiator fragments, initiator decomposition products, and direct interaction with the substrate. With many dyestuffs these side reactions are serious since they result in the decomposition of the dye. This leads to non-reproducible results in terms of shade and levelness of dyeing.

With few exceptions the use of acrylonitrile, irrespective of the treatment given (C–H), improves the light fastness and/or the wash fastness of the dyed wool specimens. However, great benefits are gained from the use of radiation induced processes (F–H) and especially treatment (F). In process (F) we are concerned with the irradiation of moist wool, exposure of the irradiated wool to the aqueous/monomer solution and then transfer of the grafted wool to the dyebath, whence the wool is dyed as usual. No problems with homopolymerization arise and there is no reduction in the dye uptake.

In those treatments involving copolymerization of wool with acrylonitrile before dyeing, very bright shades are obtained. This phenomenon is probably associated with a reduction in the yellowing tendency of the wool, though Rattee and Singh⁸ have noted that acrylic monomers enhanced the yellowing of wool when transition metal ion catalysts are used with peroxydisulphates as the initiating system. It was found that the addition of formaldehyde to the reaction mixture considerably reduced the tendency to yellowing. Such yellowing leads to dullness of shade on dyeing.

The noted improvements in the wool's fastness properties are surprising. Earlier work, using higher levels of grafting (up to 25% by wt of wool) gave wash fastness results which were disappointing. Reduction of the level of grafting to approximately 1–2% gave improved wash fastness though it is appreciated that the grafting is unlikely to be homogeneous. Further work is needed before a satisfactory explanation of such improvements can be offered.

As expected, the presence of polyacrylonitrile in wool dyed with basic dyes improved the light fastness though to varying extents, depending on the dye. Less anticipated was the superior light fastness, obtained with the acid leveling dyes, especially for samples containing no residual initiator or initiator fragments (processes F–H). Marginal improvements with the acid milling dyes and the reactive dyes suggest that polyacrylonitrile has potential as an anti-fading agent even for dyes with nominally good light fastness.

The complex nature of the systems and of the light fastness properties of dyes on wool is shown by these observations of improved light fastness even in the absence of the acrylonitrile, and has been noted by operators in related work¹⁶. This opens up an area of research into the effects of radiation on wool in relation to the light fastness of subsequently dyed samples and may be indicative of the destruction of centres which might otherwise take part in fading processes. Whilst the marginal nature of these improvements makes any conclusions highly speculative, it does suggest that further work could be pursued along similar lines.

Work is now in progress to find out if the improvements noted with grafted samples are particular to the polyacrylonitrile modified system and are a feature of the grafted polymer, or whether such improvements are obtained using other grafted polymer–wool composites, suggesting that the improved fastness properties arise from reaction with those sites in wool which would otherwise become involved in secondary reactions resulting in poor light fastness by some type of complex mechanism. One possibility involves the reaction between the acrylic monomer and reactive groups such as the amino-acid end-groups in the wool. This would reduce any electron transfer between the wool and the dye which would otherwise lead to eventual breakdown of the chromophore. If this mechanism is valid then protection of the chromophore should be possible using a variety of acrylic monomers. Hence, we are not limited to acrylonitrile. This proposed mechanism is supported by the data given in *Table 1* since improvements observed with

samples which were dyed before deposition of polymer occurred (condition E) were negligible compared with those obtained by simultaneous dyeing and deposition or by deposition of monomer followed by dyeing. However much remains to be done before proven satisfactory explanations can be offered.

The application of high energy, radiation induced processes on an industrial basis would be much simpler than those dependent on chemical initiation. Such a process could operate on lines similar to those proposed for the treatment of cellulose, about which much more has been written. This approach would require considerable changes in outlook when compared with conventional wool pre-treatment. The problems are far from insurmountable though they do exist. The low levels of grafting required to achieve significant improvements suggest that vapour-phase grafting processes offer potential though such modifications would present technological problems.

ACKNOWLEDGEMENT

We acknowledge the financial support given to one of us (N. S. B.) by the Perkin Bequest.

REFERENCES

- 1 Batty, N. S. and Guthrie, J. T. *Polymer* 1975, **16**, 43
- 2 Batty, N. S. and Guthrie, J. T. *Polymer* 1975, **16**, 370
- 3 Benson, R., Guthrie, J. T. and Lartey, R. B. *Polymer* 1975, **16**, 903
- 4 Hoffman, A. S. and Stannett, V. *Am. Dyest. Rep.* 1968, **57**, 998
- 5 Campbell, D., Williams, J. L. and Stannett, V. *Adv. Chem. Ser.* 1967, **16**, 221
- 6 Stannett, V., Araki, K., Gervasi, J. A. and McLeskey, S. W. *J. Polym. Sci. (A)* 1965, **3**, 3763
- 7 Park, J. *J. Soc. Dyers Colour.* 1974, **90**, 73
- 8 Rattee, I. D. and Singh, G. S. *Text. Res. J.* 1974, **44**, 600
- 9 Guthrie, J. T. *PhD Thesis* University of Salford (1971)
- 10 'Standard methods for the determination of colour fastness of textiles', Soc. Dyers Colour, 3rd Edn, 1962, p 57, BS 1006: 1961, British Standards Institution
- 11 ISO Recommendation R. 105, part 2, BS 2662: 1961, British Standards Institution
- 12 BS 2684: 1961, British Standards Institution
- 13 Guthrie, J. T. *Polymer* 1975, **16**, 134
- 14 Moore, P. W. *Rev. Pure Appl. Chem.* 1970, **20**, 139
- 15 Hoffman, A. S. *Isot. Radiat. Technol.* 1970, **8**, 84
- 16 Beever, R. B. *Colloid. Polym. Sci.* 1974, **252**, 367

Palladium / π - complexes as catalysts for olefin polymerization

Fereidun Hojabri, Mir-Mohammad Mohaddes and Afiat Talab

Department of Chemistry, Arya Mehr University of Technology, Tehran, Iran
(Received 18 September 1975)

Polymerization of different types of olefins was investigated with a palladium/ π -allylic complex as catalyst. Polymerization was possible only with those olefins which have a bicyclo structure. Compounds with two double bonds reacted as easily as mono-olefins. The effect of temperature on reaction rate was studied and an activation energy of 21.3 kcal/mol calculated for the polymerization reaction of bicyclohepta-2,5-diene.

INTRODUCTION

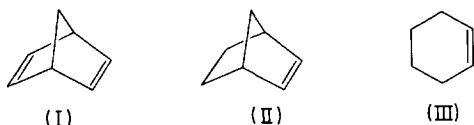
Palladium chloride has been used before for the polymerization of cyclo-olefins^{1,2}. Since palladium in the form of PdCl₂ is not very active, we applied a π -allylic complex of palladium to the polymerization. The π -allylic complex was prepared from β -pinene and Pd(C₆H₅CN)₂Cl₂³. We tried to polymerize different types of olefins to find out if the higher activity of palladium in this catalyst system would allow the polymerization of simpler olefins. Ethylene and propylene are not polymerized with palladium chloride under normal conditions^{4,5}.

EXPERIMENTAL

Palladium complex was dissolved in 200 ml of an aromatic solvent such as benzene or toluene. 100 ml of olefin were added and the mixture heated in a one litre autoclave equipped with stirrer and temperature control. In experiments with propylene the autoclave and solvent were first cooled to -40°C and the propylene in liquid form was added. Samples were taken from the reaction mixture at different stages of polymerization and the content of olefin was determined by gas chromatographic analysis. The polymer was precipitated by addition of polar solvents to the viscous liquid product. Molecular weights for the polymers were determined with a vapour pressure osmometer.

RESULTS AND DISCUSSION

In a series of experiments bicyclohepta-2,5-diene (I), norbornene (II), cyclohexene (III) and 1-hexene were used in polymerization with palladium- π -allylic complex.



The results of polymerization of these compounds are summarized in Table I. Polymerization of bicyclohepta-2,5-diene (I) and norbornene (II) was fast between 140° and 200°C. Cyclohexene which has only one ring showed only a very small amount of polymerization after long reaction times. 1-Hexene which is an open-chain olefin showed under the same reaction conditions no polymerization at all with palladium/ π -complex.

Bicyclohepta-2,5-diene polymer was decomposed to monomeric diene and gave, by hydrogenation, a compound with the same structure as the polymer obtained from norbornene. Figure 1 shows the n.m.r. spectra of bicyclohepta-2,5-diene polymer (A), hydrogenated polymer (B) and norbornene polymer (C). The last two compounds are saturated and have no double bond in their polymer chain. The strong band at 3060 cm⁻¹ in the infra-red spectrum of the polymer, indicating the presence of a carbon-carbon double bond, also disappeared in the hydrogenated polymer (Figure 2). Hydrogenation was only possible at higher temperatures and pressures (70°C, 20 atm), using Pd/C as catalyst. At normal pressure and temperature and with Raney nickel no hydrogenation took place. These results indicate that bicyclohepta-2,5-diene and

Table I Polymerization of different types of olefins with 1 mmol palladium complex; 20 ml olefin; 15 ml toluene

Olefin	Temperature (°C)	Time (h)	Product (g)	MW
Bicycloheptadiene	140	16	13.1	4800
Norbornene	140	16	9.6	4200
Cyclohexene	148	36	0.6	—
1-Hexene	145	48	—	—

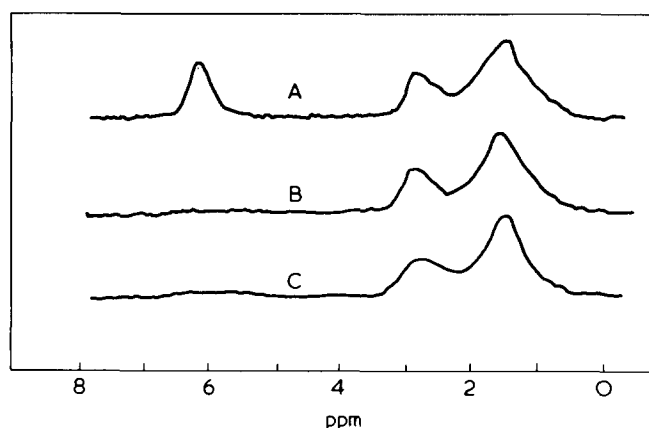


Figure 1 Nuclear magnetic resonance spectra at 60 MHz of: A, bicyclohepta-2,5-diene polymer; B, hydrogenated polymer; C, norbornene polymer

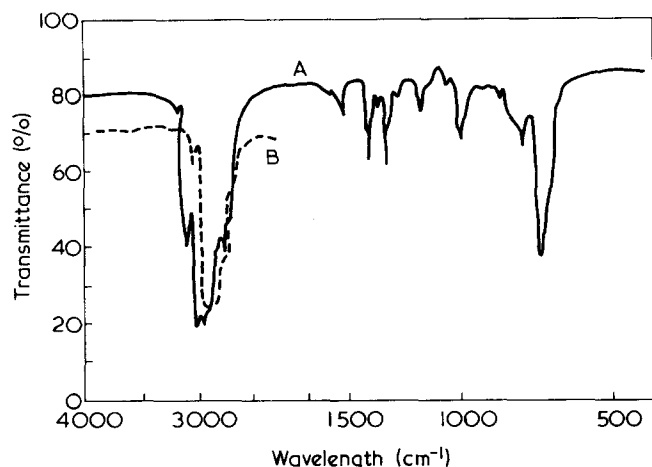


Figure 2 Infra-red spectra of: A, bicyclohepta-2,5-diene polymer; B, hydrogenated polymer

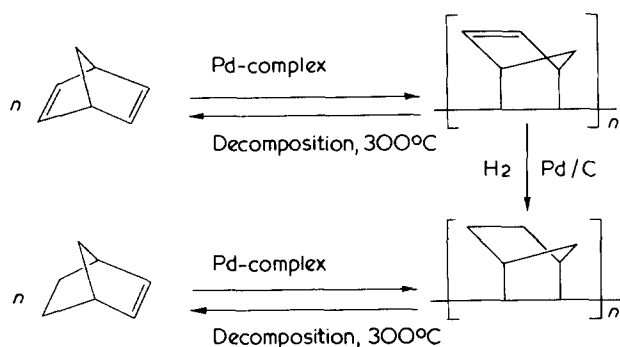


Figure 3 Polymerization pattern of bicyclohepta-2,5-diene and norbornene

norbornene display the same polymerization pattern (Figure 3).

The fact that norbornene was polymerized easily, but cyclohexene only to a very small extent, suggests that a rigid structure is necessary for an olefin to polymerize with palladium complexes. Apparently, this is an important feature for the formation of π -complexes as intermediate between the double bond and palladium. Because of the lack of a rigid structure, formation of these intermediates needs higher activation energy with cyclohexene than with norbornene. Rotation of the chain hinders the formation of these intermediates in the case of 1-hexene and therefore no polymerization can occur.

Propylene, like 1-hexene, did not show any tendency to polymerize with palladium/ π -allylic complexes. Only small amounts of dimers and trimers of propylene were obtained at 60 atm and up to 130°C. Addition of HCl (1 cm³, 1 M) to the catalyst system did not change its activity and only promoted the formation of chloropropane.

Table 2 Polymerization at 140°C, 1 mmol catalyst

No.	Time (min)	Temperature (°C)	BCHD (mol %)	BCHD (mol/l)	1/BCHD (l/mol)
1	0	140	24.6	2.1355	0.468
2	25	140	23.0	1.9966	0.501
3	45	140	24.0	2.0834	0.480
4	75	140	23.1	2.0053	0.499
5	105	140	21.7	1.8838	0.531
6	135	140	20.9	1.8143	0.551
7	150	140	20.9	1.8143	0.551

Table 3 Polymerization at 175°C, 1 mmol catalyst

No.	Time (min)	Temperature (°C)	BCHD (mol %)	BCHD (mol/l)	1/BCHD (l/mol)
1	0	165	12.5	1.080	0.925
2	30	175	10.2	0.885	1.13
3	60	175	7.3	0.633	1.58
4	80	175	6.5	0.563	1.77
5	95	175	4.0	0.347	2.88
6	150	173	2.6	0.298	3.35

Table 4 Polymerization at 200°C, 1 mmol catalyst

No.	Time (min)	Temperature (°C)	BCHD (mol %)	BCHD (mol/l)	1/BCHD (l/mol)
1	0	180	21.4	1.8577	0.536
2	10	201	20.0	1.7362	0.576
3	20	202	15.4	1.3363	0.748
4	30	200	12.2	1.0591	0.944
5	40	199	9.54	0.8262	1.207
6	55	198	6.32	0.5486	1.823
7	70	198	5.7	0.4948	2.021
8	85	197	4.35	0.3776	2.648
9	105	199	3.6	0.3125	3.200
10	125	199	3.6	0.3125	3.200

Table 5 Polymerization at 170°C with 0.3 mmol, 1 mmol and 2 mmol catalyst

No.	Time (min)	BCHD (mol/l)			1/BCHD (l/mol)		
		0.3 mmol	1 mmol	2 mmol	0.3 mmol	1 mmol	2 mmol
1	15	2.439	2.0450	2.118	0.399	0.487	0.472
2	30	2.504	2.0043	1.780	0.410	0.494	0.562
3	45	2.214	1.7835	1.645	0.452	0.561	0.608
4	60	2.283	1.6797	1.280	0.438	0.595	0.781
5	75	2.135	1.6061	1.143	0.468	0.623	0.875
6	90	2.096	—	0.981	0.477	—	1.091
7	105	1.992	1.5674	0.853	0.502	0.658	1.127
8	120	1.997	—	—	0.501	—	—
9	135	2.057	1.5238	—	0.486	—	—
10	150	1.918	1.4043	—	0.521	—	—

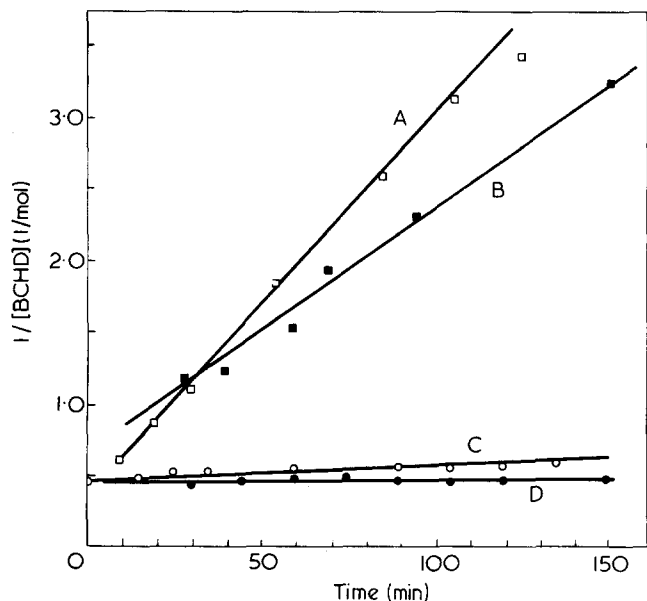


Figure 4 Variation of polymerization rate with temperature, 1 mmol catalyst. Curve A, 200°; B, 175°; C, 140°; D, 110° C

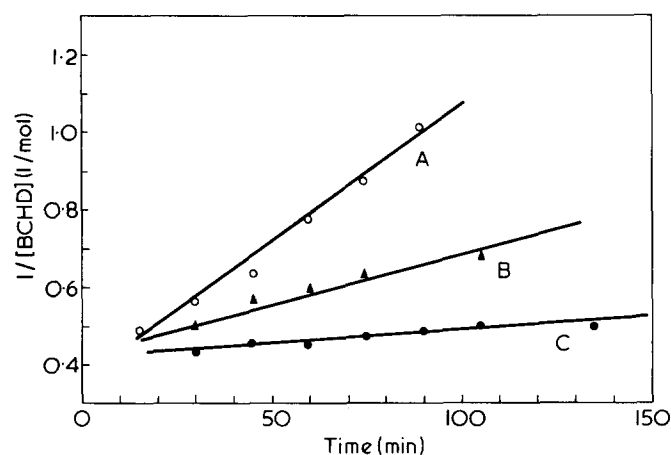


Figure 5 Variation of polymerization rate with catalyst concentration, 140° C. Curve A, 2; B, 1; C, 0.3 mmol

Table 6 Rate constants at different temperatures

t (°C)	$1/T$ (K ⁻¹)	k' (l/mol min)	Log k' (l/mol min)
110	2.61×10^{-3}	2.32×10^{-4}	-3.6340
140	2.42×10^{-3}	7.4×10^{-4}	-3.1300
175	2.25×10^{-3}	1.67×10^{-2}	-1.7730
200	2.11×10^{-3}	2.79×10^{-2}	-1.5540

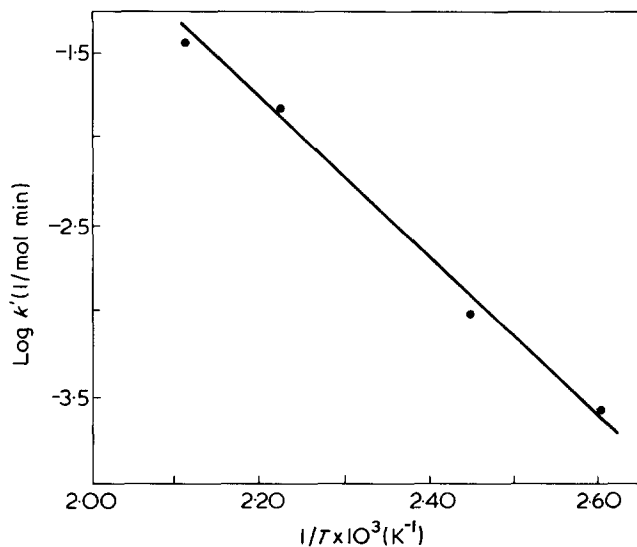


Figure 6 Plot of log k' versus $1/T$

KINETICS OF POLYMERIZATION

Polymerization of bicyclohepta-2,5-diene (BCHD) was carried out at 110°, 140°, 175° and 200°C with different amounts of catalyst. Tables 2–5 show the results of these experiments. The rate of polymerization increased with increasing temperature and concentrations (Figures 4 and 5). The linearity of variation of $1/[BCHD]$ with time at constant temperature and constant catalyst concentration shows that the polymerization reaction is second-order for bicyclohepta-2,5-diene. The reaction rate follows equation (1):

$$r = -\frac{d[BCHD]}{dt} = k'[BCHD] \quad (1)$$

$$k' = k [\text{catalyst}]^m$$

Calculated k' for different temperatures are shown in Table 6. The plot of log k' versus $1/T$ is represented in Figure 6. From this plot an activation energy of 21.3 kcal/mol was calculated for the polymerization reaction.

REFERENCES

- Schulz, R. G. *J. Polym. Sci. (B)* 1966, 4, 541
- McKeon, J. E. and Stracher, P. S. US Pat. 3 330 815 (1967)
- Hojabri, F. *J. Appl. Chem. Biotechnol.* 1973, 23, 205
- Ketley, A. D., Fisher, L. P., Berlin, A. J., Morgan, C. R., Gorman, E. H. and Steadman, T. R. *Inorg. Chem.* 1967, 6, 657
- Ketley, A. D. and Braatz, J. A. *J. Polym. Sci. (B)* 1968, 6, 341

Distribution of abnormal groups in natural rubber

D. R. Burfield, L. C. Chew and S. N. Gan

Department of Chemistry, University of Malaya, Kuala Lumpur 22-11, Malaysia
(Received 18 February 1976)

Fresh samples of natural rubber were fractionated and the distribution of epoxy and amine groups over the molecular weight range was investigated. The origin of these abnormal groups is suggested. A scheme is proposed to explain the formation of lactone groups from the reaction products of the rubber epoxide and simple amino-acids. The presence of other functional groups is discussed.

INTRODUCTION

Natural rubber, although predominantly hydrocarbon, is known to contain definite proportions of oxygen and nitrogen as integral parts of the macromolecule. The oxygen content has variously been interpreted as owing to the presence of hydroxyl^{1,2}, carboxyl², aldehyde³⁻⁶, lactone⁷, and epoxide^{8,9} groups, whilst the nitrogen content is generally assumed to be owing to proteinous material either tenaciously held or chemically bonded to the rubber. These abnormal groupings are not uniformly distributed over the whole molecular weight range but appear to be concentrated in the very low and high (or gel) molecular weight fractions. The intermediate fractions are relatively pure hydrocarbon.

Comparison of the results of different workers is hampered by the fact that the nature, number and distribution of such groups may be affected by several factors including: (a) clonal source of rubber; (b) use of fresh or stored rubbers; (c) storage conditions, i.e. whether stored as dry rubber or ammonia preserved latex; (d) conditions of isolation. In addition natural rubber is very prone to oxidation which can readily affect the molecular weight distribution and simultaneously introduce oxygen groups into the macromolecule. It is tempting to assume that the oxygen content arises as a result of oxidation of rubber subsequent to its isolation from the tree, but work with fresh rubber latex, taking stringent precautions to preclude oxidation, show this is not the case².

Recently it has been fairly conclusively shown that rubber contains epoxide groups⁹. It was speculated that the epoxide content was predominantly located in the lower molecular weight fractions because of discrepancy in the number of such groups as determined by a direct titration technique⁹ and a degradation method⁸.

This paper describes the fractionation of a fresh rubber sample and the subsequent determination of the variation of epoxide group content with molecular weight.

EXPERIMENTAL

Isolation of rubber

The natural rubber used in these experiments was isolated from freshly tapped rubber latex, clone RRIM 600, and used immediately. The rubber was precipitated by diluting the latex with an equal quantity of water and slowly adding the diluted latex, with stirring, to excess methanol. The precipitated rubber was extensively washed

with water, pressed into thin sheets and dried under vacuum at 50°C.

Fractionation

Fractionation was performed on a 1% w/v solution of rubber in toluene, stabilized with 1% w/v 2,6-di-(*t*-butyl)-*p*-cresol. The fractionation apparatus consisted of a 2 litre pear-shaped flask, equipped with stirrer, nitrogen inlet and exit, and dropping funnel for the methanol precipitant. The whole assembly was mounted in a thermostat bath at 30.00° ± 0.02°C and was continuously purged with a slow stream of oxygen-free nitrogen.

Methanol, as non-solvent, was added dropwise to the vigorously stirred solution, until a definite turbidity was observable. The temperature of the solution was first increased by 4°–5°C so as to redissolve the precipitate and subsequently returned to the original temperature overnight. The resultant precipitate was then run out of the fractionation apparatus (via a stopcock mounted at the bottom of the flask) and centrifuged for 10 min. The supernatant was tipped back into the flask, while the precipitate was added to excess methanol. The rubber was then filtered off and dried under vacuum.

The fractionation was repeated so as to obtain all together 5 molecular weight fractions, designated F₁ to F₅. The intrinsic viscosity of each fraction together with that of the unfractionated rubber was determined by viscosity measurements on dilute solutions of rubber in benzene at 30°C.

Determination of epoxide and amine group content

The number of epoxide and amine groups in each fraction was determined by a direct titration technique previously described⁹.

RESULTS AND DISCUSSION

The rubber isolated from freshly tapped latex dissolved readily in toluene, on gentle stirring overnight. There was no observable gel fraction. This is in contrast to the partial solubilities and high gel contents generally observed with samples from ammonia preserved latices and crepe rubbers¹⁰. The gel content thus presumably arises through crosslinking reactions in rubber which occur on storage either in latex, or dry rubber⁹. The intrinsic viscosity of the initial unfractionated rubber (6.66 cm³/g) is close to the value of 6.95 cm³/g determined recently for this clonal rubber by other workers⁶.

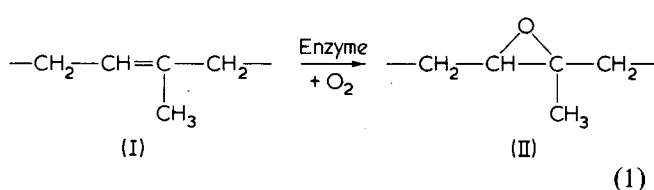
Table 1 Fractionation data

Fraction	Weight fraction, W_i	$[\eta]$	Amine concentration		Epoxide concentration		Amine/Epoxide
			mol/10 ⁶ g rubber	mol % ^a	mol/10 ⁶ g rubber	mol % ^a	
Original rubber	—	6.66	38	0.25	78	0.53	0.49
F ₁	0.217	9.36	57	0.39	111	0.75	0.51
F ₂	0.369	9.08	50	0.34	84	0.57	0.60
F ₃	0.218	5.27	10	0.07	29	0.20	0.34
F ₄	0.098	2.45	9	0.06	20	0.14	0.45
F ₅	0.107	2.26	5	0.03	21	0.14	0.24

^a mol % \equiv mol of functional group per 68g of rubber \times 100;
 $\sum W_i = 1.009$

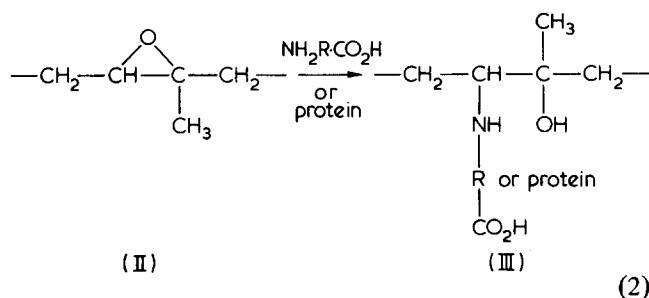
The results (Table 1) clearly show that the epoxide content of natural rubber is predominantly, although not exclusively, associated with the higher molecular weight fraction of natural rubber and is not the same as the low molecular weight 'oxide' fraction previously reported^{2,11}. In addition the amine content appears to be related to the epoxide content, being on average over the fractions approximately half its value, although lower molecular fractions show a tendency towards a smaller proportion of amine groups (see Table 1). The presence of both epoxide and amine groups and their inter-relationship can be rationalized in the following way.

Epoxidation of the macromolecule may occur within the tree at the same time as the biosynthesis, or, alternatively the two reactions may not be related. It seems likely that the epoxidation occurs enzymatically since enzyme catalysed epoxidation reactions are well known¹², and rubber latex is an ideal medium for such enzyme activity. The reaction may be represented as:



If the higher molecular weight fractions represent 'older' rubber molecules this would then explain the predominance of epoxide groups in these fractions since the epoxide content would presumably increase with reaction time. Alternatively the epoxide content might be connected with the actual biosynthesis.

Subsequent reactions of proteins or free amino-acids with some of the epoxide groups would lead to the incorporation of detectable amine groups, e.g.



This would explain the parallel relationship between the epoxide and amine content, and the tendency for the ratio amine/epoxide to increase with the higher molecular weight fraction.

That reaction (2) is feasible has been demonstrated by the reaction of amylene oxide with glycine, in aqueous media, which is shown to proceed to completion within about 36 h at room temperature¹³. Further supporting evidence that this reaction can occur in latex is provided by the addition of ³H labelled glycine to rubber latex. The labelled glycine is found to be incorporated into the rubber, to a level which approaches the concentration of epoxide groups (Table 2). Further details of these experiments are to be reported. Fractionation of rubber treated with labelled glycine shows that the incorporation is predominantly in the high molecular weight fraction (Table 3), which is again consistent with the above proposals. It should be pointed out that this latter fractionation is not directly comparable with the results presented in Table 1 since, although rubber from the same clonal source was used, amino-acids have been shown to cause crosslinking of the rubber¹⁴, and this may well affect the molecular weight distribution.

It seems likely that the high molecular weight fraction in which these abnormal groups are concentrated is equivalent to the insoluble (gel) fraction in which lactone groups were observed⁷. These apparently unrelated observations may be brought together since Gregg⁷ has presented evidence that base hydrolysis of the gel fraction (i.e. the high molecular weight fraction containing the major portion of structure III) shows the presence of the salt of a carboxylic

Table 2 Incorporation of ³H labelled glycine into rubber

Clonal source	Epoxide concentration (mol/10 ⁶ g rubber)	Amount of glycine incorporated (mol/10 ⁶ g rubber)
RRIM 600	93	89
PR 107	69	60
PB 49	46	20

Reaction conditions: $T = 30^\circ\text{C}$; $t = 4$ days; [glycine ³H] = 0.016 mol/dm³; [rubber] = 30 g/dm³; pH of latex = 8.1 ± 0.2

Table 3 Fractionation of ³H-glycine treated rubber

Fraction	$[\eta]$	Amount of glycine incorporated (mol/10 ⁶ g rubber)
F ₁	9.82	34
F ₂	6.11	6
F ₃	4.44	4
F ₄	2.38	4
F ₅	0.72	5

Clonal rubber = RRIM 600; conditions for glycine incorporation same as Table 2

markedly reduce the solubility of the rubber in non-polar solvents is shown by Gregg⁷, who found that rubber, resulting from base hydrolysis of the gel fraction, and thus presumably containing carboxylic salt residues only gelled in benzene. However, acidification of the solution with acetic acid allowed ready dissolution of the rubber.

If the above reasoning is correct the pH at which the rubber is isolated could have a profound influence on the subsequent fractionation behaviour of the rubber, since the presence of free acid or salt would markedly affect the solubility of the different rubber fractions. Thus low molecular weight fractions containing appreciable quantities of acid groupings could be readily relegated to the insoluble gel fractions.

Recently, in a comprehensive g.p.c. study of the effect of clonal variations on molecular weight distribution Subramaniam⁶ has shown that clonal rubbers exhibit distinctly bimodal distributions. In particular, 'soft' rubbers of low average molecular weight show the presence of a sizeable low molecular weight fraction. The presence of such a low molecular weight fraction was noted earlier by Westall¹⁶, who speculated that this fraction might be a basic building block for higher molecular weight macromolecules. What makes these observations of particular interest is that it is the same 'soft' rubbers which provide significant amounts of both this low molecular weight fraction and the low molecular weight oxide fraction observed by Bloomfield². Thus if there is any substance to Westall's hypothesis it is quite possible that the building-up process involves the abnormal oxygen groups discovered by Roberts¹ and Bloomfield². The nature of these groups thus definitely merit further investigation.

The presence of carbonyl or more specifically aldehyde groups in natural rubber has yet to be unambiguously established. The presence of such groups has been inferred by the inhibiting effect of amines and dimedone on cross-linking reactions in natural rubber, which were purportedly caused by these functional groups³⁻⁵. As has been pointed out amines are not specific reagents for carbonyl groups⁸, and the action of dimedone is not unequivocally established since it may well react with other non-rubber substances present in rubber, which catalyse the crosslinking reaction⁶. Recently reported estimations of carbonyl groups in natural rubber by reaction with 2,4-dinitrophenylhydrazine⁶, suffer from the same drawback that this reagent cannot be considered a specific reagent for carbonyls, for example,

reaction products with epoxides have been reported¹⁷. Further work is obviously necessary in this area.

It needs to be emphasized that the oxygenated groups discussed in this paper are restricted to those already present in rubber as it leaves the tree. Without doubt oxidation of rubber subsequent to this event will lead to the incorporation of additional oxygen functional groups including hypoperoxide groups which have not been considered in the above discussion. Analysis of stored rubber samples may thus lead to erroneous conclusions since not only may the functional groups already present in the rubber be modified by chemical reaction, but additional oxygenated groups may also be introduced.

CONCLUSIONS

The epoxide content of natural rubber is concentrated in the higher molecular weight fractions. The presence of lactone groups in the same fraction can be attributed to ring closure of the reaction product between amino-acids and the macromolecular epoxide.

REFERENCES

- 1 Roberts, K. C. *J. Chem. Soc.* 1938, **215**, 219
- 2 Bloomfield, G. F. *Rubber Chem. Technol.* 1951, **24**, 737
- 3 Sekhar, B. C. *J. Polym. Sci.* 1960, **48**, 133
- 4 Sekhar, B. C. *Proc. Nat. Rubber Res. Conf. Kuala Lumpur* 1960, p512
- 5 Sekhar, B. C. *Proc. IVth Rubber Technol. Conf. London* 1962, p460
- 6 Subramaniam, A. *Prep. Int. Rubber Conf. Kuala Lumpur* 1975
- 7 Gregg, Jr. E. C. and Macey, J. H. *Rubber Chem. Technol.* 1973, **46**, 47
- 8 Burfield, D. R. *Nature* 1974, **249**, 29
- 9 Burfield, D. R. and Gan, S. N. *J. Polym. Sci.* 1975, **13**, 2725
- 10 Kemp, A. R. and Peters, H. *J. Phys. Chem.* 1939, **43**, 923
- 11 Bloomfield, G. F. and Farmer, E. H. *Trans. Inst. Rubber Ind.* 1940, **16**, 69
- 12 Abbot, B. J. and Hou, C. T. *Appl. Microbiol.* 1973, **26**, 86
- 13 Burfield, D. R., Gan, S. N. and Smithers, R. H. to be published
- 14 Gregory, M. J. and Tan, A. S. *Prepr. Int. Rubber Conf. Kuala Lumpur* 1975
- 15 March, J. 'Advanced Organic Chemistry', McGraw-Hill, New York, 1968, p320
- 16 Westall, B. *Polymer* 1968, **9**, 243
- 17 Byers, A. and Hickinbottom, W. J. *J. Chem. Soc.* 1948, 1329

Time-dependent failure of poly(methyl methacrylate)

Robert J. Young* and Peter W. R. Beaumont

Department of Engineering, University of Cambridge, Cambridge CB2 1PZ, UK

(Received 25 February 1976; revised 22 March 1976)

A theory has been developed to explain the time-dependent failure of poly(methyl methacrylate) (PMMA) (and possibly all glassy polymers). The analysis uses the concepts of linear elastic fracture mechanics and it has been shown that by making simple assumptions it is possible to predict the lifetimes of PMMA specimens under static load from the strain-rate dependence of Young's modulus for the material.

INTRODUCTION

Many structural materials, when subjected to a static load, fracture after a period of time which varies inversely with the magnitude of the applied load. This phenomenon is sometimes called 'static fatigue' or 'creep rupture'. The Griffith theory of fracture is based on a classical elastic model which cannot, unless modified, account for the observed behaviour. It predicts that a stress only infinitesimally less than the fracture strength of the material would be sustained for an infinite period of time. The theory may be extended to explain creep rupture in several ways: (a) the size of flaws present in the material may be increased by chemical attack until the crack reaches critical dimensions, and (b) the environment may reduce the fracture-surface energy of the material by adsorption of chemical species at the crack tip.

Many theories based upon the time-dependent fracture of polymers have approached the problem from an entirely different viewpoint (Berry¹, Beuche², Zhurkov³). They have adopted a molecular model and taken the basic premise that the failure process is characterized by an activation energy, where the height of the energy barrier is reduced by some function of the applied stress. Berry¹ has reviewed some of these theories; he criticized them for being too phenomenological in that they produce arbitrary fitting constants that have little physical meaning. It is clear that the rupture of molecular bonds is an important process but like Berry we emphasize the need for a theory of fracture in amorphous glassy polymers which includes both the microscopic and macroscopic aspects of the failure process at the tip of the crack.

In this paper we have developed a theory to explain the time-dependent failure of poly(methyl methacrylate) (PMMA) in terms of the parameters controlling the growth of a crack and that can be readily measured. It is based on a theory by Williams and Marshall^{4,5} and takes a linear elastic fracture mechanics approach to explain slow crack growth in this material. It has been shown by several groups of workers^{5,6} that in PMMA the crack growth rate (da/dt), can be described as a unique function of the stress intensity factor (K) for a given temperature and environment. Williams and Marshall^{4,5} used a constant crack opening displacement (δ) criterion to explain, at least qualitatively,

the variation of crack velocity $V(=da/dt)$ with K , in terms of the strain-rate dependence of the Young's modulus (E). Young and Beaumont⁶ have applied the $V(K)$ relationship to successfully predict the lifetimes of specimens of PMMA held at different stress levels. In this paper we have proposed an extension of these two theories to predict the lifetimes of components made from PMMA (and possibly all glassy polymers) directly from measurements of Young's modulus, E , as a function of strain-rate.

MODELS

Constant δ criterion

The constant δ criterion was first developed by Williams and Marshall⁴ to explain the relationship between V and K for PMMA. It assumes that a craze at the tip of a crack in PMMA is equivalent to a Dugdale line plastic zone⁷. The zone of length R is illustrated schematically in Figure 1 and for a non-work-hardening material is given by⁸:

$$R = \frac{\pi}{8} \left(\frac{K}{\sigma_y} \right)^2 \quad (\sigma < 0.5 \sigma_y) \quad (1)$$

under conditions of plane strain or plane stress. The value of crack opening displacement, δ_t , at the crack tip is assumed to be fixed and is given by Corten⁸ as:

$$\delta_t = \frac{K^2}{\sigma_y E} \times \phi \quad (2)$$

where $\phi = 1$ under plane stress conditions and $\phi = (1 - \nu^2)$ for conditions of plane strain, where ν is Poisson's ratio. For PMMA, ν^2 is of the order of 0.1 and so the difference between the two conditions is only of the order of 10%. Brown and Ward⁹ have shown that the assumption that a craze can be modelled by the Dugdale plastic zone is a reasonable one. For simplicity we have taken ϕ equal to 1 throughout our analysis even though the specimens used are probably too thick for plane stress conditions to prevail.

The Young's modulus, E , for the polymer is a function of the applied strain-rate, $\dot{\epsilon}$. There is evidence to suggest that the yield strain, e_y , is fairly insensitive to both strain-rate and temperature (e.g. Marshall *et al.*⁵) and so:

$$\sigma_y = e_y E(\dot{\epsilon}) \quad (3)$$

* Present address: Department of Materials, Queen Mary College, University of London, London E1 4NS, UK.

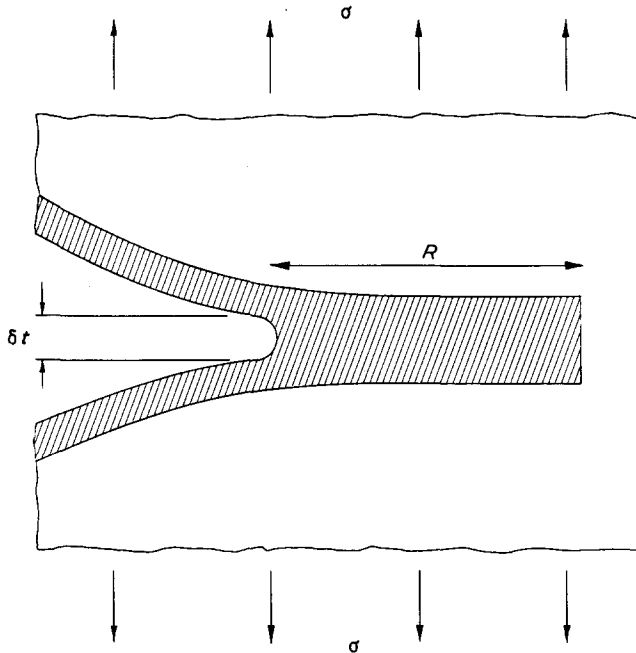


Figure 1 Dugdale line plastic zone at the tip of a crack under the action of an applied stress σ (after Williams and Marshall⁴)

Combining equations (2) and (3) gives:

$$K = (\delta_t e_y)^{1/2} \times E(\dot{\epsilon}) \quad (4)$$

In order to relate the crack velocity (V) to K it is necessary to first of all determine the relationship between $\dot{\epsilon}$ and V . If t is the time-scale of the deformation of a volume element adjacent to the crack tip, then:

$$\dot{\epsilon} \sim e_y/t \quad (5)$$

In this time, t , the crack will have moved a distance R at a velocity, V , and so:

$$t \sim R/V \quad (6)$$

Combining equations (1), (2) and (3) gives:

$$R = \frac{\pi}{8} \frac{\delta_t}{e_y} \quad (7)$$

and therefore:

$$t \sim \frac{\pi}{8} \frac{\delta_t}{e_y} \frac{1}{V} \quad (8)$$

Combining equations (5) and (8), then:

$$\dot{\epsilon} \sim \frac{8}{\pi} \frac{e_y^2}{\delta_t} V \quad (9)$$

which shows a direct proportionality between $\dot{\epsilon}$ and V [since $(8/\pi)(e_y^2/\delta_t)$ is a constant]. Equation (9) describes the relationship between $\dot{\epsilon}$ and V that is required to predict the variation of K with $E(\dot{\epsilon})$ and hence to determine the relationship between K and V .

The values of e_y , δ_t and $E(\dot{\epsilon})$ are known or can be readily measured. It should be possible therefore to construct a plot of $V(K)$ with no fitting parameters.

Time-to-failure predictions

Fracture involves two processes both of which may be time-sensitive; (a) crack initiation and (b) crack propagation. The lifetime of a PMMA specimen can be considered to be the sum of the times for the completion of these two processes. This means that:

$$\psi_f = \psi_i + \psi_p$$

where ψ_f is the time-to-failure, ψ_i and ψ_p are the times to initiate and propagate a crack to some critical size respectively, at which point catastrophic failure occurs.

Notched specimens. For notched or precracked specimens the initial crack will be present and so ψ_i will be zero. This means that the time-to-failure of such a specimen will be governed entirely by the time taken to propagate the crack and so:

$$\psi_f = \psi_p$$

The time-to-failure, ψ_f , at constant stress is given in this case therefore by the integral¹⁰:

$$\psi_f = \int_{a_i}^{a_c} \frac{1}{V(K)} da \quad (10)$$

where a_i is the initial (or inherent) crack size and a_c is the crack size at which the crack becomes unstable. The definition of the stress intensity factor, K_I is given by:

$$K_I = \sigma_a Y(a)^{1/2} \quad (11)$$

where Y is a geometrical factor (equal to $(\pi)^{1/2}$ for infinitely wide specimens) and σ_a is the applied stress. The subscript I refers to the crack opening mode of failure. Combining equations (10) and (11) gives:

$$\psi_f = \frac{2}{\sigma_a^2 Y^2} \int_{K_{Ii}}^{K_{Ic}} \frac{K_I}{V(K_I)} dK_I \quad (12)$$

where K_{Ii} is the initial value of K_I and K_{Ic} is the value of K_I at which the crack becomes unstable. In polymers K_{Ic} may be the value of K_I at which there is an adiabatic-iso-thermal transition⁴. K_{Ic} is normally called the 'plane strain fracture toughness' of the material.

All the parameters in equation (12) can be determined experimentally and the integration can be performed either analytically or numerically depending upon the complexity of the relationship between V and K_I .

Unnotched specimens. Calculation of the time-to-failure in this case is more complicated since ψ_i must also be taken into account. It is possible to obtain a conservative prediction of ψ_f by assuming ψ_i is negligible. However, this may lead to a gross underestimation of specimen lifetimes.

EXPERIMENTAL

Materials

The material used throughout this investigation was commercial Perspex (manufactured by ICI Ltd) acrylic

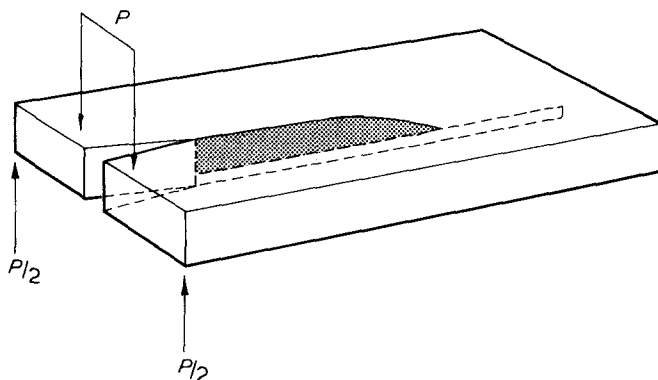


Figure 2 Schematic representation of the Double-Torsion specimen. The shaded area represents the fracture surface

sheet. 6.4 mm thick sheet was used for the Young's modulus determinations, 5.0 mm thick sheet was used for the slow crack growth measurements, and 3.2 mm thick sheet was used for the time-to-failure measurements.

Young's modulus determinations

The Young's modulus, E , of PMMA was determined as a function of strain-rate using a 3-point bend test performed on an Instron mechanical testing machine. The relationship between the applied load, P , and the displacement of the centre of the specimen, y , is given by:

$$P = \frac{4Ebh^3}{L^3} \times y \quad (13)$$

for specimens of rectangular cross-section, (thickness h and breadth b). L is the distance between the supports. The Young's modulus, E , was determined from the slope of a plot of P against y and the specimen dimensions. The plot was linear over the range of strain investigated (up to 0.005).

$V(K)$ determination

Measurements of crack velocity, V , as a function of stress intensity factor, K_I , were made at $20 \pm 2^\circ\text{C}$ using the Double-Torsion (DT) test, (Figure 2). This test and its applicability to PMMA have been described in detail elsewhere⁶. It can be shown¹¹ that the stress intensity factor, K_I , is independent of crack length, a , and for an elastic material is given by:

$$K_I = PW_m \left[\frac{3(1 + \nu)}{Wt^3t_n} \right]^{1/2} \quad (14)$$

where P is the applied load, W_m is the moment arm, ν is Poisson's ratio (~ 0.33 for PMMA), W is the bar width, t is the bar thickness and t_n is the plate thickness in the plane of the crack.

Measurements of crack velocity may be made quite simply by following a growing crack with a travelling microscope. However other, more convenient methods may also be employed which have the advantage of removing the necessity of directly observing the crack. Marshall *et al.*⁵ have favoured a constant displacement-rate method. Under conditions of constant displacement rate, the crack propagates at a constant load, P , and it can be shown that¹¹:

$$\left(\frac{dy}{dt} \right) = BPV = \text{constant} \quad (15)$$

where B is a constant related to the slope of a compliance calibration curve for the material.

The approach that has been used primarily in this paper is the constant displacement method. With the specimen held at constant displacement, the load falls off gradually as the crack extends in a controlled manner. The crack growth rate is given by¹⁰:

$$\left(\frac{da}{dt} \right) = V = \frac{-P_{i,f}}{P^2} \left(a_{i,f} + \frac{C}{B} \right) \left(\frac{dP}{dt} \right)_y \quad (16)$$

where $P_{i,f}$ is the initial (or final) load, P is the instantaneous load, $a_{i,f}$ is the initial (or final) crack length, and B and C are constants relating to the slope and intercept of a compliance analysis calibration curve for the DT specimen, $(y/P)f(a)$, respectively. The values of B and C were 7×10^{-5} and 8×10^{-4} mm/N respectively for 5 mm thick Perspex sheet.

The crack velocity can be found therefore directly from the rate of load relaxation $(dP/dt)_y$, providing the material does not suffer from mechanical relaxation as a result of, for example, molecular rearrangements in the arms of the DT specimen. This source of error may be reduced by pre-loading the sample to a value of load where the crack growth rate is very low ($V < 10^{-10}$ m/sec).

Observations of the crack front profile show that the crack extends further along the lower face of the specimen than the upper one⁶. The crack velocity is therefore smaller than that given by equation (16) by a factor which is dependent on the crack front profile¹⁰ and is of the order of 0.4 for 5 mm thick sheet.

Time-to-failure measurements

Time-to-failure measurements were made upon single edge-cracked tensile specimens 25 mm wide and loaded to a value of σ_a of 2.7 ± 0.1 MN/m². Cracks were introduced into the specimens by sawing a notch into one edge of the specimen and forcing a razor blade into the root of the notch. The cracks formed were between 9 mm and 13 mm long giving a range of values of stress intensity factor (K_{Ii}). For this particular range of crack lengths the geometrical factor Y , in equation (11) was of the order of 4.

RESULTS AND DISCUSSION

Young's modulus measurements

The measured variation of Young's modulus, E , with crosshead speed is given in Figure 3 in the form of a log-log plot. The crosshead speed has also been converted to an 'average' strain-rate corresponding to the rate of strain in the specimen half way between the neutral axis and the specimen surface. It can be seen that although the data is presented in the form of a log-log plot, the slope of the curve, n , is continually changing indicating that at this temperature (20°C) the material is near to a relaxation peak. This may correspond to the β -transition⁶.

$V(K)$ measurements

The data points in Figure 4 are measured values of V as a function of K_I for PMMA in air at $20 \pm 2^\circ\text{C}$. The different symbols refer to points obtained from various relaxation experiments on the same and different specimens. The solid curve in Figure 4 is a $V(K)$ curve derived from the $E(\dot{\epsilon})$ curve in Figure 3 using the analysis described

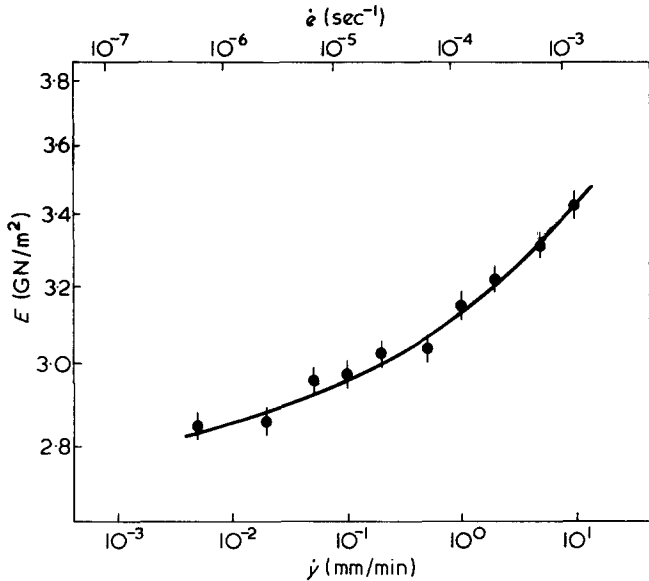


Figure 3 The Young's modulus of PMMA at $20 \pm 2^\circ\text{C}$ as a function of crosshead speed and strain-rate

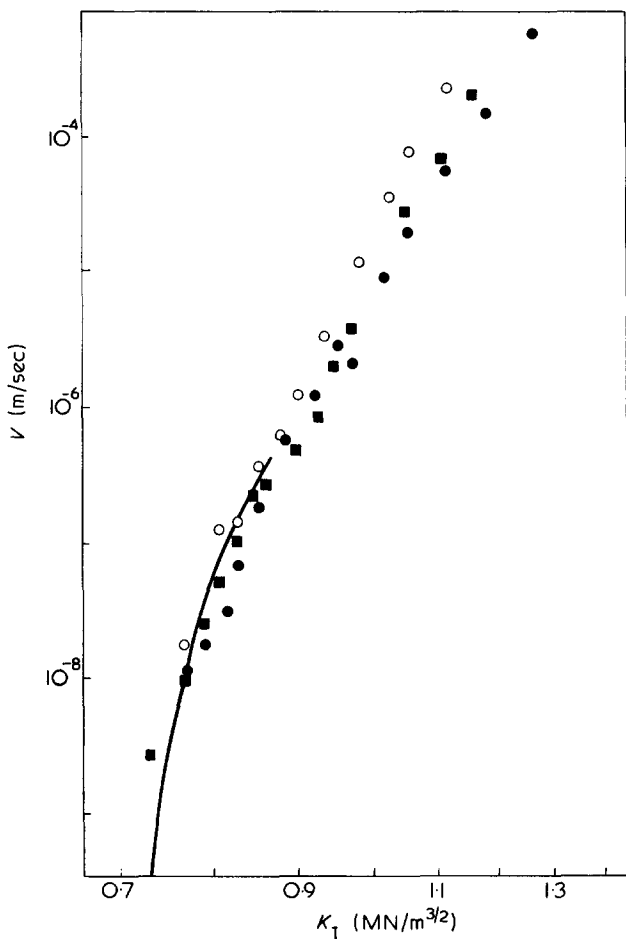


Figure 4 $V(K)$ diagram for PMMA at $20 \pm 2^\circ\text{C}$. —, theoretical line derived from the $E(\dot{\epsilon})$ data in Figure 3 using the values of the constants: $\delta_f = 1.73 \times 10^{-6}$ m; $e_y = 0.038$

earlier. The Young's modulus E has been converted to K_I using equation (4). The crack opening displacement (δ_f) for PMMA has been determined by Brown and Ward⁹ to be 1.73×10^{-6} m. The yield strain e_y , has been chosen so that the theoretical curve follows the measured data. This gives a value for e_y of 0.038. A compressive stress-strain

curve for PMMA is given in ref 12. The point of maximum stress, which is conventionally taken to be the yield point, occurs at a strain of the order of 0.08. The curve deviates from linearity well below this strain and plastic deformation takes place at values of stress below the maximum¹². A value of yield strain of the order of 0.04 is therefore not unreasonable. The strain-rate, $\dot{\epsilon}$, has been converted into a crack velocity V through equation (9) using the same values of e_y and δ_f as before.

It can be seen that the fit of the theoretical line to the measured data is very good. However, the range of crack velocities over which the curves and the data overlap is small. This is because the crack velocities corresponding to strain-rates that can easily be measured using an Instron are rather low ($<10^{-6}$ m/sec). Williams¹³ and Marshall *et al.*⁵ have shown qualitatively that the slopes of the predicted and measured $V(K)$ curves would be of the same order. Now by evaluating the $V(K)$ relationship at very low crack velocities we have shown that good quantitative agreement between the data and the theory can be obtained.

Time-to-failure measurements

Pre-cracked specimens. As well as using the constant δ criterion to explain slow crack growth in PMMA it can be used for the prediction of times-to-failure of pre-cracked PMMA specimens held under conditions of constant stress. In this case it was shown earlier that ψ_f is controlled by the time for crack propagation ψ_p . Figure 5 gives the measured times-to-failure of pre-cracked tensile specimens of PMMA as a function of initial stress intensity factor. The solid line in Figure 5 is the time-to-failure curve predicted from the $V(K)$ relationship (Figure 4) which in turn had been obtained from the $E(\dot{\epsilon})$ measurements (Figure 3). The $V(K)$ relationship was used in equation (12) with a value of K_{Ic} of $1.6 \text{ MN/m}^{3/2}$ (Young and Beaumont⁶). The broken line in Figure 5 is the predicted time-to-failure curve obtained in a similar way but using the experimentally obtained $V(K)$ data presented in Figure 4. It can be seen that all the measured points lie on or above the theoretical predictions. This shows that it is possible to integrate the $V(K)$ function [obtained from the $E(\dot{\epsilon})$ relationship] and obtain a conservative estimate of the times-to-failure.

Some of the scatter may be due to the variation in crack front profile following cracking or bifurcating of the craze

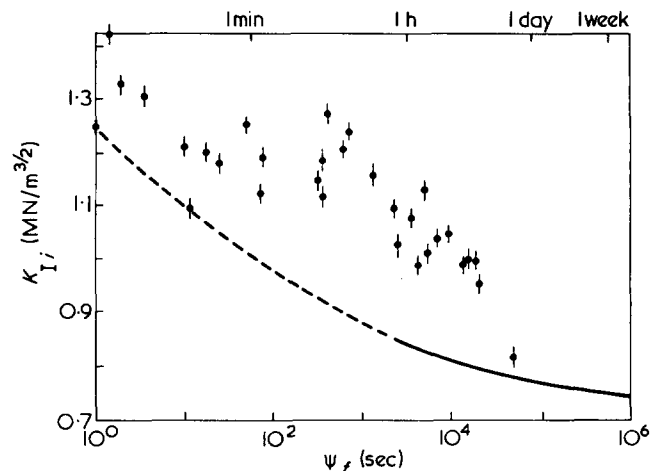


Figure 5 Time-to-failure data for pre-cracked PMMA specimens at $20 \pm 2^\circ\text{C}$. - - - -, predicted ψ_f derived from the data points in Figure 4; —, prediction from the $E(\dot{\epsilon})$ in Figure 3

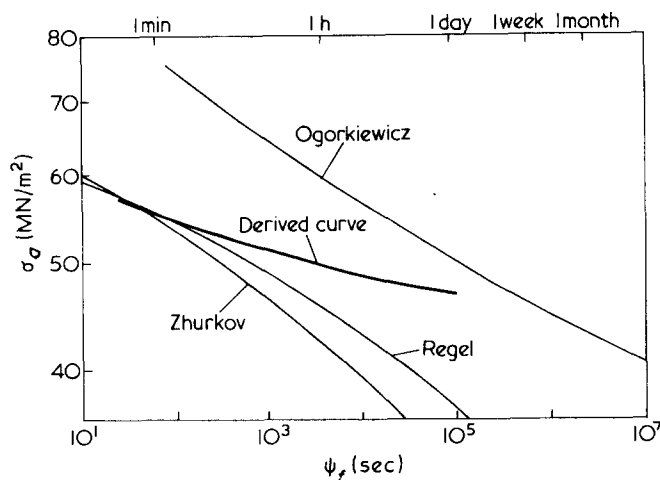


Figure 6 Time-to-failure data for PMMA as a function of applied stress σ . The data was obtained by Regel¹⁴ at 25°C, Zhurkov³ at 18°C and that given by Ogorkiewicz¹⁶ was measured at 20°C. The heavy line is the predicted time-to-failure curve for 20°C derived from the $E(\dot{\epsilon})$ data in Figure 3 and using an inherent flaw size for PMMA of 0.075 ± 0.005 mm (Berry¹⁵)

at the crack tip. The predictions presented here are for a crack with a single craze at the crack tip and any imperfections at the crack tip will lead to failure at times longer than those predicted by the analysis.

Unnotched specimens. Some experimental time-to-failure curves for unnotched specimens of PMMA are given in Figure 6. The curve of Zhurkov was used in a previous publication where it was shown that for ψ_f in the range 10^{-3} to 10^3 sec agreement could be obtained between the measured ψ_f values and ψ_f predicted solely from crack propagation using the measured $V(K)$ relationship. The analysis predicted a value of the inherent flaw size, a_0 , of 0.073 ± 0.005 mm, which is close to the value obtained by Berry¹⁵ for PMMA at 20°C. The ψ_f curve obtained by ICI Ltd for Perspex and presented by Ogorkiewicz¹⁶ is given in Figure 6. It does not agree particularly well with the experimentally determined curves of Zhurkov³ or Regel¹⁴, which are also presented in Figure 6. For a given level of applied stress the values of ψ_f given by Ogorkiewicz are approximately two orders of magnitude longer. This may be due to differences in the grade of PMMA used. Indeed, Berry¹ has shown that large differences in flaw size and fracture surface energy may be found between different grades of nominally the same material. This implies that comparisons between measured and predicted values of ψ_f should only be made for the same material. This means that in this present investigation direct comparisons should only be made for data on Perspex.

The heavy line in Figure 6 is the calculated ψ_f curve for specimens of Perspex containing inherent flaws of 0.075 ± 0.005 mm (Berry¹⁵) and using the $V(K)$ relationship (Figure 4) derived from the $E(\dot{\epsilon})$ curve in Figure 3. The time to initiate these inherent flaws, ψ_i , has been assumed to be zero and ψ_f has been calculated solely from ψ_p . The calculated line has a shallower slope and falls to the left of the measured curve for Perspex. This implies that the assumption that ψ_i is zero is incorrect and means that there must be an incubation period during which the inherent flaws are formed. It is thought (Andrews¹⁷) that the inherent flaws are crazes which have grown to a critical length

at which point they begin to break down and act as cracks of a length equivalent to the inherent flaw size. It is known that an incubation period is needed for crazes to nucleate and grow (A. Argon; personal communication). Oxborough and Bowden¹⁸ have shown that the formation of crazes in polystyrene is stress and time-dependent. It is clear therefore that the formation of the inherent flaws will be time-dependent. The results of Regel¹⁴ would appear to confirm this since he found that well before the PMMA specimens finally fractured, cracks or crazes appeared on their surfaces after an initial incubation period.

Limitations of the theory

It is clear that this theory can only be applied to polymers in which crack propagation takes place by the extension of a single craze which may be modelled as a Dugdale plastic zone. It will not be directly applicable to polymers such as polystyrene where the crack and crazes at the crack tip may be branched¹⁹.

The assumption that the crack opening displacement, δ_f , and the yield strain, e_y , are insensitive to both strain-rate and temperature will only be an approximation. The variation of these two parameters could be incorporated into the theory but the extra complication involved would probably not be worthwhile.

The time-to-failure for unnotched samples requires careful consideration. It is clear that even the experimental data is not in very good agreement. Even so it is essential that in order to accurately predict the time-to-failure of unnotched PMMA specimens we must have a complete knowledge of both the craze and crack growth kinetics.

CONCLUSIONS AND IMPLICATIONS

It has been shown that the relationship between the crack velocity, V , and the stress intensity factor, K_I , for PMMA can be explained quantitatively in terms of a critical crack opening displacement criterion. It has been possible, using simple assumptions, to construct a $V(K)$ diagram for PMMA from measurements of the Young's modulus as a function of strain-rate. Good agreement is found between the derived $V(K)$ curve and the measured data.

The analysis has been extended to predict the lifetimes of PMMA specimens held under constant stress. For specimens containing sharp cracks, it has been possible to make a conservative prediction of their times-to-failure. For unnotched samples the agreement is not so good and it appears that an incubation period is required during which time the inherent flaws must grow. A complete analysis for this case would have to include knowledge of both the craze and crack growth kinetics.

It has been shown that knowing the yield strain, crack opening displacement and initial crack length it is possible, with certain precautions, to predict the lifetime of PMMA components under stress by measuring the strain-rate dependence of the Young's modulus. This could eliminate the necessity of measuring crack velocities and may be a valuable method of predicting the time-dependent strength of other glassy polymers.

REFERENCES

- 1 Berry, J. P. 'Fracture VII', (Ed. H. Liebowitz), Academic Press, New York, 1972, Ch 2
- 2 Beuche, F. *J. Appl. Phys.* 1957, **28**, 784
- 3 Zhurkov, *Int. J. Fract. Mech.* 1965, **1**, 311
- 4 Williams, J. G. and Marshall, G. P. *Polymer* 1974, **15**, 251
- 5 Marshall, G. P., Coutts, L. H. and Williams, J. G. *J. Mater. Sci.* 1974, **9**, 1409
- 6 Young, R. J. and Beaumont, P. W. R. *J. Mater. Sci.* 1975, **10**, 1334
- 7 Dugdale, D. S. *J. Mech. Phys. Solids* 1960, **8**, 100
- 8 Corten, H. T. 'Fracture VII', (Ed. H. Liebowitz), Academic Press, New York, 1972, Ch 9
- 9 Brown, H. R. and Ward, I. M. *Polymer* 1973, **14**, 469
- 10 Evans, A. G. *J. Mater. Sci.* 1972, **7**, 1137
- 11 Evans, A. G. *Int. J. Fract.* 1973, **9**, 267
- 12 Bowden, P. B. and Raha, S. *Phil. Mag.* 1974, **29**, 149
- 13 Williams, J. G. *Int. J. Fract. Mech.* 1972, **8**, 393
- 14 Regel, V. R. *Sov. Phys. Tech. Phys.* 1956, **1**, 353
- 15 Berry, J. P. 'Fracture Processes in Polymeric Solids', (Ed. B. Rosen), Interscience, New York, 1964, Ch 2
- 16 Ogorkiewicz, R. M. 'Engineering Properties of Thermoplastics', Wiley, London, 1970
- 17 Andrews, E. H. 'The physics of Glassy Polymers', (Ed. R. N. Haward), Applied Science, London, 1973, Ch 7
- 18 Oxborough, R. J. and Bowden, P. B. *Phil. Mag.* 1973, **28**, 547
- 19 Marshall, G. P., Culver, L. E., and Williams, J. G. *Int. J. Fract.* 1973, **9**, 295

A thermoanalytical comparison between ram and screw extruded polypropylene

F. W. Hampson and T. R. Manley

Department of Materials Science, Newcastle upon Tyne Polytechnic, Newcastle upon Tyne NE1 8ST, UK

(Received 20 October 1975; revised 12 March 1976)

Thermoanalytical methods are useful in comparing the effects of extrusion on talc filled polypropylene. Differential thermal analysis, either by the conventional technique, or in an atmosphere initially of nitrogen to which oxygen is introduced, is the most convenient way of studying the extruded polymers. The polymer is more degraded by screw extrusion than by ram extrusion. Critical oxygen index measurements confirm the d.t.a. results.

INTRODUCTION

Extrusion is the most widely used technique for processing polymers¹. A screw feed is usually employed but recently there has been considerable interest in ram extruders. Work on ram extruded polyethylene has already been reported in this series². Thermoanalytical techniques are well established for the characterization of polymers³ and the critical oxygen index flammability test has been found to be of value in quality control studies⁴. It was decided, therefore, to compare these with the conventional quality control tests to monitor differences in the properties of polypropylene that had been extruded by ram and screw techniques.

EXPERIMENTAL

For differential thermal analysis a Dupont 900 apparatus in the so called DSC mode was used. Samples of approximately 15 mg were heated to 400°C at 8°C/min in still air, with an empty aluminium cup as the reference cell. In the second series of experiments, the polypropylene was initially heated under static nitrogen and oxygen was instantaneously introduced at a flow rate of 8 ml/sec near 200°C as indicated in *Figure 3*.

The critical oxygen index (COI) was measured on a Stanton Redcroft FTA. The results are the mean of ten samples. Each sample was a semi-circular rod 75 mm long and 6.35 mm radius. A gas flow of 4 cm/sec was used with butane ignition (30 sec, 15 mm flame). This is substantially the method of ASTM D 20863-70.

The polypropylene was a powder HS6 10E (ICI Ltd) containing a tertiary butyl type as an anti-oxidant and was used as supplied, 35% by wt of talc was added to the polypropylene in a tumbler dry powder mixer before extrusion, in order to provide economical reinforcement. It can be seen that the mechanical shearing action of the screw raises the temperature of the screw extruded polymer by 22°C, in spite of the fact that the polymer stays for a much shorter period in the heated zones than the ram extruded polymer does.

A prepactor (ram controlled compactor unit) assisted the feeding of the powder to the screw extruder to ensure that the product was homogeneous.

Operating conditions were as follows:

	Single ram extruder	Single start screw extruder
Ratio length to diameter of barrel	96:1	20:1
Diameter of die orifice	0.375 in (9.53 mm)	0.375 in (9.53 mm)
Temperature of orifice (°C)	230	230
Temperature of barrel (°C) ±2°C	Zone 1 137 Zone 4 230	Zone 1 190 Zone 4 215
Temperature of polymer (°C) (a) at orifice (b) after cooling	230 ± 2 15	252 ± 3 15
Take-off speed for polymer (m/min) (extrudate cooled with water)	0.456	4.56

Tensile strength and extension under load were determined at 20°C on an Instron Model TT-DM. In both cases the extension rate was 100 mm/min. Specimens were rods 75 mm long and 9.5 mm in diameter.

In the COI studies of talc filled polypropylene samples a hard crust may form on the test sample surface during the initial ignition period (before the onset of uniform cone burning surface). If this char is removed from the softened surface of the sample and the test recommenced on the softened cone surface produced, a steady flame and reproducible results are obtained.

RESULTS

Differential thermal analysis

The d.t.a. curves for the polypropylene powder before and after ram extrusion are shown in *Figure 1*. *Figure 2* shows the d.t.a. of the screw extruded material and in *Figure 3* the d.t.a. curves are seen of the polypropylene powder, before and after extrusion by both methods examined by heating in an atmosphere of static nitrogen with the admission of oxygen around 200°C. The unextruded powder in *Figure 1*, curve A and the talc filled powder, *Figure 1*, curve B, both show evidence of premelting which is usually attributed to the presence of material of less

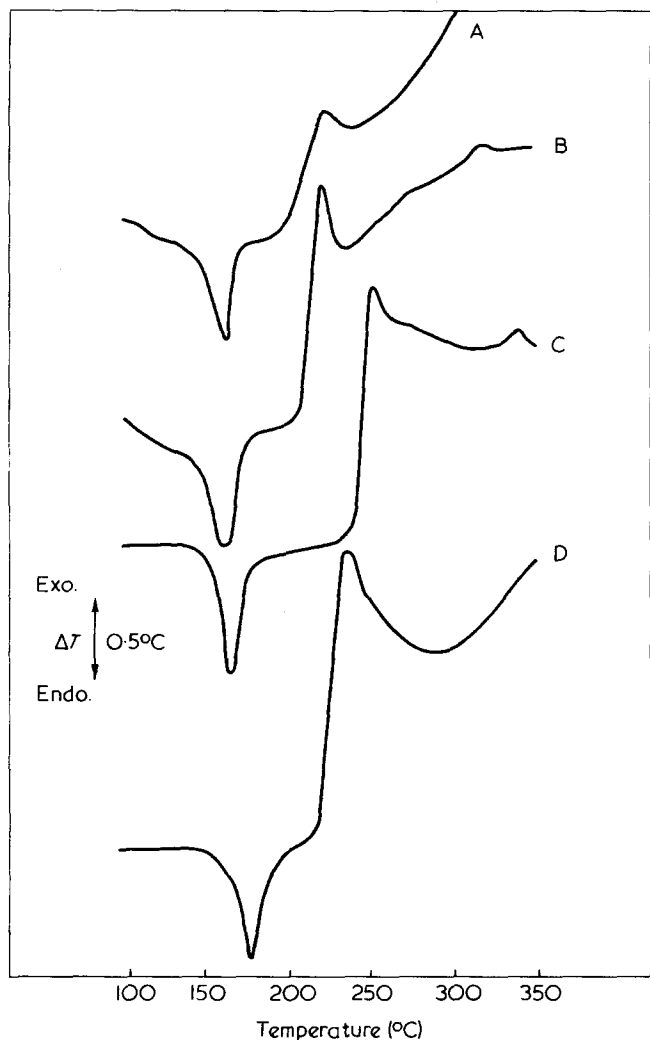


Figure 1 D.t.a. of powder and ram extruded polypropylene + talc. A, Powdered polypropylene, not extruded; B, powdered polypropylene + talc, not extruded; C, ram extruded polypropylene, aged 12 days at 155°C; D, ram extruded polypropylene, aged 21 days at 155°C

ordered structure than the normal crystalline polymer. The samples after extrusion, Figure 1, curves C and D and Figure 2 having had heat treatment do not show this initial premelting. In the unextruded talc filled powder, the oxidation begins to occur around 200°C. It is noticeable that the onset of oxidation is later in the extruded samples and this is attributed to the better mixing of the inhibitor in the extruded material. The d.t.a. curves both in still and flowing atmospheres were closely reproducible except above 450°C by which time most of the polymer had been consumed.

We now come to a significant difference between the two techniques. The sample in Figure 1, curve C was ram extruded and then aged in still air for 12 days at 155°C; the curve obtained is similar to that for shorter ageing periods of eight and five days respectively which are therefore not shown. The corresponding curves, Figure 2, curve C, for screw extruded material held for 12 days for 155°C shows that the ram extruded material is significantly more stable after this ageing period, as seen in Table 1. After the ram extruded material has been aged for 21 days, Figure 1, curve D, it can be seen that the inhibitor is beginning to be used up and ageing is occurring around 200°C. This curve is very similar to that of Figure 2, curve B of a screw extruded material after 8 days. After 21 days ageing, oxidation is occurring almost immediately after the melting

endotherm and it is obvious that the useful life of the screw extruded material has already been completed. In Figure 3 we present the results for the differential thermal analysis of the original polypropylene, the powder plus the talc filler, and for samples that were extruded on the ram and screw machines and subsequently aged for 21 days at 155°C. These samples were initially heated in static nitrogen and then oxygen was introduced at the point indicated on the graph to obtain the exotherm. The technique has been widely used to study the effect of inhibitors on the oxidation of polyolefins⁵. The change in scale of the ΔT after the introduction of the oxygen should be noted. In addition after such a vigorous reaction the base-line will not be that of the original polypropylene. It is clearly seen that the sample in Figure 3, curve C that had been ram extruded still retains much material for oxidation whilst for the screw extruded material, Figure 3, curve D, the reaction is almost complete before the oxygen is introduced. This difference is also seen between Figure 1, curve D and Figure 2, curve D but is greatly enhanced by the introduction of oxygen. This technique of introducing oxygen into d.t.a. conducted under nitrogen is a very sensitive and rapid method for determining the amount of oxidation that a sample has undergone and this could well be the preferred way of quality control testing by d.t.a. of extruded materials.

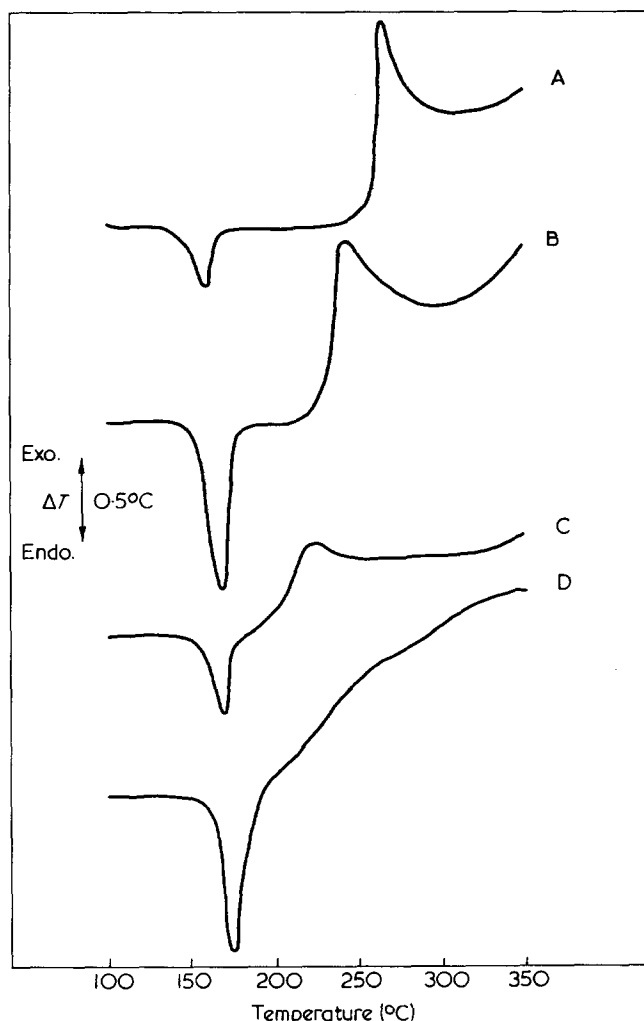


Figure 2 D.t.a. of screw extruded polypropylene + talc. A, Screw extruded polypropylene unaged; B, screw extruded polypropylene aged 8 days at 155°C; C, screw extruded polypropylene aged 12 days at 155°C; D, screw extruded polypropylene aged 21 days at 155°C

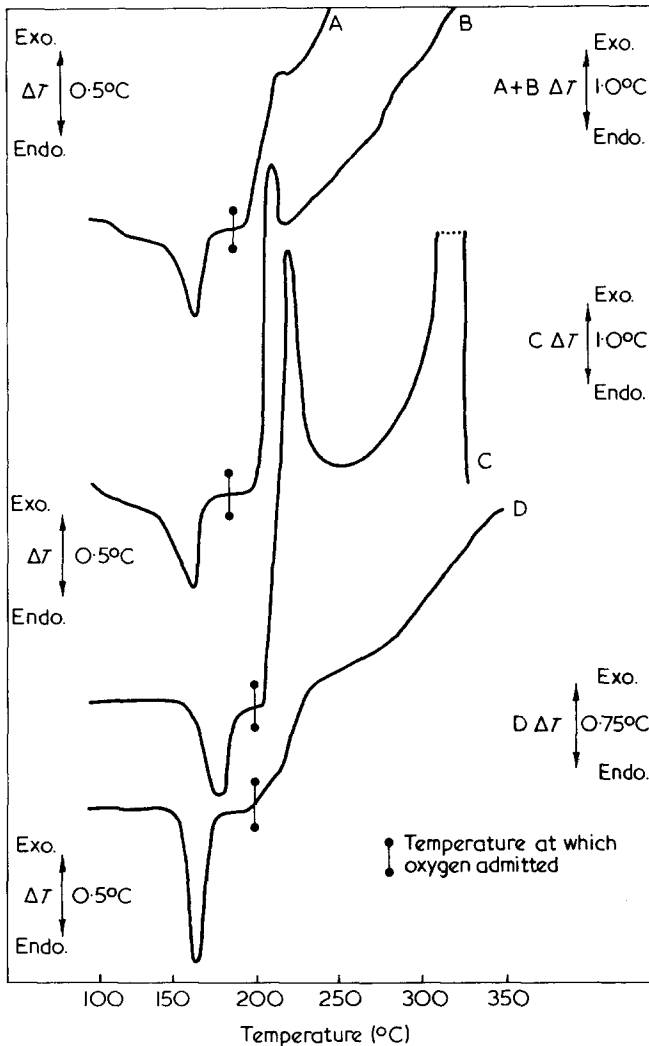


Figure 3 D.t.a. on polypropylene + talc, in nitrogen with subsequent admission of oxygen. A, Powdered polypropylene, not extruded; B, powdered polypropylene + talc, not extruded; C, ram extruded polypropylene, aged 21 days at 155°C; D, screw extruded polypropylene, aged 21 days at 155°C. Note change of scale

CRITICAL OXYGEN INDEX

Samples were examined after various periods of ageing in air on a metal free surface at 155°C. In addition, a further sample was aged for 21 days at 155°C in contact with copper, in order to get a figure for the COI of the fully oxidized material.

The results of the critical oxygen index are shown in Table 2. The improvement in oxidation stability of the ram extruded material over the screw extruded material is clearly seen. A COI of 21.27 for material oxidized in the presence of copper, is the maximum COI value. It can be seen from Table 2 that the critical oxygen index is not sufficiently sensitive to distinguish between extruded material that had been aged for 21, 12, 8 or 5 days. On the other hand, it clearly shows the difference between the ram and screw extruded material. The screw extruded polypropylene is nearing the end of its useful mechanical efficiency as shown by a COI of 20.73% close to the maximum value. In an industrial process involving repetitive heating to 155°C and cooling to ambient temperatures over periods of 2 h the screw extruded material withstands only 2 or 3 2 h cycles before mechanical failure occurs. The ram extruded material shows no oxidative degradation (COI 17.82%) and remains mechanically serviceable for

50 to 60 2 h cycles. It is interesting to note that the critical oxygen index indicates the onset of degradation before any physical discolouration of samples is seen.

TENSILE STRENGTH AND DENSITY

The ram extruded material had a density of 1.15 compared to 1.08 in the screw extruded material. For 100% sample compactness using polypropylene of SG 0.892 and talc of SG 2.65, a density of 1.176 would be anticipated. The maximum possible consolidation has thus not been achieved by either process, and small voids were seen in the screw extruded material, but were not visible at 20x magnification in the ram extruded polypropylene.

The tensile strengths of the two materials after ageing are shown in Table 3. The ram extruded material retains its tensile strength longer, as would be expected since the d.t.a. indicates that it has degraded less. The latter technique is much simpler than tensile testing and is therefore preferable for quality control work.

The screw extruded material exhibits drawing effects by necking under excess loads prior to fracture. The ram ex-

Table 1 Temperature of initial degradation exotherm (°C) of samples of polypropylene

Extruder	Aged for 21 days at 155°C		
	Aged for 12 days at 155°C	Without oxygen	Oxygen introduced at 200°C
Screw	192	181	186
Ram	219	202	206

The corresponding temperature for unaged, unextruded polypropylene powder was 188°C, and for the talc filled powder 200°C.

Table 2 Critical oxygen index measurements on extruded polypropylene after being aged at 155°C for several days. COI results are the mean of 10 specimens

Days	Ram extrusion		Screw extrusion	
	COI	SD	COI	SD
0	17.97	0.16	20.70	0.10
5	17.81	0.13	20.89	0.09
8	17.73	0.06	20.66	0.07
12	17.87	0.09	20.94	0.06
21	17.71	0.21	20.45	0.09
Mean	17.82		20.73	

Table 3 Tensile strength of talc filled polypropylene after ageing at 155°C

Tensile strength polypropylene (kg/cm ²)			Ageing period (h)
Ram extruder	Screw extruder		
59.2	57.4		0
16.5	15.0		24
20.5	18.0		48
20.5	18.25		72
21.0	18.5		96
20.75	19.5		168
21.0	16.25		192
20.75	1.5		240
20.75	Nil		264

truded material remains as a fused structure which shows a brittle fracture with no necking under breaking load conditions.

CONCLUSIONS

Thermoanalytical methods give information on flammability, dispersion, degradation and thermal history. It is possible with controlled ageing, to obtain results indicative of the component life of an extrudate before the onset of visible degradation. This is particularly valuable when pigmented materials are in use and coloured oxidation product formation is masked.

Differential thermal analysis is a useful means of detecting and following the onset of oxidative degradation and exhaustion of antioxidant, without the need for testing large samples of material with heavy test machinery and is thus a convenient quality control test for prognostication of the life of extruded materials. D.t.a., with controlled admission of oxygen into an initially inert atmosphere is the better quality control technique.

Critical oxygen index results show insufficient ageing differential to be of value for process control purposes.

The screw extruder appears to cause greater degradation than the ram extruder. This indicates that the mechanical shearing action of the screw is much more destructive than the longer time spent at high temperatures and pressure within the ram extruder. The effect of the extrusion

process on antioxidant effectiveness is demonstrated; d.t.a. is a useful analytical tool to study these effects.

If a ram extrusion process with less degradative action from processing could be developed to achieve the same speed throughout as is obtainable by screw extrusion methods, valuable savings in material usage could be obtained as less scrap was lost by degradation during processing and recycling. Continuous ram extrusion is now being extensively investigated⁶.

ACKNOWLEDGEMENTS

We thank Mr B. R. Glennie for experimental assistance. We acknowledge the assistance of the Science Research Council and thank Dunlop Ltd for permission to publish.

REFERENCES

- 1 Fisher, E. G. 'Extrusion of Plastics', Iliffe Press, London, 1964, pp 8-15
- 2 Manley, T. R. and Qayyum, M. M. *Polymer* 1971, **12**, 176
- 3 'Polymer Characterisation by Thermal Methods', (Ed J. Chiu), Marcel Dekker, New York, 1974
- 4 Hampson, F. W. and Manley, T. R. *J. Appl. Polym. Sci.* 1975, **19**, 2347
- 5 Marshall, D. I., George, E. G. and Turnipseed, J. M. *Polym. Eng. Sci.* 1973, **13**, 415
- 6 Yi, B. and Fenner, R. T. *Plast. Polym.* 1975, **43**, 224

Failure criterion for the fracture of structural adhesive joints

R. A. Gledhill and A. J. Kinloch

Ministry of Defence, Explosives Research and Development Establishment, Waltham Abbey, Essex
EN9 1BP, UK

(Received 19 February 1976; revised 26 March 1976)

The long-term strength of stressed, structural adhesive joints, consisting of aluminium alloy substrates bonded with an epoxide adhesive, has been investigated. The applied adhesive fracture energy, G_{Ic} , is shown to be linearly dependent upon the logarithmic time-to-failure; the failure time decreases as the value of G_{Ic} is increased. The fracture of these joints over eight decades of time is uniquely described by the hypothesis that there is a critical plastic-zone size developed at the crack tip at failure.

INTRODUCTION

Structural adhesives are relatively brittle, high modulus, thermosetting materials, usually based upon epoxide resins, and are being increasingly used in many diverse engineering applications. This has generated a need for the mechanical properties of bonded structures to be ascertained and for pertinent failure criteria to be established. The efficient design of bonded structures, and the accurate prediction of safe-working life, are dependent upon such data being available.

Structural joints fail by progressive crack growth and thus no failure criterion based on average stress or modulus (reflecting, for example, gross yielding or buckling) is appropriate, and the failure criterion must be founded upon the initiation and propagation of flaws inherent in the joint. Since the basic tenet of continuum fracture mechanics theory¹ is that the strength of most real solids is governed by the presence of flaws, and since the theory enables the manner in which they propagate under stress to be analysed mathematically, the application of fracture mechanics to adhesive joint failure has recently received considerable attention.

It has been shown^{2,3} that the concepts of continuum fracture mechanics are applicable to the failure of structural adhesives joints but the measured adhesive fracture energies, G_{Ic} , are orders of magnitude greater than expected from theoretical considerations of solely brittle fracture⁴. This is in accord with fracture studies on other glassy polymers¹ and arises from the energy that must be dissipated in producing local plastic deformation at the tip of the crack, in addition, to that required for the rupture of molecular bonds. It has subsequently been shown that the value of G_{Ic} is not a 'joint constant' but is a function of test temperature⁵, crack velocity⁶⁻⁸ and test environment^{8,9}. However, all this work has been concerned with relatively short-term tests; the present investigation examines the long-term stability of structural joints under imposed stresses. A main aim is to develop a failure criterion, for such joint fracture, by employing a continuum fracture mechanics analysis.

EXPERIMENTAL

Determination of G_{Ic}

The specimen geometry employed in this investigation was a tapered double cantilever beam joint and is shown

schematically in *Figure 1*. The substrate material was aluminium alloy, to specification British Standard 1474 NE4, which was machined into cantilever beams, 152 mm long, 6.4 mm thick and with a height, h , varying between 16.0 and 31.5 mm. The surfaces to be bonded were first subjected to a liquid- and vapour-degreasing bath of trichloroethane, then grit-blasting with 180–220 mesh alumina, then degreasing again and finally were allowed to air-dry. The epoxide adhesive employed was a diglycidyl ether of bisphenol A crosslinked with 9.4 mass per cent of a tertiary amine curing agent [tri-2-ethyl hexanoate of 2,4,6-tris(dimethylamino-methyl)phenol]. Immediately prior to joint preparation the aluminium alloy substrates were treated as described above, adhesive spread on the treated faces and the two beams pressed lightly together; small pieces of plastic sheet, previously inserted in the adhesive at the far ends of the joint, were employed to control the thickness of the epoxide resin layer to 0.50 ± 0.06 mm. Further, a piece of Teflon tape, about 30 mm long, 6.4 mm wide and 0.08 mm thick, was previously placed, approximately in the centre of the adhesive layer and at the narrow end of the joint, to assist in propagating a 'starter' crack later. Excess adhesive on the beam sides was wiped off and to effect cure of the adhesive the joint was held at 23°C for 96 h, followed by 1½ h at 100°C and finally 2½ h at 180°C, and then allowed to cool slowly. The specimens were then conditioned at 23°C and 56% r.h. for a few days prior to testing.

To obtain a natural, sharp, starter crack for subsequent experiments the arms of the specimen were separated at a constant rate of 8.5×10^{-3} mm/sec using an Instron tensile

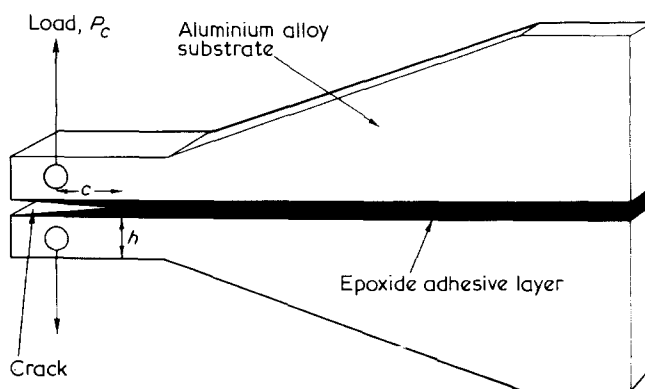


Figure 1 Sketch of tapered double cantilever beam specimen

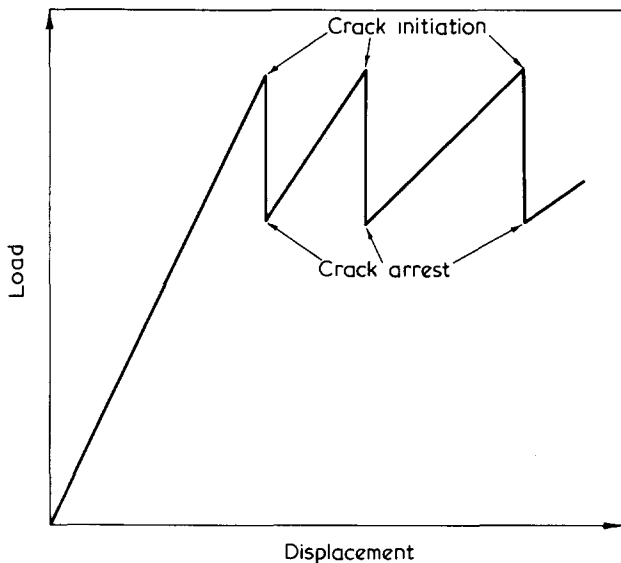


Figure 2 Typical schematic load-displacement record for stick-slip crack growth

testing machine. Now, for this particular adhesive and joint geometry, crack propagation occurs intermittently⁶, in a stick-slip manner, as is shown schematically in Figure 2. The fundamental reasons why unstable, stick-slip crack growth, rather than continuous, stable crack growth, is observed in this material/geometry combination is not fully understood. Similar differences in fracture behaviour have previously been ascribed to geometry effects¹⁰, β -relaxation transitions occurring in the polymer¹¹, a change from isothermal to adiabatic crack propagation (e.g. ref 12), environmental effects^{8,10} and the morphology of the material¹. Further, our current work¹³ suggests that the shape and sharpness of the crack tip, and the strain distribution in the immediate vicinity of the crack tip, prior to crack propagation may be of some importance.

After several crack initiation/arrest cycles, when the crack length was between 50 and 90 mm, the specimen was removed from the tensile testing machine and the sharpness of the crack tip examined using transmission optical microscopy. Initial observations indicated, however, that it was not possible to insert reproducibly sharp cracks; similar difficulties have been experienced by other workers¹⁴⁻¹⁶. Indeed, using the technique described above crack tip radii ranged between 1 and 200 μm and improvement in the reproducibility was not obtained by employing other techniques such as cooling the specimen in liquid nitrogen prior to crack insertion, propagating a longer crack, using a razor blade instead of the Teflon tape to initiate the blunt starter crack, etc. To ensure minimum, reproducible values of the adhesive fracture energy the technique as described was employed but only the sharp cracks, having tip radii of $1.5 \pm 0.5 \mu\text{m}$, were selected for subsequent testing. Initial work showed that the value of G_{Ic} was not significantly dependent upon the crack tip radius within these limits.

The tapered double cantilever beam joint was then placed in a creep machine (a 'Unisteel Stress Corrosion' apparatus, manufactured by W. H. Mayes and Son Ltd.) and the required load gently applied via a double lever system giving a 30:1 loading ratio. The test temperature and humidity were maintained at 23°C and 56% r.h. The crack tip was frequently observed using a travelling microscope, fitted with an eyepiece graticule unit which permitted a minimum crack growth increment of 0.01 mm to be detected. The failure time was taken as the time between the application

of the total load and the time when the crack had propagated completely through the specimen.

The adhesive fracture energy, G_{Ic} , was ascertained from the relationship¹⁷:

$$G_{Ic} = \frac{4P_c^2 m}{E_s b^2} \quad (1)$$

where P_c is the applied load, E_s is the modulus of the substrate (68.9 GPa), b is the specimen thickness and m is a geometry factor given by¹⁸:

$$m = \frac{3c^2}{h^3} + \frac{1}{h} \quad (2)$$

where c is the crack length corresponding to a height of substrate beam, h . Values of m are shown as a function of crack length in Figure 3 and are in good agreement with values ascertained from experimental calibrations^{18,19}.

Determination of the creep modulus

The method of determining the creep modulus, $E(t)$, as a function of time has been described in detail elsewhere^{20,21} and it is sufficient to note that values of $E(t)$ for samples of the epoxide resin, cured as detailed above, were ascertained at stress-levels of 18.5, 36.1, 48.0 and 53.4 MPa.

Uniaxial stress-strain measurements

Dumb-bells of the epoxide resin were cast in silicone-rubber moulds and cured as described previously. The

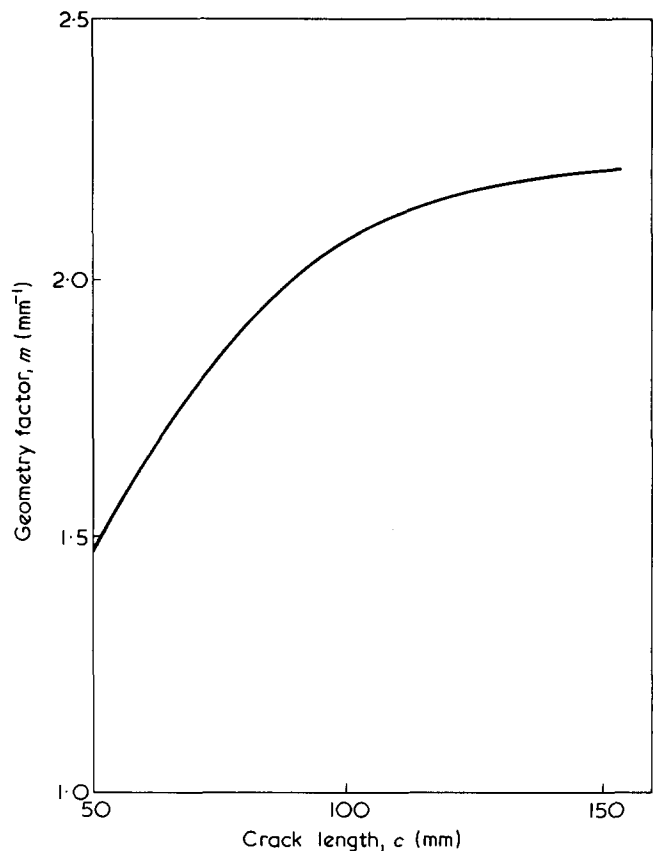


Figure 3 The geometry factor, m , as a function of crack length, c , for the tapered double cantilever beam specimen

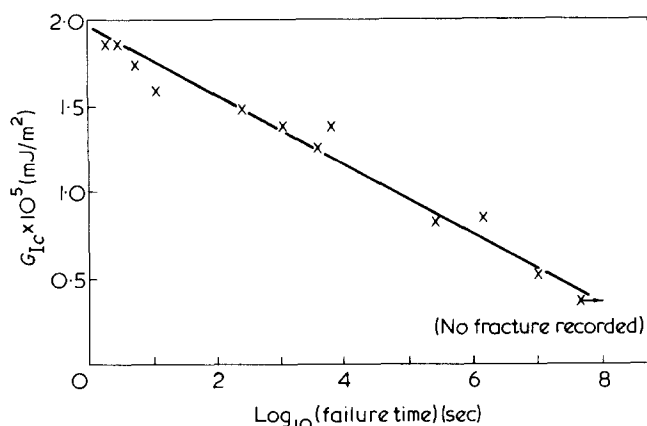


Figure 4 The relationship between the applied adhesive fracture energy, G_{1c} , and joint failure time

dumb-bells had a gauge-length of 30 mm and a cross-sectional area of about 10 mm^2 . Uniaxial stress-strain curves were obtained at 23°C and at strain-rates from $7.1 \times 10^{-3} \text{ sec}^{-1}$ to $2.8 \times 10^{-5} \text{ sec}^{-1}$, using an Instron tensile testing machine and a strain-gauge extensometer.

RESULTS

Determination of G_{1c}

The relationship between the applied adhesive fracture energy, G_{1c} , and the resulting failure time is shown in Figure 4; a linear relation exists between G_{1c} and logarithmic failure time with the failure time decreasing as the value of G_{1c} is increased. Several other interesting observations were recorded during the course of these determinations. First, the locus of joint failure was cohesive in the epoxide adhesive, with the crack propagating along the centre of this layer. Second, the failure time represented an incubation period; the original starter crack was never observed to propagate until the very end of the experiment, at the instant of fracture, when it propagated extremely rapidly. The part of the total failure time during which the crack was actually growing was confined, therefore, approximately to milliseconds. This is in accord with previous work⁶ where the short-term, initiation, adhesive fracture energy was studied as a function of initial crack velocity. For this particular geometry and adhesive it was found that the velocity of crack growth was always greater than about 20 m/sec; crack velocities slower than this were never observed. In the present experiments, however, even though unstable crack growth occurred, no crack arrest was observed. This was probably due to (a) the relatively high crack velocities and short specimen length; (b) the fact that a constant load, rather than a constant displacement, was applied to the specimen during crack growth and thus no decay in the applied load occurred as the crack length increased during crack propagation, obviously a fall in the applied load would assist crack arrest; (c) the tapered-double-cantilever-beam specimen has a poor geometrical stability factor which hinders the attainment of stable crack growth¹⁰, especially when a relatively large crack-length to specimen-length ratio is employed²², as in the present experiments. Third, within the time-scale of the current experiments, there was no discernible minimum value of G_{1c} , below which joint failure did not occur.

Determination of the creep modulus

The creep modulus, $E(t)$, of the epoxide adhesive is

shown as a function of time in Figure 5 and these results clearly demonstrate that $E(t)$ is also a function of the applied stress level, i.e. the epoxide material exhibits non-linear viscoelastic behaviour. An empirical, curve-fitting exercise revealed that the value of $E(t)$ in GPa could be represented by:

$$E(t) = 2.27361 + 0.33261 \ln t - 0.02076 (\ln t)^2 + 0.02192 \sigma - 0.01175 \sigma \ln t + 0.00052 \sigma (\ln t)^2 \quad (3)$$

where σ is the applied stress level (MPa) and t the time (sec). The average difference between the experimental values of $E(t)$ shown in Figure 5 and values calculated from equation (3) is 7.0%.

DISCUSSION

A failure criterion

It had been hoped that the adhesive fracture energy would prove to be a working criterion for the long-term stability of these structural adhesive joints upon being stressed. However, while it had been expected that the value of G_{1c} might well have been dependent upon such variables as test temperature and crack velocity, its dependence on a parameter such as an incubation time cast grave doubts as to its usefulness as a failure criterion.

Nevertheless, a unique failure criterion may be derived by considering the fracture behaviour from the viewpoint of the crack opening displacement model of an elastic-plastic material²³⁻²⁵ the deformation of which is elastic up to the yield stress, σ_y , and then becomes fully plastic. The plastic zone at a crack tip, according to this model, is shown schematically in Figure 6, where δ is the crack opening displacement and r_y is the radius of the plastic zone at the crack tip.

Now, in plane-strain, the plastic zone size, r_{1y} , is given by²³:

$$r_{1y} = \frac{K_I^2}{6\pi\sigma_y^2} \quad (4)$$

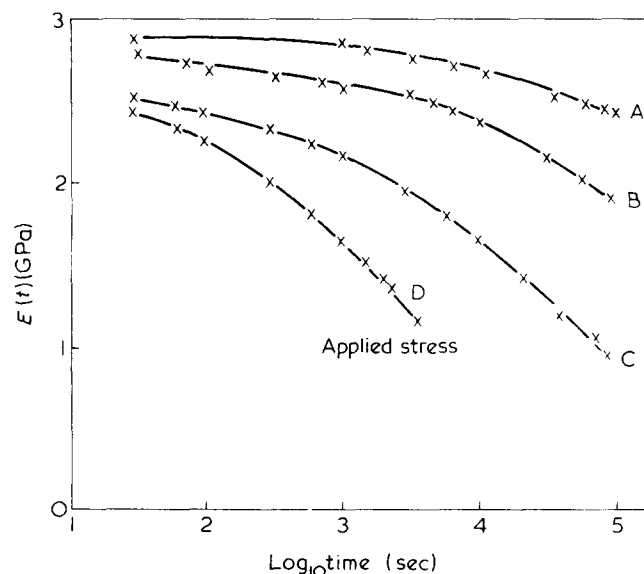


Figure 5 The creep modulus, $E(t)$, of the epoxide adhesive as a function of time: A, 18.5; B, 36.1; C, 48.0; D, 53.4 MPa

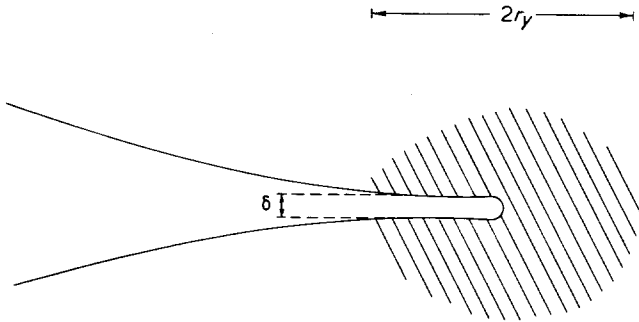


Figure 6 Schematic drawing of the crack opening displacement model of an elastic-plastic material

where K_I is the stress-intensity factor, related to G_I by^{19,23,24}:

$$K_I^2 = \frac{EG_I}{(1-\nu^2)} \quad (5)$$

where E is the modulus of the adhesive and ν its Poisson's ratio. By combining equations (4) and (5) to eliminate K_I :

$$r_{Iy} = \frac{G_I E}{6\pi(1-\nu^2)\sigma_y^2} \quad (6)$$

Now for many polymers^{26,27}, including epoxide resins²⁸, it has been shown that the yield strain, ϵ_y , is largely insensitive to both strain rate and temperature and thus equation (6) may be simplified if ϵ_y is taken as constant and

$$\sigma_y = E\epsilon_y \quad (7)$$

Substituting equation (7) into (6):

$$r_{Iy} = \frac{G_I}{6\pi(1-\nu^2)\epsilon_y^2 E} \quad (8)$$

At fracture, $r_{Iy} = r_{Iyc}$ and $G_I = G_{Ic}$. Now it has been shown that both G_{Ic} and E are time-dependent. Therefore:

$$r_{Iyc} = \frac{1}{6\pi(1-\nu^2)\epsilon_y^2} \cdot \frac{G_{Ic}}{E(t)} \quad (9)$$

Thus, if the value of $G_{Ic}/E(t)$ is a constant over the time-scale of the experiments, a constant value of r_{Iyc} might be deduced which would provide a unique failure criterion for the fracture of these structural adhesive joints. Indeed Williams and coworkers^{12,27} have recently shown that a constant r_{yc} criterion, derived from a Dugdale line-plastic-zone model, is valid for poly(methyl methacrylate) and polycarbonate over a wide range of test temperatures and rates.

Calculations of r_{Iyc}

To calculate a value of r_{Iyc} values of $E(t)$, G_{Ic} , ϵ_y and ν are required.

Now, since the epoxide adhesive exhibits non-linear viscoelastic behaviour, derivation of pertinent values of $E(t)$, from either Figure 5 or from equation (3), requires that an appropriate value for the applied stress level, σ , be selected. A typical uniaxial stress-strain curve for the epoxide resin is shown in Figure 7 and, since the material is relatively brittle, with no evidence of bulk yielding, no yield-load drop is recorded. A 'yield point' was therefore

defined as the point of intersection of two tangent lines on the stress-strain curve²⁹ and this value, σ_c , taken as the appropriate value of σ to use for deducing $E(t)$. The value of σ_c from Figure 7 is 42 MPa and was not significantly dependent upon the strain-rate employed.

Experimentally obtained values of G_{Ic} were taken from Figure 4 and values of $E(t)$, at a stress-level of 42 MPa and at a corresponding time, t , ascertained either by interpolation of Figure 5 or from equation (3). Values of G_{Ic} and $E(t)$ so determined are plotted in Figure 8 and both

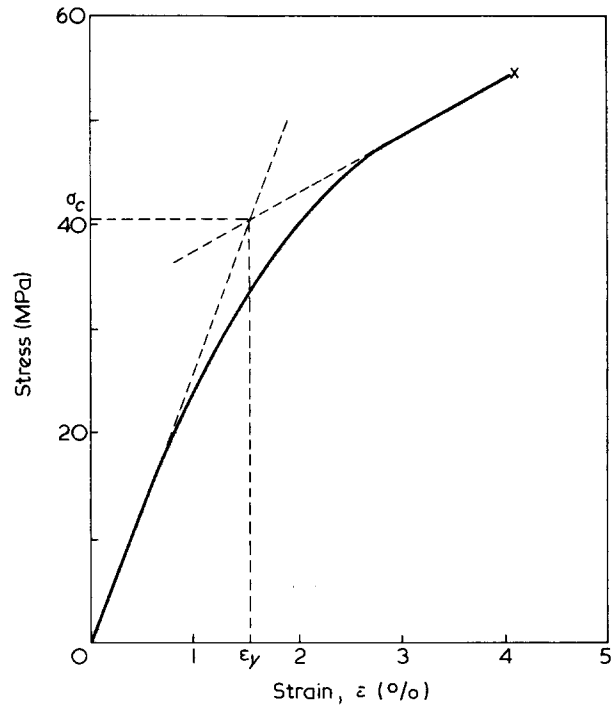


Figure 7 Typical uniaxial stress-strain curve of the epoxide material

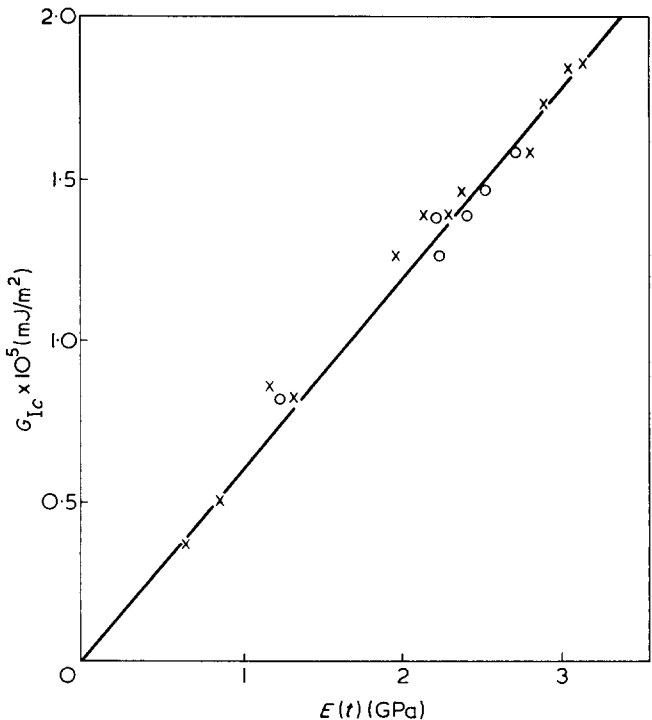


Figure 8 The adhesive fracture energy, G_{Ic} , as a function of the corresponding value of the creep modulus, $E(t)$, of the adhesive. O, for values of $E(t)$ interpolated from Figure 5. X, for values of $E(t)$ calculated from equation (3)

Table 1 Yield-strain, ϵ_y , as a function of strain-rate

Log_{10} (strain-rate) (sec^{-1})	Yield strain, ϵ_y
-2.15	0.016
-2.55	0.013
-2.85	0.015
-3.15	0.015
-4.15	0.018
-4.55	0.014

methods of deducing $E(t)$ yield a linear proportionality between G_{Ic} and $E(t)$ (having a combined correlation coefficient of 0.984). $G_{Ic}/E(t)$ is therefore constant and has a value of $0.059 \pm 0.006 \mu\text{m}$. This means that the value of r_{Iyc} is a constant over the entire time-scale of eight decades, over which the fracture experiments were conducted, and thus provides a unique failure criterion.

Values of 'yield strain' were determined from the uniaxial stress-strain curves as exemplified in Figure 7, and are shown in Table 1. The yield strain, ϵ_y is not significantly dependent upon the strain-rate employed and its mean value is 0.015.

Thus, taking the value of ν of the epoxide adhesive as 0.35, the value of r_{Iyc} from equation (9) is $16 \mu\text{m}$. If, in ascertaining the values of $E(t)$, a stress-level, σ_c , of, say, 36 or 48 MPa had been chosen, (instead of the 42 MPa value used above) a constant value of r_{Iyc} would still have been obtained, but its value would have been $13 \mu\text{m}$ or $19 \mu\text{m}$ respectively. Thus, the hypothesis that a constant value of r_{Iyc} provides a unique failure criterion, is not dependent upon the value of σ_c chosen for deducing values of $E(t)$.

Furthermore, a constant r_{Iyc} criterion implies that there is also a critical crack opening displacement, δ_c , for fracture which may be deduced from¹²:

$$\delta_c = \frac{G_{Ic}}{E(t)\epsilon_y(1-\nu^2)} \quad (10)$$

The value of δ_c so determined is $4.5 \mu\text{m}$.

Finally, the wider implications of the proposed constant r_{Iyc} criterion may be considered. This is a criterion for the onset of crack propagation but the total time-to-failure, t_f , of a pre-cracked structural adhesive joint is given by:

$$t_f = t_i + t_p \quad (11)$$

where t_i is the incubation time and t_p the time the crack takes to propagate through the specimen. In the present experiments $t_i \gg t_p$, and hence $t_i \approx t_f$, and thus the attainment of the critical value of r_{Iy} not only provides a criterion for the onset of crack propagation but also provides one for total fracture of the structure. However, for other adhesive/geometry combinations, t_p may well not be negligible and, in such cases, G_{Ic} as a function of t_i , rather than t_f , must be used to deduce the value of r_{Iyc} .

CONCLUSIONS

The long-term strength of stressed, structural adhesive joints has been investigated and the following main conclusions reached:

(a) A linear relationship exists between the applied adhesive fracture energy, G_{Ic} , and the logarithmic failure time; the failure time decreases as the value of G_{Ic} is increased.

(b) Within the time-scale of the present experiments no discernible minimum value of G_{Ic} , below which joint failure did not occur, was recorded.

(c) From a fracture mechanics analysis it has been demonstrated that there is a critical value of the plastic zone size, r_{Iyc} , at the crack tip at which fracture occurs. This gives a unique failure criterion for the fracture of these joints over eight decades of failure time. A value for r_{Iyc} of $16 \mu\text{m}$ is indicated.

ACKNOWLEDGEMENTS

The authors wish to thank Mr B. V. Howes and Mr M. Bergh for their assistance in obtaining the creep modulus data and also Mr W. A. Dukes for helpful discussions.

[© Crown copyright. Reproduced with permission of the Controller, HMSO, London, 1976.]

REFERENCES

- Andrews, E. H. 'Fracture in Polymers', Oliver & Boyd, London, 1968
- Ripling, E. J., Mostovoy, S. and Patrick, R. L. *Mater. Res. Stand.* 1964, 4, 129
- Malyshev, B. M. and Salganik, R. L. *Int. J. Fract. Mech.* 1965, 1, 114
- Berry, J. P. *J. Polym. Sci.* 1961, 59, 197
- Mostovoy, S. and Ripling, E. J. *Appl. Polym. Symp.* 1972, 19, 395
- Gledhill, R. A. and Kinloch, A. J. *J. Mater. Sci.* 1975, 10, 1261
- Phillips, D. C. and Scott, J. M. *J. Mater. Sci.* 1974, 9, 1205
- Mai, Y. W. *J. Adhes.* 1975, 7, 141
- Ripling, E. J., Mostovoy, S. and Bersch, C. *J. Adhes.* 1971, 3, 145
- Mai, Y. W. and Atkins, A. G. *J. Mater. Sci.* 1975, 10, 2000
- Radon, J. C. and Johnson, F. A. *J. Polym. Sci. (A-1)* 1973, 11, 1995
- Marshall, G. P., Coutts, L. H. and Williams, J. G. *J. Mater. Sci.* 1974, 9, 1409
- Gledhill, R. A. and Kinloch, A. J. to be published
- Di Benedetto, A. T. *J. Macromol. Sci. (B)* 1973, 7, 657
- Selby, K. and Miller, L. E. *J. Mater. Sci.* 1975, 10, 12
- Griffiths, R. and Holloway, D. G. *J. Mater. Sci.* 1970, 5, 302
- Mostovoy, S., Ripling, E. J. and Bersch, C. F. *J. Adhes.* 1971, 3, 125
- Mostovoy, S., Crosley, P. and Ripling, E. J. *J. Mater.* 1967, 2, 661
- Trantina, G. G. *J. Compos. Mater.* 1972, 6, 192
- Howes, B. V. *ERDE Tech. Rep.* 170, 1974
- Howes, B. V. *ERDE Tech. Memo* 166, to be published
- Mai, Y. W., Atkins, A. G. and Caddell, R. M. *Int. J. Fract.* 1975, 11, 939
- Knott, J. F. 'Fundamentals of Fracture Mechanics', Butterworths, London, 1973
- Williams, J. G. 'Stress Analysis of Polymers', Longmans, London, 1973
- Bascom, W. D., Cottingham, R. L., Jones, R. L. and Peyser, P. *J. Appl. Polym. Sci.* 1975, 19, 2545
- Williams, J. G. *Int. J. Fract. Mech.* 1972, 8, 393
- Marvin, M. and Williams, J. G. *J. Mater. Sci.* 1975, 10, 1883
- Moehlenpach, A. E., Ishai, O. and Di Benedetto, A. T. *J. Appl. Polym. Sci.* 1969, 13, 1231
- Ward, I. M. *J. Mater. Sci.* 1971, 6, 1397

Photoelastic non-equilibrium behaviour of natural rubber networks

F. de Candia, A. Tagliatela and V. Vittoria

Laboratorio di Ricerche su Tecnologia dei Polimeri e Reologia, CNR, 80072 Arco Felice (Napoli), Italy

(Received 9 December 1975; revised 22 March 1976)

INTRODUCTION

In previous papers¹⁻⁴ we have reported results from studying the elastic and thermoelastic behaviour of rubber-like networks obtained by vulcanizing elastomers such as natural rubber and *cis*-polybutadiene in the presence of a solvent, and analysing the mechanical behaviour in the bulk dry state. A feature of such materials is that they follow the Gaussian equation for the rubber elasticity^{5,6} very closely.

This feature is related to the particular vulcanization technique and thus to the topology of the network. The conformational state of the network chains which in the preswollen rubbers are in a supercoiled state^{1,2}, is particularly relevant. Taking into account this property, a working hypothesis has been given, which suggests that in the monodirectional elongation the chain supercoiling is a direct cause of a smaller degree of orientation in the strain direction, when compared to a conventional vulcanizate at the same strain value. Therefore, the tendency for chain-chain interactions or chain-chain aggregations induced by the strain to arise is smaller in a preswollen network than in a conventional vulcanizate. Moreover, the supercoiling, and the consequent high concentration of crosslinking points may be, in the same way, a direct cause of a smaller degree of order in the rubber-like network, such as an order resembling chain bundles.

This hypothesis is related to the main hypothesis that deviations from the rubber elasticity theory can be related to the presence in the amorphous material of some degree of order present before or induced by the strain^{7,8}.

In other papers^{9,10} our aim was to give experimental support to the suggested effects of the supercoiling on the mechanical behaviour. Results ob-

tained by analysing the viscoelastic behaviour of an ethylene-propylene copolymer⁹, and the crystallization kinetics under stress of natural rubber¹⁰ seem to give support to our hypothesis.

In the present paper we have studied the photoelastic behaviour in strain cycles where the maximum strain is increased step by step. The materials used were natural rubber vulcanized both in bulk and in the swollen state. The results are discussed in the light of these two different vulcanization techniques and give more direct evidence to our model.

EXPERIMENTAL AND RESULTS

The networks analysed were prepared in the usual way¹⁻⁴. The preswollen network, denoted as Gaussian-NR, was vulcanized in a chlorobenzene solution with the following composition: 0.3 rubber, 0.7 solvent.

The initiator was dicumylperoxide (3% of the polymer weight), and vulcanization was carried out at 120°C for 2 h. The conventional network, denoted as normal-NR, was vulcanized at 145°C for 45 min using 0.3% of dicumylperoxide as initiator. The stress-strain plots for these two samples reported in terms of the Mooney-Rivlin equation⁵, and corrected for the effect of the solvent during vulcanization¹, give values of the same order for the molecular weight of the network chains, M_c . In particular M_c is 10 800 and 8100 for the normal-NR and Gaussian-NR, respectively.

The photoelastic measurements were carried out using a system that gives the force and the birefringence values. The force was measured with a force transducer, and the birefringence was detected following the Senarmont method¹¹. The hysteresis photoelastic loops were obtained by stretching and relaxing the sample step by step with

5 min intervals between two successive points. For each sample four hysteresis loops were obtained with a gradually increased maximum strain value. In the first loop α_{\max} was 2, 3 in the second, and so on up to 5, where α_{\max} is the maximum strain ratio in a given hysteresis loop.

In *Figure 1* results obtained with the normal-NR are shown. The birefringence Δn is plotted vs. the true stress $\tau\alpha$. The arrows indicate the increasing and decreasing strain. In *Figure 2*, results obtained with the Gaussian-NR are reported. In *Table 1* we report the quantitative data for the photoelastic hysteresis loops in terms of the functions ϕ and ϕ_{rel} . ϕ is the hysteresis area, while ϕ_{rel} is the relative amount of ϕ with respect to the total integral of the function Δn vs. $\tau\alpha$.

DISCUSSION

The photoelastic measurements, as carried out in this paper, can give evidence of irreversibility phenomena in the time scale of the experiment. In fact, the birefringence is a physical quantity which is a direct measure of the optical anisotropy of the sample, where the optical anisotropy is the effect of the chain orientation in the strain direction. As is well known in the literature⁵, and as explained in a previous paper¹², if the chain orientation is partly irreversible in the time scale of the experiment, we observe an hysteresis loop in the photoelastic plots. The irreversibility of the chain orientation is related to a reduced conformational freedom, which can be an effect of chain interaction or aggregation induced by the deformation, or, in more drastic situations, due to chain crystallization.

Considering the present work, the photoelastic hysteresis loops can promise a direct support to our picture regarding the topology of the preswollen networks and the relation between the particular topology and the Gaussian mechanical behaviour observed for these materials. In the light of these few considerations we can analyse the

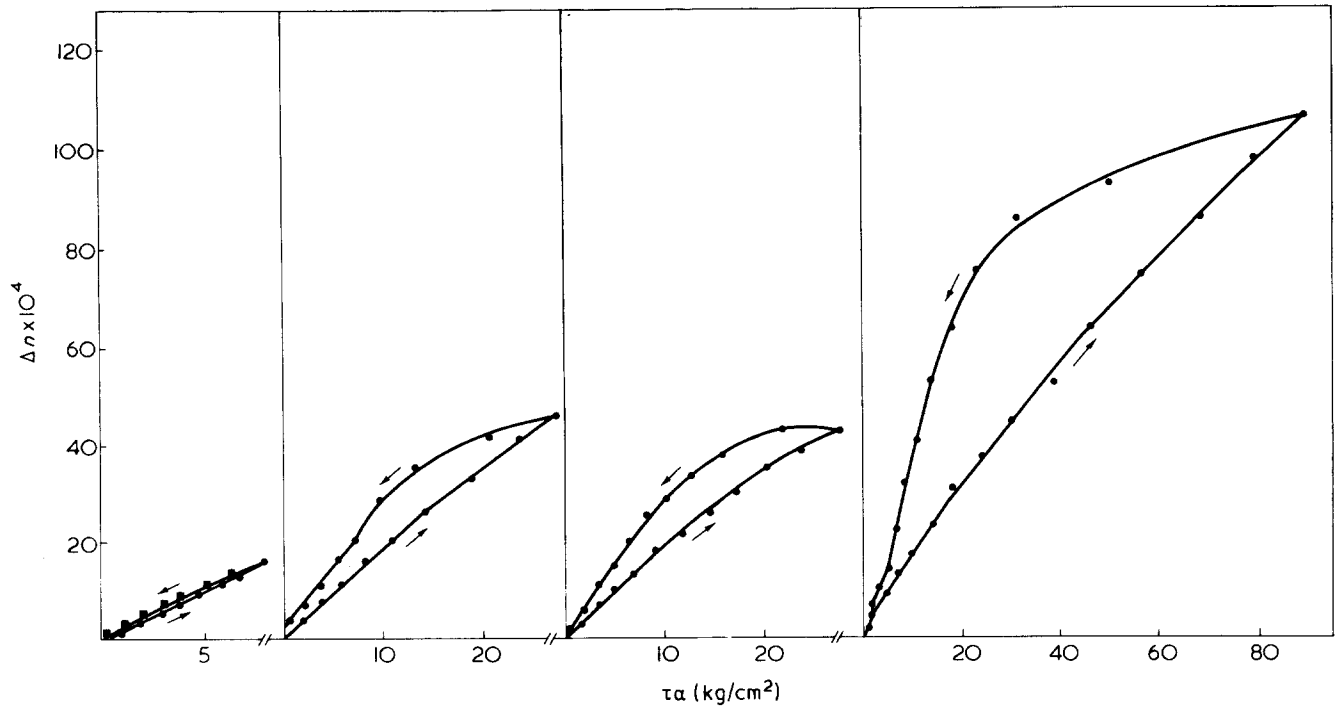


Figure 1 Photoelastic hysteresis loops obtained with the normal-NR. The maximum value of the strain is increased from 2 to 5 going from left to right. The birefringence $\Delta n \times 10^4$ is reported versus the true stress $\tau\alpha$ in kg/cm^2 . The arrows indicate the increasing and decreasing strain

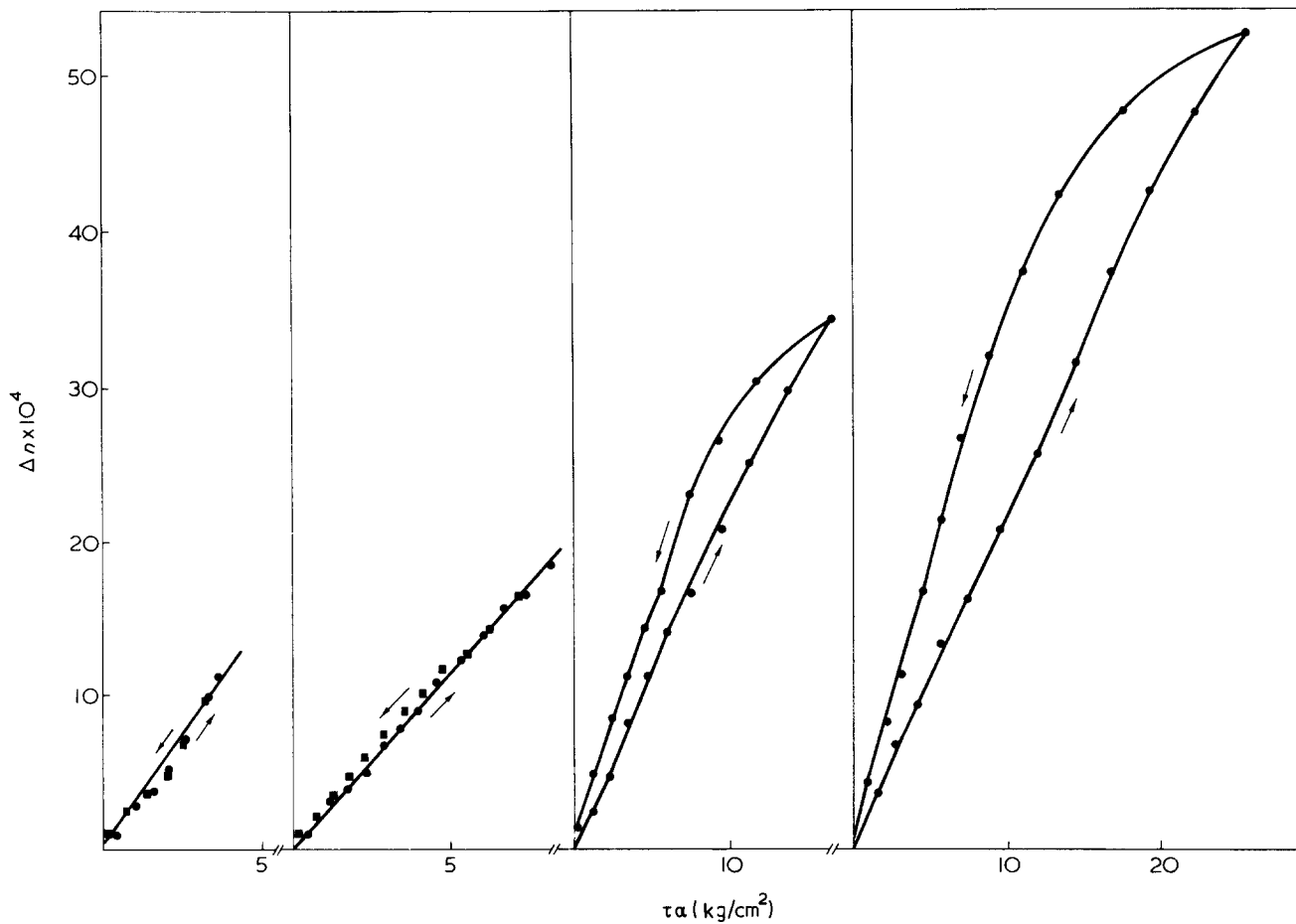


Figure 2 Photoelastic hysteresis loops obtained with the Gaussian-NR. Maximum strain values as in Figure 1 from 2 to 5 going from left to right

Table 1 Numerical values relative to the photoelastic hysteresis loops

Sample	α_{\max}	$\phi \times 10^4$ (kg/cm ²)	ϕ_{rel}
Normal-NR	2	6.77	0.10
	3	167.60	0.18
	4	223.54	0.22
	5	1914.88	0.28
Gaussian-NR	2	0	0
	3	0	0
	4	54.92	0.13
	5	203.80	0.24

results obtained in the summarized form of *Table 1*. The term ϕ in *Table 1* is a quantitative measure of the degree of irreversibility of the deformation process.

As shown in *Table 1* the experimental data indicate a drastic difference between the normal-NR and the Gaussian-NR. For the latter, in fact, at α_{\max} 2 and 3, a completely reversible behaviour is observed, while at α_{\max} 4 and 5, even if ϕ indicates the presence of a deformation mechanism irreversible in the time scale of the experiment, the numerical values for ϕ are clearly smaller than the corresponding values detected for the normal-NR sample. The effect is not so drastic, but equally evident, on ϕ_{rel} , for which the difference seems to decrease on increasing the strain.

This is in good agreement with the crystallization data previously pub-

lished¹⁰. In other words the samples of normal-NR and Gaussian-NR give evidence of a very different degree of irreversibility of the photoelastic behaviour in the time scale of the experiment. In the light of this evidence it seems possible to state that the ideal mechanical behaviour of the preswollen samples is related to higher degree of reversibility of the deformation mechanism.

Considering the particular topology of the preswollen samples, and the significance of the photoelastic data, these results support our model, suggesting the ideal behaviour to be a consequence of the smaller tendency of these materials to give rise to chain-chain aggregations, or, in general, to interaction before or induced by the strain. In fact, even if other mechanisms of relaxation can give effects of irreversibility, the photoelastic measurements indicate that an important role is played on relaxation by a residual orientation of the chains with a smaller conformational mobility, related to chain-chain effects induced on stretching.

Finally, we wish to pay some attention to another feature of the preswollen networks, i.e. the number of physical entanglements. In fact, this particular vulcanization technique is the cause of a reduced concentration of entanglements in the volume unit^{1,13}. We believe that this property plays a role at

the level of the mechanical behaviour¹³, but, at the same time, the interaction effects are believed to have greater relevance.

Results of this and of a previous paper¹⁰ seem to give firm support to the last hypothesis.

REFERENCES

- Price, C., Allen, G., de Candia, F., Kirkham, M. and Subramanian, A. *Polymer* 1970, **11**, 486
- de Candia, P. *Macromolecules* 1972, **5**, 102
- de Candia, F., Amelino, L. and Price, C. *J. Polym. Sci. (A-2)* 1972, **10**, 975
- Price, C., Evans, K. A. and de Candia, F. *Polymer* 1973, **14**, 338
- Treolar, L. R. G. 'The Physics of Rubber Elasticity', 3rd edn, Clarendon Press, Oxford, 1975
- Flory, P. J. *J. Am. Chem. Soc.* 1956, **78**, 5222
- Kargin, V. A., Ya Berestneva, Z. and Kalashnikova, V. G. *Usp. Khim.* 1967, **36**, 203
- Dusek, K. and Prins, W. *Adv. Polym. Sci.* 1969, **6**, 1
- de Candia, F. and Vittoria, V. *J. Appl. Polym. Sci.* 1973, **17**, 3243
- de Candia, F., Romano, G. and Vittoria, V. *Makromol. Chem.* 1974, **175**, 2983
- Flügge, S. 'Encyclopedia of Physics', Springer Verlag, Berlin, 1958, Vol 6
- de Candia, F., Tagliatalata, A. and Vittoria, V. *J. Appl. Polym. Sci.* in press
- Ong, C. S. M. and Stein, R. S. *J. Polym. Sci. (Polym. Phys. Edn)* 1974, **12**, 1599

Filler enhancement of rubber modulus

David W. Southwart

Dunlop Ltd, Precision Rubbers Division, Shephed, Loughborough, Leicestershire LE12 9EQ, UK

(Received 28 February 1976; revised 2 April 1976)

Many attempts have been made to relate the modulus of filled vulcanizates, showing the phenomenon termed reinforcement, to the modulus of the unfilled vulcanizate and the filler concentration.

Several modifications of the Einstein viscosity equation have been developed and applied, including the introduction of a shape factor to allow for the asymmetric nature of carbon black aggregates¹.

Many workers have chosen to express data in the form of 'modulus enhancement', equal to E/E_0 where E and E_0 are the modulus of filled and unfilled vulcanizates respectively. Not

only is modulus dependent on such factors as type of filler, strain, deformation history, test method etc., but so also is the modulus enhancement. Mullins and Tobin's² static Young's modulus data obtained at small extensions, on initial extension of natural rubber vulcanizates filled with HAF black, fit the equation:

$$E/E_0 = 1 + 0.67fc + 1.62f^2c^2 \quad (1)$$

where c is the volume fraction of filler, when f the shape factor is given a value of 6.5 (*Table 1*).

Payne's³ data from his study of the dynamic properties of rubbers in shear

show that the enhancement of in-phase modulus is reduced markedly as strain amplitude is increased; they further show how heat treatment of the mix reduces the enhancement. His data for butyl rubber filled with HAF black are given in *Table 2*, in comparison with theoretical values now calculated from equation (1) after putting $f = 6.5$. With normally compounded vulcanizates it is clearly the enhancement at high strain which approximates to the theoretical relationship. Heat treatment enormously reduces the effect of strain except at very high filler concentration.

Sircar and Lamond⁴ have obtained data on a wide range of elastomers filled with a high-structure HAF black. Their dynamic shear moduli values differed slightly from those of Payne, in showing a slight increase to a maximum modulus with very small increases

Table 1 Numerical values relative to the photoelastic hysteresis loops

Sample	α_{\max}	$\phi \times 10^4$ (kg/cm ²)	ϕ_{rel}
Normal-NR	2	6.77	0.10
	3	167.60	0.18
	4	223.54	0.22
	5	1914.88	0.28
Gaussian-NR	2	0	0
	3	0	0
	4	54.92	0.13
	5	203.80	0.24

results obtained in the summarized form of *Table 1*. The term ϕ in *Table 1* is a quantitative measure of the degree of irreversibility of the deformation process.

As shown in *Table 1* the experimental data indicate a drastic difference between the normal-NR and the Gaussian-NR. For the latter, in fact, at α_{\max} 2 and 3, a completely reversible behaviour is observed, while at α_{\max} 4 and 5, even if ϕ indicates the presence of a deformation mechanism irreversible in the time scale of the experiment, the numerical values for ϕ are clearly smaller than the corresponding values detected for the normal-NR sample. The effect is not so drastic, but equally evident, on ϕ_{rel} , for which the difference seems to decrease on increasing the strain.

This is in good agreement with the crystallization data previously pub-

lished¹⁰. In other words the samples of normal-NR and Gaussian-NR give evidence of a very different degree of irreversibility of the photoelastic behaviour in the time scale of the experiment. In the light of this evidence it seems possible to state that the ideal mechanical behaviour of the preswollen samples is related to higher degree of reversibility of the deformation mechanism.

Considering the particular topology of the preswollen samples, and the significance of the photoelastic data, these results support our model, suggesting the ideal behaviour to be a consequence of the smaller tendency of these materials to give rise to chain-chain aggregations, or, in general, to interaction before or induced by the strain. In fact, even if other mechanisms of relaxation can give effects of irreversibility, the photoelastic measurements indicate that an important role is played on relaxation by a residual orientation of the chains with a smaller conformational mobility, related to chain-chain effects induced on stretching.

Finally, we wish to pay some attention to another feature of the preswollen networks, i.e. the number of physical entanglements. In fact, this particular vulcanization technique is the cause of a reduced concentration of entanglements in the volume unit^{1,13}. We believe that this property plays a role at

the level of the mechanical behaviour¹³, but, at the same time, the interaction effects are believed to have greater relevance.

Results of this and of a previous paper¹⁰ seem to give firm support to the last hypothesis.

REFERENCES

- Price, C., Allen, G., de Candia, F., Kirkham, M. and Subramanian, A. *Polymer* 1970, **11**, 486
- de Candia, P. *Macromolecules* 1972, **5**, 102
- de Candia, F., Amelino, L. and Price, C. *J. Polym. Sci. (A-2)* 1972, **10**, 975
- Price, C., Evans, K. A. and de Candia, F. *Polymer* 1973, **14**, 338
- Treolar, L. R. G. 'The Physics of Rubber Elasticity', 3rd edn, Clarendon Press, Oxford, 1975
- Flory, P. J. *J. Am. Chem. Soc.* 1956, **78**, 5222
- Kargin, V. A., Ya Berestneva, Z. and Kalashnikova, V. G. *Usp. Khim.* 1967, **36**, 203
- Dusek, K. and Prins, W. *Adv. Polym. Sci.* 1969, **6**, 1
- de Candia, F. and Vittoria, V. *J. Appl. Polym. Sci.* 1973, **17**, 3243
- de Candia, F., Romano, G. and Vittoria, V. *Makromol. Chem.* 1974, **175**, 2983
- Flügge, S. 'Encyclopedia of Physics', Springer Verlag, Berlin, 1958, Vol 6
- de Candia, F., Tagliatalata, A. and Vittoria, V. *J. Appl. Polym. Sci.* in press
- Ong, C. S. M. and Stein, R. S. *J. Polym. Sci. (Polym. Phys. Edn)* 1974, **12**, 1599

Filler enhancement of rubber modulus

David W. Southwart

Dunlop Ltd, Precision Rubbers Division, Shephed, Loughborough, Leicestershire LE12 9EQ, UK

(Received 28 February 1976; revised 2 April 1976)

Many attempts have been made to relate the modulus of filled vulcanizates, showing the phenomenon termed reinforcement, to the modulus of the unfilled vulcanizate and the filler concentration.

Several modifications of the Einstein viscosity equation have been developed and applied, including the introduction of a shape factor to allow for the asymmetric nature of carbon black aggregates¹.

Many workers have chosen to express data in the form of 'modulus enhancement', equal to E/E_0 where E and E_0 are the modulus of filled and unfilled vulcanizates respectively. Not

only is modulus dependent on such factors as type of filler, strain, deformation history, test method etc., but so also is the modulus enhancement. Mullins and Tobin's² static Young's modulus data obtained at small extensions, on initial extension of natural rubber vulcanizates filled with HAF black, fit the equation:

$$E/E_0 = 1 + 0.67fc + 1.62f^2c^2 \quad (1)$$

where c is the volume fraction of filler, when f the shape factor is given a value of 6.5 (*Table 1*).

Payne's³ data from his study of the dynamic properties of rubbers in shear

show that the enhancement of in-phase modulus is reduced markedly as strain amplitude is increased; they further show how heat treatment of the mix reduces the enhancement. His data for butyl rubber filled with HAF black are given in *Table 2*, in comparison with theoretical values now calculated from equation (1) after putting $f = 6.5$. With normally compounded vulcanizates it is clearly the enhancement at high strain which approximates to the theoretical relationship. Heat treatment enormously reduces the effect of strain except at very high filler concentration.

Sircar and Lamond⁴ have obtained data on a wide range of elastomers filled with a high-structure HAF black. Their dynamic shear moduli values differed slightly from those of Payne, in showing a slight increase to a maximum modulus with very small increases

Table 1 Young's modulus enhancement for natural rubber vulcanizates filled with HAF black

Filler volume fraction	As determined	From equation (1)
0.0383	1.30	1.27
0.0611	1.49	1.52
0.0954	2.01	2.04
0.144	3.12	3.05
0.233	8.77	5.73

Data from ref 2

in dynamic strain amplitude. The data in *Table 3* show that modulus enhancement is dependent on both the strain and the polymer type. Values calculated from equation (1), with $f = 6.5$, depend on the polymer density but range from 5.6 to 8.0, and fall between those quoted for enhancement at the two strains (*Table 3*).

Other data confirm the dependence involved on strain and polymer type but indicate that the modulus variation from polymer to polymer for a given filler and concentration, may be less than the variation of the modulus enhancement value (*Table 4*). This is particularly noticeable with a filler such as Aerosil 300 which gives values far in excess of those predicted by equation (1) with $f = 6.5$.

Previous workers^{5,6} have had some success in fitting a modified Einstein equation to their data by making some allowance for bound rubber determined on the unvulcanized polymer/filler mixture. The bound rubber, with a particular filler, depends on the polymer and may at least qualitatively explain the differences in modulus enhancement; but neither the decrease in dynamic modulus with increase of strain amplitude, nor the decrease due to heat treatment (*Table 2*), can be attributed to a decrease in bound rubber.

Unvulcanized silicone rubber/silica mixes, at low strains, are sufficiently elastic to allow Young's modulus values to be determined⁷. Some such mixes on remilling show a decrease of Young's modulus with no significant change in bound rubber; other mixes on remilling and subsequent storage show an increase of Young's modulus accompanied by an increase in bound rubber.

These several effects and anomalies can, however, be explained in terms of three types of structure which are assumed to be present: adsorbed rubber, interparticular rubber and filler-filler structure^{8,9}.

Generally, straining temporarily

Table 2 Dynamic modulus enhancement for butyl rubber vulcanizates filled with HAF black

Filler volume concentration	Normally compounded		Heat treated		From equation (1)
	Low strain (<0.1%)	High strain (>100%)	Low strain (<0.1%)	High strain (>100%)	
0.092	3.00	2.04	2.00	1.70	1.98
0.132	5.26	2.39	2.30	2.04	2.77
0.168	8.70	3.04	2.65	2.17	3.66
0.202	19.3	3.91	4.13	2.96	4.67
0.232	42.6	4.35	6.26	3.52	5.69
0.288	62.6	5.43	27.0	5.00	7.93
0.336	113.0	6.52	95.7	6.09	10.2
0.388	217.4	13.0	221.7	12.6	13.0

Data from ref 3

Table 3 Dynamic modulus, and modulus enhancement, for vulcanizates filled with high structure HAF black (60 phr)

Polymer type	Low strain (~0.2%)		High strain (200%)	
	Maximum modulus (MPa)	Modulus enhancement	Modulus (MPa)	Modulus enhancement
SBR	23.8	11.9	5.0	2.00
BR	16.0	8.0	4.75	1.85
NR	17.2	8.6	4.40	2.00
IR	14.4	6.9	3.5	2.14
NBR	43.6	15.6	5.0	2.17
CR	37.5	15.6	5.5	8.50
EPDM	31.7	10.2	4.8	1.60
CI-IIR	31.3	24.1	3.2	1.68

Data from ref 4

Table 4 The effect of filler (50 phr) and polymer type on modulus, and modulus enhancement, of vulcanizates

Polymer type	Modulus enhancement							
	Young's modulus (MPa)			From equation (1)				
	No filler	SAF black	Aerosil 300	Actual	SAF black	Aerosil 300	SAF black	Aerosil 300
Natural rubber	0.9	2.3	22.5	2.6	25	4.7	3.8	
Nitrile rubber	1.2	4.9	22.8	4.1	19	5.1	4.1	
Silicone rubber	0.5	5.0	~27*	10	~54	5.1	4.1	

Data from ref 8; *value obtained by extrapolation of data for 0 to 40 phr of Aerosil 300

disturbs any three-dimensional filler-filler structure present and, in a vulcanizate, reversibly reduces the contribution of this structure to the modulus without any change in the other two structures. This may be the explanation of the quoted dynamic results, and of the comparable effects in a silicone rubber/silica vulcanizate⁸.

More severe straining, while decreasing the number of contacts, or near contacts, between filler particles, may expose hitherto unreacted sites on the filler surface to active sites on the

polymer. This can lead to an increase of adsorbed rubber and/or interparticular rubber, and consequently to an increase in modulus and bound rubber; it occurs in the case of the remilling of the second class of silicone rubber/silica mixes mentioned above.

Improvement of filler dispersion e.g. by hot milling of butyl rubber/HAF black mixes, reduces the extent of filler-filler structure and its contribution to modulus; there may be a concurrent increase in polymer-filler interaction, exhibited as an increase in bound rubber etc.

If filler dispersion is good, and no unreacted filler sites exist, filler–filler structure is at a low level and a high degree of straining will lead to the re-arrangement of the interparticular rubber chains (as postulated by Boonstra¹⁰), or to their scission. The former will allow partial reversibility, the latter irreversibility, of modulus reduction; bound rubber is not significantly changed because any broken chain ends will still be present as adsorbed rubber. This is the situation occurring in many systems and the remilling of the first class (see above) of unvulcanized silicone rubber/silica mixes provides a good example of the phenomenon.

The properties of a vulcanizate depend upon the concentrations of the three structures when crosslinking

takes place, polymer in the form of adsorbed rubber, interparticular rubber and matrix rubber being involved.

Until methods can be found for quantifying the structures, and the various changes, during vulcanization, it appears unlikely that the problem of modulus enhancement will be solved.

ACKNOWLEDGEMENTS

Thanks are due to the Directors of Dunlop Limited for permission to publish this Note, and to Dr C. M. Blow for help in its preparation.

REFERENCES

- 1 Guth, E. *J. Appl. Phys.* 1945, 16, 20; *Proc. 2nd Rubber Technol. Conf.* 1948 p 353; *Rubber Chem. Technol.*

- 1950, 23, 635
- 2 Mullins, L. and Tobin, N. R. *J. Appl. Polym. Sci.* 1965, 9, 2993; *Rubber Chem. Technol.* 1966, 39, 799
- 3 Payne, A. R. 'Reinforcement of elastomers', (Ed. G. Kraus), Interscience, New York 1965, Ch 3
- 4 Sircar, A. K. and Lamond, T. G. *Rubber Chem. Technol.* 1975, 48, 79
- 5 Brennan, J. J., Jermyn, T. E. and Boonstra, B. B. *J. Appl. Polym. Sci.* 1964, 8, 2687
- 6 Medalia, A. I. *J. Colloid. Interface. Sci.* 1970, 32, 115; *Rubber Chem. Technol.* 1972, 45, 1171; 1973, 46, 877
- 7 Southwart, D. W. and Hunt, T. *J. Inst. Rubber Ind.* 1970, 4, 74
- 8 Southwart, D. W. *PhD Thesis* Loughborough University (1974)
- 9 Southwart, D. W. *Polymer* 1976, 17, 147
- 10 Boonstra, B. B. 'Reinforcement of elastomers', (Ed. G. Kraus), Interscience New York 1965, Ch 16

A re-examination of the necessity of the mosaic concept in polymer crystals

I. R. Harrison

Department of Materials Science, Pennsylvania State University, Pennsylvania 16802, USA

A. Keller and D. M. Sadler

H. H. Wills Physics Laboratory, University of Bristol, Bristol BS8 1TL, UK

and E. L. Thomas

Department of Engineering and Material Science, University of Minnesota, Minneapolis, Minnesota 55455, USA

(Received 18 February 1976; revised 15 April 1976)

We would like to suggest a reappraisal of the notion of mosaic blocks within polymer crystals in the light of the implications of recent diffraction results. The concept has an importance with regard to the fundamental nature of polymer crystals^{1–3} and in addition has a wider significance, since it has become influential in the interpretation of polymer deformation⁴ and mechanical behaviour⁵.

The X-ray diffraction pattern from polymers, ever since their first observations⁶ were noted for their broad diffraction maxima. In view of considerations of inherent polymer disorder, these peak widths were interpreted quite naturally in terms of small crystallite (or 'micelle') size. Polymer crystals were first directly observed by crystallization from dilute solution and subsequently also in the bulk^{7–9}. The crystal entities have been identified as lamellae, with the polymer chains either parallel or at a particular angle ϕ to the lamellar normals. ϕ can have

a value of up to 45°; in polyethylene single crystals it is usually around 30°.

As is well known, the thickness of these lamellae is in the range of 100–300 Å and corresponds to the fold length. Hence the limited size of the crystals along the chain direction has acquired a very specific molecular interpretation and is satisfactorily accounted for by the chain folding behaviour. However, the solution grown crystals were seen to extend laterally over many microns, even tens of microns. In spite of this the X-ray reflections from planes parallel to the chain directions (i.e. $(hk0)$) of collected assemblies of such crystals were still broadened — even if to a somewhat lesser extent — than in the usual polycrystalline bulk material. This indicates that what are seen as single crystals by microscopy do not yield $hk0$ X-ray reflections as sharp as expected from extended regions of a coherent crystal lattice. Nevertheless, when the crystals are extended in the thickness

direction (the so-called chain extended crystals grown under pressure) the $hk0$ reflections are sharp¹⁰.

Measurement of successive orders of diffraction enabled a separation of the line broadening effect into crystal distortion and crystal size components^{1,2}. Although some contribution from the former was established, an effective mosaic size not much greater than the lamellar thickness was found (e.g. 300 Å mosaic size for 130 Å thick polyethylene single crystals). It has now been suggested that there is an intrinsic structural unit corresponding to a mosaic block within the lamellae^{1–3,10,11}. To reach this conclusion it has been assumed¹² that one of the three principle axes which are necessary to describe a mosaic unit is parallel to the chains (along (001) , i.e. $\phi = 0$).

The effective block size assessed in this way increases in proportion with the lamellar thickness, which has led to the postulate of an equilibrium block shape satisfying a Wulff surface criterion¹¹. The blocks themselves are visualized as having slightly differing c axes orientations; the boundaries separating them would thus be twist boundaries¹.

More recently an electron microscope investigation was undertaken in order to observe the postulated blocks directly. It was believed that owing to the misorientations in question the

If filler dispersion is good, and no unreacted filler sites exist, filler–filler structure is at a low level and a high degree of straining will lead to the re-arrangement of the interparticular rubber chains (as postulated by Boonstra¹⁰), or to their scission. The former will allow partial reversibility, the latter irreversibility, of modulus reduction; bound rubber is not significantly changed because any broken chain ends will still be present as adsorbed rubber. This is the situation occurring in many systems and the remilling of the first class (see above) of unvulcanized silicone rubber/silica mixes provides a good example of the phenomenon.

The properties of a vulcanizate depend upon the concentrations of the three structures when crosslinking

takes place, polymer in the form of adsorbed rubber, interparticular rubber and matrix rubber being involved.

Until methods can be found for quantifying the structures, and the various changes, during vulcanization, it appears unlikely that the problem of modulus enhancement will be solved.

ACKNOWLEDGEMENTS

Thanks are due to the Directors of Dunlop Limited for permission to publish this Note, and to Dr C. M. Blow for help in its preparation.

REFERENCES

- 1 Guth, E. *J. Appl. Phys.* 1945, 16, 20; *Proc. 2nd Rubber Technol. Conf.* 1948 p 353; *Rubber Chem. Technol.*

- 1950, 23, 635
- 2 Mullins, L. and Tobin, N. R. *J. Appl. Polym. Sci.* 1965, 9, 2993; *Rubber Chem. Technol.* 1966, 39, 799
- 3 Payne, A. R. 'Reinforcement of elastomers', (Ed. G. Kraus), Interscience, New York 1965, Ch 3
- 4 Sircar, A. K. and Lamond, T. G. *Rubber Chem. Technol.* 1975, 48, 79
- 5 Brennan, J. J., Jermyn, T. E. and Boonstra, B. B. *J. Appl. Polym. Sci.* 1964, 8, 2687
- 6 Medalia, A. I. *J. Colloid. Interface. Sci.* 1970, 32, 115; *Rubber Chem. Technol.* 1972, 45, 1171; 1973, 46, 877
- 7 Southwart, D. W. and Hunt, T. *J. Inst. Rubber Ind.* 1970, 4, 74
- 8 Southwart, D. W. *PhD Thesis* Loughborough University (1974)
- 9 Southwart, D. W. *Polymer* 1976, 17, 147
- 10 Boonstra, B. B. 'Reinforcement of elastomers', (Ed. G. Kraus), Interscience New York 1965, Ch 16

A re-examination of the necessity of the mosaic concept in polymer crystals

I. R. Harrison

Department of Materials Science, Pennsylvania State University, Pennsylvania 16802, USA

A. Keller and D. M. Sadler

H. H. Wills Physics Laboratory, University of Bristol, Bristol BS8 1TL, UK

and E. L. Thomas

Department of Engineering and Material Science, University of Minnesota, Minneapolis, Minnesota 55455, USA

(Received 18 February 1976; revised 15 April 1976)

We would like to suggest a reappraisal of the notion of mosaic blocks within polymer crystals in the light of the implications of recent diffraction results. The concept has an importance with regard to the fundamental nature of polymer crystals^{1–3} and in addition has a wider significance, since it has become influential in the interpretation of polymer deformation⁴ and mechanical behaviour⁵.

The X-ray diffraction pattern from polymers, ever since their first observations⁶ were noted for their broad diffraction maxima. In view of considerations of inherent polymer disorder, these peak widths were interpreted quite naturally in terms of small crystallite (or 'micelle') size. Polymer crystals were first directly observed by crystallization from dilute solution and subsequently also in the bulk^{7–9}. The crystal entities have been identified as lamellae, with the polymer chains either parallel or at a particular angle ϕ to the lamellar normals. ϕ can have

a value of up to 45°; in polyethylene single crystals it is usually around 30°.

As is well known, the thickness of these lamellae is in the range of 100–300 Å and corresponds to the fold length. Hence the limited size of the crystals along the chain direction has acquired a very specific molecular interpretation and is satisfactorily accounted for by the chain folding behaviour. However, the solution grown crystals were seen to extend laterally over many microns, even tens of microns. In spite of this the X-ray reflections from planes parallel to the chain directions (i.e. $(hk0)$) of collected assemblies of such crystals were still broadened — even if to a somewhat lesser extent — than in the usual polycrystalline bulk material. This indicates that what are seen as single crystals by microscopy do not yield $hk0$ X-ray reflections as sharp as expected from extended regions of a coherent crystal lattice. Nevertheless, when the crystals are extended in the thickness

direction (the so-called chain extended crystals grown under pressure) the $hk0$ reflections are sharp¹⁰.

Measurement of successive orders of diffraction enabled a separation of the line broadening effect into crystal distortion and crystal size components^{1,2}. Although some contribution from the former was established, an effective mosaic size not much greater than the lamellar thickness was found (e.g. 300 Å mosaic size for 130 Å thick polyethylene single crystals). It has now been suggested that there is an intrinsic structural unit corresponding to a mosaic block within the lamellae^{1–3,10,11}. To reach this conclusion it has been assumed¹² that one of the three principle axes which are necessary to describe a mosaic unit is parallel to the chains (along (001) , i.e. $\phi = 0$).

The effective block size assessed in this way increases in proportion with the lamellar thickness, which has led to the postulate of an equilibrium block shape satisfying a Wulff surface criterion¹¹. The blocks themselves are visualized as having slightly differing c axes orientations; the boundaries separating them would thus be twist boundaries¹.

More recently an electron microscope investigation was undertaken in order to observe the postulated blocks directly. It was believed that owing to the misorientations in question the

mosaic blocks should be directly visible by diffraction contrast within the electron microscopic image¹³. However, the crystals proved to be uniform in diffraction contrast. The same investigation also examined the electron diffraction patterns and quantified the observation, (noted ever since the discovery of polymer single crystals) that the reflections appear unusually sharp for a polymer. An effective block size of more than 2000 Å was obtained from the diffraction peak width. Thus not only has the mosaic itself remained unobserved within the crystals, but the actual diffraction effects produced by these crystals denied their existence. Admittedly, different types of radiation, sample mounting and recording geometries were used. Nevertheless it is indisputable that while there can be various extraneous sources which may contribute to broadening, there is nothing but the intrinsic perfection of the crystal which can make reflections sharp. It follows that polymer crystals can be highly perfect in the lateral direction, and it remains to be discovered why they produce line broadening in the usual X-ray diffraction pattern.

Recent X-ray measurements have revealed one extraneous source of broadening¹⁴. It was found that the reflections are broader if the solution grown single crystals are dried into a mat, as usually carried out for X-ray diffraction studies, than if they are in the form of a sludge in mineral oil. The same was observed in subsequent experiments where the crystals were left as a sludge in their original liquor (xylene)¹⁵. Clearly sedimentation and drying introduces a mosaic character of the crystal in addition to any present after growth. Nevertheless, even without drying there is still appreciable line broadening, as compared with electron diffraction. It is then pointed out that this residual broadening would correspond to diffraction from thin crystals with oblique chains in a 'powder diagram', where the effective crystallite size as determined by the Scherrer equation is a measure of the perpendicular distance through the set of crystallographic planes, i.e. $T/\sin \phi$ where T is the length of the crystalline stem within the lattice¹⁴.

It will be clear at this juncture that a fundamental re-examination of the basis of the mosaic concept is needed. This is the principle purpose of the present note. No new discovery is being claimed besides the examination of familiar principles of diffraction in the

context relevant to established structural features of polymer crystals.

The argument as evolved in discussion between the authors of this note is based on the reciprocal lattice construction pertaining to a lamellar crystal of finite thickness but with long range crystalline register laterally. In this case each reciprocal lattice point will be broadened into a spike along the direction of the lamellar normal. This spike will only coincide with c^* , the chain direction, if $\phi = 0$. It should be emphasized that at no time have any polyethylene crystals been verified as having ϕ exactly zero degrees when the crystals are in suspension or in aggregates. Thus the spike should be inclined at a finite angle ϕ to $\langle 001 \rangle$. The rest of the argument relates to the different possible modes of intersection of the spikes and the Ewald sphere.

If only one well defined crystal orientation exists within the sample the intersection can only be a point, whatever the value of ϕ (Figure 1). As discussed below, this situation can only be realized in electron diffraction. The more usual situation, which always pertains for X-ray diffraction, is when more than one crystal orientation is present. Consider first that the crystals are all random such as would give a 'powder' pattern. The observed signal is now the consequence of a superposition of reciprocal lattice points of different crystals, i.e. the spikes superimpose to give a shell of finite thickness in reciprocal space and hence a broadened reflection (Figure 2). Approximating the spike as being length $1/T$, where T is the crystal thickness, the shell width b which will govern the total breadth of the ring in a powder pattern will be

$$b = \frac{\sin \phi}{T} \quad (1)$$

where b is inversely related to the mosaic size (Figure 2). Note first that this line broadening only occurs if $\phi \neq 0$. Secondly, note that full randomization is not necessary to give this line width. Within sedimented aggregates, single crystals acquire a spread of orientation with relation to the plane of sedimentation, and a misorientation of only a very few degrees is sufficient to produce a line width of similar magnitude to that in a powder pattern. This is simplest to show analytically for small curvatures of the Ewald sphere in which case the minimum range 2α (Figure 2b) is approximated by

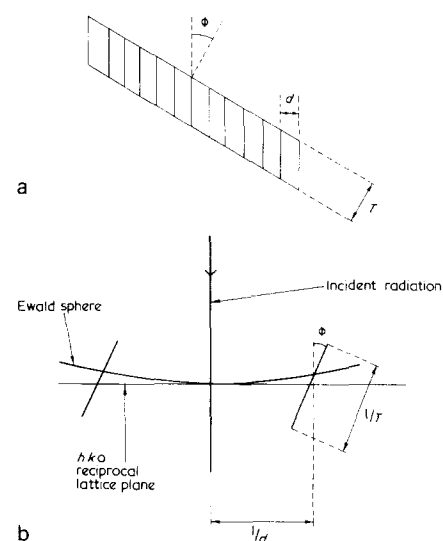


Figure 1 (a) Schematic section through a polymer crystal, as seen along one set of $h k 0$ planes of spacing d . T is the thickness of the crystal, and ϕ defines chain obliquity. (b) Corresponding reciprocal lattice construction, the lattice points being approximated as spikes. The incident radiation direction is vertical; a section through the Ewald sphere is shown intersecting the spikes in points. (Both spikes can intersect simultaneously in the case of electron diffraction)

$$\tan \alpha = \frac{d \cos \phi}{2T} \quad (2)$$

For a typical strong $h k 0$ reflection and a typical value of ϕ and T ¹⁶ 2α would be about 2° . This description of 'powder' type diffraction is entirely equivalent to the rigorous derivation of the modified Scherrer equation¹⁷ whereby the 'effective mosaic size' for a reflection is given by the interaction length through a crystallite in a direction perpendicular to the reflecting planes in question.

Hence we identify two well defined situations, depending on whether or not the precision of crystal lattice orientation is within the few degrees described by equation (2) or not. The former case can only occur for individual polymer crystals in electron diffraction as selected under the electron microscope, though in practice, the precision of orientation may not be sufficient even here (e.g. if Bragg fringes are visible, a whole range of orientation must be present)*.

The latter case, namely that the precision of crystal orientation is lower than defined by equation (2) will apply to all X-ray work which is always on aggregates.

* Footnote given on p738

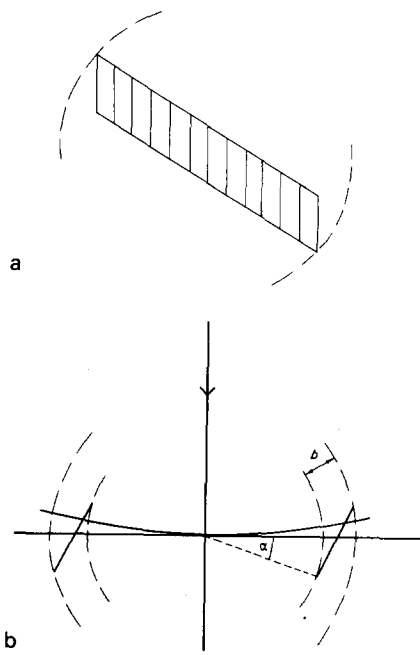


Figure 2 (a) As Figure 1a but with a range of orientations. (b) The corresponding reciprocal lattice construction; the intersections now define a line on the Ewald sphere whose length is related to $T/\sin \phi$

On the basis of X-ray evidence alone therefore there are two possible explanations for line broadening even as confined to the 'crystal size' contribution alone (i.e. lattice distortion apart). If one assumes that the lamellar normals are parallel to the chains the extension of the lattice register in the lateral direction will need to be limited to a few 100 Å and from this the mosaic block structural unit would follow. As an alternative, we can account for the same line broadening effect on the basis of the well established structural feature of chain obliquity in the way described above. We consider that the electron microscope results are deci-

* The structure of the crystal as observed in the electron microscope is not always as in suspension owing to changes occurring when the crystals are dried down on to the support film. It is then possible for crystals to collapse by chain slip so that ϕ becomes zero, although the original chain tilt can be demonstrated by special methods¹⁶. Alternatively the crystal may collapse by tilt, such that tent shaped crystals show characteristic pleats. There is evidence from wide-angle X-ray diffraction that in this case the original value of ϕ is retained when macroscopic aggregates are dried¹⁶. In the first case all principal $hk0$ reflections will be visible in the usual setting of the sample where the beam is perpendicular to the support. In the latter case (collapse by tilt) only some particular reflections, if any, are seen unless the sample plane is tilted. Whichever the case, it does not affect the issue that a sharp reflection is obtained as long as the orientation is uniform within the crystal or sufficiently large portions of it.

sively in favour of the latter interpretation. This alternative also explains the decrease in X-ray $hk0$ 'crystal size' broadening with lamella thickness¹⁸ with no need to invoke the equilibrium Wulff shape¹¹ in a system not normally considered as being in equilibrium in any case.

It would follow that sharp reflections might be observable for polymers where there is no such chain obliquity as in polyethylene. This prediction has been strikingly verified by recent observations on polyoxymethylene¹⁴ and isotactic polystyrene¹⁹; here the $hk0$ reflections were very much narrower than in polyethylene. In fact in the better explored polyoxymethylene system close numerical correspondence was found between the peak broadening crystal size and the crystal size determined from the slope of the observed shallow pyramid (2°) ('mosaic size' of 2300 against 2500 Å predicted).

We would in this way question the necessity of the mosaic concept as an intrinsic feature in polymer crystallization. To avoid possible misrepresentations, we are anxious to stress that we do not question the existence of small crystal blocks, which may produce X-ray line broadenings, due to genuine size limitations to the coherently diffracting lattice under appropriate circumstances, such as are likely to be present in the more complex and yet partly unexplored morphologies of the bulk where X-ray reflections are usually broad. Also, they are likely to arise in systems which results from deformation as in drawn fibres etc. What we do question is the necessity for invoking an intrinsic structure unit of a specific size and shape as a necessary attribute of polymer crystallization. Neither do we question the self-consistency of the existing theoretical treatment of line broadening. All we wish to point out is that these treatments have derived analytical results on certain assumptions, which imply a particular model, and that different physical consequences can be deduced on the basis of an alternative model which requires no postulate beyond established structural knowledge. What is more, the interpretation that we advocate does not imply any contradiction between different diffraction techniques in the particular case of single crystals.

To conclude we may sum up the various factors which could contribute to the crystal size component of the X-ray line broadening as we feel this

has not been done before in its entirety:

Broadening with coherent lattice

(1) Thin crystals with oblique chains coupled with at least slight misorientation (the subject of the present note).

(2) Different lattice spacings in different crystal sectors. This item under the term 'subcell distortion' is documented throughout the literature on polymer single crystals²¹ and is attributed to the distorting effect of the folds. It produces multiplicity of spots in electron diffraction patterns in individual crystals (e.g. Figure 21 ref 7). It is clear that in principle it will contribute to the broadening of appropriate lines when the crystals are in the form of aggregates even if no other source of broadening is present. On the basis of existing data²¹ this effect, however, should be small.

Broadening by genuine limitation of lateral crystal size (incoherent lattice)

(1) Induced by the process of sedimentation and drying. This may be a total artefact, but it may well relate to some fine-structural feature we do not yet know about. It has been so far only recorded for X-ray work, but may also occur on individual crystals in the electron microscope.

(2) A genuine limit to lateral chain register. This is clearly the case when the crystals are genuinely small in such a direction. This will be the case for thin bundles in fringed micelles which act as tie points for physical gelation²⁰. The same is expected from thin fibres produced by flow orientation.

When all the foregoing causes of mosaic-type line broadening are absent, sharp reflections are observed. In these circumstances, the evidence may be judged to leave no scope for the mosaic block concept as an intrinsically general feature of polymer crystallization.

REFERENCES

- Hosemann, R., Wilke, W. and Baltá Calleja, F. J. *Acta Crystallogr.* 1966, **21**, 118
- Wilke, W., Vogel, W. and Hosemann, R. *Kolloid Z. Z. Polym.* 1970, **237**, 317
- Hosemann, R. *Makromol. Chem. Suppl.* 1975, **1**, 559
- Peterlin, A. *J. Mater. Sci.* 1971, **6**, 490
- Kajima, T., Okada, T. and Takayanagi, M. *J. Macromol. Sci. (B)* 1974, **9**, 35
- 'Die Physik der Hochpolymeren', (Ed. H. A. Stuart), Springer-Verlag, Berlin, 1955, Vol 3, p 202-3
- Keller, A. *Rep. Prog. Phys.* 1968, **31**, 623

- 8 Geil, P. H. 'Polymer single crystals', Interscience, New York, 1973
- 9 Wunderlich, B. 'Macromolecular Physics', Academic Press, London, 1974
- 10 Schonfeld, A. and Wilke, W. *Kolloid Z. Z. Polym.* 1972, **250**, 496
- 11 Čačković, H., Hosemann, R. and Wilke, W. *Kolloid Z. Z. Polym.* 1969, **234**, 1000
- 12 Schonfeld, A., Wilke, W., Hohne, G. and Hosemann, R. *Kolloid. Z. Z. Polym.* 1972, **250**, 102
- 13 Thomas, E. L., Saas, S. L. and Kromer, E. J. *J. Polym. Sci. (Polym. Phys. Edn)* 1975, **12**, 1015
- 14 Harrison, I. R. and Runt, J. *J. Polym. Sci. (Polym. Physics Edn)* in press
- 15 Wright, T., Keller, A. and Sadler, D. M. unpublished
- 16 Bassett, D. C., Frank, F. C. and Keller, A. *Phil. Mag.* 1963, **8**, 1753
- 17 Bertaut, E. F. *Acta Crystallogr.* 1950, **3**, 14
- 18 Kavesh, S. and Schultz, J. M. *J. Polym. Sci. (A-2)* 1971, **9**, 85
- 19 Overbergh, N., Keller, A. and Sadler, D. M. unpublished
- 20 Girolamo, M., Keller, A., Miyasaka, K. and Overbergh, N. *J. Polym. Sci. (Polym. Phys. Edn)* in press
- 21 Bassett, D. C. *Phil. Mag.* 1964, **10**, 595

The glass transition temperature of poly(*N*-vinyl pyrrolidone) and the effect of water

Y. Y. Tan and G. Challa

Department of Polymer Chemistry, State University of Groningen, Groningen, The Netherlands

(Received 15 January 1976; revised 5 April 1976)

In the literature several conflicting values of a glass transition temperature (T_g) of poly(*N*-vinylpyrrolidone)* (PVP) were found¹⁻⁸, ranging from 54° to 175°C (Table 1). These may be attributed to the large influence of sorbed moisture due to the hygroscopic nature of the material, as will be shown by the present measurements.

PVP samples containing various known amounts of water were scanned in a Perkin-Elmer DSC-1B differential scanning calorimeter. The PVP was a commercial sample, Luviskol K-90 BASF (Germany), having a viscosity-average molecular weight of 750 000. The results are shown in Figure 1.

The onset of the transitions were taken as the T_g values (see inset in Figure 1). If the best fitting curve was drawn through these T_g values, on extrapolation to zero water content a T_g value for PVP of $175 \pm 1^\circ\text{C}$ (448K) was obtained. The effect of diluents and plasticizers on the T_g of a polymer may be expressed by the equation^{9,10}:

$$1/T_g = w_1/T_{g1} + w_2/T_{g2}$$

where the subscripts 1 and 2 pertain to

* Poly[1-(2-oxo-1-pyrrolidiny)ethylene]

Table 1 T_g values of PVP

T_g (°C)	Literature reference
54	1
86	2,3
145	4,5,6
140-160	7
175	6,8

Details mentioned in ref 2

polymer and diluent or plasticizers, respectively. Applied to the PVP/H₂O system the equation becomes:

$$1/T_g = w_{\text{PVP}}/T_{g\text{PVP}} + w_{\text{H}_2\text{O}}/T_{g\text{H}_2\text{O}}$$

where $T_{g\text{H}_2\text{O}}$ represents the glass transition temperature of water, $w_{\text{H}_2\text{O}}$ the weight fraction of water, and $w_{\text{PVP}} = 1 - w_{\text{H}_2\text{O}}$.

A plot of $1/T_g$ in K⁻¹ versus $w_{\text{H}_2\text{O}}$ appeared to be linear over the whole range (0-16.1% H₂O). As $T_{g\text{PVP}}$ was

found to be 448K it can be derived that $T_{g\text{H}_2\text{O}} = 128\text{K}$ (-145°C), a value which agrees well with 135K¹¹ and 134K^{12,13} found by other means.

This extremely low value provides water with a very effective T_g depressing activity if it is homogeneously absorbed in a polymer.

Hence for hydrophilic polymers such as PVP, careful drying at the highest temperature possible, preferably under a nitrogen blanket, is necessary in order to obtain correct T_g values.

REFERENCES

- Jenckel, E. *Kolloid-Z* 1942, **100**, 163
- Sugiura, M. and Fujii, E. *Kogyo*

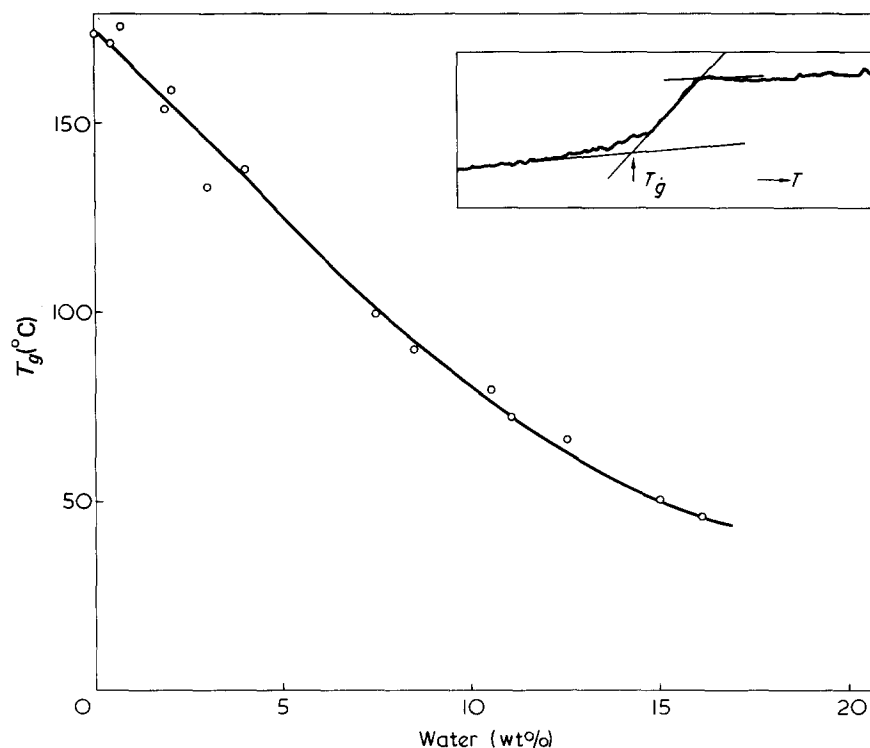


Figure 1 The lowering effect of water content (wt%) on the glass transition temperature, T_g (°C) of PVP. Inset: a typical d.s.c. thermogram; scan speed 8°C/min; sensitivity range 1

- 8 Geil, P. H. 'Polymer single crystals', Interscience, New York, 1973
- 9 Wunderlich, B. 'Macromolecular Physics', Academic Press, London, 1974
- 10 Schonfeld, A. and Wilke, W. *Kolloid Z. Z. Polym.* 1972, **250**, 496
- 11 Čačković, H., Hosemann, R. and Wilke, W. *Kolloid Z. Z. Polym.* 1969, **234**, 1000
- 12 Schonfeld, A., Wilke, W., Hohne, G. and Hosemann, R. *Kolloid. Z. Z. Polym.* 1972, **250**, 102
- 13 Thomas, E. L., Saas, S. L. and Kromer, E. J. *J. Polym. Sci. (Polym. Phys. Edn)* 1975, **12**, 1015
- 14 Harrison, I. R. and Runt, J. *J. Polym. Sci. (Polym. Physics Edn)* in press
- 15 Wright, T., Keller, A. and Sadler, D. M. unpublished
- 16 Bassett, D. C., Frank, F. C. and Keller, A. *Phil. Mag.* 1963, **8**, 1753
- 17 Bertaut, E. F. *Acta Crystallogr.* 1950, **3**, 14
- 18 Kavesh, S. and Schultz, J. M. *J. Polym. Sci. (A-2)* 1971, **9**, 85
- 19 Overbergh, N., Keller, A. and Sadler, D. M. unpublished
- 20 Girolamo, M., Keller, A., Miyasaka, K. and Overbergh, N. *J. Polym. Sci. (Polym. Phys. Edn)* in press
- 21 Bassett, D. C. *Phil. Mag.* 1964, **10**, 595

The glass transition temperature of poly(*N*-vinyl pyrrolidone) and the effect of water

Y. Y. Tan and G. Challa

Department of Polymer Chemistry, State University of Groningen, Groningen, The Netherlands

(Received 15 January 1976; revised 5 April 1976)

In the literature several conflicting values of a glass transition temperature (T_g) of poly(*N*-vinylpyrrolidone)* (PVP) were found¹⁻⁸, ranging from 54° to 175°C (Table 1). These may be attributed to the large influence of sorbed moisture due to the hygroscopic nature of the material, as will be shown by the present measurements.

PVP samples containing various known amounts of water were scanned in a Perkin-Elmer DSC-1B differential scanning calorimeter. The PVP was a commercial sample, Luviskol K-90 BASF (Germany), having a viscosity-average molecular weight of 750 000. The results are shown in Figure 1.

The onset of the transitions were taken as the T_g values (see inset in Figure 1). If the best fitting curve was drawn through these T_g values, on extrapolation to zero water content a T_g value for PVP of $175 \pm 1^\circ\text{C}$ (448K) was obtained. The effect of diluents and plasticizers on the T_g of a polymer may be expressed by the equation^{9,10}:

$$1/T_g = w_1/T_{g1} + w_2/T_{g2}$$

where the subscripts 1 and 2 pertain to

* Poly[1-(2-oxo-1-pyrrolidiny)ethylene]

Table 1 T_g values of PVP

T_g (°C)	Literature reference
54	1
86	2,3
145	4,5,6
140-160	7
175	6,8

Details mentioned in ref 2

polymer and diluent or plasticizers, respectively. Applied to the PVP/H₂O system the equation becomes:

$$1/T_g = w_{\text{PVP}}/T_{g\text{PVP}} + w_{\text{H}_2\text{O}}/T_{g\text{H}_2\text{O}}$$

where $T_{g\text{H}_2\text{O}}$ represents the glass transition temperature of water, $w_{\text{H}_2\text{O}}$ the weight fraction of water, and $w_{\text{PVP}} = 1 - w_{\text{H}_2\text{O}}$.

A plot of $1/T_g$ in K⁻¹ versus $w_{\text{H}_2\text{O}}$ appeared to be linear over the whole range (0-16.1% H₂O). As $T_{g\text{PVP}}$ was

found to be 448K it can be derived that $T_{g\text{H}_2\text{O}} = 128\text{K}$ (-145°C), a value which agrees well with 135K¹¹ and 134K^{12,13} found by other means.

This extremely low value provides water with a very effective T_g depressing activity if it is homogeneously absorbed in a polymer.

Hence for hydrophilic polymers such as PVP, careful drying at the highest temperature possible, preferably under a nitrogen blanket, is necessary in order to obtain correct T_g values.

REFERENCES

- Jenckel, E. *Kolloid-Z* 1942, **100**, 163
- Sugiura, M. and Fujii, E. *Kogyo*

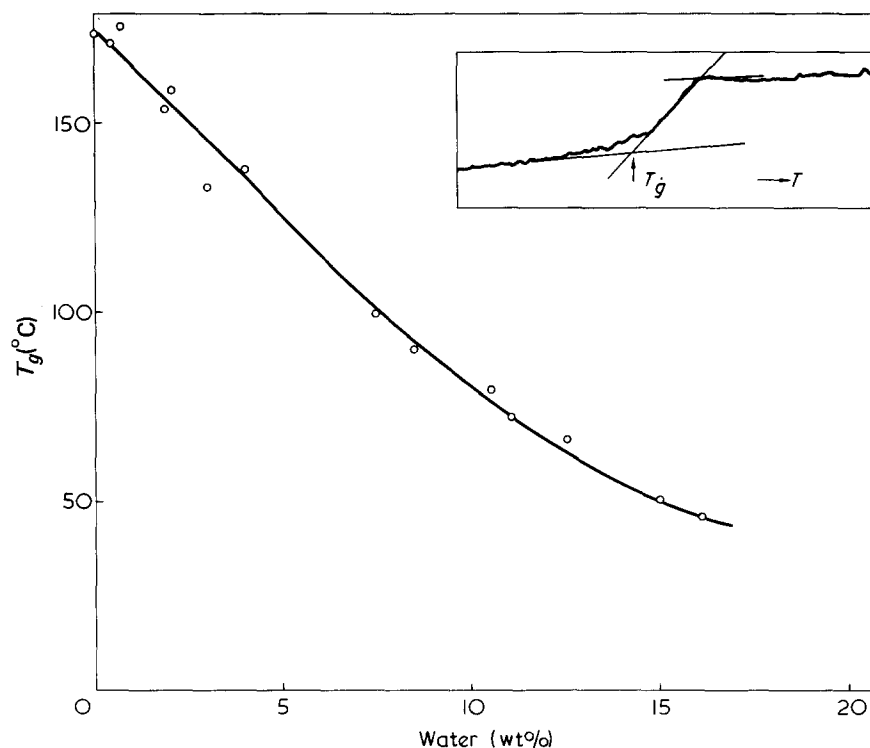


Figure 1 The lowering effect of water content (wt%) on the glass transition temperature, T_g (°C) of PVP. Inset: a typical d.s.c. thermogram; scan speed 8°C/min; sensitivity range 1

- Kagaku Zasshi* 1963, **66**, 1228; *Chem. Abstr.* 1964, **60**, 9369
- 3 Brandrup, J. and Immergut, E. H. 'Polymer Handbook', 2nd edn, Wiley, New York, 1975, p III-155
- 4 Kinsinger, J. B., Panchak, J. R., Kelso, R. L., Bartlett, J. S. and Graham, R. K. *J. Appl. Polym. Sci.* 1965, **9**, 429
- 5 Griffin-Lewis, O. 'Physical Constants of Linear Homopolymers', Springer Verlag, Berlin, 1968, pp 128-9
- 6 Van Krevelen, D. W. and Hoftijzer, P. J. 'Properties of Polymers, Correlations with Chemical Structure', Elsevier, Amsterdam, 1972, p 387
- 7 Sidelkovskaya, F. P. 'The Chemistry of *N*-vinylpyrrolidone and its Polymers', Moscow, 1970, p 99
- 8 Nielsen, L. E. 'Mechanical Properties of Polymers', Reinhold, New York, 1962, p 21
- 9 Nielsen, L. E. 'Mechanical Properties of Polymer', Reinhold, New York, 1962, p 27
- 10 Miller, M. L. 'The Structure of Polymers', Reinhold, New York, 1966, p 291
- 11 Sugisaki, M., Suga, H. and Seki, S. *Bull. Chem. Soc. Japan* 1968, **41**, 2591
- 12 Korosi, A. and Fabus, B. M. *Anal. Chem.* 1968, **40**, 157
- 13 'Water', (Ed R. Frank), Plenum Press, New York, 1972, vol 1, 116, 127, 407, 408

Distribution and desorption of free radicals in the emulsion polymerization of styrene

B. W. Brooks and M. K. Qureshi

Department of Chemical Engineering, Loughborough University of Technology, Loughborough, Leicestershire LE11 3TU, UK
(Received 19 March 1976)

INTRODUCTION

The emulsion polymerization of styrene is often regarded as one of the few emulsion polymerization systems that conforms to 'case 2' of the Smith-Ewart model¹. A number of reasons have been suggested for this conformity; one of these is the apparent absence of radical migration from the polymer particles. Thus, the average number of radicals per particle, \bar{n} , would be ≥ 0.5 for styrene polymerization.

In this paper some experiments are described in which the emulsion polymerization of styrene, which has attained a constant polymerization rate, is subjected to step-changes in the supply rate of free radicals. These experiments provide information on the value of \bar{n} and show that radical desorption from polystyrene particles takes place.

THEORY

Prediction of \bar{n}

The present experiments deal with the region where the conversion of monomer to polymer is a linear function of time. Therefore, it is valid to assume that the distribution of radical populations in the particles has reached a steady state. If radicals are able to desorb from the particles they must be subsequently re-absorbed by the particles (assuming that mutual reaction of radicals in the continuous aqueous phase is negligible). Thus the number of particles which contain n free radicals, N_n , is given by the recursion expression¹:

$$\begin{aligned} &BN_{n-1} + m(n+1)N_{n+1} \\ &+ (n+1)(n+2)N_{n+2} \\ &= N_n[n(n-1) + mn + B] \end{aligned}$$

where

$$B = m\bar{n} + E, \quad E = \nu q_w/k_t N_w$$

$$\text{and } m = k_0 a/k_t$$

In these expressions ν is the volume and a is the area of a polymer particle, k_t is the rate coefficient for radical-radical termination reactions in the particles, k_0 is the rate coefficient for radical desorption from the particles, N_w is the total number of particles per unit volume of emulsion and q_w is the rate of production of new free radicals from the decomposition of initiator.

A general solution to the recursion expression may be obtained if it is first transformed into an ordinary second-order differential equation. This technique was used by Stockmayer² and also Ugelstad *et al.*³ who also allowed for radical re-absorption. For a given value of m , \bar{n} can be obtained as a function of E . This function contains the ratio of two modified Bessel functions the values of which are obtained from series expressions. Thus, this mathematical procedure, although elegant, eventually requires numerical manipulations and the approximation of series. In view of this, an alternative and simpler procedure for solving the recursion equation is now obtained by allowing the maximum value of n to be 4. This transforms the recursion expres-

sion into a set of linear equations which can be solved exactly for given values of E and m . Since the value of \bar{n} in the present work (and in many other cases also) is $\gg 1$, the assumption that $n \leq 4$ is at least as good as the assumptions made in previous treatments.

Examples of the solutions resulting from this simpler procedure are shown in Figure 1. In Figure 1, \bar{n} was obtained from individual values of n_1 , n_2 , n_3 and n_4 by using the relationship $\bar{n} = \sum n N_n / \sum N_n$.

EXPERIMENTAL

Styrene was freed from inhibitor by washing with aqueous sodium hydroxide. The initial composition of all reaction mixtures was as follows (parts by weight): styrene, 100; water, 214; sodium laurylsulphate, 7; ammonium persulphate, 5; sodium hydroxide, 5. Polymerizations were carried out in agitated glass vessels under nitrogen. Conversion to polymer was monitored by periodically extracting samples of the reaction mixture and weighing the recovered polymer. The polymerizations were carried out in three different ways: (a) at 30°C; (b) at 30°C with post-addition of extra initiator; (c) initiated at 60°C and subsequently cooled to 30°C. Cooling of reaction mixtures from 60° to 30°C was achieved by rapid replacement of water in the thermostated bath. In some cases, precalculated amounts of cold oxygen-free water were also added to the reactor. This cold water contained ammonium persulphate and sodium hydroxide in the same concentrations as those initially present in the reactor. No extra surface-active agent was added. A new constant polymerization rate was attained in ~5 min.

- Kagaku Zasshi* 1963, **66**, 1228; *Chem. Abstr.* 1964, **60**, 9369
- 3 Brandrup, J. and Immergut, E. H. 'Polymer Handbook', 2nd edn, Wiley, New York, 1975, p III-155
- 4 Kinsinger, J. B., Panchak, J. R., Kelso, R. L., Bartlett, J. S. and Graham, R. K. *J. Appl. Polym. Sci.* 1965, **9**, 429
- 5 Griffin-Lewis, O. 'Physical Constants of Linear Homopolymers', Springer Verlag, Berlin, 1968, pp 128-9
- 6 Van Krevelen, D. W. and Hoftijzer, P. J. 'Properties of Polymers, Correlations with Chemical Structure', Elsevier, Amsterdam, 1972, p 387
- 7 Sidelkovskaya, F. P. 'The Chemistry of *N*-vinylpyrrolidone and its Polymers', Moscow, 1970, p 99
- 8 Nielsen, L. E. 'Mechanical Properties of Polymers', Reinhold, New York, 1962, p 21
- 9 Nielsen, L. E. 'Mechanical Properties of Polymer', Reinhold, New York, 1962, p 27
- 10 Miller, M. L. 'The Structure of Polymers', Reinhold, New York, 1966, p 291
- 11 Sugisaki, M., Suga, H. and Seki, S. *Bull. Chem. Soc. Japan* 1968, **41**, 2591
- 12 Korosi, A. and Fabus, B. M. *Anal. Chem.* 1968, **40**, 157
- 13 'Water', (Ed R. Frank), Plenum Press, New York, 1972, vol 1, 116, 127, 407, 408

Distribution and desorption of free radicals in the emulsion polymerization of styrene

B. W. Brooks and M. K. Qureshi

Department of Chemical Engineering, Loughborough University of Technology, Loughborough, Leicestershire LE11 3TU, UK
(Received 19 March 1976)

INTRODUCTION

The emulsion polymerization of styrene is often regarded as one of the few emulsion polymerization systems that conforms to 'case 2' of the Smith-Ewart model¹. A number of reasons have been suggested for this conformity; one of these is the apparent absence of radical migration from the polymer particles. Thus, the average number of radicals per particle, \bar{n} , would be ≥ 0.5 for styrene polymerization.

In this paper some experiments are described in which the emulsion polymerization of styrene, which has attained a constant polymerization rate, is subjected to step-changes in the supply rate of free radicals. These experiments provide information on the value of \bar{n} and show that radical desorption from polystyrene particles takes place.

THEORY

Prediction of \bar{n}

The present experiments deal with the region where the conversion of monomer to polymer is a linear function of time. Therefore, it is valid to assume that the distribution of radical populations in the particles has reached a steady state. If radicals are able to desorb from the particles they must be subsequently re-absorbed by the particles (assuming that mutual reaction of radicals in the continuous aqueous phase is negligible). Thus the number of particles which contain n free radicals, N_n , is given by the recursion expression¹:

$$\begin{aligned} &BN_{n-1} + m(n+1)N_{n+1} \\ &+ (n+1)(n+2)N_{n+2} \\ &= N_n[n(n-1) + mn + B] \end{aligned}$$

where

$$B = m\bar{n} + E, \quad E = \nu q_w/k_t N_w$$

$$\text{and } m = k_0 a/k_t$$

In these expressions ν is the volume and a is the area of a polymer particle, k_t is the rate coefficient for radical-radical termination reactions in the particles, k_0 is the rate coefficient for radical desorption from the particles, N_w is the total number of particles per unit volume of emulsion and q_w is the rate of production of new free radicals from the decomposition of initiator.

A general solution to the recursion expression may be obtained if it is first transformed into an ordinary second-order differential equation. This technique was used by Stockmayer² and also Ugelstad *et al.*³ who also allowed for radical re-absorption. For a given value of m , \bar{n} can be obtained as a function of E . This function contains the ratio of two modified Bessel functions the values of which are obtained from series expressions. Thus, this mathematical procedure, although elegant, eventually requires numerical manipulations and the approximation of series. In view of this, an alternative and simpler procedure for solving the recursion equation is now obtained by allowing the maximum value of n to be 4. This transforms the recursion expres-

sion into a set of linear equations which can be solved exactly for given values of E and m . Since the value of \bar{n} in the present work (and in many other cases also) is $\gg 1$, the assumption that $n \leq 4$ is at least as good as the assumptions made in previous treatments.

Examples of the solutions resulting from this simpler procedure are shown in *Figure 1*. In *Figure 1*, \bar{n} was obtained from individual values of n_1 , n_2 , n_3 and n_4 by using the relationship $\bar{n} = \sum n N_n / \sum N_n$.

EXPERIMENTAL

Styrene was freed from inhibitor by washing with aqueous sodium hydroxide. The initial composition of all reaction mixtures was as follows (parts by weight): styrene, 100; water, 214; sodium laurylsulphate, 7; ammonium persulphate, 5; sodium hydroxide, 5. Polymerizations were carried out in agitated glass vessels under nitrogen. Conversion to polymer was monitored by periodically extracting samples of the reaction mixture and weighing the recovered polymer. The polymerizations were carried out in three different ways: (a) at 30°C; (b) at 30°C with post-addition of extra initiator; (c) initiated at 60°C and subsequently cooled to 30°C. Cooling of reaction mixtures from 60° to 30°C was achieved by rapid replacement of water in the thermostated bath. In some cases, precalculated amounts of cold oxygen-free water were also added to the reactor. This cold water contained ammonium persulphate and sodium hydroxide in the same concentrations as those initially present in the reactor. No extra surface-active agent was added. A new constant polymerization rate was attained in ~5 min.

RESULTS

In all isothermal experiments the polymerization rate was constant between 0 and 65% conversion. The two methods of cooling from 60° to 30°C produced substantially the same results. It can be seen from *Table 1* that the addition of extra amounts of ammonium persulphate at 30°C does not change the polymerization rate. The data in *Table 1* show that the polymerization rate at 60°C is 6.77 times faster than that at 30°C. Also, polymerizations which are carried out at 30°C throughout are 1.96 times faster than those started at 60°C and subsequently cooled to 30°C. By taking the propagation rate constant for styrene as 332 l/mol sec at 60°C and 52.6 l/mol sec at 30°C⁴ and by assuming the monomer concentration in the particles to be 5.07 mol/l at 60°C and 5.76 mol/l at 30°C⁵ we obtain the following values for the stationary number of growing free radicals: $9.23 \times 10^{17} \text{ l}^{-1}$ for polymerization at 60°C; $7.47 \times 10^{17} \text{ l}^{-1}$ for polymerization at 30°C and $3.82 \times 10^{17} \text{ l}^{-1}$ for polymerization started at 60°C and cooled to 30°C.

DISCUSSION

Since the addition of extra persulphate at 30°C had no effect on the polymerization rate, we may deduce from *Figure 1* that $\bar{n} \approx 0.5$ under these conditions (because \bar{n} is almost independent of E and q_w when $\bar{n} \approx 0.5$). If this was the case, N_w would be $1.49 \times 10^{18} \text{ l}^{-1}$ which leads to a value of E of about 1.6×10^{-2} before the addition of extra persulphate (assuming the rate constant for persulphate decomposition at 30°C = $3.60 \times 10^{-8} \text{ sec}^{-1}$ ⁶ and $k_t = 2.24 \times 10^7 \text{ l/mol sec}^4$). This value is in the region where $\bar{n} \approx 0.5$ providing $m \gg 10^{-2}$ (see *Figure 1*); thus the assumptions are self consistent.

The results of previous workers (who used the same chemicals as are used here) indicate that for any given recipe, the number of particles produced at 60°C is about 3 times greater than the number produced at 30°C^{7,8}. Consequently polymer particles which are produced in isothermal experiments at 30°C will be larger (and less numerous) than the particles produced in the experiments which are started at 60°C and subsequently cooled to 30°C.

Thus, in comparing these two sets of experiments, it can be seen that E is about 9 times smaller in the 'thermally quenched' experiments than in the isothermal experiments (v is inversely proportional to N_w). This lowering of E

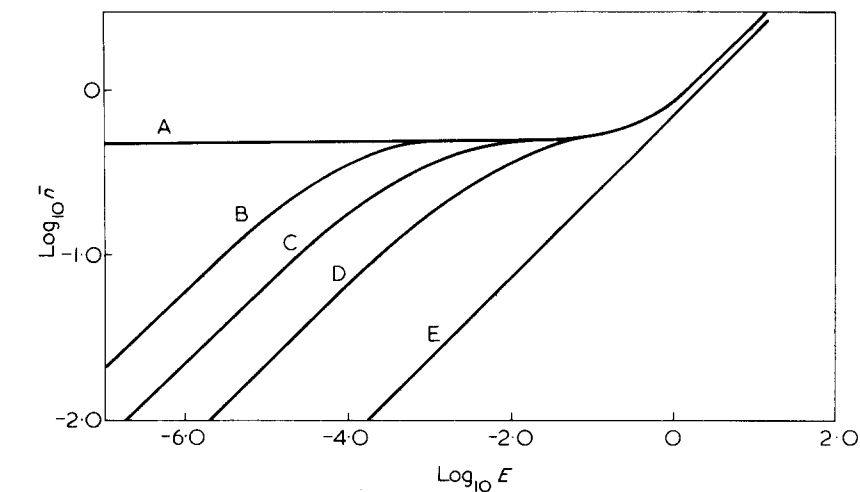


Figure 1 Variation of \bar{n} with E for various values of m : A, $m = 0$; B, $m = 10^{-4}$; C, $m = 10^{-3}$; D, $m = 10^{-2}$; E, $m = 10$

Table 1 Effect of step-changes on polymerization rate

Initial temperature (°C)	Change introduced	Conversion at change (%)	Polymerization rate before change (%/min)	Polymerization rate after change (%/min)
30	none	—	0.757	—
30	a	35	0.725	0.725
30	b	38	0.750	0.750
30	b	45	0.725	0.725
30	b	60	0.750	0.750
60	none	—	5.00	—
60	c	52	4.76	0.350
60	c	50	4.80	0.414
60	d	54	5.40	0.370
60	d	33	5.00	0.474
60	d	48	5.10	0.281

a, addition of twice the original initiator; b, addition of 4 times original initiator; c, external cooling to 30°C; d, internal cooling to 30°C

causes the value of \bar{n} to be reduced by a factor of about 6. From *Figure 1* it can be seen immediately that m must be >0 at 30°C. Since a four-fold increase in E produces no change in \bar{n} while a nine-fold decrease in E reduces \bar{n} by about 85% we can see from *Figure 1* that the value of m for styrene polymerization at 30°C is in the region of 10^{-2} . Precise values of m are difficult to obtain because the value of a (and therefore m) is not exactly the same in the two sets of experiments. With reference to *Figure 1* it can be seen that the value of \bar{n} may not change markedly during the period of particle growth because the values of both E and m are increasing during this period. Since \bar{n} at 60°C appears to be less than \bar{n} at 30°C (in the isothermal experiments) and the value of E is probably larger at 60°C, it seems that the value of m increases with temperature.

It may be concluded that the desorption rate of free radicals from polystyrene particles is low (k_0 is about $2 \times 10^{-8} \text{ m/sec}$ at 30°C). However, even this low desorption rate can have an appreciable effect on the value of \bar{n} and the polymerization rate.

REFERENCES

- Smith, W. V. and Ewart, R. H. *J. Chem. Phys.* 1948, **16**, 592
- Stockmayer, W. H. *J. Polym. Sci.* 1957, **24**, 314
- Ugelstad, J., Mork, P. C. and Aasen, *J. Polym. Sci. (A-1)* 1967, **5**, 2281
- Brandrup, J. and Immergut, E. H. 'Polymer Handbook', 2nd edn, Wiley, New York, 1975
- Van der Hoff, B. M. E. *J. Polym. Sci.* 1960, **44**, 241
- Kolthoff, I. M. and Miller, I. K. *J. Am. Chem. Soc.* 1951, **73**, 3055
- Paolletti, K. P. and Billmeyer Jr., F. W. *J. Polym. Sci.* 1964, **2**, 2049
- Gardon, J. L. *Br. Polym. J.* 1970, **2**, 1

Polymerization of *N*-vinylcarbazole in systems containing maleic anhydride and benzoyl peroxide

Polymerization of *N*-vinylcarbazole (NVC) in benzene can be initiated at 60°C by benzoyl peroxide (BPO) or azoisobutyronitrile (AIBN) but the kinetics of the reactions promoted by the two initiators and the characteristics of the resulting polymers are quite different^{1,2}. Mixtures of BPO and AIBN give rise to polymers having bimodal distributions of molecular weight, confirming that the initiators give rise to polymerizations of fundamentally different types. It is believed that BPO is involved in a one-electron transfer with NVC and gives rise to a cationic polymerization. It has been shown³ that, when monomer of very high purity is used with BPO, about 4% of the polymer differs from the remainder, resembling the polymer made using AIBN and having the characteristics expected for the product of a radical polymerization. Confirmation of the nature of the main polymerization promoted by BPO might be obtained by initiating with mixtures of BPO and substances known to form charge-transfer complexes with NVC giving rise to cationic polymerization. It seemed that maleic anhydride (MAH) might be suitable for this purpose but the first experiments revealed anomalies meriting close attention. Polymer precipitated as it was formed when both MAH and BPO were present but initial rates could be measured. *Figure 1* shows that the rate of polymerization for a system containing both initiators considerably exceeds the sum of the rates produced by them separately.

The amounts of MAH incorporated in the polymeric products of low conversion experiments were found using ¹⁴C-MAH. Systems without added initiator gave products completely soluble in chloroform and containing only one MAH unit for approximately 100 NVC units. Systems including BPO gave products only partly soluble in chloroform although completely soluble in pyridine; they contained appreciable quantities of MAH but unexpectedly the proportion decreased con-

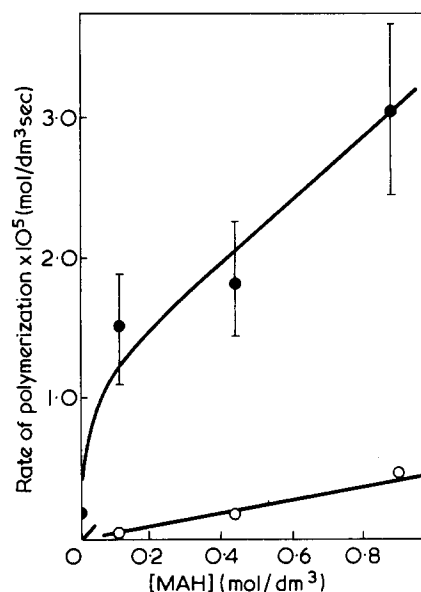


Figure 1 Effect of MAH on rate of polymerization at 60°C of NVC at 1 mol/dm³ in benzene. ○, Systems free from added initiator; ●, systems containing BPO at 2.07 × 10⁻³ mol/dm³

tinuously as the mole fraction of MAH in the NVC/MAH mixture was increased from 0.1 to 0.9 (see *Figure 2*). The compositions were unaltered by performing the polymerizations in complete darkness using (MAH + BPO) and NVC solutions previously stored in the dark. The proportion of MAH in the product was increased by the presence during polymerization of a small amount of ammonia but was unaffected by replacing BPO with AIBN.

Polymers produced from mixtures NVC/MAH/BPO in benzene were subjected to prolonged Soxhlet extraction with chloroform. They split into two fractions: the soluble fraction was a homopolymer of NVC containing very little combined MAH, and the other a copolymer of NVC with MAH at a mole fraction of about 0.40 (see *Figure 2*).

These results disagree with a statement⁴ that NVC and MAH with AIBN at 50°C do not undergo copolymerization. It appears that benzene solutions

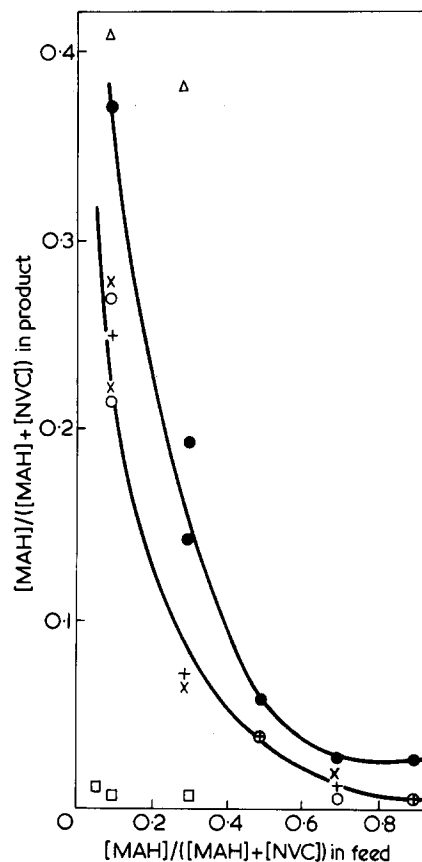


Figure 2 MAH contents of polymers made at 60°C with NVC at 1 mol/dm³ in benzene. □, Systems free from added initiator; ○, BPO at 2.07 × 10⁻³ mol/dm³; ●, as for (○) but small amount of ammonia present during polymerization; +, as for (○) but reaction performed in darkness; X, BPO replaced by AIBN; △, chloroform-insoluble fractions from products from systems (○)

of NVC with MAH containing either BPO or AIBN give rise to the simultaneous formation of a homopolymer of NVC and a copolymer which may not be far removed from an alternating copolymer of MAH with NVC. The system NVC/MAH resembles those of NVC with fumaronitrile or diethyl fumarate⁵ and vinylidene cyanide with unsaturated ethers⁶, in that homopolymers can be formed spontaneously while copolymers can be

made using additives known to dissociate to radicals. Further studies are in progress.

Acknowledgement

The work described here was performed while C. J. D. was the holder of a Research Studentship awarded by the Science Research Council.

J. C. Bevington and C. J. Dyball

Department of Chemistry,
The University,
Lancaster, UK
(Received 5 May 1976)

References

- 1 Jones, R. G., Catterall, E., Bilson, R. T. and Booth, R. G. *Chem. Commun.*

1972, 22

- 2 Bevington, J. C. and Dyball, C. J. *JCS Faraday Trans. 1* 1975, 71, 2226
- 3 Bevington, J. C. and Dyball, C. J. *J. Polym. Sci. (A)* in the press
- 4 Hyde, P., Kricka, L. J. and Ledwith, A. *Polymer* 1973, 14, 124
- 5 Tada, K., Shirota, Y. and Mikawa, H. *J. Polym. Sci. (B)* 1972, 10, 691
- 6 Stille, J. K. and Chung, D. C. *Macromolecules* 1975, 8, 115

Book Reviews

Advances in Polymer Friction and Wear
Volumes 5A and 5B
Edited by Lieng-Huang Lee
Plenum, New York, 1975, 840 pp. \$35.50

This two-volume set, the fifth volume of the series of Polymer Science and Technology provides a unique survey of both theoretical and practical aspects of polymer tribology. It reports the First International Symposium on the subject held in Los Angeles, which was sponsored by the Division of Organic Coatings and Plastics Chemistry and co-sponsored by the Division of Cellulose, Wool and Fibre Chemistry and Colloid and Surface Chemistry of the American Chemical Society. The proceedings contains all revised or expanded papers together with discussions, introductory remarks by session chairman, the plenary lectures and the symposium address.

Following the sequence of the sessions the book consists of eight parts:

- (1) Mechanisms of Polymer Friction and Wear
- (2) Polymer Properties and Friction
- (3) Characterisation and Modification of Polymer Surfaces
- (4) Polymer Surface Lubrication and Solid Lubricants
- (5) Polymer Properties and Wear
- (6) Friction and Wear of Polymer Composites
- (7) Polymer Tribology Research in the USSR
- (8) Trends in Polymer Tribology Research

The first three parts are in volume 5A and the remaining five in volume 5B.

For the benefit of polymer chemists, in most parts there is a state-of-the-art review. Most papers present recent research results in science or technology pertaining to the subject matter. A general discussion devoted to the future of polymer tribology research is included. Thus the book covers the past, the present and the future of this important branch of interdisciplinary science.

Part one introduced by L. H. Lee contains the plenary lecture of D. Tabor on 'Friction, adhesion and boundary lubrication of polymers' a survey of the effects of surface energetics on polymer friction and wear and papers on the adhesion mechanism of rubbers, the interaction between PTFE and iron and fracture mechanics aspects of polymer wear.

T. L. Thomson introduces the six papers on the nature of polymer friction in part two which illustrates some of the complexities of the problem of friction. J. J. Bikerman discusses the nature of polymer friction and the other papers cover the effects of deformation on friction in the context of extrusion, studies of solid film lubrication, studies of relating polymeric molecular structure to friction and the effects of velocity and temperature.

Part three introduced by D. V. Keller contains six papers which demonstrate that the surface characterization of polymers is well underway. The plenary lecture by D. T. Clark on 'The application of ESCA to studies of structure and bonding in polymers' reviews most of the current areas of applicability to polymers and the potential of the technique for the investigation of friction and wear phenomena.

The six papers of part four introduced by D. Dowson cover polymer surface lubrication and solid lubricants and indicate that the fundamental and applied problems posed by the newer solid lubricants and composites provide a formidable challenge to physi-

cists, chemists and engineers by the multidisciplinary approach required.

Polymer properties and wear are covered in part five by five papers introduced into the background of the subject by G. J. J. Griffin. The papers deal with the wear topic from a variety of viewpoints and are all concerned with 'ordinary functional' rather than exotic materials. Two of the contributors deal with the problem of polymer wear in the human machine and emphasize the increasing importance of bio-engineering.

D. H. Buckley introduces the six papers of part six concerned with friction and wear of polymeric composites. These cover thermally anisotropic plastics bearing materials, wear of phenolic resin - asbestos friction materials, wear mechanisms of polymers at cryogenic temperatures, wear characteristics of fluoropolymer composites, wear of nylon by paper and wear of dental restoratives.

Part seven introduced by K. C. Ludema contains five papers covering polymer tribology research in the USSR which outline the current state-of-the-art and offer a better understanding of the terminology, apparatus and equipment used in the USSR.

The last part, 'Trends in polymer technology' contains three contributions; the symposium address, 'Probing the effects of entanglements in rubber networks' by J. D. Ferry, 'Chemical and physical effects associated with polymer tribology' by M. O. W. Richardson and an overview of the conference and closing remarks by K. C. Ludema as well as some general discussion.

Short biographical sketches of many of the contributors are given and a complete author and subject index for both volumes is given at the end of each volume.

The books are well produced and attractively bound and should be a valuable reference source for all concerned with polymer science and technology.

As to be expected with this modern method of publication some tables are difficult to read e.g. p 674, 675 and 676 and some electron micrographs have suffered in quality in reproduction.

D. Scott

Degradation and Stabilisation of Polymers
Edited by G. Geuskens
Applied Science, Barking, 1975, £8.00

This book consists of nine papers given at a conference in Brussels under the above title. It is not as the title appears to imply, a systematic review of the field, although there are some valuable review papers dealing with particular aspects of polymer degradation and stability, notably Grassie on present trends in polymer degradation, Braun on PVC degradation and Wright on heat-resistant organic polymers. The latter is a particularly valuable systematic review, not only of recent developments but also of the principles underlying the development of thermally stable polymers.

The remaining papers (Hawkins on polyolefins, Chien on hydroperoxides in polymer degradation, Geuskens and David on polystyrene, Wiles on fibre-forming polymers, Sohma on e.s.r. studies of mechano-chemical degradation and Guillet on polymer photochemistry) are not critical reviews but accounts of research originating in the laboratories of the authors. As such they present

made using additives known to dissociate to radicals. Further studies are in progress.

Acknowledgement

The work described here was performed while C. J. D. was the holder of a Research Studentship awarded by the Science Research Council.

J. C. Bevington and C. J. Dyball

Department of Chemistry,
The University,
Lancaster, UK
(Received 5 May 1976)

References

- 1 Jones, R. G., Catterall, E., Bilson, R. T. and Booth, R. G. *Chem. Commun.*

1972, 22

- 2 Bevington, J. C. and Dyball, C. J. *JCS Faraday Trans. 1* 1975, 71, 2226
- 3 Bevington, J. C. and Dyball, C. J. *J. Polym. Sci. (A)* in the press
- 4 Hyde, P., Kricka, L. J. and Ledwith, A. *Polymer* 1973, 14, 124
- 5 Tada, K., Shirota, Y. and Mikawa, H. *J. Polym. Sci. (B)* 1972, 10, 691
- 6 Stille, J. K. and Chung, D. C. *Macromolecules* 1975, 8, 115

Book Reviews

Advances in Polymer Friction and Wear
Volumes 5A and 5B
Edited by Lieng-Huang Lee
Plenum, New York, 1975, 840 pp. \$35.50

This two-volume set, the fifth volume of the series of Polymer Science and Technology provides a unique survey of both theoretical and practical aspects of polymer tribology. It reports the First International Symposium on the subject held in Los Angeles, which was sponsored by the Division of Organic Coatings and Plastics Chemistry and co-sponsored by the Division of Cellulose, Wool and Fibre Chemistry and Colloid and Surface Chemistry of the American Chemical Society. The proceedings contains all revised or expanded papers together with discussions, introductory remarks by session chairman, the plenary lectures and the symposium address.

Following the sequence of the sessions the book consists of eight parts:

- (1) Mechanisms of Polymer Friction and Wear
- (2) Polymer Properties and Friction
- (3) Characterisation and Modification of Polymer Surfaces
- (4) Polymer Surface Lubrication and Solid Lubricants
- (5) Polymer Properties and Wear
- (6) Friction and Wear of Polymer Composites
- (7) Polymer Tribology Research in the USSR
- (8) Trends in Polymer Tribology Research

The first three parts are in volume 5A and the remaining five in volume 5B.

For the benefit of polymer chemists, in most parts there is a state-of-the-art review. Most papers present recent research results in science or technology pertaining to the subject matter. A general discussion devoted to the future of polymer tribology research is included. Thus the book covers the past, the present and the future of this important branch of interdisciplinary science.

Part one introduced by L. H. Lee contains the plenary lecture of D. Tabor on 'Friction, adhesion and boundary lubrication of polymers' a survey of the effects of surface energetics on polymer friction and wear and papers on the adhesion mechanism of rubbers, the interaction between PTFE and iron and fracture mechanics aspects of polymer wear.

T. L. Thomson introduces the six papers on the nature of polymer friction in part two which illustrates some of the complexities of the problem of friction. J. J. Bikerman discusses the nature of polymer friction and the other papers cover the effects of deformation on friction in the context of extrusion, studies of solid film lubrication, studies of relating polymeric molecular structure to friction and the effects of velocity and temperature.

Part three introduced by D. V. Keller contains six papers which demonstrate that the surface characterization of polymers is well underway. The plenary lecture by D. T. Clark on 'The application of ESCA to studies of structure and bonding in polymers' reviews most of the current areas of applicability to polymers and the potential of the technique for the investigation of friction and wear phenomena.

The six papers of part four introduced by D. Dowson cover polymer surface lubrication and solid lubricants and indicate that the fundamental and applied problems posed by the newer solid lubricants and composites provide a formidable challenge to physi-

cists, chemists and engineers by the multidisciplinary approach required.

Polymer properties and wear are covered in part five by five papers introduced into the background of the subject by G. J. J. Griffin. The papers deal with the wear topic from a variety of viewpoints and are all concerned with 'ordinary functional' rather than exotic materials. Two of the contributors deal with the problem of polymer wear in the human machine and emphasize the increasing importance of bio-engineering.

D. H. Buckley introduces the six papers of part six concerned with friction and wear of polymeric composites. These cover thermally anisotropic plastics bearing materials, wear of phenolic resin - asbestos friction materials, wear mechanisms of polymers at cryogenic temperatures, wear characteristics of fluoropolymer composites, wear of nylon by paper and wear of dental restoratives.

Part seven introduced by K. C. Ludema contains five papers covering polymer tribology research in the USSR which outline the current state-of-the-art and offer a better understanding of the terminology, apparatus and equipment used in the USSR.

The last part, 'Trends in polymer technology' contains three contributions; the symposium address, 'Probing the effects of entanglements in rubber networks' by J. D. Ferry, 'Chemical and physical effects associated with polymer tribology' by M. O. W. Richardson and an overview of the conference and closing remarks by K. C. Ludema as well as some general discussion.

Short biographical sketches of many of the contributors are given and a complete author and subject index for both volumes is given at the end of each volume.

The books are well produced and attractively bound and should be a valuable reference source for all concerned with polymer science and technology.

As to be expected with this modern method of publication some tables are difficult to read e.g. p 674, 675 and 676 and some electron micrographs have suffered in quality in reproduction.

D. Scott

Degradation and Stabilisation of Polymers
Edited by G. Geuskens
Applied Science, Barking, 1975, £8.00

This book consists of nine papers given at a conference in Brussels under the above title. It is not as the title appears to imply, a systematic review of the field, although there are some valuable review papers dealing with particular aspects of polymer degradation and stability, notably Grassie on present trends in polymer degradation, Braun on PVC degradation and Wright on heat-resistant organic polymers. The latter is a particularly valuable systematic review, not only of recent developments but also of the principles underlying the development of thermally stable polymers.

The remaining papers (Hawkins on polyolefins, Chien on hydroperoxides in polymer degradation, Geuskens and David on polystyrene, Wiles on fibre-forming polymers, Sohma on e.s.r. studies of mechano-chemical degradation and Guillet on polymer photochemistry) are not critical reviews but accounts of research originating in the laboratories of the authors. As such they present

Book Reviews

carefully argued points of view which are not, however, necessarily accepted by other workers in the field.

There are some important omissions from the book which detract from its general value. There is no mention at all of the degradation and stabilization of elastomers or of rubber modified thermoplastics, both of which are of considerable interest to polymer scientists and technologists. Nor is there any discussion of high temperature processing operations and their effect on subsequent service stability of polymers and one is left with the impression that many of the degradation processes discussed are carried out under conditions which bear little relation to those to which polymers are subjected in practice.

In spite of these shortcomings, the book will be of considerable value to the research specialist since it is a major function of a conference of this nature to stimulate the presentation of original work in a rapidly advancing field.

G. Scott

Polymer—Plastics Technology and Engineering Volume 4

Edited by L. Naturman

Marcel Dekker, New York, 1975, 249 pp. \$32.50

The editorial policy in this volume has been to maintain the shift of emphasis from polymer characterization and properties to polymer engineering and processing. To this end a series of review articles have been presented mainly on the state of art in the various branches of polymer technology and engineering.

The articles range from rather specific topics such as epoxy resin casting processes, reduction of creep in high acrylonitrile and other polymers, interpretation of gel permeation chromatography, to urethane elastomers, asbestos in polymers, and then more general papers on elastic fracture mechanics and continuum mechanics of solid polymers. Although all of these topics were meant to be covered by review type articles, there is a wide disparity between the various presentations. Some are so specific as to materials and processing as to be more in the nature of technical reports of limited interest. Others were more what one expects of a review article. In any case a review will always be useful if it contains up to date references to the research literature. Sadly one of the articles 'Asbestos in polymers' contains no references, while others were certainly not up to date. For example the latest reference in 'continuum mechanics' was for a book published in 1971.

As a whole this volume of the series lack coherence in the choice of review papers. The only feature that they loosely have in common is that they deal mainly with polymer processing and engineering, but perhaps this is what the editor had in mind. The price \$32.50 for 249 pages is rather high even in these of high inflation.

M. G. Brereton

Heparin, Structure, Function and Clinical Implications

Edited by Ralph A. Bradshaw and Stanford
Wessler

Plenum Press, New York, 1975, 422 pp. \$39.1

Polysaccharides encompass the plant and animal kingdoms: they exhibit astonishing diversity in nature, intermeshing structurally and interacting on a molecular level with numerous other biological macromolecules. Of those polysaccharides known to be essentially linear in construction the relative complexity (or simplicity) of the repeating chemical sequence lies within reasonable bounds. Thus, for example, the plant celluloses, mannans, xylans and the insect cuticle chitins, just to name a few, are all relatively straightforward homopolymers, whereas the bacterial capsular polysaccharides are more complex, often involving four to six different saccharide units per repeat sequence. The animal connective tissue polysaccharides, with which heparin may be loosely associated, are intermediate in the spectrum of complexity: they are polysaccharides with molecular weights in the range 10^3 to over 10^6 Daltons. Heparin is the most highly charged of this group, drenched with sulphate appendages, and preferring a molecular weight close to the lower end of this scale. It occurs as packets of polymeric material in mast cells and is released as and when required.

The blood anti-coagulant properties associated with heparin and its role as an anti-lipemic (fat-clearing) agent have aroused considerable medical interest and its clinical application has encouraged pharmacological preparation and standardization. Thus scientific interest in heparin and its behaviour embraces medicine, biochemistry, chemistry plus a little physics, and with so many aspects of heparin being investigated simultaneously, often involving specialized techniques, a conference was organized in an attempt to correlate this wealth of information. The book represents the proceedings of the International Symposium on Heparin, held in St. Louis, Missouri in May 1974.

The collected contributions are segregated into three main sections. The first deals with the structural aspects of heparin covering the molecular properties, biosynthesis, biological properties and including analytical and pharmacological considerations. The first part discusses the chemistry of heparin and its molecular architecture. It is near this point that the related macromolecule heparan sulphate (also confusingly referred to as heparitin sulphate) creeps into the text. The nomenclature is somewhat novel, to say the least, since heparan sulphate is 'heparin-like' but contains on average approximately 70% less sulphate groups! This substance has generated considerable interest recently since it appears on cell surfaces and may have a controlling influence on intercellular adhesion. However, returning to heparin, the evidence accumulated relating to the biosynthetic process strongly favours polymerization followed by epimerization of the sugar residue D-glucuronic acid to L-iduronic acid coupled with, or followed by sulphation of the polymer.

This is a further example in the polysaccharide field where post-polymerization modifications are carried out to suit particular biological roles. Synthetic polymer chemists might well be enlightened by examining the inherent shrewdness in the manufacture of some of these natural polymers.

The biological properties of heparin certainly change as a function of the varying chemical structures that occur, especially from different sources, but no clear correlation has yet emerged. The ambiguities in this area certainly create unforgivable headaches for those responsible for standardization of such an important drug.

The second section covers the functional aspects of heparin: parts of the complex 'waterfall' process of blood clotting are examined in detail. My only criticism of the book relates to this section, — nowhere can one find a concise layout of this 'waterfall' or 'cascade' process which involves about eight steps, where A interacts with B and which in turn controls conversion of C to D etc. As Macfarlane pointed out in 1964 the whole blood clotting process may be likened to a multistage amplifier probably with positive and/or negative feedback — after all, when we cut ourselves we do not wish to clot to death! Thus, I judge, many readers will be lured into details about such substances as antithrombin (one of the factors involved in the process) without first having the opportunity of grasping the gist of the blood clotting sequences and the relevance of heparin. One can eventually pull out some of the essentials from the text. During the coagulation of blood thrombin is produced from its precursor, prothrombin, on lipid surfaces and in the presence of calcium ions. Thrombin, which is a proteolytic enzyme, interacts with fibrinogen and initiates the development of the fibrin clot. The outsider in this arena is antithrombin, which as its name implies, neutralizes thrombin thus safeguarding fibrinogen. Heparin accelerates this neutralization between thrombin and antithrombin by a couple of orders in magnitude. As mentioned earlier heparin is also a fat-clearing agent. Intravenous injections of heparin triggers the release of the enzyme lipase into the circulating blood which can then fragment the fatty lipoproteins.

In the final section relating to the clinical aspects of heparin Dr Stanford Wessler points out the frightening fact that about 15% of Americans are hospitalized every year and one sixth of these die from venous thromboembolism! Heparin, when administered in carefully controlled doses, behaves as an effective anticoagulant for the prevention of the possibly fatal formation of blood clots after surgery. Additionally heparin has a potential role in inhibiting the clotting process in the early stages without increasing the danger of excessive bleeding, and may well reduce the risk of clotting in women using oral contraceptives.

This book, consisting of some thirty-three papers on selected aspects of heparin in 422 pages, is an excellent reference text for those wishing to familiarize themselves with the heparin macromolecule. The editors have made an excellent job of juxtapositioning the individual contributions to produce a coherent text. The bright red textured dust cover is almost appropriate.

Edward Atkins

made using additives known to dissociate to radicals. Further studies are in progress.

Acknowledgement

The work described here was performed while C. J. D. was the holder of a Research Studentship awarded by the Science Research Council.

J. C. Bevington and C. J. Dyball

Department of Chemistry,
The University,
Lancaster, UK
(Received 5 May 1976)

References

- 1 Jones, R. G., Catterall, E., Bilson, R. T. and Booth, R. G. *Chem. Commun.*

1972, 22

- 2 Bevington, J. C. and Dyball, C. J. *JCS Faraday Trans. 1* 1975, 71, 2226
- 3 Bevington, J. C. and Dyball, C. J. *J. Polym. Sci. (A)* in the press
- 4 Hyde, P., Kricka, L. J. and Ledwith, A. *Polymer* 1973, 14, 124
- 5 Tada, K., Shirota, Y. and Mikawa, H. *J. Polym. Sci. (B)* 1972, 10, 691
- 6 Stille, J. K. and Chung, D. C. *Macromolecules* 1975, 8, 115

Book Reviews

Advances in Polymer Friction and Wear

Volumes 5A and 5B

Edited by Lieng-Huang Lee

Plenum, New York, 1975, 840 pp. \$35.50

This two-volume set, the fifth volume of the series of Polymer Science and Technology provides a unique survey of both theoretical and practical aspects of polymer tribology. It reports the First International Symposium on the subject held in Los Angeles, which was sponsored by the Division of Organic Coatings and Plastics Chemistry and co-sponsored by the Division of Cellulose, Wool and Fibre Chemistry and Colloid and Surface Chemistry of the American Chemical Society. The proceedings contains all revised or expanded papers together with discussions, introductory remarks by session chairman, the plenary lectures and the symposium address.

Following the sequence of the sessions the book consists of eight parts:

- (1) Mechanisms of Polymer Friction and Wear
- (2) Polymer Properties and Friction
- (3) Characterisation and Modification of Polymer Surfaces
- (4) Polymer Surface Lubrication and Solid Lubricants
- (5) Polymer Properties and Wear
- (6) Friction and Wear of Polymer Composites
- (7) Polymer Tribology Research in the USSR
- (8) Trends in Polymer Tribology Research

The first three parts are in volume 5A and the remaining five in volume 5B.

For the benefit of polymer chemists, in most parts there is a state-of-the-art review. Most papers present recent research results in science or technology pertaining to the subject matter. A general discussion devoted to the future of polymer tribology research is included. Thus the book covers the past, the present and the future of this important branch of interdisciplinary science.

Part one introduced by L. H. Lee contains the plenary lecture of D. Tabor on 'Friction, adhesion and boundary lubrication of polymers' a survey of the effects of surface energetics on polymer friction and wear and papers on the adhesion mechanism of rubbers, the interaction between PTFE and iron and fracture mechanics aspects of polymer wear.

T. L. Thomson introduces the six papers on the nature of polymer friction in part two which illustrates some of the complexities of the problem of friction. J. J. Bikerman discusses the nature of polymer friction and the other papers cover the effects of deformation on friction in the context of extrusion, studies of solid film lubrication, studies of relating polymeric molecular structure to friction and the effects of velocity and temperature.

Part three introduced by D. V. Keller contains six papers which demonstrate that the surface characterization of polymers is well underway. The plenary lecture by D. T. Clark on 'The application of ESCA to studies of structure and bonding in polymers' reviews most of the current areas of applicability to polymers and the potential of the technique for the investigation of friction and wear phenomena.

The six papers of part four introduced by D. Dowson cover polymer surface lubrication and solid lubricants and indicate that the fundamental and applied problems posed by the newer solid lubricants and composites provide a formidable challenge to physi-

cists, chemists and engineers by the multidisciplinary approach required.

Polymer properties and wear are covered in part five by five papers introduced into the background of the subject by G. J. J. Griffin. The papers deal with the wear topic from a variety of viewpoints and are all concerned with 'ordinary functional' rather than exotic materials. Two of the contributors deal with the problem of polymer wear in the human machine and emphasize the increasing importance of bio-engineering.

D. H. Buckley introduces the six papers of part six concerned with friction and wear of polymeric composites. These cover thermally anisotropic plastics bearing materials, wear of phenolic resin - asbestos friction materials, wear mechanisms of polymers at cryogenic temperatures, wear characteristics of fluoropolymer composites, wear of nylon by paper and wear of dental restoratives.

Part seven introduced by K. C. Ludema contains five papers covering polymer tribology research in the USSR which outline the current state-of-the-art and offer a better understanding of the terminology, apparatus and equipment used in the USSR.

The last part, 'Trends in polymer technology' contains three contributions; the symposium address, 'Probing the effects of entanglements in rubber networks' by J. D. Ferry, 'Chemical and physical effects associated with polymer tribology' by M. O. W. Richardson and an overview of the conference and closing remarks by K. C. Ludema as well as some general discussion.

Short biographical sketches of many of the contributors are given and a complete author and subject index for both volumes is given at the end of each volume.

The books are well produced and attractively bound and should be a valuable reference source for all concerned with polymer science and technology.

As to be expected with this modern method of publication some tables are difficult to read e.g. p 674, 675 and 676 and some electron micrographs have suffered in quality in reproduction.

D. Scott

Degradation and Stabilisation of Polymers

Edited by G. Geuskens

Applied Science, Barking, 1975, £8.00

This book consists of nine papers given at a conference in Brussels under the above title. It is not as the title appears to imply, a systematic review of the field, although there are some valuable review papers dealing with particular aspects of polymer degradation and stability, notably Grassie on present trends in polymer degradation, Braun on PVC degradation and Wright on heat-resistant organic polymers. The latter is a particularly valuable systematic review, not only of recent developments but also of the principles underlying the development of thermally stable polymers.

The remaining papers (Hawkins on polyolefins, Chien on hydroperoxides in polymer degradation, Geuskens and David on polystyrene, Wiles on fibre-forming polymers, Sohma on e.s.r. studies of mechano-chemical degradation and Guillet on polymer photochemistry) are not critical reviews but accounts of research originating in the laboratories of the authors. As such they present

Book Reviews

carefully argued points of view which are not, however, necessarily accepted by other workers in the field.

There are some important omissions from the book which detract from its general value. There is no mention at all of the degradation and stabilization of elastomers or of rubber modified thermoplastics, both of which are of considerable interest to polymer scientists and technologists. Nor is there any discussion of high temperature processing operations and their effect on subsequent service stability of polymers and one is left with the impression that many of the degradation processes discussed are carried out under conditions which bear little relation to those to which polymers are subjected in practice.

In spite of these shortcomings, the book will be of considerable value to the research specialist since it is a major function of a conference of this nature to stimulate the presentation of original work in a rapidly advancing field.

G. Scott

Polymer—Plastics Technology and Engineering Volume 4

Edited by L. Naturman

Marcel Dekker, New York, 1975, 249 pp. \$32.50

The editorial policy in this volume has been to maintain the shift of emphasis from polymer characterization and properties to polymer engineering and processing. To this end a series of review articles have been presented mainly on the state of art in the various branches of polymer technology and engineering.

The articles range from rather specific topics such as epoxy resin casting processes, reduction of creep in high acrylonitrile and other polymers, interpretation of gel permeation chromatography, to urethane elastomers, asbestos in polymers, and then more general papers on elastic fracture mechanics and continuum mechanics of solid polymers. Although all of these topics were meant to be covered by review type articles, there is a wide disparity between the various presentations. Some are so specific as to materials and processing as to be more in the nature of technical reports of limited interest. Others were more what one expects of a review article. In any case a review will always be useful if it contains up to date references to the research literature. Sadly one of the articles 'Asbestos in polymers' contains no references, while others were certainly not up to date. For example the latest reference in 'continuum mechanics' was for a book published in 1971.

As a whole this volume of the series lack coherence in the choice of review papers. The only feature that they loosely have in common is that they deal mainly with polymer processing and engineering, but perhaps this is what the editor had in mind. The price \$32.50 for 249 pages is rather high even in these of high inflation.

M. G. Brereton

Heparin, Structure, Function and Clinical Implications

Edited by Ralph A. Bradshaw and Stanford
Wessler

Plenum Press, New York, 1975, 422 pp. \$39.1

Polysaccharides encompass the plant and animal kingdoms: they exhibit astonishing diversity in nature, intermeshing structurally and interacting on a molecular level with numerous other biological macromolecules. Of those polysaccharides known to be essentially linear in construction the relative complexity (or simplicity) of the repeating chemical sequence lies within reasonable bounds. Thus, for example, the plant celluloses, mannans, xylans and the insect cuticle chitins, just to name a few, are all relatively straightforward homopolymers, whereas the bacterial capsular polysaccharides are more complex, often involving four to six different saccharide units per repeat sequence. The animal connective tissue polysaccharides, with which heparin may be loosely associated, are intermediate in the spectrum of complexity: they are polysaccharides with molecular weights in the range 10^3 to over 10^6 Daltons. Heparin is the most highly charged of this group, drenched with sulphate appendages, and preferring a molecular weight close to the lower end of this scale. It occurs as packets of polymeric material in *mast* cells and is released as and when required.

The blood anti-coagulant properties associated with heparin and its role as an anti-lipemic (fat-clearing) agent have aroused considerable medical interest and its clinical application has encouraged pharmacological preparation and standardization. Thus scientific interest in heparin and its behaviour embraces medicine, biochemistry, chemistry plus a little physics, and with so many aspects of heparin being investigated simultaneously, often involving specialized techniques, a conference was organized in an attempt to correlate this wealth of information. The book represents the proceedings of the International Symposium on Heparin, held in St. Louis, Missouri in May 1974.

The collected contributions are segregated into three main sections. The first deals with the structural aspects of heparin covering the molecular properties, biosynthesis, biological properties and including analytical and pharmacological considerations. The first part discusses the chemistry of heparin and its molecular architecture. It is near this point that the related macromolecule heparan sulphate (also confusingly referred to as heparitin sulphate) creeps into the text. The nomenclature is somewhat novel, to say the least, since heparan sulphate is 'heparin-like' but contains on average approximately 70% less sulphate groups! This substance has generated considerable interest recently since it appears on cell surfaces and may have a controlling influence on intercellular adhesion. However, returning to heparin, the evidence accumulated relating to the biosynthetic process strongly favours polymerization followed by epimerization of the sugar residue D-glucuronic acid to L-iduronic acid coupled with, or followed by sulphation of the polymer.

This is a further example in the polysaccharide field where post-polymerization modifications are carried out to suit particular biological roles. Synthetic polymer chemists might well be enlightened by examining the inherent shrewdness in the manufacture of some of these natural polymers.

The biological properties of heparin certainly change as a function of the varying chemical structures that occur, especially from different sources, but no clear correlation has yet emerged. The ambiguities in this area certainly create unforgivable headaches for those responsible for standardization of such an important drug.

The second section covers the functional aspects of heparin: parts of the complex 'waterfall' process of blood clotting are examined in detail. My only criticism of the book relates to this section, — nowhere can one find a concise layout of this 'waterfall' or 'cascade' process which involves about eight steps, where A interacts with B and which in turn controls conversion of C to D etc. As Macfarlane pointed out in 1964 the whole blood clotting process may be likened to a multistage amplifier probably with positive and/or negative feedback — after all, when we cut ourselves we do not wish to clot to death! Thus, I judge, many readers will be lured into details about such substances as antithrombin (one of the factors involved in the process) without first having the opportunity of grasping the gist of the blood clotting sequences and the relevance of heparin. One can eventually pull out some of the essentials from the text. During the coagulation of blood thrombin is produced from its precursor, prothrombin, on lipid surfaces and in the presence of calcium ions. Thrombin, which is a proteolytic enzyme, interacts with fibrinogen and initiates the development of the fibrin clot. The outsider in this arena is antithrombin, which as its name implies, neutralizes thrombin thus safeguarding fibrinogen. Heparin accelerates this neutralization between thrombin and antithrombin by a couple of orders in magnitude. As mentioned earlier heparin is also a fat-clearing agent. Intravenous injections of heparin triggers the release of the enzyme lipase into the circulating blood which can then fragment the fatty lipoproteins.

In the final section relating to the clinical aspects of heparin Dr Stanford Wessler points out the frightening fact that about 15% of Americans are hospitalized every year and one sixth of these die from venous thromboembolism! Heparin, when administered in carefully controlled doses, behaves as an effective anticoagulant for the prevention of the possibly fatal formation of blood clots after surgery. Additionally heparin has a potential role in inhibiting the clotting process in the early stages without increasing the danger of excessive bleeding, and may well reduce the risk of clotting in women using oral contraceptives.

This book, consisting of some thirty-three papers on selected aspects of heparin in 422 pages, is an excellent reference text for those wishing to familiarize themselves with the heparin macromolecule. The editors have made an excellent job of juxtapositioning the individual contributions to produce a coherent text. The bright red textured dust cover is almost appropriate.

Edward Atkins

POLYMER in the USA

Many of POLYMER's readers will have noticed various changes in the appearance of the journal over the years. Some of these have been minor and of little importance (such as the recent change to a three column format for the *Notes to the Editor* and *Letters* sections). Others, such as the change in page size in 1972 and the introduction of more modern printing methods in 1975 have made a bigger impact, allowing more material to be published and some reduction in the inflationary spiral of increased production costs. The observant reader of *this issue* will have noticed a change in appearance to the inside front cover of far greater significance than anything previously – the appointment of a group of Editors for the USA.

However, this change is more than just an appearance and should be seen as a fresh and positive approach by the journal. The presence of these Editors will hopefully encourage more authors in North America to submit contributions to POLYMER in the knowledge that each submission will be refereed by their immediate contemporaries to the standard expected of this journal. This will also help to minimize delays in the refereeing procedure so that publication to a worldwide audience can be made quickly and accurately; our previous performance should testify to that. It is understandable that many potential authors in the past have felt reluctant to break with tradition by publishing outside their own country. Now, by placing POLYMER's new facilities and current reputation before the North American polymer community on the same level as our competitors already based there, we ask to be judged not as direct competitors but as complementary publishers whose aim is to continue to serve the international interests of polymer research. By having the services of such eminent scientists to act as US Editors for POLYMER, their range of experience and specialist knowledge will cover most areas of the field. Inevitably new techniques, new technologies, fresh developments as well as different materials will evolve with the need for academic debate in public (the biomaterials and biopolymers field is one area with an exciting potential). Thus an ever-increasing group of specialists will become involved with the refereeing process and this will ensure that POLYMER remains a living organ in dynamic equilibrium with its environment ('constantly changing yet constantly unchanged').

Growth is another aspect of the living process and these changes will represent further growth for POLYMER so that some of the great wealth of polymer research from the USA can be published alongside the present existing material.

Airspeeding service

We are pleased to announce that from the July 1976 issue, all copies of POLYMER destined for North America have been airfreighted to New York and posted from there *at no additional cost to subscribers*. This should mean that readers will receive their copy during the period of the cover date where before it had been taking anything from 2 to 6 months to reach a library in the USA. The publishers would be interested to hear how the system works in practice.

Directional diffusion rates in keratin

Ian C. Watt

*Division of Textile Physics, CSIRO, Ryde, New South Wales 2112, Australia
(Received 8 December 1975; revised 20 April 1976)*

The kinetics of sorption of water vapour have been measured for keratin prepared by slicing horsehairs into discs so that the major part of the external surface of the discs was composed of cross-sections of the original fibres perpendicular to the fibre direction. For diffusion-controlled absorption no significant difference in the diffusion coefficients of the horsehair discs or intact keratin was detected indicating that diffusion in the longitudinal or lateral directions in keratin fibres, occurs at similar rates. However, the initial rate of absorption by the discs was faster by a factor equivalent to the increased surface to volume ratio. The rates of absorption approached similar values for anomalous sorption where stress relaxation in the keratin contributes largely to the water uptake and the rate of stress relaxation is sufficiently fast to occur concurrently with diffusion into the keratin. This occurs at high penetrant concentrations and for large integral absorption steps. The similar rates of absorption, despite the difference in surface areas, is not evidence that diffusion is more rapid in a lateral direction but supports the concept of a coupled diffusion—relaxation sorption mechanism.

INTRODUCTION

Keratin is not isotropic with respect to swelling in water and this had led to speculation that diffusion rates in wool fibres may be dependent upon the direction of travel of the penetrant. However, no conclusive evidence on this question is available. The geometry of wool fibres is such that there is a large surface to volume ratio. The molecular chains are oriented in the direction of the fibre axis and since orientation in the direction of travel is thought to be responsible for decreased rates of absorption in amorphous polymers with continued sorption cycles¹, the ability of water molecules to diffuse longitudinally may be considerably less than their ability to diffuse laterally in the fibres.

Penetration initially occurs perpendicular to the surface and the basic assumption that all diffusion takes place in a direction perpendicular to the surface probably provides a reasonable approximation in calculation of diffusion rates. The present paper reports on experiments designed so that the calculated rates of diffusion of water vapour longitudinally and laterally into horsehair keratin could be compared. Horsehair was sectioned perpendicular to the fibre axis, to form flat discs; the surface area of the discs being composed of new surface created by the sectioning, and the original surface of the horsehair. Thus, diffusion perpendicular to the flat surfaces of the discs would be in the longitudinal direction of the original fibres while diffusion across the curved surface would be perpendicular to the fibre direction.

EXPERIMENTAL

Preparation of materials

The keratins used were horsehair, taken from the tail, and Merino wool fibres cleaned by six washes in cold petroleum ether followed by thorough soaking in distilled water until the pH of the wash water was unchanged by the keratin. Successive sections of average thickness 20 μm were microtomed from a number of horsehairs embedded in parallel array in a paraffin wax, using a Cambridge rotary rocking microtome. Another portion of horsehair, of dry

diameter the same as the average diameter of the microtomed horsehairs, was kept intact.

Apparatus and procedure

Sorption measurements were carried out by a gravimetric technique using quartz spiral spring balances (sensitivity 500 cm/g) mounted in evacuable sorption chambers, the whole apparatus being enclosed in an air thermostat. Two identical chambers were set up side by side and connected to the same reservoir of water vapour and to a wide-bore differential mercury manometer. The temperature was controlled to $\pm 0.01^\circ\text{C}$ and the spring extensions read to 0.01 mm with cathetometers. A length of horsehair weighing 8 mg was suspended from one spring and from the other an equivalent weight of horsehair discs, each 20 μm thick, was suspended by spreading the sections thinly on a non-sorbing plastic sheet attached to the end of the spring.

The dry diameter of the intact horsehair and the average dry diameter of the sliced horsehair discs was 170 μm . Thus, the surface area, A , of an x cm length of this horsehair would be $A = 2\pi 85x \times 10^{-4} \text{ cm}^2$. The additional surface exposed by microtoming an equivalent length of horsehair of this diameter into 20 μm sections would be:

$$2 \frac{x}{20 \times 10^{-4}} \times \pi(85 \times 10^{-4})^2 \text{ cm}^2 = \pi x 85^2 \times 10^{-5} \text{ cm}^2 \\ = 4.25A \text{ cm}^2$$

Thus, the total surface of the microtomed sections was $5.25A \text{ cm}^2$ of which $A \text{ cm}^2$ was the original surface lying parallel to the fibre axis and $4.25A \text{ cm}^2$ was new surface perpendicular to the fibre axis.

RESULTS AND DISCUSSION

Interval sorption

Rates of uptake of water vapour by keratin are dependent on the initial concentration of water and the size of

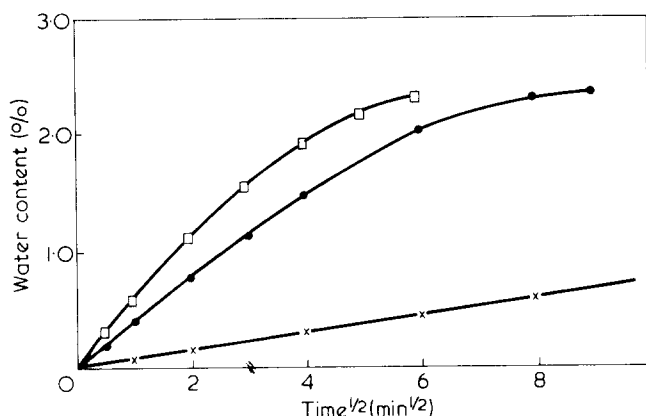


Figure 1 Uptake of water vapour by keratin at 35°C as a function of $(\text{time})^{1/2}$ following a 0–4.5% r.h. humidity increment. ●, Horsehair snippets; X, intact horsehair; □, Merino wool fibres

the concentration increment². Sorption over a large concentration range has been termed integral sorption and over a small concentration range, interval sorption. For such small concentration increments absorption may occur in two stages; the second stage much slower than the first³. The uptake during the first stage of absorption occurs by a Fickian mechanism with a concentration-dependent diffusion coefficient. Accordingly, in order to determine diffusion coefficients the horsehair samples were equilibrated with water vapour at various concentrations and subjected to small increments of vapour pressure.

Low humidities. Initially the samples were evacuated to attain an equilibrium dry weight and subjected to a 0–4.5% r.h. humidity increment at 35°C. The uptake curve for the intact horsehair and the corresponding uptake for the horsehair snippets are shown in Figure 1 where the water contents of the keratin samples are plotted as a function of $(\text{time})^{1/2}$. The uptake curve for 20 μm diameter Merino wool fibres is included for comparison.

Fickian sorption is characterized by an initially linear plot of absorption or desorption as a function of $(\text{time})^{1/2}$. Crank⁴ has given mathematical solutions for the amount of penetrant entering a cylinder, or a thin film, at any time following an instantaneous change of surface concentration to a constant value and assuming an infinite supply of penetrant. The two cases yield different shaped uptake curves because of the different geometry. When plotted as a function of $(\text{time})^{1/2}$ the linear portion of the uptake curve for the plane film persists to as much as 50% of the equilibrium value, while the uptake for the cylinder becomes concave to the abscissa soon after the commencement of absorption and reaches equilibrium at half the value for the plane for a sample of equivalent surface area. Thus it is essential to consider only initial rates of uptake.

The diffusion coefficient for water vapour into intact horsehair over the range 0–4.5% r.h. was calculated from the data presented in Figure 1 to be $2.7 \times 10^{-10} \text{ cms}^2/\text{sec}$. This is in good agreement with the value of $2.4 \times 10^{-10} \text{ cms}^2/\text{sec}$ obtained for the diffusion of water vapour into Merino wool fibres for the same concentration increment. The greater surface to volume ratio for the snippets compared to the intact horsehair allows the uptake of water vapour to approach equilibrium more quickly in the former case. The coefficient of diffusion into the two parallel surfaces of the discs can be calculated from the appropriate expression for a plane film if the initial uptake is considered uniform over the whole surface, and yields a value of $2.5 \times 10^{-10} \text{ cms}^2/\text{sec}$.

A simpler comparison can be obtained from the initial slopes of the uptake curves for horsehair; these differ by a factor of 5 whereas the ratios of surface area in the two cases is 5.25:1. If the original surface is assumed to absorb at the same rate in both cases, the difference in rate of uptake over the two surfaces is less than 7% and must be considered within the experimental error. Thus, the diffusion of water into keratin at low concentrations is virtually isotropic. Similar results were obtained for desorption when the samples were evacuated to dryness after equilibration at 4.5% r.h.

Intermediate humidities. At intermediate humidities, and for small increments of humidity, absorption into wool fibres occurs in two distinct phases. An increasing proportion of the uptake occurs in the second stage as the initial water content is increased and reaches a maximum for wool conditioned at around 50% r.h.⁵ Similar data were obtained for the horsehair samples equilibrated at 50% r.h. and subjected to a 4% r.h. increment of humidity. The fractional change in water content for the step is plotted in Figure 2 as a function of $(\text{time})^{1/2}$ for the intact horsehair and the snippets. The ratio of the initial rates of uptake is 4.7:1 but the second stage uptake which continued for 5 days occurs at the same rate in the two cases. This supports the contention that the mechanism of absorption in the second stage is not diffusion-controlled and is consistent with the notion that it results from a relaxation mechanism which occurs uniformly throughout the keratin following the entry of water during the first stage of uptake⁵.

High humidities. As the water content of the horsehair samples increased a continued reduction was observed in the difference in the rates of uptake of the snippets and the intact horsehair. For the small increment of 83–86% r.h. the ratio of the initial rates of uptake was reduced to 2.25:1. However, it must be emphasized that the uptake in this region displays anomalous sorption characteristics over the whole range and the comparison of rates is only an estimate in that uptake is not strictly linear as a function of $(\text{time})^{1/2}$ and there is no clear separation into two stages.

Integral sorption

Integral sorption embraces the two mechanisms of sorption mentioned previously, i.e. a diffusion-controlled entry of water vapour and an additional uptake of water as a result of stress relaxation in the keratin. In such a coupled diffusion-relaxation system the relative contribution of each of these mechanisms to the total uptake will vary according to the concentration range of the step. The dependence of uptake on sample thickness is also variable according to the concentration range. A better comparison,

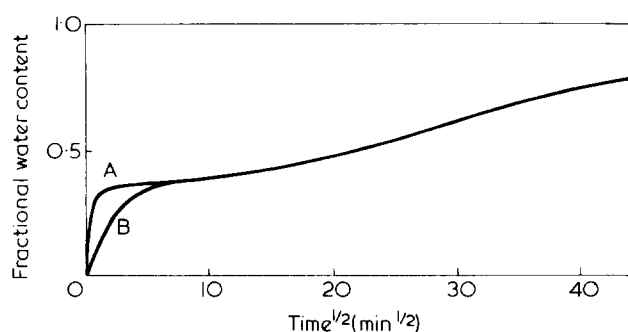


Figure 2 Interval absorption. Fractional water content change as a function of $(\text{time})^{1/2}$ for horsehair subjected to a 50.0–54.0% r.h. humidity increment. A, Horsehair snippets; B, intact horsehair

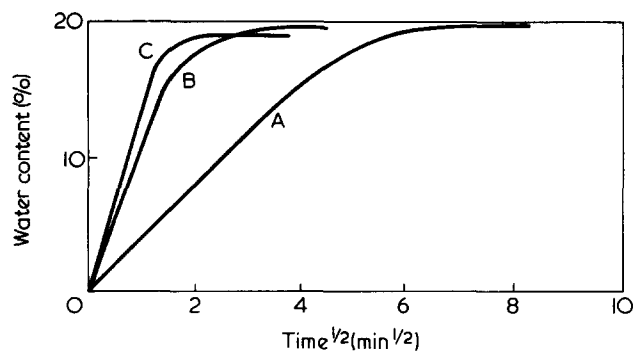


Figure 3 Integral absorption. Uptake of water vapour by keratin as a function of $(\text{time})^{1/2}$ for the humidity range of 0–80% r.h. at 35°C. A, Intact horsehair; B, horsehair snippets; C, Merino wool fibres

therefore, is obtained by considering the rates of uptake by Merino wool fibres of 20 μm diameter and the horsehair snippets over the same concentration range. If the wool fibres are considered as cylinders and the snippets as infinite plane films, the wool fibres should have double the surface area for the same weight of sample. Because the curved surfaces of the snippets contribute appreciably to their total surface area this ratio is less for the snippets used here; the surface area of the 20 μm diameter wool fibres is 1.67 times the surface area of the horsehair snippets for the same weight of keratin.

For the sorption steps of 0–25% r.h. and 0–50% r.h. the rate of uptake by horsehair snippets was approximately 60% of the initial rate of uptake by Merino wool fibres. Sorption into the intact horsehair was much slower because of the increased diameter of the sample and the consequent reduction in surface to volume ratio. Thus, there is little evidence that absorption in the longitudinal direction occurs at a different rate from absorption perpendicular to the original surface of the fibre.

For integral absorption at humidities approaching saturation the situation changes. The rate differences become progressively less as the humidity range is increased and at high humidities the intact horsehair absorbs water vapour at a rate which approaches the rate of uptake by the snippets despite the difference in surface area. In Figure 3 the uptake curves for the intact horsehair, horsehair snippets and the Merino wool fibres for the humidity step of 0–80% r.h. show the greatly decreased differences in uptake rates compared to the corresponding absorption curves of Figure 1.

Desorption of the samples by evacuation to dryness showed that the discs desorbed rapidly at a rate similar to that for Merino wool fibres while the intact horsehair, after an initial rapid desorption, approached equilibrium slowly such that the time to reach dryness became proportional to $(\text{diameter})^2$.

CONCLUSIONS

The rate of diffusion of water into keratin fibres is similar in the directions parallel to, and perpendicular to the fibre direction. However, the uptake of water is influenced by the ability of the keratin to stress relax after swelling. For small increments of water vapour pressure the diffusion process and the stress relaxation process can be separated; the former leads to rates of uptake proportional to the surface area and the latter to rates of uptake independent of surface area. When stress relaxation occurs concurrently with diffusion the contribution of the stress relaxation mechanism becomes the rate controlling step throughout the sample and the dimensions of the sample become less important in determining the rate of uptake. The apparent slower rate of uptake in the direction parallel to the fibre direction at higher humidities follows from the rapid rate of stress relaxation in this region.

A further deduction which may be made from these results is that because diffusion coefficients for the two samples of horsehair and the wool fibres are similar, it appears to be a reasonable assumption to consider wool fibres as smooth cylinders for purposes of treatment of sorption data, despite the surface irregularities present.

ACKNOWLEDGEMENT

The author wishes to thank Mr R. Morris for the careful preparation of the keratin samples used in this study.

REFERENCES

- 1 Drechsel, P., Hoard, J. L. and Long, F. A. *J. Polym. Sci.* 1953, **10**, 241
- 2 Watt, I. C. *Text. Res. J.* 1960, **30**, 443
- 3 Downes, J. G. and Mackay, B. H. *J. Polym. Sci.* 1958, **28**, 45
- 4 Crank, J. 'Mathematics of Diffusion', Clarendon Press, Oxford, 1956, Ch 4 and 5
- 5 Watt, I. C. *Text. Res. J.* 1960, **30**, 644

Small-angle neutron scattering studies of molten and crystalline polyethylene

J. Schelten*, D. G. H. Ballard, G. D. Wignall, G. Longman and W. Schmatz*

Imperial Chemical Industries Limited, Corporate Laboratory, The Heath, Runcorn, Cheshire WA7 4QE, UK

(Received 4 March 1976)

Small-angle neutron scattering studies have been made of molten and crystalline polyethylene using samples containing small amounts of deuterated polyethylene (PED) in a protonated polyethylene (PEH) matrix. Careful studies were made of PED aggregation effects, and by a combination of solution blending techniques and rapid quenching from the melt, it was possible to prepare samples with a statistical distribution of PED molecules in the PEH matrix. Measurements of radius of gyration ($\langle S^2 \rangle_w^{1/2}$ at low κ [$\kappa = (4\pi/\lambda) \sin \theta \leq 2 \times 10^{-2} \text{ \AA}^{-1}$] in the melt and in the solid state gave very similar values which may be summarized as $\langle S^2 \rangle_w^{1/2} = (0.46 \pm 0.05)M_w^{1/2}$ for both phases. This correspondence of values indicates that on a rapid quench, diffusion is sufficiently slow that the molecule crystallizes with a similar spatial distribution of mass elements to that possessed in the melt. Measurements of scattering data over a wide κ range ($6 \times 10^{-3} \leq \kappa \leq 0.12 \text{ \AA}^{-1}$) have also been made from samples showing no aggregation effects. Calculations indicate that it is difficult to fit this data in terms of models which postulate adjacent chain re-entry in one crystallographic plane for this type of sample.

INTRODUCTION

Small-angle neutron scattering (SANS) using the D-H system has proved successful in studying amorphous polymers in the solid state¹ and above T_g^2 , and crystalline polymers above their melting point^{3,4}. When applied to the study of crystalline polymers in the solid state several experimental problems were encountered which were associated with voids of sub-microns dimensions formed between the crystalline and amorphous regions and the segregation into clusters of the tagged molecules during sample preparation³.

The first of these problems is overcome in the case of polyethylene, by using deuterated polyethylene (PED) in a matrix of protonated polyethylene (PEH). Normally void scattering dominates low-angle X-ray scattering from polyethylene, but in the case of neutron scattering from PEH, cancellation between the positive scattering length of C ($b_C = +0.66 \times 10^{-12} \text{ cm}$) and the negative scattering from ¹H ($b_H = -0.37 \times 10^{-12} \text{ cm}$) means that the coherent neutron scattering is almost completely eliminated. In PED on the other hand no such cancellation is possible since the scattering lengths of carbon and deuterium are nearly of the same magnitude and the same sign.

The second problem, the formation of clusters of tagged molecules, can be overcome by a combination of appropriate solution blending techniques and rapid quenching from the melt as described below. The segregation of PED chains within the PEH matrix was first mentioned by Stehling *et al.*⁵, who measured the difference in melting points in two series of deuterated and protonated alkanes. They showed that PED has a melting point $\sim 6^\circ\text{C}$ below that of PEH and discussed how this might arise from differences in the entropy or enthalpy of the two polymers. They pointed out that there was a danger of segregation and that a statistical distribution of tagged molecules could not be assumed.

EXPERIMENTAL

The first samples prepared were solution blended in boiling xylene and precipitated into methanol at room temperature. The resultant powders were washed in methanol and dried in a vacuum oven at 70°C and subsequently compression moulded at 190°C into sheets $\sim 1 \text{ mm}$ thick, suitable for neutron measurements. After compression moulding the samples were removed from the press and quenched into water at room temperature. Further details of sample preparation, the experimental SANS technique, together with the measured SANS data, are given in refs 3 and 6. It was concluded from an analysis of this data that clusters of 15–30 PED molecules had occurred in the solid state, and that the clustering was reduced or eliminated by thermodynamic mixing when performing measurements in the melt over periods of several hours^{3,6}.

In order to reduce or eliminate the clustering problem in the solid state, the method of sample preparation was varied, and it was eventually found that virtually unclustered solid samples could be prepared by substituting *ortho*-dichlorobenzene (*o*-DCB) for xylene in the above procedure, and quenching from the melt after compression moulding. *o*-DCB has a boiling point $\approx 180^\circ\text{C}$ (compared to xylene $\approx 140^\circ\text{C}$), which is well above the melting point of polyethylene ($\approx 135^\circ\text{C}$) and will therefore enhance the probability of complete dissolution of the two polymers. By this method samples coded A3, A6, PE 18, 21, 22, 23, 24 and 25 (*Table 1*) were made. *Table 1* shows the molecular weights of the matrix and deuterated molecules and also the polydispersity and concentration of the tagged PED molecules. The scattering parameters found in *Table 1* are defined and discussed below.

For all these samples the matrix was linear unbranched PEH and the crystallinity indices of this series, as measured by X-ray diffraction and density flotation methods, were typically $65 \pm 2\%$. In order to further characterize the morphology of the rapidly quenched material, typical samples were analysed by small-angle X-ray scattering (SAXS)

* Institut für Festkörperforschung der Kernforschungsanlage GmbH, D-5170 Jülich 1, Postfach 1913, Germany.

Table 1 Neutron scattering data for polyethylene with PEH matrix and PED tagged molecules

Sample No.	PEH		Polydispersity M_w/M_n	c (g/g)	PED (linear)		$(S^2)^{1/2}$ (Å)	$(S^2)^{1/2}/M_w^{1/2}$	Q	Comments
	$M_w \times 10^{-3}$	$M_w \times 10^{-3}$			$(M_w)_{app} \times 10^{-3}$					
Rapidly quenched measurements at 23°C										
A3Q	78	60	1.54	0.03	53	146	0.52	—	Matched sample with branched PEH matrix	
A6Q	78	60	1.54	0.06	46	133	0.46	2.4	Matched sample with branched PEH matrix	
A6Q	78	60	1.54	0.06	46	132	0.46	—	Matched sample with branched PEH matrix	
PE18	112	43	2.8	0.03	50	136	0.53	—	Linear PEH matrix	
PE18	112	43	2.8	0.03	55	150	0.59	—	Linear PEH matrix	
PE21	100	140	2.1	0.10	344	307	0.66	2.3	Linear PEH matrix	
PE21	100	140	2.1	0.10	338	313	0.68	2.3	Linear PEH matrix	
PE22	100	140	2.1	0.05	121	197	0.43	—	Linear PEH matrix	
PE23	100	140	2.1	0.03	143	189	0.41	—	Linear PEH matrix	
PE24	100	383	2.1	0.05	275	276	0.36	—	Linear PEH matrix	
PE25	100	54	2.1	0.05	58	142	0.54	—	Linear PEH matrix	
Measurements at 150°C										
PE21	100	140	2.1	0.10	114	215	0.46	2.3	Linear PEH matrix	
Slow cooled clustered PED, measurements at 25°C										
A3SC	78	60	1.54	0.03	343	313	1.10	—	Matched sample with branched PEH matrix	
A6SC	78	60	1.54	0.06	693	368	1.29	2.4	Matched sample with branched PEH matrix	

methods. The measurements were performed on a SAXS scattering facility which utilized a 5 kW rotating anode, pin-hole collimation and a position sensitive proportional counter⁷. The $\text{CuK}\alpha$ radiation was monochromatized before scattering and very well collimated in both directions. No resolution corrections were therefore necessary and the differential scattering cross-section, $d\Sigma/d\Omega$, was measured in absolute units. A typical scattering pattern is shown in Figure 1 and shows a well resolved first maximum at $\kappa = 4\pi\lambda^{-1} \sin \theta = 0.024 \text{ \AA}^{-1}$. Typical Bragg-law 'spacings' calculated from the position of the first maximum are in the range $254 \pm 10 \text{ \AA}$ for fast quenched samples. The occurrence of well resolved maxima in the SAXS patterns is good evidence for the existence of lamellar structures in the samples.

If samples are slow cooled from the melt it is to be expected that separation could again occur due to the well established separation mechanism by which the higher melting component will crystallize first on slow cooling. It was to avoid this separation mechanism that samples were initially quenched rapidly from the melt. We attempted to check by thermal analysis for possible segregation on slow cooling, the measurements being made in a Perkin-Elmer DSC-2 differential scanning calorimeter. As thermal methods cannot easily detect PED at the normal level of 1–10%, measurements were made on a 50:50 mixture. The mixture (components as PE 25) was solution blended (*o*-DCB) and precipitated into methanol. As prepared, this showed a single melt endotherm on heating to 160°C. Subsequent cooling relatively rapidly from the melt at 5°C/min gave a single crystallization exotherm and the anticipated single melt endotherm on reheating. There is no evidence to suggest that phase separation has occurred. However, cooling from the melt slowly at 0.62°C/min resulted in two clearly resolvable crystallization peaks, (Figure 2a) and a distinct shoulder in the subsequent melt endotherm at a temperature consistent with the melting point

of the deuterated material (Figure 2b). From this data we can conclude that fast quenching from the melt consider-

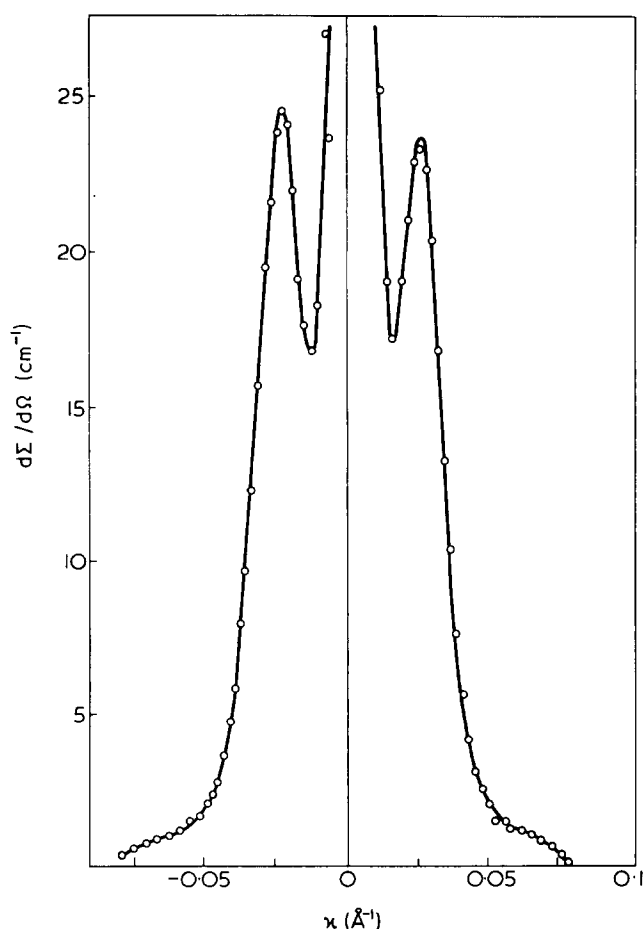


Figure 1 SAXS pattern from bulk polyethylene, rapidly quenched from the melt

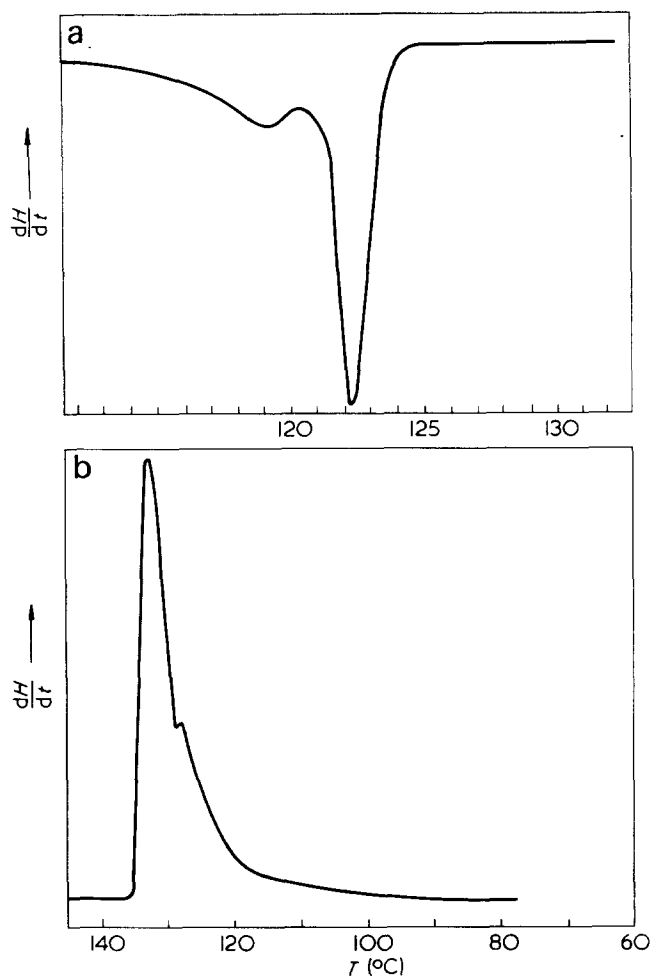


Figure 2 (a) Crystallization exotherm; (b) re-melt exotherm of 50:50 PEH/PED mixture slow cooled at $0.62^{\circ}\text{C}/\text{min}$ from the melt

ably reduces the possibility of phase segregation of the molecules.

We have attempted to reduce the probability of segregation in *slow cooled* samples by choosing a slightly branched PEH polymer, whose thermal characteristics match those of the deuterated material. The temperatures for the start of crystallization, T_s , and peak crystallization rate, T_p , were $T_s = 113.7^{\circ}\text{C}$ and $T_p = 111.7^{\circ}\text{C}$; and $T_s = 113.5^{\circ}\text{C}$ and $T_p = 112^{\circ}\text{C}$ for the PEH and PED materials respectively. These materials were then solution blended in *ortho*-dichlorobenzene as described above, and slow cooled from the press at $\sim 1^{\circ}\text{C}/\text{min}$ after compression moulding. It will be seen from the subsequent discussion that although the matching procedure reduced the segregation or clustering effect, it was not eliminated completely. It is our opinion therefore that it is virtually impossible to prepare unclustered samples of unmatched (i.e. linear) PEH and PED, when these samples are cooled slowly from the melt.

It is important to understand, not only the morphology of melt crystallized polyethylene, but also solution crystallized polymer. For this reason we attempted to also make samples of solution crystallized material. However, d.s.c. measurements on the 50:50 blend of linear PEH and PED, crystallized slowly from *ortho*-dichlorobenzene at 65°C indicated a well resolved shoulder on the d.s.c. endotherm $\sim 8^{\circ}\text{C}$ below the peak of the endotherm (Figure 3). The equivalent melt endotherm of PEH crystallized from solution in the same manner showed no such shoulder. This again indicated the strong possibility of phase separation in

samples of solution crystallized mixtures, and for this reason we did not attempt to proceed with solution crystallized samples at this stage.

For both melt and solution crystallized systems, it is clear that unambiguous conclusions on chain configuration can only be drawn from data which originates from a homogeneous specimen (no phase segregation), where the tagged molecules are statistically distributed throughout the matrix. Fortunately, it is possible to check the latter in a homogeneous specimen as shown in the next section.

SEGREGATION OF TAGGED MOLECULES

The extrapolated forward scattering cross-section, measured in absolute units is a very sensitive indicator as to whether the tagged molecules are clustered or statistically distributed. For the latter case it has been shown^{2,3} that:

$$\frac{1}{cK_N} \left(\frac{d\Sigma}{d\Omega} \right)_{\kappa=0} = \frac{1}{M_w} \quad (1)$$

where

$$K_N = \rho \left[2X \frac{1}{M_{(\text{CD}_2)_x \text{H}_2(1-x)}} (b_D - b_H) \right]^2 N \quad (2)$$

where $\rho = 0.94 \text{ g/cm}^2$ is the density, X is the degree of deuteration of PED chains, $M_{(\text{CO}_2)_x \text{H}_2(1-x)}$ is the mass of a chain segment, N is Avogadro's number, b_D and b_H are the scattering lengths of ^2D and ^1H . The extrapolated forward scattering cross-section is obtained from the usual linear plots of $d\Sigma^{-1}/d\Omega$ vs. κ^2 . Where there is no clustering, M_w determined from the neutron measurement (equation 1) should equal the known molecular weight of the tagged molecules determined by g.p.c. or osmometry prior to blending. When clustering does occur, curves obtained by plotting $d\Sigma^{-1}/d\Omega$ against κ^2 are still linear over a wide range as can be seen by corresponding Figures 4 and 5 but the values of the slope and intercept are changed. In this case the apparent molecular weight obtained from the forward scattering, $(M_w)_{\text{app}}$, is larger than the real molecular weight M_w . The ratio $(M_w)_{\text{app}}/M_w$ is a measure of the number of molecules in a cluster (n).

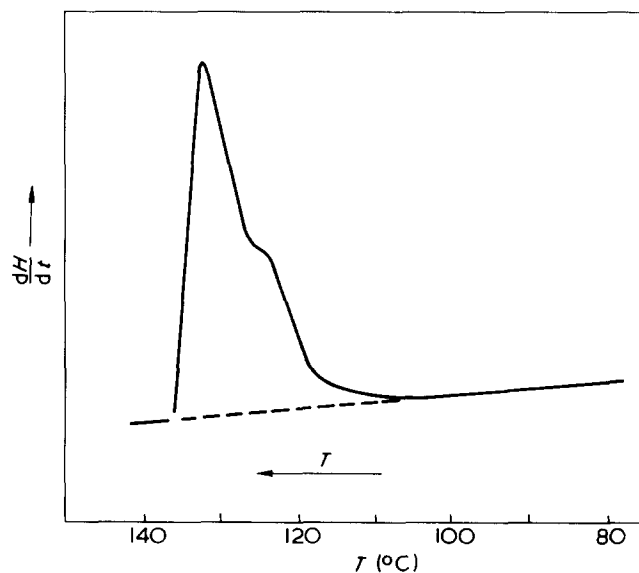
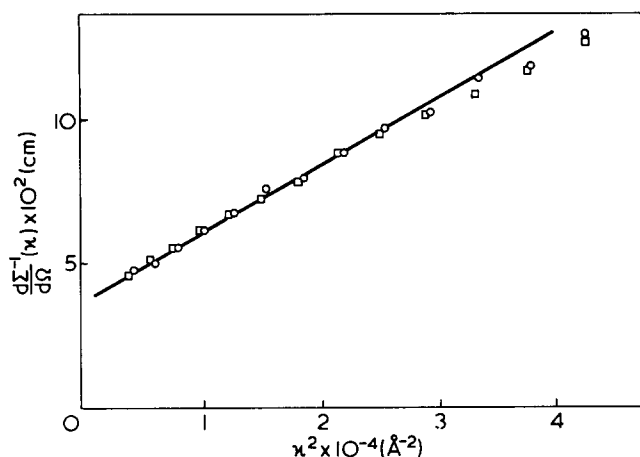
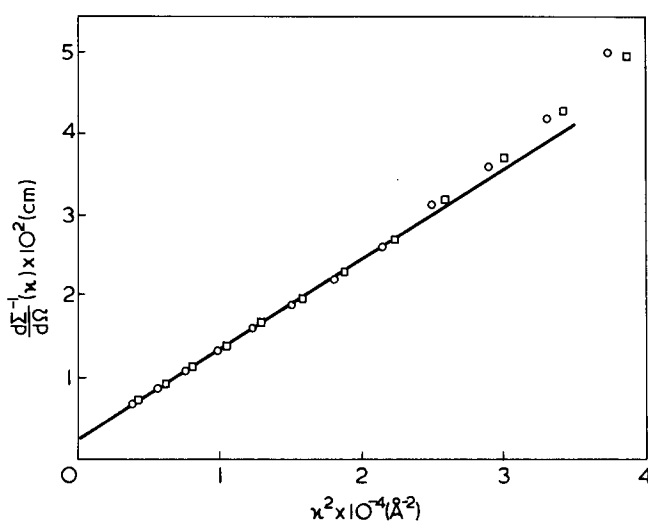


Figure 3 Melt endotherm of a 50:50 PEH/PED mixture after crystallizing from *o*-DCB solution at 65°C

Figure 4 Plot of $d\Sigma/d\Omega$ vs. κ^2 for sample A6QFigure 5 Plot of $d\Sigma/d\Omega$ vs. κ^2 for sample A6SC

In Table 1 we have summarized the neutron scattering data on polyethylene. Comparing $(M_w)_{app}$ with M_w , there is generally good agreement showing that clustering has been substantially eliminated. The combined error of the comparison is $\sim 25\%$ due to uncertainties in the calibration of g.p.c., SANS and the polydispersity correction¹. One exception to the agreement is sample PE 21 which contains a high concentration (10%) of tagged molecules. It may also be seen that clustering occurs even for matched samples (A3 SC, A6 SC) which are slow cooled from the melt.

MEASUREMENTS OF RADIUS OF GYRATION

For samples without clustering, obtained by rapid quenching from the melt, we obtain from the slopes of the curves such as Figure 4 values of the radius of gyration of statistically distributed molecules in the solid state. In Table 2 we compare values of $\langle S^2 \rangle^{1/2} / M_w^{1/2}$ obtained in the solid state, with those obtained in the melt⁴ and in a θ -solvent. The close agreement between these values shows that the overall size of the molecule is the same in all these systems. The values of radius of gyration measured in the melt are in excellent agreement with the measurements of Lieser *et al.*⁴ and this provides a useful cross-check on the accuracy of the data.

HOMOGENEITY OF THE DISTRIBUTION OF TAGGED MOLECULES IN THE MATRIX

We were concerned to test whether the tagged molecules were preferentially occupying the amorphous regions, as this might have been one explanation for the close agreement between results in the solid and liquid states. To do this we rapidly quenched samples as thin films and etched a selection of this material with nitric acid. This process preferentially removes the amorphous regions of the sample and we would expect a reduction in the deuterium content if this kind of segregation had occurred. The initial and etched samples were therefore analysed using an ARL Multi-Element Plasma Detector, which gives a signal proportional to the deuterium content. Within the experimental error of the measurement ($\frac{1}{2}\%$ in the concentration of tagged molecules, c) no differences was observed. The etched sample showed an increase ($\sim 6\%$) in crystallinity indicating that the amorphous regions had been preferentially removed. Therefore it may be concluded that the deuterated molecules were uniformly distributed throughout the amorphous and crystalline regions.

NEUTRON SCATTERING AT HIGHER ANGLES

We have studied the scattering behaviour at high angles in a similar way to our studies with polystyrene². The most convenient way to present this data is shown in Figure 6 for samples PE 21 at 150°C . It is evident that the results are similar to those obtained for polystyrene. Moreover, sample A6Q, when cooled rapidly at 23°C gives a similar curve as can be seen by comparing Figure 7 with Figure 6. Both curves tend to a constant value at $\kappa \sim 0.15 \text{ \AA}^{-1}$, which may be characterized as follows. Let us define the quantity

$$Q = \lim_{\kappa \rightarrow 0.15 \text{ \AA}^{-1}} \left[\frac{\kappa^2 \langle S^2 \rangle_w \frac{d\Sigma}{d\Omega}(\kappa)}{c K_N M_w} \right] = \lim_{\kappa \rightarrow 0.15 \text{ \AA}^{-1}} [\kappa^2 \langle S^2 \rangle^{1/2}] [|F(\kappa)|]^2 \quad (3)$$

where $F(\kappa)$ is the form factor of the polymer molecule and c is the concentration of tagged molecules. Q is thus a measure of the asymptotic value of the ordinates of Figures 6 and 7. Listed in Table 1 we see that at 150°C and 23°C (for the rapidly quenched material) $Q = 2.3$, very close to that derived from the Debye function⁹ for which $Q \rightarrow 2$ for large κ . The sample PE 21, which contains clusters of tagged molecules, shows a scattering behaviour which is different in the intermediate κ range ($0 \leq \kappa \leq 0.04 \text{ \AA}^{-1}$). Figure 8 shows that in this range the presence of clusters leads to an overshoot of the simple Debye-like curve observed in Figure 7. This overshoot dis-

Table 2 Values of $\alpha = \langle S^2 \rangle_w^{1/2} / M_w^{1/2}$

Temperature ($^\circ\text{C}$)	State	α	Origin
23	Crystalline	0.46 ± 0.05	This paper
150	Molten	0.46 ± 0.05	This paper
150	Molten	0.45	Ref 4
150	Solution	0.45 ± 0.08	Ref 8
	θ -solvent		

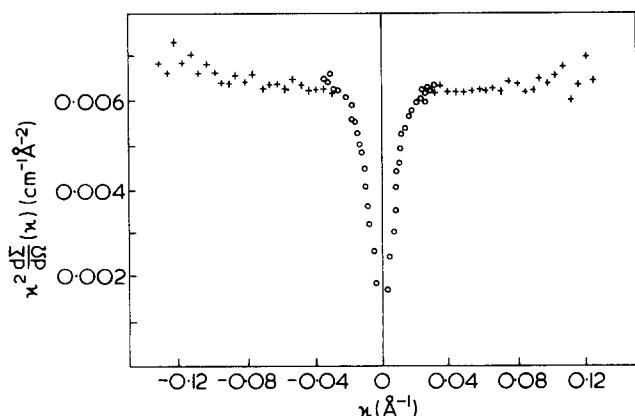


Figure 6 Kratky plot for scattering from 10% PED molecules (sample PE 21 at $T = 150^\circ\text{C}$)

appears when the sample is melted (Figure 6) and the clusters are dispersed (Table 1).

MODEL CALCULATIONS AND DISCUSSION

It has been shown that the random coil model can fit the neutron data, in the solid state, both with regard to radius of gyration and the whole small-angle scattering function (Figure 7). However, this model is in conflict with the known crystallinity and the SAXS evidence (Figure 1), which shows that long straight sections of the molecule (~ 100 Å) exist. Thus such an extreme model cannot be used to describe the scattering data and other properties of solid polyethylene.

At the opposite extreme of models which might be used to fit the data there are models postulating folding within a given crystallographic plane of the lamella. Such a model has been put forward by Bank and Krimm¹⁰ on the basis of adjacent re-entry. Generally the scattering function of such a configuration would also lead to the observed κ^{-2} behaviour and we have therefore performed model calculations, in which the basic requirement is that the chain folding must occur within a given plane. The molecule is therefore constrained within a plane height, w , length, l , with negligible width. The density of CD_2 molecules of one chain is therefore $\rho_x(x)\rho_y(y)\delta(z)$ with $\rho_x(x)$ and $\rho_y(y)$ constant over distances l and w respectively and zero elsewhere. $\rho_x(x)$ and $\rho_y(y)$ are the mass distribution functions, x and y are the rectangular coordinates within the folding plane, and z is perpendicular to it. The form factor of this chain molecule is:

$$F_x(q_x)F_y(q_y) = \frac{\sin\left(q_x \frac{w}{2}\right)}{q_x \frac{w}{2}} \times \frac{\sin\left(q_y \frac{l}{2}\right)}{q_y \frac{l}{2}} \quad (4)$$

if F_x and F_y are the Fourier transforms of ρ_x and ρ_y of argument q with components q_x and q_y in the x and y directions. The differential cross-section $d\Sigma/d\Omega$ of tagged molecules folded in planes with their normals statistically oriented in space is:

$$\frac{d\Sigma}{d\Omega}(\kappa) = cM_w K_N |F(\kappa)|^2 / |F(0)|^2 \quad (5)$$

with

$$|F(\kappa)|^2 = \frac{1}{4\pi} \int \int d\phi \sin \psi d\psi |F_x(q_x)F_y(q_y)|^2 \quad (6)$$

and

$$q_x = \kappa \sin \psi \cos \phi \quad (7)$$

$$q_y = \kappa \sin \psi \sin \phi$$

The radius of gyration $\langle S^2 \rangle_w^{1/2}$ corresponding to $(d\Sigma/d\Omega)(\kappa)$ is resolvable into two components:

$$\langle S^2 \rangle_w = R_{gx}^2 + R_{gy}^2 = \frac{l^2}{12} + \frac{w^2}{12} \quad (8)$$

where R_{gx} and R_{gy} are the second moments of the mass distributions ρ_x and ρ_y , respectively.

For each chosen pair of mass distribution functions the scattering cross-section $d\Sigma/d\Omega$ was calculated for R_{gy}/R_{gx} ratios of 1, 2, 4 and 8, and hence a value of Q was calculated for each of these ratios. These values of Q are shown in Figure 9, and show that only for a value of $R_{gy}/R_{gx} = 4$, can this model give the measured value of $Q = 2.3$. Using this value of R_{gy}/R_{gx} , Figure 10 shows the curve of $\kappa^2(d\Sigma/d\Omega)(\kappa)$ predicted by the model. The function shows some oscillations which are not important to the main argument, and gives a reasonable agreement to the

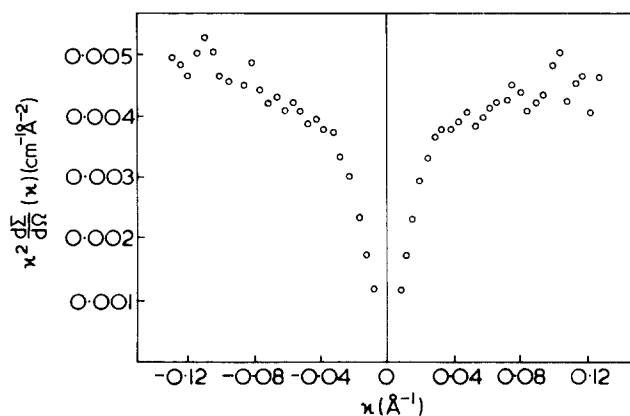


Figure 7 Kratky plot for scattering from 6% PED molecules (sample A6Q at $T = 23^\circ\text{C}$)

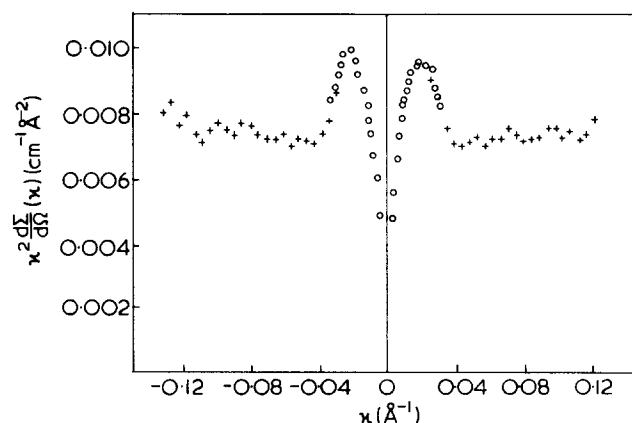


Figure 8 Kratky plot for scattering from 10% PED molecules (sample PE 21 at 23°C) $[(M_w)_{\text{app}}/M_w] = 2$

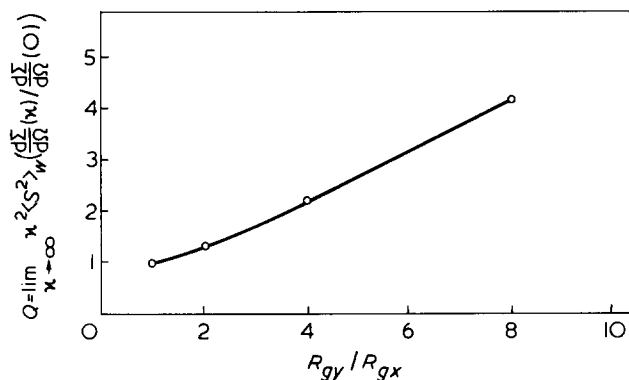


Figure 9 Model calculation of Q vs. R_{gy}/R_{gx} for folding in one plane $R_{gy}/R_{gx} = w/l$

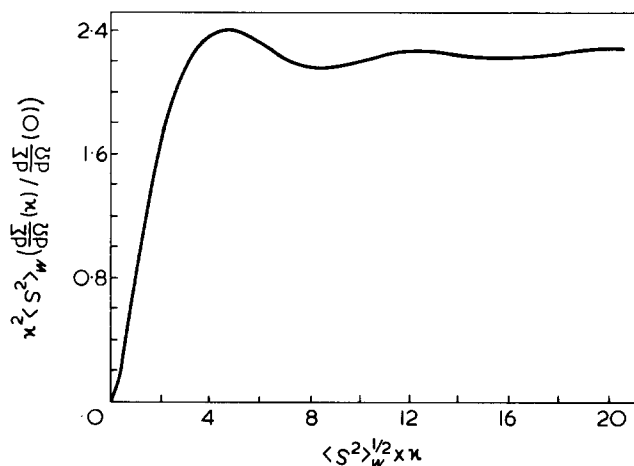


Figure 10 Plot of $\kappa^2 \langle S^2 \rangle_w^{1/2} (d\Sigma/d\Omega) (K) / (d\Sigma/d\Omega) (O)$ vs. κ for model with $R_{gy}/R_{gx} = 4$

measured scattering data (Figure 7). For a typical chain with molecular weight $M \approx 140\,000$, the length L , is $\approx 12\,500 \text{ \AA}$ and the radius of gyration $\langle S^2 \rangle^{1/2} = 0.46 M^{1/2} \approx 168 \text{ \AA}$. Thus, assuming $w/l = 4$ we calculate from equation (8) that $l \approx 138 \text{ \AA}$, $w \approx 565 \text{ \AA}$. The distance between adjacent folding segments is then calculated to be:

$$d = \frac{w}{L/l} = 6 \rightarrow 10 \text{ \AA} \tag{9}$$

depending on whether one assumes that all the molecule is within the folding plane, or whether 35% of it is in the amorphous region. Thus this distance of the same order of magnitude to a value of 4.9 \AA calculated by Bank and Krimm¹⁰ for adjacent re-entry within the (200) plane.

According to equation (8), however, $\langle S^2 \rangle = 0.46^2 M_w = l^2/12(1 + 4^2)$ or

$$l = 0.38 M_w^{1/2} \tag{10}$$

This implies a molecular weight dependent fold length, and for a chain with molecular weight $M \approx 60\,000$ we calculate $l \approx 93 \text{ \AA}$; $d = 6 \rightarrow 10 \text{ \AA}$. This raises a particular difficulty for this model because in the neutron experiments l is effectively fixed by the matrix, and yet it is seen that Q remains 2.3, while the tagged molecular weight changes from $60\,000 \rightarrow 140\,000$ (Table 2). It therefore seems that although the model can be made to give a reasonable fit to the data at a given molecular weight, it does not seem

capable of describing the variation of the measured parameters over the whole molecular weight range.

In order to remove the molecular weight dependence of l , which arises from equation (8), the model might plausibly be re-formulated to allow the molecule to pass through several different lamellae. To maintain the κ^{-2} behaviour of $d\Sigma/d\Omega$, the chain would have to crystallize in each lamella in a plane whose dimensions obeyed the relation $w/l = 4$. This relaxes the constraint of equation (8), as the radius of gyration of the molecule is determined by the overall mass distribution of the molecule rather than by equation (8). Such a molecular configuration is shown schematically in Figure 11, for a molecule passing through 4 lamellae. However, a serious argument against this kind of configuration is that l has to be approximately the same as before as this is determined by the matrix. Hence as the ratio w/l has to remain 4 in order to give $Q = 2.3$ (Figure 9), it follows that each folding plane has to have approximately the same dimensions (w, l) as in the previous formulation. Hence the chain has to be distributed over four planes (in the case of Figure 11), of approximately the same size as the original plane. This means that the interchain distance d , has to increase by a factor of 4 and one cannot, therefore, maintain the adjacent re-entry mode of folding.

It seems that the basic problem of this type of model lies in the assumption that the measured value of $Q = 2.3$ in the solid arises from the fact that the molecules fold in planes maintaining $w/l = 4$. This seems a very artificial assumption, which leads to the problems discussed above. It is thus difficult to see therefore how the correspondence with the melt, both in radius of gyration in (Table 2) and the whole scattering function (Figure 7), can be plausibly explained on the basis of adjacent re-entry within a given crystallographic plane for rapidly quenched samples.

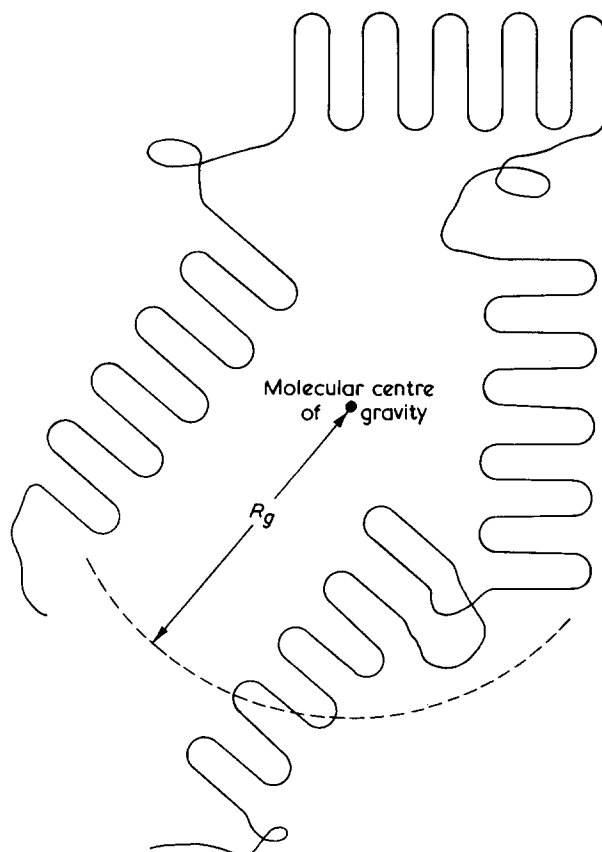


Figure 11 Schematic reformulation of model with molecules folding in one crystallographic plane in each lamella

It seems much more reasonable to propose that the reason for the correspondence of $\langle S^2 \rangle^{1/2}$ with the melt, lies in the fact that on a fast quench, the molecule cannot diffuse sufficiently rapidly to adopt a very different mass distribution of chain elements to that adopted in the melt. The correspondence of Q values in the melt probably arises from a retention in the crystalline state of some of the randomness of the melt.

Beyond these general assertions, we are not in a position of being able to propose a unique configuration for the molecule from the data of *Figure 7*. This is because two extreme models can be fitted mathematically to this data, and hence it is to be expected that there are a whole variety of further models between these extremes which might generate a similar function. It is clear that further data over a wider κ range would be useful for determining the configuration, and such experiments are currently in progress.

In conclusion, it is relevant to discuss the work of Sadler and Keller on single crystal mats¹¹. *Figure 4b* in ref 11 is typical of the results obtained for single crystal mats 0.1 mm thick. The results shown correspond to the translucent material obtained by pressing at 60°C. Sadler and Keller were unable to measure the molecular weight of the tagged molecules from the forward scattering because of the presence of a 'void artefact'. No check for clustering was therefore made, and the evidence from the studies described in this paper would suggest that the system is highly aggregated. A maximum at a value $\kappa \approx 0.08 \text{ \AA}^{-1}$ was observed in the Kratky plots, though we are of the opinion that the shape of this curve is in no way a feature of the structure of PE but a consequence of aggregation

of PED chains. A similar feature was found in sample PE 21 (*Figure 8*) and was shown to be due to clustering of small numbers (2 to 3) of PED molecules. This feature is absent in unclustered samples (*Figure 7*), and the strength of this overshoot in Sadler and Keller's data suggests even greater aggregation effects.

REFERENCES

- 1 Kirste, R. G., Kruse, W. A. and Schelten, J. *Makromol. Chem.* 1972, **162**, 299; Ballard, D. G. H., Schelten, J. and Wignall, G. D. 'Symposium on Molecular Weight Characterisation of Industrial Polymers, National Physical Laboratory', (Eds J. H. S. Green and R. Dietz), Transcripta, London, 1973; *Eur. Polym. J.* 1973, **9**, 965; Benoit, H., Cotton, J. P., Decker, D., Farnous, B., Higgins, J. S., Jannink, G., Ober, R. and Picot, C. *Nature* 1973, **245**, 13
- 2 Wignall, G. D., Ballard, D. G. H. and Schelten, J. *Eur. Polym. J.* 1974, **10**, 861
- 3 Schelten, J., Wignall, G. D. and Ballard, D. G. H. *Polymer* 1974, **15**, 682
- 4 Lieser, G., Fischer, E. W. and Ibel, K. *J. Polym. Sci.* 1975, **13**, 39
- 5 Stehling, F. S., Ergos, E. and Mandelkern, L. *Macromolecules* 1971, **4**, 672
- 6 Schelten, J., Wignall, G. D., Ballard, D. G. H. and Schmatz, W. *Colloid Polym. Sci.* 1974, **252**, 749
- 7 Schelten, J. and Hendricks, R. W. *J. Appl. Crystallogr.* 1975, **8**, 421
- 8 Brandup, J. and Immergut, E. H. 'Polymer Handbook', Interscience, New York, 1969
- 9 Debye, P. *J. Appl. Phys.* 1944, **15**, 338; 1946, **17**, 392; *J. Phys. Colloid Chem.* 1947, **51**, 18
- 10 Bank, M. I. and Krimm, J. *Polym. Sci. (A-2)* 1969, **67**, 1785
- 11 Sadler, D. M. and Keller, A. *Polymer* 1976, **17**, 37

Effect of molecular oxygen on the n.m.r. relaxation times of some aromatic polymers

Michael F. Froix and Andreas O. Goedde

Xerox Corporation, Webster, New York, USA

(Received 5 April, 1976)

Proton spin-lattice (T_1) and spin-spin (T_2) relaxation times are reported for poly(2-vinylpyridine), poly(1-vinylanthracene) and polycarbonate in air, oxygen and *in vacuo*. The results substantiate earlier findings that oxygen complexes with the aromatic rings giving rise to T_1 minima which are not intrinsic to the polymers. This effect appears to be fairly general for aromatic containing polymers. For those polymers containing low temperature relaxations intrinsic to the polymer, the oxygen paramagnetic effect can complicate the relaxation behaviour and, in some cases, totally mask the intrinsic processes. The transitions in T_1 and T_2 , due to the torsional oscillation of the anthracene side group in poly(1-vinylanthracene), is much better defined than the corresponding transitions for previously reported aromatic vinyl polymers. The activation energy for the motion of the side group is comparable to that of polystyrene and poly(*N*-vinylcarbazole).

INTRODUCTION

Recently, it has been shown that some aromatic polymers exhibit anomalous n.m.r.¹⁻⁴ and dielectric^{5,6} relaxations in the presence of oxygen. Prior to this discovery, the origins of these relaxations were the source of much uncertainty. Polyvinylcarbazole (PNVC), poly(*N*-ethyl-3-vinylcarbazole) and polystyrene (PS) were found to complex with molecular oxygen giving rise to low temperature n.m.r. relaxations due to the dipole-dipole interaction with, and spin-diffusion to the paramagnetic oxygen. N.m.r.¹⁻⁴ and dielectric^{5,6} measurements have also shown low temperature relaxations due to the motion of the aromatic side groups which are only observed on interaction with oxygen. In the absence of oxygen, these motions are either of too low amplitude or about a symmetry axis and, consequently, are not observed in the n.m.r. and dielectric data. However, on interaction with oxygen, a dipolar field due to the unpaired electrons of the paramagnetic species is experienced by the polymer protons. At the onset of oscillation of the aromatic ring, the lifetime of the interaction is reduced and transitions in n.m.r. and dielectric relaxations are observed with activation energies corresponding to the intrinsic motions of the polymers.

In this paper, the nuclear spin-lattice (T_1) and spin-spin (T_2) relaxation times are reported for a series of aromatic polymers. The relaxation behaviour of thoroughly evacuated samples is compared with that of samples in air and oxygen, and the results are discussed in terms of the influences of paramagnetic oxygen on the polymer proton relaxation behaviour.

EXPERIMENTAL

The polycarbonate (PC), poly(2-vinylpyridine), and poly(1-vinylanthracene) (PA) samples were obtained from various sources. The relevant data are given in Table 1. All samples were reprecipitated several times before using. Evacuated samples were obtained by pumping the samples to $\sim 10^{-5}$ mmHg at 80°C for 12 h. The n.m.r. tubes were

attached to nylon valves so that samples could be re-equilibrated with oxygen or air at a later time.

The n.m.r. relaxation times were obtained on a Bruker SXP NMR Spectrometer at 90 MHz. The magnetic field was generated by a 12 in shimmed electromagnet operated in the current regulated mode. The temperature was controlled by a gas-flow system thermostatted with a copper constantan thermocouple and controlled to an accuracy of $\pm 1^\circ\text{C}$.

Spin-lattice relaxation times were measured by the $180^\circ - \tau - 90^\circ$ pulse technique⁷. Values of T_1 were derived from a least squares analysis of plots of $\ln[A(\infty) - A(T)]$ as a function of the interval τ between the 180° and 90° pulses, where $A(T)$ is the amplitude of the free induction decay following the 90° pulse and $A(\infty)$ is the value of $A(T)$ for infinite time.

Spin-spin relaxation times were obtained from the free induction decays following the 90° pulse. T_2 was taken as $t_{1/2}/\ln 2$ where $t_{1/2}$ is the time for the magnetization to decay to one-half of its original value. Both values of T_1 and T_2 were determined using a computer program⁸ in which the free induction decays were stored in a Nicolet 1080 computer.

RESULTS

Figure 1 is a plot of T_1 versus temperature for degassed poly(2-vinylpyridine) and poly(2-vinylpyridine) in oxygen. The high temperature T_1 come together at the minimum due to the glass transition. At low temperatures, the sample in oxygen shows a minimum at 210K which is not pre-

Table 1

Sample	M_w	MWD	Source
Polycarbonate	38 000	2.36	General Electric ¹⁶
Poly(2-vinylpyridine)			Polysciences
Poly(1-vinylanthracene)	152 000	1.8	This laboratory ¹⁶

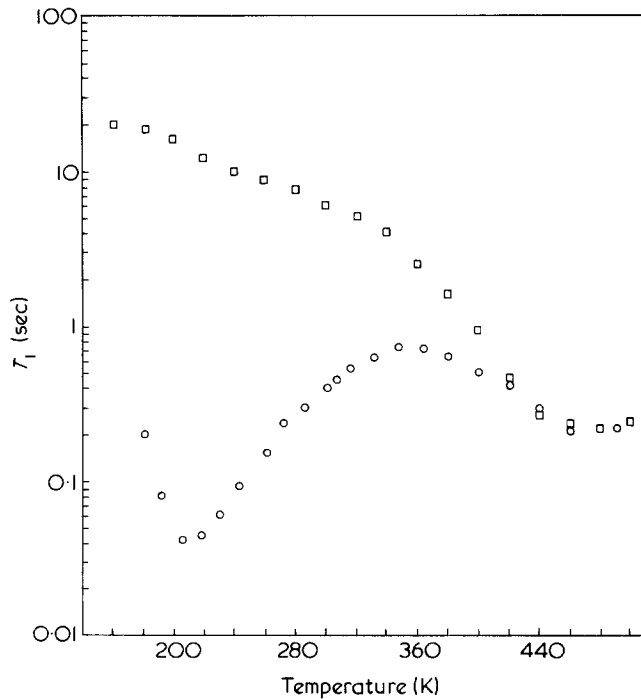


Figure 1 A plot of T_1 vs. temperature for an evacuated sample of poly(2-vinylpyridine) (\square) and poly(2-vinylpyridine) in oxygen (\circ)

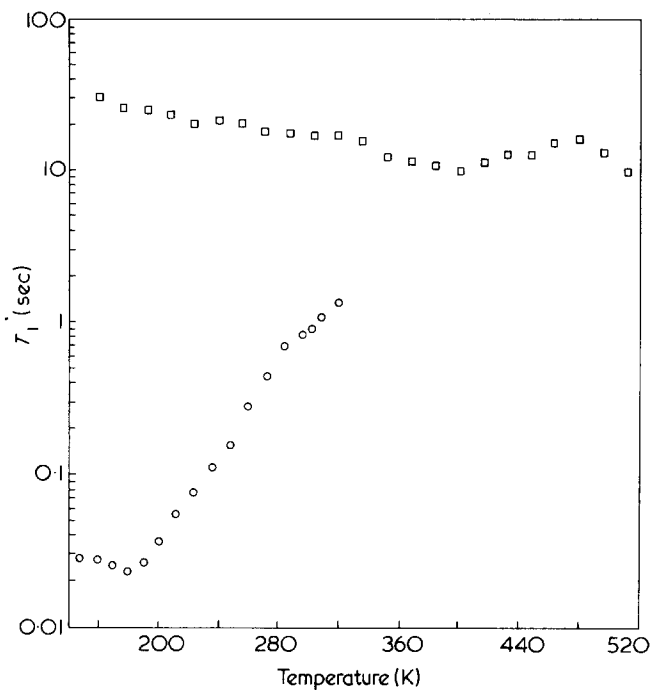


Figure 2 A plot of T_1 vs. temperature for PA evacuated (\square) and in air (\circ)

sent in the evacuated sample. The T_1 behaviour of PA in air and *in vacuo* is given in Figure 2. The evacuated sample shows a shallow minimum at 400K and the approach to another minimum beginning at 480K. There is no minimum in T_1 for this sample below room temperature; however, the sample in air shows a minimum at 180K three orders of magnitude smaller than the degassed sample. A transition in T_2 at 220 K is observed in Figure 3. The transition in air is slightly more pronounced than that of the evacuated sample. Figure 4 gives T_1 plots of evacuated PC and PC in air. The evacuated sample shows a minimum at 280K while the sample in air exhibits a minimum at 190K and a less in-

tense minimum at 280K which is almost totally masked by the lower temperature minimum. All samples exhibit anomalous minima in air and oxygen. The magnetization recovery on the low temperature side of these minima is non-exponential. This magnetization recovery can be described by a $(\text{time})^{1/2}$ dependence at short times and the plots consist of two straight line segments¹.

DISCUSSION

The low temperature T_1 behaviour of polycarbonate, poly(2-vinylpyridine) and poly(1-vinylanthracene) exhibit enhanced relaxation in the presence of air and oxygen accompanied by the appearance of new minima which are not observed for the evacuated samples. The anomalous minima are accompanied by a non-exponential magnetization recovery on the low temperature side of the minima. The limiting cases of diffusion-limited and rapid diffusion of nuclear spin energy to paramagnetic oxygen have been dealt with previously¹⁻⁴. In diffusion-limited relaxation, the initial magnetization recovery is described by a $(\text{time})^{1/2}$ dependence at short times which gives rise to an exponential dependence at longer times⁹. All of the polymers examined in this study exhibit this type of behaviour in both

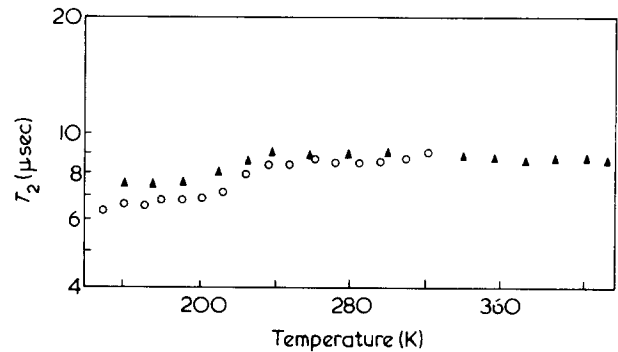


Figure 3 A plot of T_2 vs. temperature for PA evacuated (\blacktriangle) and in air (\circ)

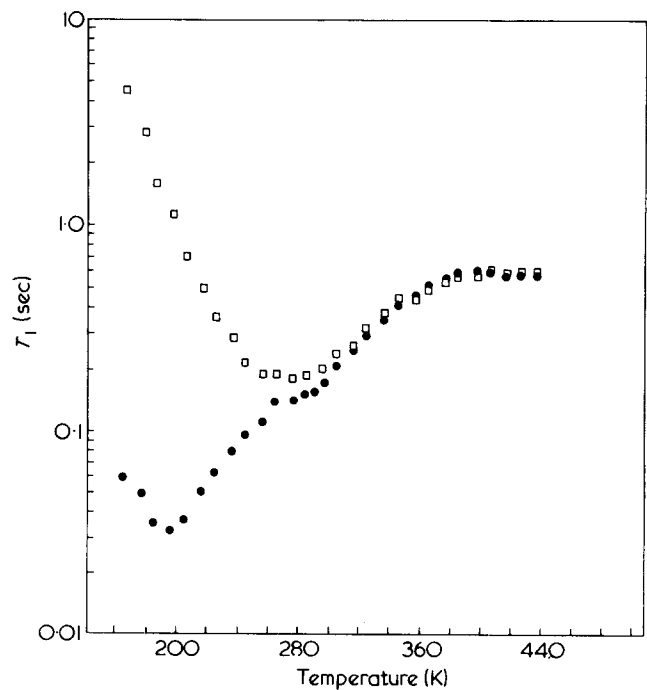


Figure 4 A plot of T_1 vs. temperature for PC evacuated (\square) and in air (\bullet)

air and oxygen below the low temperature T_1 minimum. Plots of fractional magnetization recovery are composed of two regions which have been demonstrated to result from surface and bulk oxygen effects¹. Polyvinylcarbazole and polystyrene have been shown to complex with oxygen^{1,3,10} and it appears from the results of this study that this is a general feature of aromatic ring containing polymers. The polymers absorb oxygen both at the surface and in the bulk; however, there appears to be a preference for surface adsorption giving rise to larger concentrations of oxygen on the surface than in the bulk¹. Higher surface area materials have been shown to exhibit shorter values of T_1 in the presence of oxygen and the minimum due to this effect occurs at lower temperatures reflecting the change from diffusion-limited relaxation on the low temperature side of the minimum to rapid diffusion above the minimum¹.

The T_1 minimum at 400K and the corresponding transitions in T_2 at 220K for PA are consistent with maxima in $\tan \delta$ observed for poly(2-vinylanthracene) and poly(α -methyl-2-vinylanthracene)¹¹. Polystyrene^{3,12} and polyvinylcarbazole¹ have been shown to exhibit fairly ill defined minima in T_1 due to torsional oscillation of the aromatic side group. In degassed samples, the corresponding transitions in T_2 are not observed due to the low amplitude of the motion. However, in the presence of oxygen in these systems, changes in T_2 are observed at the onset of re-orientation of the rings due to the averaging of the small dipolar field arising from the proton interaction with the unpaired electrons^{1,3}. In PA, both the T_1 and T_2 transitions are well defined. The T_2 transition is small and is accentuated in air. It is concluded that the T_1 and T_2 transitions correspond to a low amplitude torsional oscillation with an activation energy of approximately 8 kcal/mol. Above 480K, the beginning of another transition in T_1 is apparent. The temperature was not taken any higher in order to avoid sample degradation. The approaching relaxation is probably the $\alpha\beta$ process associated with the glass-transition.

The minimum in T_1 at 280K for degassed PC has been observed previously and is ascribed to methyl group re-orientation¹³⁻¹⁵. Since the position and depth of the T_1 minimum due to the paramagnetic oxygen is known to be a function of the surface area of the sample^{1,3} the position and width of the low temperature minimum can be vastly altered (if T_1 measurements are made in air) depending on the physical state of the sample. This has been shown to be the case for low molecular weight, small particle size polystyrene in air where two minima in T_1 are observed at low temperatures due to the oxygen effect and to the motion of chain ends. When this sample is quenched from the melt, thereby reducing the surface area, both minima merge to form a broad minimum³. Poly(2-vinyl-*N*-ethyl-carbazole) and poly(3-vinyl-*N*-ethylcarbazole) also exhibit a low temperature T_1 minimum due to motion of the ethyl group. It has been shown that in the presence of air, this minimum is totally masked and, as a result, is not observed; however a minimum due to the interaction of oxygen does appear at a lower temperature². In view of these facts, it is not surprising that the minimum due to the methyl group motion is somewhat overshadowed in the PC sample in air. Taking these observations into

account, we have been able to regenerate some previously published T_1 data^{14,15} and to account for their unusually wide and more intense T_1 minimum in terms of the above mentioned oxygen effects.

CONCLUSIONS

Spin-lattice relaxation time measurements have been made on evacuated samples of polycarbonate, poly(2-vinylpyridine) and poly(1-vinylanthracene) and on these polymers in air and oxygen. The results agree with those previously obtained for carbazole containing polymers^{1,2,4} and polystyrene³ in which oxygen is found to complex with the aromatic ring giving rise to a T_1 minimum in these atmospheres which are not intrinsic to the polymers. This effect now appears to be fairly general for aromatic containing polymers. Like low molecular weight polystyrene³ and poly(2-vinyl-*N*-ethylcarbazole)² which exhibit low temperature relaxations due to chain-ends and side chains respectively the oxygen effect in polycarbonate can complicate the low temperature behaviour, in some instances masking the intrinsic processes altogether.

Poly(1-vinylanthracene) exhibits a T_1 minimum and a transition in T_2 due to torsional oscillation of the anthracene side chain. The transitions are more easily discernible than for previously reported aromatic vinyl polymers¹⁻⁶ reflecting either a larger amplitude motion of the side group or a narrower distribution of correlation times associated with that motion. The activation energy for torsional oscillation of poly(1-vinylanthracene) agrees with that of polystyrene and poly(*N*-vinylcarbazole)^{1,3}.

ACKNOWLEDGEMENT

The authors wish to thank John Yanus for providing the polycarbonate and poly(1-vinylanthracene) samples and for all the pertinent data concerning their molecular weights and molecular weight distributions.

REFERENCES

- 1 Froix, M. F., Williams, D. J. and Goedde, A. O. *J. Appl. Phys.* 1975, **46**, 4166
- 2 Froix, M. F., Williams, D. J. and Goedde, A. O. *Macromolecules* to be published
- 3 Froix, M. F., Williams, D. J. and Goedde, A. O. *Macromolecules* submitted
- 4 Froix, M. F., Williams, D. J., Pochan, J. M. and Goedde, A. O. *Polym. Prepr.* 1975, **16**, 576
- 5 Pochan, J. M. and Hinman, D. F. *J. Appl. Phys.* 1975, **46**, 4155
- 6 Pochan, J. M., Hinman, D. F., Froix, M. F. and Nash, R. W. *Polym. Prepr.* 1975, **16**, 570
- 7 Hahn, E. L. *Phys. Rev.* 1950, **80**, 580
- 8 Goedde, A. O., Froix, M. F. and Williams, D. J. to be published
- 9 Blumberg, W. E. *Phys. Rev.* 1960, **119**, 79
- 10 Tsubomura, H., Yamaoto, N. and Kaishi, N. A. *Kobunshi Kagaku* 1972, **29**, 657
- 11 Pochan, J. M. and Hinman, D. F. to be published
- 12 Connor, T. M. *J. Polym. Sci. (A-2)* 1970, **8**, 191
- 13 McCall, D. W. and Falcone, D. R. *Trans. Faraday Soc.* 1970, **66**, 262
- 14 Stefan, D. and Williams, H. L. *J. Appl. Polym. Sci.* 1974, **18**, 1279
- 15 Stefan, D., Williams, H. L., Renton, D. R. and Dintar, M. M. *J. Macromol. Sci. (B)* 1970, **4**, 853

Pulsed n.m.r. studies of molecular motion in wet nylon-6,6 fibres

Edward G. Smith

Unilever Research Port Sunlight Laboratory, Port Sunlight, Wirral, Merseyside L62 4XN, UK
(Received 3 February 1976; revised 20 April 1976)

The influence of water molecules on molecular motion in commercial nylon-6,6 fibres has been investigated by pulsed n.m.r. techniques. Transient n.m.r. signals, T_2 and T_1 relaxation times for the fibre protons were measured as a function of temperature and moisture (D_2O) content. Above the glass transition temperature, T_g , of the fibre, separation of the signal into two components, a 'rigid' and 'non-rigid' fraction, was possible. For wet fibres, the temperature at which the 'non-rigid' or 'mobile' component appeared was reduced as the water content was increased and the 'mobile fraction' increased with temperature. This behaviour is explained in terms of the mobilization of amorphous chain segments above the T_g and their ability to be 'plasticized' by water molecules. The effect of D_2O molecules and paramagnetic Mn^{2+} ions on T_1 relaxation of rigid and mobile segments provided further information on the properties of accessible chain segments between and on the crystallite surfaces. A chain folded model of semi-crystalline morphology has been adopted throughout the discussion.

INTRODUCTION

The semi-crystalline structure and properties of polymeric fibres are important in many aspects of textile preparation and applications. It is well known, for example, that the strength, crease recovery and dyeing characteristics of fabrics¹⁻³ depend on the crystallinity and state of orientation in the fibres. Moreover, for fibres such as nylon or rayon, the influence of moisture on these properties is determined by the behaviour of fibre polymer chains in the accessible regions and therefore ultimately by the semi-crystalline morphology. Although numerous correlations have been established between the properties and structure of fibre forming polymers in terms of their degree of crystallinity and orientation^{4,5} more information is required on the dynamic configurational behaviour of the polymer chain segments in both the crystalline and amorphous states. However, the non-crystalline or amorphous structures are of particular interest since it is in these regions that the processes leading to fibre distortions originate^{6,7}, either through mechanical disruption of inter-chain attractions or by the influence of the glass transition temperature, T_g , on molecular mobility. Furthermore, it is known that the penetration of liquids and other low molecular weight substances into fibres⁸ takes place via the inter-crystalline regions and that the rate of penetration is increased above the T_g ⁹. The most popular theory of fibre structure at present is one in which the crystalline or elementary fibril is formed by a polymer chain folding back and forth in a regular manner along its own length¹⁰ with chain ends, loops and tie molecules between crystallite surfaces forming the amorphous regions. Hence, in this case the extent of mobility of an amorphous chain segment above the T_g , unlike that in a completely amorphous polymer depends on its mode of attachment to the crystallite¹¹.

Of the many techniques employed to examine the physical properties and transition behaviour in solid polymers¹²⁻¹⁴ the n.m.r. method is perhaps the one most suited for obtaining direct information on the various molecu-

lar motion processes involved¹⁵⁻²³. The broad-line n.m.r. investigations of Zachmann¹⁸ and of Bergmann¹⁹ on poly(ethylene terephthalate) are representative of recent attempts to analyse the mobility behaviour of the different amorphous arrangements of chain segments in semi-crystalline polymers, while Olf and Peterlin have used the same technique to study orientation²² and the effects of moisture²³ on mobility transitions in nylon-6,6 fibres. Although there have been several pulsed n.m.r. relaxation time studies on polyamides^{21,24} to our knowledge this method has not been used to study chain mobility and thermal transitions in wet nylon fibres. This paper examines the influence of temperature and moisture on chain motion in commercial nylon-6,6 fibres. The n.m.r. relaxation behaviour of polymer segments resulting from penetration of water (D_2O) molecules and paramagnetic electrolyte into the fibres is discussed with reference to the features of a chain folded morphology.

EXPERIMENTAL

Sample preparation

Commercial nylon-6,6 fibres (1.5 denier) were obtained from ICI Fibres Ltd. Fibres were washed several times in distilled water but no attempt was made to remove opacifier or carry out any other purification treatment which might have changed the original morphology. For dry samples oxygen and other volatile materials were removed by maintaining the samples under vacuum for several days. Samples of different water content were achieved by equilibrating fibre samples in various relative humidity chambers (saturated salt solutions in D_2O)²⁵ for about 6 weeks (at 25°C). Saturated fibres and fibres containing manganese sulphate were prepared by soaking fibres in appropriate solutions.

N.m.r. measurements

Pulsed n.m.r. signals and proton relaxation times were measured using a Bruker (BKR 322S) pulsed n.m.r. spectro-

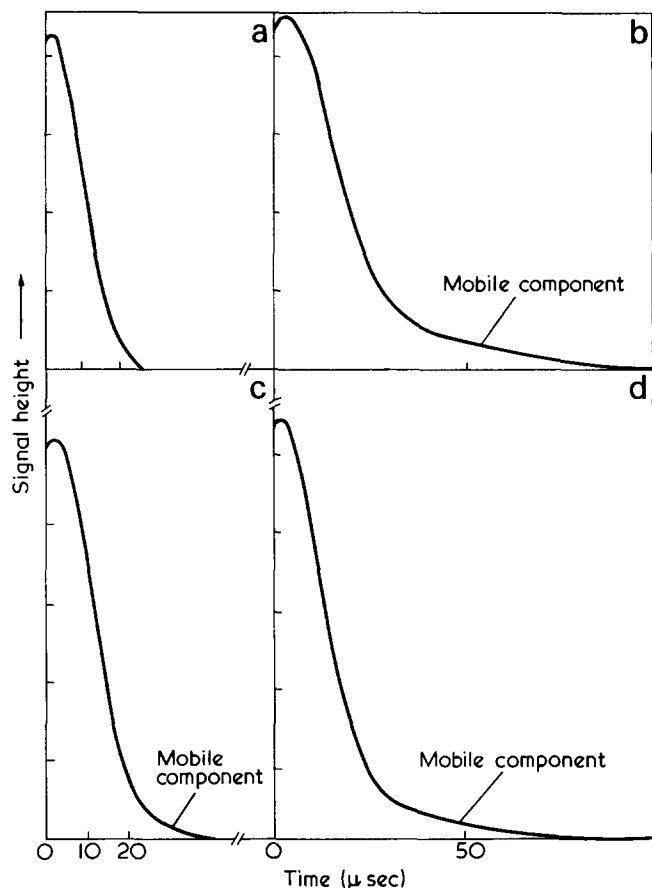


Figure 1 Form of pulsed n.m.r. induction signals for protons of nylon-6,6 fibres (showing 'solid-echo' signals; $t = 0$, end of pulse II.) Dry fibres: (a) at 45°C; (b) at 165°C. Wet fibres: (c) at 45°C, 4% D₂O; (d) at 45°C, 12% D₂O

meter operating at 60 MHz. The temperature was controlled to within ± 1 K. Loss of signal during the pulse and receiver dead time was minimized by examining the induction signals in the form of a 'solid-echo'²⁶ using a $90^\circ - \tau - 90^\circ - 90^\circ$ pulse sequence, where τ , the pulse separation is of the order of several microseconds. Two component signals were found to fit reasonably well the superposition of a Gaussian and an exponential curve of the form:

$$h = h_R \exp [-t^2/2T_{2R}] + h_M \exp [-t/T_{2M}]$$

where h is the signal intensity at time t after the signal maximum and h_R and h_M are proportional to the numbers of chain segments in the 'rigid' and 'mobile' states, respectively. T_{2M} , the spin-spin relaxation time for the mobile component was deduced from the linear portion of the plot of $\log h$ against t and T_{2R} , a relaxation time related to the second moment of 'rigid', Gaussian, component, was estimated from a plot of $\log (h - h_M)$ versus t^2 . T_1 , the spin-lattice relaxation time was determined from the recovery of signal amplitude following a $90^\circ - \tau - 90^\circ$ sequence as τ , the pulse separation, is varied. T_1 values for each signal component could be measured separately.

RESULTS AND DISCUSSION

Influence of water on n.m.r. signals and transitions

Pulsed n.m.r. signals were recorded as a function of temperature for dry fibres and fibre samples containing different amounts of water; a signal contribution from the

water was avoided by using D₂O. The main variations in signal shape obtained for the nylon-6,6 fibres are illustrated in Figure 1, which shows solid echo signals formed after the second 90° pulse ($t = 0$); signal amplitudes are proportional to the total number of protons in the sample. In the dry fibres at temperatures above about 100°C a broader component indicating an increase in molecular motion appears in the signal. This is connected with the α_a process or the onset of 'liquid-like' motions of the amorphous chain segments above their glass transition temperature, T_g . The interesting feature of the n.m.r. behaviour for the wet fibres is that a similar mobile signal component is present at much lower temperatures. Olf and Peterlin²³ have recently investigated a mobile component in broad-line n.m.r. studies of wet nylon filaments which they suggest is a manifestation of the process causing a narrow line in the dry fibres at high temperatures i.e. the α_a process. By comparison we therefore conclude that the pulsed n.m.r. behaviour in the wet fibres is due to mobilization of chain segments in the amorphous regions by water molecules. The temperature at which the mobile component appeared, was found to depend on water content. In an arbitrary manner, transition temperatures for each sample have been deduced from plots of decay time ($1/4$ life) of the bulk signal versus temperature, these curves are presented in Figure 2. It can be seen that the transition occurs at lower temperatures as the water content is increased and in saturated fibres determination of a value below 0°C is probably limited by some freezing of water. From detailed studies of sorption in nylon by Puffr and Šebenda^{27,28} it has been proposed that the progressive uptake of water by nylon occurs in several stages involving water strongly bound across CO groups, loosely bound water forming bridges between neighbouring amide groups and, after further disruption of inter-chain bonds^{29,30}, clustering of water molecules as 'capillary' or included water. Therefore it is not expected that a single mechanism of segment mobilization applies throughout the entire sorption range; the tightly bound water is thought to cause local plasticization of segments connected to CO groups³¹, only above about 3% water content³² can plasticization by water be considered to be of a polymer-diluent type described by free-volume theories^{33,34}.

Apart from recent indications that the transition α_c in the crystalline regions of nylon-6,6 is affected by water²³, it is often accepted that the penetration of water into

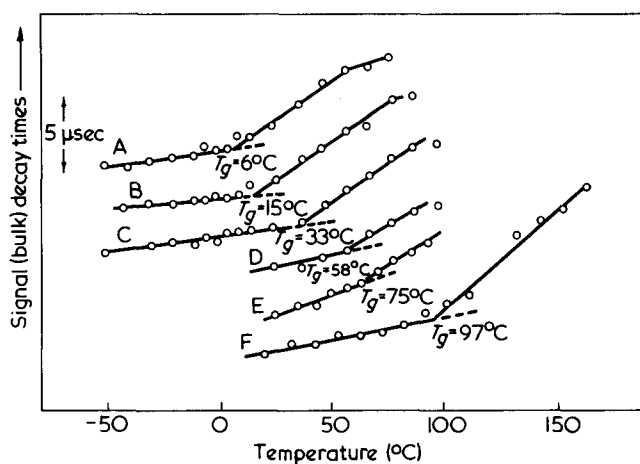


Figure 2 Variation of bulk signal decay times (arbitrary scale) with temperature for nylon-6,6 fibres containing different amounts of water (D₂O). Estimation of T_g (n.m.r.). D₂O content: A, 12%; B, 6%; C, 4%; D, 2%; E, 0.6%; F, dry fibres

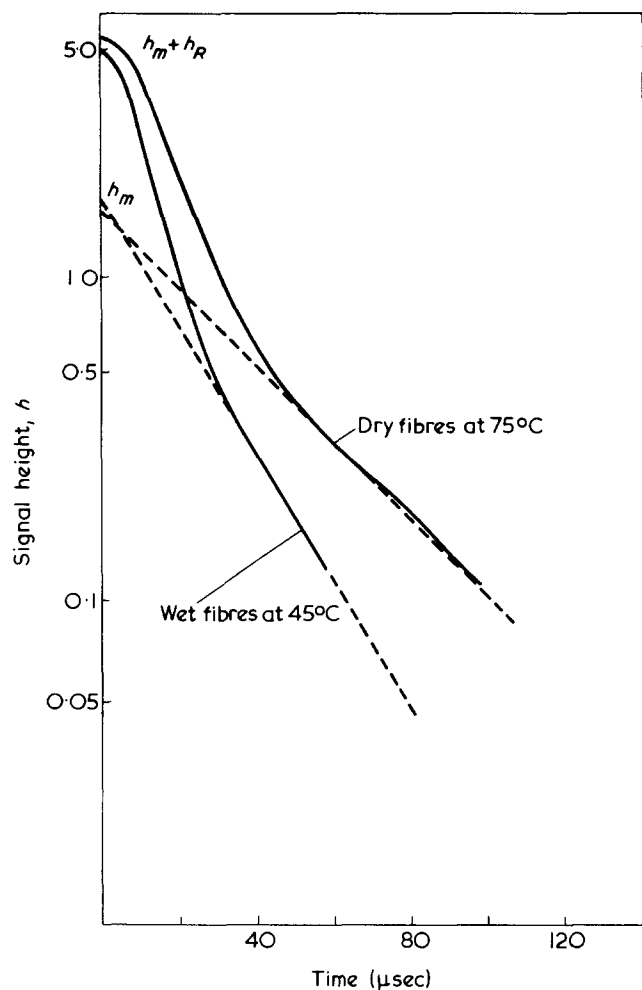


Figure 3 Estimation of mobile fraction, MF , for nylon-6,6 fibres from analysis of pulsed n.m.r. signal ($t = 0$, end of pulse II). $MF = h_M / (h_M + h_R)^{-1}$ where h_M = mobile component; h_R = rigid component

nylon fibres takes place via the amorphous regions and therefore the molecular motion processes associated with these segments alone are influenced by water. In addition to the influence of water on the normal T_g process it is believed that the firmly bound water gives rise to another transition in the amorphous regions at a somewhat lower temperature, sometimes called the β -transition; (Kapur³¹ *et al* propose that the β -process in wet nylon-6 at low water contents is similar to the mechanical and dielectric transition in ice associated with LI defects). The other important motional process in the non-crystalline regions which can be affected by water is that associated with local movement of the CH_2 groups, as in polyethylene, namely the γ -process^{22,35}. Olf and Peterlin²³ have observed a reduction in hindrance of the γ -motion in wet nylon above -75°C by wide-line n.m.r. due to mobilization of water molecules at this temperature. In the present work, at low water contents it is difficult to determine the relative importance of each mobility process from the signal shape alone, except that at a water content of 2%, which must represent bound water at normal temperatures, a mobile component is produced in the n.m.r. signal at a temperature about 30°C lower than in the dry fibres.

Mobile fraction

At higher water contents and temperatures where the 'rigid' and 'mobile' components can be separated more easily it is possible to estimate the fraction of material

undergoing significant segmental motion and its characteristic decay or relaxation time T_{2M} , as in Figure 3. In this analysis it has been assumed that the 'mobile' component can be extrapolated as a single exponential beneath the 'rigid' signal component and h_M has been taken from the end of the second 90° pulse (the exact position of $t = 0$ for the exponential component probably lies between the two pulses, separation $\sim 4 \mu\text{sec}$, therefore our estimates of h_M will be slightly low). The mobile fraction, defined as the amplitude of mobile signal divided by total signal was plotted against temperature for several water contents, (Figure 4). From these curves it is evident that not all segments in the amorphous regions are able to commence motion at the same temperature and also that the presence of water shifts the curves to lower temperature. This behaviour must be related to the influence of fibre morphology on the properties of chains forming the amorphous regions between the crystallites. Present theories of structures of semi-crystalline fibres, such as chain folding, require that some of the amorphous chain segments belong to chains having at least one end embedded in the crystallites^{11,18} as represented in Figure 5. Hence, in contrast to the beha-

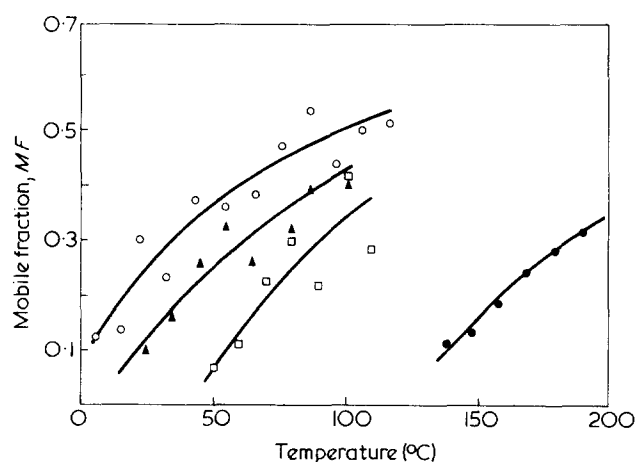


Figure 4 Dependence of mobile fraction, MF , on temperature for nylon-6,6 fibres containing different amounts of water (D_2O): \circ , saturated fibres; \blacktriangle , 12% D_2O ; \square , 2% D_2O ; \bullet , dry fibres

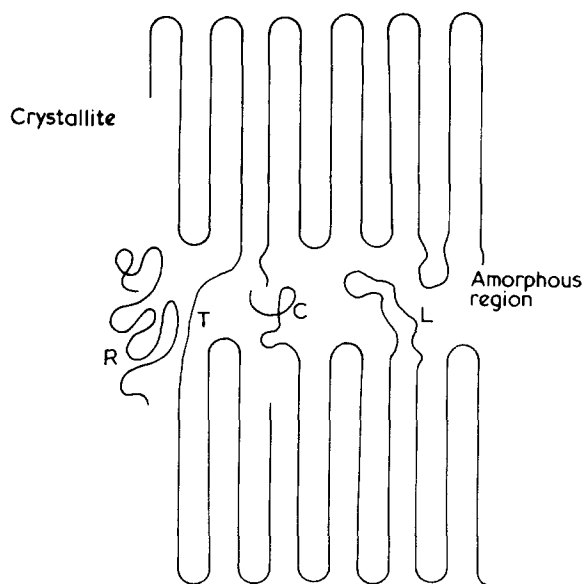


Figure 5 Schematic representation of chain folded structures in a semi-crystalline fibre. C, Cilia (chain end); T, tie molecule; R, rejected chain; L, loop

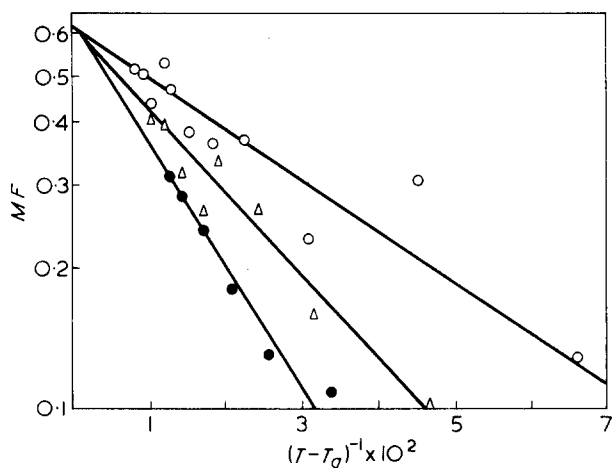


Figure 6 Plot of log MF against $(T - T_g)^{-1}$ for dry and wet nylon-6,6 fibres: ○, saturated fibres; △, 12% D₂O; ●, dry fibres

viour in completely amorphous materials the presence of the crystalline regions in nylon fibres impose permanent constraints on the ends of amorphous chains at temperatures below the melting point of the crystallites. Zachmann¹⁸ proposes that in poly(ethylene terephthalate), loops of amorphous chain segments (L in Figure 5) protruding from the surfaces of chain folded crystallites take part in significant motion above the T_g only if the ratio of end-end separation to extend length of the loop is less than about 0.5 (in this model, rejected chains and chain ends emerging from crystallite surfaces would, of course, be capable of such motion). Using simple free-volume theories³⁶ to relate n.m.r. mobile fraction to free volume increase viz.:

$$MF = MF_{\infty} \exp [-A(T - T_g)^{-1}]$$

(where T_g is the temperature at which the mobile component first appears and A is a constant which includes the coefficient of expansion) Zachmann extrapolated his n.m.r. data to 'infinite temperature' and obtained estimates of the maximum fraction of chains, MF_{∞} , capable of taking part in motion above the T_g . Our data has been plotted in this form and, for comparison, the curves obtained for dry and wet nylon-6,6 fibres are shown in Figure 6; within experimental error linear relationships were obtained. Although, due to the specific water-polymer interactions in the nylon system, quantitative interpretation of the temperature behaviour becomes difficult, extrapolation of the curves to 'infinite temperature' demonstrates that the fraction of non-crystalline chain segments able to participate in the motion is independent of the method of introducing free volume i.e. whether solvent or thermally induced. The concept of moisture-temperature superposition has been used elsewhere in studies of nylon fibres^{37,38} and in general could be applied to these results, however the method of introducing D₂O into the samples does not preclude the possibility of some droplet formation between individual fibres in the staple pack thereby yielding uncertainties in amounts of water actually absorbed in a fibre.

Relaxation in dry fibres

For dry nylon-6,6 fibres both the T_1 and T_2 processes could be described as single component below the T_g (~100°C); the results are presented in Figure 7. The T_1 behaviour is similar to that found by McCall and Anderson²¹ for dry nylon filaments. The main feature between -100°C

and 100°C is a pronounced T_1 minimum occurring at about 40°C which is attributed to the γ -process in the non-crystalline regions. That T_1 relaxation of the whole sample is influenced by the γ -process suggests that a spin diffusion process³⁹ operates between the crystalline and amorphous regions whereby spin energy of 'rigid' chain segments is propagated by mutual 'spin-flips' between pairs of nuclei to mobile sites capable of relaxing via the normal spin-lattice mechanism. The behaviour is compatible with the arrangements of chains outlined previously in Figure 5 in which the non-crystalline segments are located on the surfaces of the crystallites as chain loops, rejected chains, chain ends or tie molecules adjoining the crystalline regions. These segments, by virtue of either their γ - or α_d -motion, will be able to act as the 'sinks' for the drain of spin energy from the chain folded material to produce an average T_1 for the system. The steady increase in T_2 with increasing temperature up to 100°C is also associated with the γ -process, the signal components of the crystalline and amorphous phases being inseparable in this temperature range. Above ~100°C the T_1 /temperature curve begins to form a second minimum which is accompanied by the appearance of the 'mobile' T_2 component. Here the T_1 values for the two components were determined separately and found to be practically equal, again demonstrating the efficiency of the spin diffusion process between crystalline and mobile amorphous segments above their T_g . (There is likely to be a contribution to the drop in T_1 at this temperature due to the α_c -process²² associated with motion of segments about long chain axes in the crystalline regions.) Approximate T_2 values for each component at the higher temperatures have been determined and are included in Figure 7.

Relaxation in wet fibres

In Figure 8 is shown the recovery of magnetization after the second 90° pulse in a typical T_1 measurement for wet

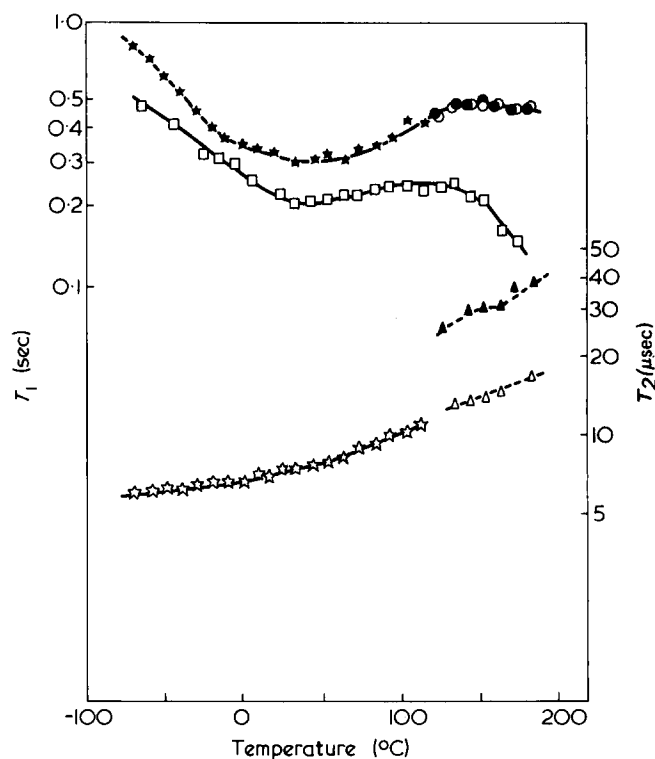


Figure 7 Dependence of proton relaxation times, T_1 and T_2 , on temperature for dry nylon-6,6 fibres: total signal, ★ (T_1), ☆ (T_2); mobile signal, ● (T_1), ▲ (T_{2M}); rigid component, ○ (T_1), △ (T_{2R}); fibres containing MnSO₄ (□)

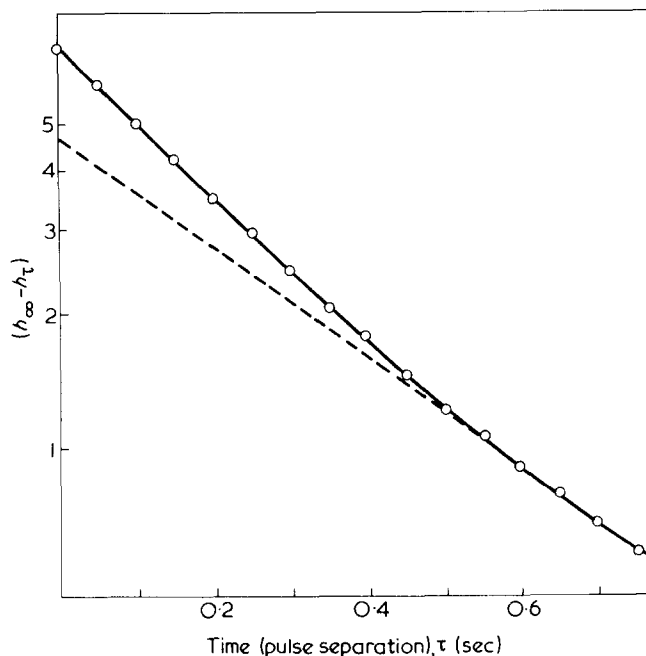


Figure 8 Recovery of signal intensity in a typical T_1 experiment ($90^\circ - \tau - 90^\circ$ pulse sequence) for wet nylon-6,6 fibres (at 55°C), $h(\tau)$ = signal intensity at time τ ; $h(\infty)$ = signal intensity as $\tau \rightarrow \infty$. \circ , Wet nylon-6,6 fibres; ----, single exponent

nylon fibres (saturated in D_2O). It can be seen that the form is non-exponential; examination of the curves obtained between 0° and 100°C suggests a distribution of T_1 values⁴⁰. Therefore it appears that in this temperature range spin diffusion is not completely effective in producing an average \bar{T}_1 when some D_2O molecules are present between the chains in the accessible regions. The dependence of relaxation times on temperature is presented in Figure 9. After about 0°C the appearance of the 'mobile' signal component enabled both T_1 and T_2 for the amorphous regions to be measured separately. It is interesting to observe that the lower T_1 curve referring to relaxation of the 'rigid' component retains the minimum characteristic of that produced by the γ -process in the dry fibres. In view of the nature of the morphology being considered this is not surprising since non-crystalline segments contributing to this component over most of the temperature range are those segments capable of acting as 'sinks' in spin diffusion relaxation of crystallite protons i.e. those forming tight loops on the crystallite surface. (The existence of a strong γ -relaxation in highly crystalline nylon-6,6 has recently been noted by Ito, Tanaka and Kayamoto²⁴ and interpreted as arising from crystal defects.) The γ -process may also be responsible for the steady increase in T_2 with temperature for this component although it is possible that the increase includes a contribution from the influence of water on the α_c -process, as indicated in the n.m.r. second moment data of Olf and Peterlin²³. Because of the ability of both moisture and temperature to mobilize chain segments in the amorphous regions it is reasonable to claim that the T_1 minimum observed (Figure 9) for the plasticized segments is a low temperature version of the minimum for the α_c -process commencing after the T_g in the dry fibres. However, in addition, it is realized that the T_1 behaviour for the amorphous component includes relaxation of more and more segments as the temperature is increased. Unfortunately, it is impossible to resolve separate T_1 data for the different types of amorphous chain segments and at present no quantitative treatment can be applied to deter-

mine the relative influences of water on their α_c - and γ -processes.

Effect of paramagnetic ions

When paramagnetic Mn^{2+} ions are introduced into the wet fibre sample only one T_1 is apparent and the T_1 /temperature behaviour is modified considerably as shown in Figure 9. Since there is a reduction in T_1 over the whole temperature range and the fibre diameter is in excess of $10\ \mu\text{m}$ the effect is considered to be due to penetration of some paramagnetic ions into the water accessible regions⁴¹. Below about 0°C some water responsible for plasticization at normal temperatures is frozen; as the temperature is raised above 0°C there must be a dramatic change in correlation frequency for the ions as this water melts. The drop in T_1 as the temperature is further increased arises from the influence of increasing chain mobility in the presence of paramagnetic ions. It is possible that the increase in free-volume with increase in temperature allows more ions to reach tight loops near the crystallite surfaces. The structural features thought to determine relaxation of chain segments between two chain folded crystalline regions are represented schematically in Figure 10. In this model it is expected that amorphous segments plasticized by D_2O molecules remote from the crystallite surface will have a different average motional correlation time, $\bar{\tau}_A$, to those in the chain folded material forming the crystallites (correlation time $\bar{\tau}_C$). The action of D_2O molecules between mobilized chains will result in an inefficient spin diffusion

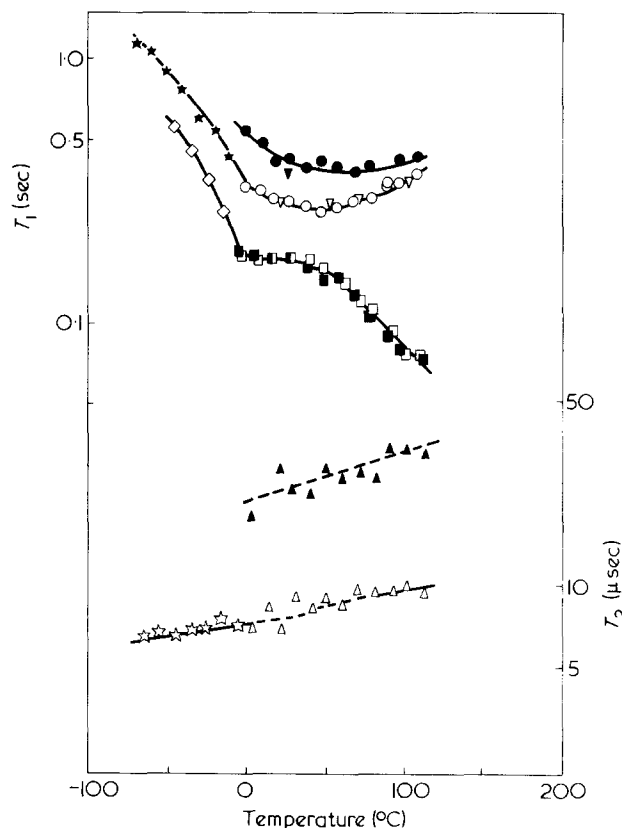


Figure 9 Dependence of proton relaxation times, T_1 and T_2 , on temperature for wet nylon-6,6 fibres. Fibres soaked in D_2O : total signal, \star , (T_1); \star , (T_2); mobile component, \bullet , (T_1); \blacktriangle , (T_{2M}); rigid component, \circ , (T_1); \triangle , (T_{2R}). Fibres soaked in $\text{MnSO}_4/\text{D}_2\text{O}$ solution (0.2M): total, \diamond , (T_1); mobile, \square , (T_1); rigid, \square , (T_1). Fibres soaked in $\text{MgSO}_4/\text{D}_2\text{O}$ solution (0.2M): mobile, \blacktriangledown , (T_1); rigid, \triangledown , (T_1)

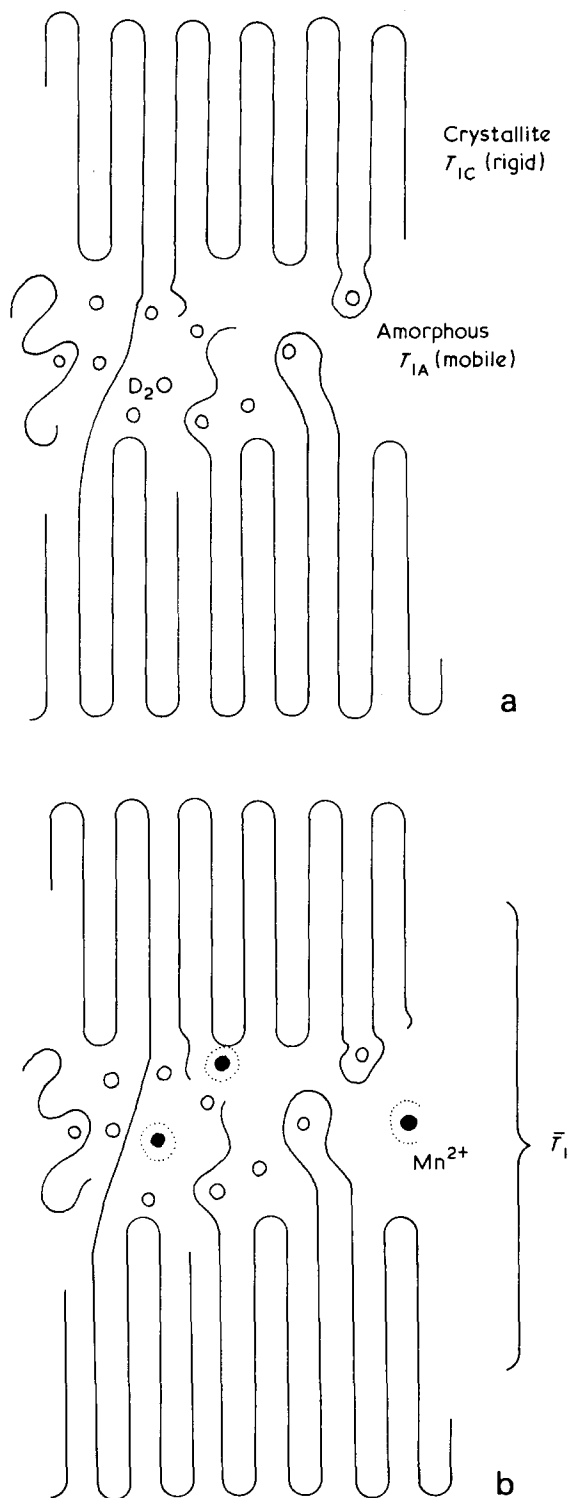


Figure 10 Schematic representation of morphology of wet fibres showing penetration of D_2O (○) molecules and Mn^{2+} (●) ions into accessible regions between crystallites. (a) Fibre and water (D_2O); (b) fibre, water and Mn^{2+} ions

process across the amorphous regions and hence prevent complete averaging of the T_1 process, i.e. T_{1C} for the crystallites and T_{1A} for mobilized amorphous segments. However, a distribution of Mn^{2+} ions in the amorphous regions, as shown in Figure 10 will relax directly all protons between and on the crystallite surfaces. A single T_1 process is obtained because these ions also determine the relaxation of chain folded material via spin diffusion through the crystallite surface. The influence of paramagnetic sources on the relaxation of chain segments in the region of the transition

for a fibre sample in which the bulk of the water had been removed is shown in Figure 7. Spin diffusion is still effective in producing a single T_1 and it can be seen that compared to the pure dry fibres the drop in T_1 accompanying the increase in chain motion in the vicinity of the T_g is more pronounced. Finally, in order to confirm that paramagnetic effects were responsible for relaxation behaviour in fibres containing manganous sulphate, T_1 values obtained at several temperatures for a sample with non-magnetic Mg^{2+} ions have been included in Figure 9. It can be seen that the presence of these ions has little, if any, effect on T_1 relaxation behaviour.

CONCLUSIONS

For wet nylon-6,6 fibres at ambient temperatures a mobile component is present in the pulsed n.m.r. signal which is similar to that observed in the dry fibres above $100^\circ C$. The temperature at which the mobile component appears was found to depend on water content, the depression in the transition being about $100^\circ C$ on saturating the fibres. This behaviour is due to plasticization of the amorphous regions of the fibre by water molecules corresponding to mobilization of 'non-crystalline' chain segments above their glass transition temperature i.e. the α_g -process. The growth of mobile fraction with increase in temperature and moisture indicates that in contrast to the behaviour for completely amorphous polymers more segments take part in the α_g -process as the free volume is increased after the transition. This is consistent with some of the morphological features of recent chain folded models of fibre structure in which chain loops, chain ends and tie molecules forming the non-crystalline material are constrained to different extents through their attachments to crystallites. The influence of fibre morphology on the mobility properties of chain segments is also reflected in the relaxation behaviour of the fibres. T_1 relaxation of the crystalline segments in dry fibres is dominated by processes occurring in the amorphous regions such as the γ -process, which shows an efficient spin diffusion or relaxation averaging process between both arrangements of chain segments. In D_2O soaked fibres it is concluded that spin diffusion only operates between crystallites and those amorphous segments which are not plasticized by D_2O molecules, i.e. some of the folds on the crystallite surface. When Mn^{2+} ions are introduced into the fibre samples the relaxation behaviour of both the amorphous and crystalline segments is strongly influenced by paramagnetic effects, indicating that some of these ions are able to reach the water accessible segments between and on the surfaces of the crystallites.

REFERENCES

- 1 Bell, J. P. *J. Appl. Polym. Sci.* 1968, **12**, 627
- 2 Sisson, W. *Text. Res. J.* 1960, **30**, 153
- 3 van der Meer, S. J. *J. Text. Inst.* 1974, **65**, 288
- 4 Hearle, J. W. S. and Peters, R. H. 'Fibre Structure', Butterworths, London, 1963
- 5 *Enc. Polym. Sci. Technol.* 1967, **6**, 505
- 6 Ribnick, A. S., Weigmann, H. D. and Rebenfeld, L. *Text. Res. J.* 1973, **43**, 176
- 7 Dumbleton, J. H. *Text. Res. J.* 1970, **40**, 1035
- 8 Balczyk, E., Kozłowski, W. and Włodarski, G. *Text. Res. J.* 1969, **39**, 835
- 9 Gur-Arich, Z. and Ingamells, W. *J. Soc. Dyers Colour.* 1974, **90**, 3
- 10 Watanabe, S., Hayashi, J. and Akahori, T. *J. Polym. Sci.* 1974, **12**, 1065

- 11 Boyer, R. F. *J. Macromol. Sci. (B)* 1973, **8**, 503
 12 Boyer, R. F. *Rubber Chem. Technol.* 1963, **36**, 1303
 13 McCrum, N. G., Read, B. E. and Williams, G. 'Anelastic and Dielectric Effects in Polymeric Solids', Wiley, London, 1967
 14 Woodward, A. E. *Rev. Pure Appl. Chem.* 1966, **12**, 341
 15 Powles, J. G. *Polymer* 1960, **1**, 219
 16 Slichter, C. P. *J. Polym. Sci. (C)* 1966, **14**, 33
 17 McCall, D. W. and Falcone, D. R. *Trans. Faraday Soc.* 1970, **66**, 262
 18 Zachmann, H. G. *J. Polym. Sci. Polym. Symp.* 1973, 111
 19 Bergmann, K. *Kolloid Z. Z. Polym.* 1973, **251**, 962
 20 McCall, D. W. and Douglass, D. C. *Polymer* 1963, **4**, 433
 21 McCall, D. W. and Anderson, E. W. *Polymer* 1963, **4**, 93
 22 Olf, H. G. and Peterlin, A. *J. Polym. Sci. (A-2)* 1971, **9**, 1449
 23 Olf, H. G. and Peterlin, A. *J. Polym. Sci. (A-2)* 1971, **9**, 2033
 24 Ito, M., Tanaka, K. and Kanamoto, T. *Rept. Prog. Polym. Phys. Japan* 1973, **16**, 249
 25 Stokes, R. H. and Robinson, R. A. *Ind. Eng. Chem.* 1949, **41**, 2013
 26 Powles, L. G. and Mansfield, P. *Phys. Lett.*, 1962, **2**, 58
 27 Puffr, R. and Šebanda, L. *J. Polym. Sci. (C)* 1965, 16
 28 Puffr, R. and Šebanda, L. *J. Polym. Sci. (C)* 1967, **16**, 79
 29 Kawasaki, K. and Sekita, Y. *J. Polym. Sci. (A-2)* 1964, **2**, 2437
 30 Illers, K. H. and Kosfeld, R. *Makromol. Chem.* 1960, **42**, 44
 31 Kapur, S., Rogers, E. and Baer, E. *J. Polym. Sci.* 1972, **10**, 2297
 32 Papir, Y. S., Kapor, S., Rogers, E. and Baer, E. *J. Polym. Sci. (A-2)* 1972, **10**, 1305
 33 Bueche, F. 'Physical Properties of Polymers', Interscience, New York, 1962
 34 Ferry, J. D. and Stratton, R. A. *Kolloid-Z* 1960, **171**, 107
 35 Olf, H. G. and Peterlin, A. *J. Polym. Sci. (A-2)* 1970, **8**, 771
 36 Cohen, M. H. and Turnbull, D. *J. Chem. Phys.* 1959, **31**, 1164
 37 Howard, W. H. and Williams, M. L. *Text. Res. J.* 1968, **36**, 691
 38 Andrews, R. D. and Buchoff, L. S. *J. Polym. Sci. Polym. Symp.* 1974, 191
 39 Abragam, A. 'Principles of Nuclear Magnetism', OUP, London, 1961, p 138
 40 Odajima, A. *J. Phys. Soc. Japan* 1959, **14**, 1574
 41 Smith, E. G. and Robb, I. D. *Polymer* 1974, **15**, 713

Dissolution of polypropylene in organic solvents: 2. The steady state dissolution process

D. A. Blackadder and G. J. Le Poidevin*

Department of Chemical Engineering, University of Cambridge, Cambridge CB2 3RA, UK
(Received 31 March 1976)

This paper is part of a series describing the dissolution of solid polypropylene in organic solvents. A previous paper distinguished between two types of dissolution. (a) At sufficiently low temperatures dissolution is partial and only a limited amount of polymer dissolves, the rate of dissolution falling to zero. (b) At higher temperatures and in suitable solvents dissolution occurs continuously at a constant rate. The present paper is concerned with the details of (b). Steady state dissolution is preceded by an induction period during which solvent penetrates the solid polymer to some characteristic depth. The rate of dissolution is measured by gravimetric analysis of the dilute solution surrounding a rotating disc of solid polymer. The variables considered include polymer density, stirring speed and temperature. From the results it is possible to identify the rate-determining stage of the dissolution. Depending on the conditions this is either the rate at which polymer molecules escape from a solvent-swollen surface layer, or the rate at which solvent penetrates and destroys crystallites in the solid polymer.

INTRODUCTION

Substantial differences exist between the dissolution behaviour of micromolecular and macromolecular substances. The former have been studied in great detail and it is well known that dissolution takes place through a liquid boundary layer with little or no penetration of the solid matrix by the solvent. The concentration of solute at the solid/liquid interface is that of an equilibrium saturated solution at the temperature of the system, and this concentration falls through the boundary layer to the bulk solution value which may be effectively zero.

The molecular entanglement characteristic of high polymers has a pronounced effect on the dissolution rate. Solvent may penetrate deeply into the solid structure while molecules at the surface disentangle themselves sufficiently to 'float' out into the solution. There is certainly a polymer-rich mixed phase in the solid as well as a liquid boundary layer, and some degree of swelling is often observed in the form of a surface gel. Most of the work on polymers so far has been concerned with polystyrene¹⁻⁹ or poly(methyl methacrylate)², both amorphous, or with the very low crystallinity polymer poly(vinyl chloride)¹⁰. The semi-crystalline ester poly(ethylene succinate) has also received some attention^{2,11} and a few results are available concerning the partial dissolution of polyethylene¹². In the present paper it will be convenient to interpret the dissolution of polypropylene on the basis of a comparison with the well-documented features of the dissolution of amorphous polymers. It is therefore necessary to summarize briefly the findings of other authors.

An amorphous polymer dissolves in two stages: an induction period^{1,8,10,13} during which the rate of dissolution build up is followed by a steady state regime where the rate is essentially constant for a fixed area of dissolving polymer. Ueberreiter and Asmussen have identified the

induction period or swelling time as being related to the thickness of the total surface layer system and to an average diffusion coefficient for the solvent penetrant⁸. The stationary state would be represented by a straight line on a plot of penetration depth of solvent into polymer against time, the depth, s , being measured from a fixed reference plane parallel to the flat surface of the receding solid. The slope of the line is \dot{s} , the velocity of penetration, and extrapolation gives the induction time as an intercept on the t axis. Alternatively it is possible to measure m , the mass of polymer dissolved at time t , and this approach would lead to \dot{m} as the measure of steady state dissolution rate. Ueberreiter and Asmussen⁴ have painstakingly described the complicated steady-state system of layers which is built up near the surface of the dissolving polymer, and their model takes account of the influence of temperature. It appears that the flow temperature, glass temperature and gel temperature of the polymer are of particular importance in defining regimes, the last-named being the temperature below which no surface gel is formed.

The dissolution of a semi-crystalline polymer is altogether more difficult to achieve than that of an amorphous polymer, and fewer solvents are suitable. The parallel between crystallization and dissolution has been discussed by many authors since the original suggestions of Tamman¹⁴. In the polymer context it has been shown that under appropriate conditions single crystals of polyethylene will first undergo some dissolution then the dissolved material recrystallizes with a longer fold length than previously^{15,16}. Steiner *et al.*¹¹ used poly(ethylene succinate) to demonstrate a marked correspondence between the temperature of the maximum rate of crystallization¹⁷ and the maximum rate of dissolution. Some work on the effect of hot toluene on polypropylene¹⁸ has shown a dependence on morphology, which is at least qualitatively in line with expectations based on the rate of crystallization.

The present paper considers the steady state dissolution of polypropylene in hot organic solvents, with special refer-

* Now at the Electricity Council Research Centre at Capenhurst, Chester, UK.

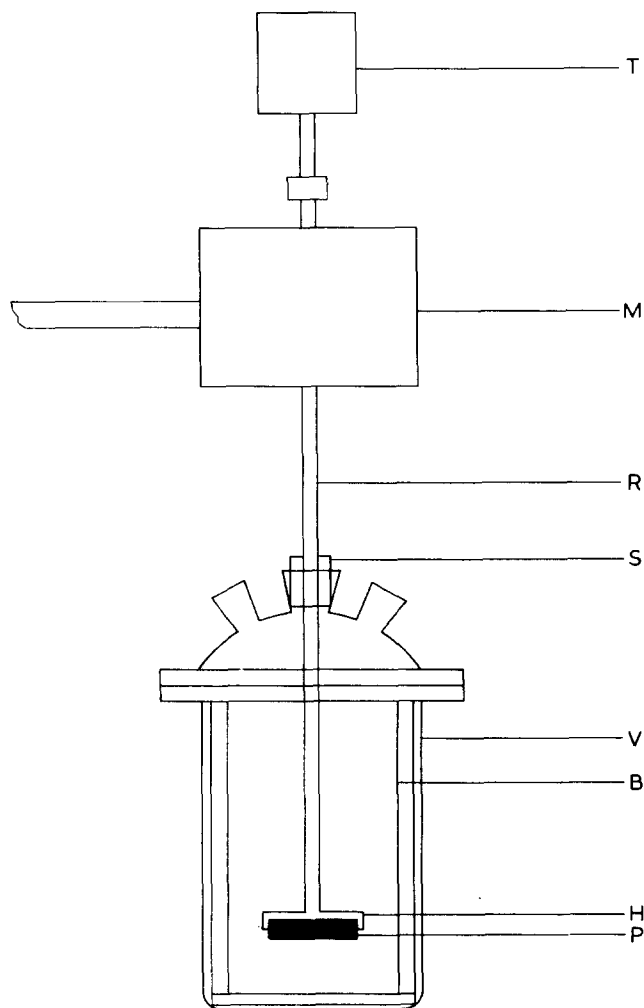


Figure 1 The dissolution apparatus: P, polymer specimen; H, metal holder; B, steel baffles; V, glass vessel; S, Teflon seal; R, stirrer rod; M, stirrer motor; T, tachometer

ence to the effects of stirring rate, crystallinity, and temperature. The first paper of the series¹⁹ provided a description of the processes involved in the induction period, and a further paper will discuss the importance of polymer-solvent compatibility on a thermodynamic basis, as well as the effect of the molecular weight of the polymer.

EXPERIMENTAL

Materials

Polymer. The polymer used was a homopolymer, GXM 43, kindly supplied by ICI Plastics Division. The amount of atactic material present was estimated to be about 2 wt %, and the polymer contained the usual small amounts of antioxidant and stabilizer. In view of the relatively high temperatures used in some of the experiments these additives were welcome and no attempt was made to remove them. The polymer was quoted as having a melt flow index of 2.16 and a melt viscosity of 5.0×10^3 N sec/m at 190°C.

Solvents. The *p*-xylene was a 99% product obtained from ICI. The other organic solvents, of SR or AR grade, were used as received.

Procedures

Fabrication of specimens. For the main dissolution experiments it was necessary to prepare polypropylene discs

50 mm in diameter and 4.5 mm thick. 8 g of polymer chips were melted at 210°C for 1 h under vacuum in a special mould. The mould and contents were then quench cooled by immersion in a water bath. Cooling was not particularly rapid and the specimens were typically of density 905 kg/m³. For some purposes specimens were slow cooled from the melt temperature by controlling the input to the heater of the mould assembly. Another method of obtaining higher densities was to anneal quenched specimens for 2 h in the mould itself at an appropriate temperature followed by slow cooling.

Check on polymer degradation. The polypropylene was inevitably subjected to fairly severe conditions during fabrication of specimens and in the dissolution experiments involving hot solvents. It was therefore desirable to check for degradation, and a technique was not adopted on a routine basis until it had been shown that no detectable degradation was caused by the use of that technique. The test was to measure the specific viscosity of a solution of the polymer in a given solvent at fixed temperature and concentration.

Characterization of specimens. Infra-red and density measurements were carried out to assess crystallinity. For the former a Perkin-Elmer Infracord Spectrometer was used, and for the latter a density gradient column with *p*-xylene and chlorobenzene as the column liquids.

Apparatus for dissolution measurements

The apparatus is shown in Figure 1. The flat-bottomed cylindrical vessel was provided with a set of stainless steel baffles designed to prevent the formation of a vortex beneath the spinning disc. The baffle assembly was removable for thorough cleaning between runs. The disc of polypropylene was held in a rimmed plate by means of three retaining screws in the rim. The disc protruded about 1 mm beyond the rim, a slight ambiguity concerning the area of the dissolving polymer being preferable to the possibility of stagnant zones forming if the disc were significantly recessed. Dissolution was assumed to occur over the area represented by one side of the disc. The rimmed plate was attached to one end of an axle with the other end being driven by a variable speed motor.

It was important not to expose a polymer disc to heat or solvent unduly before the start of a timed experiment, having characterized the specimen. The lower surface of the disc was about 40 mm above the bottom of the vessel which held about half a litre of solvent and was thermostatted in an oil bath to $\pm 0.05^\circ\text{C}$. In general runs were terminated when no more than 30% of the original specimen had dissolved.

After reviewing the methods of following the dissolution process used by other workers^{1,10,13,20} and trying a few of these, it was decided to rely on a very simple gravimetric procedure. Up to 10 samples of solution were withdrawn at intervals into a 20 cm³ pipette and transferred to weighed aluminium foil dishes. The solvent was evaporated off in an oven for 12 h at 80°C. The amount of polymer was then found by reweighing. The time of each sample was taken as the midpoint of the 10 sec required for sampling. The initial volume of solvent was generally 550 cm³ measured at room temperature, and corrections were applied to allow for expansion to the operating temperature. The amount of solvent, even after removal of all the samples, was sufficient to ensure that the solution was always very dilute with respect to polymer. Indeed the polymer was

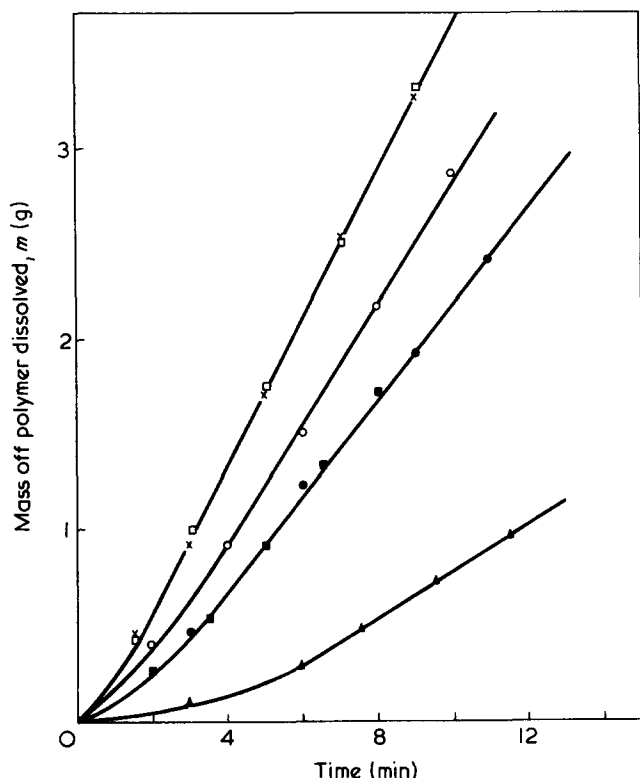


Figure 2 Dissolution of polypropylene in *p*-xylene at 120°C for various densities; stirring speed 1000 rev/min, disc diameter 50 mm. □, Run 1, 904.7 kg/m³; X, Run 2, 909.0 kg/m³; ○, Run 3, 910.8 kg/m³; ●, Run 4, 913.5 kg/m³; ■, Run 5, 913.0 kg/m³; ▲, Run 6, 914.7 kg/m³

virtually dissolving into pure solvent all the time. It is easily shown that m , the amount dissolved after time t , is given by:

$$m = \left[\frac{Vd_A}{vd_B} - (n-1) \right] m_n + \sum_{x=1}^{n-1} m_x$$

In this equation:

- V = initial volume of solvent at room temperature,
- d_A = density of solvent at room temperature,
- v = volume of sample at temperature of experiment,
- d_B = density of solvent at temperature of experiment,
- n = number of samples taken up to time t ,
- m_n = mass of polymer in n th sample,
- m_x = mass of polymer in x th sample.

The weight of polymer in each extracted sample was in the range 5 to 150 mg, increasing with t . Near time zero the error was about $\pm 2\%$ but much less in the later stages of an experiment.

The results of an experiment are in the form of values of m for different values of t and, where appropriate, the slope of a plot of the data, \dot{m} , may be regarded as a good measure of the rate of dissolution. Values of \dot{m} from different experiments are directly comparable because, with the exception of experiments designed to test the effect of disc size, the same type of disc was used throughout. The reproducibility of \dot{m} in separate experiments was better than 5%.

RESULTS AND DISCUSSION

General aspects of the dissolution

Figure 2 shows the dependence of m , the mass of polypropylene dissolved, on the immersion time, t , in *p*-xylene at 120°C for a range of specimen densities, each measured at 23.6°C in the gradient column prior to a dissolution experiment. After an initial period during which the dissolution rate gradually increases, the process enters a steady state in which the rate, \dot{m} , holds constant for several minutes. (Some experiments were continued into a further period of accelerating dissolution rates but these experiments do not appear in Figure 2. Discs subjected to this final stage were deeply pitted by erosion which increased the effective area of exposed surface in an irregular way.) The existence of an induction period followed by a steady rate of dissolution suggests a similarity between the behaviour of amorphous and semi-crystalline polymers. There is, however, a difference in the significance of density for the two kinds of polymers. At any given temperature the density of an amorphous polymer is more or less fixed and predictable, whereas the density of a semi-crystalline polymer is dependent upon its thermal history and is controllable within limits. Figure 2 shows that the dissolution rate of polypropylene tends to increase with decreasing density but in a non-simple manner due to the intrusion of other effects.

Runs 1 and 2 gave similar values of \dot{m} yet the densities of the specimens were different. Since the specimen for Run 1 was prepared by quench cooling it might be thought that a substantial density increase occurred as a result of annealing during the dissolution experiment itself. However, subsidiary experiments with i.r. showed that the crystallinity of both specimens remained unchanged on heating to the temperature of the dissolution experiments. Only on subsequent cooling to room temperature at the end of the experiment did the specimen used in Run 1 show a rise in density, while the density of the specimen from Run 2 remained substantially the same on cooling. The latter observation is explained by the fact that the specimen had experienced a higher temperature (130°C) during the dry annealing which formed part of its initial fabrication than in the subsequent dissolution (120°C). For sufficiently low densities it would therefore appear that the rate of dissolution is actually independent of density and this is borne out by the more detailed results which appear later on.

Runs 4 and 5 also require special comment. The specimens had the same density but were prepared by different methods. (The specimen for Run 4 was quench cooled then annealed at 155°C, while the other was slow cooled from the melt at 10°C/h). The results suggest that for densities of this magnitude the effect of preparative method is wholly subordinate to the effect of density in determining the rate of dissolution.

Figure 3 shows the effect of initial specimen density on the steady dissolution rate, \dot{m} , at various temperatures. Each curve has been extrapolated to intersect the density axis at zero dissolution rate, though it is known from Part 1 of the series¹⁹ that partial dissolution can occur at a slow and ever-diminishing rate even at densities greater than the 'intercept' value for a given temperature. Figure 3 is nevertheless correct in that it shows steady state dissolution rates, and these do genuinely tend to zero at characteristic densities. For a given temperature the dissolution which

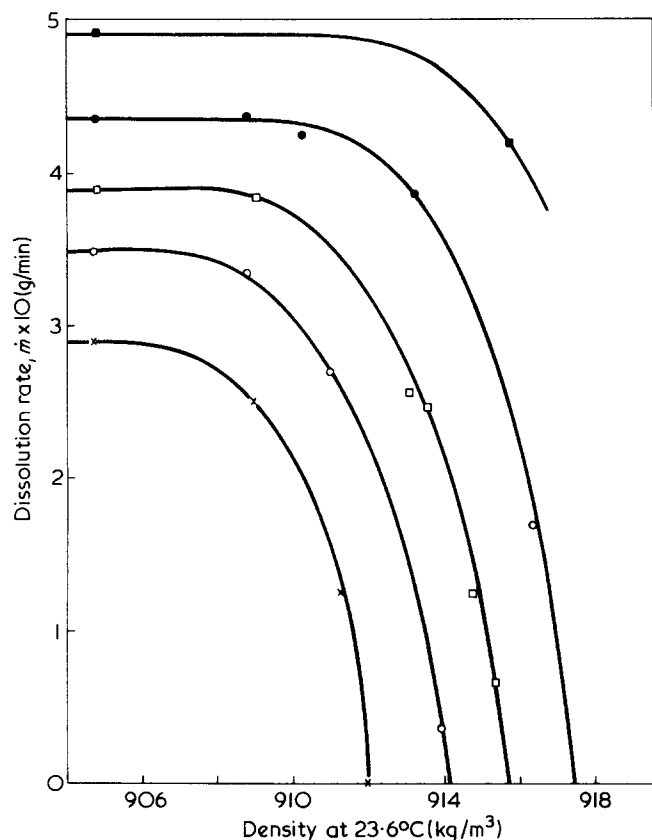


Figure 3 Rate of dissolution of polypropylene in *p*-xylene at various temperatures as a function of density; stirring speed 1000 rev/min, disc diameter 50 mm. ■, 130°; ●, 125°; □, 120°; ○, 115°; X, 110°C

can occur at densities above the intercept value is fractional rather than wholesale, and its rate eventually falls to zero for any given specimen.

Figure 4 shows schematically the dependence of dissolution rate on density for both steady state dissolution and fractional dissolution. For the latter runs, characterized by the plot of m against t being concave to the time axis, the recorded \dot{m} is the slope of the tangent at time zero, and it was noticeable that the surfaces of the discs did not recede. Some material evidently dissolved out but the overall structure was maintained by the larger insoluble molecules. The gradual slowing up of any fractional dissolution is due to the fact that removal of soluble polymer becomes increasingly difficult as it has to be leached from deeper levels in the disc.

Figure 5 provides an example where the specimen density of 917.9 kg/m³ slightly exceeded the intercept density of 915.7 kg/m³ read off Figure 3 for the temperature concerned. It is interesting to note that 120°C is virtually the thermodynamic dissolution temperature, T_s , for polymer having the intercept density.

A further demonstration of the nature of fractional dissolution is provided by the following simple experiment. A disc of density 916.2 kg/m³ was suspended motionless in excess *p*-xylene at 120°C. Figure 3 would predict the absence of steady state dissolution for such a specimen. After 4 days the original disc outline remained despite a weight loss of 33%, but the specimen was probably on the verge of dissolving completely in view of the replacement of the smooth surface by a rough gel which could be scraped off easily. Viscometric measurements were carried out on specimens obtained from the original polymer, the interior of the disc after dissolution, and dissolved polymer. For

0.25% w/v solutions in decahydronaphthalene at 135°C the values of η_{sp} were 0.692, 0.738 and 0.250 respectively, thus providing clear evidence for fractionation.

It must be emphasized that the intercepts on Figure 3 have a significance only for relatively short experiments. Considerable morphological changes occur on annealing polypropylene in solvents at temperatures between ambient and T_s (see ref 19). If the dissolution were slow enough it is conceivable that solvent could penetrate right to the back of a disc during an experiment with ambiguous consequences. In addition the excessive swelling so caused could lead to buckling of the disc in its holder. Indeed this tended to occur after 30 min or so however high the dissolution rate, which is a further reason why data such as in Figure 3 should be based on fairly short experiments.

For homopolymers the linear growth rate, G , of spherulites in the vicinity of T_m , the melting point, follows a relation of the form:

$$\ln G = \text{constant} - \frac{C_1 T_m^n}{RT_c(T_m - T_c)^2}$$

where $n = 1$ or 2, C_1 is a term involving interfacial energy and heat of fusion terms, and T_c is the temperature of the crystallization. Qualitatively the curves on Figure 3 appear to follow a similar relationship if T_c and T_m are replaced by

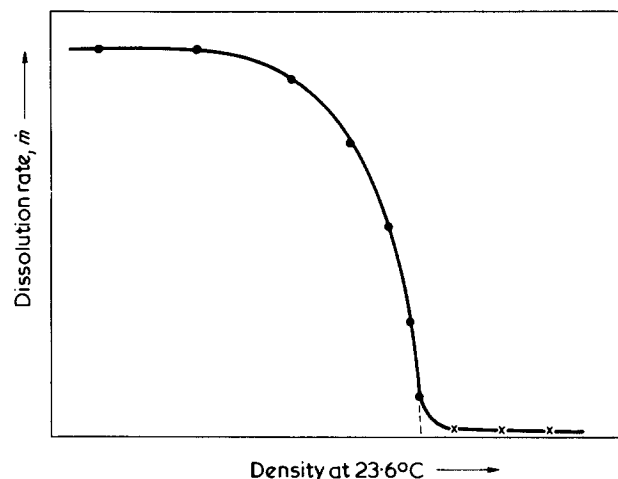


Figure 4 Schematic diagram of dissolution rate as a function of density showing regimes of wholesale and fractional dissolution. ●, Wholesale dissolution; X, fractional dissolution

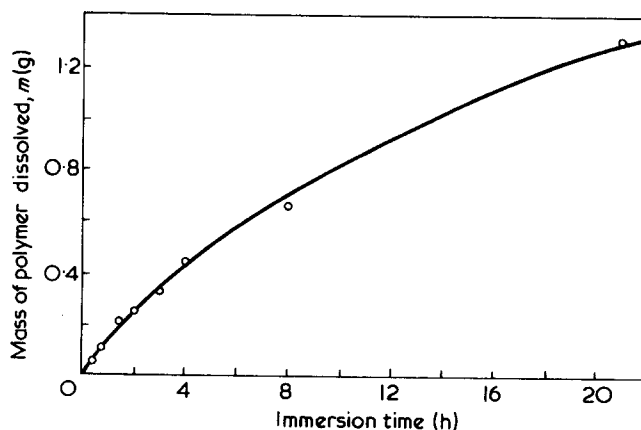


Figure 5 Fractional dissolution of polypropylene in *p*-xylene at 120°C; specimen density 917.9 kg/m³

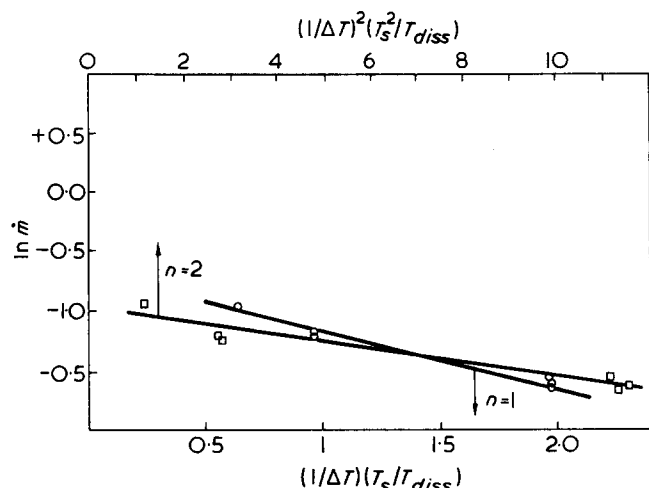


Figure 6 Effect of T_{diss} and T_s on the rate of dissolution of polypropylene in *p*-xylene; stirring speed 1000 rev/min, disc diameter 50 mm

T_{diss} and T_s , where T_{diss} is the actual temperature of a dissolution experiment and T_s is the thermodynamic dissolution temperature. Modification of the above equation, putting $n = 1$, gives:

$$\ln \dot{m} = \text{constant} - \frac{KT_s}{(T_{diss} - T_s)T_{diss}}$$

and this is plotted in Figure 6. A good straight line is obtained, but regrettably this does not exclude fractional powers of n around unity, and indeed the fit is only marginally less satisfactory for $n = 2$. It well illustrates the difficulty of matching theory to experiment in this context.

In their work on poly(ethylene succinate) Steiner *et al.*^{2,11} were able to show quite an impressive correlation between the maximum rate of dissolution and the maximum rate of crystallization. In the present work there was no evidence of an identifiable maximum rate of dissolution of polypropylene which is known to crystallize most rapidly round about 75°C²¹. This could well be because it was not possible to cool the relatively massive specimens quickly enough to prevent most of the crystallization occurring at temperatures well above 75°C. If typical water cooled discs were annealed at 110°C there was no change in density and even at 130°C the density change was very small, thus confirming the view that the original cooling allowed crystallization at quite high temperatures.

Modelling the dissolution process

The dissolution process may be described broadly in terms of the following steps which, at the steady state, are occurring at characteristic depths in the dissolving polymer. (a) Penetration and swelling of the non-crystalline regions by solvent. (b) Penetration of the crystalline regions by solvent with subsequent destruction of crystallites. (c) Dilution, disentanglement and final escape of the polymer molecules into solution.

The first step is certainly not rate-controlling: it has been shown previously¹⁹ that the rate of penetration actually increases with specimen density, whereas quite the opposite trend is observed for the rate of dissolution. If step (c) controls, the previous thermal history should be unimportant since the polymer which is exposed to the bulk solvent is essentially in the amorphous state. On the other hand if step (b) dominates, the structure of the specimen

should assert itself and the dissolution rate should be a function of annealing temperature or density. Evidence for separate regimes for control by (b) and (c) is discussed in detail in the next section. At this point it is appropriate to try to identify the fundamental parameter involved in a crystallite destruction controlling step.

The thermodynamic dissolution temperature, T_s , is controlled by fold length as shown by Flory²², and one would certainly suppose that material with a longer fold length would be more resistant to solvent attack. Furthermore, Farrow²³ has established a correlation between fold length and annealing temperature for polypropylene. A six-fold change in fold length was also accompanied by a change of about 20°C in T_s according to the Flory equation. The present results are compatible with these facts since T_s was observed to cover a range of 20°C depending on specimen density or annealing temperature, and the changing fold length can explain this variation if Flory's analysis is sound.

Effect of stirring speed on dissolution rate

For the dissolution of microcrystalline solids many authors have obtained relationships of the form:

$$\dot{m} = n^x + C$$

where \dot{m} is the dissolution rate, C is its value at zero stirring speed and n is the actual rate of stirring. The exponent x lies between 0.4 and 1, with most values around 0.5.

Spalding²⁰ has shown from theoretical considerations that in the laminar regime the rate of a diffusion controlled dissolution is proportional to $n^{0.5}$, all other parameters being fixed. The exponent of 1 sometimes observed²⁴ for higher stirring speeds is probably an indication of non-laminar flow.

Figure 7 shows the effect of stirring speed on the dissolution of polypropylene in *p*-xylene at 120°C. All of the discs were prepared by annealing quenched specimens, and their densities were 909, 913 and 914 kg/m³. There are two distinct dissolution regimes, one in which the rate of dissolution rises with stirring speed and another in which the rate of dissolution is constant.

The fact that the plot of rate of dissolution against stirring speed is linear for the specimen of density 909 kg/m³ suggests that the flow is turbulent. The Reynold's number for a rotating disc is given by

$$\text{Re}_{\text{rot}} = \frac{\Omega \rho d^2}{\eta}$$

where Ω is the rotation speed in radians per unit time, ρ is the fluid density, d is the disc diameter and η the liquid viscosity. Taking η to be the viscosity of the pure solvent, Re_{rot} varied from 1.1×10^5 at 150 rev/min to 7.2×10^5 at 1000 rev/min. For other systems turbulent flow is known to occur²⁰ when Re_{rot} is about 8×10^5 , and in the present apparatus turbulence could be induced at lower values by the presence of flow-disturbing baffles and vibration in the stirrer. It is likely, therefore, that turbulent flow existed.

Ueberreiter and Kirchner¹ have shown that for amorphous polymers the dissolution rate rises with stirring speed. This was attributed to a reduction in the thickness of the swollen layer, rather than to a change in the average diffusion coefficient of the permeant into the polymer since the latter is presumably independent of stirring rate. Likewise crystallite destruction should not depend on stirring speed. In a sense the interplay between disentanglement

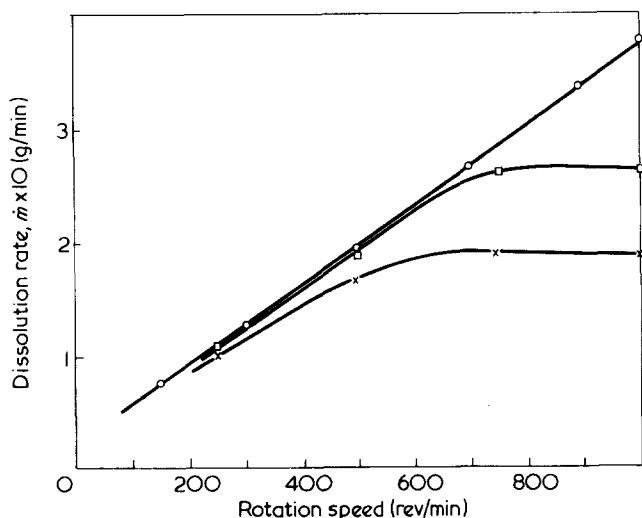


Figure 7 Effect of stirring speed on the rate of dissolution of polypropylene in *p*-xylene at 120°C for various densities; disc diameter 50 mm. ○, 909 kg/m³; □, 913 kg/m³; X, 914 kg/m³

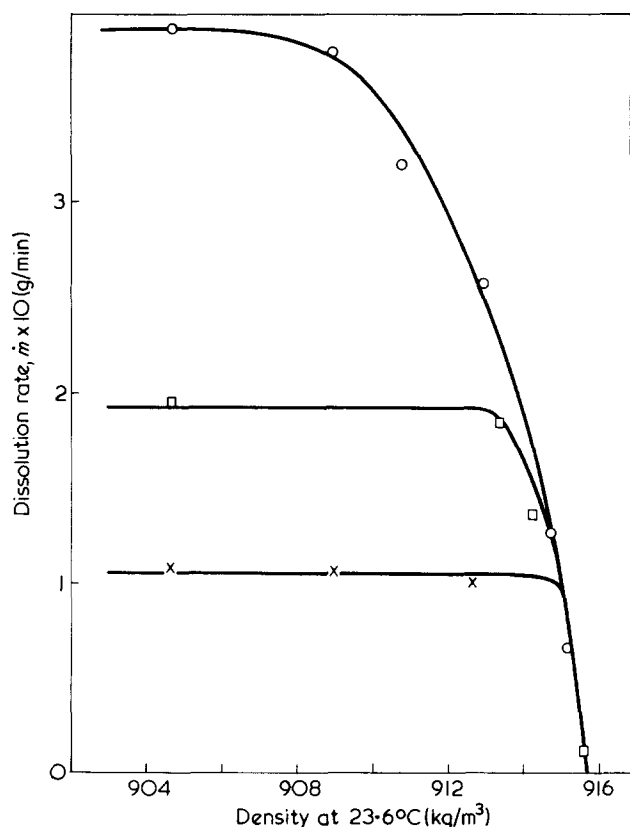


Figure 8 Effect of density on the rate of dissolution of polypropylene in *p*-xylene at 120°C for various stirring speeds; disc diameter 50 mm. ○, 1000 rev/min; □, 500 rev/min; X, 250 rev/min

and crystallite destruction mechanisms gives rise to a situation similar to that involving transport processes and chemical reaction, with the destruction of crystallites replacing chemical reaction. At high enough stirring speeds the dissolution rate should flatten off, and this is observed for the 913 and 914 kg/m³ curves on Figure 7. The existence of a regime of rising dissolution rate with stirring speed indicates that the controlling step under these conditions is the disentanglement of polymer chains. It will appear later that this is accompanied by the formation of a gel layer and the polymer therefore resembles amorphous polymer in its behaviour. The similarity is reinforced by Figure 8

which shows the effect of density on dissolution rate at three stirring speeds. At 250 and 500 rev/min the dissolution rate is virtually constant over the density range 905 to 914 kg/m³. This is not the case at 1000 rev/min, though there are signs of flattening out at the lower densities. In regions of constant dissolution rate the fraction of crystalline material (and fold length) does not affect the rate because the stirring speed is too low. It can be imagined that solvent penetrates the polymer very quickly and destroys the crystalline structure, but the amorphous phase so created is still in a very tangled state and the disentanglement process is rate controlling. A result of this is the formation of a gel layer whose thickness actually controls the rate. In other circumstances the rate of destruction of crystallites is the slowest process and so rate controlling. The overall rate of dissolution will decrease with increasing density in this regime because the rate of destruction of crystallites is sensitive to density or fold length. The extent of the gel layer should decrease with increasing density and there is direct experimental evidence for this. A quenched disc, removed from the holder of the dissolution apparatus immediately after a run at 500 rev/min and 120°C, had a surface layer which was extremely tacky and easily scraped off. In addition there were whorls on the surface suggesting bulk movement of a highly viscous gel layer. The amount of polymer which could be scraped off denser discs was smaller and on the specimen of highest density whorls were conspicuously absent. Indeed there may have been no gel layer whatever.

Figure 9 shows schematically the surface layer structure of dissolving polypropylene where ρ_t refers to the density at the transition between constant and changing dissolution rate at a given temperature. The layers are not, of course, individually homogeneous. In the swollen crystalline layer, for example, the crystallinity varies from the dry polymer value on the extreme left to zero at the next interface whatever it might be. It is plausible that when a large amount of solvent is present in the swollen crystalline layer ($T_{diss} \approx T_s$) the macromolecules may be sufficiently disentangled at the outer face of this layer to pass directly into solution without forming a gel layer. Conversely, when the solvent content of the swollen crystalline layer is everywhere fairly low, a gel layer will become necessary to round off the process.

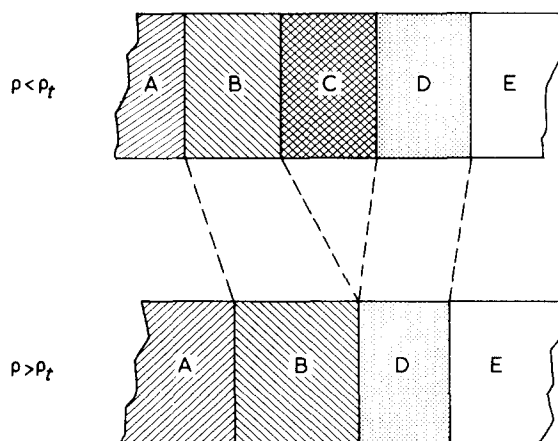


Figure 9 Schematic representation of the layer structure of polypropylene dissolving in solvent. A, Dry crystalline polymer; B, swollen crystalline polymer; C, amorphous gel layer; D, liquid boundary layer; E, bulk solvent

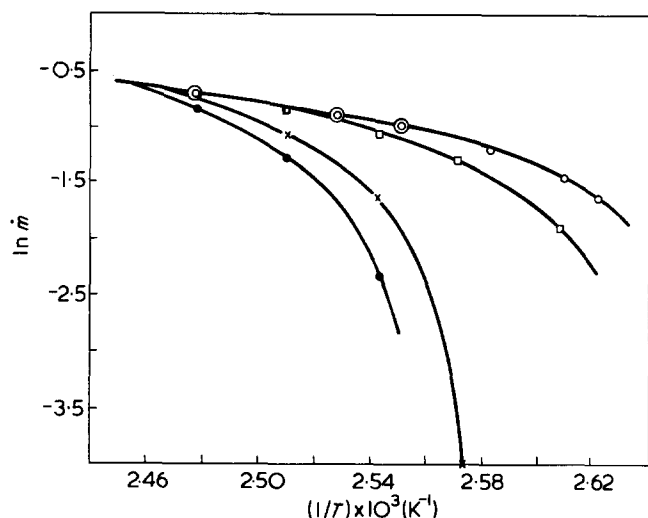


Figure 10 Effect of temperature on the rate of dissolution of propylene in *p*-xylene for various densities; stirring speed 1000 rev/min, disc diameter 50 mm. ○, 904.7 kg/m³; □, 911.0 kg/m³; X, 914.0 kg/m³; ●, 915.0 kg/m³

Effect of temperature on the dissolution rate

Figure 10 shows an Arrhenius plot of $\ln \dot{m}$ against $1/T_{diss}$ for polypropylene and *p*-xylene. Ueberreiter and Asmussen⁴ and Lapčik and Valko¹⁰ have shown that the systems polystyrene–toluene, polystyrene–amyl acetate and poly(vinyl chloride)–cyclohexanone give straight lines when the data are plotted in this manner. For a semi-crystalline polymer such as polypropylene the situation is rather more complicated. It is significant that for a density of 904.7 kg/m³ (the lowest available density, obtained by quench cooling) a straight line can be drawn through the points for the three highest temperatures. In this region each run was repeated at each temperature and the reproducibility was very good.

It is interesting to compare values of the apparent activation energy of dissolution, E_S , for amorphous polymers and polypropylene. E_S can be determined from $\dot{m} = \dot{m}_0 \exp(-E_S/RT)$ where \dot{m} is the observed dissolution rate at temperature T_{diss} and \dot{m}_0 is the value at infinite temperature. For polystyrene–toluene and polystyrene–amyl acetate Ueberreiter and Asmussen⁸ obtained 15.9 and 25.1 kJ/mol for E_S , and Figure 10 gives a value of 31.4 kJ/mol for quenched polypropylene at the higher temperatures. For the poly(vinyl chloride)–cyclohexanone system Lapčik and Valko obtained values of E_S ranging from 30 to 50 kJ/mol depending on the molecular weight¹⁰. When, as in the present work, E_S usually varies with temperature it is instructive to consider the form of the variation. Figure 10 shows clearly that E_S , considered in terms of point values, increases with density at any selected temperature, and varies with temperature for quenched polymer below 120°C and at all temperatures if the density exceeds 909 kg/m³. This can be explained as follows. Higher densities, produced at higher crystallization or annealing temperatures, are associated with crystallites having longer fold lengths^{23,25}. These crystallites may be expected to present larger energy barriers to diffusing molecules.

As the temperature increases the curves on Figure 10 appear to converge, though it is not possible to be sure from the data available. If there is indeed a common line above 137°C or so this would imply that the disentanglement step is controlling regardless of density.

Effect of disc size on dissolution rate

Figure 11 shows $\ln \dot{m}$ plotted against $1/T_{diss}$ for disc diameters of 25 and 50 mm and stirring rates of 500 and 1000 rev/min. Good straight lines of similar slopes can be drawn through the higher temperature points and the values of E_S so obtained range from 27.2 to 31.4 kJ/mol, with an average of 28.9 kJ/mol. The variation is within experimental error, the range of accessible temperatures being only 15°C. Temperatures higher than 135°C were not practicable because *p*-xylene boils at 138°C. Table 1 shows how disc size affects the dissolution rate at fixed stirring speed and temperature. The subscripts refer to the disc diameter in mm. If the local rate of dissolution were the same at all points on the surface of a disc, then doubling the diameter would simply quadruple the exposed surface area and produce a $\dot{m}_{50}/\dot{m}_{25}$ ratio of 4:1. In fact the ratio is about 4.9:1 and direct observation provided an explanation in terms of varying local rates. The 25 mm discs dissolved evenly over the whole surface, while 50 mm discs were noticeably thinned at the edges compared with the centres of the discs.

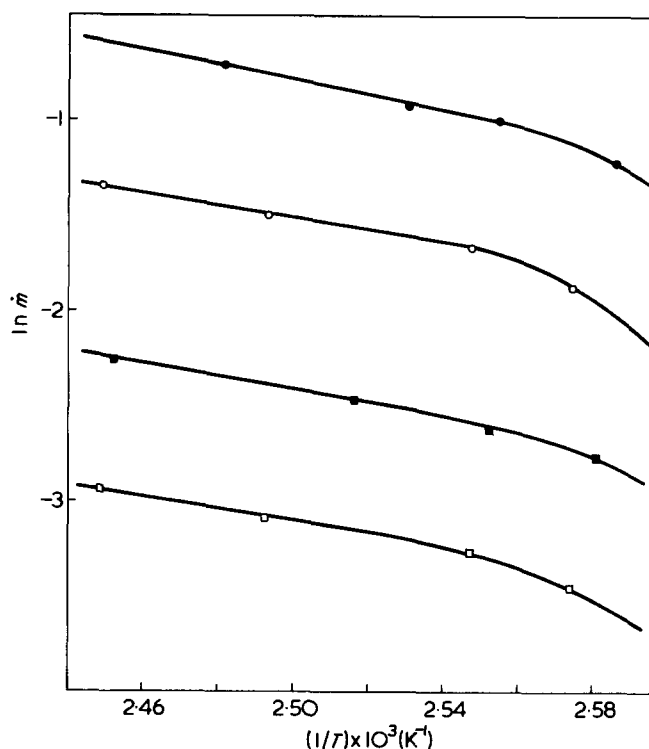


Figure 11 Effect of disc diameter and stirring speed on the rate of dissolution of polypropylene in *p*-xylene over a range of temperatures. Average specimen density 904.7 kg/m³. ●, 50 mm, 1000 rev/min; ○, 50 mm, 500 rev/min; ■, 25 mm, 1000 rev/min; □, 25 mm, 500 rev/min

Table 1 The effect of temperature on the dissolution rates of polypropylene discs, 25 and 50 mm diameter, rotated in *p*-xylene at 500 rev/min

Temperature of dissolution, T_{diss} (K)	Dissolution rate, \dot{m} (g/min)		
	25 mm disc	50 mm disc	$\dot{m}_{50}/\dot{m}_{25}$
387.5	0.0317	0.154	4.85
392.7	0.0383	0.190	4.96
401.1	0.0458	0.223	4.87
408.4	0.0533	0.259	4.85

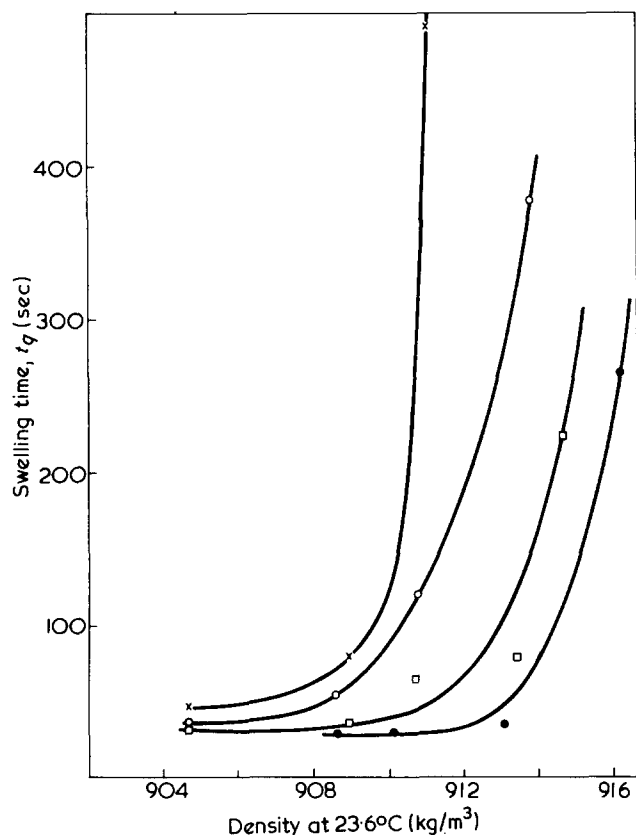


Figure 12 Swelling time for polypropylene in *p*-xylene at various temperatures as a function of density; stirring speed 1000 rev/min, disc diameter 50 mm. ●, 125°C; □, 120°C; ○, 115°C; X, 110°C

Effect of temperature and density on the swelling time

Figure 12 shows the swelling time, t_q , plotted against the density. (t_q was obtained by extrapolating the linear portion of the plot of m against t to make an intercept at zero m .) Decreasing the temperature and increasing the density both lengthen the swelling time. At low densities t_q is clearly very small (30–50 sec) even with an error of ± 15 sec. At sufficiently high temperatures the induction period for dissolution of poly(vinyl chloride) was virtually non-existent, an important clue to the behaviour of polypropylene. The relative flatness of the curves on Figure 12 at low densities may be associated with the fact that disentanglement controls the ensuing steady state just as for amorphous polymers. On the other hand, as the density increases so does t_q , crystallite destruction being dominant in the resulting steady state. If the crystallites are more resistant to solvent attack when the density is higher, then more swelling is required to bring about their destruction. In its general shape Figure 12 is seen to be an inverted mirror image of Figure 3, thus illustrating a connection between an induction period and the steady state to which it leads.

There are at least two effects which indicate caution in the interpretation of absolute values of t_q . First it might be thought that there are structural differences between the surface of a disc and its interior, but thin sections cut from these places showed that density, at least, was independent of position. Secondly, since discs were not pre-heated before plunging them into hot solvent at the start of a run it might be that swelling time and heating up time are connected. The surface of the disc will heat up almost instantaneously, but there will certainly be a small drop in the liquid temperature due to the thermal capacity of the poly-

mer disc and its holder. In practice it was convenient to set the solvent temperature about 2°C above that actually required for a run, since this offset the fall in temperature. The desired temperature was maintained by adjusting the bath heater. At worst the thermal capacity effect could introduce an uncertainty into t_q of less than 30 sec, and the trend of increasing t_q with increasing density and decreasing temperature is too marked to be obscured by these experimental shortcomings.

CONCLUSIONS

(1) Like amorphous polymers, polypropylene dissolves according to a two-part rate curve. There is first an induction period during which the rate of dissolution gradually increases, and this is followed by a period in which the rate is essentially constant. The length of the induction period increases with increasing density and decreasing temperature.

(2) The rate of wholesale dissolution at a given temperature is constant only over a limited range of lower densities, the breadth of this range being greater at higher temperatures. For any fixed temperature the rate eventually falls for specimens of sufficiently high density, and the rate curve extrapolates to zero at a density value which increases with temperature. This behaviour can be best explained in terms of an increase in the fold length of the chains which accompanies an increase in density. Specimens whose densities exceed the 'zero-rate intersection density' for a given temperature dissolve to some extent, though the process is quite different being a matter of fractionation or selective leaching rather than wholesale dissolution. The rate of a fractional dissolution process inevitably falls off with time since the soluble material (atactic and low molecular weight isotactic) must be leached out from ever deeper levels of the specimen.

(3) For polypropylene discs dissolving in *p*-xylene at 120°C there is a linear relationship between dissolution rate and stirring speed for a specimen density of 909 kg/m³. In these circumstances the rate controlling step appears to be molecular disentanglement in a gel-like surface layer of swollen polymer. At higher densities the linear relationship is visible only at low stirring speeds. When the rate becomes independent of stirring speed it appears that the rate of destruction of crystallites controls the overall rate of the dissolution.

(4) The temperature dependence of the dissolution rate of polypropylene is such that it resembles amorphous polymers only at the highest temperatures and for specimens of lowest density. Otherwise the activation energy for dissolution varies a good deal, and curvature of the Arrhenius plots is attributed to the controlling influence of crystallite destruction.

(5) T_s and T_{diss} are important for dissolution in just the way that T_m and T_c are important for crystallization.

ACKNOWLEDGEMENT

One of the authors (G. J. Le P.) is indebted to the Science Research Council for a studentship.

REFERENCES

- 1 Ueberreiter, K. and Kirchner, P. *Makromol. Chem.* 1965, 87, 32

Dissolution of propylene in organic solvents (2): D. A. Blackadder and G. J. Le Poidevin

- 2 Ueberreiter, K. in 'Diffusion in Polymers', (Eds J. Crank and G. S. Park), Academic Press, London, 1968
- 3 Ueberreiter, K. and Asmussen, F. *J. Polym. Sci.* 1957, **23**, 75
- 4 Ueberreiter, K. and Asmussen, F. *Makromol. Chem.* 1961, **43**, 324
- 5 Ueberreiter, K. and Asmussen, F. *J. Polym. Sci.* 1962, **57**, 187
- 6 Asmussen, F. and Ueberreiter, K. *J. Polym. Sci.* 1962, **57**, 199
- 7 Asmussen, F. and Ueberreiter, K. *Makromol. Chem.* 1962, **52**, 164
- 8 Asmussen, F. and Ueberreiter, K. *Kolloid-Z* 1962, **185**, 1
- 9 Asmussen, F. and Ueberreiter, K. *Kolloid-Z* 1968, **223**, 6
- 10 Lapčik, L. and Valko, L. *J. Polym. Sci. (A-2)* 1971, **9**, 633
- 11 Steiner, K., Engelbart, W., Asmussen, F., and Ueberreiter, K. *Kolloid-Z* 1969, **233**, 849
- 12 Blackadder, D. A. and Keniry, J. S. *J. Appl. Polym. Sci.* 1972, **16**, 1261
- 13 Machin, D. A. and Rogers, C. E. *Polym. Eng. Sci.* 1970, **10**, 300
- 14 Tamman, G. 'Kristallisieren und Schmelzen', Verlag Barth, Leipzig, 1903
- 15 Holland, V. F. *J. Appl. Phys.* 1964, **35**, 59
- 16 Blackadder, D. A. and Schleinitz, H. M. *Polymer* 1966, **7**, 603
- 17 Ueberreiter, K., Kanig, G. and Brenner, A. S. *J. Polym. Sci.* 1955, **16**, 53
- 18 Leugering, H. J. *Makromol. Chem.* 1967, **109**, 204
- 19 Blackadder, D. A. and Le Poidevin, G. J. *Polymer* 1976, **17**, 387
- 20 Spalding, D. B. 'Convective Mass Transfer', Arnold, London, 1963
- 21 Magill, J. H. *Polymer* 1962, **3**, 35
- 22 Flory, P. J. *J. Chem. Phys.* 1949, **17**, 223
- 23 Farrow, G. *Polymer* 1963, **4**, 191
- 24 King, C. V. and Bravermann, M. M. *J. Am. Chem. Soc.* 1932, **54**, 1744
- 25 Wunderlich, B. 'Macromolecular Physics', Academic Press, London, 1973, Vol 1, p196

Relative rate constants during the hydrolysis of syndiotactic poly(methyl methacrylate) with base*

Volker Barth and Ernst Klesper

*Institut für Makromolekulare Chemie, Universität Freiburg, D-78 Freiburg, W. Germany
(Received 8 January 1976; revised 5 March 1976)*

The relative rates of appearance and disappearance of triads of monomer units during the hydrolysis of syndiotactic methyl methacrylate/methacrylic acid copolymers in aqueous solution with excess base are studied by proton n.m.r. The relative rate constants are determined from these data using a graphical method. The measured relative rates and rate constants are consistent with a mechanism wherein COO^- retards the attack of OH^- . There is, however, a mechanism change indicated on consumption of OH^- during hydrolysis. The COOH which are then formed apparently participate in an intramolecular mechanism. The change of mechanism is accompanied by a change in copolymer statistics, i.e. from alternation tendency to block character. The lack of temperature dependence of the relative rate constants during the hydrolysis with OH^- as the active species leads to the conclusion that enthalpies of activation are equal for the three reacting triads. Thus the differences found between the relative rate constants are entropic in origin.

INTRODUCTION

Diesters and monoesters of dicarboxylic acids may serve as model substances for the hydrolysis of polymeric esters. Particularly during the hydrolysis of monoesters large cooperative effects influence the kinetics in many instances. These cooperative effects may also be present during the hydrolysis of polymeric esters since with progressive hydrolysis an increasing number of carboxyl or carboxylate groups is introduced. The hydrolysis of the esters of dicarboxylic acids has been frequently studied¹⁻³ and it was found that alkyl esters have widely differing rates for the hydrolysis of the first and the second ester group⁴⁻⁶. This was explained by the electrostatic repulsion between COO^- and the OH^- reacting with the second ester group^{3,7-10}. General base catalysis and nucleophilic attack by neighbouring COO^- appears not to have been found in the alkaline range with alkyl esters of saturated aliphatic dicarboxylic acid. This is in keeping with the known ineffectiveness of COO^- as a general base or nucleophile for the hydrolysis of alkyl esters of saturated monocarboxylic acids¹¹.

For the hydrolysis of atactic methyl methacrylate/methacrylic acid copolymers in aqueous solution with excess base, it has been postulated that the slowing down of the rate and limiting conversion is due to the electrostatic repulsion between the negatively charged carboxylate on the chain and the OH^- attacking the ester groups¹². Copolymers were used as starting materials because poly(methyl methacrylate) is insoluble in aqueous base. For the hydrolysis of syndiotactic methyl methacrylate/methacrylic acid copolymers it was shown by n.m.r. determination of the triads of monomer units that the hydrolysis leads to a statistics of monomer units with a pronounced tendency of alternation^{13,14}. This was attributed also to electrostatic repulsion between the carboxylate and the OH^- attacking the next neighbouring ester group. With

some exceptions^{13,14} most studies of reactions on vinyl polymers relied on measurements of the gross composition of the polymer during the reaction. The probabilities of triads for tactic methyl methacrylate/methacrylic acid copolymers can be evaluated by ^1H n.m.r. and ^{13}C n.m.r.¹³⁻¹⁶. The probabilities of the sequences during hydrolysis gives information on the distribution of hydrolysed and unhydrolysed monomer units along the chain and this is intimately linked with the basic features of the mechanism of hydrolysis. Also, more reliable determinations of the rate constants for the individual sequences might be possible than with measurements of the change of gross composition alone. In this communication the conversion dependent rates of the hydrolysis of triads are studied in detail, (a short account has been previously published¹⁷) and the conversion dependent (relative) rates are evaluated to yield the relative rate constants.

RESULTS

The kinetic runs were carried out with a syndiotactic methyl-methacrylate/methacrylic acid (MMA/MAA) copolymer, possessing Bernoullian (random) compositional statistics. The use of 'prehydrolysed' syndiotactic PMMA, instead of PMMA itself, is necessary to obtain a homogeneous solution of the polymer in the aqueous base. Having Bernoullian compositional statistics is an advantage since it is uniquely defined, easily calculated, and because any cooperative character of the kinetics will be revealed immediately during the kinetic runs by a deviation of the measured sequence probabilities from calculated Bernoullian sequence probabilities. The starting copolymers are characterized by the probability of A-monomer units, $P(\text{A})$, ($\text{A} = \text{MMA}$) the probabilities of configurational triads, $P(\text{ss}) = 0.92$ and $P(\text{is}^+) = 0.08$, and the weight-average molecular weight \bar{M}_w ($s = \text{syndiotactic placement}$, $i = \text{isotactic placement}$; the $^+$ sign indicates inclusion of both forms of the sequence, in this case is and si). The copolymers are then dissolved in aqueous KOH and the kinetic

* Dedicated to Professor H. Kämmerer on the occasion of his 65th birthday.

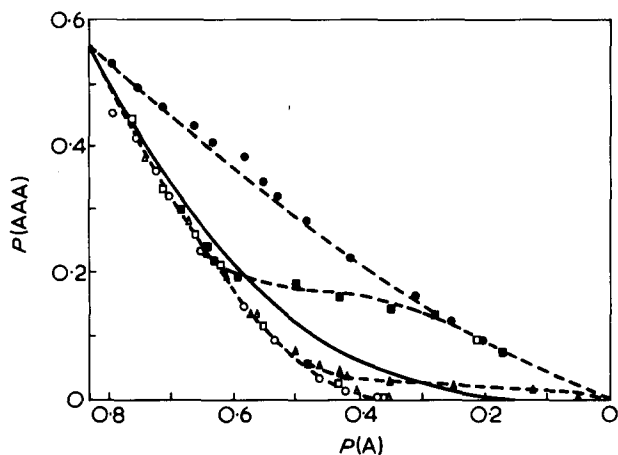


Figure 1 Probabilities of triad AAA, $P(AAA)$, versus conversion parameter, $P(A)$. Initial Bernoullian copolymer $P(A) = 0.83$. \bullet , 0.5; \blacksquare , 1; \blacktriangle , 1.5; \circ , 3; \square , 5; \triangle , 7 mmol KOH. —, Calculated for Bernoullian statistic from experimental $P(A)$

runs carried out by heating a number of ampoules to 145°C for specified periods. The products were characterized by determining $P(A)$ and the probabilities of the compositional triads [$P(X_sX_sX)$ ($X = A, B$; $B = \text{MAA monomer units}$)] from the α -methyl resonance of the ^1H n.m.r. spectra^{13,14}. In the following, the $P(X_sX_sX)$ are simply written as $P(XXX)$ since only syndiotactic triads are considered. The small amount of $X_iX_sX^+$ is assumed to possess only a small kinetic effect. Plots of $P(XXX)$ versus $P(A)$, the latter being chosen as a convenient conversion parameter, results in graphs which are dependent on relative rates and relative rate constants, but not on absolute rates and absolute rate constants¹⁸.

Starting with a Bernoullian copolymer of $P(A) = 0.83$ with $\bar{M}_w = 100\,000$ (copolymer No. 6 of Table 4) the kinetic runs resulted in $P(XAX)$ vs. $P(A)$ data which are shown as points in Figures 1 to 3. The total amount of KOH (mmol) indicated, is present at the start of the hydrolysis run and includes the amount of KOH necessary for the neutralization of the $-\text{COOH}$ groups of the MAA-units. The broken curves were drawn to give the best fit through the experimental points and, at the same time, to obey the statistically necessary relations¹⁹:

$$P(A) = P(AAA) + P(AAB^+) + P(BAB) \quad (1a)$$

$$P(B) = 1 - P(A) = P(BBB) + P(ABB^+) + P(ABA) \quad (1b)$$

$$P(ABB^+) + 2P(ABA) = 2P(BAB) + P(AAB^+) \quad (2)$$

Equations (1) and (2) are independent of the mode of formation of a copolymer, and are therefore suitable for correcting the experimental triad probabilities for errors which stem from the n.m.r. measurements, particularly the errors caused by incorrect separation of areas of overlapping triad peaks. The full curves in Figures 1 to 3 represent Bernoullian $P(XAX)$ calculated from the measured $P(A)$.

The conversion dependent kinetic behaviour does not depend on the initial amount of KOH, if the amount of KOH is 3, 5 and 7 mmol. Some data collected with 10 and 20 mmol KOH indicated that this appears to hold also for these much higher KOH concentrations. The kinetic behaviour does, however, depend on the amount of KOH when only 0.5, 1.0 and 1.5 mmol KOH are initially present. This dependence of the relative rates on the initial amount of

KOH, at low KOH concentrations, is due to a change in relative rate constants which in turn is due to a change in the cooperative mechanism. The dependence is clearly connected with the consumption of OH^- during the kinetic runs. With 1.0 and 1.5 mmol KOH the excess of OH^- initially present at $P(A) = 0.83$ ($t = 0$) can be calculated to be consumed at $P(A) = 0.61$ and $P(A) = 0.41$. Inspecting Figures 1 to 3 shows that up to these conversions the experimental points for 1.0 and 1.5 mmol KOH follow the main curve, i.e. the common curve for 3, 5, and 7 mmol KOH, and then form separate branches. With 0.5 mmol KOH at $P(A) = 0.83$, there is no excess OH^- present from the start, since all KOH is needed for the neutralization of $-\text{COOH}$. Thus the experimental points immediately form a branch. In summary, it may be concluded that the relative rates are independent of $[\text{OH}^-]$, as long as OH^- is present in excess.

The branches of the main curve, occurring with 0.5, 1.0, and 1.5 mmol KOH, are connected with the fact that not all carboxyl groups of the MAA-units are present as $-\text{COO}^-$ but some are present as $-\text{COOH}$. The proportion of $-\text{COOH}$ increases with increasing hydrolysis, that of $-\text{COO}^-$ remaining constant. The unneutralized MAA-units can partake in the reaction leading to a change in reaction mechanism and relative rates. Comparison with the Bernoullian curves shows that the main curves for excess of OH^- indicate a tendency towards alternation of the A- and B- units, while the branches indicate block character. More AAA and less BAB than corresponds to the Bernoullian curves may be taken as indicating block character and less AAA and more BAB as indicating a tendency towards alternation (Figures 1 and 3). However, no such simple connection apparently exists for AAB^+ (Figure 2). It is worth noting, that a unique relation between

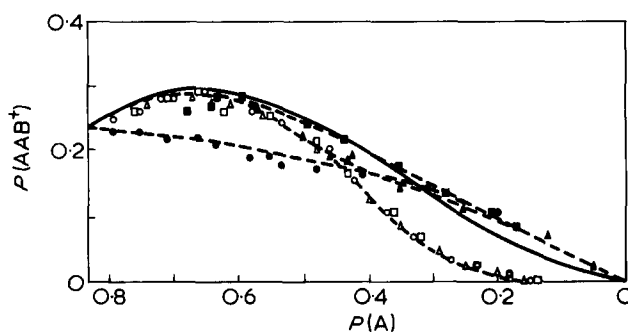


Figure 2 Probabilities of triad AAB^+ , $P(\text{AAB}^+)$, versus conversion parameter, $P(A)$. Initial Bernoullian copolymer $P(A) = 0.83$. Symbols as for Figure 1

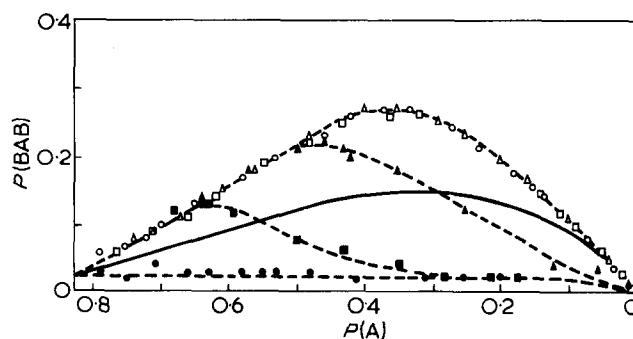


Figure 3 Probabilities of triad BAB, $P(\text{BAB})$, versus conversion parameter, $P(A)$. Initial Bernoullian copolymer $P(A) = 0.83$. Symbols as for Figure 1

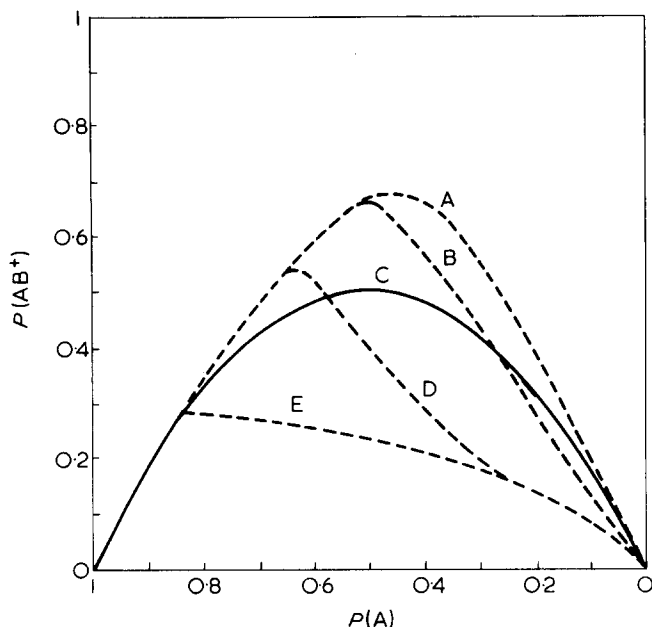


Figure 4 Probabilities of dyad AB^+ , $P(AB^+)$, versus $P(A)$. Initial Bernoullian copolymer $P(A) = 0.83$. A, 3–7 mmol KOH; B, 1.5 mmol KOH; C, calculated from Bernoullian statistics from experimental $P(A)$; D, 1 mmol KOH; E, 0.5 mmol KOH

$P(\text{sequence})$ and a tendency towards alternation or block character may only be assumed for the behaviour of dyads. This may be seen as follows:

$$P(A) = P(AA) + P(AB) \quad (3)$$

$$P(A) = P(AA)_r + P(AB)_r \quad (4)$$

Where the $P(XX)_r$ are the Bernoullian probabilities. On subtraction:

$$0 = \Delta P(AA) + \Delta P(AB) \quad (5)$$

The $\Delta P(XX) = P(XX) - P(XX)_r$ are the deviations from Bernoullian probabilities at a given $P(A)$. Similarly one obtains:

$$0 = \Delta P(BB) + \Delta P(BA) \quad (6)$$

It follows with $\Delta P(AB) = \Delta P(BA)$ and $\Delta P(AB) + \Delta P(BA) = \Delta P(AB^+)$:

$$\Delta P(AA) = \Delta P(BB) = -0.5\Delta P(AB^+) \quad (7)$$

The deviation of each $P(XX)$ from the corresponding $P(XX)_r$ determines the deviations of the probabilities of the other two dyads at a given $P(A)$. Thus there is a unique relation between the experimentally found deviations from Bernoullian curves and the terms 'tendency toward alternation' and 'block character'. An equation similar to equation (7) does not exist for $P(XXX)$ for the most general case since at a given $P(A)$ the probabilities of three of the triads are independent while only the probability of one dyad is independent.

In Figure 4 the dyad probability $P(AB^+)$ is plotted versus $P(A)$. The $P(XX)$ have been obtained from the $P(XXX)$ by the usual relations based on the principle of stationarity^{20,21}. For $P(AB^+)$ there are two possibilities of reducing the triads to dyads:

$$P(AB^+) = 2P(ABA) + P(ABB^+) = 2P(BAB) + P(AAB^+) \quad (8)$$

for average values equation (9) was employed:

$$P(AB^+) = P(ABA) + 0.5P(ABB^+) + P(BAB) + 0.5P(AAB^+) \quad (9)$$

Inspection of the $P(XX)$ versus $P(A)$ data reveals that the necessary relation equation (7) is reasonably well obeyed. The $P(XX)$ vs. $P(A)$ plots are, together with the $P(XXX)$ data, necessary for the evaluation of relative rate constants.

A second set of kinetic runs was carried out with a Bernoullian copolymer of $P(A) = 0.60$ (copolymer No. 9 of Table 4), in order to show that the relative rate constants do not change when another starting copolymer is used.

In Figure 5 data are plotted for runs with 3, 5 and 7 mmol initial KOH in a similar way as for Figures 1 to 3. The scatter of the points in Figure 5 is reasonable and they are well fitted by the broken curves which have been drawn according to equations (1) and (2). As with Figures 1 to 3, there is no dependence of the data on the amount of excess OH^- .

The conversion dependent kinetics of the triads with excess OH^- , as shown in Figures 1–3, 5, could in principle be dependent on the molecular weight of the copolymers, the ionic strength of the solution, the concentration of the copolymer and the temperature. The molecular weight was varied from $\bar{M}_w = 100\,000$ to 650 000 and the ionic strength changed by the addition of 2 mmol KCl. Moreover, the concentration of copolymer was reduced to 1/2 or 1/4 and the temperature varied from 115° to 175°C. Within the investigated range, none of these variables appears, however, to influence the kinetics to any extent, which is outside the error of measurement.

Assuming that the A-centred triads are the kinetic units for the cooperative hydrolysis, then, if for a given A-centred triad the conformation and/or the solvation state changes with conversion, the rate constants might also change with conversion. A change in conformation and solvation should, however, make itself felt through the ^1H n.m.r. chemical shifts of the copolymers, if the spectra are recorded under conditions similar to hydrolysis. Figure 6 shows the ^1H n.m.r. spectra from $\text{D}_2\text{O}/\text{KOD}$ solutions of syndiotactic copolymers with Bernoullian compositional statistics. The copolymers cover the range of conversion with $P(A) = 0.83; 0.60; 0.37; 0.16; 0.00$. The spectra are recorded from solutions of 100 mg copolymer ($P(A) = 0.83; 0.60; 0.37$) or 50 mg polymer ($P(A) = 0.16; 0.00$) in 1 ml 0.8 N KOD. This is sufficient KOD for an excess of OH^- to prevail after neutralization of all MAA-units. The copolymer concentration is about 5 or 2.5 times the concentration used for hydrolysis, and, the temperature 80°C instead of 145°C. It is unlikely, however, that a change in conformation and solvation with conversion, if present, will appear less strongly at the higher concentration and the lower temperature used for the n.m.r. spectra.

Spectral trace A of Figure 6 shows that at $P(A) = 0.83$ the $-\text{OCH}_3$, $\beta\text{-CH}_2-$ and $\alpha\text{-CH}_3$ resonances are very broad. Decreasing the $P(A)$, however, shows that an acceptable resolution of sequences is possible. A maximum of three peaks appears in the $\beta\text{-CH}_2-$ and a maximum of four peaks in the $\alpha\text{-CH}_3$ resonance. The assignment of the $\beta\text{-CH}_2-$ peaks to dyads is straightforward by observing the change in intensity with changing $P(A)$. On the other hand, the assignment of the $\alpha\text{-CH}_3$ peaks is complicated by coin-

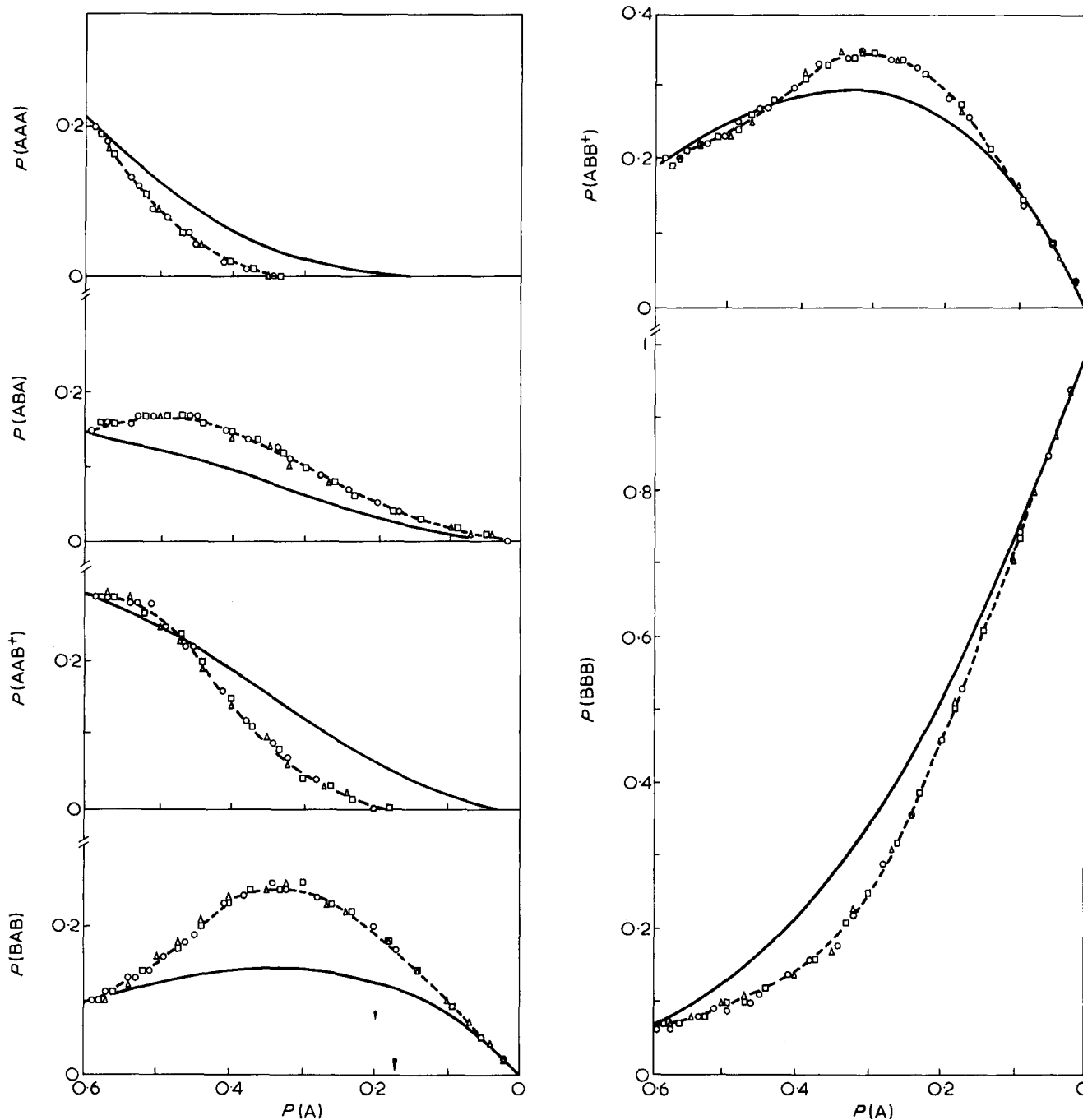


Figure 5 Probabilities of triads versus $P(A)$. Symbols as for Figure 1

cidence of triad resonances. In Table 1 the chemical shifts and relative peak intensities are shown for the peaks in the α -CH₃ resonance of the Bernoullian copolymers and a number of copolymers with alternation character which have been obtained from the kinetic runs. The agreement between the observed relative peak intensities and the expected peak intensities for the proposed assignment leaves little doubt that the assignment of the triads is correct as in Table 1 and trace B of Figure 6. The only strong deviation is seen for the Bernoullian copolymer of $P(A) = 0.60$. This may be connected with the inferior resolution of trace B but also with the possibility that the assignment changes at $P(A) = 0.60$. There exists a self-consistent set of shift differences governing the assignment. Both the replacements $XAX \rightarrow XB X$ (Table 1) ($X = A, B$) and replacements

$BXX \rightarrow AXX$ (Table 1) produce an upfield shift of 0.10 ppm. Having ascertained that the chemical shifts of the triads do not change with the $P(A)$ of the copolymers in the range $0.6 > P(A) > 0$, it is reasonable to assume an absence of change in conformation and solvation of triads in that range. Therefore, an invariance of rate constants with conversion may also be assumed. However, the broadening of the resonances at $P(A) = 0.83$ points to a collapse of the coiled chains with a concomitant reduction in conformational mobility. This collapse is apparently caused by poor solvation of longer blocks of A-units and raises the question of the accessibility of these A-units by the attacking OH^- . Consequently, the reaction rate constants may possibly be variable in the conversion range of $P(A) > 0.60$.

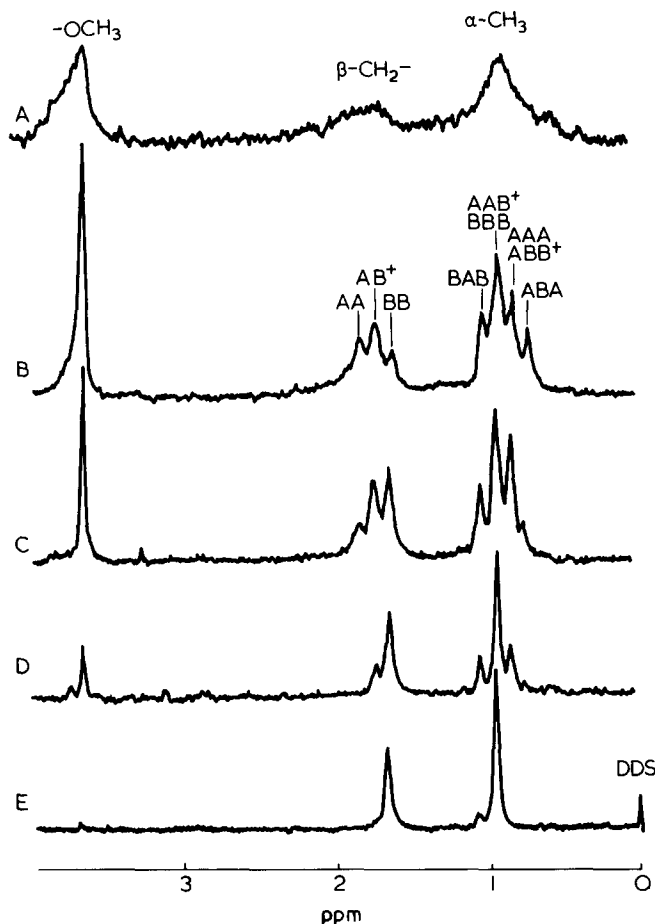
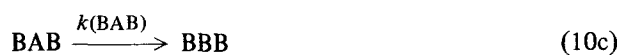


Figure 6 ^1H n.m.r. spectra of syndiotactic MMA/MAA copolymers of Bernoullian compositional statistics and different $P(\text{A})$. A, $P(\text{A}) = 0.83$; B, $P(\text{A}) = 0.60$; C, $P(\text{A}) = 0.37$; D, $P(\text{A}) = 0.16$; E, syndiotactic PMAA, $P(\text{A}) = 0$

DISCUSSION

The treatment of data is limited to that obtained with excess OH^- . The data obtained with less KOH than necessary to neutralize the MMA/MAA copolymers will be the subject of a future communication. With an OH^- excess statistics are obtained which deviate from Bernoullian pointing to cooperative kinetics, i.e. to a kinetic influence of neighbouring monomer units on the hydrolysis of central A-monomer units. Considering only the next nearest monomer units to have kinetic influence and in view of the fact that ester hydrolysis with base is irreversible, the polymer analogous hydrolysis reaction may be reduced to three individual reactions involving the three A-centred triads and their rate constants k , i.e.



From the kinetics of the saponification of low molecular weight alkyl esters it is well known^{2,11} that the rate is first order both in ester and in OH^- . The rate laws in terms of probabilities for overall second order reactions of triads have been established previously^{17,18,22}:

$$\frac{dP(\text{AA})}{dt} = -2k(\text{AAA})[\text{R}]P(\text{AAA}) - k(\text{AAB}^+)[\text{R}] \times P(\text{AAB}^+) \quad (11)$$

$$\frac{dP(\text{AB}^+)}{dt} = 2k(\text{AAA})[\text{R}]P(\text{AAA}) - 2k(\text{BAB})[\text{R}] \times P(\text{BAB}) \quad (12)$$

$$\frac{dP(\text{BB})}{dt} = k(\text{AAB}^+)[\text{R}]P(\text{AAB}^+) + 2k(\text{BAB})[\text{R}] \times P(\text{BAB}) \quad (13)$$

where $[\text{R}]$ is the concentration of reactant, in this case $[\text{OH}^-]$.

There are two more rate laws for the reactions of triads but unfortunately their differential coefficients are written in terms of two triads and may not be simply reduced to

Table 1 Chemical shifts assignment and relative peak intensities (normalized)^d in the $\alpha\text{-CH}_3$ resonance of nearly Bernoullian^a and 'alternating'^b copolymers from 10% solutions in D_2O with an excess of OD^-

	$P(\text{A})$	Chemical shifts (ppm) ^c			
		1.05	0.95	0.85	0.75
		BAB	BBB	ABB ⁺	ABA
			AAB ⁺	AAA	
Bernoullian copolymers	0.83 ^e	—	—	—	—
	0.60 ^f	0.14 (0.096)	0.46 (0.352)	0.26 (0.408)	0.14 (0.144)
	0.52	0.12 (0.120)	0.41 (0.370)	0.34 (0.380)	0.13 (0.130)
	0.37	0.15 (0.147)	0.45 (0.422)	0.32 (0.345)	0.08 (0.086)
	0.28	0.18 (0.145)	0.48 (0.487)	0.29 (0.312)	0.05 (0.056)
	0.16	0.14 (0.113)	0.63 (0.636)	0.20 (0.230)	0.03 (0.021)
	0.009	0.08	0.92	—	—
Copolymers with tendency toward alternation	0.72 ^e	—	—	—	—
	0.50	0.17 (0.22)	0.33 (0.28)	0.25 (0.28 ₅)	0.25 (0.21 ₅)
	0.42	0.23 (0.25 ₅)	0.27 (0.26)	0.32 (0.29 ₅)	0.18 (0.19)
	0.36	0.29 (0.27)	0.22 (0.26 ₅)	0.34 (0.30 ₅)	0.15 (0.16)
	0.32	0.28 (0.26 ₅)	0.24 (0.28 ₅)	0.34 (0.31 ₅)	0.14 (0.13 ₅)
	0.24	0.26 (0.22 ₅)	0.31 (0.39 ₅)	0.36 (0.30)	0.07 (0.08)
	0.14	0.18 (0.14)	0.52 (0.60)	0.26 (0.23 ₅)	0.04 (0.02)

^aBernoullian copolymers of $P(\text{A}) \geq 0.60$ prepared by hydrolysis of syndiotactic PMMA [$P(\text{ss}) = 0.92$; $P(\text{is}^+) = 0.08$] in dioxane/methanol/ KOH . Bernoullian copolymers of $P(\text{A}) < 0.60$ prepared by hydrolysis in concentrated H_2SO_4 ¹⁹. ^bCopolymers with a tendency toward alternation prepared under conditions of a kinetic run by hydrolysis of a Bernoullian copolymer with $P(\text{A}) = 0.83$ with an excess of OH^- at 145°C . ^cMeasured at 80°C relative to $(\text{CH}_3)_3\text{Si}(\text{CH}_2)_3\text{SO}_3\text{Na}$ (DDS) as internal standard. ^dValues in parentheses are expected probabilities for Bernoullian copolymers calculated from $P(\text{A})$, for alternating copolymers obtained from spectra in pyridine of the same copolymer¹³. ^ePeaks not resolved. ^fPeaks not well resolved. ^gSyndiotactic PMMA of $P(\text{ss}) = 0.92$, $P(\text{is}^+) = 0.08$.

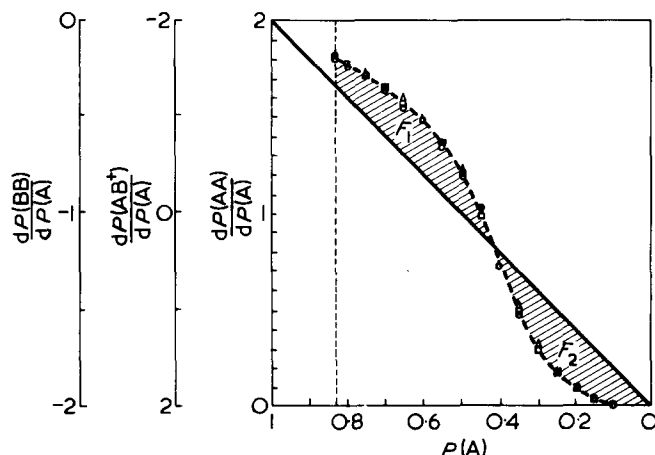


Figure 7 Slopes of the $P(XX)$ vs. $P(A)$ curves as obtained from tangents (points). Composition $P(A) = 0.83$ of Bernoullian starting copolymer indicated by broken vertical line. —, Valid for a non-cooperative reaction starting from a homopolymer or Bernoullian copolymer. \circ , $dP(AA)/dP(A)$ vs. $P(A)$; \square , $dP(AB^+)/dP(A)$ vs. $P(A)$; \triangle , $dP(BB)/dP(A)$ vs. $P(A)$

differential quotients of dyads. The differential quotient of the monad A

$$\frac{dP(A)}{dt} = -k(AAA)[R]P(AAA) - k(AAB^+)[R]P(AAB^+) - k(BAB)[R]P(BAB) \quad (14)$$

In order to obtain rate laws which are compatible with the conversion plots, equations (11) to (13) should be divided by equation (14).

$$\frac{dP(AA)}{dP(A)} = \frac{-2k'(AAA)P(AAA) - k'(AAB^+)P(AAB^+)}{N} \quad (15)$$

$$\frac{dP(AB^+)}{dP(A)} = \frac{2k'(AAA)P(AAA) - 2k'(BAB)P(BAB)}{N} \quad (16)$$

$$\frac{dP(BB)}{dP(A)} = \frac{k'(AAB^+)P(AAB^+) + 2k'(BAB)P(BAB)}{N} \quad (17)$$

with

$$N = -k'(AAA)P(AAA) - k'(AAB^+)P(AAB^+) - k'(BAB)P(BAB)$$

The kinetic behaviour shown in Figures 1, 2, 3 and 5 demonstrates that there exists no dependence on $[OH^-]$, as long as an excess of OH^- is available. This lends support to the reaction model embodied in equations (11) to (17). The differential quotients in equations (15) to (17) are affected only by relative rate constants and not the rate constants themselves. For the relative rate constants we choose arbitrarily the definition:

$$k'(AAA) + k'(AAB^+) + k'(BAB) = 1 \quad (18)$$

with, for instance:

$$k'(AAA) = \frac{k(AAA)}{k(AAA) + k(AAB^+) + k(BAB)} \quad (19)$$

The sequence probabilities of a copolymer prepared by a polymer analogous reaction depend only on the relative rate constants and a specified $P(A)$ (and on the sequence probabilities of the starting polymer), but not on the reaction time needed to reach that $P(A)$. Furthermore, only one of equations (15) to (17) is independent since at a given $P(A)$ only one $P(XX)$ is independent. Thus at least two copolymers of differing $P(A)$, prepared under analogous conditions, are needed to determine the two independent relative rate constants. The rate equations (15) to (17), could either be used as such or in their integrated form. We choose to use the former, since it is not simple to establish even the differential equation for a given model of polymer analogous reactions^{22,23}, while it is a formidable task to obtain an integration in closed form without approximations²⁴. Also, an available solution for the irreversible case is difficult to handle²⁵. Thus the differential equations for polymer analogous reactions are important in evaluating kinetic data, particularly with new models. The situation is similar to that for enzyme kinetics where the differential equations are often employed²⁶. The inaccuracy in the determination of the differential quotients by constructing tangents can be kept to levels comparable to or below the inaccuracies caused by the n.m.r. determination of the kinetic curves; both inaccuracies being compared in their effect on the determination of the relative rate constants.

As only one of the equations (15) to (17) is independent, equation (15) has been arbitrarily chosen for evaluating the relative rate constants. Setting $dP(AA)/dP(A) = S$ and substituting $k'(BAB)$ by $[1 - k'(AAA) - k'(AAB^+)]$ one obtains:

$$k'(AAA) = c_1 + c_2 k'(AAB^+) \quad (20)$$

with:

$$c_1 = -\frac{SP(BAB)}{SP(AAA) - SP(BAB) - 2P(AAA)} \quad (21)$$

$$c_2 = \frac{SP(BAB) - SP(AAB^+) + P(AAB^+)}{SP(AAA) - SP(BAB) - 2P(AAA)} \quad (22)$$

Although c_1 and c_2 are functions of $P(A)$, at a given $P(A)$ i.e. for a given copolymer equation (20) yields a linear plot of $k'(AAA)$ versus $k'(AAB^+)$. In order to determine S by the tangent method, not only $dP(AA)/dP(A)$ was determined but also $dP(AB^+)/dP(A)$ and $dP(BB)/dP(A)$, all of them over the available range of $P(A)$ at intervals of $\Delta P(A) = 0.05$. These values are plotted in Figure 7 for the starting copolymer of $P(A) = 0.83$. Differentiating the two generally valid equations $P(A) = P(AA) + 0.5P(AB^+)$ and $P(B) = P(BB) + 0.5P(AB^+)$ with respect to $P(A)$ and $P(B)$, respectively, and considering $dP(A) = -dP(B)$:

$$\frac{dP(AA)}{dP(A)} = 1 - 0.5 \frac{dP(AB^+)}{dP(A)} = 2 + \frac{dP(BB)}{dP(A)} \quad (23)$$

Equation (23) states that the values for the three differential quotients trace out a common curve (broken curve in Figure 7) if a corresponding triple ordinate is used. Any experimental scatter is then due only to errors in constructing the tangents on the $P(XX)$ vs. $P(A)$ curves and on deviations of the $P(XX)$ vs. $P(A)$ curves themselves from the principle of stationarity.

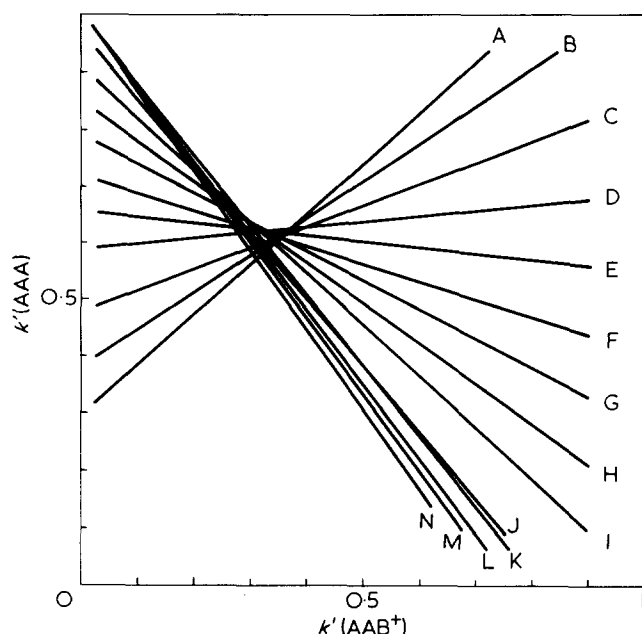


Figure 8 Relative rate constants $k'(AAA)$ and $k'(AAB^+)$ as intersections of straight lines plotted according to equation (20). Bernoullian starting copolymer of $P(A) = 0.83$. $P(A)$ values: A, 0.83; B, 0.80; C, 0.75; D, 0.70; E, 0.65; F, 0.60; G, 0.55; H, 0.50; I, 0.45; J, 0.40; K, 0.20; L, 0.35; M, 0.30; N, 0.25

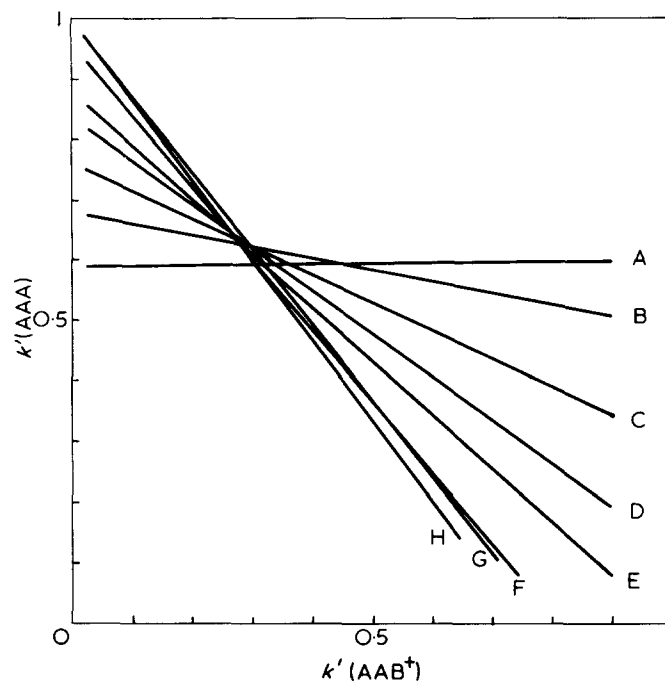


Figure 9 Relative rate constants $k'(AAA)$ and $k'(AAB^+)$ as intersections of straight lines plotted according to equation (20). Bernoullian starting copolymer of $P(A) = 0.60$. $P(A)$ values: A, 0.60; B, 0.55; C, 0.50; D, 0.45; E, 0.40; F, 0.35; G, 0.20; H, 0.25/0.35

For a random polymer analogous reaction, for which $k'(AAA) = k'(AAB^+) = k'(BAB)$, equation (15) becomes:

$$\frac{dP(AA)}{dP(A)} = \frac{2P(AA)}{P(A)} = 2P(A) \quad (24)$$

However, the second equality holds only if the copolymers formed are Bernoullian, which is always the case for $k'(AAA) = k'(AAB^+) = k'(BAB)$ when the starting polymer

is either a homopolymer or a Bernoullian copolymer. The straight line of equation (24) is seen as the diagonal in Figure 7. As a further test of the precision of the differential quotients the shaded areas F_1 and F_2 must be equal. Considering two polymer analogous reactions, 1 and 2, which differ in their sets of k' but start from the same $P(A)_{start}$ and $P(AA)_{start}$ and end at the same $P(A)_{end}$ and $P(AA)_{end}$, it holds with $P(AA)_{start} - P(AA)_{end} = \Delta P(AA)$:

$$\Delta P(AA)_1 = \Delta P(AA)_2 \quad (25)$$

and

$$\int_{P(A)_{start}}^{P(A)_{end}} dP(AA)_1 = \int_{P(A)_{start}}^{P(A)_{end}} dP(AA)_2 \quad (26)$$

whence:

$$\int_{P(A)_{start}}^{P(A)_{end}} \frac{dP(AA)_1}{dP(A)} dP(A) = \int_{P(A)_{start}}^{P(A)_{end}} \frac{dP(AA)_2}{dP(A)} dP(A) \quad (27)$$

According to equation (27) the areas under the curves traced out in a plot of $dP(AA)/dP(A)$ vs. $P(A)$ for reactions 1 and 2 must be equal. One may regard the hydrolysis with excess OH^- as reaction 1 and the hypothetical hydrolysis with $k'(AAA) = k'(AAB^+) = k'(BAB)$ as reaction 2, because they start from the same $P(A)$ and $P(AA)$ and both end at $P(AA) = P(A) = 0$. The equality holds for Figure 7 with $F_1/F_2 = 1.03$.

The averaged S of Figure 7 (broken curve) and the $P(XAX)$ of $P(XAX)$ versus $P(A)$ curves are taken at intervals of $\Delta P(A) = 0.05$ to plot $k'(AAA)$ vs. $k'(AAB^+)$ according to equation (20). In Figure 8 (starting copolymer of $P(A) = 0.83$) and in Figure 9 (starting copolymer of $P(A) = 0.60$) it becomes apparent that the intersections of the straight lines of differing $P(A)$ show only a reasonable amount of scatter or systematic change. Moreover, the areas in which the intersections occur are about the same for both starting copolymers. In order to evaluate the coordinates of the intersections more closely, the results of Figure 8 are summarized in Table 2; the $k'(AAA)$ values are in the upper right half and the $k'(AAB^+)$ values in the lower left half, the diagonal separating the areas. The intersections of the straight lines of different $P(A)$ in Figure 8 are seen in Table 2 as the intersections of columns and rows. The $k'(AAA)$ and $k'(AAB^+)$ values at the intersections of the columns and rows of $P(A) = 0.60$ to 0.40 can be considered as particularly characteristic for two reasons. First, they stem from a conversion range where Figure 6 shows well resolved spectra with constant chemical shifts of the triad peaks, and second, in this range the difference between different sets of relative rate constants is about the largest both with respect to $P(XXX)$ and $dP(XX)/dP(A)^{18}$. Comparing the fluctuation of the values $k'(AAA)$ and $k'(AAB^+)$ within the rectangle of Table 2 with that of the other values of the same Table, it is apparent that the fluctuation is about the same. The data may be inspected by comparing the $k'(AAA)$ or $k'(AAB^+)$ values running parallel to the diagonal. Immediately adjacent to the diagonal, the values are obtained by intersections of lines which are only $\Delta P(A) = 0.05$ apart. These values are not very reliable since the

Table 2 Values for $k'(AAA)$ and $k'(AAB^+)$ for the intersections of Figure 8, representing the data obtained from a starting copolymer of $P(A) = 0.83$. The intersections of two straight lines of different $P(A)$ in Figure 8 are represented in Table 2 by the intersections of columns and rows of the same $P(A)$.

$P(A)$	0.83	0.80	0.75	0.70	0.65	0.60	0.55	0.50	0.45	0.40	0.35	0.30	0.25	0.20
0.83		0.63	0.61	0.63	0.62	0.61	0.61	0.60	0.60	0.59	0.58	0.58	0.57	0.59
0.80	0.37		0.61	0.63	0.62	0.61	0.61	0.61	0.60	0.60	0.59	0.59	0.58	0.60
0.75	0.35	0.34		0.63	0.62	0.61	0.61	0.61	0.60	0.60	0.60	0.59	0.59	0.60
0.70	0.37	0.37	0.40		0.62	0.62	0.62	0.62	0.62	0.62	0.62	0.62	0.62	0.62
0.65	0.36	0.35	0.37	0.33		0.62	0.62	0.62	0.62	0.63	0.63	0.63	0.63	0.62
0.60	0.35	0.35	0.35	0.32	0.30		0.61	0.62	0.62	0.63	0.63	0.63	0.64	0.62
0.55	0.35	0.35	0.35	0.33	0.33	0.35		0.64	0.64	0.65	0.66	0.66	0.67	0.64
0.50	0.34	0.34	0.34	0.32	0.32	0.33	0.30		0.64	0.66	0.66	0.68	0.69	0.65
0.45	0.34	0.33	0.33	0.32	0.31	0.32	0.30	0.30		0.70	0.70	0.72	0.74	0.66
0.40	0.33	0.32	0.32	0.30	0.29	0.29	0.27	0.26	0.23		0.70	0.67	0.82	0.41
0.35	0.32	0.31	0.31	0.31	0.28	0.28	0.26	0.26	0.23	0.23				
0.30	0.31	0.31	0.30	0.29	0.28	0.27	0.25	0.24	0.21	0.17				
0.25	0.31	0.30	0.29	0.27	0.27	0.26	0.24	0.22	0.18	0.13				
0.20	0.33	0.32	0.32	0.31	0.30	0.30	0.29	0.28	0.27	0.48				

angles with which the lines intersect are very acute (Figure 8). Once or twice removed from the diagonal, the intersecting lines are $\Delta P(A) = 0.10$ and $\Delta P(A) = 0.15$ apart and the angles less acute, although still far from 90° . A systematic change of the k' values with conversion should appear along these lines parallel to the diagonal. There appears indeed a relatively small increase of $k'(AAA)$ and a corresponding decrease in $k'(AAB^+)$, but in view of the accuracy of the data it is not clear whether one should attach significance to this trend. It should finally be pointed out that intersections for which only lines of $P(A) = 0.35$ to 0.20 participate are those for which the hydrolysis has so far progressed that $P(AAA) = 0$. Then c_1 of equation (21) becomes 1 and the intersections of two such lines becomes meaningless (blank space, lower right corner of Table 2). If, however, only one of these lines participates in a given intersection the values are still useful, although possibly less reliable, since $P(AAB^+)$ has already become small at $P(A) \leq 0.35$ and can only be inaccurately measured (values in broken line rectangles).

In view of the foregoing it appears justified to simply take the median of the values for lines from $P(A) = 0.60$ to $P(A) = 0.40$ for both starting copolymers of $P(A) = 0.83$ and $P(A) = 0.60$ to result in $k'(AAA) = 0.62$ and $k'(AAB^+) = 0.33$. This in turn yields $k'(BAB) = 0.05$. Similar values are obtained when all intersections are evaluated. In view of the experimental error this result may be rounded to 0.6, 0.3, and 0.1, respectively. Apparently, next neighbouring $-\text{COO}^-$ retards the attack of OH^- by electrostatic repulsion. This retardation amounts to about 2 for $k(AAA)/k(AAB^+)$ and to at least 6 for $k(AAA)/k(BAB)$. In view of the relative constancy of the k' values with $P(A)$ it may also be concluded that repulsion by $-\text{COO}^-$ situated on monomer units further removed is not large. It is, of course, also possible to use, besides equation (15), equations (16) and (17) to plot $k'(AAA)$ vs. $k'(AAB^+)$ diagrams. However, the expressions for the intercept and the slopes of the corresponding straight lines are identical with those of equations (21) and (22), as shown for equations (16) and (17) and in accordance with equation (23).

The relative rate constants are not significantly changed in the temperature range 115°C (T_1) to 175°C (T_2). Using the Eyring equation one obtains for T_1 :

$$\left(\frac{k(AAA)}{k(AAB^+)}\right)_{T_1} = \left(\frac{k'(AAA)}{k'(AAB^+)}\right)_{T_1}$$

$$= \frac{(kT_1/h) \exp(\Delta S_1^\ddagger/R) \exp(-\Delta H_1^\ddagger/RT_1)}{(kT_1/h) \exp(\Delta S_2^\ddagger/R) \exp(-\Delta H_2^\ddagger/RT_1)} \quad (28)$$

where S_1^\ddagger and S_2^\ddagger are, for instance, the activation entropies valid for the reaction 1, ($AAA \rightarrow ABA$) and the reaction 2, ($AAB^+ \rightarrow ABB^+$), respectively. Similarly for temperature T_2 :

$$\left(\frac{k(AAA)}{k(AAB^+)}\right)_{T_2} = \left(\frac{k'(AAA)}{k'(AAB^+)}\right)_{T_2} = \frac{(kT_2/h) \exp(\Delta S_1^\ddagger/R) \exp(-\Delta H_1^\ddagger/RT_2)}{(kT_2/h) \exp(\Delta S_2^\ddagger/R) \exp(-\Delta H_2^\ddagger/RT_2)} \quad (29)$$

presupposing, as usual, that ΔS_1^\ddagger , ΔS_2^\ddagger , ΔH_1^\ddagger , and ΔH_2^\ddagger are invariant over a limited temperature range. Since it was found that the approximation:

$$\left(\frac{k'(AAA)}{k'(AAB^+)}\right)_{T_1} = \left(\frac{k'(AAA)}{k'(AAB^+)}\right)_{T_2} \quad (30)$$

holds, it follows from equations (28) and (29) that:

$$\Delta H_1^\ddagger = \Delta H_2^\ddagger \quad (31)$$

and analogously to equations (28) to (30) that:

$$\Delta H_1^\ddagger = \Delta H_3^\ddagger \quad (32)$$

where the subscript 3 is valid for reaction 3 ($BAB \rightarrow BBB$). Thus the activation enthalpies are all equal. From equation (28) it follows that:

$$\frac{k(AAA)}{k(AAB^+)} = \exp \frac{\Delta S_1^\ddagger - \Delta S_2^\ddagger}{R} \quad (33)$$

and similarly that:

$$\frac{k(AAA)}{k(BAB)} = \exp \frac{\Delta S_1 - \Delta S_3}{R} \quad (34)$$

Equations (33) and (34) state that the ratios of the rate constants are determined only by the differences of the activation entropies. From $k'(AAA)/k'(AAB^+) = 0.6/0.3 = 2$

Table 3 Preparation of syndiotactic poly(methyl methacrylate)

PMMA No.	AlEt ₃ (ml)	TiCl ₄ (ml)	Aging time (min)	MMA (ml)	Reaction time (h)	Polymer yield (%)	Tacticity <i>P</i> (ss) ^a	Molecular weight \bar{M}_w ^b
1	17.5	2.8	30	70	38	55	0.92	651 000
2	17.5	2.8	30	70	18	30	0.92	525 000
3	17.5	2.8	45	70	5	4	0.92	210 000
4	25	2.8	90	70	40	65	0.92	292 000
5	17.5	2.8	60	70	40	69	0.90	243 000
6	12.5	2.0	60	70	18	51	0.90	364 000
7	13	2.8	60	70	18	49	0.90	274 000
8	17.5	2.8	60	50	18	51	0.90	179 000
9	25	4	60	70	18	66	0.90	192 000
10	25	2.8	60	40	7	35	0.92	100 000

^aAs determined from the α -CH₃ resonance of the ¹H n.m.r. spectra recorded from pyridine solution (100°C) at 220 MHz. For all polymers $P(ii) = 0$ and $P(is^+) = 1 - P(ss)$. ^bAs determined from $[\eta] = 5.2 \cdot 10^{-5} \bar{M}_w^{0.76}$, a relation which has been established for radical initiated (predominantly syndiotactic) PMMA of $\bar{M}_w \geq 35\,000$ at 30°C in benzene²⁹

and $k'(AAA)/k'(BAB) = 0.6/0.1 = 6$ the differences of the activation entropies are found as $\Delta S_1^\ddagger - \Delta S_2^\ddagger = 1.4$ cal/mol K and $\Delta S_1^\ddagger - \Delta S_3^\ddagger = 3.6$ cal/mol K, respectively. The cooperativity of the kinetics is therefore entropic in origin.

EXPERIMENTAL

Syndiotactic poly(methyl methacrylate) (PMMA) was prepared using Ziegler-Natta initiator at -75° to -78°C in toluene, according to the method of Abe *et al.*²⁷ Table 3 lists experimental conditions for 10 preparative runs. The PMMA was prehydrolysed in dioxane/methanol/KOH mixture as described previously¹³. Table 4 lists the copolymers prepared. With one exception the hydrolysis solutions were homogeneous up to the end of reaction time, with the same extent of hydrolysis for all polymer chains. Comparison with Table 3 shows that the \bar{M}_w of the re-esterified copolymers in Table 4 (values without parentheses) are not greatly affected by the prehydrolysis. Moreover, the ¹H n.m.r. spectra of the re-esterified products were the same as those of the corresponding precursor PMMA.

For some copolymers obtained after prehydrolysis it was shown by fractionation, carried out by the incremental addition of HCl from aqueous solution²⁸, that within error of measurement, no heterogeneity with respect to $P(A)$ and $P(XXX)$ ($X = A, B$) existed (Table 5). Thus the copolymers are compositionally homogeneous starting materials for the kinetic runs. For the copolymers obtained after the kinetic runs with excess of OH⁻ it could likewise be shown (Table 5) that no heterogeneity exists with respect to $P(A)$ and $P(XXX)$. Therefore, the sequence data obtained during the kinetic runs with excess of OH⁻ are representative of the statistics of the individual chains¹³. Also, the \bar{M}_w after the kinetic runs are not very different from that of the precursor PMMA or precursor Bernoullian copolymers. The n.m.r. spectra of the PMMA obtained by esterification of the copolymers from kinetic runs are identical with those of the precursor PMMA, showing that side reactions are absent.

For the kinetic runs, 1N KOH was added to multiples of 250 mg prehydrolysed copolymer in an alkali resistant glass ampoule (the amount of KOH specified in this communication always applies to 250 mg of starting copolymer). Sufficient water was added to bring the volume of aqueous KOH to 12 ml for each 250 mg copolymer. As

noted, part of the water was substituted by aqueous KCl solution. The ampoule was flushed with N₂, sealed, and transferred to a circulating air oven at 115°C and after a maximum of 1 h, and shaking every ten minutes, the polymer had dissolved. The $P(A)$ had not changed measurably as determined by n.m.r. The content of the ampoule was then distributed into several smaller ampoules of Duran glass (12 ml solution into each) which contained Teflon thimbles to completely prevent contact of the alkaline solutions with the glass. For the kinetic runs, these ampoules were inserted into well fitting holes of an aluminium block and inserted in a thermostatically controlled oil bath. The time at this instance was taken as $t = 0$; the time needed for the ampoules to reach 145°C (115°C, 175°C) being assumed to be compensated to some extent by the time spent dissolving the copolymer in the dissolution step. The copolymers were isolated after the kinetic runs by diluting

Table 4 Prehydrolysis of syndiotactic poly(methyl methacrylate) to methyl methacrylate/methacrylic acid copolymers of Bernoullian statistics^a

Copolymer No.	Prehydrolysis time (h)	$P(A)$	Molecular weight ^b , \bar{M}_w	Derived from PMMA No.
1	15	0.85	(525 000) 437 000	2
2	18	0.83	(651 000) 630 000	1
3	18	0.83	(364 000)	6
4	18	0.83	(179 000)	8
5	18	0.83	(243 000) 241 000	5
6	18	0.83	(100 000) 100 000	10
7 ^c	40	0.62	(292 000)	4
8	40	0.60	(192 000) 190 000	9
9	40	0.60	(100 000) 100 000	10

^aSyndiotactic PMMA (1 g), dioxane which had been treated with NaOH and Na wire (32 ml), and 20% w/w KOH in methanol (16 ml) were purged with N₂ in an ampoule. After sealing, it was heated at 85°C, tumbling thereby the ampoule. After the specified prehydrolysis time it was poured into water (1 l) with stirring, heated to 80°–100°C, precipitated by slow addition of a just sufficient amount of concentrated HCl, filtered and washed with small amounts of hot water. Drying to constant weight *in vacuo* at 50°C. ^bValues in parentheses are \bar{M}_w determined from the precursor PMMA by viscosity, values without parentheses obtained by re-esterification of copolymers to PMMA with diazomethane¹⁵ and determination of \bar{M}_w by viscosity (see Table 3). ^cBecause of its higher molecular weight this copolymer started to precipitate before 40 h, explaining the somewhat lower degree of hydrolysis as compared to copolymers 8 and 9.

Table 5 Fractionation of copolymers obtained after prehydrolysis and of copolymers obtained after kinetic runs with excess OH⁻

	Copolymer ^a and fraction No.	Molecular weight ^b \bar{M}_w	Amount (mg)	$P(A)^c$	$P(AAA)$	$P(ABA)$	$P(AAB^+)$	$P(ABB^+)$	$P(BAB)$	$P(BBB)$	
After prehydrolysis	6	(100 000)	500	0.83	0.57	0.11	0.23	0.05	0.03	0.01	
	I	97 000	160								
	II	97 000	230								
(Bernoullian copolymers)	8	(181 000)	500	0.60	0.22	0.14	0.29	0.19	0.10	0.06	
	I	200 000	260								
	II	182 000	170								
After kinetic run (copolymers with tendency toward alternation)	d	(100 000)	500	0.62	0.21	0.19	0.26	0.16	0.14	0.04	
	I	95 000	350								
	II	95 000	140								
	e	(100 000)	500	0.46	0.03	0.20	0.20	0.26	0.23	0.08	
		I	87 000								270
		II	83 000								230
	f	(100 000)	500	0.23	0	0.06	0.02	0.32	0.21	0.39	
		I	91 000								220
		II	79 000								240

^aArabic numerals 6 and 8 refer to whole (unfractionated) copolymers, of Table 4. d-f refer to whole copolymers, and I and II signify first and second fraction derived from the corresponding whole copolymers. ^b \bar{M}_w in parentheses are determined by viscosimetry from the precursor PMMA, the \bar{M}_w without parentheses apply to fractions which have been determined by re-esterifying with CH₂N₂ to PMMA and determining \bar{M}_w by viscosimetry. ^cThe P values were identical for the whole copolymer and its two fractions. Values of P in parentheses calculated from the experimental $P(A)$ for a Bernoullian statistics. ^dAlternating copolymer, obtained from random copolymer No. 6 (Table 4) with 5 mmol KOH after 4 h at 145°C. ^eAlternating copolymer, obtained from random copolymer No. 6 (Table 4) with 3 mmol KOH after 18 h at 145°C. ^fAlternating copolymer, obtained from random copolymer No. 6 (Table 4) with 5 mmol KOH after 48 h at 145°C

with a ten-fold amount of water and precipitating with concentrated HCl at 80° to 100°C.

The ¹H n.m.r. spectra were recorded on a Varian HR-220 spectrometer operated at 220 MHz. For all the copolymers pyridine was used as solvent; a temperature of 100°C, a concentration of ~10% w/v, and TMS as internal standard were employed. The gross composition of the copolymers was obtained by:

$$P(A) = \frac{\frac{5}{3}I(-OCH_3)}{I(-CH_2-) + I(-CH_3)} \quad (39)$$

where the I values are the areas of the resonance regions indicated in parentheses. The $P(XXX)$ were obtained from the α -CH₃ resonance region by either separating the triad peak areas by hand and measuring the areas by planimeter, or, in most cases, by a Du Pont Curve Resolver 310. For the latter procedure the peak shape was derived from the undisturbed high field flank of the AAA peak which is the α -CH₃ peak situated to highest field. The skew of the peaks was adjusted by observing the skew of the TMS signal.

ACKNOWLEDGEMENTS

Thanks are due to the Deutsche Forschungsgemeinschaft for financial support and to Professor H.-J. Cantow for providing the use of the n.m.r. spectrometer. Spectra were recorded with assistance of H. Bodenstern, H. Bührer, H. Erler, A. Hasenbühl and M. Seiter. Experimental assistance by A. Disch and J. Glaser is gratefully acknowledged.

REFERENCES

- Capon, B. *Q. Rev. Chem. Soc.* 1964, 18, 45
- Euranto, E. K. 'The Chemistry of Carboxylic Acids and Esters', (Ed S. Patai) Interscience, New York, 1969, Ch 11
- Ingold, C. K. *J. Chem. Soc.* 1930, 1375 and references cited therein
- Meyer, J. *Z. Phys. Chem.* 1909, 67, 257
- Knoblauch, O. *Z. Phys. Chem.* 1898, 26, 96
- Goldschmidt, H. *V. Scholz Ber.* 1903, 36, 1333
- Ingold, C. K. *J. Chem. Soc.* 1931, 2170
- Ingold, C. K. *J. Chem. Soc.* 1931, 2179
- Ingold, C. K. and Mohrhenn, H. G. G. *J. Chem. Soc.* 1935, 1482
- Westheimer, F. H. and Shookhoff, M. W. *J. Am. Chem. Soc.* 1940, 62, 269
- Schwetlick, K. 'Kinetische Methoden zur Untersuchung von Reaktionsmechanismen', VEB Deutscher Verlag der Wissenschaften, Berlin, 1971, p 214
- Smets, G. and DeLoecker, W. *J. Polym. Sci.* 1959, 41, 375
- Klesper, E., Gronski, W. and Barth, V. *Makromol. Chem.* 1970, 139, 1
- Klesper, E., Barth, V. and Johnsen, A. *Pure Appl. Chem. Suppl.* 1971, 8, 151
- Klesper, E., Johnsen, A., Gronski, W. and Wehrli, F. W. *Makromol. Chem.* 1975, 176, 1071
- Johnsen, A., Klesper, E. and Wirthlin, T. *Makromol. Chem.* in press
- Klesper, E., Strasilla, D. and Barth, V. in 'Reactions on Polymers', (Ed J. A. Moore), D. Reidel, Dordrecht, Holland, 1973, p 137
- Klesper, E., Gronski, W. and Barth, V. *Makromol. Chem.* 1971, 150, 223
- Klesper, E. *J. Polym. Sci. (B)* 1968, 6, 663
- Ito, K. and Yamashita, Y. *J. Polym. Sci. (A-1)* 1965, 3, 2165
- Gronski, W., Klesper, E. and Cantow, H.-J. *J. Polym. Sci. Polym. Symp.* 1973, 217
- Klesper, E., Johnsen, A. and Gronski, W. *Makromol. Chem.* 1972, 160, 167
- Silberberg, A. and Simha, R. *Biopolymers* 1968, 6, 479
- Lacombe, R. H. and Simha, R. *J. Chem. Phys.* 1974, 61, 1899
- McQuarrie, D. A., McTague, J. P. and Reiss, H. *Biopolymers* 1965, 3, 657
- Laidler, K. J. and Bunting, P. S. 'The Chemical Kinetics of Enzyme Action', Clarendon Press, Oxford, 1973, p 35
- Abe, H., Imai, K. and Matsumoto, M. *J. Polym. Sci. (B)* 1965, 3, 1053
- Klesper, E., Strasilla, D. and Regel, W. *Makromol. Chem.* 1974, 175, 523
- Cohn-Ginsberg, E., Fox, T. G. and Mason, H. F. *Polymer* 1962, 3, 97

Rate constants during the hydrolysis of syndiotactic poly(methyl methacrylate) with base*

Ernst Klesper and Volker Barth

Institut für Makromolekulare Chemie, Universität Freiburg, D-78 Freiburg, W. Germany

(Received 5 March 1976)

A procedure is presented for the determination of rate constants for the reaction of triads during the reaction on polymers and the method applied to the base hydrolysis of syndiotactic methyl methacrylate/methacrylic acid copolymers.

INTRODUCTION

For reactions of polymers the relative rate constants for individual sequences are sufficient to determine the distribution of sequence probabilities at a given gross composition for present reaction models. The rate constants themselves yield the same information and in addition the time necessary to obtain a given gross composition and distribution of sequences. The relative rate constants of triads have been determined¹ for the hydrolysis of syndiotactic methyl methacrylate/methacrylic acid copolymers with excess base in aqueous solution. In the present communication a procedure is given for the determination of the rate constants of triads for this hydrolysis reaction. It was found that the values for the rate constants and relative rate constants are compatible and that the rate constants are not greatly affected by conversion, e.g. by the total charge on the chain or by a kinetic effect of pendants.

RESULTS AND DISCUSSION

Syndiotactic methyl methacrylate/methacrylic acid (MMA/MAA) copolymers of Bernoullian distribution of monomer units are used for the kinetic runs in aqueous KOH. PMMA itself could not be employed since it is not soluble in aqueous KOH. Unless otherwise stated, aliquots of 250 mg of copolymer in 12 ml aqueous KOH of specified concentration are kept at 145°C under N₂ in sealed ampoules for periods of time to effect the hydrolysis. The experimental details for obtaining the kinetic data have been described¹. Two gross compositions are selected for the starting MMA/MAA copolymers, i.e. one with a probability of finding A of $P(A) = 0.83$ (copolymer No. 6 of Table 4 in reference 1) and $P(A) = 0.60$ (copolymer No. 9 of Table 4 in reference 1) (A = MMA monomer unit). The molecular weight of the starting copolymers is $\bar{M}_w = 100\,000$, unless otherwise indicated. The probabilities of the configurational triads are $P(ss) = 0.92$ and $P(is^+) = 0.08$ in all cases, where s = syndiotactic and i = isotactic placement. The + sign indicates that both forward and reversed forms of the sequence are included, e.g. is and si. Part of the $P(XXX)$ and $P(XX)$ data presented in this communication (X = A, B; B = MAA monomer unit) have already been evaluated for their dependence of $P(A)$ in a previous communication¹ in which the same hydrolysis reaction was studied,

* Dedicated to Professor H. Kämmerer on the occasion of his 65th birthday.

but with the interest centring on relative rates and relative rate constants. In this communication the time dependent behaviour of $P(XXX)$, $P(XX)$, and also $P(A)$, is of primary concern in order to evaluate the rate constants themselves.

Figure 1 shows the change of gross composition, $P(A)$, with time for the copolymer of $P(A) = 0.83$ with different initial amounts of KOH (at $t = 0$). An amount of 3, 5, and 7 mmol KOH/250 mg copolymer is sufficient to maintain a significant concentration of OH⁻ during the whole course of the reaction, since [KOH] used is more than is needed for the transformation of all -COOH and -COOCH₃ to -COO⁻. The kinetic curves for these OH⁻ concentrations show a monotonous decrease of $P(A)$ with time which depends greatly on [OH⁻]. The runs with 3 mmol initial KOH are considerably slower at the end range of conversion than those with 5 and 7 mmol KOH because a greater percentage of the OH⁻ has then been consumed in the former run.

Kinetic runs are also shown for 0.5, 1.0, and 1.5 mmol initial KOH. With 0.5 mmol KOH, the [KOH] is only slightly in excess of that necessary to transform all carboxyl groups of the starting copolymer to carboxylate (calculated: 0.435 mmol KOH). The kinetic behaviour approximates to that of a straight line. The kinetic curves for 1.0 and 1.5 mmol initial KOH, however, exhibit two points of inflection. During the first part of the reaction the rate de-

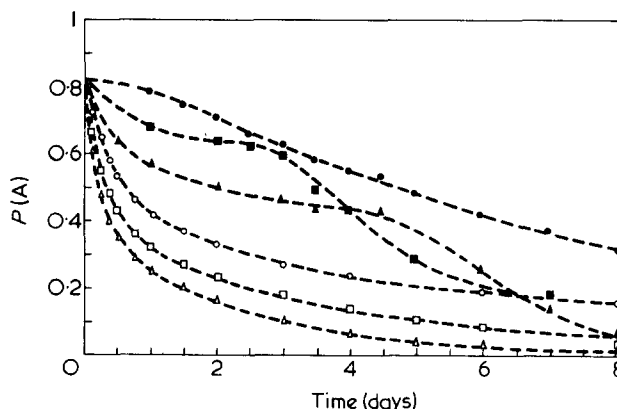


Figure 1 Change of gross composition, $P(A)$, with reaction time during hydrolysis of syndiotactic methyl methacrylate methacrylic acid (MMA/MAA) copolymer of Bernoullian compositional statistics and $P(A) = 0.83$. ●, 0.5; ■, 1; ▲, 1.5; ○, 3; □, 5; △, 7 mmol KOH

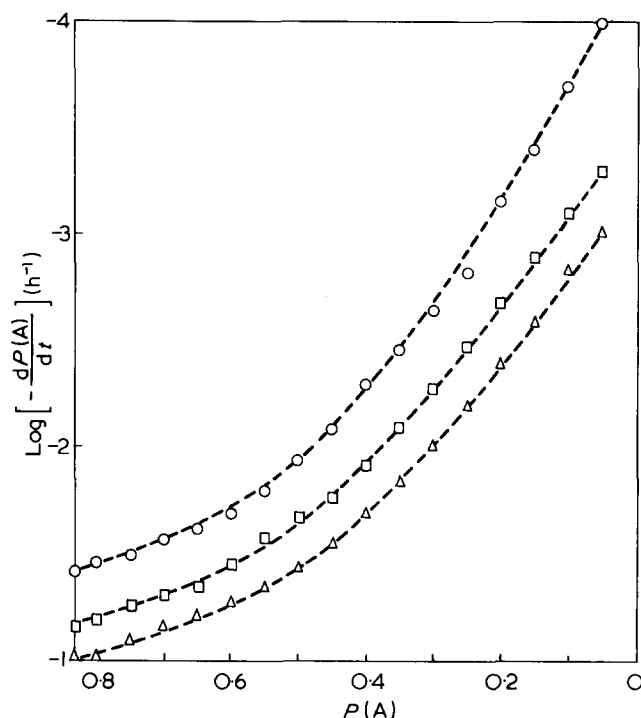


Figure 2 Slopes of $P(A)$ versus t curves, $dP(A)/dt$, of the curves of Figure 1 for \circ , \square , \triangle , 7 mmol KOH. Slopes are obtained graphically at $\Delta P(A) = 0.05$ intervals

increases greatly to a point which nearly coincides with the point where the excess KOH is consumed during hydrolysis by newly formed $-\text{COO}^-$, i.e. where $[\text{OH}^-] \approx 0$. The calculated points of consumption are $P(A) = 0.61$ with initially 1.0 mmol KOH and $P(A) = 0.41$ with initially 1.5 mmol KOH. The points of consumption are approached slowly, as to be expected for an overall second order reaction in which OH^- partakes, the curves forming thereby a plateau of small slope. The plateau indicates also, that the $-\text{COO}^-$ alone does not sustain the hydrolysis and the slow hydrolysis still prevailing at the plateau leads to an autocatalytic phase which at the end of the reaction levels off again. It is suspected that the active species present after the plateau is connected with the $-\text{COOH}$ formed during the hydrolysis. The final levelling off is connected with the exhaustion of A-units in the copolymer chains. Thus $P(A)$ versus time behaviour is in keeping with the previous finding¹ that at the point of consumption of OH^- the compositional statistics of the copolymers changes from one with alternation character to one with block character. Apparently the plateau separates the hydrolysis with OH^- as the attacking species to one in which the $-\text{COOH}$ partakes in some way. The electrostatic repulsion between OH^- and $-\text{COO}^-$ is likely to create alternation character, while the active species related to $-\text{COOH}$, by being bound to the chain and attacking preferably next neighbouring A-units, will tend to form block character. The following results refer to the hydrolysis in the presence of excess OH^- .

The rate for the hydrolysis of A-units with excess base may be written¹⁻³:

$$\frac{dP(A)}{dt} = -k(\text{AAA}) [\text{OH}^-]^x P(\text{AAA}) - k(\text{AAB}^+) [\text{OH}^-]^x P(\text{AAB}^+) - k(\text{BAB}) [\text{OH}^-]^x P(\text{BAB}) \quad (1)$$

where the $P(\text{XAX})$ designate probabilities in the copolymer chains and the $[\text{OH}^-]$ concentrations in solution. The ex-

ponent x is the reaction order with respect to $[\text{OH}^-]$ and the $k(\text{XAX})$ are the rate constants of the three individual reactions. On transferring $[\text{OH}^-]^x$ to the left of equation (1), the right hand side should be a constant at a given $P(A)$, provided the $P(A)$ uniquely determines the $P(\text{XAX})$, which is the case with a given set of $k(\text{XAX})$ and a given starting copolymer. Then the left hand side of equation (1) can be equated for different $[\text{OH}^-]$:

$$\left[\left(\frac{dP(A)}{dt} \right)_3 \times \frac{1}{[\text{OH}^-]_3^x} \right]_{P(A)_3} = \left[\left(\frac{dP(A)}{dt} \right)_7 \times \frac{1}{[\text{OH}^-]_7^x} \right]_{P(A)_7} \quad (2)$$

where the subscripts 3 and 7 indicate reactions with 3 and 7 mmol KOH and where $P(A)_3 = P(A)_7$. $[\text{OH}^-]_3$ and $[\text{OH}^-]_7$ refer to the momentary $[\text{OH}^-]$ at $P(A)_3 = P(A)_7$. Equation (2) leads to

$$x = \left[\log \frac{\left(\frac{dP(A)}{dt} \right)_3}{\left(\frac{dP(A)}{dt} \right)_7} / \log \frac{[\text{OH}^-]_3}{[\text{OH}^-]_7} \right]_{P(A)_3=P(A)_7}$$

The $dP(A)/dt$ values obtained graphically as slopes from Figure 1 at $\Delta P(A) = 0.05$ intervals are shown in Figure 2 for 3, 5, and 7 mmol KOH. The accuracy of the slope measurements appears to be good since there is little scatter around the broken curves which have been drawn visually through the points for best fit. The $[\text{OH}^-]$ (mol/l) which remains from the initial amount of KOH after hydrolysis to a given $P(A)$ is calculated by:

$$[\text{OH}^-] = \frac{\text{mmol KOH}_{\text{initial}} - \text{mmol KOH}_{\text{consumed}}}{12 \text{ ml}} \quad (4a)$$

The $\text{mmol KOH}_{\text{consumed}}$ is the KOH needed for the neutralization of all MAA units present at a given $P(A)$. Therefore:

$$\text{mmol KOH}_{\text{consumed}} = \frac{250[1 - P(A)_2]}{100P(A)_1 + 86[1 - P(A)_1]} \quad (4b)$$

The $P(A)_1$ is that of the starting copolymer (0.83 or 0.60), while $P(A)_2$ is that of the copolymer for which the $[\text{OH}^-]$ is to be calculated. The $[\text{OH}^-]$ so calculated agreed with the $[\text{OH}^-]$ titrated for a number of copolymers hydrolysed to high conversion. The results for the reaction order x of $[\text{OH}^-]$ are shown in Table 1 for both sets starting from $P(A) = 0.83$ and $P(A) = 0.60$, combining the data for 3 and 7 mmol KOH as well as 5 and 7 mmol KOH. Based on these results, the reaction order is taken to be $x = 1$ and it is interesting that $x \neq 1$ goes unnoticed when evaluating the relative rates as expressed by equations (15) to (17) in ref 1, because $[\text{OH}^-]^x$ has been cancelled in these equations. Also, the determination of x from $dP(\text{XX})/dt$ by equations (13) to (15) is equally possible.

The initial rates of the probabilities do not depend greatly on the concentration of polymer. This can be deduced from Figure 3a where some $P(A)$ vs. t points are shown for 125 and 62.5 mg starting copolymer of $P(A) = 0.83$ hydrolysed

Table 1 Reaction order x for $[\text{OH}^-]$ with copolymers of $P(A) = 0.83$ and $P(A) = 0.60$. The data were combined according to equation (3) for 3 and 7 mmol initial KOH as well as for 5 and 7 mmol initial KOH. The constant C (l/mol h) for transforming relative rate constants $k'(XAX)$ to $k(XAX)$ ($X = A, B$)

$P(A)^b$	Reaction order x of $[\text{OH}^-]$				Constant C^c	
	$P(A) = 0.83^a$		$P(A) = 0.60^a$		$P(A) = 0.83^a$	$P(A) = 0.60^a$
	3 and 7 mmol KOH	5 and 7 mmol KOH	3 and 7 mmol KOH	5 and 7 mmol KOH	3, 5, and 7 mmol KOH	3, 5, and 7 mmol KOH
0.83	0.99	1.03			0.42	
0.80	1.03	1.04			0.44	
0.75	1.01	1.05			0.46	
0.70	1.00	1.04			0.51	
0.65	0.97	1.04			0.54	
0.60	0.97	1.01	0.91	1.00	0.55	0.59
0.55	0.94	1.02	0.92	1.03	0.59	0.58
0.50	0.95	1.04	0.95	1.02	0.60	0.55
0.45	0.98	1.13	0.97	1.07	0.64	0.54
0.40	1.00	1.17	0.99	1.12	0.63	0.54
0.35	1.03	1.27	1.00	1.12	0.61	0.57
0.30	1.03	1.29	1.04	1.11	0.55	0.55
0.25	1.04	1.29	1.00	1.10	0.48	0.55
0.20	1.07	1.29	1.06	1.10	0.45	0.52
0.15	1.06	1.29	1.05	1.14	0.40	0.47
0.10	1.06	1.20	1.11	1.13	0.36	0.40
0.05	1.10	1.21	1.07	1.17	0.44	0.40

^a $P(A)$ of starting copolymer; ^b $P(A)$ during hydrolysis run; ^ccalculation based on $k'(AAA) = 0.60$, $k'(AAB^+) = 0.30$, and $k'(BAB) = 0.10$. Average value of reaction order x of $[\text{OH}^-] = 1.06$; average value of constant $C = 0.51$

by 5 mmol KOH in 12 ml solution. The points may be compared with the drawn out curve of the standard run with 250 mg copolymer under the same reaction conditions.

Since $x = 1$ and the chosen definition for the relative rate constants $k'(XAX)^1$, equation (1) may be written simply as:

$$\frac{dP(A)}{dt[\text{OH}^-]C} = -k'(AAA)P(AAA) - k'(AAB^+)P(AAB^+) - k'(BAB)P(BAB) \quad (5)$$

where C is given by:

$$k'(AAA)C = k(AAA) \quad (6a)$$

$$k'(AAB^+)C = k(AAB^+) \quad (6b)$$

$$k'(BAB)C = k(BAB) \quad (6c)$$

The relative rate constants were previously found to be $k'(AAA) = 0.6$, $k'(AAB^+) = 0.3$, and $k'(BAB) = 0.1$ at 145°C and are not detectably dependent on temperature in the range 115° to 175°C or on the extent of hydrolysis¹. Using the known values for the $k'(XAX)$ equation (5) can be employed to obtain the constant C . The $dP(A)/dt[\text{OH}^-]$ data needed for this purpose are plotted in Figure 4. The $dP(A)/dt[\text{OH}^-]$ obtained for runs with a starting copolymer of $P(A) = 0.83$ are shown in Figure 4a and those for a starting copolymer of $P(A) = 0.60$ in Figure 4b. Because $dP(A)/dt[\text{OH}^-]$ is found invariant with $[\text{OH}^-]$ at a given $P(A)$, averaging curves may be drawn through the experimental points obtained with 3, 5, and 7 mmol initial KOH. The $P(XAX)$ data shown in Tables 2 to 4 however, contain only the primary kinetic data for runs with a starting copolymer of $P(A) = 0.83$. The primary data for $P(XAX)$ of Tables 2 to 4 are not taken as such for the evaluation of C , but are plotted versus time for averaging and interpolation. The C values calculated

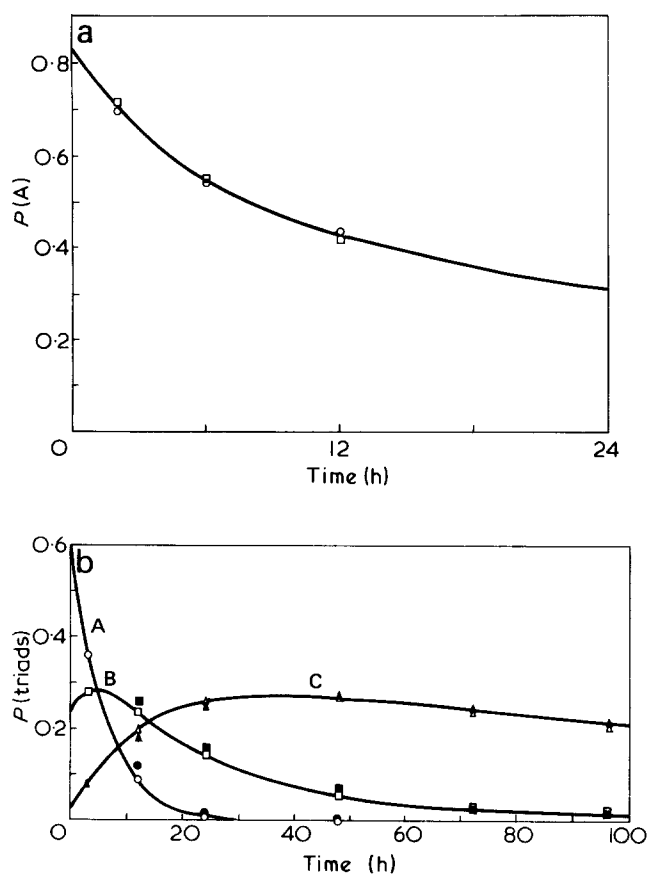


Figure 3 (a) Change of gross composition, $P(A)$, with reaction time (h) during hydrolysis of syndiotactic MMA/MAA copolymer of Bernoullian compositional statistics of $P(A) = 0.83$. \square , 125; \circ , 62.5 mg initial copolymer; —, 250 mg initial copolymer from Figure 1. (b) Change of probabilities of A-centred triads, $P(XAX)$, with hydrolysis time. Initially 3 mmol KOH + 2 mmol KCl: \bullet , \circ , $P(AAA)$; \blacksquare , \square , $P(AAB^+)$; \blacktriangle , \triangle , $P(BAB)$ where \bullet , \blacksquare , \blacktriangle represent $\bar{M}_w = 651\,000$ and \circ , \square , \triangle represent $\bar{M}_w = 243\,000$; —, —, —, Represents 3 mmol KOH, $\bar{M}_w = 100\,000$: A, $P(AAA)$; B, $P(AAB^+)$; C, $P(BAB)$

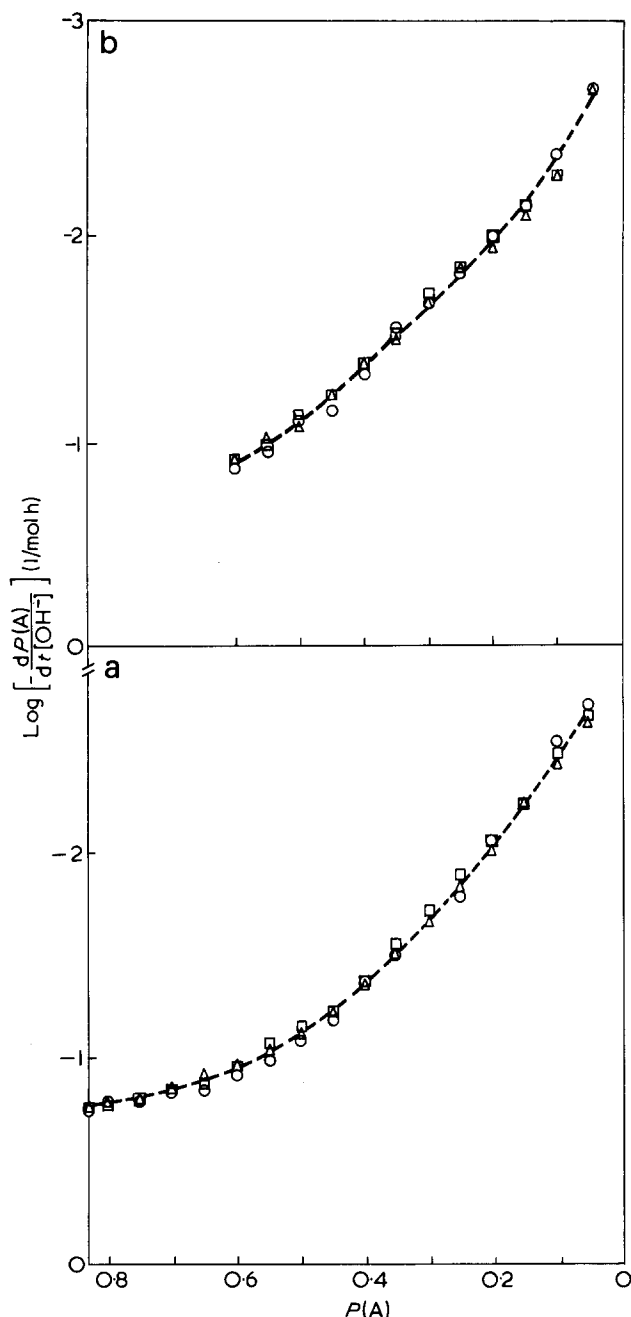


Figure 4 Slopes $dP(A)/dt$ from $P(A)$ versus t curves for: \circ , 3; \square , 5; \triangle , 7 mmole KOH. Data obtained at 145°C from a starting copolymer: (a) $P(A) = 0.83$; (b) $P(A) = 0.60$

for a given $P(A)$ are shown in Table 1. The fluctuation of C with $P(A)$ and with the two starting copolymers of $P(A) = 0.83$ and $P(A) = 0.60$ is within the limits probably to be expected for the errors inherent in the determination of $P(XAX)$. It should be noted that the invariance of C with $P(A)$ excludes the presence of a strong repulsion of attacking OH^- by $-\text{COO}^-$ removed further than one monomer unit along the chain.

The independence of $dP(A)/dt[\text{OH}^-]$ from $[\text{OH}^-]$, was also found for $dP(\text{XX})/dt[\text{OH}^-]$. It should be pointed out that this independence is a test for the chosen kinetic model as embodied in equations (1), (13)–(15) and excludes the presence of a significant overall first order reaction of triads connected with a hydrolysis by neighbouring $-\text{COO}^-$ or by H_2O . An overall first order reaction in the presence of the postulated overall second order reaction with OH^- can be written with respect to kinetic behaviour of A as

$$\begin{aligned} \frac{dP(A)}{dt[\text{OH}^-]} = & - \left[k(\text{AAA})_2 + \frac{k(\text{AAA})_1}{[\text{OH}^-]} \right] \times P(\text{AAA}) \\ & - \left[k(\text{AAB}^+)_2 + \frac{k(\text{AAB}^+)_1}{[\text{OH}^-]} \right] \times P(\text{AAB}^+) \\ & - \left[k(\text{BAB})_2 + \frac{k(\text{BAB})_1}{[\text{OH}^-]} \right] \times P(\text{BAB}) \end{aligned} \quad (7)$$

where the subscripts 1 and 2 denote the rate constants for the overall first and second order reactions. Clearly $dP(A)/dt[\text{OH}^-]$ cannot be independent of $[\text{OH}^-]$ according to equation (5) if the $k(\text{XAX})_1$ possess significant magnitude. Equations analogous to equation (7) may be written for $dP(\text{XX})/dt[\text{OH}^-]$.

Figure 3b shows the averaged $P(\text{XAX})$ of Table 2 (3 mmol KOH and starting copolymer of $P(A) = 0.83$). The points from runs carried out with addition of 2 mmol KCl to starting copolymers of different \bar{M}_w , using otherwise the same reaction conditions show neither a great dependence on molecular weight nor a salt effect. First results (not shown), however, indicate that the counterion might be an influence on the kinetics since with LiOH the rate appears to increase. From the $P(\text{XXX})$ versus t data of Tables 2 to 4 the $P(\text{XX})$ versus t are calculated by the principle of stationarity^{4,5}. The result is shown in Figure 5 as points for the run with 5 mmol KOH. The curves are drawn for best fit and are utilized for graphical determination of $dP(\text{XX})/dt$. A procedure was adopted which allows checking and averaging of the graphically determined differential quotients. On differentiation of the generally valid relations $P(\text{AA}) + 0.5P(\text{AB}^+) = P(A)$ and $P(\text{BB}) + 0.5P(\text{AB}^+) = 1 - P(A)$:

$$\frac{dP(\text{AA})}{dt} = \frac{dP(A)}{dt} - 0.5 \frac{dP(\text{AB}^+)}{dt} \quad (8)$$

$$\begin{aligned} \frac{dP(\text{AB}^+)}{dt} &= 2 \left[\frac{dP(A)}{dt} - \frac{dP(\text{AA})}{dt} \right] \\ &= -2 \left[\frac{dP(A)}{dt} + \frac{dP(\text{BB})}{dt} \right] \end{aligned} \quad (9)$$

$$\frac{dP(\text{BB})}{dt} = -\frac{dP(A)}{dt} - 0.5 \frac{dP(\text{AB}^+)}{dt} \quad (10)$$

From equations (8) and (10) it follows

$$\frac{dP(\text{AA})}{dt} = 2 \frac{dP(A)}{dt} + \frac{dP(\text{BB})}{dt} \quad (11)$$

$$\frac{dP(\text{BB})}{dt} = -2 \frac{dP(A)}{dt} + \frac{dP(\text{AA})}{dt} \quad (12)$$

So, each $dP(\text{XX})/dt$ may be obtained in two additional ways thus compensating the error in drawing the $P(\text{XX})$ versus t curves and in slope measurement.

Table 2 Primary data at 145°C with a syndiotactic, Bernoullian copolymer of $P(A) = 0.83$ and 3 mmol initial KOH

Time (h)	$P(A)$	$P(AAA)$	$P(ABA)$	$P(AAB^+)$	$P(ABB^+)$	$P(BAB)$	$P(BBB)$
0	0.83	0.57	0.11	0.23	0.05	0.03	0.01
1	0.79 ^a	0.45	0.15	0.25	0.08	0.06	0.01
2	0.75 ^a	0.41	0.16	0.26	0.08	0.07	0.02
3	0.72	0.36	0.17	0.28	0.09	0.08	0.02
4	0.70	0.32	0.18	0.28	0.09	0.10	0.03
6	0.65 ^a	0.23	0.18	0.29	0.14	0.12	0.04
9	0.58 ^a	0.14	0.20	0.26	0.19	0.17	0.04
12	0.53	0.09	0.21	0.24	0.20	0.20	0.06
18	0.46 ^a	0.03	0.20	0.20	0.26	0.23	0.08
24	0.42	0.01	0.18	0.15	0.29	0.26	0.11
36	0.37 ^a	0	0.15	0.10	0.32	0.27	0.16
48	0.33	0	0.14	0.06	0.31	0.27	0.22
72	0.27	0	0.09	0.03	0.32	0.24	0.32
96	0.23	0	0.06	0.02	0.32	0.21	0.39
144	0.18	0	0.04	0.01	0.27	0.17	0.51
192	0.15	0	0.03	0	0.25	0.15	0.57
240	0.13	0	0.02	0	0.23	0.13	0.62
480	0.07	0	0.01	0	0.13	0.07	0.79
720	0.03	0	0	0	0.06	0.03	0.91

^aResult of duplicate runs, reproducibility ± 0.01 Table 3 Primary data at 145°C with a syndiotactic, Bernoullian copolymer of $P(A) = 0.83$ and 5 mmol initial KOH

Time (h)	$P(A)$	$P(AAA)$	$P(ABA)$	$P(AAB^+)$	$P(ABB^+)$	$P(BAB)$	$P(BBB)$
0	0.83	0.57	0.11	0.23	0.05	0.03	0.01
1	0.76 ^a	0.44	0.15	0.26	0.08	0.06	0.01
2	0.71	0.33	0.17	0.28	0.11	0.09	0.02
3	0.66	0.26	0.18	0.29	0.13	0.11	0.03
4	0.62 ^a	0.21	0.19	0.26	0.16	0.14	0.04
6	0.55	0.11	0.20	0.25	0.20	0.19	0.05
9	0.48	0.05	0.21	0.21	0.24	0.22	0.07
12	0.43	0.02	0.18	0.16	0.28	0.25	0.11
18	0.36	0	0.15	0.10	0.32	0.26	0.17
24	0.32	0	0.12	0.06	0.33	0.26	0.23
36	0.27	0	0.09	0.03	0.32	0.24	0.32
48	0.23 ^a	0	0.06	0.02	0.32	0.21	0.39
72	0.18 ^a	0	0.03	0.01	0.28	0.17	0.51
96	0.14	0	0.02	0	0.24	0.14	0.60
120	0.11	0	0.01	0	0.20	0.11	0.68
144	0.09	0	0.01	0	0.17	0.09	0.73
192	0.05	0	0.01	0	0.09	0.05	0.85
264	0.02	0	0	0	0.04	0.02	0.94
360	0.00 ₅	0	0	0	0.01	0.00 ₅	0.98 ₅

^aResult of duplicate runs, reproducibility ± 0.01 Table 4 Primary data at 145°C with a syndiotactic, Bernoullian copolymer of $P(A) = 0.83$ and 7 mmol initial KOH

Time (h)	$P(A)$	$P(AAA)$	$P(ABA)$	$P(AAB^+)$	$P(ABB^+)$	$P(BAB)$	$P(BBB)$
0	0.83	0.57	0.11	0.23	0.05	0.03	0.01
1	0.74	0.38	0.16	0.27	0.09	0.08	0.02
2	0.67	0.28	0.18	0.28	0.12	0.11	0.03
3	0.61	0.19	0.19	0.27	0.16	0.15	0.04
4	0.56	0.13	0.20	0.25	0.19	0.18	0.05
6	0.48 ^a	0.05	0.19	0.20	0.25	0.23	0.08
9	0.40 ^a	0.01	0.17	0.12	0.31	0.27	0.12
12	0.35	0	0.15	0.08	0.31	0.27	0.19
18	0.29	0	0.11	0.04	0.31	0.25	0.29
24	0.25	0	0.08	0.02	0.31	0.23	0.36
36	0.20 ^a	0	0.05	0.01	0.29	0.19	0.46
48	0.16	0	0.03	0	0.25	0.16	0.56
72	0.10	0	0.01	0	0.18	0.10	0.71
96	0.07	0	0.01	0	0.13	0.07	0.79
120	0.04	0	0	0	0.08	0.04	0.88
144	0.03	0	0	0	0.06	0.03	0.91
192	0.01	0	0	0	0.02	0.01	0.97
240	0	0	0	0	0	0	1.00

^aResults of duplicate runs, reproducibility ± 0.01

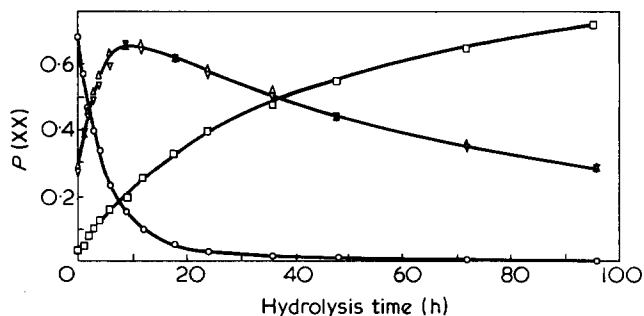


Figure 5 Change of probabilities of dyads with time of hydrolysis. \circ , $P(AA) = P(AAA) + 0.5 P(AAB^+)$; \triangle , $P(AB^+) = P(AAB^+) + 2P(BAB)$; ∇ , $P(AB) = P(ABB^+) + 2P(ABA)$; \square , $P(BB) = P(BBB) + 0.5 P(ABB^+)$

The appropriate differential equations¹ for $dP(XX)/dt$ are:

$$\frac{dP(AA)}{dt} = -2k(AAA)[OH^-]P(AAA) - k(AAB^+)[OH^-]P(AAB^+) \quad (13)$$

$$\frac{dP(AB^+)}{dt} = 2k(AAA)[OH^-]P(AAA) - 2k(BAB)[OH^-]P(BAB) \quad (14)$$

$$\frac{dP(BB)}{dt} = k(AAB^+)[OH^-]P(AAB^+) + 2k(BAB)[OH^-]P(BAB) \quad (15)$$

Equations (13) to (15) assume first order reaction with respect to $[OH^-]$ and absence of an additional, overall first order reaction of triads.

Equation (13) may be rearranged to the straight line form:

$$k(AAA) = c_1 k(AAB^+) + c_2 \quad (16)$$

with

$$c_1 = -\frac{P(AAB^+)}{2P(AAA)} \quad (17)$$

$$c_2 = -\frac{S_1}{2P(AAA)} \quad (18)$$

where $S_1 = dP(AA)/dt[OH^-]$, and where S_1 , c_1 and c_2 refer, of course, to data at the same time or $P(A)$. Equations (14) and (15) may be rearranged similarly to:

$$k(AAA) = \frac{P(BAB)}{P(AAA)} k(BAB) + \frac{dP(AB^+)/dt[OH^-]}{2P(AAA)} \quad (19)$$

$$k(AAB^+) = -\frac{2P(BAB)}{P(AAB^+)} k(BAB) + \frac{dP(BB)/dt[OH^-]}{P(AAB^+)} \quad (20)$$

In Figure 6 the $k(AAA)$ vs. $k(AAB^+)$ plot of equation (16) is shown for the run with 5 mmol KOH and starting from $P(A) = 0.83$. The $P(XAX)$ for equation (16) are obtained

from $P(XXX)$ vs. t curves drawn through the data of Table 3. Similarly, Figures (7) and (8) show the $k(AAA)$ versus $k(BAB)$ and the $k(AAB^+)$ versus $k(BAB)$ plots. The lines are labelled by their reaction time and vertical parallel lines refer to special cases. When $P(AAA)$ becomes zero during hydrolysis, then according to equations (13) and (14):

$$k(AAB^+) = -\frac{dP(AA)/dt[OH^-]}{P(AAB^+)} \quad (21)$$

$$k(BAB) = -\frac{dP(AB^+)/dt[OH^-]}{2P(BAB)} \quad (22)$$

and $k(AAB^+)$ or $k(BAB)$ can be immediately obtained without plotting. However, additional information is obtained by drawing corresponding vertical lines on the

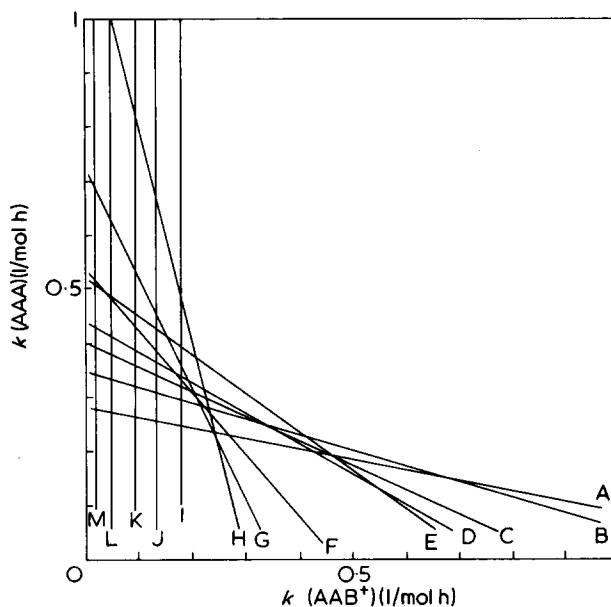


Figure 6 Determination of $k(AAA)$ and $k(AAB^+)$ according to equation (16). Reaction time (h): A, 0; B, 1; C, 2; D, 3; E, 4; F, 6; G, 9; H, 12; I, 18; J, 24; K, 36; L, 72; M, 48

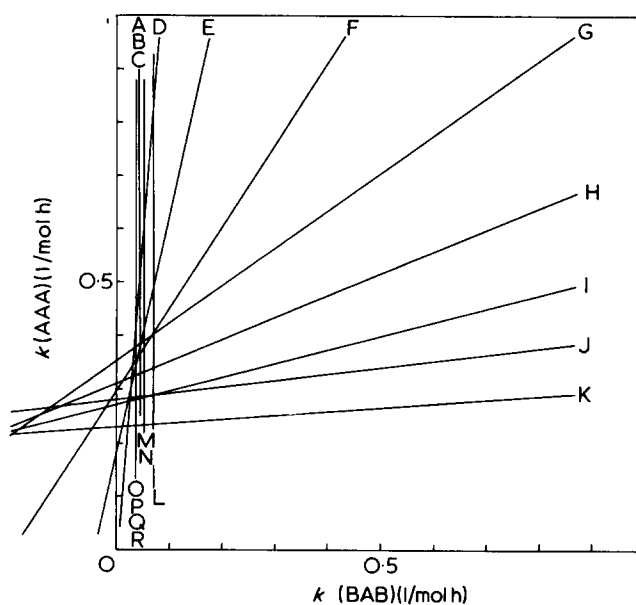


Figure 7 Determination of $k(AAA)$ and $k(BAB)$ according to equation (19). Reaction time (h): A, 18; B, 36; C, 48; D, 12; E, 9; F, 6; G, 4; H, 3; I, 2; J, 1; K, 0; L, 240; M, 24; N, 192; O, 72; P, 96; Q, 120; R, 144

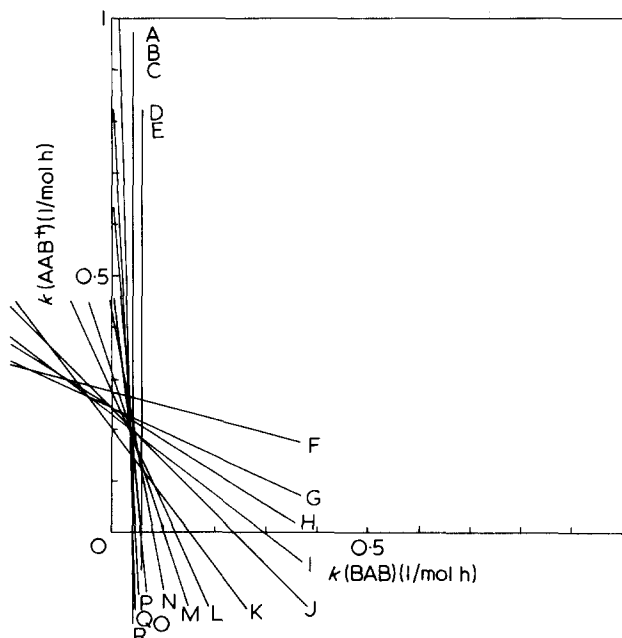


Figure 8 Determination of $k(\text{AAB}^+)$ and $k(\text{BAB})$ according to equation (20). Reaction time (h): A, 96; B, 120; C, 144; D, 192; E, 240; F, 0; G, 1; H, 2; I, 3; J, 4; K, 6; L, 9; M, 12; N, 18; O, 24; P, 36; Q, 48; R, 72

$k(\text{AAB}^+)$ or $k(\text{BAB})$ axis. When $P(\text{AAB}^+) = 0$, in addition to $P(\text{AAA}) = 0$, then equation (15) becomes:

$$k(\text{BAB}) = \frac{dP(\text{BB})/dt[\text{OH}^-]}{2P(\text{BAB})} \quad (23)$$

Again, $k(\text{BAB})$ may be obtained directly and plotted as vertical on the $k(\text{BAB})$ axis.

There is considerable scatter of the intersections particularly in Figure 6, indicating the limits of accuracy in determining the triad probabilities. Since the two coordinates of the intersections are not normally distributed, the median and the 95% confidence limits of the median were determined. For Figure 6 it was found that $k(\text{AAA}) = 0.34$ (from 0.30 to 0.38) and $k(\text{AAB}^+) = 0.16$ (from 0.10 to 0.18). For Figure 7 it was found that $k(\text{AAA}) = 0.33$ (0.28 to 0.35) and $k(\text{BAB}) = 0.04$ (range less than 0.01), while for Figure 8 the values $k(\text{AAB}^+) = 0.21$ (0.20 to 0.21) and $k(\text{BAB}) = 0.04$ (0.03 to 0.04) were obtained, all rate constants being in (1/mol h). The lack of overlap of the confidence ranges for $k(\text{AAB}^+)$ indicates a systematic error for the triad probabilities.

Plotting the three graphs corresponding to equations (16), (19) and (20) for the data obtained with 3 and 7 mmol KOH (Tables 2 and 4) yields similar values for the rate constants and the same applies to runs starting with a copolymer of $P(\text{A}) = 0.60$ at 3, 5, and 7 mmol initial KOH. Moreover, the value $C_{\text{average}} = 0.51$ of Table 1 agrees reasonably, because this value yields $k(\text{AAA}) = 0.30$, $k(\text{AAB}^+) = 0.15$, and $k(\text{BAB}) = 0.05$ when applied to $k'(\text{AAA}) = 0.6$, $k'(\text{AAB}^+) = 0.3$, and $k'(\text{BAB}) = 0.1$.

The rate constants were determined not only at 145°C but also at 115°C and 175°C, using 5 mmol KOH and a starting copolymer of $P(\text{A}) = 0.83$. The rate constants at 115°C were found as $k(\text{AAA}) = 1.1 \times 10^{-5}$, $k(\text{AAB}^+) = 5.5 \times 10^{-6}$, and $k(\text{BAB}) = 1.9 \times 10^{-6}$, those at 175°C as $k(\text{AAA}) = 6.7 \times 10^{-4}$, $k(\text{AAB}^+) = 3.3 \times 10^{-4}$, and $k(\text{BAB}) = 1.1 \times 10^{-4}$, which compares with $k(\text{AAA}) = 8.3 \times 10^{-5}$, $k(\text{AAB}^+) = 4.2 \times 10^{-5}$, and $k(\text{BAB}) = 1.4 \times 10^{-5}$ at 145°C,

all in (1/mol sec). The set of values for 145°C corresponds to $k(\text{AAA}) = 0.30$, $k(\text{AAB}^+) = 0.15$, and $k(\text{BAB}) = 0.05$ (1/mol h) as derived from $k'(\text{XAX})$ and C .

According to the Eyring equation one may write for the rate constant of each individual reaction (A) $\text{AAA} \rightarrow \text{ABA}$, (B) $\text{AAB}^+ \rightarrow \text{ABB}^+$, and (C) $\text{BAB} \rightarrow \text{BBB}$

$$\log \frac{k}{T} = \log \frac{k}{h} + \frac{\Delta S^\ddagger}{2.303R} + \frac{\Delta H^\ddagger}{2.303RT} \quad (24)$$

The plots of $\log k/T$ vs. $1/T$ are shown in Figure 9 for three temperatures 115°, 145°, and 175°C. The lines for the three rate constants are parallel, i.e. of identical slope, indicating the same ΔH^\ddagger for each of the three reactions. The same conclusion has been reached from the relative rate constants¹. The ΔH^\ddagger was derived from:

$$\text{Slope} = -\frac{\Delta H^\ddagger}{4.576} \quad (25)$$

and found to be 22.9 kcal/mol for the three individual reactions. The ΔS^\ddagger for the three reactions (A), (B), and (C) are then $\Delta S_1^\ddagger = -23.0$; $\Delta S_2^\ddagger = -24.4$, and $\Delta S_3^\ddagger = -26.5$ cal/mol K. This yields $\Delta S_1^\ddagger - \Delta S_2^\ddagger = 1.4$ eu and $\Delta S_1^\ddagger - \Delta S_3^\ddagger = 3.5$ eu which compares with 1.4 and 3.6 eu obtained previously for these differences from the relative rate constants¹. The ΔH^\ddagger possesses a value which is in a higher range than usually found for ester hydrolysis with base⁶. In view of the finding that ΔH^\ddagger is independent of the reacting triad, i.e. its charge, this higher value should be attributed to steric constraints for the attacking OH^- . Clearly, the difference in rates for the three individual re-

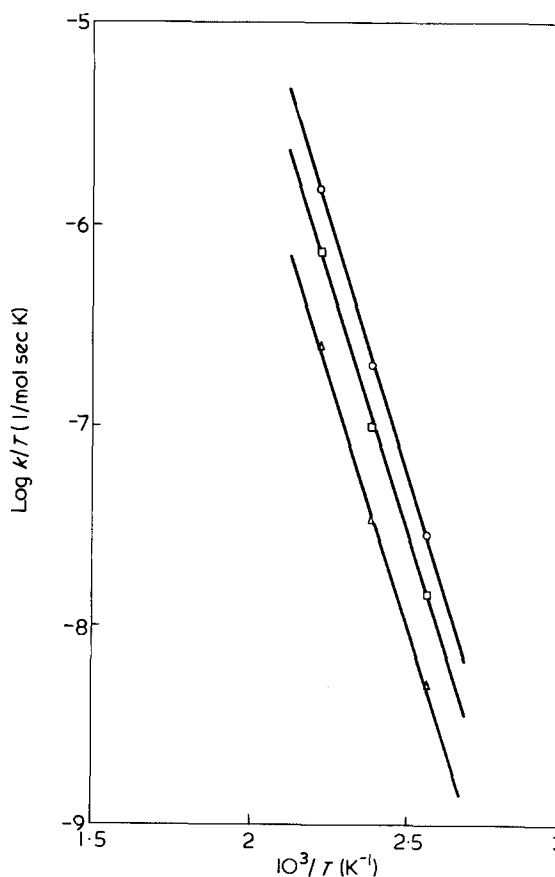


Figure 9 Eyring plot (equation 24) for temperature dependence of $k(\text{AAA})$, $k(\text{AAB}^+)$, and $k(\text{BAB})$. \circ , AAA $k(\text{AAA})$; \square , AAB^+ $k(\text{AAB}^+)$; \triangle , BAB $k(\text{BAB})$

actions is due to entropic changes occurring when OH^- is approaching the charged chain to form the transition state. The entropy loss increases from reaction (A) to (C) which indicates that the gain in conformational, and possibly also solvational order of the reacting triads increases with increasing charge of the triad.

ACKNOWLEDGEMENT

Financial support by the Deutsche Forschungsgemeinschaft is gratefully acknowledged.

REFERENCES

- 1 Barth, V. and Klesper, E. *Polymer*, 1976, 17, 777
- 2 Klesper, E., Gronski, W. and Barth, V. *Makromol. Chem.* 1971, 150, 223
- 3 Klesper, E., Johnsen, A. and Gronski, W. *Makromol. Chem.* 1972, 160, 167
- 4 Coleman, B. D. and Fox, T. G. *J. Polym. Sci. (A)* 1963, 1, 3183
- 5 Frisch, H. L., Mallows, C. L. and Bovey, F. A. *J. Polym. Sci.* 1966, 45, 1565
- 6 Euranto, E. K. in 'The chemistry of carboxylic acids and esters' (Ed S. Patai), Interscience, New York, 1969

Effect of solvent on the crystallization from dilute polyethylene solutions

E. Riande and J. M. G. Fatou

Sección de Fisicoquímica y Física de Polímeros, Instituto de Plásticos y Caucho, Juan de la Cierva 3, CSIC, Madrid-6, Spain

(Received 15 March 1976; revised 10 May 1976)

The influence of the thermodynamic interaction parameter on the crystallization of very dilute solutions of polyethylene in decalin, tetralin, α -chloronaphthalene and *p*-xylene has been studied. Depending on the solvent, quantitative kinetics data were obtained at different temperature intervals. In comparison with the crystallization in bulk, higher crystallinity levels were obtained. The overall rate temperature coefficient has been analysed according to the nucleation theory pertinent to polymer-diluent mixtures and the results show that the basal free energy for nucleation is independent of the solvent.

INTRODUCTION

Long chain molecules crystallize in the form of lamellar-like structures of platelets when precipitated from dilute solutions¹⁻³. It has been shown that for linear polyethylene the crystallite size in the chain direction is governed by the nucleation process. In a previous work⁴, the influence of molecular weight and concentration on the crystallization kinetics has been analysed, using a new approach to the nucleation theory for finite chain molecules. It has been shown that the crystallization process in these systems is governed by the nucleation act, so that, when the variation in the interfacial free energy in the (001) face of the crystal with molecular weight is stipulated, the phase transformation is described by a function of the free energy required for nucleation. This analysis was later extended to very dilute solutions⁵ of polyethylene in α -chloronaphthalene and it was found that the basal interfacial free energy of the critical nucleus increases slightly with molecular weight.

Renewed attention has been given in recent years to the effect of solvents on the crystallization of polymers. The relation between the crystallite size and the crystallization temperature^{6,7} and between the dissolution temperature and the mature crystal⁸⁻¹¹ have been studied.

In the present paper we analyse the crystallization kinetics of a high molecular weight fraction of polyethylene in several solvents, utilizing the theory for polymer diluent mixtures. Special emphasis is given to the influence of the thermodynamic interaction parameter on the crystallization conditions.

EXPERIMENTAL

Materials

A linear polyethylene fraction was obtained from unfractionated Marlex 50 using the column fractionation technique¹². The viscosity-average molecular weight was determined from the relation given by Chiang¹³ for decalin at 135°C and corresponds to $M = 100\,000$.

The four solvents used in this work, *p*-xylene, chloronaphthalene, tetralin and decalin, were of high purity

Crystallization

An accurately weighed amount of polymer was introduced into the bulk of the dilatometer and the desired amount of solvent was added to obtain a polymer volume fraction of 0.0030. The dilatometers were so constructed that, after adding the solvent, the bulk was sealed and filled with mercury in a high vacuum line. The total change in the mercury height upon the completion of the crystallization was about 4 cm. Prior to the isothermal crystallization, the polymer in the dilatometer was dissolved by heating overnight at 220°C in the case of α -chloronaphthalene and at about 140°C for the other three solvents. The crystallization was conducted in silicone oil thermostats with the temperature controlled to within $\pm 0.01^\circ\text{C}$. After shaking and complete dissolution of the sample, the dilatometer was quickly transferred to the thermostat set at a preassigned temperature. About 10 min were required for the dilatometer to achieve thermal equilibrium.

RESULTS AND DISCUSSION

Depending on the solvent, quantitative kinetic data could be obtained at different temperature intervals. At this very high dilution ($\nu_2 = 0.003$) comparatively large undercoolings are necessary to obtain kinetics data in a reasonable time period and these undercoolings depend on the solvent. All the isotherms display the same characteristic sigmoidal behaviour.

In order to examine the shape of the isotherms, we analysed the data according to the Gōler-Sachs or free growth approximation¹⁴. For the initial portion of the transformation it is found that:

$$\begin{aligned}1 - \lambda(t) &= (k_3 t)^4 / 4 \\1 - \lambda(t) &= (k_2 t)^3 / 6 \\1 - \lambda(t) &= (k_1 t)^2 / 2\end{aligned}\tag{1}$$

for three, two or one dimensional growth. In these equations $1 - \lambda(t)$ is the degree of crystallinity, k_1 , k_2 and k_3

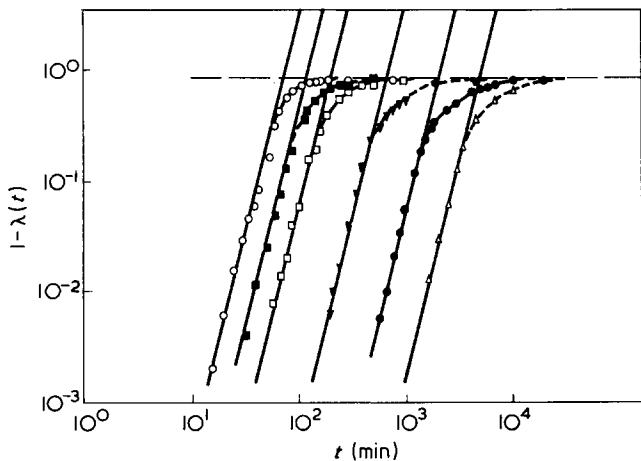


Figure 1 Double logarithmic plot of degree of crystallinity against t , at different crystallization temperatures, for polyethylene in decalin: \circ , 81.8°; \blacksquare , 82.8°; \square , 83.7°; \blacktriangledown , 85.2°; \bullet , 86.4°; \triangle , 87.2°C

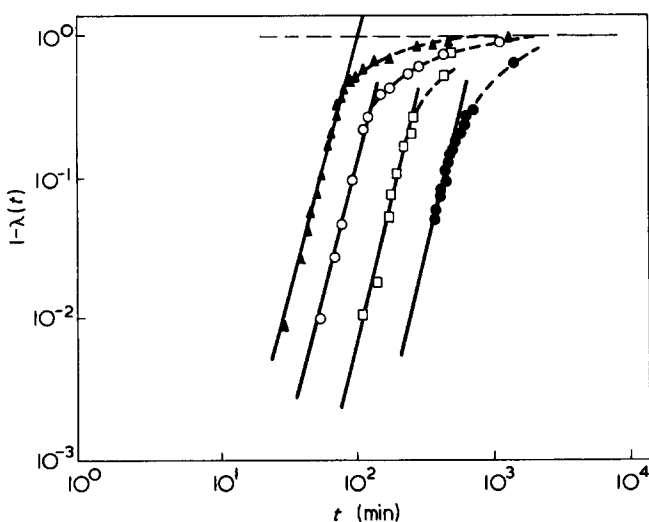


Figure 2 Double logarithmic plot of degree of crystallinity against t , at different crystallization temperatures, for polyethylene in xylene: \blacktriangle , 87.2°; \circ , 88.1°; \square , 89.0°; \bullet , 90.0°C

are the rate constants and t is the time. Equation (1) suggests, that as the simplest analysis, a double logarithmic plot be made of $1 - \lambda(t)$ against time.

Figures 1 to 4 show the experimental results for the four solvents. There is a good adherence of the experimental data to this theoretical development and a linear relation is obtained for a significant portion of the total transformation. At the lower crystallization temperatures, this formulation holds for about 50–60% of the transformation, independent of the solvent. The level of agreement decreases somewhat as the crystallization temperature is increased.

The agreement of the experimental data with the Avrami equation, $\ln(1 - x) = kt^n$, is about the same as with the G6ler–Sachs theory and deviations from either of the theories occurs at about the same level of crystallinity. This conclusion is similar to that obtained previously in the crystallization in bulk¹⁵.

In comparison with the crystallization in bulk, higher crystallinity levels are obtained in solution. For the fraction used in this work, the total crystallinity varies from 90 to 95% and does not depend on the solvent. The slope of the linear portion of the G6ler–Sachs plot, corresponds to the

exponent in the Avrami equation, and these slopes are dependent on solvent. For decalin and *p*-xylene n is four and for α -chloronaphthalene and tetralin n is three. The differences in the exponent n is made clear in Figure 5 where we have superimposed points from two different solvents, decalin and tetralin. Previously, the Avrami exponent for *p*-xylene, decalin and *n*-hexadecane was found to be $n = 4$ in all cases⁶. The simplest interpretation of the exponent $n = 4$ is the occurrence of an homogeneous nucleation accompanied by three-dimensional growth and for $n = 3$, an homogeneous nucleation with a two-dimensional growth. The first fact must be reconciled with the lamella-like crystallites that are observed. The fact that integral values of 3 are obtained in α -chloronaphthalene and tetralin is very important. There is no correlation between the interaction polymer solvent and n and differences observed must remain unexplained at present. How-

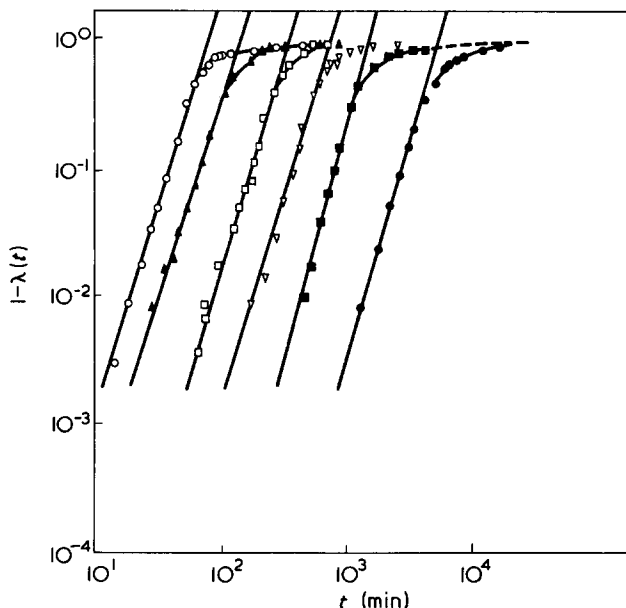


Figure 3 Double logarithmic plot of degree of crystallinity against t , at different crystallization temperatures, for polyethylene in tetralin: \circ , 87.9°; \blacktriangle , 89.4°; \square , 90.5°; \blacktriangledown , 91.5°; \blacksquare , 92.4°; \bullet , 93.7°C

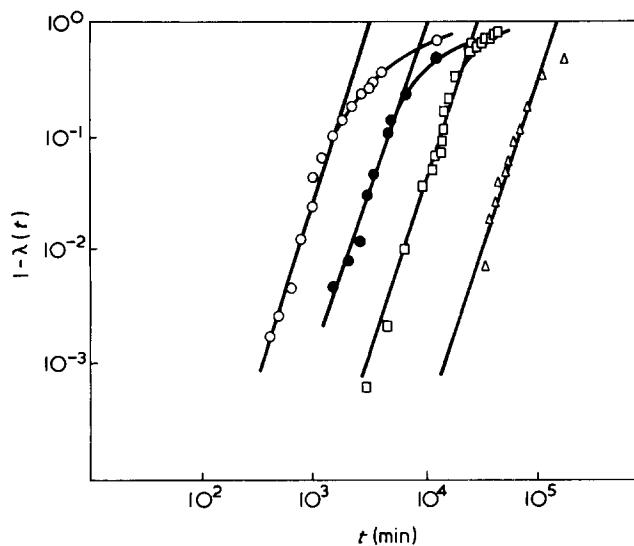


Figure 4 Double logarithmic plot of degree of crystallinity against molecular weight, at different crystallization temperatures, for polyethylene in α -chloronaphthalene: \circ , 98.9°; \bullet , 100.0°; \square , 100.9°; \triangle , 102.0°C

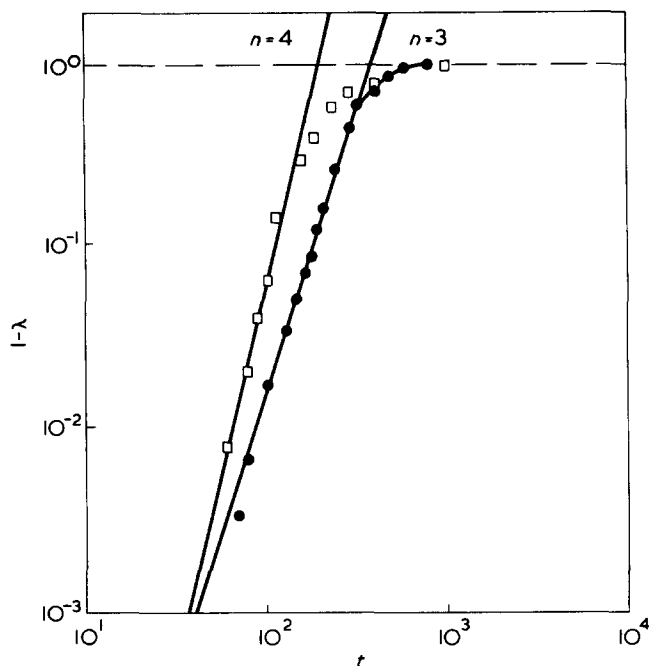


Figure 5 Superimposed isotherms of decalin (□) and tetralin (●). T_c of decalin 83.7°C ; T_c for tetralin 90.5°C

ever, the exponent $n = 3$ looks as if it corresponds to poor solvents, in which the molecules freely interpenetrate one another, and the exponent $n = 4$ corresponds to better solvents.

The crystallization rate depends strongly on the solvent. Thus the time necessary for 10% of the transformation to occur at 87.2°C is ~ 3000 min for the polyethylene fraction in decalin while in xylene the time is reduced by a factor of 6. It is tempting to relate this difference to the intensity of polymer-solvent interaction embodied in the parameter χ_1 . Most of the values of χ_1 reported in the literature for these systems, were calculated on the basis of the familiar relationship:

$$\frac{1}{T_m} - \frac{1}{T_m^0} = \frac{R}{\Delta H_u} \frac{V_u}{V_1} v_1(1 - \chi_1 v_1) \quad (2)$$

where T_m^0 is the melting temperature of the undiluted polymer, of infinite molecular weight. As it has been pointed out³ the validity of equation (2) is questionable for very dilute solutions and although it describes the equilibrium, the appropriate thermodynamic quantities may no longer remain constant because of the non-uniform polymer segment distribution throughout the medium. Only when the solvent is sufficiently poor may these aspects be neutralized.

Although different investigations have led to different absolute values for the interaction parameter, they rank in the same order for different solvents, as can be seen in Table 1. Decalin has the lowest value for χ_1 and xylene the highest. Therefore, the crystallization rate, at a given temperature, is lower in the better solvent. However, it is difficult to find a correlation between χ_1 and the magnitude of the crystallization rate as can be seen in Table 1 where χ_1 and the temperature at which 10% of the crystallization occurs in 100 min has been represented for polyethylene in several solvents. The lack of correlation may be due to the fact that the estimation with sufficient accuracy of χ_1 presents serious difficulties. This point will be discussed later.

Nucleation free energy

The free energy of melting of crystalline polymers was calculated by Flory¹⁷ using the lattice model. One of the main contributions to the free energy of melting is the free enthalpy of mixing which for a quasibinary system (single solvent plus multicomponent homologous polymer) is given by:

$$\Delta F/RT = n_1 \ln v_1 + \sum n_i \ln v_i + g n_1 v_2 \quad (3)$$

In the above equation n_1 , n_i are the number of moles and v_1 , v_i the volume fractions of solvent and polymer species i , respectively, $v_2 = \sum v_i$ is the whole polymer volume fraction and RT has its usual meaning. The dimensionless interaction function g is allowed to depend on temperature, pressure and concentration, but not on the molecular weight of any of the species. According to equation (3) the chemical potential of the solvent, referred to its value in the pure liquid is given by¹⁸:

$$\Delta\mu/RT = \ln(1 - v_2) + (1 - x^{-1})v_2^2 + \chi v_2^2 \quad (4)$$

where $\chi = g - v_1 \delta g / \delta v_2$. Moreover, the concentration dependence of χ can be expressed in series form:

$$\chi = \chi_1 + \chi_2 v_2 + \dots \quad (5)$$

A molecular weight dependent contribution to g are the end-group contributions^{19,20} as well as the well-known inherent non-uniformity²¹ of local polymer segment concentration at high dilutions. It has long been recognized that an interaction function g independent of chain length cannot describe the thermodynamic properties of dilute polymer solutions; e.g. the second and third virial coefficients are known to depend on molecular weight. As it is well known two extremes of polymer solutions behaviour can be distinguished. At sufficiently high concentration, we have an enmeshed, intertwined and entangled assembly of chains. Under these conditions, an essentially uniform polymer segment concentration may be assumed throughout the solution and the theoretical treatment leads to equation (2) with an interaction coefficient g that is independent of chain length except for the specific end-group effects. At high dilutions, however, the macromolecules are more or less isolated from each other, only occasionally interacting in small clusters.

Koningsveld *et al.*¹⁸ have considered the dependence of g on molecular weight, by assuming g for a polymer solution of arbitrary concentration as a simple linear combination of the two extreme cases described above. For a strictly binary polymer solution these authors obtain:

$$g = g_{\text{conc}} + \left(\frac{1}{2} - \chi_1 \right) (1 - h(Z))(1 + \lambda)^{-1} \exp(-\lambda_0 x^{1/2} v_2) \quad (6)$$

Table 1 Values of the interaction parameter for different solvents

Solvents	χ_1	T_c
Decalin	0.10 ^{10,11}	84
Xylen	0.41 ^{8,10,11,16}	88
Tetraline	0.39 ^{10,11} ; 0.20 ^{8,16}	89
Chloronaphthalene	0.30 ^{8,16}	96
Hexadecane*	0.15 ^{10,11}	105

*Kinetic data from ref 6

The factor $h(z)$ is always less than unity above the θ -temperature and is theoretically related to the average number of nearest neighbour segment-segment contacts between two polymer chains of a binary cluster. λ_0 is given by:

$$\lambda_0 = 4\pi a N_A b^3 V_1^{1/2} / 3 \bar{v}_2^{3/2} \quad (7)$$

where $b = S_i M_i^{-1/2}$, S_i^2 being the mean square polar radius of gyration, a is a geometric factor of order unity and \bar{v}_2 is the effective specific volume of polymer.

The free energy change involved in forming a cylindrically arranged crystalline array of ξ units long and ρ sequences in cross-section, for a diluted system containing N polymer molecules each comprised of x repeating units, in which the volume fraction of polymer is v_2 , is given by⁴:

$$\Delta F_D = 2\pi^{1/2} \sigma_u \xi - 2\rho \sigma_e \ln v_2 - \xi \rho \Delta f'_u + \xi \rho \frac{RT}{x} v_2 - \rho RT \ln \frac{x - \xi + 1}{x} \quad (8)$$

where σ_e is the lateral interfacial free energy per repeating unit as it emerges from the crystal face normal to the chain direction. The third term in equation (8) represents the depressed energy of fusion for the units involved in the transformation. By taking into account equation (6) $\Delta f'_u$ can be written in the following way:

$$\Delta f'_u = \Delta f_u - RT \frac{V_u v_1}{V_1} \left\{ 1 - \left[g_{\text{conc}} + \left(\frac{1}{2} - \chi_1 \right) \times (1 - h(z)) (1 + \lambda)^{-1} \exp(-\lambda_0 x^{1/2} v_2) \right] v_1 \right\} \quad (9)$$

where Δf_u is the energy of fusion per repeating unit for a chain of infinite molecular weight, V_u is the volume unit per repeating unit of the polymer and V_1 is the molar volume of the diluent.

As has been described in a previous work⁴, the surface described by equation (8) contains a saddle point and the coordinates of this point prescribe the dimensions of a nucleus of critical size. These dimensions are given by the relations:

$$\begin{aligned} \rho^{1/2} &= \frac{2\pi^{1/2} \sigma_u}{\Delta f'_u - (RT/x) v_2 - RT/(x - \xi + 1)} \\ \frac{\xi}{2} &\left(\Delta f'_u - \frac{RT}{x} v_2 + \frac{RT}{x - \xi + 1} \right) \\ &= 2\sigma_e - RT \ln v_2 - RT \ln \frac{x - \xi + 1}{x} \\ &= 2\sigma'_e - RT \ln \frac{x - \xi + 1}{x} \quad (10) \end{aligned}$$

and the free energy change, ΔF , involved in forming the critical nucleus is given by:

$$\Delta F = \pi^{1/2} \xi \rho^{1/2} \sigma_u \quad (11)$$

If a bidimensional nucleation is assumed and we use the concepts and notation of a previous analysis, the change in

free energy that accompanies the formation of a bidimensional nucleus, ξ units long and ρ sequences breadth is given by:

$$\Delta F = 2\sigma_u \xi \quad (12)$$

where ξ is expressed by the equation:

$$\xi = \frac{2\sigma'_e - RT \ln \frac{x - \xi + 1}{x}}{\Delta f'_u - \frac{RT}{x} v_2} \quad (13)$$

It is quite clear, independent of the type of nucleation assumed, that the free energy is strongly dependent on the depressed energy of fusion and this magnitude depends on the polymer-diluent interaction. The analysis of g according to the treatment of Koningsveld *et al.*¹⁸ is perfectly feasible in principle, but for its practical implementation a precise specification of the dependence of the second virial coefficient on molecular weight distribution is required. Present experimental and theoretical knowledge is quite limited. We are thus not in a position to evaluate the dependence of g on molecular weight and will use the approximation $g = \chi_1$ in further calculation. Moreover, we should stress that the estimation of χ_1 is a difficult task indeed; as a consequence, different authors obtain different values and the difference between these values are perhaps greater than the contribution to g of the corrections due to the excluded volume effects.

Temperature coefficient

The characteristic strong negative temperature coefficient found in the crystallization of polymer suggests a nucleation controlled crystallization. Taking, $\tau_{0,1}$, the time required for 10% of the crystallization to occur, as a measure of the rate constant and assuming for simplicity that only one type of nucleation process is rate controlling, the data can be analysed by the equation:

$$\ln \tau_{0,1}^{-1} = (\ln \tau_{0,1}^{-1})_0 - \frac{\Delta F}{RT} \quad (14)$$

where T is the crystallization temperature and ΔF is the energy required for the formation of a critical nucleus. If the rate determining step requires the formation of a two dimensional nucleus, then for chains of high molecular weight:

$$\ln \tau_{0,1}^{-1} = \ln (\tau_{0,1}^{-1})_0 - \frac{2\sigma_u \sigma'_e}{T \Delta f'_u} \quad (15)$$

It is clear that $2\sigma_u \sigma'_e$ can be obtained from the straight lines in the plot $\ln \tau_{0,1}^{-1}$ vs. $1/T \Delta f'_u$. The slopes of these lines are clearly dependent on the value taken for χ_1 . Taking as a typical example the polyethylene-tetralin system, if χ_1 for tetralin were taken to be 0.39 as reported by Nakajima *et al.*¹⁰ instead of 0.20, the earlier value given by Quinn and Mandelkern¹⁶, then σ'_e would increase from 3.000 cal/mol, to 4.800 cal/mol (Figure 6) if σ_u is equal to 58 ± 2 cal/mol, as it has been suggested by Mandelkern *et al.*⁶. Similar variations are observed in the other solvents. Therefore it is possible that within the uncertainty of the present

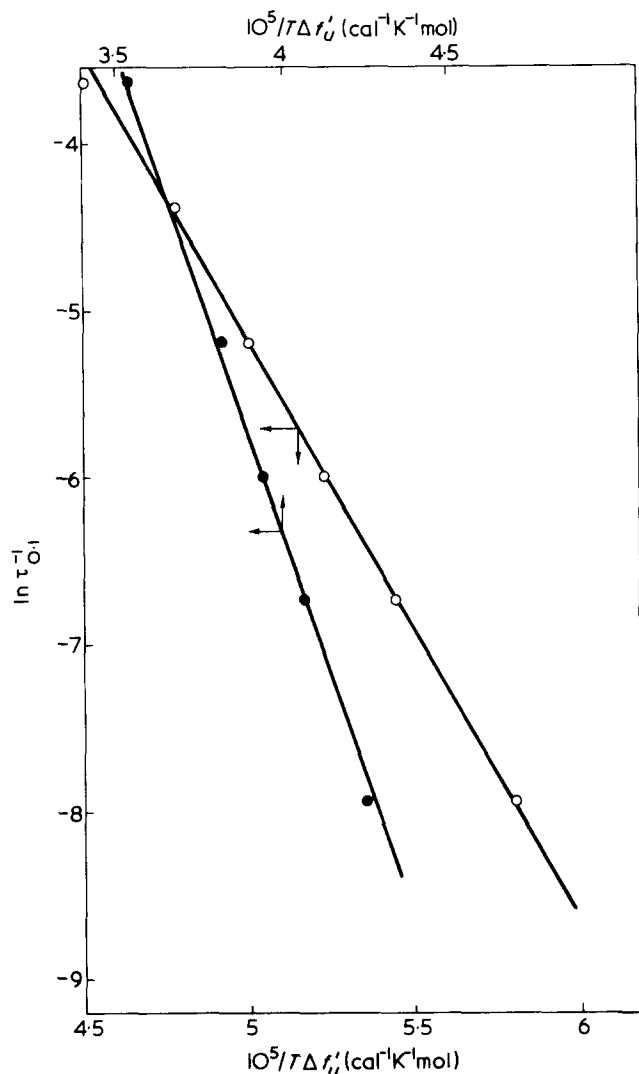


Figure 6 Influence of χ_1 in the coefficient temperature for polyethylene in tetralin

assignment of χ_1 , different values could be obtained for the slopes for each solvent. Consequently relatively high differences in the product of the interfacial free energies cannot be ruled out of this procedure.

It is thus paramount to assign a correct value to the thermodynamic interaction parameter χ_1 . From nucleation theory it is easily shown that equation (15) can be written in the following way:

$$\ln \tau_{0,1}^{-1} = \ln (\tau_{0,1}^{-1})_0 - \frac{2\sigma_u \sigma'_e}{\Delta H_u} \frac{T_s^0}{T \Delta T} \quad (16)$$

where ΔH_u is the enthalpy of fusion per repeating unit and T_s^0 , the equilibrium melting temperature (or dissolution temperature) of the dilute solution. As has been discussed in the literature^{3,8}, this quantity has evaded direct experimental determination and it has been obtained by various extrapolation procedures. The most reliable values of T_s^0 are represented in Table 2. Using these quantities a value of σ'_e equal to 4.800 cal/mol is obtained for polyethylene in different solvents when $\ln \tau_{0,1}^{-1}$ is plotted against $T_s^0/T \Delta T$ (Figure 7). This is the same value obtained by Mandelkern *et al.*⁶ from kinetic analysis and from the crystallite size-crystallization temperature relation⁸.

In order that the plots of Figures 6 and 7 for tetralin are consistent with one another the thermodynamic interaction parameter χ_1 should be 0.39 as has been reported by Nakajima *et al.*¹⁰. For the same reason of consistency we have used for other solvents the values of χ_1 which are summarized in Table 3. These chosen values completely agree with the values reported for decalin, xylene and tetralin and they are higher for chloronaphthalene and hexadecane. By using these values in equations (12) and (13), a set of parallel lines are obtained, and from the slopes a value σ'_e of 4.800 cal/mol is obtained.

The fact that solvents with different interaction parameter χ_1 , such as decalin and tetralin, are characterized by the same slopes in Figure 8 indicates that the interfacial free energies controlling the kinetics of crystallization are independent of the nature of the medium. A similar conclusion has been made earlier by other investigators^{6,7}. This is a very important finding as it enables the temperature solution T_s^0 and the interaction parameter χ_1 for any

Table 2 Values of T_s^0 , the dissolution temperature, for different solvents

Solvent	T_s^0 ^a (°C)	T_s^0 ^b (°C)
Decalin	112.6 ± 2	113.0 ± 1.5
Xylene	118.6 ± 2	118.6 ± 2
Tetralin	118.6 ± 2	—
n-Hexadecane	131.7 ± 2	133.1 ± 2

^aObtained from crystallite sizes (ref 7); ^bobtained from nucleation theory (ref 7)

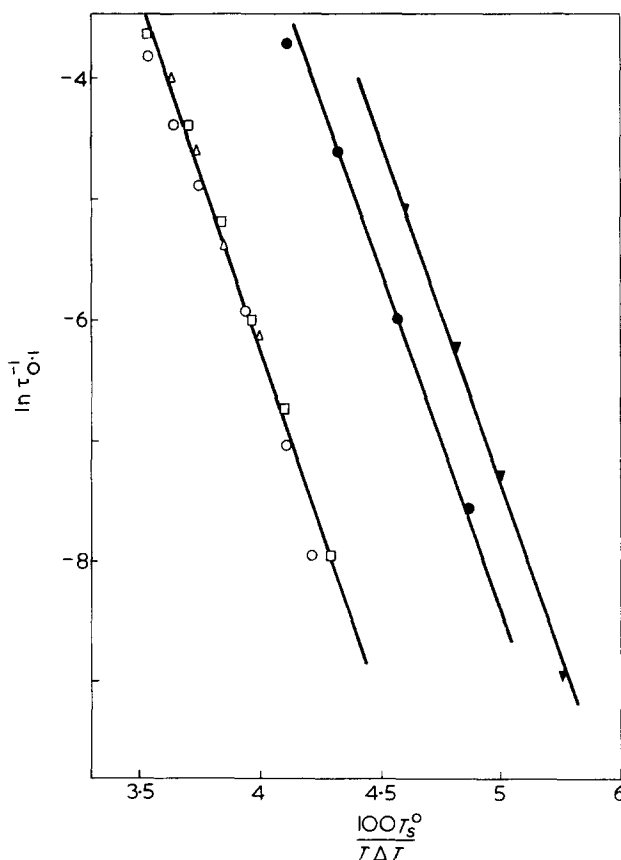


Figure 7 Plot of $\ln \tau_{0,1}^{-1}$ against $T_s^0/T \Delta T$ for the indicated solvents: \circ , decalin; \square , tetralin; \triangle , xylene; \bullet , n-hexadecane; \blacktriangledown , chloronaphthalene

Table 3 Calculated values of thermodynamic parameters for different solvents

Solvent	V_1 (cm ³ /mol)	T_s^0 (°C)	χ_1	T_c^a (°C)	$\frac{1 - \chi_1}{V_1}$
Decalin	170	112.6	0.10	84	5.29×10^{-3}
Xylene	131	117.0	0.38	88	4.73×10^{-3}
Tetralin	143	118.6	0.39	89	4.27×10^{-3}
Chloronaphthalene	144	122.0	0.43	96	3.90×10^{-3}
Hexadecane*	315	131.7	0.35	105	2.06×10^{-3}

^aTemperature at which 10% of crystallization occurs in 100 min. *The kinetic data for the analysis were taken from ref 6

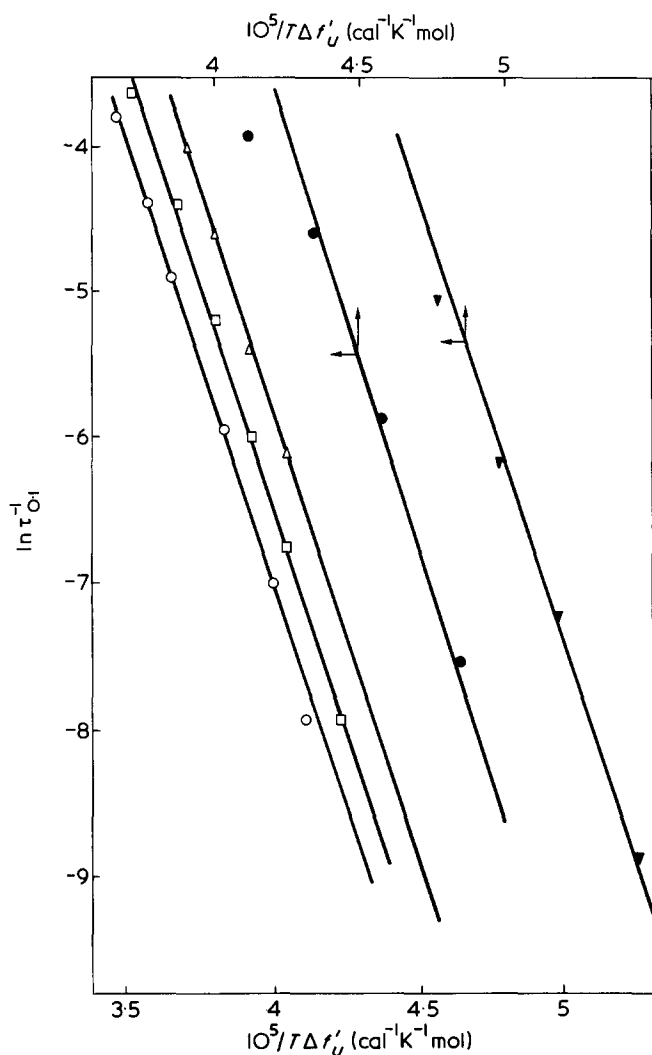


Figure 8 Plot of $\ln \tau_{0,1}^{-1}$ against $10^5/T\Delta f'_U$ for the indicated solvents: \circ , decalin; \square , tetralin; \triangle , xylene; \bullet , n-hexadecane; \blacktriangledown , chloronaphthalene

given polyethylene-solvent system to be established if kinetic data are available. Thus, for instance, from our kinetic data we conclude that the equilibrium melting temperature of polyethylene in α -chloronaphthalene should be equal to 122.0°C and χ_1 equal to 0.43. On the same basis, $T_s^0 = 117.6^\circ\text{C}$ and $\chi_1 = 0.38$ for polyethylene in xylene.

It is interesting to analyse the influence of the solvent on the crystallization. The crystallization temperature for 10% of the transformation to occur in a given time, has

been indicated in Table 3. For any given crystallization temperature the depressed free energy of melting depends on $(1 - \chi_1)/V_1$ and as a consequence, the change of free energy involved in forming a critical nucleus increases as $(1 - \chi_1)/V_1$ increases. Therefore, the crystallization temperature should increase as $(1 - \chi_1)/V_1$ decreases as our results show.

With the establishment of the equilibrium dissolution temperature or the thermodynamic interaction parameter χ_1 , it is possible to assess the influence of the crystallizing medium and the temperature on the size of the critical nucleus in the chain direction. By assuming bidimensional nucleation, ξ is given by equation (13) and depends strongly on $(1 - \chi_1)/V_1$. With the values of χ_1 from Table 3, ξ can be calculated from equation (13). It is worthwhile stressing that these values calculated coincide quite well with the mature crystallite thicknesses, which have already been measured as a function of the crystallization temperature¹⁰.

In the analysis of the temperature coefficient of the crystallization process which has been carried out above, we have assumed the same temperature coefficient for both initiation and growth nucleation. This is a fairly standard assumption commonly used. In order to confirm this assumption we compare our results, based on overall temperature coefficient analysis, with the recent results of Cooper and Manley²³, who have measured the growth rates of polyethylene single crystals in xylene as a function of solution concentration, molecular weight and crystallization temperature using the self-seeding method. On increasing the concentration from 0.001 to 0.1%. Cooper and Manley found that the free energy product $\sigma_u \sigma_e$ increases with molecular weight in agreement with our earlier results of polyethylene in chloronaphthalene⁵. If a two dimensional process is assumed, the product $2\sigma_e \sigma_u$ is found to be $5 \times 10^5 \text{ cal}^2/\text{mol}^2$ when the concentration is 0.1%. Although this quantity is about 12% lower than the corresponding one deduced here for overall crystallization, the values can be considered comparable. Therefore, the suggestion is that the temperature coefficient of the overall process is a reflection of the temperature coefficient of lateral crystallite growth.

ACKNOWLEDGEMENT

We thank Professor L. Mandelkern for several helpful discussions on this work.

REFERENCES

- 1 Keller, A. *Phil. Mag.* 1957, 2, 1171
- 2 Fischer, E. W. *Z. Naturforsch (A)* 1957, 12, 753
- 3 Mandelkern, L. 'Crystallization of Polymer', McGraw-Hill, New York, 1964

- 4 Fatou, J. G., Riande, E. and Valdecasas, R. G. *J. Polym. Sci. (Polym. Phys. Edn)* 1975, **13**, 2103
- 5 Riande, E. and Fatou, J. G. *Polymer* 1976, **17**, 99
- 6 Devoy, C., Mandelkern, L. and Bourland, L. *J. Polym. Sci. (A-2)* 1970, **8**, 869
- 7 Ergoz, E. and Mandelkern, L. *J. Polym. Sci. (Polym. Lett. Edn)* 1973, **11**, 73
- 8 Jackson, J. F. and Mandelkern, L. *Macromolecules* 1968, **1**, 546
- 9 Sharma, R. K., Mandelkern, L. and Jackson, J. F. *Am. Chem. Soc. Meeting, New York* 1969
- 10 Nakajima, A., Hamada, F., Hayashi, S. and Sumida, T. *Kolloid Z.* 1968, **222**, 10
- 11 Nakajima, A., Hayashi, S., Korenaga, T. and Sumida, T. *Kolloid Z.* 1968, **222**, 124
- 12 Fatou, J. G. and Mandelkern, L. *J. Phys. Chem.* 1965, **69**, 71
- 13 Chiang, R. *J. Polym. Sci.* 1959, **36**, 91
- 14 Göler, V., Sachs, F. and Sachs, G. *Z. Phys.* 1932, **77**, 281
- 15 Ergoz, E., Fatou, J. G. and Mandelkern, L. *Macromolecules* 1972, **5**, 147
- 16 Quinn, F. A. and Mandelkern, L. *J. Am. Chem. Soc.* 1958, **80**, 3178
- 17 Flory, P. J. *J. Chem. Phys.* 1949, **17**, 223
- 18 Koningsveld, R., Stockmayer, W. H., Kennedy, J. W. and Kleintjens, L. A. *Macromolecules* 1974, **7**, 73
- 19 Tompa, H. 'Polymer Solutions', Butterworths, London, 1956
- 20 Huggins, M. L. *Ann. N.Y. Acad. Sci.* 1942, **43**, 1
- 21 Flory, P. J. 'Principles of Polymer Chemistry' Cornell University Press, New York, 1953
- 22 Mandelkern, L. *Polymer* 1964, **5**, 637
- 23 Cooper, M. and Manley, R. St. J. *Macromolecules* 1975, **8**, 219

Effect of intra-chain double bonds on the melt crystallization of aliphatic polyesters

A. Di Meo, G. Maglio, E. Martuscelli and R. Palumbo

Laboratorio di Ricerche su Tecnologia dei Polimeri e Reologia, CNR, Arco Felice (Napoli), Italy

(Received 16 March 1976; revised 10 May 1976)

The influence of intra-chain double bonds on the crystallization rate of a series of linear aliphatic polyesters was investigated. The free energy of formation of a nucleus of critical dimensions decreases with the percentage of double bonds along the chain. The values of the free energy of folding drastically decreases with an almost linear trend with increase in the amount of unsaturation. The results may be interpreted assuming that the increasing chain flexibility decreases the free energy of formation of a nucleus of critical dimensions mainly because of a lamellar surface effect.

INTRODUCTION

The influence of intra-chain double bonds, introduced along the chain of polyamides and linear polyethylene, on the crystallization rate from the melt has been reported previously^{1,2}. The results have shown that both kinetic and thermodynamic quantities such as the half time of crystallization, kinetic rate constant, the free energy of formation of a nucleus of critical dimensions and the surface free energy of lamellar fibrillae of spherulites are dependent upon the chain flexibility, i.e. upon the amount of double bonds distributed along the macromolecular chain.

This investigation has been extended to include crystallization rate measurements for a series of linear aliphatic polyesters with various amounts of double bonds along the chain.

The whole research is part of a general project leading to the study of the properties of some important class of polymers whose chemical structure has been modified³.

EXPERIMENTAL

Materials

The polyesters were prepared by melt polycondensation of 1,16-hexadecandiol with the acid chlorides⁴. They are reported in *Table 1*, along with their composition, inherent

Table 1 Composition, inherent viscosity and molecular weight of the prepared polyesters

Polyester ^a	Name	Molar fraction of 4-OD	η_{inh} (dl/g) ^b	\bar{M}_n ^c
SUB-1,16-HDD	P _s	0	0.99	—
SUB-4-OD-1,16-HDD	P ₁	0.20	1.06	11,000
SUB-4-OD-1,16-HDD	P ₂	0.57	1.30	11,000
SUB-4-OD-1,16-HDD	P ₃	0.75	0.80	10,500
4-OD-1,16-HDD	P _i	1.00	1.16	—

^aSUB = suberic acid; 4-OD = *trans*-4-octen-1,8-dioic acid; 1,16-HDD = 1,16-hexadecandiol. ^bIn tetrachloroethane/phenol mixture (60/40 by wt) at 30°C, C = 0.5 g/dl. ^cNumber-average molecular weight determined in CHCl₃ by vapour pressure osmometry at 40°C

Table 2 Crystallinity X_c , apparent enthalpy of fusion ΔH_F^* and thermodynamic enthalpy of fusion ΔH_F of the investigated polyesters

Sample	Molar fraction of 4-OD	ΔH_F^* (cal/g)	X_c (%)	ΔH_F (cal/g)
P _s	0	26.7	67	40
P ₁	0.20	23.2	66	35
P ₂	0.57	18.7	59	32
P ₃	0.75	18.4	56	33
P _i	1.00	18.6	57	33

viscosity and number-average molecular weight. From the data reported in *Table 1* it may be deduced that effects of the molecular weight on the crystallization kinetics should be negligible.

Calorimetry

All the measurements were carried out using a Perkin-Elmer DSC-2 differential scanning calorimeter operating under N₂ atmosphere with samples of 4 to 8 mg by wt.

The temperature scale was calibrated against the melting temperature of high purity standards for each of the individual heating rates. For the determination of the heat of fusion indium was used as the standard material. The following procedure was used to record the crystallization exotherm: the sample was kept for 10 min at a temperature 20°C higher than the melting temperature T_m and then cooled rapidly to the predetermined crystallization temperature T_c and the exothermic curve of crystallization was recorded. Furthermore the melting thermograms of the crystals formed in the isothermal crystallization were performed after each crystallization run. The maxima of the melting endotherms were taken to be the melting temperatures. The method used for the determination of the weight fraction of crystallized material at time t , X_t , has been described in detail in previous papers^{1,2}.

Measurement of X-ray diffraction patterns

The wide-angle X-ray diffraction patterns were recorded at room temperature over the range of diffraction angles (2θ) from 2° to 50° with nickel filtered CuK α radiation by

RESULTS AND DISCUSSION

Kinetics and thermal data

Typical examples of crystallization isotherms obtained by plotting X_t versus time are shown in Figure 1. From these curves the half life time of crystallization $t_{1/2}$ was calculated. The variation of $t_{1/2}$ with T_c is given in Figure 2 for each of the polyesters investigated.

For every T_c and for each sample the Avrami exponent n was calculated from the slopes of the lines obtained by plotting the quantity $\log[-\log(1 - X_c)]$ against $\log t^6$ and thereafter the rate constant Z was calculated according to the relation:

$$Z = \frac{\ln 2}{(t_{1/2})^n} \quad (2)$$

Typical Avrami plots are shown in Figure 3.

The values of the equilibrium melting temperature were graphically determined by plotting the melting temperature T_m versus the crystallization temperature T_c by using the well known relation⁷:

$$T_m = T_m^0 \left(\frac{\gamma - 1}{\gamma} \right) + \frac{T_c}{\gamma} \quad (3)$$

where γ is constant.

In Table 3 the values of n and $\log Z$ are given as functions of T_c together with T_m^0 for each polyester examined. The values of n range from 2.8 to 4.1. T_m^0 decreases linearly with the increase in the amount of 4-OD units along the chain. This trend is shown in Figure 4.

For sample P_s, T_m^0 is equal to 382K while for sample P_i the value is reduced to 358K with a percentage lowering of 6.3%. Assuming that the crystallization of polymers from melt is of lamellar type then overall rate constant of crystallization Z can be described in terms of a classical equation^{7,8} which can be written as:

$$\frac{1}{3} \log Z + \frac{\Delta F^*}{2.3KT_c} = A_0 - \frac{\Delta \Phi^*}{2.3KT_c} \quad (4)$$

where ΔF^* is the activation energy for the transport of a chain unit across the liquid-crystal interface and $\Delta \Phi^*$ can be written:

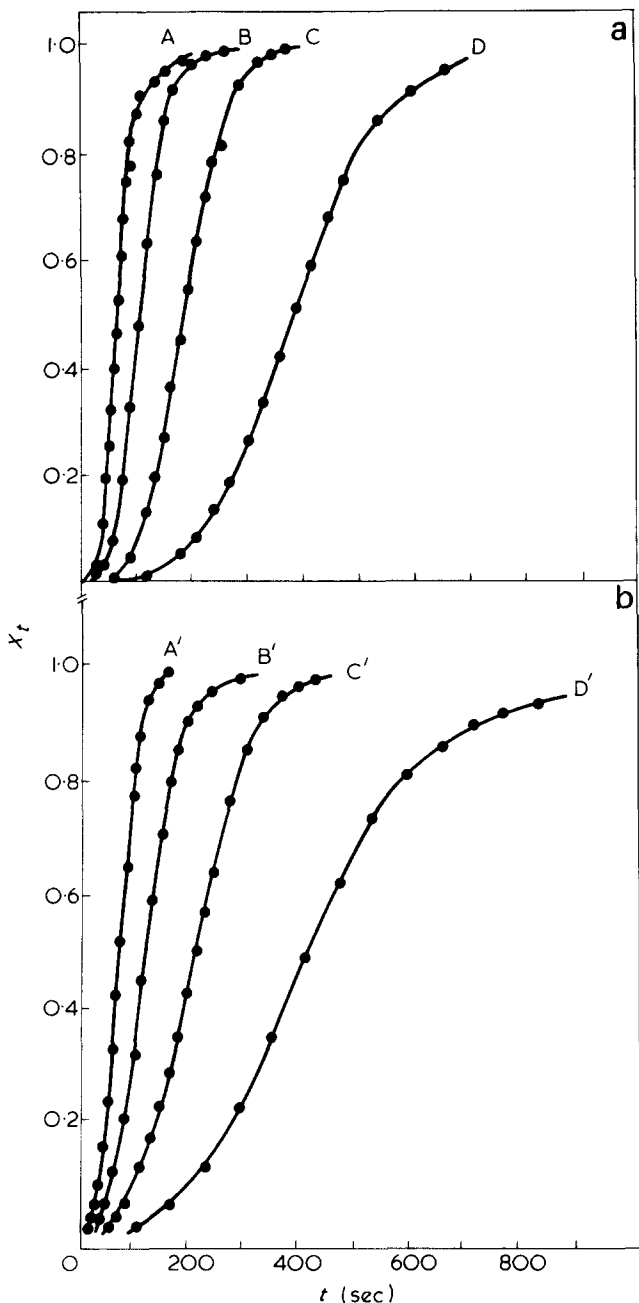


Figure 1 Crystallization isotherms of polyesters with different composition at various crystallization temperatures. (a) Sample P_s, T_c values: A, 346.5K; B, 347.5K; C, 348.4K; D, 349.4K. (b) Sample P_i, T_c values: A', 341.7K; B', 342.6K; C', 343.6K; D', 344.6K

using a Philips diffractometer. The scattering intensities of the crystalline part were obtained by subtracting the contribution of the amorphous part and the incoherent scattering from the total scattering intensity. To separate the contribution of the crystalline part and to calculate the mass crystallinity conventional methods were followed⁵.

The thermodynamic enthalpy of melting ΔH_F has been calculated by means of the simplified relation:

$$\Delta H_F = \frac{\Delta H_F^*}{X_c} \quad (1)$$

where ΔH_F^* is the apparent enthalpy of fusion as deduced from d.s.c. traces and X_c is the X-ray mass crystallinity. In Table 2 the quantities ΔH_F^* , X_c and ΔH_F are reported for each of the samples examined.

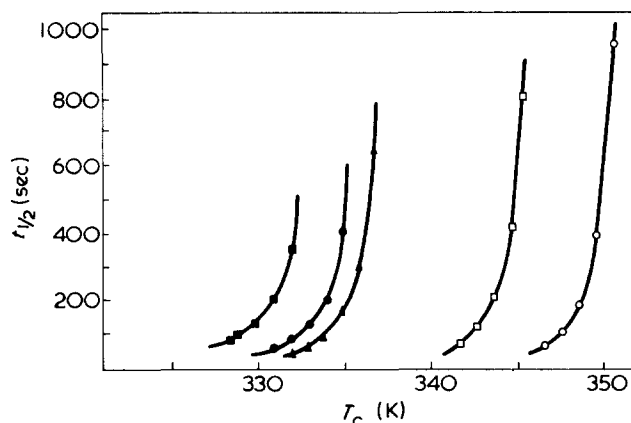


Figure 2 Variation of half time of crystallization $t_{1/2}$ with crystallization temperature for aliphatic polyesters. \blacksquare , P₁; \bullet , P₃; \blacktriangle , P₂; \square , P_i; \circ , P_s

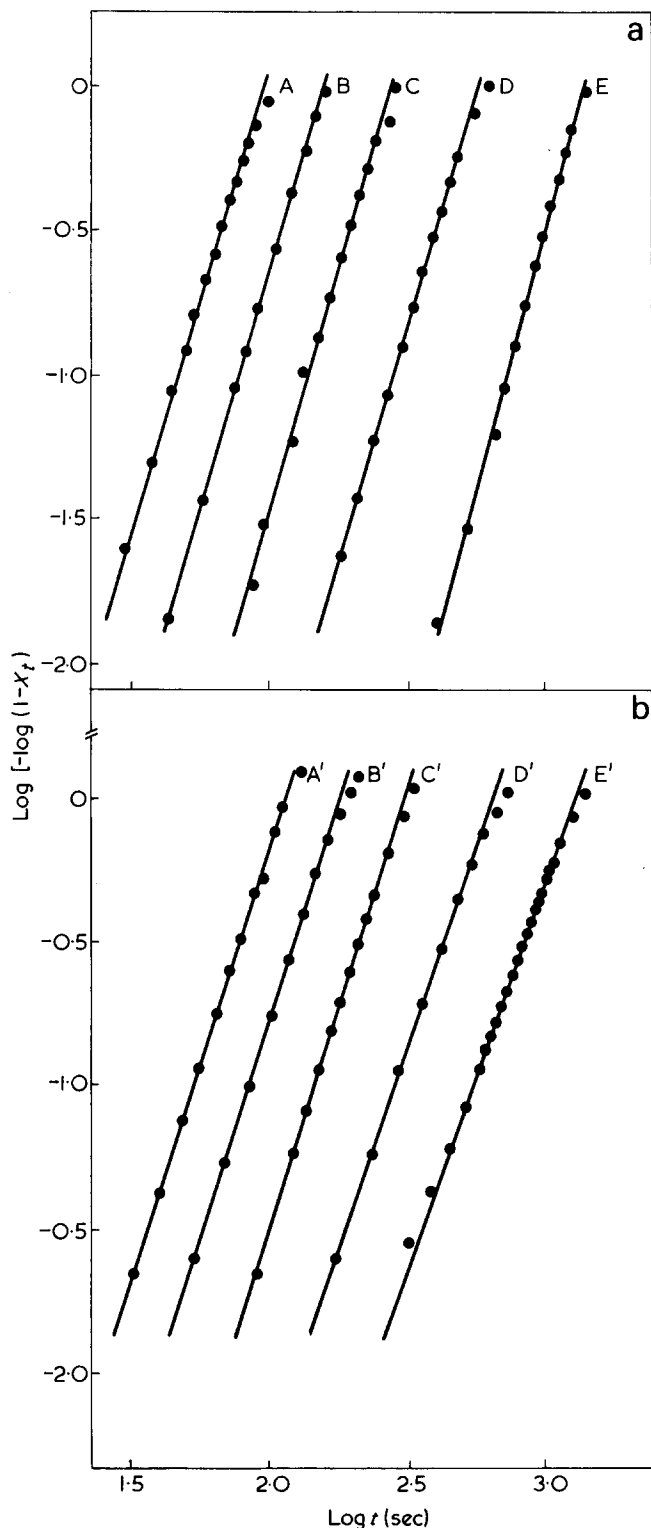


Figure 3 Avrami plots for copolyesters with different composition at various crystallization temperature. (a) Sample P_s, T_c values: A, 346.5K; B, 347.5K; C, 348.4K; D, 349.4K; E, 350.4K. (b) Sample P₁, T_c values: A', 341.7K; B', 342.6K; C', 343.6K; D', 344.6K; E', 345.3K

$$\Delta\Phi^* = \frac{4b_0\sigma\sigma_e T_m^0}{\Delta H_F(T_m^0 - T_c)} = \frac{4b_0\sigma\sigma_e T_m^0}{\Delta H_F\Delta T} \quad (5)$$

where b₀ is the distance of two adjacent fold planes and σ and σ_e are the free energies of formation per unit area of the lateral and end interfaces of the lamellar crystal respectively.

Equation (4) may be rewritten as:

$$\frac{1}{3} \log Z = A_0 - \frac{\Delta F^*}{2.3KT_c} - \frac{4b_0\sigma\sigma_e T_m}{\Delta H_F 2.3KT_c \Delta T} \quad (6)$$

According to equation (6) and taking the term A₀ and ΔF^{*}/KT_c to be relatively insensitive to temperature in the vicinity of the melting point, a plot of 1/3 (log Z) against T_m⁰/T_cΔT should be a straight line of slope 4σσ_eb₀/2.3KΔH_F. Such plots for the series of polyesters investigated are given in Figure 5. A linear trend is observed for all samples of polyesters. The values of the slopes of the straight line drawn through the experimental points are reported in Table 4. The free energy of formation of a nucleus of critical dimensions calculated from the slopes of Table 4 decreases with the percentage of 4-OD units along the chain of the polyesters. This trend is shown in Figure 6 for two different values of the undercooling.

Table 3 Values of the exponent of Avrami n and of the rate constant Z, at various crystallization temperatures. The equilibrium melting temperatures T_m⁰ are also reported

Sample	T _m ⁰ (K)	T _c (K)	n	\bar{n}	-log Z
P _s	382	346.5	3.3	3.54	6.57
		347.5	3.3		7.35
		348.5	3.6		8.21
		349.4	3.4		9.33
		350.4	4.1		10.51
P ₁	377	341.7	3.2	3.0	5.82
		342.6	3.2		6.45
		343.6	3.1		7.17
		344.6	2.8		8.07
		345.3	2.8		8.93
P ₂	368	331.9	4.0	3.9	6.39
		332.9	3.6		7.08
		333.9	4.0		7.86
		334.9	4.1		8.85
		335.9	3.8		9.61
P ₃	364	336.8	4.0	3.8	10.29
		330.9	3.5		6.93
		331.9	3.9		7.56
		332.9	4.0		8.28
P _i	358	333.9	3.9	3.9	9.00
		328.5	3.5		7.50
		328.9	3.5		7.89
		329.9	4.1		8.49
		330.9	4.2		9.15
		331.9	4.2		10.10

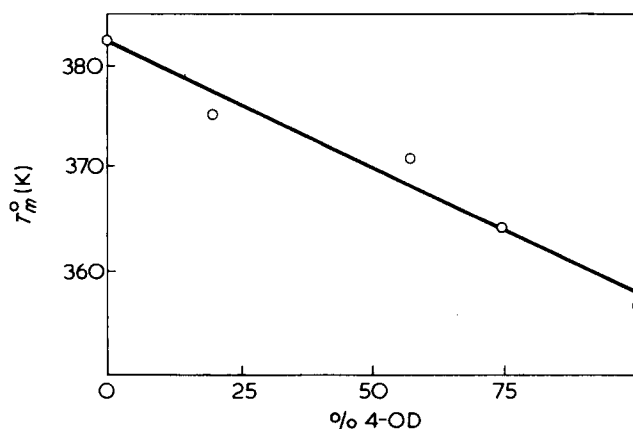


Figure 4 Variation of the equilibrium melting temperature, T_m⁰ with the percentage of 4-OD

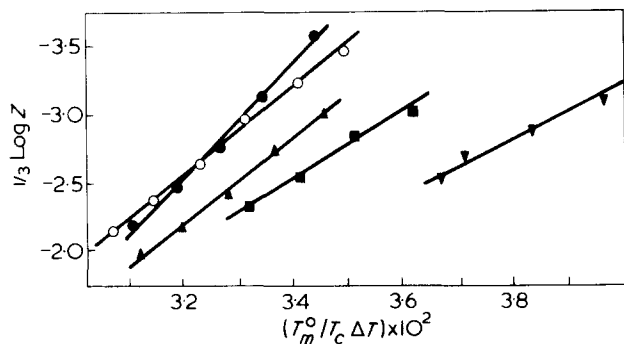


Figure 5 Plots of $1/3 \log Z$ against $T_m^0/T_c \Delta T$ for the samples of polyesters: ●, P_s ; ○, P_1 ; ▲, P_2 ; ■, P_3 ; ▼, P_i

Table 4 Values of the quantity $4b_0\sigma\sigma_e/\Delta H_F 2.3K$ obtained from the slopes of the lines of Figure 6

Sample	Molar fraction of 4-OD	$\frac{4b_0\sigma\sigma_e}{\Delta H_F 2.3K}$
P_s	0	384
P_1	0.20	320
P_2	0.57	310
P_3	0.75	246
P_i	1.00	201

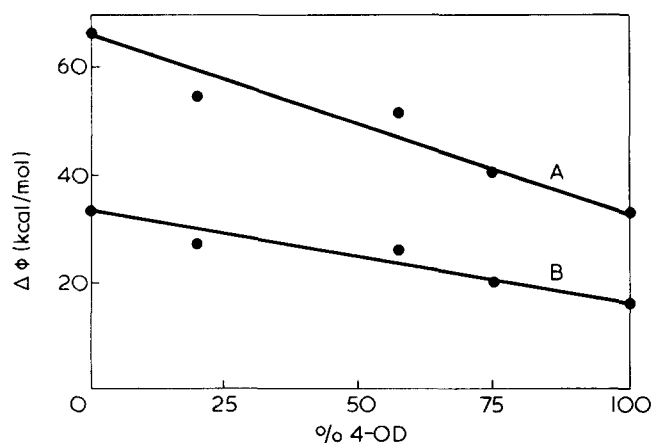


Figure 6 Variation of the free energy of formation of a nucleus of critical dimensions $\Delta\Phi^*$, as function of the copolyesters composition. The value of $\Delta\Phi^*$ are compared under the same values of ΔT . A, $\Delta T = 10$; B, $\Delta T = 20$

Wide-angle X-ray diffraction analysis of polyesters

Wide-angle X-ray diffraction traces of the polyesters under examination are given in Figure 7. It is well known from literature data⁹ that aliphatic polyesters generally crystallize according to a polyethylene-like monoclinic unit cell with the chains in a *trans* planar conformation.

For sample P_s we assumed a unit cell similar to that of 10–16 aliphatic polyester ($a = 6.47 \text{ \AA}$; $b = 7.38 \text{ \AA}$; $c = 37 \text{ \AA}$; $\beta = 115^\circ$) except for the length of the \bar{c} axis assumed equal to $37 - 2.5 \text{ \AA}$ where 2.5 \AA is the shortening due to the absence of two methylenic groups. According to this consideration it is possible to calculate for the equatorial (110) and (020) reflections; values of spacing of 4.14 and 3.69 \AA , respectively. These values agree very well with the observed spacings of the two most intense reflections on the X-ray traces of the P_s sample, 4.12 and 3.69 \AA , respectively.

These planes are also the most probable fold planes in the case of linear aliphatic polyesters. Sample P_1 shows an X-ray spectrum similar to that of P_s , only a shift toward smaller angles being observed for the (020) reflection.

The unsaturated polyester, sample P_i , has an X-ray diffraction pattern that is totally different from that of the sample P_s . This result is an indication that this polyester crystallizes in a different crystalline unit cell. The X-ray diffraction patterns of the P_2 and P_3 samples (0.57 and 0.75 molar fractions of 4-OD respectively) still show the reflection characteristic of the fully saturated polyester P_s together with some of the more intense reflections characteristic of the fully unsaturated polyester P_i . As observed in the case of the P_1 sample, the (020) reflection of the P_s -like phase shows also for P_2 and P_3 an increasing shift toward smaller angles indicating an expansion of the unit cell along the b -axis. This result is interpreted by assuming that unsaturated units can be incorporated in the P_s crystal lattice as defects. The relative intensities of the reflections lead us to conclude that, for the P_2 and P_3 samples, the fraction of material crystallized with a P_i -like structure is very low. This observation may account for

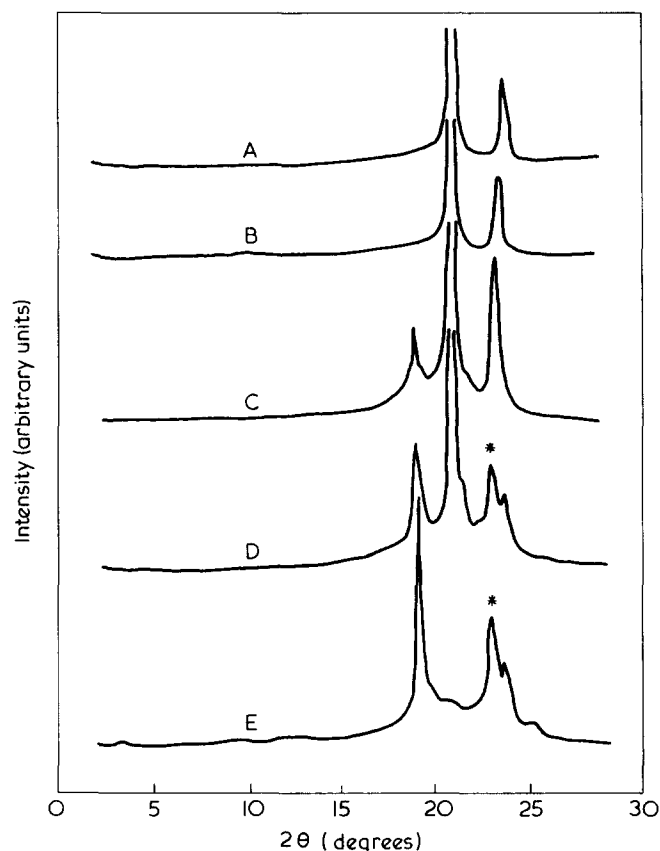


Figure 7 Wide angle X-ray diffraction traces of bulk polyesters (see text). A, P_s ; B, P_1 ; C, P_2 ; D, P_3 ; E, P_i

Table 5 Values of b_0 , $\sigma\sigma_e$, σ and σ_e for the investigated polyesters

Sample	$b_0(\text{\AA})$	$\sigma\sigma_e(\text{erg}^2/\text{cm}^4)$	$\sigma(\text{erg}/\text{cm}^2)$	$\sigma_e(\text{erg}/\text{cm}^2)$
P_s	3.69	2334	10.4	224
P_1	3.74	1692	9.3	182
P_2	3.77	1656	9.6	172
P_3	3.78	1198	8.8	136
P_i	3.83	964	8.8	110

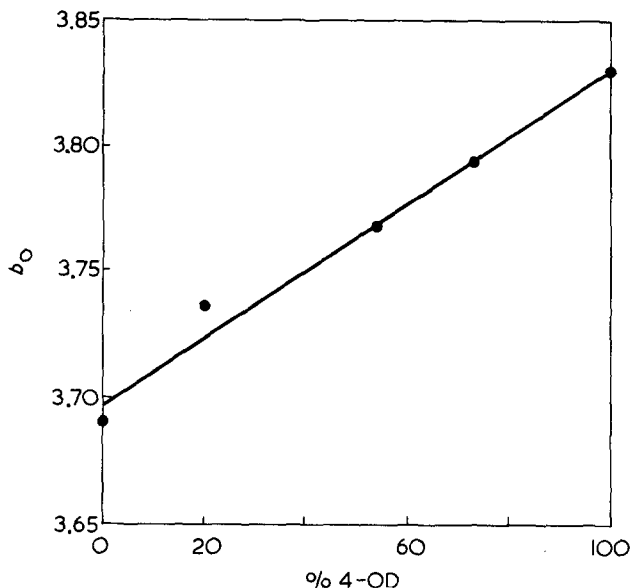


Figure 8 Variation of b_0 with the composition of the polyesters

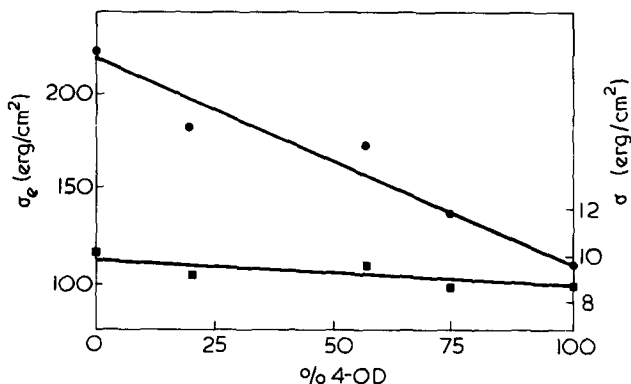


Figure 9 Effect of the copolyesters composition on the value of σ_e (●) and σ (■)

the absence of double peaks both in the fusion endotherm and in the crystallization exotherm.

Moreover to neglect the contribution of the very low amount of the P_i -like phase in the treatment of the thermal and kinetic data should not affect the qualitative trend of the thermodynamic parameters investigated as function of the composition.

For all the polyesters we assumed that the equatorial plane has a smaller spacing than the fold plane. These planes were identified by means of fibre spectra. The fold planes are coincident with the (020) reflection of the saturated polyester phase in the case of sample P_s , P_1 , P_2 , P_3 . For sample P_i we assumed as fold phase that corresponding to the marked peak in Figure 7.

The variation of this spacing, that is coincident with the term b_0 in equation (5), is shown in Figure 8 as function of the percentage of 4-OD units in the sample.

Surface free energies calculation

From the values of $4b_0\sigma\sigma_e/2.3K\Delta H_F$ of Table 4, b_0 and ΔH_F being determined for every samples, it was possible to calculate the quantity $\sigma\sigma_e$. The values are reported in Table 5.

The free energy σ of surfaces parallel to the chain axis of the lamellar crystals was calculated by means of the well known empirical relation⁷:

$$\sigma = \Delta H_F b_0 \alpha \quad (7)$$

where α for polymeric material is assumed equal to 0.1. From the values of $\sigma\sigma_e$ and σ the surface free energy of folding σ_e was obtained. The values of σ and σ_e are reported in Table 5.

As shown in Figure 10 σ_e drastically decreases with an almost linear trend with increase in the amount of unsaturation, whilst σ is practically constant. Values of σ_e of 224 and 110 erg/cm² are obtained for samples P_s and P_i respectively with a percentage reduction of 51%.

It can be concluded that the higher chain flexibility of the more unsaturated chains¹⁰ decreases the free energy of formation of a nucleus of critical dimension mainly because of a lamellar surface effect. This surface effect is probably due to an increase in the values of the surface entropy of folding σ_e . The same result was observed in the case of linear aliphatic copolyamides¹.

REFERENCES

- 1 Maglio, G., Martuscelli, E., Palumbo, R. and Soldati, I. *Polymer* 1976, 17, 185
- 2 Amelino, L. and Martuscelli, E. *Polymer* 1975, 16, 864
- 3 Martuscelli, E. and Pracella, M. *Polymer* 1974, 15, 306; Marchetti, A. and Martuscelli, E. *J. Polym. Sci. (Polym. Phys. Edn)* 1974, 12, 1649; Martuscelli, E. *J. Macromol. Sci. (B)* 1975, 11, 1
- 4 Wing Foot Corp., US Pat. 2 589 687 (1952); Flory, P. J. and Leutner, F. S. *Chem. Abstr.* 1952, 46, 5891a; Maglio, G., Marchetta, C., Palumbo, R. and Riva, F. to be published
- 5 Hermans, P. H. and Weidenger, A. *Makromol. Chem.* 1961, 44, 24; 1961, 50, 98
- 6 Sharples, A. 'Introduction of Polymer Crystallization', Arnold, London, 1966
- 7 Hoffman, J. D. *SPE Trans.* 1964, 4, 315
- 8 Hoffman, J. D. and Weeks, J. *J. Chem. Phys.* 1962, 37, 1723
- 9 Kanamoto, T., Tanaka, K. and Nagai, H. *J. Polym. Sci. (A-2)* 1971, 9, 2043
- 10 Martuscelli, E. *Acta Crystallogr.* 1967, 23, 1086; Corradini, P., Frasci, A. and Martuscelli, E. *Chem. Commun.* 1969, p779; Martuscelli, E. and Frasci, A. *Acta Crystallogr. (B)* 1969, 25, 2547

Chain conformation of poly-(tetramethylene terephthalate) and its change with strain

I. H. Hall and M. G. Pass*

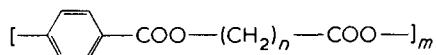
Department of Pure and Applied Physics, University of Manchester Institute of Science and Technology, Manchester M60 1QD, UK

(Received 1 March 1976; revised 21 April 1976)

In monofilaments of poly(tetramethylene terephthalate) the chain conformation changes reversibly between two forms as the fibre is strained. Both forms and their packing have been determined using the techniques of X-ray diffraction. In the unstrained form the methylene section of the chain has the conformation *gauche-trans-gauche*; on straining this changes to *trans-trans-trans*. The consequences of this change on other structural parameters are discussed in detail.

INTRODUCTION

Poly(tetramethylene terephthalate) is a member of the family of polymers having the structural formula:



and abbreviated n-GT. The best known member of this series is 2GT [poly(ethylene terephthalate)] which has been extensively studied. Other members have received much less attention. The series is of particular interest with regard to relationships between structure and properties of polymers, and previous publications have dealt with comparisons of melting points and glass transitions^{1,2}, with studies of molecular mobility using broad-line nuclear magnetic resonance²⁻⁴ and in a very limited way with crystallographic structure^{2,3,5}.

The present investigation forms part of a study of the relationship between the structure and properties of n-GT for $n = 3, 4$, and 5 , using the techniques of X-ray diffraction and Laser-Raman spectroscopy. It has already been reported that the chain conformation of 3- and 4GT varies by a surprisingly large amount with strain⁶. The conformation of 4GT undergoes a discontinuous change at strains in the region of 4–6%, and in a preliminary publication the unstrained conformation has been described⁷ together with provisional indications of the way it changes with strain. The present paper is a detailed account of the determination of these structures. When it was in an advanced state of preparation the structure of 4GT was published⁸, but it is still of interest to compare the two independent sets of results.

EXPERIMENTAL

Material

4GT polymer chip with an intrinsic viscosity of 0.75 dl/g was made available for this study by ICI Fibres Ltd. It was spun into monofilament at 252°C, the collec-

tion speed being adjusted to give a filament of suitable diameter. The monofilament was drawn over a hot pin (90°C) and plate (170°C), giving a final diameter of 200 μm . A filament as coarse as this was chosen in order that a single fibre could be used in the experiments in which it was strained, and reasonably short X-ray exposures used. The final draw ratio of the fibre was 7:1.

Following drawing, the monofilaments were mounted, just taut, on a frame and annealed for at least 4 h at 202°C. They then had extremely well developed crystallinity and high orientation. After annealing, the birefringence was 0.183 ± 0.007 .

Recording of diffraction data

X-ray diffraction photographs were taken using nickel filtered $\text{CuK}\alpha$ radiation with a camera of the type described by Elliott⁹ and manufactured by G. and D. Searle Ltd. The essential feature of this camera is that a high-intensity, highly monochromatic beam of X-rays of about 40 μm diameter is focused at the film position giving a diffraction photograph of good resolution with comparatively short exposure time. A cylindrical film holder was used and the camera evacuated to eliminate air scatter.

The photographs of the unstrained material revealed biaxial orientation. This has been interpreted qualitatively, but in order to generate true cylindrical symmetry in the photographs used for structural analysis the fibre was spun about its axis whilst the exposure was being made. The specimen holder in which this could be carried out only became available later in the investigation. Some of the intensities were measured from photographs in which the fibre was stationary and may therefore contain some error due to biaxial effects.

To obtain diffraction photographs of the strained fibre, it was strained by 10% whilst mounted in the specimen holder used during the X-ray exposure. This value of strain was chosen because separate experiments had revealed that it was sufficient for most of the material to have adopted the strained conformation, and that diffuseness of the pattern increased at higher strains. The strained fibre was allowed to stand for a few hours so that major relaxation effects could occur before the exposure was made. Experiments

* Present address: ICI Fibres Ltd, Hookstone Road, Harrogate, Yorks, UK.

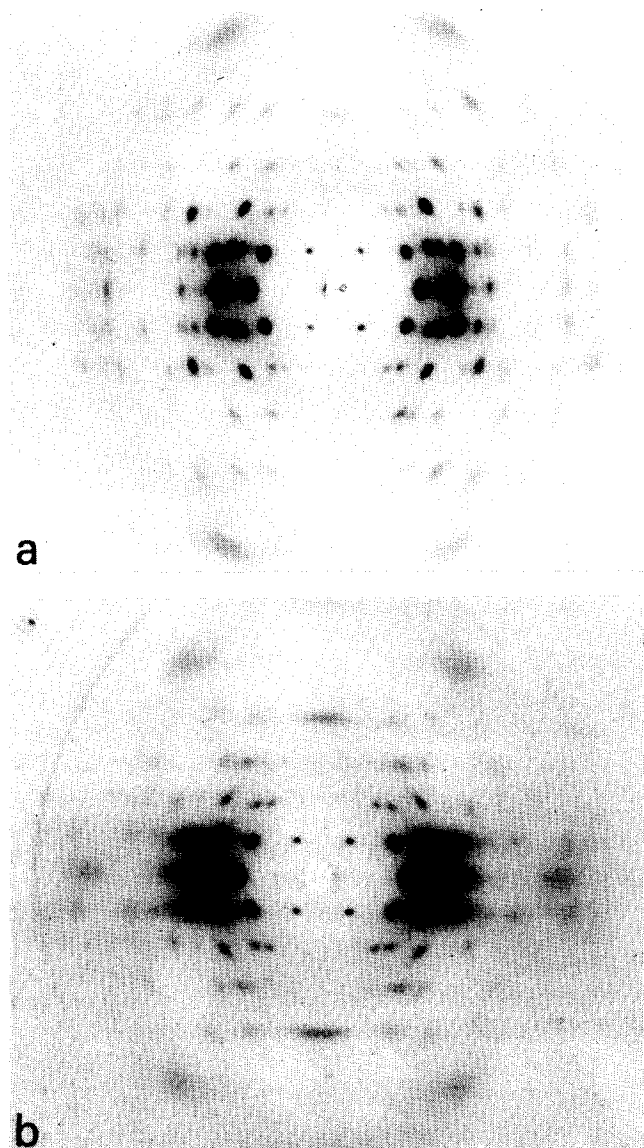


Figure 1 X-ray diffraction patterns of 4GT fibre. (a) Relaxed; (b) strained at 10%

in which the fibre was re-annealed whilst strained produced negligible improvement in the clarity of the diffraction pattern, and so this procedure was not adopted.

Biaxial orientation persisted in the strained state, and so the fibre was spun on its axis during the exposure. A diffraction pattern of each state of the fibre is shown in Figure 1.

Determination of unit cell parameters

The location of all the diffraction spots on the film was measured, and a reciprocal unit cell that would fit these was determined by trial and error. In the diffraction pattern of the unstrained fibre, the reflections were displaced up and down from the mean layer line positions, indicating that the molecular chain axes were systematically misoriented from the fibre axis by a few degrees, (i.e. the *c*-axis of the unit cell was slightly tilted with respect to the fibre axis). Similar behaviour was reported by Daubeny *et al.* for 2GT¹⁰ and following the method he described, the magnitude and direction of tilt was determined, and it was shown that displacement of all reflections could be explained this way, thereby confirming the correctness of the unit cell. This tilting persisted in the strained form, but not to such a

marked extent. Daubeny *et al.* found with 2GT that annealing under tension would remove the tilt. This did not occur with 4GT.

The unit cell parameters were refined by minimizing the sum of the differences between the squares of the *d*-spacings calculated from the location of the diffraction spots and those calculated from the unit cell. Since a *d*-spacing can be determined directly from the location of a reflection, even though it is displaced from a layer-line, this procedure was particularly convenient.

Determination of intensity of X-ray diffraction spots

The integrated intensity of each reflection was determined using an Optronix 'Photoscan' digital microdensitometer in conjunction with an Optronix 'Photowrite' machine. The technique has been fully described elsewhere¹¹. As far as possible, allowance was made for background intensity, and intensity was apportioned between partly overlapping reflections. Where this could not be done the reflections were treated as an overlapping group.

Determination of chain conformation

Relaxed form. Comparison of the density calculated from the unit cell dimensions with the measured value confirmed that there was one monomer of one molecular chain per cell. This monomer is illustrated in Figure 2 which also defines the symbols used to specify particular angles and bonds. It was assumed that the conformation was centro-symmetric about the points marked. An attempt to confirm this using intensity statistics was inconclusive.

Because of the small quantity and relatively poor quality of the intensity data, it was considered unlikely that a complete structural determination would be possible. Therefore bond lengths and angles were assumed to be the same as those in comparable low molecular weight compounds. Only the chain conformation angles and the orientation of the molecule in the unit cell then remain to be determined.

Bailey¹² and Ohrt *et al.*¹³ have determined the structures of compounds containing many similar bonds to those found in 4GT. Daubeny *et al.*¹⁰ attempted to determine bond lengths and angles in their structural analysis of poly(ethylene terephthalate) as did Tomashpol'skii and Markova¹⁴ from electron diffraction data. Very recently Pérez and Brisse¹⁵⁻¹⁷ have published the structures of ethylene glycol dibenzoate, ethylene glycol di-*para*-chlorobenzoate, and trimethylene glycol di-*para*-chlorobenzoate, all of which closely resemble the 4GT monomer. Bond lengths and angles from all these studies are listed in Table 1 and defined in Figure 2 (values obtained by Tomashpol'skii *et al.* have been omitted because some seem very questionable). Our own choice of assumed values is also given in this Table. Where discrepancies between the various values

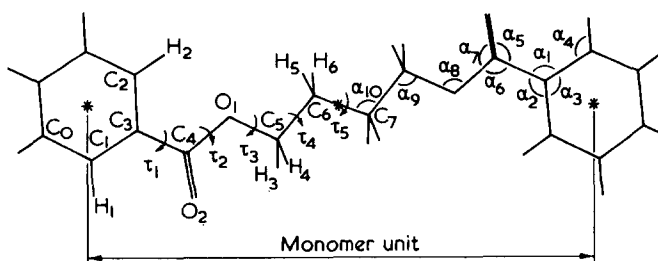


Figure 2 Monomer of 4GT. *Centre of symmetry

Table 1 Values of bond lengths and bond angles

Bond	Length (Å)							
	1	2	3	4	5	6	7	8
C ₀ -C ₁	1.39	1.36	1.41	1.38	1.38	1.37	1.40	1.38
C ₁ -C ₃	1.40	1.41	1.34	1.38	1.40	1.38	1.40	1.38
C ₂ -C ₃	1.38	1.39	1.41	1.39	1.40	1.39	1.40	1.39
H ₁ -C ₁				1.11	0.95	0.94	1.08	1.07
H ₂ -C ₂				1.10	0.99	0.93	1.08	1.07
C ₄ -C ₃	1.48	1.47	1.48	1.48	1.48	1.48	1.49	1.48
O ₂ -C ₄	1.28	1.22	1.26	1.21	1.20	1.21	1.23	1.21
O ₁ -C ₄	1.32	1.34	1.36	1.34	1.34	1.33	1.26	1.34
C ₅ -O ₁	1.51	1.47	1.45	1.44	1.45	1.49	1.41	1.44
H ₃ -C ₅				1.03	1.01	0.97	1.09	1.03
C ₆ -C ₅	1.55		1.48	1.50	1.49	1.50	1.53	1.50
C ₇ -C ₆							1.53	1.54/1.50
	Angle (degrees)							
α ₁	124	119	125	119	118	120	119	119
α ₂	118	123	118	121	123	121	119	121
α ₃	118	119	117	120	123	119	121	120
α ₄					116			120
α ₅	120	125	127	125	125	124	121	125
α ₆	115	113	110	113	113	113	119	113
α ₇	125	123	122	122	123	123	120	122
α ₈	117	117	114	116	116	117	119	116
α ₉	105		104	105	108	107	104	106
α ₁₀						115	105	109.5

1, From structure of diethyl terephthalate¹²; 2, from structure of *trans*-4-*t*-butyl cyclohexanol *para*-bromobenzoate¹³; 3, calculated from atomic coordinates of poly(ethylene terephthalate)¹⁰; 4, from structure of ethylene glycol dibenzoate¹⁵; 5, from structure of ethylene glycol di-*para*-chlorobenzoate¹⁶; 6, from structure of trimethylene glycol di-*para*-chlorobenzoate¹⁷; 7, assumed by Mencik⁸ in structural analysis of 4GT; 8, assumed in the present work.

For identification of bonds, see Figure 2. A blank has been left where no comparable bond exists in the model compound, or where it has not been possible to determine a value from the data given

exist we have used ones similar to those of Pérez and Brisse which are likely to be the most relevant to our work. No bond comparable with C₇-C₆ exists in any of the model compounds and we investigated two possibilities in our trial structures: (a) 1.54 Å which is comparable with the C-C bond in the methylene chain, and (b) 1.50 Å which is comparable with the value found by Pérez and Brisse¹⁵⁻¹⁷ in compounds where the C-C bond is adjacent to an O-C bond. A similar uncertainty exists in the value chosen for α₁₀. The only comparable bond in the compounds listed was in trimethylene glycol di-*para*-chlorobenzoate and was larger than similar bond angles in the methylene chain. The latter value was chosen but the effect of varying it was investigated.

The values chosen by Mencik⁸ are also listed in Table 1. It will be seen that several differ significantly from those chosen by us.

The terephthaloyl residue contributes most of the scattering power of the molecule and is likely to be almost planar. There is only one of these in each unit cell and so its centre was placed at the origin of coordinates, and, assuming it to be planar, the inclination found which gave best agreement between observed and calculated structure factors. Once the inclination of this unit is fixed there are only four different ways in which the section of chain O₁-C₅-C₆-C₇ can be added which will preserve the centre of symmetry, chain repeat length, bond lengths and bond angles. Hence four trial models were generated and the final conformation was found by refinement of these models.

If bond lengths and bond angles are fixed the only degrees of freedom available to the system are the chain conformation angles, τ₁ to τ₄ in Figure 2 (from the as-

sumption of centro-symmetry τ₅ = 180°), and angles which define the inclination of the molecule within the unit cell. This complete set of angles must satisfy the constraints of symmetry and chain repeat length, but subject to this requirement may be varied to minimize the sum of the squares of the differences between the observed and calculated structure factors, these differences being weighted according to some suitable scheme¹⁸. This technique of refinement of polymer structures was described by Arnott and Wonacott¹⁹ and a computer program for performing it was kindly made available for the present investigation by Professor Arnott (The Linked Atom Least Squares Structure Refinement System for Helical Polymers).

For the purpose of computation a model of the chain is built by successively adding atoms, starting at H₁ and proceeding to C₇ (Figure 2). Suppose the atom C₄ has been reached and O₁ is about to be laid down. Its position will be determined by three parameters, the bond length C₄-O₁, the bond angle α₆, and the conformation angle τ₁. The manner in which τ₁ is measured may be understood by reference to Figure 3. In this Figure the section of chain C₂-C₃-C₄-O₁ is held so that C₃-C₄ (the bond about which τ₁ is being measured) is normal to the plane of the diagram with C₂-C₃ (the section already built) above the plane of the diagram and C₄-O₁ (the section about to be built) below. τ₁ is then measured as shown. It is positive if measured clockwise, negative if anticlockwise.

When the chain conformation has been fixed, the molecule still has to be placed in the unit cell. Its location is totally, and its orientation partly, determined by the fact that the centre of a benzene ring lies at the cell origin, and the chain axis coincides with the C-axis. However, the rotation of the chain about its axis is still undetermined. This

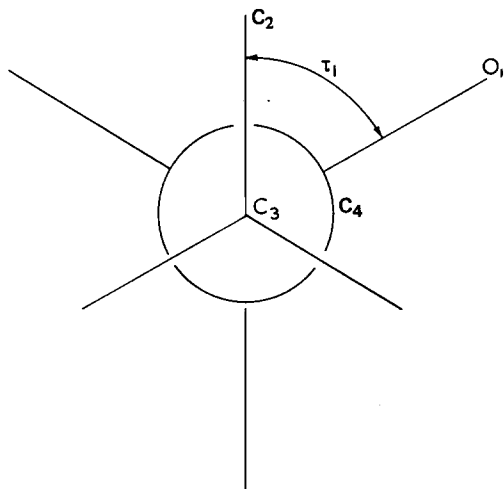


Figure 3 Convention for measuring the conformation angle τ

Table 2 Unit cell parameters

Parameter	Relaxed	Strained	Relaxed (from ref 8)
a (Å)	4.8(9)	4.7	5.96
b (Å)	5.9(5)	5.8	4.83
c (Å)	11.6(7)	13.0	11.62
α (degrees)	98.0	102	115.2
β (degrees)	116.(6)	121	99.9
γ (degrees)	110.0	105	111.3

The chain axis is in the c -direction

is specified by the angle θ . The molecule is placed in the unit cell so that the normal to the plane of the benzene ring lies in the (010) plane. θ is the rotation about the chain axis required to bring the molecule into its correct orientation and is positive if this rotation is anticlockwise looking in the negative C direction.

The uncertainty concerning the value of α_{10} has already been mentioned. In general bond-angles might be expected to vary more between compounds than bond lengths. Consequently, when the best models had been obtained by refining τ_1 – τ_4 , α_8 – α_{10} were refined. The choice between 1.50 and 1.54 Å for the bond C_6 – C_7 was based on the results from these final models.

Unobserved reflections were omitted from the refinement procedure and R -factors calculated using only observed reflections.

Strained form. In general the same procedure was followed as with the relaxed form, differences being dictated by the fact that the quality of the intensity data was much poorer in this case.

Refinement of bond angles and lengths was less likely to be conclusive, and so the final refined values from the relaxed form were used. A refinement was attempted, but the results are only quoted to indicate possible changes, not to define a conformation.

Unobserved reflections were included at threshold intensity and only omitted from the refinement if the calculated value was less than this. However, so that R -factors should be directly comparable with those from the relaxed form, the values quoted are calculated on observed reflections only.

RESULTS

Unit cell

The unit cells of both the relaxed and strained fibre were triclinic and the parameters are given in Table 2. Whilst experimental results show conclusively that the change in c occurs discontinuously, they do not show whether the much smaller changes in the other parameters take place discontinuously or not.

The transformation between the two structural forms is known to commence at a fibre strain of about 2%, and as strain is increased above this value progressively more material is transformed until a strain of about 10% is reached at which the transformation is complete²⁰.

At about 6% fibre strain near-equatorial reflections are blurred whilst near-meridional ones remain sharp. This blurring might be due to disorder in the lateral packing of chains, or because two species of unit cell with only slightly differing lateral dimensions are present.

At about 10% strain the 100 reflection remains blurred, but other equatorial ones have sharpened. The (100) planes are fairly close to those of the benzene rings, suggesting that the stacking of these rings is somewhat disordered in the strained state.

A value of 1.286 g/cm³ has been reported for the density of a specimen of 4GT which shows negligible evidence of crystallinity in its X-ray diffraction pattern²¹. The density calculated from the unit cell dimensions of the relaxed material was 1.39(0) g/cm³ and the measured value of the sample used was 1.336 g/cm³. These values correspond to a crystallinity by density of 48%. Since it was not possible to measure the density of the strained sample, no value can be given for this state.

Systematic misorientation of chain axes

The crystallites are tilted by rotation about an axis which lies in the a^*b^* plane at an angle of 42° from the line of intersection of this plane with the ac plane, the angle being measured anticlockwise looking in the negative

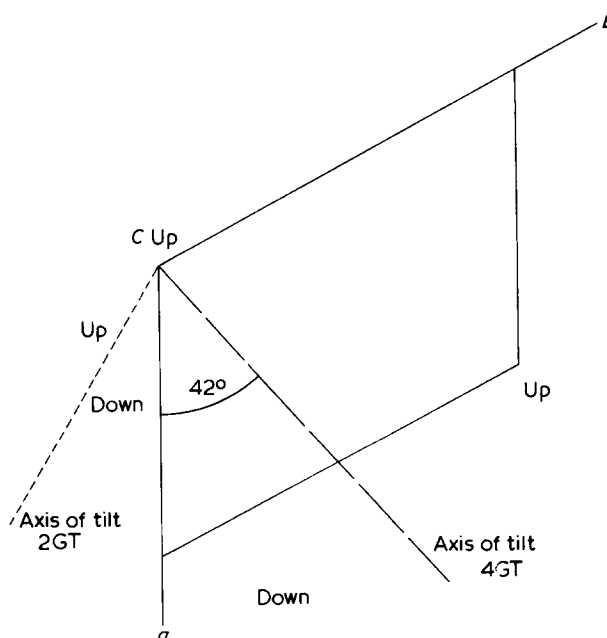


Figure 4 Projection of 4GT unit cell down c -axis showing axis about which tilting occurs

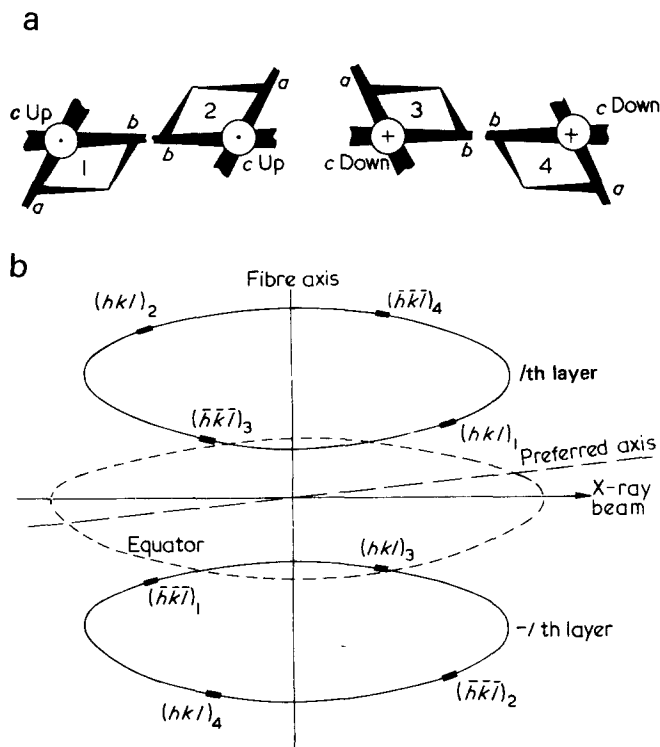


Figure 5 An example, showing four different unit cell orientations having two axial directions common. (a) Projections of the four cells down the c -axis. (It is assumed in this diagram that c and b -projected are the common directions. The direction of tapering indicates the directions in which the axes recede from the observer.) (b) Positions in reciprocal space of the same reciprocal lattice point for each cell

C direction. The magnitude of the tilt is such that the chain axes are, on average, inclined at an angle of $2^\circ \pm 0.2^\circ$ to the fibre axis. Its sense is such that the positive b -axis moves up, whilst the positive a -axis moves down (see Figure 4).

The (310) plane is almost normal to the tilt axis and so will remain vertical on tilting.

Biaxiality

The cross-section of the fibres was elliptical and photographs of stationary (not rotated) fibres showed indications of an axis of a preferred orientation of the crystallites in addition to the c -axis. Since the unit cell is triclinic, in this situation there can be four different possible orientations of the unit cell within the specimen. An example is illustrated in Figure 5a which shows projections of the cell edges on a plane normal to the c -axis and assumes that c and b -projected are the axes of preferred orientation. The plane containing these directions (100) (to be called the preferred plane) has the same orientation in each cell.

Figure 5b shows the positions of equivalent reciprocal lattice spots for each of these cell orientations [$(hkl)_1$ and $(\bar{h}\bar{k}\bar{l})_1$ are equivalent spots for the orientation labelled 1 in Figure 5a, and others are denoted similarly]. If it is assumed that all four orientations are equally probable, then the intensity of each of the illustrated reciprocal lattice points will be the same. Therefore, on a diffraction photograph of a stationary specimen (not rotated), equivalent spots above and below the equator (such as $(hkl)_1$ and $(\bar{h}\bar{k}\bar{l})_2$ in Figure 5b) will have the same intensity. In the general case, this will not be true for equivalent spots either side of the meridian; the relative intensities of these

will depend on their position relative to the sphere of reflection, i.e. on the orientation of the preferred plane relative to the X-ray beam. Their intensities will be equal only in the special case in which the beam is either parallel or perpendicular to this plane.

The intensity of equivalent spots above and below the equator was not equal on the diffraction photographs of the 4GT fibre used in this investigation. Thus the proportion of unit cells in an orientation such as 1 in Figure 5a was different from that in an orientation such as 2, and the proportion in an orientation such as 3 was different from that in 4.

On the other hand intensities of equivalent spots across the centre of the diffraction pattern tended to be similar. This cannot be interpreted without more detailed knowledge of the distribution of intensity in reciprocal space, but if the X-ray beam had been either parallel or perpendicular to the preferred plane, then it would imply that either the proportions in orientations such as 1 and 3 are similar, as are those in 2 and 4, or that the proportions in 1 and 4 are similar, as are those in 2 and 3. Both of these are consistent with the conclusion of the previous paragraph.

These results therefore indicate that there are two directions of preferred orientation in the fibre and that the four different unit cell orientations which are consistent with this do not occur in equal proportion.

To investigate biaxiality further, a sheet was prepared by melting polymer between hot plates under pressure. A section of this sheet was cold-drawn on a tensile testing machine and then annealed under vacuum for 24 h at 202°C . A Weissenberg photograph of the zero layer line showed that the b^* axis lay in the plane of the sheet or was, at most, inclined to it by a few degrees. Comparison of intensities in the different quadrants of a stationary-film photograph showed that all four possible cell orientations were present in approximately equal proportions. The biaxial texture was much more pronounced than with the fibre.

Chain conformation

Relaxed form. After preliminary refinement of the four trial models, it was clear that one gave much closer agreement between observed and calculated structure factors than the others. Subsequent investigations were confined to this model.

In the first stage of refinement, bond angles and lengths were kept constant at the values given in Table 1 and $\tau_1 - \tau_4$ allowed to vary. The values obtained for these angles at the end of this stage are given in columns 1 and 2 of Table 3 for both values of $C_6 - C_7$. In the second stage the bond angles $\alpha_8 - \alpha_{10}$ were allowed to vary as well as $\tau_1 - \tau_4$ and the values obtained at the end of this stage are listed in columns 3 and 4 of Table 3.

In this Table two parameters are given in addition to those defined already. These are not essential to defining the structure but help in visualizing the orientation of the terephthaloyl residue. ϕ is the angle between the bond $C_3 - C_4$ and the c -axis; ψ is the angle the normal to the benzene ring makes with the c -axis.

The different lengths for the bond $C_6 - C_7$ result in negligibly different conformations. If the values of α are kept constant during refinement R increases from 17.2 to 17.3 as the length of $C_6 - C_7$ is reduced from 1.54 to 1.50 Å. If the values of α are allowed to vary then R decreases from

Table 3 Parameters defining chain conformation

	Relaxed					Strained	
	1	2	3	4	5	6	7
τ_1 (degrees)	179.(8)	179.(3)	179.(7)	179.(3)	174.8	172.(9)	171.(3)
τ_2 (degrees)	-178.(6)	-179.(5)	-177.(3)	-177.(8)	-177.5	-178.(6)	-175.(3)
τ_3 (degrees)	-96.(3)	-96.(3)	-94.(5)	-94.(5)	-90.6	-159.(1)	-157.(1)
τ_4 (degrees)	-77.(6)	-79.(3)	-77.(9)	-79.(3)	-88.4	162.(2)	144.(4)
α_8 (degrees)	116.0	116.0	118.(8)	119.(0)	119	119.0	126.(1)
α_9 (degrees)	106.0	106.0	105.(2)	105.(1)	104	105.0	111.(1)
α_{10} (degrees)	109.5	109.5	112.(3)	112.(9)	109.5	113.0	112.(6)
C_6-C_7 (Å)	1.54	1.50	1.54	1.50	1.53	1.50	1.50
θ (degrees)	4.(8)	5.(2)	4.(2)	4.(4)		19.(5)	17.(8)
ϕ (degrees)	27.(4)	27.(4)	27.(7)	27.(7)		26.(4)	27.(6)
ψ (degrees)	74.(0)	74.(1)	73.(7)	73.(7)		86.(9)	86.(8)
R	17.2	17.3	17.0	16.8	14.8	22.3	21.8

In columns 1, 2 and 6, $\alpha_8-\alpha_{10}$ were fixed at the values given, in columns 3, 4 and 7 they were allowed to vary during the refinement procedure. Column 5 are the values found by Mencik⁸

Table 4 Amount by which atomic separations are less than sum of Van der Waals' radii

(a) Within a molecule		
Atom pair	(Sum of radii) - separation (Å)	
	Relaxed	Strained
O ₂ -C ₁	0.2(5)	0.2(5)
O ₁ -C ₂	0.3(8)	0.3(8)
O ₁ -H ₂	0.0(2)	0.0(2)
C ₅ -O ₂	0.4(1)	0.4(2)
H ₃ -C ₄	0.2(1)	0.1(6)
H ₃ -O ₂	0.0(7)	
C ₆ -C ₄	0.2(6)	

(b) Between molecules		
Atom pair	Unit cell translations between molecules	(Sum of radii) - separation, Strained model
H ₁ -C ₂	$a = 0, b = 1$	0.1(8)

17.0 to 16.8 with the same variation in C_6-C_7 . These differences are too small to be significant. However since the conformation in column 4 of Table 3 gave the lowest value of R , these parameters were used in the strained model. Tables and diagrams which refer to the relaxed form, and in which the particular conformation is not defined, are derived from the parameters in column 4.

It was assumed that the Van der Waals radius of the carbon atom was 1.7 Å, of oxygen was 1.4 Å, and of hydrogen was 1.0 Å. Using these values the separations of all pairs of non-bonded atoms were compared with the sums of their radii. Between molecules, all such separations were greater than this sum; within molecules, a few were less and these are listed in Table 4.

The chain conformation and packing within the unit cell is illustrated in Figures 6a-9a.

Strained form. Using values of bond lengths and angles modified according to experience with the relaxed form, four trial models were constructed as already described. Refinement of these again produced one which appeared better than the others. In this case, other factors were introduced as well as agreement between observed and calculated structure factors. (For example, τ_4 is known to move from a *gauche* towards a *trans* conformation²⁰ in

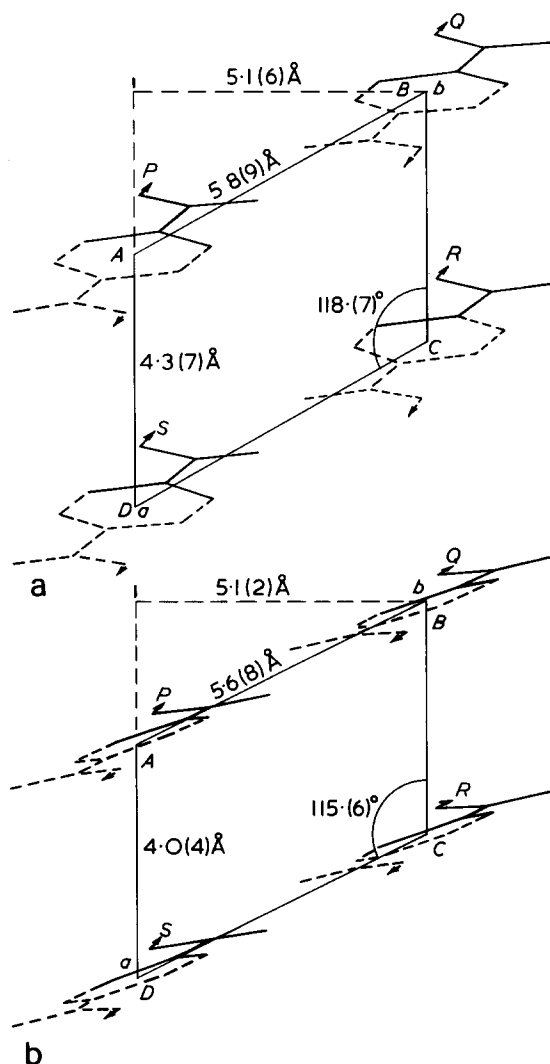


Figure 6 Projection of unit cell and terephthaloyl residue on to plane normal to c -axis. (a) Relaxed; (b) strained at 10%. (The methylene part of the molecule has been omitted from this diagram for clarity)

the transformation from the relaxed form, and the changes in other conformation angles must appear to be reasonable in experiments with molecular models.)

This model was refined by varying $\tau_1 - \tau_4$ but keeping bond angles constant and the values at the end of this stage

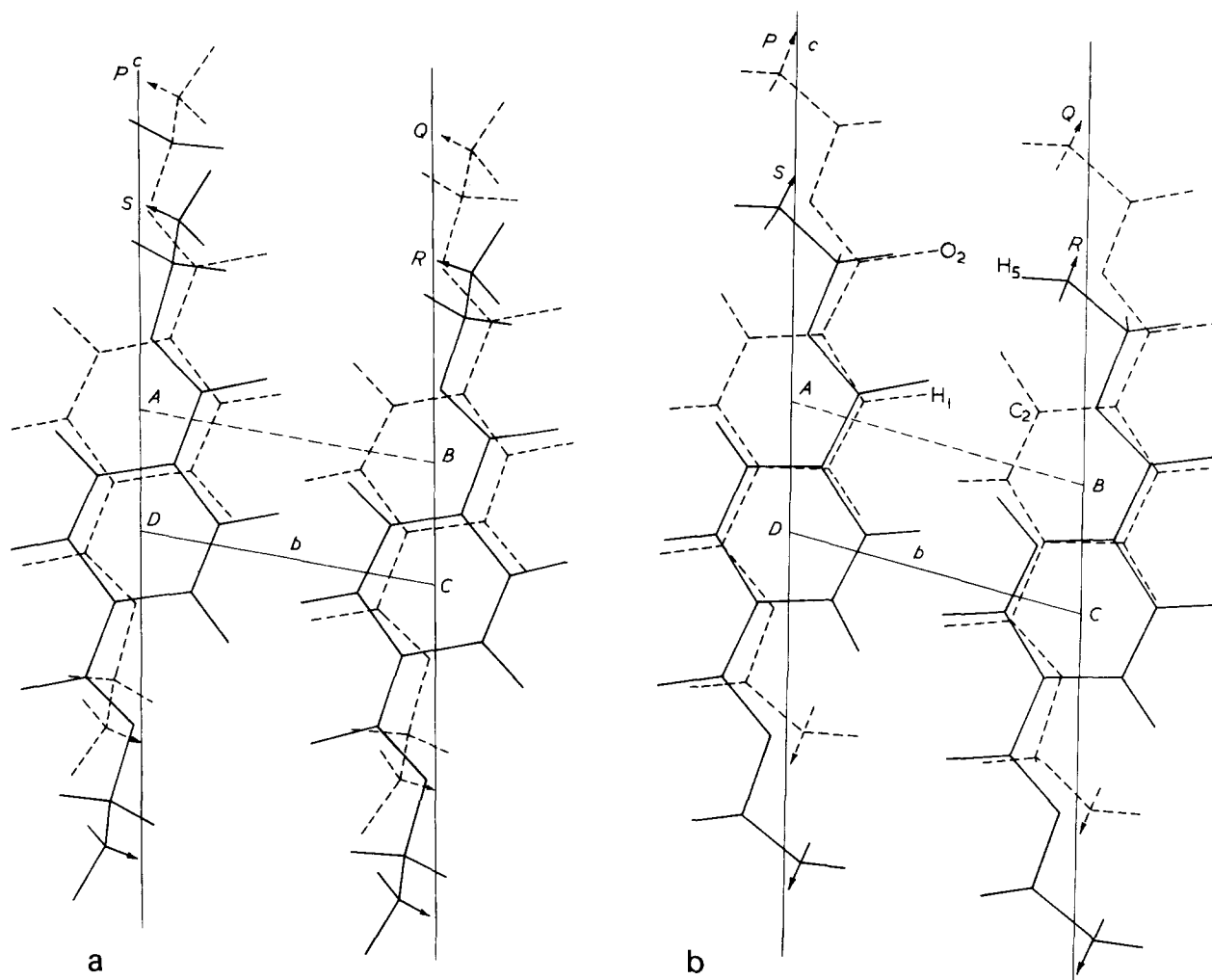


Figure 7 Projection of unit cell and contents onto b^*c plane. (a) Relaxed; (b) 10% strain

are given in column 6 of Table 3. Bond angles α_8 – α_{10} were then allowed to vary as well as τ_1 – τ_4 and the values obtained are given in column 7 of Table 3.

Because of the poor quality of the intensity data, this last conformation is unlikely to be any more accurate than that obtained with the bond angles fixed. It is only included to indicate possible variations in the parameters. Diagrams and Tables refer to the fixed bond-angle model.

The separations of all pairs of non-bonded atoms were compared with the sums of their Van der Waals radii. All cases in which the separation is less than the sum of the radii are listed in Table 4.

The chain conformation is illustrated in Figures 6b–9b.

DISCUSSION

From Table 3 it is clear that the orientation and shape of the terephthaloyl residue is almost the same for each of the relaxed and for each of the strained models. Most of the scattering power of the molecule is concentrated in this residue and so it is likely that this part of the structure has been determined fairly accurately. The other parts of the molecule complete the molecular chain within the constraints imposed, and variations in their parameters have a fairly small effect on the structure factors. Hence there is more doubt about this part of the structure, particularly for the strained form for which fewer reflections were recorded,

and (since they were more diffuse) for which intensities were measured less accurately.

For these reasons, the model of the strained form in which bond angle strain was allowed (column 7 of Table 3) will not be considered here, although this does suggest that bond angles α_8 and α_9 are opened by a few degrees on straining.

With the relaxed form, the terephthaloyl residue is planar, though Daubeny *et al.*¹⁰ found that in 2GT the carbonyl unit was about 10° out of the plane of the benzene ring. Tonelli²² has calculated the potential barrier to rotation about this bond and found it to be low. Deviations from planarity of 10° – 20° might not be surprising. However, in low molecular weight compounds containing this arrangement of atoms^{12–17} the unit is planar.

It has been assumed that there is a centre of symmetry, at the middle of the three bonds joining the methylene groups. Hence this central one must be *trans*, but the others are close to a *gauche* conformation. The conformation of this part of the molecule is shown in Figure 9a.

In 2GT the rotation about the only methylene bond is *trans* but Pérez and Brisse^{15,16} have investigated two low molecular weight analogues and found that in ethylene glycol dibenzoate it is *trans*, whereas it is *gauche* in ethylene glycol di-*para*-chlorobenzoate. In both of these materials τ_3 is nearly 180° whereas it is about -90° in 4GT. In 2GT it is -160° but in poly(ethylene adipate)²³ it is -114° . (In both of these cases the authors quoted values

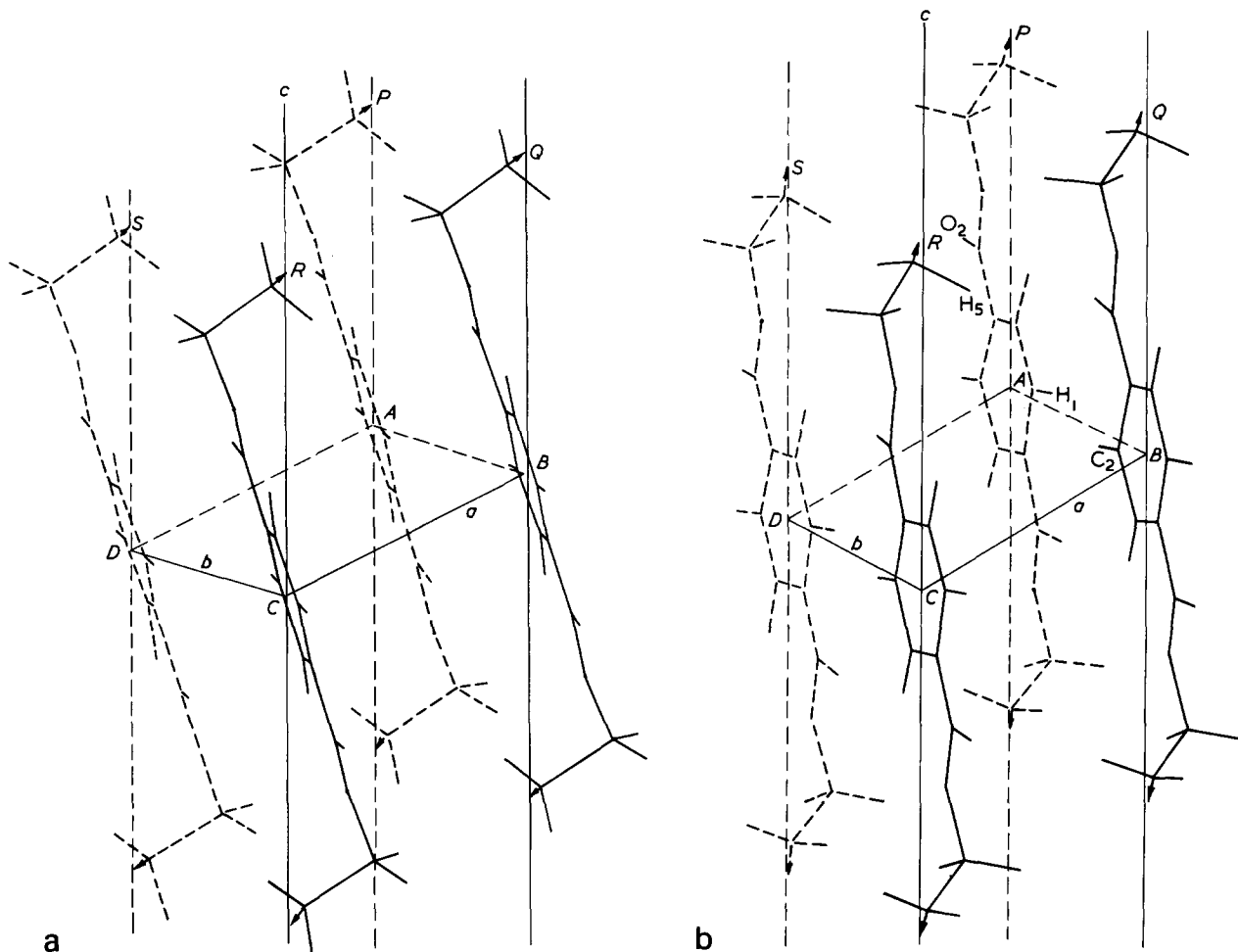


Figure 8 Projection of unit cell and contents onto ac plane. (a) Relaxed; (b) 10% strain

have been transformed to agree with the conventions used in this paper). These two disparate values suggest a low potential barrier to rotation about this bond which is confirmed by our value. τ_2 is close to 180° in this and all similar structures.

If the structure reported here is compared with that given by Mencik⁸, there is a strong overall similarity with some differences of detail. The unit cells are in close agreement, (see Table 2) except that Mencik has made a different choice of a and b directions from us. Since our cell was the first to be published⁶ we propose to keep to our original convention.

There are some differences in the choice of bond angles and lengths. These are quantities which cannot be determined with high accuracy from studies in the polymeric state, and there must be some doubt in values assumed from similar atomic groups in low molecular weight compounds. However, since the values we take come from studies on compounds which bear a closer resemblance to 4GT than any others yet reported, where differences exist between ourselves and Mencik our values are likely to be the more reliable.

The major differences between the conformation angles found in the two studies are that we find the terephthaloyl residue to be more closely planar and rotation about methylene bond to be closer to *gauche*. To ascertain whether these differences followed from the choice of bond angles and lengths, the parameters given by Mencik

were used to construct a model which was then refined against our intensity data. The final model thus obtained had a closely planar terephthaloyl residue in agreement with our original model, but the methylene conformation angle was roughly midway between the values given by ourselves and Mencik.

Since most of the scattering power of the molecule is concentrated in the terephthaloyl residue the differences in this part probably follow from differences between the two sets of intensity data, but the difference in the methylene conformation is likely to follow from the choice of model parameters and the non-planarity of the terephthaloyl residue.

The R -factor of 14.8 obtained by Mencik was lower than the value of 16.8 obtained by us. However he applied independent scaling to each layer line, whereas we scaled them all by the same factor, and he also used a different formula to calculate R . (We use $R = \Sigma|F_0 - F_c|/\Sigma F_0$ whereas Mencik uses $R = [\Sigma(F_0 - F_c)^2/\Sigma F_c^2]^{1/2}$). The two values are not, therefore, comparable.

The shortest of the interatomic distances, that between O_2 and C_5 (Figure 2 and Table 4) is controlled by the conformation angle τ_2 and the bond angle α_8 (non-planarity in the bonds radiating from C_4 , which was not allowed in our refinement procedure, could also change this distance). τ_2 is nearly 180° which is common to all similar structures. 116° is a typical value for α_8 from similar structures; after refinement we get 119° which should increase this distance.

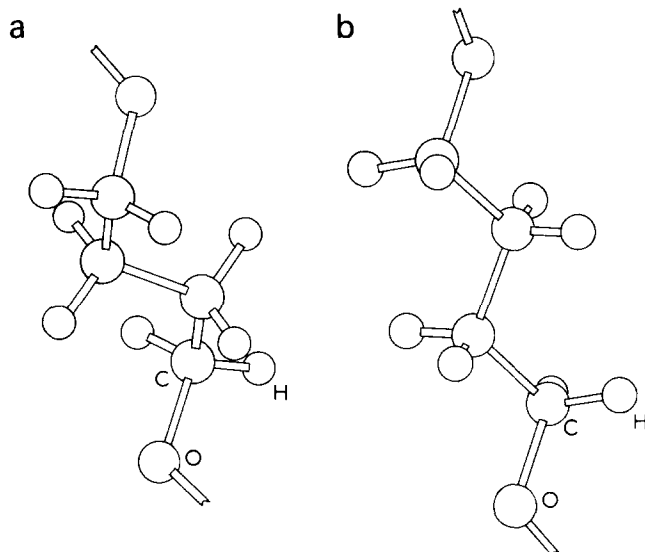


Figure 9 Conformation of methylene part of molecule. (a) Relaxed; (b) 10% strain

This short distance must, therefore, be a common feature of these structures as are the distances O_2-C_1 and O_1-C_2 which arise from the planarity of the terephthaloyl residue. The other short distances, H_3-C_4 and C_6-C_4 are controlled by the angle τ_3 . As has been pointed out, this varies widely between similar structures indicating a low potential barrier to rotation. Presumably movement to ease these contacts will cause an increase in energy due to the proximity of other atoms, not necessarily in the same molecule.

The main differences between the strained and relaxed conformations are in the values of τ_3 and τ_4 (see Figure 9), and in the planarity of the terephthaloyl residue (τ_1); τ_1 and τ_3 take values very similar to those of equivalent angles in 2GT. The parameters quoted for the strained model are likely to be subject to greater error than those of the relaxed because of the poorer quality of the intensity data.

On transition from the relaxed to the strained form, the unit cell distorts by simple shear along $a-c$ planes accompanied by a reduction in the chain spacings in the a -direction (see Figure 6). There is also some translation of chains in the c -direction. The volume of the unit cell increases from 262.8 \AA^3 in the relaxed state to 268.9 \AA^3 in the strained.

Figure 7 shows that the translation of chains maintains neighbouring terephthaloyl residues in similar positions relative to each other. Thus R and S (Figure 7), which lie alongside each other maintain a position in which the hydrogen atoms on the respective benzene rings interleave. P and S maintain relative positions in which the benzene ring of one sits behind the carboxyl unit of the other. This form of packing is also characteristic of 2GT¹⁰ indicating that the terephthaloyl part of the molecule exerts the controlling influence on their packing.

On straining, the inclination of the plane of the benzene ring changes so that the angle its normal makes with the c -axis increases from 73.7° to 86.9° (Table 3). Thus the perpendicular separation of planes of adjacent rings would increase if the spacing of chains along the a -axis was maintained. This spacing contracts from $4.3(7) \text{ \AA}$ to $4.0(4) \text{ \AA}$ (Figure 6) and the ring normal rotates through 15.1° about the c -axis towards the $b-c$ plane (Table 3). These changes result in the perpendicular separation increasing by a very small amount (from $3.5(7) \text{ \AA}$ to $3.6(7) \text{ \AA}$).

In the relaxed state the plane of the terephthaloyl residue of molecule R (Figure 6) lies roughly midway between those of S and P . The shearing of the unit cell and the rotation of the molecular plane makes S and R more nearly coplanar on straining. From Figures 6–8 it is seen that in the strained state there is a close contact between atoms O_2 and H_5 of molecules P and R . (This is not listed in Table 5a because the atomic separation is about 0.1 \AA greater than the sum of Van der Waals radii.) The shearing movement and twisting would help relieve this contact. These movements, however, cause a close contact between atoms H_1 and C_2 of molecules P and Q . The final positions and orientations of the molecules, therefore, balance these contacts. However, a rotation of the benzene ring in a sense which would improve the planarity of the terephthaloyl residue would also relieve the H_1-C_2 contact. This non-planarity does not, therefore, appear to arise as a consequence of the chain packing.

From the above discussion it is clear that the unit cell dimensions change on straining so as to restore the main features of intramolecular packing with the new conformation.

Since the conformation angles of the strained form are close to those of 2GT, this form might be expected to be stable. The fact that it is not suggests that each conformation represents an energy minimum the relaxed form being the lowest, with the barrier between them being sufficiently low for thermal activation to transform most material to the unstrained form at normal temperatures. The presence of tension reverses the relative heights of these energy levels. Confirmation of this hypothesis must await calculation of the energy of the system, taking into account the proximity of near neighbours. The present study shows that the volume of unit cell of the shortened, relaxed, form is smaller than that of the other, indicating a more economically packed, lower energy, form. However it gives no indication as to why this should be so for 4GT, but not 2GT.

The result from the investigation of biaxiality in a pressed sheet may be combined with the results of the structure determination. It then follows that the chain axis lies in the plane of the sheet, and the plane of the terephthaloyl residue intersects this plane in a line which is within a few degrees of the perpendicular to the chain axis. That is, the two planes are as close as possible to coincidence subject to the constraint that the chain axis also lies in the sheet plane. This finding is in agreement with Menciuk, although he produced his films by a different method.

Consideration of the relative intensity of equivalent diffraction spots has led to the conclusion that the proportions of unit cells in an orientation such as, for example, 1 (Figure 5a) must be different from that in 2, but could be similar to that in either 3 or 4. This suggests that the crystalline objects in 4GT might comprise an orientation such as 1 twinned with either 3 or 4. If this is so the twin plane is likely to be the plane of preferred orientation (which is (100) in the example illustrated in Figure 5), and a twin satisfying this condition is illustrated in Figure 10. It will be seen that this comprises orientations 1 and 3 of Figure 5 (because of the assumed centre of symmetry, the molecular conformation is the same, whether the positive c -axis points up or down) and will so satisfy the requirement that these are present in similar proportions. If an axis normal to the twin plane has a preferred orientation, biaxiality will occur. This axis will correspond to a positive unit cell direction on one side of the twin plane and a nega-

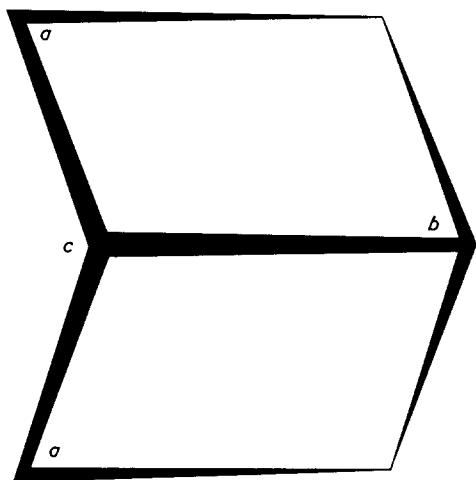


Figure 10 Projection down c -axis of a twin on (100) plane

tive on the other. Should it point with equal probability in both directions along the line of preferred orientation, there will be four unit cell orientations in roughly equal proportions. This was the situation observed in the sheet. Should different proportions point in these directions, one pair of unit cell orientations will occur in greater abundance than the other. This was observed in the fibre.

(It must be emphasized that the choice of preferred plane used in Figure 5a and followed in the above discussion, and in Figure 10, was made solely for convenience of illustration. As already shown, the plane of preferred orientation in 4GT is close to that of the terephthaloyl residue, and if the above suggestion of twin formation is correct, this will be the plane on which twins are formed.)

The cross-section of the fibre was elliptical, and this, together with the biaxiality, was probably caused by lateral compression during drawing at the pin. A longitudinal section containing the major axis of the cross-section might be expected to be equivalent to the sheet plane as far as biaxial orientation is concerned. During pin-drawing there would be a gradient in temperature and pressure normal to this plane which would not occur when pressing a sheet. This might account for the difference in orientation in this direction between the two test-pieces.

There is no apparent relationship between crystalline structure and the tilt of the c -axis with respect to the fibre axis. This is illustrated in Figure 4. Since, on projection down the c -axis, the angles between a and b are similar in 2- and 4GT, it is possible to mark on the diagram the tile axis for 2GT as well as for 4GT. The plane of the terephthaloyl residue, which is the main structure-determining feature, is similar with respect to the a and b axes in each case, but it is seen that the direction of the axis of tilt is very different in the two cases.

ACKNOWLEDGEMENTS

The authors wish to thank Professor I. M. Ward and Dr R. Jakeways of Leeds University for many stimulating discussions and for making the results of their own work readily available. They also gratefully acknowledge the help given by Professor S. Arnott of Purdue University in making a copy of the 'Linked Atom Least Squares' computer program available, and in providing instruction in its use.

One of us (MGP) gratefully acknowledges tenure of a Science Research Council Cooperative Award in Pure Science sponsored by ICI Fibres Ltd, who provided the facilities for making the fibres used in this work.

REFERENCES

- 1 Farrow, G., McIntosh, J. and Ward, I. M. *Makromol. Chem.* 1960, **38**, 147
- 2 Goodman, I. *Angew. Chem.* 1962, **74**, 606
- 3 Bateman, J., Richards, R. E., Farrow, G. and Ward, I. M. *Polymer* 1960, **1**, 63
- 4 Ward, I. M. *Trans. Faraday Soc.* 1960, **56**, 648
- 5 Joly, A. H. *PhD Thesis* University of Lyons (1970)
- 6 Jakeways, R., Ward, I. M., Wilding, M. A., Hall, I. H., Desborough, I. J. and Pass, M. G. *J. Polym. Sci. (Polym. Phys. Edn)* 1975, **13**, 799
- 7 Jakeways, R., Ward, I. M. and Hall, I. H. *Proc. Shirley Inst. Seminar* December, 1974
- 8 Mencik, Z. *J. Polym. Sci. (Polym. Phys. Edn)* 1975, **13**, 2173
- 9 Elliott, A. *J. Sci. Instrum.* 1965, **42**, 312
- 10 de P. Daubeny, R., Bunn, C. W. and Brown, C. J. *Proc. Roy. Soc. (A)* 1954, **226**, 531
- 11 Hall, I. H. and Pass, M. G. *J. Appl. Crystallogr.* 1975, **8**, 60
- 12 Bailey, M. *Acta Crystallogr.* 1949, **2**, 120
- 13 Ohrt, J. and Parthasarathy, R. *J. Cryst. Mol. Struct.* 1972, **2**, 213
- 14 Tomashpol'skii, Y. Y. and Markova, G. S. *Polym. Sci. USSR.* 1964, **6**, 316
- 15 Pérez, S. and Brisse, F. *Acta Crystallogr.* in press
- 16 Pérez, S. and Brisse, F. *Can. J. Chem.* in press
- 17 Pérez, S. and Brisse, F. in press
- 18 Rollett, J. S. 'Computing Methods in Crystallography', Pergamon, London, 1965, p114
- 19 Arnott, S. and Wonacott, A. J. *Polymer* 1966, **7**, 157
- 20 Jakeways, R., Smith, T., Ward, I. M. and Wilding, M. A. *J. Polym. Sci. (Polym. Lett. Edn.)* in press
- 21 Marrs, W. personal communication
- 22 Tonelli, A. E. *J. Polym. Sci. (Polym. Lett. Edn)* 1973, **11**, 441
- 23 Turner-Jones, A. and Bunn, C. W. *Acta Crystallogr.* 1962, **15**, 105

Note added in proof

After this paper had been accepted for publication, a structural determination of the two forms of poly(tetramethylene terephthalate) was published (Yokouchi, M., Sakakibara, Y., Chatani, Y., Tanaka, T. and Yoda, K. *Macromolecules*, 1976, **9**, 266). The two accounts agree substantially for the relaxed form, but there appear to be significant differences between the proposed structures of the strained form.

Block polymers of poly(*para*-xylelene) and polystyrene or poly(vinyl pyridine) prepared by anionic polymerization

P. K. Wong, A. E. Zachariades and M. Szwarc

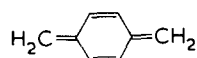
Department of Chemistry, State University of New York, College of Environmental Science and Forestry, Syracuse, New York 13210, USA

(Received 6 April 1976)

Anionic polymerization of *para*-xylelene, *p*-X, may be initiated in solution at a low temperature ($\sim -70^\circ\text{C}$) by electron-transfer process. The spontaneous formation of diradicals through dimerization of *p*-X monomers is too slow at these temperatures to initiate the radical polymerization of *p*-X. The anionic polymerization yields a living poly(*p*-xylelene) which is capable of growing further by the addition of vinyl pyridine, VP. In this way block polymers PVP-PpX-PVP were prepared. Alternatively, the addition of *p*-X monomers to living polystyrene, PS, or living poly(vinyl pyridine), PVP, yields at low temperatures the block polymers PpX-PS-PpX or PpX-PVP-PpX. The block polymers prepared by this approach were isolated and characterized. Even small blocks of PpX attached to polystyrene or poly(vinyl pyridine) make the resulting polymers insoluble in boiling solvents below 200°C .

INTRODUCTION

The quinonoid *p*-xylelene hydrocarbon,



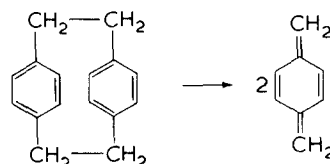
discovered by one of us as a product of pyrolysis of *p*-xylene¹, is a highly reactive species which spontaneously polymerizes on any surface exposed to its vapour. Such a surface becomes coated by a tough, crystalline film of poly(*p*-xylelene). In spite of its high reactivity, the *p*-xylelene persists in highly dilute vapour in monomeric form; its stable solutions may be obtained at low temperatures ($\sim -70^\circ\text{C}$) by condensing the dilute vapour of this monomer into a well stirred and chilled solvent², e.g. hexane or toluene, kept at -70°C .

The spontaneous polymerization of *p*-xylelene proceeds through a radical mechanism initiated by the dimerization yielding diradicals, $2\text{CH}_2=\text{C}_6\text{H}_4=\text{CH}_2 \rightarrow \cdot\text{CH}_2-\text{C}_6\text{H}_4-\text{CH}_2\text{CH}_2-\text{C}_6\text{H}_4-\text{CH}_2\cdot$. Low temperature presumably inhibits the latter reaction as well as slows down the subsequent propagation. The high intrinsic reactivity of *p*-xylelene prevents its copolymerization with the conventional vinyl or vinylidene monomers, and hence all attempts of obtaining such copolymers or block polymers were virtually in vain³. However, we expected that the preparation of block polymers of *p*-xylelene with conventional vinyl monomers could be feasible through anionic mode polymerization and, as shown in this paper, this expectation turned out to be correct.

Preparation of *p*-xylelene from *p*-cyclophane

High temperatures of about 800°C – 1000°C are needed to afford the pyrolysis *p*-xylene into *p*-xylelene. Moreover, the resulting monomer vapour is then mixed with an excess of unpyrolysed *p*-xylene and contaminated by some undesirable by-products of pyrolysis. A pure monomer is conveniently obtained by pyrolysing *para*-cyclophane⁴.

Such a pyrolysis takes place at about 600°C , and the vapour of the precursor, maintained at low pressure, is then decomposed cleanly and quantitatively into *p*-xylelene, i.e.



This method has been utilized therefore in the present work.

EXPERIMENTAL

The apparatus used in our studies is depicted in *Figure 1*. *Para*-cyclophane, kindly provided by the Union Carbide Corp., was freshly sublimed in vacuum and placed in the sublimation zone (A). The wide portion (P) of the quartz tube was inserted into an electrically heated furnace, and a thermocouple, placed in a pocket tube, measured the temperature of pyrolysis. The outlet (K) was connected to a pyrex double walled tube (F) through a quartz-to-pyrex graded joint and heated with electric tape to avoid any condensation and polymerization of the monomer on the walls of the outlet system. For the same reason the inner tube of the pyrex double walled tube (F) was also electrically heated. The double walled tube (F) fitted into a round flask reactor (R) equipped with a magnetic stirrer and connected to a high vacuum line. Two evacuated ampoules (B) and (C), or more if necessary, contained the required reagents or solvents. These were equipped with breakseals and magnetic hammers which allowed the introduction of the reagents at the proper time.

After placing a weighed sample of *para*-cyclophane in (A), the left outlet of the pyrolysis tube is sealed and the furnace brought to a desired temperature. The whole unit is then thoroughly evacuated. A solvent, or a solution of a

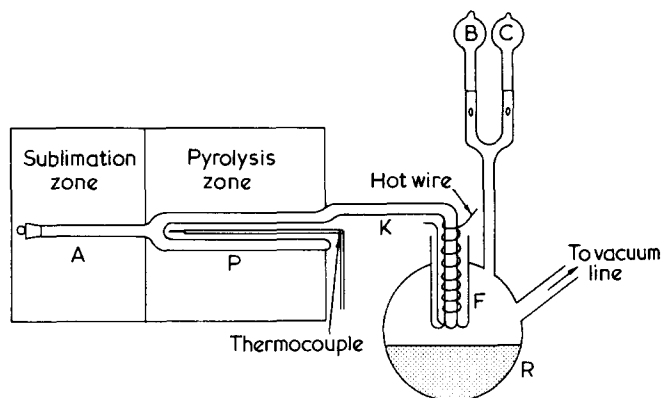


Figure 1 The schematic drawing of the apparatus used in the preparation of block polymers of PpX

living polymer, is then introduced into the reactor (R) by crushing the appropriate breakseal and the contents are cooled with solid carbon dioxide–isopropanol mixture. The sublimation zone is then heated to about 200°C with electric tape and subsequently the pyrolysis ensues. The resulting monomer vapour passes through (K) and (F) into the reactor (R) where it is dissolved in the stirred liquid that half filled the reactor. Some of the vapour reaches the upper walls of the reactor, above the level of the liquid, coating them with a coherent and insoluble film of poly(*p*-xylene). After completion of the pyrolysis the furnace is switched off and, if desired, the additional reagents are introduced into the reactor by crushing the breakseal of the appropriate ampoule. Finally, air is introduced into the unit, the reactor detached from the outlet of the pyrolysis tube, and its content analysed.

RESULTS

We confirmed that the monomer vapour, *p*-X, when introduced into cold (−70°C) tetrahydrofuran (THF) does not polymerize but forms a clear solution stable as long as the liquid is kept at −70°C. The presence of *p*-X monomer in the solution was demonstrated by pouring the solution into a precooled hexane solution of iodine. The excess of iodine was reduced with thiosulphate, and thereafter 2.2 g of CH₂I.C₆H₄CH₂I were isolated from the organic layer. The amount of the isolated di-iodide shows that 66% of the pyrolysed *para*-cyclophane (1.0 g) was dissolved in THF. The weight of the poly(*p*-xylene) film coating the walls of the reactor was 0.30 g, and hence the material balance is satisfactory.

The identity of the purified di-iodide was established by its n.m.r. spectrum in CDCl₃, δ4.35, (bs, 4), and 7.24 (bs 4).

After establishing the reliability of our procedure the pyrolysis of *para*-cyclophane was repeated and its vapour was introduced into a THF solution of sodium naphthalenide. The dark green solution of the naphthalenide turned rapidly into a light tan suspension. The reaction was completed after 2 h and thereafter the resulting lightly coloured precipitate of apparently living poly(*p*-xylene) was bleached by adding methanol to the reactor yielding a white, dead polymer.

The precipitate was filtered, washed, and dried in a vacuum oven. The conversion of the dissolved *p*-X into the polymer was virtually quantitative and the X-ray diffraction demonstrated that the precipitated poly(*p*-xylene) is in the α-form. We conclude that the electron-transfer initiated

anionic polymerization of *p*-X monomer proceeds rapidly in THF at −70°C, while the initiation of its radical polymerization is too slow to be observed under comparable conditions.

Preparation of block polymers of PpX and styrene

Samples of PpX–PS–PpX block polymers were prepared by introducing the vapour of *p*-X monomer into a THF solution of living sodium polystyryl kept at −70°C. The polystyryl used in these experiments was prepared by the well known anionic technique⁵, initiating the polymerization with sodium naphthalenide. Its molecular weight and molecular weight distribution, determined by the gel-chromatography, were 110 000–120 000 and 1.1–1.2, respectively.

The *p*-X vapour was introduced by the previously described procedure. The red solution of the living polystyrene turned into a redish-brown suspension as the reaction ensued. The pyrolysis was completed after 2 h and the living polymers were terminated then by the addition of methanol to the reactor. The resulting white suspension was then separated from the homo-poly(*p*-xylene) film coating the walls of the reactor. The latter formed 30–40% of the pyrolysed *para*-cyclophane. Repeated centrifugation and decantation yielded a gel that coagulated on addition of water. The coagulate was filtered, washed, and dried for 12 h in a vacuum oven at 110°C. Alternatively, the resulting suspension was gently heated until all the solvent evaporated. This procedure yields white granules from which the soluble fraction (up to 20%) could be extracted with THF, benzene, or toluene. The extractable material, or the solid residue isolated from the decanted THF liquor, was shown to be homo-polystyrene, presumably resulting from the ‘killing’ of some living polystyrene in the course of manipulation preceding the addition of the *p*-X monomer.

The polymers left after extraction were insoluble in boiling benzene, toluene, or chloroform. They could be dissolved in boiling methylnaphthalene (~250°C) but precipitated as the temperature of the solution dropped to about 200°C. The results of the individual experiments are summarized in Table 1. The first two columns give, the respective amounts of pyrolysed *para*-cyclophane and of polystyrene introduced into the reactor. The total amount of the collected polymer, excluding the homo-PpX film, is given in the third column, while the fourth column

Table 1 Preparation of the block polymers PpX–PS–PpX. The polystyrene block, PS, has DP ~ 100

Weight of pyrolysed <i>para</i> -cyclophane (g)	Weight of introduced polystyrene (g)	Total weight of insoluble polymer (g)	Total weight of extractable polymer (g)	Insoluble polymer	
				PS (%)	PpX (%)
1.0	1.0	1.22	0.2	66	34
1.0	1.0	1.19	0.4	50	50
1.0	1.0	1.30	0.2	62	38
1.0	0.5	1.13	0.2	27	73
1.5	0.5	1.10	0.2	27	73

Mechanical losses in the isolation amount often to 10% of the total feed. The percentages are calculated on the assumption that the extractable polymer is a pure PS, subtracting this amount from the PS feed and dividing by the total weight of the isolated, insoluble block polymer. This kind of calculation gives the upper limit for the % of PS

Table 2 Preparation of block polymers of 2-vinyl pyridine and *p*-xylene

	Sample 1, PpX-PVP-PpX	Sample 2, PpX-PVP-PpX	Sample 3, PVP-PpX-PVP
Feed (g) <i>p</i> -X	0.5	0.7	1.0
Feed (g) VP	1.0	0.7	0.5
Total (g)	1.5	1.4	1.5
Film of homo-PpX (g)	0.20	0.28	0.32
Insoluble co-polymer (g)	0.80	0.66	0.70
Extractable polymer (g)	0.15	0.16	0.18
PVP calc. (%)	73	53	29
N calc. (%)	9.7	7.1	3.9
N analysed (%)	10.1	6.1	4.9

gives the amount of the insoluble block polymer left after extraction of the THF or benzene soluble fraction. The wt% PPX blocks and PS blocks are given in the last two columns and are derived on the basis of material balance.

No attempts were made to prepare block polymers by starting with a suspension of living PpX and feeding it with monomeric styrene. It is known that the initiation of anionic polymerization of styrene by a primary carbanion, e.g. $\text{PhCH}_2^- \text{Na}^+$, is slow as compared with the subsequent propagation, and hence the initiation by $\sim\text{CH}_2-\text{C}_6\text{H}_4-\text{CH}_2^- \text{Na}^+$ was expected to be inefficient. Instead, we decided to produce the two kinds of block polymers, viz. those terminated by the PpX blocks and the other possessing a middle PpX block, by using a monomer that reacts very rapidly with the $\sim\text{CH}_2-\text{C}_6\text{H}_4-\text{CH}_2^- \text{Na}^+$ end groups. 2-Vinyl pyridine was chosen for this purpose.

Preparation of block polymers of *p*-X and vinyl pyridine, VP

Two kinds of block polymers of 2-vinyl pyridine (VP) and *para*-xylene were prepared. The technique used in the preparation of PpX-PS-PpX was applied also in the preparation of PpX-PVP-PpX block polymers. Living poly(2-vinyl pyridine) was prepared in THF by initiating the polymerization with sodium naphthalenide⁶. The solution of the resulting polymer of $DP \sim 100$ was introduced into the reactor and the *p*-X vapour was fed thereafter in the way previously described. The resulting precipitate was extracted with methanol in a Soxhlet and the residue dried in a vacuum oven. The results of two typical experiments are summarized in Table 2. Alternatively, a living PpX was prepared, as described earlier, by initiating the polymerization of *p*-X monomer with sodium naphthalenide. Thereafter, 2-vinyl pyridine was added to the cold solution of the living PpX and the insoluble residue extracted with methanol, dried in vacuum oven and then weighed. A typical result of such a preparation is included in Table 2 (sample 3).

The percentage of PVP in the insoluble fraction was calculated by assuming that the mechanically lost material was proportionally divided between the insoluble and extractable fractions, the latter being assumed to be pure PVP. Thus the composition of the insoluble fraction was calculated as:

$$\text{PpX} = p\text{-X (fed in)} - p\text{-X (in the film of homo-}p\text{-X)}$$

$$\text{PVP} = \text{VP (fed in)} - (\text{corrected weight of the extractable material}).$$

The results of such calculations are given in Table 2 and on this basis we calculated the percentage of N in the block polymers. The calculated results, given in the line before the last, compare satisfactorily with those listed in the last line and obtained by the analysis of the pertinent samples.

I.r. spectra of the studied polymers

All the i.r. spectra reported in this paper were obtained by dispersing the investigated polymers (~ 1 wt%) in KBr and pressing pellets from the mixture. The i.r. spectrum of anionically prepared homo-polystyrene is shown in Figure 2. The two strong absorption bands centred at 758 and 696 cm^{-1} are characteristic of that polymer and distinguish it from the anionically prepared homo-poly(*p*-xylene), the i.r. spectrum of which is shown in Figure 2. The latter has an intense absorption band centred at 819 cm^{-1} .

A typical i.r. spectrum of PpX-PS-PpX block polymer is shown in Figure 3. The absorption bands due to the blocks PpX and PS are clearly seen, proving that both blocks are present in the investigated polymer. To demon-

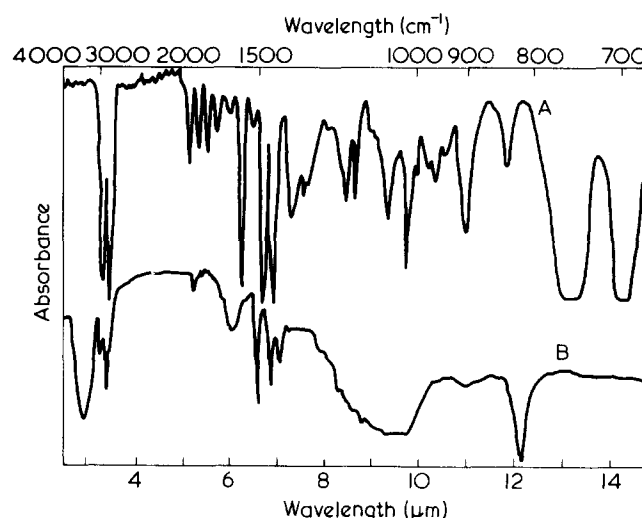


Figure 2 I.r. spectra of anionically prepared polystyrene (A) and poly(*p*-xylene) (B)

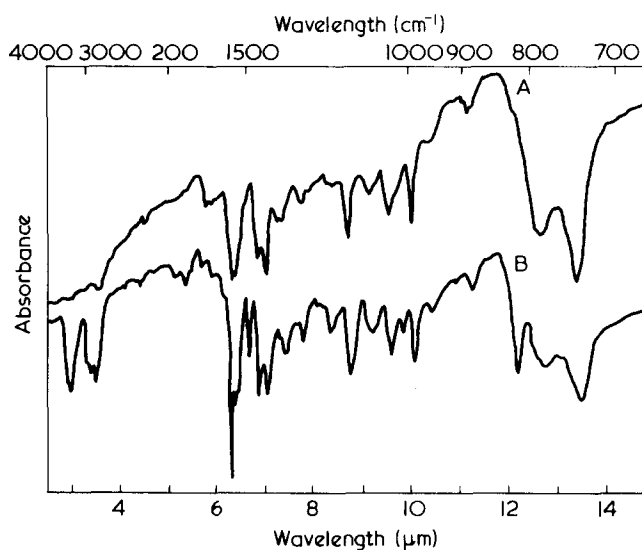


Figure 3 I.r. spectra of block polymers, PpX-PS-PpX. A, the originally isolated polymer; B, the spectrum of the same material after its precipitation from α -methylnaphthalene solution. The block polymer was dissolved in α -methylnaphthalene at 250°C and began to precipitate when the solution was cooled to $\sim 200^\circ\text{C}$

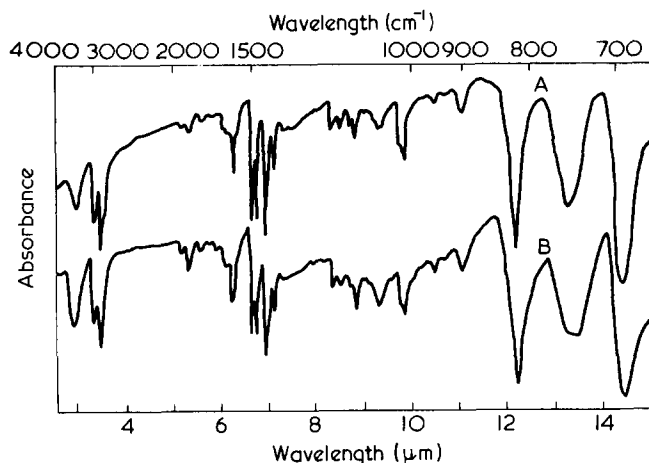


Figure 4 I.r. spectra of block polymers PpX-PVP-PpX (A) and PVP-PpX-PVP (B)

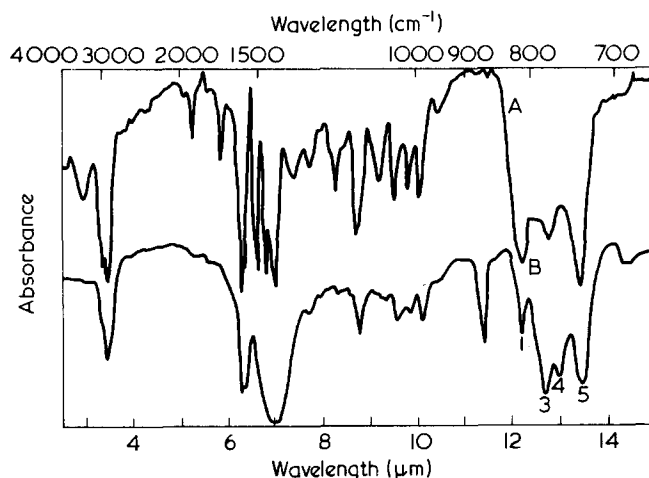


Figure 5 I.r. spectra of PVP-PpX-PVP polymer before (A) and after (B) its precipitation from α -methylnaphthalene solution

strate that the investigated sample contains block polymers and is not a blend of homo-PpX and homo-PS, the following tests were performed. A mixture of homo-PS and homo-PpX, both prepared by anionic technique, were dissolved in boiling α -methylnaphthalene. Precipitation occurred instantly after cooling the solution to about 200°C. The precipitate was isolated and its i.r. analysis showed that it contained PpX only. A similar solution of the PpX-PS-PpX sample afforded on cooling a precipitate, the i.r. spectrum of which is shown also in Figure 3, and its inspection clearly demonstrates the presence of both blocks. Since polystyrene is not occluded in the poly(*p*-xylene) when the latter precipitates from the α -methylnaphthalene solution of the blend, its presence in the precipitate formed from the solution of the block polymer provides an un-

equivocal proof of its block nature. Of course, this test does not preclude the presence of some homo-poly(*p*-xylene) in the material containing a block polymer PpX-PS-PpX.

Comparison of the two i.r. spectra shown in Figure 3 suggests that the percentage of PpX in the dissolved and then precipitated material seems to be higher than that in the original sample. This observation was confirmed by repeating such tests with other samples of the PpX-PS-PpX polymers. The enrichment in PpX could be due to the presence of some homo-PpX in the block polymer, and while the former is insoluble in the cold solvent, the latter could be partly soluble.

The i.r. spectra of the block polymers of PVP and PpX are shown in Figure 4. The presence of the PVP blocks is manifested by the strong absorption bands centred at 745 cm^{-1} and 785 cm^{-1} characteristic for the homo-poly(vinyl pyridine). It is significant to note the presence of poly(vinyl pyridine) in the PVP-PpX-PVP block polymer, an observation confirming the ability of living poly(*p*-xylene) to continue the growth by the addition of vinyl pyridine.

Finally, a sample of PVP-PpX-PVP block polymer was dissolved in boiling α -methylnaphthalene and precipitated by cooling the solution. The i.r. spectra of the original sample and of that obtained from the precipitate are shown in Figure 5. The presence of the PVP blocks in the latter proves again that the original material contained the PVP-PpX-PVP block polymers and not a blend of homo-PVP and homo-PpX.

We tried to develop a quantitative i.r. method of analysis of block polymers. However, these attempts were not yet met with success.

ACKNOWLEDGEMENT

We wish to thank the National Science Foundation for the financial support of these investigations.

REFERENCES

- 1 Szwarc, M. *Discuss. Faraday Soc.* 1947, 2, 39; Szwarc, M. *J. Polym. Sci.* 1951, 6, 319
- 2 Errede, L. A. and Landrum, W. *J. Am. Chem. Soc.* 1957, 79, 4952
- 3 Errede, L. A., Gregorian, R. S. and Hoyt, J. M. *J. Am. Chem. Soc.* 1960, 82, 5218; Errede, L. A. and Szwarc, M. *Quart. Rev. Chem. Soc.* 1958, 12, 301
- 4 Gorham, W. F. *J. Polym. Sci. (A-1)* 1966, 4, 3027; Gorham, W. F. *Adv. Chem. Ser.* 1969, 91, 643
- 5 Szwarc, M. 'Carbanions, Living Polymers and Electron Transfer Processes', Interscience, New York, 1968
- 6 Fisher, M. *PhD Thesis* State University College of Forestry (1970)

Stereoelective polymerization of racemic propylene oxide using a diethylzinc-chiral-1,2-diol system as initiator

Christian Coulon, Nicolas Spassky and Pierre Sigwalt

Laboratoire de Chimie Macromoléculaire associé au CNRS, Université Pierre et Marie Curie, 75230 Paris Cedex 05, France

(Received 4 March 1976)

The polymerization of racemic propylene oxide was performed using a chiral initiator obtained from the reaction of diethylzinc with (–) 3,3-dimethyl-1,2-butanediol. With this initiator *R*(+) enantiomer is preferentially incorporated into the polymer with a stereoelectivity ratio *r* equal to 1.8, the *r* value remaining constant during the polymerization. The polymer was fractionated into a crystalline isotactic part and an amorphous heterotactic part, both optically active. Partial stereoelectivities were determined for both fractions and found to be equal to 2.6 and 1.6 respectively for polymerization at 80°C. Two types of sites, stereospecific and non-stereospecific, formed in the first reaction between monomer and initiator are both active for the stereoelective polymerization. The stereospecificity of the monomer–initiator system increased at low temperatures, but the overall stereoelectivity remained constant and seemed to be an intrinsic property of the system.

INTRODUCTION

Propylene oxide was the first heterocyclic monomer to be polymerized in its optically active form by Price and Osgan in 1956¹, giving an optically active polymer. It was also the first monomer to be involved in an asymmetric selective or stereoelective polymerization in which a racemic monomer is polymerized using an asymmetric catalyst².

Over the last ten years the Japanese school with the groups of Furukawa and Tsuruta have investigated various features of these processes and this work has been reviewed in several papers^{3,4}. The initiator systems which were used in such polymerizations are derived from the reaction between an organometallic compound, usually diethylzinc, and chiral compounds with active hydrogens such as alcohols², amino-acids⁵ or other derivatives.

Most of the results reported up to now were run with a low polymer conversion (generally less than 30%) and under these conditions a linear relationship between optical purity and conversion was established by Furukawa *et al.*⁶ defining the asymmetric selectivity of the catalytic system.

A few years ago we investigated the stereoelective* polymerization of propylene sulphide, and it was found that the initiator systems obtained from the reaction of diethylzinc with chiral 1,2-diols were much more efficient than those obtained using chiral alcohols⁸. We also investigated the stereoelective process at various conversions and have established a theoretical relationship which fitted well with experimental data⁹.

It was interesting therefore to see if this type of initiator was more efficient in the case of propylene oxide than the initiators used previously and also to study the stereoelective process up to high conversions.

EXPERIMENTAL

Materials

Commercial racemic propylene oxide was stored on potassium hydroxide, then distilled on a spinning band column and purified under vacuum on calcium hydride. It was chromatographically pure. A commercial solution of diethylzinc in heptane (Orgmet) was used. It was redistilled and distributed in graduated ampoules under vacuum. The classical EDTA method was used for the zinc content titration; (–) 3,3-dimethyl-1,2-butanediol was prepared as described elsewhere²³.

Polymerizations

All the experiments were carried out in sealed apparatus using high vacuum technique. Diethylzinc was allowed to react with chiral 1,2-diol in heptane solution for 2 h at 80°C, the solvent was evaporated and the initiator dried at 80°C under vacuum for several hours. Then, the monomer was introduced by distillation and the polymerization carried out at a convenient temperature. At the end of the polymerization unreacted monomer was recovered by vacuum distillation. Chloroform and a few drops of acetic acid were added to the residual polymer. The catalyst residue was separated by centrifugation and the solution washed several times with water in order to eliminate all traces of diol. The chloroformic solution was dried on sodium sulphate and finally the polymer recovered and dried under vacuum. Optical activities were measured on a Perkin–Elmer P 141 Polarimeter. ¹³C n.m.r. spectra were observed in CCl₄–C₆D₆ (90:10) solutions on a JEOL PS 100 FT spectrometer.

* Using the terminology introduced by Pino *et al.*⁷ in the case of olefins.

Table 1 Polymerization of racemic propylene oxide at 80°C in bulk using diethylzinc (–) 3,3-dimethyl-1,2-butanediol (1:1 molar ratio) as initiator system

No.	[C] [M] (mol %)	Polymer- ization Time (h)	Polymer yield (%)	α_D^{25} unreacted monomer neat, dm	$[\eta]$ C ₆ H ₆ (dl/g)	$[\alpha]_D^{25}$ whole polymer C ₆ H ₆ C = 1
12‡	2.62	7	12	–0.42	1.39	–9.2
5*	1	42	14	–0.49		–9.6
14‡	2.47	5	17	–0.64	0.92	–8.6
9†	2.72	15	23.5	–0.97	1.41	–8.5
7†	2.80	24	42	–1.87	1.74	–7.7
8*	1.35	52	63	–3.5	3.48	–6.0
6†	2.1	41	65.5	–3.6	3.0	–5.7
11†	2.64	48	93	–8.2	2.07	–2.4
13‡	2.46	29	94	–8.7	3.31	–1.7
10†	2.72	63	96	–9.0	1.87	–1.3

*Polymerization carried out in heptane; †initiator dried 2 h at 80°C; ‡initiator dried 10 h at 80°C

POLYMERIZATION USING DIETHYLZINC/(–) 3,3-DIMETHYL-1,2-BUTANEDIOL (1:1) SYSTEM

Stereoselectivity of the system

Racemic propylene oxide was polymerized using the initiator system derived from the reaction between diethylzinc and (R) (–) 3,3-dimethyl-1,2-butanediol (DMBD) in equimolar ratio. The preparation of the catalyst was carried out under conditions described elsewhere¹⁰ and in all cases we have used an initiator in which the ratio R–M–O/O–M–O between alkylalcoholate and dialcoholate species, was equal to 0.24. The polymerization was carried out in bulk at 80°C. The experimental data are given in Table 1. As one can see, the optical activity α_m of unreacted monomer increases with conversion to polymer, while the optical activity of the polymer α_p is decreasing. The signs of unreacted monomer in pure liquid form and of polymer in benzene solution are both levorotatory. This means that (R)-enantiomer was preferentially incorporated into the polymer chain [poly(|R| propylene oxide) is levorotatory in benzene solution¹] leaving an excess of S(–) enantiomer in the unreacted monomer. This corresponds to the so-called ‘homosteric’ type process as was defined in the case of propylene sulphide¹¹.

If one plots the optical activities of unreacted monomer versus the conversion to polymer as shown in Figure 1, one can see that the experimental data fit well on a curve which corresponds to the following theoretical equation (1), established previously for the stereoselective process⁹:

$$(1-x)^{r-1} = \frac{1 + \alpha/\alpha_0}{(1 - \alpha/\alpha_0)r} \quad (1)$$

where α is the optical activity of unreacted monomer, α_0 the optical activity of pure enantiomer, x the conversion and r the stereoselectivity ratio.

α and x are directly obtained from experimental data and α_0 was deduced from n.m.r. data on the polymer¹² and was taken to be 11.9° (neat, dm). The best theoretical curve fitting the experimental data corresponds to a value of the stereoselectivity r equal to 1.8 as shown in Figure 1.

Similar calculations could be made for the polymer giving the same r value. In all cases we have checked that the optical balance between the recovered monomer and the polymer satisfies the relation (2) proposed previously by Inoue et al.¹³:

$$M[\alpha_m] = \frac{\alpha_{m_0}}{\alpha_{p_0}} P[\alpha_p] \quad (12)$$

where α , α_p , α_{m_0} and α_{p_0} are the optical activities of unreacted monomer, obtained polymer, pure enantiomer and pure polyenantiomer respectively. M is the ratio of recovered to starting monomer and P the yield (%) of optically active polymer. This is shown in Figure 2. The slope of the straight line corresponding to the ratio $\alpha_{m_0}/\alpha_{p_0}$ was found to be 0.34 which is identical to the calculated theoretical value $11.9/35 = 0.34$.

The stereoselectivity ratio found ($r = 1.8$) is one of the highest obtained for propylene oxide. Comparison with the results of Tsuruta and Furukawa is not very easy, because they have usually worked at low conversions where very small variations of optical activity of the monomer produce strong variations in the r value. One can estimate however, that for ZnEt₂/(+) borneol system the stereo-

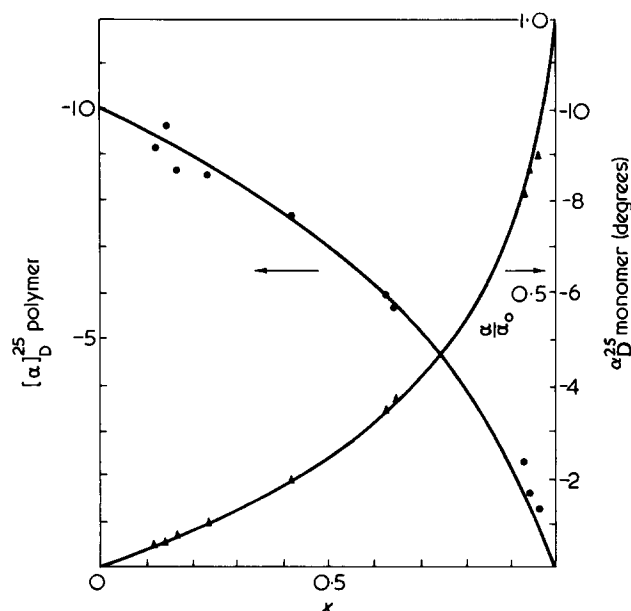


Figure 1 Stereoselective polymerization of racemic propylene oxide using diethylzinc/(–) 3,3-dimethyl-1,2-butanediol as initiator system. Polymerization carried out at 80°C, $r = 1.8$. ▲, optical activity of unreacted monomer (neat, dm); ●, optical activity of whole polymer (C = 1, benzene); —, theoretical curves according to equation (1)

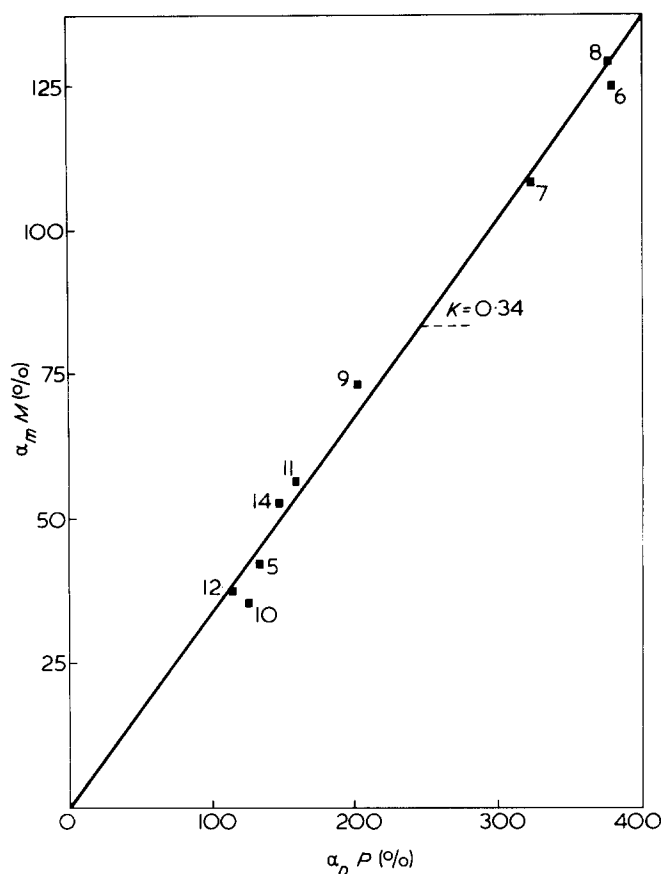


Figure 2 Relation between optical activities of recovered monomer and whole polymer. $\alpha_{m0}/\alpha_{p0} = 12/35 = 0.34$

electivity should be close to $1.5-1.6^3$ and the best result for $\text{ZnEt}_2/\text{amino-acid}$ system was found equal to 1.2^5 . A single result for $(\text{FeCl}_3/\text{propylene oxide})$ complex- H_2O catalyst containing *d*-bornylethylether corresponds to $r = 1.71$, however in this case the polymer obtained was optically inactive⁶. In our case both unreacted monomer and resulting polymer fitted satisfactory with the proposed $r = 1.8$ value.

A few experiments were performed in heptane solution. These experimental data fit on the same theoretical curve with $r = 1.8$. The polymerization times are however much longer in solution than in bulk, as expected.

Fractionation of the polymer

Crude polymers were fractionated into crystalline, semi-crystalline and amorphous fractions using selective solubility in acetone at different temperatures.

Using this procedure the following fractions were isolated: a crystalline polymer insoluble in acetone at room temperature; a semi-crystalline polymer insoluble at -20°C and an amorphous polymer, soluble in acetone below -20°C .

Crystalline fractions were of high molecular weight (an intrinsic viscosity of $|\eta| = 7.7$ corresponds to $800\,000\text{ MW}$) and high melting points (varying from 69° to 72°C). Semi-crystalline fractions were of lower molecular weights and lower melting points.

Results of the fractionation are given in Table 2. If one plots $[\alpha]_D^{25}$ of polymers versus conversion one can see that data for the crystalline and semi-crystalline fractions fall on the same curve corresponding to a stereoelectivity ratio equal to 2.6. The data for amorphous fractions, on the other hand, fit well on a theoretical curve corresponding to a much lower stereoelectivity ratio equal to 1.6 (Figure 3).

Effect of temperature on polymerization

A lowering of the temperature from 80° to -8°C (see Table 3) decreased the rate of polymerization by a factor of one hundred if comparing times of polymerization necessary to reach similar yields. The overall stereoelectivity of the system r was not changed significantly. However, distributions between crystalline and amorphous fractions and their corresponding 'partial' stereoelectivities, were considerably modified. Thus, as much as 65% of the crystalline fraction was isolated in the polymerization run at -8°C against only 10% in the polymerization carried out at 80°C . The proportion of semi-crystalline fraction does not alter much as a function of temperature, this fraction resulting probably from an imperfect fractionation. As expected, the proportion of amorphous fraction increased as the temperature increased (Figure 4).

The stereoelectivities of all fractions decreased with decrease in temperature, while overall stereoelectivity remained nearly constant. The semi-crystalline fraction obtained at low temperature has a stereoelectivity very similar to the amorphous fraction, in contrast to their stereoelectivities at 80°C .

Table 2 Fractionation of poly(propylene oxides) obtained in stereoselective polymerizations. Experimental conditions as described in Table 1

No.	$[\alpha]_D^{25}$ whole polymer*	Fraction insoluble in acetone						Fraction soluble in acetone		
		At room temperature			At -20°C			At -20°C		
		(%)	$[\alpha]_D^{25}$ *	$[\eta]$ †	(%)	$[\alpha]_D^{25}$ *	$[\eta]$ †	(%)	$[\alpha]_D^{25}$ *	$[\eta]$ †
5	-9.6	8	-14.4					67	-7.6	
14	-8.6	12	-14.1	3.60	10	-14.9	1.40	78	-7.1	0.95
9	-8.5	9.4	-14.0	4.62	9.2	-14.4	1.76	81.4	-7.2	0.98
7	-7.7	10.3	-12.5	4.2	12.3	-12.6	1.63	73.5	-6.5	1.0
8	-6.0	16.6	-10.5	8.1	9.1	-10.7	2.58	74.2	-5.8	2.05
6	-5.7	15	-9.9	7.9				82	-5.1	
11	-2.4	12.4	-2.8	5.63	6.1	-3.0	1.9	81.0	-2.0	1.53
13	-1.7	18.2	-2.4	5.50	7.4	-2.5	2.0	72.4	-1.5	2.24
10	-1.3	12.0	-1.5	3.72	6.2	-2.0	1.8	79.6	-1.0	1.15

*In benzene $C = 1$; †dl/g in benzene

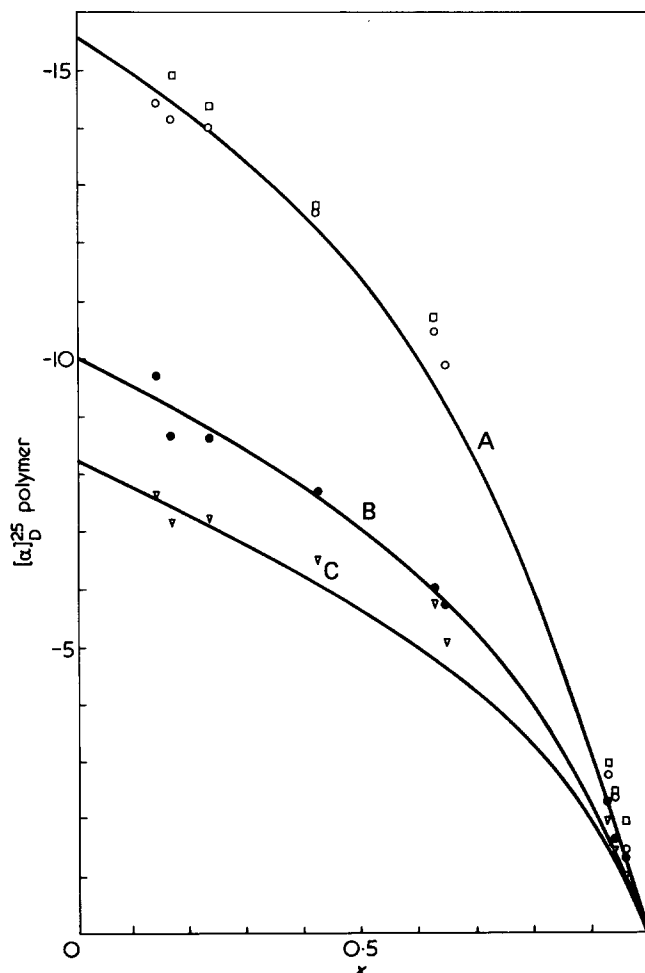


Figure 3 Stereoselective curves for whole polymer and its crystalline and amorphous fractions. Polymerization carried out at 80°C. A, $r = 2.6$; B, $r = 1.8$; C, $r = 1.6$; ●, whole; ○, crystalline; □, semi crystalline; ▽, amorphous

According to Tsuruta *et al.*¹⁴ and Furukawa *et al.*¹⁵, racemic stereoregular poly(propylene oxide) could be separated into two fractions of opposite signs with predominant *R*- and *S*-units. The crystalline fraction is therefore a mixture of poly-*R* type chains and poly-*S* type chains in different amounts formed on enantiospecific sites. For other fractions Tsuruta considered a full spectrum of sites having more or less *R* or *S* character^{3,4}.

It is possible to make an estimation of the distribution of various sites knowing the proportion of different fractions and the partial stereoselectivities.

At the beginning of the polymerization the enantiomeric composition of the polymer first formed directly reflects the stereoselective choice of the initiator.

$$[\alpha_p]_r^0 / [\alpha_p^0] = \frac{R/S - 1}{R/S + 1} \sim \frac{r - 1}{r + 1}$$

where $[\alpha_p]_r^0$ is the optical activity of the polymer extrapolated to the origin for a given r ; $[\alpha_p^0]$ is the optical activity of optically pure polymer [we have taken $[\alpha_p^0] = 35(C_6H_6, C = 1)$].

Therefore it is possible to determine the distribution of *R*- and *S*-type species for each fraction of polymer, corresponding to a partial r . Then knowing the amount of each fraction in the whole polymer, one can calculate the percentage of polymer corresponding to different stereoregularities and different chiralities. Calculations were performed using experimental data obtained at various temperatures. Although there is no direct indication that amorphous polymer may be separated into fractions of opposite signs, we have introduced such fractions of both chiralities in our scheme.

Indeed, with a decrease in the temperature of polymerization there is an increase in the stereoregular fraction and with an increase in the temperature a substantial decrease. We consider that there is a full spectrum of sites having different *R*-type and *S*-type characters. The distribution of stereospecific and non-stereospecific sites depends on the experimental conditions, namely on the temperature. At a high temperature (80°C) only 10–15% of active sites are highly stereospecific (giving a crystalline fraction), but the existence of a semi-crystalline polymer fraction is an indication that other sites have potential stereospecificity. With a decrease in the temperature many more sites become stereospecific giving rise to a crystalline polymer (65% of crystalline fraction at –8°C). The latter requires sequences of approximately at least ten successive monomer units of the same configuration incorporated in the polymer chain.

The overall stereoselectivity is not affected by this change in distribution, but a continuous variation of the amounts of different fractions is observed when changing the temperature. The estimated distributions of different polymer fractions calculated from the experimental data are given in Table 4.

As one can see an almost symmetric variation of the percentage of fractions is observed when changing the temperature from –8° to +80°C. Such distributions could directly reflect the spectra of active sites of both chiralities and of different degrees of stereospecificity existing in the polymerization system for given experimental conditions.

Table 3 Effect of the temperature on stereoselective polymerization of racemic propylene oxide

t (°C)	Polymerization time (h)	Yield (%)	α_D^{25} unreacted monomer neat, dm (degrees)	$[\alpha_p]_D^{25*}$ whole polymer	$[\eta]$ †	r	Fractionation in acetone								
							Insoluble at room temperature		Insoluble at –20°C		Soluble at –20°C				
							(%)	$[\alpha_p]_D^{25*}$	r	(%)	$[\alpha_p]_D^{25*}$	r	(%)	$[\alpha_p]_D^{25*}$	r
–8	426	14.6	–0.50	–8.3	5.8	1.8	65	–10.5	2.0	6.5	–5.6	1.4	27.5	–3.9	1.2
28	63.5	53	–2.4	–6.0	4.9	1.72	38	–11.5	2.7	5	–5.9	1.6	57	–3.3	1.35
50	40	80	–5.1	–4.1	2.8	1.72	26	–7.0	3.0	6.5	–4.0	1.8	67.5	–2.9	1.5
80	5	17	–0.64	–8.6	0.92	1.8	12	–14.1	2.6–2.5	10	–14.9	2.6	78	–7.1	1.6
80	63	96	–9.0	–1.3	1.87	1.75	9	–1.5	2.6–2.7	8.2	–2.0	2.6	82.6	–1.0	1.6

*In benzene $C = 1$; †dl/g in benzene

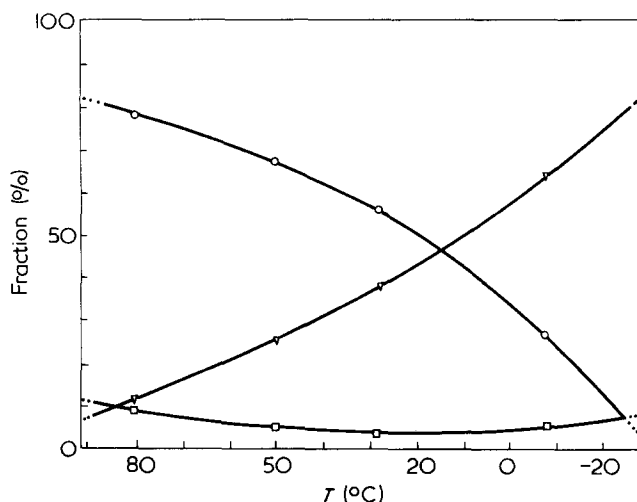


Figure 4 Variation of the percentage of crystalline and amorphous fractions as a function of the temperature of polymerization. ∇ , crystalline part; \square , semi-crystalline part; \circ , amorphous part

Stereoregularity of polymers

The stereoregularity of the different polymer fractions were used as a tool for the study of the stereospecificity of sites in the mechanism of polymerization.

^{13}C n.m.r. was used for the study of the stereoregularity. Schaefer¹⁶ has shown that the tertiary carbon of the poly(propylene oxide) chain is sensitive to triad effects and the methylenic carbon to dyad effects only. The assignment of peaks was reconsidered by Oguni *et al.*¹⁷ and confirmed with the use of optically active monomers by Uryu *et al.*¹⁸ and ourselves¹².

For a random polymer in CCl_4 solution, the i , ($h_i + h_s$) and s triads of tertiary carbon were respectively located at 75.5, 75.4 and 75.3 ppm, while the m and r dyads, corresponding to methylenic carbon, found at 73.5 and 73.1 ppm (from TMS). The methyl carbon was observed as a singlet at 17.6 ppm. The crystalline and the semi-crystalline fractions showed only one type of peak for each carbon, e.g. at 75.5, 73.5 and 17.6 ppm, which indicates that these polymers are highly isotactic. The amorphous fractions, on the contrary, showed a heterotactic structure with predominance of i peak and m peak in triads and dyads respectively (Figure 5).

It was interesting to discover if the tacticity found corresponded to a statistical distribution of R and S units in the chain, the R/S ratio being directly related to the optical activity of the polymer, or whether there was some kind of preferential sequence of units in the chain.

In the first case the arrangement of units should correspond to a Bernoulli type formation of dyads and triads, in

the second case the tacticity found would be higher (or different from) than statistical distribution.

In previous work on propylene sulphide¹⁹ it was demonstrated that the triad distribution could be calculated easily from the enantiomeric composition of a polymer obtained by a non-specific initiation. Thus, if the starting monomer mixture has an enantiomeric composition $R/S = 1/p$ the relative amounts of triads and dyads in the polymer are given by:

$$i = \frac{p^3 + 1}{(p + 1)^3}; \quad s = h_s = h_i = \frac{p(p + 1)}{(p + 1)^3}$$

and

$$m = \frac{p^2 + 1}{(p + 1)^2}; \quad r = \frac{2p}{(p + 1)^2}$$

The enantiomeric composition R/S could be obtained simply from the optical activity of the polymer. Indeed, a linear relationship was found between optical activities of the polymer and of the monomer²⁰ and moreover the optical purity of the latter was determined¹².

The calculation of theoretical amounts of triads and dyads could be carried out easily for our amorphous samples and the comparison with experimental data obtained from ^{13}C spectra showed (Table 5) a satisfactory agreement with tacticity derived from a statistical Bernoulli type process.

Therefore the amorphous fraction is very probably due to non-specific stereoelective sites.

MECHANISM OF POLYMERIZATION

Some mechanistic aspects of stereoelective polymerization of propylene oxide using chiral catalysts have already been described by Tsuruta^{2,3} and Furukawa⁶. The ring-opening occurs almost exclusively at the primary carbon-oxygen bond and a polymer having some stereoregularity is produced.

Using our chiral initiator, we preferentially polymerized the $R(+)$ enantiomer which corresponds to a so-called 'homosteric' choice, i.e. the configuration of the chosen enantiomer is identical to that of the chiral agent used. The result is similar to the result observed previously for propylene sulphide using the same initiator¹¹. Anti-steric type initiators for propylene sulphide in which $R-M-O/O-M-O$ ratio is higher than 3 (excess of alkylalcoholates species) were not able to polymerize racemic propylene oxide under the same conditions. The stereoelectivity found was lower in the case of propylene oxide ($r = 1.8$)

Table 4 Variation of the percentage of polymer fractions of different stereoregularities and chiralities as a function of the temperature of polymerization. Experimental conditions as described in Table 3

Polymerization temperature (°C)	R-type polymer			S-type polymer		
	Stereoregular (a)	Stereoregular (b)	Stereoirregular (c)	Stereoirregular (c)	Stereoregular (b)	Stereoregular (c)
-8	43	3.7	15	12.5	2.7	22
28	27	3	33	24	2	11
50	19.5	4.2	40	27.5	2.3	6.5
80	8.6	7.2	48	30	2.8	3.4

(a) Crystalline fraction; (b) semi-crystalline fraction; (c) amorphous fraction

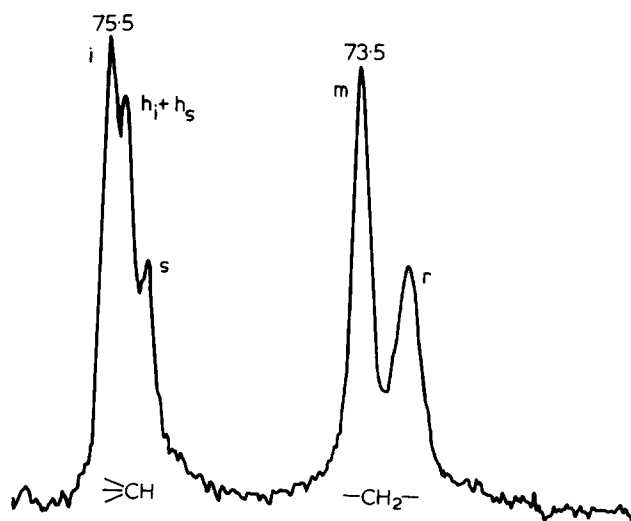


Figure 5 ^{13}C n.m.r. spectra of the amorphous part of poly(propylene oxide) obtained is stereoelective polymerization. Amorphous polymer $[\alpha]_D^{25} = -5.8$ ($C = 1$, C_6H_6); spectra run in $\text{CCl}_4/\text{C}_6\text{D}_6$ (90:10) solution at 40°C

than in the case of propylene sulphide ($r = 2.4$). A possible explanation of this result could be found in the difference of 'hardness' or 'softness' of both systems.

The oxygen atom of the oxirane cycle is a 'hard' element, according to the classification of Pearson²¹, while the sulphur is much softer. The association of the latter with the zinc, a soft element, is more favourable and this could play a role in the monomer-initiator interaction during polymerization steps.

The fractionation of poly(propylene oxide) into crystalline (isotactic) and amorphous (heterotactic) parts is a strong support for the existence of different kinds of sites: one, stereospecific, giving isotactic polymer, others, non-specific but stereoelective, giving heterotactic polymer.

Stereospecific sites are enantiomorphic with R -type and S -type chirality. They give through homopolymerization of each enantiomer R -type chains and S -type chains which are in principle separable.

Non-stereospecific sites present an overall electivity corresponding to the preferential choice of one enantiomer.

If one calls C , C_R and C_S the concentrations of non stereospecific sites, or stereospecific R -type sites and S -type sites respectively and k'_R , k'_S , k_R and k_S the global rate constants of polymerization on these sites, one obtains the following kinetic equations for R and S enantiomers:

$$\frac{-d|R|}{dt} = k'_R |C| |R| + k_R |C_R| |R|$$

$$\frac{-d|S|}{dt} = k'_S |C| |S| + k_S |C_S| |S|$$

then

$$\frac{d|R|}{d|S|} = \frac{k'_R |C| + k_R |C_R|}{k'_S |C| + k_S |C_S|} \times \frac{|R|}{|S|} = r \frac{|R|}{|S|} \quad (3)$$

where

$$r = \frac{k'_R |C| + k_R |C_R|}{k'_S |C| + k_S |C_S|}$$

The stereoelectivity ratio r is constant during all the polymerization and equal to 1.8 in our system.

Therefore equation (3) can be integrated and gives the theoretical relation (1) given previously. 'Partial' stereoelectivities could be defined for each type of sites.

The change in the relative proportion of stereospecific and non-stereospecific sites according to polymerization conditions, and particularly temperature, seems to show that there exists a whole spectrum of sites, stereospecific or non-stereospecific, having a relative preference for one of the enantiomers, the rate of each type of site being $\sum_i k'_{iR} C_i$ for non-stereospecific sites choosing preferentially R , $\sum_i k_{iR} C_{iR}$ for stereospecific sites choosing R , and so on.

For pure stereospecific sites, if k_R and k_S are supposed equal, the partial stereoelectivity is:

$$r_{sp} = \frac{|C_R|}{|C_S|}$$

and stereoelection results from unbalanced concentration of R -type and S -type sites

$$|C_R| > |C_S|$$

In our case r_{sp} is equal to 2.6.

For non-stereospecific process the stereoelectivity is given by the ratio:

$$r_{nsp} = \frac{\sum_i k_{iR} C_i}{\sum_i k_{iS} C_i}$$

which is equal to 1.6 for our system.

Table 5 Calculated and experimental dyads and triads for amorphous fractions of poly(propylene oxides) prepared by stereoelective polymerization

$[\alpha_p]_D^{25a}$	R/S^b	>C Triads						$-\text{CH}_2-\text{ Dyads}$			
		i		h		s		m		r	
		Calc.	Found	Calc.	Found	Calc.	Found	Calc.	Found	Calc.	Found
-5.8	58.3/41.7	0.273	0.27	0.486	0.49	0.243	0.24	0.514	0.51	0.486	0.49
-13.2 ^c	68.9/31.1	0.36	0.35	0.42	0.43	0.21	0.21	0.57	0.56	0.43	0.44
-16.6 ^c	73.7/26.3	0.385	0.38	0.41	0.40	0.205	0.22	0.59	0.60	0.41	0.40
+6.3 ^c	41.0/59.0	0.285	0.28	0.475	0.47	0.24	0.25	0.524	0.52	0.476	0.48
+8.5 ^c	37.9/62.1	0.29	0.30	0.47	0.48	0.235	0.22	0.53	0.55	0.47	0.45

^aIn benzene $C = 1$; ^bbased on $[\alpha]_D^{25} = 35$ for an optically pure monomer $\alpha_0 = 11.9$ (neat, dm)¹²; ^camorphous part of polymers taken from ref 22

Preliminary results recently reported for propylene oxide and propylene sulphide²² show that the stereoelectivity ratio changed with the enantiomer composition of the monomer used. However, the r values remained constant during the polymerization. This would seem to indicate that active sites are formed only after a reaction of pre-existing sites with the monomer at the beginning of the polymerization.

More data are needed in order to explain the relationship between the global ratio r and partial ratios r_{sp} and r_{nsp} .

Particularly, it is not yet clear why the overall selectivity is constant with temperature and seems to be an intrinsic property of a monomer–initiator system.

CONCLUSIONS

The polymerization of racemic propylene oxide was performed using a chiral initiator derived from the reaction of diethylzinc with (–) 3,3-dimethyl-1,2-butanediol. During the polymerization and up to high conversions, the stereoelectivity ratio, e.g. the preferential choice of the initiator for one of the enantiomers, was constant and a simple relation between the conversion and the optical purity of unreacted monomer remained valid.

The stereoelectivity is equal to 1.8, which is the highest value found up to now for propylene oxide. However this stereoelectivity is lower than that found for propylene sulphide for the same initiator.

The polymer could be fractionated into a crystalline isotactic part and an amorphous heterotactic part both optically active. Partial stereoelectivities could be determined for both fractions, the crystalline one corresponding for example at 80°C to a ratio of 2.6 against 1.6 for the amorphous part.

Two types of sites, stereospecific and non-stereospecific, probably formed in the first reaction between monomer and initiator, are both active for the stereoelective polymerization.

The proportion of stereospecific and non-stereospecific sites depends on the temperature of the polymerization, but the overall stereoelectivity remains constant and seems

to be an intrinsic property of this monomer–initiator system.

REFERENCES

- 1 Price, C. C. and Osgan, M. *J. Am. Chem. Soc.* 1956, **78**, 4787
- 2 Inoue, S., Tsuruta, T. and Furukawa, J. *Makromol. Chem.* 1962, **55**, 215
- 3 Tsuruta, T. 'The stereochemistry of Macromolecules', (Ed A. D. Ketley), Marcel Dekker, New York, 1967, Vol 2, p 177
- 4 Tsuruta, T. *J. Polym. Sci. (D)* 1972, **6**, 179
- 5 Furukawa, J., Kumata, Y., Yamada, K. and Fueno, T. *J. Polym. Sci. (C)* 1968, 711
- 6 Furukawa, J., Akutsu, S. and Saegusa, T. *Makromol. Chem.* 1965, **81**, 100
- 7 Pino, P. *Adv. Polym. Sci.* 1965, **4**, 236
- 8 Spassky, N. and Sigwalt, P. *Eur. Polym. J.* 1971, **7**, 72
- 9 Sepulchre, M., Spassky, N. and Sigwalt, P. *Macromolecules* 1972, **5**, 92
- 10 Deffieux, A., Sepulchre, M. and Spassky, N. *J. Organomet. Chem.* 1974, **80**, 311
- 11 Deffieux, A., Sepulchre, M., Spassky, N. and Sigwalt, P. *Makromol. Chem.* 1974, **175**, 339
- 12 Lapeyre, W., Cheradame, H., Spassky, N. and Sigwalt, P. *J. Chim. Phys.* 1973, **5**, 838
- 13 Inoue, S., Tsuruta, T. and Yoshida, N. *Makromol. Chem.* 1964, **79**, 34
- 14 Tsuruta, T., Inoue, S. and Tsukuma, I. *Makromol. Chem.* 1965, **84**, 298
- 15 Furukawa, J., Akutsu, S. and Saegusa, T. *Makromol. Chem.* 1966, **94**, 68
- 16 Schaefer, J. *Macromolecules* 1969, **2**, 533
- 17 Oguni, N., Lee, K. and Tani, H. *Macromolecules* 1972, **5**, 819
- 18 Uryu, T., Shimazu, H. and Matsuzaki, K. *J. Polym. Sci. (B)* 1973, **11**, 275
- 19 Sepulchre, M., Spassky, N., van Ooteghem, D. and Goethals, E. J. *J. Polym. Sci. (Polym. Chem. Edn)* 1974, **12**, 1683
- 20 Tsuruta, T., Inoue, S., Yoshida, N. and Yokota, Y. *Makromol. Chem.* 1965, **81**, 191
- 21 Pearson, R. G., *Science* 1966, **151**, 172; Seyden-Penne, J., *Bull. Soc. Chim.* 1968, 3871
- 22 Sepulchre, M., Coulon, C., Spassky, N. and Sigwalt, P. *Prepr. 1st Int. Symp. Polymerization Heterocycles Warsaw-Jablonna* 1975, p 80
- 23 Guette, J. P. and Spassky, N. *Bull. Soc. Chim.* 1972, 4217

Salt effect on cationic copolymerization between *cis*- and *trans*-ethyl propenyl ethers

Kenji Yamamoto and Toshinobu Higashimura

Department of Polymer Chemistry, Faculty of Engineering, Kyoto University, Kyoto 606, Japan

(Received 15 March 1976)

In order to study the common-ion effect on monomer reactivity ratios, cationic copolymerization between *cis*- and *trans*-ethyl propenyl ethers was carried out at 0°C by using iodine or acetyl perchlorate as initiator. In toluene, the *cis* isomer was several times more reactive than the *trans* isomer regardless of the kind of initiators employed. When a common-ion salt (tetra-*n*-butylammonium iodide, triiodide, or perchlorate) was added to the copolymerization system in ethylene dichloride, the monomer reactivity ratios were changed approaching those observed in a non-polar solvent such as toluene. On the other hand, in nitroethane the monomer reactivity ratios were only slightly affected by the addition of common-ion salts. These noticeable common-ion effects on monomer reactivity ratios in the '*cis*-*trans*' copolymerization were satisfactorily explained on the basis of the steric hindrance between the substituents of monomers and a bulky propagating chain end.

INTRODUCTION

Recently the common-ion effect has been examined with the cationic copolymerizations between vinyl ethers and styrene derivatives and between styrene derivatives initiated by iodine¹ or acetyl perchlorate². When a common-ion salt was added to the copolymerization systems in a polar solvent, it was found that the monomer reactivity ratios approached those observed in a non-polar solvent. These changes in monomer reactivity ratios were interpreted in terms of the depression of the dissociation of propagating species by a common-ion salt, and hence the selectivity of propagating species is dependent upon its dissociation state.

In the cationic copolymerization between *cis*- and *trans*-ethyl propenyl ethers initiated by BF₃OEt₂, it has been reported that the relative reactivities of the two monomers depend greatly on the solvent polarity³⁻⁵. In a non-polar solvent the *cis* isomer is several times more reactive than the *trans* isomer, while in a polar solvent both isomers show nearly the same reactivities.

The addition of a common-ion salt to a polymerization system will vary the degree of dissociation of propagating species without changing its counter-ion in a given solvent^{1,2}. If the change in monomer reactivity ratios by the solvent polarity in the '*cis*-*trans*' copolymerization results from that in the dissociation state of propagating species, the addition of the common-ion salt is also expected to change the monomer reactivity ratios. Therefore, in the present investigation, the common-ion effect on the cationic copolymerization of *cis*- and *trans*-ethyl propenyl ethers in several solvents was examined and the propagation mechanism was discussed on the basis of the experimental results obtained.

EXPERIMENTAL

Materials

Ethyl propenyl ether (EPE) was synthesized by the elimination of ethanol from the corresponding acetal

which was prepared from propionaldehyde and ethanol⁶. The *cis* and *trans* isomers of EPE were separated by fractional distillation through a spinning-band column of over 70 theoretical plates. The *cis* and *trans* isomers were identified by i.r. and n.m.r. spectroscopy. The boiling points of *cis*- and *trans*-EPE were 69° and 75°C, respectively. The spin-spin coupling constants of olefinic α - and β -protons were 6.8 Hz for the *cis* isomer and 13.2 Hz for the *trans* isomer; these values being similar to those for other propenyl ethers⁷. The two monomers were distilled over calcium hydride and then over metallic sodium just before use. The geometric purities of *cis*- and *trans*-EPE were found by gas chromatography to be 99.0% and 98.0%, respectively; each purified monomer containing only its geometric isomer as impurity.

Solvents (toluene, ethylene dichloride, and nitroethane) and *n*-heptane as an internal standard for gas chromatography were purified by the usual methods. Iodine (Merck, Guaranteed Reagent) was used without further purification. Acetyl perchlorate (AcClO₄) was synthesized by the same methods as described in the previous paper⁸. Tetra-*n*-butylammonium iodide (*n*-Bu₄NI) (Wako Pure Chemicals, Guaranteed Reagent) and tetra-*n*-butylammonium perchlorate (*n*-Bu₄NClO₄) (Nakarai Chemicals, Guaranteed Reagent) were used after drying overnight *in vacuo*. Tetra-*n*-butylammonium triiodide (*n*-Bu₄NI₃) was synthesized from *n*-Bu₄NI and iodine⁹.

Procedures

Copolymerizations were carried out under dry nitrogen in the same manner as reported previously¹⁰. The concentration of residual water in the copolymerization system was found to be 0.2–0.3 mmol/l by the Karl-Fischer titration. *n*-Heptane (5 vol%) was added to the reaction mixture as the internal standard for gas chromatography. Copolymer compositions were determined from the amount of residual monomers measured by gas chromatography. Monomer reactivity ratios were calculated according to an improved Fineman-Ross method¹¹. Molecular weights of

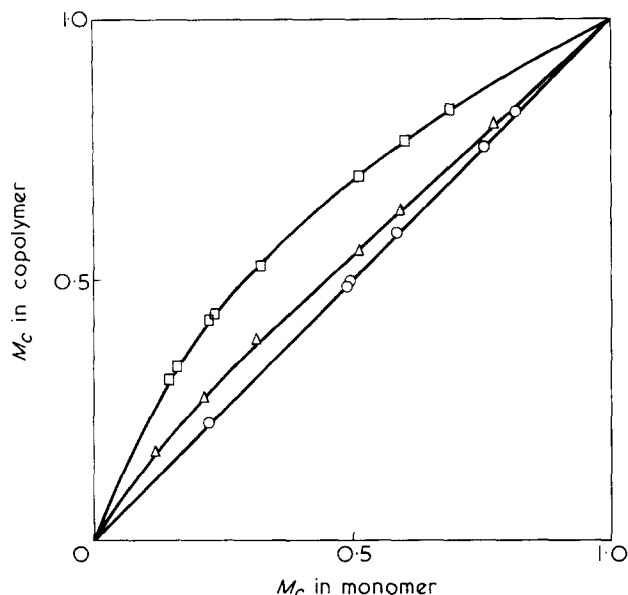


Figure 1 Effect of solvent on the copolymerization of *cis*-EPE (M_c) with *trans*-EPE (M_t) by I_2 at 0°C , $[M]_0 = 10 \text{ vol\%}$. \circ , $\text{C}_2\text{H}_5\text{NO}_2$; \triangle , $(\text{CH}_2\text{Cl})_2$; \square , $\text{C}_6\text{H}_5\text{CH}_3$

Table 1 Monomer reactivity ratios in the copolymerization of *cis*-EPE (M_c) with *trans*-EPE (M_t) at 0°C ($[M]_0 = 10 \text{ vol\%}$)

Solvent	Salt	r_c	r_t
Initiator: I_2 (1.0 mmol/l)			
$\text{C}_6\text{H}_5\text{CH}_3^a$	—	2.08 ± 0.13	0.41 ± 0.03
$(\text{CH}_2\text{Cl})_2$	—	0.99 ± 0.03	0.68 ± 0.02
$\text{C}_2\text{H}_5\text{NO}_2$	—	1.02 ± 0.01	0.97 ± 0.01
$(\text{CH}_2\text{Cl})_2$	$n\text{-Bu}_4\text{NI}$ (1.0)	1.22 ± 0.04	0.57 ± 0.02
$(\text{CH}_2\text{Cl})_2$	$n\text{-Bu}_4\text{NI}_3$ (1.0)	1.29 ± 0.06	0.52 ± 0.03
$(\text{CH}_2\text{Cl})_2$	$n\text{-Bu}_4\text{NI}_3$ (5.0)	1.48 ± 0.09	0.51 ± 0.03
$\text{C}_2\text{H}_5\text{NO}_2$	$n\text{-Bu}_4\text{NI}$ (1.0)	1.09 ± 0.02	0.95 ± 0.01
$\text{C}_2\text{H}_5\text{NO}_2$	$n\text{-Bu}_4\text{NI}_3$ (1.0)	1.18 ± 0.04	0.87 ± 0.02
Initiator: AcClO_4 (0.01 mmol/l)			
$\text{C}_6\text{H}_5\text{CH}_3$	—	1.62 ± 0.03	0.29 ± 0.01
$(\text{CH}_2\text{Cl})_2$	—	1.18 ± 0.03	0.78 ± 0.02
$(\text{CH}_2\text{Cl})_2$	$n\text{-Bu}_4\text{NClO}_4$ (1.0)	1.40 ± 0.05	0.53 ± 0.02

^a $[I_2]_0 = 10.0 \text{ mmol/l}$

Values in parentheses represent the concentration of salt in mmol/l

all the copolymers obtained were found to be about 3×10^3 (vapour pressure osmometry). Therefore, the conventional copolymer composition equation can be safely applied.

RESULTS

Copolymerization of *cis*-EPE (M_c) with *trans*-EPE (M_t) by iodine

The effect of solvent polarity on the copolymerization of *cis*- and *trans*-EPE was investigated by using iodine as initiator at 0°C . Copolymerizations proceeded relatively slowly in the three solvents. Figure 1 shows the copolymer composition curves. Monomer reactivity ratios (r_c and r_t) are summarized in Table 1. *Cis*-EPE was more reactive than *trans*-EPE regardless of the solvent polarity. As the solvent polarity decreased, r_c increased and r_t decreased.

A common-ion salt for iodine was added to the copolymerization system in a polar solvent. Since it is uncertain whether a counter anion is I^- or I_3^- in the cationic polymerization initiated by iodine¹²⁻¹⁴, both $n\text{-Bu}_4\text{NI}$ and

$n\text{-Bu}_4\text{NI}_3$ were tentatively used as common-ion salts in the present investigation.

Figure 2 shows the copolymer composition curves for the copolymerization in ethylene dichloride and in nitroethane in the presence of $n\text{-Bu}_4\text{NI}$ or $n\text{-Bu}_4\text{NI}_3$. Monomer reactivity ratios are summarized in Table 1. The addition of the common-ion salts in ethylene dichloride affected the monomer reactivity ratios and the resultant copolymer composition curves approached that observed in toluene. Although the effect of $n\text{-Bu}_4\text{NI}$ is not so large as that of $n\text{-Bu}_4\text{NI}_3$, it is clear that the monomer reactivity ratios are changed by the addition of both salts. In nitroethane, a more polar solvent than ethylene dichloride, the monomer reactivity ratios were little affected by the addition of the common-ion salts.

Copolymerization of *cis*-EPE (M_c) with *trans*-EPE (M_t) by AcClO_4

Cis- and *trans*-EPE were copolymerized by AcClO_4 at 0°C . Figure 3 shows the effects of the solvent polarity and of the addition of $n\text{-Bu}_4\text{NClO}_4$. Monomer reactivity ratios are summarized in Table 1. When AcClO_4 was used as initiator, *cis*-EPE was more reactive than *trans*-EPE regardless of the solvent polarity as in the copolymerizations by iodine. As the solvent polarity decreased, r_c increased and r_t decreased. Furthermore, in ethylene dichloride, the addition of $n\text{-Bu}_4\text{NClO}_4$ one hundred times as much as AcClO_4 affected the monomer reactivity ratios and the resultant copolymer composition curve approached that observed in toluene. In nitroethane the copolymerization rate was so large that the monomer reactivity ratios could not be determined.

DISCUSSION

In the cationic copolymerization between *cis*- and *trans*-EPE initiated by iodine or by AcClO_4 , the monomer re-

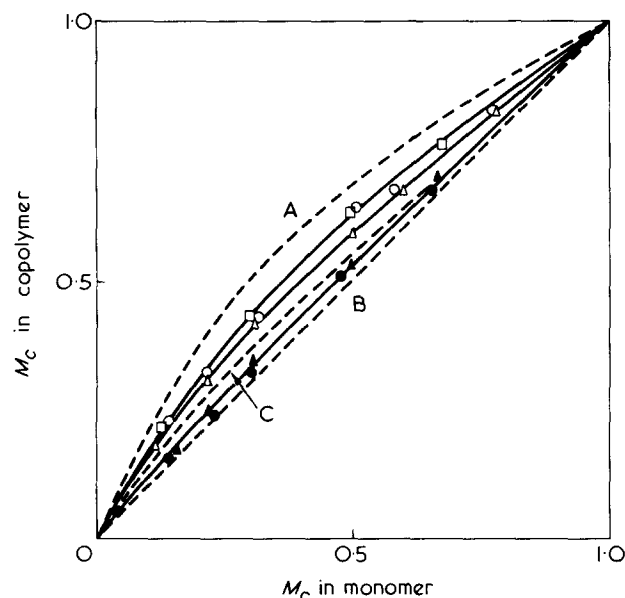


Figure 2 Effect of $n\text{-Bu}_4\text{NI}$ or $n\text{-Bu}_4\text{NI}_3$ on the copolymerization of *cis*-EPE (M_c) with *trans*-EPE (M_t) by I_2 at 0°C , $[M]_0 = 10 \text{ vol\%}$, $[I_2]_0 = 1.0 \text{ mmol/l}$: \triangle , $(\text{CH}_2\text{Cl})_2$, $[n\text{-Bu}_4\text{NI}]_0 = 1.0 \text{ mmol/l}$; \circ , $(\text{CH}_2\text{Cl})_2$, $[n\text{-Bu}_4\text{NI}_3]_0 = 1.0 \text{ mmol/l}$; \square , $(\text{CH}_2\text{Cl})_2$, $[n\text{-Bu}_4\text{NI}_3]_0 = 5.0 \text{ mmol/l}$; \bullet , $\text{C}_2\text{H}_5\text{NO}_2$, $[n\text{-Bu}_4\text{NI}]_0 = 1.0 \text{ mmol/l}$; \blacktriangle , $\text{C}_2\text{H}_5\text{NO}_2$, $[n\text{-Bu}_4\text{NI}_3]_0 = 1.0 \text{ mmol/l}$. Broken lines show the salt-free copolymer composition curves in various solvents (from Figure 1): A, $\text{C}_6\text{H}_5\text{CH}_3$; B, $\text{C}_2\text{H}_5\text{NO}_2$; C, $(\text{CH}_2\text{Cl})_2$

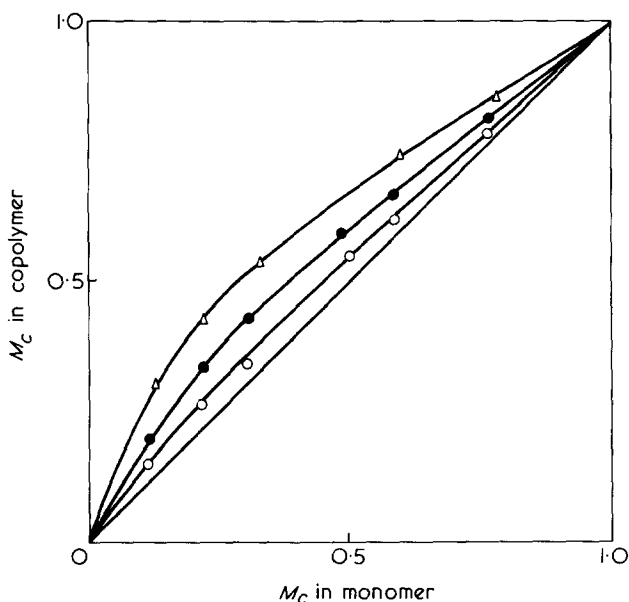


Figure 3 Effect of solvent and $n\text{-Bu}_4\text{NClO}_4$ on the copolymerization of *cis*-EPE (M_c) with *trans*-EPE (M_t) by AcClO_4 at 0°C . $[M]_0 = 10 \text{ vol}\%$, $[\text{AcClO}_4]_0 = 0.01 \text{ mmol/l}$: \circ , $(\text{CH}_2\text{Cl})_2$, salt free; \bullet , $(\text{CH}_2\text{Cl})_2$, $[n\text{-Bu}_4\text{NClO}_4]_0 = 1.0 \text{ mmol/l}$; \triangle , $\text{C}_6\text{H}_5\text{CH}_3$, salt free

activity ratios were changed by the addition of a common-ion salt in ethylene dichloride, and the resultant copolymer composition curves approached those obtained in toluene. This may be the first example of the cationic copolymerization of α,β -disubstituted olefins, in which the monomer reactivity ratios are affected by the addition of a common-ion salt. The addition of a common-ion salt to a reaction mixture is expected to depress the dissociation of propagating species through the mass-law effect. The propagating species will exist in the form of ion pairs and free ions in ethylene dichloride. When a common-ion salt is added, some of the free ions will be changed to ion pairs and hence the relative reactivities of monomers will approach those in a non-polar solvent such as toluene, in which ion pairs will be the propagating species exclusively.

On the other hand, in the iodine initiated copolymerization in nitroethane the monomer reactivity ratios were little affected by the addition of $n\text{-Bu}_4\text{NI}$ or $n\text{-Bu}_4\text{NI}_3$. The propagating species in nitroethane must be ion pairs in the presence of a common-ion salt. Therefore, the above results suggest that the nature of these ion pairs is similar to that of free ions. The present explanation is based on the same viewpoint as that presented in our previous paper².

It has been shown by ^{13}C n.m.r. measurements and molecular orbital calculations that the π -electron densities of α - and β -carbons are similar to *cis*- and *trans*-EPE¹⁵.

Therefore, it is safe to assume that the magnitude of electrostatic interaction between the propagating carbocation and its counterion does not depend on the geometric structure of monomers. In spite of these, the relative reactivities of *cis*- and *trans*-EPE changed considerably according to the dissociation state of propagating species. This suggests that a factor other than the electrostatic one plays an important role in the determination of relative reactivities in the '*cis*-*trans*' copolymerization.

In a non-polar solvent, the propagating carbocation forms a tight ion pair with its counter-ion, hence the growing chain end must be very crowded. In this circumstance it is probably more difficult for the propagating carbocation to attack *trans*-EPE than *cis*-EPE, because the former carries two bulky substituents on both sides of its olefinic double bond. This will lead to the higher reactivity of *cis*-EPE than that of *trans*-EPE in a non-polar solvent. It is therefore concluded that the changes in relative reactivities of EPE by the addition of common-ion salts result from the difference in steric hindrance of the propagating species in different dissociation states. The above explanation is essentially consistent with the propagation mechanism proposed in our previous paper concerning the solvent effect on the cationic copolymerization between *cis*- and *trans*-EPE initiated by BF_3OEt_2 ⁵.

REFERENCES

- 1 Yamamoto, K. and Higashimura, T. *J. Polym. Sci. (Polym. Chem. Edn)* in press
- 2 Higashimura, T. and Yamamoto, K. *J. Polym. Sci. (Polym. Chem. Edn)* in press
- 3 Okuyama, T., Fueno, T., Furukawa, J. and Uyeo, K. *J. Polym. Sci. (A-1)* 1968, 6, 1001
- 4 Higashimura, T., Kusudo, S., Ohsumi, Y. and Okamura, S. *J. Polym. Sci. (A-1)* 1968, 6, 2523
- 5 Higashimura, T. and Yamamoto, K. *Makromol. Chem.* 1974, 175, 1139
- 6 Mizote, A., Kusudo, S., Higashimura, T. and Okamura, S. *J. Polym. Sci. (A-1)* 1967, 5, 1727
- 7 Higashimura, T., Kusudo, S., Ohsumi, Y., Mizote, A. and Okamura, S. *J. Polym. Sci. (A-1)* 1968, 6, 2511
- 8 Masuda, T. and Higashimura, T. *J. Macromol. Sci. (A)* 1971, 5, 549
- 9 Buckles, R. E. and Yuk, J. P. *J. Am. Chem. Soc.* 1953, 75, 5048
- 10 Yamamoto, K. and Higashimura, T. *J. Polym. Sci. (Polym. Chem. Edn)* 1974, 12, 613
- 11 Ezrielev, A. I., Brokhina, E. L. and Roskin, E. S. *Vysokomol. Soedin.* 1969, 11, 1670
- 12 Eley, D. D. and Richard, A. W. *Trans. Faraday Soc.* 1949, 42, 425, 436
- 13 Eley, D. D., Isack, F. L. and Rochester, C. H. *J. Chem. Soc. (A)* 1968, 872
- 14 Okamura, S., Kanoh, N. and Higashimura, T. *Makromol. Chem.* 1961, 47, 19
- 15 Masuda, T. *J. Polym. Sci. (Polym. Chem. Edn)* 1973, 11, 2713

Mechanism of fibrillation in the flow of molten polymer mixtures

M. V. Tsebrenko, A. V. Yudin and T. I. Ablazova

Chemical Fibers Laboratory, Kiev Technological Institute of the Light Industry, Kiev 252011, Ukrainian SSR, USSR

and G. V. Vinogradov*

Polymer Rheology Laboratory, Institute of Petrochemical Synthesis, USSR Academy of Sciences, Moscow 117071, USSR

(Received 10 February 1976)

Experiments on the flow of melts of mixtures of thermodynamically incompatible polymers show that ultra-fine fibrils of one of the polymers form in the matrix of the other in the entrance to the extrusion orifice.

INTRODUCTION

Earlier published papers¹⁻⁵ show that in the flow of melts of mixtures of thermodynamically incompatible polymers under certain conditions ultra-thin fibrils of one of the components form in the mass of the other. Melts of mixtures of polyoxymethylene (POM) with a copolyamide (CPA) show the phenomenon clearly (*Figure 1*).

The experimental results seek answers to the following questions: is the length of elementary ultra-thin fibrils determined by the dimensions of the individual particles of the fibril-forming polymer or are fibrils of considerable length obtained due to the coalescence of the particles of the fibril-forming polymer deformed in the flow? Where does fibrillation take place, at the entrance to the duct, in the duct, or at its exit?

EXPERIMENTAL

The series of extrudates of a mixture of POM + 70% CPA was obtained in a constant pressure gas capillary viscosimeter at temperatures of 173°, 177° and 190°C. The melting point of the POM was determined by d.t.a. and was taken as the melting peak at 171°C. The melting peak at a heating rate of 4°C/min is rather wide⁶, covering the range from 158° to 180°C. The characteristics of the polymers and the conditions under which they were mixed have been described before⁷. Conditions of deformation were as follows: the shear stress at capillary wall was $5.25 \cdot 10^4$ N/m²; diameter of capillary, 0.92 mm; capillary length to diameter ratio, 6. The outflowing extrudate was passed into a mixture of isopropyl alcohol and dry ice (temperature -70°C) or into liquid nitrogen. The copolyamide was extracted from the set extrudate with ethyl alcohol at 75°C in a Soxhlet apparatus. After the removal of CPA the microstructure of thin sections of the extrudates and the remnants of POM were examined under an optical or electron microscope.

RESULTS AND DISCUSSION

Formation of fibrils begins at a temperature 2°C above the melting point of POM: the smallest particles become extended, forming the fibrils (*Figure 2*), but the bulk of POM remains in the shape of undeformed particles. At 177°C fibril formation becomes more pronounced, but large POM particles (=100 μm) still do not stretch, but aggregate. It is from such POM aggregates at increasing volume output, that films form (*Figure 3*). The largest particles do not appear to take part in fibril formation at all, but move in the stream from its axis to the periphery (*Figure 4*) and settle mainly in concentric rings. Conditions can probably be found under which POM in the CPA mass forms only thick films in the shape of concentric cylinders.

The results show that the process of fibrillation takes

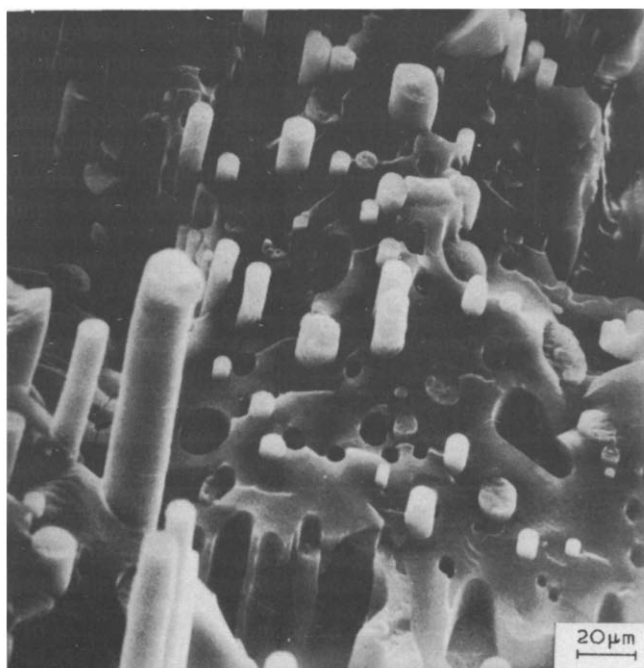


Figure 1 Electron microphotograph of an extrudate transversal fracture POM + 70% CPA mixture

* To whom correspondence should be addressed.

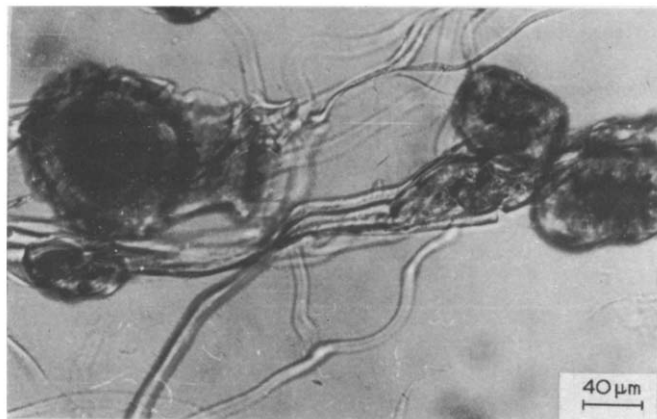


Figure 2 Microphotograph of POM after extraction of CPA from the extrudate produced at 173°C

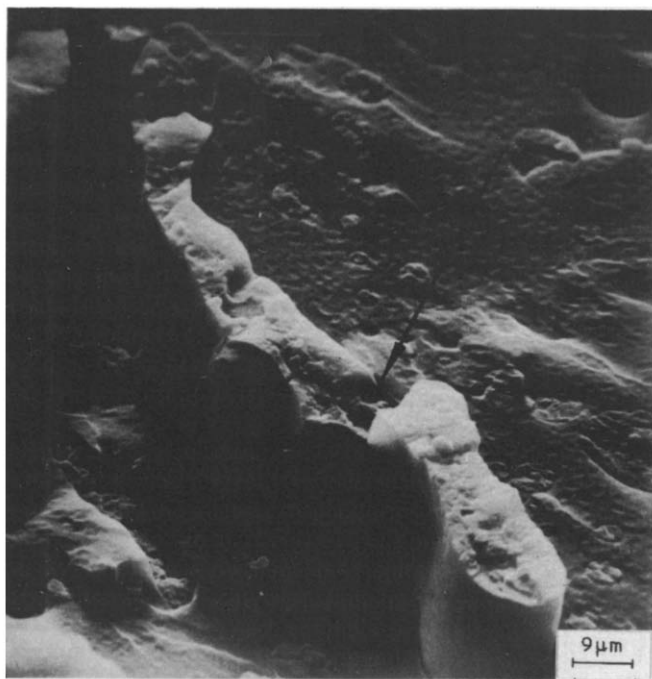


Figure 3 Electron microphotograph of an extrudate fracture. Arrow indicates particle aggregates in the form of films

place by the stretching of POM particles in the direction of the stream and is accompanied by their coalescence, which is the necessary prerequisite for producing long uniform continuous fibrils.

Microscopic analysis of longitudinal sections of extrudates obtained at 177°C confirm the deformation of the particles (Figure 5), and an electron microphotograph clearly shows coalescence of the particles which seem to form a chain of 'Vienna sausages' (Figure 6).

In the case of well pronounced fibrillation the bundles obtained contain $\sim 10^5$ ultra-thin fibrils. Since it is not possible to measure the length of an individual fibril in the bundle, we examined microscopically the POM after the extraction of CPA from the extrudates formed at 177°C, when only a small number of POM particles take part in fibril formation. The individual fibrils, so obtained were several millimetres in length and simple calculations show that the formation of a fibril about 20 μm in diameter and 3.2 mm long requires coalescence of 12 POM particles with a mean diameter of 53 μm . Proof of the coalescence of deformed POM particles in the direction of the stream

is provided also by the formation of ultra-thin fibrils with POM powder of particle diameter $\sim 2 \mu\text{m}$. In this case a bundle of fibrils, obtained after the extraction of CPA from the extrudate, contains no separate particles or short fibrils indicating that the fibrils are continuous in length.

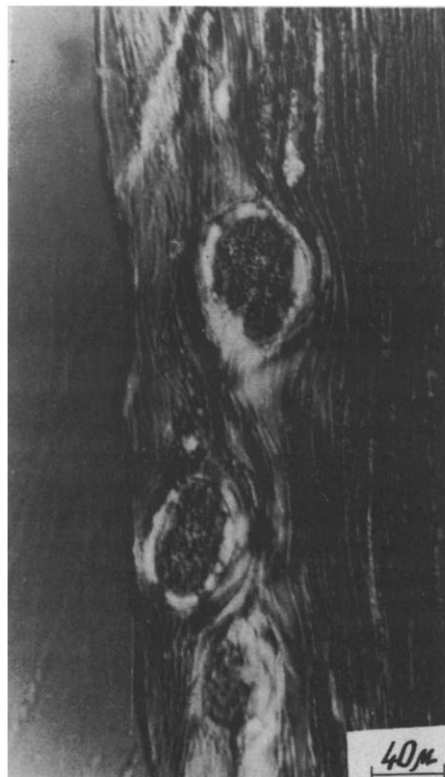


Figure 4 Microphotograph of a longitudinal section of an extrudate produced at 177°C

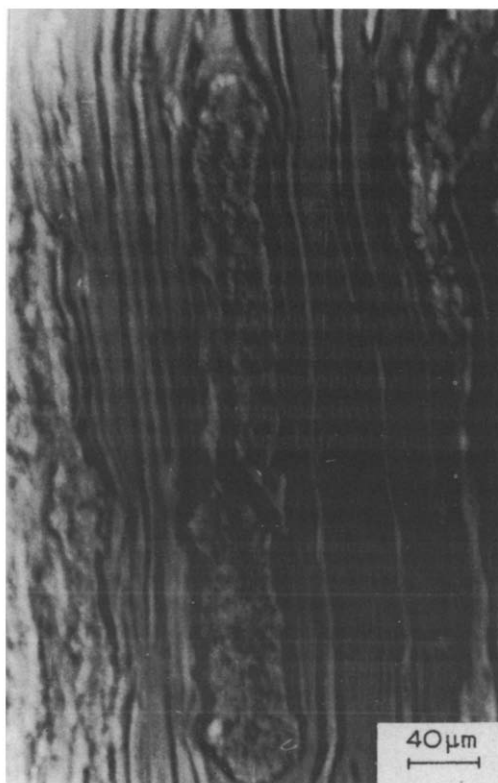


Figure 5 Microphotograph of a longitudinal section of an extrudate produced at 177°C, illustrating stretching and coalescence of stretched POM particles



Figure 6 Electron microphotograph of individual POM fibrils after extraction of CPA from the extrudate

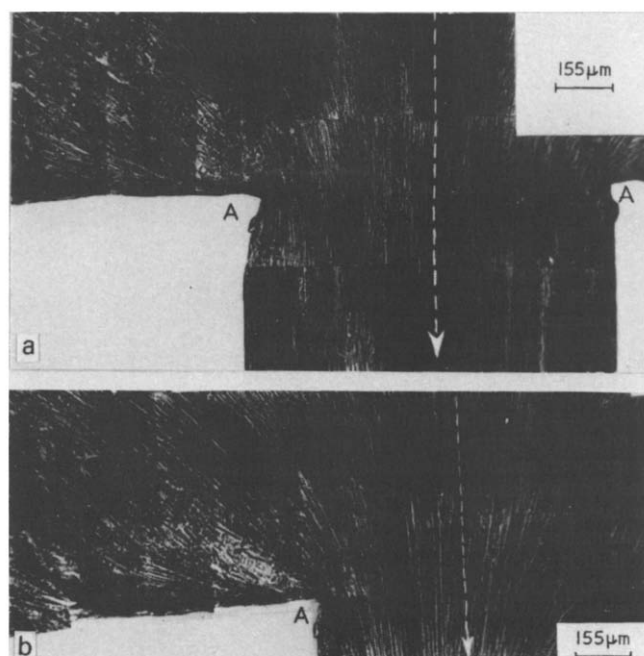


Figure 7 Microphotographs of a longitudinal section of a frozen sample from the entrance zone area: (a) along stream axis; (b) parallel to the axis at distance of 200 μm from it. A, entrance to capillary. Arrow indicates direction of the flow

Experiments in which the extrudated stream was frozen in liquid nitrogen were carried out to ascertain the place where formation of ultra-thin fibrils takes place. For this purpose a dismountable capillary consisting of semi-cylinders fastened to the viscometric container charged with polymer mixture was used. The container and capillary were placed in a thermostat at 190°C, a pre-set pressure applied and when the regime of flow stabilized, the container with the capillary was rapidly immersed in liquid nitrogen. Examination of such chilled samples enables the character of POM particle and fibril distribution in the CPA mass, during the flow of the melt in the viscosimetric container, in the entrance zone and in the capillary to be studied.

Figure 7a shows a microphotograph of a longitudinal section of a frozen sample in the entrance zone area, while Figure 7b presents the same results for a section which is parallel to the former, but is situated at a distance of 200 μm away from the stream axis. These data show convincingly that fibrillation takes place in the entrance zone and is due to the effect of tensile stresses which extend and coalesce the POM particles in the direction of the stream lines.

In the zone adjacent to the entrance to the capillary the stream lines form concentric cone-like funnels in which the fibrillation is very pronounced (Figure 8). Nearer to the walls the process becomes weaker and peters out in the dead zones of the container.

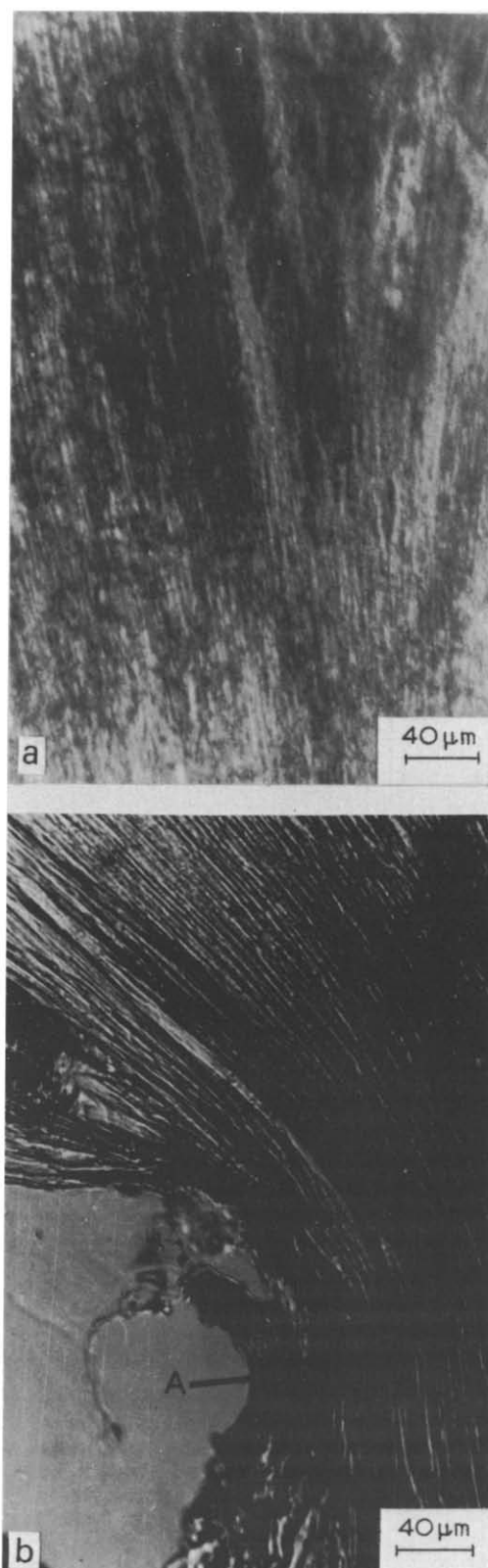


Figure 8 Microphotographs of longitudinal sections of a frozen sample, illustrating formation of funnel in entrance zone: (a) along stream axis; (b) parallel to the axis at distance of 0.5 mm from it

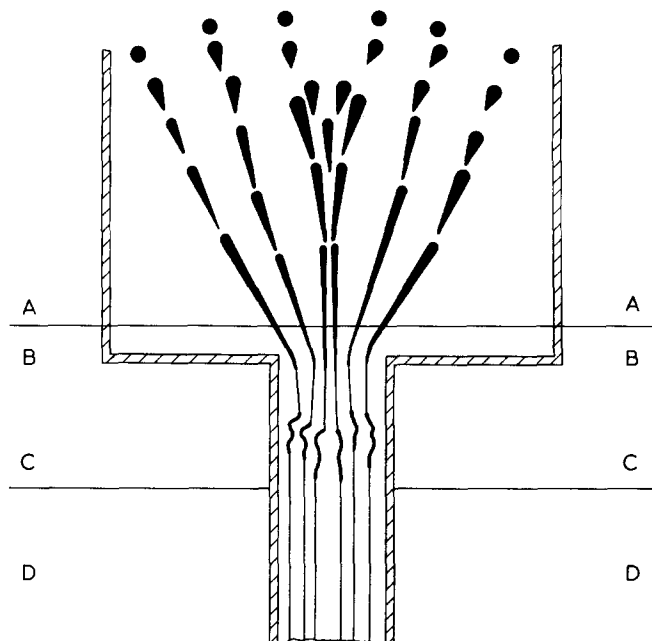


Figure 9 Representation of the fibrillation process in the entrance zone and in the ducts



Figure 10 Microphotograph of a longitudinal section of a frozen sample, illustrating the process of fibril shrinkage and loss of parallelism

On the basis of microscopic examinations the fibrillation process can be presented schematically as shown in Figure 9. Under the effect of tensile stresses acting in the direction of the stream the stretching and coalescence of the particles of the fibrillation component takes place in the entrance zone (Figure 9, A). Close to the entrance to the duct the stream narrows sharply (Figure 9, B) and at a definite distance from the entrance (Figure 9, C) the influence of its walls becomes manifest, leading to the intensive development of shear and retardation of the stream. This is apparent in shrinkage (enlargement of diameters) of the fibrils and loss of parallelism in their mutual arrangement as shown in Figure 10. In the zone of shear flow the fibrils become parallel once again (Figure 9, D; Figure 11).



Figure 11 Microphotograph of a longitudinal section of a frozen sample at a zone of stabilized flow

These results show that the formation of ultra-thin fibrils takes place in the entrance zone of the ducts and the effect of tensile stress on the particles and their coalescence in the entrance zone is a prerequisite for the production of continuous fibrils.

ACKNOWLEDGEMENT

The authors are indebted to Dr B. V. Yarlykov, who helped them to stage the tests with the dismantable capillary.

REFERENCES

- 1 Tsebrenko, M. V., Yudin, A. V., Kuchinka, M. Yu., Vinogradov, G. V. and Zubovich, K. A. *Vysokomol. Soedin. (B)* 1973, 15, 566
- 2 Yudin, A. V., Tsebrenko, M. V., Kuchinka, M. Yu. and Vinogradov, G. V. *Abstr. Compl. Res. Work. Ukr. Higher Sch.* 1974, 7, 3
- 3 Tsebrenko, M. V., Yakob, M., Kuchinka, M. Yu., Yudin, A. V. and Vinogradov, G. V. *Int. J. Polym. Mater.* 1974, 3, 99
- 4 Vinogradov, G. V., Yarlykov, B. V., Tsebrenko, M. V., Yudin, A. V. and Ablazova, T. I. *Polymer* 1975, 16, 609
- 5 Ablazova, T. I., Tsebrenko, M. V., Yudin, A. V., Vinogradov, G. V. and Yarlykov, B. V. *J. Appl. Polym. Sci.* 1975, 19, 1781
- 6 Vlasenko, V. I., Mel'nikov, B. N., Blinicheva, I. B., Yudin, A. V. and Tsebrenko, M. V. *Proc. Higher Sch. Chem. Chem. Technol.* 1973, 16, 760
- 7 Ablazova, T. I., Tsebrenko, M. V., Yudin, A. V., Vinogradov, G. V. and Yarlykov, B. V. *Vysokomol. Soedin. (A)* 1975, 17, 1385

Swelling of linear polymers in mixed swelling agents; predictability by means of solubility parameters

P. E. Froehling, D. M. Koenhen, A. Bantjes and C. A. Smolders
Laboratory for Macromolecular Chemistry, Twente University of Technology, PO Box 217, Enschede, The Netherlands
 (Received 26 March 1976; revised 19 May 1976)

INTRODUCTION

The solubility behaviour of polymers can be predicted to a reasonable extent by applying the Hildebrand relation¹ which connects the energy of mixing of two compounds to their individual energies of vaporization:

$$\frac{\Delta E_{\text{mix}}}{\Phi_1 \Phi_2} = V(\delta_1 - \delta_2)^2 \quad (1)$$

where ΔE_{mix} is the energy of mixing; Φ_1 and Φ_2 , the volume fractions of the components; V , the total volume of one mole of the mixture and δ_1, δ_2 , the Hildebrand solubility parameters of both components, defined by:

$$\begin{aligned} \delta &= (\text{cohesive energy density})^{1/2} \\ &= \left(\frac{\Delta E_{\text{vap}}}{V_m} \right)^{1/2} \end{aligned} \quad (2)$$

where ΔE_{vap} is the energy of vaporization and V_m is the molar volume. From equation (1) it is clear that a smaller difference in δ between two compounds results in a diminished energy of mixing. A decrease in ΔE_{mix} gives a higher degree of swelling and eventually complete solubility may result. The applicability of equation (1) has been extended by Hansen², who divided the solubility parameter into contributions from disperse (δ_d), dipole (δ_p) and donor/acceptor or hydrogen-bond (δ_h) interactions, and represented δ as:

$$\delta^2 = \delta_d^2 + \delta_p^2 + \delta_h^2 \quad (3)$$

which may be taken as a vector sum.

It is possible to express each of the solubility parameter components for a mixture of two solvents as:

$$\delta_{m,i} = \Phi_1 \delta_{1,i} + \Phi_2 \delta_{2,i}; \quad i = d, p, h \quad (4)$$

This relation can be used only when there are no specific interactions upon mixing, since these interactions (e.g. additional donor/acceptor interactions) do not obey the geometric mean rule.

The values of the components of δ have been reported for numerous compounds, and methods to calculate them from other physico-chemical properties of solvents and polymers are progressing rapidly³.

The often encountered enhanced interaction of polymers with solvent pairs can be explained by the vector concept of the solubility parameter, of which a representation is given in *Figure 1*.

The affinity of a solvent mixture X (on the line A-B) with respect to a polymer is inversely proportional to its distance to P, the location of the polymer in the $\delta_d, \delta_p, \delta_h$ space. It is evident that for the given spatial configuration of A, B and P there exists a point M at which the energy of mixing is at a minimum and swelling should reach a maximum. The application of the solubility parameter concept to the interaction of polymers with solvent mixtures has been confined up to now to qualitative aspects of the solubility of linear polymers^{2,4} and the swelling behaviour of cross-linked elastomers⁵. We wish to report here on the application of the same concepts to the swelling of linear polymers by swelling agent/non-solvent mixtures.

The systems studied are shown in *Table 1*. Toluene, trichloroethylene and n-butyl acetate are well-known swelling agents for poly(vinyl chloride), while methanol and nitromethane are strict non-solvents². For the combina-

tion n-butylacetate/nitromethane a deviating behaviour may be expected, as these solvents show mutual interaction on account of their respective electron donating and accepting character⁶. The other two solvent pairs do not show specific interactions which may cause deviations.

EXPERIMENTAL

Poly(vinyl chloride), Breon S 110/10 (BP Ltd), was a very pure preparation according to i.r. spectrum and elementary analysis. From gel permeation chromatography (solvent tetrahydrofuran, stationary phase Styragel-Waters Associates) the molecular weight distribution was calculated as^{7,8} $\bar{M}_n = 28\,000$, $\bar{M}_w = 56\,000$ using calibration samples of PVC from Pressure Chemical Co. All solvents were analytical grade quality.

PVC films were cast from a 15% so-

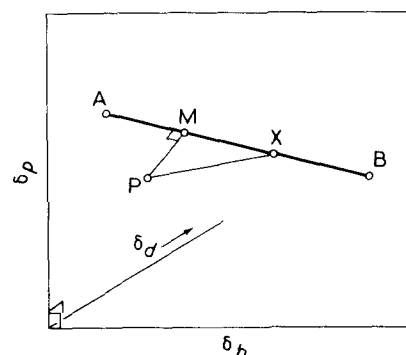


Figure 1 Spatial representation of solvent mixture/polymer interaction

Table 1 Solubility parameters of PVC and solvents. Values are taken from ref 3

Compound	δ_d	δ_p	δ_h
PVC	9.15	4.9	1.5
Toluene	8.82	0.7	1.0
Trichloroethylene	8.78	1.5	2.6
n-Butylacetate	7.67	1.8	3.1
Nitromethane	7.70	9.2	2.5
Methanol	7.42	6.0	10.9

lution in tetrahydrofuran. The dry films (about 0.5 mm thick) was cut into pieces of ~200 mg. The pieces were immersed in the solvent mixtures, and (after rapid blotting with filter paper) weighed after 2, 6 and 20 h immersion. Equilibrium was attained after 6 h at 20°C. All experiments were carried out in triplicate.

RESULTS

The results of the swelling experiments are plotted in Figures 2–4, together with the calculated polymer/solvent distances in the δ space:

$$\Delta = [(\delta_{p,S} - \delta_{p,P})^2 + (\delta_{d,S} - \delta_{d,P})^2 + (\delta_{h,S} - \delta_{h,P})^2]^{1/2} \quad (5)$$

where the subscripts S and P refer to solvent and polymer respectively.

Values of δ were taken from Koenhen³. The values of the solvent mixtures were calculated according to equation (4). It is clear that for the solvent pairs toluene/methanol and trichloroethylene/nitromethane which do not show donor/acceptor interactions upon mixing, the maximum in the swelling curve coincides with the calculated composition at which the distance in δ -space is minimal. The magnitude of the relative increase in swelling with relation to the pure solvents appears to be proportional to the calculated decrease in Δ .

It should be pointed out that the δ values for PVC as given by Hansen² result in a poorer agreement between the calculated and measured extreme values of Δ and degree of swelling. In the case of the donor/acceptor solvent pair

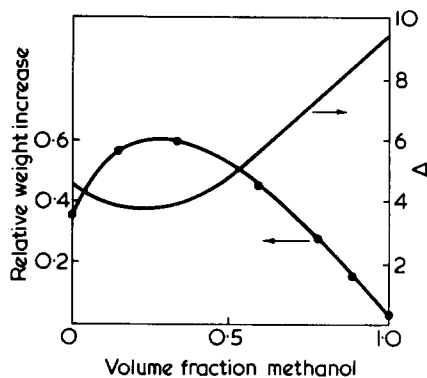


Figure 2 Calculated interaction parameter Δ and measured relative weight increase of PVC in toluene/methanol mixtures

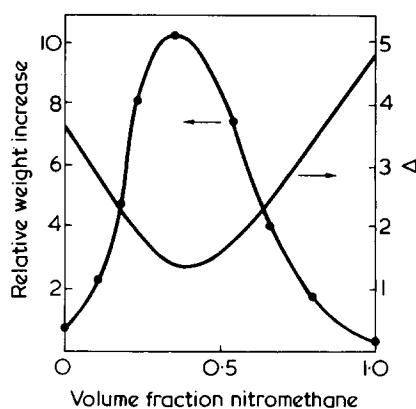


Figure 3 Calculated interaction parameter Δ and measured relative weight increase of PVC in trichloroethylene/nitromethane mixtures

n-butyl acetate/nitromethane no maximum occurs in the swelling curve, contrary to expectation.

Caution should therefore be exercised in the application of the solubility parameter concept in mixtures of solvent which may interact through donor/acceptor forces.

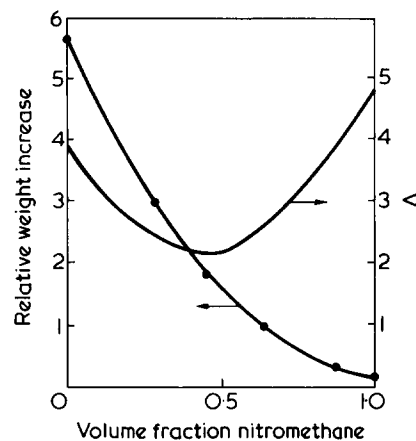


Figure 4 Calculated interaction parameter Δ and measured relative weight increase of PVC in n-butylacetate/nitromethane mixtures

ACKNOWLEDGEMENT

The g.p.c. measurements were carried out by G. van de Ridder.

REFERENCES

- Hildebrand, J. H. and Scott, R. L. 'The Solubility of Non-Electrolytes', Dover, New York, 1949
- Hansen, C. M. *J. Paint Technol.* 1967, 39, 104
- Koenhen, D. M. and Smolders, C. A. *J. Appl. Polym. Sci.* 1975, 19, 1163
- Chen, S. A. *J. Appl. Polym. Sci.* 1971, 15, 1247
- Beerbower, A. and Dickey, J. R. *ASLE Trans.* 1969, 12, 1
- McClellan, A. and Pimental, G. 'The Hydrogen Bond', Freeman, San Francisco, 1960
- Evans, J. M. *Polym. Eng. Sci.* 1973, 13, 401
- Cardenas, J. N. and O'Driscoll, K. F. *J. Polym. Sci. (Polym. Lett. Edn)* 1975, 13, 657

A method for the calculation of optimum filler content in amorphous and semi-crystalline polymers

S. C. Shea*

Department of Polymer and Fibre Science, University of Manchester Institute of Science and Technology, Manchester, UK
(Received 22 March 1976; revised 13 May 1976)

INTRODUCTION

Currently more and more additives are being used in polymers, particularly the polyolefins. These additives include fillers, flame retardants, pig-

ments etc. Consequently, it is desirable to be able to predict the concentration of additive above which the mechanical properties significantly deteriorate. This communication details a method of calculating an optimum filler concentration using principles well known in the surface coat-

ing industry. While this proposed technique will be illustrated using high density polyethylene, it is thought that since the equations presented here are of a general nature, they may be more widely applicable. Of the many tests available elongation at break is probably the most sensitive and will be used here to compare experimental results with theory.

THEORY

Consider a polymeric material to which

* Present Address: Van Leer Research Laboratories, Passfield, Hampshire, UK

lution in tetrahydrofuran. The dry films (about 0.5 mm thick) was cut into pieces of ~200 mg. The pieces were immersed in the solvent mixtures, and (after rapid blotting with filter paper) weighed after 2, 6 and 20 h immersion. Equilibrium was attained after 6 h at 20°C. All experiments were carried out in triplicate.

RESULTS

The results of the swelling experiments are plotted in Figures 2–4, together with the calculated polymer/solvent distances in the δ space:

$$\Delta = [(\delta_{p,S} - \delta_{p,P})^2 + (\delta_{d,S} - \delta_{d,P})^2 + (\delta_{h,S} - \delta_{h,P})^2]^{1/2} \quad (5)$$

where the subscripts S and P refer to solvent and polymer respectively.

Values of δ were taken from Koenhen³. The values of the solvent mixtures were calculated according to equation (4). It is clear that for the solvent pairs toluene/methanol and trichloroethylene/nitromethane which do not show donor/acceptor interactions upon mixing, the maximum in the swelling curve coincides with the calculated composition at which the distance in δ -space is minimal. The magnitude of the relative increase in swelling with relation to the pure solvents appears to be proportional to the calculated decrease in Δ .

It should be pointed out that the δ values for PVC as given by Hansen² result in a poorer agreement between the calculated and measured extreme values of Δ and degree of swelling. In the case of the donor/acceptor solvent pair

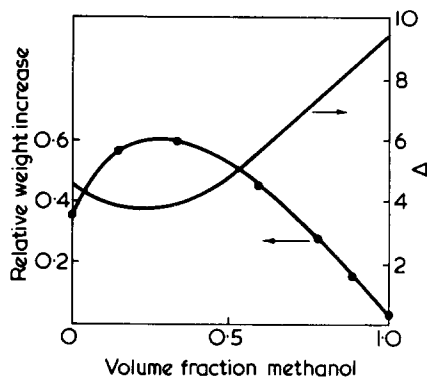


Figure 2 Calculated interaction parameter Δ and measured relative weight increase of PVC in toluene/methanol mixtures

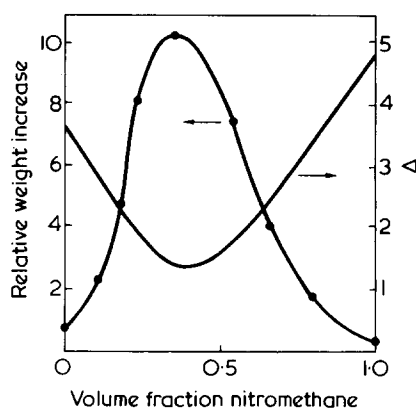


Figure 3 Calculated interaction parameter Δ and measured relative weight increase of PVC in trichloroethylene/nitromethane mixtures

n-butyl acetate/nitromethane no maximum occurs in the swelling curve, contrary to expectation.

Caution should therefore be exercised in the application of the solubility parameter concept in mixtures of solvent which may interact through donor/acceptor forces.

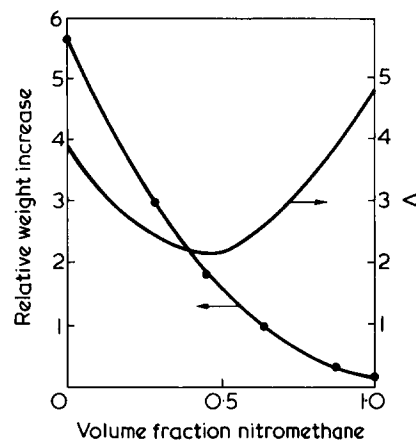


Figure 4 Calculated interaction parameter Δ and measured relative weight increase of PVC in n-butylacetate/nitromethane mixtures

ACKNOWLEDGEMENT

The g.p.c. measurements were carried out by G. van de Ridder.

REFERENCES

- Hildebrand, J. H. and Scott, R. L. 'The Solubility of Non-Electrolytes', Dover, New York, 1949
- Hansen, C. M. *J. Paint Technol.* 1967, 39, 104
- Koenhen, D. M. and Smolders, C. A. *J. Appl. Polym. Sci.* 1975, 19, 1163
- Chen, S. A. *J. Appl. Polym. Sci.* 1971, 15, 1247
- Beerbower, A. and Dickey, J. R. *ASLE Trans.* 1969, 12, 1
- McClellan, A. and Pimental, G. 'The Hydrogen Bond', Freeman, San Francisco, 1960
- Evans, J. M. *Polym. Eng. Sci.* 1973, 13, 401
- Cardenas, J. N. and O'Driscoll, K. F. *J. Polym. Sci. (Polym. Lett. Edn)* 1975, 13, 657

A method for the calculation of optimum filler content in amorphous and semi-crystalline polymers

S. C. Shea*

Department of Polymer and Fibre Science, University of Manchester Institute of Science and Technology, Manchester, UK
(Received 22 March 1976; revised 13 May 1976)

INTRODUCTION

Currently more and more additives are being used in polymers, particularly the polyolefins. These additives include fillers, flame retardants, pig-

ments etc. Consequently, it is desirable to be able to predict the concentration of additive above which the mechanical properties significantly deteriorate. This communication details a method of calculating an optimum filler concentration using principles well known in the surface coat-

ing industry. While this proposed technique will be illustrated using high density polyethylene, it is thought that since the equations presented here are of a general nature, they may be more widely applicable. Of the many tests available elongation at break is probably the most sensitive and will be used here to compare experimental results with theory.

THEORY

Consider a polymeric material to which

* Present Address: Van Leer Research Laboratories, Passfield, Hampshire, UK

pigment is added in increasing amounts. Ultimately a point is reached where just sufficient polymer (binder) is present to fill the voids between pigment particles. This point is defined as the Critical Pigment Volume Concentration (*CPVC*). The term pigment is used here rather loosely and is taken to mean, pigments, fillers and extenders. The term *CPVC*, has been 'borrowed' from the paint industry and hence it is convenient to retain their terminology. According to Patton¹ the *CPVC* represents the densest packing of the particles commensurate with the degree of dispersion and is found to be relatively independent of the binder used (except for polymer emulsions). Hence it can be argued that the *CPVC* is a basic property of the pigment.

Above the *CPVC* insufficient polymeric material is available to bind all the pigment particles, while below the *CPVC* a state of excess binder exists. Associated with this transition, changes can be expected in terms of paint performance, thus for example, high gloss can be achieved below the *CPVC* while above it matt finishes result. Other properties like flexibility and permeability are also affected. It should be appreciated that the *CPVC* is not a sharp point of inflection; properties change gradually, and in general follow sigmoidal shaped curves.

One method of determining the *CPVC* values for pigments and fillers is to use oil absorption figures. The oil absorption (*OA*) is defined as the amount of oil required to wet a particular pigment and depends on particle size distribution and degree of dispersion. It is usually expressed as grams of oil per hundred grams of pigment and can be simply determined by adding oil drop-wise to a known weight of pigment, rubbing with a spatula and considering the end point to be when a uniform film forms. Various other methods to measure oil absorption have been described by Gardner and Sward² and results are slightly dependent on the method used.

The relationship between oil absorption and *CPVC* is given by:

$$CPVC = \frac{100}{\frac{\rho_f}{OA} + \frac{100}{\rho_o}} \times 100\% \quad (1)$$

where ρ_f is the density of filler (pig-

ment); *OA*, the oil absorption (g/100 g) and ρ_o is the density of oil used.

Since oil absorption values are known to be additive¹ it follows that in a blend consisting of many pigments or fillers the following holds:

$$(CPVC)_{Blend} = \frac{V_1(CPVC)_1 + V_2(CPVC)_2 + V_3(CPVC)_3 + \dots + V_n(CPVC)_n}{V_1 + V_2 + V_3 + \dots + V_n}$$

or

$$(CPVC)_{Blend} = \frac{\sum V_i(CPVC)_i}{\sum V_i} \quad (2)$$

where V_i is the volume fraction of a particular pigment or filler.

On applying these equations to polyethylene, it is assumed that the filler is distributed throughout the amorphous regions only, hence if the degree of crystallinity (by volume) of

the base polymer is ϕ it follows that the critical volume fraction of filler, $V_{f\text{crit}}$ is given by:

$$V_{f\text{crit}} = CPVC \times (1 - \phi) \quad (3)$$

This can readily be converted to critical weight fraction of filler, $W_{f\text{crit}}$ by:

$$W_{f\text{crit}} = \frac{(V_{f\text{crit}})\rho_f}{\rho_m(1 - V_{f\text{crit}}) + (V_{f\text{crit}})\rho_f} \quad (4)$$

where ρ_f is the density of filler; ρ_m is the density of polymer matrix and $(1 - V_{f\text{crit}}) = V_m$ (volume fraction of polymer).

In a blend of many pigments and fillers it is necessary to replace ρ_f in equation (4) by $\bar{\rho}_f$ where $\bar{\rho}_f$ is a weighted average density.

The following assumptions are basic to the argument and are discussed in more detail below.

It is assumed that the filler is distributed in the amorphous regions only. In the case of polyethylene the size of the crystallite would appear to exclude any foreign material; with other semi-crystalline polymers some disruption of the crystallites may occur. Other

Table 1 Materials specification

(A) Polyethylene:	
Viscosity-average molecular weight	110 000
<i>MF1</i> (ISO R292A)	0.25 g/10 min
Density	959 kg/m ³
Melting range (polarized microscope)	132°–135°C
(B) Antimony trioxide:	
Density	5500 kg/m ³
Purity	>99%
Oil absorption* (g/100g)	12
Refractive index	2.09–2.29
(C) Chlorinated hydrocarbon [†] :	
Approximate chemical formula	C ₂₃ H ₂₈ Cl ₂₀
Approximate molecular weight	1010
Amount of chlorine (w/w)	68–72%
Density	1630 kg/m ³
Oil absorption** (g/100g)	35
(D) Alumina trihydrate [‡] :	
Density	2400 kg/m ³
Oil absorption (g/100g)	40
Purity	>99%
Chemical formula	Al ₂ O ₃ ·3H ₂ O
Refractive index	1.58

* Boiled linseed oil (density 935 kg/m³) is commonly used to measure oil absorption; ** measured by author; [†] typically Cereclor 70[®] from ICI Ltd; [‡] typically Trihydrate E[®] from Plasticchem

assumptions include no volume change on the introduction of the filler and that oil absorption is an accurate measure of the CPVC. Strictly both these statements are incorrect, however they are adequate approximations for this simple theory.

Clearly care should be exercised in using the above equations, which are intended to be a rough guide only.

APPLICATION OF THEORY

The above theory was studied using high density (linear) polyethylene (HDPE) as a matrix together with two different fillers viz. antimony trioxide/chlorinated hydrocarbon in the molar ratio Sb:Cl of 1:3 and alumina trihydrate. Properties of polyethylene and the fillers used are shown in Table 1, the data being taken from the manufacturer's information sheets.

In the case of the antimony/chlorine system the theoretical calculations detailed above gave a critical weight frac-

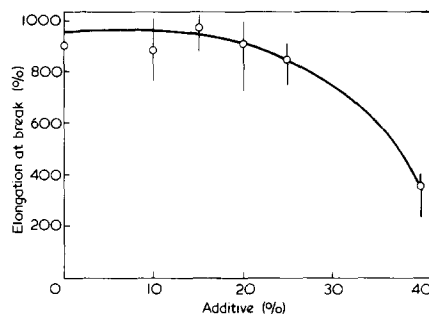


Figure 1 Elongation at break as a function of amount of additive at Sb:Cl ratio of 1:3

tion of filler of 29%, while from consideration of Figure 1 it can be seen that the elongation at break decreases rapidly after 25% additive.

Regarding alumina trihydrate a critical weight fraction was calculated to be 24%, while Figure 2 indicates a value of 26%.

Thus, while the assumptions used in the theoretical model are somewhat crude it would appear that their use is justified as the practical results indicate.

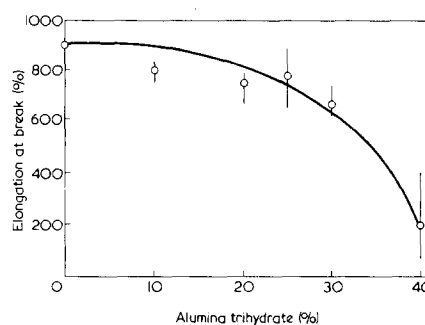


Figure 2 Elongation at break as a function of amount of alumina trihydrate

Although the theory has only been tested on HDPE it is thought that it could be applied to all polymers as the equations used are of a general nature.

REFERENCES

- 1 Patton, T. C. 'Paint Flow and Pigment Dispersion', Interscience, New York, 1964
- 2 Gardner, H. A. and Sward, G. G. 'Physical Examination of Paints, Varnishes, Lacquers and Colours' 10th Edn, Henry A. Gardner Labs, Maryland, 1946

Letter

Laser-Raman spectroscopic studies of mechanically-loaded polymers

There has recently been interest in the effect of mechanical stress on the vibrational spectra of polymers with the prime aim of obtaining some insight on the fracture mechanism of polymers. In particular Zhurkov and co-workers^{1,2} using infra-red transmission spectroscopy have examined the effect on skeletal vibrational modes of applying small stresses to thin polymer films or fibres. They observed small frequency shifts which were a linear function of applied stress and agreed with theoretical predictions of Gubonov³; such stress-sensitivity has been confirmed in the i.r. by Roylance and De Vries⁴ and by Wool and Statton⁵.

Recent work in our laboratories has shown that laser-Raman spectroscopy can be used in a similar, but more convenient way to i.r. for the investigation of the effect of stress on polymers. This letter outlines the application, briefly compares the results with the i.r. data, and highlights the advantages which Raman offers for

such studies.

Our investigations have included polypropylene (PP), polycarbonate (PC), polystyrene and nylon-6,6. The samples used are standard 4 in ASTM tensile testing dumbbells which thus allow direct correlations to be made with tensile test data. The dumbbells are stretched *in situ* in a mechanical jig with the orientation shown in Figure 1 and with almost no restrictions of sampling area.

The spectrometer used was the Spex Ramalog 4 with triple monochromator. The 514.5 and 488.0 nm exiting lines of a CRL Ar⁺ laser were used, with Claassen filtering, at a power level of ~200 mW at the sample. Fluorescence presented no problem with PP but PC samples required about an hour to 'burn' out. To check the effect of the laser beam on the polymers some samples were left in the beam for up to three days with neither visible effect nor any further changes in the Raman spectra. The draw direction is

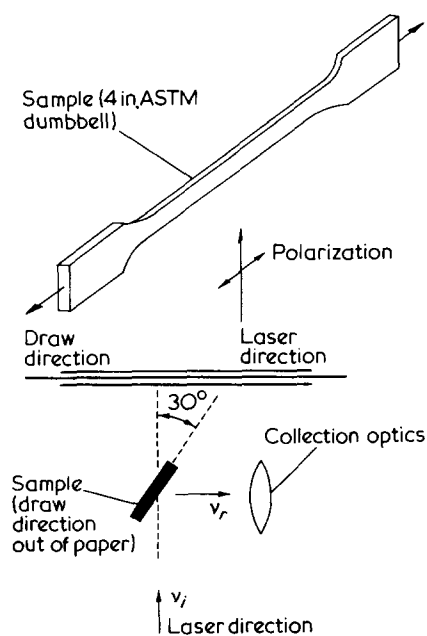


Figure 1 Sample orientation in Raman spectrometer (Spex Ramalog 4)

assumptions include no volume change on the introduction of the filler and that oil absorption is an accurate measure of the CPVC. Strictly both these statements are incorrect, however they are adequate approximations for this simple theory.

Clearly care should be exercised in using the above equations, which are intended to be a rough guide only.

APPLICATION OF THEORY

The above theory was studied using high density (linear) polyethylene (HDPE) as a matrix together with two different fillers viz. antimony trioxide/chlorinated hydrocarbon in the molar ratio Sb:Cl of 1:3 and alumina trihydrate. Properties of polyethylene and the fillers used are shown in Table 1, the data being taken from the manufacturer's information sheets.

In the case of the antimony/chlorine system the theoretical calculations detailed above gave a critical weight frac-

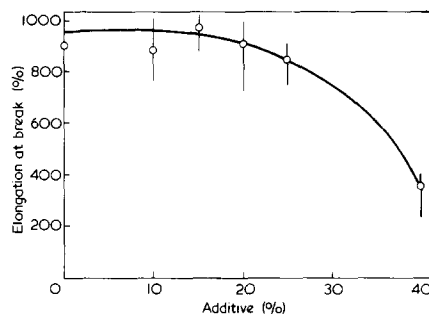


Figure 1 Elongation at break as a function of amount of additive at Sb:Cl ratio of 1:3

tion of filler of 29%, while from consideration of Figure 1 it can be seen that the elongation at break decreases rapidly after 25% additive.

Regarding alumina trihydrate a critical weight fraction was calculated to be 24%, while Figure 2 indicates a value of 26%.

Thus, while the assumptions used in the theoretical model are somewhat crude it would appear that their use is justified as the practical results indicate.

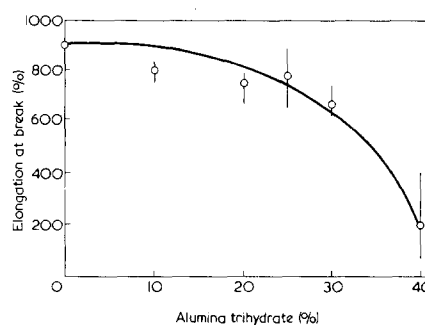


Figure 2 Elongation at break as a function of amount of alumina trihydrate

Although the theory has only been tested on HDPE it is thought that it could be applied to all polymers as the equations used are of a general nature.

REFERENCES

- 1 Patton, T. C. 'Paint Flow and Pigment Dispersion', Interscience, New York, 1964
- 2 Gardner, H. A. and Sward, G. G. 'Physical Examination of Paints, Varnishes, Lacquers and Colours' 10th Edn, Henry A. Gardner Labs, Maryland, 1946

Letter

Laser-Raman spectroscopic studies of mechanically-loaded polymers

There has recently been interest in the effect of mechanical stress on the vibrational spectra of polymers with the prime aim of obtaining some insight on the fracture mechanism of polymers. In particular Zhurkov and co-workers^{1,2} using infra-red transmission spectroscopy have examined the effect on skeletal vibrational modes of applying small stresses to thin polymer films or fibres. They observed small frequency shifts which were a linear function of applied stress and agreed with theoretical predictions of Gubonov³; such stress-sensitivity has been confirmed in the i.r. by Roylance and De Vries⁴ and by Wool and Statton⁵.

Recent work in our laboratories has shown that laser-Raman spectroscopy can be used in a similar, but more convenient way to i.r. for the investigation of the effect of stress on polymers. This letter outlines the application, briefly compares the results with the i.r. data, and highlights the advantages which Raman offers for

such studies.

Our investigations have included polypropylene (PP), polycarbonate (PC), polystyrene and nylon-6,6. The samples used are standard 4 in ASTM tensile testing dumbbells which thus allow direct correlations to be made with tensile test data. The dumbbells are stretched *in situ* in a mechanical jig with the orientation shown in Figure 1 and with almost no restrictions of sampling area.

The spectrometer used was the Spex Ramalog 4 with triple monochromator. The 514.5 and 488.0 nm exiting lines of a CRL Ar⁺ laser were used, with Claassen filtering, at a power level of ~200 mW at the sample. Fluorescence presented no problem with PP but PC samples required about an hour to 'burn' out. To check the effect of the laser beam on the polymers some samples were left in the beam for up to three days with neither visible effect nor any further changes in the Raman spectra. The draw direction is

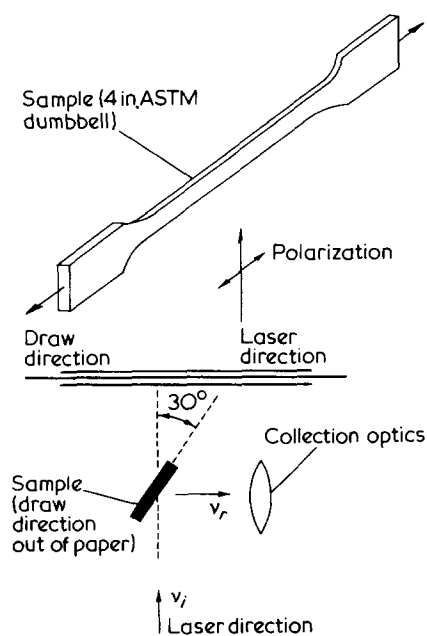


Figure 1 Sample orientation in Raman spectrometer (Spex Ramalog 4)

along the direction of polarization of the laser radiation.

We have made an extensive study of all the Raman-active modes in the region 4000 to 10 cm⁻¹ of polycarbonate and polypropylene and preliminary studies on polystyrene and nylon-6,6. We have examined frequency changes, band intensity changes and depolarization ratios for small stresses and large stresses up to the yield point.

In general our experimental results are in agreement with the i.r. data but our much wider coverage of all vibrational modes and to larger stresses suggests that caution must be taken over the early interpretation^{1,2} of the observed changes. Table 1 lists our results for some of the bands of PP, in all cases the data being taken as the average of at least three replicate runs. From this it is clear that the skeletal modes are not the only modes which are stress-sensitive. For the skeletal modes, in concordance with the i.r. studies, we observe a slight decrease in frequencies with applied stress up to neck. After neck we find an increase in frequency often to higher than their initial values. Additionally we have found significant intensity changes usually very sudden at the necking-point, which is not accompanied by a sudden frequency change, the latter being a gradual change between limits. With depolarization ratios we have found a sudden drop in the ratio with small amounts of stress with no change thereafter.

The interpretation of our results will be discussed later in a full paper. However, we feel that the Zhurkov/Gubanov¹⁻³ theory of the stressing of the interatomic bonds in the molecule is an unlikely mechanism and that the modification of intermolecular forces is of greater importance. We thus favour a mechanism along the lines of changes in molecular conformations proposed by Cunningham *et al.*⁶ for

Table 1 Frequencies (cm⁻¹) of selected bands in the Raman spectrum of mechanically loaded polypropylene

Unstressed	Stressed		Band assignment
	Prior to neck	Prior to break	
2923.5	2923	2923	νC-H (CH ₂ anti)
2883	2883.5	2881.5	νC-H (CH ₃ sym)
2867.5	2867	2868.5	νC-H (CH ₂ sym)
2839.5	2839	2838	νC-H (CH ₂ sym)
1459	1458.5	1459.5	CH ₂ bending
1435	1434	1435	CH ₃ antisym bending
1151.5	1151	1152.5	Skeletal C-C
973.0	972.8	972.5 ^a	Skeletal C-C
808.5	807.5	807.0	Skeletal C-C
320.0	320.0	321.5	Skeletal C-C bending
105.5	104.5	Absent	Lattice vibration?

^aFor comparison purposes this peak has been studied on scale expansion and values are quoted to 0.1 cm⁻¹ and are the mean of 10 runs. Other values are quoted to 0.5 cm⁻¹ and are mean of at least 3 runs.

the polarized i.r. spectral changes occurring in poly(ethylene terephthalate) on drawing. From the depolarization ratio measurements it would appear that orientation occurs very early in the stress process and changes very little thereafter. The sudden intensity changes are thought to be a conformational change at neck the preferred conformer on necking being more 'streamlined' than the other.

We hope to have shown the value of laser-Raman as a research tool for stress analysis. The convenience of using bulk samples, in particular standard dumbbells, together with almost no restrictions on sampling area, which allows the ready use of sophisticated stress- and strain-measuring equipment, gives it many advantages over the i.r. technique. However, it should be emphasized that the two methods are complementary rather than competitive and that the use of both i.r. and Raman on the same system is likely to lead to a better understanding of the stress-sensitive phenomena.

Acknowledgements

We are most grateful for the support given for this project by the Ministry of Defence Procurement Executive.

R. A. Evans and H. E. Hallam

Department of Chemistry,
University College of Swansea,
Swansea, SA2 8PP, UK
(Received 14 June 1976; revised 28 June 1976)

References

- Zhurkov, S. N., Vettergren, V. I., Korsukov, V. E. and Novak, I. I. *Proc. 2nd Int. Conf. Fracture. Brighton* 1969, pp 545-550
- Korsukov, V. E. and Vettegren, V. I. *Strength Mater. (USSR)* 1971, 2, 51
- Gubanov, A. I. *Mekh. Polim.* 1967, 3, 771
- Roylance, D. K. and De Vries, K. L. *J. Polym. Sci. (B)* 1971, 9, 443
- Wool, R. P. and Statton, W. O. *J. Polym. Sci. (A-2)* 1974, 12, 1575
- Cunningham, A., Ward, I. M., Willis, H. A. and Zichy, V. *Polymer* 1974, 15, 749

ERRATA

'Annealing effects of polymers and their underlying molecular mechanisms' by G. S. Y. Yeh, R. Hosemann, J. Loboda-Čačković and H. Čačković, *Polymer* 1976, 17, 309-318.

Page 317, left hand column, equation (15) should read:

$$I_p = (\Delta\rho)^2 \gamma V [\sin\pi l_c / (l_a + l_c)]^2 \times \frac{l_a + l_c}{\pi^2} Z_{3p}$$

The authors apologise for this error.

along the direction of polarization of the laser radiation.

We have made an extensive study of all the Raman-active modes in the region 4000 to 10 cm⁻¹ of polycarbonate and polypropylene and preliminary studies on polystyrene and nylon-6,6. We have examined frequency changes, band intensity changes and depolarization ratios for small stresses and large stresses up to the yield point.

In general our experimental results are in agreement with the i.r. data but our much wider coverage of all vibrational modes and to larger stresses suggests that caution must be taken over the early interpretation^{1,2} of the observed changes. Table 1 lists our results for some of the bands of PP, in all cases the data being taken as the average of at least three replicate runs. From this it is clear that the skeletal modes are not the only modes which are stress-sensitive. For the skeletal modes, in concordance with the i.r. studies, we observe a slight decrease in frequencies with applied stress up to neck. After neck we find an increase in frequency often to higher than their initial values. Additionally we have found significant intensity changes usually very sudden at the necking-point, which is not accompanied by a sudden frequency change, the latter being a gradual change between limits. With depolarization ratios we have found a sudden drop in the ratio with small amounts of stress with no change thereafter.

The interpretation of our results will be discussed later in a full paper. However, we feel that the Zhurkov/Gubanov¹⁻³ theory of the stressing of the interatomic bonds in the molecule is an unlikely mechanism and that the modification of intermolecular forces is of greater importance. We thus favour a mechanism along the lines of changes in molecular conformations proposed by Cunningham *et al.*⁶ for

Table 1 Frequencies (cm⁻¹) of selected bands in the Raman spectrum of mechanically loaded polypropylene

Unstressed	Stressed		Band assignment
	Prior to neck	Prior to break	
2923.5	2923	2923	νC-H (CH ₂ anti)
2883	2883.5	2881.5	νC-H (CH ₃ sym)
2867.5	2867	2868.5	νC-H (CH ₂ sym)
2839.5	2839	2838	νC-H (CH ₂ sym)
1459	1458.5	1459.5	CH ₂ bending
1435	1434	1435	CH ₃ antisym bending
1151.5	1151	1152.5	Skeletal C-C
973.0	972.8	972.5 ^a	Skeletal C-C
808.5	807.5	807.0	Skeletal C-C
320.0	320.0	321.5	Skeletal C-C bending
105.5	104.5	Absent	Lattice vibration?

^aFor comparison purposes this peak has been studied on scale expansion and values are quoted to 0.1 cm⁻¹ and are the mean of 10 runs. Other values are quoted to 0.5 cm⁻¹ and are mean of at least 3 runs.

the polarized i.r. spectral changes occurring in poly(ethylene terephthalate) on drawing. From the depolarization ratio measurements it would appear that orientation occurs very early in the stress process and changes very little thereafter. The sudden intensity changes are thought to be a conformational change at neck the preferred conformer on necking being more 'streamlined' than the other.

We hope to have shown the value of laser-Raman as a research tool for stress analysis. The convenience of using bulk samples, in particular standard dumbbells, together with almost no restrictions on sampling area, which allows the ready use of sophisticated stress- and strain-measuring equipment, gives it many advantages over the i.r. technique. However, it should be emphasized that the two methods are complementary rather than competitive and that the use of both i.r. and Raman on the same system is likely to lead to a better understanding of the stress-sensitive phenomena.

Acknowledgements

We are most grateful for the support given for this project by the Ministry of Defence Procurement Executive.

R. A. Evans and H. E. Hallam

Department of Chemistry,
University College of Swansea,
Swansea, SA2 8PP, UK
(Received 14 June 1976; revised 28 June 1976)

References

- Zhurkov, S. N., Vettergren, V. I., Korsukov, V. E. and Novak, I. I. *Proc. 2nd Int. Conf. Fracture. Brighton* 1969, pp 545-550
- Korsukov, V. E. and Vettegren, V. I. *Strength Mater. (USSR)* 1971, 2, 51
- Gubanov, A. I. *Mekh. Polim.* 1967, 3, 771
- Roylance, D. K. and De Vries, K. L. *J. Polym. Sci. (B)* 1971, 9, 443
- Wool, R. P. and Statton, W. O. *J. Polym. Sci. (A-2)* 1974, 12, 1575
- Cunningham, A., Ward, I. M., Willis, H. A. and Zichy, V. *Polymer* 1974, 15, 749

ERRATA

'Annealing effects of polymers and their underlying molecular mechanisms' by G. S. Y. Yeh, R. Hosemann, J. Loboda-Čačković and H. Čačković, *Polymer* 1976, 17, 309-318.

Page 317, left hand column, equation (15) should read:

$$I_p = (\Delta\rho)^2 \gamma V [\sin\pi l_c / (l_a + l_c)]^2 \times \frac{l_a + l_c}{\pi^2} Z_{3p}$$

The authors apologise for this error.

Book Reviews

Structural Studies of Macromolecules by Spectroscopic Methods

Edited by K. J. Ivin

Wiley, London, 1976, 339 pp. £14.50

This volume is based largely on the contributions to a meeting held at Cranfield Institute of Technology, England, in July 1974. The object of the meeting, and also that of this volume, was to bring together information about the application of some of the more recently developed spectroscopic methods to the study of macromolecules. It consists of sixteen individual chapters, which vary in length from 8 to 69 pages and which may be divided into five groups, of roughly equal total length, dealing with neutron scattering, far infra-red and Raman spectroscopy, X-ray photoelectron spectroscopy (ESCA), n.m.r. (^{13}C and ^1H) and e.s.r. The character of the individual chapters varies quite widely, from one in the review-style on ESCA, which forms the longest chapter of the book, to rather specialized chapters such as that on ^{13}C n.m.r. studies of α -methylstyrene-alkane copolymers. This variation is not a weakness, since the different spectroscopic methods involved are in different stages of development both in terms of their general application and of their more specific application to polymers, and by avoiding any attempt at a rigid style of coverage it has been possible to produce a book of modest length with stimulating and reasonably up-to-date contributions on all the techniques considered.

The book deals with experiments on nearly 100 macromolecules. Most of them are synthetic polymers but very brief descriptions are given of neutron diffraction from collagen, of the overall vibrations of polypeptide chains and protein molecules and of some ^{13}C studies of biopolymers. The techniques described allow information to be obtained about the detailed chemical structure and conformations of macromolecules, about their radii of gyration in the bulk and their segmental and side-chain motions in bulk and in solution, about the rate of collision between the ends in solution and about the vibrational frequencies, crystallinity, lamellar thickness and surface composition in the bulk. Most of the chapters have extensive lists of references.

This is a well-produced book in which all polymer spectroscopists, and indeed most polymer scientists, will find much of interest and value.

D. I. Bower

Macromolecules in Solution

Volume 21: High Polymers, 2nd Edition

Herbert Morawetz.

Wiley, London, 1975, 549 pp. £15.00

The second edition of this well known book is an expanded and updated version of its predecessor but does not deviate from the underlying philosophy of the original volume. As the author makes clear in his introduction, his aim is to present a unified view of macromolecular behaviour in solution regardless of whether the macromolecule is a synthetic polymer or a biopolymer. This eminently desirable aim does carry with it the difficulty of adequately covering a very wide field.

Professor Morawetz starts the book with a chapter entitled 'General Considerations' which deals with the classification, dimensions, dispersity and shape of macromolecules in solution. There follows a chapter on thermodynamic aspects of polymer solutions and one dealing with conformation and the statistics of polymer chains. The next three chapters respectively entitled 'Equilibrium Properties of Dilute Solution'; 'Spectroscopy, Optical Activity and the Scattering of Light and X-rays'; 'Frictional Properties of Dissolved Macromolecules'; present the theoretical but no experimental background into the technique on which we largely base our knowledge of macromolecules in solution. The final three chapters discuss Polyelectrolytes, Molecular Association, and Chemical Kinetics in Macromolecular Solution. Throughout the book considerable

weight is given to biopolymers as illustrative of the various phenomena discussed.

Because of the extent of the field, the author has had to be selective and this has resulted in the omission or scant coverage of certain topics. The author has eschewed the discussion of experimental details, but on occasion missed or insufficiently stressed aspects of theory. Thus, although there is good coverage of the thermodynamic aspects of solubility and miscibility, its underlying importance in the practice of polymer fractionation is not explicitly discussed. There is brief mention of gel-permeation chromatography, but one is left with the impression that this technique inevitably requires the viscometric determination of the molecular weight of the eluted fractions, since there is no mention that columns may be calibrated or even that the Walter's Q factor method may on occasion prove useful. In the chapter on frictional properties there is no mention of the dangers of intrinsic viscosity calibrations when used with samples of differing molecular weight distributions, and the viscosity-average molecular weight is not mentioned. There is some coverage of relaxation techniques, and viscoelasticity is given a brief mention, but dielectric relaxation is hardly touched upon and the use of dipole moment measurements as a tool in studying polymer flexibility not at all.

The author presents numerous interesting examples with references to illustrate the various facets of the field but such mathematical derivations as are given are often over brief. In the case of light scattering the author initially related molecular polarizability to the dielectric constant rather than to the square of the refractive index, not making it clear when these differ, or as an alternative, using the optical frequency form of the Clausius-Mossotti relation and thereby avoiding dielectric constant altogether.

There are a few minor typographical errors, but on the whole the book is well produced and illustrated. Because the author makes extensive use of examples, the book will prove valuable as a source book and reference work. It is a worthwhile acquisition for anyone involved with work on polymers or biopolymers, provided the field is not completely new to the reader. However, for the student embarking for the first time into an understanding of the behaviour of macromolecules in solution, the book is difficult and in some places misleading.

H. Block

Conference Announcement

IUPAC INTERNATIONAL SYMPOSIUM ON MACROMOLECULES

Dublin, Eire, 17-22 July 1977

The IUPAC International Symposium on Macromolecules will be held in Dublin on 17-22 July 1977.

The symposium will cover the following topics:

(1) Homogeneous Polymerizations, Zwitterions and Coordination Complexes; (2) Fine Structure of Polymers including Biopolymers; (3) Polymers as Reagents and Catalysts and (4) Polymer Chemistry in Polymer Engineering. These topics have been chosen in order to avoid overlapping those proposed for the Macromolecular section of IUPAC XXVI Congress in Tokyo in September 1977. Further details about registration, social events and the full programme may be obtained from: Symposium Officer, Macro Dublin 77, Institute for Industrial Research and Standards, Ballymun Road, Dublin 9, Eire.

Synthesis and characterization of poly(acryloyl morpholine) xerogel networks suitable for the gel permeation chromatography of small molecules

R. Epton, S. R. Holding and J. V. McLaren

Department of Physical Sciences, Wolverhampton Polytechnic, Wolverhampton WV1 1LY, UK
(Received 30 April 1976)

The synthesis and characterization of a crosslinked poly(acryloyl morpholine) network, Enzacryl® Gel KO, calculated to be effective as a matrix for the g.p.c. of small molecules, is described. Chromatographic performance was evaluated in water, chloroform, dimethylformamide and pyridine. Characteristic g.p.c. behaviour was observed for all standards tested although 'additional exclusion' was observed in the case of aliphatic hydrocarbons in the three organic solvents and with aromatic hydrocarbons in chloroform and pyridine. Similar molecular weight fractionation ranges were obtained for poly(ethylene glycols) in the four solvents investigated the molecular weight exclusion limit being less than 1500.

INTRODUCTION

For a polymer network to be effective as a column packing in the gel permeation chromatography (g.p.c.) of small molecules it is essential that the network undergoes gelation in the chromatographic solvent selected as eluent. Matrices which undergo gelation in both water and organic solvents are particularly useful and may be termed 'universal' g.p.c. supports. Three such networks are commercially available. These are the hydroxypropyl ether of crosslinked dextran (Sephadex® LH 20)¹, a crosslinked poly(hydroxyethyl methacrylate) (Spheron® 1)² and a crosslinked poly(acryloyl morpholine) (Enzacryl® Gel K1)³⁻⁴. In water and the more useful organic solvents the exclusion limits of these packings lie in the 3000–4000 molecular weight range. This is rather high for the efficient fractionation of most small organic molecules.

In this paper we report the synthesis of a poly(acryloyl morpholine) network of greatly reduced mean pore diameter. The g.p.c. evaluation of this new bead polymerized column packing (Enzacryl Gel KO) is described. Water, chloroform, dimethylformamide and pyridine were used as chromatographic solvents.

EXPERIMENTAL

Synthesis of Enzacryl Gel KO

The polymerization vessel and stirrer blade used are depicted in *Figure 1*. Stirring was effected by a Citenco continuously variable (0–300 rev/min) stirrer motor (Citenco Ltd, UK).

The bulk phase for the polymerization consisted of light liquid paraffin (5 l) ($\rho^{20} = 0.85 \text{ g/cm}^3$; $\eta^{20} = 3.5\text{--}4.0 \text{ sec/m}^2$) and the surfactant (100 cm³) which was usually sorbitan trioleate (Koch-Light Ltd, UK). In some runs a surfactant mixture (100 cm³) consisting of sorbitan trioleate and polyoxyethylene (20) sorbitan trioleate (Koch-

Light Ltd, UK), volume ratio 19:1, was used. The bulk phase was placed in the polymerization vessel and freed of oxygen by vigorously bubbling nitrogen from a fine jet (0.5 mm) over 3 h with stirring. Subsequently the length of the nitrogen inlet was adjusted to maintain a nitrogen atmosphere over the liquid.

The monomer solution, consisting of acryloyl morpholine (470 g, 3.33 mol), (Koch-Light Ltd, UK), crosslinker, *N,N'*-methylene diacrylamide (52 g, 0.33 mol) and water (500 cm³) as diluent, was deoxygenated by nitrogen bubbling for 1.5 h. The appropriate amount of initiator, potassium persulphate, was dissolved in water (50 cm³) and deoxygenated. Polymerization was started by mixing the initiator solution with the rest of the monomer phase. This mixture was added to the bulk phase in the polymerization vessel and dispersed as droplets by a short period of rapid stirring (100 rev/min). The stirring rate was reduced (25–30 rev/min) and adjusted periodically to maintain most of the droplets within a size range of 50–100 μm .

To ensure complete polymerization, the suspension was left stirring under nitrogen overnight. The hydrated beads of Enzacryl Gel KO so obtained were washed free of paraffin with petroleum spirit (40–60°), further washed with ethanol and dispersed in water.

Preliminary bulk polymerizations were necessary in order to determine optimum initiator concentration. These were carried out using a reciprocating gel timer (Tecam, UK)⁵. An initiator concentration which would cause the gel timer to stop in 10 to 20 min was considered ideal. A temperature maximum was observed in 0.5 to 1 h in the corresponding suspension polymerization at this concentration.

Gradation of Enzacryl Gel KO

Bead gradation was effected by wet elutriation. Up to 1 litre bed volume of the swollen beads was placed in a uniform bore glass elutriation column (9 × 200 cm) fitted with

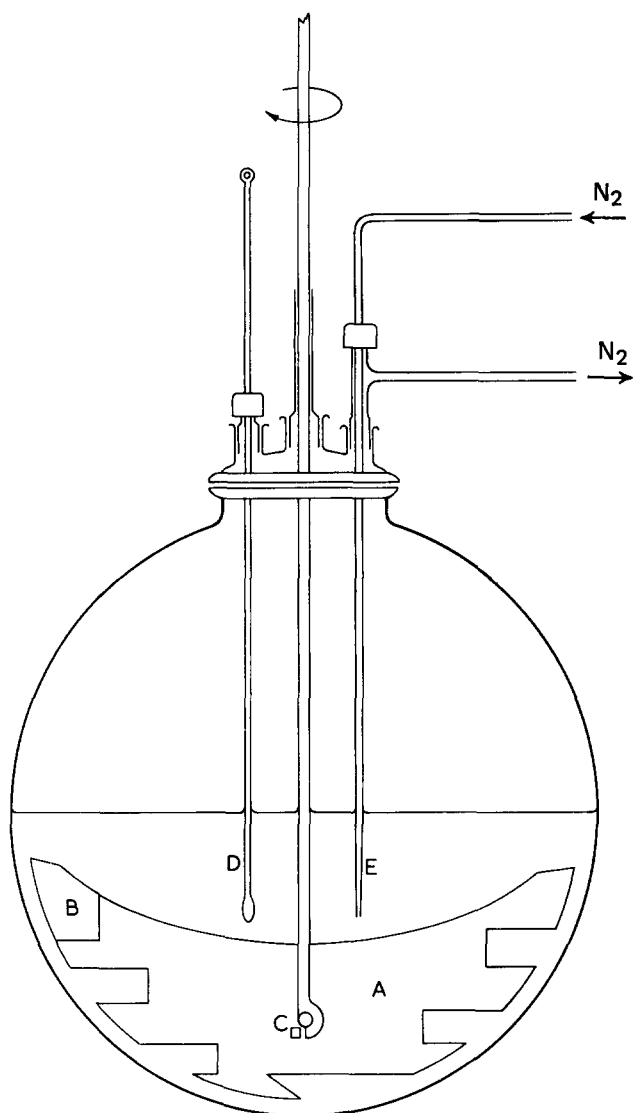


Figure 1 Polymerization vessel showing stirrer blade geometry: A, polystyrene stirrer blade; B, polystyrene counterweight; C, pivot stop; D, thermometer; E, nitrogen inlet. For clarity, the dropping funnel and stirrer motor have been omitted

a water inlet at the base. The bed was mechanically stirred by means of a polypropylene paddle situated immediately over the water inlet. The paddle (depth 20 cm) had horizontal rectangular slats (1×2.5 cm) cut at 2 cm intervals along each vertical side and each set of slats was staggered with respect to the other. A stirring rate of 40 rev/min was found to give adequate bed fluidization with minimal swirling. The aqueous suspension of graded gel beads was conducted from the top of the column, via a number of siphon tubes, to a wide collecting vessel where the beads settled out. Elutriation times, flow rates and bead size ranges obtained are presented in Table 1.

Gel permeation chromatography

Chromatographic standards. The principle standards used were poly(ethylene glycols) (Carbowaxes) (\bar{M}_n 200, 400, 600, 750, 1000, 1500 and 4000) (Phase Separations Ltd, UK), triethylene glycol, diethylene glycol and ethylene glycol (British Drug Houses Ltd, UK). In addition polystyrene (\bar{M}_n 585), (Digby Chemicals Ltd, UK), t-stilbene, styrene and n-alkanes (pentane, heptane, decane and hexadecane) (British Drug Houses Ltd) were used in organic solvents. Saccharides (stachyose, raffinose, maltose and

glucose) (Koch-Light Ltd, UK) were employed as standards in water.

Column packing. A funnel was attached to the top of each column and the whole assembly filled with a slurry of pre-swelled Enzacryl Gel KO (40–80 μm dry diameter) in the appropriate solvent. In the case of chloroform, packing was effected using an approximate flow rate of $150 \text{ cm}^3/\text{h cm}^2$ throughout. This was necessary in order to prevent flotation of the beads. With other solvents the beads were allowed to settle under gravity for a few minutes before completing packing under flow.

Jobling liquid chromatography columns (1.5 \times 100 cm) (Jobling Ltd, UK) fitted with PTFE end fittings were used throughout.

Elution of columns and effluent analysis. The precise column lengths and flow rates used are given in Table 2. Elution was performed at ambient temperature. Sample volumes applied did not exceed 1 cm^3 and solute concentrations were generally less than 2%.

For aqueous g.p.c. the column was incorporated in a Technicon Auto-Analyzer (Technicon, USA). The proportionating pump of the Auto-Analyzer was used both to operate the column and to regulate the analysis of the column effluent. Analysis was effected by the automatic five-fold dilution of effluent samples with chromic acid reagent⁶, heating and monitoring the colour produced at 440 nm. The flow rate used for column elution was the maximum practical with the Auto-Analyzer.

An alternative system was used with organic solvents. This consisted essentially of a Type R401 Waters differential refractometer (Water Associates, USA), a constant displacement pump (Milton Roy Co., USA) and an injection valve (Jobling Ltd, UK). The flow rates used for elution were those which gave a pressure drop of 14 kg/cm^3 across the column.

The deuterated solvents CDCl_3 , $\text{C}_5\text{D}_5\text{N}$ and $(\text{CD}_3)\text{NCHO}$ were detected in column effluents directly by the differential refractometer. Deuterated water was detected by mass spectrometry⁴.

Table 1 Elutriation parameters used for the gradation of Enzacryl Gel KO

Flow rate (cm^3/min)	Elutriation time (h)	Bead diameter (μm)	
		Hydrated	Dry
70	48	<60	<40
200	24	60–120	40–80
420	8	110–175	70–120
1450	4	>175	>120

Table 2 Column and elution parameters for Enzacryl Gel KO

Solvent used for elution	Column parameter			Bead volume available to solvent (cm^3/g dry polymer)
	Length (cm)	Efficiency (plates/m)	Flow rate ($\text{cm}^3/\text{cm}^2 \text{ h}$)	
Water	95.5	8387	19	1.16
Chloroform	87.5	2354	37	1.42
Dimethylformamide	90.0	3356	12	0.90
Pyridine	93.0	904	30	1.06

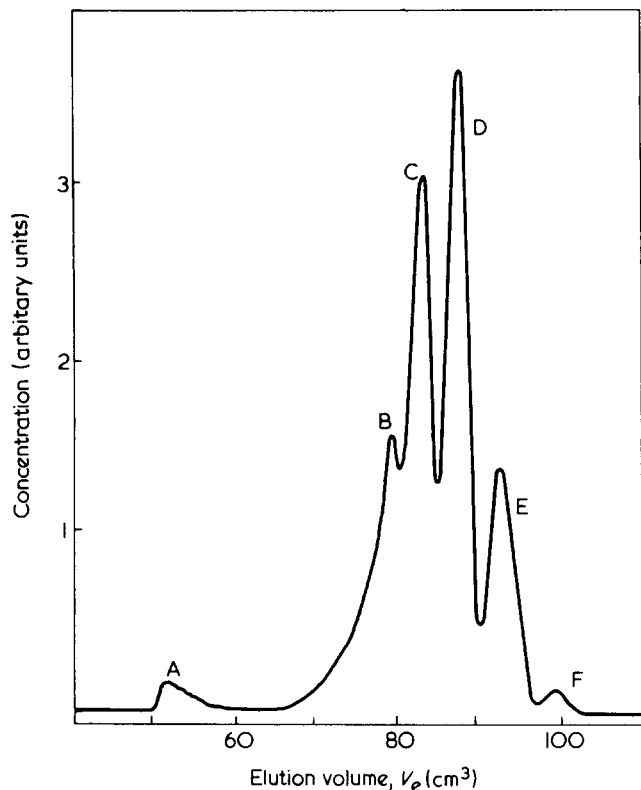


Figure 2 Aqueous g.p.c. fractionation of Carbowax 200 on Enzacryl Gel KO. Column dimensions and flow rate are given in Table 2. A, Breakthrough peak; B, $\text{H}(\text{OCH}_2\text{CH}_2)_5\text{OH}$; C, $\text{H}(\text{OCH}_2\text{CH}_2)_4\text{OH}$; D, $\text{H}(\text{OCH}_2\text{CH}_2)_3\text{OH}$; E, $\text{H}(\text{OCH}_2\text{CH}_2)_2\text{OH}$; F, $\text{HOCH}_2\text{CH}_2\text{OH}$

Distribution coefficients. The Wheaton and Baumann⁷ absolute distribution coefficient, K_d , was calculated in the case of all standards chromatographed from the relationship:

$$K_d = \frac{V_e - V_o}{V_i} = \frac{V_e - V_o}{V_s - V_o}$$

where V_e is the elution volume of the given standard, V_o the void volume of the column and V_i the internal volume of the xerogel packing available to a solute able to penetrate the gel with equal facility to the solvent. The void volume, V_o , was determined as the elution volume of Blue Dextran ($M_w 2 \times 10^6$) (Pharmacia Ltd, UK) or polystyrene ($M_n 4 \times 10^5$) (Digby Chemicals Ltd). It was assumed that V_i corresponded to the difference between the solvent elution volume, V_s , and V_o .

Column efficiency. The number of theoretical plates per metre, n , was calculated for appropriate solutes by applying the equation⁸:

$$n = \frac{16}{L} \left(\frac{V_e}{w} \right)^2$$

where L is the column length and w the peak width. The latter was calculated by producing tangents through the points of inflection of a given peak and measuring the distance between the points of intersection with the baseline.

RESULTS AND DISCUSSION

Aqueous suspension polymerization of acryloyl morpholine and N,N' -methylene diacrylamide at the high monomer

concentration necessary to obtain beads of low mean pore diameter proved much more difficult than in the case of other poly(acryloyl morpholine) networks³⁻⁵. The suspension was difficult to stabilize and the aqueous droplets had a marked tendency both to settle and to fuse during polymerization to give 'grape-like' agglomerates.

After numerous empirical trials it was found that the best approach was to use the moderately efficient surfactant, sorbitan trioleate (Span 85) together with slow but very efficient stirring. The geometry of the stirrer blade (Figure 1) and stirrer speed are critical. Inefficient stirring results in a plug of xerogel at the bottom of the reaction vessel whereas stirring too rapidly results in the production of very small droplets at the extremities of the paddle. With some batches of acryloyl morpholine, it was necessary to add a small amount of the more efficient surfactant, polyoxyethylene(20)sorbitan trioleate (Tween 85), to the continuous phase in order to prevent bead agglomeration. Too much Tween 85 resulted in beads too small for chromatographic application.

Enzacryl Gel KO forms denser xerogels in water than the more expanded poly(acryloyl morpholine) networks. Consequently, comparatively high flow rates were required to displace a given bead size range during wet elutriation (Table 1). This was a considerable advantage because grading efficiency is related to the number of column volumes of water which can be passed through the elutriation column during a practical time scale.

A preliminary separation of a poly(ethylene glycol) sample, Carbowax 200, into its constituent oligomers indicated that Enzacryl Gel KO was effective in the g.p.c. of small molecules in water (Figure 2). Aqueous characterization was completed with a series of higher molecular weight poly(ethylene glycols) and oligosaccharides. Chloroform, dimethylformamide and pyridine were selected to complete the g.p.c. evaluation because these solvents all swell the packing efficiently while differing widely in physico-chemical properties. Poly(ethylene glycols) together with aliphatic and aromatic hydrocarbons were employed as g.p.c. standards in these solvents.

For all four solvents used, plots of logarithm solute molecular weight versus K_d were indicative of chromatographic separation by molecular sieving (Figure 3a-3d). Oligosaccharides and aromatic hydrocarbons, being more compact molecules, had relatively higher K_d values than the less compact poly(ethylene glycols) and n-alkanes of similar molecular weight. Late elution of compact solutes in gel permeation chromatography is well established⁹. The fractionation range for poly(ethylene glycols) was similar in all four solvents the molecular weight exclusion limit being less than 1500.

Although reasonable separations were obtained in all four solvents, marked variation in column efficiency was observed (Table 2). The aqueous xerogel derived from Enzacryl Gel KO is considerably softer than those obtained with organic solvents. This allows distortion of the beads on column packing and results in maximal capacity ratio, V_i/V_o , and hence efficiency. The rigidity of the xerogel derived from dimethylformamide was intermediate between that of the aqueous xerogel and xerogels derived from chloroform and pyridine. This is reflected in the efficiency of Enzacryl Gel KO in dimethylformamide even though the internal bead volume corresponding to dimethylformamide is less than that occupied by the solvent component in other xerogels.

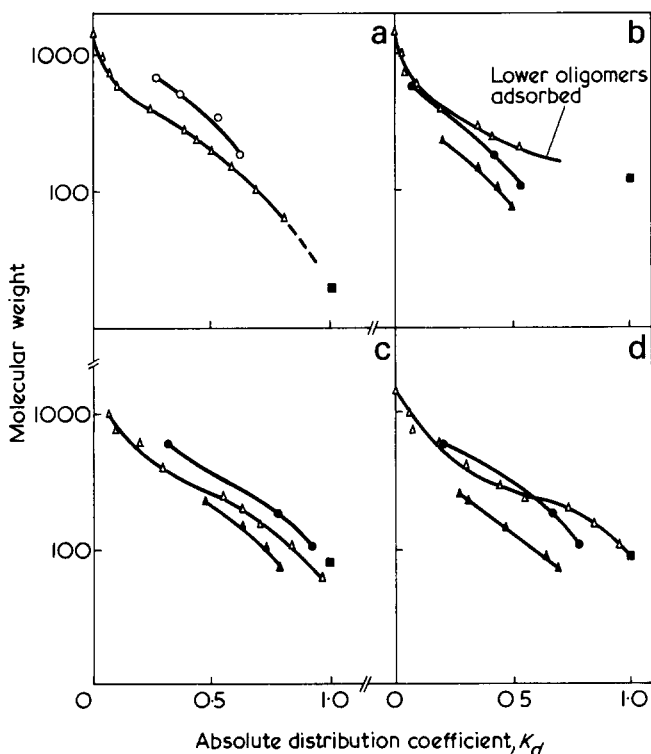


Figure 3 Logarithm molecular weight versus K_d relationships for poly(ethylene glycols) (Δ); oligosaccharides (\circ); aliphatic hydrocarbons (\blacktriangle); aromatic hydrocarbons (\bullet) and deuterated eluent (\blacksquare) obtained using Enzacryl Gel KO in different solvents: (a) water; (b) chloroform; (c) dimethylformamide; (d) pyridine

When volumetric parameters alone determine the elution volume of homologous solutes then a plot of logarithm molecular weight versus K_d will extrapolate back through a point close to the coordinates for the isotopically labelled solvent. A linear (isotopically labelled) solvent molecule should emerge from the column slightly earlier than a compact solute molecule of a similar molecular weight. Conversely a compact solvent molecule should emerge from the column later than that of a linear solute. It is clear (Figure 3a–3d) that poly(ethylene glycols) exhibit ideal g.p.c. behaviour in water, dimethylformamide and possibly pyridine. Weak adsorption of ethylene glycol ($K_d = 1.17$) occurs in this solvent. Low molecular weight ethylene glycol oligomers are adsorbed in chloroform.

Marked early elution is apparent in the case of aliphatic hydrocarbons in all three organic solvents and aromatic hydrocarbons in chloroform and pyridine. This is indicative of an 'additional exclusion' mechanism^{10,11} being operative as well as molecular sieving. Altgelt¹¹ has suggested that, in the case of polymeric solutes, 'additional exclusion' arises as a result of the low entropies of mixing between the solvated macromolecular species involved, i.e. between the solvated polymeric solute and the solvated gel matrix. Early elution arises if the entropy term is too small to overcome a positive heat of mixing. We have noted previously that a sufficiently low entropy term is only likely to arise with macromolecular solutes³. We have suggested that 'additional exclusion' of small molecules may be a more subtle, related phenomenon involving solute micropartition being regions of the gel beads consisting of more or less pure solvent and other regions consisting of the constrained solvated polymer chains comprising the gel matrix. The present results are explicable also on this hypothesis.

ACKNOWLEDGEMENTS

The authors wish to thank Koch-Light Laboratories Ltd, for general support and a studentship (S. R. H.).

REFERENCES

- 1 'Sephadex LH-20', Technical Booklet, Pharmacia AB, Uppsala, 1972
- 2 Coupek, J., Krivakova, M. and Pokorny, S. *J. Polym. Sci. (C)* 1973, **48**, 185
- 3 Epton, R., Holloway, C. and McLaren, J. V. *J. Appl. Polym. Sci.* 1974, **18**, 179
- 4 Epton, R., Holloway, C. and McLaren, J. V. *J. Chromatogr.* 1974, **90**, 249
- 5 Epton, R., Holding, S. R. and McLaren, J. V. *J. Chromatogr.* 1975, **110**, 327
- 6 Johnson, S. and Samuelson, O. *Anal. Chim. Acta* 1966, **36**, 1
- 7 Wheaton, R. M. and Baumann, W. C. *Ann. N. Y. Acad. Sci.* 1953, **57**, 159
- 8 Martin, A. J. P. and Synge, R. L. M. *Biochem. J.* 1941, **35**, 1358
- 9 Churms, S. C. *Adv. Carbohydr. Chem. Biochem.* 1970, **25**, 13
- 10 Altgelt, K. H. *Macromol. Chem.* 1965, **88**, 75
- 11 'Gel Permeation Chromatography', (Eds K. H. Altgelt and L. Segal), Marcel Dekker, New York, 1971, p 193

Synthesis and characterization of poly(ϵ -carbobenzoxy-L-lysyl- γ -benzyl-L-glutamate)

I. Omura*, D. C. Lee**, S. Itou, A. Teramoto, and H. Fujita

Department of Polymer Science, Osaka University, Toyonaka, Osaka 560, Japan

(Received 17 December 1975; revised 26 February 1976)

An alternating copolypeptide poly(ϵ -carbobenzoxy-L-lysyl- γ -benzyl-L-glutamate) was synthesised by polymerizing the *p*-nitrophenyl ester of ϵ -carbobenzoxy-L-lysyl- γ -benzyl-L-glutamate. The highest molecular weight obtained was 570 000 (2370 peptide residues), which had not yet been attained by the active ester method. The polymers were soluble in various organic solvents including those solvents in which the parent polymers were insoluble, i.e. poly(ϵ -carbobenzoxy-L-lysine) and poly(γ -benzyl-L-glutamate), and their conformations were essentially α -helical except in strong acids such as dichloroacetic acid.

INTRODUCTION

According to well-established theories¹, typical average quantities, such as the helical fraction, the number of helix portions, and so forth, which characterize homopolymer conformations in dilute solution, can be expressed in terms of three parameters s , σ , and N , where s is the equilibrium constant between helix and random coil residues, σ is the cooperativity parameter for the formation of a helix sequence, and N is the degree of polymerization of the polymer. Much effort has been made to establish practical methods which allow the parameters s and σ to be evaluated from measurements of thermally or solvent induced helix-coil transition curves, and now little remains to be developed further in this direction, as can be seen for example from our recent review articles^{2,3}.

For both theoretical and experimental studies with copolypeptides one has to face the complexity of two additional factors influencing their conformation. These factors are the composition of different peptide residues and their distribution (or geometric arrangement) in the polymer chain. Furthermore, in general, these factors fluctuate among a bunch of polypeptide molecules in the system under consideration, and this introduces an added complication. To approach the problem of copolypeptides it is therefore desirable to start with systems which involve such complexities as little as possible. One of these systems is an alternating sequential copolymer consisting of two peptide residues A and B, which may be schematically represented by ...ABABAB... In this case, the composition and arrangement of the constituent residues are fixed not only in a particular chain but also among all the individual chains in the system. Thus none of the complexities mentioned appear. The sole effect that distinguishes such sequential copolymers from homopolymers is expected to arise from the interaction between A and B in a given solvent, and it is certainly of interest to investigate either theoretically or experimentally the consequences from this

interaction. The work described in the present paper deals with the synthesis of an alternating copolypeptide and its preliminary characterization.

Since 1963 when DeTar *et al.*⁴ reported a successful synthesis of sequential polypeptides using *p*-nitrophenyl esters, a number of active esters have proved useful for synthesising this class of polypeptides. An obvious motivation of such syntheses has been the hope of acquiring model compounds for the proteins, and much attention has been paid to the preparation of water-soluble species and to the investigation of their conformations in aqueous media. Conformation studies of sequential polypeptides in organic solvents have not always proved easy. Most of the copolypeptides so far obtained were poorly soluble in ordinary organic solvents, making it difficult to characterize them satisfactorily. In fact, dichloroacetic acid (DCA), trifluoroacetic acid (TFA), and their mixtures with chloroform, for example, were the only solvents effective for them. Further, their molecular chains were usually quite short, consisting of at the most 100 peptide residues. It is now well recognized that there is a marked difference in conformation between oligomers and high molecular weight homologues. For this reason it is an important prerequisite for the conformation study of a polypeptide to have samples covering a wide span of molecular weights. To be more precise, such samples must be as homogeneous as possible in molecular weight. The work of Sakakibara *et al.*⁵ on sequential polypeptides of L-prolyl-L-prolyl-glycine is a very impressive example on this point.

The alternating sequential polypeptide chosen for the present study was poly(ϵ -carbobenzoxy-L-lysyl- γ -benzyl-L-glutamate). The choice was made for two reasons. Firstly, there were detailed investigations available on conformational characteristics of the homopolypeptides of its constituent residues, i.e. poly(γ -benzyl-L-glutamate) (PBLG) and poly(ϵ -carbobenzoxy-L-lysine) (PCBL) in various organic solvents^{2,3,6-11}. It was thus hoped that when compared with the data for these parent polymers, measurements on the copolypeptide would provide clear information about the interaction between neighbouring different peptide units. Secondly, Ledger and Stewart¹² had already reported synthesis of this sequential polypeptide by the active ester

* Present address: The Central Research Laboratory, Kurarei Co. Ltd, Kurashiki, Japan.

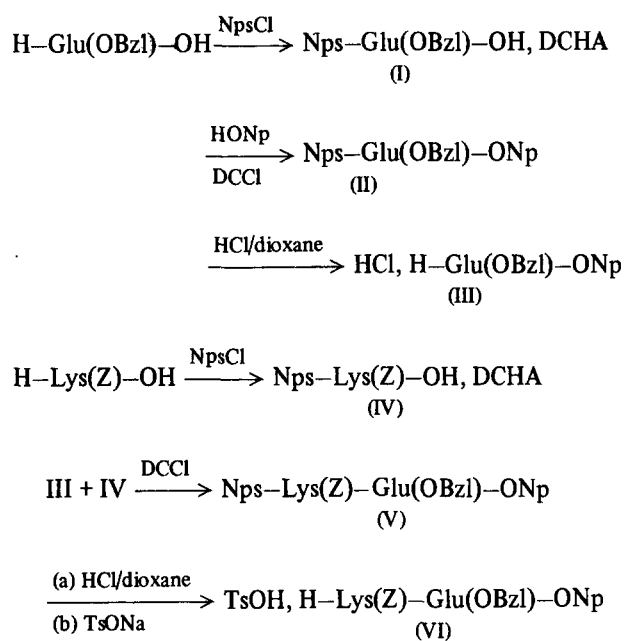
** On leave of absence from the Department of Polymer Science and Technology, School of Engineering, Inha University, Incheon, Korea.

method and its conformation in the solid state, but little had been mentioned in their paper about the conformation in solution and molecular weight. It is shown below that certain modifications of their method yield samples of poly[Lys(Z)-Glu(OBzl)]* which not only cover a wide range of molecular weight but are also soluble in many organic solvents.

RESULTS AND DISCUSSION

Synthesis of ϵ -carbobenzoxy-L-lysyl- γ -benzyl-L-glutamate *p*-nitrophenyl ester *p*-toluenesulphonate

The scheme of Ledger and Stewart¹² for the synthesis of a dipeptide monomer unit ϵ -carbobenzoxy-L-lysyl- γ -glutamate *p*-nitrophenyl ester *p*-toluenesulphonate (VI) is:



We found that some modifications of this procedure were effective for obtaining the final compound VI in a form of high purity. The modified procedure was as follows.

Cleavage of the Nps-group from the compound II was achieved by treatment with excess HCl, according to Ledger and Stewart¹². The resulting HCl, H-Glu(OBzl)-ONp (III) melted over a rather broad range of temperature. This, together with the result from elemental analysis, suggested that the protecting groups on the side chains might have been partly cleaved. Recrystallization of the crude product from acetonitrile gave the compound III, melting point 157°–160°C, which Ledger and Stewart had described as a hemihydrate. However, our compound III, in agreement with Brack and Spach¹⁴, showed no sign of hydration.

Nps-Lys(Z)-OH (IV) and H-Glu(OBzl)-ONp (III) were coupled to obtain the compound V by the DCCI procedure of Bodanszky and Vigneaud¹⁵ with use of THF or

THF/dioxane as solvent. This choice of solvent was made because racemization of the Glu(OBzl) residue and undesirable side reactions were least likely to occur¹⁶. The compound V recrystallized from acetone/isopropanol had a melting point 10°C higher than the reported melting point for the same compound obtained by the mixed carbonic anhydride method¹². Removal of the Nps-group from the compound V was made by treatment with two equivalents of HCl to the protected peptide, and the resultant hydrochloride was converted to the *p*-toluenesulphonate (VI). The product VI, recrystallized from 0.5% acetonitrile solution, had a melting point of 181.5°–182°C, which indicated its high purity.

Polycondensation

Experimental evidence has indicated that, among various active esters suggested so far for polycondensation, *N*-succinimidyl esters^{14,17–23} and 2-hydroxyphenyl esters^{17,18,24,25} may be least liable to induce racemization. However, the use of these esters yielded polymers which had relatively low molecular weights, at least not high enough for our present purpose. The synthesis of the latter esters involved a lengthy path with relatively poor yields. Although *p*-nitrophenyl esters^{14,22,26–29} and pentachlorophenyl esters^{14,17,22,29,30} were effective for the production of high molecular weights, they induced racemization. The former esters were more satisfactory than the latter with respect to racemization^{14,17,22,29}. Therefore, as a compromise between molecular weight and racemization, we chose *p*-nitrophenyl ester VI.

Recently, König and Geiger^{31–34} have shown that addition of 1-hydroxybenzotriazole (HOBt) was not only largely effective for the condensation of amino-acids and peptides with repressed racemization but also accelerated reactions of active esters to form amide bonds. With the expectation of a similar effect on the polycondensation of active esters, we allowed the active ester VI to polymerize in DMF by treatment with an approximately equimolar amount of base and varying amounts of HOBt. Preparative data are summarized in Table 1.

Samples LG-1 to LG-4 were synthesised under similar conditions in order to observe the effect of HOBt. It was found from an increase in viscosity that the polymerization for LG-1 (with an 0.1 equivalent of HOBt added) was fastest in the initial rate and gave the highest molecular weight when terminated. The polymerization for LG-3 (with no HOBt added) was slower than that for LG-1. These observations appear to substantiate the predicted effect of HOBt on polymerization reaction. Other samples synthesised under similar conditions gave essentially the same results. Furthermore, it was noticed that addition of one equivalent of HOBt had no detectable effect on accelerating polymerization and resulted in a low molecular weight (LG-2). This was probably due to the acidity of HOBt, which is comparable to that of acetic acid.

During the course of these polymerization experiments, we observed that the molecular weights of samples LG-2, LG-3, and LG-4 were quite low when the polymers were precipitated from the reaction mixtures. However the precipitates underwent a remarkable increase in molecular weight when allowed to stand in the solid state. This interesting observation suggests that the precipitated polymers retained the polymerizing activity even in the solid state; the reason for which is as yet unknown to us, because no other samples showed such behaviour.

* Abbreviations used in this article are those recommended by the IUPAC IBU Commission in Biochemical Nomenclature¹³, except that the side chains attached to the α -carbon atom are given in parentheses. All amino-acids referred to in the text are of L-configuration; Bzl, benzyl; Nps, *o*-nitrophenylsulphenyl; Np, *p*-nitrophenyl; TsO, *p*-toluenesulphonate; DCCI, dicyclohexylcarbodiimide; DCHA, dicyclohexylamine; THF, tetrahydrofuran; DMF, *N,N*-dimethylformamide; DCA, dichloroacetic acid; PBLG, poly(γ -benzyl-L-glutamate); PCBL, poly(ϵ -carbobenzoxy-L-lysine); Ala, alanine; Tyr, tyrosine.

Table 1 Preparative data for poly(ϵ -carbobenzoxy-L-lysyl- γ -benzyl-L-glutamate)

Sample code	Equivalent of NEt ₃ ^b	Equivalent of HOBt	Yield (%)	$\bar{M}_v \times 10^{-4}$	$[\alpha]_{546}$	Reaction time (days)
LG-1	1.0	0.1	80	49	-23.4	6
LG-2 ^a	1.0	1.0	56	23	-22.4	3
LG-3 ^a	1.0	0	68	57	-23.2	3
LG-4 ^a	1.0 ^c	0.1	73	32	—	3
LG-9	1.0	0	—	3	-18.2	5
LG-10-I	1.0	0.1	83	9.7	—	7
LG-10-II	1.0	0.1	—	8	—	4
LG-11	1.0	0.1	84	19	—	7
LG-12	0.99	0.5	84	15	-21.9	4
LG-13	1.00	0.5	93	9.1	-22.3	4
LG-14	1.01	0.5	94	13	-22.3	4
LG-15	1.00	0	90	5.5	-19.8	6
LG-16	1.00	0.4	91	9.5	-21.4	6
LG-17	1.00	1.0	90	10	-21.6	6
LG-18	1.03	0.5	80	32	-23.0	9
LG-19	1.02	0.5	86	30	-23.2	11
LG-20	1.01	0.5	64	53	-22.6	11

^a $[\eta]$ and $[\alpha]_{546}$ measured after three days of polymerization; ^bNEt₃ = triethylamine; ^cN-methylmorpholine

Polymerization of LG-19 was followed by g.p.c. Figure 1 shows the g.p.c. diagrams taken at three intervals of polymerization. It can be seen that the polymerization continued for as long as 7–11 days, with the peak molecular weight increasing gradually from 70 000 to 300 000 and that the low molecular weight oligomers almost disappeared in one week. Other crude samples yielded similarly broad g.p.c. patterns. Thus the samples obtained were quite broad in molecular weight distribution, as expected for polycondensates. A quantitative analysis of these g.p.c. diagrams is deferred until the calibration curve with absolute molecular weights becomes available.

Molecular weights

The molecular weight of 570 000 for LG-3 is the highest of the reported values for polypeptides synthesised by the active ester method. In fact, it far exceeds, e.g. 160 000 for poly[Glu(OBzl)]¹⁴ and 62 600 for poly(Tyr-Ala-Gly)³⁵. Many other samples listed in Table 1 also have molecular weights of a few hundred thousands. This success in attaining high molecular weights may be attributed primarily to the fact that, as observed from its narrow melting range, the crystallizable active ester VI was of high purity and that the resulting polypeptide was very soluble in DMF, the solvent used for polymerization.

Optical purity of polypeptide samples

As is shown below, poly[Lys(Z)-Glu(OBzl)] assumes random coil in DCA, so that the specific rotation $[\alpha]_{546}$ in this solvent may be taken as a measure of the optical purity of the polypeptide. The values of $[\alpha]_{546}$ listed in Table 1 then indicate that all the samples but LG-9 and LG-15 had essentially the same optical purity. Closeness of these $[\alpha]_{546}$ values to those of the parent polypeptides, PBLG and PCBL (Table 2), suggests that polymerization was accompanied by little racemization. In fact, optical rotation measurements on acid hydrolysates gave optical purities of $97 \pm 1\%$ and $98.5 \pm 1\%$ for LG-2 (with a 0.1 equivalent of HOBt added) and $96 \pm 1\%$ for LG-3 (with no HOBt added). These estimates should be accepted with some reservations, because racemization on acid hydrolysis is known to differ between amino-acids and peptides³⁶. Samples LG-9 and FF-3 (fractionated sample) showed somewhat lower optical purities. This is partly because

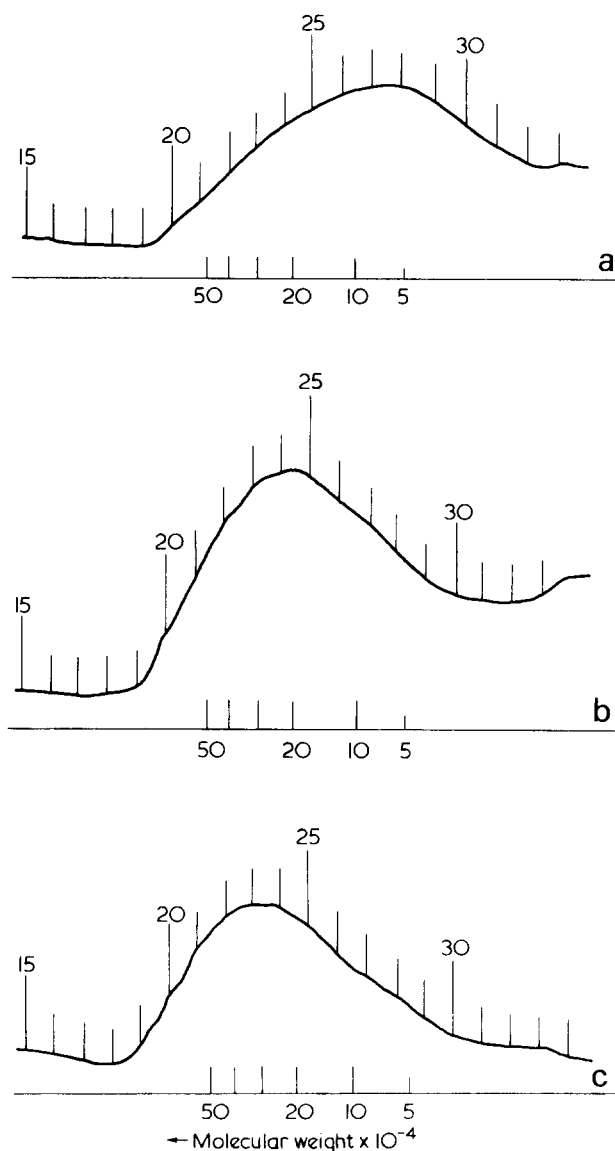


Figure 1 G.p.c. diagrams for LG-19 taken at the indicated intervals of polymerization: (a) 143; (b) 163; (c) 212 h

Table 2 Results from racemization tests

Sample code	$[\alpha]_{546}^a$	Optical purity (%) ^b
LG-2	-22.4	97 \pm 1
LG-3	-22.3	98.5 \pm 1
LG-9	-18.2	91
FF-3	-19.7	93
PBLG ^c	-21 \pm 1	(100)
PCBL ^c	-21.3	(100)

^a $[\alpha]_{546}$ = specific rotation for the wavelength 546 nm in DCA at 25°C; ^b derived from optical rotation measurements on acid hydrolysates; ^c synthesised by the NCA method

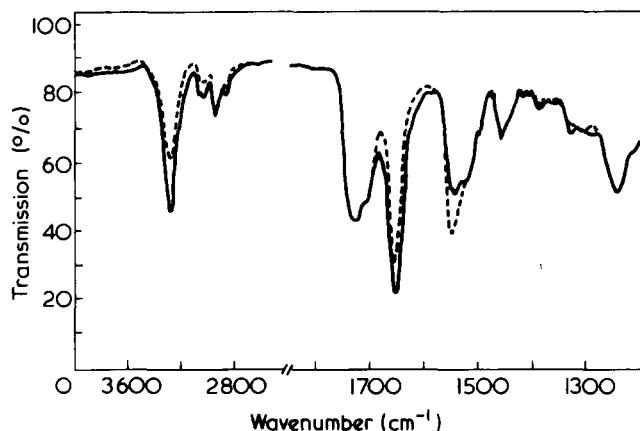


Figure 2 Polarized infra-red spectra of an oriented film of poly[Lys(Z)-Glu(OBzl)] (LG-4): —, parallel; - - -, perpendicular

these samples contained low molecular weight impurities, as revealed by g.p.c.

Overall, the present polymerization experiments did not introduce more than a few percent racemization, a conclusion compatible with the previous results from the polymerization of *p*-nitrophenyl esters of γ -benzyl glutamates^{14,17,22,29}. Although HOBt has shown to accelerate polycondensation of compound VI, it had no detectable effect on repressing racemization.

Conformation in solid and in solution

Figure 2 shows the polarized infra-red spectra taken on an oriented film of LG-4. The frequencies and dichroisms of amide I and II bands are recorded in Table 3. From the reported infra-red spectra of synthetic polypeptides³⁷, these data may be viewed as exhibiting characteristic features of the α -helical conformation. Ledger and Stewart¹² have reported essentially the same result, but, differing from their finding, the present spectra show no band attributable to the β -structure or diketopiperazine. This difference is probably ascribed to the fact that the samples used by Ledger and Stewart were of low molecular weight and contained cyclic compounds. Infra-red spectra of LG-4 in ethylene dichloride (EDC) were also characteristic of the α -helical conformation. Thus we conclude that poly[Lys(Z)-Glu(OBzl)] can assume the α -helical conformation in solution as well as in the solid state.

The fact that the intrinsic viscosities of LG-1 were 2.13 dl/g in DCA and 7.13 dl/g in DMF, both at 25°C, suggested that the conformations in these solvents are different. The Moffitt parameters b_0 for LG-1 were 39 in DCA and -575 in DMF at 25°C. The literature values of b_0 for the parent polypeptides are 45 in DCA⁶ and -630 in DMF³⁸ for PBLG, and 3 in DCA and -550 for PCBL⁹. From these

data we may conclude that the conformations of poly[Lys(Z)-Glu(OBzl)] are α -helical in DMF and random coil in DCA, as is the case with PBLG and PCBL. Figure 3 illustrates the o.r.d. curve of LG-1 in trifluoroethanol at 25°C, which displays a negative Cotton effect with a trough at 234 \pm 2 nm ($[m']_{234} = -18\ 600$). The position and depth of this trough are also consistent with the α -helical conformation^{39,40}.

Solubility

Unexpectedly and fortunately, the copolypeptide samples synthesised dissolved in a number of organic solvents, which included either non-solvents or partial solvents for their parent homopolypeptides PBLG and PCBL. Examples of such solvents were THF, methylethyl ketone, and ethyl acetate. This unexpected feature must be a consequence of the interaction between neighbouring different peptide residues, since such interaction is absent in the parent homopolymers. The observation⁴¹ that in CHCl₃ about two thirds of urethane NH groups in the side chains of PCBL were left unbonded would probably account for its poor solubility in less polar solvents. However, the present copolypeptide dissolved in such solvents, despite the fact that the infra-red spectra of LG-4 in EDC suggested the presence of unbonded NH groups comparable in quantity to those of PCBL in CHCl₃. At present, no adequate explanation of the unexpected solubility in terms of molecular concepts comes to mind. For the sake of reference, the intrinsic viscosities and Moffitt parameters of LG-1 in typical solvents at 25°C are compared in Table 4. From these data the conformation of the copolypeptide in the listed solvents except for DCA are supposed to be α -helical. The large intrinsic viscosities obtained might be expected to be largely due to molecular association in these solvents. However, this may be ruled out because the Huggins viscosity constant k' was quite normal (0.4-0.5). Recent light scattering measurements on fractionated samples⁴⁶ have provided more direct evidence for the absence of association in one of the helicogenic solvents, MEK. They have also confirmed the correctness of the molecular weights reported in this paper.

Table 3 Characteristic amide bands for LG-4

Dichroism	Amide I (cm ⁻¹)	Amide II (cm ⁻¹)
Parallel	1648	-
Perpendicular	1651	1544

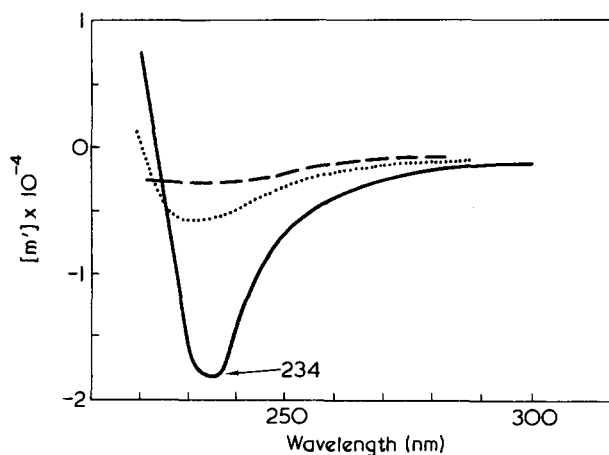
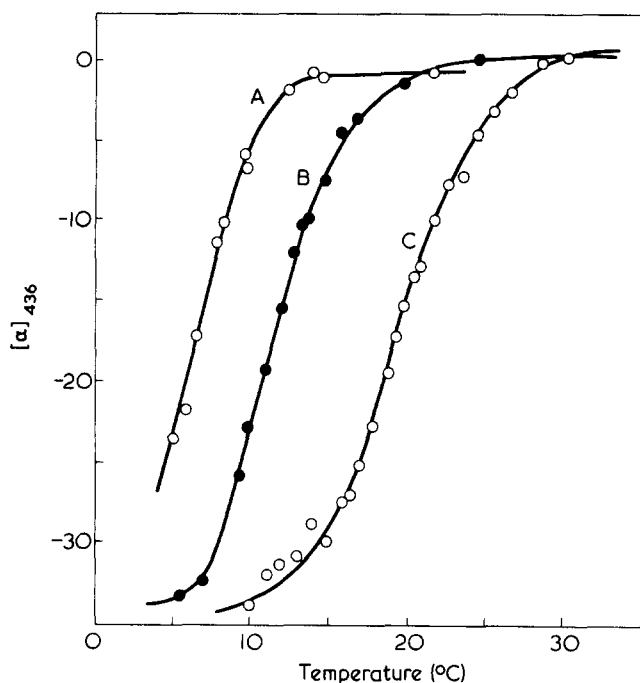


Figure 3 O.r.d. spectrum of poly[Lys(Z)-Glu(OBzl)] (LG-1) in trifluoroethanol at 25°C: - - -, random coil; ····, β -structure

Table 4 Intrinsic viscosity $[\eta]$ and Moffitt parameter b_0 of LG-1 in various solvents at 25°C

Solvent	$[\eta]$ (dl/g)	k'	b_0
DCA	2.13	0.20	39
DMF	7.13	0.47	-575
CHCl ₃	8.00	0.50	-549
THF	8.75	0.44	-619
MEK ^a	8.75	0.36	-632
PBLG (in DMF)			-630
PCBL (in DMF)			-550

^aMethyl ethyl ketone**Figure 4** Plots of $[\alpha]_{436}$ against temperature for poly[Lys(Z)-Glu(OBzl)] (FF-2) in DCA-EDC mixtures of the indicated vol% of DCA: A, 53; B, 55; C, 58

Helix-coil transition

Figure 4 shows plots of $[\alpha]_{436}$ against temperature for a fractionated sample FF-2 in DCA-EDC mixtures with the indicated DCA volume compositions. It can be seen that the polypeptide undergoes an inverse thermal helix-coil transition in these mixed solvents. For example, the transition temperature in the 58 vol% mixture is about 20°C. Table 5 compares this composition with those of DCA-EDC mixtures for which the transition temperatures of PBLG and PCBL appear at about 20°C. It also includes the transition temperature for an equimolar random BLG-CBL copolymer in CHCl₃ containing 54.4 vol% DCA⁴². The conclusion from this Table is that the stability of the helix of poly[Lys(Z)-Glu(OBzl)] is intermediate between those of PBLG and PCBL and comparable with that of the equimolar random copolymer. Detailed spectroscopic data and an analysis of helix-coil transition curves will be reported in a forthcoming publication.

EXPERIMENTAL

Reagent and solvents

γ -Benzyl-L-glutamate, ϵ -carbobenzoxy-L-lysine, and dicyclohexylcarbodiimide were purchased from the Protein

Research Foundation, Osaka, and used without further purification. *p*-Nitrophenol (the Protein Research Foundation) was recrystallized from toluene. 1-Hydroxybenzotriazole⁴³ was synthesised from *o*-nitrochlorobenzene and hydrazine hydrate, melting point 156°–157°C. *N*-Methylmorpholine and triethylamine were refluxed over sodium metal and fractionally distilled. Other chemicals were purified according to the standard procedures. All the melting points reported below were uncorrected.

γ -Benzyl-L-glutamate *p*-nitrophenyl ester hydrochloride (III)

α -*o*-Nitrophenylsulphenyl- γ -benzyl-L-glutamate, DCHA (I) was synthesised from γ -benzyl-L-glutamate⁴⁴ and recrystallized from dichloromethane, m.p. 160°–164°C, $[\alpha]_D^{25} = -38.4^\circ$ (*c* 1.62, CHCl₃). Literature⁴⁴: m.p. 168°C, $[\alpha]_D = -34.0^\circ$ (*c* 1.2, CHCl₃). The compound I was coupled with *p*-nitrophenol following the procedure of Bodanszky and Vigneaud¹⁵ to give α -*o*-nitrophenylsulphenyl- γ -benzyl-L-glutamate *p*-nitrophenyl ester (II)^{12,44}. The product was recrystallized from EtAc/ether, m.p. 77°–80.5°C, $[\alpha]_D^{25} = -121.3^\circ$ (*c* 1.2, CHCl₃). Literature⁴⁴: m.p. 77°–78°C, $[\alpha]_D = -121.0^\circ$ (*c* 3, CHCl₃). The compound II (69.8 g, 0.136 mol) was dissolved in warm anhydrous dioxane (310 ml), and 4.8 N HCl/dioxane (83 ml, 0.4 mol) was added in one portion to the solution cooled to room temperature. After 3 min, 1.5 l of anhydrous ethyl ether were added to the solution. A white precipitate appeared immediately. The precipitate was washed with ether, dried under reduced pressure, and recrystallized from acetonitrile, yielding 43 g (80%) of the product III, m.p. 157°–160°C, $[\alpha]_D^{25} = 35.2^\circ$ (*c* 1.87, methanol). Literature¹²: m.p. 149°–151°C, $[\alpha]_D = 35.6^\circ$ (*c* 2.0, methanol). Analysis calculated for C₁₈H₁₉N₂O₆Cl: C, 54.76; H, 4.85; N, 7.10; Cl, 8.98. Found: C, 54.5; H, 4.86; N, 7.03; Cl, 8.98; Literature¹⁴: C, 54.43; H, 4.95; N, 6.87; Cl, 9.09; Literature¹²: C, 53.5; H, 5.0; N, 6.9.

α -*o*-Nitrophenylsulphenyl- ϵ -carbobenzoxy-L-lysyl- γ -benzyl-L-glutamate *p*-nitrophenyl ester (V)

α -*o*-Nitrophenylsulphenyl- ϵ -carbobenzoxy-L-lysine, DCHA (IV)⁴⁴ was obtained from ϵ -carbobenzoxy-L-lysine, m.p. 176°–181°C, $[\alpha]_D^{25} = -30.6^\circ$ (*c* 0.61, DMF). Literature⁴⁴: m.p. 184°–187°C, $[\alpha]_D = -29.1$ (*c* 0.7, DMF). α -*o*-Nitrophenylsulphenyl- ϵ -carbobenzoxy-L-lysine isolated from 30.7 g (0.05 mol) of the compound IV was dissolved in THF (250 ml), in which γ -benzyl-L-glutamate *p*-nitrophenyl ester hydrochloride (III) (19.74 g, 0.05 mol) was suspended and cooled to 0°C. Dicyclohexylcarbodiimide (10.3 g, 0.05 mol) dissolved in a small volume of dioxane was added with vigorous stirring, and the suspension was kept stirred for 30 min. *N*-Methylmorpholine (5.06 g, 0.05 mol) diluted with 50 ml of THF was added dropwise

Table 5 Helix-coil transitions in DCA-EDC mixtures

Polypeptide	Transition temperature (°C)	Solvent composition (vol% DCA)
PBLG ^a	20	71
BLG-CBL ^b	16	54.4 (DCA-CHCl ₃)
FF-2 ^c	20	58
PCBL ^d	20	34

^aTaken from Norisuye et al.^{6,7}; ^bdata for an equimolar random copolymer of γ -benzyl-L-glutamate and ϵ -carbobenzoxy-L-lysine in a DCA-CHCl₃ mixture⁴²; ^cfractionated sample of poly[Lys(Z)-Glu(OBzl)]; ^dtaken from Matsuoka et al.⁹

to the suspension in 40 min. The reaction was then allowed to proceed at 0°C for 10 h. The precipitates formed were filtered, and the filtrate was concentrated at reduced pressure almost to saturation. Addition of isopropanol to the solution gave yellow crystals, which were dried at reduced pressure. The product was recrystallized from acetone/isopropanol to yield needle crystals of the compound V in 70% yield, m.p. 143.5°–145.5°C, $[\alpha]_D^{25} = -48.3^\circ$ (*c* 0.77, EtAc). Literature¹²: yield 39% (the mixed carbonic anhydride method), m.p. 134°–136°C, $[\alpha]_D = -49.4^\circ$ (*c* 2.0, EtAc).

Analysis calculated for C₃₈H₃₉N₅O₁₁S: C, 58.98; H, 5.08; N, 9.05; S, 4.14. Found: C, 58.81; H, 5.09; N, 9.25; S, 4.06.

ϵ -Carbobenzoxy-L-lysyl- γ -benzyl-L-glutamate p-nitrophenyl ester p-toluenesulphonate (VI)

The procedure of Ledger and Stewart¹² with some modifications was used to obtain the compound VI. α -o-Nitrophenylsulphenyl- ϵ -carbobenzoxy-L-lysyl- γ -benzyl-L-glutamate p-nitrophenyl ester (V) (15.86 g, 0.0205 mol) was dissolved in 55 ml of anhydrous dioxane at 60°C. To the solution cooled to room temperature was added 4.8 N HCl/dioxane (0.0408 mol). After 7 min, ether was added to the solution, which was kept overnight in a refrigerator. The precipitate was washed with ether, dried at reduced pressure, and dissolved in methanol. To the solution sodium p-toluenesulphonate (8 g, 0.041 mol) was added. Precipitated sodium chloride was filtered. The filtrate was concentrated to saturation, cooled in ice, and diluted with cold water. The precipitated p-toluenesulphonate (VI) was collected, washed with ether, and dried. The product, recrystallized from 0.5% acetonitrile solution, gave colourless needle crystals of the compound VI in 78% yield, m.p. 181.5–182°C, $[\alpha]_D^{25} = -5.5^\circ$ (*c* 1.6, methanol). Literature¹²: 170°–173°C, $[\alpha]_D = -6^\circ$ (*c* 2.0, methanol).

Analysis calculated for C₃₉H₄₄N₄O₁₂S: C, 59.08; H, 5.59; N, 7.07; S, 4.04. Found: C, 58.97; H, 5.60; N, 7.04; S, 4.03.

Polycondensation

ϵ -Carbobenzoxy-L-lysyl- γ -benzyl-L-glutamate p-nitrophenyl ester p-toluenesulphonate (VI) (1.301 g, 1.64 mmol) and HOBt (0.022 g, 0.16 mmol) were dissolved in DMF (1.5 ml). Triethylamine (0.227 ml, 1.64 mmol) was added to this solution with stirring. An appreciable increase in solution viscosity was observed after 1 h, and the viscosity continued to increase for four days, so that subsequently the solution was diluted with DMF. The solution finally diluted to 5% was poured onto 200 ml of water–methanol mixture, yielding a thread-like precipitate LG-1. The product LG-1 was purified by repeated precipitation from DMF solutions and freeze-dried from a dioxane solution in 80% yield. Polymerizations of other samples were performed in a similar way. Aliquots were taken at suitable intervals from the polymerization mixture for LG-19 and the polymers precipitated from them in water–methanol were analysed by g.p.c.

Racemization test

In a sealed tube, a given amount of the polymer mixed with 5.7 N hydrochloric acid or an acetic acid/5.7 N hydrochloric acid mixture (1:1 by volume) was heated at 111°C for 24 h. The optical rotation of the hydrolysate was then measured, after removal of benzyl chloride by centrifuga-

tion if necessary, and compared with that of a similarly treated solution of an equimolar mixture of γ -benzyl-L-glutamate and ϵ -carbobenzoxy-L-lysine. For example, the acid hydrolysate of 0.06 g of LG-2 in 6 ml of 5.7 N HCl gave an optical rotation of $0.343 \pm 0.002^\circ$ for the wavelength 436 nm; $[\alpha]_{436} = 34.4^\circ$. The hydrolysate of the corresponding amino-acid mixture gave $0.318 \pm 0.002^\circ$, which, corrected for the residue weights, led to $[\alpha]_{436} = 34.8^\circ$.

Characterization

Molecular weights were estimated from intrinsic viscosities $[\eta]$ in DCA at 25°C with the use of the $[\eta]$ – degree of polymerization relation for PBLG⁴⁵ as the calibration standard. They actually correspond to the viscosity-average degrees of polymerization multiplied by mean residue molecular weight 241. The accuracy of the estimated molecular weights was confirmed by molecular weight determination of several fractionated samples by osmometry, light scattering, and sedimentation equilibrium⁴⁶. G.p.c. measurements were made on a gel-permeation chromatograph HLC-801A (Toyo Soda) equipped with two columns 2 feet long packed with polystyrene gels of nominal porosities, $1 \times 10^4 \text{ \AA}$ and $1 \times 10^6 \text{ \AA}$, respectively. THF was used as solvent and the molecular weight calibration of the chromatogram was made by using several fractionated samples of known weight-average molecular weights. Infra-red spectra were taken on a Jasco Model 402G spectrophotometer. Optical rotatory dispersion (o.r.d.) and optical rotation measurements were carried out in the manner described previously^{6–9}. O.r.d. data were analysed by means of the Moffitt–Yang equation, with λ_0 being taken to be 212 nm.

ACKNOWLEDGEMENTS

Acknowledgement is made to the Japan Society for the Promotion of Science for the research fellowship awarded to D. C. L. The authors wish to thank Professor H. Yuki and Dr S. Sakakibara for their valuable discussion.

REFERENCES

- 1 Poland, D. and Scheraga, H. A. 'Theory of Helix-Coil Transitions in Biopolymers', Academic Press, New York, 1970
- 2 Teramoto, A. and Fujita, H. *Adv. Polym. Sci.* 1975, **18**, 65
- 3 Teramoto, A. and Fujita, H. *J. Macromol. Sci. (C)* in press
- 4 DeTar, D. F., Honsberg, W., Honsberg, U., Wieland, A., Gouge, M., Bach, H., Tahara, A., Briniger, W. S. and Rogers, F. F. *J. Am. Chem. Soc.* 1963, **85**, 2873
- 5 Sakakibara, S., Kishida, Y., Kikuchi, Y., Sakai, R. and Kakiuchi, K. *Bull. Chem. Soc. Japan* 1968, **41**, 1273
- 6 Norisuye, T., Matsuoka, M., Teramoto, A. and Fujita, H. *Polym. J.* 1970, **1**, 691
- 7 Sayama, N., Kida, K., Norisuye, T., Teramoto, A. and Fujita, H. *Polym. J.* 1972, **3**, 538
- 8 Norisuye, T., Teramoto, A. and Fujita, H. *Polym. J.* 1973, **4**, 323
- 9 Matsuoka, M., Norisuye, T., Teramoto, A. and Fujita, H. *Biopolymers* 1973, **12**, 1515
- 10 Urnes, P. and Doty, P. *Adv. Protein Chem.* 1961, **16**, 401
- 11 Fasman, G. D. 'Poly- α -amino acids', (Ed. G. D. Fasman), Marcel Dekker, New York, 1967, Ch 11
- 12 Ledger, R. and Stewart, F. H. C. *Aust. J. Chem.* 1967, **20**, 2509
- 13 'IUPAC–IBU Commission on Biochemical Nomenclature Symbols for Amino Acids Peptides Recommendations', *Biochem.* 1971, **11**, 1726

- 14 Brack, A. and Spach, G. *Bull. Soc. Chim. France* 1971, **12**, 4481
- 15 Bodanszky, M. and du Vigneaud, V. *Biochem. Prep.* 1962, **9**, 110
- 16 Williams, A. W. and Joung, J. T. *JCS Perkin Trans. 1* 1972, 1194
- 17 Trudelle, Y. *Chem. Commun.* 1971, 639
- 18 Trudelle, Y. *JCS Perkin Trans. 1* 1973, 1001
- 19 Hardy, P. M., Haylock, J. C. and Rydon, H. N. *JCS Perkin Trans. 1* 1972, 606
- 20 Ali, A., Hardy, P. M. and Rydon, H. N. *JCS Perkin Trans. 1* 1972, 1070
- 21 Hardy, P. M., Rydon, H. N. and Storey, H. T. *JCS Perkin Trans. 1* 1972, 1523
- 22 Spach, G. and Brack, A. *C.R. Acad. Sci. (C)* 1967, **264**, 2023
- 23 Katakai, R., Oya, M., Toda, F. and Uno, K. *Macromolecules* 1973, **4**, 827
- 24 Jones, J. H. and Walker, J. *JCS Perkin Trans. 1* 1972, 2923
- 25 Cowell, R. D. and Jones, J. H. *J. Chem. Soc. (C)* 1971, 1082
- 26 Fairweather, R. and Jones, J. H. *Immunology* 1973, **25**, 241
- 27 Fraser, R. D. B., Harrap, B. S., MacRae, T. P., Stewart, F. H. C. and Suzuki, E. *J. Mol. Biol.* 1965, **12**, 482
- 28 Takahashi, S. *Bull. Chem. Soc. Japan* 1969, **42**, 521
- 29 Heitz, F. and Spach, G. *Macromolecules* 1971, **4**, 429
- 30 Kovacs, J. and Kapoor, A. *J. Am. Chem. Soc.* 1965, **87**, 118
- 31 König, W. and Geiger, R. *Chem. Ber.* 1970, **103**, 788
- 32 König, W. and Geiger, R. 'Chemistry and Biology of Peptides', (Ed J. Meinenhofer), Ann Arbor Science, Michigan, 1972, p 343
- 33 König, W. and Geiger, R. *Chem. Ber.* 1973, **106**, 3626
- 34 Munakata, H. and Sakakibara, S. *J. Syn. Org. Chem.* 1973, **31**, 853
- 35 Ramachandran, J., Berger, A. and Katchalski, E. *Biopolymers* 1971, **10**, 1829
- 36 Manning, J. M. and Moore, S. *J. Biol. Chem.* 1968, **243**, 5591
- 37 Miyazawa, T. and Blout, E. R. *J. Am. Chem. Soc.* 1961, **83**, 712
- 38 Matsumoto, T. and Teramoto, A. *Biopolymers* 1974, **13**, 1347
- 39 Yang, J. T. in 'Poly- α -amino Acids', (Ed. G. D. Fasman), Marcel Dekker, New York, 1967, Ch 6
- 40 Parrish, J. R. and Blout, E. R. *Biopolymers* 1971, **10**, 1491
- 41 Hatano, M. and Yoneyama, M. *J. Am. Chem. Soc.* 1970, **92**, 1392
- 42 Roig, A., Blanco, F. G. and Cortijo, M. *Biopolymers* 1971, **10**, 329
- 43 Nietzki, R. and Braunschweig, E. *Ber. Dtsch. Chem. Ges.* 1894, **27**, 3381
- 44 Zervas, L., Borovas, D. and Gazis, E. *J. Am. Chem. Soc.* 1963, **85**, 3660
- 45 Norisuye, T. *PhD Thesis* Osaka University (1973)
- 46 Lee, D. C., Itou, S., Teramoto, A. and Fujita, H. to be published

Theory of gelatinization in a starch–water–solute system

J. Lelievre

Agricultural and Food Chemistry Division, Department of Agriculture, Queen's University, Belfast BT9 5PX, UK

(Received 16 June 1975; revised 19 January 1976)

In an attempt to understand the effect of solutes on starch gelatinization the theory of polymer–amorphous phase transitions has been developed to consider melting in a three component system consisting of polymer, diluent and solute. An expression has been derived according to this theory which relates melting temperatures to composition. It is suggested that the expression may be used to explain certain features of gelatinization. However while the theory successfully predicts some of the effects of various solutes on gelatinization temperatures, the fact that the analysis is based on an idealized model of the relatively complex gelatinization transition is emphasized.

INTRODUCTION

When an aqueous suspension of starch granules is heated above a certain temperature the granules swell to form a viscous paste, this process is known as gelatinization. The gelatinization temperature may be defined as the point at which all, or a fraction, of the granules have undergone transformation. Since different experimental techniques for determining this stage give varying results, gelatinization temperatures have arbitrary values when determined by conventional methods. Detailed reviews of starch gelatinization are available in several texts^{1,2}. Many investigators have demonstrated that if gelatinization occurs in the presence of low molecular weight solutes the course of the transition may be altered. For example, polyhydric alcohols raise gelatinization temperatures by an amount that increases as the molarity of the solute is increased³. In the case of monohydric alcohols results are more complicated since lower concentrations of alcohol decrease the values of the temperature at which the transitions occur while in more concentrated solutions these values are raised³. Pasting of starch granules is also possible in non-aqueous systems⁴. Under commercial conditions, gelatinization frequently takes place in solutions containing sugars. The precise effect obtained depends on the concentration of starch and sugar examined^{5,6}. In general, sugar concentrations of less than about 20% w/w appear to have relatively little influence, though in certain instances the temperature at which gelatinization occurs appears to be slightly decreased. As the concentration of sugar is raised above this level gelatinization temperatures are increased, with higher concentrations of sugar producing a disproportionate increment in the temperature at which conversion to a paste occurs^{5,6}. In concentrated sugar solutions there may be relatively large changes in the course of gelatinization. Thus D'Appolonia reported that with a 9% w/w starch suspension the point at which 98% of granules had gelatinized was 24°C higher in an 80% w/w sucrose solution compared to a control⁵. If more concentrated starch suspensions are examined, it is found that sugars tend to cause a greater increase in gelatinization temperatures. Some evidence suggests that disaccharides may cause a larger change in the course of gelatinization than monosaccharides⁷. Despite the industrial significance of starch, the mechanism by

which non-electrolytes influence gelatinization is incompletely understood.

In order to resolve the uncertainties as to how organic solutes influence gelatinization, a detailed knowledge of the structural changes occurring during this process is required. The starch grain consists largely of extensively branched and virtually linear polymers of D-glucose. The chains of these polysaccharides associate to form zones possessing different degrees of order within each granule. However the precise distribution of the numerous types of amylose and amylopectin molecules in the various crystalline and amorphous domains is unknown⁸. In many respects granule structure appears to be quite similar to that of a spherulite crystallized from molten polymer; this might not be expected since polysaccharides are deposited in the starch grain under conditions which are very different from those operating during the crystallization of the synthetic material⁹. Gelatinization occurs when higher temperatures cause the crystalline regions in granules to melt¹⁰, and since these zones possess different degrees of order the transition takes place over a temperature range. When starches are completely gelatinized polymer chains are in an amorphous state, though a fraction of the amylose may complex with traces of lipid^{1,2}. Thus gelatinization entails a change in structure from a partly crystalline to an amorphous form. Previous work has demonstrated that the theory of crystalline–amorphous phase transitions in polymer–diluent mixtures¹¹ may be used to explain certain features of this behaviour in starch¹². The theory provides a means of analysing an idealized model of the gelatinization process, namely that of melting of a partly crystalline polymer in the presence of diluent. The following report describes an attempt to develop the analysis to consider the case of a three component system consisting of polymer, diluent and low molecular weight solute.

THEORY OF MELTING IN POLYMERS

Let the subscripts 1, 2 and 3 refer to diluent, polymer and solute respectively. The expression describing crystalline–amorphous phase transitions relates the melting temperature, T_m , at which liquid crystalline polymer repeat units are in equilibrium, to the composition of the liquid phase.

T_m is the temperature at which the last traces of crystallinity disappear when melting is performed using an extremely slow heating schedule. The condition for equilibrium may be stated as follows:

$$\mu_u^c - \mu_u^0 = \mu_u - \mu_u^0 \quad (1)$$

where μ_u is the chemical potential of the liquid polymer repeat unit with μ_u^c and μ_u^0 the chemical potentials of the polymer in crystalline form and in the standard state. According to Flory¹¹, the left-hand side of equation (1), i.e. the difference in the chemical potential of the crystalline repeat unit and the unit in the standard state may be expressed thus:

$$\mu_u^c - \mu_u^0 = -\Delta H_u(1 - T/T_m^0) \quad (2)$$

where T is the absolute temperature, T_m^0 is the melting temperature of pure polymer and ΔH_u is the heat of fusion of polymer repeat unit. The right-hand side of equation (1) represents the lowering of the chemical potential of the unit in the liquid phase owing to the presence of diluent. For a tertiary system, this may be derived from the following general formula¹¹:

$$\begin{aligned} \mu_2 - \mu_2^0 = RT[\ln \nu_2 + (1 - \nu_2) - \nu_1(x_2/x_1) - \nu_3(x_2/x_3) \\ + (\chi_{21}\nu_1 + \chi_{23}\nu_3)(\nu_1 + \nu_3) - \chi_{13}(x_2/x_1)\nu_1\nu_3] \end{aligned}$$

where μ_2 and μ_2^0 represent the chemical potentials of liquid polymer and polymer in the standard state; R is the gas constant; ν_1 , ν_2 and ν_3 the volume fractions; x_1 , x_2 and x_3 the number of segments per molecule in the respective species and χ_{ij} the pair interaction parameters corresponding to χ_1 in the two component system. An equation for the chemical potential per mole of repeat unit rather than per mole of polymer is required. Dividing by the number of units per polymer molecule, i.e. $x_2 V/V_u$, where V and V_u are the molar volumes of segment and structural unit respectively:

$$\begin{aligned} \mu_u - \mu_u^0 = \frac{RTV_u}{V} [(\ln \nu_2)/x_2 + (1 - \nu_2)/x_2 - \nu_1(x_2/x_1)/x_2 \\ - \nu_3(x_2/x_3)/x_2 + (\chi_{21}\nu_1 + \chi_{23}\nu_3)(\nu_1 + \nu_3)/x_2 - \chi_{13} \times \\ (x_2/x_1)\nu_1\nu_3/x_2] \end{aligned}$$

This expression for the right-hand side of equation (1) may be simplified by making assumptions analogous to those used in deriving the melting point equation for a two component system¹¹. Thus by considering the case of large values of x_2 , and relatively high concentrations of polymer, the expression reduces to:

$$\begin{aligned} \mu_u - \mu_u^0 = RT \frac{V_u}{V} [-\nu_1 x_1 - \nu_3/x_3 + (\chi_{21}\nu_1 + \chi_{23}\nu_3) \times \\ (\nu_1 + \nu_3)/x_2 - \chi_{13}\nu_1\nu_3/x_1] \end{aligned}$$

Let $V = V_1$, and the number of segments per solvent molecule be 1, i.e. $x_1 = 1$. Then:

$$\begin{aligned} \mu_u - \mu_u^0 = RT \frac{V_u}{V} [-\nu_1 - \nu_3/x_3 + (\chi_{21}\nu_1 + \chi_{23}\nu_3) \times \\ (\nu_1 + \nu_3)/x_2 - \chi_{13}\nu_1\nu_3] \end{aligned}$$

The formula may be further simplified by using the relation:

$$\chi_{ji} = \chi_{ij}(x_j)/(x_i)$$

Therefore:

$$\chi_{21} = \chi_{12} \frac{x_2}{x_1} = \chi_{12} x_2$$

Substitution gives:

$$\begin{aligned} \mu_u - \mu_u^0 = \frac{RT}{V_1} V_u \{-\nu_1 - \nu_3/x_3 + [\chi_{12}\nu_1 + (\chi_{32}\nu_3/x_3)] \times \\ (\nu_1 + \nu_3) - \chi_{13}\nu_1\nu_3\} \quad (3) \end{aligned}$$

Combining equation (2) and (3), replacing T by T_m , and rearranging gives:

$$\begin{aligned} \frac{1}{T_m} - \frac{1}{T_m^0} = \frac{R}{\Delta H_u} \frac{V_u}{V_1} \{\nu_1 + \nu_3/x_3 + \chi_{13}\nu_1\nu_3 \\ - [\chi_{12}\nu_1 + (\chi_{32}\nu_3)/x_3] (\nu_1 + \nu_3)\} \quad (4) \end{aligned}$$

This expression relates the melting temperature to the composition as represented by the volume fractions of solvent and monomeric solute. The depression of the melting point is a function of the heat of fusion per repeat unit, the ratio of the molar volumes of this unit and of diluent, the interaction parameters χ_{12} , χ_{13} , χ_{32} and the number of segments per solute molecule.

APPLICATION OF THEORY

While equation (4) provides a means of analysing the effects of solutes on melting temperatures, the expression contains a number of unknown constants and is therefore difficult to use to evaluate experimental situations in an unambiguous manner. Certain of the terms in the equation can be established by considering the case of a two component system; the equilibrium temperature, T_m , is then related to the concentration of diluent by¹⁰:

$$\frac{1}{T_m} - \frac{1}{T_m^0} = \frac{R}{\Delta H_u} \times \frac{V_u}{V_1} (\nu_1 - \chi_{12}\nu_1^2) \quad (5)$$

Values of T_m determined at various volume fractions, ν_1 , may be substituted into this equation and ΔH_u and χ_{12} calculated if T_m^0 is known. However pure starch, like many other naturally occurring polymers, decomposes before melting and hence T_m^0 cannot be determined directly. In this situation it is advantageous to rearrange equation (5) into the form¹³:

$$\left(1 - \frac{T_m}{T_m^0}\right) \frac{1}{\nu_1^2} = \frac{RV_u}{\Delta H_u V_1} \times \frac{T_m}{\nu_1} - \frac{R}{\Delta H_u} \times \frac{V_u}{V_1} \chi_{12} T_m \quad (6)$$

If ΔH_u and the product $\chi_{12} T_m$ are assumed to be constant over the temperature range of concern¹¹, then according to equation (6) the term $[1 - (T_m/T_m^0)]/\nu_1^2$ should be a linear function of T_m/ν_1 . On substituting known values of T_m and ν_1 the magnitude of T_m^0 that gives the best fit to a

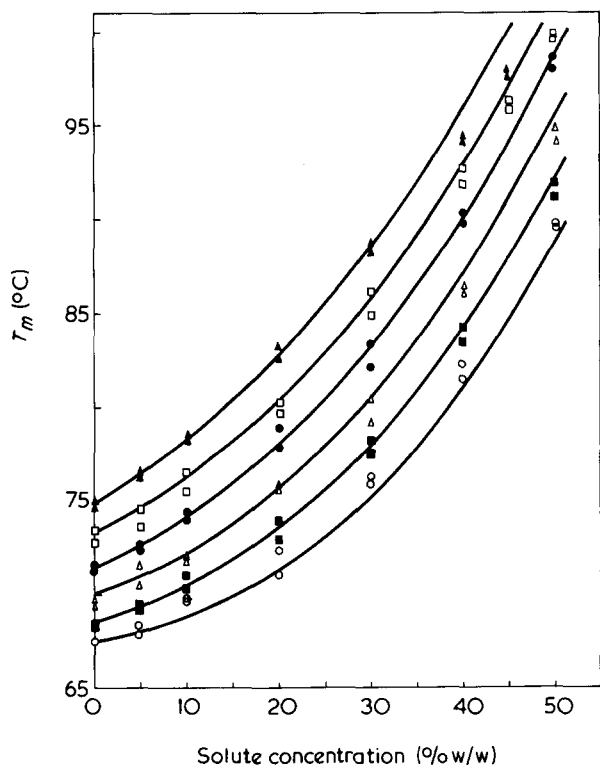


Figure 1 Graph of predicted melting temperature as a function of maltose concentration for various starch concentrations. From left to right the curves correspond to suspensions of 110, 100, 90, 80, 70, and 60 g starch in 100 g solution containing the percentage of solute indicated. The symbols refer to corresponding experimentally determined melting temperatures

linear relationship may be established and ΔH_u and χ_{12} can then be calculated.

Two constants remain unknown in equation (4), namely χ_{13} and χ_{32} . However in certain instances it is possible to make assumptions about the values of these parameters. For example, in the particular case of a sugar such as glucose, χ_{32} is approximately zero. In other words, there is a negligible difference between energy of a glucose molecule immersed in starch polymer and the energy of the same molecule surrounded by glucose monomer. On letting χ_{32} equal zero, equation (4) simplifies to:

$$\frac{1}{T_m} - \frac{1}{T_m^0} = \frac{R}{\Delta H_u} \frac{V_u}{V_1} [\nu_1 + \nu_3/x_3 + \chi_{13}\nu_1\nu_3 - \chi_{12}\nu_1(\nu_1 + \nu_3)] \quad (7)$$

Furthermore, for a hexose sugar, χ_{12} is approximately equal to χ_{13} , i.e. the difference between the energy of a solvent molecule in the environment of starch polymer and one surrounded by molecules of its own kind is similar to the difference when a solvent molecule is first in the situation of pure polymer and then pure solvent. Thus in the special case of a sugar, equation (7) may be used to predict the effect of solute on melting temperatures.

The possibility of using equations (7) and (4) to describe certain aspects of gelatinization in starch-water-solute systems was examined in the present study.

EXPERIMENTAL

Starch was isolated from wheat grains according to the method of Adkins and Greenwood¹⁴. Melting temperatures

were determined for starch-water and starch-water-solute systems. Starch suspensions containing Thiomersal (0.01%) to inhibit microbial growth¹⁵ were first annealed by holding at 50°C for at least 72 h. Samples were then heated at a rate of 1°C/3 h. Melting points were detected by loss of birefringence. A minimum of two measurements of T_m were made, results generally agreed to within $\pm 1^\circ\text{C}$. The effects of maltose and glucose on gelatinization were examined.

Equation (7) was used to calculate T_m values as a function of solute concentration when χ_{32} was zero and χ_{13} was equal to χ_{12} . In a further analysis the situation where χ_{13} and χ_{12} had different values was examined. The effect of changing the size of the solute molecule, i.e. varying x_3 was also studied. Finally the case where χ_{32} was not equal to zero was tested. Results were computed using volume fractions calculated from density values of 1.55, 1.50 and 1.0 g/ml for starch, sugar and water respectively.

RESULTS AND DISCUSSION

Results from the starch-water system were analysed according to equation (6) by computing the value of T_m^0 that gave the best fit of the melting temperature and diluent volume fraction data to a linear relationship. Comparison of the experimentally determined melting points with the fitted melting temperatures obtained from this analysis indicated that the expression described results more accurately when diluent volume fractions were of relatively small magnitude. This would be expected as equation (6) was designed to apply to more concentrated polymer solutions. In the range where ν_1 was greater than 0.9 the fitted melting temperatures passed through a minimum as ν_1 increased. Since this was not observed experimentally the expression does not adequately describe melting at such volume fractions as far as the starch examined is concerned. Equation (6) could be modified to consider crystalline-amorphous phase transitions in the presence of relatively large quantities of diluent, however the resultant expression would be more complicated. As the situation where diluent volume fractions have relatively large values is of commercial interest the compromise of analysing data obtained when the diluent volume fraction was less than 0.7 was employed in the present study. From such data T_m^0 was found to be 495 K, ΔH_u to be 6000 cal/mol and χ_{12} to be 0.5, these results are similar to those obtained previously¹². The value of the solvent-polymer interaction coefficient is in agreement with that obtained by other investigators when using different methods of measurement^{16,17}. The similarity between experimental and fitted melting temperatures in the situation where ν_1 is less than 0.7 is illustrated on the y-axis of Figure 1.

The polymer-diluent-solute system was examined in the range of polymer volume fractions where equation (6) was found to describe the behaviour of polymer-diluent mixtures. Equation (7) was used to calculate melting temperatures as a function of solute and polymer concentrations. Figure 1 shows values obtained for the case where the solute was a sugar with a molar volume similar to that of maltose. Results were computed using the assumption that χ_{32} was zero and χ_{12} was equal to χ_{13} . The Figure shows that according to equation (7) sugars increase T_m values under the range of conditions studied, the precise effect depending on starch concentration. Experimentally determined melting points are also illustrated in this diagram. The computed and experimental values are quite

Table 1 Melting temperatures predicted for different molar volumes

Weight water (g)	Weight sugar (g)	Weight starch (g)	Melting temperature (°C)	
			Molar volume 120 ml	Molar volume 228 ml
100	0	65	68.0	68.0
90	10	65	69.0	69.7
80	20	65	70.9	72.6
70	30	65	74.1	76.7
60	40	65	79.0	82.6
50	50	65	86.0	90.8
100	0	75	69.4	69.4
90	10	75	70.8	71.5
80	20	75	73.2	74.8
70	30	75	77.0	79.4
60	40	75	82.4	85.8
50	50	75	89.8	94.3
100	0	85	70.8	70.8
90	10	85	72.7	73.4
80	20	85	75.7	77.1
70	30	85	79.9	82.1
60	40	85	85.7	88.8
50	50	85	93.5	97.6
100	0	95	72.4	72.4
90	10	95	74.8	75.4
80	20	95	78.1	79.4
70	30	95	82.7	84.8
60	40	95	88.9	91.8
50	50	95	97.1	100.9
100	0	105	74.2	74.2
90	10	105	76.9	77.4
80	20	105	80.6	81.8
70	30	105	85.5	87.5
60	40	105	92.0	94.7
50	50	105	100.5	103.9

similar though there is some disagreement at high concentrations of polymer in the presence of relatively large quantities of sugar. The melting points of certain starch suspensions were found to be greater than the boiling point of water as required by theory. When equation (7) was used to predict melting points for smaller sugar molecules such as glucose i.e. molecules having decreased molar volumes but similar solute-polymer and solute-solvent interaction coefficients, the results resembled those in Figure 1 but the curves were shifted to slightly lower temperatures (see Table 1). The computed melting points did not fit the experimentally determined values as well as the results for maltose did, however the discrepancy was usually less than 2°C except at relatively high sugar and starch concentrations where the difference was of the order of 4°C. The assumptions used in deriving equation (7) from equation (4) are probably more accurate for maltose than for glucose, and this may explain the better fit obtained with the former sugar.

The effect of assuming that χ_{32} was zero when calculating melting points was examined. Values of $\chi_{32} \leq \pm \chi_{12}/10$ were substituted into equation (4), this altered results by less than 1°C in all cases. Hence provided χ_{32} is of relatively small magnitude predicted melting temperatures are not significantly changed. Table 2 shows typical results obtained when χ_{32} was zero but χ_{13} and χ_{12} were not equal. In general, if $\chi_{13} > \chi_{12}$ then T_m decreases, and it was only in solutions containing the greatest amount of solute that values increase. When $\chi_{13} \leq \chi_{12}$ or $\chi_{13} < 0$, melting temperatures are increased at all solute concentrations in the range of conditions analysed. As the negative value of χ_{13} increases T_m values increase.

The above results suggest that a theory of crystalline-amorphous phase transitions may be used to explain certain features of gelatinization in a starch-water-sugar system. With other solutes gelatinization temperatures (defined by the point at which the last traces of crystallinity melt) and calculated melting temperatures may correspond when appropriate values of the solute-polymer and solvent-solute interaction coefficients are substituted into the melting point expression. Hence from an analysis based on an idealized model of starch behaviour various qualitative and quantitative aspects of the effect of solutes on gelatinization temperatures may be predicted. However the melting temperature is not strictly identical to the gelatinization point unless suitable experimental conditions are adopted. The term T_m refers to the temperature at which crystalline polymer units are in equilibrium with material in the liquid state. In order to obtain such a condition it is necessary to adopt a very slow heating schedule when melting the polymer. If a slow heating schedule is used annealing occurs which results in the apparent melting temperature increasing in value.

Studies by Kempf¹⁸, Sair¹⁹ and also by Gough and Pybus²⁰ indicate that such a recrystallization process occurs in the starch granule²¹. However the crystallization of starch is a relatively complicated process with high temperatures and low water contents favouring A-type crystallization whereas low temperatures and high water contents favour B-type crystallization²². In addition, branched starch polymers appear to interfere with the crystallization of the linear polymer fraction²³. Thus it is possible that a true equilibrium melting is not achieved even under controlled laboratory conditions. It is clear that with the more rapid heating schedules used under commercial conditions the equilibrium

Table 2 Predicted melting temperatures for various χ_{13} values when $\chi_{32} = 0$

Weight water (g)	Weight solutes (g)	Weight starch (g)	$\chi_{12} =$	$\chi_{13} =$	$\chi_{13} =$	$\chi_{13} =$
			$\frac{1}{2}\chi_{12}$	$\frac{1}{2}\chi_{12}$	$\chi_{13} = \chi_{12}$	$2\chi_{12}$
100	0	60	67.4	67.4	67.4	67.4
90	10	60	75.1	71.0	68.9	64.8
80	20	60	83.5	75.5	71.5	63.5
70	30	60	92.6	81.1	75.4	63.9
60	40	60	102.7	88.3	81.1	66.7
50	50	60	113.9	97.3	89.0	72.4
100	0	70	68.7	68.7	68.7	68.7
90	10	70	76.4	72.5	70.6	66.8
80	20	70	84.7	77.4	73.7	66.3
70	30	70	94.0	83.4	78.1	67.5
60	40	70	104.1	90.8	84.2	71.0
50	50	70	115.3	100.1	92.5	77.3
100	0	80	70.1	70.1	70.1	70.1
90	10	80	77.8	74.3	72.5	68.9
80	20	80	86.2	79.4	76.0	69.1
70	30	80	95.5	85.7	80.8	71.0
60	40	80	105.6	93.4	87.3	75.1
50	50	80	116.9	102.9	96.0	82.0
100	0	90	71.6	71.6	71.6	71.6
90	10	90	79.4	76.1	74.4	71.1
80	20	90	87.8	81.5	78.3	71.9
70	30	90	97.1	88.0	83.5	74.4
60	40	90	107.3	96.0	90.3	79.0
50	50	90	118.5	105.7	99.3	86.4
100	0	100	73.3	73.3	73.3	73.3
90	10	100	81.1	78.0	76.4	73.3
80	20	100	89.5	83.6	80.6	74.7
70	30	100	98.8	90.4	86.1	77.7
60	40	100	109.0	98.5	93.2	82.8
50	50	100	120.3	108.4	102.4	90.5

state is not achieved and hence the point at which gelatinization occurs is not the same as the equilibrium melting temperature.

The application of equation (1) to the analysis of gelatinization is complicated by the fact that the crystalline phase may contain diluent. In this situation, an additional requirement is imposed for equilibrium, namely that the chemical potentials of water in the liquid and crystalline phases be equal. Flory²⁴ has discussed this case with respect to the collagen–gelatin transition and suggested that at the completion of melting part of the diluent is firmly solvated to polar groups while the remainder is in solution, i.e. in the amorphous phase. Under these circumstances, the condition in equation (1) is sufficient to describe the equilibrium and hence equation (5) gives the melting point relation. However T_m now refers to the polymer in a hydrated state. The behaviour of the diluent in the starch crystalline structures is likely to be analogous to that described by Flory for the collagen–gelatin system. There is also the uncertainty as to the precise effect of solutes on the annealing process. In the present study it has been assumed that solutes do not interfere with annealing, however some evidence suggests that in the particular instance of high concentrations of sugars this may not be the case²⁵. A further general problem is that the traces of lipid contained in starch grains may complex with polymer in solution²⁶. The presence of such complexes would influence the chemical potential of the amorphous phase and hence the temperature at which melting occurs would be altered. Lipids complex with approximately ten times their own weight of starch polymer²⁶ and hence the magnitude of the effect may be greater than anticipated from the absolute amount of lipid in the granule. Finally, there is the problem that the analysis is, of necessity, based on a simplified model of the starch granule. This is since the precise distribution and structure of the various amylose and amylopectin molecules in the crystalline and amorphous regions of starch particles is unknown, and hence the framework necessary for a comprehensive treatment of gelatinization is unavailable. Furthermore, even if the required information were available the resultant equations would be too complicated to solve explicitly. Other investigators have also used model structures to interpret crystalline–amorphous transformations in relatively complicated polymers, their results indicate that the principles by which phase transitions in simple polymer systems may be understood apply equally well to more complex situations²⁷.

The results of the present study indicate that some aspects of gelatinization may be explained by treating the process as a general problem in phase equilibria. In particular, the theory of melting in a three component system consisting of polymer, diluent and low molecular weight solute appears to provide a means of analysing certain of the effects of sugars on the starch transition. However the fact that the

analysis is based on an idealized concept of the relatively complex gelatinization process must be stressed. While the foregoing explanation of gelatinization is speculative, it is suggested that the analysis serves to emphasize the fact that starch exhibits crystal–liquid transitions which are analogous to those occurring in other polymeric substances.

ACKNOWLEDGEMENTS

Thanks to Mr John Scott and Mr G. Stevenson for assistance with computing.

REFERENCES

- 1 Leach, H. W. 'Starch: Chemistry and Technology', (Eds R. L. Whistler and E. F. Paschall), Academic Press, New York, 1965, Vol 1, pp 289–307
- 2 Collison, R. 'Starch and its derivatives', (Ed J. A. Radley), Chapman and Hall, London, 1968, pp 168–193
- 3 Gerlsma, S. Y. *Stärke* 1970, **22**, 3
- 4 Taft, R. *J. Phys. Chem.* 1930, **34**, 2792
- 5 D'Appolonia, B. L. *Cereal Chem.* 1972, **49**, 532
- 6 Freke, C. D. *J. Food Technol.* 1971, **6**, 273
- 7 Bean, M. M. and Yamazaki, W. T. *Cereal Sci. Today* 1974, **19**, 400
- 8 Banks, W. and Greenwood, C. T. *Ann. N.Y. Acad. Sci.* 1973, **210**, 17
- 9 Banks, W., Greenwood, C. T. and Muir, D. D. 'Molecular structure and function of food carbohydrate', (Eds G. G. Birch and L. F. Green), Applied Science, London, 1973, pp 177–194
- 10 French, D. *J. Anim. Sci.* 1973, **37**, 1048
- 11 Flory, P. J. 'Principles of Polymer Chemistry', Cornell University Press, New York, 1953
- 12 Lelievre, J. *J. Appl. Polym. Sci.* 1974, **18**, 293
- 13 Flory, P. J., Garrett, R. R., Newman, S. and Mandelkern, L. *J. Polym. Sci.* 1954, **12**, 97
- 14 Adkins, G. K. and Greenwood, C. T. *Stärke* 1966, **18**, 213
- 15 Colwell, K. H., Axford, D. W. E., Chamberlain, N. and Elton, G. A. H. *J. Sci. Food. Agric.* 1969, **20**, 550
- 16 Foster, J. F. 'Starch Chemistry and Technology', (Eds R. L. Whistler and E. F. Paschall), Academic Press, New York, 1965, Vol 1, pp 349–389
- 17 Hollinger, G., Kuniak, L. and Marchessault, R. H. *Biopolymers* 1974, **13**, 879
- 18 Kempf, W. *Stärke* 1955, **7**, 161
- 19 Sair, L. *Cereal Chem.* 1967, **44**, 8
- 20 Gough, B. M. and Pybus, J. N. *Stärke* 1971, **23**, 210
- 21 Banks, W. and Greenwood, C. T. 'Starch and its components', Edinburgh University Press, Edinburgh, 1975
- 22 Hellman, N. N., Fairchild, B. and Senti, F. R. *Cereal Chem.* 1954, **31**, 495
- 23 Lampitt, L. H., Fuller, C. H. F. and Goldenberg, N. *J. Soc. Chem. Ind.* 1941, **60**, 675
- 24 Flory, P. J. and Garrett, R. R. *J. Am. Chem. Soc.* 1958, **80**, 4836
- 25 Hester, E. E., Briant, A. M. and Personius, C. J. *Cereal Chem.* 1956, **33**, 91
- 26 Senti, F. R. and Erlander, S. R. 'Non-Stoichiometric compounds', (Ed L. Mandelkern), Academic Press, London, 1964, pp 568–587
- 27 Mandelkern, L. 'Crystallization of Polymers', McGraw-Hill, New York, 1964

Glass transition temperature of ideal polymeric networks

F. Rietsch, D. Daveloose and D. Froelich

Laboratoire de Physique Macromoléculaire, Université des Sciences et Techniques de Lille, 59650 Villeneuve d'Ascq, France

(Received 9 March 1976)

Measurements of the glass transition temperature (T_g) have been carried out on polystyrene networks prepared by the anionic copolymerization of styrene and divinylbenzene, and star-shaped polystyrene of varying functionality. The results show a linear variation of T_g versus M_n^{-1} in all cases. The value of the slope interpreted in terms of the free volume theory shows that the glass transition temperature depends closely on the average functionality of the crosslinks. In order to study the influence of free chains on the glass transition of crosslinked polymers a series of networks were contaminated with increasing ratios of linear polystyrene chains, slightly polydisperse.

INTRODUCTION

The glass transition temperature (T_g) of polymers is an important parameter, as their physical and mechanical properties vary greatly at this temperature. This is why the variation of T_g with molecular parameters has been the subject of numerous experiments¹. In particular, it is well known that the glass transition temperature is a decreasing function of the molecular weight for a linear polymer and of the crosslinking density for crosslinked polymers.

The results published up to now on the variation of T_g with crosslinking density were obtained with samples prepared by a radical process. These samples are poorly defined and their molecular weight between crosslinks, obtained by indirect measurements, is to a great extent polydisperse. In addition to this, the functionality of these networks, i.e. the number of elastic chains produced at each crosslink is a constant figure determined by the chemical nature of the reaction at crosslinking.

The samples studied here are ideal networks prepared by anionic copolymerization². This technique makes it possible to obtain networks for which the molecular weight between crosslinks is only slightly polydisperse and experimentally measurable. It also makes possible the preparation of star-shaped polymers in which the functionality and the molecular weight of the star-points can be varied³. Studies of the temperature variation of glass transition with these two parameters have been carried out. Results have been compared to those obtained on linear polystyrenes and interpreted with the help of existing theories.

EXPERIMENTAL

Polystyrene samples were prepared by anionic copolymerization following the method of Rempp and coworkers². The polymerization of styrene is initiated by the disodium tetramer of α -methylstyrene and gives by the nucleophilic attack of the double bonds, a 'living' polystyrene with reactive organo sodium sites at both ends. The network is obtained by the addition of divinylbenzene (DVB) whose copolymerization is initiated by styryl carbanion. The reactions were carried out in a mixture of 50% toluene and

tetrahydrofuran (THF) at -78°C , in order to obtain a good dispersion of the DVB in the mixture before crosslinking. The gels obtained in this way were deactivated by a solution containing 10% THF and tetrahydrofurfuryl alcohol; its alcoholates were removed by successive washings. Before adding the DVB a calculated amount of linear polystyrene was taken in order to determine the molecular weight and the polydispersity of the chains between crosslinks.

The gels obtained in this way consist of nodules of DVB which are strongly crosslinked and link chains of polystyrene of known molecular weight and slightly polydisperse. It has been shown⁴ that the functionality of the network thus obtained depends on the concentration of DVB per living end. Two series of gels were prepared, with 3 and 10 molecules of DVB per living end. A third series was prepared following the method of Herz⁵ which gives a functionality of three.

In order to study the simultaneous influence of the free ends of the chain and of the crosslink points, we also measured the glass transition of star-shaped polymers with different molecular weight and functionality which were prepared by Rempp and coworkers³. The method used by these researchers consists of preparing living polymers with a reactive organo sodium site at one end only, initiated by a monofunctional initiator. The formation of a star-shaped polymer is obtained by the addition of a variable amount of DVB. The determination of the molecular weight of the initial linear polystyrene and of the star-shaped polystyrene makes it possible to determine the average functionality.

In addition to this, and so as to study the influence of free chains on the glass transition of crosslinked polymers, a series of networks were contaminated with increasing amounts of polystyrene chains of a molecular weight resembling that of the network.

The glass transition temperatures of the polymers were determined on a Perkin-Elmer differential scanning calorimeter (DSC-2). The values of T_g were obtained by the intersection on the baseline of the tangent at the inflection point on the representative curve. It is well known that the glass transition temperature, deduced by calorimetric analysis, depends on the thermal history of the polymer and on the speed of heating and cooling. So as to make the measurements among the different samples comparable, each

Table 1 Experimentally determined T_g values for linear and crosslinked polymers

\bar{M}_n	Linear T_g (°C)	Crosslinked				
		T_g (°C) ($f = 5-7$)	\bar{M}_n	T_g (°C) ($f = 3$)	T_g (°C) ($f = 10-12$)	
7500	77.7		9600	98.5	8000	109.5
10450	83	103	12100	98	20000	103.5
10660		102.5	27550	97.7	36000	102
13200	84.9	101.7				
19100	90					
19900	92	100.7				
30000	93.5	99				
45600	94.5	98.6				
75000	95.3	97.7				
110000	97.4					
$K \times 10^{-5}$	1.5	0.55		0.13		0.78
$\rho N_A \xi$	6	4		1		6
M_0						

Table 2 Experimental values for linear crosslinked and star-shaped polymers

	\bar{M}_n / branched	T_g (°C)	K_{measured} $\times 10^{-6}$	$K_L \times 10^{-5}$	$K_R \times 10^{-5}$	$\Delta T_g \bar{M}_n^{\text{measured}}$ $\times 10^{-5}$	$1/2(K_L + K_R)$ $\times 10^{-5}$
$f = 3$	10880	93.5					
	23200	95.5					
	50450	96.3	-0.41	1.50	0.13	1.09	0.82
	80000	96.7					
	319000	97.1					
$f = 4$	16670	96.2					
	61900	96.9					
	134300	97.1	-0.27	1.50	0.30	1.23	0.90
	200000	97.5					
	480000	97.6					
$f = 6-7$	35200	98.1					
	52270	97.7					
	100000	97.9	+0.1	1.50	0.55	1.60	1.05
	518200	98.7					
$f = 10-12$	56360	98.2					
	54540	98.1	0.26	1.50	0.78	1.76	1.14
	172700	97.8					

of the samples was maintained at 460K for 10 min, then cooled at 40°C/min. With the intention of increasing the reproducibility of the measurements, the T_g were measured for different values of heating-rate and extrapolated at low rate, although this extrapolation has no physical meaning.

RESULTS AND DISCUSSION

Twenty years ago, Fox and Flory⁶ showed that for a series of fractioned linear polystyrene, the glass transition temperature varied linearly with the inverse of the number-average molecular weight of polymers and they proposed an equation of the type:

$$T_g = T_{g\infty} - \frac{K_L}{\bar{M}_n} \quad (1)$$

in which $T_{g\infty}$ is the glass transition temperature of an infinite molecular weight polymer and K_L is a constant. Ueberreiter and Kanig⁷ showed that this equation was an approximation valid for molecular weights up to 2000.

In the same way, Fox and Loshaek⁸ proposed the following semi-empirical equation for crosslinked polymers obtained by radical polymerization:

$$T_g = T_{g\infty} + \frac{K_x \Gamma}{N_A}$$

in which N_A , Γ , K_x represent the Avogadro's number, the crosslink density and a constant characteristic of the polymer. In this equation, the molecular weight of chains between crosslinks does not appear because it is not directly accessible through experiments for this type of network. In our case, where we can measure this molecular weight, we can express the variation of T_g in relation to \bar{M}_n by an equation similar to equation (1):

$$T_g = T_{g\infty} + \frac{K_R}{\bar{M}_n} \quad (2)$$

where $T_{g\infty}$ represents the value of T_g for a network of infinite molecular weight. All the experimental results on linear crosslinked and star-shaped polymers are included in Tables 1 and 2. Following equations (1) and (2) we have plotted in Figures 1 and 2 the values of T_g versus \bar{M}_n^{-1} for linear, cross-linked and star-shaped polymers. In this way we obtained a cluster of straight lines, all passing through $T_{g\infty} = 97.5^\circ\text{C}$ for infinite molecular weight. The convergence of these different straight lines indicates that struc-

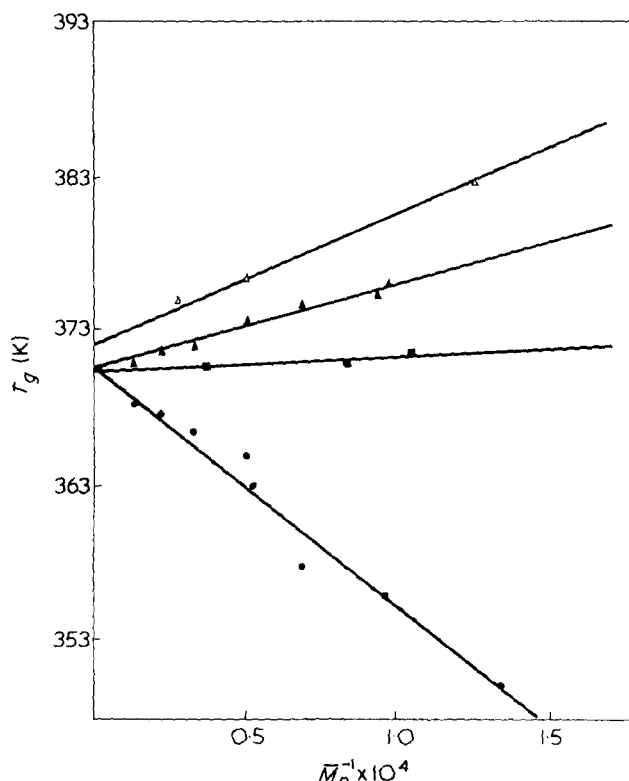


Figure 1 Network: Δ , $f = 10-12$; \blacktriangle , $f = 5-7$; \blacksquare , $f = 3$. Linear, \bullet

tural parameters become negligible when the molecular weight \bar{M}_n is high.

The physical interpretation of the value of the slope of these straight lines, in the case of linear and crosslinked polymers, has been the subject of a great many studies based either on the concept of free volume¹, or on statistical theories⁹⁻¹¹. Recently Chompff¹² proposed a theory using the concept of the additivity of free volume, which can be relatively well applied to the experimental results obtained.

The calculation is based on a model made up of three distinct structural elements: free chain ends (index 1), chain segments (index 2) and branch points (index 3). Assuming the additivity of free volumes, we can write:

$$f = \sum_{i=1}^3 f_i \phi_i$$

and $f_i = f_{gi} + \alpha f_i (T - T_{gi})$ with $i = 1, 2, 3$

where f_i are the fractions in free volume of elements i at a given temperature; f_{gi} are the fractions in free volume of elements i at $T = T_{gi}$; T_{gi} are the temperatures of glass transition of elements i ; αf_i are the coefficients of volumic expansion of elements i ; ϕ_i are the fractions in effective volume of elements i and f is the total fraction of free volume.

Considering as Chompff did, that f_3 is negligibly small for $T = T_g$

$$T_g = \frac{\alpha f_1 \phi_1 T_{g1} + \alpha f_2 \phi_2 T_{g2} + f_{g3} \phi_3}{\alpha f_1 \phi_1 + \alpha f_2 \phi_2} \quad (3)$$

Linear polymer

For a linear polymer, the volume fraction ϕ_3 is zero, which enables the volume fraction, ϕ_1 , to be defined by

the equation:

$$\phi_1 = \frac{2\rho N_A \zeta_1}{\bar{M}_n} \quad (4)$$

where ρ is the density of the polymer; N_A is Avogadro's number and ζ_1 represents the effective volume of one chain end.

This equation combined with equation (3) leads to the variation of T_g as a function of \bar{M}_n^{-1} :

$$\begin{aligned} \left(\frac{\partial T_g}{\partial \bar{M}_n^{-1}} \right)_{\substack{\phi_3=0 \\ \phi_1 \rightarrow 0}} &= \left(\frac{\partial T_g}{\partial \phi_1} \right) \left(\frac{\partial \phi_1}{\partial \bar{M}_n^{-1}} \right) \\ &= - \frac{\alpha f_1}{\alpha f_2} (T_{g2} - T_{g1}) 2\rho N_A \zeta_1 = K_L \quad (5) \end{aligned}$$

As is indicated in equation (3), the variation of T_g with \bar{M}_n^{-1} or ϕ_1 is not linear, and equation (5) is an approximation valid only when the molecular weight \bar{M}_n is sufficiently high ($\phi_1 \rightarrow 0$).

From the curve relating to the linear polymer in Figure 1, we have obtained the experimental value of $K_L = 1.5 \times 10^5$. The results obtained by other authors are scattered between 0.70 and 2.1×10^5 ^{6-8,13-16}. This disparity may be linked either to the choice in experimental methods, or to the way in which the results were plotted, or even to the dispersity in the molecular weight of the sample¹⁵.

By identifying the experimental and theoretical values of K_L (equations 1 and 5), it is possible to determine the value of ϕ_1 and thus to know the number of monomer units included in a free end of the chain. To this end, we used the experimental values published by Ueberreiter and Kanig⁷ and by Fox and Loshaek⁸, who obtained respectively the characteristic parameters T_{g1} and αf_1 for oligomers of varying molecular weight.

In Table 3 we have plotted the value of the different parameters appearing in equation (5) as a function of the number of monomer units $\rho N_A \zeta_1 / M_0$ (M_0 is the molecular weight of a monomer unit). The result nearest to the experimental value is obtained when:

$$\rho N_A \zeta_1 = 6M_0$$

This value is twice as great as that obtained by Chompff¹². This difference is essentially due to the experimental value of K_L which was used and to the physical interpretation

Table 3 Parameters from equation (5) as a function of the number of monomer units

$\rho N_A \zeta_1 / M_0$	T_{g1} (°C)	T_{g2} (°C)	$\alpha f_1 \times 10^4$	$\alpha f_2 \times 10^4$	$K_L \times 10^{-5}$
1	-158	97.5	10.08	3.9	1.37
2	-78	97.5	7.05	3.9	1.32
3	-41	97.5	5.96	3.9	1.32
4	-25	97.5	5.44	3.9	1.42
5	-10	97.5	5.14	3.9	1.47
6	3	97.5	4.93	3.9	1.49
7	12	97.5	4.71	3.9	1.525
8	20	97.5	4.67	3.9	1.544
9	26.5	97.5	4.59	3.9	1.564
10	32	97.5	4.52	3.9	1.579

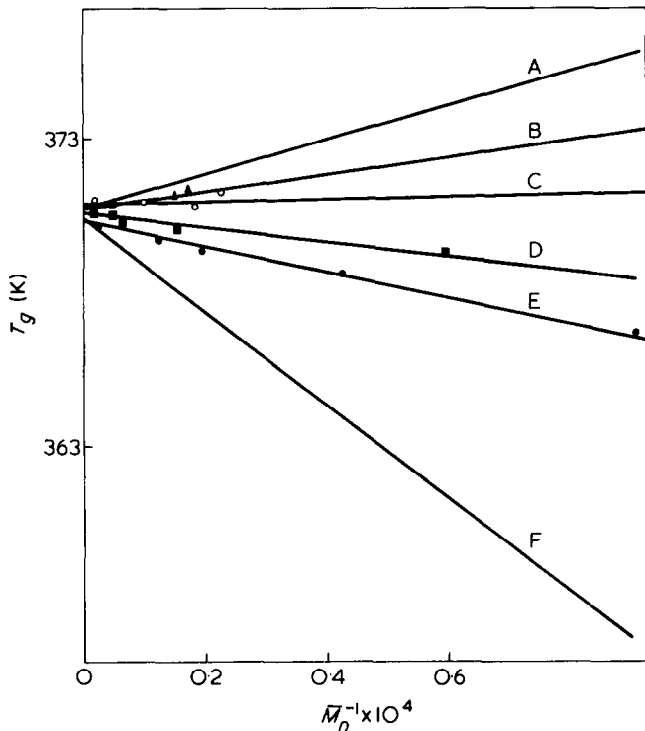


Figure 2 Network: A, $f = 5-7$. Star-shaped: B, $f = 10-12$; C, $f = 6-7$; D, $f = 4$; E, $f = 3$. Linear F

of the characteristic parameters T_{g1} and αf_1 . Clearly this value has no real physical meaning and is only related to the model and its parameters that we have used. It can only be used to compare among themselves the results obtained with different types of polymers.

Crosslinked polymers

For networks obtained by anionic copolymerization we can suppose that $\phi_1 = 0$ (ideal networks) when all the active chain ends have reacted. The volume fraction ϕ_3 is then defined by the equation:

$$\phi_3 = \frac{2\rho N_A \zeta_3}{\bar{M}_n} \tag{6}$$

where ζ_3 represents the effective volume of the crosslinked chain ends. The variation of T_g versus \bar{M}_n^{-1} is expressed by an equation similar to equation (5), with the aid of equations (2), (3) and (6):

$$\left(\frac{\partial T_g}{\partial \bar{M}_n^{-1}} \right)_{\substack{\phi_1=0 \\ \phi_3 \rightarrow 0}} = \left(\frac{\partial T_g}{\partial \phi_3} \right) \left(\frac{\partial \phi_3}{\partial \bar{M}_n^{-1}} \right) = \frac{f_g}{\alpha f_2} 2\rho N_A \zeta_3 = K_R \tag{7}$$

where $f_g = f_{g1} = f_{g2} = f_{g3}$ for $T = T_g$.

This equation is an approximation valid only when the molecular weight \bar{M}_n is sufficiently high ($\phi_3 \rightarrow 0$).

In Table 1 we have included the results obtained for gels of functionality 3, 5-7, 10-12. These results suggest the following remarks.

The slope K_R , as well as the number of segments of ϕ_3 depends closely on the average functionality of the crosslinks. This parameter, which does not appear in an explicit

way in the theory of free volume, reflects the intermolecular interactions near the crosslink points, these are all the more remarkable the higher the functionality. It is therefore very probable that the orientation of the chain segments, near the crosslink nodules is imposed by a volume effect among different chains of the same nodule.

The results we obtained seem to agree with those of other authors^{7,17,18} if we suppose, as Chomppf¹² suggests, that crosslinks prepared by radical means have an average functionality $f = 4$ (Figure 3).

Star-shaped polymers

It is interesting to know the variation of glass transition temperature ΔT_g induced by total or partial crosslinking of linear chains of known molecular weight \bar{M}_n . The T_g increase due to the crosslinking process can be written for a small change in ϕ_1 and ϕ_3 :

$$\Delta T_g = \left(\frac{\partial T_g}{\partial \bar{M}_n^{-1}} \right) \left(\frac{\partial \bar{M}_n^{-1}}{\partial \phi_1} \right) \Delta \phi_1 + \left(\frac{\partial T_g}{\partial \bar{M}_n^{-1}} \right) \times \left(\frac{\partial \bar{M}_n^{-1}}{\partial \phi_3} \right) \Delta \phi_3$$

As T_g is a linear function of \bar{M}_n^{-1} (for ϕ_1 or ϕ_3 small), the variation $\Delta \phi_1$ and $\Delta \phi_3$ for star-shaped polymers is given by:

$$\Delta \phi_1 = -\frac{\rho N_A \zeta_1}{\bar{M}_n}; \Delta \phi_3 = \frac{\rho N_A \zeta_3}{\bar{M}_n}$$

then:

$$\Delta T_g = \frac{1}{2} (K_L + K_R) \bar{M}_n^{-1} \tag{8}$$

In Table 2 the values obtained for star-shaped polymers of functionality 3, 4, 6-7, 10-12, as well as experimental and theoretical (equation 8) values for ΔT_g . \bar{M}_n are given. In Figure 2 the experimental values of T_g versus \bar{M}_n^{-1} are plotted.

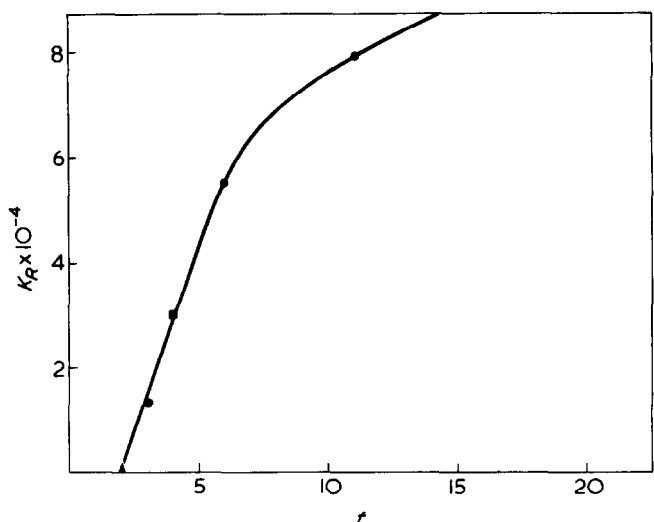


Figure 3 ●, Gel anionic; ■, gel radical; ▲, extrapolation to $f = 2$

Table 4 Values of T_g for contaminated gels

$\bar{M}_n = 10450$ $\bar{M}'_n = 7500$	C	C/2	C/5	C/11
Initial concentration $\times 10^2$ (g/cm)	4.20	2.16	0.70	0.38
ρ (%)	13.89	7.52	3.11	2.8
$T_{g\text{contaminated}}$ (found) ($^{\circ}\text{C}$)	98.5	101	102	102.5
$T_{g\text{contaminated}}$ (calculated) ($^{\circ}\text{C}$)	99	100.9	102.1	102.2

Concerning samples of functionality $f = 3$ and $f = 4$, the agreement is still satisfactory, whereas for star-shaped polymers of higher functionality, the disagreement is very important. For all cases the calculated values are lower than the experimental values. This discrepancy can only be interpreted by architectural factors in relation to functionality.

This can be explained if we suppose that the star-shaped molecules the segment density is higher in the vicinity of the nodule than in crosslinked systems where the chains are more extended.

Contaminated gels

In order to study the influence of free chains present in a network on glass transition temperature, we contaminated a sample having a molecular weight between crosslinks $\bar{M}_n = 10450$ at increasing ratio of linear polystyrene with a molecular weight of $\bar{M}'_n = 7500$, slightly polydisperse.

The free polystyrene chains were introduced into the network by a diffusion process in the swollen state. Samples prepared with different concentrations are shown in Table 4.

From the additivity of free volume it is obvious that:

$$T_{g\text{contaminated}} = T_{g\text{linear}}\rho + (1 - \rho)T_{g\text{network}}$$

where ρ is the weight fraction of linear polystyrene in the sample.

As linear polystyrene with a molecular weight \bar{M}'_n slightly different from the network molecular weight \bar{M}_n , has been used, the following correction must be introduced:

$$T_{g\text{contaminated}} = T_{g\text{network}} \left(1 - \rho \frac{\bar{M}_n}{\bar{M}'_n} \right) + \rho \frac{\bar{M}_n}{\bar{M}'_n} T_{g\text{linear}}$$

The results are included in the Table 4. We can see that the agreement between experimental and calculated values is quite good within the experimental errors and justify the assumption of additivity of free volume.

ACKNOWLEDGEMENTS

We wish to thank Dr P. Rempp, Dr J. Herz and Dr C. Strazielle from CRM in Strasbourg for providing us with some gel samples.

REFERENCES

- 1 Kovacs, A. J. *Fortschr. Hochpolym. Forsch.* 1963, 3, 394
- 2 Weiss, P., Hild, G., Herz, J. and Rempp, P. *Makromol. Chem.* 1970, 135, 249
- 3 Zilliox, J. G., Rempp, P. and Parrod, J. *J. Polym. Sci. (C)* 1968, 22, 145
- 4 Rietsch, F. and Froelich, D. *Polymer* 1975, 16, 873
- 5 Belkebir, Mrani, A. *Thesis* Strasbourg (1976)
- 6 Fox, T. G. and Flory, P. J. *J. Appl. Phys.* 1950, 21, 581
- 7 Ueberreiter, K. and Kanig, G. *J. Colloid Sci.* 1952, 7, 569
- 8 Fox, T. G. and Loshaek, S. *J. Polym. Sci.* 1955, 15, 371
- 9 Gibbs, J. H. *J. Chem. Phys.* 1956, 25, 185
- 10 Gibbs, J. H. and Di Marzio, E. A. *J. Chem. Phys.* 1958, 28, 373
- 11 Di Marzio, E. A. *J. Res. Nat. Bur. Stand (A)* 1964, 68, 611
- 12 Chompff, A. J. 'Polymer Networks', (Eds. A. J. Chompff and S. Newman), Plenum Press, New York, 1971, 145
- 13 Fox, T. G. and Flory, P. J. *J. Polym. Sci.* 1954, 14, 315
- 14 Pierson *Thesis* Strasbourg (1969)
- 15 Blanchard, L. P., Hesse, J. and Malhotra, S. L. *Can J. Chem.* 1974, 52, 3170
- 16 Rudin, A. and Burein, D. *Polymer* 1975, 16, 291
- 17 Ueberreiter, K. and Kanig, G. *J. Chem. Phys.* 1950, 18, 399
- 18 Nielsen, L. E. *J. Macromol. Sci (C)* 1969, 3, 69

Conformation and thermodynamics of adsorbed macromolecules at the liquid/solid interface

Erwin Killmann

Institut für Technische Chemie der Technischen Universität München, 8 München, W. Germany

(Received 20 April 1976)

Calorimetric measurements and results of the adsorption of poly(ethylene glycols) on Aerosil out of solution are reported. With the aid of conformation models for the adsorbed macromolecules and by comparing with the results on low molecular weight model substances, the measured values and their dependence on coverage, molecular weight and solvent are discussed. The resulting structure of the polymer layer, characterized by the adsorbed amount, the number of adhesive segments, the adsorption enthalpy, the thickness and the concentration of the adsorbed layer is verified by i.r. spectroscopic and ellipsometric data.

INTRODUCTION

Most of the experimental work concerning adsorption of macromolecules has dealt with the determination of the amount of adsorption, which is basically necessary for the interpretation of all results from other methods to characterize the conformation of the adsorbed macromolecules. In some adsorption systems information has been successfully obtained on the structure of the layer by spectrometric measurements of the number of adhesive units, and in some other systems by ellipsometric measurement of the thickness and the concentration of the adsorbed layer.

Besides the adsorption layer characterizing parameters, the adsorption enthalpy is also very important in characterizing adsorption behaviour. As we know, direct calorimetric measurements of the enthalpy of adsorption on solid surfaces for polymers were rare until recently¹⁻³. In some investigations enthalpy of adsorption was obtained from the temperature dependence of the adsorption isotherms⁴⁻⁶. The plot of the equilibrium concentration in solution against the reciprocal of the absolute temperature at constant amount of adsorption yields the isosteric Clausius-Clapeyron adsorption enthalpy. This method is very problematical, as the conditions of isostericity and also of reversibility are not fulfilled in the case of polymer adsorption. To demonstrate this an example is given later.

MEASUREMENTS AND DISCUSSION

The enthalpy values reviewed here were measured with an isoperibolic calorimeter (LKB), which is useful for measurements up to 30 minutes. Aerosil 175 and Aerosil 200 were used for the adsorption experiments to achieve the necessary conditions for the method. The Aerosil is non-porous as shown by electron microscopy and has a high specific surface, $\sim 200 \text{ m}^2/\text{g}$. After heating at 10^{-2} – 10^{-1} Torr and 300°C for 6 h the Aerosil was immersed in a solvent or transferred to ampoules under nitrogen and melted off. This procedure yields reproducible adsorbents, shown by i.r. spectroscopy and by calorimetric measurements of the wetting enthalpy in pure solvents. The opti-

imum temperature for preconditioning was found to be 300°C . The wetting enthalpies and the extinction band of the SiOH groups at 3695 cm^{-1} show a maximum (Figure 1). The extinction band of the hydrogen bonds at 3500 cm^{-1} still existing is based partly on hydrogen bonds between neighbouring silanol groups and partly on adsorbed water.

For the calorimetric adsorption measurements poly(ethylene glycols) of different molecular weight were used in comparison with some low molecular weight substances^{1,2}. The solvents were carbon tetrachloride, benzene, water and methanol. Carbon tetrachloride is most important for comparison with i.r. spectroscopic measurements of the number of adhesive segments.

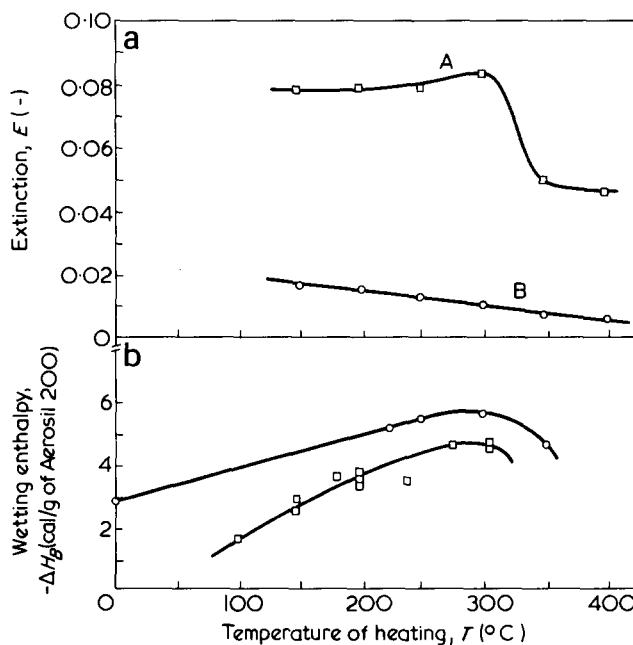


Figure 1 (a) Extinction of the hydrogen bonds $E_{\text{O}-\text{H}-\text{O}}$ and of the SiOH groups $E_{\text{O}-\text{H}}$ versus temperature of heating of Aerosil 200. A, $E_{\text{O}-\text{H}} = 3695 \text{ cm}^{-1}$; B, $E_{\text{O}-\text{H}-\text{O}} = 3500 \text{ cm}^{-1}$. (B) Wetting enthalpies in CCl_4 (○) in benzene (□) versus temperature of heating of Aerosil 200

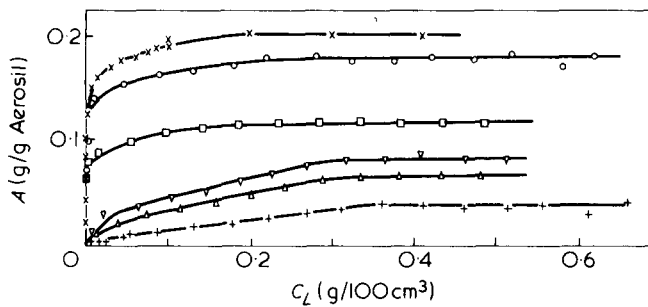


Figure 2 Adsorption isotherms of adsorbed amount A of poly(ethylene glycols); M_w 40 000 (X), M_n 6000 (○), M_n 600 (□), ethyl glycol (▽), ethanol (△), diethyl ether (+). CCl_4 -25°C-Aerosil 200

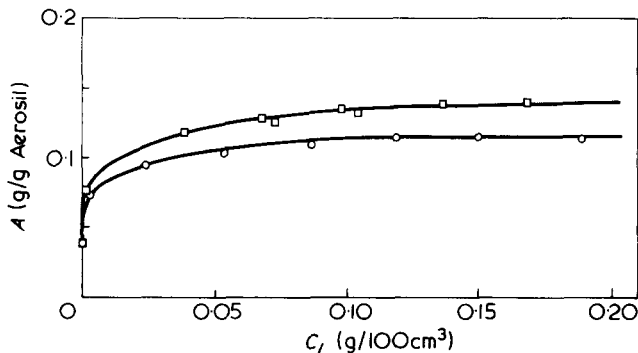


Figure 3 Adsorption isotherms of adsorbed amount A of PEG 6000-benzene at 25°C (○) and 40°C (□)

The adsorbed amounts from CCl_4 and C_6H_6 solutions were measured in the usual way from the difference between the initial concentration weighed in and the equilibrium concentration in the supernatant solution using C-H stretching vibration at 2900 cm^{-1} in CCl_4 and the C-OC valence vibration (oscillation) at 1107 cm^{-1} in C_6H_6 . Figure 2 shows some adsorption isotherms measured in carbon tetrachloride.

The measured adsorption isotherms of poly(ethylene glycol) 6150 in benzene at two different temperatures are given in Figure 3 yielding with the Clausius-Clapeyron evaluation an isosteric endothermic adsorption enthalpy. In contrast to this all calorimetrically measured adsorption enthalpies in all solvents are negative, representing exothermic adsorption. This discrepancy shows that it is impossible to use the temperature dependence of the isotherms and to calculate the adsorption enthalpies according to Clausius-Clapeyron. The reason for this is that the conditions of isostericity and irreversibility are not fulfilled in the case of polymer adsorption, because the conformation of the adsorbed macromolecules is independent of coverage and temperature; this is demonstrated by the i.r. spectrometry and the enthalpy measurements discussed later and by desorption measurements. In the Clausius-Clapeyron evaluation of the adsorption, determination of the enthalpy shows that at the same amount of adsorption the state of adsorption is independent of temperature. This means that at different temperatures at the same amount adsorbed, the macromolecules are adsorbed in the same conformation with the same number of adhesive segments. This condition is not guaranteed by the conformation of the adsorbed macromolecules. The Clausius-Clapeyron enthalpy therefore does not correspond to the enthalpy of adsorption. It contains rather entropic factors, caused

by the variation in conformation and in the number of adhesive segments.

The adsorption enthalpy was measured by breaking an ampoule of 1 ml concentrated polymer solution in an Aerosil suspension of 50 or 100 ml. The desired polymer concentration is given by the amount of the polymer in the ampoule. To obtain the adsorption enthalpy the measured enthalpy must be corrected with the dilution enthalpy, which is measured by separate experiments shown in Figure 4. One can see the strong dependence of the dilution enthalpies on the polymer weight resp. the fraction of OH end groups to the ether groups in the molecules. An example for the correction of the measured enthalpies with the dilution enthalpy to obtain the adsorption enthalpy is given in Figure 5.

The immersion enthalpy was measured by breaking a 1 ml ampoule with the Aerosil under nitrogen gas in a 50 or 100 ml vessel filled with polymer solution. From these procedures one can formulate for the adsorption enthalpy:

$$-\Delta H(\theta) = -n\Delta H_{P,A} + n\Delta H_{L,A} + n\Delta H_{L,P} + \Delta H_{P,P} \quad (1)$$

and for the immersion enthalpy:

$$-\Delta H_I(\theta) = -n\Delta H_{P,A} - (n_0 - n)\Delta H_{L,A} + n\Delta H_{L,P} + \Delta H_{P,P} \quad (2)$$

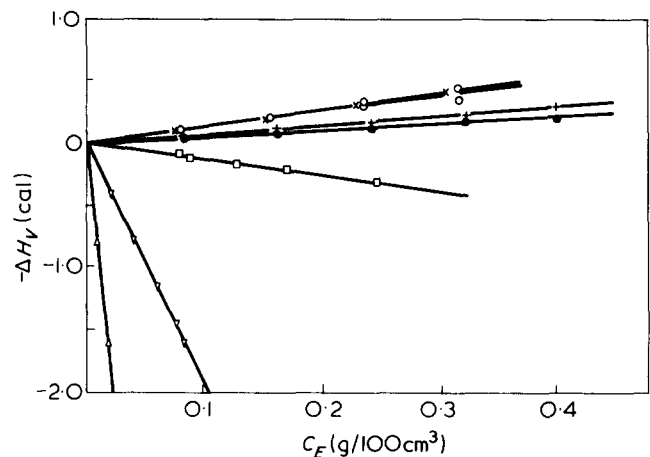


Figure 4 Dilution enthalpies $-\Delta H_V$ of poly(ethylene glycols): M_w 40 000 (X), M_n 6000 (○), M_n 2000 (●), M_n 600 (□), diethyl ether (+), ethyl glycol (▽), ethanol (△)- CCl_4 -25°C

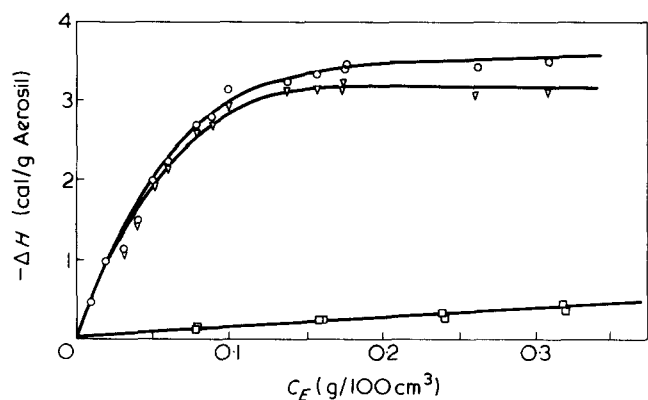


Figure 5 Measured enthalpy $\Delta H_{\text{Meas.}}$ (○), dilution enthalpy ΔH_V (□), adsorption enthalpy ΔH (▽) versus concentration, C_E

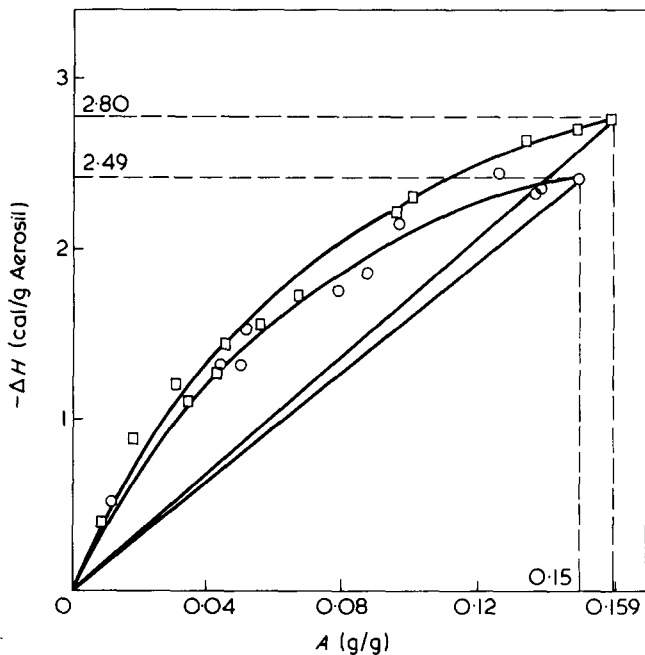


Figure 6 Adsorption enthalpy $-\Delta H$ of PEG 40000-Aerosil 200- C_6H_6 versus adsorbed amount A at $25^\circ C$ (\square), at $40^\circ C$ (\circ)

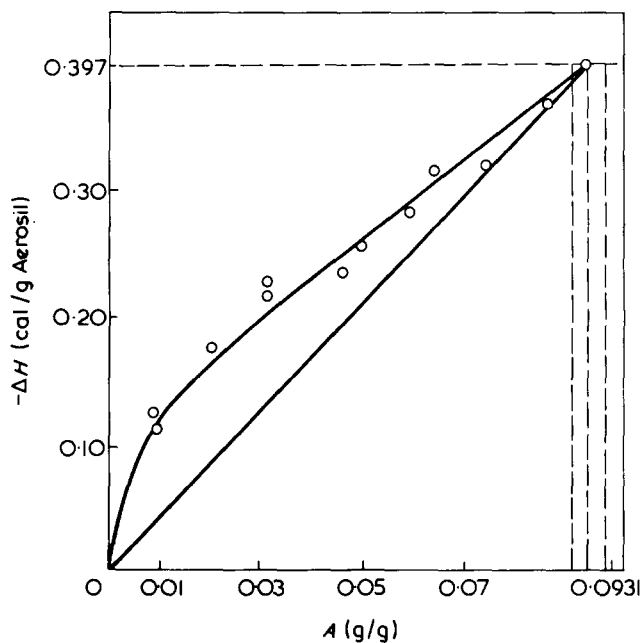


Figure 7 Adsorption enthalpy $-\Delta H$ of PEG 40000-Aerosil 200- H_2O versus adsorbed amount A at $25^\circ C$ (\circ)

which leads to the general rule:

$$H_I(\theta) = \Delta H(\theta) + n_0 \Delta H_{L,A} \quad (3)$$

The integral adsorption enthalpy equation (1) results from the binding of polymer segments $n\Delta H_{P,A}$ simultaneous displacement of the solvent from the surface $n\Delta H_{L,A}$ and the desolvation of the solvent from the solvation shell $n\Delta H_{L,P}$. In addition to these contributions a possible interaction between polymer segments $\Delta H_{P,P}$ must be regarded. The immersion enthalpy (equation 2) results from the sum of the adsorption enthalpy and the wetting enthalpy of the adsorbent with solvent molecules (equation 3). Neglecting the polymer-polymer interaction the equation states that the integral adsorption enthalpy is proportional to the molar number, n , of adsorbed segments at a defined degree of coverage and to an enthalpy difference ($\Delta H_{P,A} - \Delta H_{L,A} -$

$\Delta H_{L,P}$). The differential adsorption enthalpy, D_M , deviating from equation (1) is proportional to dn/dN ; this means that D_M is a measure of the fraction of adhered segments dn/dN .

In Figures 6-9 the values of adsorption enthalpies obtained are plotted against the adsorbed amount for some different solvents and molecular weights. Because of the convex bent curves the adsorption enthalpies do not increase proportionally with the adsorbed amount. The differential adsorption enthalpy D_M decreases with increasing amount of adsorption. From this one can conclude

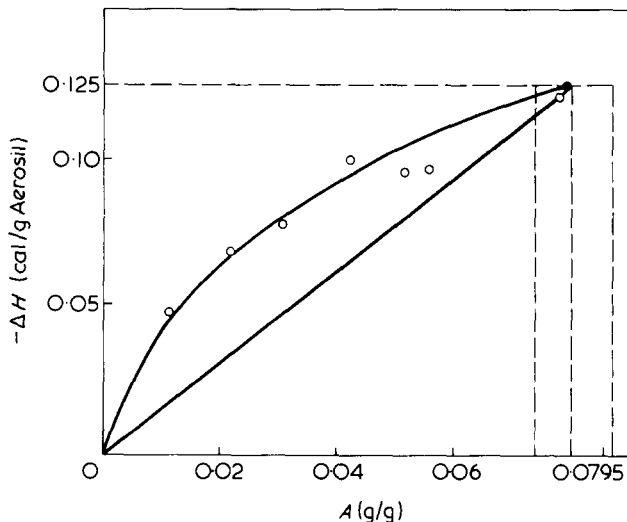


Figure 8 Adsorption enthalpy $-\Delta H$ of PEG 40000-Aerosil 200-methanol versus adsorbed amount A at $25^\circ C$ (\circ)

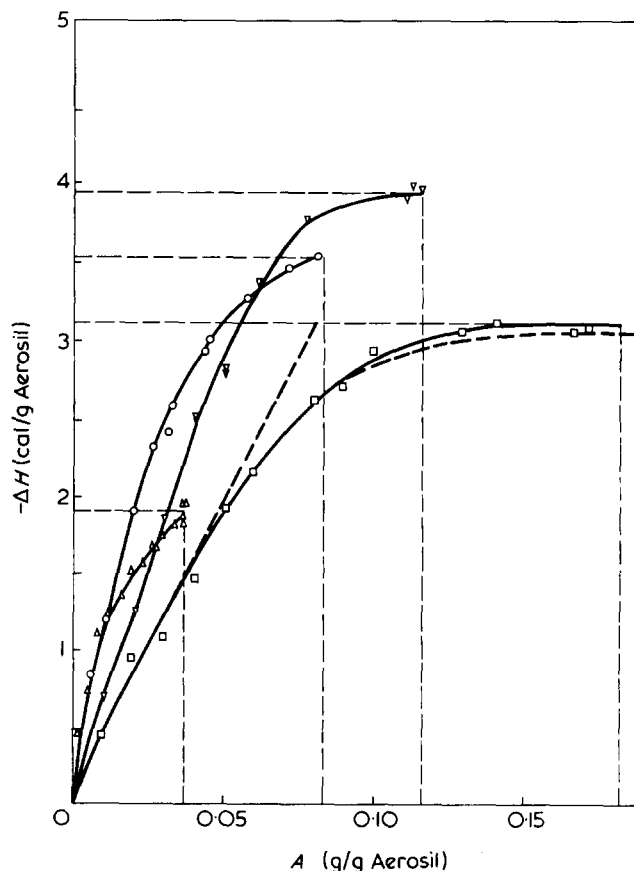


Figure 9 Adsorption enthalpy $-\Delta H$ versus adsorbed amount A of poly(ethylene glycols) 40000, 6000 (\square), 600 (∇), ethyl glycol (\circ), diethyl ether (\triangle)- CCl_4 - $25^\circ C$ -Aerosil 200

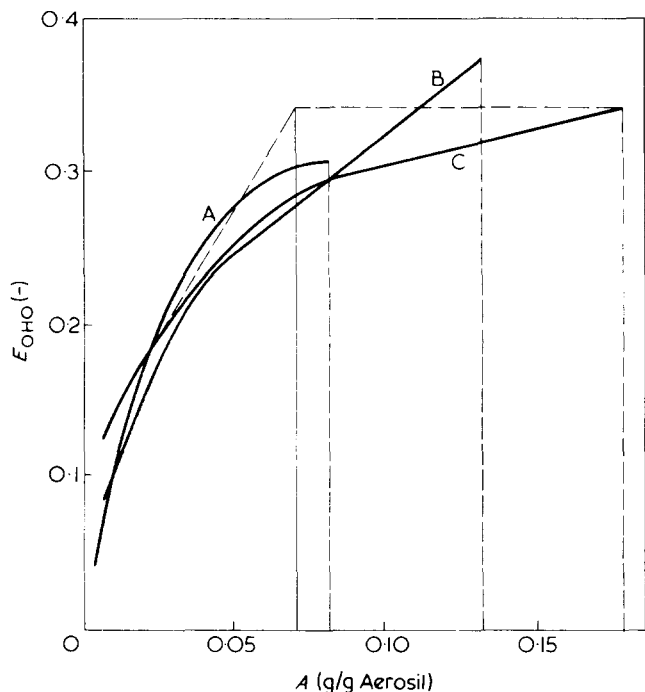


Figure 10 Extinction E_{OHO} of the hydrogen bonds at 3300 cm^{-1} versus adsorbed amount A of poly(ethylene glycols) 6000 (C), 600 (B) and ethyl glycol- CCl_4 - 25°C -Aerosil 200 (A)

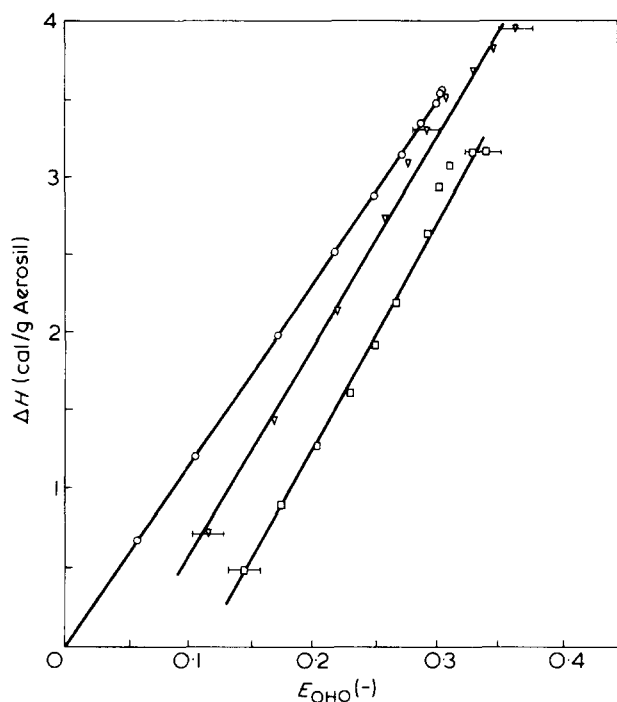


Figure 11 Adsorption enthalpy $-\Delta H$ versus extinction E_{OHO} of the hydrogen bonds of poly(ethylene glycols)- CCl_4 - 25°C -Aerosil 200. \circ , Ethyl glycol; ∇ , poly(ethylene glycol) 600; \square , poly(ethylene glycol) 6000

that the fraction of adhered segments decreases with increasing amount of adsorption, respectively with increasing coverage. This is confirmed by the i.r. spectroscopic measurements of the number of adhered segments on the same Aerosil in CCl_4 ⁷. The plot of the extinction of the hydrogen bonds at 3300 cm^{-1} , responsible for the adsorption of the polyethers, against the adsorbed amount also shows a convex curvature (Figure 10).

The plot of the hydrogen bond extinction against the adsorption enthalpy in Figure 11 shows a straight line. This proves that the adsorption enthalpy and the number or the fraction of adhered segments are proportional. This justifies the neglect of the polymer-polymer interaction contribution in the adsorbed layer in comparison with other enthalpy contributions because the polymer-polymer interaction should increase with coverage, yielding a concave ΔH versus A curve if essentially; but the contrary is measured.

From the analogue curvature of the i.r. measured hydrogen bonds and the adsorption enthalpy it follows clearly that the fraction of adsorbed segments decreases with rising coverage—the conformation of the adsorbed macromolecule depends on coverage. At low coverage the macromolecule on average is bound with more adhered segments in a more flat conformation than at high coverage. At low coverage the macromolecules adsorb unhindered by each other with highest possible contact points, simultaneously desorbing the solvent molecules from the surface and producing the highest exotherm adsorption enthalpy.

With increasing coverage the new adsorbing macromolecule segments are in contact not only with surface places covered with solvent, but also those covered with polymer segments. The number of new contact points decreases. The exchange of segments of adsorbed macromolecules with segments of new adsorbing macromolecules, changing the average conformation of the adsorbed macromolecules, gives no enthalpy contribution. Of course only those segments which adsorb on new solvent covered places give a contribution to the adsorption enthalpy. This change of conformation independent of the concentration of the solution respectively of the coverage also takes effect in the time dependence of the adsorbed amount, demonstrated in Figure 12^{2,7}. At high concentrations normal behaviour is observed: the solution concentration C_L , represented by the extinction of the CH-band, decreases with time indicating the normal increase of the adsorbed amount with time. At low concentrations the opposite behaviour is observed: the solution concentration increases with time indicating a decrease of the adsorbed amount. This behaviour can only be explained by conformation change in the same way as before.

In the solvents CCl_4 , C_6H_6 , CH_3OH and H_2O the immersion enthalpy in polymer solution with adsorption saturation is practically the same, $\Delta H_\infty = 7.2\text{ cal/g}$ adsorbent (equation 2). The wetting enthalpies of the polar solvents H_2O , 6.78 cal/g and CH_3OH , 7.06 cal/g nearly correspond with the immersion enthalpies, the adsorption enthalpy

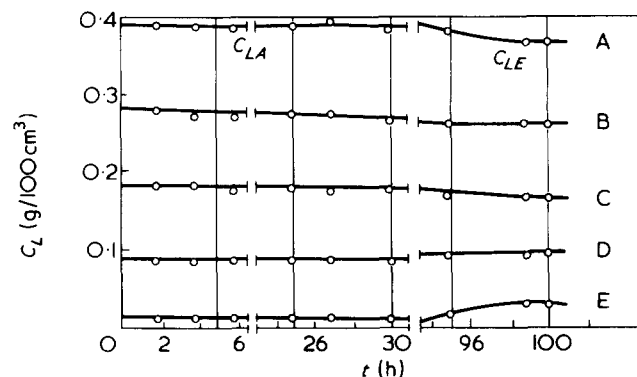


Figure 12 Concentration of the supernatant solution C_L versus time t at different concentrations in C_E ($\text{g}/100\text{ cm}^3$): A, 0.55; B, 0.45; C, 0.35; D, 0.25; E, 0.15

therefore is very low. The wetting enthalpies of the non-polar solvents CCl_4 , 3.75 cal/g and C_6H_6 , 4.6 cal/g are on the contrary much lower than the immersion enthalpies, the adsorption enthalpy therefore is higher (equation 1).

From the solvent independent immersion enthalpy it therefore follows from equation (2) that the solvent dependent terms $(n_0 - n)\Delta H_{L,A}$ and $n\Delta H_{L,P}$ nearly vanishes in the saturation case. It is considered that this is only possible in the different solvents if both terms are nearly zero. This means that the desolvation contribution for all solvents is small in comparison to the other terms and could be neglected and that in saturation nearly all places are covered with polymer segments, so that $n = n_0$. This interpretation is confirmed by the finding that in case of saturation in CCl_4 practically no more extinction of hydroxyl groups is recognized by i.r.⁷ This interpretation also means that the adsorbed enthalpy of poly(ethylene glycol) on Aerosil in CCl_4 is influenced predominantly by the binding enthalpy and in competition to this, the desorption enthalpy of the solvent. The competition by the desolvation and the polymer-polymer interaction must be of second order.

Relating the measured immersion enthalpy to the number of silanol groups, 2.7 SiOH/100 Å² on the Aerosil surface a binding enthalpy of 9.9 kcal/mol SiOH groups results^{1,7} in good agreement with the enthalpy values of hydrogen bonds in the literature. The value of 9.9 kcal/mol is also confirmed by the fact that also for the low molecular weight substances ethyl glycol, diethyl ether, ethyl alcohol the binding enthalpies are nearly 10 kcal/mol².

From the linear ascent of the adsorption enthalpies with low coverage e.g. in CCl_4 , one can calculate an adsorption enthalpy of 1.76 kcal/mol base units of the polymer. In comparison the adsorbed enthalpy of ethyl glycol at saturation is 4.0 kcal/mol. This consideration shows that at low coverage the fraction of adhered segments of the polymers is $p = 0.5$. This means that the polymer in this state is adsorbed in an extremely flat conformation with 50% adsorbed base units.

In the saturation region from the adsorbed amount and the measured adsorption enthalpy it follows that the frac-

tion of the attached segments is about $p = 0.2-0.25$. This indicates a conformational change of the adsorbed polymer chain with coverage.

The consequences of the high fractions of adsorbed base units are: (1) an extremely flat adsorption layer confirmed by the ellipsometric thicknesses on chrome which are found to be less than 20 Å in the whole coverage region⁸; (2) the extremely small dependence of the adsorbed saturation amounts from the molecular weight²; (3) the state that poly(ethylene glycol) adsorbs almost irreversibly when the molecular weight is high enough, which is demonstrated by desorption measurements⁷.

This paper is restricted mainly to the calorimetric part of our work on polymer adsorption. Extensive i.r. spectroscopic measurements have also been carried out on the same PEG- CCl_4 systems and on low molecular weight materials to obtain direct information about the number of adhesive segments^{2,7}. Also ellipsometric measurements for determining the thickness and the concentration of poly(ethylene glycol), polystyrene, poly(vinyl pyrrolidone), poly(methyl methacrylate), polyisobutylene and poly(vinyl acetate) layers on chrome, platinum and gold surfaces in different solvents have been carried out^{8,9}.

REFERENCES

- 1 Killmann, E. and Eckart, R. *Makromol. Chem.* 1971, **144**, 45
- 2 Killmann, E. and Winter, K. *Angew. Makromol. Chem.* 1975, **43**, 53
- 3 Tadros, T. F. Personal Communication *Discuss. Meet. Polym. Liquid-Solid Interface Loughborough* 1975
- 4 Koral, J., Ullmann, R. and Eirich, F. R. *J. Phys. Chem.* 1958, **62**, 541
- 5 Killmann, E. and Schneider, G. *Makromol. Chem.* 1962, **52**, 212
- 6 Lipatov, Y. U. S. and Sergeeva, L. M. *Kolloid Z.* 1965, **27**, 217
- 7 Killmann, E. and Strasser, H. J. *Angew. Makromol. Chem.* 1973, **31**, 169
- 8 Killmann, E. and Kuzenko, M. V. *Angew. Makromol. Chem.* 1974, **35**, 39
- 9 Gebhard, G. and Killmann, E. *Angew. Makromol. Chem.* 1976, **53**, 17

On the reproducibility of T_g measurements on polystyrene using d.s.c.

Marion D. Griffiths and L. J. Maisey

*Rubber and Plastics Research Association of Great Britain, Shawbury, Shrewsbury SY4 4NR, UK
(Received 27 January 1975; revised 29 April 1976)*

In determining the reproducibility of T_g data of a standard polystyrene measured by differential scanning calorimetry (d.s.c.), the effects of d.s.c. trace interpretation method, extrapolation to zero scan rate, polymer sample form, a thermal treatment and a thermal cycling procedure on the results were examined. The results showed that data from scanning at $8^\circ\text{C}/\text{min}$ are preferred to those from extrapolation to zero scan rate while the overall reproducibility was unaffected by the d.s.c. trace interpretation method used. However, the onset of the transition step was selected to define T_g in this work. Similarly, no differences in the reproducibility of data were noted between the overall results for granular or sheet samples, although certain treatments of specific samples did produce changes in some instances. The mean value for T_g at $8^\circ\text{C}/\text{min}$ was found to be 102.3°C . Imposing the thermal treatment on the samples did not significantly alter the reproducibility of the results whereas in contrast, cycling markedly improved the reproducibility of sheet sample data but left that of granules unaffected.

INTRODUCTION

The glass transition temperature (T_g) is a fundamental property of an amorphous or semi-crystalline polymer and is determined by molecular composition and structure. At this temperature, complex rate-dependent molecular processes occur which influence polymer properties both during processing and in service.

Experimental methods of measuring T_g exploit the changes in properties manifested as polymers pass from the glassy to the rubbery state and normally fall into two categories. These are stepwise, steady state methods in which properties are measured under static thermal equilibrium conditions over a temperature range encompassing T_g , and dynamic methods, in which properties are measured during heating the material through T_g . The former approach gives T_g data directly, under approximately isothermal conditions, whilst the latter relies upon an extrapolation procedure in order to generate isothermal (zero scan rate) T_g data. Dynamic methods, however, are becoming increasingly popular on account of their convenience. Differential scanning calorimetry (d.s.c.)¹ falls into this latter category and utilizes the fact that heat capacity changes are observed in a polymer with changes in temperature. Although not intended solely as a technique for determining T_g , d.s.c. is nevertheless widely used for this purpose on account of the commercial availability of suitable equipment, speed of measurement, small sample size requirements and precision of measurement². Currently, many research and development studies use d.s.c. to examine thermal characteristics, structural changes and transitions in polymers. However, no published information which defines the reproducibility of the data generated using this technique is available; it is not known, for example, whether polymer variability is sufficiently low to allow meaningful d.s.c. data to be gathered when small differences between samples are being considered.

The purpose of this paper is to examine the capability of d.s.c. for polymer characterization under normal laboratory conditions; the reproducibility of glass transition data produced for a standard polystyrene will be considered. Sample form, sample thermal history and data interpretation methods are varied. Such a study will permit certain of the polymer/d.s.c. interactions to be quantified, allow a set of data to be produced with which other laboratories may compare their own d.s.c. performances, and finally permit a method to be defined, within the limits of the variables examined, for obtaining the most reproducible d.s.c. data.

EXPERIMENT DESIGN

In an experimental programme of this nature it is important to identify the sources of error and to design the experiment so that the effect of the variables being examined can be readily observed. The present programme recognizes that variations in data result from polymer sample inhomogeneities, instrument/operator errors and data interpretation errors.

In order to minimize d.s.c. data variation due to polymer sample inhomogeneities, a standard polystyrene, supplied by the Polymer Supply and Characterisation Centre (PSCC) at RAPRA was used. This material is homogenized before issue and has a fine particle size (~ 0.5 to 1 mm beads) allowing about 40 individual beads to make up the approximately 10 mg samples used in the study.

There are varying opinions about the method of defining T_g from a d.s.c. trace³⁻⁶. Two methods were used in this work and are shown in *Figure 1*. Both T_i , the intersection point of the projection of the base line with the tangent to the step and T_s , the mid-point between the upper and lower deviations of the step from its tangent were defined. Although glass transitions occur over a temperature range, it is normal practice to quote a single temperature of transition.

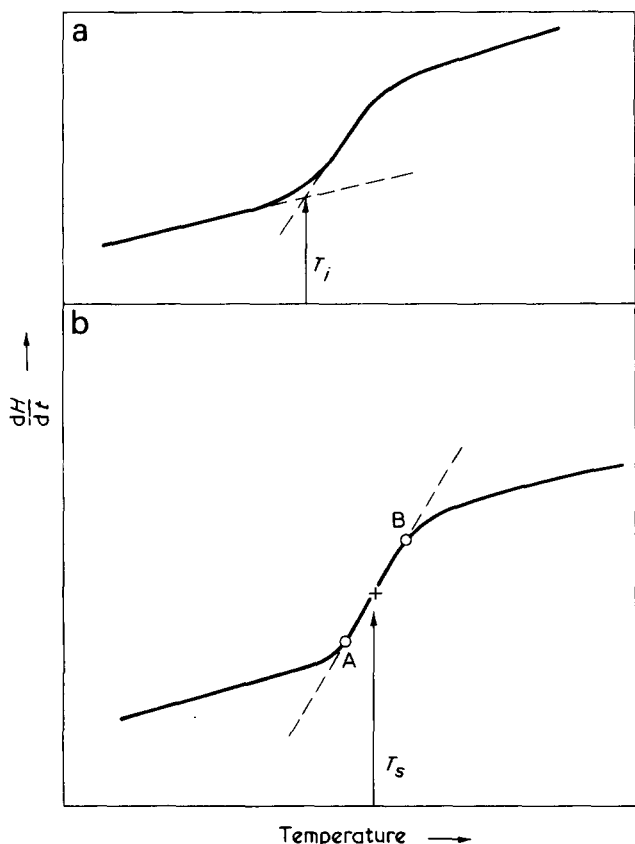


Figure 1 (a) T_g taken as the intersection of the extrapolation of the baseline with the extrapolation of the inflection. (b) T_g taken as the inflection point

Also two methods of handling the abstracted data were considered by comparing the reproducibility of the T_i or T_s values obtained at a single calibrated scan rate with those calculated from an extrapolation of transition data from four scan rates.

Amongst the several factors which may affect the reproducibility of d.s.c. data, the following were taken as the controllable variables and were examined in some detail. (A) The effect of sample form, i.e. granules or a thin sheet moulded from the granules. (B) The effect of an imposed, controlled thermal treatment. (C) The effect of thermally cycling the samples in the d.s.c.

The experimental array to examine these three factors is shown in Table 1.

The above were considered to be major practical variables and in order to increase the confidence of data handling, six replications were made of each experimental condition over a period of five months; after three replications had been completed the d.s.c. was serviced. The lengthy period over which the measurements were made, coupled with the instrument service allows the data generated to be considered as typical information, where the instrument/polymer/operator variability encountered will be maximized rather than minimized. It might be argued that the thermal and cycling treatments are not truly independent variables but from a practical point of view and for the purposes of this study they are considered independent.

EXPERIMENTAL METHOD

Material

The polymer used was PSCC polystyrene PS2, a standardized commercial material with number- and weight-

average molecular weights of 145 and 328 g/mol respectively.

Moulding sheet polystyrene

Granules of PS2 were compression moulded to give circular sheets 50 mm in diameter by 1 mm thickness using a manually operated, laboratory Moore press and a semi-positive mould of 100 mm external diameter with a plunger diameter of 50 mm, the cavity depth being 1 mm. Granules were placed in the mould which had been heated to 170°C, the mould was then closed and held at this temperature under a pressure of 18.45 MN/m² for 30 min. The mould was then cooled to and held at 100°C for a further 30 min, and finally slowly cooled to room temperature still under pressure. Three separate sheets of polystyrene were moulded.

Sample preparation

Four different forms of sample were used. These were: (a) the granules as received, samples A and B (Table 1); (b) the granules after they had been given a controlled thermal treatment in the d.s.c., samples C and D; (c) compression moulded sheet formed from the granules, samples 1 and 2; (d) compression moulded sheet as in (c) after having been given the thermal treatment of (b), samples 3 and 4.

Sample selection

Granular material was taken randomly from the stock of polystyrene while the sheet material was taken randomly from the three sheets fabricated; it is possible however that towards the end of the programme sheet sample selection did not fulfil this random condition as only small unidentified remnants of sheet were available for the last few measurements.

Instrumentation

A Perkin-Elmer DSC-1B was used in the programme. Sample size, heating and cooling rates which could be accommodated by this instrument were chosen. All measurements were made under oxygen-free (BOC white-spot) nitrogen gas at a 25 cm³/min flow rate.

D.s.c. operating method

The temperature indicated by the programmer of the d.s.c. is not the true temperature of the contents of the sample pan due to the inherent non-linear character of the programmed temperature range. To allow for this effect calibration of the instrument with pure materials of known melting point was carried out at 8°C/min scan rate and a relationship established between the known melting tem-

Table 1 The experimental array

Sample name	Sample form	Thermal Treatment	Cycled
A	Granules	No	Yes
B	Granules	No	No
C	Granules	Yes	Yes
D	Granules	Yes	No
1	Sheet	No	Yes
2	Sheet	No	No
3	Sheet	Yes	Yes
4	Sheet	Yes	No

peratures and the indicated d.s.c. programmer temperature. Results obtained after scanning the polystyrene samples at 8°C/min could then be corrected using this relationship.

As each polystyrene specimen was scanned at four different rates, viz. 64°C/min, 32°C/min, 16°C/min, and 8°C/min, pure indium was also scanned at these rates and, following Lambert⁷, correction factors to account for the thermal lags at the different scan rates were calculated.

Data abstraction and extrapolation

The transition temperatures were abstracted from the d.s.c. traces as illustrated in Figure 1; the temperatures are given to the nearest 0.5°C.

As has been mentioned previously the experiment requires a comparison of the transition data generated in two ways, viz. that of a single scan rate and that found from extrapolation which involved fitting the logarithms of the T_g values obtained from each set of four scan rates to a first order equation. The basis for this procedure is given elsewhere⁵.

Thermal treatment

The thermal treatment consisted of heating the polystyrene in an open d.s.c. pan until the sample flowed, i.e. from 30° to 200°C at 8°C/min scan rate followed immediately by cooling to 30°C at 2°C/min scan rate. After treatment, the lid was crimped on to the pan. Wunderlich and Bodily⁸ have shown that this type of treatment gives a clear transition upon reheating the sample at a fast scan rate.

Cycling

This was investigated by determining the T_g of the same sample at each of the four scan rates employed and comparing these values with those found when using a fresh sample for each scan rate. Details of these treatments are given below.

(i) The same sample was heated successively to 140°C at 64°C/min, cooled at 16°C/min; to 140°C at 32°C/min, cooled at 8°C/min; to 140°C at 16°C/min, cooled at 4°C/min and finally heated to 140°C at 8°C/min, the T_g being determined during heating at each scan rate. This method is referred to as 'cycling' and samples A, C, 1 and 3 (Table 1) were treated in this manner.

(ii) A fresh sample was used for each of the heating scans at 64°, 32°, 16° and 8°C/min. This treatment is termed 'uncycled' and samples B, D, 2 and 4 (Table 1) were so handled.

Data analysis

Variance ratio and Student's 't' tests were used as appropriate and normally applied at the 5% level of significance.

RESULTS AND DISCUSSION

Effect of extrapolation

The variance calculated from T_i and T_s replications at both the 8°C/min scan rate and the extrapolated zero scan rate are given in Table 2. It can be seen that the 8°C/min results have lower variances in 15 out of the 16 cases given; the probability that this result occurs by chance is 0.24×10^{-3} and it can be concluded that the extrapolation procedure increased the variance obtained. Consequent to this observation the remaining analyses of this work consider only the transition data from the 8°C/min scan rate measurements.

Effect of data abstraction method

Both the T_i and T_s methods of evaluation must produce errors. In order to define the lower intersection point (T_i), tangents to two slopes must be constructed. The errors involved here will be partly dependent upon the gradient of these tangents. To define the inflection point (T_s), the tangent to the transition step must be constructed, the upper and lower points of deviation of the trace from this tangent must be defined and the mid-point between these two determined. It is probable that the errors produced using this method are self-compensating i.e. referring to Figure 1, the errors associated with fixing point A are likely to be similar but in the opposite direction to those involved in fixing point B. It could be anticipated therefore that T_s definition should be more reliable than T_i definition.

Table 2 shows the variance in the replicate measurements calculated for the 8°C/min scan rate using the two graphical methods of determining the transition point. Apart from a single case, no significant differences in variance at the 5% level could be detected between results of each method. Examination at the 20% level of significance however suggests that the intersection (T_i) method may give the better reproducibility. As a result of this observation the T_i method only was adopted for the remainder of this study. It must be emphasized however, that very little difference, if any, exists between the reproducibility of the two methods of data abstraction; a choice has been made only on the grounds of expediency.

A subsidiary experiment where T_i and T_s were determined repeatedly from two different d.s.c. traces showed that T_s was fixed more reproducibly than T_i when temperatures were read to 0.5°C. This finding apparently contradicts the observation from the main experiment where T_i variability is stated to be possibly somewhat less than T_s variability. No contradiction, however, does exist as the variances determined in the main experiment include contributions from sources of error other than those of graphically fixing the T_i or T_s points. It is possible therefore

Table 2 Comparison of variances of means of results from 8°C/min scan rate with those extrapolated to 0°C/min by taking logarithms of T_g

Scan Rate (°C/min)	Data abstraction method	Variance							
		Granules				Sheet			
		A	B	C	D	1	2	3	4
8	Intersection	0.48	0.45	0.95	0.87	0.10	0.70	0.20	2.65
0	Intersection	3.55	1.04	1.45	1.27	3.55	0.75	0.37	5.75
8	Inflection	0.65	0.53	0.36	0.97	0.22	0.57	2.03	5.65
0	Inflection	2.40	3.85	0.75	1.55	0.19	1.45	4.45	7.27

that T_g is more precisely fixed than T_i for a given trace but that overall reproducibility is favoured by using T_i .

Effect of the major variables

Changes in thermal properties are produced on heating and cooling polymeric materials⁴. These are explained by both the free volume and molecular relaxation theories on the basis of molecular configurational changes. All polymer samples handled in this experiment have been subjected at some stage to heating and cooling. It has been reported⁹ that changes in the T_g of polystyrene can be produced by varying the cooling rate of the polymer from the molten condition. Also according to Wunderlich¹⁰ it is only the molten state of linear high polymers that is independent of thermal history. Although Shen and Eisenberg¹¹, in their review of glass transitions in polymers, remark that the effect of thermal history upon T_g is not well characterized, it can reasonably be assumed that differences in heating and cooling rates could lead to differences in the reproducibility of T_g data.

In the case of sample form, differences in reproducibility additionally may arise from differences in sample geometry. A thin disc of sample gives good resolution in the d.s.c. because of the maximization of heat transfer between the sample pan and the sample and this results in more straightforward interpretation of the d.s.c. trace. With a granular material good heat transfer exists only at and near point contacts with the sample pan and unless the granules are extremely fine, the quality of the trace may suffer.

From the above considerations it was expected that the reproducibility of results would be affected by the treatments the polymer received in this work. The effects of the major variables were investigated by calculating and comparing the variances associated with the major variables themselves and also their various interactions. This is shown in Table 3 where F_1 and F_2 represent the two levels of sample form considered i.e. granules and sheet, Th_1 and Th_2 represent thermally untreated and treated samples respectively and C_1 and C_2 represent uncycled and cycled samples respectively.

Considering first the effect of sample form (i.e. F_1

Table 3 The effect of the major variables

Results pooled		Sample condition		Variance			Degrees of freedom		5% level of significance	Ratio significant
Sample name		F_1	F_2	F_1	F_2	Variance ratio	F_1	F_2		
ABCD	1234	$Th_1Th_2C_1C_2$	$Th_1Th_2C_1C_2$	0.93	1.11	1.19	23	23	2.0	No
AB	12	$Th_1C_1C_2$	$Th_1C_1C_2$	0.84	0.98	1.17	11	11	2.8	No
CD	34	$Th_2C_1C_2$	$Th_2C_1C_2$	0.83	1.34	1.61	11	11	2.8	No
BD	24	$Th_1Th_2C_1$	$Th_1Th_2C_1$	0.61	1.75	2.88	11	11	2.8	Yes
AC	13	$Th_1Th_2C_2$	$Th_1Th_2C_2$	1.07	0.41	2.60	11	11	2.8	No
B	2	Th_1C_1	Th_1C_1	0.45	0.71	1.57	5	5	5.1	No
D	4	Th_2C_1	Th_2C_1	0.87	2.66	3.07	5	5	5.1	No
A	1	Th_1C_2	Th_1C_2	0.48	0.10	4.80	5	5	5.1	No
C	3	Th_2C_2	Th_2C_2	0.96	0.20	4.80	5	5	5.1	No

Results pooled		Sample condition		Variance			Degrees of freedom		5% level of significance	Ratio significant
Sample name		Th_1	Th_2	Th_1	Th_2	Variance ratio	Th_1	Th_2		
AB12	CD34	$C_1C_2F_1F_2$	$C_1C_2F_1F_2$	0.89	1.08	1.21	23	23	2.0	No
B2	D4	$C_1F_1F_2$	$C_1F_1F_2$	0.57	1.72	3.03	11	11	2.8	Yes
A1	C3	$C_2F_1F_2$	$C_2F_1F_2$	0.27	0.52	1.97	11	11	2.8	No
AB	CD	$C_1C_2F_1$	$C_1C_2F_1$	0.84	0.83	1.01	11	11	2.8	No
12	34	$C_1C_2F_2$	$C_1C_2F_2$	0.98	1.34	1.37	11	11	2.8	No
B	D	C_1F_1	C_1F_1	0.45	0.86	1.91	5	5	5.1	No
A	C	C_2F_1	C_2F_1	0.48	0.96	2.00	5	5	5.1	No
2	4	C_1F_2	C_1F_2	0.71	2.66	3.75	5	5	5.1	No
1	3	C_2F_2	C_2F_2	0.10	0.20	2.00	5	5	5.1	No

Results pooled		Sample condition		Variance			Degrees of freedom		5% level of significance	Ratio significant
Sample name		C_1	C_2	C_1	C_2	Variance ratio	C_1	C_2		
BD24	AC13	$F_1F_2Th_1Th_2$	$F_1F_2Th_1Th_2$	1.13	0.71	1.60	23	23	2.0	No
BD	AC	$F_1Th_1Th_2$	$F_1Th_1Th_2$	0.61	1.07	1.76	11	11	2.8	No
24	13	$F_2Th_1Th_2$	$F_2Th_1Th_2$	1.75	0.41	4.26	11	11	2.8	Yes
B2	A1	$F_1F_2Th_1$	$F_1F_2Th_1$	0.57	0.27	2.14	11	11	2.8	No
D4	C3	$F_1F_2Th_2$	$F_1F_2Th_2$	1.72	0.52	3.30	11	11	2.8	Yes
B	A	F_1Th_1	F_1Th_1	0.45	0.48	1.07	5	5	5.1	No
D	C	F_1Th_2	F_1Th_2	0.86	0.96	1.12	5	5	5.1	No
2	1	F_2Th_1	F_2Th_1	0.71	0.10	7.10	5	5	5.1	Yes
4	3	F_2Th_2	F_2Th_2	2.66	0.20	13.30	5	5	5.1	Yes

versus F_2), the first row of Table 3 gives the variances of the results pooled over the two levels of both the remaining major variables; the next four rows give the variances of the results pooled over the two levels of one of the remaining variables with one level of the other variable, each being considered in turn. The final four rows represent the separate variances for the individual sets of replicates.

The same treatment was given to each of the major variables in turn to complete the array of Table 3.

Those pairs of conditions which display a significant difference at the 5% level can be identified from the Table and the conditions associated with the larger variance in each of these pairs may therefore be taken as those which should be avoided when minimum variance in the data is being sought. These particular conditions are:

- $F_2Th_2C_1$ uncycled, thermally treated sheet,
- $F_2Th_1C_1$ uncycled, thermally untreated sheet,
- $F_2Th_1Th_2C_1$ uncycled sheet,
- and $F_1F_2Th_2C_1$ uncycled, thermally treated material.

Table 3 also shows variance ratios which are suspiciously large indicating that the following conditions possibly should not be used:

- $F_1Th_1Th_2C_2$, $F_1Th_1C_2$ and $F_1Th_2C_2$ (i.e. cycled granules).

The condition $F_2Th_1Th_2C_1$ appears with both of its components $F_2Th_1C_1$ and $F_2Th_2C_1$ and it is clear that uncycled sheet must never be used. It follows therefore from the experimental design that if sheet is used it must be cycled. The position with $F_1F_2Th_2C_1$ however is less clear as only $F_2Th_2C_1$ appears as a separately identified, undesirable component. Since the other component $F_1Th_2C_1$ does not appear as undesirable the use of uncycled, thermally treated granules cannot be excluded on this evidence.

The above treatment of the data merely shows which conditions should not be employed when the best reproducibility of T_g data is being considered. To determine the most favourable experimental conditions a comparison of the lowest values of the variances displayed in Table 3 should be made. This is carried out in the next section.

Minimum variance conditions

By taking the minimum variance shown in Table 3 and comparing it with all the other variances of the array in turn, it may be seen that only five other sets of conditions show a variance ratio which is not significantly different at the

5% level. These are $F_2Th_1Th_2C_2$, $F_1Th_1C_1$, $F_1F_2Th_1C_2$, $F_1Th_1C_2$, $F_2Th_2C_2$, the minimum variance condition being $F_2Th_1C_2$. Using the variance ratio test it is not possible to discriminate further between these six sets of conditions to isolate the one providing the best reproducibility.

It is observed that the condition $F_1Th_1C_2$ appears as both a minimum variance condition and, from above, as one which should possibly be avoided. This apparent contradiction is due to the fact that $F_1Th_1C_2$ possesses a variance which is only suspiciously large when compared with the minimum variance of the array but which is nevertheless a low variance in absolute terms. In fact the variances of all the conditions examined apart from those associated with cycled sheet show up as suspiciously large or significant at the 5% level due to the low variances of the cycled sheet samples.

Preferred experimental conditions

Additional information, which can aid in the choice of experimental procedure, was obtained by a statistical examination of the actual mean values given in Table 4. It was found that the means of samples A ($F_1Th_1C_2$) and 1 ($F_2Th_1C_2$) are significantly different at the 5% level from the remaining means of the array. These particular sets of conditions which lead to anomalous mean values are therefore excluded from those leading to minimum variance. Since experimental simplicity in addition to experimental reliability is desirable, the conditions $F_2Th_2C_2$, $F_2Th_1Th_2C_2$ and $F_1F_2Th_1C_2$ can be eliminated as experimentally complex. Thus the favoured experimental condition giving rise to the best reproducibility is suggested as $F_1Th_1C_1$ i.e. the simple case of uncycled, thermally untreated granules.

It should be noted that elimination of the two anomalous mean values (samples A and 1) does not greatly influence the grand mean value for the whole array. The grand mean for the T_g of PS2 at 8°C/min scan rate using the intersection method of trace interpretation is 102.3°C; exclusion of the two anomalous means shifts this mean value up to 102.6°C.

CONCLUSIONS

None of the major variables of sample form, thermal treatment or thermal cycling of themselves produced a significant difference at the 5% level in the reproducibility of the T_g data. Certain interactions between these variables however are evident and the following conclusions can be drawn from the study.

Table 4 Corrected glass transition data at 8°C/min scan rate, found from the intersection method

Group	Transition temperature (°C)						Mean
	1	2	3	4	5	6	
Sample							
A	102.0	101.5	100.5	102.0	100.5	101.5	101.33
B	102.0	102.0	102.0	103.0	103.0	103.5	102.58
C	101.0	103.5	103.5	102.0	102.5	103.0	102.58
D	103.5	101.5	102.0	103.0	102.5	104.0	102.75
1	101.5	101.5	102.0	101.5	101.5	101.0	101.50
2	103.0	102.5	102.0	103.0	103.0	104.5	103.00
3	102.0	102.0	103.0	102.5	103.0	102.5	102.50
4	99.5	101.5	101.5	102.5	103.5	104.0	102.08
							Grand mean = 102.29

(a) The sheet samples used in the experiment are sensitive to cycling but not to the thermal treatment. It is clear that thermally cycling the sheet samples gives an enhanced reproducibility to the results.

(b) The granules used in the study are not sensitive to cycling or the thermal treatment.

(c) The best reproducibility is associated with an $8^\circ\text{C}/\text{min}$ scan rate as opposed to an extrapolated zero scan rate.

(d) Trace interpretation by the intersection method is preferred.

(e) For experimental convenience uncycled, thermally untreated granules can be used without increasing the variability of the results.

ACKNOWLEDGEMENTS

The authors are grateful to Mr R. H. Norman for his advice on statistics and to Mr C. D. Price for all the experimental work.

REFERENCES

- 1 Watson, E. S. *et al. Anal. Chem.* 1964, **36**, 1233
- 2 Thomson, M. D. *RAPRA Bulletin* September 1972
- 3 Pezzin, G. *et al. Eur. Polym. J.* 1970, **6**, 1053
- 4 Ali, M. S. and Sheldon, R. P. *J. Appl. Polym. Sci.* 1970, **14**, 2619
- 5 Strella, S. *J. Appl. Polym. Sci.* 1963, **7**, 569
- 6 Strella, S. and Erhardt, P. F. *J. Appl. Polym. Sci.* 1969, **13**, 1373
- 7 Lambert, A. *Polymer* 1969, **10**, 319
- 8 Wunderlich, B. and Bodily, D. M. *J. Polym. Sci. (C)* 1964, **6**, 137
- 9 Ichihara, S. *et al. Polym. J.* 1971, **2**, 644
- 10 Wunderlich, B. *J. Thermal Anal.* 1973, **5**, 117
- 11 Shen, M. C. and Eisenberg, A. *Rubber Chem. Technol.* 1970, **43**, 95
- 12 Cassels, B. *Pittsburgh Conf. Anal. Chem. Cleveland, Ohio* March 1974
- 13 Illers, K. H. *Macromol. Chem.* 1969, **127**, 1

APPENDIX

Although the analysis of d.s.c. trace shape was not one of the objectives of this experiment, it was observed that some of the traces showed endothermal peaks superimposed upon the high temperature side of the transition step. The appearance of such peaks has been observed in polystyrene^{4,12} and in PVC where Illers¹³ has presented an

extensive discussion of the phenomenon. Insufficient information is available from our work to allow a critical comparison of our observations with those from Illers' carefully controlled experiments which were specifically designed to study this particular effect. However some of our experimental observations are in agreement with those of Illers and in addition it is probable that some form of correlation exists between the appearance of endothermal peaks and the thermal treatment of PS2. Large peaks appeared on the d.s.c. traces of almost all the granular and moulded sheet samples which had not been thermally conditioned. Cycled and thermally treated samples showed a reduction in both the size and the frequency of occurrence of these endothermal peaks.

It is recognized that the fixing of the mid-point of the T_g step (T_g) will be influenced by the presence of such peaks, with a consequent effect upon the accuracy and precision of the measurement.

As is usually the case in an experiment of this nature, several interesting phenomena have been observed in the course of the study which fall outside the scope of the narrow objectives of the work and which cannot be explained adequately because of the experiment design.

These can be summed up in the questions of why does cycling have such a marked effect upon the reproducibility of results from sheet materials but not upon the reproducibility of results from granules and why does the thermal treatment, which causes melting and flow in both sheet and granules, have no significant effect upon the reproducibility of data? All the materials used in the study have a thermal history whether it has been imposed by the polymerization or moulding stages or by the thermal conditions of the experiment and yet only in certain instances do the differences in thermal history show up as differences in the reproducibility of data.

These observations suggest that the thermal history of the polystyrene samples used is unimportant apart from the single case where sheet is cycled. The only difference between the cycled sheet and cycled granular samples is that the sheet material has been held under pressure in a mould while in the molten state and during cooling.

One is led therefore to the conclusion that the thermal treatment of the experiment maintains but does not improve the reproducibility of the data but that samples which have been melted and cooled once under pressure in some way become more homogeneous when cycled to above T_g but below the polymer melting temperature. Further studies into this specific area are required in order to confirm and explain this particular observation.

Structure-property relationships in amorphous polyamides

John G. Dolden

British Petroleum Co. Ltd, Great Burgh, Epsom, Surrey, UK

(Received 16 May 1974; revised 20 May 1976)

New methods are put forward to explain the numerical values of some useful bulk physical properties of amorphous copolyamides, in terms of parameters related to monomer structure. Polyamides based on adipic, tetramethylsuberic, iso- and tere-phthalic acids, and diamines including isophorone, xylylene, cyclohexane, hexamethylene and its trimethyl derivatives, methylnonane and dodecamethylene diamines were studied. ϵ -Caprolactam and 12-aminododecanoic acid were also used as comonomers. In Part I, an empirical rule is proposed, based on experimental observations which predicts whether a copolyamide has an amorphous or crystalline character. The rule is based on the individual stereochemical contributions of the constituent monomers to the overall polymer chain structure. A relationship between Vicat softening point and monomer composition is derived from experimental data, which seems to be generally applicable to all amorphous polyamides of the diacid/diamine type. Each monomer makes a molar contribution which has been determined experimentally for all the materials studied. An arbitrary set of simple structural rules has been devised which enables the molar contributions of monomers to be related to their chemical structure. This procedure provided a method of predicting the contributions of other monomers for which molar constants had not been measured, and was successfully tested for a limited number of materials. A modified relationship was obtained experimentally to explain the effect of amino-acids on Vicat softening point.

In Part II, the relationships outlined in Part I are combined on the basis of experimental evidence to provide an empirical relationship between composition and impact strength. This relationship predicted the impact strengths of the majority of eighty copolyamides, of widely different chemical structure, with a reasonably good accuracy. Substantial inaccuracy occurred only when a large proportion of a long chain aliphatic monomer was present in the polyamide. Tentative correlations between tensile strength and carbon chain length were observed from a limited number of measurements which suggests that tensile strength may be a constitutive property. The main conclusions of this work are: (a) polyamides are naturally crystalline with high melting points if more than 80% of the monomer units are symmetrical; (b) Vicat softening point and tensile strength decrease linearly with increasing monomer chain length; the softening point is particularly affected by the presence of substituent groups; (c) amino-acids reduce symmetry, impact strength and Vicat softening points of copolyamides; (d) Charpy impact strength increases with the proportion of symmetric monomer units, the rigidity of the acid and flexibility of the diamine structures; (e) tensile strength and flexural modulus correlate with each other in copolyamides of diacids and diamines and both increase as the amount and chain length of aliphatic monomer is reduced; (f) by using the empirical relationships developed in this work, it has proved possible to formulate amorphous polyamides with outstanding combinations of physical properties, when compared with commercially available polymers.

PART I: AMORPHOUS STATE AND VICAT SOFTENING POINT

INTRODUCTION

Polyamides containing aromatic residues are normally very high melting, practically insoluble crystalline materials which are difficult to process. In recent years, a number of more easily processed amorphous polyamides, based on iso- and tere-phthalic acids have been claimed in the patent literature¹⁻¹⁰. Dynamit Nobel market an amorphous polyterephthalamide (Trogamid T) which is suitable for injection moulding¹¹. In general, amorphous polyamides can possess a wide range of good mechanical properties including high tensile and impact strength and high specific modulus which are desirable for engineering applications.

The stereochemistry and the rigidity of the constituent monomer structures will not only determine the bulk physical and mechanical properties of the polyamide, but also

whether it is crystalline or amorphous. There is little published information on the relationship between chemical structure and bulk physical properties of polyamides. Gabler *et al.*¹² reported the effect of using different alkyl substituted hexamethylenediamines on the melting point and physical state of corresponding polyterephthalamides. Ridgeway¹³ showed that incorporating a minimum of 20% of the asymmetric phenylindane dicarboxylic acid into nylon-6,6 rendered the polymer amorphous. Weyland *et al.*¹⁴ discussed a method for predicting the T_g of polymers including some polyamides.

In order to determine the quantitative relationships between chemical composition and bulk physical properties of polyamides, a large number of copolyamides containing from two to five monomers were prepared by melt conden-

sation. The monomers selected for study were chosen principally on the basis of availability, and with the exception of ϵ -caprolactam and 12-aminododecanoic acid, were diacids or diamines. A number of bulk physical properties, including Vicat softening point, tensile strength and notched Charpy impact strength were determined for each polymer. Polyamides were produced to a high molecular weight ($M_n > 20\,000$) in order to minimize the effect of molecular weight on bulk properties. Molecular weight was screened by measuring the inherent viscosity of the polyamides in concentrated sulphuric acid at 25°C. Physical properties were normally measured on polymers with values of $[\eta]_I \geq 0.1 \text{ m}^3/\text{kg}$, as this value corresponded to $M_n \sim 20\,000$ in a few test cases. It was impractical to measure the $[\eta]_I$ versus M_n relationship in every case.

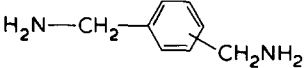
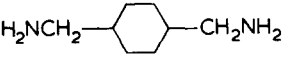
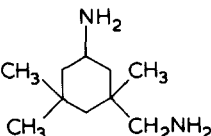
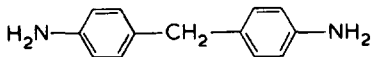
Primary data for about 130 copolyamides are set out in Tables 1–5. Each Table contains a set of polymers with a common acid present.

EXPERIMENTAL

Monomers

All the monomers used in the preparation of polyamides were obtained from commercial sources, with the exception of 12-aminododecanoic acid, 5-methylnonanediamine and 2,2,7,7-tetramethylsuberic acid, which were synthesised in the laboratory.

Abbreviations of monomers studied

PDA	1,3-diaminopropane,
BDA	1,4-diaminobutane,
2-MePMD	2-methylpentanediamine,
3-EtHMD	3-ethylhexamethylenediamine,
3-MeHMD	3-methylhexamethylenediamine,
2,5-DMeHMD	2,5-dimethylhexamethylenediamine,
2,2,4-TMeHMD	2,2,4-trimethylhexamethylenediamine,
2,4,4-TMeHMD	2,4,4-trimethylhexamethylenediamine,
5-MeNDA	5-methylnonanediamine,
DMD	dodecamethylenediamine,
HMD	hexamethylenediamine,
MXD	<i>m</i> -xylylenediamine,
MPXD	<i>m</i> - and <i>p</i> -xylylenediamine,
	
DACH	<i>cis</i> or <i>trans</i> -diaminomethyl cyclohexane,
	
IPD	isophoronediamine,
	
DAPM	4,4'-diaminodiphenylmethane,
	
AA	adipic acid,
2,2,4-TMeAA	2,2,4-trimethyladipic acid,
2,2,7,7-TMeSA	2,2,7,7-tetramethylsuberic acid,
AZA	azelaic acid,
SA	sebacic acid,
DDA	dodecanedioic acid,

12-ADA	12-aminododecanoic acid,
TPA	terephthalic acid,
IPA	isophthalic acid,
CAP	caprolactam,
PIDA	1,1,3-trimethyl-5-carboxy-3-(<i>p</i> -carboxyphenyl) indane.

Polycondensation

Nylon salts were used as the starting material for the preparation of polyamides. These salts were prepared by dissolving equimolar concentrations of diacid and diamine in water at 60°–95°C, precipitating with isopropanol at ambient temperature and drying overnight under vacuum.

Polymerization was carried out in a 250 cm³ round bottomed flask fitted with a vertical fractionating column, water-cooled condenser and receiver. 0.2 g-mol of salts containing 1% w/w ammonium hypophosphite (reaction catalyst and colour stabilizer), 10 ml water and optionally 0–1.0 mol % benzoic acid to control molecular weight, were charged to the reaction flask. The charge was stirred with a stainless steel rod and heated to a temperature of 270°–300°C under nitrogen over a period of 2 h. Diamine loss was minimized by retaining the fractionating column for a further 2 h at the reaction temperature. The final traces of water of condensation were then removed by venting the flask to the atmosphere for a further hour. The molten polyamide was allowed to cool and recovered by breaking the flask.

This procedure was modified for the preparation of polyterephthalamides, which were difficult to polymerize to a high molecular weight. A precondensation step was introduced, in which the terephthalic acid salts were held under reflux at 220°C for up to 2 h before raising the temperature to 270°–300°C. A small excess (≤ 1 mol %) of diamine was sometimes added to the reaction flask. This method produced polyterephthalamides of very high molecular weight.

Polymer test methods

Test specimens were compression moulded at 220°C using a cycle of 4 min at 0 ton followed by 4 min at 20 ton applied to the 4 in press ram.

Vicat softening point was measured in accordance with BS 2782 1965 Method 102B (Part I), using moulded discs 12.7 mm in diameter and 3.2 mm thick.

Impact strength was measured by the Hounsfield Charpy method at 20°C using compression moulded bars 41.4 mm by 3.8 mm, which were notched after moulding (notched radius = 0.94 mm, notch depth = 0.56 mm). The average value obtained from testing six specimens was taken as the impact strength of the polymer.

Tensile strength was measured at 20°C according to BS 2782, method 301C on an Instron tensile machine at a crosshead speed of 20 mm/min. Dumb-bell specimens 53.4 mm long and between 0.51 and 1.27 mm thick (the actual thickness being recorded) with a control width of 5.39 mm were used in the test. The average value obtained from testing six specimens was taken as the tensile strength of the polymer.

Flexural modulus was measured in accordance with ASTM 790 at 20°C using 6 cm by 1 cm by 0.47 cm specimens with 5 cm between supports and the beam centrally loaded at a rate of 0.127 cm/min.

The following method was used to measure inherent viscosity: ~ 0.04 g of polymer was dissolved in 25 ml of

Table 1 Polyadipamides and polydodecamides

Polymer no.	Composition (mol %)									Physical property				
	AA	DDA	IPA	TPA	HMD	TMe-HMD	IPD	MPXD	DMD	Inherent viscosity (m ³ /Kg)	Vicat soft. pt (°C)	Impact strength (kJ/m ²)	Tensile strength (MN/m ²)	Flexural modulus (MN/m ²)
I	50						50			0.165	167	7	77.5	
II	37.5		12.5				50			0.104	179	8		
III	37.5			12.5			50			0.105	184	9		
IV	50						15	35		0.088	127	9		
V	37.5			12.5			25	25		0.123	143	12		
VI	50				17		33			0.095	134	13	94	2580
VII	50				25		25					17		
VIII	50				42.5		7.5			0.155	230	29	69.5	2890
IX	20		30		25		25			0.144	134	19		
X	25			25	25		25			0.156		34	97.0	
XI	40			10			50						93	
XII		50					50				122	4		
XIII		50			25		25			0.120	74	10		
XIV		35		15			50			0.105	139	18		
XV		20	30		42.5			7.5		0.096	96	26		
XVI		10	40				30		20	0.098	152	27		
XVII		20	10	20	30				20			23		
XVIII		10	40						50	0.108	142	13		
XIX		6	24	20	42.5		7.5			0.096	135	37		
XX		4	30	16	42.5		7.5			0.110	139	36		
XXI		8	30	12	42.5		7.5			0.117	126			
XXII		12	30	8	42.5		7.5			0.093	115	32		
XXIII		16	30	4	42.5		7.5			0.112	107	29		
XXIV		20	30		42.5		7.5			0.096	96	26		
XXV		10	24	16	42.5		7.5			0.103	122	35		
XXVI		20	18	12	42.5		7.5			0.130	100	30		
XXVII		30	12	8	42.5		7.5			0.189		28		
XXVIII		40	6	4	42.5		7.5			0.133		25		
XXIX		50			42.5		7.5			0.113	191	17		
XXX		12	18	20	42.5		7.5			0.087	153			
XXXI		18	12	20	42.5		7.5			0.103	184	25		
XXXII		24	6	20	42.5		7.5			0.104	179	20		
XXXIII		30		20	42.5		7.5				200	34		

Table 2 Copolyamides of caprolactam and 12-aminododecanoic acid

Polymer no.	Composition (mol %)									Physical property				
	Cap	12-ADA	IPA	TPA	HMD	DMD	TMe-HMD	IPD	MPXD	Inherent viscosity (m ³ /Kg)	Vicat soft. pt (°C)	Impact strength (kJ/m ²)	Tensile strength (MN/m ²)	Flexural modulus (MN/m ²)
XXXIX	20			40		20		20		0.155	147	48		
XL	28.4		17.9	17.9	17.9			17.9			144			
XLI	10			45			45				140	55	88.5	2980
XLII	10			45		15.5	18	11.5				68	72.6	1880
XLIII	10			45			35	10			158	36	88.5	2800
XLIV	33.3		6.7	26.6				33.3			178	14		
XLV	42.8			28.6					28.6				91.5	
XLVI	50			25				25					87.5	
XLVII	60				20				20				84	
XLVIII	60			20					20			7	91.5	
XLIX	66.7			16.7				16.7					78	
L	100 (quenched to amorphous state)												47	
LI	50	50											58	
LII	66.7	33.3											50	
LIII		11.1	31.1	13.3				44.4		0.118	211	57		
LIV		17.7	24.7	16.5				41.2		0.068	193			
LV		30	24.5	10.5				35		0.102	155	19		
LVI		43	20	8.6				28.5		0.125	116	24		
LVII		66.4	11.8	5				16.8		0.092	74	23		
LIX		30		35				35				26		
LX		17.7	24.7	16.5	35			6.2				38		
LXI		54	13.8	9.2	19.5			3.4				21		
LXII		10	27	18	39.3			5.7		0.177		39	79	2120
LXIII		20	20	20					40		133	7	67.5	2980

Table 3 Polyisophthalamides

Polymer no.	Composition (mol %)								Physical property				
	IPA	TPA	HMD	DMD	TMe-HMD	IPD	MPXD	5-Me-NDA	Inherent viscosity (m ³ /Kg)	Vicat soft. pt (°C)	Impact strength (kJ/m ²)	Tensile strength (MN/m ²)	Flexural modulus (MN/m ²)
LXIV	50		50							143	38	86.5	
LXV	50							50	0.105	105	29		
LXVI	50		42.5			7.5			0.116	151	28	101	
LXVII	50		37.5			12.5			0.096	164	17	103	
LXVIII	50		25			25			0.124	192	17	111	
LXIX	50		30	10		10			0.139	146	34		
LXX	50		12.5	20		17.5			0.085	149	27		
LXXI	50					5		45	0.076	117	27		
LXXII	50		30				20		0.103	149	22	106	
LXXIII	30	20	17			33			0.109	217	10		3003
LXXIV	30	20	42.5			7.5			0.120	152	46	95	2600
LXXV	30	20	42.5				7.5		0.107	140	50	102	2500
LXXVI	50		40				10		0.098	137	30		
LXXVII	30	20	30				20		insoluble	151	45	106	
LXXVIII	30	20	37.5				12.5		0.195	143	41	98	
LXXIX	30	20	32.5				17.5		0.114	145	38		
LXXX	30	20	5		37.5		7.5		0.107	148	28		
LXXXI	30	20	32.5		10		7.5		0.099	140	26		
LXXXII	30	20		30		20			0.118	152	47	70	2140
LXXXIII	30	20		42.5		7.5			0.085	115	58		
LXXXIV	30	20	47.5			2.5			0.254	141	59		
LXXXV	30	20						50	0.107	107	46		
LXXXVI	30	20	30	10		10			0.136	151	58	82	2360
LXXXVII	30	20			50				0.152	146	17		
LXXXVIII	30	20	10		32.5		7.5		0.099	140	26		
LXXXIX	30	20	15	20		15			0.120	153	46		

Table 4 Polyterephthalamides

Polymer no.	Composition (mol %)							Physical property				
	TPA	HMD	DMD	TMe-HMD	IPD	MPXD	5-Me-NDA	Inherent viscosity (m ³ /Kg)	Vicat soft. pt (°C)	Impact strength (kJ/m ²)	Tensile strength (MN/m ²)	Flexural modulus (MN/m ²)
XC	50			50				0.136	155	68	81	2570
XCI	50						50	0.168	>200	131		
XCII	50		30		20			0.297	160	98	70	1920
XCIII	50		15	35					131	126	89	
XCIV	50				10		40	0.110	143	82		1990
XCV	50				5		45	0.122	125		64	1960
XCVI	50				16.5		33.5	0.081	158	54	73	
XCVII	50				20		30	0.112	166	55		
XCVIII	50			40		10		0.138	162	62	92	2520
XCIX	50	5		45					155	60	82	2470
C	50			42.5	7.5				171	50	89	2400
CI	50	10		32.5	7.5				171	65		
CII	50		10	32.5	7.5				160	80	77	2230
CIII	50		20	15	15				162	85		
CIV	50		25	10	15					77		
CV	50			40	10					50	90	
CVI	50		7.5	35	7.5				164	63	89	2390
CVII	50	10		32.5		7.5			156	69	91	2430
CIX	50	15		27.5		7.5			155	115		3010
CX	50	15		25		10			158	79		
CXI	50	10		30		10		insoluble	159	69	93	2550
CXII	50		5	37.5		7.5			151	70		
CXIII	50		10	25		15			157	68		
CXIV	50		10	30		10		0.155	148	90	82	2340
CXV	50		15	25		10			145	119		
CXVI	50		15	27.5		7.5			154	131	77	
CXVII	50		20	22.5		7.5			147	135		
CXVIII	50				50				245	<1		
CXIX	50		15	27.5	7.5			0.142	153	121	77	2230

Table 5 Miscellaneous polyamides

Polymer no.	Composition (mol %)														Physical property		
	AZA	2,2,7,7-TMeSA	SA	DDA	IPA	PDA	BDA	2-Me-PMD	HMD	TMe-HMD	5-Me-NDA	DAPM	IPD	cis-DACH	trans-DACH	Inherent viscosity (m ³ /kg)	Vicat soft. point (°C)
CXX	50									50						0.082	50
CXXI	50									50						0.01	51
CXXII		50							50							0.032	70
CXXIII			50										50				135
CXXIV				50		25							25			0.063	76
CXXV				50			25						25			0.071	74
CXXVI				50				35					15			0.095	54
CXXVII				50				35					15			0.060	56
CXXVIII				15	35							50				insoluble	185
CXXIX				50						35				15		0.115	49
CXXX				50						35				15			54
CXXXI				22.5	27.5					8.5				41.5		0.151	128
CXXXII				22.5	27.5					8.5					41.5	insoluble	133

Analar sulphuric acid, ($SG = 1.84$) overnight on a rotating shaker, and subsequently diluted to 0.15% w/v. Flow times were measured in BS 188/U Type D Ostwald viscometers suspended in a viscometer bath controlled at $25^\circ \pm 0.015^\circ\text{C}$. No correction was made for kinetic energy effects etc.

Inherent viscosity was determined from the equation:

$$[\eta]_I = \ln \frac{(t/t_0)}{c}$$

where c , is the concentration (g/100 ml); t , the solution flow time and t_0 is the solvent flow time.

The physical state of polyamides is described in the text as 'amorphous' if the polymer was transparent and possessed a relatively low softening point ($<200^\circ\text{C}$); 'crystalline' is used to describe white opaque polymers which were normally characterized by very high softening points ($>200^\circ\text{C}$). The transition from amorphous to crystalline state normally occurred over a narrow range of composition and was accompanied by a rapid loss of transparency and increase in softening point. It was outside the scope of this work to study these changes by X-ray techniques.

RELATIONSHIP BETWEEN STRUCTURE AND AMORPHOUS STATE IN POLYAMIDES

The objective of the following discussion set out below is to develop an empirical relationship based on experimental data, which will allow the amorphous or crystalline character of a polyamide to be determined on the basis of the individual stereochemical contribution of the constituent monomers to the overall polymer chain structure.

The various degrees of crystallinity found in polyamides prepared from aliphatic diacids and diamines, or ω -aminoacids, and the high melting points which characterize such materials, are the result of the ability of the linear chains to pack in a regular crystal lattice and of the hydrogen bonding which exists between interchain amide links. The inclusion in such materials of in-chain structural units which prevent the formation of crystalline regions within which regular chain packing can occur leads to formation of an amorphous material of generally much lower melting point.

The ability of individual monomers to inhibit crystallization in polyamides can be gauged from the data pre-

sented in Table 6 which has been compiled from published literature. The first two sections of Table 6 show that the structurally planar benzene ring can be accommodated within the polymer chain without interfering with the overall crystalline character of the polyamide formed, and the mono-methyl substitution of an in-chain carbon atom in a linear aliphatic monomer has likewise no effect on the general physical state of the polyamide. The last two sections of the same Table show, however, that the introduction of ethyl or higher substituents along a linear aliphatic chain, or the attachment of more than one methyl group to the same in-chain carbon member, prevents crystallization.

The ability of isophoronediamine to inhibit crystallization is immediately obvious from its structure. The ability of isophthalic acid to do so is less obvious, until it is recalled that the stereochemical configuration of the carbonyl groups adjacent to the benzene ring must introduce a point of inflection into the polymer chain, this being such as to prevent regular chain packing and hence crystallization.

It is interesting to compare the photographs of molecular models of isophthalic acid/hexamethylenediamine units and adipic acid/meta-xylylenediamine units shown in

Table 6 Effect of monomer symmetry upon the form of the solid state of homopolyamides

Polyamide	Asymmetric monomer	Physical state of the polyamides
AA/HMD	—	Crystalline
AA/PXD	—	
TPA/DMD	—	
TPA/2-MePMD	2-MeHMD	Crystalline
TPA/3-MeHMD	3-MeHMD	
TPA/5-MeNDA	5-MeNDA	
TPA/2,5-DMeHMD	2,5-DMeHMD	
(AA)TPA/MXD	MXD	
TPA/3-EtHMD	3-EtHMD	Amorphous
TPA/3-iPrHMD	3-iPrHMD	
TPA/2-Et-4-MeHMD	2-Et-4-MeHMD	
TPA/2,4,4-TMeHMD	2,4,4-TMeHMD	
TPA/IPD		
IPA/HMD(DMD)	IPA	Amorphous
2,4,4-TMeHMD	2,4,4-TMeAA	
2,2,7,7-TMeSA/HMD	2,2,7,7-TMeSA	
PIDA/AA/HMD	PIDA	

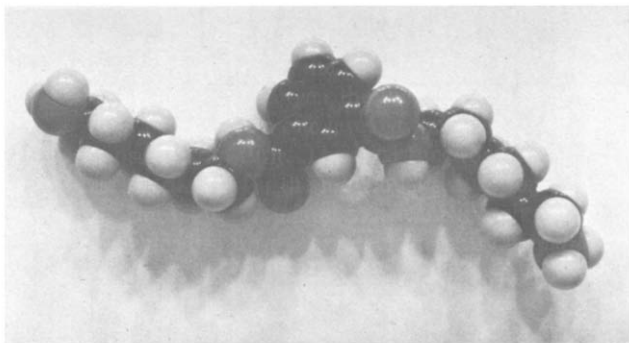


Figure 1 Molecular model of an isophthalic acid/hexamethylenediamine unit in a polyamide chain

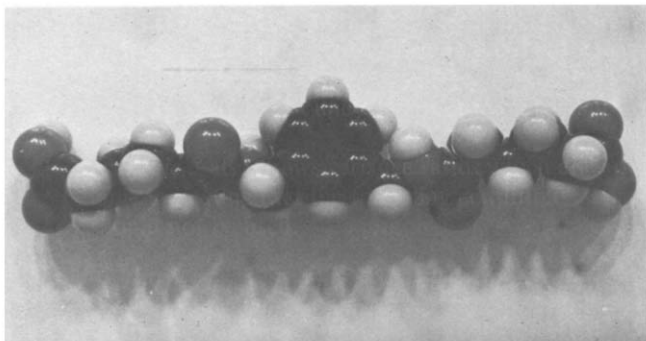


Figure 2 Molecular model of an adipic acid/meta-xylylenediamine unit in a polyamide chain

Figures 1 and 2. In the former case the point of inflection in the chain caused by the stereochemical configuration of isophthalic acid is clearly demonstrated and contrasts with the linear configuration preserved in the xylylenediamine linkages. In both cases, the benzene ring is asymmetrically positioned with respect to the main chain axis and must interfere with the ordered packing of layers within the polyamide crystalline regions. The additional point of inflection created in the linear polyamide chain by isophthalic acid must prevent the growth of ordered layers of crystallite and increase the amorphous character of the polyamide. Since monomers which prevent crystallization all possess some measure of stereochemical asymmetry, it will be convenient to refer to these as asymmetric monomers.

The minimum molar concentration of asymmetric monomers required to produce amorphous polyamides in a number of formulations studied in this work are listed in Table 7.

The number of formulations studied in this way was very limited. Nevertheless it was interesting to note that whereas only 20 mol % of isophoronediamine was required to render the formulations studied amorphous, 30 mol % of trimethylhexamethylenediamine or isophthalic acid were needed to accomplish the same effect, while monomers such as meta-xylylenediamine or 5-methylnonanediamine failed to give rise to amorphous materials at the limit set by their diamine function.

On the basis of this somewhat tentative observation, and a knowledge of the physical state, i.e. amorphous or crystalline, of the polymers listed in Table 6, it was decided to attempt a speculative classification of asymmetric monomers into three groups, and attach to this classification a summative numerical index based on type and molar concentration from which the physical state of the polyamide could be predicted. The following three groups of asymmetric monomers, AM, were distinguished,

Type AM1: Monomers whose presence alone, either as a diacid or diamine, do not seriously interfere with the linearity of the polyamide chain and hence do not affect the crystallinity of the polyamides, e.g. linear aliphatic diamine having one or more monomethyl substituted carbon atoms in the main chain—3-MeHMD, 2,5-DMeHMD etc. and MXD (Table 6).

Type AM2: Monomers whose presence alone, either as a diacid or diamine, would interfere stereochemically with the ability of the linear polyamide chains to pack in a crystalline manner e.g. linear aliphatic diacids or diamines having ethyl or higher substituents along the linear aliphatic chain, or the attachment of more than one methyl group to the same in-chain carbon member—3-EtHMD, 2,2,7,7-TMeSA and 2,4,4-TMeHMD (Table 6). Aromatic diacids also come within this group because of the stereochemical restriction imposed by the rigid benzene nucleus flanked by two carbonyl groups.

Type AM3: Monomers whose stereochemical configuration causes a gross distortion of the linear polyamide chain e.g. isophoronediamine and 1,1,3-trimethyl-5-carboxy-3-(*p*-carboxyphenyl) indane (PIDA). The latter at a concentration of 20 mol % prevents crystallization in nylon-6,6¹³.

The results already presented in Table 7 have shown that different amounts of each type of monomer are required to produce amorphous properties, and hence the transition point between the amorphous and crystalline state cannot be related to the simple sum of the molar concentrations of the so called asymmetric monomers. It was decided intuitively to sum the molar concentrations of the asymmetric monomers expressed in percentages according to the relationship:

$$\Sigma[\text{AM}] = [\text{AM1}] + 2[\text{AM2}] + 3[\text{AM3}] \quad (1)$$

A contribution from the asymmetric monomers of Type AM1 has been included here in order to allow for the possibility of an amorphous product being produced as the result of the combination of diacids and diamines of this type in the same polymer chain. The result of carrying out this procedure is shown in Table 8, from which it can be seen that polymers with a summed asymmetry value of less than 60 are crystalline, while materials with a higher molar asymmetry contribution are amorphous. Examples where the value given by equation (1) was used to predict the physical state of a polyamide before it had been prepared are indicated by an asterisk.

It is interesting to compare formulations 2 and 7 in Table 8. The former contains dodecamethylenediamine in

Table 7 Comparative values of asymmetric monomer concentration required to produce the amorphous state in polyamides

Polyamide formulation	Asymmetric monomer	Critical concentration to yield amorphous state (%)
TPA/DMD/IPD	IPD	20
AA/TPA/HMD/IPD	IPD	20
DDA/HMD/IPD	IPD	20
TPA/HMD/TMeHMD	TMeHMD	30
TPA/DMD/TMeHMD	TMeHMD	30
IPA/TPA/HMD	IPA	30
DDA/HMD/MXD	MXD	>50
TPA/5-MeNDA	5-MeNDA	>50

Table 8 Relationship between the asymmetry index and the amorphous-crystalline transition of polyamides

No.	Polyamide composition	Asymmetric monomer (mol %)			Asymmetry index, Z(AM)	Solid state
		Type AM1	Type AM2	Type AM3		
1	TPA/5-MeNDA AA/MXD	50			50	Crystalline
2	TPA/DMD/IPD			20 17.5	60 52.5	Transparent Crystalline
3	DDA/HMD/IPD			20 15	60 45	Semi-transparent Crystalline
4	*TPA/HMD/ TMeHMD		31.6 30		63.2 60	Transparent Crystalline
5	TPA/DMD/TMeHMD		35 30		70 60	Transparent Semi-transparent
6	†IPA/TPA/HMD		35 30		70 60	Transparent Crystalline
7	TPA/5-MeNDA/IPD	45 40		5	60 50	Transparent Crystalline
8	†IPA/TPA/HMD/ IPD		23 25	6 2.5	64 57.5	Transparent Crystalline
9	*†IPA/TPA/HMD/ MXD	7.5 10	30 25		67.5 60	Transparent Crystalline
10	*TPA/HMD/TMeHMD/ IPD		25 20	5 5	65 55	Transparent Crystalline
11	*TPA/DMD/TMeHMD/ IPD		22.5 17.5	7.5 7.5	67.5 57.5	Transparent Crystalline
12	DDA/IPA/TPA/HMD/ IPD		24 18	7.5 7.5	70.5 58.5	Transparent Crystalline
13	TMeSA/TPA/HMD		50 25		100 50	Transparent Crystalline

*Solid state predicted by equation (1); †IPA: TPA = 30:20

Table 9 Effect of monomer composition on the physical properties of polyamides

Composition (mol %)				Physical State	Vicat soft. pt (°C)
IPA	TPA	HMD	IPD		
50		40	10	Amorphous	155
40	10	40	10	Amorphous	156
30	20	40	10	Amorphous	159
20	30	40	10	Crystalline	219
20	30	35	15	Amorphous	172

combination with isophoronediamine, and the latter 5-methylnonanedi-amine in combination with isophoronediamine. The last mentioned only required the addition of 5 mol % isophoronediamine to render it amorphous, whereas the other material did not become amorphous till almost 20% isophoronediamine had been added. This would seem to indicate that monosubstituted monomers do make a finite contribution towards the amorphous state.

Insufficient data are available at the time of writing to extend this concept to polyamides containing caprolactam as a comonomer. Values of the asymmetry index have been calculated for about one hundred experimental polymers. These values have been transformed into the more convenient concept of a symmetry index (*SI*), which is defined by the relationship:

$$SI = 1 - \frac{\Sigma(AM)}{300}$$

From the former discussion, it is clear that we should expect a polymer with a symmetry index >0.80 to be crystalline. From the data presented in Table 11, this normally appears to be the case.

There is a simple rule for deciding to which group an asymmetric monomer should be assigned. If the monomer can interfere with chain packing by distortion in one direc-

Table 10 Vicat constants of monomers studied

Monomer	Vicat constant (°C/mol)
PDA	53
BDA	51
2-MePMD	53
HMD	40
2,2,4-TMeHMD	50
2,4,4-TMeHMD	50
5-MeNDA	15
DMD	0
MPXD	80
DACH	103
IPD	140
DAPM	125
AA	30
2,2,7,7-TMeSA	30
AZA	1
SA	-5
DDA	-20
TPA	105
IPA	90

Table 11

Polymer no.	Symmetry index	Physical state	Vicat soft. pt (°C)		Polymer no.	Symmetry index	Physical state	Vicat soft. pt (°C)	
			Measured	Predicted				Measured	Predicted
I	0.50	A	167	170	LXXII	0.60	A	149	146
II	0.42	A	179	185	LXXIII	0.47	A	217	203
III	0.50	A	184	189	LXIV	0.73	A	152	152
IV	0.73	A	127	128	LXXV	0.78	A	140	142
V	0.67	A	143	159	LXXVI	0.63	A	137	138
VI	0.67	A	134	136	LXXVII	0.73	A	151	152
VIII	0.93	C	230	80	LXXVIII	0.76	A	143	146
IX	0.55	A	134	156	LXXVIX	0.74	A	145	150
XII	0.50	A	122	120	LXXX	0.53	A	148	155
XIII	0.50	A	74	70	LXXXI	0.71	A	140	144
XIV	0.50	A	139	149	LXXXII	0.60	A	152	152
XV	0.74	A	96	96	LXXXIII	0.73	A	115	117
XVI	0.43	A	152	152	LXXXIV	0.77	A	141	141
XVIII	0.57	A	142	148	LXXXV	0.63	A	107	111
XIX	0.77	A	135	143	LXXXVI	0.70	A	151	148
XX	0.71	A	139	141	LXXXVII	0.47	A	146	146
XXI	0.71	A	126	131	LXXXVIII	0.56	A	140	149
XXII	0.71	A	115	121	LXXXIX	0.65	A	153	153
XXIII	0.71	A	107	111	XC	0.67	A	155	155
XXIV	0.71	A	96	101	XCI	0.83	C	>200	120
XXV	0.77	A	122	128	XCII	0.80	A	160	161
XXVI	0.81	A	100	105	XCIII	0.77	A	131	140
XXIX	0.93	C	191	35	XCIV	0.77	A	143	145
XXX	0.81	C	153	134	XCVI	0.80	A	125	133
XXXI	0.85	C	184	126	XCVII	0.70	A	166	170
XXXII	0.87	C	179	117	XCVIII	0.70	A	162	161
XXXIII	0.93	C	200	109	XCIX	0.70	A	155	154
XXXIX		A	147	147	C	0.63	A	171	169
XL		A	144	145	CI	0.71	A	171	167
XLI		A	140	143	CII	0.71	A	160	159
XLIII		A	158	161	CIII	0.75	A	162	162
XLIV		A	178	178	CVI	0.69	A	164	161
LIII		A	211	205	CVII	0.76	A	156	158
LIV		A	193	194	CIX	0.79	A	155	157
LV		A	155	164	CX	0.80	A	158	158
LVI		A	116	134	CXI	0.77	A	159	159
LVII		A	74	79	CXII	0.73	A	151	155
LXIII		A	133	155	CXIII	0.78	A	157	153
LXIV	0.67	A	143	130	CXIV	0.77	A	148	151
LXV	0.50	A	105	105	CXV	0.80	A	145	146
LXVI	0.59	A	151	143	CXVI	0.79	A	157	154
LXVII	0.54	A	164	169	CXVII	0.82	A	147	149
LXVIII	0.42	A	192	180	CXVIII	0.79	A	245	245
LXIX	0.57	A	146	142	CXXI	0.67	A	51	51
LXX	0.49	A	149	149	CXXVI	0.73	A	54	58
LXXI	0.47	A	117	118	CXXXI	0.76	A	128	134

A = amorphous; C = crystalline

tion only, either along the chain or at right angles to it, then it belong to Type AM1. If it can interfere with chain packing by causing distortion in two different directions at right angles to each other, irrespective of how it is rotated about the chain axis, then it belongs to Type AM2. Similarly if the stereochemical configuration of the monomer causes distortion in three different non-coplanar directions it must belong to Type AM3.

STRUCTURE-VICAT SOFTENING POINT RELATIONSHIP IN AMORPHOUS POLYAMIDES

Review of experimental data and derivation of molar constant concept

A linear relationship between Vicat softening point and composition for a series of amorphous copolyamides containing ϵ -caprolactam and six of the nine salts which can be prepared from adipic, terephthalic, and isophthalic acids with isophorone-, trimethylhexamethylene- and *m*-xylylene-

diamines is shown in *Figure 3* and demonstrates that the softening point decreases linearly as the proportion of ϵ -caprolactam in the copolyamides is raised. This dependence of softening point upon the caprolactam molar concentration can be described by the equation:

$$V = V_0(1 - \alpha m) \quad (2)$$

where V is the Vicat softening point of the copolyamide; V_0 , the Vicat softening point of the corresponding polyamide containing no caprolactam; m , the molar concentration of caprolactam and α is a constant.

Similar behaviour is observed for copolyamides containing 12-aminododecanoic acid (*Figure 4*).

A linear dependence of softening point upon molar composition has also been observed for multi-component copolyamides prepared from mixtures of diacids and diamines. This is shown graphically in *Figure 5* for the dodecanedioic acid/hexamethylenediamine/isophoronediamine system, in which the ratio of the two diamines is varied, and in

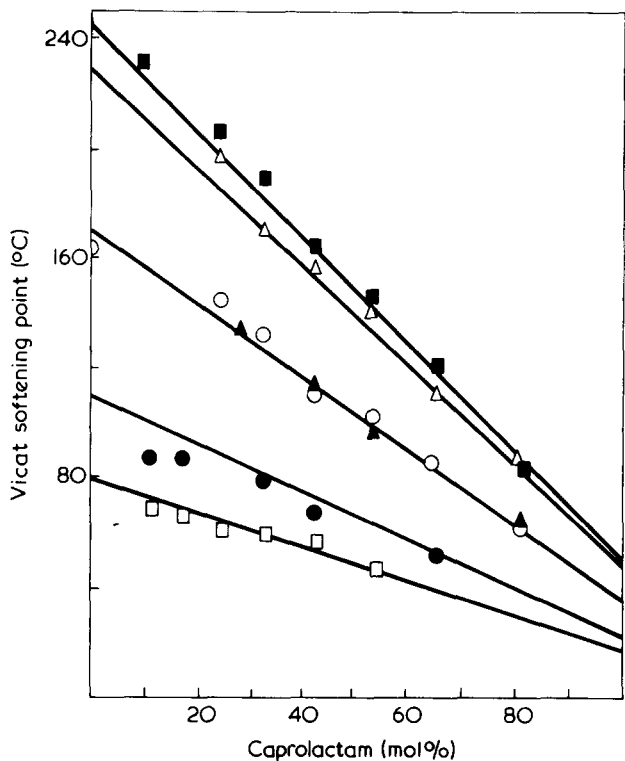


Figure 3 A comparison of Vicat softening point data measured for caprolactam copolymers with the calculated linear relationship $V = V_0 (1 - 0.8 [\text{CAP}])$. \circ , AA/IPD; \square , AA/TMeHMD; \bullet , AA/MXD; \triangle , IPA/IPD; \blacksquare , TPA/IPD; \blacktriangle , IPA/MXD

Figure 6 for the dodecanedioic acid/isophthalic acid/terephthalic acid/hexamethylenediamine/isophoronediamine system in which the ratio of dodecanedioic acid to terephthalic acid is varied.

A statistical analysis was carried out on the relationship between composition and physical properties of the iso-

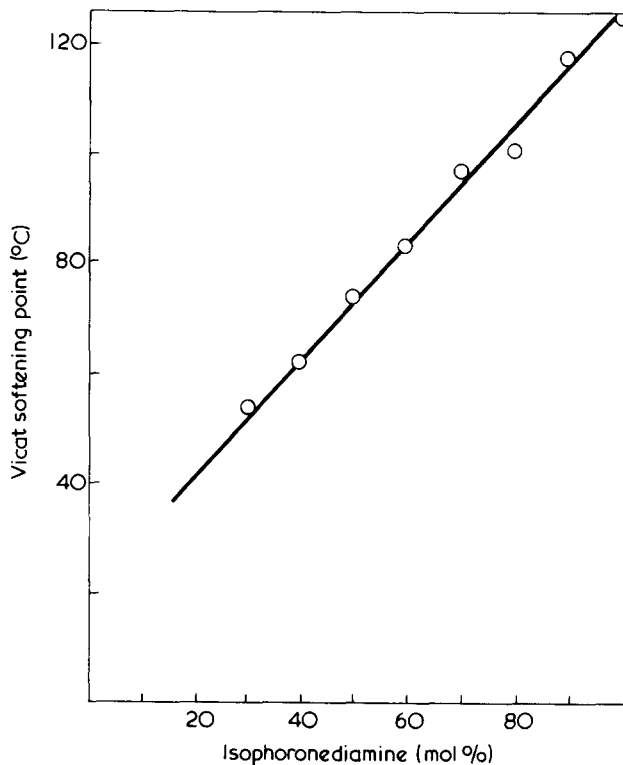


Figure 5 The effect of isophoronediamine concentration on the Vicat softening point of DDA/HMD/IPD copolyamides

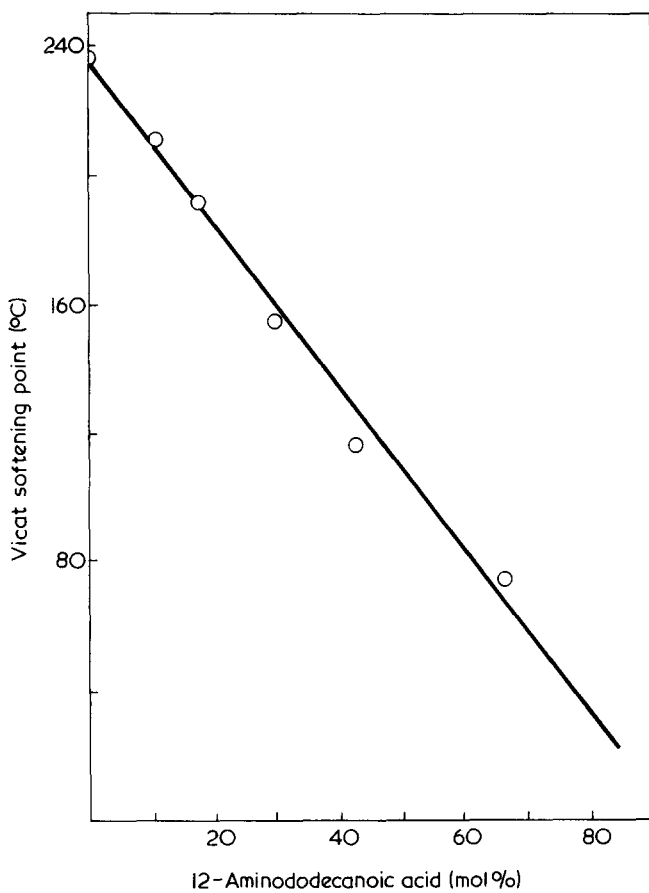


Figure 4 The effect of the molar concentration of 12-aminododecanoic acid on the Vicat softening point of IPA/TPA/IPD polyamides. Ratio of IPA/TPA 30:20

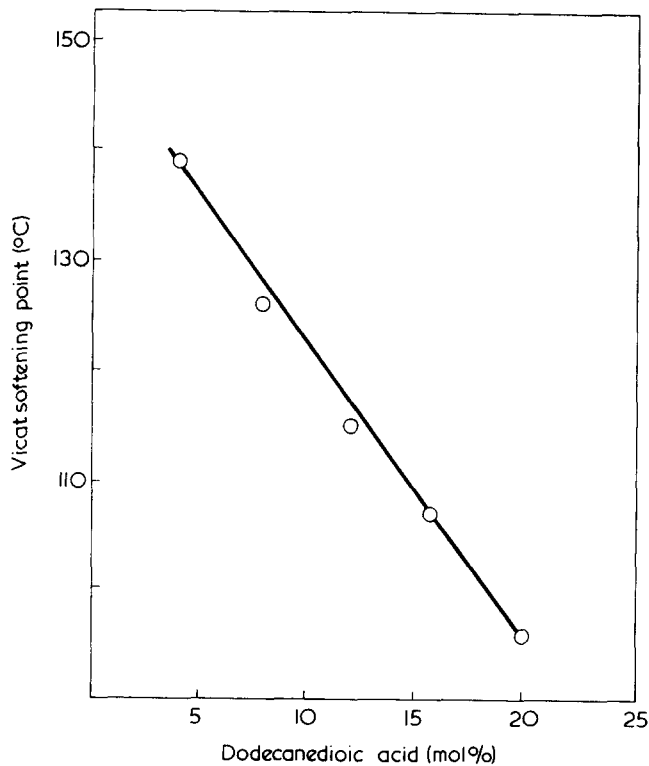


Figure 6 Variation of Vicat softening point with % substitution of dodecanedioic acid for terephthalic acid in IPA/TPA/HMD/IPD polyamides

phthalic acid/terephthalic acid/hexamethylenediamine/isophoronediamine system, using concentration ranges of terephthalic acid and isophoronediamine which yielded amorphous products. A relationship was established between softening point and composition of the form:

$$V = b_0 + b_1(\text{TPA}) + b_2(\text{IPD}) \quad (3)$$

Values of 0.143 and 1.38 were found for b_1 and b_2 respectively.

The softening point is therefore not only related to the concentration of a single diacid/diamine pair, as in the caproamide copolymers referred to earlier, and to the linear combination of two or more such diacid/diamine pairs (see *Figures 3-6*), but also to a linear combination of the individual diacids and diamines in the polyamide formulation. It follows that the softening point of an amorphous copolyamide is related to its constituent diacid/diamine pairs by the expression:

$$V = m_1V_1 + m_2V_2 + \dots + m_nV_n \quad (4)$$

where m_1, m_2, \dots, m_n are the mole fractions of the diacid/diamine pairs which form polyamides of softening points V_1, V_2, \dots, V_n .

In addition:

$$V_n = (K_a)_n + (K_b)_n \quad (5)$$

where $(K_a)_n$ is the molar constant of the diacid in the n th diacid/diamine pair and $(K_b)_n$ is the molar constant of the diamine in the n th diacid/diamine pair.

Substituting equation (5) into equation (4) yields:

$$V = m_1(K_a)_1 + m_2(K_a)_2 + \dots + m_n(K_a)_n + m_1(K_b)_1 + m_2(K_b)_2 + \dots + m_n(K_b)_n \text{ etc.}$$

which can be written more conveniently in the form:

$$V = \sum m_a K_a + \sum m_b K_b \quad (6)$$

K_a and K_b values for terephthalic acid and isophoronediamine are given in equation (3) as b_1 and b_2 respectively. Since K_a and K_b values can be derived from the softening points of polyamides, it is only necessary to assign a unique value to one such component in order to calculate values for all other diacids and diamines. From the data contained in *Table 9* it can be seen that isophoronediamine has a much more marked effect on the Vicat softening point than terephthalic acid, and for this reason the value of b_2 quoted for isophoronediamine was considered to be the better reference standard. It will be convenient in the discussion to follow to write K_b as $100b_2$.

The K_b values for isophoronediamine can now be used to calculate the K_a values for diacids in two component polyamides, and the procedure progressed through other polyamide formulations to yield further K_a and K_b values. Unfortunately, a large number of salts cannot be easily polymerized due to the formation of polymers of very high softening points, e.g. terephthalic acid/isophoronediamine, and reliable softening point measurements cannot be made. In many cases a crystalline polymer is formed and the softening point is not a true measure of the monomer contributions because of crystal lattice forces. In both cases molar constants can be calculated from ternary copoly-

amide softening point data. The extrapolation of softening point to zero concentration of ϵ -caprolactam in copolyamides is a particularly useful method of obtaining molar constants.

Molar constants are listed in *Table 10* and are quoted in $^{\circ}\text{C}/\text{mol}$, to an accuracy of $\pm 5^{\circ}\text{C}$. By using these values to determine the intercepts of the best straight lines through the experimental points shown in *Figure 3* for copolycaproamides, it was found that a slope of -0.8 satisfactorily characterizes the relationship between softening point and ϵ -caprolactam concentration in every series of copolycaproamide studied. The softening point of these polymers can therefore be predicted from the equation:

$$V = V_0(1 - 0.8[\text{CAP}]) \quad (7)$$

providing V_0 is known or can be predicted from molar constants.

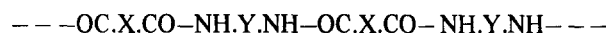
Table 11 compares softening points calculated from equation (5) using the values of the molar constants given in *Table 10* with measured softening points of polyamides containing up to five monomers. The predicted values agreed to within 5% of the experimental values in most cases except when the polyamide was crystalline, and amply demonstrate the utility of the molar constant concept for amorphous polyamides.

The simple additivity of the molar constant concept would appear to indicate that the rigidity and cohesive energy forces of the polymer chains are determined solely by the number and frequency of different monomeric structural units present in the molecular chain. From the data contained in *Figures 3* and *4* there is also evidence to indicate that a reversal in the arrangement of amide groups by the introduction of an amino-acid into the diacid/diamine copolymer creates additional steric hindrance which further reduces the ability of chains to pack together and lowers the softening point of the polymer. Because of a much more regular and closer packing arrangement in crystalline polyamides the cohesive energy between chains is much greater, and the softening points are much higher than for amorphous polyamides.

Extension of the molar constant concept to the prediction of Vicat softening point from functional group contributions

The Vicat constants K_a and K_b of a range of diacids and diamines have been calculated in the manner described above. The chemical structure of the various diacids and diamines, together with their associated Vicat constants, are presented in *Table 10*. The objective of the discussion to follow will be to determine whether the individual groups within these monomers can be assigned a constant fractional contribution to the already characterized monomer Vicat constant.

The chemical formula of a linear polyamide chain may be written in the form:



In the discussion, it is proposed to consider the polyamide chain as being built up of structural units $\text{---NH.O.C.X.CO.NH---}$ and ---Y--- . These units were chosen in order to simplify the discussion.

Linear polyamides derived from aliphatic diacids and diamines contain structural units in which X and Y repre-

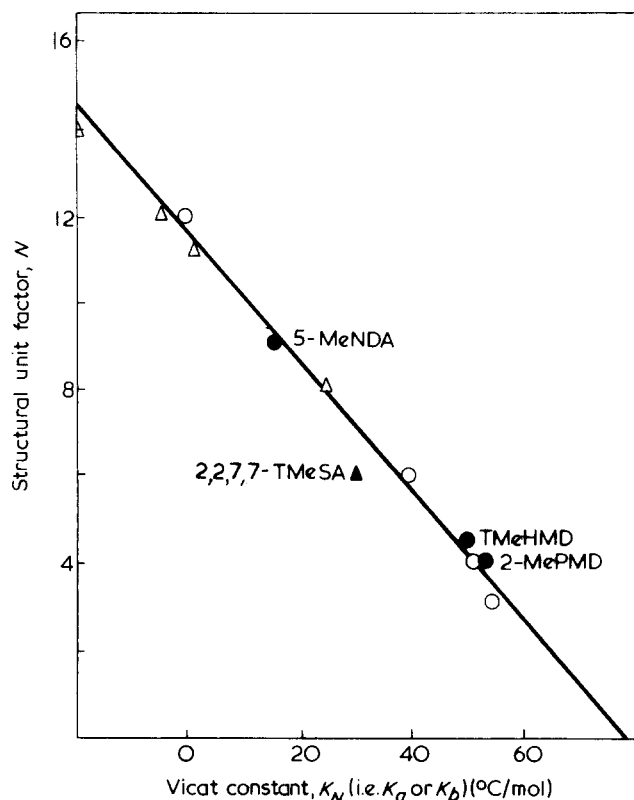


Figure 7 Relationship between the Vicat constant K_N and the monomer structural unit factor N . \circ , Linear diamine unit; Δ , linear diacid unit; \bullet , branched diamine unit; \blacktriangle , branched diacid unit

sent a chain of methylene groups $(-\text{CH}_2-)_n$. If the total number of atoms in a structural unit which lie along the chain axis of the polyamide is given by N , then $N = n + 4$ for the linear structural unit $-\text{NH}.\text{OC}.\text{X}.\text{CO}.\text{NH}-$ and $N = n$ for the linear structural unit $-\text{Y}-$.

Figure 7 shows that a linear relationship exists between the Vicat constants for the various aliphatic diacids and diamines listed in Table 5, and their individual N values derived as above. The line shown is fitted by the equation:

$$K_N = 78 - 6.7N \quad (8)$$

where K_N is the Vicat constant characterizing both diacids and diamines in terms of the common structural unit factor N .

The monosubstitution of in-chain atoms remote from the polar amide groups, would not be expected to significantly affect the value of K_N . This is found to be the case with 5-MeNDA whose K_N value is close to that predicted for the unsubstituted nonanediamine. On the other hand, methyl substitution at in-chain carbon atoms adjacent to the amide groups would be expected to cause a steric effect, and hence some change in K_N relative to the value of N computed from the number of in-chain atoms within the structural units. This is indeed observed when the data contained in Figure 7 for 2-MePMD and 2,2,4-TMeHMD are plotted against the respective diamine N values. However, if for such monomers the apparent chain length N is reduced by the number of methyl groups substituted on in-chain carbon atoms which occupy the α or β position relative to the amide bond, agreement with the previously established relationship is obtained. The same rule when applied to 2,2,7,7-TMeSA reduces the apparent chain length from 10 to 6, and as can be seen from Figure 7, gives a better fit to the linear relationship proposed.

Additional empirical rules which might govern the application of equation (8) to cyclic diacids and diamines should next be considered. Since only six such monomers are listed in Table 10, two being alicyclic and four aromatic, it will not be possible to test adequately any proposed structural rule.

Applying equation (8) to diaminomethylcyclohexane yields a value of $N = -4$. Since from the previously established rule for aliphatic diamines the two exocyclic methylene groups contributed $n = 2$, the alicyclic ring must contribute $n = -6$ to the overall value of N . Thus for isophoronediamine, the alicyclic ring must contribute $n = -6$, tetra-substitution of the two ring atoms $n = -4$, and the exocyclic methylene group $n = 1$. Isophoronediamine has therefore a derived structural unit factor $N = -9$, and coordinates $K_N = 140$, $N = -9$ which allow placement in Figure 8 according to the relationship given in equation (8). In neither of these calculations has any account been taken of the nature of the ring substitution. The general application of the proposed group contribution to the structural unit factor, N , cannot be further tested here because of the lack of experimental data on other alicyclic diamines.

In considering how aromatic monomer might be placed on the same K_N versus N relationship, it is convenient to make the purely arbitrary selection of terephthalic acid as the aromatic standard. Terephthalic acid has a K_d value of 105, and therefore to fit the required data line it must have a structural unit factor of $N = -4$. If instead of assigning an arbitrary value to the aromatic ring we count each carbon atom in the shortest chain through the aromatic nucleus as -1 , and add -1 for each carbonyl group directly attached to the aromatic ring, terephthalic acid can be assigned a structural unit factor of -4 (by previous rules each of the nitrogen atoms attached to the carbonyl groups

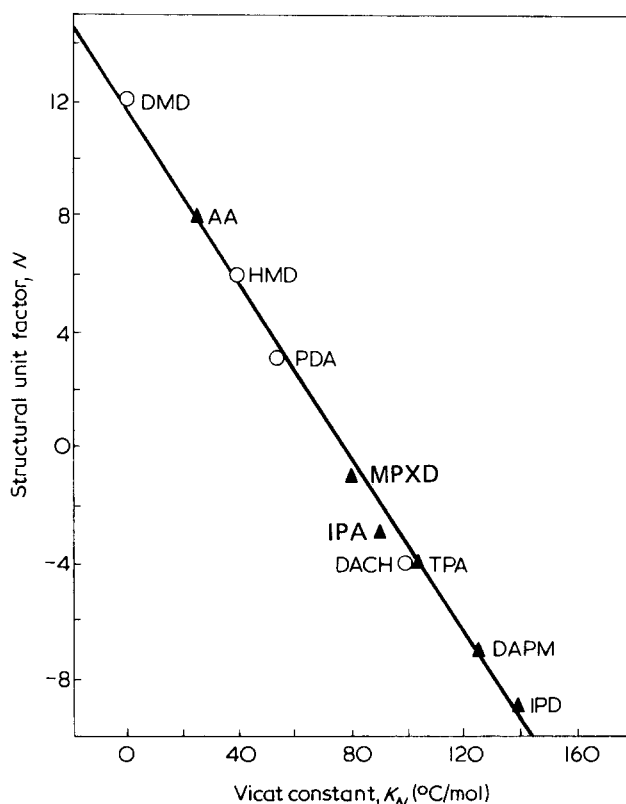


Figure 8 Extension of the relationship between the Vicat constant K_N and the monomer structural unit factor N to cyclic monomers

must be counted as +1). In the same way isophthalic acid yields a structural unit factor $N = -3$, and 4,4'-diaminodiphenylmethane a factor $N = -7$, both of which fit the desired relationship fairly well. *m*- and *p*-Xylylenediamine with a Vicat constant $K_b = 80$ and a *m*-/*p*-ratio of 70/30 also provides a fairly close fit to the K_b against N plot contained in Figure 8, by having a calculated value of $N = -1.3$.

From the discussion set out above it is clearly possible from the simple structural rules derived to calculate the Vicat constant for a diamine or a diacid, and hence predict the Vicat softening point of a polyamide containing that component. The computational procedure adopted is arbitrary. Nevertheless, a limited amount of success has been achieved in predicting values for the structural unit N

which would have yielded by interpolation, values of K_a and K_b close to the values derived from experimental observation. Most of the polyamides listed in Table 5 were prepared to provide additional data to support the relationship shown in Figure 7.

A procedure similar to the above has been published by Weyland *et al.* which uses numerical increments for constitutional molecular groups to predict the glass transition temperature of polymers from the chemical structure¹⁴.

The scheme proposed in this paper is better suited for use with polyamides which Weyland *et al.* found did not conform to their general structural principles for other polymer types.

PART II: IMPACT STRENGTH, TENSILE STRENGTH AND FLEXURAL MODULUS

IMPACT STRENGTH

Two empirical relationships proposed in Part I relate (a) the asymmetry of the monomeric units to the physical nature (amorphous or crystalline) of the polyamide and (b) the chemical structure of the monomeric units to the Vicat softening point of the polyamide. The objective of the discussion below is to demonstrate that the impact strength (IS) of an amorphous polyamide is related, in a simple way, to the chemical structure, frequency of occurrence, and symmetry of the structural units in the polyamide chain. It is shown that the empirical relationships referred to above can be combined in a particular way which enables the impact strength of a polyamide to be computed with reasonable accuracy. The effect of molecular weight on impact strength has been ignored since the polyamides studied had a molecular weight level ($>20\,000$) above which their impact strength remained fairly constant.

Comparative effect of acids and diamines on impact strength

The examples of polyamides set out in Table 1 are arranged in pairs to illustrate the dependence of impact strength upon the nature of the acid(s) employed, when the diamine residues are fixed. The results of substituting one acid for another upon the impact strength is summarized in the final column of Table 1. Reference to this column will verify that the acids studied can be arranged in a particular order in which substitution increases impact strength: TPA $>$ IPA \approx AA $>$ DDA $>$ TMeSA.

The relationship between the diamine composition of the polyamide and its impact properties has been studied extensively, particularly in high impact resins containing iso- and/or tere-phthalic acids. The examples given in Table 2 are again set out in pairs, in which only the ratios of the diamines common to each pair have been varied.

An example of every possible substitution* of one diamine by another is given, and the data are arranged in five sections to show that impact strength is increased by diamine substitution in the order DMD $>$ HMD $>$ 5-MeNDA $>$ MPXD $>$ 2,2,4-TMeHMD $>$ IPD.

Monomer structure and impact strength

The significance of the comparative influence of the diacids and diamines upon the impact strength has been examined. In Part I monomers were divided into three

*Except the substitution of MPXD by DMD.

types: AM1, AM2 and AM3. It will now be convenient for the following discussion to classify all symmetric diacids or diamines studied, e.g. terephthalic acid, adipic acid, hexamethylenediamine etc., into a single group designated SM. In Part I, a symmetry index was defined by the relationship:

$$\text{Symmetry index} = 1 - \frac{\Sigma [\text{AM}]}{300} \quad (1)$$

where

$$\Sigma [\text{AM}] = [\text{AM1}] + 2[\text{AM2}] + 3[\text{AM3}] \quad (2)$$

[AM1], [AM2], [AM3] are the percentage molar concentrations of asymmetric monomers in the three groups.

The symmetry index (SI) is more conveniently calculated from the relationship:

$$SI = (3[\text{SM}] + 2[\text{AM1}] + [\text{AM2}])/300 \quad (3)$$

Each of the six diamines studied has been placed in Table 3 in the column corresponding to its symmetry group and in the row corresponding to its relative position in the order listed above (Vicat constants are quoted in parentheses). Reference to this Table indicates that impact strength is decreased by substituting a diamine with lower symmetry and/or higher Vicat constant.

The first observation was tested by plotting impact strength against the symmetry index for several series of polymers in which the composition of the acids were kept constant. Figure 1 shows linear plots of impact strength versus symmetry index, which are all statistically significant, for polydodecamides, polyadipamides, polyisophthalamides, polyterephthalamides and mixed polymers (IPA: TPA = 3:2). Furthermore, the slope of the line increases with the Vicat constant of the acid in the order TPA $>$ IPA $>$ AA $>$ DDA and confirms the conclusions drawn from Table 1.

The second observation was demonstrated by plotting the impact strength of polyterephthalamides against Vicat softening point. In spite of some variations in the symmetry index, of these polymers, (0.70–0.80) a significant relationship was obtained (Figure 2) which showed that

Table 1 Effect of interchanging diacids in polyamide formulations on impact strength

TMeSA	Composition (mol %)									Charpy /S (kJ/m ²)	Effect of acid substitution on impact strength
	DDA	AA	IPA	TPA	HMD	IPD	5-MeNDA	TMeHMD	MPXD		
				50				50		68	TPA > IPA
			50					50		35	
		25		25	25	25				34	TPA > AA
		50			25	25				17	
	20		30	20	42.5	7.5				46	TPA > DDA
			30		42.5	7.5				26	
			50		25	25				17	IPA ~ AA
		50			25	25				17	
			50		42.5	7.5				28	IPA ~ AA
					42.5	7.5				29	
	20		30	20	30				20	45	IPA > DDA
			10	20	30				20	23	
50			50		50					38	IPA > TMeSA
					50					<1	
		50			42.5	7.5				29	AA > DDA
	50				42.5	7.5				17	
50		50			50					37	AA > TMeSA
					50					<1	

Table 2 Effect of interchanging diamines in polyamide formulations on the impact strength

DDA	Composition (mol %)									[η] _i (m ³ /kg)	Vicat soft. pt (°C)	Charpy /S (kJ/m ²)	Comparative effect of diamines on impact strength
	IPA	TPA	HMD	DMD	5-MeNDA	MPXD	TMeHMD	IPD					
		50	10			10	30			insoluble	159	69	DMD > HMD
		50		10		10	30			insoluble		90	
		50			30			20		0.112	166	55	DMD > 5-MeNDA
		50		30				20		0.297	161	98	
		50					42.5	7.5		0.136	171	50	DMD > TMeHMD
		50		15			27.5	7.5		0.169	153	131	
	30	20		30				20		0.119	152	47	DMD > IPD
	30	20		42.5				7.5		0.085	115	58	
	50				50					0.105	105	29	HMD > 5-MeNDA
	50		50								143	38	
	30	20	32.5			17.5					145	38	HMD > MPXD
	30	20	42.5			7.5				0.107	140	50	
	30	20	5			7.5	37.5			0.107	148	28	HMD > TMeHMD
	30	20	42.5			7.5				0.107	140	50	
	50		25					25		0.124	192	17	HMD > IPD
	50		50								143	38	
10	50					50				0.074		brittle	5-MeNDA > MPXD
	40					50				0.108	142	13	
	50				50					0.105	105	29	
		50					50			0.136	155	68	5-MeNDA > TMeHMD
		50			50					0.163	>200	131	
		50			30			20		0.112	166	55	5-MeNDA > IPD
		50			40			10		0.11	143	83	
	30	20	32.5			7.5	10			0.099	140	26	MPXD > TMeHMD
	30	20	32.5			17.5				0.114	145	38	
		50					42.5	7.5		0.136	171	50	MPXD > IPD
		50					40			0.146	160	62	
		50					42.5	7.5		0.136	171	50	TMeHMD > IPD
		50					50			0.136	155	68	

Table 3 Diamines arranged according to symmetry group and order of substitution which diminishes impact strength

Type	Type AM1	Type AM2	Type AM3
DMD (0)			
HMD (40)			
	5-MeNDA (15) MPXD (80)		
		TMeHMD (50)	
			IPD (140)

Values in parentheses are values of K_N , the Vicat constant

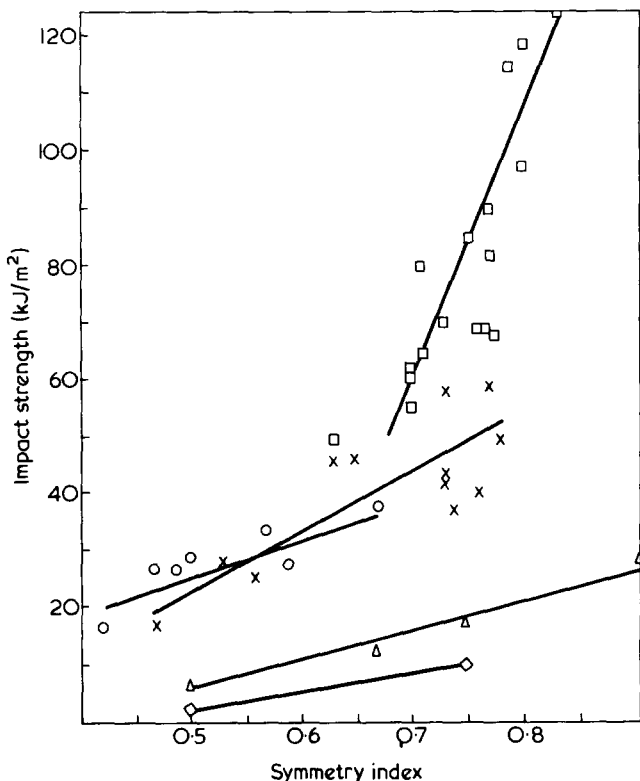


Figure 1 Relationships between impact strength and symmetry index for polyamides of various acids:

	K_a	Slope	% Significance
□ Polyterephthalamides	105	488	0.1
X IPA/TPA = 30/20	96	108	0.1
○ Polyisophthalamides	90	65	5
△ Polyadipamides	30	52	2
◇ Polydodecamides	-20	24	-

impact strength does increase with a decline in softening point (i.e. longer diamine chain length). The correlation between impact strength and Vicat softening point does not hold for the other series of polyamides based on other acids, the data for which covers a wider symmetry range.

The interaction between symmetry and softening point is better understood by referring to the schematic arrangement shown in Table 3. Impact strength can be decreased by substituting a diamine of higher Vicat constant from the same symmetry group or by substituting a diamine from a lower symmetry group. If the substitution is made from within the same symmetry group then a correlation

between impact strength and Vicat softening point can be expected. However, this correlation breaks down when the substitution is made from different symmetry groups. For example, the substitutions of 5-MeNDA by HMD or 2,2,4-TMeHMD by MPXD increase not only the symmetry and the impact strength but also the Vicat softening point. The effect of diacid structure on impact strength can also be appreciated better by a similar schematic arrangement (Table 4). The order in which the diacids were ranked, on the basis of the data given in Table 1 is broadly confirmed by the data plotted in Figure 1. The slope of the best straight line relating impact strength to symmetry index increases with the numerical value of the acid Vicat constant. The slope obtained in the series containing IPA is lower than would be expected, on the basis of Vicat constant only, and must be due to the asymmetry of this acid. This information is summarized qualitatively in Table 4.

The effect of amino-acids has not been studied in detail. Nevertheless, the data given in Table 5 clearly show that a reduction in impact strength occurs as the level of ϵ -caprolactam or 12-ADA in the polyamide is increased.

Prediction of impact strength

More information is needed about the interaction between monomer symmetry and Vicat constant before a quantita-

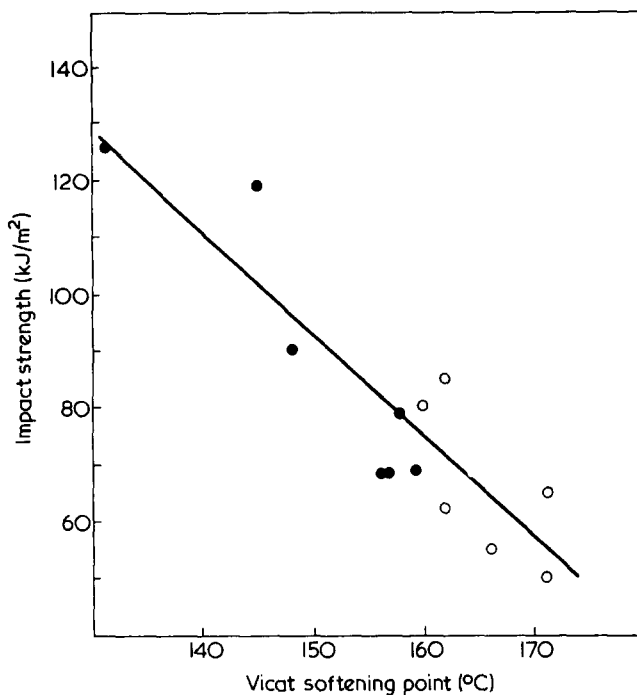


Figure 2 Linear relationship between impact strength and Vicat softening point for polyterephthalamides with symmetry indices in the range 0.70-0.80 (1% significant). ○, SI = 0.70-0.75; ●, SI = 0.75-0.80

Table 4 Diacids arranged according to symmetry group and order of substitution which diminishes impact strength

Type SM	Type AM1	Type AM2	Type AM3
TPA (105)			
AA (30)		IPA (90)	
DDA (-20)			
		TMeSA (30)	

Values in parentheses are values of K_N , the Vicat constant

Table 5 Comparison of predicted and measured values of impact strength of amorphous polyamides containing amino-acids

Composition (mol %)								Average measured Charpy I_S (kJ/m ²)	Predicted Charpy I_S (kJ/m ²)
Amino-acids		Diacids		Diamines					
ϵ -CAP	12-ADA	IPA	TPA	TMeHMD	HMD	DMD	IPD		
0			50	50				68	68
10			45	45				55	60
10			45	18			15.5	68	65
20			40				20	48	40
50			25				25	19	14
	0	30	20		42.5		7.5	46	48
	17.7	24.7	16.5		35		6.2	38	38
	54	13.8	9.2		19.5		3.4	21	21
	30		35				35	26	22

tive prediction of impact strength can be made using these parameters. Nevertheless, an empirical equation has been devised which has been applied to the experimental data with surprising accuracy. For polyamides containing symmetric acids only, equation (4) can be used.

$$\text{Impact strength} = \frac{150K}{V} [SI] V_A \quad (4)$$

where $[SI]$ is the symmetry index of the polyamide; V_A , the molar contribution of the acids to the Vicat softening point (in °C); V , the Vicat softening point (in °C) and K is a constant.

In Part I, it was shown that:

$$V = V_A + V_B = \sum m_a K_a + \sum m_b K_b \quad (5)$$

where m_a , m_b are mole fractions of diacids and diamines and K_a , K_b are contributions to v.s.p./mol of diacid or diamine.

Equation (4) is in accordance with the experimental observation discussed above.

In order to predict the impact strength of polyamides containing isophthalic acid, it has been necessary to introduce an additional assumption, viz. that impact strength depends on the sum of the products of symmetric monomer content and Vicat acid constant in the directions of the chain axis and two other planes mutually at right angles to each other and the chain axis. This equation takes the form:

$$\text{Impact strength (kJ/m}^2\text{)} = \frac{100K}{V} [\sum [SM]_x V_x + \sum [SM]_y V_y + \sum [SM]_z V_z] \quad (6)$$

where $[SM]$ is the mole fraction of symmetric monomer, and x , y , z denote each of the three non-coplanar directions. V_x , V_y , V_z are the Vicat contributions of diacids symmetrical in the planes x , y , z (°C).

Equation (6) simplifies to the form of equation (4) when only symmetric acids are employed. Both equations are applicable only if the Vicat constants are expressed in °C and are limited to those polyamides where $V_A > 0$. The direction of symmetry for each monomer was decided by its symmetry groups (SM, AMI etc.).

To avoid ambiguity, and to obtain the most accurate prediction asymmetric diacids and diamines in the same polymer were awarded the *least* number of possible coincident directions of symmetry.

The value of K in equations (4) and (5) was computed by inserting reproducibly established values of impact strength for two reference polymers (TPA/2,2,4-TeHMD = 68 kJ/m²; IPA/TPA/HMD/IPD = 46 kJ/m²) and found to approximate to unity. The equation was applied to polyamides containing amino-acids, by regarding these as completely asymmetric (Type AM3), (because they cause serious disruption to symmetry by reversing the order of amide groups along the polymer chain).

Table 6 Comparison of measured and predicted Charpy impact strengths of amorphous polyamides

Polymer no.	Impact strength (kJ/m ²)		Polymer no.	Impact strength (kJ/m ²)	
	Measured	Predicted		Measured	Predicted
I	7	13	LXXVIII	41	51
III	9	10	LXXIX	38	47
VI	13	23	LXXX	28	32
VII	17	28	LXXI	26	48
IX	19	19	LXXXII	47	39
X	34	48	LXXXIII	58	61
XVIII	13	17	LXXXIV	59	53
XIX	37	49	LXXXV	46	50
XX	36	43	LXXXVI	58	46
XXII	32	33	LXXXVII	17	29
XXIII	29	25	LXXXVIII	26	36
XXIV	26	17	LXXXIX	46	42
XXV	35	44	XC*	68	68
XXVI	30	36	XCI	131	110
XXVII	28	20	XCII	98	79
XXXIX	48	51	XCIII	126	92
XLI	55	61	XCIV	82	84
XLII	68	65	XCVII	55	66
XLIII	36	51	XCVIII	62	68
XLIV	14	15	XCIX	60	69
XLVIII	7	4	C	50	59
LV	19	9	CI	65	65
LVII	23	3	CII	80	70
LIX	26	22	CIII	85	69
LX	38	38	CIV	77	69
LXI	21	21	CV	50	58
LXIV	38	32	CVI	63	66
LXV	29	22	CVII	69	77
LXVI	28	28	CIX	115	80
LXVII	17	24	CX	79	79
LXVIII	17	18	CXI	69	76
LXIX	34	28	CXIII	68	79
LXXVII	45	45	CXII	70	76
LXX	27	25	CXIV	90	82
LXXI	27	19	CXV	119	87
LXXII	22	24		77	
LXXIV*	46	46	CXVI	120	87
LXXV	50	53		131	
LXXVI	30	30	CXVII	135	83

*Reference polymers

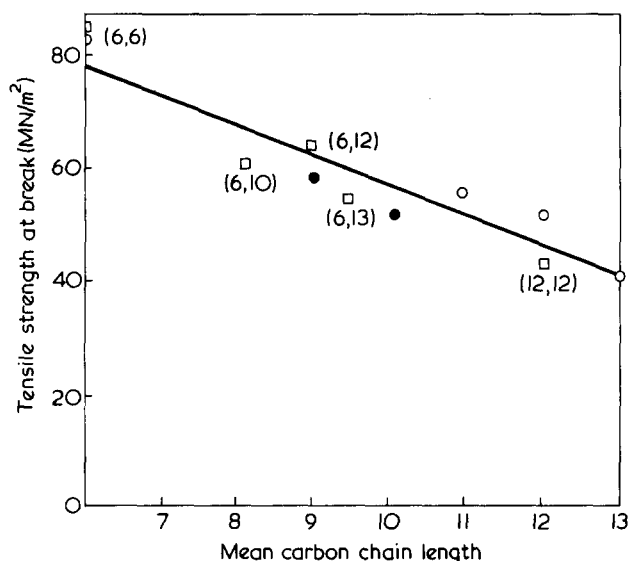


Figure 3 Relationship between the tensile strength and carbon chain length of the monomer unit in crystalline aliphatic polyamides. ○, Amino-acid homopolymers; ●, caprolactam/12-ADA copolymers; □, diamine/diacids homopolymers

The predictions made with equation (6) agree fairly well with the experimental values over a wide range of impact values. The predicted and average measured values of seventy five polyamides are compared in Table 6, for impact values ranging from 7 to 135 kJ/m². The agreement between these values was good, particularly in the range 20–80 kJ/m² but the equation tends to underestimate very high values by a substantial margin. Most of the high impact polyamides contain a substantial proportion of C₁₂-diamine, which appears to increase the impact strength rather more than it reduces softening point. The prediction of impact strength for polyamides containing amino-acids is also surprisingly good (see Table 5) and justifies the inclusion of these monomers in symmetry group AM3.

Worked examples of equation (6) are included in the Appendix. The reasonable agreement between equation (5) and experimental values indicates the impact strength of polyamides may be a constitutive property. Optimum impact strength depends on raising the symmetry of the polymer chain to the limit permitted without loss of amorphous nature, and by using a rigid acid structure alternating between flexible diamine links to absorb the shock of impact. Energy of impact is readily delocalized through the bonding in the carbonyl group, particularly when the carbonyl groups form part of a conjugated system with an aromatic ring, e.g. in terephthalamide units, and is dissipated through the long flexible diamine chains.

TENSILE STRENGTH AND FLEXURAL MODULUS

Crystalline polyamides

The tensile strength of linear crystalline polyamides is plotted as a function of the average number of carbon atoms in the monomeric unit, in Figure 3. The data were obtained from literature sources^{15–16} measured according to ASTM D238 and from measurements made in our laboratories.

A linear relationship was observed, the tensile strength decreased with increasing carbon number and was independent of whether the polyamide was derived from an amino-acid or from a diacid/diamine combination.

Amorphous polyamides

During the course of our research programme in amorphous polyamides, the tensile strength of a wide variety of formulations have been measured according to BS 2782, method 301C. The formulations which were most extensively studied contained one or more of the following monomers, each of which contained a linear backbone of six carbon atoms: adipic acid, hexamethylenediamine, a 1:1 isomeric mixture of 2,2,4- and 2,4,4-trimethylhexamethylenediamine, caprolactam. These monomers were copolymerized with at least one of the following cyclic monomers: isophthalic acid, terephthalic acid, a 7:3 mixture of *meta*- and *para*-xylylenediamines, isophorone diamine. The tensile strength of this type of formulation was found to be linearly dependent upon the molar concentration of the aliphatic monomers with a backbone of six carbon atoms, irrespective of the nature or combination of the linear monomers or of the cyclic monomers (see Figure 4). It was concluded that even substantial differences in the chemical structure of cyclic or linear monomers had relatively little effect on the tensile strength of amorphous polyamides. The tensile strength of a few amorphous polymers containing C₉- and C₁₂-monomers have been measured (see Tables 2–4, Part I). When those results are compared against those of polymers containing only C₆-aliphatic monomers it is evident that tensile strength does fall off with increasing chain length of monomer unit for amorphous polymers as well, as might be expected.

A linear relationship between tensile strength and flexural modulus (0.1% significant) was obtained by plotting values for polyamides containing terephthalic, isophthalic or adipic acids (see Figure 5). Results obtained for polyamides containing ϵ -caprolactam or 12-aminododecanoic acid did not fit this relationship.

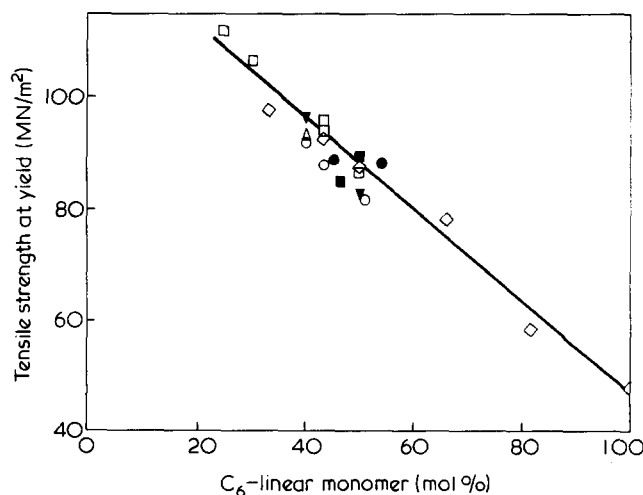


Figure 4 Relationship between tensile strength and the molar concentration of aliphatic monomer units containing 6 carbon atoms in copolyamides with cyclic monomers. C₆-monomer combination: □, HMD; ○, TMeHMD; △, AA; ◇, CAP; ●, CAP/TMeHMD; ■, CAP/HMD; ▼, TMeHMD/HMD

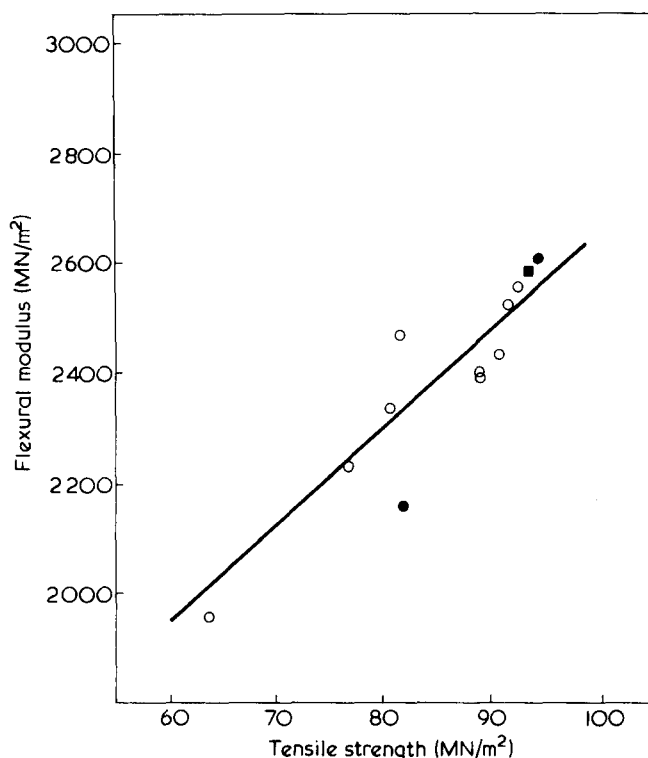


Figure 5 Linear relationship between tensile strength and flexural modulus (0.1% significant). Acid: ○, TPA; ●, IPA/TPA = 3/2; ■, AA

CONCLUSIONS

The observations set out in Parts I and II demonstrate that a number of bulk physical properties of amorphous polyamides can be described by simple structural parameters which relate them to the chemical structure, symmetry and molecular concentration of the monomer units which build the polymer chain. Amorphous polyamides may therefore be regarded as an 'ideal class of polymers' because interactions between polymer chains have a negligible effect on the relationship between the chain structure and bulk properties.

Vicat softening point was shown to be a constitutive property which should be calculated from the contributions of individual constituent groups within the molecule. This treatment has been combined with a simple symmetry concept to predict impact strength in the amorphous state. It was shown that impact strength could be optimized by maintaining the highest level of structural symmetry compatible with an amorphous nature in a polymer chain composed of alternating rigid acid and flexible diamine structures. This type of structure facilitated the dissipation of shock energy along the chain, and was particularly effective when the carbonyl groups were incorporated into a delocalized π -bonding system by conjugation with an aromatic ring. It was demonstrated that on average only 20% of the monomer units need to be asymmetric for the polymer to

be amorphous, and a simple method was proposed for calculating the amorphous-crystalline transition point for structures containing monomer units with different degrees of symmetry.

The tensile strength of both amorphous and crystalline polyamides was found to depend on the average number of carbon atoms in the monomer units which comprised the polymer chain.

A statistically significant positive linear correlation was obtained between tensile strength and flexural modulus for polyamides not containing amino-acids.

By utilizing the relationships outlined in Part I and Part II of this paper, it is possible to predict the compositions of polyamides which will have an outstanding combination of physical properties.

ACKNOWLEDGEMENTS

The author gratefully acknowledges the help of Dr K. Lawrence who supervised the physical testing of polymer, and is indebted to Dr W. W. Kerr for his many useful suggestions and criticisms. Thanks are also due to Dr P. S. Thukral whose work provided much useful data on polyamides and to Dr R. C. Pitkethly who carefully checked the paper. Permission to publish this work has been given by the British Petroleum Company Limited.

REFERENCES

- Grace, W. R. Br. Pat. 914 456 (1962)
- Veba-Chemie, Br. Pat. 976 007 (1964)
- Grace, W. R. Br. Pat. 977 868 (1964)
- Chemische Werke Witten, Br. Pat. 1 019 707 (1965)
- Hibernia-Chemie, Br. Pat. 1 096 908 (1967)
- Chemische Werke Witten, Br. Pat. 1 100 375 (1967)
- Veba-Chemie, Br. Pat. 1 100 972 (1967)
- ICI, Br. Pat. 1 201 652 (1970)
- BP Chemicals, Br. Pat. 1 228 761 (1971)
- BP Chemicals, Br. Pat. 1 250 877 (1971)
- Doffin, H., Pungs, W. and Gabler, R. *Kunststoffe* 1966, **56**, 546
- Gabler, R., Muller, M., Ashby, G. E., Agouri, E. R., Meyer, H. L. and Kabos, G. *Chimia* 1967, **21**, 65
- Ridgway, J. S. *J. Polym. Sci. (A-1)* 1969, **7**, 2195
- Weyland, H. G., Moftyzer, P. J. and Van Krevelen, D. W. *Polymer* 1970, **11**, 79
- Mod. Plast.* 1970, **47**, 107
- Plast. Rubber Wkly* 1970, July 17th, 13

APPENDIX

Worked examples to calculate the impact strength of an amorphous polyamide

EXAMPLE 1

IPA/TPA/HMD/MXD; mole ratio: 30:20:30:20.

(1) (2) (3) (4)

Vicat softening point

$$V = \sum m_a k_a + \sum m_b K_b; \text{ where } \sum m_a = 1, \sum m_b = 1$$

$$= (0.6 \times 90 + 0.4 \times 105 + 0.6 \times 40 + 0.4 \times 80)$$

$$= 152^\circ\text{C}$$

Symmetry

$$\Sigma(\text{SM})_x = (\text{SM})_{x1} + (\text{SM})_{x2} + (\text{SM})_{x3} + (\text{SM})_{x4}$$

$$= 0 + 0.2 + 0.3 + 0.2 = 0.7$$

$$\Sigma(\text{SM})_y = 0 + 0.2 + 0.3 + 0.2 = 0.7$$

$$\Sigma(\text{SM})_z = 0.3 + 0.2 + 0.3 + 0 = 0.8$$

Vicat acid contribution

$$V_x = \sum m_x K_a = m x_1 K_{a1} + m x_2 K_{a2}$$

$$= 0 + 0.2 \times 105 = 21$$

$$V_y = m y_1 K_{a1} + m y_2 K_{a2} = 0 + 0.2 \times 105 = 21$$

$$V_z = m z_1 K_{a1} + m z_2 K_{a2} = 0.3 \times 90 + 0.2 \times 105 = 48$$

Impact Strength (IS)

$$IS = \frac{100}{V} [\Sigma(\text{SM})_x V_x + \Sigma(\text{SM})_y V_y + \Sigma(\text{SM})_z V_z]$$

$$= \frac{100}{152} [0.7 \times 21 + 0.7 \times 21 + 0.8 \times 48] = 45 \text{ kJ/m}^2$$

EXAMPLE 2

 ϵ -CAP/TPA/IPD; mole ratio 50:25:25

(1) (2) (3)

Vicat softening point

$$V_0 = 105 + 140 = 245$$

$$V = V_0(1 - 0.8[\epsilon\text{-CAP}])$$

$$= 0.6 \times 245$$

$$= 147^\circ\text{C}$$

Symmetry

$$\Sigma(\text{SM})_x = (\text{SM})_{x1} + (\text{SM})_{x2} + (\text{SM})_{x3}$$

$$= 0 + 0.25 + 0$$

$$= 0.25$$

$$\Sigma(\text{SM})_x = \Sigma(\text{SM})_y = \Sigma(\text{SM})_z = 0.25$$

Vicat acid contribution

$$V_x = V_y = V_z = 0.25 \times 105 = 26.25$$

Impact strength (IS)

$$IS = \frac{100}{147} [3(26.25 \times 0.25)]$$

$$= 13.5 \text{ kJ/m}^2$$

Relative rate constants during the acidic hydrolysis of syndiotactic poly(methyl methacrylate)

V. Barth and E. Klesper

Institut für Makromolekulare Chemie, Universität Freiburg, D-78 Freiburg, W. Germany

(Received 29 April 1976)

The relative rates during acidic hydrolysis of triads of monomer units in syndiotactic methyl methacrylate/methacrylic acid copolymers in aqueous solution at different degrees of neutralization have been studied by proton n.m.r. Relative rate constants were determined by application of a graphical method to experimental and computer simulated relative rates of triads.

INTRODUCTION

When monoesters of dicarboxylic acids are hydrolysed in the acidic range, neighbouring group effects, i.e. anchimeric assistance by undissociated $-\text{COOH}$, has been found. This occurs, for instance, when an aryl group is directly bound to the carbonyl group of the ester moiety^{1,2}. While this general acid catalysis has also been found with the methyl monoester of a sterically hindered, aliphatic dicarboxylic acid, i.e. methyl hydrogen 2,3-di-(*t*-butyl)-succinate³, no such effect appears to be prominent with aliphatic monoesters of unhindered aliphatic dicarboxylic acids^{4,5}. However, it has been observed⁶ that an aryl ester with two neighbouring $-\text{COOH}$ groups shows a greatly enhanced rate of hydrolysis when partly neutralized to $-\text{COO}^-$, as compared to the fully unneutralized state. This points to a bifunctional, electrophilic-nucleophilic catalysis, which might also be operative for the acidic hydrolysis of the purely aliphatic acrylic acid/ethyl methacrylate copolymers⁷.

The apparent rate constants for the acid hydrolysis of tactic and atactic methyl methacrylate/methacrylic (MMA/MAA) copolymers have previously been studied by Smets^{8,9} by following the gross conversion with time at different degrees of neutralization. The rates were explained by simultaneous general acid and nucleophilic catalysis of $-\text{COOH}$ and $-\text{COO}^-$ respectively, the two catalysis mechanisms being largely independent. In the present communication we have investigated the relative rate constants of individual triads for the acidic hydrolysis of syndiotactic MMA/MAA copolymers of different degrees of neutralization by following gross conversion and change of triad probabilities by proton n.m.r.

EXPERIMENTAL

The kinetic runs were carried out as previously described¹⁰, except that with the syndiotactic, Bernoullian copolymer of $P(\text{A}) = 0.60$ for each 250 mg copolymer 1.5 mmol KOH were employed in the dissolution step and part of the KOH neutralized by titration with HCl before starting the hydrolysis, as indicated in *Figures 1* and *2*. Alternatively, runs with this copolymer were carried out in a mixture of 8 ml aqueous base and 4 ml dioxane instead of 12 ml

aqueous base for each 250 mg of starting copolymer*. The $P(\text{A})$ and $P(\text{XXX})$ were evaluated from the $\alpha\text{-CH}_3$ $^1\text{H-n.m.r.}$ resonance as before¹⁰.

For studying the reversibility of the acidic hydrolysis, 250 mg of syndiotactic poly(methacrylic acid) (PMAA) (2.91 mmol) was dissolved in 3 ml of 1 N KOH and 3 ml H_2O at 115°C . The syndiotactic PMAA was prepared by repeated hydrolysis of syndiotactic PMMA in concentrated H_2SO_4 ¹². After dissolution, 3 ml of 1 N HCl and 0.1 ml methanol (2.5 mmol) were added and the total volume brought up to 12 ml. After 144 h at 145°C a small degree of esterification of $P(\text{A}) \approx 0.01$ could be detected. The experiment was repeated adding only 1.5 ml of 1 N HCl because partly neutralized copolymer showed a greater rate of hydrolysis than unneutralized copolymer¹³. The degree of esterification was, however, not increased.

The homogeneity of the copolymers with respect to $P(\text{A})$ and $P(\text{XXX})$ was tested after acidic hydrolysis at 145°C . Starting with the Bernoullian copolymer of $P(\text{A}) = 0.83$ and 0.5 mmol KOH per 250 mg starting copolymer, the hydrolysis was stopped after 144 h at $P(\text{A}) = 0.40$. The resulting copolymer (500 mg) was fractionated from aqueous solution by incremental addition of HCl¹². Two fractions of approximately equal weight were obtained (fraction first precipitated 284 mg, final fraction 204 mg) which had the same $P(\text{A})$ and $P(\text{XXX})$. Therefore the measured data are representative of the individual chain. The fractionation was repeated starting with a copolymer of $P(\text{A}) = 0.60$ and 0.5 mmol KOH per 250 mg starting copolymer and hydrolysing for 72 h to $P(\text{A}) = 0.23$. Again, two fractions were obtained which had the same $P(\text{A})$ and $P(\text{XXX})$.

The accuracy of the determination of $P(\text{A})$ for a large number of copolymers was checked by total esterification with diazodiphenylmethane $[(\text{C}_6\text{H}_5)_2\text{CN}_2]$ ¹⁵. The copolymers were dissolved in dioxane and twice the stoichiometric amount of diazodiphenylmethane in dioxane added. After refluxing until the violet colour of the diazo compound had disappeared, the same amount of reagent was added and refluxing continued until the colour had turned again.

* In the latter case only the desired amount of KOH was used in the dissolution step, no backtitration being required before the run.

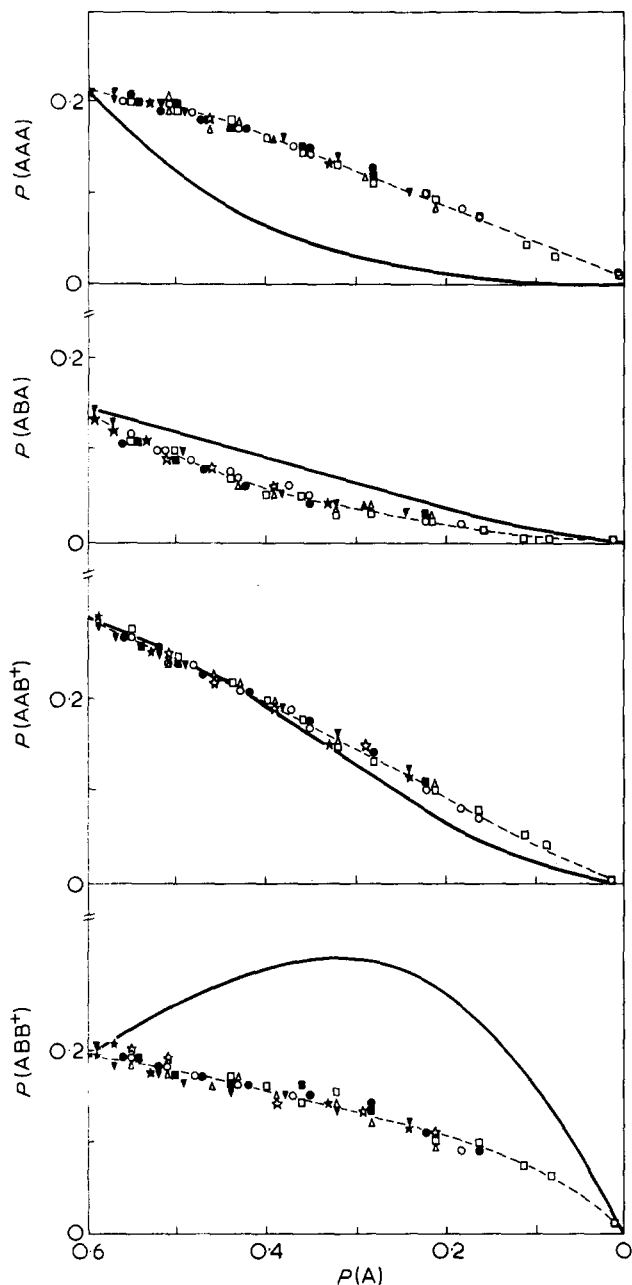


Figure 1 Dependence of triad probabilities, $P(AAA)$, $P(ABA)$, $P(AAB^+)$, $P(ABB^+)$ on conversion during the hydrolysis of a syndiotactic, Bernoullian copolymer of initially $P(A) = 0.60$. Data are from runs with different initial amounts of KOH for 250 mg copolymer in H_2O or H_2O /dioxane solution. \circ , 1.5 mmol KOH + 1.25 mmol HCl; \square , 1.5 mmol KOH + 1.00 mmol HCl; \triangle , 1.5 mmol KOH + 0.75 mmol HCl; ∇ , 1.5 mmol KOH + 0.50 mmol HCl; \bullet , 0.25 mmol KOH + 4 ml dioxane; \blacksquare , 0.50 mmol KOH + 4 ml dioxane; \star , 0.75 mmol KOH + 4 ml dioxane; \star , 1.00 mmol KOH + 4 ml dioxane. —, Calculated Bernoullian triad probabilities

After precipitation with methanol the fully esterified product was soluble in $CHCl_3$. The copolymer was reprecipitated from $CHCl_3$ solution with methanol and dried at $50^\circ C$ *in vacuo*. The 1H -n.m.r. spectra were recorded from $CHCl_3$ solution at $60^\circ C$ and $P(A)$ evaluated by:

$$P(A) = \frac{(5/3)I(-OCH_3)}{I(-CH_2-) + I(-CH_3)} \quad (1)$$

$$P(B) = 1 - P(A) = \frac{(5/11)I(-CH(C_6H_5)_2)}{I(-CH_2-) + I(-CH_3)} \quad (2)$$

where I are the relative areas of the resonances indicated in parentheses. The $P(A)$ values of equations (1) and (2) agree with each other and the $P(A)$ obtained directly from the precursor MMA/MAA copolymer to within ± 0.01 .

RESULTS AND DISCUSSION

In two previous communications^{10,11} the rates and rate constants as well as the relative rates and relative rate constants of triads have been studied for the hydrolysis of syndiotactic methyl methacrylate/methacrylic acid (MMA/MAA) copolymers of Bernoullian compositional statistics. The hydrolysis was carried out in aqueous solution, predominantly at $145^\circ C$, with more KOH than necessary to neutralize all carboxyl groups of the MAA-units, either present at start or formed during the hydrolysis. In the present study

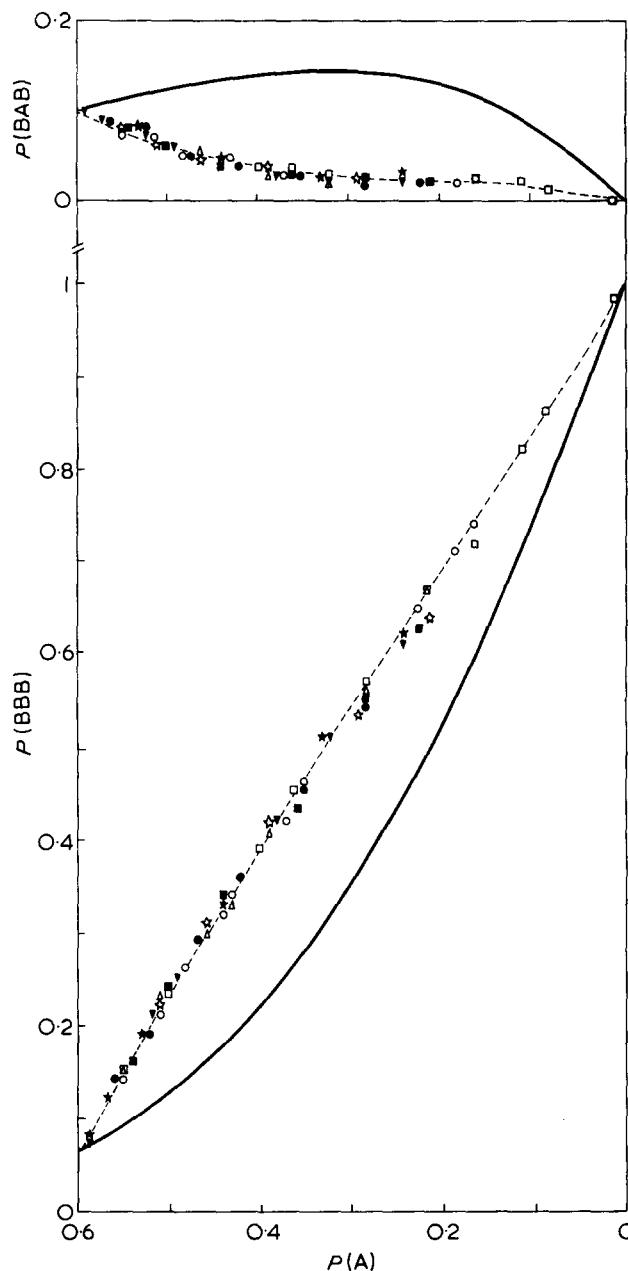


Figure 2 Dependence of triad probabilities $P(BAB)$ and $P(BBB)$ on conversion starting with a copolymer of initially $P(A) = 0.60$. Data were obtained with different initial amounts of KOH in H_2O or H_2O /dioxane solution. Symbols as in Figure 1. Calculated Bernoullian triad probabilities shown for comparison (—)

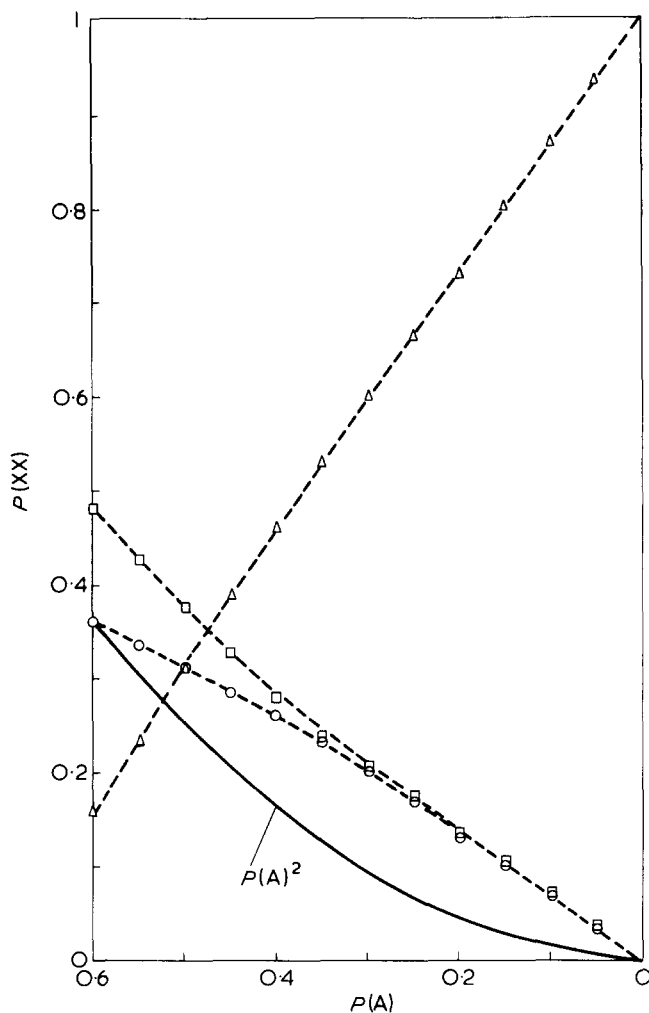


Figure 3 Dependence of dyad probabilities, $P(AA)$, $P(AB^+)$ and $P(BB)$ on conversion. Data derived from curves of best fit in Figures 1 and 2. Calculated Bernoullian dyad probability $P(AA)$ shown for comparison and labelled $P(A)^2$. \circ , $P(AA)$; \square , $P(AB^+)$; \triangle , $P(BB)$

the amount of KOH was reduced to investigate the hydrolysis in the acidic range. Starting with a copolymer of $P(A) = 0.60$ ($A = \text{MMA}$, $P(A)$ is the probability of finding an A monomer unit) 1.06 mmol KOH is required for a 250 mg aliquot of copolymer in 12 ml H_2O to neutralize all the MAA-units at $t = 0$. Accordingly, runs were carried out with 1.0, 0.75, 0.50 and 0.25 mmol KOH at $t = 0$. All kinetic measurements were carried out in KOH, because the copolymer is insoluble in water. Because of slow dissolution, the copolymer was dissolved in excess KOH (1.5 mmol) and then titrated with HCl to the desired amount of KOH. Other kinetic runs were carried out by substituting one third of the volume of water by dioxane (4 ml), adding only the desired amount of KOH without titration with HCl. An additional reason for using dioxane is the possibility that the limited solubility of MMA/MAA copolymers in purely aqueous solution with small amounts of KOH may lead to the formation of aggregates, e.g. microgels, which in turn might influence the kinetics. It was found, however, that the kinetic results are almost the same with or without dioxane.

In Figures 1 and 2 the conversion dependent behaviour of the six possible triads is shown. The triad probabilities, $P(XXX)$, ($X = A, B$) and the conversion parameter, $P(A)$, have been determined by ^1H -n.m.r. at 220 MHz¹⁰. The points represent the experimental data, while the curves

of best fit have been drawn on the basis of generally valid statistical relations¹⁰. Barring the experimental scatter, all points trace out the same curve, regardless of the degree of neutralization or whether pure water or water/dioxane was the hydrolysis medium. Thus at a given $P(A)$

$$\left[\frac{dP(AA)}{dP(A)} \right]_{\alpha_1} = \left[\frac{dP(AA)}{dP(A)} \right]_{\alpha_2}$$

where α_1 and α_2 are any two degrees of neutralization, or in more general terms, states of ionization. From equation (15) of ref 10 this gives for a given $P(A)$:

$$\frac{-2k'(AAA)_{\alpha_1}P(AAA) - k'(AAB^+)_{\alpha_1}P(AAB^+)}{N_{\alpha_1}} = \frac{-2k'(AAA)_{\alpha_2}P(AAA) - k'(AAB^+)_{\alpha_2}P(AAB^+)}{N_{\alpha_2}} \quad (3)$$

the $k'(XAX)$ being relative rate constants and

$$N_{\alpha} = -k'(AAA)_{\alpha}P(AAA) - k'(AAB^+)_{\alpha}P(AAB^+) - k'(BAB)_{\alpha}P(BAB) \quad (4)$$

Because the $P(XAX)$ at a given $P(A)$ are shown to be the same at α_1 and α_2 , equation (3) leads to:

$$k'(XAX)_{\alpha_1} = k'(XAX)_{\alpha_2} = k'(XAX) \quad (5)$$

at a given $P(A)$. Thus the $k'(XAX)$ are invariant with α but may depend on $P(A)$.

Equation (15) of ref 10 is valid for irreversible, overall first order and overall second order reactions of triads. However, some other conceivable models for the polymer analogous reaction would also give equation (5) considering Figures 1 and 2.

Comparison of the data in Figures 1 and 2 with the calculated Bernoullian $P(XXX)$ indicates that the copolymers change from Bernoullian to block character during the course of hydrolysis. This finding is corroborated by the behaviour of dyads in Figure 3. The $P(XX)$ of Figure 3 (points) have been obtained from the broken curves of Figures 1 and 2, applying the principle of stationarity at intervals of $P(A) = 0.05$. The block character indicates that the carboxyl groups in different ionization states which are next neighbours to MMA units partake in the mechanism of the hydrolysis of these MMA-units. Figures 1 and 2 also show that the hydrolysis may be almost complete which would not be possible if the reaction was significantly reversible. The essential irreversibility of the reaction has also been shown using syndiotactic poly (methacrylic acid) with a corresponding amount of methanol (see experimental section). It has been demonstrated that the $P(XXX)$ measured by n.m.r. represent the probabilities for individual chains by fractionating the copolymers by a procedure which was previously shown¹² to fractionate according to $P(A)$.

In Figure 4 the graphically determined slopes $dP(XX)/dP(A)$, are shown for the $P(XX)$ versus $P(A)$ plot of Figure 3. A triple ordinate is employed as before¹⁰ for averaging the errors which originate by the deviations of the $P(XX)$ versus $P(A)$ curves from the principle of stationarity and/or by the graphical evaluation of slopes. As

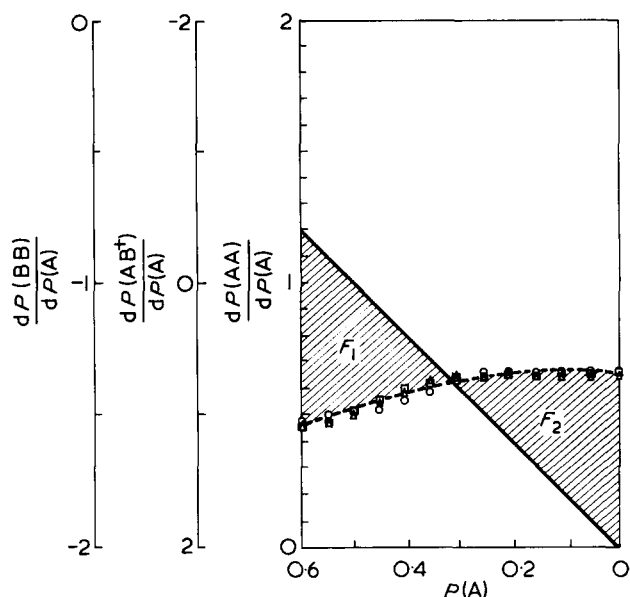


Figure 4 Slopes $dP(XX)/dP(A)$ of $P(XX)$ versus $P(A)$ curves of Figure 3. Diagonal is $2P(A)$, valid for a hypothetical hydrolysis with $k'(AAA) = k'(AAB^+) = k'(BAB) = 0.33$. Shaded areas F_1 and F_2 as an additional test for correct slope measurement. Δ , $dP(BB+)/dP(A)$ vs. $P(A)$; \square , $dP(AB^+)/dP(A)$ vs. $P(A)$; \circ , $dP(AA)/dP(A)$ vs. $P(A)$

to be expected¹⁰, the ratio of areas $F_1/F_2 = 0.96$ is close to 1 in Figure 4.

Besides using a Bernoullian copolymer of $P(A) = 0.60$ (copolymer no. 9 of Table 4 in ref 10) with different initial α , a Bernoullian copolymer of $P(A) = 0.83$ was employed (copolymer no. 6 of Table 4 in ref 10) as a starting material. Using 0.5 mmol KOH initially, $\alpha = 1$ is reached almost immediately during the run. With 1.0 mmol KOH, however, the hydrolysis progresses first by attack of OH^- . At the point of consumption of OH^- ($\alpha = 1$), the hydrolysis continues by the acidic mechanism. Correspondingly, with 1.0 mmol KOH only the part of the data obtained by acidic hydrolysis is of relevance here. The $P(XAX)$ versus $P(A)$ data obtained with a starting copolymer of $P(A) = 0.83$ have already been discussed in connection with the change of mechanism from the basic to the acidic range¹⁰. The evaluation of $P(XX)$ and $dP(XX)/dP(A)$ was carried out analogously to that of the starting copolymer of $P(A) = 0.60$. No data are available with different α at the beginning of the acidic hydrolysis, contrary to the case of the starting copolymer of $P(A) = 0.60$. However, for the evaluation of the $k'(XAX)$ one may find for a given $P(A) - \alpha$ state during a run starting from $P(A) = 0.83$, the same state for the runs starting from $P(A) = 0.60$ if the first runs have reached $P(A) = 0.60$ or below and if the latter runs are considered to be invariant with α .

For the determination of the relative rate constants equation (20) of ref 10 was used. The intersections of the corresponding straight lines in the $k'(AAA)$ versus $k'(AAB^+)$ plot demonstrated that the values for $k'(AAA)$ are only small, while the $k'(AAB^+)$ are larger. Using all available $P(XAX)$ and $dP(AA)/dP(A)$ data, the data were replotted therefore in the equivalent $k'(AAB^+)$ versus $k'(BAB)$ diagram by means of equation (6).

$$k'(AAB^+) = C_1 + C_2 k'(BAB) \quad (6)$$

$$C_1 = - \frac{(S - 2)P(AAA)}{S[P(AAB^+) - P(AAA)] + 2P(AAA) - P(AAB^+)} \quad (7)$$

$$C_2 = \frac{(S - 2)P(AAA) - SP(BAB)}{S[P(AAB^+) - P(AAA)] + 2P(AAA) - P(AAB^+)} \quad (8)$$

where $S = dP(AA)/dP(A)$. In the corresponding plot of Figure 5 the first arabic numeral indicates the runs from which a given line originates, i.e. (1) initial $P(A) = 0.83$, with 0.5 mmol initial KOH; (2) $P(A) = 0.83$, with 1.0 mmol KOH, and (3) $P(A) = 0.60$, with 1.0, 0.75, 0.50 and 0.25 mmol KOH. The second numeral indicates the $P(A)$, e.g. 6 means $P(A) = 0.60$. Lines of the same run exhibit usually only small differences in slope, their intersects are therefore less reliable. However, lines belonging to different runs possess often less acute angles at their intersects. Nevertheless the latter intersects scatter also in a relatively large range of $k'(XAX)$ reflecting significant inaccuracy of the data. Taking the average of the intersects results in $k'(BAB) \approx 0.80$, $k'(AAB^+) \approx 0.15$ and $k'(AAA) = 1 - k'(AAB^+) - k'(BAB) \approx 0.05$. From these values it appears already that the acidic hydrolysis of A monomer units relies primarily on the attack of neighbouring B-units. This is in contrast to the hydrolysis with base where the attack of OH^- is retarded by neighbouring B due to electrostatic repulsion between OH^- and negatively charged B.

The ratio $k'(BAB)/k'(AAB)$ is much larger than two, which indicates that neither general acid catalysis by $-\text{COOH}$ nor nucleophilic catalysis by $-\text{COO}^-$ alone or simultaneously are primarily responsible for the hydrolysis. A concerted electrophilic-nucleophilic catalysis by $-\text{COOH}$ and $-\text{COO}^-$ seems to be operating. This conclusion is supported by the time dependent rates which exhibit a maximum between $\alpha = 0$ and $\alpha = 1$ ¹³.

In order to demonstrate that the similar slopes for a given run in Figure 5 are a property of the statistics of monomer units for the runs in question, several runs of 1000 monomer units each were simulated by computer as previously described¹⁴. The simulated runs started from the homo-

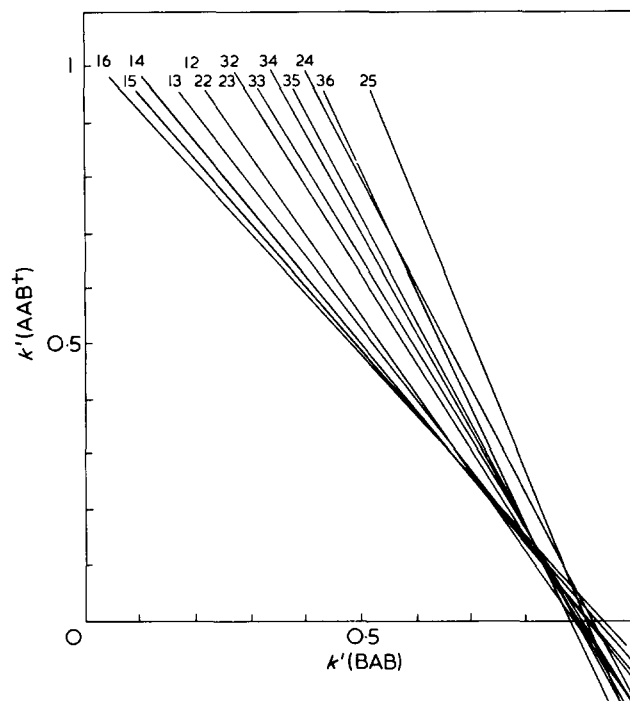


Figure 5 Relative rate constants $k'(AAB^+)$ versus $k'(BAB)$ according to equation (6). Lines identified by type of run (first digit) and $P(A)$ (second digit). Runs 1 and 2 start from $P(A) = 0.83$ with 0.5 and 1.0 mmol KOH in H_2O , respectively. Run 3 starts from $P(A) = 0.60$ with different amounts of KOH in H_2O or $\text{H}_2\text{O}/\text{dioxane}$

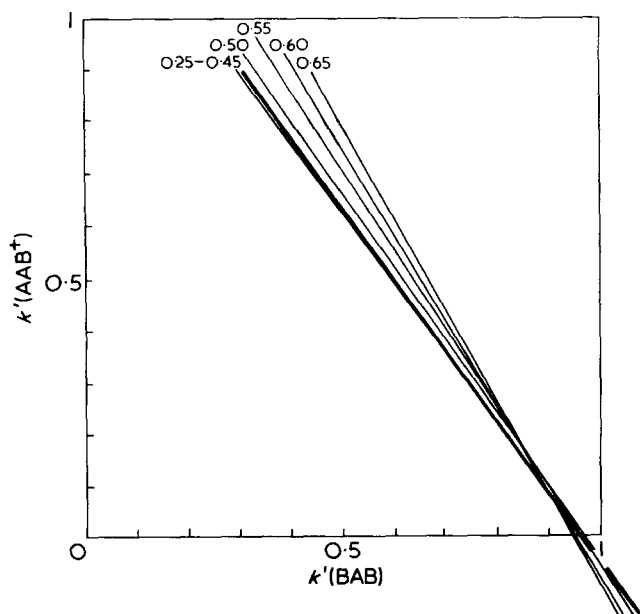


Figure 6 Relative rate constants $k'(AAB^+)$ versus $k'(BAB)$ according to equation (6) from the block-like part of computer runs of 1000 monomer units simulated with $k'(AAA) = 0.01$, $k'(AAB^+) = 0.10$, $k'(BAB) = 0.90$. Curves for values of $P(A)$ 0.25–0.65 are shown in the Figure

polymer with the Bernoullian set of relative rate constants $k'(AAA) = k'(AAB^+) = k'(BAB) = 0.33$ until $P(A) = 0.67$ was reached. The set of rate constants was changed at this point to $k'(AAA) = 0.01$, $k'(AAB^+) = 0.09$, $k'(BAB) = 0.90$ which is similar to the experimentally found set of rate constants. The resulting block part of the simulated curves of $P(XXX)$ was evaluated in analogy to the experimental curves yielding the $k'(AAB^+)$ versus $k'(BAB)$ plot of Figure 6. The random errors incurred with 1000 monomer units amount to $\Delta P(XXX) = \pm 0.01$ selecting individual runs at random at a given $P(A)$, and as compared to the average of a larger number of runs with 1000 monomer units each. This error, and the errors in drawing curves

through the selected points, as well as in measuring the slopes of the curves, suffice, in conjunction with the small slope differences of the straight lines in Figure 6, to distribute the intersects over a relatively large range. Thus a plot of the type of Figure 6 indicates the errors inherent in the evaluation of $k'(XAX)$, including the random errors in measuring the $P(XXX)$. Comparison with a plot of the type of Figure 5 indicates then the magnitude of the systematical errors in measuring $P(XXX)$ and/or the possible true variation of the $k'(XAX)$, provided the $k'(XAX)$ are the same or similar between the Figures.

ACKNOWLEDGEMENT

Thanks are due to the Deutsche Forschungsgemeinschaft for financial support. Spectra were recorded with assistance of H. Bodenstein, H. Bührer, H. Erler, A. Hasenhiindl and M. Seiter.

REFERENCES

- 1 Thanassi, J. W. and Bruice, T. C. *J. Am. Chem. Soc.* 1966, **88**, 747
- 2 Ebersson, L. *Acta Chem. Scand.* 1964, **18**, 2015
- 3 Ebersson, L. *Acta Chem. Scand.* 1962, **16**, 2245
- 4 Bender, M. L. *Chem. Rev.* 1960, **60**, 53
- 5 Capon, B. *Quart. Rev. Chem. Soc.* 1964, **18**, 45
- 6 Morawetz, H. and Oreskes, I. *J. Am. Chem. Soc.* 1958, **80**, 2591
- 7 Smets, G. and van Humbeeck, W. *J. Polym. Sci. (A)* 1963, **1**, 1227
- 8 DeLoecker, W. and Smets, G. *J. Polym. Sci.* 1959, **40**, 203
- 9 Smets, G. and DeLoecker, W. *J. Polym. Sci.* 1960, **45**, 461
- 10 Barth, V. and Klesper, E. *Polymer* 1976, **17**, 777
- 11 Klesper, E. and Barth, V. *Polymer* 1976, **17**, 787
- 12 Klesper, E., Strasilla, D. and Regel, W. *Makromol. Chem.* 1974, **175**, 523
- 13 Klesper, E. *et al.* unpublished results
- 14 Klesper, E., Gronski, W. and Barth, V. *Makromol. Chem.* 1971, **150**, 223
- 15 Strasilla, D. and Klesper, E. *Makromol. Chem.* 1974, **175**, 535

Phosphonitrilic chloride : polymerization behaviour of some hexaalkoxycyclotriphosphazenes

M. Kajiwara, Y. Mori, and H. Saito

Department of Applied Chemistry, Faculty of Engineering, Nagoya University, Nagoya, Japan

(Received 6 February 1976)

Electron conductivity of hexaalkoxycyclotriphosphazenes $N_3P_3(OR)_6$ is temperature dependent; the conductivity of the n-propoxy derivatives is dramatically raised at elevated temperature. $\tan \delta$ values of hexa-n-propoxy- and hexa-n-butoxy-cyclotriphosphazene increase appreciably at room temperature at high frequency. A chemical shift with ^{31}P -n.m.r. spectra of hexa-n-propoxycyclotriphosphazene appears at the lowest field compared with other hexaalkoxycyclotriphosphazenes. Dipropyl ether or dibutyl ether, respectively, were detected when hexa-n-propoxy- or hexa-n-butoxy-cyclotriphosphazene were heated. It is assumed that a polymerization rather than a rearrangement reaction occurs on heating with the elimination of ethers.

INTRODUCTION

The preparation of hexaalkoxycyclotriphosphazenes¹⁻³ and their pK'_a values have been reported^{4,5}. Shaw *et al.*⁶⁻⁸ observed that some hexaalkoxycyclotriphosphazenes are transformed to *N*-alkylcyclotriphosphazenes under certain conditions. Godfrey⁹ found that hexa-n-propoxycyclotriphosphazene is the best flameproofing agent of the series for rayon, and many patents¹⁰ describe its use for this purpose. In this paper some characteristic properties of several hexaalkoxycyclotriphosphazenes are presented.

EXPERIMENTAL

Materials

Hexachlorocyclotriphosphazene $(NPCl_2)_3$ was prepared by the modified method of Kajiwara¹². Pure trimer was obtained by repeated fractional crystallization from light petroleum.

Hexaalkoxycyclotriphosphazenes $N_3P_3(OR)_6$ (R = CH_3 , C_2H_5 , $n-C_3H_7$, $n-C_4H_9$) were prepared by the method of Shaw¹.

Methods

Ultra-violet spectra were measured with a Hitachi-124 type spectrometer in n-hexane, methanol and ethanol. ^{31}P -n.m.r. spectra were measured with a Nihon Denshi JNMC-60HL type spectrometer using dioxane as solvent and H_3PO_4 as standard. Electron conductivity measurements were carried out following the method of Kajiwara¹³ and dielectric constants were measured with a Shibayama Kagaku SS-802 type apparatus.

RESULTS AND DISCUSSION

The u.v. characteristics of hexaalkoxycyclotriphosphazenes are summarized in Table 1. The maximum absorption of hexaalkoxycyclotriphosphazenes appears at 215–217 nm in n-hexane. The maxima are not shifted with different

alkyl groups, but they change their position in methanol or ethanol. A slight blue shift is due to $n-n^*$ of nitrogen atoms rather than to $\pi-\pi^*$ transitions in the triphosphazene ring.

Dipole moments may indicate the planarity or non-planarity of a ring system. Results for some hexaalkoxycyclotriphosphazenes determined by dielectric constant measurements are given in Table 2.

High dipole moments suggest the presence of a relatively inflexible ring at 25°C whereas low dipole moments are consistent with a slightly planar ring at 95°C. Differences in dipole moments directly attributable to side groups have not been observed.

The $\tan \delta$ curves for some hexaalkoxycyclotriphosphazenes at room temperature are shown in Figure 1.

At lower frequencies a decrease in $\tan \delta$ results from dipole relaxation, deformation or electron polarization losses. At high frequencies an increase in $\tan \delta$ for hexa-n-

Table 1 Ultra-violet absorption maxima, λ_{max} , ϵ (nm), of hexaalkoxycyclotriphosphazenes

Alkyl	n-Hexane		Methanol		Ethanol	
	λ_{max}	ϵ (nm)	λ_{max}	ϵ (nm)	λ_{max}	ϵ (nm)
CH_3			201	40		
C_2H_5	215	120	205	120	206	120
$n-C_3H_7$	217	810	203	60	205	90
$n-C_4H_9$	217	910	203	90	205	100

Table 2 Dielectric Constant, dipole moment and conductance of hexaalkoxycyclotriphosphazene

Alkyl	Dielectric constant		Dipole moment		Conductance (sec/cm $\times 10^{-9}$)	
	25°C	95°C	25°C	95°C	25°C	120°C
	C_2H_5	6.7	4.2	3.3	2.3	6.3
$n-C_3H_7$	5.3	3.5	3.1	2.2	1.9	2100
$n-C_4H_9$	4.5	3.2	3.1	2.1	1.1	38

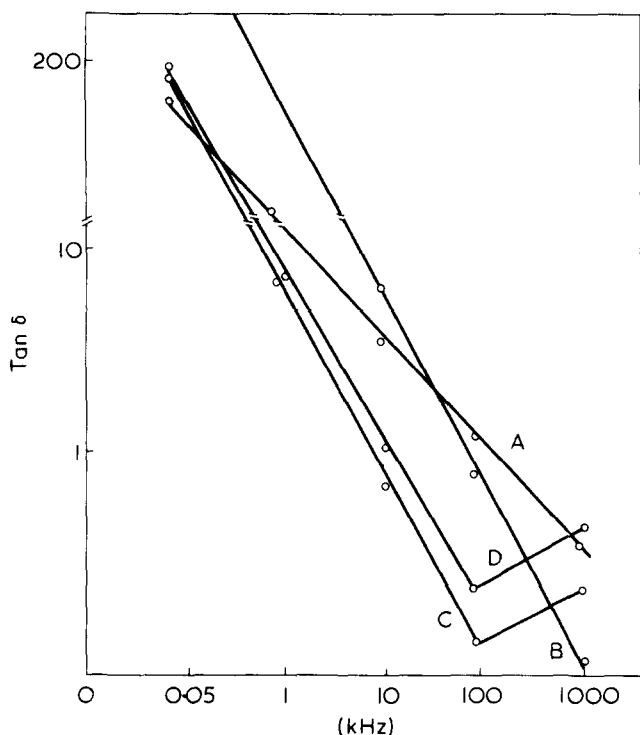


Figure 1 Tan δ of hexaalkoxycyclotriphosphazenes $[\text{NP}(\text{OR})_2]_3$ at room temperature. A, R = Me; B, R = Et; C, R = Prⁿ; D, R = Buⁿ

Table 3 ³¹P-n.m.r. chemical shift values, δ , for hexaalkoxycyclotriphosphazenes in dioxane

Alkyl	δ (ppm)
CH ₃	-21.3 ^a
C ₂ H ₅	-15.3 ^b
n-C ₃ H ₇	-34.2
n-C ₄ H ₉	-16.9

^a-21.7 (Allcock, H. R. *Inorg. Chem.* 1966, 5, 1709). ^b-15.3 (Allcock, H. R. *Inorg. Chem.* 1966, 5, 1709)

propoxy- or hexa-*n*-butoxy-cyclotriphosphazene is attributed to an ion split off from their R groups. However, this is not observed with hexamethoxy- or hexaethoxycyclotriphosphazene. The electron conductivity of some hexaalkoxytriphosphazene (Table 2) shows that the conductivity of hexa-*n*-propoxycyclotriphosphazene shows the largest increase with increasing temperature. Allcock and Best¹¹ found that above 200°C the conductivity of molten hexachlorocyclotriphosphazene increased dramatically with temperature, and ascribed this to dissociation of chloride ion from phosphorus, with concurrent polymerization of the trimer. Consequently, the highest conductivity of hexa-*n*-propoxycyclotriphosphazene obtained at 120°C is attributed to dissociation of an ion from R groups in hexa-*n*-propoxycyclotriphosphazene.

As shown in Table 3 ³¹P-n.m.r. spectra of some hexaalkoxycyclotriphosphazenes display a singlet peak, and the chemical shift of hexa-*n*-propoxycyclotriphosphazene appears at the lowest field. For this reason, it is believed that the electron density around phosphorus atoms is lowered by the deshielding effect, i.e. the electron may centre on nitrogen atoms.

A change in viscosity of some hexaalkoxycyclotriphosphazenes on heat treatment is shown in Figure 2.

It can be seen that the viscosity of hexa-*n*-propoxycyclo-

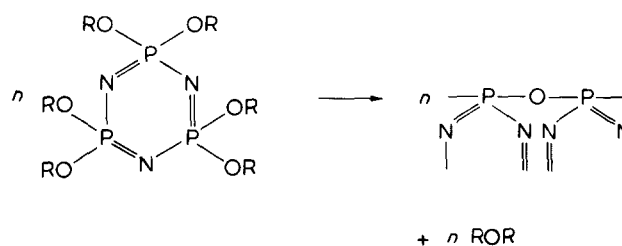
triphosphazene rapidly increases with temperature, and a crystalline product, *N*-ethylcyclotriphosphazene having a melting point of 61°C is obtained from hexaethoxycyclotriphosphazene.

The molecular weights of hexaalkoxycyclotriphosphazenes increases on heating as shown in Figure 3. The rapid change with hexa-*n*-propoxycyclotriphosphazene parallels the corresponding increase in viscosity.

The products formed from hexa-*n*-propoxycyclotriphosphazene on heating were collected in a glass tube cooled by dry ice, and were identified by gas chromatography or ¹H-n.m.r. spectra as propyl ether or butyl ether; other products were not observed.

From the analytical data it can therefore be estimated that polymerization rather than rearrangement becomes the predominant reaction on heating hexa-*n*-propoxycyclotriphosphazene or hexa-*n*-butoxycyclotriphosphazene.

Consequently, it can be presumed that the polymerization reaction proceeds as follows:



R = *n*-CH₂CH₂CH₃, *n*-CH₂CH₂CH₂CH₃

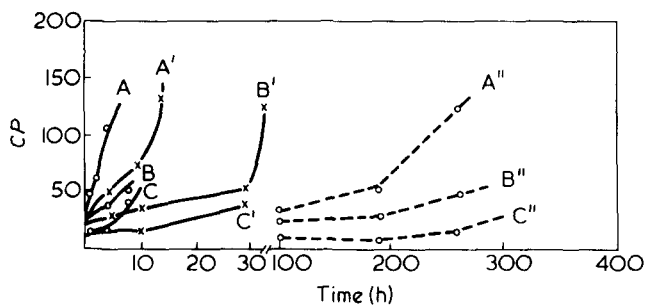


Figure 2 The time curves of viscosity of hexaalkoxytriphosphazenes $[\text{NP}(\text{OR})_2]_3$ during heating: O, 155°C; X, 135°C; ---, 110°C. A, A', A'', Prⁿ; B, B', B'', Buⁿ; C, C', C'', Et

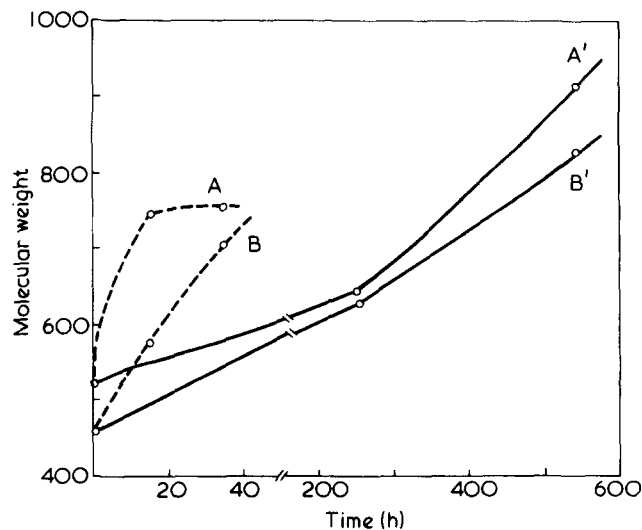


Figure 3 The time course curves of molecular weight of hexaalkoxytriphosphazenes $[\text{NP}(\text{OR})_2]_3$ during heating: ---, 150°C; —, 110°C. A, A', Buⁿ; B, B', Prⁿ

However, products insoluble in organic solvents are formed when hexa-n-propoxy- or hexa-n-butoxy-cyclotriphosphazene are heated for a long time and glass-like products are obtained at the final stage.

REFERENCES

- 1 Fitzsimmons, B. W. and Shaw, R. A. *J. Chem. Soc.* 1964, 1735
- 2 Allcock, H. R., Caputo, R., Kalmus, A., Roberts, C. W. and McBee, E. T. *US Gov. Res. Rep.* 1959, 209, 669
- 3 Kajiwara, M. and Saito, H. *J. Inorg. Nucl. Chem.* 1974, 36, 738
- 4 Feakins, D., Last, W. A., Neemuchwala, N. and Shaw, R. A. *Chem. Ind. (London)*, 1963, 164
- 5 Feakins, D., Last, W. A., Neemuchwala, N. and Shaw, R. A. *J. Chem. Soc.* 1965, 2804
- 6 Fitzsimmons, B. W. and Shaw, R. A. *Proc. Chem. Soc.* 1961, 258
- 7 Fitzsimmons, B. W., Hewlett, C. and Shaw, R. A. *J. Chem. Soc.* 1964, 4459
- 8 Fitzsimmons, B. W., Hewlett, C. and Shaw, R. A. *J. Chem. Soc.* 1965, 7432
- 9 Godfrey, L. E. A. and Schappel, J. W. *Ind. Eng. Chem. Prod. Res. Dev.* 1970, 9, 426
- 10 Ger. Pat. 2 245 079, 2 056 619, 2 306 510, 2 341 739; US Pat. 3 799 526, 3 732 683, 3 455 713; Br. Pat. 1 153 955; Fr. Pat. 2 021 440
- 11 Allcock, H. R. and Best, R. J. *Can. J. Chem.* 1964, 42, 477
- 12 Saito, H. and Kajiwara, M. *J. Chem. Soc. Japan Ind. Chem. Sect.* 1966, 66, 618
- 13 Kajiwara, M., Hashimoto, M. and Saito, H. *Polymer* 1973, 14, 488

^{13}C n.m.r. study of optically active polymers: poly(4-methyl-1-hexene)

F. Conti and L. Acquaviva

Istituto di Chimica Fisica, Università di Roma, Rome, Italy

E. Chiellini and F. Ciardelli

Centro di Studio del CNR per le Macromolecole Stereordinate ed Otticamente Attive, Istituto di Chimica Organica Industriale, Università di Pisa, Pisa, Italy

and M. Delfini and A. L. Segre

Laboratorio di Chimica e Tecnologia dei Radioelementi, CNR, Padova, Italy

(Received 2 April 1976; revised 24 May 1976)

Isotactic polymers of optically active and racemic 4-methyl-1-hexene, obtained by polymerization with Ziegler–Natta catalysts, were studied by ^{13}C n.m.r. Polymer fractions with different stereoregularity and molecular weight, derived from the monomer with high optical purity, show in their ^{13}C n.m.r. spectra differences which are tentatively associated with possible conformation effects. Stereoselectivity is observed in polymers obtained from the racemic monomer.

INTRODUCTION

The investigation of the microstructure of vinyl polymers from chiral olefins led to a better knowledge of the nature and mechanism of steric control in stereospecific¹ and stereoselective^{2,3} polymerizations. Moreover information on the relation between microstructure and conformation in solution was obtained by studying chiroptical properties of the above polymers and by comparing experimental values of rotatory power with the calculated ones, according to Brewster's method⁴. For the detailed determination of the macromolecular conformation in the solid state, X-ray studies were essential. In the case of poly[(*S*)-3-methyl-1-pentene]⁵ and poly[(*S*)-5-methyl-1-heptene]⁶, the crystal structure shows the existence of macromolecules having helical conformation with the left screw sense only, while for poly[(*S*)-4-methyl-1-hexene] main chain helical conformation of both screw senses has been found in the stable form, a second metastable form existing with the left handed screw sense only⁷. Statistical models^{8–11} in addition allowed one to obtain indications of the most probable conformation in solution. All the authors agree on the general feature of the model which consists of a succession of main chain sections spiralled in both the possible screw senses with one screw sense largely prevailing. N.m.r. has proved to be a powerful tool for studying configuration and conformation of polymers in solution, and we have therefore examined 4-methyl-1-hexene polymers obtained with Ziegler–Natta catalysts by ^{13}C n.m.r. The results constitute the object of the present paper.

EXPERIMENTAL

Monomers

(*S*)-4-methyl-1-hexene, (*R*)-4-methyl-1-hexene with different optical purity and racemic 4-methyl-1-hexene were obtained as described previously^{12,13}.

Polymers

Polymerization experiments were carried out in the presence of TiCl_3 'ARA', or VCl_4 and $\text{Al}(\text{iso-C}_4\text{H}_9)_3$, and the polymers obtained were fractionated by extraction with different solvents as previously reported¹⁴. In Table 1 the characteristics of some typical analysed samples are collected.

Polymers were characterized by their optical rotation at 589 nm, viscosity-average molecular weight, and crystallinity by X-rays.

^{13}C n.m.r. spectra were run on 5% solutions in CDCl_3 at room temperature and at 70°C, on a Varian FTXL 100 and on a Bruker HF90, using TMS (tetramethylsilane) as an internal reference. The spectral conditions were as follows: spectral width, 5000 Hz; acquisition time, 0.4 sec; pulse width, 30 μsec ; sensitivity enhancement factor, 0.3 sec; K transients 10 to 50. The results obtained with the two spectrometers were absolutely reproducible.

RESULTS AND DISCUSSION

Assignment of the spectra

The ^{13}C n.m.r. spectrum of poly[(*S*)-4-methyl-1-hexene] (sample E_{1,2}, Table 1) is given in Figure 1. Apart from variation of the intensities, and the width of the lines of the two signals at 11.51 and 31.72 ppm, all polymers from monomers having high optical purity show identical spectra.

Let us consider the monomeric residue:

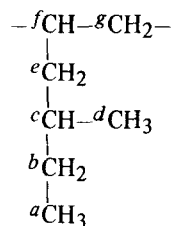


Table 1 Properties of the poly(4-methyl-1-hexene) samples obtained from optically active and racemic monomer analysed by ¹³C n.m.r.

Monomer absolute configuration	Polymeric sample	Catalyst	Fraction				
			Solvent for extraction	Weight %	[α] _D ²⁵ ^a	[η] ^b (dl/g)	$\bar{M}_v \times 10^{-3}$
S ^c	E _{0,2} E _{0,3}	VCl ₄ /Al(iso-C ₄ H ₉) ₃	Diethyl ether	52.5	+257	1.64	425
			Chloroform	47.5	+272	6.85	2365
	E _{1,2} E _{5,2}	TiCl ₃ 'ARA'/Al(iso-C ₄ H ₉) ₃	Diethyl ether	42.9	+258	0.67	145
			Diethyl ether	46.0	+268	0.94	215
R ^d	E _{5,3} E _{R,3}		Cyclohexane	54.0	+270	4.39	1395
			Di-isopropyl ether	24.5	-248	1.69	440
R,S	E _{R0,3}	VCl ₄ /Al(iso-C ₄ H ₉) ₃	Cyclohexane	55.8	—	3.60	1105

^aMeasured in chloroform solution; ^bmeasured in tetralin at 120°C; ^cmonomer with optical purity 93.5%¹² was polymerized; ^dmonomer with optical purity 87.0%¹² was polymerized

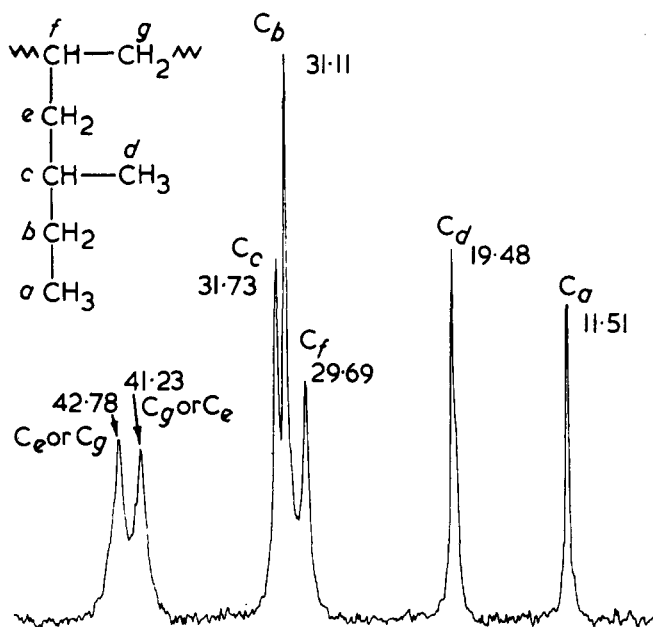


Figure 1 ¹³C n.m.r. spectrum of poly[(S)-4-methyl-1-hexene] (sample E_{1,2}) at room temperature

Table 2 Assignment of ¹³C n.m.r. spectra of poly(4-methyl-1-hexene) obtained from high optical purity and racemic monomer

Assignment	Average δ-value (ppm) of the signals observed for polymer from:		
	Optically active monomer	Racemic monomer	Calculated δ-value (ppm)
C _a	11.51	11.41	10.87
C _b	31.13	*30.87†	29.60
C _c	31.74	*31.72†	32.52
C _d	19.52	19.59 20.35	19.63
C _e or C _g	42.77 broad	43.00	41.67
C _f	29.72	*30.00 broad high intensity	30.84
C _g or C _e	41.20 broad	41.70 intensity	39.98

*In the 30.00 ppm band of the polymer from racemic monomer, peaks due to C_b and C_c should overlap the C_f signal due to very strong intensity of this band; †with other signals at 30.00 ppm

The assignment of the peaks is made accordingly to the rules of Lindemann and Adams¹⁵, as well as on the basis of 'Off Resonance' experiments (Table 2).

The three signals at 29.70 ppm, 31.13 ppm and 31.70 ppm are due to the methine carbons C_f and C_c and to the

methylenic C_b respectively. The assignment of the peak at 31.13 ppm to C_b was obtained by an 'Off Resonance' experiment. The assignment of the peaks at 29.70 ppm and 31.70 ppm to methines C_f and C_c respectively is made on the basis of the application of Lindemann and Adams rules, and is supported by the observation that in polymers obtained from the racemic monomer, which show quite different spectra due to the broadening and overlapping of some resonances (Figure 2), the signal at 29.70 ppm does not change while the signal at 31.70 ppm is split; this splitting (present also in the signals due to C_d and C_b) can be related to the variation in the configuration of the asymmetric carbon atom C_c (see Table 2).

The peaks at 41.20 ppm and 42.70 ppm, due to methylenic carbon atoms C_e and C_g cannot be assigned unequivocally because of their broadness in all the samples examined*. Clearly optically active polymers obtained from the (R) monomer show spectra identical to those obtained from the (S) monomer¹⁶.

Conformational effects on poly[(S)-4-methyl-1-hexene]

In Figure 3 spectra of fractions of poly[(S)-4-methyl-1-hexene], extracted with diethyl ether and cyclohexane, run at room temperature and at 70°C are reported. The polymers, previously extracted with acetone and ethyl acetate, have a rather high isotactic content.

The spectra of different fractions, run at the same temperature, show some peculiar differences. The resonance line due to C_c, at 31.72 ppm and to a lesser extent that due to C_a at 11.41 ppm, show different line widths which seem to indicate a difference in the correlation times. If this difference in the spectra were due to differences of steric configuration about carbon C_f, one might expect that the signal due to this carbon atom would be split at least in the less stereoregular fraction. However it would seem that the more affected resonances are for C atoms (C_a and C_c) quite far away (6 and 4 bonds) from the hypothetical centre of irregularity C_f. Because of the high optical purity of the monomers used, and the very close values of the optical rotation of the two fractions, conformational effects on the side chain must be ruled out.

Consequently a possible explanation should be related to conformational effects on the side chain; different con-

* These assignments are confirmed recently by the elegant work of Neuenschwander in which the assignments of the methine carbons were obtained with ¹³C enriched (in position f) monomers. *Makromol. Chem.* 1976, 177, 1231
We thank Professor P. Pino and Dr P. Neuenschwander, for sending us the manuscript before publication.

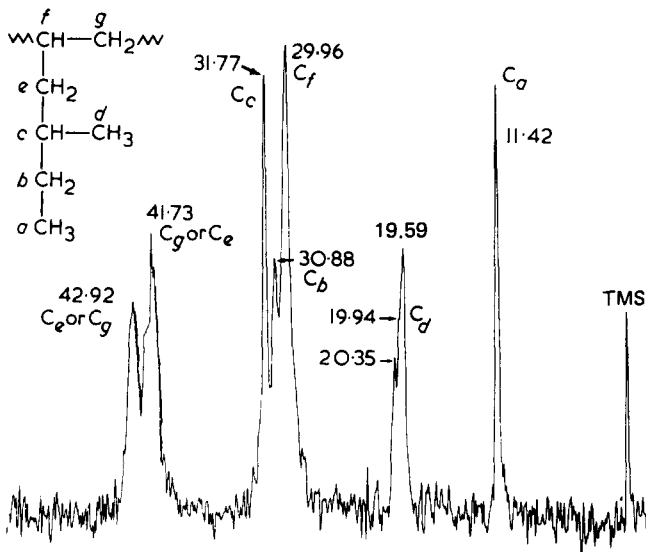


Figure 2 ¹³C n.m.r. spectrum of poly[(*R*)(*S*)-4-methyl-1-hexene (sample E_{70,3}) at room temperature

formers for units of poly[(*S*)-3-methyl-1-pentene]⁵ and poly[(*S*)-4-methyl-1-hexene]⁷ have been observed in the solid state.

The similarity of the spectra at 70°C of sample E_{5,3} and of the spectra of sample E_{5,2} at room temperature strongly support this explanation.

Taking into account the slight stereoregularity difference between examined samples it might be possible that the extraction is controlled by molecular weight. So far it cannot be excluded that steric defects are present in similar amounts but have different distribution in the two fractions.

Configurational effects

Let us consider isotactic polymers obtained by polymerization of racemic 4-methyl-1-hexene with a Ziegler–Natta catalytic system or more generally isotactic polymers in which macromolecules consisting of both the monomer enantiomers may be present.

With respect to the side chain asymmetric C atom which can have *R* or *S* configuration, it is possible to have in terms of triads the following situation:

- | | |
|--------------|--------------|
| <i>R R S</i> | <i>R S S</i> |
| (1a) | (1b) |
| <i>S R R</i> | <i>S S R</i> |
| (2a) | (2b) |
| <i>S R S</i> | <i>R S R</i> |
| (3a) | (3b) |
| <i>R R R</i> | <i>S S S</i> |
| (4a) | (4b) |

The triads a and b are equivalent being in an enantiomeric relation.

The spectrum of the E_{70,3} sample (Figure 2) shows the splitting of the resonances due to the methyl C_d in three different peaks at 19.59 ppm, 19.94 ppm, 20.35 ppm. The analysis of these peaks in terms of triads is straightforward since the signal at 19.59 ppm is also observed in polymers obtained from the optically pure monomer. Hence the peak

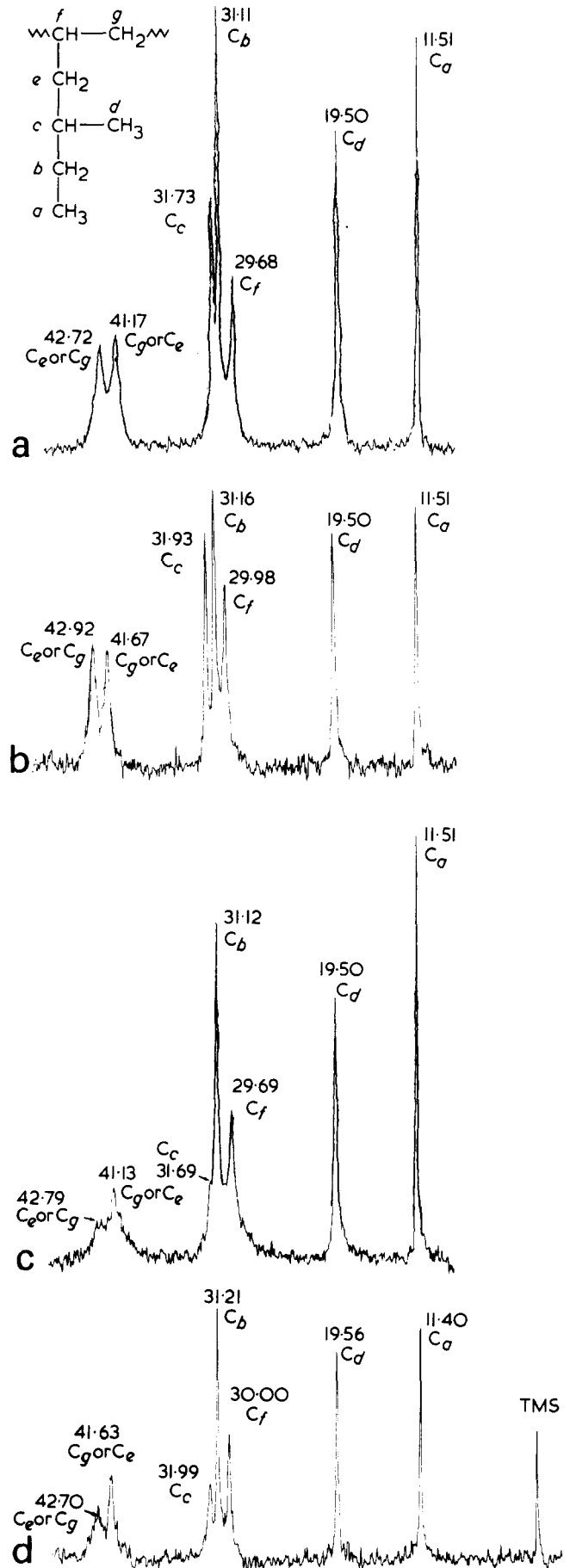


Figure 3 ¹³C n.m.r. spectra of poly[(*S*)-4-methyl-1-hexene]: (a) ether soluble fraction (sample E_{5,2}) at room temperature; (b) ether soluble fraction (sample E_{5,2}) at 70°C; (c) cyclohexane soluble fraction (sample E_{5,3}) at room temperature; (d) cyclohexane soluble fraction (sample E_{5,3}) at 70°C

at 19.59 ppm has been assigned to the triads (4a) and (4b). Because of the inversion of configuration of both the side units it is reasonable to think that the shifts for the triads (3a) and (3b) differ to a larger extent from the shifts for the triads (4a) and (4b) than those for the triads (1a), (1b) and (2a), (2b). With this hypothesis it is possible to attribute the peak at 20.35 ppm to the triads (3a) and (3b).

This assignment is in agreement with the fact that in absence of structure of the type:



the intensity of signals due to triads (3) are lower than the intensity of the triads (1) and (2). The signals at 19.94 ppm can be then assigned to the triads (1) and (2). Quantitative analysis is unreliable since the signals are partly overlapped. However it seems that the process of polymerization is stereoselective³.

In fact, in a non-stereoselective polymerization, the probability (and as a consequence the intensity of the corresponding signals) of triad (4a) would be 1/8, and, due to the magnetic equivalence of the *SSS* and *RRR* triads, the probability of the peak at 19.59 ppm should be 1/4 of the total which does not correspond to the experimental results.

ACKNOWLEDGEMENTS

This work was supported by Consiglio Nazionale delle

Ricerche. We thank Dr F. Wehrli of Varian A. G. Zug who ran some of the spectra.

REFERENCES

- 1 Pino, P. *Adv. Polym. Sci.* 1965, **4**, 393
- 2 Mazzanti, G., Corradini, P. and Giannini, U. *Rend. Accad. Naz. Lincei* 1955, **19**, 397
- 3 Pino, P., Oschwald, A., Ciardelli, F., Carlini, C. and Chiellini, E. 'Coordination Polymerization', (Ed. J. C. W. Chien), Academic Press, New York, 1975, p 25
- 4 Pino, P., Ciardelli, F. and Zandomenighi, M. *A. Rev. Phys. Chem.* 1970, **1**, 561
- 5 Petraccone, V., Ganis, P., Corradini, P. and Montagnoli, G. *Eur. Polym. J.* 1972, **8**, 99
- 6 Corradini, P., Martuscelli, E., Montagnoli, G. and Petraccone, V. *Eur. Polym. J.* 1970, **6**, 1201
- 7 Bassi, I. W., Bonsignori, O., Corradini, P., Lorenzi, G. P., Pino, P. and Temussi, P. A. *J. Polym. Sci (A-2)* 1971, **9**, 193
- 8 Birshtein, T. M. and Luisi, P. L. *Vysokomol. Soedin.* 1964, **6**, 1238
- 9 Allegra, G., Corradini, P. and Ganis, P. *Makromol. Chem.* 1966, **90**, 60
- 10 Abe, A. *J. Am. Chem. Soc.* 1968, **90**, 2205
- 11 Luisi, P. L. *Polymer* 1972, **13**, 232
- 12 Pino, P., Lardicci, L. and Centoni, L. *Gazz. Chim. Ital.* 1961, **91**, 428
- 13 Carlini, C., Pini, D., Bonsignori, O. and Neuenschwander, P. *Gazz. Chim. Ital.* 1973, **103**, 1297
- 14 Ciardelli, F., Montagnoli, G., Pini, D., Pieroni, O., Carlini, C. and Benedetti, E. *Makromol. Chem.* 1971, **147**, 53
- 15 Lindemann, L. P. and Adams, J. Q. *Anal. Chem.* 1971, **43**, 1245
- 16 Bovey, F. A. 'High resolution NMR of Macromolecules' Academic Press, New York, 1972

Melting in single screw extruders

J. Shapiro*, A. L. Halmos†, and J. R. A. Pearson

Department of Chemical Engineering and Chemical Technology, Imperial College, London SW7 2AZ, UK

(Received 10 March 1976)

A model for the melting of granules in a single screw extruder is presented in Part I. It is consistent with observations of earlier workers and retains some of the ideas introduced by Tadmor in his model; however, it assumes that the solid bed of granules cannot stand large differences of principal stresses and so account has to be taken explicitly of the downstream force balance on the solid bed and in the melt pool. Detailed quasi-analytic results are given for a Newtonian (constant viscosity) fluid in Part II. These illustrate the model for a particularly simple case and have relevance for some materials. A more elaborate numerical scheme is described in Part III for a non-Newtonian model and results are presented for comparison with the predictions of other theories and with experiments.

PART I: The Mathematical Model

INTRODUCTION

There is as yet no rational nor fully satisfactory mathematical model for the melting process in single screw extruders. Reliable predictive calculations that are based on fundamental physical principles cannot yet be carried out. However, experimental evidence obtained by several workers¹⁻⁵ on small to medium extruders had provided a fairly clear kinematic description of the process. Various physical and mathematical models have been described^{3,5-8} based on these observations, and comparisons have been made between calculations based on these models and experiment. In most cases the models are partly empirical, or fail to satisfy the full set of conservation laws that are generally accepted to govern mechanical phenomena, namely conservation of mass, momentum and energy⁹.

A new model attempting to satisfy all of these conservation laws was described at a meeting of an EFCE Working Party (1970) and was presented by Shapiro¹⁰. This model will be further developed here in relatively general form. It derives from the original observations of Maddock and Street and from the elementary model of Tadmor, the main difference from the last named being that the stress field is considered explicitly as part of the problem formulation. It is thus a full dynamical model and not merely a kinematical model.

The utility of the model must depend upon the approximations that can be shown to be relevant, because otherwise even numerical solution of the full governing equations is impracticable. Two particular approximation schemes are described and discussed in Parts II and III.

It is important to emphasize that a kinematical model for the process is needed and that it is not sufficient merely to write down the conservation equations for the whole system and to hope that the observed flow pattern will be predictable from first principles. A completely general approach would have to distinguish, for example, between a suspen-

sion of isolated granules in a molten matrix and the discrete solid bed observed in practice; it is not clear that the latter would be inevitably predicted.

THE 5-ZONE MODEL

Figure 1 provides in diagrammatic form the geometrical basis for the model we shall develop. The diagram relates to a cross-section of the screw channel taken perpendicular to the screw flights. The various geometrical approximations leading to this rectangular 'unrolled' form of the problem are now well known (see for example ref 11 pp.78-80, ref 12 and ref 13) and will not be discussed further. We choose a suitable Cartesian coordinate system with the x -axis parallel to the axis of the channel and the y -axis normal to the plane of the barrel (and to the floor of the screw

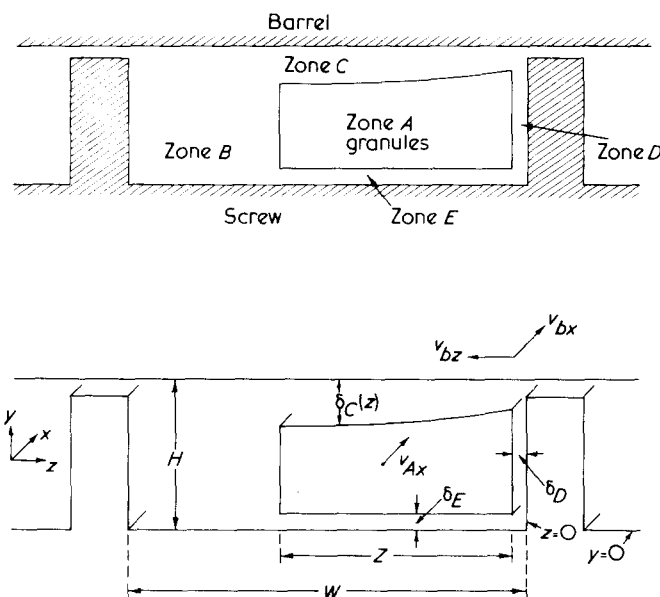


Figure 1 Geometry of the melting zone

* Present address: Canadian Industries Ltd, Quebec, Canada.

† Present address: Department of Chemical Engineering, Monash University, Clayton, Victoria 3168, Australia.

channel). The z -axis is thus normal to the screw flights. Curvature has been neglected.

The material flowing in the channel is divided into 5 zones, marked A to E . Zone A is formed of unmelted granular material, while zones B to E are regions of molten polymer. One essential feature of the model is that sharp interfaces exist between the solid and molten material, and that the cross-sectional shape of zone A is very nearly rectangular and fills most of the 'right-hand' side of the channel. The bulk of the mass flow in the downstream x direction takes place in the solid bed A and the melt pool B . Zones C , D and E are treated as relatively thin layers of molten polymer which 'lubricate' the surfaces of the solid bed, and across which heat to melt the solid bed can be conducted from the hot barrel and screw surfaces.

The cross-sectional shape shown in Figure 1 for a fixed value of x is assumed to vary slowly downstream, i.e. Z , the bed width, is a slowly varying (usually decreasing) function of x . Melting of the solid material at its interfaces with melt is a slow process. This means that no velocity gradient in the solid bed need be large. This is consistent with a second essential feature of the model, namely that the solid bed moves downstream with a velocity v_{Ax} that is independent of y and z and varies slowly with x . The y and z velocities in the bed are assumed very small everywhere.

It will be seen that the prime cause for any motion in the (y, z) -plane is provided by the crosschannel velocity v_{bz} of the barrel relative to the screw. This leads to a dragging of melt from zone C into zone B : put differently, the material that is melted at the AC interface is swept away by the barrel into the melt pool. Because of this, it may be anticipated that the thickness of the melt layer C will be small, and hence that both heat generation in and conduction across the layer C will be larger than similar effects in the other molten zones. Furthermore, the thickness will vary with z .

Zones D and E are treated as molten on the assumption that the screw temperature is higher than the melting point of the polymer. This need not necessarily be so: if the screw were kept cold enough, the bed of granules A would be in direct unlubricated contact with the metal screw, and frictional forces would replace the viscous ones that we shall be considering here. Because there is no significant motion of the bed A relative to the screw in the (y, z) -plane, the thicknesses of zones D and E will be treated as independent of y and z respectively at any station x , and the velocity in these zones as in the x direction only.

Because rheological forces are much larger than gravitational or inertial forces the momentum conservation equation degenerates to a stress equilibrium equation. A third essential feature of the model is that the rheological behaviour of the molten material is that of a temperature-dependent inelastic viscous liquid, while that of the solid bed is not specified in advance but is assumed to be consistent with the simple kinematics already presumed to apply in the solid bed. The stress equilibrium equation can therefore be satisfied locally everywhere in the molten material, i.e. in zones B – E , but only in an integrated form over the cross-section of the solid bed.

The consequences of these assumptions will become clear when we discuss the equations that are relevant in each zone treated separately, and when we then consider the overall relation that links the variables describing each zone. As with many such complex situations, it is difficult to decide which features of the model to treat as basic assumptions and which as consequences of the assump-

tions. What is important is to ensure that the model is self-consistent: this can only be done satisfactorily after numerical values have been calculated.

The relevant conservation laws and boundary conditions have been set out by Pearson¹¹. To these must be added those that apply at the solid bed–melt interfaces within the flow region. We shall require the velocity vector, the temperature and the stress tensor to be continuous. A discontinuity in the heat flux is permitted, which provides the heat necessary to melt the polymer at the interface.

Zone A: the solid bed

We have already stated that the solid bed's downstream velocity v_{Ax} and its width Z are to be treated as slowly varying functions of x only. To these variables we add the mass flowrate M_{Ax} and the melting rate R , also slowly varying functions of x . Formally

$$M_{Ax} = v_{Ax} \int_{-Z}^{-\delta_D} \left(\int_{\delta_E}^{H-\delta_C} \rho_A dy \right) dz \quad (1)$$

ρ_A can be regarded as temperature (T) and pressure (p) dependent and hence a function of y and z . However, since the pressure dependence is likely in practice to be more important than the temperature dependence, and our model treats (see below) the pressure as a function of x only, we can take ρ_A outside the integral. We note for later reference that if δ_C , δ_D and δ_E are taken to be $\ll H$, then

$$M_{Ax} \approx \rho_A v_{Ax} H Z \quad (1a)$$

where

$$\rho_A = \rho_A(p) \quad (2)$$

The mass melting rate, R , can again formally be written as

$$R = R_B + R_C + R_D + R_E \quad (3)$$

where the subscripts B – E refer to the melting taking place at the interfaces AB – AE . We shall take up the question of providing relations for each of these when we consider zones C – E .

The mass conservation equation for zone A then becomes, trivially,

$$\frac{dM_{Ax}}{dx} = -R \quad (4)$$

So far, there is no difference from all previous models.

We now consider the stress equilibrium equation for zone A . The kinematical model that we have chosen allows us to make use of the x component equation as a governing equation of the system; in particular, it effectively provides the extra equation needed to determine v_{Ax} in terms of the other variables that depend on x only. Formally we define the total shear stress/unit length in the x direction acting in the x direction over the interfaces AB – AE as S_{ABx} – S_{AEx} , so that the total shear force/unit length on the solid bed is given by

$$S_x = S_{ABx} + S_{ACx} + S_{ADx} + S_{AEx} \quad (5)$$

Note that this is the force caused by viscous shear stresses in the deforming molten material. Relations for S_{ABx} etc. will be derived in later subsections. This force will be balanced by the downstream variation in isotropic pressure p ($1/3$ the trace of the stress tensor) which is assumed to be a slowly varying function of x only, and to dominate all other 'normal' forces. We obtain

$$S_x = \frac{dp}{dx} \left[\int_{-Z}^{-\delta_D} \left(\int_{\delta_E}^{H-\delta_C} dy \right) dz \right] \quad (6)$$

or, using the same approximation as earlier,

$$S_x \approx \left(\frac{dp}{dx} \right) HZ \quad (6a)$$

The geometry is given in Figure 2.

The approximations inherent in equation (6) are completely equivalent to those usually made in dealing with the fully molten zone (metering or melt pumping section) and the dry granular zone (feed section), where an effective pressure p is used as the relevant dynamical variable at any station x . Gradients in p are balanced by viscous or frictional forces caused by local shear rates or slip velocities, the former being calculated in terms of a purely viscous fluid model and the latter using a coefficient of friction. Normal stress differences are neglected in the metering zone models, and in the simplest¹⁴ of the dry feed models, and are simply parametrized in the more complex feed zone models of Schneider¹⁵ and Lovegrove and Williams¹⁶.

We do not explicitly consider here the local stress equilibrium conditions within the slowly deforming solid bed A . Thus we do not need to specify its rheology. Because of the shear stresses imposed at the interfaces AB – AE , the implied stress state within the solid bed cannot be purely isotropic. However, if the absolute magnitude of p is large enough, we can assume that the stress tensor will be nearly isotropic. This is an assumption that we can check *a posteriori*. What we have assumed is that the almost isotropic stress state will be compatible with the small velocity gradients needed to cause the AB interface to move slowly towards the trailing flight $z = 0$ and the AC interface to remain sensibly fixed relative to the moving barrel, i.e. material is slowly squashed up towards the hot barrel surface. One rheological idealization that is compatible with this approach is that of an almost freely deforming hard granular bed, i.e. one with a low (and suitably variable!) angle of internal friction. However, it is not necessary for this to be the case: indeed, a relatively rigid viscoelastic local model may well be far more appropriate, provided that large (comparable with $|p|$) differences of normal stresses do not arise and so lead to significant modification of the overall balance relation equation (6).

The same arguments allow us to neglect detailed consideration of even the integrated y and z components of the stress equilibrium equation. Clearly there will be a z shear stress on the bed A , caused by the lubricated motion of the barrel sliding over the melting face AC . This must be balanced largely by variations of the normal stress (pressure) across the interfaces AB and AD , since we cannot expect comparable z shear stresses in zone E . Similar consideration of the balance of moments acting about a z -axis on the bed A lead to pressure differences between zones C

and E . What we are assuming is that these differences are small in absolute magnitude compared to the local pressure p and, as we shall see later, are therefore too small to provide significant pressure driven fluid motions in zones C , D , and E . All of these assumptions must be checked *a posteriori*.

Nothing has been said so far about the temperature field within the bed. This has been treated by previous authors^{3,6} in terms of a straightforward solution of the heat conduction equation. Shapiro¹⁰ and Pearson¹⁷ have made the coarse assumption that the solid bed remains at essentially the entry (feed pocket) temperature T_A everywhere and that solid granules are raised to the melting temperature in a thin layer near the melting interface. The relevant equations are derived later. Insofar as the layer may be relatively thick, then physical arguments show that the melting rate will be overestimated in the early stages of melting and underestimated in the later stages. The total amount of heat needed to melt the entire solid bed will however be correctly calculated.

Zone B: the melt pool

The flow in this region is very similar to the flow in relatively deep channels already analysed by Martin¹⁵. Two differences arise:

(1) The fixed trailing screw flight surface (at $z = 0$ in our notation here) is replaced by the interface AB (at $z = -\delta_D - Z$) moving downstream with velocity v_{Ax} .

(2) The outflow/unit length, m_{Fz} , over the leading flight edge (at $z = -W$) is no longer balanced by the inflow over the trailing flight edge (at $z = 0$); instead the mass inflow, m_{Cz} from zone C (at $z = -\delta_C - Z$) causes the downstream flow, M_{Bx} to increase according to

$$\frac{dM_{Bx}}{dx} + m_{Cz} - m_{Fz} = 0 \quad (7)$$

Note that m_{Cz} and m_{Fz} are both negative for the coordinate system chosen.

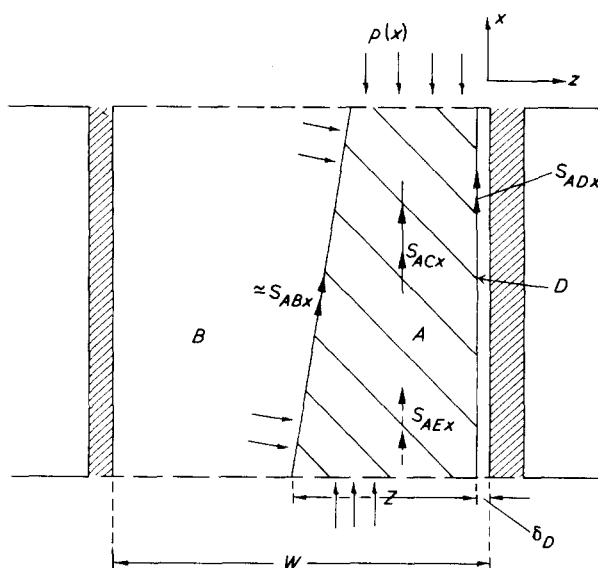


Figure 2 The force balance on the moving solid bed A ; the upper (barrel) and lower (screw) stresses S_{ACx} and S_{AEx} are both shown. The shear stress $\approx S_{ABx}$ is shown clearly inclined to the x -axis but the effect of the cosine of dZ/dx is assumed negligible. The equivalent $\sin(dZ/dx)$ term on the normal p forces is not negligible however. In practice, S_{ADx} and S_{AEx} will be negative

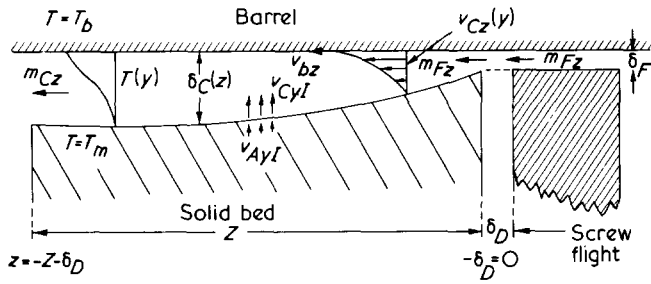


Figure 3 The flow region in zone C. The thickness of δ_F and δ_C is exaggerated. Typical velocity and temperature profiles are shown. Main development of depth δ_C is in z-direction

A full solution to the problem requires a local solution everywhere for the field variables $v(x, y, z)$, $p(x, y, z)$ and $T(x, y, z)$. Martin has already shown that at best one can hope to calculate fully developed solutions (independent of x , except that $\partial p/\partial x$ can be a non-zero constant) and that even so heavy numerical computation is in general required. The often relevant case of high cross-channel Graetz number¹¹ leads to simplifications that could allow in principle of developing solutions but the influx m_{Cz} and the consequential open streamlines would be difficult to cope with.

Hence we shall assume that the mechanics of flow in zone B leads to a single dynamical equation that we write here formally as

$$M_{Bx} = \hat{\rho}_B f \left(W - Z - \delta_D, v_{Ax}, \frac{dp}{dx}; H, v_{bx}, v_{bz} \right) \quad (8)$$

where f is also dependent on the material properties of the melt. Thus there is an implicit dependence in equation (8) on the viscous properties of the melt and hence on the temperature field. We defer any further consideration of the function f in equation (8) until we consider specific approximate models.

We note that our discussion of zone A left S_{ABx} and R_B unspecified; we should defer consideration of these also until a specific model for f is chosen, but it is convenient to assume here that they can be taken as negligible.

Zone C: the swept melting layer

Zone C is the most important region of all from the point of view of heat transfer and hence of melting. Except very near the beginning of the melting section, δ_C will be smaller than δ_E or δ_D unless the screw temperature is much closer to the melting temperature than the barrel temperature is. Certainly R_C will be the dominant component of R , and for a very good reason: if it were not so, then melting in an extruder would not be significantly more rapid than in a static reservoir with heated metal walls, which can easily be shown to be unacceptably slow.

We shall therefore analyse the flow and temperature distribution in zone C as precisely as possible. The problem is intrinsically more difficult than that in a fully-molten metering section, say, because of the more complex boundary conditions that apply at the melting interface. The matter has been discussed at some length by Shapiro¹⁰ and Pearson¹⁷ and so we try here to summarize the most important points of the arguments given there. The geometry is illustrated in Figure 3.

We first introduce the geometrical assumption, which will have to be verified later, that:

$$\frac{\partial \delta_C}{\partial z}, \frac{\partial \delta_C}{\partial x} \ll 1 \quad (9)$$

and hence that

$$v_{Cy} \ll v_{Cz}, \quad v_{Cx}(v_{bz}, v_{bx}) \quad (10)$$

(However we note that v_{Cy} cannot necessarily be neglected completely because its convective contribution to heat transfer must be important. What we shall seek to do here is to take account of its effect implicitly rather than explicitly, so as to retain as far as possible the advantages of a full lubrication approximation.) Thus we are led, using equations (9) and (10) to the stress equilibrium equations:

$$\frac{\partial p}{\partial x} = \frac{\partial}{\partial y} \left(\mu \frac{\partial v_{Cx}}{\partial y} \right) \quad (11)$$

$$\frac{\partial p}{\partial z} = \frac{\partial}{\partial y} \left(\mu \frac{\partial v_{Cz}}{\partial y} \right) \quad (12)$$

and may neglect $\partial p/\partial y$. We may note at once that the assumptions we made earlier, i.e. that the stress field in zone A is dominated by the isotropic component $p(x)$, requires us to make the equivalent assumption here that $\partial p/\partial z \approx 0$. This result can be reached in a quite different manner^{10,17} by considering flow in zone C alone, and using the further geometrical approximation that:

$$\delta_C \ll H \quad (13)$$

In simple terms, we showed that any significant departure from drag flow in zone C would lead to unacceptably large pressure variations [i.e. of the order of the mean pressure $p(x)$] around the surface of the solid bed. This result is consistent with the hypothesis of a freely but very slowly deforming solid bed in zone A if (see Figure 3)

$$\left. \begin{aligned} v_{Cx} &= v_{Ax} \\ v_{Cz} &= 0 \end{aligned} \right\} \quad (14)$$

at the interface AC, i.e. at $y = H - \delta_C$.

The other boundary conditions for equations (11) and (12) are provided by 'no slip' at the barrel,

$$v_{Cx}(H) = v_{bx}; \quad v_{Cz}(H) = v_{bz} \quad (15)$$

The viscosity μ in equations (11) and (12) must be specified by a constitutive relation. Following previous authors, we shall use

$$\mu = 2^{-2s} C_0 \exp[-b(T - T_0)] (I_2)^{-s} \quad (16)$$

where the second invariant I_2 of the deformation rate tensor is given by

$$I_2 = \frac{1}{4} \left[\left(\frac{\partial v_{Cx}}{\partial y} \right)^2 + \left(\frac{\partial v_{Cz}}{\partial y} \right)^2 \right] \quad (17)$$

$C_0(T_0)$, s and b are parameters for any particular molten polymer in a given range of temperature and shear rate.

The energy, or heat balance, equation can be written as

$$\rho_C C_C \left(v_{Cx} \frac{\partial T}{\partial x} + v_{Cz} \frac{\partial T}{\partial z} + v_{Cy} \frac{\partial T}{\partial y} \right) = k_C \frac{\partial^2 T}{\partial y^2} + 4\mu l_2 \quad (18)$$

where convection, conduction and generation are all accounted for, bearing in mind the obvious consequences of equation (9) on the conduction term. Two obvious boundary conditions to apply are

$$T(H) = T_b; T(H - \delta_C) = T_m \quad \text{all } z \quad (19)$$

We now have to account for the effect of melting at the interface AC . Formally, we obtain

$$\begin{aligned} \lambda \rho_A v_{Ay}(y = H - \delta_C) &\equiv \lambda \rho_C v_{Cy}(y = H - \delta_C) \\ &= k_C \left(\frac{\partial T}{\partial y} \right)_{y=H-\delta_C^+} - k_A \left(\frac{\partial T}{\partial y} \right)_{y=H-\delta_C^-} \end{aligned} \quad (20)$$

where we have assumed the position of the interface, i.e. δ_C , to be independent of time and of x . More precisely, it is the material derivative

$$\frac{d\delta_C}{dt} = \frac{\partial \delta_C}{\partial t} + v_{Ax} \frac{\partial \delta_C}{\partial x}$$

that is taken to be zero. λ is the latent heat of fusion of the polymer.

Earlier, we argued that

$$\left(\frac{\partial T}{\partial y} \right)_{y=H-\delta_C^+} \gg \frac{T_m - T_A}{H} \quad (21)$$

so that most of the solid bed would remain at the entry temperature T_A . This will be the case provided that

$$\rho_A C_A v_{Ay} \gg k_A/H \quad (22)$$

in which case

$$k_A \left(\frac{\partial T}{\partial y} \right)_{y=H-\delta_C^-} \simeq \rho_A C_A v_{Ay} (T_m - T_A) \quad (23)$$

We are thus able to represent the term describing heat transfer into zone A —in equation (2)—in a very elementary fashion, and it is convenient to write

$$\Lambda = \lambda + (T_m - T_A) C_A \quad (24)$$

to give

$$k_C \left(\frac{\partial T}{\partial y} \right)_{y=H-\delta_C} = \Lambda \rho_C v_{CyI}, \quad v_{CyI} = v_{Cy}(H - \delta_C) \quad (25)$$

as the relevant additional boundary condition for equation (18). Here Λ is an effective latent heat of fusion.

Equation (18) still contains v_{Cy} as an unknown field variable. Equations (11)–(13) need to be supplemented by the continuity equation

$$\frac{\partial v_{Cy}}{\partial y} + \frac{\partial v_{Cx}}{\partial x} + \frac{\partial v_{Cz}}{\partial z} = 0 \quad (26)$$

for the set of field equations to be determinate. The boundary conditions become complete if we include the obvious condition

$$v_{Cy}(H) = 0 \quad (27)$$

and a sufficient set of entry conditions on v_C and T along $z = 0$ and $x = 0$.

We could, with care and sufficient computing power, obtain numerical solutions to this governing set of equations. However, without further simplifications, the task would be more formidable than those we have already rejected as too expensive for other regions of the flow, e.g. the metering section, zone B or zone A . This is largely because δ_C is an initially unknown function of x and z .

The key to simplification is the convection term in the energy equation, i.e. the left-hand side of equation (18). We shall first suppose that

$$\frac{\partial \delta_C}{\partial x} \ll \frac{\partial \delta_C}{\partial z} \quad (28)$$

and that

$$\frac{\partial T}{\partial x} \ll \frac{\partial T}{\partial z} \quad (29)$$

For this to be a rational approximation, we need dv_{Ax}/dx to be sufficiently small, e.g.

$$\frac{dv_{Ax}}{dx} \ll \frac{v_{Ax}}{Z} \quad (30)$$

We note that the initial conditions at $z = 0$, which will be determined by the leakage flow over the flight, are likely to be very slowly varying functions of x . Thus the assumptions equations (28) and (29) are inherently plausible.

Physically this means that the material that is melted at the AC interface is effectively swept in the z -direction into the melt pool B : the v_{bz} sweeping velocity is more effective than the $(v_{bx} - v_{Ax})$ relative sweeping velocity because $dZ/dx \ll 1$. The full set of field equations for v and T in zone C are now functions of y and z only, with dp/dx and v_{Ax} as parameters. We are therefore looking for a local (i.e. fixed x) solution. Furthermore, v_{Cx} and hence v_{Ax} is only coupled to the equations for v_{Cy} , v_{Cz} and T very weakly through l_2 .

We have therefore effectively reached the starting point of Pearson¹⁷. There it was shown that a useful approximation to the solution of equations (12), (18) and (26) with $v_{Cx} \equiv 0$ can, in certain circumstances, be obtained by using

$$k_C \frac{\partial^2 T}{\partial y^2} + 4\mu l_2 = 0 \quad (18a)$$

instead of equation (18) to give T rather simply in terms of δ_C using boundary conditions equation (19). The relevant dimensionless group is

$$M = \Lambda / C_C (T_b - T_m) \quad (31)$$

If M^{-1} is sufficiently small, then equation (18a) can be used provided the local melting rate (given by v_{Cy} at the interface) is calculated from equation (25) using a modified value

Λ^* for Λ . Formally we can write

$$\Lambda^* = \Lambda + FC_C(\bar{T} - T_m) = \lambda + C_A(T_m - T_A) + FC_C(\bar{T} - T_m) \quad (32)$$

where F is a pure number and \bar{T} is some average value of the temperature in $H < y < H - \delta_C$. Shapiro¹⁰ took \bar{T} to be the mixing cup mean

$$\hat{T} = \frac{\int_{H-\delta_C}^H T v_{Cz} dy}{\int_{H-\delta_C}^H v_{Cz} dy} \quad (33)$$

and $F = 1$. Pearson¹⁷ showed that $F = 1/2$ would be a more obvious general choice, and also gave results for certain special cases.

When solving the simplified problem for zone C , we find that the relevant set of equations become equation (12) subject to equations (14) and (15), equation (18a) subject to boundary conditions equations (19) and (25) using Λ^* from equation (32) and the integrated mass conservation relation

$$v_{CyI} = \frac{\partial}{\partial z} \left(\int_{H-\delta_C}^H v_{Cz} dy \right) \quad (34)$$

which follows directly from equations (26) and (27). Equation (34) yields δ_C implicitly. The solution is dependent on v_{Ax} and on the initial condition

$$m_{Fz} = \rho_C \int_{H-\delta_C}^H v_{Cz}(z = -\delta_D) dy$$

Here we have assumed that all the molten material is flowing over the flight and no more enters zone C ; clearly $\delta_C(z = -\delta_D) \approx \delta_F$, the flight clearance. The solution is very weakly dependent on dp/dx through equation (11) and I_2 . The solution yields

$$m_{Cz} = \rho_C \int_{H-\delta_C}^H v_{Cz}(z = -Z - \delta_D) dy \quad (35)$$

which is required in equation (7) for zone B . We see at once that

$$R_C = m_{Fz} - m_{Cz} \quad (36)$$

which is required for estimating R in equation (4) using equation (3). Finally we note that

$$S_{ACx} = \int_{-Z-\delta_D}^{-\delta_D} \left(\mu \frac{\partial v_{Cx}}{\partial y} \right)_{y=H-\delta_C} dz \quad (37)$$

which is needed in equation (5).

Zones D and E : the lubricating layers

An analysis of flow in the lubricating layers D and E follows that of zone C in many respects. Equations (9) and (10) become

$$\frac{\partial \delta_D}{\partial x}, \frac{\partial \delta_E}{\partial x} \ll 1 \quad (38)$$

$$v_{Dz} \ll v_{Dx}, v_{Ey} \ll v_{Ex} \quad (39)$$

where v_{Dx} and v_{Ex} are of order v_{Ax} . Equation (13) is retained, i.e.

$$\delta_D, \delta_E \ll H \quad (40)$$

We shall see that a breakdown of equation (40) will prove to be the strongest constraint on our calculations for the melting process. Again, to be compatible with the assumptions made above, we treat p as a function of x only. Thus $\partial p / \partial y = 0$ in the analogue of equation (12) for v_{Dy} and for $\partial p / \partial z = 0$ in that for v_{Ez} . The zero boundary conditions

$$v_{Dy}(z = 0) = v_{Dy}(z = -\delta_D) = 0 \quad (41)$$

and

$$v_{Ez}(y = 0) = v_{Ez}(y = -\delta_E) = 0 \quad (42)$$

ensure that $v_{Dy} = v_{Ez} \equiv 0$. The flow pattern shown in Figure 4 for zone D is therefore the relevant 2-dimensional situation exactly equivalent to that considered by Pearson¹⁷. Thus

$$\frac{\partial}{\partial z} \left(\mu \frac{\partial v_{Dx}}{\partial z} \right) = \frac{\partial p}{\partial x} \quad (43)$$

with

$$v_{Dx}(0) = 0; v_{Dx}(-\delta_D) = v_{Ax} \quad (44)$$

μ still obeys equation (16) where now

$$I_2 = \frac{1}{4} \left(\frac{\partial v_{Dx}}{\partial z} \right)^2 \quad (45)$$

We obtain T from

$$k_D \frac{\partial^2 T}{\partial z^2} + 4\mu I_2 = 0 \quad (46)$$

with

$$T(0) = T_s; T(-\delta_D) = T_m \quad (47)$$

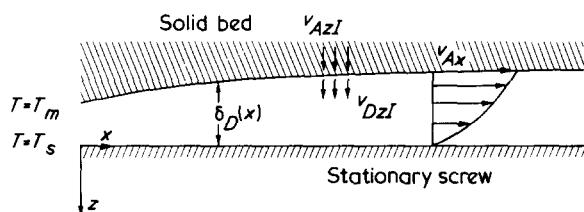


Figure 4 The flow region in zone D . A typical velocity profile is shown with development of depth δ_D in the x -direction

v_{Dz} is given by

$$k_D \left(\frac{\partial T}{\partial z} \right)_{z=-\delta_D} = \Lambda^* \rho_D v_{Dz} \quad (48)$$

where Λ^* is given by equation (32), \bar{T} being interpreted as the relevant average temperature in $-\delta_D < z < 0$.

The solution is obtained by 'marching' forward from some initial $\delta_{D0}(m_{Dx0})$ using

$$v_{Dz} = \frac{d}{dx} \left(\int_{-\delta_D}^0 v_{Dx} dz \right) \equiv \frac{d}{dx} (m_{Dx}/\rho_D) \quad (49)$$

Note that here, as elsewhere, variations in ρ across the layer have been neglected. The information needed for the overall calculation is provided by $\delta_D(x)$,

$$R_D = \frac{dm_{Dx}}{dx} [H - \delta_C(-\delta_D) - \delta_E] \quad (50)$$

and

$$S_{ADx} = \left(\mu \frac{\partial v_{Dx}}{\partial z} \right)_{z=-\delta_D} [H - \delta_C(-\delta_D) - \delta_E] \quad (51)$$

Similarly

$$R_E = \left(\frac{dm_{Ex}}{dx} \right) Z \quad (52)$$

and

$$S_{AEx} = \left(\mu \frac{\partial v_{Ex}}{\partial y} \right)_{y=\delta_E} Z \quad (53)$$

If $\delta_{D0} = \delta_{E0}$, then $\delta_D = \delta_E$ for all x and the solutions for v_{Dx} and v_{Ex} are essentially identical.

Summary of governing equations

The important quantities from an overall point of view are the major mass fluxes of solid and melt, namely M_{Ax} and M_{Bx} , the width and the downstream velocity of the solid bed, Z and v_{Ax} respectively and the downstream pressure gradient dp/dx . All of these are slowly varying functions of x . They are connected through the five approximated balance equations

$$M_{Ax} = \rho_A v_{Ax} H Z \quad (1a)$$

$$\frac{dM_{Ax}}{dx} = - (R_C + R_D + R_E) \quad (4a)$$

$$H Z \frac{dp}{dx} = S_{ACx} + S_{ADx} + S_{AEx} \quad (6b)$$

$$\frac{dM_{Bx}}{dx} = R_C \quad (7a)$$

$$M_{Bx} = \hat{\rho}_B f \left(Z, v_{Ax}, \frac{dp}{dx} \right) \quad (8a)$$

Clearly initial values M_{Ax0} , M_{Bx0} and p_0 and relations for R_K , S_{AKx} ($K = C, D, E$) and f in terms of Z , v_{Ax} and dp/dx are needed to make the problem determinate.

We have noted that R_K and S_{AKx} are only weakly dependent on dp/dx and involve the important ancillary variables δ_K ($K = C, D, E$). The basic equations needed to obtain these R_K and S_{AKx} functions are given above, and they are formally expressed as equations (35)–(37) and (49)–(53). The procedure for obtaining these functions is discussed at greater length by Shapiro¹⁰ and Pearson¹⁷. No detailed discussion of the functional form of f has yet been given, nor of means to calculate it numerically.

The complex non-linear nature of these equations implies step-by-step and iterative numerical procedures. Equations (4a) and (7a) carry forward information from one section x to the next section $x + \Delta x$, as do the subsidiary relations equations (50) and (52) for m_{Dx} and m_{Ex} . At any particular station x , the x -mass fluxes in each zone are treated as given, and equations (1a), (6b) and (8a) are solved iteratively for Z , v_{Ax} and dp/dx , using the ancillary relations relevant in zones C , D and E which yield the R_K and S_{AKx} implicitly in terms of Z and v_{Ax} .

Particular examples of solutions are given in Parts II and III of this paper.

DISCUSSION

A self-consistent 5-zone model has been described above which is based on a large number of interlocking assumptions. It might be possible to justify all of the approximations made by means of formal rational mechanical analysis. However, such severely analytical expansion methods usually appear to restrict the applicability of the formal theory to a far smaller range of situations than is ever met in practice. We argue here that the only sensible way to assess the model is to apply it in typical industrial or laboratory contexts. Once having obtained numerical solutions based on the model, it is a relatively simple matter to estimate the order of magnitude of the errors involved in the various approximations that have been made, and so to put limits on the applicability of the model. Such *a posteriori* estimates should also suggest modifications to the model to overcome its limitations far better than *a priori* argument.

We consider this first in Part II for the particularly simple case of a constant viscosity (Newtonian) fluid, choosing a viscosity which is representative, for the rates of shear encountered in the flow, of the apparent viscosity of commercial polymer melts. The adequacy of the various approximations made is examined, and within quite reasonable limits, they are found to be valid. The effect of using the approximations used for zone C on a representative non-Newtonian fluid are also examined and the basic contention of Pearson¹⁷, that a similarity solution is rapidly established, is found to be self-consistent. The advantage of using a Newtonian approximation for the full problem is that many of the relevant intermediate results, e.g. for δ_D , are analytic.

The full non-linear (non-Newtonian) problem is considered in Part III, where the elements of a numerical solution scheme and an associated computer program are described. Representative results are presented and discussed briefly, particularly a *post hoc* analysis of the initial assumptions.

INTRODUCTION

Part I of this paper has described a 5-zone mathematical model for the melting process in single screw extruders. It was based on a number of intuitive assumptions concerning the dominant geometrical and mechanical features of the flow. However, even with the simplifications imposed in Part I, a complex computational problem results. As a preliminary to providing computational results for a fully non-Newtonian (shear and temperature dependent) melt, a representative set of results will be given here for the much simpler case of a melt of constant viscosity. Various other approximations, not essential in the basic model, are also made here for convenience.

SIMPLIFIED SOLUTION SCHEME

The three equations (1a), (4a) and (6b) relating to zone A given in Part I are retained, with the added assumption that $\rho_A = \rho_S$ and H are constant. The two equations (7a) and (8a) relating to zone B are also retained, where now an exact solution can be given for f in the case where δ_F , δ_C , δ_D and δ_E are neglected in comparison with H and W . Thus, using Rowell and Finlayson¹⁹

$$f = v_{bx} \left(\frac{8(W-Z)^2}{\pi^3} \sum_{n=1}^{\infty} \frac{1}{n^3} \tanh \frac{n\pi H}{2(W-Z)} \right) + v_{Ax} \left(\frac{8H^2}{\pi^3} \sum_{n=1}^{\infty} \frac{1}{n^3} \tanh \frac{n\pi(W-Z)}{2H} \right) - \frac{1}{\mu} \frac{dp}{dx} \left(\frac{(W-Z)^3 H}{12} - \frac{16(W-Z)^4}{\pi^5} \sum_{n=1}^{\infty} \frac{1}{n^3} \times \tanh \frac{n\pi H}{2(W-Z)} \right) \quad (54)$$

We also assume that the density ρ_m , the specific heat C_m and thermal conductivity k_m of the melt are constant everywhere. All we need now are expressions for R_K and S_{AKx} ($K = C, D, E$). We note at once that equation (16) is replaced by $\mu = \text{constant}$.

Putting $\partial p / \partial z = 0$ in equation (12) gives

$$\frac{\partial^2 v_{Cz}}{\partial y^2} = 0 \quad (55)$$

with solution, using boundary conditions equations (14) and (15),

$$v_{Cz} = v_{bz} \frac{(y - H + \delta_C)}{\delta_C} \quad (56)$$

Similarly, neglecting dp/dx in equation (11)—the drag flow assumption—yields

$$v_{Cx} = v_{Ax} + (v_{bx} - v_{Ax})(y - H + \delta_C) / \delta_C \quad (57)$$

We now make the further assumption that the generation term in equation (18a) can be neglected. This is not, in any case, essential to this development but happens to be an approximation that is moderately well justified in the numerical case to be presented here. Thus

$$\frac{\partial^2 T}{\partial y^2} = 0; \quad T(H) = T_b; \quad T(H - \delta_C) = T_m \quad (58)$$

giving

$$T = T_m + (T_b - T_m)(y - H + \delta_C) / \delta_C \quad (59)$$

From equation (56)

$$v_{CyI} = \frac{k_m(T_b - T_m)}{\delta_C \rho_m \Lambda^*} \quad (60)$$

where, using equation (33) and putting $F = 1$

$$\Lambda^* = \lambda + (T_m - T_A)C_A + \frac{2}{3} C_m(T_b - T_m) \quad (61)$$

From equation (34) and equation (56) above we obtain directly

$$v_{CyI} = \frac{1}{2} v_{bz} \frac{\partial \delta_C}{\partial z} \quad (62)$$

whence

$$\delta_C = \left(\frac{4k_m(T_b - T_m)z}{\rho_m \Lambda^* v_{bz}} + \delta_F^2 \right)^{1/2} \quad (63)$$

where δ_D has been neglected in comparison with Z and $\delta_C(0)$ has been equated with δ_F . R_C is obtained immediately as

$$R_C = -\frac{1}{2} \rho_m v_{bz} \left\{ \left(\frac{-4k_m(T_b - T_m)Z}{\rho_m \Lambda^* v_{bz}} + \delta_F^2 \right)^{1/2} - \delta_F \right\} \quad (64)$$

and

$$S_{ACx} = -\frac{1}{2} \frac{\rho_m v_{bz} \Lambda^* \mu (v_{bx} - v_{Ax})}{k_m(T_b - T_m)} \times \left\{ \left(\frac{-4k_m(T_b - T_m)Z}{\rho_m \Lambda^* v_{bz}} + \delta_F^2 \right)^{1/2} - \delta_F \right\} \quad (65)$$

Similarly, for zones D and E we obtain

$$S_{ADx} = \mu v_{Ax} H / \delta_D \quad (66)$$

$$S_{AEz} = \mu v_{Ax} Z / \delta_E \quad (67)$$

Table 1

Geometry of the screw:	
Diameter, D_b	63 mm
Helix angle, β	0.31 rad
Screw channel depth (feed section)	9.4 mm
Screw channel width (normal to the flight)	54.15 mm
Screw flight clearance	76.3 μm
Physical properties of polymer (LDPE):	
Melting temperature	110°C
Viscosity	294.2 N sec/m ²
Thermal conductivity of melt	0.178 W/m°C
Thermal conductivity of pellets	0.178 W/m°C
Density of melt	760 kg/m ³
Bulk density of pellets	490 kg/m ³
Heat of fusion of the polymer	130 kJ/kg
Heat capacity of solid	2.76 kJ/kg°C
Heat capacity of melt	2.60 kJ/kg°C
Operating conditions:	
(standard conditions given first)	
Speed of rotation	2 π ; π , (4/3) π rad/sec
Temperature of barrel	230°C; 180°C, 280°C
Temperature of screw	130°C; 120°C, 140°C, 160°C
Temperature of feed	30°C; 20°C, 50°C, 80°C
Flowrate through the extruder	0.01; 0.015, 0.02, 0.03 kg/sec

where

$$\delta_E = \delta_D = \left(\delta_{D0}^2 + \int_0^x \frac{4k_m(T_s - T_m)}{\rho_m v_{Ax} \Lambda^{**}} dx \right)^{1/2} \quad (68)$$

and

$$\Lambda^{**} = \lambda + (T_m - T_A)C_A + \frac{2}{3} C_m(T_s - T_m) \quad (69)$$

No account is taken of R_D and R_E , since δ_D and δ_E are neglected in comparison with Z and H .

The five governing equations given in Part I, for zones A and B , can now be reduced at a given x to the three equations

$$\frac{dp}{dx} = - \frac{\mu}{HZ} \left\{ \frac{(v_{bx} - v_{Ax})v_{bz}\rho_m\Lambda^*}{2k_m(T_b - T_m)} \times \left[\left(- \frac{4k_m(T_b - T_m)Z}{\rho_m\Lambda^*v_{bz}} + \delta_F^2 \right)^{1/2} - \delta_F \right] - v_{Ax}(H + Z) \left(\delta_{D0}^2 + \int_0^x \frac{4k_m(T_s - T_m)}{\rho_m v_{Ax} \Lambda^{**}} dx \right)^{-1/2} \right\} \quad (70)$$

$$M_{Ax} = \rho_A v_{Ax} HZ \quad (71)$$

$$v_{Ax} = (M_T - \rho_m f) / \rho_A HZ \quad (72)$$

with f given by equation (54), and only 3 unknowns dp/dx , Z and v_{Ax} . Iterative numerical solution is necessary but not difficult. These equations give the solution for any given value of x , M_{Ax} being treated as known. The value of M_{Ax} at a new value of x is provided by

$$\frac{dM_{Ax}}{dx} = -R_C \quad (73)$$

where R_C is given by equation (64).

TYPICAL SOLUTIONS

Table 1 gives geometrical, physical and operating parameters for a 'typical' polymer and screw. The solution scheme given above requires additionally that δ_{D0} and δ_{E0} be specified. Shapiro¹⁰ showed that results obtained for $\delta_{D0} = 100, 200$ and $300 \mu\text{m}$ were virtually indistinguishable, and for convenience, he then took

$$\delta_{D0} = \delta_{E0} = \delta_F$$

Results are given in the Figures for separate variation about the 'standard' operating conditions of (a) barrel temperature, T_b ; (b) screw temperature, T_s ; (c) total flowrate, M_T ; (d) screw revolution rate, N ; (e) solid feed temperature, T_A ; (f) solid feed density, ρ_A .

A careful analysis of the dimensionless groups relevant in the very simplified circumstances considered here shows that only 3 of these need be varied to provide all possible dimensionless solutions. However, since more realistic cases introduce further dimensionless variables, the exercise of writing all the results in dimensionless form has not been undertaken here.

It is convenient to plot results as v_{Ax} , Z and dp/dx as functions of x for various values of the operating conditions. These are given as Figures 6–11. However, the performance of the melting section is more easily understood in terms of p and M_{Ax} which are also shown for the standard case and a few variations in Figure 5. Little need be said about the results obtained in that they contain no surprises, given the model used.

VERIFICATION OF ASSUMPTIONS

We now return to a consideration of the original assumptions, whose validity can now be assessed quantitatively in terms of our numerical solution.

δ_C values

The maximum value for δ_C using Table 1, i.e. with $Z = W$, and equation (63) is 0.44 mm. Hence $(\delta_C/H)_{\text{max}} = 0.047$. From equation (63) we have that:

$$\frac{\partial \delta_C}{\partial z} = \frac{2k_m(T_b - T_m)}{\rho_m \Lambda^* v_{bz}} \cdot \frac{1}{\delta_C} \quad (74)$$

which has a maximum value, when $\delta_C = \delta_F$, of 0.012. In our problem $\partial \delta_C / \partial x \equiv 0$. Thus δ_C is small as required.

δ_D, δ_E values

The maximum value for δ_D or δ_E using Table 1 and equation (68) with $x = 2$ m can be approximated by taking v_{Ax} as constant and equal to 0.06 m/sec. This yields $\delta_{E_{\text{max}}} = 1$ mm. Thus $\delta_E/H \sim 0.1$. The assumption that δ_E is negligible in going from equation (1) to equation (1a) or from equation (6) to equation (6a) clearly introduces a significant (10–15%) error which could have been eliminated; however, in simple geometrical terms, no major error is

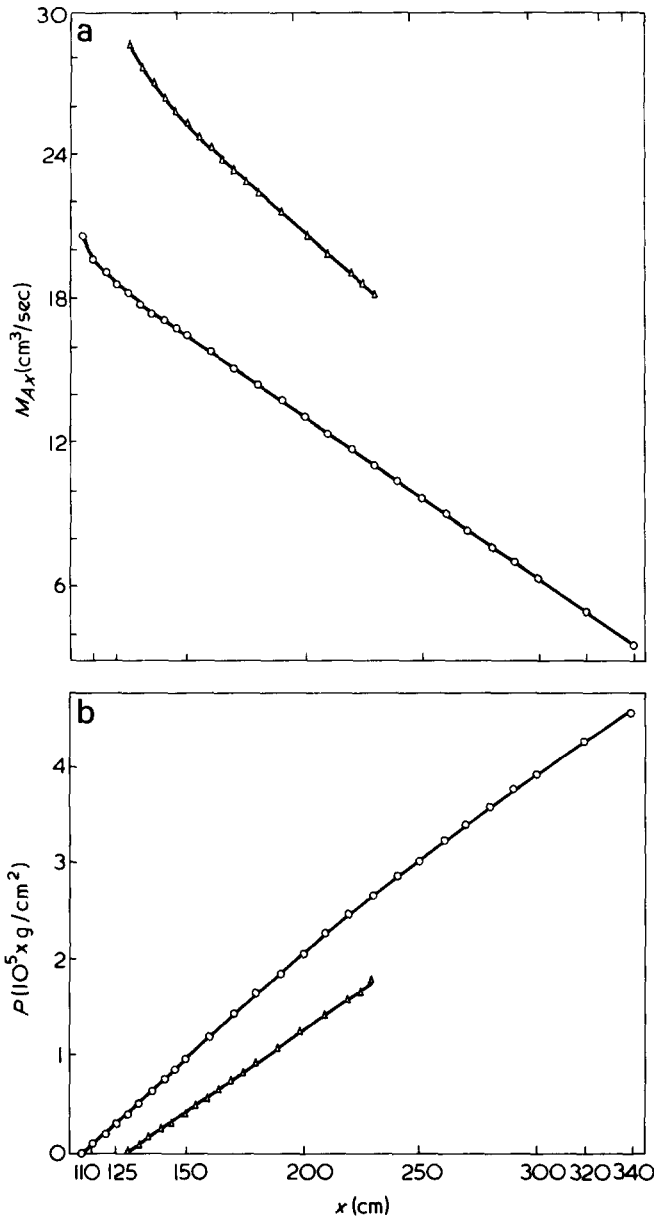


Figure 5 (a) M_{Ax} vs. x ; (b) p vs. x . \circ , Standard operating conditions; \triangle , $T_b = 280^\circ$, $M_T = 0.02$ kg/sec, $N = \pi$ rad/sec

likely to have arisen. The consequences are likely to be much more important when investigating the assumption that $\partial p/\partial z$ and $\partial p/\partial y$ can be neglected. It can simply be verified that $\partial \delta_D/\partial x$ is quite negligible.

v_{Ax} , Z values

The lubrication approximation for zones C, D and E had assumed that

$$\frac{\delta_K}{v_{Ax}} \cdot \frac{\partial v_{Ax}}{\partial x} \ll 1 \tag{75}$$

Putting in the values used above, the ratio is readily seen to be $< 10^{-3}$. It is quite clear therefore that the lubrication approximation for zones C, D, and E is entirely justified and leads to insignificant error.

The stress balance equation (6a) has the largest length scale, namely W , and is based on the principle that v_{Ax} and Z are slowly varying functions of x . We can easily show that

$$\max \left(\frac{W}{v_{Ax}} \cdot \frac{dv_{Ax}}{dx}, \frac{W}{Z} \cdot \frac{dZ}{dx} \right) \approx 0.1 \tag{76}$$

A careful analysis of the equations shows that this is effectively very small and that v_{Ax} and Z (and likewise M_{Ax} and R) can indeed be regarded as very slowly varying.

R , S_x values

From equations (34) and (48) or equation (64) we can compare R_D or R_E with R_C . Using representative values for δ_C and δ_D we find that

$$\frac{R_D + R_E}{R_C} < 0.15 \tag{77}$$

and so neglect of R_D and R_E implied in equation (20) is

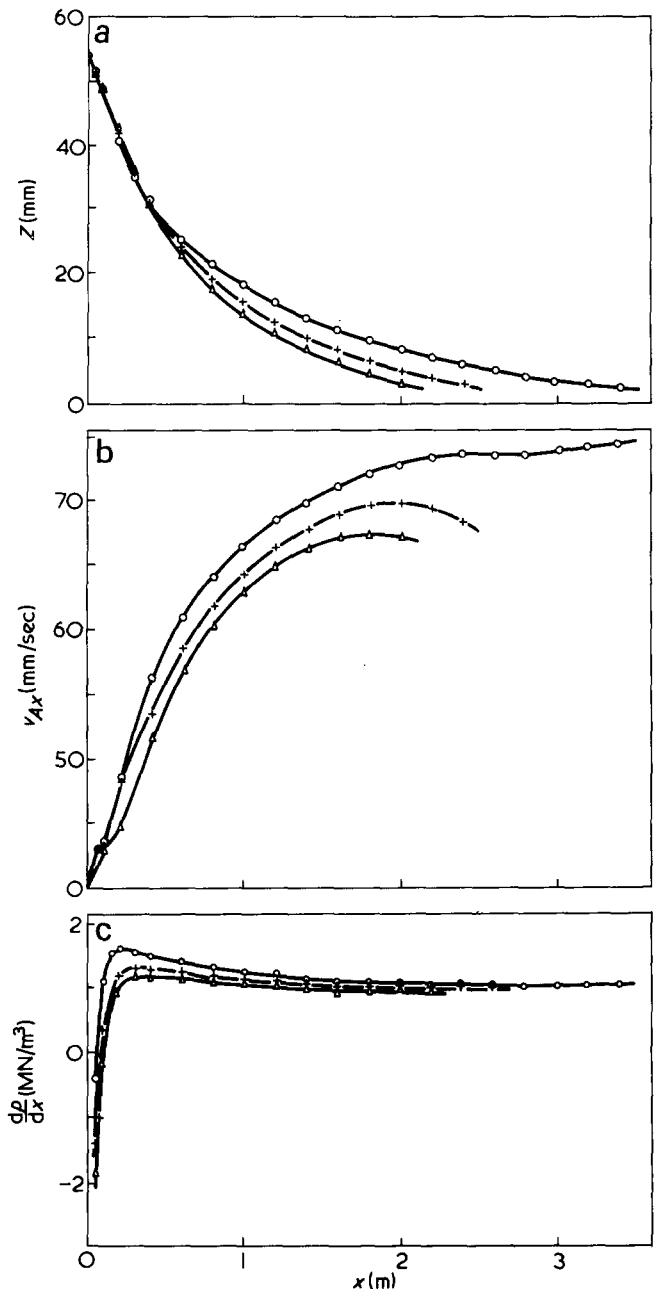


Figure 6 Effect of varying T_b . (a) Effect of T_b on Z . T_b values: \triangle , 280°C ; \circ , 230°C ; \square , 180°C . (b) Effect of T_b on v_{Ax} . T_b values: \circ , 280°C ; $+$, 230°C ; \triangle , 180°C . (c) Effect of T_b on dp/dx . T_b values: \circ , 280°C ; $+$, 230°C ; \triangle , 180°C

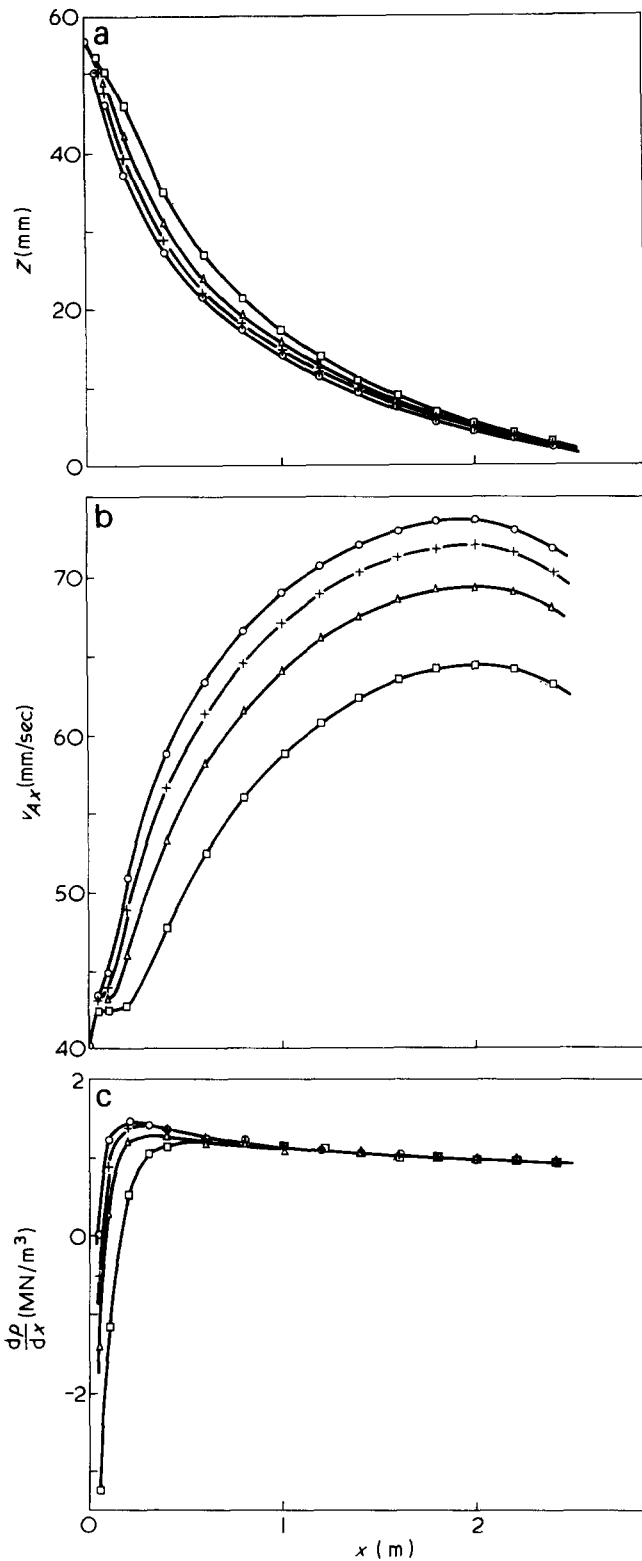


Figure 7 Effect of varying T_s . (a) Effect of T_s on Z ; (b) effect of T_s on v_{Ax} ; (c) effect of T_s on dp/dx . T_s ($^{\circ}\text{C}$): \circ , 150° ; $+$, 140° ; \triangle , 130° ; \square , 120°

comparable with the errors made in neglecting δ_E and δ_D in equations (1a) and (6a). Indeed, to a large extent they are mutually compensating. R_B is readily seen to be completely negligible.

Similarly

$$\left| \frac{S_{AE_x} + S_{AD_x}}{S_{AC_x}} \right| < 0.25 \quad (78)$$

which shows that the dynamical effect of the layers E and D is not far from one of free lubrication. Small variations in δ_E and δ_D would not therefore alter the solution at all significantly. Clearly S_{AB_x} is negligible.

M, Λ^* values

By the definition given in equation (31)

$$M^{-1} \approx 2.4 \quad (79)$$

The discussion given by Pearson²⁰ was partly based on an expansion in powers of M^{-1} (see ref 20, Appendix). Relation (79) might be interpreted as suggesting that the simplification implied by equations (18a) and (32) was inapplicable in the case considered here as standard. However experience in cases where the full convective equation (18) is used (ref 11, p 81) suggests that M^{-1} (a Graetz number) has to be $O(10)$ rather than $O(1)$ before convective terms become comparable with conduction terms. To this extent, 2.4 may be sufficiently small for the approximation used to be a good one. What is wrong is the value chosen here for F , namely 1, which is probably a factor of 4 too

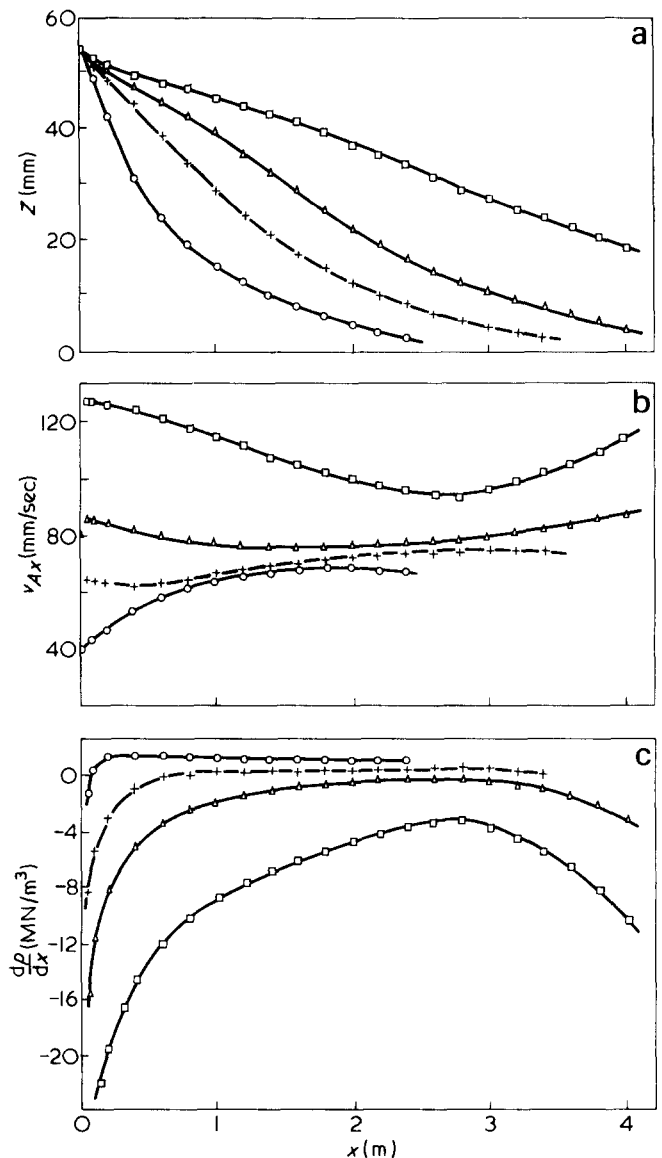


Figure 8 Effect of varying M_T . (a) Effect of M_T on Z ; (b) effect of M_T on v_{Ax} ; (c) effect of M_T on dp/dx . M_T (g/sec): \circ , 10; $+$, 15; \triangle , 20; \square , 30

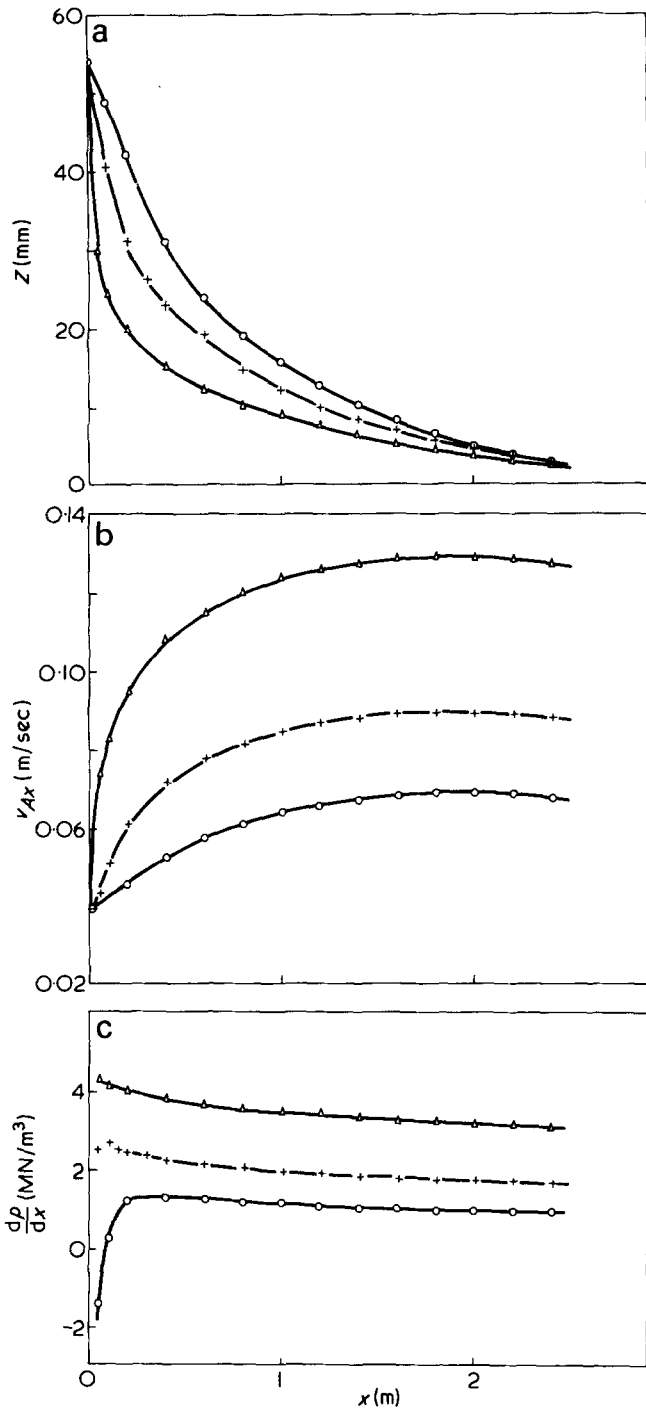


Figure 9 Effect of varying N . (a) Effect of N on Z ; (b) effect of N on v_{Ax} ; (c) effect of N on dp/dx . N (rad/sec): \circ , 0.5; $+$, 0.667; \triangle , 1.0

large. Putting $F = 1/4$ would reduce Λ^* by a little over 15% and Λ^{**} by less than 10% and so significantly increase the rate of melting.

Generation

If generation is included, then its effect is simply to replace the coefficient of Z in equation (64) by

$$2[2k_m(T_b - T_m) + \mu\{v_{bz}^2 + (v_{bx} - v_{Ax})^2\}]/\rho_m\Lambda^*v_{bz}$$

This leads to an increase in melting rate of a further 8% in zone C. Combining this with the result from the previous section, we see that the largest error made is in underesti-

ating the melting rate by a factor of up to 25%. This however is not sufficient to invalidate any of our earlier arguments relating to the basic assumptions; for more accurate calculations, both $F = 0.25$ and generation could be included in either the Newtonian or the full 5-zone model, and so eliminate this numerically large error in the melting rate.

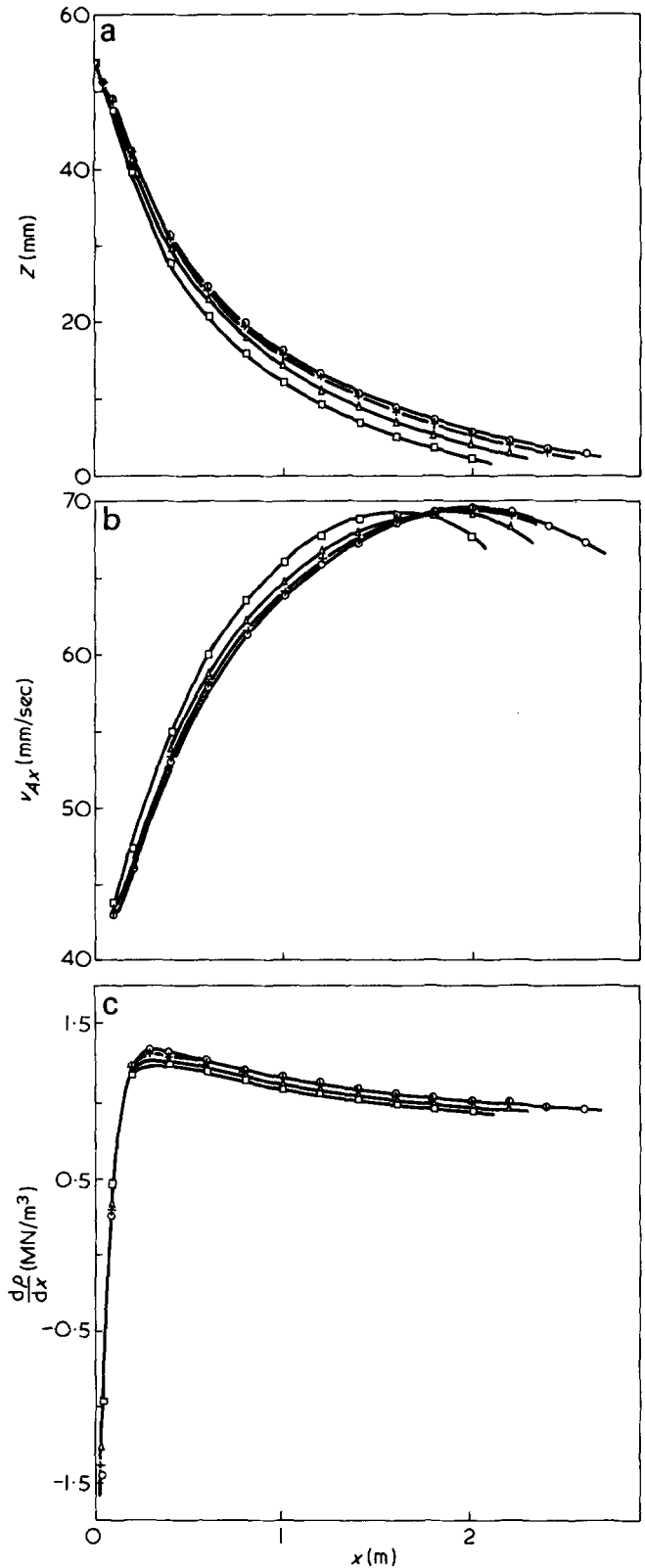


Figure 10 Effect of varying T_A . (a) Effect of T_A on Z ; (b) effect of T_A on v_{Ax} ; (c) effect of T_A on dp/dx . T_A ($^{\circ}\text{C}$): \circ , 20; $+$, 30; \triangle , 50; \square , 80

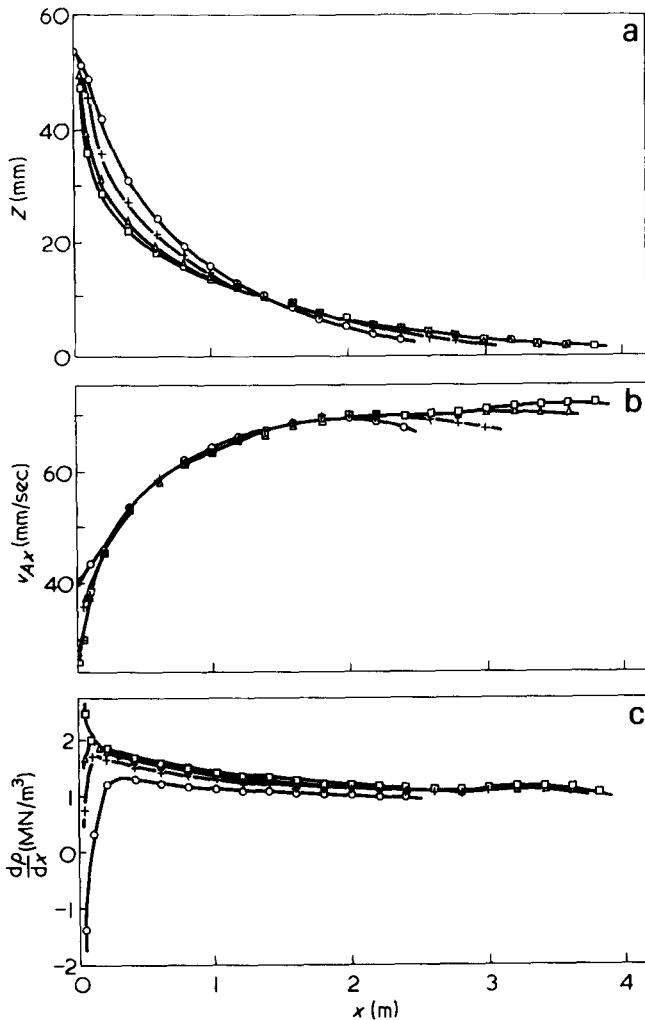


Figure 11 Effect of varying ρ_A . (a) Effect of ρ_A on Z ; (b) effect of ρ_A on v_{Ax} ; (c) effect of ρ_A on dp/dx . ρ_A (kg/m^3): \circ , 490; $+$, 600; \triangle , 700; \square , 760

p and dp/dx values

Although absolute values of p have been shown in Figure 5, it is important to recognize that the melting section is preceded by a feed zone in which no melt pool arises, and for which dry friction may be relevant at all or some of the metal-polymer interfaces. A relatively large pressure may therefore be developed by the beginning of the melting zone ($x = 0$ in our coordinate system). In practice, for a given screw $p(x = 0)$ and M_T are not independently variable. It is therefore difficult to specify a representative value of p . We shall take 10 MN/m^2 as not unreasonable. We then see that

$$\frac{W}{p} \frac{dp}{dx} \approx \frac{1}{20} \quad (80)$$

which goes a long way to justifying the assertion made in Part I that differences in normal stress would be small compared with the isotropic pressure.

We now try to estimate the value of $\partial p/\partial z$ by considering the z balance of stress on zone A . We can obtain, analogously to equation (65) above,

$$S_{ACz} = -\frac{\rho_m v_{bz}^2 \Lambda^*}{2k_m(T_b - T_m)} \left[\left(-\frac{4k_m(T_b - T_m)Z}{\rho_m \Lambda^* v_{bz}} + \delta_F^2 \right)^{1/2} - \delta_F \right] \quad (81)$$

By equating this to $p(Z) - p(0)$ we get an estimate

$$\frac{\partial p}{\partial z} = \frac{S_{ACz}}{ZH} \quad (82)$$

which is, of course, of the same order of magnitude as dp/dx , namely 10 MN/m^3 . Hence the argument given after equation (80) still applies.

We now turn to the question of whether a drag flow approximation in zones C , D and E is justifiable. We use the result that a pressure gradient G in a channel of depth h yields a mass flowrate

$$m_p = \frac{\rho h^3 G}{12\mu} \quad (83)$$

This is to be compared with a drag flow

$$m_D = \frac{1}{2} \rho v h \quad (84)$$

The ratio is given by $Gh^2/6\mu v$. Putting $G = 10 \text{ MN/m}^3$, $h = 10^{-3} \text{ m}$, $v = 0.05 \text{ m/sec}$ and $\mu = 200 \text{ Nsec/m}^2$ gives

$$m_p/m_D \approx 0.1 \quad (85)$$

If we take $h = 0.4 \times 10^{-3} \text{ m}$, the ratio falls to less than 2%, and so the drag flow approximation was justified in our case.

The last question is whether the pressure difference acting between zones D and B could squeeze a significant amount of fluid from zones D and E into zone B and so cause the two-dimensional flow assumption in zones D and E to be inappropriate. The first thing we discover is that the pressure gradient would, if anything, cause flow towards zone D and so increase its thickness*. We have already decided that the mechanics are essentially those of a solid block unconstrained by the screw and so this would not lead to serious error. Simple calculations however, based on the constant values of δ_E and δ_D obtained above, and taking the z force balance above, predict the melt pool to form on the opposite side of the solid block to that which is observed. It is therefore clear that the actual pressure distribution in zones D and E is more complex. We have already argued that the x moment of forces on zone A must be zero. This may result in δ_E becoming very small near $z = -Z$ and so inhibit flow from zone E into zone B . Further progress in this matter can only be made when a full rheological analysis is made of zone A . This remains an outstanding problem.

The errors inherent in assuming that μ is constant are obviously large. We therefore consider a more realistic rheological model in Part III of this paper.

It should be pointed out that the results obtained here should not be interpreted as being always relevant. Assuming the polymer in question to be LDPE, the barrel temperatures chosen are on the high side, and so in practice generation would be more significant in zone C than here.

* Lindt²¹ has already shown that under certain circumstances, the melt pool model does not apply and that, instead, a rigid tongue of compacted granular solid advanced down the screw channel. He shows that this can be explained in terms of the z stress balance.

NOMENCLATURE

b	a material constant in a constitutive (temperature sensitivity of apparent viscosity),	S_x	total shear stress on solid bed in x direction,
$C_{A,C}$	specific heat of melt in zones A (solid bed) and C respectively,	s	material constant in the constitutive equation (power-law index),
C_m	specific heat of melt,	T	temperature,
C_0	material constant in the constitutive equation,	T_A	solid feed entry temperature,
F	constant introduced in equation (32)	T_b	barrel temperature,
f	a scalar function used in equation (8),	T_m	melting temperature of polymer,
G	pressure gradient,	T_0	base temperature for viscosity measurement,
H	depth of screw channel,	T_s	screw temperature,
I_2	second invariant of the rate-of-strain tensor,	t	time,
$k_{A,C,D}$	thermal conductivity of melt in zones A (solid bed), C and D respectively,	v	local velocity vector,
k_m	thermal conductivity of the melt,	$v_{Ax,Ay}$	velocity components of the solid bed (zone A)
M	ratio of apparent latent heat of fusion to change in heat content between barrel and melting temperatures,	$v_{bx,bz}$	velocity components of the barrel
M_{Ax}	mass flowrate in bed A in x direction,	$v_{Cx,Cy,Cz}$	velocity components in zone C ,
M_{Bx}	mass flowrate in melt pool B in x direction,	$v_{Dx,Dz}$	velocity components in zone D ,
$M_{Dx,Ex}$	mass flowrates in zones D and E in x direction respectively,	$v_{Ex,Ey}$	velocity components in zone E ,
$m_{Cz,Fz}$	mass outflow in z direction per unit length in x direction in zone C and under flight respectively,	$v_{CyI,DzI}$	velocities at AC and AD interface,
M_T	total mass flux in extruder,	W	width of screw channel,
N	rate of revolution of the screw,	x	Cartesian coordinate—downstream,
p	isotropic pressure,	y	Cartesian coordinate—radial,
R	total melting rate at the solid—melt interface per unit downchannel area,	Z	width of zone A ,
$R_{B,C,D,E}$	melting rates at the AB , AC , AD , and AE interfaces respectively,	z	Cartesian coordinate—cross-stream,
$S_{ABx,ACx,ADx,AEEx}$	forces due to x shear stress on the AB , AC , AD and AE interfaces per unit downchannel distance,	β	helix angle of the screw,
		δ_x	thickness of melt film in any of zones C , D , or E ,
		$\delta_{C,D,E}$	thickness of zones C , D and E ,
		$\delta_{D0,E0}$	initial thickness of zones D and E ,
		δ_F	screw flight clearance,
		$\Lambda, \Lambda^*, \Lambda^{**}$	'effective' latent heats of fusion,
		λ	latent heat of fusion,
		μ	viscosity function,
		ρ_A	density of solid bed (zone A),
		$\hat{\rho}_B$	mean density of melt in melt pool,
		$\rho_{C,D}$	density of melt in zones C and D ,
		ρ_m	density of the melt.

REFERENCES

- Maddock, B. H. *SPE J.* 1959, 383
- Street, L. F. *Int. Plast. Eng.* 1961, 1, 289
- Tadmor, Z. *Polym. Eng. Sci.* 1966, 6, 185; Tadmor, Z., Duvdevani, H. and Klein, I. *Polym. Eng. Sci.* 1967, 7, 198
- Marshall, D. I. and Klein, I. *Polym. Eng. Sci.* 1966, 6, 191
- Fenner, R. T. and Edmondson, I. R. *Polymer* 1975, 16, 49
- Chung, C. I. *Mod. Plast.* 1968, 45, 178; 1968, 45, 110
- Hinrichs, D. R. and Lilleht, L. V. *Paper presented at the AIChE 67th Nat. Meet. Atlanta, Georgia* 1970
- Donovan, R. C. 'A theoretical melting model for plasticating extruders', Internal Report, Western Electric Co., New Jersey, 1970
- Martin, B., Pearson, J. R. A. and Yates, B. *University of Cambridge Polymer Processing Research Report No. 5*, 1969
- Shapiro, J. *PhD Thesis* University of Cambridge (1973)
- Pearson, J. R. A. 'Prog. in Heat and Mass Transfer' (Ed. W. R. Schowalter), Pergamon Press, New York, 1972, p 73
- McKelvey, J. M. 'Polymer Processing', Wiley, New York, 1962, Ch 11
- Tadmor, Z. and Klein, I. 'Engineering Principles of Plasticating Extrusion', Reinhold, New York, 1970
- Darnell, W. H. and Mol, E. A. J. *SPE J.* 1956, 20
- Schneider, K. *Chem. Ing. Tech.* 1969, 41, 364
- Lovegrove, J. G. A. and Williams, J. G. *J. Mech. Eng. Sci.* 1973, 15, 114
- Pearson, J. R. A. *Int. J. Heat Mass Transfer* 1976, 19, 405
- Martin, B. *PhD Thesis* University of Cambridge (1969)
- Rowell, H. S. and Finlayson, D. *Engineering* 1922, 114, 606; 1928, 126, 249, 385
- Pearson, J. R. A. *Imperial College Dep. Chem. Eng. Chem. Technol. Polym. Sci. Eng. Rep. No. 4*, 1974
- Lindt, J. T. *Polym. Eng. Sci.* 1976, 16, 284

Osmotic pressures of moderately concentrated poly(γ -benzyl-L-glutamate) solutions in *N,N*-dimethylformamide

Kenji Kubo, Kenji Kubota, and Kazuyoshi Ogino

Department of Pure and Applied Sciences, University of Tokyo, Meguro-ku, Tokyo, Japan
(Received 5 April 1976; revised 13 May 1976)

INTRODUCTION

It is known that poly(γ -benzyl-L-glutamate) (PBLG) exists in a rod-like conformation in helicogenic solvents, such as *N,N*-dimethylformamide (DMF) and chloroform. Below some concentration (A-point) PBLG solutions are isotropic, while above another concentration (B-point) they are anisotropic (liquid crystalline). The coexistence of these isotropic and anisotropic phases is observed in an intermediate concentration range¹. Flory² proposed the theory of solutions of rod-like molecules based on a lattice treatment. The results predicted that rate of change in solvent activity for the anisotropic phase is much less than for the isotropic phase. Osmotic pressure measurements provide a means for determining the solvent activities in the moderately concentrated region, extending sufficiently over the two phases. Osmotic pressures for the PBLG-chloroform system have been determined in the concentration range up to $c = 0.19 \text{ g/cm}^3$ at 29°C ³. The difference between the solvent activities for the two phases was sufficiently small for a smoothed curve to be drawn for the range in contrast with the results predicted by Flory. Recently, the curve for the data on solvent activities has been found to correspond with that in the range above $c = 0.21 \text{ g/cm}^3$ at 30°C ⁴. The data in the concentration range below approximately $c = 0.5 \text{ g/cm}^3$ can be semi-quantitatively explained by the Wee-Miller theory, in which modification of Flory's lattice theory to allow for side chain flexibility has been made.

The present investigation was undertaken with the object of detecting the difference between the solvent activities for the two phases. The results of osmotic pressure for the PBLG-DMF system are reported in

the moderately concentrated region at 45°C . The results are compared with those predicted by the Wee-Miller theory.

EXPERIMENTAL

The PBLG used in the experiments was obtained by polymerizing γ -benzyl-L-glutamate-*N*-carboxy anhydride with triethylamine as an initiator and then refluxing with hot ethanol to remove low molecular weight impurities. The solvent, DMF was dried with MgSO_4 and then purified by vacuum-distillation before use. The semi-permeable membranes were prepared from regenerated cellulose membranes (Zartrius-Membranefilter Co., type Ultrafilter). Osmotic pressure was obtained in the concentration range up to $c = 0.23 \text{ g/cm}^3$ at 45°C . A high pressure osmometer described previously³ was used for solutions in the concentration range above $c = 0.05 \text{ g/cm}^3$. The solution charged in a solution cell was stirred as little as possible to avoid air-bubble formation in a solvent cell⁵. The rate of movement of solvent in a capillary was observed under a selected pressure. Osmotic pressure was determined by interpolating the relation between the pressure and the rate of meniscus movement to the null rate. The pressure was read using a mercury manometer. An equilibrium pressure was ordinarily attained within 6 h. The concentration was determined after the run, assuming no volume change on mixing. The specific volume of PBLG was taken to be $0.787 \text{ cm}^3/\text{g}$. After the osmotic pressures were determined for a few solutions of higher concentrations, solvent was removed from the solvent cell and tested for the presence of polymer; no polymer was detected. As the PBLG solution was gradually diluted with DMF, the following procedures were

necessary in order to maintain a high level of accuracy in the osmotic pressure measurements. (1) The solvent above the membrane was removed thoroughly with a blotter immediately before charging the solution. (2) In order to avoid dilution or concentration of the solution near the membrane due to the transport of the solvent through it, the external pressure was readjusted as frequently as possible until equilibrium pressure was attained. Osmotic pressure was determined in a low concentration range below $c = 0.02 \text{ g/cm}^3$ using a high-speed membrane osmometer (Hewlett-Packard Co., model 503). The molecular weight of the sample was 160 000.

For the determination of biphasic compositions at 45°C ten solutions of $c = 0.1$ to 0.25 g/cm^3 were prepared in glass tubes (i.d. 6 mm). The solutions were allowed to stand at 45°C for at least three weeks, and then observed over a wide temperature range using a polarizing microscope. The concentration at the A-point was found to be $c = 0.131 \text{ g/cm}^3$. Although it was difficult to determine accurately the point when no dark areas remained between crossed polars, we considered the concentration at the B-point to be $c = 0.17$ – 0.18 g/cm^3 .

RESULTS AND DISCUSSION

The dependence of osmotic pressure π on concentration c is shown in *Figure 1*. The biphasic compositions are satisfactorily within the range of the present osmotic pressure measurements. The osmotic pressure does not increase monotonously with increase in concentration within this range, unlike the ordinary curves of solutions of randomly-coiled polymers. It is evident from the form of the Figure that the osmotic pressure data show three regions of thermodynamic behaviour. It is reasonable to consider that the region below $\sim c = 0.13 \text{ g/cm}^3$ is the isotropic region, that the region above $\sim c = 0.17 \text{ g/cm}^3$ is the anisotropic region, and that the intermediate region is the coexistence region of the two phases. The change in thermodynamic

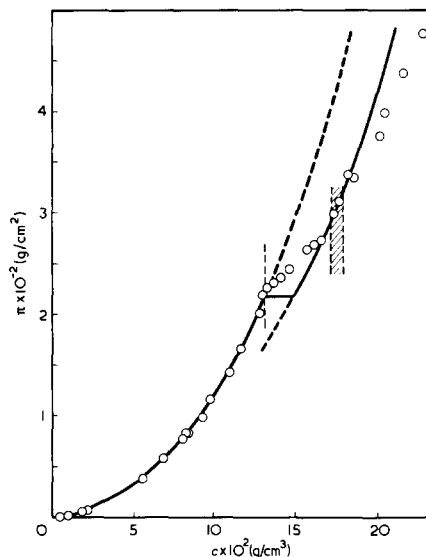


Figure 1 Osmotic pressure π versus concentration c (in g/cm^3) for PBLG solutions in DMF at 45°C . Curves were calculated from the Wee-Miller theory with $\chi = 0.462 + 0.213\nu_2$, $x = 376$, and $a = 1219$. Vertical broken line indicates position of A-point. B-point lies in vertical zone

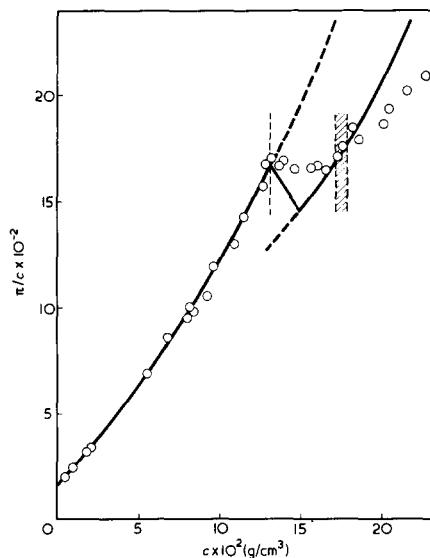


Figure 2 Reduced osmotic pressure π/c versus concentration c (in g/cm^3) for PBLG solutions in DMF at 45°C . Curves were calculated from the Wee-Miller theory with $\chi = 0.462 + 0.213\nu_2$, $x = 376$, and $a = 1219$. Vertical broken line indicates position of A-point. B-point lies in vertical zone

behaviour between the regions is more clearly evident from the plot of π/c versus c , which is shown in *Figure 2*.

PBLG can be assumed to be a polymer composed of a rigid main chain and flexible side chains. Several studies have shown that the side chains of PBLG have some flexibility in the solid state⁶⁻⁸ and that they become

increasingly flexible as solvent is added⁹. Wee and Miller extended the Flory lattice theory for rigid rods by arranging rigid units and flexible ones on a lattice^{4,7}. Solvent activity a_1 for the isotropic phase is given:

$$\ln a_1 = \ln(1 - \nu_2) + [(x + a - 1)/(x + a)] \nu_2 + \chi \nu_2^2 \quad (1)$$

and that for the anisotropic phase by:

$$\ln a_1 = \ln(1 - \nu_2) + [(y + a - 1)/(x + a)] \nu_2 + 2/y + \chi \nu_2^2 \quad (2)$$

where ν_2 is the volume fraction of polymer, x the axial ratio of main chain, a the total number of side chain segments per main chain, y the disorientation index, and χ the parameter which is related to the interaction between the polymer and solvent. The value of y is given by:

$$\nu_2 = [(x + a)/(x - y)] \times [1 - \exp(-2/y)] \quad (3)$$

The parameter χ is assumed to be independent of whether the system is in the isotropic or anisotropic phase.

In order to allow these equations to be applicable to actual solutions, x and a are taken as adjustable parameters. Because $\ln a_1/\ln(1 - \nu_2)$ must approach the ratio of the molar volumes of solvent and polymer at infinite dilution, it is reasonable to take $x + a$ as the reciprocal of the ratio. The solvent activity is related to osmotic pressure by:

$$\ln a_1 = -\pi V_1/RT \quad (4)$$

where V_1 is the molar volume of solvent. The value of χ is estimated using equations (1) and (4). In *Figure 3* the χ values calculated using $x + a = 1595$ are plotted against the volume fraction of polymer. The χ value for the isotropic phase may be linearly related to the volume fraction regardless of whether the concentration is low or high. In *Figure 3* the straight line is drawn as $\chi = 0.462 + 0.213\nu_2$.

In view of the thermodynamic equilibrium between the isotropic and anisotropic phases, the biphasic compositions are calculated for given x and a from equations (1)–(3) together with equations⁴ for activity of polymer for the two phases. The concen-

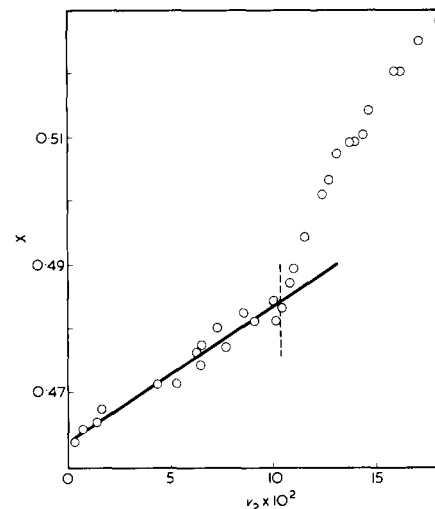


Figure 3 Experimental values of χ plotted against volume fraction of polymer ν_2 for PBLG solutions in DMF at 45°C . Vertical broken line indicates position of A-point

tration at the A-point observed by the microscopic measurements can be fitted to the point calculated using $x = 376$, $a = 1219$, and $\chi = 0.462 + 0.213\nu_2$. The plots of π and π/c versus c calculated with these values are shown in *Figures 1* and *2*, respectively. The osmotic pressure data shown in *Figures 1* and *2* show that the rate of change in the solvent activity for the anisotropic phase is considerably less than that indicated by extrapolation of the curves for the isotropic phase. The horizontal line in *Figure 1* shows the region of the thermodynamic equilibrium between the two phases. However, the present data demonstrate that the solvent activity in the biphasic region is not constant, but increases with increase in concentration. The results may be due to the polydispersity of the polymer used. Above $c = 0.131 \text{ g}/\text{cm}^3$ the longer rods separated first of all from the isotropic phase. The shorter ones separated at higher concentrations. This polydispersity might, perhaps, exert some effect on the width of the biphasic region and the curve of solvent activity for the anisotropic phase. *Figures 1* and *2* indicate the discrepancies between the calculated values and experimental data for the width and the solvent activity. The discrepancies may be partly removed by applying the Wee-Miller theory to rods of different lengths, provided that a form on the dispersity of the polymer used is given. However, attempts to calculate this have not been considered meaningful, because the PBLG-DMF system is not perfectly within the limits of applicability of the lattice

model.

Equations (1)–(3) in the case of $\alpha = 0$ lead back to the original Flory equations². The Flory equations with the value of χ estimated here showed that the concentration at the A-point is small while the volume fraction at the B-point is near unity, so the present results cannot be accounted for by the Flory theory.

ACKNOWLEDGEMENT

The authors thank Dr A. Hatano of their Department for helpful discussions.

REFERENCES

- 1 Robinson, C., Ward, J. C. and Beevers, R. B. *Discuss. Faraday Soc.* 1958, **25**, 29
- 2 Flory, P. J. *Proc. Roy. Soc. (A)* 1956, **234**, 73
- 3 Okamoto, A., Kubo, K. and Ogino, K.

- 4 Kubo, K. and Ogino, K. *Polymer* 1975, **16**, 629
- 5 Carter, S. R. and Record, B. R. *J. Chem. Soc.* 1939, 660
- 6 Flory, P. J. and Leonard, Jr, W. J. *J. Am. Chem. Soc.* 1965, **87**, 2102
- 7 Rai, J. H. and Miller, W. G. *Macromolecules* 1972, **5**, 45
- 8 Rai, J. H. and Miller, W. G. *Macromolecules* 1973, **6**, 257
- 9 Rai, J. H., Miller, W. G. and Bryant, R. G. *Macromolecules* 1973, **6**, 262

Study of polymer crosslinking by thermally stimulated current

P. K. C. Pillai, P. K. Nair and Rabinder Nath

Department of Physics, Indian Institute of Technology, New Delhi 110029, India
(Received 24 February; revised 11 May 1976)

Thermally stimulated current (TSC) has become a powerful tool in the investigations of dielectric relaxation in polymers. The relaxation time, activation energy and the distribution function of dipolar relaxation, attempt-to-escape frequency and capture cross-section have been successfully evaluated for many polymers^{1–4}.

In the present Note, the use of TSC for the study of crosslinking mechanism in polymers is illustrated with reference to poly(vinyl cinnamate) (PVCn). The crosslinking in PVCn, achieved by u.v. irradiation, is believed to cause photocyclodimerization of cinnamic groups with formation of cyclobutane bridges between polymer chains through the excited triplet state of the cinnamic groups and/or through the free radicals generated by the u.v. radiations⁵.

PVCn used in the present investigations was supplied by Polyscience Inc., USA. The benzene solution of PVCn, cast on plane glass sheets was allowed to solidify under saturated benzene atmosphere. The PVCn layer (6.25 cm² × 0.025 cm) was held between two Al electrodes forming a sandwich cell configuration. The crosslinked product was obtained by u.v. irradiation with 125 W, 220 V mercury discharge lamp for 3 h and the crosslinking was evidenced by the increased opacity of the film and its insolubility in benzene. Before the polarization and TSC measurements, the samples were preheated to 120°C (the maximum temperature used in TSC measurements) for 2 h. The satisfactory reproducibility of the a.c. capacitance measurements carried out during repeated heating and cool-

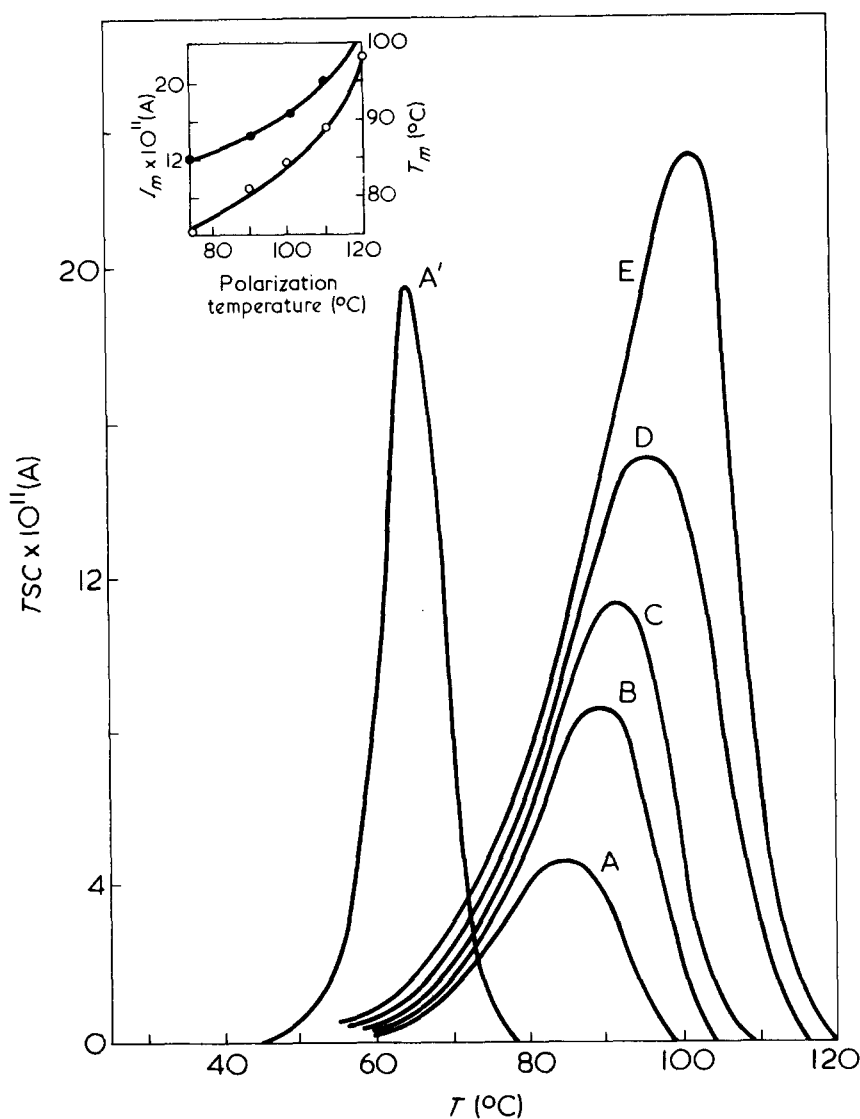


Figure 1 TSC of photocrosslinked PVCn for $V_b = 1.95$ kV and different polarization temperature T_b : A, 75°C; B, 90°C; C, 100°C; D, 110°C; E, 120°C. A', TSC of uncrosslinked sample for $V_b = 1.95$ kV and $T_b = 100^\circ\text{C}$. Inset: \bullet , T_m ; \circ , I_m

model.

Equations (1)–(3) in the case of $\alpha = 0$ lead back to the original Flory equations². The Flory equations with the value of χ estimated here showed that the concentration at the A-point is small while the volume fraction at the B-point is near unity, so the present results cannot be accounted for by the Flory theory.

ACKNOWLEDGEMENT

The authors thank Dr A. Hatano of their Department for helpful discussions.

REFERENCES

- 1 Robinson, C., Ward, J. C. and Beevers, R. B. *Discuss. Faraday Soc.* 1958, **25**, 29
- 2 Flory, P. J. *Proc. Roy. Soc. (A)* 1956, **234**, 73
- 3 Okamoto, A., Kubo, K. and Ogino, K.

- Bull. Chem. Soc. Japan* 1974, **47**, 1054
- 4 Kubo, K. and Ogino, K. *Polymer* 1975, **16**, 629
 - 5 Carter, S. R. and Record, B. R. *J. Chem. Soc.* 1939, 660
 - 6 Flory, P. J. and Leonard, Jr, W. J. *J. Am. Chem. Soc.* 1965, **87**, 2102
 - 7 Rai, J. H. and Miller, W. G. *Macromolecules* 1972, **5**, 45
 - 8 Rai, J. H. and Miller, W. G. *Macromolecules* 1973, **6**, 257
 - 9 Rai, J. H., Miller, W. G. and Bryant, R. G. *Macromolecules* 1973, **6**, 262

Study of polymer crosslinking by thermally stimulated current

P. K. C. Pillai, P. K. Nair and Rabinder Nath

Department of Physics, Indian Institute of Technology, New Delhi 110029, India
(Received 24 February; revised 11 May 1976)

Thermally stimulated current (TSC) has become a powerful tool in the investigations of dielectric relaxation in polymers. The relaxation time, activation energy and the distribution function of dipolar relaxation, attempt-to-escape frequency and capture cross-section have been successfully evaluated for many polymers^{1–4}.

In the present Note, the use of TSC for the study of crosslinking mechanism in polymers is illustrated with reference to poly(vinyl cinnamate) (PVCn). The crosslinking in PVCn, achieved by u.v. irradiation, is believed to cause photocyclodimerization of cinnamic groups with formation of cyclobutane bridges between polymer chains through the excited triplet state of the cinnamic groups and/or through the free radicals generated by the u.v. radiations⁵.

PVCn used in the present investigations was supplied by Polyscience Inc., USA. The benzene solution of PVCn, cast on plane glass sheets was allowed to solidify under saturated benzene atmosphere. The PVCn layer (6.25 cm² × 0.025 cm) was held between two Al electrodes forming a sandwich cell configuration. The crosslinked product was obtained by u.v. irradiation with 125 W, 220 V mercury discharge lamp for 3 h and the crosslinking was evidenced by the increased opacity of the film and its insolubility in benzene. Before the polarization and TSC measurements, the samples were preheated to 120°C (the maximum temperature used in TSC measurements) for 2 h. The satisfactory reproducibility of the a.c. capacitance measurements carried out during repeated heating and cool-

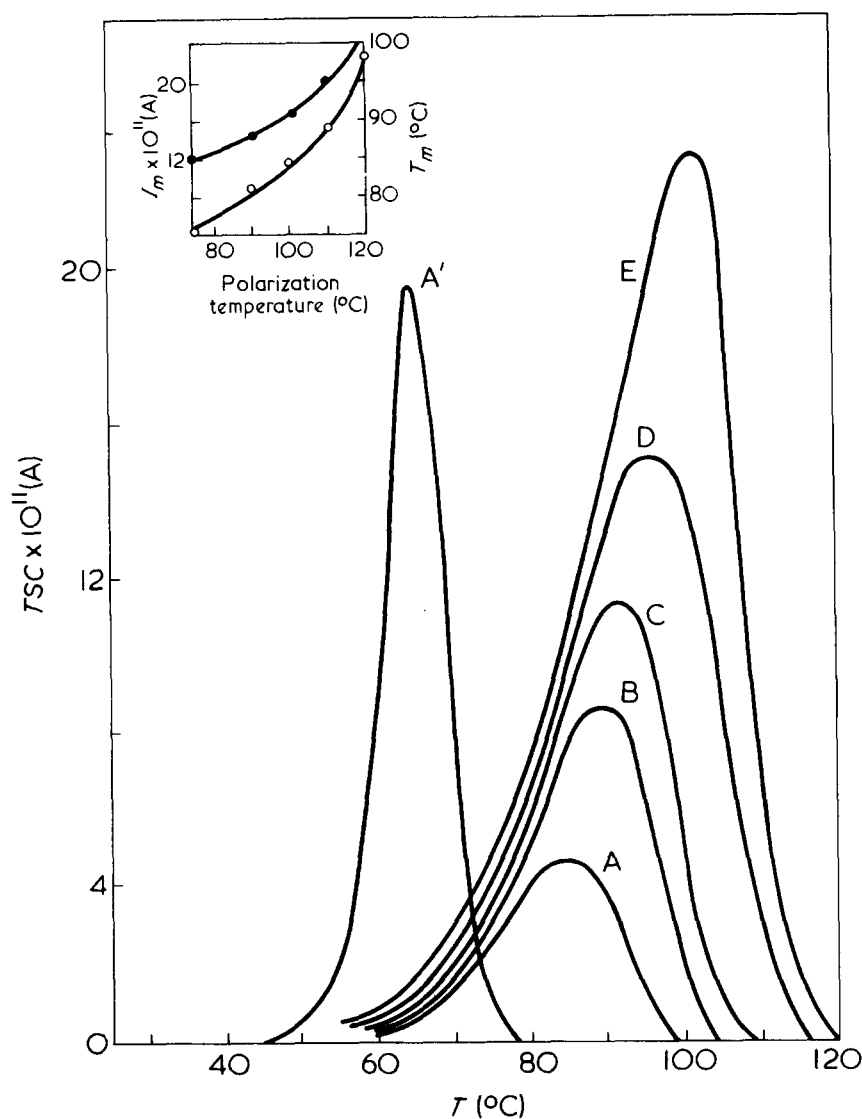


Figure 1 TSC of photocrosslinked PVCn for $V_b = 1.95$ kV and different polarization temperature T_b : A, 75°C; B, 90°C; C, 100°C; D, 110°C; E, 120°C. A', TSC of uncrosslinked sample for $V_b = 1.95$ kV and $T_b = 100^\circ\text{C}$. Inset: \bullet , T_m ; \circ , I_m

ing cycles (30°–110°C) of the same sample, suggests that the chemical degradation is not significant. A heating rate of 1.5°C/min was kept constant throughout the measurements.

The results of TSC on uncrosslinked and crosslinked products are shown in Figure 1. The crosslinking in polymers increases the glass transition temperature (until the gel-point is reached)⁶ and so the shift of the TSC peak towards the high temperature-side upon crosslinking of PVCn is understandable. As the heating rate is low, one also expects the TSC peak temperature T_m to correspond to the glass transition temperature. Since T_m is found to vary by about 16°C in the biasing temperature (T_b) range used (inset Figure 1), the glass transition in the photocrosslinked sample should be a slow transition. This can happen, because, the degree of crosslinking in the sample may not be uniform on a microscopic scale and the gelation on the surface may start before crosslinking has been initiated in the interior, particularly in the present study of solid state crosslinking where the movement of polymer chains is not possible. The width of the TSC peak and shift of T_m with T_b for the crosslinked samples are in marked contrast with PVCn which shows neither of these phenomena (Figure 1, curve A'). The activation energies for dipole relaxation calculated by the initial rise method⁷ for PVCn (2.48 eV) and the photocrosslinked product (1.43 eV) show a significant difference.

The evaluations of capture cross-section (σ_n) and attempt-to-escape frequency (ν) made from Grossweiner's formula⁸ are shown in Table 1

$$\sigma_n = \frac{\nu}{2.9 \times 10^{24} T_m} \text{ (m}^2\text{)}$$

$$\nu = \frac{3T' \exp(E/kT_m)}{2(T_m - T')T_m} \text{ (sec}^{-1}\text{)}$$

where β is the heating rate and T' is the half width temperature on the left of TSC peak.

It is seen that in the crosslinked product, the capture cross-section σ_n decreases with the increase of T_b (Table I). The dipolar relaxation times calculated using these values of activation energy are given in Figure 2, along with those obtained using the full curve method⁹. The agreement is good in the case of PVCn, but in the case of the crosslinked product the points are scattered towards the high

Table 1 Evaluation of capture cross-section, σ_n , and attempt-to-escape frequency, ν , made from Grossweiner's formula⁸

T_b (K)	T_m (K)	Activation energy, E (eV)	Escape frequency, ν (sec ⁻¹)	Capture cross-section, σ_n (m ²)	Crosslinked (CL) or uncrosslinked (UCL)
373.0	337.0	2.48	3.37×10^{34}	1.20×10^5	UCL
348.0	358.0	1.43	6.16×10^{17}	1.66×10^{-12}	CL
363.0	362.0	1.43	2.53×10^{17}	6.66×10^{-13}	CL
373.0	364.5	1.43	1.96×10^{17}	5.08×10^{-13}	CL
383.0	369.0	1.43	8.01×10^{16}	2.02×10^{-13}	CL
393.0	375.0	1.43	3.86×10^{16}	9.46×10^{-14}	CL

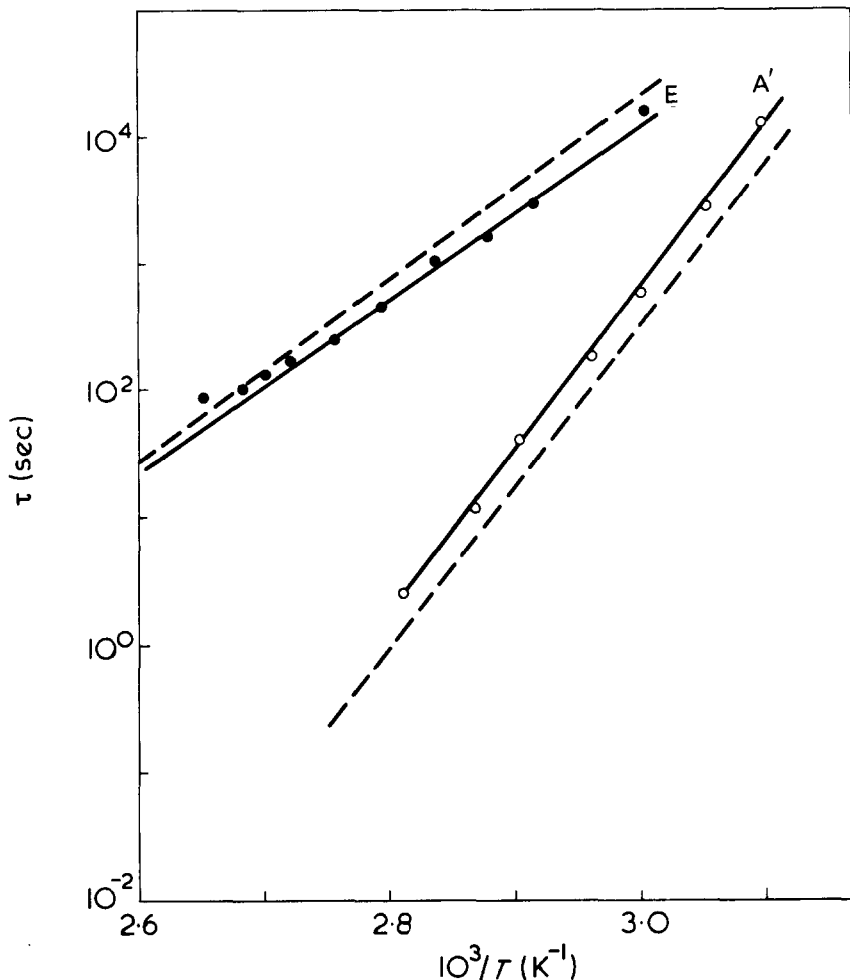


Figure 2 Relaxation time (τ) for PVCn (A') and its photocrosslinked product (E) obtained by the full curve method (—) and initial rise method (---) from Figure 1

temperature region, showing that the same relaxation process cannot be operative throughout the temperature range of TSC curve in photocrosslinked product.

ACKNOWLEDGEMENT

One of the authors (R. N.) gratefully acknowledges the financial support given by CSIR, India.

REFERENCES

1 Turnhout, J. V. *PhD Thesis* Central

Laboratory, TNO, The Netherlands (1972)

- Pillai, P. K. C., Jain, K. and Jain, V. K. *Phys. Status Solidi (A)* 1972, 13, 341
- Hino, T. *J. Appl. Phys.* 1975, 46, 1956
- Jain, V. K., Gupta, C. L., Agarwal, S. K. and Tyagi, R. C. *Thin Solid Films* 1975, 30, 245
- Delzenne, G. A. 'Reviews in Polymer Technology', (Ed I. Skeist), Marcel Dekker, New York, 1971, Vol 1
- Fox, T. G. and Loshaek, S. *J. Polym. Sci.* 1955, 15, 371
- Garlick, G. F. J. and Gibson, A. F. *Proc. Phys. Soc.* 1948, 60, 574
- Grossweiner, L. I. *J. Appl. Phys.* 1953, 24, 1306
- Bucci, C., Fieschi, R. and Guidi, G. *Phys. Rev.* 1966, 48, 816

Optical observations of partly molten fibres of poly(ethylene terephthalate)

Enrico Pedemonte, Giovanni Carlo Alfonso and Giovanni Dondero
Istituto di Chimica Industriale dell'Università, via Pastore 3, 16132 Genova, Italy

and Girolamo Coppola and Piero Fabbri
Centro Sperimentale 'F. Marinotti' della Snia Viscosa, Cesano Maderno (Milano), Italy
(Received 20 April 1976; revised 10 June 1976)

The relevant interest for the fibrous state is well evidenced by the original investigations in fibre forming long chain polymers¹ and by the theoretical and experimental studies on the oriented crystallization, both from solution and from the melt²⁻⁸.

Some attempts have been made to classify the fibrous materials. Very recently Keller⁹ suggested a rather simple criterion which divides samples

into two classes 'according to the manner in which the fibrous nature was achieved even in the case of one and the same polymer', Class 1 comprises fibres formed from molecules pre-extended in an elongational flow field^{10,11}, i.e. for instance by particular stirring of solutions¹² or by very high speed melt spinning¹³. Class 2 includes the fibrous materials obtained by solid state deformation of preformed crystalline textures, i.e. for example by cold drawing⁶, where the original folded structure is disrupted and rebuilt in 'extended chain' crystals.

Optical observation of fibres is a well known and widely employed technique to obtain quickly fundamental information about their structure. Also according to Keller⁹ the shrinking test can be carried out on the hot stage of a polarizing microscope.

We have carried out some observations on fibres heated very close to the melting range; at these temperatures it can be seen that the filaments are only partly fused; individual birefringent fibrils are clearly visible inside the original fibre (*Figure 1*).

The polymer studied was a commercial poly(ethylene terephthalate), supplied by Snia Viscosa Co. under the trade name of Wistel.

Filaments were obtained by melt spinning followed by drawing at 107°C (stretching ratio: 1.70). The section of the single filament was triangular and the lateral size dimensions were ~20 μm. The density of the filaments was 1.3740 g/cm³, which corresponds to a crystallinity value of about 20%¹⁴; wide-angle X rays diffraction implies a good orientation of the crystalline phase.

The fibrils still present at high temperature (*Figure 1*) are very long and have a diameter of about 2 μm. They are oriented along the fibre axis and seem to be rather straight.

Scanning the specimen from 260° to 276°C at a heating rate of 1°C/min shows that the fibrils are stable well above the d.s.c. melting point of the sample ($T_m = 261^\circ\text{C}$). *Figure 2* shows that at 268°C the structure is very similar to that one observed at 260°C; only some connections between the fibrils seem to be disrupted. By increasing the temperature more and more polymer is melted; up to 276°C the birefringent filamentous entities are still visible in the inner core of the fibre, which is completely melted.

Incidentally it should be emphasized that the melting point of these fibrils is very close to the equilibrium melting temperature reported in literature by some authors^{15,16} but is higher than that quoted by Wunderlich (270°C)¹⁷.

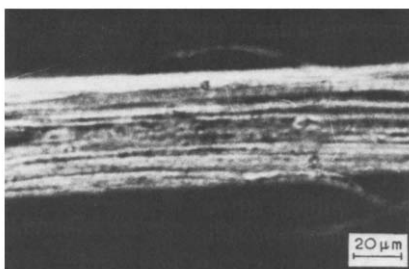


Figure 1 PET fibre heated close to the melting range and rapidly quenched. Crossed polaroids (Heating rate, 3°C/min up to 260°C; storage time at 260°C, 10 min; quenching temperature, 214°C)

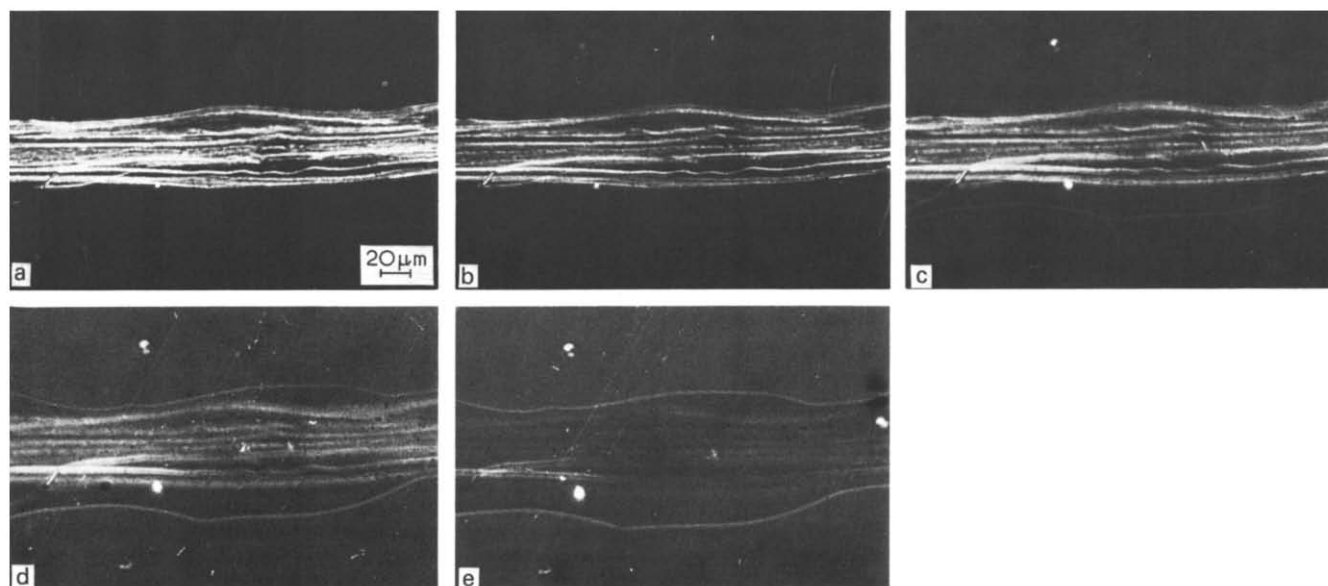


Figure 2 PET fibre scanned from 260.0° to 276.0°C. Heating rate: 1°C/min. (a) 260.0°C; (b) 268.0°C; (c) 272.0°C; (d) 274.0°C; (e) 276.0°C. Crossed polaroids

Keller¹⁸ has reported some similar data for polyethylene samples prepared from the melt by extrusion through, and crystallization in a capillary.

The thermal stability of the fibrils is in agreement with the expectations coming from the Peterlin model¹⁹. Actually Peterlin suggests that each fibril is made up of bundles of parallel microfibrils that differ slightly in the average draw ratio from the adjacent bundles; the packing of microfibrils within each fibril being more perfect than the lateral packing of fibrils¹⁹⁻²².

Nevertheless the fibrils observed in the present study are longer and have lateral size larger than those previously reported for linear polyethylene¹⁹. This result still fits with the Peterlin model if we take into account that the starting structure of the PET is certainly more complicated than that of polyethylene, i.e. the texture is approaching a defective crystal rather than a lamellar one. It would imply that the drawing would generate fibrils in which several tie molecules connect bundles of crystallites and therefore the boundaries of the microfibrils become partly lost.

Besides this, neither the fibres nor the fibrils shrink during the annealing in the hot stage of the polarizing microscope. According to Keller's criterion, our material should be assigned to Class 1; this is in disagreement with the preparative method of the specimens. As a matter of fact a contraction of about 10% can be mea-

sured by dipping the fibres in boiling water.

In order to justify the different behaviour of the two classes of materials we must take into account the morphology of the samples. We believe that in the Class 1 fibres many extended chain crystals are present; they are highly stable to temperature and consequently the whole structure is frozen in: the oriented non-crystalline sequences of the macromolecules having no possibility to relax. The specimen does not shrink. On the other hand, the structure of a Class 2 fibre is very different: the crystallites are defective and therefore the amorphous and oriented molecules can be easily pulled off from the paracrystallites by increasing the temperature. In this way a measurable shrinkage can occur. The shrinking test can never be fully satisfactory because the non-crystalline and oriented molecules of fibrous samples can crystallize very rapidly² and consequently the crystallization can take place before the relaxation occurs. The experimentally observed shrinkage is an undervaluation of the potential contraction or the molecules; if the relaxation time is very high in comparison with the crystallization time no shrinkage would occur².

REFERENCES

- 1 *J. Macromol. Sci. (A)* 1973, 7
- 2 Ziabicki, A. *Colloid Polym. Sci.* 1974, 252, 207

- 3 Ziabicki, A. *Colloid Polym. Sci.* 1974, 252, 433
- 4 McHugh, A. J. *J. Appl. Polym. Sci.* 1975, 19, 125
- 5 Porter, R. S., Southern, J. H. and Weeks, N. *Polym. Eng. Sci.* 1975, 15, 213
- 6 Capaccio, G. and Ward, I. M. *Polymer* 1974, 15, 233
- 7 Peterlin, A. *Polym. Prepr.* 1975, 16, 315
- 8 Spruiell, J. E. and White, J. L. *Appl. Polym. Symp.* 1975, 27, 121
- 9 Barham, P. and Keller, A. *J. Polym. Sci. (Polym. Lett. Edn)* 1975, 13, 197
- 10 Peterlin, A. *Pure Appl. Chem.* 1966, 12, 563
- 11 Frank, F. C., Keller, A. and Mackley, M. R. *Polymer* 1971, 12, 468
- 12 McHugh, A. J. and Forrest, E. H. *J. Polym. Sci. (Polym. Phys. Edn)* 1975, 13, 1643
- 13 Nakamura, K., Watanabe, T., Katayama, K. and Amano, T. *J. Appl. Polym. Sci.* 1972, 16, 1077
- 14 Pedemonte, E., Alfonso, G. C., Dondero, G., Coppola, G. and Fabbri, P. *Tecnopolim. (Milan)* to be published
- 15 Taylor, G. W. *Polymer* 1962, 3, 543
- 16 Ikeda, M. and Mitsuishi, V. *Kobunshi Kagaku* 1967, 24, 378
- 17 Wunderlich, B. 'Macromolecular Physics', Academic Press, New York, 1973, Vol 1
- 18 Grubb, D. T., Keller, A. and Odell, J. A. *J. Mater. Sci.* in press
- 19 Peterlin, A. and Sakaoku, K. *J. Appl. Phys.* 1967, 38, 4152
- 20 Peterlin, A. 'Advances in Polymer Science and Engineering', Plenum Press, New York, 1972, Vol 1, p1
- 21 Sakaoku, K., Morosoff, N. and Peterlin, A. *J. Polym. Sci. (A-2)* 1973, 11, 31
- 22 Peterlin, A. *Adv. Chem. Ser.* 1975, 142, 1

Polymer chain cross-section and the Mooney–Rivlin constants

It is widely recognized that the stress–strain curves of real elastomers, even when tested under near equilibrium conditions, may depart to varying degrees from the theory of rubber elasticity¹. Instead, particularly under uniaxial tension at low extension ratios, they follow the Mooney–Rivlin equation^{2,3}

$$f = 2C_1(\lambda - \lambda^{-2}) + \frac{2C_2}{\lambda} (\lambda - \lambda^{-2}) \quad (1)$$

where f is the force of retraction at extension ratio $\lambda = l/l_0$ and C_1 and C_2 are the Mooney–Rivlin constants. Details of data treatment and numerical values of $2C_1$ and $2C_2$ for many elastomers have recently been summarized⁴.

An investigation of the variation of C_2/C_1 with chemical structure suggested an inverse correlation between cross-sectional area per polymer chain and C_2/C_1 ⁵. A more critical examination of the data has now been completed⁶.

Figure 1 shows a log–log plot of C_2/C_1 (at a fixed value of $2C_1 = 0.2 \text{ N/mm}^2$) against cross-sectional areas per chain in nm^2 . (Abbreviations used for polymer names and relevant data are given in Table 1.) The latter were calculated from lattice parameters of crystalline polymers⁷ on the assumption that they would not differ significantly for the amorphous elastomers. An averaging method was used for copolymers.

There is considerable controversy in the literature about the molecular significance of the Mooney–Rivlin constants⁴. This controversy will be discussed later⁶. Figure 1 seems to indicate an intermolecular rather than an intramolecular origin for $2C_2$.

Figure 1 predicts that an elastomer such as di(*n*-propyl siloxane) with a cross-sectional area of 90 nm^2 should have a substantially lower value of $2C_2$ and might indeed be indistinguishable from an ideal elastomer. However, from Vincent's⁸ correlation between strength and cross-sectional area, this same elastomer might have no practical utility.

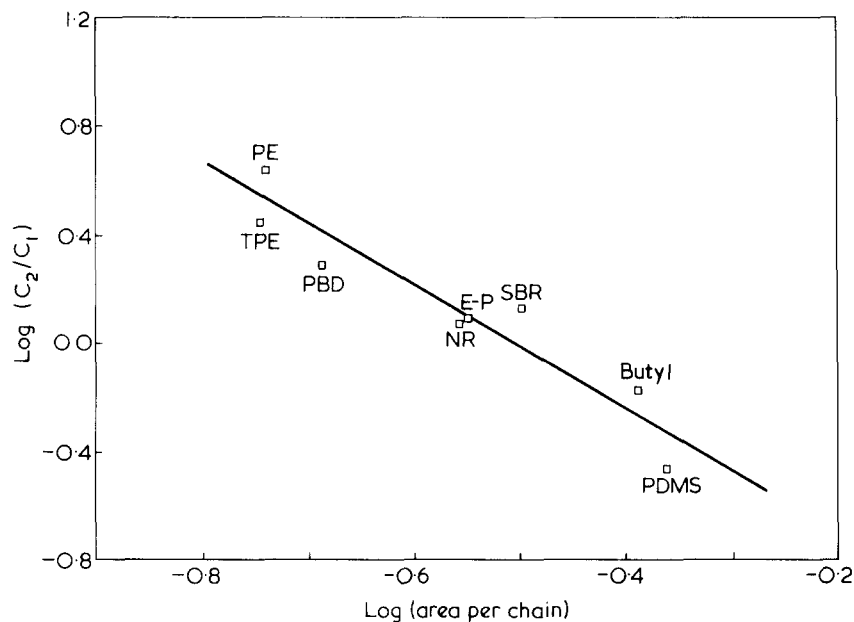


Figure 1 Variation of C_2/C_1 at $2C_1 = 0.2 \text{ N/mm}^2$ as a function of cross-sectional area in nm^2 per polymer chain. The curve for $2C_2$ is parallel to the trend line

Table 1 Mooney–Rivlin constants and cross-sectional areas per chain

Polymer family	Area per chain (nm^2)	C_2/C_1 at $2C_1 = 0.2 \text{ N/mm}^2$
Polyethylene (PE)	0.183	4.3
Trans-polybutadiene (TPE)	0.181	2.75
Polybutadiene (<i>cis</i> and <i>cis-trans</i>) (PBD)	0.207	1.90
Ethylene–propylene rubber (E 60 wt%) random (E–P)	0.285	1.2
Styrene–butadiene rubber (25% S) (SBR)	0.32	1.3
Hevea rubber (NR)	0.280	1.15
Butyl	0.41	0.64
Poly(dimethyl siloxane) (PDMS)	0.436	0.33

We have found correlations of other physical parameters with cross-sectional area. Details of these correlations will be published in due course.

ACKNOWLEDGEMENT

Acknowledgement is made to Professor Treloar who suggested that comparison of C_2/C_1 for different elastomers be made at constant $2C_1$.

R. F. Boyer and Robert L. Miller

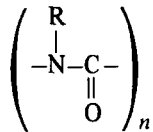
Midland Macromolecular Institute,
1910 West St. Andrews Drive,
Midland, Michigan 48640, USA
(Received 15 June 1976)

References

- Treloar, L. R. G. 'Physics of Rubber Elasticity', 2nd Edn, Clarendon Press, Oxford, 1958; 3rd Edn, 1975
- Mooney, J. *J. Appl. Phys.* 1940, **11**, 582
- Rivlin, R. S. *ibid.* 1947, **18**, 444
- Mark, J. E. *Rubber Chem. Technol.* 1975, **48**, 495
- Boyer, R. F. *J. Macromol. Sci. (B)* in press
- Boyer, R. F. and Miller, R. L. manuscript in preparation
- Miller, R. L. in 'Polymer Handbook,' 2nd Edn. Interscience–Wiley, New York, 1975
- Vincent, P. I. *Polymer* 1972, **13**, 558

Properties of nylon-1 polymers and copolymers

Since Shashoua^{1,2} first showed that nylon-1 polymers of the type



could be prepared from alkyl or aryl isocyanates, several such polymers and copolymers have been prepared³⁻⁸ and their solution properties have been studied extensively⁹. In this way it has been shown that these polymers have an extended, nearly linear, chain in solution with a persistence length of 40–100 nm, and in this respect are more to be compared with the cellulose esters than with conventional vinyl polymers.

However, although the preparation of these polymers is well known there have been few, if any studies of their mechanical properties. This appeared to us to be unfortunate since considerable interest is attached to the question of the relation of chain configuration to physical and especially mechanical properties. For example, work on the yielding and post-yield deformation of polymers has postulated that these properties may be related to the number of deformable bonds in the

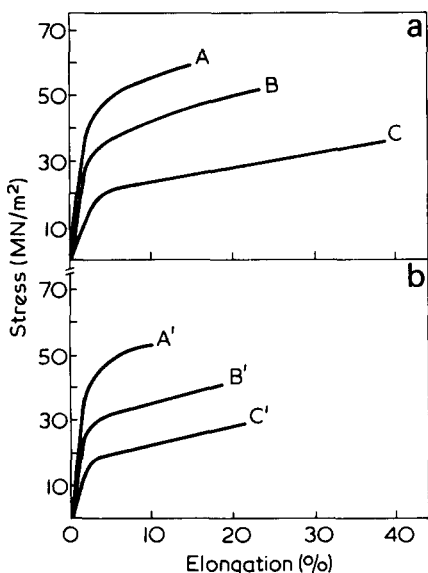


Figure 1 Stress-strain curves for butyl nylon-1 polymer and copolymer. (a) Homopolymer 30–40% crystalline, $[\eta] = 7.25$ dl/g, $M_v = 175,000$. A, -20°C ; B, 0°C ; C, 23°C . (b) Copolymer with $\sim 40\%$ molar ethyl isocyanate. Amorphous $[\eta] = 4.9$ dl/g (in benzene, 30°C). A', -20°C ; B', 0°C ; C', 23°C .

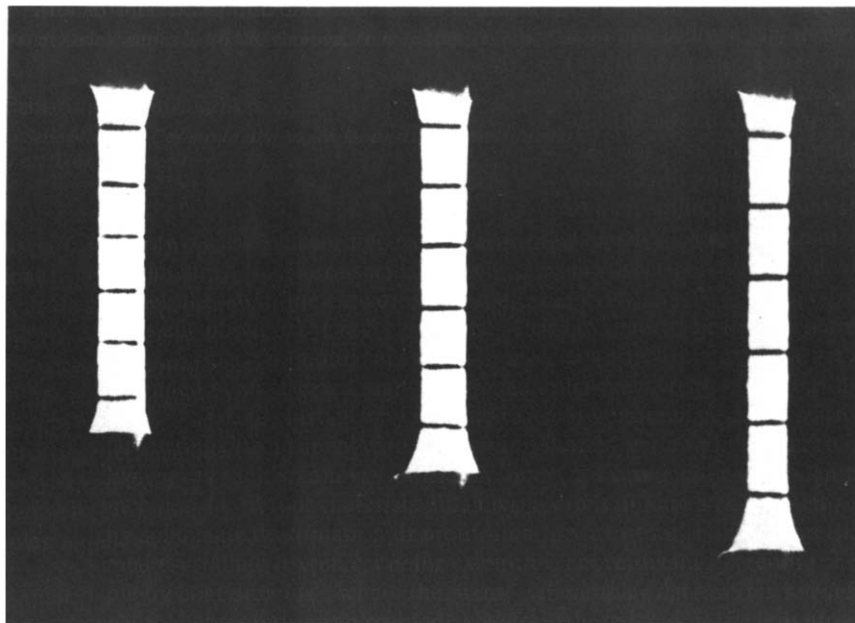


Figure 2 Photographs of poly(butyl isocyanate) test-piece showing uniform tensile deformation without necking. The sample on the left is the undeformed polymer

polymer chain^{10,11}. Thus polymers with straight chains would not be expected to undergo such large deformations as other polymers and orientation hardening (due to the exhaustion of deformable bonds) should set in at lower strains, thus counteracting the effect of strain softening. According to these theories therefore such polymers would show relatively uniform deformation in tension and 'necking' would be unlikely.

We have now made stress-strain measurements on cast films of poly(butyl isocyanate) (partly crystalline) and a butyl-ethyl isocyanate copolymer (amorphous). The polymers were cast from a 1:2 (v/v) mixture of toluene and chloroform. The curves obtained are shown in *Figures 1a* and *1b*. They clearly have a form similar to that reported for isotropic cellulose¹² and for cellulose ester films¹⁰. They also extend uniformly as shown in *Figure 2*.

Further studies at higher temperatures have shown that these polymers also differ from conventional vinyl polymers in other ways. Although, as shown in *Figure 3* they exhibit a damping peak at the temperature where the Young's modulus starts to fall, which may be regarded as a glass transition

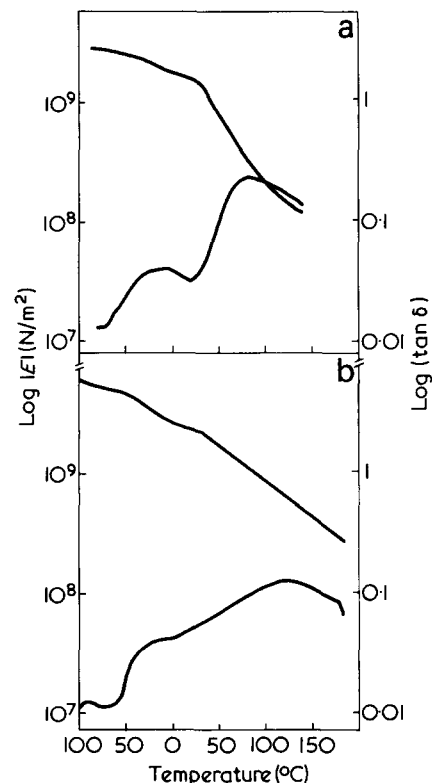


Figure 3 Modulus and damping measurements on butyl nylon-1 polymer and copolymer. $|E|$, elastic modulus. (a) Poly(butyl isocyanate) (as for *Figure 1a*). (b) Poly(butyl-ethyl isocyanate) (as for *Figure 1b*). Measured on a Rheovibron Viscoelastometer DDV II

A. A. J. Owadh, I. W. Parsons,
J. N. Hay and R. N. Haward

Department of Chemistry,
University of Birmingham,
PO Box 363,
Birmingham B15 2TT, UK
(Received 27 July 1976)

References

- 1 Shashoua, V. E. *J. Am. Chem. Soc.* 1959, **81**, 3156
- 2 Shashoua, V. E., Sweeny, W. and Tietz, R. F. *ibid.* 1960, **82**, 866
- 3 Natta, G., DiPietro, M. and Cambini, M. *Makromol. Chem.* 1962, **56**, 200
- 4 Tiga, R. P., Sarymina, L. I. and Entelis, S. G. *Russ. Chem. Revs.* 1972, **41**, 734
- 5 Takida, H. and Noro, K. N. *Kobunshi Kagaku* 1965, **22**, 463
- 6 Raes, M. C., Karabinos, J. V. and Kietrich, H. J. *J. Polym. Sci. (A-1)* 1968, **6**, 1067
- 7 Odian, G. and Hiraoka, L. S. *J. Polym. Sci. (A-1)* 1970, **8**, 1309
- 8 Burchard, W. *Makromol. Chem.* 1963, **67**, 182
- 9 Berger, M. N. *J. Macromol. Sci. (C)* 1973, **9**, 269
- 10 Thackray, G. and Haward, R. N. *Proc. Roy. Soc. (A)* 1968, **302**, 453
- 11 Argan, A. S. *Phil. Mag.* 1973, **28**, 839
- 12 Hermans, P. H. 'Cellulose and Cellulose Derivatives Part III', (Eds. E. Ott, H. M. Sparlin and M. W. Griffin), Interscience, New York, 1955, p 1333

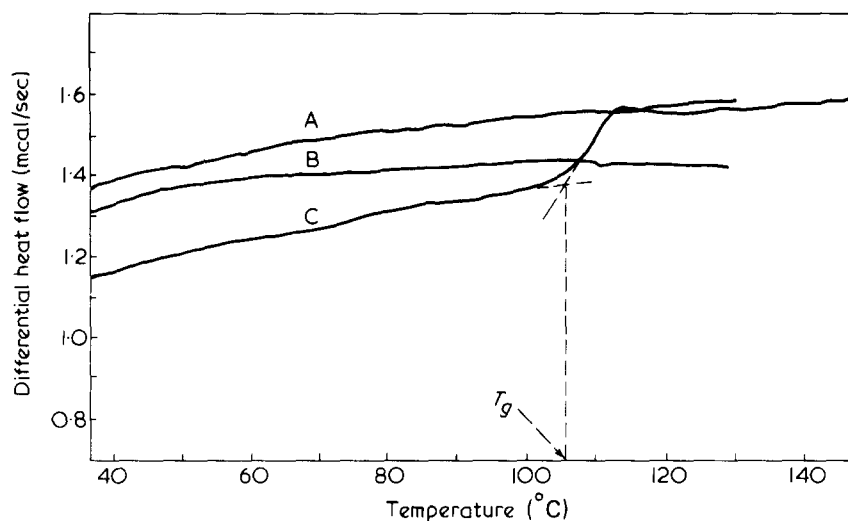
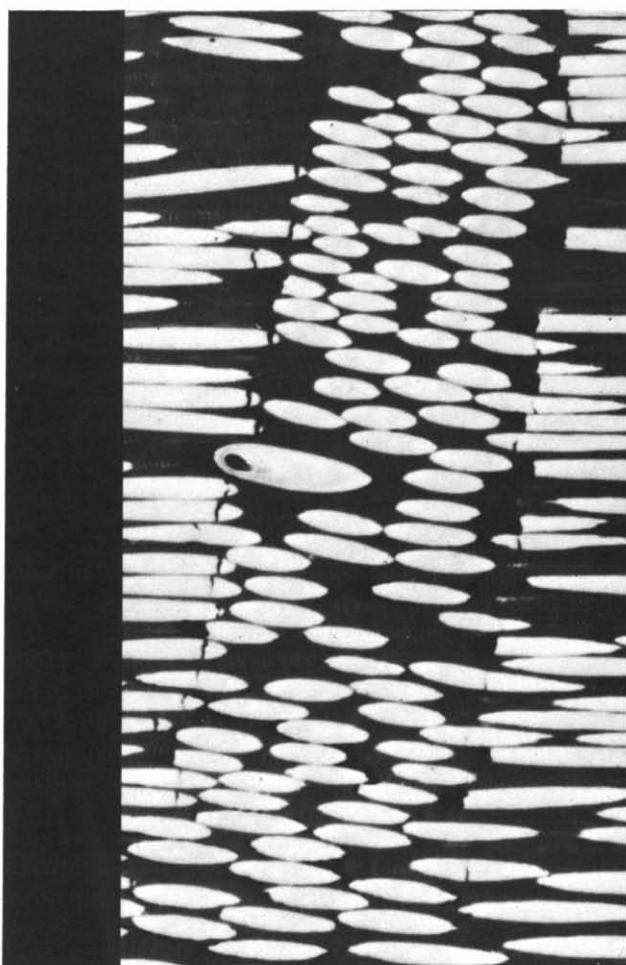


Figure 4 Differential scanning calorimetric measurements with butyl nylon-1 polymer and copolymer compared with polystyrene. (A) Homopolymer (as for Figure 1a); (B) copolymer (as for Figure 1b); (C) polystyrene. Experiments carried out on Perkin-Elmer DSC-2 at 10°C/min and 5 m cal sensitivity

temperature (T_g) the fall in modulus with temperature is rather slow and the damping peak rather flat compared with more conventional polymers. This is accompanied by a very much reduced change in specific heat at ' T_g ' as shown by the d.s.c. curves in Figure 4, where the measurements recorded

for the two nylon-1 polymers are compared with those for polystyrene. It will be seen that on a scale in which ΔC_p (at T_g) is easily observed with polystyrene there is no significant effect with the nylon-1 polymers.

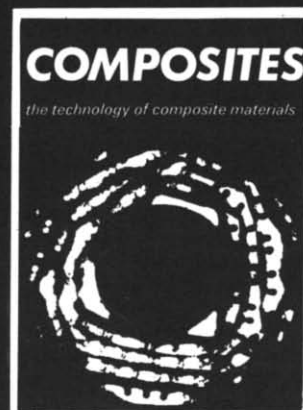
We hope to publish full details of this work at a later date.



COMPOSITES

the technology of composite materials

COMPOSITES is the only journal devoted to the science and technology of composite materials. All materials which can be classed as composites are included. The approach is therefore interdisciplinary, covering fields such as metallurgy and timber research, polymer chemistry and glass technology. Published quarterly, each issue of COMPOSITES contains a selection of news, conference reports and calendar, book reviews and abstracts of relevant articles and patents, in addition to papers on applications and current research and development work.



COMPOSITES subscription (4 issues)
£22 UK, £28 Overseas

For full details write to:
IPC Science and Technology Press Ltd
IPC House, 32 High Street, Guildford,
Surrey GU1 3EW, UK

Book Reviews

Emulsion Polymerization: Theory and Practice

D. C. Blackley

Applied Science, London, 1975, 566 pp. £16.00

It is 20 years since the only previous monograph in English on emulsion polymerization was published. Bovey, Kolthoff, Medalia, and Meehan summarized the work carried out under the Office of Rubber Reserve in the United States during the war on the development of synthetic rubber. Subsequently the emulsion polymerization of other monomers has become important: vinyl chloride, vinyl acetate for emulsion paints, butyl acrylate for leather finishes, vinylidene chloride, ethylene, and tetrafluoroethylene. These differ between themselves and from the much studied styrene model system. Although one or two reviews have appeared each year in the meantime, an up-to-date monograph was overdue. The field is thoroughly reviewed in this book although in a rather verbose style. A few previously unpublished results from the author's laboratory are included. Chapters explain the Smith-Ewart Theory and Gardon's revision of it in detail. The history of the topic, the effects of initiators, emulsifiers, modifiers, electrolyte additions, variation of aqueous phase composition, sequestering agents, and shortstoppers are all covered. There is a chapter on non-aqueous dispersion polymerization: the final chapter points out 'Some Unresolved Problems'. Continuous reactors for emulsion polymerization, emulsion copolymerization, and applications of polymer latices are excluded. Literature references are confined to those in English or available in English translation but these will cover 90% of the relevant material and readers may be encouraged to follow up references although most will find as much as they need to know in the book itself.

There are indications (mentioned in the last chapter) that the theory of emulsion polymerization is now due for a major revision. The importance of the micellization of emulsifiers and the solubilization of monomers in micelles has been exaggerated and the question of the stabilization of polymer latex particles has been neglected. So this account, written from the viewpoint of the classical theory of Smith and Ewart, may only just have appeared in time. Undoubtedly the Smith-Ewart theory accounts for most features of the emulsion polymerization of styrene and (when effects of transfer to monomer are taken into account) for those of the vinyl chloride and vinyl acetate too. But there has been a tendency for workers to force their results into the mould provided by the only available theory when an unbiased assessment would have shown that the results did not really fit the theoretical relations at all! It is greatly to be hoped that the advent of this admirable work may stimulate rather than delay the development of an alternative theory.

A. S. Dunn

Deformation Kinetics

A. S. Krausz and H. Eyring

Wiley, New York, 1975, 398 pp. £13.50

The object of this book is to explain and describe plastic deformation and fracture processes in solids in terms of the kinetics of bond rupture. The point is made, cogently, that any deformations (other than purely elastic ones) in a condensed phase of matter involve the rupture and repair of inter-atomic bonds; to quote 'plastic deformation is a process *identical* to the isomerization of a giant molecule - the specimen'.

The philosophy having been established, the book launches into part I—The theory of deformation kinetics. The basic idea of thermally activated atomic processes is developed and applied briefly to viscoelasticity and, much more extensively, to dislocation mobility in crystals. This section contains a considerable amount of experimental data e.g. on dislocation velocities and the stress dependence of strain rate in creep. In all cases the experimental results can be described satisfactorily by rate-theory equations.

Turning from the microscopical to a continuum approach, the rate theory of thermally activated plastic flow is introduced, featuring as major parameters the apparent activation energy and the acti-

vation volume, both of which betray the underlying atomicity of the phenomena.

Part II, titled 'The analysis of deformation processes', introduces the familiar mechanical (spring and dashpot) models for inelastic processes. Having derived the relevant equations, the authors apply them to experimental phenomena such as yield (the Johnson-Gilman analysis), creep and recovery and stress relaxation. A refreshing feature of this section is the catholic treatment of materials, examples being taken from among metals, thermoplastics and thermosetting resins. Continuing the use of model analysis under 'special topics' the authors next consider mechanical hysteresis, vibration, and the effects of hydrostatic pressure on yield and flow.

A section on the interaction of deformation and chemical reactivity is mainly limited to effects on hair and natural fibres and an opportunity to include stress-corrosion processes seems to have been missed. The final section is devoted to the kinetic theory of fracture and includes reference to the direct observation of bond breakage in polymers by e.s.r. Appendices cover Boltzmann statistics, partition functions and the theory of absolute reaction rates for solids.

This is altogether a most useful, thorough and up-to-date book, eminently readable and thought-provoking on account of its synoptic approach to a wide range of physical phenomena. It is expensive at £13.50 but represents excellent value for money.

E. H. Andrews

Advances in Polymer Science

Volume 18: Macroconformation of Polymers

Springer-Verlag, Berlin, 1975, 149 pp. \$29.70

This volume comprises two authoritative highly specialized review articles which fall within the sub-title 'Macroconformation of Polymers'.

The first, on 'Long-Chain Branching in Polymers', by P. A. Small, runs to 64 pages with 208 references. It opens with a general introduction, followed by eight sections which deal with generalized aspects of the subject, viz. the general effects of long branches, the dimensions of branched molecules, the hydrodynamic properties of branched polymers, the melt viscosity of branched polymers, the thermodynamics of solutions of branched polymers, synthetically branched polymers as models and methods for the estimation of long branching. These are followed by three chapters in which long branching in specific polymers, viz. polyethylene, poly(vinyl acetate), polystyrene, poly(methyl methacrylate) and poly(vinyl chloride), is discussed. In a brief conclusion the author draws attention to the difficulties of applying theoretical treatments to branched polymers and discusses the origins of these difficulties.

The second article, by A. Teramoto and H. Fujita, deals with 'Conformation-Dependent Properties of Synthetic Polypeptides in the Helix-Coil Transition Region'; it occupies 83 pages and includes 137 references. Attention is drawn to the restrictions which the authors have imposed on themselves; they deal here only with non-electrolyte poly(amino-acids) and only in the helix-coil transition region, in which the conformation can be regarded as an 'interrupted helix'. The article opens with an outline of the statistical-mechanical formulation of polypeptides conformation in terms of the degree of polymerization, N , and the Zimm-Bragg-Nagai parameters s and σ . It then proceeds to discuss three properties of interrupted-helical poly(amino-acids), viz. molecular dimensions, intrinsic viscosity and translational friction coefficient, and mean-square dipole moment and mean rotational relaxation time derived from dielectric dispersion measurements. In all three cases, a theoretical treatment is followed by a discussion of experimental results. As the authors state, the article is to some extent a summary of the work of their own school, although it is by no means restricted to this.

A must for specialist polymer laboratories, the price of this volume will probably put it out of the reach of most individuals; it is not for the non-specialist reader.

H. N. Rydon

Professor Geoffrey Gee FRS—A Tribute

Geoffrey Gee's attachment to polymer science began soon after he had graduated with distinction at Manchester University in 1931. He had come under the ubiquitous wing of the Dye-stuffs Division of ICI and was promptly sent to work with Professor Eric Rideal in the Colloid Science Laboratory at Cambridge. This was probably the most exciting centre for physical chemistry in the country at the time because Rideal was adept at attracting a mixed bag of lively researchers from near and far, encouraged a catholicity of interests, and gave people their heads. In this nurturing environment, polymer synthesis and behaviour was becoming a main topic of interest, and Gee with a fellow ICI colleague swelled this stream by studying the kinetics of polymerizations relevant to the production of synthetic rubbers.

His career took a new turn in 1938. The British Rubber Producers' Research Association had just been founded to provide technical backing to the natural rubber industry in the shape of consumption research and development to complement the substantial agricultural effort that had been going on for some time. The first Director, Mr J. Wilson, was recruiting the start-up staff and, by a combination of luck and judgement, he assembled a small team that proved to be of more than ordinary ability. A star performer was Geoffrey Gee who, on Rideal's recommendation, had been invited to head and build up a physical chemistry cum physics group. Mr Wilson, happily still with us, was a decidedly unconventional character who, although coming from an entirely industrial background, had acquired as passionate a fervour for fundamental research as John Knox had for Calvinism. When, as years passed, remonstrances were sometimes voiced as to whether the emphasis on fundamental research was perhaps being overdone, his come-back was much in the colloquial vein of 'you've seen nothing yet'. But whatever the power and persuasion of this particular and, as it turned out, well justified spirit, somebody has to give it flesh and bones if it is to be credible and purposeful and this is where Gee's efforts in the early years of the BRPRA's existence have an enduring value. Amid the fog which shrouded rubber science at the time, and with any number of false trails to confuse and confound, he saw with acute perception where fundamental research on a modest scale could make worthwhile break-throughs. The outcome was that within a decade or two he and his colleagues had made major contributions to the remarkable advances in knowledge of this general field that occurred in the period and thereby set up the scaffolding on which developments of great commercial impact were later to be built.

To gauge the measure of this achievement one must recall the state of basic polymer science nearly forty years ago—though I doubt if anyone who was not around and involved at the time can quite visualize today how embryonic and murky it then was. Certainly Staudinger had revealed the general topography of the domain of high polymers and a few other pioneers such as K. H. Meyer and H. F. Mark had located important landmarks, but most explorers made little inroads and often managed to obscure rather than clarify the detailed features. This unsatisfactory state of affairs was thrown into greater relief by the striking developments coming forward on the technological and industrial fronts. PVC, Perspex, polyethylene, chloroprene and nylon were at different stages of large-scale commercialization and other synthetic rubbers were soon to be. These developments were broadly science based of course, but as regards polymer science *per se* the input was of 'inspired empiricism', to use W. J. S. Naunton's apt expression, rather than much by way of guiding principles. But the need for back-up basic knowledge was increasingly being felt and the flowering of polymer science and polymer scientists, notably in the USA, that soon followed in the wake of this stimulus is a matter of history.

For his own work Gee chose to tackle two truly basic problems in rubber science, namely to put the determination of molecular size on a sound basis and to rationalize the behaviour in solvents and swelling agents. Finding that the key to the latter lay in thermodynamics, he set himself to become thoroughly proficient in a subject of but limited familiarity to him hitherto. One recollection from those days is of him at his desk in the utilitarian laboratory he shared with other senior and junior staff working his way imperturbably through tomes and papers on thermodynamics, seemingly oblivious of the day-long comings and goings and the incessant clatter of vacuum pumps. By a combination of theory so absorbed and of elegantly simple experiments designed to dig out cleanly the data that mattered, the problems mentioned were clarified in out-

line within a handful of years and highways opened up for understanding vulcanizate behaviour and elasticity theory that are still being travelled today.

At the same time, Gee took any amount of trouble to help along the work of his colleagues—and did so to real effect. In particular, as no-one knows better than myself, he played a big part in resolving the mechanistic details of olefin and polyisoprenoid autoxidation—another piece of work which changed the face of knowledge and was to have important spill-offs later on.

In 1949 Gee succeeded to the Directorship of the Association and was confronted with problems of a different kind. More critical questioning of the 'dollars and cents' impact of the work was entering the scene and so, without fuss or upset and while ever concerned to sustain the scientific élan, he proceeded to put a more practical slant into the BRPRA's activities. Illustrative of this was his own analysis made in 1949, little known and barely remembered, of what the natural rubber industry needed to do by way of improved marketing and technical standardization of its product if this were to compete with synthetic rivals. His recommendations prompted action at the plantations and, while others in practising the art of the possible have since had to modify the approaches and emphases, the sequel to his early initiative is that something like a million tons of modern presentation natural rubber are currently being marketed annually—this representing one of the most dramatic technical achievements in up-dating a traditional agricultural, and high polymeric, product from developing countries.

Having put his distinctive imprint on the Association in ways such as this, Geoffrey Gee was obviously gratified to receive in 1953 an invitation to occupy the Chair of Physical Chemistry at his *alma mater*. He, and others, saw as an important objective in this appointment the bringing into being of a school of polymer chemical physics, and this was immediately turned to. But the going was not to be easy. In a year or so the Senior Professor moved to more cloistered pastures and Gee, a relatively raw recruit to the university scene, had perforce to assume the responsibility of managing a large department at a testing time of change. Expansion was then the thing; high student intakes had to be coped with, staff at all levels recruited when practically every university was doing likewise, and new buildings planned and organized—and all within the particular context of the massive redevelopment of the enlarged university site at Manchester. Becoming involved in these matters to a degree that both the pressures and his conscientiousness dictated he had to be, it is no wonder that the prosecution of his own research interests came under constraints. Nevertheless, work in his main speciality of seeking better descriptions of solution and kindred properties of polymers was soon put under way and a supporting team built up. From this has since come notable contributions to the deeper understanding now prevailing of the thermodynamics of polymer—solvent and polymer—polymer mixing, of intermolecular forces between polymers in solution, and of the structural and configurational features determining chain flexibility. With his collaborators and associates, the newer physical techniques of nuclear magnetic resonance and neutron scattering have been exploited with positive effect to supplement the traditional, though increasingly refined data obtained from older investigational methods such as calorimetry. Of special value in this general effort has been simply the existence of a strong group in the field, having close contacts with the polymer industry and critically familiar with work going on elsewhere, with whom Paul Flory has been happy to spend sabbatical leave, and which has served as a 'reference base' for polymer scientists in Europe with cognate interests.

Geoffrey Gee's original papers and review articles are in the literature to testify to his perceptive intellect and to his enviable clarity in analysis and exposition. But not on record are the finely sifting queries, the shrewdly pointed suggestions to measure this or work out that, and the rare skill to penetrate the perplexing that have placed so many who have worked alongside him so much in his debt. It is in the sum of his work and of his influence, so self-effacingly exerted, that the full worth of his conspicuous contribution to polymer science over four decades is to be found.

L. Bateman

Theory of glasses*

S. F. Edwardst

Science Research Council, State House, High Holborn, London WC1R 4TA, UK

(Received 19 May 1976)

It is argued that it is possible to define a 'perfect glass' which is both preparable experimentally and understandable theoretically. Some basic conditions and statistical thermodynamics are derived. Polymerized glasses are complex substances but it is argued that progress may be possible by considering them to have short range properties, and long range properties. Examples are given of models of glasses with such properties and their behaviour is shown to be amenable to theory.

INTRODUCTION

It is a pleasure to contribute a paper in honour of Professor Geoffrey Gee, for it was he who suggested to me that polymerized glasses present a great challenge to the theorist. The trouble with the study of such glasses lies not only in the irreducible difficulties which separate them from simpler systems, but also in their specification. From the point of view of a theorist, or indeed any investigator, one just does not know the nature of the substance under study. It is therefore worthwhile asking if there is possibly a 'perfect' glass, or perhaps a 'theorist's ideal glass' (*TIG*), where well founded calculations can be made of the thermodynamic properties. I believe this to be the case, and indeed some *TIG*'s already exist, and confirm strikingly the predictions of theory.

Polymerized glasses are bound to be more complex than these examples, but one must walk before one can run.

STATISTICAL MECHANICS OF A *TIG*

Suppose one could order the motions of a substance at a particular temperature and density, so that a label can be put on each of them, and any particular state built up from them. Suppose that at a certain temperature one or more of these motions are clearly slower than the rest. Suppose finally that it is possible to suddenly reduce the temperature or pressure of the system so that one maintains the population of the different modes of motion into the region where certain modes are very slow; so slow that they scarcely change over a period where all the other modes reach thermal equilibrium. Then one has a *TIG* in which some modes are characterized by the current temperature and density (or pressure), and others by previous conditions.

It is easy to find examples which can be made. For example if one has 1% of Cu dissolved in Au, and cools it from the melt, the rate at which it orders into crystallinity is much faster than the rate of migration of the Cu about in the Au lattice. So, although in the fullness of time atoms will migrate and either nucleate, or if they remain dissolved do so with the correlation functions of the CuCu CuAu etc. determined by the thermal equilibrium distribution, it is easy to obtain a specimen in which the Cu atoms are distributed with a distribution appropriate to a high

temperature (in fact virtually at random) whilst the specimen is at say 10K.

How can one describe such a system? Consider the problem, at constant volume for simplicity, with the glass formation due to temperature changes. Suppose the degrees of freedom of the system are arranged into the fast modes, called x_α and slow modes called X_α . The energy of the system is given by a Hamiltonian $H(X, x)$ and in thermal equilibrium the probability of finding... X_α ... x_α ... is:

$$P(\dots X_\alpha \dots; \dots x_\alpha \dots) = \exp[F - H(X, x)]/kT \quad (1)$$

where the normalization condition of the probability

$$\int P \Pi dX dx = 1 \quad (2)$$

gives the Helmholtz free energy F from

$$\exp -F(T)/kT = \int \exp[-H(X, x)/kT] \Pi dX dx \quad (3)$$

One may also introduce the probability of finding X with no restraint on x

$$P'(\dots X_\alpha \dots) = \int \exp\{[\hat{F}(X) - H(X, x)]/kT\} \Pi dx \quad (4)$$

where

$$\exp[-\hat{F}(X, T)/kT] = \int \exp[-H(X, x)/kT] \Pi dx \quad (5)$$

By putting equations (3) and (5) together, one has also:

$$\exp(-F/kT) = \int \exp(-\hat{F}(X)/kT) \Pi dx \quad (6)$$

Suppose the material is at T_0 , and is cooled to T_1 , in such a way that the distribution of the X is unchanged, and is therefore still

$$P'(X) = \int \exp\{[\hat{F}(X, T_0) - H(X, x)]/kT_0\} \Pi dx \quad (7)$$

The x variables thermalize at T_1 , whilst the X variables are no longer part of the dynamics of the system, being frozen at their T_0 values. It follows that the free energy of the glass is given, for a definite set of X 's by

* Presented at the Sixth Biennial Manchester Polymer Symposium, UMIST, Manchester, March 1976.

† Also at Cavendish Laboratory, Cambridge, UK.

$$\exp[-F_g(X, T_1)/kT_1] = \int \exp[-H(X, x)/kT_1] \Pi dx \quad (8)$$

i.e.

$$F_g(X, T_1) = -kT_1 \log \int \exp[-H(X, x)/kT_1] \Pi dx \quad (9)$$

But the X 's have the distribution (7), so the experimentally observed free energy will be

$$F_g(T_0, T_1) = -kT \int \{ \exp([\hat{F}(X, T_0) - H(X, y)]/kT_0) \Pi dy \times \log \int \exp[-H(X, x)/kT_1] \Pi dx \} \Pi dX \quad (10)$$

This is much more difficult to handle than the straightforward Gibbs formula, equations (1) and (2), but it must be emphasized that it is the *simplest* formula possible for a glass, and will be only applicable under *TIG* conditions.

The formula (10) already has applications in polymer science. The grand example is that of a rubber. In a rubber a set of crosslinks are established in the entangled polymer melt. Their positions are now fixed and their mobility essentially nil. The rubber is now sheared say, but the crosslinks are distributed in a way appropriate to the unsheared material, so a modulus of elasticity results. Notice that the Gibbs equations (1) and (2) cannot give a resistance to shear. It is surprising that text books do not generally discuss this point. When they study the transition from a liquid to a solid, the crystal axes of the solid are put in without comment. But the Gibbs formula, strictly interpreted, would integrate over these axes as well. In such a case $F = F(T, V, N)$ only, and cannot sustain shear.

The analogous formula to equation (10) has been given by the author (Edwards^{1,2}) and provides (at least to the author's mind!) a firm basis for calculations of higher detail of the elastic equation of state (see for example Deam and Edwards³).

Examples will now be given applying these ideas to models with short range order and long range order. The suggestion is that a polymerized glass will have both the properties of local difficulties in fitting together, and long range effects carried along the molecular chain by which atoms remote from each other can nevertheless interact. Such long range interaction is well known in polymer solution and gel studies, but harder to develop for glasses.

GLASSES WITH SHORT RANGE ORDER: THE SPIN GLASS

Suppose one dissolves a little Fe in Au. One can think of the Fe atom as a little magnet, but solid state physics shows that if the interaction energy is written as

$$\sum_{ij} J_{ij} s_i \cdot s_j$$

where the i th little magnet points in direction s_i , and the j th in direction s_j , then J_{ij} oscillates with the distance $R_i - R_j$ between the sites i and j . Roughly speaking this is why some materials like pure Fe are ferromagnets i.e.

the spacing between Fe neighbours hits an attractive value for J and all the little magnets line up parallel whilst other materials e.g. MnF_2 are antiferromagnets, where the lattice spacing hits a repulsive value for J and the Mn magnets line up alternately up and down. Such a material will not show external magnetism but will have anomalies in the specific heat showing the existence of a phase change when the random directions at high temperatures are replaced by the alternate up and down positions below the critical temperature.

In a spin glass, the magnetic atoms are placed at random, so any pair will interact with J positive or negative according to the distance. This is adequately described, since the distances between atoms is random being fixed by the high temperature from which the alloy was cooled, by taking J_{ij} to itself be a random distribution, albeit decreasing with distance. In other words one can model the problem by saying that:

$$H = \sum_{ij} J_{ij} s_i \cdot s_j \quad (11)$$

but J_{ij} have fixed values, by a probability distribution:

$$P(J_{ij}) = [\exp -(\frac{1}{2} J_{ij}^2 / J_0^2 \epsilon_{ij})] (J_0 \epsilon_{ij} \pi)^{-1/2} \quad (12)$$

where ϵ_{ij} is some monotonic decreasing function of distance. Thus equation (10) in this case is translated into a somewhat simpler form:

$$F_g = \int \Pi dJ_{ij} P(J_{ij}) kT \log \int \exp[(J_{ij} s_i - s_j)/kT] \Pi ds_i \quad (13)$$

This is equation (10) with the X being J_{ij} and with $T_0 = \infty$, P being given by equation (12).

Now one may ask what one would expect to happen. At a high temperature, the magnets will point at random i.e. paramagnetically. At a very low temperature there must be a position, or positions, of equilibrium and the magnets will settle into one of these. In one of these states they will still be pointing in different directions since their local fields will all be different, built out of the J 's of their neighbours. Thus one can expect a phase change from the paramagnetic state in which the direction of the little magnet varies over the whole 4π available to it, to a state in which the direction of each little magnet oscillates about some mean definite direction. The change will show up in a susceptibility anomaly and in a specific heat anomaly. These are found and a theory based on equation (13) has been given by Edwards and Anderson⁴. That this theory explains the particular experimental phenomena is of course to be confirmed by more detailed experimentation, but there seems no doubt that if solid is aptly described by equations (11) and (12) then it will show a phase change into a 'glassy' spin state.

The device which makes equation (13) a basis for calculation is the observation that

$$\log A = \text{coefficient of } n \text{ in } A^n \quad (14)$$

Hence if we think of n 'replicas' of our system, and evaluate

$$\mathcal{F}(n) = \int \prod J_{ij} P(J) \times \exp \left(\sum_{\alpha} \sum_{ij} J_{ij} s_i^{\alpha} \cdot s_j^{\alpha} / kT \right) \prod_{\alpha, i} ds_i^{\alpha} \quad (15)$$

then

$$\mathcal{F}(n) = \mathcal{F}(0) + nF_g \quad (16)$$

It turns out that with approximations it is possible to study equation (15) in n dimensions and evaluate equation (16). The mathematics is not far from the familiar mean field theory, but instead of a mean field, one makes the hypothesis that:

$$\langle s_i^{\alpha} \cdot s_i^{\beta} \rangle = 0 \quad T > T_c \quad (17)$$

$$= q(T) \quad T < T_c \quad (18)$$

$$\text{with } q(0) = 1 \quad (19)$$

There is some analogy with the fact that molecules in a polymer chain which is disordered will have an orientational interaction with their neighbours, although the analogy is by no means perfect. There is perhaps a stronger analogy with rod-like molecules, but these will normally have a potential energy which is doubly periodic whereas magnets are singly periodic.

LONG RANGE INTERACTIONS

At once one meets the difficulty that whereas the simplest theory of ferromagnetism produces an intuitive feeling for the spin glass, there is no simple theory of the simplest model of the long range effect, that of the liquid/solid transition; at least no simple theory which produces the crucial feature of a first order transition. It is argued for example in Landau and Lifschitz' text⁵ that the first order transition is a phenomenon requiring a transition between states of symmetry and no symmetry. I do not believe this is true, and will now develop an admittedly crude theory of the liquid/solid transition in which the crystal structure of the perfect solid is not introduced, and which does not indeed give a first order transition*.

The theory will follow many crude but successful theories of statistical mechanics in which the phase change is attributed to a phenomenon and the magnitude of the physical manifestation of the phenomenon, q say, is a parameter to be determined by the equilibrium condition:

$$\frac{\partial F}{\partial q} = 0 \quad (20)$$

Equation (20) represents a relation between T , N , V , q and the phase change comes when two roots of equation (20) cross over and the value of F which is the minimum corresponds to phase 1 for $T > T_c$ and phase 2 for $T < T_c$. The q of equation (17) is an example, but a much more familiar

one is the mean field of the Weiss theory of ferromagnetism. One assumes that such a field exists and calculates the value which makes F a minimum. For $T > T_c$ the mean field is zero, and the material paramagnetic. For $T < T_c$ the mean field is non-zero, and saturates as $T \rightarrow 0$ to the value obtained when every atom is aligned parallel.

The reference state will be taken to be the perfect solid, and the liquid state will be viewed as a solid which contains faults. It is well known that the simplest classification of faults in a solid is into dislocation and point defects. Point defects are fairly straightforward and local, whilst dislocations have long range effects and are difficult to create or destroy. The model will then assume that the solid state has no dislocations, whereas the liquid state does. Now a real solid does have dislocations of course, but these are the analogue of ferromagnetic fluctuations in a ferromagnet and can be ignored in the crude theory studied here. The idea of treating a liquid as a network of dislocations is not new, but the calculation to be reported on here will contain new features. The free energy of the perfect solid is taken to be known $F_0(V, T, N)$ and will be used as a given function. It will be taken to have the normal property appropriate to a solid under zero (or effectively zero) pressure i.e.

$$P_0(V) = - \frac{\partial F_0}{\partial V} = 0 \quad (21)$$

$$\frac{\partial P_0(V)}{\partial V} \quad (22)$$

At this point one may catalogue the changes expected when a dislocation density q appears.

An expansion

The dislocation will carry volume, say a^3 per unit length, total dislocation length being q . Then $F_0(V)$ becomes $F_0(V + qVa^3)$. Thus:

$$F_0(V + qVa^3) = F_0(V) + qa^3 \frac{\partial F_0}{\partial V} + q^2 \frac{a^6}{2} \frac{\partial^2 F_0}{\partial V^2} \quad (23)$$

to second order. Hence:

$$F_0(V + qVa^3) = F_0(V) + \frac{c}{2} \rho^2 \quad (24)$$

where $c = -\partial P_0 / \partial V$ and will be assumed approximately constant, i.e.

$$\Delta F_1 = \frac{c}{2} \rho^2 \quad (25)$$

Entropy

The dislocation edge will give rise to an entropy corresponding to the choices of direction open to it on formation. One immediately has the difficulty of the non-Markovian nature of the 'random walk' of the edge, and also by the fact that although energy effects are not strictly separable from the entropy, the effective step length of the system can involve local elastic energy and make sharp bends infrequent. Nevertheless the first approximation will be to associate an entropy per unit length of the dislocation, say

* Professor P. W. Anderson made substantial contributions to this work and Mr Mark Warner helped work out the details.

$$\Delta F_2 = -TS = -Tq\sigma \quad (26)$$

Elastic energy

The local elastic energy will simply be proportional to q , ϵq say. More tricky is the long range elastic field (of which ϵ is just the cut off term). A full calculation involves detailed elasticity theory as given by the books of Friedel⁶ or Nabarro⁷, but it will suffice here to consider an electro-magnetic analogy. Suppose one has a unit current j flowing along the dislocation line. The energy will be:

$$H = \mu \iint \frac{j(s_1) \cdot j(s_2)}{|r(s_1) - r(s_2)|} ds_1 ds_2 \quad (27)$$

where s is considered as the arc length of the locus of the line $r(s)$ and for unit current:

$$j = \frac{\partial r}{\partial s} \quad (28)$$

One must now evaluate $\exp(-H/kT)$ taken over a random distribution of dislocation lines being random walks of step length say l (of the order of a few lattice spacings). (The full elastic theory uses stress tensors but does not have an essentially different energy function.)

The calculation of $\int \exp(-H/kT)$ now can be performed after the Debye-Huckel theory of screened Coulomb interactions. It need not be reproduced here except in the final form that it gives rise to a free energy contribution:

$$\frac{\partial \Delta F_3}{\partial q} = \frac{2\pi^2 \mu b^2}{b + \left(\frac{q\mu}{kT}\right)^{1/2}} \quad (29)$$

where b is the point at which equation (2) is an inadequate description, so that as $q \rightarrow 0$ the contribution is:

$$\Delta F_3 \rightarrow 2\pi^2 \mu b^2 q$$

The term ϵq compensates for any errors in this expression due to short range detail.

$$F = F_0 + \Delta F_1 + \Delta F_2 + \Delta F_3$$

The condition of equilibrium is

$$\frac{\partial F}{\partial q} = 0$$

or

$$0 = cq - \sigma kT + \epsilon + \frac{\mu'}{b + \left(\frac{q\mu}{kT}\right)^{1/2}} \quad (30)$$

The perfect solid is $q = 0$ and q must always be ≥ 0 . A sketch of the right hand side $-P(q)$ of equation (30) shows three cases (Figure 1). Possible values of q are marked by crosses. In Figure 1a the perfect solid is the only solution and $q = 0$. Figure 1b is critical and $q_c \neq 0$. Finally in Figure 1c the right hand value gives the q for which F is a minimum.

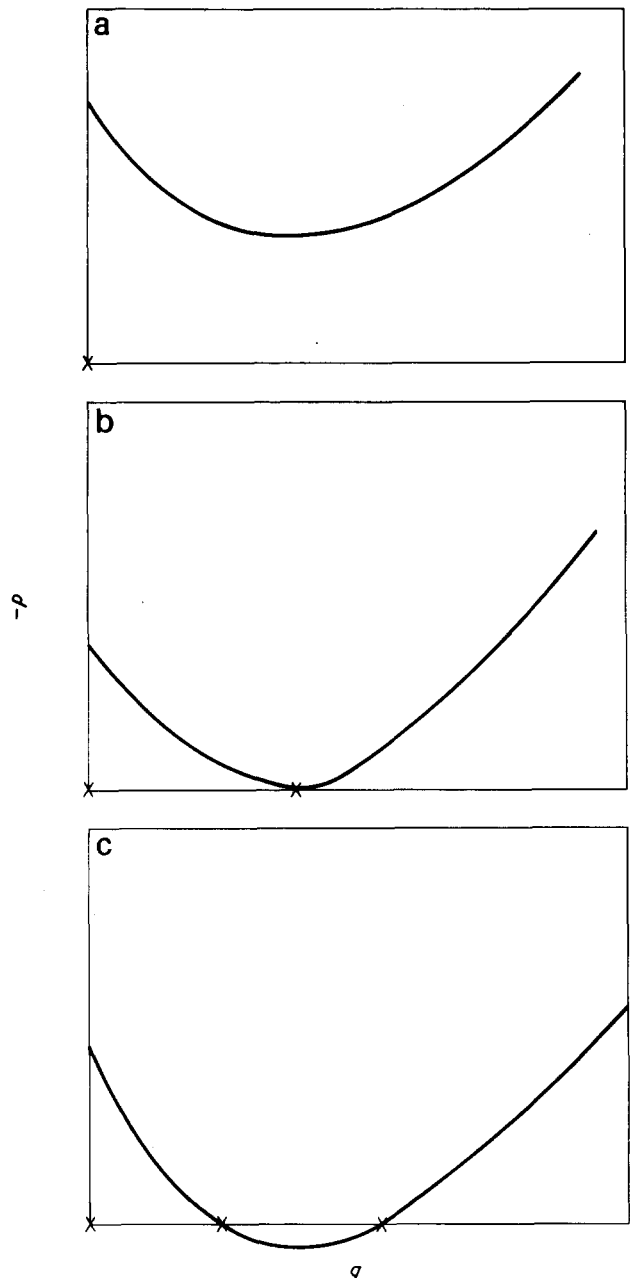


Figure 1 Free energy curves

Thus a first-order transition has been obtained. The cases are in ascending temperature Figure 1a, 1b, 1c for constant volume.

GLASS WITH LONG RANGE ORDER

The work of the section above, crude as it is, will give a model of a glass. The view is that q represents a slow motion. When the glass is quenched from T_0 with q_0 , to T_1 , q remains the same. Clearly the identification of q with a dislocation density may be an oversimplification, but from a TIG point of view one now has a framework to employ (equation 10) and derive say the specific heat as a function not only of T_1 but T_0 . It will be seen that what in fact is derived is:

$$(C_v)_{\text{glass}} - (C_v)_{\text{perfect solid}}$$

since all the work is relative to the perfect glass free energy which is taken to be known.

It is possible to make sense of the various curves describing the behaviour of C_v through the glass transition by extending these ideas, and it is hoped to report fully on them (and some new experiments aimed to make the glass quickly rather than slowly) later.

I hope however to have shown that both local molecular orientation and long range effects may both be important contributors to glass behaviour, and doubtless polymerized glass contains elements of both of these phenomena.

REFERENCES

- 1 Edwards, S. F. in '4th International Conference on amorphous materials', (Eds R. W. Douglas and B. Ellis), Wiley, New York, 1970
- 2 Edwards, S. F. in 'Polymer networks: structural and mechanical properties', (Eds A. J. Chompff and S. Newman), Plenum Press, New York, 1971
- 3 Deam, R. T. and Edwards, S. F. *Phil. Trans. Roy. Soc. (A)* 1976, **280**, 317
- 4 Edwards, S. F. and Anderson P. N. *J. Phys. (F)* 1975, **5**, 965; 1976, **6**, in press
- 5 Landau, L. D. and Lifschitz, E. M. 'Statistical Physics', Pergamon, Oxford, 1970
- 6 Friedel, J. 'Dislocations', Pergamon, Oxford, 1964
- 7 Nabarro, F. R. N. 'Theory of Crystal Dislocations', Oxford University Press, London, 1967

Structure and properties of block polymers and multiphase polymer systems: an overview of present status and future potential*

S. L. Aggarwal

The General Tire & Rubber Company, Akron, Ohio 44329, USA

(Received 13 July 1976)

Work on the block polymers of styrene and butadiene indicates the potential of multiphase polymers of controlled solid state structure. The effect of chemical composition, molecular architecture (multichain 'star' shaped *versus* linear), block sequence length, processing conditions, and blending of homopolymer with the block polymers on their solid state morphology is discussed. Results on these block polymer systems indicate the future research directions in certain areas. Implications of these areas for polymers of controlled solid state structure to provide materials of desirable combination of properties are also considered.

INTRODUCTION

The scientific and technological advances resulting from the work on block polymers have constituted a major milestone in polymer science during the last decade. The exciting aspect of the block polymers and other multiphase polymers is that in a number of important cases, it has been found possible to control the morphology in the solid state and to be able to vary it over a broad spectrum through control of their molecular structure and composition. The scientific foundation for the advances in block and multiphase polymers goes back to early fundamental studies of Professor Geoffrey Gee, particularly the work in such areas as the preparation of polymers of controlled structure, thermodynamics of polymer solutions and phase separation, and the relation between chemical structure

and mechanical properties. Future advances in multiphase polymer materials, particularly in those polymers that are generally referred to as thermoplastic rubbers, are likely to depend on the scientific framework that the work of Professor Gee and his group provided in the area of network structure and rubber elasticity.

This paper is in two parts: Part I is an overview of the solid state morphology and combination of desirable properties that are attainable by the control of the chemical and molecular structure of block polymers. Part II is a brief discussion of a few of the recent research directions that appear particularly promising for multiphase materials of controlled structure with desirable combinations of properties.

PART I: STRUCTURE AND MORPHOLOGY OF MULTIPHASE POLYMERS — AN OVERVIEW

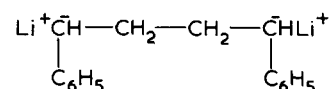
MORPHOLOGY OF STYRENE/BUTADIENE BLOCK POLYMERS

Preparation of styrene/butadiene/styrene triblock polymers by anionic polymerization

The system that has been studied in detail is that of block polymers of styrene and butadiene (or of isoprene in place of butadiene)¹⁻⁷. The polymerization chemistry that has made possible the preparation of block polymers of controlled structure is based on anionic catalysts such as butyllithium⁸⁻¹¹. The reactive species from such initiators, with suitable monomers, are long-lived carbanions^{11,12}. Thus, one may polymerize a monomer A (styrene) to completion, followed in sequence by polymerization of another monomer B (butadiene or isoprene) to obtain a diblock polymer. The triblock ABA block polymer may then be

prepared by adding monomer A to the diblock polymer with the active end, or the diblock polymer active species may be coupled by a chemical coupling agent^{10,13}. The scheme of preparing block polymers by sequential anionic polymerization is shown schematically in *Figure 1*. However, a number of kinetic and preparative details must be considered in the preparation of triblock polymers from styrene and butadiene, to eliminate the homopolymer and diblock impurities during polymerization and coupling reactions. These have recently been discussed by several authors¹⁴⁻¹⁶.

An especially convenient, and perhaps better controlled, method for the preparation of styrene/butadiene/styrene triblock polymers is by the use of difunctional catalysts such as 1,4 dilithio-1,1,4,4-tetraphenylbutane¹⁷⁻¹⁹.



* Presented at the Sixth Biennial Manchester Polymer Symposium, UMIST, Manchester, March 1976.

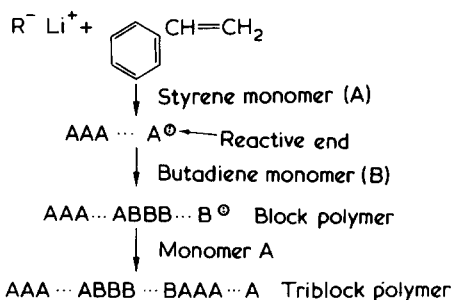


Figure 1 Scheme for preparing block polymers by anionic polymerization

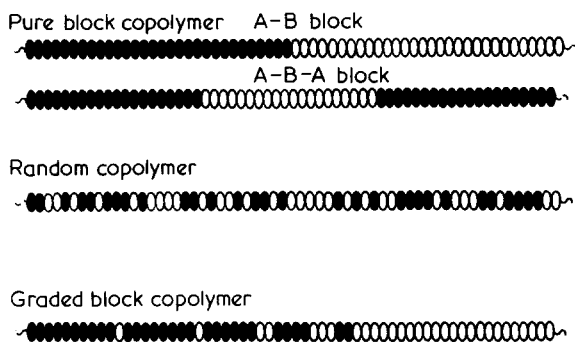


Figure 2 Schematic representation of copolymer structures

Butadiene is first polymerized at each terminal active end, followed by the polymerization of styrene to form the terminal blocks. This procedure was also used to prepare the triblock ABA polymers of α -methylstyrene (A) and isoprene (B)¹⁹.

Another aspect of anionic polymerization that makes it a very useful method for obtaining copolymers of controlled sequence length is the broad range of reactivity ratios that are possible in copolymerization of such monomers as styrene and the common dienes either in different solvents (e.g. benzene *versus* tetrahydrofuran) or in the presence of different concentrations of weakly basic ethers (e.g. diphenyl ether and anisole)²⁰⁻²⁵. Based on these features of anionic polymerization, using an organo-lithium compound as an initiator, a number of block polymers of styrene and the common dienes (butadiene and isoprene) have been prepared.

Styrene/butadiene/styrene thermoplastic rubbers

Figure 2 shows schematically the various block polymer structures that can be prepared. The graded block structures result when the comonomers are added together initially and the reactivity ratios are controlled by carrying out the polymerization in benzene containing a suitable concentration of a weakly basic ether such as diphenyl ether²⁴⁻²⁷. It results in long sequences of styrene at each end. The sequence length of the styrene units gradually decreases away from the terminal blocks, so that the central block may have only sequences of one or two styrene units, but it has long sequences of butadiene units.

The first block polymer that attracted wide interest was Kraton thermoplastic rubber by Shell^{2,3,28}. It consists of approximately 70% butadiene and 30% styrene by weight. The central block is of butadiene units, and the terminal blocks are of styrene units. At room temperature it is a strong rubber^{29,30}, can be processed as a thermoplastic at elevated temperatures and requires no crosslinking for

coverable large deformations characteristic of common vulcanized rubbers.

In Tables 1 and 2 are given the comparative strength and fatigue-to-failure properties of Kraton thermoplastic rubber and typical vulcanized rubbers at room temperature. At higher temperatures there is of course a large decrease in these properties for the thermoplastic rubber.

The model⁵ proposed to explain the above properties is shown schematically in Figure 3. It shows polystyrene domains segregating as glassy domains that act both as reinforcing filler and also provide physical crosslinks that are thermally labile. This model in its essential features, has been shown to be the correct one by the work of a number of workers³¹⁻⁴¹. The most direct evidence has been from the electron micrographs of such block polymers, stained by osmium tetroxide which stains the rubber phase, and thus appears dark in the electron micrographs. Figure 4 is one of the early electron micrographs from our laboratory

Table 1 Comparative strength values of typical vulcanized rubbers and Kraton 101 thermoplastic rubber

	Tensile strength (lb/in ²)	Elongation (%)
Triblock thermoplastic rubber (Kraton 101)	40 300	740
Natural rubber (carbon black reinforced and cured)	28 200	560
SBR synthetic rubber (carbon black reinforced and cured)	29 800	590

Data with typical rubber formulations and at room temperature. Tensiles based on true cross-section at break (1 lb/in² = 6.894 × 10³ N/m²)

Table 2 Comparative fatigue-to-failure values* at approximately equal strain energy for Kraton thermoplastic rubber and typical vulcanized rubbers

	Cycles to failure
Triblock thermoplastic rubber (Kraton 101)	145 000
Natural rubber (carbon black reinforced and cured)	48 000
SBR synthetic rubber (carbon black reinforced and cured)	45 000

Data with typical rubber formulations and at room temperature. * Monsanto Fatigue Tester, ~110% elongation

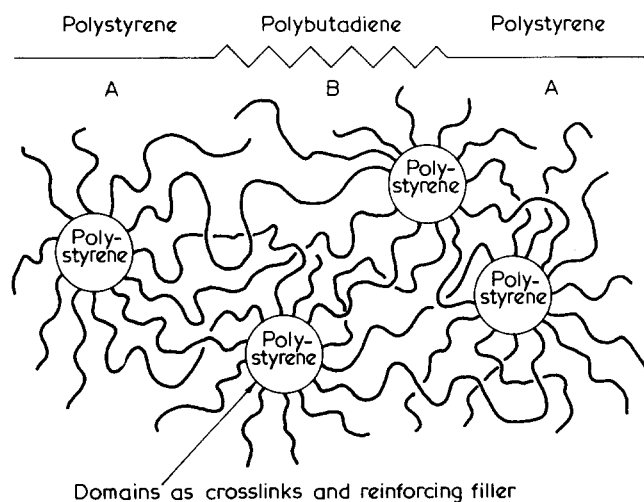


Figure 3 Schematic of the domain structure of styrene/butadiene/styrene triblock thermoplastic rubbers

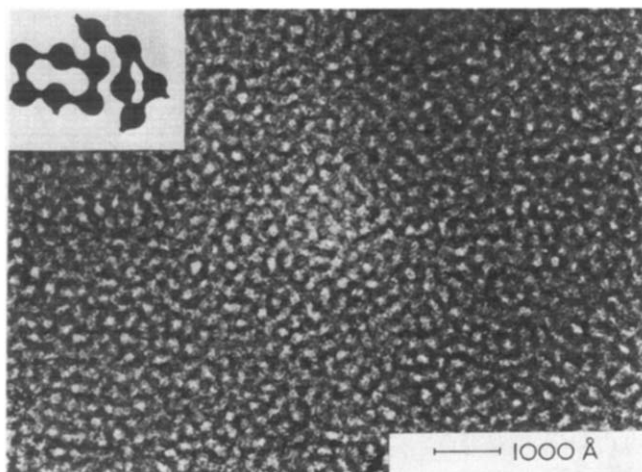


Figure 4 Electron micrograph of Kraton 101 Cast from THF/MEK 90/10 solution

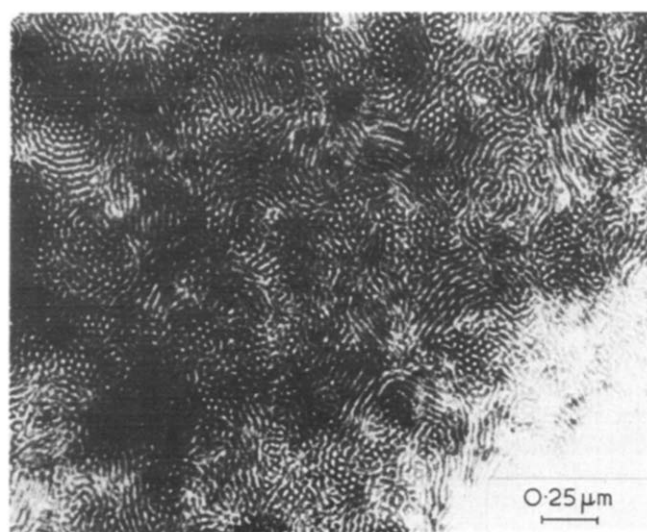


Figure 5 Electron micrograph showing short range order and morphology of styrene/butadiene/styrene (styrene/butadiene 25/75) block polymer

which shows the spherical polystyrene domains of approximately 100 Å dispersed in the polybutadiene matrix³⁵. Further studies revealed additional details in the electron micrograph that are important in understanding properties of such block polymers. Results of these studies may serve as a model for other block polymers that may not have as well defined structure as the block polymers from styrene and butadiene.

The electron micrograph, Figure 5, shows that between the polystyrene domains there are frequent interconnections, and there is an apparent short range order between the polystyrene domains. A consequence of such short range order, as shown in Figure 6, is that during the first stress-strain cycle, the material shows a high modulus typical of a plastic rather than that of a rubber (i.e. steep slope of the stress-strain plot), followed by a yield point and considerable cold-drawing^{25,35}. The short range order breaks down beyond the yield point during the first extension cycle. Consequently, during the second and subsequent cycles, the behaviour is that of a crosslinked rubber. Interestingly, the behaviour is completely reversible on annealing. The domains are thus shown to have appreciable elastic memory.

Another interesting aspect of the behaviour of polystyrene glassy domains in these polymers is shown in Figure 7. The polystyrene glassy domains in these block polymers are markedly ductile. The spherical domains present in the original sample are deformed to elliptical domains³⁵ at elongations above 300%. The high strength of styrene/butadiene/styrene triblock polymers mentioned above, may be attributed to the ductility of the glassy domains. On annealing a stretched sample, the elliptical domains revert to their original shape.

Phase separation in block polymers results in two distinct transition temperatures that correspond nearly to that of the two phases⁴²⁻⁴⁴. Figure 8 shows the transition behaviour of Kraton 101 triblock polymer from measurements of damping as a function of temperature^{25,35}. The transition peaks in the vicinity of -80°C and 100°C are close to the transition temperatures of polybutadiene and polystyrene respectively. How complete the phase separation is, depends also upon the nature of the solvent from which the film is deposited. Whenever there is appreciable mixing of phases, there is an intermediate transition peak, as is the case for the sample deposited from carbon tetrachloride. The completeness of phase separation, or the lack of it in films deposited from different solvents, has marked effect on their stress-strain behaviour^{25,35}.

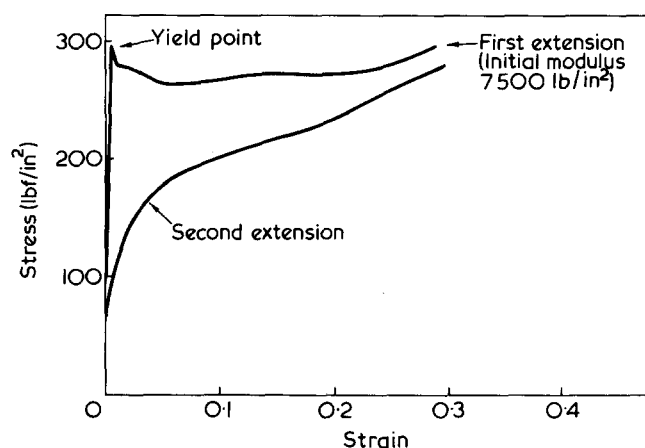


Figure 6 Stress-strain curve of Kraton 101 styrene/butadiene/styrene triblock polymer cast from THF/MEK 90/10 solution

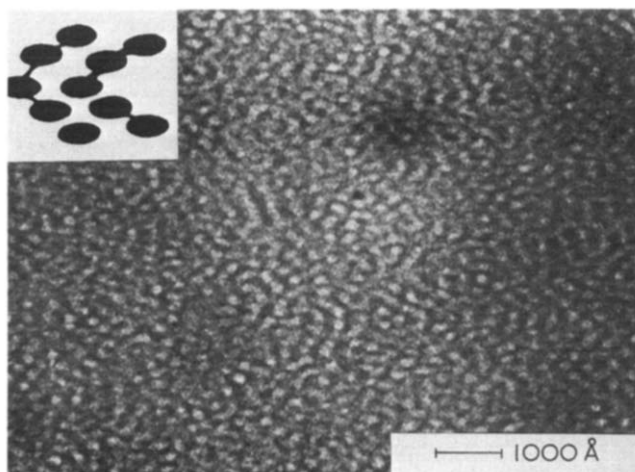


Figure 7 Deformation of polystyrene domains in styrene/butadiene/styrene triblock polymers on stretching 300 %

Effect of composition and structure on the block polymers of styrene and butadiene

The range of solid state structure, i.e. the nature of morphology of the dispersed phase, and thus the useful combination of properties that can be realized in block polymer systems^{32,39,45}, is well illustrated by the examples discussed below for the block polymer of styrene and the common dienes.

In *Figure 9* are shown electron micrographs of those styrene/butadiene/styrene triblock polymers that contain increasing wt % styrene. In the block polymer that has butadiene as the major component, the dispersed phase is that of polystyrene spheres. As the amount of styrene increases, the morphology changes to short rods, lamellar structure of polybutadiene and polystyrene layers, and finally as styrene in the block polymer becomes the major component, the dispersed phase is that of polybutadiene in the matrix of polystyrene. The high styrene triblock polymers are glassy high impact materials, and are optically clear because of the submicroscopic size of the dispersed phase. The effect of composition on the morphology of block polymers is seen more clearly from the electron micrographs in *Figure 10* of styrene/isoprene/styrene block polymers from the work of Kawai and his associates^{39,46}. The block polymer that contains almost equal amounts of styrene and isoprene (*Figure 10c*) has a layered structure of polystyrene and polyisoprene domains. The composition

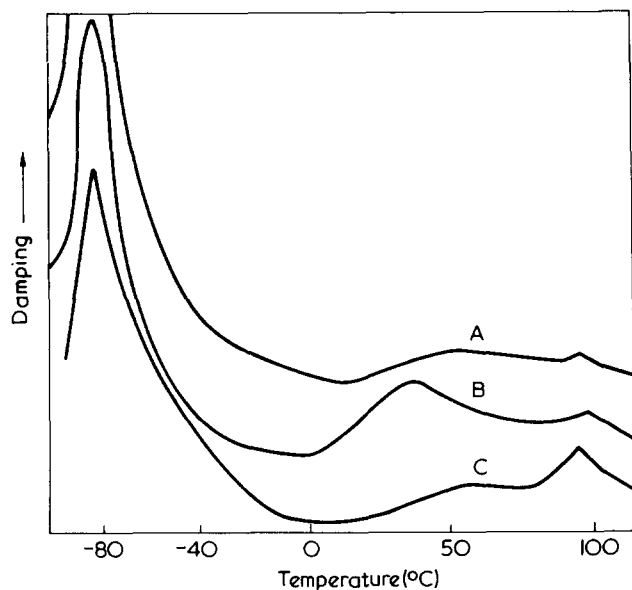


Figure 8 Transition behaviour of styrene/butadiene/styrene triblock polymers cast from different solvents: A, benzene/heptane; B, carbon tetrachloride; C, THF/MEK

of the triblock polymers is shown in *Figure 10* caption.

The morphology is also dependent upon the solvents in which the block polymer is prepared because of the effect of the solvent on the polymer morphology during work-up and isolation from solutions in different solvents. The two electron micrographs in *Figure 11* are for triblock polymers of the same composition (40% styrene and 60% butadiene), but one was prepared in toluene and the other was prepared in heptane. The difference in morphology results from toluene being a good solvent for the polystyrene terminal blocks, while heptane is a good solvent for the central block and a rather poor solvent for the terminal blocks.

Figure 12 shows the electron micrographs of styrene/isoprene/styrene triblock polymers of the same styrene/isoprene composition (75% styrene and 25% isoprene). The difference is that the pure block has terminal blocks of long styrene sequences, while in the graded block the styrene sequence length of the terminal blocks is smaller and the sequence length of the styrene blocks gradually decreases from each end toward the centre. The diffuse boundary of the dispersed phase for the graded block polymer results from the favourable conditions for phase mixing in block polymers of such structure.

Effect of processing on the morphology of block polymers

The morphology of the domains, for a particular composition and molecular structure of the block polymers, depends markedly on the flow conditions during processing and fabrication. *Figure 13a* is an electron micrograph of a thin section of a rod of Kraton 101 (styrene/butadiene/styrene block polymer containing 28% styrene terminal blocks marketed by Shell Chemical Company) extruded into the capillary of the Instron Rheometer, annealed in the capillary and then forced out. The electron micrograph shows long cylindrical polystyrene domains parallel to the direction of extrusion in contrast to the spherical or short cylindrical polystyrene domains present in samples of the polymer cast as films from solutions. When the sample is prepared by milling and then pressing the milled sheet under conditions of minimum flow, the morphology of polystyrene domains in the surface layers of the sheet is shown in *Figure 13b*. The domains in the surface layers are oriented parallel to the milling direction. The top and bottom layers thus may be regarded as 'macrodomains' of polystyrene with preferential orientation parallel to the milling direction. Optical birefringence measurement showed that as one goes away from the surface towards the mid-plane of the sheet, there is an increased tendency of the macrodomains to orient out of the plane of the sheet, and there is increasing disorder in the orientation of the principal direction of the macrodomains with respect to the mill-

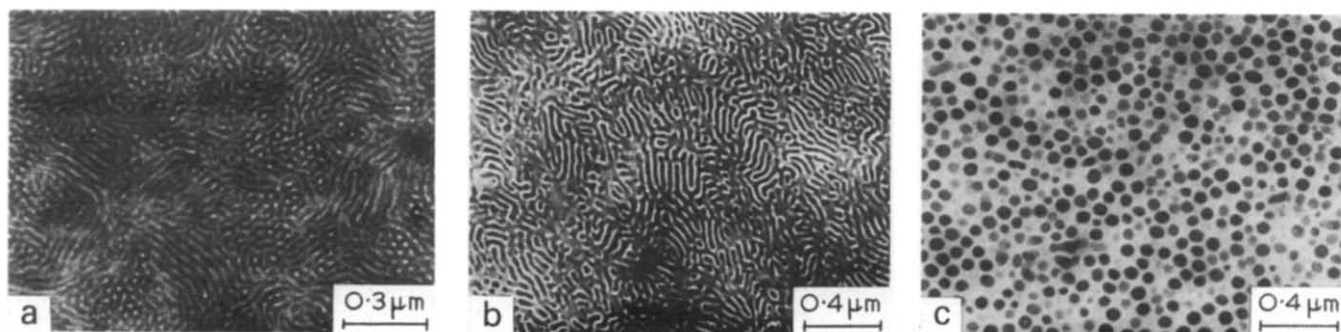


Figure 9 Effect of chemical composition on the domain structure of styrene/butadiene/styrene block polymers: (a) styrene/butadiene, 25/75; (b) styrene/butadiene, 60/40; (c) styrene/butadiene, 90/10

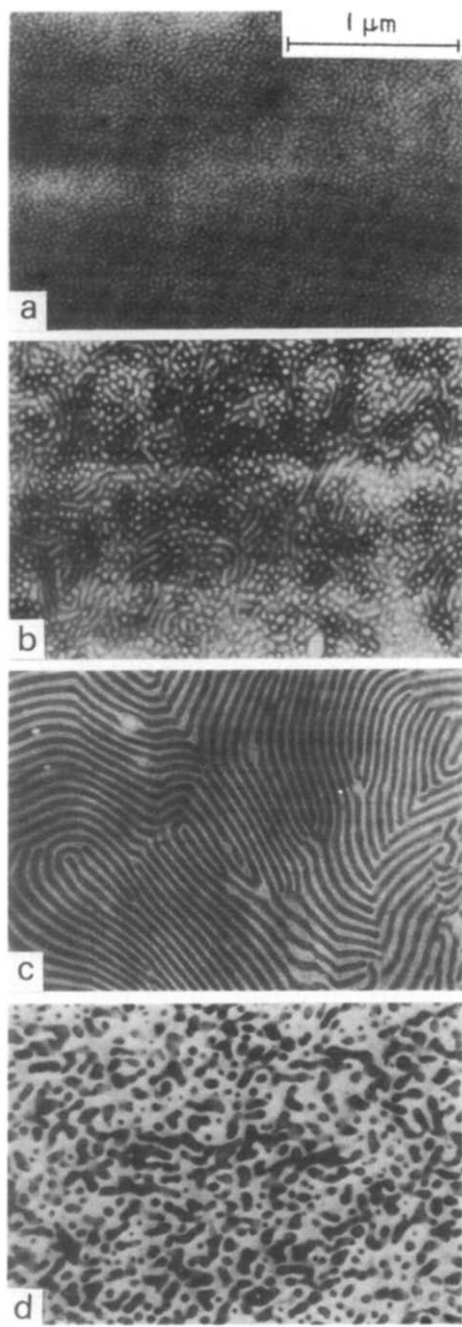


Figure 10 Effect of chemical composition on the domain structure of styrene/isoprene/styrene triblock polymers. (a) SIS-1, 5/90/5 S-I-S; (b) SIS-2, 10/80/10 S-I-S; (c) SIS-3, 25/50/25 S-I-S; (d) SIS-4, 35/30/35 S-I-S. [Reproduced from: Kawai, H., Soen, T., Inoue, T., Ono, T. and Uchida, T. *Mem. Fac. Eng. Kyoto Univ.* 1971, **33**, 421 by permission of the Faculty of Engineering, Kyoto University, Japan ©]

ing direction. Because of preferential orientation of the polystyrene domains, these samples show highly anisotropic mechanical properties, and are discussed later. Orientation of lamellar domains is observed in triblock polymers which contain approximately equimolar amounts of styrene and butadiene. The electron micrograph in *Figure 13c* is that of a sample cast rotationally from a triblock polymer containing styrene and butadiene in the ratio of 60:40.

Keller and his collaborators in a series of papers^{47,48} have reported that it is possible to obtain an almost perfect hexagonal arrangement of polystyrene domains as con-

tinuous rods arranged parallel to the direction of extrusion, in a rod sample of Kraton, if extruded slowly as a plug and the plug allowed to cool slowly. *Figure 14* is an electron micrograph of an ultra-thin section cut parallel to the extruded and annealed plug. *Figure 15* is an electron micrograph of the cross-section of such an extruded rod, and shows the uniformity of the cross-section of these cylindrical domains and their regular hexagonal packing.

Effect of molecular architecture on the morphology of block polymers

The molecular architecture of the block polymers apparently has a marked effect on the regularity of the domain structure, and on the comparative ease with which such domain regularity develops. This is most dramatically demonstrated by the 'star' or 'radial' block copolymers prepared by Fetters and his associates⁴⁹⁻⁵¹. Schematically, the structure of such radial block polymers is shown at the bottom of *Figure 16*. Each arm of this poly-

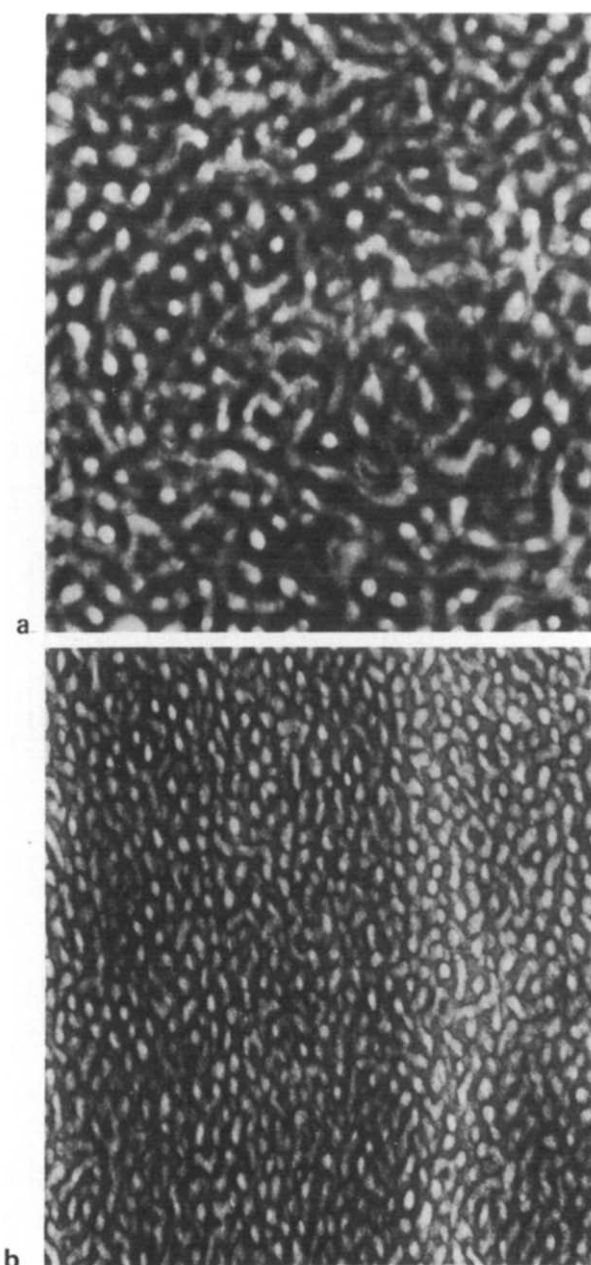


Figure 11 Effect on morphology of the styrene/butadiene/styrene triblock polymer by the solvent used for polymerization and isolation. (a) Toluene; (b) heptane

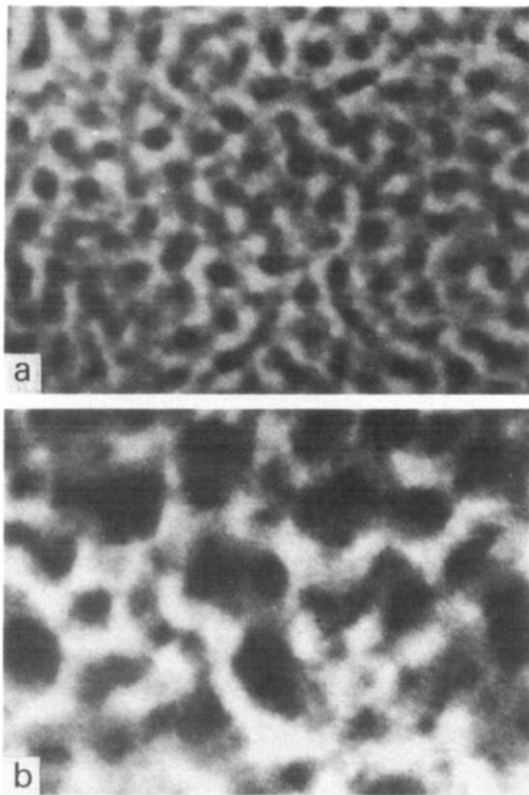


Figure 12 Morphology of 'pure' and 'graded' styrene/butadiene/styrene block polymers. Micrographs for block polymers of styrene/isoprene 75/25 by wt: (a) pure block polymer (75/25, styrene/isoprene); (b) graded block polymer (75/25, styrene/isoprene)

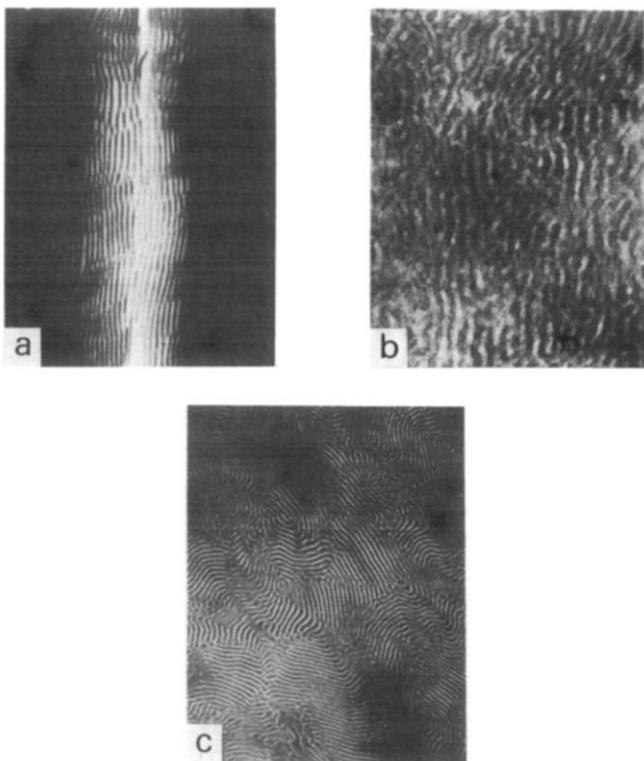


Figure 13 Effect of processing conditions on the morphology of polystyrene domains in styrene/butadiene block polymers: (a) cylindrical polystyrene domains in extruded rod—high tensile modulus with low torsion modulus; (b) domains in a milled sheet—polystyrene domains parallel to direction of milling; (c) domain morphology in rotationally moulded sample—60/40 styrene/butadiene triblock polymer

mer is an AB diblock polymer, and the total average number of arms may be controlled from four to as many as twenty-nine. The electron micrograph in Figure 16 shows the morphology of domains formed in a film of styrene/isoprene radial block polymer containing 30% styrene, and



Figure 14 Electron micrograph of an ultrathin section cut parallel to the extrusion direction of extruded and annealed rod of styrene/butadiene/styrene block polymer—Kraton 101. [Reproduced from Dlugosz, A., Keller A. and Pedemonte, E. *Kolloid Z. -Z. Polym.* 1970, 242, 1125 by permission of Dietrich Steinkopff Verlag ©]

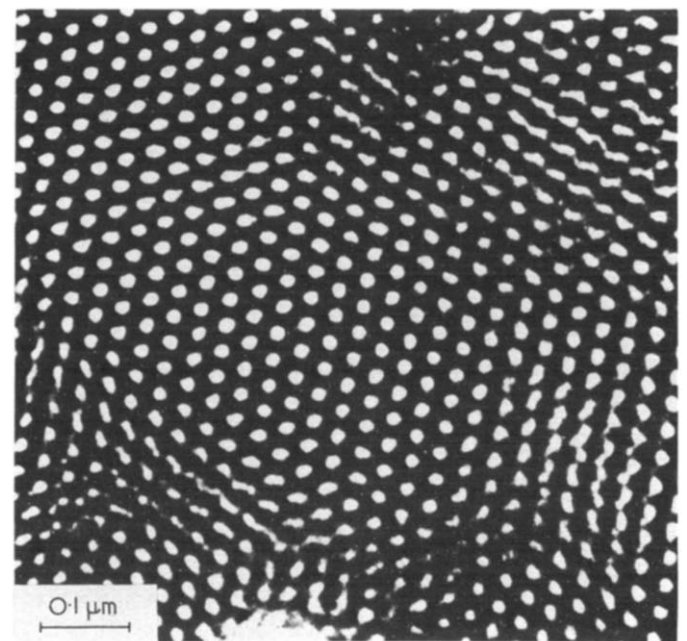


Figure 15 Electron micrograph of cross-section of same sample as used for electron micrograph in Figure 14

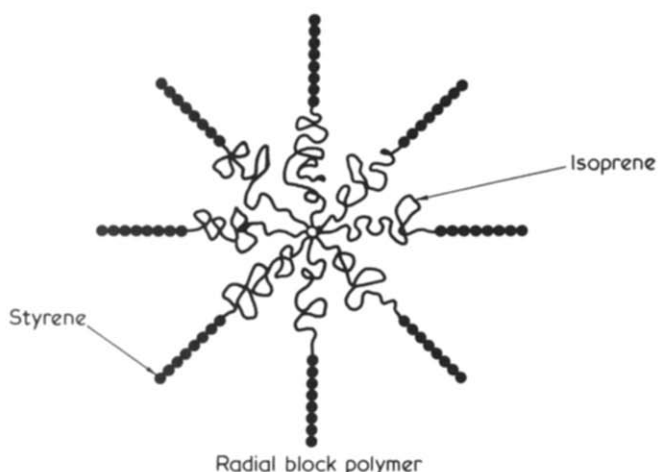
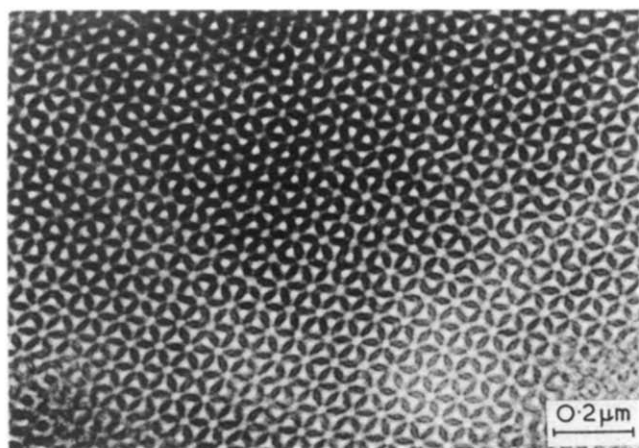


Figure 16 Morphology of polystyrene domain in a film of 'radial' block polymer

having 15 number average arms with each arm having $M_n = 71\ 000$. The noteworthy point is the regularity of the domains and that this regularity is easily achieved in solvent-cast films. In Figure 17, morphology in cast films of linear triblock polymers is compared with that of multichain 'star' polymers of the same styrene/butadiene composition. These micrographs demonstrate the effect of the molecular architecture of the block polymers (linear triblock *versus* radial) on the morphology of the cast films.

BLOCK POLYMERS AS MICROCOMPOSITES

Similarity between multiphase structure of block polymers and of macrocomposites

The multiphase domain structure of block polymers, and the orientation of such domains under suitable processing conditions, results in materials that are analogous to macrocomposite materials fabricated by combining two types of materials. Some of the common examples of macrocomposites of technological importance because of the useful combination of properties, are the filled plastics and rubbers for high modulus and strength, glass fibre reinforced plastics, and laminated structure of fibre cord/rubber in pneumatic tires. Composite materials in general may be considered under three broad classes: (a) isotropic particulate composites (particles of one phase randomly dispersed in the matrix of another phase); (b) uniaxial oriented composites (fibres or similar shaped particles with uniaxial orientation in a matrix); and (c) laminated composites (layers of various

materials, or structures). In block polymer systems, some of which were referred to in the preceding discussion, similarities to each of these classes of composite materials are noted. In block polymer systems, the size of the phases may be of submicroscopic dimensions.

There has been considerable activity and significant progress in recent years in developing micromechanic theories of composite materials to calculate the various moduli of the composites, from the knowledge of the properties of the constituents and the geometry of the phases in the composite. Such theories have been successfully applied to block polymer systems. They serve as an important guide to understand and interpret the mechanical behaviour of block polymers, and to obtain a broad variation in composite properties by manipulating morphology and properties of phases. Following is a brief review of some of the theories of micromechanics of composite materials, and a discussion of their applicability to some of the block polymer systems.

Theories of micromechanics of composites

Particulate composites. Hashin, in a classical set of papers, made use of variational energy methods to establish the upper bound and lower bound for the moduli of composite systems of irregular phase geometry, for systems of randomly dispersed spheres and for systems containing uniaxially oriented fibres⁵²⁻⁵⁴. For a random assemblage of spheres, the system is isotropic and only two material parameters are needed to characterize the system completely. He found that the upper and lower

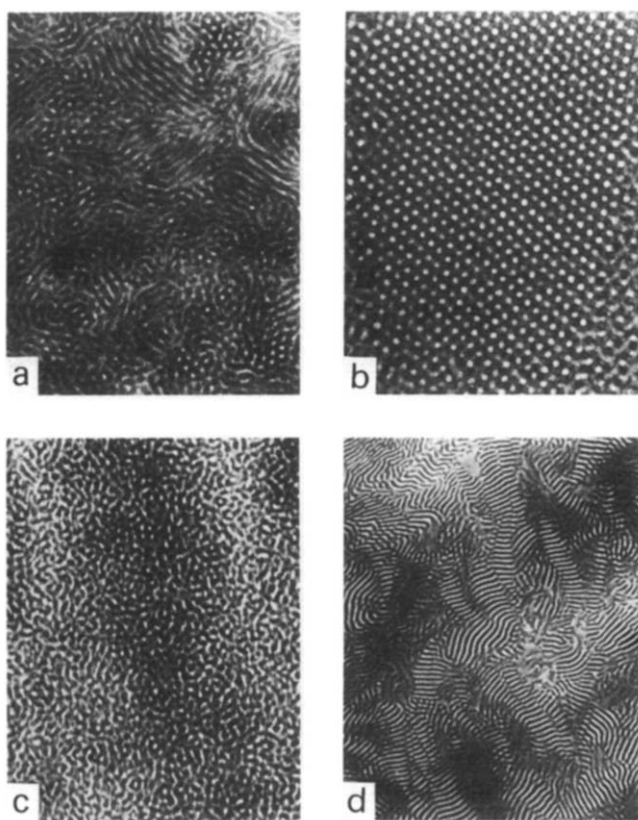


Figure 17 Comparison of morphology of polystyrene domains for the linear triblock *versus* multichain 'star' block polymers. 30/70 Styrene/butadiene block polymers: (a) linear triblock; (b) 'star' multichain, 40/60 styrene/butadiene block polymers; (c) linear triblock; (d) 'star' multichain

bounds for bulk and compression moduli were almost identical. For shear moduli, these bounds are close only when the moduli of matrix and particle are close. The lower bound for the shear modulus is:

$$\frac{G}{G_1} = 1 + \frac{15(1 - \nu_1) \left(\frac{G_2}{G_1} - 1 \right) \Phi_2}{7 - 5\nu_1 + (8 - 10\nu_1) \left[\frac{G_2}{G_1} - \left(\frac{G_2}{G_1} - 1 \right) \Phi_2 \right]} \quad (1)$$

where G is the shear modulus of composite, G_1 and G_2 are the shear moduli of the matrix and of the dispersed phase, and subscripts 1 and 2 refer to matrix and dispersed phase respectively. ν_1 is the Poisson ratio of the matrix, and Φ_2 is the volume fraction of the dispersed phase. This equation is equivalent to Kerner's equation derived by an entirely different method.

When the dispersed phase is much more rigid than the polymer matrix, equation (1) reduces to:

$$\frac{G}{G_1} = 1 + \frac{15(1 - \nu_1)\Phi_2}{8 - 10\nu_1\Phi_1} \quad (2)$$

We used this equation to calculate the shear modulus of Kraton 101 SBS triblock polymer films²⁵.

Halpin and Tsai have shown that Kerner's equation and other equations for moduli of composites, such as equation (1) above, can be put in a more general form for the particulate composites⁵⁶⁻⁵⁸. Nielsen⁵⁹, and then Lewis and Nielsen⁶⁰, further generalized the Halpin and Tsai equations to take account of the maximum packing fraction ϕ_m of the dispersed phase. For composites such as polystyrene domains in the matrix of polybutadiene, the shear modulus for the isotropic composite is given by the following modified Halpin-Tsai equations for the lower bound value of the modulus:

$$\frac{G}{G_1} = \frac{1 + AB\Phi_2}{1 - B\psi\Phi_2}$$

where

$$A = \frac{7 - 5\nu_1}{8 - 10\nu_1}$$

and

$$B = \frac{\frac{G_2}{G_1} - 1}{\frac{G_2}{G_1} + A} \quad (3)$$

A takes into account the morphology of the dispersed phase and the Poisson ratio of the matrix. For dispersed spheres in an elastomeric matrix, $A = 1.5$, for instance. ψ is a function of the maximum packing fraction, ϕ_m , of the dispersed phase:

$$\psi = 1 + \frac{1 - \phi_m}{\phi_m^2} \cdot \Phi_2 \quad (4)$$

Similar equations apply for those systems in which the dispersed phase is elastomeric in a rigid matrix, such as SBS block polymers containing a high amount of styrene, and give the upper bound value of the modulus. They are written in a form that takes into account that the continuous phase is more rigid than the dispersed phase. In systems where both phases may be continuous, such as in the case of SBS block polymers containing equal amounts of styrene and butadiene, the equations giving the upper and lower bounds have to be combined in some manner. Nielsen used a logarithmic rule of mixtures to combine the upper and lower bound values^{61,62}:

$$\log M = \phi_U \log M_U + \phi_L \log M_L \quad (5)$$

where M_U and M_L are the upper and lower bounds for the modulus respectively, at a given composition; ϕ_U is the fraction of the low modulus material that is in a continuous phase in the overlap region where both phases are almost continuous, and ϕ_L is the fraction of the rigid material in the overlap region.

Uniaxially oriented fibre composites and laminated composites. Uniaxially oriented fibre composite materials are transversely isotropic, i.e. properties perpendicular to the fibre axis are direction independent. The basic geometry of this system is shown in Figure 18. Five independent elastic constants are needed to characterize completely the elastic behaviour of such systems. There are two tensile moduli: E_{11} and E_{22} ; two shear moduli: G_{12} for shear parallel to the fibre direction, and G_{23} for shear normal to the fibre direction; bulk modulus, and two Poisson ratios. One Poisson ratio, ν_{12} , gives the transverse strain caused by the imposed strain in the longitudinal direction, and the second Poisson ratio, ν_{21} , gives the longitudinal strain caused by the strain in the transverse direction.

Material constants for the uniaxial composites are most conveniently calculated by Halpin and Tsai's equations⁵⁷ given below:

$$E_{11} = E_f V_f + E_m V_m \quad (6)$$

$$\nu_{12} = \nu_f V_f + \nu_m V_m \quad (7)$$

$$\frac{P}{P_m} = \frac{(P_f/P_m) + \mathcal{L} [1 + (P_f/P_m - 1)V_f]}{P_f/P_m - V_f(P_f/P_m - 1) + \mathcal{L}} \quad (8)$$

where E_f , E_m = Young's modulus of fibre and matrix, respectively; ν_f , ν_m = Poisson ratio of fibre and matrix, respectively; V_f , V_m = volume fraction of fibre and matrix; $P = E_{22}$, G_{12} or G_{23} for the composite; $P_m = E_m$, G_m or

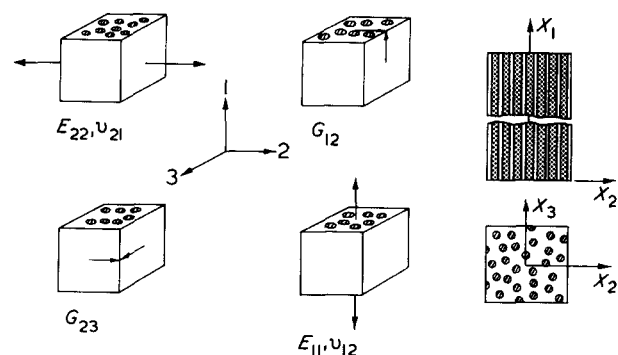


Figure 18 Basic geometry of uniaxial composite and reference coordinate system (right) and corresponding elastic constants

ν_m for the matrix; $P_f = E_f, G_f$ or ν_f for the fibre, and $\mathcal{L} =$ a parameter which accounts for the geometry of the filler and the mode of deformation.

Equations (6) and (7) are the familiar 'Law of Mixtures' for principal Young's modulus and principal Poisson ratio, respectively. Equation (7) is a condensed formula for determining the elastic constants, E_{22} , G_{12} or G_{23} . Use of equations (6), (7) and (8) is not restricted to uniaxial continuous fibre composites. Halpin and Tsai⁵⁷ have shown that:

(a) Equation (8) can be applied to the calculation of the axial modulus of discontinuous composites by choosing an appropriate constant \mathcal{L} , which depends upon the particle shape and aspect ratio.

(b) The above equations can be extended to balanced ply laminates of discontinuous or continuous fibre composites, by application of laminated plate theory⁵⁹ and taking into account the angles between the ply orientation and the principal directions of the composite.

(c) These concepts can be extended to randomly oriented fibre composites which are treated as quasi-isotropic materials⁶⁴, that is, the material is treated as a many-ply laminated structure having equal probability of all orientations.

Experimental moduli and comparison with values calculated from theories of micromechanics of composites

The above equations and concepts for the composite materials moduli have been applied to a number of block polymers of definable morphology and geometry, considering them as composite materials.

Equation (1) was used to calculate the shear modulus of Kraton 101 SBS triblock polymer, considering it as a microcomposite with spherical polystyrene domains in a matrix of polybutadiene²⁵. The shear modulus of Kraton was assumed to be 1.13×10^{10} dyne/cm². Modulus of the rubber can be estimated on the basis that all rubbery chains are tied down at each end in the glassy domains of polystyrene. The modulus is then determined by the entanglement network, which for polybutadiene would give a value of about 1×10^7 dyne/cm². Using these values of moduli for polystyrene and polybutadiene in equation (1) gives a composite modulus for Kraton 101 equal to 1.85×10^7 dyne/cm². The experimental values are found to be much higher than this. For a film of Kraton 101 cast from benzene-heptane solution, a shear modulus of 10^8 dyne/cm² is obtained. This large discrepancy between the experimental and theoretical value can be ascribed to three possible factors: (a) the polystyrene domains are not strictly spherical and show some connectivity; (b) the effective size of the domains is larger than that observed in the electron micrograph because of the interfacial region; and (c) the modulus of the matrix is higher than the rubbery modulus value, which will of course be the case in the interfacial region near the domain boundaries. As referred to in the preceding discussion the studies on morphology and transition behaviour suggest that all the three factors are important considerations in the cast films of Kraton 101 block polymers.

The Young's moduli of block polymers of styrene and butadiene as a function of composition cover a range of almost four decades — from ~ 10 to 10^4 kg/cm². Nielsen has shown that, the moduli of such diverse polymers — from elastomers to rigid plastics, calculated from equations (3–5) fit the experimental values over a broad range of composi-

tions of the styrene/butadiene block polymers⁶¹. In block polymers of low styrene content (such as Kraton 101 discussed above), polystyrene domains appear to be either aggregates of six spheres or rods with an aspect ratio of 6 to 1. This corresponds fairly well with the morphology observed in samples of Kraton 101. The volume fraction of styrene, over which both polystyrene and polybutadiene

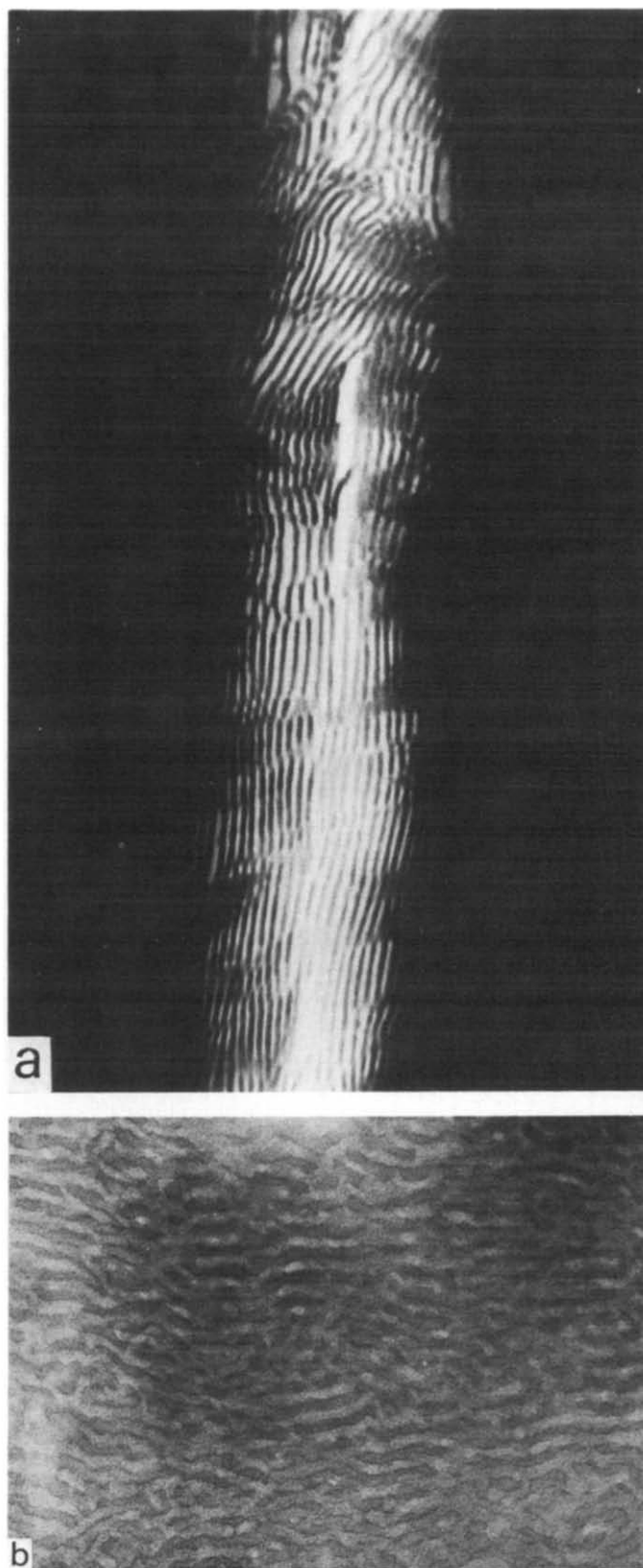


Figure 19 (a) Fibrous polystyrene domains of polystyrene in an extruded rod of Kraton 101; (b) oriented polystyrene domain in the outer layers of a milled sample of Kraton 101

phases in the block polymer are almost continuous, ranges from about 0.15 to 0.8. Outside this region, either spherical domains of polystyrene or polybutadiene are the dispersed phase⁶⁵.

As discussed above the polystyrene domains in a sample of Kraton 101 extruded into the capillary of a rheometer, and then annealed in the capillary have cylindrical polystyrene domains parallel to the extrusion direction. The morphology of a thin section cut parallel to the length of the rod is included in *Figure 13a*, and is shown in more detail in *Figure 19a*. Moduli of the extruded rod were measured in tension, bending and torsion. It was modelled as an uniaxial composite and the moduli were calculated from equations (6–8) for different geometries of the dispersed fibrous polystyrene domains. The experimental and calculated values for this sample are given in *Table 3*.

The ratio of tensile modulus to shear modulus is about 80 for this sample. The rod sample is therefore quite stiff under bending and tensile loading, but has comparatively very low torsion modulus typical of an elastomer. At loads of greater than 10.5 kg/cm², there appears to be a yield process which results in a five-fold decrease in tensile modulus. The torsion (shear) modulus shows a small but significant increase. On loading, there is some breaking up of the cylindrical domains which results in a decrease in tensile modulus and a slight increase in the torsion modulus. The calculated value of the tensile modulus for the composite of continuous polystyrene cylindrical domains is about twice that of the experimental value. The calculated shear modulus is appreciably lower than the experimental value. For a composite of discontinuous cylinders with $L/D = 750$, which appears reasonable from the electron micrograph, the calculated value of the tensile modulus is close to that obtained experimentally. The calculated shear modulus is still appreciably lower than the experimental value, but calculations show that only five percent of disorder in orientation of the fibres should account well for this discrepancy, without much effect on the calculated value of the tensile modulus.

In the sheet sample of Kraton 101 thermoplastic rubber prepared by pressing the milled sheet under conditions of minimum flow, the polystyrene domains in the outer layers are oriented parallel to the milling direction, as shown in *Figure 19b*. Optical birefringence measurements showed that in this sample, away from the surface layers, there is less preferred orientation of the cylindrical polystyrene domains. This sample may be modelled as a layered laminate composite of uniaxially oriented sheets with a core of quasi-isotropic material. Flexural, tensile, and torsional moduli of sheets cut both parallel and perpendicular to the direction of milling, measured according to the methods described in ref 25, are given in *Table 4*. The values of shear modulus are the same for the samples cut parallel and perpendicular to the milling direction. However, the flexural

Table 4 Experimental and calculated moduli of mill oriented Kraton 101 sheet

Modulus (and test method)	Experimental values (dyne/cm ²) × 10 ⁹		Calculated values laminated plate theory (dyne/cm ²) × 10 ⁹	
	MD	⊥ MD	MD	⊥ MD
Flexural modulus, E_B (vibrating beam)	1.655	0.331	1.72	0.103
Tensile modulus, E_T (longitudinal resonance)	0.538	0.331	0.504	0.076
Shear modulus (torsion pendulum)	0.241	0.241		
E_B/E_T	3.1	1.0		

modulus value parallel to the milling direction (*MD*) is about five times that perpendicular to the milling direction. Also, for the sample cut parallel to the milling direction, the bending and tensile moduli are in the ratio of 3:1. In the absence of longitudinal shear, the values would be the same for any homogeneous material. The observed difference, we attribute to the outer layers consisting of unidirectionally oriented high modulus material, while the centre is less well oriented and is of lower modulus. The outer layers from the neutral plane make a disproportionately large contribution to the flexural modulus, while they do not play as important a role in the tensile experiment.

The experimental values are compared with the calculated moduli based on the laminated plate theory. The agreement between the calculated and experimental values of the bending and tensile moduli for samples cut parallel to the milling direction is surprisingly good. However, in the transverse direction, the flexural and tensile moduli have about the same ratio as that predicted, but the experimental values of these moduli are much higher than predicted. This is to be expected because, in these modes of deformation, the moduli are very much dependent upon the transverse orientation of the cylindrical polystyrene domains. Considering the uncertainty in describing precisely the details of orientation of the polystyrene domains, especially away from the outer layers towards the centre, this discrepancy is not serious. Better agreement of values calculated from the laminated plate theory will be expected if the solid structure could be described more accurately.

In summary, the theories for composite materials can be useful in estimating the moduli of block polymer materials if information on morphology and orientation of domains is available. They can be useful in explaining the mechanical properties of block polymers. The noteworthy point is that, using theories developed for macroscopic composites, and using macroscopic bulk properties of the constituent

Table 3 Experimental and calculated moduli of extruded Kraton 101 rod

	Experimental (dyne/cm ²)		Composite theory calculations (dyne/cm ²)		
	Before loading	After loading 10.5 kg/cm ²	Orthotropic continuous rods	Orthotropic discontinuous rods, $L/D = 750$	Quasi-isotropic
Tensile modulus, E_{11}	4.28×10^9	0.93×10^9	7.55×10^9	5.0×10^9	$E = 1.5 \times 10^9$
Shear modulus, G_{12}	5.4×10^7	6.5×10^7	1.66×10^7	1.66×10^7	$G = 0.5 \times 10^9$

$$E_{11}/G_{12} = 79$$

materials, mechanical properties of block polymer samples in which the size of phases is of such submicroscopic dimensions, can be calculated with a fair degree of dependability.

BLENDS OF BLOCK POLYMERS AND HOMOPOLYMERS

Another class of composite materials based on block polymers, of both fundamental and technological interest, are the blends of block polymers with one or both of the corresponding homopolymers. Either the homopolymer may be solubilized in the corresponding domains of the block polymer, or the block polymer may act as a surface active material, in which case blocks of one particular type may be incorporated at the interfacial boundary between the homopolymer and the block polymer. In the latter case, blocks act as an 'alloying' agent by preventing the separation of

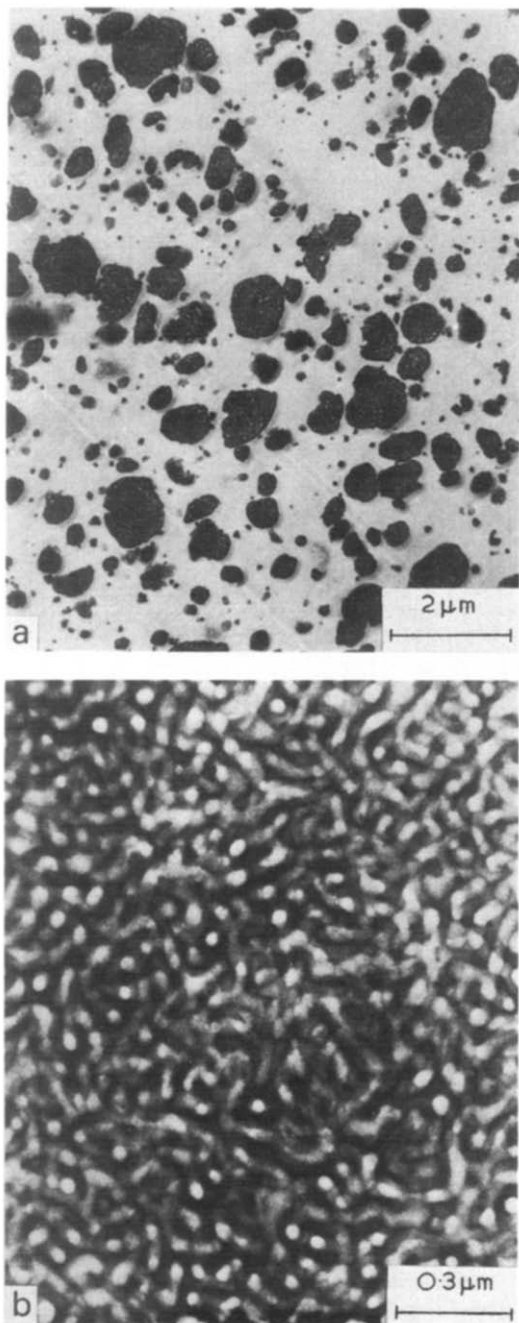


Figure 20 (a) Morphology of a polyblend of 60/40 styrene/butadiene triblock polymer (25 parts) and polystyrene (75 parts); (b) morphology of 60/40 styrene/butadiene triblock polymer

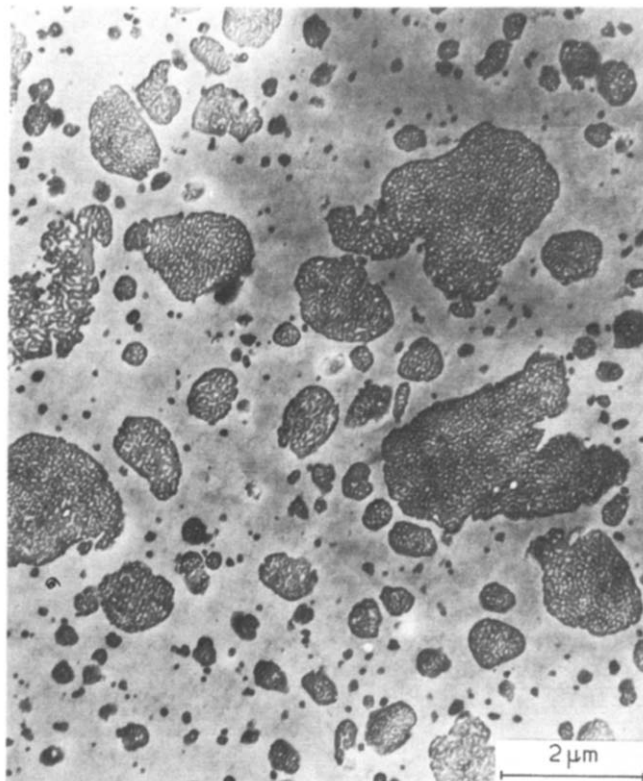


Figure 21 Morphology of the dispersed phase in the polyblend of 60/40 butadiene/styrene triblock polymer and polystyrene

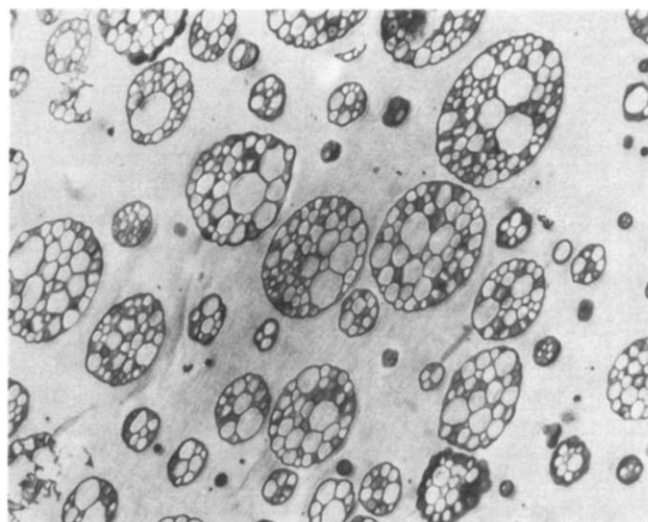


Figure 22 Electron micrograph of high impact polystyrene, Styron 495

the incompatible homopolymers into macroscopic phases.

Kawai and his coworkers^{36,46,66,67}, in a series of studies with AB type block polymers of styrene and isoprene, showed that when the molecular weight of the added homopolymer is less than or comparable to that of the corresponding block of the copolymer, the solubilization of the homopolymer into domains of the corresponding block takes place. In such cases, the size of the domains increases in relation to the amount of the added homopolymers, and in some cases, morphology of the domains may also change. However, when the molecular weight of the added homopolymer is larger than that of the corresponding block poly-

mer, the block polymer behaves as if it were incompatible with the corresponding homopolymer. However, in such cases, the blocks in the interfacial region between the homopolymer and the block polymer are preferentially anchored in the homopolymer phase, and thus help to form a stable interface.

A technologically important application of the above concept is in the blends of a styrene/butadiene/styrene block polymer of overall 60/40 butadiene/styrene composition with homopolymer styrene^{68,69}. These blends have higher impact strength than the commercial high impact polystyrene, or rubber modified polystyrene materials. This is achieved without adversely affecting the flexural modulus, the softening temperature, and hardness. *Figure 20b* is an electron micrograph of the block polymer and shows the morphology and the domains of polystyrene. *Figure 20a*, an electron micrograph of the blend of polystyrene and the block copolymer, shows that the dispersed phase is that of the block polymer in a polystyrene matrix. *Figure 21* shows in more detail that the dispersed phase is itself a block polymer and has in it the two-phase structure of the block polymer. It has similarity with the electron micrograph of high impact polystyrene in which the dispersed phase is itself also a two-phase system of polystyrene and rubber (*Figure 22*), and it is dispersed in the polystyrene matrix. In the blend of the block polymer with polystyrene, the polystyrene domains in the dispersed block polymer

Table 5 Comparison of physical properties of polyblend containing block polymer to commercial high impact polystyrene and ABS materials

	Polyblend (85% total polystyrene)	High impact polystyrene (Styron 495)	ABS resin (Cycolac GSE 1000)
Unnotched Izod (ft lb/in)	22.0	14.0	25.0
Notched Izod (ft lb/in)	7.5	2.2	7.0
Flexural modulus \times 10^{-5} , (lb/in ²)	3.0	2.3	2.9
Deflection tempera- ture ($^{\circ}$ C) samples annealed at 73 $^{\circ}$ C. (60 mm deflection under 264 lb/in ²)	93.0	82.0	94.0

phase are of submicroscopic dimension, in contrast to that in the dispersed phase of high impact polystyrene. In *Table 5*, are given the comparative values of impact strength, flexural modulus, and heat distortion temperature of the polyblend of polystyrene and block polymer, a high impact polystyrene, and an ABS (acrylonitrile/butadiene/styrene) resin, showing that in the desirable combination of these properties, the polyblend properties are superior to those of high impact polystyrene, and approach those of ABS.

PART II: RECENT RESEARCH DIRECTIONS AND OUTLOOK ON THE FUTURE OF BLOCK POLYMERS AND MULTIPHASE POLYMER SYSTEMS

The discussion above is an overview of the recent work in block polymers and multiphase systems. Projection into the research areas in which future important advances of both scientific and technological interest in block polymers and multiphase polymer systems are likely to occur can only be subjective and to a large extent biased by personal experience and research interests. I have selected six research areas which I believe will play an important role in the development of advanced microcomposite materials and multiphase polymers of controlled solid state structure.

THERMODYNAMICS OF PHASE SEPARATION

Heading the list should be the basic understanding of the thermodynamics of phase separation in block polymers. Two dissimilar homopolymers are usually incompatible, because the heat of mixing is generally positive (endothermic process), while the only driving force towards compatibility is the entropy of mixing, which in polymers is generally very small. In block polymers, the blocks of A and of B units tend to separate because they are incompatible, but are prevented from doing so by the chemical bonds linking the blocks together. The important consequence of arranging the chains in this way is that the phases cannot grow indefinitely if the density of packing of the molecules in each of the phases is to remain uniform. The sizes of the domains in the block polymers is thus much smaller than aggregates found in a mixture of homopolymers

exhibiting phase separation. The restrictions arising from the small size of the domains and from the attachment of the blocks, cause a drastic reduction of the entropy of a polymer molecule in a phase separated system as compared to that of a free chain. The important entropy terms that need to be considered in calculating free energy differences between the completely mixed block polymer system and the system separating into domains of discrete size may be summarized with reference to the model shown in *Figure 23* for the case in which the domains are lamellar. In this model for an ABA triblock polymer, all

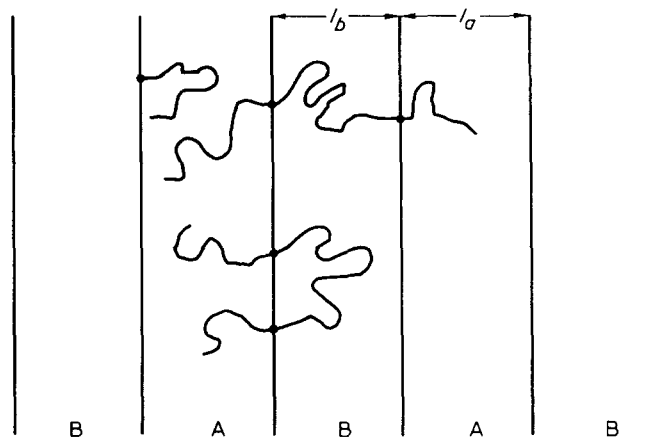


Figure 23 Model for phase separated domains in triblock polymers

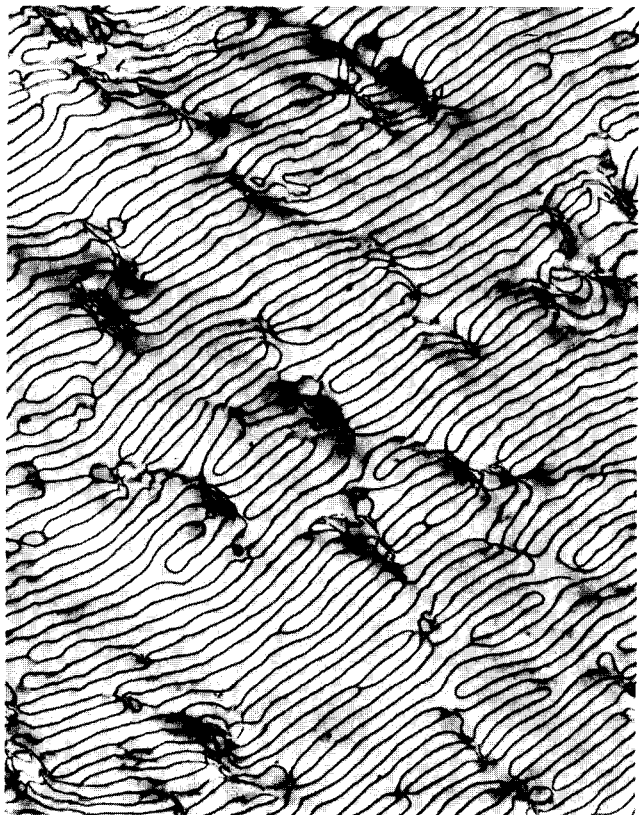


Figure 24 Electron micrograph of sample from polymerization of a 10% solution of Kraton 1101 in styrene monomer. Dark lamellae are of polybutadiene phase. Magnification 30 000X

B chains start at the phase boundary, and terminate at either the same boundary, or the opposite boundary of the B domain. All A chains start at the boundary and end in the A domain. The principal entropy terms are the following: (a) the limit in entropy due to restricted volume of the domain; (b) the limit in entropy because the chain is constrained to start at the boundary; (c) the limit in entropy due to the placement of one block junction point in the vicinity of the interfacial boundary; (d) the limit in configuration entropy arising from the restriction of the second end of the B segment to lie at an interfacial boundary; (e) the entropy of mixing term, which is comparatively small and decreases with increasing molecular weight.

The entropy decrease due to the above factors is a serious restriction against phase separation of block polymers into discrete domains as compared to a completely mixed system. However, there is a large bonus in entropy over the increase in interfacial energy or heat of mixing if we relax the restriction of sharp interfacial boundary, and consider an interfacial region in which phase mixing is allowed. Thus, the interfacial boundary of mixed phases in which there is a gradient of composition seems to be necessary for a stable phase separated system as compared to completely mixed or completely incompatible systems. The size of this interfacial region, the composition gradient in this region, and how they are affected by the molecular weight and composition of the blocks, and presence of different solvents, and diluent molecules, controls many of the important properties of block polymers.

A number of workers, notably Meier, Krause, and Helfand, have developed thermodynamic analysis of block polymer systems to describe quantitatively the dependence of the size and shape of the domains on molecular weights and

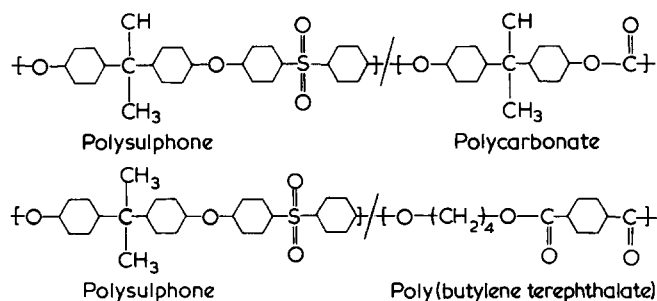
composition of the blocks, and on the concentration gradient in and size of the interfacial regions⁷⁰⁻⁸³. Recently, Meier has extended his thermodynamic analysis to the consideration of factors that govern the solubilization of homopolymers in the domains of block polymers, and to the block polymers as surface active materials⁸⁴. Further advances in theory and detailed thermodynamic analysis of block polymer systems will guide the development of methods for the control of their solid state structure, and their applications.

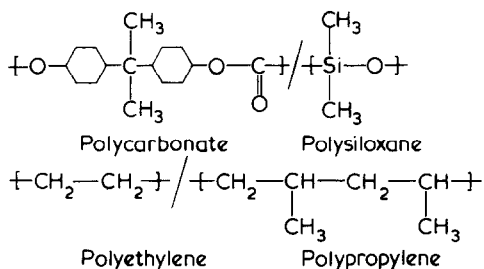
Block polymer solutions which show liquid crystalline structure have many important implications. The thermodynamics of such solutions needs greater attention. Even more important are the solutions of block polymers in which the solvent is one of the monomers. In such solutions, block polymers form fairly organized micellar structure⁸⁵. After polymerization of such block polymer/monomer solution, the final solid has interesting morphology, particularly when the polymerization is carried out under controlled shear flow conditions. Figure 24 shows the lamellar regularity achieved when a 10% solution of styrene/butadiene/styrene block polymer (Kraton 101) in styrene monomer is polymerized under a small shear field. The regularity in thickness of the rubber domains is a consequence of the micellar structure of the block polymer in the styrene monomer solvent.

BLOCK POLYMERS OF CONTROLLED STRUCTURE

Control of block length and of the number of blocks is possible only in a limited number of systems: block polymers of styrene/butadiene (or isoprene), as discussed above being one of the notable examples. The glassy domains in styrene/butadiene block polymers lose their integrity at about 80°-90°C, and are susceptible to solvents. Block polymers in which the domains have higher glass transition temperature, and are less susceptible to solvents, will have a broader range of usefulness. Such block polymers offer an important area of future research.

Considerable effort in recent years has been directed to studies of block polymers in which the component blocks have either higher glass transition temperature, or better solvent resistance, or better thermal stability. Some of these materials have already achieved technological importance. Notable among them are the block polymers of poly(butylene terephthalate)/poly(tetramethylene ether terephthalate)^{86,87}, polysulphone/poly(dimethyl siloxane)^{88,89}, polycarbonate/polysiloxane⁹⁰, and polyethylene/polypropylene⁹¹. An important area for future research is the development of synthetic methods to obtain a similar type of control on the size and number of blocks as is now possible for styrene/butadiene block polymers. Block polymers of controlled structure in the following systems appear to be promising:





MULTILAYERED MACROCOMPOSITES

Alfrey and coworkers have shown that multilayer composites of high and low modulus materials exhibit mutual interlayer reinforcement^{92,93}. A multilayer composite film of polystyrene and polyethylene was shown to undergo 75% elongation without fracture, while the polystyrene by itself failed at 3.5% elongation. The high elongation layers act to prevent the propagation of transverse cracks across the brittle layers. Such multilayer composites consisting of as many as 300 alternate layers can be prepared through rotation of annular die boundaries during coextrusion of two polymers^{94,95}.

Recently, Shen and his coworkers have applied a similar concept to block polymer systems, and have obtained some very interesting results⁹⁶. They prepared, by spin casting, multilayer composites consisting of three to eleven alternate layers of a polymer blend of 60% polystyrene and 40% by weight of Kraton 1101 triblock SBS polymer, and polystyrene; and of polystyrene and Kraton 1101. The stress-strain behaviour of the 11-layer laminates is shown in Figure 25 from the results made available to the author by Professor Shen for this paper. The noteworthy feature is that these laminates can be stretched to 600% without fracture. This stress-strain behaviour is in contrast to fracture of polystyrene beyond 3% strain. Block polymers, which, as discussed above may be considered as microcomposites by themselves, may further be combined as multilayer macroscopic composites for useful applications. Considering that block polymers from a particular set of monomers or starting materials can be prepared over a broad range of modulus, they offer a promising area for advanced materials, when they are combined as multilayer composites. Multilayer composites may be prepared either by using non-diffusive multiple extrusion of two molten polymer streams, or by sequential spin casting of thin layers.

Another type of similar layered composites that appears interesting has been suggested by Shen and Beaver⁹⁷. A polymerizing monomer may be diffused into a sheet of block polymer. Concentration of the polymerizing monomer in the block polymer thus varies uniformly from the outer surface towards the centre. On later polymerization of such a sample, a multilayered structure having a gradient in composition and perhaps in morphology should result. Mechanical properties, particularly impact and fracture properties of such materials, offer interesting possibilities.

SEGMENTED POLYURETHANES

Segmented polyurethanes are a class by themselves of block and multiphase polymers. Because of the broad range of structural variations, both controlled and uncontrolled, that are possible in these systems, the spectrum of mechanical properties they show is surpassed by few classes of polymers. The molecular units and sequences in segmented poly-

urethanes are commonly divided into 'hard segments' and 'soft segments'. The hard segments consist of groups that are rigid and/or capable of strong intermolecular interaction, such as aromatic rings, urea and urethane groups. When hard segments crystallize, they do so generally by intermolecular aggregation, but systems containing long sequences of such segments may form crystalline lamellae by chain folding. The soft segments generally consist of long chain polyethers or polyesters, and are flexible. Figure 26 shows schematically a typical 'hard' and 'soft' segment in a segmented polyurethane. The soft segments in such a polymer are formed by the reaction of diphenylmethane-4,4'-di-isocyanate (MDI) with poly(propylene ether glycol) oligomer. When this reaction is carried out in the presence of excess di-isocyanate, a prepolymer with isocyanate terminal group is formed. This prepolymer is then extended with additional di-isocyanate and ethylene glycol (chain extender), resulting in the final segmented polyurethane with 'soft' and 'hard blocks'. Considerable literature has developed upon the structural variations and their effect on mechanical and performance properties by varying the structure of the oligomer, the di-isocyanate, and the chain extender used for the preparation of segmented polyurethanes⁹⁸⁻¹⁰¹.

Crystallization of soft segments can occur in certain cases, particularly when its molecular weight is large, and is enhanced by stretching¹⁰¹. However, it is the molecular aggregation and phase separation of the hard segments that has marked influence on the properties of the segmented polyurethanes. Phase separation of the hard segments in these systems comes about even when the sequence length of units in each hard segment is comparatively short. Strong intermolecular interaction and crystallizability of the units enhances phase separation^{78,82}. Such phase separation, often results in multiphase systems that exhibit multiple transition

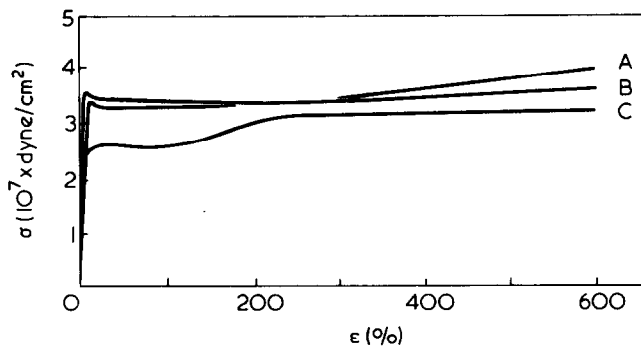


Figure 25 Stress-strain plots of multilayered composites: L_1 : 11 layer laminate of blend of 40% SBS triblock polymer (Kraton 1101) and 60% polystyrene ($\bar{M}_n = 30\,000$), and SBS triblock polymer; L_{4A} and L_{4B} are 11 layer laminates of polystyrene ($\bar{M}_n = 30\,000$) and Kraton 1101 triblock polymer; L_{4A} and L_{4B} have innermost layer of polystyrene and triblock polymer respectively. A, L_{4A} ; B, L_{4B} ; C, L_1

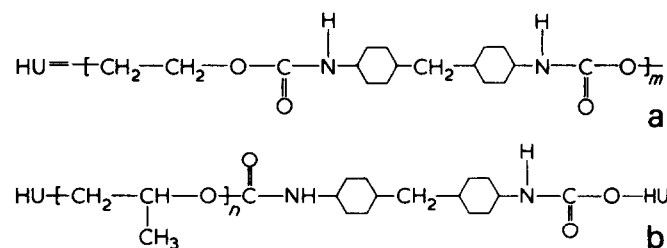


Figure 26 (a) Hard and (b) soft segments in a typical segmented polyurethane

temperature. Transitions in these systems are traditionally labelled as α , β , and γ in order of decreasing temperature. Generally speaking, the γ -transition (or a lower transition) is attributed to a Schastzki type mechanism¹⁰², the β -transition is associated with the glass transition for the more flexible part of the chain, and the higher temperature α -transition, is associated with the hard segments. The α -transition temperature depends upon the concentration of the hard segments in the chain. As the hard segment concentration increases, this transition shifts to considerably higher temperature, and merges with the fusion temperature of the crystallinities of the hard segments. A number of studies have recently been reported on the transition behaviour of segmented polyurethanes and its relation with their molecular structure¹⁰³⁻¹⁰⁷

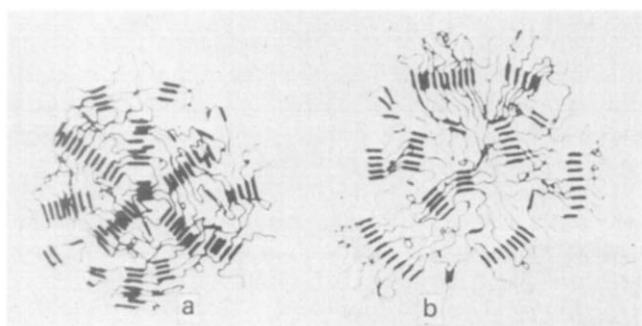


Figure 27 Schematic of spherulite structures in segmented polyurethanes: (a) hard segments crystallize radially, chain orientation is tangential; (b) hard segments crystallize tangentially, chain orientation is radial

The multiphase structure of segmented polyurethanes has been studied by a number of workers¹⁰⁸⁻¹²³. The general picture that emerges from studies of these polymers by differential scanning calorimetry, infra-red absorption, rheo-optical (low-angle light scattering), low-angle X-ray diffraction, and thermomechanical analysis, is that hard segments do not separate as discrete domains. Instead, the hard segments domains consist of two phases: crystallites or aggregates of hard segments in a matrix of soft segments. These domains are separated by elastomeric material richer in soft segments and which may also contain some uncrystallized hard segments. The domains of hard segments are likely to form spherulitic structure under suitable conditions. Figure 27 shows schematically the structure of spherulites proposed for the hard segment domains in segmented polyurethanes.

Direct observation by electron microscopy of the segmented polyurethanes appears possible by staining with a solution of phosphotungstic acid. This technique is similar to that used so successfully for studying the morphology of polyester-polyether block polymers^{124,125}. Figure 28 is an electron micrograph of a segmented polyurethane containing the oligomer, poly(propylene ether glycol) as the soft segment, and MDI and ethylene glycol as hard segments. The staining was done by immersing a microtomed section in a 10% aqueous solution of phosphotungstic acid. The elastomeric phase absorbs the stain, but not uniformly. The crystalline domains are visible as light fibrillar regions.

In spite of the extensive work in segmented polyurethanes, only a few studies have been made with controlled block length and number distribution of the blocks in the polymer chain^{118,126,127}. Our understanding of the structural factors that control the multiphase solid state structure in these

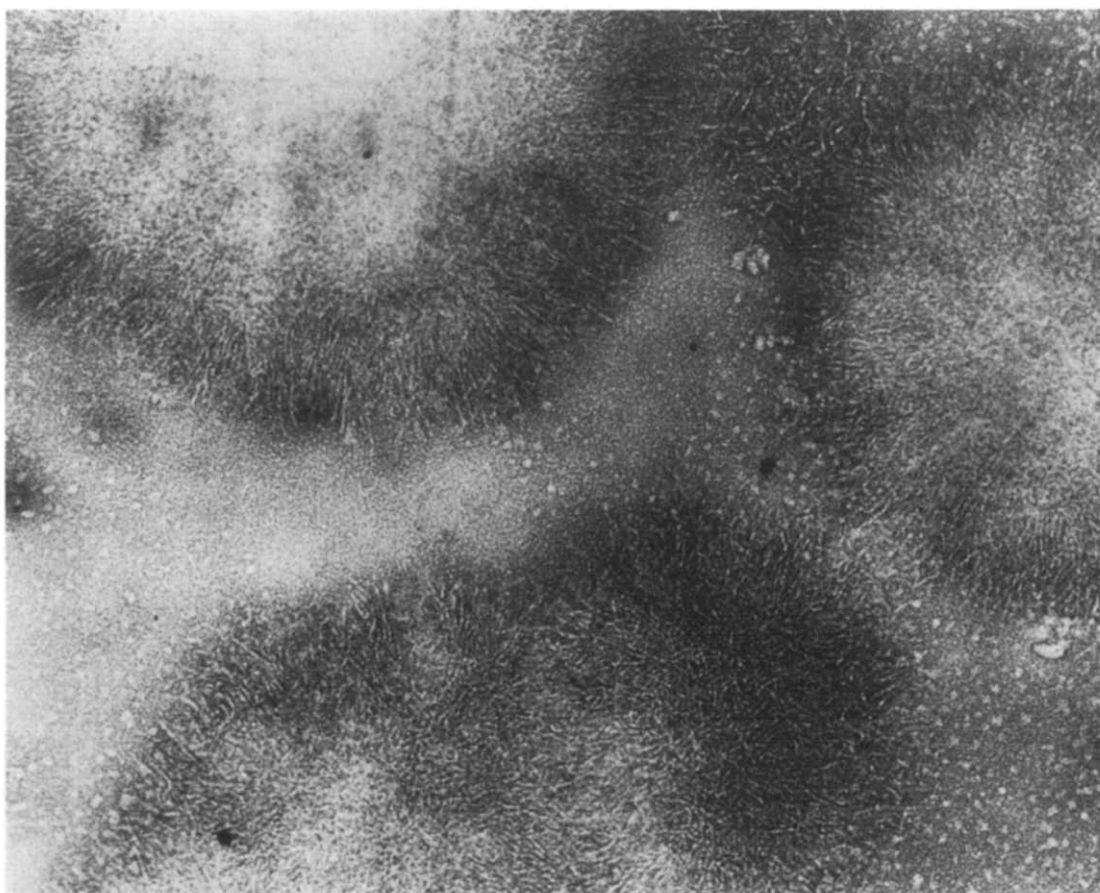


Figure 28 Electron micrograph of segmented polyurethane: poly(propylene ether glycol) (as soft segments); MDI and ethylene glycol as hard segments. Stained by 10% solution of phosphotungstic acid

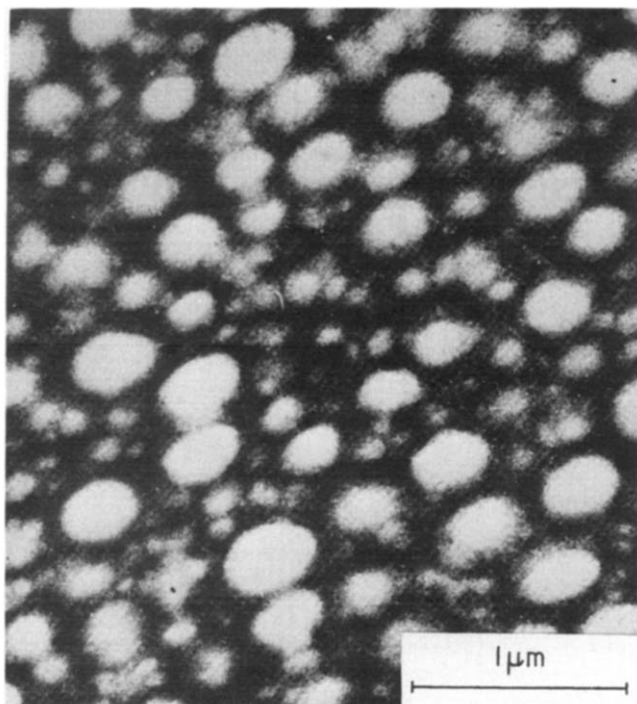


Figure 29 Electron micrograph of an 80/20 PMMA/PU interstitial composite. Polyurethane phase from polybutadiene diol stained by OsO_4

systems, and how this relates to their performance is indeed embryonic. Studies on segmented polyurethanes in which the block lengths can be well controlled offer a promising research area. Use of moieties other than the commonly used low molecular weight diols and diamines, for use in hard segments, offers a number of promising approaches for materials with interesting properties. The moieties that are likely to enhance intermolecular hydrogen bonding and crystallization should be especially interesting. Only limited work has so far been done with soft segments that undergo strain-induced crystallization, and this should also be a fruitful research area. Thus, segmented polyurethanes offer a number of promising research directions for multiphase and microcomposite materials.

INTERSTITIAL POLYMERS

Another type of multiphase polymers based on polyurethanes, that seem to have intriguing possibilities, have been reported recently from the work in the laboratories of Professor Allen at the University of Manchester and in the Corporate Laboratory of Imperial Chemical Industries¹²⁸⁻¹³³. These polymers are prepared by the interstitial polymerization of vinyl monomers within polyurethane elastomer gels. The precursors for preparation of a polyurethane elastomer network (mixture of an oligomer diol and triol, and di-isocyanate), are mixed with a vinyl monomer (methyl methacrylate, acrylonitrile were most suitable). The crosslink points are introduced by the trifunctional polyol. Using dibutyltin dilaurate as the catalyst to promote polyurethane (PU) formation, a polyurethane network swollen in the vinyl monomer is formed. Subsequent polymerization of the vinyl monomer in the swollen polyurethane network results in a composite material: vinyl polymer and polyurethane being the two submicroscopic phases.

Figure 29 is an electron micrograph of an interstitial polymer composite from 80 parts of methyl methacrylate poly-

merized interstitially in a polyurethane network from polybutadiene diol. Osmium tetroxide stain was used to stain the polybutadiene elastomeric phase¹²⁹. The spherical domains of PMMA are clearly seen in the matrix of the elastomer. The size of the PMMA domains, for a given PMMA/PU composition is almost independent of factors connected with the vinyl polymerization, but is very sensitive to the physical condition and molecular details of the swollen PU network and on the state of gelation at the time of polymerization. Thus, it is quite sensitive to \bar{M}_c of the PU network. If the gel is 'loose', the domain size is larger than the domain size from a 'tight' network.

The systems amenable to interstitial polymerization must clearly have two important prerequisites: (1) the precursors for the PU network must be soluble in the vinyl monomer, and (2) there must be a mechanism for formation of an elastomer network prior to the polymerization of the vinyl monomer¹²⁸. Further, the solubility interaction parameter between the monomer and the gel should be such that the maximum swelling capacity of the gel is not exceeded, and that the density of crosslinks is high enough to prevent macroscopic phase separation during subsequent polymerization of the monomer.

A composite from interstitial polymerization containing 80:20 PMMA/PU was found to have notched impact strength and shear modulus of $12.5 \pm 1.0 \text{ kJ/m}^2$ and $0.65 \pm 0.05 \text{ GN/m}^2$ respectively, compared to $1.2 \pm 0.2 \text{ kJ/m}^2$ and $1.47 \pm 0.03 \text{ GN/m}^2$ in PMMA homopolymer¹²⁸. The impact strength is increased ten-fold with only a decrease in modulus to about one-half. The composites from interstitial polymerization of acrylonitrile in a polyurethane network were found to have the desirable combination of high notched impact strength and high modulus.

These interstitial polymer composites may also be treated as microcomposites. The equation for composite materials that is most suitable for calculating the moduli of these systems takes into account the interaction of the two phases in the interfacial layer. The experimental values of the shear modulus over a broad composition range of PMMA/PU interstitial composites was found to fit well the equation proposed by Davies^{132,134}.

The two-phase structure of the interstitial composites is also supported by their transition behaviour. Two transition temperatures associated with T_g of PMMA and PU are observed. The shift in the position of PU α process from that normally seen in the corresponding PU bulk polymer is in support of the phase mixing in the interfacial region between the vinyl polymer domains¹²⁹.

Interstitial polymer composites, similar to the systems that have been studied, are likely to play an important part in the future development of multiphase polymers and microcomposite materials.

IN SITU CRYSTALLIZATION

One of the intriguing ways of obtaining microcomposites is by crystallization of low molecular weight crystalline compounds or suitable crystalline polymers, in a polymer matrix, notably in the matrix of slightly crosslinked rubber. Only a few studies on *in situ* crystallization of one phase in the matrix of a rubber or plastic have been reported, but such investigations offer interesting possibilities for future research.

One of the early studies on the *in situ* crystallization of low molecular weight crystalline compounds in rubber^{135,136} showed that crystallization of only 5% phenyl- β -naphthyl-

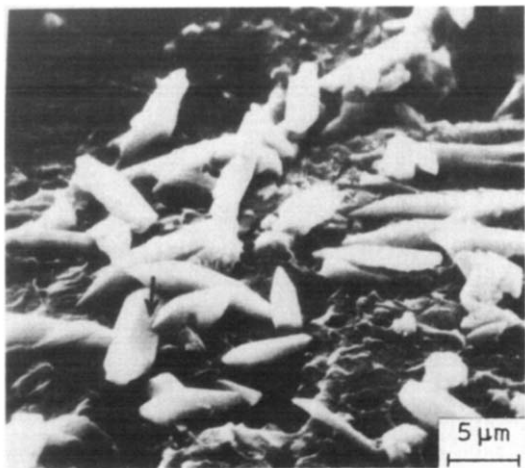


Figure 30 Scanning electron micrograph of a cut section of a sample containing 30 vol % of acetanilide in butadiene-acrylonitrile rubber

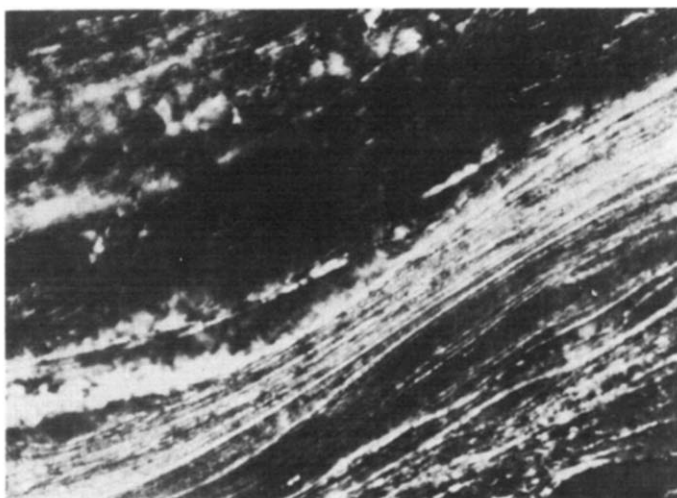


Figure 31 Photomicrograph of polypropylene crystallizing in EPDM rubber

mine produced the same increase in modulus of rubber as 30–40% carbon black, commonly used for reinforcement and stiffening of gum rubber.

Kardos and his workers^{137,138} studied the *in situ* crystallization of acetanilide in a styrene/acrylonitrile copolymer (SAN) and in an acrylo rubber (butadiene/acrylonitrile copolymer). Figure 30 is a scanning electron micrograph of a cut surface of a sample containing 30 vol % of acetanilide (from ref 138). The needle-like crystals were shown to have excellent adhesion with the matrix. The arrow in Figure 30 points to the interlocking of two crystals, probably by twinning. There is a significant increase in the modulus of the composite relative to that of the matrix. Over a fairly broad filler loading range crystallized at 25°C, the modulus can be predicted by the Halpin-Tsai equation^{57,58}. At higher filler volume fraction (~0.3), because of the interlocking effect of the crystals, a Halpin-Tsai equation modified by Nielsen⁵⁹ is more appropriate since it takes into account the maximum packing fraction which the filler can achieve.

Figure 31 is a photomicrograph of a sample of EPDM rubber in which polypropylene was allowed to crystallize. It shows the fibrous structure of polypropylene crystallizing in a matrix of rubber.

The systems of the crystallizing filler and the matrix suitable for microcomposites of controlled solid state structure need to satisfy the criteria: (a) crystallizing polymer

should show solubility in the matrix at a temperature below the degradation temperature of each of the components; (b) broad range of temperature between the dissolution temperature of the crystallizing filler and the glass transition temperature of the matrix; (c) no chemical interaction of the crystallizing filler with the matrix, and low volatility at the fabrication and processing temperature^{137,138}. These are difficult requirements to satisfy, but a systematic application of these concepts appears promising. It offers the prospect for developing composite materials with good adhesion between the dispersed phase and the matrix, and for controlling the morphology of the dispersed phase, and thus the mechanical properties, by controlling the temperature at which the system is allowed to crystallize and by the volume fraction of the crystallizing filler.

CONCLUSION

In conclusion, the recent work on block and multiphase polymers has already resulted in a number of materials with unique combinations of properties. We have, however, barely scratched the surface in this area of polymer science. Further progress will depend upon systematic studies in the above areas. In addition, we need to develop a scientific base for the understanding of the strength properties of multiphase polymers, because the main interest in such materials is the promise they offer for strong and tough materials. To guide the development of such materials, we need also to develop our understanding of the yield and failure mechanism of multiphase materials of controlled structure and morphology, including the study of creep and crazes that relate to the toughening of multiphase materials.

ACKNOWLEDGMENTS

I wish to express my special appreciation to Professor Geoffrey Allen of Imperial College of Science and Technology, who made the facilities of his personal office available to me during my two weeks stay in the United Kingdom. The outline and major part of this manuscript was completed during this stay at Imperial College, London.

REFERENCES

- 1 Shell Oil Co. Ltd. S. Afr. Pat. 280 712 (1963)
- 2 Shell Oil Co. Ltd. US Pat. 3 265 765 (1966)
- 3 Bailey, J. T., Bishop, E. T., Hendricks, W. R., Holden, G. and Legge, N. R. *Rubber Age* 1966, 98, 69
- 4 Holden, G., Bishop, E. T. and Legge, N. R. *Proc. Int. Rubber Conf. MacLaren* 1967
- 5 Holden, G., Bishop, E. T. and Legge, N. R. *J. Polym. Sci. (C)* 1969, 26, 37
- 6 Morton, M., McGrath, J. E. and Juliano, P. C. *J. Polym. Sci. (C)* 1969, 26, 99
- 7 Robinson, R. A. and White, E. F. T. 'Block Polymers' (Ed. S. L. Aggarwal), Plenum Press, New York, 1970, pp 123–136
- 8 Szwarc, M., Levy, M. and Milkovich, R. *J. Am. Chem. Soc.* 1956, 78, 2656
- 9 Schlick, S. and Levy, M. *J. Phys. Chem.* 1960, 64, 883
- 10 Zelinski, R. P. and Childers, C. W. *Rubber Rev.* 1968, 41, 161
- 11 Hsieh, H. L. and Glaze, W. H. *Rubber Chem. Technol.* 1970, 43, 22
- 12 Szwarc, M. 'Block and Graft Copolymers', (Eds John J. Burke and Volker Weiss), Syracuse University Press, New York, 1973, pp 1–16
- 13 Adams, H. E., Bebb, R. L., Forman, L. E. and Wakefield, L. B. *Rubber Chem. Technol.* 1972, 45, 1252
- 14 Morton, M. 'Block Polymers' (Ed. S. L. Aggarwal), Plenum Press, New York, 1970, pp 1–10

- 15 Prud-homme, J. and Bywater, S. 'Block Polymers', (Ed. S. L. Aggarwal), Plenum Press, New York, 1970, pp 11-17
- 16 Morton, M. and Fetters, L. J. *Rubber Chem. Technol.* 1975 **48**, 359
- 17 Reed, P. J. and Urwin, J. R. *J. Organomet. Chem.* 1972, **39**, 1
- 18 'Analysis, Handling, and Reactions of Difunctional Organolithium Initiators', Product Bulletin 194 'DiLi', Lithium Corporation of America, Bessemer City, USA
- 19 Fetters, L. J. and Morton, M. *Macromolecules* 1969, **2**, 453
- 20 Kelly, D. J. and Tobolsky, A. V. *J. Am. Chem. Soc.* 1959, **81**, 1597
- 21 Tobolsky, A. V. and Rogers C. E. *J. Polym. Sci.* 1959, **40**, 73
- 22 Spirin, Yu. L., Polyakov, D. K., Gantmakber, A. R. and Medvedev, S. S. *Polym. Sci. USSR* 1962, **3**, 233
- 23 Korotkov, A. A. and Rakova G. V. *Polym. Sci. USSR* 1962, **3**, 990
- 24 Livigni, R. A., Marker, L. F., Shkapenko, G. and Aggarwal, S. L. *Am. Chem. Soc. Div. Rubber Chem. Symp. Struct. Properties Elastomers, Montreal, Canada* 1967
- 25 Aggarwal, S. L., Livigni, R. A., Marker, Leon F. and Dudek, T. J. 'Block And Graft Copolymers', Syracuse University Press, New York, 1973, pp 157-194
- 26 Phillips Petroleum Co. Ltd, US Patent 3 287 333 (1966)
- 27 Phillips Petroleum Co. Ltd US Patent (1962),
- 28 Deanin, R. D. *SPE J.* 1967, **23**, 45
- 29 Smith, T. L. in 'Block Polymers', (Ed. S. L. Aggarwal) Plenum Press, New York, 1970, pp 137-152
- 30 Smith, T. L. and Dickie, R. A. *J. Polym. Sci. (C)* 1969, **26**, 163
- 31 Hendus, H., Illers, K. H. and Ropte, E. *Kolloid-Z.* 1967, **216-217**, 110
- 32 Matsuo, M., Ueno, T., Horino, H., Chujiyo, S. and Asai, H. *Polymer* 1968, **9**, 425
- 33 Henderson, J. F., Grundy, K. H. and Fisher, E. *J. Polym. Sci. (C)* 1968, **16**, 3121
- 34 Wilkes, Garth L. and Stein, R. S. *J. Polym. Sci. (A-2)* 1969, **7**, 1525
- 35 Beecher, J. F., Marker, L., Bradford, R. D. and Aggarwal, S. L. *J. Polym. Sci. (C)* 1969, **26**, 117
- 36 Inoue, T., Soen, T., Hashimoto, T. and Kawai, H. in 'Block Polymers' (Ed. S. L. Aggarwal), Plenum Press, New York, 1970, pp 53-79
- 37 Lewis, P. R. and Price, C. *Polymer* 1971, **12**, 258
- 38 Inoue, T., Moritani, M., Hashimoto, T. and Kawai, H. *Macromolecules* 1971, **4**, 500
- 39 Uchida, T., Soen, T., Inoue, T. and Kawai, H. *J. Polym. Sci. (A-2)* 1972, **10**, 101
- 40 McIntyre, D. and Campos-Lopez, E. in 'Block Polymers', (Ed. S. L. Aggarwal), Plenum Press, New York, 1970, pp 19-30
- 41 LeFlair, R. T. 'XXIIIrd International Congress of Pure and Applied Chemistry', Butterworths, London, 1971, Vol.8. p 195
- 42 Dawkins, J. V. in 'Block Copolymers', (Eds D. C. Allport and W. H. Janes), Wiley, New York, 1973, pp 391-397
- 43 Fedors, R. F. *J. Polym. Sci. (C)* 1969, **26**, 189
- 44 Childers, C. W. and Kraus, G. *Rubber Chem. Technol.* 1967, **40**, 1183
- 45 Matsuo, M. *Japan Plast.* 1968, p 6
- 46 Kawai, H., Soen, T., Inoue, T., Ono, T. and Uchida, T. Mem. Fac. Eng. Kyoto Univ. 1971, **33**, 421
- 47 Folkes, M. J. and Keller, A. *Polymer* 1971, **12**, 222
- 48 Dlugosz, A., Keller, A. and Pedemonte, E. *Kolloid Z. -Z. Polym.* 1970, **242**, 1125
- 49 Bi, Le-Khac and Fetters, L. J. *Macromolecules* 1975, **8**, 90
- 50 Bi, Le-Khac *PhD Dissertation* University of Akron (1975)
- 51 Bi, Le-Khac and Fetters, L. J. to be published
- 52 Hashin, Z. *J. Appl. Mech.* 1965, **32**, 630
- 53 Hashin, Z. in 'Mechanics of Composite Materials', (Eds F. W. Wendt, H. Liebowitz and W. Perrone), Pergamon Press, New York, 1970, p 201
- 54 Hashin, Z. and Rosen, B. W. *J. Appl. Mech.* 1964, **31**, 233
- 55 Kerner, E. H. *Proc. Phys. Soc. (B)* 1956, **69**, 802
- 56 Tsai, S. W. US Gov. Rep. (1968) AD834851
- 57 Ashton, J. E., Halpin, J. C. and Petit, P. H. 'Primer on Composite Analysis', Technomic Press, Stamford, 1969, Ch. 5
- 58 Halpin, J. C. *J. Compos. Mater.* 1969, **3**, 720
- 59 Nielsen, L. E. *J. Appl. Phys.* 1970, **41**, 4626
- 60 Lewis, T. B. and Nielsen, L. E. *J. Appl. Polym. Sci.* 1970, **14**, 1449
- 61 Nielsen, L. E. *Rheol. Acta* 1974, **13**, 86
- 62 Nielsen, L. E. *Chem. Tech.* 1974, p 486
- 63 Lekhnitskii, S. G. 'Anisotropic Plates', (Eds S. W. Tsai and T. Cheron), Gordon and Breach, New York, 1968, p 195
- 64 Pagano, N. J. and Tsai, S. W. 'Progress in Materials Science, Technomic Press, Stamford, 1968, Vol 1, p 233
- 65 Lewis, T. B. and Nielsen, L. E. *Trans. Soc. Rheol.* 1968, **12**, 421
- 66 Inoue, T., Soen, T., Hashimoto, T. and Kawai, H. *Macromolecules* 1970, **3**, 87
- 67 Kawai, H. and Inoue, T. *Japan Plast.* 1970, p 12
- 68 Durst, R. R., Griffith, R. M., Urbanic, A. J. and van Essen, W. J. *Symp. Toughness Brittleness Plast. 168th Am. Chem. Soc. Meet. Atlantic City 1974*; to be published in *Adv. Chem. Ser.*
- 69 Durst, R. R. US Pat. 3 906 057; 3 906 058; 3 907 929; 3 907 931 (1975)
- 70 Meier, D. J. *J. Polym. Sci. (C)* 1969, **26**, 81
- 71 Meier, D. J. *Polym. Prepr.* 1970, **11**, 400
- 72 Meier, D. J. *Polym. Prepr.* 1973, **14**, 280
- 73 Meier, D. J. in 'Block and Graft Copolymers', (Eds John J. Burke and Volker Weiss), Syracuse University Press, New York, 1973, pp 105-120
- 74 Meier, D. J. *Polym. Prepr.* 1974, **15**, 171
- 75 Meier, D. J. *Appl. Polym. Symp.* 1974, **24**, 67
- 76 Helfand, E. *Polym. Prepr.* 1973, **14**, 970
- 77 Helfand, E. in 'Recent Advances in Blends, Grafts and Blocks', (Ed. L. H. Sperling), Plenum Press, New York, 1974
- 78 Helfand, E. *Acc. Chem. Res.* 1975, **8**, 295
- 79 Krause, S. *J. Polym. Sci. (A-2)* 1969, **7**, 249
- 80 Krause, S. *Macromolecules* 1970, **3**, 84
- 81 Krause, S. *Polym. Prepr.* 1970, **11**, 568
- 82 Krause, S. in 'Block and Graft Copolymers', (Eds John J. Burke and Volker Weiss), Syracuse University Press, New York, 1973, pp 143-55
- 83 Krause, S. and Reismiller, P. A. *J. Polym. Sci. (A-2)* 1975, **13**, 1975
- 84 Meier, D. J. Personal communication; unpublished results
- 85 Molau, G. E. and Wittbrodt, W. M. *Macromolecules* 1968, **1**, 261
- 86 Witsiepe, W. K. in 'Polymerization Reactions and New Polymers', (Ed. N. A. J. Platzer), Am. Chem. Soc., Washington, 1973, p 39
- 87 Brown, M. and Witsiepe, W. K. *Rubber Age* 1972, **104**, 35
- 88 Noshay, A., Metzner, M. and Merriam, C. N. *Polym. Prepr.* 1971, **12**, 1
- 89 Robeson, L. M., Noshay, A., Metzner, M. and Merriam, C. N. *Angew. Makromol. Chem.* 1973, **29/30**, 47
- 90 Kambour, R. P. in 'Block Polymers', (Ed. S. L. Aggarwal), Plenum Press, New York, 1970, p 263
- 91 Kontos, E. G., Esterbrook, E. K. and Gilbert, R. D. *J. Polym. Sci.* 1962, **61**, 69
- 92 Schrenk, W. J. and Alfrey, T. Jr., *Polym. Eng. Sci.* 1969, **9**, 393
- 93 Schrenk, W. J. *Appl. Polym. Symp.* 1974, **24**, 9-12
- 94 Schrenk, W. J. and Alfrey, T. Jr. *SPE J.* 1973, **29**, 38
- 95 Schrenk, W. J. and Alfrey, T. Jr. *SPE J.* 1973, **29**, 43
- 96 Akovali, G., Diamant, J. and Shen, M. to be published
- 97 Shen, M. and Beaver, M. B. *J. Mater. Sci.* 1972, **7**, 741
- 98 Saunders, J. H. and Frisch, K. C. 'Polyurethanes: Chemistry and Technology', Interscience - Wiley, New York, 1962
- 99 Trappe, G. in 'Advances in Polyurethane Technology' (Eds J. M. Buist and H. Gudgeon), Interscience - Wiley, New York, 1968, Chs 2 and 3
- 100 Wright, P. and Cumming, A. P. C. 'Solid Polyurethane Elastomers' Maclaren, London, 1969, Ch 2
- 101 Puett, D. *J. Polym. Sci. (A)* 1967, **25**, 839
- 102 Schatzki, T. F. *J. Polym. Sci.* 1962, **57**, 496
- 103 Becker, G. W. and Oberst, H. *Kolloid Z.* 1957, **152**, 1
- 104 Ferguson, J., Hourston, D. J., Meredith, R. and Patsavoudis D. *Eur. Polym. J.* 1972, **8**, 369
- 105 Ferguson, J. and Patsavoudis, D. *Eur. Polym. J.* 1972, **8**, 385
- 106 McCrumb, N. G., Read, B. E. and Williams, G. 'Anelastic and Dielectric Effects in Polymeric Solids', Wiley, New York, 1967
- 107 Schneider, N. S., Sung, C. S., Paik, Matton, R. W. and Illinger, J. L. *Macromolecules* 1975, **8**, 62
- 108 Clough, S. B., Schneider, N. S. and King, A. O. *J. Macromol. Sci. (B)* 1968, **2**, 641
- 109 Clough, S. B. and Schneider, N. S. *J. Macromol. Sci. (B)* 1968, **2**, 553
- 110 Bonart, R. *J. Macromol. Sci. (B)* 1968, **2**, 115

- 111 Bonart, R., Morbitzer, L. and Hentze, G. *J. Macromol. Sci. (B)* 1969, 3, 337
- 112 Estes, G. M., Seymour, R. W., Huh, D. S. and Cooper S. L. *Polym. Eng. Sci.* 1969, 9, 383
- 113 Kimura, I., Ishihara, H., Saito, K., Tamaki, K. and Ono, H. *Rep. Prog. Polym. Phys. Japan* 1970, 13, 209
- 114 Seymour, R. W., Estes, G. M. and Cooper, S. L. *Macromolecules* 1970, 3, 579
- 115 Kimura, I., Ishihara, H., Ono, H., Yoshihara, N., Nomura, S. and Kawai, H. *Macromolecules* 1974, 7, 355
- 116 Wilkes, C. E. and Yusek, Chloe S. *J. Macromol. Sci. (B)* 1973, 7, 157
- 117 Samuels, S. L. and Wilkes, G. L. *J. Polym. Sci. (C)* 1973, 43, 149
- 118 Wilkes, G. L. and Samuels, S. L. in 'Block and Graft Copolymers', (Eds John J. Burke and Volker Weiss), Syracuse University Press, New York, 1973, pp 225-277
- 119 Seymour, R. W., Allegrezza, A. E. and Cooper, S. L. *Macromolecules* 1973, 6, 896
- 120 Ng, H. N., Allegrezza, A. E., Seymour, R. W. and Cooper, S. L. *Polymer* 1973, 14, 255
- 121 Allegrezza, A. E. Jr., Seymour, R. W. and Cooper, S. L. *Polym. Prepr.* 1974, 15, 631
- 122 Chang, Yeong P. and Wilkes, G. L. *J. Polym. Sci. (Polym. Phys. Edn)* 1975, 13, 455
- 123 Sung, Chong-Sook P. and Schneider, N. S. *Macromolecules* 1975, 8, 68
- 124 Cella, R. J. *J. Polym. Sci. Polym. Symp.* 1973, 42, 727
- 125 Buck, W. H., Cella, R. J. Jr., Gladding, E. K. and Wolfe, J. R. Jr. *J. Polym. Sci. Polym. Symp.* 1974, 48, 47
- 126 Harrel, L. L. Jr. in 'Block Polymers' (Ed. S. L. Aggarwal), Plenum Press, New York, 1970, pp 213-24
- 127 Harrel, L. L. Jr. *Macromolecules* 1969, 2, 607
- 128 Allen, G., Bowden, M. J., Blundell, D. J., Hutchinson, G., Jeffs, G. M. and Vyvoda, J. *Polymer* 1973, 14, 597
- 129 Allen, G., Bowden, M. J., Blundell, D. J., Jeffs, G. M., Vyvoda, J. and White, T. *Polymer* 1973, 14, 604
- 130 Allen, G., Bowden, M. J., Lewis, G., Blundell, D. J. and Jeffs, G. M. *Polymer* 1974, 15, 13
- 131 Allen, G., Bowden, M. J., Lewis, G., Blundell, D. J., Jeffs, G. M. and Vyvoda, J. *Polymer* 1974, 15, 19
- 132 Allen, G., Bowden, M. J., Todd, S. M., Blundell, D. J., Jeffs, G. M. and Davies, W. E. A. *Polymer* 1974, 15, 28
- 133 Blundell, D. J. Longman, G. W., Wignall, G. D. and Bowden, M. J. *Polymer* 1974, 15, 33
- 134 Davies, W. E. A. *J. Phys. (D)* 1971, 4, 318
- 135 Linnig, F. J., Parks, E. J. and Stiehler, R. D. *Rubber Chem Technol.* 1966, 39, 1041
- 136 Payne A. R. *Rubber Chem. Technol.* 1968, 41, 1203
- 137 Joseph, J. R. Kardos, J. L. and Nielsen L. E. *J. Appl. Polym. Sci.* 1968, 12, 1151
- 138 Kardos W. L., McDonnell W. L. and Raisoni, J. *J. Macromol. Sci. (B)* 1972, 6, 397

Molecular complexes in polymer synthesis – from Lewis acid adducts to exiplexes*

A. Ledwith

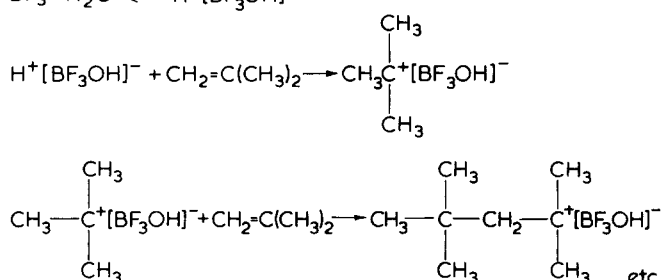
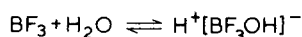
Department of Inorganic, Physical and Industrial Chemistry, University of Liverpool, Liverpool L69 3BX, UK

(Received 14 June 1976)

Specific intermolecular forces have been important to the development of many methods of polymer synthesis. This theme is developed so as to encompass major discoveries in ionic and complex organo-metallic polymerizations and the more recent utilization of Lewis acid adducts for control of copolymerization. In a final section, the rather weaker forces involved in charge transfer and exciplex binding are discussed in the light of existing and possible future mechanisms for polymer synthesis.

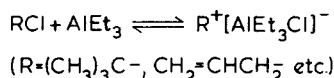
It is self evident that intermolecular forces and intermolecular complexes play an important role in a very wide range of chemical reactions, including synthesis of polymers. On the other hand, there are a number of rather specific molecular interaction phenomena of particular importance to the synthetic polymer chemist which provide the foundation for this survey. Many of these intermolecular complexes have been recognized and characterized during the time in which Geoffrey Gee has occupied the Sir Samuel Hall Chair of Physical Chemistry at the University of Manchester, and it is particularly appropriate to honour his retirement with a review of this nature as the first, and perhaps the simplest form of, molecular complex utilized in polymer synthesis was characterized in the same Department shortly before his arrival.

In the late 1940s the research group led by Polanyi showed conclusively that rigorously purified, dry, isobutylene failed to polymerize when in contact with dry BF_3 and/or TiCl_4 . Immediate polymerization ensued upon the introduction of traces of water¹. These observations established the requirement for a Lewis acid–cocatalyst complex as an initiating species for what is now termed a cationic polymerization, e.g.

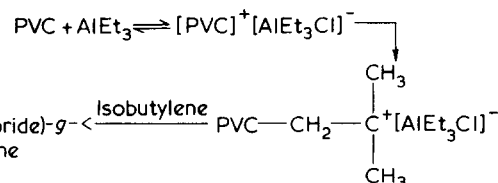
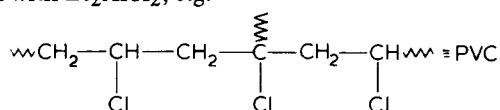


Similar Lewis acid complexes are now widely employed for initiation of many types of cationic polymerizations and, whilst precise details of some reaction mechanisms remain to be elucidated, afford opportunities for synthe-

sis of new block and graft polymeric materials. Much of the recent development in this area is due to the work of Kennedy², following the commercial exploitation of butyl rubber (a random cationically prepared copolymer of isobutylene and isoprene) by the Standard Oil Development Co. (now Exxon Research and Engineering Co.). A particularly important development by the Kennedy group was the utilization of aluminium alkyls as Lewis acids in formation of catalytically active initiator complexes³. Whereas the more usual Lewis acid–cocatalyst complexes employed protic agents such as water or HCl as cocatalysts (and hence the ultimate source of initiating protons), it was demonstrated that carbocation precursors such as t-butyl chloride, allyl chloride, benzyl chloride etc. became extremely effective cocatalysts when complexed with trialkyl aluminiums and alkyl aluminium chlorides e.g.

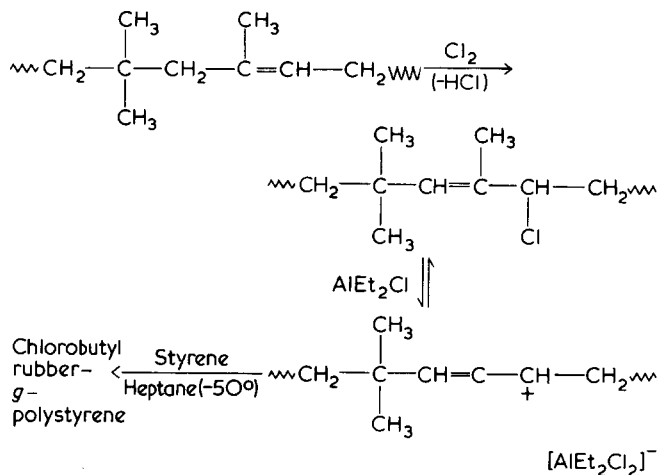


It is well known that tertiary alkyl chloride units are present in commercially prepared samples of poly(vinyl chloride), as a result of side reactions during polymerization, and these abnormal structures may thus be used to co-initiate graft polymerization when activated by complex formation with Et_2AlCl_2 , e.g.

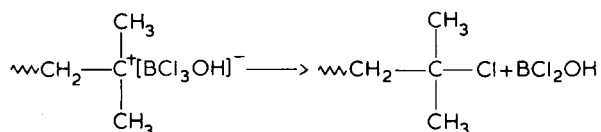


Similarly, chlorobutyl rubber (obtained commercially by partial chlorination of isobutylene–isoprene copolymers) possesses allylic chloride units in the main chain which are readily activated to graft copolymerization by complex formation with Et_2AlCl :

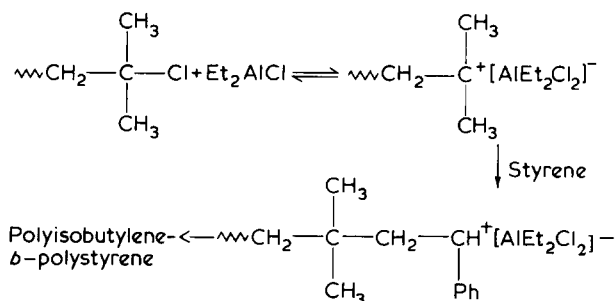
* Presented at the Sixth Biennial Manchester Polymer Symposium, UMIST, Manchester, March 1976.



We have already noted¹ that BF_3 was one of the first Lewis acids to be activated as an initiator for cationic polymerization by protic agents etc. and, until very recently, it was the only boron trihalide which appeared to function in the required manner even though BF_3 is formally the 'weakest' Lewis acid among BF_3 , BCl_3 , BBr_3 and BI_3 ⁴. Clarification of this apparent anomaly has become available again through the work of Kennedy and collaborators⁵. It is now known that the essential differences between cationic homopolymerization of isobutylene initiated by $\text{BF}_3/\text{H}_2\text{O}$ and $\text{BCl}_3/\text{H}_2\text{O}$ combinations respectively, arise because the former catalyst system gives rates of polymerization governed largely by rates of initiation, which decrease with decrease in temperature, whilst the $\text{BCl}_3/\text{H}_2\text{O}$ system gives rise to very rapid rates of initiation at all temperatures and rates of polymerization which increase with decrease in temperature as a result of much diminished termination rates. In contrast to the $\text{BF}_3/\text{H}_2\text{O}$ system where molecular weight is largely governed by chain transfer to monomer, polymerizations initiated by $\text{BCl}_3/\text{H}_2\text{O}$ exhibit spontaneous termination with transfer of chlorine from counterion to growing chain e.g.

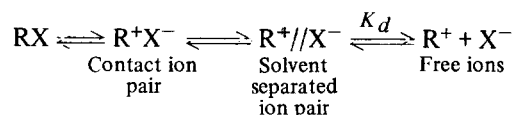


In an elegant series of experiments, Kennedy and collaborators⁵ have established the termination mechanism indicated, and simultaneously generated a new technique for synthesis of block copolymers, by subsequent activation of the terminal tertiary alkyl chloride unit with diethyl aluminium chloride in the presence of styrene e.g.



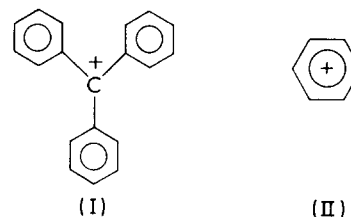
Thus by suitable choice of catalyst or complexing cocatalyst homopolymer structures may be modified to provide a new range of graft and block polymers from readily available monomers.

As indicated in the foregoing paragraphs, molecular complexes between Lewis acids and a variety of cointiating species have dominated initiation processes in cationic polymerizations. However, there is a further complex equilibrium of equal importance to be considered, namely that of ion pair dissociation. Whatever the nature of Lewis acids and cointiators, an initiating complex, and the actual chain propagating cationic entity, will be subject to ion pair dissociation equilibria possibly involving covalently bound, ion paired, solvent separated, and freely dissociated ionic species, e.g.



Whether or not contact and/or solvent separated ion pairs are intermediates will depend on the particular system being considered but it is clear that full characterization of the effects of ion pair dissociation equilibria can only be successfully accomplished in the absence of cation forming equilibria such as those between typical Lewis acids and the usual cocatalysts.

In our own work⁶ we have sought to minimize complications due to cation forming equilibria by utilizing as initiators, thermally stable crystalline complexes of appropriate Lewis acids with comparatively stable carbocations such as triphenylmethyl (I) and tropylium (II). Hexachloroantimonate (SbCl_6^-) ion was the most convenient counterion.

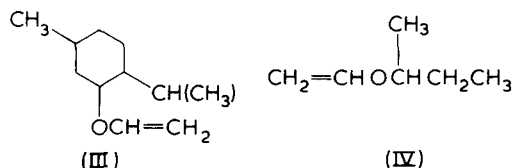


Use of these types of stable salts offers many advantages not least of which is the convenience of measurement of ion pair dissociation equilibria⁷. Knowledge of the latter (e.g. for $\text{C}_7\text{H}_7^+\text{SbCl}_6^-$ in CH_2Cl_2 at 0°C , $K_d = 3 \times 10^{-5}$ M) is important in that it permits regulation of catalyst concentrations so as to ensure cationic propagation exclusively by free carbocations^{6,8,9}. Representative data for free carbocation propagation rate coefficients are given in Table 1. More recently we have used tropylium hexachloroantimonate in studies designed to evaluate the effects of chiral substituents on the stereochemistry of chain growth in propagation by free carbocations. This work is being pursued in collaboration with Chiellini and Solaro at the University of Pisa, in a group which owes its origins to Professor Pino who surveyed the effects of chiral substituents on the stereochemistry of polymerization at the Manchester symposium¹⁰.

Table 1 Propagation rate coefficients (k_p^+) for polymerization of $\text{RCH}=\text{CH}_2$ in CH_2Cl_2 at 0°C initiated by $\text{C}_7\text{H}_7^+\text{SbCl}_6^-$

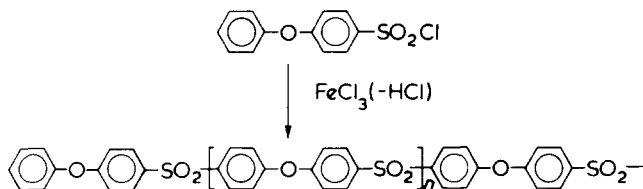
R	$k_p^+ \times 10^{-3}$ ($\text{dm}^3/\text{mol sec}$)	E_a (kcal/mol)
$\text{CH}_3\text{O}-$	0.14	14
$\text{ClCH}_2\text{CH}_2\text{CHO}-$	0.2	7
$\text{CH}_3\text{CH}_2\text{O}-$	1.5	10
$(\text{CH}_3)_2\text{CHCH}_2\text{O}-$	4.1	6
Cyclohexyl-O-	3.3	9
$(\text{CH}_3)_3\text{CO}-$	3.5	<2
N-carbazyl-	340	6

In summary we find¹¹ that polymerization of (–)menthyl vinyl ether ($[\alpha]_D^{25} = -73.6$) (III) by $C_7H_7^+SbCl_6^-$ (10^{-5} M) in CH_2Cl_2 at $0^\circ C$ gives a product polymer ($M_n = 15\,000$) having highly enhanced optical activity ($[\alpha]_D^{25} = -206$). Highly isotactic poly[(–)menthyl vinyl ether] produced with more complex catalysts¹² has $[\alpha]_D^{25} = -198$. Polymerization initiated by $C_7H_7^+SbCl_6^-$ involves only freely dissociated ions, at the concentrations employed, and hence the high degree of stereoregulation observed must arise from steric, and chiral, effects between monomer and growing chains.



Very similar polymerizations of the less bulky monomer (*S*)-(1-methylpropyl)vinyl ether ($[\alpha]_D^{25} = +13$) (IV), yielded a polymer ($M_n = 6000$) having enhancement of optical activity ($[\alpha]_D^{25} = +142$) approximately 40% of that exhibited by the highly isotactic product ($[\alpha]_D^{25} = +312$) obtained at lower temperatures with more complex catalysts¹². Clearly the smaller alkyl substituent in IV (compared with III) leads to a lower degree of stereoregularity in the polymer. Nevertheless the fact that the freely growing carbocation can interact with monomer with significant stereoregulation requires modification of the usual mechanisms put forward to explain stereoregular polymerization of alkyl vinyl ethers by complex catalyst systems¹³.

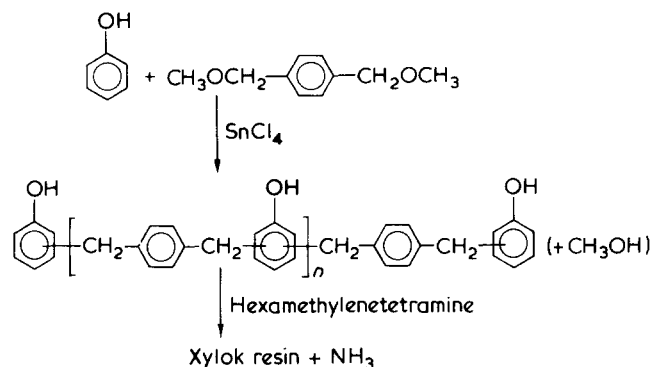
The Lewis acid complexes used in initiation of cationic polymerization of olefins are, of course, special examples of the more usually encountered Friedel–Crafts complexes, important in many organic alkylation, acylation and sulphonation procedures. Whereas Friedel–Crafts reactions in organic synthesis normally employ large (i.e. equimolar) amounts of the Lewis acid component, the synthetic polymer chemist has been able to develop reaction conditions in which Friedel–Crafts complexes play a truly catalytic role. A good example is provided by the synthesis, developed by ICI, of various types of polyarylsulphones from cationic step growth polymerizations of arylsulphonyl chlorides, e.g.



Polyarylsulphones prepared in this way are now important commercial thermoplastic materials¹⁴.

Another important example of the use of Friedel–Crafts complexes to produce resins having good combinations of electrical properties, chemical resistance and good thermal stability, is provided by the recently commercialized Xylok resins, developed by Albright and Wilson¹⁵. In this case the Friedel–Crafts reaction is used to synthesise a range of prepolymers from phenol and α,α' -dimethoxy-*p*-xylene in the presence of $SnCl_4$. The prepolymer (soluble) materials are eventually converted into cross-linked resins by the conventional phenolic resin curing

agents such as epoxy compounds or, more particularly, hexamethylenetetramine, viz.:



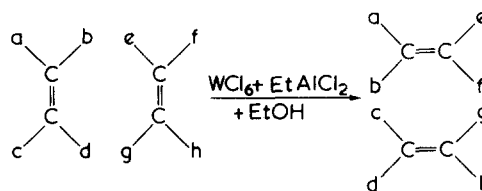
Formation of Xylok resins is important in that it indicates how related cationic polymerizations of readily available monomeric units, which frequently give rise to products of low molecular weights may, in future developments, be readily converted to more useful products.

Ion-pair dissociation equilibria are perhaps the most common forms of intermolecular complex important in polymer synthesis and there can be little doubt that anionic polymerizations provide the best examples (both quantitative and qualitative) of specific ion–solvent interactions¹⁶. However these phenomena have been widely reviewed and will not be discussed further; a particularly lucid and revealing survey has been given by Szwarc¹⁷, who was the first to recognize these important effects. It is worth noting that the polymerization of olefin oxides, especially propylene oxide, to high molecular weight and sometimes stereoregular polymers might also be classified as anionic¹⁸ and involves molecular complexes of iron, zinc, and aluminium alkoxides. Indeed it is fitting to recall that the role of water as activating cocatalyst in several of these systems was first recognized by Gee and his colleagues¹⁹.

Similarly, the general area of Ziegler–Natta polymerization provides outstanding examples of molecular complex formation, notably between alkyl aluminium compounds and transition metal derivatives. Here again the subject matter has been extensively reviewed¹⁶ and will not be discussed further in so far as polymerization of olefin and diene monomers is concerned. Olefin metathesis however, is a development of studies in the general area of Ziegler–Natta polymerization and transition metal complex formation which is not only recent, but which could become increasingly important in polymer synthesis with the continuing improvement in types and yields of hydrocarbon structures from refining of petroleum.

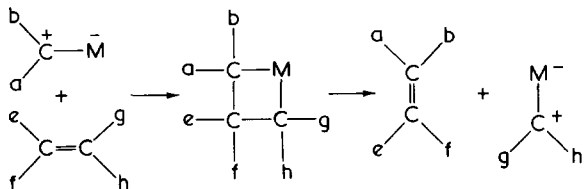
OLEFIN METATHESIS

As developed initially by the Goodyear Co., olefin metathesis^{20,21} was a term used to describe a redistribution reaction in olefins e.g.

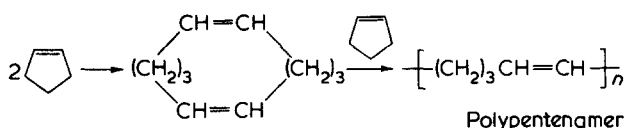


These truly remarkable transformations can be accom-

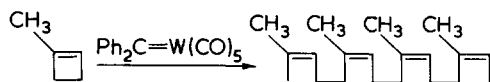
plished with a wide variety of catalysts but most readily by complexes derived from tungsten or molybdenum halides. A particularly good catalyst is formed from appropriate combination of tungsten hexachloride, ethylaluminum dichloride and ethanol. Many reaction mechanisms have been proposed to explain the course of olefin metathesis but there is now convincing evidence²² in favour of the metal-carbene complex chain reaction, originally proposed by Herrison and Chauvin²³ as illustrated schematically:



Applied to strained cyclic olefins such as cyclopentene, the reaction gives high molecular weight polypentenamer, a useful elastomer e.g.



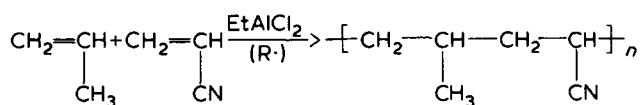
Very recent work by Katz and collaborators²⁴ indicates how well known polymeric materials may be synthesised from new monomers. Application of the metal-carbene chain reaction to 1-methylcyclobutene yields a polymer having essentially the same structure as *cis*-1,4-polyisoprene. It is interesting that the most effective metathesis catalyst for this polymerization is a preformed tungsten-carbene complex $\text{Ph}_2\text{C} = \text{W}(\text{CO})_5$.



ALTERNATING COPOLYMERIZATION

Molecular complexes of the ubiquitous alkyl aluminium compounds are important in yet another area of polymer synthesis, in which completely new alternating copolymers are produced from the common polymerizable monomers.

It was first reported by Hirooka *et al.*²⁵ that free radical copolymerization of propylene and acrylonitrile in the presence of ethyl aluminium dichloride gave good yields of a 1:1 alternating copolymer:



Since the publication of Hirooka's observations, there have been a large number of similar reports for other monomer combinations and with other Lewis acid complexing agents. Typical examples include styrene/acrylonitrile/ ZnCl_2 ²⁶; vinyl chloride/acrylonitrile/ EtAlCl_2 ²⁷; butadiene and isoprene/acrylonitrile—with many Lewis acids²⁸. These types of copolymerization show the following general features:

(1) 1:1 alternating copolymer is formed over a wide range of monomer feed compositions, usually in complete contrast to the behaviour observed in the corresponding conventional free radical systems.

(2) The reactions are often spontaneous on addition of the donor monomer to a preformed Lewis acid-acceptor monomer complex, but may be promoted by conventional free radical initiation techniques to give copolymers of the same composition²⁹.

(3) Monomers which homopolymerize and copolymerize poorly by free radical techniques (e.g. propylene³⁰, allyl monomers)³¹ copolymerize readily in the presence of Lewis acids.

(4) The copolymerizations are usually affected by conventional free radical inhibitors (DPPH, hydroquinone)³² and are frequently complicated by competitive cationic homopolymerization of one of the monomers³³.

Thus, although these systems exhibit many of the characteristics of free radical copolymerizations, the nature of the end products shows the powerful directing effect of the complexing agent. Lewis acids most commonly used are ZnCl_2 , SnCl_4 , EtAlCl_2 and $\text{Et}_3\text{Al}_2\text{Cl}_3$. Acceptor monomers tend to be those with polar substituents (acrylonitrile, methacrylonitrile, MMA) and the donor monomers are generally neutral hydrocarbons such as styrene, propylene, butadiene and isoprene. Alternating copolymerization in the presence of Lewis acids is undoubtedly of practical importance and can be expected to feature prominently in the future design of copolymers. However, there is still considerable uncertainty as to the precise role of the Lewis acid component³⁴ and a full explanation must also account for the much earlier reports of the effects of metal salts on free radical homopolymerization of vinyl monomers, e.g. LiCl /acrylonitrile³⁵ and ZnCl_2 /methyl methacrylate³⁶.

Complexes of Lewis acids with monomers containing electron withdrawing groups such as acrylonitrile and methyl methacrylate, where the unshared electron pairs on oxygen or nitrogen supply Lewis base activity, are readily characterized by accompanying changes in the u.v. or i.r. absorption spectra of the olefinic compound. The complexes will certainly be more electrophilic, overall, than the uncomplexed olefin and would be expected to interact further with typical donor monomers, such as styrene, to promote alternating copolymerization. However, it is not at all clear whether the Lewis acid (which is usually present in large amounts) acts to complex a reacting monomer or a propagating radical. Both types of complex have been suggested³⁴. Bamford³⁷ has given an enlightened analysis of kinetic and mechanistic aspects with consideration of the complete range of monomer-Lewis acid phenomena and has suggested the more general description 'regulated copolymerization'. The latter implies copolymerization in which a change in monomer reactivity ratios is brought about by a Lewis acid, regardless of mechanistic implications.

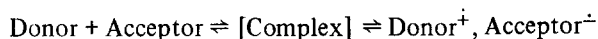
Alternating copolymers were initially obtained from free radical polymerizations of mixtures of monomers having strong electron donor and acceptor character; important examples include styrene/maleic anhydride and alkyl vinyl ethers/maleic anhydride. In most of these cases there is evidence (usually spectroscopic) of ground state association between donor and acceptor monomer pairs, leading to the suggestion that alternating copolymers arise directly by free radical polymerization of monomer complexes. However, association constants for monomer complexes are frequently small and it is not yet clear how such weak forces of association could increase the polymerization reactivity of the complex (present in comparatively low concentration) relative to homopolymerization of the

monomers (where appropriate). A further difficulty with the concept of reactive monomer complexes arise because measurements of association constants indicate formation of molecular complexes for pairs of monomers which do not yield alternating copolymers. Proton magnetic resonance studies³⁸ of complexes between maleic anhydride and the monomers styrene, methyl acrylate, and methyl methacrylate give association constants 0.28 dm³/mol at 30°C, 0.32 dm³/mol at 60°C and 0.43 dm³/mol at 60°C respectively. Only the first monomer gives alternating polymers with maleic anhydride. Despite these anomalies there is a continuing interest in donor acceptor interactions in polymer chemistry especially those exhibiting charge transfer phenomena.

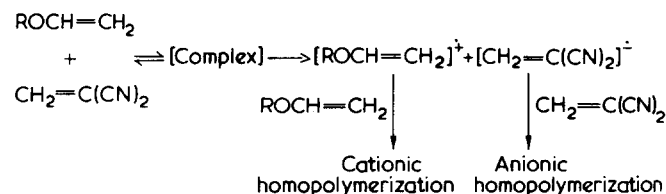
CHARGE TRANSFER COMPLEXES IN POLYMER SYNTHESIS

In principle, monomers exhibiting donor or acceptor function i.e. having low ionization potentials (I_D) and high electron affinities (E_A) respectively, should be polymerizable via charge transfer interactions with a suitable partner³⁴. There are comparatively few examples of homopolymerizable olefins having the required high electron affinity (vinylidene cyanide being a notable exception) but there are many examples of homopolymerizable electron donor monomers including *N*-vinylcarbazole, alkyl vinyl ethers vinyl derivatives of naphthalene and anthracene, and cyclic ethers such as tetrahydrofuran. Useful, natural, organic electron acceptors include tetracyanoethylene (TCNE), tetracyanoquinodimethane (TCNQ), chloranil, and maleic anhydride.

The simplified Mulliken scheme for charge transfer interaction i.e.

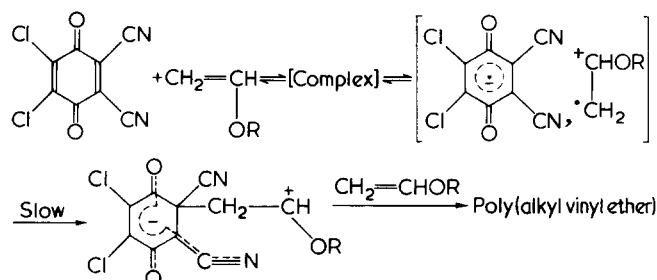


suggests the possibility of utilizing polymerizable olefins, as both donor and acceptor, in order to generate more than one type of polymerizing intermediate. Olefins having donor character polymerize best by cationic processes, and those having electron acceptor character by anionic or free radical processes. This distinction was first made use of by Gilbert *et al.*³⁹ who showed that mixtures of alkyl vinyl ethers (donors) and 1,1-dicyanoethylene (vinylidene cyanide) spontaneously polymerized to give products consisting mainly of poly(alkyl vinyl ethers) (known to form by cationic processes only) and poly(vinylidene cyanide) (known *not* to polymerize by cationic processes). A simple explanation for these observations although not generally known at the time, is that the reacting olefins undergo mutual oxidation and reduction with production of small amounts of initiating cations and anions respectively, e.g.

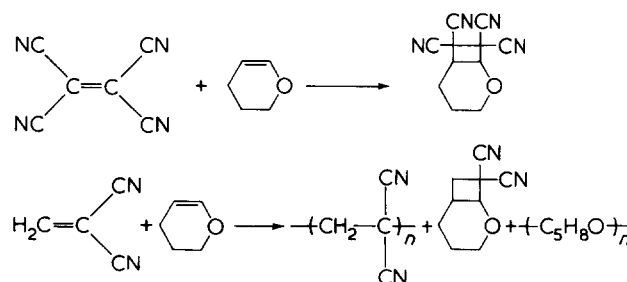


The early observations by Gilbert *et al.*³⁹ have been confirmed and substantially extended by Stille and colla-

borators⁴⁰ who have reported detailed studies of the mechanisms of interaction between a variety of unsaturated⁴¹ and saturated cyclic⁴² ethers with strong electron acceptors. Thus although in the presence of TCNE alkyl vinyl ethers form intermediate donor-acceptor complexes which ultimately collapse to 2 + 2 cycloadducts, the same monomers readily polymerize cationically in the presence of catalytic quantities of TCNQ and 2,3-dichloro-5,6-dicyano-*p*-benzoquinone (DDQ). Neither TCNQ nor DDQ can readily undergo facile 2 + 2 cycloaddition. E.s.r. experiments and quenching of reaction intermediates by methanol have established the following (typical) mechanism for initiation via a charge transfer complex:



The reactions of TCNE and vinylidene cyanide with dihydropyran are illustrative of the diversity of products which may be obtained in charge transfer initiated polymerizations; TCNE gives only the 2 + 2 cycloadduct while vinylidene cyanide gives the two homopolymers as well as the 2 + 2 cycloadduct:

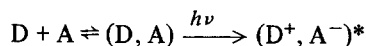


Similar complications arise in the reactions of TCNE with *N*-vinylcarbazole⁴³ where the products include poly(*N*-vinylcarbazole) and 2 + 2 cycloadduct with the latter also being able to initiate polymerization in the presence of excess monomer.

Apart from the well documented studies by Stille and collaborators⁴⁰, there is considerable uncertainty as to the reaction mechanisms pertaining in many other charge transfer initiation processes. The topic has been fully surveyed by Hyde and Ledwith³⁴ and although it may be fairly said that charge transfer initiation of polymerization has not proved of any general value, despite considerable efforts, the closely related phenomenon of exciplex formation appears to hold promise for significant commercial exploitation.

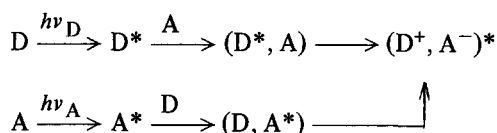
EXCIPLEX INTERACTION IN PHOTOINITIATED POLYMERIZATION

Excited states of charge-transfer complexes have structures resulting from a considerable degree of electron transfer in comparison to their ground states, e.g.



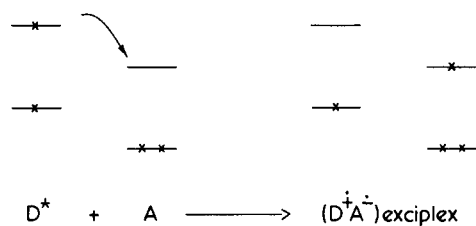
Nevertheless, the excited states of a charge-transfer complex should not be equated with a thermally-equilibrated pair of ion radicals, a point which was first highlighted in the early, but stimulating, review by Kosower⁴⁴.

More recently, mainly as a result of the pioneering studies of Weller and his associates⁴⁵, it has become apparent that excited states, having structures equivalent to those of photoexcited charge-transfer complexes, may be formed by local excitation of one or the other component (i.e. D or A) in systems which do not give evidence of ground-state complex formation, e.g.

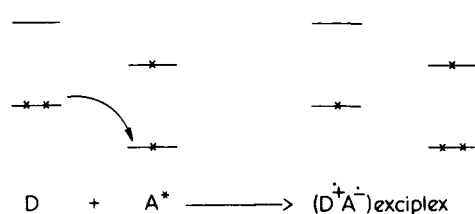


Here the excited state having the most electron-transfer character $(D^+, A^-)^*$ is termed an exciplex and its formation may be preceded by a variety of collisional complexes (encounter complexes) between an excited donor and ground-state acceptor or *vice versa*, e.g. (D^*, A) and (D, A^*) .

A simple molecular orbital treatment due to Weller⁴⁵ assumes that an electron is transferred from an excited state of one component to the ground state of another as illustrated below:



Molecular orbital treatment of exciplex formation (donor excited)

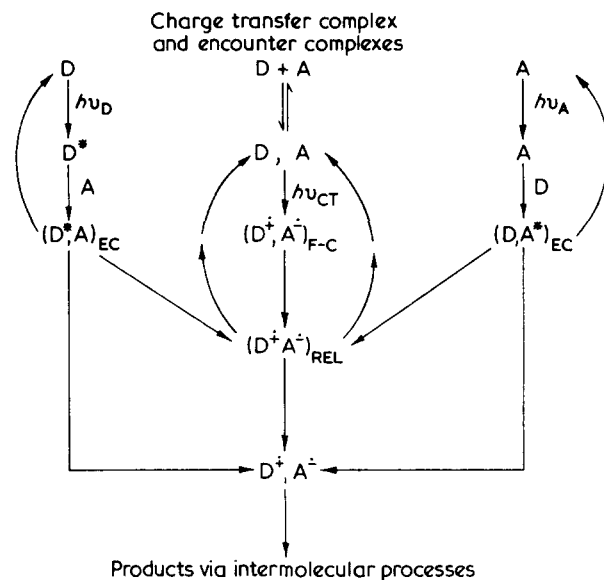


Molecular orbital treatment of exciplex formation (acceptor excited)

Since the ionization potential (I_D) and electron affinity (E_A) are measures of the energies of the highest bonding and lowest antibonding molecular orbitals respectively, ΔG , the energy of formation of the separated ions D^+ and A^- from D and A in their ground states is $I_D - E_A$. Since we actually start with an excited state (e.g. A^*), the energy of formation is diminished by the excitation energy of A^* . Bringing the separated ions D^+ and A^- to their equilibrium distance (r) in the exciplex reduces ΔG by an electrostatic term ($-e^2/r$). It follows therefore⁴⁶ that the free energy of exciplex formation is given by:

$$\Delta G = I_D - E_A - h\nu - \frac{e^2}{r}$$

where $h\nu$ is the excitation energy of A^* or D^* as appropriate. Because a molecule in its excited state is both a better electron donor and a better electron acceptor than in its ground state, exciplex formation should be a widespread phenomenon. The topic is the subject of a recent review monograph⁴⁷. A particular advantage of ion radical formation via exciplexes rather than ground state charge transfer complexes is that a much wider range of substrates may be employed, including many compounds which do not interfere with commercially important polymerization systems. However it must be stressed that molecules having ionization potentials or electron affinities typical of those observed in formation of ground state charge transfer complexes can equally well participate in exciplex formation with partners which do not give rise to ground state adducts. Likewise it is not necessarily the case that the photoexcited state of a ground state charge transfer adduct is the same as an exciplex formed by collisional interaction of an excited (uncomplexed) component⁴⁸. Interrelationships between charge transfer (CT) complexes and exciplexes are illustrated below:

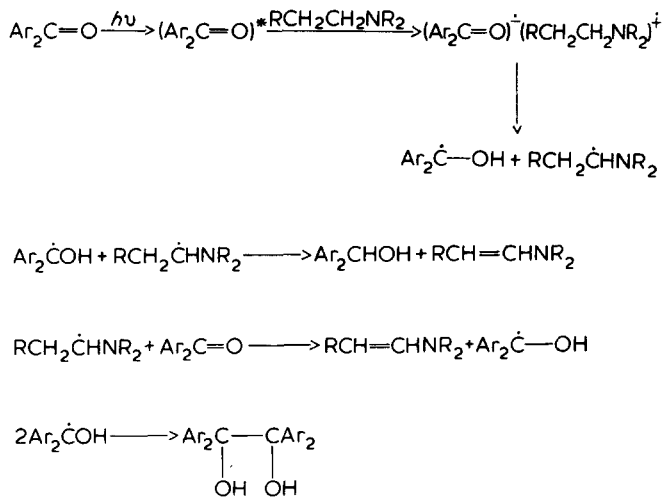


Any distinction between collisional encounter complexes (denoted by EC) and exciplexes is indicated, in the diagram, by the potential interconversions of the two possible EC complexes to a pair of ion radicals $[(D^+, A^-)_{REL}]$ having a solvation shell considerably relaxed from the Franck-Condon state $[(D^+, A^-)_{F-C}]$ formed on direct excitation of a ground state CT complex between the same components. Either of the encounter complexes, or the solvent relaxed exciplex, could be responsible for formation of the solvent equilibrated pair of ion radicals leading to ultimate photochemistry in the system. Reversion back to the neutral starting components will be an important competing process at any stage of the equilibria indicated and, although the diagram uses a common donor D and acceptor A for both CT complexation and exciplex formation, there is no requirement for ground state association prior to EC or exciplex formation.

Exciplex formation between the excited states of most aromatic carbonyl compounds (acceptors) and a wide range of organic amines (donors) has been particularly useful as a

means of photoinitiating free radical polymerization^{48,49}.

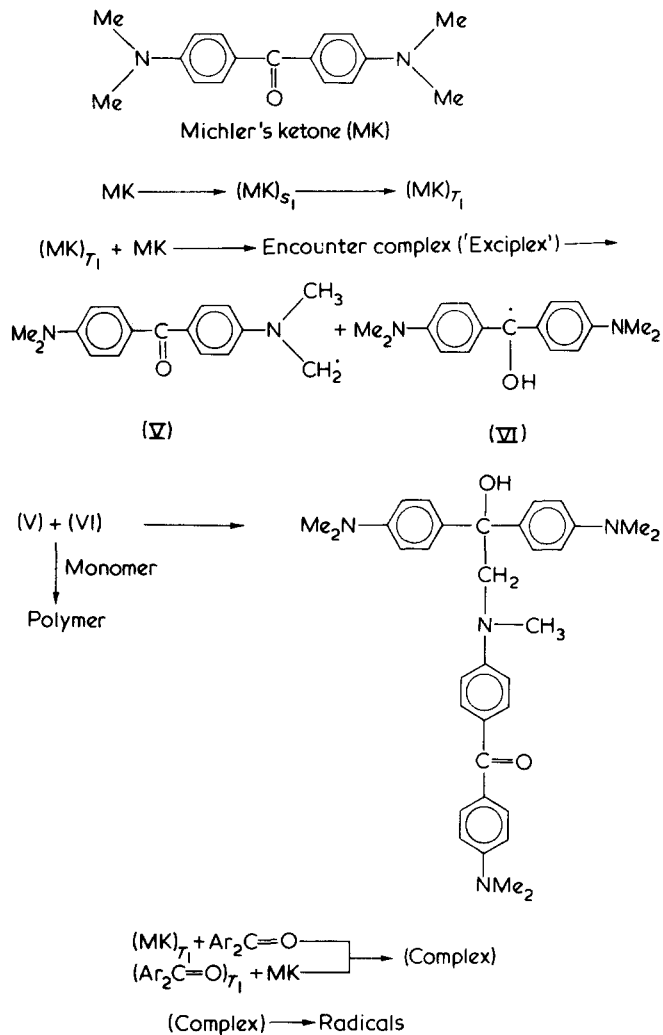
Singlet and triplet states of aromatic ketones are efficiently quenched by a wide variety of amino compounds and a general correlation exists between quenching efficiency and ionization potential of the amine, for a particular class of amine^{50,51}. In many cases tertiary amines are more effective than the corresponding secondary and primary derivatives although specific solvation phenomena may change this order of reactivity. Products from these various photo-redox processes are related and, for the photo-oxidation of amines, may be generalized as follows:



Fluorenone is one of the most useful of aromatic ketones having lowest lying π , π^* triplet excited states and its photophysical characteristics have been extensively characterized⁴⁸.

Ionization potentials of amines are important in determining quenching ability towards both singlet and triplet excited fluorenone but it appears that *photoreduction* is consequent upon interaction of triplet excited fluorenone with amine donors⁵⁰, the main effect of singlet state quenching being to reduce triplet yields. Evidence for the existence of both ion-radical pairs and free radicals is available from detailed CIDNP studies of photoreduction of benzophenones by tertiary amines. Such combinations afford a useful initiation system for radical polymerization of methyl acrylate⁵³ and we have demonstrated^{49,54} that photoreduction of fluorenone by tertiary amines is also an effective free radical initiating system for polymerization of methyl methacrylate, styrene, and acrylonitrile.

Exciplexes produced on irradiation of naphthalene in the presence of acrylonitrile initiate polymerization of the latter⁵⁵, a reaction which helps to illustrate the wide range of organic structures which may be expected to participate in such processes. For initiation of radical polymerizations however, exciplexes of aryl ketones have been most widely employed and a particular interesting case arises from the use of Michlers' ketone (MK) (4,4'-dimethylaminobenzophenone) which possesses both carbonyl acceptor group and amine donor unit⁵⁶. It is also quite remarkable that Michlers' ketone enhances the light sensitivity of initiator systems derived from other ketones⁵⁷. There is experimental evidence⁵⁸ for the photoinduced self condensation of Michlers' ketone, presumably via an intermolecular exciplex, and similar exciplexes are probable intermediates in systems based on mixtures of Michlers ketone and other carbonyl compounds e.g.



During the past five years there has been an enormous upsurge in interest in photoinitiated polymerization for the hardening of decorative and protective surface coatings and soft mouldings as well as for the manufacture of printed circuits and relief printing plates^{59,60}. Exciplex interaction has provided the means of improving both light absorption and wavelength sensitivity of photoinitiator components and will continue to be important for the future, especially since a number of economic and environmental factors now demand the development of pigmented, photocurable, printing inks based on fully polymerizable components.

REFERENCES

- 1 Evans, A. G., Holden, D., Plesch, P. H., Polanyi, M., Skinner, H. A. and Weinberger, W. A. *Nature* 1946, **157**, 102; Evans, A. G., Meadows, G. W. and Polanyi, M. *Nature* 1946, **158**, 94; Evans, A. G. and Polanyi, M. *J. Chem. Soc.* 1947, 252
- 2 Kennedy, J. P. 'Cationic Polymerization of Olefins: A Critical Inventory', Wiley-Interscience, New York, 1975
- 3 Kennedy, J. P. and Smith, R. R. 'Recent Advances in Polymer Blends, Grafts and Blocks', (Ed L. H. Sperling), Plenum Press, New York, 1974, p 303
- 4 Brown, H. C. and Holmes, R. R. *J. Am. Chem. Soc.* 1975, **78**, 2173; Mente, D. C., Mills, J. L. and Mitchell, R. E. *J. Inorg. Chem.* 1975, **13**, 1484
- 5 Kennedy, J. P., Feinberg, S. C. and Huang, S. Y. *Polymer Prepr.* 1976, **17**, 194
- 6 Ledwith, A. and Sherrington, D. C. *Adv. Polym. Sci.* 1975, **19**, 1; Ledwith, A. *Makromol. Chem.* 1974, **175**, 1117
- 7 Bower, P. M., Ledwith, A. and Sherrington, D. C. *J. Chem. Soc. (B)* 1971, 1511

- 8 Chung, Y. J., Rooney, J. M., Squire, D. R. and Stannett, V. *Polymer* 1975, **16**, 31
- 9 Goka, A. M. and Sherrington, D. C. *Polymer* 1975, **16**, 819
- 10 Pino, P. *Polymer* 1976, **17**, 000
- 11 Chiellini, E., Ledwith, A. and Solaro, R. to be published
- 12 Chiellini, E. *Macromolecules* 1970, **3**, 527
- 13 Bawn, C. E. H. and Ledwith, A. *Quart. Rev.* 1962, **16**, 361; 'The Stereochemistry of Macromolecules', (Ed A. D. Keiley), Marcel Dekker, New York, 1967, Vols 1 and 2
- 14 ICI Br. Pat. 1 016 245; Ivin, K. and Rose, J. B. *Adv. Macromol. Chem.* 1968, **1**, 336
- 15 Harris, G. I., Edwards, A. G. and Huckstep, B. G. *Plast. Polym.* 1974, 239
- 16 Jenkins, A. D. and Ledwith, A. 'Reactivity, Mechanism and Structure in Polymer Chemistry', Wiley, New York, 1974
- 17 Szwarc, M. in 'Molecular Behaviour and the Development of Polymeric Materials', (Eds A. Ledwith and A. M. North), Chapman and Hall, London, 1975, p 1
- 18 Teyssie, P., Ouhadi, T. and Bioul, J. P. in 'Macromolecular Science', (Ed C. E. H. Bawn), M. T. P. Series Two, 1975, Vol 8, p 191
- 19 Colclough, R. C. and Gee, G. *J. Polym. Sci.* 1959, **34**, 153, 171; Colclough, R. C. and Gee, G. *J. Polym. Sci.* 1960, **48**, 273
- 20 Calderon, N. *Acc. Chem. Res.* 1972, **5**, 127
- 21 Dall'asta, G. and Motroni, G. *Angew Makromol. Chem.* 1971, **16/17**, 51
- 22 Mocella, M. T., Busch, M. A. and Muetterties, E. L. *J. Am. Chem. Soc.* 1976, **98**, 1283; Katz, T. J. and McGinnis, J. *J. Am. Chem. Soc.* 1975, **97**, 1592
- 23 Herrisson, J. L. and Chauvin, Y. *Makromol. Chem.* 1970, **141**, 161
- 24 McGinnis, J., Katz, T. J. and Hurwitz, S. *J. Am. Chem. Soc.* 1976, **98**, 606
- 25 Hirooka, M., Yabuuchi, H., Iseki, J. and Nakai, Y. *J. Polym. Sci. (A-1)* 1968, **6**, 1381
- 26 Yabumoto, S., Ishii, K. and Arita, K. *J. Polym. Sci. (A-1)* 1969, **7**, 1577; Gaylord, N. G. and Patnaik, B. K. *J. Polym. Sci. (B)* 1970, **8**, 401
- 27 Wentworth, G. and Sechrist, J. R. *J. Polym. Sci. (B)* 1971, **9**, 539
- 28 Koma, Y., Imura, K. and Takeda, M. *J. Polym. Sci. (Polym. Chem. Edn)*, 1972, **10**, 2983; Kurau, W., Pasykiewicz, S. and Florjanezyk, Z. *Makromol. Chem.* 1972, **154**, 71; *ibid.* 1972, **162**, 53; Furukawa, J., Kobayashi, E. and Iseda, Y. *J. Polym. Sci. (B)* 1970, **8**, 47; Taniguchi, M., Kawashaki, A. and Furukawa, J. *J. Polym. Sci. (B)* 1969, **7**, 411
- 29 Armstrong, G. H. and Harwood, H. J. *J. Polym. Sci. (B)* 1970, **8**, 627
- 30 Hirooka, M., Yabuuchi, H., Morita, S., Kawasumi, S. and Nakaguchi, K. *J. Polym. Sci. (B)* 1967, **5**, 47
- 31 Kornil'eva, V. F., Masterova, M. N., Garina, Ye. S., Zubov, V. P., Kabanov, V. A., Polak, L. S. and Kargin, V. A. *Vysokomol. Soedin (A)* 1971, **13**, 1830
- 32 Yabumoto, S., Ishii, K. and Arita, K. *J. Polym. Sci. (A-1)* 1969, **7**, 1577
- 33 Ikegami, T. and Hirai, H. *J. Polym. Sci. (A-1)* 1970, **8**, 195
- 34 Hyde, P. and Ledwith, A. in 'Molecular Complexes', (Ed R. Foster), Elek Science, London, 1974, Vol 2, p 174
- 35 Bamford, C. H., Jenkins, A. D. and Johnson, R. *Proc. Roy. Soc. (A)* 1957, **239**, 214
- 36 Bamford, C. H. and Brumby, S. *Makromol. Chem.* 1970, **134**, 159
- 37 Bamford, C. H. in 'Molecular Behaviour and the Development of Polymeric Materials', (Eds A. Ledwith and A. M. North), Chapman and Hall, London, 1975, p 51
- 38 Dodgson, K. and Ebdon, J. R. *Makromol. Chem.* 1974, **175**, 3173
- 39 Gilbert, H., Miller, F. F., Averill, S. J., Carlson, E. H., Folt, V. L., Heller, H. J., Steward, F. D., Schmidt, R. F. and Trumbull, H. L. *J. Am. Chem. Soc.* 1956, **78**, 1669
- 40 Stille, J. K., Oguni, N., Chung, D. C., Tarvin, R. F., Aoki, S. and Kamachi, M. *J. Macromol. Sci. (A)* 1975, **9**, 745
- 41 Stille, J. K. and Chung, D. C. *Macromolecules* 1975, **8**, 114; Tarvin, R. F., Aoki, S. and Stille, J. K. *Macromolecules* 1972, **5**, 663
- 42 Oguni, N., Kamachi, M. and Stille, J. K. *Macromolecules* 1974, **7**, 435
- 43 Bawn, C. E. H., Ledwith, A. and Sambhi, M. *Polymer* 1971, **12**, 209; Nakamura, T., Soma, M., Onishi, T. and Tamura, K. *Makromol. Chem.* 1970, **135**, 341
- 44 Kosower, E. M. *Prog. Phys. Org. Chem.* 1967, **3**, 81
- 45 Weller, A. *Pure Appl. Chem.* 1968, **16**, 115
- 46 Barltrop J. A. and Coyle, J. D. 'Excited States in Organic Chemistry', Wiley, New York, 1975
- 47 'The Exciplex', (Eds M. Gordon and W. R. Ware) Academic Press, London, 1975
- 48 Ledwith, A. in 'The Exciplex', (Eds M. Gordon and W. R. Ware), Academic Press, London, 1975, p 209
- 49 Ledwith, A. *Proc. IUPAC Meet. Photochem. Processes Polym. Leuven* 1976
- 50 Cohen, S. G., Parola, A. and Parsons, G. H. *Chem. Rev.* 1973, **73**, 141
- 51 Davidson, R. S. in 'Molecular Association', (Ed R. Foster), Academic Press, London, 1975, Vol 1, p 216
- 52 Roth, H. D. and Manion, M. L. *J. Am. Chem. Soc.* 1975, **97**, 6886
- 53 Sandner, M. R., Osborne, C. L. and Trecker, D. J. *J. Polym. Sci. (A-1)* 1972, **10**, 3173
- 54 Ledwith, A. and Purbrick, M. D. *Polymer* 1973, **14**, 521
- 55 Barton, J., Kapek, I. and Hrdlovič, P. *J. Polym. Sci. (Polym. Chem. Edn)* 1975, **13**, 2671
- 56 US Pat. 3 673 140; 3 661 588; McGinniss, V. D. and Dusek, D. M. *Polymer Prepr.* 1974, **15**, 480
- 57 Wamser, C. C., Hammond, G. S., Chang, C. T. and Bayler, C. *J. Am. Chem. Soc.* 1970, **92**, 6362; Pappas, S. D. and Chattopadhyay, A. K. *J. Am. Chem. Soc.* 1973, **95**, 6484
- 58 Koch, T. H. and Jones, A. H. *J. Am. Chem. Soc.* 1970, **92**, 7503; Schuster, D. I. and Goldstein, M. D. *J. Am. Chem. Soc.* 1973, **95**, 986
- 59 Ledwith, A. *J. Oil Colour Chem. Assoc.* 1976, **59**, 157
- 60 Ledwith, A. in 'Macromolecular Science', (Ed C. E. H. Bawn), M.T.P. Series Two, 1975, Vol 8, p 253

Molecular design of polymers*

Anthony H. Willbourn

Imperial Chemical Industries Ltd, Plastics Division, Welwyn Garden City, Hertfordshire, UK

(Received 14 May 1976)

This presentation is centred on what the chemist can achieve by control of molecular structure to achieve the 'simple properties' in linear, synthetic polymers which make them useful in a modern industrial environment. Transparency is a desirable property, readily accessible with amorphous polymers. Rather special structures are required to produce transparent crystalline polymers in the bulk state. The utility of many polymers is restricted by their susceptibility to chain scission, leading to a drop in molecular weight and hence loss of mechanical strength. A structural approach to defeating this effect is to make 'ladder' structures. An approach to the synthesis of novel ladder structures by bi-nuclear regulated copolymerization is suggested. Although copolymerization has been widely studied, little systematic work has been carried out on copolymer systems, which are more difficult to attain, to study the effect of copolymer composition on physical properties. The results are not always those expected, as illustrated by the acrylonitrile/styrene system. An example for further research of this type is proposed. The problems of correlating molecular structure with mechanical properties in any quantitative way are formidable, although much progress has been made on the phenomenological level in the understanding of the physical behaviour of polymers. Attention is drawn to a correlation which has been observed between modulus and certain structural parameters which may open the way to quantitative studies. Toughness is a more difficult property even to define, let alone correlate with structure. Nevertheless qualitative correlations may provide a useful starting point for future research.

INTRODUCTION

Design is for a purpose. Design comes after the recognition of the need for what is to be achieved, and after a satisfactory answer to the question: why do it? It leads on to the question: how is it to be done?

It is only in a mature field of science that these questions can be posed and answered at all, because they presuppose a wealth of knowledge about what it is possible to achieve and the ability either to do so, or to discover means of so doing by pursuing lines of research of known promise. Hence the fact that it is possible to talk on 'molecular design of polymers' is itself a tribute to the many able scientists who have, over the past 50 years or so, provided this wealth of background knowledge and who have discovered many remarkable ways of making polymers of all sorts of shapes and sizes. These different shapes and sizes result in an equal diversity of properties, and it is particularly in striving for understanding of some of these properties that Professor Geoffrey Gee has contributed so significantly.

This discussion will be restricted to a consideration of the relationship between the molecular design of synthetic linear polymers and some of those simple properties which are relevant to their usefulness to man. This will be the unifying theme, which may not be scientifically very defensible but in practice it is among the most powerful motivators of scientific research.

The 'simple properties' that are useful are not always simple in scientific terms and the future direction of much polymer research will be governed by efforts the better to

understand these properties and to improve on them. In reviewing what has been done, and what might be done in the future, emphasis will be placed on what can be achieved by the *chemist* by the control of the molecular architecture of polymers. There are other ways of changing properties, e.g. by adding plasticizers, stabilizers, 'reinforcing' agents, etc., which are often the only practicable means of producing polymeric compositions (plastics) with the processing characteristics and final properties to suit particular needs. However, on this occasion attention will be focused on what the chemist can do.

MOLECULAR ENGINEERING

Transparency

Water-white transparency is on the face of it a very simple property. All that is required is that the material should neither absorb nor scatter radiation of wavelengths between 4000 and 7000 Å. In principle the former should be no great problem with polymers based on carbon chemistry, since the electronic states of the ordinary simple carbon bonds in synthetic polymer do not give rise to significant absorption of this radiation. In practice however there are two major problem areas.

The first problem is that most polymers when first made turn out to be coloured – usually dark brown, or at best yellow – and even if they start colourless they discolour on heating or on exposure to light. The pure scientist may dismiss this unfortunate result as due to an aberration – the use of impure reagents, the formation of ionic complex chromophores from metallic contamination, thermal or photochemical degradation of the polymer to form conjugated

* Presented at the Sixth Biennial Manchester Polymer Symposium, UMIST, Manchester, March 1976.

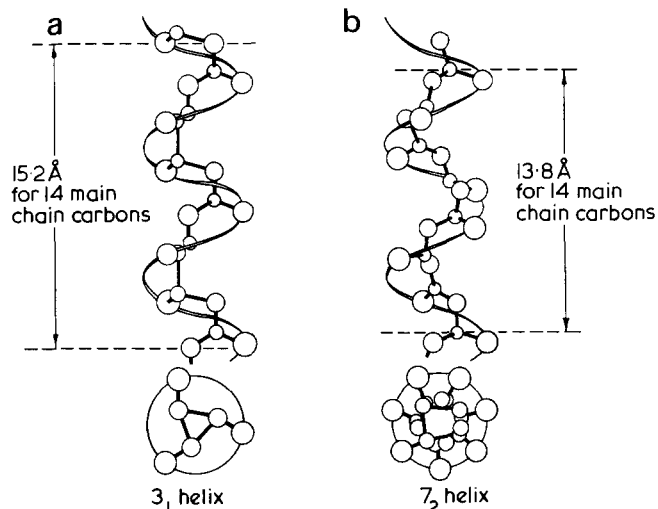


Figure 1 Helical structures of (a) isotactic polypropylene and (b) isotactic poly(4-methylpentene-1). [Reproduced from Caunt, A.D. and Rose, J. B. 'Kirk-Othmer Encyclopaedia of Chemical Technology Supplement Volume', 2nd Edn, Wiley, New York, 1971, pp 773-807 by permission of John Wiley and Sons Inc., New York, ©]

diene sequences in the chain, and so on. He will be right, but nevertheless a vast amount of both industrial and academic research has been, and will be, aimed at eliminating colour in polymers, and in devising stabilizers to prevent the formation of chromophores (or to eliminate them by reacting with them). The problem arises not only from thermal decomposition during synthesis and processing, but from photochemical and thermal reactions during service. There is however one very helpful empirical rule to comfort the industrial chemist: the yellowness of a moulded thermoplastic polymer decreases with each increase in the scale and volume of commercial production and tends asymptotically to zero.

This comes about for many reasons, the main one being that much effort is devoted to achieving it. Qualitatively the evidence for this 'law' may be seen in the history of PVC, polystyrene and polycarbonate among other commercial plastics.

The second problem area is more fundamental and arises because, in general, those polymers having geometrically regular repeat units will crystallize to form crystalline domains larger than the wavelength of visible light.

In polymer samples prepared by melting and forming (as most of them are), the individual lamellae are small, typically 100-300 Å in thickness with lateral dimensions that can be up to several thousand Å. But the lamellae aggregate in twisted ribbons to form spherulitic structures of sizes from about a micron up to units easily visible in the microscope. Therefore crystalline polymers are opaque, or at best translucent, in the bulk state. In forming these polymers into films they can be made more transparent which is fortunate considering how important these materials are in such uses as photography. The rapid quenching which a thin film is subjected to produces some improvement in transparency since rapid quenching from the melt reduces the degree of crystallinity and retards aggregation into spherulites. More drastic modification is achieved by orientation which not only results in the absence of spherulites but can produce lamellar structures in which the orientation is correlated over distances large in relation to the wavelength of light, resulting in a marked decrease in intensity of scattered light¹. For example when

polypropylene film is biaxially oriented, the spherulitic structure is completely disrupted and the final film has no visible structure and is highly transparent. However there are crystalline polymers which are transparent in the bulk state because of their molecular architecture, which is something that the chemist can control.

An unusual method of achieving transparency is exemplified by poly(4-methylpentene-1). It is taken for granted that a polymer crystal has a greater density than the amorphous phase, a larger refractive index and is optically anisotropic. These things are not true for poly(4-methylpentene-1)². For instance the polymer chain in the crystalline unit cell forms a fairly open helix (less tightly coiled than the polypropylene helix, see Figure 1), and the packing of the large isobutyl side groups is such that the total assembly of bonds is vectorially quite well randomized. The result is that individual crystallites have low anisotropy and polymer spherulites exhibit unusually low birefringence compared, for instance, with polypropylene or polyethylene (Table 1). A second crucial and unusual factor is the fact that the specific volumes of the crystalline and amorphous regions are very close to each other; in fact at room temperature the specific volume of the crystalline phase is greater (1.208 cm³/g) than that of the amorphous polymer (1.193 cm³/g). But the system is more complicated, otherwise the polymer would not crystallize at all. The amorphous polymer has a larger coefficient of thermal expansion than the crystalline phase, and has a greater specific volume above 60°C (Figure 2). The difference is large at around 200°C which is the temperature region at which the polymer crystallizes on cooling slowly from the melt (m.p. = 245°C). Under these conditions large spherulites are formed, and in forming they produce voids and the optical transmission drops to about 20%. If however the samples are quenched, such crystallization as occurs is at a lower temperature; voiding is reduced, and transparency is good (~80% transmission). In practice quenching produces other problems and is not always practicable, and in fact the need to quench can be eliminated by some delicate molecular engineering. Copolymerization with a minor amount (~2%) of a linear 1-olefin helps, probably by lowering the temperature at which crystallization sets in. If in addition a very small amount (<1%) of a high melting polyolefin is incorporated as a fine dispersion, to provide nuclei which persist in the molten polymer, then moulded parts can be made in which the average spherulite size is less than 5 μm, with optical transmissions around 97% (Table 2).

There is another industrially important way chemically to affect the transparency of crystalline polymers if they can be made with ionizable groups. Examples are polyethylenes and polyoxymethylenes containing small molar percentages of carboxylic acid groups which, when neutral-

Table 1 Spherulite birefringence of some polyolefins

Polymer	Birefringence, $n_r - n_t$
Polyethylene (low density)	-0.003
Polypropylene:	
Type I	0.003
Type II	-0.002
Type III	-0.007
Typical mouldings	Varying from 0.003 to -0.002
Poly(4-methylpentene-1)	0.0005

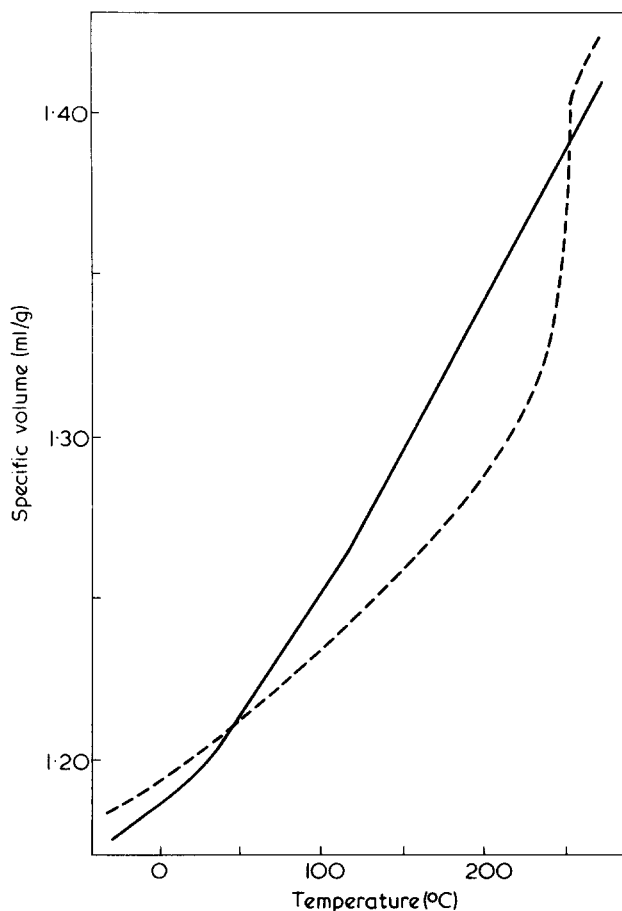


Figure 2 Specific volume—temperature curves for poly(4-methylpentene-1) samples: —, quenched (more amorphous); ---, annealed (more crystalline). [Reproduced from Griffith, J. H. and Ranby, B. G. *J. Polym. Sci.* 1960, 44, 369 by permission of John Wiley and Sons Inc., New York ©]

Table 2 Optical transmission of 1-olefin copolymers of 4-methylpentene-1

Comonomer (2 wt %)	Nucleation	Mean spherulite size (μm)	Optical transmission of mouldings (%)	
			Quenched	Slow-cooled
None	No	>25	84	20
	Yes	< 2	95	88
1-Hexene	No	>25	80	38
	Yes	< 2	98	93
1-Decene	No	>25	90	47
	Yes	< 2	98	97

ized with metallic cations, exhibit markedly increased transparency⁴. These 'ionomers' (as they are known) are complex structures with many unusual features which can be illustrated by the Surlyn* range of plastics: these are ionomers based on ethylene copolymerized with methacrylic acid and (partly) neutralized with Na^+ or Zn^{++} ions. The acid copolymers themselves with up to about 4 mol% of acid are structurally not very different from the parent low density polyethylenes, being translucent with typical spherulitic crystallinity (Figure 3). The introduction of cations however destroys the spherulitic structure (Figure 4), and the process is reversible. The 'ionomerized' structure is still crystalline (as shown by X-ray diffraction) and

* Registered trademark, E. I. Du Pont de Nemours and Co. Inc.

the ions form clusters a few tens of Angstroms in diameter. Other properties change also: ionomers are generally more transparent than the parent acid copolymers, depending on the type and concentration of the cation; they have greatly increased water absorption (which can be up to 25% by weight), the water presumably solvating the ionic clusters; ionomers are tougher than polyethylene, and are resistant to stress-cracking agents but they start to soften at quite low temperatures. In fact ionomers show some of the properties of crosslinked structures, but the 'crosslinks' are labile because ionomers are melt processable although they have much higher viscosities than the parent copoly-

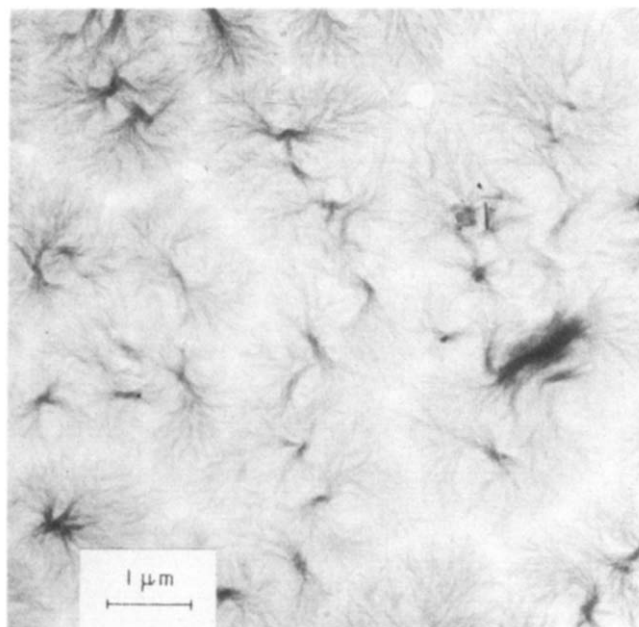


Figure 3 Electron micrograph of an acid copolymer [Reproduced from Longworth, R. 'Ionic Polymers', (Ed. L. Holliday), Applied Science, London, 1975, Ch 2, pp 69-172 by permission of Applied Science Publishers Ltd, Barking ©]

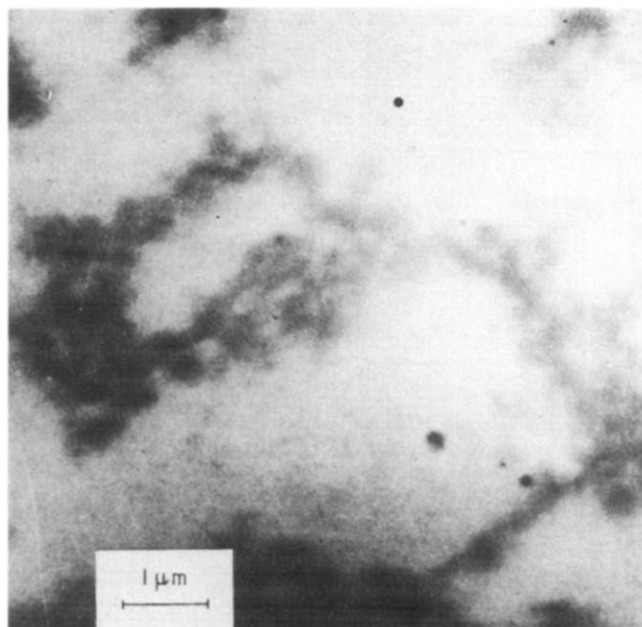


Figure 4 Electron micrograph of an acid copolymer after ionomerization. [Reproduced from Longworth R. 'Ionic Polymers', (Ed. L. Holliday), Applied Science, London, 1975, Ch 2, pp. 69-172 by permission of Applied Science Publishers Ltd, Barking ©]

mers. Studies of other properties: dielectric relaxations, mechanical relaxations, thermal behaviour, X-ray diffraction etc. display a complex dependence of properties on composition and no very convincing correlation with molecular structure. There seems to be plenty of scope for further research to understand these effects and to seek novel combinations of properties in such systems.

Seemingly simple uses often demand unusual property combinations. Consider the laminated windscreen as used in motor cars. All that is apparently required to make such a windscreen is a transparent, colourless tough plastic foil, which can be sandwiched between two sheets of (curved) glass. Further study shows that the optical quality of the interlayer foil must be of a very high order so that a glass laminate made with it has a minimum light transmission of 70%, negligible haze (i.e. wide-angle scattered light) and low optical distortion. The foil must also be tough over a wide temperature range so that laminates are highly resis-

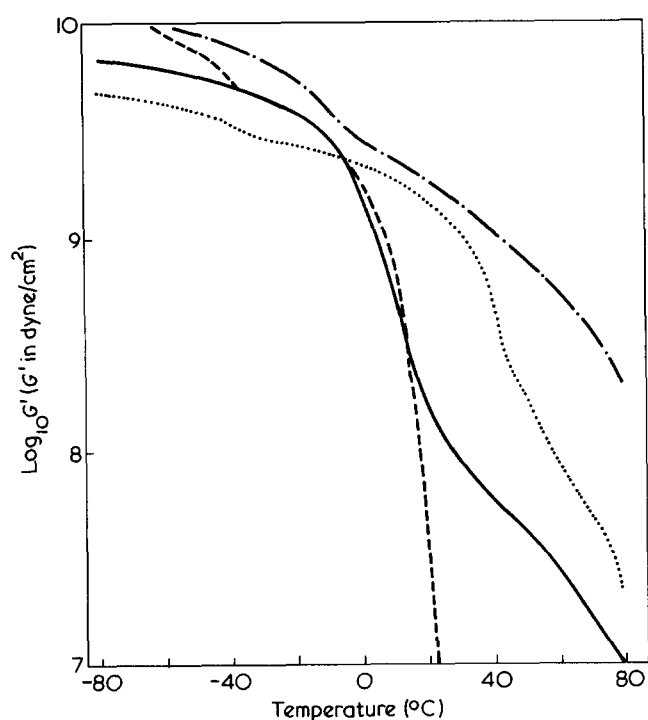


Figure 5 Variation of dynamic shear modulus G' with temperature. Method: torsion pendulum 0.3–3 cycles/sec. — — —, LDPE; ·····, ionomer B; —, Terpolymer X; — · — ·, plasticized poly(vinyl butyral)

tant to penetration over the temperature range -20° to $+40^{\circ}\text{C}$, but at the same time the laminate must yield on impact to give controlled deceleration below the threshold value causing brain damage. On top of all that, when the windscreen is broken, the glass fragments should still adhere to the foil. To achieve these effects, the adhesion between foil and glass must be closely controlled, not too great, and not too small. There is only one foil material which has been found satisfactory on a commercial scale for this use. It is poly(vinyl butyral) (PVB), an amorphous polymer, compounded with a specific plasticizer, which was introduced some 30 years ago and which has of course been gradually improved over this period. A crucial requirement of PVB foil for this use is that its water content shall be carefully controlled at near 0.4%, because this governs not only the adhesion behaviour of laminates, but also the ability to make laminates and their integrity in service. PVB when saturated takes up 3 to 5% of water.

Various commercial ethylene copolymers and ionomers, which are partly crystalline, have some of the right sorts of properties for the windscreen application but none have the right balance. For example, ethylene/vinyl acetate copolymers may have the desired stiffness and toughness but have poor adhesion to glass and inadequate optical properties. Ionomers tend to be fairly transparent and give better adhesion to glass but are likely to be too stiff and to show too high a sensitivity to ambient relative humidity (r.h.). A much more suitable foil can be made by specific design of an ethylene/methacrylic acid terpolymer system. The level of acid copolymerized sets adhesion characteristics, while optical and mechanical characteristics can be optimized by controlling the content of a third monomer which can for instance be methyl methacrylate⁵. It turns out that a system with 4 mol% of each comonomer (Terpolymer X) possesses the right balance of properties: comparison of these materials is shown in Figure 5 and Table 3. An additional advantage of this terpolymer is that, unlike PVB, it has low water absorption and hence low sensitivity to ambient r.h. (Figure 6). One final thing is needed to achieve the highest transparency and minimum haze: the terpolymer foil should be cooled rapidly from the molten state during the process of making the windscreen. This quenching process renders the foil practically amorphous. Figure 7 shows what happened when a car fitted with a windscreen* made using Terpolymer X was involved in an (accidental) head-on collision, and illustrates the advantage of laminated screens. The driver's head impacted onto the

* Experimental windscreen made by Triplex Safety Glass Co. for BLMC 1800 car.

Table 3 Comparison of foil materials and glass laminates made from them

Material	Cation	Methacrylic acid (mol%)	Methyl methacrylate (mol%)	Impact strength of laminate* (ft)		Adhesion behaviour: glass retention after breakage	Transparency of laminate
				at -20°C	at 25°C		
PVB	—	—	—	8	18	Good	Clear
Ionomer A	Na^+	4	—	15	14	Poor	Hazy
Ionomer B	Zn^{++}	6	—	5	16	Fair	Clear
Ionomer C	Na^+	7	—	10	15	Fair	Hazy
Terpolymer X	—	4	4	8	20	Good	Clear

* Expressed as mean penetration height (ft) of a 1 ft square laminate (foil 0.030 in thick and glass 1/8 in thick) for a 5 lb steel ball

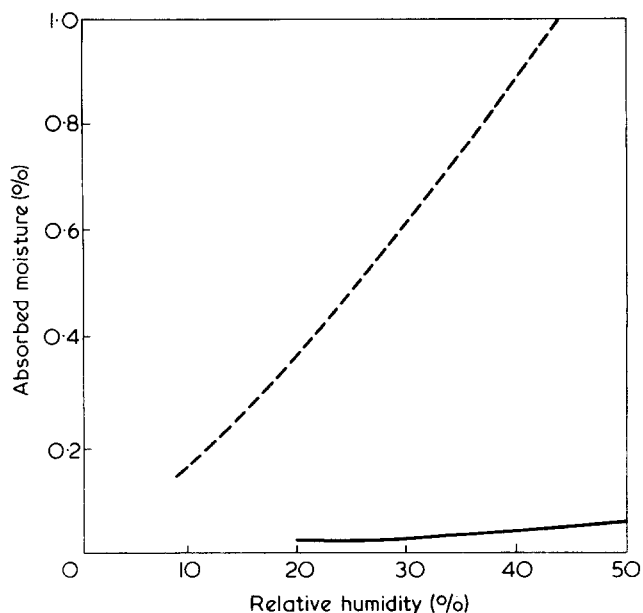


Figure 6 Variation of equilibrium moisture content with relative humidity. Temperature 20°–50°C. —, Terpolymer X; --- plasticized poly(vinyl butyral)

screen, but he emerged without a scratch on his face (although he did break his arm!).

Glass transition temperatures of crystalline polymers

No discussion of the temperature dependence of physical properties can be coherent without agreement about the nature of the glass transition temperature, T_g , and its relationship to features of molecular structure. This has been a fruitful field for research, and there is no need to emphasize its continuing importance. There is however one recent development worth drawing attention to because of its wider implications. For the simplest of polymers, viz. polyethylene, there is still controversy about its glass transition temperature: values of T_g are variously quoted as either around -120°C , or around -30°C ⁶. This disagreement leads to great confusion in the abundant literature on the properties of polyethylene and of related polymers (including the ionomers). Part of the problem undoubtedly arises because the 'glass transition temperature' can be defined in different ways which lead to different criteria for recognition and measurement of T_g . A definition favoured by the author (although it is admittedly incomplete) is 'that temperature at which the main polymer chain acquires large-scale mobility'. Following this definition there is a simple criterion for T_g for those crystalline polymers that can be quenched from the melt into the fully amorphous glassy state: T_g is that temperature at which crystallization occurs⁷. Crystallization must involve fairly large scale chain movement, translational as well as rotational, especially as we now know that lamellae of folded chains are formed in the process.

This criterion was of no value in the case of polyethylene because amorphous linear polyethylene had never been produced despite many efforts to do so. Quite recently however Hendra has succeeded in quenching a linear high density polyethylene to the fully amorphous state in which it is stable at -150°C . He has followed the onset of crystallization by observing infra-red spectra, Raman spectra and X-ray diffraction and has concluded that crystallization sets in at around -100°C which sets an upper limit for T_g , using this criterion^{8,9}. This work opens up a new

and fruitful field of research on the properties in their amorphous states of normally crystalline polymers, since this quenching technique can no doubt be applied to other crystalline polymers such as the aliphatic nylons, polyacetal and perhaps to polytetrafluoroethylene, polymers which have never been reported in the amorphous glassy state.

Ladder polymers

Permanence in physical behaviour is very desirable but most polymers are restricted in their utility by degradation, by light or by heat or by oxidation or by a combination of these. Typically such degradative reactions cause random chain scission, which results in a rapid drop in average molecular weight and this in turn results in a rapid fall in those properties dependent on average MW : impact strength, tensile strength and elongation at break. However there has been little work published on the quantitative aspects of this very important phenomenon. Adams has published data on MW changes of (unstabilized) polypropylene caused by thermal oxidation, photo-oxidation and by melt processing, and noted that samples were quite brittle by the time their MW were halved¹⁰. The effect is quite dramatic: polypropylene of $M_n = 84\,000$ becomes brittle after 2 h exposure at 138°C if it is not stabilized. Similar data have been presented by Birley and Brackman on the photo-degradation of low density polyethylene¹¹.

Most commercially available thermoplastics are produced with molecular weights as low as is safe and reasonable to confer the required mechanical properties, in order to make fabrication by moulding, extrusion, etc. as easy as possible by keeping the melt viscosity low. With this in mind, and taking account of the published data, it seems that when degradation has proceeded to the extent of about one bond broken per molecule present (thus halving M_n) the mechanical strength of the polymer has been effectively destroyed.

A means of defeating this effect by redesign of molecular structure is to form ladder polymers in which two parallel chains are connected together at regular intervals. An individual chain in a ladder polymer can undergo cleavage of any single bond without any effect on MW . If cleavage is a random process, then only after extensive degradation will two bonds in the same section of the ladder be cleaved



Figure 7 Car fitted with Terpolymer X windscreen after head-on collision



Figure 8 A ladder structure can withstand many bond cleavages without reduction in overall length

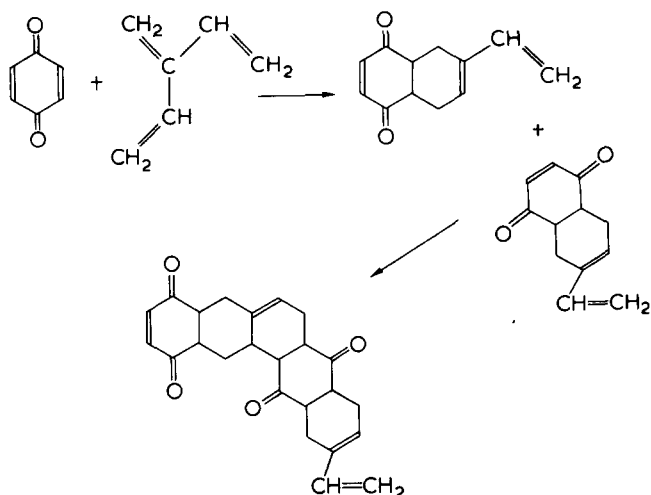


Figure 9 Diels-Alder condensation and polymerization of 2-vinylbutadiene and benzoquinone

and the chain itself be broken, with consequent drop in MW and in related physical properties (Figure 8). The first deliberate synthesis of a ladder polymer was by Bailey and Economy in 1954^{12,13} of the polymer from 2-vinylbutadiene and benzoquinone by Diels-Alder condensation (Figure 9). A proportion of the product was of fairly high MW , softening at over 340°C and soluble only in powerful solvents such as hexafluoroisopropanol. Many such ladder polymers have since been made, often containing condensed heterocyclic rings and giving intractable infusible solids¹⁴. However some polyester types with a significant aliphatic content have been synthesised, and degradation studies on these and other systems have demonstrated that these ladder structures are more resistant to degradation than the analogous single-strand polymers^{15,16}.

This is a tantalizing field because there are polymers it would be interesting to examine but synthetic methods to make them have yet to be devised. One such is a polyethylene-type ladder polymer with the 'rungs' irregularly spaced at intervals with an average of around 4 per 100 chain atoms, i.e. at about the same frequency at the short branches in low density polyethylene (Figure 10). It is interesting to speculate what its properties would be. It is likely to be not very crystalline, the rungs not being regularly spaced, and also it is difficult to see such a ladder structure being incorporated in a chain-folded lamellar structure. A small amount of copolymerization with an α -olefin (say propylene or butene-1) to introduce some random short branches (R in Figure 10) might be expected to produce a completely amorphous polymer. Its thermal stability (and light stability) should be good, and although its melt viscosity would presumably be high for a given 'ladder length', it should be processable at high temperatures without significant degradation. What its mechanical properties would be depends on one's view of the T_g of polyethylene (hence the comments above on this matter).

Taking the view that the T_g is below -100°C , then this amorphous branched polyethylene-type ladder polymer will have an effective T_g around -70°C and (if lightly cross-linked) will be elastomeric over a wide temperature range, say from -60°C up to its limit of stability which could be well over 100°C depending on the conditions, the life required and the effectiveness of stabilizing systems.

Clearly some very advanced molecular engineering will be needed to synthesise a polyethylene ladder polymer. The obvious elegant way is to persuade, say 1,7-octadiene to copolymerize regularly, and coincidentally, between the same two growing polyethylene chains. Whilst this looks to be impossible to achieve in the way set out in Figure 11, published work on transition metal compounds which are catalysts for olefin polymerization¹⁷ perhaps provides the basis of a possible synthesis. These catalysts function by 'growing' the polymer chain from the metal atom, the monomer being first coordinated to the metal and then being inserted into the polymer chain. Thus zirconium tetrabenzyl is such a catalyst, and it retains its activity when bonded to a silica surface as a siloxy-tribenzyl zirconium. Under the right conditions structures of this

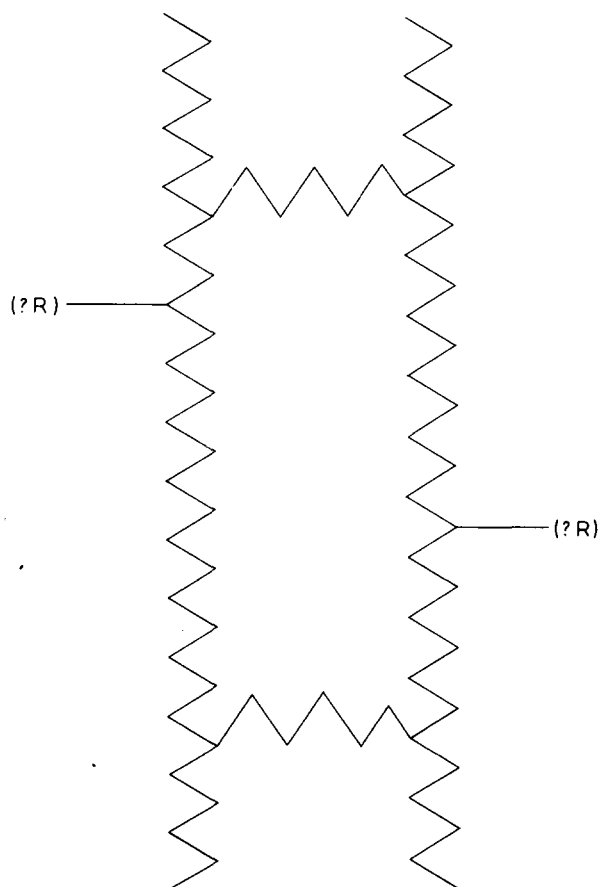


Figure 10 A polyethylene-type ladder structure

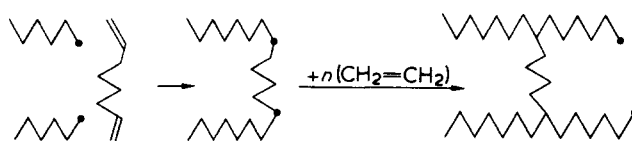


Figure 11 Growth of polyethylene-type ladder structure by bi-copolymerization with 1,7-octadiene (schematic)

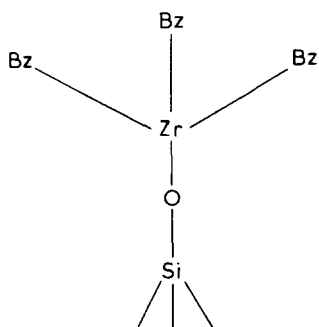


Figure 12

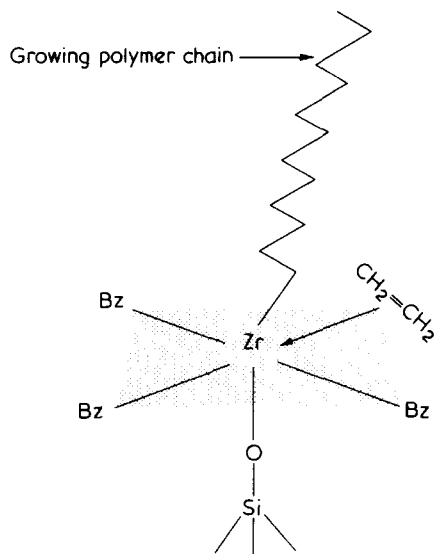


Figure 13

type can indeed be formed (Figure 12).

In this state the bonds are tetrahedrally disposed, but it is probable that during polymerization the zirconium is 6 coordinated with an octagonal structure (Figure 13).

Now the procedure would be to synthesise a binuclear catalyst, joining two Zr (Bz)₃ moieties with a *para*-xylyl ligand to form (Bz)₃Zr.CH₂.C₆H₄.CH₂.Zr(Bz)₃. This binuclear complex is then reacted onto a silica surface previously heated to about 400°C so as to leave the surface only sparsely covered with OH groups (so that paired structures like those in Figure 12 are formed). When ethylene is presented to the system, polyethylene chains will grow from each of the paired Zr nuclei, and the problem is: how to join these two growing chains together? In principle this might be done by copolymerizing with 1,4-diallylbenzene if the two allyl groups could be placed simultaneously next to the two neighbouring Zr nuclei. To achieve this some 'template' mechanism must be provided to attract 1,4-diallylbenzene molecules onto the surface in between the paired Zr nuclei, so that their relative concentration is much greater there than at any other surface site. Such a mechanism could be the formation of a weak complex between diallylbenzene and the *para*-xylyl ligand by appropriate substitution of the respective aromatic nuclei by attracting groups X and Y. The complete system is shown in Figure 14. It would clearly be a formidable task to realize this system, but one might suggest an approach using X = F and Y = NR₂ (R = alkyl), or *vice versa*. The effect of the substituent X on the stability of the xylyl ligand and on the polymerizing activity of the Zr nuclei may well be an important factor.

Novel copolymer systems

Copolymerization is one of the most direct and widely used techniques of molecular engineering and the kinetics of copolymerization have rightly been the subject of extensive academic study. The principles of the free-radical copolymerization of vinyl monomers are to be found in standard texts, with tables of reactivity ratios, and *Q* - *e* diagrams. From these data it is apparent that there are many copolymers which are difficult to make. It is somewhat surprising that more of these systems have not been taken as projects in, say, chemical engineering, the objective being to make significant quantities of truly random, thermally stable copolymers using the special monomer composition control and feeding techniques now practicable with the advent of on-line process instrumentation and real-time computer control. It should be possible to make enough of these copolymers in laboratory scale apparatus to study their properties as a function of composition¹⁸. These properties sometimes turn out to be quite different from what was expected.

Examples of 'difficult' copolymers which have become industrially important are the truly random copolymers of styrene and acrylonitrile (AN) containing 75 and higher mol% AN. This is a system in which¹⁹:

$$\text{AN is monomer 1, } r_1 = 0.04$$

$$\text{Styrene is monomer 2, } r_2 = 0.4$$

The copolymer composition plot is skew sigmoidal, as shown in Figure 15. This reflects the fact that over much of the range of monomer compositions the copolymer (instantaneously) formed has a very different composition from the monomer mixture. Inevitably therefore if such a monomer mixture is fully polymerized, the copolymer formed will be structurally heterogeneous. This is illustrated in Figure 16 for a 25:75 molar mixture of styrene and AN. The properties of these heterogeneous copolymers are dreadful: thermal stability is poor and they are so brittle that the properties can hardly be measured. If however the monomer composition is controlled during reaction to produce a truly

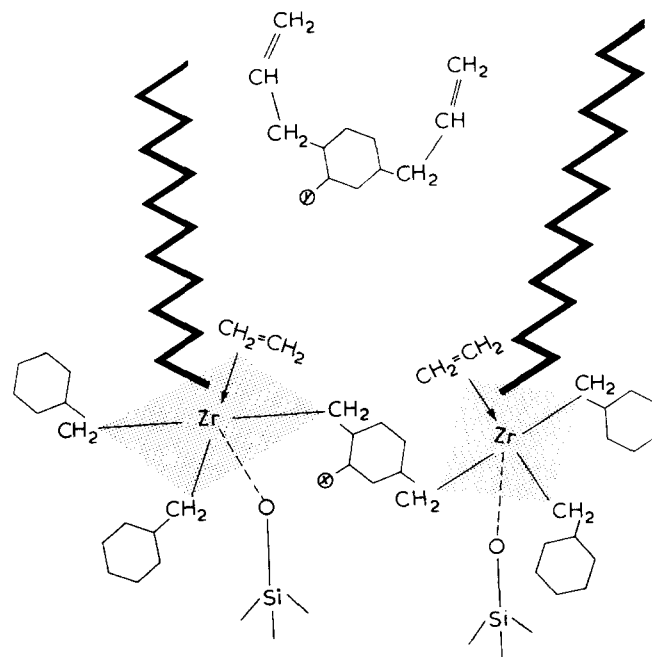


Figure 14 System for polyethylene-type ladder polymer synthesis

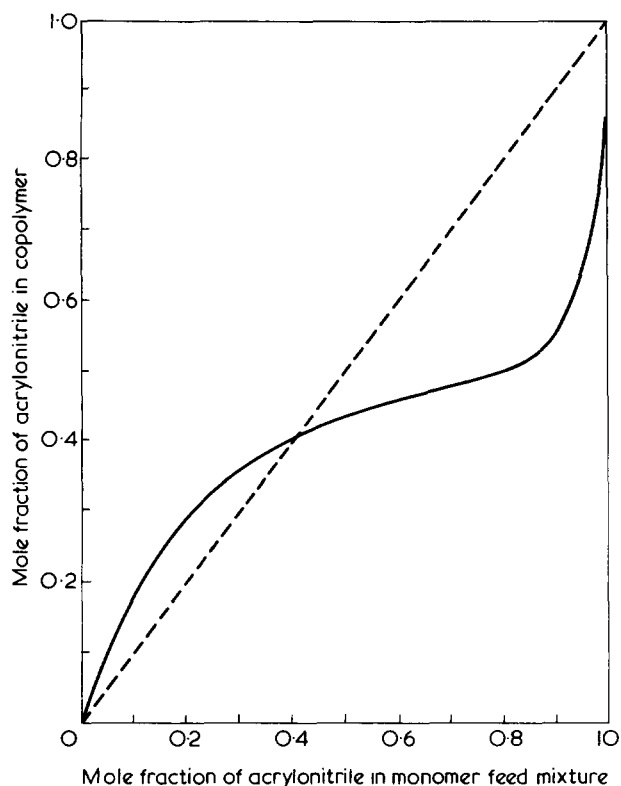


Figure 15 The relationship between monomer mixture composition and copolymer composition for acrylonitrile and styrene

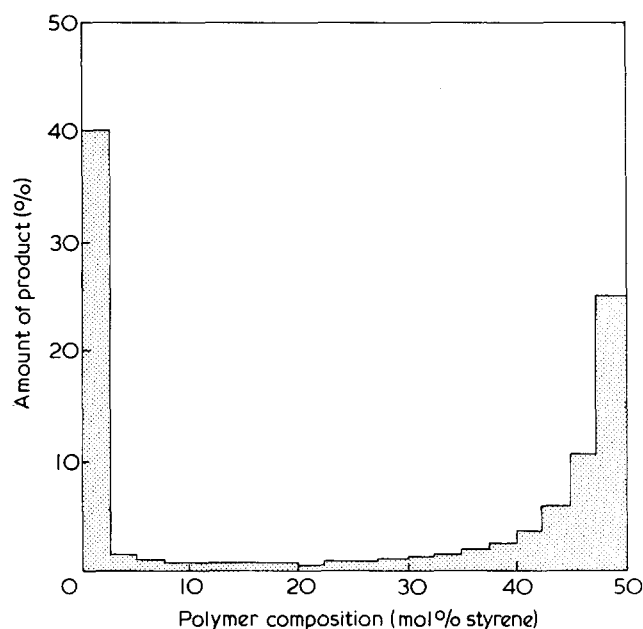


Figure 16 The composition of the product resulting from the batch copolymerization of acrylonitrile (75 mol %) and styrene (25 mol %). [Reproduced from HENDY, B. N. 'Copolymers, Polyblends and Composites', Advances in Chemistry Series, No. 142, Am. Chem. Soc., Washington D.C., 1975, pp. 115-128 by permission of The American Chemical Society, Washington D.C. ©]

random copolymer having even as much as 80 mol% AN, then a strong, clear and thermally stable copolymer can be made¹⁸. The contrast in properties is indicated in Table 4.

These particular copolymers, with high AN contents, are important because of their very low permeability to permanent gases and in particular to CO₂ and oxygen (Table 5). Such copolymers are classed industrially as 'barrier resins',

and are used in the manufacture of bottles for carbonated beverages.

Permeability is an important property which governs the use of many polymers in film form to protect foodstuffs, chemicals, and agricultural products. In its simplest terms, permeability is a function of both the solubility (*S*) of a gas in the polymer and of its rate of diffusion (*D*). Both *S* and *D* are dependent on polymer structure in ways that are qualitatively understood, but there is certainly scope for better understanding and there are structural effects which are still mysterious. One of these is the relatively low permeability of vinylidene polymers, shown by for instance polyisobutene compared with natural rubber and poly(vinylidene chloride) compared with poly(vinyl chloride) (Table 5). An interesting research project would be to synthesise a range of vinylidene chloride¹/isobutene² copolymers, truly random composition. This is likely to be difficult since one can guess that for this system $r_1 \sim 3$, $r_2 \sim 0$.

The structures, and hence the properties, of these copolymers might well show some interesting and unusual features. The methyl group, although slightly larger than the Cl atom and not spherically symmetrical, is not very different in size from the Cl atom. The available evidence suggests that the chain configurations of the two polymers in their individual unit cells are somewhat similar. Polyisobutene (PIB) only crystallizes on stretching; however in the unit cell the conformation of the molecule is a 8₃ distorted helix with a repeat distance of 2.32 Å per monomer unit²⁰; the corres-

Table 4 Styrene: acrylonitrile copolymers (20:80 mol ratio). Comparison of homogeneous and heterogeneous copolymers

Copolymer	Vicat softening point (°C)	Un-notched impact strength (kJ/m ²)	Appearance	X-ray observations
Heterogeneous	123	2.4	Yellow, translucent	Appreciable two-dimensional order
Homogeneous	108	24	Pale yellow, clear	Amorphous

Table 5 Permeability of some polymers to oxygen and carbon dioxide

	Permeability coefficient at 25°C ($\frac{\text{cm}^3 \text{ (STP) cm}}{\text{cm}^2 \text{ sec atm}} \times 10^{10}$)	
	Oxygen	Carbon dioxide
(a) Thermoplastics:		
Polyethylene (low density)	180	900
Polypropylene	90	300
ABS	45	450
PVC (unplasticised)	5	11
Nylon-6,6 (dry)	2	7
Nitrile barrier resin (AN: styrene, 75:25)	2	5
Oriented polyester film [poly(ethylene terephthalate)]	2	11
Saran film [poly(vinylidene chloride) copolymer]	0.5	4
(b) Rubbers:		
Natural rubber	1500	11 000
Butyl rubber	100	400

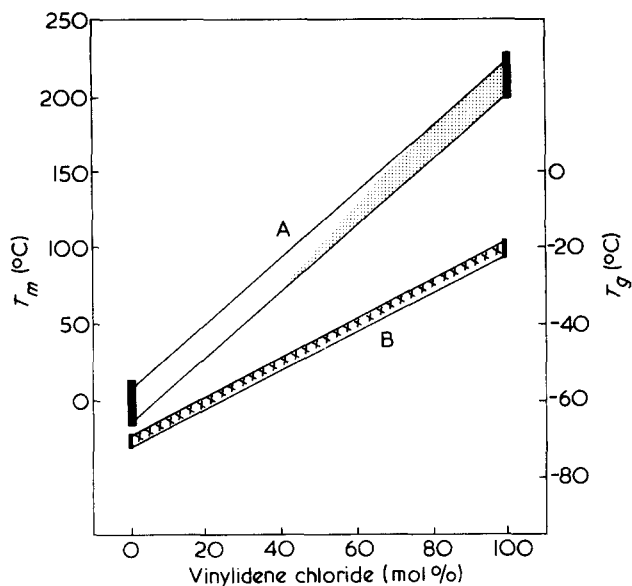


Figure 17 Vinylidene chloride/isobutene copolymers: dependence (hypothetical) of melting point (T_m) and of glass transition temperature (T_g) on composition. A, T_m ; B, T_g

ponding conformation for poly(vinylidene chloride) (PVdC) is a 2_1 helix with a repeat distance of 2.34 Å per monomer unit²¹. Both molecules are very overcrowded in any configuration, so much so that the main chain bond angles at the CH_2 groups are opened up from the tetrahedral 109.5° to 128° for PIB and 123° for PVdC; the difference in bond angle at the CX_2 group is rather greater, the angle being 110° for PIB and 120° for PVdC. These molecules are therefore rather similar in size and in preferred conformation, and in random copolymers of low isobutene content the comonomer units might be expected to cocrystallize.

Some estimates can be made of the properties of such a cocrystallizing system. Although PIB does not crystallize unless stretched, from observations of the melting point of PIB at different elongations it appears that its notional melting point is around 0°C ; the T_g of PIB is -70°C . For poly(vinylidene chloride) $T_m \sim 210^\circ\text{C}$ and $T_g \sim -20^\circ\text{C}$. Hence one would expect a random, cocrystallizing, copolymer of 80:20 VdC/IB composition to have (Figure 17): $T_m \sim 175^\circ\text{C}$; and $T_g \sim -30^\circ\text{C}$.

Quite apart from this being an interesting academic research project, these random copolymers should have technologically useful properties, especially if their lower melting points could be combined with thermal stability adequate to permit fabrication by melt processing. They should have good mechanical properties and be tough and extensible (the amorphous phase having such a low T_g), and might be expected to retain low permeability to CO_2 and oxygen.

MECHANICAL PROPERTIES

Problem of structure correlation

It is evident that, however desirable may be properties such as transparency, resistance to degradation, low dielectric loss, low flammability and low permeability, these are of little practical value unless they can be combined with 'good mechanical properties' in a polymer which can be readily processed into desired shapes — mouldings, extrusions, sheet and film. It is impossible really to define 'good mechanical properties' because what is acceptable in practice is the result of a compromise between properties which

are essential for a particular application, adequate performance in other respects, and the overall cost involved. However, prescinding from specific properties and applications, it is reasonable to generalize to the extent of stating that for structural uses one is seeking for high strength, rigidity, toughness and a wide usable temperature range.

Although the dependence of mechanical behaviour on a variety of parameters (time, stress, geometry, environment, temperature), has been the subject of detailed investigation and some progress has been made in an understanding in phenomenological terms, understanding at the level of molecular design is still qualitative, fragmentary and imperfect, and compares unfavourably with the state of knowledge about low molecular weight compounds, metals and even of elastomers.

This point has recently been emphasized by Flory²². He points the way to a rigorous mathematical approach to the calculation of physical properties using such basic data as energy barriers to bond rotation, intermolecular forces, the dimensions of chain links and of sub-units, the distribution of chain lengths, and the conformations of the long chain molecules. While in principle possible, this is a daunting task for the ordinary polymer scientist, if only because of the large amount of quantitative information needed for each polymer before a start can be made with the calculations, and also the difficulty of formulating the mathematical functions and programming the computations.

A complementary approach is to consider the total system and to concentrate on those essential molecular features which determine a few basic properties. If one can establish some real correlations then these will point the way to profitable lines for future research, both practical and theoretical. Two examples of such correlations are proposed for consideration.

Toughness and structure

A tough material fails in ductile fashion, at large strains. Why is it that some glassy, amorphous (linear) polymers exhibit ductile failure, while others are brittle? Of course distinctions are not all clear cut, and are dependent on temperature, strain rate, etc. but the reality is quite recognizable in contrasting polystyrene with polycarbonate. There is no real correlation with modulus, glass transition temperature or secondary mechanical transitions. One clue is perhaps to be found in the shape of the molecule.

In the 1930s and the 1940s when free-radical polymerization of vinyl compounds was the only readily available synthetic route to high molecular weight polymers, and most of these were amorphous being of the types $-(\text{CH}_2-\text{CHX})-$ or $-(\text{CH}_2-\text{CXY})-$, much effort was put into seeking useful polymers with softening points above 110°C which was the top limit of T_g values for the polymers then in general use [polystyrene, poly(vinyl chloride), poly(methyl methacrylate)]. A favoured approach was to incorporate large side groups (X) in the vinyl $(-\text{CH}_2-\text{CHX}-)_n$ chain units, but the effect of this was invariably to make brittle materials. Perhaps the ultimate example was polyvinylcarbazole, which has been used commercially because of its excellent dielectric properties and high softening point:

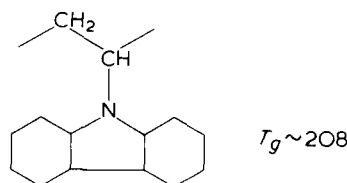


Table 6 Effect of structure on impact behaviour of aromatic sulphone polymers

Structure	Impact behaviour
	Tough
	Brittle
	Tough
	Brittle
	Tough
	Brittle
	Brittle

In more recent years conditions for carrying out a variety of coupling and condensation reactions have been devised (and intermediates of the requisite purity have been synthesised) to produce a wide range of macromolecular structures. These routes have been exploited to make high softening amorphous polymers by synthesising more rigid chain structures in which large aromatic groups are incorporated in the main chain itself. If one compares these with polymers having bulky pendant groups, the striking difference is that the ring-in-the-chain polymers combine higher softening points (T_g) with increased toughness over vinyl polymers. They fail in ductile fashion, even at temperatures well below T_g , and therefore are able to absorb and dissipate mechanical energy: they are tough.

It is in this context that the simple concept of *shape* becomes significant. Put in its crudest terms large pendant groups interlock. This inhibits relative movement of neighbouring chain segments and the dissipation of elastically stored energy and the redistribution of stresses over the system thereby, thus leading to sequential failure at local high stress concentrations and to brittle failure of the total system. This mechanism is widely accepted as relevant on the macroscopic scale.

The ring-in-the-chain amorphous polymers which are tough have chain structures without protuberances. It is interesting to note that if large side groups are introduced

into these structures, then they become brittle also as was exemplified by Rose²³ for a series of aromatic sulphone polymers (Table 6). He also found that with the poly-(phenylene ethersulphone) series of polymers the all *para*-linked polymer was tough but the *ortho*-*para* and the *meta*-*para* structures resulted in polymers which were brittle (Table 6). This is not inconsistent with the reasoning suggested, in that the *ortho* and *meta* linkages result in abrupt 'kinks' in the chains which could be envisaged as causing neighbouring chains to interlock.

This approach to the understanding of 'toughness' is clearly much over-simplified but it does suggest that a systematic study of the failure behaviour of glassy amorphous polymers of widely different structures could be rewarding.

Modulus and structure

There is no satisfactory quantitative correlation between parameters dependent on molecular structure and elastic modulus, although in qualitative terms it is clear that modulus must be dependent on the energy of interaction between molecules and hence on parameters such as internal energy and coefficient of thermal expansion. Recognition of this has prompted a number of basic simple approaches to the problem.

Combining a standard thermodynamic approach to the derivation of an equation of state of a simple molecular crystal with the Lennard-Jones model for the dependence of the energy of interaction between molecules on their distance of separation, gives for the bulk modulus (B) of a face-centred cubic lattice at 0K²⁴:

$$B^0 = 8.04 \left(\frac{E_{\text{vap}}^0}{V^0} \right) \text{ dyne/cm}^2 \quad (1)$$

where E_{vap}^0 is the molar energy of vaporization at 0K (erg/mol) and V^0 is the molar volume (cm^3/mol).

This equation holds well for neon, argon and nitrogen at cryogenic temperatures.

Tobolsky²⁴ suggested that equation (1) would be a fair approximation at higher temperatures, and might even be relevant to amorphous polymers in the glassy state. The term (E_{vap}/V) is the cohesive energy density (CED), and this is 83 cal/ cm^3 at 25°C for polystyrene. With CED expressed in cal/ cm^3 equation (1) becomes:

$$B = 3.37 (CED) \times 10^8 \text{ dyne/cm}^2 \quad (2)$$

which gives a modulus value for polystyrene of 2.8×10^{10} dyne/ cm^2 . The experimental value is 3.5×10^{10} dyne/ cm^2 , and at first sight this seems to be a very promising measure of agreement.

A test of the general applicability (and utility) of equation (1) is to plot modulus vs. CED for a number of polymers. Nielsen²⁵ collected such data but noted that there was no correlation. His data are plotted in Figure 18.

Lack of interest in this approach is therefore understandable. However a broader consideration of the structural parameters which will determine modulus, combined with a similar approach to the glass transition temperature, enables one to demonstrate by an empirical procedure that there does indeed seem to be a relationship between modulus and cohesive energy density.

Consider the simplest case of a linear, amorphous polymer of very high molecular weight (so that chain ends can be ignored) in the glassy state at temperature $T < T_g$. The indi-

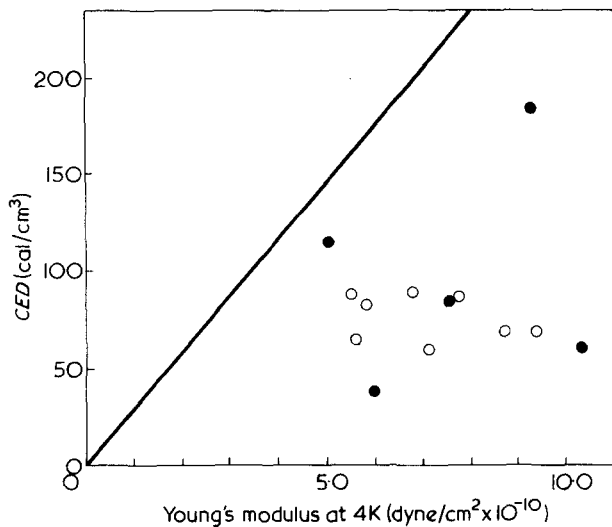


Figure 18 Cryogenic Young's modulus and cohesive energy density for various polymers. \circ , Amorphous polymers; \bullet , crystalline polymers. —, $E = 3.37 (CED) \times 10^8$

vidual macromolecules will take up completely random configurations, such as they assume in infinitely dilute solution²². The force per unit area needed to produce uniaxial deformation at vanishingly small strain (i.e. the Young's modulus, E at zero strain) will in the ultimate be determined by three parameters:

- (1) A molecular flexibility parameter, $F(T, t)$, which is a function of temperature, T , and of the time scale of the experiment, t ;
- (2) a parameter which is a measure of interchain forces, assumed to be of the form of equation (2);
- (3) a parameter which is a measure of bond angle distortion, assumed to be negligible at temperatures significantly $>0K$.

The glass transition temperature is clearly determined by two of the same parameters, namely molecular flexibility and interchain forces. At the glass transition temperature the Young's modulus of amorphous plastics drops from $>1.0 \text{ GN/m}^2$ to $\sim 0.01 \text{ GN/m}^2$, the lower limit being set by the value for an ideal rubber—

$$E \sim 3\rho RT/M_c \quad (3)$$

which typically will be around 0.001 GN/m^2 . So for amorphous linear polymers at their glass transition temperatures $E \sim 0.01 \text{ GN/m}^2$.

What this means is that, in a sense, T_g is a 'normalized' temperature and it suggests an approach to identifying the individual parameters which determine the modulus. Assume as an approximation that at temperatures just below T_g the parameter F (molecular flexibility) has the same dependence on temperature for all polymers, and hence that in this temperature region differences in modulus are determined by interchain forces (the contribution from the flexibility parameter F being constant). Pursuing this hypothesis, Figure 19 shows a plot of E'_{50} versus δ_{50}^2 from data currently available on amorphous polymers, where: E'_{50} is the dynamic modulus in GN/m^2 at $\sim 300 \text{ Hz}$ measured at the temperature T_{50} ; T_{50} is the temperature 50°C below the T_g ; δ_{50}^2 is the cohesive energy density at T_{50} .

The key to the data plotted is:

- PAN polyacrylonitrile,
PEX polyethylene (amorphous, crosslinked, see ref 7),

- NR natural rubber,
PVAc poly(vinyl acetate),
PET poly(ethylene terephthalate) (amorphous),
PVC poly(vinyl chloride),
PC polycarbonate (of Bisphenol A),
PS polystyrene,
PMMA poly(methyl methacrylate),
PES poly(phenylene ethersulphone),
PSA polysulphone (of Bisphenol A),
PPO poly(dimethylphenylene oxide).

The E'_{50} values were taken from dynamic mechanical data measured in these laboratories between the years 1955 and 1965 except for the value for polysulphone (from Bisphenol A) which is a static modulus value and may therefore be slightly low relative to the other data. CED values were derived from solubility parameter values at 25°C calculated by the additive scheme proposed by Small²⁶ and collated by van Krevelen and Hoftyzer²⁷ who also give the specific heat data needed to make the derivations²⁸, except for values for the two aromatic sulphone polymers which were estimated by Small²⁹. T_g values were taken as generally quoted in the literature, except that T_g for (amorphous) polyethylene was taken as -120°C .

The line of slope 0.034 drawn in Figure 19 is simply the theoretical proportionality coefficient in equation (2), corrected for a change in units ($1 \text{ GN/m}^2 = 10^{10} \text{ dyne/cm}^2$) and assuming that the bulk modulus is (approximately) equal to the Young's modulus:

$$E \approx 0.034 (CED) \text{ GN/m}^2 \quad (4)$$

In contrast to Figure 18, it is apparent that the data plotted in Figure 19 do indicate a significant correlation between

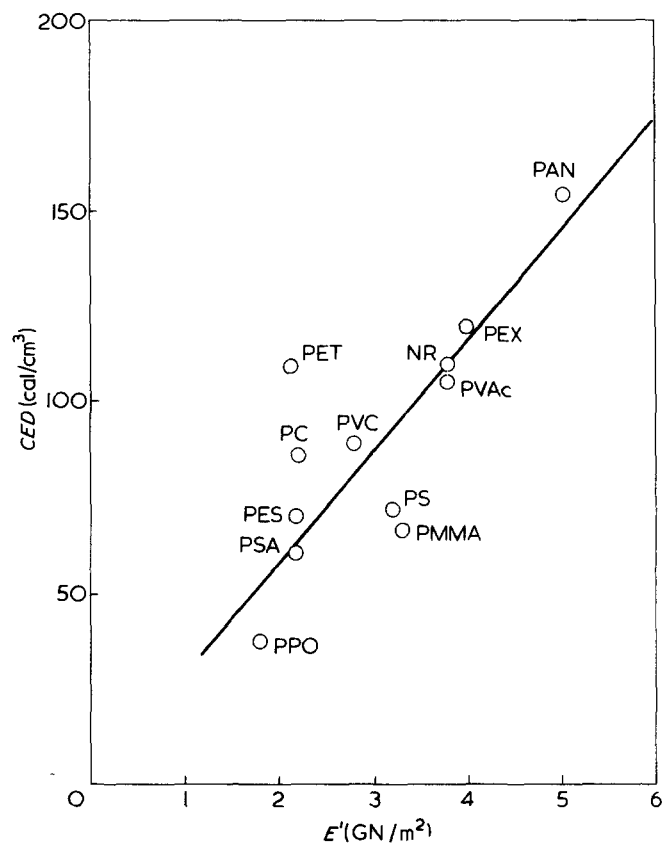


Figure 19 Relation between dynamic Young's modulus (E') and cohesive energy density (CED) for some amorphous polymers at $(T_g - 50)^\circ\text{C}$. $E'/CED = 0.034$

E'_{50} and CE_D which is not very different from equation (4). It is interesting to note that the T_{50} values range from -170° to $+175^\circ\text{C}$.

While some relationship between the relaxed Young's modulus and short-range intermolecular forces (of which CE_D is a measure) is to be expected, the excellence of the particular correlation observed is surprising and is further discussed elsewhere³⁰. In the meantime it is clear that further work to explore the scope of these observations is called for, and it would be particularly interesting to obtain modulus data for the amorphous states of those polymers which are normally crystalline.

ACKNOWLEDGEMENTS

The author is indebted to his colleagues in the Research Department of the Plastics Division of ICI for helpful discussions and assistance in preparing this paper, and in particular to Mr I. T. Barrie, Dr D. J. Blundell, Dr J. D. Burnett, Dr A. D. Caunt, Mr P. R. Hendy, Mr A. Pajaczkowski, Dr J. E. Priddle, Dr J. B. Rose, Dr F. M. Willmouth and Dr D. G. M. Wood. The author would also like to thank Dr R. Longworth for permission to reproduce Figures from ref 4.

REFERENCES

- 1 Stein, R. S. and Prud'homme, R. *J. Polym. Sci. (Polym. Lett. Edn)* 1971, 9, 595
- 2 Caunt, A. D. and Rose, J. B. 'Kirk-Othmer Encyclopaedia of Chemical Technology, Supplement Volume', 2nd Edn Wiley, New York, 1971, pp 773-807
- 3 Griffith, J. H. and Ranby, B. G. *J. Polym. Sci.* 1960, 44, 369
- 4 Longworth, R. 'Ionic Polymers' (Ed L. Holliday), Applied Science, London, 1975, Ch 2, pp 69-172
- 5 Priddle, J. E., Pajaczkowski, A. and Vincent, P. I. Br. Pat. 1 406 703 (1975)
- 6 Boyer, R. F. *Plast. Polym.* 1973, 41, 15; *Macromolecules* 1973, 6, 288
- 7 Willbourn, A. H. *Trans. Faraday Soc.* 1958, 54, 717
- 8 Hendra, P. J. *J. Polym. Sci. (Polym. Lett. Edn)* 1975, 13, 365
- 9 Hendra, P. J. unpublished results
- 10 Adams, J. H. *J. Polym. Sci. (A-1)*, 1970, 8, 1077, 1269, 1279
- 11 Birley, A. W. and Brackman, D. S. *Proc. Conf. Degradability Polym. Plast. Plast. Inst.*, November 1973
- 12 Bailey, W. J. and Economy, J. *126th Meet. Am. Chem. Soc. Div. Polym. Chem. New York*, September 1954
- 13 Bailey, W. J., Economy, J. and Hermes, M. E. *J. Org. Chem.* 1962, 27, 3295
- 14 Okada, M. and Marvel, C. S. *Polym. Prepr.* 1967, 8, 229
- 15 Bailey, W. J. and Feinberg, B. D. *Polym. Prepr.* 1967, 8, 165
- 16 Bailey, W. J. and Volpe, A. A. *Polym. Prepr.* 1967, 8, 292
- 17 Ballard, D. G. H. 'Advances in Catalysis' (Eds D. D. Eley, H. Pines and P. B. Weisz), Academic Press, New York and London, 1973, pp 263-325
- 18 Hendy, B. N. 'Copolymers, Polyblends and Composites', *Advances in Chemistry Series*, No. 142, Am. Chem. Soc., Washington D.C., 1975, pp 115-128
- 19 Fordyce, R. G. and Chapin, E. C. *J. Am. Chem. Soc.* 1947, 69, 581
- 20 Tanaka, T., Chatani, Y. and Tadokoro, H. *J. Polym. Sci. (Polym. Phys. Edn)* 1974, 12, 515
- 21 Coiro, V. M., De Santis, P., Liquori, A. M. and Ripamonte, A. *Ric. Sci. (2A)* 1963, 3, 1043
- 22 Flory, P. J. *Chem. Eng. News*, 1974, 36
- 23 Rose, J. B. *Polymer* 1974, 15, 464
- 24 Tobolsky, A. V. 'Properties and Structure of Polymers', Wiley, New York and London, 1960
- 25 Nielsen, L. E. 'Mechanical Properties of Polymers and Composites', Marcel Dekker, New York, 1974, pp 205-207
- 26 Small, P. A. *J. Appl. Chem.* 1953, 3, 71
- 27 van Krevelen, D. W. and Hoftyzer, P. J. 'Properties of Polymers: Correlations with Chemical Structure', Elsevier, 1972, Ch 8, p 140
- 28 van Krevelen, D. W. and Hoftyzer, P. J. *ibid* Ch 5, p 69
- 29 Small, P. A. personal communication
- 30 Willbourn, A. H. in press

Some aspects of stereoregulation in the stereospecific polymerization of vinyl monomers*

Piero Pino and Ulrich W. Suter

Swiss Federal Institute of Technology, Department of Industrial and Engineering Chemistry, 8092 Zurich, Switzerland

(Received 19 July 1976)

Stereoregularity in vinyl polymers, although theoretically foreseen since 1929, became one of the main topics in polymer research after the discovery of the stereospecific polymerization of α -olefins in 1954. The theoretical and practical significance of a thorough knowledge of stereoregulation became immediately evident; however, in spite of extensive efforts made by different industrial and academic research groups, the mechanism of stereoregulation is far from being understood and the control of stereoregulation, particularly in Ziegler–Natta polymerization, is still carried out on a purely empirical basis. In this review, after a short survey of the methods used to determine polymer stereoregularity and a discussion of the information which can be obtained from examination of the microtacticity of the polymer chains, some of the factors which can influence the stereoregulation in radical, ionic and Ziegler–Natta polymerization will be considered. For the last type of polymerization, in which the nature of the catalyst seems to have an overwhelming importance, some analogies with the transition metal catalysed asymmetric reactions will be discussed. Finally, an attempt will be made to identify the main difficulties in further improving our knowledge of the control of stereoregulation.

INTRODUCTION

In 1929 Staudinger *et al.*¹ pointed out that in vinyl polymers, even in those of completely regular chemical structure of the macromolecular main chain, steric irregularities should be expected, since the tertiary carbon atoms were indeed asymmetric and could assume both possible absolute configurations.

Unfortunately, no methods were available at that time to control the configuration of the newly formed asymmetric carbon atoms during polymerization. The first attempts in this direction were made by Marvel *et al.*², who used optically active initiators in radical polymerization; the resulting polymers, however, were not optically active and were found to have similar properties to polymers prepared with the usual initiators. A paper by Huggins³, in which he attributed the different solution properties of polystyrenes produced at different temperatures to a different stereoregularity, did not induce polymer chemists to investigate possible stereospecific polymerization processes. Schildknecht and collaborators⁴, investigating the cationic polymerization of vinyl ethers with boron trifluoride in different solvents, found two different types of polymers, one of which showed some crystallinity. Unfortunately, the crystallinity was low and the authors apparently assumed that all polymer chains in the sample had a similar steric structure. Therefore, they did not look for a suitable method of separation of polymers in a crystalline and in an amorphous fraction. Since the crystallinity of the polymers was too small to establish the actual type of stereo-

regularity, and since the properties of the crystalline samples were not excitingly different from those of amorphous polymers, this research did not persuade polymer chemists to look for polymerization processes having a high degree of stereospecificity. Furthermore, the possibility that the properties of stereoregular polymers could be entirely different from those of the amorphous materials known at the time was not seriously considered.

A few years later, styrene was polymerized using 'Alfin' catalysts⁵. Although the 'Alfin' systems were shown to be highly stereospecific in the butadiene polymerization, yielding almost exclusively 1,4-*trans* polymers, the polystyrenes were not investigated in detail. It was only after the synthesis of isotactic polystyrene with Ziegler–Natta catalysts⁶, that the above polymers were again considered and it was shown that they were isotactic⁷.

The concept that a catalyst could produce both stereoregular and non-stereoregular chains was so far from the mind of polymer scientists that some α -olefin polymers obtained with heterogeneous catalysts containing chromium⁸ or cobalt⁹ in the early fifties, which showed a slight crystallinity, were treated as if each macromolecule contained some stereoregular sections able to crystallize and some stereoirregular non-crystallizable sections. Therefore, no systematic attempt was made to separate crystalline and amorphous components.

Only when Natta and his group⁶ obtained a partly crystalline polypropylene, using catalytic systems similar to that proposed by Ziegler for ethylene polymerization, the way of looking at partly crystalline vinyl polymers changed. In this case the first polymer obtained was clearly non-homogeneous, and a successful attempt was made to separate

* Presented at the Sixth Biennial Manchester Polymer Symposium, UMIST, Manchester, March 1976.

crystalline and amorphous polymers. In this way highly stereoregular polymers of propylene and other α -olefins were obtained⁶ which had completely different properties than both the non-fractionated and the amorphous material.

These results opened a broad field of research, including the synthesis and the properties of stereoregular vinyl polymers. The investigation of the crystalline structure and of the properties of these macromolecular materials have proceeded rapidly. The research on the origin of the stereospecificity in polymerization processes and on the stereoregulating factors, however, is proceeding much more slowly and still has a largely empirical character.

In our opinion there are two reasons that are mainly responsible for the persistent ignorance about stereoregulating factors in vinyl polymerization. First, the tools available for the separation of the raw materials in fractions having different stereoregularity and for the quantitative determination of the stereostructure of the fractions thus obtained are limited. For the separation, no large progress has been made since 1954⁶, when the boiling solvents extraction technique was first used for this purpose. This is still the most widely used method, even if many evident disadvantages and failures have been pointed out⁷⁵. For the determination of the stereostructure, proton and ¹³C n.m.r. have replaced some relative methods such as determination of the crystallinity by X-ray diffraction or intensity measurement of i.r. bands connected with crystallinity or stereoregularity¹⁰. Very interesting results have been obtained with high resolution proton n.m.r., but ¹³C n.m.r. promises to become even more useful, although there are at present still some disadvantages connected with the difficulty in relating signal intensity to concentration. In any case, experimental uncertainties do not allow in general the detection of less than ~2% steric irregularities in a polymer chain¹¹. Furthermore, the amount of information obtained is restricted by the limited length of the observable sequences, usually 2 or 3, exceptionally 4 or 5 monomeric units. The second reason for our lack of knowledge on the stereoregulating factors in vinyl polymerization lies in the nature of the process leading to highly stereoregular polymers. Most of these processes are in fact heterogeneous, and the most important ones in practice involve heterogeneous catalysts containing a very small number of catalytic centres, the nature of which cannot be suitably investigated by direct methods. Under these conditions the work carried out in most industrial laboratories has an empirical character and, even though it has been very successful in identifying catalytic systems with very high stereospecificity and, recently, exceptionally high reactivity, has not contributed remarkably to the basic knowledge on stereoregulation. In an academic environment, on the other hand, this type of research is not carried out easily, since it requires a rather advanced knowledge of polymer chemistry, n.m.r. spectroscopy and catalysis; a combination of specialties not readily achievable by graduate students during the relatively short period assigned for the preparation of a thesis.

In the following, we will try to summarize briefly the state of our knowledge on the stereoregulating factors in vinyl polymerization and to identify the main directions for future development for the research in this field. However, it must be emphasized that no attempt has been made to prepare a complete survey of the literature, which is very extensive indeed and even very important contributions may have been overlooked.

THERMODYNAMIC AND KINETIC ASPECTS OF STEREOREGULATION

The relative thermodynamic stability of isotactic and syndiotactic sequences in vinyl polymers has never been experimentally investigated. Some data have been obtained for 'oligomers'¹²⁻¹⁸ and are shown in *Table 1*. Racemic dyads (i.e. couples of monomeric units arranged in a syndiotactic way), denoted by (r), are thermodynamically slightly favoured over meso dyads, denoted by (m), in all cases investigated. The free energy differences involved are apparently so small, however, that under equilibrium conditions highly stereoregular polymers would never be formed. The formation of stereoregular chains must therefore be kinetically controlled and the stereoregularity is controlled by the difference in activation energy for the insertion of a monomeric unit in the growing chain yielding an isotactic or a syndiotactic dyad. In radical polymerization, for instance, the situation can be schematized as in *Figure 1*, if none of the preceding units in the chain has an effect on the reactivity of the chain end (i.e. in the case of a Bernoullian propagation process). The degree of stereoregularity of the polymer formed depends on the difference in the free energies of activation for the two processes leading to isotactic (II) or syndiotactic (III) diads, $\Delta\Delta G^\ddagger$ ($\Delta G_i^\ddagger - \Delta G_s^\ddagger$) (see *Figure 2*). Thus, to obtain a polymer at room temperature that contains more than 97% syndiotactic (or isotactic) dyads, i.e. whose stereoregular sequences have an average length of at least 33, $\Delta\Delta G^\ddagger$ must be larger than 2 kcal/mol.

This description of a single step in vinyl polymerization is analogous to that of a diastereoselective synthesis. Of course, for most polymerization reactions, e.g. ionic and especially Ziegler-Natta polymerization, the reaction path will be much more complicated than the one shown in *Figure 1*. However, the stereoregulation will always be connected with the difference in free energy of activation between the two non-reversible steps of the growth reaction leading to the isotactic or syndiotactic dyads. This step can, but does not need to be the rate determining step of the growth reaction.

Unfortunately, conventional kinetic measurements yield only the sum of the rates of formation of isotactic and syndiotactic dyads, and ΔG_i^\ddagger and ΔG_s^\ddagger cannot be determined separately. This situation is analogous to the one existing for instance in catalytic asymmetric synthesis. The information obtained there from the enantiomeric purity of the products is extracted, in the case of vinyl polymerization, from the microtacticity of the synthesized polymer chains. In fact, in the most simple case (e.g. radical polymerization) the ratio between the relative amounts of isotactic and syndiotactic dyads, (m)/(r), corresponds to the ratio between the rate constants of the reaction steps leading to the respective sequences, k_i/k_s . Then, the ratio (m)/(r) gives the difference in free energy of activation, $\Delta\Delta G^\ddagger$, as noted above, and the difference between the enthalpies of activation ($\Delta\Delta H^\ddagger = \Delta H_i^\ddagger - \Delta H_s^\ddagger$) and the difference between the entropies of activation ($\Delta\Delta S^\ddagger = \Delta S_i^\ddagger - \Delta S_s^\ddagger$) can be determined by plotting $\ln(k_i/k_s)$ measured at different temperatures versus $1/T$ ^{10,20}. As expected, in free radical polymerization, a linear relationship between $\Delta\Delta G^\ddagger$ and T has often been observed²¹.

STERIC ASPECTS OF STEREOREGULATION

Besides yielding information on the difference in activation

Table 1 Stereochemical equilibrium in model compounds of vinyl polymers

$$\text{CH}_3-\overset{\text{R}}{\underset{|}{\text{CH}}}-\text{CH}_2\text{)}_x\text{H}$$

R	T (°C)	Solvent	Catalyst	Equilibrium composition					Reference
				x = 2		x = 3			
				(m)	(m)	(mm)	(mr)	(rr)	
-CN	25	MeOH	NaOH	0.40	—	—	—	—	12
-COOMe	25	MeOH	MeONa	0.455	0.453	0.198	0.509	0.293	12
-COOEt	25	EtOH	EtONa	—	0.431	0.178	0.506	0.314	12
-COO(iso-Pr)	25	iso-PrOH	iso-PrONa	—	0.360	0.117	0.485	0.398	12
-COOH	180	H ₂ O	HCl	—	0.483	0.242	0.482	0.274	12
-COONH ₄	180	H ₂ O	NH ₄ OH	—	0.487	0.244	0.486	0.271	12
-COONa	180	H ₂ O	NaOH	—	0.449	0.197	0.504	0.299	12
-Phenyl	25	DMSO	t-BuOK	0.486	—	—	—	—	13
	70	DMSO	t-BuOK	—	0.467	0.217	0.499	0.284	14
-Cl	25	CS ₂	AlCl ₃	0.29	—	—	—	—	15
	70	DMSO	LiCl	0.364	0.342	0.111	0.462	0.427	16, 17

R	T (°C)	Solvent	Catalyst	Equilibrium composition					Reference
				x = 4		x = 5			
				(m)	(m)	(mm)	(mr)	(rr)	
-CH ₃	-75	Pentene	ClSO ₃ H	0.459	—	—	—	—	18
	270	Octane	Pd/C	0.485	0.487	0.237	0.500	0.263	18

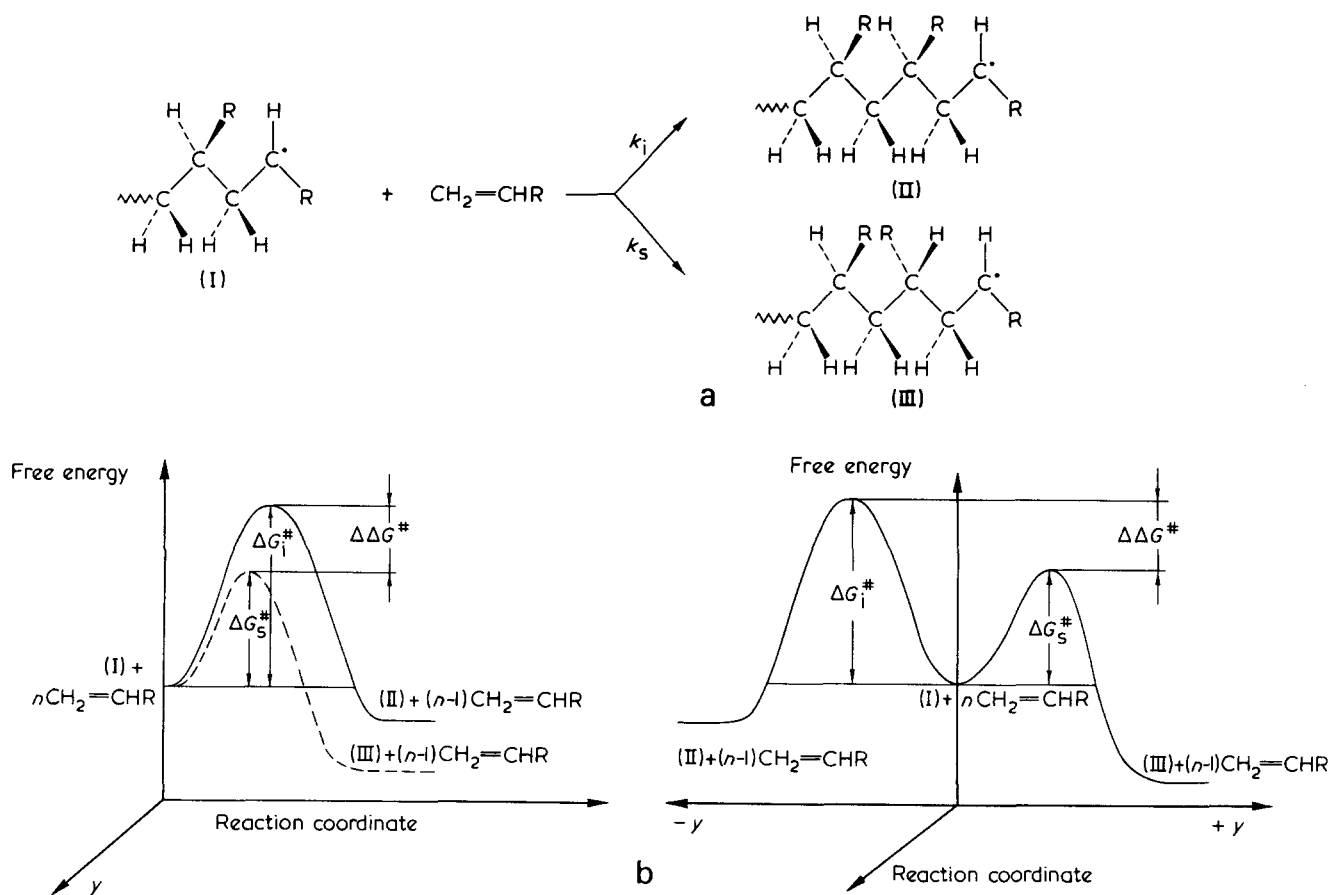


Figure 1 Possible reaction paths for the addition of a vinyl monomer unit to a growing chain by a radical mechanism

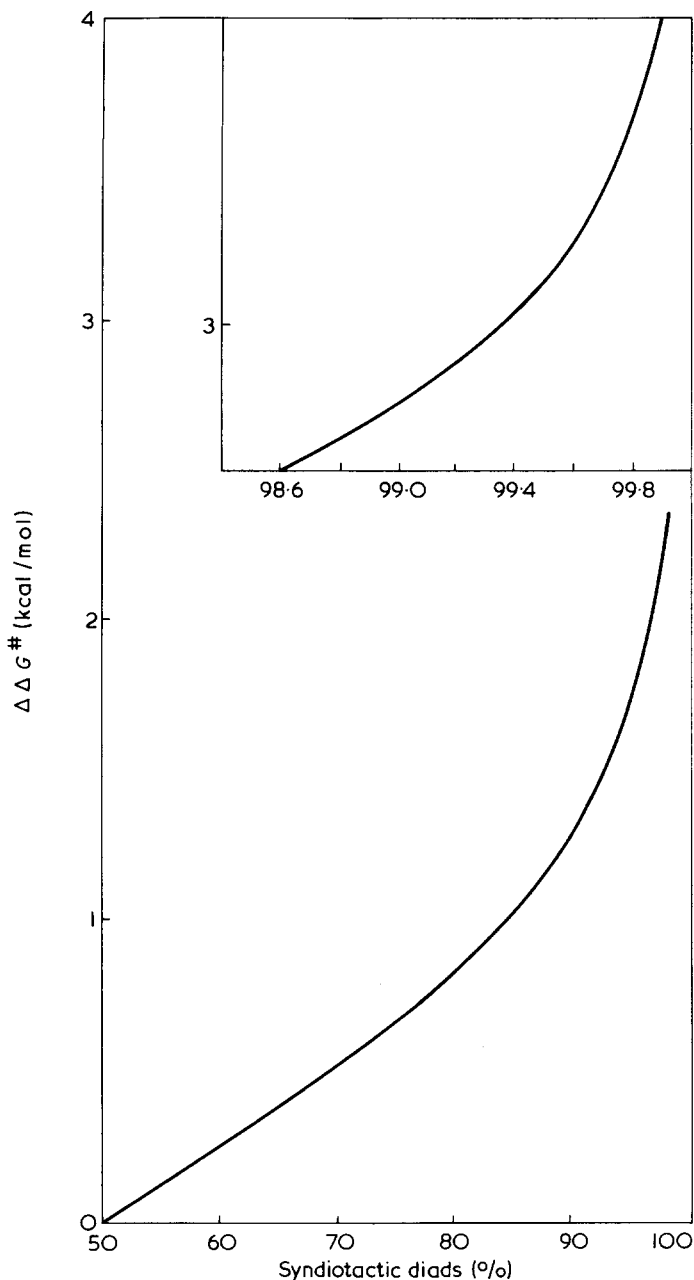
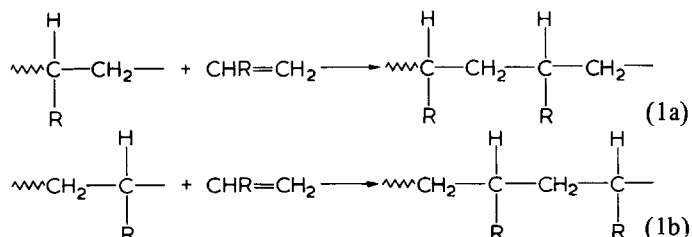


Figure 2 Difference in the free energies of activation (at 25°C) for the formation of isotactic and syndiotactic dyads in a Bernoullian propagation process, required to obtain a given degree of stereoregularity

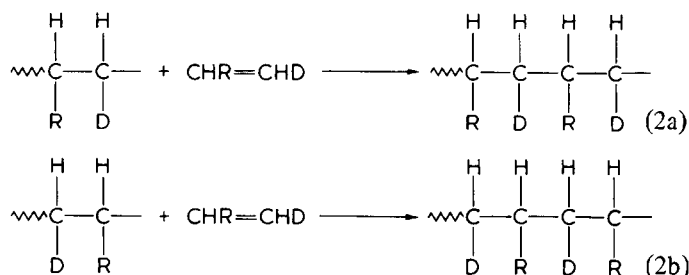
parameters for the formation of isotactic dyads, n.m.r. experiments can also give interesting insight into the steric course of the growth reaction. Depending on the polymerization mechanism, the growth of, for instance, an isotactic chain in vinyl polymerization can occur according to the two paths depicted in scheme (1). In the first case (1a),



which has been verified in the Ziegler–Natta polymerization to isotactic chains, the configuration of the asymmetric carbon atom of the new monomeric unit that forms in each polymerization step is decided at the very moment of the addition. Therefore, it is possible to speculate about steric interactions between the R group of the entering monomer and the growing chain. Nothing can be said on this basis about the type of opening (*cis* or *trans*) of the monomeric double bond or about the side of the growing chain, approached by the entering monomer the growing chain terminal group being a CH₂ group.

In the second case (1b), which occurs for instance in radical polymerization, the configuration of the asymmetric carbon atom of the ultimate monomeric unit of the chain is defined when the new monomer joins the growing chain. In this case, information on the side of the ultimate carbon atom (assumed as planar) of the growing chain which is attacked by the newly arriving monomer can be obtained, but nothing can be said about which prochiral face of the monomer is attacked or about the type of the double bond opening.

More information can be obtained if deuterated monomers with known stereochemistry are used. In scheme (2)



formation of a diisotactic dyad is shown. In both cases of addition, labelled (a) and (b) in analogy to scheme (1) steric information concerning both the side of the growing chain which is approached by the monomer and the prochiral face of the monomer preferentially attacked can be obtained from a knowledge of the microtacticity of the polymer. Furthermore, the type of double bond opening can be established if the growth reaction occurs simultaneously at the two unsaturated carbon atoms of the entering monomer. Unfortunately, most of the research up to now has involved non-deuterated vinyl monomers, but some cases of radical, cationic, anionic and Ziegler–Natta polymerization using deuterated monomers have been described and have yielded very important indications on stereoregulation^{22–33}.

STEREOREGULATION IN FREE RADICAL POLYMERIZATION

Free radical polymerization occurs substantially as shown in equation (1b). We can think of the terminal group with the unpaired electron as being substantially planar or a rapidly inverting trigonal pyramid. Then the stereoregulating effect is connected with the prochiral side of the terminal trisubstituted carbon atom to which the new monomer is joined. The stereoregulating effect must originate from the steric interaction of the entering monomer with the R group of the penultimate unit of the chain. Interaction of the CHR group of the entering monomer with the growing chain apparently does not contribute to the stereoregulating effects, since experiments with monomers having a CHD

Table 2 Stereoregularity in radical polymers of monosubstituted ethylenes

Monomers	Initiator ^a	T (°C)	Solvent	Dyads (m)	Triads			4(mm)(rr)	Reference
					(mm)	(mr)	(rr)	(mr) ²	
Styrene	BPO	80	Toluene	0.29	—	—	—	—	35, 36
	—*	—*	—*	0.3	—	—	—	—	37
β,β - <i>d</i> ₂ -Styrene	AIBN	100	Bulk	(0.26)	0.06	0.40	0.55	0.83	22
<i>d</i> ₇ -Styrene	AIBN	18	Bulk	~0.8	—	—	—	—	24
Vinyl chloride	AIBN	25	Bulk	0.435	0.21	0.45	0.34	1.41	38
	—*	—*	—*	0.43	0.186	0.489	0.325	1.01	39
α - <i>d</i> ₁ -Vinyl chloride	AIBN	50	Butyraldehyde	0.33	—	—	—	—	40
	AIBN	0	Cyclohexanone	0.43	—	—	—	—	25
	AIBN	100	Cyclohexanone	0.46	—	—	—	—	25
β,β - <i>d</i> ₂ -Vinyl chloride	CPO	40	Bulk	(0.434)	0.191	0.487	0.322	1.04	26
(<i>E</i>)- α,β - <i>d</i> ₂ -Vinyl chloride	BPO	70	CCl ₄	0.45	—	—	—	—	27
Vinyl formate	AIBN	30	Bulk	(0.50)	0.30	0.40	0.30	2.25	41
	AIBN	30	Acetaldehyde	(0.50)	0.30	0.40	0.30	2.25	41
	AIBN	40	Bulk	(0.52)	0.301	0.444	0.255	1.56	42
	AIBN	40	Acetone	(0.53)	0.333	0.393	0.274	2.36	42
Vinyl acetate	AIBN/h ν	30	Bulk	0.42	0.29	0.39	0.32	2.44	43
	AIBN	90	Amyl acetate	0.42	—	—	—	—	43
	—*	—*	Bulk	0.46	0.207	0.498	0.296	0.99	44
Menthyl vinyl ketone	AIBN	40	Bulk	0.44	—	—	—	—	45
Ethyl vinyl ketone	AIBN	50	Bulk	0.47	—	—	—	—	45
Phenyl vinyl ketone	AIBN	50	Bulk	0.47	—	—	—	—	45
[(<i>S</i>)-1-methyl propyl]-vinyl ketone	AIBN	50	Bulk	0.48	—	—	—	—	45
[(<i>S</i>)-2-methyl butyl]-vinyl ketone	AIBN	50	Bulk	0.43	—	—	—	—	45
4-Vinylpyridine	AIBN	60	MeOH	(0.29)	0.06	0.45	0.49	0.58	46
2-Vinylpyridine	AIBN	60	MeOH	(0.20)	0.02	0.36	0.62	0.38	46
Acrylonitrile	B(Butyl) ₃ + O ₂	35	Bulk	0.5	—	—	—	—	47
	BPA	120	Bulk	0.5	—	—	—	—	47
α - <i>d</i> ₁ -Acrylonitrile	AIBN	50	DMSO	0.5	—	—	—	—	28
Methyl acrylate	BPO/h ν	0	Toluene	0.53	—	—	—	—	48
	γ -Rays	40	Bulk	0.53	—	—	—	—	48
iso-Propyl acrylate	—*	—*	—*	~0.3	—	—	—	—	49, 50

*Exact conditions are not known. †BPO, benzoyl peroxide; AIBN, azobisisobutyronitrile; CPO, cumylhydroperoxide; BPA, t-butylperacetate. Values in parentheses are calculated from triad data.

group show, that no preference for one of the prochiral faces of the entering monomer exists³⁴.

The stereoregulating effect of the CHR group of the penultimate unit (or CRR' in 1,1-disubstituted ethylenes) could be due to a conformational effect along the growing chain, causing a preferential orientation of the terminal CHR (or CRR') group with respect to the chain already formed, and hence to a preferential orientation of the CH₂ group of the newly incoming monomer toward one or the other side of the terminal CHR (or CRR') group (compare Figure 1a).

The extent of this type of regulation is very small, as expected. Experimental data, some of which are collected in Tables 2 and 3, show that a slight prevalence of syndiotactic dyads exists in most cases, especially in polymers of 1,1-disubstituted ethylenes. The polymers obtained from monosubstituted ethylenes can be divided roughly into two groups: those with aromatic substituents (phenyl or pyridyl groups) that are quite syndiotactic, (m) = 0.2 to 0.3, and all other ones, which are very nearly atactic. Poly(iso-propyl acrylate) seems to be an exception to this rule. No similar simple rule is obvious for the polymers from 1,1-disubstituted ethylenes.

In most cases where the content of dyads and triads could be determined experimentally, the polymerization

appears to follow Bernoullian statistics. This is a confirmation of the statement that the type of dyads already existing in the growing chain does not influence the stereochemistry of the addition of the new monomer unit, but that only the configuration of the ultimate tertiary (or quaternary) carbon atom in the chain has an influence. The only polymers that according to the value of the ratio $4(mm)(rr)/(mr)^2$ are non-Bernoullian¹⁰ have extremely large side groups, i.e. the polymers from diphenylmethyl methacrylate and triphenylmethyl methacrylate⁵⁶, and perhaps (2,4,6-triphenylbenzyl) methacrylate⁵⁷ in Table 3. Poly(triphenylmethyl methacrylate) is also the only one that is distinctly isotactic.

The quantity $4(mm)(rr)/(mr)^2$ is a test for Bernoullian statistics with triad data only¹⁰. It is listed in Tables 2 and 3 whenever triad data were available. As Bovey has pointed out⁶³, this criterion is extremely sensitive and can deviate substantially from the Bernoullian value of 1, if the triad data used are not very accurate. In general, a value of $4(mm)(rr)/(mr)^2$ between ~2 and ~½ seems not to contradict the assumption of Bernoullian statistics.

Attempts to improve stereoregulation by polymerization in different solvents were made, but very poor results were obtained. In the polymerization of methyl methacrylate in bulk and 13 different solvents at 70°C, for instance, the

Table 3 Stereoregularity in radical polymers of 1,1-disubstituted ethylenes

Monomer	Initiator†	T (°C)	Solvent	Dyads † (m)	Triads			4(mm)(rr)	Reference
					(mm)	(mr)	(rr)	(mr) ²	
α -Methylstyrene	AIBN/6000 atm	100	Bulk	(0.26)	0.06	0.40	0.55	0.83	22
Methyl methacrylate	—*	—*	—*	0.26	0.04	0.36	0.60	0.74	51
	—*	—*	—*	(0.15)	0.03	0.24	0.73	1.52	52
	None‡	60	Toluene	0.30	0.08	0.33	0.59	1.73	53
	BPO	50	Bulk	(0.24)	0.085	0.315	0.600	2.05	54
Benzyl methacrylate	BPO	60	Bulk	(0.26)	0.07	0.37	0.56	1.15	55
Diphenylmethyl methacrylate	AIBN	60	Toluene	(0.23)	0.02	0.41	0.57	0.27	56
Triphenylmethyl methacrylate	AIBN	60	Toluene	(0.75)	0.64	0.22	0.14	7.40	56
(2,4,6-Triphenyl benzyl) methacrylate	AIBN	80	Toluene	0.32	0.16	0.33	0.51	3.00	57
iso-Propenyl acetate	BPO	60	Bulk	(0.44)	0.20	0.47	0.33	1.20	58
Methacrylonitrile	AIBN	60	Bulk	0.46	0.19	0.47	0.33	1.14	59
	AIBN	80	Bulk	(0.45)	0.20	0.50	0.30	0.96	60
Methyl- α -chloroacrylate	BPO	60	Toluene	(0.26)	0.08	0.35	0.57	1.49	61
	BPO	70	Bulk	0.30	0.12	0.35	0.53	2.08	62
Ethyl- α -chloroacrylate	BPO	70	Bulk	0.19	0.05	0.29	0.66	1.57	62
iso-Propyl- α -chloroacrylate	BPO	60	Bulk	0.37	0.14	0.44	0.42	1.21	62

*Exact conditions are not known. †AIBN, azobisisobutyronitrile; BPO, benzoylperoxide. ‡Thermally initiated. Values in parentheses are calculated from triad data

meso dyad content (m) varied between 0.257 and 0.319⁶⁴. Having in mind the mechanism outlined above, it is clear that strong changes can only be expected between solvents that include drastically different chain (or chain end) conformations.

A decrease in temperature generally increases the relative number of syndiotactic dyads. The case of methyl methacrylate, where (r) increases from 0.64 at 250°C to 0.87 at -78°C, has been particularly well investigated^{54,65,66}. Similar observations have been made for many other monosubstituted and 1,1-disubstituted ethylene compounds. Accurate analysis of the experimental data still leaves questions open¹⁰. However, in general a small difference in activation entropy seems to favour syndiotactic placements. The difference in activation enthalpy also seems to work in favour of the syndiotactic dyads, in many cases of monosubstituted ethylenes, however, this factor seems to be very small^{10,67}.

The stereoregulating factors in free radical polymerization are thus relatively well known. The possibility of good stereocontrol seems at the present time to be really scarce, considering the points mentioned above. The only real success has been obtained on a different route, by ordering the monomer molecules prior to the polymerization using inclusion complexes^{19,68} and then initiating the polymerization by X-rays; however, this method has not found practical application up to now. Template polymerization of the type found in methyl methacrylate⁶⁹, does not seem to be very promising at the present time, although it offers very interesting possibilities, in principle.

STEREOREGULATION IN IONIC POLYMERIZATION

Polymers with marked stereoregularity have been produced both with cationic and anionic initiators from monosubstituted and 1,1-disubstituted ethylenes. Although this stereoregulation was often achieved under homogeneous conditions, the best results were obtained where either the catalyst or the polymer or both were insoluble in the reac-

tion medium. From literature data, however, it is not always clear if the system under consideration is homogeneous or heterogeneous, and we will list the data in common Tables regardless of the physical state of the components in the reaction mixture, although the existence of only one or two phases can be significant for stereoregulation. Results on polymers obtained from the most investigated monomers are listed in Tables 4 to 10. Tables 4 to 7 concern monosubstituted ethylenes, the others show results for 1,1-disubstituted ethylenes.

Table 4 summarizes some results on styrene. Here, in the non-stereoregular polymers, investigation of the microtacticity is hindered by the high band width of the n.m.r. peaks¹⁰. Only in very recent publications it was claimed that a detailed analysis of the microtacticity was performed, using ¹³C n.m.r.^{35,36}. Cationic systems in toluene seem to yield polymers with low crystallinity and meso dyad contents similar to the value measured in free radical polymers^{23,36}. On the other hand it appears that with anionic initiators isotactic polymers can be produced under homogeneous conditions in apolar solvents, such as toluene^{70,71}. Even better results are obtained with heterogeneous systems containing anylsodium or Alfin catalysts^{7,71-73}. In polar solvents, such as ethers, however, no highly stereoregular materials were formed^{23,36,70}.

Vinyl ketones (Table 5) polymerize with anionic initiators in hydrocarbon solvents to isotactic macromolecules^{45,74}, some fractions having very high stereoregularities, (m) >0.95⁴⁵. Often, the highly isotactic fractions amount to more than 80% of the total material. While lithium aluminum hydride gives an inherently heterogeneous system, the polymerization with dialkyl zinc start homogeneously but a part of the polymer begins to precipitate already at low conversions⁴⁵.

Cationic polymerization of vinyl ethers is illustrated by the data shown in Table 6. In homogeneous systems, polymerization in hydrocarbon solvents yields predominantly isotactic chains, whereas almost atactic polymers are obtained in polar solvents such as methylene chloride⁷⁷⁻⁷⁹.

Table 4 Ionic polymerization of styrene

Catalyst	System	T (°C)	Solvent	Stereoregularity	Polymer insoluble in boiling heptane (%)	m.p. (°C)	Reference
C ₄ H ₉ Li	Homogeneous	-40	Toluene	Isotactic*	—	—	70
C ₄ H ₉ Li	Homogeneous	-78	Ethyl ether	Atactic*	—	—	70
C ₄ H ₉ Li	Homogeneous	30	THF	Atactic, (m) = 0.35	—	—	36
C ₅ H ₁₁ Na/NaCl 'Alfin't	Heterogeneous	-40	Hexane	Isotactic*	61	215–217	71
	Heterogeneous	-20	Hexane	Isotactic*	98	215	71
BF ₃	Homogeneous	-78	Toluene	Atactic [†]	—	—	23
BF ₃ ·OEt ₂	Homogeneous	-78	Toluene	Atactic, (m) = 40	—	—	36
Na	Heterogeneous	-20	THF	Predicted syndiotactic [‡]	—	—	23

*Stereoregularity from X-ray analysis. [†]Allylsodium/sodium-iso-propoxide (1:1)/NaCl. [‡] β,β -d₂-styrene as monomer, stereoregularity from n.m.r. measurements

Table 5 Anionic polymerization of vinyl ketones, R—COCH=CH₂. Solvent: toluene

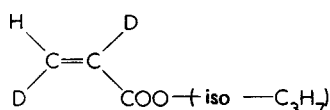
R	Catalytic system		T (°C)	Highly isotactic polymer*	Dyads (m)	Reference
—CH ₃	Zn(iso-C ₄ H ₉) ₂	Heterogeneous	-78	50	>0.95	45
—C ₂ H ₅	Zn(iso-C ₄ H ₉) ₂	Heterogeneous	-78	27	0.81	45
(S)—CH(CH ₃)C ₂ H ₅	LiAlH ₄	Heterogeneous	-78	94	0.96	45
(S)—CH ₂ —CH(CH ₃)C ₂ H ₅	Zn(iso-C ₄ H ₉) ₂	Homogeneous	-78	41	0.82	45
—Phenyl	Zn(C ₂ H ₅) ₂	Homogeneous	-25	23	0.85	74

* Insoluble in acetone

Table 6 Ionic polymerization of vinyl ethers and acrylates

Monomer	Catalytic system	T (°C)	Solvent	Fraction	Dyads (m)	Triads			Reference
						(mm)	(mr)	(rr)	
Methyl vinyl ether	BF ₃ ·OEt ₂ (Homogeneous)	-78	Toluene	n.f.	0.79	0.65	0.27	0.08	77
	BF ₃ ·OEt ₂ (Homogeneous)	-78	Toluene	n.f.	(0.71)	0.54	0.34	0.12	78
	BF ₃ ·OEt ₂ (Homogeneous)	0	CH ₂ Cl ₂	n.f.	0.64	0.45	0.40	0.15	77
	BF ₃ ·OEt ₂ (Homogeneous)	-78	CHCl ₃ /toluene	n.f.	(0.60)	0.41	0.37	0.22	78
	BF ₃ ·OEt ₂ (Heterogeneous)	-78	Toluene/hexane	n.f.	1	1	0	0	78
Ethyl vinyl ether	BF ₃ ·OEt ₂ (Homogeneous)	-78	Toluene	n.f.	0.75	0.56	0.36	0.08	77
	BF ₃ ·OEt ₂ (Homogeneous)	0	CH ₂ Cl ₂	n.f.	0.65	0.38	0.50	0.12	77
t-Butyl vinyl ether	BF ₃ ·OEt ₂ (Homogeneous)	-78	Toluene	n.f.	0.82	0.70	0.24	0.06	77
	BF ₃ ·OEt ₂ (Homogeneous)	-78	Toluene	n.f.	(0.69)	0.497	0.388	0.155	79
	BF ₃ ·OEt ₂ (Homogeneous)	-78	CH ₂ Cl ₂	n.f.	0.45	0.16	0.58	0.26	77
	BF ₃ ·OEt ₂ (Homogeneous)	-78	CH ₂ Cl ₂	n.f.	0.44	0.186	0.500	0.314	79
α,β -d ₂ -Methyl acrylate	LiAlH ₄	-78	Toluene	n.f.	~0.9	—	—	—	34
(E)- α,β -d ₂ -iso-Propyl acrylate	Phenyl MgBr/Et ₂ O (1:2)	-78	Toluene	pet.ether insol.*	1.00	—	—	—	29
	Phenyl MgBr	-78	Toluene	pet.ether insol.	0.95	—	—	—	29
	Fluorenyl Li/THF (~1:2)	-78	Toluene	pet.ether insol.	0.86	—	—	—	29
β -d ₁ -iso-Propyl acrylate	Phenyl MgBr/Et ₂ O (1:2)	-78	Toluene	n.f.	~1	—	—	—	30

*This polymer is completely insoluble in petroleum ether. Values in parentheses are calculated from triad data. n.f. = not fractionated

Table 7 Anionic polymerization of (*Z*)- α,β -*d*₂-iso-propylacrylate²⁹

 In toluene at -78°C , petroleum ether insoluble fractions

Initiator	Ratio initiator ether	(m)	
		COOR D C — C — C D H D	COOR C D
Phenyl MgBr/Et ₂ O	1:0.05	0.95	0.28
	1:0.5	0.79	0.51
	1:2	~1.00	0.50
	1:9	0.73	0.64
Fluorenyl Li/THF	1:2.5	0.86	0.39
	1:16	0.83	0.20
	1:32	0.82	0.09

* Fraction of dyads that are meso and have the deuterium on the methylene group in *threo* position

Temperature does not seem to change these results drastically. In both cases mentioned, it would not seem unreasonable to assume Bernoullian statistics⁷⁷.

Isotactic polymers can be obtained with heterogeneous systems, e.g. with boron trifluoride etherate in toluene/saturated hydrocarbon mixtures^{4,78} or with a catalyst obtained from aluminium oxide and sulphuric acid using aluminium alkyls as activators^{80,81,102}. The latter system, in addition to being stereospecific, is also stereoselective⁸⁰ and stereoelective⁸¹.

A few results for polyacrylates are also listed in Table 6. These monomers polymerize anionically to isotactic chains in pure hydrocarbon solvents^{29,30,34}. In oxygenated solvents, predominantly syndiotactic chains are obtained²⁹. Table 7 shows the results of a particularly detailed study of the stereochemistry of anionic acrylate polymerization with (*Z*)- α,β -*d*₂-iso-propyl acrylate. It shows that the portion of meso dyads decreases somewhat with added ether, but that the stereochemistry of the methylene group is much more sensitive to this factor. With a Grignard initiator in virtually ether-free hydrocarbon solvent the *erythro* configuration is preferred at CHD in meso dyads, and this preference changes to the one for the *threo* placement as ether is added. With aryl lithium as initiator and otherwise unchanged conditions the preferential stereochemistry at the methylene group (in meso dyads) is reversed.

For the 1,1-disubstituted ethylenes we begin the tabulation of selected experimental values (Table 8) with poly(α -methylstyrene) and some polymers obtained from *para*-substituted α -methylstyrenes. Polymers obtained with cationic initiators in polar or aromatic media, such as methylene chloride or toluene, are strongly syndiotactic^{22,82,85}. In saturated hydrocarbons, syndiotactic chains of somewhat lower stereoregularity are obtained^{62,84}. The presence of a substituent in the *para* position and, in polar solvents, the type of initiator, have only little influence on the stereoregularity. Anionic initiators also lead to syndiotactic chains, but less so in polar solvents than in hydrocarbons^{22,83}.

Also reported in Table 8 are some values for α -chloroacrylates. The usual anionic initiators, e.g. alkyl lithium or Grignard reagents, yield nearly atactic polymers^{72,86}.

Breslow and Kutner⁸⁷ found in 1971 that the solid product of the 1,4-addition of a Grignard reagent to an α,β -unsaturated ketone such as benzalacetophenone converts methyl methacrylate and methyl- α -chloroacrylate quantitatively to higher isotactic polymers. Application to several α -chloroacrylates show an equal stereospecificity^{62,86}.

The most intensely investigated monomer in ionic polymerization is methyl methacrylate. Table 9 shows a selection of published data. With Grignard reagents in hydrocarbons highly isotactic chains are obtained. Addition of ethers lowers the isotacticity²⁹. With small amounts of ether, stereoblock structures are formed²⁹. Under most conditions, chains with different types of steric structure are formed, and the polymers must be fractionated before investigation⁸⁸. As in the case of α -chloroacrylates, the addition products of Grignard reagents to conjugated ketones give highly isotactic polymers in quantitative yield⁸⁷. With alkyl or aryl lithium as initiator, isotactic polymers are obtained in hydrocarbon solvents. Solvents with higher ability to solvate the lithium cation give polymers with lower isotacticity. In the presence of amines substantially syndiotactic chains have been obtained^{29,89-91}.

Triad data in Table 9 indicate clearly non-Bernoullian statistics in toluene [where $4(\text{mm})(\text{rr})/(\text{mr})^2 \approx 8$] and increasingly more Bernoullian behaviour as the solvation power increases [the quantity $4(\text{mm})(\text{rr})/(\text{mr})^2$ is 0.9 for ethylamine and 1.4 for ammonia as solvents]. Counterion size plays a clear role. In hydrocarbon solvents stereoregulation decreases with increasing size of the counterion ($\text{Li} < \text{Na} < \text{K}$), the decrease is smaller in pyridine and practically absent in amines^{89,91}. Finally, with lithium aluminium hydride as initiator, highly isotactic polymers are obtained in ethyl ether and toluene, while in tetrahydrofuran predominantly syndiotactic chains are produced⁵⁷.

With (*E*)- α -ethyl- β -*d*₁-methyl acrylate, Fowells, Schuerch, Bonvy, and Hood obtained information on the stereochemistry of the methylene group (Table 10)²⁹. They polymerized this monomer in the presence of various amounts of tetrahydrofuran in toluene, using alkyl or aryl lithium as initiator. In the absence of tetrahydrofuran the process was highly stereospecific, both for the quaternary chain carbon atoms and for the CHD groups, yielding *threo*-diisotactic chains. Addition of ~2 molecules of tetrahydrofuran per lithium atom resulted in virtually no change. By further addition of THF, stereoblock polymers are obtained at first (at least at the low temperature listed in Table 10) and finally, predominantly syndiotactic structures with random configuration of the methylene group are formed. With Grignard initiator systems one obtains a reversed stereochemistry, since *erythro*-meso placements predominate at low ether concentrations and *threo*-meso structures in the presence of larger ether concentration.

Finally, recent work on anionically polymerized methyl- α -ethyl acrylate shows an unusually strong dependence of stereoregularity on temperature for the butyllithium/toluene system⁹². In contrast to observations on methacrylates, here (m) changed from 0.51 at -78°C to 0.99 at 0°C . The authors suggested that the low temperature material is actually a mixture of isotactic and syndiotactic chains. Similar to alkyl methacrylates, syndiotactic polymers form in tetrahydrofuran and isotactic ones in ethyl ether.

The data of Tables 4 to 10 suggest some general lines that seem to be valid for stereoregulation in both, anionic and cationic polymerization. The ionic species can occur in several different forms in equilibrium with each other⁷⁶,

Table 8 Ionic polymerization of α -methylstyrenes and α -chloroacrylates

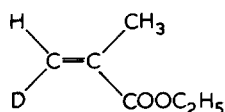
Monomer	Catalytic system	T (°C)	Solvent	Dyads (m)	Triads			Reference
					(mm)	(mr)	(rr)	
α -Methylstyrene	TiCl ₄	-78	CH ₂ Cl ₂	(0.05)	0.02	0.06	0.92	62
	Triphenylmethyl ZrCl ₅	-78	Methylcyclo- hexane + CH ₂ Cl ₂	(0.28)*	—*	—*	—*	82
	BF ₃	-78	Toluene	(0.06)	0	0.12	0.88	62
	BF ₃	-78	Toluene	(0.06)	0	0.11	0.89	22
	BF ₃	-78	Hexane	(0.27)	0.11	0.32	0.57	62
	Naphthyl Na	-78	THF	(0.35)	0.10	0.50	0.40	83
	Na	0	THF	(0.34)	0.11	0.45	0.44	22
	C ₄ H ₉ Li	4	Cyclohexane	(0.16)	0	0.31	0.69	22
p -Chloro- α -methylstyrene	TiCl ₄	-78	CH ₂ Cl ₂	(0.11)	0.04	0.13	0.83	62
	TiCl ₄	-78	Hexane	(0.34)	0.10	0.48	0.42	62,84
p -Methyl- α -methylstyrene	TiCl ₄	-78	CH ₂ Cl ₂	(0.03)	0	0.05	0.95	62
p -Trifluoromethyl- α - methylstyrene	TiCl ₄	-78	CH ₂ Cl ₂	(0.33)	0.10	0.45	0.45	62
p -iso-Propyl- α - methylstyrene	Triphenylmethyl- hexafluorophos- phate	-25	Cl(CH ₂) ₂ Cl	(0.43)	0.22	0.42	0.36	85
	C ₄ H ₉ Li — H ₂ N(CH ₂) ₄ NH ₂	-25	Cl(CH ₂) ₂ Cl	(0.25)	0.13	0.24	0.63	85
Methyl- α -chloroacrylate	Phenyl MgBr	-60	Toluene	(0.48)	0.30	0.36	0.34	86
	EtMgBr	30	Heptane	(0.41)	0.22	0.37	0.41	86
	EtMgBr—benzalaceto- phenone	30	Heptane	(0.91)	0.87	0.07	0.06	86,87
Ethyl- α -chloroacrylate	Phenyl MgBr	0	Heptane	(0.50)	0.34	0.33	0.33	86
	EtMgCl	30	Heptane	(0.40)	0.24	0.31	0.45	86
	EtMgCl—benzalaceto- phenone	30	Heptane	(0.91)	0.87	0.07	0.06	86

* Dyads are calculated from triad data, but these are not given in the original paper. Values in parentheses are calculated from triad data

Table 9 Ionic polymerization of methyl methacrylate

Catalytic system	Solvent	T (°C)	Fraction	Dyads [†] (m)	Triads			Reference
					(mm)	(mr)	(rr)	
Phenyl MgBr	Toluene	0	{ n.f. (100%) pet. ether insol. (90%)	(0.84)	0.58	0.26	0.16	88
Phenyl MgBr	Toluene	30		—*	(1)	1	0	0
EtMgBr—benzalaceto- phenone	Heptane	30	n.f.	(0.99)	0.99	0.01	0	90
				(1)	1	0	0	87
C ₄ H ₉ Li	Toluene	-70	pet. ether insol.	(0.77)	0.670	0.205	0.125	89
Fluorenyl Li/THF (1:1) [‡]	Toluene	-78	pet. ether insol.	(0.79)	0.70	0.19	0.11	29
C ₄ H ₉ Li	THF	-78	—*	(0.47)	0.31	0.32	0.37	90
C ₄ H ₉ Li	Pyridine	-60	pet. ether insol.	(0.24)	0.074	0.332	0.594	89
Fluorenyl Li	EtNH ₂	-60	—*	(0.16)	0.023	0.275	0.702	91
Fluorenyl Li	NH ₃	-68	—*	(0.14)	0.026	0.232	0.742	91
C ₄ H ₉ Li	Toluene	0	pet. ether insol.	(0.81)	0.720	0.173	0.107	89
C ₄ H ₉ Li	THF	0	—*	(0.25)	0.06	0.38	0.56	90
C ₄ H ₉ Li	Pyridine	0	pet. ether insol.	(0.24)	0.082	0.318	0.600	89
Fluorenyl Li	EtNH ₂	9	—*	(0.25)	0.073	0.347	0.580	91
C ₅ H ₁₁ Na	Toluene	0	pet. ether insol.	(0.72)	0.567	0.309	0.124	89
C ₅ H ₁₁ Na	Pyridine	0	pet. ether insol.	(0.35)	0.119	0.458	0.423	89
Fluorenyl Na	EtNH ₂	10	—*	(0.32)	0.146	0.300	0.554	91
C ₈ H ₁₇ K	Toluene	0	pet. ether insol.	(0.56)	0.346	0.421	0.233	89
C ₈ H ₁₇ K	Pyridine	0	pet. ether insol.	(0.40)	0.140	0.529	0.331	89
Fluorenyl K	EtNH ₂	10	—*	(0.30)	0.096	0.410	0.494	91
LiAlH ₄	Et ₂ O	-70	MeOH insol.	(1.00)	1.00	0	0	57
LiAlH ₄	THF	-70	MeOH insol.	(0.15)	0.07	0.16	0.77	57

* Fractionation is not described; [†] values are calculated from triad data; [‡] with (*E*)- β - δ -1-methyl methacrylate. n.f. = not fractionated

Table 10 Anionic polymerization of (Z)- α -ethyl- β - d_1 methyl acrylate²⁹Temperature -78°C , petroleum ether insoluble fractions

Catalytic system	Solvent	(m)				(mm)	(mr)	(rr)
			0.80	0.77	0.76			
$\text{C}_4\text{H}_9\text{Li}$	Toluene	0.96	0.80	0.77	0.76	0.91	0.08	0.01
Fluorenyl Li	Toluene	0.87	0.77	0.77	0.76	0.79	0.16	0.04
Fluorenyl Li/THF(1:2.5)	Toluene	0.91	0.76	0.76	0.76	0.85	0.12	0.03
Fluorenyl Li/THF(1:7.5)	Toluene	0.64	0.07	0.07	0.07	0.55	0.18	0.27
Fluorenyl Li	THF	0.15	0.07	0.07	0.07	0.05	0.21	0.74
Phenyl MgBr/Et ₂ O (1:9)	Toluene	0.96	0.92	0.92	0.92	0.94	0.04	0.02

* Fraction of dyads that are meso and have the deuterium in threo position

and each form has an individual behaviour for polymerization and stereoregulation⁹³⁻⁹⁵. Most polar solvents exhibit a specific solvent effect by solvating the cation or the ion pair, e.g. pyridine, ethers or amines; in this case either free ions or solvated ion pairs are formed. On the other hand, in apolar solvents, for instance in hydrocarbons, contact ion pairs occur predominantly. Additionally, different ion pairs might aggregate here to form unreactive species⁹⁶. Depending on the type of charged chain end (carbonium ion or carbanion) and on the state of solvation of the ions or ion pair, a different behaviour might be anticipated.

Under homogeneous conditions, in solvents with high 'solvating power' where solvent separated ion pairs or even solvated free ions exist^{93,97}, the polymers formed contain atactic or prevalingly syndiotactic structures, similar to those found in free radical polymerized chains. In the case of free ions we expect principally the same stereoregulating factors to exist as in the case of free radicals, except for differences in solvation of the chain ends. In the case of solvent separated ion pairs, which occur in the media of lower 'solvating power' and seem to predominate under usual polymerization conditions in polar solvents, a very small influence of the counterion seems to exist. If 2- d_1 -monosubstituted ethylenes are used, we expect the configuration of the CHD groups to be random, as was observed in the case of free radical polymers³⁴. Indeed, in the case of (Z)- α -ethyl- β - d_1 -methacrylate, polymerized with aryllithium in tetrahydrofuran, such a random stereostructure has been observed (see Table 10)²⁹.

In solvents having little 'solvating power', the polymers formed are in general isotactic. Here, the charged chain ends are involved predominantly in contact with ion pairs. These seem to be somewhat less reactive than the more separated species encountered above^{94,95}, but a stereoregulating influence of the counterion seems to exist during the polymerization process. Different models have been proposed to explain the occurrence of isotactic structures, and several factors are probably important. Many authors have made the assumption of a cyclic and/or chelated chain end. Many authors believe that poly(vinyl ethers), for instance, have a ring structure as suggested in Figure 3 the oxygenated chain acting as a specific solvating agent itself⁹⁹. For the anionic polymerization of methacrylic esters a propagating chain end structure like the one in Figure 4 was proposed^{29,98}; other authors however, regard such structures as unreactive^{100,101}. Also, for anionic metha-

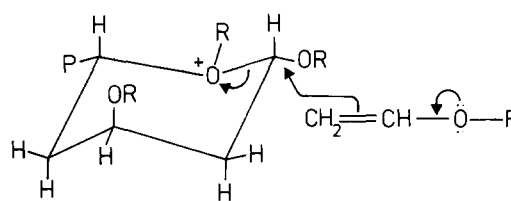


Figure 3 Cyclic transition state proposed for the polymerization of vinyl ethers to isotactic polymers in solvents having little 'solvating power'

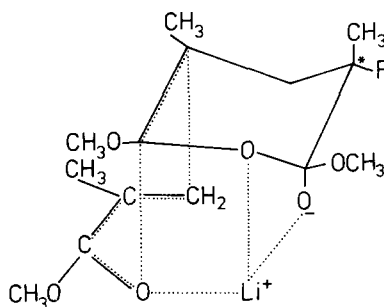


Figure 4 Cyclic transition state proposed for the polymerization of methyl methacrylate to isotactic polymers in solvents having little 'solvating power'

crylate polymerization a specific interaction between entering monomer and counterion has been postulated⁸⁹. None of these models seems to suit the case of styrene, however, with which one can still obtain isotactic structures under apparently homogeneous conditions (see Table 4).

Under the same conditions, for instance in the system styrene/perchloric acid in methylene chloride at room temperature and below, it seems that at least part of the growing chain end contains a covalent bond between 'chain end' and 'counterion'^{95,103-105}. This structure and the free ion model are the extrema in the concept of the growing species of ionic polymerization. They form the bridges to free radical polymerization and coordinative polymerization respectively.

If small amounts of good solvent are added to systems with low 'solvating power', stereoblock structures can appear, that are characterized by relatively high (mm) and

Table 11 Stereoregulating factors in ionic polymerization

Prevailing stereoregulating factor	Stereoregulating capacity		Prevailing stereoregularity	Examples				
	Mono-substituted ethylenes	Disubstituted ethylenes		Monomer	Initiator	Solvent	Temperature (°C)	Reference
Interaction between solvated growing chain end and monomer	Low	Medium	Syndiotactic	Styrene	LiC ₄ H ₉	THF	30	36
Interaction between non-solvated chain end and monomer	Medium	Medium	Isotactic	Methyl vinyl ether	BF ₃ ·O(C ₂ H ₅) ₂	Toluene/hexane	-78	78
Interaction between contact ion pair and monomer	High	High	Isotactic	Methyl methacrylate	LiC ₄ H ₉	Toluene	0	89
Interaction between asymmetric counterion and monomer	High		Isotactic	1-Methyl propyl vinyl	Al(O-iso-C ₃ H ₇) ₃ -H ₂ SO ₄ Al(iso-C ₄ H ₉) ₃ .THF	Ethyl acetate	25	80

(rr) triad contents as compared with (mr). Table 10 shows an example²⁹, with aryllithium/tetrahydrofuran (1:7.5) in toluene as initiator for (*Z*)- α -ethyl- β -*d*₁-methacrylate. There, (mm), (rr) > (mr) and 4(mm)(rr)/(mr)² is larger than 18. These facts have been explained by assuming two different, simultaneously active propagating species in equilibrium with each other, solvent separated ion pairs and 'peripherally solvated' contact ion pairs²⁹. The former are thought to propagate yielding predominantly syndiotactic chains, the latter generated isotactic structures. Here, as well as in all other cases where different propagating species are thought to compete, a strong temperature effect is observed, and assumed to originate in the changing equilibria between the ionic species. The above mentioned case of methyl- α -ethyl acrylate⁹² is a drastic example. In contrast to this, temperature effects are relatively small whenever one single species is responsible for polymer formation.

The experiments with acrylates and methacrylates, stereospecifically monodeuterated at the methylene carbon, show that the stereochemistry of propagation in solvents where contact ion pairs predominate, i.e. where isotactic structures are formed, is not the same for all systems. While the case of alkyl lithium or aryl lithium in toluene is relatively well understood²⁹, the mechanistic speculations are less well founded for Grignard reagents^{29,30,106} or lithium aluminum hydride^{34,107} as initiators.

The fact that the polymerization of vinyl ethers under certain (heterogeneous) conditions is stereoselective⁸⁰ seems to indicate that chiral catalytic centres, possibly formed by interaction of a chiral monomer with a counterion, can play an important role in stereoregulation in ionic polymerization. Since the stereoselectivity persists even in chains with relatively large numbers of steric irregularities (5–10%), a chiral counterion seems very probable. The fact that these initiators are also stereoselective⁸¹ suggests, that this chiral counterion contains one or more monomeric units.

From the large amount of the experimental data the picture schematized in Table 11 seems to emerge for the stereoregulating factors in ionic polymerization of mono- and disubstituted ethylenes. The interaction between solvated growing chain and monomer gives in general polymers having a low to medium stereoregularity degree of syndiotactic type. Stronger interactions between non-

solvated chain ends and monomers seem to lead to a prevalence of isotactic structure. However, a really large stereoregulating capacity seems to be connected with interactions between ionic couples and monomers and lead to prevalently isotactic structures. As a special case the stereoregulating capacity of ionic couples must be considered in which an asymmetric counterion exists which might be responsible of the stereoselectivity and stereoselectivity phenomena observed for instance in the racemic vinyl ethers cationic polymerization.

STEREOREGULATION IN TRANSITION METAL CATALYSED POLYMERIZATION

Catalytic systems or initiators containing transition metal compounds are known to polymerize olefins and other unsaturated monomers. These polymerizations are believed (and to a large extent proved) to occur through a monomer insertion on a metal-carbon bond. We shall not consider the polymerization of monomers containing polar groups carried out in the presence of the above catalysts or initiators as polar groups react very easily with organometallic catalysts. For this reason the nature of the catalytic species is in general not well understood and the existence and role of the metal to carbon bonds in the polymerization can be questioned.

The first indications concerning the possibility of polymerizing ethylene and α -olefins in the presence of transition metal catalysts appear in some patent applications between 1952 and 1954 in which these monomers are claimed to polymerize in the presence of chromium oxides supported on SiO₂/Al₂O₃ or nickel and cobalt supported on molybdenum oxides^{8,9,108}. Although the formation of solid polymers was reported in some cases, the structure of the polymers was not well understood and only some years later the possibility of obtaining stereoregular polymers with particular catalytic systems of this type was shown¹¹⁸. The real breakthrough in the field of α -olefins stereospecific polymerization came in 1954 when Natta and his group discovered the high stereoregulating capacity of some Ziegler catalysts obtained by reacting transition metal halides with an organometallic component⁶, the best organometallic com-

Table 12 Polymerization of propylene with different catalytic systems

Catalysts components	Type of prevailing stereoregularity	Polymer fraction considered	(m)	Reference
Soluble catalysts:				
Zr(C ₂ H ₅) ₄	Isotactic	Toluene insol. (64%)	0.81	109
Zr(CH ₂ -C ₆ H ₅) ₄	Isotactic	Heptane insol.	—	110
Ti(CH ₂ -C ₆ H ₅) ₄ /Al(CH ₂ -C ₆ H ₅) ₃	Atactic	—	—	110
VCl ₄ /Al(C ₂ H ₅) ₂ Cl/Anisole	Syndiotactic	—	<0.10	111,112
Insoluble catalysts:				
TiCl ₄ /Al(C ₂ H ₅) ₃	Isotactic	Heptane insol. (40%)	>0.97	113
TiCl ₄ /NaC ₈ H ₁₇	{ Isotactic Syndiotactic	Ether insol.	—	114
TiCl ₃ /Al(C ₂ H ₅) ₂ Cl	Isotactic	Heptane insol. (90%)	>0.97	115,116
Supported catalysts:				
CrO ₃ /Al ₂ O ₃ /SiO ₂	Isotactic	Benzene insol.	—	118
SiO ₂ /Zr(C ₂ H ₅) ₃ Br	Isotactic	Toluene insol. (45%)	0.84	109
TiCl ₄ /MgCl ₂ /Al(C ₂ H ₅) ₃	Isotactic	Heptane insol. (83%)	>0.97	117
C ₆ H ₅ COOC ₂ H ₅				

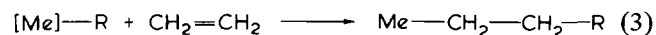
ponents being the ones (e.g. BeR₂, AlR₃, LiR) which polymerize ethylene also in the absence of transition metal components.

In the following years it was confirmed that supported and non-supported organometallic complexes of transition metals can act as active polymerization catalysts also in the absence of non-transition metal organometallic components. Today we can distinguish for the polymerization of olefins three classes of catalysts having a certain degree of stereoregulating capacity in the α -olefins polymerization: the first class consists of soluble catalysts which in general have a relatively low stereoregulating capacity and in the case of propylene can yield both isotactic and syndiotactic polymers. The second class consists of the typical Ziegler-Natta catalysts which are insoluble in the reaction medium and in which the catalytic centres are supported on the transition metal compounds used to prepare the catalyst or on other products arising from these compounds in general by alkylation and reduction. The third class consists of transition metal compounds supported on non-transition metal compounds such as SiO₂, Al₂O₃ or MgCl₂. In Table 12 some examples of catalysts active in propylene polymerization are given with the type and the maximum degree of stereoregulation which have been achieved in the most stereoregular fractions.

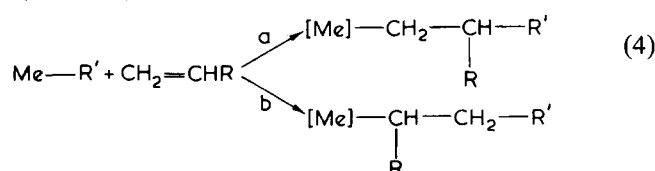
Most of the investigations on stereoregulation in α -olefins polymerization have been carried out on Ziegler-Natta catalytic systems and the knowledge thus arising has been very often unduly extended to other catalytic systems which do not appear to be deeply investigated up to now; this is particularly true for the supported catalysts. Therefore we shall limit our remarks to the Ziegler-Natta catalytic systems and after a brief survey of some facts concerning the polymerization mechanism we shall discuss separately the isotactic and the syndiotactic type of stereoregulation.

Nature of the growth reaction

The nature of terminal groups in ethylene polymerization demonstrates beyond any doubt that Ziegler-Natta polymerization occurs through an insertion of the monomer in a metal to carbon bond (scheme 3) similarly to the insertion of ethylene in a Li-C, Al-C or Be-C bond (growth reaction)¹¹⁹⁻¹²¹.



When propylene is used two possibilities exist for the insertion of a new monomer molecule into a Me-C bond (scheme 4):



As shown by the existence of crystallinity as well as by i.r. and n.m.r. spectra, stereoregular polymers of propylene possess a very high chemical regularity corresponding to a head-to-tail enchainment. This chemical structure is in principle possible with insertion of both types (schemes 4a and 4b), the important factor in obtaining the chemical regularity being only that the type of insertion remains constant during the formation of each chain.

In 1956 it was proved by i.r. investigation of the terminal groups that in the case of the most used Ziegler-Natta catalysts (TiCl₄-AlR₃ or TiCl₃-AlR₃) the fractions having the highest stereoregularity are formed according to an insertion of type (4a)¹²². This regioselectivity was shown to be smaller, but still very large, in the formation of the non-stereoregular polymers¹²².

These results have been unduly generalized and for about a decade the general belief has been that the insertion in transition metal catalysed polymerization always occurs according to scheme (4a). However, dimerization of propylene with Ziegler type catalysts prepared from nickel^{123,124} or palladium¹²⁵ compounds and aluminium dichloro monoalkyls has shown that both types of insertion are possible¹²³⁻¹²⁵, that catalytic systems exist where regioselectivity is very poor¹²⁴ and that regioselectivity can be regulated using appropriate ligands^{123,125}.

Furthermore, it has been shown that, using a VCl₄/Al(C₂H₅)₂Cl/Anisol catalytic system which yields syndiotactic polypropylene having a relatively high stereoregularity, insertion of α -olefins according to scheme (4a) or (4b) might be possible^{126,127}, although no proof has been given that a macromolecular chain can grow after an insertion of type (2b). Some n.m.r.^{129,130} and i.r.¹²⁸ evidence shows, however, that in the case of syndiotactic propylene polymerization a chain growth according to scheme (4b) is not unlikely.

No evidence has been provided up to now concerning

Table 13 Stereoregulation in polymerization of deuterated propylenes to isotactic polymers*

Monomer	(m)		Reference
		$\begin{array}{c} R & H & R \\ & & \\ C & -C & -C \\ & & \\ H/D & D & H/D \end{array} \quad \ddagger$	
$\begin{array}{c} CD_3 & & H \\ & \backslash & / \\ & C=C \\ & / & \backslash \\ D & & D \end{array}$ (E)-1,2,3,3,3-d ₅ -Propylene	>0.98	<0.02	11
$\begin{array}{c} CD_3 & & D \\ & \backslash & / \\ & C=C \\ & / & \backslash \\ D & & H \end{array}$ (Z)-1,2,3,3,3-d ₅ -Propylene	>0.98	>0.98	11
$\begin{array}{c} CD_3 & & D \\ & \backslash & / \\ & C=C \\ & / & \backslash \\ H & & H \end{array}$ (Z)-1,3,3,3-d ₄ -Propylene	>0.95	>0.95 erythro diisotactict	32
$\begin{array}{c} CD_3 & & H \\ & \backslash & / \\ & C=C \\ & / & \backslash \\ H & & D \end{array}$ (E)-1,3,3,3-d ₄ -Propylene	>0.95	<0.05 threo diisotactict	32
$\begin{array}{c} CH_3 & & H \\ & \backslash & / \\ & C=C \\ & / & \backslash \\ D & & H \end{array}$ 2-d ₁ -Propylene	>0.98	—	11

* Catalytic system: TiCl₃/Al(C₂H₅)₂I, in n-heptane at 0°C, n-heptane insoluble fractions; † assignment confirmed by infra-red spectroscopy (ref 33); ‡ fraction of dyads that are meso and have the deuterium in threo position

the possibility of obtaining isotactic poly(α-olefins) according to scheme (4b). On the other hand, catalytic systems are known which produce polypropylene chains with long individual sections of isotactic and syndiotactic structure^{114,131,132,162}. In conclusion the present state of our knowledge seems to indicate that, in the case of propylene, isotactic polymers are formed only according to scheme (4a), while syndiotactic polymers are formed both according to scheme (4a) and (4b). The type of insertion has been very little investigated with other α-olefins and even in the case of styrene the type of insertion in the formation of isotactic polymers with Ziegler–Natta catalysts is still open to discussion.

Stereochemistry of the growth reaction

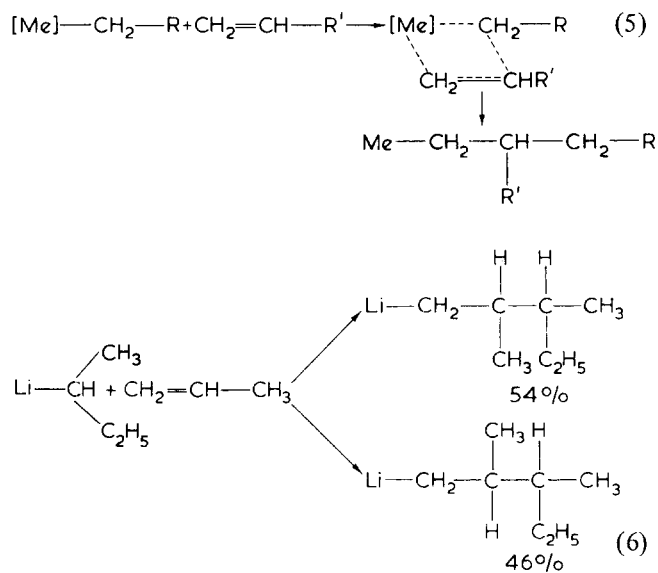
Polymerizing (Z)- or (E)-1-deutero-propylene with Ziegler–Natta catalysts to isotactic polymers *erythro*- or *threo*-diisotactic polymers¹³³, respectively has been performed (see Table 13). If the reaction at the two carbon atoms of the olefinic double bond is simultaneous this fact proves that the type of addition during the insertion reaction is *cis*. If, however, the above reaction does not occur simultaneously, an attack to one olefinic carbon atom, being followed by a rotation around the remaining single bond of the former olefinic group and finally by a *trans* addition

to the second carbon atom of the olefinic group would yield the same result as simultaneous *cis* addition.

As the isotactic type stereoregularity requires a constant type of addition which might be difficult to achieve admitting the occurrence of rotations between the attack to the first and to the second olefinic carbon atom, and in view of the fact that *cis* addition is a rather common feature in the reactions between organometallic compounds and double bonds, it seems likely today that insertion in Ziegler–Natta polymerization to isotactic polymers occurs with a *cis* stereochemistry. Some evidence mainly based on n.m.r. data has been published indicating that also propylene polymerization to syndiotactic polymers occurs according to a *cis* mechanism³².

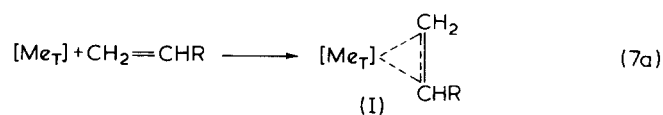
Mechanism of the insertion reaction

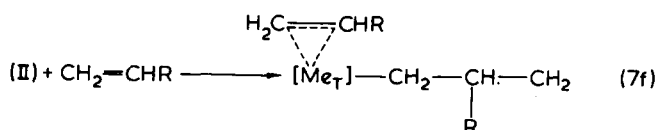
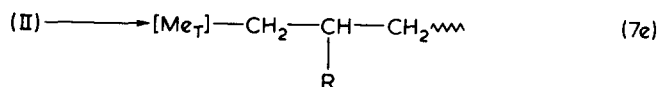
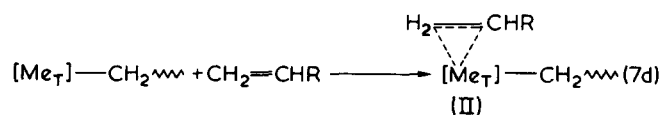
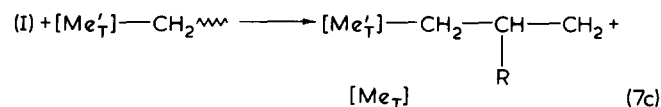
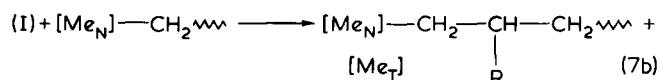
There is no direct experimental evidence concerning the mechanism of the insertion reaction. A one step reaction occurring through a four centre intermediate or transition state (scheme 5) has not found experimental support. On the other hand, addition of propylene to *sec*-butyllithium¹⁴² which is believed to occur through a four centre intermediate or transition state¹³⁹, although a highly regioselective process, shows a poor stereospecificity (scheme 6). Therefore the hypothesis of a four centre intermediate or transition state is not attractive, from a stereochemical point of view, to explain the formation of isotactic chains.



For these reasons, and in view of similarities with other transition metal catalysed reactions such as hydrogenation or hydroformylation, a two step mechanism involving formation of a π-olefin complex followed by the insertion of the complexed olefin into a metal–carbon bond is preferred at present, although the experimental evidence for the first step is still very scarce^{140,141}.

Taking into account that in the typical Ziegler–Natta catalysts both a transition metal [Me_T] and a non-transition metal [Me_N] are present, the mechanism can be formulated as in scheme (7).



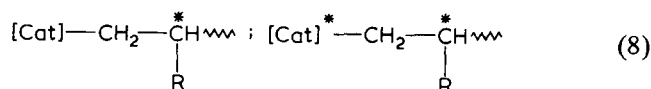


The mechanism (7a + 7b) is often described as a bimetallic mechanism¹³⁸ while the mechanism (7a + 7c) involving two transition metal atoms Me_T and Me_T' , which is also possible and for which some evidence exists^{135,136}, is mostly ignored. The mechanism (7d + 7e) is described in general¹³⁸ as a monometallic mechanism but (7d + 7f) is equally possible. A molecular orbital description of centres (equation 2) and of reaction (7e) has been published¹³⁷ but all attempts to polymerize olefins with complexes containing only one metal atom as for instance $TiCl_3CH_3$ ¹³⁶ or $Cp_2Ti(C_6H_5)_2$ ¹³⁵ failed. $Ti(CH_2-C_6H_5)_4$ or $Zr(CH_2-C_6H_5)_4$ show a very poor activity in the propylene polymerization¹¹⁰ and only very few of the metal atoms present are catalytically active as shown from the average molecular weight of the polymers obtained. On the other hand as mixtures of $TiCl_3CH_3$ and $TiCl_3$ ¹³⁶ and of $Cp_2Ti(C_6H_5)_2$ and $TiCl_4$ ¹³⁴ give moderately active catalysts, it is possible that also in the case of $Ti(CH_2-C_6H_5)_4$ the catalytically active complexes contain more than one metal atom.

For the above reasons bimetallic centres involved in mechanism [(7a + 7b) or (7a + 7c)] seem more probable than monometallic centres involved in the other mechanisms, (7d + 7e) or (7d + 7f); it must be emphasized that mechanism (7a + 7c) in which only transition metal atoms are involved is certainly possible as shown since 1957¹³⁵ but does not exclude mechanism (7a + 7b).

Stereoregulation in Ziegler-Natta polymerization of α -olefins to isotactic polymers

As previously discussed the formation of an isotactic polymer seems to involve a *cis* addition always to the same prochiral face of the α -olefin; therefore the catalyst-growing chain complex must be able to distinguish between the two prochiral faces of the α -olefin, the difference in the activation energy for the insertion reaction being more than 2 kcal/mol when an highly isotactic polymer is formed (see Figures 1 and 2). This type of stereospecific polymerization can be considered an asymmetric reaction as either one or the other prochiral face of the α -olefin must be preferred by the couple growing chain-catalyst. The pair must therefore be chiral. Considering the growing chain-catalyst pair the chirality of the centre can be connected only with the presence of asymmetric carbon atoms in the last unit or units of the growing chain, or with the presence of a chiral catalyst or with both factors (scheme 8).

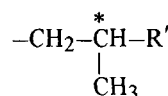


The following facts indicate that the presence of chiral catalytic centres play the principal role in stereoregulation:

(a) The polymerization of racemic α -olefins in the presence of heterogeneous catalysts to highly isotactic polymers is stereoselective, when the asymmetric carbon atom is in α or β position with respect to the double bond (scheme 9).

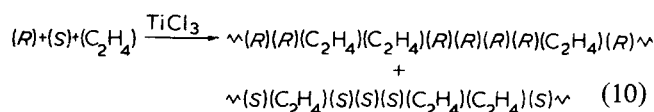


Frequent inversion of configuration in the main chain does not cancel or appreciably alter stereoselectivity^{143,146} and starting of the chains with alkyl groups of the type

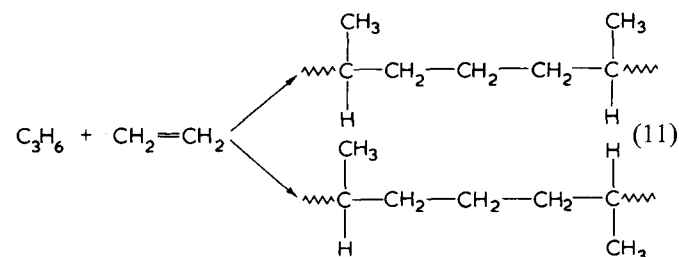


of a single chirality type does not induce preferential (stereoselective) polymerization of one antipode of the monomer¹⁴⁴. The polymerization of the same racemic olefins with soluble catalysts is not stereoselective¹⁴⁵. These facts show that the chirality of the asymmetric carbon atoms in the main chain is not an important factor in determining stereoselectivity. Therefore, the ability to distinguish between two antipodes must be connected with the chiral character of the heterogeneous catalyst.

(b) Copolymerization of racemic olefins with ethylene is stereoselective^{147,148} (scheme 10) confirming that the chiral character of the tertiary carbon atoms of the main chain is not decisively important for the distinction between the two antipodes implicit in stereoselective polymerization.



(c) The copolymerization of a large excess of propylene with $^{13}C_3H_6$ in the presence of catalyst $TiCl_3/AlR_2Cl$ yields copolymers with only two bands in the ^{13}C n.m.r. spectrum attributable to isolated $-CH_2-CH_2-$ (scheme 11)¹⁴⁹. In the same experiment carried out with non-stereospecific catalyst $[VCl_4-Al(C_2H_5)_3]$, five of the expected six peaks have been detected¹⁵⁰.



If the catalyst is chiral and accepting the previously dis-

cussed two-step mechanism for the polymerization of propylene (scheme 7), the stereoregulation might occur in the first step (formation of the π -complex) or in the second step (insertion reaction) or in both steps. Up to now no sufficient experimental evidence exists to decide between the three hypotheses. Based on the fact that stereospecific complexation to transition metals (e.g. platinum) is known¹⁵¹, it can be assumed as a working hypothesis that the two π -complexes arising from the attack of the catalyst to one or the other face of the α -olefin are in equilibrium. They may have a sufficient difference in free energy of formation ($\Delta\Delta G^0$) to justify the synthesis of highly isotactic poly(α -olefins), even if the free energy of activation for the insertion reaction yielding isotactic or syndiotactic diads are not very different (see Figure 4 in ref 143). Work is in progress to find experimental support in favour of this hypothesis.

The known dependence of the degree of stereoregularity on the structure of the alkyl group in the α -olefin [using typical Ziegler–Natta catalyst ($\text{TiCl}_4/\text{AlR}_3$), *t*-butylethylene does not polymerize; 3-methylbutene gives only isotactic polymers; propylene gives a mixture of isotactic, partly isotactic and atactic polymers¹⁴⁰] is well explained by the above hypothesis as the structure of the alkyl group of the olefinic ligand has been shown to influence remarkably the complexation equilibrium in *cis* (dichloro)(amino)(olefin) Pt^{II} complexes¹⁵².

An independent control of the hypothesis that the chirality of the catalyst is the main stereoregulating factor can be obtained from the investigation of the few steric irregularities in the isotactic polypropylene fractions. In fact if the main stereoregulating factor is the chiral catalytic centre, the insertion of a monomer molecule with an opposite stereochemistry with respect to the preceding one would remain isolated (Figure 5a). On the contrary, if the main stereoregulating factor is the growing chain, the growth would continue maintaining the configuration of the unit causing the first steric irregularity until another irregularity occurs in the insertion (Figure 5b).

In the first case couples of syndiotactic dyads would occur while in the second case isolated syndiotactic dyads should exist. Unfortunately, many possible mechanisms exist by which a change in the stereochemistry of an isotactic chain can occur. While all the authors agree that both types of irregularities can be observed with n.m.r. techniques, discrepancies exist concerning the prevalence of (rr)

or isolated (r) dyads. In a recent paper in which the different pentads of polypropylene have been investigated¹⁵³ a larger amount of pairs of syndiotactic dyads than of isolated ones has been found in a number of highly isotactic polymers prepared with different catalysts, confirming that the chirality of the catalyst is the main stereoregulating factor. Similar investigation on other poly(α -olefins) has not appeared in the literature up to now and even the simple quantitative determination of the degree of stereoregularity is in many cases difficult because of the very small chemical shift difference between the methylene signals of the isotactic and syndiotactic diads.

Research is in progress on poly(4-methyl-1-pentene) using specifically deuterated monomers and high resolution n.m.r. techniques.

Control of stereoregulation in the Ziegler–Natta polymerization of α -olefins to isotactic polymers

Although the factors determining the formation of the isotactic polypropylene are reasonably well known, very little is known about the structure of the chiral catalytic centres. The n.m.r. investigation of the polypropylenes produced with $\text{TiCl}_4/\text{AlR}_3$ catalysts shows that the degrees of isotactic stereoregularity in different fractions continuously change from more than 98% to about 50% of isotactic dyads showing that centres having a different stereoregulating capacity exist. However, the detailed planning of a modification of the structure of the centres leading to a predetermined change of stereoregularity is still not possible and changes in stereoregulating capacity of the catalysts can be obtained only empirically.

Back in 1955 Natta and his group thoroughly investigated the factors causing a change in the ratio between highly stereospecific and non-stereospecific centres. Among these factors the nature of the transition metal compound used for the preparation of the catalyst seems to be overwhelmingly important. However, other factors such as the nature of the non-transition metal component¹⁵⁴ and the addition of Lewis bases to the catalyst¹⁵⁵ seem also to be effective. The last factor brings dramatic changes in the stereospecificity of titanium catalysts supported on magnesium chloride¹⁵⁶ as shown in Table 14.

The effect of the Lewis base is still not well understood; in fact, it has been supposed¹³⁸ that the Lewis base, which in general causes a decrease of the activity of the catalysts, simply inactivates the non-stereospecific centres thus causing an increase in the ratio between stereospecific and non-stereospecific catalytic centres and hence an increase of the highly isotactic polymer fraction. However, on the basis of the experimental results it is not possible to exclude that the stereospecific catalytic centres have a complicated structure in which the Lewis base plays an important role influencing the complexation equilibrium of the

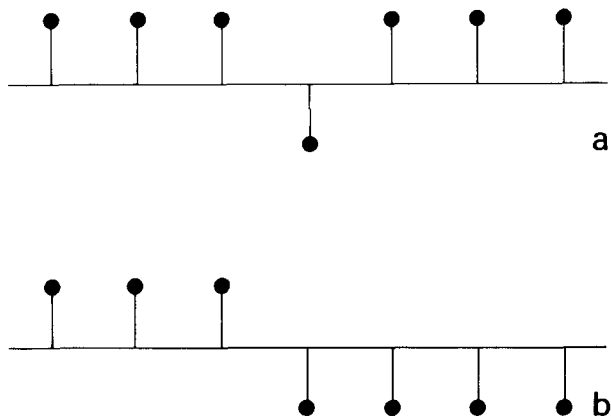


Figure 5 Principal possibilities for defects in highly isotactic polymers. (a) Isolated error, leading to a pair of racemic dyads. (b) The defect leads to a further polymerization with reversed stereochemistry, yielding an isolated racemic dyad

Table 14 Influence of Lewis bases on stereoregulation in propylene polymerization with supported $\text{MgCl}_2/\text{TiCl}_4/\text{AlR}_3$ catalytic system

Catalytic system	Boiling heptane insoluble polymer (%)	Reference
$\text{TiCl}_4/\text{MgCl}_2/\text{Al}(\text{iso-C}_4\text{H}_9)_3$	21	156
$\text{TiCl}_4[(\text{CH}_3)_2\text{N-CH}_2]_2/\text{MgCl}_2/\text{Al}(\text{C}_2\text{H}_5)_3(\text{C}_6\text{H}_5)$	93.5	117

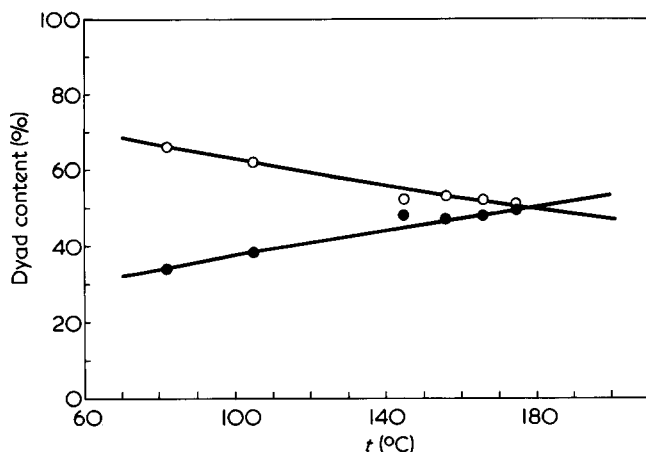


Figure 6 Content of meso and racemic dyads in 'atactic' (ether soluble) polypropylene as a function of polymerization temperature. Catalyst: $\text{TiCl}_3/\text{Al}(\text{iso-C}_4\text{H}_9)_3$ (1:4). Polymerization in decalin at 6 atm. ●, % i-dyad placements; ○, % s-dyad placements. $\Delta H^\ddagger_M - \Delta H^\ddagger_R = 2.2$ kcal/mol; $\Delta S^\ddagger_M - \Delta S^\ddagger_R = 5.0$ cal/mol K

monomer with the catalyst. Similar hypotheses are at the present formulated to explain the enantioselectivity of nickel catalysts on which chiral compounds are adsorbed¹⁵⁷.

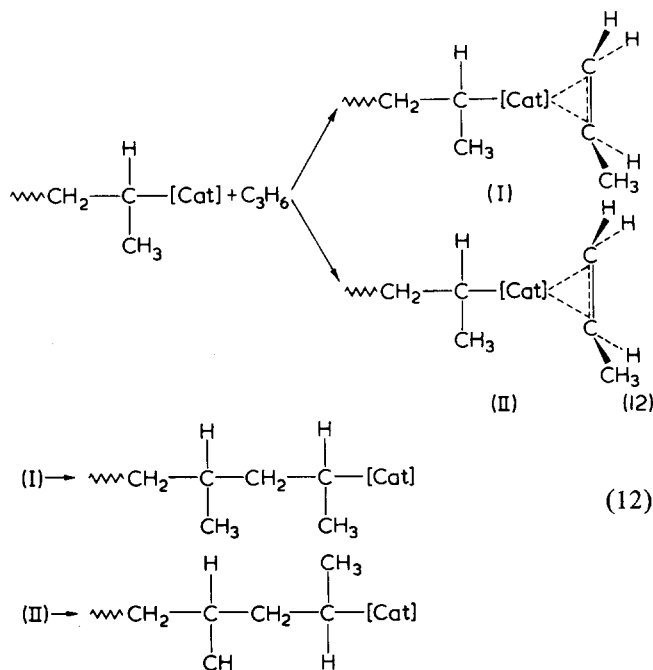
By increasing the temperature of polymerization of propylene both a decrease of the highly isotactic polymer¹⁵⁸ and an increase in the percentage of isotactic dyads in the polymers having a lower isotacticity have been noticed (Figure 6)¹⁵⁹. The result might be taken as an indication of a decrease, with increasing temperature, of the number of highly stereospecific catalytic centres and of a larger free energy of activation for the isotactic insertion than for syndiotactic insertion at the non-stereospecific catalytic centres. However, by increasing the polymerization temperature the average molecular weight decreases and the solvent fractionation does not yield a sharp separation according to stereoregularity. Therefore, the increase in content of isotactic dyads in the diethyl ether soluble fraction might be due to the formation (at high temperature) of highly isotactic but low molecular weight polypropylene. In any case, the propylene polymerization at high temperature has shown that some catalytic centres have a remarkable stability at temperatures up to 180°C, since, even at that temperature, they yield a highly isotactic polymer. The large decrease of the heptane insoluble polymers with temperature (even considering, that part of the highly isotactic polymer has such a low molecular weight that it becomes soluble in boiling heptane or ether) seems to indicate that the stereospecificity of some centres, that is, according to the previously formulated hypothesis, the capacity to discriminate between the two prochiral faces of the olefins, decreases with temperature as in other asymmetric catalysts. Polymerization temperature remains therefore the parameter which can be best used for fundamental investigation of the stereoregulating capacity of the catalytic centres.

STEREOREGULATION IN POLYMERIZATION OF PROPYLENE WITH ZIEGLER-NATTA CATALYSTS TO SYNDIOTACTIC POLYMERS

The polymerization of α -olefins to syndiotactic polymers, because of its limited scope, as only propylene and butadiene have been shown to yield polymers with a high syn-

diotacticity, has been much less investigated. The polymerization was first believed to occur with a regioselectivity similar to that demonstrated for the isotactic polymerization¹¹² and with a *cis* type of addition¹⁶⁰. Then some chemical^{126,127}, n.m.r.^{129,130} and i.r.¹²⁸ indications have been obtained showing that with vanadium catalysts the regioselectivity could be opposite in syndiotactic and isotactic type of propylene polymerization respectively (see above). However, no investigation has been carried out on regioselectivity in the synthesis of syndiotactic polymers obtained with typical isospecific catalysts $[\text{TiCl}_3/\text{Al}(\text{C}_2\text{H}_5)_2\text{F}]$ ¹⁶² or catalysts obtained from TiCl_4 and sodium-alkyls¹¹⁴. The problem of regioselectivity being not yet completely settled, and the maximum degree of syndiotactic stereoregularity achievable being not systematically investigated, only speculations are possible concerning stereoregulating factors in propylene polymerization yielding highly syndiotactic polymers. As a possible working hypothesis, the following can be suggested for the syndiotactic polymerization at low temperature with soluble catalysts, which is at least in part in agreement with the recent literature and is not in contrast with n.m.r. data on ethylene-propylene copolymers (scheme 11). Propylene would still insert into a metal to carbon bond but with a regioselectivity opposite to that proved for the isotactic polymerization; the stereoregulation is not connected with the chirality of the catalyst but with the chirality of the last monomeric unit, the asymmetric carbon atom of which is bound to the metal atom of the catalyst and does not racemize during the insertion reactions*.

Two limiting cases are possible (scheme 12): (a) an equilibrium between π -complexes exists, regulated by the asymmetric carbon atom of the growing chain bound to the metal, the position of the equilibrium being sufficiently displaced toward one of the complexes to justify the maximum degree of stereoregularity observed (90–95% of (r) dyads); or (b) the free energy of formation of I and



* Insertions of carbon monoxide into a bond between an asymmetric carbon atom and a metal atom without racemization are known¹⁶¹.

II is the same but the activation energy for the insertion of the olefin bound to the metal with one or with the other prochiral face is sufficiently different to justify the stereoregularity achieved. The diastereomeric composition obtained in the insertion of propylene in a Li to *sec*-butyl bond (46% of *erythro* and 54% of *threo*) which can be taken as a proper model for syndiotactic polymerization, seems to indicate that the first hypothesis is at the present more acceptable. The above totally speculative scheme for the steric control in syndiotactic polymerization of propylene at low temperature has the merit of explaining why the steric factors, which do not hinder inversion of configuration during the polymerization to atactic polymers with typical Ziegler–Natta catalysts of α -olefins with alkyl groups other than methyl group (1–2 type of insertion), can hinder completely the low temperature syndiotactic polymerization (2–1 type of insertion) of the same monomers.

PERSPECTIVES OF STEREOREGULATION IN VINYL POLYMERS

As it results from the topics discussed in the present review the problem of the control of stereoregularity in vinyl polymers is far from being solved.

The perspectives for stereocontrol in free radical polymerization are not very promising and research in this field should mainly be directed to polymers in which large attractive interactions exist between the last monomeric unit containing the unpaired electron and the preceding units of the growing chain. A further direction for research would be the radical polymerization of monomers regularly adsorbed on a surface¹⁶³ simulating the polymerization of monomers included in solid matrixes which seem to be today the only way to obtain highly stereoregular polymers with radical polymerization.

The stereoregulating factors in ionic polymerization are fairly well understood and by varying the polymerization conditions, and particularly the type of solvent and temperature, the degree of stereoregulation can be fairly well controlled. Further progress will lead to improvement of the degree of stereoregularity, and is bound to give a more detailed knowledge of the type of coordination around the counterions and of the structure of the growing chain ends. This type of knowledge requires both a clever choice of the system to be studied and improvements in the methods for the investigation of structures of complex ions in solution.

More complicated is the situation in the case of transition metal catalysed polymerization. Here much basic knowledge of the chemical aspects of the growing reaction and on the nature of the catalytic centres is still lacking. Therefore, a thorough discussion of the stereoregulating factors is not possible and we are still in the stage in which we try to improve our knowledge of the polymerization processes by investigating the stereoregularity of the polymers obtained. In this field the success of the industrial production of isotactic polypropylene shows how enormous progress can be made on a purely empirical basis. Progress in the basic knowledge of transition metal catalysed polymerization and on the stereoregulating forces will probably be very slow in the future because of the complexity of the problems. A purely empirical approach will probably yield more results of practical interest in a relatively short time.

Possible lines of development of the basic research in

the field of transition metal catalysed polymerization are further studied on model systems to obtain a better understanding of the role of the different components of the catalysts as well as attempts to synthesize catalytically active chiral transition metal complexes. Attention should be given also to a thorough investigation of the kinetics of the polymerization in homogeneous systems. One of the most fascinating and important fields is the investigation of the stereoregulating effects of bases in the Ziegler–Natta catalysts supported on $MgCl_2$. However, here, despite extensive progress in the techniques of investigating heterogeneous catalysts, a final proof of the structure of the stereospecific catalytic centres is not likely to come very soon.

REFERENCES

- 1 Staudinger, H., Ashdown, A. A., Brunner, M., Bruson, H. A. and Wehrli, S. *Helv. Chim. Acta.* 1929, **12**, 934
- 2 Marvel, C. S., Frank, R. L. and Prill, E. *J. Am. Chem. Soc.* 1943, **65**, 1647
- 3 Huggins, M. L. *J. Am. Chem. Soc.* 1944, **66**, 1991
- 4 Schildknecht, C. E., Gross, S. F., Davidson, H. R., Lambert, J. M. and Zoss, A. O. *Ind. Eng. Chem.* 1948, **40**, 2108
- 5 Morton, A. A. *Ind. Eng. Chem.* 1950, **42**, 1488
- 6 Natta, G., Pino, P., Corradini, P., Danusso, F., Mantica, E., Mazzanti, G. and Moraglio, G. *J. Am. Chem. Soc.* 1955, **77**, 1708; Natta, G. *J. Polym. Sci.* 1955, **16**, 143
- 7 Williams, J. L. R., Van Den Berghe, J., Dulmage, W. J. and Dunham, K. R. *J. Am. Chem. Soc.* 1956, **78**, 1260; Williams, J. L. R., Van Den Berghe, J., Dunham, K. R. and Dulmage, W. J. *J. Am. Chem. Soc.* 1957, **79**, 1716
- 8 Hogan, J. P. and Banks, R. L. US Pat. 2 825 721 (1958)
- 9 Feller, M. and Field, H. *Ind. Eng. Chem.* 1957, **49**, 1883;
- 10 Feller, M. and Field, H. *Ind. Eng. Chem.* 1959, **51**, 155
- 11 Bovey, F. A. 'High Resolution NMR of Macromolecules', Academic Press, New York, 1972, Ch 3–8
- 12 Zambelli, A., Segre, A. L., Farina, M. and Natta, G. *Makromol. Chem.* 1967, **110**, 1
- 13 Clark, H. G. *J. Polym. Sci. (C)* 1968, **16**, 3455
- 14 Williams, A. D., Brauman, J. I., Nelson, N. J. and Flory, P. J. *J. Am. Chem. Soc.* 1967, **89**, 4807
- 15 Williams, A. D. and Flory, P. J. *J. Am. Chem. Soc.* 1969, **91**, 3111
- 16 Billups, W. E. and Kurtz, A. N. *J. Am. Chem. Soc.* 1968, **90**, 1361
- 17 Flory, P. J. and Williams, A. D. *J. Am. Chem. Soc.* 1969, **91**, 3118
- 18 Flory, P. J. and Pickles, C. J. *J. Chem. Soc. Faraday Trans. 2* 1973, **69**, 632
- 19 Suter, U. W., Pucci, S. and Pino, P. *J. Am. Chem. Soc.* 1975, **97**, 1018
- 20 White, D. M. *J. Am. Chem. Soc.* 1960, **82**, 5678
- 21 Fordham, J. W. *J. Polym. Sci.* 1959, **39**, 321
- 22 Elias, H. G. and Göldi, P. *Makromol. Chem.* 1971, **144**, 85
- 23 Brownstein, S., Bywater, S. and Worsfold, D. J. *Makromol. Chem.* 1969, **48**, 127
- 24 Brownstein, S., Bywater, S. and Worsfold, D. J. *J. Phys. Chem.* 1962, **66**, 2067
- 25 Segre, A. L., Ferruti, P., Toja, E. and Danusso, F. *Macromolecules* 1969, **2**, 35
- 26 Bovey, F. A., Hood, F. P., Anderson, E. W. and Kornegay, R. L. *J. Phys. Chem.* 1967, **71**, 312
- 27 Cavalli, L., Borsini, G. C., Carraro, G. and Confalonieri, G. *J. Polym. Sci. (A-1)* 1970, **8**, 801
- 28 Yoshino, T. and Komigama, J. *J. Polym. Sci. (B)* 1965, **3**, 311
- 29 Yoshino, T., Kono, H. and Kuno, K. *J. Polym. Sci. (B)* 1967, **5**, 703
- 30 Fowells, W., Schuerch, C., Bovey, F. A. and Hood, F. P. *J. Am. Chem. Soc.* 1967, **89**, 1396
- 31 Yoshino, T. and Kuno, K. *J. Am. Chem. Soc.* 1965, **87**, 4404
- 32 Zambelli, A., Segre, A. L., Farina, M. and Natta, G. *Makromol. Chem.* 1967, **110**, 1

- 32 Zambelli, A., Giongo, M. G. and Natta, G. *Makromol. Chem.* 1968, **112**, 183
- 33 Miyazawa, T. and Ideguchi, T. *J. Polym. Sci. (B)* 1963, **1**, 389
- 34 Yoshino, T., Komiyama, J. and Shinomiya, M. *J. Am. Chem. Soc.* 1964, **86**, 4482
- 35 Matsuzaki, K., Uryu, T., Osada, K. and Kawamura, T. *Macromolecules* 1972, **6**, 816
- 36 Matsuzaki, K., Uryu, T., Seki, T., Osada, K. and Kawamura, T. *Makromol. Chem.* 1975, **176**, 3051
- 37 Bovey, F. A. 'High Resolution NMR of Macromolecules', Academic Press, New York, 1972, p 129
- 38 Pham, Q. T., Millan, J. L. and Madruga, E. L. *Makromol. Chem.* 1974, **175**, 945
- 39 Heatley, F. and Bovey, F. A. *Macromolecules* 1969, **2**, 241
- 40 Hassan, A. M. *J. Polym. Sci. (Polym. Phys. Edn)* 1974, **12**, 655
- 41 Ramey, K. C., Lini, D. C. and Statton, G. L. *J. Polym. Sci. (A-1)* 1967, **5**, 257
- 42 Elias, H. G., Riva, M. and Göldi, P. *Makromol. Chem.* 1971, **145**, 163
- 43 Friedlander, H. N., Harris, H. E. and Pritchard, J. G. *J. Polym. Sci. (A-1)* 1966, **4**, 649
- 44 Wu, T. K. and Ovenall, D. W. *Macromolecules* 1973, **6**, 582
- 45 Allio, A. and Pino, P. *Helv. Chim. Acta* 1974, **57**, 616
- 46 Lukovkin, G. M., Komarova, O. P., Torchilin, V. P. and Kirsch, Yu. E. *Vysokomol. Soedin (A)* 1973, **15**, 443, p 503 of the English Translation
- 47 Svegliado, G., Talamini, G. and Vidotto, G. *J. Polym. Sci. (A-1)* 1967, **5**, 2875
- 48 Matsuzaki, K., Uryu, T., Ishida, A., Ohki, T. and Takeuchi, M. *J. Polym. Sci. (A-1)* 1967, **5**, 2167
- 49 Heatley, F. and Bovey, F. A. *Macromolecules* 1968, **1**, 303
- 50 Bovey, F. A. 'High Resolution NMR of Macromolecules', Academic Press, New York, 1972, p 92
- 51 Frisch, H. L., Mallows, C. L., Heatley, F. and Bovey, F. A. *Macromolecules* 1968, **1**, 533
- 52 Ferguson, R. C. *Macromolecules* 1969, **2**, 237
- 53 Hatada, K., Ota, K. and Yuki, H. *J. Polym. Sci. (B)* 1967, **5**, 225
- 54 Bovey, F. A. *J. Polym. Sci.* 1960, **46**, 59
- 55 Matsuzaki, K., Kanai, T., Yamawaki, K. and Rung, K. P. S. *Makromol. Chem.* 1973, **174**, 215
- 56 Yuki, H., Hatada, K., Niinomi, T. and Kikuchi, Y. *Polym. J.* 1970, **1**, 36
- 57 Tsuruta, T., Makimoto, T. and Kanai, H. *J. Macromol. Chem.* 1966, **1**, 31
- 58 Matsuzaki, K., Kawamura, T. and Saito, K. *J. Polym. Sci. (Polym. Chem. Edn)* 1975, **13**, 253
- 59 Suzuki, T., Koshiro, S. and Takegami, Y. *Polymer* 1973, **14**, 549
- 60 Inoue, Y., Koyama, K., Chûjô, R. and Nishioka, A. *Makromol. Chem.* 1974, **175**, 277
- 61 Matsuzaki, K., Urgu, T. and Ito, K. *Makromol. Chem.* 1969, **126**, 292
- 62 Lenz, R. W. *J. Macromol. Sci. (A)* 1975, **9**, 945
- 63 Bovey, F. A. 'High Resolution NMR of Macromolecules', Academic Press, New York, 1972, p 158
- 64 Göldi, P. and Elias, H. G. *Makromol. Chem.* 1973, **153**, 81
- 65 Fox, T. G. and Schnecko, H. W. *Polymer* 1963, **3**, 575
- 66 Otsu, T., Yamada, B. and Imoto, M. *J. Macromol. Chem.* 1966, **1**, 61
- 67 Elias, H. G. and Göldi, P. *Makromol. Chem.* 1971, **144**, 85
- 68 Farina, M., Natta, G., Allegra, G. and Löffelholz, M. *J. Polym. Sci. (C)* 1967, **16**, 2517; Farina, M., Isio, G. A. and Natta, G. *J. Am. Chem. Soc.* 1967, **89**, 5071
- 69 Liquori, A. M., Anzuino, G., D'Alagni, M., Vitagliano, V. and Costantino, L. *J. Polym. Sci. (A-2)* 1968, **6**, 509; Miyamoto, T., Tomoshige, S. and Inagaki, H. *Makromol. Chem.* 1975, **176**, 3035
- 70 Kern, R. J. *Nature* 1960, **187**, 410
- 71 Braun, D., Herner, M. and Kern, W. *Makromol. Chem.* 1960, **36**, 232
- 72 Kern, W., Braun, D. and Herner, M. *Makromol. Chem.* 1958, **28**, 66
- 73 Braun, D., Betz, W. and Kern, W. *Makromol. Chem.* 1961, **42**, 89
- 74 Merle-Aubry, L., Merle, Y. and Selegny, E. *Makromol. Chem.* 1975, **176**, 709
- 75 Fuchs, O. *Makromol. Chem.* 1962, **58**, 247
- 76 Winstein, S. and Robinson, G. C. *J. Am. Chem. Soc.* 1958, **80**, 169
- 77 Matsuzaki, K., Ho, H., Kawamura, T. and Urgu, T. *J. Polym. Sci. (Polym. Chem. Edn)* 1973, **11**, 971
- 78 Brownstein, S. and Wiles, D. M. *J. Polym. Sci. (A)* 1964, **2**, 1901
- 79 Moritani, T., Kuruma, I., Shibatani, K. and Fujiwara, Y. *Macromolecules* 1972, **5**, 577
- 80 Chiellini, E., Montagnoli, G. and Pino, P. *J. Polym. Sci. (B)* 1969, **7**, 121
- 81 Chiellini, E. *Macromolecules* 1970, **3**, 527
- 82 Kunitake, T. and Tsugawa, S. *Macromolecules* 1975, **8**, 709
- 83 Elias, H. G. and Kamat, V. S. *Makromol. Chem.* 1968, **117**, 61
- 84 Lenz, R. W., Regel, W. and Westfelt, L. *Makromol. Chem.* 1975, **176**, 781
- 85 Leonard, J. and Malhotra, S. L. *J. Polym. Sci. (Polym. Chem. Edn)* 1974, **12**, 2391
- 86 Urgu, T., Ohaku, K. I. and Matsuzaki, K. *J. Polym. Sci. (Polym. Chem. Edn)* 1974, **12**, 1723
- 87 Breslow, D. S. and Kutner, A. *J. Polym. Sci. (Polym. Lett. Edn)* 1971, **9**, 129
- 88 Bovey, F. A. and Tiers, G. V. D. *J. Polym. Sci.* 1960, **44**, 173
- 89 Braun, D., Herner, M., Johnsen, U. and Kern, W. *Makromol. Chem.* 1962, **51**, 15
- 90 Yuki, H., Hatada, K., Ohta, K. and Okamoto, Y. *J. Makromol. Sci. (A)* 1975, **9**, 983
- 91 Kawak, J., Pham, Q. T., Pillot, C. and Pascault, J. P. *Eur. Polym. J.* 1974, **10**, 997
- 92 Hatada, K., Kokan, S., Niinomi, T., Miyaji, K. and Yuki, H. *J. Polym. Sci. (Polym. Chem. Edn)* 1975, **13**, 2117
- 93 Smid, J. in 'Structure and Mechanism in Vinyl Polymerization', (Eds T. Tsuruta and K. R. O'Driscoll), Marcel Dekker, New York, 1969, Ch. 11
- 94 Swarc, M. 'Carbanious, Living Polymers and Electron-Transfer Processes', Interscience, New York, 1968
- 95 Morton, M. in 'Macromolecular Science', (Ed. C. E. H. Bawn), Butterworth, London, 1974, p 4
- 96 Bywater, S. *Adv. Polym. Sci.* 1965, **4**, 66
- 97 Hogen-Esch, T. E. and Smid, J. *J. Am. Chem. Soc.* 1966, **88**, 318
- 98 Leitereg, T. J. and Cram, D. J. *J. Am. Chem. Soc.* 1968, **90**, 4019
- 99 Cram, D. J. and Kopecky, K. R. *J. Am. Chem. Soc.* 1959, **81**, 2748
- 100 Glusker, D. L., Lystoff, I. and Stiles, E. *J. Polym. Sci.* 1961, **49**, 315
- 101 Wiles, D. M. and Bywater, S. *Trans. Faraday Soc.* 1965, **61**, 150
- 102 Christman, D. L. and Vandenberg, E. J. US Pat. 3 025 282 (1962); *Chem. Abstr.* 1963, **57**, 2415d
- 103 Pepper, D. C. and Reilly, P. J. *J. Polym. Sci.* 1962, **58**, 639
- 104 Gandini, A. and Plesch, P. H. *J. Chem. Soc.* 1965, 4765
- 105 Higashimura, T. in 'Structure and Mechanism in Vinyl Polymerization', (Eds T. Tsuruta and K. F. O'Driscoll), Marcel Dekker, New York, 1969, Ch. 10
- 106 Schuerch, C., Fowells, W., Yamada, A., Bovey, F. A., Hood, F. P. and Anderson, E. W. *J. Am. Chem. Soc.* 1964, **86**, 4481
- 107 Yoshino, T., Shinomiya, M., and Komiyama, J. *J. Am. Chem. Soc.* 1965, **87**, 387
- 108 Gaylord, N. G. and Mark, H. F. 'Linear and Stereoregular Polymers', Interscience, New York, 1959
- 109 Ballard, D. G. H. *Adv. Catal.* 1973, **23**, 263
- 110 Giannini, U., Zucchini, U. and Albizzati, E. *J. Polym. Sci. (Polym. Lett. Edn)* 1970, **8**, 405
- 111 Zambelli, A., Pasquon, I., Signorini, R. and Natta, G. *Makromol. Chem.* 1968, **112**, 160
- 112 Zambelli, A., Natta, G., and Pasquon, I. *J. Polym. Sci. (C)* 1963, **4**, 411
- 113 Natta, G., Pino, P. and Mazzanti, G. *Gazz. Chim. Ital.* 1957, **87**, 528
- 114 Longi, P. and Roggero, A. *Ann. Chim.* 1961, **51**, 1013
- 115 Natta, G., Pasquon, I., Zambelli, A. and Gatti, G. *J. Polym. Sci.* 1961, **51**, 387
- 116 Natta, G., Mazzanti, G., Crespi, G. and Moraglio, G. *Chim. Ind.* 1957, **39**, 275
- 117 Giannini, U., Cassata, A., Longi, P. and Mazzocchi, R. Belg. Pat. 785 332 (1972)

- 118 Hogan, J. P. and Banks, R. L. *Can. Pat.* 956 748 (1974)
- 119 Natta, G., Fino, P., Mazzanti, G., Giannini, U., Mantica, E. and Peraldo, M. *J. Polym. Sci.* 1957, **26**, 120
- 120 Natta, G., Corradini, P. and Bassi, I. W. *J. Am. Chem. Soc.* 1965, **80**, 755
- 121 Natta, G., Pino, P., Mazzanti, G. and Giannini, U. *J. Inorg. Nucl. Chem.* 1958, **8**, 612
- 122 Natta, G., Pino, P., Mantica, E., Danusso, F., Mazzanti, G. and Peraldo, M. *Chim. Ind.* 1956, **38**, 124
- 123 Wilke, G., Bogdanović, B., Hardt, P., Heimbach, P., Keim, W., Kröner, M., Oberkirch, W., Tanaka, K., Steinbrücke, E., Walter, D. and Zimmermann, H. *Angew. Chem.* 1966, **78**, 157
- 124 Bogdanović, G., Henc, B., Karman, H. G., Nüssel, H. G., Walter, D. and Wilke, G. *Ind. Eng. Chem.* 1970, **62**, 34
- 125 Henrici-Olivé, G. and Olivé, S. *Angew. Chem.* 1975, **87**, 110
- 126 Takegami, Y. and Suzuki, T. *Bull. Chem. Soc. Japan* 1969, **42**, 848
- 127 Suzuki, T. and Takegami, Y. *Bull. Chem. Soc. Japan* 1970, **43**, 1484
- 128 Zambelli, A., Tosi, C. and Sacchi, C. *Macromolecules* 1972, **5**, 649
- 129 Zambelli, A., Wolfsgruber, C., Zannoni, G. and Bovey, F. A. *Macromolecules* 1974, **7**, 750
- 130 Bovey, F. A., Sacchi, M. C. and Zambelli, A. *Macromolecules* 1974, **7**, 752
- 131 Natta, G. *J. Polym. Sci.* 1959, **34**, 531
- 132 Zambelli, A. and Tosi, C. *Adv. Polym. Sci.* 1974, **15**, 31
- 133 Natta, G., Farina, M. and Peraldo, M. *Rend. Accad. Naz. Lincei* 1958, **25**, 424; *Chim. Ind.* 1960, **42**, 255
- 134 Pino, P. and Mazzanti, G. *Ital. Pat.* 583 219 (1958); *Chem. Abstr.* 1959, **53**, 23094
- 135 Natta, G., Pino, P., Mazzanti, G. and Lanzo, R. *Chim. Ind.* 1957, **39**, 1032
- 136 Beermann, C. and Bestian, H. *Angew. Chem.* 1959, **71**, 618
- 137 Cossee, P. *Recl. Trav. Chim. Pays Bas* 1966, **85**, 1151
- 138 Boor, J. *Macromol. Rev.* 1967, **2**, 115
- 139 Braude, E. A. *Prog. Org. Chem.* 1955, **3**, 172
- 140 Boor, Jr. J. *Ind. Eng. Chem. Prod. Res. Dev.* 1970, **9**, 437
- 141 Henrici-Olivé, G. and Olivé, S. *Adv. Polym. Sci.* 1969, **6**, 429
- 142 Pino, P. *et al.* unpublished results
- 143 Pino, P., Oschwald, A., Ciardelli, F., Carlini, C. and Chiellini, E. 'Coordination Polymerization', (Ed. J. C. W. Chien), Academic Press, New York, 1974, p 25
- 144 Pino, P., Ciardelli, F. and Lorenzi, G. P. *J. Polym. Sci. (C)* 1973, **4**, 21
- 145 Oschwald, A. *Dissertation* ETH, Zürich (1974)
- 146 Pino, P. *Adv. Polym. Sci.* 1965, **4**, 393
- 147 Pieroni, O., Stigliani, G. and Ciardelli, F. *Chim. Ind. (Milan)* 1970, **52**, 289
- 148 Ciardelli, F., Locatelli, P., Marchetti, M. and Zambelli, A. *Makromol. Chem.* 1974, **175**, 923
- 149 Zambelli, A. 'NMR Basic Principles and Progress', Springer-Verlag, Heidelberg, 1971, Vol 4, p 101
- 150 Zambelli, A., Gatti, G., Sacchi, C., Crain, Jr. W. O. and Roberts, J. D. *Macromolecules* 1971, **4**, 475
- 151 Corradini, P., Paiaro, G., Panunzi, A., Mason, S. F. and Searle, G. H. *J. Am. Chem. Soc.* 1966, **88**, 2863
- 152 Lazzaroni, R., Salvadori, P., Bertucci, C. and Veracini, C. A. *J. Organomet. Chem.* 1975, **99**, 475
- 153 Wolfsgruber, C., Zannoni, G., Rigamonti, E. and Zambelli, A. *Makromol. Chem.* 1975, **176**, 2765
- 154 Natta, G. *J. Inorg. Nucl. Chem. Suppl.* 1958, **8**, 589
- 155 Mitsubishi Petrochemical Co. Br. Pat. 1 092 390
- 156 Longi, P., Giannini, U. and Cassata, A. Belg. Pat. 774 600 (1971)
- 157 Ozaki, H., Tai, A. and Izumi, Y. *Chem. Lett.* 1974, 935
- 158 Natta, G., Mazzanti, G. and Longi, P. *Chim. Ind.* 1958, **40**, 183; Mazzanti, G. and Longi, P. *Rend. Ist. Lomb. Sci. Lett.* 1957, **91**, 755
- 159 Atteya, E. and Pino, P. unpublished results
- 160 Zambelli, A. *Chem. Commun.* 1967, 1252
- 161 Whitesides, G. M. and Boschetto, D. J. *J. Am. Chem. Soc.* 1969, **91**, 4313; Hines, L. F. and Stille, J. K. *J. Am. Chem. Soc.* 1974, **92**, 485
- 162 Natta, G., Pasquon, I., Corradini, P., Peraldo, M., Pegoraro, M. and Zambelli, A. *Atti Accad. Naz. Lincei. Cl. Sci. Fis. Mat. Nat. Rend.* 1960, **28**, 539
- 163 Blumstein, A., Malhotra, S. L. and Watterson, A. C. *Polymer Prepr.* 1968, **9**, 167

Mechanical motions in amorphous and semi-crystalline polymers*

Raymond F. Boyer

Midland Macromolecular Institute, 1910 West St. Andrews Drive, Midland, Michigan 48640, USA

(Received 14 May 1976)

Ten areas of the field, all with some special interest to the author, were selected for predictions about the near future. In order to gain perspective, a brief review is presented of some key developments which occurred after the publication of the book 'Anelastic, and Dielectric Effects in Polymeric Solids' by McCrum, Read and Williams in 1967. The following predictive areas are then discussed in varying degrees of detail. (1) Apparatus: current status and the need for automation and more sophistication. (2) Extending the temperature range above T_g or T_M and the molecular weight range down to the oligomers. (3) Study of rarefied polymers (higher than normal free volume). (4) Nature of the in-chain β relaxation ($T < T_g$) in addition polymers. (5) Use of nitroxide probes as an auxiliary tool to study amorphous phase relaxations in highly crystalline polymers. (6) Computer simulation of molecular motion at sub-group relaxations. (7) Nature of the amorphous state and its possible effect on mechanical relaxations other than through free volume. (8) Correlation between mechanical strength of glassy polymers and secondary, glassy state relaxations. (9) The need to prepare highly crystalline polymers in the completely amorphous state. (10) The impact of new polymer types. It is concluded that mechanical spectroscopy is still a quite viable field with exciting potentialities. A synergism between automation of apparatus, new materials, new techniques (not necessarily in the field of mechanical spectroscopy) and theory is anticipated.

INTRODUCTION

Historical perspective

Any considerations about the future prospects for the mechanical spectroscopy of polymers should start properly with recognition of the land-mark book by McCrum, Read and Williams¹ followed by a precis of key events between the 1967 publication of this book and the current time. This book presented six elements of the subject: historical perspective; definitions of terms; theory; experimental techniques; numerous relaxation spectra on all major polymers; relaxation maps, where data warranted, showing plots of log frequency $-1/T$ for two or more of the major loss peaks in a given polymer. Granting authors the privilege of knowing and citing their own most recent work, including papers in press, one must conclude from the bibliography section that literature references terminated sometime prior to 1965, when this subject was accelerating in interest and number of publications.

Today, there are three commonly used dynamic mechanical loss instruments: torsional pendulum in several variants; the Rheovibron (dynamic tensiometer); and to a much more limited extent, the torsional braid apparatus (t.b.a.) which is a form of torsion pendulum using an impregnated glass braid rather than a strip of polymer. In the book by McCrum *et al.*¹, the torsion pendulum was treated in detail, the then new Rheovibron method was mentioned in one sentence; and the t.b.a. not at all. Some Rheovibron data were included. We have summarized elsewhere the salient features of these three methods². Since that time Sternstein³ has modified the torsion pendulum technique by applying a

tensile force along the length of the specimen which is then under both shear and tensile deformation. Gillham⁴ has presented a comprehensive review on t.b.a., including his current completely automated instrument. Tabor *et al.* have miniaturized a torsion pendulum and placed it inside a hydrostatic pressure vessel to measure the effect of pressure on mechanical relaxations^{5,6}.

It is not possible within the scope or space limitations of this article to summarize all of the key developments in mechanical spectroscopy between 1965 and the present. Some of them will emerge in subsequent discussion. The following selections are in some measure subjective, having in mind topics to be covered later.

(1) Takayanagi has reviewed his extensive studies on dynamic properties of mats prepared by compression of polymer single crystals^{7,8}. Many other relevant topics are included. These papers serve as an introduction to many subsequent articles by him in the English language technical literature.

(2) Sauer *et al.*⁹ prepared an extensive review on deformation and relaxation behaviour of polymer single crystals, showing in effect that this is a very mature area of study.

(3) McCall¹⁰ published a series of relaxation maps for all key polymers with special emphasis on n.m.r. data.

(4) The work of Heijboer¹¹ on mechanical loss in saturated ring ester of poly(methyl acrylic acid) constitutes a definitive study correlating both temperature and intensity of the group motion with chemical structure of the unsubstituted and substituted rings from C₅ to C₈. The five types of experimental apparatus developed by Heijboer and/or his collaborators to cover the frequency range from $\sim 10^{-4}$ Hz (torsional creep) to $\sim 10^7$ Hz (wave propagation) are described, and typical results presented.

(5) Lamb¹²⁻¹⁴ and his colleagues have approached dyna-

* Presented at the Sixth Biennial Manchester Polymer Symposium, UMIST, Manchester, March 1976.

mic viscoelastic behaviour of liquids and polymers from the viewpoint of electrical circuitry. Analogies with circuit theory have allowed them to analyse and resolve the several key components playing a role in viscoelastic processes. Ultrasonic absorption (up to 1–2 GHz) and dielectric loss (low frequency) apparatus have recently been added.

(6) Simha and his students^{15,16} have measured thermal expansion of amorphous and semi-crystalline polymers, in some cases from 4.2K upwards, and shown in many examples a one to one correspondence between multiple step-jumps in coefficient of linear thermal expansion and peak heights of torsion pendulum loss curves. The latter represent their own data as well as literature data, in some cases on identical samples as, for example, the C₅ to C₈ cycloalkyl methacrylates prepared and measured by Heijboer¹¹.

(7) Ward and collaborators have made a systematic study of the effect of orientation on mechanical relaxation in polyethylene^{17,18} supplementing such studies with dielectric¹⁹ and n.m.r.²⁰ results. Orientation permits a correlation between loss peaks and direction of crystallographic axes, thereby helping to define molecular motion occurring at specific loss peaks. Takayanagi *et al.*²¹ have also reported a systematic study of Rheovibron data on oriented PE.

(8) Illers, in a series of detailed studies on branched and linear polyethylenes^{22–25} has resolved and clarified the detailed nature of the various amorphous and crystalline loss peaks lying in the temperature range between liquid N₂ and the melting point. His conclusions about $T_g = 195–200\text{K}$ for amorphous polyethylene are not universally accepted and the controversy continues. We consider this work definitive and the most sophisticated use yet made of the torsion pendulum in analysing an exceedingly complex problem.

(9) Eisenberg²⁶ has carried out extensive mechanical loss measurements on a new class of polymers, the ionomers, which contain relatively small amounts (usually less than 10%) of metal salts of acrylic or methacrylic or other acids present in the polymer chain.

(10) Several pertinent review papers might be cited, both comparing results from mechanical and other types of relaxation measurements. We refer to book chapters by Roberts and White²⁷ and by North²⁸. The present author has reviewed in some detail special problems related to multiple loss spectra of semi-crystalline polymers²⁹.

(11) Jansson^{30–32} has developed a new viscoelastic function which facilitates frequency or time–temperature transformations, calculation of creep compliance from complex compliance, and separation of viscoelastic mechanisms.

(12) Gisolf has discussed the relationship between the applied mechanical field and the moving groups in the polymer in terms of mechanical–dipole relaxation³³. He concludes that compliance rather than modulus is the proper function to use³⁴. Gray and McCrum³⁵ had earlier stressed the importance of considering the proper viscoelastic function to use for crystalline polymers.

Future trends: the outlook

Any scientific discipline advances in an erratic fashion caused by the unexpected advent of new theories and new techniques; one need only consider the characterization of polymers prior to the advent of light scattering, the laser or gel permeation chromatography. Our personal philosophy is that by reviewing the recent past as above and in refs 2–35, one can draw a tangent to the curve of progress at this moment in time and extrapolate to what might happen in the absence of unpredictable break-throughs. Hence, we

confine ourselves to listing some areas where problems exist and where specific types of studies might be conducted.

THE OUTLOOK FOR DYNAMIC MECHANICAL SPECTROSCOPY

Apparatus

Several trends can be foreseen with considerable confidence based on activities already present in specific laboratories.

Automation of data acquisition and reduction, with plotting either directly on an $X-Y-Y'$ recorder or as a computer printout, is inevitable. Automation of all instrumental techniques is occurring rapidly. Dynamic mechanical testing has seemed to lag in this regard, presumably because of some inherently difficult problems. Gillham has automated his torsional braid analysis equipment to the point that temperature programming is completely controlled in any desired logical sequence while an $X-Y-Y'$ recorder plots out as a function of temperature at ~ 1 Hz log decrement and log (period⁻²), the latter being a measure of relative modulus of rigidity. This has now been described in detail⁴. Since t.b.a. is inherently a torsion pendulum, this means that the technique for automating any torsion pendulum is at hand. In principal, the digital printouts⁴ can be punched onto tape. All viscoelastic functions can be calculated and printed out.

Du Pont has just announced a new type of automated dynamic mechanical analyser, Model 980^{36,37}. It prints out on an $X-Y-Y'$ recorder, X being the temperature scale, the resonant frequency of the specimen, which can be related to modulus, and damping on a decibel scale. Temperature is programmed from -150° to 500°C at various linear rates in heat–cool cycles or isothermal modes. The modulus range is 0 to 10^{11} dyne/cm² so that metals, polymers, and other materials can be studied. While frequency varies along the temperature scale as modulus decreases, the variation is generally in the range from 150 to 3.5 Hz, and in specific instances, such as linear PE, from 20 to 3.5 Hz. The output information from the unit can be fed to various outside data handling devices and computers. In this way modulus can be calculated directly from the frequency–temperature data.

An automated Rheovibron developed by the Monsanto Company has been described by Kenyon^{38,39}. Stress, strain phase angle, sample length and temperature are recorded continuously while the data are fed to an off-line computer to give storage modulus, loss modulus and $\tan \delta$. Tension is controlled with loadings as low as 0.015 g. Such low loading permits going well above T_g . $\tan \delta$ measurements are made to ± 0.001 . Minor transitions and relaxations are now seen in a reproducible fashion.

One automated instrument originally developed by Simpson *et al.*⁴⁰ for mechanical loss in metals deserves consideration for polymers. As originally conceived and used, the driven metal specimen forms one plate of a parallel plate condenser. Electrical circuitry permits plotting of logarithmic decrement and Young's modulus, currently as a function of time, but alternately as a function of temperature. According to Soisin⁴¹, the apparatus works on a polymer sample coated with an electrically conducting paint. Frequencies in the range of 0.1 to 5 kHz can be attained.

Increased experimental sophistication. While a given investigator may use a single dynamic mechanical testing apparatus for general characterization, it is apparent that complete characterization of mechanical spectra requires a range

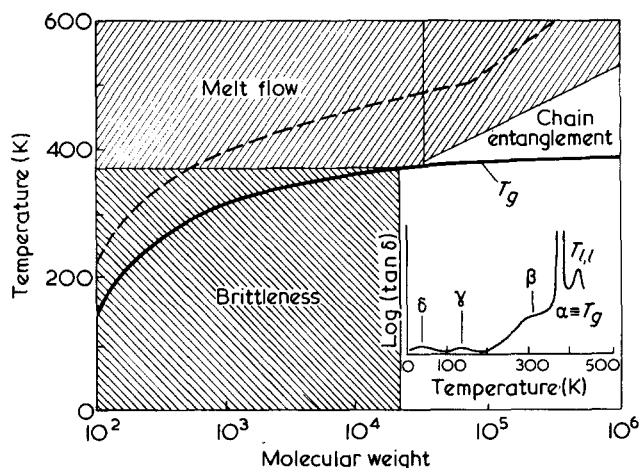


Figure 1 T_g -molecular weight plot for a polymer such as PS or PMMA. The shaded area above T_g is not normally available for dynamic mechanical tests because of excessive melt flow. The shaded area to the left of molecular weight $\sim 20\,000$ gives, for PS, polymers too weak and brittle to be tested. The inset shows a dynamic loss spectrum at 1 Hz for atactic PS of molecular weight in the range $1-2 \times 10^5$

of instruments^{11,42}, namely: torsional creep for $\sim 10^{-5}$ to $\sim 10^0$ Hz; torsional pendulum for ~ 0.1 to ~ 20 Hz; flexural resonance for $\sim 10^2$ to $\sim 10^4$ Hz; long resonance for $\sim 10^3$ to $\sim 10^5$ Hz; wave propagation for $\sim 10^6$ Hz. The resulting range of 11 decades permits a precise determination of apparent energies of activation, especially for secondary relaxations⁴³.

In general, mechanical relaxation measurements should be supplemented with one or more of the following techniques: dielectric, n.m.r., neutron scattering, and dynamic viscoelasticity. One such multidisciplinary study by Allen *et al.* on the glassy state of polymers containing *para*-phenylene linkages might be cited⁴⁴.

Extension of mechanical relaxation measurements to higher temperatures and to lower molecular weights

The Problem. Figure 1 is a generalized dilatometric, d.s.c. or d.t.a. determined glass temperature-log (molecular weight) plot for an atactic polymer whose limiting T_g , $T_g(\infty)$, is around 400K such as PS or PMMA. The insert is a schematic 1 Hz torsion pendulum loss curve on an atactic PS of molecular weight $\sim 100\,000$. (A schematic curve is used because no single investigator has reported for one specimen the five loss peaks shown.) The dynamic loss curve usually ends at a temperature corresponding to the minimum in $\tan \delta$ just above T_g . Very careful torsion pendulum work by Turley⁴⁵ has revealed on several specimens the $T_{l,l}$ loss peak indicated. In general, dynamic measurements normally must cease slightly above T_g because of excessive melt flow in the specimen. Thus, the shaded region above T_g is inaccessible to torsion pendulum (or Rheovibron) measurements because of viscous flow. However melt flow measurements by Ueberreiter and Orthmann⁴⁶ show some kind of viscoelastic relaxation behaviour above T_g (broken line) for both atactic PS and atactic PMMA. This broken line appears to represent an iso-viscous state associated with the time scale of their instrument. Nevertheless, there have been in the literature enough scattered reports about events in the liquid state above T_g in atactic polymers and above the melt in crystalline polymers to suggest that an *a priori* dismissal of this area is inadvisable.

At the same time, Turley⁴⁵ found it impossible to make coherent moulding of atactic polystyrene at molecular

weights of 20 000 or below. Hence the crosshatched area below the T_g line and to the left of molecular weight $\sim 20\,000$ is inaccessible for measurement by torsion pendulum or Rheovibron as those instruments are normally used. The lower limiting molecular weight will vary from polymer to polymer. In brief, both the liquid state above T_g at all molecular weights and the oligomeric region for T_g and below at less than some critical molecular weight are not available for examination by conventional dynamic mechanical spectroscopy.

We first recognized this situation in about 1969 when trying to prepare a review article on polystyrene⁴⁷. It then became apparent to us that the torsional braid analysis technique being perfected by Gillham⁴ offered the possibility of examining the entire molecular weight range as well as the entire temperature range up to the thermal decomposition temperature. A collaborative study on anionic PS from 600 to 2×10^6 molecular weight and on a fractionated thermal PS over a more limited molecular weight range has been mostly completed, using the temperature range from liquid N_2 to 300°C. Certain parts of the data are in press^{48,49} while other parts are being withheld because of some uncertainties about interpretation. The following summary can be made of both types of data.

(a) A dynamic T_g for anionic PS of molecular weight between 600 and 2×10^6 is available⁴⁸. The points lie consistently above the dilatometric values, as is normal for a dynamic test.

(b) The $T_{l,l}$ loss peak noted by Turley is found on both heating and cooling cycles and is completely reproducible. Below M_c , $T_{l,l}$ (K) $\sim 1.2 T_g$ (K) and $T_{l,l} \sim \bar{M}_n^{-1}$ ^{48,49}. Both facts suggest an iso-free volume state at $T_{l,l}$, which is consistent with an iso-viscous state

(c) The β loss peak is always below T_g being ~ 300 K for molecular weights down to 20 000 and as low as 190K for 600 molecular weight. As normally seen, it is a shoulder on the low temperature side of the T_g loss curve and hence must be approximated. Moreover, it shows marked hysteresis, being much more intense on reheating from liquid N_2 than on cooling below T_g . Since the curves are reproducible on subsequent cooling and heating, Gillham has postulated that crazing occurs at very low temperatures, with crazes being removed on heating back to T_g ⁵⁰. The large free volume existing in craze matter (up to 50%) is presumably responsible for the enhanced loss. The subject of crazes will be discussed later.

(d) The γ peak around 150K is not seen as such at any molecular weight⁵¹. The loss curves start to rise again below the normal γ region for all molecular weights and reach, at the lowest molecular weights, a maximum around 190–200K with height increasing as \bar{M}_n^{-1} . This loss peak might arise from catalyst end-groups, as first suggested by the n.m.r. measurements of Connor⁵² and later clearly assigned to CH_3 -rotation by Crist⁵³. However, a thermal PS fraction of molecular weight 3100 also shows such a low peak but at 100–110K⁵¹. It is also possible that the peak seen is somehow related to the δ loss mechanism normally occurring at 40–50K (1 Hz)¹. Again, because of such uncertainties, this data is being withheld from publication.

Meanwhile, Cowie and McEwen⁵⁴ have reported torsional braid values of T_g on PDMS oligomers. Since this polymer does not appear to have a β peak (see Table 1) and since crystallinity at about $1.2 T_g$ would suppress and/or hide a $T_{l,l}$, only T_g was reported (and presumably was the only peak to be observed). The apparatus used was an earlier non-automated torsional braid equipment.

Table 1 Dynamic studies of supported low molecular weight substances^a

Substance investigated	Support	Dynamic method	References
Various	Steel sheet	Vibrating reed	b
Alcohols	Porous crosslinked styrene-divinylbenzene films	Torsion pendulum (t.p.)	Illers ^c
Alcohols	Cellulose blotter	t.p.	Faucher and Koleske ^d
Oligomeric propylene glycols and butylene glycols	Cellulose blotter	t.p.	Faucher ^e
Oligomeric ethylene glycols	Cellulose blotter	t.p.	Faucher <i>et al.</i> ^f
Polyoxetanes	Cellulose blotter Al Foil sandwiches	t.p.	Stratta <i>et al.</i> ^g
Lactones	Bleached cellulose	t.p.	Koleske and Lundberg ^h
Plasticizers, curing systems	Glass braid	t.b.a.	Gillham ⁱ
Oligomeric PS	Glass braid	t.b.a.	Gillham <i>et al.</i> ^{48,49}
Oligomeric siloxanes	Glass braid	t.b.a.	Cowie and McEwen ⁵⁴
Itaconic acid esters above T_g	Glass fibre circles	Rheovibron	Cowie <i>et al.</i> ⁵⁶
Polybutadiene (PBD)	PBD of 10^6 MW	Forced shear vibrations	Sidorovitch <i>et al.</i> ^j

^a A low molecular weight substance is one which is too weak mechanically and/or which is too fluid to be used unsupported in conventional equipment. ^b See footnote 1, Table 1, ref 2. ^c Illers, K.-H. *Rheolog. Acta* 1964, 3, 13. ^d Faucher, J. A. and Koleske, J. V. *Phys. Chem. Glasses* 1966, 7, 202. ^e Faucher, J. A. *J. Polym. Sci. (B)* 1965, 3, 143. ^f Faucher, J. A., Koleske, J. V., Santee, E. R., Stratta, J. J. and Wilson, C. W. *J. Appl. Phys.* 1966, 37, 3962. ^g Stratta, J. J., Reding, F. P. and Faucher, J. A. *J. Polym. Sci. (A)* 1964, 2, 5017. ^h Koleske, J. V. and Lundberg, R. D. *J. Polym. Sci. (A-2)* 1972, 10, 323. ⁱ See ref 4 for general background and references. ^j See item 4 of Table 2

It is clear then that torsional braid analysis provides one solution to covering both the oligomeric range of molecular weights as well as the liquid region above T_g and/or T_M . While its frequency can be carried by using pendulums with different moments of inertia, the frequency range available is limited. The Rheovibron offers a more extended range of frequencies but cannot use the inextensible Gillham braid⁵⁵. Cowie *et al.*⁵⁶ have demonstrated the use on the Rheovibron of polymer-impregnated strips cut from non-woven glass fibre circles (Watmann GFC) to go above T_g with t.b.a. on some semi-crystalline polymers. The results obtained were similar to those using t.b.a. We used some GFC material supplied by Cowie⁵⁶ to study anionic PS of molecular weight 37 000, but appreciable flow occurred in the Rheovibron just above T_g . Inspired by Cowie, we used woven stainless-steel mesh strips cut at an angle of 45° to the warp and weft directions. This permitted obtaining well defined loss curves at several frequencies, showing T_{β} , T_g and $T_{l,l}$ on anionic PS of molecular weight 37 000^{57a}.

This section will be closed by reviewing two pertinent areas. The first concerns the fact that there have been many successful attempts reported in the literature to measure dynamic mechanical properties of low molecular weight compounds and of oligomeric polymer series. Because of our general interest in this area for reasons cited above, and because such a tabulation might inspire future work, we list in Table 1 the examples readily culled from our files. In all cases the low molecular weight substance is on or within a substrate that can withstand the applied mechanical force over the desired temperature range, while contributing little or no background loss.

The second point is that the scientific community has expressed friendly scepticism about the so-called $T_{l,l}$ transition first named and explained some years ago by us Gillham⁵⁰ and the present author both agree that since the braid may generate an artifact and since the event is not seen by conventional viscoelastic tests, scepticism is deserved until certain key issues are completely resolved, and answers

made available. Since the present author is proposing the liquid region above T_g as a fruitful area for future study, it is important that the joint Gillham-Boyer attitude be clearly stated*. Briefly:

(1) While we do not profess to understand the molecular basis for the t.b.a. observations, it is quite clear how the phenomenon can be observed with t.b.a. at will, and reversibly on heating and cooling, via the use of essentially monodisperse polymers having M_n values $\leq 100\,000$.

(2) The unambiguous dependence of $T_{l,l}$ on M_n^{-1} for molecular weights of narrow polymers and bimodal blends below M_c suggests a basic molecular mechanism, even if an interaction between glass braid and molten polymer is involved.

(3) However, several bodies of systematic data (variation of molecular weight) are now available in the literature on three atactic polymers using four different experimental methods. All agree that something with relaxational character occurs above T_g (Table 2).

(4) In one instance, a fraction of PMMA (25 000 MW) tested by one non-braid method in Germany was furnished to the t.b.a. programme. Essentially identical values were obtained for T_g and $T_{l,l}$ by both techniques, the braid values being slightly higher because of frequency^{57b}.

Table 2 is a summary of these eight systematic bodies of data. We believe that this tabulation should serve to encourage study of dynamic mechanical loss in the region above T_g in amorphous polymers and above T_M in crystalline ones.

Mechanical spectra of rarefied polymers

The mechanical spectra of amorphous and semi-crystalline polymers have been studied as a function of hydrostatic pressure by Zogel⁵⁸ and more recently by Tabor

* A position paper is currently being prepared and will appear as a long abstract in *Polymer Preprints* 1976, 17, (ACS San Francisco Meeting August 1976). This seems to answer all major objections thus far made against $T_{l,l}$ and the t.b.a. method.

Table 2 Systematic evidence for relaxation phenomena above T_g

Polymer (all atactic)	Molecular weight range	Support for polymer	Method	Reference
1 Polystyrene	500–5 x 10 ⁵	Glass plates	Melt fusion under pressure	Ueberreiter and Orthmann ⁴⁶
2 PMMA	1200–1.1 x 10 ⁶	Glass plates	Melt fusion under pressure	Ueberreiter and Orthmann ⁴⁶
3 PMMA	200–1.1 x 10 ⁶	None ^a	Thermal diffusivity	Ueberreiter and Naghizadeh ^{b,c}
4 <i>cis</i> – <i>trans</i> polybutadiene ^d	10 000–3.1 x 10 ⁵	PBD of <i>MW</i> 10 ⁶	Dynamic mechanical loss	Sidorovitch, Marei and Gashtol'd ^e
5 Anionic PS	600–2 x 10 ⁶	Glass braid	t.b.a.	Stadnicki, Gillham and Boyer ⁴⁸
6 Anionic PS		Al pan	d.t.a. ^f	Stadnicki, Gillham and Boyer ⁴⁸
7 Thermal PS fractions	1800–1.1 x 10 ⁵	Glass braid	t.b.a.	Glandt, Toh, Gillham and Boyer ⁴⁹
8 Thermal PS fractions		Al pan	d.t.a. ^f	Glandt, Toh, Gillham and Boyer ⁴⁹

^a Sample in form of a rod. ^b Ueberreiter, K. and Naghizadeh, J. *Kolloid. Z. Z. Polym.* 1972, 250, 927. ^c A fraction of PMMA, molecular weight 25 000 has been tested with t.b.a. Both methods essentially agree concerning T_g and a second event above T_g . ^d ~ 40% *cis*, 40% *trans*, 10% vinyl-1,2. Similar results were obtained but not reported on hevea rubber and a poly(propylene oxide) elastomer. ^e Sidorovitch, E. A., Marei, A. I. and Gashtol'd, N. S. *Rubber Chem. Technol.* 1971, 44, 166. See also *Polym. Sci. USSR* 1974, 16, 993. ^f Seen only on heating cycle of specimens in finely divided form.

It should be recalled that Cox, Isaksen and Mers, *J. Polym. Sci.* 1960, 44, 149 found a minimum in damping lying above T_g but below what we call $T_{1,1}$ which they could not observe. The temperature of this minimum increased with M_n while the magnitude of damping at the minimum decreased. Similar results for PBD are found in the references in footnote e

and his collaborators^{5,6}. Both amorphous and crystalline loss peaks are shifted to higher temperatures, as might be expected because of the decrease in free volume with pressure. Densified polystyrene prepared by the application of hydrostatic pressure in the melt above T_g with subsequent cooling under pressure has been measured at room temperature by Dale and Rogers⁵⁹, as well as by Price *et al.*⁶⁰.

The densification achieved in this latter reference was quite small, being only 1% at 3000 bars. The intensity of a secondary and the T_g peak of atactic polystyrene appeared to be suppressed in intensity by this densification. One cannot be certain if the effect arises from a decrease in free volume alone, or from different ordering parameters, i.e. different isomer content frozen in above T_g or both.

We suggest for the future that there may be some merit in studying polymers whose densities are less than normal and hence, with enhanced free volume. This is achieved to a very limited extent by quenching from above T_g which gives, at least for polystyrene, an enhanced β ($T < T_g$) amorphous loss peak⁶¹. This peak height is suppressed by annealing. We have in mind far greater volume changes than this.

Illers and Jenckel⁶² showed that the β peak in crosslinked styrene–DVB copolymers increased as the divinyl benzene content was raised from zero to 1 to 3 and to 9%. The effect was far greater than that normally achieved by quenching. Subsequent unpublished torsion pendulum results by Turley⁴⁵ on a styrene–1% DVB copolymer confirmed the enhanced β peak.

While one normally expects crosslinking to increase density and decrease free volume, the exact opposite can occur in some instances. For example, Ueberreiter and Otto-Laupenmüehlen⁶³ cast a series of styrene–DVB rods containing 5, 10, and 15% DVB. These cast rods were cooled slowly from 200°C to room temperature at which tempera-

ture densities of 1.047, 1.021 and 1.005 g/cm respectively were measured. Presumably the normal shrinkage, which occurs both during polymerization and subsequent cooling, was inhibited by crosslinks and a substantial decrease in density resulted.

A further but less dramatic indication of this same effect is afforded in the data of Millar⁶⁴ on S–DVB 18–50 mesh beads prepared in suspension. The density goes through a slight minimum at 2 to 4% DVB before starting to climb sharply. This could result from a competition between the shrinkage effect already discussed and the normal tendency of crosslinkers to increase density. This shrinkage effect should be smaller, the smaller the dimensions of the polymerized system.

It might be thought that the presence of physical crosslinks would drastically alter glassy state relaxation processes, and this may in fact prove true. However, with one crosslink every 10 or 20 monomer units, and with the β process involving only one or two monomers along the chain¹, it does not appear too likely that effects other than from free volume will be effective. Takayanagi and coworkers⁶⁵ have clearly shown that high levels of crystallinity (which we consider to act as physical crosslinks) do not appreciably affect either the temperature or the intensity of the β relaxation in poly(ethylene terephthalate).

If one assumes a value of 10% as the effective free volume at T_g , and presumably in the glassy state not too far below T_g then a 5% decrease in density is a 50% increase in free volume. Correspondingly a 1% increase in density by densification means a 10% decrease in free volume.

Further it is known from the studies of Lloyd and Alfrey⁶⁶ that addition of an inert diluent to a styrene–DVB system prior to polymerization, and subsequent removal of the diluent, leads to a control of porosity (and even the shape of the pores depending on amount and type of diluent)

Table 3 Relative intensities of β (local mode)^a amorphous relaxation peaks

Polymer	Crystalline form ^b	Strength of β peak ^c	Reference
Polyethylene	Planar zig-zag	Strong	(l), h
Poly(vinyl fluoride)	Planar zig-zag	Strong	d
Poly(vinylidene fluoride)	Planar zig-zag	Strong	e
	Helical	Weak	e
Isotactic PS	Helical	Weak	f
Atactic PS	Mixed iso-syndio-hetero	Strong	f
Isotactic PMMA	Isotactic	Weak	g
Syndiotactic PMMA	Syndiotactic	Strong	g
Isotactic polypropylene	Helical	Weak	h
Polyisobutylene	Helical	Absent	i, j
PDMS	Helical	Absent	k, l
<i>Cis</i> -polybutadiene	No crankshaft ⁿ	Weak	m
<i>Trans</i> -polybutadiene	Crankshaft ⁿ	Strong	m

^a The β (local mode) loss peak arises in the amorphous phase as well as in crystal defect regions. ^b It is assumed that some tendencies for the indicated conformation will persist in amorphous regions where β peak occurs. ^c Strength of a sub-group relaxation is not well defined. In general, we use whatever measure appears in the literature. See also Figure 2. ^d Osaki, S., Nemura, S. and Ishida, Y. *J. Polym. Sci. (A-2)* 1971, 9, 585; Kawasaki, N. and Hashimoto, J. *J. Polym. Sci. (A-2)* 1971, 9, 2095. ^e Kakutani, H. *J. Polym. Sci. (A-2)* 1970, 8, 1177. ^f Reference 45. ^g Figure 5 of ref 4. ^h Flöcke, H. A. *Kolloid Z.* 1962, 180, 118. Data on PE also appears in this article. ⁱ Morgan, R. J., Nielsen, L. E. and Buchdahl, R. J. *Appl. Phys.* 1971, 42, 4653. There is methyl group rotation below T_g . See Figure 9 of ref 10. ^j It is not known if symmetrical substitution plays some role. As mentioned in the text the β peak may lie under the T_g peak. ^k Figure 34 of ref 10. ^l Symmetrical substitution again. ^m Figure 2 of footnote i. ⁿ Morgan *et al.* (footnote i) above suggest that a slightly imperfect crankshaft is possible in the amorphous phase for the *trans* but not for the *cis* isomer

Small amounts of diluent might be removed from linear polymers by freeze drying techniques although such porosity would almost certainly collapse on heating the specimen near T_g . The porosity induced in crosslinked polymers by diluents is probably much more stable near and above T_g .

We also note that 'popcorn' polymers prepared by proliferous polymerization⁶⁷ as with S-DVB, can naturally attain densities as low as 0.3–0.4 g/cm, with apparently a complete range in densities possible up to ~ 1.05 ⁶⁸.

Finally, controlled crazing offers another technique for introducing microvoids. This crazing may be developed under simple tension on the glassy polymer as was carried out by Maxwell and Rahm⁶⁹ on polystyrene or on a rubber modified glassy polymer such as rubber modified polystyrene, in which crazes developed at each rubber particle on flexing⁷⁰. Such crazes tend to heal themselves and disappear when the specimen is heated above T_g . As indicated earlier crazes induced in PS by deformation at low temperature definitely enhance the intensity of the β peak.

One might rationalize the enhanced β peak with increased free volume as follows: the opportunity for local mode relaxation is probably much greater at the surface than in the interior of a specimen. Generation of large amounts of internal voids would be expected to enhance the intensity of the β peak and possibly to shift its location and/or breadth along the temperature scale.

In summary, we suggest that control of free volume by one or more of the techniques just enumerated offers new opportunities for investigating the nature of relaxation processes in the rarefied glassy state.

Nature of the in-chain β relaxation in addition polymers

The in-chain β relaxation is an amorphous phase process lying below T_g . For addition polymers (vinyl, vinylidene, ring opening, and some self condensing monomers such as 2,6-dimethylphenol) in which the motion about the chain axis must be similar in type but smaller in extent than the motion at T_g , we know from the original finding of Matsuoka and Ishida⁷¹ as later modified and refined by Boyer^{2,29} that:

$$T_{\beta}(100 \text{ Hz}) \equiv (T < T_g)(100 \text{ Hz}) \cong 0.75 T_g(100 \text{ Hz}) \quad (1)$$

for a large number of examples but not all. It seems true for many amorphous and semi-crystalline polymers. The author has interpreted this relationship to imply that the motion occurring at T_{β} is a precursor of that which will occur at T_g ⁷². The presumption here is that the local mode motion (see pp 182–85 of ref 1 for definition) associated with T_{β} occurs in isolated pockets of free volume and that these pockets coalesce at T_g . Moreover Goldstein⁷³ has predicted on theoretical grounds that every T_g should have a $T < T_g$ or T_{β} process.

The key question which remains for the future is: why is this β process missing completely or exceedingly weak in many common polymers? For example, it is missing in PIB, PVDCI, PDMS, isotactic PMMA, isotactic PS, etc. Janssen has concluded^{30,32} that in some cases T_{β} is hidden under the T_g loss peak and can be resolved by suitable data treatment techniques which he has developed. Even so, it would seem that the Goldstein hypothesis, equation (1), and the precursor argument all fail in such instances.

Even though the detailed answers are not available, Table 3 assembles some literature data indicating that both chain geometry as well as chemical structure may play a role in the intensity of the β peak. In pairs of cases where the chemistry is identical, planar zig-zag vs. helical, *trans* vs. *cis* and syndiotactic vs. isotactic appear to be crucial with the first of the two giving a stronger β peak. This is further developed numerically in Table 4 for a few polymers using definitions shown in Figure 2. We show two measures for intensity of the β peak: absolute height on a given loss scale (whatever used by the investigator) and difference between peak height and an assumed background. Heijboer¹¹ has recommended for such weak secondary loss peaks an integration of the area between peak and background vs. $1/T$ but present circumstances do not warrant such detail. Table 4 gives some quantitative feeling for the qualitative statements made in several cases cited in Table 3.

Heijboer⁷⁴ has concluded that apparent activation energies, ΔH_a , for these secondary or β loss peaks are determined by

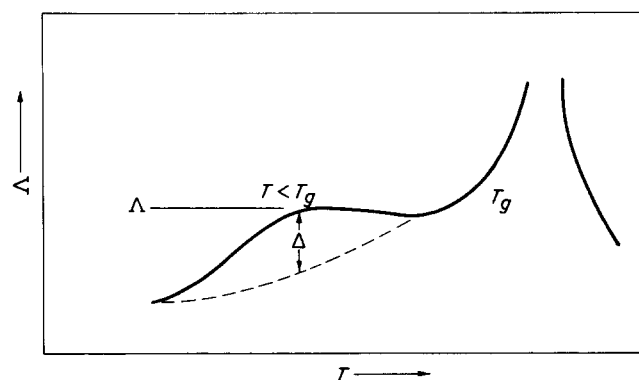


Figure 2 Two definitions of β peak intensity used in connection with Table 4

Table 4 Relative intensities of β ($T < T_g$) peak as defined in Figure 2

System	f (Hz)	Structural comparison	$\Delta/\Delta_{\text{helical}}$	$\Lambda/\Lambda_{\text{helical}}$	Data source
Poly-styrene	1	Anionic/ quenched isotactic	2	4	Turnley ^a
PMMA	1	Atactic/ isotactic	3.6	2	Gillham ^b
PE/PP	1	Planar zig- zag/helical ^c	6	4	Flöcke ^d
PVF ₂	10	Planar zig-zag ^e helical ^f	-9	2	Kakutani ^h

^a Ref 45; ^b Figure 5 of ref 4; ^c comparison based on specimens of about equal crystallinity; ^d Flöcke, H. A. *Kolloid. Z.* 1962, **180**, 118. ^e oriented or cast from solvent; ^f unorientated; ^g $T < T_g$ loss peak not well defined; ^h Kakutani, H. J. *Polym. Sci. (A-2)* 1970, **8**, 1177

local intramolecular barriers to motion about the chain axis. Strong intermolecular steric hindrance decreases the intensity of the loss maxima but leaves ΔH_a unchanged. These conclusions raise several problems. If T_β is indeed a precursor for T_g , a heavy intramolecular component to T_g is implied. This is consistent with the fact that the methyl side group in PMMA raises T_g 100K over the value for poly(methyl acrylate). Heijboer's view is substantiated by the findings of Amrhein *et al.*⁷⁵ that dielectric loss in PMMA solutions still shows the β loss peak because, they conclude, it has an intramolecular origin.

On the other hand, an intense dielectric β peak has been reported for the relatively rigid coplanar molecule, σ -terphenyl⁷⁶. This would appear more in harmony with Goldstein's view of the nature of the glassy state than of Heijboer's internal energy barrier.

Molecular probes for motion in highly crystalline polymers

Introduction. Highly crystalline polymers such as linear PE, POM, isotactic polypropylene, PVF, PVDF etc. are composites consisting of three types of interconnected material in either the chain folded or fringed micelle models: high modulus crystallites; lower modulus crystalline defect regions, amorphous regions with low modulus above T_g , high modulus below T_g . Some amorphous material may be unconnected to the crystallites, or possibly adsorbed on them⁷⁷.

Dynamic mechanical measurements of necessity yield the properties of the composite at any temperature and frequency, with the amount of crystallinity and overall morphology being very important. From an engineering point of view, dynamic properties of the composite are important because they should correlate with end use behaviour. However, this composite structure greatly complicates a thorough understanding of molecular motions in the several regions named above. There are three key problems:

- identification of the phase in which each loss peak occurs;
- effect of fractional crystallinity, χ_c , on the temperature of amorphous and crystalline relaxations and transitions;
- effect of χ_c on the intensities of each relaxation. This in turn assumes knowledge of how to define and measure intensity.

In spite of 20 years or more of efforts to resolve these problems, much controversy still exists, especially in regard to the value of T_g for such highly crystalline polymers (see Figure 1 of ref 29). Therefore, it seems pertinent to review briefly the approaches taken in the past before proposing how one might proceed in the future. The examples deal mainly with PE, POM and PP.

McCrum and his colleagues varied thermal history to control relative amounts of amorphous and crystalline phase, and morphology¹. They were also concerned with the proper mechanical loss function ($\tan \delta$, decrement loss, modulus loss, compliance etc.) to use in describing the dynamic behaviour of crystalline composites as a function of χ_c ³⁵. Recently McCrum has worked with the so-called T jump method⁷⁸, as well as the effect of annealing *versus* quenching on mechanical loss in PE⁷⁹.

Takayanagi and his colleagues extended this work in several directions including modelling, i.e. series models, parallel models and mixed series-parallel models for the two phases; and secondly, study of single crystal mats in which the amorphous phase was extremely small in volume^{7,8,21,65}.

Illers has varied branching, crystallinity, morphology, radiation crosslinking and the use of diluents in studying the relaxation behaviour of polyethylene²²⁻²⁵.

Ward¹⁷⁻²⁰ has studied mechanical spectroscopy, coupled with other techniques, for highly oriented polyethylene. Takayanagi *et al.*²¹ have also used orientation as a tool in studying molecular motion as have Buckley and McCrum.

Kardos and Raison⁸¹ have proposed using very specific models based on analogues with two-component engineering composites. Thus, for the crystalline phase in PE, the spherulite is modelled as a two-dimensional disc whose radius is the lamellar crystal length. The bulk polymer is considered to consist of many such spherulites whose lamellae lengths are oriented principally in one plane of the flat specimen. Observed values of stiffness and thermal expansion vary with crystallinity and morphology in a manner consistent with such a model.

This listing by no means exhausts the names of workers or techniques devoted to mechanical loss in highly crystalline polymers. For example, we have proposed⁸² two simple models to describe respectively the effect of crystallinity on the glass temperature(s) of polymers and the variation in strength of the T_g and $T < T_g$ or T_β relaxations with crystallinity. Dielectric and n.m.r. studies have been reported extensively in the literature as an adjunct to mechanical loss.

However, all of the above considerations convince us that mechanical spectroscopy must be supplemented in the future by one or more techniques not currently in common use. The nature of the problems and the likely origins of the continuing controversy about T_g have been discussed in detail by McCrum⁸³. He concludes *inter alia* that the amorphous forms of linear crystalline polymers are not in all respects identical to the amorphous forms of other polymers and hence one must first define what is meant by the T_g of crystalline polymers.

For purposes of continuing discussion of this problem, we include Figure 3. This Figure shows three types of experimental results. The upper curve is the 0.2 Hz torsion pendulum plot for the T_g of ethylene-propylene copolymers as measured by Tuijman⁸⁴ and further modified in Figure 10.14 of ref 1. To the right of the minimum, as pure PE is approached, T_g is more generally known in the literature as T_β . The lower curve is a plot made by Illers⁸⁵ of dilatometric T_g values for another series of E-P copolymers,

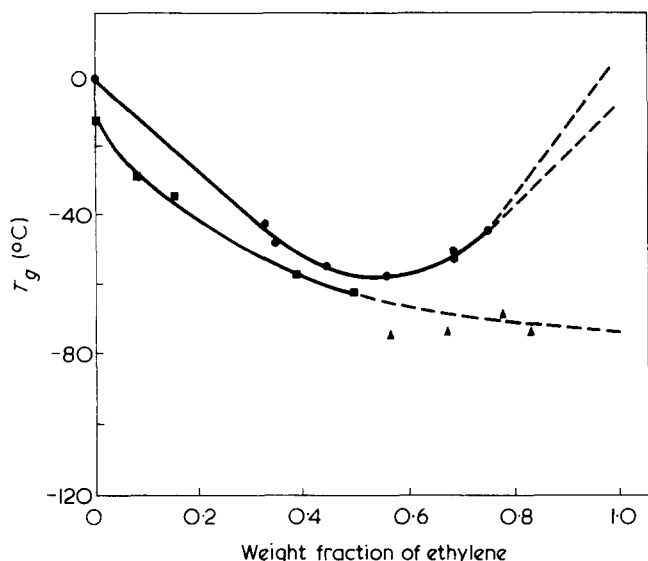


Figure 3 Glass temperatures of ethylene/propylene copolymers as measured by 0.2 Hz torsion pendulum (●)⁸⁴; dilatometry with extrapolation to 100% amorphous PE by the Gordon–Taylor equation (■)⁸⁵; and e.s.r. spin probe technique (▲)^{87–89}

with extrapolation to a value for amorphous PE by the Gordon–Taylor copolymer equation. This places T_g of amorphous PE at Iller's well known value of 196K. The broken straight line is one sometimes found in the literature as the proper extrapolation to a T_g around 150K. We have argued elsewhere⁸⁶ against such a conclusion because the γ relaxation is found independently of T_g in all E–P copolymers for which there is no ambiguity about T_g , as well as in PE for which there is doubt.

The four square points at high ethylene content were obtained by an e.s.r. technique employing a nitroxide probe^{87–89}. We will comment more on this later but suggest for the moment that this probe technique reinforces the Iller's extrapolation via the Gordon–Taylor equation by measuring motion in the amorphous regions over small volume regions.

The main conclusion from Figure 3 is that a dynamic mechanical test on PE gives the T_g of a composite specimen. This T_g is real and is the proper value for such a highly crystalline two phase material. This is the T_g of amorphous material connected to the crystalline material probably at both ends, as in a loop²⁹. It is not the T_g of free (rejected) molecules or of cilia connected at only one end to the chain folded crystal²⁹. It is our belief that the T_g of such amorphous material within a composite semi-crystalline polymer can best be seen only with some type of molecular probe.

Molecular probes. There is nothing novel about proposing molecular probes to study motion in highly crystalline polymers. Bergmann⁹⁰ has demonstrated the power of the n.m.r. technique in revealing the onset of proton mobility in PE and other semi-crystalline polymers; North⁹¹ has recently reviewed the use of luminescence techniques, among which that of Guillet⁹² is prominent. Our own interest is in the use of nitroxide free radical probe molecules to detect the onset of molecular motion in amorphous and semi-crystalline polymers. There are several reasons for this choice: (a) ready availability of a variety of nitroxide probes of different molecular weights and shapes; (b) low level of additive needed (10–50 ppm) because of the extreme sensitivity of the e.s.r. technique; (c) ease of constructing calibration curves between a characteristic e.s.r. signal from a large probe and T_g values of known polymers^{87,89,93,94}; (d) indica-

tions are that smaller probes may be used to calibrate for the onset of motion at secondary relaxations⁹⁵.

A rather sophisticated application of the e.s.r. technique has been reported for PE by Bullock *et al.*⁹⁶ who have used the same nitroxide molecule both as a free probe and as a tag or label chemically bound to the backbone chain. This probe is smaller than any studied by us^{87–89}. It appears from their Figure 6 that this small probe may be responding to the γ relaxation even though the mechanical relaxation peak is normally insensitive to crystallinity variation^{22–25}. However, it may be responding to the amorphous phase T_g around 195K, which is presumably sensitive to crystallinity level. A firm conclusion about T_γ or T_g is not warranted in the absence of a calibration curve for this specific probe.

Finally, it appears from their Figure 5 as if the nitroxide tag is observing the β relaxation, i.e. the T_g of the composite. This would be the case if, for example, the tag were carried on a loop because it has been rejected by the chain folded crystal. It would then follow the motion of the loop, the motion we associate with T_β ²⁹. Bullock *et al.*⁹⁶ appear to believe that this label can rotate freely about the backbone chain, although forced to rotate anisotropically. In our experience, the drop in line width starting at about 250K would be consistent with seeing β motion.

Figure 4 is a schematic plot for PE combining the probe and label data of Bullock *et al.*⁹⁶ with results on two sizes of probes (both larger in size than Bullock's) by Rabold⁹³, as subsequently confirmed by the author and colleagues^{87–89,95}.

Figure 4 is intended to suggest possibilities for understanding complex relaxation spectra in semi-crystalline polymers by using free probes of different size in addition to tags.

Our current experience in using free nitroxide probes in semi-crystalline polymers is not free from problems^{87–89}. Four samples of PE gave T_g values of 201, 201, 220, and 233K, suggesting that probes are not always immune to morphological influences. Experience with POM, PEO and PVF have been satisfactory; that with PVDF is a complete failure for reasons not yet elucidated but probably connected with morphology^{87–89}.

In conclusion, we suggest that the e.s.r. probe and tag techniques will be a valuable adjuncts to, but not replacements for, mechanical spectroscopy. Other probe techniques

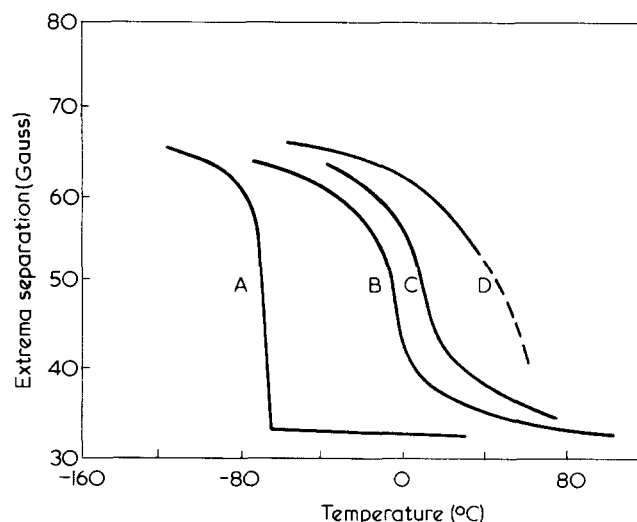


Figure 4 Line width vs. temperature by e.s.r. technique in PE for: A, very small probe showing either T_γ or amorphous T_g ⁹⁶; B and C, probes of increasing size showing amorphous T_g ⁹³; D, spin label⁹⁶ which appears to reveal T_β

are not thereby rejected. In fact, the dielectric probe studies of Davies and Edwards⁹⁷ for polystyrene might be cited. Although higher quantities of added probe are required, the essentially spherical molecule, camphor, *MW* 136, lies on a common curve with our nitroxide probes of molecular weight 172 and higher.

It will be suggested later that availability of high molecular weight fractions which are slow to recrystallize will permit examination of PE, PEO, POM and other such polymers by mechanical spectroscopy with no or only minor complications from crystallinity. The work of Illers²² suggests that moderate amounts of crystallinity may have little effect on the loss spectra of PE.

Computer simulation of in-chain sub-group molecular motions for addition polymers

As above, this section is concerned only with cases where the relaxing subgroup is identical in structure to the rest of the chain, as for example in linear PE for which the γ subgroup relaxation at $\sim 150\text{K}$ involves $-(\text{CH}_2)_n-$ where n is a small number, perhaps ≤ 7 . Boyd and Breiting have developed computer techniques involving both intra-chain and inter-chain barriers for simulating the motion of small units in the polymer backbone. This was first demonstrated for PIB only as an exercise in possible backbone chain motions, not in activated relaxation processes⁹⁸.

Such techniques were then extended to a conformational analysis of crankshaft motions in polyethylene⁹⁹⁻¹⁰⁰, namely the γ relaxation. Different proposals for crankshaft motion reported in the literature, such as the Schatzki or the Boyer crankshafts (Figure 5.8 of ref 1) could be examined rigorously. It is possible to calculate the intra-chain energetics and also to simulate the possible effects of the surrounding matrix. Even more recently a simulation has been made for the energetics of kinks in PE, using crystalline arrays of C_{14} , C_{18} and C_{22} linear paraffins¹⁰¹.

These simulation methods would appear to be limited ultimately by computer time and ingenuity in devising computational routines to shorten this time.

We are not concerned here with the important parallel task of devising models for specific sub-group motions such as the glycol unit in PET¹⁰², the phenyl side group in PS¹⁰³ or the generalized local mode motion in addition polymers¹⁰⁴, and analysing such motion either experimentally or theoretically or both.

Structure of the amorphous state and its possible effect on mechanical loss spectra

There is currently considerable world wide interest in the nature of the amorphous state in polymers¹⁰⁵⁻¹⁰⁹. One prevailing opinion, based on recent neutron scattering experiments, is that an amorphous polymer such as atactic PS or PMMA; or the melt of a crystallizable polymer; or an amorphous elastomer consists of an assembly of randomly coiled inter-penetrating molecules with each polymer chain having essentially theta dimensions¹⁰⁵⁻¹⁰⁷. Still uncertain is the extent of short range or local order, such as whether there might be a correlation of molecular orientation among neighbouring chains greater than expected for random coils but still less than will show long range order by scattering of X-rays, electrons or visible light. One study shows PS of *MW* 21 000 to 1.1×10^6 to be random to 10 \AA ¹¹⁰.

Now the mechanical relaxations with which we are concerned (with the possible exception of the $T_{l,1}$ process) involve relatively short sections of a polymer chain i.e. 20-30 monomers at T_g , 1-2 monomers at T_β and less than an

entire monomer unit at T_γ and T_δ . Hence, the question must be whether such local relaxations are sensitive to local order, if such exists.

We have studied on several occasions²⁹ a hypothesis by Bunn¹¹¹ that the empirical rule, $T_g(\text{K}) \cong (2/3)T_M(\text{K})$, is consistent with the presence of short range order in the amorphous phase. While one cannot prove this hypothesis conclusively, a number of facts are in harmony with it.

However as mentioned above, Amrhein *et al.*⁷⁵ have shown that dielectric loss curves of either iso- or syndiotactic PMMA in concentrated solutions (15 and 48%) in toluene occur at lower temperatures but are essentially similar to those of the bulk polymer. They conclude that intra-chain barriers to rotation are playing the dominant role in such motion. This would seem to suggest that the nature of the bulk state in these polymers plays no significant role beyond affecting free volume and hence the temperature at which a relaxation will occur. Presumably the relative intensities are also affected. Regions of demixing occur in the 15 and 40% solutions and act as crosslinks.

Ito and Hatakeyama^{112,113} have attempted to introduce local order into PET¹¹² and into polycarbonate¹¹³ by controlled orientation. Dielectric and mechanical loss do change in a very definite pattern with draw ratio. The frequency of the maximum in dielectric loss changed in the same manner at T_β as at T_g . They consider that the local mode process does reflect the structure of the glassy state. We cite these two papers as indicative of concern about relaxation spectra and structure of the glassy state.

We have attempted¹¹⁴ to explain the extreme breadth of the β relaxation in atactic polystyrene, namely from about 170 to 370K at 1 Hz, as arising from the extremes of variation of free volume in the glassy state. Following an argument of Robertson¹¹⁵, it has been assumed that a random array of matchsticks (polymer chains) will have only about 60% of the density of a regular parallel array, with many polymers showing an amorphous to crystalline density ratio of about 0.9. Therefore, one can visualize a free volume range from 0 to 40% with an average around 10%. An increase in T_g of 500 to 700K per cm^3/g decrease in free volume has also been estimated. We assume similar values might hold for T_β . Thus a range in free volumes from 0 to 40% might correspond to a spread in the β peak of 175-250K, in agreement with the observed value for atactic PS.

Finally it has been noted many low molecular weight glasses show β and T_g relaxations not too dissimilar in overall characteristics from those in polymers. For such glasses there can be only a short range, local liquid-like order with no long range physical connectivity between different parts of the glass, as in the case of polymers. It would appear from these simple considerations that local structure of the amorphous state other than distribution of free volume, may not play a role in glassy state relaxations. However, we mainly pose the problem for the future to answer.

Room temperature impact of glassy polymers in relation to glassy state relaxations

It is now known that the room temperature impact strength of polymers whose T_g is above room temperature may vary by several orders of magnitude. It is also known from the classical work of Bohn and Oberst¹¹⁶, as well as Staverman and Heijboer¹¹⁷, that for certain polymers room temperature impact is higher if a strong $T < T_g$ relaxation, a β peak in amorphous polymers, exists below room temperature (provided this is due to an in-chain and not a side

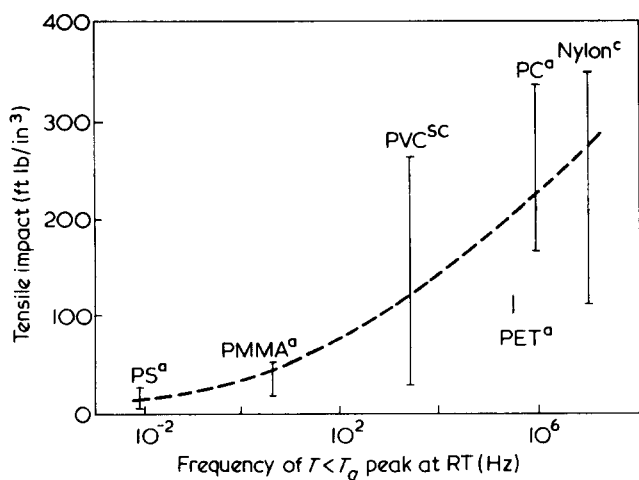


Figure 5 Tensile impact at room temperature plotted against the estimated frequency of the glassy state β or local mode relaxation at room temperature. The latter can be estimated from relaxation maps in ref 1. They may have torsion pendulum 1 Hz relaxation peaks at very low temperatures, i.e. nylon, 150–160K; PC, 180K. a, Amorphous; sc, slightly crystalline, c, crystalline

chain motion). This general topic has been reviewed both by Heijboer¹¹⁸ and by the present author¹¹⁹.

We have recently tried to refine the basic ideas of Bohn and Oberst with the hypothesis that room temperature impact should correlate with the measured or calculated frequency at room temperature of the most dominant subgroup in-chain motion. This frequency, determined dielectrically and/or mechanically, will be higher the lower is the temperature of the $T < T_g$ relaxation at 1 Hz and the higher its apparent energy of activation. Using scattered data from the literature on Izod, tensile impact and elongation at break, one could observe that high frequency of the subgroup motion at room temperature correlated well with high toughness. These data were presented in tabular form¹²⁰. Figure 5 shows a plot of tensile impact strength against log frequency. The scatter is considerable, which is not unusual in view of the nature of catastrophic tests and their sensitivity to flaws. Moreover, the data came from a variety of investigators.

Manson *et al.*¹²¹, aware of the above correlations, found that one characteristic parameter in fatigue studies, namely fatigue crack sensitivity, FCS , (rate of change of fatigue crack propagation per decade change in test frequency at room temperature) correlated with the room temperature jump frequency of the β process.

Sacher¹²² has shown a good correlation between toughness evaluated from stress-strain curves (Instron) and dynamic $\tan \delta$ (Rheovibron) at 11 Hz and 10°C.

It is evident in the two cases^{121,122} where one investigator(s) collects the data that the correlation found is significantly better than that shown in Figure 5. This clearly points out a future need.

Deformation and rupture processes in tough, glassy polymers pose a number of complex problems. We have enumerated some of them on a prior occasion (pp 342–347 ref 114). There is, however, a simple rationale for behaviour such as that shown in Figure 5. Application of a tensile stress generates a bias favouring rearrangement of bonds by rotation over energy barriers and/or free volume barriers. A high frequency of rotation in the absence of stress presumably facilitates such motion, leading to facile glassy state deformation in the presence of a stress. Argon has treated

the problem of deformation in glassy polymers in some detail (pp 411 ref 114).

There is now a rather dramatic new development in n.m.r. which can have a profound impact on the subject matter of this section. Schaefer *et al.*¹²³ have shown that by use of ¹³C n.m.r. with magic angle spinning, the motion of chemically unique carbon atoms in the main chain and side chain of bulk polymers can be followed in detail. Thus, they have been able to differentiate between the frequencies of motion of the 5 carbon atoms of a monomer residue in the PMMA chain. Each one has a characteristic frequency and some of the frequencies are quite high (especially $-\text{CH}_2-$ and $\text{CH}_3-\text{O}-$ groups) in comparison with the normal 1 Hz mechanical motion associated with the β relaxation. Thus far, such measurements have not been made as a function of temperature¹²⁴.

Schaefer and his associates^{125,126} have now extended this work to obtain a correlation between motions of carbon atoms in a selected group of polymers and notched impact strength. They observe crosspolarization relaxation times, T_{CH} , which contain information in the near zero frequency range; and ¹³C rotating frame relaxation times, $T_{1\rho}$, which contain information about motion in the 10–50 kHz range. An empirical correlation shows that a high ratio of $T_{\text{CH}}/T_{1\rho}$ is associated with high notched impact strength and *vice versa*. It seems clear that a technique such as this which follows motion of individual carbon atoms in bulk polymers can really help to clarify all types of mechanical behaviour problems such as crazing, shear band yielding, creep and impact strength, especially once such measurements are made over a range of temperatures.

Amorphous state of rapidly crystallizing polymers and copolymers

This topic naturally relates to the section on molecular probes for highly crystalline polymers but has been deferred because of required background material in subsequent sections.

We have stated on an earlier occasion²⁹ that certain questions relating to T_g for the amorphous state of highly crystalline polymers such as PE, PEO, POM, etc. will not be answered unambiguously until the amorphous state of such systems is achieved experimentally. Several recent events have revived our interest in this topic as one for much consideration in the future.

The first is that Hendra *et al.*¹²⁷ have reported the preparation via rapid quenching of amorphous PE and its subsequent recrystallization as a function of temperature. I.r. crystalline bands at 720 and 730 cm^{-1} were used as the measure for crystallinity. They conclude from the development of these bands with temperature of subsequent annealing that T_g of amorphous PE must lie below 190K, presumably because recrystallization normally occurs only above T_g . While we accept their experimental findings without reservation, some caution is indicated concerning their conclusion on T_g in view of material produced above especially Figures 3 and 4, and considerations introduced.

Without trying to pre-judge this matter categorically, we suggest that their results are not inconsistent with an amorphous T_g of about 195K for the following reasons.

(1) Order present in the crystalline material is not necessarily completely destroyed by a simple melting regime. Short range order reported by Zachmann¹²⁸ for PE melts could then be preserved in the quenched specimens, predisposing them to recrystallize, especially with the marked undercooling.

(2) Semi-crystalline PE shows²²⁻²⁵ 1 Hz torsion pendulum loss peaks at 108K in the crystalline regions and at 138 and 163K in amorphous regions which may be subject to some restraint by the crystallites. As noted above, especially in regard to Figure 5, 1 Hz loss peaks at low temperature can move much more rapidly at elevated temperatures. Hence frequencies of 10^4 – 10^6 Hz in the region of 180–200K are not unlikely. An e.s.r. spin probe (Figure 6, ref 96) is probably rotating at 10^6 Hz at 190K and 10^8 Hz at 210K. This does not prove, of course, that chain segments are moving this rapidly.

(3) The absence of side groups favours recrystallization.

(4) Their PE specimen is a commercial material and, hence, heterodisperse. Limited evidence above suggests that all glassy transitions decrease in temperature with decreasing molecular weight so that transition temperatures just given may be considerably lower for short chains and effective frequencies at 180–200K higher than estimated.

(5) Nylon-6,6 recrystallizes at temperatures some 80K below its nominal T_g ¹²⁹, which most likely is a result of the prominent 1 Hz γ loss peak in nylons around 150–160K*.

The issues we have raised are amenable to experimental attack but would seem to require a high molecular weight monodisperse PE (a fraction) with a carefully controlled history in the melt.

The other recent development is that MacLaine and Booth¹³⁰ have succeeded in preparing by fractionation amorphous high molecular weight PEO and following its rate of recrystallization. A fraction of MW 1.6×10^6 had a limiting fractional crystallinity of 0.4 when recrystallized at 57°C.

We were able to obtain a small amount of a fraction having MW 1.1×10^6 in order to check T_g by several methods¹³¹. A preliminary d.s.c. run on a Perkin–Elmer II unit by MacDonald¹³² showed no evidence for a T_g but did give a strong endotherm at T_M . It appears that the specimen had become highly crystalline while held at ambient temperature for four months. The maximum rate of recrystallization for PEO occurs at 20°–25°C¹³³, consistent with the d.s.c. observations. Quenching from just above the melt generated a small amount of amorphous material. Other parallel studies of melting for 2½ h at 100°C and for 10 min at 130°C were insufficient to remove all crystallinity. Thus high molecular weight and monodispersity slow down recrystallization and also remelting.

Our experience with e.s.r. at a frequency of 10^7 Hz indicates that since T_{50G} is usually 40°–50°C above T_g , rapid recrystallization may occur during e.s.r. measurements, entrapping the probe molecule and leading to a high estimate of T_g .

At the moment enough has been done to demonstrate the preparation of amorphous PE and PEO. Dynamic mechanical measurements on such amorphous materials remain for the future.

New polymer types

One can predict the appearance of challenging new polymer types without being specific. One need only consider the challenges presented by two-phase polymer systems: block, graft, interpenetrating polymer networks, and poly-

blends. The advent of a class of synthetic polymers with rings in the chain (polycarbonates, poly(phenylene oxides), polysulphones, etc.) generated a new set of problems, especially when considering mechanical properties via a vis relaxation spectra. The ionomers²⁶ were mentioned very briefly above as possibly being at the threshold of some surprising new developments, especially in view of unpublished work by Eisenberg¹³⁴ as, for example, a new peak above T_g which correlates in intensity with ion content.

CONCLUSIONS

The areas chosen as likely candidates for future effort in mechanical spectroscopy cover apparatus, materials and experimental as well as theoretical techniques. Most of them, understandably, are areas in which we have had a strong interest and/or some measure of interaction in the recent past. It is evident that progress made on the mechanical spectroscopy of polystyrene^{48,49}, both above T_g and at low molecular weights, was heavily dependent first on the automation of the t.b.a. equipment⁴ and second on the commercial availability of anionic polystyrenes from 600 to 2×10^6 MW. Many polymers, such as PMMA, are not readily amenable to preparation by living polymer techniques. Until sizeable fractions (1–10 g) of narrow distribution atactic, isotactic and syndiotactic PMMA are available by any means, progress in studying these materials will lag far behind PS. The same can be said of poly(vinyl acetate), poly(isobutylene), polypropylene, PVC and many other polymers. Any simple technique to give high molecular weight fractions of PE, PEO, POM, PVDF, PVF and other rapidly crystallizing polymers will be tremendously important. Therefore, the pace of progress in the near future – five to ten years – will rest heavily on automation of mechanical spectroscopy to simplify acquisition of data; on easy availability of good, relatively monodisperse materials; on new polymer types; and on characterization breakthroughs, in related fields, as in ¹³C n.m.r.^{123–126} and e.s.r.^{87–96}.

Failure to include any results based on dielectric techniques was dictated almost entirely by a need to limit the scope of this article, and not by any lack of appreciation for this powerful tool. If one could cite a single example, it is the dielectric study by Irvine and Work¹³⁵ on copolymers of *para*-methyl- and *para*-chloro-styrenes in order to elucidate the nature of the δ relaxation mechanism in polystyrene. North¹³⁶ has a recent review on dielectric relaxation, with special reference to two phase systems.

REFERENCES

- 1 McCrum, N. G., Read, B. E. and Williams, G. 'Anelastic and Dielectric Effects in Polymeric Solids', Wiley, New York, 1967
- 2 Boyer, R. F. *J. Macromol. Sci. (B)* 1974, 9, 187
- 3 Sternstein, S. S. and Ho, T. C. *J. Appl. Phys.* 1972, 43, 4370; Paterno, J. J. *Dissertation* Rensselaer Polytechnic Institute (1970)
- 4 Gillham, J. K. *AIChE J.* 1974, 20, 1066
- 5 Billingham, P. R. and Tabor, D. *Polymer* 1971, 12, 101
- 6 Parry, E. J. and Tabor, D. *Polymer* 1973, 14, 617, 623, 628; *J. Phys (D)* 1973, 6, 1328
- 7 Takayanagi, M. *Pure Appl. Chem.* 1967, 15, 555
- 8 *Idem. ibid.* 1970, 23, 151
- 9 Sauer, J. A., Richardson, G. C. and Morrow, D. R. *J. Macromol. Sci. (C)* 1973, 9, 149
- 10 McCall, D. W. in 'Molecular Dynamics and Structure of Solids', (Eds R. S. Carter and J. J. Rush), Nat. Bur. Stand. Special Publication 301, Washington D.C., 1969, pp 475–537

* Personal discussions with Hartley and Lord in Manchester in March 1976 reveals that they consider the above results to be based on an artifact. A recent paper, Lord, F. W. (*Polymer* 1974, 15, 42) shows ordering but not recrystallization in the glass state below T_g i.e. from 20°–40°C. Crystallization occurs only some 30°–40°C above T_g . Nylons are dominated by hydrogen bonding which is absent in PE.

- 11 Heijboer, J. 'Mechanical Properties of Glassy Polymers Containing Saturated Rings', Uitgereij Waltman, Delft, 1972
- 12 Lamb, J. 'Molecular Motion in Liquids', (Eds J. Lascombe and D. Reidel), Dordrecht, Holland, 1974
- 13 Lamb, J. personal communication
- 14 Barlow, J. and Aynur, E. *Polymer* 1975, **16**, 110
- 15 Roe, J. M. and Simha, R. *Int. J. Polym. Mater.* 1974, **3**, 193
- 16 Lee, S. and Simha, R. *Macromolecules* 1974, **7**, 909
- 17 Ward, I. M. *Polymer* 1974, **15**, 379
- 18 Stachurski, Z. H. and Ward, I. M. *J. Macromol. Sci. (B)* 1969, **3**, 427, 445
- 19 Davies, G. R. and Ward, I. M. *Polym. Lett.* 1969, **7**, 353
- 20 Smith, J. B., Manuel, A. J. and Ward, I. M. *Polymer* 1975, **16**, 57
- 21 Takayanagi, M., Imada, K., and Kajiyama, T. *J. Polym. Sci. (C)* 1966, **15**, 263
- 22 Illers, K.-H. *Kolloid Z. Z. Polym.* 1969, **231**, 622
- 23 *Idem. ibid.* 1972, **250**, 426
- 24 *Idem. ibid.* 1973, **251**, 394
- 25 *Idem. ibid.* 1974, **252**, 1
- 26 Eisenberg, A. *Polym. Prepr.* 1973, **14**, 871 (this paper is the introduction to a symposium on ion-containing polymers which includes other papers on viscoelastic behaviour); 'IUPAC Jerusalem', Butterworth, London, 1976
- 27 Roberts, G. E. and White, E. F. T. 'The Physics of Glassy Polymers', (Ed R. N. Haward), Applied Science, London, 1973, Ch 3, pp. 153-222
- 28 North, A. M. 'Molecular Behaviour and The Development of Polymeric Materials', (Eds A. Ledwith and A. M. North), Chapman-Hall, London, 1974, Ch 11, pp 368-403
- 29 Boyer, R. F. *J. Polym. Sci. Polym. Symp.* 1975, p 189
- 30 Jansson, J. F. 'Amorphous Materials', (Eds R. W. Douglas and B. Ellis), Wiley-Interscience, New York, 1972, Ch 15, pp 141-150
- 31 Jansson, J. F. *J. Appl. Polym. Sci.* 1973, **17**, 2965, 2977, 2987, 2997
- 32 Jansson, J. F. *Acta Polytechnica Scandinavica Series 115*, Helsinki, 1974, pp 1-39
- 33 Gisolf, J. H. *Kolloid Polym. Sci.* 1975, **253**, 185
- 34 Gisolf, J. H. *Delft Progr. Rep.* 1974, **1**, 85-89
- 35 Gray, R. W. and McCrum, N. G. *Polym. Lett.* 1966, **4**, 639
- 36 Instrument Products Division, E. I. Du Pont de Nemours and Co., Wilmington, Del. 19898, USA. Additional information relating to refs 36-39 appears in *Polym. Prepr.* 1976, **17**, 1
- 37 Dr Philip S. Gill, Product Manager, Thermal Analysis Section, has kindly supplied us with preliminary literature on this instrument prior to its general release. The instrument was announced at The Pittsburgh Instrument Conference, Cleveland, Ohio, March, 1976
- 38 Kenyon, A. S. *West Coast Gordon Polym. Conf. Santa Barbara California USA* January 1976
- 39 Dr Kenyon, Monsanto Company, Corporate Research Department, 800 N. Lindbergh Blvd, St. Louis, Missouri 63166, USA has supplied us with some details about this instrument prior to publication.
- 40 Simpson, H. M., Soisin, A. and Johnson, D. F. *Phys. Rev. (B)* 1972, **5**, 1393
- 41 Professor A. Soisin, Department of Materials Science, University of Utah has advised us of current successful efforts to use polymeric materials in this apparatus
- 42 Struik, L. C. E., Bree, H. W. and Tak, A. G. M. 'A Survey of Equipment for The Mechanical Testing of Polymers at The Central Laboratory TNO', TNO, Delft, 1975, pp 75-61
- 43 Heijboer, J. 'Mechanical Properties of Glassy Polymers containing Saturated Rings', Uitgereij Waltman, Delft, 1972, Figure 5.5
- 44 Allen, G., John, R. M., Jeffs, G. M. and McAinsh, J. A. 'Amorphous Materials', (Eds R. W. Douglas and B. Ellis), Wiley-Interscience, London, New York, 1972, Ch 39, pp 389-398
- 45 Turley, S. G. personal communication
- 46 Ueberreiter, K. and Orthmann, H. *J. Kunststoffe* 1958, **48**, 525
- 47 Boyer, R. F. 'Encyclopedia of Polymer Science and Technology', (Ed. N. Bikales), Wiley-Interscience, New York, 1970 Vol 13, p 291
- 48 Stadnicki, S. J., Gillham, J. K. and Boyer, R. F. *J. Appl. Polym. Sci.* 1976, **20**, 1245
- 49 Glandt, C., Toh, H. K., Gillham, J. K. and Boyer, R. F. *J. Appl. Polym. Sci.* 1976, **20**, 1277
- 50 Gillham, J. K. personal communication
- 51 Stadnicki, S. J. unpublished data
- 52 Connor, T. M. *J. Polym. Sci. (A-2)* 1970, **8**, 191
- 53 Crist Jr, B. *ibid.* 1971, **9**, 1719
- 54 Cowie, J. M. G. and McEwen, I. J. *Polymer* 1973, **14**, 423
- 55 Meier, D. J. and Boyer, R. F. unpublished results
- 56 Cowie, J. M. G., McEwen, I. J. and Velickovic, J. *Polymer* 1975, **16**, 869
- 57 (a) Burmester, A. and Boyer, R. F. unpublished results; (b) Gillham, J. K. and Boyer, R. F. Experiments carried out at Princeton University June 1975 and briefly mentioned in footnote c, Table 2
- 58 Zosel, A. *Kolloid Z.* 1964, **199**, 113
- 59 Dale, W. C. and Rogers, C. E. *J. Appl. Polym. Sci.* 1972, **16**, 21
- 60 Price, C., Williams, R. C. and Ayerst, R. C. 'Amorphous Materials', (Eds R. W. Douglas and B. Ellis), Wiley-Interscience, London, New York, 1972, Ch 12, pp 117-124
- 61 Goldbach, G. and Rehage, G. *Kolloid Z. Z. Polym.* 1967, **216**, 56
- 62 Illers, K.-H. and Jenckel, E. *Rheolog. Acta* 1958, **1**, 322
- 63 Ueberreiter, K. and Otto-Lüpenmühlen, E. *Kolloid Z.* 1953, **133**, 26
- 64 Millar, J. R. *J. Chem. Soc.* 1960, p 1311
- 65 Takayanagi, M., Yoshino, M. and Minami, S. *J. Polym. Sci.* 1962, **61**, 5; McCrum, N. G., Read, B. E. and Williams, G. 'Anelastic and Dielectric Effects in Polymeric Solids, Wiley, New York, 1967, Figure 13.2
- 66 Lloyd, W. G. and Alfrey Jr, T. A. *J. Polym. Sci.* 1962, **62**, 159, 301; Dow Chemical Co. US Pat. 3 322 695 (1967)
- 67 Breitenbach, J. W. 'Encyclopedia of Polymer Science and Technology' (Ed. N. Bikales), Wiley-Interscience, New York, 1969, Vol 11, pp 587-597
- 68 Density figures are not given in ref 67. The values cited are based on personal observations of L. C. Rubens and R. F. Boyer
- 69 Maxwell, B. and Rahm, L. F. *Ind. Eng. Chem.* 1949, **41**, 1990
- 70 Schmidt, J. A. and Keskkula, H. *J. Appl. Polym. Sci.* 1960, **3**, 132; Boyer, R. F. and Keskkula, H. in 'Encyclopedia of Polymer Science and Technology' (Ed. N. Bikales), Wiley-Interscience, 1970, Vol 13, pp 375-394
- 71 Matsuoka, S. and Ishida, Y. *J. Polym. Sci. (C)* 1966, **14**, 247
- 72 Boyer, R. F. *J. Polym. Sci. Polym. Symp.* 1975, pp 195-198, Figures 2 and 3
- 73 Goldstein, M. *J. Chem. Phys.* 1969, **51**, 3728
- 74 Heijboer, J. *Atti del 2° Convegno della Societa Italiana de Reologia Siena May 1973* pp 307-329; Communication No. 508, Central Laboratorium, TNO
- 75 Amrhein, E. M., Bayer, R. K., Hentze, G. and Muller, F. H. *Kolloid Polym. Sci.* 1974, **252**, 66
- 76 Johari, G. P. and Goldstein, M. *J. Chem. Phys.* 1970, **53**, 2372
- 77 Hoffman, J. D. and Davis, G. T. *J. Res. Nat. Bur. Stand. (A)* 1975, **79**, 613
- 78 Hutchinson, J. M. and McCrum, N. G. *Nature Phys. Sci.* 1972, **236**, 115
- 79 Cooper, J. W. and McCrum, N. G. *J. Mater. Sci.* 1972, **7**, 1221
- 80 Buckley, C. P. and McCrum, N. G. *J. Polym. Sci. (A-2)* 1971, **9**, 369
- 81 Kardos, J. L. and Raison, J. *J. Polym. Eng. Sci.* 1975, **15**, 183
- 82 Boyer, R. F. *J. Polym. Sci. Polym. Symp.* 1975, pp 212-218, Figures 12-14
- 83 McCrum, N. G. *Midland Macromol. Inst. Michigan, USA* February 1975, to be published
- 84 Tuijman, C. A. F. *J. Polym. Sci. (C)* 1967, **16**, 2379
- 85 Illers, K.-H. *Kolloid Z. Z. Polym.* 1963, **190**, 16
- 86 Boyer, R. F. *Plast. Polym.* 1973, **41**, 15
- 87 Kumler, P. L. and Boyer, R. F. *Polym. Prepr.* 1975, **16**, 572
- 88 Keinath, S. E., Kumler P. L. and Boyer, R. F. *Polym. Prepr.* 1975, **16**, 120
- 89 Kumler, P. L. and Boyer, R. F. *Macromolecules* 1976, in press
- 90 Bergmann, K. *Kolloid Z. Z. Polym.* 1973, **251**, 962
- 91 North, A. M. *Br. Polym. J.* 1975, **7**, 119
- 92 Somersall A. C., Dan, E. and Guillet, J. E. *Macromolecules* 1974, **7**, 233
- 93 Rabold, G. P. *J. Polym. Sci. (A-1)* 1969, **7**, 1203
- 94 Boyer, R. F. *Macromolecules* 1973, **6**, 288
- 95 Kumler, P. L. and Boyer, R. F. unpublished results
- 96 Bullock, A. T., Cameron, G. G. and Smith, P. M. *Eur. Polym. J.* 1975, **11**, 617
- 97 Davies, M. and Edwards, A. *Trans. Faraday. Soc.* 1967, **63**, 2163

- 98 Boyd, R. H. and Breitling, S. M. *Macromolecules* 1972, **5**, 1
- 99 Boyd, R. H. and Breitling, S. M. *Macromolecules* 1974, **7**, 855
- 100 Boyd, R. H. *Coat. Plast. Prepr. Am. Chem. Soc.* 1975, **35**, 215
- 101 Boyd, R. H. *J. Polym. Sci. (Polym. Phys. Edn)* 1975, **13**, 2345
- 102 Sacher, E. J. *Macromol. Sci. Phys. (B)* 1971, **5**, 739
- 103 Reich, S. and Eisenberg, A. *J. Polym. Sci. (A-2)* 1972, **10**, 1397
- 104 Hayakawa, R. and Wada, Y. *J. Polym. Sci. (Polym. Phys. Edn)* 1974, **12**, 2119
- 105 *Polym. Prepr.* 1974, **15**, 1, 324
- 106 The above long abstracts are to appear in *J. Macromol. Sci. (B)* 1976
- 107 *Kolloid Z. Z. Polym.* 1973, **251**, Many papers in this issue are related to structure of the amorphous state
- 108 Robertson, R. E. *Ann. Rev. Mater. Sci.* 1975, **5**, 73
- 109 Arzhakov, S. A., Bakeev, N. F. and Kabanov, V. A. *Vysokomol. Soedin (A)* 1973, **15**, 1154
- 110 Cotton, J. P., Decker, D., Benoit, H., Farnoux, B., Higgins, J., Jannink, G., Ober, R., Pecot, C. and des Cloizeaux, J. *Macromolecules* 1974, **7**, 863
- 111 Bunn, C. 'Molecular Behaviour and The Development of Polymeric Materials' (Eds A. Ledwith and A. M. North), Chapman-Hall, London, 1974, pp 337-367
- 112 Ito, E. and Hatakeyama, T. *J. Polym. Sci. (Polym. Phys. Edn)* 1974, **12**, 1477
- 113 *Idem. ibid.* 1975, **13**, 2313
- 114 Boyer, R. F. 'Polymeric Materials: Relationship Between Structure and Mechanical Behaviour', (Eds E. Baer and S. V. Radcliffe), Am. Soc. Metals, Ohio, 1974, Ch 6, pp 277-368
- 115 Robertson, R. E. *J. Phys. Chem.* 1965, **69**, 1575
- 116 Bohn, L. and Oberst, H. *Acustica*, 1959, **9**, 431
- 117 Staverman, A. J. and Heijboer, J. *Kunststoffe* 1960, **50**, 23
- 118 Heijboer, H. J. *Polym. Sci. (C)* 1968, **16**, 3755
- 119 Boyer, R. F. *Polym. Eng. Sci.* 1968, **8**, 161
- 120 Boyer, R. F. 'Polymeric Materials: Relationship between Structure and Mechanical Behaviour', (Eds E. Baer and S. V. Radcliffe), Am. Soc. Metals, Ohio, 1974, pp 348, Table 8
- 121 Manson, J. A. Hertzberg, R. W., Kim, S. L. and Skibo, M. *Polymer* 1975, **16**, 850
- 122 Sacher, E. J. *Appl. Polym. Sci.* 1975, **19**, 1421
- 123 Schaefer, J., Stejskal, E. O. and Buchdahl, R. *Macromolecules* 1975, **8**, 291
- 124 Schaefer, J. personal communication
- 125 Schaefer, J., Stejskal, E. O. and Buchdahl, R. *Midland Macromol. Inst. Michigan USA* January 1976; *Macromolecules*, in press
- 126 Schaefer, J. *Bull. Am. Phys. Soc.* 1976, **21**, 443
- 127 Hendra, P. J., Jobic, H. P. and Holland-Moritz, K. *J. Polym. Sci. (Polym. Lett. Edn)*, 1975, **13**, 365
- 128 Zachmann, H. G. *J. Polym. Sci. (C)* 1973, **43**, 111
- 129 Hartley, F. D., Lord, F. W. and Morgan, L. B. *Rec. Sci.* 1955, **25**, 577
- 130 MacLaine, J. Q. G. and Booth, C. *Polymer* 1975, **16**, 191, 679
- 131 Booth, C. personal communication
- 132 McDonald, R. A. personal communication
- 133 Kovacs, A. J. and Gonthier, A. *Kolloid Z. Z. Polym.* 1972, **250**, 530; Kovacs, A. J. personal communication
- 134 Eisenberg, A. unpublished results; 'IUPAC Jerusalem', Butterworth, London, 1976
- 135 Irvine, J. D. and Work, R. N. *J. Polym. Sci. (Polym. Phys. Edn)* 1973, **11**, 175
- 136 North, A. M. *J. Polym. Sci. (C)* 1975, **50**, 345

Syntheses and conformational studies of poly(*S*-menthyloxycarbonylmethyl L- and D-cysteines)

Tadao Hayakawa, Yoshiyuki Kondo and Masayo Matsuyama

Institute of High Polymer Research, Faculty of Textile Science and Technology, Shinshu University, Ueda 386, Japan

(Received 14 May 1976)

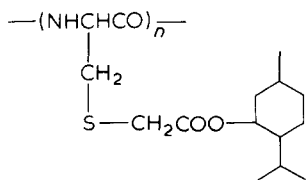
S-menthyloxycarbonylmethyl L- and D-cysteines were prepared by the reaction of L- or D-cysteine and (–)-menthyl chloroacetate in liquid ammonia and were then polymerized to poly(*S*-menthyloxycarbonylmethyl L- and D-cysteines) by the *N*-carboxyanhydride (NCA) method. From the results obtained by means of infra-red spectra, X-ray diffractions, optical rotatory dispersions (o.r.d.), and circular dichroisms (c.d.), poly(*S*-menthyloxycarbonylmethyl-L-cysteine) was found to be a right-handed α -helix in the solid state and in ethyl ether/chloroform and chloroform solutions. Similarly, poly(*S*-menthyloxycarbonylmethyl-D-cysteine) was a left-handed α -helix. The helix–coil transition of these polymers was observed in the vicinity of 3–4% trifluoroacetic acid (TFA) in chloroform/TFA mixtures.

INTRODUCTION

Considerable interest has recently been shown in the conformation of many synthetic poly(α -amino-acids) and proteins in the solid state and in solution. The conformation of a polypeptide is intrinsically dependent on its amino-acid composition, and it can form an α -helix, a β -structure, or a random coil conformation. It has been reported that polypeptides with a hetero-atom (oxygen or sulphur) attached directly to the β -carbon atom, such as poly(L-cysteine) and poly(L-serine) derivatives form a stable β -structure¹; in coil promoting solvents, such as DCA and TFA, they are in a random coil. However, poly(L-homocysteine) derivatives with a hetero-atom attached to the γ -carbon in the side chains, assume the α -helix conformation^{2,3}.

Poly(*S*-benzylthio-L-cysteine)⁴ and poly(*S*-benzylpenicillamines)⁵ are in the ω -helical conformation due to the steric interference between the side chain and main chain. Since polycysteine derivatives are hardly soluble in most common organic solvents, o.r.d. and c.d. measurements in the far ultra-violet region are very difficult.

In the present study, *S*-menthyloxycarbonylmethyl L- and D-cysteines were prepared by the reaction of L- or D-cysteine with (–)-menthyl chloroacetate and were polymerized to poly(*S*-menthyloxycarbonylmethyl L- and D-cysteines) by the NCA method. The forms of the poly(*S*-menthyloxycarbonylmethyl L- and D-cysteines) are as follows:



The polymers were soluble in many organic solvents, such as chloroform, methylene chloride, benzene, dioxane, DCA and TFA, were slightly soluble in diethyl ether and

n-hexane, and were insoluble in water and alcohols. The conformations of the polymers were studied by o.r.d., c.d., infra-red spectra, and X-ray diffractions, in order to investigate the effect of their side chains with optically active groups on the polypeptide structure.

EXPERIMENTAL

Materials

(–)-Menthyl chloroacetate. 9.45 g of monochloroacetic acid, 15.2 g of (–)-menthol, and 1.88 g of *p*-toluenesulphonic acid monohydrate were mixed with 150 ml of benzene. The mixture was heated under reflux, and the nascent water was removed azeotropically by means of a Dean and Stark distillation apparatus. After the solvent was removed, the residue was distilled under reduced pressure; yield 19.0 g (83.0%); b.p. 140°–144°C at 25 mmHg; $[\alpha]_D^{25^\circ\text{C}} = -112.2$ ($c = 0.13\%$ in EtOH).

S-menthyloxycarbonylmethyl-L-cysteine. 5.7 g of L-cysteine in 150 ml of liquid ammonia were treated with small pieces of metallic sodium, with stirring until a lasting blue colour was obtained. To this solution 10.0 g of (–)-menthyl chloroacetate were slowly added. 4.8 g of ammonium chloride were then added, the solvent was allowed to evaporate, and the residue was taken up in 200 ml of water and brought to pH 6.8 under cooling. The crystals thus precipitated were filtered and dried yielding 9.8 g, and were then recrystallized from methanol and ether; yield 6.5 g (52.2%); m.p. 149°C; $[\alpha]_D^{25^\circ\text{C}} = -64.1$ ($c = 0.55\%$ in MeOH). Calculated for C₁₅H₂₇O₄NS: C = 56.75%; H = 8.57%; N = 4.41%; found: C = 56.31%; H = 8.38%; N = 4.49%.

S-menthyloxycarbonylmethyl-D-cysteine was prepared from the D-cysteine and (–)-menthyl chloroacetate by the same procedure as above; yield 4.38 g (27.6%); m.p. 156°C; $[\alpha]_D^{25^\circ\text{C}} = -27.0$ ($c = 0.56\%$ in MeOH). Calculated for C₁₅H₂₇O₄NS: C = 56.75%; H = 8.57%; N = 4.41%; found:

Table 1 Characteristic absorption bands of poly(*S*-menthyloxycarbonylmethyl *L*- and *D*-cysteines) at 22°C

Assignment	Wavenumber (cm ⁻¹)			
	L-polymer		D-polymer	
	Solid*	in CHCl ₃	Solid*	in CHCl ₃
Amide I	1667	1665	1663	1665
Amide II	1548	1544	1549	1548

*KBr disks

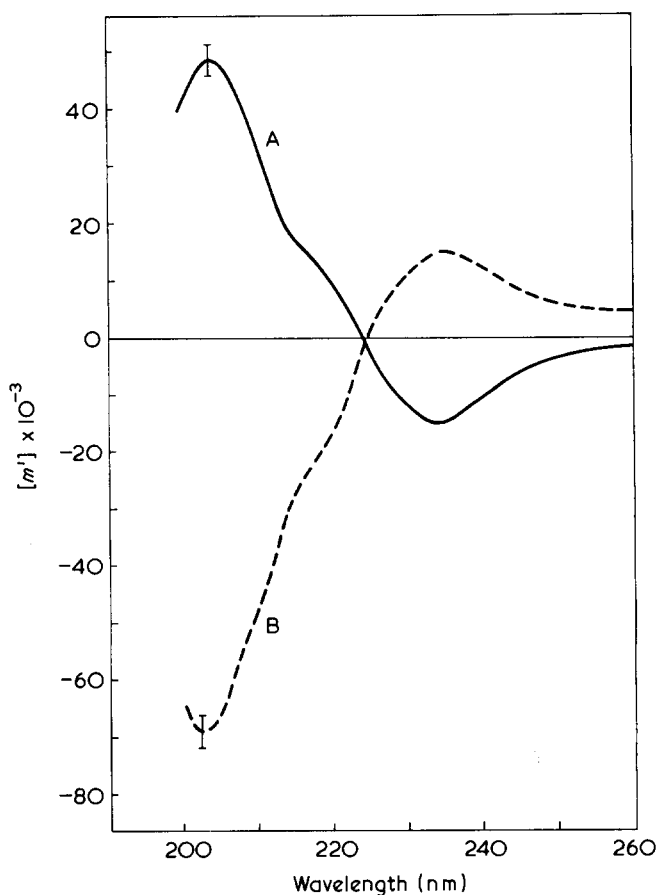


Figure 1 O.r.d. spectra of poly(*S*-menthyloxycarbonylmethyl *L*- and *D*-cysteines) in an ethyl ether/chloroform, 95/5 (v/v) mixture at 22°C. A, Poly(*S*-menthyloxycarbonylmethyl-*L*-cysteine); B, poly(*S*-menthyloxycarbonylmethyl-*D*-cysteine)

C = 57.27%; H = 8.57%; N = 4.12%.

S-menthyloxycarbonylmethyl-*L*-cysteine NCA. *S*-menthyloxycarbonylmethyl-*L*-cysteine NCA was prepared from the corresponding cysteine derivative and phosgene by the usual procedure; yield 58.2%; m.p. 95.5°C. Calculated for C₁₆H₂₅O₅NS: C = 55.95%; H = 7.33%; N = 4.08%; found: C = 55.87%; H = 7.32%; N = 4.00%. *S*-menthyloxycarbonylmethyl-*D*-cysteine NCA was prepared by the same procedure; yield 83.3%; m.p. 77.0°C. Calculated for C₁₆H₂₅O₅NS: C = 55.95%; H = 7.33%; N = 4.08%; found: C = 55.78%; H = 7.30%; N = 4.03%.

Poly(*S*-menthyloxycarbonylmethyl-*L*-cysteine). The above NCA (1.9 g) was polymerized in benzene with triethylamine as an initiator at NCA/initiator ratios of 50/1; yield 1.02 g (61.9%). Calculated for (C₁₅H₂₅O₃NS)_n:

C = 60.11%; H = 8.35%; N = 4.68%; found: C = 59.78%; H = 8.42%; N = 4.61%. $[\eta] = 0.243$ (in DCA at 25°C ± 0.05°C). N-terminal titration, $MW = 25\,600$ ($DP = 80$). Poly(*S*-menthyloxycarbonylmethyl-*D*-cysteine) was prepared by the same method as mentioned above; yield 54.8%. Calculated for (C₁₅H₂₅O₃NS)_n: C = 60.11%; H = 8.35%; N = 4.68%; found: C = 59.58%; H = 8.65%; N = 4.52%. $[\eta] = 0.213$ (in DCA at 25°C ± 0.05°C). N-terminal titration, $MW = 12\,000$ ($DP = 40$).

Methods

The molecular weights were determined from the titration of the polymer in benzene with HClO₄/acetic acid, using crystal violet as the indicator. The viscosities were measured in DCA at 25°C using an Ubbelohde viscometer. Infra-red spectra were measured with a JASCO Model DS-301 spectrophotometer at 22°C. Infra-red spectra of the solutions of the polymers were measured in a tube of polyethylene film. X-ray diffraction photographs were taken using a Rigaku-Denki Geigerflex with a Cu target. C.d. and o.r.d. were measured with a JASCO ORD/UV-5 spectropolarimeter with a c.d. attachment at 22°C. The c.d. and o.r.d. measurements were performed with 0.1 and 1 mm cells from 260 to 200 nm, and with 10 and 50 mm cells in the visible region. The concentration of the polymers was between 0.1 and 1.0 vol%. The c.d. and o.r.d. were expressed, respectively by the molecular ellipticity, $[\theta]$, and the reduced residual rotation, $[m']$.

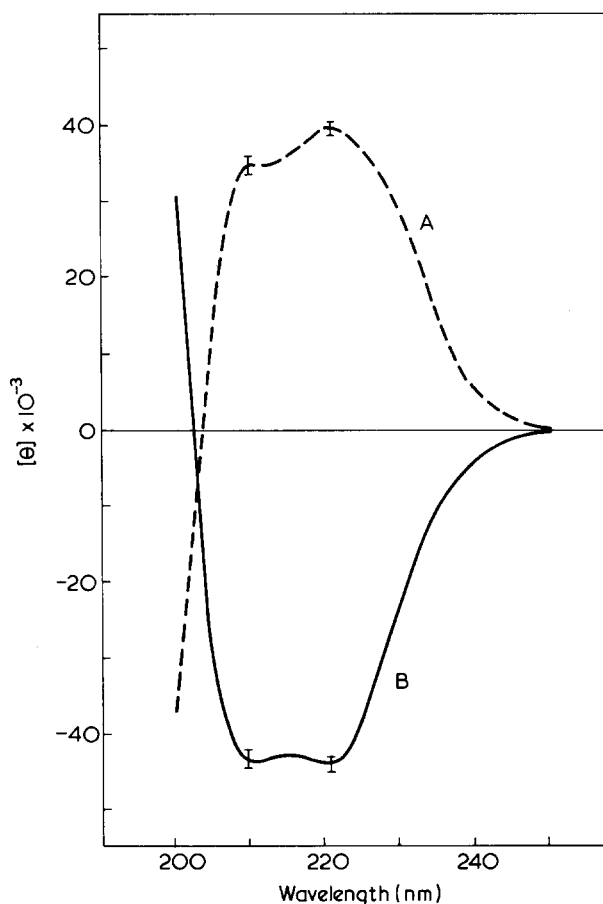


Figure 2 C.d. spectra of poly(*S*-menthyloxycarbonylmethyl *L*- and *D*-cysteines) in an ethyl ether/chloroform, 95/5 (v/v) mixture at 22°C. A, Poly(*S*-menthyloxycarbonylmethyl-*D*-cysteine); B, poly(*S*-menthyloxycarbonylmethyl-*L*-cysteine)

RESULTS AND DISCUSSION

Infra-red studies and X-ray analyses

Poly(S-menthyloxycarbonylmethyl L- and D-cysteines) showed infra-red absorption bands characteristic of polypeptides both in the solid state and in chloroform solution (Table 1). Both the L- and D-polymers gave almost the same infra-red spectra. The amide I and the amide II bands were found at about 1660 cm^{-1} and 1550 cm^{-1} , respectively. The X-ray diffraction patterns of the L- and D-polymers indicated the presence of a 13.6 \AA reflection. The marked spacing at 13.6 \AA corresponds to the helix-helix interval of the α -helical polypeptides, as has been reported by Bamford *et al.*⁶ The result of the X-ray diffraction diagram coincides well with that of the infra-red spectra.

Optical rotatory dispersion and circular dichroism

The o.r.d. and c.d. of poly(S-menthyloxycarbonylmethyl L- and D-cysteines) in ethyl ether/chloroform, 95/5 (v/v) were measured. Figure 1 shows the o.r.d. curves of the L- and D-polymers in ethyl ether/chloroform 95/5 (v/v). The L-polymer exhibits a broad trough at 233–235 nm with $[m']_{233} = -14\,500$ degree cm^2/dm , a crossover point of $[m']$ at 224 nm, a strong peak near 204 nm with $[m']_{204} = 49\,000$ and a shoulder near 217 nm with $[m']_{217} = 13\,000$. The c.d. curves are shown in Figure 2. The o.r.d. and the c.d. spectra correspond well with each other. Two negative dichroism bands at 221 nm and

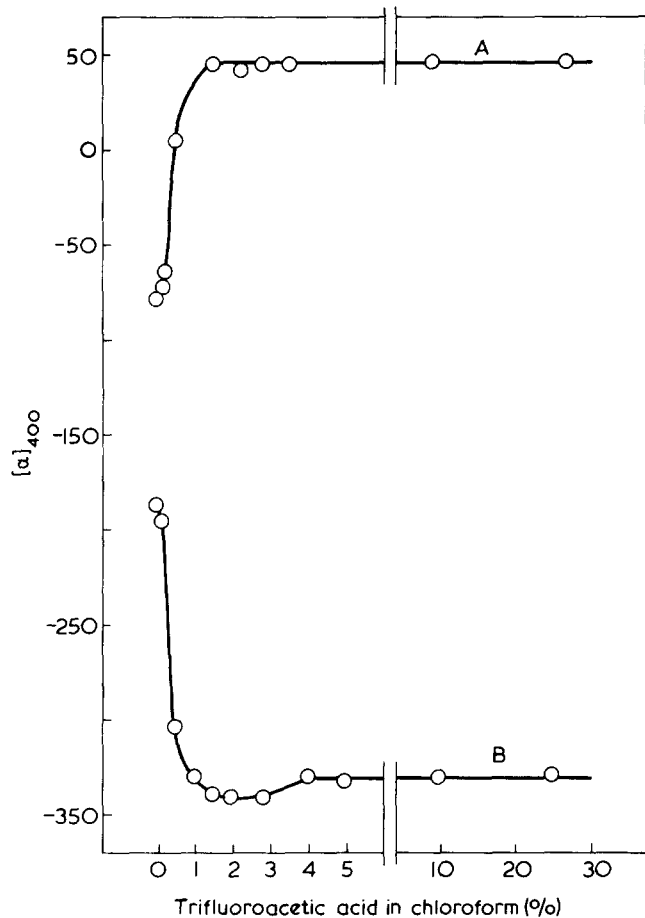


Figure 3 Helix-coil transition of poly(S-menthyloxycarbonylmethyl L- and D-cysteines) in chloroform/TFA mixtures at 22°C . A, Poly(S-menthyloxycarbonylmethyl-D-cysteine); B, poly(S-menthyloxycarbonylmethyl-L-cysteine)

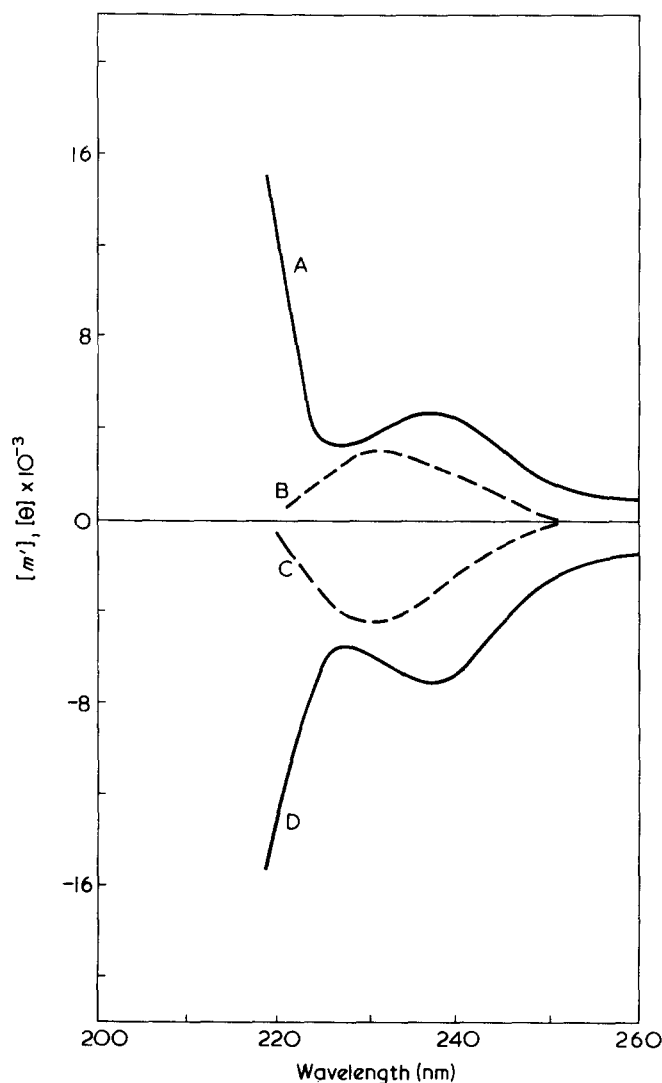


Figure 4 O.r.d. and c.d. spectra of poly(S-menthyloxycarbonylmethyl L- and D-cysteines) in a chloroform/TFA 96/4 (v/v) mixture at 22°C . Poly(S-menthyloxycarbonylmethyl-D-cysteine): A, o.r.d.; B, c.d. Poly(S-menthyloxycarbonylmethyl-L-cysteine): C, c.d.; D, o.r.d.

210 nm, with $[\theta]_{221} = -44\,000$ and $[\theta]_{210} = -43\,000$ and a zero point at 203 nm were observed for the L-polymer; a positive dichroism band below 200 nm can be expected. The polymer gave also similar curves in chloroform solution. From these o.r.d. and c.d. measurements, the L-polymer can be considered to have a right-handed α -helical conformation in an ethyl ether/chloroform mixture and in chloroform solution⁷. On the other hand, the o.r.d. and c.d. curves of the D-polymer have a peak at 233–235 nm with $[m']_{235} = 15\,200$ and the positive dichroism bands at 221 nm and 210 nm, with $[\theta]_{221} = 39\,500$ and $[\theta]_{210} = 35\,100$. This result suggests that the D-polymer can be considered to have a left-handed α -helical conformation in solution⁷. The o.r.d. trough (or peak) at about 233–235 nm, and the magnitude of the negative (or positive) c.d. band of $[\theta]_{210}$, is somewhat different for the L-polymer and the D-polymer. This result signifies that the asymmetry of the (–)-menthyl chromophore in their side chains causes an extraordinary rotational strength. The conformational changes of the L- and D-polymers in chloroform and in a chloroform/TFA mixture have been studied. The plots of the specific rotation $[\alpha]_{400}$ values versus the solvent composition of these

polymers in solution are shown in *Figure 3*. In 100% chloroform, the $[\alpha]_{400}$ of the L-polymer is -190 . When TFA is added to the chloroform solution, its levorotation increases markedly. In a chloroform/TFA mixture 98/2 (v/v), it decreases to a minimum value of -341 , finally reaching the $[\alpha]_{400} = -332$ at about 4% TFA. On the other hand, in 100% chloroform, that of the D-polymer is -78 . With the addition of TFA, it increases to a maximum value of $+46.3$ at 1.5% TFA, finally reaching $+44.0$ at above 2.5% TFA. *Figure 4* shows the o.r.d. and c.d. curves of the L- and D-polymers in a chloroform/TFA mixture 96/4 (v/v), characteristic of the random coil conformation. There is a 237 nm trough (or peak), a 226 nm peak (or trough), and a trough (or peak) below 210 nm in the o.r.d. curves, and a small negative (or positive) dichroism band at 230 nm in the c.d. curves. This means that a small amount of TFA causes a drastic conformational transition from an α -helix to a random coil conformation. However, the absolute magnitude of the $[m']_{237}$ and $[\theta]_{230}$ are larger than those of usual polypeptides^{7,8}, and differ for the L-polymer and the D-polymer. This may be due to the influence of the (-)-menthyl groups in their side chains.

As described above, the o.r.d., c.d., infra-red spectra, and X-ray results suggest that poly(*S*-menthyloxycarbonylmethyl L- and D-cysteines) in helix promoting solvents take the α -helical conformation. This could be interpreted as indicating that these polymers form an α -helix because of the stacking of the menthyl groups in their side chains. In the case of poly(*S*-alkyl cysteine), the steric interference between the side chains and the main chain forms a stable

β -structure⁹⁻¹³, however, it is interesting that poly(*S*-menthyloxycarbonylmethyl L- and D-cysteines) form an α -helix because of the influence of the menthyl groups in their side chains.

REFERENCES

- 1 Blout, E. R. 'Polyamino Acids, Polypeptides and Proteins', (Ed. M. A. Stahman), University of Wisconsin Press, 1962, p 275
- 2 Hayakawa, T., Kondo, Y. and Kobayashi, N. *Polym. J.* 1975, 7, 538
- 3 Hayakawa, T. *et al.* unpublished data
- 4 Fraser, R. D. B., MacRae, T. P. and Stapleton, I. W. *Nature* 1962, 193, 573
- 5 Hayakawa, T., Kondo, Y., Yamamoto, H. and Aoe, T. *Polym. J.* 1974, 6, 515
- 6 Bamford, C. H., Elliot, A. and Hanby, W. E. 'Synthetic Polypeptides', Academic Press, New York, 1965, p 263; Mitsui, Y., Iitaka, Y. and Tsuboi, M. *J. Mol. Biol.* 1967, 24, 15
- 7 Holzwarth, G. and Doty, P. *J. Am. Chem. Soc.* 1965, 87, 218
- 8 Davidson, B. and Fasman, G. D. *Biochemistry* 1967, 6, 1616
- 9 Kamashima, K. *J. Phys. Soc. Japan* 1966, 21, 1781
- 10 Harrap, B. S. and Stapleton, I. W. *Biochim. Biophys. Acta* 1963, 75, 31
- 11 Ikeda, S., Maeda, H. and Isemura, T. *J. Mol. Biol.* 1964, 10, 223
- 12 Anufrieva, E. V., Bolotina, I. A., Volchek, B. Z., Illarionova, N. G., Kalikhevich, V. I., Korotkina, O. Z., Mitin, Yu. V., Ptitsyn, O. B., Purkina, A. V. and Eskin, V. E. *Biofizika* 1965, 10, 918
- 13 Hayakawa, T., Kondo, Y. and Murakami, Y. *Polym. J.* 1974, 6, 424

Phosphonitrilic chloride : 34. Electrical conductivity of polybisaminophosphazenes

M. Kajiwara and H. Saito

Department of Applied Chemistry, Faculty of Engineering, Nagoya University, Nagoya, Japan

(Received 10 May 1976)

The electrical conductivity of polybisaminophosphazenes investigated over a range of temperatures was found to obey the general relation for semi-conductors. The resistivity decreased or increased when a side group having a high inductive effect or bulky group was linked in the polymers. The electrical conductivity of polybisaminophosphazenes containing primary amine, secondary amine and aromatic amine ranged from 1.3×10^{10} to 2.8×10^{10} Ω -cm, 9.3×10^{10} to 8.5×10^{11} Ω -cm and above 9.1×10^{14} Ω -cm, respectively.

INTRODUCTION

Eley and Wills¹ and Reucroft² described the electrical conductivity of single crystals or powdery dichlorocyclophosphazene (NPCl₂)₃ and dichlorocyclophosphazene (NPCl₂)₄. Allcock and Best³ reported electrical conductivity of liquid dichlorocyclophosphazene and thereby explained its polymerization mechanism. Recently, the conductivity of some phosphazene chelating polymers was described by Kajiwara^{4,5}. This paper describes the conductivity of polybisaminophosphazenes.

EXPERIMENTAL

Dichlorocyclophosphazene (NPCl₂)₃ was prepared by a method previously described⁶ and polymerized as described by Gimblet⁷.

Polybis(ethylamino)phosphazene [NP(NHC₂H₅)₂]_n (I), polybis(n-propylamino)phosphazene [NP(n-NHC₃H₇)₂]_n (II), polybis(n-butylamino)phosphazene [NP(n-NHC₄H₉)₂]_n (III), polybis(hexylamino)phosphazene [NP(NHC₆H₁₃)₂]_n (IV), polybis(allylamino)phosphazene [NP(NHCH₂CHCH₂)₂]_n (V), polybis(dimethylamino)phosphazene {NP[N(CH₃)₂]₂]_n (VI), polyaminodiethylaminophosphazene [NP(NH₂)N(C₂H₅)₂]_n (VII) and polybis(phenylamino)phosphazene [NP(NHC₆H₅)₂]_n (VIII) were synthesised by the methods of Allcock^{8,9}.

The electron conductivity of polybisaminophosphazenes

was investigated using the apparatus described by Kajiwara⁴.

The value of the electrical conductivity (ρ) was estimated by equation (1):

$$\rho = RA V/L \quad (1)$$

where R is the electrical resistance, A the plate area (1.3773 cm²), L the sample thickness (cm), and V is the volume fraction. Polybisaminophosphazenes were moulded under pressures 200–300 kg/cm².

Infra-red (i.r.) spectra of the polymers were obtained using the pressed KBr disc technique with a Shimadzu Co. IRG-2 type spectrometer.

RESULTS AND DISCUSSION

Yield and appearance of the polymers formed from the reaction of polydichlorophosphazene (NPCl₂)_n with each amino compound are summarized in Table 1.

The polybisaminophosphazenes were soluble in THF and the P = N frequency in P₃N₃ ring of the polymers appeared in the region of 1200 to 1300 cm⁻¹.

The relationship between the resistivity of the polymers I–V and temperature is shown in Figure 1 and the energy gaps of the polymers calculated from the general relation of semi-conductors are summarized in Table 2.

The glass transition temperature of the polymers I, IV and V appears at about 45°–80°C as shown by the drastic

Table 1 Yield and appearance of polybisaminophosphazenes [NP(NHR)₂]_n

Polydichlorophosphazene (g)	Amine compounds (g)	Polybisaminophosphazene	Yield (%)	Appearance
3.96	3.10	[NP(NHC ₂ H ₅) ₂] _n	23	White, powder
7.10	23.3	[NP(NHC ₃ H ₇) ₂] _n		White, powder
9.65	17.0	[NP(NHC ₄ H ₉) ₂] _n		White, powder
3.68	25.0	[NP(NHC ₆ H ₁₃) ₂] _n	25	White, powder
7.20	56.5	[NP(NHCH ₂ CHCH ₂) ₂] _n	10.8	White, powder
8.98	20.5	{NP[N(CH ₃) ₂] ₂] _n	37.4	Orange, adhesive
5.35	16.1	[NP(NH ₂)N(C ₂ H ₅) ₂] _n	27.0	Brown, adhesive
7.0	5.0	[NP(NHC ₆ H ₅) ₂] _n	20.0	Brown, adhesive
8.45	46.8	[NP(NHCH ₂ C ₆ H ₅) ₂] _n	3.0	White, powder

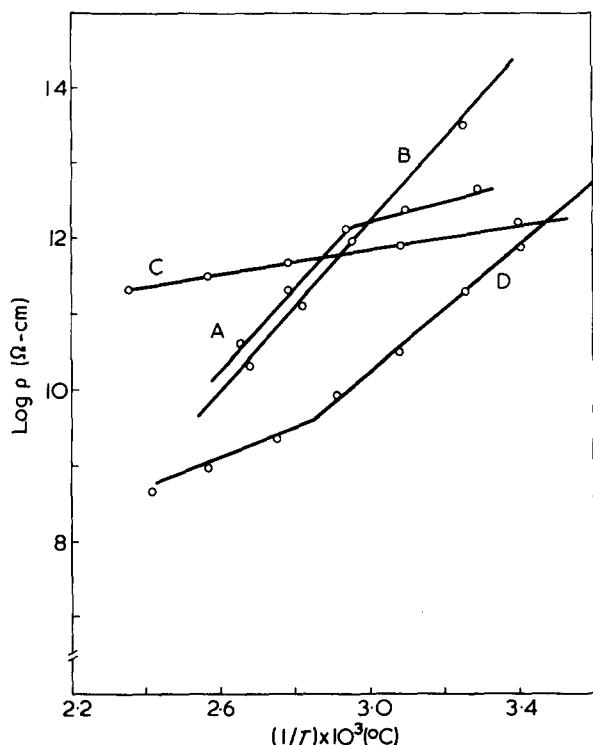


Figure 1 Electrical conductivity of polybisaminophosphazenes: A, $[\text{NP}(\text{NHC}_2\text{H}_5)_2]_n$ (I); B, $[\text{NP}(\text{n-NHC}_3\text{H}_7)_2]_n$ (II); C, $[\text{NP}(\text{n-NHC}_4\text{H}_9)_2]_n$ (III); D, $[\text{NP}(\text{NHC}_6\text{H}_{13})_2]_n$ (IV)

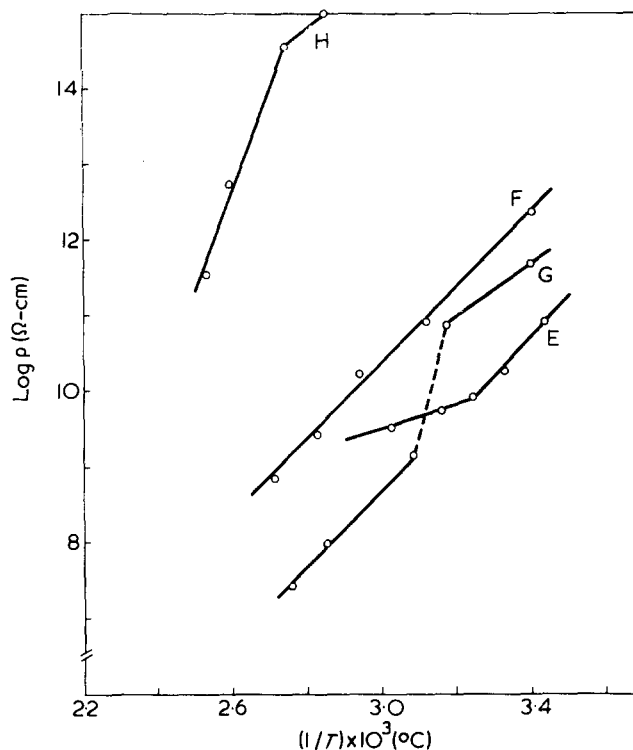


Figure 2 Electrical conductivity of polybisaminophosphazenes: E, $[\text{NP}(\text{NHCH}_2\text{CHCH}_2)_2]_n$ (V); F, $\{\text{NP}[\text{N}(\text{CH}_3)_2]_2\}_n$ (VI); G, $[\text{NP}(\text{NH}_2)\text{N}(\text{C}_2\text{H}_5)_2]_n$ (VII); H, $[\text{NP}(\text{NHC}_6\text{H}_5)_2]_n$ (VIII)

Table 2 Energy gaps and the value of resistivity of polybisaminophosphazenes $[\text{NP}(\text{NHR})_2]_n$

Polybisaminophosphazenes $(\text{NPR}_2)_n$	Temperature (°C)	(ρ) (25°C) ($\Omega\text{-cm}$)	E (eV)
NHC_2H_5	70–100	1.0×10^{13}	2.1
	35–115		2.2
$\text{n-NHC}_3\text{H}_7$	20–150	2.0×10^{12}	0.35
$\text{NHC}_6\text{H}_{13}$	20–85	10×10^{11}	1.90
	85–115		0.54
$\text{NHCH}_2\text{CHCH}_2$	20–40	1.41×10^{10}	1.13
	40–110		0.11
$\text{N}(\text{CH}_3)_2$	20–90	9.3×10^{10}	1.62
	50–90		1.80
$(\text{NH}_2)\text{N}(\text{C}_2\text{H}_5)$	20–40	2.2×10^{11}	1.35
	70–90		1.90
NHC_6H_5	70–90	9.1×10^{14}	1.90
	90–120		5.69

change of resistivity with increasing temperature. The resistivity at 25°C is decreased since the inductive effect is increased with increasing number of carbon atoms in the pendant group.

The activation energies and the resistivity of secondary

amino phosphazene polymers is lower than the values of primary amino phosphazene polymers, and this may be ascribed to the inductive effect of secondary amine linked in a side group. Furthermore the resistivity of the anilinophosphazene polymer, at room temperature is so high that it is difficult to measure. However, the resistivity decreased on heating and the polymer showed a glass temperature of 91°C. The resistivity of the benzylaminophosphazene polymer was too high to measure even with the heated polymer.

REFERENCES

- Eley, D. D. and Wills, M. R. *J. Chem. Soc.* 1963, 1543
- Reucroft, P. J., Kronick, P. L., Scott, M. and Labes, M. *Nature*, 1964, 4919
- Allcock, H. R. and Best, R. J. *Can. J. Chem.* 1964, 42, 447
- Kajiwara, M. and Saito, H. *Polymer* 1973, 14, 488
- Kajiwara, M. and Saito, H. *Polymer* 1975, 16, 861
- Saito, H. and Kajiwara, M. *J. Chem. Soc. Japan (Ind. Chem. Sect.)* 1963, 66, 618
- Gimblet, F. G. R. *Polymer* 1960, 1, 418
- Allcock, H. R. and Forgione, P. S. *Inorg. Chem.* 1966, 5, 1716
- Allcock, H. R. and Kugel, R. L. *Inorg. Chem.* 1972, 11, 2584

Use of differential scanning calorimetry to study polymer crystallization kinetics

J. N. Hay*, P. A. Fitzgerald† and M. Wiles‡

Department of Chemistry, University of Birmingham, Birmingham B15 2TT, UK

(Received 17 March 1976; revised 1 June 1976)

The use of differential scanning calorimetry to determine accurate crystallization parameters is reconsidered by direct comparison with dilatometry. Two calorimeters are compared: Perkin-Elmer DSC models 1B and 2. Fractions of polyethylene are studied since their rate constants have a marked temperature dependence which enables the accuracy of setting and calibrating the temperature of the calorimeters to be gauged. The resolutions of the calorimeters are compared from their abilities to detect secondary crystallization. The limitations of d.s.c. and the choice of operating conditions are discussed.

INTRODUCTION

In a previous publication¹ the limitations of a differential scanning calorimeter, DSC-1B, in measuring directly isothermal crystallization data were discussed. It was concluded that the d.s.c. was not as sensitive as precision dilatometry in detecting low rates of crystallization, but nevertheless the time dependence of crystallization could be obtained at higher rates with sufficient accuracy to test the validity of rate equations. Care, however, was necessary in setting and calibrating the temperature, as rate variations between repeated isothermal crystallizations were consistent with an error of $\pm 0.3\text{K}$.

Since this report, d.s.c. has been considerably improved with the introduction of the Perkin-Elmer DSC-2. We now report on its use in crystallization kinetics.

EXPERIMENTAL

Materials

Polyethylene (Marlex 60) fractions, supplied by Phillips Petroleum Co. Ltd, were used. Their characteristics are listed in Table 1.

Apparatus

Dilatometry has been described previously². Perkin-Elmer Differential Scanning Calorimeters, models DSC-1B and DSC-2, were used with powder samples (1.0–30.0 mg) weighed to 0.01 mg on a microbalance, and sealed in aluminium sample holders. An empty aluminium sample holder was used as a reference.

DSC-2 could be used at a constant temperature (preset to 0.1K) by heating or cooling from temperatures also preset to 0.1K at rates from 0.312 to 320 K/min. For comparison the DSC-1B rates were from 0.50 to 64 K/min and temperatures set to 1K. The temperature scale of the DSC-2 was calibrated for the effect of sample size and rate of heating from the melting characteristics of zone refined

stearic acid (343.2K) dibenzyl (325.3K) and ultra-pure metals, indium (429.8K) and tin (505.0K). Extrapolation to zero rate of heating was used to calibrate constant temperature. Over this range (340–500K) temperature corrections were linear with temperature. This was a considerable improvement over that of the DSC-1B, which exhibited pronounced curvature¹. For calibration, the heat of fusion of indium was taken as 28.45 J/g.

Analysis of the crystallization isotherms

The crystallization–time dependence was analysed by means of the Avrami equation:

$$(X_{\infty} - X_t)/(X_{\infty}) = \exp(-Z_1 t^n) \quad (1)$$

where X_t and X_{∞} are the weight fraction of crystallized material at time t , and ∞ ; Z_1 is the rate constant and n the exponent.

Accordingly,

$$\log\{\ln[(X_{\infty})/(X_{\infty} - X_t)]\} = n \log t + \log Z_1 \quad (2)$$

and

$$n = -t(dX_t/dt)/\{(X_{\infty} - X_t) \ln[(X_{\infty} - X_t)/(X_{\infty})]\} \quad (3)$$

The rate constant Z_1 was calculated from the half life, $t_{1/2}$, and the average value of n , since:

$$Z_1 = \ln(2)/t_{1/2}^n \quad (4)$$

D.s.c. measures the rate of evolution of the enthalpy of

Table 1 Polyethylene characteristics

Serial no.	Molecular weight $\times 10^{-3}$		D^*
	\bar{M}_n	\bar{M}_w	
A	19.0	142.0	7.4
B	25.0	41.0	1.6
C	32.0	99.0	3.1
D	78.0	165.0	2.1

* G.p.c. molecular weight, $D = \bar{M}_w/\bar{M}_n$

* To whom all communications should be addressed:

† Present address: ICI Mond Division, Runcorn, Cheshire, UK.

‡ Present address: British Vinyl Products Ltd, Carshalton, Surrey, UK.

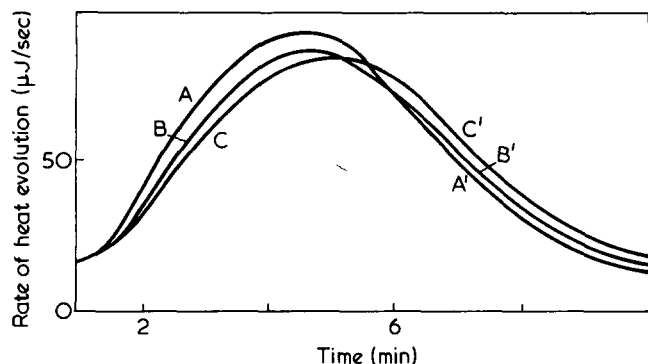


Figure 1 Temperature dependence of crystallization isotherms. AA', 396.1K; BB', 396.0K; CC', 395.9K

Table 2 Primary crystallization parameters for sample B

Method	Crystallization temperature (K)	<i>n</i>	<i>t</i> ^{1/2} (min)	<i>Z</i> ₁ (min ^{-<i>n</i>)}
DSC-2	397.5	2.6	1.6	2.04 × 10 ⁻¹
	398.5	2.3	2.9	6.0 × 10 ⁻²
	399.5	2.2	4.7	2.3 × 10 ⁻²
	400.5	2.6	10.6	1.5 × 10 ⁻³
	401.0	2.9	13.5	3.6 × 10 ⁻⁴
	402.0	2.4	35	1.4 × 10 ⁻⁴
	402.5	3.0	70	2.0 × 10 ⁻⁶
DSC-1B	399.5	3.2	3.8	9.7 × 10 ⁻³
	400.5	2.9	7.2	2.3 × 10 ⁻³
	401.5	3.1	31.0	1.7 × 10 ⁻⁵
Dilatometry	400.5	2.8	9.5	1.3 × 10 ⁻³
	401.5	3.2	36.0	7.3 × 10 ⁻⁶
	402.0	3.2	77.0	6.4 × 10 ⁻⁷
	402.5	3.3	187	2.2 × 10 ⁻⁸

crystallization (dH_t/dt) as a function of time. The rate curves were processed by integrating to determine the relative extent of crystallization as a function of time, i.e. by assuming:

$$X_t/X_\infty = \frac{\int_0^t (dH_t/dt) \cdot dt}{\int_0^\infty (dH_t/dt) \cdot dt} \quad (5)$$

RESULTS AND DISCUSSION

Primary crystallization

Rate measurements were restricted by the sensitivity of the calorimeter (0.4–8.5 μJ/sec), sample size (up to 30 mg), and the enthalpy of crystallization (300 J/g). For polyethylene this limited the study to crystallization with half lives between 2–200 min, and to a range of 5–7K. With polymers which crystallize less readily than polyethylene, these restrictions severely limit their study. Dilatometry is not so restricted since it measures the extent of crystallization directly rather than the rate.

The isothermal extent of crystallization–time plots obtained with the DSC-2 was similar in most details to those obtained with DSC-1B and by dilatometry (see Figure 1 of ref 1). The reproducibility of the plots, however, was improved compared with those obtained with the DSC-1B, since the automatic temperature control enabled the temperature to be reproduced to 0.1K. Figure 1 exhibits the

effect of varying the temperature of crystallization by ±0.1K at 396.0K (sample B). The crystallization at 396.0K was repeated 10 times and the scatter in the superimposed rate curves used as a measure of the error in setting the temperature. This was ±0.025K. The method must be considered a maximum error since it attributes all variations, recorder speed and setting the initial onset of crystallization, to an error in temperature.

Analysis of the crystallization rate–time dependences by equations (1) to (5) indicated that two processes were present² which could be separated on a time scale. Following Banks *et al.*³, X_∞ for the primary stage was used as an adjustable parameter and a value was selected which gave a constant value of *n* over most of the primary process. Rate constants, Z_1 , and values of *n* obtained in this way are listed in Table 2. Dilatometry and both DSC's gave similar rate constants with the same temperature dependence, indicating that the primary process was being measured to a similar extent by the methods.

Variations in the rate constants were considered to be due to errors in the procedures adopted for calibrating and setting temperature (0.3K in DSC-1B). This can be seen by directly comparing the crystallization rate curves. For this purpose the time interval between attainment of constant temperature and maximum crystallization rate, t_{max} , was selected as an experimental parameter independent of the choice of X_∞ and the analyses procedure adopted. No sample size dependence was observed with the DSC-2 in the weight range (1–30 mg), (see Figure 2) and all three methods exhibited the same temperature dependence.

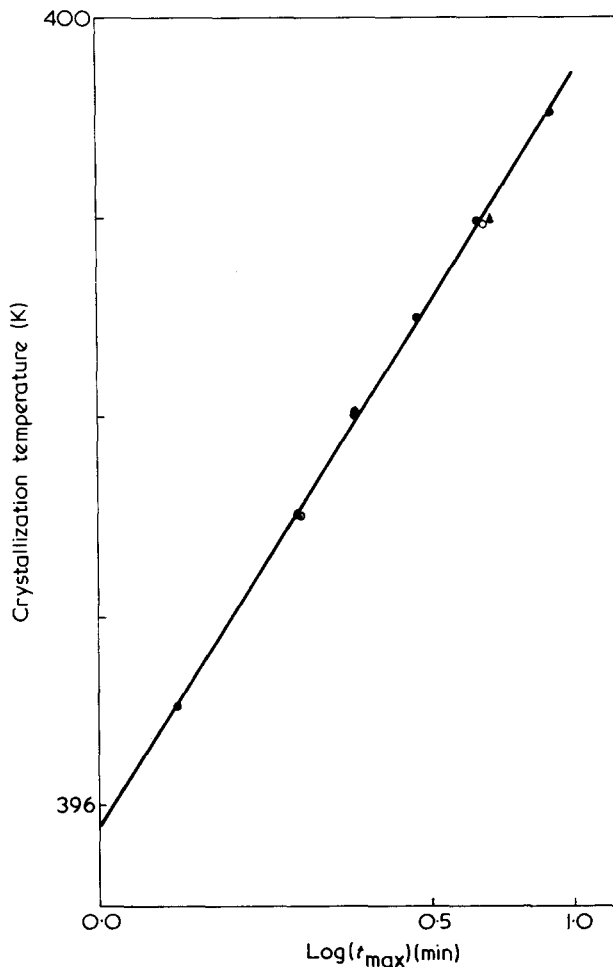


Figure 2 Sample size effects: ●, 15.0 mg; ▲, 10.0 mg; ○, 5.2 mg

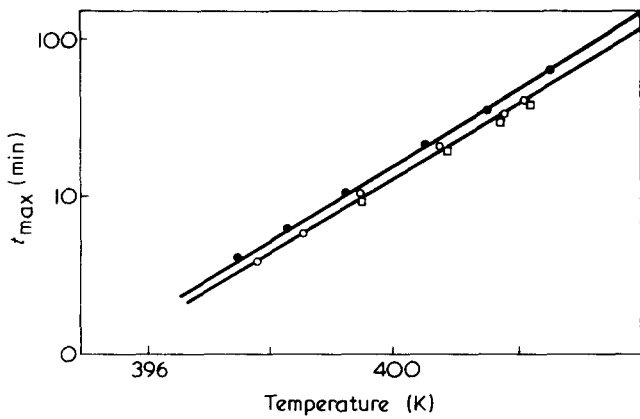


Figure 3 Reproducibility of crystallization characteristics within the methods: ●, DSC-1B; ○, DSC-2; □, dilatometry

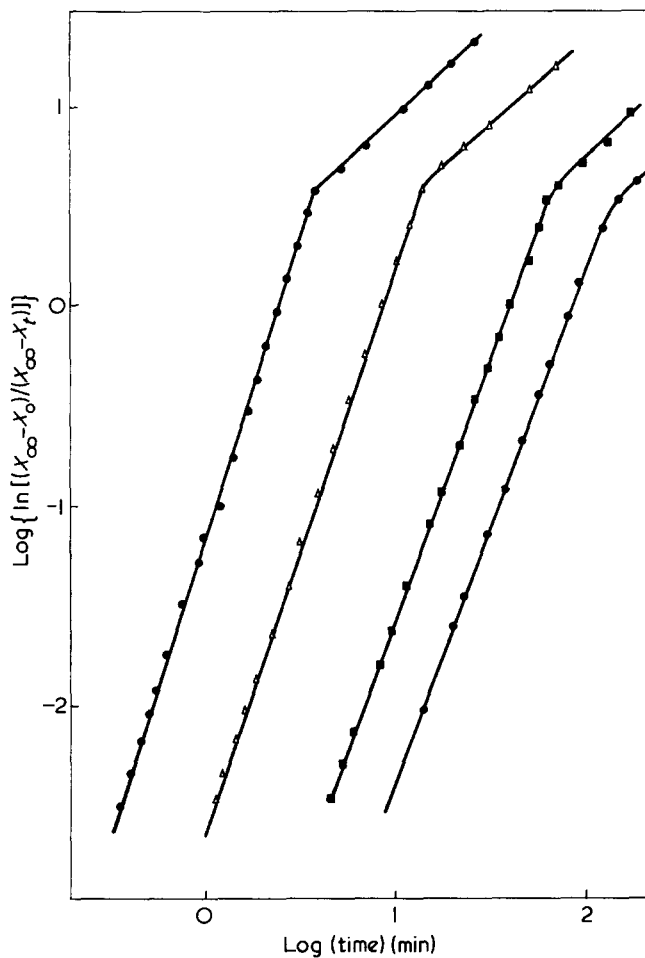


Figure 4 Analysis of crystallization isotherms for sample B from equation (2). ●, 398.8K; △, 399.3K; ■, 399.8K; ●, 400.8K

Assumption of an error of 0.3K in the DSC-1B temperature calibration alone was sufficient to superimpose all the data, (see Figure 3).

It would also appear that t_{max} might be a more accurate means of calibrating constant temperature of the calorimeters than linear extrapolation of the melting points of zone-refined materials determined at various rates of heating to zero rate.

Secondary crystallization

It was observed previously¹ that differences existed between the integrated DSC-1B and dilatometric crystalliza-

tion extent-time plots, in that the slow increase in crystallinity with time attributed to secondary crystallization was not present in the calorimeter determined plots. Despite this, analyses of the DSC-2 determined plots by equation (2) indicated that there was a change in mechanism at about 85–95% of the measured crystallinity in that the exponent changed from 2.5–3.0 to about 1.0, (see Figure 4). The lower rates, inherent in secondary crystallization, meant that the process could only be followed over a limited time period and also a limited temperature range. The rate parameters, obtained from equations (2) and (4) using $n = 1.0$, are listed in Table 3. Apparently conflicting results were

Table 3 Secondary crystallization parameters

Sample no.	Method	Crystallization temperature (K)	n	Z_2^* (min ⁻¹)
B	DSC-2	397.5	0.8	0.27
		398.8	1.0	0.13
		399.8	1.1	0.08
	Dilatometry	400.5	1.0	0.02
		401.5	1.0	0.007
C	DSC-2	399.5	1.0	0.12
		400.5	1.0	0.16
		402.0	1.0	0.0014
	Dilatometry	400.5	1.0	0.0048
		401.5	1.0	0.0021

* Assuming $n = 1.0$

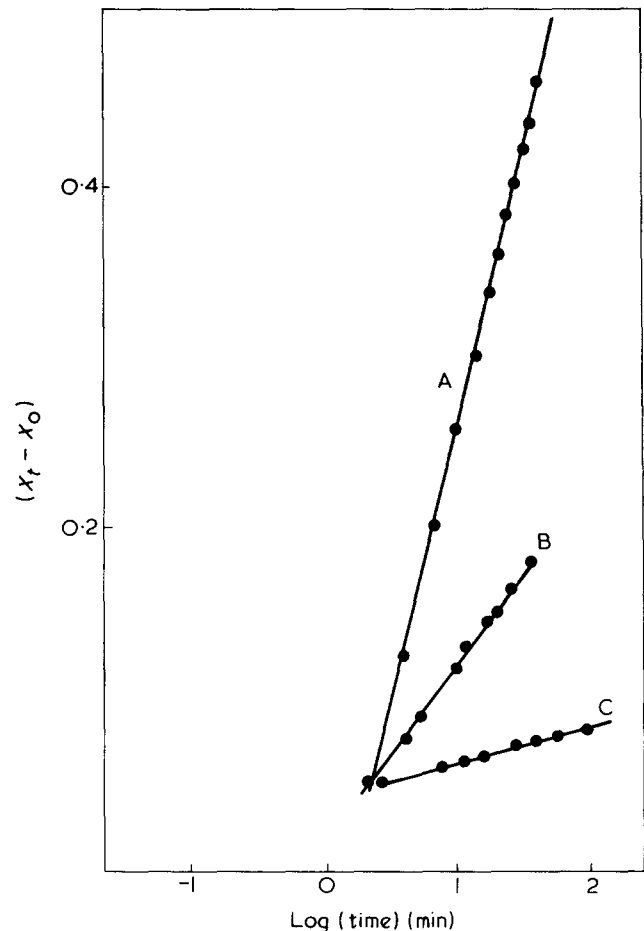


Figure 5 Secondary crystallization for sample B. A, 399.8K; B, 398.8K; C, 397.5K

obtained, in that with sample B, both dilatometric and calorimetric measured rate constants are very similar, and with sample C, very different values were obtained. However, dilatometry indicates that the secondary process of sample C is much slower than that of B, to such an extent that it would not be detected to any appreciable conversion by DSC-2. Furthermore, it is unlikely that it could be separated from the final traces of the primary process.

The sensitivity of the calorimeter required to determine the primary process severely restricted the use of the calorimeter to detect secondary crystallization, and no faith could be placed on the rate parameters determined. An alternative procedure was adopted by which the crystallization was followed to 80–90% apparent completion, and then the sensitivity of the calorimeter increased to a maximum ($0.4 \mu\text{J}/\text{sec}$). The remaining rates of crystallization were followed to completion at this increased sensitivity. As before, the increased crystallinity was obtained by integrating [from the arbitrary initial point (X_∞) to the experimental point (X_c, t)]. An increase in crystallinity with logarithmic time was observed with sample B which closely paralleled the dilatometric observation² (see *Figure 5*) and indicated that secondary crystallization was present but its extent limited by the calorimeter sensitivity.

CONCLUSIONS

DSC-2 can be applied to the study of isothermal crystallization kinetics provided the rate is sufficiently large. Rates can be measured to lower values ($\times 0.1$) than can be measured by DSC-1B.

The isothermal crystallization–time curves are more reproducible with DSC-2 because of the improved temperature setting (to 0.1K), and the maximum variation in temperature setting is $\pm 0.025\text{K}$.

Despite the improved sensitivity of DSC-2, it is more restricted than dilatometry in measuring low rate of crystallinity. This severely limits its use in studying secondary crystallization processes. Its main advantages, however, are in the speed and accuracy of use, and also the small samples required (1–2 mg). This has obvious advantages in characterizing the crystallization behaviour of polymer fractions for which small samples may only be available.

There may also be some advantage in using the crystallization rate characteristics of standard polymer samples to calibrate the temperature of the calorimeter.

REFERENCES

- 1 Booth, A. and Hay, J. N. *Polymer* 1969, **10**, 95
- 2 Hay, J. N. *J. Polym. Sci. (A)* 1965, **3**, 433
- 3 Banks, W., Gordon, M., Roe, R.-J. and Sharples, A. *Polymer* 1963, **4**, 61

Contributions to the proton relaxation of poly(ethylene oxide) in benzene solutions

F. Heatley and I. Walton

Chemistry Department, University of Manchester, Manchester M13 9PL, UK
(Received 27 May)

It is clear from recent studies of polymer motion in solution using nuclear magnetic relaxation¹⁻³ that the auto-correlation functions for reorientation of internuclear vectors are often far from exponential, and full characterization of the motion requires the measurement of several relaxation parameters. Because of the simplicity of interpretation, ¹³C spin-lattice relaxation times (T_1) and nuclear Overhauser enhancements (NOE) are extremely valuable for this purpose^{1,3}, but it has been shown³ that further data is required to distinguish between various models of the reorientation process. An obvious source of such data is ¹H relaxation, since almost all synthetic polymers contain ¹H nuclei and general application is possible. However whereas ¹³C relaxation is practically entirely intramolecular in origin, ¹H relaxation may also have substantial intermolecular contributions from interactions with solvent, polymer and dissolved oxygen. Each of these contributions must either be removed or determined separately in order to isolate the intramolecular contribution which is the significant quantity in studying chain dynamics. The interaction with dissolved oxygen is easily eliminated by vacuum degassing, but the interactions with other molecules can only be removed by expensive deuteration of both polymer and solvent. In order to determine whether intermolecular interactions are sufficiently important to require the use of the deuteration technique, we have measured the ¹H relaxation times of poly(ethylene oxide) in benzene solutions of concentrations from 5 to 30% w/w.

Three series of solutions were run: (a) fully protonated polymer (PEOH) in C₆H₆; (b) PEOH in C₆D₆; (c) C₆H₆ solutions of polymer consisting of 20% PEOH and 80% fully deuterated polymer (PEOD). The PEOD available had a fairly wide molecular weight distribu-

tion ($M_n = 3500, M_w = 7000$). To ensure that replacing PEOH by PEOD left the solution properties unchanged, the PEOH employed was a mixture of sharp fractions which reproduced the PEOD distribution. All solutions were degassed and the polymer and solvent ¹H relaxation times measured on a Varian Associates HA-100 spectrometer using the adiabatic rapid passage with sampling technique⁴. The results are presented in Table 1.

It is clear that the polymer ¹H relaxation times are affected very little by deuteration of either solvent or polymer, and are therefore determined almost entirely by intramolecular interactions. As expected the largest increase in T_1 is observed on replacing C₆H₆ by C₆D₆ for the 5% solution, but the increase is small and not far outside the combined experimental errors. The smallness of the polymer-solvent contribution is also shown by the minor increase in the solvent T_1 on deuteration of the polymer. The largest increase is shown by the 30% solution. Using the formula:

$$\left(\frac{1}{T_1}\right)_{\text{PS}} = \left(\frac{1}{T_1}\right)_{\text{S,PEOH}} - \left(\frac{1}{T_1}\right)_{\text{S,PEOD}}$$

where $(T_1)_{\text{PS}}$ is the polymer-solvent contribution and $(T_1)_{\text{S,PEOH}}$ and $(T_1)_{\text{S,PEOD}}$ are the solvent relaxation

times for the PEOH and PEOH/PEOD solutions respectively, we calculate a value of 70 ± 30 sec for $(T_1)_{\text{PS}}$ in the 30% solution. Such a contribution would lead to a change of only 0.08 sec in the polymer T_1 of about 1.5 sec, which is well within the experimental error. The effect on the polymer relaxation in the more dilute solution would be even smaller. The insignificance of solvent-polymer interactions in polymer relaxation is in accord with earlier measurements⁵ on aqueous PEO solutions.

The conclusion drawn from these results is that in PEO solutions, ¹H relaxation arises almost entirely from intramolecular causes, and is therefore an accurate indicator of the chain motion. This data may thus be combined with ¹³C relaxation data to define the nature of the motion more precisely. We have measured the ¹³C T_1 of PEOH in C₆D₆ at 30°C and 25.14 MHz using a Varian Associates XL-100 spectrometer. The results are given in Table 2, together with correlation times, τ_c , obtained using

$$\frac{1}{T_{1C}} = \frac{2\gamma_H^2\gamma_C^2\hbar^2}{r_{CH}^6} \times \tau_c \quad (1)$$

where r_{CH} is the C-H bond length (0.11 nm). This equation assumes isotropic motion in the extreme narrowing limit. ¹H relaxation times were then calculated using the equation:

$$\frac{1}{T_{1H}} = \frac{3}{2} \gamma_H^4 \hbar^2 \tau_c \left[\frac{1}{r_m^6} + P_T \times \left(\frac{1}{r_t^6} + \frac{1}{r_g^6} \right) + \frac{P_G}{2} \left(\frac{1}{r_t^6} + \frac{3}{r_g^6} \right) \right] \quad (2)$$

Table 1 ¹H spin-lattice relaxation times (sec) for solutions of PEO in benzene at 35°C

Concentration (% w/w)	PEOH/C ₆ H ₆		PEOH/C ₆ D ₆ Polymer	PEOH/PEOD/C ₆ H ₆	
	Polymer	Solvent		Polymer	Solvent
5	1.66 ± 0.08	18.8 ± 1.0	1.84 ± 0.11	1.54 ± 0.11	19.3 ± 0.7
10	1.61 ± 0.05	17.0 ± 1.0	1.52 ± 0.1	1.55 ± 0.1	17.7 ± 1.0
20	1.55 ± 0.06	17.0 ± 1.1	1.59 ± 0.1	1.7 ± 0.10	18.5 ± 1.0
30	1.51 ± 0.05	12.0 ± 0.8	1.37 ± 0.06	1.52 ± 0.07	14.7 ± 0.7

Table 2 ^{13}C spin—lattice relaxation times, average correlation times and calculated ^1H relaxation times for PEOH in C_6D_6

Concentration (% w/w)	$T_{1\text{C}}^{\text{a}}$ (sec)	τ_{C} (psec)	$T_{1\text{H}}$ (sec)	
			Calculated	Found
5	1.56	15.8	2.02	1.84 ± 0.1
10	1.40	17.6	1.80	1.52 ± 0.1
20	1.14	21.6	1.47	1.59 ± 0.1
30	0.99	24.9	1.28	1.37 ± 0.06

^aError in $T_{1\text{C}} \pm 10\%$

where P_T and P_G are the relative populations of the rotational isomers of the C—C bond with the oxygen atoms *trans* and *gauche* respectively, and r_m , r_t and r_g are distances between protons in respectively *geminal*, *trans* vicinal and *gauche* vicinal orientations. $T_{1\text{H}}$ is in fact dominated by the *geminal* interaction, and the uncertainty in assuming equal weighting of the isomers ($P_T = P_G/2 = 1/3$) amounts to only 2.5%. A comparison of calculated and experimental values of $T_{1\text{H}}$ is also made in Table 2.

The correspondence between the two sets of values is quite close, apparently justifying the isotropic rotational model used to derive equations (1) and

(2). It is known¹⁻³ however that polymer motion is often better represented by a distribution of correlation times, and τ_{C} should be interpreted as an average correlation time. The conclusion to be drawn is that the C—H interactions causing the ^{13}C relaxation, and the H—H interactions causing the ^1H relaxation have the same average correlation time and presumably also the same autocorrelation function.

In PEO, the major contribution to ^1H relaxation arises from mutual interaction of *geminal* protons separated by 0.18 nm. It is therefore highly probable that one can ignore intermolecular contributions to the relaxation of CH_2 groups in other polymers. However, relaxation of methine protons is due to vicinal interactions over distances of 0.25 nm or more, which are at least 10 fold less effective. In a vinyl polymer $(-\text{CH}_2-\text{CHX}-)_n$, each CH proton has four vicinal neighbours, so its relaxation time should be about 3 or 4 times greater than the CH_2 relaxation time. In a hypothetical vinyl polymer with the same motional properties as PEO, the methine $T_{1\text{H}}$ would therefore be about 5 sec. The polymer—solvent contribution of 70 sec estimated above would cause a significant decrease of 7% from 5 to 4.67 sec. However, vinyl

polymers are generally much less flexible than PEO, so that at the same temperature the relaxation times in vinyl polymers would be much less than in PEO and therefore the effect of intermolecular interactions would be as insignificant for CH protons as it is for CH_2 .

Finally, it is worth noting that the relaxation times presented here are in agreement with previous studies⁵⁻⁷ of polymer motion, which showed that the polymer motions causing n.m.r. relaxation are independent of concentration until monomer/solvent mole ratios of about 5 are reached^{5,6}, and that the motions of solvent molecules are essentially unaffected by the presence of polymer up to quite high concentrations of 20–30%⁷.

REFERENCES

- Schaefer, J. *Macromolecules* 1973, **6**, 882
- Hermann, G. and Weill, G. *Macromolecules* 1975, **8**, 171
- Heatley, F. and Begum, A. *Polymer* 1976, **17**, 399
- Parkes, R. G. and Jonas, J. *Rev. Sci. Instrum.* 1970, **41**, 319
- Liu, K. J. and Ullman, R. *J. Chem. Phys.* 1968, **48**, 1158
- Heatley, F. *Polymer* 1975, **16**, 493
- Heatley, F. *Polymer* 1975, **16**, 489

Preparation and reactions of polymeric Grignard compounds

F. J. Burgess and D. H. Richards

Explosives Research and Development Establishment, Ministry of Defence, Waltham Abbey, Essex EN9 1BP, UK

(Received 14 June 1976)

INTRODUCTION

The synthesis of mono- and difunctional living polymers was first described in full by Szwarc^{1,2} in 1956, although the idea of terminationless polymerization systems had been proposed by Ziegler³⁻⁵ in the 1930s. In recent years academic and commercial interest in these anionic techniques has developed rapidly; in particular the methods have allowed the synthesis of terminally functional polymers of narrow molecular weight distributions. Polymeric carbanions have been reacted with carbon dioxide to give carboxy end groups, and with ethylene oxide to give hydroxy end groups (equation 1)⁶. This approach

has been particularly valuable in the preparation of di-terminally functional (telechelic) liquid polybutadienes⁷, which may be subsequently chain extended and crosslinked by the addition of suitable reagents.

Other methods, which rely on the reaction of living polymers with an excess of a difunctional reagent, have been developed to prepare terminally functional polymers. Thus epoxy terminated polymer has been synthesised by reaction with excess epoxy resin⁸ and, perhaps more importantly, bromine terminated polymer has been prepared by reaction with excess bromine or with excess of an α,α' -dibromoxylene⁹ (equation 2). However, in both the latter cases the resulting mate-

rial contained appreciable quantities of non-functional polymer, the maximum yield of brominated chain ends never exceeding 75%. It was shown that when monofunctional living polystyrene was used, the non-brominated material was double the molecular weight of that brominated, and so it was concluded that the efficiency of the reaction was limited by the prevalence of the Wurtz condensation reaction, as represented generally by equation (3).

The latter process appears to be so rapid that attempts to reduce its contribution by rapid stirring or increase in the halide excess all failed.

Clearly this high rate of reaction is controlled by the extreme reactivity of the organometallic end group and, if this could be reduced, it should result in a corresponding decrease in the rate of coupling. Further, if this rate were lowered to a point where the reagents could be efficiently mixed be-

Table 2 ^{13}C spin—lattice relaxation times, average correlation times and calculated ^1H relaxation times for PEOH in C_6D_6

Concentration (% w/w)	$T_{1\text{C}}^a$ (sec)	τ_c (psec)	$T_{1\text{H}}$ (sec)	
			Calculated	Found
5	1.56	15.8	2.02	1.84 ± 0.1
10	1.40	17.6	1.80	1.52 ± 0.1
20	1.14	21.6	1.47	1.59 ± 0.1
30	0.99	24.9	1.28	1.37 ± 0.06

^aError in $T_{1\text{C}} \pm 10\%$

where P_T and P_G are the relative populations of the rotational isomers of the C—C bond with the oxygen atoms *trans* and *gauche* respectively, and r_m , r_t and r_g are distances between protons in respectively *geminal*, *trans* vicinal and *gauche* vicinal orientations. $T_{1\text{H}}$ is in fact dominated by the *geminal* interaction, and the uncertainty in assuming equal weighting of the isomers ($P_T = P_G/2 = 1/3$) amounts to only 2.5%. A comparison of calculated and experimental values of $T_{1\text{H}}$ is also made in Table 2.

The correspondence between the two sets of values is quite close, apparently justifying the isotropic rotational model used to derive equations (1) and

(2). It is known¹⁻³ however that polymer motion is often better represented by a distribution of correlation times, and τ_c should be interpreted as an average correlation time. The conclusion to be drawn is that the C—H interactions causing the ^{13}C relaxation, and the H—H interactions causing the ^1H relaxation have the same average correlation time and presumably also the same autocorrelation function.

In PEO, the major contribution to ^1H relaxation arises from mutual interaction of *geminal* protons separated by 0.18 nm. It is therefore highly probable that one can ignore intermolecular contributions to the relaxation of CH_2 groups in other polymers. However, relaxation of methine protons is due to vicinal interactions over distances of 0.25 nm or more, which are at least 10 fold less effective. In a vinyl polymer $(-\text{CH}_2-\text{CHX}-)_n$, each CH proton has four vicinal neighbours, so its relaxation time should be about 3 or 4 times greater than the CH_2 relaxation time. In a hypothetical vinyl polymer with the same motional properties as PEO, the methine $T_{1\text{H}}$ would therefore be about 5 sec. The polymer—solvent contribution of 70 sec estimated above would cause a significant decrease of 7% from 5 to 4.67 sec. However, vinyl

polymers are generally much less flexible than PEO, so that at the same temperature the relaxation times in vinyl polymers would be much less than in PEO and therefore the effect of intermolecular interactions would be as insignificant for CH protons as it is for CH_2 .

Finally, it is worth noting that the relaxation times presented here are in agreement with previous studies⁵⁻⁷ of polymer motion, which showed that the polymer motions causing n.m.r. relaxation are independent of concentration until monomer/solvent mole ratios of about 5 are reached^{5,6}, and that the motions of solvent molecules are essentially unaffected by the presence of polymer up to quite high concentrations of 20–30%⁷.

REFERENCES

- Schaefer, J. *Macromolecules* 1973, **6**, 882
- Hermann, G. and Weill, G. *Macromolecules* 1975, **8**, 171
- Heatley, F. and Begum, A. *Polymer* 1976, **17**, 399
- Parkes, R. G. and Jonas, J. *Rev. Sci. Instrum.* 1970, **41**, 319
- Liu, K. J. and Ullman, R. *J. Chem. Phys.* 1968, **48**, 1158
- Heatley, F. *Polymer* 1975, **16**, 493
- Heatley, F. *Polymer* 1975, **16**, 489

Preparation and reactions of polymeric Grignard compounds

F. J. Burgess and D. H. Richards

Explosives Research and Development Establishment, Ministry of Defence, Waltham Abbey, Essex EN9 1BP, UK

(Received 14 June 1976)

INTRODUCTION

The synthesis of mono- and difunctional living polymers was first described in full by Szwarc^{1,2} in 1956, although the idea of terminationless polymerization systems had been proposed by Ziegler³⁻⁵ in the 1930s. In recent years academic and commercial interest in these anionic techniques has developed rapidly; in particular the methods have allowed the synthesis of terminally functional polymers of narrow molecular weight distributions. Polymeric carbanions have been reacted with carbon dioxide to give carboxy end groups, and with ethylene oxide to give hydroxy end groups (equation 1)⁶. This approach

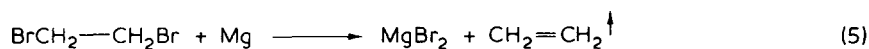
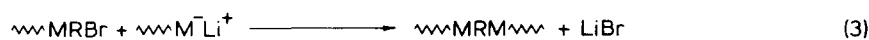
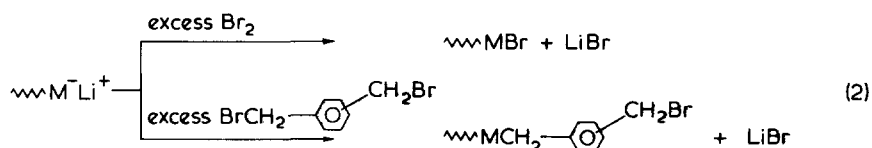
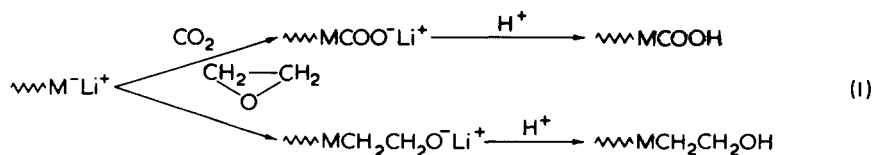
has been particularly valuable in the preparation of di-terminally functional (telechelic) liquid polybutadienes⁷, which may be subsequently chain extended and crosslinked by the addition of suitable reagents.

Other methods, which rely on the reaction of living polymers with an excess of a difunctional reagent, have been developed to prepare terminally functional polymers. Thus epoxy terminated polymer has been synthesised by reaction with excess epoxy resin⁸ and, perhaps more importantly, bromine terminated polymer has been prepared by reaction with excess bromine or with excess of an α,α' -dibromoxylene⁹ (equation 2). However, in both the latter cases the resulting mate-

rial contained appreciable quantities of non-functional polymer, the maximum yield of brominated chain ends never exceeding 75%. It was shown that when monofunctional living polystyrene was used, the non-brominated material was double the molecular weight of that brominated, and so it was concluded that the efficiency of the reaction was limited by the prevalence of the Wurtz condensation reaction, as represented generally by equation (3).

The latter process appears to be so rapid that attempts to reduce its contribution by rapid stirring or increase in the halide excess all failed.

Clearly this high rate of reaction is controlled by the extreme reactivity of the organometallic end group and, if this could be reduced, it should result in a corresponding decrease in the rate of coupling. Further, if this rate were lowered to a point where the reagents could be efficiently mixed be-



fore significant reaction occurred, then the effect of the excess halide would be maximized as would the yield of brominated product.

We have previously shown that living polymers react smoothly with metal halides such as triethyl lead chloride¹⁰, and mercuric bromide¹¹ to give the corresponding polymeric adducts, and so it was expected that a similar reaction would occur with excess magnesium bromide to form a polymeric Grignard compound (equation 4). By analogy with the behaviour of small molecule Grignard compounds, these species should be very much less reactive than their parent living polymers but still retain sufficient activity to react clearly with the reagents cited¹². It is the results of such experiments which are the subject of this communication.

EXPERIMENTAL

The preparation of benzene/THF solution of 2000 molecular weight monofunctional polystyryl lithium was carried out under nitrogen, and is an adaptation of a high vacuum technique described by Altares *et al.*¹³. This adaptation has been described previously⁹, as has the reaction of aliquots of the living polymer with ten-fold excess bromine and with ten-fold excess α,α' -dibromoxylene.

The preparation of the polystyrene Grignard has not been previously re-

ported and is briefly outlined here.

The reaction scheme shown in equation (4) requires that an anhydrous solution of magnesium bromide be prepared, preferably in THF so that the final Grignard reaction is carried out in the presence of an ethereal solvent. The most convenient method of preparing this is by the reaction of 1,2-dibromoethane with magnesium turnings in THF, which goes quantitatively by equation (5)¹⁴.

Typically, 37 g (0.2 mol) of 1,2-dibromoethane was added gradually to 6 g (0.25 mol) of magnesium turnings in 350 ml of refluxing THF. Reaction was carried out under nitrogen with rapid stirring to prevent uncontrolled frothing. After completing the addition the mixture was further refluxed for half an hour before filtering through a porosity 3 sinter whilst just below the boiling point of THF. The filtered solution was clear and colourless, but much magnesium bromide crystallized out on cooling to room temperature. Its solubility was determined as being ~ 0.25 M at 25°C (titration with 0.1 N silver nitrate using phenosafranine as indicator¹⁵).

A known volume of the polystyryl lithium solution was transferred into an appropriate container fitted with a septum, and through which nitrogen was passing. A quantity of saturated magnesium bromide solution in slight excess of that required to react with the carbanion ends according to equa-

tion (4) was added with a syringe, and this resulted in the immediate and total loss of the characteristic red colour of the living ends.

The reaction of polystyrene Grignard both with excess bromine and with excess α,α' -dibromoxylene was conducted in a manner identical to that previously described for the analogous reactions with living polymer⁹, and will therefore not be described again here.

RESULTS AND DISCUSSION

Living polystyrene of about 2000 molecular weight with one active end per chain was prepared. A sample of this solution was protonated with methanol, and examination of the polymer by g.p.c. showed it to be of the anticipated molecular weight, and to possess a narrow molecular weight distribution ($M_w/M_n \approx 1.05$) (Figure 1).

The remaining solution was divided into three parts, two being of equal volume and half the volume of the third. This largest sample was then reacted with magnesium bromide before again dividing into two equal parts.

One of the living polymer solutions was added slowly to a rapidly stirred solution containing ten-fold excess bromine, and the other was added similarly to a solution containing the same excess of α,α' -dibromo-*m*-xylene. These operations were repeated under identical conditions using the two polymeric Grignard solutions, and the four polymers were then isolated and examined by g.p.c. The traces of the two polymers resulting from the direct bromination reaction are compared

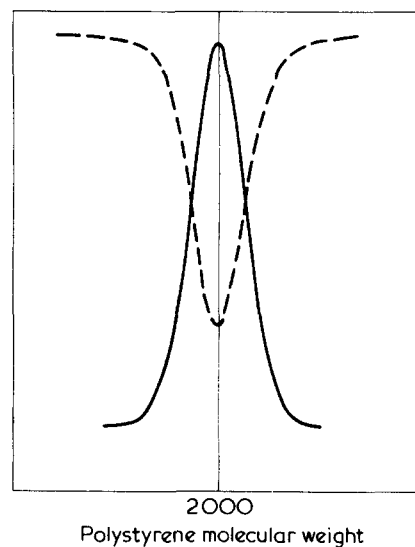


Figure 1 G.l.c. trace of protonated polystyryl lithium

in Figure 2, and those of the two produced by reaction with α,α' -dibromo-*m*-xylene are illustrated in Figure 3. The traces are all typical of a number of repeat experiments carried out under these conditions.

All the four traces in Figures 2 and 3 show the presence of coupled polystyrene of 4000 molecular weight. This is in contrast to the protonated material (Figure 1) which exhibits a single sharp peak at 2000 molecular weight. Thus the coupling must have resulted from the bromination reactions employed.

The degree of coupling has been very much reduced, however, in both reactions when the Grignard reagent is employed. In the direct bromination reaction the percentage of bromine terminated polystyrene is increased from about 58 to 93% by this means. Similarly, with α,α' -dibromo-*m*-xylene the percentage is increased from 25 to 77%. Undoubtedly the bromine content can be increased fur-

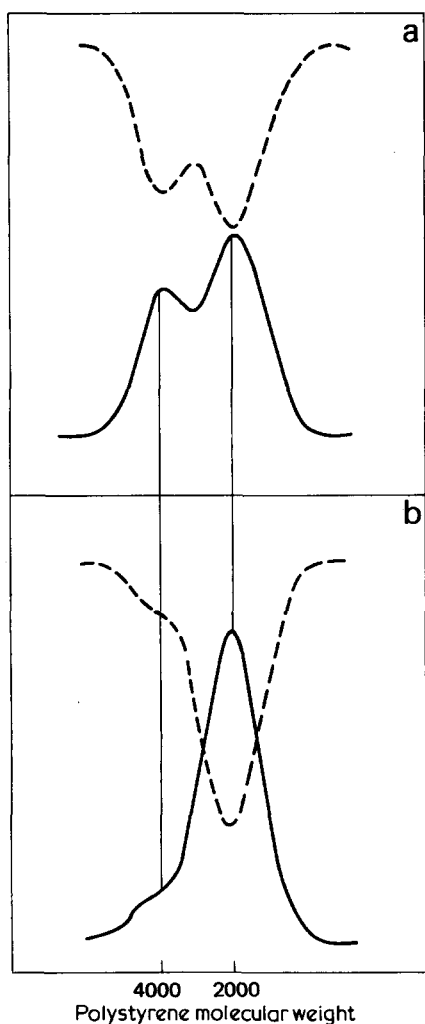


Figure 2 G.I.c. traces of products of (a) polystyryl lithium and (b) polystyryl Grignard reaction with ten-fold excess bromine

ther by a more refined technique of addition and so these figures are not meant to represent an upper limit for bromination. These increases do, however, illustrate the principle of reducing reactivity in order to improve selectivity.

It is at first sight somewhat surprising that the degree of coupling with either polymeric reagent should be much more pronounced when α,α' -dibromo-*m*-xylene is used than in the direct bromination reaction. This trend may perhaps be explained in the following manner. The initial bromination reaction is expected to be appreciably faster with bromine than with the dihalide and in both cases the polymeric bromides formed are benzylic in character and therefore should be of comparable intrinsic reactivities. The product from direct bromination should react less readily with further living polymer, however, because it is more shielded initially and on coupling produces a more sterically hindered bond (equations 6 and 7).

This idea of reducing reactivity of the polymer end groups to a required level may have much wider application than that listed here. Preliminary experiments in our laboratories indicate that the reaction of polybutadiene dianions with carbon dioxide or with ethylene oxide to produce telechelic carboxy or hydroxy liquid polymers (equation 1) may benefit by prior reaction to form Grignard analogues. Under these conditions we have found that the polymer may be mixed at room tem-

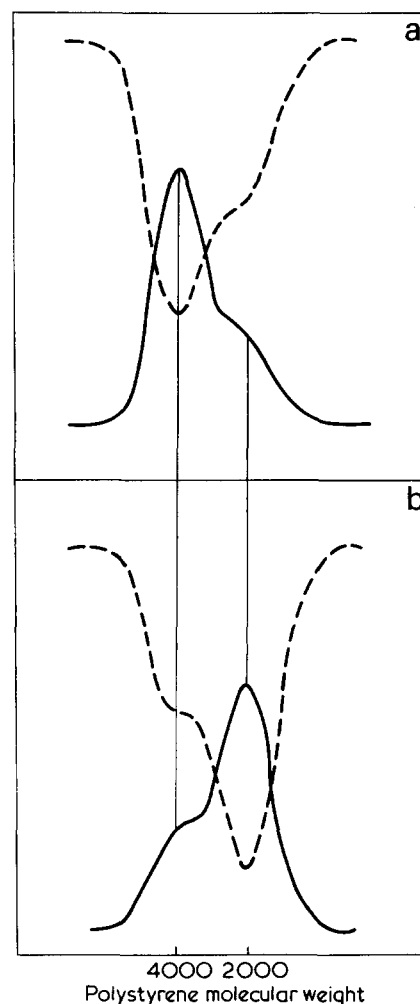
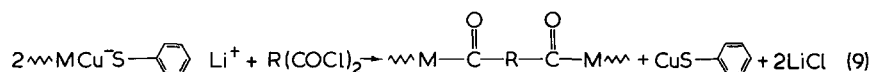
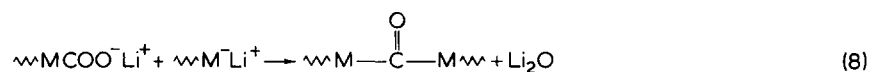
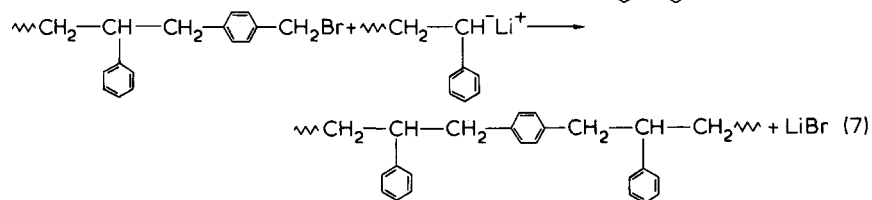
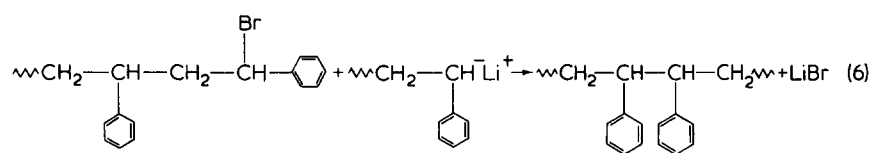


Figure 3 G.I.c. traces of products of (a) polystyryl lithium and of (b) polystyryl Grignard reaction with ten-fold excess α,α' -dibromo-*m*-xylene



perature with ethylene oxide without significant reaction occurring. Reaction takes place at elevated temperatures¹⁶ as evinced by the gelling of the solution due to alkoxide ion pair association⁶, and this may be subsequently destroyed by hydrolysis. When living polymer is mixed directly with ethylene oxide immediate reaction occurs and the resulting gel delays completion of the reaction for hours or days. The efficiency of the Grignard-ethylene oxide reaction has not as yet been studied.

Similarly, in the reaction with carbon dioxide it is very probable that the prior formation of the polymeric Grignard would reduce the production of ketone groups by the unwanted side reaction shown in equation (8).

Of course, living polymers may be reacted with other metallic salts, either in excess or stoichiometrically, to generate organometallic terminal groups possessing a variety of reactivities and properties. We have prepared end groups of the Grignard type such as $-\text{HgX}$, $-\text{CdX}$, $-\text{ZnX}$ etc, and have also prepared the dipolymeric derivatives of metals such as these. We are currently investigating the behaviour of such species, and we have already shown

that high yields of bromine terminated polymer may be obtained by reacting the mercury derivatives directly with bromine.

Another intriguing possibility is that of preparing polydiketone systems by reacting polymeric cadmium¹⁷ or copper complexes¹⁸ with diacylchlorides (neither of these species are reactive toward ketones) as illustrated in equation (9).

It appears that this approach of generating polymers with end groups of controlled reactivity allows a much greater freedom in the choice of subsequent reactions to produce new polymers and copolymers of well defined structure.

ACKNOWLEDGEMENT

We wish to thank Mr R. J. Pace for the gel permeation chromatographic measurements.

[© Crown Copyright. Reproduced with permission of the Controller, HMSO, London, 1976]

REFERENCES

- 1 Szwarc, M. *Nature* 1956, **178**, 1168
- 2 Szwarc, M., Levy, M. and Milkovich,

- 3 R. *J. Am. Chem. Soc.* 1956, **78**, 2656
- 4 Ziegler, K. *et al. Annalen*, 1934, **511**, 13, 45, 64
- 5 Ziegler, K. *Angew. Chem.* 1936, **49**, 499
- 6 Ziegler, K., Grimm, H. and Willer, R. *Annalen*, 1940, **542**, 90
- 7 Brody, H., Richards, D. H. and Szwarc, M. *Chem. Ind.* 1958, p 1473
- 8 French, D. M. *Rubber Chem. Technol.* 1969, **42**, 71
- 9 Cunliffe, A. V., Huglin, M. B., Pearce, P. J. and Richards, D. H. *Polymer* 1975, **16**, 654
- 10 Burgess, F. J., Cunliffe, A. V., Richards, D. H. and Sherrington, D. C. *Polym. Lett.* 1976, **14**, 471
- 11 Abadie, M., Burgess, F. J., Cunliffe, A. V. and Richards, D. H. *Polym. Lett.* 1976, **14**, 477
- 12 Cunliffe, A. V., Hayes, G. F. and Richards, D. H. *Polym. Lett.* in press
- 13 Kharasch, M. S. and Reinmuth, O. 'Grignard Reactions of Organometallic Substances', Constable, London, 1954, Ch 16
- 14 Altare Jr, T., Wyman, D. P. and Allen, V. R. *J. Polym. Sci. (A-2)* 1964, **2**, 4533
- 15 Tissier, A. and Grignard, V. C. R. *Acad. Sci.* 1901, **132**, 835
- 16 Vogel, A. I. 'A Textbook of Quantitative Inorganic Analysis', Longmans, London, 1964, p 81
- 17 Vogel, A. I. 'Practical Organic Chemistry', Longmans, London, 1956, p 253
- 18 Cason, J. *Chem. Rev.* 1947, **40**, 15
- 19 Posner, G. H., Whitten, C. E. and Sterling, J. J. *J. Am. Chem. Soc.* 1973, **95**, 7788

A new quarterly journal

APPLIED MATHEMATICAL MODELLING

environmental, social and engineering systems

APPLIED MATHEMATICAL MODELLING is the new international journal providing a multidisciplinary medium for publishing and discussing recent advances and thinking pertinent to mathematical modelling and practical systems analysis. In addition to methodology — its validation and reliability — emphasis is also given to the practical applications of both novel and successful models.

Some articles published in early issues

Computation of long-term average SO_2 concentration in the Venetian area
E. Runca et al. (IBM Italia, Venice, Italy)

A simple model of economic growth or decline under the influence of resource depletion
Bent Sørensen (Niels Bohr Institute, Copenhagen, Denmark)

Evaluating environmental quality management programmes in which dischargers are grouped
E. Downey Brill Jr. et al. (University of Illinois, USA)

Mathematical modelling of flows in recessed wall flame holder
D. Bhaduri and A. K. Majumdar (CMERI, Durgapur, India)

Manuscripts for publication should be sent to the Editor-in-Chief:
Dr C. A. Brebbia, University of Southampton, Southampton, England SO9 5NH
ISSN: 0307-904X
One years subscription (four issues) £25.00 (\$65.00)

For more details, please write to:

IPC Science and Technology Press Limited,
IPC House, 32 High Street, Guildford, Surrey, England GU1 3EW
Telephone: 0483-71661 Telex: Scitec Gd 859556

Book Review

Synthetic Paper from Fibers and Films

M. G. Halpern

Noyes Data Corporation, Park Ridge, New Jersey, 1975, \$36.00

This volume is essentially a summary of the content of 122 US Patents issued during the period 1957–1974. Paraphrasing the author's words, 'legal jargon and juristic phraseology have been eliminated' giving a book that is much more readable by the average scientist than would be the original patents.

Perhaps inevitably the book title does not adequately describe its contents. Basic information on both polymer technology and papermaking is lacking. Patents issued prior to 1957 have apparently been ignored and no account has been taken of information available from other sources such as technical journals and trade literature. A number of highly important recent developments in both materials and processes are not at present covered by patents, in some cases possibly because the innovators are not prepared to meet the Patent Office requirement of 'sufficient disclosure' or because the innovation is not considered sufficient to warrant the issue of a patent, and these are not referred to. Admittedly, the Foreword makes it clear that the volume is effectively a patent review covering a limited period of time, but this is not clear from the title.

Although this is still the subject of some controversy, the author's description of paper in the Introduction as a nonwoven fabric can be criticized. Furthermore, his statement of the advantages of synthetic papers, also given in the Introduction, must be regarded as an over-simplification. For instance, not all synthetic fibres have good chemical durability and the dimensional stability of synthetic fibres is sometimes much worse than that of cellulose fibres. It is suspected that the author was here referring primarily to moisture effects, but paper is also subjected to heat (during manufacture, conversion and usage) and the dimensional stability of cellulose fibres to heat is much better than that of some synthetic fibres and other materials.

There must also be some reservation with regard to the use by the author of the term 'synthetic paper'. Agreed terminology in

this field is inadequate. However, the current internationally accepted definition of paper requires that the material should be produced from fibres (thus disqualifying those paper-like materials manufactured in film form), but permits the use of synthetic fibres in any quantity. Rigid application of these criteria would require a complete change in the title of the book, but the reviewer has encountered the same terminology problems himself when preparing technical papers on this subject and cannot suggest a better title.

The patent field covered by the author includes the use of chemical derivatives of cellulose (in both fibrous and non-fibrous forms) and of chemically modified natural cellulose fibres in papermaking. It also includes the papermaking use of fibres manufactured from polymers such as polyolefins, polyamides and polyacrylonitriles, and the manufacture of non-fibrous synthetic papers from polyolefins and other polymers.

The patents described in the text will obviously vary considerably in their importance. Some have been exploited commercially and in a few cases the reviewer, from personal knowledge of products manufactured using the process described, is satisfied that the information given would be very useful to interested scientists and technologists. Others might be considered to be of very doubtful merit but, bearing in mind the constantly changing technological requirements for paper and paper products and the state of flux in the availability and relative costs of materials, more critical selection of the patents included would have been very difficult.

The descriptions of the patents are clear and concise although in some cases the terminology used is somewhat unorthodox. Adequate diagrams are included and the amount of tabulated numerical data given is gratifyingly greater than might have been expected. It is interesting to note, however, the wide variety of test methods and units for expression of results used by the different workers. For instance, no fewer than 15 different units are used for tensile strength, apart from several patents where numerical values for this property are given without units. This must be viewed as a criticism not of the author of this book, but of the original workers and of the lack of progress towards standardization.

Although not without its limitations, this book is considered to be a very useful addition to the available literature, most particularly for papermakers, but also for polymer and textile technologists. Its publication at this stage of the development of synthetic pulps and papers is particularly well timed. Technical papers in this area have tended to concentrate on the properties and performance of these materials and have usually ignored the basic production technologies. This gap has now at least partially been filled.

F. D. Munday

Conference Announcement

Polymer Processing

Massachusetts Institute of Technology, Cambridge, Massachusetts, USA, 15–18 August 1977

An international conference on 'Polymer Processing' will be held at M.I.T., Cambridge, Massachusetts, 15–18 August, 1977. The purpose of the conference is to establish the state of fundamental knowledge in polymer processing and to assess the nature of major problems to be solved in the field. The topics to be covered are: basic considerations in polymer processing, polymer melt processing, liquid reaction processing, processing of composites, processing of foamed plastics, processing related to surface phenomena, polymers for non-traditional applications, recent advances in polymer processing, characterization and properties of polymers, quality control and accelerated testing and needs and opportunities in polymer processing. Those interested in presenting papers are invited to submit abstracts of not more than 500 words on subjects related to one of the topics above. Abstracts should be sent by 30 November, 1976 to: Professor Nam P. Suh, Conference Chairman, Massachusetts Institute of Technology, Room 34–134, Cambridge, Massachusetts 02139, USA.

Conference Announcement

Polymer Surfaces Symposium

University of Durham, 21–24 March 1977

The Macromolecular Group of the Chemical Society are organizing the symposium 'Polymer Surfaces' to be held at the University of Durham, 21–24 March 1976. Particular emphasis is being placed on plenary and keynote lectures to review and highlight work of both an applied and academic nature. The topics to be discussed include the formation; chemical, physical, electrical and mechanical properties and modifications thereof; characterization and uses of polymer surfaces. Contributed papers are solicited and abstracts are requested by the end of November 1976. Further details may be obtained from: Dr W. J. Feast, Department of Chemistry, University of Durham, South Road, Durham DH1 3LE.

Configuration of cellulose trinitrate in solution

C. Holt*, W. Mackie and D. B. Sellen

Astbury Department of Biophysics, University of Leeds, Leeds LS2 9JT, UK

(Received 1 March 1976; revised 19 May 1976)

Cellulose trinitrate was prepared from cotton (*Deltapine*) under a variety of conditions and investigated in solution with ethyl acetate as solvent using the techniques of light scattering, osmometry and viscometry. The more mildly nitrated samples (e.g. 1 h at 20°C) exhibited downward curvature in the Zimm plots and a fractional precipitation experiment showed that this was due to the presence of large gel-like aggregates. Light scattering, viscometry, infra-red and ultracentrifuge measurements were made on the fraction of gel-like material and the effect of further nitration investigated. The possible nature of the aggregates is discussed. Light scattering measurements made on a mildly nitrated sample with this fraction removed yielded a straight line Zimm plot from which chain statistics similar to those found by other authors could be deduced. Samples obtained by more extensive nitration (2–25 h at 20°C) were considerably degraded but yielded straight line Zimm plots and osmotic pressure measurements showed the polydispersities to be low ($DP_w/DP_n \sim 1.3$). Values of effective bond length, b , calculated from these Zimm plots (4.6 to 5.6 nm) were much larger than those found for the more mildly nitrated samples and those found by other authors. Also, in contrast to the results of other authors, second virial coefficients obtained by light scattering and osmotic pressure were found to be in fair agreement. The effect of gel-like material on measured second virial coefficients is discussed. It is suggested that the discrepancy in b arises because gel-like material remains in more mildly nitrated samples even after the larger aggregates have been removed by fractional precipitation. This material consists of particles denser than the single coils but of comparable or smaller size so that values obtained for the effective bond length are too low. The results of previous investigations on all the cellulosic polymers which have been investigated are discussed in the light of the present work with particular reference to the effect of gel-like material. It is suggested that the apparent disagreement between the conformational analysis of cellulose and experimental results arises from the presence of gel-like material in solutions rather than any fault in the molecular model.

INTRODUCTION

Although the degree of polymerization and polydispersity of native cellulose has been investigated by a number of workers over many years, the nature of native cellulose in this respect remains a matter for speculation. An extensive re-investigation of this problem has therefore been carried out in this department¹ and a brief report of the results obtained has already been published². During this investigation, cellulose trinitrate was prepared from cotton cellulose and investigated in solution with ethyl acetate as solvent, using the techniques of light scattering, osmometry and viscometry. The chain statistics of cellulose trinitrate, calculated from the results of the experiments, were similar to those obtained by other authors^{3–6}, when similar procedures of nitration and fractionation were adopted, and similar assumptions made about polydispersity. However it was discovered that direct nitration of cotton for periods of from 2 to 25 h at 20°C yielded samples of low polydispersity with $M_w/M_n \sim 1.3$ and the chain statistics calculated from the results of experiments on these samples indicated a much stiffer chain. It is this aspect of the work which forms the subject of the present paper. The biological aspects of the work will be discussed elsewhere. Gel permeation chromatography measurements were also made

on the cellulose trinitrate solution but in view of the complex behaviour discovered these also will be the subject of a separate publication.

EXPERIMENTAL

Preparation of cellulose trinitrate solutions

In all the work to be discussed in the present paper, cotton (*Deltapine*) was obtained from freshly opened bolls and was air dried prior to nitration with the mixture of Alexander and Mitchell⁷. Stock solutions of the nitrate were made up in redistilled ethyl acetate at concentrations of $\sim 1 \text{ kg/m}^3$. The good solvent ethyl acetate was used for three reasons (a) microgel formation is less likely in a good solvent, (b) for instrumental reasons osmotic pressure measurements were not possible in acetone and (c) gel permeation chromatography measurements were made concurrently with this investigation and a good solvent was found to be necessary for this technique. The solutions were made up by slowly agitating for 24 h and then centrifuging for 1 h at $30\,000 \times g$ to remove any undissolved material. The time of nitration required to achieve complete solubility was found to be a function of temperature and was approximately 20 min at 20°C, 1 h at 0°C and 24 h at –20°C. The nitrogen content of all the fully soluble samples was found by a semi-micro Kjeldahl method to be

* Present address: The Hannah Research Institute, Ayr, Scotland KA6 5HL, UK.

13.8 ± 0.1% (14.1% represents full substitution). The nitrogen content of the soluble components of samples obtained by nitration for shorter periods was also 13.8 ± 0.1% whilst the insoluble components had a nitrogen content ranging from 1 to 12%.

Light scattering measurements

Light scattering measurements were made by using a semi-cylindrical cell in an Aminco apparatus (American Instrument Co. Inc., Silver Spring, Maryland, USA). The apparatus was tested and calibrated as already described⁶ except that the Ludox calibration was checked by measurements on the pure liquids carbon tetrachloride, benzene and carbon disulphide. Assuming the Rayleigh ratios for these liquids based on a literature survey by Kratochvil *et al.*⁸ and making the usual correction for the refractive index of the liquids^{9,10} the Ludox calibration was confirmed to be correct within experimental error (±5%).

An adequate degree of clarification prior to light scattering measurements is especially difficult to achieve with solutions of cellulose derivatives because centrifugation is the only effective means of removing dust and because the low refractive index increment and high dissymmetry of scatter make it necessary to work at concentrations where the solute scatter is sometimes less than that due to the solvent. In this work solutions were centrifuged for 2 h at 30 000 × g and the top 20% of each volume used for light scattering measurements. Both the syringe used for transferring the solution to the light scattering cell and the cell itself were rinsed in a stream of condensing distilled ethyl acetate immediately before use. In this way an adequate degree of clarification was achieved once in every three attempts. The solute concentration was determined after each set of light scattering measurements by taking a 2 ml volume of solution from the light scattering cell and evaporating to dryness.

Zimm plots were made in the usual way. It was found however that repeated experiments at a given concentration yielded KC/R_θ against $\sin^2\theta/2 + kC$ plots (where the symbols have their usual meaning) in which the slope at high angles varied by about 10% although constant intercepts at $\theta = 0$ were obtained. Higher slopes were obtained more frequently at the lower concentrations. The Zimm plots presented in this paper were constructed by taking at each concentration the set of measurements yielding the highest slopes at high angles. This procedure was found to yield self-consistent Zimm plots with linear extrapolation to zero concentration. A justification of this procedure will be given in the Results and Discussion section of this paper.

The refractive index increment dn/dC was measured using a 10 mm cell in a Rayleigh differential refractometer. The cellulose trinitrate sample used for this purpose was one obtained by nitration for 1 h at 20°C. This was divided into three fractions by precipitation from solution in ethyl acetate with n-hexane and the middle fraction used for refractive index measurements. This was done to ensure that measurements were made on cellulose trinitrate chains and not upon microgel or low molecular weight material. It was found that due to it being slightly hygroscopic the refractive index of ethyl acetate could vary by several parts in 10⁵. The errors resulting from this can be minimized by using ethyl acetate from the same distillation batch both for making up the solution and as reference solvent. In this way dn/dC was found to be 0.105 ± 0.001 ml/g at both 546 and 436 nm. This is in good agreement with the values found by Holtzer *et al.*³ and Huque *et al.*⁵ but 5% lower than that found by Penzel and Schulz¹¹.

Membrane osmometry

Osmotic pressure measurements were made in a Mechrolab apparatus (model 503 Hewlett-Packard Ltd, Slough, UK) at 25°C using type 08 membranes. In this apparatus a negative pressure head of solvent is applied with the aid of a servo-mechanism so as just to counteract the flow of solvent through the membrane. Solvent flow is detected by means of a photocell which is set to receive light passing through an air bubble. The apparatus was found usually to reach equilibrium within 5 min and no permeation of the membrane by the solute was observed. By continuously recording the pressure with the aid of a pen recorder until 15 min after equilibrium had been reached, it was found possible to integrate out purely random fluctuations (thermal and instrumental) and to obtain osmotic pressures correct to 0.05 mm of ethyl acetate. Prior to making measurements the stock solutions were centrifuged for 2 h at 100 000 × g and decanted.

Viscometry

Viscosity measurements were made at 20°C using two Cannon-Fenske viscometers each with two bulks thus giving four rates of shear in the range 900 to 3000 sec⁻¹. In each case the reduced specific viscosity was extrapolated first to zero rate of shear and then to zero concentration in the manner previously described¹².

RESULTS AND DISCUSSION

Mildly nitrated samples

Table 1 shows data derived from Zimm plots represent-

Table 1 Light scattering measurements upon cellulose trinitrate obtained by mildly nitrating cotton (Deltapine). Ethyl acetate as solvent

Sample	Time and temperature of nitration	λ (nm)	Second virial coefficient $B \times 10^4$ (mol m ³ /kg ²)	Interpretation in terms of the theory of Benoit <i>et al.</i> ¹³ for a polydisperse solution of Gaussian coils			Interpretation in terms of a gel-coil mixture (see text)			
				DP_w	DP_n	b (nm)	DP_c	S_g (nm)	S_c (nm)	b^* (nm)
I	1 h at 20°C	436	6.2	11 000	2800	3.3	5700	270	120	3.6
		546	7.0	10 500	2700	3.5	5400	270	130	3.9
II	1 h at -20°C	436	4.3	11 000	2400	3.0	4800	240	100	3.3
		546	3.8	10 500	2600	3.5	5200	290	120	3.9
III	24 h at -20°C	436	8.8	13 500	3300	3.4	6600	290	130	3.7
		546	7.5	13 500	3200	3.0	6400	290	120	3.3

* Assuming a Schulz-Zimm distribution for the single coils with $DP_w/DP_n = 1.3$ (see text)

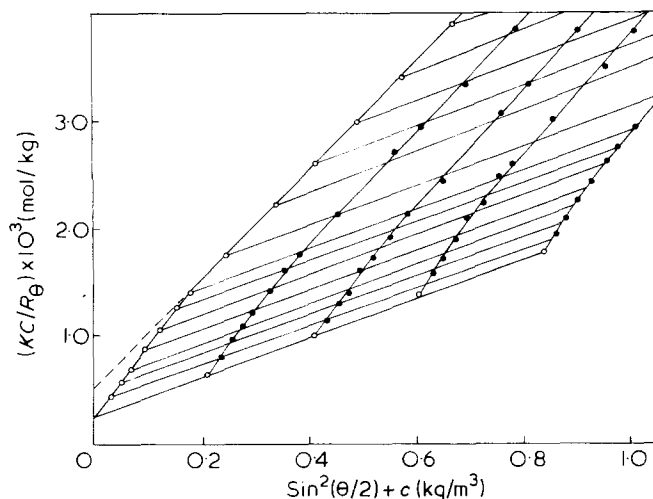


Figure 1 Zimm plot for cellulose trinitrate derived from cotton (Deltapine), sample III (Table 1). $\lambda_0 = 436$ nm; solvent, ethyl acetate

ing light scattering experiments on samples which had been obtained by nitration for relatively short periods, i.e. long enough to yield a high proportion of soluble material, (sample II was 84% soluble), without severe degradation. A representative Zimm plot is shown in Figure 1. All the Zimm plots exhibited downward curvature at low angles and Table 1 shows their interpretation in terms of the theory of Benoit *et al.*¹³ for a polydisperse solution of Gaussian coils. This interpretation indicates highly polydisperse material with weight-average degrees of polymerization in the range 10 000 to 14 000. b is given by $b^2 = r^2/DP$, where r^2 is the mean square end to end distance of the cellulose chain. The mean value of b obtained, 3.3 ± 0.3 nm (calculated from the asymptotic slopes⁶) agrees well with that found by Hunt *et al.*⁴ for cellulose trinitrate in ethyl acetate and other authors for cellulose trinitrate in acetone. It is somewhat lower than that found by Huque *et al.*⁵ for cellulose trinitrate in ethyl acetate (4.3 nm).

The interpretation of the Zimm plots as representing a polydisperse solution of Gaussian coils does not however stand up to close inspection. The number-average degrees of polymerization so derived are about 3000. Systematic errors arising because the Zimm plots are not truly asymptotic at high angles would make these higher than the true values. Thus the number-average degrees of polymerization should be low enough to be determined by osmotic pressure measurements. An attempt to make such a measurement on one of the samples showed that the number-average degree of polymerization was much higher than 3000. It could not be determined with any accuracy because solutions at concentration greater than 1 kg/m^3 could not be conveniently handled owing to their high viscosity.

An alternative explanation of the downward curvature in the Zimm plots is that the solutions contained supermolecular aggregates or gel-like material. In order to ascertain whether this was so, fractional precipitation experiments were carried out. A series of fractions was obtained by adding *n*-hexane to a 0.1% solution of sample I. Precipitates were removed by centrifugation at $3000 \times g$ after sufficient *n*-hexane had been added to produce a permanent cloudiness. In order to avoid local excesses of precipitant, and hence obtain a narrower fraction, the cloudy solutions were raised 5°C above ambient temperature for 24 h and then allowed to cool prior to centrifugation. On heating, the

cloudiness disappeared for all the fractions except the first. All the fractions were completely resolvable in ethyl acetate except the first which was only 68% soluble. The first fraction had a lower intrinsic viscosity than the second, (Table 2), indicating the presence of denser particles and Figure 2 shows the corresponding Zimm plot. The virtually zero second virial coefficient indicates a high density particle, and the form of the reciprocal particles scattering factor indicates some sort of supermolecular aggregate, with molecular weight and polar radius of gyration $\geq 10^4 \text{ kg/mol}$ and $\geq 200 \text{ nm}$ respectively. It was thought unlikely that the solution consisted entirely of aggregates however and an attempt was made to separate aggregates from single chains by centrifuging for 4 h at $100\,000 \times g$. This resulted in the removal of $\sim 15\%$ of the material from solution. Light scattering measurements on the supernatant however yielded a qualitatively similar Zimm plot to that obtained previously although the molecular weight and polar radius of gyration fell to $4 \times 10^3 \text{ kg/mol}$ and 150 nm respectively. An experiment with the first fraction using an analytical centrifuge running at $100\,000 \times g$ confirmed that there was no separation into two components. A single sharp Schlieren peak was obtained and the sedimentation constant increased markedly with decreasing concentration in a manner characteristic of single cellulose chains; the extrapolated value at infinite dilution ($S \sim 2 \times 10^{-12} \text{ sec}$) corresponding to a degree of polymerization of ~ 7000 on the

Table 2 Fractionation of cellulose trinitrate derived from cotton (Deltapine), sample I (see Table 1)

Fraction number	Intrinsic viscosity (m^3/kg)	Huggin's constant	Weight fraction
1	3.6	1.08	0.17
2	5.8	0.71	0.09
3	4.5	0.50	0.28
4	4.6	0.45	0.25
5	2.3	0.33	0.13
6	1.1	0.38	0.05
7	0.54	0.30	0.03

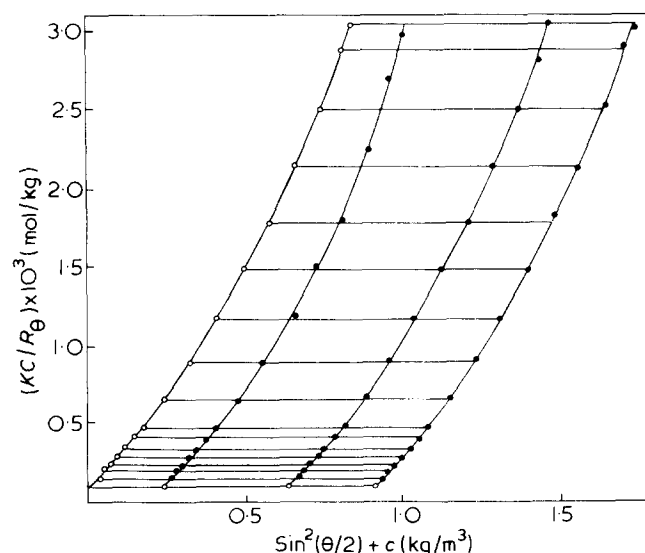


Figure 2 Zimm plot for cellulose trinitrate derived from cotton (Deltapine), sample I (Table 1), fraction 1 (Table 2). $\lambda_0 = 436$ nm; solvent, ethyl acetate

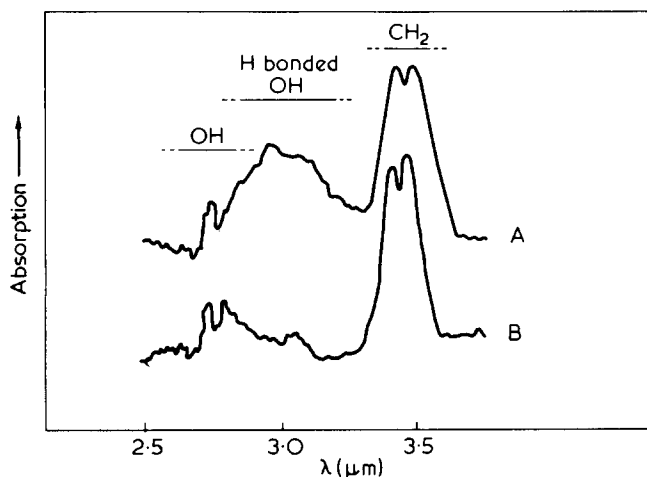


Figure 3 Infra-red spectrum for cellulose trinitrate derived from cotton (Deltapine), sample I (Table 1) fraction 1 (Table 2) before (A) and after (B) renitration

basis of the relationship given by Hunt *et al.*⁴. A possible explanation of this is that the aggregates are *like* branched polymers, rather than swollen gel particles, with just a few *effective* branch points, each formed by a number of inter-chain hydrogen bonds acting cooperatively. In this case the sedimentation constant of the aggregates might not differ greatly from that of their constituent chains and if single chains were also present the difference would be diminished due to the Johnston–Ogston effect¹⁴. The nitrogen content of the first fraction, 13.2%, indicated incomplete substitution, and the infra-red spectrum (Figure 3) showed high absorption in the range characteristic of hydrogen bonded hydroxyl groups. After precipitating with *n*-hexane, drying and renitration for 1 h at 20°C, the nitrogen content rose to 13.9% and the absorption characteristic of hydrogen bonds disappeared (Figure 3). On redissolving in ethyl acetate and centrifuging at $100\,000 \times g$ for 30 min to remove a small amount of insoluble material, the intrinsic viscosity was found to have risen to $3.9 \text{ m}^3/\text{kg}$, the Huggins constant to have fallen to 0.59, and a straight line Zimm plot (Figure 4) was obtained consistent with single cellulose chains of low polydispersity having weight-average degree of polymerization 4500 and polar radius of gyration, $[(\bar{S}^2)_z]^{1/2}$, 130 nm. The second virial coefficient was $8.5 \times 10^4 \text{ mol m}^3/\text{kg}$. Thus the properties of the gel fraction after renitration are consistent with the model proposed above, the aggregates breaking down into single chains.

Light scattering measurements were also made upon sample I with the first fraction removed. The fractional precipitation experiment was repeated, the first fraction in this case representing 14% by weight of the material. The remaining solute was precipitated with *n*-hexane, air dried and heated *in vacuo* at 50°C for 4 h to remove all traces of hydrocarbon. It was then redissolved in ethyl acetate, centrifuged at $100\,000 \times g$ for 1 h and decanted. Figure 5 shows the Zimm plot obtained from this sample. It exhibits no downward curvature and yields the data $DP_w = 5800$, $B = 9.2 \times 10^{-4} \text{ mol m}^3/\text{kg}^2$, $[(S^2)_z]^{1/2} = 140 \text{ nm}$. The way in which this sample was prepared is similar to the way in which most authors have obtained their highest molecular weight fraction. In the case of straight line Zimm plots it is common practice to assume a Schulz–Zimm distribution with $DP_z : DP_w : DP_n = 3 : 2 : 1$ as theory predicts a straight line in this case³. If this is assumed a value of $b = 3.8 \text{ nm}$ is obtained. This is in agreement with other

authors, as is the intrinsic viscosity of this sample, $4.4 \text{ m}^3/\text{kg}$, which corresponds to degrees of polymerization of 5300 and 6700 according to the expressions given by Hunt *et al.*⁷ and Huque *et al.*⁵ respectively. A similar agreement may be obtained with the results for the renitrated first fraction. However Kratochvil¹⁶ has shown that reciprocal particle scattering factors are in practice indistinguishable from straight lines over a very wide range of polydispersities. The data of Table 2, yield $DP_w/DP_n = 1.1$ if each fraction is assumed to be monodisperse. The true value is therefore much less than 2 and it will be shown in the next section that $1.3 > DP_w/DP_n > 1.1$, yielding $4.5 \text{ nm} > b > 4.2 \text{ nm}$.

Figures 2 and 5 show that at high angles the scattered intensity per unit concentration due to aggregates is of the same order as that due to single coils. In the unfractionated sample the weight fraction of aggregates is small. As a result values of degree of polymerization and radius of gyration obtained by ignoring the downward curvature in Figure 1 and extrapolating high angle data to zero angle differ little from those obtained from Figure 5. Table 1 shows values for the coil component, DP_c and S_c calculated in this way for all three samples, together with values for the radius of gyration of the aggregates, S_g , found using the relation:

$$S_g^2 \sim \frac{(\bar{S}^2)_z M_w - S_c^2 M_c}{M_w - M_c} \quad (1)$$

$(\bar{S}^2)_z$ and M_w relate to the whole sample and are found from the low angle data in the usual way. In all cases squares of radii of gyration are *z* averages and molecular weights weight-averages. The definition of the aggregates is here somewhat arbitrary however. Whereas there appears to be a fairly well defined fraction of gel-like material, the Huggins constants shown in Table 2 decrease continuously with fraction number and only for low molecular weights approach the value of 0.3 characteristic of polymers in a good solvent¹⁷. Thus it is likely that the Zimm plot of Figure 5 contains a contribution from residual gel-like material, the particles of which are not large enough to cause any downward curvature. The extent to which the

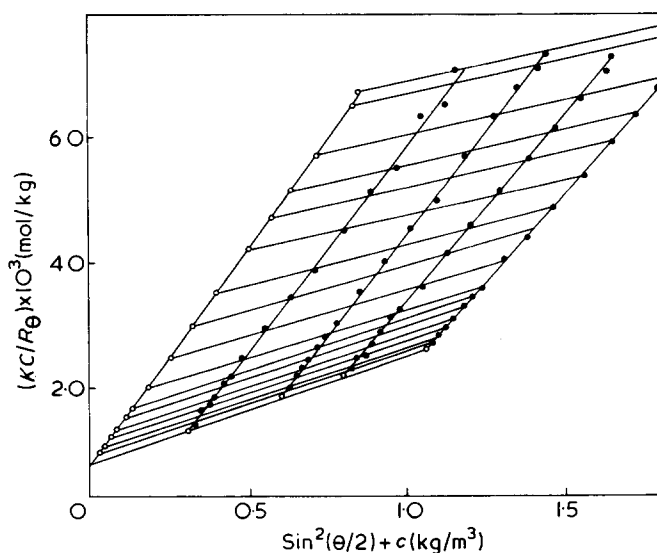


Figure 4 Zimm plot for cellulose trinitrate derived from cotton (Deltapine), sample I (Table 1), fraction 1 (Table 2), after renitration. $\lambda_0 = 436 \text{ nm}$; solvent, ethyl acetate

parameters calculated for the coil component (DP_c, M_c, S_c, b) are thereby in error depends upon the distribution of sizes of the residual gel-like particles. It will be argued later that S_c and b are seriously affected but M_c and DP_c much less so.

More extensively nitrated samples

Table 3 shows data derived from Zimm plots representing light scattering measurements on samples which had been obtained by nitration for longer periods. These samples were considerably degraded. Their Zimm plots (e.g. Figure 6) however, exhibited no downward curvature indicating the absence of large aggregates. There are probably two reasons for this. First, aggregates were broken down into single chains after longer periods of nitration and second, any remaining aggregates were more easily removed during the light scattering clarification procedure due to the lower solution viscosity. After 25 h of nitration some downward curvature reappeared in the Zimm plot although this was easily removed by centrifuging the sample for 4 h at $100\,000 \times g$ and decanting. Still longer periods of nitra-

tion, however, produced even greater downward curvature and the material causing this is clearly different in origin from the aggregates in the mildly nitrated samples. It is likely that all the samples contain some very dense particles which are highly resistant to nitration but are normally easily removed during the light scattering clarification procedure. Very long periods of nitration however turn these into swollen gel particles which are not so easily removed. It is thought that the two types of gel-like material arise from different components of the cell wall and the biological significance of this will be discussed elsewhere.

Table 3 and Figure 7 show the results of osmotic pressure measurements. These were made possible by virtue of the lower degrees of polymerization and the fact that the lower solution viscosities enabled higher concentrations to be used. The polydispersities are low with $DP_w/DP_n \sim 1.3$. It is very unlikely therefore that the coil components of the more mildly nitrated samples had a higher polydispersity than this. Values of b calculated for the more extensively nitrated samples are considerably greater than those found for the more mildly nitrated samples and those found by other authors. This cannot be explained

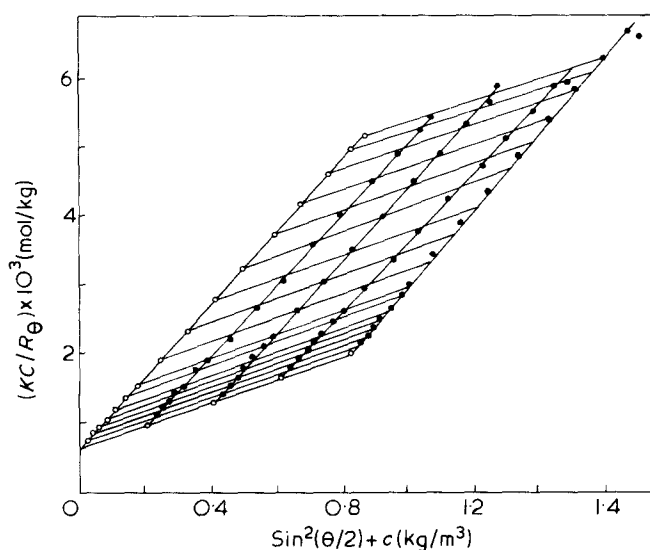


Figure 5 Zimm plot for cellulose trinitrate derived from cotton (Deltapine), sample I (Table 1), with fraction 1 (Table 2) removed. $\lambda_0 = 436$ nm; solvent, ethyl acetate

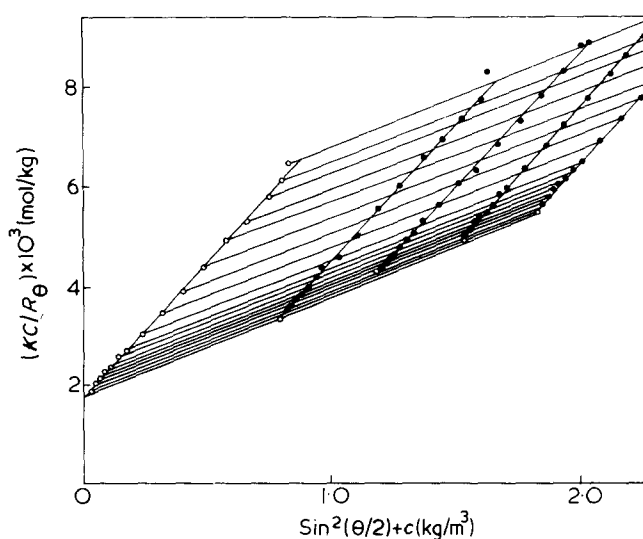


Figure 6 Zimm plot for cellulose trinitrate derived from cotton (Deltapine), sample VIII (Table 3). $\lambda_0 = 546$ nm; solvent, ethyl acetate

Table 3 Measurements in solution made on cellulose trinitrate obtained by nitrating cotton (Deltapine) for various extensive periods. Ethyl acetate as solvent

Sample	Time of nitration at 20°C (h)	λ (nm)	Light scattering results			Osmotic pressure results				Diffusion constant $\times 10^6$ (mm ² /sec) [†]
			$B \times 10^4$ (mol m ³ /kg ²)	DP_w	$(S^2)^{1/2}$	$B \times 10^4$ (mol m ³ /kg ²)	DP_n	b^* (nm)	$[\eta]$ (m ³ /kg)	
IV	2	436	8.0	3300	140	10	2600	5.6		5.9
		546	7.0	3000	180					
V	3								3.6	4200 [‡] 5200 [§]
VI	4	436	10.0	3300	140	10	2600	5.6		
		546	9.0	3300	140					
VII	6	436	9.8	2700	120	9	2100	5.1	2.6	3050 [‡] 3550 [§]
		546	9.5	2600	130					
VIII	25	436	9.8	2400	110	16	1600	4.6	2.1	2450 [‡] 2750 [§]
		546	10.0	1900	98					

* Assuming a Schulz-Zimm distribution¹⁶. † Light scattering Rayleigh Linewidth measurements¹⁸. ‡ Using the expression of Hunt *et al.*⁴. § Using the expression of Huque *et al.*⁵.

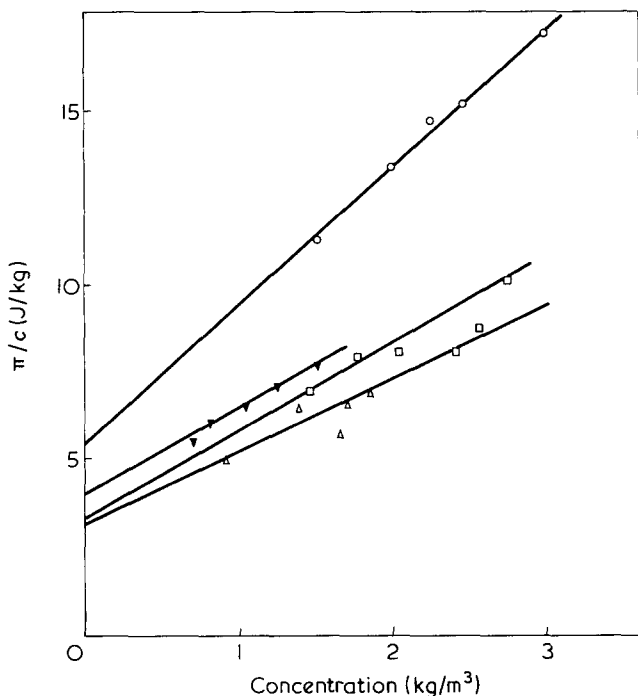


Figure 7 Osmotic pressure measurements on cellulose trinitrate derived from cotton (Deltapine). Solvent, ethyl acetate. □, sample IV; △, sample VI; ▽, sample VII; ○, sample VIII (Table 3)

in terms of experimental errors (the calculation of b depends only on the square root of the slope of the Zimm plot and the square root of the estimate of polydispersity). The intrinsic viscosities are also higher than those found by other authors and the dispersity in intrinsic viscosity may be correlated with the disparity in b . The second virial coefficients obtained by light scattering (B_{ls}) and osmometry (B_{op}) are in fair agreement in contrast to the results of other authors who have usually obtained much lower values for B_{ls} comparable to the values obtained in the present work for the unfractionated mildly nitrated samples. All of these discrepancies may be explained in terms of residual gel-like material in the mildly nitrated samples and the samples of other authors. The general effects of the presence of gel-like material will now be discussed.

Effects of the presence of gel-like material on the solution properties of cellulose trinitrate

Particle scattering factors. Numerical calculations using particle scattering factors similar to that obtained from Figure 2 show that the presence of small numbers of large aggregates not only causes downward curvature in the Zimm plot at low angles of scatter, but also produces a slight decrease in the slope at high angles. This decrease is due to the fact that the aggregates are denser than the coils and is mitigated by the downward curvature at low angles resulting from the large disparity in size between coil and aggregate. Gel-like material comprised of smaller particles would not necessarily cause downward curvature and when this is the case a greater decrease in the slope of the Zimm plot would be expected. This decrease could be considerable if a significant proportion of the gel-like material were comprised of particles comparable in size to or smaller than the single coils. If this sort of material remained in sample I after the larger aggregates had been removed by fractional precipitation, as in fact the viscosity measurements on the fractions

(Table 2) have already suggested, then this would account for the discrepancy in the values of b calculated for the mildly and more extensively nitrated samples. On this basis the highest value of b obtained is nearest the true value, i.e. $b \geq 5.6$ nm, showing that the flexibility of the cellulose trinitrate chain has been overestimated by other workers. The optimum period of nitration from the point of view of investigating chain statistics appears to be in the range 2 to 6 h. After very long periods of nitration additional gel-like material becomes soluble leading once again to lower apparent values of b .

It is the contention of the authors that the variability observed in the high angle slopes of plots of KC/R_θ against $\sin^2\theta/2 + kC$ for given concentrations is entirely due to the removal of varying amounts of gel-like material during the light scattering clarification procedure. It is on the basis of the above discussion that data yielding the highest slopes were selected to construct Zimm plots. However the observed variability would in any case affect the calculated values of b by only $\pm 5\%$.

Second virial coefficients. An analysis of the effect of polydispersity on the second virial coefficients as determined by light scattering and osmometry is given in the Appendix. B_{ls} and B_{op} should be the same for a solution of single coils unless the polydispersity is very high. It is also shown that when gel-like material is present:

$$\frac{B_{ls}}{B_{op}} \sim \frac{M_c}{M_w} \quad (2)$$

where M_c is the true weight-average molecular weight of the coil component and M_w is that for the whole sample.

In practice B_{ls} may be even lower due to the fact that less gel-like material is removed at the higher concentrations during the light scattering clarification procedure. In either case serious disagreement between B_{ls} and B_{op} is a sure indication that the results are affected by the presence of a gel-like component, quite apart from whether or not downward curvature in the Zimm plot is observed. Agreement between B_{ls} and B_{op} however merely indicates that $M_c \sim M_w$ showing that any gel-like material present does not contain sufficient heavy particles to affect the measured molecular weight. The high value of B_{ls} obtained for sample I with the first fraction removed would indicate that the value for DP_c obtained is reliable. However as already argued the value of b obtained from the slope of the Zimm plot is not correct.

Intrinsic viscosity and diffusion constants. Intrinsic viscosity is a measure of effective partial specific volume. For a given sample molecular weight therefore, the effect of the presence of a gel-like component is to lower the intrinsic viscosity as well as lowering the experimentally determined value of b . The observed correlation in Table 3 is therefore to be expected.

A diffusion constant is an inverse measure of effective hydrodynamic diameter so that for a given sample molecular weight the effect of the presence of a gel-like component is to increase the diffusion constant. The straight line which best fits a double logarithmic plot of diffusion constant against degree of polymerization obtained from data in Table 3 has a slope somewhat less than -1^{18} . It is likely that this arises from a systematic variation in the amount of gel-like material present, the diffusion constants for the lower degrees of polymerization being too high.

Comparison of the experimentally determined chain statistics of cellulosic polymers in general with conformational analysis

In order to compare experimental results with the results of conformational analysis it is necessary to correct experimental data so as to obtain the value of b , b_0 corresponding to the unperturbed chain statistics. In the present work the only method available is to apply the expression of Orofino and Flory¹⁹, which, by taking account of excluded volume, gives the expansion factor, α , in terms of the second virial coefficient. For the sample yielding the highest value of b (5.6 nm) α can be calculated in this way to be 1.04. In view of the experimental errors involved, this correction is not considered to be significant.

No detailed theoretical work has been carried out on the conformation of cellulose derivatives. Cellulose itself has been investigated. The results however depend very much on the value, τ , assumed for the angle at the bridge oxygen atom and also on the type of potential energy function and the associated parameters used to estimate the permitted degrees of rotation about the C—O bonds. Assuming free rotation, b_0 varies from 0.89 nm for $\tau = 118^\circ$ to 0.77 nm for $\tau = 110^\circ$ ^{20,21}. Using Lennard—Jones potentials and Van der Waals radii obtained from crystallographic data to take account of hindered rotation, Cleland²¹ obtained $b_0 = 2.1$ nm for $\tau = 118^\circ$ and $b_0 = 4.3$ nm for $\tau = 110^\circ$. However by increasing the Van der Waals radii by 0.02 nm (which Cleland considers more realistic) the values $b_0 = 4.6$ nm for $\tau = 118^\circ$ and $b_0 = 4.8$ nm for $\tau = 110^\circ$ are obtained. Using Kitaigorodsky potentials Yathindra and Rao²⁰ have obtained $b_0 = 3.8$ nm for $\tau = 118^\circ$ and $b_0 = 5.2$ nm for $\tau = 110^\circ$, Cleland obtaining $b_0 = 3.5$ nm for the former figure. Yathindra and Rao have suggested that τ could be different in different solvents.

The solution properties of cellulose have been investigated in cadoxen^{22,23} and iron sodium tartrate²⁴. Numerous investigations of the solution properties of various derivatives have also been made viz. the hydroxyethyl,^{25,26} hydroxypropyl-²⁷, ethyl(hydroxyethyl)-^{28,29}, methyl-³⁰, ethyl-^{31,32}, sodium (carboxymethyl)-^{33,34} derivatives, and also the acetate^{35–37}, tricaproate³⁸, tricarbanilate^{39–44}, tributrylate⁴⁵, tricaprilate⁴⁵ and trinitrate^{2–6,11}. An extensive review of these publications has been given elsewhere¹. Values of b_0 range from 1.5 to 4.5 nm but in general agreement between different authors for the same derivative is not good, and only the values for cellulose trinitrate (excluding those presented in the present paper) consistently fall within the range predicted by the conformational analysis for cellulose. Most other work has suggested that cellulose and its derivatives are highly flexible polymers. Brown, Henley and coworkers for instance have obtained results for cellulose and the hydroxyethyl-, ethyl(hydroxyethyl)- and sodium (carboxymethyl)- derivatives which indicate that all have the same flexibility with a persistence length equal to about four monomer units, comparable in fact to synthetic polymers such as polystyrene.

Previously reported experimental data is therefore clearly at variance with conformational analysis and Brant and Goebel⁴⁶ have suggested that this might result from a fault in the molecular model, in that glucose residues in the cellulose chain might occasionally adopt conformations other than C1. It is the contention of the present authors however that nearly all previously reported values of b_0 are too low and that the true values of b_0 for cellulose and many derivatives probably lie within the range predicted

by the conformational analysis of cellulose, whilst the true value for cellulose trinitrate is somewhat higher.

The above assertions are based on the authors' belief in the light of experience gained in the present work, that gel-like material in the samples investigated by most other authors has seriously affected their results. Second virial coefficients as determined by light scattering and osmometry have nearly always been in serious disagreement (by factors as much as three²⁵), B_{12} often varying widely and at random with molecular weight. B_{12} can often be correlated with the biological source of material, a fact never commented on by the authors concerned which can only be explained by the presence of varying amounts of gel-like material, and in one case B_{12} has been correlated with the degree of nitration⁵. It might be expected that using a low value for B_{12} in the Orofino—Flory equation would lead to an underestimate of α and thus tend to compensate for the effect of a gel-like component on the measured value of b . However the form of the Orofino—Flory equation is such that substitution of a too low value for the radius of gyration tends to counteract this. Huggins constants reported for cellulosic polymers are often very high, again indicating the presence of gel-like material. Nevertheless it might be expected that chain statistics calculated from viscosity measurements would be less affected by the presence of a gel-like component than those calculated from Zimm plots. In fact values of b_0 calculated from the former tend to be even lower than those calculated from the latter. This arises because the various methods used to calculate b_0 ^{47–50} involve the extrapolation of intrinsic viscosity data to zero molecular weight, i.e. into a region where the theories themselves do not apply and in which the effective value of b_0 would be lower than the true value.

Finally it must be mentioned that the work of Mackie and Sellen on the nitrates of mannan and xylan^{12,51} is open to all the criticisms levelled here against other authors. The purely relative conclusions of these publications that the chain statistics of the trinitrate of β -1,4 linked mannan are similar to those of cellulose trinitrate whilst the dinitrate of β -1,3 linked xylan is a much more flexible polymer still stand. The absolute values of b quoted are however almost certainly much too low.

CONCLUSIONS

The results of solution experiments on cellulose trinitrate obtained by mild nitration procedures are very much affected by the presence of gel-like material even when the larger aggregates are removed by fractional precipitation so as to yield straight line Zimm plots. Gel-like material remaining consists of particles denser than the single coils but of comparable or smaller size so that values obtained for the effective bond length are too low. Experiments on more extensively nitrated samples indicate that the effective bond length is at least 5.6 nm. It is suggested that all previous investigations of cellulosic polymers have yielded too low values for the effective bond length and that this has led to the apparent disagreement with conformational analysis.

ACKNOWLEDGEMENTS

This work was supported in part by the Science Research Council and in part by Hickson and Welch Ltd, to whom the authors owe their thanks.

REFERENCES

- 1 Holt, C. *PhD Thesis* University of Leeds (1973)
- 2 Holt, C., Mackie, W. and Sellen, D. B. *J. Polym. Sci. (C)* 1973, **42**, 1505
- 3 Holtzer, A. M., Benoit, H. and Doty, P. *J. Phys. Chem.* 1954, **58**, 624
- 4 Hunt, M. L., Newman, S., Scheraga, A. H. and Flory, P. J. *J. Phys. Chem.* 1956, **60**, 1278
- 5 Huque, M. M., Goring, D. A. and Mason, S. G. *Can. J. Chem.* 1958, **36**, 952
- 6 Sellen, D. B. and Levi, M. P. *Polymer* 1967, **8**, 633
- 7 Alexander, W. J. and Mitchell, R. L. *Anal. Chem.* 1949, **21**, 1497
- 8 Kratochvil, J. P., Dezelic, C., Kerker, M. and Matijevic, E. *J. Polym. Sci.* 1962, **57**, 59
- 9 Hermans, J. J. and Levinson, S. *J. Opt. Soc. Am.* 1951, **41**, 460
- 10 Billmeyer, F. W., Levine, H. I. and Livesey, P. J. *J. Colloid Interface Sci.* 1971, **35**, 204
- 11 Penzel, E. and Schulz, G. V. *Makromol. Chem.* 1968, **112**, 260; *ibid.* 1968, **113**, 64
- 12 Mackie, W. and Sellen, D. B. *Polymer* 1969, **10**, 621
- 13 Benoit, H., Holtzer, A. M. and Doty, P. *J. Phys. Chem.* 1954, **58**, 635
- 14 Johnston, J. P. and Ogston, A. G. *Trans. Faraday Soc.* 1946, **42**, 789
- 15 Schulz, G. V. *Z. Phys. Chem. (B)* 1939, **43**, 25; Zimm, B. H. *J. Chem. Phys.* 1948, **16**, 1099
- 16 Kratochvil, P. *J. Polym. Sci. (C)* 1968, **23**, 143
- 17 Moore, W. H. *Prog. Polym. Sci.* 1967, **1**, 1
- 18 Sellen, D. B. *Polymer* 1975, **16**, 169
- 19 Orofino, T. A. and Flory, P. J. *J. Chem. Phys.* 1957, **26**, 1067
- 20 Yathindra, N. and Rao, V. S. R. *Biopolymers* 1970, **9**, 783
- 21 Cleland, R. L. *Biopolymers* 1971, **10**, 1925
- 22 Henley, D. *Ark. kemi* 1961, **18**, 327
- 23 Brown, W. and Wikström, R. *Eur. Polym. J.* 1965, **1**, 1
- 24 Valtasaari, L. *Makromol. Chem.* 1971, **150**, 117
- 25 Brown, W. *Ark. kemi* 1961, **18**, 227
- 26 Brown, W. and Henley, D. *Makromol. Chem.* 1963, **64**, 49
- 27 Wirick, M. G. and Waldman, M. H. *J. Appl. Polym. Sci.* 1970, **14**, 579
- 28 Manley, R. St. J. *Ark. kemi* 1956, **9**, 519
- 29 Brown, W. and Henley, D. *Makromol. Chem.* 1964, **75**, 179
- 30 Nealy, W. B. *J. Polym. Sci. (A)* 1963, **1**, 311
- 31 Scherer, P. C., Tanenbaum, A. and Levi, D. W. *J. Polym. Sci.* 1960, **43**, 531
- 32 Meyerhoff, G. and Sutterlin, N. *J. Polym. Sci. (C)* 1973, **42**, 943
- 33 Schneider, N. S. and Doty, P. *J. Phys. Chem.* 1954, **58**, 762
- 34 Brown, W., Henley, D. and Ohman, J. *Makromol. Chem.* 1963, **62**, 164
- 35 Flory, P. J., Spurr, O. K. and Carpenter, D. K. *J. Polym. Sci.* 1958, **27**, 231
- 36 Sharples, A. and Swinton, F. L. *J. Polym. Sci.* 1961, **50**, 53
- 37 Shakhparanov, M. I., Zakurdayeva, N. P. and Podgorodetski, Ye. X. *Polym. Sci. USSR (A)* 1967, **9**, 1349
- 38 Krigbaum, W. R. and Sperling, L. H. *J. Phys. Chem.* 1960, **64**, 99
- 39 Burchard, W. and Husemann, E. *Makromol. Chem.* 1961, **44**, 358
- 40 Shanbhag, V. P. *Ark. kemi* 1969, **29**, 1, 33, 139, 163
- 41 Burchard, W. *Z. Phys. Chem.* 1964, **42**, 293
- 42 Burchard, W. *Makromol. Chem.* 1965, **88**, 11
- 43 Ohman, J. *Ark. kemi* 1969, **31**, 125
- 44 Shanbhag, V. P. and Ohman, J. *Ark. kemi* 1969, **31**, 137
- 45 Mandelkern, L. and Flory, P. J. *J. Am. Chem. Soc.* 1952, **74**, 2517
- 46 Brant, D. A. and Goebel, K. D. *Macromolecules* 1973, **5**, 536
- 47 Stockmayer, W. H. and Fixman, M. *J. Polym. Sci. (C)* 1963, **1**, 137
- 48 Kurata, M. and Stockmayer, W. H. *Fortschr. Hochpolym. Forsch.* 1963, **3**, 196
- 49 Ptitsyn, O. B. and Eizner, Yo. E. *Sov. Phys. Tech. Phys.* 1960, **4**, 1020
- 50 Bauman, H. *J. Polym. Sci. (B)* 1965, **3**, 1069
- 51 Mackie, W. and Sellen, D. B. *Biopolymers* 1971, **10**, 1
- 52 Brinkman, H. C. and Hermans, J. J. *J. Chem. Phys.* 1949, **17**, 574
- 53 Kirkwood, J. G. and Goldberg, R. J. *J. Chem. Phys.* 1950, **18**, 54
- 54 Stockmayer, W. H. *J. Chem. Phys.* 1950, **18**, 58

APPENDIX

It is not possible to obtain general expressions which relate the values of B obtained from light scattering and osmotic pressure measurements to the values which would be obtained for constituent components if each were in solution alone⁵²⁻⁵⁴. B_{op} and B_{ls} are in fact given by:

$$B_{op} = \frac{\sum_i \sum_j C_i C_j B_{ij}}{\sum_i \sum_j C_i C_j}, \quad B_{ls} = \frac{\sum_i \sum_j C_i C_j M_i M_j B_{ij}}{\sum_i \sum_j C_i C_j M_i M_j} \quad (A1)$$

If $B_{ij} = (B_i + B_j)/2$, an assumption which will not lead to appreciable error if B_i and B_j are not too different*, then $B_{op} = B_w$ and $B_{ls} = B_z$. B is not expected to vary greatly with molecular weight for single chain polymers and unless the polydispersity is very high, values of B obtained by the two methods should agree. This is not the case when a gel-like component is present however. Equation (A1) may be written:

$$\frac{B_{ls}}{B_{op}} = \frac{1}{M_w^2} \frac{\sum_i \sum_j C_i C_j M_i M_j B_{ij}}{\sum_i \sum_j C_i C_j B_{ij}} \quad (A2)$$

If the second virial coefficients corresponding to all mutual interactions between gel-like particles are assumed to be zero due to their high density and/or low solubility, and if the polydispersity of the coil component is low enough for all mutual coil interactions to be characterized by a single value B_c then:

$$\frac{B_{ls}}{B_{op}} = \frac{M_c (w_c M_c B_c + 2w_g M_g B_{cg})}{M_w^2 (w_c B_c + 2w_g B_{cg})} \quad (A3)$$

where w indicates weight fraction. This formula is oversimplified since B_{cg} will be different for each gel-coil interaction and there are no real criteria for saying what the effective value of B_{cg} in equation (A3) is, as in this case the second virial coefficients of the two components are very different. However, crude calculations made on data obtained from *Figures 2* and *5* by adopting a hard sphere model in which the equivalent radius is proportional to the radius of gyration, indicate that the foregoing assumption is still approximately true, i.e. $B_{cg} \sim B_c/2$. Substituting this in equation (A3) yields equation 2†.

* For a hard sphere model in which the radius of the equivalent hard sphere is assumed to be proportional to $(r^2)^{1/2}$ and in which r^2 is proportional to molecular weight:

$$B_{ij} = \frac{3}{8} (B_i + B_j) + \frac{1}{8} \left(\frac{B_i^2}{B_j} + \frac{B_j^2}{B_i} \right)$$

† A more rigorous but less useful expression may be obtained by putting $B_{cg} > 0$ which yields $B_{ls}/B_{op} > (M_c/M_w)^2$.

Dynamics of solutions of entangled polymers

D. A. Maclnnes

Department of Pure and Applied Chemistry, University of Strathclyde, Glasgow G1 1XL, UK

(Received 22 March 1976)

A simple network model for the relaxation dynamics of entangled polymer fluids is presented. It has been assumed that entanglement friction is the principal dissipative mechanism for all but the longest wavelength modes in the entanglement region, and this gives rise to a peak in the relaxation spectrum. This model is shown to predict viscoelastic response functions whose qualitative features agree well with those observed experimentally, and in particular the well-known, 'C²' effect of entanglement coupling is derived in a natural manner.

INTRODUCTION

The phenomenon of entanglement coupling in polymer fluids is well known and has been studied many times¹. Most of the work has concentrated on explaining the response in terms of a spectrum of relaxation modes and the experimental indications are that the major portion of the response derives from a relatively narrow region, known as the terminal region, of the spectrum.

The purpose of this paper is to propose a very simple model, for the dynamics of an entangled polymer fluid, which reproduces some of the major features of the response in a physically transparent manner. This work depends greatly on the work of Edwards², Edwards and Grant³ and de Gennes⁴. The standard assumption is made that the normal relaxational modes of the fluid can be separated into two groups – single chain modes and entanglement modes – and that with the transition between these groups a characteristic relaxation time T_c can be associated. It is further assumed that there is a disentanglement time⁴ T_d such that for motion on a time scale $t \gg T_d$ the polymer fluid will simply flow showing no elasticity. The primary concern in the present study is with modes with relaxation times τ such that $T_d < \tau < T_c$ i.e. the terminal spectrum. It is assumed that there are no relaxation modes with $\tau > T_d$. The spectrum and response of single chain modes (i.e. those with relaxation times $< T_c$) have already been studied⁵⁻⁷, and given certain assumptions it has been shown that the relaxation spectrum contains a peak. The present study shows that the terminal spectrum should show a similar peak, and that this feature is crucial in the interpretation of the experimental data.

DYNAMICS OF THE TERMINAL REGION

For $T_d > \tau > T_c$ (i.e. for relaxation in the terminal region) the motion of the polymer fluid is taken to be that of an elastic network with two dissipative mechanisms: polymer–polymer (entanglement) friction and polymer–solvent friction. The equation of motion is assumed to be:

$$\zeta \frac{\partial \mathbf{u}(\mathbf{r}t)}{\partial t} - \zeta_e \frac{\partial}{\partial t} \nabla_{\mathbf{r}}^2 \mathbf{u}(\mathbf{r}t) - \epsilon \nabla_{\mathbf{r}}^2 \mathbf{u}(\mathbf{r}t) = \phi(\mathbf{r}t) \quad (1)$$

where $\mathbf{u}(\mathbf{r}t)$ is the position vector of the network element labelled \mathbf{r} ; ζ is the polymer–solvent friction constant; ζ_e is the entanglement friction; ϵ is the 'elastic constant' of the network and $\phi(\mathbf{r}t)$ is a random force such that:

$$\langle \phi(\mathbf{r}t) \phi(\mathbf{r}'t') \rangle = f(\mathbf{r} - \mathbf{r}') \delta(t - t') \quad (2)$$

where $f(\mathbf{r})$ is an unknown function and $\delta(y)$ is the Dirac delta function. The average is over an equilibrium ensemble. To find the relaxation times implicit in equation (1) the author has followed the procedure of Edwards² and Edwards and Grant³ in calculating the second moment:

$$\langle [\mathbf{u}(\mathbf{r}t) - \mathbf{u}(\mathbf{r}'t')]^2 \rangle$$

Writing

$$\mathbf{u}(\mathbf{r}t) = \iint \bar{\mathbf{u}}(\mathbf{k}\omega) \exp [i(\mathbf{k} \cdot \mathbf{r} + \omega t)] d\mathbf{k} d\omega$$

gives

$$\langle [\mathbf{u}(\mathbf{r}t) - \mathbf{u}(\mathbf{r}'t')]^2 \rangle = 2 \iint \langle \bar{\mathbf{u}}(\mathbf{k}\omega) \bar{\mathbf{u}}^*(\mathbf{k}\omega) \rangle \times \{1 - \cos[\mathbf{k} \cdot (\mathbf{r} - \mathbf{r}') + \omega(t - t')]\} d\mathbf{k} d\omega \quad (3)$$

(unimportant normalization constants are omitted throughout). This is obtained by observing that:

$$\iint \exp(i\mathbf{k} \cdot \mathbf{r}) \exp(i\mathbf{k}' \cdot \mathbf{r}') d\mathbf{k} d\mathbf{k}' \propto \cos[\mathbf{k} \cdot (\mathbf{r} - \mathbf{r}')]$$

Carrying out a Fourier transform on equation (1) gives:

$$\zeta i\omega \bar{\mathbf{u}}(\mathbf{k}\omega) + \zeta_e i\omega k^2 \bar{\mathbf{u}}(\mathbf{k}\omega) + \epsilon k^2 \bar{\mathbf{u}}(\mathbf{k}\omega) = \bar{\phi}(\mathbf{k}\omega) \quad (4)$$

so

$$\bar{\mathbf{u}}(\mathbf{k}\omega) = \bar{\phi}(\mathbf{k}\omega) / [i\omega(\zeta + \zeta_e k^2) + \epsilon k^2] \quad (5)$$

Inserting equation (5) into equation (2) gives:

$$\langle [\mathbf{u}(rt) - \mathbf{u}(r't')]^2 \rangle = 2 \iint \frac{\langle \bar{\phi}(\mathbf{k}\omega) \bar{\phi}^*(\mathbf{k}\omega) \rangle \{1 - \cos [k \cdot (r - r') + \omega(t - t')]\}}{\omega^2(\zeta + \zeta_e k^2)^2 + \epsilon^2 k^4} d\mathbf{k} d\omega$$

Now equation (2) implies:

$$\langle \bar{\phi}(\mathbf{k}\omega) \bar{\phi}^*(\mathbf{k}\omega) \rangle = \bar{f}(\mathbf{k}) \quad (7)$$

so equation (5) becomes:

$$\begin{aligned} \langle [\mathbf{u}(rt) - \mathbf{u}(r't')]^2 \rangle &= 2 \iint \frac{\bar{f}(\mathbf{k}) \{1 - \cos [\omega(t - t')]\}}{\omega^2(\zeta + \zeta_e k^2)^2 + \epsilon^2 k^4} d\mathbf{k} d\omega \\ &= \frac{1}{2\pi} \int \frac{\bar{f}(\mathbf{k})}{k^2(\zeta + \zeta_e k^2)} \left\{ 1 - \exp \left[-\frac{\epsilon k^2}{\zeta + \zeta_e k^2} |t - t'| \right] \right\} d\mathbf{k} \end{aligned} \quad (8)$$

The integration over ω is carried out by complex variable methods⁸ and the result is standard. Thus it is clear from equation (8) that the dispersion relation of the terminal spectrum is:

$$\tau(k) = \zeta + \zeta_e k^2 / \epsilon k^2 \quad (9)$$

Equation (9) is the principal result of this section.

SPECTRUM OF RELAXATION TIMES

The spectrum is assumed to be divided into three separate regions: (a) $\tau > T_d$; (b) $T_d > \tau > T_c$ and (c) $T_c > \tau$.

Region (c) has already been discussed⁵⁻⁷, and has been shown, given certain conditions, to contain a peak (at $\tau \equiv \omega_s^{-1}$).

Region (a) is of little interest, since it is assumed that there are no relaxation modes in this region.

Region (b) is the terminal region with dispersion relation given by equation (9). The entanglement friction is taken to be the dominant resistance for almost all the motion in the terminal region. This implies $\zeta_e k^2 \gg \zeta$ for most values of k such that $\tau(k) < T_d$ which gives a peak in the relaxation spectrum at $\tau \approx \zeta_e / \epsilon$. To obtain an estimate of the number, N , of modes in the peak it is assumed that nearly all of the modes of the network which cannot be described by single chain dynamics are concentrated round $\tau \approx \zeta_e / \epsilon$. By following Graessley¹ it is found that N is the number of modes in the 'shifted Rouse' spectrum i.e. $N \sim C^2 M^0$, or by following de Gennes⁴ by means of essentially the same procedure but with excluded volume taken into account, it is found that $N \sim C^{2.25} M^0$. In the present study we have taken $N \sim C^{2\alpha}$ where $0 < \alpha < 1$.

Thus the predominant features of the spectrum are two peaks, one with $\tau > T_c$ and one with $\tau < T_c$.

VISCOELASTIC RESPONSE

To calculate the response it is necessary to know the visco-

elastic weighting factor of a normal mode. The author has shown this to be proportional to the relaxation time of the normal mode for the principal viscoelastic modes in single chain dynamics⁷, and has assumed it to be so for network dynamics. An argument is given to support this claim but this has been relegated to an appendix, for two reasons: (a) the result is what we would intuitively expect; (b) the argument contains features which, although plausible on physical grounds, will require further analysis to become totally justified.

The zero frequency response will come almost entirely from the terminal peak. This will give for the steady-state viscosity, η_0 , and the equilibrium compliance, J_e :

$$\eta_0 = \sum_{k=1}^N \tau(k) \approx N\tau_0 \quad (\tau_0 \equiv \zeta_e / \epsilon)$$

and

$$\begin{aligned} J_e &= \lim_{\omega \rightarrow 0} \{G'(\omega) / [G''(\omega)]^2\} \\ &\approx N\tau_0^2 / N^2\tau_0^2 \\ &= N^{-1} \end{aligned}$$

Thus

$$\eta_0 \sim C^{2\alpha} \tau_0$$

and

$$J_e \sim C^{-2\alpha} \quad (10)$$

Equation (10) compares well with similar expressions quoted by Graessley¹.

The principal features of the dynamical response can be seen from $G'(\omega)$ and $G''(\omega)$

$$\left\{ G'(\omega) = \sum_k \frac{\omega^2 \tau(k)^2}{1 + \omega^2 \tau(k)^2}; G''(\omega) = \sum_k \frac{\omega \tau(k)}{1 + \omega^2 \tau(k)^2} \right\}$$

$G'(\omega)$ will clearly have a plateau stretching from $\omega \approx \epsilon / \zeta_e$ to $\omega = \omega_s$ and the magnitude of the plateau modulus will be proportional to N i.e. to $C^{2\alpha} M^0$. $G''(\omega)$ will appear to contain a separate relaxation region at $\omega = \epsilon / \zeta_e$. These results bear close resemblance to those quoted by Graessley¹ and those reported by Riande *et al.*⁹. The magnitude of the maximum in $G''(\omega)$ at $\omega = \epsilon / \zeta_e$ should be proportional to N i.e. to $C^{2\alpha} M^0$. The author is unaware of any experimental results against which to test this prediction.

CONCLUSION

A simple model for the dynamics of a fluid of entangled polymers has been proposed, and it has been shown how this model predicts a viscoelastic response whose qualitative features agree well with experiment, in particular the 'C²' effect attributed to entanglement coupling occurs naturally and is a result of a peak in the relaxation spectrum.

The principal features lacking in the model are considered to be: (a) Mathematical rigour—many assumptions

are introduced with only physical intuition as a guide. (b) The quantities ϵ , ζ and ζ_e are introduced as parameters. To obtain the full theory of the viscoelastic response (i.e. the molecular weight dependence) it will probably be necessary to relate equation (1) to a more detailed molecular theory.

It is felt that these omissions are justified in that the present work is only a first step. The analysis of (a) and (b) would seem to contain very difficult but perhaps not intractable mathematical difficulties.

To obtain an idea of the M dependence of the response we need to know the M dependence of τ_0 . It would be consistent with the present analysis to assume $\tau_0 \sim T_d$. de Gennes found $T_d \sim M^3$ which would give $\tau_0 \sim M^3$ in close agreement with experiment. However this feature is grafted on to the present model rather than occurs naturally, and should not be taken too seriously.

ACKNOWLEDGEMENT

It is a pleasure to acknowledge receipt of financial support from the Science Research Council as part of the programme concerning molecular motion in polymers currently under study at Strathclyde University.

REFERENCES

- 1 Graessley, W. W. *Adv. Polym. Sci.* 1974, **16**, 1
- 2 Edwards, S. F. *J. Phys. (A)* 1974, **7**, 318
- 3 Edwards, S. F. and Grant, J. W. V. *J. Phys. (A)* 1973, **6**, 1169
- 4 de Gennes, P. G. 'Dynamics of Entangled Polymer Solutions I and II', preprints
- 5 Pugh, D. and MacInnes, D. A. *Chem. Phys. Lett.* 1975, **34**, 139
- 6 MacInnes, D. A. *J. Polym. Sci.* to be published
- 7 MacInnes, D. A. *J. Polym. Sci.* submitted for publication
- 8 Whittaker, E. T. and Watson, G. N. 'Modern Analysis', Cambridge Univ. Press, Cambridge, 1950
- 9 Riande, E., Markovitz, H., Plazek, D. J. and Raghupathi, N. 'Viscoelastic Behaviour of Polystyrene-Tricresyl Phosphate Solutions', preprint
- 10 Yamakawa, H. 'Modern Theory of Polymer Solutions', Harper and Row, New York, 1971
- 11 Peterlin, A. *J. Polym. Sci. (A-2)* 1967, **5**, 179

APPENDIX

Response of the entangled network

The purpose of this Appendix is to give justification to the claim that each viscoelastic mode is weighted according to its relaxation time. The argument is not rigorous, rather it is carried out by analogy with those in refs 7 and 10.

The viscosity is taken as:

$$\eta = - \left\langle \int_v \mathbf{u}_y(\mathbf{r}t) \mathbf{F}_x(\mathbf{r}t) d\mathbf{r} \right\rangle \quad (\text{A1})$$

where $\mathbf{F}_x(\mathbf{r}t)$ is the elastic force on the element of network labelled \mathbf{r} at time t . The average is over the non-equilibrium distribution of the network, in a shear field, given by the function ψ which is determined by a diffusion equation. The secular force in a shear field $\mathbf{V}_0(\mathbf{r}t)$ on an element of network is taken as:

$$\zeta \left[\frac{\partial \mathbf{u}(\mathbf{r}t)}{\partial t} - \mathbf{V}_0(\mathbf{r}t) \right] - \zeta_e \left[\frac{\partial}{\partial t} \nabla_{\mathbf{r}}^2 \mathbf{u}(\mathbf{r}t) - \nabla_{\mathbf{r}}^2 \mathbf{V}_0(\mathbf{r}t) \right] - \epsilon \nabla_{\mathbf{r}}^2 \mathbf{u}(\mathbf{r}t) \equiv f_s(\mathbf{r}t) \quad (\text{A2})$$

where $\nabla_{\mathbf{r}}$ is the gradient with respect to \mathbf{r} .

The principal difference between equations (A2) and (1) is that in equation (A2) velocities are taken relative to the local shear velocity. We have no proof that this is the correct procedure but adopt it by analogy with ref 7. If $\mathbf{V}_0(\mathbf{r}t)$ is omitted in the entanglement resistance term there would appear, in a manner identical to ref 11, a non-relaxing component of the fluid viscosity and this is taken to be unphysical.

The diffusion equation for the network is:

$$\frac{\partial \psi}{\partial t} = - \int \nabla_{\mathbf{u}(\mathbf{r}t)} \cdot \left[\psi \frac{\partial \mathbf{u}(\mathbf{r}t)}{\partial t} \right] d\mathbf{r} \quad (\text{A3})$$

Fourier transform the $\mathbf{u}(\mathbf{r}t)$, $\mathbf{V}_0(\mathbf{r}t)$ and $\nabla_{\mathbf{u}(\mathbf{r}t)}$ to normal coordinates by writing:

$$\mathbf{u}(\mathbf{r}t) = \int \cos(\mathbf{k} \cdot \mathbf{r}) \bar{u}_c(\mathbf{k}t) d\mathbf{k} + \int \sin(\mathbf{k} \cdot \mathbf{r}) \bar{u}_s(\mathbf{k}t) d\mathbf{k}$$

Similarly for $\mathbf{V}_0(\mathbf{r}t)$ and:

$$\nabla_{\mathbf{u}(\mathbf{r}t)} = \int \cos(\mathbf{k} \cdot \mathbf{r}) \nabla_{\bar{u}_c(\mathbf{k}t)} d\mathbf{k} + \int \sin(\mathbf{k} \cdot \mathbf{r}) \nabla_{\bar{u}_s(\mathbf{k}t)} d\mathbf{k}$$

where the bar, $\bar{\quad}$ denotes 'transformed function'. Unimportant normalization factors are omitted throughout.

Thus in normal coordinates the diffusion equation becomes:

$$\frac{\partial \psi}{\partial t} = - \sum_{\alpha} \int \nabla_{\bar{u}_{\alpha}(\mathbf{k}t)} \left\{ \psi \left[\bar{V}_{0\alpha}(\mathbf{k}t) - \frac{\epsilon k^2}{\zeta + \zeta_e k^2} \bar{u}_{\alpha}(\mathbf{k}t) \right] - \frac{k_B T}{\zeta + \zeta_e k^2} \nabla_{\bar{u}_{\alpha}(\mathbf{k}t)} \psi \right\} d\mathbf{k} \quad (\text{A4})$$

where α represents c or s . Take

$$\bar{V}_{0\alpha}(\mathbf{k}t) \equiv (g \bar{u}_{y\alpha}(\mathbf{k}t), 0, 0)$$

The viscosity

$$\eta = - \left\langle \int \mathbf{u}_y(\mathbf{r}t) \mathbf{F}_x(\mathbf{r}t) d\mathbf{r} \right\rangle = \sum_{\alpha} \int \epsilon k^2 \langle \bar{u}_{y\alpha}(\mathbf{k}t) \bar{u}_{x\alpha}(\mathbf{k}t) \rangle d\mathbf{k}. \quad (\text{A5})$$

The $\langle \bar{u}_{y\alpha}(\mathbf{k}t) \bar{u}_{x\alpha}(\mathbf{k}t) \rangle$ can be found in a manner similar to that given by Yamakawa¹⁰, i.e. by the construction from equation (A4) of a closed set of first order linear differential equations. This is carried out as follows:

$$\begin{aligned} \frac{\partial}{\partial t} \langle \bar{u}_{y\alpha}(kt) \bar{u}_{x\alpha}(kt) \rangle &= - \sum_{\beta} \int dk' \langle g \bar{u}_{y\beta}(kt) \times \\ &\frac{\partial \psi}{\partial \bar{u}_{x\beta}(k't)} \bar{u}_{y\alpha}(kt) \bar{u}_{x\alpha}(kt) - \frac{\epsilon k'^2}{(\zeta + \zeta_e k'^2)} \bar{u}_{y\alpha}(kt) \times \\ &\bar{u}_{x\alpha}(kt) \nabla_{\bar{u}_{\beta}(k't)} \cdot \{ \bar{u}_{\beta}(k't) \psi \} - \\ &\frac{k_B T}{(\zeta + \zeta_e k^2)} \bar{u}_{y\alpha}(kt) \bar{u}_{x\alpha}(kt) \nabla_{\bar{u}_{\beta}(k't)}^2 \psi \rangle \\ &= g \langle \bar{u}_{y\alpha}^2(kt) \rangle - \frac{2\epsilon k^2}{(\zeta + \zeta_e k^2)} \langle \bar{u}_{y\alpha}(kt) \bar{u}_{x\alpha}(kt) \rangle \end{aligned} \quad (A6)$$

where β is summed over c and s .

This results, as in ref 10, by the application of boundary conditions on ψ and by the independence of the normal coordinates.

Similarly

$$\begin{aligned} \frac{\partial}{\partial t} \langle \bar{u}_{y\alpha}^2(kt) \rangle &= - 2 \frac{\epsilon k^2}{(\zeta + \zeta_e k^2)} \langle \bar{u}_{y\alpha}^2(kt) \rangle + \\ &2 \frac{k_B T}{(\zeta + \zeta_e k^2)} \end{aligned} \quad (A7)$$

The equations (A5), (A6) and (A7) are identical in form to those of Yamakawa¹⁰ apart from the replacement of the ordinary friction constant ζ by an effective friction constant $(\zeta + \zeta_e k^2)$. Thus the expression for the viscosity will have the same form as in ref 10 i.e.

$$\eta(\omega)_{\alpha} \sum_k \left[\frac{\tau(k)}{1 + i\omega\tau(k)} \right]$$

where $\tau(k) = \zeta + \zeta_e k^2 / \epsilon k^2$ giving that the viscoelastic weighting factor of each mode is the relaxation time of that mode.

Effect of macromolecular length on anisotropic scattering of light in an electric field*

M. Dębska-Kotłowska and S. Kielich

Nonlinear Optics Division, Institute of Physics, A. Mickiewicz University, 60-780 Poznań,

Grunwaldzka 6, Poland

(Received 9 April 1976)

Light scattering by monodisperse solutions of rigid rod-like anisotropic macromolecules, with linear dimensions l of the order of incident wavelength λ , oriented in an external d.c. electric field, E has been analysed. The relative variations δV_v^E , δH_v^E , δV_h^E , δH_h^E of the scattered light components are discussed for the three values $[l/\lambda] = 1, 0.5, 2$, and various reorientation parameters, $p = [\mu E/kT]$ of the permanent dipole moment μ and $q = [(\alpha_3 - \alpha_1)E^2/2kT]$ of the moment induced by the principal polarizabilities $\alpha_1 = \alpha_2 \neq \alpha_3$. The saturation orientation field strength has been calculated for certain macromolecules with the aim of determining their optical anisotropy numerically.

INTRODUCTION

Relative intensity variations of the components of light scattered by monodisperse solutions of macromolecules, oriented in an external d.c. electric field, are a source of abundant data concerning their optical, electric and geometrical properties¹. The field effect has been considered for large macromolecules, of linear dimensions comparable with the incident light wavelength, for particular cases of the Rayleigh-Debye-Gans approximation^{2,3}. Wippler and Benoit⁴ analysed theoretically the influence of a d.c. electric field on the particle interference scattering factor, $P(\theta)$, with an accuracy to the square of the field strength E . Stoylov^{5,6} extended their analysis to intense fields, including electric saturation. Ravey⁷ gave a description of the effect of arbitrary orientations of macromolecules having the shape of spheres, rods, discs and Gaussian chains in a d.c. electric field, acting in the direction of the external bisector of the observation angle.

In the present study, on the basis of previous theory^{8,9}, we give an analysis of the relative variations δV_v^E , δH_v^E , δV_h^E and δH_h^E of the respective components of light scattered by solutions of large rod-like macromolecules, oriented by a d.c. electric field applied perpendicularly to the plane of observed scattered light. Our results are obtained by numerical computer calculation of the relative variations for the three values $[l/\lambda] = 1, 0.5$ and 2 , and for various values of the reorientation parameters of the permanent dipole moments and polarizability ellipsoids.

THEORY

Consider dilute, monodisperse solutions of rigid, aniso-

tropic, non-absorbing macromolecules in the shape of rods, of rotation-ellipsoidal symmetry. We have assumed that the symmetry axis of their electric and optical properties coincides with their geometrical axis. Thus, the principal electric polarizability, α_3 , and optical polarizability, a_3 , are parallel to the symmetry axis, the principal 3-axis of the macromolecule, whereas the principal polarizabilities $\alpha_1 = \alpha_2$ and $a_1 = a_2$ are perpendicular. The permanent dipole moment is also assumed to lie along the symmetry axis.

Relative variations in scattered light intensity can be defined as follows^{5,6}:

$$\delta I^E = \frac{I^E - I^0}{I^0} \quad (1)$$

where I^E and I^0 represent the intensity of light scattered in the presence and absence of the d.c. field E . Considering the experimental arrangement shown in Figure 1, and taking into account equation (1) and the expression for I^E and I^0 proposed by Kielich⁹ and Horn², respectively, one can write the relative variations of the vertical (V) and horizontal (H) components of scattered light when the incident light beam is polarized vertically (v), or horizontally (h), as follows:

$$\delta V_v^E = \frac{1}{V_v^0} \times \left[\int_0^\pi \int_0^{2\pi} [1 + 2\kappa(3 \cos^2 \nu - 1) + \kappa^2(9 \cos^4 \nu - 6 \cos^2 \nu + 1)] |R(\nu, \phi)|^2 \times \exp(p \cos \nu + q \cos^2 \nu) \sin \nu d\nu d\phi \right] - 1$$

$$\frac{2\pi \int_0^\pi \exp(p \cos \nu + q \cos^2 \nu) \sin \nu d\nu}{0} \quad (2)$$

* Reported in part at the International Symposium on Electro-optical Properties of Macromolecular Solutions, Liège, September 1974.

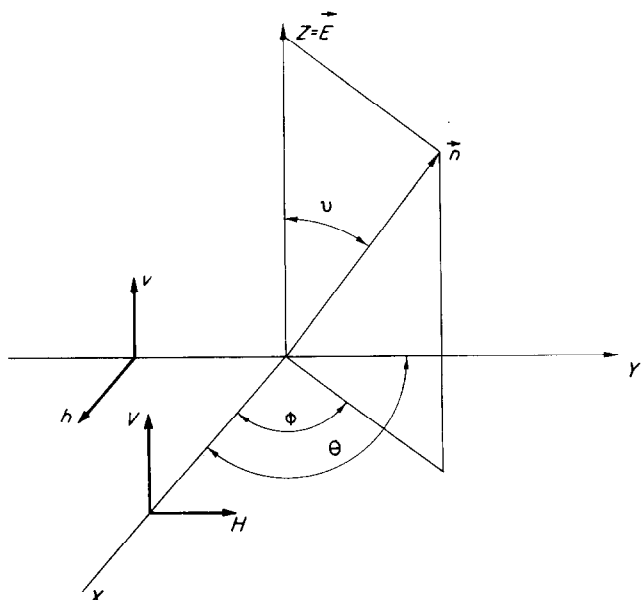


Figure 1 The light beam is incident in the Y-direction with its electric vector $\vec{E}(\omega)$ vibrating in the XZ-plane (the direction of the electric vector vibrations defines the light polarization direction: ν , vertical; h horizontal). The scattered light is observed in the x-direction (observation angle $\Theta = 90^\circ$), with the vertical and horizontal component of scattered light denoted by V and H , respectively. θ is the angle between the Z-axis and the macromolecular symmetry axis \vec{n} , whereas ϕ is the azimuth of \vec{n} . The orienting electric field \vec{E} is directed along Z

$$\delta V_h^E = \frac{1}{V_h^0} \times \frac{9\kappa^2 \int_0^\pi \int_0^\pi \cos^2 \nu \sin^2 \nu \cos^2 \phi |R(\nu, \phi)|^2 \times \exp(p \cos \nu + q \cos^2 \nu) \sin \nu d\nu d\phi}{2\pi \int_0^\pi \exp(p \cos \nu + q \cos^2 \nu) \sin \nu d\nu} - 1 \quad (3)$$

$$\delta H_v^E = \frac{1}{H_v^0} \times \frac{9\kappa^2 \int_0^\pi \int_0^\pi \cos^2 \nu \sin^2 \nu \sin^2 \phi |R(\nu, \phi)|^2 \times \exp(p \cos \nu + q \cos^2 \nu) \sin \nu d\nu d\phi}{2\pi \int_0^\pi \exp(p \cos \nu + q \cos^2 \nu) \sin \nu d\nu} - 1 \quad (4)$$

$$\delta H_h^E = \frac{1}{H_h^0} \times \frac{9\kappa^2 \int_0^\pi \int_0^\pi \sin^4 \nu \cos^2 \phi \sin^2 \phi |R(\nu, \phi)|^2 \times \exp(p \cos \nu + q \cos^2 \nu) \sin \nu d\nu d\phi}{2\pi \int_0^\pi \exp(p \cos \nu + q \cos^2 \nu) \sin \nu d\nu} - 1 \quad (5)$$

where²:

$$V_v^0 = (1 - \kappa)^2 \left[\frac{Si(2K)}{K} - \left(\frac{\sin K}{K} \right)^2 \right] + 3\kappa(1 - \kappa) \left[\frac{Si(2K)}{K} + \frac{\sin 2K}{4K^3} - \frac{1}{K^2} + \frac{\cos 2K}{2K^2} \right] + \frac{27}{8} \kappa^2 \left[\frac{Si(2K)}{K} - \frac{4}{3K^2} - \frac{\cos 2K}{4K^4} - \frac{\sin 2K}{4K^3} + \frac{\cos 2K}{2K^2} + \frac{\sin 2K}{8K^5} \right] \quad (6)$$

$$V_h^0 = H_v^0 = 9\kappa^2 \left[\frac{Si(2K)}{16K} + \frac{\cos 2K}{32K^2} + \frac{\sin 2K}{64K^3} + \frac{3 \cos 2K}{64K^4} - \frac{3 \sin 2K}{128K^5} \right] \quad (7)$$

$$H_h^0 = 9\kappa^2 \left[\frac{3Si(2K)}{32K} - \frac{1}{6K^2} + \frac{3 \cos 2K}{64K^2} - \frac{5 \sin 2K}{128K^3} - \frac{19 \cos 2K}{128K^4} + \frac{19 \sin 2K}{256K^5} \right] \quad (8)$$

where,

$$\kappa = \frac{a_3 - a_1}{a_3 + 2a_1} \quad (9)$$

defines the optical anisotropy of the macromolecule, whereas

$$p = \frac{\mu E}{kT} \text{ and } q = \frac{(\alpha_3 - \alpha_1)}{2kT} E^2 \quad (10)$$

are dimensionless reorientation parameters of the permanent dipole moment, μ , and electric polarizability ellipsoid; k is Boltzmann's constant and T the absolute temperature. For rod-like macromolecules, in the Rayleigh-Debye-Gans approximation, the function $R(\theta, \phi)$ is of the form³:

$$R(\theta, \phi) = \frac{\sin \left[K \sin \theta \cos \left(\phi + \frac{\Theta}{2} \right) \right]}{K \sin \theta \cos \left(\phi + \frac{\Theta}{2} \right)} \quad (11)$$

where $K = [(2\pi l \sin \Theta / 2) / \lambda]$ is a parameter dependent on the length l of the object, the observation angle, Θ and the wavelength, λ , of incident light.

DISCUSSION

In the case of small macromolecules, the component variations, equations (2)–(5) can be expressed in the variables p and q in terms of generalized Langevin functions⁹. In the case under consideration, which is that of large macromolecules, it is more simple to proceed by way of numerical computer calculations of $\delta H_v^E = \delta V_h^E$, δH_h^E and δV_v^E in the integral form of equations (2)–(5) versus the reorientation parameters q and p , for $[l/\lambda] = 1, 0.5, 2$.

As can be seen from Figures 2–11, $\delta H_v^E = \delta V_h^E$ (Figures 2 and 3) is negative for almost all the positive q values; δH_h^E (Figures 4 and 5) is negative for all $q > 0$; whereas δV_v^E (Figures 6–11) is positive at practically all $q > 0$. This is because the orienting field, here, is applied perpendicularly to the plane of observation causing a weakening

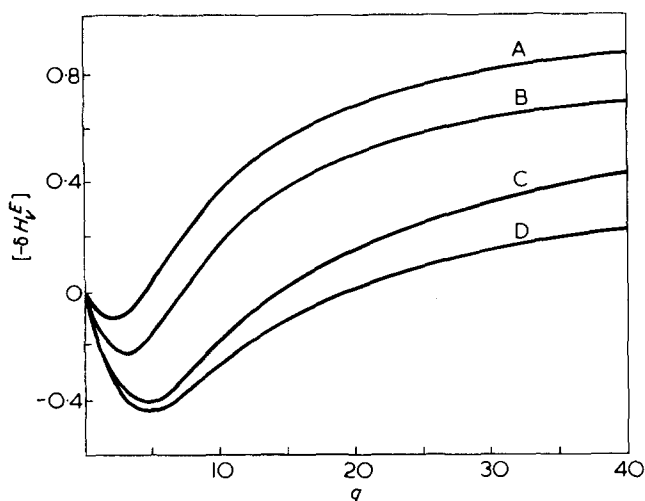


Figure 2 The relative variation $[-\delta H_v^E]$ as a function of the reorientation parameter q , at $p = 0$. A, $l < (1/20)\lambda$; B, $l = \lambda/2$; C, $l = \lambda$; D, $l = 2\lambda$

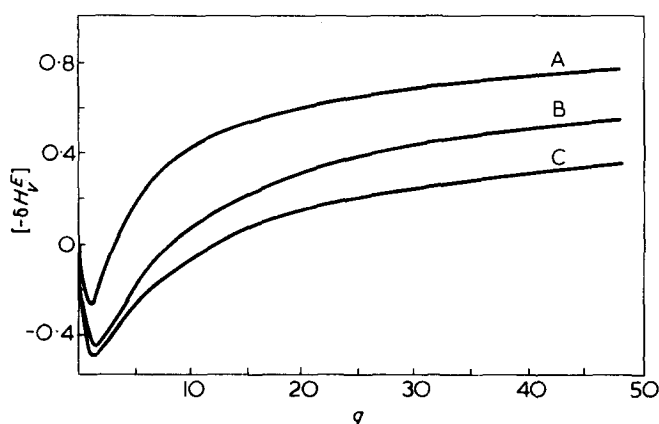


Figure 3 The relative variation $[-\delta H_v^E]$ versus the reorientation parameter q , at $p = 4\sqrt{q}$. A, $l = \lambda/2$; B, $l = \lambda$; C, $l = 2\lambda$

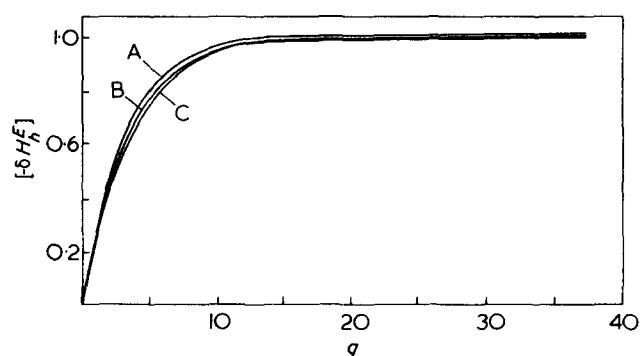


Figure 4 The relative variation $[-\delta H_h^E]$ versus the reorientation parameter q , at $p = 0$. A, $l < (1/20)\lambda$; B, $l = \lambda$; C, $l = 2\lambda$

of the horizontal scattered light components and an enhancement of the vertical ones.

The relative variations $\delta V_h^E = \delta H_h^E$ and δV_v^E (Figures 2, 3, 6–11) are strongly dependent on the macromolecular length l . The longer the macromolecule, the larger are the variations, because the scattered light intensity undergoes a weakening due to intramolecular interferences. The weakening is considerably larger if scattered light is observed in the absence of a reorienting field. The depen-

dence on l is less strong in the case of δH_h^E (Figures 4 and 5) since δH_h^E is very small in comparison with δH_h^0 even for macromolecules with $l = 2\lambda$; at very low field strengths, some influence of l on δH_h^E is still apparent, but as E increases δH_h^E very rapidly attains a constant value ($\delta H_h^E \rightarrow -1$), which is now independent of the length of the macromolecule.

With increasing q (i.e. with growing field strength), all relative variations, equations (2)–(5) tend to a finite value when saturation sets in. The saturation phenomenon consists of the complete ordering of the macromolecules in the

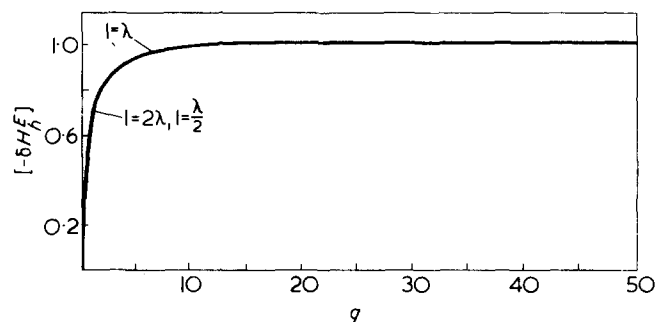


Figure 5 The relative variation $[-\delta H_h^E]$ versus the reorientation parameter q , at $p = 4\sqrt{q}$

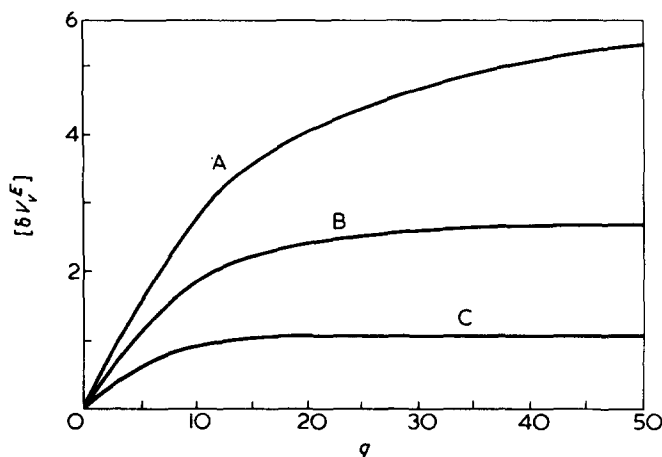


Figure 6 The relative variation $[\delta V_v^E]$ as a function of the reorientation parameter q , at $p = 0$ and $\kappa = 0.1$. A, $l = 2\lambda$; B, $l = \lambda$; C, $l = \lambda/2$

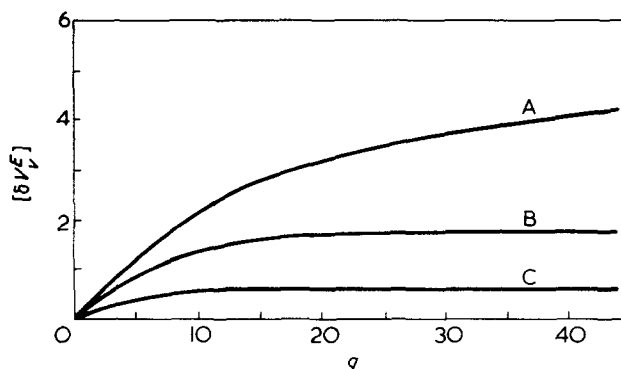


Figure 7 The relative variation $[\delta V_v^E]$ versus the reorientation parameter q , at $p = 0$ and $\kappa = 0$. A, $l = 2\lambda$; B, $l = \lambda$; C, $l = \lambda/2$

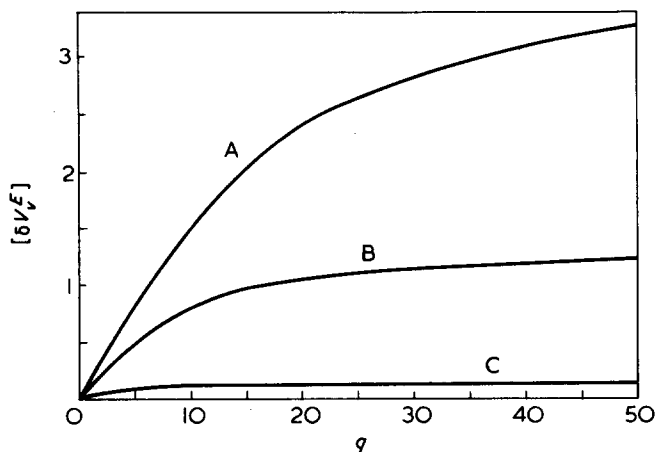


Figure 8 The relative variation $[\delta V_v^E]$ vs. the reorientation parameter q , at $p = 0$ and $\kappa = -0.1$. A, $l = 2\lambda$; B, $l = \lambda$; C, $l = \lambda/2$

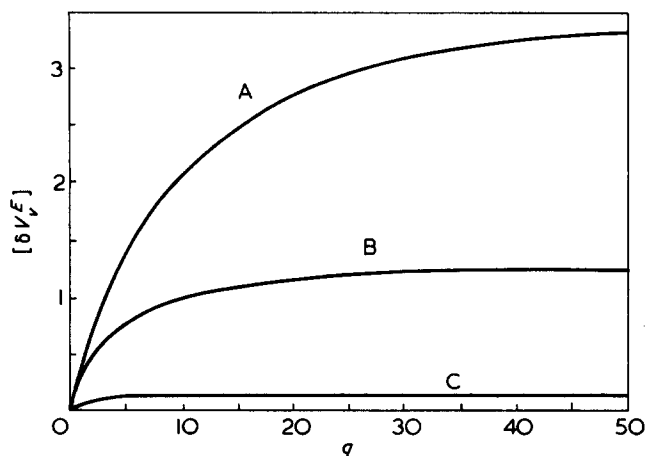


Figure 11 The relative variation $[\delta V_v^E]$ vs. q , at $p = 4\sqrt{q}$ and $\kappa = -0.1$. A, $l = 2\lambda$; B, $l = \lambda$; C, $l = \lambda/2$

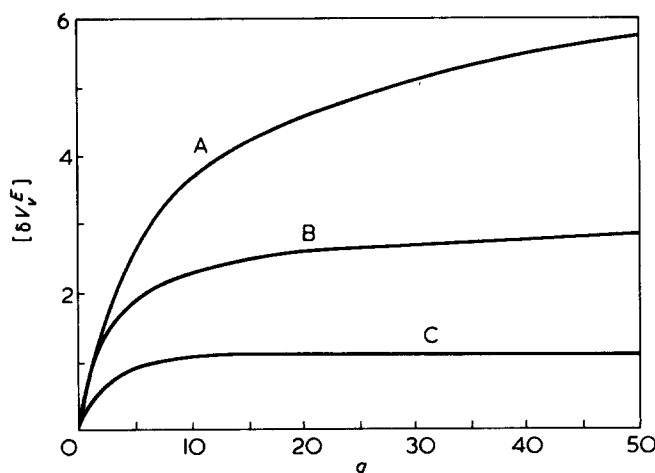


Figure 9 The relative variation $[\delta V_v^E]$ vs. the reorientation parameter q , at $p = 4\sqrt{q}$ and $\kappa = 0.1$. A, $l = 2\lambda$; B, $l = \lambda$; C, $l = \lambda/2$

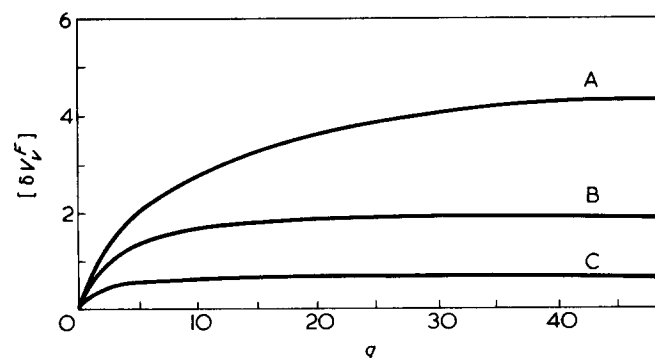


Figure 10 The relative variation $[\delta V_v^E]$ vs. the reorientation parameter q , at $p = 4\sqrt{q}$ and $\kappa = 0$. A, $l = 2\lambda$; B, $l = \lambda$; C, $l = \lambda/2$

external orienting field. At a given temperature T , macromolecules with a given value of electric anisotropy, $(\alpha_3 - \alpha_1)$, attain the completely ordered state more readily the smaller their length l .

In calculating the electric field strength when saturation occurs, the incident wavelength, λ , as well as the electric anisotropy value, $(\alpha_3 - \alpha_1)$, plays a highly essential role. For example, in the case of collagen at a wavelength of the order of 5600 Å the relative variation $\delta H_h^E = \delta V_v^E$ attains the value corresponding to saturation in a field of 30 e.s.u.

whereas δH_h^E attains its saturation value at a field strength of 17 e.s.u.

It is also worth stating that, in absolute values, $|\delta V_v^E| = |\delta H_h^E|$, $|\delta V_v^E|$ and $|\delta H_h^E|$ are always largest for macromolecules possessing a permanent electric dipole moment.

The numerical analysis of the components (equations 2–4) is also applicable to the reorientation of macromolecules by the electric field of laser light, of intensity I_L and frequency ω ¹⁰, when $p = 0$ and $q(\omega) = [(\alpha_3 - \alpha_1)I_L/2kT]$. Optical molecular reorientation in polymers¹¹ and liquid crystals^{11–14} has, in fact, successfully been observed a short time ago.

Studies of this kind are of considerable importance for the determination of the optical anisotropy of macromolecules, since the relevant formulae involve relative variations, defined by the phenomenon of electric and optical saturation^{9,15}.

In recent years, electric light scattering observations in synthetic and biological polymers^{16,17} as well as liquid crystals¹⁸ have provided abundant, interesting data on the dipole moments of macromolecules and their polarizability anisotropies. Lately, first observations have been reported¹⁹ of the effect of electric fields on the depolarization ratio of light, scattered by molecular liquids.

REFERENCES

- 1 Stoylov, S. P. *Adv. Colloid Interface Sci.* 1971, 3, 45
- 2 Horn, P. *Thesis* Strasbourg (1954)
- 3 Van de Hulst, H. C. 'Light Scattering by Small Particles', Moscow, 1961
- 4 Wippler, C. and Benoit, H. *Macromol. Chem.* 1954, 13, 7; Wippler, C. *J. Chim. Phys.* 1956, 53, 316
- 5 Stoylov, S. P. *Collect. Czech. Chem. Commun.* 1966, 31, 3052; *J. Polym. Sci. (C)* 1967, 16, 2435
- 6 Stoylov, S. P. and Sokerov, S. *Bulg. Acad. Sci. Commun. Chem.* 1969, 2, 191; Stoylov, S. P. and Stoimenova, M. *J. Colloid Interface Sci.* 1972, 40, 154
- 7 Ravey, J. C. *J. Chim. Phys.* 1970, 67, 1787; *J. Polym. Sci. Polym. Symp.* 1973, 1131; *Thèse Nancy* (1973)
- 8 Kielich, S. *J. Colloid Interface Sci.* 1968, 27, 432; 1968, 28, 214; 1970, 34, 228
- 9 Kielich, S. *Acta Phys. Pol. (A)* 1970, 37, 447; *Opt. Commun.* 1970, 1, 345
- 10 Kielich, S. *Acta Phys. Pol. (A)* 1970, 37, 719; Farinato, R. S. *J. Colloid Interface Sci.* 1975, 53, 402
- 11 Jennings, B. R. and Coles, H. J. *Nature* 1974, 252, 33

- 12 Wong, G. K. L. and Shen, Y. R. *Phys. Rev. (A)* 1974, **10**, 1277
- 13 Prost, J. and Lalanne, J. R. *Phys. Rev. (A)* 1973, **8**, 2090; Lalanne, J. R. *Phys. Lett. (A)* 1975, **51**, 74
- 14 Lalanne, J. R., Martin, F. B., Pouligny, B. and Kielich, S. to be published
- 15 Stoimenova, M. V. and Dębska, M. *J. Colloid Interface Sci.* 1975, **52**, 265
- 16 Jennings, B. R. and Schweitzer, J. R. *Eur. Polym. J.* 1974, **10**, 459
- 17 Jennings, B. R. and Plummer, H. *Biopolymers* 1970, **9**, 1361; Plummer, H. and Jennings, B. R. *Eur. Polym. J.* 1970, **6**, 171; Jennings, B. R. and Morris, V. J. *J. Colloid Interface Sci.* 1974, **49**, 89; 1975, **50**, 352; Morris, V. J., Rudd, P. J. and Jennings, B. R. *ibid.* 1975, **50**, 379
- 18 Bertolotti, M., Daino, B., Di Porto, P., Scudieri, F. and Sette, D. *J. Phys. (Paris)* 1972, **33**; Izuka, E., Keira, T. and Wada, A. *Mol. Cryst. Liq. Cryst.* 1973, **23**, 13
- 19 Aussenegg, F., Lippitsch, M., Möller, R. and Wagner J. *Phys. Lett. (A)* 1975, **55**, 199

Thermal degradation of poly(butylene terephthalate)

V. Passalacqua, F. Pilati, V. Zamboni*, B. Fortunato and P. Manaresi
Istituto Chimico della Facoltà di Ingegneria, Università di Bologna, Bologna, Italy
(Received 6 July 1976)

The thermal degradation of poly(butylene terephthalate) between 240° and 280°C has been studied by measurements of intrinsic viscosity, carboxyl end groups and weight loss. A first-order mechanism of fission, followed by elimination of butadiene, is proposed. The values of the kinetic constant and activation energy are in good agreement with those obtained for simple esters and poly(ethylene terephthalate).

INTRODUCTION

Among the linear polyesters of terephthalic acid with aliphatic diols, poly(butylene terephthalate) (PBT) has found applications in recent times, especially in the field of thermoplastics for injection moulding and films. At the temperatures of processing (250° to 280°C) various degradation effects (thermal, oxidative and hydrolytic) may occur, and while for poly(ethylene terephthalate) (PET) such phenomena have been studied extensively¹⁻¹¹, nothing on this subject has appeared in the literature, to our knowledge, for PBT. Therefore, we have studied the mechanism of the thermal degradation of PBT, between 240° and 280°C. The study was carried out by measurements of viscosity, weight loss and number of carboxyl end groups.

EXPERIMENTAL

Samples were commercial or laboratory products. They were obtained according to the well known technique of condensation of aromatic polyesters¹², i.e. by transesterification of dimethyl terephthalate with 1,4-butanediol at 180°C in the presence of titanium tetrabutyltitanate as catalyst, and subsequent polycondensation in the molten state, at 260°C *in vacuo*.

All samples were free from additives and stabilizers, and the ash content was less than 200 ppm.

The products were of different molecular weights; their properties are shown collectively in *Table 1*. All samples were ground and dried *in vacuo* at 120°C for 6 h before each experiment; under these conditions moisture was reduced to less than 400 ppm.

Degradation technique

Dried samples of PBT were placed in glass tubes, 6 mm i.d., which were placed horizontally in an electrically heated furnace. The variance of the sample temperature was controlled by means of a Philips 'Plastomatic' system, and kept to within $\pm 0.5^\circ\text{C}$.

The temperature difference between the centre and the ends was $\sim 1^\circ\text{C}$.

Degradation was carried out at various temperatures, and special care was taken to prevent the effect of oxygen:

Table 1 Properties of various PBT

PBT samples	$[\eta]_{\text{P/TCE}}^{30}$ (dl/g)	\bar{M}_n^*	-COOH end groups (g equiv./10 ⁶ g)	$\frac{\Delta[\eta]^\dagger}{[\eta]} \times 100$
L1	1.00	26 900	80	15.6
L2	1.05	28 700	—	15.0
L3	1.14	31 900	—	16.4
C4	0.98	26 200	72	16.0
C5	1.10	30 500	56	12.4
C6	1.18	33 400	58	13.0
C7	1.36	40 300	—	15.8

* Calculated from $[\eta] = 4.3 \times 10^{-4} \bar{M}_n^{0.76}$

† Values obtained after degradation in a flow of nitrogen for 1 h at 260°C

some preliminary tests were carried out at 260°C in a slight flow of preheated nitrogen; a second group of tests was carried out on tubes which had been repeatedly filled with nitrogen and evacuated, and eventually sealed under vacuum.

Identification of the products

In order to identify the gaseous degradation products the tube was connected to an evacuated gas cell, optical path length 70 mm, in which gases were collected at room temperature. Those degradation products which were liquid and solid at room temperature were generally recovered on the cold wall of the tube out of the furnace; the infra-red spectra were recorded on capillary films or nujol mulls. N.m.r. measurements of the liquid and solid degradation products were performed in CDCl_3 solutions.

Viscosity measurements

Viscosity measurements were carried out using Ubbelohde viscometers on solutions in the solvent mixture phenol/s-tetrachloroethane (50:50 by wt) at $30^\circ \pm 0.05^\circ\text{C}$.

End group analysis

Carboxyl content was determined according to the method of Pohl¹³, using freshly distilled aniline instead of benzyl alcohol as solvent.

An attempt was made also to identify and evaluate quantitatively the -OH end groups by means of infra-red spectroscopy, since the absorption band at 3620 cm^{-1}

* Montedison Spa, Centro Ricerche Bollate, Milan, Italy.

corresponds to the stretching vibration of the free -OH group. However, this method can yield only indicative data, because of experimental difficulties and of the small concentration of the -OH groups.

Weight loss determinations

A Perkin-Elmer thermogravimetric balance model TGS-1 was used for weight loss measurements. These isothermal tests were carried out in nitrogen on small samples (a few mg); special care was taken to avoid losses of those degradation products which are solid or liquid at room temperature. The temperature was calibrated with the Curie points of some selected magnetic materials.

RESULTS

Some preliminary tests, made on different samples in a flow of preheated nitrogen, showed that at 260°C PBT undergoes significant degradation. We found that $[\eta]$ decreases, and also that the ratio $\Delta[\eta]/[\eta]$, after 1 h, varies between 0.124 and 0.164, and does not depend upon the initial value of $[\eta]$ (Table 1); moreover, it seems irrespective of the preparation method.

For a more complete study of the mechanism and kinetics of decomposition we have taken into consideration the sample L₁.

During the degradation tests, volatile products are evolved and some discoloration of PBT occurs. The gas collected up to 280°C was essentially butadiene. The products condensed on the tube wall appeared to be a mixture of two solids and one liquid. One of the solids proved to be terephthalic acid, the other showed a m.p. of 124°C. The liquid distilled at reduced pressure (K_{p5} , 184°C). The i.r. and n.m.r. spectra support the suggestion that the last two are unsaturated esters of terephthalic acid. The elemental analysis and spectral data are reported in Table 2.

In order to ascertain that these degradation products are terephthalic acid mono-3-butenyl (I) and di 3-butenyl-(II) esters, the latter have been prepared by reacting 1-buten-4-ol and terephthalic acid dichloride in the correct

proportions. The spectra of these compounds coincided with those of the degradation products.

Tables 3 and 4 list respectively the viscosity data and the -COOH group content, obtained from samples degraded under vacuum. The \bar{M}_n values were calculated from the relationship¹⁴: $[\eta] = 4.3 \times 10^{-4} \bar{M}_n^{0.76}$.

By thin layer chromatography low molecular weight and volatile products were recognized to be present in the polymer bulk. Viscosity measurements and carboxyl determinations were performed without any previous extraction of these substances.

Table 3 Molecular weight data for sample L1 from viscosity measurements

Degradation temperature (°C)	Time (min)	$[\eta]$ (dl/g)	\bar{M}_n	$1/\bar{x}_n \times 10^3$
—	—	1.00	26 700	8.2
240	120	0.77	19 100	11.5
240	180	0.72	17 500	12.6
240	305	0.62	14 300	15.4
240	365	0.59	13 400	16.4
250	20	0.99	26 500	8.3
250	40	0.91	23 700	9.3
250	60	0.89	23 100	9.5
250	105	0.77	19 100	11.5
250	180	0.66	15 600	14.1
250	240	0.64	14 900	14.8
250	300	0.56	12 500	17.6
250	480	0.48	10 200	21.6
250	898	0.36	7 000	31.5
250	1320	0.29	5 300	41.6
250	1800	0.26	4 600	47.9
260	30	0.81	20 400	10.8
260	60	0.73	17 800	12.4
260	90	0.64	14 900	14.8
260	150	0.58	13 100	16.8
260	180	0.53	11 700	18.8
260	240	0.50	10 800	20.4
260	300	0.42	8 600	25.6
280	60	0.46	9 700	22.7
280	120	0.35	6 800	32.3
280	180	0.25	4 350	50.6
280	240	0.20	3 250	67.8

Calculated from $[\eta] = 4.3 \times 10^{-4} \bar{M}_n^{0.76}$

Table 2 Analytical and spectroscopic data of degradation products

Compound	M.p. (°C)	Formula	Analysis (%)				I.r. (ν)* (cm ⁻¹)	N.m.r. (δ)†
			H		C			
			Found	Calculated	Found	Calculated		
(I)	124	C ₁₂ H ₁₂ O ₄	5.55	5.49	65.86	65.45	1719 (vs), 1693 (vs), 1642 (w), 1576 (w), 1507 (w), 1435 (m), 1410 (m), 1367 (w), 1314 (m), 1283 (vs), 1131 (m), 1121 (sh), 1108 (ms), 1017 (m), 918 (m), 880 (m), 730 (s)	2.59(2H, q, OCH ₂ CH ₂ CH=CH ₂ , J = 7 Hz), 4.52(2H, t, OCH ₂ CH ₂ , J = 7 Hz), 5.25(2H, m, CH=CH ₂), 5.92(1H, m, CH=CH ₂), 8.30(4H, d, arom.), 10.65(1H, broad, OH)
(II)	—	C ₁₆ H ₁₈ O ₄	6.59	6.62	69.67	70.05	1723 (vs), 1643 (w), 1410 (w), 1383 (w), 1270 (vs), 1255 (sh), 1120 (s), 1103 (s), 1085 (sh), 1019 (m), 990 (w), 970 (w), 920 (mw), 877 (w), 730 (ms)	2.58(4H, q, OCH ₂ CH ₂ CH=CH ₂ , J = 7 Hz), 4.48(4H, t, OCH ₂ , J = 7 Hz), 5.25(4H, m, CH=CH ₂), 5.93(2H, m, CH=CH ₂), 8.22(4H, m, arom.)

* Spectra were recorded between 2000 and 650 cm⁻¹.

† In CDCl₃ solution

Table 4 —COOH end group data, for sample L1, after degradation at various temperatures

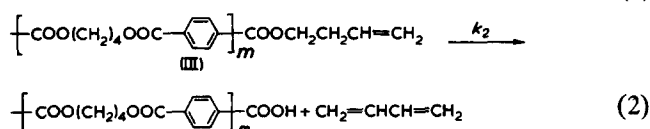
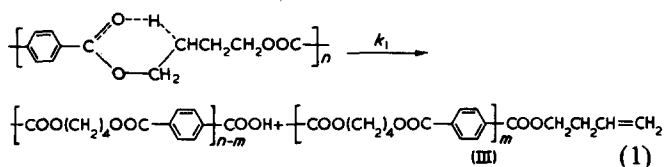
Degradation temperature (°C)	Time (min)	—COOH end groups (g equiv./10 ⁶ g)
—	—	80
239	60	80
239	120	93
239	160	100
239	232	108
239	300	108
239	360	119
250	5	87
250	30	88
250	60	96
250	120	108
250	180	123
250	240	133
250	300	143
250	360	160
260	30	93
260	60	100
260	120	142
260	240	194
260	300	229
260	360	234
280	62	213
280	121	305
280	174	409
280	246	555
280	301	637
280	360	759

Table 5 lists the weight losses at various temperatures; the weight losses were transferred into butadiene moles per mole of repeat unit: it was assumed that all gas was butadiene and that all butadiene was in the gaseous phase, because of its low solubility in the polymer¹⁵.

DISCUSSION

The presence of unsaturated esters and butadiene among the degradation products suggests that fission takes place at the ester linkage, as found for carboxylic esters^{16–24} and for the first step of PET degradation^{1–11}.

On the basis of the experimental data the most likely mechanism can be outlined as follows:



Once it is assumed, as is usual, that fissions occur randomly, for the proposed mechanism we obtain:

$$-\frac{d(N \text{ ester linkages})}{dt} = k_1(N \text{ ester linkages}) \quad (3)$$

$$\frac{d[N(-\text{COOH})]}{dt} = k_1(N \text{ ester linkages}) + k_2[N(\text{III})] \quad (4)$$

Table 5 Weight loss data for sample L1

Temperature (°C)	Time (min)	Weight loss %, $\frac{\Delta\rho}{\rho} \times 100$	Butadiene evolution $\times 10^3$ (moles/mole of repeat unit)
260	60	0.2	8.2
260	120	0.3	12.2
260	180	0.35	14.3
260	240	0.4	16.3
280	60	0.3	12.2
280	120	0.7	28.5
280	180	1.1	44.9
300	60	1.1	44.9
300	120	3.0	122.4
300	180	5.7	232.5

$$\frac{d[N(\text{III})]}{dt} = k_1(N \text{ ester linkages}) - k_2[N(\text{III})] \quad (5)$$

$$\frac{d(N \text{ butadiene})}{dt} = k_2[N(\text{III})] \quad (6)$$

where: (*N* ester linkages) = moles of ester linkages/moles of repeat units; [*N*(—COOH)] = moles of —COOH end groups/moles of repeat units; [*N*(III)] = moles of 3-butenyl ester end groups/moles of repeat units; [*N* butadiene] = moles of butadiene/moles of repeat units. According to this mechanism, only the first-order reaction (1) is the rate-controlling step with respect to the degree of polymerization.

This reaction can be described by a kinetic treatment of the Tuckett type²⁴ which results in a linear relationship between $1/\bar{x}_n$ and *t*, if $\bar{x}_n \gg 1$ (where \bar{x}_n is the number-average degree of polymerization). Figure 1 shows the experimental data.

The splitting of butadiene from the unsaturated end groups occurs, according to reaction (2), via a cyclic intermediate contiguous to a double bond.

This reaction may be favoured by resonance with the double bond, and takes place at a higher rate than the primary fission. In this way it is reasonable to apply the steady-state hypothesis to equation (5). Then, from equation (4), the initial rate of formation of butadiene is constant up to 280°C, as shown in Figure 2.

According to this hypothesis, the number of —COOH end groups must also be found linearly increasing with time. This is verified in Figure 3. The steady-state approximation yields:

$$\frac{d[N(\text{III})]}{dt} = 0; k_1(N \text{ ester linkages}) = k_2[N(\text{III})] \quad (7)$$

from which we obtain

$$\begin{aligned}
 \frac{d[N(-\text{COOH})]}{dt} &= \frac{d(N \text{ butadiene})}{dt} \\
 &= -\frac{d(N \text{ ester linkages})}{dt} = \frac{d(1/\bar{x}_n)}{dt} \\
 &= k_1(N \text{ ester linkages}) \quad (8)
 \end{aligned}$$

The values of *k*₁, the kinetic constant, calculated from Figures 1–3, are listed in Table 6; the data obtained from the different methods of measurements are fairly consis-

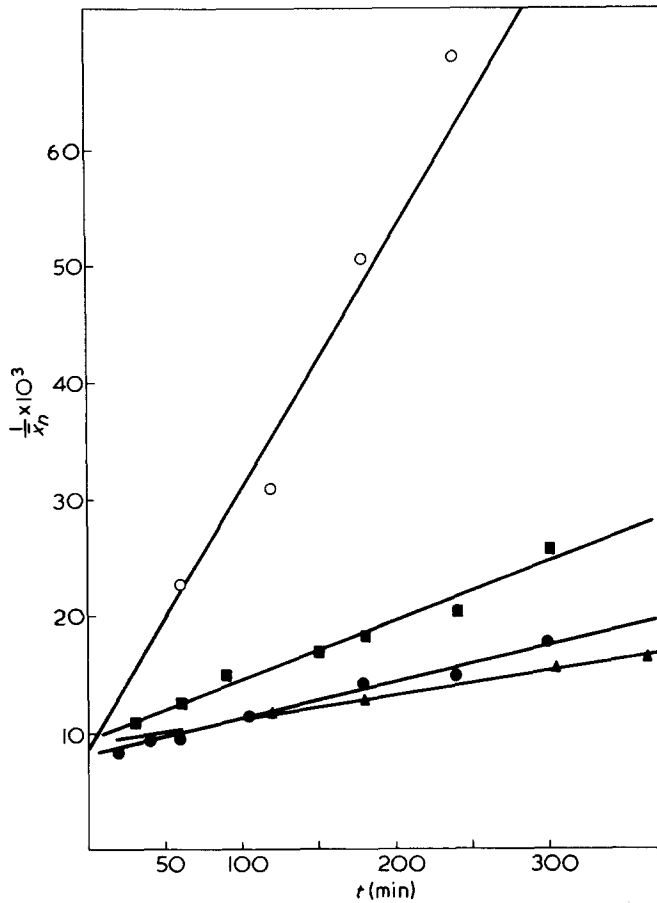


Figure 1 $1/\bar{x}_n$ versus t plots for sample L₁, degraded at various temperatures, from viscosity data. \blacktriangle , 240°; \bullet , 250°; \blacksquare , 260°; \circ , 280° C

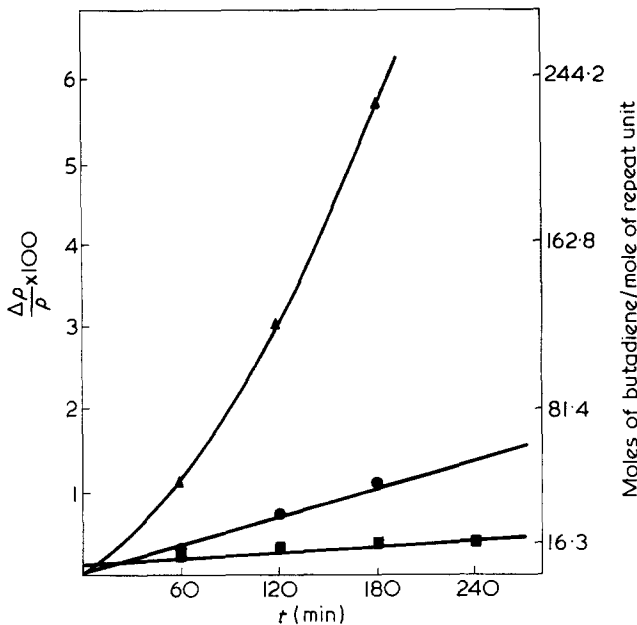


Figure 2 Weight loss data, at various temperatures, for sample L₁: $\Delta p/p \times 100$ versus t and moles of butadiene/moles of repeat unit versus t . \blacksquare , 260°; \bullet , 280°; \blacktriangle , 300° C

tent for temperatures between 240° and 280° C.

The calculated Arrhenius activation energy is $E = 41$ kcal/mol in good agreement with the values reported for PET²⁻⁴ and carboxylic esters¹⁸⁻¹⁹ under analogous conditions. Some tests at higher temperatures (300° C or more) suggest

that side reactions or different mechanisms are possible. This can be inferred from the weight loss data and from the presence of carbonyl compounds and small quantities of water and tetrahydrofuran in the gaseous degradation products.

CONCLUSIONS

In the temperature range of processing, the thermal degradation of PBT takes place by ester-linkage fission, as is the case for carboxylic esters and for the first step of the PET degradation; the value of the activation energy is also in good agreement with those reported for these.

The chain fissions of PBT are followed by an evolution of butadiene, while carboxyl end groups increase and unsaturated terminal groups disappear. This justifies the absence of those secondary reactions which take place in PET, where unsaturated compounds are more stable and acetaldehyde more soluble in the polymer bulk.

The presence of carboxyl end groups, as well as of other reactive fragments in degraded PBT might favour contamination by metal traces due to corrosion, and affect reactivity towards additives and fillers, added for the fabrication stage (stabilizers, flame-retardants and reinforcing

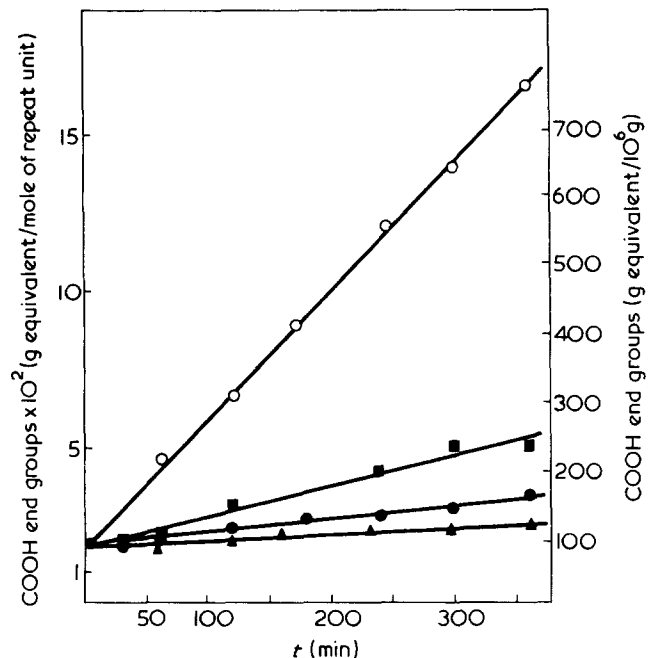


Figure 3 $-\text{COOH}$ end groups data at various temperatures for sample L₁. \blacktriangle , 240°; \bullet , 250°; \blacksquare , 260°; \circ , 280° C

Table 6 Values of the kinetic constant at various temperatures

Temperature (°C)	$k_1 \times 10^7$ (sec ⁻¹)		
	Viscosity measurements	$-\text{COOH}$ end group measurements	Weight loss measurements
240	3.3	2.0*	—
250	4.8	4.0	—
260	8.4	8.4	8.7
280	37.1	34.5	39.1

* Measured at 239° C

agents). Furthermore, degradation might have an influence upon the water adsorption and some physical properties such as crystallization kinetics.

ACKNOWLEDGEMENTS

We thank Dr E. de Fornasari and Professor L. Marchetti for many helpful suggestions and Dr M. Poloni for assistance in preparing terephthalic acid esters.

REFERENCES

- 1 Pohl, H. A. *J. Am. Chem. Soc.* 1951, **73**, 5660
- 2 Marshall, I. and Todd, A. *Trans. Faraday Soc.* 1953, **49**, 67
- 3 MacMahon, W., Birdsall, H. A., Johnson, G. R. and Camilli, C. T. *J. Chem. Eng. Data* 1959, **57**, 4
- 4 Goodings, E. P. *Soc. Chem. Ind.* 1961, **13**, 211
- 5 Zimmermann, H. *Faserforsch. Textiltech.* 1962, **13**, 481
- 6 Zimmermann, H. and Leibnitz, E. *Faserforsch. Textiltech.* 1965, **16**, 282
- 7 Zimmermann, H. and Dao duy Chu *Faserforsch. Textiltech.* 1973, **24**, 445
- 8 Zimmermann, H. and Becker, D. *Faserforsch. Textiltech.* 1973, **24**, 479
- 9 Schaaf, E. and Zimmermann, H. *Faserforsch. Textiltech.* 1974, **25**, 434
- 10 Zámorsky, Z. *Faserforsch. Textiltech.* 1963, **14**, 271
- 11 Buxbaum, L. H. *Angew. Chem. Internat. Edn Engl.* 1968, **7**, 182
- 12 Polybutyleneterephthalate SRI, Stanford Report No 96, 1975
- 13 Pohl, H. A. *Anal. Chem.* 1954, **26**, 1614
- 14 Zamboni, V. and Ajroldi, G. Scientific communication, 1^o Convegno Italiano di Scienza delle Macromolecole, San Donato Milanese, 1975
- 15 Battino, R. *Chem. Rev.* 1966, **6**, 395
- 16 Allan, R. J. P., Forman, R. L. and Ritchie, P. D. *J. Chem. Soc.* 1955, p 2717
- 17 Hurd, C. D. and Blunck, F. H. *J. Am. Chem. Soc.* 1938, **60**, 2419
- 18 O'Connor, G. L. and Nace, H. R. *J. Am. Chem. Soc.* 1953, **75**, 2118
- 19 Sommers, E. E. and Crowell, T. I. *J. Am. Chem. Soc.* 1955, **77**, 5443
- 20 Iengar, H. V. R. and Ritchie, P. D. *J. Chem. Soc.* 1956, p 3563
- 21 Allan, R. J. P., Jones, E. and Ritchie, P. D. *J. Chem. Soc.* 1957, p 524
- 22 Allan, R. J. P., Iengar, H. V. R. and Ritchie, P. D. *J. Chem. Soc.* 1957, p 2107
- 23 Iengar, H. V. R. and Ritchie, P. D. *J. Chem. Soc.* 1957, p 2556
- 24 Mackinnon, H. M. and Ritchie, P. D. *J. Chem. Soc.* 1957, p 2564
- 25 Tuckett, R. F. *Trans Faraday Soc.* 1945, **41**, 351

Glass transition temperature in nylons

R. Greco and L. Nicolais*

Laboratorio di Ricerche su Tecnologia dei Polimeri e Reologia del CNR, Arco Felice (Napoli), Italy

(Received 24 May 1976; revised 12 July 1976)

The determination of the glass transition temperature of semi-crystalline polymers is a controversial problem in the literature, because of the complexity of the phenomenon and of the different methods used for its measurement. In this work the glass transition temperatures of five commercial nylons (nylon-6, nylon-6,6, nylon-6,10, nylon-11, nylon-12) have been measured by both thermal and mechanical methods. The behaviour observed during thermal measurements is analogous to that observed by Gordon, who found that the transition detected in the heating cycle disappeared in the subsequent cooling cycle and appeared again only after a sufficient rest period of the samples, and at a temperature different from the initially measured one. He attributed this behaviour to the structure of the amorphous regions of the material, where the hydrogen bonding groups form an irregular network. The delay in reforming the above mentioned network is the main cause of the dependency of the observed transition on the thermal history imposed on the samples. Mechanical measurements give results that are quite insensitive to the thermal treatment of the materials, and thus provide very reproducible values of the transition. This feature allows the possibility of attributing to the transition obtained the character of a true glass transition where the main cause of the phenomenon is the increased mobility of the chain backbone in the amorphous regions of the materials with increasing temperature. This character was also confirmed by dilatometry, with results in agreement with Boyer's criteria for a true glass transition temperature.

INTRODUCTION

The glass transition is a well known phenomenon, especially to people working in the area of polymer science and technology, even though it occurs in several other classes of materials. It has a multidimensional character, i.e. once certain critical conditions have been achieved, it is possible, keeping all the variables constant but one to define many critical variables, such as glass transition temperature, glass transition pressure, molecular weight, frequency, and so on. The most technologically important is the glass transition temperature (T_g), which will be analysed here focusing our attention on a particular class of semi-crystalline polymers, the nylons.

It is known that going through such a transition a large number of properties of the material undergo a more or less drastic change, due to the onset of motions of the chain backbone involving long sequences of carbon atoms¹. Step changes in properties such as the coefficient of thermal expansion, specific heat, compressibility, modulus of elasticity, etc. give the glass transition the apparent behaviour of a second order thermodynamic transition, but its kinetic character is clearly shown by the dependency on time², dependency on rate of heating or cooling, hysteresis phenomena³, etc. Among all these properties, T_g has been analysed by two thermal techniques: differential thermal analysis (d.t.a.) and differential scanning calorimetry (d.s.c.), and two mechanical methods: volume dilatometry and the so-called 'Tobolsky method'^{4,5}.

In d.t.a. measurements^{6,7} a differential temperature between the sample and a reference material is recorded at steadily increasing temperature. The temperatures are determined by means of two thermocouples embedded one

in the sample and the other in the reference material and it is not very easy to relate the differential temperature to the step change in the specific heat of the polymer.

In d.s.c.^{6,7}, it is the differential heat flowing from the sample and from the reference, individually controlled and kept at the same temperature, while the temperature of the entire system is steadily increased, that is essentially measured.

In volume dilatometry a plot of specific volume vs. temperature shows a breakpoint indicating the value of T_g . Sometimes there is a region of smooth curvature and the value of T_g is taken at the intersection of two limiting straight lines, the lower one representing glass-like and the upper one rubber-like behaviour.

In the so-called 'Tobolsky method' a log-log plot of the elastic isochronal shear (tensile) modulus is plotted against temperature and the glass transition temperature is defined as the temperature corresponding to the following value of the modulus:

$$\log G(K) = \frac{\log G_1 + \log G_2}{2} \quad (1)$$

where G_1 and G_2 are the values of the modulus corresponding to the glassy and the rubbery plateau, respectively and K is a fixed time after starting the experiment. Generally K is equal to 10 sec as suggested by Tobolsky and the glass transition temperature is represented by T_i^{10} . It is possible to show, by applying the Boltzmann superposition principle and the WLF superposition procedure⁸, that the T_g obtained by volumetric measurements, and T_i^{10} obtained by the Tobolsky method, are closely related by⁹:

$$T_i(10) = T_g + 4^\circ\text{C} \quad (2)$$

* Also with the Istituto di Principi di Ingegneria Chimica, University of Naples, Italy.

The above relation is only approximate as the values of the coefficients have been calculated from average values obtained on different polymers, and different techniques.

In the case of semi-crystalline polymers and in particular nylons, some authors¹⁰ suggest the occurrence of T_g at -65°C , based on penetrometer studies and on crystallization kinetics considerations, whereas other authors¹⁰ accept the transition occurring in the range of $40^\circ\text{--}50^\circ\text{C}$, as satisfying most of the criteria for T_g , even though some unusual behaviour seems to be associated with it.

EXPERIMENTAL

The materials used were commercial samples of nylon-6 (Renyl B/V, produced by Montedison) nylon-6,6 (produced by Rhodiatocce), nylon-6,10, nylon-11 and nylon-12 (produced by BASF). The crystallinity of the samples was calculated by measuring the peak areas of the melting zone

Table 1 Crystallinities and melting temperatures for nylons investigated

Materials	H_f	H_f^0 (kJ/kg)	Crystallinity (%)	T_f
Nylon-6	51.7	193	27	224
Nylon-6,6	52.8	193	27	265
Nylon-6,10	31.5	165	19	225
Nylon-11	41.2	222	19	184
Nylon-12	58.7	225	26	172

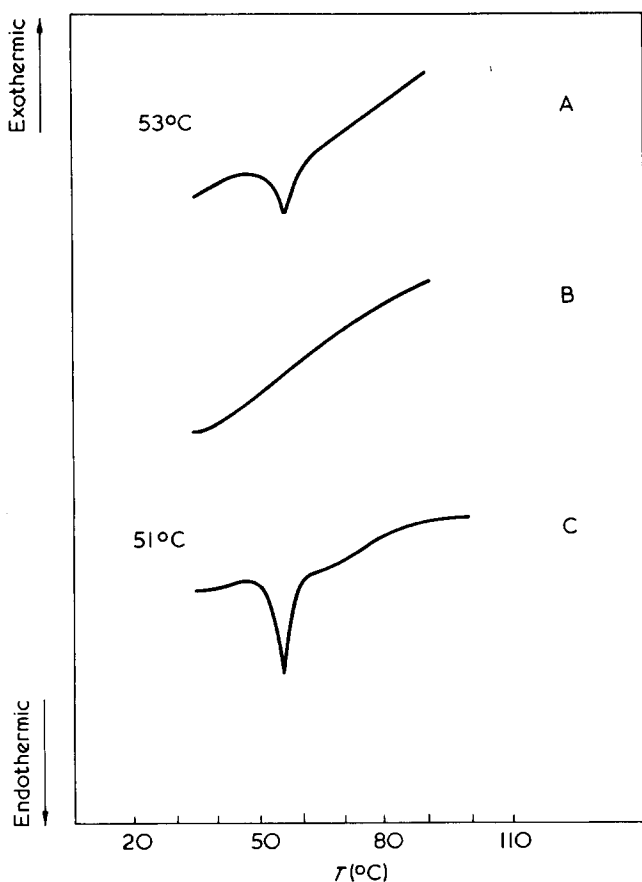


Figure 1 D.s.c. measurements on nylon-6: A, first run; B, immediate rerun; C, rerun after one week of rest

obtained by means of a previously calibrated Perkin-Elmer DSC-2 apparatus. The values of H_f (Table 1) so obtained were divided by the enthalpy of fusion H_f^0 relative to samples with 100% crystallinity. The latter values were calculated by the group contribution method¹¹. In the same Table the melting temperatures are also shown in the last column.

Thermal measurements have been made on a Perkin-Elmer DSC-2 (Figure 1) and the results are very similar to the ones obtained by Gordon on a d.t.a. apparatus¹². The transition present in the initial heating cycle, disappeared in the subsequent cooling and also in an immediate rerun; it began to reappear only after few hours rest of the samples, but at a lower temperature than the initial one. Only after about a weeks rest did the transition appear again at the initial temperature. This behaviour was similar for all the nylons studied. Another feature was the shift of the observed transition towards higher temperature due to the annealing of the samples. Furthermore in an infra-red spectrum the absorption band attributable to unbonded NH groups disappeared after heating the samples at 85°C for 15 min. This behaviour cannot be explained in terms of the classical understanding of T_g . In fact if the transition is due to the onset of motion of long segments of the chain backbone, the disappearance of the transition on cooling and also the other effects mentioned should not occur. In fact in the case of polystyrene in spite of a little hysteresis due to the kinetic character inherent in the T_g , the transition is still present in the cooling cycle and never disappears¹². Therefore Gordon postulated the existence of an irregular network formed in the amorphous region of the polymer by hydrogen bonding groups. Since bonding sites occur at a certain distance along the chain, there are some steric factors which hinder the formation of the network, and this can explain the long delay in reforming the network. The shifting on annealing is due to the formation of a new network, which is stable at higher temperatures, and the disappearance of the absorption band for unbonded NH groups is also due to the formation of the network at a temperature of 85°C . Even though this explanation seems very plausible, we found different results by performing mechanical measurements with a Clash-Berg creep torsional tester. The apparatus is very simple and very easy to use; it consists of a torsion drum to which two weights are suspended. A push button releases the weights applying to the sample a certain torque, at the start of the experiment. After a fixed time, generally 10 sec, the creeping of the sample is stopped and the angle of torsion is measured. Changing weights with decreasing modulus (at increasing temperature) allowed us to maintain torsion angles to within $20\text{--}30^\circ$ and hence to restrict, the experiments within the range of linear viscoelasticity.

The samples were obtained by compression moulding at a temperature of 20°C above the corresponding melting temperature and at a pressure of 100 kg/cm^2 . The plates of the moulding machine were water cooled. The results for nylon-6 and nylon-6,6 are shown in Figures 2 and 3 for samples subjected to heating and cooling cycles. It can be seen that the transition is very well reproduced. Furthermore since the thermal measurements (d.s.c.) are made at faster speeds, we increased the heating rate by immersing the sample of nylon-6,6, at room temperature, into a bath at 87°C , and then quenching to room temperature, therefore obtaining a very high cooling rate. Also in this case the points fall on the curve showing no dependency of the observed transition on thermal histories.

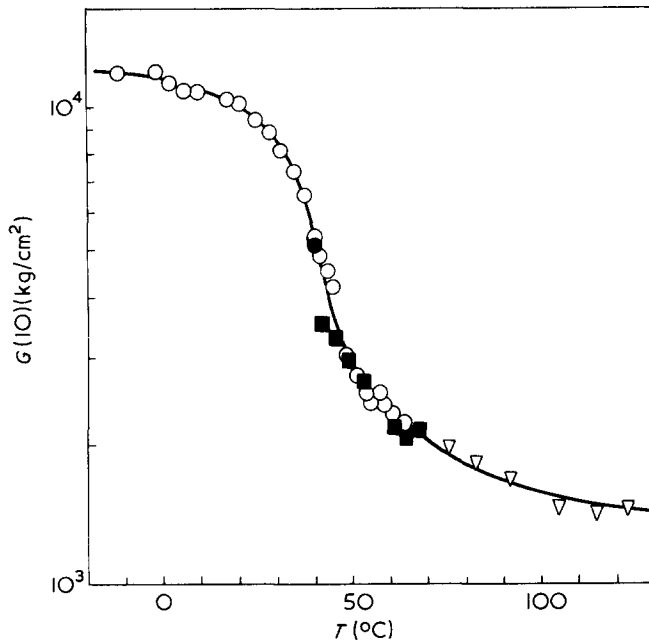


Figure 2 Plot of isochronal shear modulus after 10 sec, $G(10)$ vs. temperature for nylon-6, for different thermal histories. \circ , With increasing temperature up to 60°C; \blacksquare , subsequent cooling down to 40°C; \bullet , quenching from 125° to 40°C; ∇ , sudden heating up from room temperature to 70°C and further heating to 125°C

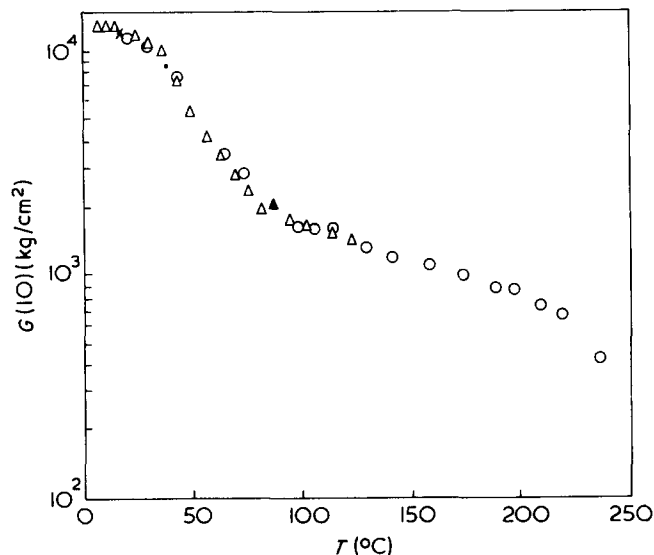


Figure 3 Plot of $G(10)$ vs. temperature for nylon-6,6 for different thermal histories: \triangle , before quenching; \times , quenching down to room temperature; \circ , after quenching; \blacktriangle , sudden heating up to 87°C

RESULTS AND DISCUSSION

The shape of the curves shown in Figures 2 and 3 is similar to that obtained in the case of non-crystalline polymers¹³, i.e. a glassy plateau, a transition zone, a rubbery plateau and a liquid-like terminal zone. The only difference is that the rubbery modulus has a value of 2–3 orders of magnitude higher than the corresponding value for a non-crystalline polymer, but this is clearly due to the presence of crystalline regions that stiffen the polymer making it leathery rather than rubbery. However it seems clear that the observed transition is due to the onset of motions of the chain backbone in the amorphous region of the material.

The independence of the transition from thermal treatments can also be seen from the dilatometric measurements shown in Figure 4 where the transition is present in both the heating and the cooling cycle.

To judge the character of the above observed transition we will apply Boyer's criteria for a true glass transition in the case of non-crystalline polymers¹⁴:

$$\alpha_e T_g = 0.16$$

$$\Delta\alpha T_g = 0.113 \quad (3)$$

$$\alpha_g = 2 \times 10^{-4} \text{ (degree}^{-1}\text{)}$$

where α_e is the expansion coefficient of the rubbery-like liquid:

$$\alpha_e = \frac{1}{V_g} \left(\frac{dV}{dT} \right)_e \quad (4)$$

α_g is the expansion coefficient of the glassy solid:

$$\alpha_g = \frac{1}{V_g} \left(\frac{dV}{dT} \right)_g \quad (5)$$

and

$$\Delta\alpha = \alpha_e - \alpha_g \quad (6)$$

These criteria are based on the concept that the glass transition is an iso-free-volume state.

In Table 2 the parameters given previously for Boyer's criteria are reported for the nylons analysed. It is clear that $\Delta\alpha T_g < 0.113$; $\alpha_e T_g < 0.16$ and $\alpha_g > 2 \times 10^{-4}$ degree⁻¹ and therefore we fall into case IV as described by Boyer¹⁵ for semi-crystalline polymers: in fact $\alpha_e T_g$ is lower than 0.16 because of the presence of crystallinity; α_g is larger than 2×10^{-4} degree⁻¹ because of the existence of secondary relaxation at temperature lower than T_g . Hence $\Delta\alpha$ must

Table 2 Physical parameters of the nylons tested

Materials	T_i	T_g (data from literature)	$\alpha_e T_g$	$\Delta\alpha T_g$	α_g	T_g (d.s.c.)
Nylon-6	54	50–75	0.115	0.03	2.6×10^{-4}	53
Nylon-6,6	58	57				57
Nylon-6,10	45	50				45
Nylon-11	42	46	0.115*	0.029*	3.6×10^{-4} *	42
Nylon-12	40	37	0.118*	0.022*	3.8×10^{-4} *	43

* Data from Champetier, G. and Pied, J. P. *Makromol. Chem.* 1961, 44, 64 where T_i is the glass transition temperature detected by means of the Tobolsky method; T_g is the glass transition temperature detected by differential thermal analysis; α_e and α_g are the expansion coefficients of the rubbery-like liquid and the glassy solid respectively; $\Delta\alpha = \alpha_e - \alpha_g$

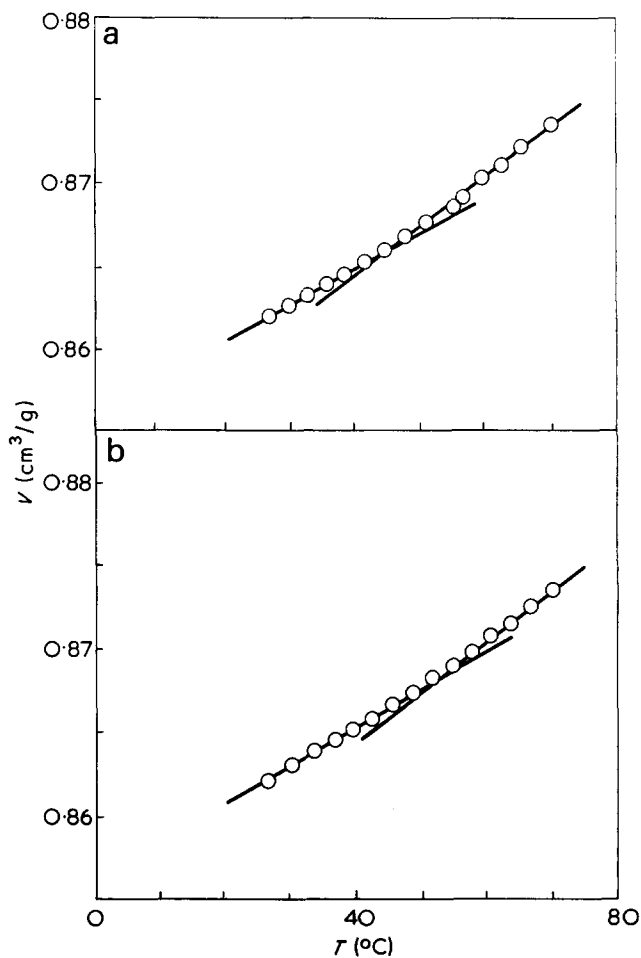


Figure 4 Plot of specific volume vs. temperature for (a) heating and (b) cooling cycles for nylon-6. \circ , Heating; \blacksquare , cooling; \bullet , quenching

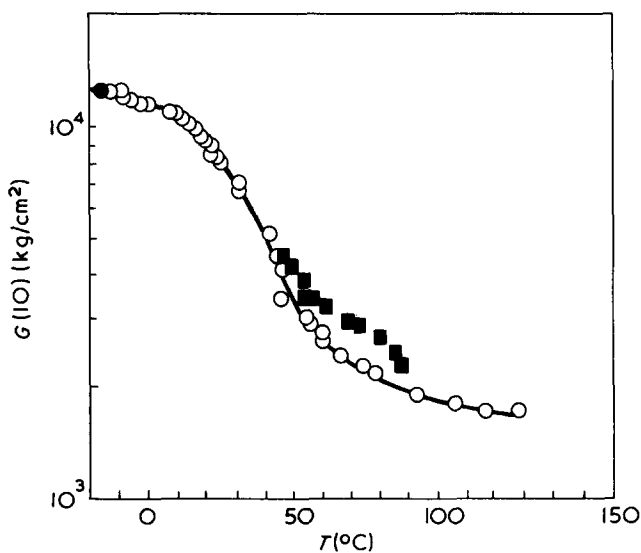


Figure 5 Plot of $G(10)$ vs. temperature for nylon-6,10. The points are obtained after annealing at 150°C for 2 h and subsequent quenching of the sample at -10°C . \circ , Heating; \blacksquare , cooling

be lower than the indicated value valid in the case of amorphous polymers. Therefore it is confirmed also from dilatometric data that the transition lying in the region of $40^\circ\text{--}50^\circ\text{C}$ is a true glass transition in its classical meaning. In Figures 5–7 the isochronal curves obtained with the Clash–Berg apparatus for nylon 6,10, nylon-11 and nylon-12

are shown. The behaviour is very similar to that already discussed for nylon-6 and nylon-6,6. Of course, this technique does not have the necessary sensitivity to detect the existence of multiple glass transition as suggested by Boyer¹⁶ and it can only give an average glass transition temperature. However if there is a change in crystallinity, some shift in the transition can occur, as qualitatively shown in the Figures 5–7. In these the full symbols are relative to the cooling cycle made on specimens maintained at temperatures very close to the melting temperatures (nylon-11 and nylon-12) for at least 10 h. It would be possible, in principle at least, to see how the change in crystallinity affects the change in the glass transition temperature, but so far this can be only a very rough, indirect and qualitative evi-

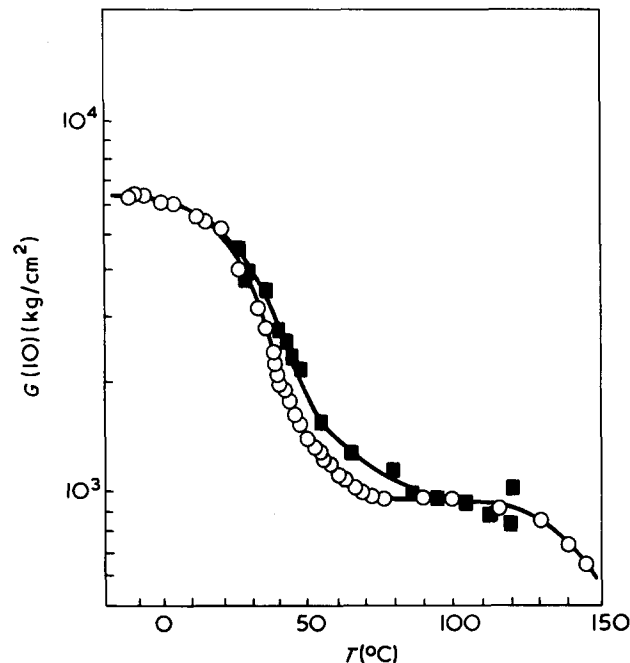


Figure 6 Plots of $G(10)$ vs. temperature for nylon-11. The cooling curve shows a variation in the value of T_g due to a change in crystallinity

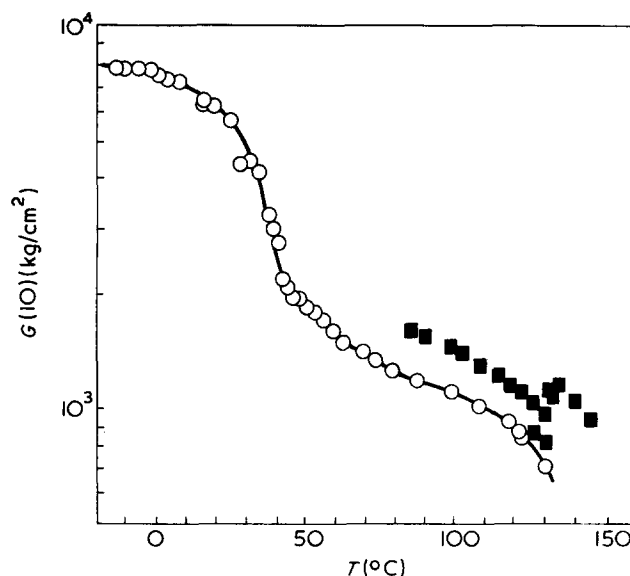


Figure 7 Plot of $G(10)$ vs. temperature for nylon-12 showing variation of T_g with increasing crystallinity. \circ , Heating; \blacksquare , cooling

dence of the presence of multiple glass transitions in nylons.

In conclusion, we have seen that transition of nylons lying in the range of 40°–50°C is a glass transition in its classical meaning, where the amorphous regions of the polymer undergo a glassy–rubbery change. Furthermore the reliability of mechanical measurements compared to the thermal techniques has been shown, at least in cases where hydrogen bonding groups are present. We have also shown that the Tobolsky method is a very convenient method, from a technological point of view, providing the T_g and also the two glassy and rubbery values of the modulus whose difference tells the importance of the glassy transition for that particular polymer.

REFERENCES

- 1 Shen, M. C. and Eisenberg, A. *Prog. Solid State Chem.* 1966, **3**, 407
- 2 Kovacs, A. J. *J. Polym. Sci.* 1958, **30**, 131
- 3 Jones, G. O. 'Glass', Methuen, 1956
- 4 Shen, M. C. and Eisenberg, A. *Prog. Solid State Chem.* 1966, **3**, 407
- 5 Tobolsky, A. V. 'Properties and Structure of Polymers', Wiley, New York, 1960
- 6 Collins, E. A., Bares, J. and Billmeyer, Jr, F. W. 'Experiments in Polymer Science', New York, Wiley, 1973
- 7 Gray, A. P. in 'Analytical Calorimetry', (Eds R. S. Porter and J. F. Johnson), Plenum Press, New York, 1968, pp 209–218
- 8 Williams, M. L., Landel, R. F. and Ferrit, J. D. *J. Am. Chem. Soc.* 1955, **77**, 3701
- 9 Mercier, J. P. and Aklonis, J. J. *J. Paint Technol.* 1971, **43**, 44
- 10 Boyer, R. F. *Rubber Chem. Technol.* 1963, **36**, 1303
- 11 'Polymer Handbook', (Eds J. Braundrup and F. H. Immergut), Wiley, London, 1975
- 12 Gordon, G. A. *J. Polym. Sci. (A-2)* 1971, **9**, 1963
- 13 Billmeyer Jr, F. W. 'Textbook of Polymer Science', 2nd Edn, Wiley, New York, 1971
- 14 Boyer, R. F. *Macromolecules* 1973, **6**, 288
- 15 Boyer, R. F. *Plast. Polym.* 1973, pp 15, 71, 77
- 16 Boyer, R. F. *J. Macromol. Sci. (B)* 1973, **8**, 503

Rheological behaviour of blends of narrow molecular weight distribution polystyrenes in the molten state: dynamic viscoelastic properties in the terminal zone

J. P. Montfort

Laboratoire de Thermodynamique, Université de Pau, 64016-Pau, France

(Received 12 May 1976)

Narrow molecular weight distribution polystyrenes and their blends, with molecular weights exceeding M_c , have been measured in the molten state by means of a Contraves–Kepes balance rheometer. The vertical and the horizontal shift factors are the same for the fractions and their blends. In the terminal zone, the effect of blending on the complex viscosity η^* and its imaginary part η'' results in the appearance of two fields representing the respective contributions of both components to the blend. The importance of the coupling between both fields as a function of the weight ratio of both components is discussed. The zero-shear viscosity η_0 is equal to that of a narrow molecular weight distribution polystyrene having the same weight-average molecular weight M_w , measured at the same temperature.

INTRODUCTION

Many investigations have revealed that the viscoelastic properties of amorphous polymers, in the terminal and plateau zones, are strongly affected by the molecular weight distribution.

This effect can be studied, for example, using binary blends of the same species of polymers having different molecular weights: blends of poly(methyl methacrylates)¹, monodisperse polystyrenes^{2–4}, poly(vinyl acetates)⁵, polyethylenes⁶. The studies dealing with the binary blends of monodisperse polystyrenes have shown that, in the terminal zone, the storage shear modulus G' and loss modulus G'' undergo only a mere translation. On the other hand, Masuda and his collaborators⁴ have shown that, if the weight ratio of the two components is high enough – higher than about four – in the rubbery zone, the curves G' of the blends show a two-step plateau and the curves G'' show two peaks seeming to correspond to those of the components. This behaviour is also found in the aspect of the relaxation spectrum which, under the same conditions as G' and G'' , can present two maxima. The peak on the long time side seems to be shifted slightly to the short time side; the other peak, on the short time side, is shifted to the long time side.

In the present study, we will show a similar behaviour with binary blends of monodisperse polystyrenes of weight-average molecular weight higher than M_c , in the terminal zone. For this purpose we have used a directly measurable viscoelastic function: the complex viscosity η^* .

EXPERIMENTAL

Materials

Narrow molecular weight distribution polystyrenes obtained by anionic polymerization and manufactured by the Waters Associates Corporation were used. The polydisper-

Table 1 The weight-average molecular weights for the narrow-molecular weight distribution polystyrene samples

Sample	M_w
PS 11	110 000
PS 20	200 000
PS 40	400 000

Table 2 Features of the binary blends

Components	Sample	ϕ^a	M_w
PS 11	M 114005	0.05	124 500
	M 114010	0.10	139 000
+	M 114015	0.15	153 500
	M 114025	0.25	182 500
	M 114050	0.50	255 000
PS 40			
PS 11			
+	M 112030	0.30	137 000
PS 20			

^a ϕ is the weight fraction of the component with the highest molecular weight

sity, determined by gel permeation chromatography, was lower than 1.1. Table 1 shows the weight-average molecular weights of the fractions used.

The blending of components was carried out by dissolving a suitable mixture of narrow molecular weight distribution polystyrenes in benzene. The solvent was then removed by freeze-drying and the blends obtained were dried in a vacuum oven at 60°C over two days. Features of the blends are given in Table 2.

Measurements

The dynamic measurements were achieved with a Contraves–Kepes balance rheometer. Complex viscosity η^* was measured at four temperatures: 156°, 166°, 176° and

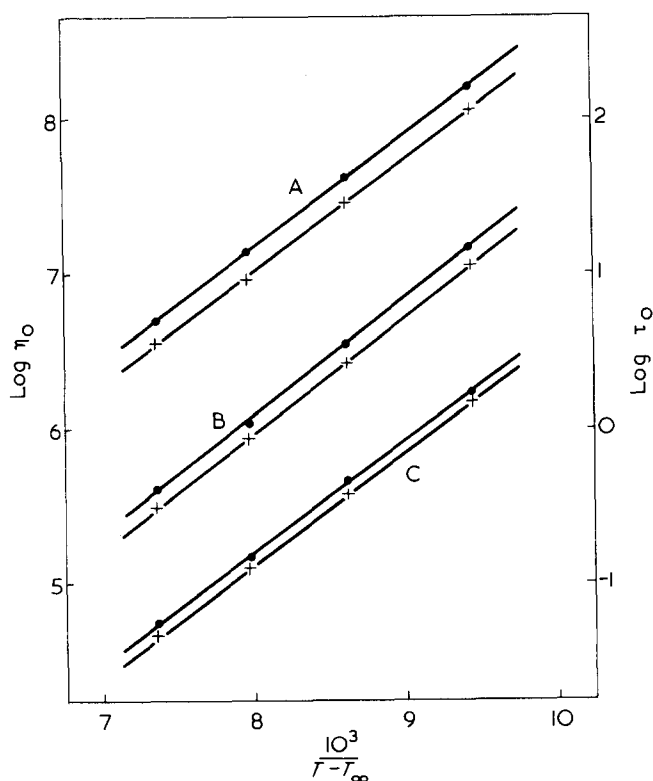


Figure 1 Temperature dependence of terminal relaxation time τ_0 (●) and zero-shear viscosity (+) for the narrow molecular weight distribution polystyrene samples: A, PS 40; B, PS 20; C, PS 11. ($T_\infty = 50^\circ\text{C}$)⁹

186°C for all samples. Frequencies varied from 10^{-4} to 20 Hz.

Superposition time-temperature

The variations of the complex viscosity η^* as a function of frequency at the various temperatures of measurement can be shown in the form of some master curves.

In fact, Marin⁷ and Labaig⁸ have shown that the analytical expression of complex viscosity can be written in the form:

$$\eta = \eta_0 z(\omega\tau_0, h) \quad (1)$$

where z is a complex function such that $z(0, h) = 1$; h is a parameter independent of time and temperature, but possibly dependent on the nature of the polymer; η_0 is the zero-shear viscosity such that $\eta_0 = \lim_{\omega \rightarrow 0} \eta^*$; and τ_0 is a terminal relaxation time as defined by $\tau_0 = 1/\omega_m$, ω_m being the pulsation corresponding to the maximum of η'' .

Therefore, for the fractions of polystyrene, the parameter h will be the same and the use of the reduced variables η/η_0 and $\omega\tau_0$ will permit the superposition of the curves relating to various temperatures.

Figure 1 shows that the thermal variations of η_0 and τ_0 follow a Vogel-type law:

$$\log \eta_0 = a_1 + \frac{b}{T - T_\infty}$$

$$\log \tau_0 = a_2 + \frac{b}{T - T_\infty}$$

where $b = 715^\circ\text{C}$ is independent of M_w , and $T_\infty = 50^\circ\text{C}$ ⁹.

If we want to bring back the variations of the reduced complex viscosity η^*/η_0 from the measuring temperature T to a reference temperature T_0 , the measuring pulsation ω_T will have to be assorted with a shift factor $a_T = (\tau_{0T}/\tau_{0T_0})$.

By using the law of thermal variation of τ_0 , it can be shown that:

$$\begin{aligned} \log a_T &= \log \tau_{0T} - \log \tau_{0T_0} \\ &= b \cdot \frac{T_0 - T}{(T - T_\infty)(T_0 - T_\infty)} \end{aligned}$$

The WLF equation is actually confirmed if we put

$$c_1^0 = -\frac{b}{T_0 - T_\infty}$$

Thus, if the reference temperature is $T_0 = 186^\circ\text{C}$, the shift factors a_T are determined by $\log a_{176} = 0.42$; $\log a_{166} = 0.91$ and $\log a_{156} = 1.49$. All the master curves are obtained using these values.

The vertical shift factor b_T will be such that $b_T = \eta_{0T_0}/\eta_{0T}$. Now, the laws of thermal variation of η_0 and τ_0 show that, in the temperature range studied:

$$\frac{\eta_{0T_0}}{\eta_{0T}} = \frac{\tau_{0T_0}}{\tau_{0T}}$$

Thus,

$$b_T = \frac{1}{a_T}$$

We notice that the same shift factors can be applied to the fraction and to their binary blends.

RESULTS AND DISCUSSION

Effect of weight ratio

Figure 2a shows the development of the curves in the complex plane, representing the points with the affix η^*/η_0 .

For the pure components (PS 11 and PS 40), the curves can be assimilated to arcs of circles, where the centre is located below the x -axis¹⁰. The location of the centre is the same for all three fractions studied.

For the binary blends of PS 11 and PS 40, the curves reveal two fields. The field corresponding to the lower frequencies increases as the weight fraction ϕ of the component with the highest molecular weight increases, while the field corresponding to the higher frequencies decreases. The coupling between both fields is sufficiently important to ensure that whatever the pulsation ω and the weight fraction ϕ may be, the curve does not present a minimum separating both fields.

This notion of coupling between the contributions of each component to the properties of the blend is also noticeable in Figure 2b, which shows the variations of the imaginary part η''/η_0 of the reduced complex viscosity.

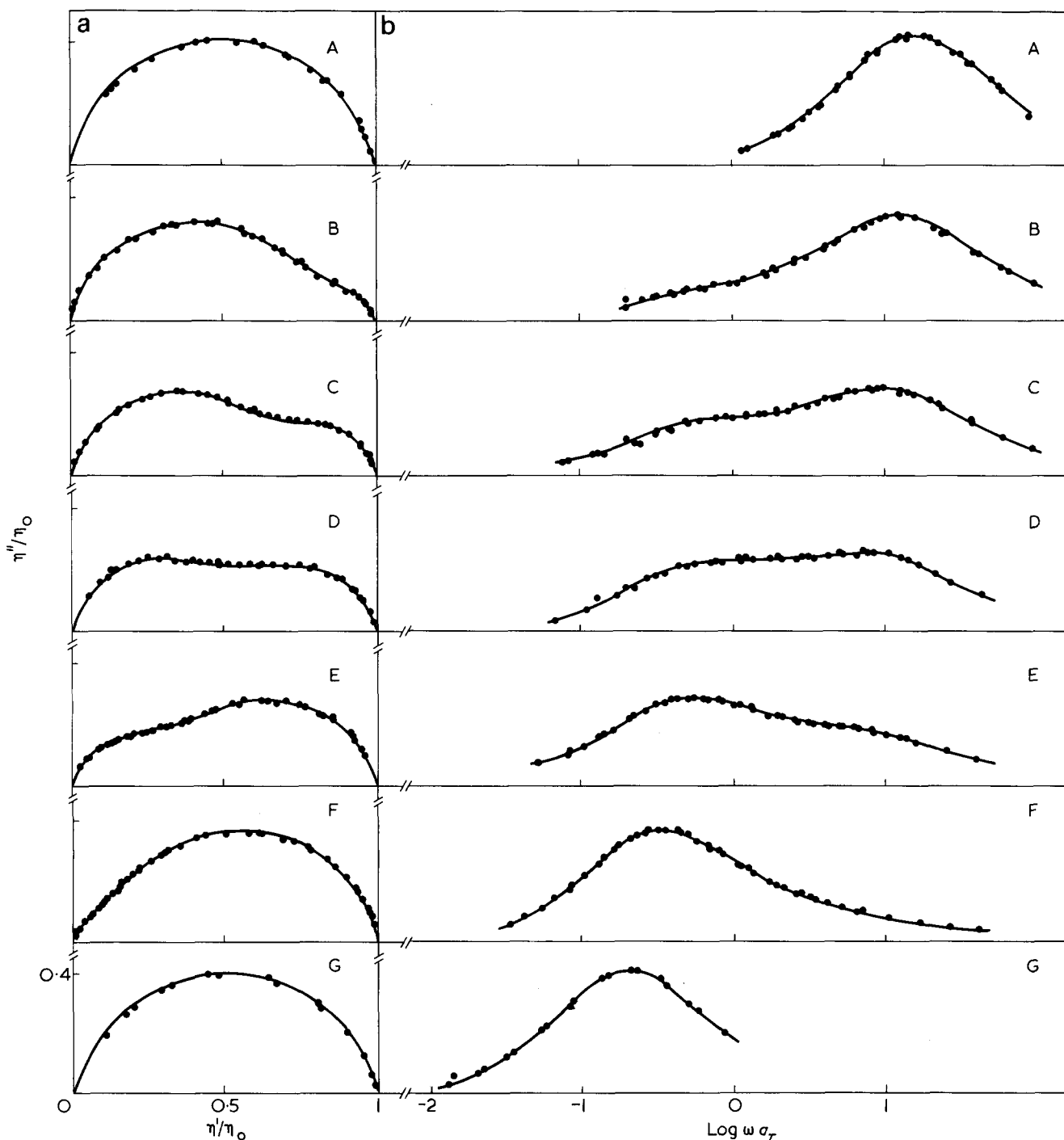


Figure 2 (a) Master curves of reduced complex viscosity and (b) reduced imaginary part for binary blends of PS 11 and PS 40 with values of ϕ : A, 0; B, 0.5; C, 0.10; D, 0.15; E, 0.25; F, 0.50; G, 1.00. ($T_0 = 186^\circ\text{C}$)

As ϕ increases, we can observe: for $\phi = 0$, a maximum at the higher frequencies; for $0 < \phi < 1$, the high frequency maximum decreases and shifts towards the lower frequencies, at the same time as a second maximum appears which increases and also shift towards the lower frequencies; or for $\phi = 1$, a maximum at the lower frequencies.

The development of the curves corresponding to the blend M 112030 (Figure 3) shows that the coupling is all the closer as the weight ratio—hence the ratio of the zero-shear viscosities and of the terminal relaxation times τ_0 —of both components is lower.

The variations of the real part η'/η_0 as a function of ϕ

show a gradual distortion of the curves as well as a shift of all points together towards the lower frequencies (Figure 4).

It should be noted that for blends, it is impossible to determine a relaxation time τ_0 having the same definition as that of fractions. In fact, τ_0 has been defined as the inverse of the pulsation ω_m corresponding to the maximum of η'' . It can be determined accurately when the curve can be assimilated to the arc of a circle^{7,8}. However, for the blends studied, the complex viscosity cannot be represented by the arc of a circle and, if the weights of the components are sufficiently distant, the distribution of ter-

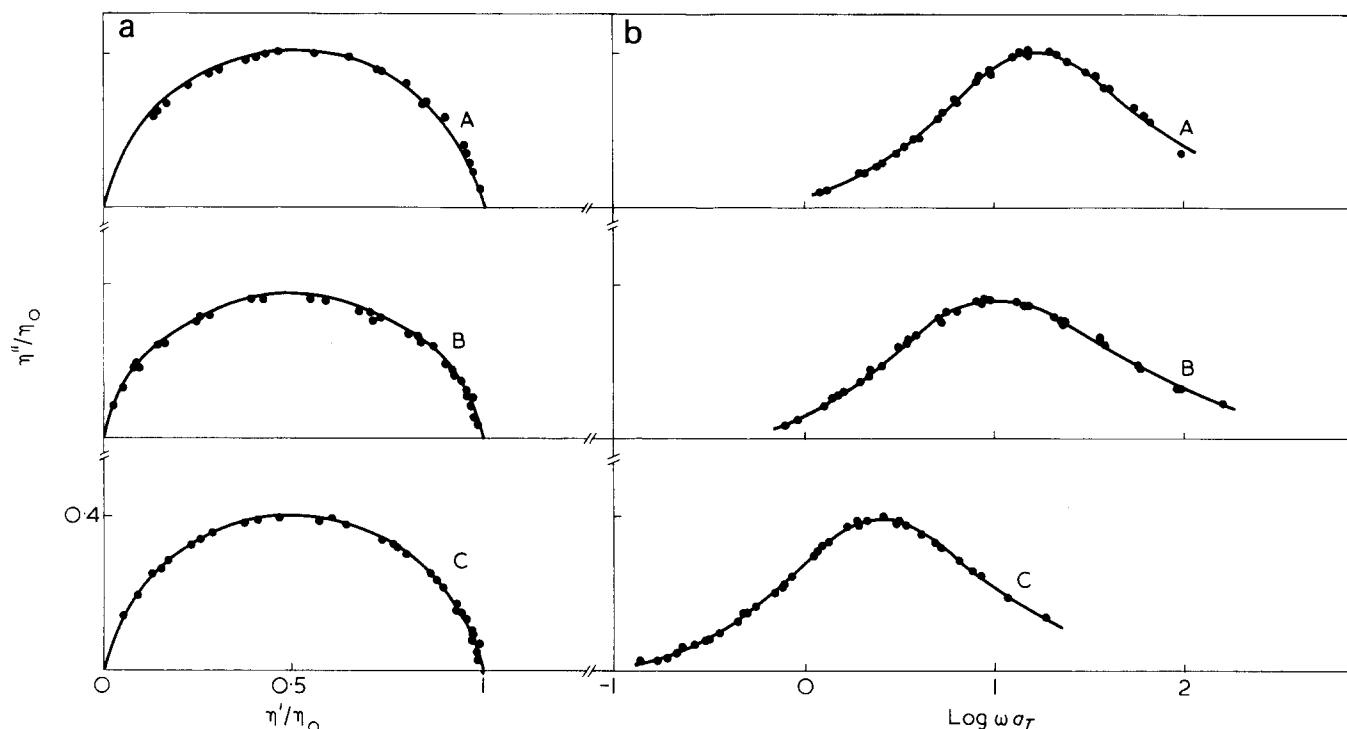


Figure 3 (a) Master curves of reduced complex viscosity and (b) reduced imaginary part for: A, PS 11; B, M 112030; C, PS 20; reduced to 186°C

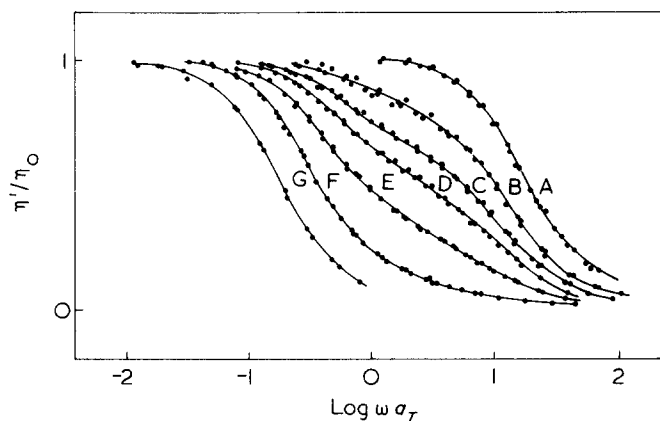


Figure 4 Master curves of reduced dynamic viscosity for the same samples as Figure 2

minimal relaxation time is a bimodal one, and a more probable relaxation time cannot be defined.

Effect of temperature and molecular weight

Figure 5 shows that the variations of η_0 as a function of temperature are the same for the pure fractions and their binary blends. This is connected with the fact that the vertical shift factor b_T is the same for the fractions and their blends. The same applies for the variations of η_0 as a function of the weight-average molecular weight M_w . The molecular weight M_w of the blends is calculated by means of the following equation:

$$M_w = (1 - \phi)M_1 + \phi M_2 \quad (2)$$

since each component presents a polydispersity very close to 1.

In equation (2), ϕ and M_2 represent the weight fraction and the molecular weight of the component with the highest weight, respectively and M_1 represents the molecular weight of the component with the lower weight.

The points relating to the blends are precisely located on the line of the points relating to the fractions (Figure 5). Therefore, the zero-shear viscosity η_{0b} of the blends obeys the law:

$$\eta_{0b} = kM_w^{3.4} \quad (3)$$

where k depends on temperature.

Thus, we notice that, as has been shown by Friedman and Porter¹¹, viscosity depends only upon the weight-average molecular weight and no other moment.

So the variations of a zero-shear viscosity of the fractions of linear atactic polystyrene and of their binary blends in the molten state, with a molecular weight higher than M_c can be represented by the expression:

$$\log \eta_0 = 3.4 \log M_w + \frac{715}{T - T_\infty} - 17.73 \quad (4)$$

The blending law on zero-shear viscosity can be easily inferred from relations (1) and (2) in the form:

$$\eta_{0b} = [(1 - \phi)\eta_{01}^{1/3.4} + \phi\eta_{02}^{1/3.4}]^{3.4} \quad (5)$$

An extension of this blending law to the complex viscosity of the blend may be contemplated in the general form:

$$\eta_{0b} = [(1 - \phi)\eta_{01}^{1/3.4} f_1(z_1, z_2, z_b) + \phi\eta_{02}^{1/3.4} f_2(z_1, z_2, z_b)]^{3.4} \quad (6)$$

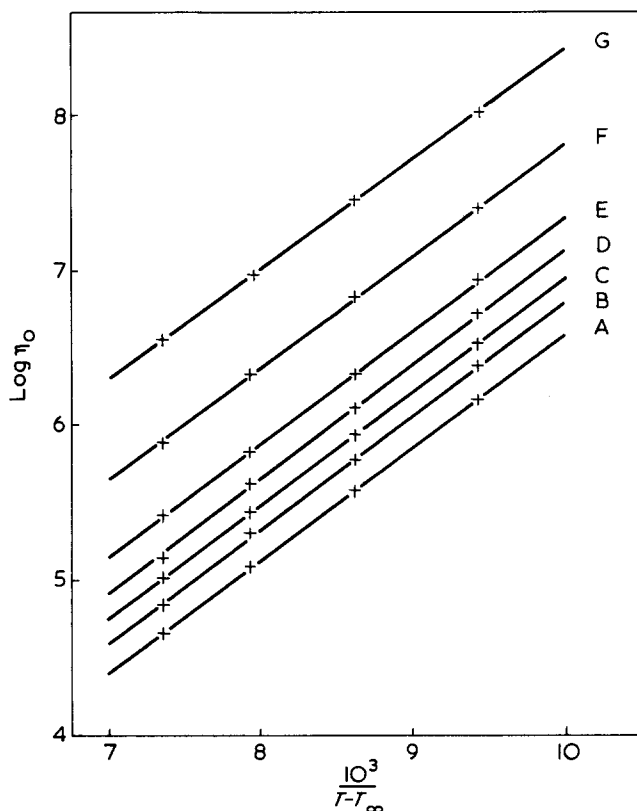


Figure 5 Temperature dependence of zero-shear viscosity for the same samples as Figures 2 and 4

where z_1 , z_2 and z_b are the reduced complex viscosities of the components 1 and 2 and the blend, respectively as defined in relation (1); f_1 and f_2 are two functions of z_1 , z_2 and z_b such that they obey the following relations:

$$\lim_{\omega \rightarrow 0} f_i = 1$$

$$f_1(z_1, z_2) = f_2(z_2, z_1)$$

Thus, relation (6) is compatible with relation (5), in that it obeys the principle of superposition time-temperature and takes into account the symmetric part of the two components.

CONCLUSIONS

We have shown that the binary blends of narrow molecular weight distribution of linear atactic polystyrene with a molecular weight higher than the critical weight M_c , in the molten state, presented an interesting rheological behaviour in the terminal zone when the variations of the complex viscosity were examined.

We have observed that, in the complex plane, the arc of a circle characteristic of the pure fractions, became distorted when these were blended and that the contribution of each component to the blend could be identified. The coupling between the two corresponding fields becomes closer as the molecular weights of the elements are nearer.

The identification of all parameters conditioning this coupling and particularly the expression of the functions f_1 and f_2 in relation (6) could provide a better knowledge of the nature of entanglements between molecular chains and of the effect of the polydispersity affecting the viscoelastic properties in the plateau and terminal zones.

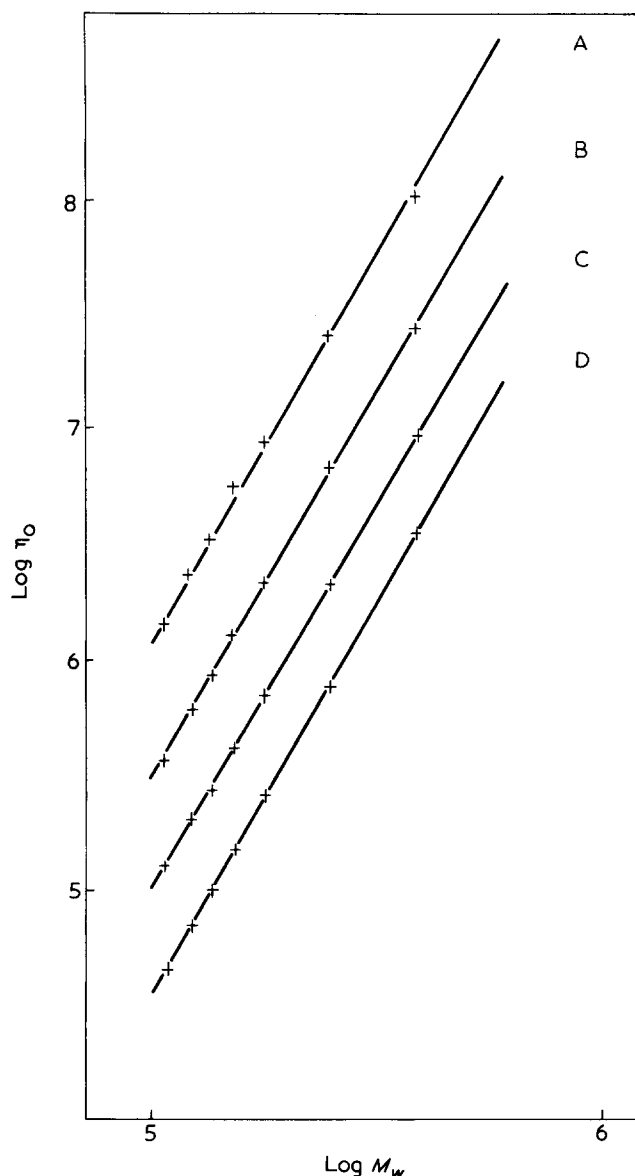


Figure 6 Zero-shear viscosity plotted logarithmically against the molecular weight at four temperatures: A, 156°; B, 166°; C, 176°; D, 186°C

ACKNOWLEDGEMENT

Financial support for the present work was provided by the Société Nationale des Pétroles d'Aquitaine. The support is gratefully acknowledged.

REFERENCES

- 1 Onogi, S., Masuda, T., Toda, N. and Koga, K. *Polym. J.* 1970, 1, 542
- 2 Prest, Jr, W. M. *Polym. J.* 1973, 4, 163
- 3 Murakami, K., Ono, K., Shiina, K., Ueno, T. and Matsuo, M. *Polym. J.* 1971, 2, 698
- 4 Masuda, T., Kitagawa, K., Inoue, T. and Onogi, S. *Macromolecules* 1970, 3, 116
- 5 Ninomiya, K., Ferry, J. D. and Oyanagi, Y. *J. Phys. Chem.* 1963, 67, 2297
- 6 Horio, M., Fujii, T. and Onogi, S. *J. Phys. Chem.* 1964, 68, 778
- 7 Marin, G. *Thesis Université de Pau* (1975)
- 8 Labaig, J. J. *Thesis Université de Pau* (1973)
- 9 Pierson, J. F. *Thesis Université de Strasbourg* (1968)
- 10 Marin, G., Labaig, J. J. and Monge, P. *Polymer* 1975, 16, 223
- 11 Friedman, E. M. and Porter, R. S. *Trans. Soc. Rheol.* 1975, 19, 493

X-ray studies of surface melting in single crystals of linear polyethylene

K. Suehiro*, H. Tanizaki and M. Takayanagi

Department of Applied Chemistry, Faculty of Engineering, Kyushu University, Fukuoka 812, Japan
(Received 8 December 1975; revised 5 July 1976)

X-ray diffraction by annealed single crystal mats of linear polyethylene was studied as a function of temperature. The intensity of small-angle scattering changed reversibly with temperature, but the long-period remained constant. The crystal thickness along the molecular chain, which was evaluated from the line width of the wide-angle 002 reflection, began to decrease in the vicinity of 60°C. The change in the intensity of the 002 reflection also indicated the decrease in the number of crystal lattices. From these facts surface melting of the crystal was inferred.

INTRODUCTION

Variation of small-angle X-ray scattering intensity above room temperature has been studied for many polymers such as polyethylene¹⁻⁶, polypropylene², nylon-6^{2,8}, polyoxymethylene^{8,9}, and others^{7,8}. According to these investigations, the intensity of the small-angle X-ray scattering changes reversibly with temperature so long as the measuring temperature does not exceed the crystallization or annealing temperature. In addition, the long-period varies reversibly in bulk and oriented polymers^{2,7,8}, but such a phenomenon has not been observed in the case of single crystals except for branched polyethylene⁵. The reversible change of the intensities has been interpreted mainly by a concept of reversible change in the ratio of the crystalline and amorphous regions due to the surface melting of the crystal.

In this paper the temperature dependence of wide-angle as well as small-angle X-ray scattering was investigated over a range of temperatures from room temperature to the melting point for annealed single crystal mats of linear polyethylene to obtain further evidence of the surface melting of the crystal lamellae.

EXPERIMENTAL

Sample preparation

The sample used in this study was a commercial grade high density linear polyethylene, Hizex 1200J, provided by Mitsui Petro-Chemical Industries Co. Ltd with a viscosity-average molecular weight (\bar{M}_v) of 30 800 and a degree of branching of 2 CH₃/1000 CH₂.

Single crystals were prepared by the following method. A hot concentrated xylene solution of polyethylene was gradually dropped into xylene, which was kept at the crystallization temperature of 80°C, to obtain finally a 0.05% solution. The solution was maintained at 80°C for more than 24 h. The precipitated single crystals were then filtered and formed into oriented mats with thickness of 0.2 mm. After drying they were annealed at 125°C for 24 h *in vacuo*.

Measurements

X-ray diffraction diagrams were obtained with Ni-filtered CuK α radiation using a counter technique. The small-angle X-ray scattering was measured over the temperature range 16°–120°C. The specimen was heated in a Rigaku–Denki hot stage. The diffraction profile from the (002) plane was measured by the reflection method using a diffractometer.

The infra-red absorption spectra were also taken in order to estimate crystallinity by using a Japan Spectroscopic Company heating cell at various temperatures from room temperature to 120°C.

Data analysis

If the single crystal mat consists of alternating crystalline and amorphous layers with no intermediate transition regions, the peak intensity of the n th order small-angle X-ray scattering is given by¹²:

$$I_n = K(\Delta\rho)^2 \sin^2(\pi nd/L) / (\pi n/L)^2 \quad (1)$$

where K is a constant, $\Delta\rho$ is the electron density difference between two layers, d is the thickness of the amorphous layer and L is the long-period. Providing that the amorphous regions are mainly located adjacent to the lamellar surfaces and those not are considered negligible, d/L may be substituted for χ , because the crystalline and amorphous regions are interchangeable as far as X-ray diffraction is concerned. Equation (1) can be written thus:

$$I_n = K(\Delta\rho)^2 \sin^2(\pi n\chi) / (\pi n/L)^2 \quad (2)$$

When the long-period does not change with temperature, the following relation can be derived from equation (2):

$$\frac{I_2(T)}{I_2(T_0)} \bigg/ \frac{I_1(T)}{I_1(T_0)} = \frac{\cos^2\pi\chi(T)}{\cos^2\pi\chi(T_0)} \quad (3)$$

where T_0 represents a standard temperature. Therefore, if $\chi(T_0)$ is known, the crystallinity at a temperature T can be evaluated⁴.

The long-periods were calculated directly applying Bragg's law to the position of the maximum intensity of the first order small-angle scattering.

The sizes of the crystalline layers along the molecular

* Present address: Department of Industrial Chemistry, Faculty of Science and Engineering, Saga University, Saga 840, Japan.

chain axis, D_{001} , were estimated from the integral line width of the 002 reflection by use of Scherrer's formula:

$$D_{001} = K\lambda/(\beta \cos \theta) \quad (4)$$

where λ is the wavelength; β is the true line width corrected for broadening due to the instrument and the $K\alpha_1$ and $K\alpha_2$ radiations; θ is the Bragg angle for the 002 reflection. The shape factor K was taken as equal to unity. The method of correction for spectral broadening was principally based on the Jones procedure¹¹. Quartz powder was used as an instrumental standard. A diffraction diagram of the 002 reflection of polyethylene is shown in Figure 1. The foot of the peak is superimposed on the 231, 511, and 112 reflections. This effect was subtracted for convenience by a straight line which was in contact with reflection curve at $\sim 73^\circ$ and 76° in 2θ . As the diffraction line profiles of polyethylene and quartz were nearer to a Gaussian rather than a Cauchy distribution, the Gaussian profile was assumed for both line shape. The true line width β is given by¹⁴:

$$\beta = (B^2 - b^2)^{1/2} \quad (5)$$

where B and b are the line widths of the specimen and quartz corrected for the spectral broadening, respectively.

The crystallinity was also determined from infra-red absorption spectra. One crystalline band, 1894 cm^{-1} , and two amorphous bands, 1352 and 1368 cm^{-1} , were used according to the method proposed by Okada and Mandelkern¹⁰ to evaluate the crystallinity of a thick polyethylene sample.

RESULTS AND DISCUSSION

The relative intensities of the first and second order peaks of the small-angle X-ray scattering are plotted against measuring temperatures in Figure 2. Both intensities increased with increasing temperature, but the degree of change in the second order scattering was less than that in the first. They decreased reversibly to their initial values on cooling from a maximum temperature of 117.5°C which did not exceed the annealing temperature of the specimen.

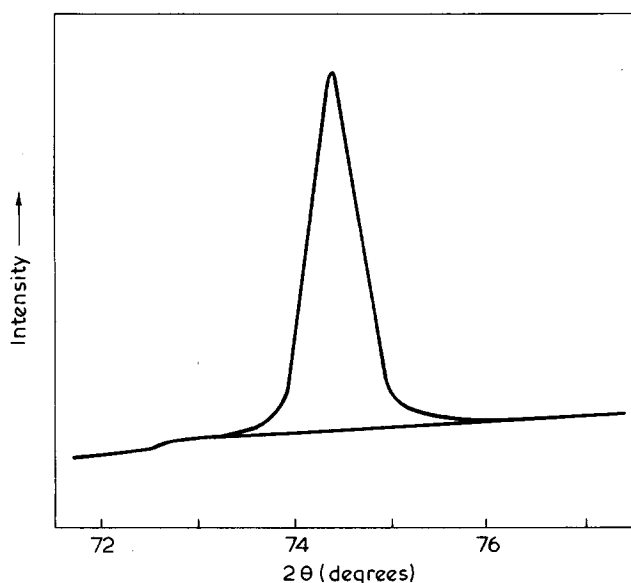


Figure 1 Diagram of the 002 reflection of polyethylene. Region below the straight line represents background

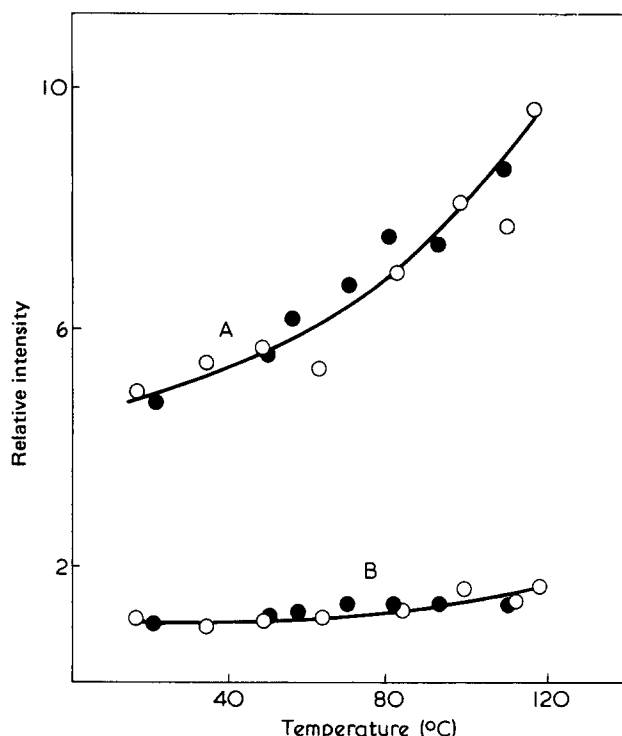


Figure 2 Variation in the peak intensities of A, the first (I_1) and B, second (I_2) order small-angle X-ray scattering with temperature: \circ , heating; \bullet , cooling

According to equation (2), the scattering intensities depend upon the density difference between the crystalline and amorphous layers and upon the volume crystallinity. The ratio of $I_1(117.5)$ to $I_1(16)$ was as large as 1.99. On the other hand, $[\Delta\rho(117.5)/\Delta\rho(16)]^2$ was found to be 1.48 by using the specific volumes of the crystalline (\bar{v}_c) and amorphous (\bar{v}_a) polyethylene, which were determined by Richardson *et al.*¹³:

$$\bar{v}_c = 0.993 + 3.0 \times 10^{-4}T$$

$$\bar{v}_a = 1.152 + 8.8 \times 10^{-4}T$$

where $T(^{\circ}\text{C})$ is the temperature. Therefore, as indicated first by Nukushina *et al.*¹, the increase of the scattering intensities can not be explained by the increase of the electron density difference alone, but is also concerned with the change in the crystallinity.

The volume crystallinity determined from density at 16°C was 0.792. By substituting this value into equation (3) as $\chi(T_0)$, the volume crystallinities at other temperatures were calculated. The results are shown in Figure 3 together with those evaluated by the infra-red method. They were in good agreement with each other. As a matter of course, these crystallinities decreased with increasing temperature. Long-period, L , was nearly constant at 418 \AA throughout a heating and cooling cycle as shown in Figure 4, although reversible changes of long-period with temperature have been observed for many bulk polymers^{2,7,8} and single crystal mats of branched polyethylene⁵. The constancy of the long-period and the decrease of the crystallinities indicate that the thickness of the amorphous layers increased. Indeed, the crystalline size along the molecular chain, D_{001} , changed reversibly with temperature decreasing gradually, increasing as the temperature was raised. The values of the ratio D_{001}/L are markedly lower

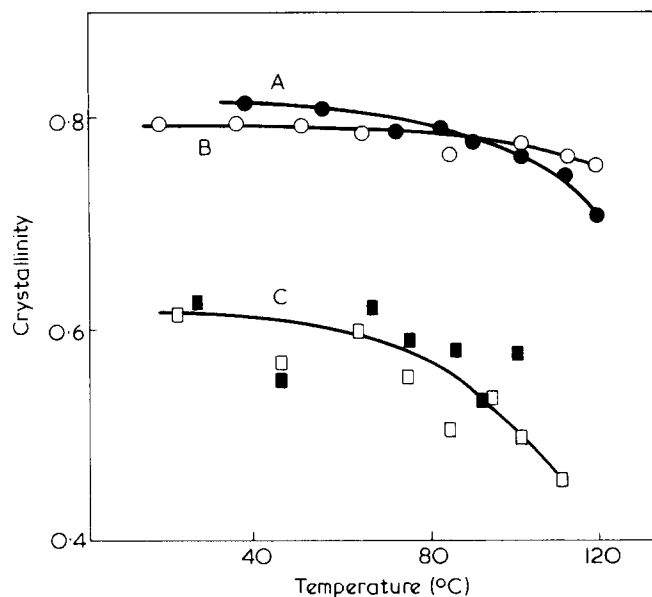


Figure 3 Crystallinities determined by A, infra-red (i.r.); B, small-angle X-ray scattering (SAXS), and C, D_{001}/L vs. temperature: □, heating; ■, cooling

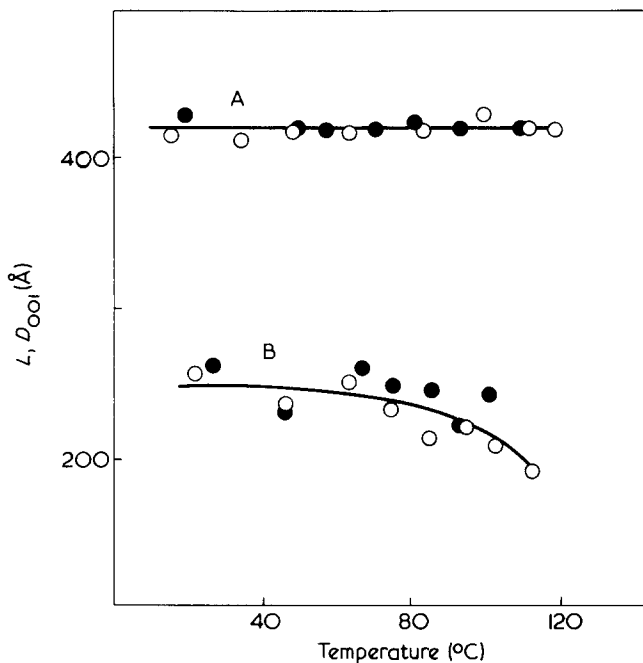


Figure 4 Temperature dependence of A, the long-period (L) and B, the crystal thickness (D_{001}) in the direction of the c -axis: ○, heating; ●, cooling

than those of SAXS and i.r. crystallinities. If any transition region of ~ 80 Å thick is assumed between the amorphous and crystalline layers which is regarded as crystalline by the infra-red and small-angle X-ray scattering measurements, those three sets of values agree fairly well.

Another reason for the discrepancy is the following. The line broadening is not corrected precisely, because the line profiles are not necessarily exactly Gaussian. Consequently, the values of D_{001} in Figure 4 may be apparent ones and the true values larger.

Furthermore, the intensity change of the 002 reflection was investigated to make sure the change of the crystallinity with temperature. The observed integrated intensities of the 002 reflection are plotted against the temperatures in Figure 5. Decrease in the intensity was observed

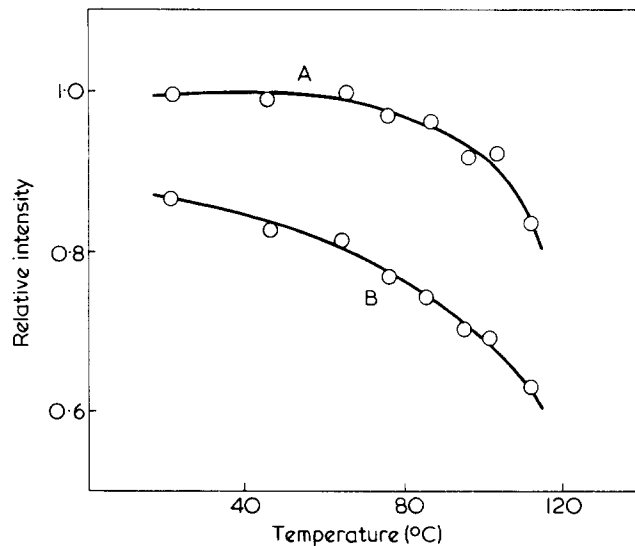


Figure 5 Relative intensity of 002 reflection vs. temperature. The corrected intensity is determined by multiplying the observed one by $[\exp 8\pi^2 U_{cc}(\sin\theta/\lambda)^2]^2$. A, Corrected; B, observed

from room temperature. Two factors may be considered as the cause: decrease in the number of crystal lattices and thermal vibration of the atoms in the crystal. The observed intensities were multiplied by $[\exp 8\pi^2 U_{cc}(\sin\theta/\lambda)^2]^2$ to eliminate the effect of the thermal vibration of the atoms. U_{cc} gives the amplitude of atomic displacement in the direction of c -axis and $8\pi^2 U_{cc}$ represents the temperature factor. The values determined by Iohara *et al.*¹⁵ were used for U_{cc} . The corrected intensities decreased markedly from the temperature in the vicinity of 60°C as shown in Figure 5. Premelting of the crystal seems to begin at this temperature.

Bergmann and Navotki separated broadline n.m.r. spectra of polyethylene samples into three components, i.e. narrow, intermediate, and broad, and they have proposed a three phase model for polyethylene¹⁶. The intermediate component is considered to originate from a boundary region where the crystal changes to the amorphous part. The molecular chains in the intermediate region must be more irregular than those in the crystal. According to the potential energy calculation of the fold conformation given by Oyama *et al.*¹⁷, the internal rotation angles of eight bonds succeeding to the fold part deviated somewhat from precise *trans* conformation. This region will correspond to the intermediate region suggested by Bergmann and Nawotki¹⁶. Intermolecular forces in the intermediate region especially with approach to the fold part are weaker than those in the crystal so that the chains in the intermediate region are relatively easy to move. On heating they will melt before those in the crystal. This fact results in the melting of the crystal from the lamellar surface to the interior.

REFERENCES

- 1 Nukushina, Y., Itoh, Y. and Fischer, E. W. *J. Polym. Sci. (B)* 1965, 3, 383
- 2 Zubov, Y. A. and Tsvankin, D. Y. *Vysokomol. Soedin* 1965, 7, 1848
- 3 Schultz, J. M., Robinson, W. H. and Pound, G. M. *J. Polym. Sci. (A-2)* 1967, 5, 511
- 4 Hara, T. and Seto, T. *Rep. Progr. Polym. Phys. Japan* 1969, 12, 189
- 5 Dawkins, J. V., Holdsworth, P. J. and Keller, A. *Makromol. Chem.* 1968, 118, 361

X-ray studies of surface melting in single crystals of linear polyethylene: K. Suehiro et al.

- | | | | |
|----|---|----|---|
| 6 | Kavesh, S. and Schultz, J. M. <i>J. Polym. Sci. (A-2)</i> 1971, 9 , 85 | 12 | Hosemann, R. and Baguchi, S. 'Direct Analysis of Diffraction by Matter', North Holland, Amsterdam, 1962 |
| 7 | Krigbaum, W. B., Balta, Y. I. and Via, G. H. <i>Polymer</i> 1966, 7 , 61 | 13 | Richardson, M. J., Flory, P. J. and Jackson, J. B. <i>Polymer</i> 1963, 4 , 221 |
| 8 | O'leary, K. and Geil, P. H. <i>J. Macromol. Sci. (B)</i> 1967, 1 , 147 | 14 | Warren, B. E. and Biscoe, J. <i>J. Am. Ceram. Soc.</i> 1938, 21 , 49 |
| 9 | Aoki, Y., Chiba, A. and Kaneko, M. <i>Rep. Prog. Polym. Phys. Japan</i> 1971, 14 , 279 | 15 | Iohara, K., Imada, K. and Takayanagi, M. <i>Polym. J.</i> 1972, 3 , 357 |
| 10 | Okada, T. and Mandelkern, L. <i>J. Polym. Sci. (A-2)</i> 1967, 5 , 239 | 16 | Bergmann, K. and Navotki, K. <i>Kolloid Z. Z. Polym.</i> 1967, 219 , 132 |
| 11 | Jones, F. W. <i>Proc. Roy. Soc. (A)</i> 1938, 166 , 16 | 17 | Oyama, T., Shiokawa, K. and Ishimaru, T. <i>J. Macromol. Sci. (B)</i> 1974, 8 , 229 |

Deformation mechanism of 'hard elastic polyethylene films'

Takeji Hashimoto, Kikuo Nagatoshi[†], Akira Todo[‡], and Hiromichi Kawai

Department of Polymer Chemistry, Faculty of Engineering, Kyoto University, Kyoto 606, Japan

(Received 23 February 1976)

Film specimens were prepared from extra-high molecular weight linear polyethylene (commercial grade, Sholex super 5551 H and 4551 H) as well as ordinary high and medium molecular weight polyethylenes (commercial grade, Hizex 7000 F and Sholex 4002) by using a calender manufacturing method, which involves the important processing problem of crystallization from a stressed polymer melt. The films crystallized from the extra-high molecular weight polyethylene, as compared with those crystallized from the lower molecular weight polyethylene, underwent a large elastic deformation on stretching along the machine direction, characteristic of the specific morphology of the so-called 'row structure' or 'hard elastic structure'. Deformation mechanism of the submicroscopic crystalline superstructure of the hard elastic films was investigated by means of small- and wide-angle X-ray scattering and diffraction, as well as electron microscopy.

INTRODUCTION

There have been many reports on the morphology and crystallization of polyethylene crystallized from stressed polymer melts and solutions. Pennings *et al.* crystallized polyethylene from stirred polyethylene solutions¹⁻³. Andrews *et al.*^{4,5} crystallized polyethylene after cooling stretched crosslinked polymer melts below their melting points. The crystallization was also achieved by applying shear stress to the polymer melts in between two plates followed by cooling below their melting points^{2,6}, and by applying tubular extrusion (blown film)^{2,7} or injection moulding to the polymer melts.

Polyethylene crystallized from stirred solutions produces the row-nucleated shish-kebab structures which contain irregular lamellar platelets held together by a central fibre. The shear stress produces the fibre acting as row nuclei on which lamellar overgrowth occurs to result in the formation of the usual lamellar crystal.

Crystallization from a stressed melt similarly produces stacks of oriented lamellae, their plane normals being parallel to the machine direction⁴⁻⁹. In order to explain the particular morphology, Keller and Machin demonstrated the row structure²; nucleation occurred from 'rows' of nucleating points, and as with crystallization from stirred solutions, growth was restricted only to the plane perpendicular to the row of nucleating points. The row nuclei were considered to be fibres formed as a result of the shear stress. Characteristics of row structure such as number of row nucleating lines, crystal and lamellar orientations were also shown to be a function of shear stress²; e.g. crystal *a*- and *c*-axes preferentially orient along the machine direction when the films are crystallized under low and high shear stresses, respectively.

On the other hand, Kobayashi¹⁰ suggested that the stacking of oriented lamellae in the machine direction results from numerous spiral growths of lamellae. The angle between the axes of the spiral and the machine direction, which varies with film preparation conditions affects crystal orientations with respect to the machine direction. Drawing the films along the machine direction has been shown to result in a pulling apart of the spiral growths in a fashion similar to that which occurs when a helical spring is stretched.

It has been found, recently, that several polymers form, under specific conditions of crystallization, highly crystalline fibres or films which exhibit markedly elastic behaviour, the so-called 'hard elastic' property, i.e. a high degree of length recovery from large extensions and additional unusual properties such as a marked reduction of apparent density, and generation of very large amounts of internal volume and surface area on stretching along the machine direction^{9,11-16}. These polymers are polypropylene, poly(3-methylbutene-1) and some of its 1-olefin copolymers, and acetal copolymer, Celcon, in particular specimens of nylon-6, nylon-6,6, polyethylene, poly(4-methylpentene-1), and poly(ethylene sulphide). The elastic nature of these polymers results from a specific morphology produced by crystallization from sheared polymer melts, i.e. the stacks of oriented lamellae, their normals being parallel to the machine directions.

It is not fully understood what the criteria are in terms of morphology or crystallization conditions for a given polymer leading to such unusual long range elasticity. The morphological studies on the 'hard elastic' fibres or films, however, indicated that the tilting and splaying apart of the lamellar network result in creating the void and surface area on stretching and that the bending of lamellae between the links in a manner analogous to a leaf spring¹¹ is related to the long range elasticity which is non-rubber-like, i.e. energetic but not entropic in origin^{9,11,14}.

In this work we adopted a calender manufacturing method to prepare high density polyethylene films as a method of crystallization from stressed melts. The method is efficient especially in moulding extra-high molecular

* Published in part in *Rep. Prog. Polym. Phys. Japan*, 1974, 17, 285

† On leave from present address: the Central Research Laboratory, Idemitsu Kosan Co. Ltd, Sodegaura-cho, Kimitsu-gun, Chiba-ken, Japan.

‡ On leave from the Research Center, Mitsui Petrochemical Industries, Ltd, Waki-cho, Kuga-gun, Yamaguchi-ken, Japan.

Table 1

Specimen code	Sample grade	Melt index	Molecular weight ($\times 10^{-4}$)		Moulding condition			
			\bar{M}_w^e	\bar{M}_v^f	Temp. ($^{\circ}\text{C}$) ^g	Take-up/extruded velocities (m/min)	Film density ^h (g/cm ³)	Film crystallinity ⁱ (%)
HMW1-L	Sholex super				145–130	6/5	0.950	66.0
HMW1-H	5551H ^a	5.0 ^c	34.9	—	170–150	6/5	0.951	66.6
HMW2-H1	Sholex Super				170–150	8/4	0.941	60.1
HMW2-H2	4551H ^a	5.0 ^c	29.1	28.4	170–150	6/5	0.940	59.5
HMW2-L					145–130	6/5	0.940	59.5
MMW-H	Hizex 7000F ^b	0.04 ^d	23.5	27.9	170–150	6/5	0.948	64.9
LMW-L	Sholex 4002 ^a	0.20 ^d	19.9	14.1	145–130	6/5	0.941	60.2

^aSupplied by Japan Olefin Chemical Ind. Ltd, prepared by the Philips method. ^bSupplied from Mitsui Petrochemical Ind. Ltd; prepared by the Ziegler method. ^cMeasured at 190°C and 21.6 kg. ^dMeasured at 190°C and 2.16 kg. ^eWeight-average molecular weights are measured by light scattering measurements using α -chloronaphthalene as a solvent at 125°C. ^fViscosity-average molecular weights are measured by using decalin as solvent at 135°C and by using a relationship $[\eta] = 6.80 \times 10^{-4} \times M_v^{0.67}$ (Chiang, R. J. *Polym. Sci.* 1959, 36, 91). ^g145–130 designates that temperatures of the first to third drums are 145°C and that of the fourth drum is 130°C (see Figure 1). ^hMeasured in methanol–water system at 25°C by using density gradient tube. ⁱVolume-average crystallinity calculated by assuming densities of crystal and amorphous being 1.000 and 0.852 g/cm³, respectively

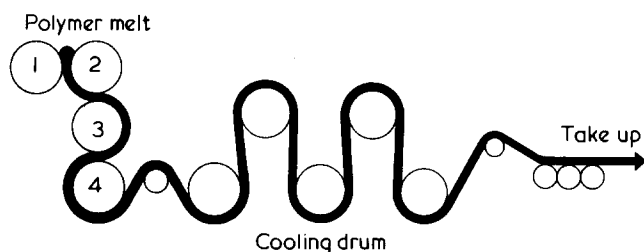


Figure 1 A schematic diagram of calender moulding process

weight polyethylene compared with conventional blowing (tubular extrusion) technique. Under a given film preparing condition, the films crystallized from the extra-high molecular weight polyethylenes showed crystal *c*-axis preferentially oriented along the machine direction (*MD*) and exhibited unusually long range elasticity (hard elastic property) of the type described above, whereas those crystallized from polyethylenes having conventional molecular weights showed crystal *a*-axis preferentially oriented along the *MD* and exhibited usual mechanical properties accompanied by necking and low degree of length recovery from large extensions. In order to understand this phenomenon, we investigated the crystalline superstructure of these films in submicroscopic scales by using various techniques such as wide-angle X-ray diffraction, small-angle X-ray scattering, and electron microscopy.

TEST SPECIMENS

Four kinds of linear polyethylenes were calendered under different conditions as shown in Table 1. Series of HMW1 and HMW2 specimens have extra-high molecular weights, while those of MMW and LMW have ordinary molecular weights. Polyethylene pellets were fed into a bumbury mixer where the pellets were melted for about 4 min. The melt, with a temperature $\sim 150^{\circ}$ to 170°C at the exit of the mixer was fed into a mixing roll controlled at 150°C . The melt was then calendered into sheets as schematically shown in Figure 1. Temperatures of the first to the fourth rolls were controlled as in Table 1, while those of the other rolls were at ambient temperature.

The friction ratios of the rolls were set so that the ratio of surface velocities of the first to the fourth rolls were 1:1.25:1.30:1.32. The surface velocity of the fourth roll

was set 5 m/min, and the films were taken up at velocity of 6 m/min. Under this condition, the whitening of the specimens due to crystallization was visible immediately after the fourth roll. The ratio of the surface velocities of the first to the fourth rolls as well as the velocities themselves are important factors which decide the shear rate of the melt.

EXPERIMENTAL

Stress–strain behaviour was measured at 20°C and at a rate of 100% elongation/min with a tensile tester, Shimadzu autograph type IM 100.

Wide-angle X-ray diffraction (WAXD) patterns were obtained at 40 kV and 20 mA, using nickel filtered $\text{CuK}\alpha$ radiation. Small-angle X-ray scattering (SAXS) patterns were obtained with nickel filtered $\text{CuK}\alpha$ radiation at 50 kV and 100 mA using a Rotaflex RU-100 PL (Rigaku–Denki) and with a point focusing system under the following collimating conditions: distances of the second pinhole, specimen and photographic films are 250, 310 and 610 mm from the first pinhole, respectively, and the size of the first and second pinholes are 0.5 and 0.2 mm in diameter, respectively.

The SAXS patterns were recorded from three directions: 'end' patterns taken with the incident X-ray beam parallel to the *MD* (machine direction); 'through' patterns with the beam normal to the film surface, and 'edge' patterns with the beam normal to the *MD* but parallel to the film surface. The end scattering was very weak and usually required a long exposure time (~ 10 h), six to seven times longer than the through and edge scattering patterns under equivalent conditions. Since the film specimen is thin, about 100 to 200 μm , the patterns were taken after stacking the specimens to an appropriate thickness (about 1 mm). In the edge and end patterns, the incident radiation is nearly parallel to the film surfaces. This situation often produces a sharp streak-like scattering in a direction parallel to the film normal due to total reflection of the X-rays at sample–air interfaces as pointed out by Hashimoto *et al.*¹⁷. In order to reduce the extra scattering arising from the reflection, the stack of specimens were immersed in liquid paraffin which replaces sample–air interfaces by sample–liquid paraffin interfaces¹⁷.

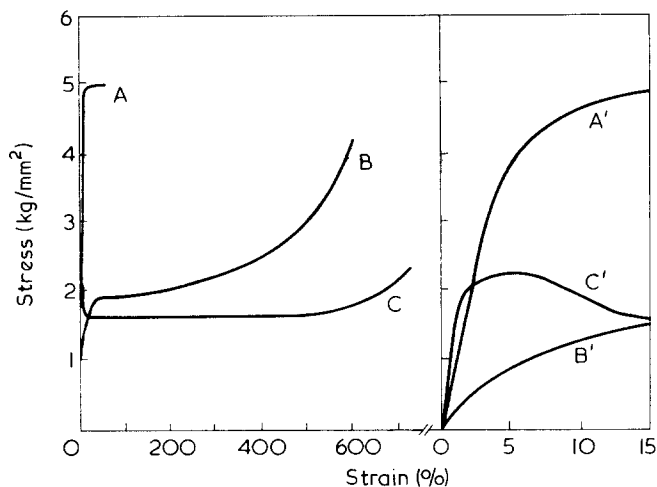


Figure 2 The stress-strain diagram of the HMW2-L specimens. A, A', 0°; B, B', 45°; C, C', 90°

The SAXS intensity distributions were measured along the meridional direction, i.e. a direction parallel to the machine direction (*MD*) with line focusing under the following collimating system: the second slit, the third slit, the specimen and the receiving slit were placed at 250, 290, 310, and 610 mm from the first slit, respectively, and the sizes of the first, second, solar, and receiving slits were 0.1×10 , 0.05×10 , 0.1×15 , and 0.05×15 mm², respectively. The length direction of the slit was set normal to the *MD*, i.e. parallel to the stack of lamellae. The intensity was measured with a scintillation counter and a Rigaku-Denki Rotaflex RU-100PL generator at 50 kV and 100 mA, and with nickel filtered ($21 \mu\text{m}$ thick) $\text{CuK}\alpha$ radiation and pulse height analyser.

The second order orientation factors of crystal *a*, *b* and *c* axes (f_a , f_b , and f_c , respectively) were evaluated by measuring the azimuthal angle dependence of integrated intensities under diffraction peaks corresponding to (110), (200), and (020) crystal planes. The intensity distributions were measured with a scintillation counter and a Rigaku-Denki Rotaflex RU-100PL at 50 kV and 100 mA. The intensity was measured with point focusing and with Ni-filtered $\text{CuK}\alpha$ radiation and pulse height analyser. The intensity was corrected according to the conventional method for air scattering, polarization factor and amorphous scattering.

RESULTS

Mechanical studies

Figures 2 and 3 demonstrate typical stress-strain behaviour of the extra-high molecular weight linear polyethylenes (HMW2-L) and polyethylenes having conventional molecular weights (LMW-L) specimens, respectively, where curves A, B and C in Figures 2 and 3 show the behaviour at small strain. The stress in the ordinate is the so-called nominal stress and is measured as a function of the angle between the *MD* and stretching direction. Under the same moulding conditions, HMW1 and HMW2 series show greater mechanical anisotropy than MMW and LMW polyethylenes in terms of Young's modulus, yield stress, ultimate strength, and ultimate elongation as is clearly seen by comparing Figures 2 and 3. The HMW1 and HMW2 series exhibit, in general, somewhat smaller ultimate elon-

gations at a given stretching direction than the MMW and LMW series. The yield strengths and ultimate strengths of the HMW1 and HMW2 are higher than those of the MMW and LMW series.

On stretching the HMW1 and HMW2 series along the *MD*, the film specimens start to whiten uniformly at $\sim 10\%$ elongation and the whitening is completed at $\sim 20\%$. On further stretching, the specimens exhibit no trace of macroscopic necking to result in a break at $\sim 75\%$. On releasing the tension, the whitening disappears almost completely unless the initial elongation is larger than 20% . At initial elongations greater than 20% , the whitening remains to some extent, although only a little. On the other hand, on stretching the MMW and LMW series, the film specimens exhibit a clear macroscopic necking where the whitening is localized.

Length recovery of the HMW1 and HMW2 series is extremely good compared with the MMW and LMW series. Figure 4 shows typical stress-strain behaviours under a cyclic tensile loading mode for the HMW1 and HMW2 series. The solid lines correspond to the specimens crystallized under calender moulding, while the broken lines correspond to the specimens crystallized from the isotropic melt.

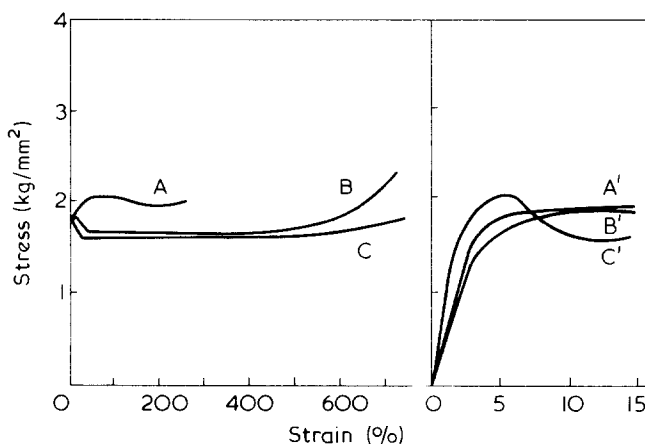


Figure 3 The stress-strain diagram of the LMW-L specimens. A, A', 0°; B, B', 45°; C, C', 90°

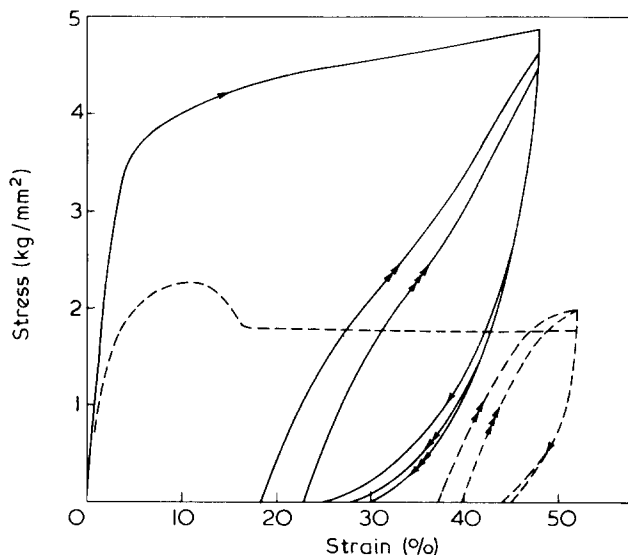


Figure 4 The stress-strain behaviours under cyclic tensile loading the specimens moulded by the calender method (—) and the specimens crystallized from isotropic melt of the same polymer grade (---). The elongation rate was 100%/min and measuring temperature was 25°C. The tensile loading is applied parallel to the machine direction

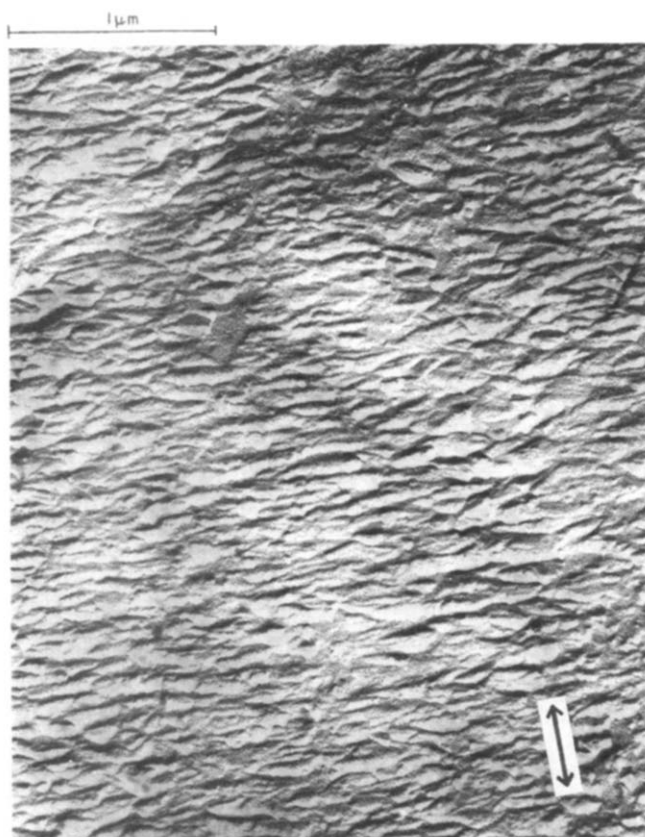


Figure 5 Typical electron micrograph of the HMW2 series. Surface replica. The arrow in the micrograph indicates the MD

The elongation rate and measuring temperature were 100% min. and 25°C, respectively. As is shown in the Figure the stress-strain behaviour of the calender films stretched parallel to the machine direction (MD) showed considerably large length recovery compared with the isotropic films. The stress-strain behaviour of MMW and LMW series along the MD are roughly similar to that of the isotropic films shown in Figure 4.

The unusual mechanical properties as observed in the HMW1 and HMW2 series are apparently similar to those found by Clark *et al.*^{9,11}, and Quynn *et al.*¹²⁻¹⁶ for 'hard elastic' films or fibres.

Morphology of as-prepared calender films

Electron microscopic studies. Figure 5 shows a typical electron micrograph of the free surface of the HMW1 and HMW2 series. As is typical for film crystallized from oriented melts, the stack of crystal lamellae are seen to highly orient with their normals parallel to the MD. The orientation of the lamellae corresponds to the two-point SAXS patterns (Figures 6 and 7) and a high degree of negative *b*-axis orientation (Figure 14) as will be discussed later. Therefore the surface structure is considered to be representative of the bulk. Some degree of lamellar twisting is shown in the micrograph, which is also important in explaining the observed degree of crystal *c*-axis orientation (Figure 14) and the preliminary results of dynamic birefringence (Figure 15). Similar but more distorted arrays of lamellae were observed on the electron micrographs of free surfaces of the MMW and LMW series.

X-ray studies. In Figures 6 and 7 are shown typical WAXD and SAXS patterns for HMW1 and HMW2 series and LMW and MMW series, respectively. In these Figures the through and edge patterns are identical, and the end

patterns are cylindrically symmetrical with respect to the incident beam axis. This indicates that orientation of both crystallites and lamellar crystals are uniaxially symmetric with respect to the MD in these specimens. The SAXS patterns for all these specimens show a typical two-point pattern, indicating that the crystalline texture is essentially the stacks of oriented lamellae, their normals being parallel to the MD. The WAXD and SAXS patterns of the other HMW1 and HMW2 series and those of the HMW-H specimens were almost identical to those of the HMW1-L and LMW-L specimens, respectively, so that their patterns are not included in this paper. The end patterns in SAXS patterns did not exhibit any appreciable distinct scattering maxima for all the specimens. This is probably because only a few lamellar edges are emerging parallel to the MD and/or lamellae having this type of orientation are stacked less regularly compared with those having their normals parallel to the MD.

The orientation of crystallites for the HMW1 and HMW2 series is, however, quite different from that for the MMW and LMW series. The former shows a preferential *c*-axis orientation along the MD, while the latter shows crystal *a*-axis orientation (Figures 6 and 7). The second order orientation factors of crystal *b*-axis, $f_b = (3\langle \cos^2 \theta_b \rangle_{av} - 1)/2$ (θ_b being the angle between the crystal *b*-axis and the MD), are close to -0.5 for all these specimens, indicating that the crystal *b*-axis orients almost perfectly normal to the MD. This is in accordance with a high degree of lamellar orientation with their normals being parallel to the MD and thus with the observed two-point SAXS patterns. The difference of the crystal *a*- or *c*-axis orientation may be therefore interpreted in terms of the difference in degree of rotation of crystal *a*- and *c*-axes around *b*-axis, i.e. a degree of lamellar twisting around its axis. For the HMW1 and HMW2 series the rotation of lamellae around their axes (i.e. *b*-axes) occurs less to give positive and negative *c*- and *a*-axis orientation, respectively, while for the MMW and LMW series it occurs much more than the HMW1 and HMW2 to give positive *c*- and *a*-axis orientations, although *a*-axis orientation factor is larger than *c*-axis orientation factor¹⁸.

Keller and Machin² demonstrated that the manner of lamellar orientation or degree of twisting of lamellae grown from the row nuclei depends upon shear stress in the melt: crystallization under high shear stress giving rise to the preferential *c*-axis orientation, while that under low shear stress gives rise to the preferential *a*-axis orientation.

According to the above result, the crystal orientation of the extra-high molecular weight HMW1 and HMW2 series is typical of that resulting from crystallization under high shear stress, while that of the MMW and LMW series is typical of that resulting from crystallization under low shear stress. This is quite reasonable because under a given manufacturing condition with a fixed temperature and shear rate, the higher molecular weight series are subjected to a greater shear stress due to a greater viscosity. The degree of crystal *c*-axis orientation, or the degree of lamellar twisting is apparently related to the 'hard elastic' properties.

Deformation mechanism along the MD

In this study, a particular specimen designated as HMW2-L was used as a test specimen having the hard elastic property. Deformation behaviour of the superstructure was again investigated by means of wide-angle X-ray diffraction, small-angle X-ray scattering, and electron microscopy techniques.

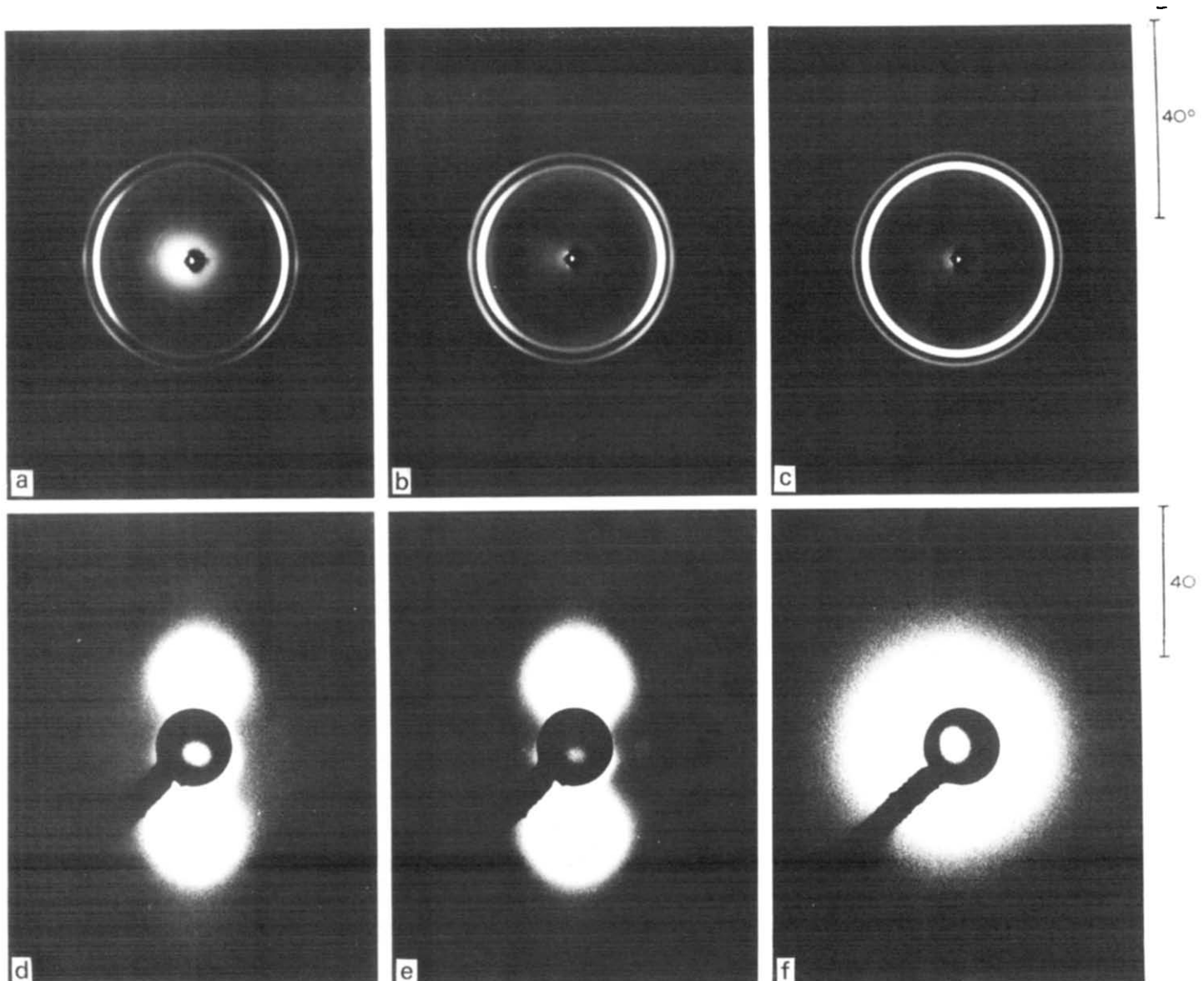


Figure 6 (a), (b), (c), WAXD and (d), (e), (f) SAXS patterns for the HMW1-L specimens. The machine direction is vertical for the through and edge patterns. (a), (d), Through; (b), (e), edge; (c), (f), end

Electron microscopy. Figure 8 shows electron micrographs of the surface replica of the specimen stretched along the MD, this particular specimen also shows increased tendencies of splaying apart, tilting and bending of the lamellar network of the type which is reported for other typical elastic hard fibres and films¹¹⁻¹⁶.

Small-angle X-ray scattering. The deformation of the lamellar network can be quantitatively investigated by detecting the change of SAXS patterns and intensity distributions during the stretching process. In Figures 9a-g and 10 the change of SAXS patterns upon stretching along the MD, which is in the vertical direction of the Figures are shown. The patterns in Figure 9 are for dry specimens, while those in Figure 10 are for specimens stretched by a given percentage and then immersed in liquid paraffin (SG, 0.855).

On increasing the stretching, the following changes in the lamellar network may be seen from Figure 9: (a) increase of interlamellar spacing, which is associated with shifting the position ($2\theta_{\max}$) of the meridional SAXS intensity maximum to a lower scattering angle; (b) increase of interlamellar void formation as a consequence of the

process (a), which is associated with increase of the SAXS intensity especially at lower angles than $2\theta_{\max}$; (c) increasing degree of lamellar bending and irregular deformation of lamellae, which is associated with increase of the lateral breadth of two-point SAXS patterns. The increase of the SAXS intensity and the appearance of the equatorial streak at large elongations are related to a phenomenon of whitening of specimen as pointed out earlier.

In Figure 10 the SAXS patterns after immersing the stretched specimens in the liquid paraffin are shown. As shown in the Figure, the SAXS intensity decreases due to a reduction in scattering arising from the void as a consequence of the penetration of the liquid paraffin into the interlamellar void region. Therefore the mechanisms (a) and (c) described above can be more clearly seen in the immersed specimens.

Figures 11a and 11b show changes of the meridional SAXS intensity distributions upon stretching for dry specimens and for specimens stretched and then immersed in the liquid paraffin, respectively. Each scattering curve shows the first and the second order scattering maxima (or shoulders). On stretching, positions of the scattering maxi-

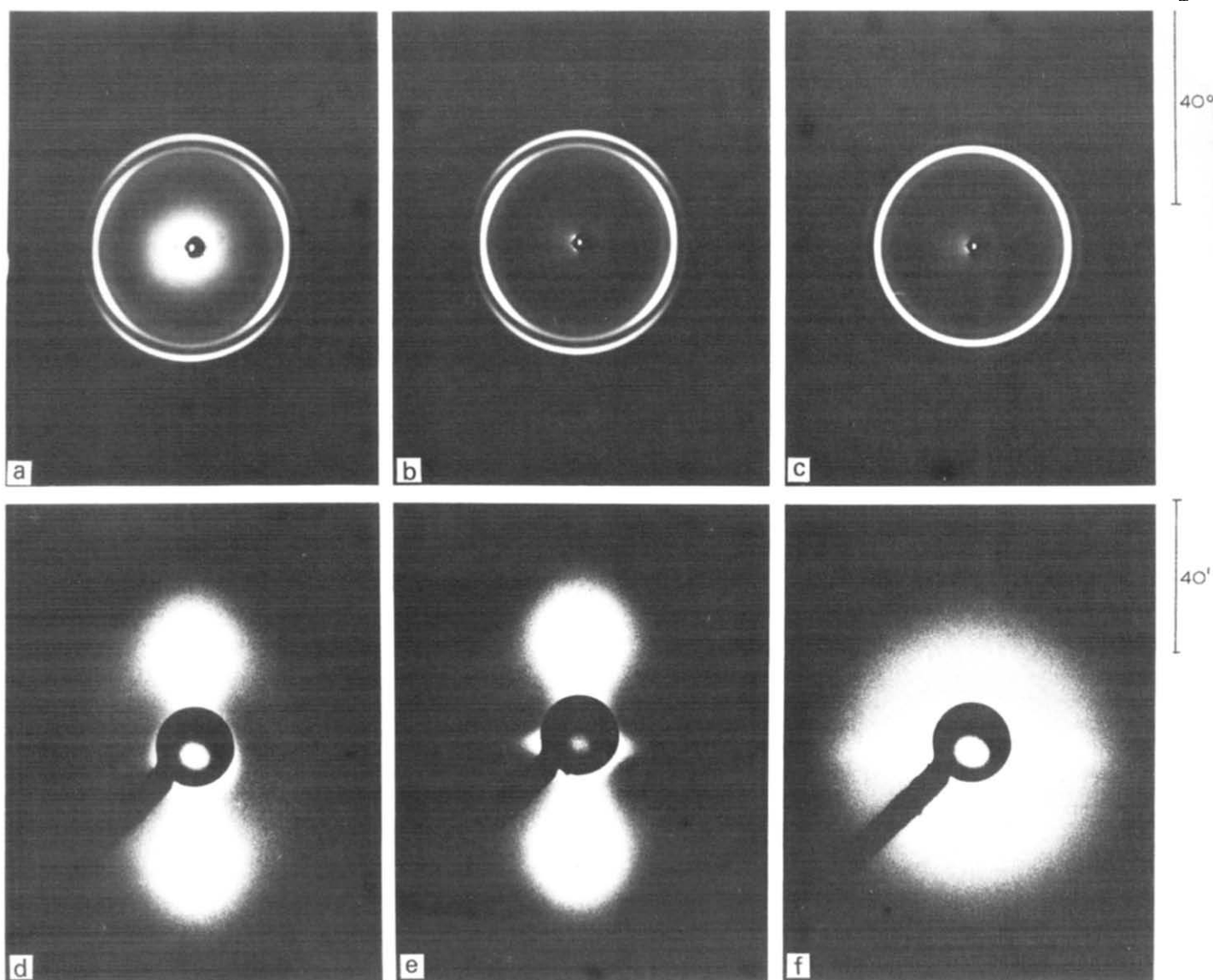


Figure 7 (a), (b), (c), WAXD and (d), (e), (f) SAXS patterns for the LMW-L specimens. The machine direction is vertical for the through and edge patterns. (a), (d), Through; (b), (e), edge; (c), (f), end

ma are seen to shift to lower angles, and the scattering intensity is seen to increase tremendously at scattering angles smaller than $\sim 20^\circ$ (Figure 11a).

The extra-intensity that appeared at the lower angles disappears upon immersing the specimens in the liquid paraffin. This is ascribed to the large interlamellar void which is accessible to the liquid paraffin. A small decrease in intensity at small angles on immersing in the liquid paraffin is also observed for unstretched specimens, which indicates that the interlamellar void exists even for unstretched specimens, though its amount is less compared with the stretched specimens. It should be noted that the peak positions themselves do not change before and after immersion, indicating that the liquid paraffin does not swell the specimens at all and thus does not affect the morphology.

Figure 12 shows change of long spacing as a function of elongation. The long spacings are evaluated from peak positions of the first and second order scattering maxima in Figure 11b by using Bragg's law. As shown in the Figure, the long spacing observed from the first maximum is greater than that observed from the second maximum. The ratio P_2/P_1 of the second to first peak positions is also plotted

in Figure 12 as a function of elongation. The ratio is seen to be greater than 2 and to increase slightly with increasing elongation. The discrepancy of the two long spacings or deviation of the ratio from 2 may be interpreted in terms of an asymmetric distribution of the interlamellar distances as proposed by Reinhold, Fischer and Peterlin²³. According to their model, the results in Figure 12 may be interpreted in terms of the positively skewed distribution of interlamellar distances. The width parameter γ corresponds to ~ 0.4 for unstretched specimens and tends to increase upon further stretching. This is partly associated with the lamellar bending.

Figure 13 shows elongation of the long spacing calculated from the position of the first meridional SAXS maximum and residual strain of the bulk specimens as a function of bulk elongation. As seen in the Figure, the deformation of submicroscopic structure as observed from the change of the spacing affinely occurs with the bulk deformation at elongations less than $\sim 10\%$. However at larger elongations, the increase in the spacing is much retarded to the bulk elongations, indicating that the submicroscopic deformation becomes increasingly heterogeneous and localized.

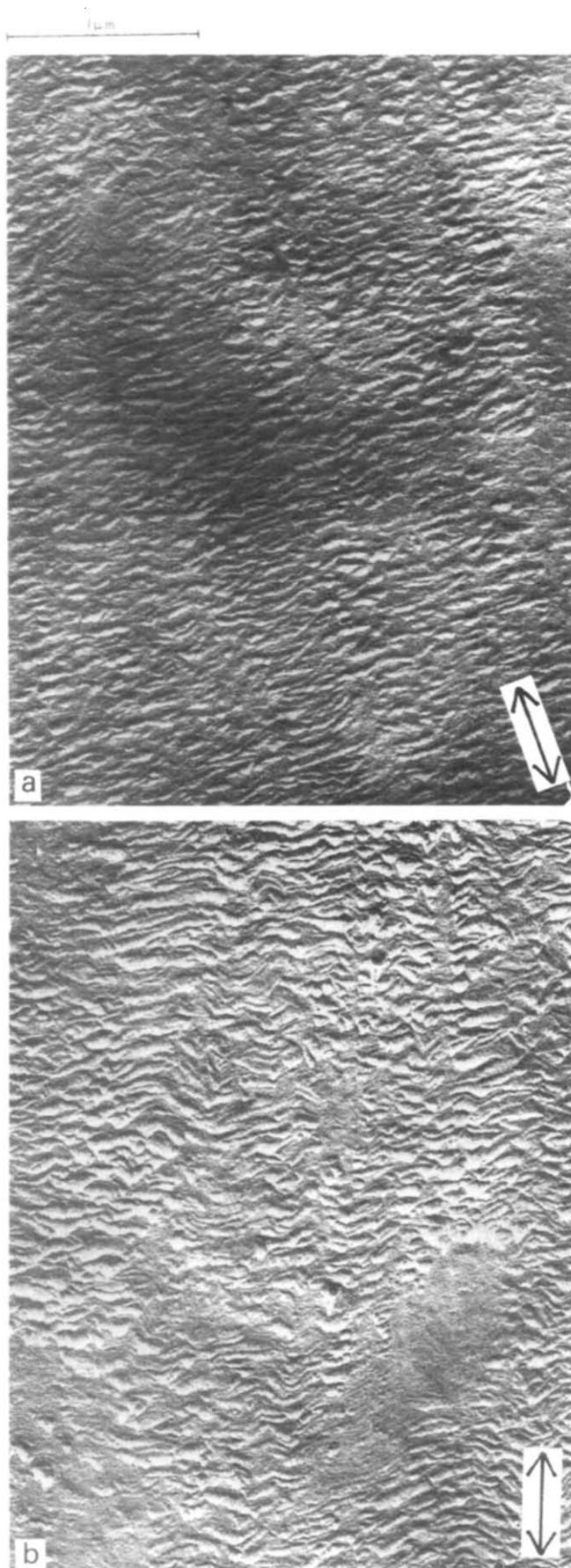


Figure 8 The change of surface structure of the specimens as a function of elongation (surface replica). Arrows indicate the stretching direction which is parallel to the MD. (a) 10%; (b) 40%

This is closely related to the whitening of the stretched specimens, and to the increasing SAXS power at the low angles (Figures 9a, 9c, 9e, 9g).

Wide-angle X-ray diffraction. Figure 14 shows the second order orientation factors of crystal a , b , and c axes as a function of elongation. The orientation factor of the i th axis is defined by $f_i = (3\langle \cos^2 \theta_i \rangle_{av} - 1)/2$, where θ_i is the angle between the stretching direction and the i th crystal axis. The orientation factors were measured both for stretched specimens and for specimens stretched and then relaxed. For the relaxed specimens, the orientation factors were plotted as a function of residual elongation. The arrows in the upper part of Figure 14 indicate changes of f_c upon relaxing the specimens from given elongations. The relationship between the residual and initial elongation is shown in Figure 13.

As is shown in Figure 14, the original unstretched specimens show almost perfect orientation of the crystal b -axis perpendicular to the MD, i.e. $f_b \cong -0.5$. This corresponds to an orientation of lamellar axes normal to the MD, which is in good agreement with evidence from electron microscopy (Figure 5) and SAXS (Figure 6) studies. On the other hand, the a - and c -axis orientations are less perfect, which is associated with some degree of lamellar twisting, i.e. rotation of crystal a - and c -axes with respect to the b -axis.

On stretching, the orientation factor f_c increases while f_a decreases, indicating that crystal c - and a -axes orient towards the stretching direction (SD) and the direction perpendicular to the SD (TD), respectively. On the other hand the orientation factor f_b changes only a little compared with f_a and f_c . These changes of the orientation factors should result primarily from a lamellar detwisting process which gives rise to rotation of crystal a - and c -axes around the crystal b -axis (lamellar axis). The detwisting (or so called interlamellar slip) makes the crystal c - and a -axes orient more towards the SD and TD, respectively.

A minor change of f_b occurs in that f_b slightly increases with increasing elongation. The increase of f_b may be attributed to a process of lamellar bending between tie links of the type as described in Figure 9 of ref 11 which may give rise to rotation of crystal c - and b -axes around crystal a -axis in a way that the c - and b -axes (originally oriented along SD and TD, respectively) tend to orient toward TD and SD directions, respectively. Therefore the entire change of orientation factors can be well interpreted in terms of the two processes, lamellar detwisting (interlamellar shearing) and lamellar bending (intralamellar shearing of mosaic blocks constituting lamellae or intralamellar chain slip). The contribution of the former to the orientation factors is greater than that of the latter, at least for the static deformation. We will discuss briefly the time-dependence of the relative contribution, later.

Recoverability of deformation of structure upon releasing the strain. The recoverability of deformation upon releasing the applied strain was investigated in terms of (a) deformation of interlamellar spacing (see Figure 13) and (b) orientation of crystallographic axes (see Figure 14). The recoverability of deformation of the interlamellar spacing is considerably high even at large elongations. The residual strain involved in the interlamellar spacing is approximately equal to the residual strain involved in the bulk. Thus in this sense the residual strain in the bulk is interpreted in terms of irreversible deformation of the submicroscopic structure, i.e. lamellae.

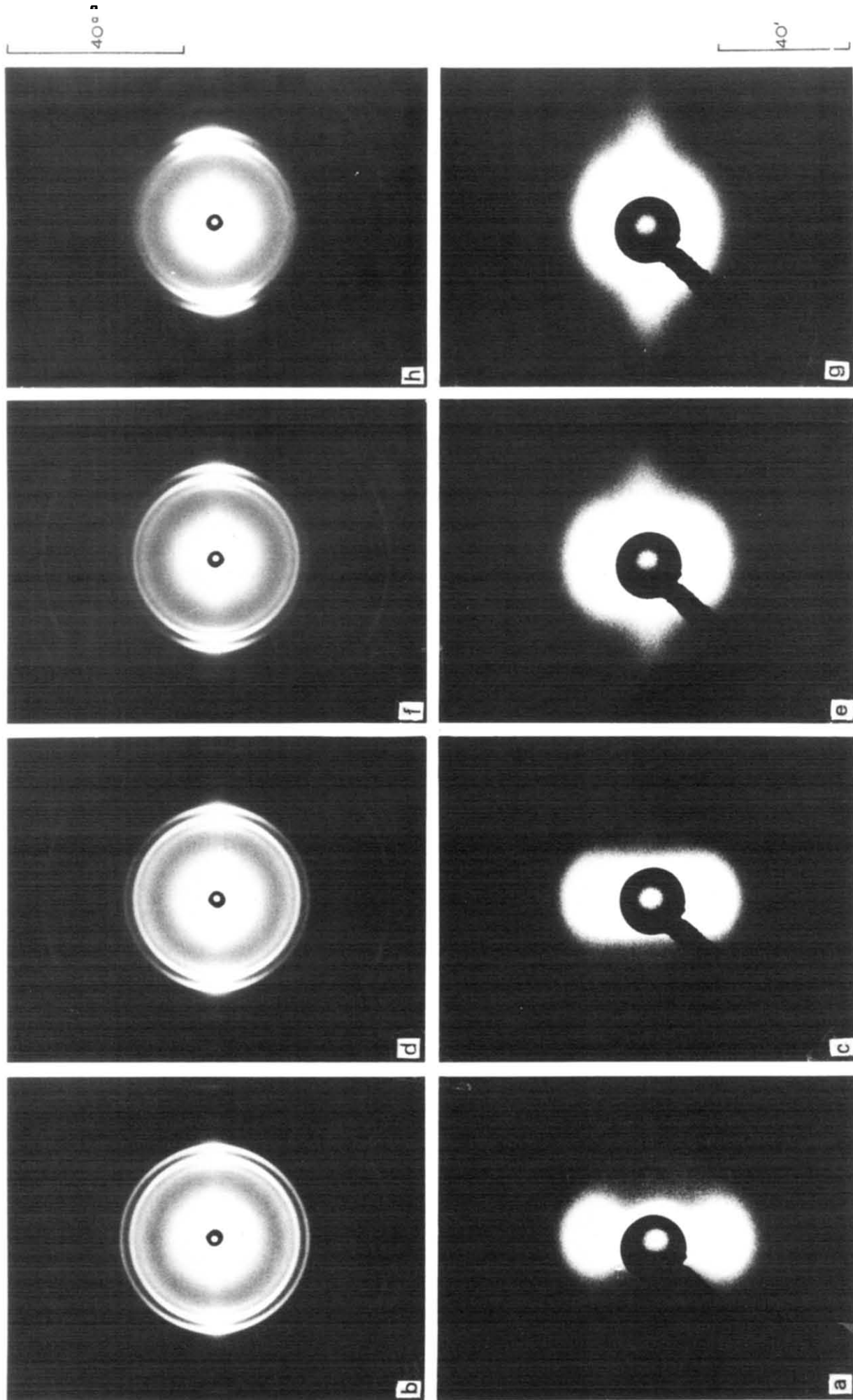


Figure 9 (b)–(h) change of WAXD and (a)–(g) change SAXS patterns upon stretching the specimens along the MD. The stretching direction is vertical. (a), (b) 10%; (c), (d) 20%; (e), (f) 40%; (g), (h) 60%

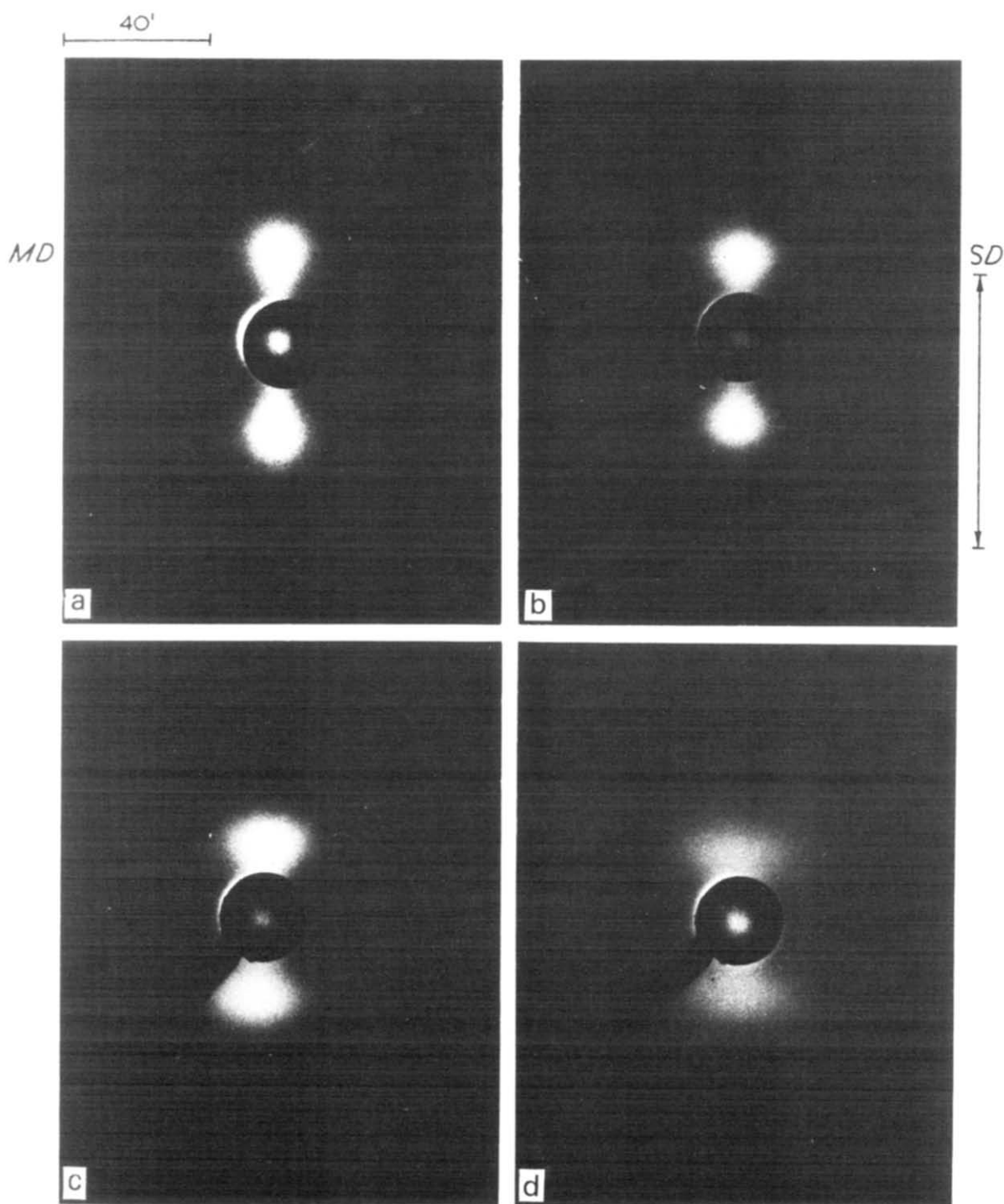


Figure 10 The change of SAXS patterns upon stretching the specimens along the *MD*. The patterns were taken for the specimens stretched by a given elongation and then immersed by liquid paraffin (*SG* 0.855). (a) 0%; (b) 20%; (c) 30%; (d) 50%

As a possible mechanism of irreversible lamellar deformation, one may consider a chain slip within the lamellae of the type as described in Figure 10 of ref 11, lamellar destruction, and destruction of interlamellar tied links. All these processes are irreversible and increasingly important with increasing bulk elongations. At large elongations, the submicroscopic residual strain is slightly smaller than the bulk residual strain. This must be associated with an irreversible deformation process involved on a much larger scale than in the interlamellar spacing. In our subsequent papers, we have discussed its origin¹⁹.

Figure 14 also shows recoverability of orientation of

the crystal *a*, *b*, and *c* axes upon releasing the applied stress. The degree of residual crystal orientation again corresponds to the bulk residual strain. Thus the lamellar bending and interlamellar slip processes involve plastic deformation of crystal such as chain slip of the type [001] (100)^{21,22}, which becomes increasingly important with elongations and is closely related to the irreversible deformation of interlamellar spacing.

Time-dependence of deformation

In the preceding sections, we discussed the static deformation mechanism of the hard elastic polyethylene films

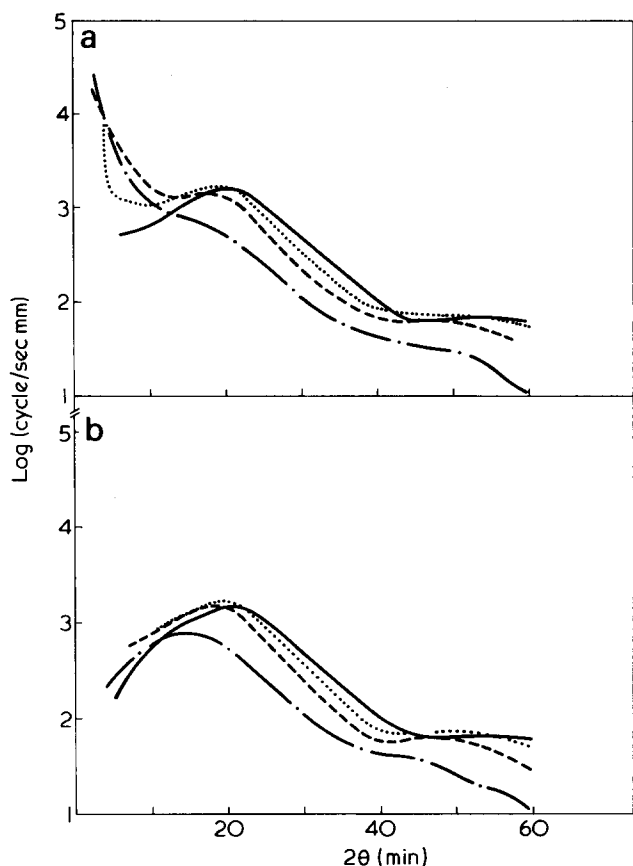


Figure 11 The meridional SAXS intensity distributions for specimens stretched by various elongations. (a) Dry specimens; (b) the specimens immersed by liquid paraffin. —, Unstretched; ····, 10% stretched; ---, 20% stretched; - · - ·, 50% stretched

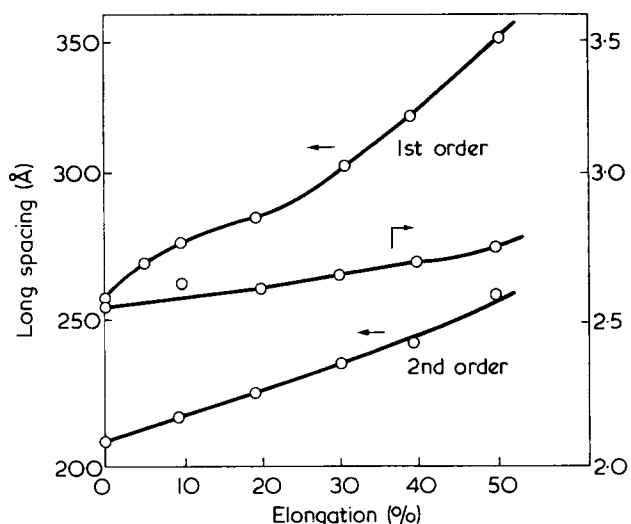


Figure 12 The change of long spacing upon stretching the specimens along the MD. The long spacings are estimated from the first and second order scattering maxima. P_2/P_1 is the ratio of the second to first peak position

along the MD. Relative contributions of the various deformation processes involved are expected to be time-dependent. The analysis of the time-dependence is very important in understanding its dynamic mechanical properties.

Figure 15 shows a preliminary result of dynamic birefringence experiments where master curves of real ($K' + P_T$) and imaginary parts ($-K'' - P_T$) of strain-optical coefficient were plotted as a function of a reduced frequency f_0T .

In order to obtain the master curves a slight vertical shift (shift factor P_T) was necessary as well as the conventional horizontal shift (shift factor o_T).

Static strain 3.3% and dynamic strain 0.25% were imposed on the specimens along the MD²⁴⁻²⁶. The strain-optical coefficient is defined as the ratio of dynamic variation of birefringence to applied dynamic strain amplitude. As seen in the Figure the real part of the strain-optical coefficient increases from negative to positive value with decreasing frequency or increasing temperature. The transition of the coefficient from negative to positive values is related to the change of molecular orientation mechanism, i.e. negative to positive molecular orientation.

As discussed earlier, the negative molecular orientation is associated with the lamellar bending process, while the positive molecular orientation is associated with the lamellar detwisting process. The frequency or temperature dependence of the coefficient is then interpreted qualitatively in terms of the frequency or temperature dependence of a

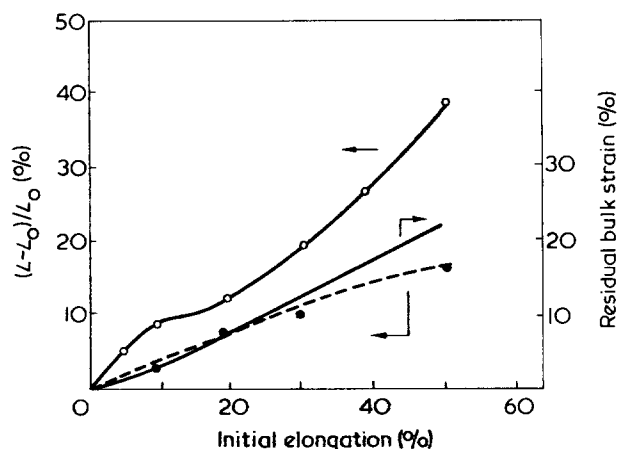


Figure 13 The deformation of the submicroscopic structure, $(L - L_0)/L_0$, as a function of bulk elongation (O). ●, Corresponds to its residual deformation when the applied stress is released. The Figure also indicates a relationship between applied bulk elongation and residual elongation in bulk

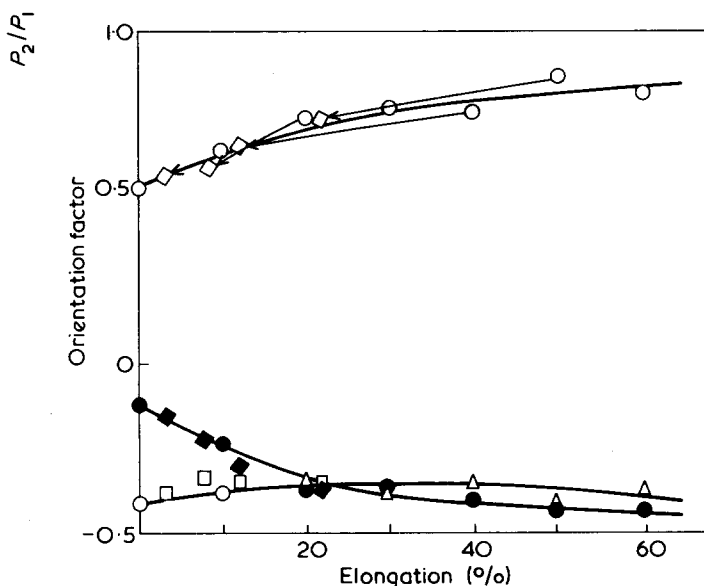


Figure 14 The second order orientation factors of crystal a, b, and c axes as a function of elongation. For the specimens stretched and then released, the orientation factors were plotted as a function of residual elongation. Stretched: ●, f_a ; △, f_b ; ○, f_c . Relaxed: ◆, f_a ; □, f_b ; ◇, f_c .

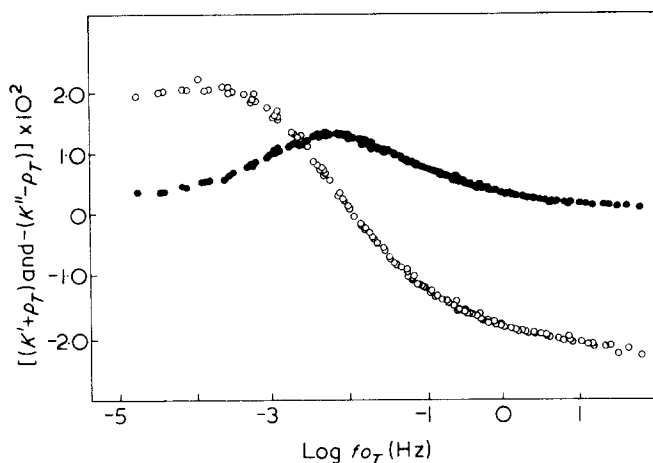


Figure 15 The master curve of the real ($K' + P_T$) and imaginary parts $-(K'' - P_T)$ of the strain-optical coefficients when static (3.3%) and dynamic strains (0.25%) were applied along the MD . The quantities σ_T and P_T are horizontal and vertical shift factors, respectively. The reference temperature is set at 50°C. ●, $-(K'' - P_T)$; ○, $(K' + P_T)$

relative contribution of the two deformation processes. In a more quantitative discussion one must take into account contributions of amorphous orientation and form birefringence to the total birefringence, the discussion of which is beyond the scope of this paper.

In other words, at high frequency or at low temperature, the lamellar bending is activated but the lamellar detwisting is not, and so the contribution of the former is greater compared with the latter. Consequently the coefficient is negative. On the other hand with decreasing frequency or increasing temperature, the lamellar detwisting is increasingly activated, and so the contribution of the latter becomes predominant to the former. Therefore the coefficient becomes positive.

The lamellar bending process is accompanied by only a small amount of negative imaginary part, and thus the phase difference between the dynamic birefringence and applied strain is very small, indicating that the process is elastic in nature. On the other hand the detwisting process is accompanied by a relatively large phase lag to the applied strain as seen in a large phase lag between the dynamic birefringence and strain at low values of $f_0 T$, indicating that the process is viscous in nature and time-dependent.

More detailed discussion including dynamic birefringence in other directions and dynamic mechanical spectra is reported elsewhere²⁰.

CONCLUSIONS

(1) High density polyethylene films crystallized by a calender processing method exhibit a submicroscopic structure typical of that found for films crystallized from oriented polymer melts. Stacks of crystal lamellae are oriented with their normals parallel to the MD . Corresponding to this, the SAXS patterns show a two-point pattern, and the second order orientation factor for the crystal b -axis is close to $-1/2$.

(2) Under a given moulding condition with fixed temperature and shear rate, the films prepared from extra-high molecular weight polyethylenes and from high and medium molecular weight polyethylenes showed a preferential c - and a -axis orientation, respectively. In either case crystal b -axis orients almost perpendicular to the MD . The differ-

ence of the orientation may be attributed to a difference of shear stress in polymer melt. The proposal by Keller and Machin² that the c - and a -axis orientation result, respectively, from crystallization under high and low shear stresses turned out to be applicable also to our system.

(3) The manner of crystal orientation is apparently related to the mechanical properties of bulk specimens. Specimens having preferential c -axis orientation exhibit the hard elastic properties, while the specimens having preferential a -axis orientation do not show such unusual elasticity but exhibit usual yielding and necking, and a relatively small degree of length recovery from large extensions. This may occur partly because the interlamellar slip process involves a plastic deformation of the type $[001] (100)$ chain slip. The interlamellar slip process which orients crystal c -axis towards the SD occurs more extensively for the specimens having a -axis orientation than for those having c -axis orientation.

(4) The deformation of specimens along the MD involves lamellar bending and interlamellar slip processes. The bending process opens up interlamellar spacing to generate voids. The expansion of the interlamellar spacing affinely occurs with bulk elongation at small elongations. At larger elongations the increase of the spacing is less than that expected for the affine deformation due to increasing localization of interlamellar deformation which is associated partly with beginning of the sample whitening.

(5) The interlamellar slip involves rotation of crystal c - and a -axes around crystal b -axis (lamellar axis) towards the stretching direction (MD) and direction normal to the stretching direction (TD), respectively. The lamellar bending, on the other hand, involves rotation of crystal b and c axes around crystal a axis towards the SD and TD , respectively.

(6) Time-dependence of the two orientation mechanisms i.e. lamellar bending and interlamellar slip were studied by means of dynamic birefringence. The results indicated that the former mechanism is associated with a small phase difference to the applied strain, and is elastic in nature, while the latter mechanism is accompanied by a large phase lag to the strain, and is viscous in nature and time-dependent.

(7) Recoverability of deformation of the lamellar network, and crystal orientation was also studied. The results indicated that the lamellar bending and interlamellar slip processes involves, to some extent, a plastic deformation of crystals (irreversible intralamellar chain slip).

ACKNOWLEDGEMENT

Part of this work was supported by a grant from Idemitsu Kosan Co. Ltd, Japan, and a grant from Mitsui Petrochemical Industries Ltd, Japan.

REFERENCES

- 1 Pennings, A. J. and Kiel, A. M. *Kolloid-Z.* 1965, **205**, 160
- 2 Keller, A. and Machin, M. J. *J. Macromol. Sci. (B)* 1967, **1**, 41
- 3 Kawai, T., Matsumoto, T., Kato, M. and Maeda, H. *Kolloid-Z. Z. Polym.* 1968, **222**, 1
- 4 Andrews, E. H. *Proc. Roy. Soc. (A)* 1964, **277**, 562; *J. Polym. Sci. (A-2)* 1966, **4**, 668
- 5 Judge, J. T. and Stein, R. S. *J. Appl. Phys.* 1961, **32**, 2357
- 6 Williamson, R. B. and Busse, W. F. *J. Appl. Phys.* 1967, **38**, 4187
- 7 Kobayashi, K. and Nagasawa, T. *J. Polym. Sci. (C)* 1966, **15**, 163

Deformation mechanism of 'hard elastic polyethylene films': T. Hashimoto et al.

- 8 Vill, M. J. and Keller, A. *J. Macromol. Sci. (B)* 1969, **3**, 153
- 9 Garber, C. A. and Clark, E. S. *J. Macromol. Sci. (B)* 1970, **4**, 499
- 10 Kobayashi, K. in 'Polymer Single Crystals', (Ed. P. H. Geil), Interscience, New York, 1963
- 11 Clark, E. S. in 'Structure and Properties of Polymer Films', (Eds R. W. Lenz and R. S. Stein), Plenum Press, New York, 1973
- 12 Quynn, R. G. and Sprague, B. S. *J. Polym. Sci. (A-2)* 1970, **8**, 1971
- 13 Quynn, R. G., Brody, H., Sobering, S. E., Park, I. K., Foley, R. L., Noether, H. D., Whitney, W., Pritchard, R., Sieminski, M. A., Hutchinson, J. D., Wagner, H. L., Sakaoku, K. and Corneliussen, R. *J. Macromol. Sci. (B)* 1970, **4**, 953
- 14 Quynn, R. G. and Brody, H. *J. Macromol. Sci. (B)* 1971, **5**, 721
- 15 Cayrol, B. and Petermann, J. *J. Polym. Sci. (Polym. Phys. Edn)* 1974, **12**, 2169
- 16 Sprague, B. S. *J. Macromol. Sci. (B)* 1973, **8**, 157
- 17 Hashimoto, T., Nagatoshi, K., Todo, A., Hasegawa, H. and Kawai, H. *Macromolecules* 1974, **7**, 367
- 18 Murakami, Y., Ishido, S., Hashimoto, T. and Kawai, H. *Rep. Prog. Polym. Phys. Japan* 1974, **17**, 293
- 19 Nagatoshi, K., Todo, A., Hashimoto, T. and Kawai, H. *Polymer*, 1976, **17**, 1075
- 20 Hashimoto, T., Yasuda, N., Suehiro, S., Nomura, S. and Kawai, H. *Polym. Prepr.* 1976, **17**, 118
- 21 Oda, T., Nomura, S. and Kawai, H. *J. Polym. Sci. (A)* 1965, **3**, 1993
- 22 Hay, I. L. and Keller, A. *Kolloid Z. Z. Polym.* 1965, **204**, 43
- 23 Rheinhold, C., Fischer, E. W. and Peterlin, A. *J. Appl. Phys.* 1964, **35**, 71
- 24 Stein, R. S., Onogi, S. and Keedy, D. A. *J. Polym. Sci.* 1962, **57**, 801
- 25 Stein, R. S., Onogi, S. and Sasaguri, K. and Keedy, D. A. *J. Polym. Sci.* 1962, **57**, 801
- 26 Kyu, T., Yasuda, N., Tabushi, M., Nomura, S. and Kawai, H. *Polym. J.* 1975, **7**, 108

Superstructure of high density polyethylene film crystallized from stressed polymer melts as observed by small-angle light scattering

Takeji Hashimoto, Kikuo Nagatoshi*, Akira Todo† and Hiromichi Kawai

Department of Polymer Chemistry, Faculty of Engineering, Kyoto University, Kyoto 606, Japan
(Received 23 February 1976)

The crystalline superstructure of high density polyethylene films prepared by a calender manufacturing method was investigated by means of polarizing light micrographs and light scattering patterns. Results show that optically anisotropic rod-like units exist which orient at preferential angles $+\alpha_0$ and $-\alpha_0$ with respect to the machine direction to form a network type superstructure. The rod-like unit is considered to be a row-nucleated cylindrite or a parallel assembly of them. The angle α_0 is associated with a preferred orientation of axes of the cylindrites with respect to the machine direction, and found to be dependent upon manufacturing condition. Existence of such a super-structure was shown to be important in accounting for whitening of the specimens on stretching along the machine direction and for deformation behaviour of the specimens.

INTRODUCTION

In a previous paper¹, we prepared various high density polyethylene films by a calender manufacturing process which involved crystallization from stressed polymer melts. Morphology and deformation mechanism of the submicroscopic structures were studied by means of small-angle X-ray scattering, wide-angle X-ray diffraction, and electron microscopy.

The X-ray data and electron micrographs were in agreement with general concepts obtained for tubular extruded^{2,3}, injected and hard elastic material⁴⁻⁸, and other material crystallized from oriented melts^{9,10}. For example, the submicroscopic structure consists of stacks of oriented lamellae, their plane normals being parallel to the machine direction (*MD*), which gives rise to two-point low-angle X-ray scattering patterns and the second order orientation factor of the crystal *b*-axis nearly equal to $-1/2$.

Under given manufacturing conditions with a fixed temperature, shear rate etc., the polyethylenes with higher molecular weights (e.g. HMW1 and HMW2 series in ref 1) result in a texture giving rise to preferential *c*-axis orientation, while those with lower molecular weights (e.g. LMW and MMW series in ref 1) result in a texture giving rise to *a*-axis orientation. This again is in agreement with the general concepts of material crystallized from oriented melt, because the material with higher molecular weights are subjected to a greater shear stress (due to greater viscosity) than those with lower molecular weights under the given conditions. The difference in the manner of crystal orientation can be interpreted in terms of the differences in number of row nuclei and in the degree of lamellar twisting overgrowth on the nuclei².

The polyethylene with higher molecular weights exhibited so-called 'hard elastic' properties⁸, i.e. a high degree of length recovery from large extensions, a marked reduction of apparent density, generation of very large amounts of internal volume and surface area on stretching along the *MD*, etc. The results obtained for our polyethylene films of morphology, deformation mechanism, and mechanical properties etc. are again in agreement with the general concepts of other hard elastic films or fibres⁴⁻⁸. The elasticity is energetically driven due to a bending type deformation of lamellae (see Figure 9 of ref 5). However in the case of polyethylene, the degree of lamellar twisting is large and thus the deformation mechanism associated with it (e.g. interlamellar slip) is markedly involved compared with poly(α -olefin). This makes the hard elasticity of polyethylene less pronounced, because the deformation will probably involve some irreversible chain slip of the type (100) [001]^{11,12} within the lamellae.

In this paper we have extended our study further, from the submicroscopic scale to the microscopic scale to investigate superstructure of the lamellae, if any, by means of polarizing microscope and light scattering. This work also should be of importance in investigating clarity of film specimens as-prepared and stretched, and to understand the deformation mechanism of the bulk specimens. It is one of our purposes in this work to study how the superstructure of the lamellae of these particular specimens is reconciled with our X-ray data and electron micrographs described in the previous paper¹ and with the concept of row-nucleated cylindrites proposed by Keller and Machin², and other workers.

TEST SPECIMENS

In this study, we used a particular linear polyethylene film designated as HMW2-L in our previous paper¹. The polyethylene (commercial grade, Sholex Super 4551H supplied

* On leave from present address, the Central Research Laboratory, Idemitsu Kosan Co. Ltd, Sodegaura-cho, Kimitsu-gun, Chiba-ken, Japan.

† On leave from the Research Center, Mitsui Petrochemical Industries Ltd, Waki-cho, Kuga-gun, Yamaguchi-ken, Japan

from Japan Olefin Chemical Ind. Ltd, and prepared by the Philips method) has weight-average molecular weight 2.9×10^5 by light scattering (measured in α -chloronaphthalene solution at 125°C), and a melt index of 5.0 at 190°C and 21.6 kg.

The film specimens were prepared by a calender processing method as described in detail in the previous paper¹. Temperatures of the first to third drums were kept at 145°C and that of the fourth drum was at 130°C (see Figure 1 of ref 1). Crystallization took place immediately after the fourth drum. The ratio of take-up to extruded velocities was controlled to 6/5. The density of the films thus prepared was 0.940 g/cm^3 (measured in methanol-water system at 25°C with a density gradient tube). The volume-average crystallinity evaluated was 59.5% by assuming densities of crystal and amorphous to be 1.000 and 0.852 g/cm^3 , respectively. Other specimens prepared from the HMW1 and HMW2 polyethylenes as described in the previous paper¹ showed a similar trend to the HMW2-L specimens.

EXPERIMENTAL

Light scattering patterns were obtained with a 1 mW He-Ne gas laser as a light source. Diffuse surface scattering was avoided by sandwiching the specimens in between the microcover glasses with silicone oil as an immersion fluid having an appropriate refractive index. The scattering patterns were taken with H_V and V_V polarizations where the polarization directions of the analyser were set horizontally and vertically, respectively, under a vertically polarized incident beam as well as with H_H polarization where both polarizer and analyser were set horizontally. The machine direction of the specimens was always set vertically. Typical exposure times were 1/30 to 1/8 sec for H_V , and 1/60 to 1/25 sec for V_V and H_H patterns.

Particular care was taken in obtaining the patterns, since as was shown in the previous paper, the specimen begins to whiten at elongations greater than $\sim 10\%$, when the specimen is stretched along the MD ¹. At these elongations the sample transparency becomes poor, in general, and as a consequence scattering patterns will be distorted due to a multiple scattering effect¹³. In order to minimize this effect the specimen stretched by a given elongation was immersed in a silicone oil (whose refractive index was matched to the average refractive index of the specimen) for at least a week prior to obtaining the patterns. Upon immersing the specimen into the silicone oil, the transparency of the stretched specimen became as high as that of the undrawn specimen. It should be noted that it takes a few hours, at least, before the stretched specimen becomes transparent after immersion in silicone oil.

Texture of the film specimens was also studied by means of polarizing light and electron microscopy.

RESULTS AND DISCUSSIONS

Polarizing light micrographs

Figure 1 shows a typical light micrograph observed under crossed polaroids. Close observation of the micrograph suggests that the texture is composed of rod-like units a few microns in diameter. These units are oriented at a particular angle of $\sim \pm 22.5^\circ$ with respect to the MD to form a network structure. It should be noted that the network structure composed of the anisotropic rod-like units

can be distinguished from the submicroscopic network structure composed of a stack of oriented lamellae linked by tie molecules of relatively short length. The deformation of the latter network was discussed by Hashimoto et al.¹ in relation to the hard elastic properties of bulk specimens. When the specimens were rotated between crossed polaroids, the brightness and the retardation colour of the units varied in such a way as to indicate that the average orientation of the optical axes of the rod-like units was parallel to the MD . The network structure was preserved and rotated. The angle that the rod-like units make to each other was also kept constant at $\sim 45^\circ$.

When the specimens are stretched parallel to the MD , the rod-like units orient toward the stretching direction (SD) and thus the angle between the units decreases from 45° . With a further increase in elongation identification of the units becomes increasingly difficult; this is associated with decreasing continuity or integrity of the units with elongations.

The observations under polarizing light microscope seem to suggest that the rod-like units reflect some morphological detail existing in the interior of the specimens. As will be discussed below, we consider that these units correspond to a single row-nucleated cylindrite or an assembly of them (see Figure 13). Although the axes of the cylindrites are usually found or considered to orient parallel to the MD , the axes orient at $\pm 22.5^\circ$ with the MD in these particular films. The boundaries between the adjacent cylindrites become a part of amorphous phase having zero birefringence similar to a volume-filling spherulitic system.

It should be noted that the network structure could also result from surface structure which is nothing to do with the morphological entity in the interior of the specimen. The surface structure causes variation of sample thickness which, in turn, gives rise to variation of retardation to result in the network structure under crossed polaroids. However, we can rule out this possibility for the light scattering data as will be discussed below.

Light scattering patterns

We consider the light scattering experiments to be very important and useful in studying the origin of the rod-like units or the network as observed under the polarizing light microscope. By treating the film specimens with silicone oils whose refractive indices are matched with the specimens, we can effectively avoid the surface scattering.

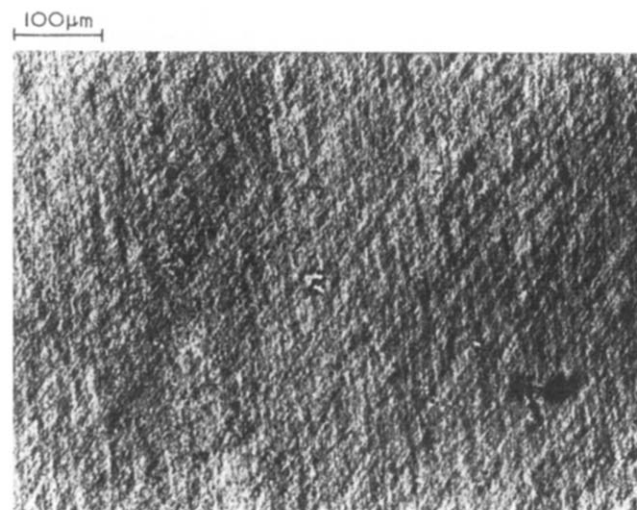


Figure 1 A typical polarizing light micrograph of the specimens

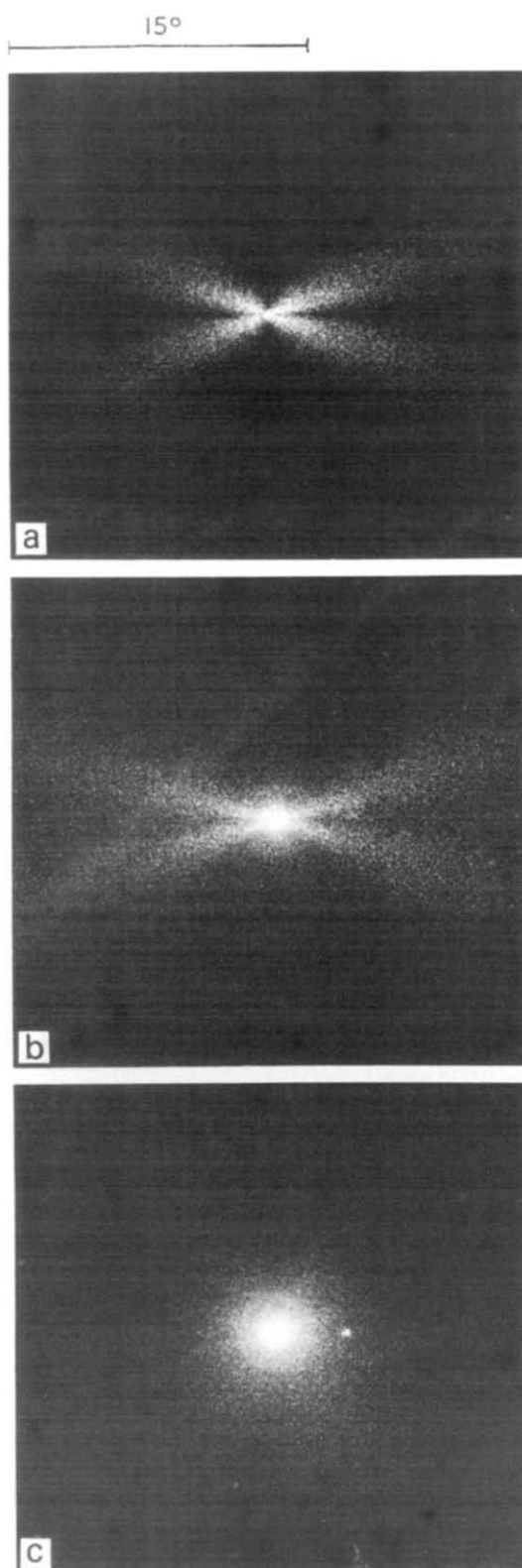


Figure 2 (a) H_V ; (b) V_V , and (c) H_H light scattering patterns of the specimens. The scale indicates the scattering angle

Therefore the scattering patterns are considered to be representative of the interior superstructure. The scattering patterns under crossed polaroids are particularly insensitive to the surface scattering.

In Figure 2 typical low-angle H_V , V_V , and H_H light scattering patterns are shown. It is observed that the patterns for other specimens (the HMW1 and HMW2 series) are essentially the same and consequently essentially identi-

cal crystalline superstructures are formed in these films. In all these patterns the scattered intensity at a given azimuthal angle continuously decreases with increasing scattering angle. In this regard the patterns are those typical of an oriented assembly of anisotropic rods¹⁴⁻¹⁶ as will be discussed below, but are not those typical of spherulitic texture.

The H_V scattering depends upon anisotropy and orientation of the rods, while the V_V and H_H scattering also depend upon density fluctuation between or within the rods and their surrounding medium. Since the scattering arising from the density fluctuation is isotropic in origin, it therefore does not depend upon a polarization direction under parallel nicols. Hence H_H and V_V scattering patterns are equivalent, if the scattering arises purely from the density fluctuations. The difference in the two patterns suggests that the orientation and anisotropy contributions are predominant in the density fluctuation. In the case of the V_V scattering the polarization direction is parallel to the MD and therefore to the molecular chain axis¹, so that the orientation and anisotropy contributions to the scattering are maximized, while in case of the H_H scattering these contributions are minimized and the scattering predominantly arises from the density fluctuation. The cylindrically symmetric H_H scattering intensity distribution with respect to the incident beam axis indicates that density fluctuation is isotropic. Therefore the density fluctuation between the rods and their boundary region turns out to be small, because if the fluctuation is large, then the H_H pattern becomes anisotropic in shape as in the V_V pattern. On the other hand the strong azimuthal angle dependence of H_V and V_V scattering arises from anisotropic orientation and anisotropy fluctuations as will be discussed later.

The angle that the H_V and V_V scattering lobes make with respect to the equator is $\sim 22.5^\circ$ and is apparently related to the angle that the optically anisotropic rod-like units make with respect to the MD . Therefore from the light scattering patterns also we can show that there exists an anisotropic rod-like entity oriented at a particular angle with respect to the MD as an internal superstructure of the film specimens. The rod-like entity giving rise to the scattering patterns should be essentially identical to the units observed under the polarizing microscope. We will discuss later a relationship between the units and the scattering patterns in a more quantitative manner by model calculation of the scattering patterns.

Orientation of the optical axis within the rod-like units may be qualitatively determined by observing the change in H_V scattering patterns upon rotation of the MD as shown in Figure 3. On rotating the MD of the specimens while keeping the polarization directions constant as in the Figure, the pattern also rotated through the angle α , since orientation of the rod-like units is changed by the angle α . An additional change is also seen in the intensity distributions in the rotated patterns. This arises from two factors which are mutually interrelated: (a) change of induced dipole moment which affects an absolute intensity, the intensity being maximum at $\alpha = 45^\circ$ because of the preferential c -axis orientation as shown in the previous paper¹, and (b) change of birefringence effect on light scattering¹⁵, the effect being maximized at $\alpha = 45^\circ$.

The fact that four lobes of the pattern change in an equivalent manner upon rotating the MD through an angle α demonstrates that the two rod-like units having $+\alpha_0$ and $-\alpha_0$ ($\alpha_0 \cong 22.5^\circ$) orientation with respect to MD have equivalent optical condition for all values of α under the given polarization condition. This may rule out the pos-

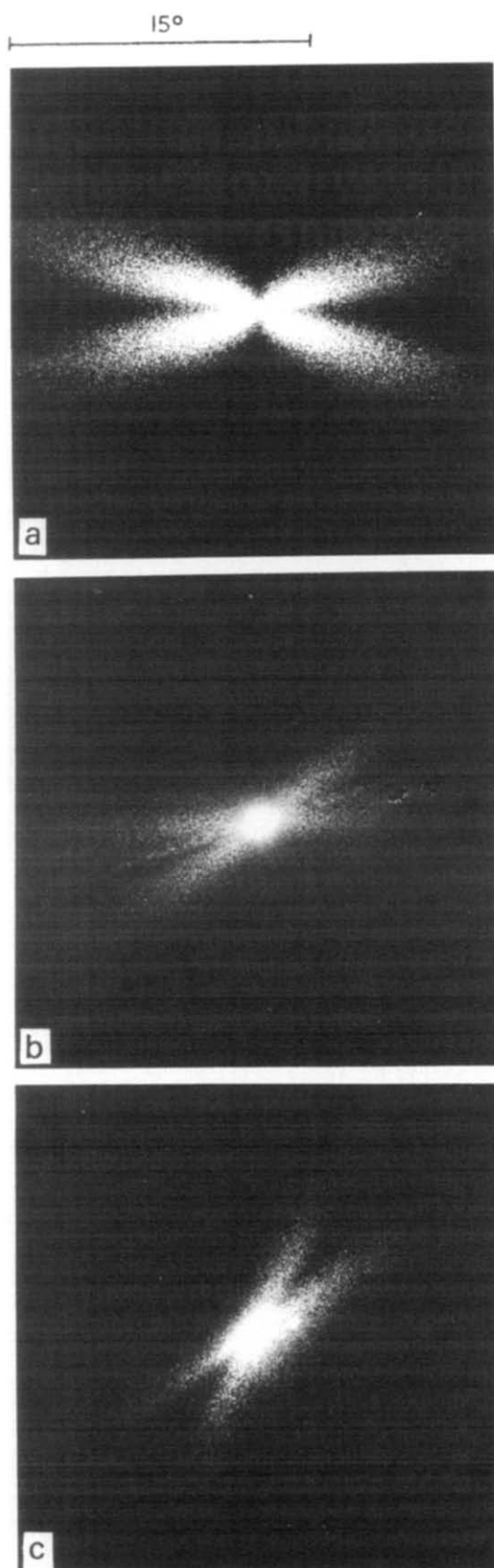


Figure 3 The change of H_V light scattering patterns upon rotating the MD by the angle α under crossed nicols. The polarization directions of polarizer (P) and analyser (A) are set in vertical and horizontal positions, respectively. (a) 0° ; (b) 22.5° ; (c) 45°

sibility that the orientation of the principal optical axis is parallel to the longitudinal direction of the rod-like units. This fact together with the preferential c -axis orientation

suggests that the optical axis is preferentially oriented along the MD , and therefore it makes an angle $\alpha_0 (= 22.5^\circ)$ or $-\alpha_0$ with respect to the longitudinal direction of the rod-like units as schematically shown in Figure 13b. Moreover the two-point SAXS patterns as described in the previous paper¹ demonstrate that the rod-like unit is composed of a stack of lamellae with their normals making also the angle $+\alpha_0$ or $-\alpha_0$ with respect to the longitudinal direction.

Integrity of the anisotropic rod-like units

Continuity or integrity of the anisotropic rod-like units which are now considered to exist as an internal superstructure were investigated by observing the change of the scattering patterns on treating the specimens with fuming nitric acid and on stretching the specimens.

Figure 4 shows the change of H_V , V_V , and H_H light scattering patterns of the specimens on treating with fuming nitric acid. Approximately 1 g of the polyethylene films was treated with 100 cm^3 of a fuming nitric acid ($SG 1.54$) for 4 and 8 h at $80^\circ \pm 2^\circ\text{C}$. The specimens were then washed with water and put into acetone for a day and subsequently dried. The film specimens obtained were brittle and opaque. On increasing the time of the treatment, the H_H pattern becomes angularly dependent with respect to the azimuthal angle and becomes similar to the V_V pattern, indicating that the density contribution becomes predominant to those of orientation and anisotropy. The change of V_V and H_H patterns indicates that the treatment increases the density difference between the rod-like units and their surrounding medium. This occurs because nitric acid first attacks boundaries between the rod-like units. On the other hand the H_V patterns of the treated specimens are essentially identical to that of the untreated original specimens. This demonstrates that the integrity or continuity of the rod-like unit itself is maintained even after the treatment. This result again suggests existence of the network superstructure which is built up from the anisotropic rod-like units as an internal superstructure of the film specimens.

As mentioned earlier in this paper and also in a previous paper, the specimen uniformly whitens during the course of stretching and becomes opaque at elongations greater than $\sim 10\%$. The stretched specimens were, therefore, treated with a silicone oil for a certain period of time prior to recording their scattering. The silicone oil acts in two ways; (a) to avoid surface scattering, and (b) to increase the transparency of specimens as a result of penetration of oil into the internal void region responsible for the whitening. For the specimens stretched by an amount smaller than 20%, the patterns were taken immediately after immersing the stretched specimens in silicone oil, so that the silicone oil essentially minimized surface diffuse scattering only. On the other hand for the specimens stretched by an amount greater than or equal to 20%, the patterns were taken after the specimens had been immersed in silicone oil for a few weeks. Thus in this case the silicone oil minimized both the surface diffuse scattering and the internal void scattering.

Figure 5 shows the change of H_V , V_V , and H_H scattering patterns on treating the specimens stretched by 20% with the silicone oil. The patterns in Figures 5a, 5b and 5c were taken immediately after the specimens had been treated with silicone oil, while Figures 5d, 5e and 5f were taken after treating the specimens with silicone oil for a few weeks. As seen in Figures 5b and 5c, V_V and H_H

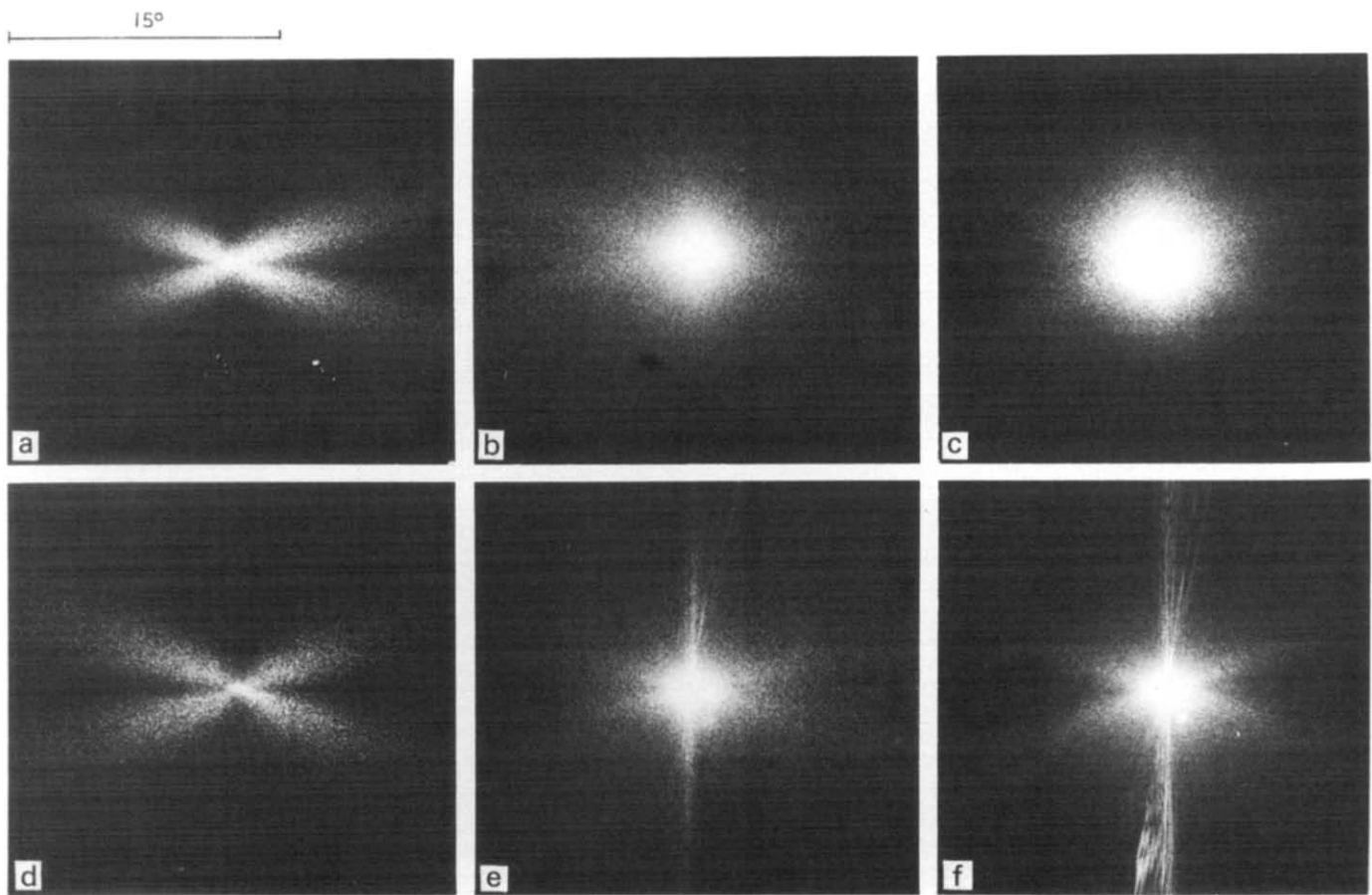


Figure 4 The change of H_V , V_V , and H_H light scattering patterns of the specimens treated with fuming nitric acid for 4 h (a, b, c) and 8 h (d, e, f). (a), (d) H_V ; (b), (e), V_V ; (c), (f), H_H

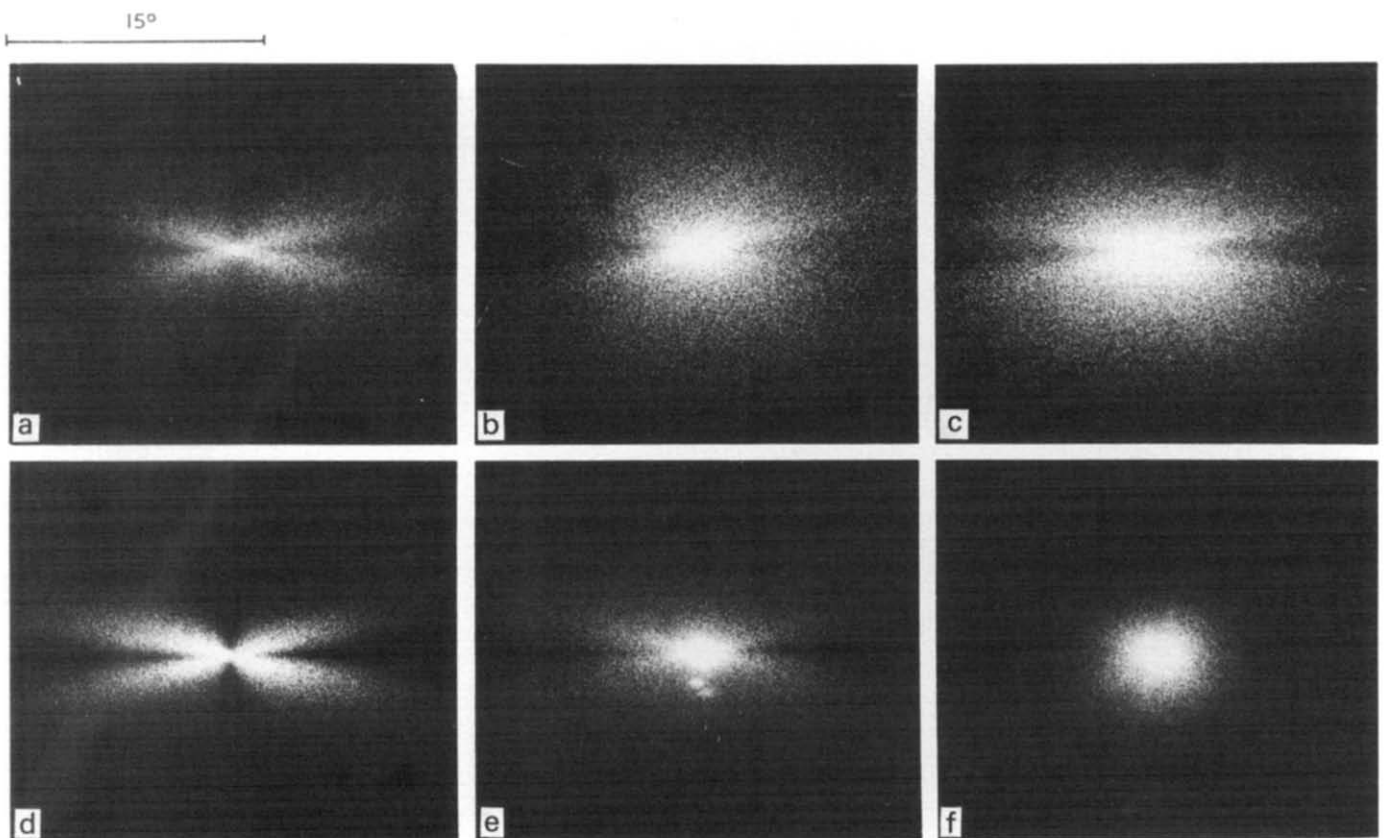


Figure 5 The change of H_V , V_V , and H_H scattering patterns upon treating the specimens stretched by 20% with the silicone oil. The patterns (a)–(c) were taken immediately after the specimens were treated with silicon oil, while (d)–(f) were taken after the specimens were treated for a few weeks. (a), (d), H_V ; (b), (e), V_V ; (c), (f), H_H

patterns are essentially identical, indicating that the scattering arises primarily from density fluctuation, since the scattering from density fluctuation is independent of polarization directions in parallel polarizers. The density fluctuation, in turn, arises from density lowering or void formation at the interrod region, i.e. at boundaries between adjacent row-nucleated cylindrites.

Upon immersing the stretched specimens in the silicone oil for a sufficient time, the silicone oil penetrates into the void region and decreases the density fluctuation along the interrod region. This results in increased transparency of the specimens and in the patterns shown in *Figures 5d, 5e* and *5f*. The difference in V_V and H_H patterns suggests that the orientation contribution is now predominant to the density fluctuation. Thus the V_V pattern is primarily dependent upon anisotropy of the rod-like units and orientation distribution of the units with respect to the MD as in the H_V pattern. On the other hand the H_H pattern primarily depends on the density fluctuation, as polarization directions of polarizer and analyser are perpendicular to molecular chain axes. The circular type of H_H pattern suggests that the density fluctuation is spherically symmetric in contrast to the pattern in *Figure 5c* where the fluctuation occurs preferentially along the interrod region. Therefore the whitening of the specimens arises primarily from the void formation at boundaries between the cylindrites and from a long range correlation of fluctuations produced by interlamellar void formation. The generation of the interlamellar voids was discussed in detail in the previous paper¹. The H_V pattern in *Figure 5a* is diffuse compared with that in *Figure 5d* due to a multiple scattering effect¹³, but is essentially identical before and after immersion, suggesting that the silicone oil does not affect the morphology except for the fact that it interpenetrates the void region.

Figure 6 shows the change of H_V , V_V , and H_H patterns on stretching the specimens along the MD . With increasing elongation the H_V scattering lobes orient towards the equatorial direction. This results from orientation of anisotropic rod-like units towards the SD as discussed previously.

On increasing the elongation, the density difference between the rod-like units and their surrounding medium increases. Consequently, the anisotropic H_H pattern appears, and the V_V and H_H patterns become identical as shown in *Figure 6* for the specimens stretched by 7, and 14% and in *Figures 5b* and *c* for the specimens stretched by 20%. The disappearance of the anisotropic V_V lobes which is especially remarkable at elongations greater than $\sim 30\%$ may be associated with a decrease of continuity or integrity of the rod-like units. The tendency is also seen in H_V patterns in that the intensity distribution becomes sufficiently broader, and in polarized light micrographs the identification of the rod-like units becomes increasingly harder.

Figure 7 shows recoverability of the H_V scattering patterns upon releasing strain from given elongation percentages. It is seen that the patterns are almost completely recoverable if the initial elongations are less than $\sim 30\%$. However at larger elongations recovery of the pattern was not complete as seen typically in the pattern released from 50% elongation. This can be associated with decreasing continuity or integrity of the rod-like unit is considerably high.

Figure 8 shows the relationship between bulk elongation and elongation of the microscopic structural units i.e. the rod-like units. The angles between the MD and the rod-like units α_0 and α before and after stretching were evaluated by measuring the angles between the equator and one of

the H_V scattering lobes. The solid line indicates the change of the $(\alpha_0 - \alpha)/\alpha_0$ if the unit affinely orients toward the SD . From the Figure the units turned out to orient affinely even at relatively large elongations. At large elongations greater than $\sim 40\%$, the deformation of the microscopic structure is retarded to the bulk elongations. This is related to some localization of strain, especially at the interrod amorphous region, which may be followed by a disruption of integrity or continuity of the rod-like units as suggested from the change of the light scattering patterns.

Hashimoto *et al.*¹ previously investigated the residual strain, i.e. the strain which is observed even after the stress applied to the specimens is released as a function of initial elongations. At low initial elongations, the residual strain in bulk turned out to be identical to the submicroscopic residual strain which is analysed in terms of the long spacings measured by low-angle X-ray scattering. At large initial elongations greater than $\sim 40\%$, the bulk residual strain cannot be uniquely interpreted in terms of the submicroscopic residual strain. The former is shown to be appreciably greater than the latter. The excess residual strain in bulk can be associated with an irreversible deformation process involved on a much larger scale than the interlamellar spacing. The irreversible deformation, in turn, may occur due to the localization of strain at the interrod amorphous region described above.

At elongations greater than 40%, $(\alpha_0 - \alpha)/\alpha_0 \cong 0.4$ thus α is approximately 10° . By taking the orientation distribution of the rod-like units into account, the interrod void is considered to exist virtually parallel to the MD , and therefore it partly accounts for the equatorial streak-like scattering in the SAXS patterns as shown in *Figure 9* of the previous paper¹. The change of the orientation of the unit α with elongations is qualitatively in agreement with that observed directly under polarizing microscope. This again confirms that the network structure of the rod-like units observed under the microscope reflects a morphological detail existing in the interior of the specimens.

Origin of anisotropic rod-like units

In order to obtain better microscopic evidence showing existence of the rod-like units as crystalline superstructure of the film specimens, we investigated electron micrographs of the free surface. The typical micrographs obtained were shown in *Figure 5* in the previous paper¹. No micrographs were obtained which showed clearly boundaries between adjacent rod-like units. This may be due to the small density difference between the rod-like units and their boundaries as predicted by the circular type H_H scattering pattern.

Since it is well known that there are anisotropic rod-like units oriented at $\sim \pm 22.5^\circ$ with the MD , our problem is now to understand the origin of the superstructure. There may be two ways to approach this problem: (a) the superstructure is essentially formed as a consequence of crystallization from oriented melts, and (b) the superstructure is eventually formed by stress exerted to crystallized texture when the films are taken up. The latter may be less probable since for this particular manufacturing condition the stress should not be so large as to change texture which has been already crystallized (probably spherulitic in nature) into the network of the oriented rod-like units. The continuity or integrity of the units also may support the fact that the former is more probable than the latter. Therefore the oriented melts are considered to be crystallized into the network of the oriented rod-like units which are followed

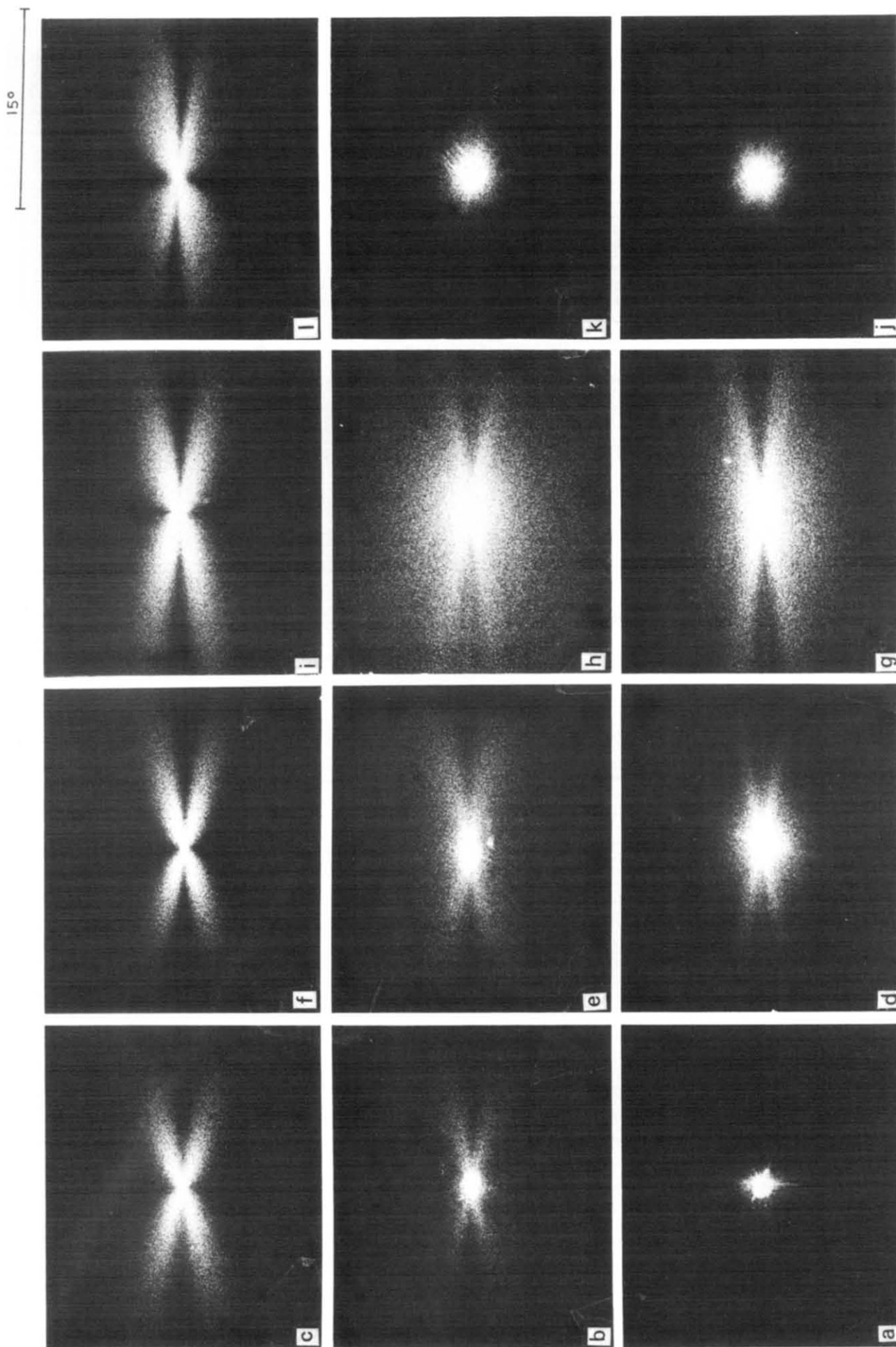


Figure 6 The change of HV , VV , and HH light scattering patterns upon stretching the specimens along the MD . The stretching direction is vertical. (a) 0%, HH ; (b) 0%, VV ; (c) 0%, HH ; (d) 7%, HH ; (e) 7%, VV ; (f) 7%, HH ; (g) 14%, HH ; (h) 14%, VV ; (i) 14%, HH ; (j) 15%, HH ; (k) 50%, VV ; (l) 50%, HH .

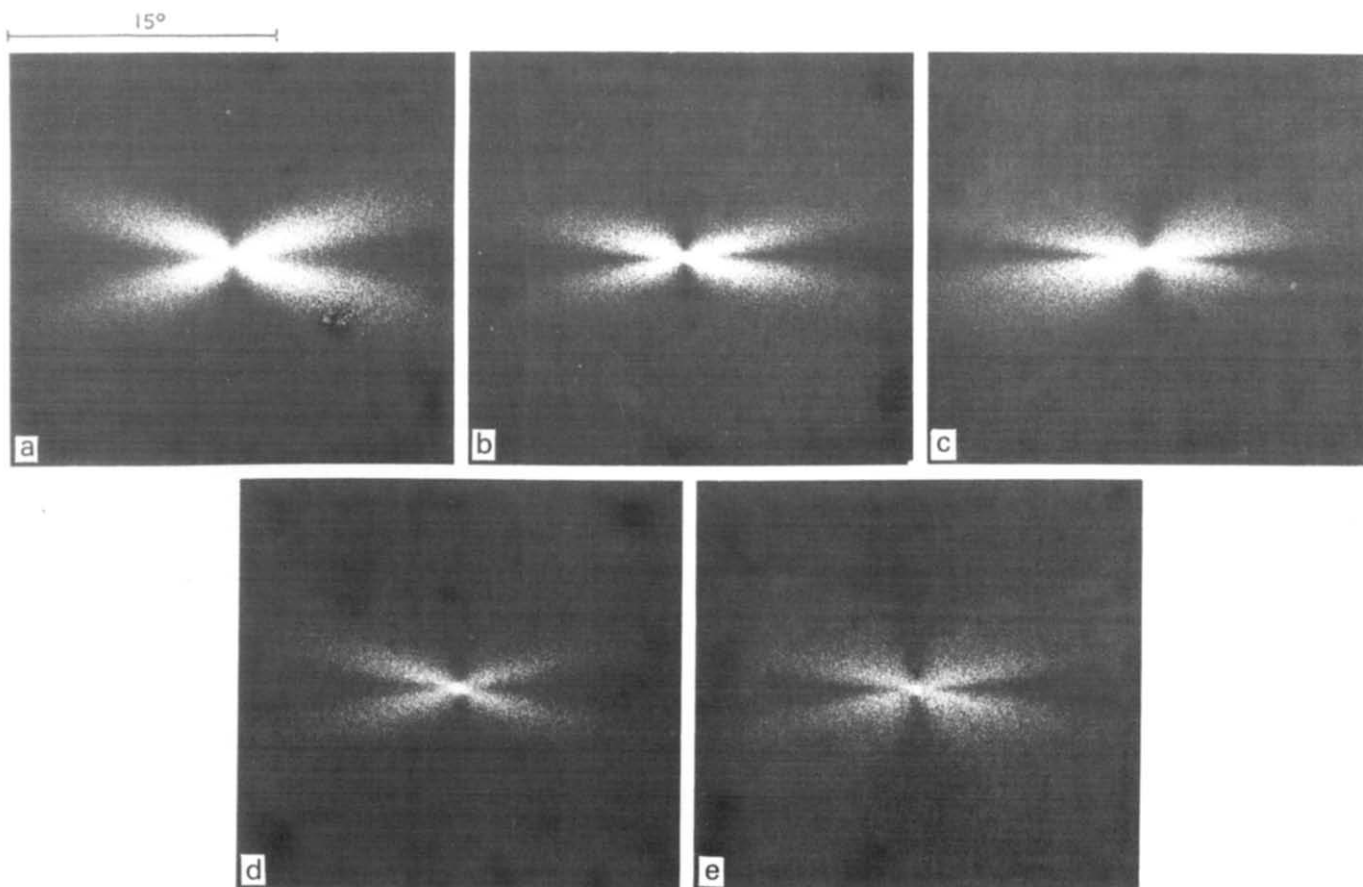


Figure 7 The recoverability of the H_V light scattering patterns upon releasing the deformation from given elongations. The patterns (a)–(c) were obtained upon stretching the specimens along the MD by a given elongation, while (d) and (e) were obtained after releasing the strain from the given elongation. (a) 0%; (b), (d) 20%; (c), (e) 50%

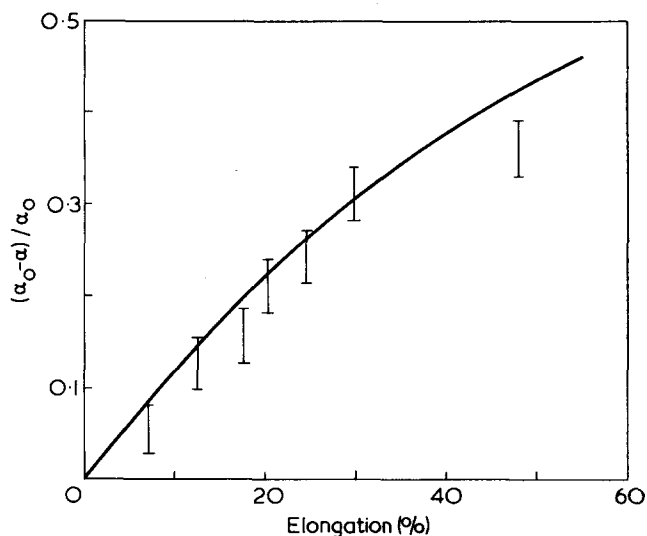


Figure 8 The change of the angle between the MD and the rod-like unit as a function of elongation

by a minor deformation by the stress exerted when the films are taken up.

The anisotropic rod-like units as observed by the scattering patterns and the light micrographs should then correspond to a row-nucleated cylindrite or parallel assembly of them. However, the axes of the cylindrites which are found or considered to be usually parallel to the MD are now inclined by angles of $\sim \pm 22.5^\circ$ with respect to the MD , though there should be some orientation distribution around the

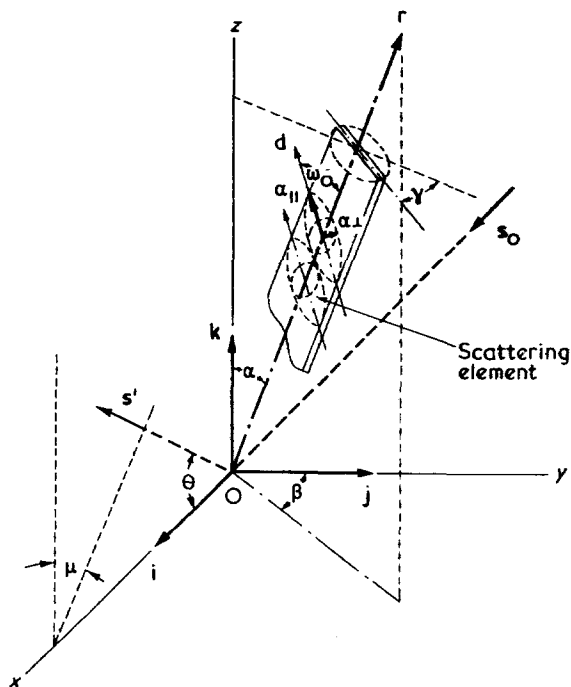


Figure 9 The model of an anisotropic rod-like unit as a scattering entity

preferred direction. It is not clearly understood at present why the axes should be inclined to the MD . A possible interpretation may be drawn by assuming that the row nuclei are formed in the preferred direction due to a particular mode of flow involved in this manufacturing method.

In fact the angle of $\sim \pm 22.5^\circ$ turned out to coincide roughly with flow directions of polymer melt by adding intentionally lower molecular weight impurity (dye) to the melt and observing its flow line.

The angle of 22.5° was found to vary with processing conditions adopted in this work. For example the angle turned out to be 15° and 20° for the HMW2-H1 and the HMW2-H2 specimens designated in the previous paper¹, respectively.

Model calculation of light scattering patterns

In order to confirm further that the scattering patterns shown in Figures 2 to 7 arise from anisotropic rod-like units observed under polarizing microscope (Figure 1), we made calculations on the scattering patterns based upon a simplified model of an oriented assembly of anisotropic cylindrical units (Figure 9).

The coordinate $oxyz$ is a cartesian coordinate where oz is parallel to the MD and ox is the film normal along which the incident beam is irradiated. The vectors $i, j,$ and k are the unit vectors along ox, oy and $oz,$ respectively, and s_0 and s' are those along propagation directions of incident and scattered light beams, respectively. The scattered light is observed as a function of the scattering angle θ and azimuthal angle μ . The axis of cylinder (unit vector r) having length L and radius R is oriented at angles α and β with respect to the coordinate. The cylinder is assumed to be composed of uniaxially anisotropic scattering element with polarizabilities α_{\parallel} and α_{\perp} parallel and perpendicular to the optical axis, respectively. The optical axis whose unit vector is given by d makes a polar angle ω_0 with respect to r .

In our special case, the orientation distribution function $N(\alpha, \beta)$ of the rod axes r has maximum values at α equal to $\alpha_0, \pi - \alpha_0, \pi + \alpha_0,$ and $2\pi - \alpha_0,$ and the value of ω_0 is nearly equal to α_0 . The radius R is roughly 0.5 to $1 \mu\text{m}$.

Some assumptions were introduced in order to simplify the calculation: (a) the radius R is negligibly small compared with length L ; (b) the distribution function $N(\alpha, \beta)$ is uniaxially symmetric with oz axis, i.e. independent of β ; (c) the angle ω_0 is zero, and (d) interrod interference is negligible, and the rod-like unit is dispersed in an isotropic medium having polarizability α_s .

The assumption (a) turned out to be reasonable from the light micrograph (Figure 1). Moreover the lateral size of the rod-like unit was previously shown to affect the pattern only in a quantitative manner^{17,18}. The assumption (b) may be reasonable from experimental evidences of uniaxially symmetric orientations of crystallographic axes and lamellar crystals¹. The assumptions (c) and (d) will be legitimate only if the qualitative shape of the patterns is of importance.

Under these assumptions, H_V and V_V scattering intensities I_{H_V} and I_{V_V} are given by

$$\begin{pmatrix} I_{H_V} \\ I_{V_V} \end{pmatrix} = C \int_{\beta=0}^{2\pi} \int_{\alpha=0}^{\pi} N(\alpha) \begin{pmatrix} E_{H_V}^2 \\ E_{V_V}^2 \end{pmatrix} \sin\alpha d\alpha d\beta \quad (1)$$

where C is a proportional constant related to the absolute intensity, and $N(\alpha)$ is an orientation distribution of the vector r . E_{H_V} and E_{V_V} are amplitudes of H_V and V_V scattering given by:

$$\begin{pmatrix} E_{H_V} \\ E_{V_V} \end{pmatrix} = \begin{pmatrix} (\mathbf{M} \cdot \mathbf{O})_{H_V} \\ (\mathbf{M} \cdot \mathbf{O})_{V_V} \end{pmatrix} F(L; \alpha, \beta) \quad (2)$$

where $(\mathbf{M} \cdot \mathbf{O})_{H_V}$ is an induced dipole moment under H_V polarization condition given by:

$$(\mathbf{M} \cdot \mathbf{O})_{H_V} = E_0(b_r - b_t) \sin\alpha \cos\alpha \cos\beta \quad (3a)$$

similarly

$$(\mathbf{M} \cdot \mathbf{O})_{V_V} = E_0[(b_r - b_t) \cos^2\alpha + b_t] \quad (3b)$$

E_0 is the amplitude of incident light, and b_r and b_t are polarizability differences defined by:

$$b_r = \alpha_{\parallel} - \alpha_s, \quad b_t = \alpha_{\perp} - \alpha_s \quad (4)$$

Now the function F is the structure amplitude of an isolated, homogeneous rod of length L having infinitesimally thin lateral dimension oriented at a given direction and is given by:

$$F(L; \alpha, \beta) = \int_{-L/2}^{L/2} \cos k(\mathbf{r}_1 \cdot \mathbf{s}) d\mathbf{r}_1 = \frac{\sin UW}{UW} \quad (5)$$

where $k = 2\pi/\lambda'$, s is so called scattering vector, and \mathbf{r}_1 is a displacement vector indicating position of a scattering element in the rod. The variables U and W are defined by:

$$U = 4\pi(L/\lambda') \sin(\theta/2) \quad (6)$$

$$W = \sin\alpha \sin\beta \sin(\theta/2) - \sin\alpha \cos\beta \cos(\theta/2) \sin\mu - \cos\alpha \cos(\theta/2) \cos\mu \quad (7)$$

The quantity λ' is a wavelength of light in the medium.

The scattered intensities can be numerically calculated by using equations (1) to (7), if a functional form $N(\alpha)$ is known. In this work $N(\alpha)$ is assumed to be:

$$N(\alpha) = \exp[-\sigma^2(|\sin\alpha| - \sin\alpha_0)^2] \quad (8)$$

where α_0 is related to a peak position and σ to a sharpness of the orientaton distribution. Figure 10 shows the typical

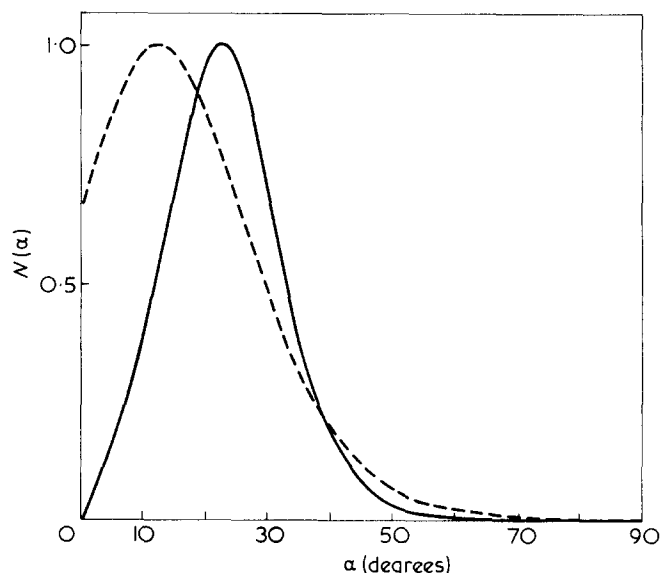


Figure 10 Assumed orientation distribution $N(\alpha)$ for a set of parameters: $\sigma = 5.0$ and $\alpha_0 = 22.5^\circ$ (—); $\sigma = 3.0$ and $\alpha_0 = 12.25^\circ$ (-----)

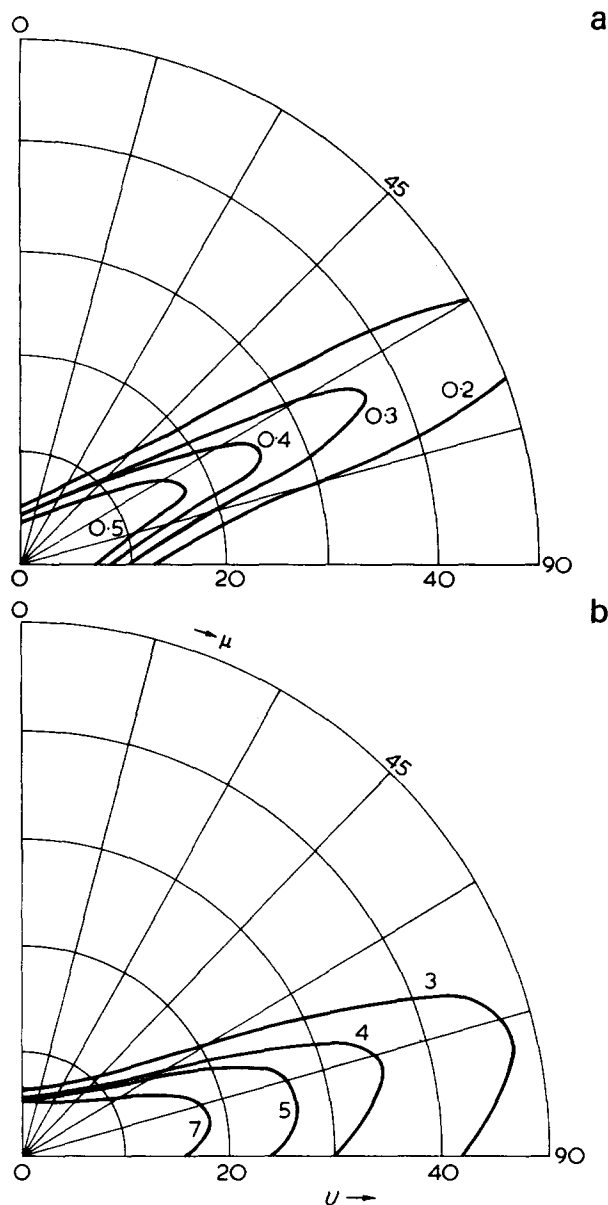


Figure 11 (a) Calculated H_V and (b) calculated V_V scattering patterns for a set of parameters: $\sigma = 5.0$, $\alpha_0 = 22.5^\circ$, $L/\lambda' = 40$, and $p = b_t/(b_r - b_t) = -0.27$

behaviour of $N(\alpha)$ for a set of parameters, ($\sigma = 5.0$, $\alpha_0 = 22.5^\circ$; solid line) and ($\sigma = 3.0$, $\alpha_0 = 12.25^\circ$; broken line).

Figure 11 shows the typical result of calculated H_V and V_V contour patterns for $\sigma = 5.0$, $\alpha_0 = 22.5^\circ$, $L/\lambda' = 40$, and $p = b_t/(b_r - b_t) = -0.27$. The intensity of the calculated H_V patterns passes through a maximum value at $\mu = 65^\circ$, which is in good agreement with that experimentally observed. The relative contribution of density and orientation fluctuations to the V_V scattering pattern is determined by a parameter $p (= -0.27)$, the value of which roughly corresponds to a case where the orientation contribution is predominant to the density contribution. Although splitting of the lobes of the calculated V_V pattern is less than that of the experimental patterns, agreement of the calculated and experimental patterns is fairly good. The intensity of the calculated V_V pattern passes through a maximum value at $\mu = 75^\circ$, which is in agreement with that of the experimental pattern. The difference in the values of μ where the H_V and V_V intensities are maximized is clearly understood by comparing $(\mathbf{M} \cdot \mathbf{O})_{H_V}$ and $(\mathbf{M} \cdot \mathbf{O})_{V_V}$ in equation (3). The deviation between the calculated and

experimental patterns in terms of the splitting of the lobes may arise from an interrod interference effect which is neglected in the present calculation.

Figure 12a shows the calculated H_V pattern for another set of parameters, $\sigma = 3$ and $\alpha_0 = 12.25^\circ$. Although the pattern well agrees with the experimental pattern, the fit of the V_V pattern is less satisfactory compared with the case of $\sigma = 5$ and $\alpha_0 = 22.5^\circ$. Figure 12b shows the calculated H_V pattern for a slightly modified model where $N(\alpha)$ linearly increases from 0 to 1 with increasing α from 0° to α_0° , and decreases according to equation (8) upon further increase of α . The pattern was calculated for a set of parameters, $\alpha_0 = 22.5^\circ$ and $\sigma = 5$ as in the previous case (Figure 11a). Upon modifying the function $N(\alpha)$, the calculated pattern at large W is shown to be slightly skewed towards the equator, the tendency of which is in better agreement with the experimental patterns.

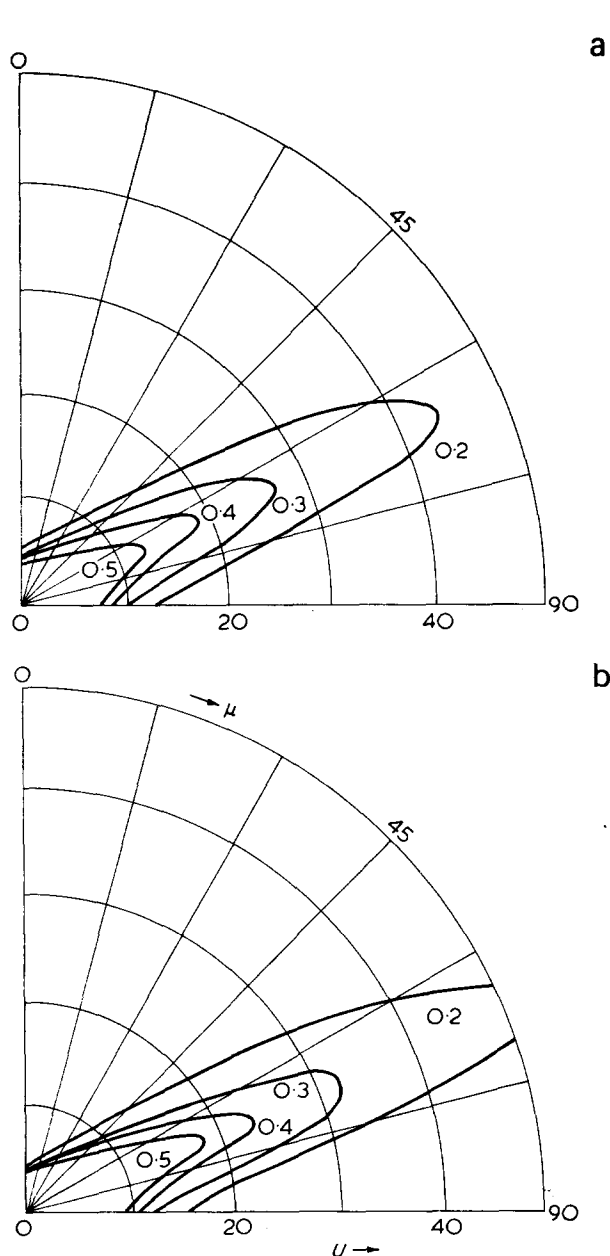


Figure 12 The calculated H_V scattering patterns: (a) $\sigma = 3$, $\alpha_0 = 12.25^\circ$, and $L/\lambda' = 40$, and (b) $N(\alpha)$ being linearly increasing from 0 to 1 with increasing α from 0° to α_0° , and decreasing according to equation (8) for a set of parameter $\alpha_0 = 22.5^\circ$, $\sigma = 5$, and $L/\lambda' = 40$

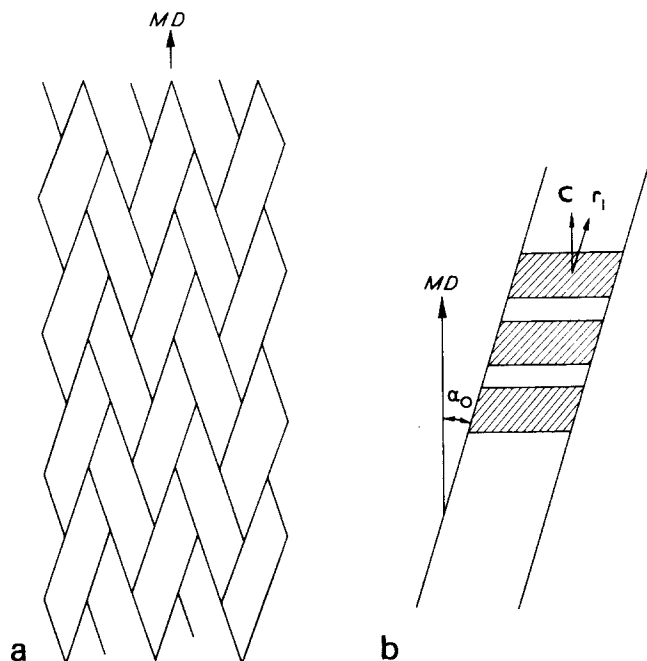


Figure 13 Schematic diagram of the network (a) composed of optically anisotropic rod-like units. The units is composed of a row-nucleated cylindrites or a parallel assembly of them. The axes of the cylindrites or the units (vector r_1) are oriented on average at angles $\pm\alpha_0$ with respect to the machine direction (MD) as in (b), while the average orientations of the chain axis and lamellar normal (vector c) are parallel to the MD

CONCLUSIONS

The high density polyethylene films crystallized by a calendar processing method exhibit a submicroscopic structure typical of that found for films crystallized from oriented melt; stack of crystal lamellae oriented with their normals parallel to the MD , giving rise to a two-point small-angle X-ray scattering patterns and to the second-order orientation factors of the crystal b -axis close to $-1/2$. Simultaneous observations of the light scattering patterns and polarized light micrographs revealed existence of a microscopic structure, i.e. a superstructure of the lamellae (Figure 13). The superstructure is composed of optically anisotropic rod-like units whose axes are preferentially oriented at angle of $\pm\alpha_0$ (22°) with respect to the MD to result in a sort of network structure as schematically shown in Figure 13a.

The rod-like unit is considered to be composed of a row-nucleated cylindrite or a parallel assembly of them. The axes of the cylindrites which are usually found to be

parallel to the MD are inclined with respect to the MD by $\sim\pm 22^\circ$ in this particular processing condition. The average orientations of the chain axis and lamellar normal is parallel to the MD and thus make angles of $\sim\pm 22^\circ$ with respect to the axes of cylindrites as shown in Figure 13b. The angle α_0 is dependent upon manufacturing conditions such as temperatures of the first to the fourth drums and the ratio of extruded and taken-up velocities. The existence of such superstructure plays an important role in the deformation behaviour of specimens and to their mechanical properties, especially at large deformation. It is also important in accounting for whitening of the specimens when they are stretched parallel to the MD .

ACKNOWLEDGEMENT

Part of this work was supported by a grant from Idemitsu Kosan Co. Ltd, Japan, and a grant from Mitsui Petrochemical Industries, Ltd, Japan.

REFERENCES

- 1 Hashimoto, T., Nagatoshi, K., Todo, A. and Kawai, H. *Polymer*, 1976, **17**, 1063
- 2 Keller, A. and Machin, M. J. *J. Macromol. Sci. (B)* 1967, **1**, 41
- 3 Kobayashi, K. and Nagasawa, T. *J. Polym. Sci. (C)* 1966, **15**, 163
- 4 Garber, C. A. and Clark, E. S. *J. Macromol. Sci. (B)* 1970, **4**, 499
- 5 Clark, E. S. in 'Structure and Properties of Polymer Films', (Eds R. W. Lenz and R. S. Stein), Plenum Press, New York, 1973
- 6 Quynn, R. G. and Sprague, B. S. *J. Polym. Sci. (A-2)* 1970, **8**, 1971
- 7 Quynn, R. G. and Brody, H. *J. Macromol. Sci. (B)* 1971, **5**, 721
- 8 Sprague, B. S. *J. Macromol. Sci. (B)* 1973, **8**, 157
- 9 Pennings, A. J. and Kiel, A. M. *Kolloid-Z.* 1965, **205**, 160
- 10 Kawai, T., Matsumoto, T., Kato, M. and Maeda, H. *Kolloid Z. Z. Polym.* 1968, **222**, 1
- 11 Oda, T., Nomura, S. and Kawai, H. *J. Polym. Sci. (A)* 1965, **3**, 1993
- 12 Hay, I. L. and Keller, A. *Kolloid Z. Z. Polym.* 1965, **204**, 43
- 13 Prud'homme, R. E. and Stein, R. S. *J. Polym. Sci. (Polym. Phys. Edn)* 1974, **12**, 1805
- 14 Rhodes, M. B. and Stein, R. S. *J. Polym. Sci. (A-2)* 1969, **7**, 1539
- 15 Hayashi, N., Murakami, Y., Moritani, M., Hashimoto, T. and Kawai, H. *Polym. J.* 1973, **4**, 560
- 16 Samuels, R. J. *J. Polym. Sci. (A-2)* 1969, **7**, 1197
- 17 Hashimoto, T., Murakami, Y., Hayashi, N. and Kawai, H. *Polym. J.* 1974, **6**, 132
- 18 Matsuo, M., Nomura, S., Hashimoto, T. and Kawai, H. *Polym. J.* 1974, **6**, 151

Studies of the chemical degradation of polysiloxanes by hydrofluoric acid: 1. Poly(tetramethyl-*p*-silphenylene siloxane)

N. Okui and J. H. Magill*

Metallurgical and Materials Engineering, University of Pittsburgh, Pittsburgh, Pennsylvania 15261, USA

(Received 1 June 1976)

Hydrofluoric acid solution selectively degrades poly(tetramethyl-*p*-silphenylene siloxane) (TMpS) through scission of the Si—O bonds. The crystallinity of self-seeded single crystals of TMpS is significantly enhanced on degradation as the fold surfaces are removed. For 48% HF at 30°C the crystallinity change is from 73 to 95%. This corresponds to removal of two or more monomeric units from each crystal surface. Acid concentration and treatment temperature are very significant factors in the degradation reactions. The observed molecular weight change with time also depends on these details. The molecular weight distribution of a fraction at first broadens and then narrows with degradation time. At relatively long reaction times, the molecular weight (by g.p.c.) is reduced by more than an order of magnitude over that of the starting polymer fraction. In the early stages of chemical degradation the reaction is heterogeneous presumably because of poor wetting of the siloxane polymer by the HF reagent.

INTRODUCTION

Many years ago chemical etching techniques were first used in the analysis of cellulose by acid hydrolysis in water or ethanol¹³. Since then numerous studies using chemical degradation methods have been used to investigate the nature of the crystal surface structure of polymers. Examples are the degradation of polyethylene with nitric acid¹⁻³ or ozone^{4,5}, isotactic polypropylene with nitric acid^{6,7} and poly(hexamethylene adipamide) with sodium hydroxide⁸ as well as the degradation of cellulose by acid hydrolysis⁹ or poly(ethylene terephthalate) with monoethylamine^{10,11,23} or water vapour¹². Over the last decade polyethylene in particular, has been the subject of very intense investigations, but the precise details of the crystal surface and the mode of chain-folding is still not well understood. However, very recent work on the chemical etching of solution grown polyethylene has provided further insight into the extent of fold region and of the crystalline core^{14,15}. From all studies made to date it is clear that there is a real need to use definitive etching techniques which have a minimum of side reactions in such studies. Recent studies¹⁶ of the surface topography of polyoxymethylene single crystals suggest that they may have an absorbed layer of 'amorphous' material which may have far reaching implications¹⁷ with regard to many solution grown polymer crystals.

It has already been established¹⁸ that TMpS and related siloxanes selectively degrade thermally through Si—O bond cleavage. More recently it has been demonstrated that HF has (a) the ability to selectively cleave Si—O bonds of siloxanes, and (b) the ability to preferentially attack, under certain conditions, the non-crystalline regions of the polymeric solid. From this vantage point the polysiloxanes are amenable to investigation by chemical degradation in a way that will provide useful information about the topography of the chain-fold surface in solution grown crystals.

* Present address: Department of Physics, University of Bristol, Bristol BS8 1TL, UK.

EXPERIMENTAL

Solution grown crystals of poly(tetramethyl-*p*-silphenylene siloxane) (TMpS), molecular weight $M_w = 6.20 \times 10^4$, were crystallized from 0.1% solution in a mixture ethyl acetate and methanol (volume ratio 2:1) using the self-seeding procedure²⁰. The single crystal nature of these samples was confirmed by electron microscopy. The crystalline samples so obtained were then dried overnight *in vacuo* at room temperature. Selective chemical degradation was carried out subsequently by treatment with hydrofluoric acid to which a few drops of a solution of an anionic dispersing agent were added to facilitate wetting of the crystal surfaces. The reaction was carried out in polyethylene vessels which are not attacked by HF. Degradation experiments were conducted at several HF concentrations, at three different temperatures and for various reaction times.

The degraded polymer was carefully washed, first with distilled water and then with methanol in which it was insoluble. Complete removal of HF from the crystals was affected by an overnight soaking and further washing in an excess of methanol. Samples were later dried to constant weight *in vacuo* at room temperature.

Molecular weights and molecular weight distributions were obtained from conventional g.p.c. analysis. A Water Associates G.P.C. was used with tetrahydrofuran as solvent. Aliquots of 0.5 ml of 0.25 wt % polymer solution in tetrahydrofuran were injected into a series arrangement of four columns having porosity ratings of 3×10^6 , 1.5×10^5 , 10^4 , 10^3 Å. The melting temperature and heat of fusion were obtained on degraded and original polymer by Perkin—Elmer (d.s.c.) calorimetry. X-ray small-angle scattering (Rigaku—Denki) was used for determining the crystalline long spacing.

RESULTS

Figure 1 shows the weight loss of poly(TMpS) as a function

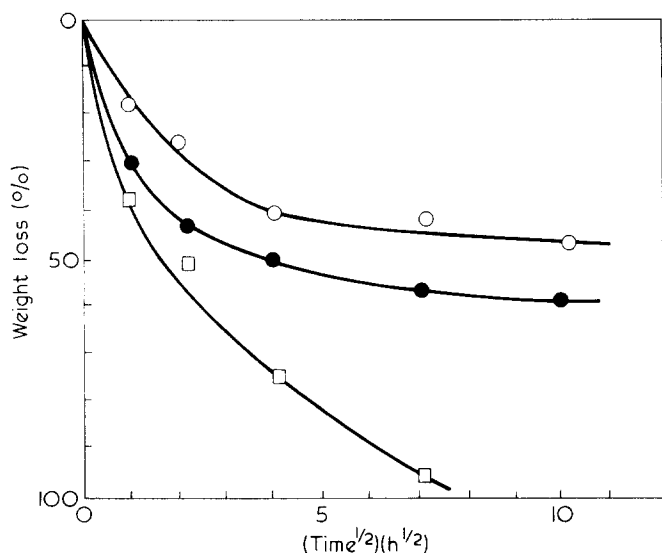


Figure 1 Weight loss (%) of poly (TMpS) on etching with 48% HF at three different temperatures: ○, 20°; ●, 30°; □, 50°C

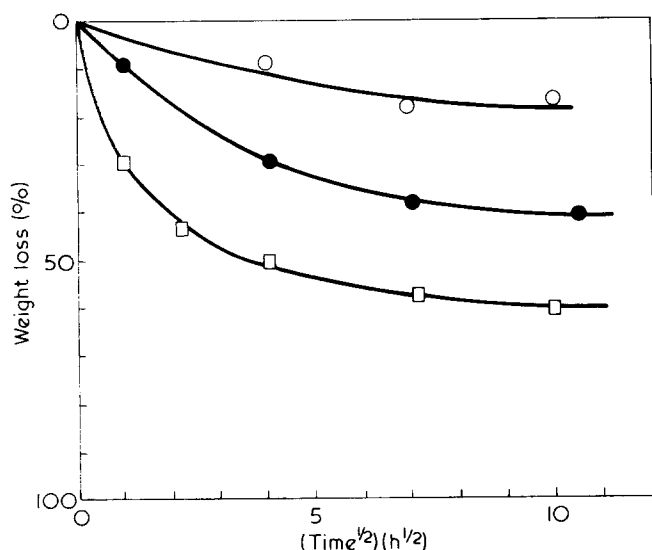


Figure 2 Weight loss (%) of poly (TMpS) on etching at 30°C with three different HF concentrations: ○, 28%; ●, 32%; □, 48%

of time when it was selectively degraded with 48% HF at three different temperatures (20°, 30°, 50°C). It was found that at 50°C, the crystals were etched away very quickly and were completely destroyed in less than 80 h of treatment. At 20° and 30°C, the reaction was less rapid and the weight loss curves show a levelling off after the first few hours of reaction. Figure 2 illustrates how the HF concentration affects the weight loss of poly(TMpS) at 30°C. These curves clearly show that weight loss is very sensitive to both the concentration of the HF and the treatment temperature. Polymer treated with 24% HF at 30°C for 100 h showed no measurable evidence of reaction since the molecular weight and specimen melting point changed very little by this treatment. However, upon etching with 28 and 32% HF at 30°C, there was some loss in weight, but no appreciable change in molecular weight or melting point was detected under these conditions. Contrast, however, the drastic molecular weight decrease with the time during degradation with 48% HF (see Figure 3) where saturation levels are rapidly reached at relatively shorter reaction times.

Typical g.p.c. traces (Figure 4) of the degraded samples show only a single peak. The molecular weight distribution was ascertained from the spread of the g.p.c. peaks for different extents of reaction. In Figure 5, the molecular weight distributions (M_w/M_n) of the resultant g.p.c. curves are plotted vs. the square root of time. At first the molecular weight of the polymer fraction broadens with the time of the reaction in the early stages, after a few polymer

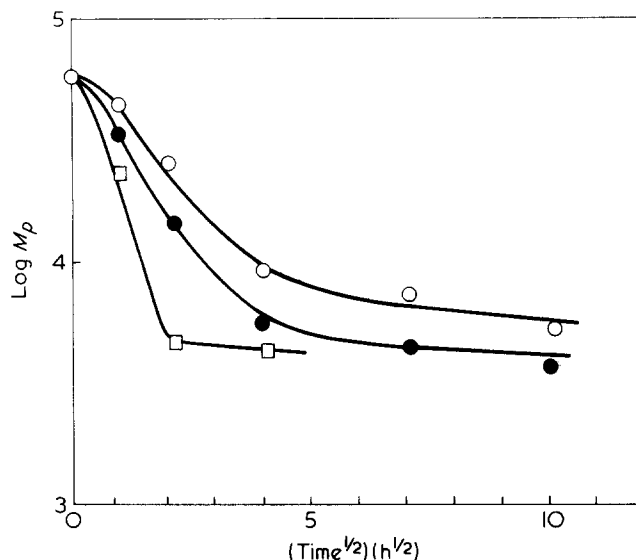


Figure 3 Time dependence of the g.p.c. molecular weight on etching with 48% HF at three different temperatures: ○, 20°; ●, 30°; □, 50°C

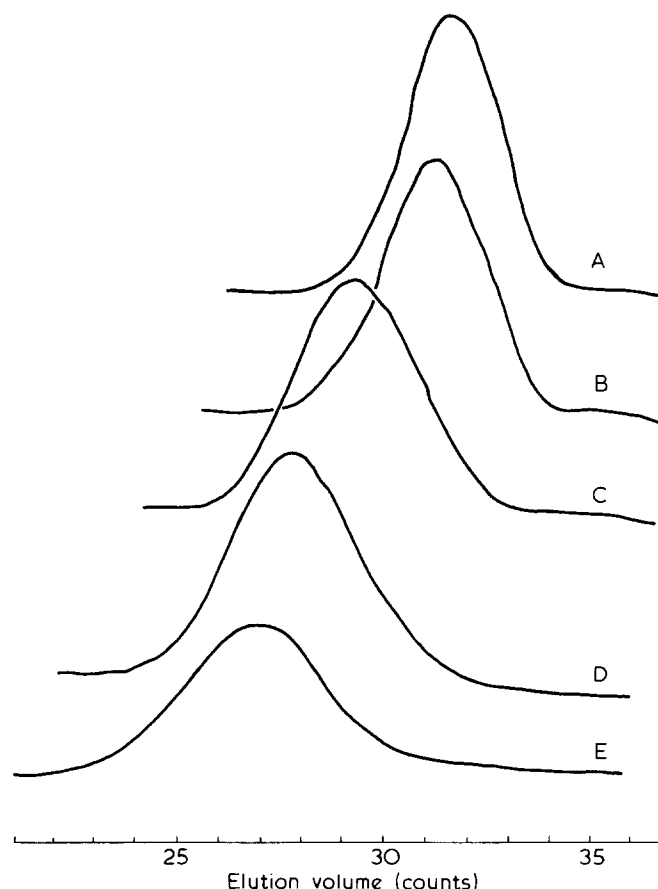


Figure 4 G.p.c. traces of poly(TMpS) degraded with 48% HF at 30°C for various periods of time: A, 100 h; B, 16 h; C, 5 h; D, 1 h; E, 0 h

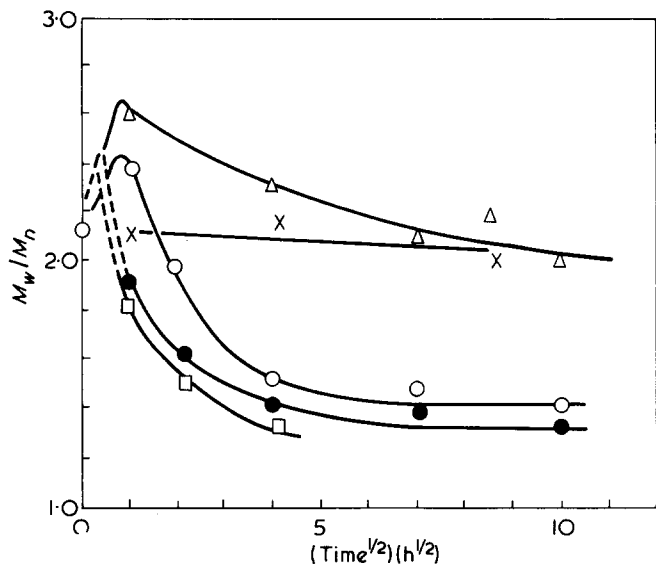


Figure 5 Plot of the molecular weight distribution (M_w/M_n) against the treatment time for poly(TMpS) degraded with HF under the conditions: \circ , 20°C, 48% HF; \bullet , 30°C, 48% HF; \square , 50°C, 48% HF; \triangle , 30°C, 28% HF; \times , 30°C, 32% HF

chains have been cut. For this reason M_w/M_n initially rises as the molecular distribution broadens as observed for 20°C, 48% HF and 30°C, 28% HF treatment conditions. For the 48% HF at 30° and 50°C, and 32% at 30°C specimens, where the degradation is faster, similar M_w/M_n rises are expected (but not measured) as much shorter reaction times (see Figure 5, broken line) are suggested. The molecular weight distribution then narrows as the treatment time and temperature are increased.

Crystal stem lengths determined by small-angle X-ray scattering, make as a function of treatment conditions, are shown in Figure 6. Little change in the long period was found at short etching times using 48% HF. However, beyond a certain reaction time for a given temperature, the crystals were rapidly attacked by HF and solution (i.e. the fold surface was readily removed by HF) and the small-angle long period decreased by about 6~13% approaching constant values at long times of reaction.

DISCUSSION

The increase in the molecular weight distribution, invariance in the molecular weight and the relatively small weight loss change during etching with 28 or 32% HF at 30°C can be explained by the relatively mild reaction conditions that all the surfaces of the aggregations of the single crystals were not equally exposed simultaneously to the etchant. This behaviour is not exclusive to these mild conditions. At very long reaction times when the HF etchant can penetrate more deeply a significant weight loss occurs. Clearly degradation must be incomplete within the reaction times investigated under mild conditions of treatment where the rate is slower and only the readily accessible surfaces of the crystals in the aggregations will be etched with HF. Under such circumstances, a somewhat superficial levelling-off of the weight loss is noted with time because of the slow rate of degradation. A model depicting this type of mechanism of degradation is given in Figure 7. Molecular weight measurements indicate as a function of degradation time that the molecular weight of the specimens changes (increases) only

slightly when the chemical attack occurs at the surfaces of the aggregates of crystals. Support for this behaviour follows from the fact that both the melting point and X-ray long spacing of the samples did not change significantly, supporting the idea of the inaccessibility of the chemical reagent to the crystal surfaces.

The somewhat unexpected trends in behaviour have been noted in other polymer systems too. The dependence of the treatment temperature, degradation reagent and specimen history have all featured in the weight loss (and/or the molecular weight changes) reported for polyethylene [solution grown crystal^{13,21,22}, bulk crystal^{1,2,23}, high oriented²⁴ and copolymers^{25,26}, isotactic polypropylene^{6,7}, poly(ethylene terephthalate)^{11,27} and cellulose⁹]. For instance in the early stages of acid treatment, a negative weight loss was observed for polyethylene crystals due to the addition of heavy chemical groups through the oxidation reaction with HNO_3 ^{21,24}. However, this gain in weight is found to be dependent on the treatment condition²³ (i.e. temperature or acid concentration). Polyethylene crystals etched with HNO_3 show a much more drastic molecular weight change for a few per cent weight loss, because the chain scission occurred mainly on the folded lamellae surface. Degradation varies with sample history because of the extent to which the acid can diffuse or penetrate into the amorphous or more disordered parts of the crystals²³.

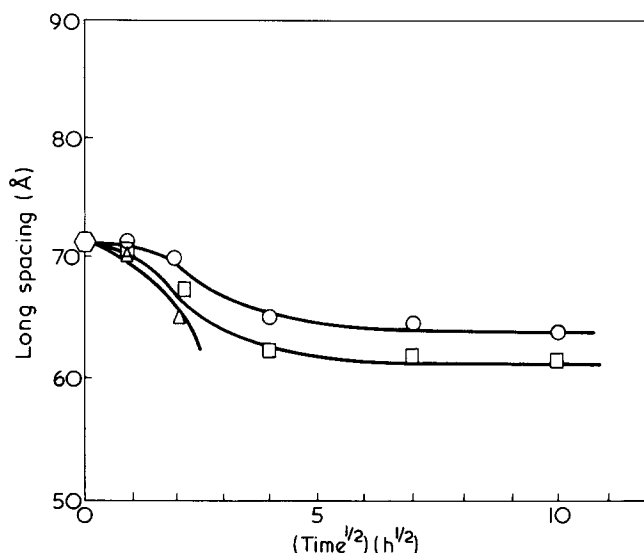


Figure 6 Time dependence of X-ray long spacing on etching with 48% HF at temperatures: \circ , 20°; \square , 30°; \triangle , 50°C

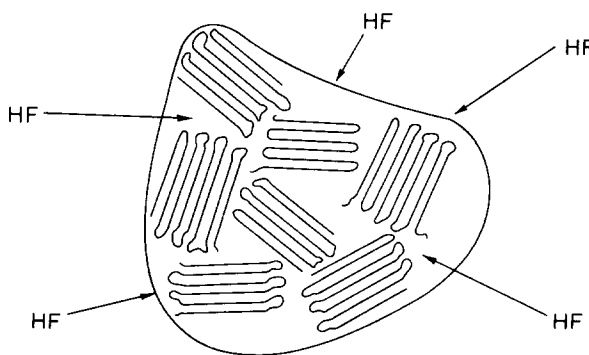


Figure 7 Model depicting the mode of attack of HF on TMpS single crystal clusters. Initially HF attacks accessible peripheral areas (arrowed), later permeating to the 'shielded' interior

Selective chain scission of polyethylene single crystal gave g.p.c. multiple peaks corresponding to the single stem traverse, double traverses and triple traverses of the lamellae²⁸. This evidence is supportive of a chain-folded morphology with a lamella texture. However, it was found that the multiple g.p.c. peaks were ill-defined for the fibrillar crystals^{9,24,29,30} and for branched polymers²⁶. Here degraded residues have inherently broad distributions because of (a) a wider distribution of crystalline lengths than in the lamellar crystal and (b) geometrical constraints associated with accessibility to the etchant.

In poly(TMpS) the molecular weight of unfractionated material is narrow ($M_w/M_n \sim 2.2$) relative to polyethylene ($M_w/M_n \sim 40$) so that the polydispersity of polyethylene usually improves with the acid treatment time tending towards a most probable distribution independent of the original chain length distribution^{31,32}. This trend is illustrated in a theoretical analysis polymer chain scission by Kothiar³³.

Figure 8 summarizes some aspects of the degradation of TMpS by HF. The molecular weight and the crystallinity variations are small until the sample weight loss reaches about 25%. Beyond this point the molecular weight and the crystallinity exhibit a drastic 25% weight loss (as indicated by the broken lines). From here on the molecular weight decrease is small but the crystallinity decrease is still comparatively large. This pattern of behaviour before the weight loss reached 25%, is attributed to limited ingress of HF where diffusion of the etchant is intimately connected with both geometrical (surface area) and wettability considerations. Later in the degradation process, the surface of the single crystals (particularly fold surfaces) are selectively cut very quickly by HF with relatively small weight loss (as indicated by the broken lines in Figure 8 about the 25% level). After the HF has removed most of the fold surface, the acid can then penetrate and attack the crystalline core and progressively remove monomer units from the crystal surfaces causing a further weight loss and crystallinity change.

Crystallinity assessed by d.s.c. from heat of fusion data

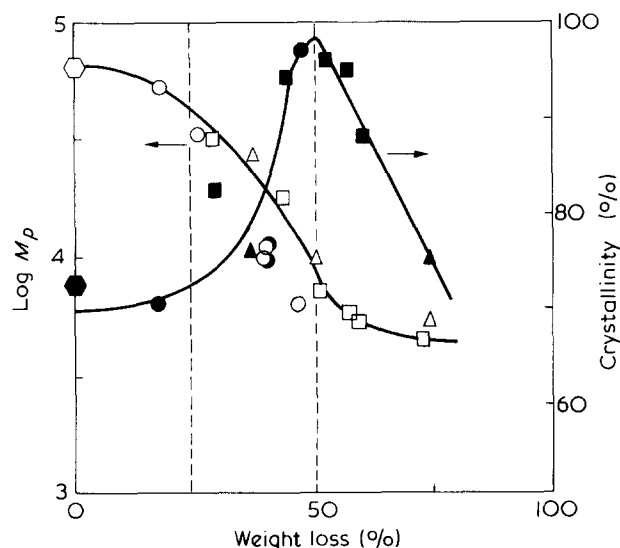


Figure 8 Plot of the molecular weight against the weight loss of the degraded poly(TMpS) under the conditions: ○, 20°C, 48% HF; ●, 30°C, 48% HF; □, 50°C, 48% HF. Plot of the degree of crystallinity against weight loss of the degraded poly(TMpS) under the conditions: ○, 20°C, 48% HF; △, 30°C, 48% HF; ▲, 50°C, 48% HF

reaches levels of 95% after selective degradation with 48% HF at 30°C for 50 h. Originally poly(TMpS) crystals have approximately 73% crystallinity and a 71 Å long period. It was found from long period measurements (Figure 6), that the crystalline core is about 52 Å (consisting of 6 monomer units) with an amorphous fold surface estimated at 9.5 Å (comprised of 2 monomer units). At this point little can be said about the unevenness of the surfaces or indeed if there are adsorbed chains on the crystal surfaces¹⁷. However it is clear that HF removes this surface resulting in a 25% loss of weight—a fact which is consistent with the proposed model and is in good agreement with the measured weight loss, molecular weight measurements and degree of crystallinity (Figure 8).

Still, in all chemical degradative studies it seems that the physical dimensions of the surface actually accessible to the acid must feature somehow in assessing the degradation rate. To date the role of geometrical factors stemming from different morphologies have largely been ignored in the literature. However it is worth mentioning that fibres and bulk crystallized specimens are naturally expected to have less accessible amorphous regions than single crystals or well dispersed aggregates of crystals. At this point the type of crystal must also be important (i.e. whether the morphology is platelet, axialite, hedrite or terraced) within a given specimen. The diffusion or penetration rate of etchant²², as well as sample area vulnerable to attack, deserves further consideration. Some of these problems will be tackled in later papers on the degradation of polysiloxanes. Highly drawn fibres will undoubtedly be more receptive to etchants than unoriented fibres because of the higher sorption and diffusion transverse to the draw direction, that is a consequence of a more open microfibrillar morphology consisting of taut tie molecules³⁴.

CONCLUSIONS

All results can be explained by assuming that aqueous HF preferentially attacks the less ordered surface layer of the crystalline material and removes it through severing selectively the Si—O bonds of poly(TMpS)¹⁹. The molecular weight decreases by 10 ~ 14 times compared to the original specimens. However, current g.p.c. curves did not show multiple peaks corresponding to single, double or triple chain traverses. This may be due to limited g.p.c. resolution or to the presence of degraded molecular fragments having broad distributions. Further investigations are aimed at this problem.

ACKNOWLEDGEMENTS

This work was supported in part by the National Science Foundation under contract GH 32581. The authors are grateful to Professor G. C. Berry of the Mellon Institute of Science for kindly placing his g.p.c. facilities at their disposal. They also wish to thank Dr J. Stejny, University of Bristol, for his helpful comments on the manuscript.

REFERENCES

- Palmer, R. P. and Cobbold, A. J. *Makromol. Chem.* 1964, 74, 174
- Keller, A. and Sawada, S. *Makromol. Chem.* 1964, 74, 190
- Peterlin, A. and Meinel, G. *J. Polym. Sci. (B)* 1965, 3, 9, 105

Chemical degradation of polysiloxanes by hydrofluoric acid (1): N. Okui and J. H. Magill

- 4 Priest, D. J. *J. Polym. Sci. (A-2)* 1971, 9, 1777
- 5 Keller, A. and Priest, D. J. *J. Macromol. Sci. (B)* 1968, 2, 479
- 6 Hock, C. W. *J. Polym. Sci. (B)* 1965, 3, 573
- 7 Hock, C. W. *J. Polym. Sci. (A-2)* 1966, 4, 227
- 8 Koenig, J. L. and Agboatwalla, M. C. *J. Macromol. Sci. (B)* 1968, 2, 391
- 9 Manley, R. St. J. *J. Polym. Sci. (Polym. Phys. Edn)* 1974, 12, 1347
- 10 Koenig, J. L. and Hannon, M. *J. Macromol. Sci. (B)* 1967, 1, 119
- 11 Matsumoto, T., Ikegami, N., Ehara, K., Kawai, T. and Maeda, H. *Kogyo Kagaku Zasshi* 1970, 73, 2441
- 12 Miyagi, A. and Wunderlich, B. *J. Polym. Sci. (Polym. Phys. Edn)* 1972, 10, 2085
- 13 Ranby, B. G. and Ribi, E. D. *Experimentia* 1950, 6, 12
- 14 Keller, A., Martuscelli, E., Priest, D. J. and Udagawa, Y. *J. Polym. Sci. (A-2)* 1971, 9, 1807
- 15 Patel, G. N. and Keller, A. *J. Polymer Sci. (Polym. Phys. Edn)* 1975, 13, 2259
- 16 Breedon Jones, J. and Geil, P. H. *J. Res. Nat. Bur. Stand. (A)* 1975, 79, 609
- 17 Hoffman, J. D. and Davis, G. T. *J. Res. Nat. Bur. Stand. (A)* 1975, 79, 613
- 18 Funt, J. M., Parekh, R. D., Magill, J. H. and Shah, T. Y. *J. Polym. Sci. (Polym. Chem. Edn)* 1975, 13, 2181
- 19 Monroe-Snyder, A. Jr, Okui, N. and Magill, J. H. unpublished results
- 20 Kojima, M., Magill, J. H. and Merker, R. L. *J. Polym. Sci. (Polym. Phys. Edn)* 1974, 12, 319
- 21 Blundell, D. J., Keller, A. and Connor, T. M. *J. Polym. Sci. (A-2)* 1967, 5, 991
- 22 Kawai, T., Goto, T. and Maeda, H. *Kolloid Z. Z. Polym. (Polym. Phys. Edn)* 1968, 223, 117
- 23 Illers, K. H. *Makromol. Chem.* 1968, 118, 88
- 24 Weeks, N. E., Mori, S. and Porter, R. S. *J. Polym. Sci. (Polym. Phys. Edn)* 1975, 13, 2031
- 25 Holdsworth, P. J. and Keller, A. *Makromol. Chem.* 1969, 125, 82
- 26 Holdsworth, P. J., Keller, A., Ward, I. M. and Williams, T. *Makromol. Chem.* 1969, 125, 70
- 27 Farrow, G., Ravens, D. A. S. and Ward, I. M. *Polymer* 1962, 3, 17
- 28 Williams, T., Blundell, D. J., Keller, A. and Ward, I. M. *J. Polym. Sci. (A-2)* 1968, 6, 1613
- 29 Williams, T., Keller, A. and Ward, I. M. *J. Polym. Sci. (A-2)* 1968, 6, 1621
- 30 Williams, F. M., Keller, A., Ward, I. M. and Williams, T. *J. Polym. Sci. (A-2)* 1968, 6, 1627
- 31 Matsumoto, M. *Kobunshi Ronbunshu* 1949, 6, 40
- 32 Hamada, H. *Kobunshi Ronbunshu* 1962, 19, 451
- 33 Kotliar, A. M. *J. Polym. Sci. (A-2)* 1964, 2, 4303, 4327
- 34 Peterlin, A. *Pure Appl. Chem.* 1974, 39, 239

Confirmation of the role of radicals in energy transfer resulting in induced phosphorescence of irradiated doped poly(methyl methacrylate)

C. S. Bilen and D. J. Morantz

London College of Printing, London SE1, UK

(Received 10 June 1976)

Transient species, in irradiated doped poly(methyl methacrylate) (PMMA), enhance the transfer of energy to the triplet state of the dopant. Production of these transients enables a strong, induced, phosphorescence to occur even at room temperature. This is inhibited by the use of a radical scavenger or the presence of oxygen, which results in reduction of the phosphorescence intensity in the post-irradiation period. E.s.r. analysis of u.v. and X-ray irradiated doped PMMA samples, showing induced phosphorescence, identifies such transients as PMMA radicals. The correlation between induced phosphorescence and thermoluminescence, previously reported, is extended by a further correlation between induced phosphorescence and e.s.r. measurements. It is concluded that the PMMA radicals are involved in the induced phosphorescence as well as the thermoluminescence.

INTRODUCTION

The presence of radicals in irradiated polymers is well established^{1,2}. However, there has been some controversy^{3,4} as to whether, in irradiated PMMA samples, there is only one type of radical with the same decay rate for various e.s.r. lines (5th and 7th lines are generally used for these arguments) or whether more than one kind of radical is present having different decay rates for the 5th and 7th lines. More recent studies⁵ indicate that various types of radical may be produced under different irradiation conditions, however, at room temperature one type only of propagation radical predominates over other types. This radical is characterized by a strong (so-called 9 line) e.s.r. spectrum. We have studied the luminescence of doped PMMA which has been irradiated by X-ray, u.v. light and visible laser light respectively and also by prolonged heating, at 473K, of this system in the absence of air. In each case this results in *induced phosphorescence*^{6,7}, emitted by the affected regions of these samples.

We have demonstrated⁶ the role of transient species as providing an alternative route for the transfer of energy to the triplet state. Other studies⁸ correlated the thermoluminescence and induced phosphorescence of the irradiated systems and helped to narrow the possible range of transient species responsible for these two effects. Our present findings concerning the reaction of transient species with atmospheric oxygen yields an estimate of the activation energy for oxygen sensitized decay of phosphorescence which is not inconsistent with the reported value⁹ for radical recombination. Furthermore, inhibition of the induced phosphorescence, through the use of a radical scavenger (diphenylamine) during u.v. irradiation, also indicates the presence of radicals in the irradiated regions. Although radicals have been demonstrated in u.v. and X-ray irradiated PMMA using e.s.r. spectroscopy, such studies did not relate to the effects of induced phosphorescence or

thermoluminescence. The present paper reports direct, e.s.r., evidence which confirms that PMMA radicals (propagation type) occur in u.v. and X-ray irradiated samples exhibiting induced phosphorescence and we find a strong correlation between the induced phosphorescence intensity and the e.s.r. signals for the u.v. irradiated samples.

EXPERIMENTAL

PMMA (BDH) was of low molecular weight and average particle size, 170 μm . Triphenylene (purity 98%) and dibenzothiophene (95%) dopants were obtained from Ralph N. Emanuel Ltd. The diphenylamine radical scavenger was laboratory reagent grade from BDH. The samples were prepared as described elsewhere⁶ and the radical scavenger, diphenylamine powder, was mixed with the doped or undoped PMMA by a similar method. Details of the emission spectrophotometer have also been mentioned in earlier papers⁸. X-ray irradiation of samples was undertaken in a steel irradiation chamber fixed at a point focus window of an Elliot Automation Cu target tube (type no. 315/Tx/6 Cu). This was generally operated using an accelerating potential of 30 kV at 16 mA beam current. X-ray spots of about 8 mm diameter were produced. U.v. irradiation of doped PMMA samples was carried out using an unfiltered high pressure mercury lamp with quartz windows (MED Mazda, powdered by an a.c. supply) at a distance of about 10 cm. Irradiations were of 5–10 min intervals, the total exposure being up to ~ 130 min.

E.s.r. analysis was undertaken at room temperature in air using a Varian E-12 X-band spectrometer and scans were carried out immediately after the completion of each u.v. irradiation period. The emission spectra for induced phosphorescence were also recorded using the same u.v. lamp in a similar arrangement.

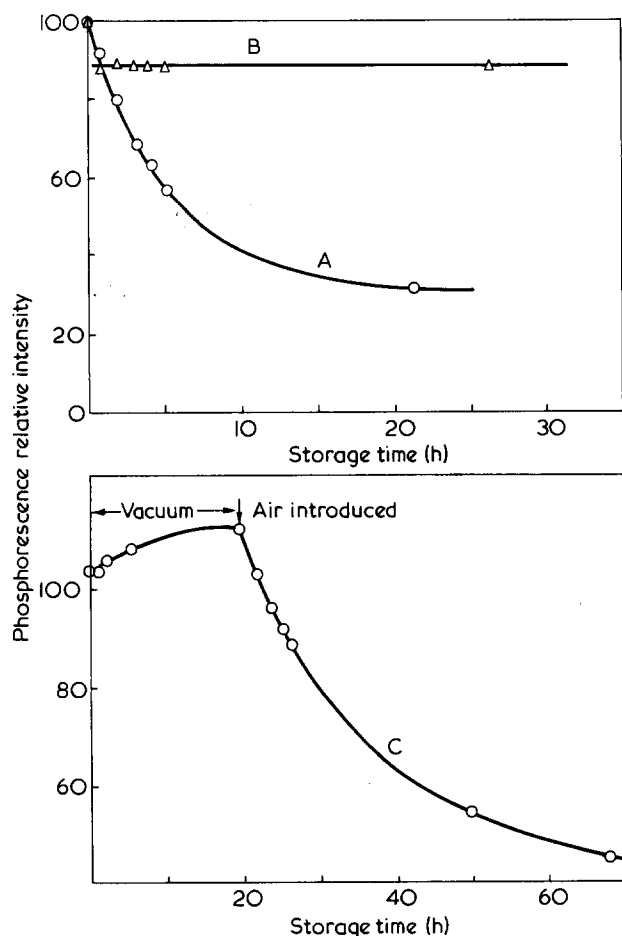


Figure 1 Effect of air on phosphorescence decay ratios. Curves A and B are for X-ray irradiated dibenzothiophene doped PMMA samples during the post irradiation period. A, Sample stored in air; B, sample stored in nitrogen; C, shows phosphorescence intensity changes of a u.v. irradiated triphenylene doped PMMA sample stored in vacuum and after the introduction of air

RESULTS

Figure 1 shows the sensitivity of the induced phosphorescence to the oxygen of the air. The intensity (curve A) falls, after 20 h, to about 30% of the value obtained immediately after the X-ray irradiation. The induced phosphorescence intensity remains high, however, when the irradiated samples are stored in oxygen-free nitrogen gas (curve B) or in a vacuum (curve C). Curve C again emphasizes how the induced phosphorescence is affected by the introduction of air to the storage dessicator. We believe that the induced phosphorescence intensity decreases when oxygen reacts with the transient species to form peroxides. The sensitivity towards oxygen of the transient species is also indicated by our observation that the induced phosphorescence in doped PMMA samples is only generated when the air (oxygen) is excluded from these samples during prolonged heating. Furthermore in u.v. irradiated samples the induced phosphorescence effect is restricted to surface layers as opposed to X-ray irradiation where the effect is in the whole thickness of the sample. The surface layers (u.v. irradiated) show a much faster decrease with storage in air, than do the thicker, bulk, (X-ray irradiated) samples.

The radical character of the transient species is further supported by the results shown in Figure 2. Curves A and B (Figure 2a) show the emission from a triphenylene doped

PMMA sample before and after u.v. irradiation. Note the development of an emission peak at 460 nm in curve B, corresponding to induced phosphorescence of the dopant in addition to the normal fluorescence peaks in the region of 360 nm. Curves C and D (Figure 2b) show the emission of triphenylene doped PMMA sample also containing a radical scavenger diphenylamine, before and after irradiation respectively. Before irradiation, the scavenger slightly reduces the fluorescence emission and suppresses the vibrational structure corresponding to triphenylene. After the u.v. irradiation (similar exposure to that in the case of curve B above) the sample does not show induced phosphorescence but does give a strong fluorescence peak in the region of 400 nm. The curves E and F show the emissions of PMMA samples containing only the radical scavenger compound diphenylamine before and after u.v. irradiation. Noting the similarity of emission after u.v. irradiation, and bearing in mind that no such emission takes place when the PMMA sample is without any additive and irradiated with u.v. light, one can only conclude that these emission bands (at 400 nm) are related to the radical scavenger diphenylamine dopant when it interacts with the transient species in PMMA. Furthermore the presence of primary dopant triphenylene does not affect this interaction.

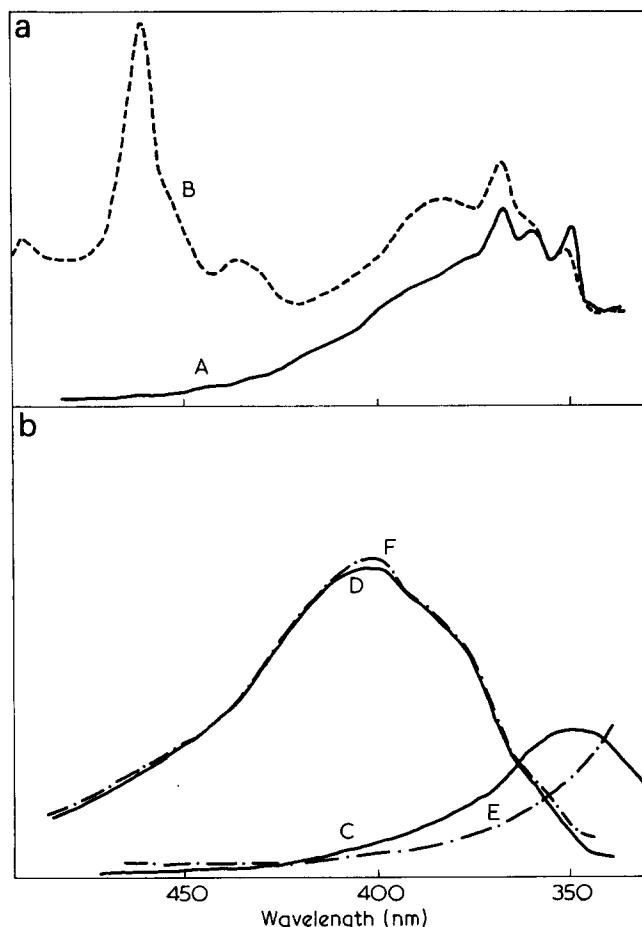


Figure 2 (a) Emission spectra of triphenylene doped PMMA sample before (A) and after u.v. irradiation (B). (b) Emission spectra of triphenylene doped PMMA sample also containing diphenylamine radical scavenger (—) before (C) and after u.v. irradiation (D); emission spectra of PMMA sample without triphenylene but containing radical scavenger (- · - ·) before (E) and after u.v. irradiation (F).

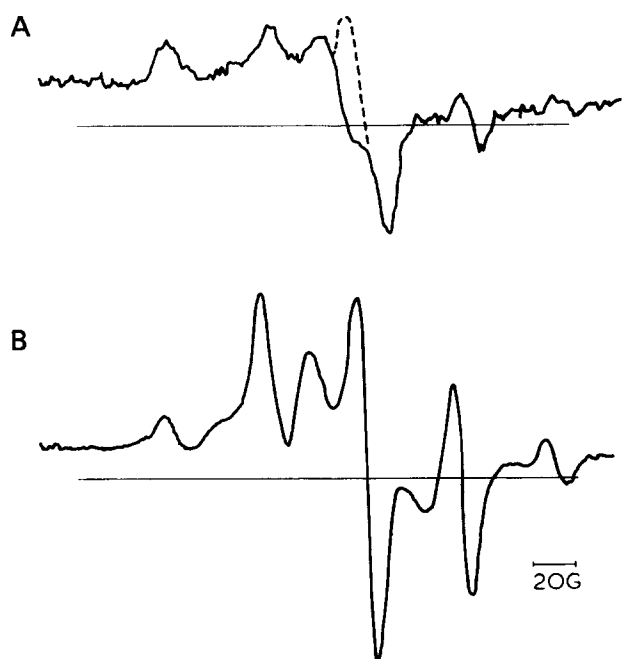


Figure 3 A, E.s.r. spectrum of X-ray irradiated dibenzothiophene doped PMMA sample scanned after 5½ h storage in air; B, e.s.r. spectrum of dibenzothiophene doped PMMA sample u.v. irradiated for 40 min and scanned immediately after irradiation

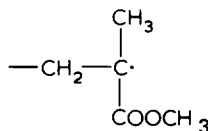
Curve A of Figure 3 shows the e.s.r. spectrum obtained, when dibenzothiophene doped PMMA, showing induced phosphorescence under u.v. inspection, was placed in the Varian E-13 cavity. This sample was irradiated, with the X-ray beam (16 mA at 30 kV accelerating potential) from a Cu target for 1 h; the sample was, however, left in air for 5½ h. As a result of this long exposure to air and because the X-ray beam spot only covered about 1/10 of the cavity area, the e.s.r. signal is relatively weak. Curve B shows the typical sharp e.s.r. spectrum, immediately after a 40 min period of u.v. irradiation for a dibenzothiophene doped PMMA sample. This spectrum is similar to those obtained by Wong¹⁰ for u.v. irradiation of evacuated PMMA films and X-ray and γ -irradiated PMMA samples^{3,5}. The line attributed to a signal from the quartz container¹⁰ did not appear in our scan, as solid samples without quartz containers were used.

Figure 4, curve A shows the variation of the e.s.r. signal, for a dibenzothiophene doped PMMA sample, with increasing u.v. irradiation. The curve shows a linear increase at first, followed after a maximum by a non-linear fall. A corresponding induced phosphorescence intensity behaviour is shown by curve B. The curves have similar shapes but with a slight shift in the relative position of the peaks for the two curves. We recall that such shifts were also present when induced phosphorescence and thermoluminescence curves were compared in our earlier studies⁸.

DISCUSSION

The results shown in Figures 1 and 2 clearly indicate that the transient species responsible for induced phosphorescence in doped PMMA are sensitive to both oxygen and radical scavengers. This points strongly to the possibility that the transients are radicals derived from the PMMA matrix. Moreover, we have estimated the activation energy for the decay, caused by oxygen, of induced phosphore-

scence (from the decay rates at 295K, 307K and 314K). The value obtained, 16.6 kcal, may be compared with half of the reported values (which range from 28–32 kcal) for PMMA radical pair recombination reported by Ohnishi and Nitta⁹. In the latter case two radicals need to be detrapped (in the absence of oxygen) compared with one only in our case in the presence of oxygen. This strengthens our earlier conclusions that the transient species are the PMMA radicals, which predominate at room temperature, of the type:



The e.s.r. spectra of Figure 3 for X-ray and u.v. irradiated doped PMMA samples clearly identify the transients as the above mentioned species of PMMA radicals by their characteristic line spectrum. The spectrum for the X-ray irradiated sample corresponds to a low signal, however, and probably for the reasons previously mentioned, namely small spot size and long exposure to air. Nevertheless there remained sufficient signal to identify it as belonging to PMMA radical. This scan of the X-ray sample, however, does not show the central line (indicated by the broken line). This has been nullified by the cavity signal. This effect is also seen in the reduction of the amplitude of the same central line for the stronger signal, in the case of the u.v. irradiated samples (Figure 3, curve B).

The strong similarity of the curves in Figure 4 supports the argument that these radicals, measured by the e.s.r. signal, play an essential role in induced phosphorescence. The slight shift in the peak positions for the two curves in Figure 4 may be explained as follows: the induced phosphorescence emission is recorded using a weak excitation source (312 line) which only affects the topmost layers of the irradiated regions near the surface of the irradiated samples. The e.s.r. signal and this would be the case as well for thermoluminescence (we have reported, elsewhere⁸, the correlation of thermoluminescence and induced phosphorescence) is derived from all the affected layers including deeper layers. Thus the weighted average for the e.s.r. signal (and for thermoluminescence) would reach saturation after a small time lag as compared with the induced phosphorescence measurements.

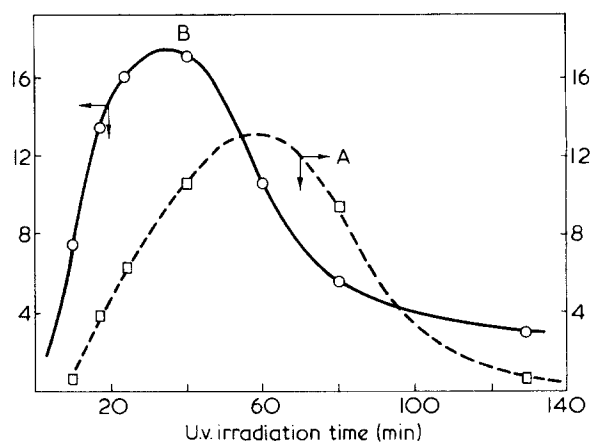


Figure 4 Comparison of e.s.r. signal amplitude (A) and induced phosphorescence intensity (B) for increasing u.v. irradiation periods

Our conclusion concerning the role of PMMA radicals in energy transfer is further supported by the anomalous thermal behaviour of induced phosphorescence. Such energy transfer as well as induced phosphorescence was reduced drastically as the irradiated doped PMMA sample was cooled below the γ -transition of PMMA. Below this transition the rotational freedom of the ester group¹² is reduced and we believe that loss of such freedom affects the energy transfer of these radicals. However, other types of radicals of PMMA origin may also be produced under other conditions⁵, and their role and participation in energy transfer processes were quite different⁸ from those of the PMMA radicals now identified by the sharp line spectra in *Figure 3*. The evidence for the role of PMMA radicals in energy transfer to the triplet state of the dopant, is we believe, quite conclusive.

ACKNOWLEDGEMENTS

We acknowledge an ILEA Research Fellowship to one of us (C. S. B.). We are also grateful to Professor J. C. Anderson and Dr J. Gibson for arranging the use of the Varian E112

spectrometer at Imperial College London; furthermore we acknowledge Mr G. M. Lack's assistance during the e.s.r. experiments.

REFERENCES

- 1 Charlesby, A. 'Atomic Radiations and Polymers', Pergamon, Oxford, 1960
- 2 Chapiro, A. 'Radiation Chemistry of Polymeric Systems', Interscience, New York, 1962
- 3 Symons, M. C. R. *J. Chem. Soc.* 1963, 2, 1186
- 4 Piette, H. 'NMR and EPR Spectroscopy', Pergamon, Oxford, 1960, pp 218
- 5 Geuskens, C. and David, C. *Makromol. Chem.* 1973, 165, 273
- 6 Morantz, D. J. and Bilen, C. S. in 'Reactivity of Solids', (Eds J. S. Anderson, M. W. Roberts and F. S. Stone), Chapman and Hall, London, 1972, p 525
- 7 Morantz, D. J. and Bilen, C. S. *8th Int. Symp. Reactivity of Solids Gothenburg* June 1976
- 8 Morantz, D. J. and Bilen, C. S. *Polymer* 1975, 16, 745
- 9 Ohnishi, S. I. and Nitta, I. *J. Polym. Sci.* 1959, 38, 451
- 10 Wong, P. K. *Polymer* 1974, 15, 60
- 11 Bilen, C. S. and Morantz, D. J. *Nature* 1975, 258, 66
- 12 Wundrich, K. *J. Polym. Sci. (A-2)* 1974, 12, 201

Some aspects of flame retardancy in high density polyethylene*

S. C. Sheat and J. P. Berry

Department of Polymer and Fibre Science, University of Manchester Institute of Science and Technology, Manchester, UK

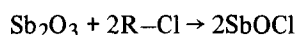
(Received 9 June 1976; revised 1 July 1976)

The influence of the flame retardant agents, antimony trioxide and a chlorinated hydrocarbon, on the mechanical and flammability properties of high density polyethylene has been studied. Flammability was assessed by means of the limiting oxygen index test, whilst mechanical properties were measured in the tensile mode on compression moulded samples. An optimum in terms of flame resistance was found at a Sb:Cl mole ratio of 1:3 which tends to confirm that the actual flame retardant is the volatile antimony trichloride. The modulus, yield and drawing behaviour, and ultimate properties of the unoriented samples did not show significant change (< 10%) until the combined level of additive exceeded 25% by wt. Above this level it was found that the samples could not be oriented and that the elongation to break decreased markedly. Alumina trihydrate was studied as an alternative flame retardant but was found to be unsuitable for use in HDPE, since to obtain an adequate level of fire retardancy a high concentration (40%) of additive was required, which resulted in a significant deterioration in the mechanical properties.

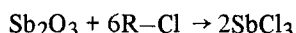
INTRODUCTION

In the study of fire retardant additives it is desirable to include the effect of these substances on other properties, notably mechanical, as these determine to a large extent the end use to which a particular formulation can be put. It is the purpose of this paper to apply these ideas to the antimony/chlorine system and to alumina trihydrate, using high density polyethylene (HDPE) as the matrix.

Although well known, the antimony/halogen synergism is highly controversial in terms of optimum ratios of antimony to halogen. Little¹ in 1947 made what is considered to be the first attempt at explaining this synergism. He claimed that hydrogen chloride was evolved from the chlorinated hydrocarbon which reacted with antimony trioxide to yield antimony oxychloride (SbOCl) *in situ*. This implies an optimum flame retardancy when the mole ratio of Sb:Cl is close to 1:1, according to the following simplified reaction:



More recently^{2,3} claims were made implying an optimum at ~28% (w/w) Sb₂O₃ and ~15% chlorinated hydrocarbon, while Raff and Allison⁴ claimed that 6% chlorinated hydrocarbon is sufficient. Pitts⁵ reviewed recent evidence and while conceding that the oxychlorides of antimony (SbOCl and Sb₄O₅Cl₂) are powerful flame retardants, suggested that the real flame retardant is the volatile antimony trichloride (SbCl₃) according to the following simplified reaction:



In 1966 Fenimore and Martin^{6,7} reported saturation in terms of oxygen index above certain mole ratios of Sb:Cl in polyethylene. Unfortunately their results are somewhat difficult to interpret and it was the purpose of the work reported in this paper to repeat their results.

Regarding alumina trihydrate, which has gained popularity as a fire retardant, in recent years, owing largely to its relatively low cost, this has been described by Hopkins⁸ and functions by the endothermic release of water at temperatures above 180°C resulting in flame cooling.

EXPERIMENTAL

Materials

Commercial grade materials were used throughout this investigation and their properties are shown in *Table 1*, the data being taken from the manufacturers' information sheets.

Sample preparation

To ensure good dispersion of the flame retardant a two-stage mixer process was adopted. The polyethylene was heated to 145°C in a Banbury mixer, the additives added over a period of 4 min and mixing continued for another 4 min at 125 rev/min. After discharging, the hot blend was rapidly transferred to a two-roll hot mill and intensively mixed for another 5 min before sheeting off, a differential speed of 1:1.14 was used to ensure shear in the nip, and roller temperatures were set at 145°C front, and 127°C rear.

Sheets moulded from 100% HDPE subjected to the above conditions showed no significant difference in tensile and flammability properties to those of sheets produced under identical moulding conditions from virgin polymer chips. On the basis of this it was assumed that no significant degrada-

* Presented at the SCI Conference Flammability, Loughborough, January 1976.

† Present address: Van Leer Research Laboratories, Passfield, Hampshire, UK.

Table 1 Materials specification

(A) Polyethylene:	
Viscosity-average molecular weight	110 000
MFI (ISO R292A)	0.25 g/10 min
Density	959 kg/m ³
Melting range (polarized microscope)	132°–135° C
(B) Antimony trioxide:	
Density	5500 kg/m ³
Purity	>99%
Oil absorption (g/100 g)*	12
Refractive index	2.09–2.29
(C) Chlorinated hydrocarbon†:	
Approximate chemical formula	C ₂₃ H ₂₈ Cl ₂₀
Approximate molecular weight	1010
Amount of chlorine (w/w)	68–72%
Density	1630 kg/m ³
Oil absorption (g/100 g)‡	35
Softening point	>85° C
(D) Alumina trihydrate§:	
Density	2400 kg/m ³
Oil absorption (g/100 g)	40
Purity	>99%
Chemical formula	Al ₂ O ₃ ·3H ₂ O
Refractive index	1.58

* Boiled linseed oil (density 935 kg/m³) is commonly used to measure oil absorption; † typically Cereclor 70® ex ICI; ‡ measured by authors; § typically Trihydrate E® ex Platichem

tion of the HDPE occurred during the blending and moulding cycles.

Compression moulded sheets of nominal thickness, 0.8 mm, were produced at 190°C and slowly cooled to room temperature over a period of 8 min. Moulded sheets were not annealed following the experience of Anderton and Treloar⁹ who found that annealing HDPE sheets gave poor drawing characteristics.

In view of its reproducibility it was decided to use the limiting oxygen index test for flammability as originally proposed by Fenimore and Martin¹⁰. Basically this test measures the concentration of oxygen (by volume) in an oxygen/nitrogen atmosphere to just sustain combustion and is interpreted on the basis of air containing ~21% oxygen. Thus, materials with an oxygen index (OI) less than 21 can be expected to burn in air, while materials with a higher OI will generally be self-extinguishing.

Samples cut from the compression moulded sheets were subjected to this test as per ASTM D2863-74 with one modification. This specification recommends that for material in the form of thin sheet the criterion for sustained combustion shall be the burning of a sample of length 100 mm. In view of the size of the compression moulded sheets (150 × 150 mm) it was decided to adopt the criterion for a rod, which is burning for a length of 50 mm or 3 min, whichever occurs first. This enabled more samples to be tested from one moulded sheet. Consequently while OI results quoted here are comparative with each other they will be slightly low when compared with results obtained by other authors. Results indicate the mean and range of five samples.

Dumbbell shaped specimens 80 mm long were used for the tensile tests, thickness being measured at three points along the length of the parallel section. Five samples per variable were tested at a clamp separation rate of 50 mm/min and an initial strain rate of 100% per min. The tests were conducted at room temperature (19°–23° C) and all samples except those at 40% additive level necked and drew. Since dumbbell specimens were used it was decided to use a

corrected initial length of 35 mm in the calculation of mechanical properties in an attempt to overcome the problems posed by this shape. Accordingly results are comparative only.

Theoretical boundary conditions, corresponding to uniform stress and uniform strain were calculated as detailed by Broutman and Krock¹¹, assuming moduli for antimony trioxide and the chlorinated hydrocarbon of 2×10^{10} Pa and 2×10^9 Pa respectively. The iso-stress modulus is calculated from:

$$1/E = \sum \frac{V_i}{E_i}$$

where E is the composite modulus; E_i is the modulus of components; V_i is the volume fraction of components: while the iso-strain modulus is obtained from:

$$E = \sum V_i E_i$$

DISCUSSION

Regarding the antimony/chlorine system it is convenient to plot results as a function of mole fraction of chlorine. This has the advantage of indicating the effects of different total concentrations on the same graph, however the graphs become somewhat compressed in that a Sb:Cl ratio of 1:3 is shown as a mole fraction of chlorine of 0.750 while a Sb:Cl ratio of 1:30 becomes 0.968.

Results for 10% and 20% total additive concentrations are shown in Figure 1 and considering these graphs it would appear that two discontinuous regions exist, corresponding to undiluted antimony trioxide and chlorinated hydrocarbon respectively. Some synergism can be seen to exist in that the oxygen index obtained in a blend is higher than that obtainable by the individual components, antimony trioxide and chlorinated hydrocarbon. It can be seen that this synergism is relatively small; an effect which has been ascribed to the relatively high degree of crystallinity of the base polymer¹².

In view of this synergism it would appear logical to consider the points at 100% Sb₂O₃ and 100% chlorinated hydrocarbon as not belonging to these curves, because of the lack of synergism at these two points. Both curves, at 10% and 20% total additive concentration, show points of inflection at mole ratios Sb:Cl of just greater than 1:3 which tends to confirm that the actual flame retardant is

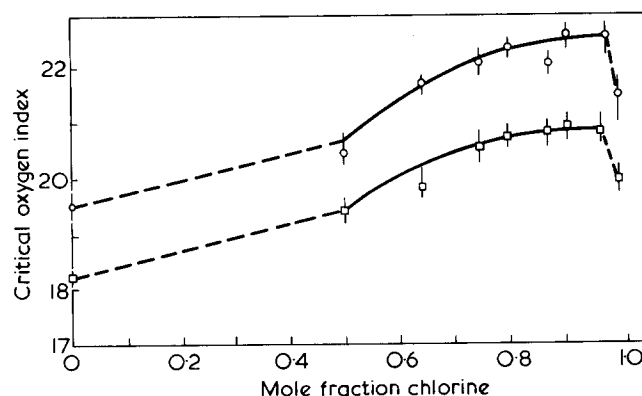


Figure 1 Oxygen index vs. amount of chlorine at different total additive levels: □, 10% total additive; ○, 20%, total additive

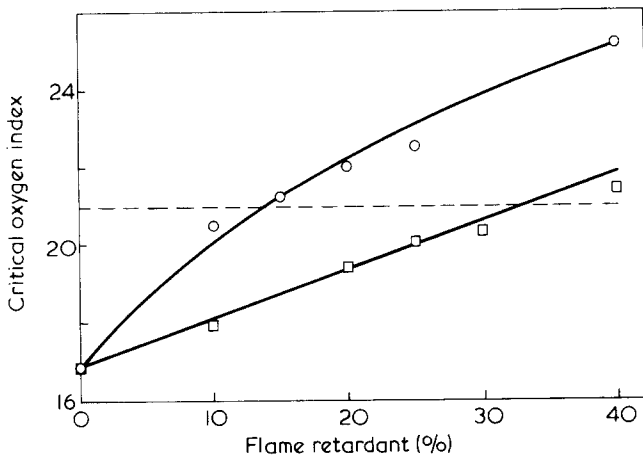


Figure 2 Comparison of different flame retardants. \circ , Sb:Cl of 1:3; \square , alumina trihydrate

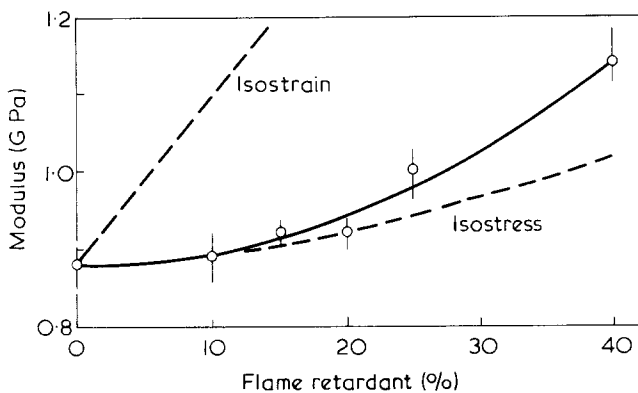


Figure 3 Modulus as a function of amount of flame retardant at Sb:Cl of 1:3

the antimony trichloride (SbCl_3). It was found that in the range Sb:Cl of 1:3 to Sb:Cl of 1:30 saturation occurred in that the oxygen index levelled off, which confirms the findings of Fenimore and Martin. The reason for this saturation is not however known at this stage.

On the basis of Figure 1 an optimum could be selected at a Sb:Cl ratio of 1:3. Figure 2 shows the effect of varying the total additive concentration at this fixed mole ratio. It is apparent from this Figure that a vast improvement of flame retardancy is not possible owing to the low efficiency as previously mentioned. From these results it can be seen that at 40% additive the OI is still fairly low at ~25. Consequently it is thought that in a real fire situation HDPE so stabilized will burn and that protection is only afforded against the dropped cigarette end etc. This can be ascribed to the fact that in a real fire situation high temperatures will be encountered, resulting in a decrease in the oxygen index as has been previously described^{13,14}. It is thought that this decrease may be sufficient to reduce the value of the oxygen index to below 21 in which case it can be expected to burn. Experimental evidence regarding the size of this oxygen index reduction with increasing temperature, in HDPE stabilized with antimony/chlorine, is not available as yet.

It was found that the oxygen index of unstabilized HDPE was 16.8 and as explained earlier this figure is expected to be low. Most authors¹⁵⁻¹⁸ quote figures for polyethylene of ~17.4.

Regarding the mechanical properties the effect on modulus and elongation to break are shown in Figures 3 and 4 respectively. It was found that an increase in the amount of additive caused an increase in modulus and a decrease in ultimate strain. Boundary conditions, corresponding to uniform strain and uniform stress are shown by the broken lines and it can be seen that the results obtained are fairly close to the iso-stress boundary, indicating that this is the controlling parameter. As a result of this close proximity to iso-stress, this condition can be used as a practical basis to determine theoretical moduli to within 10%. Above 25% total additive the elongation to break decreased markedly and it is thought that this would represent a maximum flame retardant loading for a commercial plastic.

Alumina trihydrate was compared with the antimony/chlorine system and results are shown in Figure 2. It can be seen that the antimony/chlorine system is far more efficient compared to alumina trihydrate, in HDPE. To achieve an oxygen index of 21 with the latter additive concentrations of ~40% are required, however the elongation to break decreases above levels of ~25% as shown in Figure 4. The effect of alumina trihydrate on modulus is shown in Figure 5; as before results are close to the iso-stress boundary.

CONCLUSIONS

From the available results it can be inferred that the opti-

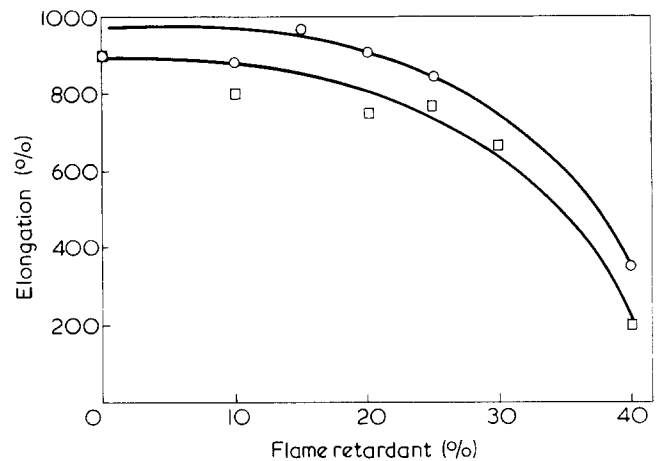


Figure 4 Elongation at break as a function of amount of flame retardant. \circ , Sb:Cl of 1:3; \square , alumina trihydrate

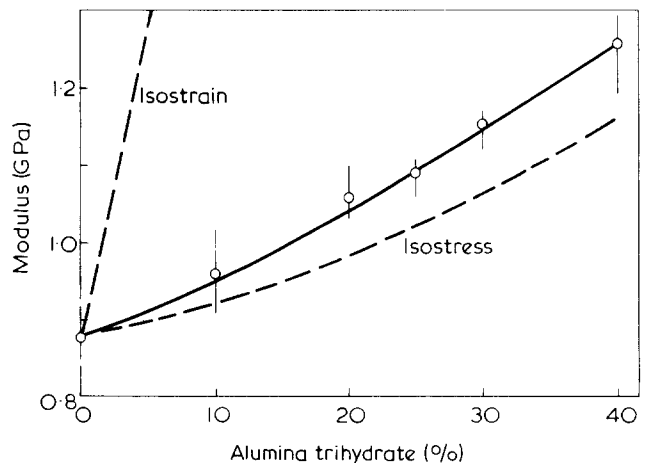


Figure 5 Modulus as a function of amount of alumina trihydrate

mum ratio of Sb:Cl is 1:3, which tends to confirm that the significant flame retardant in this system is the volatile antimony trichloride (SbCl₃). The synergistic effect of antimony/chlorine was found to be small in HDPE and it is thought that this may be due to the high crystallinity of the base polymer. In a real fire situation, even at high levels of additive (~40%) the material could be expected to burn vigorously with the evolution of dense black smoke which would cause (toxicological) problems. In practice this high level of additive could not be used since the mechanical properties (notably elongation at break and ultimate stress) showed a marked decrease at concentrations above 25%.

Alumina trihydrate, studied as an alternative to antimony/chlorine was found to have poor flame retardancy compared to the Sb:Cl system in HDPE.

ACKNOWLEDGEMENTS

One of the authors (S. C. S.) would like to thank the management of Van Leer for permission to publish this paper.

REFERENCES

- 1 Little, R. W. 'Flame Proofing Textile Fibres', Reinhold, New York, 1947
- 2 Field, G. B. US Pat. 2 962 464 29 (1960)
- 3 Walker, A. G. Br. Plast. 1969, 42, 7
- 4 Raff, R. A. V. and Allison, J. B. 'Polythene', Interscience, New York, 1956
- 5 Pitts, J. 'Flame Retardancy of Polymeric Materials', (Eds W. C. Kuryla and A. J. Papa), Marcel Dekker, New York, 1973, Vol 1
- 6 Fenimore, C. P. and Martin, F. J. *Mod. Plast.* 1966, p 141
- 7 Fenimore, C. P. and Martin, F. J. *Combust. Flame* 1966, 10, 135
- 8 Hopkins, R. C. *Polym. Age* 1975, p 130
- 9 Anderton, G. E. and Treloar, L. R. G. *J. Mater. Sci.* 1971, 6, 562
- 10 *Idem. ibid.* 1971, 6, 7
- 11 'Modern Composite Materials', (Eds L. J. Broutman and R. H. Krock), Addison-Wesley, Massachusetts, 1967
- 12 Schwarz, R. J. 'Flame Retardancy of Polymeric Materials', (Eds W. C. Kuryla and A. J. Papa), Marcel Dekker, New York, 1973, Vol 2
- 13 Di Pietro, J. and Slepniczka, H. *SPE J.* 1971, 27, 23
- 14 Day, A. J. *Plast. Polym.* 1975, p 64
- 15 *Idem. ibid.* 1975, p 8
- 16 Abbot, C. *Europlast. Mon.* 1973, p 68
- 17 Walker, A. G. *Europlast. Mon.* 1973, p 72
- 18 Warren, P. G. *SPE J.* 1971, 27, 17

Impact yielding of high density polyethylene

B. J. Briscoe and I. M. Hutchings

Physics and Chemistry of Solids, Cavendish Laboratory, University of Cambridge, Cambridge CB3 0HE, UK

(Received 14 May 1976; revised 23 July 1976)

We have used a projectile impact method to estimate the flow stress of high density polyethylene at a strain rate of $\sim 3 \times 10^3 \text{ sec}^{-1}$. The technique was developed initially by Taylor and applied successfully by Whiffin and others to ductile metals. The data from this experiment have been compared with data obtained in more conventional compression and drop hammer tests at lower strain rates at 20°C and 100°C. The flow stress of high density polyethylene deduced from the impact test at 20°C is significantly higher than that anticipated from a simple extrapolation of the low strain rate data at 20°C. The data at 100°C are however in good agreement. The technique has also been used to estimate the flow stress of high density polyethylene as a function of temperature over the range -20° to $+105^\circ\text{C}$. These data indicate that the discrepancy in the data for 20°C arises from a real discontinuity in the response of the polymer rather than from an inadequacy in the theoretical analysis of the impact experiment as applied to polymeric solids. We conclude that the impact method described is a useful technique for estimating the flow stress of polymers. It is however limited to a relatively narrow range of strain rates.

INTRODUCTION

A deformable cylinder (*Figure 1a*) impacted axially against a rigid plane at a high velocity will suffer permanent deformation. In the case of an ideal rigid-plastic material the deformation is of the form shown in *Figure 1b*. For this case Taylor¹ showed that the yield stress, σ , of the material may be estimated from the geometry of the impacted specimen, using the following formula:

$$\sigma \approx \frac{\rho V^2(L_0 - X)}{2(L_0 - L) \ln(L_0/X)} \quad (1)$$

where (*Figure 1*) ρ is the density of the specimen; V is the impact velocity; L_0 is the original length of the cylinder; L is the final length and X is the length of the undeformed portion of the cylinder. The mean rate of strain, $\dot{\epsilon}$, during the impact was shown¹ to be

$$\dot{\epsilon} \approx V/2(L_0 - X) \quad (2)$$

Equation (1) has been used successfully by Whiffin² and others to estimate the flow stress of metals at high strain rates. Taylor's analysis was based on a momentum exchange calculation for an ideal rigid-plastic material; more recent treatments^{3,4} which take account of strain hardening and elastic deformation predict yield stresses which differ only slightly from the value given by equation (1).

We have used Taylor's method to estimate the yield stress of high density polyethylene at a mean strain rate of about $3 \times 10^3 \text{ sec}^{-1}$ *. The result is compared with mea-

surements obtained by uniaxial compression in conventional compression tests and drop-weight impact tests at lower strain rates (up to $3 \times 10^2 \text{ sec}^{-1}$). The projectile impact experiment gives a yield stress significantly higher than that anticipated from a simple Eyring extrapolation of the lower strain rate data. The reason for this anomaly is uncertain; it may be due either to a real change in yield properties of the polymer at these high rates of strain or to an inadequacy in the interpretation of the impact response of polymers using the Taylor method.

This impact method has also been used to study the apparent yield stress of high density polyethylene over the temperature range -20° to $+105^\circ\text{C}$. While the yield strength decreases rapidly with temperature the variation cannot be simply explained using an Eyring flow model.

EXPERIMENTAL

Taylor impact method

A commercial grade of high density polyethylene (Rigidex 075-65) was used in the form of 16 mm diameter rod (density 953 kg/m^3). Plane-ended cylindrical specimens ~ 40 mm in length were accelerated using a compressed-gas gun⁵ and allowed to impact axially against a massive smooth-faced steel anvil. Two high speed photographic sequences are shown in *Figure 2*. *Figure 2a* shows the impact for a typical velocity (120 m/sec) at 100°C and thus corresponds to the maximum observed deformation of the cylinder. The surface of the cylinder was lubricated with MoS₂ grease to reduce frictional losses during impact. The impact velocity was about 110 m/sec and was measured to within 1% by timing the interruption of two light beams crossing the barrel⁶.

The polymer specimens could be heated before impact by means of an electrical heating element around the breech of the gun. The temperature of the barrel surface immed-

* Although in principle the strain rate may be readily varied by changing the impact velocity, in practice at low velocities the deformation is too small for accurate measurement, and at high velocities it is too gross for the theoretical assumptions to be valid. The usefulness of the method is therefore restricted to strain rates of around $3 \times 10^3 \text{ sec}^{-1}$ for high density polyethylene.

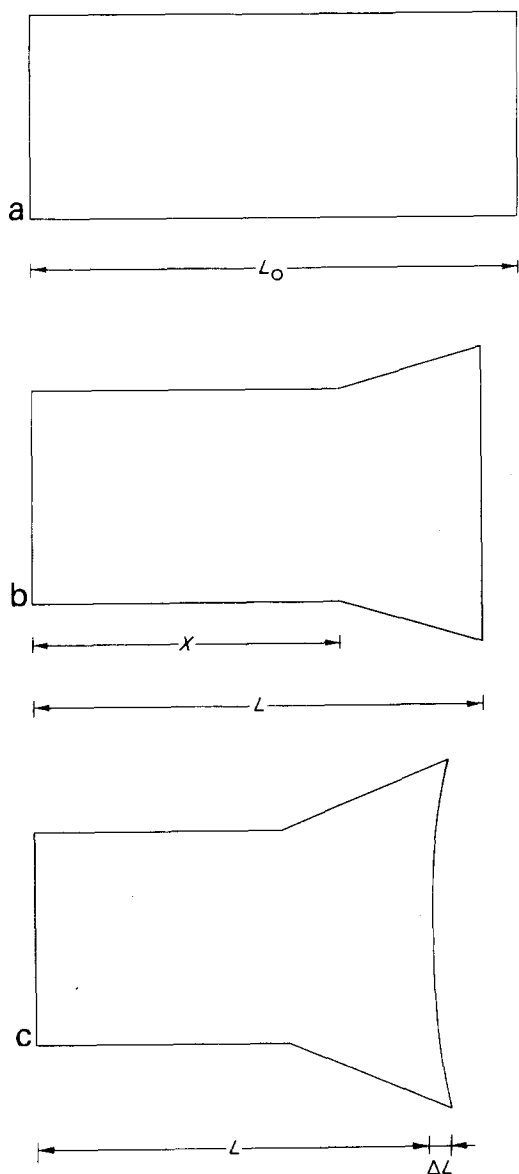


Figure 1 Projectiles used for the Taylor impact experiment: (a) before impact; (b) after impact; (c) shows the concavity which forms after impact at 100°C. This concavity is less pronounced at lower temperatures

ately above the specimen was measured by means of a thermocouple; the reading of this thermocouple was compared in a series of calibration experiments with the temperature measured by a thermocouple at the centre of a dummy polyethylene cylinder in the barrel when a steady-state temperature had been achieved. In all experiments at elevated temperatures the specimen was allowed to reach thermal equilibrium in the heated breech for 15 min before firing; we estimate that with these precautions the quoted temperatures are accurate to $\pm 2\text{K}$ and that the maximum non-uniformity of temperature is of a similar order. A few experiments were performed at below room temperature, in which specimens were cooled in a refrigerator before firing; the estimated temperature of -20°C is accurate to $\pm 10\text{K}$.

In some experiments the rebound velocity was measured by a similar photoelectric timing method to the one described above; the rebound velocity was found to be $30 \pm 2 \text{ m/sec}$ and to be essentially independent of specimen temperature and impact velocity over the range -20°C

to $+100^\circ\text{C}$ and 90 to 125 m/sec. The rebound energy was therefore $\sim 7\%$ of the initial kinetic energy of the projectile†.

The final dimensions of the specimens were measured with a micrometer screw gauge. The impacted specimens showed various degrees of concavity on the impacted surface. This is shown schematically in Figure 1c. In all cases the length L was measured along the axis of the cylinder.

The concavity becomes more extreme at the highest impact temperature where $\Delta L/(L_0 - L)$ approached 0.8. Figure 2b shows the rebound of a specimen impacted at 100°C and at a velocity of 170 m/sec. The deformation of the cylinder is extremely pronounced and indeed much greater than observed in cylinders where yield stress measurements were made. At this velocity the concavity of the specimen end is accentuated. The photographs indicate that this concavity, ΔL , is produced as the cylinder rebounds from the anvil; the axial length L remains sensibly constant during rebound. It is not clear why this post-impact deformation occurs but it may be due to a combination of factors including momentum effects, hydrostatic effects and elastic recovery.

The mean flow stress and the mean rate of strain were calculated from equations (1) and (2). After impact several specimens were cut along their axes and sections of the cylinder were microtomed. These sections were examined for stress birefringence and local tensile failure.

Hammer impact method

The instrumented drop-weight apparatus described by Heavens and Field⁷ was used. The measurements were carried out at 20°C and the mean calculated strain rate was

† No correction was made for this effect in the data quoted below. At present the theoretical treatment of such a correction is unclear. However a simple argument suggests that the calculated values of σ (equation 1) might be reduced by up to 7%.

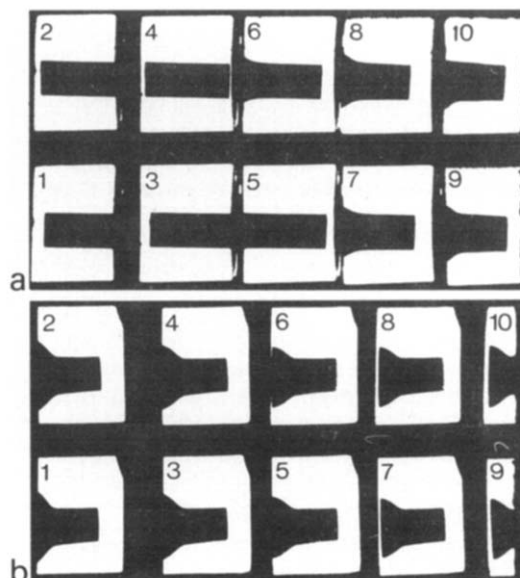


Figure 2 Two sequences of high speed photographs; interframe time 19 μsec . Frames are numbered sequentially. Initial impact is from right to left. (a) Impact of a HDPE cylinder at 100°C and 120 m/sec. Cylinder diameter 16 mm. (b) Rebound of an HDPE cylinder after impact at 100°C and 170 m/sec. Elastic recovery and formation of the concavity on the impacted face occur between frames 1 and 5; the projectile breaks contact between frames 5 and 6. Rebound velocity 30 m/sec

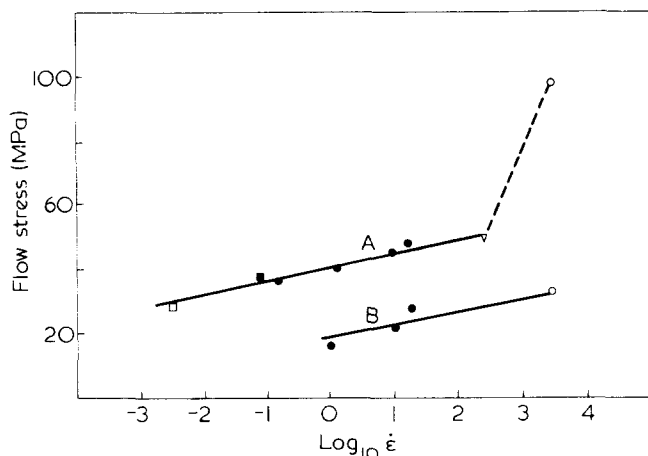


Figure 3 Flow stress of high density polyethylene measured by several techniques, plotted against log (strain rate) for two different temperatures: A, 20°C; B, 100°C. Note the sudden increase in flow stress at 20°C above $\dot{\epsilon} \approx 3 \times 10^2$, which does not appear in the results at 100°C. This work: \square , uniaxial compression; ∇ , drop-weight; \circ , Taylor impact uniaxial compression; \bullet , Amuzu and Briscoe¹¹; \blacksquare Bowden and Jukes⁸

$\sim 3 \times 10^2 \text{ sec}^{-1}$. The specimens were cylindrical and somewhat smaller than those used in the impact tests (diameter 6 mm, length 6 mm) and a certain amount of barrelling was detected in the deformed specimens.

Low strain rate tests

Low strain rate compressive tests were carried out using a commercial testing machine (Instron) in the range 10^{-3} to 1 sec^{-1} . The yield stress was taken to correspond to 10% strain following Bowden and Jukes⁸.

EXPERIMENTAL DATA AND DISCUSSION

Figure 3 shows our data and that of other workers for the influence of strain rate, $\dot{\epsilon}$, on the compressive flow stress, σ , of various grades of high density polyethylene at 20°C and 100°C. Following the classical analysis based on the high stress limit of an Eyring-type stress-modified thermally activated flow process^{9,10} we have plotted $\log_{10} \dot{\epsilon}$ against σ . With the exception of one data point, that for Taylor impact at 20°C, the data for each temperature show a similar monotonic increase in the value of σ with increasing values of $\log_{10} \dot{\epsilon}$. It appears that the Taylor impact technique gives a reasonable value of σ at 100°C. However the value of σ calculated from the impact technique at 20°C is at least twice that anticipated from the linear extrapolation of the low strain rate data. This discrepancy seems to arise from a change in the mode of deformation of the polymer at strain rates above about $3 \times 10^2 \text{ sec}^{-1}$ at 20°C. There is evidence for this in the stress birefringence of the sections of polymer cut from the impacted specimen. At 20°C the impact specimen shows a diffuse region of deformation which penetrates into the cylinder to a depth of the order of one quarter of the diameter of the cylinder. At 100°C however the deformation is more localized in a region close to the impact surface and penetrates to a depth of only about one eighth of the diameter. In addition these specimens show evidence of gross tensile rupture close to the impact surface. The deformation observed at 100°C was with the exception of the gross failure region very similar to that obtained in the slip region during conventional compression tests at both 20°C and 100°C.

A change in the mode of deformation at the high impact strain rates is also indicated by a marked difference in the temperature dependence of the flow stress at high and low strain rates. In **Figure 4** we show our data for the temperature dependence of the flow stress at two strain rates. In both cases the flow stress decreases linearly with temperature. However the temperature dependence at the high strain rate is about three times greater than at the low strain rate. In **Figure 4** we show low strain rate data for $\dot{\epsilon} = 20 \text{ sec}^{-1}$. Similar temperature dependences have been observed at strain rates down to 1 sec^{-1} ¹¹. At about 100°C the higher strain rate data (by the impact technique) are very similar to the lower strain rate uniaxial compression data. It is not clear from the present data whether the results at the two strain rates become coincident or cross over at about 100°C. The data obtained from the impact technique become very inaccurate above 120°C due to excessive concavity in the impacted specimens and thus this question cannot be answered using Taylor's method. However these data do indicate that the discontinuity in the $\log_{10} \dot{\epsilon}$ against σ plot at 20°C (**Figure 3**) is due to a change in the physical properties of the polymer rather than to an artefact inherent in the impact technique. We have no unequivocal explanation for the discontinuity or for the different temperature dependences. The onset of crystallite melting occurs at about 100°C in high density polyethylene. It therefore seems that these effects are associated with the crystalline nature of high density polyethylene. In the absence of data at higher strain rates and temperatures it is probably not sensible to speculate on their origin. Nevertheless the data do indicate that the Taylor impact technique forms a useful method for estimating the flow stress of polymers, although unfortunately limited to a very narrow range of strain rates.

ACKNOWLEDGEMENTS

We thank Professor D. Tabor for his support and encouragement during the course of this study. We are also grateful for the award of Research Fellowships from the Oppenheimer Fund (B. J. B.) and St. John's College, Cambridge (I.M.H.).

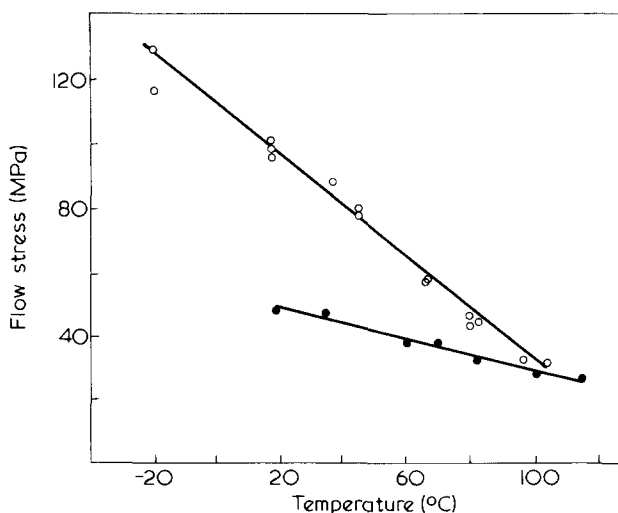


Figure 4 Flow stress of high density polyethylene as a function of temperatures. \circ , $\dot{\epsilon} \approx 3 \times 10^3 \text{ sec}^{-1}$, Taylor impact method; \bullet , $\dot{\epsilon} \approx 20 \text{ sec}^{-1}$, unpublished results of Amuzu and Briscoe¹¹ obtained in uniaxial compression

REFERENCES

- 1 Taylor, G. I. *Proc. R. Soc. (A)* 1948, **194**, 289
- 2 Whiffin, A. C. *Proc. R. Soc. (A)* 1948, **194**, 300
- 3 Hawkyard, J. B. *Int. J. Mech. Sci.* 1969, **11**, 313
- 4 Lee, E. H. and Tupper, S. J. *J. Appl. Mech.* 1954, **21**, 63
- 5 Hutchings, I. M. and Winter, R. E. *J. Phys. (E)* 1975, **8**, 84
- 6 Hutchings, I. M. *Rev. Sci. Instrum.* in press
- 7 Heavens, S. N. and Field, J. E. *Proc. R. Soc. (A)* 1974, **338**, 77
- 8 Bowden, P. B. and Jukes, J. A. *J. Mater. Sci.* 1972, **7**, 52
- 9 Ward, I. M. *J. Mater. Sci.* 1971, **6**, 1397
- 10 Bauwens-Crowet, C., Bauwens, J. C. and Homés, G. *J. Polym. Sci. (A-2)* 1969, **7**, 735
- 11 Amuzu, J. K. A. and Briscoe, B. J. unpublished data

Notes to the Editor

Cooling of a polymer sheet

R. Pollard* and J. D. Perkins

Department of Chemical Engineering, University of Cambridge, Pembroke Street, Cambridge CB2 3RA, UK

(Received 20 November 1975; revised 17 June 1976)

This Note presents some results from a digital simulation study of one typical polymer processing operation (see *Figure 1*). Molten polymer sheet cools by heat transfer to metal rollers and to the atmosphere, and as it cools it crystallizes. The crystallization process liberates heat which is removed by both conduction through the sheet and heat transfer at the surface. By a suitable choice of processing conditions it is possible to affect the final state of the polymer sheet.

Heat transfer through the sheet may be represented by:

$$\frac{\partial}{\partial t} \left(\frac{cT}{V} \right) = \frac{\partial}{\partial z} \left(k \frac{\partial T}{\partial z} \right) + \frac{L}{V} \frac{\partial X}{\partial t} \quad (1)$$

Neither heat conduction in the flow direction nor end effects due to finite sheet width have been included.

For polymer surfaces in contact with air, a suitable boundary condition for equation (1) is:

$$\left(\frac{\partial T}{\partial z} \right)_S = \frac{-h}{k} (T_S - T_A) \quad (2)$$

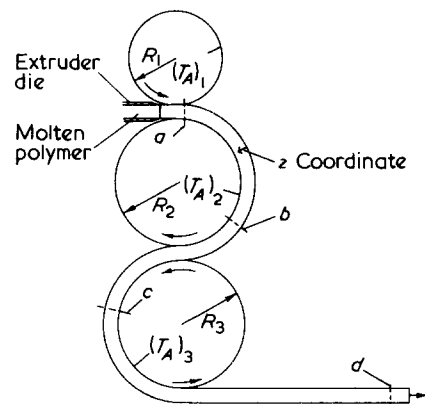


Figure 1 Schematic diagram of a common crystallization process (cross-section). Typical system parameters: $T_0 = 473.2\text{K}$; $(T_A)_1 = 368.2\text{K}$; $(T_A)_2 = 373.2\text{K}$; $(T_A)_3 = 378.2\text{K}$; $R_1 = 0.1\text{ m}$; $R_2 = R_3 = 0.15\text{ m}$; $n = 3$; $A = 0.9$; $B = -2.5$; $C = 408.2\text{K}$

* Present address: Department of Chemical Engineering, University of California, Berkeley, California 94720, USA.

Local heat transfer coefficients have been evaluated from standard correlations where heat transfer results from both free and forced convection¹.

Different correlations are used to calculate point-value heat transfer coefficients in cylindrical and flat regions. For polymer surfaces in contact with rollers, perfect thermal contact has been assumed:

$$T_S = T_A \quad (3)$$

The Avrami analysis² has been extended to predict the kinetics of the non-isothermal crystallization process³. The relative crystallinity, x , may be obtained from:

$$1 - x = \exp \left[- \left(\int_0^t K(\tau) d\tau \right)^n \right] \quad (4)$$

where $x = X/X_\infty$.

Previous workers^{3,4} have neglected X_∞ and have computed x directly. With this approach the latent heat is defined as heat released per unit mass of polymer. This quantity would seem to be a function of temperature and crystallinity, and not the constant which both Sifleet and Nakamura assume. It seems better to work in terms of the absolute crystallinity, X ; then L has the standard definition of heat released per unit mass of polymer crystallized. An empirical expression has been used to predict the temperature dependence of X_∞ ($T < C$):

$$X_\infty = A \exp \left(\frac{B}{T - C} \right) \quad (5)$$

Some evidence suggests that X_∞ is also dependent on cooling conditions⁵, but quantitative predictions are not available. The choice of parameters A , B , and C for a particular process should be made to reflect dependence on cooling rate. A linear relationship was employed to describe the dependence of

polymer properties on the temperature, and a linear mixing law of the type:

$$P = P_M(1 - X) + P_C X \quad (6)$$

was used to describe the dependence on crystallinity. Data for the polyethylene MARLEX 50 were used in this study (*Table 1*).

Estimation of the parameters in equation (4) presents difficulties: only isothermal data are readily available and generally the experiments are performed at slow rates of crystallization for ease of measurement. Thus, extrapolation is necessary to predict fast rates of crystallization common in industrial processes. *Figure 2* shows experimental half-life results⁶ and two equations fitted to these data. Both equations are of a form normally used to represent kinetic data but they lead to greatly different rate predictions in the temperature range of interest in this study. To assess the importance of this uncertainty, simulations were performed with both the fitted equations which are referred to below as 'slow' and 'fast' kinetic models.

The non-linearities in equation (1) make numerical techniques the only feasible method of solution. An explicit finite difference scheme⁷ has been used in a computer program that performs steps in time, computing new polymer temperature profiles at each step. (For constant polymer speeds,

Table 1 Physical properties for MARLEX 50

Polymer property	Temperature dependence (e.g. $C_M = q + rT$)	
	q	r
V_M	9.12×10^{-4}	8.80×10^{-7}
k_M	4.61×10^{-2}	5.02×10^{-4}
c_M	3.22×10^3	0.0
V_C	9.11×10^{-4}	3.00×10^{-7}
k_C	1.24	-2.09×10^{-3}
c_C	2.09×10^3	0.0
L	2.41×10^5	0.0
V_m	1.20×10^{-3}	0.0
k_m	0.30	0.0
c_m	2.70×10^3	0.0

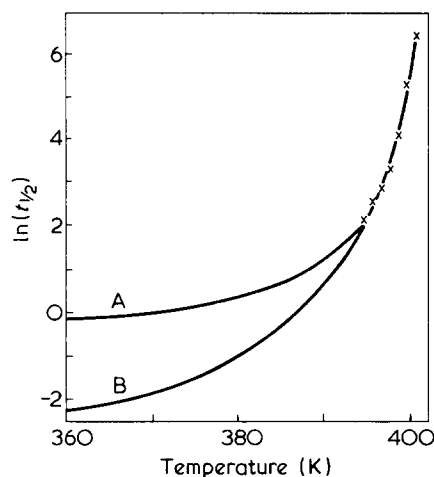


Figure 2 Temperature dependence of crystallization half-life for MARLEX 50: Data points⁶: A, 'slow' kinetic model: $t_{1/2} = 0.690 \exp[611.7/(410.7 - T)^2]$ min; B, 'fast' kinetic model: $t_{1/2} = 0.015 \exp[96.4/(410.7 - T)]$ min

the time variable, t , and the distance coordinate, y , are directly related). Also crystallinity profiles within the polymer are computed from equations (4) and (5), using successive applications of Simpson's rule to calculate the integral in equation (4). The step sizes were decreased until negligible change (<0.1 K) was observed in computed temperatures. It was found that a time step of 5.0×10^{-3} sec and a step length in z of 6.25×10^{-5} m were sufficient. All computations were performed on a PDP 11/45 computer in single-precision.

RESULTS AND DISCUSSION

The processing conditions that were simulated are shown in Figure 1, together with values for the constants in equations (4) and (5) used in this study. The linear sheet velocity is 5 cm/sec and its thickness is 2.5 mm. The calculated temperature profiles at the labeled points in Figure 1 are shown in Figure 3, for the slow kinetic model. The effect of the kinetic model on the predicted temperature profiles was found to be very small for the processing conditions chosen. There was negligible difference between the 'slow' and 'fast' temperature profiles until after the end of the rollers, when the fast model permits more crystallization. It was found that the final, essentially uniform, sheet temperature was about 5K higher for the fast kinetics than for the slow.

The final degree of crystallinity predicted by the two kinetic models is shown in Figure 4. It can be seen that

the slow model predicts negligible crystallization. The order of magnitude difference in crystallinity predicted by the fast model results in a small difference in calculated temperature profiles. The latent heat released during crystallization does not appear to be an important factor in this heat transfer problem.

Previous workers^{3,4} have assumed that polymer physical properties are independent of temperature and degree of crystallinity. To test the validity of this assumption for the process under consideration, constant mean values of the physical properties (Table I) were used in the computer program. The predicted temperature profiles never differed from the variable properties solution by more than 5K for either kinetic model. Thus it seems that the assumption of constant physical properties is reasonable for this process.

Consequently it seems admissible to simplify the equations used to describe the process. By neglecting the latent heat term in equation (1) and assuming constant physical properties, we have:

$$\frac{\partial T}{\partial t} = \frac{kV}{c} \frac{\partial^2 T}{\partial z^2} \quad (7)$$

for which analytical solutions are easily obtainable provided the boundary conditions are linear⁸. However, the boundary condition for polymer-air contact is non-linear because of the dependence of the heat transfer coefficient on the temperature difference, $T_S - T_A$. Detailed examination of the predicted temperature profiles shows that the temperature gradient, $\partial T/\partial z$, at a polymer-air interface is always small, which suggests that little heat is transferred to the air. Therefore, in this case, it is reasonable to omit the contribution of air cooling; this results in the boundary condition:

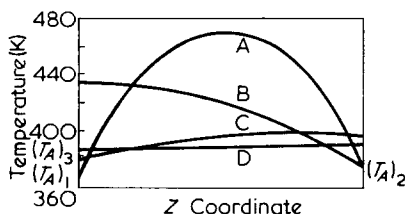


Figure 3 Temperature profiles at different points in process simulated with equation (1) and 'slow' kinetic model. Time (sec) after start of process: A, 1; B, 7; C, 15; D, 30

$$\left(\frac{\partial T}{\partial z}\right)_S = 0 \quad (8)$$

for polymer-air contact. A dimensionless form of equation (7) may be readily solved analytically with boundary conditions of the form of equations (3) and (8). The resulting temperature profile predictions are shown in Figure 5. By comparison with Figure 3, it can be seen that the simplified description of the process approximates the full description reasonably well; errors are always less than 5K.

With the simpler model it is easy to make preliminary estimates of the process configuration and roller temperatures needed to obtain a specified product. However, the detailed model should always be used to check the validity of the initial results because the simplified approach might not be acceptable for other sets of processing conditions.

Uncertainties in the data can be overcome to some extent by using a sensitivity approach. For example, the range of possible predicted rates of crystallization could be accounted for by using a 'slow' and a 'fast' model

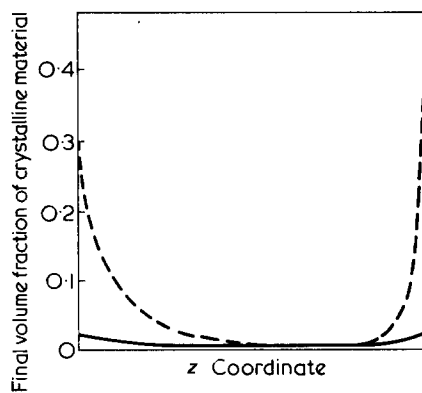


Figure 4 Variation in volume fraction of crystalline material across sheet at end of process. —, 'Slow' kinetic model; ---, 'fast' kinetic model

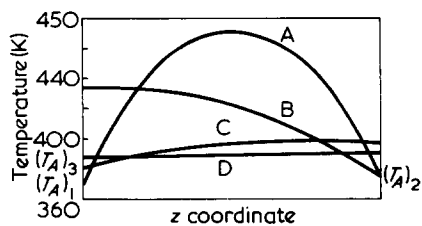


Figure 5 Temperature profiles at different points in process simulated with equation (7) and 'slow' kinetic model. Time (sec) after start of process: A, 1; B, 7; C, 15; D, 30

for the kinetics and comparing the results. In some circumstances the representation of the kinetic data will not influence the results significantly. However, in general, there is no substitute for better data. In this context, it seems that more effort should be concentrated on non-isothermal crystallization kinetics and on the measurement of higher rates of crystallization of the type usually found in industry.

NOMENCLATURE

A	} parameters in equation (5)
B	
C	
c	specific heat of polymer (J/kg K)
h	heat transfer coefficient for polymer-air contact (W/m ² K)
K	modified crystallization kinetic rate constant
k	thermal conductivity of polymer (W/m K)
L	latent heat of crystallization of polymer (J/kg)

n	Avrami index
P	polymer physical property
R	radius of cylindrical roller
T	temperature of polymer
t	residence time of polymer in process
V	specific volume of polymer (m ³ /kg)
X	fractional crystallinity of polymer
X_{∞}	final fractional crystallinity of polymer
x	fraction of final crystallinity of polymer
y	distance coordinate (measured from extruder head along polymer sheet)
z	thickness coordinate
τ	time-like integration variable

Subscripts

A	in cooling medium
C	of crystallized polymer
M	of uncrystallized polymer
m	mean value

O	at start of process
S	at surface of polymer

ACKNOWLEDGEMENTS

The authors would like to acknowledge the assistance and encouragement of Mr E. Atkinson and Dr D. A. Blackadder.

REFERENCES

- Menges, G. and Michaelis, W. *Conf. Eng. Des. Plast. Proc. Machinery, J. Mech. E./B. P. F. Bradford* April 1974
- Mandelkern, E. 'Crystallization of Polymers', Wiley, New York, 1964
- Nakamura, K., Watanabe, T., Katayama, K. and Amano, T. *J. Appl. Polym. Sci.* 1972, 16, 1077; 1973, 17, 1031; 1974, 18, 615
- Sifleet, W. L., Dinos, N. and Collier, J. R. *Polym. Eng. Sci.* 1973, 13, 10
- Sharples, A. 'Introduction to Polymer Crystallization', Arnold, London, 1966
- Mandelkern, E. in 'Growth and Perfection of Crystals', Wiley, New York, 1964
- Forsythe, G. E. and Wasow, W. R. 'Finite Difference Methods for Partial Differential Equations', Wiley, New York, 1960
- Bird, R. B., Stewart, W. E. and Lightfoot, E. N. 'Transport Phenomena', Wiley, New York, 1960

Conformational study of poly(O-carbobenzoxy-L-tyrosine) in solution

Hiroyuki Yamamoto

Institute of High Polymer Research, Faculty of Textile Science and Technology, Shinshu University, Ueda 386, Japan
(Received 23 June 1976)

The conformational properties of polypeptides having aromatic side-chain chromophores in organic solvents have been investigated by many workers; poly(L-phenylalanine)¹, poly(L-benzyl-L-histidine)², poly(L-tryptophan)³⁻⁶ and poly(O-carbobenzoxy-L-tyrosine) (PCLT)⁷⁻⁹. In most cases, the interpretation of optical rotatory dispersion and circular dichroism (c.d.) spectra in terms of conformation is rather difficult since there are overlapping contributions to the total activity both from the peptide chromophores and from the side-chain chromophores. PCLT has been shown to have a right-handed α -helical conformation from the change of b_0 with copolymer composition⁷, the c.d. spectrum in solution^{8,9} and the X-ray diffraction pattern in the solid state¹⁰. These studies, however, did not include recent improvements in apparatus and new sol-

vents which are transparent to below 200 nm. The actual conformation of PCLT in various solvents remains unresolved. The author wishes to report here the detailed conformational features and the helix-coil transition of PCLT in pure or mixed solvents.

EXPERIMENTAL

PCLT was prepared by the method described in previous papers¹¹⁻¹³; $[\eta] = 0.62$ dl/g in dichloroacetic acid (DCA) at 25°C. The molecular weight was estimated to be 95 000 (degree of polymerization = 320) from an empirical equation⁷;

$$[\eta] = 3.2 \times 10^{-2} M_w^{0.66}$$

in DCA at 25°C. The rotation properties were measured at 25°C on a Jasco

ORD/UV-5 spectropolarimeter with a c.d. attachment, using cells with light paths of between 0.1 and 10 mm (polypeptide concentration, 0.20-0.60%).

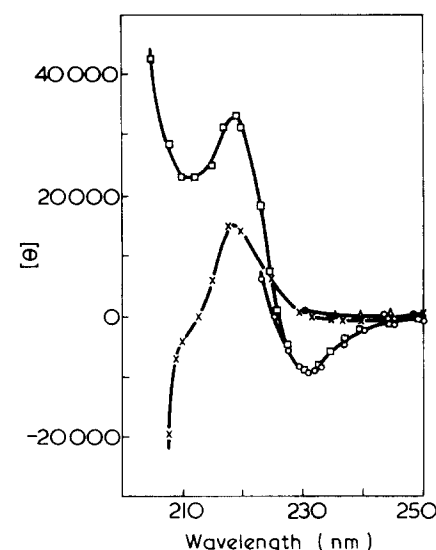


Figure 1 C.d. spectra of PCLT in the ultraviolet region at 25°C: ○, in chloroform; □, in dioxane; ●, in TFA; X, in hexafluoroacetone sesquihydrate; △, in hexamethylphosphoramide

for the kinetics and comparing the results. In some circumstances the representation of the kinetic data will not influence the results significantly. However, in general, there is no substitute for better data. In this context, it seems that more effort should be concentrated on non-isothermal crystallization kinetics and on the measurement of higher rates of crystallization of the type usually found in industry.

NOMENCLATURE

A	} parameters in equation (5)
B	
C	
c	specific heat of polymer (J/kg K)
h	heat transfer coefficient for polymer-air contact (W/m ² K)
K	modified crystallization kinetic rate constant
k	thermal conductivity of polymer (W/m K)
L	latent heat of crystallization of polymer (J/kg)

n	Avrami index
P	polymer physical property
R	radius of cylindrical roller
T	temperature of polymer
t	residence time of polymer in process
V	specific volume of polymer (m ³ /kg)
X	fractional crystallinity of polymer
X_{∞}	final fractional crystallinity of polymer
x	fraction of final crystallinity of polymer
y	distance coordinate (measured from extruder head along polymer sheet)
z	thickness coordinate
τ	time-like integration variable

Subscripts

A	in cooling medium
C	of crystallized polymer
M	of uncrystallized polymer
m	mean value

O	at start of process
S	at surface of polymer

ACKNOWLEDGEMENTS

The authors would like to acknowledge the assistance and encouragement of Mr E. Atkinson and Dr D. A. Blackadder.

REFERENCES

- 1 Menges, G. and Michaelis, W. *Conf. Eng. Des. Plast. Proc. Machinery, J. Mech. E./B. P. F. Bradford* April 1974
- 2 Mandelkern, E. 'Crystallization of Polymers', Wiley, New York, 1964
- 3 Nakamura, K., Watanabe, T., Katayama, K. and Amano, T. *J. Appl. Polym. Sci.* 1972, 16, 1077; 1973, 17, 1031; 1974, 18, 615
- 4 Sifleet, W. L., Dinos, N. and Collier, J. R. *Polym. Eng. Sci.* 1973, 13, 10
- 5 Sharples, A. 'Introduction to Polymer Crystallization', Arnold, London, 1966
- 6 Mandelkern, E. in 'Growth and Perfection of Crystals', Wiley, New York, 1964
- 7 Forsythe, G. E. and Wasow, W. R. 'Finite Difference Methods for Partial Differential Equations', Wiley, New York, 1960
- 8 Bird, R. B., Stewart, W. E. and Lightfoot, E. N. 'Transport Phenomena', Wiley, New York, 1960

Conformational study of poly(O-carbobenzoxy-L-tyrosine) in solution

Hiroyuki Yamamoto

Institute of High Polymer Research, Faculty of Textile Science and Technology, Shinshu University, Ueda 386, Japan
(Received 23 June 1976)

The conformational properties of polypeptides having aromatic side-chain chromophores in organic solvents have been investigated by many workers; poly(L-phenylalanine)¹, poly(L-benzyl-L-histidine)², poly(L-tryptophan)³⁻⁶ and poly(O-carbobenzoxy-L-tyrosine) (PCLT)⁷⁻⁹. In most cases, the interpretation of optical rotatory dispersion and circular dichroism (c.d.) spectra in terms of conformation is rather difficult since there are overlapping contributions to the total activity both from the peptide chromophores and from the side-chain chromophores. PCLT has been shown to have a right-handed α -helical conformation from the change of b_0 with copolymer composition⁷, the c.d. spectrum in solution^{8,9} and the X-ray diffraction pattern in the solid state¹⁰. These studies, however, did not include recent improvements in apparatus and new sol-

vents which are transparent to below 200 nm. The actual conformation of PCLT in various solvents remains unresolved. The author wishes to report here the detailed conformational features and the helix-coil transition of PCLT in pure or mixed solvents.

EXPERIMENTAL

PCLT was prepared by the method described in previous papers¹¹⁻¹³; $[\eta] = 0.62$ dl/g in dichloroacetic acid (DCA) at 25°C. The molecular weight was estimated to be 95 000 (degree of polymerization = 320) from an empirical equation⁷;

$$[\eta] = 3.2 \times 10^{-2} M_w^{0.66}$$

in DCA at 25°C. The rotation properties were measured at 25°C on a Jasco

ORD/UV-5 spectropolarimeter with a c.d. attachment, using cells with light paths of between 0.1 and 10 mm (polypeptide concentration, 0.20-0.60%).

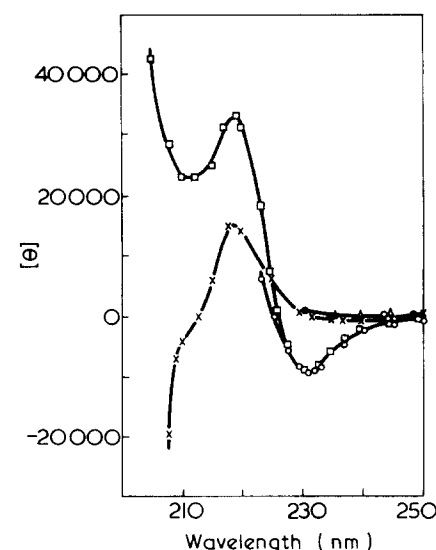


Figure 1 C.d. spectra of PCLT in the ultraviolet region at 25°C: ○, in chloroform; □, in dioxane; ●, in TFA; X, in hexafluoroacetone sesquihydrate; △, in hexamethylphosphoramide

The dimension of $[\theta]$ is degree cm^2/dmol . The nuclear magnetic resonance (n.m.r.) spectra were recorded on a Jeol 60-MHz JNM-c-60HL spectrometer and peak positions were measured relative to the internal tetramethylsilane (polypeptide concentration, 5%).

RESULTS AND DISCUSSION

Figure 1 shows the c.d. spectra of PCLT in five solvents at 25°C. PCLT has a right-handed α -helix conformation in chloroform or dioxane. Approximately the same c.d. spectrum to 200 nm is obtained in trimethylphosphate, 2-chloroethanol or 1,1,1,3,3,3-hexafluoro-2-propanol. The polypeptide has a random coil structure in trifluoroacetic acid (TFA), hexamethylphosphoramide or hexafluoroacetone sesquihydrate. As shown in Table 1, the molar ellipticity values are $-6000 \sim -8700$ (at 229–231 nm) in helix-promoting solvents and less than -700 (at 237 nm) in coil-promoting solvents. The assignment of the two Cotton effects, the first negative and centred at ~ 230 nm, the second positive at 218 nm, have been discussed by Goodman *et al.*⁸ PCLT is insoluble in 2,2,2-trifluoroethanol, *N,N*-dimethylformamide, dimethyl sulphoxide, formic acid and methylsulphonic acid.

Figure 2 shows the helix-coil transition of PCLT in chloroform/DCA (or TFA) or dioxane/DCA (or TFA) mixed solvents at 25°C with midpoint at 8% (or 4%) or 62% (or $\sim 35\%$) DCA (or TFA), respectively. This suggests that the right-handed helix of PCLT is more stable in dioxane/DCA (or TFA) mixed solvents than in chloroform/DCA (or TFA) mixed solvents and less TFA is necessary to destroy the helical conformation than DCA. The author was partly unable to measure the transition since the solubility of PCLT decreased and precipitated at solvent compositions between 35 and 88% TFA in dioxane.

Figure 3 shows the behaviour of the chemical shift and b_0 values for PCLT with change of solvent composition in chloroform/TFA mixed solvents at 25°C. The b_0 value was calculated from the optical rotatory dispersion curve using $\lambda_0 = 212 \text{ nm}$ ^{7,14} and is between 150 and 175 in chloroform or dioxane. Vollmer and Spach reported a larger b_0 value in a methylene dichloride/DCA (1%) mixed solvent (no c.d. data)⁷. As for the specific rotation, $[\alpha]_{546}^{25} = 200$ in dioxane

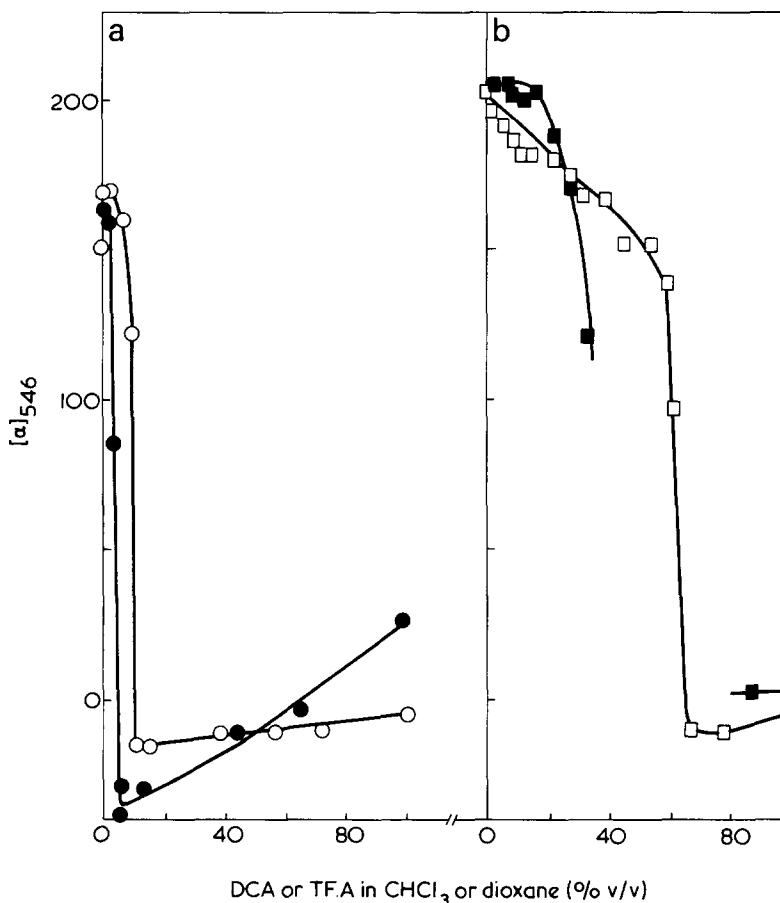


Figure 2 Helix-coil transition of PCLT with change of solvent composition at 25°C. (a): \circ , In chloroform/DCA mixed solvents; \bullet , in chloroform/TFA mixed solvents. (b): \square , In dioxane/DCA mixed solvents; \blacksquare , in dioxane/TFA mixed solvents

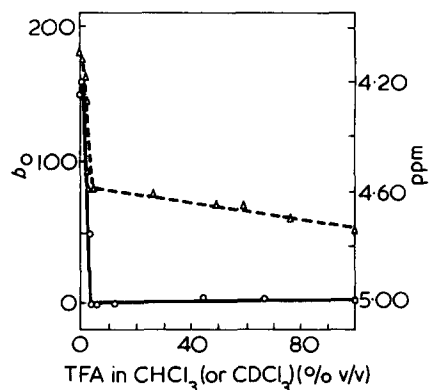


Figure 3 α -CH chemical shift (Δ) and b_0 values (\circ) of PCLT in chloroform (or chloroform- d_1)/TFA mixed solvents at 25°C

and $[\alpha]_{546}^{25} = 167$ in a chloroform/DCA (1%) mixed solvent are obtained and these values agree with a specific rotation reported by Vollmer and Spach ($[\alpha]_{500} = 165$ in a methylene dichloride/DCA (1%) mixture)⁷. Addition of 4% TFA to the chloroform solution causes a sudden drop in the value of b_0 to zero. In DCA or TFA the b_0 value is zero (random coil). In chloroform- d_1 , the α -CH resonance of PCLT

Table 1 Residue ellipticities and chemical shifts for PCLT

Solvent	$[\theta]^a$ (degree cm^2/dmol)	α -CH (ppm)
Chloroform	-8700 (231)	4.10 ^b
Dioxane	-8400 (231)	4.05 ^b
Trimethylphosphate	-7100 (230) ^c	
2-Chloroethanol	-6000 (230)	
Pyridine		4.06 ^b
1,1,1,3,3,3-Hexafluoro-2-propanol	-6000 (229)	
TFA		4.75
Hexafluoroacetone sesquihydrate	-700 (237)	4.60 ^b
1,3-Dichlorotetrafluoroacetone 2,5 hydrate	-560 (237)	

^aValues in parentheses show a trough position (nm); ^bmeasured in deuterated solvent; ^c $[\theta]_{232} \sim -7000$ was reported in ref 8

appears at 4.10 ppm (helix), whereas in TFA this proton appears at 4.75 ppm (random coil). 4% TFA changes the chemical shift from 4.10 to 4.55 ppm (Figure 3). Thus, the conformational relationship between the α -CH resonance and the rotation properties

is clearly demonstrated. As summarized in *Table 1*, the conformation of PCLT is a right-handed α -helix in chloroform, dioxane, trimethylphosphate, 2-chloroethanol, pyridine or 1,1,1,3,3,3-hexafluoro-2-propanol and a random coil in DCA, TFA, hexamethylphosphoramide, hexafluoroacetone sesquihydrate or 1,3-dichlorotetrafluoroacetone 2,5 hydrate.

ACKNOWLEDGEMENT

The author wishes to express his gratitude to Professor Tadao Hayakawa of

the Institute for his valuable discussions and suggestions.

REFERENCES

- 1 Peggion, E., Verdini, A. S. and Scoffone, E. *Macromolecules* 1969, **2**, 170
- 2 Terbojevich, M., Acampora, M., Conasi, A., Peggion, E. and Scoffone, E. *Macromolecules* 1970, **3**, 618
- 3 Fasman, G. D., Landsberg, M. and Buchwald, M. *Can. J. Chem.* 1965, **43**, 1588
- 4 Cosani, A., Peggion, E., Verdini, A. S. and Terbojevich, M. *Biopolymers* 1968, **6**, 963
- 5 Peggion, E., Cosani, A., Verdini, A. S., Del Pra, A. and Mammì, M. *Biopolymers* 1968, **6**, 1477
- 6 Peggion, E., Fontana, A. and Cosani, A. *Biopolymers* 1969, **7**, 517
- 7 Vollmer, J.-P. and Spach, G. *Biopolymers* 1967, **5**, 337
- 8 Goodman, M., Toniolo, C. and Peggion, E. *Biopolymers* 1968, **6**, 1691
- 9 Yamamoto, H. and Hayakawa, T. *Macromolecules* 1976, **9**, 532
- 10 Del Pra, A. and Gilli, G. *Biopolymers* 1975, **14**, 1769
- 11 Katchalski, E. and Sela, M. *J. Am. Chem. Soc.* 1953, **75**, 5284
- 12 Overall, B. G. and Petrow, V. *J. Chem. Soc.* 1955, p 232
- 13 Noguchi, J. and Yamamoto, H. *J. Biochem.* 1969, **65**, 123
- 14 Moffitt, W. and Yang, J. T. *Proc. Nat. Acad. Sci. USA* 1956, **42**, 596

Crown ether catalysed modification of partly chloromethylated polystyrene

J. E. L. Roovers

Division of Chemistry, National Research Council of Canada, Ottawa K1A 0R9, Canada
(Received 11 June 1976)

In the course of the preparation of well characterized narrow molecular weight distribution poly(styrene-*g*-isoprenes) partly chloromethylated polystyrene had to be converted to poly(vinylbenzyl acetate-styrene) random copolymer¹. The published method^{2,3}, using potassium acetate in dimethyl sulphoxide gave variable reaction yields and broadening of the molecular weight distribution. The former observation can be accounted for by the heterogeneity of the reaction medium, the latter is ascribed to the presence of oxidation products of dimethyl sulphoxide. Therefore, a new method using crown ethers to solubilize and activate potassium acetate in non-polar solvents⁴ was adapted to the acetylation of partly chloromethylated polystyrene.

Typically, 1 g anionically prepared⁵ and chloromethylated⁶ polystyrene containing 0.37 mmol chlorine is dissolved in 20 ml of a 50/50 (v/v) mixture of benzene and acetonitrile. To this, 135 mg dicyclohexyl-18-crown-6 (Aldrich) and 365 mg potassium acetate (3.7 mmol) are added. The mixture is magnetically stirred at 75°C. The reaction is quenched by cooling and the addition of benzene. The mixture is filtered and the polymer precipitated in excess methanol. The carbonyl absorption band at 1740 cm⁻¹ is used to monitor the acetylation. (Figure 1). The final acetate content of the polymer agrees with X-ray fluo-

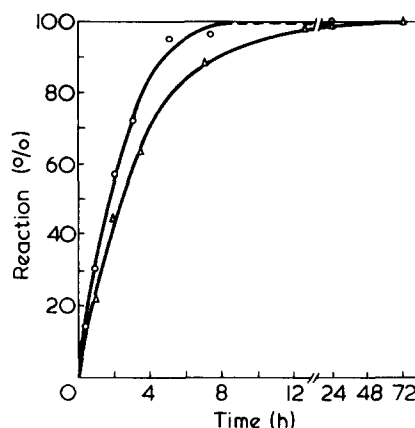


Figure 1 Progress of the substitution reaction of chlorine in partly chloromethylated polystyrene. For the reaction conditions, see the text. O, Substitution by acetate; Δ, substitution by one-ended poly(styrene carboxylate)

rescence analysis of chlorine in the original polymer, indicating that the substitution reaction goes to completion^{4,7}.

The 50/50 mixture of benzene and acetonitrile constitutes a near θ -solvent for polystyrene at room temperature. The reaction is quite slow in pure benzene at 70°C. Dibenzo-18-crown-6 is only about half as efficient as dicyclohexyl-18-crown-6. *Table 1* illustrates the generality of the substitution reaction with the same chloromethylated polystyrene. Gel permeation chromatograms indicate that the substituted polystyrenes retain the origi-

nal narrow molecular weight distribution. The substitution of chlorine by stearate is slower than by acetate, presumably because the large amount of stearate lowers the dielectric constant of the reaction medium. When potassium *p*-(2-chloroethyl) benzoate is the substituent the chloroethyl group is available for further substitution by benzoate. An average of three ester links were formed per polymer chlorine. Neither potassium 2,4-dinitrophenolate nor potassium phenolate reacted under these reaction conditions.

The reaction of chloromethylated polystyrene with potassium 1-phenyl propionate is a prototype for the reaction with one ended potassium carboxylated polystyrene. As an example of crown ether catalysed grafting, 0.30 g chloromethylated polystyrene (0.11 mmol Cl, $M_n = 143\ 000$, $M_w = 157\ 000$) is reacted with 0.655 g of polystyrene capped with one potassium carboxylate group* (0.218 mmol

* The one-ended polystyrene-COOK is prepared with sec-butyllithium in benzene. The living polymer is terminated under vacuum in the presence of 1.5 equivalent tetramethylethylenediamine with a large excess of solid carbon dioxide. The benzene solution of the polymer is acidified with aqueous hydrogen chloride, washed repeatedly with distilled water and freeze dried. The polystyrene is redissolved in benzene and the acid groups are neutralized with potassium methoxide in benzene-methanol (5:1) using the thymol blue end point⁸. The polymer is then recovered by freeze drying. During carboxylation a variable amount of polymer (less than 10%) dimerizes⁹, but this fraction does not interfere in the subsequent coupling reaction.

is clearly demonstrated. As summarized in *Table 1*, the conformation of PCLT is a right-handed α -helix in chloroform, dioxane, trimethylphosphate, 2-chloroethanol, pyridine or 1,1,1,3,3,3-hexafluoro-2-propanol and a random coil in DCA, TFA, hexamethylphosphoramide, hexafluoroacetone sesquihydrate or 1,3-dichlorotetrafluoroacetone 2,5 hydrate.

ACKNOWLEDGEMENT

The author wishes to express his gratitude to Professor Tadao Hayakawa of

the Institute for his valuable discussions and suggestions.

REFERENCES

- 1 Peggion, E., Verdini, A. S. and Scoffone, E. *Macromolecules* 1969, **2**, 170
- 2 Terbojevich, M., Acampora, M., Conasi, A., Peggion, E. and Scoffone, E. *Macromolecules* 1970, **3**, 618
- 3 Fasman, G. D., Landsberg, M. and Buchwald, M. *Can. J. Chem.* 1965, **43**, 1588
- 4 Cosani, A., Peggion, E., Verdini, A. S. and Terbojevich, M. *Biopolymers* 1968, **6**, 963
- 5 Peggion, E., Cosani, A., Verdini, A. S., Del Pra, A. and Mammì, M. *Biopolymers* 1968, **6**, 1477
- 6 Peggion, E., Fontana, A. and Cosani, A. *Biopolymers* 1969, **7**, 517
- 7 Vollmer, J.-P. and Spach, G. *Biopolymers* 1967, **5**, 337
- 8 Goodman, M., Toniolo, C. and Peggion, E. *Biopolymers* 1968, **6**, 1691
- 9 Yamamoto, H. and Hayakawa, T. *Macromolecules* 1976, **9**, 532
- 10 Del Pra, A. and Gilli, G. *Biopolymers* 1975, **14**, 1769
- 11 Katchalski, E. and Sela, M. *J. Am. Chem. Soc.* 1953, **75**, 5284
- 12 Overall, B. G. and Petrow, V. *J. Chem. Soc.* 1955, p 232
- 13 Noguchi, J. and Yamamoto, H. *J. Biochem.* 1969, **65**, 123
- 14 Moffitt, W. and Yang, J. T. *Proc. Nat. Acad. Sci. USA* 1956, **42**, 596

Crown ether catalysed modification of partly chloromethylated polystyrene

J. E. L. Roovers

Division of Chemistry, National Research Council of Canada, Ottawa K1A 0R9, Canada
(Received 11 June 1976)

In the course of the preparation of well characterized narrow molecular weight distribution poly(styrene-*g*-isoprenes) partly chloromethylated polystyrene had to be converted to poly(vinylbenzyl acetate-styrene) random copolymer¹. The published method^{2,3}, using potassium acetate in dimethyl sulphoxide gave variable reaction yields and broadening of the molecular weight distribution. The former observation can be accounted for by the heterogeneity of the reaction medium, the latter is ascribed to the presence of oxidation products of dimethyl sulphoxide. Therefore, a new method using crown ethers to solubilize and activate potassium acetate in non-polar solvents⁴ was adapted to the acetylation of partly chloromethylated polystyrene.

Typically, 1 g anionically prepared⁵ and chloromethylated⁶ polystyrene containing 0.37 mmol chlorine is dissolved in 20 ml of a 50/50 (v/v) mixture of benzene and acetonitrile. To this, 135 mg dicyclohexyl-18-crown-6 (Aldrich) and 365 mg potassium acetate (3.7 mmol) are added. The mixture is magnetically stirred at 75°C. The reaction is quenched by cooling and the addition of benzene. The mixture is filtered and the polymer precipitated in excess methanol. The carbonyl absorption band at 1740 cm⁻¹ is used to monitor the acetylation. (*Figure 1*). The final acetate content of the polymer agrees with X-ray fluo-

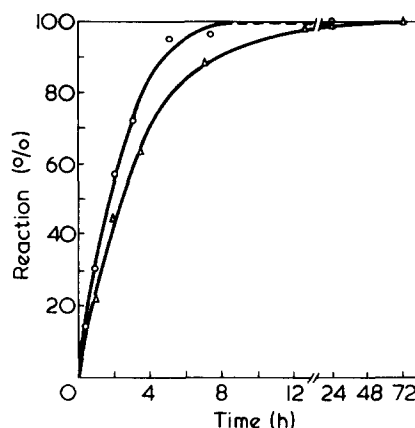


Figure 1 Progress of the substitution reaction of chlorine in partly chloromethylated polystyrene. For the reaction conditions, see the text. O, Substitution by acetate; Δ, substitution by one-ended poly(styrene carboxylate)

rescence analysis of chlorine in the original polymer, indicating that the substitution reaction goes to completion^{4,7}.

The 50/50 mixture of benzene and acetonitrile constitutes a near θ -solvent for polystyrene at room temperature. The reaction is quite slow in pure benzene at 70°C. Dibenzo-18-crown-6 is only about half as efficient as dicyclohexyl-18-crown-6. *Table 1* illustrates the generality of the substitution reaction with the same chloromethylated polystyrene. Gel permeation chromatograms indicate that the substituted polystyrenes retain the origi-

nal narrow molecular weight distribution. The substitution of chlorine by stearate is slower than by acetate, presumably because the large amount of stearate lowers the dielectric constant of the reaction medium. When potassium *p*-(2-chloroethyl) benzoate is the substituent the chloroethyl group is available for further substitution by benzoate. An average of three ester links were formed per polymer chlorine. Neither potassium 2,4-dinitrophenolate nor potassium phenolate reacted under these reaction conditions.

The reaction of chloromethylated polystyrene with potassium 1-phenyl propionate is a prototype for the reaction with one ended potassium carboxylated polystyrene. As an example of crown ether catalysed grafting, 0.30 g chloromethylated polystyrene (0.11 mmol Cl, $M_n = 143\,000$, $M_w = 157\,000$) is reacted with 0.655 g of polystyrene capped with one potassium carboxylate group* (0.218 mmol

* The one-ended polystyrene-COOK is prepared with sec-butyllithium in benzene. The living polymer is terminated under vacuum in the presence of 1.5 equivalent tetramethylethylenediamine with a large excess of solid carbon dioxide. The benzene solution of the polymer is acidified with aqueous hydrogen chloride, washed repeatedly with distilled water and freeze dried. The polystyrene is redissolved in benzene and the acid groups are neutralized with potassium methoxide in benzene-methanol (5:1) using the thymol blue end point⁸. The polymer is then recovered by freeze drying. During carboxylation a variable amount of polymer (less than 10%) dimerizes⁹, but this fraction does not interfere in the subsequent coupling reaction.

COOK, $M_n = 3000$) in 6 ml of a benzene-acetonitrile (50/50) mixture in the presence of 40 mg dicyclohexyl-18-crown-6 at 75°C. Potassium chloride precipitates out from the initially homogeneous reaction medium. The reaction is monitored by gel permeation chromatography. Progress is calculated from the relative amounts of polymer in the comb and that present as free branch material. (Figure 1). Excess branch material can be removed easily by fractionation. The i.r. carbonyl absorption of the fractionated comb is compared with the absorption in fully acetylated or 1-phenyl propionated backbone polymer. It can be used to determine the extent of branching independently of the molecular weight of the comb polymer¹⁰. Similarly, hydrolysis of the ester links with sodium hydroxide in dioxane/water³ and gel permeation chromatography of the product permits calculation of λ , the fraction of polymer in the backbone and, therefrom, the average number of branches per chain. For the comb polymer described $\lambda_{Cl} = 0.472$, $\lambda_{ir} = 0.471$, $\lambda_{hydr} = 0.458$, $\lambda_{M_w} = 0.456$. With the same backbone polymer and a branch poly-

Table 1 Substitution on partly chloromethylated polystyrene

Substituent	Yield (%)	Remarks
$CH_3(CH_2)_{16}COOK$	100 (36)	Weight increase of polymer I.r. absorption at 1740 cm^{-1} P.m.r. aliphatic/aromatic = 0.91; calculated 0.89
C_6H_5COOK	100 (24)	I.r. absorption at 1720 cm^{-1} ; compared with benzyl benzoate
<i>trans</i> - $C_6H_5CH=CHCOOK$	87 (64)	I.r. absorption at 1720 and 1635 cm^{-1} U.v. absorption at $275\text{ }\mu\text{m}$
$p(Cl-CH_2CH_2)C_6H_4COOK$	(72)	I.r. absorption indicates 3 carbonyls per Cl
$CH_3CH(C_6H_5)COOK$	100 (48)	I.r. absorption at 1740 cm^{-1}
KCN	—	I.r. absorption at 2270 cm^{-1}

Values in parentheses represent reaction times (h)

mer of $M_n = 18\,700$ a comb polymer was obtained having $\lambda_{Cl} = 0.126$, $\lambda_{ir} = 0.146$, $\lambda_{hydr} = 0.138$, and $\lambda_{M_w} = 0.145$.

REFERENCES

- Rahlwes, D., Roovers, J. E. L. and Bywater, S. to be published
- Ayres, J. T. and Mann, C. K. *Polym. Lett.* 1965, 3, 505
- Bamford, C. H. and Lindsay, H. *Polymer* 1973, 14, 330
- Liotta, C. L., Harris, H. P., McDermott, M., Gonzalez, T. and Smith, K. *Tetrahedron Lett.* 1974, 28, 2417
- Roovers, J. E. L. and Bywater, S. *Macromolecules* 1972, 5, 384
- Pepper, K. W., Paisley, H. M. and Young, M. A. *J. Chem. Soc.* 1953, p 4097
- Durst, H. D., Milano, M., Kikta, E. J., Connelly, S. A. and Grushka, E. *Anal. Chem.* 1975, 47, 1797
- Fritz, J. S. 'Acid-Base Titrations in non-aqueous Solvents', G. Frederick Smith Chem. Co., 1952
- Wyman, D. P., Allen, V. R. and Altares, T. *J. Polym. Sci. (A)* 1964, 2, 4545
- Roovers, J. E. L. *Polymer* 1975, 16, 827

Grafting on to poly(vinyl alcohol): a new spectral method to estimate the extent of grafting*

T. Vasudevan[†], H. Kothandaraman and M. Santappa

Department of Physical Chemistry, University of Madras, Madras 600025, India
(Received 29 March 1976; revised 27 April 1976)

Studies of grafting onto polymer backbones are numerous¹⁻⁵. In most cases, the grafting rates are obtained by gravimetric procedures; the complete precipitation, filtering and drying to constant weight is a cumbersome procedure, in which it is very difficult to eliminate experimental error. The use of spectral techniques obviates such a gravimetric procedure, once a correlation is established between gravimetric and spectral techniques. Though much

work has been carried out on spectroscopic investigations of vinyl copolymerizations, the method has been applied for graft polymers in only a few cases^{6,7}. In this work, grafting is carried out in a homogeneous solution under both thermal and photochemical conditions.

EXPERIMENTAL

Materials

Poly(vinyl Alcohol) (PVA) ($DP = 1000$) supplied by BDH Laboratories was used as received. Acrylamide (LR BDH) was purified by recrystallizing it from AR Chloroform twice. Ferric chloride (AR BDH) and ceric ammonium sulphate (AR BDH) were used as received without further puri-

fication. The PVA solution and other solutions used in the spectroscopic investigations were prepared according to the procedure reported in a previous paper⁸. A typical absorption spectrum of the PVA/boric acid/iodine complex was recorded using a SPECORD UV-VIS Spectrophotometer (Figure 1).

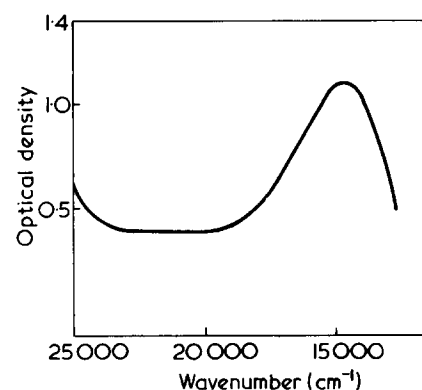


Figure 1 Typical absorption spectrum of the PVA/boric acid/iodine complex

* This work was presented at the Chemistry Symposium, Indian Institute of Technology, Madras, March 1976.

[†] Present address: Central Laboratory, Bharath Heavy Electricals Ltd, Tiruchivappalli - 620 014, India.

COOK, $M_n = 3000$) in 6 ml of a benzene-acetonitrile (50/50) mixture in the presence of 40 mg dicyclohexyl-18-crown-6 at 75°C. Potassium chloride precipitates out from the initially homogeneous reaction medium. The reaction is monitored by gel permeation chromatography. Progress is calculated from the relative amounts of polymer in the comb and that present as free branch material. (Figure 1). Excess branch material can be removed easily by fractionation. The i.r. carbonyl absorption of the fractionated comb is compared with the absorption in fully acetylated or 1-phenyl propionated backbone polymer. It can be used to determine the extent of branching independently of the molecular weight of the comb polymer¹⁰. Similarly, hydrolysis of the ester links with sodium hydroxide in dioxane/water³ and gel permeation chromatography of the product permits calculation of λ , the fraction of polymer in the backbone and, therefrom, the average number of branches per chain. For the comb polymer described $\lambda_{Cl} = 0.472$, $\lambda_{ir} = 0.471$, $\lambda_{hydr} = 0.458$, $\lambda_{M_w} = 0.456$. With the same backbone polymer and a branch poly-

Table 1 Substitution on partly chloromethylated polystyrene

Substituent	Yield (%)	Remarks
$\text{CH}_3(\text{CH}_2)_{16}\text{COOK}$	100 (36)	Weight increase of polymer I.r. absorption at 1740 cm^{-1} P.m.r. aliphatic/aromatic = 0.91; calculated 0.89
$\text{C}_6\text{H}_5\text{COOK}$	100 (24)	I.r. absorption at 1720 cm^{-1} ; compared with benzyl benzoate
<i>trans</i> - $\text{C}_6\text{H}_5\text{CH}=\text{CHCOOK}$	87 (64)	I.r. absorption at 1720 and 1635 cm^{-1} U.v. absorption at $275\text{ }\mu\text{m}$
$\rho(\text{Cl}-\text{CH}_2\text{CH}_2)\text{C}_6\text{H}_4\text{COOK}$	(72)	I.r. absorption indicates 3 carbonyls per Cl
$\text{CH}_3\text{CH}(\text{C}_6\text{H}_5)\text{COOK}$	100 (48)	I.r. absorption at 1740 cm^{-1}
KCN	—	I.r. absorption at 2270 cm^{-1}

Values in parentheses represent reaction times (h)

mer of $M_n = 18\,700$ a comb polymer was obtained having $\lambda_{Cl} = 0.126$, $\lambda_{ir} = 0.146$, $\lambda_{hydr} = 0.138$, and $\lambda_{M_w} = 0.145$.

REFERENCES

- Rahlwes, D., Roovers, J. E. L. and Bywater, S. to be published
- Ayres, J. T. and Mann, C. K. *Polym. Lett.* 1965, 3, 505
- Bamford, C. H. and Lindsay, H. *Polymer* 1973, 14, 330
- Liotta, C. L., Harris, H. P., McDermott, M., Gonzalez, T. and Smith, K. *Tetrahedron Lett.* 1974, 28, 2417
- Roovers, J. E. L. and Bywater, S. *Macromolecules* 1972, 5, 384
- Pepper, K. W., Paisley, H. M. and Young, M. A. *J. Chem. Soc.* 1953, p 4097
- Durst, H. D., Milano, M., Kikta, E. J., Connelly, S. A. and Grushka, E. *Anal. Chem.* 1975, 47, 1797
- Fritz, J. S. 'Acid-Base Titrations in non-aqueous Solvents', G. Frederick Smith Chem. Co., 1952
- Wyman, D. P., Allen, V. R. and Altares, T. *J. Polym. Sci. (A)* 1964, 2, 4545
- Roovers, J. E. L. *Polymer* 1975, 16, 827

Grafting on to poly(vinyl alcohol): a new spectral method to estimate the extent of grafting*

T. Vasudevan[†], H. Kothandaraman and M. Santappa

Department of Physical Chemistry, University of Madras, Madras 600025, India
(Received 29 March 1976; revised 27 April 1976)

Studies of grafting onto polymer backbones are numerous¹⁻⁵. In most cases, the grafting rates are obtained by gravimetric procedures; the complete precipitation, filtering and drying to constant weight is a cumbersome procedure, in which it is very difficult to eliminate experimental error. The use of spectral techniques obviates such a gravimetric procedure, once a correlation is established between gravimetric and spectral techniques. Though much

work has been carried out on spectroscopic investigations of vinyl copolymerizations, the method has been applied for graft polymers in only a few cases^{6,7}. In this work, grafting is carried out in a homogeneous solution under both thermal and photochemical conditions.

EXPERIMENTAL

Materials

Poly(vinyl Alcohol) (PVA) ($DP = 1000$) supplied by BDH Laboratories was used as received. Acrylamide (LR BDH) was purified by recrystallizing it from AR Chloroform twice. Ferric chloride (AR BDH) and ceric ammonium sulphate (AR BDH) were used as received without further puri-

fication. The PVA solution and other solutions used in the spectroscopic investigations were prepared according to the procedure reported in a previous paper⁸. A typical absorption spectrum of the PVA/boric acid/iodine complex was recorded using a SPECORD UV-VIS Spectrophotometer (Figure 1).

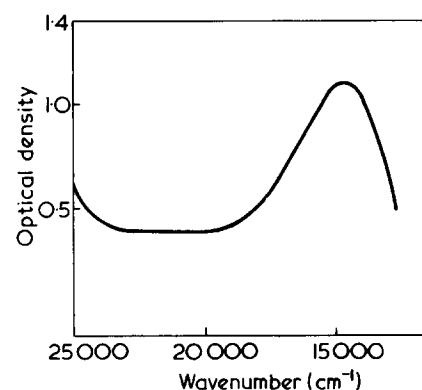


Figure 1 Typical absorption spectrum of the PVA/boric acid/iodine complex

* This work was presented at the Chemistry Symposium, Indian Institute of Technology, Madras, March 1976.

[†] Present address: Central Laboratory, Bharath Heavy Electricals Ltd, Tiruchivappalli - 620 014, India.

$$\text{Percentage grafting} = \frac{100 \times \text{Weight of grafted polymer} - \text{Weight of backbone polymer}}{\text{Weight of backbone polymer}} \quad (1)$$

Grafting procedure

Thermal. Grafting of acrylamide onto PVA was carried out in a reaction vessel having an inlet and outlet, in an atmosphere of nitrogen at a constant temperature of $50 \pm 0.1^\circ\text{C}$ using ceric ammonium sulphate as initiator. After a definite period of the reaction, the monomer concentration was estimated by bromometry. AR methanol was added to an aliquot of the solution to precipitate the PVA which was then filtered through a G₄ sintered glass crucible, washed with 2% ice cold boric acid solution and dried at 60°C , to constant weight. The percentage of grafting is calculated by equation (1).

Photochemical. The grafting of acrylamide onto PVA was carried out in an all quartz cylindrical cell under an atmosphere of nitrogen, at a constant temperature of $30 \pm 0.1^\circ\text{C}$ using ferric chloride as a photoredox initiator. A high pressure mercury vapour lamp was used for irradiation. The percentage grafting was determined using the same method as for thermal grafting. Samples with varying extents of grafting were prepared by varying the time and concentration of the initiator.

Spectral estimation

To an aliquot of the solution (5 ml) after the reaction was complete, boric acid (0.129 M) was added followed by iodine ($3.565 \times 10^{-4}\text{M}$) solution. The total volume was made up to 25 ml. The visible absorption spectrum was measured in the wavelength region $17\,000\text{--}13\,000\text{ cm}^{-1}$. The absorbance maximum occurred at $14\,500\text{ cm}^{-1}$, and was measured for the various reaction mixtures after the reaction (Figure 2). A plot of these absorbance values against the gravimetrically estimated percentage graftings is given in Figure 3.

RESULTS

Samples of varying extents of grafting were analysed spectroscopically and gravimetrically. Figure 3 represents the correlation between the percentage grafting on initial weight against absorbance, in the case of cerium (IV) and in the case of iron (III) as initiators; these values were checked against the gravimetric values using samples up to 30% grafting and the agreement was excellent.

DISCUSSION

In the PVA/boric acid/iodine complex, the function of boric acid is to wind the linear PVA in a radical conformation^{9,10} i.e. the -OH groups of PVA are held in this conformation by electrostatic interaction with boric acid and not by any covalent type of bond formation as suggested by Finch¹¹. This becomes clear from the high salting out constants of the multiply charged anions such as sulphate, citrate, borate etc.¹¹. The molecular weight and the extinction coefficient of the complex were found to be 106 000 and 55 550 respectively. The stability constant of the complex was found to be $\log k = 7.66$. In a trial study, it has been found that two different grades of PVA at the same concentration, one with no acetyl content and the other with 20% acetyl content,

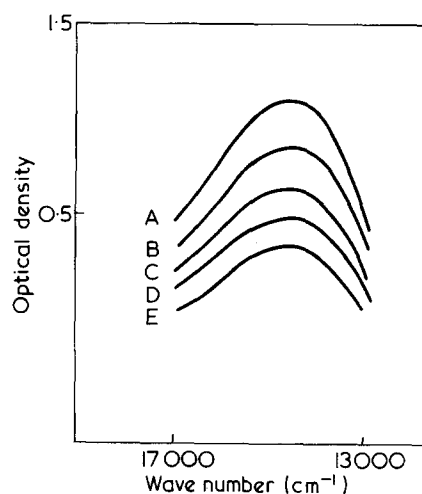


Figure 2 Absorption spectra for the complexes formed by PVA with different extents of grafting: A, 14% grafted; B, 19.4% grafted; C, 23.25% grafted; D, 26.8% grafted; E, 31.25% grafted

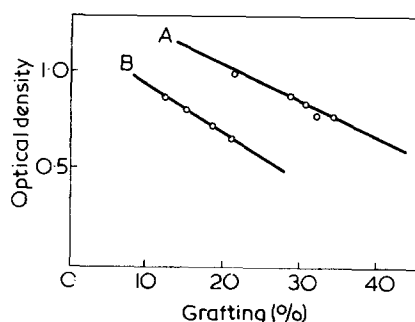
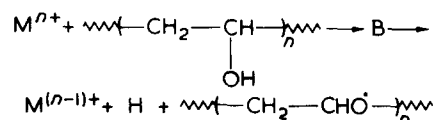


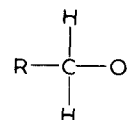
Figure 3 Relation between the optical density of the complexes and extent of grafting. (A) Thermal; initiator: ceric ammonium sulphate; (B) photochemical; initiator: ferric chloride

under identical conditions gave different absorbances, the latter having a lower absorbance than the former, in proportion to the acetyl content for the complex formed with boric acid and iodine. Thus the number of -OH sites in PVA is proportional to the absorbance. Any change in the absorbance is thus related to the number of -OH groups in PVA.

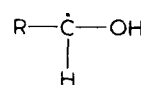
The mechanism of oxidation of secondary alcohols and that of grafting can be compared fairly well. In both cases a hydrogen atom is first abstracted. Since the latter is a polymerization reaction, the hydrogen abstraction is by a radical mechanism. The mechanism generally accepted for grafting onto PVA is that it forms a complex with the initiator which decomposes to give a radical site on the backbone polymer^{3,12}. The radical



is generally denoted by $\text{RCH}_2\dot{\text{O}}$. Palit *et al.*³, suggest that the radical is formed by the abstraction of the hydrogen atom attached to the carbon. However, according to Mino *et al.*¹³, even if the radical is formed by the removal of the hydrogen atom attached to oxygen, the radical



rearranges to



In the cases of grafting onto cellulose derivatives, the grafting takes place via the oxygen atom of the -OH group¹⁴⁻¹⁶. Also not all the oxidants appear to attack secondary alcohols through C-H bond fission¹⁷⁻²⁰. Cobalt (III) and chromium (VI) seem to remove preferentially at the hydrogen atom attached to oxygen^{21,22} whereas vanadium (V) removes the hydrogen atom attached to carbon²³. In the case of cerium (IV) and iron (III) it is evident

from this work that they attack the hydrogen atom of the —OH group and the grafting proceeds via the oxygen atom of the —OH group. Thus the low absorbance of the grafted PVA gives indirect evidence for the location of the grafted site.

REFERENCES

- 1 Krassig, H. A. and Stannett, H. A. *Adv. Polym. Sci.* 1965, 4, 3
- 2 Guthrie, J. T. *Polymer* 1975, 16, 134
- 3 Mukhopadyay, S. et al. *J. Polym. Sci. (A-1)* 1969, 7, 2079
- 4 Takahashi, A. and Takahashi, S. *Polym. J.* 1974, 5, 201
- 5 Prabakar Rao, S. and Santappa, M. *Curr. Sci.* 1965, 34, 176; *J. Sci. Ind. Res.* 1967, 26, 76; *J. Polym. Sci. (A-1)* 1967, 5, 2681
- 6 Guthrie, J. T. and Haq, Zia. *Polymer* 1974, 15, 133
- 7 Takahashi, A. and Takahashi, S. *Kobunshi Kagaku* 1973, 30, 239
- 8 Vasudevan, T., Balakrishnan, T., Kothandaraman, H. and Santappa, M. *J. Polym. Sci. (Polym. Chem. Edn)* in press
- 9 Schildkencht, C. E. *138th Meet. Am. Chem. Soc. New York* 1960
- 10 Brown, J. F. *Sci. Am.* 1962, 207, 82
- 11 'Polyvinyl Alcohol: Applications and Properties', (Ed. C. A. Finch), Wiley, London, 1973, p 41
- 12 Mukhopadyay, S., Prasad, J. and Chatterji, S. R. *Makromol. Chem.* 1975, 186, 1
- 13 Mino, G., Kaizermann, S. and Ramussen, E. J. *Am. Chem. Soc.* 1959, 81, 1494
- 14 Takahashi, A. and Takahashi, S. *Kogyo Kagaku Zasshi* 1971, 74, 2541
- 15 Guthrie, J. T., Pootle, N. S. and Margovio, M. F. *Am. Dyest. Rep.* 1964, 53, 626
- 16 Volgina, S. A., Kryashev, Y. G. and Rogivin, Z. A. *Polym. Sci. USSR (A)* 1965, 7, 1275
- 17 Water, W. A. *Prog. Org. Chem.* 1965, 5, 1
- 18 Hoare, D. G. and Waters, W. A. *J. Chem. Soc.* 1962, pp 65, 971
- 19 Best, P. A., Littler, J. S. and Waters, W. A. *J. Chem. Soc.* 1962, p 822
- 20 Littler, J. S. *J. Chem. Soc.* 1962, pp 827, 832
- 21 Kemp, T. J. and Waters, W. A. *Proc. R. Soc. (A)* 1965, 274, 480
- 22 Viswanathan, S. *PhD Thesis Madras University* (1970)
- 23 Saccubai, S. and Santappa, M. *Indian J. Chem.* 1970, 8, 533

Application of gas chromatography to the analysis of thermal decomposition products of some sulphur containing polyurethanes

T. Lesiak, J. Hetper*, J. Pielichowski†, A. Prewysz-Kwinto and K. Marzec

Institute of Chemistry, N. Copernicus University, Toruń, Poland
(Received 1 June 1976)

INTRODUCTION

In continuing earlier studies¹⁻³ on the synthesis of new types of polyurethane resins Lesiak, Pielichowski and Prewysz-Kwinto recently pointed out the possibility of applying 4,4'-dihydroxydibutyl thioether for that purpose⁴. Polyurethanes prepared using this compound show exceptionally high mechanical strength, a good thermal resistance and excellent adhesion to metals, wood and other materials. Their practical applications are of great promise and therefore it seemed appropriate to develop a simple method for their analysis. Among several possibilities, the method described by Hetper and Zagórski⁵ was chosen. They showed, that several polyurethane resins could be identified by pyrolytic gas chromatography. Basically, the method depends on a certain selection of gas chromatographic separation conditions for the polyurethane pyrolysis product, to obtain on a pyrogram, peaks of the key components derived exclusively from the destruction of the 'polyol' part of the resin mentioned. This method has

been found to give much better results than other methods of that type^{6,7} including the 'Attenuated Total Reflection' method (ATR method)⁸.

A procedure, which complements this method was used by Takeuchi and coworkers⁹ who characterized in a similar way, diisocyanates used for the synthesis of polyurethanes. The present study was undertaken in order to determine the key thermal degradation products of 4,4'-dihydroxydibutyl thioether bonded in the polyurethane resins and to elucidate the mechanism of their formation.

For comparison, similar analyses of the decomposition products of the polyol constituent of polyurethane prepared using 4,4'-dihydroxydibutyl ether were performed. In all the cases studied, pyrolysis of resins investigated was carried out at 770°C.

The products were separated using gas chromatography and identified by mass spectrometry. The method was found to be suitable for the identification of pyrolysis products of thioetherdiol constituents of polyurethanes, since the decomposition products of isocyanic acid derivatives were held in the chromatographic column. It was found that tetrahydrothiophene was the main pyrolysis product of resins ob-

Table 1 Polyurethane resins investigated and compounds used for their syntheses

Sample number	Symbol of resins	Starting materials	
		Diol	Diisocyanate
1	TT-24	4,4'-Dihydroxydibutyl thioether	Tolylene-2,4-diisocyanate
2	TT-26	4,4'-Dihydroxydibutyl thioether	Tolylene-2,6-diisocyanate
3	TT-24-26	4,4'-Dihydroxydibutyl thioether	Mixture of tolylene-2,4- and 2,6-diisocyanates in ratio 4:1
4	TP-5	4,4'-Dihydroxydibutyl thioether	Pentamethylenediisocyanate
5	TBP-44	4,4'-Dihydroxydibutyl thioether	Diisocyanato-4,4'-biphenylmethane
6	TBC-44	4,4'-Dihydroxydibutyl thioether	Diisocyanato-4,4'-bicyclohexylmethane
7	ET-24	4,4'-Dihydroxydibutyl ether	Tolylene-2,4-diisocyanate

* Institute of Heavy Organic Synthesis 'Blachownia', Kędzierzyn, Poland.

† Institute of Organic Chemistry and Technology, Technical University, Kraków, Poland.

from this work that they attack the hydrogen atom of the —OH group and the grafting proceeds via the oxygen atom of the —OH group. Thus the low absorbance of the grafted PVA gives indirect evidence for the location of the grafted site.

REFERENCES

- 1 Krassig, H. A. and Stannett, H. A. *Adv. Polym. Sci.* 1965, 4, 3
- 2 Guthrie, J. T. *Polymer* 1975, 16, 134
- 3 Mukhopadyay, S. et al. *J. Polym. Sci. (A-1)* 1969, 7, 2079
- 4 Takahashi, A. and Takahashi, S. *Polym. J.* 1974, 5, 201
- 5 Prabakar Rao, S. and Santappa, M. *Curr. Sci.* 1965, 34, 176; *J. Sci. Ind. Res.* 1967, 26, 76; *J. Polym. Sci. (A-1)* 1967, 5, 2681
- 6 Guthrie, J. T. and Haq, Zia. *Polymer* 1974, 15, 133
- 7 Takahashi, A. and Takahashi, S. *Kobunshi Kagaku* 1973, 30, 239
- 8 Vasudevan, T., Balakrishnan, T., Kothandaraman, H. and Santappa, M. *J. Polym. Sci. (Polym. Chem. Edn)* in press
- 9 Schildkencht, C. E. *138th Meet. Am. Chem. Soc. New York* 1960
- 10 Brown, J. F. *Sci. Am.* 1962, 207, 82
- 11 'Polyvinyl Alcohol: Applications and Properties', (Ed. C. A. Finch), Wiley, London, 1973, p 41
- 12 Mukhopadyay, S., Prasad, J. and Chatterji, S. R. *Makromol. Chem.* 1975, 186, 1
- 13 Mino, G., Kaizermann, S. and Ramussen, E. J. *Am. Chem. Soc.* 1959, 81, 1494
- 14 Takahashi, A. and Takahashi, S. *Kogyo Kagaku Zasshi* 1971, 74, 2541
- 15 Guthrie, J. T., Pootle, N. S. and Margovio, M. F. *Am. Dyest. Rep.* 1964, 53, 626
- 16 Volgina, S. A., Kryashev, Y. G. and Rogivin, Z. A. *Polym. Sci. USSR (A)* 1965, 7, 1275
- 17 Water, W. A. *Prog. Org. Chem.* 1965, 5, 1
- 18 Hoare, D. G. and Waters, W. A. *J. Chem. Soc.* 1962, pp 65, 971
- 19 Best, P. A., Littler, J. S. and Waters, W. A. *J. Chem. Soc.* 1962, p 822
- 20 Littler, J. S. *J. Chem. Soc.* 1962, pp 827, 832
- 21 Kemp, T. J. and Waters, W. A. *Proc. R. Soc. (A)* 1965, 274, 480
- 22 Viswanathan, S. *PhD Thesis Madras University* (1970)
- 23 Saccubai, S. and Santappa, M. *Indian J. Chem.* 1970, 8, 533

Application of gas chromatography to the analysis of thermal decomposition products of some sulphur containing polyurethanes

T. Lesiak, J. Hetper*, J. Pielichowski†, A. Prewysz-Kwinto and K. Marzec

Institute of Chemistry, N. Copernicus University, Toruń, Poland
(Received 1 June 1976)

INTRODUCTION

In continuing earlier studies¹⁻³ on the synthesis of new types of polyurethane resins Lesiak, Pielichowski and Prewysz-Kwinto recently pointed out the possibility of applying 4,4'-dihydroxydibutyl thioether for that purpose⁴. Polyurethanes prepared using this compound show exceptionally high mechanical strength, a good thermal resistance and excellent adhesion to metals, wood and other materials. Their practical applications are of great promise and therefore it seemed appropriate to develop a simple method for their analysis. Among several possibilities, the method described by Hetper and Zagórski⁵ was chosen. They showed, that several polyurethane resins could be identified by pyrolytic gas chromatography. Basically, the method depends on a certain selection of gas chromatographic separation conditions for the polyurethane pyrolysis product, to obtain on a pyrogram, peaks of the key components derived exclusively from the destruction of the 'polyol' part of the resin mentioned. This method has

been found to give much better results than other methods of that type^{6,7} including the 'Attenuated Total Reflection' method (ATR method)⁸.

A procedure, which complements this method was used by Takeuchi and coworkers⁹ who characterized in a similar way, diisocyanates used for the synthesis of polyurethanes. The present study was undertaken in order to determine the key thermal degradation products of 4,4'-dihydroxydibutyl thioether bonded in the polyurethane resins and to elucidate the mechanism of their formation.

For comparison, similar analyses of the decomposition products of the polyol constituent of polyurethane prepared using 4,4'-dihydroxydibutyl ether were performed. In all the cases studied, pyrolysis of resins investigated was carried out at 770°C.

The products were separated using gas chromatography and identified by mass spectrometry. The method was found to be suitable for the identification of pyrolysis products of thioether-diol constituents of polyurethanes, since the decomposition products of isocyanic acid derivatives were held in the chromatographic column. It was found that tetrahydrothiophene was the main pyrolysis product of resins ob-

Table 1 Polyurethane resins investigated and compounds used for their syntheses

Sample number	Symbol of resins	Starting materials	
		Diol	Diisocyanate
1	TT-24	4,4'-Dihydroxydibutyl thioether	Tolylene-2,4-diisocyanate
2	TT-26	4,4'-Dihydroxydibutyl thioether	Tolylene-2,6-diisocyanate
3	TT-24-26	4,4'-Dihydroxydibutyl thioether	Mixture of tolylene-2,4- and 2,6-diisocyanates in ratio 4:1
4	TP-5	4,4'-Dihydroxydibutyl thioether	Pentamethylenediisocyanate
5	TBP-44	4,4'-Dihydroxydibutyl thioether	Diisocyanato-4,4'-biphenylmethane
6	TBC-44	4,4'-Dihydroxydibutyl thioether	Diisocyanato-4,4'-bicyclohexylmethane
7	ET-24	4,4'-Dihydroxydibutyl ether	Tolylene-2,4-diisocyanate

* Institute of Heavy Organic Synthesis 'Blachownia', Kędzierzyn, Poland.

† Institute of Organic Chemistry and Technology, Technical University, Kraków, Poland.

tained from 4,4'-dihydroxydibutyl thioether. In addition, tetrahydrofuran and small amounts of n-butanol as well as 3-buten-1-ol were also formed. Polyurethanes obtained from 4,4'-dihydroxydibutyl ether, decomposed under these conditions to give tetrahydrofuran and the above mentioned alcohols. A mechanism of formation of these compounds is proposed below.

EXPERIMENTAL

Polyurethanes used in this study were obtained from equimolar amounts of 4,4'-dihydroxydibutyl thioether and various organic diisocyanates using the method described in ref 4. One sample was prepared in the same way using 4,4'-dihydroxydibutyl ether. Symbols for these polymers and a list of components used for their syntheses are shown in Table 1.

Instrumentation and measurement techniques

A gas chromatograph, Pye 104 provided with a pyrolysis accessory working on the principle of the Curie point was used with a mass spectrometer, LKB type GC/MS 2091 connected.

Polymers were pyrolysed in a micro-

reactor connected to the gas chromatograph. The pyrolysis was carried out in a stream of carrier gas at 770°C with a heating time of 5 sec. The pyrolysis products were separated on a glass chromatographic column packed with poly(ethylene glycol) 1000 (15%) on Chromosorb P 60/80 mesh; column length, 3 m; temperature, 100°C; carrier gas, helium; flow rate, 30 ml/min. Under these conditions the high boiling components were adsorbed, practically irreversibly, in the first section of the chromatographic column. Mass spectra of the main components were measured at the top of their chromatographic peaks with ionization energy, 70 eV and temperature of the ion source, 200°C.

Results and discussion

The pyrogram of polyurethane TT-24 is shown in Figure 1. Identical pyrograms, which are not shown here, were obtained for all polyurethanes synthesised from 4,4'-dihydroxydibutyl thioether and other aromatic diisocyanates (TT-26, TT-24-26 and TBP-44). Figure 1 indicates, that under the conditions of chromatographic separation used in this study, pyrograms show only those products which are formed from the diol part of the polymer (decomposition products of thioether bonded in polyurethane). According to the literature data⁹ systems formed from aromatic diisocyanates decompose mainly to amines, nitriles and mono-isocyanates. These compounds are held in the chromatographic column under the conditions used.

In the case of polyurethane obtained from an aliphatic diisocyanate (TP-5) the basic character of the pyrogram is not changed except that peaks corresponding to C₁-C₄ hydrocarbons are increased (Figure 2). On the other hand, the alicyclic system present in TBC 44 polyurethane gives as a result of pyrolysis a series of aliphatic hydrocarbons with higher molecular weights. Peaks of these hydrocarbons overlap with peak number 2, but even in this case the characteristic pattern of 3,4 and 5 peaks, remains unchanged (Figure 3). The main components present in all pyrolysis products investigated, were identified on the basis of their mass spectra. The results are presented in Table 2.

The results of this study show, that tetrahydrothiophene is the main pyrolysis product of the thioether component of polyurethane. However in addi-

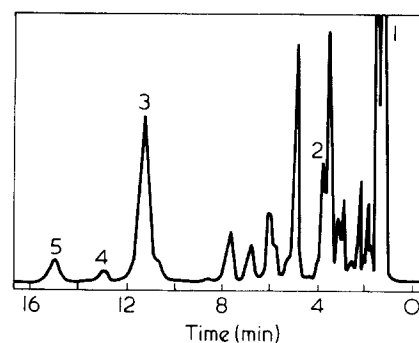


Figure 3 Pyrogram of polyurethane obtained from 4,4'-dihydroxydibutyl thioether and diisocyanato-4,4'-bicyclohexylmethane (TBC-44)

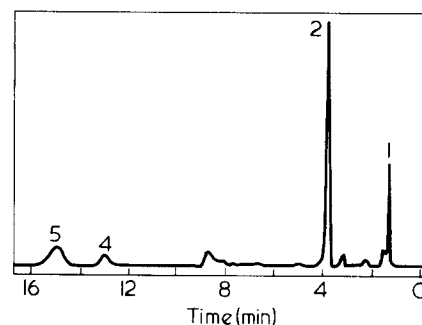


Figure 4 Pyrogram of polyurethane obtained from 4,4'-dihydroxydibutyl ether and tolylene-2,4-diisocyanate (ET-24)

Table 2 Results of analyses of the polyurethane pyrogram peaks obtained

Peak number	Compounds identified
1	C ₁ -C ₄ Hydrocarbons, carbon dioxide
2	Tetrahydrofuran
3	Tetrahydrothiophene
4	n-Butanol
5	3-Buten-1-ol

tion to this compound, tetrahydrofuran and small amounts of n-butanol and 3-buten-1-ol are formed too. Pyrolysis of polymer ET-24 (not containing sulphur) gives the same products except for tetrahydrothiophene. The main product in this case is tetrahydrofuran (Figure 4).

Mechanism of formation of the above mentioned compounds, can be explained on the basis of the characteristic property of higher esters which easily undergo the pyrolytic decomposition to carbon dioxide and the highly reactive free radicals. Thus in this case, the radical I, (scheme 1), adopting a suitable conformation, can cyclize to five membered systems. Elimination of a molecule of heterocycle II gives again a radical which can lead to tetrahydrofuran III. Scheme (1) illustrates these reactions. R,R' represent fragments of the polymer molecule and Y a hetero-

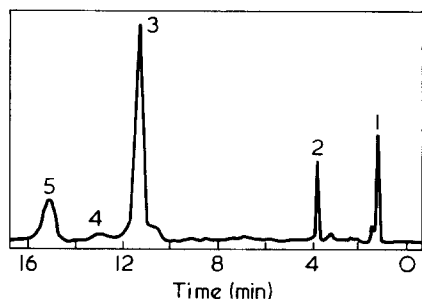


Figure 1 Pyrogram of polyurethane obtained from 4,4'-dihydroxydibutyl thioether and tolylene-2,4-diisocyanate (TT-24)

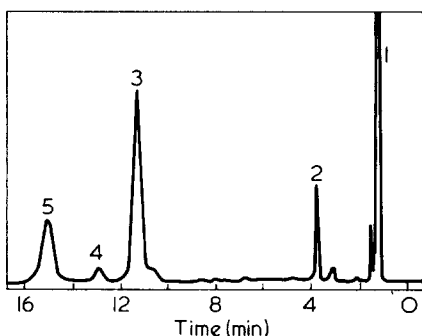
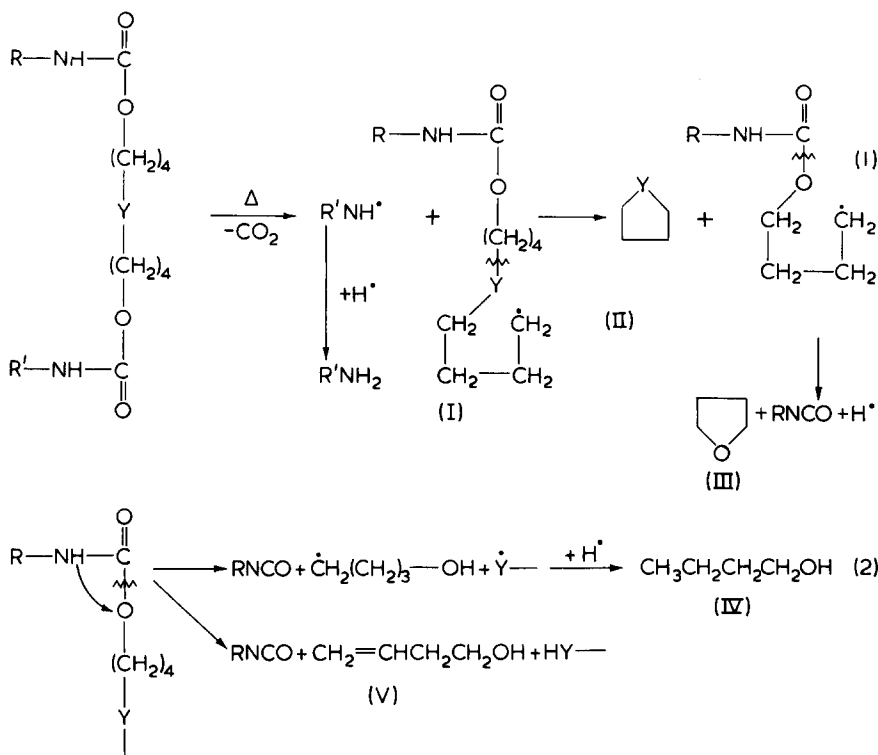


Figure 2 Pyrogram of polyurethane obtained from 4,4'-dihydroxydibutyl thioether and pentamethylenediisocyanate (TP-5)

Letters



atom (sulphur in the case of thioether and oxygen in the case of ethers used).

If the bond $\geq\text{C}-\text{O}-$ in polyurethane undergoes cleavage with subse-

quent hydrogen migration, instead of decarboxylation, a chain with OH groups at the ends can be formed. This prevents the cyclization reactions and

can lead to formation of alcohols with four carbon atoms (IV or V, scheme 2). This procedure can be accompanied by the Y-C bond cleavage with or without hydrogen atom migration as shown in scheme (2). The method presented here has been found useful for the identification of the diol constituent degradation products of polyurethanes of the type described. This makes possible a partial qualitative characterization of polyurethane composition.

REFERENCES

- 1 Lesiak, T. and Prewysz-Kwinto, A. *Chem. Stosow.* 1972, 16, 259
- 2 Lesiak, T. and Prewysz-Kwinto, A. *Chem. Stosow.* 1974, 18, 471
- 3 Lesiak, T. and Prewysz-Kwinto, A. *Chem. Stosow.* 1975, 19, 477
- 4 Lesiak, T., Pieliowski, J. and Prewysz-Kwinto, A. *Chem. Stosow.* 1975, 19, 221
- 5 Hetper, J. and Zagórski, W. *Polimery* 1973, 18, 327
- 6 Newell, J. E. 'Theory and Application of Gas Chromatography in Industry and Medicine', (Eds H. S. Kroman and S. R. Bender), Grune and Stratton, New York, 1968
- 7 Groten, B. *Anal. Chem.* 1964, 36, 1206
- 8 Corish, P. J. *Anal. Chem.* 1959, 31, 1298
- 9 Takeuchi, T., Tsuge, S. and Okumoto, T. *J. Gas Chromatogr.* 1968, 6, 542

Letters

Chain atoms between entanglements and cross-sectional area per chain

We recently demonstrated a linear log-log correlation of slope -3 between the ratio C_2/C_1 of the Mooney-Rivlin constants (at $2C_1 = 0.2 \text{ N/mm}^2$) and cross-sectional area per polymer chain^{1,2}. It was suggested² that either strain induced local order or chain entanglements might be involved in what appeared to be an intermolecular effect.

Kraus and Mocvgemba³ had proposed that the molecular origin of the C_2 term was a result, at least in part, of chain entanglements. Preliminary examination of an extensive tabulation by Porter and Johnson⁴ of entanglement distances indicated a positive correlation with cross-sectional area per polymer chain. However, the scatter in data points was so great as to discourage any firm conclusions. The entanglement data in the literature

have now been examined in detail and a preliminary strong correlation has been made.

A specific tabulation by Fox and Allen⁵ was used as a source of N_c , the number of chain atoms between entanglement points determined from concentrated or bulk viscosity measurements as a function of molecular weight. Cross-sectional areas per polymer chain were calculated by a method described previously², which differs only in minor details from that used by Vincent⁶ for a different purpose.

Figure 1 shows a log-log correlation between N_c and chain areas in nm^2 . The line as drawn has a slope of approximately 0.5. The marked deviation of atactic PMMA from the trend line is considered to arise because of molecular association between iso- and syndio-tactic species present in a

PMMA⁷. Porter and Johnson note that any form of association tends to promote low values of N_c .

A detailed study of this subject will be presented elsewhere⁸. As one in-

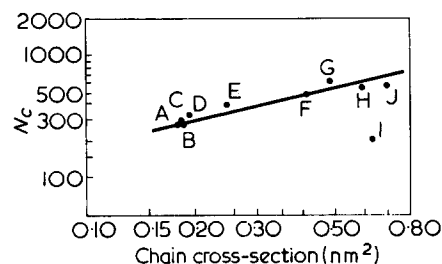
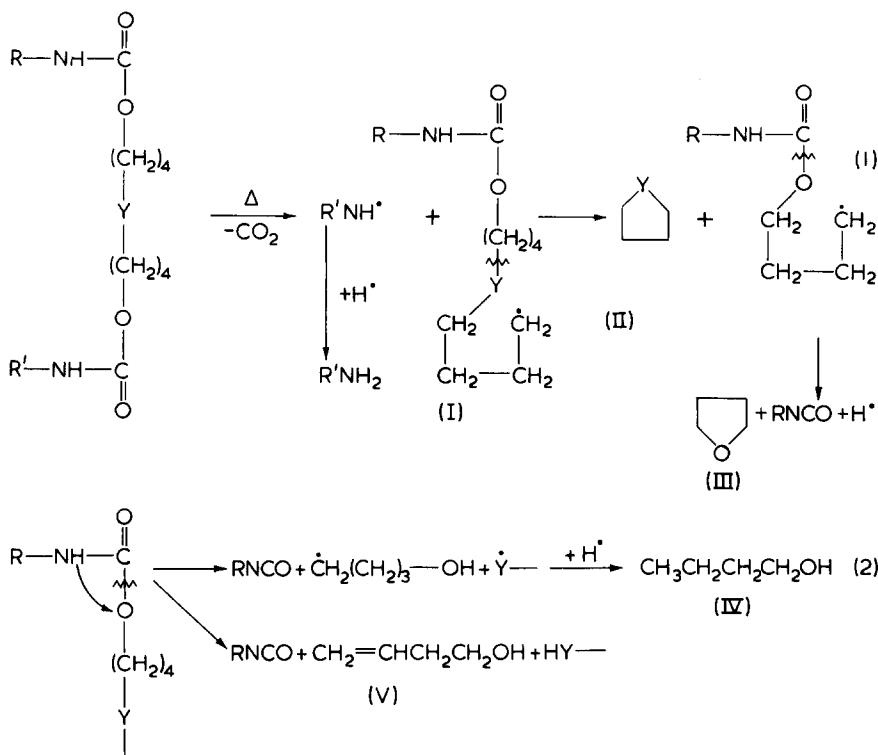


Figure 1 Number of chain atoms, N_c , between entanglements from data of Fox and Allen⁵ vs. chain cross-section in nm^2 . A, PE; B, poly(decamethylene adipate); C, poly(decamethylene sebacate); D, poly(ε-caproamide); E, poly(propylene oxide); F, PIB; G, PDMS; H, PVAc; I, atactic PMMA; J, atactic PS.

Letters



atom (sulphur in the case of thioether and oxygen in the case of ethers used).

If the bond $\geq\text{C}-\text{O}-$ in polyurethane undergoes cleavage with subse-

quent hydrogen migration, instead of decarboxylation, a chain with OH groups at the ends can be formed. This prevents the cyclization reactions and

can lead to formation of alcohols with four carbon atoms (IV or V, scheme 2). This procedure can be accompanied by the Y-C bond cleavage with or without hydrogen atom migration as shown in scheme (2). The method presented here has been found useful for the identification of the diol constituent degradation products of polyurethanes of the type described. This makes possible a partial qualitative characterization of polyurethane composition.

REFERENCES

- 1 Lesiak, T. and Prewysz-Kwinto, A. *Chem. Stosow.* 1972, 16, 259
- 2 Lesiak, T. and Prewysz-Kwinto, A. *Chem. Stosow.* 1974, 18, 471
- 3 Lesiak, T. and Prewysz-Kwinto, A. *Chem. Stosow.* 1975, 19, 477
- 4 Lesiak, T., Pieliowski, J. and Prewysz-Kwinto, A. *Chem. Stosow.* 1975, 19, 221
- 5 Hetper, J. and Zagórski, W. *Polimery* 1973, 18, 327
- 6 Newell, J. E. 'Theory and Application of Gas Chromatography in Industry and Medicine', (Eds H. S. Kroman and S. R. Bender), Grune and Stratton, New York, 1968
- 7 Groten, B. *Anal. Chem.* 1964, 36, 1206
- 8 Corish, P. J. *Anal. Chem.* 1959, 31, 1298
- 9 Takeuchi, T., Tsuge, S. and Okumoto, T. *J. Gas Chromatogr.* 1968, 6, 542

Letters

Chain atoms between entanglements and cross-sectional area per chain

We recently demonstrated a linear log-log correlation of slope -3 between the ratio C_2/C_1 of the Mooney-Rivlin constants (at $2C_1 = 0.2 \text{ N/mm}^2$) and cross-sectional area per polymer chain^{1,2}. It was suggested² that either strain induced local order or chain entanglements might be involved in what appeared to be an intermolecular effect.

Kraus and Moczygemba³ had proposed that the molecular origin of the C_2 term was a result, at least in part, of chain entanglements. Preliminary examination of an extensive tabulation by Porter and Johnson⁴ of entanglement distances indicated a positive correlation with cross-sectional area per polymer chain. However, the scatter in data points was so great as to discourage any firm conclusions. The entanglement data in the literature

have now been examined in detail and a preliminary strong correlation has been made.

A specific tabulation by Fox and Allen⁵ was used as a source of N_c , the number of chain atoms between entanglement points determined from concentrated or bulk viscosity measurements as a function of molecular weight. Cross-sectional areas per polymer chain were calculated by a method described previously², which differs only in minor details from that used by Vincent⁶ for a different purpose.

Figure 1 shows a log-log correlation between N_c and chain areas in nm^2 . The line as drawn has a slope of approximately 0.5. The marked deviation of atactic PMMA from the trend line is considered to arise because of molecular association between iso- and syndio-tactic species present in a

PMMA⁷. Porter and Johnson note that any form of association tends to promote low values of N_c .

A detailed study of this subject will be presented elsewhere⁸. As one in-

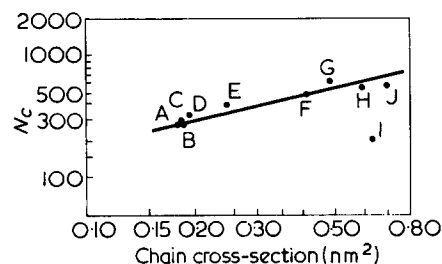


Figure 1 Number of chain atoms, N_c , between entanglements from data of Fox and Allen⁵ vs. chain cross-section in nm^2 . A, PE; B, poly(decamethylene adipate); C, poly(decamethylene sebacate); D, poly(ε-caproamide); E, poly(propylene oxide); F, PIB; G, PDMS; H, PVAc; I, atactic PMMA; J, atactic PS.

cludes more bodies of data, and especially other measures of chain entanglement to be found in ref 4, the scatter increases significantly. However, the trend shown in *Figure 1* is not lost.

Since both C_2/C_1 and N_c correlate with a common variable, area in nm^2 , it follows that one should expect a linear correlation between C_2/C_1 and N_c . This indeed is the case with five data points for PE, *cis-trans* PBD, NR, PIB, and PDMS⁸. This correlation does not necessarily mean that chain entanglements are solely responsible for the

C_2 term.

The correlation line of *Figure 1* on a homogeneous set of data provides a criterion for judging and/or selecting from discordant literature values for these and other polymers.

Raymond F. Boyer and Robert L. Miller

Midland Macromolecular Institute,
1910 W. St. Andrews Drive,
Midland, Michigan 48640, USA
(Received 19 July 1976)

References

- 1 Boyer, R. F. and Miller, R. L. *Polymer* 1976, **17**, 925
- 2 Boyer, R. F. and Miller, R. L. *Rubber Chem. Technol.* in press
- 3 Kraus, G. and Moczvgemba, G. A. *J. Polym. Sci. (A-2)* 1964, 277
- 4 Porter, R. S. and Johnson, J. F. *Chem. Rev.* 1966, **66**, 1
- 5 Fox, T. G. and Allen, V. R. *J. Chem. Phys.* 1964, **41**, 344
- 6 Vincent, P. I. *Polymer* 1972, **13**, 558
- 7 Feitsma, E. L., de Boer, A. and Challa, G. *Polymer* 1975, **16**, 515. This paper refers to earlier literature.
- 8 Boyer, R. F. and Miller, R. L. *Rubber Chem. Technol.* in press

The involvement of singlet oxygen in the sensitized photodegradation of cellulose

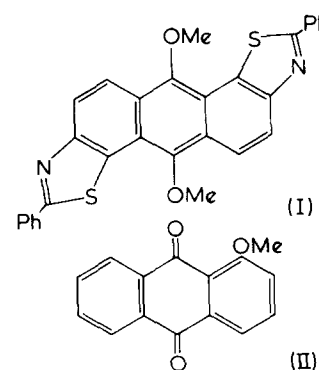
The dye sensitized photo-oxidative degradation of cellulose has long been an area of practical and theoretical interest, but the mechanism of this process is still a controversial subject¹. Of the two principal mechanisms that have been proposed, namely the singlet oxygen theory² and the hydrogen (or electron) abstraction theory³, the former has received relatively little credence. This is probably because it is relatively easy to demonstrate that a dye will photochemically abstract hydrogen or an electron from cellulose, whereas it is much more difficult to show unambiguously that singlet oxygen will react with this substrate. Almost all efficient sensitizers of singlet oxygen are good hydrogen abstractors (e.g. the quinonoid vat dyes, heterocyclic cationic dyes, and porphins), thus photodegradation studies with these compounds are ambiguous. The few known sensitizers that do not photoreduce (e.g. the acenes) are of little value because of their reactivity towards singlet oxygen. Non-photochemical sources of singlet oxygen are also suspect, as these systems are contaminated with other oxidizing species that could play an uncertain role in cellulose degradation.

We have looked for new stable singlet oxygen sensitizers that have a minimal tendency to undergo photochemical reduction. A particularly suitable compound is (I), which is obtained by the reductive methylation of Vat Yellow 2 (*CI* 67 300), using zinc and methyl-*p*-toluenesulphonate in alkaline solution. This compound, which was characterized by elemental analysis, is soluble in benzene (λ_{max} 408, 422 nm; $\log \epsilon$ 4.36, 4.29), and gives weakly fluorescent solutions. It

is particularly resistant to photo-oxidation, and no decomposition was observed after irradiating an oxygen saturated solution for 48 h (600 W tungsten lamp). The compound was an efficient sensitizer of singlet oxygen, as shown by the rapid photo-oxidation of tetraphenylcyclopentadienone when solutions of the two were exposed to visible light⁴. The reaction could be suppressed by the known singlet oxygen quencher, diazabicyclo[2,2,2]-octane⁵.

As (I) is an aromatic system that is, in effect, a prerduced form of a known photodegrading dye, it is unlikely to take part in further photoreduction processes with any degree of efficiency. To verify this, comparison experiments were carried out with (I) and 1-methoxyanthraquinone (II), an efficient hydrogen abstractor. The latter compound undergoes photoreduction in degassed isopropanol with a quantum yield of 0.53⁶. In isopropanol-benzene mixtures (3:2 by vol) under nitrogen the dimethoxy compound (I) underwent only a slow irreversible fading, in contrast to the rapid reversible photoreduction of (II). Under conditions of equal light absorption, photoreduction of (II) was at least 200 times more rapid than the fading of (I). Thus (I) can be regarded as a useful sensitizer of singlet oxygen that is free from the usual complications of competing hydrogen abstraction.

Photodegradation of regenerated cellulose film was most conveniently followed by measurement of the intrinsic viscosity $[\eta]$ of solutions in Cadoxen. Measurements were carried out at 30°C with an Ubbelohde suspended-level dilution viscometer, and the viscosity of solutions measured



over a range of concentrations. The intrinsic viscosity of the undergraded samples had an average value of 1.30 dl/g.

Cellulose films freed from plasticizer were immersed in benzene solutions of (I) (4×10^{-4} M) and were irradiated with a fluorescent lamp (8W) for 530 h. Control samples containing no sensitizer were irradiated at the same time. The unsensitized samples showed a 13% decrease in intrinsic viscosity, whereas the sensitized samples showed a corresponding decrease of 30%. Thus it can be concluded that singlet oxygen causes degradation of cellulose.

It was of interest to examine the relative efficiencies of the singlet oxygen and hydrogen abstraction mechanisms, and thus a comparison experiment was carried out with (I) and (II).

These two compounds absorb over roughly the same region of the spectrum above 350 nm, and so rate differences due to different light absorption characteristics could be minimized by using appropriate concentrations of the two compounds. Cellulose films were immersed in benzene solutions of (I)

cludes more bodies of data, and especially other measures of chain entanglement to be found in ref 4, the scatter increases significantly. However, the trend shown in *Figure 1* is not lost.

Since both C_2/C_1 and N_c correlate with a common variable, area in nm^2 , it follows that one should expect a linear correlation between C_2/C_1 and N_c . This indeed is the case with five data points for PE, *cis-trans* PBD, NR, PIB, and PDMS⁸. This correlation does not necessarily mean that chain entanglements are solely responsible for the

C_2 term.

The correlation line of *Figure 1* on a homogeneous set of data provides a criterion for judging and/or selecting from discordant literature values for these and other polymers.

Raymond F. Boyer and Robert L. Miller

Midland Macromolecular Institute,
1910 W. St. Andrews Drive,
Midland, Michigan 48640, USA
(Received 19 July 1976)

References

- 1 Boyer, R. F. and Miller, R. L. *Polymer* 1976, **17**, 925
- 2 Boyer, R. F. and Miller, R. L. *Rubber Chem. Technol.* in press
- 3 Kraus, G. and Moczvgemba, G. A. *J. Polym. Sci. (A-2)* 1964, 277
- 4 Porter, R. S. and Johnson, J. F. *Chem. Rev.* 1966, **66**, 1
- 5 Fox, T. G. and Allen, V. R. *J. Chem. Phys.* 1964, **41**, 344
- 6 Vincent, P. I. *Polymer* 1972, **13**, 558
- 7 Feitsma, E. L., de Boer, A. and Challa, G. *Polymer* 1975, **16**, 515. This paper refers to earlier literature.
- 8 Boyer, R. F. and Miller, R. L. *Rubber Chem. Technol.* in press

The involvement of singlet oxygen in the sensitized photodegradation of cellulose

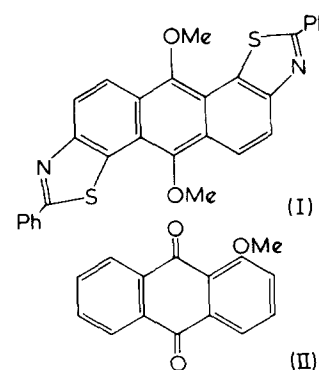
The dye sensitized photo-oxidative degradation of cellulose has long been an area of practical and theoretical interest, but the mechanism of this process is still a controversial subject¹. Of the two principal mechanisms that have been proposed, namely the singlet oxygen theory² and the hydrogen (or electron) abstraction theory³, the former has received relatively little credence. This is probably because it is relatively easy to demonstrate that a dye will photochemically abstract hydrogen or an electron from cellulose, whereas it is much more difficult to show unambiguously that singlet oxygen will react with this substrate. Almost all efficient sensitizers of singlet oxygen are good hydrogen abstractors (e.g. the quinonoid vat dyes, heterocyclic cationic dyes, and porphins), thus photodegradation studies with these compounds are ambiguous. The few known sensitizers that do not photoreduce (e.g. the acenes) are of little value because of their reactivity towards singlet oxygen. Non-photochemical sources of singlet oxygen are also suspect, as these systems are contaminated with other oxidizing species that could play an uncertain role in cellulose degradation.

We have looked for new stable singlet oxygen sensitizers that have a minimal tendency to undergo photochemical reduction. A particularly suitable compound is (I), which is obtained by the reductive methylation of Vat Yellow 2 (*CI* 67 300), using zinc and methyl-*p*-toluenesulphonate in alkaline solution. This compound, which was characterized by elemental analysis, is soluble in benzene (λ_{max} 408, 422 nm; $\log \epsilon$ 4.36, 4.29), and gives weakly fluorescent solutions. It

is particularly resistant to photo-oxidation, and no decomposition was observed after irradiating an oxygen saturated solution for 48 h (600 W tungsten lamp). The compound was an efficient sensitizer of singlet oxygen, as shown by the rapid photo-oxidation of tetraphenylcyclopentadienone when solutions of the two were exposed to visible light⁴. The reaction could be suppressed by the known singlet oxygen quencher, diazabicyclo[2,2,2]-octane⁵.

As (I) is an aromatic system that is, in effect, a prerduced form of a known photodegrading dye, it is unlikely to take part in further photoreduction processes with any degree of efficiency. To verify this, comparison experiments were carried out with (I) and 1-methoxyanthraquinone (II), an efficient hydrogen abstractor. The latter compound undergoes photoreduction in degassed isopropanol with a quantum yield of 0.53⁶. In isopropanol-benzene mixtures (3:2 by vol) under nitrogen the dimethoxy compound (I) underwent only a slow irreversible fading, in contrast to the rapid reversible photoreduction of (II). Under conditions of equal light absorption, photoreduction of (II) was at least 200 times more rapid than the fading of (I). Thus (I) can be regarded as a useful sensitizer of singlet oxygen that is free from the usual complications of competing hydrogen abstraction.

Photodegradation of regenerated cellulose film was most conveniently followed by measurement of the intrinsic viscosity $[\eta]$ of solutions in Cadoxen. Measurements were carried out at 30°C with an Ubbelohde suspended-level dilution viscometer, and the viscosity of solutions measured



over a range of concentrations. The intrinsic viscosity of the undergraded samples had an average value of 1.30 dl/g.

Cellulose films freed from plasticizer were immersed in benzene solutions of (I) (4×10^{-4} M) and were irradiated with a fluorescent lamp (8W) for 530 h. Control samples containing no sensitizer were irradiated at the same time. The unsensitized samples showed a 13% decrease in intrinsic viscosity, whereas the sensitized samples showed a corresponding decrease of 30%. Thus it can be concluded that singlet oxygen causes degradation of cellulose.

It was of interest to examine the relative efficiencies of the singlet oxygen and hydrogen abstraction mechanisms, and thus a comparison experiment was carried out with (I) and (II).

These two compounds absorb over roughly the same region of the spectrum above 350 nm, and so rate differences due to different light absorption characteristics could be minimized by using appropriate concentrations of the two compounds. Cellulose films were immersed in benzene solutions of (I)

Letters

(4×10^{-4} M) and (II) (2×10^{-3} M), and were irradiated under oxygen as described previously. It was found that (I) caused an 18% decrease in the intrinsic viscosity of the cellulose, whereas (II) caused a 23% decrease. The small difference indicates that the two mechanisms are of comparable efficiency.

Because of the low affinity of (I) and (II) for cellulose, it was necessary to use two-phase systems for these experiments. It might be argued that this does not give a true reflection of the conditions operating in dyed cellulose, and might favour the singlet oxygen mechanism. However, cellulose films dyed with Vat Yellow 2 (2% based on weight of film), which is a very effective photodegrading dye for cellulose, underwent degradation at comparable rates to the two-phase systems under conditions of similar light intensity. Thus whether the dye is in intimate contact with the cellulose or is dissolved in a solvent appears to have little influence on the rate of degradation.

As singlet oxygen is an intermediate in cellulose photodegradation, we have examined the protecting effect of a singlet oxygen quencher. Cellulose films dyed with Vat Yellow 2 (2% of the film weight) were impregnated with diazabicyclo[2,2,2]octane (0.5%), and these were found to undergo photo-oxidative degradation more slowly than films containing no quencher. Thus after 300 h exposure to a 200 W tungsten lamp, the protected films showed 5–11% decrease in intrinsic viscosity, whereas the unprotected films showed a decrease of 22–23%. A nickel ketoxime chelate has also been found to afford protection in some cases⁷, and

this may be due to the quenching of singlet oxygen⁸ or the triplet state of the sensitizer.

The reaction of singlet oxygen with cellulose possibly involves hydrogen abstraction from one of the CH groups, with rapid recombination of the radical fragments to form a hydroperoxide. Thus the process would closely parallel the degradation pathway involving direct hydrogen abstraction by the photoexcited sensitizer. The introduction of a hydroperoxide function at positions 1 or 4 of a glucose unit could then be followed by a homolytic process, causing chain scission at the carbon–oxygen bridging bond, and the formation of a carbonyl group. However, the secondary processes involved in the photodegradation of cellulose are still a subject of speculation. Although singlet oxygen is a reactive dienophile, and normally attacks alkenes, there is good evidence that it can in certain instances, take part in hydrogen abstraction reactions⁹. Whether such processes could involve the higher excited state of singlet oxygen ($^1\Sigma_g$) is still uncertain¹⁰. It should be noted that the quantum yield of dye sensitized chain scission of cellulose is very low ($\sim 10^{-5}$)¹¹, and thus the mode of attack by singlet oxygen on cellulose need not involve processes regarded as more characteristic of that species.

In conclusion, it is evident that singlet oxygen can cause degradation of cellulose at a rate at least comparable to the hydrogen abstraction mechanism. As it has been demonstrated that various dyes active towards the photodegradation of cellulose are also efficient sensitizers of singlet oxygen⁴, it must be assumed that singlet oxygen plays a

significant role in the degradation of vat-dyed cotton fabrics, although not necessarily in every case⁷. It is important in interpreting experimental results that one mechanism should not be considered to the exclusion of the other, as has often been done in the past.

Acknowledgement

We thank the Science Research Council for a research studentship (to C. H.).

J. Griffiths and C. Hawkins

Department of Cobur Chemistry,
University of Leeds,
Leeds LS2 9JT, UK

(Received 16 August 1976;
revised 9 September 1976)

References

- 1 Phillips, G. O. and Arthur, J. C. *Text. Res. J.* 1964, **34**, 497, 572; McKellar, J. F. *Radiat. Res. Rev.* 1971, **3**, 141; Egerton, G. S. and Morgan, A. G. *J. Soc. Dyers Colour.* 1971, **87**, 268
- 2 Egerton, G. S. *J. Soc. Dyers Colour.* 1949, **65**, 764
- 3 Bamford, C. H. and Dewar, M. J. S. *J. Soc. Dyers Colour.* 1949, **65**, 674
- 4 Griffiths, J. and Hawkins, C. *J. Soc. Dyers Colour.* 1973, **89**, 173
- 5 Ouannès, C. and Wilson, T. *J. Am. Chem. Soc.* 1968, **90**, 6527
- 6 Ahmed, M., Davies, A. K., Phillips, G. O. and Richards, J. T. *J. Chem. Soc. Perkin Trans. 2*, 1973, p 1366
- 7 Davies, A. K., Gee, A. G., McKellar, J. F. and Phillips, G. O. *Chem. Ind.* 1973, p 431
- 8 Carlsson, D. J., Mendenhall, G. D., Suprunchuk, T. and Wiles, D. M. *J. Am. Chem. Soc.*, 1972, **94**, 8960
- 9 Matsuura, T., Yoshimura, N., Nishinaga, A. and Saito, I. *Tetrahedron Lett.* 1969, p 1669
- 10 Kearns, D. R. *Chem. Rev.* 1971, **71**, 395
- 11 Bamford, C. H. and Dewar, M. J. S. *J. Soc. Dyers Colour.* 1949, **65**, 674

ERRATA

'Molecular motion of poly(methyl methacrylate), polystyrene and poly(propylene oxide) in solution studied by ^{13}C n.m.r. spin–lattice relaxation measurements: effects due to distributions of correlation times' by F. Heatley and Afrozi Begum, *Polymer* 1976, **17**, 399–408.

Page 401, left hand column, line 1:

for reference 12 read reference 20

Page 401, left hand column, line 16,
first term on second line of equation
(11) should read:

$$\left[\frac{(1 + \omega^2 \tau_0^2)^{1/2} + 1}{1 + \omega^2 \tau_0^2} \right]^{1/2}$$

Page 403, left hand column line 16:

for reference 20 read reference 22

Page 403, Figures 6 and 7, captions:

for CDCl_3 read PCE

We apologise for these errors.

Letters

(4×10^{-4} M) and (II) (2×10^{-3} M), and were irradiated under oxygen as described previously. It was found that (I) caused an 18% decrease in the intrinsic viscosity of the cellulose, whereas (II) caused a 23% decrease. The small difference indicates that the two mechanisms are of comparable efficiency.

Because of the low affinity of (I) and (II) for cellulose, it was necessary to use two-phase systems for these experiments. It might be argued that this does not give a true reflection of the conditions operating in dyed cellulose, and might favour the singlet oxygen mechanism. However, cellulose films dyed with Vat Yellow 2 (2% based on weight of film), which is a very effective photodegrading dye for cellulose, underwent degradation at comparable rates to the two-phase systems under conditions of similar light intensity. Thus whether the dye is in intimate contact with the cellulose or is dissolved in a solvent appears to have little influence on the rate of degradation.

As singlet oxygen is an intermediate in cellulose photodegradation, we have examined the protecting effect of a singlet oxygen quencher. Cellulose films dyed with Vat Yellow 2 (2% of the film weight) were impregnated with diazabicyclo[2,2,2]octane (0.5%), and these were found to undergo photo-oxidative degradation more slowly than films containing no quencher. Thus after 300 h exposure to a 200 W tungsten lamp, the protected films showed 5–11% decrease in intrinsic viscosity, whereas the unprotected films showed a decrease of 22–23%. A nickel ketoxime chelate has also been found to afford protection in some cases⁷, and

this may be due to the quenching of singlet oxygen⁸ or the triplet state of the sensitizer.

The reaction of singlet oxygen with cellulose possibly involves hydrogen abstraction from one of the CH groups, with rapid recombination of the radical fragments to form a hydroperoxide. Thus the process would closely parallel the degradation pathway involving direct hydrogen abstraction by the photoexcited sensitizer. The introduction of a hydroperoxide function at positions 1 or 4 of a glucose unit could then be followed by a homolytic process, causing chain scission at the carbon–oxygen bridging bond, and the formation of a carbonyl group. However, the secondary processes involved in the photodegradation of cellulose are still a subject of speculation. Although singlet oxygen is a reactive dienophile, and normally attacks alkenes, there is good evidence that it can in certain instances, take part in hydrogen abstraction reactions⁹. Whether such processes could involve the higher excited state of singlet oxygen ($^1\Sigma_g$) is still uncertain¹⁰. It should be noted that the quantum yield of dye sensitized chain scission of cellulose is very low ($\sim 10^{-5}$)¹¹, and thus the mode of attack by singlet oxygen on cellulose need not involve processes regarded as more characteristic of that species.

In conclusion, it is evident that singlet oxygen can cause degradation of cellulose at a rate at least comparable to the hydrogen abstraction mechanism. As it has been demonstrated that various dyes active towards the photodegradation of cellulose are also efficient sensitizers of singlet oxygen⁴, it must be assumed that singlet oxygen plays a

significant role in the degradation of vat-dyed cotton fabrics, although not necessarily in every case⁷. It is important in interpreting experimental results that one mechanism should not be considered to the exclusion of the other, as has often been done in the past.

Acknowledgement

We thank the Science Research Council for a research studentship (to C. H.).

J. Griffiths and C. Hawkins

Department of Cobur Chemistry,
University of Leeds,
Leeds LS2 9JT, UK

(Received 16 August 1976;
revised 9 September 1976)

References

- 1 Phillips, G. O. and Arthur, J. C. *Text. Res. J.* 1964, **34**, 497, 572; McKellar, J. F. *Radiat. Res. Rev.* 1971, **3**, 141; Egerton, G. S. and Morgan, A. G. *J. Soc. Dyers Colour.* 1971, **87**, 268
- 2 Egerton, G. S. *J. Soc. Dyers Colour.* 1949, **65**, 764
- 3 Bamford, C. H. and Dewar, M. J. S. *J. Soc. Dyers Colour.* 1949, **65**, 674
- 4 Griffiths, J. and Hawkins, C. *J. Soc. Dyers Colour.* 1973, **89**, 173
- 5 Ouannès, C. and Wilson, T. *J. Am. Chem. Soc.* 1968, **90**, 6527
- 6 Ahmed, M., Davies, A. K., Phillips, G. O. and Richards, J. T. *J. Chem. Soc. Perkin Trans. 2*, 1973, p 1366
- 7 Davies, A. K., Gee, A. G., McKellar, J. F. and Phillips, G. O. *Chem. Ind.* 1973, p 431
- 8 Carlsson, D. J., Mendenhall, G. D., Suprunchuk, T. and Wiles, D. M. *J. Am. Chem. Soc.*, 1972, **94**, 8960
- 9 Matsuura, T., Yoshimura, N., Nishinaga, A. and Saito, I. *Tetrahedron Lett.* 1969, p 1669
- 10 Kearns, D. R. *Chem. Rev.* 1971, **71**, 395
- 11 Bamford, C. H. and Dewar, M. J. S. *J. Soc. Dyers Colour.* 1949, **65**, 674

ERRATA

'Molecular motion of poly(methyl methacrylate), polystyrene and poly(propylene oxide) in solution studied by ^{13}C n.m.r. spin–lattice relaxation measurements: effects due to distributions of correlation times' by F. Heatley and Afrozi Begum, *Polymer* 1976, **17**, 399–408.

Page 401, left hand column, line 1:

for reference 12 read reference 20

Page 401, left hand column, line 16,
first term on second line of equation
(11) should read:

$$\left[\frac{(1 + \omega^2 \tau_0^2)^{1/2} + 1}{1 + \omega^2 \tau_0^2} \right]^{1/2}$$

Page 403, left hand column line 16:

for reference 20 read reference 22

Page 403, Figures 6 and 7, captions:

for CDCl_3 read PCE

We apologise for these errors.

Book Reviews

The Permeability of Plastic Films and Coatings to Gases, Vapours and Liquids

Edited by H. P. Hopfenberg

Plenum Press, New York, 1975, \$35.10

This book records the proceedings of a symposium arranged to mark the presentation of the Borden Award of the American Chemical Society's Division of Organic Coatings and Plastics Chemistry to Vivian Stannett in 1974. It consists of thirty two separate papers in the general area described by the title. The authors include many of the currently most active US workers in this field and there are five papers in the 'Fundamental' section from European laboratories.

The papers are grouped into three sections: Fundamental (17), Industrial (10) and Biomedical (5). Thus more than half the volume is devoted to fundamental considerations. Here the standard of work is high and most of the authors are highly distinguished and recognized authorities. Seven of the papers are primarily reviews and cover a considerable area of diffusion in polymers and, together, they form a useful collection. Ten contain a substantial content of new work, four theoretical and six experimental. In several cases these have enough general interest to justify inclusion but one or two are highly specific and more appropriate to a research journal.

In the industrial section the style and content is far more variable. Several papers describe well constructed and carried out research on technological problems. They make interesting reading. There are two reviews predicting rather different future trends in reverse osmosis membrane development. The remaining papers are either less relevant or describe technological studies containing little exact science.

Three of the biomedical papers are reviews: on the controlled release of drugs from capsules, on the preparation of grafted hydrogel membranes for biomedical devices and on ultrafiltration through

asymmetric hollow fibres. Two papers contain new work concerning dialysis and blood compatibility of membranes of potential use in haemodialysis.

The symposium must have been a great occasion for those who attended it. That this was so is made apparent by the editor's preface about Professor Stannett. The justification for publishing this volume is more arguable. It is a fitting form of recognition of the contribution that Professor Stannett has made over some twenty five years but the papers could, in some cases with advantage, have been as well published through the normal research journal channels. Some of them probably will be. However, the decision has been taken and the volume has been published. Its quality should certainly earn for it a place in libraries of polymer science and plastics technology. Although reproduced from the authors' typescripts the output of the many anonymous typists is of very high standard and the variety of type faces used did not disconcert this reader.

Patrick Meares

Textile Chemistry

Volume III: The Physical Chemistry of Dyeing

R. H. Peters

Elsevier, Amsterdam, 1975, 902 pp. \$112.50

It is now a quarter of a century since Vickerstaff's 'The Physical Chemistry of Dyeing' was first published and although major books on this topic have appeared since then, the comprehensive treatise on the subject that Professor Peters has produced is still welcome.

Nominally this volume forms the third, and last, of a series on Textile Chemistry, hence the title 'The Physical Chemistry of Dyeing' appears only as a subtitle to the main work. This is in some ways to be regretted as the author is acknowledged to be an expert in the subject matter of the present volume, whereas in the first two volumes which dealt with a series of rather disjointed topics he sometimes betrayed the fact that he was not always familiar with the particular topic under discussion.

The present work extends outside the strict range of the title. Thus four introductory chapters cover such topics as dyeing machinery, including 13 detailed diagrams, tests devised by the Society of Dyers and Colourists for assessing dyeing properties, and the estimation of dyes and their purification, including a brief introduction to the laws of light absorption.

The next 15 chapters, which comprise the heart of the book, describe the properties of various dye classes (dispersed, acid, direct, vat, reactive, etc.). An analysis of the equilibrium sorption behaviour is given for each dye/fibre system which is complemented by a description of the kinetics of sorption which are analysed in terms of diffusion processes.

The final eight chapters deal with a series of specialized topics such as solvent dyeing, dye aggregation and the dyeing of specialized fibres such as polypropylene.

The author is to be congratulated on producing such a detailed and well presented work. Throughout the book theoretical aspects of a particular process are supplemented copiously by experimental data in the form of tables and graphs. The book is excellently produced but the writer does not quite do himself justice by failing to provide an Author Index. Such an addition would have increased the value of the book as a source of references since it is particularly well provided for in this respect.

The major adverse criticism of this book is its price. Volume I of the series (published 1963) was £3.75, volume II (published 1967) cost £5.00 whereas the present volume is £50. Even allowing for the fact that it is a much larger book than its predecessors and the publisher is not responsible for the poor performance of the pound against foreign currencies, this price is still very high. This book will be beyond the reach of virtually all students and most private buyers. It will probably be purchased by libraries if only to complete the series, but since many of these are operating on nearly static budgets, the future of such high priced books must be very doubtful.

C. Earland

Conference Announcement
**6th Europhysics Conference on
Macromolecular Physics
Phase Transition in Bulk Polymers
Varna, Bulgaria, 26–29 September 1977**

The Macromolecular Physics section of the European Physical Society together with the Bulgarian Academy of Science are organizing the 6th EPS Conference on Macromolecular Physics—Phase Transitions in Bulk Polymers, to be held at Varna, Bulgaria, 26–29 September 1977. The topics to be discussed include: (1) crystallization and melting of polymers, thermodynamics, kinetics and mechanisms; (2) phase transitions in polymer liquid crystals, including oligomers; (3) conformational changes in bulk polymers: folding and unfolding of molecular nascent polymers obtained by polymerization reactions. A limited number of contributed papers can be accepted and those interested are invited to submit abstracts on subjects related to the topics above by 1 January 1977. Prospective contributors and those interested in attending the conference should write for further details to: Professor M. Mihailov, Bulgarian Academy of Sciences, Central Laboratory for Polymers, EPS Conference, 1113 Sofia, Bulgaria.

Classified Contents

- Anionic polymerization, block polymers of poly(*para*-xylelene) and polystyrene or poly(vinyl pyridine) prepared by, 817
- Anisotropic materials, effect of sample geometry on the measurement of mechanical properties, 495
- Anisotropic scattering of light in an electric field, effect of macromolecular length, 1039
- Anisotropy, optical and orientation of structural units, 167
- Anisotropy, optical, of polyisobutene, 511
- Annealing effects of polymers and their underlying molecular mechanisms, 309
- Anomalous diffusion of water in glassy polymers, 690
- Block polymers and multiphase polymer systems, structure and properties of: an overview of present status and future potential, 938
- Block polymers of poly(*para*-xylelene) and polystyrene or poly(vinyl pyridine) prepared by anionic polymerization, 817
- Bound rubber and swelling in silicone rubber/silica mixes and in silicone rubber vulcanizates, comparison, 147
- Brillouin scattering study of gelatin gel using a double passed Fabry-Perot spectrometer, 573
- Carboxylic acids and the peptide group, interaction between, 563
- Catalysis, Ziegler-Natta: 7. The settling period, 130
- Cellulose, the involvement of singlet oxygen in the sensitized photodegradation, 1113
- Cellulose acetate, small-angle X-ray scattering from ultrathin films, 93
- Cellulose tricarbaniolate, non-Newtonian viscosity and non-linear flow birefringence of, 155
- Cellulose tricarbaniolate, persistence length of, by small-angle neutron scattering, 363
- Cellulose trinitrate, configuration of, in solution, 1027
- Chain atoms between entanglements and cross-sectional area per chain, 1112
- Chain conformation of poly(tetramethylene terephthalate) and its change with strain, 807
- Chain structure, effect of, on the melting of low molecular weight poly(ethylene oxide), 109
- Chemorheology of irradiation-cured natural rubbers: 2. Stress relaxation mechanisms of sulphur-containing cured systems in air, 325
- Configurational and dynamic flexibility of polymer chains, 395
- Conformation and thermodynamics of adsorbed macromolecules at the liquid/solid interface, 864
- Cooling of a polymer sheet, 1103
- Copolymers, block, ethylene-propylene oxide type P(EP)_n, melting of, 105
- Copolymers, butene/propylene, monomer sequence distribution by ¹³C nuclear magnetic resonance, 548
- Copolymers of α -methylstyrene and maleic anhydride, relationship of temperature to composition, 21
- Copolymerization, radical, of styrene and methyl methacrylate, radiochemical study, 217
- Crack growth in plastic panels under biaxial stress, 627
- Craze growth and crack growth in poly(vinyl chloride) under monotonic and fatigue loading, 335
- Craze kinetics for PMMA in liquids, 439
- Creep behaviour of annealed UPVC and PMMA, 77
- Crotamine, optical rotatory dispersion: effect of denaturants, 638
- Crown ether catalyzed modification of partly chloromethylated polystyrene, 1107
- Crystallization of dilute polyethylene solutions: influence of molecular weight, 99
- Crystallization and isothermal thickening, study of in polyethylene using SAXD, low frequency Raman spectroscopy and electron microscopy, 471
- Crystallization kinetics, polymer, use of differential scanning calorimetry to study, 1015
- Crystallization rates, comparative study by d.s.c. and depolarization microscopy, 12
- Deformation mechanism of hard elastic polyethylene films, 1063
- Dielectrics, anisotropic, reaction field in, 7
- Dielectric and viscoelastic properties of two poly(propylene glycol) liquids, comparison, 665
- Differential refractometry and light scattering on nylon-6 and poly(methyl acrylate) in mixed solvents, 587
- D.s.c. and depolarization microscopy, comparative study of crystallization rates by, 12
- D.s.c. studies on phase transition of glucose and cellulose oligosaccharides, 559
- D.s.c., use of to study polymer crystallization kinetics, 1015
- Diffusion of large molecules in polymers: a measuring technique based on microdensitometry in the infrared, 481
- Diffusion rates, directional, in keratin, 748
- Diimide reduction of *cis*-1,4-polyisoprene with *p*-toluenesulphonylhydrazide, 117
- 1,1-Diphenylethyl methacrylate, stereospecific anionic polymerization and copolymerization, 618
- Drag reduction effectiveness of macromolecules, 81
- Dynamics of solutions of entangled polymers, 1035
- Elastic modulus in the crystalline region of poly(*p*-phenylene terephthalamide), 517
- Elasticity, stored, in flowing solutions of polyisobutylene as measured by recoil, 246
- Elastin, bovine, solubilization of, by a formic acid + salt method, 173
- Electric birefringence of aqueous solutions of methyl cellulose, 508
- Electro-optic Kerr birefringence of polystyrenes in dilute solutions, 651
- Equilibrium ring concentrations and the statistical conformations of polymer chains: 14. Calculation of the concentrations of medium sized cyclics in poly(dimethyl siloxane) equilibrates, 601
- Cis*- and *trans*- Ethyl propylene ethers, salt effect on cationic copolymerization between, 828
- Extruders, single screw, melting in, 905
- Fabry-Perot spectroscopy, multi-pass, of polymers, 501
- Failure criterion for the fracture of structural adhesive joints, 727
- Failure, time-dependent of poly(methyl methacrylate), 717
- Fibrillation mechanism in the flow of molten polymer mixtures, 831
- Filler enhancement of rubber modulus, 734
- Flame retardancy, some aspects of, in high density polyethylene, 1095
- Fracture surface energy in notched tension, influence of the molecular weight of poly(methyl methacrylate), 161
- Free radicals, distribution and desorption of, in the emulsion polymerization of styrene, 740
- G.p.c., differential, determination of concentration dependence of the hydrodynamic dimensions by, 455

- Gelatin gel, Brillouin scattering study of, using a double passed Fabry—Perot spectrometer, 573
- Gelatinization, theory of, in a starch—water—solute system, 854
- Glass transition temperature determination of poly(ethylene sulphide), poly(isobutylene sulphide) and their random copolymers, 348
- Glass transition temperature of ideal polymeric networks, 859
- Glass transition temperature in nylons, 1049
- Glass transition temperature of poly(*N*-vinyl pyrrolidone) and the effect of water, 739
- Glasses, theory of, 933
- Glow discharge polymerization of hexamethylcyclotrisilazane, mechanism of polysilazane thin film formation, 673
- Glucose and cellulose oligosaccharides, differential scanning calorimetric studies on phase transition, 559
- Grafting onto poly(vinyl alcohol): a new spectral method to estimate the extent of grafting, 1108
- Grignard compounds, polymeric, preparation and reactions, 1020
- Hafnium polythioethers, synthesis and thermal characterization, 231
- Heterocycles, coordinate polymerization: 1. Oligomerization of epichlorohydrin by TiCl_4 , 519. 2. Oligomerization of tetrahydrofuran by TiCl_4 in the presence of acetyl chloride or epichlorohydrin, 528. 3. Oligomerization of tetrahydrofuran induced by TiCl_4 in the presence of acetyl chloride and epichlorohydrin, 535
- Hydrodynamic dimensions, determination of concentration dependence of by differential g.p.c., 455
- Impact yielding of high density polyethylene, 1099
- Infra-red studies, polarized far, of hot-drawn polytetrafluoroethylene, 153
- I.r. study of poly(1-pentene) and poly(4-methyl-1-pentene), 121
- Initiators, new thermal, of free-radical polymerization and block copolymerization, 94
- Interesterification of starch with methyl palmitate, 555
- Intra-chain double bonds, effect of on the melt crystallization of aliphatic polyesters, 802
- Intra-chain *trans* double bonds, influence of, on the melt crystallization of polyamides, 185
- Intra-chain double bonds, influence of, on the properties of solution grown single crystals of polyethylene, 541
- Ion-clustering and viscoelastic properties in poly(butadiene—styrene—4-vinylpyridine) crosslinked by nickel chloride, 382
- Keratin, directional diffusion rates in, 748
- Laser flash photolysis investigations on primary processes of the sensitized polymerization of vinyl monomers: 1. Experiments with benzophenone, 419
- Laser—Raman spectroscopic studies of mechanically-loaded polymers, 838
- Liquid/solid interface, conformation and thermodynamics of adsorbed macromolecules, 864
- Lithium polystyryl and iodinated polystyrene, reaction between, 351
- Mechanical motions in amorphous and semi-crystalline polymers, 996
- Melt crystallization of polyamides, influence of intra-chain *trans* double bonds, 185
- Melt rheology of some aliphatic polyamides, 377
- Melting of polymers in narrow annular shear devices, 443
- Melting in single screw extruders, 905
- Methyl cellulose, electric birefringence of aqueous solutions, 508
- Molecular complexes in polymer synthesis—from Lewis acid adducts to exiplexes, 957
- Molecular design of polymers, 965
- Molecular motion of poly(methyl methacrylate), polystyrene and poly(propylene oxide) in solution studied by ^{13}C n.m.r. spin—lattice relaxation measurements: effects due to distributions of correlation times, 399
- Molecular motions and segmental size of vulcanized natural and acrylonitrile-butadiene rubbers by the spin-probe method, 448
- Molecular orientation, a study of, in drawn and shrunk poly(ethylene terephthalate) by means of birefringence, polarized fluorescence and X-ray diffraction measurements, 25
- Molecular weight, effect of, on the thermal properties of polycarbonates, 51
- Morphological aspects of AB cross-linked polymers, 367
- Morphological study of chain-extended growth in polyethylene: 1. Crystallization, 275.2. Annealed bulk polymer, 284. 3. Annealing of solution-grown lamellae, 291
- Mosaic concept in polymer crystals, a re-examination of the necessity, 736
- Networks, ideal polymeric, glass transition temperature, 859
- Neutron scattering, low angle, trajectory of polyethylene chains in single crystals by, 37
- Neutron scattering studies, small-angle, of molten and crystalline polyethylene, 751
- Non-Newtonian viscosity and non-linear flow birefringence of cellulose tricarbaniolate, 155
- N.m.r., broad line resonance, interpretation of in poly(ethylene terephthalate), 125
- N.m.r., ^{13}C , determination of monomer sequence distribution in butene/propylene copolymers, 548
- N.m.r., ^{13}C and i.r. spectroscopy, determination of chain branching in low density polyethylene by, 345
- N.m.r., ^{13}C spectra of some poly(*N*-acyliminoalkenes), 656
- N.m.r., ^{13}C , spin—lattice relaxation measurements, molecular motion of poly(methyl methacrylate), polystyrene and poly(propylene oxide) in solution studied by: effects due to distributions of correlation times, 399
- N.m.r., ^{13}C , study of optically active polymers: poly(4-methyl-1-hexene), 901
- N.m.r., pulsed, of a SBS 'macroscopic single crystal', 41
- N.m.r. relaxation times of some aromatic polymers, effect of molecular oxygen, 758
- N.m.r. studies, pulsed, of molecular motion in wet nylon-6,6 fibres, 761
- Nylon-1 polymers and copolymers, properties, 926
- Nylon-6 and poly(methyl acrylate), differential refractometry and light scattering in mixed solvents, 587
- Nylon-6,6 fibres, wet, pulsed n.m.r. studies of molecular motion, 761
- Nylons, glass transition temperature in, 1049
- Oligourethanes, structure: 6. Fine structure of melt crystallized oligourethanes, 3
- Optical rotatory dispersion of crota-mine: effect of denaturants, 638
- Optically active polymers, ^{13}C n.m.r. study of: poly(4-methyl-1-hexene), 901
- Optimum filler content in semi-crystalline polymers, a method for the calculation, 836
- Osmotic pressures of moderately concentrated poly(γ -benzyl-L-glutamate) solutions in *N,N*-dimethylformamide, 919
- Oxygen, molecular, effect of on the n.m.r. relaxation times of some aromatic polymers, 758
- Palladium/ π -catalysts, effect of phosphine ligand on the activity, 58
- Palladium/ π -complexes as catalysts for olefin polymerization, 710
- Permeation chromatography calibration, a new approach, 90

Classified Contents

- Persistence length of cellulose tricarbani-
late by small-angle neutron scatter-
ing, 363
- Phase transition and morphology of
bulk poly(*trans*-1,4-butadiene),
effect of pressure on, 249
- Phosphine ligand, effect of, on the
activity of palladium/ π -catalysts, 58
- Phosphonitrilic chloride: 33. Cyclomat-
rixphosphazene polymers formed
from hexachlorocyclotriphospha-
zene and metal acetates, 319. Elec-
trical conductivity of polybisamino-
phosphazenes, 1013
- Phosphonitrilic chloride: polymeriza-
tion behaviour of some hexaalkoxy-
cyclotriphosphazenes, 898
- Photoconduction, field dependent, in
poly(*N*-vinylcarbazole), 646
- Photodegradation of cellulose, sensi-
tized, the involvement of singlet
oxygen, 1113
- Photoelastic non-equilibrium behaviour
of natural rubber networks, 732
- Photoinitiating systems and photoactive
polymers, new, and their applica-
tions, 321
- Polarization studies, persistent internal,
in poly(*N*-vinylcarbazole)/trinitro-
fluorenone charge complex, 192
- Poly(acryloyl morpholine) xerogel net-
works, synthesis and characteriza-
tion, suitable for the gel permeation
chromatography of small molecules,
843
- Poly(*N*-acyliminoalkenes), ^{13}C n.m.r.
spectra, 656
- α -Poly(L-alanine), potential energy cal-
culations about the chain folding,
257
- Poly(γ -*N*-alkyl-L- α,γ -diaminobutyric
acids) and their carbobenzoxy deri-
vatives, syntheses and conforma-
tional studies, 429
- Poly(*N*-alkyl maleimides), thermal
stabilities, 199
- Polyamidation process, new solid state,
409
- Polyamides, amorphous, structure—
property relationships in, 875
- Polyamides, melt crystallization of,
influence of intra-chain *trans* double
bonds, 185
- Polybenzazoles, cobalticinium-bridged:
1. Low temperature solution poly-
merization, 423
- Poly(γ -benzyl-L-glutamate), osmotic
pressures of moderately concentra-
ted solutions in *N,N*-dimethylfor-
mamide, 919
- Poly(*trans*-1,4-butadiene), bulk, effect
of pressure on phase transition and
morphology, 249
- Poly(butylene terephthalate), thermal
degradation, 1044
- Poly(ϵ -carbobenzoxyl-L-lysyl- γ -benzyl-
L-glutamate), synthesis and charac-
terization, 847
- Poly(*O*-carbobenzoxy-L-tyrosine), con-
formational study of, in solution, 1105
- Polycarbonates, effect of molecular
weight on the thermal properties, 51
- Polyepichlorohydrin, multiple endo-
therms in, 551
- Polyesters, aliphatic, effect of intra-
chain double bonds on the melt
crystallization, 802
- Polyester binder, loaded unsaturated,
studies on the curing of, 611
- Polyester resin, unsaturated, radiation
curing, 261
- Polyethylene chains, trajectory of in
single crystals by low angle neutron
scattering, 37
- Polyethylene, chain-extended, in con-
text: a review, 460
- Polyethylene films, hard elastic, de-
formation mechanism, 1063
- Polyethylene film, high density, super-
structure of, crystallized from stres-
sed polymer melts as observed by
small-angle light scattering, 1075
- Polyethylene, high density, some aspects
of flame retardancy in, 1095
- Polyethylene, linear, X-ray studies of
surface melting in single crystals,
1059
- Polyethylene, molten and crystalline,
small-angle neutron scattering stu-
dies, 751
- Polyethylene, molten, radial distribu-
tion functions by X-ray diffraction,
485
- Polyethylene, morphological study of
chain-extended growth in: 1. Crystal-
lization, 275. 2. Annealed bulk poly-
mer, 284. 3. Annealing of solution-
grown lamellae, 291
- Polyethylene and polytetrafluoroethy-
lene crystals: chain folding entropy
of fusion and lamellar thickness, 695
- Polyethylene solutions, dilute, crystal-
lization of: influence of molecular
weight, 99
- Polyethylene solutions, dilute, effect
of solvent on the crystallization
from, 795
- Polyethylene, study of crystallization
and isothermal thickening using
SAXD, low frequency Raman spec-
troscopy and electron microscopy,
471
- Polyethylene, ultra-high modulus, by
high temperature drawing, 644
- Poly(ethylene glycol) solutions, upper
and lower critical solution tempera-
tures, 685
- Poly(ethylene oxide), in benzene solu-
tion, contributions to the proton
relaxation of, 1019
- Poly(ethylene oxide), crystalline,
Raman scattering from the longitu-
dinal acoustic mode, 354
- Poly(ethylene oxide), low molecular
weight, effect of chain structure on
the melting, 109
- Poly(ethylene oxide), microstructure of
directionally solidified, 581
- Poly(ethylene terephthalate), branch-
ed, correlations between viscosi-
metric properties and polymeriza-
tion parameters, 595
- Poly(ethylene terephthalate), drawn and
shrunk, a study of molecular orien-
tation in, by means of birefringence,
polarized fluorescence and X-ray dif-
fraction measurements, 25
- Poly(ethylene terephthalate) fibres,
heat set, thermal analysis, 241
- Poly(ethylene terephthalate), optical
observations of partly molten fibres,
923
- Poly(ethylene terephthalate), studies
on the formation: 6. Catalytic acti-
vity of metal compounds in polycon-
densation of bis(2-hydroxyethyl)
terephthalate, 221
- Polyisobutene, optical anisotropy, 511
- Polyisobutylene, stored elasticity in
flowing solutions of, as measured by
recoil, 246
- cis*-1,4-Polyisoprene, diimide reduction
of with *p*-toluenesulphonylhydra-
zide, 117
- Polyisoprenes, sequence distribution
of *cis*-1,4- and *trans*-1,4-units, 113
- Polyisoprenes, sequence distribution,
413
- 3,4-/*cis*-1,4-Polyisoprene, structure of
by ^{13}C n.m.r., 358
- Poly(*S*-menthyloxycarbonylmethyl L-
and D-cysteines), syntheses and con-
formational studies, 1009
- Polymer chain cross-section and the
Mooney—Rivlin constants, 925
- Polymer in the USA—*Editorial*, 747
- Polymerization of ethylene by *n*-butyl
lithium, 613
- Polymerization, stereospecific anionic,
and copolymerization of 1,1-dipheny-
lethyl methacrylate, 618
- Polymerization of styrene to polyethy-
lene, radiation graft, dependence of
rate on monomer concentration, 171
- Polymerization of tetrafluoroethylene
in acetic acid photoinitiated by metal
carbonyls, 225
- α -Poly(L-methionine), structure refine-
ment of: X-ray and conformational
analysis, 267
- Poly(methyl methacrylate), influence of
the molecular weight of, on fracture
surface energy in notched tension, 161
- PMMA, irradiated doped, confirmation
of the role of radicals in energy trans-
fer resulting in induced phosphore-
scence, 1091
- Poly(methyl methacrylates), stereoregu-
lar, association of: 3. Thermal beha-
viour and composition of stereo-
complex, 633
- PMMA, syndiotactic, rate constants
during the hydrolysis with base, 787
- PMMA, syndiotactic, relative rate con-
stants during the hydrolysis with
base, 777
- PMMA, syndiotactic, relative rate con-
stants during the acidic hydrolysis,
893
- PMMA, time-dependent failure, 717
- Poly(4-methyl-1-pentene), kinetics of
the thermal oxidation, 137
- Poly(1-pentene), thermal oxidation of:
1. Identification of products and
mechanisms, 61

- Polypeptides, sequential, and sodium deoxycholate, interaction between 259
- Poly(ρ -phenylene terephthalamide), elastic modulus in the crystalline region, 517
- Polypropylene, dissolution in organic solvents: 1. Partial dissolution, 38. 2. The steady state dissolution process, 768
- Polypropylene, isotactic, monoclinic macrolattice of quenched and cold-drawn sheets, 303
- Polypropylene, a thermoanalytical comparison between ram and screw extruded, 723
- Polypropylene, time dependent effects of pressure on the shear modulus, 329
- Polysaccharides, spin-labelling of hydroxyl groups in, 91
- Polysilazane thin film formation, mechanism of, during glow discharge polymerization of hexamethylcyclotrisilazane, 673
- Polysilazane thin films, glow discharge, structure of, 678
- Polysiloxanes, studies of the chemical degradation of, by hydrofluoric acid: 1. Poly(tetramethyl- p -silphenylene siloxane), 1086
- Polystyrene, comparison of the unperturbed dimension, for endothermal and exothermal heats of dilution within the same system, 605
- Polystyrene, low molecular weight, configuration of, in deuterated cyclohexane, 349
- Polystyrenes, narrow molecular weight distribution, rheological behaviour of blends of, in the molten state: dynamic viscoelastic properties in the terminal zone, 1054
- Polystyrene, the reproducibility of T_g measurements on, using d.s.c., 869
- Polystyrene, simple and direct assignment of the methylene and methine ^{13}C resonances, 170
- Polytetrafluoroethylene, hot-drawn, polarized far infra-red studies, 153
- Polytetrahydrofuran, narrow distribution, synthesis, 205
- Poly(tetramethylene terephthalate), chain conformation and its change with strain, 807
- Poly(trimethylene oxide) chains, dimensions of, in a theta-solvent, 670
- Polyurethane networks, model, 65
- Polyurethanes, sulphur containing, application of gas chromatography to the analysis of thermal decomposition products of some, 1110
- Poly(vinyl alcohol, grafting onto, a new spectral method to estimate the extent of grafting, 1108
- Poly(N -vinylcarbazole), field dependent photoconduction, 646
- Poly(N -vinylcarbazole)/trinitrofluorenone charge transfer complex, persistent internal polarization studies in, 192
- PVC, crystalline, intermolecular forces and the Raman spectrum, 355
- Poly(vinyl chloride), craze growth and crack growth in, under monotonic and fatigue loading, 335
- Poly(2-vinylpyridine), microstructure of: correlation between ^{13}C and ^1H n.m.r. determinations, 254
- Poly(N -vinyl pyrrolidone), glass transition temperature of and the effect of water, 739
- Professor Geoffrey Gee — a tribute — *Editorial*, 931
- Propylene oxide, racemic, stereoelective polymerization of, using a diethylzinc-chiral-1,2-diol system as initiator, 821
- Radial distribution functions from molten polyethylene by X-ray diffraction, 485
- Radiochemical study of the radical copolymerization of styrene and methyl methacrylate, 217
- Ram and screw extruded polypropylene, a thermoanalytical comparison between, 723
- Raman scattering from the longitudinal acoustic mode in crystalline poly(ethylene oxide), 354
- Rate constants during the hydrolysis of syndiotactic poly(methyl methacrylate) with base, 787
- Rate constants, relative, during the hydrolysis of syndiotactic poly(methyl methacrylate) with base, 777
- Rate constants, relative, during the acid hydrolysis of syndiotactic poly(methyl methacrylate), 893
- Reaction field in anisotropic dielectrics, 7
- Relaxation controlled (case II) transport of lower alcohols in poly(methyl methacrylate), 195
- Relaxation processes in methacrylate polymers, analysis of by thermally stimulated discharge, 212
- Rheological behaviour of blends of narrow molecular weight distribution polystyrenes in the molten state: dynamic viscoelastic properties in the terminal zone, 1054
- Rheometer, new slit die: some results with a butadiene-styrene block copolymer, 235
- Rubbers, chemorheology of irradiation-cured natural: 2. Stress relaxation mechanisms of sulphur-containing cured systems in air, 325
- Rubber, natural, distribution of abnormal groups, 713
- Rubber, natural, time effects on the thermochemical behaviour, 87
- Rubber networks, natural photoelastic non-equilibrium behaviour, 732
- Rubber/resin adhesive films, composition of: 1. Surface composition as determined by ATR spectroscopy, 699
- Rubbers, vulcanized natural and acrylonitrile-butadiene, molecular motions and segmental size of by the spin-probe method, 448
- Salt effect on cationic copolymerization between *cis*- and *trans*-ethyl propylene ethers, 828
- Sequence distribution of polyisoprenes, 413
- Shear gradients, response of macromolecular structure to, 435
- Shear modulus of polypropylene, time dependent effects of pressure on, 329
- Silicone rubber/silica mixes and silicone rubber vulcanizates, comparison of bound rubber and swelling in, 147
- Solvent, theoretical estimation of the effect of on unperturbed dimensions: 1. Isotactic poly(vinyl alcohol), 298
- Sonic pulse propagation study of phase separation in certain block copolymers, 577
- Spin-labelling of hydroxyl groups in polysaccharides, 91
- Starch, interesterification of, with methyl palmitate, 555
- Starch-water-solute system, theory of gelatinization, 854
- Stereoelective polymerization of racemic propylene oxide using a diethylzinc-chiral-1,2-diol system as initiator, 821
- Stereoregulation, some aspects of, in the stereospecific polymerization of vinyl monomers, 977
- Stop-and-go g.p.c. and i.r., a rapid technique for the qualitative analysis of polymers and additives, 17
- Structure of a compatible mixture of two polymers as revealed by low-angle neutron scattering, 640
- Styrene-butadiene block copolymers, cruciform, correlation between physical-mechanical properties and morphological features, 72
- Styrene, distribution and desorption of free radicals in the emulsion polymerization, 740
- Superstructure of high density polyethylene film crystallized from stressed polymer melts as observed by small-angle light scattering, 1075
- Swelling of bonded-rubber cylinders, 142
- Swelling of linear polymers in mixed swelling agents: predictability by means of solubility parameters, 835
- Tetrafluoroethylene, polymerization of, in acetic acid photoinitiated by metal carbonyls, 225
- Thermal analysis of heat set poly(ethylene terephthalate) fibres, 241
- Thermal degradation of poly(butylene terephthalate), 1044
- Thermal oxidation of poly(1-pentene): 1. Identification of products and mechanisms, 61
- Thermal stabilities of poly(N -alkyl maleimides), 199

Classified Contents

- Thermally stimulated discharge, analysis of relaxation processes in methacrylate polymers by, 212
- Thermally stimulated discharge, study of polymer crosslinking by, 921
- Thermochemical behaviour of natural rubber, time effects on, 87
- Thermodynamics of α , ω -methoxy-poly(ethylene oxide)/*n*-alkane systems by gas-liquid chromatography, 374
- Transition metal impurities in crystalline conjugated polymer, 623
- Universality approach to the expansion factor of a polymer chain, 179
- Upper and lower critical solution temperatures in poly(ethylene glycol) solutions, 685
- 2-Vinylanthraquinone, novel synthesis, 643
- N*-Vinylcarbazole, polymerization of in systems containing maleic anhydride and benzoyl peroxide, 742
- Vinyl chloride polymers, heat treated, structural order in, 44
- Vinyl monomers, some aspects of stereoregulation in the stereospecific polymerization, 977
- Vinyl polymers, optically active, containing fluorescent groups: 1. Synthesis and properties of copolymers of *N*-vinylcarbazole with optically active monomers, 641
- Viscosity-molecular weight concentration relationships beyond the critical region in polymer solutions and melts, 570
- Wool, dyed, modification of the fastness properties of through grafting, 705
- X-ray diffraction patterns, wide-angle, of aligned glassy polymers, analysis of with particular references to polystyrene, 488
- X-ray scattering, small-angle, from ultrathin films of cellulose acetate, 93
- X-ray studies of surface melting in single crystals of linear polyethylene, 1059

an international journal

bimonthly in English

POLYMER JOURNAL

of significant original papers on new research and studies
in the fields of polymer chemistry, physics and biopolymers
for quick beautiful publication with world-wide circulation;
appreciated in 50 countries

● **Editor in Chief** Teiji Tsuruta (University of Tokyo)

● **Subscription Rate** US \$ 85.00 per volume (calendar year)



The Society of Polymer Science, Japan

HONSHU BUILDING 5-12-8 GINZA CHUO-KU TOKYO 104 JAPAN

An exclusive sales agent **U.S. - Asiatic Co., Ltd.**

13-12 Shimbashi 1-Chome Minato-ku Tokyo 105 Japan

Author Index

- Ablazova, T. I.: *see* Tsebrenko, M. V., Yudin, A. V., Ablazova, T. I. and Vinogradov, G. V.
- Acquaviva, L.: *see* Conti, F., Acquaviva, L., Chiellini, E., Ciardelli, F., Delfini, M. and Segre, A. L.
- Adam, G. A., Hay, J. N., Parsons, I. W. and Haward, R. N.: Effect of molecular weight on the thermal properties of polycarbonates, 51
- Agarwal, S. K.: *see* Pillai, P. K. C., Agarwal, S. K. and Nair, P. K.
- Aggarwal, S. L.: Structure and properties of block polymers and multiphase polymer systems: an overview of present status and future potential, 938
- Ahuja, R. C.: *see* Pillai, P. K. C. and Ahuja, R. C.
- Aida, H.: *see* Matui, S. and Aida, H.
- Alfonso, Giovanni Carlo: *see* Pedemonte, Enrico; Alfonso, Giovanni Carlo and Dondero, Giovanni
- Allen, G., Egerton, P. L. and Walsh, D. J.: Model polyurethane networks, 65
- Alper, Turhan; Barlow, A. John and Gray, R. Walter: Comparison of the dielectric and viscoelastic properties of two poly(propylene glycol) liquids, 665
- Ando, D. J.: *see* Stevens, G. C., Ando, D. J., Bloor, D. and Ghotra, J. S.
- Araimo, L., de Candia, F. and Vittoria, V.: Time effects on the thermochemical behaviour of natural rubber, 87
- Arridge, R. G. C. and Folkes, M. J.: Effect of sample geometry on the measurement of mechanical properties of anisotropic materials, 495
- Ashman, P. C. and Booth, C.: Melting of ethylene-propylene oxide type P(EP)_n block copolymers, 105
- Ashman, P. C.: *see* Maclaine, J. Q. G., Ashman, P. C. and Booth, C.
- Ballard, D. G. H.: *see* Schelten, J., Ballard, D. G. H., Wignall, G. D., Longman, G. and Schmatz, W.
- Ballard, D. G. H., Rayner, M. G. and Schelten, J.: Configuration of low molecular weight polystyrene in deuterated cyclohexane, 349. Structure of a compatible mixture of two polymers as revealed by low-angle neutron scattering, 640
- Bamford, C. H.: New photoinitiating systems and photoactive polymers and their applications, 321
- Bamford, C. H. and Mullik, S. U.: New thermal initiators of free-radical polymerization and block copolymerization, 94. Polymerization of tetrafluoroethylene in acetic acid photoinitiated by metal carbonyls, 225
- Bantjes, A.: *see* Froehling, P. E., Koenhen, D. M., Bantjes, A. and Smolders, C. A.
- Bantjes, A.: *see* Gaymans, R. J., Tijsen, J., Harkema, S. and Bantjes, A.
- Barlow, A. John: *see* Alper, Turhan; Barlow, A. John and Gray, R. Walter
- Barrall, Edward, M.: *see* Mirabella, Francis, M., Barrall, Edward M. and Johnson, Julian F.
- Barrett, A. J.: *see* Domb, C. and Barrett, A. J.
- Barth, Volker: *see* Klesper, Ernst and Barth, Volker
- Barth, Volker and Klesper, Ernst: Relative rate constants during the hydrolysis of syndiotactic poly(methyl methacrylate) with base, 777. Relative rate constants during the acidic hydrolysis of syndiotactic poly(methyl methacrylate), 893
- Bartick, Edward, G. and Johnson, Julian F.: Determination of concentration dependence of the hydrodynamic dimensions by differential g.p.c., 455
- Bassett, D. C.: *see* Khalifa, B. A. and Bassett, D. C.
- Bassett, D. C.: Chain-extended polyethylene in context: a review, 460
- Bassett, D. C. and Khalifa, B. A.: Morphological study of chain-extended growth in polyethylene: 1. Crystallization, 275
- Bassett, D. C., Khalifa, B. A. and Olley, R. H.: Morphological study of chain-extended growth in polyethylene: 2. Annealed bulk polymer, 284
- Batty, N. S., Gradwell, A. J. and Guthrie, J. T.: Modification of the fastness properties of dyed wool through grafting, 705
- Beamish, A. and Hourston, D. J.: A sonic pulse propagation study of phase separation in certain block copolymers, 577
- Beaumont, Peter, W. R.: *see* Young, Robert, J. and Beaumont, Peter W. R.
- Bedborough, D. S. and Jackson, D. A.: Brillouin scattering study of gelatin gel using a double passed Fabry-Perot spectrometer, 573
- Beevers, R. B.: Solubilization of bovine elastin by a formic acid + salt method, 173
- Begum, Afrozi: *see* Heatley, F. and Begum, Afrozi
- Benoit, H.: *see* Gupta, A. K., Cotton, J. P., Marchal, E., Burchard, W. and Benoit, H.
- Berndt, H.-J. and Bossmann, Adelgund: Thermal analysis of heat set poly(ethylene terephthalate) fibres, 241
- Berry, J. P.: *see* Shea, S. C. and Berry, J. P.
- Bevington, J. C. and Dyball, C. J.: Polymerization of *N*-vinylcarbazole in systems containing maleic anhydride and benzoyl peroxide, 742
- Bieringer, H. F.: *see* Wolf, B. A., Bieringer, H. F. and Breitenbach, J. W.
- Bilen, C. S. and Morantz, D. J.: Confirmation of the role of radicals in energy transfer resulting in induced phosphorescence of irradiated doped poly(methyl methacrylate), 1091
- Birch, J. R.: *see* Jones, R. G., Nicol, Elisabeth A., Birch, J. R., Chantry, G. W., Fleming, J. W., Willis, H. A. and Cudby, M. E. A.
- Blackadder, D. A. and Le Poidevin, G. J.: Dissolution of polypropylene in organic solvents: 1. Partial dissolution, 387. 2. The steady state dissolution process, 768
- Bleha, T. and Valko, L.: Theoretical estimation of the effect of solvent on unperturbed dimensions: 1. Isotactic poly(vinyl alcohol), 298
- Bloor, D.: *see* Stevens, G. C., Ando, D. J., Bloor, D. and Ghotra, J. S.
- Bontà, Giorgio; Gallo, Bianca, M.; Russo, Saverio and Uliana, Claudio: Radiochemical study of the radical copolymerization of styrene and methyl methacrylate, 217
- Booth, C.: *see* Ashman, P. C. and Booth, C.
- Booth, C.: *see* Hartley, A., Leung, Y. K., Booth, C. and Shepherd, I. W.
- Booth, C.: *see* Maclaine, J. Q. G., Ashman, P. C. and Booth, C.
- Bossmann, Adelgund: *see* Berndt, H.-J. and Bossmann, Adelgund
- Bower, D. I.: *see* Nobbs, J.H., Bower, D. E. and Ward, I. M.
- Bower, D. I.: *see* Robinson, M. E. R., Bower, D. I. and Maddams, W. F.
- Boyer, Raymond F.: Mechanical motions in amorphous and semi-crystalline polymers, 996
- Boyer, R. F. and Miller, Robert L.: Polymer chain cross-section and the Mooney-Rivlin constants, 925. Chain atoms between entanglements and cross-sectional area per chain, 1112
- Bradbury, E. M.: *see* Stephens, R. M. and Bradbury, E. M.
- Brietenbach, J. W.: *see* Wolf, B. A., Bieringer, H. F. and Breitenbach, J. W.
- Brereton, M. G. and Rusli, A.: Configurational and dynamic flexibility of polymer chains, 395
- Brigodiot, M., Cheradame, H., Fontanille, M. and Vairon, J. P.: Microstructure of poly(2-vinylpyridine): correlation between ¹³C and ¹H n.m.r. determinations, 254
- Briscoe, B. J.: *see* Klein, J. and Briscoe, B. J.
- Briscoe, B. J. and Hutchings, I. M.: Impact yielding of high density polyethylene, 1099
- Brooks, B. W. and Qureshi, M. K.: Dis-

Author Index

- tribution and desorption of free radicals in the emulsion polymerization of styrene, 740
- Bunn, A.: *see* Cudby, M. E. A. and Bunn, A.
- Bunn, A. and Cudby, M. E. A.: Monomer sequence distribution in butene/propylene copolymers by ^{13}C nuclear magnetic resonance, 548
- Burchard, W.: *see* Gupta, A. K., Cotton, J. P., Marchal, E., Burchard, W. and Benoit, H.
- Burfield, D. R., McKenzie, I. D. and Tait, P. J. T.: Ziegler-Natta catalysis: 7. The settling period, 130
- Burfield, D. R., Chew, L. C. and Gan, S. N.: Distribution of abnormal groups in natural rubber, 713
- Burgess, F. J. and Richards, D. H.: Preparation and reactions of polymeric Grignard compounds, 1020
- Čačković, H.: *see* Loboda-Čačković, J., Hosemann, R., Čačković, H., Ferrero, F. and Ferracini, E.
- Čačković, H.: *see* Yeh, G. S. Y., Hosemann, R., Loboda-Čačković, J. and Čačković, H.
- Cafe, Michael C., Pryce, Norman G. and Robb, Ian D.: Spin-labelling of hydroxyl groups in polysaccharides, 91
- Cantow, H. J.: *see* Gronski, W., Murayama, N., Cantow, H.-J. and Miyamoto, T.
- Capaccio, G., Crompton, T. A. and Ward, I. M.: Ultra-high modulus polyethylene by high temperature drawing, 644
- Carraher, Charles E.: Synthesis and thermal characterization of hafnium polythioethers, 231
- Challa, G.: *see* de Boer, A. and Challa, G.
- Challa, G.: *see* Tan, Y. Y. and Challa, G.
- Champion, J. V., Dandridge, A., Downer, D., McGrath, J. C. and Meeten, G. H.: Optical anisotropy of polyisobutene, 511
- Champion, J. V., Meeten, G. H. and Southwell, G. W.: Electro-optic Kerr birefringence of polystyrenes in dilute solutions, 651
- Chantry, G. W.: *see* Jones, R. G., Nicol, Elisabeth A., Birch, J. R., Chantry, G. W., Fleming, J. W., Willis, H. A. and Cudby, M. E. A.
- Chaurasia, N. M., Kumar, Anil and Gupta, Santosh, K.: Viscosity-molecular weight concentration relationships beyond the critical region in polymer solutions and melts, 570
- Cheradame, H.: *see* Brigodiot, M., Cheradame, H., Fontanille, M. and Vairon, J. P.
- Chew, L. C.: *see* Burfield, D. R., Chew, L. C. and Gan, S. N.
- Chiellini, E.: *see* Conti, F., Acquaviva, L., Chiellini, E., Ciardelli, F., Delfini, M. and Segre, A. L.
- Chiellini, E., Solaro, R., Palmieri, M. and Ledwith, A.: Optically active vinyl polymers containing fluorescent groups: 1. Synthesis and properties of copolymers of *N*-vinylcarbazole with optically active monomers, 641
- Chiu, D. S., Takahashi, Y. and Mark, J. E.: Dimensions of poly(trimethylene oxide) chains in a theta-solvent, 670
- Ciardelli, F.: *see* Conti, F., Acquaviva, L., Chiellini, E., Ciardelli, F., Delfini, M. and Segre, A. L.
- Colonna-Cesari, F. and Premilat, S.: Structure refinement of α -poly(L-methionine): X-ray and conformational analysis, 267
- Conti, F., Acquaviva, L., Chiellini, E., Ciardelli, F., Delfini, M. and Segre, A. L.: ^{13}C n.m.r. study of optically active polymers: poly(4-methyl-1-hexene), 901
- Corsi, E., D'Alagni, M. and Giglio, E.: Interaction between sequential polypeptides and sodium deoxycholate, 259
- Cotton, J. P.: *see* Gupta, A. K., Cotton, J. P., Marchal, E., Burchard, W. and Benoit, H.
- Coulon, Christian; Spassky, Nicolas and Sigwalt, Pierre: Stereoelective polymerization of racemic propylene oxide using a diethylzinc-chiral-1,2-diol system as initiator, 821
- Counsell, P. J. C.: *see* Whitehouse, R. S., Counsell, P. J. C. and Lewis, G.
- Crompton, T. A.: *see* Capaccio, G., Crompton, T. A. and Ward, I. M.
- Croucher, T. G. and Wetton, R. E.: Synthesis of narrow distribution polytetrahydrofuran, 205
- Cudby, M. E. A.: *see* Bunn, A. and Cudby, M. E. A.
- Cudby, M. E. A. and Bunn, A.: Determination of chain branching in low density polyethylene by ^{13}C nuclear magnetic resonance and infra-red spectroscopy, 345
- Cudby, M. E. A.: *see* Jones, R. G., Nicol, Elisabeth A., Birch, J. R., Chantry, G. W., Fleming, J. W., Willis, H. A. and Cudby, M. E. A.
- Culver, L. E.: *see* Leever, P. S., Radon, J. C. and Culver, L. E.
- Cunningham, A., Manuel, A. J. and Ward, I. M.: Interpretation of broad line nuclear magnetic resonance in oriented poly(ethylene terephthalate), 125
- D'Alagni, M.: *see* Corsi, E., D'Alagni, M. and Giglio, E.
- D'Alagni, M., Giglio, E. and Pavel, N. V.: Potential energy calculations about the chain folding of α -poly(L-alanine), 257
- Dandridge, A.: *see* Champion, J. V., Dandridge, A., Downer, D., McGrath, J. C. and Meeten, G. H.
- Daryanani, R.: *see* Noordermeer, J. W. M., Daryanani, R. and Janeschitz-Kriegl, H.
- Daveloose, D.: *see* Rietsch, F., Daveloose, D. and Froelich, D.
- de Boer, A. and Challa, G.: Association of stereoregular poly(methyl methacrylates): 3. Thermal behaviour and composition of stereocomplex, 633
- Dębska-Koźłowska, M. and Kielich, S.: Effect of macromolecular length on anisotropic scattering of light in an electric field, 1039
- de Candia, F.: *see* Araimo, L., de Candia, F. and Vittoria, V.
- de Candia, Francesco: *see* Pedemonte, Enrico; Dondero, Giovanni; de Candia, Francesco and Romano, Gennaro
- de Candia, F., Tagliatela, A. and Vittoria, V.: Photoelastic non-equilibrium behaviour of natural rubber networks, 732
- De Chirico, A.: *see* Sorta, E. and De Chirico, A.
- de Fornasari, E.: *see* Manaresi, P., Parrini, P., Semeghini, G. L. and de Fornasari, E.
- Delfini, M.: *see* Conti, F., Acquaviva, L., Chiellini, E., Ciardelli, F., Delfini, M. and Segre, A. L.
- Di Meo, A., Maglio, G., Martuscelli, E. and Palumbo, R.: Effect of intrachain double bonds on the melt crystallization of aliphatic polyesters, 802
- Długosz, J., Fraser, G. V., Grubb, D., Keller, A., Odell, J. A. and Goggin, P. L.: Study of crystallization and isothermal thickening in polyethylene using SAXD, low frequency Raman spectroscopy and electron microscopy, 471
- Dolden, John G.: Structure-property relationships in amorphous polyamides, 875
- Domb, C. and Barrett, A. J.: Universality approach to the expansion factor of a polymer chain, 179
- Dondero, Giovanni: *see* Pedemonte, Enrico; Alfonso, Giovanni Carlo and Dondero, Giovanni
- Dondero, Giovanni: *see* Pedemonte, Enrico; Dondero, Giovanni; de Candia, Francesco and Romano, Gennaro
- Douglass, D. C.: *see* Wardell, G. E., Douglass, D. C. and McBrierty, V. J.
- Downer, D.: *see* Champion, J. V., Dandridge, A., Downer, D., McGrath, J. C. and Meeten, G. H.
- Droli, E.: *see* Hopfenberg, H. B., Nicolais, L. and Droli, E.
- Duckett, R. A. and Joseph, S. H.: Time dependent effects of pressure on the shear modulus of polypropylene, 329
- Dyball, C. J.: *see* Bevington, J. C. and Dyball, C. J.
- Eastmond, G. C. and Smith, E. G.: Some morphological aspects of AB crosslinked polymers, 367
- Ebdon, J. R. and Huckerby, T. N.: Simple and direct assignment of

- the methylene and methine ^{13}C resonances in polystyrene, 170
- Edwards, S. F.: Theory of glasses, 933
- Egerton, P. L.: *see* Allen, G., Egerton, P. L. and Walsh, D. J.
- Epton, R., Holding, S. R. and McLaren, J. V.: Synthesis and characterization of poly(acryloyl morpholine) xerogel networks suitable for the gel permeation chromatography of small molecules, 843
- Evans, R. A. and Hallam, H. E.: Laser-Raman spectroscopic studies of mechanically-loaded polymers, 838
- Fatou, J. M. G.: *see* Riande, E. and Fatou, J. M. G.
- Fenner, R. T.: *see* Yi, B. and Fenner, R. T.
- Ferracini, E.: *see* Loboda-Čačković, J., Hosemann, R., Čačković, H., Ferrero, F. and Ferracini, E.
- Ferrero, F.: *see* Loboda-Čačković, J., Hosemann, R., Čačković, H., Ferrero, F. and Ferracini, E.
- Fitzgerald, P. A.: *see* Hay, J. N., Fitzgerald, P. A. and Wiles, M.
- Fleming, J. W.: *see* Jones, R. G., Nicol, Elisabeth A., Birch, J. R., Chantry, G. W., Fleming, J. W., Willis, H. A. and Cudby, M. E. A.
- Folkes, M. J.: *see* Arridge, R. G. C. and Folkes, M. J.
- Fontanille, M.: *see* Brigodiot, M., Cheradame, H., Fontanille, M. and Vairon, J. P.
- Fortunato, B.: *see* Passalacqua, V., Pilati, F., Zamboni, V., Fortunato, B. and Manaresi, P.
- Foweraker, A. R. and Jennings, B. R.: Electric birefringence of aqueous solutions of methyl cellulose, 508
- Fraser, G. V.: *see* Dlugosz, J., Fraser, G. V., Grubb, D., Keller, A., Odell, J. A. and Goggin, P. L.
- Froehling, P. E., Koenhen, D. M., Bantjes, A. and Smolders, C. A.: Swelling of linear polymers in mixed swelling agents: predictability by means of solubility parameters, 835
- Froelich, D.: *see* Rietsch, F., Daveloose, D. and Froelich, D.
- Froix, Michael, F. and Goedde, Andreas O.: Effect of molecular oxygen on the n.m.r. relaxation times of some aromatic polymers, 758
- Fujita, H.: *see* Omura, I., Lee, D. C., Itou, S., Teramoto, A. and Fujita, H.
- Gabbay, S. M. and Stivala, S. S.: Thermal oxidation of poly(1-pentene): 1. Identification of products and mechanisms, 61. Infra-red study of poly(1-pentene) and poly(4-methyl-1-pentene), 121. Kinetics of the thermal oxidation of poly(4-methyl-1-pentene), 137
- Gallo, Bianca M.: *see* Bontà, Giorgio; Gallo, Bianca M.; Russo, Saverio and Uliana, Claudio
- Gan, S. N.: *see* Burfield, D. R., Chew, L. C. and Gan, S. N.
- Garner, David P.: *see* Seymour, Raymond B. and Garner, David P.
- Gaymans, R. J., Tjissen, J., Harkema, S. and Bantjes, A.: Elastic modulus in the crystalline region of poly(*p*-phenylene terephthalamide), 517
- Gazicki, M.: *see* Wróbel, A. M., Kryszewski, M. and Gazicki, M.
- Ghotra, J. S.: *see* Stevens, G. C., Ando, D. J., Bloor, D. and Ghotra, J. S.
- Giglio, E.: *see* Corsi, E., D'Alagni, M. and Giglio, E.
- Giglio, E.: *see* D'Alagni, M., Giglio, E. and Pavel, N. V.
- Gilbert, M.: *see* Gray, A. and Gilbert, M.
- Gledhill, R. A. and Kinloch, A. J.: Failure criterion for the fracture of structural adhesive joints, 727
- Goedde, Andreas O.: *see* Froix, Michael F. and Goedde, Andreas O.
- Goggin, P. L.: *see* Dlugosz, J., Fraser, G. V., Grubb, D., Keller, A., Odell, J. A. and Goggin, P. L.
- Goncalves, José M.: *see* Hampe, Oscar G. and Goncalves, José M.
- Gradwell, A. J.: *see* Batty, N. S., Gradwell, A. J. and Guthrie, J. T.
- Gradwell, A. J. and Guthrie, J. T.: Novel synthesis of 2-vinylanthraquinone, 643
- Graham, I. D., Williams, J. G. and Zichy, E. L.: Craze kinetics for PMMA in liquids, 439
- Gray, A. and Gilbert, M.: Structural order in heat treated vinyl chloride polymers, 44
- Gray, R. Walter: *see* Alper, Turhan; Barlow, A. John, and Gray, R. Walter
- Greco, R. and Nicolais, L.: Glass transition temperature in nylons, 1049
- Griffiths, J. and Hawkins, C.: The involvement of singlet oxygen in the sensitized photodegradation of cellulose, 1113
- Griffiths, Marion D. and Maisey, L. J.: On the reproducibility of T_g measurements on polystyrene using d.s.c., 869
- Gronski, W., Murayama, N., Cantow, H.-J. and Miyamoto, T.: On the structure of 3,4-*cis* 1,4-polyisoprene by ^{13}C n.m.r., 358
- Grubb, D.: *see* Dlugosz, J., Fraser, G. V., Grubb, D., Keller, A., Odell, J. A. and Goggin, P. L.
- Gryte, Carl C.: *see* Lovinger, Andrew J., Lau, Chi-Ming and Gryte, Carl C.
- Gupta, A. K., Cotton, J. P., Marchal, E., Burchard, W. and Benoit, H.: Persistence length of cellulose tricarbaniolate by small-angle neutron scattering, 363
- Gupta, Santosh K.: *see* Chaurasia, N. M., Kumar, Anil, and Gupta, Santosh K.
- Guthrie, J. T.: *see* Batty, N. S., Gradwell, A. J. and Guthrie, J. T.
- Guthrie, J. T.: *see* Gradwell, A. J. and Guthrie, J. T.
- Hall, I. H. and Pass, M. G.: Chain conformation of poly(tetramethylene terephthalate) and its change with strain, 807
- Hallam, H. E.: *see* Evans, R. A. and Hallam, L. E.
- Halmos, A. L.: *see* Shaprio, J., Halmos, A. L. and Pearson, J. R. A.
- Hampe, Oscar G. and Goncalves, José M.: Optical rotatory dispersion of crodamine: effect of denaturants, 638
- Hampson, F. W. and Manley, T. R.: A thermoanalytical comparison between ram and screw extruded polypropylene, 723
- Harkema, S.: *see* Gaymans, R. J., Tjissen, J., Harkema, S. and Bantjes, A.
- Harris, D. S.: *see* Hay, J. N., Harris, D. S. and Wiles, M.
- Harrison, I. R., Keller, A., Sadler, D. M. and Thomas, E. L.: A re-examination of the necessity of the mosaic concept in polymer crystals, 736
- Hartley, A., Leung, Y. K., Booth, C. and Shepherd, I. W.: Raman scattering from the longitudinal acoustic mode in crystalline poly(ethylene oxide), 354
- Hartley, A. J.: *see* Lindsay, S. M., Hartley, A. J. and Shepherd, I. W.
- Hashimoto, Takeji; Nagatoshi, Kikuo; Todo, Akira and Kawai, Hiromichi: Deformation mechanism of hard elastic polyethylene films, 1063. Superstructure of high density polyethylene film crystallized from stressed polymer melts as observed by small-angle light scattering, 1075
- Hatada, Koichi: *see* Yuki, Heimei; Okamoto, Yoshio; Shimada, Yoshiki; Ohta, Koji and Hatada, Koichi
- Hatakeyama, Hyoe: *see* Hatakeyama, Tatsuko; Yoshida, Hiroshi; Nagasaki, Chikage and Hatakeyama Hyoe
- Hatakeyama, Tatsuko; Yoshida, Hiroshi; Nagasaki, Chikage and Hatakeyama, Hyoe: Differential scanning calorimetric studies on phase transition of glucose and cellulose oligosaccharides, 559
- Haward, R. N.: *see* Adam, G. A., Hay, J. N., Parsons, I. W. and Haward, R. N.
- Haward, R. N.: *see* Owadh, A. A. J., Parsons, I. W., Hay, J. N. and Haward, R. N.
- Hawkins, C.: *see* Griffiths, J. and Hawkins, C.
- Hay, J. N.: *see* Adam, G. A., Hay, J. N., Parsons, I. W. and Haward, R. N.
- Hay, J. N.: *see* Owadh, A. A. J., Parsons, I. W., Hay, J. N. and Haward, R. N.
- Hay, J. N., Harris, D. S. and Wiles, M.: Polymerization of ethylene by *n*-butyl lithium, 613
- Hay, J. N., Fitzgerald, P. A. and Wiles, M.: Use of differential scanning calorimetry to study polymer crystallization kinetics, 1015

Author Index

- Hayakawa, Tadao: *see* Yamamoto, Hiroyuki; Miyazaki, Mihō and Hayakawa, Tadao
- Hayakawa, Tadao; Kondo, Yoshiyuki and Matsuyama, Masayo: Syntheses and conformational studies of poly(*S*-menthyloxycarbonylmethyl L- and D-cysteines), 1009
- Heatley, F. and Begum, Afrozi: Molecular motion of poly(methyl methacrylate), polystyrene and poly(propylene oxide) in solution studied by ¹³C n.m.r. spin-lattice relaxation measurements: effects due to distributions of correlation times, 399
- Heatley, F. and Walton, I.: Contributions to the proton relaxation of poly(ethylene oxide) in benzene solution, 1019
- Hepburn, Claude: *see* Mendis, Leslie P. and Hepburn, Claude
- Hetper, J.: *see* Lesiak, T., Hetper, J., Pielichowski, J., Prewysz-Kwinto, A. and Marzec, K.
- Higashimura, Tishinobu: *see* Yamamoto, Kenji and Higashimura, Tishinobu
- Hlavacek, B., Rollin, L. A. and Schreiber, H. P.: Drag reduction effectiveness of macromolecules, 81
- Hlavacek, B. and Schreiber, H. P.: Response of macromolecular structure to shear gradients, 435
- Hobbs, S. Y.: *see* Pratt, C. F. and Hobbs, S. Y.
- Hojabri, Fereidun: Effect of phosphine ligand on the activity of palladium/ π -catalysts, 58
- Hojabri, Fereidun; Mohaddes, Mir-Mohammad and Talab, Afiat: Palladium/ π -complexes as catalysts for olefin polymerization, 710
- Holding, S. R.: *see* Epton, R., Holding, S. R. and McLaren, J. V.
- Holt, C., Mackie, W. and Sellen, D. B.: Configuration of cellulose trinitrate in solution, 1027
- Hopfenberg, H. B., Nicolais, L. and Drioli, E.: Relaxation controlled (case II) transport of lower alcohols in poly(methyl methacrylate), 195
- Horlbeck, Gernot: *see* Neuse, Eberhard, W., Horlbeck, Gernot; Siesler, Heinz W. and Yannakou, Kleantes
- Hosemann, R.: *see* Loboda-Čačković, J., Hosemann, R., Čačković, H., Ferrero, F. and Ferracini, E.
- Hosemann, R.: *see* Yeh, G. S. Y., Hosemann, R., Loboda-Čačković, J. and Čačković, H.
- Hourston, D. J.: *see* Beamish, A. and Hourston, D. J.
- Huckerby, T. N.: *see* Ebdon, J. R. and Huckerby, T. N.
- Huglin, M. B. and Richards, R. W.: Differential refractometry and light scattering on nylon-6 and poly(methyl acrylate) in mixed solvents, 587
- Hutchings, I. M.: *see* Briscoe, B. J. and Hutchings, I. M.
- Imamura, Mikio: *see* Kijima, Tsuyoshi; Imamura, Mikio and Kusumoto, Naoshi
- Ishikawa, H.: *see* Nagura, Masanobu; Ishikawa, H., Tagawa, Hiroyuki and Wada, Eiichi
- Itou, S.: *see* Omura, I., Lee, D. C., Itou, S., Teramoto, A. and Fujita, H.
- Ivin, K. J., Kuan-Essig, L. C., Lillie, E. D. and Watt, P.: ¹³C n.m.r. spectra of some (*N*-acyliminoalkenes), 656
- Jackson, D. A.: *see* Bedborough, D. S. and Jackson, D. A.
- Janeschitz-Kriegl, H.: *see* Noordermeer, J. W. M., Daryanani, R. and Janeschitz-Kriegl, H.
- Jennings, B. R.: *see* Foweraker, A. R. and Jennings, B. R.
- Johnson, Julian F.: *see* Bartick, Edward G. and Johnson, Julian F.
- Johnson, Julian F.: *see* Mirabella, Francis, M., Barrall, Edward M. and Johnson, Julian F.
- Jones, R. G., Nicol, Elisabeth, A., Birch, J. R., Chantry, G. W., Fleming, J. W., Willis, H. A. and Cudby, M. E. A.: Polarized far infra-red studies of hot-drawn polytetrafluoroethylene, 153
- Joseph, S. H.: *see* Duckett, R. A. and Joseph, S. H.
- Kajiwara, M. and Saito, H.: Phosphonitrilic chloride: 33. Cyclomatrixphosphazene polymers formed from hexachlorocyclotriphosphazene and metal acetates, 319. Phosphonitrilic chloride: 34. Electrical conductivity of polybisaminophosphazenes, 1013
- Kajiwara, M., Mori, Y. and Saito, H.: Phosphonitrilic chloride: polymerization behaviour of some hexaalkoxycyclotriphosphazenes, 898
- Kampouris, Emmanuel M.: New solid state polyamidation process, 409
- Kaneko, Motozo: *see* Saeki, Susumu; Kuwahara, Nobuhiro; Nakata, Mitsuo and Kaneko, Motozo
- Katabe, Yasuo: *see* Nang, Tran Dai; Katabe, Yasuo and Minoura, Yuji
- Kawai, Hiromichi: *see* Hashimoto, Takeji; Nagatoshi, Kikuo; Todo, Akira and Kawai, Hiromichi
- Keller, A.: *see* Dlugosz, J., Fraser, G. V., Grubb, D., Keller, A., Odell, J. A. and Goggin, P. L.
- Keller, A.: *see* Harrison, I. R., Keller, A., Sadler, D. M. and Thomas, E. L.
- Keller, A.: *see* Sadler, D. M. and Keller, A.
- Klein, J. and Briscoe, B. J.: Diffusion of large molecules in polymers: measuring technique based on microdensitometry in the infra-red, 481
- Klesper, E.: *see* Barth, V. and Klesper, E.
- Klesper, Ernst and Barth, Volker: Rate constants during the hydrolysis of syndiotactic poly(methyl methacrylate) with base, 787
- Khalifa, B. A.: *see* Bassett, D. C. and Khalifa, B. A.
- Khalifa, B. A.: *see* Bassett, D. C., Khalifa, B. A. and Olley, R. H.
- Khalifa, B. A. and Bassett, D. C.: Morphological study of chain-extended growth in polyethylene: 3. Annealing of solution-grown lamellae, 291
- Kielich, S.: *see* Debska-Kotlowska, M. and Kielich, S.
- Kijima, Tsuyoshi; Imamura, Mikio and Kusumoto, Naoshi: Effect of pressure on phase transition and morphology of bulk poly(*trans*-1,4-butadiene), 249
- Killmann, Erwin: Conformation and thermodynamics of adsorbed macromolecules at the liquid/solid interface, 864
- Kinloch, A. J.: *see* Gledhill, R. A. and Kinloch, A. J.
- Koenhen, D. M.: *see* Froehling, P. E., Koenhen, D. M., Bantjes, A. and Smolders, C. A.
- Kondo, Yoshiyuki: *see* Hayakawa, Tadao; Kondo, Yoshiyuki and Matsuyama, Masayo
- Kothandaraman, H.: *see* Vasudevan, T., Kothandaraman, H. and Santappa, M.
- Kryszewski, M.: *see* Wróbel, A. M., Kryszewski, M. and Gaziński, M.
- Kryszewski, M., Zielinski, M. and Sapieha, S.: Analysis of relaxation processes in methacrylate polymers by thermally stimulated discharge, 212
- Kuan-Essig, L. C.: *see* Ivin, K. J., Kuan-Essig, L. C., Lillie, E. D. and Watt, P.
- Kubo, Kenji; Kubota, Kenji and Ogino, Kazuyoshi: Osmotic pressures of moderately concentrated poly(γ -benzyl-L-glutamate) solutions in *N,N*-dimethylformamide, 919
- Kubota, Kenji: *see* Kubo, Kenji; Kubota, Kenji and Ogino, Kazuyoshi
- Kučera, M., Zahradníčková, A. and Majerová, K.: Coordinate polymerization of heterocycles: 1. Oligomerization of epichlorohydrin by TiCl₄, 519. 2. Oligomerization of tetrahydrofuran by TiCl₄ in the presence of acetyl chloride or epichlorohydrin, 528. 3. Oligomerization of tetrahydrofuran induced by TiCl₄ in the presence of acetyl chloride and epichlorohydrin, 535
- Kuhlmann, R. and Schnabel, W.: Laser flash photolysis investigations on primary processes of the sensitized polymerization of vinyl monomers: 1. Experiments with benzophenone, 419
- Kumar, Anil: *see* Chaurasia, N. M., Kumar, Anil and Gupta, Santosh, K.

- Kusumoto, Naoshi: *see* Kijima, Tsuyoshi; Imamura, Mikio and Kusumoto, Naoshi
- Kusumoto, N., Sano, S., Zaitso, N. and Motozato, Y.: Molecular motions and segmental size of vulcanized natural and acrylonitrile-butadiene rubbers by the spin-probe method, 448
- Kusy, R. P. and Turner, D. T.: Influence of the molecular weight of poly(methyl methacrylate) on fracture surface energy in notched tension, 161
- Kuwahara, Nobuhiro: *see* Saeki, Susumu; Kuwahara, Nobuhiro; Nakata, Mitsuo and Kaneko, Motozo
- Lau, Chi-Ming: *see* Lovinger, Andrew J., Lau, Chi-Ming and Gryte, Carl C.
- Lau, K. H. and Young, K.: Reaction field in anisotropic dielectrics, 7
- Leblanc, Jean L.: New slit die rheometer: some results with a butadiene-styrene block copolymer, 235
- Ledwith, A.: *see* Chiellini, E., Solaro, R., Palmieri, M. and Ledwith, A.
- Ledwith, A.: Molecular complexes in polymer synthesis—from Lewis acid adducts to exiplexes, 957
- Lee, D. C.: *see* Omura, I., Lee, D. C., Itou, S., Teramoto, A. and Fujita, H.
- Leevers, P. S., Radon, J. C. and Culver, L. E.: Crack growth in plastic panels under biaxial stress, 627
- Lelievre, J.: Theory of gelatinization in a starch-water-solute system, 854
- Le Poidevin, G. J.: *see* Blackadder, D. A. and Le Poidevin, G. J.
- Lesiak, T., Hetper, J., Pielichowski, J., Prewysz-Kwinto, A. and Marzec, K.: Application of gas chromatography to the analysis of thermal decomposition products of some sulphur containing polyurethanes, 1110
- Leung, Y. K.: *see* Hartley, A., Leung, Y. K., Booth, C. and Shepherd, I. W.
- Leung, Yu-Kwan: Thermodynamics of α,ω -methoxy-poly(ethylene oxide)/*n*-alkane systems by gas-liquid chromatography, 374
- Lewis, G.: *see* Whitehouse, R. S., Counsell, P. J. C. and Lewis, G.
- Lillie, E. D.: *see* Ivin, K. J., Kuan-Essig, L. C., Lillie, E. D. and Watt, P.
- Lindsay, S. M., Hartley, A. J. and Shepherd, I. W.: Multi-pass Fabry-Perot spectroscopy of polymers, 501
- Loboda-Čačković, J.: *see* Yeh, G. S. Y., Hosemann, R., Loboda-Čačković, J. and Čačković, H.
- Loboda-Čačković, J., Hosemann, R., Čačković, H., Ferrero, F. and Ferracini, E.: Monoclinic macrolattice of quenched and cold-drawn sheets of isotactic polypropylene, 303
- Longman, G.: *see* Schelten, J., Ballard, D. G. H., Wignall, G. D., Longman, G. and Schmatz, W.
- Longman, G. W., Wignall, G. D. and Sheldon, R. P.: Radial distribution functions from molten polyethylene by X-ray diffraction, 485
- Lovell, Richard and Windle, Alan H.: Analysis of wide-angle X-ray diffraction patterns of aligned glassy polymers with particular references to polystyrene, 488
- Lovinger, Andrew J., Lau, Chi-Ming and Gryte, Carl C.: Microstructure of directionally solidified poly(ethylene oxide), 581
- McBrierty, V. J.: *see* Wardell, G. E., Douglass, D. C. and McBrierty, V. J.
- McGrath, J. C.: *see* Champion, J. V., Dandridge, A., Downer, D., McGrath, J. C. and Meeten, G. H.
- McKenzie, I. D.: *see* Burfield, D. R., McKenzie, I. D. and Tait, P. J. T.
- McLaren, J. V.: *see* Epton, R., Holding, S. R. and McLaren, J. V.
- MacInnes, D. A.: Dynamics of solutions of entangled polymers, 1035
- Mackie, W.: *see* Holt, C., Mackie, W. and Sellen, D. B.
- Maclaine, J. Q. G., Ashman, P. C. and Booth, C.: Effect of chain structure on the melting of low molecular weight poly(ethylene oxide), 109
- Maddams, W. F.: *see* Robinson, M. E. R., Bower, D. I. and Maddams, W. F.
- Magill, J. H.: *see* Okui, N. and Magill, J. H.
- Maglio, G.: *see* Di Meo, A., Maglio, G., Martuscelli, E. and Palumbo, R.
- Maglio, G., Martuscelli, E., Palumbo, R. and Soldati, I.: Influence of intrachain *trans* double bonds on the melt crystallization of polyamides, 185
- Maisey, L. J.: *see* Griffiths, Marion D. and Maisey, L. J.
- Majerová, K.: *see* Kučera, M., Zahradničková, A. and Majerová, K.
- Manaresi, P.: *see* Passalacqua, V., Pilati, F., Zamboni, V., Fortunato, B. and Manaresi, P.
- Manaresi, P., Parrini, P., Semeghini, G. L. and de Fornasari, E.: Branched poly(ethylene terephthalate) correlations between viscosimetric properties and polymerization parameters, 595
- Mancarella, C., Martuscelli, E. and Pracella, M.: Influence of intrachain double bonds on the properties of solution grown single crystals of polyethylene, 541
- Manley, T. R.: *see* Hampson, F. W. and Manley, T. R.
- Manuel, A. J.: *see* Cunningham, A., Manuel, A. J. and Ward, I. M.
- Marchal, E.: *see* Gupta, A. K., Cotton, J. P., Marchal, E., Burchard, W. and Benoit, H.
- Mark, J. E.: *see* Chiu, D. S., Takahashi, Y. and Mark, J. E.
- Martuscelli, E.: *see* Di Meo, A., Maglio, G., Martuscelli, E., and Palumbo, R.
- Martuscelli, E.: *see* Maglio, G., Martuscelli, E., Palumbo, R. and Soldati, I.
- Martuscelli, E.: *see* Mancarella, C., Martuscelli, E. and Pracella, M.
- Marzec, K.: *see* Lesiak, T., Hetper, J., Pielichowski, J., Prewysz-Kwinto, A. and Marzec, K.
- Matsuyama, Masayo: *see* Hayakawa, Tadao; Kondo, Yoshiyuki and Matsuyama, Masayo
- Matui, S. and Aida, H.: Thermal stabilities of poly (*N*-alkyl maleimides), 199
- Meeten, G. H.: *see* Champion, J. V., Meeten, G. H. and Southwell, G. W.
- Meeten, G. H.: *see* Champion, J. V., Dandridge, A., Downer, D., McGrath, J. C. and Meeten, G. H.
- Mendis, Leslie P. and Hepburn, Claude: Multiple endotherms in polyepichlorohydrin, 551
- Meyer, C. T. and Pineri, M.: Ion-clustering and viscoelastic properties in poly(butadiene-styrene-4-vinylpyridine) crosslinked by nickel chloride, 382
- Miller, Robert L.: *see* Boyer, R. F. and Miller, Robert L.
- Mills, N. J. and Walker, N.: Craze growth and crack growth in poly(vinyl chloride) under monotonic and fatigue loading, 335
- Minoura, Yuji: *see* Nang, Tran Dai; Katabe, Yasuo and Minoura, Yuji
- Mirabella, Francis M., Barrall, Edward M. and Johnson, Julian F.: A rapid technique for the qualitative analysis of polymers and additives using stop-and-go g.p.c. and i.r., 17
- Miyamoto, T.: *see* Gronski, W., Murayama, N., Cantow, H.-J. and Miyamoto, T.
- Miyazaki, Miho: *see* Yamamoto, Hiroyuki; Miyazaki Miho and Hayakawa, Tadao
- Mohaddes, Mir-Mohammad: *see* Hojabri, Fereidun; Mohaddes, Mir-Mohammad and Talab, Afiat
- Montfort, J. P.: Rheological behaviour of blends of narrow molecular weight distribution polystyrenes in the molten state: dynamic viscoelastic properties in the terminal zone, 1054
- Morantz, D. J.: *see* Bilen, C. S. and Morantz, D. J.
- Mori, Y.: *see* Kajiwara, M., Mori, Y. and Saito, H.
- Motozato, Y.: *see* Kusumoto, N., Sano, S., Zaitso, N. and Motozato, Y.
- Müller, H.-G.: *see* Schurz, J. and Müller, H.-G.
- Mullik, S. U.: *see* Bamford, C. H. and Mullik, S. U.
- Murakami, Kenkichi: *see* Tamura, Saburo and Murakami, Kenkichi
- Murayama, N.: *see* Gronski, W., Murayama, N., Cantow, H.-J. and Miyamoto, T.

Author Index

- Nagasaki, Chikage: *see* Hatakeyama, Tatsuko; Yoshida, Hiroshi; Nagasaki, Chikage and Hatakeyama, Hyoe
- Nagatoshi, Kikuo: *see* Hashimoto, Takeji; Nagatoshi, Kikuo; Todo, Akira and Kawai, Hiromichi
- Nagura, Masanobu; Ishikawa, H., Tagawa, Hiroyuki and Wada, Eiichi: Structure of oligourethanes: 6. Fine structure of melt crystallized oligourethanes, 3
- Nair, P. K.: *see* Pillai, P. K. C., Agarwal, S. K. and Nair, P. K.
- Nair, P. K.: *see* Pillai, P. K. C., Nair, P. K. and Nath, Rabinder
- Nakata, Mitsuo: *see* Saeki, Susumu; Kuwahara, Nobuhiro; Nakata, Mitsuo and Kaneko, Motozo
- Nang, Tran Dai; Katabe, Yasuo and Minoura, Yuji: Diimide reduction of *cis*-1,4-polyisoprene with *p*-toluenesulphonylhydrazide, 117
- Nath, Rabinder: *see* Pillai, P. K. C., Nair, P. K. and Nath, Rabinder
- Neuse, Eberhard, W., Horlbeck, Gernot., Siesler, Heinz W. and Yannakou, Kleantes: Cobalticinium-bridged polybenzazoles: 1. Low temperature solution polymerization, 423
- Nicol, Elisabeth A.: *see* Jones, R. G., Nicol, Elisabeth A., Birch, J. R., Chantry, G. W., Fleming, J. W., Willis, H. A. and Cudby, M. E. A.
- Nicolais, L.: *see* Greco, R. and Nicolais, L.
- Nicolais, L.: *see* Hopfenberg, H. B., Nicolais, L. and Drioli, E.
- Nobbs, J. H., Bower, D. I. and Ward, I. M.: A study of molecular orientation in drawn and shrunk poly(ethylene terephthalate) by means of birefringence, polarized fluorescence and X-ray diffraction measurements, 25
- Noordermeer, J. W. M., Daryanani, R. and Janeschitz-Kriegl, H.: Non-Newtonian viscosity and non-linear flow birefringence of cellulose tricarbamate, 155
- Okamoto, Yoshio: *see* Yuki, Heimei; Okamoto, Yoshio; Shimada, Yoshiki; Ohta Koji and Hatada, Koichi
- Okui, N. and Magill, J. H.: Studies of the chemical degradation of polysiloxanes by hydrofluoric acid: 1. Poly(tetramethyl-*p*-silphenylene siloxane), 1086
- Olley, R. H.: *see* Bassett, D. C., Khalifa, B. A. and Olley, R. H.
- Omura, I., Lee, D. C., Itou, S., Teramoto, A. and Fujita, H.: Synthesis and characterization of poly(*ε*-carbobenzoxyl-L-lysyl- γ -benzyl-L-glutamate), 847
- Owadh, A. A. J., Parsons, I. W., Hay, J. N. and Haward, R. N.: Properties of nylon-1 polymers and copolymers, 926
- Palmieri, M.: *see* Chiellini, E., Solaro, R., Palmieri, M. and Ledwith, A.
- Palumbo, R.: *see* Di Meo, A., Maglio, G., Martuscelli, E. and Palumbo, R.
- Palumbo, R.: *see* Maglio, G., Martuscelli, E., Palumbo, R. and Soldati, I.
- Pannell, J.: Reaction between lithium polystyryl and iodinated polystyrene, 351
- Parrini, P.: *see* Manaresi, P., Parrini, P., Semeghini, G. L. and de Fornasari, E.
- Parrini, P., Romanini, D. and Righi, G. P.: Melt rheology of some aliphatic polyamides, 377
- Parsons, I. W.: *see* Adam, G. A., Hay, J. N., Parsons, I. W. and Haward, R. N.
- Parsons, I. W.: *see* Owadh, A. A. J., Parsons, I. W., Hay, J. N. and Haward, R. N.
- Pass, M. G.: *see* Hall, I. H. and Pass, M. G.
- Passalacqua, V., Pilati, F., Zamboni, V., Fortunato, B. and Manaresi, P.: Thermal degradation of poly(butylene terephthalate), 1044
- Pavel, N. V.: *see* D'Alagni, M., Giglio, E. and Pavel, N. V.
- Pearson, J.R. A.: *see* Shapiro, J., Halmos, A. L. and Pearson, J. R. A.
- Pedemonte, Enrico; Dondero, Giovanni; de Candia, Francesco and Romano, Gennaro: Correlation between physical-mechanical properties and morphological features of cruciform styrene-butadiene block copolymers, 72
- Pedemonte, Enrico; Alfonso, Giovanni Carlo and Dondero, Giovanni: Optical observations of partly molten fibres of poly(ethylene terephthalate), 923
- Perkins, J. D.: *see* Pollard, R. and Perkins, J. D.
- Pielichowski, J.: *see* Lesiak, T., Hetper, J., Pielichowski, J., Prewysz-Kwinto, A. and Marzec, K.
- Pilati, F.: *see* Passalacqua, V., Pilati, F., Zamboni, F., Fortunato, B. and Manaresi, P.
- Pillai, P. K. C. and Ahuja, R. C.: Persistent internal polarization studies in poly(*N*-vinylcarbazole)/trinitrofluorenone charge transfer complex, 192
- Pillai, P. K. C., Agarwal, S. K. and Nair, P. K.: On the field dependent photoconduction of poly(*N*-vinylcarbazole), 646
- Pillai, P. K. C., Nair, P. K. and Nath, Rabinder: Study of polymer cross-linking by thermally stimulated current, 921
- Pineri, M.: *see* Meyer, C. T. and Pineri, M.
- Pino, Piero and Suter, Ulrich W.: Some aspects of stereoregulation in the stereospecific polymerization of vinyl monomers, 977
- Pogany, G. A.: Anomalous diffusion of water in glassy polymers, 690
- Pollard, R. and Perkins, J. D.: Cooling of a polymer sheet, 1103
- Pourassamy, A.: *see* Rao, R. M. V. G. K. and Pourassamy, A.
- Pracella, M.: *see* Mancarella, C., Martuscelli, E. and Pracella, M.
- Pratt, C. F. and Hobbs, S. Y.: Comparative study of crystallization rates by d.s.c. and depolarization microscopy, 12
- Premilat, S.: *see* Colonna-Cesari, F. and Premilat, S.
- Prewysz-Kwinto, A.: *see* Lesiak, T., Hetper, J., Pielichowski, J., Prewysz-Kwinto, A. and Marzec, K.
- Pryce, Norman G.: *see* Cafe, Michael C., Pryce, Norman G. and Robb, Ian D.
- Qureshi, M. K.: *see* Brooks, B. W. and Qureshi, M. K.
- Rabie, Abdelgawad: *see* Odian, George and Rabie, Abdelgawad
- Radon, J. C.: *see* Leever, P. S., Radon, J. C. and Culver, L. E.
- Rao, R. M. V. G. K. and Pourassamy, A.: Studies on the curing of a loaded unsaturated polyester binder, 611
- Rayner, M. G.: *see* Ballard, D. G. H., Rayner, M. G. and Schelten, J.
- Riande, E. and Fatou, J. M. G.: Crystallization of dilute polyethylene solutions: influence of molecular weight, 99. Effect of solvent on the crystallization from dilute polyethylene solutions, 795
- Richards, D. H.: *see* Burgess, F. J. and Richards, D. H.
- Richards, R. W.: *see* Huglin, M. B. and Richards, R. W.
- Rietsch, F., Daveloose, D. and Froelich, D.: Glass transition temperature of ideal polymeric networks, 859
- Righi, G. P.: *see* Parrini, P., Romanini, D. and Righi, G. P.
- Robb, Ian D.: *see* Cafe, Michael C., Pryce, Norman G. and Robb, Ian D.

- Robinson, M. E. R., Bower, D. I. and Maddams, W. F.: Intermolecular forces and the Raman spectrum of crystalline PVC, 355
- Rollin, L. A.: *see* Hlavacek, B., Rollin, L. A. and Schreiber, H. P.
- Romanini, D.: *see* Parrini, P., Romanini, D. and Righi, G. P.
- Romano, Gennaro: *see* Pedemonte, Enrico; Dondero, Giovanni; de Candia, Francesco and Romano, Gennaro
- Rooney, M. L.: Interesterification of starch with methyl palmitate, 555
- Roovers, J. E. L.: Crown ether catalyzed modification of partly chloromethylated polystyrene, 1107
- Rusli, A.: *see* Brereton, M. G. and Rusli, A.
- Russo, Saverio: *see* Bontà, Giorgio; Gallo, Bianca M.; Russo, Saverio and Uliana, Claudio
- Sadler, D. M.: *see* Harrison, I. R., Keller, A., Sadler, D. M. and Thomas, E. L.
- Sadler, D. M. and Keller, A.: Trajectory of polyethylene chains in single crystals by low angle neutron scattering, 37
- Saeki, Susumu; Kuwahara, Nobuhiro; Nakata, Mitsuo and Kaneko, Motozo: Upper and lower critical solution temperatures in poly(ethylene glycol) solutions, 685
- Saito, H.: *see* Kajiwara, M. and Saito, H.
- Saito, H.: *see* Kajiwara, M., Mori, Y. and Saito, H.
- Sano, S.: *see* Kusumoto, N., Sano, S., Zaito, N. and Motozato, Y.
- Santappa, M.: *see* Vasudevan, T., Kothandaraman, H. and Santappa, M.
- Sapieha, S.: *see* Kryszewski, M., Zielinski, M. and Sapieha, S.
- Sato, Hisaya: *see* Tanaka, Yasuyuki and Sato, Hisaya
- Scales, L. E. and Semlyen, J. A.: Equilibrium ring concentrations and the statistical conformations of polymer chains: 14. Calculation of the concentrations of medium sized cyclics in poly(dimethyl siloxane) equilibrate, 601
- Schelten, J.: *see* Ballard, D. G. H., Rayner, M. G. and Schelten, J.
- Schelten, J., Ballard, D. G. H., Wignall, G. D., Longman, G. and Schmatz, W.: Small-angle neutron scattering studies of molten and crystalline polyethylene, 751
- Schmatz, W.: *see* Schelten, J., Ballard, D. G. H., Wignall, G. D., Longman, G. and Schmatz, W.
- Schnabel, W.: *see* Kuhlmann, R. and Schnabel, W.
- Schreiber, H. P.: *see* Hlavacek, B. and Schreiber, H. P.
- Schreiber, H. P.: *see* Hlavacek, B., Rollin, L. A. and Schreiber, H. P.
- Schurz, J. and Müller, H.-G.: Stored elasticity in flowing solutions of polyisobutylene as measured by recoil, 246
- Śędziński, K.: Radiation curing of unsaturated polyester resin, 261
- Segre, A. L.: *see* Conti, F., Acquaviva, L., Chiellini, E., Ciardelli, F., Delfini, M. and Segre, A. L.
- Sellen, D. B.: *see* Holt, C., Mackie, W. and Sellen, D. B.
- Semeghini, G. L.: *see* Manaresi, P., Parrini, P., Semeghini, G. L. and de Fornasari, E.
- Semlyen, J. A.: *see* Scales, L. E. and Semlyen, J. A.
- Seymour, Raymond B. and Garner, David P.: Relationship of temperature to composition of copolymers of α -methylstyrene and maleic anhydride, 21
- Shapiro, J., Halmos, A. L. and Pearson, J. R. A.: Melting in single screw extruders, 905
- Shea, S. C.: A method for the calculation of optimum filler content in amorphous and semi-crystalline polymers, 836
- Shea, S. C. and Berry, J. P.: Some aspects of flame retardancy in high density polyethylene, 1095
- Sheldon, R. P.: *see* Longman, G. W., Wignall, G. D. and Sheldon, R. P.
- Shepherd, I. W.: *see* Hartley, A., Leung, Y. K., Booth, C. and Shephard, I. W.
- Shepherd, I. W.: *see* Lindsay, S. M., Hartley, A. J. and Shepherd, I. W.
- Shimada, Yoshiki: *see* Yuki, Heimei; Okamoto, Yoshio; Shimada, Yoshiki; Ohta, Koji and Hatada, Koichi
- Siesler, Heinz W.: *see* Neuse, Eberhard W., Horlbeck, Gernot; Siesler, Heinz W. and Yannakou, Kleantes
- Sigwalt, Pierre: *see* Coulon, Christian; Spassky, Nicolas and Sigwalt, Pierre
- Smith, E. G.: *see* Eastmond, G. C. and Smith, E. G.
- Smith, Edward G.: Pulsed n.m.r. studies of molecular motion in wet nylon-6,6 fibres, 761
- Smolders, C. A.: *see* Froehling, P. E., Koenhen, D. M., Bantjes, A. and Smolders, C. A.
- Solaro, R.: *see* Chiellini, E., Solaro, R., Palmieri, M. and Ledwith, A.
- Soldati, I.: *see* Maglio, G., Martuscelli, E., Palumbo, R. and Soldati, I.
- Sorta, E. and De Chirico, A.: Glass transition temperature determination of poly(ethylene sulphide), poly(isobutylene sulphide) and their random copolymers, 348
- Southwart, David W.: Comparison of bound rubber and swelling in silicone rubber/silica mixes and in silicone rubber vulcanizates, 147. Filler enhancement of rubber modulus, 734
- Southwell, G. W.: *see* Champion, J. V., Meeten, G. H. and Southwell, G. W.
- Spassky, Nicolas: *see* Coulon, Christian; Spassky, Nicolas and Sigwalt, Pierre
- Stephens, R. M. and Bradbury, E. M.: Interaction between carboxylic acids and the peptide group, 563
- Stevens, G. C., Ando, D. J., Bloor, D. and Ghotra, J. S.: Transition metal impurities in crystalline conjugated polymer, 623
- Stivala, S. S.: *see* Gabbay, S. M. and Stivala, S. S.
- Stoohart, Philip H.: Small-angle X-ray scattering from ultrathin films of cellulose acetate, 93
- Suehiro, K., Tanizaki, H. and Takayanagi, M.: X-ray studies of surface melting in single crystals of linear polyethylene, 1059
- Suter, Ulrich W.: *see* Pino, Piero and Suter, Ulrich W.
- Szewczyk, Pawel: A new approach in permeation chromatography calibration, 90
- Szwarc, M.: *see* Wong, P. K., Zachariades, A. E. and Szwarc, M.
- Tagawa, Hiroyuki: *see* Nagura, Masanobu; Ishikawa, H., Tagawa, Hiroyuki and Wada, Eiichi
- Tagliatalata, A.: *see* de Candia, F., Tagliatalata, A. and Vittoria, V.
- Tait, P. J. T.: *see* Burfield, D. R., McKenzie, I. D. and Tait, P. J. T.
- Takahashi, Y.: *see* Chiu, D. S., Takahashi, Y. and Mark, J. E.
- Takayanagi, M.: *see* Suehiro, K., Tanizaki, H. and Takayanagi, M.
- Talab, Afiat: *see* Hojabri, Fereidun; Mohaddes, Mir-Mohammad and Talab, Afiat
- Tamura, Saburo and Murakami, Kenkichi: Chemorheology of irradiation-cured natural rubbers: 2. Stress relaxation mechanisms of sulphur-containing cured systems in air, 325
- Tan, Y. Y. and Challa, G.: The glass transition temperature of poly(*N*-vinyl pyrrolidone) and the effect of water, 739
- Tanaka, Yasuyuki and Sato, Hisaya: Sequence distribution of *cis*-1,4- and *trans*-1,4-units in polyisoprenes, 113. Sequence distribution of polyisoprenes, 413
- Tanizaki, H.: *see* Suehiro, K., Tanizaki, H. and Takayanagi, M.
- Teramoto, A.: *see* Omura, I., Lee, D. C., Itou, S., Teramoto, A. and Fujita, H.
- Thomas, E. L.: *see* Harrison, I. R., Keller, A., Sadler, D. M. and Thomas, E. L.
- Tijssen, J.: *see* Gaymans, R. J., Tijssen, J., Harkema, S. and Bantjes, A.
- Todo, Akira: *see* Hashimoto, Takeji; Nagatoshi, Kikuo; Todo, Akira and Kawai, Hiromichi
- Tomita, Kosuke: Studies on the formation of poly(ethylene terephthalate): 6. Catalytic activity of metal compounds in polycondensation of bis(2-hydroxyethyl) terephthalate, 221

Author Index

- Tonelli, Alan E.: Polyethylene and polytetrafluorethylene crystals: chain folding entropy of fusion and lamellar thickness, 695
- Treloar, L. R. G.: Swelling of bonded-rubber cylinders, 142
- Tsebrenko, M. V., Yudin, A. V., Ablazova, T. I. and Vinogradov, G. V.: Mechanism of fibrillation in the flow of molten polymer mixtures, 831
- Turner, D. T.: *see* Kusy, R. P. and Turner, D. T.
- Uliana, Claudio: *see* Bontà, Giorgio; Gallo, Bianca M.; Russo, Saverio and Uliana, Claudio
- Vairon, J. P.: *see* Brigodiot, M., Cheradame, H., Fontanille, M. and Vairon, J. P.
- Valko, L.: *see* Bleha, T. and Valko, L.
- Vasudevan, T., Kothandaraman, H. and Santappa, M.: Grafting onto poly(vinyl alcohol): a new spectral method to estimate the extent of grafting, 1108
- Vinogradov, G. V.: *see* Tsebrenko, M. V., Yudin, A. V., Ablazova, T. I. and Vinogradov, G. V.
- Vittoria, V.: *see* Araimo, L., de Candia, F. and Vittoria, V.
- Vittoria, V.: *see* de Candia, F.; Tagliatala, A. and Vittoria, V.
- Wada, Eiichi: *see* Nagura, Masanobu.; Ishikawa, H., Tagawa, Hiroyuki and Wada, Eiichi
- Walker, N.: *see* Mills, N. J. and Walker, N.
- Walsh, D. J.: *see* Allen, G., Egerton, P. L. and Walsh, D. J.
- Walton, I.: *see* Heatley, F. and Walton, I.
- Ward, I. M.: *see* Capaccio, G., Crompton, T. A. and Ward, I. M.
- Ward, I. M.: *see* Cunningham, A., Manuel, A. J. and Ward, I. M.
- Ward, I. M.: *see* Nobbs, J. H., Bower, D. E. and Ward, I. M.
- Wardell, G. E., Douglass, D. C. and McBrierty, V. J.: Pulsed n.m.r. of a SBS 'macroscopic single crystal', 41
- Watt, Ian C.: Directional diffusion rates in keratin, 748
- Watt, P.: *see* Ivin, K. J., Kuan-Essig, L. C., Lillie, E. D. and Watt, P.
- Wetton, R. E.: *see* Croucher, T. G. and Wetton, R. E.
- Whitehouse, R. S., Counsell, P. J. C. and Lewis, G.: Composition of rubber/resin adhesive films: 1. Surface composition as determined by ATR spectroscopy, 699
- Wignall, G. D.: *see* Longman, G. W., Wignall, G. D. and Sheldon, R. P.
- Wignall, G. D.: *see* Schelten, J., Ballard, D. G. H., Wignall, G. D., Longman, G. and Schmatz, W.
- Wiles, M.: *see* Hay, J. N., Fitzgerald, P. A. and Wiles, M.
- Wiles, M.: *see* Hay, J. N., Harris, D. S. and Wiles, M.
- Willbourn, Anthony H.: Molecular design of polymers, 965
- Williams, J. G.: *see* Graham, I. D., Williams, J. G. and Zichy, E. L.
- Willis, H. A.: *see* Jones, R. G., Nicol, Elisabeth A., Birch, J. R., Chantry, G. W., Fleming, J. W., Willis, H. A. and Cudby, M. E. A.
- Windle, Alan H.: *see* Lovell, Richard and Windle, Alan H.
- Wolf, B. A., Bieringer, H. F. and Breitenbach, J. W.: Comparison of the unperturbed dimension of polystyrene for endothermal and exothermal heats of dilution within the same system, 605
- Wong, P. K., Zachariades, A. E. and Szwarc, M.: Block polymers of poly(*para*-xylene) and polystyrene or poly(vinyl pyridine) prepared by anionic polymerization, 817
- Wright, D. C.: Creep behaviour of annealed UPVC and PMMA, 77
- Wróbel, A. M., Kryszewski, M. and Gazicki, M.: Mechanism of polysilazane thin film formation during glow discharge polymerization of hexamethylcyclotrisilazane, 673. Structure of glow discharge polysilazane thin films, 678
- Yamamoto, Hiroyuki; Miyazaki, Miho and Hayakawa, Tadao: Syntheses and conformational studies of poly(γ -*N*-alkyl-L- α , γ -diaminobutyric acids) and their carbobenzoxy derivatives, 429
- Yamamoto, Hiroyuki: Conformational study of poly(*O*-carbobenzoxy-L-tyrosine) in solution, 1105
- Yamamoto, Kenji and Higashimura, Toshinobu: Salt effect on cationic copolymerization between *cis*- and *trans*-ethyl propenyl ethers, 828
- Yannakou, Kleanthes: *see* Neuse, Eberhard, W., Horlbeck, Gernot; Siesler, Heinz W. and Yannakou, Kleanthes
- Yeh, G. S. Y., Hosemann, R., Loboda-Čačković, J. and Čačković, H.: Annealing effects of polymers and their underlying molecular mechanisms, 309
- Yi, B. and Fenner, R. T.: Melting of polymers in narrow annular shear devices, 443
- Yoshida, Hiroshi: *see* Hatakeyama, Tatsuko; Yoshida, Hiroshi; Nagasaki, Chikage and Hatakeyama, Hyoe
- Young, K.: *see* Lau, K. H. and Young, K.
- Young, Robert J. and Beaumont, Peter W. R.: Time-dependent failure of poly(methyl methacrylate), 717
- Yudin, A. V.: *see* Tsebrenko, M. V., Yudin, A. V., Ablazova, T. I. and Vinogradov, G. V.
- Yuki, Heimei; Okamoto, Yoshio; Shimada, Yoshiki; Ohta, Koji and Hatada, Koichi: Stereospecific anionic polymerization of 1,1-diphenylethyl methacrylate, 618
- Zachariades, A. E.: *see* Wong, P. K., Zachariades, A. E. and Szwarc, M.
- Zahradnicková, A.: *see* Kučera, M., Zahradnicková, A. and Majerová, K.
- Zaitso, N.: *see* Kusumoto, N., Sano, S., Zaitso, N. and Motozato, Y.
- Zamboni, V.: *see* Passalacqua, V., Pilati, F., Zamboni, V., Fortunato, B. and Manaresi, P.
- Zichy, E. L.: *see* Graham, I. D., Williams, J. G. and Zichy, E. L.
- Zielinski, M.: *see* Kryszewski, M., Zielinski, M. and Sapieha, S.
- Zoller, P.: Optical anisotropy and orientation of structural units, 167

POLYMER

*the science and technology of
polymers and biopolymers*

- 3 Structure of oligourethanes: 6. Fine structure of melt crystallized oligourethanes
Masanobu Nagura, H. Ishikawa, Hiroyuki Tagawa and Eiichi Wada
- 7 Reaction field in anisotropic dielectrics
K. H. Lau and K. Young
- 12 Comparative study of crystallization rates by d.s.c. and depolarization microscopy
C. F. Pratt and S. Y. Hobbs
- 17 A rapid technique for the qualitative analysis of polymers and additives using stop-and-go g.p.c. and i.r.
Francis M. Mirabella Jr, Edward M. Barrall II and Julian F. Johnson
- 21 Relationship of temperature to composition of copolymers of α -methylstyrene and maleic anhydride
Raymond B. Seymour and David P. Garner
- 25 A study of molecular orientation in drawn and shrunk poly(ethylene terephthalate) by means of birefringence, polarized fluorescence and X-ray diffraction measurements
J. H. Nobbs, D. I. Bower and I. M. Ward
- 37 Trajectory of polyethylene chains in single crystals by low angle neutron scattering
D. M. Sadler and A. Keller
- 41 Pulsed n.m.r. of a SBS 'macroscopic single crystal'
G. E. Wardell, D. C. Douglass and V. J. McBrierty
- 44 Structural order in heat treated vinyl chloride polymers
A. Gray and M. Gilbert
- 51 Effect of molecular weight on the thermal properties of polycarbonates
G. A. Adam, J. N. Hay, I. W. Parsons and R. N. Haward
- 58 Effect of phosphine ligand on the activity of palladium/II-catalysts
Fereidun Hojabri
- 61 Thermal oxidation of poly(1-pentene): 1. Identification of products and mechanisms
S. M. Gabbay and S. S. Stivala
- 65 Model polyurethane networks
G. Allen, P. L. Egerton and D. J. Walsh
- 72 Correlation between physical-mechanical properties and morphological features of cruciform styrene-butadiene block copolymers
Enrico Pedemonte, Giovanni Dondero, Francesco de Candia and Gennaro Romano
- 77 Creep behaviour of annealed UPVC and PMMA
D. C. Wright

(continued on next page)